Oil Recovery

Field Demonstrations

Progam Class I

Department of Energy

Contact Information

General Information

NPTO/NETL
918.699.2000

Bernadette Ward
918.699.2033

Publications & Copies

Oletha Thompson
918.699.2034

Instructions

Finding words in PDF documents

You can use the find command to **Find** a complete word or part of a word in the current PDF document. Acrobat looks for the word by reading every word on every page in the file, including text in the form fields.

To find a word using the Find command:

1. Click the Find button , or choose Edit > Find.
2. Enter the text to find in the text box.
3. Select search options if necessary:

   Match Whole Word Only finds only occurrences of the complete word you enter in the text box. For example, if you search for the word stick, the words tick and sticky will not be highlighted.

   Match Case finds only words that contain exactly the same capitalization you enter in the text box.

   Find Backwards starts the search from the current page and goes backward through the document.
4. Click Find. Acrobat finds the next occurrence of the word.

To find the next occurrence of the word:

Do one of the following:

Choose Edit > Find Again.

Reopen the Find dialog box, and click Find Again. (The word must already be in the Find text box.)

Contact: General information - NPTO 918.699.2000
Bernadette Ward 918.699.2033
Publications & Copies - Oletha Thompson 918.699.2034

Credits: Cover Photo: Mississippi River Delta - Credits: NASA photo courtesy of Dr. William Muhlburger and Dr. Paul Knox, University of Texas, Austin

Design: RMC Consultants, Incorporated, Tulsa, OK

Table of Contents

Overview

Class I Oil Recovery Projects

Amoco Exploration and Production Company
West Hackberry Tertiary Project - Louisiana
DE-FC22-93BC14963

Bureau of Economic Geology
Revitalizing a Mature Oil Play - Texas
DE-FC22-93BC14959

Columbia University
Dynamic Enhanced Recovery Technologies - Louisiana
DE-FC22-93BC14961

Diversified Operating Corporation
Advanced Secondary Recovery Project for the Sooner "D" Sand Unit - Colorado
DE-FC22-93BC14954

Hughes Eastern Corporation
The Utilization of Microflora Indigenous to Selectively Plug Porous Zones
to Increase Oil Recovery during Water Flooding - Alabama
DE-FC22-94BC14962

Lomax/Inland Resources, Incorporated
Green River Formation Waterflood - Utah
DE-FC22-93BC14958

Texaco E&P
Post Waterflood CO2 Miscible Flood in Light Oil Fluvial-Dominated
Deltaic Reservoirs - Texas
DE-FC22-93BC14960

University of Kansas
Improved Oil Recovery in Fluvial Dominated Deltaic Reservoirs - Kansas
DE-FC22-93BC14957

University of Oklahoma
Identification and Evaluation of Fluvial Deltaic Reservoirs - Oklahoma
DE-FC22-93BC14956

University of Tulsa
Glenn Pool Field - Oklahoma
DE-FC22-93BC14951

Utah Geological Survey
Increase Oil Production and Reserves from Improved Completion
Techniques in the Bluebell Field - Utah
DE-FC22-93BC14953

FIELD DEMONSTRATIONS OVERVIEW

Introduction:

The Field Demonstration Program was initiated in FY92 in response to rapidly declining domestic production and the realization that huge volumes of oil are being abandoned in reservoirs because of uneconomic production techniques. This program is just one of the critical elements of the Oil Program necessary to move improved oil recovery (IOR) technology from the conceptual stage through research, pilot scale field experiments, and full-scale field demonstrations to industry acceptance and commercialization. Both successful results and failures of the field demonstrations will provide focus to concurrent research programs. Elements of the field demonstrations that are suitable for broad industry application will be communicated to the industry through the oil program=s technology transfer.

Significant events in the oil industry during 1998-1999, including company repositioning, mergers, sale of fields, and personnel layoffs, have effected important changes in DOE's Class projects. Several projects have moved field locations and transferred the technology developed in Phase I to other nearby fields in Phase II. Mergers have caused several fields to be sold, and a few projects have terminated early because of these changes.

The value of the research remains high, and publications and technology transfer presentations by project personnel continue to contribute a significant body of knowledge on the solution of problems in producing oil from mature domestic oil fields.

Two publications on the Class projects are available through NPTO. *Class Project Summary Sheets* is updated approximately every six months. It is published by the NPTO office and posted on their Website. Included in this book are maps showing project locations, tables of technologies addressed, and an overview of each project along with project results. *Reservoir Class Field Demonstration Publication & Presentation Bibliography*, a listing of publications and presentations by the project operators, compiled by the National Petroleum Technology Office is published annually and posted on the NPTO Website. DOE reports can be ordered through NPTO (918-699-2034). To receive copies of other publications and presentations contact the project operator. Project operators, and the contact person for each project are listed in the publication.

FIELD DEMONSTRATIONS OVERVIEW

Goals and Objectives:

1) Extend the economic production of domestic fields by a) slowing the rate of well abandonments and b) preserving industry infrastructure (including facilities, wells, operating units, data, and expertise).

2) Increase ultimate recovery in known fields by demonstrating a) better methods of reservoir characterization (both rock and fluid), b) advanced oil recovery and production technologies, c) advanced environmental compliance technologies, and d) improved reservoir management techniques.

3) Use field demonstrations to broaden information exchange and technology application among stakeholders by a) expanding participation in DOE projects to include both traditional and nontraditional participants, b) increasing third-party participation and interaction throughout the life of DOE-sponsored projects, and c) making technology transfer products user-friendly.

4) Integrate Field Demonstration activities with activities of other areas of the advanced oil recovery program by a) actively pursuing demonstration activities from work developed in other program areas, b) assessing Field Demonstration efforts regarding future directions and research needs, and c) informing the research community of research needs and opportunities identified in demonstration projects.

FIELD DEMONSTRATIONS OVERVIEW

Projects:

Class I Fluvial-Dominated Deltaic reservoirs - Four mid-term and ten near-term projects were selected and awarded in FY92 and FY93. Three projects were canceled during Budget Period I. DOE will monitor contractual performance and fund the second budget period of demonstration projects that provided technically and economically feasible in the first budget period. Projects will be completed between FY94 and FY2000. All eleven Class I projects have been completed.

Class II Shallow Shelf Carbonate Reservoirs - Three mid-term and seven near-term field demonstrations in shallow-shelf carbonate reservoirs have been selected and awarded in FY94. DOE will monitor the contractual performance and fund the second budget period as necessary. One project was canceled. Six of the projects have been completed.

Class III Slope and Basin Clastic Reservoirs - Four near-term and five mid-term projects in slope and basin clastic reservoirs were selected and awarded in FY95. DOE will monitor contractual performance and fund the second budget period as approved. One project was completed in the fall of 1999, and one in mid 2001.

Advanced Class Work - Field-based reservoir characterization and recovery process projects to refine advanced technologies that were demonstrated or identified in the Class demonstration projects. In addition, technologies shown to be promising in laboratory research and development efforts - improved recovery methods and reservoir characterization technologies - were considered for demonstration in Advanced Class activities. Three projects were selected and have been completed.

Class Revisit – Ten new projects were awarded in October 1999. The ten projects include Fluvial-dominated Deltaic, Shallow Shelf Carbonate and Slope and Basin Clastic reservoirs, and both light and heavy oil projects. The projects will have three phases, reservoir characterization, field implementation and monitoring. All phases will provide Technology Transfer to the oil industry and public.

Class I Oil Recovery Projects

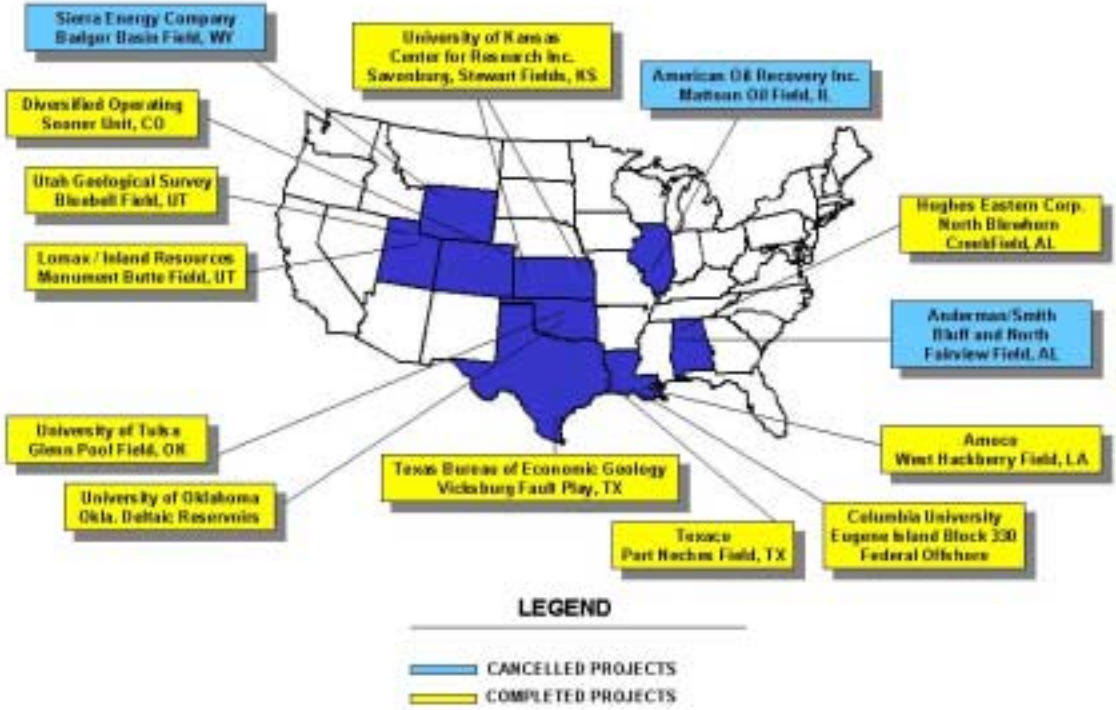

FOSSIL ENERGY

DOE/BC/14963-21
(OSTI ID: 792224)

WEST HACKBERRY TERTIARY PROJECT

Final Report
September 3, 1993-March 31, 1999

By
Kenneth A. Haley
Travis H. Gillham
Demetrios Yannimaras

Date Published: March 2002

Work Performed Under Contract No. DE-FC22-95BC14963

Amoco Production Company
Houston, Texas

National Energy Technology Laboratory
National Petroleum Technology Office
U.S. DEPARTMENT OF ENERGY
Tulsa, Oklahoma

DISCLAIMER

This report was prepared as an account of work sponsored by an agency of the United States Government. Neither the United States Government nor any agency thereof, nor any of their employees, makes any warranty, expressed or implied, or assumes any legal liability or responsibility for the accuracy, completeness, or usefulness of any information, apparatus, product, or process disclosed, or represents that its use would not infringe privately owned rights. Reference herein to any specific commercial product, process, or service by trade name, trademark, manufacturer, or otherwise does not necessarily constitute or imply its endorsement, recommendation, or favoring by the United States Government or any agency thereof. The views and opinions of authors expressed herein do not necessarily state or reflect those of the United States Government.

This report has been reproduced directly from the best available copy.

DOE/BC/14963-21
Distribution Category UC-122

West Hackberry Tertiary Project

By
Kenneth A. Haley
Travis H. Gillham
Demetrios Yannimaras
March 2002

Work Performed Under DE-FC22-95BC14963

Prepared for
U.S. Department of Energy
Assistant Secretary for Fossil Energy

Dan Ferguson, Project Manager
National Petroleum Technology Office
P.O. Box 3628
Tulsa, OK 74101

Prepared by
Amoco Production Company
P.O. Box 3092
Houston, TX 77253

Final Technical Progress Report
West Hackberry Tertiary Project

TABLE OF CONTENTS

PAGE

1.0 ABSTRACT 1
1.1 Brief Description of Research 1
1.2 Summary of Key Results and Conclusions 1
2.0 EXECUTIVE SUMMARY 2
2.1 Background 2
2.2 Conclusions 2
2.3 Recommendations 3
3.0 INTRODUCTION 3
4.0 DISCUSSION 4
4.1 Project Performance (by reservoir) 4
4.1.1 High Pressure Cam C Reservoir on the West Flank 4
4.1.2 Low Pressure Cam C Reservoir on the North Flank 5
4.1.3 Low Pressure Bol 3 Reservoir on the North Flank 6
4.1.4 Low Pressure Cam D Reservoir on the North Flank 7
4.1.5 Composite North Flank Performance 7
4.2 Operation of Wells and Surface Injection Facilities 7
4.3 SI Metric Conversion Factors 8

APPENDIX
APPENDIX A Statement of Work 9

FIGURES AND TABLES **PAGE**
Project Location Map 17
Map Depicting Location of Air Injection Units 18
Type Log 19
Structure Map: Top of Cam C-1 Sand (West Flank) 20
Plot of Cumulative Air Injected vs. Time 21
Schematic Cross-Section: Cam C (North Flank) 22
Structure Map: Top of Cam C-1 Sand (North Flank) 23
Production Plot: Cam C (North Flank) 23
Structure Map: Top of Bol 3 Sand (North Flank) 24
Production Plot: Bol 3 (North Flank) 25
Structure Map: Top of Cam D Sand (North Flank) 26
Production Plot: Cam D (North Flank) 27
Combined Production Plot for All Three North Flank Low Pressure Reservoirs 28

Final Technical Progress Report
West Hackberry Tertiary Project

1.0 ABSTRACT

1.1 Brief Description of Research

The West Hackberry Tertiary Project is a field test of the concept that air injection can be combined with the Double Displacement Process to produce a tertiary recovery process that is both low cost and economic at current oil prices. The Double Displacement Process is the gas displacement of a water invaded oil column for the purpose of recovering tertiary oil by gravity drainage. In reservoirs with pronounced bed dip such as those found in West Hackberry and other Gulf Coast salt dome fields, reservoir performance has shown that gravity drainage recoveries average 80% to 90% of the original oil in place while waterdrive recoveries average 50% to 60% of the original oil in place. The target for tertiary oil recovery in the Double Displacement Process is the incremental oil between the 50% to 60% waterdrive recoveries and the 80% to 90% gravity drainage recoveries.

In previous field tests, the Double Displacement Process has proven successful in generating tertiary oil recovery. The use of air injection in this process combines the benefits of air's low cost and universal accessibility with the potential for accelerated oil recovery from the combustion process. If successful, this project will demonstrate that utilizing air injection in the Double Displacement Process will result in an economically viable tertiary process in reservoirs (such as Gulf Coast salt dome reservoirs) where any other tertiary process is presently uneconomic.

1.2 Summary of Kev Results and Conclusions

Air injection on the West Flank began in November of 1994. Although West Flank air injection has increased reservoir pressure by 500 pounds per square inch (psi), production response has not yet occurred. The gas cap on the West Flank has not expanded sufficiently to push the oil rim down to the nearest down structure well. Cumulative injection to date is 1.6 BCF, only approximately 50% of the projected volume required to establish oil production response. Additional air injection is required to further expand the gas cap and thereby bring about oil production. Air injection rates have been restricted due to iron oxide plugging in the injectors.

To spread risk among multiple reservoirs, the project was expanded in 1996 to include air injection in low pressure reservoirs on the North Flank of the field. The project reservoirs on the West Flank are much higher pressure (2500-3300 psi) than the project reservoirs on the North Flank (300-600 psi). Air injection began on the North Flank in July of 1996. While West Flank air injection has not yet yielded oil production, air injection has increased oil production in all three low pressure North Flank reservoirs. Production increased in the North Flank after only two months of air injection, much quicker than anticipated. Between July of 1996 and July of 1999, cumulative air injection of 0.9 BCF increased North Flank oil production by 224,000 barrels above the normal decline. As of

July, 1999, air injection was generating 270 barrels of oil per day (BOPD) of incremental oil production from the three low pressure reservoirs on the North Flank of the field.

2.0 EXECUTIVE SUMMARY

2.1 Background

The following report is the Final Technical Progress Report for the West Hackberry Tertiary Project and covers the time period from September 3, 1993 to the end of Budget Period 1, March 31, 1999. The West Hackberry Tertiary Project is one of four mid-term projects selected by the United States Department of Energy (DOE) as part of the DOE's Class 1 Program for the development of advanced recovery technologies in fluvial dominated deltaic reservoirs.

Over a funding period from September 3, 1993 to March 31, 1999, Amoco and the DOE implemented a field test of the theory that air injection can be combined with the Double Displacement Process to create a tertiary oil process that is economically viable for the domestic oil industry. Air injection on the West Flank of the field is testing the process in a high pressure (2500-3300 psi) reservoir which had watered out. Although the project originally targeted the West Flank of the field, Amoco and the DOE agreed to expand the project to the North Flank during 1996. The low pressure north flank reservoirs exhibit slow water encroachment, possess low pressure gas caps and contain thin oil rims. Injection on the North Flank is testing the process in low pressure (300-600 psi) reservoirs that are approaching depletion.

As part of the project, the Petroleum Engineering Department at Louisiana State University (LSU) has been subcontracted to provide independent study and technology transfer support. The Statement of Work for the West Hackberry Tertiary Project is included as Appendix A.

West Hackberry is a salt dome oil field located in Southwestern Louisiana about 30 miles southwest of Lake Charles, Louisiana as shown on the map on Page 17. A map with the location of each of the project's four reservoir-wide units is included on Page 18. A type log for the sands in the project is shown on Page 19. Production is from Oligocene Age sandstones found at a depth 7500 to 9000 feet with bed dips in excess of 30 degrees. Average reservoir properties are a porosity of 25-28% and a permeability of 300-1000 md, with a reservoir temperature of 200 degrees F. The Hackberry crude is 33 degree API gravity with a viscosity of 0.9 centipoise at 200 degrees F and an original bubble point pressure of 3295 psi.

2.2 Conclusions

The following conclusions have been generated during the project.

1. Oil production has not yet occurred in the high pressure West Flank reservoirs since the oil rim has not moved sufficiently down structure to reach the first producing well.

The gas cap has not expanded enough to push the oil rim down to the most up structure well.

2. Air injection in each of three low pressure North Flank oil reservoirs has generated a significant increase in oil production.
3. Autoignition of the Hackberry crude with air is occurring in the reservoir based on the minimal oxygen content in the gas produced.
4. Operational challenges associated with compressor run time and well servicing (pulling jobs) have been remedied without significant incremental operating expenses.
5. Operational challenges associated with plugged injectors due to iron oxide plugging have not been successfully remedied through the use of wellhead filters.

2.3 Recommendations

The following recommendations are presented for future operations:

1) Distribute air injection between the high pressure West Flank reservoir and the three low pressure North Flank reservoirs with the ultimate goal to maximize production response throughout the project.
2) Monitor reservoir performance with production data, bottom hole pressure surveys, well tests and produced oil, gas and water analyses.
3) Utilize production response to guide the timing for workovers and to guide the injection rates for each reservoir.
4) Evaluate the economic feasibility of upgrading the air injection system. This would include the installation of new pipeline, dehydration equipment, as well as wellbore cleanout workovers.

3.0 Introduction

In the West Hackberry Tertiary Project, air was injected into a high pressure (2500-3300 psi) watered out oil reservoir on the West Flank and is injected into low pressure (300-600 psi) North Flank oil reservoirs that are nearing depletion. In both situations, air injection is combined with the Double Displacement process in an attempt to generate an economically viable tertiary recovery process for Gulf Coast oil reservoirs with pronounced bed dip. The Double Displacement Process is the gas displacement of a water invaded oil column for the purpose of recovering tertiary oil by gravity drainage. In West Hackberry Field, gravity drainage recoveries average 80% to 90% of the original oil in place while waterdrive recoveries average 50% to 60% of the original oil in place. The target for tertiary oil recovery in the Double Displacement Process is the incremental oil between the 50% to 60% waterdrive recoveries and the 80% to 90% gravity drainage recoveries. West Hackberry core studies indicate an average residual oil saturation of 26% after water flooding and an average of only 8% after *gas* flooding.

For air injection to work successfully with the Double Displacement Process, the reservoir temperature must be high enough for oxygen to be consumed through combustion with the reservoir oil. Amoco has performed laboratory tests which prove

that West Hackberry oil will spontaneously combust with oxygen in the pore space. The combustion of oxygen in the reservoir alleviates concerns relating to the presence of oxygen in the reservoir or production equipment. Oxygen in the reservoir can form viscous emulsions hindering the flow of oil in the well and in the production equipment. Oxygen that reaches the producing wells can also produce corrosion and or explosions in the production equipment. Produced gas from the air injection reservoirs indicates approximately 1% Oxygen (1% Oxygen, 77% Nitrogen, 13% carbon dioxide, 9% hydrocarbons), resulting in minimal incremental corrosion and limited risk of explosion. Also, there has been no evidence of any viscous emulsion tendencies.

In the high pressure (2500-3300 psi) west flank reservoir, the mechanics of the tertiary process involve: 1) injecting air into the crest of a watered out oil reservoir in order to fill the reservoir with a gas from the top down, 2) as the reservoir fills with air, oxygen is consumed through spontaneous combustion, 3) oil and water drain toward the base of the structure through gravity segregation and gravity drainage and 4) tertiary oil, which previously had been trapped as a residual oil saturation, is now produced in down structure wells. In this case, the economic potential of the project is enhanced by the low cost associated with using air as the injection gas.

On the North Flank of West Hackberry, low pressure (300-600 psi) oil reservoirs are found which have large low pressure gas caps, thin oil rims and slow water encroachment. In the low pressure north flank reservoirs, air injection can increase oil recovery by: 1) pushing the oil rim down structure to the structural location of existing wellbores, 2) repressurizing the reservoir and 3) obtaining tertiary oil recovery through the Double Displacement Process in the same manner as described in the preceding paragraph. Although injection of nitrogen, carbon dioxide and natural gas have been utilized to increase oil recovery in Gulf Coast reservoirs in the past, this project is unique in the use of air as the injection gas.

4.0 Discussion

4.1 Project Performance (by reservoir)

4.1.1 High Pressure Cam C Reservoir on the West Flank (WH Cam C RI SU)

A structure map for the top of the Cam C-1 sand on the West Flank of West Hackberry Field can be found on Page 20. Throughout most of the project, the Gulf Land D (GLD) No. 51 served as an air injector in the Cam C sand on the West Flank. In October of 1997, the GLD No. 51 became plugged with iron oxide after injection of almost 1.6 billion standard cubic feet (BCF) since start-up in November, 1994. On Page 21 is a plot of cumulative air injected versus time.

Throughout this three year time frame, the GLD Nos. 44 and 45 were periodically tested for evidence of production response. Neither well tested any oil production response or nitrogen breakthrough, although reservoir pressure did increase by about 500 psi.

However, reservoir modeling results predicted production response required approximately 3 BCF of injection, almost twice the actual volume injected. Therefor, the data accumulated to date does not support or condemn the application of the Double Displacement Process to this reservoir.

Efforts to clean out the GLD No. 51 were not successful. To help assess the location of the oil rim, the GLD No. 51 was sidetracked and logged. The location of the sidetrack hole is immediately adjacent to the original hole. The Cam C-1,2 was found wet and the Cam C-3 appeared to contain a small amount of oil pay. The sidetrack was completed in the Cam C-3 and initially tested nitrogen and oil with a high water cut. After several months of testing, the Cam C-3 watered out. The reason that the GLD No. 51 Sidetrack (ST) is still below the oil rim is an insufficient volume of air injected in combination with: 1)uncertainty as to the pre-injection location of the oil rim, 2)the large volume of the attic portion of the reservoir and 3)the high reservoir pressure (which inhibits the growth of the gas cap).

The GLD No. 51 ST is the highest well on structure in the Cam C sand. Using the GLD No. 51 ST as a producing well would generate the earliest possible oil production. During October of 1998, the GLD No. 45 was converted into an air injector. Although the GLD No. 45 is down structure to the GLD No. 51 ST, the GLD No. 45's location is not directly down structure to the GLD No. 51. Air injected into the GLD No. 45 is expected to migrate up structure, accumulate in the gas cap and push the oil rim down to the GLD No. 51.

The GLD No. 51 was completed in the Cam C-3 in a manner that would allow for pulsed neutron logs to be run over the Cam C-1 through tubing. Plans were to run a pulsed neutron log in GLD No. 51 each quarter to monitor the arrival of the oil rim in the Cam C-1. However, air injection in GLD No. 45 lasted only from October 1998 through March 1999 due to wellbore plugging from iron oxide. Currently, there is no injection into this reservoir.

4.1.2 Low Pressure Cam C Reservoir on the North Flank

In 1996, Amoco and the DOE agreed to expand the project to include air injection in low pressure reservoirs on the North Flank of the field. The low pressure North Flank reservoirs exhibit slow water encroachment, possess large low pressure gas caps and contain thin oil rims. In the low pressure North Flank reservoirs, air injection can increase oil recovery by: 1) pushing the oil rim down structure to the structural location of existing wellbores, 2) repressurizing the reservoir and 3)obtaining tertiary oil recovery through the Double Displacement Process.

Air injection began on the North Flank in a low pressure (300-600 psi) Cam C oil reservoir during July of 1996. Cumulative injection from July 1996 through July 1999 is 0.5 BCF. A schematic cross-section of the reservoir is included on Page 22. The SL 42 No. 155 serves as the air injector in the gas cap. A structure map for the top of the Cam C-1 is included on Page 23.

Four producing wells have exhibited increased oil production as a result of air injection in the Cam C sand. Response in the producing wells was seen almost immediately, within two months of the start of injection. A composite production plot for the four producing wells in the North Flank Cam C sand is included on Page 24. As shown on the production plot, air injection has resulted in increased oil production and reduced water cut. Air injection increased oil production to a peak response of 200 BOPD above the normal decline in the summer of 1998, with a July, 1999 response of 150 BOPD over the normal decline.

In July of 1997, air injection was interrupted when the injector, the SL 42 No. 155 became plugged with iron oxide. Repeated attempts to clean out the SL 42 No. 155 were unsuccessful. The SL 42 No. 155 was sidetracked and returned to injection in March of 1998.

Through August of 1998, the air injection project in the Cam C consisted of four producers and one injector. A hydrocarbon pore volume analysis of the reservoir suggested that an additional producer might be needed to more effectively produce the remaining reserves. The SL 42 No. 98 was sidetracked from its position in the gas cap down structure approximately 100' targeting the oil rim to serve as the fifth producer in the Cam C. The SL 42 No. 98 ST was placed on production during the last half of September, 1998. This well tested gas, indicating the difficulty in tracking the gas oil contact throughout the life of the project.

One additional injector, the SL 42 No. 221, was added to the Cam C reservoir during the fourth quarter of 1998 to increase injection rates and to provide a backup injector for the reservoir. Historically, air injection rates in the SL 42 No. 155 ST have averaged only 400 to 500 thousand standard cubic feet per day (MSCFD) due to iron oxide plugging the wellhead filter. To increase injection rates, an improved filter design utilizing a tee-type filter was installed immediately upstream of the injector wellhead. The new filters improved injectivity in the short term, but have not been a long term solution. The plugging problem still controls the amount of air delivered to the reservoir. Currently, the North Flank Cam C consists of two injectors and four producers.

4.1.3 Low Pressure Bol 3 Reservoir on the North Flank

In December of 1996, air injection was extended to a second low pressure North Flank reservoir, the Bol 3 sand. As with the Cam C reservoir, the Bol 3 reservoir has low reservoir pressure, a thin oil rim, steep bed dip and slow water encroachment. A structure map for the North Flank Bol 3 is on Page 25.

As was the case in the Cam C low pressure reservoir, production response in the Bol 3 was almost immediate. As noted on the production plot on Page 26, air injection has increased oil production in the Bol 3, with a peak response of 35 BOPD over the normal decline from two producers. Production levels have remained fairly steady over the last

two years even though air injection was stopped in December, 1997 after only 0.2 BCF of cumulative injection.

Air injection in the Bol 3 was interrupted in December, 1997, when the GLAC No. 245 became plugged and efforts to clean out the well were unsuccessful. An alternate well, the GLAC No. 42 has been chosen to replace the GLAC No. 245, but the conversion has not been done.

4.1.4 Low Pressure Cam D Reservoir on the North Flank

Air injection began in the North Flank Cam D in December of 1997. The Cam D is by far the largest of the three low pressure North Flank reservoirs and thereby contains the most reserve potential. A structure map for the Cam D is shown on Page 27. The Cam D's low pressure gas cap, thin oil rim and steep bed dip are similar to those of the North Flank Cam C and Bol 3 reservoirs. Average reservoir pressure is approximately 400 psi.

Prior to air injection, the Cam D had produced through many wells over a period of over 40 years and was in the fmal stages of depletion. The air injection project in the Cam D currently consists of one injector and two producers. As of July of 1999, air injection had increased production by 70 BOPD over the normal decline, with peak response yet to occur. The production plot for the North Flank Cam D is on Page 28.

4.1.5 Composite North Flank Performance

The West Hackberry Air Injection Project is the first successful application of the use of low cost air injection to improve oil recovery in low pressure Gulf Coast salt dome reservoirs. From July of 1996 to July of 1999, air injection in three low pressure reservoirs on the North Flank of West Hackberry Field increased oil production by 224,000 barrels over the normal decline. A composite production plot is shown on Page 29. In July, 1999, air injection generated 270 BOPD of incremental oil production.

4.2 Operation of Wells and Surface Air Injection Facilities

By far the most serious operational problem encountered to date has been the iron oxide plugging of air injection wells. After the injection well tubing strings were replaced with coated tubing, problems continued as a result of ongoing corrosion in the injection lines. Other recent high pressure air injection projects (North Dakota) have not had a problem with corrosion in the injection lines. The absence of corrosion in the other projects was thought to have been caused by carryover of synthetic compressor lubricant into the injection lines. Injection of synthetic compressor lubricant into the lines at Hackberry failed to protect the lines.

While other recent high pressure air injection projects have not had problems with corrosion in the flowlines, the other high pressure projects did not have a low pressure component. The corrosion seen in the Hackberry project appears to have been caused by water condensation associated with the pressure drop from the high pressure compressors to the low pressure lines. Both high pressure and low pressure compressed air are still required for the Hackberry project. Only water condensed in the interstage coolers is

removed from the air. The remaining vapor is sufficient to promote internal corrosion of the carbon steel line pipe.

Corrosion coupons have been placed in the air injection lines to assess the location and extent of the corrosion. To alleviate future corrosion in the injection lines, the use of a desiccant is under evaluation which would remove the moisture in the air immediately after the pressure drop into the low pressure portion of the system. However, to fully remedy this problem will require a system upgrade, including the replacement of the existing line pipe along with an air dehydration system.

Wellhead filters have been installed on the air injectors to prevent iron oxide plugging downhole in the injection wells. While the filters have reduced plugging downhole, the filters become so quickly plugged after cleaning that injection rates have been restricted to a range of 400 to 600 MCrll. To relieve the problem of restricted rates and plugged filters, tee-type filters were installed immediately upstream of the injection wellheads. These filters have had mixed success. On a positive side, they have kept the corrosion byproducts from entering the wellbore. On the negative side, the filters become plugged within hours of cleaning and injection rates are significantly restricted. Pressure drops across the filters can exceed 500 psi. It is not practical for field personnel to change out the 30 pound filters as frequently as necessary for optimum injection.

Compressor run time continues to improve compared with early project performance. The compressors were down 3 months in the summer of 1995. However, run times have improved to approximately 85% reliability over the last 12 months.

Well servicing expenses have not been significantly different than other wells in the field. The injectors require periodic acid jobs, small volumes of HCL at a cost of $1,500 per job. However, after two to three jobs, there is no longer any injectivity improvement. The producing wells are all on beam lift. These wells have seen a slightly higher failure tendency due to corrosion, but this increase is estimated at only 10-25% above the overall field failure rate.

4.3 SI Metric Conversion Factors

bbl x 1.589 873	E-01 = cubic meters
cubic feet x 2.831 685	E-02 = cubic meters
psi x 6.894 757	E+00 = kPa
Btu x 1.055 056	E+00 = kJ

APPENDIX A

STATEMENT OF WORK

STATEMENT OF WORK

WEST HACKBERRY TERTIARY PROJECT

Amoco Production company
October 16, 1992

Background and Objectives

The goal of the West Hackberry Tertiary Project is to demonstrate the technical and economic feasibility of oil recovery using air injection in the double Displacement Process. The Double Displacement Process is the gas displacement of a water invaded oil column for the purpose of recovering oil through gravity drainage. A novel aspect of this project is the use of air as the injection fluid. This technology will be applicable to reservoirs which have both sufficient bed dip for gravity drainage and sufficient reservoir temperature for the consumption of oxygen. Numerous water-drive reservoirs associated with salt dome fields along the Gulf Coast would be potential follow-up candidates for this technology. The use of air injection in this process offer the benefits of air's excellent accessibility and low cost combined with potentially greater recovery due to the combustion process. If successful, this project will demonstrate that the use of air injection in the Double Displacement Process can economically recover oil in reservoirs where tertiary oil recovery is presently uneconomical.

Based on a preliminary project design developed prior to commencement of the project, the following basic operational information has been determined for the study: injection rates; selection of reservoirs and fault blocks; required number of producing and injection wells; requirements for new wells versus re-completing existing wells; requirements for continuous injection versus intermittent injection; assessment of the disposal of produced gases by flaring or injection into low pressure reservoirs; unitization; and the design of surface production and injection facilities. The project is designed for injection into two separate fault blocks (Fault Blocks II & IV). In Fault Block IV, the technology will be assessed using a line of four producers at structurally equivalent positions in a heavily developed area. In Fault Block II, the technology will be assessed using a single producer in a sparsely developed area.

A description of each task associated with the project is provided below.

Task 1- **Environmental Study**

It is anticipated that this project will be categorically excluded from the DOE NEPA requirements. Upon DOE certification, if this project does qualify for a categorical exclusion, this task will not be required. If this project does not quality for a categorical exclusion, then this task will involve activities, such as data collection and reporting, that are required by the DOE to meet NEPA requirements.

Task 2 - Construction of Surface Facilities

The necessary permits required for construction of the surface facilities will be obtained. Based on the preliminary project design, Amoco will acquire the necessary equipment/facilities to inject 4-4.5 MMCFD of air at pressures greater than 4000 psi. Surface injection facilities will be installed which consist primarily of the air compressors and water purge system for the injection wells. The timing for the installation of production facilities will be tied to workovers on the producing wells conducted in Task 5. The production facilities will consist of flowlines, possibly a Natural Gas Liquids recovery unit, and a separate-test-and-boost (STAB) facility. After separation and testing, produced fluids will be piped to Amoco's central production facility. Undesired produced gasses will be flared or injected into low pressure reservoirs.

Task 3 - Conversion of Producing Wells to Injection Wells

Two producing wells will be converted to injection wells. Initially, a single injection well will be dedicated to each of the two fault blocks. Two additional injectors (i.e. converted producing wells) may be required to improve the economics of the process. A typical workover to convert a producing well to an injector would require cleaning out the wellbore, perforating the full prospective injection interval, and completing the well with new packers, tubing, and wellhead (i.e. valves, etc.).

Task 4 - Operations and Maintenance of Infection Facilities

The operation of the high pressure air compressors in the injection facilities requires close attention to safety issues. Synthetic lubricants and periodic cleaning of injection equipment will be conducted to prevent the possibility of a detonation resulting from the combination of high pressure air and hydrocarbon deposits. Additionally, routine maintenance of injection equipment will be conducted to avoid the possibility of catastrophic mechanical failure. Workovers to repair injection wells will be performed on an as needed basis.

Task 5 - Workovers for Monitoring and Producing Wells

A total of 9 wells will be repaired and/or re-completed to serve as producing wells and/or monitoring wells for the project. The timing of the workovers will be dictated by the advance of the flood front.. The task of monitoring the flood front is addressed in Task 6. Once the project is underway, workovers to repair producing and monitoring wells will be performed on an as needed basis.

Task 6 - Production Operations

All production operations for the project will be handled by Amoco field personnel assigned to West Hackberry Field. Produced liquids will be transported through existing collection lines to be handled at an Amoco Tank Battery. Initially, producing wells will

be gas lifted within Amoco's field-wide gas lift system. When the produced gasses become concentrated with undesirable components (e.g. nitrogen and carbon dioxide) due to breakthrough, it will be necessary to install a separate gas lift system for the project. The separate gas lift system will require a gas lift compressor. Produced gasses will either be sold, burned as fuel, flared or re-injected into low pressure reservoirs on the north flank of the field. Booster compressors may be required to generate sufficient pressure for injection of produced gasses. A flowline will be installed to the north flank of West Hackberry Field in order to carry the produced gasses to the low pressure reservoirs in that area. Monthly production tests, at a minimum, will be performed on all producing wells. Gas analyses will be conducted periodically to monitor the composition and oxygen content of the produced gasses. Produced oil and water samples will be analyzed periodically to determine their composition and physical properties. Pulsed neutron logs, bottom hole pressure surveys, temperature surveys, and spinner surveys may be run in both producing and monitoring wells in order to assess the effectiveness of the project. Periodic replacement of surface production and injection equipment (including flowlines) may also be required due to wear and tear on these items.

Task 7 - Reservoir Management

Reservoir modeling studies will be conducted to effectively manage the project. These studies will assist in assessing the following: distribution of injection volumes; timing of repairs and recompletions; and the determination of monitoring schemes and schedules. Amoco's " THERM" reservoir model will be used to history match reservoir performance and to predict future reservoir performance. Specialized combustion tests will be conducted at Amoco's Combustion Laboratory in Tulsa, Oklahoma to assist in monitoring and predicting the performance of the project. Reservoir fluid property analyses will be conducted to calibrate the reservoir model. The results of reservoir management will be continually documented and reported in a manner consistent with the DOE reporting requirements and technology transfer needs of the project.

Task 8 - Louisiana State University Technology Transfer

A yearly Amoco grant will be provided to the Petroleum Engineering Department at Louisiana State University (LSU). LSU will study various aspects of the project and report their findings. LSU will publish and make industry presentations on all results from their analyses. Amoco plans to provide LSU with all pertinent data and information from the project. Examples of typical data and information that will be made available to LSU include the following: individual well production rates; individual well injection rates; structure maps; net pay isopachs; core data; well logs; gas analyses; and fluid property data.

Task 9 - Amoco Technology Transfer

Amoco will assess the technical and economic feasibility of Double Displacement Process based on the data and information acquired from the project. These results will be

documented and submitted to various technical conferences for presentation and/or publication. Since the Double Displacement Process will probably have its greatest applicability to salt dome fields along the Gulf Coast, Amoco personnel will focus on technical conferences in the Houston, Texas and New Orleans, Louisiana areas. It is anticipated that presentations and/or papers will be completed at the beginning, middle, and end of the project. Amoco does not intend to regard any data and/or information on this project as proprietary.

FIGURES AND TABLES,

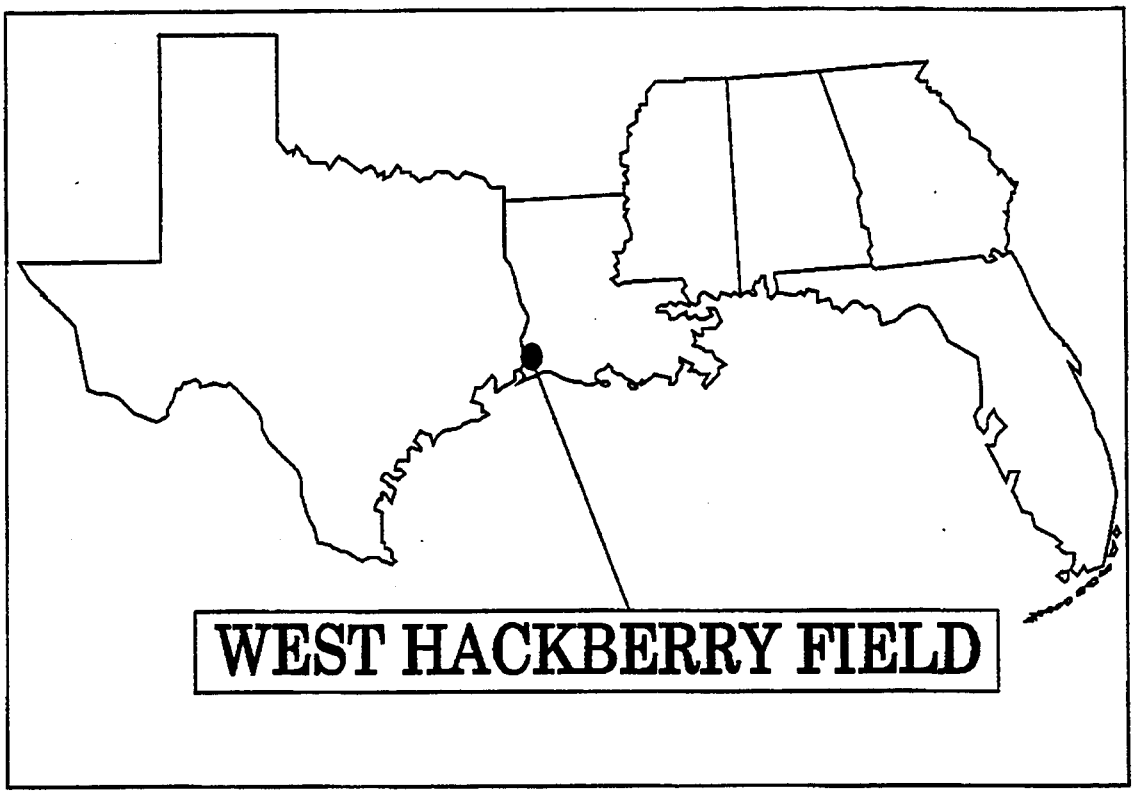
WEST HACKBERRY FIELD

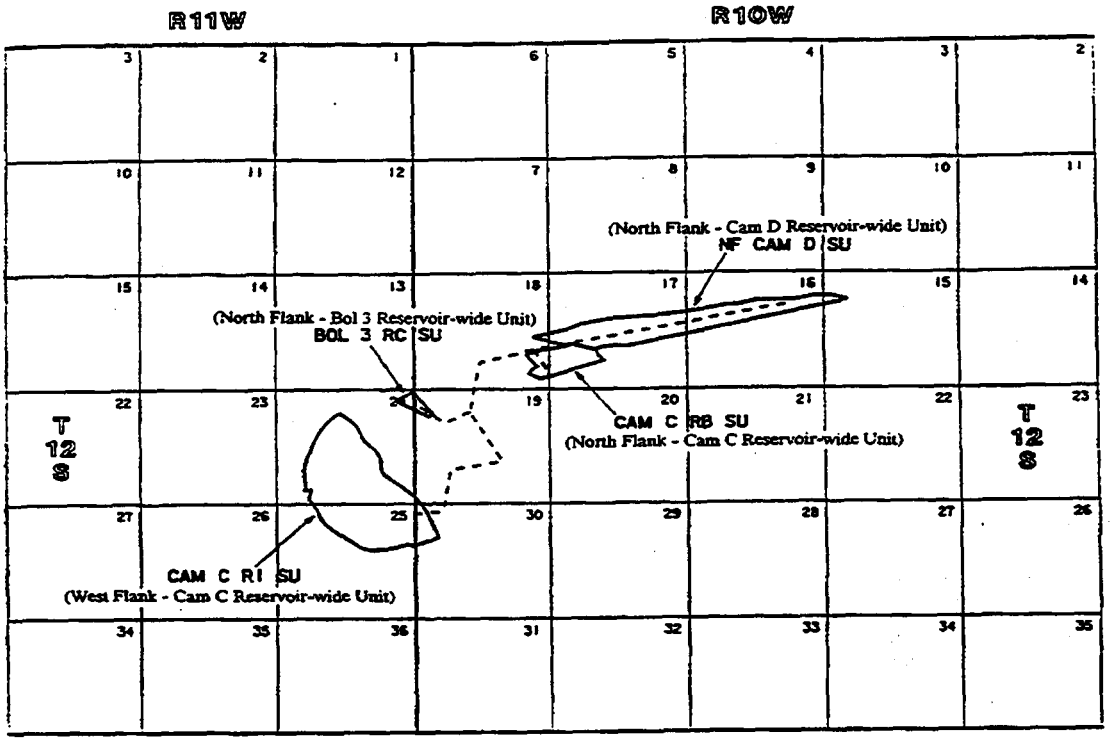

Reservoir-Wide Units
West Hackberry Air Injection Project

- - - - - Air Injection Lines

AIR COMPRESSOR LOCATED IN NE/4, NE/4 OF SECTION 25.

Amoco Production Company
WEST HACKBERRY FIELD
Cameron Parish, Louisiana

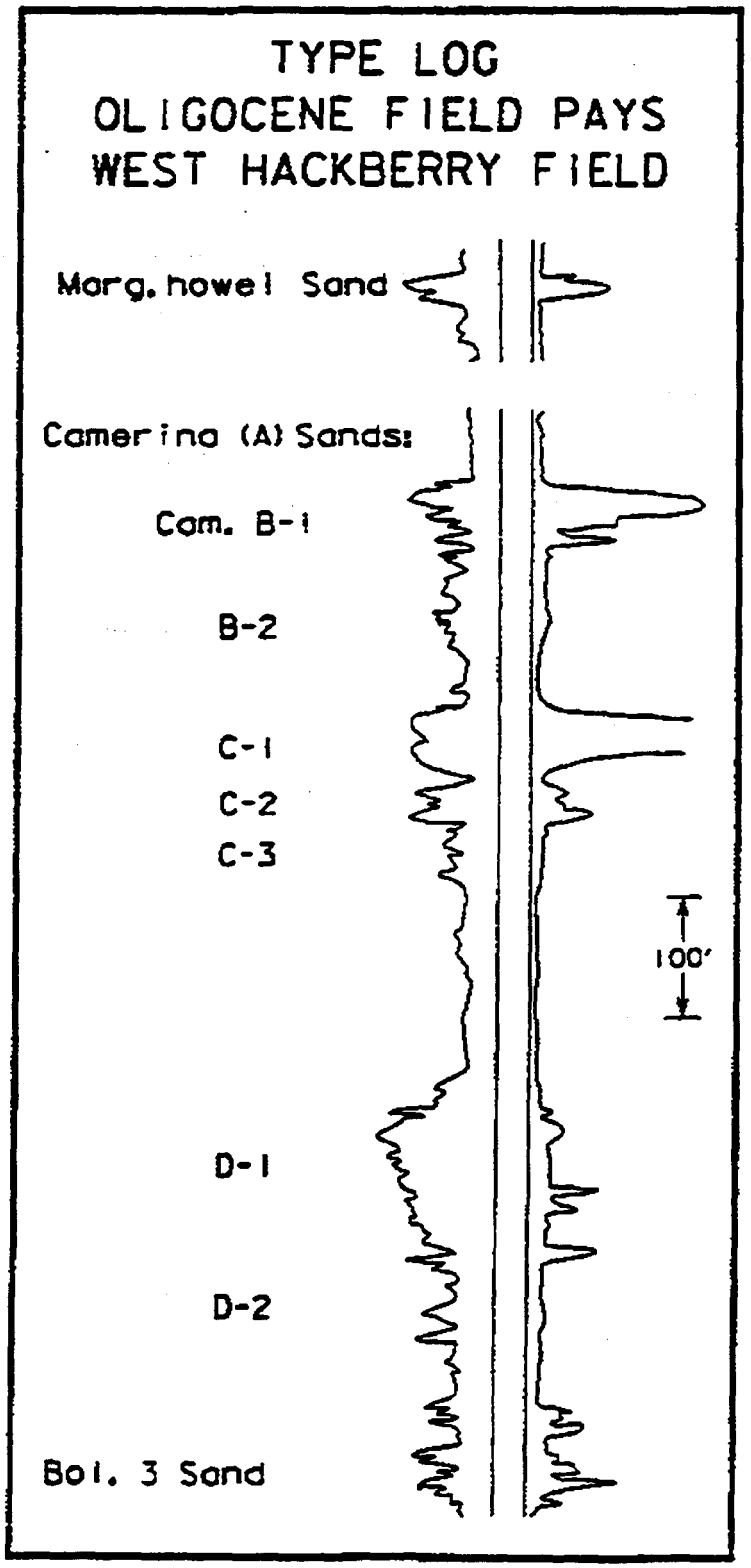
TYPE LOG
OLIGOCENE FIELD PAYS
WEST HACKBERRY FIELD
Marg. howel Sand
Camerina (A) Sands:
Cam. B-1
B-2
C-1
C-2
C-3
100'
D-1
D-2
Bol. 3 Sand

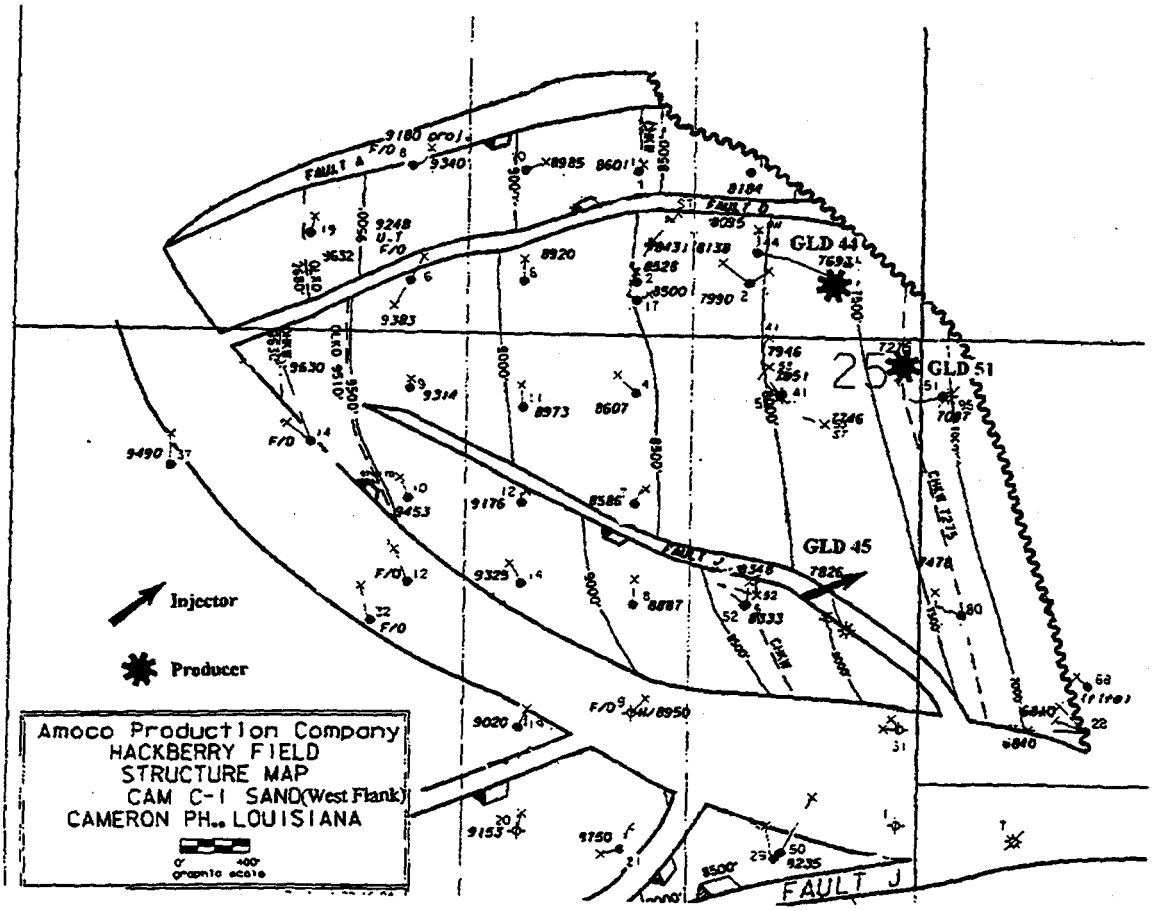
Amoco Production Company
HACKBERRY FIELD
STRUCTURE MAP
CAM C-1 SAND(West Flank)
CAMERON PH., LOUISIANA
Injector
Producer
GLD 43
GLD 51
GLD 45
FAULT J
25

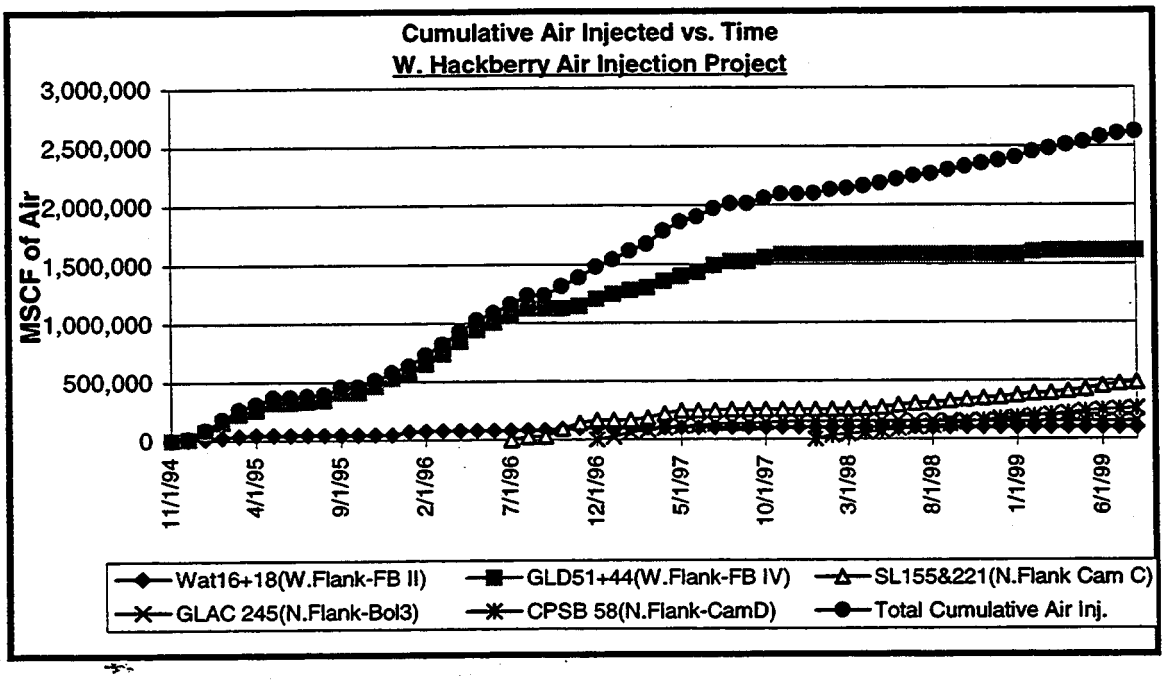
Cumulative Air Injected vs. Time
W. Hackberry Air Injection Project
MSCF of Air
3,000,000
2,500,000
2,000,000
1,500,000
1,000,000
500,000
0
11/1/94
4/1/95
9/1/95
2/1/96
7/1/96
12/1/96
5/1/97
10/1/97
3/1/98
8/1/98
1/1/99
6/1/99
Wat16+18(W.Flank-FB II)
GLD51+44(W.Flank-FB IV)
SL155&221(N.Flank Cam C)
GLAC 245(N.Flank-Bol3)
CPSB 58(N.Flank-CamD)
Total Cumulative Air Inj.

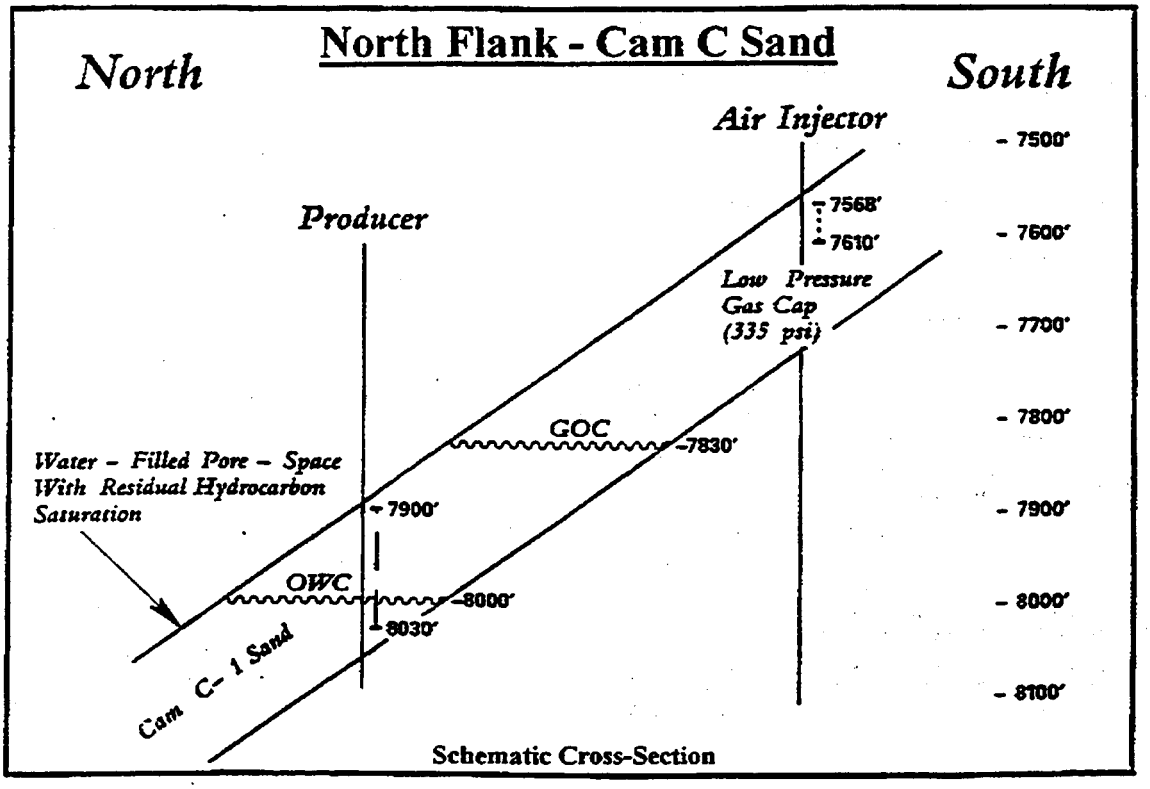
North Flank - Cam C Sand
North
South
Air Injector
Producer
7568'
7610'
Low Pressure
Gas Cap
(335 psi)
GOC
7830'
Water - Filled Pore - Space
With Residual Hydrocarbon
Saturation
7900'
OWC
8000'
8030'
Cam C- 1 Sand
- 7500'
- 7600'
- 7700'
- 7800'
- 7900'
- 8000'
- 8100'
Schematic Cross-Section

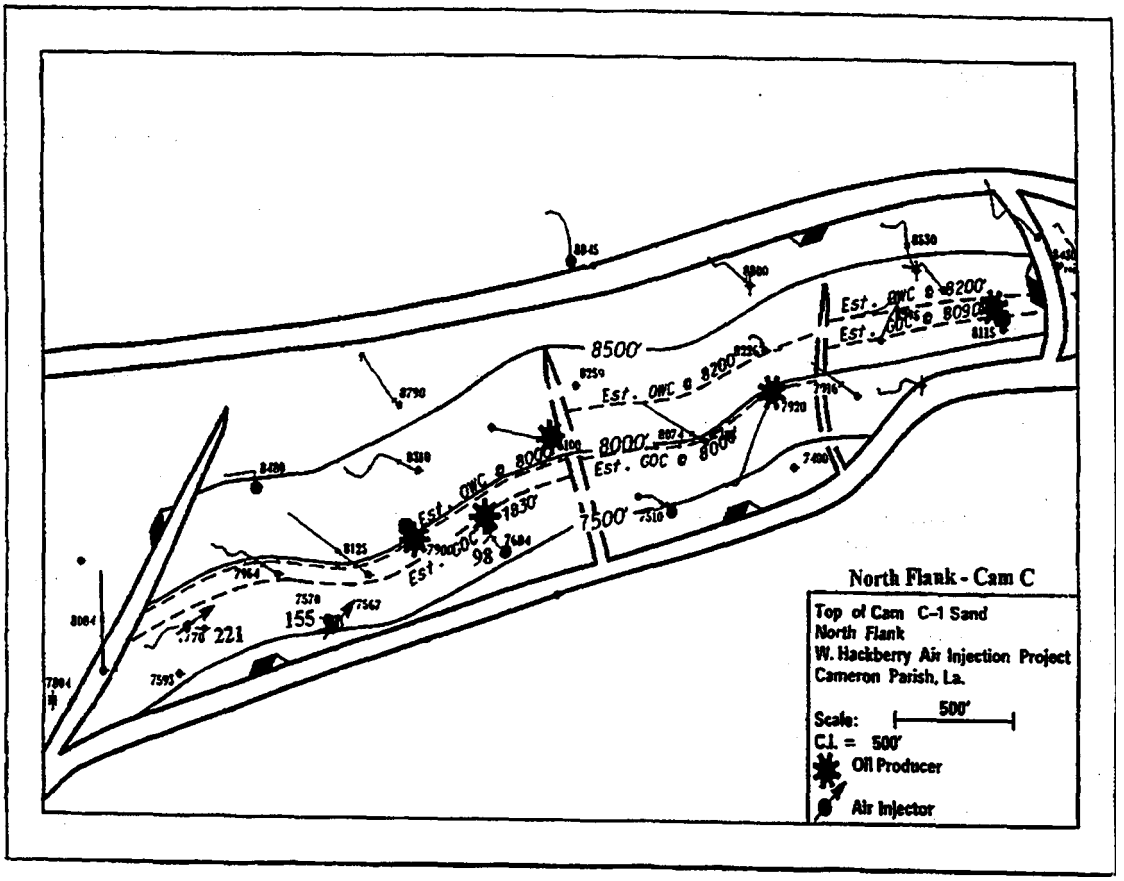
North Flank - Cam C
Top of Cam C-1 Sand
North Flank
W. Hackberry Air Injection Project
Cameron Parish, La.
Scale:
500'
C.I. = 500'
Oil Producer
Air Injector
8500'
8200'
8000'
7850'
7500'
Est. OWC @ 8200'
Est. GOC @ 8000'
Est. OWC @ 8000'
Est. GOC @ 8000'
Est. OWC @ 7900'
Est. GOC
98
155
221

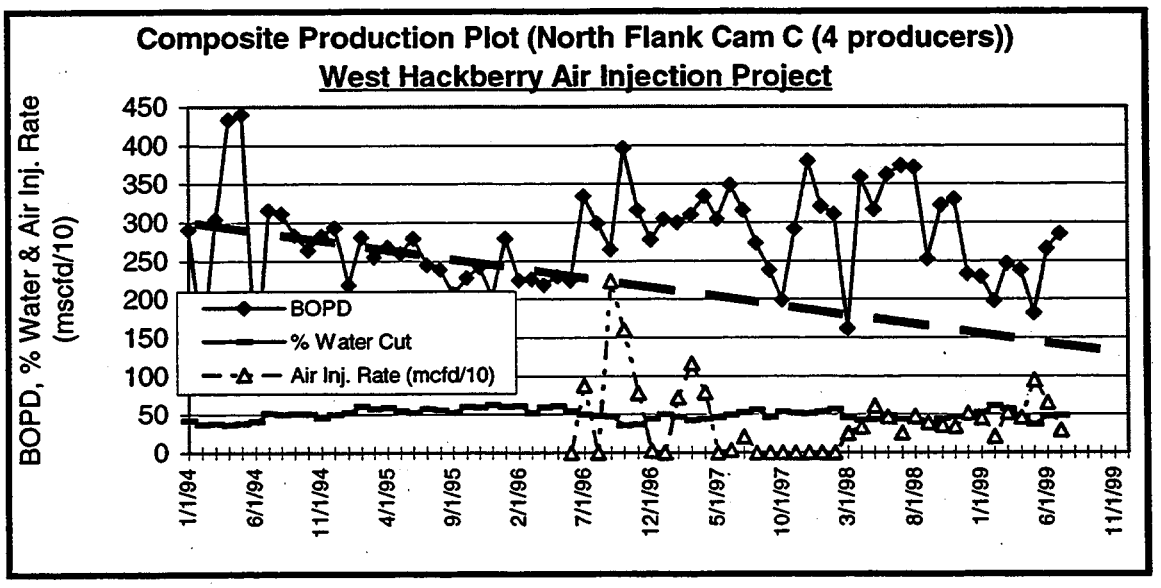
Composite Production Plot (North Flank Cam C (4 producers))
West Hackberry Air Injection Project
BOPD, % Water & Air Inj. Rate (mscfd/10)
450
400
350
300
250
200
150
100
50
0
BOPD
% Water Cut
Air Inj. Rate (mcfd/10)
1/1/94
6/1/94
11/1/94
4/1/95
9/1/95
2/1/96
7/1/96
12/1/96
5/1/97
10/1/97
3/1/98
8/1/98
1/1/99
6/1/99
11/1/99

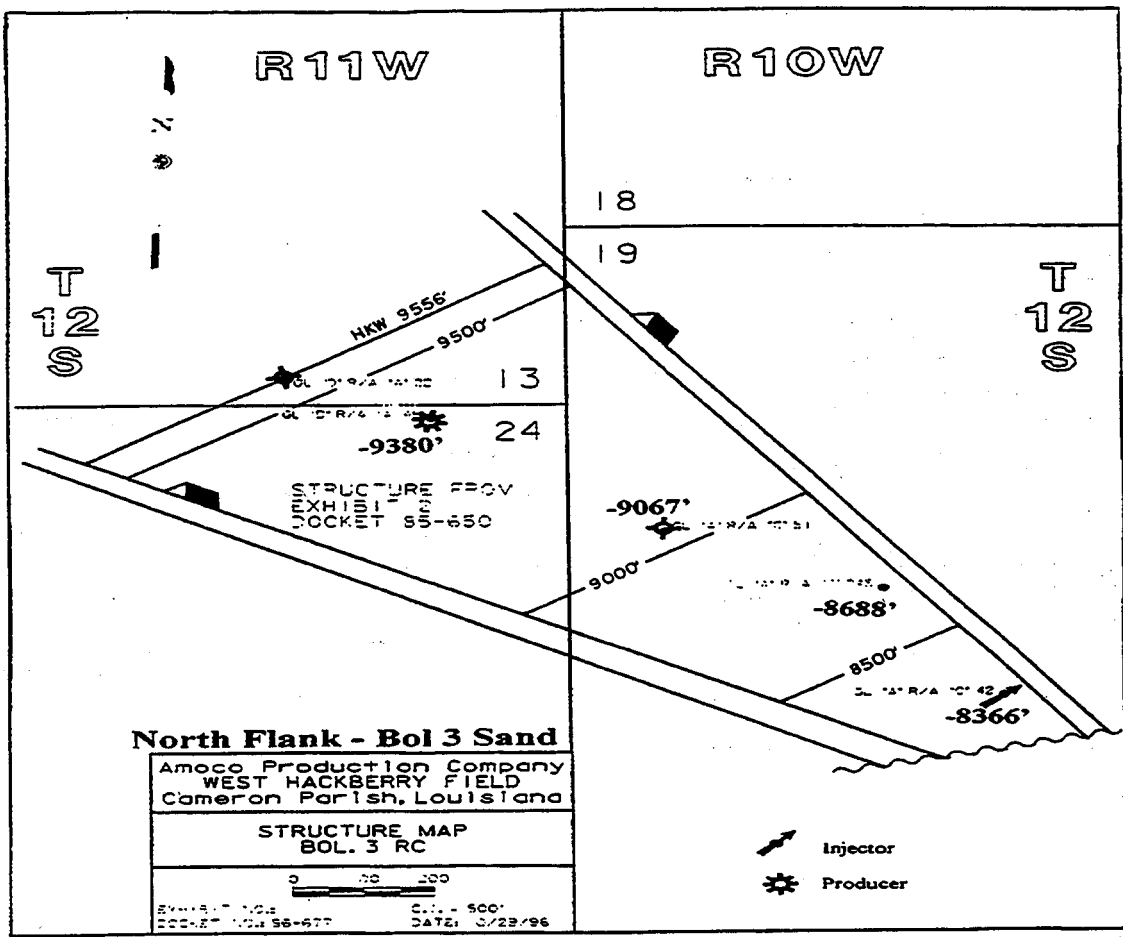
R11W
R10W
18
19
T
12
S
T
12
S
HKW 9556'
9500'
13
24
-9380'
-9067'
9000'
-8688'
8500'
-8366'
North Flank - Bol 3 Sand
Amoco Production Company
WEST HACKBERRY FIELD
Cameron Parish, Louisiana
STRUCTURE MAP
BOL. 3 RC
Injector
Producer

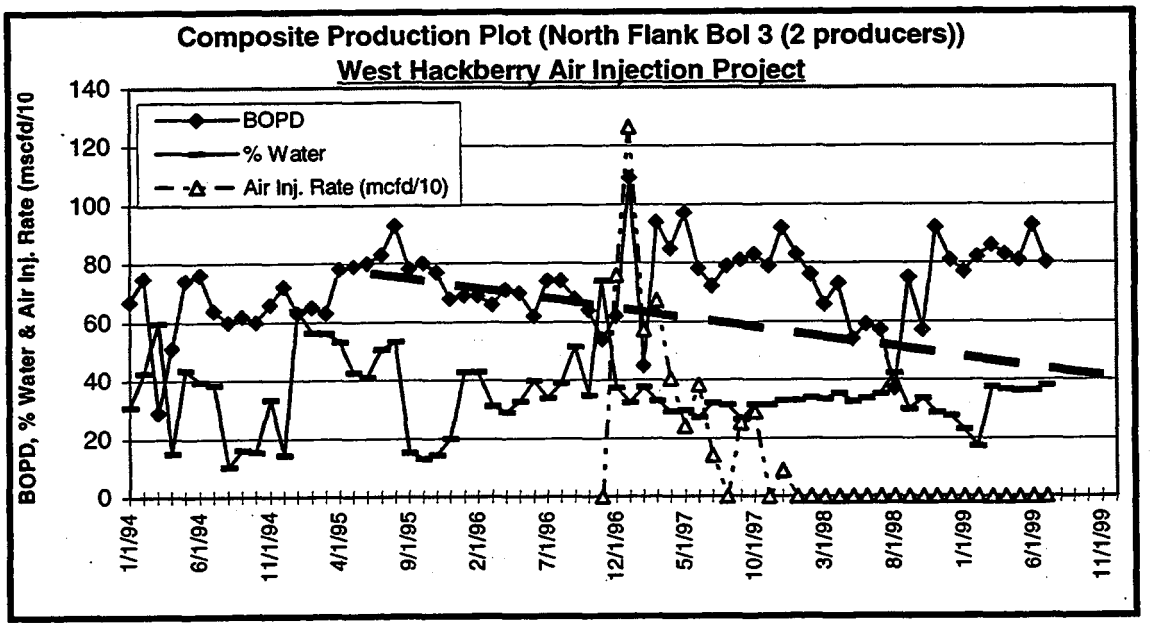
Composite Production Plot (North Flank Bol 3 (2 producers))
West Hackberry Air Injection Project
BOPD, % Water & Air Inj. Rate (mscfd/10
BOPD
% Water
Air Inj. Rate (mcfd/10)
140
120
100
80
60
40
20
0
1/1/94
6/1/94
11/1/94
4/1/95
9/1/95
2/1/96
7/1/96
12/1/96
5/1/97
10/1/97
3/1/98
8/1/98
1/1/99
6/1/99
11/1/99

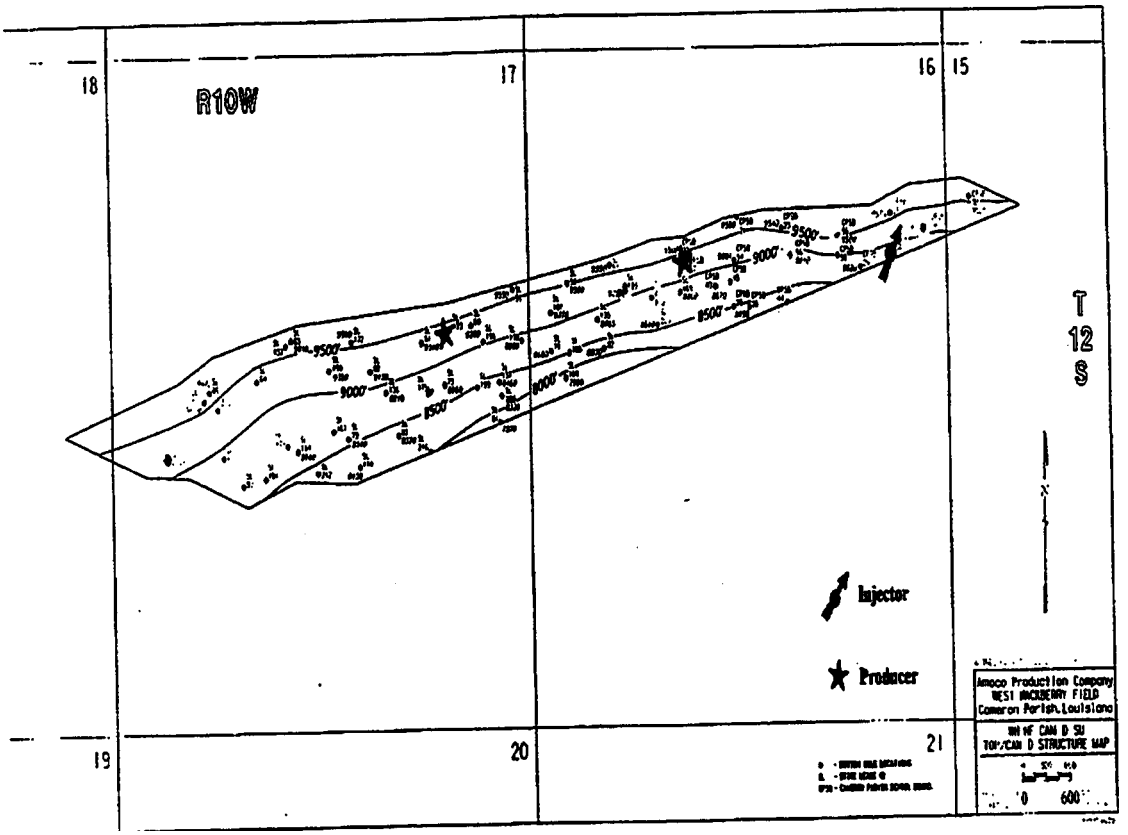
18
17
16
15
R10W
T
12
S
9500'
9000'
8500'
8000'
Injector
Producer
N
19
20
21
Amoco Production Company
WEST MACKEBEAN FIELD
Cameron Parish, Louisiana
WH HF CAM D SU
TOP/CAM D STRUCTURE MAP
0
600'

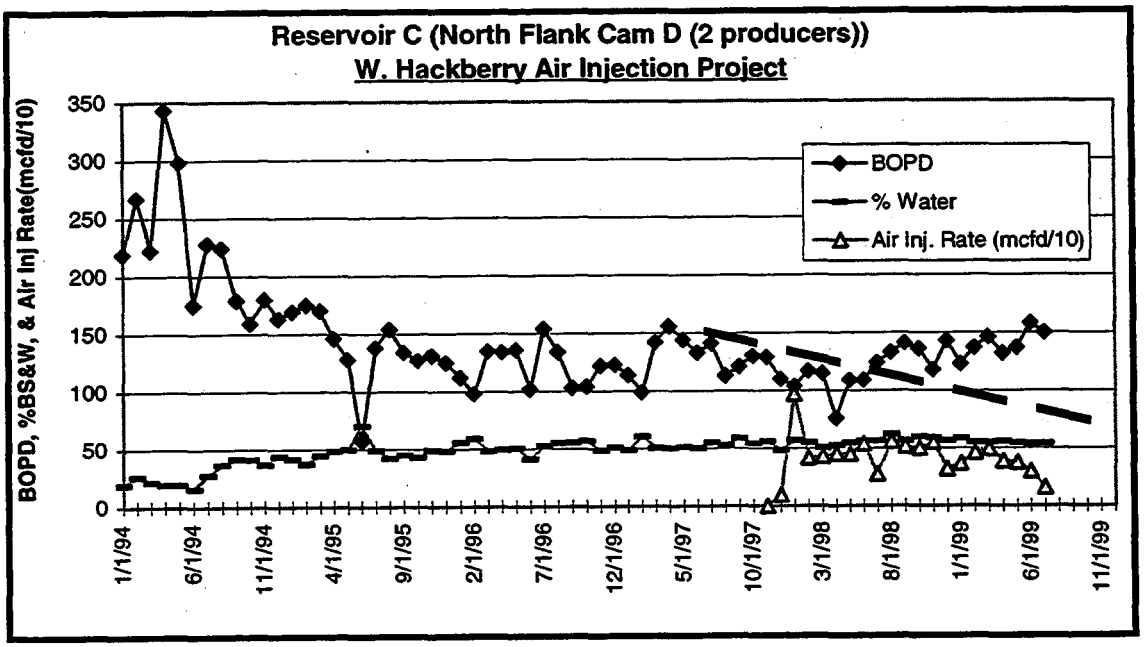
Reservoir C (North Flank Cam D (2 producers))
W. Hackberry Air Injection Project
BOPD, %BS&W, & Air Inj Rate(mcfd/10)
350
300
250
200
150
100
50
0
1/1/94
6/1/94
11/1/94
4/1/95
9/1/95
2/1/96
7/1/96
12/1/96
5/1/97
10/1/97
3/1/98
8/1/98
1/1/99
6/1/99
11/1/99
BOPD
% Water
Air Inj. Rate (mcfd/10)

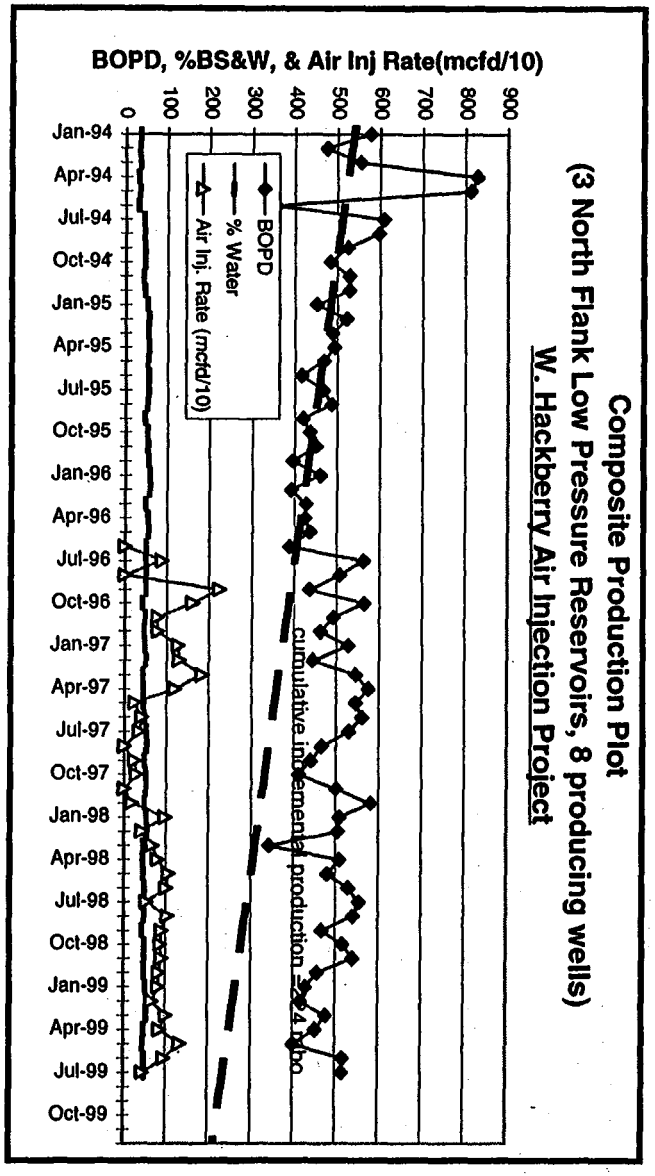
Composite Production Plot
(3 North Flank Low Pressure Reservoirs, 8 producing wells)
W. Hackberry Air Injection Project
BOPD, %BS&W, & Air Inj Rate(mcfd/10)
900
800
700
600
500
400
300
200
100
0
BOPD
% Water
Air Inj. Rate (mcfd/10)
cumulative incremental production 3.4 mbo
Jan-94
Apr-94
Jul-94
Oct-94
Jan-95
Apr-95
Jul-95
Oct-95
Jan-96
Apr-96
Jul-96
Oct-96
Jan-97
Apr-97
Jul-97
Oct-97
Jan-98
Apr-98
Jul-98
Oct-98
Jan-99
Apr-99
Jul-99
Oct-99

FOSSIL ENERGY

DOE/BC/14963-19
(OSTI_ID: 2711)

WEST HACKBERRY TERTIARY PROJECT

Annual Report
September 3, 1997 to September 2, 1998

By
Travis H. Gillham

January, 1999

Performed Under Contract No. DE-FC22-93BC14963

Amoco Production Company
Houston, Texas

National Petroleum Technology Office
U. S. DEPARTMENT OF ENERGY
Tulsa, Oklahoma

DISCLAIMER

This report was prepared as an account of work sponsored by an agency of the United States Government. Neither the United States Government nor any agency thereof, nor any of their employees, makes any warranty, expressed or implied, or assumes any legal liability or responsibility for the accuracy, completeness, or usefulness of any information, apparatus, product, or process disclosed, or represents that its use would not infringe privately owned rights. Reference herein to any specific commercial product, process, or service by trade name, trademark, manufacturer, or otherwise does not necessarily constitute or imply its endorsement, recommendation, or favoring by the United States Government or any agency thereof. The views and opinions of authors expressed herein do not necessarily state or reflect those of the United States Government.

This report has been reproduced directly from the best available copy.

Available to DOE and DOE contractors from the Office of Scientific and Technical Information, P.O. Box 62, Oak Ridge, TN 37831; prices available from (615) 576-8401.

Available to the public from the National Technical Information Service, U.S. Department of Commerce, 5285 Port Royal Rd., Springfield, VA 22161

DOE/BC/14963-19
Distribution Category UC-122

West Hackberry Tertiary Project

By
Travis H. Gillham

January 1999

Work Performed Under Contract DE-FC22-93BC14963

Prepared for
U.S. Department of Energy
Assistant Secretary for Fossil Energy

Dan Ferguson, Technology Manager
National Petroleum Technology Office
P.O. Box 3628
Tulsa, OK 74101

Prepared by:
Amoco Production Company
501 West Lake Park Blvd., Room 9.134W1
Houston, TX 77253

TABLE OF CONTENTS

1.0 ABSTRACT 1
1.1 Brief Description of Research 1
1.2 Summary of Key Results and Conclusions 1
2.0 EXECUTIVE SUMMARY 2
2.1 Background 2
2.2 Conclusions 2
2.3 Recommendations 3
3.0 INTRODUCTION 3
4.0 DISCUSSION 4
4.1 Project Performance (by reservoir) 4
4.1.1 High Pressure Cam C Reservoir on the West Flank 4
4.1.2 Low Pressure Cam C Reservoir on the North Flank 5
4.1.3 Low Pressure Bol 3 Reservoir on the North Flank 6
4.1.4 Low Pressure Cam D Reservoir on the North Flank 6
4.1.5 Composite North Flank Performance 6
4.2 Operation of Surface Injection Facilities 6
4.3 Technology Transfer Activities 7
4.4 SI Metric Conversion Factors 8

APPENDIX
APPENDIX A Statement of Work 9

FIGURES AND TABLES
Project Location Map 17
Map Depicting Location of Air Injection Units 18
Type Log 19
Structure Map: Top of Cam C-1 Sand (West Flank) 20
Plot of Cumulative Air Injected vs. Time 21
Schematic Cross-Section: Cam C (North Flank) 22
Structure Map: Top of Cam C-1 Sand (North Flank) 23
Production Plot: Cam C (North Flank) 24
Structure Map: Top of Bol 3 Sand (North Flank) 25
Production Plot: Bol 3 (North Flank) 26
Structure Map: Top of Cam D Sand (North Flank) 27
Production Plot: Cam D (North Flank) 28
Combined Production Plot for All Three North Flank Low Pressure Reservoirs 29

Annual Technical Progress Report (9/3/97-9/2/98)
West Hackberry Tertiary Project

1.0 ABSTRACT

1.1 Brief Description of Research

The West Hackberry Tertiary Project is a field test of the concept that air injection can be combined with the Double Displacement Process to produce a tertiary recovery process that is both low cost and economic at current oil prices. The Double Displacement Process is the gas displacement of a water invaded oil column for the purpose of recovering tertiary oil by gravity drainage. In reservoirs with pronounced bed dip such as those found in West Hackberry and other Gulf Coast salt dome fields, reservoir performance has shown that gravity drainage recoveries average 80% to 90% of the original oil in place while waterdrive recoveries average 50% to 60% of the original oil in place. The target for tertiary oil recovery in the Double Displacement Process is the incremental oil between the 50% to 60% waterdrive recoveries and the 80% to 90% gravity drainage recoveries.

In previous field tests, the Double Displacement Process has proven successful in generating tertiary oil recovery. The use of air injection in this process combines the benefits of air's low cost and universal accessibility with the potential for accelerated oil recovery from the combustion process. If successful, this project will demonstrate that utilizing air injection in the Double Displacement Process will result in an economically viable tertiary process in reservoirs (such as Gulf Coast salt dome reservoirs) where any other tertiary process is presently uneconomic.

1.2 Summary of Key Results and Conclusions

Air injection on the West Flank began in November of 1994. Although West Flank air injection has increased reservoir pressure by 500 pounds per square inch (psi), production response has not yet occurred. The gas cap on the West Flank has not expanded sufficiently to push the oil rim down to the nearest downstructure well. Continued air injection is expected to further expand the gas cap and thereby bring about oil production.

To spread risk among multiple reservoirs, the project was expanded in 1996 to include air injection in low pressure reservoirs on the North Flank of the field. The project reservoirs on the West Flank are much higher pressure (2500-3300 psi) than the project reservoirs on the North Flank (300-600 psi). Air injection began on the North Flank in July of 1996. While West Flank air injection has not yet yielded oil production, air injection has increased oil production in all three low pressure North Flank reservoirs. Between July of 1996 and August of 1998, air injection increased North Flank oil production by 141,000 barrels above the normal decline. As of August, 1998, air injection was generating 280 barrels of oil per day (BOPD) of incremental oil production from the three low pressure reservoirs on the North Flank of the field.

While air injection has been successful in the low pressure North Flank reservoirs, additional air injection will be required to generate production response on the West Flank of the field. During the upcoming year, air injection will be split between the high pressure West Flank reservoir and three low pressure North Flank reservoirs with the ultimate goal to maximize production response throughout the project.

2.0 EXECUTIVE SUMMARY

2.1 Background

The following report is the Annual Technical Progress Report for the fifth year of the West Hackberry Tertiary Project and covers the time period from September 3, 1997 to September 2, 1998. The West Hackberry Tertiary Project is one of four mid-term projects selected by the United States Department of Energy (DOE) as part of the DOE's Class 1 Program for the development of advanced recovery technologies in fluvial dominated deltaic reservoirs.

Over an 106 month funding period from September 3, 1993 to July 2, 2002, Amoco and the DOE are implementing a field test of the theory that air injection can be combined with the Double Displacement Process to create a tertiary oil process that is economically viable for the domestic oil industry. Air injection on the West Flank of the field is testing the process in a high pressure (2500-3300 psi) reservoir which had watered out. Although the project originally targeted the West Flank of the field, Amoco and the DOE agreed to expand the project to the North Flank during 1996. The low pressure north flank reservoirs exhibit slow water encroachment, possess low pressure gas caps and contain thin oil rims. Injection on the North Flank is testing the process in low pressure (300-600 psi) reservoirs that are approaching depletion.

As part of the project, the Petroleum Engineering Department at Louisiana State University (LSU) has been subcontracted to provide independent study and technology transfer support. The Statement of Work for the West Hackberry Tertiary Project is included as Appendix A. West Hackberry is a salt dome oil field located in Southwestern Louisiana about 30 miles southwest of Lake Charles, Louisiana as shown on the map on Page 17. A map with the location of each of the project's four reservoir-wide units is included on Page 18. A type log for the sands in the project is shown on Page 19.

2.2 Conclusions

The following conclusions have been generated during the fifth year of the project:

1) Oil production has not yet occurred on the West Flank since the oil rim has not moved sufficiently downstructure to reach the first producing well. The gas cap has not expanded enough to push the oil rim down to the most upstructure well.

2) Air injection in each of three low pressure North Flank oil reservoirs has generated a significant increase in oil production.

2.3 Recommendations

The following recommendations are presented for the upcoming year:

1) Distribute air injection between the high pressure West Flank reservoir and the three low pressure North Flank reservoirs with the ultimate goal to maximize production response throughout the project.

2) Monitor reservoir performance with production data, bottom hole pressure surveys, well tests and produced oil, gas and water analyses.

3) Utilize production response to guide the timing for workovers and to guide the injection rates for each reservoir.

4) Update future technology transfer activities with additional project performance and production response.

3.0 Introduction

In the West Hackberry Tertiary Project, air is injected into a high pressure (2500-3300 psi) watered out oil reservoir on the West Flank and into three low pressure (300-600 psi) North Flank oil reservoirs that are nearing depletion. In both situations, air injection is combined with the Double Displacement process in an attempt to generate an economically viable tertiary recovery process for Gulf Coast oil reservoirs with pronounced bed dip. The Double Displacement Process is the gas displacement of a water invaded oil column for the purpose of recovering tertiary oil by gravity drainage. In West Hackberry Field, gravity drainage recoveries average 80% to 90% of the original oil in place while waterdrive recoveries average 50% to 60% of the original oil in place. The target for tertiary oil recovery in the Double Displacement Process is the incremental oil between the 50% to 60% waterdrive recoveries and the 80% to 90% gravity drainage recoveries.

For air injection to work successfully with the Double Displacement Process, the reservoir temperature must be high enough for oxygen to be consumed through combustion with the reservoir oil. Amoco has performed laboratory tests which prove that West Hackberry oil will spontaneously combust with oxygen in the pore space. The combustion of oxygen in the reservoir alleviates concerns relating to the presence of oxygen in the reservoir or production equipment. Oxygen in the reservoir can form viscous emulsions hindering the flow of oil in the well and in the production equipment. Oxygen that reaches the producing wells can also produce corrosion and or explosions in the production equipment.

In the high pressure (2500-3300 psi) west flank reservoir, the mechanics of the tertiary process involve: 1) injecting air into the crest of a watered out oil reservoir in order to fill the reservoir with a gas from the top down, 2) as the reservoir fills with air, oxygen is consumed through spontaneous combustion, 3) oil and water drain toward the base of the structure through gravity segregation and gravity drainage and 4) tertiary oil, which previously had been trapped as a residual oil saturation, is now produced in downstructure

wells. In this case, the economic potential of the project is enhanced by the low cost associated with using air as the injection gas.

On the North Flank of West Hackberry, low pressure (300-600 psi) oil reservoirs are found which have large low pressure gas caps, thin oil rims and slow water encroachment. In the low pressure north flank reservoirs, air injection can increase oil recovery by: 1) pushing the oil rim downstructure to the structural location of existing wellbores, 2) repressurizing the reservoir and 3) obtaining tertiary oil recovery through the Double Displacement Process in the same manner as described in the preceding paragraph. Although injection of nitrogen, carbon dioxide and natural gas have been utilized to increase oil recovery in Gulf Coast reservoirs in the past, this project is unique in the use of air as the injection gas.

4.0 Discussion

4.1 Project Performance (by reservoir)

4.1.1 High Pressure Cam C Reservoir on the West Flank (WH Cam C RI SU)

A structure map for the top of the Cam C-1 sand on the West Flank of West Hackberry Field can be found on Page 20. Throughout most of the project, the Gulf Land D (GLD) No. 51 served as an air injector in the Cam C sand on the West Flank. In October of 1997, the GLD No. 51 became plugged with iron oxide after injection of almost 1.6 billion standard cubic feet (BCF). On Page 21 is a plot of cumulative air injected versus time.

Efforts to clean out the GLD No. 51 were not successful. To help assess the location of the oil rim, the GLD No. 51 was sidetracked and logged. The location of the sidetrack hole is immediately adjacent to the original hole. The Cam C-1,2 was found wet and the Cam C-3 appeared to contain a small amount of oil pay. The sidetrack was completed in the Cam C-3 and initially tested nitrogen and oil with a high water cut. After several months of testing, the Cam C-3 watered out. The reason that the GLD No. 51 Sidetrack (ST) is still below the oil rim is an insufficient volume of air injected in combination with: 1)uncertainty as to the pre-injection location of the oil rim, 2)the large volume of the attic portion of the reservoir and 3)the high reservoir pressure (which inhibits the growth of the gas cap).

The GLD No. 51 ST is the highest well on structure in the Cam C sand. When the oil rim reaches the GLD No. 51 ST, using the GLD No. 51 ST as a producing well would generate the earliest possible oil production. If the GLD No. 51 ST serves as a producer, then an alternate wellbore would be needed to serve as an injector. During late September of 1998, the GLD No. 45 will be converted into an air injector. Although the GLD No. 45 is downstructure to the GLD No. 51 ST, the GLD No. 45's location is not directly downstructure to the GLD No. 51. Air injected into the GLD No. 45 is expected to migrate upstructure, accumulate in the gas cap and push the oil rim down to the GLD No. 51.

The GLD No. 51 was completed in the Cam C-3 in a manner that would allow for pulsed neutron logs to be run over the Cam C-1 through tubing. After the GLD No. 45 begins air injection, a pulsed neutron log will be run each quarter to monitor the arrival of the oil rim in the Cam C-1. When the oil rim reaches the GLD No. 51 ST, the GLD No. 51 ST will be recompleted to the Cam C-1 and placed on production.

4.1.2 Low Pressure Cam C Reservoir on the North Flank

In 1996, Amoco and the DOE agreed to expand the project to include air injection in low pressure reservoirs on the North Flank of the field. The low pressure North Flank reservoirs exhibit slow water encroachment, possess large low pressure gas caps and contain thin oil rims. In the low pressure North Flank reservoirs, air injection can increase oil recovery by: 1)pushing the oil rim downstructure to the structural location of existing wellbores, 2)repressurizing the reservoir and 3)obtaining tertiary oil recovery through the Double Displacement Process.

Air injection began on the North Flank in a low pressure (300-600 psi) Cam C oil reservoir during July of 1996. A schematic cross-section of the reservoir is included on Page 22. The SL 42 No. 155 serves as the air injector in the gas cap. A structure map for the top of the Cam C-1 is included on Page 23. To date, four producing wells have exhibited increased oil production as a result of air injection in the Cam C sand. A composite production plot for the four producing wells in the North Flank Cam C sand is included on Page 24. As shown on the production plot, air injection has resulted in increased oil production and reduced water cut.

In July of 1997, air injection was interrupted when the injector, the SL 42 No. 155 became plugged with iron oxide. Repeated attempts to clean out the SL 42 No. 155 were unsuccessful. The SL 42 No. 155 was sidetracked and returned to injection in March of 1998. As of August, 1998, air injection had increased oil production in the North Flank Cam C by 240 BOPD above the normal decline.

Through August of 1998, the air injection project in the Cam C consisted of four producers and one injector. A hydrocarbon pore volume analysis of the reservoir suggested that an additional producer might be needed to more effectively produce the remaining reserves. The SL 42 No. 98 was sidetracked from its position in the gas cap down into the oil rim to serve as the fifth producer in the Cam C. The SL 42 No. 98 ST was placed on production during the last half of September, 1998.

Air injection rates in the SL 42 No. 155 ST have averaged only 400 to 500 thousand standard cubic feet per day (MSCFD) due to iron oxide plugging the wellhead filter. To increase injection rates, facilities modifications are underway which are expected to relieve the plugging problem. One additional injector, the SL 42 No. 221, will be added to the Cam C reservoir during the fourth quarter of 1998 to increase injection rates and to provide a backup injector for the reservoir. After the addition of one injector and one producer, the North Flank Cam C will consist of two injectors and five producers.

4.1.3 Low Pressure Bol 3 Reservoir on the North Flank

In December of 1996, air injection was extended to a second low pressure North Flank reservoir, the Bol 3 sand. As with the Cam C reservoir, the Bol 3 reservoir has low reservoir pressure, a thin oil rim, steep bed dip and slow water encroachment. A structure map for the North Flank Bol 3 is on Page 25. As noted on the production plot on Page 26, air injection has increased oil production in the Bol 3.

Air injection in the Bol 3 was interrupted in December, 1997, when the GLAC No. 245 became plugged and efforts to clean out the well were unsuccessful. In the absence of air injection, production has fallen back to the level of the previous decline. An alternate well, the GLAC No. 42 has been chosen to replace the GLAC No. 245. The GLAC No. 42 will be converted to air injection during the fourth quarter of 1998. .

4.1.4 Low Pressure Cam D Reservoir on the North Flank

Air injection began in the North Flank Cam D in December of 1997. The Cam D is by far the largest of the three low pressure North Flank reservoirs and thereby contains the most reserve potential. A structure map for the Cam D is shown on Page 27. The Cam D's low pressure gas cap, thin oil rim and steep bed dip are similar to those of the North Flank Cam C and Bol 3 reservoirs. Average reservoir pressure is approximately 400 psi.

Prior to air injection, the Cam D had produced through many wells over a period of over 40 years and was in the final stages of depletion. The air injection project in the Cam D currently consists of one injector and two producers. As of August of 1998, air injection had increased production by 40 BOPD over the established decline. The production plot for the North Flank Cam D is on Page 28. Over the next six months, workovers are planned that will add two producers and one injector to the Cam D reservoir. With these additions, the Cam D will have two injectors and four producers.

4.1.5 Composite North Flank Performance

The West Hackberry Air Injection Project is the first successful application of the use of low cost air injection to improve oil recovery in low pressure Gulf Coast salt dome reservoirs. From July of 1996 to August of 1998, air injection in three low pressure reservoirs on the North Flank of West Hackberry Field increased oil production by 141,000 barrels over the decline. A composite production plot is shown on Page 29. In August, 1998, air injection generated 280 BOPD of incremental oil production.

4.2 Operation of Surface Air Injection Facilities

By far the most serious facilities problem encountered to date has been the iron oxide plugging of air injection wells. After the injection well tubing strings were replaced with coated tubing, problems continued as a result of ongoing corrosion in the injection lines. Other recent high pressure air injection projects (North Dakota) have not had a problem with corrosion in the injection lines. The absence of corrosion in the other projects was thought to have been caused by carryover of synthetic compressor lubricant into the

injection lines. Injection of synthetic compressor lubricant into the lines at Hackberry failed to protect the lines.

While other recent high pressure air injection projects have not had problems with corrosion in the flowlines, the other high pressure projects did not have a low pressure component. The corrosion seen in the Hackberry project appears to have been caused by water condensation associated with the pressure drop from the high pressure compressors to the low pressure lines. Both high pressure and low pressure compressed air are still required for the Hackberry project.

Corrosion coupons have been placed in the air injection lines to assess the location and extent of the corrosion. To alleviate future corrosion in the injection lines, the use of a desiccant is under evaluation which would remove the moisture in the air immediately after the pressure drop into the low pressure portion of the system.

Wellhead filters have been installed on the air injectors to prevent iron oxide plugging downhole in the injection wells. While the filters have prevented plugging downhole, the filters become so quickly plugged after cleaning that injection rates have been restricted to a range of 400 to 600 MCFD. To relieve the problem of restricted rates and plugged filters, strainers have been ordered which will catch most of the iron oxide before it reaches the wellhead filters.

4.3 Technology Transfer Activities

The following is a listing of technology transfer activities from the past twelve months:

1)On October 6, 1997, a paper entitled "Keys to Increasing Production Via Air Injection in Gulf Coast Light Oil Reservoirs" was presented at the SPE Annual Technical Conference and Exhibition in San Antonio, Texas. Over 200 SPE members were in the audience.

2)On October 17, 1997, an Amoco geologist presented a paper entitled "Air Injection Enhanced Oil Recovery and 3-D Seismic: Revitalizing an Aging South Louisiana Oil Field" at the Gulf Coast Association of Geological Societies' (GCAGS) Annual Convention in New Orleans, Louisiana.

3)During the last week of October, 1997, an article discussing the West Hackberry Air Injection Project appeared in the *Enhanced Energy Recovery News.*

4)On October 30, 1997, Amoco personnel reviewed the West Hackberry project at a technology transfer event in Houston, Texas, for the Texas Railroad Commission.

5)The November, 1997, issue of *World Oil* included an article entitled "A new/economically viable EOR process for the U.S. Gulf Coast" which was co-authored by representatives from Amoco and LSU.

6)On January 23, 1998, a talk entitled "Air Injection: Low Cost IOR for Gulf Coast Reservoirs" was given at a technology transfer conference in New Orleans sponsored by LSU's Basin Research Institute.

7)On February 10, 1998, a West Hackberry talk was presented to the monthly meeting of the Mississippi Geological Society in Jackson, Mississippi.

8)The SPE/DOE Eleventh Symposium on Improved Oil Recovery was held on April 19-22, 1998, in Tulsa, Oklahoma. A paper entitled "Low Cost IOR: An Update on the West Hackberry Air Injection Project" was presented at that time.

4.4 SI Metric Conversion Factors

bbl	x 1.589 873	E-01 = cubic meters
cubic feet	x 2.831 685	E-02 = cubic meters
psi	x 6.894 757	E+00 = kPa
Btu	x 1.055 056	E+00 = kJ

APPENDIX A

STATEMENT OF WORK

STATEMENT OF WORK

WEST HACKBERRY TERTIARY PROJECT

Amoco Production company
October 16, 1992

Background and Objectives

The goal of the West Hackberry Tertiary Project is to demonstrate the technical and economic feasibility of oil recovery using air injection in the double Displacement Process. The Double Displacement Process is the gas displacement of a water invaded oil column for the purpose of recovering oil through gravity drainage. A novel aspect of this project is the use of air as the injection fluid. This technology will be applicable to reservoirs which have both sufficient bed dip for gravity drainage and sufficient reservoir temperature for the consumption of oxygen. Numerous water-drive reservoirs associated with salt dome fields along the Gulf Coast would be potential follow-up candidates for this technology. The use of air injection in this process offer the benefits of air's excellent accessibility and low cost combined with potentially greater recovery due to the combustion process. If successful, this project will demonstrate that the use of air injection in the Double Displacement Process can economically recover oil in reservoirs where tertiary oil recovery is presently uneconomical.

Based on a preliminary project design developed prior to commencement of the project, the following basic operational information has been determined for the study: injection rates; selection of reservoirs and fault blocks; required number of producing and injection wells; requirements for new wells versus re-completing existing wells; requirements for continuous injection versus intermittent injection; assessment of the disposal of produced gases by flaring or injection into low pressure reservoirs; unitization; and the design of surface production and injection facilities. The project is designed for injection into two separate fault blocks (Fault Blocks II & IV). In Fault Block IV, the technology will be assessed using a line of four producers at structurally equivalent positions in a heavily developed area. In Fault Block II, the technology will be assessed using a single producer in a sparsely developed area.

A description of each task associated with the project is provided below.

Task 1 - Environmental Study

It is anticipated that this project will be categorically excluded from the DOE NEPA requirements. Upon DOE certification, if this project does qualify for a categorical exclusion, this task will not be required. If this project does not quality for a categorical exclusion, then this task will involve activities, such as data collection and reporting, that are required by the DOE to meet NEPA requirements.

Task 2 - Construction of Surface Facilities

The necessary permits required for construction of the surface facilities will be obtained. Based on the preliminary project design, Amoco will acquire the necessary equipment/facilities to inject 4-4.5 MMCFD of air at pressures greater than 4000 psi. Surface injection facilities will be installed which consist primarily of the air compressors and water purge system for the injection wells. The timing for the installation of production facilities will be tied to workovers on the producing wells conducted in Task 5. The production facilities will consist of flowlines, possibly a Natural Gas Liquids recovery unit, and a separate-test-and-boost (STAB) facility. After separation and testing, produced fluids will be piped to Amoco's central production facility. Undesired produced gasses will be flared or injected into low pressure reservoirs.

Task 3 - Conversion of Producing Wells to Injection Wells

Two producing wells will be converted to injection wells. Initially, a single injection well will be dedicated to each of the two fault blocks. Two additional injectors (i.e. converted producing wells) may be required to improve the economics of the process. A typical workover to convert a producing well to an injector would require cleaning out the wellbore, perforating the full prospective injection interval, and completing the well with new packers, tubing, and wellhead (i.e. valves, etc.).

Task 4 - Operations and Maintenance of Injection Facilities

The operation of the high pressure air compressors in the injection facilities requires close attention to safety issues. Synthetic lubricants and periodic cleaning of injection equipment will be conducted to prevent the possibility of a detonation resulting from the combination of high pressure air and hydrocarbon deposits. Additionally, routine maintenance of injection equipment will be conducted to avoid the possibility of catastrophic mechanical failure. Workovers to repair injection wells will be performed on an as needed basis.

Task 5 - Workovers for Monitoring and Producing Wells

A total of 9 wells will be repaired and/or re-completed to serve as producing wells and/or monitoring wells for the project. The timing of the workovers will be dictated by the advance of the flood front. The task of monitoring the flood front is addressed in Task 6. Once the project is underway, workovers to repair producing and monitoring wells will be performed on an as needed basis.

Task 6 - Production Operations

All production operations for the project will be handled by Amoco field personnel assigned to West Hackberry Field. Produced liquids will be transported through existing collection lines to be handled at an Amoco Tank Battery. Initially, producing wells will be gas lifted within Amoco's field-wide gas lift system. When the produced gasses become

concentrated with undesirable components (e.g. nitrogen and carbon dioxide) due to breakthrough, it will be necessary to install a separate gas lift system for the project. The separate gas lift system will require a gas lift compressor. Produced gasses will either be sold, burned as fuel, flared or re-injected into low pressure reservoirs on the north flank of the field. Booster compressors may be required to generate sufficient pressure for injection of produced gasses. A flowline will be installed to the north flank of West Hackberry Field in order to carry the produced gasses to the low pressure reservoirs in that area. Monthly production tests, at a minimum, will be performed on all producing wells. Gas analyses will be conducted periodically to monitor the composition and oxygen content of the produced gasses. Produced oil and water samples will be analyzed periodically to determine their composition and physical properties. Pulsed neutron logs, bottom hole pressure surveys, temperature surveys, and spinner surveys may be run in both producing and monitoring wells in order to assess the effectiveness of the project. Periodic replacement of surface production and injection equipment (including flowlines) may also be required due to wear and tear on these items.

Task 7 - Reservoir Management

Reservoir modeling studies will be conducted to effectively manage the project. These studies will assist in assessing the following: distribution of injection volumes; timing of repairs and recompletions; and the determination of monitoring schemes and schedules. Amoco's "THERM" reservoir model will be used to history match reservoir performance and to predict future reservoir performance. Specialized combustion tests will be conducted at Amoco's Combustion Laboratory in Tulsa, Oklahoma to assist in monitoring and predicting the performance of the project. Reservoir fluid property analyses will be conducted to calibrate the reservoir model. The results of reservoir management will be continually documented and reported in a manner consistent with the DOE reporting requirements and technology transfer needs of the project.

Task 8 - Louisiana State University Technology Transfer

A yearly Amoco grant will be provided to the Petroleum Engineering Department at Louisiana State University (LSU). LSU will study various aspects of the project and report their findings. LSU will publish and make industry presentations on all results from their analyses. Amoco plans to provide LSU with all pertinent data and information from the project. Examples of typical data and information that will be made available to LSU include the following: individual well production rates; individual well injection rates; structure maps; net pay isopachs; core data; well logs; gas analyses; and fluid property data.

Task 9 - Amoco Technology Transfer

Amoco will assess the technical and economic feasibility of Double Displacement Process based on the data and information acquired from the project. These results will be documented and submitted to various technical conferences for presentation and/or

publication. Since the Double Displacement Process will probably have its greatest applicability to salt dome fields along the Gulf Coast, Amoco personnel will focus on technical conferences in the Houston, Texas and New Orleans, Louisiana areas. It is anticipated that presentations and/or papers will be completed at the beginning, middle, and end of the project. Amoco does not intend to regard any data and/or information on this project as proprietary.

FIGURES AND TABLES

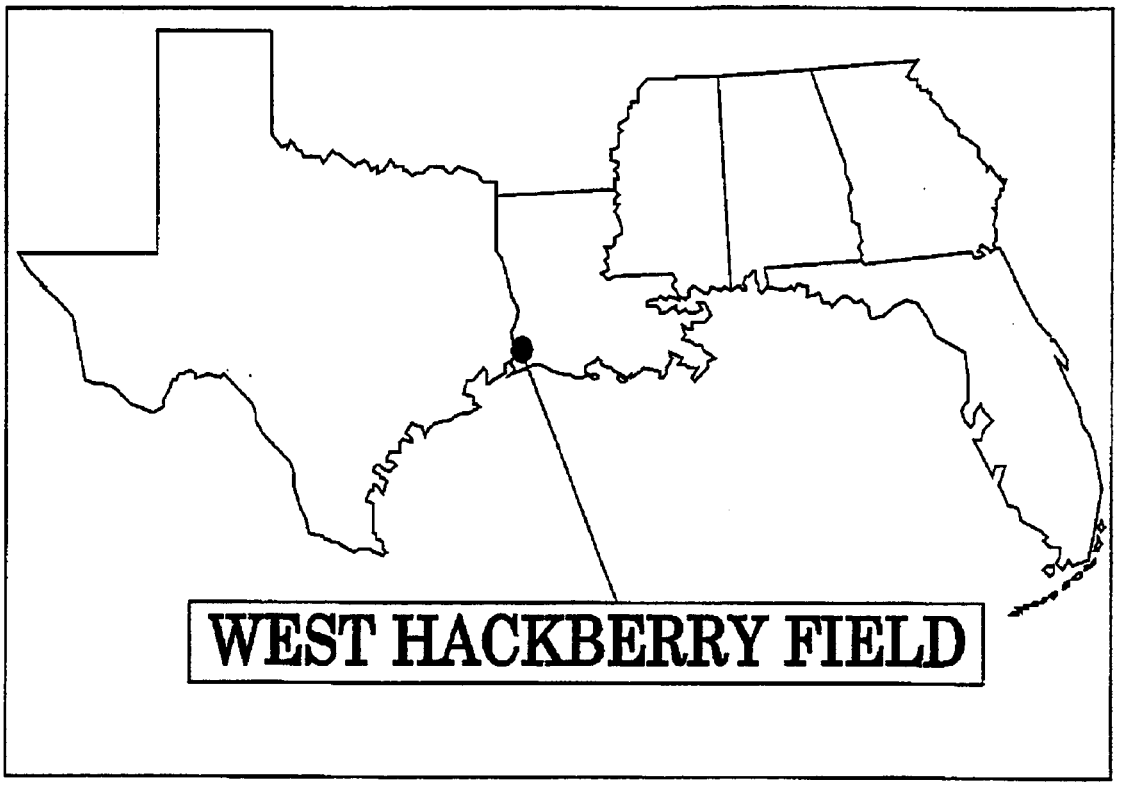
WEST HACKBERRY FIELD

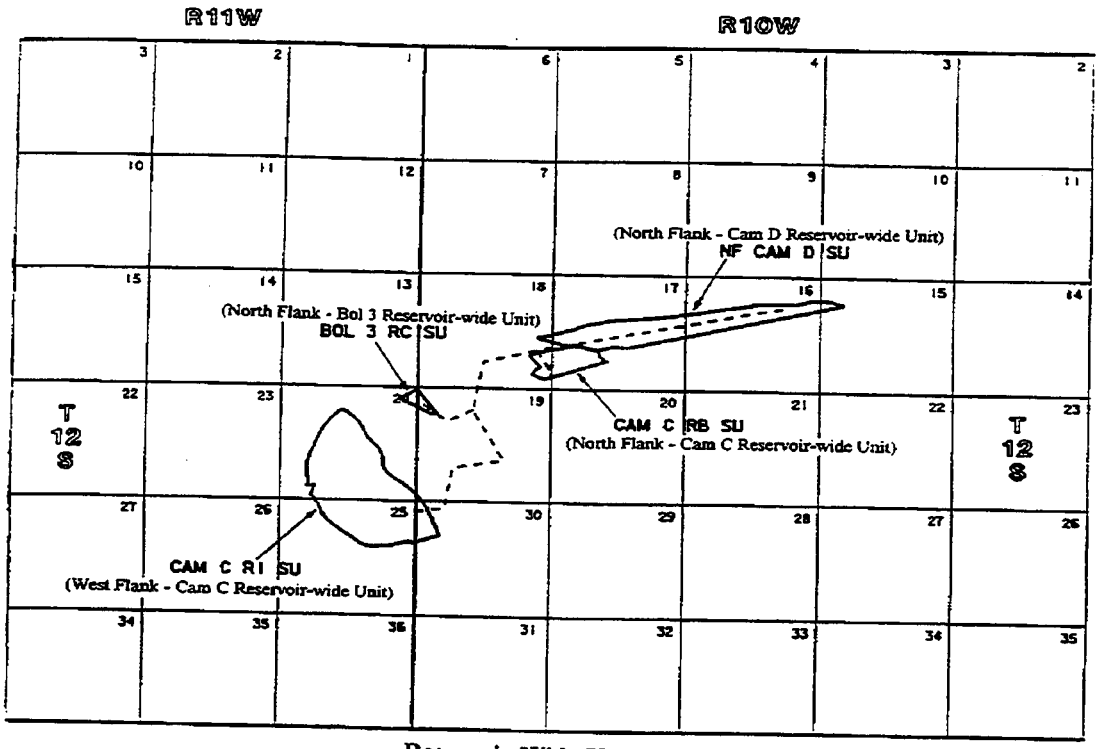

Reservoir-Wide Units
West Hackberry Air Injection Project

- - - - - Air Injection Lines

AIR COMPRESSOR LOCATED IN NE/4, NE/4 OF SECTION 25.

Amoco Production Company
WEST HACKBERRY FIELD
Cameron Parish, Louisiana

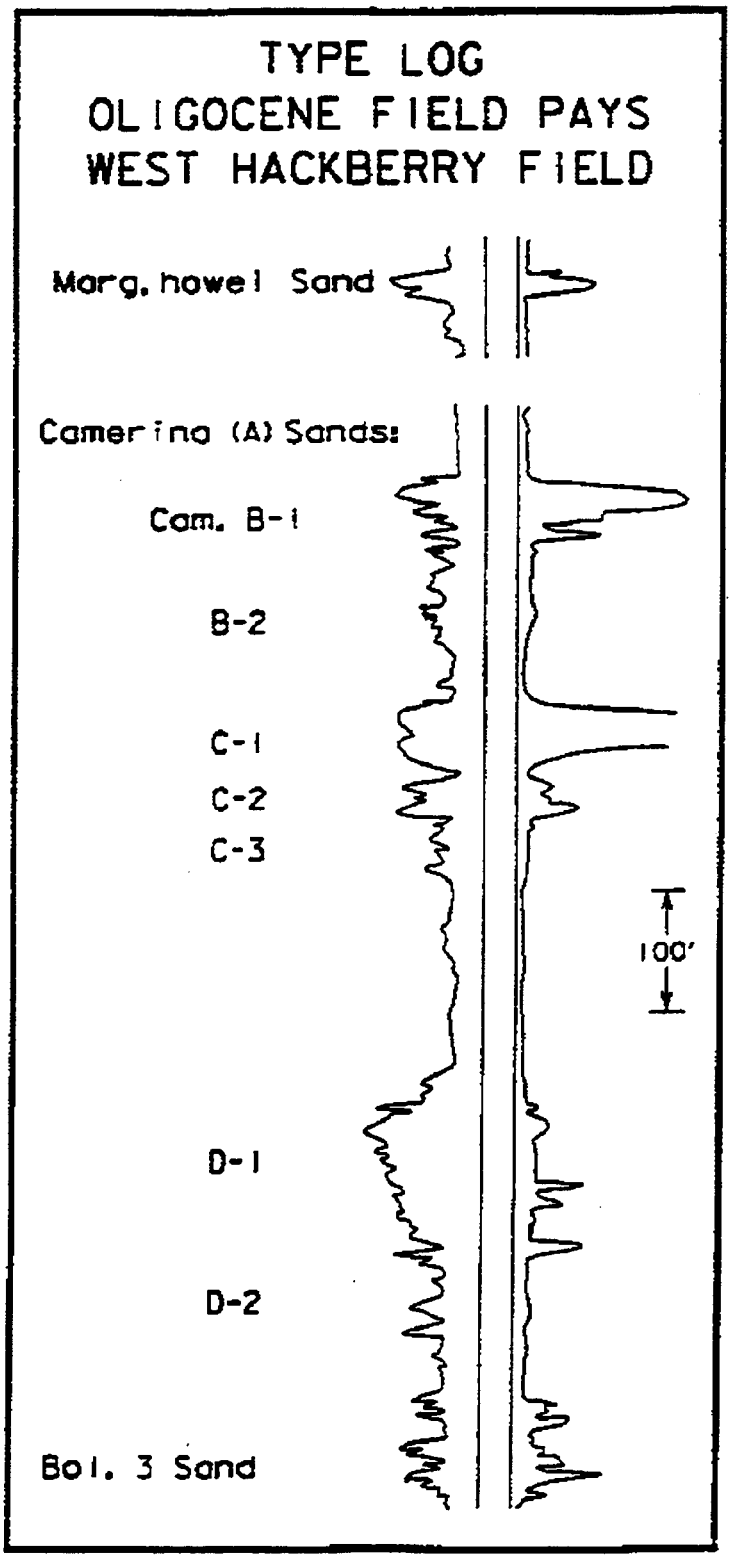
TYPE LOG
OLIGOCENE FIELD PAYS
WEST HACKBERRY FIELD
Marg. howel Sand
Camerino (A) Sands:
Cam. B-1
B-2
C-1
C-2
C-3
100'
D-1
D-2
Bol. 3 Sand

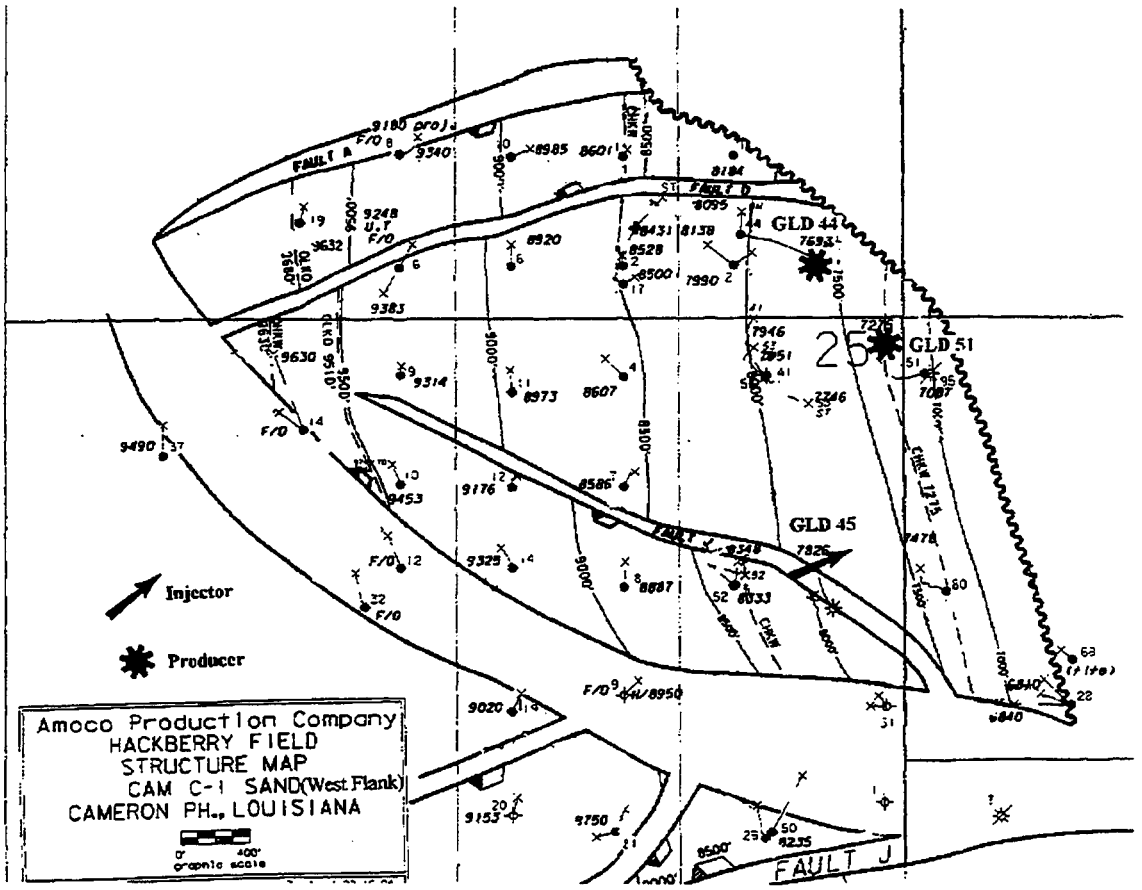
Amoco Production Company
HACKBERRY FIELD
STRUCTURE MAP
CAM C-1 SAND(West Flank)
CAMERON PH., LOUISIANA
400'
graphic scale
Injector
Producer
GLD 44
GLD 51
GLD 45
FAULT A
FAULT B
FAULT J
25

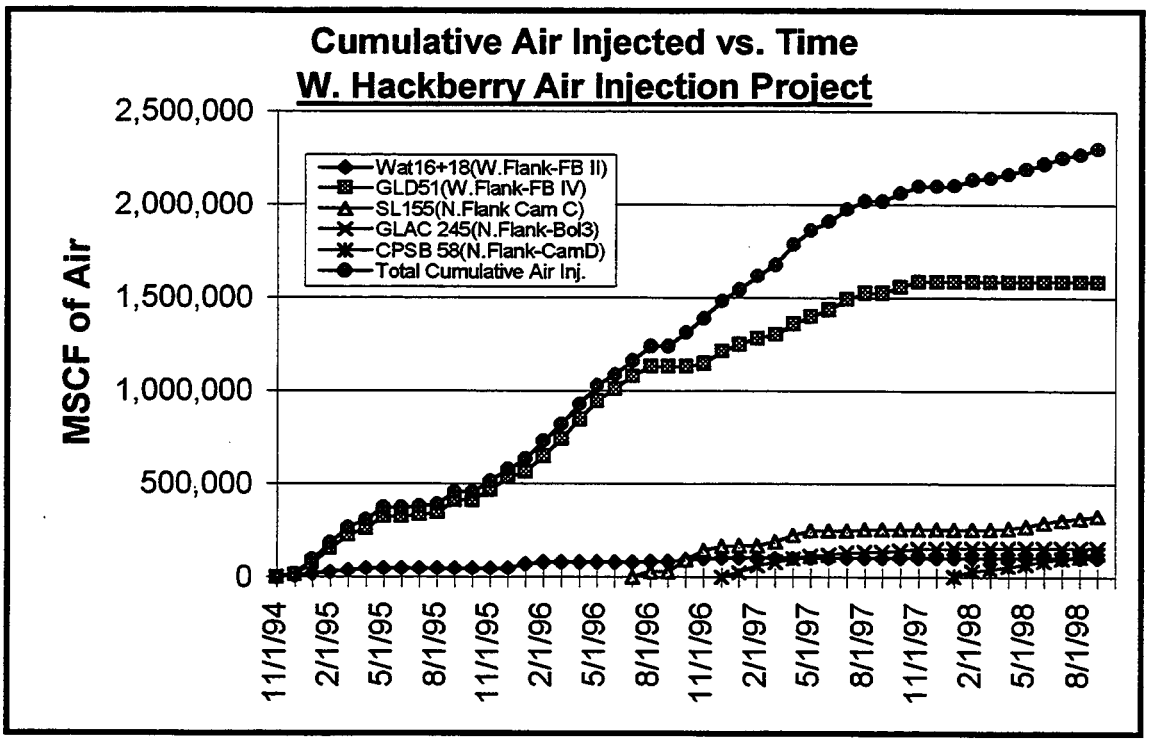
Cumulative Air Injected vs. Time
W. Hackberry Air Injection Project
MSCF of Air
2,500,000
2,000,000
1,500,000
1,000,000
500,000
0
Wat16+18(W.Flank-FB II)
GLD51(W.Flank-FB IV)
SL155(N.Flank Cam C)
GLAC 245(N.Flank-Bol3)
CPSB 58(N.Flank-CamD)
Total Cumulative Air Inj.
11/1/94
2/1/95
5/1/95
8/1/95
11/1/95
2/1/96
5/1/96
8/1/96
11/1/96
2/1/97
5/1/97
8/1/97
11/1/97
2/1/98
5/1/98
8/1/98

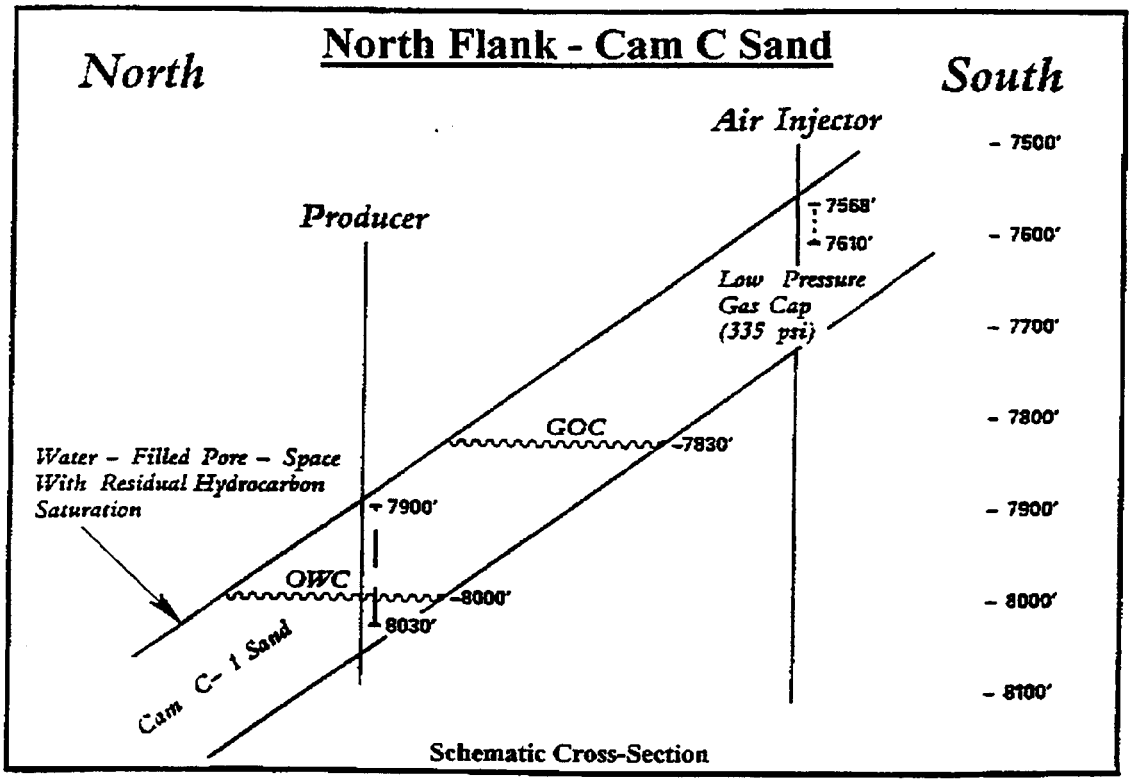
North Flank - Cam C Sand
North
South
Air Injector
Producer
7568'
7610'
Low Pressure
Gas Cap
(335 psi)
GOC
7830'
Water - Filled Pore - Space
With Residual Hydrocarbon
Saturation
7900'
OWC
8000'
8030'
Cam C- 1 Sand
- 7500'
- 7600'
- 7700'
- 7800'
- 7900'
- 8000'
- 8100'
Schematic Cross-Section

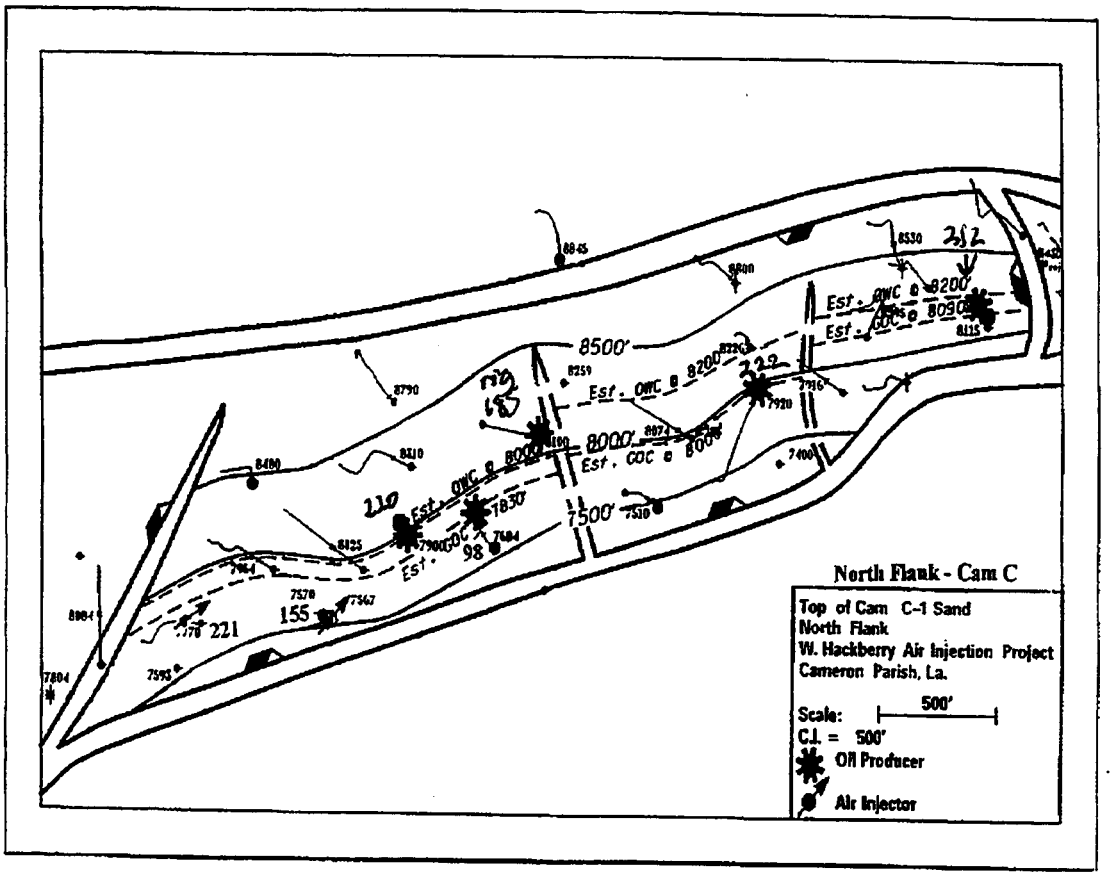
North Flank - Cam C
Top of Cam C-1 Sand
North Flank
W. Hackberry Air Injection Project
Cameron Parish, La.
Scale:
500'
C.I. = 500'
Oil Producer
Air Injector
8500'
8000'
7500'
Est. OWC @ 8200'
Est. GOC @ 8090'
Est. OWC @ 8000'
Est. GOC @ 8000'
Est. OWC @ 8000'
Est. GOC @ 7900'
252
222
183
210
98
155
221

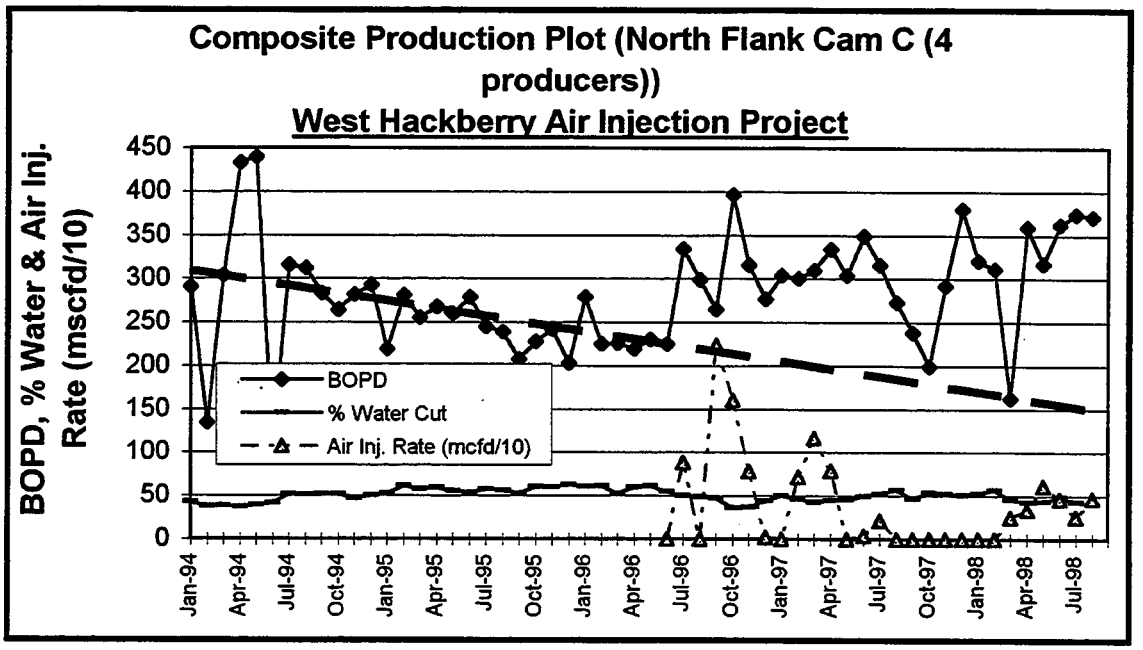
Composite Production Plot (North Flank Cam C (4 producers))
West Hackberry Air Injection Project
BOPD, % Water & Air Inj. Rate (mscfd/10)
450
400
350
300
250
200
150
100
50
0
BOPD
% Water Cut
Air Inj. Rate (mcfd/10)
Jan-94
Apr-94
Jul-94
Oct-94
Jan-95
Apr-95
Jul-95
Oct-95
Jan-96
Apr-96
Jul-96
Oct-96
Jan-97
Apr-97
Jul-97
Oct-97
Jan-98
Apr-98
Jul-98

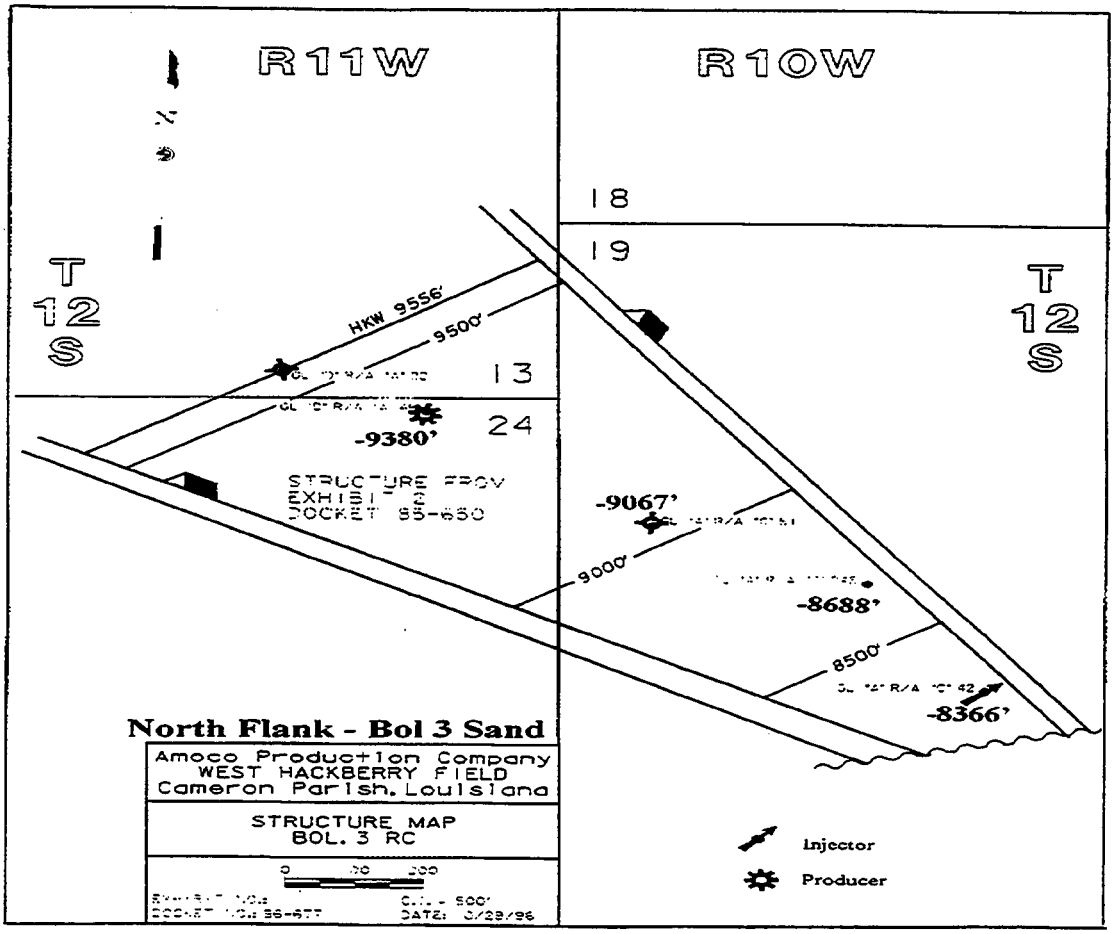
R11W
R10W
18
19
T
12
S
T
12
S
HKW 9556'
9500'
13
24
-9380'
STRUCTURE PROV
EXHIBIT 2
DOCKET 85-650
-9067'
9000'
-8688'
8500'
-8366'
North Flank - Bol 3 Sand
Amoco Production Company
WEST HACKBERRY FIELD
Cameron Parish, Louisiana
STRUCTURE MAP
BOL. 3 RC
Injector
Producer

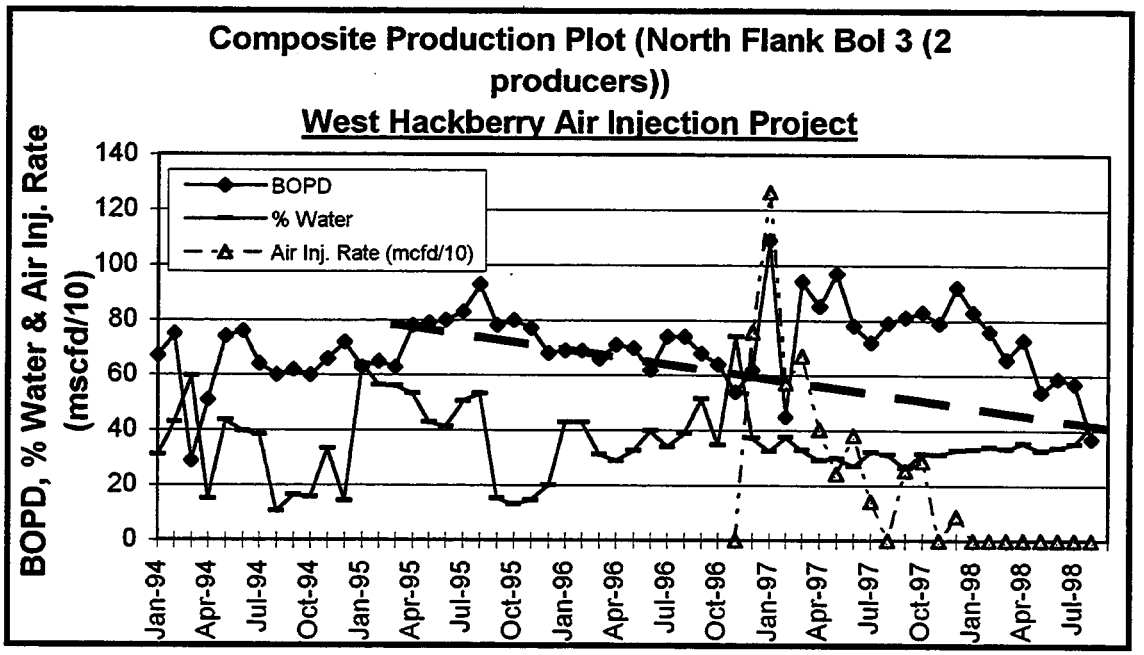
Composite Production Plot (North Flank Bol 3 (2 producers))
West Hackberry Air Injection Project
BOPD, % Water & Air Inj. Rate (mscfd/10)
BOPD
% Water
Air Inj. Rate (mcfd/10)
140
120
100
80
60
40
20
0
Jan-94
Apr-94
Jul-94
Oct-94
Jan-95
Apr-95
Jul-95
Oct-95
Jan-96
Apr-96
Jul-96
Oct-96
Jan-97
Apr-97
Jul-97
Oct-97
Jan-98
Apr-98
Jul-98

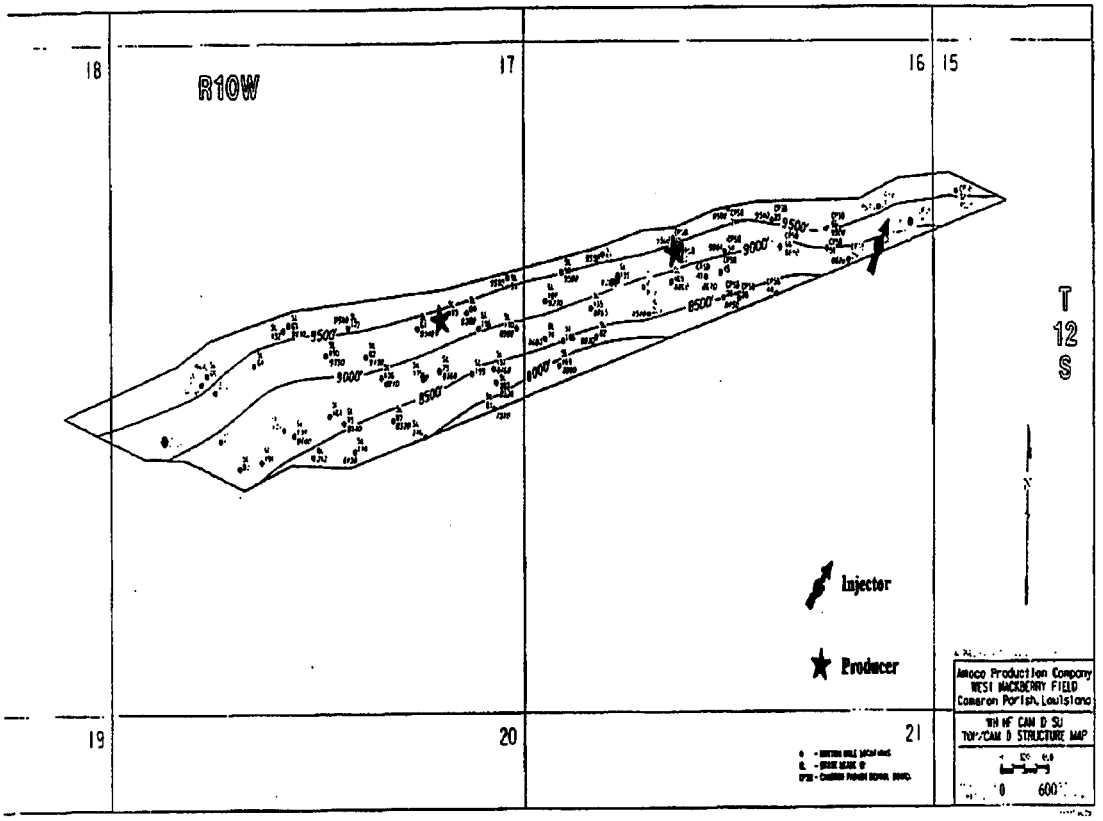
18
17
16
15
R10W
T
12
S
9500'
9000'
8500'
8000'
Injector
Producer
Amoco Production Company
WEST MACKBERRY FIELD
Cameron Parish, Louisiana
19
20
21
0
600

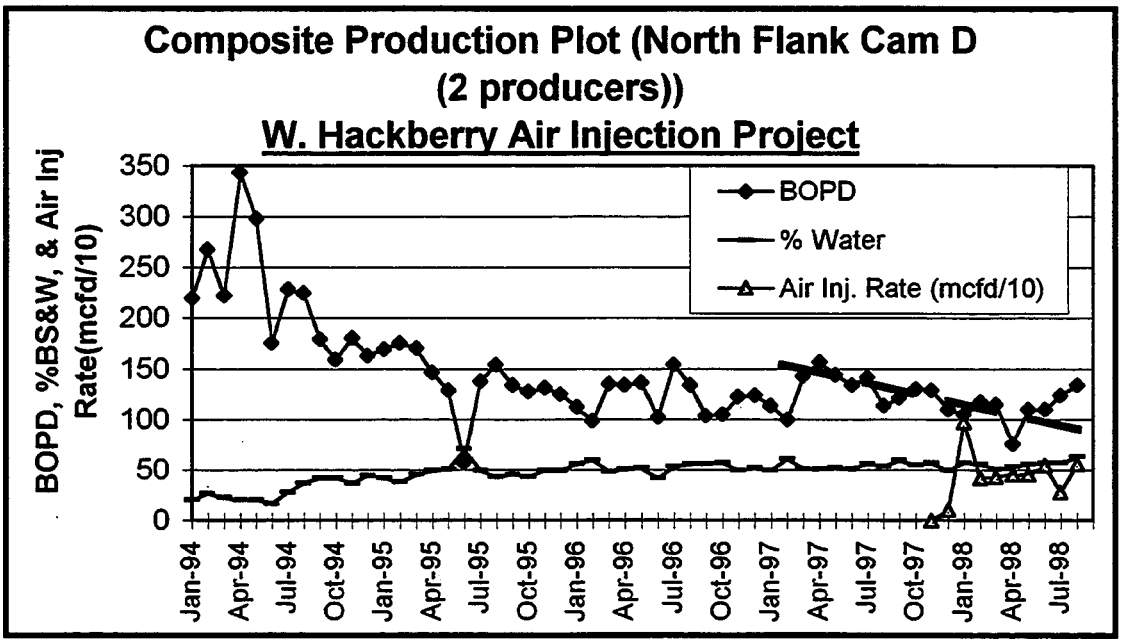
Composite Production Plot (North Flank Cam D (2 producers))
W. Hackberry Air Injection Project
BOPD, %BS&W, & Air Inj Rate(mcfd/10)
350
300
250
200
150
100
50
0
BOPD
% Water
Air Inj. Rate (mcfd/10)
Jan-94
Apr-94
Jul-94
Oct-94
Jan-95
Apr-95
Jul-95
Oct-95
Jan-96
Apr-96
Jul-96
Oct-96
Jan-97
Apr-97
Jul-97
Oct-97
Jan-98
Apr-98
Jul-98

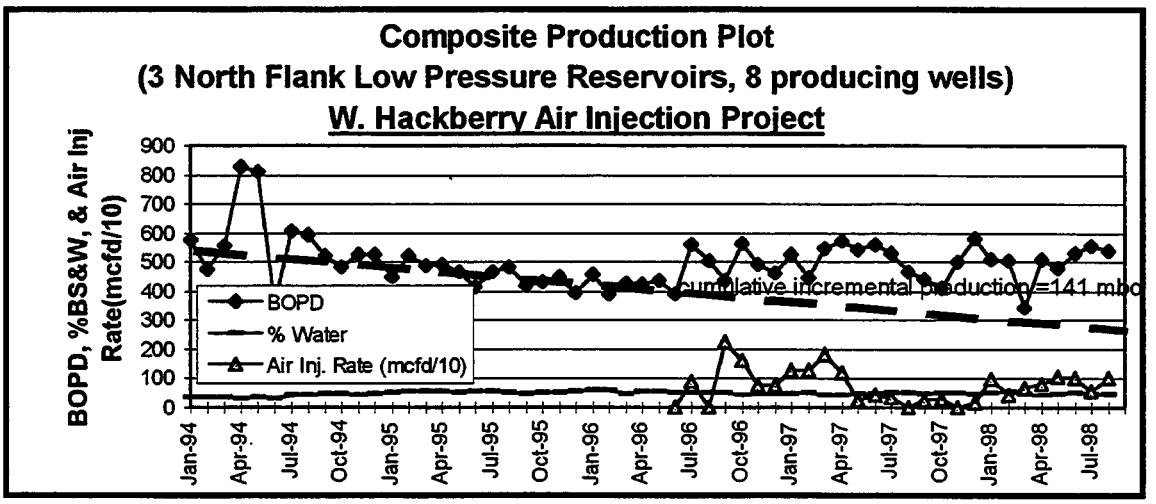
Composite Production Plot
(3 North Flank Low Pressure Reservoirs, 8 producing wells)
W. Hackberry Air Injection Project
BOPD, %BS&W, & Air Inj Rate(mcfd/10)
900
800
700
600
500
400
300
200
100
0
BOPD
% Water
Air Inj. Rate (mcfd/10)
cumulative incremental production=141 mbo
Jan-94
Apr-94
Jul-94
Oct-94
Jan-95
Apr-95
Jul-95
Oct-95
Jan-96
Apr-96
Jul-96
Oct-96
Jan-97
Apr-97
Jul-97
Oct-97
Jan-98
Apr-98
Jul-98

FOSSIL ENERGY

DOE/BC/14963-16
(DE96001287)

WEST HACKBERRY TERTIARY PROJECT

Annual Report
September 03, 1995 to September 02, 1996

By
Travis H. Gillham
Bruce Cerveny
Ed Turek

May 1997

Performed Under Contract No. DE-FC22-93BC14963

Amoco Production Company
Houston, Texas

National Petroleum Technology Office
U. S. DEPARTMENT OF ENERGY
Tulsa, Oklahoma

DISCLAIMER

This report was prepared as an account of work sponsored by an agency of the United States Government. Neither the United States Government nor any agency thereof, nor any of their employees, makes any warranty, expressed or implied, or assumes any legal liability or responsibility for the accuracy, completeness, or usefulness of any information, apparatus, product, or process disclosed, or represents that its use would not infringe privately owned rights. Reference herein to any specific commercial product, process, or service by trade name, trademark, manufacturer, or otherwise does not necessarily constitute or imply its endorsement, recommendation, or favoring by the United States Government or any agency thereof. The views and opinions of authors expressed herein do not necessarily state or reflect those of the United States Government.

This report has been reproduced directly from the best available copy.

Available to DOE and DOE contractors from the Office of Scientific and Technical Information, P.O. Box 62, Oak Ridge, TN 37831; prices available from (615) 576-8401.

Available to the public from the National Technical Information Service, U.S. Department of Commerce, 5285 Port Royal Rd., Springfield VA 22161

DOE/BC/149963-16
Distribution Category UC-122

West Hackberry Tertiary Project

Annual Report

By
Travis Gillham
Bruce Cerveny
Ed Turek

May 1997

Work Performed Under Contract No. DE-FC22-93BC14963

Prepared for
U.S. Department of Energy
Assistant Secretary for Fossil Energy

Jerry F. Casteel, Project Manager
National Petroleum Technology Office
P.O. Box 3628
Tulsa, OK 74101

Prepared by:
Amoco Production Company
501 West Lake Park Blvd.
Houston, TX 77253

Annual Technical Progress Report (9/3/95-9/2/96)
West Hackberry Tertiary Project

TABLE OF CONTENTS — PAGE

1.0 ABSTRACT 3
1.1 Brief Description of Research 3
1.2 Summary of Key Results and Conclusions 3
2.0 EXECUTIVE SUMMARY 4
2.1 Background 4
2.2 Conclusions 4
2.3 Recommendations 5
3.0 INTRODUCTION 5
4.0 DISCUSSION 6
4.1 Project Performance by Reservoir 6
4.1.1 Fault Block IV on the West Flank (WH Cam C RI SU) 6
4.1.2 Fault Block II on the West Flank (WH Cam C RI SU) 13
4.1.3 Low Pressure Reservoir on the North Flank (WH Cam C RB SU) 13
4.2 Results from Amoco's Reservoir Model 17
4.3 Ongoing Injection Strategy 17
4.4 Surface Injection Facilities 18
4.4.1 Operation and Maintenance of the Air Injection System 18
4.4.2 Installation of Air Injection Flowline to the North Flank 19
4.5 Technology Transfer Activities 19
4.6 Independent Project Study by LSU 22

LIST OF FIGURES AND TABLES — PAGE

Structure Map for the Top of the Cam C-1 (west flank-WH Cam C RI SU) 7
Plot of Air Injection Rates and Pressures (west flank) 8
Plot of Cumulative Air Injected vs. Time 9
Bottom Hole Pressure Table (west flank) 10
Plot of Bottom Hole Pressure versus Time (west flank) 11
Structure Map for the Top of the Cam C-1 (north flank-WH Cam C RB SU) 14
Schematic Cross-Section of North Flank Air Injection Reservoir 15
Production Plot for the SL 42 No.220 (north flank) 16
Maps with Route of Air Injection Flowline to the North Flank 20,21
Schematic Drawing of the Air Injection System 23

APPENDICES

APPENDIX A Statement of Work A-1
APPENDIX B Summary of LSU's Laboratory Researcy B-1
APPENDIX C Summary of LSU's Modeling Research C-1

Annual Technical Progress Report (9/3/95-9/2/96)
West Hackberry Tertiary Project

1.0 ABSTRACT

1.1 Brief Description of Research

The West Hackberry Tertiary Project is a field test of the concept that air injection can be combined with the Double Displacement Process to produce a tertiary recovery process that is both low cost and economic at current oil prices. The Double Displacement Process is the gas displacement of a water invaded oil column for the purpose of recovering tertiary oil by gravity drainage. In reservoirs with pronounced bed dip such as those found in West Hackberry and other Gulf Coast salt dome fields, reservoir performance has shown that gravity drainage recoveries average 80% to 90% of the original oil in place while waterdrive recoveries average 50% to 60% of the original oil in place. The target for tertiary oil recovery in the Double Displacement Process is the incremental oil between the 50% to 60% waterdrive recoveries and the 80% to 90% gravity drainage recoveries.

In previous field tests, the Double Displacement Process has proven successful in generating tertiary oil recovery. The use of air injection in this process combines the benefits of air's low cost and universal accessibility with the potential for accelerated oil recovery from the combustion process. If successful, this project will demonstrate that utilizing air injection in the Double Displacement Process will result in an economically viable tertiary process in reservoirs (such as Gulf Coast salt dome reservoirs) where any other tertiary process is presently uneconomic.

1.2 Summary of Key Results and Conclusions

Air injection on the west flank began in November of 1994. Although west flank air injection has increased reservoir pressure by 350 pounds per square inch (psi), production response has not yet occurred. The lack of west flank production response is attributed to the fact that the project has not injected sufficient air in the large west flank reservoir to push the oil rim down to the nearest downstructure well. While west flank air injection continues, production response is expected to occur during the upcoming 12 months.

To spread project risk among multiple reservoirs, the project was expanded in 1996 to include air injection in reservoirs on the north flank of the field. The project reservoirs on the west flank are much higher pressure (2500-3300 psi) than the project reservoirs on the north flank (350-800 psi). While west flank air injection has not yet yielded oil production, air injection in the first low pressure north flank reservoir generated an almost immediate increase in oil production. After north flank air injection began in July of 1996, the nearest downstructure well increased production from about 40 barrels of oil per day (BOPD) prior to injection to 177 BOPD in August of 1996. The additional oil production noted in August of 1996 in the low pressure north flank reservoir is: 1) the first oil production resulting from air injection in the West Hackberry Tertiary Project and 2) the

first occasion that air injection has been used to successfully increase oil production in a Gulf Coast salt dome oil reservoir.

While air injection is beginning to demonstrate success in the low pressure north flank reservoirs, additional air injection will be required before production response is seen on the west flank of the field. During the upcoming year, air injection will be split between the higher pressure west flank reservoir and several low pressure north flank reservoirs with the ultimate goal to maximize production response in as many reservoirs as possible.

2.0 EXECUTIVE SUMMARY

2.1 Background

The following report is the Annual Technical Progress Report for the third year of the West Hackberry Tertiary Project and covers the time period from September 3, 1995 to September 2, 1996. The West Hackberry Tertiary Project is one of four mid-term projects selected by the United States Department of Energy (DOE) as part of the DOE's Class 1 Program for the development of advanced recovery technologies in fluvial dominated deltaic reservoirs. Over an 82 month funding period from September 3, 1993 to July 2, 2000, Amoco and the DOE are implementing a field test of the theory that air injection can be combined with the Double Displacement Process to create a tertiary oil process that is economically viable for the domestic oil industry. As part of the project, the Petroleum Engineering Department at Louisiana State University (LSU) has been subcontracted to provide independent study and technology transfer support. To provide a further project description, the Statement of Work for the West Hackberry Tertiary Project is contained in Appendix A.

West Hackberry is a salt dome oil field located in Southwestern Louisiana about 30 miles southwest of Lake Charles, Louisiana. Although the project originally targeted Oligocene Age reservoirs on the west flank of the field, Amoco and the DOE agreed to expand the project to the north flank during 1996. Injection on the west flank of the field will test the process in higher pressure (2500-3300 psi) reservoirs which have watered out. Injection on the north flank will test the process in low pressure (350-800 psi) reservoirs that are approaching depletion. The low pressure north flank reservoirs exhibit slow water encroachment, possess low pressure gas caps and contain thin oil rims.

2.2 Conclusions

The following conclusions have been generated during the third year of the project:

1) Pressure response on the west flank noted thus far is the result of air injection and confirms the original geologic picture.

2) Oil production has not yet occurred on the west flank since the oil rim has not moved sufficiently downstructure to reach the first producing well. The lack of production response on the west flank can be attributed to the large size of the reservoir, the high reservoir pressure which inhibits the growth of the gas cap, uncertainty as to the pre-injection location of the oil rim and an insufficient volume of air injected to date.

3) Air injection in a low pressure north flank oil reservoir has generated almost immediate and promising production response. In this and other low pressure oil reservoirs, additional air injection and production response will be required to prove that air injection can economically produce improved oil recovery in low pressure Gulf Coast oil reservoirs.

2.3 Recommendations

The following recommendations are presented for the upcoming year:

1) Divide air injection between the high pressure west flank reservoirs and several low pressure north flank reservoirs with the ultimate goal to maximize production response in as many reservoirs as possible.

2) Monitor reservoir performance with production data, bottom hole pressure surveys, well tests and produced oil, gas and water analyses.

3) Utilize production response to guide the timing for workovers and the timing for rotating air injection from one reservoir to another.

4) After increased oil production has been achieved in three or more West Hackberry reservoirs, plan and coordinate a technology transfer program with LSU involving workshops, talks with industry groups, articles in industry publications and the publishing of technical papers.

3.0 Introduction

In the West Hackberry Tertiary Project, air is injected into watered out oil reservoirs on the west flank and into lower pressure north flank oil reservoirs that are nearing depletion. In both situations, air injection is combined with the Double Displacement process in an attempt to generate an economically viable tertiary recovery process for Gulf Coast oil reservoirs with pronounced bed dip. The Double Displacement Process is the gas displacement of a water invaded oil column for the purpose of recovering tertiary oil by gravity drainage. In West Hackberry Field, gravity drainage recoveries average 80% to 90% of the original oil in place while waterdrive recoveries average 50% to 60% of the original oil in place. The target for tertiary oil recovery in the Double Displacement Process is the incremental oil between the 50% to 60% waterdrive recoveries and the 80% to 90% gravity drainage recoveries.

For air injection to work successfully with the Double Displacement Process, the reservoir temperature must be high enough for oxygen to be consumed through combustion with the reservoir oil. Amoco has performed laboratory tests which prove that West Hackberry oil will spontaneously combust with oxygen in the pore space. The combustion of oxygen in the reservoir alleviates concerns relating to the presence of oxygen in the reservoir or production equipment. Oxygen in the reservoir can form viscous emulsions hindering the flow of oil in the well and in the production equipment. Oxygen that reaches the producing wells can also produce corrosion and or explosions in the production equipment.

In the higher pressure (2000-3300 psi) west flank reservoirs, the mechanics of the tertiary process involve: 1) injecting air into the crest of a watered out oil reservoir in order to fill the reservoir with a gas from the top down, 2) as the reservoir fills with air, oxygen is consumed through spontaneous combustion, 3) oil and water drain toward the base of the structure through gravity segregation and gravity drainage, and 4) tertiary oil, which previously had been trapped as a residual oil saturation, is now produced in downstructure wells. In this case, the economic potential of the project is enhanced by the low cost associated with using air as the injection gas.

On the north flank of West Hackberry, low pressure (350-800 psi) oil reservoirs are found which have large low pressure gas caps, thin oil rims and slow water encroachment. In the low pressure north flank reservoirs, air injection can increase oil recovery by: 1) pushing the oil rim downstructure to the structural location of existing wellbores, 2) repressurizing the reservoir and 3) obtaining tertiary oil recovery through the Double Displacement Process in the same manner as described in the preceding paragraph. Although injection of nitrogen, carbon dioxide and natural gas have been utilized to increase oil recovery in Gulf Coast reservoirs in the past, this project is unique in the use of air as the injection gas.

4.0 Discussion

4.1 Project Performance by Reservoir

4.1.1 Fault Block IV on the West Flank (in the WH Cam C RI SU)

On the following page is a structure map for the top of the Cam C-1 Sand on the west flank of West Hackberry Field. As noted on the structure map, the Gulf Land D (GLD) No.51 serves as the air injector for Fault Block IV and is located near the crest of the structure. From the forth quarter of 1995 through June of 1996, the project's injection strategy has been to inject all of the project's 4 million standard cubic feet per day (MMSCFD) air injection capacity into the GLD No.51. Through August 31, 1996, a total 1127 million standard cubic feet (MMSCF) of air has been injected into the GLD No.51. On Page Nos.8 and 9 are plots of air injection rate, pressure and cumulative injection versus time.

In Fault Block IV, reservoir pressure has increased about 350 psi since the start of air injection. The GLD No.44 (Cam C-1,2), GLD No.45 (Cam C-1,2), GLD No.52 (Cam C-1,2) and Watkins No.3 (Cam C-3) are future producing wells currently completed in the project interval in Fault Block IV. All of these wells have seen an increase in bottom hole pressure as a result of air injection. A table and plot of bottom hole pressure versus time are included on Page Nos.10 and 11. While the Cam C-3 in Fault Block IV has typically seen 150-200 psi lower pressure than the Cam C-1,2, the Cam C-3 has shown a similar increase in reservoir pressure as a result of air injection. The increase in reservoir pressure noted (in both Cam C-1,2 and Cam C-3) in this area appears to prove that: 1) the

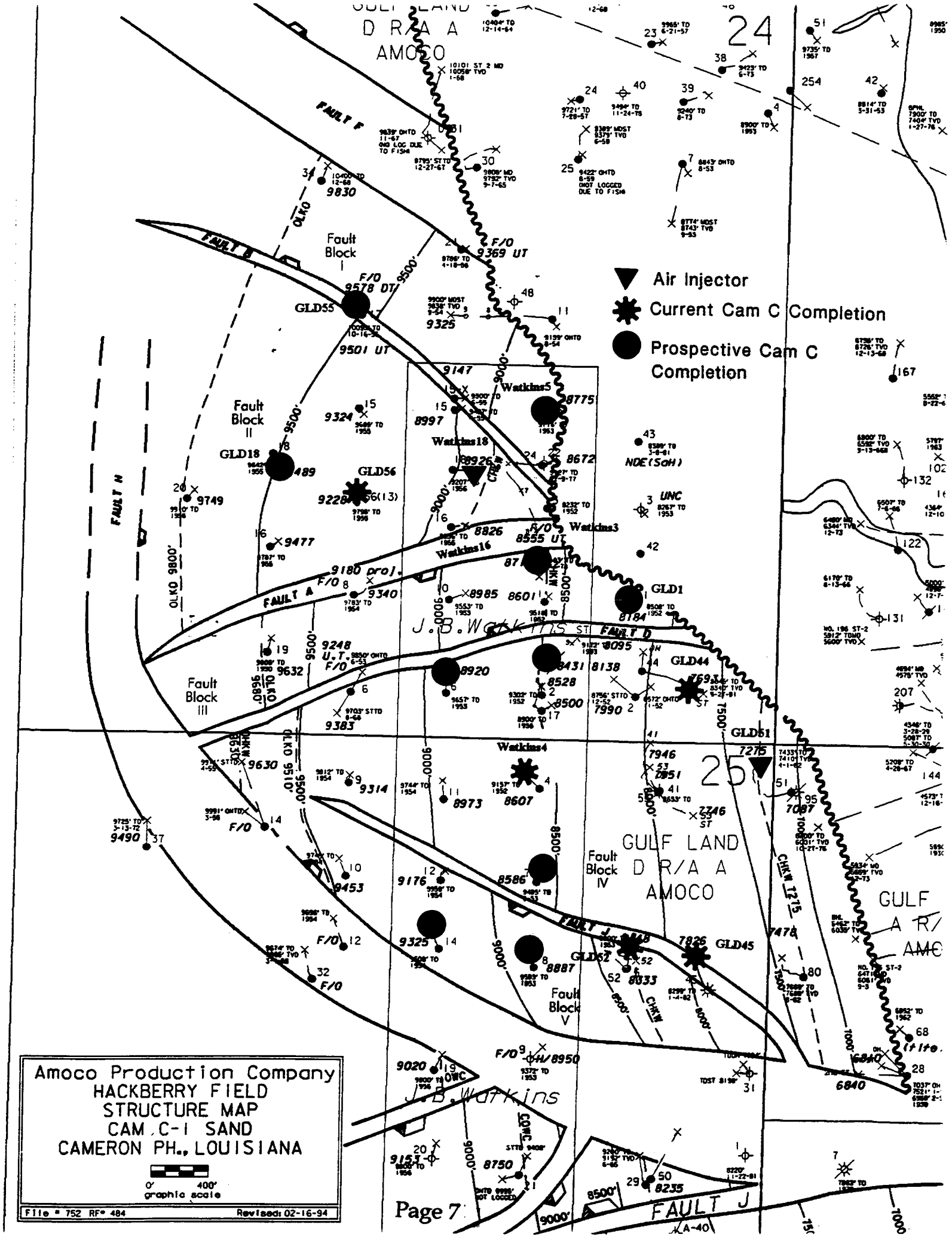
Air Injector
Current Cam C Completion
Prospective Cam C Completion
Fault Block I
Fault Block II
Fault Block III
Fault Block IV
Fault Block V
FAULT F
FAULT B
FAULT N
FAULT A
FAULT D
FAULT J
GULF LAND
D R/A A
AMOCO
J.B.Watkins
GLD55
GLD18
GLD56
GLD1
GLD44
GLD51
GLD45
GLD62
Watkins5
Watkins18
Watkins3
Watkins16
Watkins4
F/O 9369 UT
F/O 9578 DT
9501 UT
9180 proj.
9248 U.T.
NDE(SOH)
UNC
OLKO 9800'
OLKO 9680'
OLKO 9530'
OLKO 9510'
CHKW 7215
Amoco Production Company
HACKBERRY FIELD
STRUCTURE MAP
CAM C-1 SAND
CAMERON PH., LOUISIANA
0' 400'
graphic scale
File # 752 RF# 484
Revised: 02-16-94

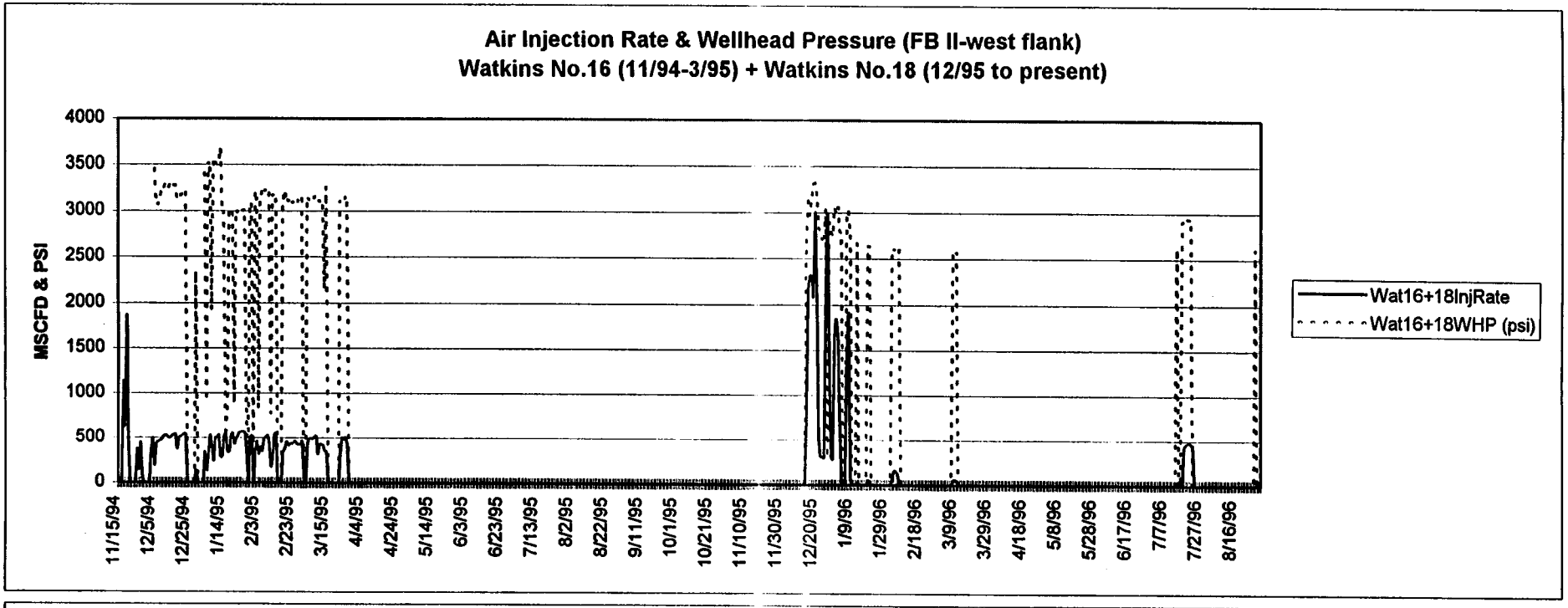
Air Injection Rate & Wellhead Pressure (FB II-west flank)
Watkins No.16 (11/94-3/95) + Watkins No.18 (12/95 to present)
MSCFD & PSI
4000
3500
3000
2500
2000
1500
1000
500
0
11/15/94
12/5/94
12/25/94
1/14/95
2/3/95
2/23/95
3/15/95
4/4/95
4/24/95
5/14/95
6/3/95
6/23/95
7/13/95
8/2/95
8/22/95
9/11/95
10/1/95
10/21/95
11/10/95
11/30/95
12/20/95
1/9/96
1/29/96
2/18/96
3/9/96
3/29/96
4/18/96
5/8/96
5/28/96
6/17/96
7/7/96
7/27/96
8/16/96
Wat16+18InjRate
Wat16+18WHP (psi)

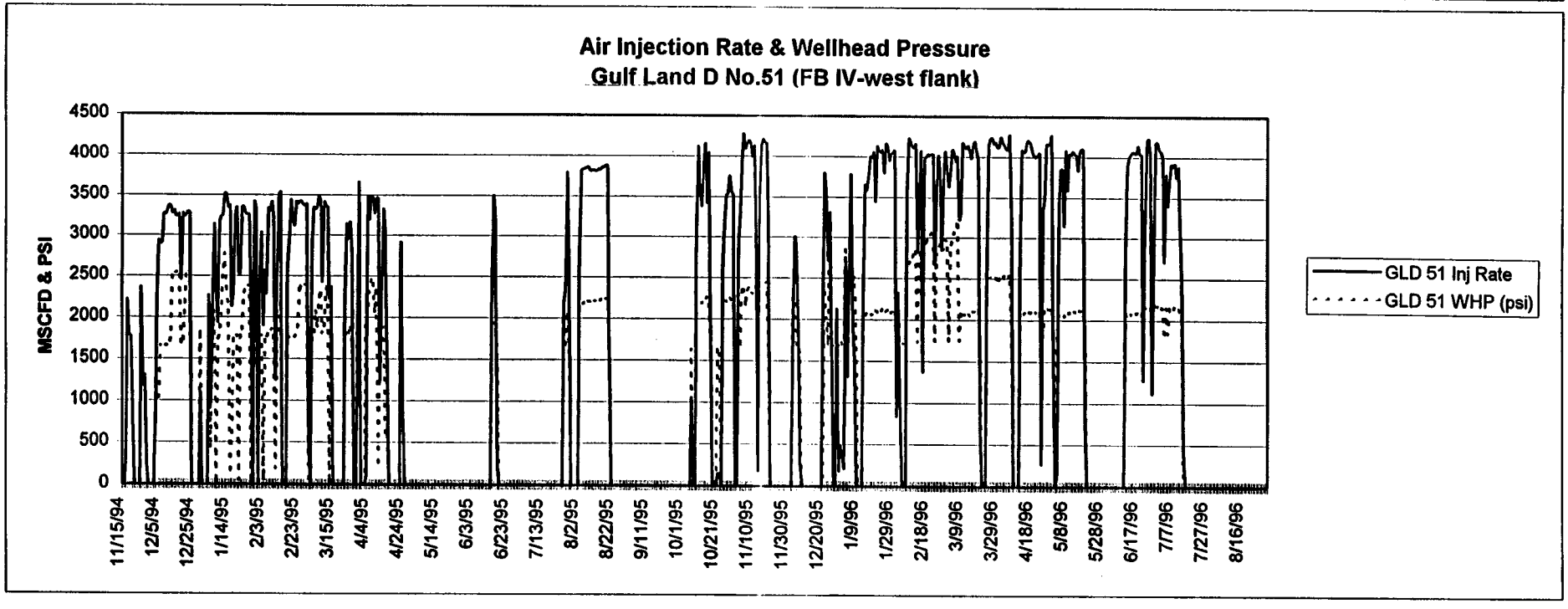
Air Injection Rate & Wellhead Pressure
Gulf Land D No.51 (FB IV-west flank)
MSCFD & PSI
4500
4000
3500
3000
2500
2000
1500
1000
500
0
11/15/94
12/5/94
12/25/94
1/14/95
2/3/95
2/23/95
3/15/95
4/4/95
4/24/95
5/14/95
6/3/95
6/23/95
7/13/95
8/2/95
8/22/95
9/11/95
10/1/95
10/21/95
11/10/95
11/30/95
12/20/95
1/9/96
1/29/96
2/18/96
3/9/96
3/29/96
4/18/96
5/8/96
5/28/96
6/17/96
7/7/96
7/27/96
8/16/96
GLD 51 Inj Rate
GLD 51 WHP (psi)

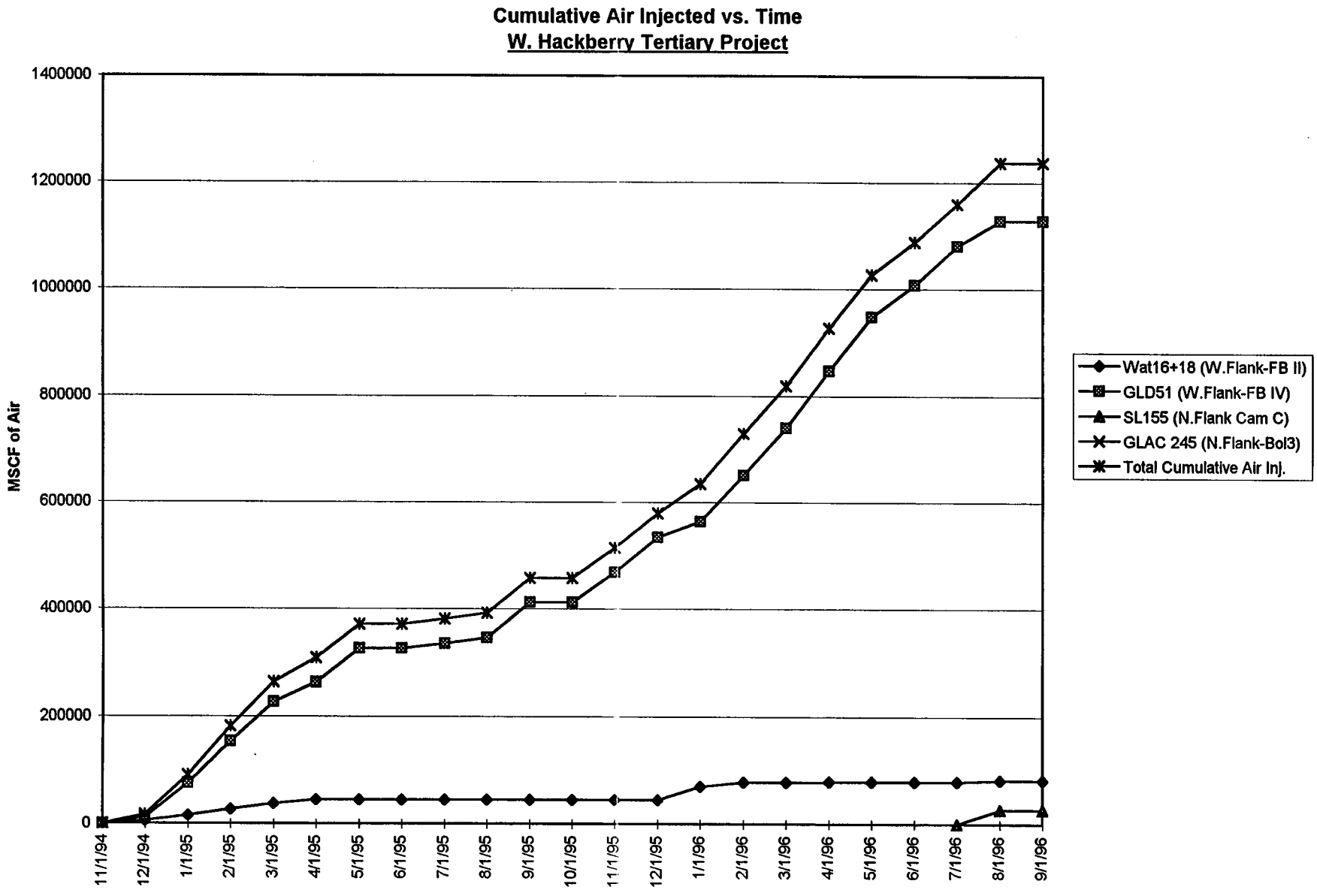
Cumulative Air Injected vs. Time
W. Hackberry Tertiary Project
MSCF of Air
1400000
1200000
1000000
800000
600000
400000
200000
0
11/1/94
12/1/94
1/1/95
2/1/95
3/1/95
4/1/95
5/1/95
6/1/95
7/1/95
8/1/95
9/1/95
10/1/95
11/1/95
12/1/95
1/1/96
2/1/96
3/1/96
4/1/96
5/1/96
6/1/96
7/1/96
8/1/96
9/1/96
Wat16+18 (W.Flank-FB II)
GLD51 (W.Flank-FB IV)
SL155 (N.Flank Cam C)
GLAC 245 (N.Flank-Bol3)
Total Cumulative Air Inj.

West Flank Bottom Hole Pressure (psi) By Reservoir By Fault Block

West Hackberry Field

Fault Block	Well	Pressure	9000'Press.	Cam C-1 Date	Depth	Temp.(F)	Pressure	9000'Press.	Cam C-2,3 Date	Depth	Temp.(F)
I	Watkins #5	3711 psi	3839 psi	6/55	8600'						
		2407 psi	2531 psi	4/83	8612'	228					
		3124 psi	3217 psi	6/91	8800'	208					
	Watkins #15x										
	Watkins #22						2943 psi	3059 psi	12/77	8751'	
	GLD #11	3880 psi	3847 psi	1/55	9100'		2974 psi	2974 psi	4/64	9000'	
		3135 psi	3415 psi	3/56	8150'						
		3160 psi	3500 psi	3/60	8000'						
		2843 psi	3125 psi	3/61	8000'						
		2909 psi	3378 psi	3/62	8000'						
	GLD #17										
	GLD #21										
	GLD #34										
II	Watkins #15										
	Watkins #16	2887 psi	2887 psi	10/76		200	2217 psi	2239 psi	7/82	8930'	209
		3233 psi	3271 psi	5/94	8911'		2150 psi	2230 psi	3/80	8750'	
							2115 psi	2134 psi	11/81	8940'	
							3156 psi	3188 psi	6/91	8899'	204
	Watkins #18	2899 psi	2922 psi	8/82	8950'	210					
		3058 psi	3168 psi	8/91	8775'	201					
		3224 psi	3271 psi	3/95	8900'	207					
	GLD #56(13)	3780 psi	3647 psi	3/56	9400'						
		3500 psi	3500 psi	3/60	9000'		3350 psi	3350 psi	6/64	9000'	
		3429 psi	3429 psi	3/61	9000'						
		3375 psi	3375 psi	3/62	9000'						
		3436 psi	3301 psi	5/94	9320'	208					
		3488 psi	3350 psi	2/95	9320'	209					
		3473 psi	3321 psi	6/95	9319'						
		3392 psi	3311 psi	8/95	9167'	208					
		3418 psi	3337 psi	11/95	9168'	207					
		3494 psi	3320 psi	3/96	9320'	208					
		3514 psi	3434 psi	10/96	9167'	205					
	GLD #15	3824 psi	3888 psi	9/55	8800'		3247 psi	3247 psi	3/62	9000'	
		3460 psi	3780 psi	3/56	8000'		3357 psi	3357 psi	6/64	9000'	
	GLD #16	3170 psi	3410 psi	3/60	8500'		3500 psi	3339 psi	11/61	9504'	
		3163 psi	3371 psi	3/61	8500'		4010 psi	3878 psi	9/55	9400'	
							3900 psi	3768 psi	3/56	9400'	
							2740 psi	2922 psi	3/62	8500'	
							3240 psi	3460 psi	6/64	8500'	
	GLD #18						3825 psi	3825 psi	3/56	9000'	
							3330 psi	3330 psi	3/60	9000'	
							3293 psi	3293 psi	3/61	9000'	
							3256 psi	3256 psi	3/62	9000'	
	GLD #20										
III	Watkins #1	4110 psi	4227 psi	5/52	8635'		2300 psi	2382 psi	11/68	8744'	
		1968 psi	2247 psi	6/78	8400'	200					
	Watkins #10	2892 psi	2878 psi	3/64	9044'		1609 psi	1702 psi	4/77	8800'	
	GLD #1	3607 psi	3985 psi	12/54	8170'						
		3505 psi	3768 psi	9/55	8170'						
		3415 psi	3694 psi	3/56	8150'						
	GLD #8										
	GLD #19	3700 psi	3700 psi	3/56	9000'						

Fault Block	Well	Pressure	9000'Press.	Cam C-1 Date	Depth	Temp.(F)	Pressure	9000'Press.	Cam C-2,3 Date	Depth	Temp.(F)
IV	Watkins #2										
	Watkins #4						2016 psi	2176 psi	7/73	8500'	
							1962 psi	2042 psi	6/91	8749'	196
							2336 psi	2470 psi	9/94	8716'	198
							2386 psi	2518 psi	2/95	8716'	198
							2487 psi	2593 psi	5/95	8769'	
							2525 psi	2643 psi	8/95	8749'	199
							2534 psi	2664 psi	11/95	8716'	195
							2592 psi	2738 psi	3/96	8706'	196
							2625 psi	2792 psi	6/96	8640'	194
							2755 psi	2871 psi	10/96	9167'	205
	Watkins #6										
	Watkins #7										
	Watkins #11						2400 psi	2364 psi	9/69	9111'	
							1476 psi	1444 psi	2/80	9100'	190
	Watkins #17										
	Watkins#17ST										
	GLD #2						3462 psi	3770 psi	12/54	8000'	
							3176 psi	3782 psi	9/55	8244'	
							3490 psi	3543 psi	3/56	8250'	
							3290 psi	3330 psi	11/57	8200'	
							3030 psi	3090 psi	3/60	8150'	
							2928 psi	2980 psi	3/61	8250'	
							2839 psi	2901 psi	3/62	8000'	
							2857 psi	2918 psi	6/64	8000'	
	GLD #6	3831 psi	3750 psi	1/55	9250'		3202 psi	3084 psi	7/62	9369'	184
		3740 psi	3660 psi	3/56	9250'		2950 psi	2905 psi	6/64	9100'	
		3230 psi	3164 psi	3/60	9200'						
		3098 psi	3003 psi	3/61	9300'						
		3013 psi	3013 psi	3/62	9000'						
	GLD #6ST										
	GLD #9	3754 psi	3754 psi	1/55			1838 psi	1691 psi	8/76	9459'	200
		3650 psi	3650 psi	3/56	9000'						
		3190 psi	3190 psi	3/60	9000'						
		3002 psi	3002 psi	3/61	9000'						
		2937 psi	2937 psi	3/62	9000'						
		2764 psi	2899 psi	1/63	8600'						
		2825 psi	2825 psi	2/64	9000'						
		2792 psi	2681 psi	2/66	9347'	228					
	GLD #12										
	GLD #14ST										
	GLD #41	1752 psi	2218 psi	7/80	7998'		1724 psi	2031 psi	7/80	8041'	
		1771 psi	2225 psi	9/81	8024'	190					
		1715 psi	2187 psi	11/81	7985'						
	GLD #44	1463 psi	3044 psi	4/96	5679'		1612 psi	2141 psi	4/88	7862'	181
		1464 psi	3042 psi	6/96	5679'						
		2511 psi	3096 psi	11/96	7771'	190					
	GLD #45	2480 psi	2967 psi	3/96	7956'	186					
		2542 psi	3023 psi	6/96	7956'	186					
	GLD #51	1898 psi	2636 psi	7/94	7312'	183	1683 psi	2375 psi	7/94	7417'	186
		1896 psi	2630 psi	7/94	7320'		1673 psi	2360 psi	7/94	7427'	187
		1939 psi	2653 psi	7/94	7367'	185					
		1857 psi	2566 psi	8/94	7377'	186					
V	Watkins #8						1975 psi	1975 psi	7/73	9000'	
	Watkins #12	2109 psi	2109 psi	4/79	9000'						
	Watkins #14										
	GLD #5	1750 psi	1959 psi	2/77			3480 psi	3676 psi	12/54	8400'	
							3440 psi	3598 psi	9/55	8400'	
							3400 psi	3751 psi	3/56	8150'	
							3290 psi	3350 psi	11/57	8400'	
							3010 psi	3070 psi	3/60	8400'	
							2843 psi	2912 psi	3/61	8000'	
							2779 psi	2937 psi	3/62	8250'	
							2660 psi	2874 psi	6/64	8250'	
							2618 psi	2858 psi	3/65	8250'	
							2339 psi	2509 psi	3/68	8470'	
							2246 psi	2415 psi	3/70	8472'	
	GLD #10	3759 psi	3759 psi	1/55	9000'						
		3560 psi	3560 psi	3/56	9000'						
		3140 psi	3140 psi	3/60	9000'						
		3049 psi	3049 psi	3/61	9000'						
		2933 psi	2933 psi	3/62	9000'						
		2833 psi	2678 psi	2/66	9485'	196					
	GLD #62	2407 psi	2675 psi	8/94	8386'	193					
		2512 psi	2803 psi	2/95	8386'						
		2577 psi	2855 psi	5/95	8386'	194					
		2594 psi	2883 psi	8/95	8386'	195					
		2629 psi	2907 psi	11/95	8406'	192					
		2713 psi	3009 psi	3/96	8386'	192					

Bottom Hole Pressure (psi) vs. Time

West Hackberry Air Injection Project (west flank)

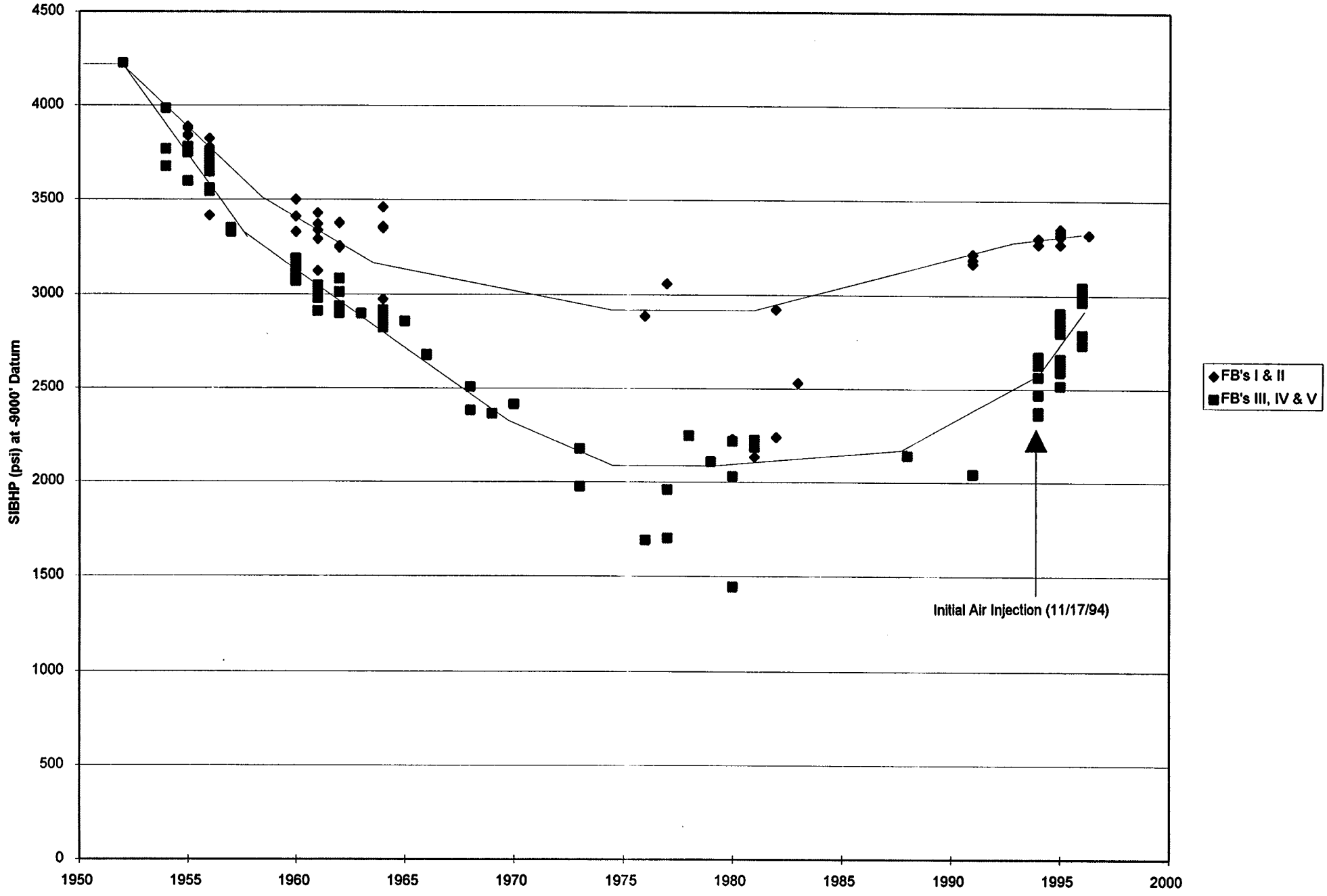

overall geologic picture for Fault Block IV is correct, and 2) air is being injected into both the Cam C-1,2 and Cam C-3 in Fault Block IV.

Oil production has not yet occurred in Fault Block IV since the oil rim has not moved sufficiently downstructure to reach the closest producing well, the GLD No.44. The lack of production response in Fault Block IV can be attributed to the large size of the reservoir, the high reservoir pressure (2500 psi) which inhibits the size of the gas cap, uncertainty as to the pre-injection location of the oil rim and an insufficient volume of air injected to date. Although oil production has not yet occurred in Fault Block IV, neither has nitrogen breakthrough which suggests that the air injection flood is proceeding as planned in a gravity stable manner. Plans are to continue air injection in the GLD No.51 in order to maintain the growth of the upstructure gas cap and to bring about oil production in the GLD No.44 within the upcoming 12 months.

The GLD No.44 is the next highest well on structure after the GLD No.51 and is expected to see the earliest oil production when it occurs. Recent tests from the GLD No.44 show production volumes that are gas lifted at a rate of 700-800 barrels of water per day(BWPD) with no gas and no oil. Amoco personnel became concerned that the source of the water production in the GLD No.44 could have been from another reservoir as a result of a casing leak or a channel behind pipe. The tubing in the GLD No.44 was pulled out of the well and the casing was pressure tested with no hint of leakage. Extraneous water production as a result of a channel behind pipe is considered highly unlikely for the following reasons: 1) water from below is not possible since the GLD No.44 encountered no permeable sands below the Cam C-1,2,3 and 2) water from above is unlikely since a low pressure (800 psi) gas sand, the Cam B-1, is immediately above the Cam C-1,2,3 and any water from above this interval would flood the lower pressure Cam B-1 (800 psi) in preference to the higher pressure (2500 psi) Cam C-1,2,3.

One added cause for concern relating to the GLD No.44 is the chlorides content of the produced water. While the chlorides content of the water from the GLD No.44 measures 131,000 parts per million (ppm), the chlorides content of the produced water from the GLD No.45 is 99,000 ppm. A water sample from the Watkins No.4 taken before the start of the project measured 120,000 ppm. Although the reason for the variation in chlorides content in Fault Block IV has not been resolved, all other available data suggests that the source of the water production in the GLD No.44 is the completion interval and that the oil rim has not yet arrived at the GLD No.44's structural position.

The GLD No.45 is the next well downstructure after the GLD No.44. During August of 1995, the GLD No.45 was recompleted to the Cam C-1,2 and tested gas lifting at a rate of 190 BOPD and 451 BWPD. The GLD No.45 had previously watered out in the same completion interval. In the face of continued air injection over the past year in which injection far exceeded withdrawals, the oil production in the GLD No.45 declined while the water cut increased to 90%-95% and the produced gas showed no nitrogen content. The source of the new oil production in the GLD No.45 is believed to be a thin sand interval that was covered with sand during the previous completion. The most recent

completion in the GLD No.45 was gravel packed to prevent sand fill while the earlier completion was not.

The GLD No.51 serves as the air injector for Fault Block IV. In July of 1996, the GLD No.51 plugged up with sand, magnetite (Fe_3O_4) and pieces of casing which prevented air injection. At least some portion of the problems with the wellbore were caused by the corrosion resulting from the previous use of potassium chloride purge water. To prevent future plugging of the well with fill and or collapsed casing, the GLD No.51 will need either a liner or a gravel pack. During August of 1996, the GLD No.51 was cleaned out in preparation to run a gravel pack inside casing. A workover to run a gravel pack and restart air injection has been deferred to the beginning of October while operating experience is gained with another gravel packed air injector, the SL 42 No.155. After the GLD No.51 is restored to injection, the injection strategy will be to divide the 4 MMSCFD injection capacity between the GLD No.51 and the air injectors in the low pressure reservoirs on the north flank of the field.

4.1.2 Fault Block II on the West Flank (in the WH Cam C RI SU)

In Fault Block II, the Watkins No.18 is the current air injector and the GLD No.56 serves the downstructure future producer. Originally, the Watkins No.16 was the air injector for Fault Block II. When the Watkins No.16 experienced casing collapse during a workover, the well was temporarily abandoned. Both the GLD No.56 and the Watkins No.18 exhibited premature nitrogen breakthrough without evidence of oil production. The nitrogen breakthrough is believed to have been caused by the nitrogen preferentially flowing through a high permeability interval near the top of the Cam C-1. Coincidentally, Fault Block II was more prone to premature nitrogen breakthrough due to the lower bed dip (23 degrees) than the other reservoirs involved in the project. The current operating strategy is to inject air into the Watkins No.18 when the other air injectors are incapable of taking the project's 4 MMSCFD capacity.

4.1.3 Low Pressure Reservoir on the North Flank(WH Cam C RB SU)

To spread project risk among multiple reservoirs, Amoco and the DOE agreed to expand the project to include air injection in low pressure reservoirs on the north flank of the field. The low pressure north flank reservoirs exhibit slow water encroachment, possess low pressure gas caps and contain thin oil rims. Air injection began on the north flank in a low pressure (350-400 psi) oil reservoir, the WH Cam C RB SU, during July of 1996. A structure map for the top of the Cam C-1 is included on the following page. In the WH Cam C RB SU, the SL 42 No.155 serves as the air injector in the gas cap and the SL 42 No.220 is currently producing oil in a downdip structural position. A schematic cross-section for the reservoir is included on Page No.15. The WH Cam C RB SU had previously undergone gas injection which improved the rate for the SL 42 No.220 from 21 BOPD and 89 BWPD in December of 1991 to 43 BOPD and 88 BWPD in April of 1993. The production rate achieved in April of 1993 remained at about that same level up to the middle of 1996. A production plot for the SL 42 No.220 is included on Page No.16. After air injection began in the WH Cam C RB SU in July of 1996, the SL 42 No.220 was tested on August 11, 1996, producing at a rate of 177 BOPD and 145

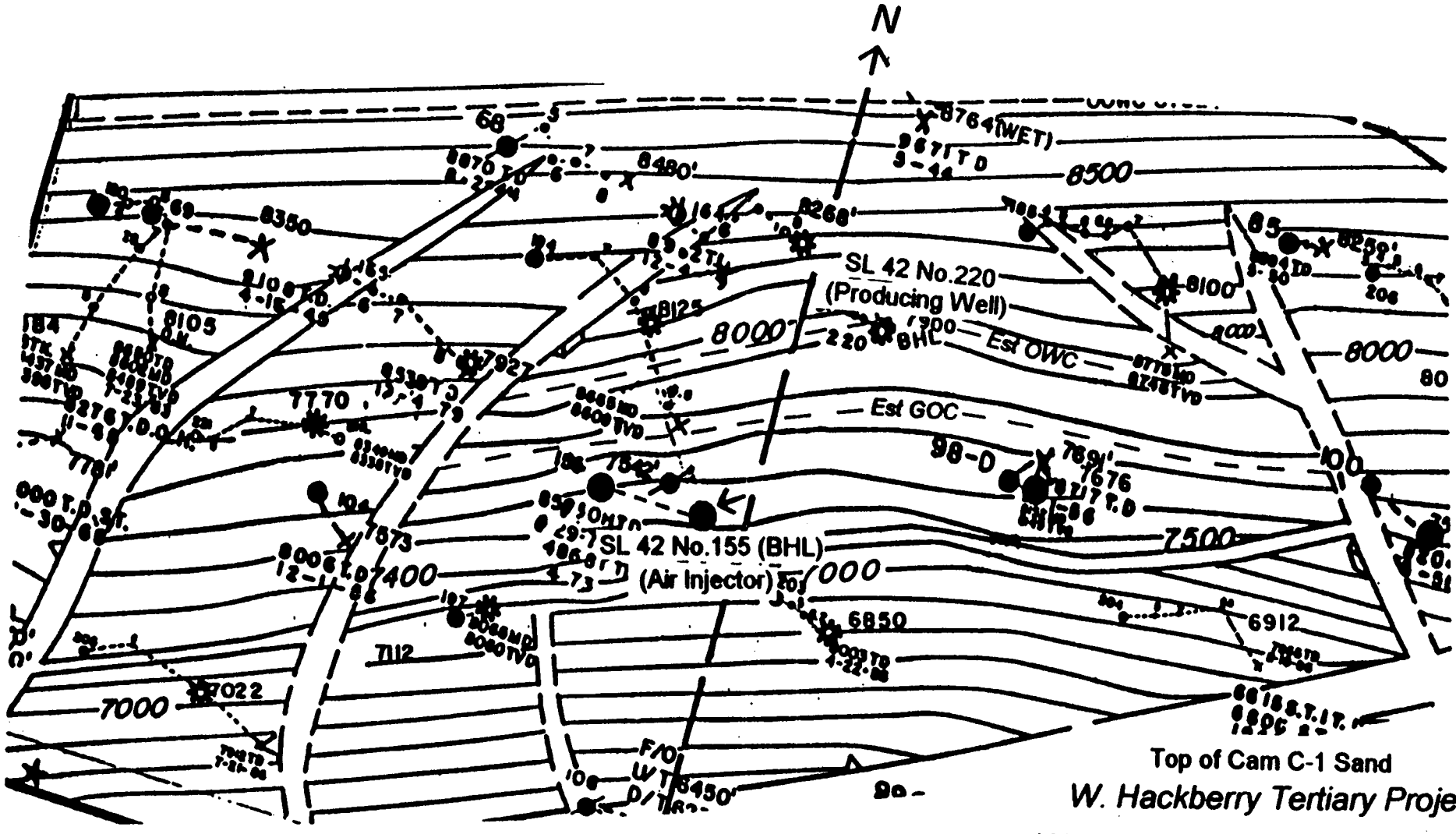

Top of Cam C-1 Sand

W. Hackberry Tertiary Project

West Hackberry Field (north flank)

Cameron Parish, La.

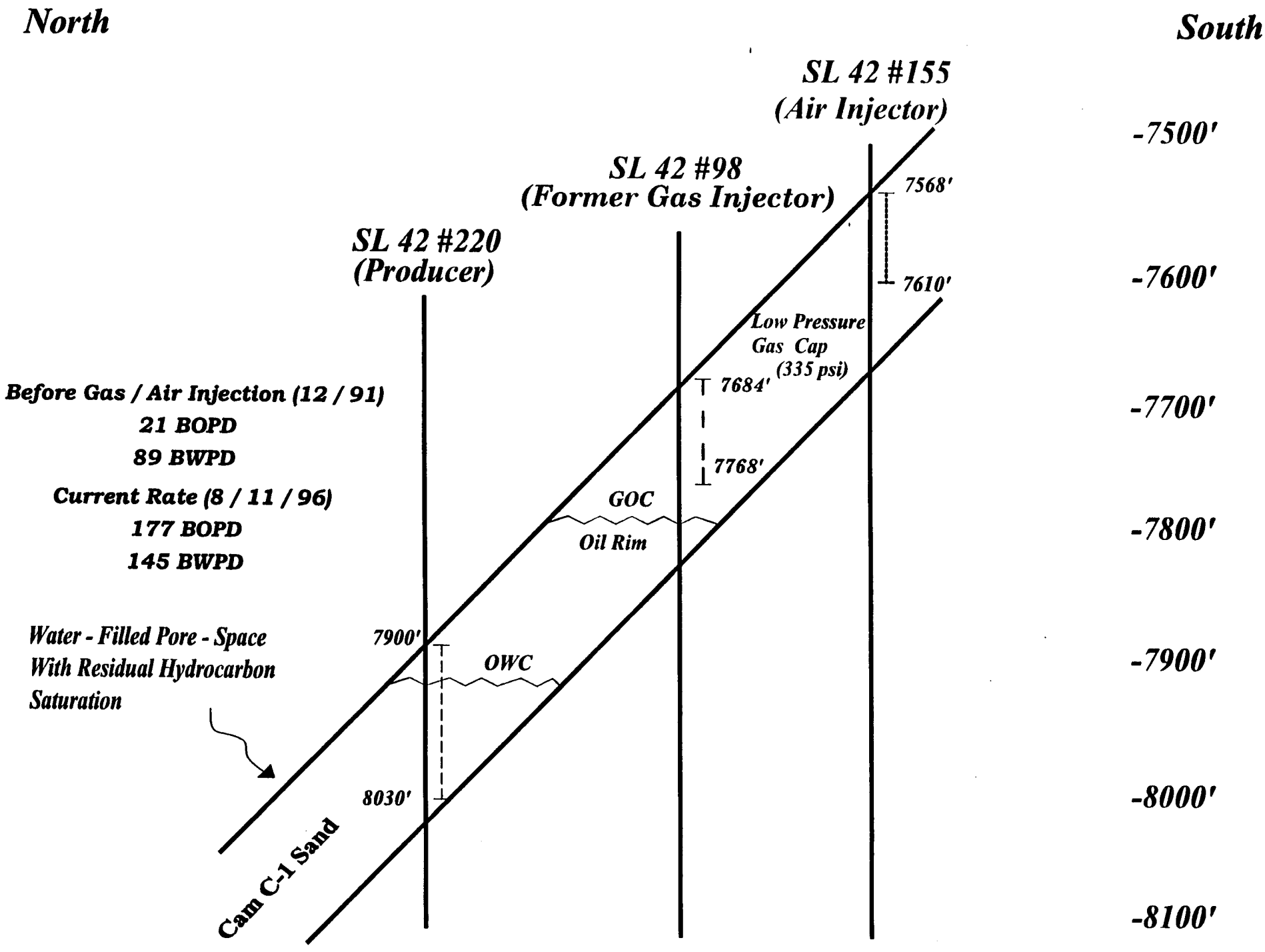

Reservoir Schematic of Cam C-1 (in the W H Cam C RB SU) on the north Flank of W. Hackberry as of August of 1996

SL 42 No.220 (WH Cam C RB SU)(north flank of W. Hackberry)
(Injected 136 mmscf of gas in updip well (5/92-3/93))
(Began air injection in updip well in 7/96 (28 mmscf))

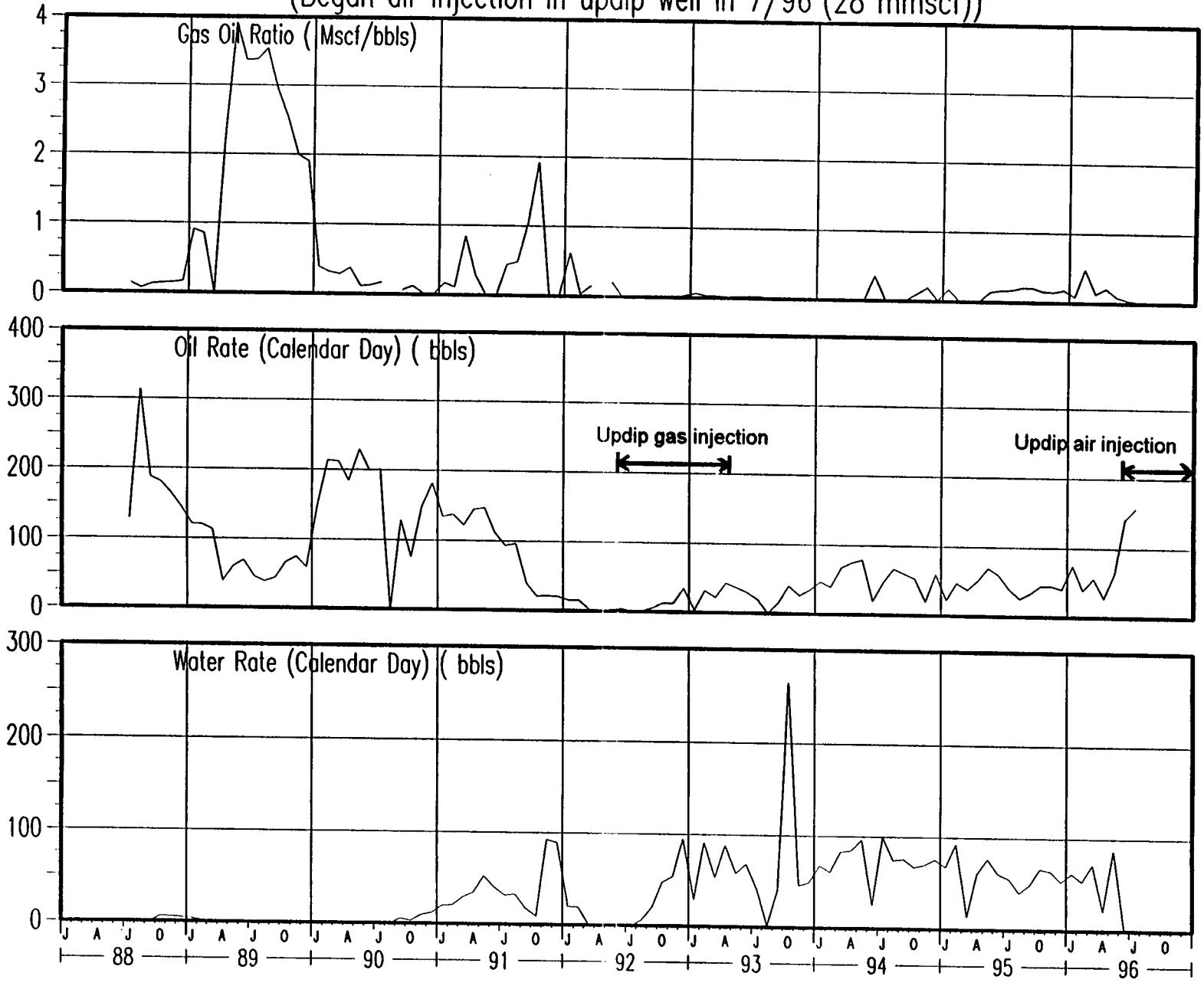

BWPD. The production increase noted in the SL 42 No.220 is the first demonstration of increased oil production as a result of air injection in the West Hackberry Tertiary Project.

Air injection on the north flank has provided almost immediate production response while prolonged injection on the west flank has only shown an increase in reservoir pressure. The two main reasons for the difference in response are that the north flank reservoir is much smaller and much lower reservoir pressure. In fact, the gas cap in the low pressure WH Cam C RB SU only contains about 100 MMSCF of gas in place. With so little gas cap volume at such a low reservoir pressure, air injection of 28 MMSCF in July would be expected to have an almost immediate impact on production in the downstructure well.

4.2 Results from Amoco's Reservoir Model

During the past year, the reservoir model for Fault Block IV on the west flank was revised to match available injection and pressure data. According to the reservoir model, production response on the west flank is controlled to a large extent by the air injection rate, not just by the cumulative volume of air injected. That is, at high injection rates the gas-oil contact and water-oil contacts are forced downstructure more on the north end of Fault Block IV(closer to the nearest producing well) than on the south end. At lower air injection rates, the gas-oil and water-oil contacts tend to be flatter across the reservoir.

By injecting air on the north flank, less air has been available for injection into Fault Block IV and therefore deferring production response in Fault Block IV. Slowing injection in Fault Block IV has also allowed more time for gravity segregation and gravity drainage. Allowing more time for gravity segregation and gravity drainage is expected to reduce the negative impact of permeability variations thereby resulting in improved vertical sweep efficiency and higher oil recovery.

Verification of reservoir model predictions will only be possible upon arrival of the tertiary oil bank at the first producer, the GLD No.44. In an effort to guide other operators, documentation and technology transfer regarding the reservoir model will occur once verification has been achieved.

4.3 Ongoing Injection Strategy

Air injection is presently split between the SL 42 No.155 (3.3-3.5 MMSCFD) on the north flank and the Watkins No.18 (0.4-0.5 MMSCFD) in Fault Block II on the west flank. After the GLD No.51 is repaired in October of 1996, the current plan is to split air injection between the GLD No.51 (2 MMSCFD) and the low pressure injectors (2 MMSCFD) on the north flank. In addition to the SL 42 No.155 in the WH Cam C RB SU, other north flank injectors that will be added to the project include: 1) the GLAC No.245 in the Bol-3 RC SU, 2) the CPSB No.56 in the WH Cam D NF SU and 3) the SL 42 No.172 in the WH Cam D NF SU. The air injection line to the north flank is connected to each of the north flank injection wells. Well workovers will be required to complete the additional north flank wells as air injectors. To take advantage of the Double Displacement Process on the north flank, more workovers may be required to enable downstructure wells to produce as the oil rims are pushed downstructure.

4.4 Surface Injection Facilities

4.4.1 Operation and Maintenance of the Air Injection System

During the last year an effort was made to further improve the reliability and run time of the air compression system. A schematic drawing of the air injection system is included on Page No.23. At the time of the last annual report, significant heat and lubrication related mechanical failures had been occurring in higher pressure stages of the reciprocating compressor. This resulted in downtime for the much of the summer of 1995 while components were redesigned, manufactured, and installed. The failures were occurring to the rod packing, piston rings, and valves of the third, fourth, and fifth stages of the reciprocating compressor; the stages of compression from 1250 psi to 4000 psi. The following is a summary of the major changes performed:

1. Installed water cooled packing cases on stages 3, 4, and 5.
2. Changed rod packing material from carbon impregnated Teflon to Cook 094 Teflon.
3. Changed rod packing backup rings from cast iron to bronze.
4. Changed 4th and 5th stage piston ring material from Teflon to Peek.
5. Added Teflon wear band to 5th stage piston.
6. Changed lubricant from Syntholube 150 to Mobil Rarus 829.
7. Installed redesigned lubrication distribution system.
8. Rebuilt valves with spring rates based on actual operating pressures.

This work has proven to be successful as no mechanical failures have reoccurred to the reciprocating compressor since this work was completed. Periodic teardown and inspections were performed this summer and no abnormal wear or problems were noted.

Over the last year two significant failures did occur on the screw compressor package. The first was a failure of the coupling which transmits power from the natural gas engine prime mover to the screw compressor. The cause of failure, as determined by the coupling manufacturer, was that a wrong sized bushing was called for on their Bill of Materials. Although this repair cost was covered by the manufacturer of the coupling it did cause over three weeks of downtime to the project. Also, some additional previous downtime caused by broken lines due to vibration could be attributed to this problem. The second failure that occurred was contamination of the lubricating oil with coolant. This problem occurred once before and was thought to be due to a leak in the oil cooler. Based on subsequent experience, Atlas-Copco diagnosed the coolant-oil communication to probably be occurring across a leaking plug in a machined port in either the low pressure or high pressure compressor assembly. Both the low and high pressure screw compressor assemblies were removed, disassembled, and inspected. The high pressure assembly was found to have the leaking plugs. Atlas-Copco installed a new high pressure screw compressor assembly under warranty and no oil contamination has been noted to date. No additional downtime was experienced due to this repair as it was performed at the time the GLD No.51 injection well was down for repair.

4.4.2 Installation of Equipment for North Flank Air Injection

When the project scope was expanded to include air injection in the North Flank reservoirs it created a problem in that the North Flank is a considerable distance from the existing compression equipment. It was decided that the most economical means of transporting air would be to split the flow at the GLD No.51 well, utilize the old GLD No.51 flowline to Central Facility No.2 and install approximately 18,000 feet of new line from C. F. No.2 across Black Lake on an existing pipe rack to serve the four North Flank injection wells. On the following two pages are maps which show the route of the air injection line to the north flank. Since the North Flank reservoirs are lower pressure and do not require injection lines with pressure integrity to 4300 psi as did the West Flank injection lines, the old GLD No. 51 flowline and thinner wall linepipe for the new section of line was used. The air flow is split downstream of the GLD No.51 wellhead scrubber and the pressure and rate is controlled through a control valve. Since the line to the North Flank does not have pressure integrity to 4300 psi, it is protected from overpressure by a pneumatically controlled safety valve and a pressure relief valve. A separator is installed at C. F. No.2 to catch any water vapor that could condense as a result of the Joule-Thompson cooling effect across the control valve as well as any liquids that could have accumulated in low spots of the old line. An orifice meter is installed immediately downstream of the separator to meter the flowrate. As of this date, approximately 90% of the installation has been completed, however, enough of the new line was completed in July 1996 to commence air injection in the SL 42 No. 155.

4.5 Technology Transfer Activities

During the past year, talks were presented at the following venues which reviewed the West Hackberry Tertiary Project:

September 19, 1996 Amoco presentation at the Fluid Imaging Workshop at BP in Houston, Texas

February 14, 1996 Amoco presentation at the Oil Industry Outreach Conference in Houston, Texas

February 21, 1996 Amoco presentation at the Time Lapse Imaging Workshop in Houston, Texas

April 21-24, 1996 At the SPE Symposium on Improved Oil Recovery in Tulsa, Oklahoma, Amoco presented an SPE Paper entitled "The Economics of Light Oil Air Injection Projects" and LSU presented an SPE Paper entitled "Second-Contact Water Displacement Oil Recovery Process"

An on-line version of Amoco's West Hackberry Tertiary Project presentation can be accessed on the Internet file server for the Society of Petroleum Engineers (SPE) at www.neosoft.com/pub/users/s/spe. In addition, Amoco, LSU and DOE personnel contributed to an article entitled "Air injection project breathes fire into aging West Hackberry oil field" which appeared in the February, 1996 edition of "Hart's Oil and Gas

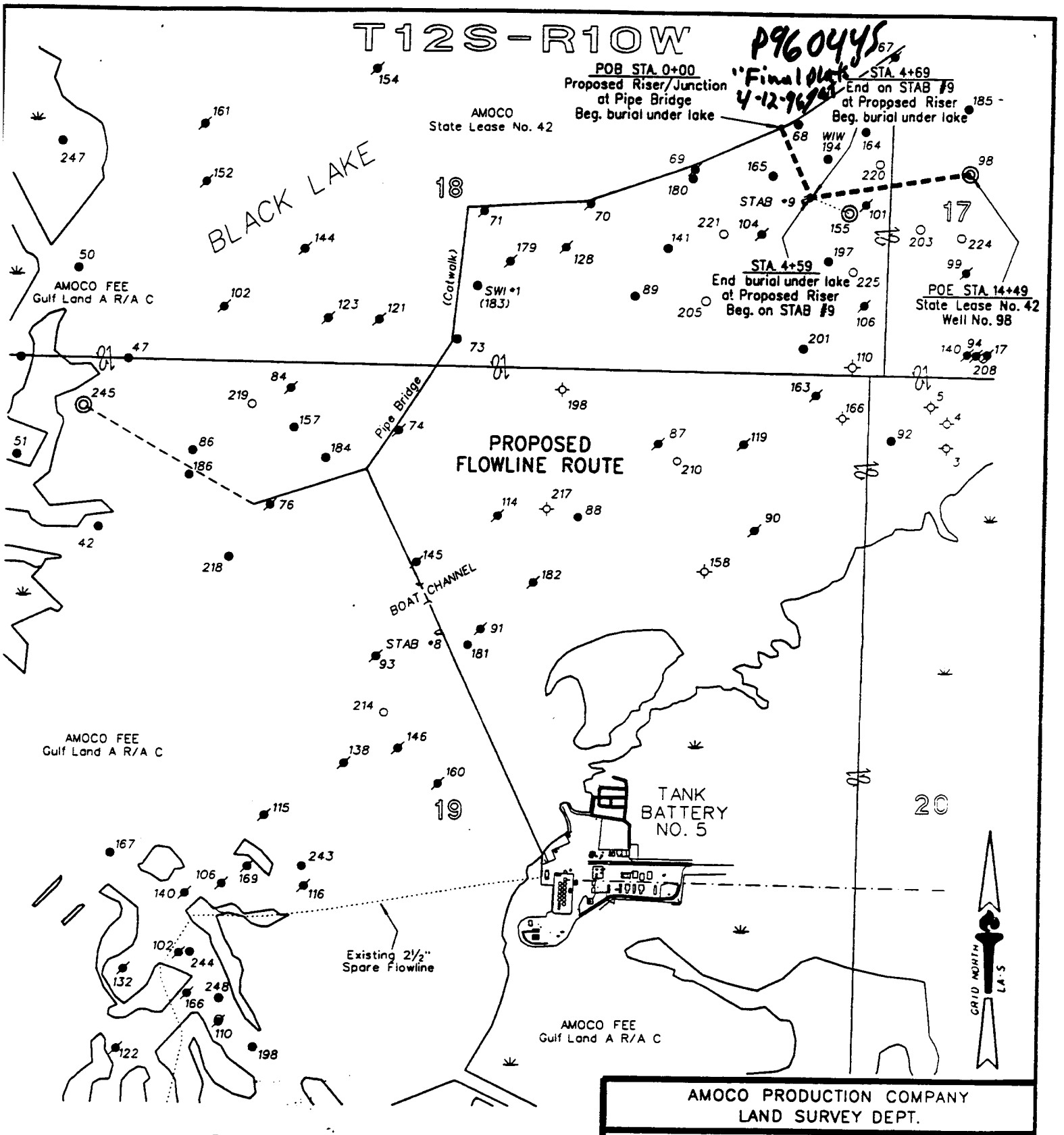

LEGEND

- Proposed Flowlines
- Existing Pipelines
- C/L Existing Roads
- Open Water Marsh

PROPOSED ROUTE - One 2½" Air Injection Flowline

NAD 27 POB: Lat.-30° 00'47.36", Lon.-93° 25'09.51"
POE: Lat.-30° 00'44.85", Lon.-93° 24'56.19"

NAD 83 POB: Lat.-30° 00'48.13", Lon.-93° 25'10.07"
POE: Lat.-30° 00'45.62", Lon.-93° 24'56.75'

AMOCO PRODUCTION COMPANY
LAND SURVEY DEPT.

Proposed Air Injection Flowline Installation to Serve State Lease 42, Well No. 98, State Lease 42, Well No. 155 and Gulf Land A R/A C, Well No. 245 as Extension to D.O.E. Tertiary Project

West Hackberry Field
Section 17, 18 & 19, T12S-R10W
Cameron Parish, Louisiana

Drw.by RWB 3/25/96	LA038123.dgn Lv 21
Scale: 1 in = 800 ft	SHEET 5 OF 9

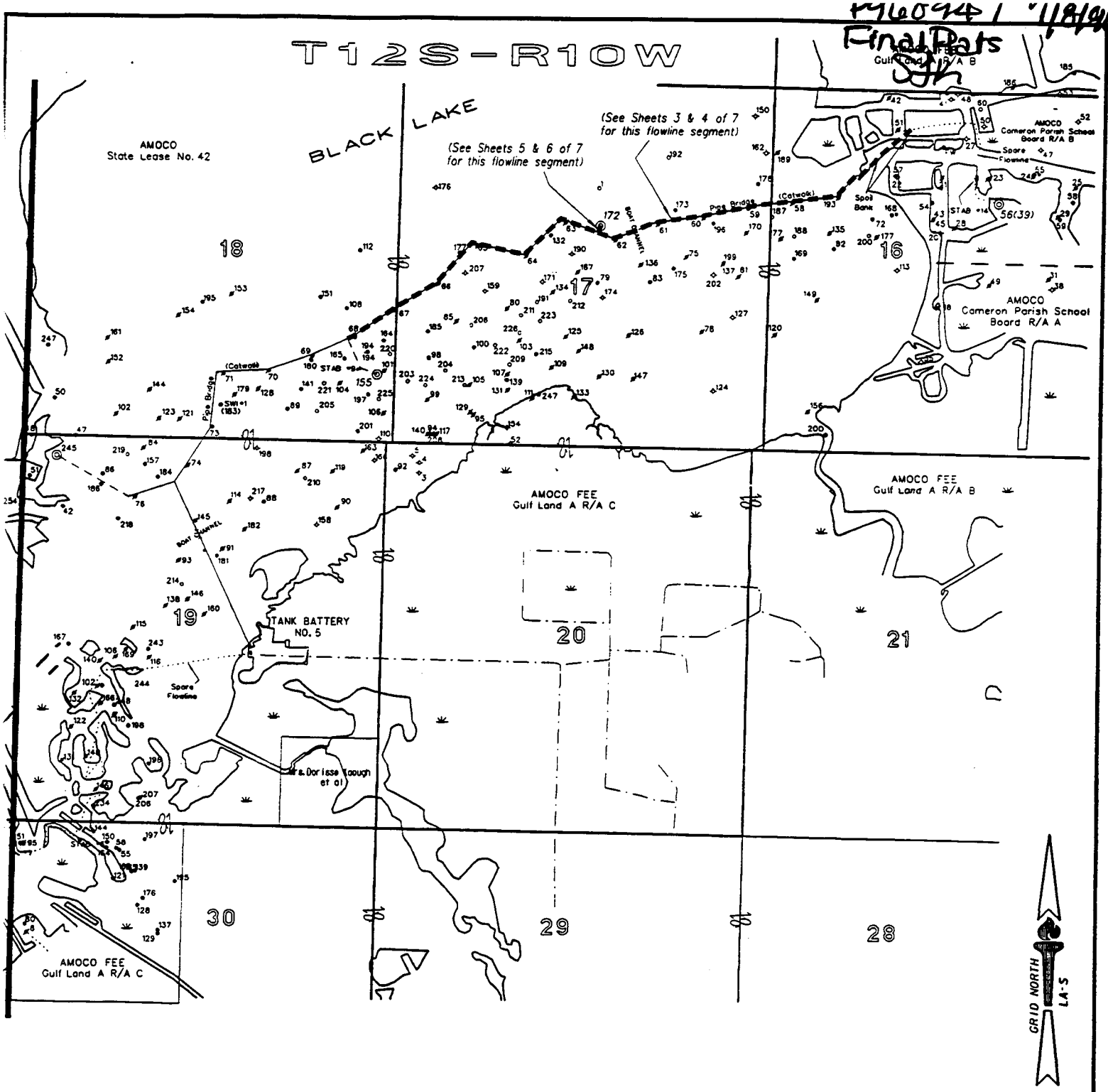

COMPOSITE VIEW

AMOCO PRODUCTION COMPANY
LAND SURVEY DEPT.

Proposed Air Injection Flowline Installation to Serve State Lease 42, Well No. 172 and Cameron Parish School Board R/A B, Well No. 56, as Extension to D.O.E. Tertiary Project

West Hackberry Field
Section 16, 17 & 18, T12S-R10W
Cameron Parish, Louisiana

Drw. by RWB 6/5/96	LA038123.dgn Lv 25
Scale: 1 in = 2000 ft	SHEET 2 OF 7

LEGEND

- Proposed Flowlines Route (D.O.E. Tertiary Project)
- Existing Flowlines (D.O.E. Tertiary Project)
- Existing Pipelines
- C/L Existing Roads
- Marsh

The total material to be excavated for the two segments of the proposed Air Injection Flowline - approx. 124 cu. yds.

The total combined length for the two segments of the proposed Air Injection Flowline - 9,475 feet.

World." Amoco personnel authored another article entitled "Field tests assess novel air-injection EOR processes" which appeared in the May 20,1996 edition of the "Oil and Gas Journal."

4.6 Independent Project Study by LSU

LSU has allocated two graduate students supported by faculty to independently study the West Hackberry Tertiary Project. Bogdan Lepski, a graduate student preparing for a master's degree in petroleum engineering, conducted core floods to simulate the Double Displacement Process in the laboratory. A vertical water-filled core was flooded with oil and then flooded with water from the bottom to a residual oil saturation. Gas was injected in the top of the core to simulate the Double Displacement Process. As the core was flooded with gas, additional oil was recovered thereby simulating the Double Displacement Process in the laboratory. After the core was flooded with gas and the added oil recovery was almost at an end, water was pumped into the bottom of the core to prepare the core for the next flood. As the water filled the core, a significant volume of additional post-Double Displacement oil was recovered. LSU named the process that recovered oil through water flooding a core after the Double Displacement Process the "Second-Contact Water Displacement" oil recovery process.

In the field, the Second-Contact Water Displacement Process could be used for improved oil recovery in two ways: 1) allowing the water level to push back up through the reservoir after the Double Displacement Process has reached depletion or, 2) injecting a gas into a watered out reservoir with a single well and then allowing the aquifer to push water back through the reservoir to recover more oil. LSU presented an SPE paper documenting the Second-Contact Water Displacement Process at the SPE Symposium on Improved Oil Recovery on April 21-24, 1996, in Tulsa, Oklahoma. A summary of Bogdan Lepski's work with the core floods is included within a proposal for a doctorial research project Appendix B.

Tammy Bourgoyne, a doctoral student in petroleum engineering, has prepared a model simulation of the core tests of the Double Displacement Process. An introduction to the modeling work performed by LSU is included in Appendix C.

AIR INJECTION SYSTEM

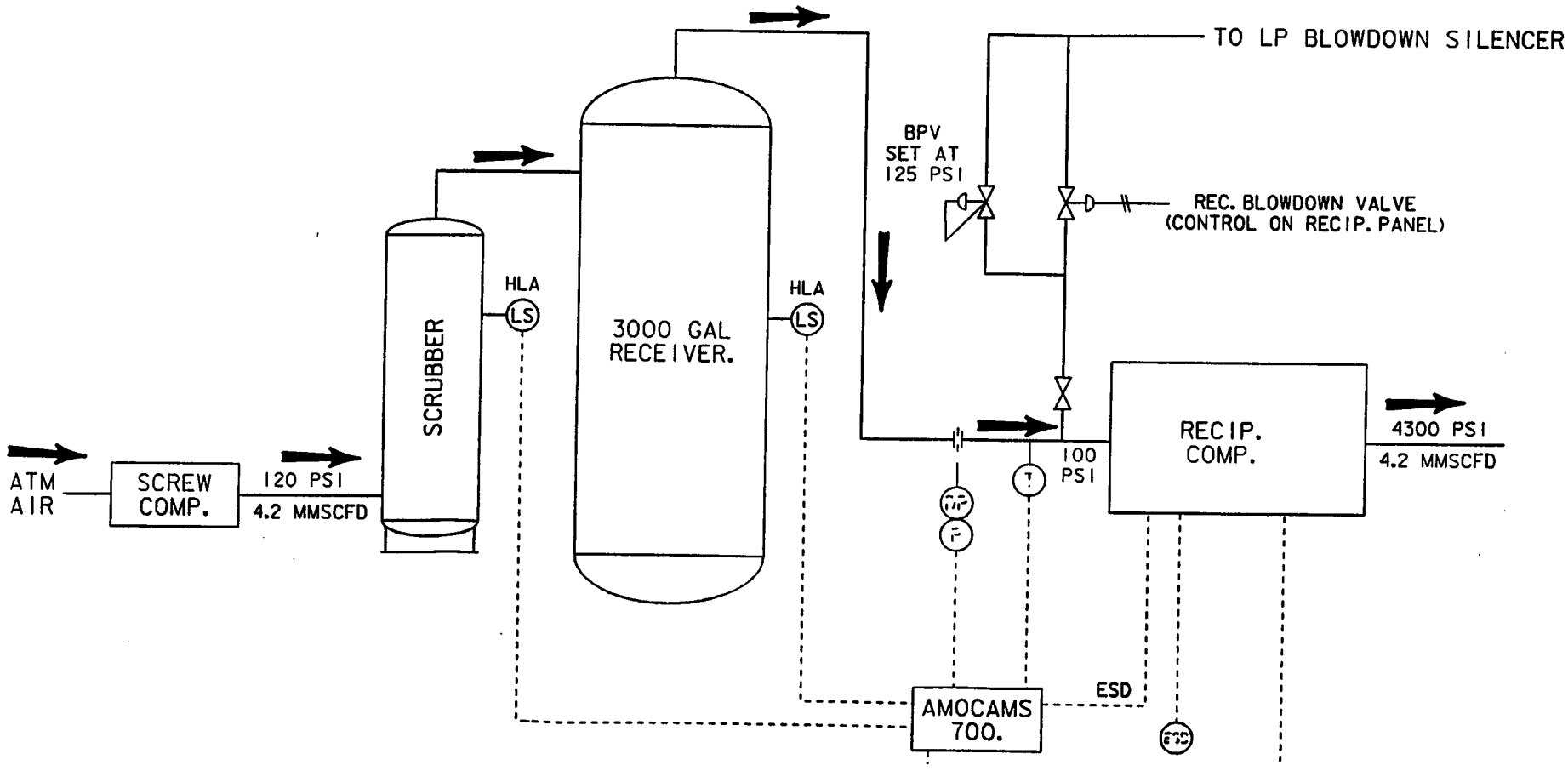

APPENDIX A

STATEMENT OF WORK

STATEMENT OF WORK

WEST HACKBERRY TERTIARY PROJECT

Amoco Production Company
October 16, 1992

Background and Objectives

The goal of the West Hackberry Tertiary Project is to demonstrate the technical and economic feasibility of oil recovery using air injection in the Double Displacement Process. The Double Displacement Process is the gas displacement of a water invaded oil column for the purpose of recovering oil through gravity drainage. A novel aspect of this project is the use of air as the injection fluid. This technology will be applicable to reservoirs which have both sufficient bed dip for gravity drainage and sufficient reservoir temperature for the consumption of oxygen. Numerous water-drive reservoirs associated with salt dome fields along the Gulf Coast would be potential follow-up candidates for this technology. The use of air injection in this process offer the benefits of air's excellent accessibility and low cost combined with potentially greater recovery due to the combustion process. If successful, this project will demonstrate that the use of air injection in the Double Displacement Process can economically recover oil in reservoirs where tertiary oil recovery is presently uneconomical.

Based on a preliminary project design developed prior to commencement of the project, the following basic operational information has been determined for the study: injection rates; selection of reservoirs and fault blocks; required number of producing and injection wells; requirements for new wells versus re-completing existing wells; requirements for continuous injection versus intermittent injection; assessment of the disposal of produced gases by flaring or injection into low pressure reservoirs; unitization; and the design of surface production and injection facilities. The project is designed for injection into two separate fault blocks (Fault Blocks II & IV). In Fault Block IV, the technology will be assessed using a line of four producers at structurally equivalent positions in a heavily developed area. In Fault Block II, the technology will be assessed using a single producer in a sparsely developed area.

A description of each task associated with the project is provided below.

Task 1 - Environmental Study

It is anticipated that this project will be categorically excluded from the DOE NEPA requirements. Upon DOE certification, if this project does qualify for a categorical exclusion, this task will not be required. If this project does not qualify for a categorical exclusion, then this task will involve activities, such as data collection and reporting, that are required by the DOE to meet NEPA requirements.

Task 2 - Construction of Surface Facilities

The necessary permits required for construction of the surface facilities will be obtained. Based on the preliminary project design, Amoco will acquire the necessary equipment/facilities to inject 4-4.5 MMCFD of air at pressures greater than 4000 psi. Surface injection facilities will be installed which consist primarily of the air compressors and water purge system for the injection wells. The timing for the installation of production facilities will be tied to workovers on the producing wells conducted in Task 5. The production facilities will consist of flowlines, possibly an Natural Gas Liquids recovery unit, and a separate-test-and-boost (STAB) facility. After separation and testing, produced fluids will be piped to Amoco's central production facility. Undesired produced gasses will be flared or injected into low pressure reservoirs.

Task 3 - Conversion of Producing Wells to Injection Wells

Two producing wells will be converted to injection wells. Initially, a single injection well will be dedicated to each of the two fault blocks. Two additional injectors (i.e. converted producing wells) may be required to improve the economics of the process. A typical workover to convert a producing well to an injector would require cleaning out the wellbore, perforating the full prospective injection interval, and completing the well with new packers, tubing, and wellhead (i.e. valves, etc.).

Task 4 - Operations and Maintenance of Injection Facilities

The operation of the high pressure air compressors in the injection facilities requires close attention to safety issues. Synthetic lubricants and periodic cleaning of injection equipment will be conducted to prevent the possibility of a detonation resulting from the combination of high pressure air and hydrocarbon deposits. Additionally, routine maintenance of injection equipment will be conducted to avoid the possibility of catastrophic mechanical failure. Workovers to repair injection wells will be performed on an as needed basis.

Task 5 - Workovers for Monitoring and Producing Wells

A total of 9 wells will be repaired and/or re-completed to serve as producing wells and/or monitoring wells for the project. The timing of the workovers will be dictated by the advance of the flood front. The task of monitoring the flood front is addressed in Task 6. Once the project is underway, workovers to repair producing and monitoring wells will be performed on an as needed basis.

Task 6 - Production Operations

All production operations for the project will be handled by Amoco field personnel assigned to West Hackberry Field. Produced liquids will be transported through existing collection lines to be handled at an Amoco Tank Battery. Initially, producing wells will be gas lifted within Amoco's field-wide gas lift system. When the produced gasses become concentrated with undesirable components (e.g. nitrogen and carbon dioxide) due to breakthrough, it will be necessary to install a separate gas lift system for the project. The separate gas lift system will require a gas lift compressor. Produced gasses will either be sold, burned as fuel, flared or re-injected into low pressure reservoirs on the north flank of the field. Booster compressors may be required to generate sufficient pressure for injection of produced gasses. A flowline will be installed to the north flank of West Hackberry Field in order to carry the produced gasses to the low pressure reservoirs in that area. Monthly production tests, at a minimum, will be performed on all producing wells. Gas analyses will be conducted periodically to monitor the composition and oxygen content of the produced gasses. Produced oil and water samples will be analyzed periodically to determine their composition and physical properties. Pulsed neutron logs, bottom hole pressure surveys, temperature surveys, and spinner surveys may be run in both producing and monitoring wells in order assess the effectiveness of the project. Periodic replacement of surface production and injection equipment (including flowlines) may also be required due to wear and tear on these items.

Task 7 - Reservoir Management

Reservoir modeling studies will be conducted to effectively manage the project. These studies will assist in assessing the following: distribution of injection volumes; timing of repairs and re-completions; and the determination of monitoring schemes and schedules. Amoco's "THERM" reservoir model will be used to history match reservoir performance and to predict future reservoir performance. Specialized combustion tests will be conducted at Amoco's Combustion Laboratory in Tulsa, Oklahoma to assist in monitoring and predicting the performance of the project. Reservoir fluid property analyses will be conducted to calibrate the reservoir model. The results of reservoir management will be continually documented and reported in a manner consistent with the DOE reporting requirements and technology transfer needs of the project.

Task 8 - Louisiana State University Technology Transfer

A yearly Amoco grant will be provided to the Petroleum Engineering Department at Louisiana State University (LSU). LSU will study various aspects of the project and report their findings. LSU will publish and make industry presentations on all results from their analyses. Amoco plans to provide LSU with all pertinent data and information from the project. Examples of typical data and information that will be made available to LSU include the following: individual well production rates; individual well injection rates; structure maps; net pay isopachs; core data; well logs; gas analyses; and fluid property data.

Task 9 - Amoco Technology Transfer

Amoco will assess the technical and economic feasibility of Double Displacement Process based on the data and information acquired from the project. These results will be documented and submitted to various technical conferences for presentation and/or publication. Since the Double Displacement Process will probably have its greatest applicability to salt dome fields along the Gulf Coast, Amoco personnel will focus on technical conferences in the Houston, Texas and New Orleans, Louisiana areas. It is anticipated that presentations and/or papers will be completed at the beginning, middle, and end of the project. Amoco does not intend to regard any data and/or information on this project as proprietary.

APPENDIX B

SUMMARY OF LSU'S LABORATORY RESEARCH

(Doctorial Research Proposal)

SCREENING WATERFLOODED OIL RESERVOIRS FOR GAS INJECTION IMPROVED OIL RECOVERY METHODS

A Proposal Submitted to General Examination Committee
September 1996

by
Bogdan Lepski

M.S. University of Mining and Metallurgy, Cracow, 1992.
M.S. in PETE Louisiana State University, Baton Rouge, 1995.

TABLE OF CONTENTS

Chapter Page

STUDY OBJECTIVES AND METHODOLOGY....1

LITERATURE REVIEW....2
Theoretical Work....2
Experimental Work....5
Field Cases....7

ACCOMPLISHED INVESTIGATIONS....9
Transparent Micromodel Experiments....9
High Pressure and Temperature Corefloods....13
Interfacial Tension Measurements (Drop Volume Method)....21
Oil Spreading Experiments....26

INVESTIGATIONS IN PROGRESS....26
Pendant Drop Method IFT Measurements....26

FUTURE INVESTIGATIONS....28
Combination of the Drop Volume and Maximum Bubble Pressure Methods....28
Screening Criteria for SCWD....30

CONCLUSIONS....31

BIBLIOGRAPHY....33

VITA....35

LIST OF FIGURES

Number		Page
Fig. 1.	Reservoir undergoing DDP	2
Fig. 2.	Pore scale gas displacement of water residual oil	4
Fig. 3.	Oil gravity drainage after gas injection	4
Fig. 4.	Schematic of the Transparent Micromodel	10
Fig. 5.	Transparent Micromodel Setup	12
Fig. 6a-6d.	Transparent cell photos of SCWD stages	13
Fig. 7.	Consolidated core setup	15
Fig. 8.	Unconsolidated core setup	16
Fig. 9.	Unconsolidated core experimental results	20
Fig. 10.	Consolidated core experimental results	21
Fig. 11.	Through Window Ruska PVT Cell	22
Fig. 12.	Drop Volume Method Schematic	23
Fig. 13.	Capillary Tip Design	23
Fig. 14.	Oil-Water IFT Measurement	24
Fig. 15.	Attempted Oil Surface Tension Measurement	25
Fig. 16.	Water Surface Tension Measurement	25
Fig. 17.	West Hackberry crude final spreading over water	27
Fig. 18.	Pendant Drop IFT Measurement Method	27
Fig. 19.	Schematic of Pendant Drop Image Processing	29
Fig. 20.	Maximum Bubble Pressure Method	30
Fig. 21.	Schematic of the Maximum Bubble Pressure Method	30

LIST OF TABLES

Number Page

Table 2.1 Rock and Fluids Properties of Weeks Island, Hawkins and West Hackberry Reservoirs....9

Table 2. Core Permeability and Saturation Summary....18

Table 3. Fluid Injection Rates, Densities and Viscosities....18

STUDY OBJECTIVES AND METHODOLOGY

Conventional production techniques leave substantial quantities of oil in the reservoir. Various IOR processes target that oil. In steeply dipping, water driven reservoirs substantial incremental production can be obtained using Double Displacement Process (DDP) and Second Contact Water Displacement (SCWD). Both processes target water displaced residual oil. Experimental work and case histories indicate that up to 95 % initial oil in place can be recovered using DDP.

DDP utilizes updip gas injection and subsequent oil gravity drainage to mobilize and displace oil left behind the waterfront. While investigating the DDP, substantial oil was recovered when the gasflooded cores were subjected to downdip water injection. High pressure, high temperature corefloods and transparent micromodel experiments were performed in order to quantify and confirm this phenomenon referred to as SCWD. The advantage of SCWD over DDP is shorter duration of the recovery process and its suitability to larger number of reservoirs.

Research is needed to establish reservoir selection criteria and practical predictive techniques for the SCWD process. The efficiency of the process depends on phase distribution in the pore space after gas injection which in turn depends on interfacial and surface tensions (IFT) of the phases involved. Part of the planned study will concern designing a practical method of IFT measurement under reservoir conditions.

LITERATURE REVIEW

Theoretical Work

The Double Displacement Process (DDP) involves updip gas injection into a water-invaded oil column in order to mobilize and produce incremental oil.[1] The incremental oil results from the difference in residual oil saturation in the presence of water as compared to that in the presence of gas. Gravity stable displacement causes the formation of an oil bank which builds up progressively as it migrates downward the reservoir towards the producing wells. A simplified schematic of a dipping reservoir subjected to DDP is shown in Figure 1.

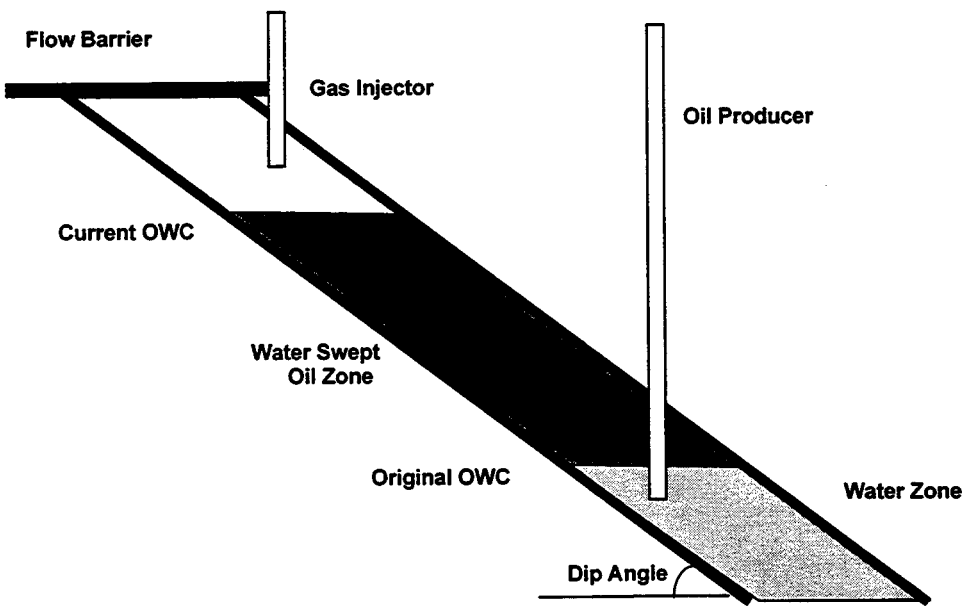

Fig. 1. Reservoir undergoing DDP.

Gas injection will help mobilize oil until the oil-water contact is lowered to its initial position at the beginning of reservoir production. Under favorable conditions, incremental oil recovery on the order of 40% of the initial oil-in-place may be recovered using DDP.[1-5]

Residual oil is left behind a waterfront because it is trapped by capillary retention forces that are greater than the forces applied during the waterflood. Residual oil may be in contact with the surface of the pore network (oil-wet rocks), trapped as globules surrounded by water contacting the pore network surface (water - wet rocks) or a combination of the preceding may occur in the case of mixed wettability.[6]

In order to recover waterflood residual oil, we must restore effective permeability to oil which is essentially zero in the water-swept zone. By injecting gas, some of the excessive water is displaced from pores where oil globules are trapped. For initially water wet systems with oil trapped in the pores, introduction of a gas phase creates conditions for three phase flow. When gas enters a pore containing a residual oil blob, capillary forces cause oil to spread between water coating the pore wall and the gas bubble occupying the center of the pore. This creates conditions allowing oil globules and blobs to reconnect. The reconnected oil film flows downward due to gravity forces and creates an oil bank. As more gas is injected, the existing oil bank flows downwards encompassing residual oil blobs as it travels. If gas front progresses slowly, no movable oil is left behind the gas front. However if the gas front advances rapidly, residual oil blobs are bypassed. These isolated oil blobs. can be reconnected to form a continuous phase which is efficiently displaced by SCWD process. Single pore scale gas displacement of waterflood residual oil is illustrated in Figure 2.

Efficiency of the DDP is governed by several different processes, including gravity drainage and the oil spreading coefficient. Gravity drainage is an oil recovery mechanism in which gravity acts as the main driving force for mobilization of oil with gas replacing the voided volume. A comprehensive description of the process was given by Hagoort.[7]

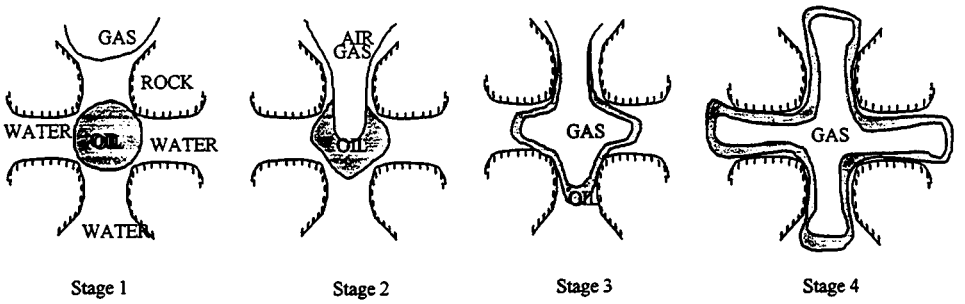

Fig. 2. Pore scale gas displacement of water residual oil.

A schematic of a reservoir subjected to gravity drainage process after gas injection is given in Figure 3.

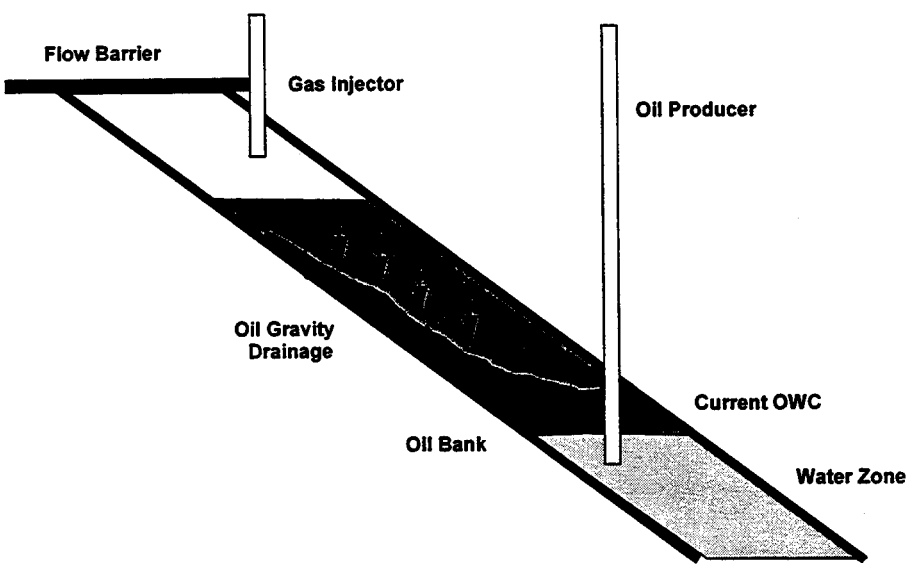

Fig. 3. Oil gravity drainage after gas injection

According to Chatzis et al[8], process efficiency is dependent on the spreading of oil over water in presence of gas. The spreading coefficient is given by:

$$S'_{o/w} = \sigma'_{wg} - \sigma'_{og} - \sigma'_{ow} \quad \text{.....(1)}$$

where:

$S'_{o/w}$ = final spreading coefficient of oil over water

σ'_{wg} = water/gas interfacial tension

σ'_{og} = oil/gas interfacial tension

σ'_{ow} = oil/water interfacial tension

When $S'_{o/w}$ is positive, oil tends to spread on water and form a continuous film. When $S'_{o/w}$ is negative, oil does not spread on water and stays discontinuous. This observations were further investigated by Oren at al[9] using a 2D glass micromodel containing a regular square network of intersecting capillaries. Soltrol 130™ was used to simulate the oil phase. Gas injection was performed with the cell positioned horizontally. Combinations of both positive were negative spreading coefficient systems were tested. Film formation and high oil recovery was observed for positive spreading coefficient systems. For negative spreading coefficient systems, the residual oil after gasflood tended to coalesce instead and form blobs occupying several pore spaces.

The spreading coefficient changes with time, as two substances initially contact than become mutually saturated. If an initially positive S' becomes negative, the initial oil film retracts and forms a lens.[10]

Experimental Work

Water-flood residual oil production has been modeled experimentally by performing floods in unconsolidated and consolidated cores, glass bead columns and glass micromodels. In general, the experiments demonstrated that a high percentage of the residual oil can be recovered for various sets of rock-fluid combinations.[2,4,5,12] Most of the studies showed that the residual oil

saturation after gas displacement was the same for waterflood residual oil and initial oil saturation in presence of irreducible water.

In 1983, Carlson[1] conducted laboratory tests to evaluate the DDP. A composite core made of 17 Dexter sand core plugs was mounted in a Hassler-type device. The core was oilflooded then waterflooded in a gravity stable manner to establish a residual oil saturation. Nitrogen was then injected at a very slow rate. All experimental steps were performed at reservoir temperature and pressure. Only 35% was recovered by waterflooding. An additional 1% was recovered by nitrogen injection. Poor flood performance was attributed to the lack of capillary continuity between core plugs. Additional experiments using Dexter sand core plugs mounted in triaxial core holders and a high speed centrifuge were performed to measure two-phase and three-phase end point saturations. An average residual oil saturation of 12% was measured for gas drive and 35% for water drive displacements.

Kantzas et al[12] evaluated the DDP using glass bead columns 0.05 to 0.10 m in diameter and 0.2 - 1.5 m in length. Experiments were carried out with "continuous oil" i.e. oil was the continuous phase in the presence of irreducible water, and "discontinuous oil" i.e. residual oil after waterflooding. Oil displacement was performed under "free drainage" and "controlled drainage" conditions. These terms refer to drainage of oil due to its own weight and due to the hindrance of a semipermeable membrane, respectively. The oil front advancement ranged from 0.01 to 0.1 m per day. A needle valve or semi-permeable membrane was used to control the flow rate. Using controlled displacement, the recovery of continuous oil approached 100% of the original oil-in-place, while the recovery of discontinuous oil was 85-95%. Under free drainage conditions, recoveries of continuous oil were lower and ranged from 73-79% of the initial oil-in-place. Reported gas injection time ranged from 350 to 2700 hours.

Kantzas et al[12] also examined the DDP in consolidated Berea sandstone (0.038 m in diameter and 0.29 m in length). The controlled drainage mode was used for Berea sandstone. Recoveries of continuous oil reached about 76% of initial oil-in place after 3200 hours of gas injection. Recoveries of discontinuous oil were lower and frequent changes of the semipermeable membrane were required to enhance oil production.

Chatzis et al[8] performed tests to visualize oil film formation and its influence on recovery efficiency. Square 500 mm and smaller capillary tubes were used to observe the flow behavior of the wetting phase. The DDP was performed in 1.2 m long, 0.038 m in diameter Berea sandstone cores with Computer-Assisted Tomography used to visualize the gas injection process and oil bank formation. The gas injection rate was 1 cc/day and the injection pressure was 34.5 kPa. About 40% of residual oil was produced at the time the report was published.

Field Cases

The DDP can be an economical IOR method for reservoirs with substantial oil left after water invasion, assuming optimum permeability, bed dip and oil viscosity for gravity drainage. As this is a gas injection project, a source of cheap gas must be readily available. Typically there is no need to drill a significant number of new wells for gas injection and oil production. The SCWD extends application of the DDP to single-well, water-driven reservoirs, where SCWD can be combined with attic oil recovery process to maximize oil recovery.

The Weeks Island field pilot DDP with CO_2 and methane was completed by Shell. The Hawkins Field DDP nitrogen injection project operated by Exxon is currently in progress, while the West Hackberry air injection project operated by Amoco is in its initial stage. A more detailed description of these reservoirs is provided in Table 1.

The Weeks Island field located in New Iberia Parish, Louisiana, is a typical Gulf Coast salt-dome field. It has a strong water drive, good sand quality and reservoir continuity with water drive sweep efficiencies ranging from 60 to 70% of initial oil-in-place. A mixture of CO_2 and natural gas was chosen to arrive at a relatively low gas density which would help achieve a stable displacement front. The gas injection started in 1978 and oil production began in 1981. Upon completion of the project in 1988, it was estimated that about 60% of the oil trapped behind the waterfront was recovered.[3]

The Hawkins Field unit was subjected initially to gas cap injection pressure maintenance between 1975 and 1987. In 1987, the DDP was initiated in the eastern part of the field which was subjected to a water drive. It was hoped that injection of a mixture of nitrogen and natural gas would lower the waterflood residual oil saturation from 35% down to 12% by the end of the project. The rate of oil bank downdip movement was originally anticipated to be approximately 25 feet per year.[5] During the early stages of the process, the gravity drainage rate was found to be about 12 ft/year. As a result, some oil remained trapped behind the gas front. After three years of project life, the oil column thickness increased by 10 ft, about 50% of the expected increase. The slower gravity drainage rate was attributed to an increase in the in-situ oil viscosity and gravity. It was found that the increase in oil viscosity was not due to gas injection, but to recovery of heavier oil that had been displaced upward during waterflooding. The reservoir oil relative permeability at low oil saturations was lower than expected, which also caused a delay in oil bank formation. Even though oil drainage was slower than expected, the DDP was considered to be successful based on the amount of oil recovered.[4]

Table 2.1 Rock and Fluids Properties of Weeks Island, Hawkins and West Hackberry Reservoirs[5]

Reservoir Property	Weeks Island	Hawkins Field	West Hackberry
Porosity, %	26	27	24 - 28
Permeability, md	1200	3400	300-1000
Swi, %	10	13	19-23
Sorw, %	22	35	26
Sorg, %	1.9	12	8 (est.)
Reservoir Temperature, °F	225	168	195-205
Dip Angle, deg	26	8	23-35
Pay Thickness, ft	186	230	30-31
API Oil Gravity	32.7	25	33
Viscosity, cp	0.45	3.7	0.9
Bubble Point Pressure, psig	6013	1985	3295
Solution GOR, SCF/STB	1386	900	500
Oil FVF at Bubble Point	1.62	1.225	1.285
Waterflood Recovery Factor, % of IOIP	78	60	60
Gasflood Recovery Factor, % of IOIP	95	85	90 (est.)

The West Hackberry field is characterized by a waterflood residual oil saturation of about 26 %. The residual oil saturation after gasflooding is expected to be 5%. Air is the injection gas. Combustion is expected at prevailing reservoir temperature producing flue gas composed of 85% nitrogen and 15% carbon dioxide. It is also expected, that carbon dioxide will go into solution and decrease the residual oil viscosity thus easing the gravity drainage process.[5]

ACCOMPLISHED INVESTIGATIONS

Transparent Micromodel Experiments

In order to visually observe the mechanisms responsible for oil mobilization and displacement, a transparent micromodel was built. The cell used in the experiment is similar to the cells described by Dahmani.[12] Figure 4 is a schematic of the transparent micromodel.

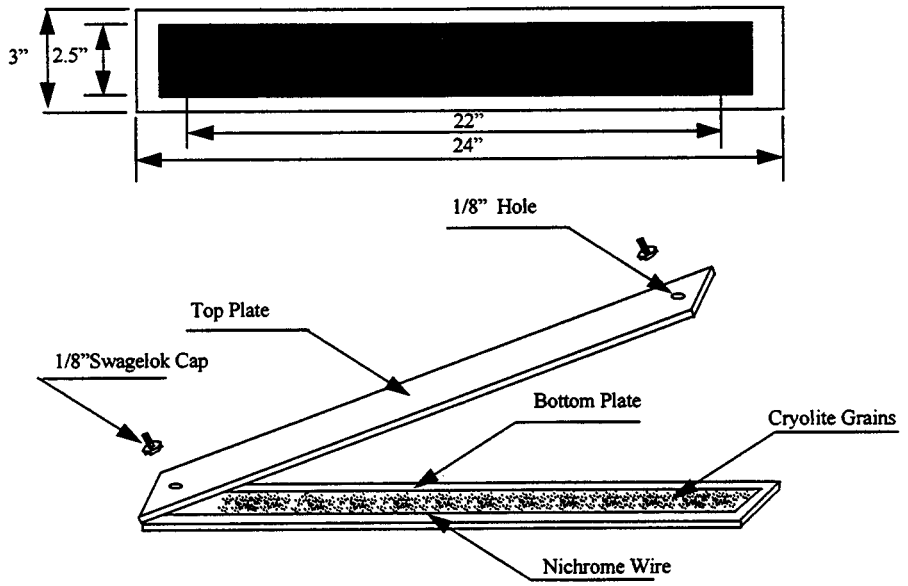

Fig. 4. Schematic of the Transparent Micromodel.

Two 24" x 3" glass plates were used as the bottom and the top of the cell. Two 1/8" holes were drilled at both ends of the top plate and stainless steel Swagelok caps (1/8" in diameter) were glued to the glass to serve as an inlet and outlet for fluid flow. The glass plates were glued together with two pieces of 28 gauge (0.015" in diameter) Ni-Cr wire serving as a spacer. The total volume of the cell was 14 cc. The glue used in the construction was Devcon 2-Ton Epoxy. To provide the cell with a porous medium, cryolite (Na_3AlF_6) granules were injected. Cryolite was chosen because it is highly water-wet. Most importantly, the cryolite refractive index is close to that of water rendering it transparent when it is in contact with water. Cryolite rocks, purchased from Ward's Natural Science Establishments, Inc, were crushed and sieved. The 100-150 mesh fraction was used to pack the cell. The cell was packed by applying a vacuum on one end of the cell; glass wool was placed in the outlet fitting, to

prevent the grains from entering the vacuum pump. The grains were consolidated by injecting a fresh mixture of 60% tetraethyl orthosilicate, 32% ethanol, and 8% 0.1 N HCl into the cell. Excess mixture was removed from the cell by flushing the cell with air. The orthosilicate mixture solidified as non-reactive silica and cemented the cryolite grains to streaks of different permeability. The transparent micromodel was incorporated in the experimental setup shown in Figure 5. For all injections, a Sage Instruments Model 355 syringe pump was used. The injection rate was adjustable. The cell was initially flooded with CO_2 to remove air from the cell. The cell was then positioned vertically and saturated with deaerated water. Residual CO_2 dissolved in the water which was subsequently displaced from the cell. About 4 PV of water were injected into the cell from each direction to remove CO_2. After the cell was saturated anew with water, oil was injected into the top of the cell until no additional water was produced and the system was allowed to stabilize for one day. The oil used was a mixture of 67% decane and 33% crude from the West Hackberry, LA, field. This opaque mixture was selected to yield a mobility ratio close to unity. Next, deaerated water was injected into the bottom of the cell until no additional oil was produced, and the cell was again stabilized for one day. Gas was then injected at the slowest possible rate of 0.08 cc/day into the top of the cell to simulate DDP. After gas breakthrough, the cell was shut-in for two days for stabilization. After the shut-in period, water was injected into the bottom of the cell to simulate the SCWD process. The experiment was filmed using a VCR camera. The VCR camera was fixed on a tripod and fitted with additional optical equipment such as a teleconverter, bellows unit, three close-up lenses and a polarizing filter. This arrangement reduced unwanted light reflections and permitted variable scales of magnification from whole cell size, down to single pore level, 450:1.[13]

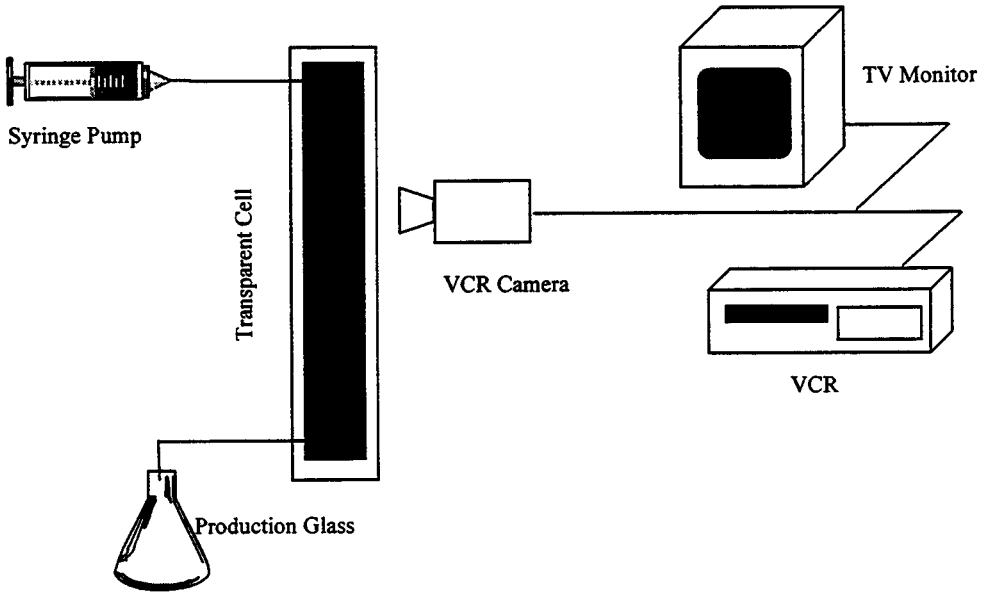

Fig. 5 Transparent Micromodel Setup.

The transparent micromodel experiments succeeded in visualizing microscopic gas-oil-water displacements, oil film development and oil bank growth. It was also observed that injected water, simulating the SCWD displaced most of the gas and remaining oil. This created an oil bank which grew with time and progressed updip. Only insignificant amount of oil was left behind the SCWD waterfront. The stages of the second contact water displacement are shown in the magnified pictures of Figures 6a-6d.

High Pressure and Temperature Corefloods

Experimental conditions were selected to be as close as possible to West Hackberry field reservoir conditions.[5] However, certain constraints were imposed by the equipment design and capabilities. The pressure and temperature selected for all floods were 2000 psig and 205°F respectively. The West Hackberry oil was used. The oil API gravity was 31.5° and its

asphaltene content was 0.52%. The asphaltene content is sufficiently low that core plugging was unlikely. Oil viscosity at 205°F was 2.15 cp, which made gas gravity drainage and SCWD investigation feasible within a reasonable time period.

Two experimental setups were used and a total of four experiments were performed. The main part of the first experimental setup, shown in Fig. 7, consisted of a consolidated Berea sandstone core 6 feet in length and two inches in diameter.

Fig. 6a. Transparent cell prior to water invasion, after gas injection. Water and cryolite grains--light, oil and gas--dark)

Fig 6b. Water invasion from the left causes oil displacement.

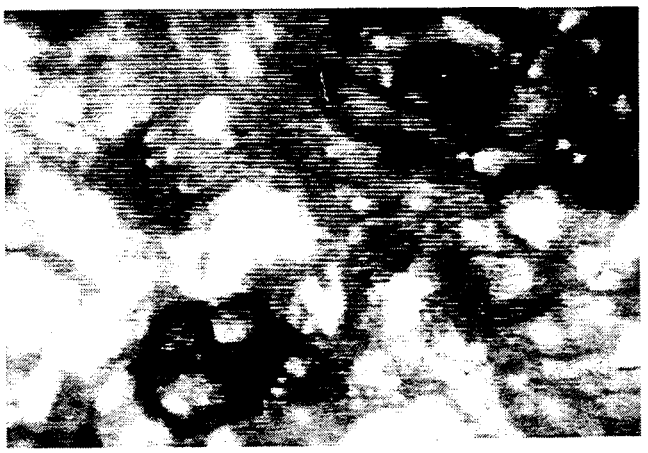

Fig. 6c. Continued water invasion from the left, further oil displacement.

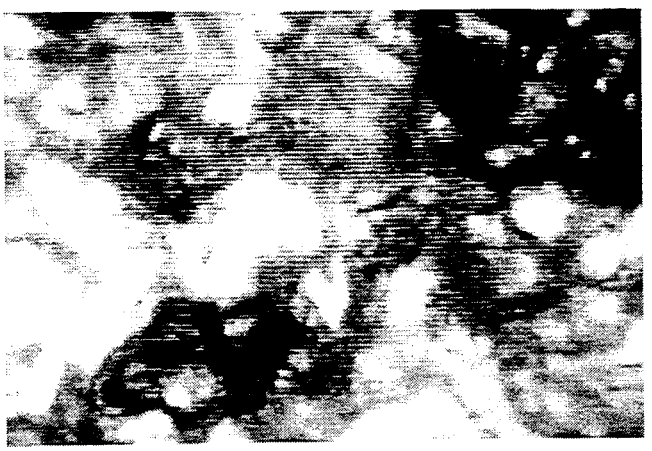

Fig. 6d. Final fluid distribution, black zones--gas bubbles left behind the waterfront.

Berea sandstone was used to simulate a heterogeneous reservoir rock with permeability streaks. The core was coated with epoxy resin and fiberglass tape and placed in a stainless steel coreholder. Stainless-steel tube coils were wrapped around the core and used to circulate a heated mixture of ethylene glycol and water to create a uniform temperature distribution. The coreholder was insulated to minimize heat losses. The annulus of the coreholder was filled with hydraulic oil and pressurized to at least 1000 psi higher than the highest pressure expected

in the core during the experiment. The goal was to keep the core under permanent compression.

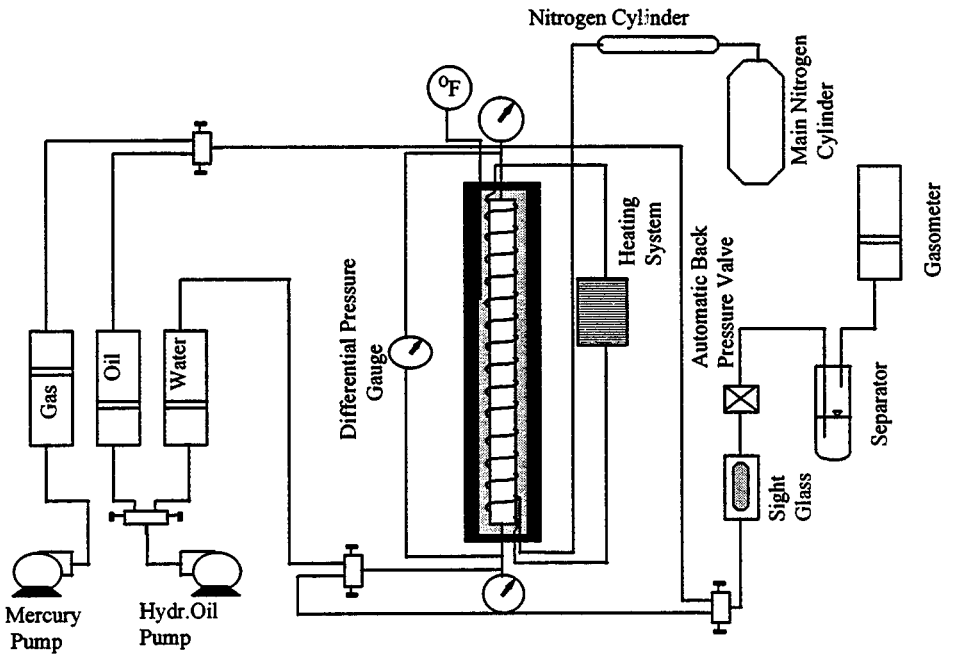

Fig. 7. Consolidated core setup

To maintain a constant pressure in the annulus of the coreholder, 500 cc and 1000 cc high pressure stainless steel cylinders filled with nitrogen were connected to the annulus. This safety device is necessary to maintain the core under compression in case of failure of the heating system when the core is saturated with gas.[13]

The core assembly was mounted vertically and both ends were connected to floating piston transfer vessels. The other ends of the transfer vessels were connected to positive displacement Ruska pumps filled with hydraulic oil. The transfer vessels were used to transfer fluids in and out of the core. The producing end of the core, which changed during the experiment, was connected to the production panel with a sight glass for visual observations at high pressure and a back pressure valve was used to maintain a preset pressure at the producing

end. Produced fluids were separated and measured in an atmospheric pressure separator connected to a gasmeter. Pressures at both ends were measured using digital-meters and Bourdon tube gauges. The differential pressure across the core was also monitored.

In order to investigate the process in a homogeneous rock environment, a second setup incorporating a sandpack apparatus with a much higher permeability and core crossectional area was also built, Figure 8.

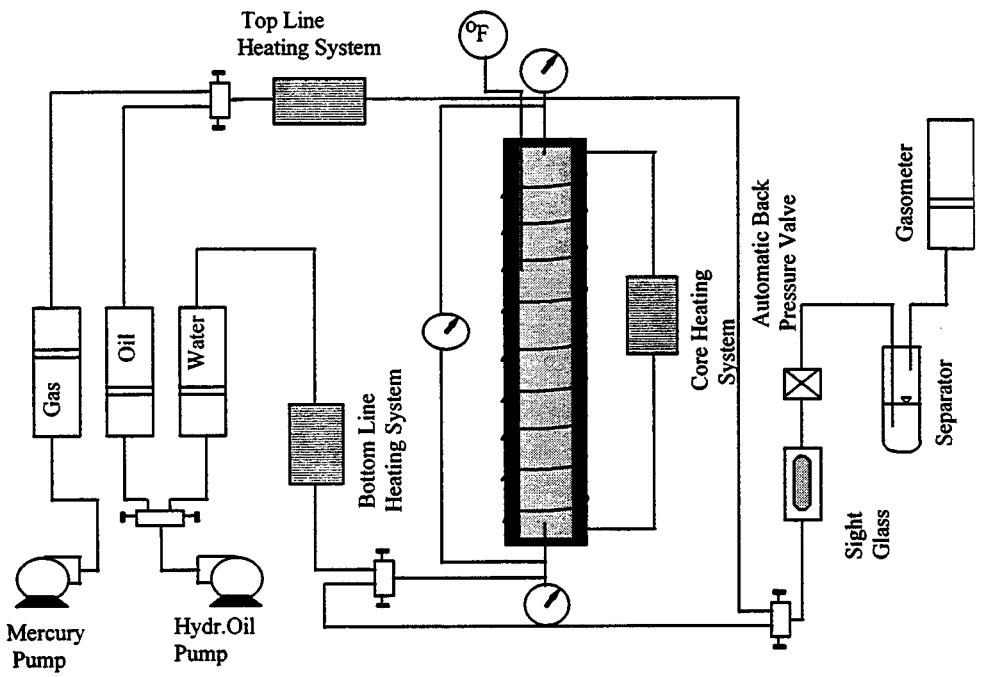

Fig. 8. Unconsolidated core setup

The apparatus consisted of a 9.5 ft long, 0.2225 ft diameter steel cylinder, packed with 80-120 mesh Ottawa sand. Sand and water were added simultaneously and the holder was vibrated to ensure a tight pack. The sandpack assembly was mounted vertically and a brass tube heating coil was wrapped around the coreholder. The system was insulated to minimize

heat losses. The flowlines closest to the core were preheated to 205°F by placing 15 feet of coiled tubing in the ethylene glycol/water mixture. This sort of preheating system was unnecessary in the Berea sandstone core since more than 5 feet of flowlines were already immersed in the coreholder annulus filled with hot hydraulic oil. The average core porosity was calculated to be 36% based on the amount of water retained by the sand pack. Pore volume was calculated to be 4785 cc.

Clean, water-saturated cores were used for each experiment. An initial permeability check was performed before each experiment by pumping water at constant flow rate and constant pressure drop across the core. Permeability was measured in both flow directions of the linear core. The absolute permeability measurements were performed at 205 °F and 2000 psig, the same conditions planned for the displacement experiment. The core was then subjected to an oilflood to establish an irreducible water saturation. The oil was injected in the top and water was produced from the bottom of the core. After one day of stabilization time, a waterflood was performed to establish residual oil saturation in the presence of water. The injection rates for oil and water ranged from 16 to 160 cc/hr. The flood ended when the fraction of the displacing fluid reached 95%. After the oilflood and the waterflood, effective permeabilities to oil and water at residual saturations were measured in both directions. Permeability and saturation values are listed in Table 2. Permeability measurements were performed in top to bottom (t-b subscript) and bottom to top (b-t subscript) directions.

Gas injection was initiated by pressurizing all lines of the production side with only the back pressure valve closed. The same gas injection rate was maintained during all cycles of gas injection. An exact measurement of the produced gas was difficult due to the very slow injection rate; therefore the cut-off point was established by observing the produced fluids

through the sight glass. After gas breakthrough, the cores were shut-in for oil mobilization. After the shut-in period, the gas injection was resumed to displace the oil mobilized during the previous shut-in period. Lastly, water was injected into the bottom of the core.

The fluids used during all coreflood experiments and their properties are listed together with gas injection rates in Table 3. Water and oil properties were measured and gas properties were interpolated from existing tables. After each experiment the core was cleaned to restore the initial strongly water-wet and water saturation conditions[13].

Table 2. Permeability and Saturation Summary.

Property	Sandpack Run #1	Berea Run #1	Sandpack Run #2	Berea Run #2
$k_{(t-b)}$	1.72 d	417 md	1.53 d	286 md
$k_{(b-t)}$	1.38 d	469 md	1.46 d	327 md
$k_{oiw(t-b)}$	1.22 d	179 md	0.78 d	250 md
$k_{oiw(b-t)}$	1.34 d	239 md	0.95 d	239 md
$k_{wor(t-b)}$	0.18 d	53 md	0.60 d	32 md
$k_{wor(b-t)}$	0.15 d	46 md	0.50 d	28 md
S_{iw}	13.88 %	44.5 %	14.13 %	43.6 %
S_{or}	15.53 %	30.3 %	15.56 %	35.0 %

Table 3. Fluid Injection Rates, Densities and Viscosities.

Experiment	Type of Fluid	Flow Rate (cc/hr)	Density (g/cc) @ 205°F	Viscosity (cp) @205°F
Sandpack Runs	Deaerated Water	96 cc/hr	0.9623	0.3873
	West Hackberry Crude (Recycled)	160 cc/hr	0.8234	2.40
	Pure Nitrogen	20 cc/hr	0.1177	0.0230
Berea Runs	30k ppm KCl Brine	16 cc/hr	0.9810	0.3721
	West Hackberry Crude	32. cc/hr	0.8182	2.1528
	Pure Nitrogen	2.5 cc/hr	0.1177	0.0230

One of the important design parameters of the experiment was the gas injection rate. Since only water was initially produced followed by the oil bank, a gravity stable displacement

must have been maintained throughout gas injection.

The critical gas injection rate (flux) was predicted using Eq. 2 proposed by Dietz.[14]

$$u_c = \frac{0.044 k_o \Delta \rho_{o/g} \sin \alpha}{\mu_o} \qquad \text{.....(2)}$$

where:

k_o = permeability to oil, Darcy

$\Delta\rho_{o/g}$ = oil/gas density difference, lbs/cu ft

α = dip angle, degrees

μ_o = oil viscosity, cp

After the first Berea sandstone experiment was completed, the same core was used in a second experiment. The goal of the second experiment was to determine if the duration of the shut-in period following gas breakthrough affected process performance. The experimental procedures were the same except for a shorter duration of the shut-in period.

All procedures in the unconsolidated core experiments were the same as in the Berea experiments, except the gas injection rate, which was 20 cc/hr. A sufficiently low gas injection rate was selected to avoid gas fingering. Fluid saturations and core permeabilities for all experiments are summarized in Table 2.

The sandpack experiments yielded significant oil production. Experiment #1 was performed with a short gas gravity drainage shut-in period of 5 days. In experiment #2, the gas gravity drainage period was extended to 38 days. The duration of the shut-in period had no effect on oil recovery. Even though the initial waterflood residual oil saturation was low in both experiments, about 15.5% PV, that value was reduced by SCWD to 11.3% PV in the first

experiment and 11.9% PV in the second. Subsequent gas injection-shut-in cycles did not yield significant oil production. The plot of oil saturation vs. time for both sandpack experiments is given in Figure 9.

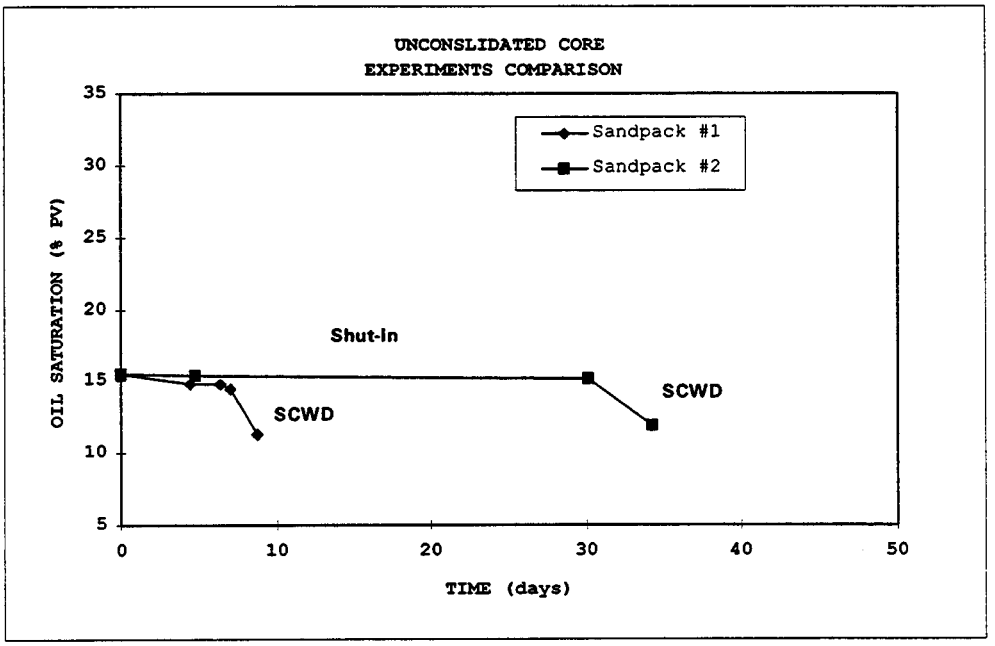

Fig. 9. Unconsolidated core experimental results

In the consolidated core experiments, unlike the sandpack experiment, significant oil production was observed prior to gas breakthrough. The increase in early oil production may be attributed to gas penetration of zones unwept by water. Only a fraction of the movable water (about 70%) was displaced before gas breakthrough. Additional water production was observed during subsequent gas injection period. The residual oil saturation after initial gas injection was lowered from 30.3% to 20.3% PV in the first Berea experiment and from 35.0% PV down to 24.2% PV in the second experiment. In the first experiment, the core was shut-in after gas breakthrough for 5 days, gas was injected again and additional oil was produced. Immediately after the second cycle of gas injection/oil production, water was injected downdip.

The oil saturation was reduced to 17.3% at the end of the experiment. SCWD resulted in an additional 3.6% PV of oil. In the second experiment, the duration of the shut-in period was extended to 38 days. Gas was injected again and additional oil was produced. Subsequent SCWD produced an additional 2.51% PV of oil bringing the final oil saturation down to 17.8% PV.

The amount of incremental oil produced prior to gas breakthrough during both Berea experiments was in good agreement with the amount obtained in DDP Berea experiments.[13] The saturation summary for both Berea experiments is shown in Figure 10.

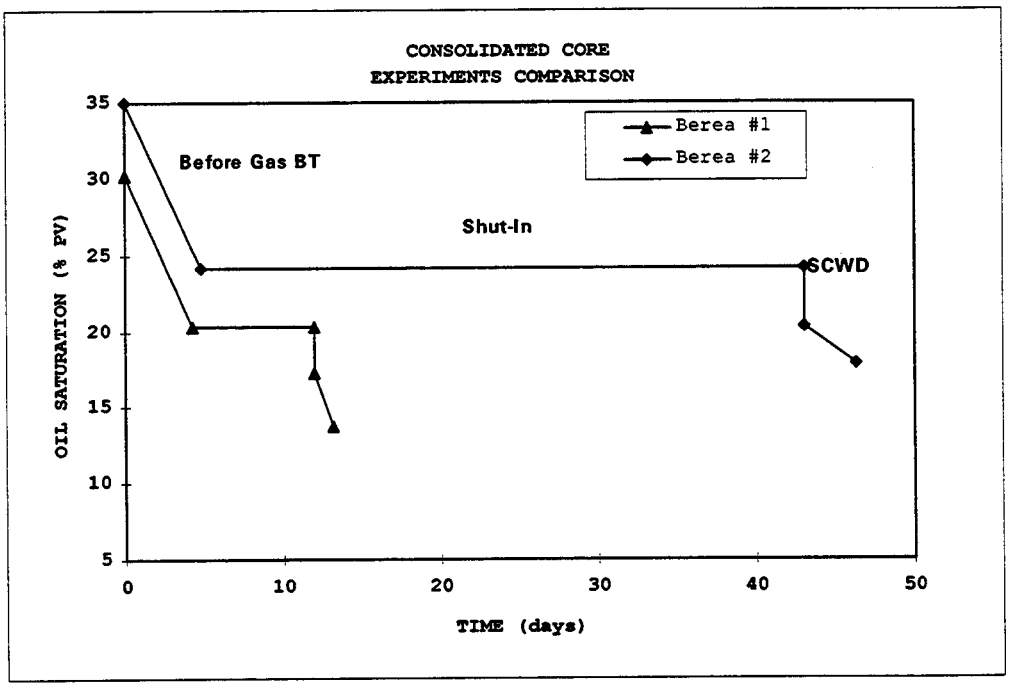

Fig. 10. Consolidated core experimental results

Interfacial Tension measurements (Drop Volume Method)

IFT measurements for spreading coefficient calculation have to be performed under reservoir conditions with recombined oil phase used. In order to achieve that, a Through Window

Ruska PVT Cell (Fig. 11) and HP Ruska mercury pump is used. Recombined oil is injected via a transfer vessel. The system is capable of going up to 5000 psi and 300 °F, thus covering reservoir conditions where SCWD is applicable.

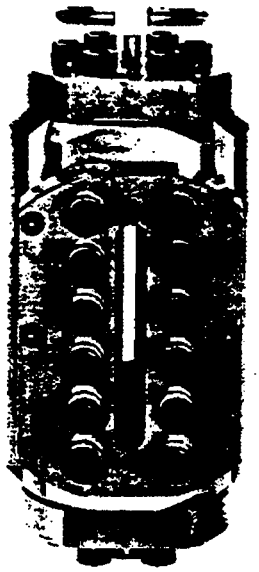

Fig. 11. Through Window Ruska PVT Cell

The IFT measurement using this method is made by pumping the light phase into the dense phase at constant flow rate. Drops form at the tip of the specially designed capillary, Fig. 12, and IFT is calculated using Eq. 3. To avoid necessary corrections due to liquid that can wet and accumulate on the tip, the tip was designed to be very sharp as shown in Fig 13.[15]

$$\sigma_i = \frac{V_{drop}(\rho_H - \rho_L)g}{\pi d} \qquad \text{.....(3)}$$

Where:

ρ_H = density of the heavy phase

ρ_L = density of the light phase

V_{drop} = volume of the drop

g = acceleration of gravity

d = inside diameter of the tip

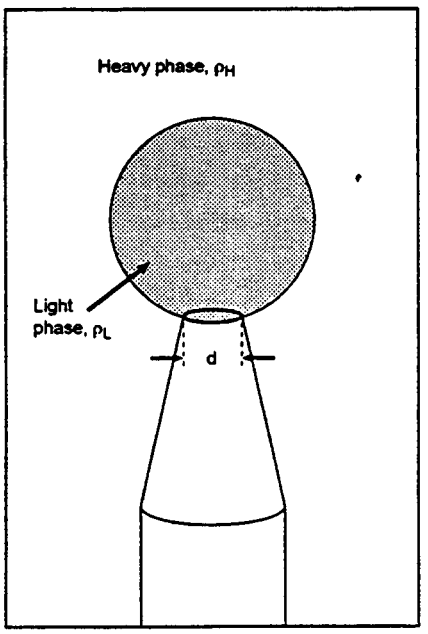

Fig. 12. Drop Volume Method Schematic (after Gilman[15]).

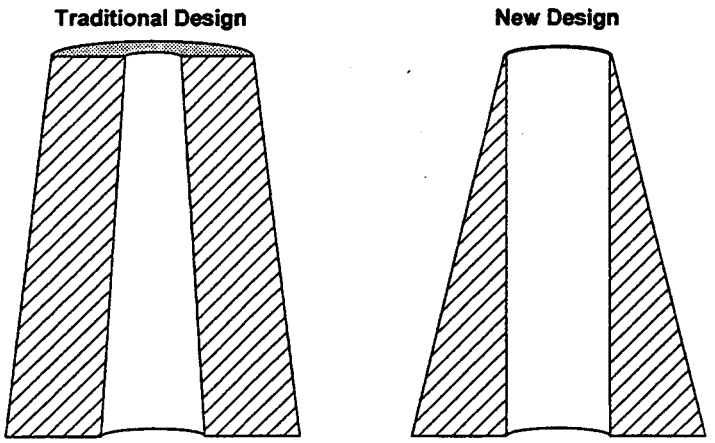

Fig. 13. Capillary Tip Design (after Gilman[15]).

Drop volume method was believed to be the simplest method available and sufficiently accurate for IFT measurements. Unfortunately, the method was originally designed to be applicable only for the measurement of liquid/liquid IFT. The measurement of IFT for heptane-distilled water system is shown in Fig. 14. Results obtained are in very good agreement with published values.[16]

Fig. 14. Oil-Water IFT Measurement.

The difficulty in using the drop volume method for liquid/gas IFT (surface tension measurements) comes from the wettability of the capillary tip in presence of gas. This phenomena causes liquid to climb over the tip instead of forming a regular shape drop Fig 15.

Fig. 15. Attempted Oil Surface Tension Measurement.

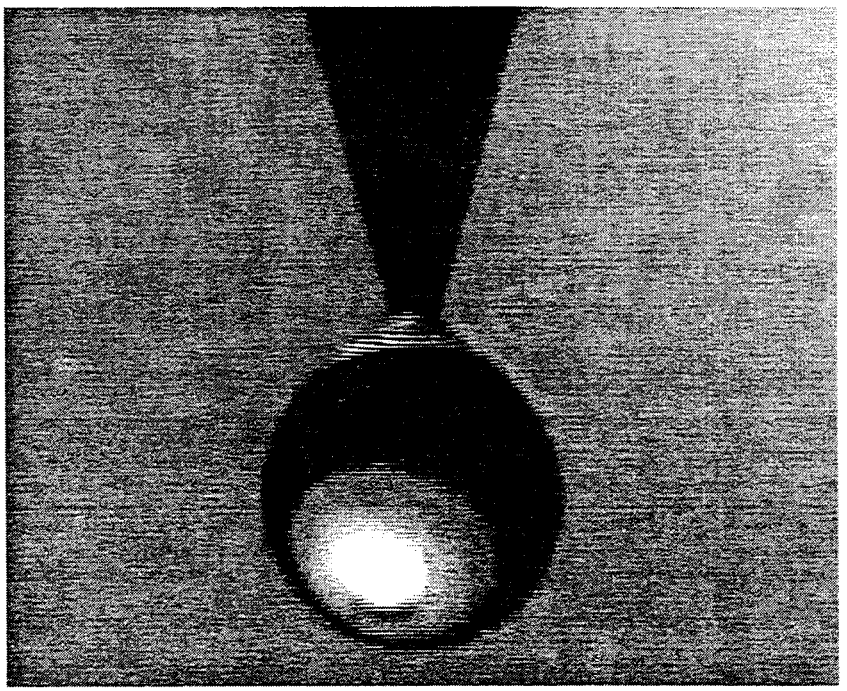

Fig. 16. Water Surface Tension Measurement.

In case of water surface tension measurement, the problem was overcome by soaking the tip in mineral oil thus forming thin oil film coating on the tip. Using oil-wet tip, injected water formed a regular shape drop (Fig.16) and detached in a way that Eq. 3 was valid again for calculation of surface tension. Results obtained were in good agreement with literature values.

Several methods were tried to change wettability of the tips used for oil/gas IFT measurements, but none succeeded in producing a regular shaped oil drop.

Oil Spreading Experiments

Estimation of the spreading coefficient was attempted by observing oil spreading observed visually under ambient conditions. The setup consisted of beaker filled with distilled water mounted on a holder, and a syringe used for oil injection. Diluted oil used for transparent micromodel experiments (66% decane and 33% West Hackberry oil) and West Hackberry oil used for coreflood experiments were investigated. The diluted oil spread over water and formed a thin film that remained the same after overnight maturation. West Hackberry crude behaved initially the same way, but the thin film contracted after overnight maturation and formed a small lens as shown in Fig. 17.

Further investigation using this method under reservoir conditions was not possible. A single oil drop spreads over an area far greater than that available within the Ruska PVT cell.

INVESTIGATIONS IN PROGRESS

Pendant Drop Method IFT Measurements

The research is now concentrated on pendant drop method of IFT measurement. A drop hanging from a capillary tip (or a clinging bubble) elongates as it grows larger. Then, the drop

shape dependent quantity $S = d_s/d_e$ (d_s measurement is taken within d_e from the bottom of the drop, Fig. 18) is used in calculation of the IFT.[17]

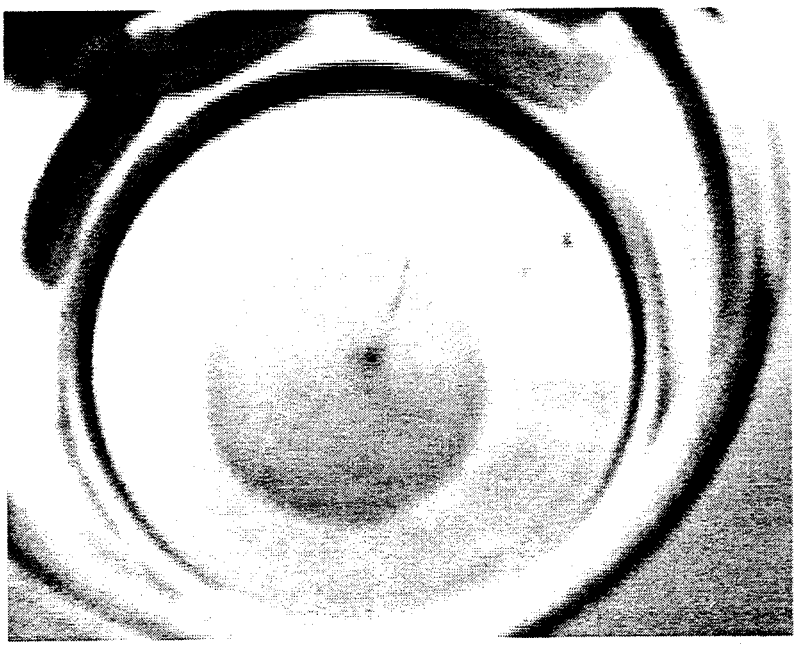

Fig. 17. West Hackberry crude final spreading over water

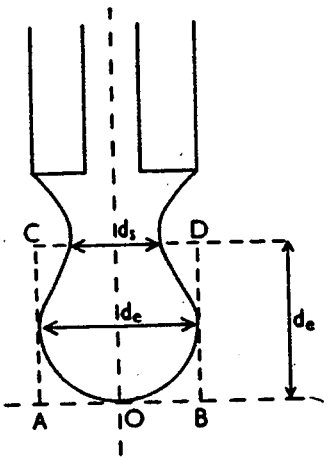

Fig. 18. Pendant Drop IFT Measurement Method (after Padday[17]).

IFT can be calculated quickly using following algorithm:[18]

$$\sigma_i = \frac{\Delta\rho g R_o^2}{\beta} \quad \text{.....(4)}$$

$$\beta = 0.12836 - 0.7577S + 1.7713S^2 - 0.5426S^3 \quad \text{.....(5)}$$

$$R_o = \frac{d_e}{2\left(0.9987 + 0.1971\beta - 0.0734\beta^{3^2} - 0.34708\beta^3\right)} \quad \text{.....(6)}$$

In order to perform the measurement with sufficient accuracy and simplicity, pendent drop will be filmed with VCR camera equipped with set of additional lenses, taped on VCR and then the image will be transferred to a computer using the frame capture software Minolta - Play Snappy. Transferred image will be then measured using Jandel SigmaScan Measuring software. Preliminary measurements performed with these two pieces of software provided sufficient accuracy for the SCWD process spreading coefficient calculation. An example measurement is illustrated in Fig. 19.

FUTURE INVESTIGATIONS

Combination of the Drop Volume and Maximum Bubble Pressure Methods

Drop volume method is not designed for surface tension measurement of liquids. When liquid is pumped through the capillary tip in presence of gas, liquids tend to wet the tip and, instead of forming regular shape drop hanging at the tip, it climbs over the tip and forms irregularly shaped drop, as demonstrated in Fig. 16. When gas is bubbled through the capillary, expansion

of the bubbles makes drop volume method calculation invalid. Due to the method's simplicity and convenience of use within the transparent PVT cell, I plan to improve drop volume method by trying to combine it with maximum bubble pressure method.

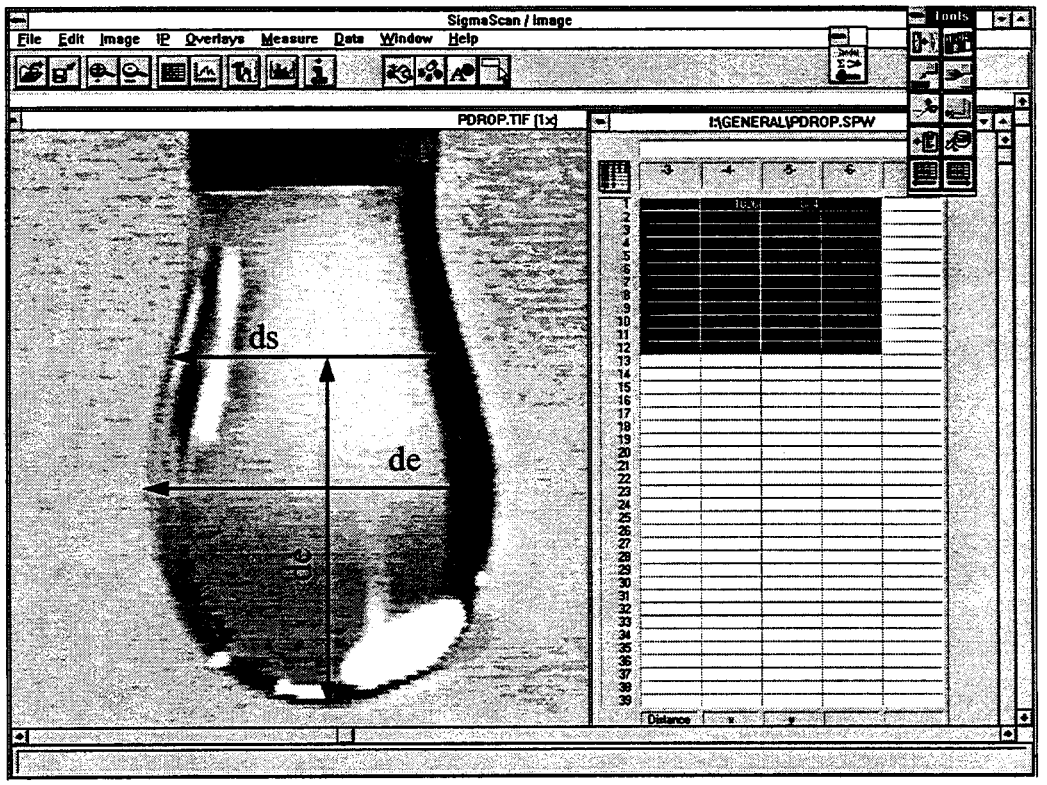

Fig. 19. Schematic of Pendant Drop Image Processing.

The procedure for maximum bubble method is to slowly blow bubbles of gas in the liquid by means of a tube projecting below the surface. For small tube, the sequence of shapes of the bubble is such that the bubble radius reaches its minimum when it reaches the inner or outer radius of the tube (depending on tube wettability), as shown in Fig. 20 and Fig. 21. At the same time, pressure needed to pump this gas bubble into a liquid reaches its maximum. The value of IFT is proportional to the value of that maximum pressure. [10]

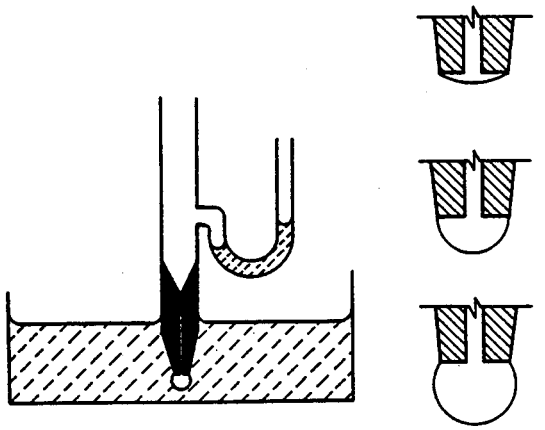

Fig. 20. Maximum Bubble Pressure Method (after Adamson[10]).

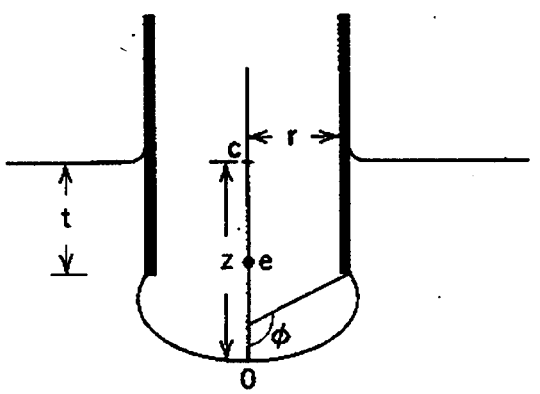

Fig. 21. Schematic of the Maximum Bubble Pressure Method (after Adamson[10]).

Under reservoir conditions where compressibility effect is less pronounced, drop volume method for liquid/gas interfaces combined with maximum bubble pressure method should provide sufficient accuracy required for spreading coefficient calculation.

Screening Criteria for SCWD

Since SCWD is a new process, little is known about screening criteria to be used for candidate reservoir selection. SCWD is an extension of DDP, thus DDP screening criteria should apply.

However, additional criteria governing water encroachment in the gasflooded oil zone are needed.

The following are some general screening criteria for DDP developed experimentally and with reservoir simulation:

- minimum of two wells in good mechanical condition,
- reservoir dip angle should be over 10°,
- reservoir permeability should be no less than 300 md,
- reservoir depth should be considered in view of optimizing gas/oil density difference.

When considered together, lower permeability has more detrimental effect on process efficiency than dip angle. [19]

It is believed that oil spreading over water in presence of gas will be one of crucial factors for predicting process performance.

Further investigation of the SCWD process will be performed with transparent micromodel and HPHT Ruska PVT cell. After a method of IFT measurement is developed, other corefloods are planned to investigate process performance for negative spreading coefficient. By the time these experiments are finished, a numerical simulator for DDP should be available to help in development of some practical screening criteria for SCWD.

CONCLUSIONS

Original contribution of this work is discovery and initial investigation of the new Improved Oil Recovery method, the Second Contact Water Displacement (SCWD). Additional contribution came from development of practical IFT measurement under reservoir conditions. Further study of the SCWD is planned including development of practical screening criteria for

the new process. Ongoing IFT experimental work has attracted attention of industry including Krüss and Dow Chemical.

BIBLIOGRAPHY

1. Carlson, L. O.: "Performance of Hawkins Field Unit Under Gas Drive-Pressure Maintenance Operation and Development of an Enhanced Oil Recovery Project", paper SPE/DOE No. 17324 presented at the SPE/DOE Enhanced Oil Recovery Symposium in Tulsa, Oklahoma, April 17-20, 1988.

2. Dullien, F. A., Catalin, L.: "Recovery of Waterflood Residual Oil by Gravity Assisted Inert Gas Injection Using a Horizontal Well in a Two-Dimensional reservoir Model", paper Petroleum Society of CIM & AOSTRA No. 94-49 presented at 45th Annual Meeting in Calgary, Canada, June 12-15, 1994.

3. Johnston, J. R.: "Weeks Island Gravity Stable CO_2 Pilot", paper SPE/DOE No. 17351 presented at the SPE/DOE Enhanced Oil Recovery Symposium in Tulsa, Oklahoma, April 17-20, 1988.

4. Langenberg, M. A., Henry, D. M., Chlebana, M. R.: "Performance and Expansion Plans for the Double Displacement Process in the Hawkins Field Unit", paper SPE No. 28603 presented at the 69th SPE Annual Technical Conference and Exhibition in New Orleans, LA, September 25-28 1994.

5. Fassihi, M. R., Gillham, T. H.: "The use of Air Injection to Improve the Double Displacement Processes", paper SPE No. 26374 presented at the 68th SPE Annual Technical Conference and Exhibition in Houston, TX, October 3-6 1993.

6. Holm, L. W.: "Mobilization of Waterflood Residual Oil by Miscible Fluids", *SPE Reservoir Engineering* (July 1986).

7. Hagoort, J.: "Oil Recovery by Gravity Drainage", *SPE Journal* (June 1980).

8. Chatzis, I., Kantzas, A., Dullien, F. A. L.: "On the Investigation of Gravity-Assisted Inert Gas Injection Using Micromodels, Long Berea Sandstone Cores, and Computer-Assisted Tomography", paper SPE No.18284 presented at the 63rd SPE Annual Technical Conference and Exhibition in Houston, TX, October 2-5 1988.

9. Oren, P. E., Billiotte, J., Pinczewski, W. V.: "Mobilization of Waterflood Residual Oil by Gas Injection for Water-Wet Conditions", *SPE Formation Evaluation* (March 1992).

10. Adamson, A.W.: Physical Chemistry of Surfaces, Interscience Publishers Inc., New York, 1960.

11. Kantzas, A., Chatzis, I., Dullien, F. A. L.: "Enhanced Oil Recovery by Inert Gas Injection", paper SPE/DOE No. 17379 presented at the SPE/DOE Enhanced Oil Recovery Symposium in Tulsa, Oklahoma, April 17-20, 1988.

12. Dahmani, M. A.: "The Effects of Alcohols and Crude Oil Composition on the Performance and Mechanisms of Alkaline Flooding of Oil reservoirs", PhD dissertation, Louisiana State University, Baton Rouge, LA (1986).

13. Lepski, B.:"Physical Modelling of the Oil Displacement by Gas in Waterflooded Zones", M.S. Thesis, Louisiana State University, Baton Rouge, LA (1995).

14. Richardson, J. G., Blackwell, R. J.: "Use of Simple Mathematical Models for Predicting reservoir Behavior", paper SPE No. 2928 presented at 45th Annual Fall Meeting of the SPE of AIME in Houston, Texas, October 4-7, 1970.

15. Gilman, L.B.: "A Review of Instruments for Static and Dynamic Surface and Interfacial Tension Measurement", Presented at the AOCS Annual Meeting and Expo, Anaheim, CA April 27, 1993.

16. Dean J.A., Lange's Handbook of Chemistry, McGraw-Hill Book Company, New York 1985.

17. Padday, J.F.: *Surface and Colloid Science*, John Wiley & Sons, New York (1969) 39.

18. Herd, M.D., Lassahn, G.D., Thomas C.P., Bala G.A.:"Interfacial Tensions of Microbial Surfactants Determined by Real-Time Video Imaging of Pendant Drops", SPE/DOE No. 24206 presented at the SPE/DOE Eight Symposium on Enhanced Oil Recovery in Tulsa, Oklahoma, April 22-24, 1992.

19.. Bensaid, F.:" Effects of Dip angle, Absolute Permeability and Relative Permeability on Double Displacement Process", M.S. Thesis, Louisiana State University, Baton Rouge, LA (1995).

VITA

Bogdan Lepski, son of Maria Lepski and Roman Lepski was born on March 22, 1966 in Paslek, Poland.

He was admitted to University of Mining and Metallurgy, Cracow, Poland in October 1986. He obtained his Master of Science and Engineering degree in June 1992 and started his career as a drilling engineer with the Polish Oil and Gas Company in Zielona Gora, Poland. After coming to USA in August 1993, he obtained his Master of Science in Petroleum Engineering in May 1995 and entered a Doctor of Philosophy program at Louisiana State University in Baton Rouge.

APPENDIX C

SUMMARY OF LSU'S MODELING RESEARCH

(Introduction to Doctorial Paper)

Summary

Currently, U. S. producers are faced with economically unfavorable conditions such as competition from less mature areas, lower oil prices, and increasing environmental regulations which lead to higher operating costs. With current technology, more than half of the oil discovered is being left in the ground. Technological improvements, which increase the recovery of bypassed oil, would further aid the aging domestic oil industry to maximize production from previously developed reservoirs. Without significant advances to improve recovery, the domestic oil and gas industry will continue to decline at the same or at a higher rate.

Oil can be bypassed on both a macroscopic scale and a microscopic scale. Oil is bypassed on a macroscopic scale when regions of the reservoir remain unswept due to well placement or reservoir inhomogeneities. Oil is bypassed on a microscopic scale when it becomes immobile within the porous medium due to capillary and wettability effects. Oil bypassed in this manner is referred to as *residual oil* and can be recovered with any process which creates conditions under which the mobility of the oil is restored. An emerging technology which targets the oil remaining after natural water influx or waterflooding is the tertiary injection of gas. The term *tertiary* refers to the recovery of oil remaining after completion of a secondary recovery process such as waterflooding. In this body of work, it implies that the original oil column has been invaded by water and that remaining oil is discontinuous. A process in which gas displaces mobile water and re-establishes the hydraulic continuity of the oil is referred to in this study as a tertiary gas injection. This is in contrast to a secondary gas injection process which involves the displacement of a continuous oil phase by gas.

Another term which is often used to refer to a particular tertiary gas injection process is the phrase *Double Displacement Process*. The term Double Displacement Process (DDP) was coined by Carlson (1988) in his discussion of the Hawkins Field operated by Exxon. Carlson (1988) defined DDP as the displacement by gas of a water-invaded oil column. In a non-horizontal system, gas is injected into the up-dip portion of the reservoir to drive the current water oil contact back to its original (pre-production) level. Gas acts to mobilize the oil trapped due to capillary pressure effects in the water invaded zone. In a steeply dipping reservoir, the density differences among the gas, oil, and water tend aid in the drainage process. The oil may accumulate between the gas (up-dip) and water-invaded oil zone (down-dip). The oil bank grows as oil drains to the bottom of the gas-invaded zone and flows down-dip. The oil bank can be produced once it reaches a down-dip production well.

The key parameters in the economic success of any enhanced oil recovery (EOR) process is the oil production rate as a function of time from the start of gas injection. A long delay between the initial injection and the initial production response and a low oil production rate will both adversely affect the economic viability of the process. Even though numerous laboratory studies have proven that oil can be efficiently displaced in this type of process, implementation in the field has been less successful. If the double displacement process is initiated in a dipping bed, the sweep efficiency should be maximized if the gas is injected slowly enough that the gas-fluid interface remains stable and approximately horizontal.

Gravity segregation of the oil and gas behind the front will tend to drive the oil down-dip and the gas up-dip behind the advancing gas front. A key parameter in conventional modelling of the drainage rate of oil in any process is the relative permeability to oil as a function of fluid saturation.

Currently, Amoco, in partnership with the U. S. Department of Energy, is conducting a field test of the Double Displacement Process in a portion of the West Hackberry Field in Cameron Parish, Louisiana. Although this is not the first time the DDP has been implemented on a field-wide level, this is the first instance of using air as the injection fluid in the DDP. In theory, the use of air should improve the economics of the process by both reducing the operating costs and accelerating recovery of the oil. Operating costs are reduced since air is less expensive and more accessible than other gases, such as carbon dioxide and natural gas. Amoco further expects that the recovery process will be accelerated by in-situ combustion of the air in the presence of hydrocarbons at high temperature and pressure. Although the past DDP projects have been a technical success in that significant volumes of tertiary oil were recovered, the projects have been less successful economically due to delayed oil recovery. Amoco hopes to demonstrate that the DDP can be both a technical and economic success if air is used as the injection fluid. To make a distinction between the DDP combined with in-situ-combustion (as for West Hackberry Tertiary Project) and the DDP without thermal effects, I will refer to the DDP at West Hackberry as the *West Hackberry Process*.

As part of a technology transfer agreement among Amoco, the U. S. Department of Energy (DOE), and Louisiana State University (LSU), independent research on regarding the tertiary recovery of oil by up-dip gas injection is currently being conducted at LSU. In 1995, a physical linear modelling study of the process was conducted at elevated temperature and pressure in both unconsolidated and consolidated vertically-oriented porous media (Lepski, 1995). The study conducted by Lepski (1995) showed that residual oil remaining after a waterflood can indeed be re-mobilized by up-dip gas injection.

The objective of the current study is to develop a method for estimating the relative permeability to oil for use in modelling of a double displacement process in a high permeability, strongly water-wet sandstone reservoir. To investigate mechanisms involved in the tertiary recovery of oil by up-dip gas injection, the published literature was surveyed for laboratory and field studies investigating the displacement of waterflood residual oil by gas and for information related to gravity drainage and surface forces among fluids. To develop a method for modelling the oil relative permeability for the double displacement process, the literature was also surveyed for existing three-phase relative permeability models and correlations. A goal strived for during the development of the proposed relative permeability model was use of a function which could be easily implemented in any of the available commercial reservoir simulators.

The review of literature revealed a series of both theoretical and laboratory studies investigating the pore-level mechanisms involved in a horizontal double displacement process and another series of both theoretical and laboratory studies investigating the relative permeability to oil during a vertical double displacement process. Based on the results reported in these studies, a simple power-law relationship relating the relative permeability of oil to the oil saturation was developed. A one-dimensional, numerical model which included the effects of gravity and capillarity was then developed to test the proposed oil relative permeability function using the data collected previously by the LSU-Amoco Technology Transfer Project Research Team (Lepski, 1995).

Once the oil relative permeability function had been tested and verified using the available experimental data, a simplified approach for applying the oil relative permeability function was developed. This simplified approach can be used to predict the oil rates which could be achieved during up-dip gas injection into a water-invaded, anisotropic, stratified reservoir. As a means of illustrating its application, this simplified approach has been applied to one of the fault blocks involved in the West Hackberry Tertiary Project. This simplified approach applies only to a gravity-stable gas injection process which is steady-state at reservoir conditions. This approach neither considers the gas solubility in the oil phase nor the resulting changes in oil properties. It also does not account for the stripping of the lighter components of the oil phase to the gas phase. Also neglected in this simplified approach are the effects of in situ combustion which may occur if air is the injected fluid.

These limitations are considered to be acceptable in view of the unusual difficulty in accurately describing the reservoir inhomogeneity, the effects of which are generally much more important. By performing a sensitivity study on those parameters which are believed to be beneficially affected by gas solubility and in situ combustion (if applicable), the beneficial effects of these factors on oil recovery may be bracketed. The other simplifying assumptions (gravity-stable, steady-state, no stripping) will tend to provide the most optimistic estimate of oil recovery. Since this approach would tend to predict an upper limit on the oil recovery which could be expected for a given reservoir lacking any unidentified inhomogeneities beneficial to the process, the techniques presented in this work could be applied as a tool for screening candidates for tertiary oil recovery by up-dip gas injection.

The following body of work includes (1) a chronological summary of previously published field and laboratory studies which pertain directly to the mobilization of residual oil by gas injection, (2) a discussion of the efficiency of oil recovery by gas injection based on both field and laboratory observations, (3) a discussion of interfacial forces and the mechanisms involved in the displacement of residual oil, (4) a summary of the currently available relative permeability correlations and models, (5) a discussion of the development of the proposed relative permeability functions for the tertiary up-dip gas injection process, (6) a discussion of the implications of the proposed relative permeability functions on oil recovery, and (7) a summary of the study which provides conclusions and recommendations for future work.

FOSSIL ENERGY

RECEIVED
OCT 30 1996
OSTI

DOE/BC/14959-21
(DE96001255)

REVITALIZING A MATURE OIL PLAY: STRATEGIES FOR FINDING AND PRODUCING UNRECOVERED OIL IN FRIO FLUVIAL-DELTAIC SANDSTONE RESERVOIRS OF SOUTH TEXAS

Final Report

By
Paul R. Knox, Mark H. Holtz, Lee E. McRae,
Tucker F. Hentz, Jeffrey G. Paine, W. Gerald White,
and Chun Yen Chang

September 1996

Performed Under Contract No. DE-FC22-93BC14959

Bureau of Economic Geology The
University of Texas at Austin
Austin, Texas

Bartlesville Project Office
U. S. DEPARTMENT OF ENERGY
Bartlesville, Oklahoma

MASTER
DISTRIBUTION OF THIS DOCUMENT IS UNLIMITED

DISCLAIMER

This report was prepared as an account of work sponsored by an agency of the United States Government. Neither the United States Government nor any agency thereof, nor any of their employees, makes any warranty, expressed or implied, or assumes any legal liability or responsibility for the accuracy, completeness, or usefulness of any information, apparatus, product, or process disclosed, or represents that its use would not infringe privately owned rights. Reference herein to any specific commercial product, process, or service by trade name, trademark, manufacturer, or otherwise does not necessarily constitute or imply its endorsement, recommendation, or favoring by the United States Government or any agency thereof. The views and opinions of authors expressed herein do not necessarily state or reflect those of the United States Government.

This report has been reproduced directly from the best available copy.

Available to DOE and DOE contractors from the Office of Scientific and Technical Information, P.O. Box 62, Oak Ridge, TN 37831; prices available from (615) 576-8401.

Available to the public from the National Technical Information Service, U.S. Department of Commerce, 5285 Port Royal Rd., Springfield VA 22161

DOE/BC/14959-21
Distribution Category UC-122

Revitalizing a Mature Oil Play: Strategies For Finding and Producing Unrecovered Oil in Frio Fluvial-Deltaic Sandstone Reservoirs of South Texas

Final Report

By
Paul R. Knox, Mark H. Holtz, Lee E. McRae,
Tucker F. Hentz, Jeffrey G. Paine, W. Gerald White,
and Chun-Yen Chang

September 1996

Work Performed Under Contract No. DE-FC22-93BC14959

Prepared for
U.S. Department of Energy
Assistant Secretary for Fossil Energy

Chandra Nautiyal, Project Manager
Bartlesville Project Office
P.O. Box 1398
Bartlesville, OK 74005

Prepared by
Bureau of Economic Geology
The University of Texas at Austin
Austin, Texas 78713-8924

DISTRIBUTION of this document is unlimited

DISCLAIMER

Portions of this document may be illegible in electronic image products. Images are produced from the best available original document.

CONTENTS

ABSTRACT 1

EXECUTIVE SUMMARY 2

INTRODUCTION 4
P.R. Knox and L.E. McRae

Importance of Integrated Characterization to U.S. Resource Base 6

Near-Term Domestic Oil Resources 6

Causes of Unrecovered Mobile Oil in FDD Reservoirs 8

Stratigraphic Architecture and Scales of Reservoir Heterogeneity 8

Compartmentalization in Fluvial-Deltaic Reservoirs 12

Recovery Potential of Fluvial-Deltaic Sandstone Reservoirs 14

Project Objectives and Approach 17

Project Description 20

PLAYWIDE RESERVOIR STUDIES 24
M.H. Holtz and L.E. McRae

Overview 24

Location and Characteristics of Fields within the Play 24

Production History 24

Regional Structural and Stratigraphic Setting 28

Upper Vicksburg-Frio Genetic Sequence 31

Preliminary Assessment of Reserve Growth Potential in Frio Oil Reservoirs 34

Stratigraphic Distribution of Additional Oil Potential 37

Methodology 37

Strategies for Reservoir Classification 38

Upper Vicksburg Reservoirs 40

Lower Frio Reservoirs 40

Middle Frio Reservoirs 42

Distribution of Remaining Recoverable Oil 42

RESERVOIR CHARACTERIZATION EXAMPLES FROM RINCON FIELD 45
L. E. McRae, M. H. Holtz, T. F. Hentz, and C. Chang

Introduction 45

Location and Geologic Setting of Rincon Field 46

Selection of Reservoirs for Detailed Study 48

Reservoir Characterization Methodology 49

Determine Reservoir Architecture 49

Importance of the Genetic Sequence Analysis Approach 49

Ascertaining Internal Reservoir Stratigraphy 51

Regional Stratigraphy 52

Upper Vicksburg reservoirs 53

Lower Frio reservoirs 53

Middle Frio reservoirs 54

Description of Lithofacies from Core 54

Mudstones 58

Sandstones 59

Petrographic Studies 61

Overview 61

Methods 61

Texture 62

Framework mineralogy 62

Detrital clay matrix 65

Cements 66

Porosity 67

Diagenetic sequence 68

Determination of Finest Scale Genetic Units 69

Correlation of bounding surfaces and reservoir genetic units 69

Sandstone Geometry and Depositional History 70

Frio E reservoir units 70

Frio D reservoir units 73

Establish Fluid-Flow Trends in the Reservoir 74

Initial Fluid Properties 74

Field Production History 74

Evaluation of Areal Trends of Past Oil Production 75

Integrating Fluid-Flow Trends in the Reservoir 78

Identifying Correspondence Between Stratigraphy, Structure, and Fluid-Flow Trends 78

Effect of Sandstone Geometry on Oil Production 78

Matching Stratigraphy with Reservoir Production 79

Reservoir development patterns within the Frio E reservoir 79

Reservoir development patterns within the Frio D reservoir 85

Reservoir Petrophysical Model Development 90

Porosity and Permeability Modeling 90

Porosity and permeability distribution for primary facies types 91

Well log analysis 93

Analysis of modern logs 94

Analysis of old logs 97

Fluid Saturation Modeling 98

Formation resistivity factor 98

Capillary pressure modeling 101

Residual oil saturation 103

Reserve Growth Potential 103

Conclusions 105

T-C-B FIELD RESERVOIR STUDIES 107
P. R. Knox and J. G. Paine

Introduction 107

Location, History, and Geologic Setting of T-C-B Field 108

Location 108
Development History 109
Stratigraphic Framework 109
Methodology 113
Outcrop-Based Models for Predicting Reservoir Architecture 113
Geological Reservoir Characterization Methods 117
Geophysical Reservoir Characterization Methods 118
Acquisition, processing, and analysis 118
Limits of horizontal and vertical resolution 119
Tying seismic data to stratigraphic markers 121
Lithologic source of amplitude peaks 125
Characterization Examples from the Scott/Whitehill Reservoir Interval 126
Genetic Stratigraphic Setting of the Scott/Whitehill Interval 126
Architecture of Reservoirs within the Scott/Whitehill Depositional Cycle 128
Geophysical Identification of Scott/Whitehill Architecture 132
Scott/Whitehill Internal Heterogeneity 135
Reserve-Growth Opportunities 137
Accommodation-Based Predictive Model for Reserve-Growth Potential in Upper Delta-Plain Fluvial Reservoirs 141
A Cautionary Note 144
Uses of the Model 144
Implications 146
RESERVOIR PRIORITIZATION 147
P. R. Knox
Quick-look Evaluation Factors 147
The Formula 151
Limitations 152

TECHNOLOGY TRANSFER ACTIVITIES 154
P. R. Knox and W. G. White

Presentations 154

Publications 156

Short Courses 157

Planned One-Day Courses 157

PTTC/TIPRO Workshop 158

GRI Ferron Field Trip 159

Reservoir Characterization Advisor Software 160

Introduction 160

Software Development 161

Distribution 162

ACKNOWLEDGMENTS 163

REFERENCES 164

APPENDICES 172

FIGURES

1. Histogram of remaining-oil-in-place and abandonment potential for U.S. clastic reservoirs, by depositional setting 5

2. Distribution of original-oil-in-place in fluvial-dominated reservoirs 7

3. Examples of scales associated with the various levels of heterogeneity present in fluvial-deltaic reservoirs 10

4. Analytical tools used in the description of reservoir heterogeneity at various scales 11

5. Schematic geologic cross section contrasting the generalized interpretation of a sandstone reservoir as a simple, laterally continuous (homogeneous) producing zone with a more detailed interpretation of the same sandstone unit as a complex heterogeneous zone consisting of multiple reservoir compartments 16

6. Diagram of work structure for this project illustrating three primary phases and a breakdown of individual tasks associated with each phase of the project 21

7. Location map of major oil and gas fields in the Frio Fluvial-Deltaic Sandstone Play in South Texas 25

8. Distribution of the oil resources within reservoirs of the Frio Fluvial-Deltaic Sandstone (Vicksburg Fault Zone) play in South Texas 26

9. Histograms illustrating trends in reservoir discovery, reservoir abandonment, and decline in annual production in the Frio Fluvial-Deltaic sandstone oil play 27

10. Stratigraphic column of Cenozoic sediments of the South Texas Gulf Coast 29

11. Schematic cross section of the South Texas Gulf Coast Basin 30

12. General distribution of the Norias delta and Gueydan fluvial depositional systems responsible for deposition of the Frio stratigraphic unit 30

13. Distribution of aggradational and progradational intervals of the Frio Formation along the Vicksburg Fault Zone oil play 32

14. Stratigraphic subdivisions for reservoirs in the Frio Fluvial-Deltaic Sandstone Play and summary of genetic sequence context, reservoir characteristics, oil production, and estimates for remaining oil potential in middle and lower Frio reservoirs 33

15. Histograms illustrating distributions for values of porosity, initial water saturation, residual oil saturation, net pay, and area from reservoirs throughout the Frio Fluvial-Deltaic Sandstone Play in South Texas 35

16. Probability distribution curves illustrating the cumulative probability of original oil in place, original residual oil, original mobile oil, and remaining mobile oil for the Frio Fluvial/Deltaic Sandstone play 37

17. Map of south Texas showing location of fields within the Frio Fluvial-Deltaic Sandstone Play along the Vicksburg Fault Zone 38

18. Cumulative frequency histograms illustrating the differences in the distribution of values of porosity, initial water saturation, net pay, and reservoir area for middle Frio, lower Frio, and Vicksburg reservoir sandstones in the Frio Fluvial-Deltaic Sandstone Play 41

19. Distribution of the location of oil resources within reservoirs of the Frio Fluvial-Deltaic Sandstone Play in South Texas 44

20. Location map of Rincon field within the Frio Fluvial-Deltaic Sandstone Play and area of field selected for detailed reservoir studies 47

21. Generalized west-to-east cross section through Rincon field illustrating structural setting of a representative field in the Frio Fluvial-Deltaic Sandstone Play 48

22. Spontaneous Potential/resistivity type logs illustrating the general depositional sequence for the productive Frio–upper Vicksburg reservoir interval, the stratigraphic context of the middle Frio reservoir sequence in Rincon field, and the reservoir nomenclature of individual producing units within the Frio D–E interval selected for detailed study 51

23. Depositional systems and reservoir attributes of the Rincon field reservoir section 52

24. General distribution of the Norias delta and Gueydan fluvial depositional systems responsible for deposition of the Frio stratigraphic unit 55

25. Graphic core log, T. B. Slick 231:149 well, Frio E reservoir zone, along with corresponding facies interpretations, core analysis data for porosity and permeability, and location of samples selected for petrographic and special core analyses 56

26. Graphic core log, T. B. Slick 231:133 well, Frio D reservoir zone, along with corresponding facies interpretations, core analysis data for porosity and permeability, and location of samples selected for petrographic and special core analyses 57

27. Graphic core log, T. B. Slick 231:133 well, Frio E reservoir zone, along with corresponding facies interpretations, core analysis data for porosity and permeability, and location of samples selected for petrographic and special core analyses 58

28. Ternary diagrams showing composition of Rincon D and E reservoir sandstones from thin-section petrography 63

29. Diagenetic sequence diagram, Rincon D and E reservoir sandstones 67

30. Representative SP/resistivity log illustrating succession of stacking patterns developed within the Frio E and D reservoir units 71

31. Series of net sandstone isopach and facies maps showing changes in the distribution of facies and sandstone facies geometry for the Frio E-4, E-3, E-2, and E-1 reservoir units and Frio D-6, D-5, D-4, and D-3 reservoir units 72

32. Comparison maps illustrating differences in overall reservoir geometry and distribution of production, Frio D and E reservoir zones 76

33. Map illustrating sandstone thickness distribution, corresponding reservoir facies geometry, productive limits, and level of development, Frio E-4 reservoir unit 80

34. Map illustrating sandstone thickness distribution, corresponding reservoir facies geometry, productive limits, and level of development, Frio E-3 reservoir unit 81

35. Map illustrating sandstone thickness distribution, corresponding reservoir facies geometry, productive limits, and level of development, Frio E-2 reservoir unit 82

36. Map illustrating sandstone thickness distribution, corresponding reservoir facies geometry, productive limits, and level of development, Frio E-1 reservoir unit 83

37. Map illustrating sandstone thickness distribution, corresponding reservoir facies geometry, productive limits, and level of development, Frio D-6 reservoir unit 86

38. Map illustrating sandstone thickness distribution, corresponding reservoir facies geometry, productive limits, and level of development, Frio D-5 reservoir unit 87

39. Map illustrating sandstone thickness distribution, corresponding reservoir facies geometry, productive limits, and level of development, Frio D-4 reservoir unit 88

40. Map illustrating sandstone thickness distribution, corresponding reservoir facies geometry, productive limits, and level of development, Frio D-3 reservoir unit 89

41. Histograms illustrating the distribution of porosity and permeability values according to each of the mapped reservoir facies 92

42. Nonlinear regression analysis on a facies-by-facies scale results in an equation to predict permeability from porosity 93

43. Core graphic log; porosity and permeability data; and gamma-ray, induction, and porosity logs, T. B. Slick 231:149 well 95

44. Comparison of shale-corrected and uncorrected cross-plot porosity versus core porosity 96

45. Results of the multiple nonlinear regression model for predicting FRF 101

46. Initial water saturation is modeled from a multi-nonlinear regression equation with porosity, permeability, and height above free-water as the independent variables 102

47. Residual oil saturation measured from core flood tests indicates a wide range of possibilities due to high and low tails on the distribution 104

48. Map of study area in T-C-B field showing lease boundaries and approximate location of geoseismic section 108

49. Location of Tijerina-Canales-Blucher (T-C-B) field within the Frio Fluvial-Deltaic Sandstone (Vicksburg Fault Zone) Play in South Texas 110

50. Representative log from T-C-B field illustrating generalized stratigraphy and nomenclature of productive reservoir sandstones 111

51. Northwest-to-southeast geoseismic dip section across T-C-B field illustrating the general structural setting of Frio and Vicksburg reservoir sections 112

52. Genetic stacking pattern and architecture of the Cretaceous (Turonian) Ferron Sandstone of central Utah 115

53. Major inlines (east-west), crosslines (north-south), well locations, and lease block boundaries within the T-C-B three-dimensional seismic data set provided by Mobil 119

54. Two-way time versus depth established from checkshot surveys in the Blucher B-3 well in the eastern part of the data volume and the Blucher 51-R well in the western part of the data volume 120

55. Frequency content for stacked data from inline 315 121

56. Effect of adding the wavelets A and B after they reflect from similar interfaces A and B that are separated by 50, 100, and 125 ft 122

57. Synthetic seismogram constructed from sonic and density logs for the Blucher B-3 well and tied to seismic data from inline 315 123

58. Representative dip line that extends east-west across the data volume 124

59. Downward changes in resistivity plotted against downward changes in acoustic impedance at the same well log level 125

60. Arbitrary seismic strike section A–A′ with overlain time-converted well logs from the Stewart-Jones 1-5, Stewart-Jones 1-7, Blucher 55, and Blucher 37 wells 127

61. Dip-oriented stratigraphic cross section A–A′ through the Frio Formation from updip of T-C-B field down to the present coastline 128

62. Dip-oriented stratigraphic cross section B–B′ of the Scott/Whitehill 4th-order reservoir interval, which contains at least four 5th-order depositional cycles 129

63. Structure, net sandstone, and infill-potential maps, Scott/Whitehill reservoirs 130

64. Upper Whitehill structure map in two-way time 133

65. Amplitude display of time slice within the Upper Whitehill interval at 1508 ms (about 6,300 ft deep) 134

66. Net sandstone and facies map for the Upper Whitehill interval derived from log data alone 135

67. Cross plot of initial water cut versus depth to top of reservoir, upper Scott zone 138

68. Map showing reservoir compartment distribution, productive limits, identified recompletion/infill opportunities, and results of one recompletion within the upper Whitehill reservoir of T-C-B field 139

69. Model for upper delta-plain fluvial architecture under the range of accommodation conditions experienced during a depositional cycle 142

70. Spectrum of upper delta-plain fluvial reservoir architecture, internal heterogeneity, production characteristics, and reserve-growth potential encountered in the Scott/Whitehill interval 145

71. The effect of past completion density on reserve growth potential 149

72. Influence of position within a depositional cycle on delta style and reservoir architecture 150

Tables

1. Scales of reservoir heterogeneity 13

2. Reservoir compartment terminology 15

3. Spectrum of reservoir heterogeneity and resulting recovery potential in clastic reservoirs 18

4. Summary of project objectives 19

5. Significant accomplishments in Project Year 1: 1992–1993 22

6. Significant accomplishments in Project Year 2: 1993–1994 22

7. Significant accomplishments in Project Year 3: 1994–1995 23

8. Strategies for play-scale reservoir characterization studies 34

9. Statistics for reservoir parameters grouped by oil and combined oil and gas data sets 36

10. List of major oil fields in the Frio Fluvial-Deltaic Sandstone Play. 39

11. Summary of petrographic data for Rincon sandstones 64

12. Representative saturation exponents from the Frio Fluvial-Deltaic Sandstone play 98

13. Special core analysis and descriptive statistics for core samples in Rincon field 100

14. Initial potential and cumulative production data for completions within the upper Scott zone 137

15. Summary of recompletion opportunities in Whitehill reservoir, T-C-B field 140

16. Potential effects on reservoir architecture of position within 4th- and 5th-order cycles 150

ABSTRACT

Domestic fluvial-dominated deltaic (FDD) reservoirs contain more than 30 Billion barrels (Bbbl) of remaining oil, more than any other type of reservoir, approximately one-third of which is in danger of permanent loss through premature field abandonments. The U.S. Department of Energy has placed its highest priority on increasing near-term recovery from FDD reservoirs in order to prevent abandonment of this important strategic resource. To aid in this effort, the Bureau of Economic Geology, The University of Texas at Austin, began a 46-month project in October, 1992, to develop and demonstrate advanced methods of reservoir characterization that would more accurately locate remaining volumes of mobile oil that could then be recovered by recompleting existing wells or drilling geologically targeted infill wells.

Reservoirs in two fields within the Frio Fluvial-Deltaic Sandstone (Vicksburg Fault Zone) oil play of South Texas, a mature play which still contains 1.6 Bbbl of mobile oil after producing 1 Bbbl over four decades, were selected as laboratories for developing and testing reservoir characterization techniques. Advanced methods in geology, geophysics, petrophysics, and engineering were integrated to (1) identify probable reservoir architecture and heterogeneity, (2) determine past fluid-flow history, (3) integrate fluid-flow history with reservoir architecture to identify untapped, incompletely drained, and new pool compartments, and (4) identify specific opportunities for near-term reserve growth. To facilitate the success of operators in applying these methods in the Frio play, geologic and reservoir engineering characteristics of all major reservoirs in the play were documented and statistically analyzed. Finally, to assist operators in identifying those reservoirs most prospective for reserve growth, and therefore most worthy of detailed characterization efforts, a quantitative quick-look methodology was developed to prioritize reservoirs in terms of reserve-growth potential.

Extensive efforts have been made to transfer the methodology and results of this study to operators within the Frio play, as well as to all operators of fluvial-deltaic reservoirs. One half-day and two full-day workshops were held in cities convenient to Frio operators to demonstrate the methodology through lectures and exercises and answer any questions or concerns about its application. Throughout the course of the study, 16 presentations and 15 publications have been completed to keep operators and researchers across the country, as well as the DOE, informed about project progress and results. Additionally, a microcomputer-based software program titled the Reservoir Characterization Advisor-Fluvial-Deltaic (RCA-FD) has captured the integrated reservoir characterization method and results in a user-friendly format that includes opportunities for input and quick-look prioritization evaluation of operator data.

EXECUTIVE SUMMARY

This volume summarizes work done by the Bureau of Economic Geology, The University of Texas at Austin, over a 46-month period as part of the U.S. Department of Energy (DOE) Oil Recovery Field Demonstration Program, Class I (Near-Term). The goal of the program, and this project, is to increase oil production from domestic fluvial-deltaic reservoirs in the near term to prevent their premature abandonment and the resulting permanent loss of resources to the United States. Specifically, this project developed and demonstrated 'an •integrated,intiltidisciplinary advanced reservoir characterization methodology that can aid operators in locating areas of untapped or incompletely drained reservoirs. These areas can then be targeted 'for near-term production through the recompletion of existing wells or the drilling of new infill wells.

Nearly 11 billion barrels (Bbbl) of mobile oil, approximately equivalent to original mobile oil in Prudhoe Bay field of Alaska, remain in domestic fluvial-dominated deltaic reservoirs despite their mature status (personal communication, Mark Young, DOE Bartlesville Project Office, 1996). Approximately 1.6 Bbbl of this resource, approximately 15 percent of the domestic total, reside in reservoirs of the Frio Fluvial-Deltaic Sandstone Play (Vicksburg Fault Zone) in Texas. The project summarized herein has provided operators within this play with models of interwellscale reservoir architecture and heterogeneity that are supported by specific examples of reserve-growth opportunities within Frio fields. These models are based on integrated geological, geophysical, and engineering characterization of stratigraphically complex Frio reservoirs and are applicable to fluvial-deltaic reservoirs throughout the United States.

A conservative estimate of mobile oil identified during this study of 12 major reservoirs is 4.7 million barrels. Numerous recompletion and infill opportunities have-been identified to operators for potential action. Results of the first action by an operator support the validity of project methodology: a recompletion recommended by this study in a well identified as being within an incompletely drained reservoir compartment has yielded economic production rates of 600 thousand cubic ft of gasper day.

The methodology developed and applied in this project requires an investment in personnel time and data acquisition that is substantial for many small operators. As a consequence, operators must make an initial effort to evaluate their reservoirs to determine which ones likely contain significant remaining resources. This project has developed a methodology by which reservoirs can be quickly and semiquantitatively ranked in terms of their reserve growth potential. Parameters used in the evaluation are designed to be readily available to the typical operator, preventing a loss of time in extensive data-gathering efforts. This methodology has been incorporated into the Reservoir Characterization Advisor-Fluvial Deltaic software package as an interactive routine that calculates reservoir priority on the basis of data input by the operator.

The technology and methodology used in this project have been transferred to Texas operators through inexpensive workshops at sites convenient to the majority of companies and through technical presentations and publications at the local level. Presentations at national technical meetings have made technologies and results available to all domestic operators, and the methodology has been made publicly available through production of the Reservoir Characterization Advisor-Fluvial Deltaic (RCA-FD), a software package for use in personal computers.

This project has met its goal of developing and demonstrating an advanced, integrated, multidisciplinary methodology of reservoir characterization to identify opportunities for near-term recovery of resources in fluvial-deltaic reservoirs. The current and expected future success of recompletions and infill wells based on this study provide convincing evidence to operators that detailed integrated characterization can revitalize mature fields and prevent the loss of domestic resources because of premature abandonment of fields.

INTRODUCTION

P.R. Knox and L.E. McRae

Data from the U.S. Department of Energy (DOE) TORTS database indicate that domestic fluvial-dominated deltaic (FDD) reservoirs contain 30 billion barrels (Bbbl) of remaining oil in place, more than almost any other reservoir type, and that more than one-third of this strategic domestic resource is in near-term danger of being lost because of premature field abandonment (Figure 1). As a consequence, the U.S. DOE has placed a high priority on activities that will preserve access to these fields by increasing production in the near future. Texas was identified as the state having the largest near-term incremental recovery potential in such reservoirs (616 million barrels total) (U.S. DOE, 1991, Ch. 2).

To respond to this urgent need for increased production from FDD reservoirs, the Bureau of Economic Geology, The University of Texas at Austin, began a 46-month project in October, 1992, to develop and demonstrate to operators methods that could quickly improve oil production. As a laboratory for demonstration, the Bureau selected the most prolific fluvial-deltaic play on the Texas Gulf Coast, the Frio Fluvial-Deltaic Sandstone,(Vicksburg Fault Zone). Because recompletion of existing wells and" drilling of infill wells is the most significant and least expensive method for improving production in FDD reservoirs, the Bureau focused its efforts on developing and demonstrating techniques for multidisciplinary advanced reservoir characterization that can identify the location and volume of unrecovered mobile oil and lead to cost-effective reserve growth.

This report summarizes the results of the Bureau's 46-month project. The introductory section is a review of project objectives and approach. In following sections, the methodology developed for integration of geology, geophysics, and engineering in reservoir characterization is demonstrated with selected examples from studied reservoirs. In addition, the distribution of values for geologic and engineering attributes of reservoirs throughout the play is provided to support estimates of the volume of oil resources remaining in the play and the reserve growth potential of reservoirs in the play. Because integrated characterization efforts consume precious

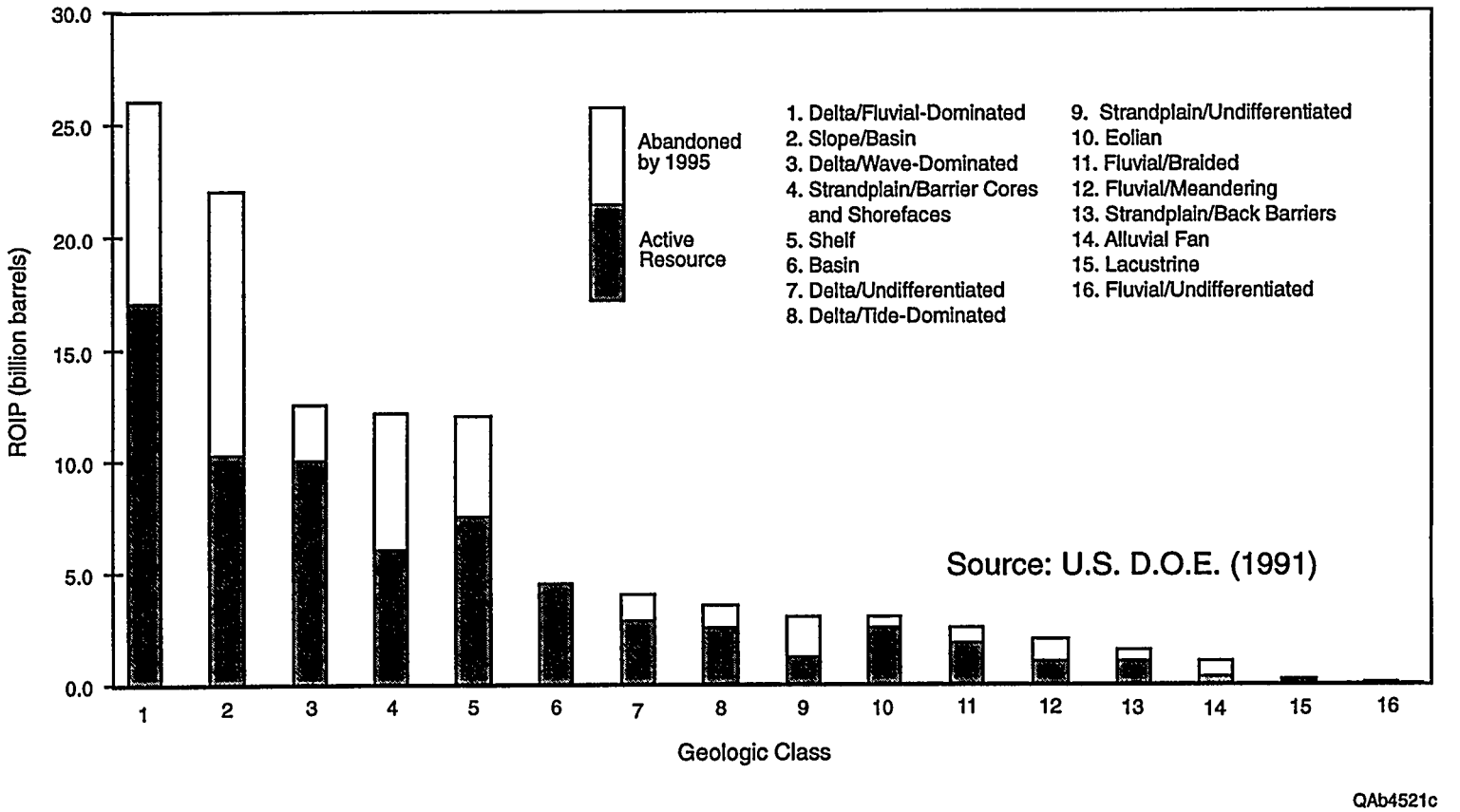

Figure 1. Histogram of remaining-oil-in-place and abandonment potential for U.S. clastic reservoirs, by depositional setting. In 1991, fluvial-dominated deltaic settings account for the greatest remaining resource, at over 25 billion barrels in place. A large percentage of this resource is threatened by premature reservoir abandonment. Once abandoned, any resources remaining are essentially lost forever because of the high cost of replacing producing infrastructure. Data from the U.S. Department of Energy (1991).

time and money for operators, some comments on criteria that can be used to select the most prospective reservoirs in a mature field for detailed study are given. Finally, our efforts to transfer this information to operators and encourage the application of this methodology to increase production are presented.

Importance of Integrated Characterization to U.S. Resource Base

Near-Term Domestic Oil Resources

Remaining domestic oil resources represent an important energy reserve for the United States. Because liquid hydrocarbons are expected to remain the principal source of energy for our society well into the coming century, and because secure inexpensive energy supplies are critical to economic growth, we must protect and husband our domestic oil resources. A large percentage of these resources reside in mature fields where production costs are inherently higher than newer fields because of greater water production and disposal costs. Under current management practices, in fact, many of these fields are nearing uneconomic status and may be abandoned, despite the fact that they contain large volumes of oil that, together, represent a critical domestic resource. Once they are abandoned, reestablishing access to these resources is rarely economically feasible because of the cost of reinstalling infrastructure. As a consequence, their loss is essentially permanent.

The U.S. DOE has recognized this danger and established a program to maintain access to these resources. This program fosters research into methods that can increase production from these fields in the near term, thus revitalizing their economic outlook and preventing premature abandonment. The DOE has divided remaining resources into classes on-the basis of the original depositional setting of the reservoir rock and prioritized these classes by volume of remaining resource and threat of premature abandonment. Classification by depositional setting was done because the setting exerts a first-order control on the reservoir nature which, in turn, controls the factors that have prevented complete recovery of the resource.

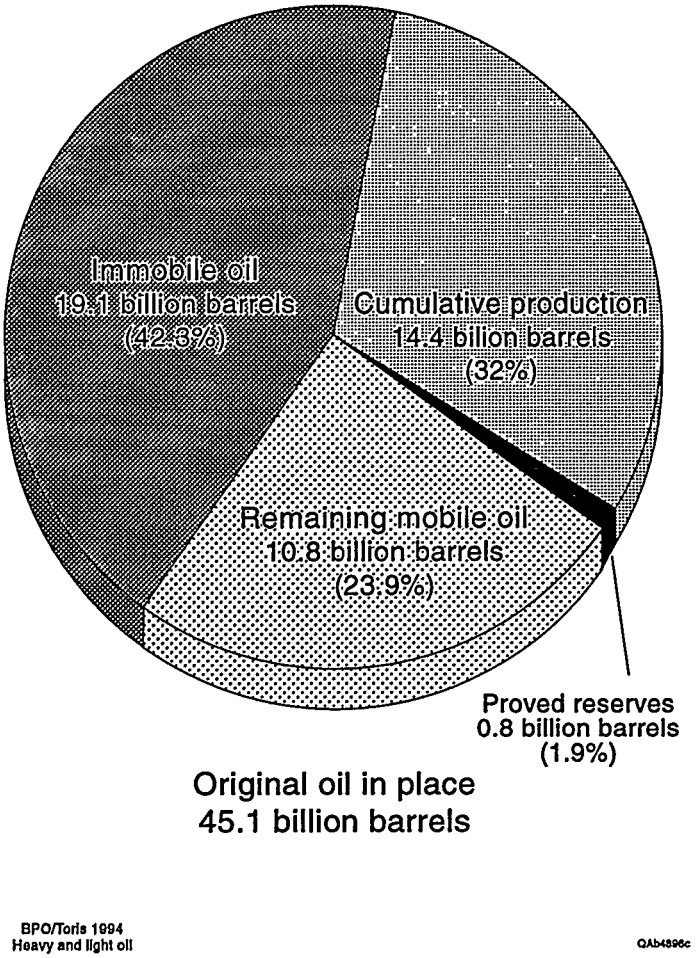

Figure 2. Distribution of original-oil-in-place in fluvial-dominated reservoirs. The volume of mobile oil remaining in these reservoirs, 10.8 billion barrels, is more than 10 times the current proved reserves and represents a resource nearly as significant to the United States as Prudhoe Bay field. Data from U.S. Department of Energy TORIS database (1994)(personal comm., Bartlesville Project Office, 1996).

In 1991, the DOE determined that reservoirs deposited in fluvial-dominated deltaic (FDD) settings (Class I) contained the highest priority resource. They represented the largest volume of remaining oil, more than 25 billion barrels (Bbbl), one-third of which was projected to be abandoned by 1995 (Figure 1). More recent estimates by the DOE were higher still. An analysis of the Tertiary Oil Recovery Information System (TORTS) in 1994 revealed that of 45 Bbbl originally in Class I reservoirs, more than 30 Bbbl remain. More than 19 Bbbl of the remaining oil are immobile (Figure 2) and unrecoverable by conventional low-cost primary or secondary recovery methods. That leaves nearly 11 Bbbl, roughly the size of the Prudhoe Bay discovery, still remaining to be targeted in the near term (Figure 2) by currently economic methods. This represents more than 40 percent of the mobile oil originally in the reservoirs, despite roughly five decades (on average) of production!

Causes of Unrecovered Mobile Oil in FDD Reservoirs

In the past, FDD reservoirs have commonly been developed with wells placed in geometric grids with predetermined spacing. Unfortunately, these reservoirs are not uniformly distributed or internally homogeneous. Instead, reservoir sandstone bodies occur in a range of shapes and sizes. Reservoirs can be separated into these bodies, or compartments, by laterally or vertically intervening shales and each compartment can be internally complex. For example, a sandstone reservoir body (compartment) deposited by a deltaic distributary channel can be narrow and elongated in the dip direction, and can contain many cross-cutting low permeability shale drapes (internal heterogeneities) that inhibit uniform flow of the oil from the reservoir toward the well bore. Consequently, wells drilled on a rigid grid may miss individual bodies in a particular reservoir interval, resulting in untapped compartments. Additionally, wells penetrating a reservoir body may be placed too far apart to efficiently drain it, leading to incompletely drained compartments. In FDD reservoirs, the most expedient way to increase production is to map reservoir compartments using geologic and geophysical information, evaluate their internal heterogeneity by applying engineering methods to production and test data, and identify untapped and incompletely drained compartments that can be targeted through recompletions of existing wells or the careful placement of infill wells. The following sections provide detail on the depositional controls on reservoir architecture and heterogeneity.

Stratigraphic Architecture and Scales of Reservoir Heterogeneity

The architecture of sandstones in clastic reservoirs has a direct impact on hydrocarbon recovery. Internal features within reservoir sandstone units define the geometry of fluid pathways that control the efficiency of hydrocarbon migration to the well bore and therefore provide fundamental constraints on the ultimate volume of conventionally recoverable oil and gas that remain in the ground when the reservoir is abandoned (Tyler and others, 1992). Understanding the details of reservoir architecture and its inherent control on fluid migration is critical to efficiently targeting the remaining recoverable oil resource in maturely developed reservoirs.

The internal geometry of sandstone bodies and the degree of interconnectedness, communication, or compartmentalization between individual reservoir sand bodies are products of the nonuniformity, or heterogeneity, of a rock reservoir (Alpay, 1972). Reservoir structure can be exceedingly complex, containing heterogeneities from scales of kilometers down to scales of less than 1 millimeter (Lasseter and others, 1986). To facilitate studies of the various types of heterogeneities present in rock reservoirs, researchers have arbitrarily divided reservoir heterogeneity into four different classes, or levels, that relate to different scales of investigation (Alpay, 1972; Weber, 1986; Tyler, 1988). These levels of heterogeneity range from the megascopic identification of variations in depositional style and sediment stacking patterns within an entire sedimentary basin sequence, to macroscopic and mesoscopic variations described within an individual depositional unit, to the microscopic study of pore throat variations between grains in a single core (Figure 3). The description and characterization of reservoir heterogeneity at each of these scales require separate methodologies, different data types, and the use of various analytical tools designed to measure and detect heterogeneity at different levels of resolution (Figure 4) (Worthington, 1991; Jackson and others, 1993).

Megascopic studies of reservoir heterogeneity address large-scale relationships between reservoirs that occur within a play trend or field area (basin scale and field scale) and are controlled by regional variations in base level that occur in response to changes in eustasy, sediment supply, subsidence, and climate (Miall, 1988). An understanding of regional-scale variations in reservoir architecture (for example, connected, laterally amalgamated fluvial channels versus isolated, vertically stacked fluvial channels) is important in identifying reservoir analogs within a play and assessing intrafield variations in reservoir quality and recovery efficiency.

Intermediate scales of reservoir heterogeneity include variations at the macroscopic level of the genetic sand unit or depositional facies (for example, point-bar versus crevasse splay deposits) and mesoscale variations within ripple laminae and beds. Microscopic heterogeneity refers to variations at the scale of grains, pores, and pore throats. These small-scale heterogeneities are responsible for variations in capillarity and local fluid-flow pathways that control the nature of oil

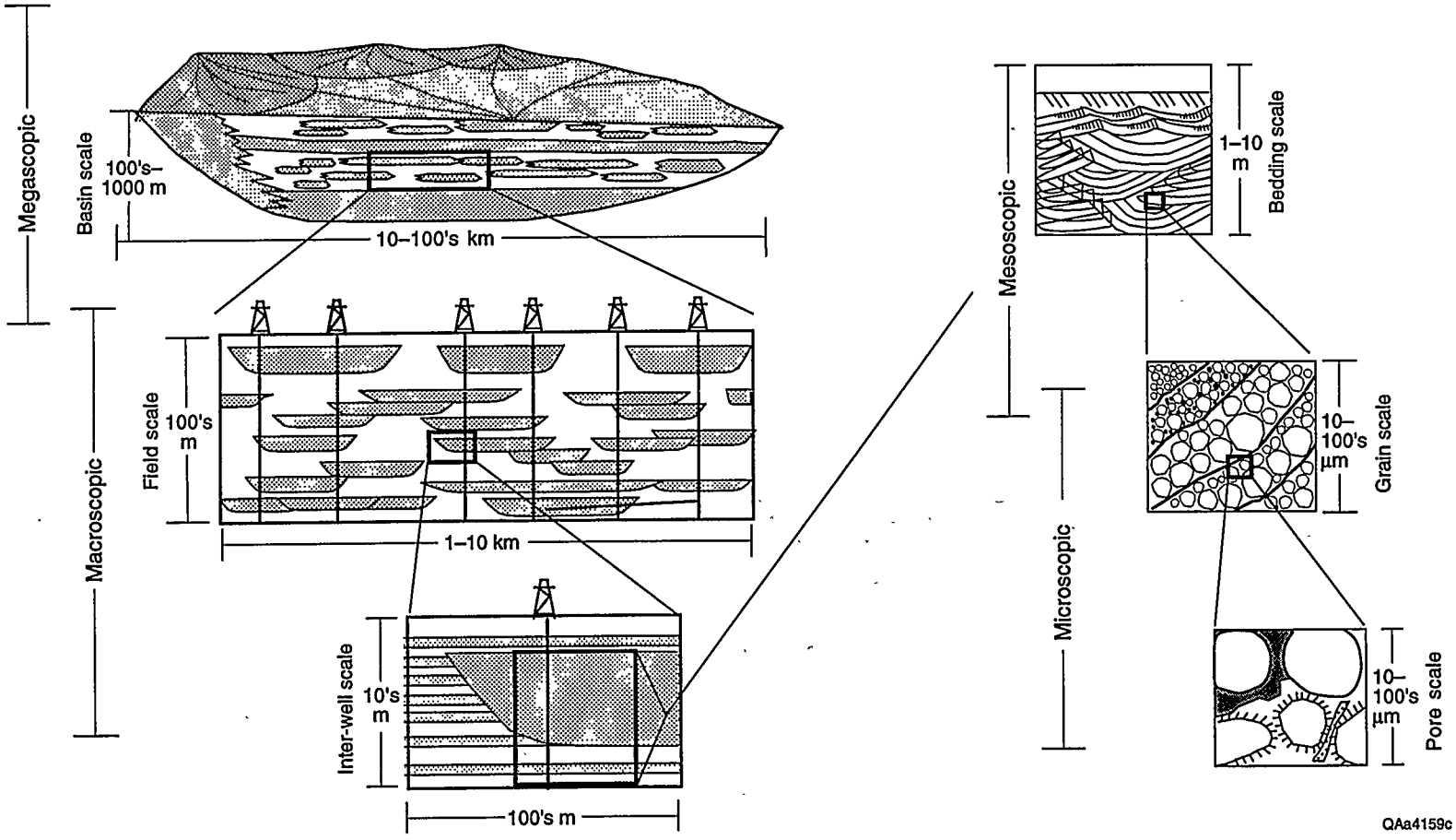

Figure 3. Examples of scales associated with the various levels of heterogeneity present in fluvial-deltaic reservoirs. Compiled from Weber (1986) and Miall (1988).

Scale	Geologic descriptors	Reservoir characterization
Mega-scale	• Basin (providence) • Sub-basin • Formation	1. Composition, grain size variations across basin 2. Reservoir size and boundaries 3. Distribution of reservoir and nonreservoir facies
Macro-scale	• Depostional system • Trap type • Faulting	1. Reservoir compartments 2. Reservoir position, geometry, connectivity 3. Spatial distribution of heterogeneities (baffles, barriers, thief zones) 4. Relationship of lithologic units to flow units
Meso-scale	• Depositional facies • Sedimentary structures • Lithology • Rock fabric (texture)	1. Mean values, ranges of reservoir attributes 2. Core facies studies, core analysis data 3. Relationship of flow units and petrophysical properties with stratigraphy
Micro-scale	• Grain size, sorting, and packing • Mineralogy • Pore size, geometry and network • Cementation Clay content	1. Diagenetic controls on porosity and permeability 2. Controls on initial and residual fluid saturations

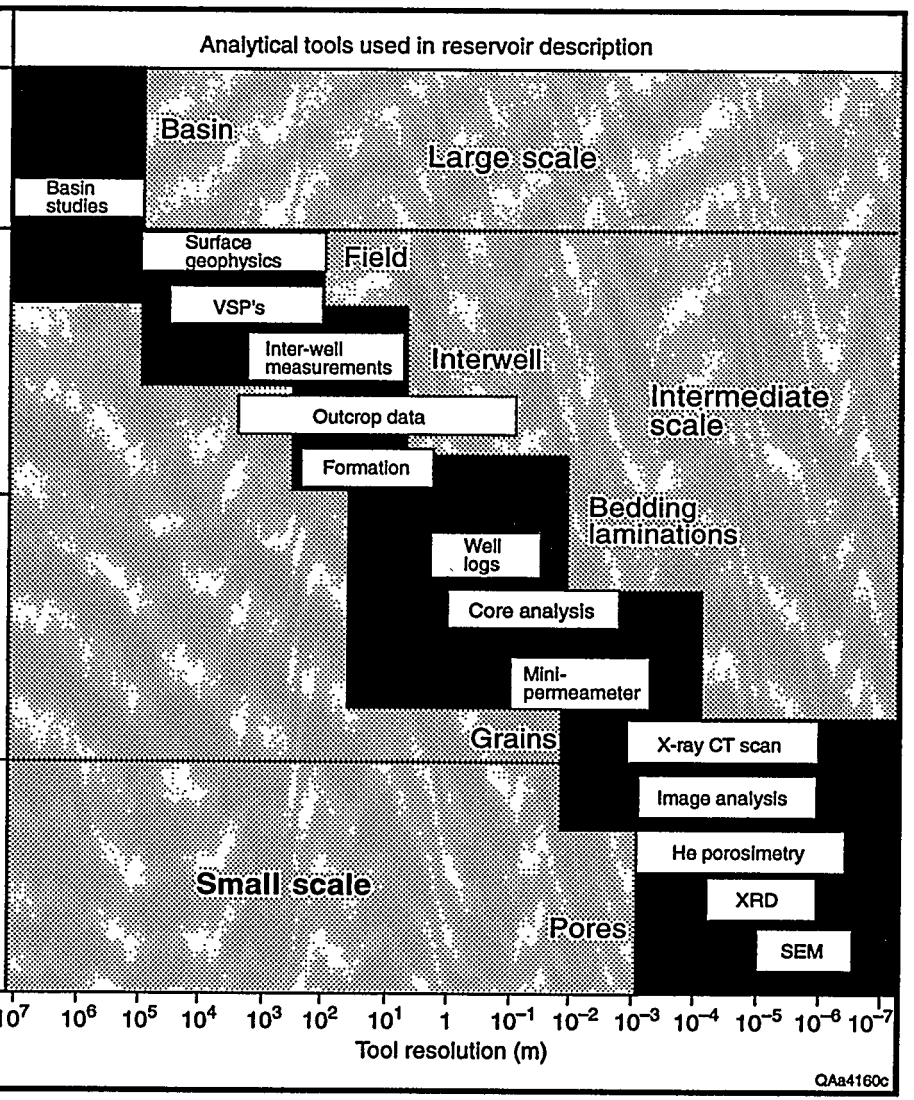

Figure 4. Analytical tools used in the description of reservoir heterogeneity at various scales. Data from Worthington (1991) and Jackson and others (1993).

saturation and the retention of residual oil in the vicinity of the well bore. This level of heterogeneity is largely a function of diagenetic processes.

Heterogeneity in fluvial sandstones has also been described in terms of a hierarchy of bounding surfaces of various scales (Miall, 1988). These range from large-scale sixth-order surfaces that separate depositional sequences; to fifth- and fourth-order surfaces defining major reservoir packages and individual channel units at the interwell level, respectively; to smaller fourth- through first-order bounding surfaces, which are small-scale features recognized at the core level, but their limited lateral extent (<25 acres) precludes correlation at the interwell level. A summary of the various scales and nomenclature associated with reservoir heterogeneity is provided in Table 1.

Compartmentalization in Fluvial-Deltaic Reservoirs

The scale of heterogeneity that is most critical in controlling fluid-flow pathways and is the key to accessing unrecovered mobile oil remaining in the reservoir is the intermediate, interwell, or macroscopic scale of heterogeneity. This level of heterogeneity most closely corresponds to the reservoir flow unit. Macroscopic features include variations in depositional and diagenetic facies that serve to compartmentalize a reservoir. Physical bounding elements that define the permeability structure of a reservoir and divide it into separate flow units include both bedding surfaces as well as nonpermeable rock types that act as intrareservoir seals between individual reservoir compartments (Tyler and Finley, 1991). The types of permeability barriers present and the style and extent of reservoir compartmentalization that they create are directly related to the depositional system. LeBlanc (1977) documented many examples of how the distribution, internal characteristics, and continuity of sandstone reservoirs are primarily controlled by the original environment of deposition.

Stratigraphic compartmentalization that is inherent in fluvial-deltaic depositional systems is responsible for the incomplete and inefficient recovery of available oil and gas resources within a developing field. Various categories of infield reservoir compartments, in addition to those

Table 1. Scales of reservoir heterogeneity.

Level of Heterogeneity and Order of Bounding Surface (Miall, 1988)	**Lateral Dimensions (Width)**	**Vertical Dimensions (Thickness)**	**Depositional Unit**	**Subsurface Correlation (Data Types and Mapping Methods)**
Basin Scale *(6th order)*	10-100's km	100's-1000's m	• Formation • Member	• Regional correlation of wireline logs
Field Scale *(5th order)*	1-10 km	100's m	• Channel (Sheet) sandstones • Channel (Ribbon) sandstones	• Intrafield correlation of wireline logs • 2-D seismic data • Closely spaced logs • 3-D seismic data
Interwell (Intrafield) Scale *(4th, 3rd, 2nd orders)*	100's m	10's m	• Macroforms • Bed cosets	• Core studies, facies analysis
Bedding Scale *(1st order)*		1-10 m	• Individual crossbeds	• Core studies
Grain Scale		10-100's mm		• Petrography
Pore Scale		10-100's mm		• Petrography • SEM • X-ray diffraction • Capillary pressure measurements

currently producing or depleted, are recognized as targets for incremental recovery in mature fields (Levey and others, 1992). These include (1) untapped reservoir compartments, (2) incompletely drained reservoir compartments, and (3) deeper pool targets. Characteristics of these various reservoir targets have been summarized in Table 2. Untapped and incompletely drained compartments are the primary targets that can be identified through detailed depositional facies analysis and the identification of interwell scale heterogeneities that divide reservoir facies into separate flow units. Lithologic heterogeneity and the presence of uncontacted and incompletely drained reservoir compartments located between existing'well spacing are illustrated in Figure 5. The present level of development within a field, described by current well spacing and the density of completions within reservoir zones, can be used as a relative indicator of remaining untapped potential.

In addition to untapped and incompletely drained reservoir targets, there may be additional resource potential present in deeper pool reservoirs, which may exist in reservoir zones already penetrated, but below previously established production. Evaluations of deeper-pool targets are based on a much less dense framework of data; therefore, they often require regional facies analysis and sequence stratigraphic studies of reservoir systems to properly assess their recovery potential.

Recovery Potential of Fluvial-Deltaic Sandstone Reservoirs

Estimates of oil recovery from reservoirs in fields across the United States average 34 percent (Tyler, 1988). A recent survey of more than 450 Texas oil reservoirs documented a well-defined trend of declining recovery efficiency with increasing heterogeneity and complexity of reservoir architecture (Galloway and others, 1983). Recovery efficiencies in clastic reservoirs range from a high of nearly 80 percent in the architecturally simple, laterally continuous, wave-dominated delta and barrier-strandplain reservoirs of East Texas, to a low of 8 percent in sandstone-poor, discontinuous basin-floor turbidite reservoirs in the Permian Basin (Tyler and others, 1984). Fluvial-deltaic reservoirs fall between these extremes, with complex channelization and abrupt

Table 2. Reservoir compartment terminology.

TYPE	DEFINITION	STRATEGIES FOR IDENTIFICATION
1. UNTAPPED RESERVOIRS	• Not contacted during original field development • Separated vertically or laterally from adjacent producing reservoirs	• Identification by stratigraphic correlation of key shale horizons • Small and narrow channels within a single operational reservoir unit exhibit high degree of variability
2. INCOMPLETELY DRAINED RESERVOIRS	• Not drained when original completions reach an economic limit • May or may not be separated vertically or laterally from adjacent reservoirs	• Correlation of marker horizons within reservoir aids in recognition of separate compartments • Pressure data can be used to identify barriers which inhibit complete drainage of a reservoir
3. DEEPER POOL RESERVOIR	• May have been contacted during original field development, but is at depth below established production	• Regional facies analysis • Development of sequence stratigraphic framework for reservoir systems • Application of field analogs

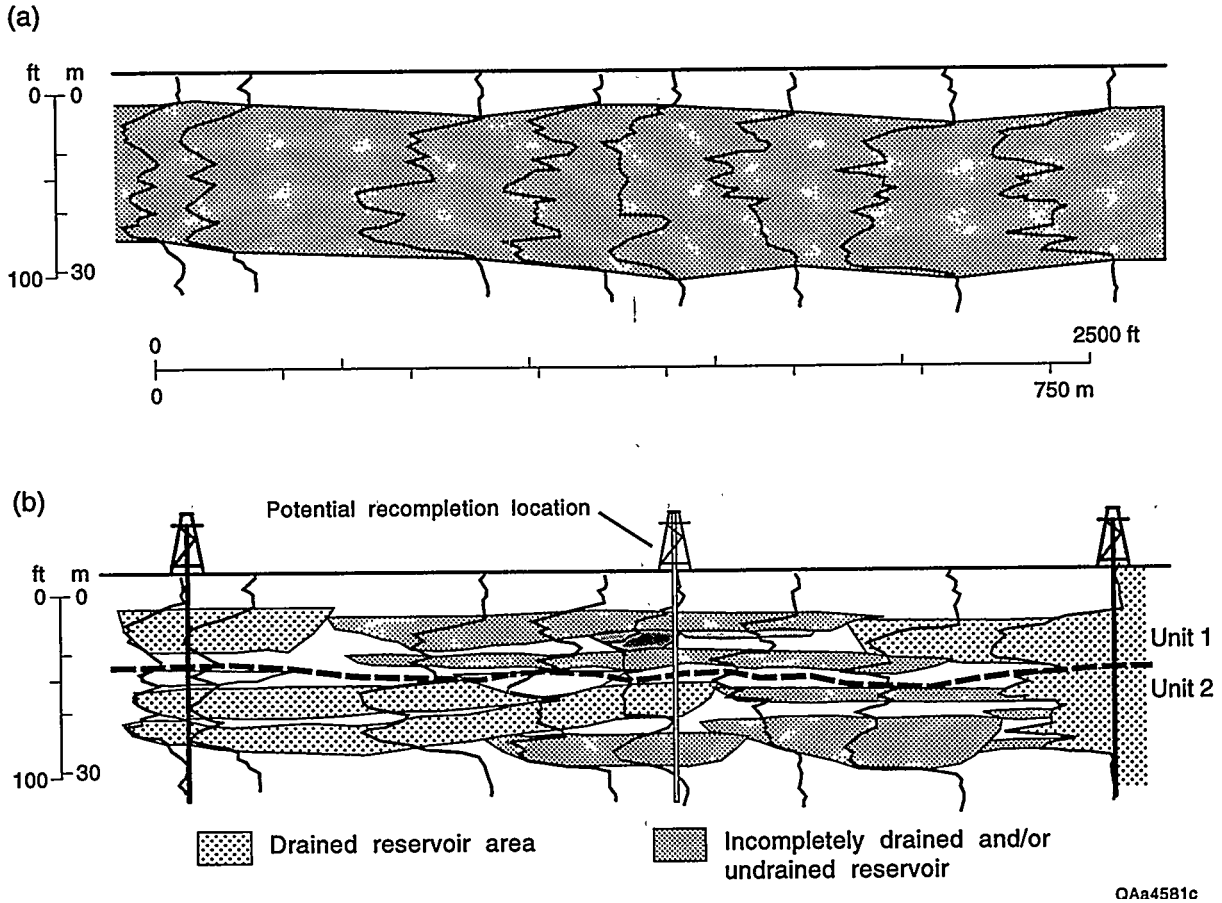

Figure 5. Schematic geologic cross section contrasting the generalized interpretation of a sandstone reservoir as a simple, laterally continuous (homogeneous) producing zone (a) with a more detailed interpretation of the same sandstone unit as a complex heterogeneous zone consisting of multiple reservoir compartments (b). In the traditional example of the simple reservoir unit (a), good reservoir continuity suggests that the reservoir can be completely drained at the current well spacing. The complex architecture illustrated in (b) suggests the presence of facies boundaries within the sandstone that create multiple compartments, some of which are only partially drained or are completely untapped at the present well spacing. Modified from Jackson and Ambrose (1989).

facies variation in some fluvial-deltaic reservoir systems responsible for recovery efficiencies as low as 20 percent. This large variation in recovery efficiency is well illustrated for Texas oil reservoirs, because populations of fluvial-deltaic, deltaic, and submarine fan reservoirs contain similar volumes of oil in place but the deltaic reservoirs account for more than 50 percent of total reservoir production (Tyler and Finley, 1991).

Lateral and vertical reservoir heterogeneity is controlled by the depositional process responsible for creating the reservoir, and this heterogeneity in turn is responsible for developing the reservoir architecture that provides the fundamental control on hydrocarbon recovery efficiency in a given reservoir unit (Tyler and Finley, 1991). Developing a detailed understanding of the processes, styles, and scales of heterogeneity that characterize a particular reservoir type can become a powerful predictive tool in the identification and delineation of additional unrecovered oil and gas resources. Using this approach, major sandstone types can be classified according to their degree of vertical and lateral heterogeneity and this classification can be used to predict recovery efficiencies and the residency of unrecovered mobile oil in the reservoir (Tyler and Finley, 1991) (Table 3).

Project Objectives and Approach

The primary objective of this project has been to develop and demonstrate advanced, integrated, multidisciplinary reservoir characterization methods that allow identification of untapped and incompletely drained compartments (Table 4), which can then be targeted for near-term recovery methods. These actions will increase production from mature fluvial-deltaic reservoirs, revitalizing mature fields and maintaining access to this class of reservoirs, thereby preventing the loss of important domestic energy resources.

To achieve our primary objective, we have integrated geological facies models with geophysical, petrophysical, and engineering data to develop an advanced, integrated characterization methodology. We have applied this methodology to selected fields and reservoirs to provide specific examples of near-term recovery opportunities (Table 4).

Our approach has been to select a trend of mature fluvial-deltaic reservoirs in danger of abandonment, assemble an overview of reservoir characteristics, select fields and reservoirs for characterization, and identify untapped and incompletely drained compartments (Table 4). We selected a prolific mature fluvial-deltaic oil play on the Texas Gulf Coast as a laboratory for the development and demonstration of characterization techniques and selected reservoirs in two

Table 3. Spectrum of reservoir heterogeneity and resulting recovery potential in clastic reservoirs (adapted from Tyler and Finley, 1991).

LATERAL HETEROGENEITY	LOW		MODERATE	HIGH	
VERTICAL HETEROGENEITY	***Depositional Environment***	***Recovery Potential***	***Depositional Environment***	***Depositional Environment***	***Recovery Potential***
LOW	Wave-dominated delta Barrier core Barrier shoreface Sand-rich strandplain	Very high recovery efficiency	Delta-front mouth bar Proximal delta front Tidal deposits Mud-rich strandplain	Meander belt *(single story)* Fluvial-dominated delta *(single story)* Back barrier *(single story)*	Low recovery efficiency Mobile oil compartmentalized, uncontacted, and laterally bypassed
MODERATE	Eolian Wave-modified delta (distal)		Shelf bars Alluvial fan Fan delta Lacustrine delta Wave-modified delta (proximal)	Braided stream Tide-dominated delta	
HIGH	Basin-floor turbidites	Low recovery efficiency Mobile oil vertically bypassed		Back barrier *(stacked units)* Fluvial-dominated delta *(stacked units)* Fine-grained meander belts *(stacked units)* Submarine fans *(stacked units)*	Very low recovery efficiency Mobile oil uncontacted and bypassed

Table 4. Summary of project objectives.

OBJECTIVE	APPROACH
1. Demonstrate the application of state-of-the-art reservoir characterization to assess the reserve growth potential in mature fluvial/deltaic oil fields of South Texas	• Utilize maturely developed fluvial and deltaic sandstone reservoirs as a laboratory for reservoir characterization techniques
2. Integrate geological facies models with petrophysical and engineering data to characterize fluvial-deltaic reservoir heterogeneity and identify controls on the location and volume of unrecovered mobile and residual oil	• Categorize engineering information by depositional and diagenetic characteristics
3. Provide examples from selected fields and reservoirs to serve as a guide for other fields and reservoirs	• Characterize major Frio reservoirs in the Vicksburg Fault Zone oil play in the Texas Gulf Coast Basin
4. Define near-term reserve growth potential in selected fields by describing the spatial distribution of remaining oil resource	• Emphasize practical field-oriented techniques to screen for reserve growth potential and develop approaches to direct strategic targeting of new infill drilling and recompletions to overcome reservoir compartmentalization

fields for detailed study. Whereas successful demonstration of these techniques will most tangibly influence production in Texas fluvial-deltaic trends, presentation of findings to national audiences will also contribute to increased production throughout the United States.

The trend selected, the Frio Fluvial-Deltaic Sandstone (Vicksburg Fault Zone) play of South Texas, has already produced nearly 1 Bbbl of oil since discovery and development in the 1930's and 1940's but still contains 1.6 Bbbl of unrecovered mobile oil. More than half of the reservoirs have already been abandoned, and thus large volumes of oil may remain unproduced unless advanced characterization techniques are applied to define untapped, incompletely drained, and new pool reservoirs as suitable targets for near-term recovery methods.

This project has developed interwell-scale geological facies models of the Frio fluvial-deltaic reservoirs and combined them with engineering assessments to characterize reservoir architecture

and fluid-unit boundaries and to determine the controls that these characteristics exert on the location and volume of unrecovered mobile oil and residual oil. These studies have lead directly to the identification of specific opportunities to exploit these heterogeneous reservoirs for incremental recovery by recompletion and strategic infill drilling.

Project Description

This project was divided into three major phases (Figure 6). The first phase included (1) the initial task of screening fields within the play to select representative reservoirs that have a large remaining oil resource and are in danger of premature abandonment (task 1), and (2) performing initial characterization studies on these reservoirs in order to identify the potential for untapped, incompletely drained, and new pool reservoirs (tasks 2-4). The second phase involved advanced characterization of the selected reservoirs in order to delineate incremental resource opportunities. This included volumetric assessments of untapped and incompletely drained oil, along with an analysis, by reservoir, of specific targets for recompletion and targeted infill drilling. The third and final phase of the project consisted of a series of tasks associated with final project documentation, technology transfer, and the extrapolation of specific results from reservoirs in this study to other heterogeneous fluvial-deltaic reservoirs within and beyond the Frio play in South Texas.

Specific accomplishments throughout the project are presented in each annual report (McRae and others, 1994, 1995and Holtz and others, 1996). Tables 5 through 7 provide summaries of these activities. Activities that postdate the last annual report consist predominantly of technology transfer events, and are summarized in that major section.

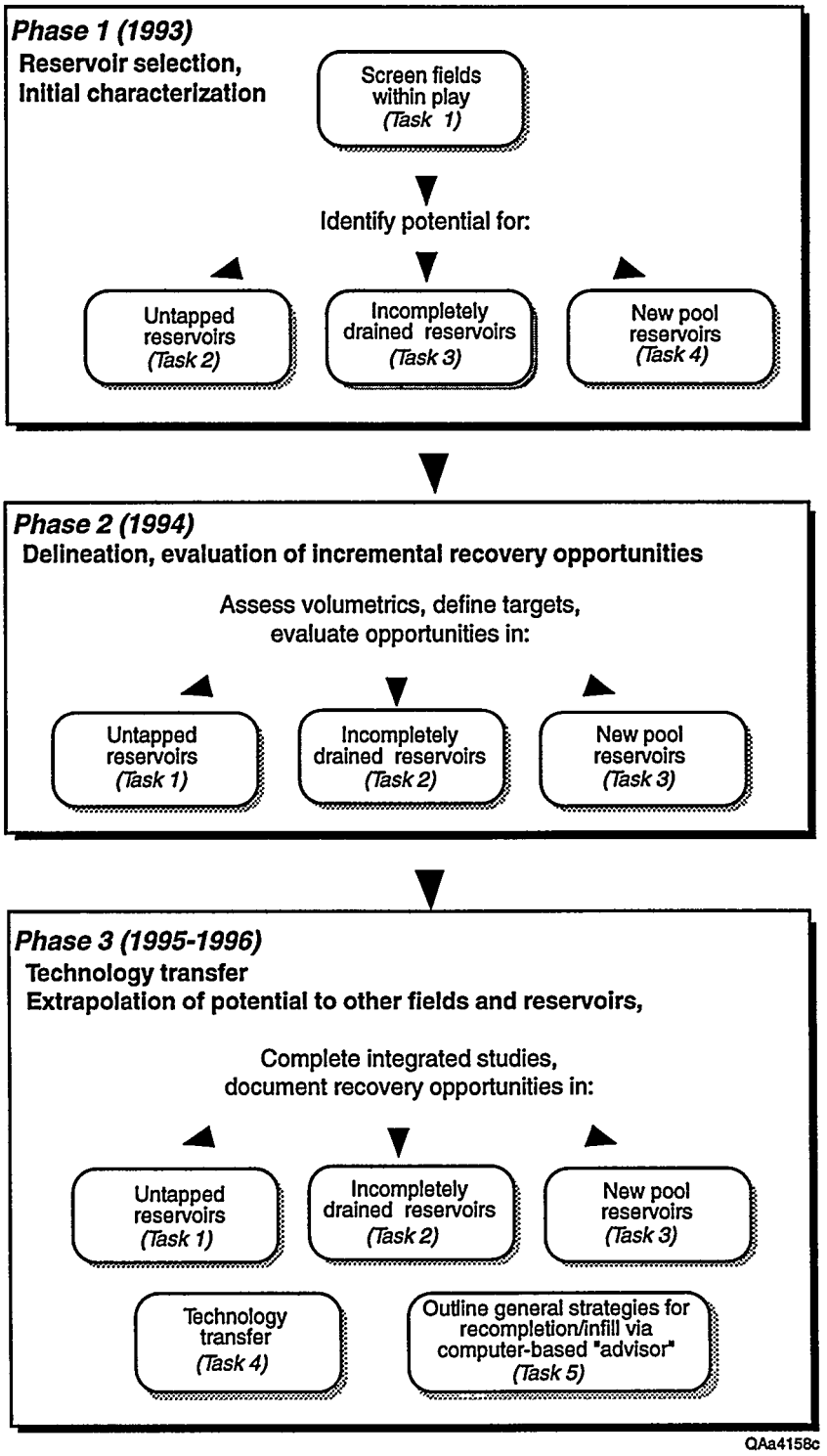

Figure 6. Diagram of work structure for this project illustrating three primary phases and a breakdown of individual tasks associated with each phase of the project.

Table 5. Significant accomplishments in Project Year 1: 1992–1993.

1. Selection of two South Texas fields for reservoir characterization studies
2. Reviews with field operators, data gathering and inventory
3. Development of digital log data bases
4. Construction of type logs for fields, establishment of regional cross-section framework
5. Preliminary synthesis of reservoir log, core, and production data
6. Synthesis of reservoir pressure and production data
7. Comparison of production histories by reservoir
8. Synthesis of core analysis data by reservoir

Table 6. Significant accomplishments in Project Year 2: 1993–1994.

1. Statistical analysis of petrophysical attributes for middle Frio (fluvial), lower Frio (fluvial-deltaic), and Vicksburg (deltaic) stratigraphic subintervals within the entire play.
2. Playwide evaluation of additional resource potential and assessment of remaining mobile oil in middle Frio fluvial, lower Frio fluvial-deltaic, and Vicksburg deltaic sandstone reservoirs.
3. Completion of regional stratigraphic framework in Rincon and T-C-B fields and documentation of general reservoir architectural styles.
4. Selection of two representative reservoirs in each field for detailed study.
5. Digitized log data for nearly 200 wells in Rincon field were depth adjusted, normalized, and flagged with associated production data, stratigraphic tops, log facies type, net sandstone thickness, percentage sandstone, wireline core porosity and permeability, vertical log facies type, and lateral depositional facies type interpreted from facies maps.
6. Log data from more than 50 wells in T-C-B field were digitized for petrophysical analysis and annotated with associated production data and stratigraphic tops.
7. Maps illustrating distribution of oil production, initial potential, log facies, net sandstone thickness, percentage sand, and permeability-thickness have been generated for 8 separate reservoir subunits in Rincon field and compared to identify differences in sandstone depositional styles and production behavior and identify zones with high potential for containing unproduced oil.
8. Stratigraphic cross sections were constructed to document subregional stratigraphic framework of reservoirs in greater T-C-B field area, identify stratigraphic hierarchy and sandstone architectural styles within field study area, and aid in the selection of specific reservoir zones for detailed study.

Table 7. Significant accomplishments in Project Year 3: 1994–1995.

1. Routine core analysis data from 100 wells in Rincon field were categorized by depositional facies, resulting in more accurate facies-based porosity-permeability relationships and correct apportioning of commingled production to each reservoir zone.

2. Special core analysis data were measured in 15 samples from Rincon reservoirs to improve calculations of original oil in place, residual oil saturation, and irreducible water saturation, resulting in a more accurate evaluation of remaining reserves.

3. A petrographic study of 22 samples from Rincon reservoirs was carried out to determine the effect of diagenesis on reservoir quality and to supplement results of the special core testing.

4. Detailed characterization of two upper delta plain fluvial reservoirs in T-C-B field was completed, resulting in the identification of 17 recompletion and 19 infill drilling opportunities.

5. An accommodation-based model was developed that improves the prediction of reservoir architecture and between-well heterogeneity and establishes a method for ranking reservoirs in terms of reserve-growth potential on a quick-look basis.

6. Geologic societies in two cities have offered to host short courses scheduled for early 1996, and work has begun on a set of course notes for attendees.

7. Methodology and results of this study have been transferred to industry in 5 technical presentations, 4 publications, and 2 related Bureau short courses.

8. Objectives and a tentative structure for a microcomputer-based geological advisor have been established, and programming of a test version has begun.

PLAYWIDE RESERVOIR STUDIES

M.H. Holtz and L.E. McRae

Overview

A geologic and engineering review of playwide characteristics was carried out to provide a summary of basic regional information to operators and to evaluate the volumes of resources remaining to be recovered by operators. The folloyviig section provides a review of production history and geologic setting, an evaluation of playwide engineering parameters and the resource estimates calculated from them, and a breakdown of engineering parameters and resources by stratigraphic interval.

Location and Characteristics of Fields within the Play

The Frio Fluvial-Deltaic Sandstone (Vicksburg Fault Zone) play (Figure *7)* is located in South Texas and extends from Starr County northeastward to Jim Wells and Nueces Counties, Texas (Galloway and others, *1983).* Fields in the play produce oil from heterogeneous fluvial and deltaic sandstones of the Oligocene Frio and upper Vicksburg Formations on the eastern, downthrown side of the Vicksburg Fault Zone. Oil-bearing traps consist predominantly of shallow rollover anticlines that formed during later stages of fault movement along the fault zone (Jackson and Galloway, *1984;* Tyler and Ewing, *1986).* Deeper structures are characterized by synthetic and antithetic faults with large displacements commonly in excess of hundreds of feet. Individual fields within the play produce from a stratigraphic interval that averages *2,000 ft* in thickness and consists of *20* to *40* separate sandstone reservoirs that are interbedded with mudstone (Stanley, *1970).*

Production History

The Frio Fluvial-Deltaic Sandstone (Vicksburg Fault Zone) has produced nearly 1 Bbbl of oil equivalent from 129 reservoirs in fields throughout the play in South Texas (Galloway and others,

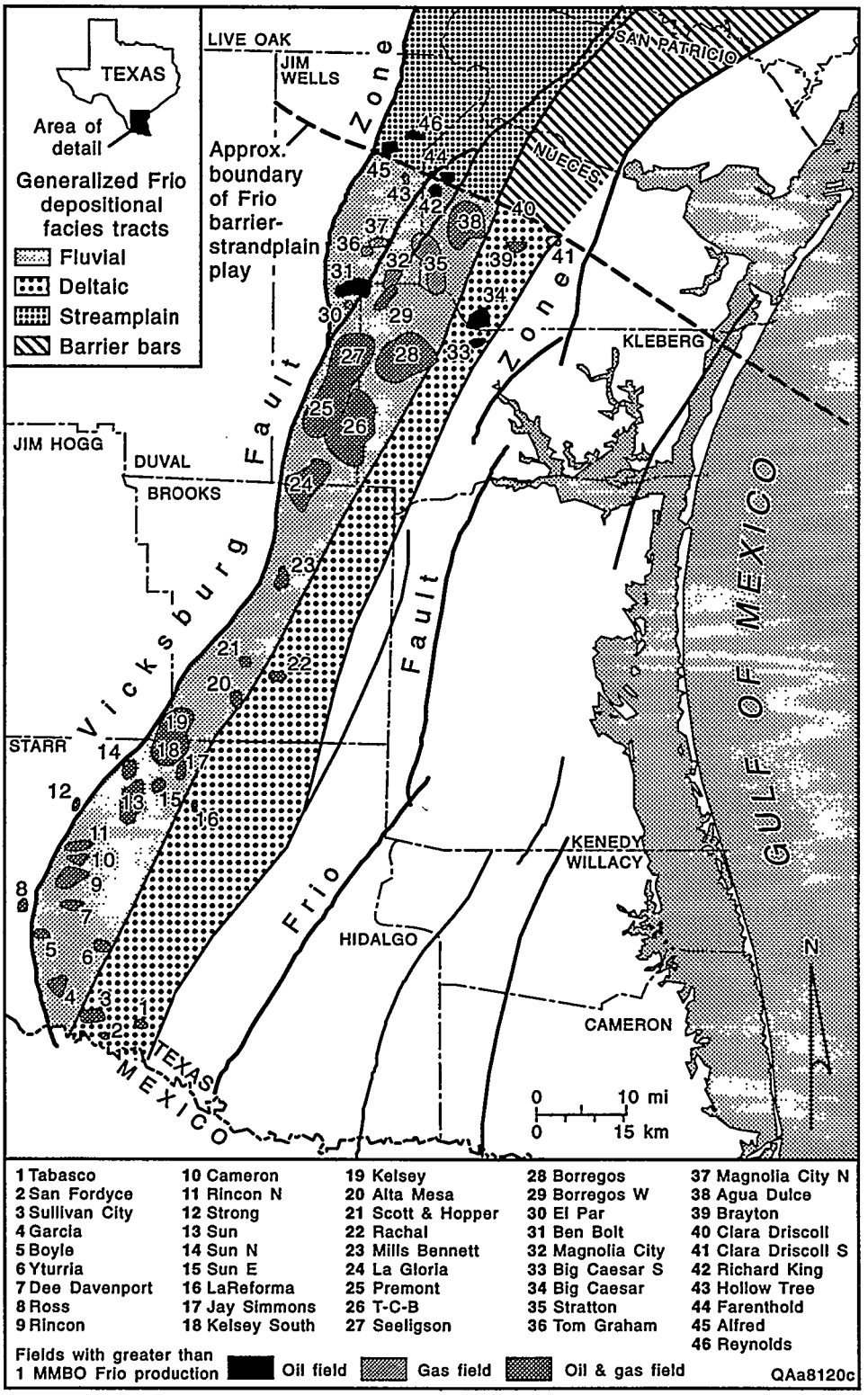

Figure 7. Location map of major oil and gas fields in the Frio Fluvial-Deltaic Sandstone Play in South Texas. Reservoirs from these fields have been subdivided according to stratigraphic position and depositional facies into middle Frio (fluvial) reservoirs and lower Frio (fluvial-deltaic) reservoirs to identify differences in heterogeneity style and better estimate remaining oil potential in each type of reservoir facies.

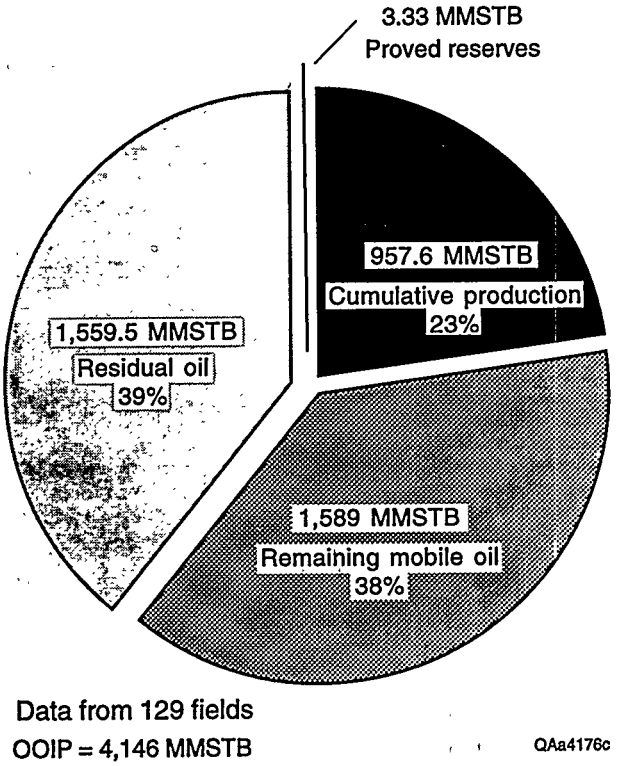

Figure 8. Distribution of the oil resources within reservoirs of the Frio Fluvial-Deltaic Sandstone (Vicksburg Fault Zone) play in South Texas. Nearly 1 Bbbl have been recovered in more than four decades of production, but nearly two-thirds of the estimated original oil in place remain.

1983; Kosters and others, 1989). Total original oil in place estimates, however, are in excess of 4 Bbbl, of which 1.6 Bbbl is classified as unrecovered mobile oil, and nearly the same amount is attributed to residual oil resources (Figure 8).

The development status of the play is classified as mature to supermature, because most of the major fields in the play were discovered in the late 1930's and early 1940's (Figure 9a). Reservoir abandonment rates increased significantly during the time period from 1987 to 1989 (Figure 9b). The number of producing wells in the play showed a precipitous decline of over 50 percent during a 5-yr period from 1974 to 1978. The play has been experiencing a steady decline in both overall production and individual flow rates throughout the 1980's (Figure 9c). By 1989, over one-half of the 129 reservoirs included in the play were no longer producing. Annual production from 376 active wells in 1989 was approximately 1.2 MMbbl. Average daily production rates from these wells had declined to 8.9 bbl/d.

Oil and natural gas reservoirs produce from the same stratigraphic interval. Production drive mechanism is dominantly gas-cap expansion. Most fields have large gas caps and have been unitized to properly develop and maintain pressure in these complex sandstone reservoirs. In

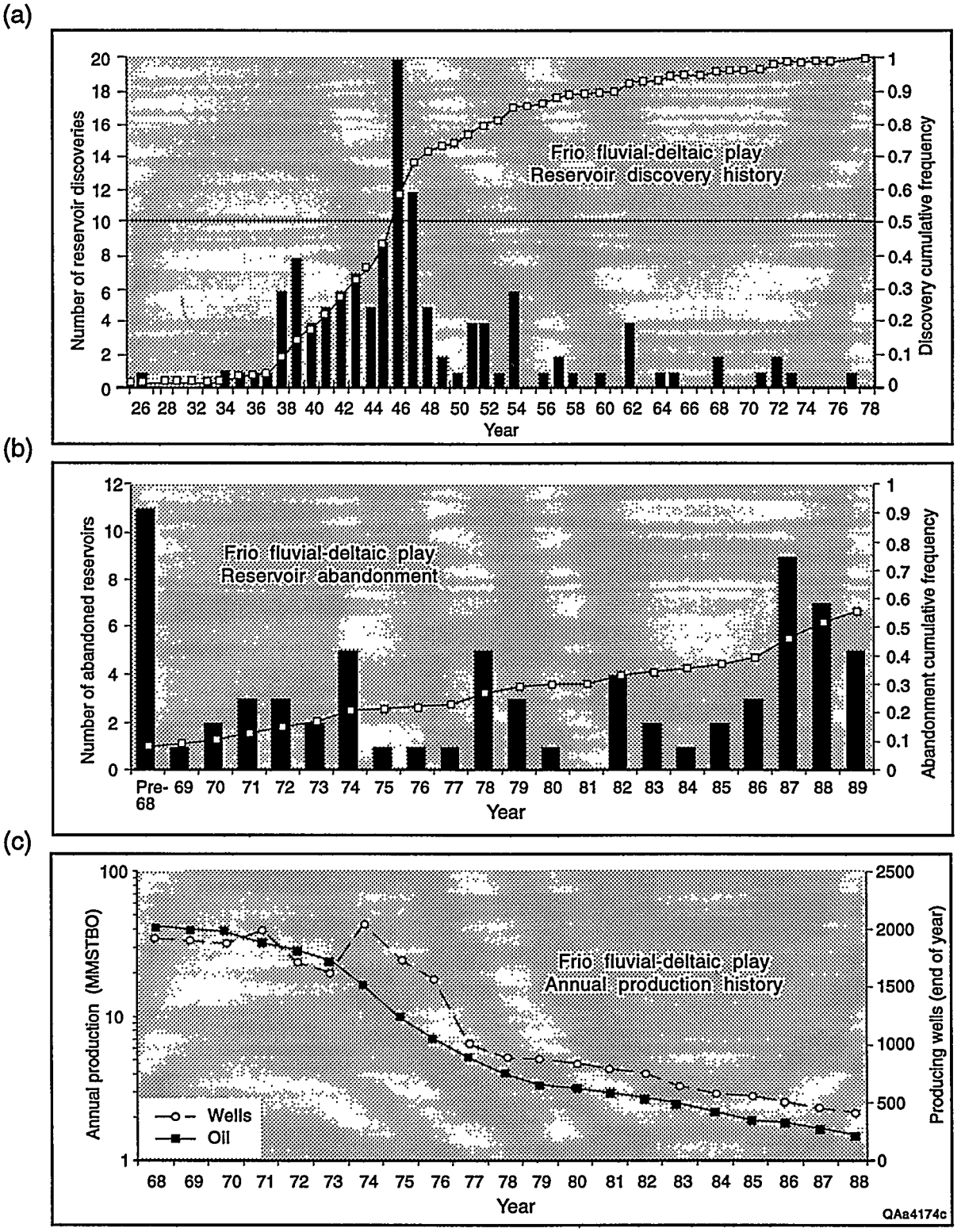

Figure 9. Histograms illustrating trends in reservoir discovery (A), reservoir abandonment (B), and decline in annual production (C) in the Frio Fluvial-Deltaic sandstone oil play. Oil production in the play has steadily declined since 1968, and as of 1991, nearly 60 percent of all producing reservoirs had been abandoned.

many cases, produced natural gas has been cycled back into some of the reservoirs to maintain production of oil.

Engineering attributes for Frio reservoirs are described in a later section. The typical reservoir is a dip-oriented fluvial or distributary-channel sandstone draped over a northeast-trending anticlinal structure. Individual sandstone reservoirs range from 10 to 50 ft in thickness and consist of individual or multiple amalgamated sandstone bodies. Porosity and permeability values average 25 percent and 430 md, respectively, and the average API gravity of produced oil is 41°. Reservoirs are internally compartmentalized by permeability baffles and barriers caused by mud-filled channel plugs, by rip-up-clast zones located between channel-on-channel contacts, and by more laterally extensive floodplain mudstone facies located in interchannel areas.

Regional Structural and Stratigraphic Setting

The entire Frio Formation in Texas has been divided into 10 plays based on regional variations in structure and depositional setting (Kosters and others, 1989). Fields in the play known as the Frio Fluvial-Deltaic Sandstone Play produce oil and gas from the eastern, downthrown side of the Vicksburg Fault Zone, a major down-to-the-coast listric normal growth fault system that parallels the Gulf coastline for over-100 mi (Figure 7). Faulting mainly offsets the Vicksburg Formation but also affects the lower portions of the overlying Frio Formation. Oil-bearing traps consist predominantly of shallow rollover anticlines that formed during later stages of movement along the fault zone (Stanley, 1970; Tyler and Ewing, 1986). Deeper structures within Vicksburg strata are characterized by synthetic and antithetic faults with large displacements commonly in excess of hundreds of feet.

Oil and gas reservoirs in this play occur within a 2,000-ft stratigraphic interval in fluvial-deltaic sandstones primarily of the Oligocene Frio Formation (Figure 10). The Frio Formation is part of a sedimentary wedge that records a major depositional offlap episode of the northwestern shelf of the Gulf of Mexico Basin (Figure 11). Frio, sediments in South Texas represent the entry of a major extrabasinal river into the Gulf basin along the axis of the Rio Grande Embayment in

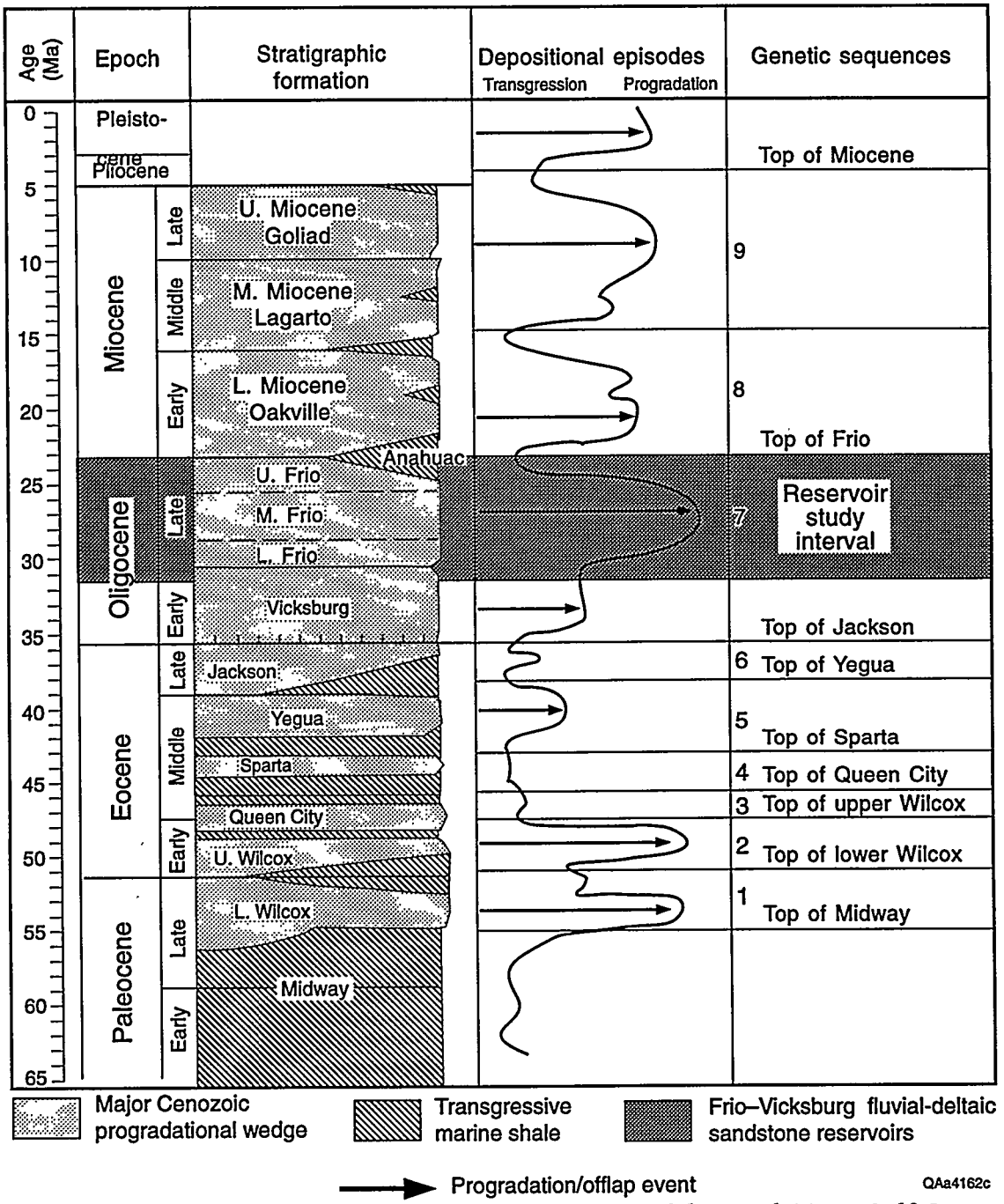

Figure 10. Stratigraphic column of Cenozoic sediments of the South Texas Gulf Coast. The sedimentary succession has been divided into a series of large-scale depositional episodes that represent major periods of progradation that occurred throughout the Cenozoic (Galloway, 1989b). Reservoirs in the Frio Fluvial/Deltaic Sandstone play are part of a larger Frio-Vicksburg genetic sequence.

Oligocene time. This ancient fluvial-deltaic complex has been divided into the Gueydan fluvial and Norias delta systems (Galloway and others, 1982). Fields within the Frio Fluvial-Deltaic Sandstone play occupy a transitional area between these two depositional systems (Figure 12). In

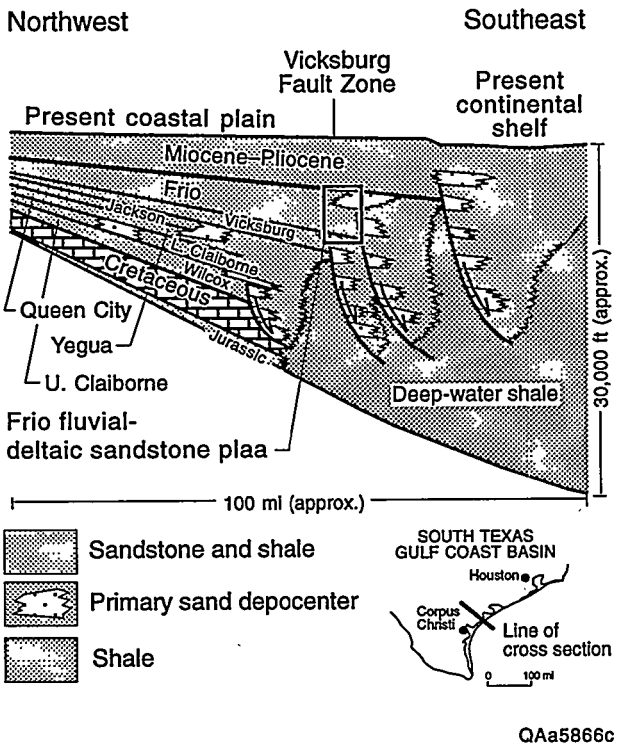

Figure 11. Schematic cross section of the South Texas Gulf Coast Basin. Modified from Bebout and others (1982).

Figure 12. General distribution of the Norias delta and Gueydan fluvial depositional systems responsible for deposition of the Frio stratigraphic unit. The Frio sediments in the vicinity of the Vicksburg Fault Zone were primarily deposited in moderate to high sinuosity mixed-load stream environments of the Gueydan Fluvial system. (Map distribution from Galloway and others, 1982). ↓

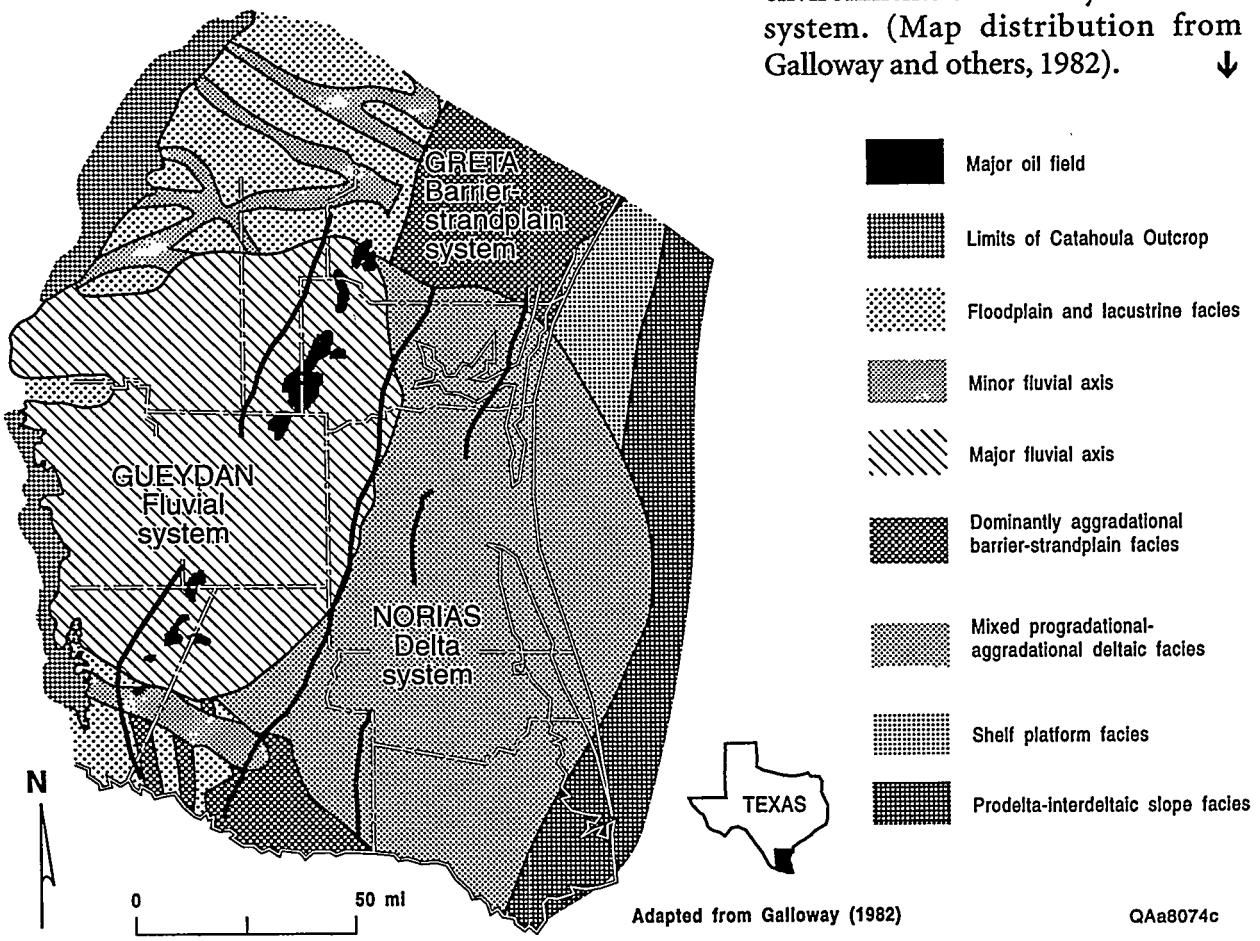

general, lower Frio sandstones represent deltaic facies of the ancestral Norias delta system, and middle and upper Frio sandstones predominantly reflect deposition in fluvial channels of the Gueydan fluvial system (Galloway and others, 1982). Important oil reservoirs in this sequence occur within progradational, fluvial-dominated deltaic depositional fades within the upper Vicksburg and lower Frio intervals and in aggradational fluvial fades in the middle Frio section (Figure 13).

Upper Vicksburg-Frio Genetic Sequence

The productive stratigraphic interval in the Frio Fluvial-Deltaic Sandstone Play is part of a larger genetic depositional sequence that reflects a series of depositional events that include strata from both Vicksburg and Frio Formations (Galloway, 1989b). These depositional events produce an overall genetic stratigraphic stacking pattern that consists of episodes of seaward-stepping deltaic progradation, vertically stacked fluvial aggradation, and landward-stepping retrogradation followed by a transgressive event (Figure 14). Reservoir sandstones within stratigraphic intervals exhibiting each sediment stacking style possess distinctive characteristics that control their pro ducibility, determine their potential for incremental recovery, and dictate which strategies should be used to best identify locations of remaining mobile oil in undeveloped compartments (McRae and Holtz, 1994).

Sediment and rocks of the upper Vicksburg Formation represent the initial progradational phase of the Vicksburg-Frio genetic stratigraphic interval (Coleman and Galloway, 1991; Xue and Galloway, 1991). Vicksburg deposition in South Texas was strongly influenced during the development of the Vicksburg Fault Zone (Coleman, 1993; Coleman and Galloway, 1991). As a result, reservoir compartmentalization is controlled to a large degree by faulting, and stratigraphic correlations necessary to document depositional heterogeneity are difficult.

Lower Frio reservoir facies are primarily delta-plain distributary-channel and delta-front channel-mouth-bar sandstones. Reservoir compartments in narrow distributary-channel sandstones isolated by low-permeability mudstone facies and channel-mouth-bar sandstones that

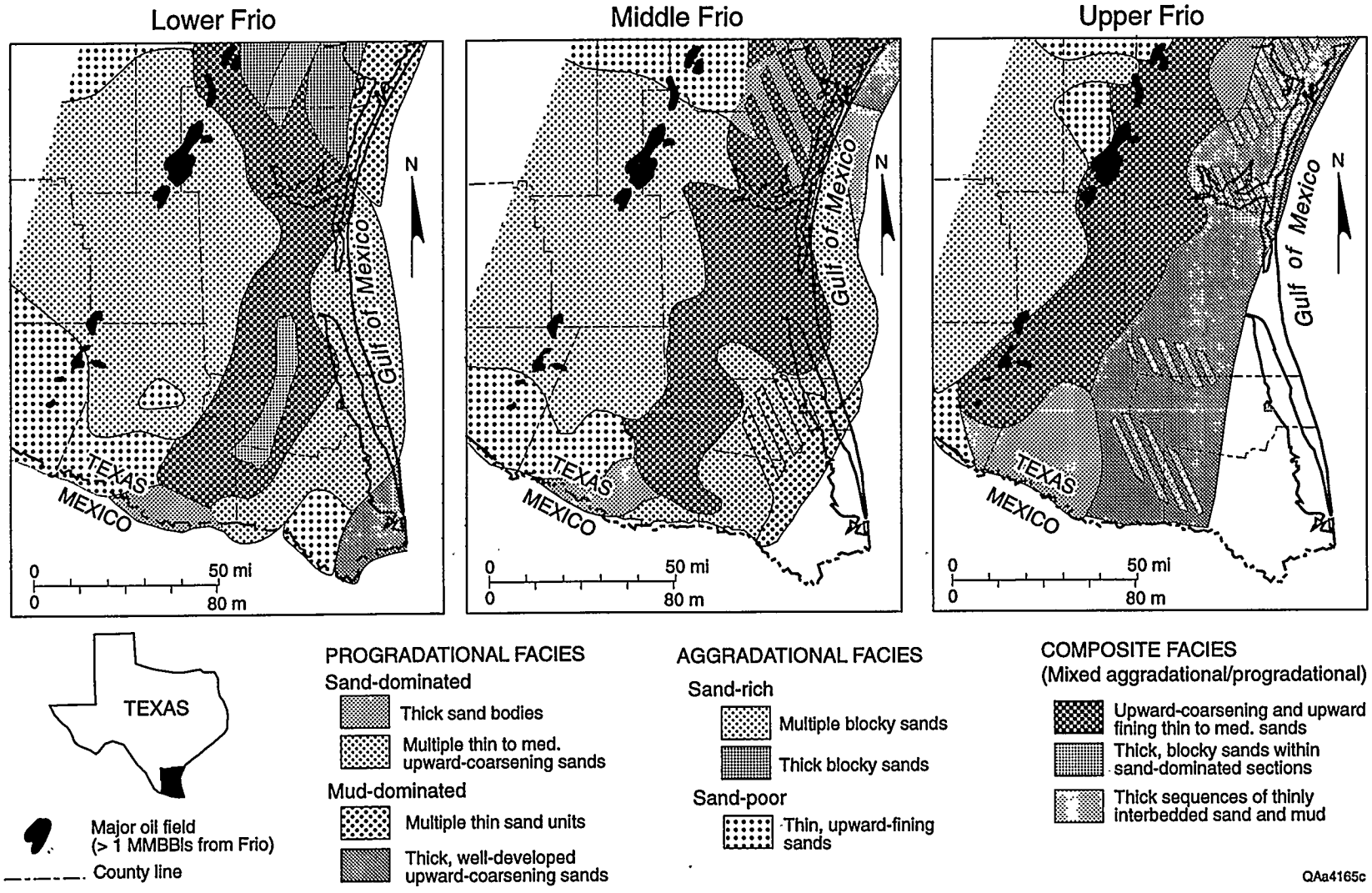

Figure 13. Distribution of aggradational and progradational intervals of the Frio Formation along the Vicksburg Fault Zone oil play. The Frio sediments near the Vicksburg Fault Zone were deposited primarily in moderate- to high-sinuosity mixed-load stream environments of the Gueydan fluvial system. Based on log facies maps by Galloway and others (1982).

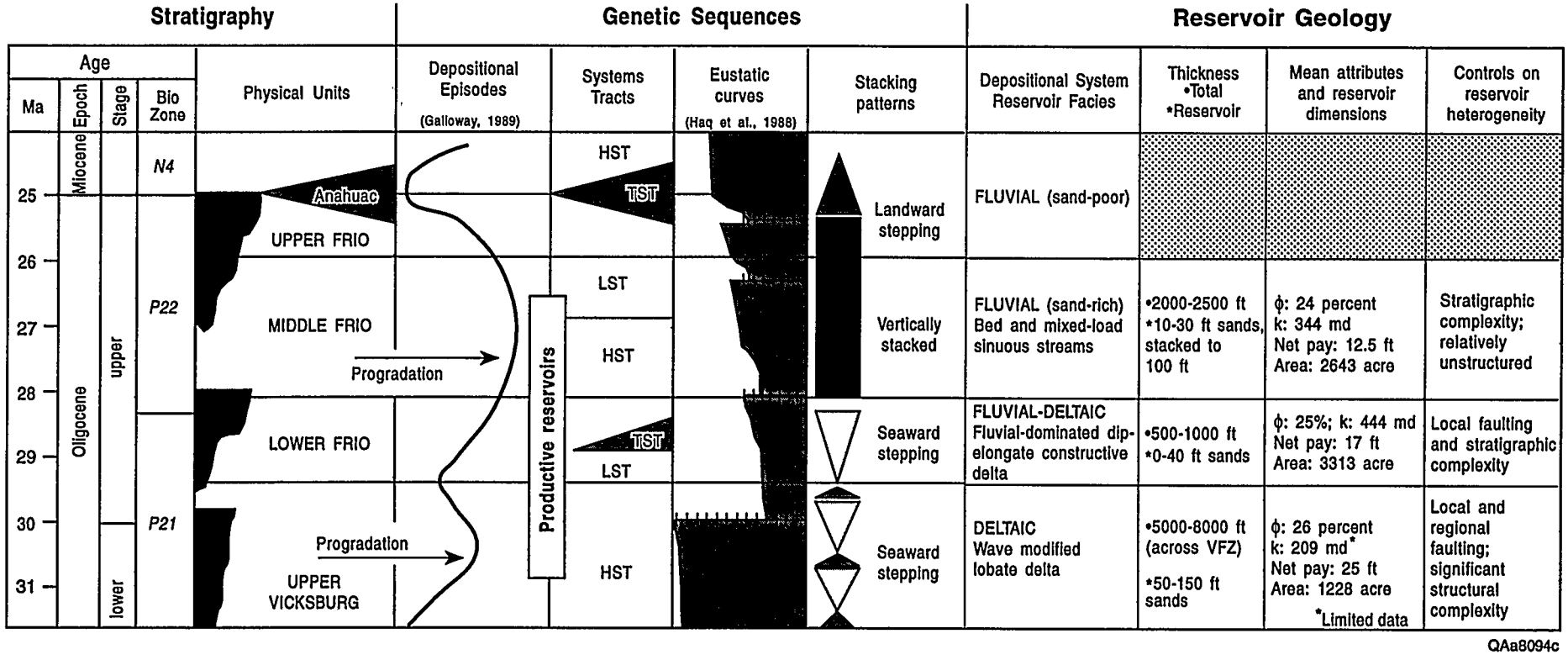

Figure 14. Stratigraphic subdivisions for reservoirs in the Frio Fluvial-Deltaic Sandstone Play and summary of genetic sequence context, reservoir characteristics, oil production, and estimates for remaining oil potential in middle and lower Frio reservoirs.

Table 8: Strategies for play-scale reservoir characterization studies.

Play-scale reservoir characterization
Goals:
• Characterize reservoir variability and degree of heterogeneity
• Develop stratigraphic context for productive reservoir interval
• Identify additional oil potential
Methodology:
• Evaluate engineering data from reservoirs in fields throughout the play trend
• Identify reservoir depositional facies and stacking patterns on a regional scale
• Perform resource calculations to estimate remaining oil volumes present in the play and distribute potential according to stratigraphic interval

pinch out into finer grained delta-front facies are the primary targets for additional oil recovery in the lower Frio section.

Reservoir facies in middle Frio units include channel-fill, point-bar, and crevasse-splay sandstones. Low-permeability subfacies within middle Frio channel fill units act as flow baffles and barriers and create isolated reservoir compartments that represent a significant opportunity for additional recovery. Crevasse-splay deposits, which are of limited areal extent and are laterally separated from channel-fill facies by low-permeability facies, are also potential targets for additional recovery of compartmentalized reserves.

Preliminary Assessment of Reserve Growth Potential in Frio Oil Reservoirs

Strategies for reservoir characterization studies at the scale of the play focused on engineering and geologic data from fields throughout South Texas and are summarized in Table 8. To optimize the calculation of remaining producible resources in the play, reservoir data from fields throughout the play were collected and screened to determine the general engineering

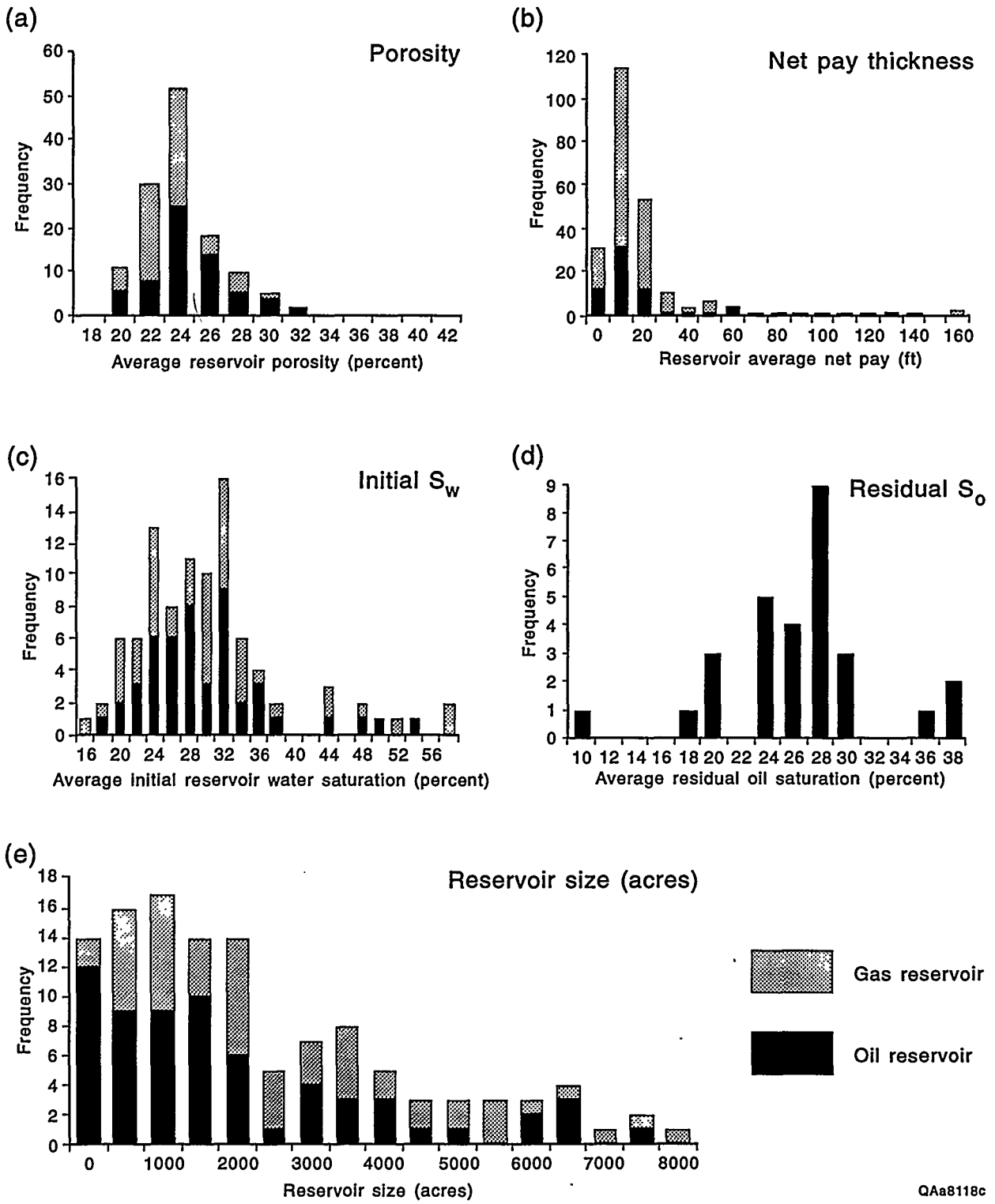

Figure 15. Histograms illustrating distributions for values of porosity (A), initial water saturation (B), residual oil saturation (C), net pay (D), and area (E) from reservoirs throughout the Frio Fluvial-Deltaic Sandstone Play in South Texas.

Table 9. Statistics for reservoir parameters grouped by oil and combined oil and gas data sets.

	Porosity (%)	Initial water saturation (%)	Residual oil saturation (%)	Net pay (feet)	Reservoir area (acres)
Oil reservoirs					
Count	64	48	29	64	65
Minimum	20	18	10	5	133
Maximum	32	54	39.8	146	7,607
Range	12	36	29.8	141	7,474
Mean	**25.3**	**30.6**	**26.9**	**22.8**	**2,170.9**
Standard deviation	2.7	7.4	5.8	25.9	1,890.2
Probability function *(best-fit)*	Normal	Beta	Logistic	Lognormal	Lognormal
Probability function *(alternative)*	Gamma or logistic	Gamma	Normal	Gamma	Exponential
All reservoirs					
Count	346	331	29	242	154
Minimum	19	11.5	10	4	40
Maximum	32	68	39.8	245	26,000
Range	13	56.5	29.8	241	25,960
Mean	**24.2**	**32.0**	**26.9**	**24.3**	**2,549.9**
Standard deviation	1.8	5.5	5.8	29.2	2,860.8
Probability function *(best-fit)*	Logistic	Lognormal	Logistic	Lognormal	Lognormal
Probability function *(alternative)*	Gamma	Beta	Normal	Gamma	Exponential

attributes of this group of fluvial-deltaic reservoirs. Reservoir attribute characteristics of Frio sandstones analyzed for determination of hydrocarbon volumes included porosity, initial water saturation, residual oil saturation, net-pay thickness, reservoir area, and volume of produced fluids (Figure 15). Statistical analysis of engineering attributes for Frio reservoirs throughout the play was completed in the first reporting period of the project (Holtz and others, 1994), and the results are summarized in Table 9.

Reservoir attributes were used to simulate volumes and create probability distributions of original oil in place, original mobile oil in place, and residual oil in place for individual reservoirs throughout the Frio Fluvial-Deltaic Sandstone play. A preliminary assessment of the oil

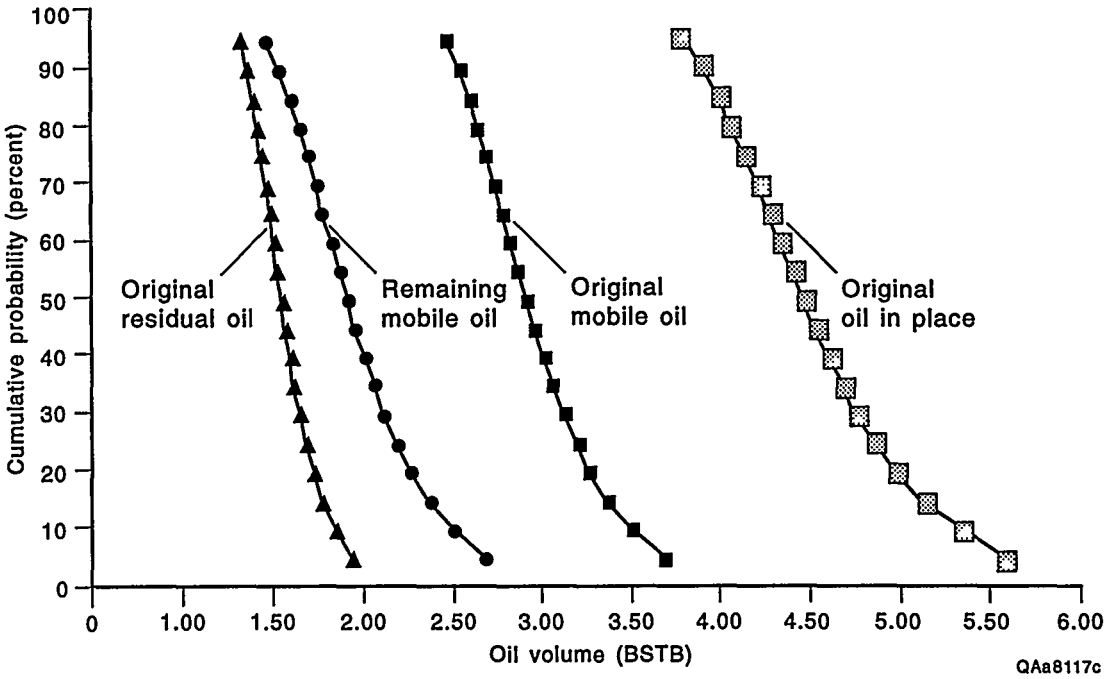

Figure 16. Probability distribution curves illustrating the cumulative probability of original oil in place, original residual oil, original mobile oil, and remaining mobile oil for the Frio Fluvial/Deltaic Sandstone play.

remaining throughout the play was based on these probability distributions (Figure 16). Oil reservoirs in the play are conservatively estimated to contain 1.2 BSTB of remaining mobile oil and 1.5 BSTB of residual oil. These volumes reside in both incompletely drained and untapped reservoirs. These two targets are a substantial volume of oil for redevelopment and reexploration.

Stratigraphic Distribution of Additional Oil Potential

Methodology

The stratigraphic positions of individual fields and reservoir units within the context of the larger scale Frio-Vicksburg genetic stacking sequence were identified to assess the importance of reservoir stratigraphy on hydrocarbon production, recovery efficiency, heterogeneity style, and the potential for compartmentalization of additional oil resources (McRae and Holtz, 1994). Reservoir data were collected from fields throughout the play to evaluate remaining potential in the play as a whole represented by each of these reservoir intervals. Most fields within the play produce from 20 to 50 individual sandstone reservoirs. Reservoirs within a single field commonly

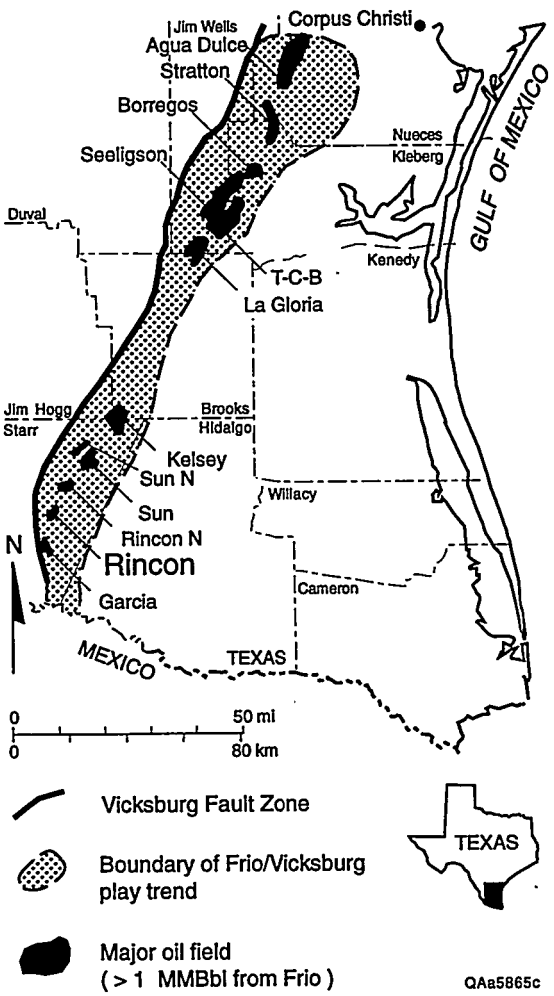

Figure 17. Map of south Texas showing location of fields within the Frio Fluvial-Deltaic Sandstone Play along the Vicksburg Fault Zone. Fields shown include those which have produced more than 1 million Bbls (Modified from Galloway and others, 1983, and Kosters and others, 1989).

include fluvial-channel, distributary-channel, and deltaic sandstones that represent a range of architectural styles, including individual, vertically stacked, and laterally amalgamated geometries. Because depositional facies is a significant control on reservoir attributes, it is important to make a distinction, whenever possible, between reservoir facies types. Subdivision of reservoirs within the play into stratigraphic facies types will result in more accurate characterization of reservoir attributes for each facies type. This analysis provides a regional context that should facilitate the transfer of results from our field-specific studies to other fields and reservoirs in the play.

Strategies for Reservoir Classification

Reservoir sandstones in fields throughout the play that have produced more than 1 MMBO (Figure 17) were identified as belonging to the middle Frio, lower Frio, or upper Vicksburg stratigraphic interval (Figure 7, Table 10). Vicksburg reservoirs are not targets for resource delineation and additional recovery in this project, but some reservoir zones originally classified within the "Frio Fluvial-Deltaic Sandstone Play" in fact represent wave-dominated deltaic sandstones belonging to the Vicksburg Formation. Classification was based on regional geologic setting as well as various other reservoir data available from files at the Railroad Commission of Texas and other nonproprietary sources. Basic criteria such as reservoir depth, geographic and structural location of the field, and depositional

Table 10. List of major oil fields in the Frio Fluvial-Deltaic Sandstone Play. Map numbers refer to figure 7.

FIELD			OIL RESERVOIR PRODUCTION HISTORY				RESERVOIR STRATIGRAPHIC SETTING		
Map No.	County	Field Name	Reservoir Name Number of zones	Disc. Year	Depth (Feet)	CumProd (MSTB)	Fault Block	Strat Unit	Reservoir Facies
1	Hidalgo	Tabasco	Heard FB2	1952	6082	2,587	VK-main+1	LF	Fluvial/Deltaic
2	Hidalgo	Sam Fordyce	Sam Fordyce	1934	2750	7934	VK-main	UF	Fluvial
3	Hidalgo	Sullivan City	Sullivan sand	1939	3437	1692	VK-main	MF	Fluvial
4	Starr	Garcia	6 zones	1942	3748-4132	36304	VK-main	MF	Fluvial
5	Starr	Boyle	Frio 3500'	1940	3500	2408	VK-main	MF	Fluvial
6	Starr	Yturria	2 reservoir zones	1941	4225-4913	4157	VK-main	LF, MF	Fluvial, Fluvial/Deltaic
7	Starr	Dee Davenport	Dee Davenport	1947	4171	1307	VK-main	MF	Fluvial
8	Starr	Ross	Vicksburg	1943	2845	2951	updip/close	V	Deltaic
9	Starr	Rincon	combined zones	1938	4000-5300	58017	VK-main	V, LF, MF	Fluvial,Fluvial/Deltaic, Deltaic
10	Starr	Cameron	lower E sand	1943	4140	3999	VK-main	MF	Fluvial
11	Starr	Rincon, North	3 zones	1940	4376-6000	10527	VK-main	V, LF, MF	Fluvial, Deltaic
12	Starr	Strong	4700 sand	1953	4670	2622	updip/close	MFM	Fluvial
13	Starr	Sun	3 zones	1941	4300-4950	27545	VK-main	LF, MF	Fluvial
14	Starr	Sun North	7 zones	1951	4315-5400	19162	VK-main	V, LF, MF	Fluvial,Fluvial/Deltaic, Deltaic
15	Starr	Sun East	F-4 Sand	1951	5068	1107	VK-main	LF	
16	Hidalgo	La Reforma	La Reforma	1941	6200	1943	VK-main	V	Deltaic
17	Starr	Jaay Simmons	Frio A-1 sand	1947	5770	6096	VK-main	LF	Fluvial
18	Starr	Kelsey South	2 zones	1938	5980	9816	VK-main	V	Deltaic
19	Brooks	Kelsey	2 zones	1938	4700-4800	14424	VK-main	LF	Deltaic
19	Brooks	Kelsey Deep	19 zones	1944	5489-6114	62025	VK-main	V	Deltaic
20	Brooks	Alta Mesa	Garcia sand	1936	2485	9426		UF	Fluvial
21	Brooks	Scott & Hopper	Scott & Hopper	1943	6875	1268	VK-main	V	Deltaic
22	Brooks	Rachal	Rachal	1946	4800	1016	VK-main	MF	Fluvial
23	Brooks	Mills Bennett	D Sand	1953	4436	1168	VK-main	MF	Fluvial
24	J. Wells	LaGloria	6 zones	1945	5950-6985	25373	VK-main	LF, MF	Fluvial , Fluvial/Deltaic
25	J. Wells	Premont	2 zones	1933	3600-3700	3555	VK-main	UF	Fluvial
26	Kleberg	T-C-B	combined 21B	1944	6900-7109	104661	VK-main	LF	Deltaic
27	Kleberg	Seeligson	13 zones	1937	5675-7090	215105	VK-main	LF, MF	Fluvial, Fluvial/Deltaic
28	Kleberg	Borregos	Combined zones	1945	7040	109744	VK-main	V, F	
29	Kleberg	Borregos West	F-82 Segment A	1961	5870	1065	VK-splay	MF	Fluvial?
30	J. Wells	Elpar	2 zones		5130-5494	7815	just updip to VFZ	Frio	Fluvial
31	J. Wells	Ben Bolt	Ben Bolt		5175	9265	just updip to VFZ	Frio	Fluvial
32	J. Wells	Magnolia City	Garcia sand	1951	5642	1980	VK-splay	MF	
33	Kleberg	Big Caesar S.	Pflueger Lower		7562	2537	VK-main	LF	Fluvial/streamplain
34	Kleberg	Bog Caesar	Pflueger Upper	1963	7440	9802	VK-main	LF	Fluvial/streamplain
35	Nueces	Stratton	12 zones	1938	6100-7000	75227	VK-main	LF, MF	Fluvial, Fluvial/Deltaic
36	J. Wells	Tom Graham	Tom Graham	1938	5400	5,721	VK-splay	V	Deltaic
37	J. Wells	Magnolia City N	2 zones	1953	4981-5040	6405	VK-splay	MF	Fluvial
38	Nueces	Agua Dulce	2 zones	1928	6850-6970	45584	VK-main	LF	Fluvial/streamplain
39	Nueces	Brayton	Brayton	1944	7196	7682	VK-main	LF	Fluvial/streamplain
40	Nueces	Clara Driscoll	Clara Driscoll	1935	3800	6913	VK-main	UF	Fluvial/streamplain
41	Nueces	Clara Driscoll S.	J or K	1937	5300	4764	VK-main	LF	Deltaic
42	Nueces	Richard King	2 zones	1937	5400-5600	20754	VK-splay	MF	Fluvial/streamplain
43	J. Wells	Hollow Tree	Hollow Tree	1949	3354	1435	VK-splay	UF	close to strandplain
44	Nueces	Farenthold	Zone L	1946	5886	1967	VK-splay	MF	Fluvial/streamplain
45	J. Wells	Alfred	Alfred	1937	4680	1577	VK-splay	MF	Fluvial/Streamplain
46	J. Wells	Reynolds	Reynolds	1939	4800	2559	VK-splay	MF	Fluvial/streamplain

environment interpreted from log profiles were used to separate Vicksburg units originally grouped within the Frio Fluvial-Deltaic Sandstone Play from Frio reservoirs that are the main focus of this study.

Upper Vicksburg Reservoirs

Data presented here from Vicksburg sandstones include only those reservoirs originally classified as belonging to the Frio Fluvial-Deltaic Sandstone Play. Vicksburg reservoirs along the play trend in South Texas have a shorter development history than do shallower Frio zones and are still actively being exploited and explored by many operators. Resource assessment in this project focused on more mature Frio reservoirs that are in danger of being abandoned before they have produced a majority of their mobile oil. Limited reservoir data from Vicksburg sandstones are shown here to illustrate some basic differences in reservoir geometry between Vicksburg reservoirs and those reservoirs in the overlying Frio section (Figure 18). Reservoir attribute value distributions for Vicksburg sandstones are statistically different than Frio reservoir values. Vicksburg reservoirs are characterized by greater net-pay thicknesses (mean value of 25 ft) and smaller reservoir areas (mean of 1,228 acres). Thicker development of reservoir sandstone facies, as compared to that observed in Frio reservoirs, is expected in delta-front facies that characterize Vicksburg sedimentation. The smaller areal distribution of these reservoir sandstones is most likely a result of the significant faulting associated with Vicksburg deposition that serves to isolate reservoirs into multiple structural compartments.

Lower Frio Reservoirs

Lower Frio reservoirs reside in the stratigraphic section immediately above the Frio-Vicksburg contact in an interval of mixed progradational and aggradational fluvial-deltaic sedimentation. Reservoir sandstones are predominantly dip-elongate, delta-plain distributary-channel sandstones that stack to combined thicknesses of up to 50 ft. These composite units

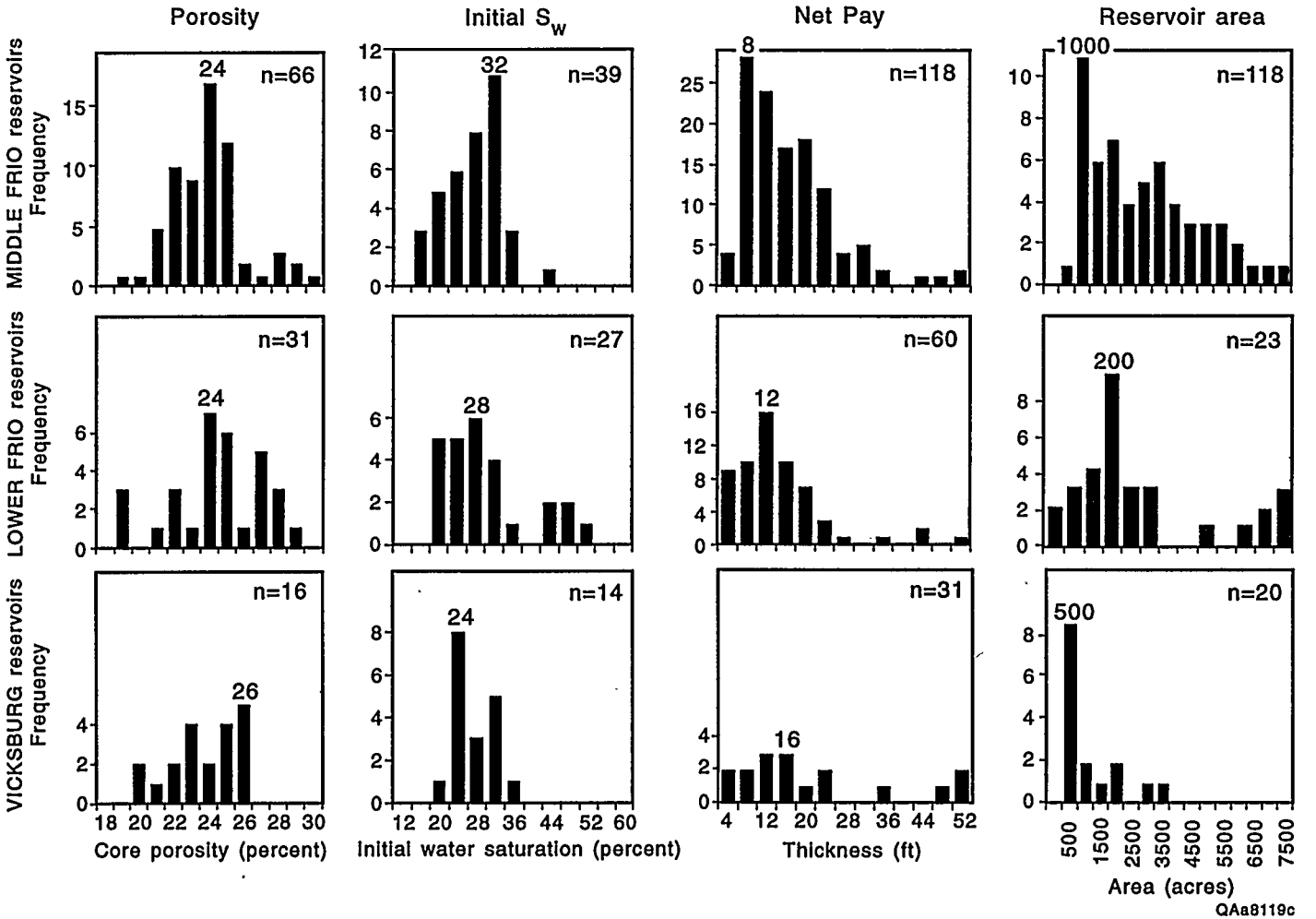

Figure 18. Cumulative frequency histograms illustrating the differences in the distribution of values of porosity, initial water saturation, net pay, and reservoir area for middle Frio, lower Frio, and Vicksburg reservoir sandstones in the Frio Fluvial-Deltaic Sandstone Play.

commonly display an upward-thickening trend that reflects net progradation of the fluvial-deltaic system. Average net pay thicknesses and reservoir areas for lower Frio sandstones are 17 ft and 3, 313 acres, respectively (Figure 18). Some of the lower Frio reservoirs included within the play during initial field classification are located rather far downdip to the Vicksburg Fault Zone (basinward from the ancient Frio shoreline) where the lower Frio section becomes expanded and is complicated by faulting. These reservoirs include more deltaic facies and are thicker than their distributary and fluvial channel counterparts located closer to the main fault zone.

Middle Frio Reservoirs

The majority of reservoir sandstones in the Frio Fluvial-Deltaic Sandstone Play are aggradational fluvial channel sandstones located within the middle Frio section. These reservoirs consist predominantly of dip-elongate, upward fining, channel-fill facies with individual thicknesses ranging from 5 to 30 ft and composite stacked thicknesses between 20 and 60 ft. Average net pay and reservoir size for 118 reservoirs from throughout the play are 12.5 ft and 2, 643 acres. Mean values for porosity (24%) and initial water saturation (Sw) (31%) are similar for both lower and middle Frio reservoir sandstones, although the distributions of values for these data are distinctive for each (Figure 18).

Distribution of Remaining Recoverable Oil

Overall estimates of the remaining mobile oil resource in reservoirs from middle and lower Frio stratigraphic intervals throughout the play trend in South Texas were calculated by subtracting the volume of oil produced and an estimated residual oil volume from an estimate of original oil in place (OOIP) calculated for each group of reservoirs in the play. OOIP and residual oil for individual reservoirs were calculated using values of acre/ft, porosity, initial water saturation, and formation volume factor (Boi) data specific to each reservoir, and where data were unavailable, mean values derived from the middle Frio and lower Frio reservoir populations were substituted. From these calculations, it is estimated that nearly 1.5 Bbbl of remaining mobile oil,

representing more than 40 percent of the OOIP, are still present in these reservoirs (Figure 19). Volumes calculated for both the lower Frio (>800 MMBO) and middle Frio (>580 MMBO) stratigraphic intervals represent significant resource targets. The larger available resource estimated to be present in lower Frio reservoirs may be in part attributed to the greater structural complexity of this deeper portion of the Frio section, which has resulted in greater compartmentalization of oil volumes and therefore reduced recovery efficiencies. Lower Frio reservoirs, because of their greater depths, also have fewer completions than those in the middle Frio and in many cases have not experienced such long production histories. This is because the shallower Frio section was the preferred focus of most early Frio reservoir development.

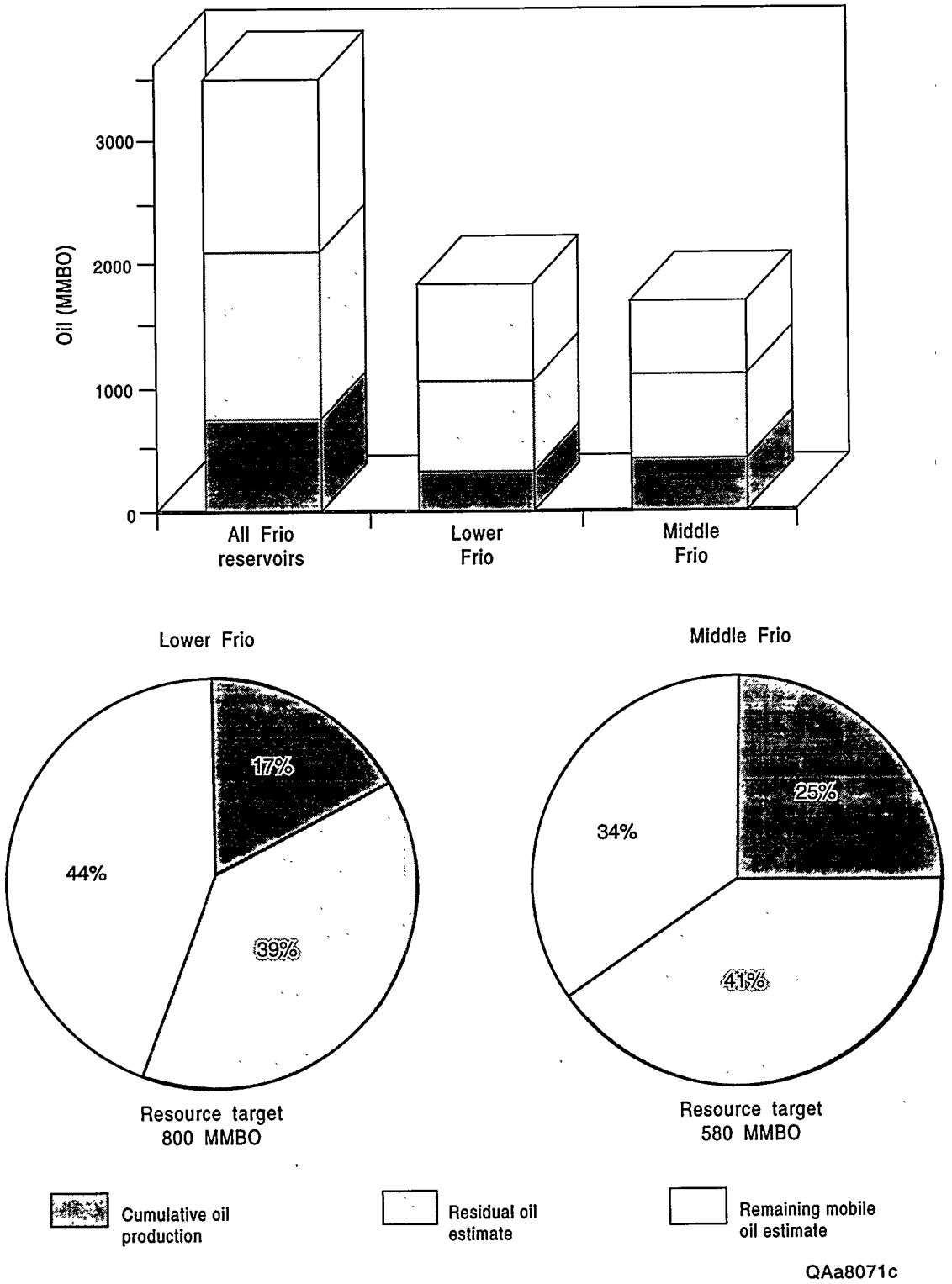

Figure 19. Distribution of the location of oil resources within reservoirs of the Frio Fluvial-Deltaic Sandstone Play in South Texas. Nearly one billion barrels have been recovered in the play, but nearly two thirds of the estimated original-oil-in-place, including more than 1.5 Bbbls of mobile oil, remain in the reservoirs.

RESERVOIR CHARACTERIZATION EXAMPLES FROM RINCON FIELD

L. E. McRae, M. H. Holtz, TF.Hentz and C. Chang

Introduction

Reservoirs throughout the Frio play were screened as candidates for detailed characterization studies. The goal of the screening was to find fields containing large infield reserve growth potential and sufficient data to support detailed studies that would demonstrate the value of multidisciplinary characterization techniques by identifying specific opportunities for recompletions or infill drilling. Screening criteria included the (1) size of the reservoir-producing area, (2) density of well completions in individual reservoirs, (3) quality and quantity of existing geologic and production data, (4) availability of 2-D or 3-D seismic coverage, and (5) current level of drilling activity. Fields that contain reservoirs with large producing areas and numerous well bores with a relatively wide completion spacing were excellent candidates for study because they present good possibilities for the identification of bypassed and untapped reservoir compartments. Fields with abundant high-quality geologic, geophysical, and production data, including conventional core and core analysis data, modern well logs, 3-D seismic coverage, and complete reservoir production histories would provide the best chance of success for identifying additional reserve potential through integrated, advanced characterization methods. Recent drilling activity in a field is an indication of an operator's current strategy for reservoir reexploration and additional field development and therefore highlights fields with the best potential for near-term implementation of recommendations resulting from this project.

Two fields, spanning the geographic extent of the play, were selected on the basis of these criteria. Tijerina-Canales-Blucher field (T-C-B) in Jim Wells County, at the north end of the play, and Rincon field in Starr County, at the south end of the play (Figure 17) both contained large reservoirs with abundant data and wide current well spacings and had experienced recent operator activity. Specifically, the Rincon field contained extensive engineering data and some conventional core while a 3-D seismic volume was made available by the T-C-B operator.

The following section describes characterization studies of Rincon reservoirs, focusing on geologic and engineering characterization founded in available core material. A later section discusses integration of geology and geophysics in T-C-B reservoirs.

Location and Geologic Setting of Rincon Field

Rincon field is located in eastern Starr County, Texas, approximately 120 mi southwest of Corpus Christi and 20 mi north of the United States-Mexico border. The entire Rincon field area covers more than 20,000 acres and contains more than 64p wells. The area of investigation covers approximately 5,000 acres in the northern portion of the field, includes nearly 200 wells, and is limited to productive reservoir sandstones within the Frio section (Fig. 20).

The general structure in the shallow Frio section at Rincon is characterized by a northeast-trending, downthrown asymmetric rollover anticline that plunges gently to the northeast and is bounded to the west by the Sam Fordyce/Vanderbilt Fault, a major growth fault associated with the large Vicksburg Fault Zone system (Fig. 21). Frio production associated with the shallow structure is both stratigraphically and structurally controlled. Hydrocarbons are trapped in zones within the rollover anticline downdip of the major growth fault and exist in multistoried and multi-lateral sandstone reservoirs that form complex stratigraphic traps draped over an anticlinal nose.

More than 50 individual productive reservoirs within the stratigraphic interval from 3,000 to 5,000 ft have been identified and mapped across the Rincon field area, and they range in dimension from only a few acres to complex, interrelated reservoir systems that are present across the entire field. Individual reservoir units occur both as narrow channel-fill sandstones isolated vertically and laterally by very low permeability overbank facies and floodplain mudstones and as large channel complexes consisting of multiple thin sandstone units that combine into a single large communicating reservoir. The variability in sandstone geometries and the complex multilateral and multistacked nature of these reservoirs provide excellent potential for identifying additional hydrocarbons that have been isolated in untapped and incompletely drained reservoir compartments. In this project our Rincon field study focused on two reservoirs as type examples.

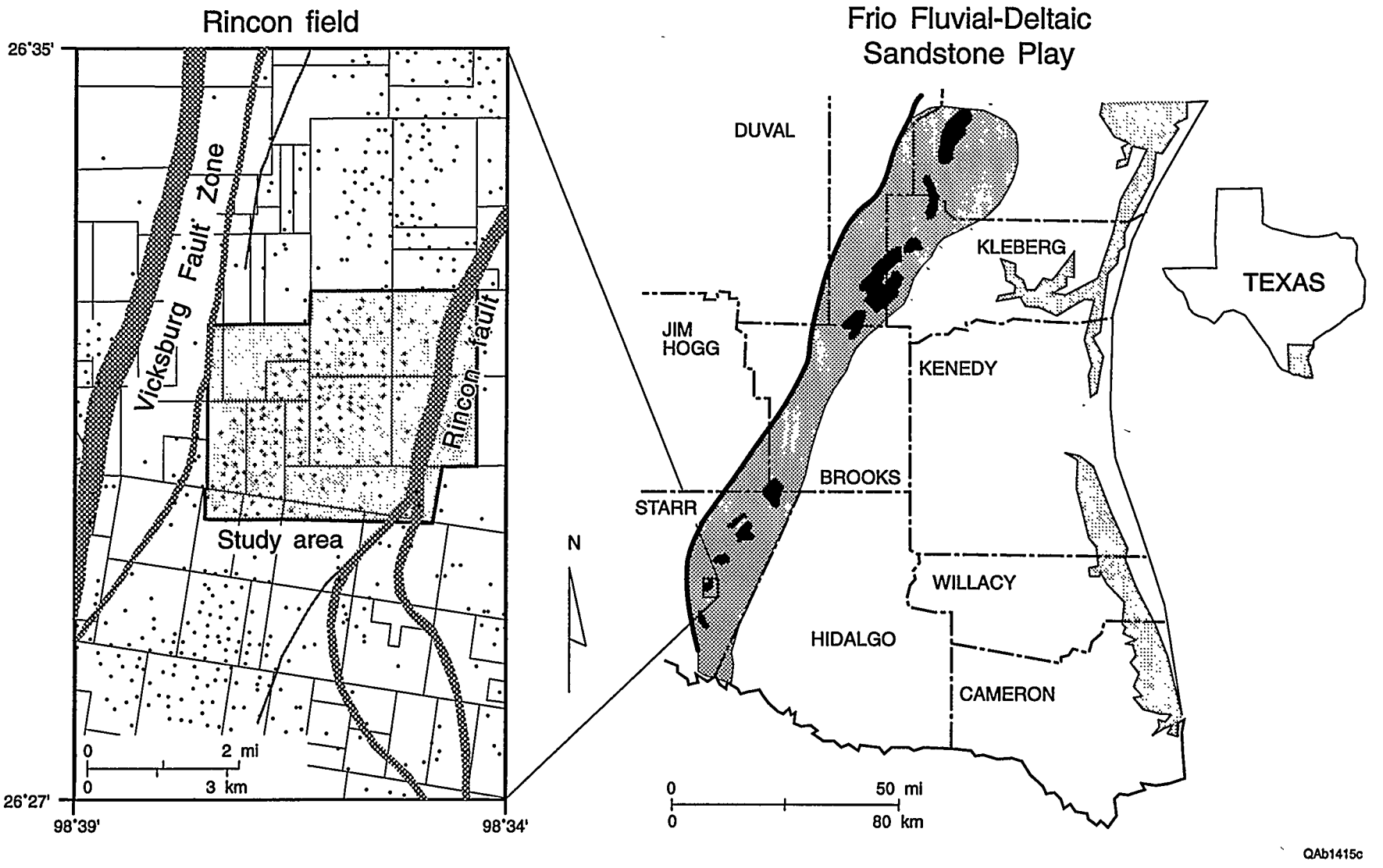

Figure 20. Location map of Rincon field within the Frio Fluvial-Deltaic Sandstone Play and area of field selected for detailed reservoir studies.

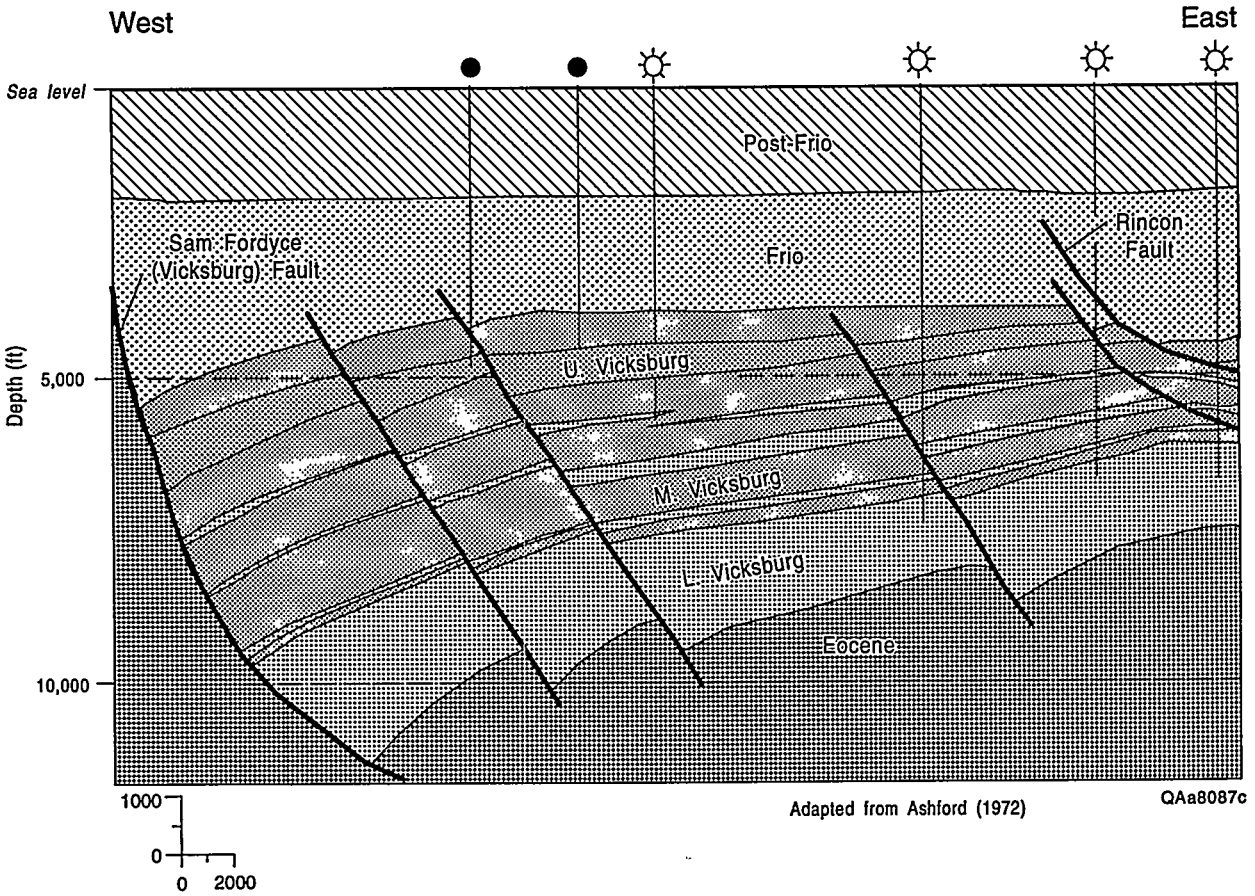

Figure 21. Generalized west-to-east cross section through Rincon field illustrating structural setting of a representative field in the Frio Fluvial-Deltaic Sandstone Play (adapted from Ashford, 1972).

Selection of Reservoirs for Detailed Study

Because of the large number of reservoirs in Rincon field and the limited nature of this study, a subset of two major reservoir intervals was selected for detailed characterization. These reservoirs, the Frio D and E intervals, are the two most highly prolific reservoir zones in Rincon field, having produced a combined 22 MMbbl of oil from the leases studied. Additionally, the stratigraphic complexity of these intervals, consisting of vertically stacked and laterally coalescing sandstone lobes, provides ideal conditions for the isolation of oil accumulations in isolated compartments, many of which are now incompletely drained or completely untapped.

The Frio D and E intervals also exhibit low recovery efficiencies. Taken together, the four reservoirs in the Frio D interval have a current recovery efficiency of only 28 percent, whereas the

four reservoirs in the E interval have a recovery efficiency of 38 percent. Both intervals were waterflooded, with substantially different results. Waterfloo ding of the E reservoirs account for 21 percent of cumulative production, whereas waterfloo ding of D reservoirs only accounts for 2 percent of total production.

Reservoir Characterization Methodology

A complete, all-encompassing reservoir characterization methodology developed during this study was presented in Holtz and others (1996). The methodology takes a systems approach, viewing geologic, geophysical, and engineering data inputs with a goal of determining reserve growth potential. The four basic steps in the methodology are to (1) determine reservoir architecture, (2) establish fluid flow trends, (3) integrate fluid flow history and reservoir architecture, and (4) evaluate reserve growth potential. As with all field studies the comprehensiveness of techniques applied is dependent on the available data. In Rincon field, only those techniques that made maximum use of available data were applied. Details of the specific methodology used on Rincon reservoirs was presented in McRae and others (1995) and pertinent information is summarized in each of the four following sections.

Determine Reservoir Architecture

Importance of the Genetic Sequence Analysis Approach

Development of a detailed regional stratigraphic and structural context for a reservoir is a critical step in evaluating its potential for secondary hydrocarbon recovery. Sequencestratigraphic concepts provide a chronostratigraphic framework in reservoir studies that is useful in delineating the structure of reservoir flow units and also provide a means of transporting results of reservoir studies to other fields in analogous stratigraphic settings. Construction of a reservoir framework at the sequence and parasequence scales provides a means for the natural packaging of strata into genetic units that correlate well to petrophysically defined units at the interwell scale (Tyler and others, 1992). Definition of lithologic and diagenetic reservoir flow-unit

architecture of fluvial-deltaic sandstones within the context of a well-defined sequence-stratigraphic framework can provide a model to predict the distribution and continuity of permeable zones in other reservoirs deposited in analogous depositional settings. Previous detailed work on the regional geology of the Frio depositional sequence in South Texas (Galloway and others, 1982; Galloway, 1977, 1982, 1989a, 1989b) and several recent reservoir characterization studies of Frio gas reservoirs (Jirik, 1990; Kerr, 1990; Kerr and Jirik, 1990; Kerr and others, 1992; Grigsby and Kerr, 1993) provide an excellent context in which to study individual facies components of oil-bearing reservoirs in the Fluvial-Deltaic Sandstone play.

In Rincon field, a prominent low-resistivity marker interpreted to be an important flooding surface separates the thicker, generally upward-coarsening progradational units in the lower Frio third-order unit from thinner, dominantly aggradational channel deposition in the middle Frio section. The majority of Frio production at Rincon occurs within a 1,000-ft interval of interstratified sandstones and mudstones. Laterally persistent low-resistivity surfaces interpreted to represent floodplain or interdeltaic mudstones separate primary reservoir sandstone zones that are commonly 50 to 150 ft thick. These fourth-order reservoir zones are, in turn, composed of several individual, 5-30-ft thick channel-fill units (Fig. 22). The major cause of stratigraphic complexity and compartmentalization of hydrocarbons in these sandstones is their variability in geometry and the multilateral and multistacked nature of individual fifth-order reservoir units. Fourth-order reservoir units at Rincon field were evaluated to identify specific reservoir styles that are representative of those observed throughout the play. Understanding the specific stratigraphic context of the reservoirs selected for study will facilitate transfer of results of this study to other reservoirs, other fields, and other analogs beyond the Frio in South Texas.

Stratigraphic positions of important reservoir units in Rincon field within the context of the larger scale genetic stacking sequence were identified to assess the importance of reservoir stratigraphy to hydrocarbon production, recovery efficiency, heterogeneity style, and the potential for compartmentalization of additional oil resources. Twenty-four low-resistivity markers representing 7 major (fourth-order) bounding surfaces and 17 secondary (fifth-order) surfaces in

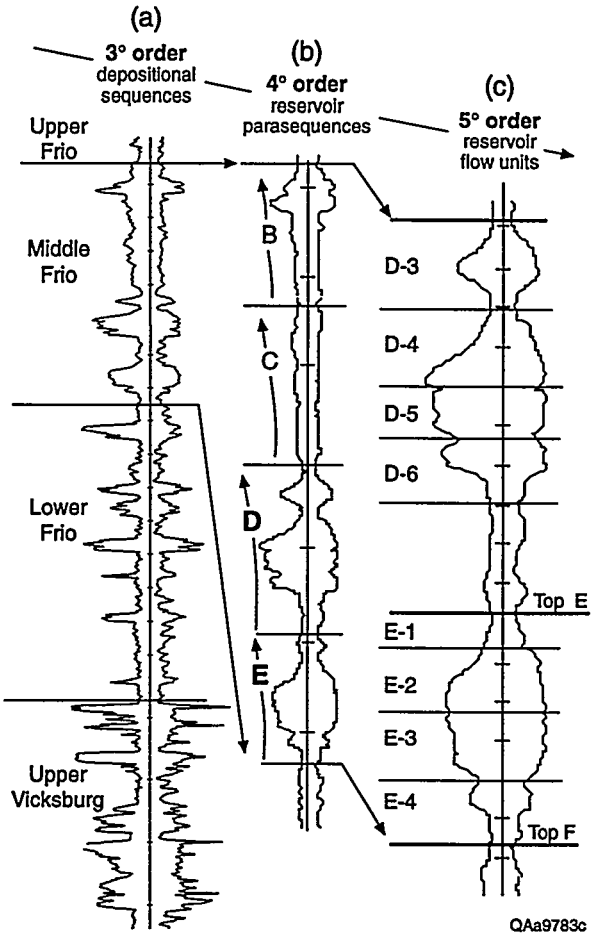

Figure 22. Spontaneous Potential/resistivity type logs illustrating (a) the general depositional sequence for the productive Frio–upper Vicksburg reservoir interval, (b) the stratigraphic context of the middle Frio reservoir sequence in Rincon field, and (c) the reservoir nomenclature of individual producing units within the Frio D–E interval selected for detailed study.

184 wells were correlated in a series of stratigraphic cross sections across the field study area. Wireline core data representing more than 1,500 analyses from more than 100 wells in the Rincon field study area were assigned to individual upper Vicksburg, lower Frio, and middle Frio reservoir subunits and evaluated to assess heterogeneity within each of these major reservoir stacking intervals.

Ascertaining Internal Reservoir Stratigraphy

Ascertaining internal reservoir stratigraphy requires five separate tasks. These include (1) identification of regional stratigraphy and preliminary fieldwide stratigraphy, (2) the identification of lithofacies from available core material, (3) petrographic examination of cores, (4) the correlation of the finest-scale genetic units resolvable with the given data, and (5) determining the geometry and depositional history of sandstones within these fine-scale genetic units.

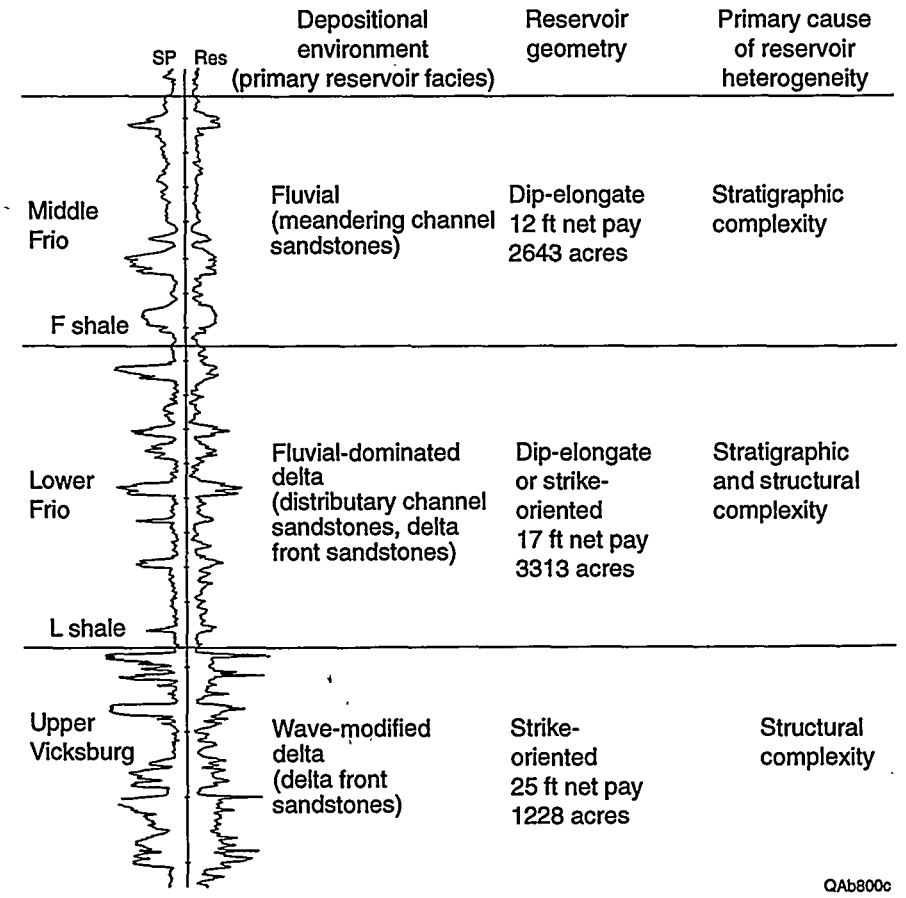

Figure 23. Depositional systems and reservoir attributes of the Rincon field reservoir section.

Regional Stratigraphy

A typical log from the productive reservoir interval in Rincon field is shown in Figure 23. The F shale marker represents the division between lower and middle Frio reservoirs, as it is located where a change in sedimentation style occurs from deposition of net progradational sandstone packages to primarily aggradational sand deposition. Reservoirs in the middle and lower Frio sections consist of multiple stacked pay sandstones. Interpretations supported by SP log profiles and whole core studies indicate that the dominant reservoir lithofacies are fluvial channel-fill deposits. Individual reservoir sandstones (fifth-order units) within each zone are commonly 5-30-ft-thick channel-fill units and have lateral dimensions ranging from 1,000 to more than 6,000 ft. The major cause of reservoir complexity and compartmentalization of hydrocarbons is a result of this variability in sandstone geometry and the multilateral and

multistacked nature of these individual reservoir units. Characteristics specific to each stratigraphic reservoir interval are discussed in more detail below.

Upper Vicksburg reservoirs

Vicksburg reservoirs in Rincon field include the sandstone unit below the L shale shown in the lower portion of the log interval illustrated in Figure 23. These reservoirs consist of thick progradational (seaward-stepping) deltaic sandstone deposits that occur in packages 50 to 150 ft thick and are separated by 50- to 200-ft-thick intervals of mudstone. Primary reservoir facies are channel-mouth-bar sandstones that are interbedded with prodelta mudstone and siltstone. Individual upward-coarsening channel-mouth-bar deposits are generally less than 50 ft thick and stack to produce repetitive cycles that can reach 150 to 200 ft in thickness.

Vicksburg reservoirs in Rincon field are not currently targets for resource delineation and additional recovery through our studies, which emphasize characterization of stratigraphic heterogeneity. This is because their deposition was strongly influenced by faulting associated with the development of the Vicksburg Fault Zone (Coleman and Galloway, 1991), and correlations necessary to document depositional heterogeneity and stratigraphic compartmentalization in these reservoirs are difficult. Our reservoir studies are focusing on the structurally uncomplicated Frio reservoir interval, where there is better potential for identifying lateral facies heterogeneity and stratigraphic compartmentalization, and there are also much more data available.

Lower Frio reservoirs

In Rincon field, the Lower Frio stratigraphic interval appears to represent deposition in an aggradational to mixed aggradational and progradational setting within the Gueydan fluvial system. The lower Frio reservoir interval shown in the log in Figure 23 is interpreted to correspond to an interval of mixed progradational and aggradational sedimentation. The F shale is taken to mark the boundary between the mixed aggradational and progradational reservoirs in the lower Frio section and the purely aggradational deposition that characterizes the middle Frio section.

Reservoir facies in the lower Frio interval are interpreted to represent predominantly fluvial channel and delta-plain distributary-channel sandstones. Channel units are distributed as elongate, dip-parallel belts. Individual, upward-fining channel sandstone packages, as evidenced by bell-shaped SP log profiles, range from 5 to 20 ft thick, and commonly stack to produce amalgamated units that have vertical thicknesses of 10 to 50 ft. These stacked sandstone packages commonly display an upward-thickening trend. Although sandstone units are, on average, thicker than in middle Frio reservoir zones, sandstone body continuity is generally less than in middle Frio fluvial channels. This may be because distributary channel-fill sandstones are commonly narrower and are flanked laterally by sandstone-poor interdeltaic fades. Low-permeability mudstone fades locally encase and compartmentalize or isolate individual reservoir sandstones and create reservoir compartments that are the primary targets for additional oil recovery in the lower Frio interval.

Middle Frio reservoirs

The depositional pattern in the middle Frio interval in Rincon field is characterized by sedimentation dominated by fluvial aggradation. Deposition in dip-elongate channel systems developed across the low-relief Oligocene Gulf Coastal Plain toward the shoreline in a direction from northwest to southeast (Fig. 24). Middle Frio reservoir fades consist primarily of dip-elongate fluvial channel-fill sandstones and are separated by nonreservoir fades that include levee siltstones and floodplain mudstones. Productive middle Frio reservoirs in Rincon field occur both as individual narrow channel-fill units isolated vertically and laterally by low-permeability overbank and floodplain fades and as large channel complexes with multiple sandstone lobes. Sandstones have individual thicknesses ranging from 5 to 30 ft but are commonly stacked into composite units with gross thicknesses between 20 and 60 ft. Low-permeability subfades within the channel fill are responsible for development of multiple reservoir compartments that may represent significant opportunities for additional recovery.

Description of Lithofacies from Core

After the regional and general fieldwide context of reservoir intervals were established, available core material was studied to tie lithofacies to log response, aid in interpreting

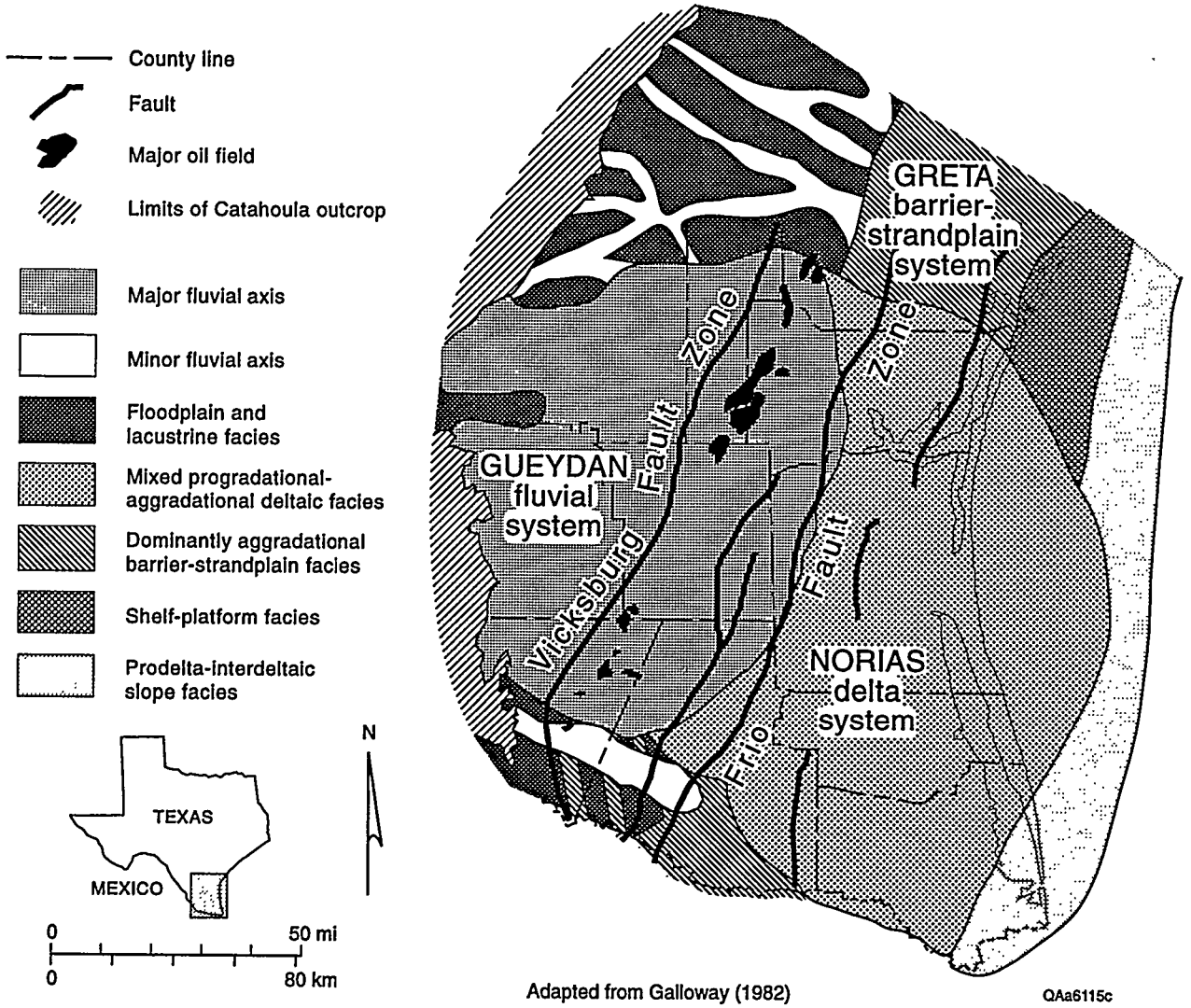

Figure 24. General distribution of the Norias delta and Gueydan fluvial depositional systems responsible for deposition of the Frio stratigraphic unit. The Frio sediments in the vicinity of the Vicksburg Fault Zone were primarily deposited in moderate- to high-sinuosity mixed-load stream environments of the Gueydan fluvial system. (Map distribution from Galloway and others, 1982.)

depositional facies, examine the petrographic character of reservoirs and acquire special petrophysical measurements. Detailed core studies were conducted on conventional core cut from the T. B. Slick A133 and A149 wells, located in lease block 231 near the center of the field study area. A total of 155 ft of core was examined. Core descriptions from both wells, along with porosity and permeability profiles derived from conventional core analysis data, are illustrated in Figures 25, 26, and 27. Detailed core description and sampling were limited to the Frio D and E reservoirs. The core from well 149 includes the stratigraphic interval through most of the

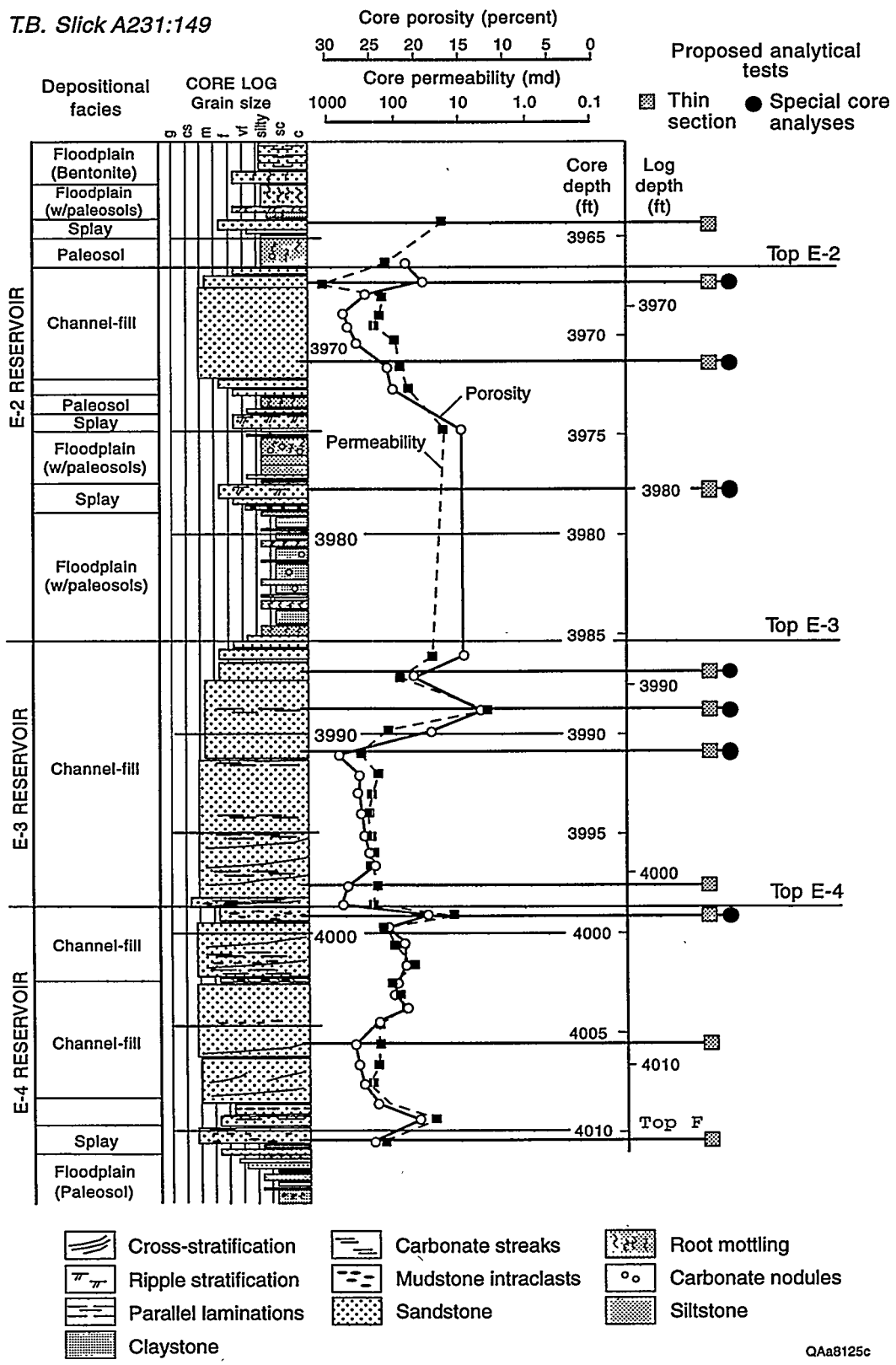

Figure 25. Graphic core log, T. B. Slick 231:149 well, Frio E reservoir zone, along with corresponding facies interpretations, core analysis data for porosity and permeability, and location of samples selected for petrographic and special core analyses.

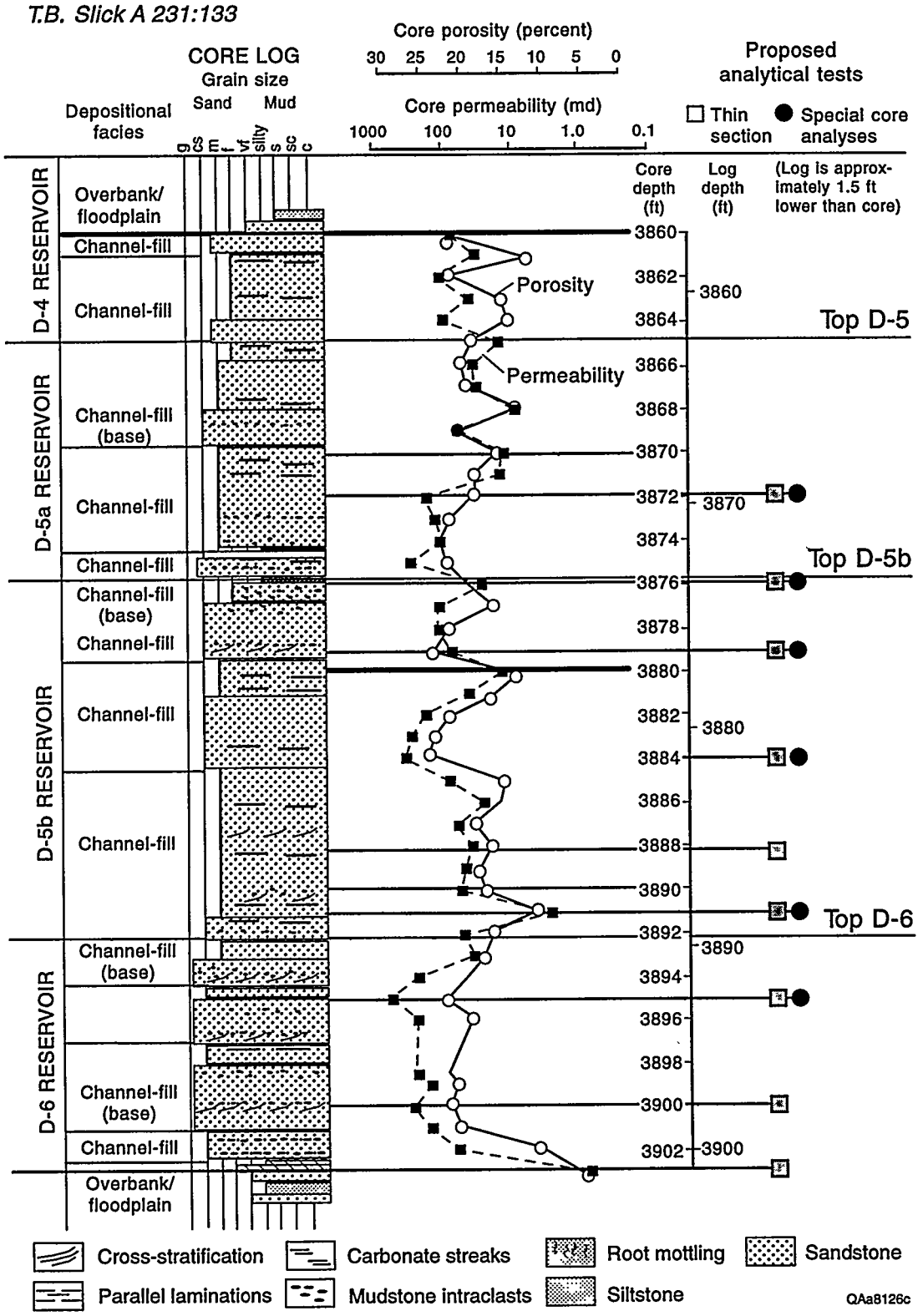

Figure 26. Graphic core log, T. B. Slick 231:133 well, Frio D reservoir zone, along with corresponding facies interpretations, core analysis data for porosity and permeability, and location of samples selected for petrographic and special core analyses.

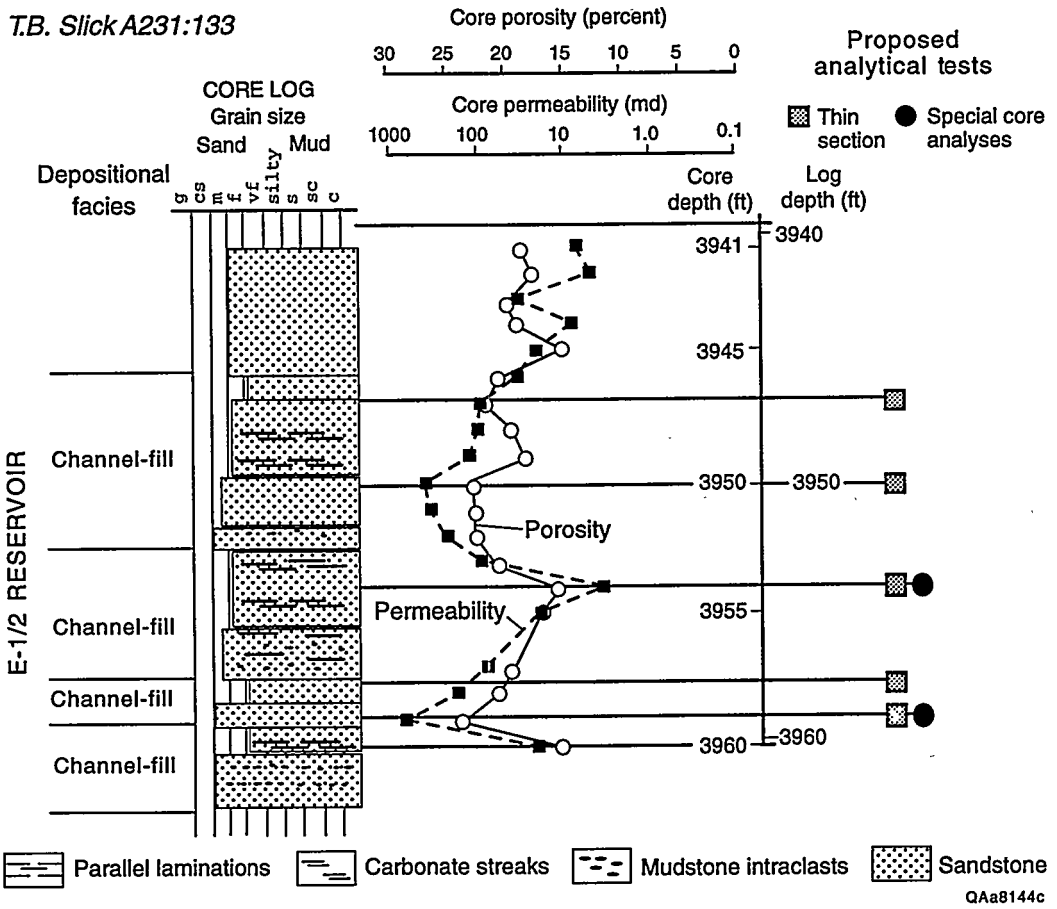

Figure 27. Graphic core log, T. B. Slick 231:133 well, Frio E reservoir zone, along with corresponding facies interpretations, core analysis data for porosity and permeability, and location of samples selected for petrographic and special core analyses.

E reservoir zone, and the well 133 core represents the depth interval through the D reservoir and the top portion of the E reservoir. Based on core observations, there are no obvious distinctive differences in sandstone mineralogy, textures, or facies types between the Frio D and E reservoir zones. Vertical facies sequences of channel-fill sandstones, splay sandstones, and floodplain mudstone units recognized in both cores support our interpretations of fluvial depositional environments determined from electric log correlations and reservoir mapping.

Mudstones

Floodplain units present between sandstone facies consist of red-brown mudstone, silty mudstone, and siltstone that commonly exhibit color variegation and various degrees of

bioturbation, root molds, and calcareous nodule development that are all diagnostic of alteration associated with soil-forming processes. Caliche formation and the reddish coloration of the mudstones reflect deposition in well-drained and sparsely vegetated floodplains and suggest semiarid climatic conditions. The abundance of pedogenic features also indicates that interchannel areas were subaerially exposed and drowned only during infrequent flooding.

Darker gray and laminated mudstones with a conspicuous lack of pedogenic features that characteristically indicate abandoned-channel facies were not observed in core. Because of the very limited whole core available, this is not surprising. Abandoned-channel facies are interpreted to be present within the field study area but cannot be distinguished solely on the basis of electric log signature. Mudstones that cannot be correlated between wells may be inferred to represent abandoned-channel facies.

Some floodplain mudstones are green-gray and possess a mottled waxy texture typical of an altered bentonite (e.g., 3,960-3,961 ft, Fig. 25). Volcanic activity was occurring in northeastern Mexico throughout the Oligocene, and other workers have noted the presence of bentonites and high concentrations of volcanic glass in the Frio reservoir section in other South Texas fields (Kerr and Jirik,1990; Grigsby and Kerr, 1993).

Sandstones

Both channel-fill sandstones and crevasse splay sandstone facies were observed in core. Individual channel-fill sandstones range from 5 to 12 ft thick, and all exhibit upward-fining textures. Splay sandstones are less than 1 ft thick (e.g., 3,964 ft, 3,974 ft, 3,980 ft, Fig. 25) and appear more uniform or slightly upward coarsening in grain size. The thin (< 2 ft) nature of these splay facies suggests that crevasse development was localized and did not provide a significant contribution to sand deposition.

In addition to these primary facies distinctions, three channel subfacies, basal, middle, and upper channel-fill, could be identified on the basis of texture and sedimentary structures. The basal channel-fill facies refers to the lowermost portion of the channel-fill unit, is commonly coarser grained than the rest of the channel-fill (medium- to coarse- grained sandstone), and may

include a gravel lag consisting of intraformational clasts of mudstone and calcareous nodules (e.g., 3,997 ft, 4,010 ft, Fig. 25, 3,875 ft, 3,894 ft, Fig. 27). The thickness of the basal facies of the channel-fill is typically less than 1 ft. The middle channel-fill facies comprises the majority of the channel-fill unit and has a grain size that normally ranges from medium to fine. Evidence of cross-stratification is very faint or not observable in core. The upper channel-fill facies consists of the top few feet of a channel-fill unit, is finer grained than the underlying middle channel-fill sandstone (fine to very fine sandstone to silty sandstone), and has rare evidence of ripple-drift stratification.

Vertical profiles of porosity and permeability values are plotted alongside each of the described cores to assist in identification of different petrophysical rock types present in the various depositional facies. These profiles also illustrate the comparison of reservoir properties between channel-fill sandstones and splay sandstones and among the various channel subfacies. Channel-fill sandstones have lower permeability in the basal channel fill, where there is commonly a well-developed mud chip zone (e.g., 3,997 ft, 4,009 ft, Fig. 25; 3,876 ft, 3,891 ft, Fig. 26). Porosity and permeability systematically increase upward through the middle portions of the sandstone unit, and then they are typically reduced near the top of a sandstone where there is a reduction in grain size (e.g., 3,970 ft to 3,967 ft, 4,009 ft to 4,003 ft, Fig. 25; 3,876 ft to 3,870 ft, Fig. 26). Thin sandstones that are interpreted to represent crevasse splays or perhaps distal channel margins are generally finer grained than channel-fill facies and therefore possess lower porosity and permeability (e.g., 3,964 ft, 3,974 ft, Fig. 25).

Commonly two sandstone units are stacked together, and the presence of a mud chip zone at the base of the upper sandstone unit results in &significant reduction of permeability (e.g.,3,997 ft, Fig. 25; 3,875 ft, Fig. 26). Another rock type that has not been designated a separate facies consists of middle or upper channel facies sandstones that contains abundant carbonate cement. Thin (<1 ft) cement zones observed in core appear to be a localized phenomenon, but where present, correspond to lower porosity and permeability values (e.g., 3,989 ft, Fig. 25; 3,871 ft, Fig. 26).

Petrographic Studies Overview

Petrographic studies on Rincon Frio sandstone samples were conducted to determine framework compositions, textures, and cement types and distribution to evaluate the degree to which diagenesis is controlling reservoir quality in the Frio D and E reservoir sandstones in Rincon field. General descriptions of pore geometry of these sandstones were also completed to supplement results from special core analyses.

Methods

The guiding approach to petrographic analyses was to conduct them within the context of the reservoir stratigraphic framework. Twenty-two representative samples from core in both wells were selected to provide good data coverage of each of the various reservoir fades and petrophysical rock types present within the Frio D and E reservoir zones in the two wells (Figs. 25, 26, and 27). Samples selected from the T. B. Slick 231/149 well were taken from the end trims of 1-inch-diameter core plugs so that petrographic parameters viewed in thin section could be directly compared to laboratory-derived porosity and permeability values. Several of these plugs were also selected for special core analyses. There are core analysis data for the T. B. Slick 231/133 core, but the original plugs from which these measurements were taken were not available. New core plugs were drilled from adjacent available core material for selected additional core measurements, and thin-section chips were taken from the ends of these new core plugs.

Composition of Frio D and E reservoir sandstones was determined by standard thin-section petrography supplemented by scanning electron microscopy (SEM) using an energy dispersive X-ray spectrometer (EDX). Petrographic characteristics, including texture (grain size, sorting), detrital mineralogy, authigenic cements, and porosity type and distribution, were observed and quantified by point counts of 21 of the 22 thin sections. A total of 200 counts was made on each thin section. Thin sections were stained for potassium feldspar and carbonates. Major categories of whole-rock volume counted include (1) primary detrital framework grains (quartz, feldspars,

and rock fragments), (2) authigenic cements, (3) accessory minerals, (4) detrital clay matrix, and (5) pore space. Size estimates of framework grains were performed by visually comparing thin sections to standardized grain-size charts. Both potassium feldspar (orthoclase) and plagioclase grains were categorized as fresh, leached, calcitized, or vacuolized/sericitized. Authigenic cements were identified by mineral composition and categorized according to their distribution within intergranular pores or within secondary pores formed by dissolution of preexisting framework constituents. Porosity was identified as primary or secondary according to similar criteria. Primary and secondary porosity were identified in the context of the inferred diagenetic history of the samples. SEM and EDX analysis of samples enabled visualization of mineral and pore morphology and precise identification of clay mineralogy.

Texture

Frio sandstone samples from Rincon field range from lower fine grained (0.15 mm) to pebbly lower medium grained (0.3 mm), with most samples being in the upper fine to lower medium sandstone range (0.21 to 0.3 mm). The mean grain size of all samples is 0.25 mm, the size that marks the border between the fine and medium sand categories. Sorting ranges from very poor to moderate; most samples are poorly sorted. Sand grains are angular to subrounded.

Framework mineralogy

All Frio sandstones examined are mineralogically immature, and most samples are classified as feldspathic litharenites by the sandstone classification of Folk (1974) (Fig. 28a). The dominant framework constituents of most Frio Rincon samples are rock fragments, which on average compose one-half of all framework grains. The average composition of essential framework grains (normalized to 100 percent) from all 21 core samples is 17 percent quartz, 33 percent feldspar, and 50 percent rock fragments (Q17F33R50). Compositions of samples from Rincon field generally coincide with compositions of other shallow (3,500 to 6,000 ft) Frio reservoir sandstones of the lower Texas Gulf Coast (Grigsby and Kerr, 1993). Deep (6,000 to 18,000 ft)

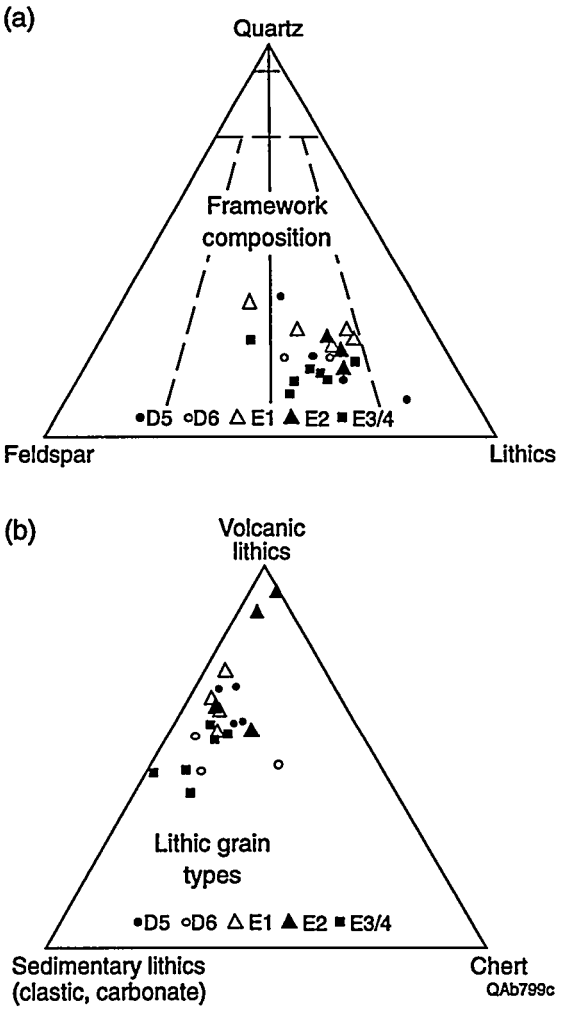

Figure 28. Ternary diagrams showing composition of Rincon D and E reservoir sandstones from thin-section petrography. (a) Percentages of quartz, feldspar, and lithic fragments. (b) Composition of lithic fragments, including volcanic rock fragments, sedimentary rock fragments, and chert.

Frio samples of the lower Texas Gulf Coast tend to be richer in quartz grains than the shallow Rincon samples, probably due to the greater degree of dissolution of feldspar and feldspar-rich rock fragments in the deep samples and resulting relative enrichment in quartz (Bebout and others, 1978; Loucks and others, 1986).

Most lithic fragments in the Frio Rincon samples are volcanic rock fragments (VRFs) (Fig. 28b), which compose an average of 59 percent of all rock fragments (range: 10 to 94 percent) and 18.7 percent of whole-rock volume (range: 6.5 to 26.0 percent). Coarser grained VRFs contain either plagioclase or predominantly orthoclase within a fine-grained groundmass and were derived from contemporaneous active volcanic areas in northern Mexico and West Texas (Loucks and others, 1986). Lindquist *(1976)* determined that most Frio VRFs from the Rio Grande Embayment are rhyolite and trachyte clasts, although numerous VRFs of basic

Table 11. Summary of petrographic data for Rincon sandstones.

Depth	Res. zone	Depositional facies	Gr. size (mm)	Phi size	Framework constituents (normalized percent) Q	F	R	Lithic grain compositions (%) Vrf	Srf	Crf	$CaCO_3$ cement (%)	Visual porosity estimates 1° Ø (%)	2° Ø (%)	Total Ø (%)	% total 2°
3872.0	D-5a	Channel-mid	0.15	2.75	11	30	59	26	1	9	7.5	1.5	20	21.5	93
3876.0	D-5a	Channel-base													
3879.0	D-5b	Channel-mid	0.21	2.25	16	41	43	19	0.5	5.5	4	0	27	27	100
3884.0	D-5b	Channel-mid	0.3	1.75	16	30	54	22	2.5	6.5	4.5	4.5	17.5	22	80
3891.0	D-5b	Channel-base	0.3	1.75	25	27	48	19	0	8.5	14	0.5	16.5	17	97
3895.0	D-6	Channel-mid	0.30	1.75	11	35	54	17	1	14.5	15	2	14	16	88
3900.0	D-6	Channel-base	0.30	1.75	13	30	57	22	4.5	10.5	22.5	2	4	6	67
3945.0	E-1	Channel-top	0.15	2.75	7	45	48	24.5	0.5	7	7.5	1	14.5	15.5	94
3950.0	E-1	Channel-mid	0.30	1.75	12	36	52	23.5	0	11	4.5	3.5	15	18.5	81
3954.0	E-1	Chan-mid (cc)	0.30	1.75	14	37	49	21.5	.05	8.5	32.5	0	1.5	1.5	100
3959.0	E-1	Channel-base	0.30	1.75	10	43	47	17.5	2	7.5	14	2	14.5	16.5	88
3964.0	E-2	Splay	0.21	2.25	21	46	33	15	0	0	0	0	2.5	2.5	100
3967.3	E-2	Channel-top	0.21	2.25	38	53	27	9.5	2	2	10.5	12.5	4.5	17	26
3969.3	E-2	Channel-mid	0.30	1.75	23	34	43	24.5	0.5	1.5	4	18.5	8	26.5	30
3974.6	E-2	Splay	0.21	2.25	15	27	58	22	4	6	24.5	5	7	12	58
3987.0	E-3	Channel-top	0.21	2.25	18	29	53	14.5	8	8	8.5	2.5	25.5	28	91
3988.7	E-3	Chan-mid (cc)	0.21	2.25	21	30	49	17.5	1	9.5	25	1	5.5	6.5	85
3990.9	E-3	Channel-mid	0.21	2.25	19	28	53	20	1.5	9.5	9	12.5	13.5	26	52
3997.5	E-3	Channel-mid	0.25	2	21	23	56	21	1	10	8	12.5	9.5	22	43
3999.6	E-3	Channel-base	0.25	2	16	34	50	16.5	4.5	11	5.5	3.5	18	21.5	84
4008.3	E-4	Channel-mid	0.30	1.75	23	25	52	13	1.5	13	9	11.5	18	29.5	61

Key: Q-quartz, F-feldspar, L-lithics, Vrf-volcanic rock fragment, Srf-sedimentary rock fragment (clastic), Crf-carbonate rock fragment (intraformational), 1° Ø-primary porosity, 2° Ø-secondary porosity, Total Ø- total visual porosity (1° + 2°), all values in counts (total 200 cts/sample), 2° Ø (% total)-percentage of total visual porosity that is secondary.

composition, such as basalt clasts, were observed in this study. In the outcrop equivalent to the Frio, sandstones contain VRFs of felsic and intermediate compositions as well as basalt grains (McBride and others, 1968). Rare VRFs in coarsest samples preserve original vesicular volcanic texture, with chert spherules now filling vesicles. Many isolated well-rounded chert and rare chalcedony grains within the Frio Rincon samples are probably vesicle fills. Sedimentary rock fragments (SRFs), which constitute an average of 41 percent of all rock fragments in Frio Rincon samples (14.7 percent of whole-rock volume), include carbonate rock fragments (CRFs), chert, and rare shale, siltstone, and sandstone clasts. CRFs and chert predominate, with only minor to trace amounts (<2 percent of whole-rock volume) of the other lithic types. CRFs are micritic and are interpreted to have been derived from caliche (Lindquist, 1976). Frio Rincon samples also contain trace amounts of metamorphic rock fragments (MRFs), generally phyllite or slate.

Plagioclase is by far the most abundant feldspar in the samples, composing an average of 82 percent of all feldspars and 17.6 percent of whole-rock volume (range: 12.0 to 27.0 percent) (Table 11). Frio samples contain an average of 3.9 percent (whole-rock volume) orthoclase (range: 1.0 to 11.0 percent). Both plagioclase and orthoclase grains occur in several states of alteration (in order of abundance): fresh, vacuolized/sericitized, leached, and calcitized. Leaching of entire feldspar grains was a prominent stage in the diagenetic evolution of the Frio Rincon reservoirs, and partially and wholly leached grains contribute to reservoir porosity and permeability. Both topics are discussed more fully in subsequent sections.

Quartz grains are third in relative abundance of all framework grains (average of 10.6 percent of whole-rock volume; range: 4.5 to 16.5 percent) (Table 11). Most quartz grains are single crystals. Rare grains in each sample, however, are polycrystalline, indicating, along with the sparse MRFs, a minor metamorphic source terrain for Frio Rincon samples.

Accessory minerals in Frio Rincon samples include, on average, only trace amounts of muscovite and biotite, and nearly 1 average whole-rock percent of patchy organic material (Table 11). Pyrite is locally finely disseminated in matrix and organics.

Detrital clay matrix

Frio Rincon reservoir rocks are low in clay matrix content, and it is not a significant factor in controlling reservoir quality. Samples contain an average whole-rock volume of 2.2 percent clay matrix (range: 0 to 9.0 percent) (Table 11). Illite and/or illite/smectite are the dominant clay minerals. One Frio Rincon sample (3964.1 ft) is notable in its abundance of detrital illite and/or illite/smectite matrix. This sample contains 48.5 whole-rock percent matrix, which is interpreted to be the alteration product of volcanic ash in a bentonite bed. Because this bed does not represent reservoir rock, its matrix content was not included in computations of the average content of the reservoir facies. Volume of pore-filling matrix (detrital clay) and clay cements is consistently low in the samples and is not considered to be a significant influence on reservoir quality.

Cements

Authigenic cements collectively constitute a range of 4.0 to 32.5 percent of the whole-rock volume in the Frio Rincon samples, with a mean value of 11.6 percent (Table 11). Authigenic cements include (in order of abundance) non-ferroan calcite, chlorite, and kaolinite. There are also trace amounts of quartz and feldspar overgrowths and illite/smectite grain-rimming cement. Calcite dominates other cements, with an average of 11.2 percent, close to the average sample content of all cements. Chlorite and kaolinite constitute an average of 0.4 and 0.1 percent of all cements, respectively.

Calcite cement occurs as an intergranular cement with a sparry, non-poikilotopic crystal habit. Most samples are only sparsely cemented and contain abundant, commonly oversized (as much as 0.45 mm in greatest dimension), pores. Isolated patches of sparry calcite with locally crenulate (corroded) rims are characteristic of most samples. In heavily calcite-cemented samples (low porosity), cemented areas are commonly as much as two framework-grain diameters wide and four grain diameters long. Some partially leached feldspar grains and VRFs contain calcite within intragranular dissolution voids; however, such grains were point-counted as calcitized feldspar and VRF, respectively, and they are relatively rare. Calcite is a significant Frio cement phase in other fields of the lower Texas Gulf Coast (Lindquist, 1977; Bebout and others, 1978; Loucks and others, 1986; Grigsby and Kerr, 1993).

The whole-rock volume of chlorite cement varies from 0 to 4.0 percent. Chlorite and illite/smectite are mostly grain-rimming cements but also fill a small percentage of intergranular pore space. Chlorite crystal morphology typically takes the form of platelets. Kaolinite, a decomposition product of feldspar, is present in only 6 of the 21 Frio Rincon samples and occurs as a patchy intergranular cement.

Quartz overgrowths are sparsely distributed in some samples and absent in others. Where present, overgrowths are consistently thin and poorly developed and probably represent incipient quartz cementation in these shallow Frio samples. Loucks and others (1986) noted that quartz overgrowths first developed in Frio sandstones between depths of 5,000 and 6,000 ft, deeper than

the 3,870- to 4,000-ft range of the Rincon field samples. In Seeligson and Stratton fields of South Texas, minor amounts of quartz overgrowths occur in Frio samples from 4,000 to 6,500 ft deep (Grigsby and Kerr, 1993). In their comparative study of Tertiary sandstones along the entire Texas Gulf Coast, Loucks and others (1986) also observed that quartz overgrowths are more abundant in samples having more quartz grains. Moreover, quartz grains are consistently the least abundant of framework grains in Frio samples from the lower Texas Gulf Coast (Bebout and others, 1978). Therefore, minimal overgrowth development in the Frio Rincon samples may also be in part due to their low quartz content. Feldspar overgrowths are rarer than quartz overgrowths in Frio Rincon samples. However, this cement is characteristic of other Frio reservoirs and is inferred to have developed at shallow depths (<4,000 ft) (Loucks and others, 1986).

Porosity

Total porosity observed in thin section varies from 2.5 to 29.5 percent of whole-rock volume, with an average value of 17.3 percent. Secondary porosity composes most of visible thin-section porosity in the Frio Rincon samples. It varies considerably from 2.5 percent of whole-rock volume in heavily calcite-cemented samples to 28.0 percent in heavily leached samples (average: 15.7 percent). Secondary porosity is developed as voids within partially dissolved framework grains (mainly feldspars and VRFs) and as oversized pores that once contained framework grains and/or calcite cement. Little primary porosity (average: 1.5 percent) is preserved in the samples.
It exists as small intergranular voids at least partially lined with chlorite or calcite crystals growing into the voids within areas of closely spaced framework grains. However, in most cases it is difficult to identify primary porosity because such textural relations are not present. The Rincon samples underwent at least two stages of dissolution of framework constituents and calcite, the dominant pore-filling cement (Fig. 29). Therefore, textural relations typically cannot be used to confidently establish whether observed porosity is original.

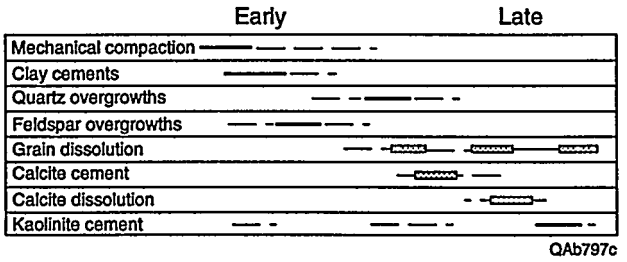

Figure 29. Diagenetic sequence diagram, Rincon D and E reservoir sandstones.

Diagenetic sequence

The primary diagenetic events in the burial history of Frio Rincon sandstones were (1) early mechanical compaction, (2) precipitation of clay (chlorite, illite/smectite) grain-rim cements, (3) development of quartz and feldspar overgrowths, (4) dissolution of primarily feldspar and feldspar-rich VRFs (probably contemporaneous with step 3 and steps 5-8), (5) calcite cementation, (6) dissolution of calcite cement, (7) migration of hydrocarbons through the reservoir rock, and (8) precipitation of kaolinite cement.

The diagenetic sequence of mineralization of the Frio Rincon samples was deduced from textural relations among the framework grains and cements observed in thin section. Where quartz and feldspar overgrowths are present, chlorite and illite/smectite grain-rimming cements lie, at least partially, between the grain and the overgrowth, thus indicating that overgrowth formation postdated clay cementation. Feldspar overgrowths probably predate, or are in part contemporaneous with, quartz overgrowths in these shallow Frio samples, although direct textural evidence is lacking. However, other studies of Frio diagenesis inferred these same temporal relations (Lindquist, 1977; Bebout and others, 1978; Loucks and others, 1986). Dissolution of the least chemically stable framework grains and rock fragments (feldspars, VRFs) began with deeper burial and continued throughout the burial history of the Rincon reservoirs. There were probably discontinuous periods of enhanced dissolution (Fig. 29), perhaps coinciding with episodes of migrating pore fluids. Loss of detrital grains from sandstones represents one of the volumetrically most important diagenetic processes that has occurred and is occurring in the Frio Formation (Milliken, 1989). In the few heavily calcite-cemented samples examined, calcite cement fills voids that are one to several grain diameters in size and are a replacive component of partially leached framework grains, all evidence that calcite cementation followed significant grain dissolution in the Rincon reservoirs. However, most Rincon samples exhibit abundant porosity due to subsequent dissolution of most of the calcite cement, as indicated by characteristic residual patches of sparry cement with corroded edges. Where calcite-cement volume is low owing to dissolution and creation of porosity, sample porosity is higher. Calcite

dissolution was a significant diagenetic stage that was magnified by the preceding and contemporaneous leaching of framework grains, particularly feldspars and VRFs. Sparse patchy kaolinite cement fills voids created by the loss of calcite cement. However, earlier kaolinite cementation is also inferred.

The petrology and ultimately the diagenesis of these Frio sandstones are primarily a function of source area and, secondarily, of original depositional environment. The presence of volcanic source terrains in northern Mexico and West Texas controlled the large volume of VRFs and feldspars in the Frio Rincon sandstones. Leaching of these abundant framework constituents created the porosity in which calcite cement precipitated and from which the cement was subsequently largely leached. Depositional environment had a secondary but important influence on porosity and permeability. Because of the fluvial depositional setting of the Rincon reservoir facies, these sands were poorly sorted and experienced minimal winnowing of the more chemically unstable and softer framework grains, such as plagioclase and VRFs. Therefore, high percentages of volcanic grains were preserved prior to burial and diagenesis.

Determination *of Finest Scale Genetic Units*

Correlation of bounding surfaces and reservoir genetic units

Subdivision of the Frio D and E reservoir interval consisted of defining correlation surfaces that are interpreted to represent a series of time slices through the reservoir zone. A primary goal in detailed reservoir characterization is to subdivide a productive reservoir interval so that any nonpermeable unit (usually mudstone) that may form a continuous barrier between two or more wells is associated with a bounding surface. In fluvial sandstone reservoirs, this objective is most often achieved by correlating mudstone units, representing primarily interchannel floodplain facies, from well to well. In many instances, floodplain mudstone units are not continuous across more than a few wells, and where equivalent mudstone is not preserved in adjacent wells, the position of a bounding surface must be defined within an interval of sandstone. Some of the mudstones used as correlation surfaces occur throughout the entire field study area. Most

mudstones are more restricted in areal extent and occur over only a portion of the study window. Some were observed in only a few wells. Identifying the distribution of all shale barriers is very important, as they are probably the most significant cause of heterogeneity in fluvial reservoirs and are responsible for the isolation and compartmentalization of parts of the reservoir, thereby preventing adequate primary drainage and efficient sweep by injected fluids.

Ten primary correlation surfaces were used to subdivide the Frio D-E reservoir zone. There are eight productive sandstone-rich reservoir zones defined within these primary surfaces. The depth of each correlation surface was defined in every well so that each surface could be interpolated throughout the study area for use in the development of a reservoir model.

Sandstone Geometry and Depositional History

Frio E reservoir units

A series of maps were constructed on each of the Frio D and Frio E reservoir subunits using net-sandstone values based on shale volume calculations from SP logs for each well and depositional facies interpreted from electric log signature. Geologic data from mature Frio reservoirs in South Texas consist primarily of pre-1950 electric logs and very limited whole core. Thus, facies studies must rely heavily on stratigraphic correlations using only these older electric logs.

The Frio E reservoir zone includes strata from the F shale marker to the E shale marker (Fig. 30). The entire zone is composed of four, predominantly upward-fining units divided by three low-resistivity marker beds. Each unit between two shale markers represents a depositional parasequence that together makes up a larger-scale, backstepping, or retrogradational cycle that took place during deposition of the entire E zone.

The onset of sand deposition in the Frio E stratigraphic interval is represented by the E-4 unit (Fig. 31). Log facies and net-sandstone thickness patterns reveal the development of two to three discrete through-going fluvial channels oriented along directional dip from northwest to southeast. Individual log facies patterns of these channels exhibit blocky and upward-fining

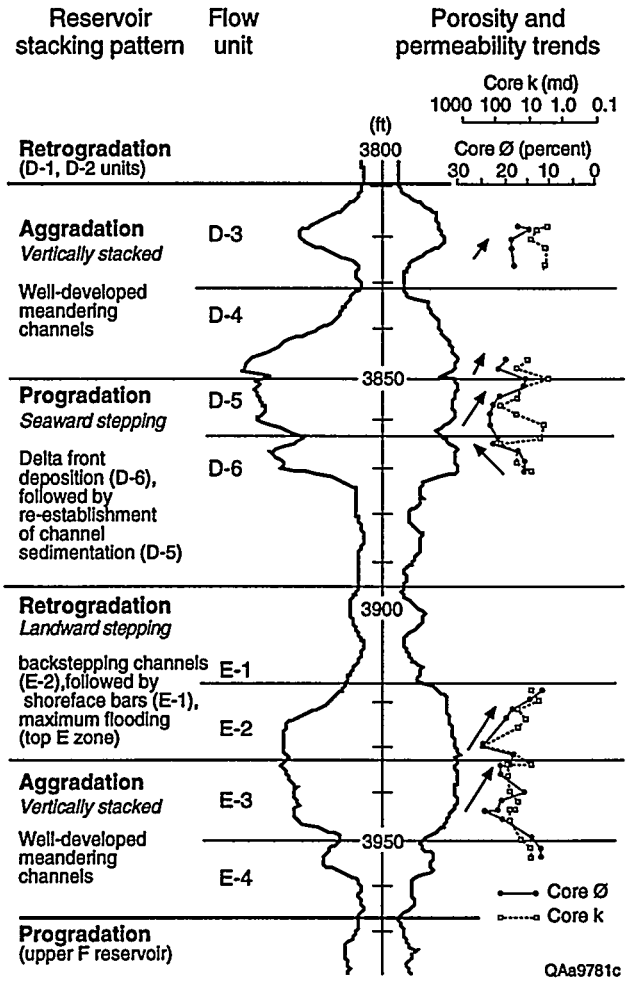

Figure 30. Representative SP/resistivity log illustrating succession of stacking patterns developed within the Frio E and D reservoir units. Conventional core analysis data posted on the right illustrate porosity and permeability trends commonly observed in each subunit that generally correspond to SP and resistivity bell and funnel curve shapes indicative of upward-fining channel sandstones and upward-coarsening bar sandstones, respectively.

responses representing channel-fill facies. The next depositional unit, the E-3 sandstone, is characterized by thicker development of sandstone, reflecting an increase of sediment supplied to this portion of the depositional system. The dip-elongate channel patterns observed in the underlying E-4 unit are still apparent. The channels are distinctly separated by floodplain facies in the downdip portion of the map area, but in the updip portion, the channels appear to be better connected, suggesting some flow-communication would be present between the two. Higher up section in the E-2 unit, dip-oriented NW to SE channel geometries still predominate. In the updip portions of these channels, some minor strike-oriented features are apparent, and maximum sand thicknesses have stacked up in a more updip position relative to earlier deposition, indicating a backstepping pattern caused perhaps by relative sea-level rise.

Figure 31. Series of net sandstone isopach and facies maps showing changes in the distribution of facies and sandstone facies geometry for the Frio E-4, E-3, E-2, and E-1 reservoir units and Frio D-6, D-5, D-4, and D-3 reservoir units.

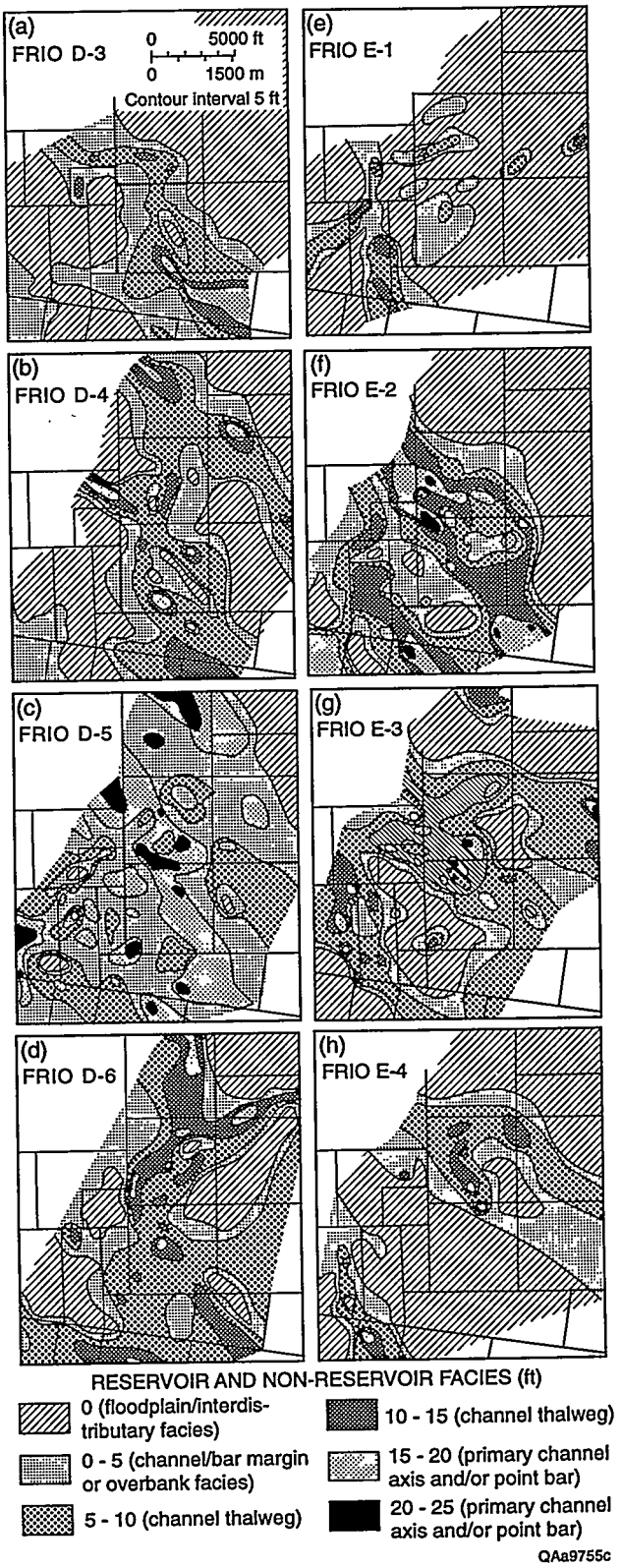

A significant change in the amount and distribution of sandstone is observed at the top of the E-zone. In the E-1 unit, mudstone facies predominate, and the majority of sandstone is distributed in strike-oriented bodies that are limited in areal extent. These small strike-oriented sandstone deposits are interpreted to represent the development of minor shoreface bars associated with continued backstepping or retrogradation. A narrow dip-elongate channel, perhaps a narrow tidal channel, is present in the far southwestern corner (bottom left) of the map area. The advance of a laterally extensive flooding surface marks the end of E zone deposition.

Frio D reservoir units

The productive D reservoir interval also consists of four discrete depositional parasequences divided by three low-resistivity shales (Fig. 30). These are identified as the D-3, D-4, D-5, and D-6 units, and together they form a larger-scale depositional sequence that includes both progradational and aggradational units. Located above the E flooding surface, the D-6 unit is the lowermost sandstone of the D reservoir zone, and follows a relatively extended period of predominantly mud deposition. The strike-elongate sandstone pattern in the D-6 unit is believed to reflect initial progradation and development of a thin delta front. Upward-coarsening and blocky log responses in many of the electric log profiles of D-6 units are further evidence that delta-front sand facies make up this strike-oriented sand body. Dip-elongate channel deposition appears to be present in the northern portion of the study area, as well as across the center of the map where the strike elongate delta front sandstone is dissected by narrow upward-fining channel facies.

Progradation continues during deposition of the D-5 unit. The overall sandstone geometry in the D-5 consists of northwest-southeast trending, dip-parallel channel facies (Fig. 31). Because of the greater thicknesses of mapped sand patterns, it is difficult to distinguish boundaries between individual channels. The thickest development of sandstone is present as a relatively narrow channel feature that runs from northwest to southeast across the study area. The D-5 zone also contains evidence of some reworked strike-oriented delta front remnants, and log correlation in some areas indicates this unit may be mapped as two discrete episodes of channel deposition.

The uppermost Frio D reservoir subunits represent a return to more discrete channels and aggradational sedimentation. Both the D-4 and D-3 units are dominated by dip-elongate fluvial channel deposition. Sediment load being carried by these channels appears to be reduced from earlier D-5 deposition, as evidenced by thinner development of sandstone and more clearly identified channel margins. The two channel systems mapped in the D-4 unit appear to be in communication in the updip portion of the map area. The D-3 unit consists of a single, relatively broad channel system. In addition to the blocky and upward-fining log patterns that characterize

channel-fill facies, serrate and thin upward-coarsening responses diagnostic of levee and crevasse splay facies are also observed adjacent to channel margins in these two units.

Establish Fluid-Flow Trends in the Reservoir

Initial Fluid Properties

Oil produced from the Rincon field is a light high-shrinkage crude. Oil gravity ranges from 40° to 48° API and formation volume factor ranges from 1.14 to 2.05 (STB/bbl). The high gravity gives the oil a favorable mobility ratio. The oil is associated with a gas cap; therefore, the oil was initially at bubble point pressure. This fluid character makes pressure maintenance important because any pressure drop causes gas to come out of solution.

Field Production History

Frio and Vicksburg reservoirs have produced more than 65 MMbbl of oil under combined natural water drive and gas cap expansion since discovery of Rincon field 55 years ago in 1939. Frio production peaked in 1944, when production averaged approximately 7,300 bbl/d. Vicksburg production began in 1950. Production from 38 separate Frio reservoirs has yielded over 45 MMbbl of oil.

Three main Frio reservoirs, the D, E, and,G sandstone units, account for 69 percent of all completions and 88 percent of the oil produced in the field area selected for study (McRae and others, 1994). Most of the Frio oil reservoirs had initial gas caps, and reservoirs have produced under a combined natural water drive and gas cap expansion. Gas injection took place during the early years of field production in order to maintain reservoir pressure and extend the flowing life of the wells. Waterfloods performed in each of these large reservoir zones met with varying degrees of success. Oil production from these major reservoirs has declined steadily since 1968 and has been accompanied by increasing abandonments of individual reservoir zones. As of 1990, there were only 27 oil wells remaining in the field that were producing or had shut-in status, and average daily rates had declined to 373 bbl of oil and 4,576 Mcf of gas.

The Frio E sandstone is the most prolific reservoir zone in the field and has produced nearly 12 MMSTB of oil since production began in 1940. The E zones are individually mapped as the E-1, E-2, E-3, and E-4 sands. Stratigraphic correlation and production data from the operator indicate that the E- 1 and E-2 sands are commonly in fluid communication, as are the E-3 and E-4 sand zones. Secondary waterflooding in the Frio E reservoir zone accounted for 2.5 MMSTB, or nearly 21 percent of total E zone production. An overall recovery efficiency of 38 percent was calculated for the combined E zone using average reservoir values of 26.5 percent porosity and 37.5 percent water saturation.

Frio D reservoirs have produced nearly 10 MMSTB oil since 1940. The main productive D sand interval consists of four units correlated as the D-3, D-4, D-5, and D-6 sands. These units are correlated as individual sandstones that combine into a complex stratigraphic channel system that covers more than 2,000 acres in the northern half of the field. Frio D sandstones have similar reservoir attributes as Frio E reservoirs (average porosity of 25.2 percent, Sw of 40.5 percent, and estimated OOIP of approximately 35 MMSTB) but a lower recovery efficiency of 29 percent. Waterflooding attempts in this reservoir zone accounted for secondary recovery amounting to only 2 percent of total D production. These disappointing results were attributed by the field operator to the heterogeneous nature of the D sandstone interval.

Evaluation of Areal Trends of Past Oil Production

Areal patterns of reservoir development identified by isoproduction contours reveal the general distribution of hydrocarbon storage capacity and degree of flow communication within a productive reservoir zone. These maps also may indicate areas where there are significant production contrasts that may be a direct result of flow barriers created by stratigraphic heterogeneity. In many cases well completions in a given reservoir include a stratigraphic interval that spans more than one flow unit, and in these situations, cumulative production data on a per-well basis provide less insight into the stratigraphic distribution of production in an individual flow unit. However, such data can provide general insights into the production behavior of the selected reservoir.

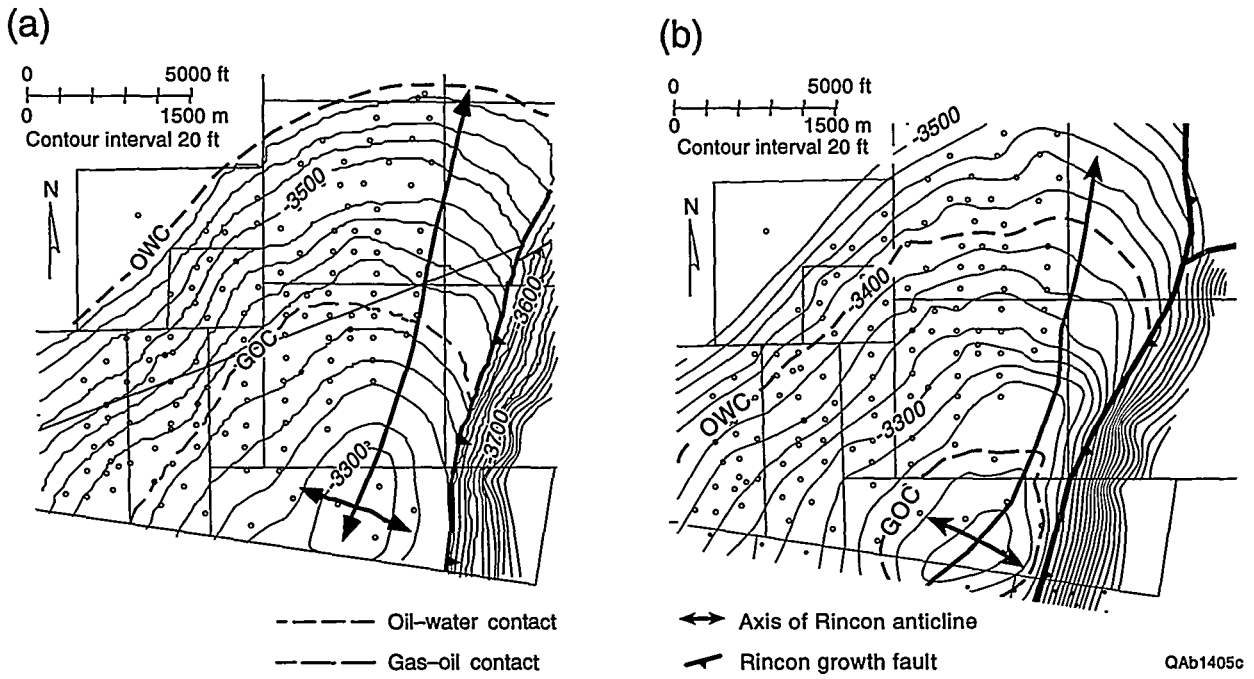

Figure 32. Comparison maps illustrating differences in overall reservoir geometry and distribution of production, Frio D and E reservoir zones. Maps on the left for the Frio E reservoir show (a) representative structure contoured on the top of the Frio E unit, showing the anticlinal pattern of the Rincon structure and location of the down-to-the-east Rincon growth fault; and (c) cumulative oil production for the combined Frio E reservoir; and (e) isopach map from the total E sandstone reservoir zone, showing distribution of net sandstone thickness and depositional geometry. The stacking of greater sandstone thicknesses in the updip portion of map area may have created increased flow communication between adjacent channels along the crest of the structure and caused the relatively high recovery efficiency of the E reservoir. Maps illustrating structure (b), distribution of cumulative oil production (d), and total net sandstone thickness (f) are presented on the right for the Frio D reservoir. In contrast to the Frio E zone, the strong dip-elongate depositional pattern and narrower geometry of Frio D channels make this reservoir appear more compartmentalized and may explain lower overall recovery efficiency.

In the Rincon field, where production from many completions was commingled, structural maps (Fig. 32 a,b) and cumulative production isopach maps (Fig. 32c,d) were constructed for both the Frio D and E reservoir zones to help identify the general distribution of oil production. Composite net sandstone thicknesses were calculated over the total Frio D and total Frio E reservoirs to serve as a comparison to the total reservoir production maps (Fig. 32e,f). The cumulative production map for the E reservoir shown in Figure 32c illustrates the trend of high

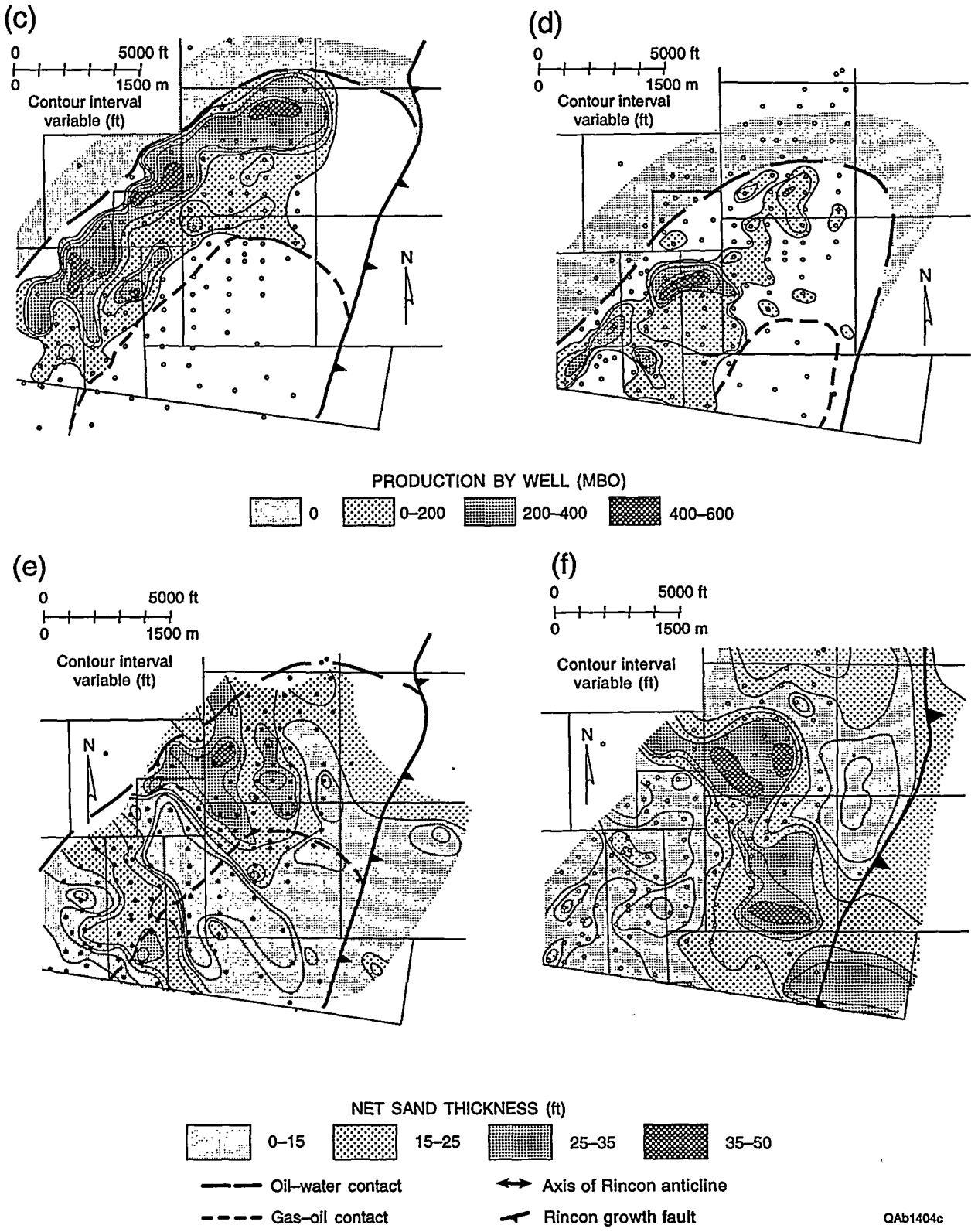

Figure 32 (cont.)

production following along the lower edge of the structure. The correspondence between better production and the downdip edge of the reservoir is due to efficient water drive in the lower portions of the reservoir. In addition to structural position, another control on cumulative production appears to be differences in net thickness. The composite E reservoir net sandstone isopach map shows greatest sand thicknesses occurring in the updip portion of channels, and comparison with the production map indicates that higher production approximately corresponds to areas of thicker net sandstone that generally follow along channel depositional axes (Fig. 32e).

Maps comparing the distribution of oil production in the D zone with structure show a similar pattern as was observed in the E reservoir zone, with production "hot spots" oriented along strike parallel to the crest of the anticlinal structure (Fig. 32d). Areas of high production within the D reservoir appear to be much more isolated than was observed on the E cumulative production map (Fig. 32f). The total net sandstone thickness map for the combined D interval shown in Figure 32e illustrates the strongly dip-oriented pattern of the composite D sandstone interval. The stratigraphic complexity of this interval of vertically stacked and laterally coalescing sandstone lobes provides ideal conditions for isolation of oil accumulations in multiple reservoir compartments, many of which may be incompletely drained or completely untapped.

Integrating Fluid-Flow Trends in the Reservoir

Identifying Correspondence Between Stratigraphy, Structure, and Fluid-Flow Trends

*Effect of **Sandstone Geometry** on Oil **Production***

The Frio D and E reservoir intervals illustrate a systematic evolution of sediment transport styles and stratigraphic stacking patterns (Fig. 30). These are: (1) aggradation in the lower Frio E-4 and E-3 reservoir units, (2) retrogradation in the upper Frio E-2 and E-1 units, (3) progradation in the lower Frio D-6 and D-5 units, and (4) a return to aggradation in the Frio D-4 and D-3 units. These different styles of deposition directly affect the reservoir geometry

present within each sandstone unit (Fig. 31). Aggradational and progradational channel sedimentation create dip-oriented channel sandstones that may or may not be in communication with each other. Strong dip-oriented geometry in the D units and the development of successively more laterally isolated channels during aggradation reduces communication between units that may be directly responsible for lower recovery efficiency. Retrogradational units such as those present in the E reservoir, in contrast, allow reworking of previously deposited sediment into long strike-oriented features that have potential for increased flow communication. Evaluation of individual map patterns suggests that the strike-oriented distribution of sandstone located in the updip portions of the map area in the E-3 and E-2 units, combined with the relative broadness (3, 500-7,000 ft) and lower sinuosity of individual channel units, may lead to greater interconnectedness of channels and increased communication between reservoir flow units. The updip stacking of sandstone thickness and lateral connectivity between E units may be controlling factors in the relatively high recovery efficiency (38 percent) of this reservoir zone.

Matching Stratigraphy with Reservoir Production

Reservoir development patterns within the Frio E reservoir

Reservoir development within each unit was indicated by identifying wells with completions within that particular stratigraphic unit. In addition, wells were identified that were not perforated within the mapped zone but were completed in a reservoir subunit stratigraphically above or below the mapped unit that may have been in partial or complete vertical communication. The series of reservoir geometry/development maps prepared for the E reservoir units are shown in Figures 33 through 36.

The Frio E-4 unit has the least number of completions of the three E reservoir units (E-4, E-3, and E-2) that are characterized predominantly by channel sedimentation. This unit consists of two discrete dip-oriented channel bodies that are separated laterally by at least 3,000 ft of non-reservoir floodplain facies (Fig. 33). The channel located in the southwest portion of the map area is narrow (1,000-1,500 ft) and contains a relatively thin channel margin facies as interpreted from

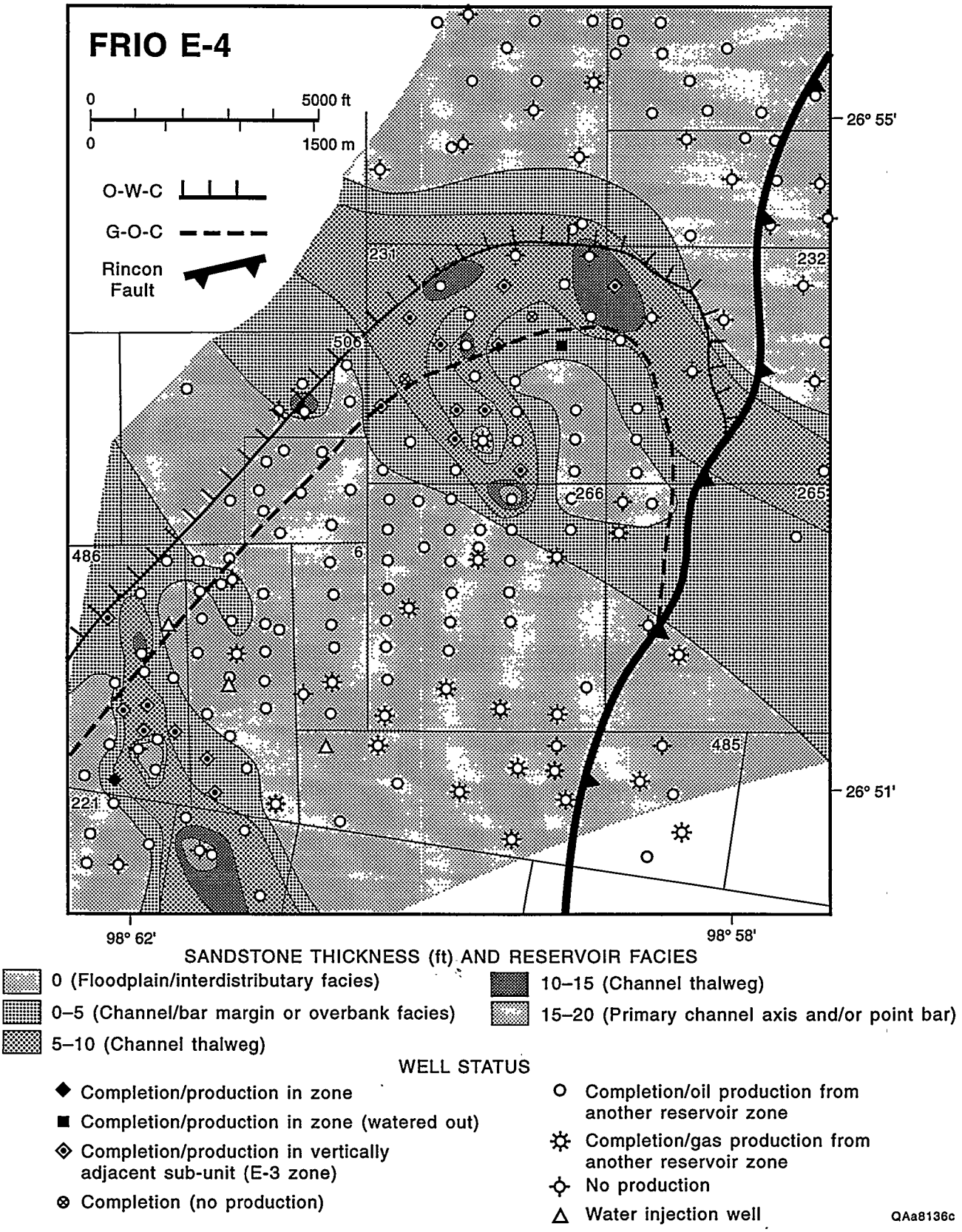

Figure 33. Map illustrating sandstone thickness distribution, corresponding reservoir facies geometry, productive limits, and level of development, Frio E-4 reservoir unit.

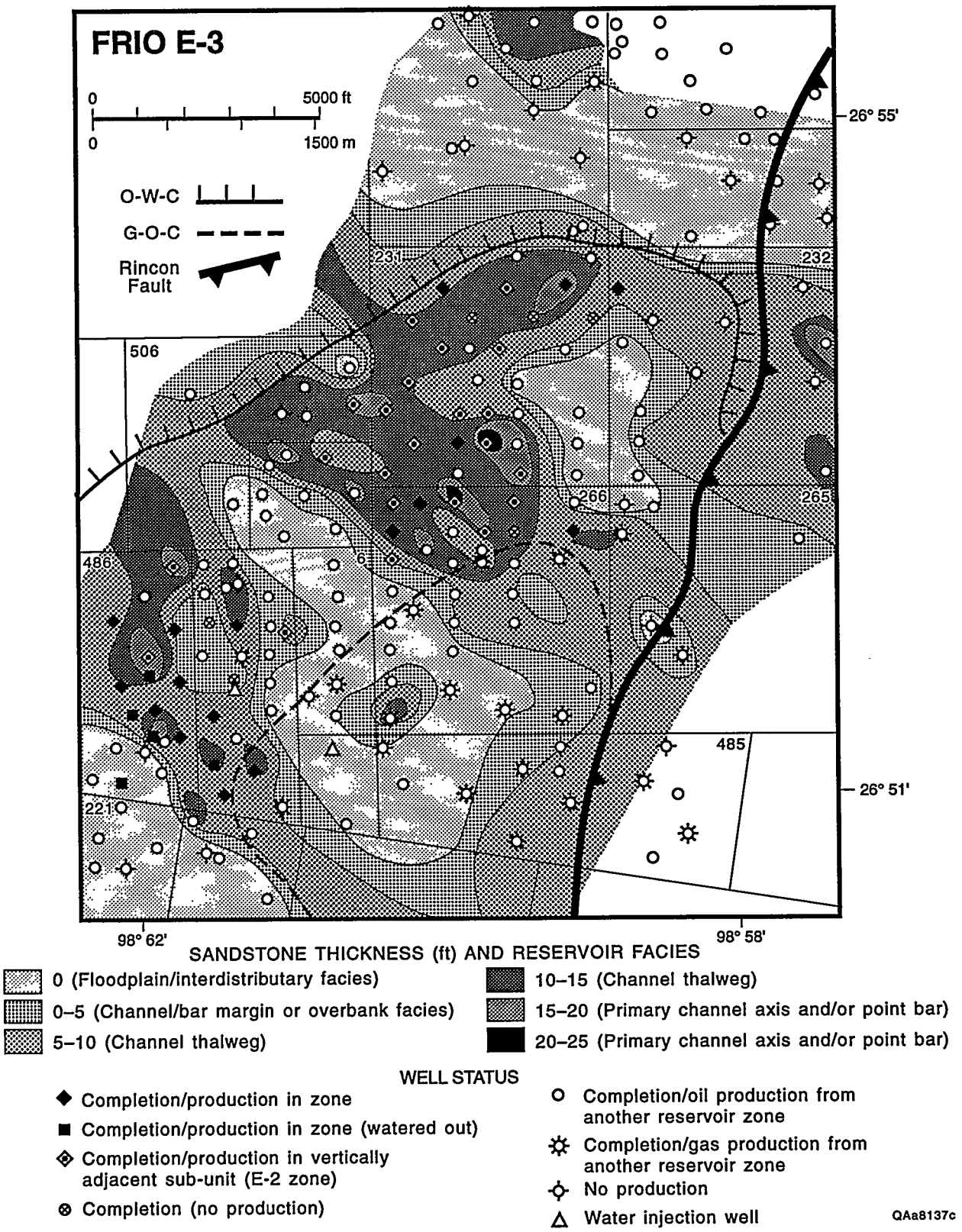

Figure 34. Map illustrating sandstone thickness distribution, corresponding reservoir facies geometry, productive limits, and level of development, Frio E-3 reservoir unit.

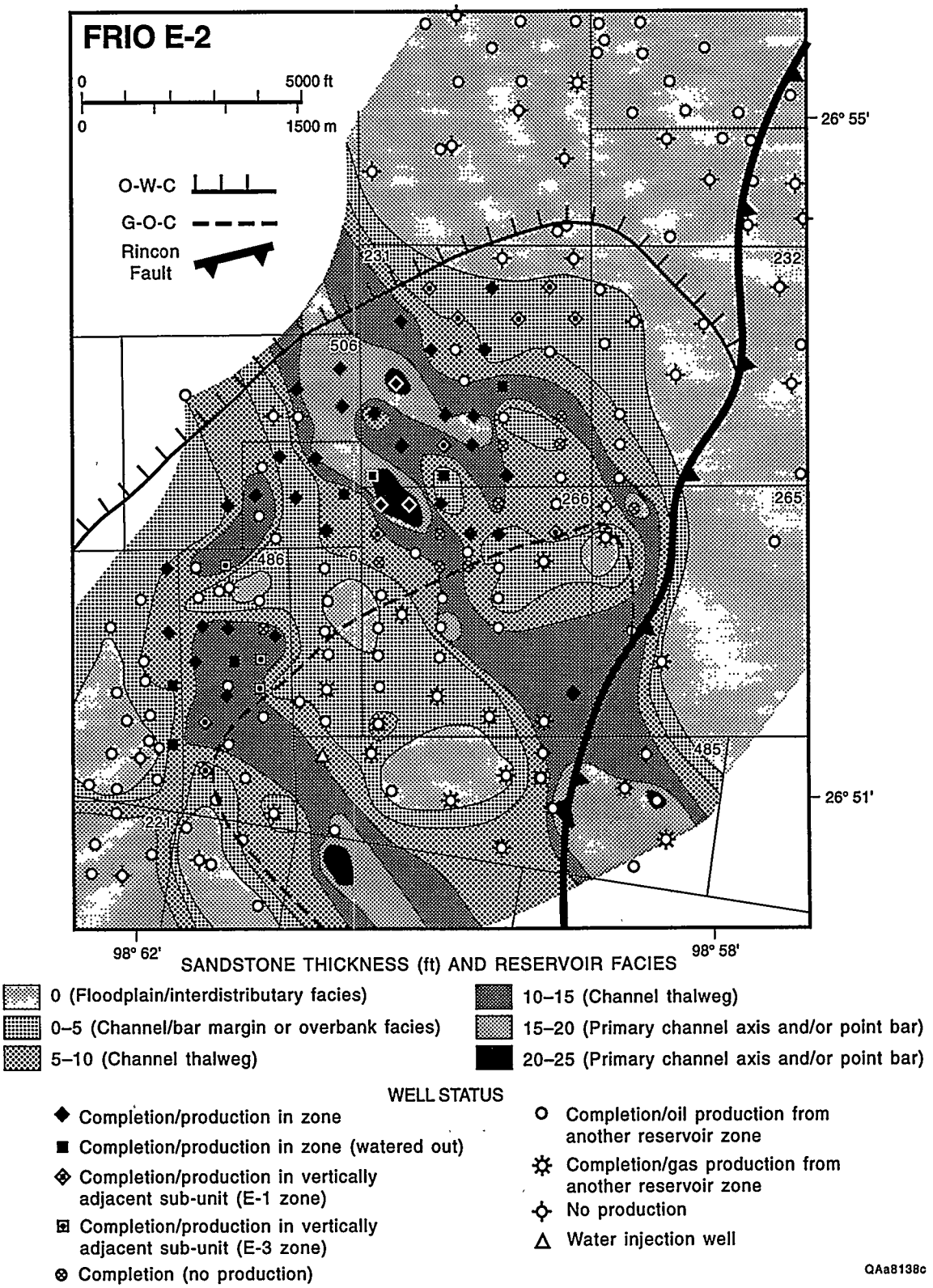

Figure 35. Map illustrating sandstone thickness distribution, corresponding reservoir facies geometry, productive limits, and level of development, Frio E-2 reservoir unit.

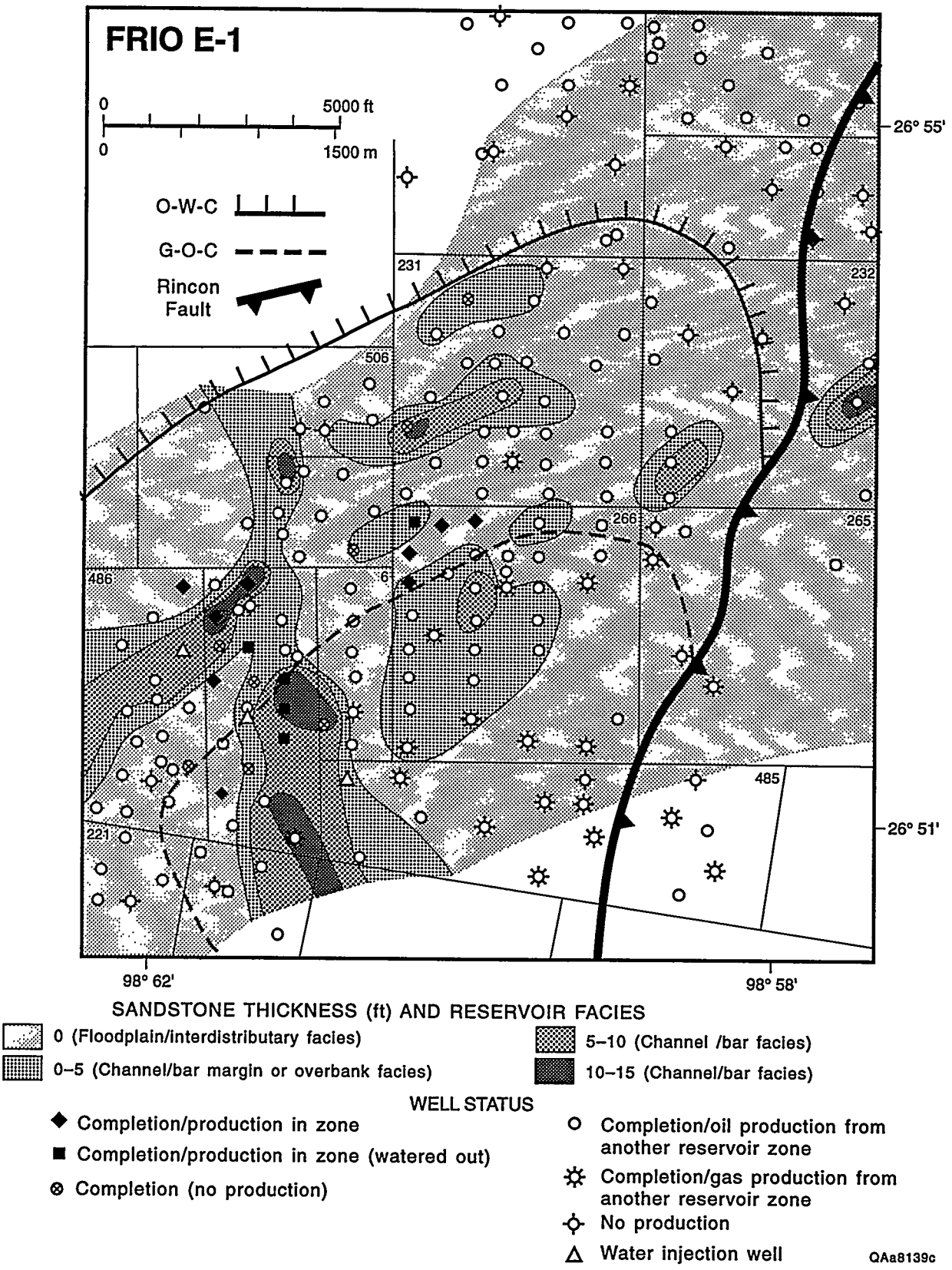

Figure 36. Map illustrating sandstone thickness distribution, corresponding reservoir facies geometry, productive limits, and level of development, Frio E-1 reservoir unit.

net sandstone isopachs. The channel system located in the central portion of the map area consists of two main channel tracts defined by thicker development of sandstone, and these are probably in flow communication. The updip, connected portion of this channel system is approximately 3,500 ft wide and narrows to 2,000-2,500 ft farther downdip, where it appears to bifurcate into two separate channel units. Forty-nine wells penetrate sandstone facies in the E-4 reservoir, and only 21 of these have been completed. Many of these completed wells may have associated production, but actual volumes are not known because all E-4 production reported by the operator was assigned to the combined E-3 & E-4 reservoir zone.

E-3 unit reservoirs appear to consist of three separate channel systems oriented northwest to southeast across the field study area (Fig. 34). The location of the oil-water contact indicates that it is likely that the southwesternmost channel is not in communication with the two channels located to the north. The two northern channels appear connected, in part, and are probably in lateral communication. The southwestern channel is approximately 2,500 ft wide and has 50 completions and 21 producing wells. The majority of completions and producing wells are located in the two northern channels. Many additional wells have been completed in a vertically subjacent zone, primarily the overlying E-2 reservoir, and have produced oil, some of which may be properly allocated to the E-3 unit. More than 3 MMBO of production has currently been assigned to the E-3 reservoir.

The Frio E-2 reservoir unit possesses the greatest number of completions (64) and producing wells (46) of all the E reservoir subunits. The mapped sandstone geometry (Fig. 35) shows two primary dip-oriented channels that are probably only in partial communication because of the floodplain facies and lower permeability channel-margin facies developed between the two channel areas. The primary channel area in the E-2 unit is relatively broad (4,000-6,000 ft) and contains sandstone facies that have some of the highest permeability values (1250 and+) measured in the field. Present production allocation indicates that the E-2 unit is also by far the most prolific oil reservoir in Rincon field, with more than 7.5 MMBO currently reported.

The uppermost E reservoir sand, the E- 1 unit, has the fewest completions of all E subunits. Part of this is attributable to the fact that the E-1 and E-2 sandstones were developed as though

they were usually in flow communication, and extensive development in the E-2 reservoir has likely produced much of the E- 1 oil. Sandstone isopach mapping and evaluation of log facies in this study suggests that the E-1 sandstone was deposited in a retrogradational cycle where pre-existing channel units have been eroded and reworked into a series of strike-elongate bar sandstones that cover most of the mapped study area (Fig. 36). Well data and log facies interpretations indicate that these bar units are thin (mean thickness of 6 ft) and not very laterally continuous (width dimensions from 1,500 to 3,000 ft). This facies interpretation indicates that there may be less vertical communication between E-2 and E-1 reservoir units than previously assumed.

Reservoir development patterns within the Frio D reservoir

Composite maps illustrating the distribution of reservoir sandstone, fades patterns, and level of development for each of the D reservoir subunits are presented in Figures 37 through 40. As discussed previously, the lowermost D reservoir unit, the D-6 sand, has been interpreted to represent part of a progradational cycle of sedimentation during which strike-elongate sandstone bars deposited during the previous retrogradational cycle are being eroded and transected by a dip-oriented channel system that trends across the center of the map area (Fig. 37). Upward-coarsening profiles observed on electric logs indicate the presence and northeast-to-southwest distribution of the bar sandstone facies that appears to be in the process of being dissected by the northwest-to-southeast oriented channel. The D-6 unit has relatively few completions (14), and although some of these completions were productive, all production was originally assigned to the composite D-5 reservoir zone.

As illustrated in Figure 38, the depositional geometry of the Frio D-5 subunit is very complex. The isopach map pattern reveals the presence of a primary axis of deposition, indicated by the thickest development of sandstone, running from northwest to southeast across the center of the map area. The relatively thick sandstone throughout this reservoir zone obscures much of the depositional pattern. The D-5 zone has more completions (60) and productive wells (39) than

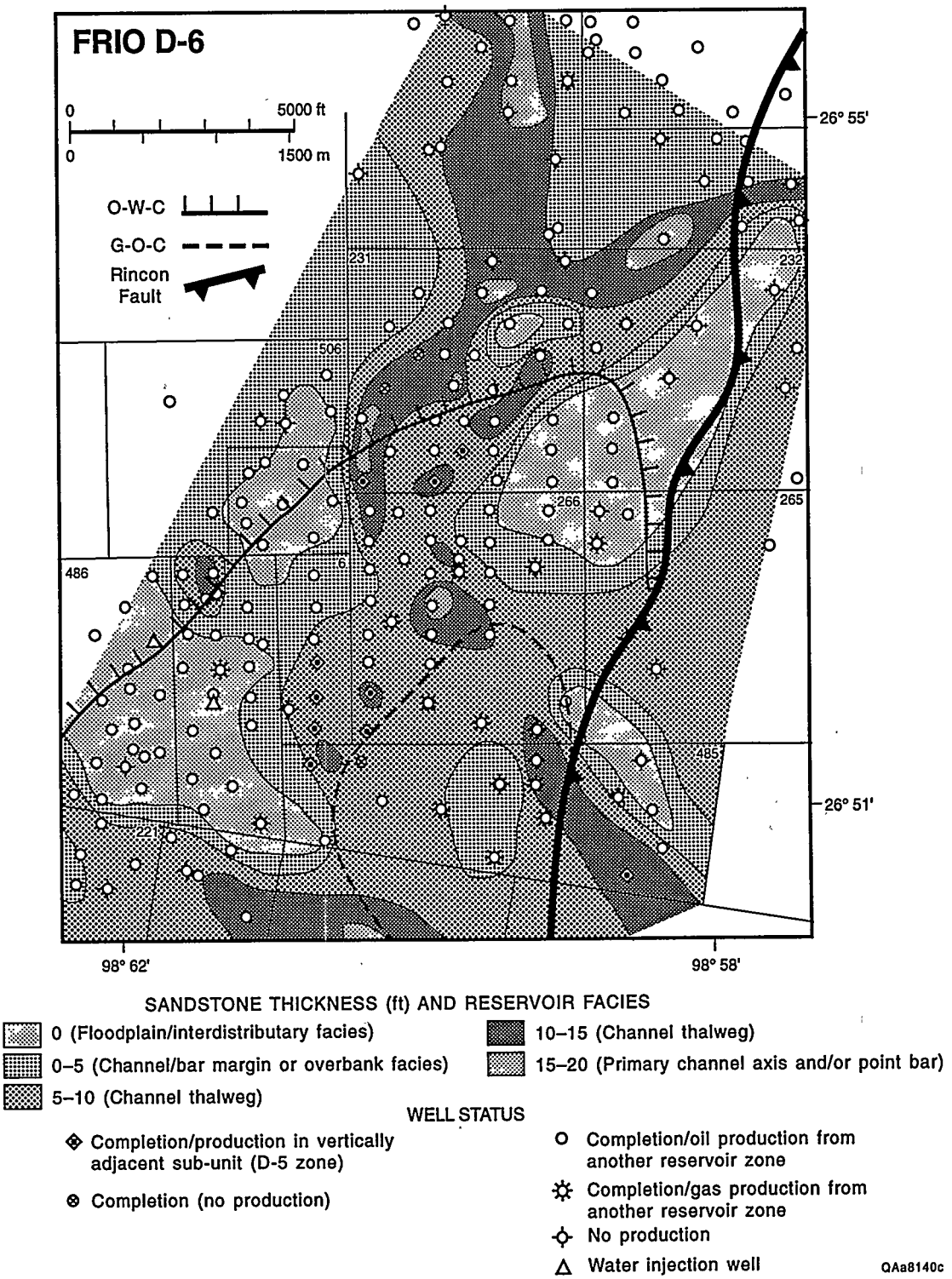

Figure 37. Map illustrating sandstone thickness distribution, corresponding reservoir facies geometry, productive limits, and level of development, Frio D-6 reservoir unit.

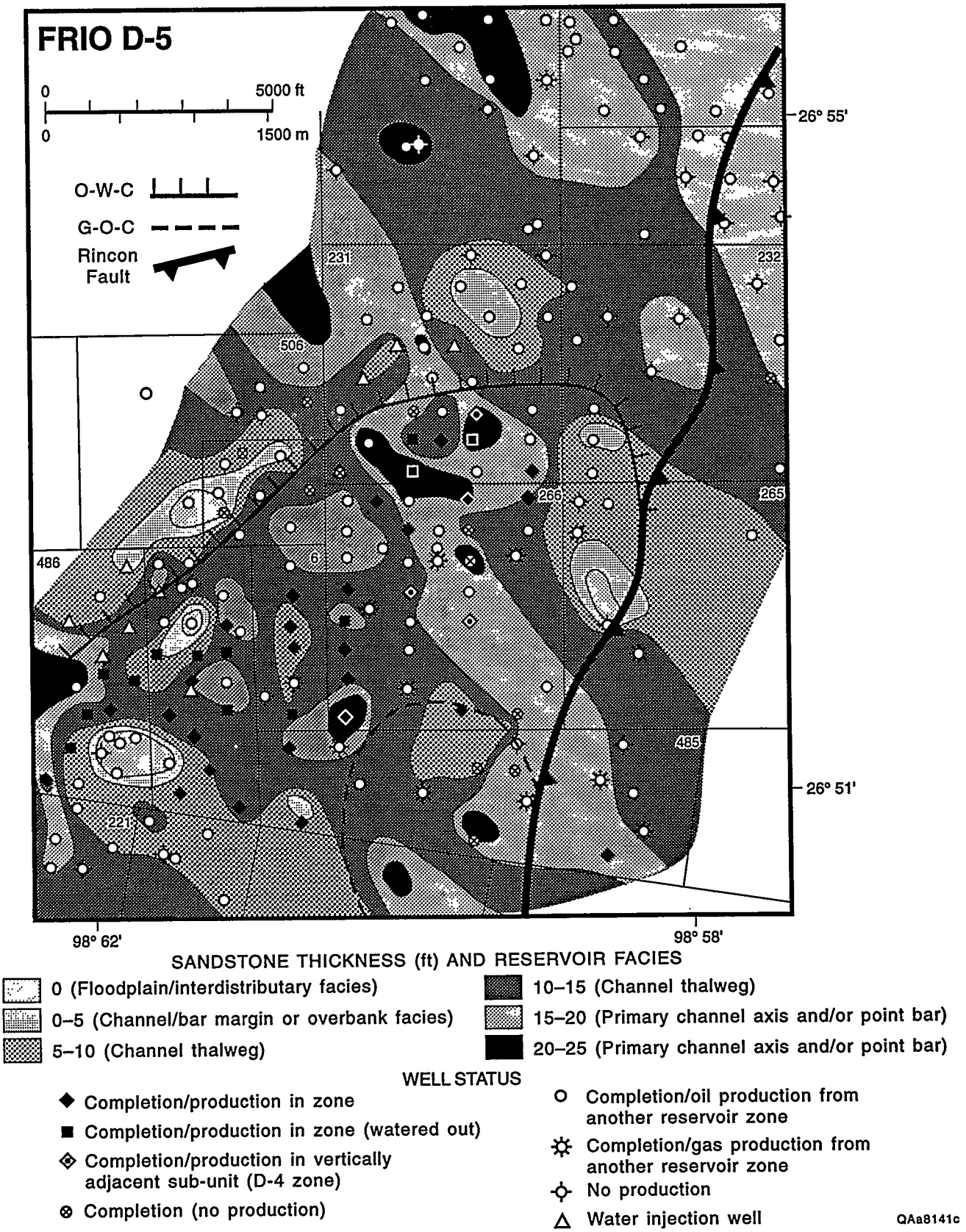

Figure 38. Map illustrating sandstone thickness distribution, corresponding reservoir facies geometry, productive limits, and level of development, Frio D-5 reservoir unit.

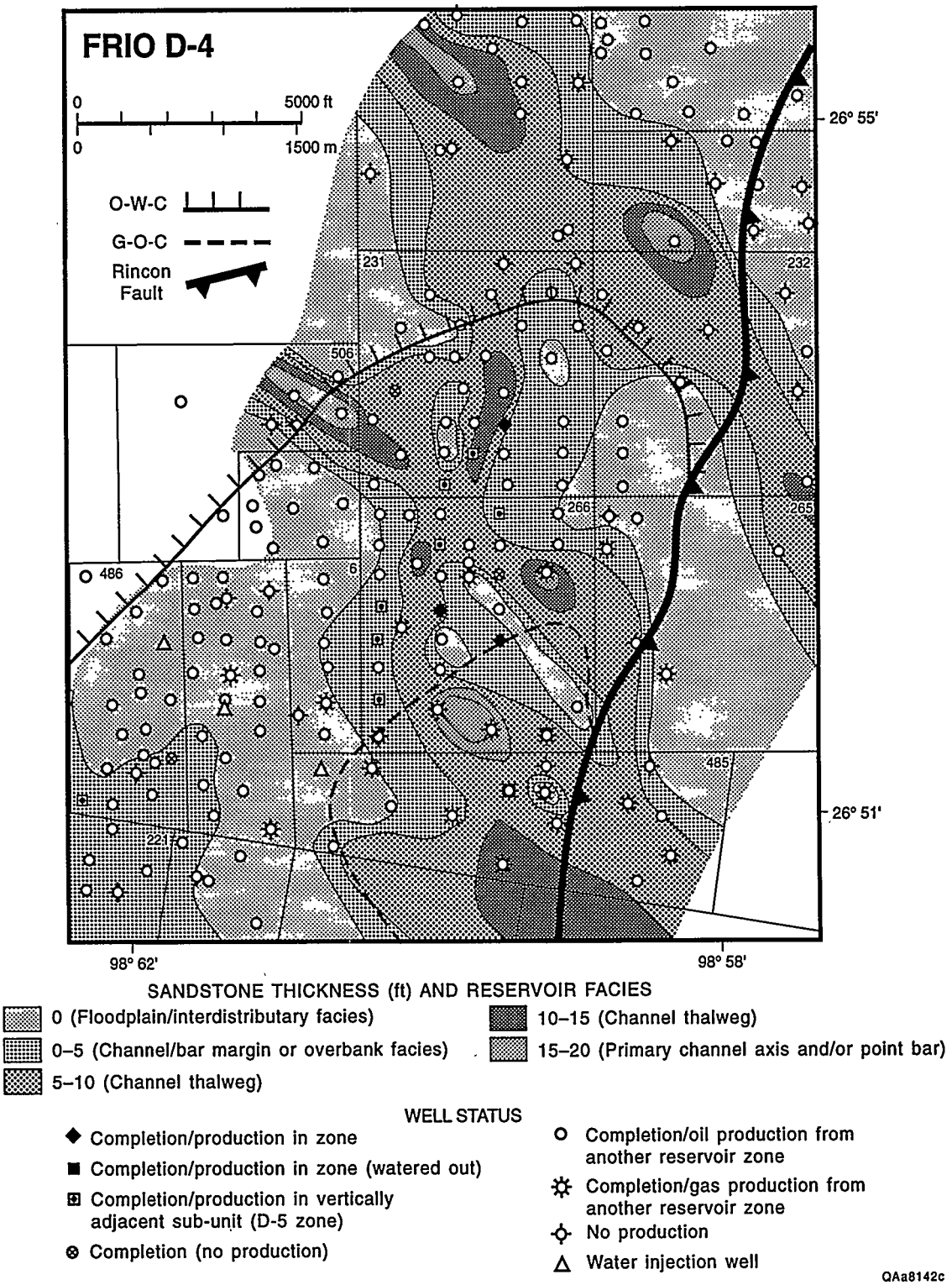

Figure 39. Map illustrating sandstone thickness distribution, corresponding reservoir facies geometry, productive limits, and level of development, Frio D-4 reservoir unit.

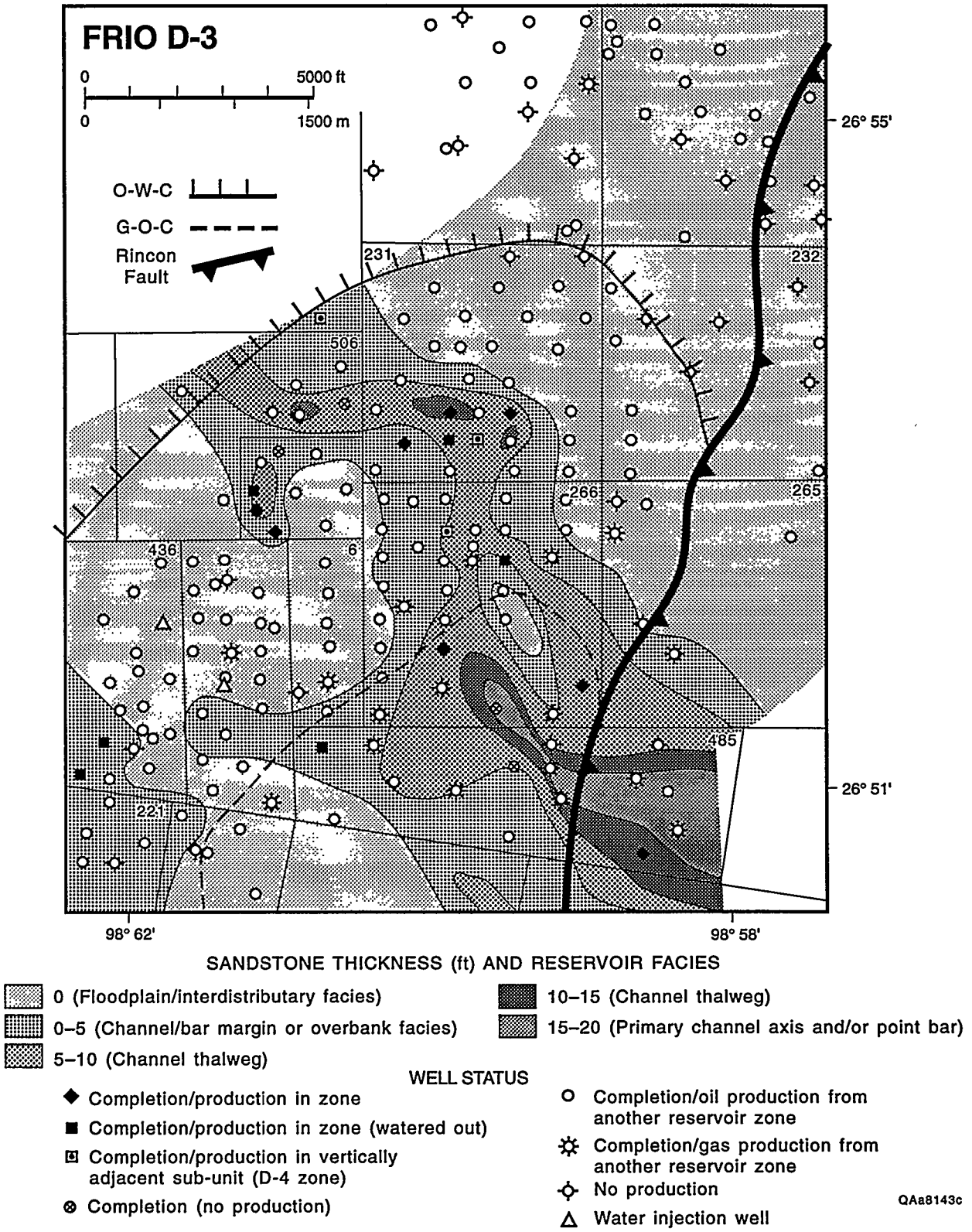

Figure 40. Map illustrating sandstone thickness distribution, corresponding reservoir facies geometry, productive limits, and level of development, Frio D-3 reservoir unit.

all other D reservoir units combined, and production reported for the composite D-4, 5, 6 reservoir zone totals in excess of 6 MMBO. Assessment of the permeability distribution within the D-5 unit suggests that there are several areas where flow baffles or barriers may exist, and this heterogeneous unit probably represents the best potential for identifying incompletely drained or completely undeveloped reservoir compartments.

The D-4 reservoir unit consists of a series of two to three dip-oriented channel units that appear to be connected in their updip portion of the map area, and they therefore are likely in lateral communication with each other (Fig. 39). Channel boundaries are clearly defined and width dimensions range from 2,000 to 3,500 ft. The number of completions within the D-4 unit (16) is few compared to those in the D-5. Vertical communication between D-4 and D-5 sandstones is probable, and it is assumed that many D-5 completions have also produced oil from the D-4 unit.

Reservoir geometry in the D-3 unit is also clearly defined, and is mapped as a single channel that transects across the center of the field area (Fig. 40). The channel dimensions are relatively narrow in the updip region (2,500 ft) but broaden significantly downdip to the southeast to more than 6000 ft wide. The D-3 unit has reported production from 10 wells of nearly 750 MBO, but some production associated with 12 additional completions has been assigned to the D-5 composite reservoir zone in wells where D-3, 4, and 5 units have been considered to be in communication.

Reservoir Petrophysical Model Development

Porosity and Permeability Modeling

Accurate characterization of porosity and permeability and their distribution within a hydrocarbon reservoir is the key to understanding past production history and is of obvious importance in designing future incremental recovery strategies to maximize resource development. Because they can be directly related to fluid transmissivity and therefore productivity, permeability values can provide a direct means to allocate total hydrocarbon

production to specific geologic units. In many older reservoirs, such as in Rincon field, production has been combined and reported for multiple sandstone units, and characterizing the vertical permeability distribution within wells and lateral distribution of permeability between wells is possible only when abundant data from routine core analyses are available. Rincon field is unusual among mature South Texas oil fields in its abundance of core data. The field was extensively cored during its early drilling phase, and although these wireline cores were not preserved, core analysis data exist from more than 100 wells within the general field study area.

The standard technique used by many operators for estimating porosity and permeability is to combine all routine core data from a reservoir to derive a general porosity/permeability relationship, and then use this derived relationship along with porosities calculated from well logs to estimate permeability in uncored wells and intervals. This method is obviously inappropriate in heterogeneous reservoirs. The use of a single relationship between porosity and permeability may result in underestimating the possible permeability contrasts present within a reservoir interval, and this will subsequently lead to incorrect calculations of original-oil-in-place volumes and inaccurate predictions of future production potential.

Porosity and permeability distribution for primary facies types

Measured porosity and permeability values from wireline cores were analyzed with their sample depths and corresponding reservoir subunit and facies types identified from patterns on sandstone isopach maps and electric log signatures, respectively. Evaluation of log facies and sandstone distribution for each of the reservoir subunits reveals three primary depositional facies types: (1) channel (dip-elongate) sandstone reservoir units, (2) bar (strike-oriented) sandstone reservoir units, and (3) overbank (levee and crevasse splay) units. Basic descriptive statistics, including histograms and linear regressions of porosity versus permeability, were calculated for each different subgroup of data. Frequency distributions of core porosity and permeability values grouped according to the three general facies types are illustrated in Figure 41. Channel units, on average, possess higher values of porosity and permeability (21% mean f, 61 and mean k) than the

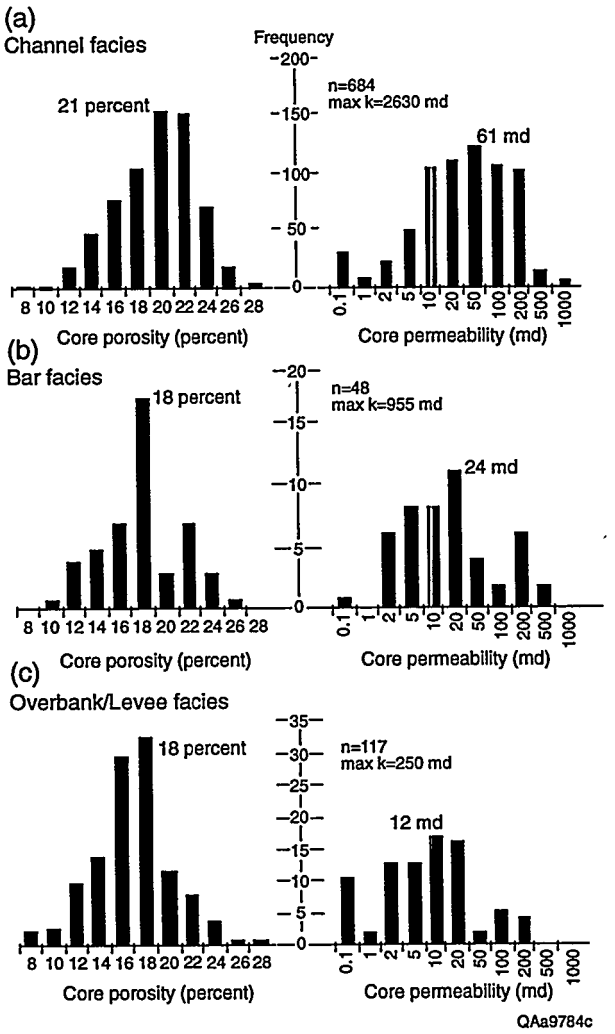

Figure 41. Histograms illustrating the distribution of porosity and permeability values according to each of the mapped reservoir facies: (a) aggradational channels, (b) retrogradational bars, and (c) overbank (splay and levee) facies.

bar sandstone units (mean f of 18%, mean k of 24 md). Overbank facies have lower porosities (mean 18%) and substantially lower permeabilities (mean 12 md) than either channel or bar sandstones. Mean permeability values'for thin upward-coarsening log patterns interpreted to bf crevasse-splays are 25 and (range 0.3-199 md) and are 5 and (range 0.1-54 md) in units with serrate log responses classified as levee facies. These poorer quality overbank facies generally are not significant reservoirs.

The porosity-permeability relationship between facies is distinctly different. Porosity and permeability for bar sandstone facies in the E-1 and D-6 reservoir subunits and for all fluvial facies types in the other reservoir units were cross plotted, and a nonlinear regression was performed for each group. The resulting equations for the regression lines demonstrate the

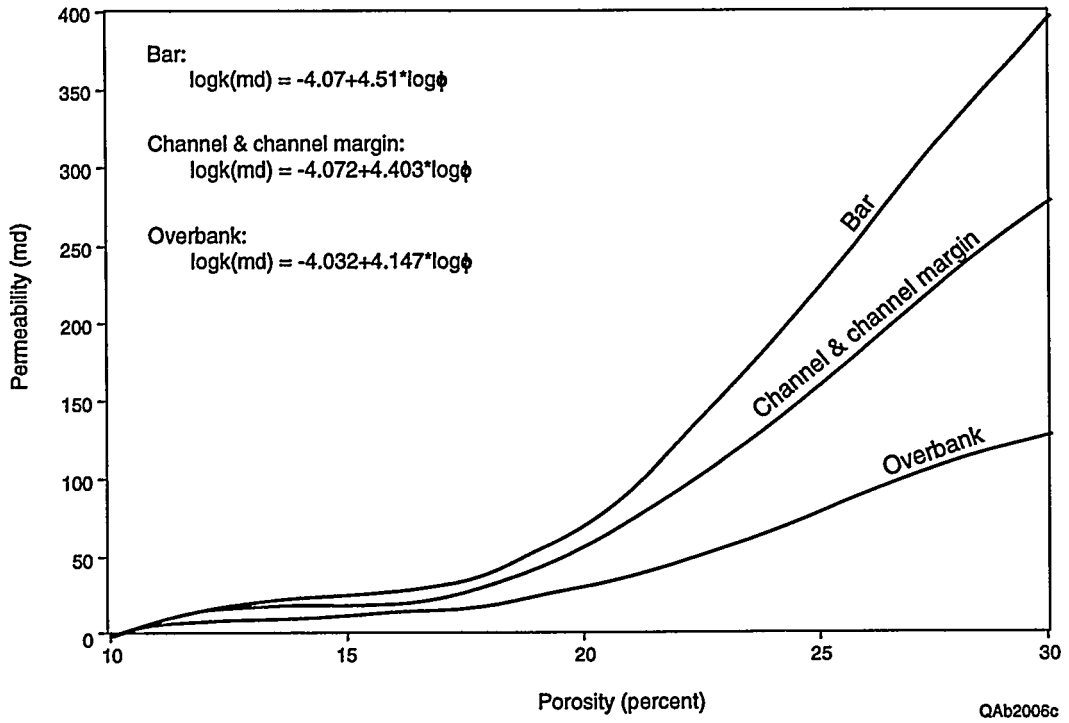

Figure 42. Nonlinear regression analysis on a facies-by-facies scale results in an equation to predict permeability from porosity.

different porosity-permeability relationships between these facies types. Similar porosity values have the lowest corresponding permeability for overbank facies, midrange for channel sandstone facies, and the highest for bar sandstone facies (Fig. 42). Therefore, greater accuracy in permeability estimation can be achieved by calculating permeability on a facies-by-facies scale.

Well log analysis

Petrophysical analysis of the Frio D and E reservoirs inRincon field includes (1) integrating core data with geophysical log data, (2) quantifying petrophysical properties from wireline logs, and (3) testing the validity of these derived properties by comparing maps of log facies and net sandstone thickness with reservoir-volumetrics maps. The development of petrophysical models to calculate porosity, permeability, and water saturation from geophysical log data is based on thorough evaluation of wireline core analysis data, results from special core analyses, petrographic identification of the type and distribution of clay minerals, and calculated shale volumes of

reservoir units. The lack of porosity log data in the field (only six wells have porosity logs) requires petrophysical characterization of porosity to be based primarily on indirect methods using non-porosity logs such as SP and resistivity.

An example of core and porosity log data over the E reservoir in the T. B. Slick A149 well is shown in Figure 43. This is one of two wells for which we have whole core, abundant conventional core analyses, and a modern log suite including gamma-ray, deep induction, density, and compensated neutron log curves. There is no spontaneous potential log for this well, and this is most unfortunate, because virtually all of the other wells in the field have SP logs (and no gamma ray), and therefore no whole core-SP log calibration can be made. Comparisons of the resistivity curve (1) with the core graphic log (2) and with porosity (3) and permeability (4) data measured on core samples show a reasonable correlation between resistivity, core facies, and porosity and permeability. Sandstones with reduced porosity and permeability correspond to locations described in core as basal channel facies, or they are carbonate cemented. These permeability variations are not readily recognizable from the log data alone.

Relationships between log resistivity and porosity were studied in order to develop a model to determine porosity from electric log data. Relationships determined for porosity and resistivity were subsequently used to calculate permeability using the appropriate porosity/ permeability relationship that has been identified for each reservoir facies type.

Analysis of modern logs

Modern well logs are uncommon in Rincon field, but it is important to develop a methodology so that new development and reexploration can be analyzed. A log suite in well 149, including gamma ray, resistivity, density and compensated neutron porosity, as well as core data, was analyzed in order to develop a strategy for wireline petrophysics.

The work-flow scheme for analyzing modern logs includes depth shifting core data to wireline depths, determining a bulk shale volume indicator (Vsh), and developing a porosity algorithm. Based on correlation with other wells, and the significant presence of radioactive lithic fragments within the sandstone, it is determined that the gamma-ray log is not a good indicator

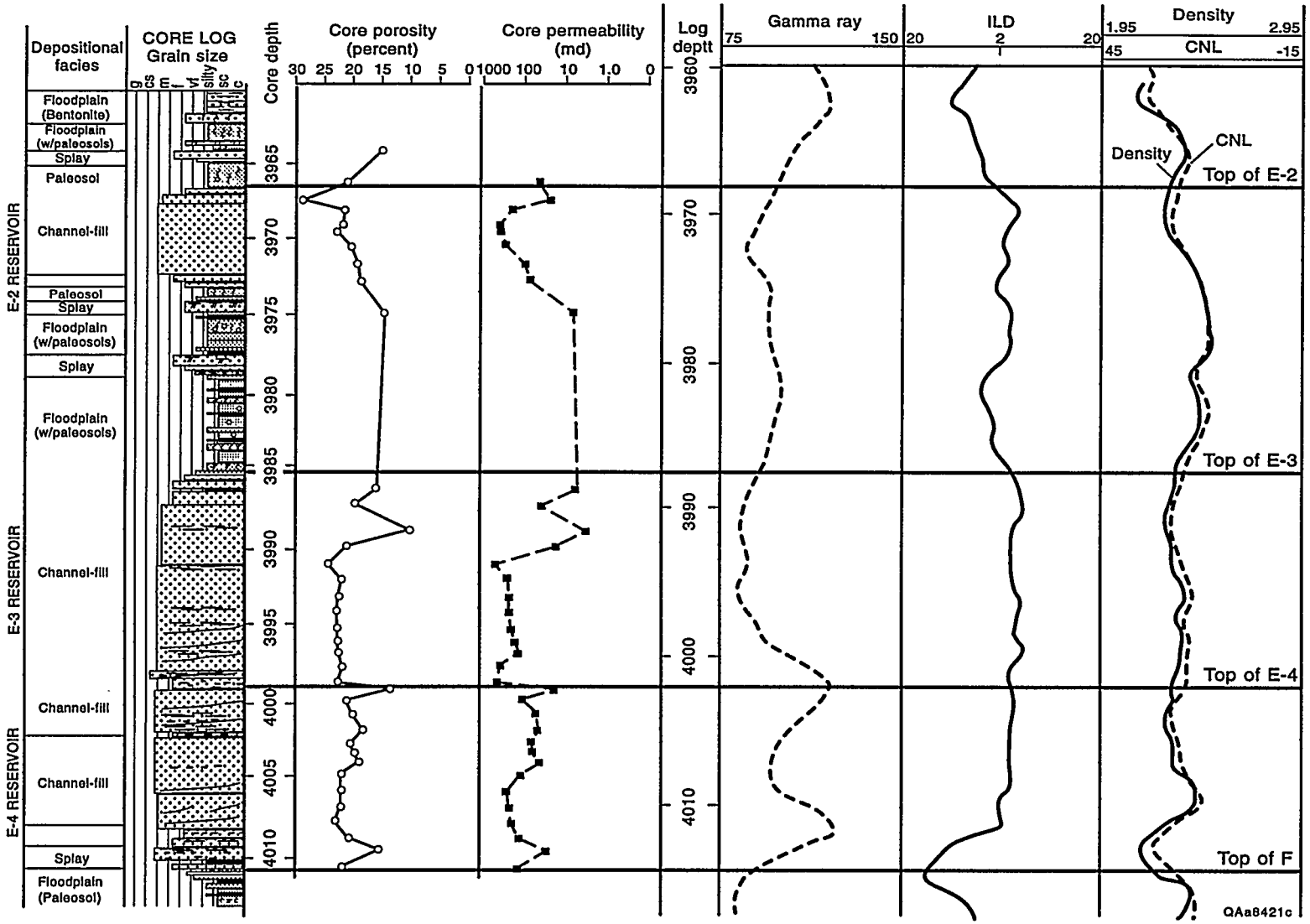

Figure 43. Core graphic log; porosity and permeability data; and gamma-ray, induction, and porosity logs, T. B. Slick 231:149 well. See Figure 25 for legend explanation.

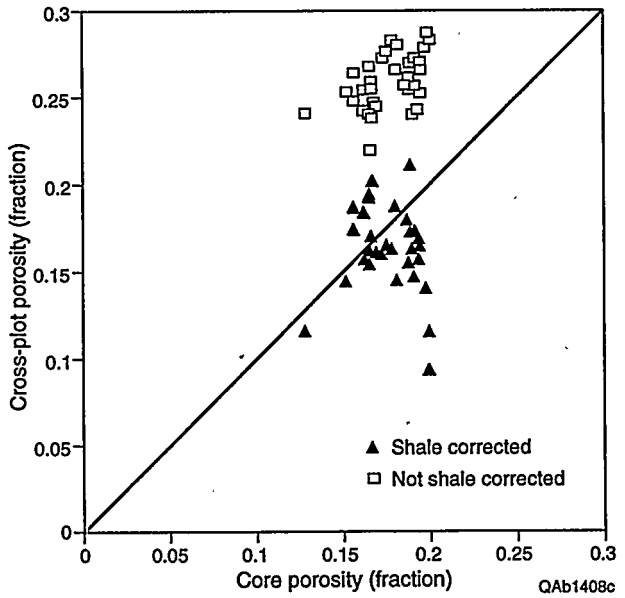

Figure 44. Comparison of shale-corrected and uncorrected cross-plot porosity versus core porosity.

of shale. Instead, the neutron log (CNL) is used as a shale indicator to calculate the shale fraction. The following equation is used to determine the shale volume:

$$Vsh = ((CNL * (CNL - CNL\ sand)) / DI)^{**}\ 0.5 \qquad (10)$$

where

DI = CNL shale * (CNL shale - CNL sand)

Vsh = bulk shale volume

CNL = CNL log value

CNL sand = the clean sand value read from the CNL log

CNL shale = the pure shale value read from the CNL log.

Shale determination is based on adjusting the CNL log reading between a pure sandstone and pure shale measurement. The clean sandstone and the pure shale values are respectively picked from local (Frio E reservoir) minimum and maximum values of the CNL log. For the Frio E interval the neutron clean sandstone value is 0.283 and the neutron shale value is 0.534, which were directly read from CNL log.

Porosity can be determined from the standard density-neutron cross plot applying a bulk volume shale correction. When calculating porosity a clay density of 2.124 g/cc and a neutron clay response of 0.534 were chosen. These values were determined from matching of density and

neutron values at the depth where the pure shale volume (100% of shale) is present. It is noted that the value for the density of clay (2.124) corresponds to the published value of 2.120 for montmorillonite. The value for neutron clay (0.534) is not very much different from the published values of 0.6 for montmorillonite, and, this value is very close to the published value of between 0. 519 and 0.500 for wet clay.

Correction for bulk volume shale is critical in determining correct porosity. The computed results for porosity without shale correction and shale corrected cross-plot porosity are compared with core porosity in Figure 44. Figure 44 clearly shows that shale corrected cross-plot porosity better represents core porosity than uncorrected cross-plot data, and the uncorrected data predicts overly optimistic porosity values.

Analysis of old logs

Resistivity measurements are used to obtain porosity from wireline logs where porosity logs are not available, for example, where wells predate the development of porosity logs. Several steps are needed to ascertain the resistivity derived porosity. These steps involve calculating Vcl in order to compensate for the conductivity of shale and then calculating a compensation for the effect of mud filtrate invasion.

Often with an old log suite, mud filtrate resistivity (Rmf) must be derived from mud resistivity (Rm). This conversion can be made by applying the equation below with C equal to 0. 847, when mud weight is less than 10.8 pounds.

Rmf C*(Rm)i.7 (11)

The first step in determining bulk volume shale is to calculate a clean sandstone SP response (SSP) for separate reservoirs. The need to derive a separate SSP for each reservoir occurs when they have different Rw values. The equation below is applied to determine SSP. When applying this equation Rw and Rmf must be at reservoir conditions and Tr must be reservoir temperature. Test the SSP value to make sure it does not exceed the minimum measured SP response. If this discrepancy occurs, the variables in the equation must be adjusted to make the minimum SP equal to the SSP.

Table 12. Representative saturation exponents from the Frio Fluvial-Deltaic Sandstone play.

Field	Cementation exponent	Saturation exponent
*Frio, South Texas	1.80	1.8
*Agua Dulce field	1.71	1.66
*Hollow Tree field	1.84	1.665
**Seeligson field	1.89	1.79
Average	**1.81**	**1.729**

$$SSP = ((0.133*Tr)+60)*\log(Rw/Rmf) \quad (12)$$

Having a reservoir specific SSP allows the determination of bulk volume shale (Vcl) from SP wireline curve. The calculation is made from the equation below.

$$Vcl = 1-(SP/SSP) \quad (13)$$

Resistivity-derived porosity is now determined by calculating resistivity of near-borehole mixing zone resistivity (Rz) and applying the previously determined Vcl. The mixing zone resistivity is determined at formation temperature from formation water resistivity (Rw) and Rmf. For shallow invasion, Rz is calculated from the equation below.

$$Rz = 1/((o.1/Rw)+(.9/Rmf)) \quad (14)$$

Resistivity porosity is then derived from the equation below.

$$fsn = (a*Rz/Rsn)^{1/m}*(1-Vcl) \quad (15)$$

Fluid Saturation Modeling

Formation resistivity factor

The saturation exponent applicable in Rincon field is taken as 1.7. Reported values range from 1.64 to 1.8 and average 1.7 (Table 12). This data source is limited, but values do not range significantly and the result of saturation calculation is not sensitive to saturation exponent in clean sandstone.

Formation resistivity measurements were conducted to define the cementation exponent m, which is used in the Archie equation to calculate formation water saturation. It has been documented in studies on the sensitivity of variables used in the Archie equation (Archie, 1942) that, unless reservoirs are characterized by low porosity (which these Frio reservoirs are not), variations in *m* will affect calculated water saturation values much more than values of *n,* the saturation exponent (Chen and Fang, 1986). Reported data on m values from the Frio in South Texas are very limited; at present we have found values ranging from 1.6 to 1.8 (Dewan, 1988). Reported Frio values are all less than the value 2.0, which is the standard default value generally used in the Archie equation for sandstones characterized by intergranular porosity. Higher values of m result in higher calculated water saturation values, which will in turn result in lower estimates for oil in place. Accurate estimates of water saturation are critical to delineating reasonable volumes of oil in place, and measurements *of m* on our own core samples will provide best possible estimates of values and variations in Sw in these Frio reservoir rock types.

Formation resistivity factor (FRF) was analyzed from laboratory measurements. A total of 14 measurements were obtained to determine the character of formation resistivity factor. The data are representative of the total range of pay as defined by porosity and permeability. Porosity ranges from 9 percent to 32 percent, and permeability ranges from 0.4 and to 747 md. Measured FRF values are also consistent with published data, ranging from 12.5 to 45.8. Converting FRF to cementation exponent values, assuming in the Archie equation a = 1, the values range from a minimum of 1.67 to a maximum is 2.4, and have a median of 1.81 (Table 13). This median is consistent with the average published cementation exponents in Table 13.

Modeling FRF for use in Archie equations was accomplished by assuming that porosity, permeability, and FRF are all interrelated. The tortuosity that the electrical path measures by FRF is a function of both porosity and permeability. Relatively high porosity but poor permeability could have a larger FRF value than a lower porosity with relatively higher permeability. Thus, modeling FRF by applying both porosity and permeability has the potential to determine more accurate values.

Table 13. Special core analysis and descriptive statistics for core samples in Rincon field.

Sample number	Depth (ft)	Porosity (%)	Permeability (md)	Formation resistivity factor	Cementation exponent (a=1)
1	3967.3	0.22	36.50	16.25	1.83
2	3974.6	0.16	7.20	25.20	1.74
3	3987	0.22	61.00	14.57	1.78
4	3988.7	0.11	3.30	44.58	1.73
5	3990.9	0.26	747.00	12.51	1.90
6	3999.6	0.23	98.00	16.82	1.90
7	4008.3	0.18	27.50	20.47	1.74
8	3872	0.30	172.00	13.85	2.18
9	3879	0.30	102.00	13.64	2.40
10	3891	0.32	320.00	15.52	2.40
11	3895	0.18	121.00	19.69	1.73
12	3950	0.22	130.00	14.78	1.80
13	3954	0.09	0.40	45.79	1.57
14	3959	0.20	370.00	14.15	1.82
Minimum		0.09	0.40	12.51	1.57
Maximum		0.32	747.00	45.79	2.40
Range		0.23	746.00	33.28	0.83
Average		0.21	156.85	20.56	1.89
Median		0.22	100.00	15.88	1.81
Skewness		–0.19	2.16	1.90	1.27

Both porosity and permeability display power relationships with FRF. Exponential, logarithmic, and power functions were all applied with porosity or permeability as the independent variable and FRF as the dependent variable. A porosity power function was determined to have a superior correlation coefficient (r square) of 0.86 and a permeability power function had a superior correlation coefficient of 0.82. Because both porosity and permeability strongly predict FRF, a multiple nonlinear regression is possible.

A robust multiple nonlinear regression model for the prediction of FRF was developed. The model in the equation below predicts FRF with porosity and permeability as input independent variables. The correlation is strong, displaying a multiple r of 0.95 and an F statistic of 53 compared to a significant F of 2.3×10^{-6}. The predictive capability is illustrated in Figure 45. Actual versus predicted values cluster closely around the 1-to-l line with the exception of one

Figure 45. Results of the multiple nonlinear regression model for predicting FRF. The strong predictive capability is displayed by the clustering of the data around the 1-to-1 line.

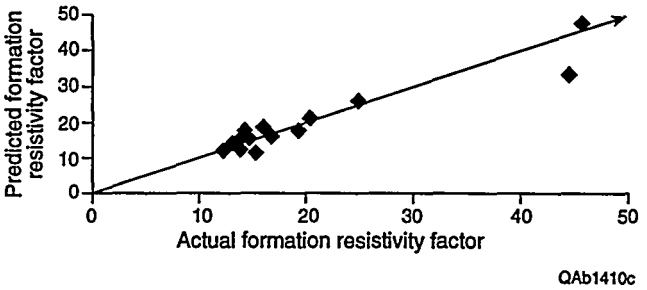

data outlier. This outlier is a data point that displays a higher FRF for the measured porosity and permeability.

$$FRF = 10^{(1.029-.58*\log(porosity)-0.095*\log(permeability))} \quad (16)$$

where porosity is a fraction and permeability is in millidarcys.

Capillary pressure modeling

The primary objective of the mercury-injection capillary pressure measurements was to determine the distribution of pore throat sizes present in each sample, and to ascertain any differences in pore types among the various rock types identified from core description and evaluation of conventional core analysis data. Thin sections were prepared for each sample selected for capillary pressure studies to provide visual description of pore geometries and estimates of pore sizes. The mercury-injection technique is the most commonly used and fastest method of capillary pressure measurement, and it yields the maximum number of data values. Pore geometry identified from these measurements will provide insight into heterogeneity present within individual samples. Pore throat size derived from capillary pressure tests will form the basis for estimates of irreducible water saturation. These estimates of Swirr will in turn be used in subsequent resource calculations. Capillary pressure results may also be used to estimate reservoir efficiency.

Initial connate water saturation was modeled from capillary pressure data as a function of porosity, permeability, and height above free water. From exploratory statistical data analysis it was found that both porosity and permeability, as well as height above free water, controlled

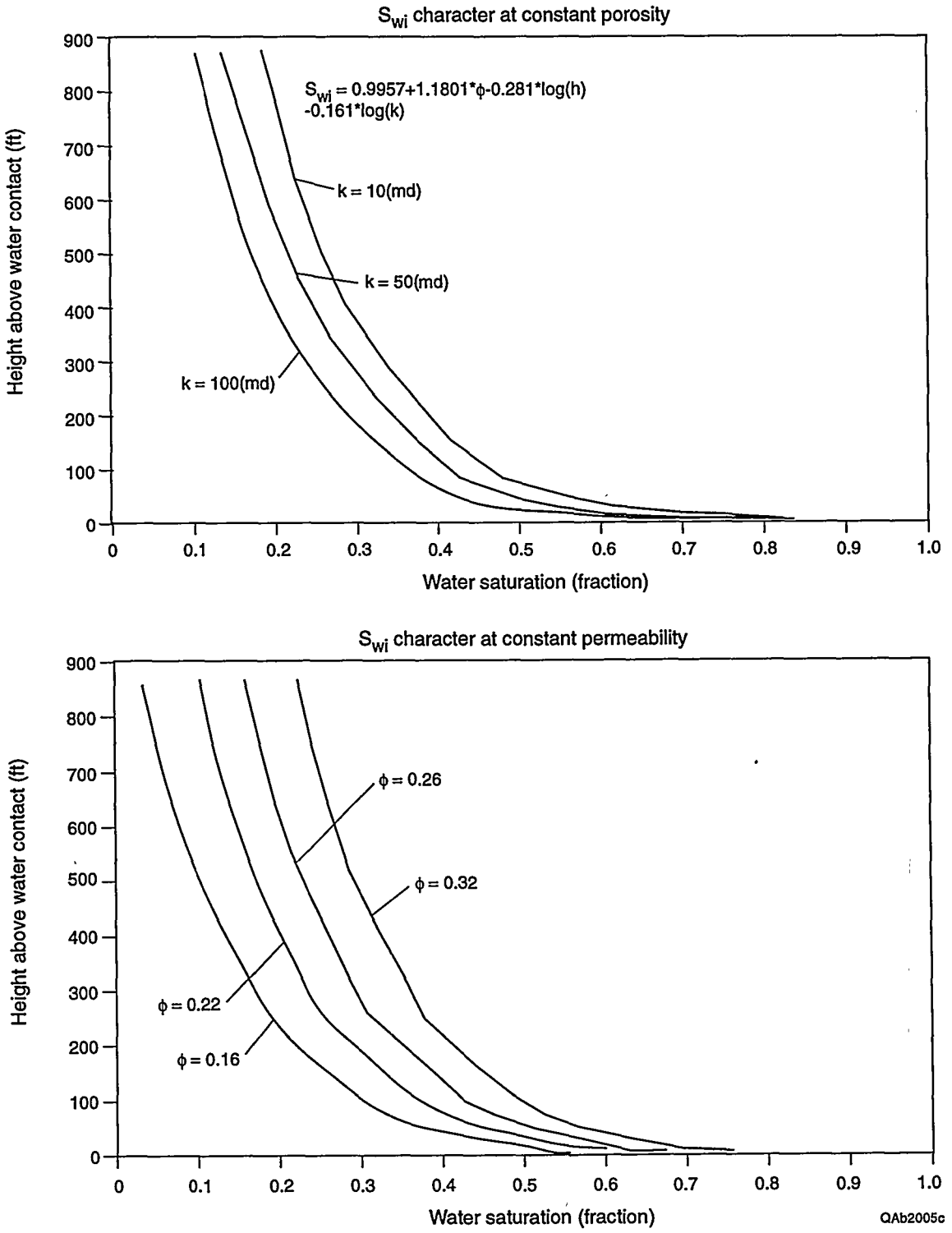

Figure 46. Initial water saturation is modeled from a multi-nonlinear regression equation with porosity, permeability, and height above free-water as the independent variables.

initial water saturation. The relationship between initial water saturation and permeability and height above free water is nonlinear, whereas the relationship between initial water saturation and porosity is linear. Multi-nonlinear regression was applied to develop an initial water saturation function. The character of this function is illustrated in Figure 46. The multi-nonlinear equation is statistically robust, having a correlation coefficient (r) of 0.88. The utility of this equation is that it can be applied when, because of lack of data, the Archie equation cannot be applied.

Residual oil saturation

Core flood tests were conducted on 15 core plugs to acquire data on residual oil saturation (Sor) and end point relative permeability. There are no good available residual oil saturation data for these reservoirs, and values for Sor reported for reservoirs throughout the Frio play range widely from 10 to 38 percent (Holtz and McRae, 1995). Sor data are obviously critical to obtaining reasonable estimates of remaining mobile oil.

Residual oil saturation can be characterized as low, with a long tail on the high side. The mean and median are nearly identical at 28.8 percent, indicating a strong central tendency. The standard deviation is a low 9 percent, although the range is large (48 percent). The large range is due to a single high outlier value of 62.5 percent. Because the data sample is small, it cannot be determined if this high data point is valid. The long tail is evident in the high skewness value of 1.74 and on the histogram shown in Figure 47.

Reserve Growth Potential

The potential for infield resource additions is a function of the original oil volume in place, the present level of development, and the degree of internal geologic complexity of the reservoir being produced. Studies of the Frio D and E reservoirs in Rincon field have identified the current level of development in individual reservoir units and documented that reservoir geometry within each stratigraphic reservoir interval is variable and provides important controls on the level of flow communication within a single reservoir unit. Stratigraphic heterogeneity and

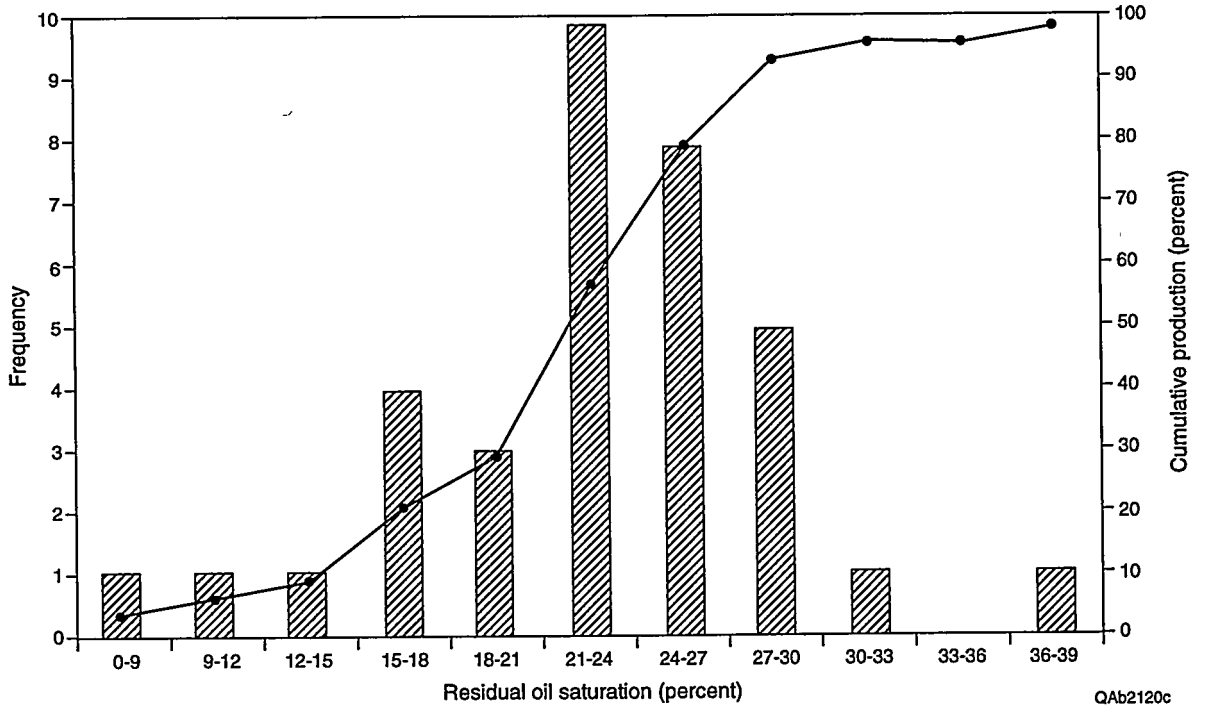

Figure 47. Residual oil saturation measured from core flood tests indicates a wide range of possibilities due to high and low tails on the distribution.

variability in reservoir quality exhibited within these reservoirs are directly responsible for the distribution of original oil in place and have also been a primary control on present recovery efficiencies. The wide range of oil volumes produced from wells completed in the same reservoir is an additional indication of the presence of interwell-scale heterogeneity.

Frio D reservoir sandstones have more complex facies patterns and a greater degree of stratigraphic variability, and, as a result, the composite reservoir zone has a significantly lower recovery efficiency than do E series reservoirs. The relatively poor recovery efficiency of the Frio D reservoir zone is caused by the fact that current well spacing is greater than the size of reservoir compartments that collectively make up the total storage space of the mobile oil resource in the Frio D reservoir zone. As a consequence, reservoirs of the Frio D zone represent a greater opportunity for future reserve growth than those of the Frio E zone.

Conclusions

Assessing the potential for incremental reserve growth in mature fields, such as those producing from Frio reservoirs in South Texas, requires identifying the location and volume of the remaining resource in the reservoir (Tyler and Finley, 1991). Detailed interwell-scale studies of selected reservoirs serve to characterize reservoir flow-unit architecture and determine the controls reservoir characteristics exert on the distribution of original oil volumes, present production trends, and locations and volumes of unrecovered mobile oil in untapped and incompletely drained zones. With an estimated 1.6 Bbbl of remaining recoverable oil, Frio reservoirs in South Texas represent a significant resource worthy of these efforts.

Different Frio reservoir architectural styles possess characteristic geometries and permeability distributions that directly impact their ability to produce hydrocarbons. Studies of the Frio D and E reservoir zones in Rincon field demonstrate that sandstone architecture is a primary control on recovery efficiency. The architectural styles exhibited by the D and E reservoirs in Rincon field include aggradational, retrogradational, and progradational stacking patterns. The D/E reservoir sequence records an evolution from aggradational, vertically stacked and more laterally isolated units in the lower E zones to retrogradational, landward-stepping units in the upper E reservoir that are also vertically stacked but have increased lateral communication that is probably responsible for higher recovery efficiencies. Frio D reservoir sandstones have more complex facies patterns and a greater degree of stratigraphic variability, and, as a result, the composite reservoir zone has a significantly lower recovery efficiency than do E series reservoirs. The relatively poor recovery efficiency of the Frio D reservoir zone is caused by the fact that current well spacing is greater than the size of reservoir compartments that collectively make up the total storage space of the mobile oil resource in the Frio D reservoir zone.

The techniques of multidisciplinary advanced reservoirs characterization that have been used in Rincon field serve as a useful template for additional recovery efforts in other mature fluvial-deltaic reservoirs throughout the Frio Fluvial-Deltaic (Vicksburg Fault Zone) Play. The specific methodologies can also be applied to other mature fluvial-deltaic reservoirs throughout

the United States because similar facies in those reservoirs will result in similar architectures. Furthermore, the basic tenets of multidisciplinary advanced reservoir characterization, including geological and engineering interpretations enhanced by high-frequency stratigraphic studies and facies-based petrophysical analysis, will enhance the understanding of any mature reservoir, regardless of its depositional setting.

T-C-B FIELD RESERVOIR STUDIES

P. R. Knox and'. G. Paine

Introduction

Objectives for the study of Tijerina-Canales-Blucher (T-C-B) field included the delineation of untapped/incompletely drained compartments and the evaluation of potential for new pools within selected reservoir intervals, as well as documentation of these features for purposes of technology transfer. The reservoir intervals studied in detail were selected on the basis of certain criteria (McRae and others, 1995) following a review of all reservoir intervals within T-C-B field. Two reservoir intervals in the Middle Frio Formation, the Scott and Whitehill, comprising a fourth-order genetic unit, were selected for detailed study because they represent significant past production, are unfaulted, and show a spectrum of fluvial upper delta plain architectures.

Advanced characterization of the Scott and Whitehill zones has been completed and specific reserve-growth opportunities have been delineated. Following subregional study to identify the bounding surfaces correlative to fourth-order marine flooding surfaces, detailed well log interpretation allowed further subdivision of the Scott/Whitehall interval into fifth-order genetic units within the T-C-B area. Facies, net sandstone, and compartment production maps were then prepared to document general compartment boundaries and past production history for each fifth-order interval. Volumetric analysis was combined with other reservoir history data to identify approximate compartment areas drained. The distribution of undrained areas was then compared with the location of open well bores to plan infill and recompletion opportunities. Results of the Scott/Whitehill study indicate that sandstones within a fourth-order genetic unit show a systematic and predictable change in architecture and internal heterogeneity from base to top, and that these relationships can be used to predict reserve-growth potential in other reservoirs on a quick-look basis.

Interpretation of reservoir compartmentalization has been presented to the field operator, along with specific recommendations for recompletion and infill drilling opportunities. Because

of various economic and operational considerations, only one recompletion has been done. This opportunity, evaluated as having moderate risk, is currently producing at economic rates.

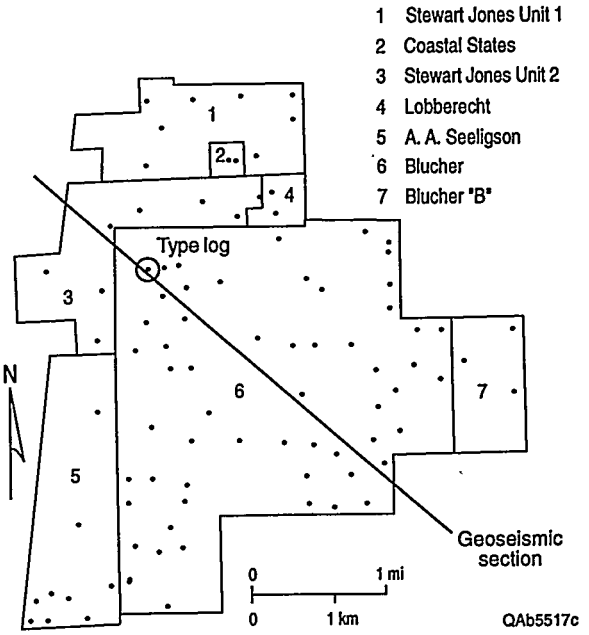

Figure 48. Map of study area in T-C-B field showing lease boundaries and approximate location of geoseismic section (Fig. 51).

Location, History, and Geologic Setting of T-C-B Field *Location*

Tijerina-Canales-Blucher field is located in the northern half of the Frio Fluvial-Deltaic Sandstone (Vicksburg Fault Zone) oil play, about 55 mi southwest of Corpus Christi, and it straddles the border between Kleberg and southern Jim Wells Counties (Fig. 17). The field lies in a structural low between large rollover anticlines in the Seeligson and La Gloria fields to the northeast and southwest, respectively. Movement on the Sam Fordyce Fault, a part of the regional Vicksburg Fault Zone, and subsidiary synthetic and antithetic faults, has generated a fault-segmented rollover structure in the lower Frio reservoir section. Accumulation of most of the sediment within the middle Frio postdates most of the fault movement, creating a low-relief unfaulted (to subtly faulted) anticline slightly offset from the crest of the underlying rollover structure.

The area selected for study is a contiguous 4,800-acre block, located at the southwest edge of the field and operated by Mobil Exploration and Producing U.S., Inc. The block is primarily composed of the 3,500-acre Blucher lease, which is adjoined by the smaller Blucher B, A. A. Seeligson, Lobberecht, and Stewart & Jones I and II leases (Fig. 48). Mobil has supplied well log, core, and production data for more than 80 wells on this lease block.

Development History

The many stacked reservoirs in the various areas of T-C-B field have been discovered and produced by several operators over the years, beginning in the late 1930's. Original operators include Sun (now Oryx), Humble (now Exxon), Texaco, and Mobil. Cumulative oil production from Frio reservoirs in the T-C-B field is reported at more than 50 MMSTB. T-C-B is in a mature stage of development, and production has declined drastically since the 1970's due, in part, to the abandonment of a large number of wells. Recent operator focus has turned to the deeper, more complexly faulted reservoirs of the Vicksburg Formation as a result of improvements in seismic technology. Consequently, the mature Frio reservoirs are suffering from a lack of investigation and are in danger of premature abandonment.

The area of T-C-B field selected for detailed study, the western Blucher portion, was discovered by Shell in 1939 and subsequently sold to La Gloria Corporation in 1942. La Gloria operated the field until Mobil purchased the leases in 1967. Recent deeper drilling by Mobil in the late 1980's targeted complex fault blocks interpreted from 2-D seismic data. During 1994, 3-D seismic data were gathered over the Mobil leases, and processing was completed in early 1995. As of 1992, there were 24 active wells, 12 idle wells, and 28 abandoned wells on the Blucher lease. Production has come from more than 40 separate reservoirs in the Vicksburg, lower Frio, and middle Frio Formations. Data from the Railroad Commission of Texas indicate that no Frio reservoir has been drilled at closer than a 40-acre spacing, an indication of substantial potential for infill drilling opportunities.

Stratigraphic Framework

A detailed discussion of the stratigraphic framework for T-C-B reservoirs can be found in McRae and others (1994). The following is a summary of the general setting of Frio reservoirs within the T-C-B area.

Frio sediments in the vicinity of T-C-B field were deposited by the Norias deltaic and Gueydan fluvial depositional systems that filled the axis of the Rio Grande structural embayment (Fig. 49).

The location of T-C-B field lies near the boundary of these two depositional systems. During early Frio times, the Norias delta occupied the T-C-B area. Because of continuous progradation, the Gueydan Fluvial system (equivalent to the upper delta plain of the Norias system) eventually encroached on the T-C-B area from the northwest, occupying the area throughout the middle Frio time.

Productive reservoir sandstones in T-C-B field range in depth from 5,500 to 8,000 ft and lie within the middle and lower members of the upper Oligocene Frio Formation and the upper part of the lower Oligocene Vicksburg Formation, as shown in the field type log (Fig. 50) . The thick massive progradational deltaic to shallow-water marine sandstones of the upper portion of the Vicksburg (Taylor and Al-Shaieb, 1986) are extensively faulted and produce mostly gas. The lower Frio Formation in T-C-B field ranges in depth from 6,600 to 7,600 ft and contains many 10- to 30-ft-thick deltaic reservoir sandstones in a dominantly shaly interval. This section is moderately faulted and produces both oil and gas, with gas predominating. The mostly oil -productive reservoirs of the middle Frio Formation range in depth from 5,500 to 6,600 ft and occur within an interval of thick and abundant fluvial sandstones interbedded with floodplain mudstones. In Seeligson field, directly northwest of T-C-B field, the contact between the Vicksburg Formation and lower Frio unit is reportedly unconformable (Ambrose and others, 1992). Because

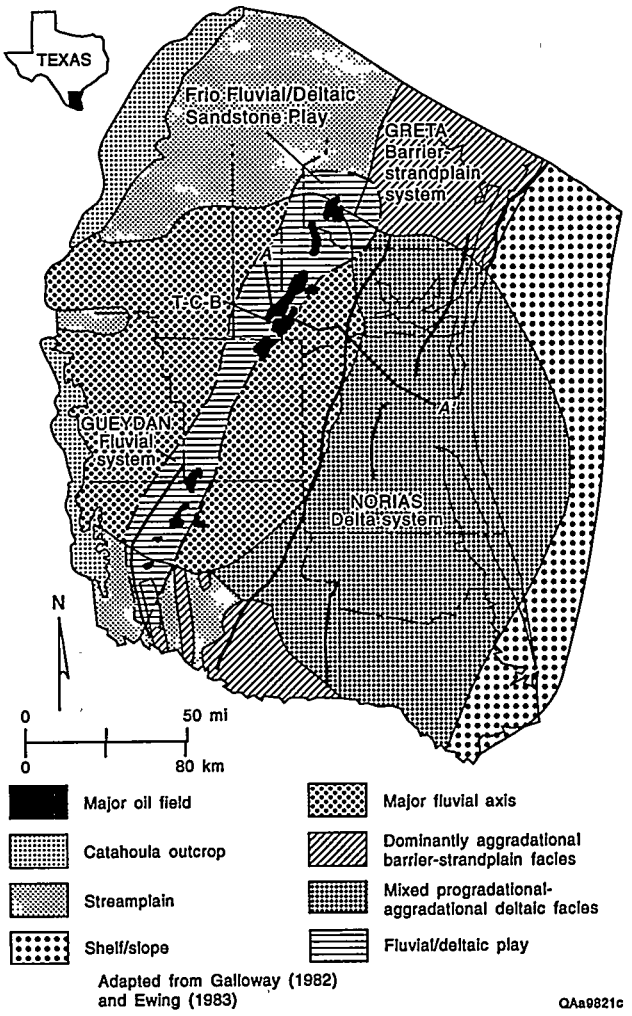

Figure 49. Location of Tijerina-Canales-Blucher (T-C-B) field within the Frio Fluvial-Deltaic Sandstone (Vicksburg Fault Zone) Play in South Texas. Also shown is the position of T-C-B field with respect to the Norias delta and Gueydan fluvial depositional systems of Galloway (1982). Cross section A–A′ is shown in Figure 61.

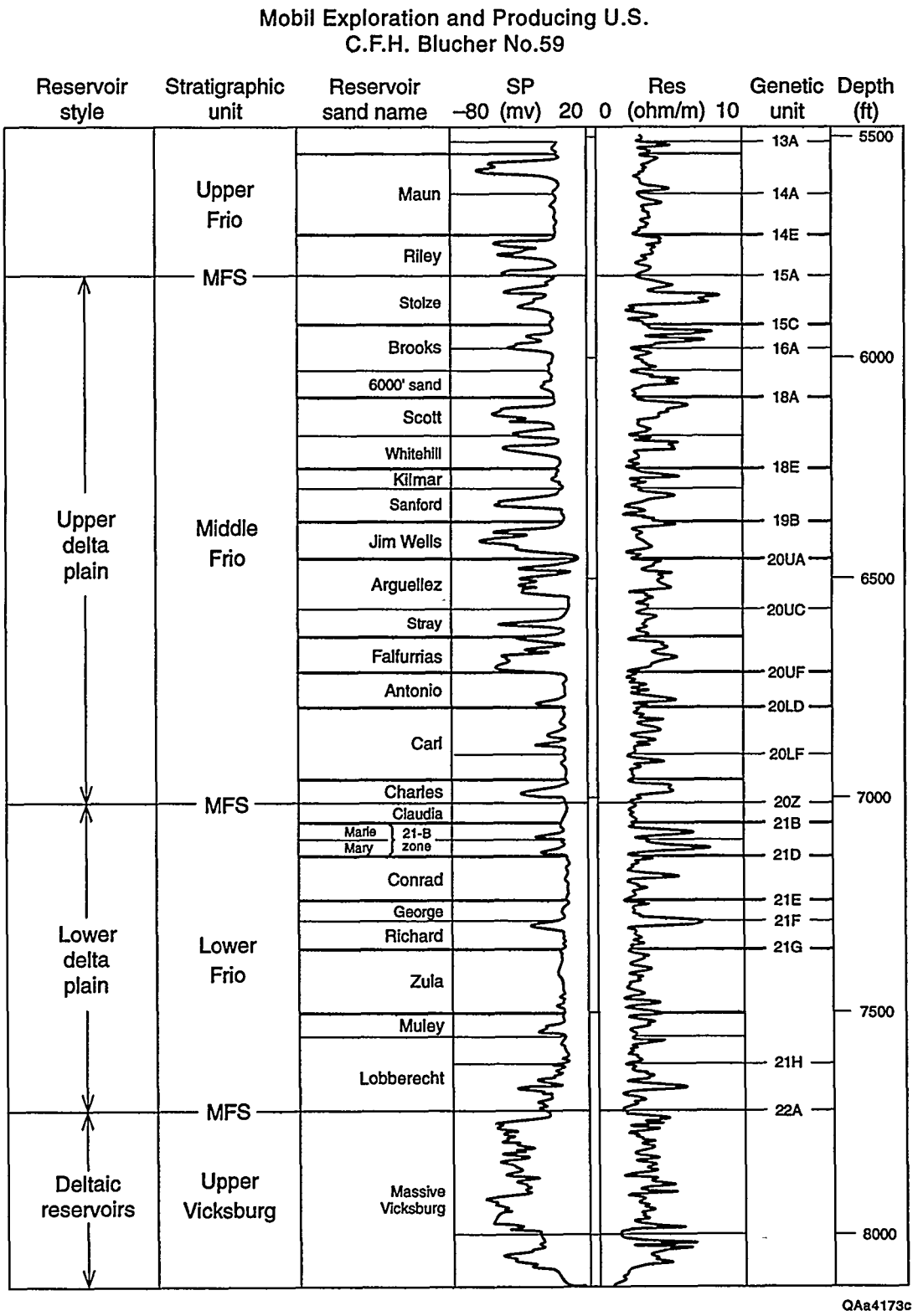

Figure 50. Representative log from T-C-B field illustrating generalized stratigraphy and nomenclature of productive reservoir sandstones.

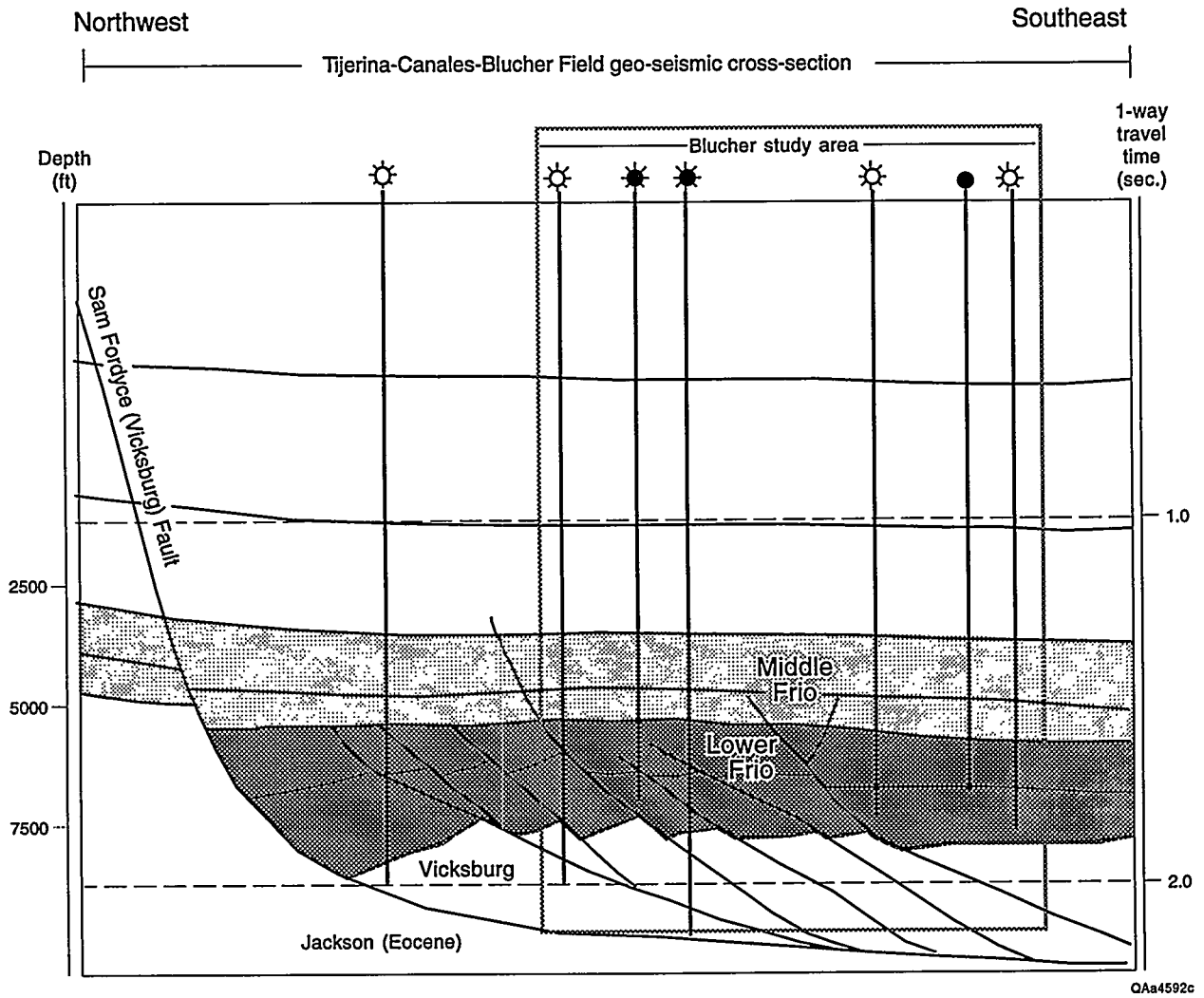

Figure 51. Northwest-to-southeast geoseismic dip section across T-C-B field illustrating the general structural setting of Frio and Vicksburg reservoir sections. The base of the middle Frio is a significant unconformity separating structurally complicated reservoirs below from less faulted reservoirs above. Seismic interpretation provided by Mobil Exploration and Producing, U.S. See Figure 48 for approximate location of section.

the Vicksburg is not a focus of this study, insufficient work has been done to confirm an unconformable relationship between the two units in T-C-B field. The contact between the lower and middle Frio is a subtle but moderately profound unconformity. Well log correlation within T-C-B field has identified mild truncation in the underlying lower Frio sediments and demonstrates the abrupt change from a sandstone-poor to a sandstone-dominated interval across the contact. However, a two-dimensional seismic line (Fig. 51) illustrates that the significance of

the surface exceeds that of minor erosion. The lower Frio is moderately growth faulted, with significant expansion of section at the updip edge of the field adjacent to the Sam Fordyce Fault, whereas the middle Frio is, at best, mildly faulted with no expansion of section. This difference in style exaggerates the appearance of truncation at the unconformable boundary.

The transition from the middle Frio to the overlying upper Frio is subtle in the T-C-B area and has not been investigated in detail. On the basis of subregional correlation, there is a significant change at the 15A marker (Figure 50) from dominantly aggradational to dominantly retrogradational architecture that may correspond to the transition from middle to upper Frio as identified by Galloway and others (1982).

Methodology

The primary objective in T-C-B field, that of identifying specific reserve-growth opportunities in selected reservoirs, required advanced technology reservoir characterization that integrated geological, geophysical, and engineering methods (the methodology is documented in Holtz and others, 1996). An important technical goal was to apply observations from a previous outcrop study of Cretaceous fluvial-deltaic sandstones of the Ferron Formation of central Utah. This study, funded by the Gas Research Institute and various industrial associates, concluded that reservoir architecture and heterogeneity varies systematically within a fourth-order genetic unit (Barton, 1994), possibly as a consequence of systematic changes in accommodation rate. The following two sections briefly review both the observations from the Ferron outcrop study and the general reservoir characterization methods used to investigate the Scott/Whitehill reservoir interval of T-C-B field.

Outcrop-Based Models for Predicting Reservoir Architecture

The Upper Cretaceous (Turonian) Ferron Sandstone of central Utah was deposited in a fluvial-deltaic depositional system that existed on the west margin of the Cretaceous Interior Seaway (Barton, 1994) and carried sediments from the rising thrust belt in the west to the rapidly

subsiding foreland basin to the east. Total accommodation rates for the Ferron are similar to those for the Frio Formation in the Texas Gulf Coast: the Ferron spans 1.6 m.y. and is 800 ft thick, whereas the Frio ranges from 800 to 4,000+ ft and accumulated in a similar time span. Gardner (1991) divided the Ferron into seven fourth-order genetic sequences, GS 1 through GS 7 (Fig. 52a), each bounded by a marine flooding surface and being equivalent to a parasequence, as defined by Van Wagoner and others (1988). These genetic sequences vary from strongly progradational or seaward stepping in the lower portion (GS 1 and 2), to aggradational or vertically stacked in the middle (GS 3 and 4), to retrogradational or landward-stepping at the top of the depositional cycle (GS 5, 6, and 7).

Barton (1994) examined, in detail, outcrops of distributary-channel deposits of two genetic sequences, GS 2 and 5, and identified two styles of deposits exhibiting distinctly different external architecture and internal heterogeneity. He determined that variable internal heterogeneity is a function of the preservation potential of different lithofacies and differences in the content of channel lag deposits.

Distributary-channel-belt deposits that formed during the strongly seaward-stepping portion of a depositional cycle (GS 2), at which time the rate of sediment influx was greater than the rate of generation of accommodation space, are typically narrow and few in number, and consequently cover little area in map view (Fig. 52b). Internally, these channel belts consist of sandy, vertically amalgamated channel deposits dominated by trough-fill cross-stratified lithofacies of basal channel deposits. The base of individual channel deposits commonly contains a lag of dispersed and rounded mudstone and sandstone clasts, creating a layer of slightly reduced permeability at the contact between vertically adjacent channels. Low-permeability lithofacies from the upper portions of individual channel deposits, such as finer grained ripple strata and siltstones, are uncommon, having been removed by erosion during the incision and filling of subsequent channels. Barton (1994) ascribed the dominance of erosion over deposition in these channels, and thus their relative internal homogeneity, to the low accommodation rates under which they were deposited. The straight, narrow configuration of these channel belts is also a

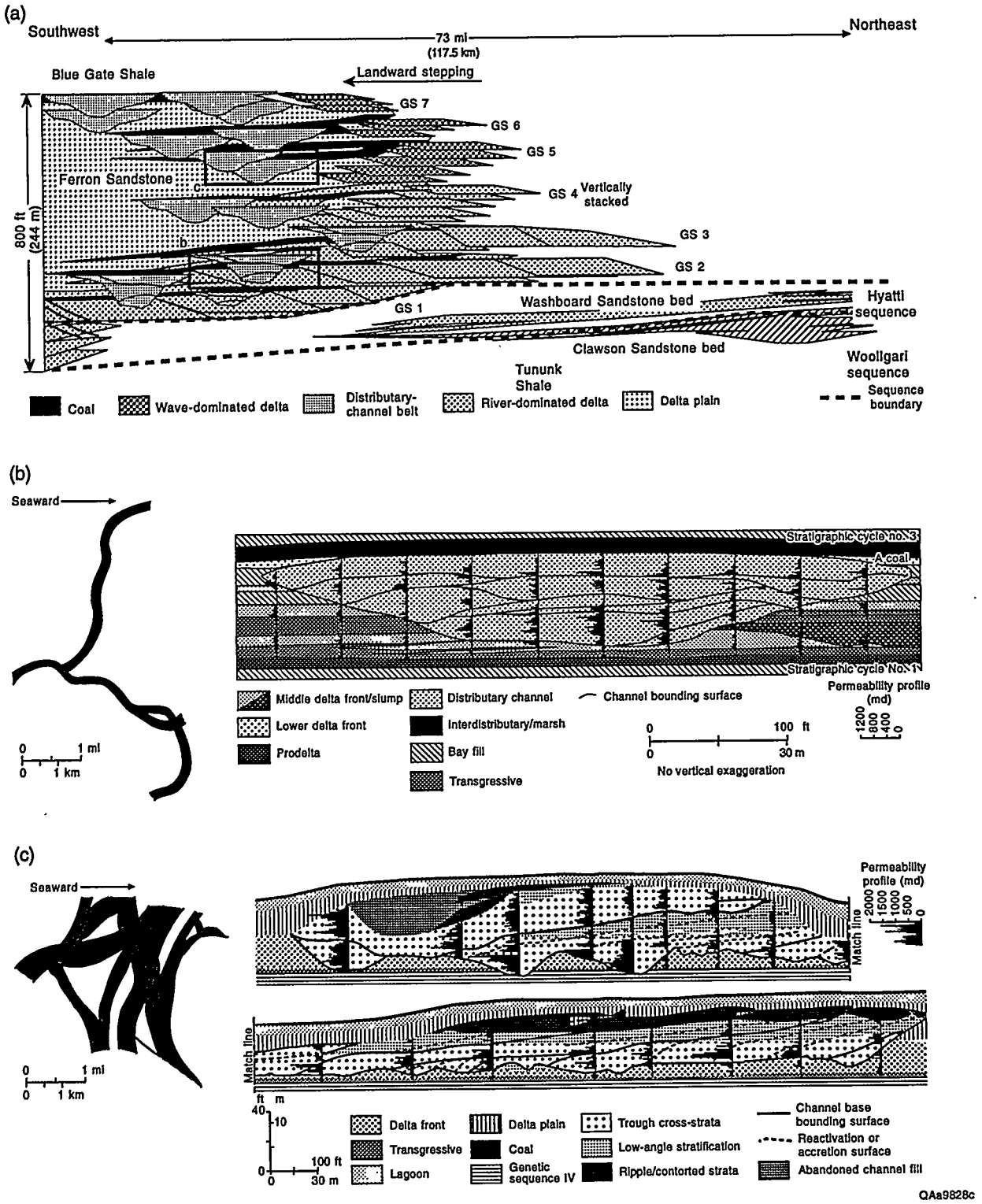

Figure 52. Genetic stacking pattern and architecture of the Cretaceous (Turonian) Ferron Sandstone of central Utah. (a) Stacking pattern for the Ferron 3rd-order depositional unit, composed of a depositional cycle of 4th-order units. Note locations of distributary channel fills detailed in (b) and (c). (b) Map view architecture and internal lithofacies of distributary channel fills in the low-accommodation seaward-stepping GS 2 4th-order unit. (c) Map view architecture and internal lithofacies of distributary channel fills in the high-accommodation landward-stepping GS 5. From Barton (1994).

consequence of low accommodation in that the channel system, previously meandering in part, must stretch to cover the increasing distance to the seaward-stepping distributary mouth, eliminating the tendency toward lateral migration and meandering. Distributaries are few because there is no opportunity for the channel to avulse, having never built substantially higher than the surrounding delta plain.

In contrast, distributary-channel-belt deposits formed during the landward-stepping portion of the Ferron depositional cycle, in which the rate of accommodation exceeded the rate of sediment influx, are broader and more numerous, covering a greater percentage of area in map view than those of the seaward-stepping unit. Internally, channel belts are more lithologically heterogeneous, containing nearly complete vertical channel deposit successions including trough cross-stratification, low-angle inclined stratification, rippled beds, and abandoned channel-fill mudstones (Fig. 52c). Channel bases are commonly draped by a lag deposit containing abundant deformed mudstone clasts that form a very low permeability layer between channel deposits that are in sandstone-on-sandstone contact. This depositional style indicates laterally migrating channels constrained within topographically high levee systems and flanked by large areas of low-lying floodplain, leading to frequent channel avulsion. This is consistent with the anticipated morphodynamic response of a distributary to rising base level, in which a channel of fixed length must increase its sinuosity as the distributary mouth steps landward. More complete preservation of individual, internally heterolithic channel deposits is a consequence of higher accommodation rates, in which subsequent channels do not cut as deeply into previous channel deposits because of a larger rise in base level (relative sea level) in the intervening period.

The two end-member distributary channel styles identified by Barton (1994) would have very different characteristics if they were subsurface oil and gas reservoirs. The narrow seaward-stepping distributary channel belts would not be effectively contacted by pattern-style drilling, but individual completions would drain considerable reservoir volumes because of the internal homogeneity of the channel belts. Conversely, the broader, more numerous distributary channel belts of the landward-stepping units would be more commonly contacted by pattern drilling, but

completions would drain smaller areas because of the internal heterogeneity resulting from more abundant low-permeability lithologies and mudclast conglomerate layers at channel boundaries.

Geological Reservoir Characterization Methods

As can be seen from the above discussion, the identification of third- and fourth-order marine flooding surfaces can provide a powerful framework in which to interpret reservoir architecture from limited well log data. Consequently, one of the first and most important steps in the reservoir characterization process is subregional correlation of the stratigraphic interval of interest far enough downdip to clearly locate fourth-order marine flooding surfaces. Once these have been defined, the more subtle fifth-order surfaces that subdivide the fourth-order unit can be identified within the field area. The fifth-order units frequently correspond to what operators identify as individual reservoir subzones.

Facies and net sandstone maps are then made for each fifth-order unit to define general reservoir architecture. Individual reservoir compartments can commonly be interpreted from these maps. Stratigraphic analysis of 3-D seismic data may help to interpret compartment boundaries at the between-well scale. Structure maps are then created for each compartment and fluid contacts are determined and annotated on the maps. Net pay maps are created for each compartment and production records are consulted to allow annotation of past drainage from the compartment. Petrophysical parameters such as porosity and water saturation are determined in order to calculate original hydrocarbons in place and area drained by each completion. A compartment status map is then created that incorporates original net pay and drainage from past production. Typical drainage radii of past completions are then compared with areas of undrained reservoir to evaluate the potential for recompletions in existing wells and the need for geologically targeted infill drilling. Expected production from economically viable recompletions and infill wells is then summed and represents reserve-growth potential.

Geophysical Reservoir Characterization Methods

Acquisition, processing, and analysis

A three-dimensional seismic data set used to analyze subtle stratigraphic features in the T-C-B field was provided to the project by Mobil. The data set, which covers 14 mi^2 in Kleberg and Jim Wells counties, consists of 347 east-west inlines and 280 north-south crosslines (fig. 53). The data were acquired in 1994 by Grant Geophysical using four vibrators, 10 Hz geophones, and a 2 ms sample interval (CGG, 1995). Stacking fold was between 22 and 24; bin size was 82 ft.

Original processing was by CGG. Problems with acquisition geometry, consistent well ties, and excessive air blast led Mobil to have EnTec Energy Consultants, Ltd. (EnTec) reprocess the data. EnTec also had problems with consistent well ties and ultimately recommended that Mobil acquire a vertical seismic profile (VSP) in the Blucher B-3 well. The VSP allowed EnTec to establish reliable time-to-depth ties and to produce time-converted log suites for four of the wells in the field. These wells were used as the control wells for our seismic horizon mapping.

The reprocessed three-dimensional seismic data volume was received in January 1996. Structural and stratigraphic analysis of the data was accomplished using the software Photon SeisX operating on Sun workstations at the Bureau of Economic Geology. Data analysis included (a) establishing time-to-depth ties between digitized log suites and the seismic data using checkshot surveys, synthetic seismograms, and the vertical seismic profile, (b) identifying key mappable seismic horizons within the stratigraphic zone of interest, (c) picking peaks, troughs, or zero crossings for the seismic horizons of interest and extending those picks across the data volume, (d) mapping faults within the heavily growth-faulted Vicksburg zone and the subtly faulted Frio section, (e) constructing structure maps (in time) for key seismic horizons, (f) creating time slices above and below key flattened horizons to show subtle stratigraphic features, and (g) creating seismic amplitude maps on various time slices and seismic horizons for comparison with net sandstone and facies maps created using well logs alone.

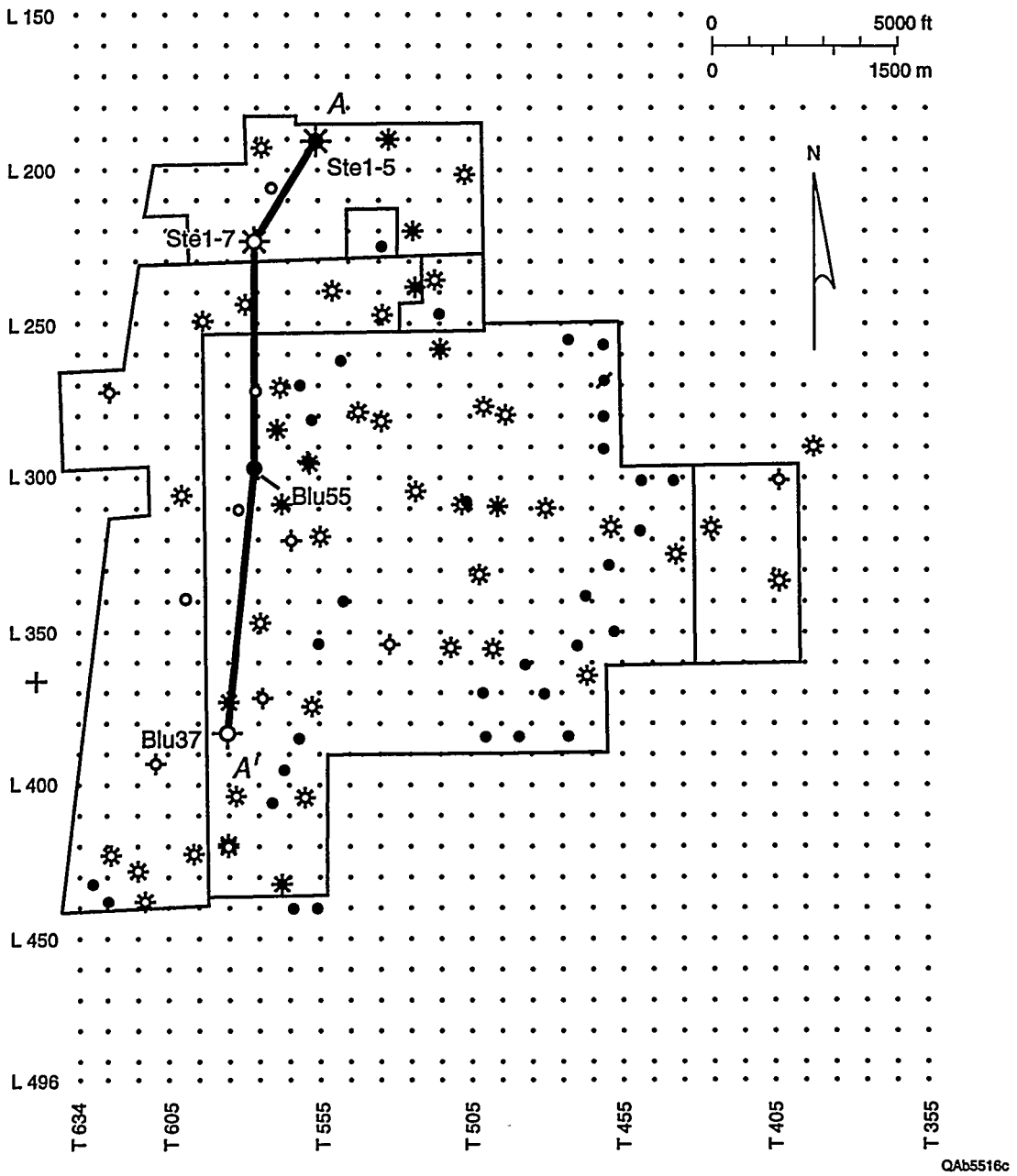

Figure 53. Major inlines (east-west), crosslines (north-south), well locations, and lease block boundaries within the T-C-B three-dimensional seismic data set provided by Mobil. Also shown are the locations of arbitrary seismic strike section A–A′ and dip section B–B′.

Limits of horizontal and vertical resolution

Analysis of acquisition geometry and seismic data characteristics allows us to establish theoretical limits for both the horizontal and vertical resolution of the T-C-B seismic data set. Aside from frequency content and rock property considerations, the practical limit of lateral

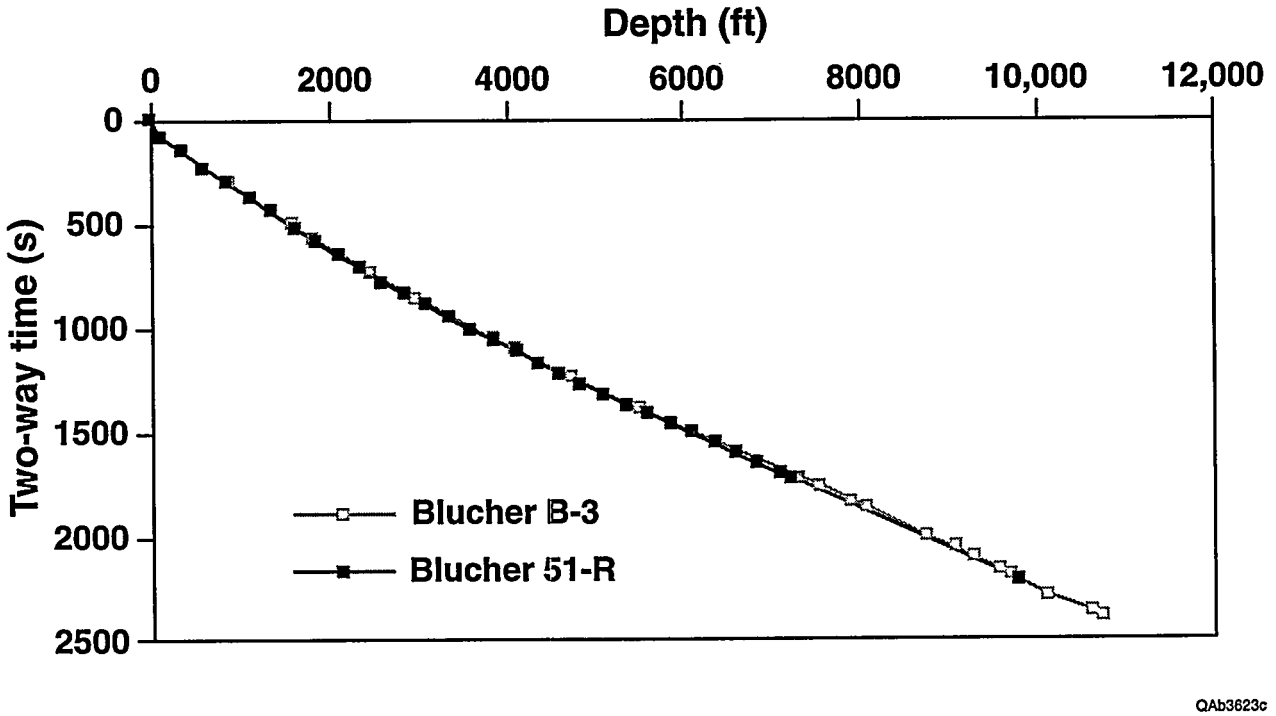

Figure 54. Two-way time versus depth established from checkshot surveys in the Blucher B-3 well in the eastern part of the data volume and the Blucher 51-R well in the western part of the data volume.

resolution is established by the fact that features smaller than three or four bins across cannot be distinguished. Bin size for the T-C-B data set is 82 ft; the smallest identifiable feature is thus 250 to 300 ft across.

Vertical resolution depends upon compressional wave velocity of the material and frequency content of the seismic signal. For the depth range of interest in the T-C-B field, which extends from the lower Frio 21B horizon at about 7,000 ft to the upper Frio 13A horizon at about 5,500 ft, seismic velocities are in the 10,000 ft/sec range (fig. 54). Frequency content of the T-C-B data is limited (fig. 55), perhaps because of acquisition geometry problems. Seismic signal is above background noise between about 10 and 50 Hz. When combined with typical seismic velocities of 10,000 ft/sec, modeling calculations illustrate that two adjacent reflectors do not begin to be resolved until their separation is about 125 ft (fig. 56). In other words, two stratigraphic horizons separated by less than this distance cannot be resolved into separate reflectors.

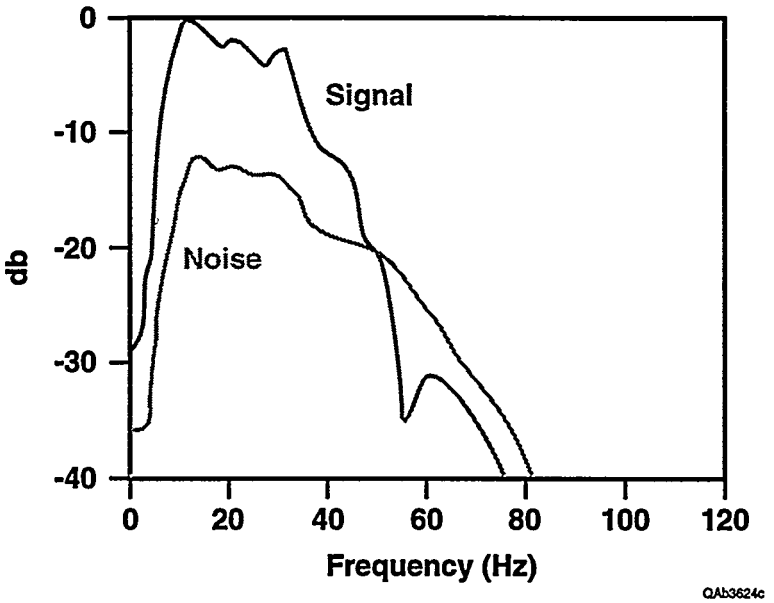

Figure 55. Frequency content for stacked data from inline 315. Adapted from EnTec (1995).

Tying seismic data to stratigraphic markers

Because this study is principally one of subtle stratigraphic traps, the depth range of interest is above the faulted Vicksburg section. Most of the seismic analysis was confined to the dominantly upper delta plain deposits of the middle Frio, although units as high as the upper Frio 13A and as deep as the lower Frio 21-B were examined (fig. 50). Synthetic seismograms constructed from sonic and density logs were used along with checkshot surveys and VSP data to tie seismic horizons to stratigraphic picks made on well logs. A synthetic seismogram constructed from Blucher B-3 well logs (fig. 57) correlates fairly well with the surface seismic data and shows that there are relatively few major reflectors within the stratigraphic zone of interest. Two-way times for this zone are typically between 1350 ms and 1700 ms.

A dip-oriented section through the data volume illustrates the general structural and stratigraphic characteristics of the stratigraphic zone of interest (fig. 58). The zone below the 21B horizon at about 1700 ms shows the complexly faulted lower Frio and Vicksburg sections and clearly shows the main Vicksburg growth fault and many sets of synthetic and antithetic faults. Between' the 13A and 21B horizons there is relatively little structural imprint, with the exception of a graben-like feature that intersects the 18E horizon and minor unmarked faulting in the structurally high areas.

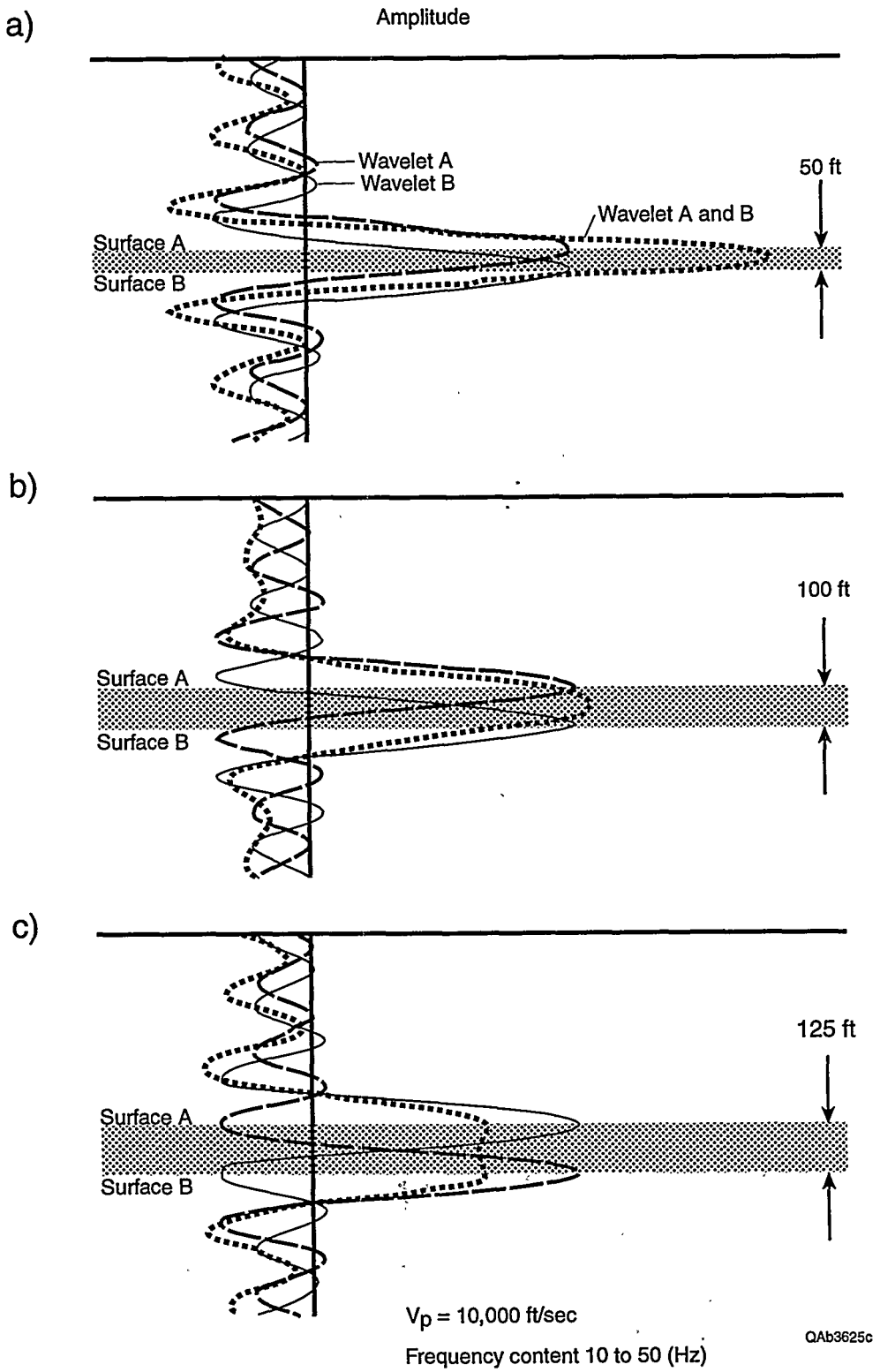

Figure 56. Effect of adding the wavelets A and B after they reflect from similar interfaces A and B that are separated by (a) 50 ft, (b) 100 ft, and (c) 125 ft. Modeled frequency content is 10 to 50 Hz and seismic velocity is 10,000 ft/sec.

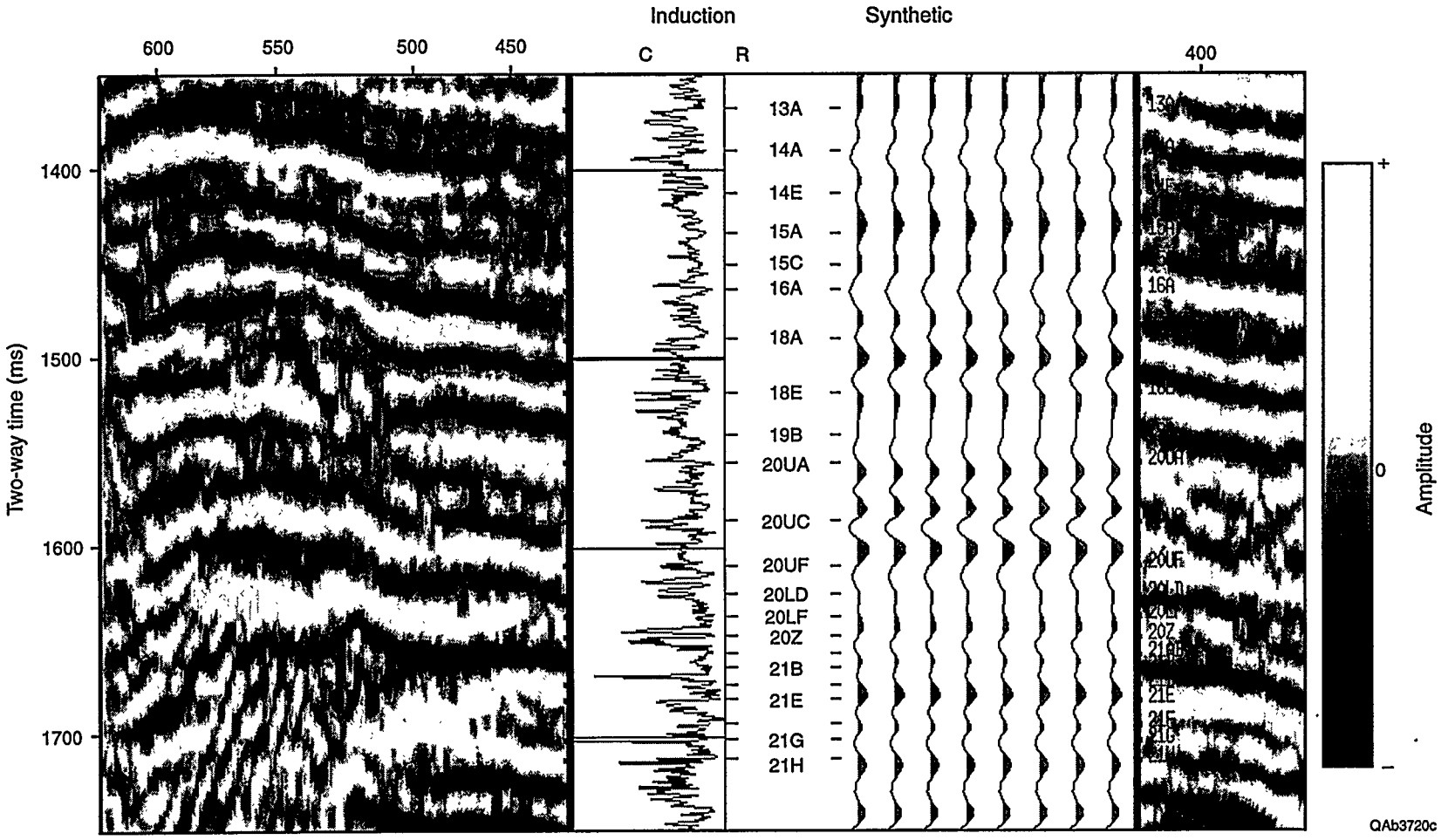

Figure 57. Synthetic seismogram constructed from sonic and density logs for the Blucher B-3 well and tied to seismic data from inline 315.

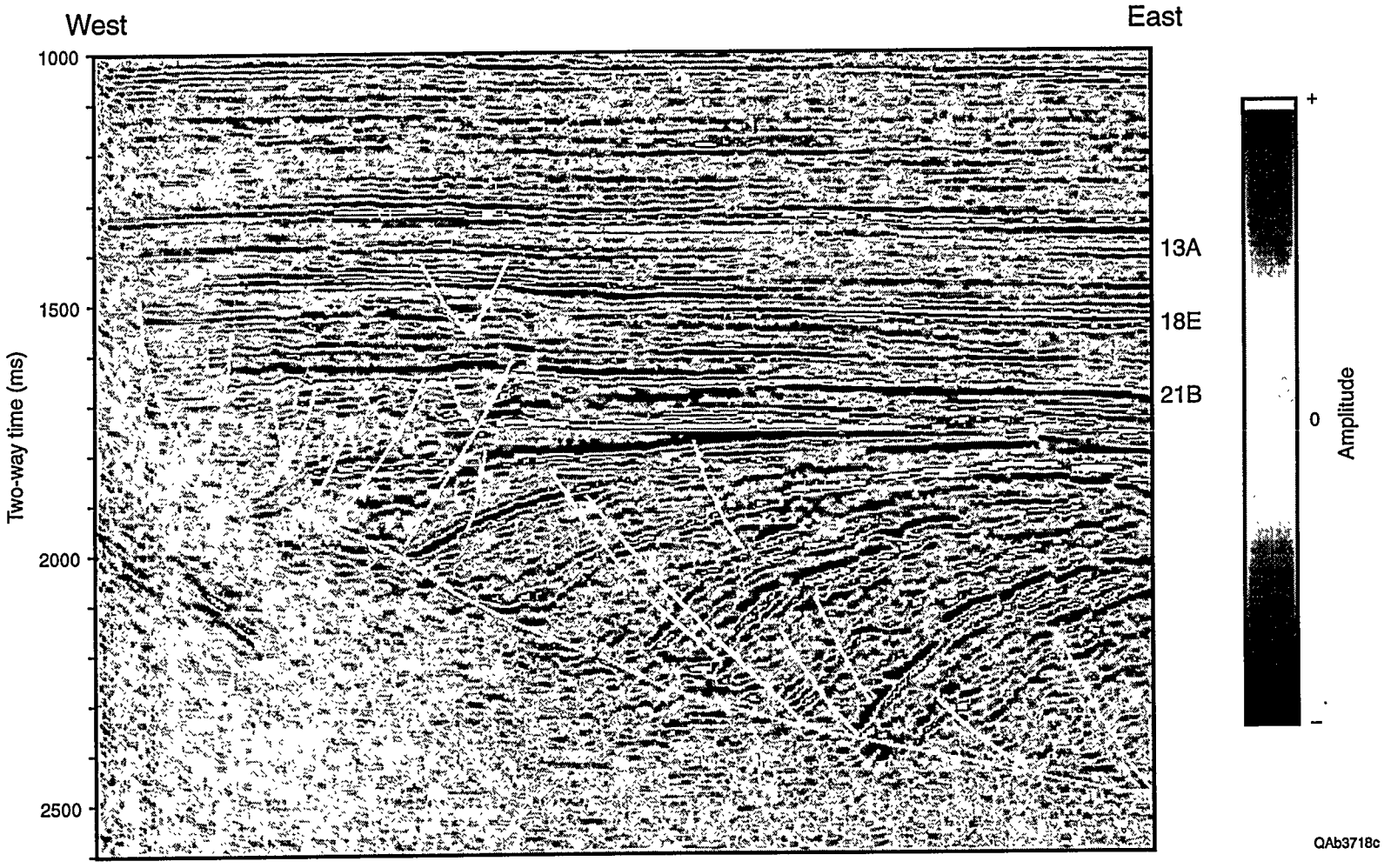

Figure 58. Representative dip line that extends east-west across the data volume. The stratigraphic zone of interest is between the 13A and 21B horizons.

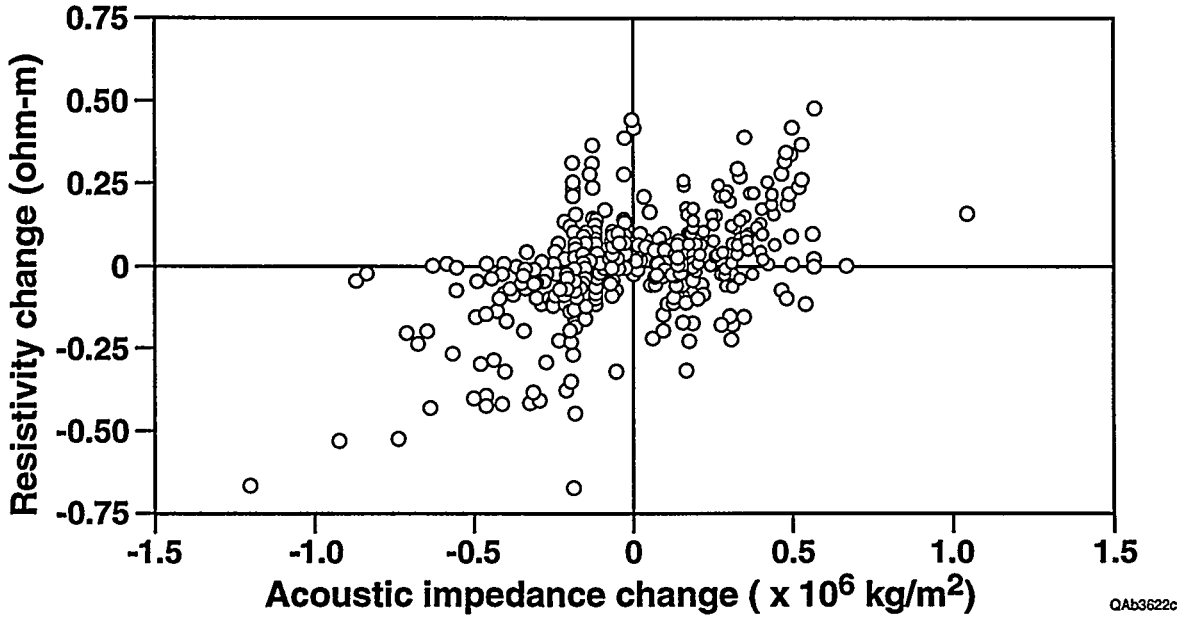

Figure 59. Downward changes in resistivity plotted against downward changes in acoustic impedance at the same well log level. Values calculated from Blucher B-3 well logs between the middle Frio Scott and Sanford intervals. Positive changes in impedance are generally accompanied by positive changes in resistivity (upper right quadrant), indicating that most positive reflections correspond to shale-to-sandstone transitions.

Lithologic source of amplitude peaks

In detailed stratigraphic reservoir analysis, it is helpful to know whether seismic amplitude peaks generally correspond to shale-to-sand or sand-to-shale transitions within the zone of interest. In the Gulf Coast region, there is much regional and vertical variation in the relative seismic velocities of shales and sands. Gamma or induction logs can be used in combination with acoustic and density logs to determine this relationship within any depth zone. For the Scott to Sanford interval within the middle Frio (fig. 50), for example, downward changes in resistivity were used as a proxy for lithology (increases in resistivity indicate increases in sand content and decreases in resistivity indicate increases in clay content). At each level where a resistivity change was calculated, an acoustic impedance (product of velocity and density) change was also calculated. These two numbers were plotted against each other (fig. 59) and show that, in general, increases in acoustic impedance correspond to increases in resistivity. In other words, seismic amplitude peaks are largely caused by the tops of sandstone bodies within this stratigraphic zone.

Further verification that amplitude peaks arise from the tops of sandstone bodies within this stratigraphic interval is obtained by converting well logs to a time scale and superimposing the logs on an arbitrary seismic section drawn through the data volume between the well log locations. Seismic section A -R (figs. 53 and 60), an arbitrary strike section drawn from north to south through the Stewart & Jones (Ste) 1-5, Stel-7, Blucher (Blu) 55, and Blu 37 wells, illustrates that (a) well logs are able to resolve sandstone beds far thinner than those resolvable with the seismic data, and that (b) most seismic amplitude peaks correlate with sand signatures of leftward deflection on the SP log and rightward deflection on the induction log (fig. 60). This section also shows that the power of 3D seismic data, though impressive in the vertical dimension, has its greatest advantage over well logs in the large increase in lateral resolution. Seismic units above the 13A horizon can be clearly seen to pinch out from right to left; difficult correlation problems presented by thin-bed reservoirs can be worked out more easily when arbitrary seismic lines can be constructed from one problem well to another.

Characterization Examples from the Scott/Whitehill Reservoir Interval

Genetic Stratigraphic Setting of the Scott/Whitehill Interval

A dip-oriented stratigraphic cross section stretching from several miles updip of T-C-B field to approximately 60 mi downdip (Fig. 61) was prepared so that these reservoirs could be placed within a depositional and stratigraphic framework. The character of spontaneous potential (SP) and resistivity logs was used to imply general depositional setting of Frio units in the cross section and identify shales that represented major (third- and fourth-order) marine flooding events in the downdip marginal marine setting. Log markers that bound the Scott/Whitehill reservoir interval above and below were correlated from an implied upper delta-plain position at T-C-B field to fourth-order marine flooding surfaces in the downdip area (Fig. 61). Thus, because the interval is bounded above and below by the nonmarine equivalent of flooding surfaces, it reflects a cycle of deposition beginning with progradation, leading to aggradation, and terminating with retrogradation.

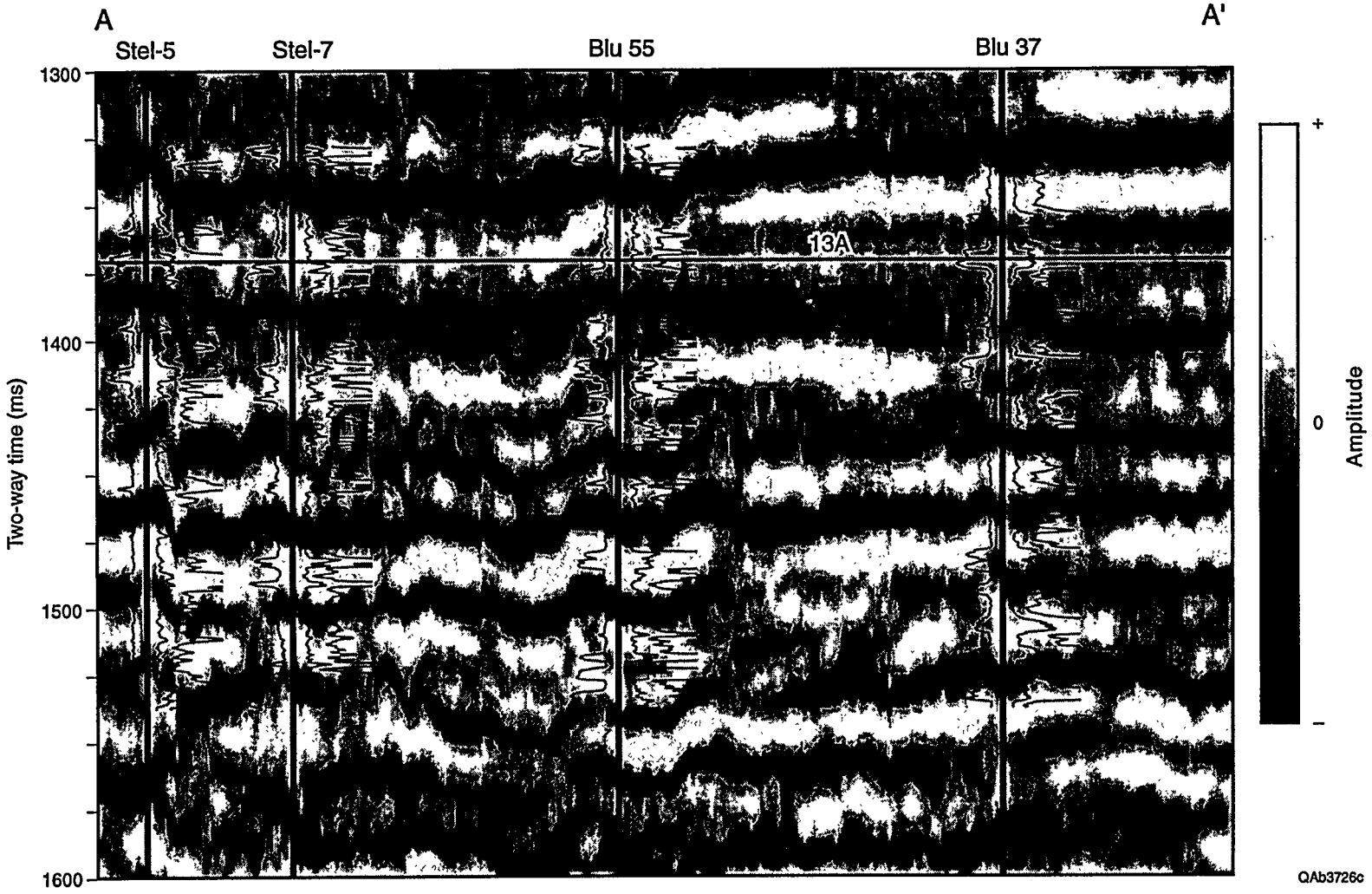

Figure 60. Arbitrary seismic strike section A–A′ with overlain time-converted well logs from the Stewart-Jones 1-5, Stewart-Jones 1-7, Blucher 55, and Blucher 37 wells. Data are flattened on the 13A seismic horizon.

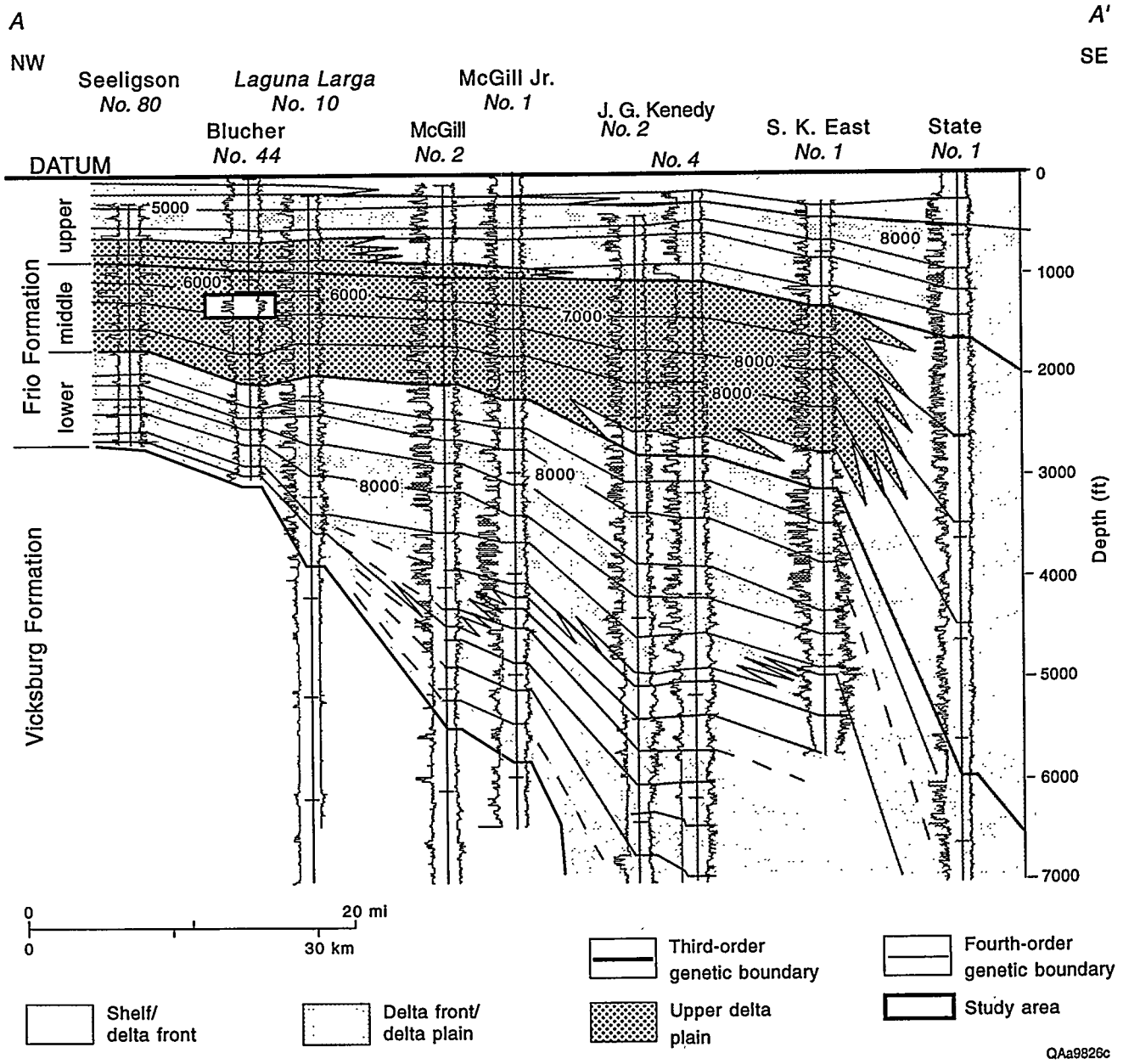

Figure 61. Dip-oriented stratigraphic cross section A–A′ through the Frio Formation from updip of T-C-B field down to the present coastline. The Frio consists of three 3rd-order depositional units, each containing 4th-order units. See Figure 49 for location of cross section.

Architecture of Reservoirs within the Scott/Whitehill Depositional Cycle

The general stratigraphy and architecture of the Scott/Whitehill reservoir interval can be deduced from careful well log correlation, and are shown in a dip-oriented stratigraphic cross section through the study area (Fig. 62) and a series of net sandstone maps (Fig. 63b,c, and d). The interval is divided into four fifth-order genetic units by laterally continuous surfaces that

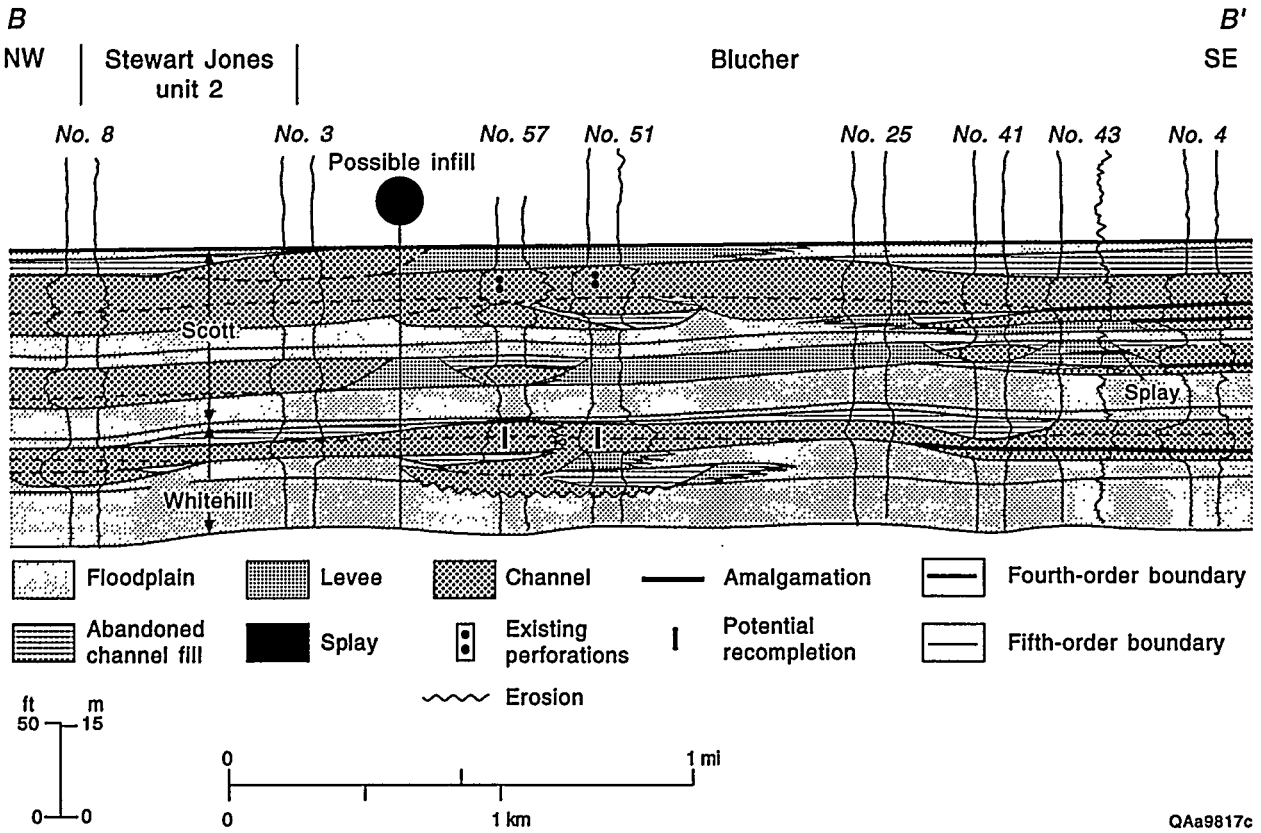

Figure 62. Dip-oriented stratigraphic cross section B–B′ of the Scott/Whitehill 4th-order reservoir interval, which contains at least four 5th-order depositional cycles. These are, from the top down, the upper and lower Scott and the upper and lower Whitehill reservoir intervals. See Figure 63a for location of cross-section.

may correspond to more minor marine flooding events. Narrow to broad dip-oriented channel belts represent major reservoir compartments. Each fifth-order genetic unit ranges in thickness from 20 to 50 ft, with each successive unit generally thickening from the lower Whitehill 20 ft at the base through the upper Scott (50 ft) (Fig. 62) at the top. Assuming equivalent time spans for each unit, this would suggest persistently increasing rates of accommodation. In addition, the percentage of net sandstone also increases upward.

Sandstones within the Scott/Whitehill interval are draped across a subtle south-plunging structural nose (Fig. 63a). They display symmetrical, blocky, or upward-fining log patterns, range in thickness from 3 ft to more than 50 ft, and are separated by siltstones and mudstones of similar thickness. Thicker sandstones consist of amalgamated individual channel deposits, each of which

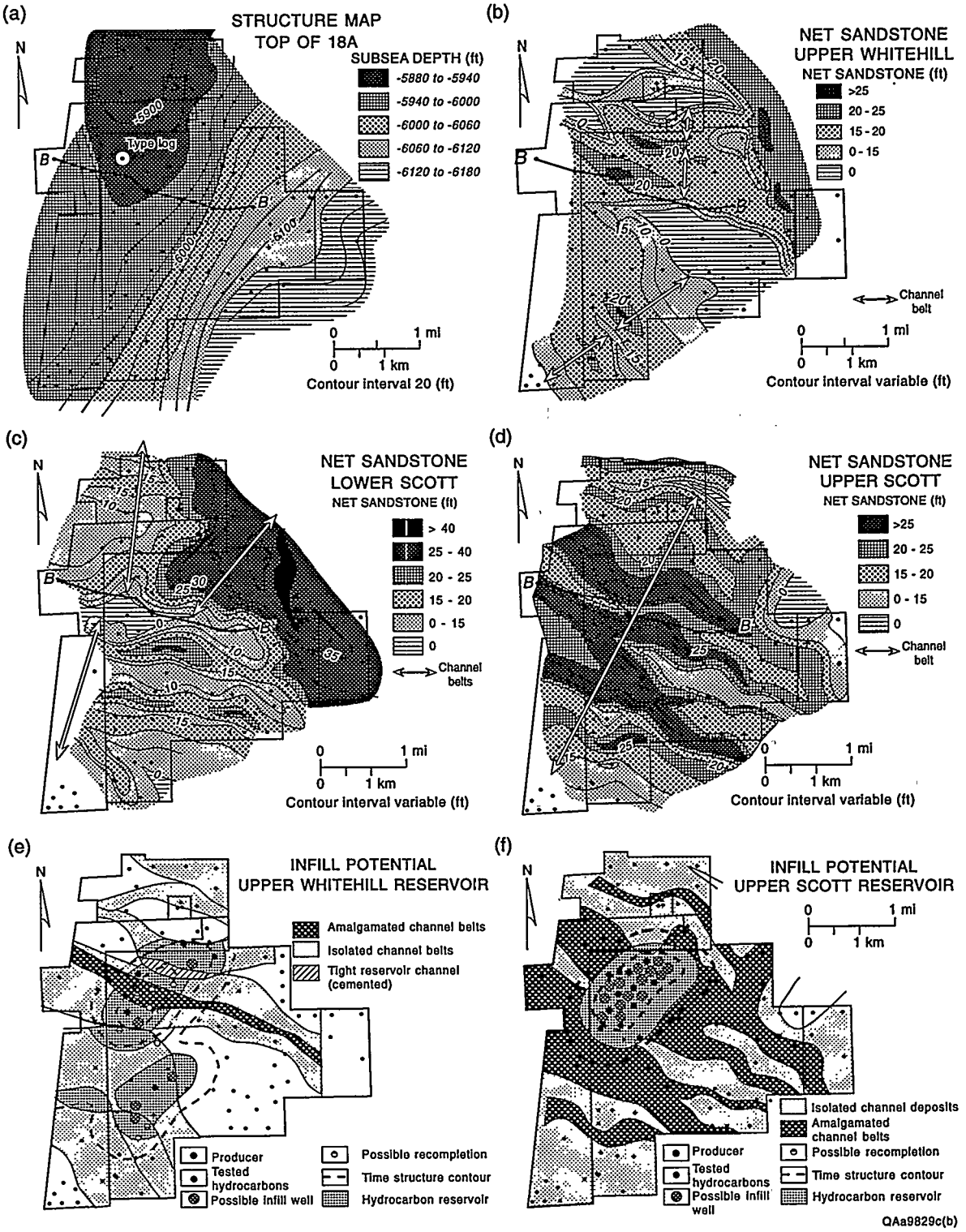

Figure 63. Structure, net sandstone, and infill-potential maps, Scott/Whitehill reservoirs. (a) Structure map on the 4th-order flooding surface that forms the upper boundary of the interval. Cross section B-B' shown in Figure 62. (b) Net-sandstone map of the upper Whitehill 5th-order interval. (c) Net-sandstone map of the lower Scott 5th-order interval. (d) Net-sandstone map of the upper Scott 5th-order interval. (e) Infill potential map of the upper Whitehill reservoir interval. (f) Infill potential of the upper Scott reservoir interval.

reaches a maximum of 20 ft. The dominance of a blocky and upward-fining log pattern, the absence of microfauna, and the regional setting all indicate that these sandstones were deposited in an upper delta-plain fluvial setting. Depositional facies identified on the basis of log character include sandy point bar channel deposits, silty to muddy abandoned channel fill, rare sandy splay deposits, silty levee deposits, and fine-grained floodplain mudstones (Fig. 62).

The lowermost fifth-order unit, the lower Whitehill, deposited at the base of the depositional cycle (low accommodation) and therefore a seaward-stepping unit, is composed entirely of floodplain mudstone throughout the study area. Correlation in the T-C-B area shows no widespread sandstones at this level, but the existence of narrow localized deposits has not been ruled out because channel bodies might be narrower than the log spacing used for regional correlation (approximately 1 mi apart).

The overlying upper Whitehill unit, in the seaward-stepping to vertically stacked portion of the depositional cycle (low to intermediate accommodation), consists of three relatively narrow (1 mi wide) but generally thin fluvial channel-belt deposits (Fig. 63b) separated by large areas of floodplain mudstone. These channel belts trend in a general dip orientation and are typically less than 20 ft in thickness. Thicknesses in excess of this are the result of vertical stacking of broader channel belts (1 mi wide) in the middle or upper portion of the interval on top of very narrow channel belts (0.3 mi wide) at the base of the interval. The comparatively broader channel belts in the middle and upper portion are each interpreted to contain two to three incomplete, vertically amalgamated channel deposits, each ranging from 5 to 10 ft in thickness. Abandoned channel mudstones are most common in the uppermost channel deposits.

The next highest unit, the lower Scott, in the vertically stacked to landward-stepping portion of the depositional cycle (intermediate to high accommodation), is similar to the upper Whitehill except that channel belts tend to be broader (1.5 mi) (Figs. 62 and 63c). In addition, the narrow channel belts that occur at the base of the interval are restricted to the northeastern portion of the study area, where an unusually thick accumulation of channel deposits may have resulted from subtle paleotopographic control. Overall, the lower Scott contains a greater volume of sandstone than the underlying upper Whitehill interval.

The upper Scott reservoir interval, at the top of the fourth-order unit and, thus, in the strongly landward-stepping portion of the depositional cycle (high accommodation), differs markedly from the underlying intervals in that it is distinctly thicker and sandier, with a single broad channel belt (3.5 mi wide) covering the entire study area, which consists of vertically amalgamated channel deposits (Figs. 62 and 63d). Dip-oriented bodies of sandstone thicknesses in excess of 20 ft are the result of two or three vertically amalgamated channel deposits, each separated from the other by abandoned channel mudstones, finer grained upper channel-fill deposits (presumably rippled silty sandstones of an upper point bar setting), or possibly thin layers of mudclast rip-up conglomerate at the bases of channels. The uppermost portion of the upper Scott interval is dominated by siltstones and mudstones of abandoned channel, levee, and floodplain deposits (Fig. 62).

In summary, from the lower Whitehill at the base of the fourth-order depositional cycle (lower accommodation) to the upper Scott at the top (highest accommodation), there is a progressive change in channel architecture and heterogeneity. Individual fifth-order units become thicker upward, and net sandstone percentage increases. Channel belts become wider in each stratigraphically higher unit, and greater volumes of fine-grained channel-fill deposits, such as upper point bar and abandoned channel fill, are present in successively higher units. These features closely correspond to observed accommodation-dependent architecture in the Ferron distributary channel deposits.

Geophysical Identification of Scott/Whitehill Architecture

The identification of reservoir architecture using only well data requires the extrapolation of sandstone body geometries between wells. The accuracy of this extrapolation is dependent upon the predictability inherent in geologic models and is limited by a lack of information between well control. The stratigraphic interpretation of 3-D seismic data can improve the identification of reservoir architecture by imaging compartment boundaries between well control.

To analyze the architecture of reservoirs in the Scott/Whitehill interval, the extensive shale above the Scott, correlative to a 4th-order flooding surface, was picked in the seismic data and the

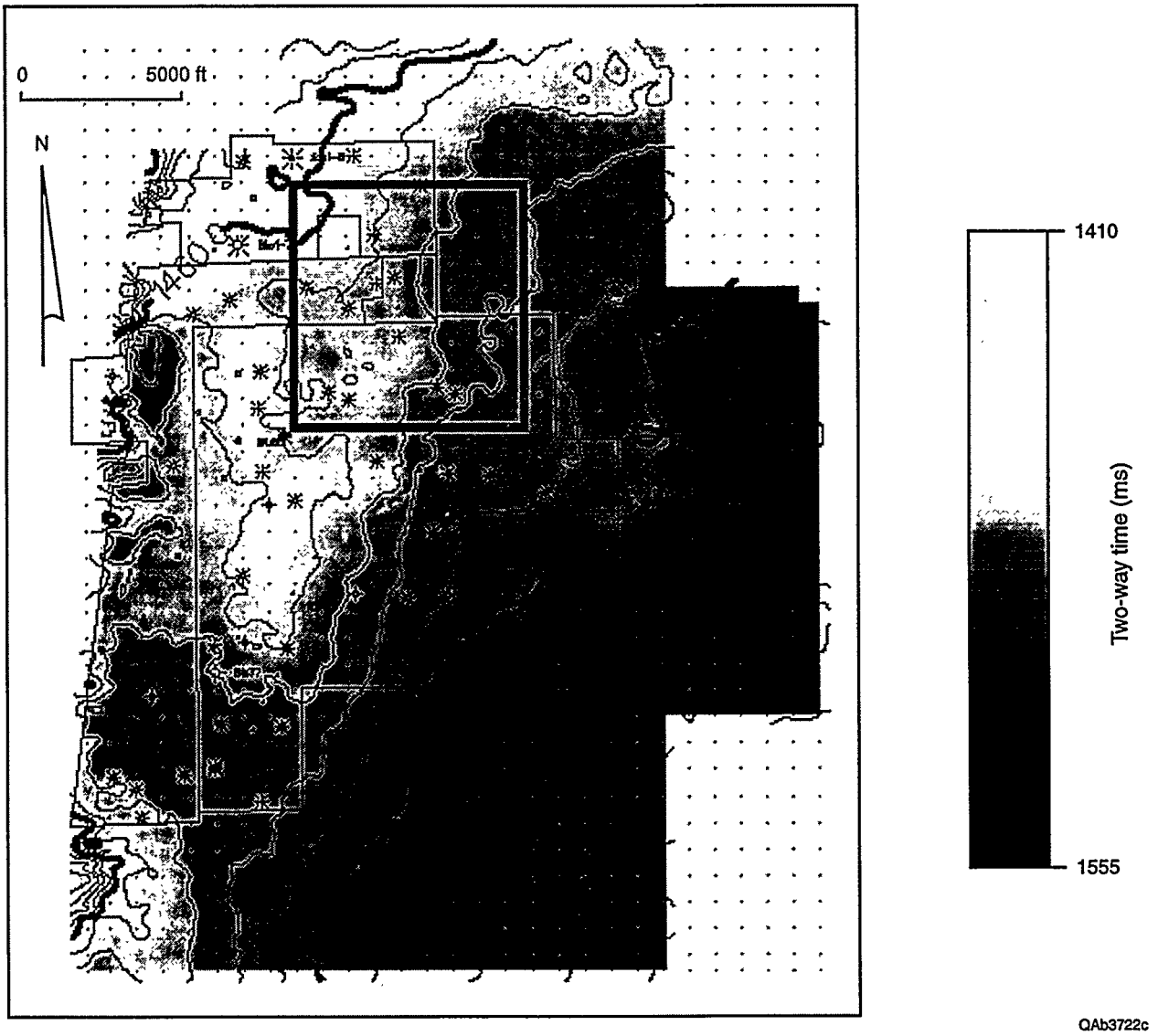

Figure 64. Upper Whitehill structure map in two-way time. Box represents area covered by Figures 65 and 66.

volume flattened on this horizon. Amplitude values across the study area were then sampled at 2 ms intervals (equivalent to approximately 10 ft in depth) below the flattened horizon, a process referred to as horizon slicing. At many horizons within this interval the combination of low frequency content and insufficient seismic contrast between sandstones and shales obscured compartment boundaries. However, detailed analysis in selected areas was successful in clarifying between-well architecture.

An example of this analysis is from the upper Whitehill interval. Figure 64 is a structural map in time on a seismic horizon closest to this stratigraphic interval and shows a north-

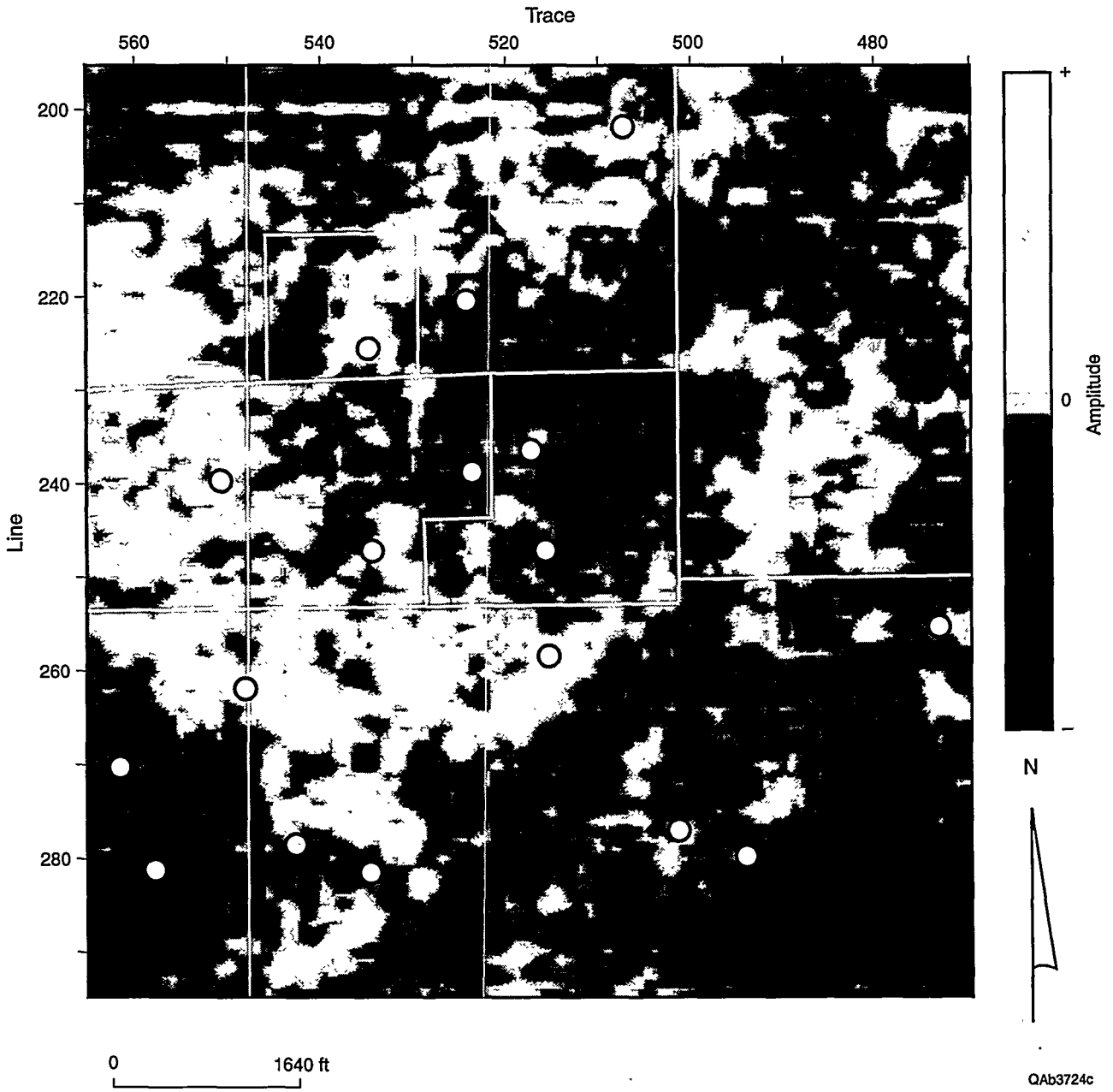

Figure 65. Amplitude display of time slice within the Upper Whitehill interval at 1508 ms (about 6,300 ft deep). See Figure 64 for location.

northeasterly striking high and a marked deepening to the southeast. Relatively little faulting is evident at this level. An amplitude map (horizon slice) of a 1 mi^2 area (Figure 65) at a two-way time of 1508 ms (about 6300 ft deep) shows the 2,000 ft wide feature that trends southeastward from the left side of the map and then bends northeastward in the bottom half of the map. This feature corresponds fairly well with a similar arcuate channel-like sand body as much as 25 ft thick that was mapped solely on the basis of well log patterns (fig. 66). A dominance of lower

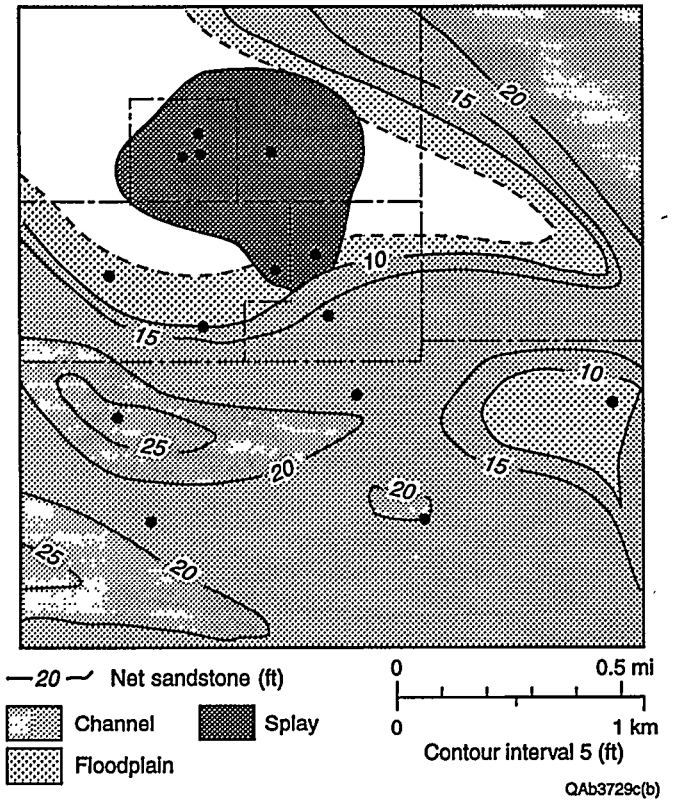

Figure 66. Net sandstone and facies map for the Upper Whitehill interval derived from log data alone. Map covers the same area as the horizon slice in Figure 65.

amplitudes in an area in the center of the northern portion marks an area interpreted as a splay from wells logs. An area to the north that was conservatively predicted from well logs to contain floodplain facies is seen to have high amplitudes in the horizon slice. This suggests that this area may instead contain a separate channel belt not encountered by well control. This increases the area of potential reservoir facies and opens up possibilities for infill potential.

Scott/Whitehill Internal Heterogeneity

Whereas the gross architecture of the reservoir compartments (channel belts) could be identified with reasonable accuracy with well log control, and augmented by 3-D seismic data, the heterogeneity within compartments is potentially much finer than the spacing between wells and is commonly beyond the resolution of seismic, being, as it likely is, controlled by the boundaries between individual channelforms. In a subsurface setting, the most reliable measure of internal heterogeneity is production performance. The relative size of areas drained in a series of

reservoirs will be a measure of the internal complexity of the reservoirs, assuming similar drive mechanisms and fluid viscosities.

We have produced compartment history maps (Figs. 63e, f) for the upper Whitehill and upper Scott intervals, documenting compartment boundaries and past completions. The following discussion summarizes the production history of the two reservoirs and estimates drainage areas for these completions.

Well control, limited 2-D seismic data, and interpretations of 3-D seismic indicate two areas of subtle structural closure (Fig. 63e) on the more prominent structural nose (Fig. 63a) in the study area. Production from the Scott/Whitehill interval is limited to gas in the upper Whitehill and oil in the upper Scott.

The upper Whitehill has produced from two wells, one on the northern structural crest and the other farther to the north in which perforations were structurally below the documented gas/ water contact on the structural crest (Fig. 63e). Resistivity measurements indicate moderate gas saturations in the southern structure, but no tests of this potential accumulation have been made. Mapping of channel belts and evidence of tightly carbonate cemented sandstone in one well suggest that the northernmost of the two completions was stratigraphically isolated from the structural crest. Evidence from wells postdating production indicates that the crestal completion drained approximately 40 acres. At present, insufficient data are available on the other well to document drainage area.

Eight wells have produced oil from the upper Scott on the main structural crest (Fig. 63f). Cumulative production has ranged from less than 1,000 bbl to more than 54,000 bbl per well (Table 14). Initial water cuts have varied widely and have been independent of structural position and offset production history, indicating a lack of communication between well locations (Table 14, Fig. 67). Approximate volumetric analyses suggest that completions have drained areas ranging from less than 1 acre to approximately 5 acres, significantly less than the completion in the Whitehill. Calculations indicate that despite completion at a 20- to 40-acre spacing, and the fact that all current completions are idle or nearly watered out, less than 10 percent of the original oil in place has been recovered from the Scott.

Table 14. Initial potential and cumulative production data for completions within the upper Scott zone.

Well no.	Comp. date	Initial potential	Top Scott (ft, subsea)	Cum. prod.
3	9/64	40 bwpd 129 Mcfd	-5933	squeezed
26	3/89	400 bwpd 400 Mcfd	-5959	squeezed
28	4/85	223 bopd 3 bwpd 281 Mcfd	-5929	54,608 bo 546,860 bw 181.6 MMcf
46	9/69	27 bopd 130 bwpd	-5929	18,773 bo 170,642 bw 87.1 MMcf
48	1/71	20 bopd 309 bwpd	-5939	11,499 bo 212,712 bw 51.2 MMcf
51	1/86	31 bopd 33 bwpd 403 Mcfd	-5943	3,485 bo 56,307 bw 67.8 MMcf
52	7/86	55 bopd 130 bwpd 114 Mcfd	-5932	8,641 bo 28,859 bw 71.5 MMcf
55	3/86	55 bopd 45 bwpd 127 Mcfd	-5940	12,989 bo 209,112 bw 88.9 MMcf
56	9/86	7 bopd 16 bwpd 21 Mcfd	-5952	856 bo 10,260 bw 26.3 MMcf
57	9/86	52 bopd 2 bwpd 288 Mcfd	-5935	12,273 bo 201,174 bw 86.5 MMcf

Although some of the discrepancy in recoveries from the Whitehill and the Scott can be attributed to the different mobility ratios of oil and gas, a significant part can be attributed to smaller compartment sizes in the Scott zone. This indicates that the upper Scott channel belt (high accommodation) is much more internally heterogeneous than the upper Whitehill channel belts (low to intermediate accommodation).

Reserve-Growth Opportunities

Because of sparse past development of the upper Whitehill interval, numerous recompletion opportunities exist, in addition to possible infill locations. Figure 68 shows the location of 16

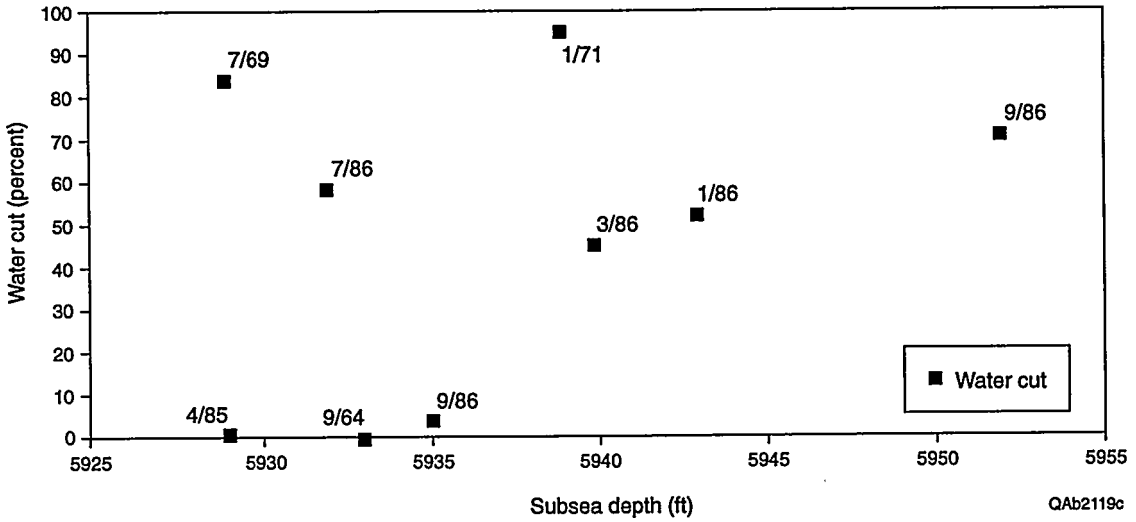

Figure 67. Crossplot of initial water cut versus depth to top of reservoir, upper Scott zone. The completion date is also annotated to document the possible effects of offset production. Note the very poor correlation of water cut versus depth or completion date, indicating laterally isolated compartments.

recompletion opportunities, which are listed in Table 15 and accompanied by a qualitative risk value and 5 infill drilling opportunities. The operator recently recompleted one well rated as moderate risk because of its proximity to a well that has produced 5 billion cubic feet (Bcf) of gas from the upper Whitehill. The recompleted well flowed moderate amounts of gas (500 Mcfd) but also is producing high volumes of water (200 bpd). The present rate is economic, despite the high water production. Three low-risk recompletions remain untested owing to a number of operating considerations such as current production from other zones in prospective wellbores. Because the drive mechanism in the upper Whitehill is a combination pressure depletion/water drive, cumulative production for proposed recompletions is anticipated to approach but not exceed 5 Bcf for each low-risk recompletion. Risk for identified infill opportunities has not'been assigned, pending results of recompletions.

Because of the greater internal heterogeneity within the upper Scott interval, reserve-growth opportunities are more problematic than those in the upper Whitehill. One low- to moderate-risk recompletion exists in Blucher 59, which has excellent resistivity with the top of the reservoir at -5933 ft subsea. Most completions in which the sandstone top occurred above -5940 ft accumulated in excess of 10,000 bo, which would justify the costs of a recompletion. The

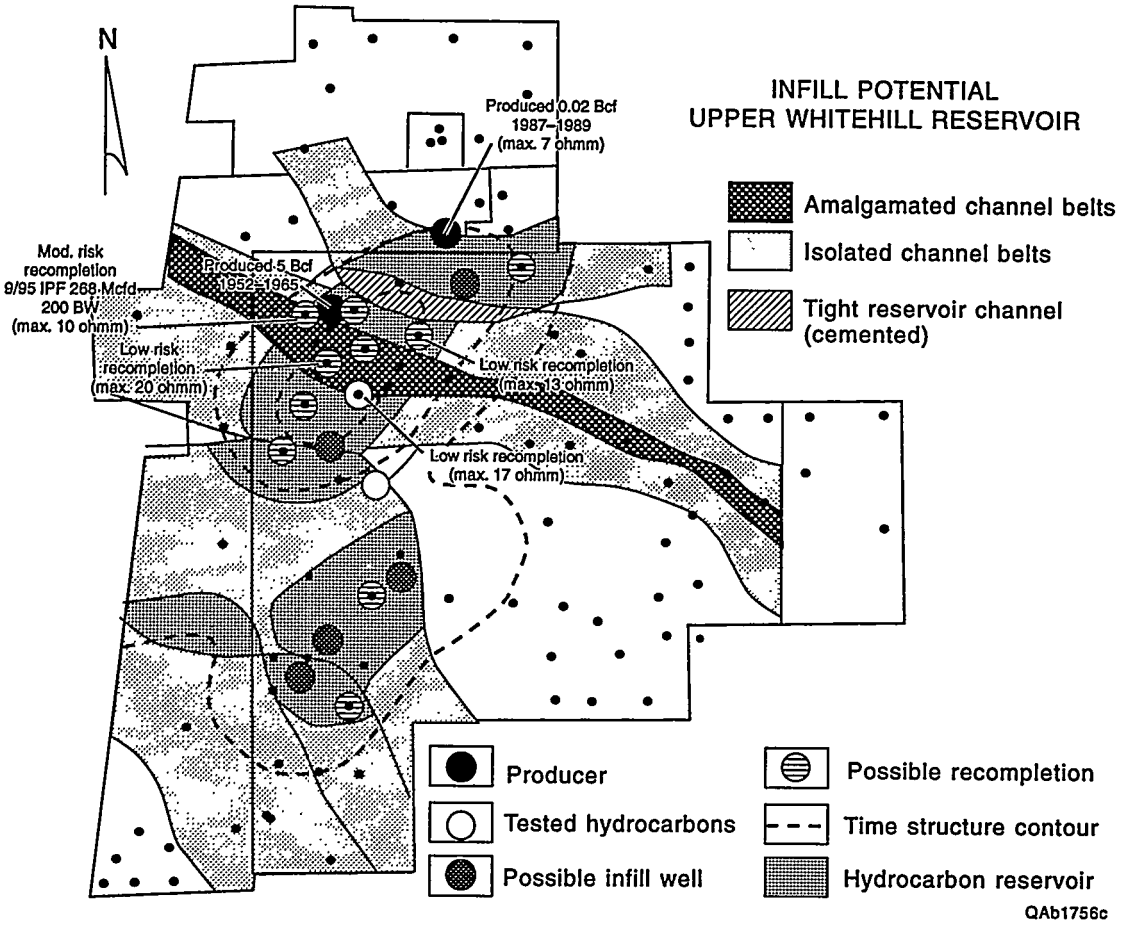

Figure 68. Map showing reservoir compartment distribution, productive limits, identified recompletion/infill opportunities, and results of one recompletion within the upper Whitehill reservoir of T-C-B field. Three recompletion opportunities evaluated as having lower risk than the current recompletion are annotated.

remainder of the opportunities in the upper Scott include 14 infill well locations. Completions on a spacing as close as 10 acres are justified on the basis of past completion performance, and each should accumulate more than 10,000 bo if it is above -5940 ft. However, such small volumes would not, by themselves, justify the cost of a new wellbore. Creative solutions are required to produce the large volume of oil remaining in the upper Scott. If other targets can be found in other reservoirs above or below the Scott that coincide with Scott infill locations, the economics of a wellb ore can be improved. Alternatively, a horizontal well that contacts a larger area, perhaps draining several individual channelforms, might prove economically viable. Without more information regarding the location of individual channelform boundaries, this approach will

Table 15. Summary of recompletion opportunities in Whitehill reservoir, T-C-B field.

Well	Evidence of Productivity	Well Status	Risk
Blucher 28	Strong log show (16 ft @ >5 ohm-m, peak of 13 ohm-m)	Open to below Whitehill (producing from Scott zone at 10 bopd)	Low
Blucher 51	Very strong log show (16 ft @ > 5 ohm-m, peak of 17 ohm-m)	Open to below Whitehill (idle in Sanford)	Low
Blucher 57	Good resistivity (22 ft @ > 5 ohm-m, peak of 20 ohm-m), 16% porosity, suppressed SP suggests tight but microlog indicates 8 ft of permeable reservoir	Open to below Whitehill (idle in Scott)	Low
Blucher 32	Strong Log show (12 ft @ > 5 ohm-m, peak of 7.5 ohm-m)	Open to below Whitehill (producing from Richard zone, 50 Mcfd)	Low-Moderate
Blucher 1	Strong log show (15 ft @ > 5 ohm-m, peak of 15 ohm-m)	Open to below Whitehill (idle in Imme zone)	Moderate
Blucher 23	Strong log show (11 ft @ >5 ohm-m, peak of 6.5 ohm-m)	Open to below Whitehill (idle in 21-B)	Moderate
Blucher 42	High resistivity in thin bed (5 ft @ > 3 ohm-m, peak of 4 ohm-m)	Idle (Stray, 6030'), 4 plugs above Whitehill	Moderate
Blucher 55	High resistivity (9 ft @ > 5 ohm-m, peak of 8.5 ohm-m) but low porosity (5 ft < 12%)	Open to below Whitehill (idle in Charles)	Moderate
Blucher 58	High resistivity (3 ft @ > 5 ohm-m, peak of 6 ohm-m), 18% porosity, RWA curve indicates 4 ft pay	Open to below Whitehill (producing X from Carl)	Moderate
Blucher 59	Strong log show (20 ft @ > 5 ohm-m, peak of 10 ohm-m)	Open to below Whitehill (idle in Charles)	Moderate
Seeligson 7	High resistivity (5 ft @ > 5 ohm-m, peak of 5.5 ohm-m)	Open to below Whitehill (producing X from Alexander)	Moderate
Blucher 25	High resistivity (10 ft @ > 4 ohm-m, peak of 4.5 ohm-m)	Open to below Whitehill (producing X from Charles)	Moderate-High
Blucher 43	High resistivity (3 ft @ > 5 ohm-m, peak of 5.2 ohm-m)	Open to below Whitehill (idle in Jim Wells)	Moderate-High
Blucher 50	High resistivity (3 ft @ 5 ohm-m), perforated and squeezed due to channeling	Open to below Whitehill (idle in Richard)	Moderate-High
Blucher 52	High resistivity (4 ft @ > 5 ohm-m, peak of 6 ohm-m), 18% porosity	Open to below Whitehill (idle in Arguellez)	Moderate-High
Blucher 53	High resistivity (7 ft @ > 5 ohm-m, peak of 6 ohm-m), 2 ft of weak RWA show	Open to below Whitehill (idle in Nicholas)	Moderate-High

contain significant technical risk. However, if the current recovery percentage of less than 10 percent of the original oil in place could be improved, through geologically targeted horizontal drilling, to just 20 percent, more than 0.5 million barrels of reserves could be added.

Accommodation-Based Predictive Model for Reserve-Growth Potential in Upper Delta-Plain Fluvial Reservoirs

Data from subsurface reservoirs in the Frio Formation, T-C-B field, deposited in an upper delta-plain fluvial setting, document a correlation between the reserve-growth.potential of mature reservoirs and reservoir architecture and internal heterogeneity, which appear to be related to position within a depositional cycle. Outcrop observations of the Ferron Sandstone supply additional evidence that architecture and internal heterogeneity are a function of rate of accommodation, which varies predictably throughout a depositional cycle. This correlation could provide a powerful predictive tool for assessing reserve growth potential and improving the confidence of reservoir characterization studies. To better explain the hypothesized link between accommodation rate, architecture, internal heterogeneity, and reserve-growth potential in upper delta-plain fluvial reservoirs, the following section summarizes the interpreted sequence of events affecting the reserve-growth potential of reservoirs in the Scott/Whitehill interval during the course of a single depositional cycle.

Figure 69 illustrates the progression envisioned for the Scott/Whitehill succession of the upper delta plain. Figure 69a represents the upper portion of the sequence underlying the Scott/ Whitehill, deposited near maximum relative sea-level highstand and under conditions of high accommodation. Frequent avulsion and meandering create a series of laterally and vertically amalgamated channels within one broad channel belt.

As sea level begins to fall, resulting in decreasing accommodation, the delta steps seaward, lengthening and straightening the fluvial system and creating a single, potentially incised, channel belt containing internally homogeneous sandy deposits (Fig. 69b). This is flanked by a broad, slowly aggrading floodplain that receives overbank muds during flood events. This stage

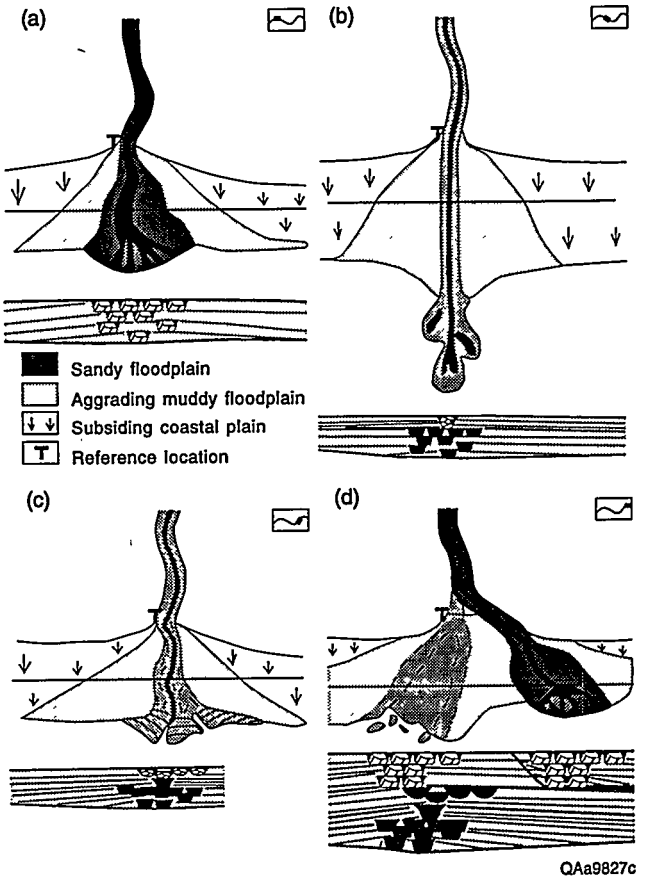

Figure 69. Model for upper delta-plain fluvial architecture under the range of accommodation conditions experienced during a depositional cycle. (a) High accommodation at maximum highstand of relative sea level results in a series of heterolithic vertically and laterally amalgamated channels. (b) Low accommodation during falling relative sea level results in a single internally homogeneous channelbelt. (c) Slightly higher accommodation during initial rise of relative sea level results in occasional avulsion and a series of laterally isolated internally homogeneous channelbelts similar to those in the upper Whitehill. (d) Highest accommodation during maximum rate of rise of relative sea level again results in a single broad heterolithic channelbelt similar to that in the upper Scott reservoir interval. This is also a period during which the fluvial system may be prone to major avulsion and switching of the deltaic depocenter.

corresponds to the deposits of the lower Whitehill, which are dominated by mudstone but may include a single primary channel deposit located outside the study area.

During initial sea-level rise (Fig. 69c), minor accommodation in the upper delta-plain results in infrequent major avulsion events, leading to the deposition of few laterally isolated channel belts. Within channel belts, the limited accommodation results in scouring and removal of much of the upper portion of most individual channel deposits. This is similar to the setting of the upper Whitehill reservoir interval and produces reservoir compartments that correspond to channel belts, laterally isolated but internally homogeneous. As in the upper Whitehill, such reservoirs can be drained effectively by larger well spacings, but infill well locations should be selected so as to avoid the broad areas of floodplain that separate channels. Also, the potential for off-crest stratigraphic accumulations should be considered.

When relative sea level is rising at a maximum rate, the rate of generation of accommodation is also greatest (Fig. 69d). Lateral channel migration and frequent avulsion result in a broad channel belt composed of many vertically and laterally amalgamated channel deposits. However, because of the preservation of finer grained upper channel and abandoned-channel-fill deposits and the abundance of low-permeability mudclast-rich basal lag deposits, the resulting reservoir deposit will be internally heterogeneous, with many barriers to fluid flow at sandstone-on-sandstone contacts.

It should be noted that observations of the Quaternary deposits of the Colorado River of Texas (Blum, 1990) suggest that periods of high accommodation may represent times when major avulsion of a fluvial system occurs, resulting in substantial shifting of the locus of deltaic deposition. The upper Scott reservoir was deposited under such conditions of high accommodation. Here, sufficient permeability between individual channel deposits exists to allow the reservoir to have a common oil/water contact because it filled over geologic time. However, enough permeability barriers or baffles exist that, over the comparatively shorter period of reservoir depletion, the reservoir responds as though it were composed of a number of isolated compartments.

In summary, a spectrum of reservoir styles exists within the upper delta-plain deposits of the Frio Formation in T-C-B field (Fig. 70). This spectrum is the result of varying amounts of accommodation during the period of deposition of the reservoir sandstones. Reservoirs range from moderately narrow, internally homogeneous channel belts deposited under conditions of low accommodation in the seaward-stepping portion of a depositional cycle to broad internally heterogeneous channel belts laid down under conditions of high accommodation in the landward-stepping phase of a depositional cycle. These reservoir styles contain varying reserve-growth potential and require very different strategies for optimum development. In general, upper delta-plain fluvial reservoirs deposited during a landward-stepping period contain the greatest reserve-growth potential and may require the tightest well spacings for optimal reservoir drainage.

A Cautionary Note

Changing fluvial style in the upper delta plain during a depositional cycle results in a pattern of upward-increasing net sandstone percentage. However, opposite patterns have been observed in the lower delta plain, where observations suggest that the highest percentage of sandstone is deposited during the lowstand. In explanation, one hypothesis is that during the early period of relative sea-level rise, fluvial gradients, which have not fully equilibrated with the rapidly rising base level, and initial backstepping of the delta favor sand deposition and preservation in the lower delta plain. During the later rising phase, deposition and preservation shift to the upper delta plain.

Uses of the Model

The model represents a significant breakthrough in reservoir characterization in that it is an inexpensive, flexible, predictive tool that is simple enough to use in a quick-look estimate of reserve-growth potential but powerful enough to guide a detailed reservoir characterization study. By placing reservoirs into a sequence stratigraphic framework of depositional cycles, the model provides rules that allow predictions of between-well architecture and sandstone continuity, degree of compartmentalization, and intracompartment heterogeneity. This tool effectively bridges the gap between routine reservoir characterization made on the basis of well-log correlations and more expensive methods utilizing stratigraphic analysis of 3-D seismic data. Specific uses include (1) estimation of relative reserve-growth potential of a group of reservoirs, leading to prioritization of these reservoirs for detailed characterization studies and (2) risk reduction of reservoir development activities through more confident understanding of reservoir complexities.

The model is an integral component of a quick-look analysis of reserve-growth potential. Reservoirs are placed within a framework of depositional cycles to predict internal stratigraphic heterogeneity. Other factors, such as initial estimates of structural heterogeneity, reservoir significance, and past completion history, are integrated. Reservoirs can then be ranked in terms

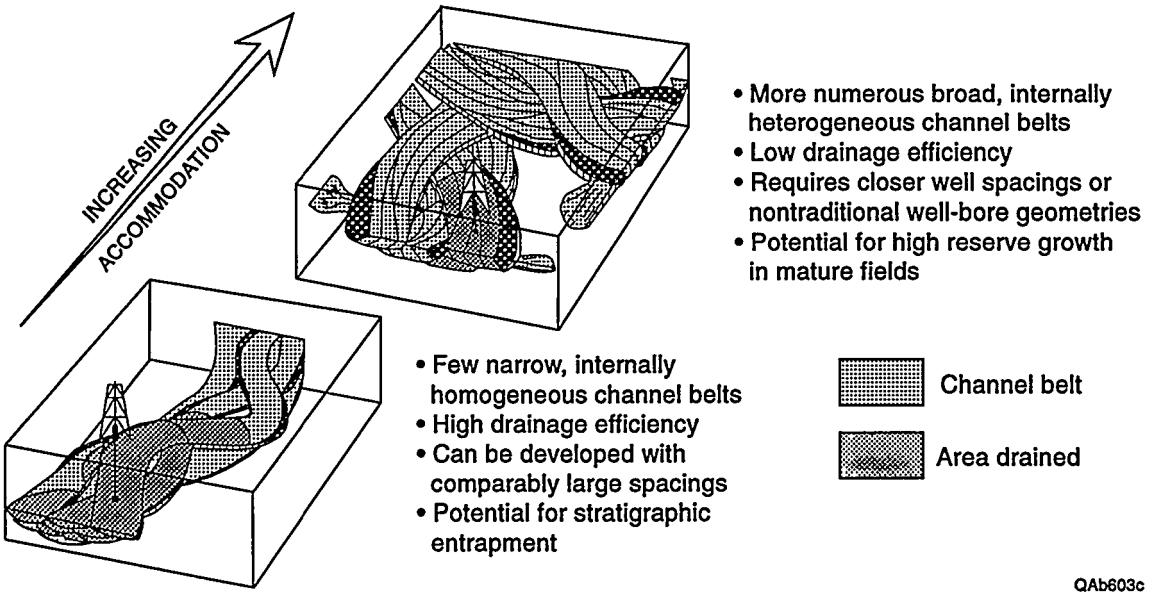

Figure 70. Spectrum of upper delta-plain fluvial reservoir architecture, internal heterogeneity, production characteristics, and reserve-growth potential encountered in the Scott/Whitehill interval.

of estimated reserve-growth potential based on this information. Significant reservoirs with sparse completions and high structural or stratigraphic heterogeneity would rank high and receive further attention to refine the estimation of reserve-growth potential. Ultimately, this leads to the informed selection of specific intervals for detailed reservoir characterization aimed at identifying the location of remaining mobile oil or gas (see Reservoir Prioritization section).

The model also provides critical assistance during detailed characterization studies by allowing a more confident interpretation of the reservoir at the between-well scale, thereby reducing the geologic risk associated with subsequent recompletions or infill drilling to target identified reserves. For example, when core material is unavailable and difficult facies interpretations and correlations must be based on log information alone, the model provides rules for the vertical progression of facies and architecture: sandstones at the base of a cycle should show a progradational architecture and contain more proximal facies than those immediately above them, whereas sandstones at the top of the cycle should show reversed relationships.

Implications

The model described here only addresses reservoirs deposited in an upper delta-plain fluvial setting. However, it represents a new generation of models for reservoir characterization. Because rates of accommodation can be demonstrated to control sandstone body architecture and internal heterogeneity, and because these effects are different for each depositional setting but can be documented from outcrop work or implied from careful subsurface study, other models must be developed for reservoirs deposited in the spectrum of depositional settings. Any such models must be based on outcrop observations because continuous lateral exposures are critical for identifying geometries and permeability characteristics of the surfaces that bound potential reservoir compartments. Further understanding of the cyclic nature of the stratigraphic record, and the controls on that cyclicity, will provide more accurate models and supply more specific guidelines for their application in various depositional settings.

The predictive nature of these new models will improve the accuracy of reservoir characterization studies and increase the use of reservoir characterization by operators of mature fields. The outcome will undoubtedly be increased recovery of oil and gas from reservoirs that otherwise might have been abandoned prematurely, preventing permanent loss of vital resources.

RESERVOIR PRIORITIZATION

P. R. Knox

The methodology of integrated multidisciplinary reservoir characterization that has been described and demonstrated in this report requires significant effort on the part of the operator. Gathering of field data and interpretation of detailed reservoir architecture and compartmentalization requires a significant commitment of time from geological, geophysical, and engineering staff, and the acquisition of seismic data and reservoir visualization software can involve a large expense. As a consequence, an initial effort should be made to insure that the reservoirs selected for detailed study have a high potential for yielding additional reserves. This effort should consist of a quick-look evaluation in which readily available parameters are used to estimate reserve growth potential and rank reservoirs from greatest to least potential.

Quick-look Evaluation Factors

On the basis of experience gained during this investigation, six factors were identified that can be used to help determine the potential for reserve growth from untapped and incompletely drained compartments in mature reservoirs. Four of these factors, (1) relative reservoir size, (2) past completion density, (3) reservoir heterogeneity, and (4) hydrocarbon mobility address the likelihood that unrecovered hydrocarbons exist in the reservoir. The two remaining factors, (5) reservoir depth and (6) operator gas/oil preference, provide indications of economic efficiency and practical company strategy.

Larger relative reservoir size indicates a greater potential for unrecovered oil because, in considering two reservoirs with equal past recovery efficiency (percentage), the larger reservoir will contain a greater volume of oil still remaining. For example, consider two reservoirs having similar characteristics except that one contains 10 MMbbl of mobile oil originally and the other 1 MMbbl originally. If 30 percent of the oil is recovered from each reservoir, the larger reservoir will still contain 7 MMbbl of mobile oil to be recovered by recompletions and infill drilling,

whereas the smaller reservoir will contain only 0.7 MMbbl. It is more likely that the cost of reservoir characterization will be recouped in the course of increased production from the larger reservoir, whereas the risk of pay out will be higher for the smaller reservoir. Relative reservoir size can be evaluated from volumetric data (e.g., OOIP), if available, or estimated by comparing cumulative production of the reservoirs being ranked. The latter approach assumes that the reservoirs have had similarly thorough development and are at a similar stage of maturity.

If past completion density in a reservoir is low (well spacing is large), the potential of that reservoir for reserve growth may be high because there is a greater chance that untapped reservoir compartments exist between well penetrations. In addition, heterogeneity within compartments may limit the size of the effective drainage area, leaving substantial portions of compartments incompletely drained (Figure 71). The greater the past completion density (the closer the well spacing), the less chance that substantial areas of the reservoir remain undrained.

The higher the reservoir heterogeneity, the greater the chance that areas exist in the reservoir that are not in good communication with current well penetrations. Reservoir heterogeneity is a function of (1) structural complexity, which creates fault-bounded compartments, (2) complex stratigraphic architecture, which results in many small stratigraphically isolated compartments (e. g., channel belts), and (3) intercompartment heterogeneity, in which lithologic contrasts within an architectural unit inhibit fluid flow through a compartment (e.g., low-permeability channelon-channel contacts) (Figure 70). Structural heterogeneity can be qualitatively deduced from existing structure maps, general structural setting, or from seismic sections or volumes. Both types of stratigraphic heterogeneity can be inferred from well log correlatability or knowledge of depositional facies and position within a depositional cycle (Figure 72). Predicting stratigraphic heterogeneity is discussed further in "Accommodation-based predictive model for reserve-growth potential" in the section covering characterization examples from T-C-B field. Table 16 provides a summary of potential heterogeneity for Gulf Coast fluvial-deltaic reservoirs.

The greater the hydrocarbon mobility, the poorer the chances of a reservoir containing significant undrained reserves, all other factors being equal between two reservoirs. Hydrocarbon

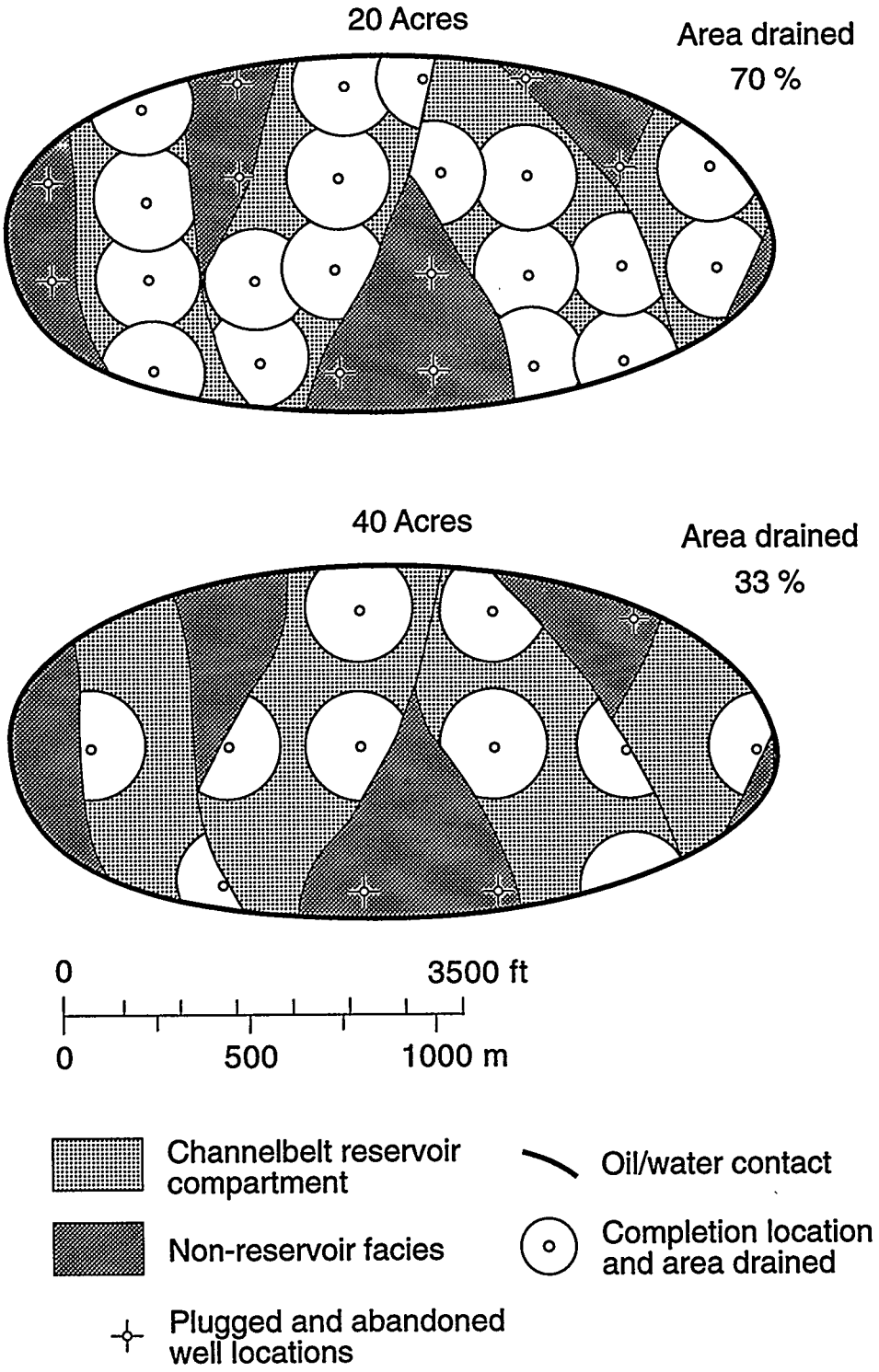

QAb4894c

Figure 71. The effect of past completion density on reserve growth potential. All other things being equal, a reservoir developed at a closer spacing has probably been more well drained than one completed at a wider spacing.

Table 16. Potential effects on reservoir architecture of position within 4th- and 5th-order cycles.

STAGE	U. DELTA PLAIN	L. DELTA PLAIN	DELTA FRONT
LANDWARD STEPPING	THICK, BROAD, HETEROGENEOUS CHANNEL BELTS	FEWER BUT THICKER HETEROGENEOUS DISTRIBUTARIES	FEWER, THICKER CHANNEL AND MOUTH BAR DEPOSITS WITH COMMON WAVE-REWORKED TOPS
VERTICALLY STACKED	BROAD, MODERATELY THICK AND HETEROGENEOUS CHANNEL BELTS	MORE THICK HETEROGENEOUS DISTRIBUTARIES	FEWER, THICKER CHANNELS, POSSIBLY SUBORDINATE TO MOUTH BAR AND DELTA FRONT BODIES
SEAWARD STEPPING	NARROW, POSSIBLY THIN AND INCISED, ISOLATED CHANNELS	MANY BROAD SHALLOW SANDY CHANNEL BELTS?	MANY LONG NARROW SANDY CHANNEL AND MOUTH BAR DEPOSITS

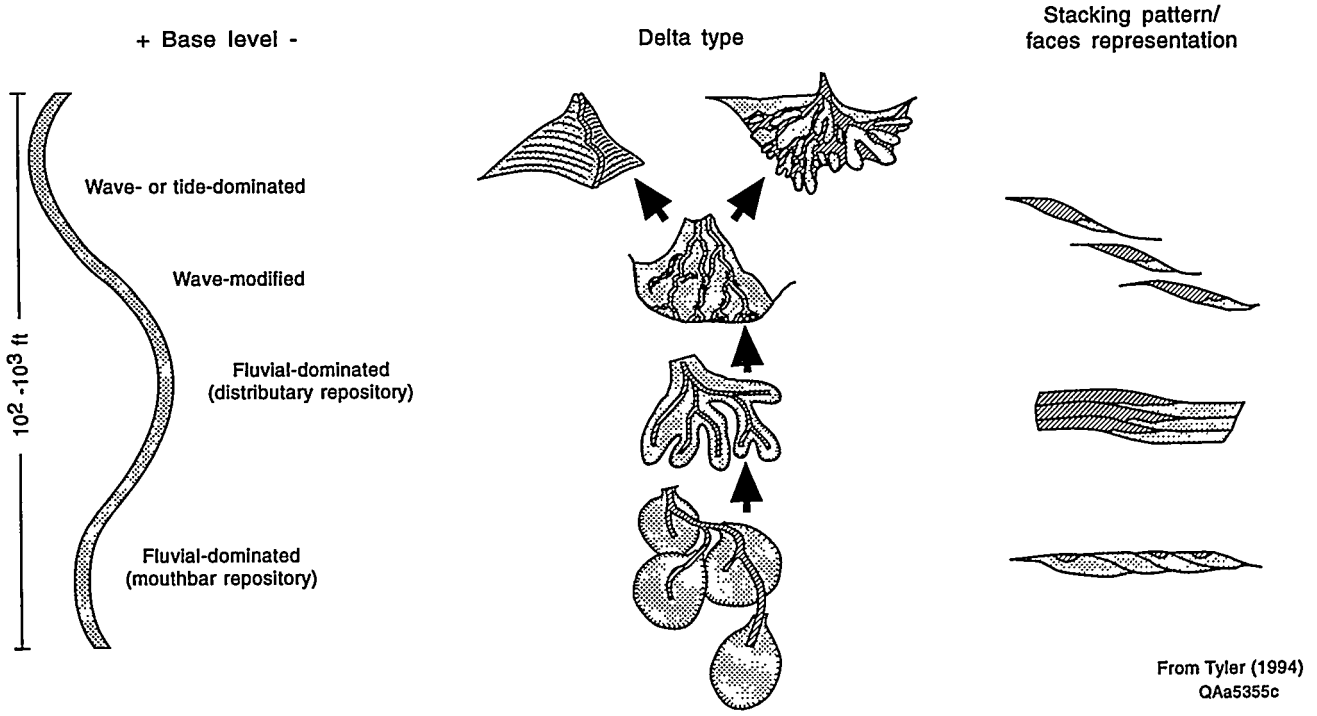

Figure 72. Influence of position within a depositional cycle on delta style and reservoir architecture. Because critical factors such as sediment supply, discharge, and shelf profile change through a depositional cycle, some change in delta morphology and facies can be expected. Periods of falling sea level may be marked by voluminous sandy sediment input because of devegetation of the source area, and may exhibit a broad shelf formed as the previous deltaic platform is exposed, resulting in an amplification of fluvial dominance. Conversely, during highstand, sediment input might be reduced (depending on climate effects in the source area) and wave energy might be dispersed by a broad, shallow shelf, increasing tidal influence on facies distribution. Modified from Tyler (1994).

mobility is a function of reservoir fluid viscosity and reservoir permeability, in which the relationship can be expressed as

$$\text{Mobility} = f(m, \log(k)) \quad (1)$$

in which m is the average viscosity of the reservoir fluid (in cp) and k represents geometric mean permeability in md. (Average permeability can be substituted, as long as that substitution is made for all reservoirs being compared.) Because the average viscosity of reservoir fluid is not typically readily available, it can be approximated by weighted averaging of separate gas and oil phases in the reservoir using the following:

$$m = f(f(12, API)\,(100 - G) + 0.02 * G, 100) \quad (2)$$

where API is the average gravity of the oil leg and G is the volume percent of the reservoir containing gas. The expression 12/API yields oil viscosity in cp on the basis of a cross plot of oil gravity versus viscosity for the Frio play and 0.02 is a mean value for gas viscosity (in cp) from the Frio play.

Reservoir depth is included as a criterion in order to compare economic viability of infill drilling that would occur during recovery of any identified resources. For a given volume of expected reserves at an infill location, shallower wells are more economic than deeper wells because of lower drilling costs. For example, a 10,000-bbl opportunity would be an economic target at a depth of 2,000 ft but would be clearly uneconomic at 8,000 ft.

Operator gas/oil preference is included in a quick-look evaluation because a given operator at a given time may be seeking to expand gas production more than oil production, or vice versa. This preference may occur because of commodity prices, infrastructure constraints, or contracted delivery goals.

The Formula

An equation has been established that incorporates readily available data from the above factors into a quantitative ranking of reservoirs in terms of their reserve growth potential. Because this formula is intended to yield a quick estimation of potential, it has several limitations, which

are enumerated in the following section. The formula is as follows, with higher rank being equated to higher potential for economically recoverable reserves:

$$RANK = f(C\ (SUH)\ (SAH)\ V\ M\ G', D) \tag{3}$$

Where
C = current well spacing (acres)
SUH = structural heterogeneity, from 1 (low) through 10 (high)
SAH = stratigraphic heterogeneity, from 1 (low) through 10 (high)
V = relative volumetric importance, ranked from 1 (smallest) to 100 (largest)
M = mobility, represented by f(m,log(k))
G' = Gas/oil bias (gas preference, G' = G (% gas in reservoir), oil preference, G' = 100-G)
D = f(Depth, 6000) (economic risk factor - higher drilling costs for deeper reservoirs)
and
k = geometric mean or estimated average permeability in md.
m = average viscosity of reservoir fluid, given by:

f((f(12,API•)(100 - G) + 0.02••G),100), where API = reservoir oil gravity in API units.

• f(12,API) yields the viscosity of the oil in cp.
•• 0.02 = viscosity of typical gas in cp.

Limitations

The quick-look prioritization equation is designed such that it utilizes input that should be readily available to an operator for almost all reservoirs. The intent is that such an evaluation should not require significant additional research or data gathering. In establishing such a relationship, many assumptions have been made. The influence of drive mechanism on recovery has been neglected, as has the variable efficacy of past reservoir management practices. Additionally, sandstones that have not been produced in the past, but that may contain future potential, are not considered.

Drive mechanism is known to affect recovery efficiency (API, 1967; Tyler and others, 1984). However, these effects are difficult to quantify and can change throughout the life of the reservoir

depending on initial gas saturation and reservoir management practices. In decreasing order of efficiency, common drive mechanisms are (1) water drive, (2) gas cap expansion, and (3) solution gas drive. However, recovery from solution gas drive reservoirs can be altered during their life by gas injection programs which approximate gas expansion drives with variable success.

Another assumption inherent in the equation is that all reservoirs have experienced a similar degree of development and reservoir management. Certainly, though, not all reservoirs have been given the same level of attention by past operators in terms of looking for recompletion/infill opportunities or identifying production anomalies that would indicate compartmentalization. In addition, past mismanagement of water or gas injection programs can affect reserve growth potential, and this history can be difficult to discern in a quick-look evaluation. For instance, injection of water into downdip wells that are in direct communication with updip wells through narrow high permeability channel facies can result in large volumes of unswept oil in lateral facies between the channels.

Another possibility that is not considered in the quick-look evaluation is the potential for reserve growth in sandstones that have not previously been economically produced. Possible scenarios include (1) unrecognized low-resistivity pay zones, caused either by anomalous mineralogy or thinly bedded nature, (2) zones that have exhibited flow rates that were lower than desired during more prolific periods of field development, and (3) zones that have been misdiagnosed as unproductive because of unrecognized formation damage or unrecognized potential to produce when stimulated. Each of these situations would not be recognized by the above quick-look evaluation because of the lack of high relative reservoir volume (they are not considered reservoirs or have a low cumulative production volume).

TECHNOLOGY TRANSFER ACTIVITIES

P. R. Knox and W G. White

The methodologies for advanced multidisciplinary reservoir characterization that have been developed and demonstrated in the Frio Fluvial-Deltaic Sandstone (Vicksburg Fault Zone) play of South Texas by the Bureau of Economic Geology, The University of Texas at Austin, exhibit tremendous potential to increase near-term production in fluvial-deltaic reservoirs throughout the play, and are broadly applicable to fluvial-deltaic resources across the United States. To achieve this objective, however, operators must be made aware of these methodologies and their proven worth. The Bureau has expended substantial effort to transfer these technologies to domestic fluvial-deltaic operators, and particularly operators of Gulf Coast fluvial-deltaic reservoirs.

Through the course of this study, eleven presentations have been made at regional or national meetings of geological, geophysical, and engineering professional societies (Appendix 1) . Results have been widely distributed in 15 publications, including articles, ' abstracts, and major contract reports (Appendix 2). Three short courses focused on study results, and results played a pivotal role in a fourth short course prepared for a project that had provided matching funds to this study (Appendix 3). The methodology and results have also been captured in an interactive software package titled the Reservoir Characterization Advisor-Fluvial-Deltaic, which could form the basis for future similar software demonstrating characteristics of reservoirs deposited in other settings such as carbonate platforms or slope and basin settings.

Presentations

Oral and poster presentations of project methods and results at regional and national technical conferences are one way to quickly transfer information, as soon as it becomes available, in a face-to-face format, to operators of fluvial-deltaic operators. Bureau scientists have provided 11 such presentations over the project life. In addition, two presentations to DOE-sponsored gatherings made other researchers aware of Bureau approaches and progress. On two occasions, a

prominent operator within the Frio play invited Bureau scientists to present methods and results to reservoir teams working in this trend. Additionally, presentations have been made to the operators of fields studied in detail to communicate specific opportunities for reserve growth identified by the Bureau. Other oral presentations given at short courses are covered under that section heading.

Audiences at presentations to technical societies have ranged from 25 senior independent oil and gas operators at a regional meeting to hundreds of geoscientists at a national meeting. All presentations received positive audience response and several have resulted in invitations to make follow-up presentations to individual operators. The eleven oral or poster presentations are listed in Appendix 1 and include:

- 1 poster presentation, joint national meeting of the American Association of Petroleum Geologists (AAPG) and SEPM (Society for Sedimentary Geology), April 1994, Denver, Colorado
- 1 oral presentation, Gulf Coast Association of Geological Societies (GCAGS), October 1994, Austin, Texas
- 2 oral and 1 poster presentation, national AAPG-SEPM, March 1995, Houston, Texas
- 2 oral presentations, GCAGS, October 1995, Baton Rouge, Louisiana
- 1 oral presentation, Society of Petroleum Engineers/DOE Improved Oil Recovery Conference, April 1996, Tulsa, Oklahoma
- 1 oral presentation, national AAPG-SEPM, May 1996, San Diego, California
- 1 oral presentation, GCAGS, October 1996, San Antonio, Texas
- 1 oral presentation, Society for Independent Professional Earth Scientists monthly meeting, May 1996, San Antonio, Texas

Bureau researchers have also been invited to present interim findings at Contractors Meetings convened by DOE. Presentations at Fountainhead, Oklahoma, in 1993 and 1995 reported interim results to the DOE and allowed for cross-fertilization among the Class I projects.

Presentations by Bureau staff at the national AAPG-SEPM meeting held in Houston precipitated two invitations from a Pennzoil team working in the Frio play. The operator covered

expenses for two day-long visits to the Houston headquarters to present methods and findings from this study. The presentations were well received and the visits allowed for working discussions on specific issues being faced by the operator.

Finally, specific opportunities for reserve growth in the two fields selected for detailed study will be presented to the operators involved. A presentation was made to the Mobil T-C-B reservoir team in early 1995 to present interim findings. Final meetings with Mobil and Conoco (Rincon field) will be held in August 1996 to present final results.

Publications

In addition to presentations, methods and results have been published in several forms to provide a more permanent and widely circulated documentation of ways to increase near-term production from mature fluvial-deltaic reservoirs. Articles in transaction volumes for meetings where presentations have been made provide details and figures so that attendees and those unable to attend can fully comprehend the more complicated aspects of characterization. Abstracts in convention volumes can entice operators to presentations and provide summaries for those unable to attend. In-depth information on project details and results has been presented in annual and topical project reports to the DOE, and project results have been highlighted in the DOE Fall, 1996 edition of the DOE publication "The Class Act"

Appendix 2 lists all publications produced by this project. These include three articles in the Transactions volumes from the 1994 and 1995 GCAGS meetings and one article in the Transactions of the SPE/DOE Improved Oil Recovery Conference, 1996. A total of six abstracts have been published in convention volumes accompanying the 1994,1995, and 1996 national AAPG-SEPM meetings and the 1996 GCAGS meeting. Project reports to the DOE have included three annual reports, two topical reports (one focused on regional play evaluation and one on detailed reservoir characterization), and this final report. A two-page article in the fall, 1996 " Class Act" newsletter that is circulated to operators of fluvial-deltaic reservoirs is anticipated to yield requests for additional copies of project reports, possibly leading to the increased

application of advanced characterization methodology and resulting increases in production from fluvial-deltaic reservoirs.

Short Courses

Short courses and workshops provide an opportunity to meet and train operators who are interested in applying integrated characterization methods to their reservoirs. It is a forum for providing detailed information and conducting question and answer sessions. This ensures a deeper understanding of the steps required in identifying remaining resources and increases the confidence of operators in applying these steps, thereby improving the likelihood of increasing near-term production. Original project goals included two short courses, to be held in cities convenient to operators in the Frio play. During the project opportunities arose for an additional one-half day course and participation in a three-day field workshop. Attendees to each of these courses were provided course notebooks containing figures and text for future reference and annotation. Topics presented at each of the workshops are given in Appendix 3 in the form of course schedules.

Planned One-Day Courses

Two one-day short courses were held in the Spring of 1996 in San Antonio and Houston in order to be convenient for operators of Gulf Coast fluvial-deltaic reservoirs. The purpose was to present (1) an overview of Frio play characteristics, (2) details of the integrated multidisciplinary reservoir characterization methodology, (3) examples of its application within the Frio play, (4) strategies for identifying reservoirs prospective for detailed characterization studies, and (5) an overview of the Reservoir Characterization Advisor-Fluvial-Deltaic (RCA-FD) software. In addition, core material from Frio fluvial-deltaic reservoirs in Rincon field was available for viewing and discussion and the RCA-FD was demonstrated during breaks.

The first course was held in San Antonio, Texas, on Monday, April 8, 1996, at the Bright Shawl restaurant and meeting complex, and was hosted by the South Texas Geological Society.

The minimal registration cost of $45 included lunch and a 3-inch-thick 3-ring binder course notebook. The notebook contained annotated handouts of slides, a bibliography of publications and articles pertinent to fluvial-deltaic reservoir characterization, copies of the latest project annual report and a Bureau publication of playwide resource assessment, and several pamphlets on seismic and well log interpretation published jointly by Gas Research Institute (GRI), DOE, and the Bureau. The course was attended by 25 operator representatives from the San Antonio area. Audience feedback was positive, with the RCA-FD software demonstration receiving high levels of interest. Special presenters included Dr. George Asquith of Texas Tech University lecturing on the interpretation of old e-logs and Dr. Bob Hardage discussing how to design a 3-D seismic survey.

The second course was held in Houston on June 6, 1996, at the Exxon Auditorium, and was hosted by the Houston Geological Society. Again, the minimal cost of $50 (at-the-door and non-member fee higher) included a complete course notebook. Paid attendance was 75. As before, cores and a RCA-FD demonstration were available at breaks and Dr. Bob Hardage served as a special presenter. Responses to a questionnaire passed out at the end of the meeting provided substantial encouragement that many operators intended to apply the methodology in mature Gulf Coast reservoirs. Nearly all of the questionnaire respondents were geologists, engineers, or geophysicists working for independent oil companies or consulting firms, with responsibilities for reservoirs on the Texas Gulf Coast. Evaluations of course content were overwhelmingly positive, with some opposing opinions regarding the ratio of time spent on methodology versus examples. The presentation of how to do 3-D geocellular modeling received all positive comments, as did the overall reservoir characterization methodology.

PTTC/TIPRO Workshop

The beneficial collaboration of the Bureau with the Texas Independent Producers and Royalty Owners Association (TIPRO) and the Petroleum Technology Transfer Council (PTTC) created an additional opportunity to meet with operators and present a methodology for

integrated reservoir characterization. A significant portion of the meeting was a discussion period in which operators expressed their opinions on factors that inhibited increased production in fluvial-deltaic reservoirs.

A total of 29 operators, geologists, engineers, and geophysicists attended the August 1995 one-half day meeting in Houston. The presentation portion of the meeting was divided into three sections. The first part was an introduction to Texas oil and gas plays and reserve growth concepts while the second and third portions discussed Frio playwide characteristics and reservoir characterization methodology, respectively. It was emphasized to the operators and independent geologists present that the great bulk of reserve growth in this play will come within already discovered reservoirs.

Questions and concerns raised by the audience during the question and answer session included the applicability of 3-D seismic in the Frio play and the cost and difficulty of obtaining production and log information from these mature fields. It was emphasized that 3-D seismic is very applicable to characterization of fluvial-deltaic reservoirs but that operators must be aware of the difference in vertical resolution between well logs and seismic data. Additionally, it was relayed that the Railroad Commission of Texas is working on computerizing production files to simplify access and that logs in the archives of the Bureau are available to operators for only the cost of reproduction.

GRI Ferron Field Trip

Results of this study were also presented to 22 geoscientists from major and large independent oil companies during a three-day field trip intended to demonstrate controls on reservoir architecture and heterogeneity at the between-well scale. This trip to see exposures of the Ferron Sandstone in central Utah was an outgrowth of an Industrial Associates (IA) program being conducted at the Bureau. This IA program has provided matching funding to the Frio study and established many relationships from the outcrop that the Frio study has then applied in the subsurface.

The evening before the first field day, participants were given an overview of observations from the Ferron study, including data indicating that reservoir architecture and heterogeneity vary in a given facies throughout a depositional cycle. The concluding presentation documented the application and testing of this concept in the subsurface study of Frio reservoirs. Specifically, it documented that, as predicted by outcrop observations, fluvial upper delta plain channels deposited during progradational or aggradational portions of a depositional cycle (e.g., upper Whitehill reservoir of T-C-B field) were less internally heterogeneous than those deposited during the retrogradational portion of a depositional cycle (e.g., upper Scott reservoir of T-C-B field). This heterogeneity controls reservoir drainage efficiency and dictates optimum well spacing in subsurface reservoirs. Thus, the talk underscored the practical utility of the outcrop studies and was well received.

Reservoir Characterization Advisor Software

Introduction

In an effort to make the results of this study available to operators on a day-to-day basis, and in a form that is most useful and flexible, we have incorporated methods and results into a microcomputer-based software package referred to as the Reservoir Characterization Advisor-Fluvial Deltaic (RCA-FD). While the basic reservoir characterization methodology is applicable to nearly all reservoirs, specific information for the fluvial deltaic setting and examples from fluvial-deltaic reservoirs have been provided. The RCA-FD has been designed in a modular format so that future versions covering other depositional settings can easily be constructed. The RCA-FD is also designed to be user-friendly and compatible with nearly any computer in use by operators within the Frio Fluvial-Deltaic Sandstone Play.

The RCA-FD will combine text and illustrations with simple calculation functions. In this way it will provide an illustrated guide to carrying out reservoir characterization studies, as well as enable operators to calculate parameters specific to their reservoirs. The various features available in this software will produce a powerful tool that will improve the efficiency and productivity of

operators of mature fluvial/deltaic reservoirs, resulting in more characterization studies undertaken and more recompletion and infill-drilling activity. Ultimately, it will lead to reserve growth and increased production and prevent the premature abandonment of mature reservoirs.

Software Development

The RCA-FD demonstrates the planning process and strategies employed in the real world when characterizing reservoirs to identify reserve growth potential and is based on actual Bureau research strategies developed over the last 15 years. The intended user audience is the independent oil exploration company, which may not have the in-house expertise available to larger companies.

The RCA-FD uses a multimedia approach, incorporating text, graphics, application tools such as spreadsheets, and animation to guide the user through the process of ranking reservoirs in terms of reserve growth, followed by the four basic steps of detailed reservoir characterization used to identify specific reserve growth opportunities. The four steps of reservoir characterization are presented as separate modules in the advisor, which build cumulatively: (1) determining reservoir architecture, (2) establishing fluid-flow trends, (3) integrating architecture and fluid-flow, and (4) combining the results of previous steps to quantify the reserve growth potential of the reservoir and delineate recompletion and infill-drilling opportunities.

The RCA-FD is written for the PC-compatible platform and requires at least a 386 CPU running Windows, and an SVGA monitor to display the graphics and animation. RCA-FD is written in Microsoft Visual Basic 4.0, which employs many user-friendly application controls to assist the user in running the software: menus, hypertext links, clickable buttons, dialog boxes, and online help. An online, searchable glossary of reservoir characterization terms will be a component of the package; the user can either call up the glossary directly and look up definitions, or click on highlighted terms which appear throughout the body of the RCA-FD text screens.

Graphics are an important component of the package as well: graphs, charts, and well log images will be displayed appropriately to illustrate and underscore points presented in the text. Simple animations will be employed to effectively communicate time-dependent processes.

The RCA-FD serves as a complete tutorial package, allowing users to work at their own pace. Users may choose to stop at any point and come back later to the same point in the tutorial or to review material already presented. Basic analysis procedures are presented so that the user can grasp the general idea. These procedures are first shown to the user with sample data developed by Bureau content experts, then, in some modules, the user can enter their data for analysis, such as in the quick-look reservoir prioritization module. When the user is prompted to enter real-world data to work through certain procedures, that data will be stored as a workbook for recall and use in later procedures as appropriate. The workbook can then be printed at the completion of the tutorial for a permanent record of the user's work.

Distribution

Each of the RCA-FD CD will be distributed on several floppy discs, accompanied by a brief publication that provides an overview of its contents and use. These items will be packaged in a 3-ring binder and priced at a cost sufficient to cover reproduction of the materials.

ACKNOWLEDGMENTS

This research was performed for and funded by the U.S. Department of Energy under contract no. DE-FC22-93BC14959. Conoco International and Mobil Exploration and Producing U.S. are gratefully acknowledged for their cooperation in providing well logs, cores, production and engineering data, and other miscellaneous geologic information. Particular appreciation is extended to B. Ackman, S. Kershner, and C. Mullenax of Conoco, and M. Poffenberger, M. Klein, C. Carpenter, C. Talash, J. Van Horn, and C. Bukowski of Mobil for their assistance. Interpretation of 3-D seismic data volume was done in SeisX workstation software provided by CogniSeis, Inc. Research was assisted by Chung-yen Chang, Shannon Crum, Douglas Dawson, Radu Boghici, and Mohammad Sattar. Drafting was assisted by Michele Bailey, William C. Bergquist, Susan Krepps, Jana S. Robinson, and Maria E. Saenz of the Bureau of Economic Geology, The University of Texas at Austin, under the direction of Richard L. Dillon and Joel Lardon. Others contributing to the publication of this report were Susan Lloyd, word processing and Jamie H. Coggin, design, and Alison Boyd, proofreading.

REFERENCES

Alpay, A. O., 1972, A practical approach to defining reservoir heterogeneity: Journal of Petroleum Technology, p. 841-848.

Ambrose, W. A., Grigsby, J. D., Hardage, B. A., Langford, R. P., Jirik, L. A., Levey, R. A., Collins, R. E., Sippel, M. A., Howard, W. E., and Vidal, JosO, 1992, Secondary gas recovery: targeted technology applications for infield reserve growth in fluvial reservoirs in the Frio Formation, Seeligson field, South Texas: The University of Texas at Austin, Bureau of Economic Geology, topical report prepared for the Gas Research Institute, GRI-92/0244, 200 p.

American Petroleum Institute (API), 1967, A statistical study of recovery efficiency: API Bulletin D 14.

Archie, G.E., 1942, The electrical resistivity log as an aid in determining some reservoir characteristics:
American Institute of Mining and Metallurgical Engineers Transactions, v. 146, p. 54-62.

Barton, M. D., 1994, Outcrop characterization of architecture and permeability structure in fluvial-deltaic sandstones, Cretaceous Ferron Sandstone, Utah: The University of Texas at Austin, Ph. D. dissertation, 260 p.

Bebout, D. G., Loucks, R. G., and Gregory, A. R., 1978, Frio sandstone reservoirs in the deep subsurface along the Texas Gulf Coast: The University of Texas at Austin, Bureau of Economic Geology, Report of Investigations No. 91, 92 p.

Blum, M. D., 1990, Climatic and eustatic controls on Gulf Coast plain fluvial sedimentation: an example from the late Quaternary of the Colorado River, Texas: GCSSEPM Foundation Eleventh Annual Research Conference Programs with Abstracts, p. 71-83.

CGG, 1995, South Texas TCB 3D: Houston, Texas, Processing report for Exxon Company, USA, not consecutively paginated.

Chen, H. C., and Fang, J. H., 1986, Sensitivity analysis of the parameters in Archie's water saturation equation: The Log Analyst, Sept.-Oct., p. 39-44.

Coleman, J. M. C., 1993, Depositional systems and tectonic/eustatic history of the Oligo cene Vicksburg episode of the northern Gulf Coast: The University of Texas at Austin, Ph.D. dissertation, 538 p.

Coleman, J., and Galloway, W. E., 1991, Sequence stratigraphic analysis of the lower Oligocene Vicksburg Formation of Texas, in Armentrout, J. W, and Perkins, R. F., eds., Sequence stratigraphy as an exploration tool: Gulf Coast Section, Society of Economic Paleontologists and Mineralogists research conference, p. 99-112.

Dewan, J. T., 1988, Log interpretation and applications: Houston, Schlumberger Educational Services course notes, unpaginated.

Folk, R. L., 1974, Petrology of sedimentary rocks: Austin, Hemphill, 182 p.

Galloway, W. E., 1977, Catahoula Formation of the Texas coastal plain-depositional systems, composition, structural development, ground-water flow history, and uranium distribution: The University of Texas at Austin, Bureau of Economic Geology Report of Investigations No. 87, 59 p.

_____1982, Depositional architecture of Cenozoic Gulf Coastal Plain fluvial systems, in Ethridge, R G., and Flores, R. M., eds., Recent and ancient nonmarine depositional environments: models for exploration: Society of Economic Paleontologists and Mineralogists, Special Publication 31, p. 127-155.

_____1989a, Genetic stratigraphic sequences in basin analysis I: architecture and genesis of flooding-surface bounded depositional units: American Association of Petroleum Geologists Bulletin, v. 73, p. 125-142.

_____1989b, Genetic stratigraphic sequences in basin analysis II: application to northwest Gulf of Mexico Cenozoic Basin: American Association of Petroleum Geologists Bulletin, v. 73, no. 2, p. 143-154.

Galloway, W. E., Hobday, D. K., and Magara, K., 1982, Frio Formation of the Texas Gulf Coast Basin -depositional systems, structural framework, and hydrocarbon origin, migration, distribution, and exploration potential: The University of Texas at Austin, Bureau of Economic Geology Report of Investigations No. 122, 78 p.

Galloway, W. E., Ewing, T. E., Garrett, C. M., Tyler, Noel, and Bebout, D. G., 1983, Atlas of major Texas oil reservoirs: The University of Texas at Austin, Bureau of Economic Geology, 139 p.

Gardner, M. H., 1991, Sequence stratigraphy of the Ferron Sandstone, east-central Utah, in N. Tyler, M. D. Barton, and R. S. Fisher, eds., Architecture and permeability structure of fluvial-deltaic sandstones: a field guide to selected outcrops of the Ferron Sandstone, east-central Utah: The University of Texas at Austin, Bureau of Economic Geology, Guidebook prepared for 1991 field trips, p. 4-55.

Grigsby, J. D., and Kerr, D. R., 1993, Gas reservoir quality variations and implications for resource development, Frio Formation, South Texas: examples from Seeligson and Stratton fields: The University of Texas at Austin, Bureau of Economic Geology Geological Circular 93-2, 27 p.

Holtz, M. H., McRae, L. E., and Tyler, Noel, 1994, Identification of remaining oil resource potential in the Frio fluvial-deltaic sandstone play, South Texas: The University of Texas at Austin, Bureau of Economic Geology, topical report prepared for the U.S. Department of Energy, Bartlesville Project Office, under contract no. DE-FC22-93BC14959, report no. DOE/BC/14959-8 (DE94000132), 67 p.

Holtz, M. H., and McRae, L. E., 1995, Modeling reservoir attributes and estimating additional hydrocarbon potential for redevelopment in fluvial-deltaic reservoirs: an example from the

Frio fluvial-sandstone play in South Texas (abs.), in AAPG Annual convention official program: Houston, American Association of Petroleum Geologists, v 4, p. 42A-43A.

Holtz, M., McRae, L. E., Knox, P. R., Hentz, T., and Chang, C., 1996, Revitalizing a mature oil play: strategies for finding and producing unrecovered oil in Frio fluvial-deltaic reservoirs of South Texas: The University of Texas at Austin, Bureau of Economic Geology, annual report prepared for the U.S. Department of Energy, Bartlesville Project Office, under contract no. DE-FC22-93BC14959, report no. DOE/BC/14959-17 (DE96001211), 178 p.

Jackson, M. P. A., and Galloway, W. E., 1984, Structural and depositional styles of Gulf Coast Tertiary continental margins: applications to hydrocarbon exploration: American Association of Petroleum Geologists, Continuing Education Course Note Series No. 25, 226 p.

Jackson, S., Chang, M. M., and Tham, M., 1993, Data requirements and acquisition for reservoir characterization: U. S. Department of Energy topical report NIPER-615, 26 p.

Jirik, L. A., 1990, Reservoir heterogeneity in middle Frio fluvial sandstones: case studies in Seeligson field, Jim Wells County, Texas: Gulf Coast Association of Geological Societies Transactions, v. 40, p. 335-352.

Kerr, D. R., 1990, Reservoir heterogeneity in the middle Frio Formation: case studies in Stratton and Agua Dulce fields, Nueces County, Texas: Gulf Coast Association of Geological Societies Transactions, v. 40, p. 363-372.

Kerr, D. R., and Jirik, L. A., 1990, Fluvial architecture and reservoir compartmentalization in the Oligocene middle Frio Formation, South Texas: Gulf Coast Association of Geological Societies Transactions, v. 40, p. 373-380.

Kerr, D. R., Grigsby, J. D., and Scott, A. R., 1992, Fluvial deposits of the Frio Formation along the Vicksburg Fault Zone: examples from Stratton and Seeligson fields, in Levey, R. A.,

Grigsby, J. D., Langford, R. P., Kerr, D. R., Guevara, E.H., Scott, A. R., and Finley, R. J., Core and log analyses of depositional systems and reservoir properties of Gulf Coast natural gas reservoirs: an integrated approach to infield reserve growth in Frio, Vicksburg, and Wilcox sandstones: The University of Texas at Austin, Bureau of Economic Geology Geological Circular 92-1, p. 7-25.

Kosters, E. C., Bebout, D. G., Seni, S. J., Garrett, C. M., Jr., Brown, L. F., Hamlin, H. S., Dutton, S. P., Ruppel, S. C., Finley, R. J., and Tyler, Noel, 1989, Atlas of major Texas gas reservoirs: The University of Texas at Austin, Bureau of Economic Geology Special Publication, 161 p.

Lasseter, T. J., Waggoner, J. R., and Lake, L. W., 1986, Reservoir heterogeneities and their influence on ultimate recovery, *in* Lake, L. W., ed., Reservoir characterization: Orlando, Academic Press, p. 545-560.

LeBlanc, R. J., 1977, Distribution and continuity of sandstone reservoirs: Journal of Petroleum Technology, p. 776-792.

Levey, R. A., Sippel; M. A., Finley, R. J., and Langford, R. P., 1992, Stratigraphic compartmentalization within gas reservoirs: examples from fluvial-deltaic reservoirs of the Texas Gulf Coast: Gulf Coast Association of Geological Societies Transactions, v. 42, p. 227-235.

Lindquist, S. J., 1976, Sandstone diagenesis and reservoir quality, Frio. Formation (Oligocene), South Texas: The University of Texas at Austin, Master's thesis, 147 p.

_____1977, Secondary porosity development and subsequent reduction, overpressured Frio Formation sandstone (Oligocene), South Texas: Gulf Coast Association of Geological Societies Transactions, v 27, p. 99-107.

Loucks, R. G., Dodge, M. M., and Galloway, W. E., 1986, Controls on porosity and permeability of hydrocarbon reservoirs in lower Tertiary sandstones along the Texas Gulf Coast: The University of Texas at Austin, Bureau of Economic Geology, Report of Investigations No. 149, 78 p.

McBride, E. F., Lindemann, W. L., and Freeman, P. S., 1968, Lithology and petrology of the Gueydan (Catahoula) Formation in South Texas: The University of Texas at Austin, Bureau of Economic Geology, Report of Investigations No. 63,122 p.

McRae, L. E., and Holtz, M. H., 1994, Integrated reservoir characterization of mature oil reservoirs: an example from Oligocene Frio fluvial-deltaic sandstones, Rincon field, South Texas, Gulf Coast Association of Geological Societies Transactions, v. 44, p. 487-498.

McRae, L. E., Holtz, M. H., and Knox, P. R., 1994, Revitalizing a mature oil play: strategies for finding and producing unrecovered oil in Frio fluvial-deltaic reservoirs of South Texas: The University of Texas at Austin, Bureau of Economic Geology, topical report prepared for the U.S. Department of Energy, Bartlesville Project Office, under contract no. DE-FC22-93BC14959, report no. DOE/ BC/14959-5 (DE94000131), 93 p.

McRae, L. E., Holtz, M. H., and Knox, P. R., 1995, Revitalizing a mature oil play: strategies for finding and producing unrecovered oil in Frio fluvial-deltaic reservoirs of South Texas: The University of Texas at Austin, Bureau of Economic Geology, annual report prepared for the U.S. Department of Energy, Bartlesville Project Office, under contract no. DE-FC22-93BC14959, report no. DOE/ BC/14959-13 (DE95000160), 155 p.

Miall, A. D., 1988, Reservoir heterogeneities in fluvial sandstones: lessons learned from outcrop studies: American Association of Petroleum Geologists Bulletin, v. 72, no. 6, p. 682-697.

Milliken, K. L., 1989, Petrography and composition of authigenic feldspars, Oligocene Frio Formation, South Texas: Journal of Sedimentary Petrology, v. 59, no. 3, p. 361-374.

Stanley, T. B., 1970, Vicksburg Fault Zone, Texas, in Halbouty, M. T., ed., Geology of giant petroleum fields: American Association of Petroleum Geologists Memoir 14, p. 301-308.

Taylor, D. A., and Al-Shaieb, Z., 1986, Oligocene Vicksburg sandstones of the Tijerina-Canales-Blucher field, a South Texas geologic jambalaya: Gulf Coast Association of Geological Societies, Transactions, v 36, p. 315-339.

Tyler, Noel, 1988, New oil from old fields: Geotimes, v. 33, p. 8-10.

Tyler, Noel, Barton, M. D., Bebout, D. G., Fisher, R. S., Grigsby, J. D., Guevara, E., Holtz, M. H., Kerans, C., Nance, H. S., and Levey, R. A., 1992, Characterization of oil and gas heterogeneity: U.S. Department of Energy final report, October 1992, 219 p.

Tyler, Noel, and Ewing, Thomas, 1986, Major oil plays of South and Central Texas, *in* Stapp, W. L., ed., Contributions to the geology of South Texas: South Texas Geological Society, p. 24-52.

Tyler, Noel, and Finley, R. J., 1991, Architectural controls on the recovery of hydrocarbons from sandstone reservoirs, *in* Miall, A. D., and Tyler, Noel, eds., The three-dimensional facies architecture of terrigenous clastic sediments and its implications for hydrocarbon discovery and recovery: Society of Economic Paleontologists and Mineralogists, Concepts in Sedimentology and Paleontology, v 3, p. 1-5.

Tyler, Noel, Galloway, W. E., Garrett, C. M., Jr., and Ewing, T. E., 1984, Oil accumulation, production characteristics, and targets for additional recovery in major oil reservoirs in Texas: The University of Texas at Austin, Bureau of Economic Geology Geological Circular 84-2, 31 p.

U.S. Department of Energy, Bartlesville Project Office, 1991, Opportunities to improve oil productivity in unstructured deltaic reservoirs, proceedings from the technical symposium, Oil Implementation Task Force, January, 154 p.

Van Wagoner, J. C., Posamentier, H. W., Mitchum, R. M., Jr., Vail, P. R., Sarg, J. F., Loutit, T. S., and Hardenbol, J., 1988, An overview of the fundamentals of sequence stratigraphy and key definitions, *in* Wilgus, C. K., Hastings, B. S., Kendall, C. G., Posamentier, H. W., Ross, C. A.,

and Van Wagoner, J. C., eds., Sea-level changes: an integrated approach: Society of Economic Paleontologists and Mineralogists Special Publication No. 42, p. 39-46.

Weber, K. J., 1986, How heterogeneity affects oil recovery, *in* Lake, L. W, and Carroll, H. B., eds., Reservoir characterization: Orlando, Florida, Academic Press, p. 487-544.

Worthington, P. F., 1991, Reservoir characterization at the mesoscopic scale, *in* Lake, L. W., Carroll, H. B., and Wesson, T. C., eds., Reservoir characterization II: San Diego, California, Academic Press, p. 123-165.

Xue, L., and Galloway, W. E., 1991, High-resolution, log-derived, genetic stratigraphic sequence profile of the Paleogene section, Central Texas Gulf Coast, *in* Armentrout, J. W., and Perkins, R. F., eds., Sequence stratigraphy as an exploration tool: Gulf Coast Section, Society of Economic Paleontologists and Mineralogists research conference, p. 399-408.

A P P E N D I X 1: LIST OF PRESENTATIONS PRODUCED BY BEG CLASS I PROJECT. *1993*

Dutton, S. P., Revitalizing a mature oil play: strategies for finding and producing unrecovered oil in Frio.fluvial-deltaic reservoirs of South Texas: presented at the Department of Energy Oil Program Contractor Review Meeting in Fountainhead, Oklahoma, July 1993.

1994

McRae, L. E., and Holtz, M. H., Targeting the unrecovered oil resource in mature field areas: an example from Oligocene Frio fluvial-deltaic reservoirs of South Texas, Rincon field, South Texas: AAPG Annual convention, May, Denver, Colorado (poster).

McRae, L. E., and Holtz, M. H., Integrated reservoir characterization of mature oil reservoirs: an example from Oligocene Frio fluvial-deltaic sandstones, Rincon field, South Texas: Gulf Coast Association of Geological Societies, October, Austin, Texas.

1995

Holtz, M. H., and McRae, L. E., Modeling reservoir attributes and estimating additional hydrocarbon potential for redevelopment in fluvial-deltaic reservoirs: An example from the Frio fluvial-sandstone play in South Texas: AAPG Annual convention, April, Houston, Texas (poster).

Knox, P. R., and McRae, L. E., High-resolution sequence stratigraphy: the key to identifying compartment styles in Frio Formation fluvial-deltaic reservoirs, T-C-B Field, South Texas: AAPG Annual convention, April, Houston, Texas. .

McRae, L. E., and Holtz, M. H., Reservoir architecture and permeability characteristics of fluvial-deltaic sandstone reservoirs in the Frio Formation, Rincon field, South Texas: AAPG Annual convention, April, Houston, Texas.

Holtz, M. H., Characterization of Frio fluvial-deltaic reservoirs, South Texas: U. S. Department of Energy Contractors meeting, Fountainhead, Oklahoma, June 1995.

Knox, P. R., Predicting reservoir architecture and internal heterogeneity in upper delta plain settings: Implications for reserve-growth potential and development strategies, presented to Pennzoil Exploration and Production Company, June, Houston, Texas.

Dutton, S. P., Revitalizing a mature oil play: strategies for finding and producing unrecovered oil in Frio fluvial-deltaic reservoirs of South Texas: presented at the Department of Energy Oil Program Contractor Review Meeting in Fountainhead, Oklahoma, July 1993.

Knox, P. R., and McRae, L. E., Application of sequence stratigraphy to the prioritization of incremental growth opportunities in mature fields: an example from Frio fluvial-deltaic sandstones, TCB field, South Texas: Gulf Coast Association of Geological Societies, October, Baton Rouge, Louisiana.

McRae, L. E., and Holtz, M. H., Strategies for optimizing incremental recovery from mature reservoirs in Oligocene Frio fluvial-deltaic sandstones, Rincon field, South Texas: Gulf Coast Association of Geological Societies, October, Baton Rouge, Louisiana.

Knox, P. R., Progress Report: T-C-B field reservoir characterization, presented to Mobil Exploration and Producing U.S., Inc., Houston, Texas.

1996

Holtz, M. H., and Hamilton, D. S., Reservoir characterization methodology to identify reserve growth potential: SPEIDOE Improved Oil Recovery Conference, April, Tulsa, Oklahoma.

Knox, P. R. , Accommodation-based controls on fluvial-deltaic reservoir compartmentalization: Examples from the Oligocene Frio Formation, South Texas: AAPG Annual convention, May, San Diego, California.

Knox, P. R., Predicting between-well reservoir architecture and heterogeneity in fluvial-deltaic sandstones on the basis of position within a depositional cycle: Society of Independent Professional Earth Scientists, May, San Antonio, Texas.

Knox, P. R., Determining Between-Well Reservoir Architecture in Deltaic Sandstones Using Only Well Data: Oligocene Frio Formation, Tijerina-Canales-Blucher Field, South Texas: Gulf Coast Association of Geological Societies, October, San Antonio, Texas.

APPENDIX 2: LIST OF PUBLICATIONS PRODUCED BY BEG CLASS I PROJECT.

1994

Holtz, M. H., McRae, L. E., and Tyler, Noel, 1994, Identification of remaining oil resource potential in the Frio fluvial-deltaic sandstone play, South Texas: The University of Texas at Austin, Bureau of Economic Geology, topical report prepared for the U.S. Department of Energy, Bartlesville Project Office, under contract no. DE-FC22-93BC14959, report no. DOE/BC/14959-8 (DE94000132), 67 p.

McRae, L. E., and Holtz, M. H., 1994, Integrated reservoir characterization of mature oil reservoirs: an example from Oligocene Frio fluvial-deltaic sandstones, Rincon field, South Texas: Gulf Coast Association of Geological Societies Transactions, v. 44, p. 487-498.

McRae, L. E., and Holtz, M. H., 1994, Targeting the unrecovered oil resource in mature field areas: an example from Oligocene Frio fluvial-deltaic reservoirs of South Texas, Rincon field, South Texas (abs.) *in* AAPG Annual convention official program: analogs for the world: Denver, American Association of Petroleum Geologists, p. 213.

McRae, L. E., Holtz, M. H., and Knox, P. R., 1994, Revitalizing a mature oil play: strategies for fmding and producing unrecovered oil in Frio fluvial-deltaic reservoirs of South Texas: The University of Texas at Austin, Bureau of Economic Geology, annual report prepared for the U.S. Department of Energy, Bartlesville Project Office, under contract no. DE-FC22-93BC14959, report no. DOE/BC/14959-5 (DE94000131), 93 p.

1995

Holtz, M. H., and McRae, L.' E., 1995, Identification and assessment of remaining oil resources in the Frio fluvial-deltaic sandstone play, South Texas: The University of Texas at Austin, Bureau of Economic Geology Report of Investigations No. 227, 46 p.

Holtz, M. H., and McRae, L. E., 1995, Modeling reservoir attributes and estimating additional hydrocarbon potential for redevelopment in fluvial-deltaic reservoirs: An example from the Frio fluvial-sandstone play in South Texas (abs.), *in* AAPG Annual convention official program: Houston, American Association of Petroleum Geologists, v. 4, p. 42A-43A.

Knox, P. R., and McRae, L. E., 1995, Application of sequence stratigraphy to the prioritization of incremental growth opportunities in mature fields: an example from Frio fluvial-deltaic sandstones, TCB field, South Texas: Gulf Coast Association of Geological Societies Transactions, v. 45, p. 341-359.

Knox, P. R., and McRae, L. E., 1995, High-resolution sequence stratigraphy: the key to identifying compartment styles in Frio Formation fluvial-deltaic reservoirs, T-C-B Field, South Texas (abs.), *in* AAPG Annual convention official program: Houston, American Association of Petroleum Geologists, v. 4, p. 51A.

McRae, L. E., and Holtz, M. H., 1995, Reservoir architecture and permeability characteristics of fluvial-deltaic sandstone reservoirs in the Frio Formation, Rincon field, South Texas (abs.), *in* AAPG Annual convention official program: Houston, American Association of Petroleum Geologists, v 4, p. 64A.

McRae, L. E., and Holtz, M. H., 1995, Strategies for optimizing incremental recovery from mature reservoirs in Oligocene Frio fluvial-deltaic sandstones, Rincon field, South Texas: Gulf Coast Association of Geological Societies Transactions, v. 45, p. 423-434.

McRae, L. E., Holtz, M., Hentz, T., Chang, C., and Knox, P. R., 1995, Strategies for reservoir characterization and identification of incremental recovery opportunities in mature reservoirs in Frio fluvial-deltaic sandstones, South Texas: an example from Rincon field, Starr County: The University of Texas at Austin, Bureau of Economic Geology, topical report prepared for the U.S. Department of Energy, Bartlesville Project Office, under contract no. DE-FC22-93BC14959, report no. DOE/BC/14959-15 (DE95000190), 111 p.

McRae, L. E., Holtz, M. H., and Knox, P. R., 1995, Revitalizing a mature oil play: strategies for finding and producing unrecovered oil in Frio fluvial-deltaic reservoirs of South Texas: The University of Texas at Austin, Bureau of Economic Geology, annual report prepared for the U.S. Department of Energy, Bartlesville Project Office, under contract no. DE-FC22-93BC14959, report no. DOE/BC/14959-13 (DE95000160), 155 p.

1996

Holtz, M., McRae, L. E., Knox, P. R., Hentz, T., and Chang, C., 1996, Revitalizing a mature oil play: strategies for fording and producing unrecovered oil in Frio fluvial-deltaic reservoirs of South Texas: The University of Texas at Austin, Bureau of Economic Geology, annual report prepared for the U.S. Department of Energy, Bartlesville Project Office, under contract no. DE-FC22-93BC14959, report no. DOE/BC/14959-17 (DE96001211), 178 p.

Holtz, M. H., and Hamilton, D. S., 1996, Reservoir characterization methodology to identify reserve growth potential: SPE Paper 35434, 12 p.

Knox, P. R. , 1996, Accommodation-based controls on fluvial-deltaic reservoir compartmentalization: Examples from the Oligocene Frio Formation, South Texas (abs.), *in* AAPG Annual convention official program: San Diego, American Association of Petroleum Geologists, v. 5, p. A76.

Knox, P. R., 1996, Determining Between-Well Reservoir Architecture in Deltaic Sandstones Using Only Well Data: Oligocene Frio Formation, Tijerina-Canales-Blucher Field, South Texas (abs.): Gulf Coast Association of Geological Societies Transactions, in press.

Knox, P. R., 1996, Integrated Characterization Yields Targeted Infill/Recompletion Opportunities: The Class Act, U.S. DOE Bartlesville Project Office, in press, 2 p.

APPENDIX 3: CONTENT OF SHORT COURSES PRODUCED BY BEG CLASS I PROJECT.

New Oil From Old Fields: Identifying Opportunities for Reserve-Growth Potential in Mature Fields of the Frio Fluvial/Deltaic Sandstone Play, Vicksburg Fault Zone

Short Course Schedule

9:00 -9:15	Welcome and Workshop Overview
9:15 - 9:45	Frio Fluvial/Deltaic Play Characteristics
9:45 - 10:00	Integrated Reservoir Characterization Methodology: Overview
10:00 - 10:15	The Geologic Advisor
10:15 - 10:30	*Break*
10:30 - 11:00	Sequence Stratigraphic Concepts, Introduction to Facies Identification in Deltaic Systems
11:00 - 12:00	Geological Identification of Reservoir Architecture
12:00 - 1:00	*Lunch*
1:00 - 1:45	The Interpretation of Old E-Logs
1:45 - 2:00	Frio Fluvial/Deltaic Petrophysical Characteristics
2:00 - 2:30	The Power and Benefits of 3-D Seismic
2:30 - 3:05	Geophysical Identification of Reservoir Architecture
3:05 - 3:20	*Break*
3:20 - 4:05	Developing the Reservoir Model–Integrating Geology, Geophysics, and Engineering
4:05 - 4:20	Identifying Reserve Growth Potential
4:20	Concluding Remarks

Hosted by the South Texas Geological Society
San Antonio, Texas, April 8, 1996

APPENDIX 3: CONTENT OF SHORT COURSES ASSOCIATED WITH BEG CLASS I PROJECT.

New Oil From Old Fields: Identifying Opportunities for Reserve–Growth Potential in Mature Fields of the Frio Fluvial/Deltaic Sandstone Play, Vicksburg Fault Zone

Short Course Schedule

8:00 – 8:10	Welcome and Workshop Overview *(Major)*
8:10 – 8:40	Frio Fluvial/Deltaic Play Characteristics *(Holtz)*
8:40 – 9:40	Sequence Stratigraphic Concepts, Introduction to Facies Identification in Deltaic Systems *(Knox)*
9:40 – 10:10	Integrated Reservoir Characterization Methodology: Overview *(Holtz)*
10:10 – 10:30	The Geologic Advisor *(White)*
10:30 – 10:45	*Break*
10:45 – 11:45	Geological Identification of Reservoir Architecture *(Knox)*
11:45 – 1:00	*Lunch*
1:00 – 2:00	Power and Benefits of 3-D Seismic *(Hardage)*
2:00 – 2:30	Geophysical Identification of Reservoir Architecture *(Paine)*
2:30 – 3:00	Frio Fluvial/Deltaic Petrophysical Characteristics *(Holtz)*
3:00 – 3:15	*Break*
3:15 – 4:15	Developing the Reservoir Model–Integrating Geology, Geophysics, and Engineering *(Holtz)*
4:15 – 4:45	Reservoir Prioritization *(Knox, Holtz)*
4:45	Concluding Remarks and Questionnaire *(Major)*

Hosted by the Houston Geological Society
Houston, Texas, June 6, 1996

☆U.S. GOVERNMENT PRINTING OFFICE: 1996 - 760-032/40035

FOSSIL ENERGY

DOE/BC/14961-9

DYNAMIC ENHANCED RECOVERY TECHNOLOGIES – CLASS I

Final Report
Part I
July 1994-October 1995

By:
Roger N. Anderson

Date Published: October 1995

Work Performed Under Contract No. DE-FC22-93BC14961

Columbia University
New York, New York

National Energy Technology Laboratory
National Petroleum Technology Office
U.S. DEPARTMENT OF ENERGY
Tulsa, Oklahoma

DISCLAIMER

This report was prepared as an account of work sponsored by an agency of the United States Government. Neither the United States Government nor any agency thereof, nor any of their employees, makes any warranty, expressed or implied, or assumes any legal liability or responsibility for the accuracy, completeness, or usefulness of any information, apparatus, product, or process disclosed, or represents that its use would not infringe privately owned rights. Reference herein to any specific commercial product, process, or service by trade name, trademark, manufacturer, or otherwise does not necessarily constitute or imply its endorsement, recommendation, or favoring by the United States Government or any agency thereof. The views and opinions of authors expressed herein do not necessarily state or reflect those of the United States Government.

This report has been reproduced directly from the best available copy.

DOE/BC/14961-9
Distribution Category UC-122

Dynamic Enhanced Recovery Technologies – Class I

By
Roger N. Anderson

October 1995

Work Performed Under DE-FC22-93BC14961

Prepared for
U.S. Department of Energy
Assistant Secretary for Fossil Energy

Chandra Nautiyal, Project Manager
National Petroleum Technology Office
P.O. Box 3628
Tulsa, OK 74101

Prepared by
Columbia University
New York, NY 10021
Edited by
National Petroleum Technology Office

ABSTRACT

We chose the Eugene Island 330 field for our oil migration study because it is the largest Pleistocene oil field in the world, it is geologically well-characterized, and most importantly, it shows a variety of indications of geologically recent hydrocarbon migration (Holland et al, 1990 and Whelan et al, 1994). The Eugene Island 330 Field is a typical Gulf of Mexico mini-basin (Alexander and Flemings, 1994). Structurally, a regional growth-fault system (the "Red Fault Zone") forms the northern boundary of alternating sequences of Plio-Pleistocene sands and shales overlying deep-water turbidities and basin-floor fan deposits from the ancestral Mississippi River delta. As the Red Fault Zone accommodated extension toward the deep-water Gulf of Mexico, the sediments in the depobasin formed rollover anticlines that are now filled with oil and gas. Extension was caused by withdrawal to the south of an extensive salt sill initially present near the surface of the mini-basin from 6 to at least 2.2 Ma (Rowan, Weimer and Flemings l994). A counter-regional, down-to-the-north fault zone forms the southern boundary of the mini-basin. A thick shale sequence separates the shallow-water shelf sands from geopressured. deep-water deposits (Alexander and Flemings, 1994). Remnant salt feeder stocks and remobilized salt diapirs bound the mini-basin, exclusively upthrown to the bounding fault system. The deep turbidities are still geopressured (He and Anderson, 1994), even after the removal of the impermeable salt seal, because high sedimentation rates combined with the thick, deepwater shale accumulations in the Pliocene resulted in rapid burial and permeabilities too low for the excess pore fluids to escape (Mello, et al, 1994).

Migration of hydrocarbons is occurring today in the Eugene Island 330 Field (Anderson. et al, 1993). Seeps are active at the sea floor outcrop of the Red Fault Zone system. Oil and gas are being produced in reservoirs as young as 400,000-years-old beneath these seeps. Geochemical monitoring over the last twenty years has recorded temporal changes in the composition of the oils being produced from the shallow reservoirs; these changes may reflect recent injection of wet gas and gasolines (Whelan, et al, 1994). Also, biodegraded oils have been replaced by less biodegraded oils over time in the shallowest reservoirs.

Executive Summary

Task One - Management Start-Up
Roger N. Anderson - Task Manager

OBJECTIVE:

The purpose of this task was to equip the project with staff and resources (computer and otherwise) to accomplish the other 6 tasks of this project; to negotiate contracts with several industry and university subcontractors to achieve the task objectives; and to initiate the technology transfer to industry and the public from the very beginning of this project

Task Two - Database Management
Roger N. Anderson - Task Manager

OBJECTIVE:

The objectives of this task were to accumulate, archive, and disseminate the geological information available within the area of research of this project; networked database creation, generation of new seismic interpretation with high-tech software, and real-time visualization of the on-line database

SUMMARY:

Fluid-Flow Monitoring Using Industry Multiple 3-D Seismic Data Sets has been one of the outstanding new discoveries of the project We have developed and submitted a patent for 4-D seismic processing software that can recognize amplitude and impedance changes caused by the addition and subtraction of oil and gas from reservoirs over time intervals as short as a few years. The technique has been developed using the 1992 Shell/Exxon data set (received in December 1994) with two previously acquired 3-D seismic surveys, the Texaco/Chevron data set (acquired in 1988) and the Pennzoil et al data set (acquired in 1985). This DOE project is one of the first Case Histories of 4-D seismic reservoir monitoring in the oil industry.

Liqing Xu developed the LDEO 4-D Software as a set of AVS modules that are networked to form a 4-D package library. He has written, modLFied, debugged and mounted more than 100,000 lines of code that form the AVS modules making up the code. He worked out the 4-D imaging and visualization requirements, and has completed a new 4-D software homepage.
Houston in October 1995. LDEO 4-D Software is copyrighted by Columbia University in the City of New York, and ownership remains with Columbia University, for whom a United States Letters Patent is pending.

Task Three - Field Demonstration Experiment
Roger N. Anderson - Task Manager

OBJECTIVE:

Task three drilled one well extension to test the Dynamic Enhanced Recovery Technologies objectives of this project In November and December, 1993, we drilled into the fault zone in Eugene Island Block 330 (A20-ST) and performed the following experiments: whole coring, wireline logging, sidewall coring, formation pressure tests, stress tests, completion with frac-pack, flow test and pressure transient test.

SUMMARY:

The A-20ST, Pathfinder well was drilled by Pennzoil Exploration and Production Co., on behalf of partners Exxon, Mobil and Cockrell, into the 01-4 reservoir just above the "Red" growth fault zone that forms the northern boundary of the Eugene Island 330 minibasin. The well was then extended across the fault zone and into the footwall. The GBRN Field Demonstration Project consisted of three phases: whole coring, extensive logging, and stress and production testing in the Pathfinder extension. Measurements were made to determine in situ conditions within and surrounding the fault zone and to test the hypothesis that hydrocarbons could be produced from a fault zone.

We found and sampled oil and gas from silty shales within the fault zone and discovered that the oils have similar chemistry to those being produced from the reservoirs directly above the fault zone. Whole coring revealed that faulting and fracturing extended at least 350 feet into the shales of the upthrown block. Many of the faults and fractures contained oil. Hydrocarbons would not flow at economically viable rates during drill-stem tests. The larger the drawdown pressure applied across the perforations, the lower the permeability of the fault zone became.

Where the A-2OST crossed the fault zone, the horizontal closure stress was 500 psi greater than the fluid pressure. An increase in the pore pressure of 500 psi was then found to induce signLFicant permeability within the fault zone.

A related well, the A-lOST, was drilled into the fault zone in Eugene Island 330 in October, 1993, in anticipation of the Pathfinder well. In contrast to the "tight" fault encountered in the Pathfinder well, fluids flowed strongly when the fault zone was penetrated by the shallower A-lOST well. Fluid flow within the high-pressured fault zone was sufficient to cause differential sticking and the loss of two bottom-hole assemblies in the well. A pulsed-neutron, Thermal Decay Time log run through the stuck drillpipe recorded increased gamma ray radiation from oxygen activation indicating that water was flowing at rates of up to 700 barrels/day within the fault zone.

Task Four - Reservoir Characterization
Peter FIemings - Task Manager

OBJECTIVE:

The purpose of this task was to integrate the geological and geophysical data to construct the minibasin and reservoir models in the Eugene Island 330 Area in order to understand the hydrodynamics of the minibasins. The minibasins are analyzed through stratigraphic interpretation, salt analysis, pressure and temperature mapping. Temporal seismic amplitude analysis is to monitor the dynamic changes occurred in the reservoir.

SUMMARY:

Though the final year of the project we continued to acquire important data for the 330 field. These included: 1) complete wire- line data for Blocks 338 and 339 (donated by Texaco), 2) fracture completion data, and leak off data for Blocks 330, 338, and 339, and 3) The entire 316 A-12 core (now housed in the Penn State Core Repository) which was recently drilled by Pennzoil.

Task Five - Modeling
Larry Cathles - Task Manager

OBJECTIVE:

The objectives of the modeling task: (1) the cause of pressure, temperature, fluid chemical, and porosity anomalies near the Red Fault; (2) the possible sources of oil and gas moving up the fault; and (3) the causes of organic and inorganic chemical alteration near the fault.

Particular attention was to be focused on: (1) porosity and excess pressure development in the RVE, (2) hydrocarbon maturation (3) detailed fluid flow near the fault focusing on the detailed distribution of high permeability sands, (4) the effects of salt diapirism on subsurface temperatures, (5) the effects of fault movement on fault permeability and fluid venting out of the fault (6) the effects of gas venting on oil migration, (7) the transport of oil as a separate phase up the fault, and (8) the effects of fluid flow (water, gas, and oil) on rock chemistry and mineralogy. The modeling was to be carried out in 3-D as well as2-D.

No computer software existed that was adequate to these tasks. In collaboration with Computational Mechanics Corp. of Knoxville, Tennessee, we developed a basin modeling system capable of investigating the highly coupled phenomena associated with hydrocarbon migration up the Red Fault of the South Eugene Island minibasin, and applied that modeling system to the geologic data collected.

The AKCESS.BASIN Modeling System was developed and applied to the South Eugene Island (SEI) Block 330 region. Preparation of the geologic data in a fashion that takes account of diapirism, overpressuring, and faulting in three dimensions, proved far more dLFficult and time

consuming than we had anticipated. Substantial effort was also devoted to developing algorithms that accurately describe critical parameters such as thermal conductivity and permeability in the data cube. A powerful modeling capability has been created that is supported by a private company and a growing group of academics spread over five separate institutions.

SUMMARY:

The principal accomplishments to date under this proposal are:

1. Development of a 3-D finite element basin modeling system with sound and fully articulated fundamentals, and accurate algorithms for thermal conductivity and sand permeability. It provides for easy input of highly detailed three-dimensional geologic data with options to infer salt diapirism from the surface pattern of sedimentation and sea level. It takes into account all major physical and chemical phenomena (e.g., isostasy, salt diapirism, faulting, overpressuring, seals, hydrocarbon maturation, fluid flow driven by haline or thermal convection, water table topography, or overpressuring, salt dissolution and transport, etc.). It solves the coupled equations with an easy to use, but versatile and controllable finite element solver, which can execute rapidly on parallel machines. It provides convenient and easy to use visualization tools at all stages.
2. Distribution of that modeling system across 5 institutions (Cornell, LSU, Michigan Tech., and Bowling Green) with appropriate training of professionals and students at each.
3. Extensive benchmarking demonstration of the validity of various aspects of the modeling system.
4 Application of the Modeling System to eight -100km long 2-D) seismic lines centered on the South Eugene Island Block 330 area of the Gulf of Mexico and one 1200km interpreted N-S sectioL The history of salt movement over the last 20 Ma inferred direcily from sedimentation shows evolution from a salt sheet to multiple minibasins and domes. The domes have a major impact on subsurface temperature (70^0C temperature anomalies above and below the salt domes).
5. Construction of highly detailed 3-D data cube in the SEI 330 area resolving all principal sands and their displacement across four NE-SW faults over the last 3.4 Ma. The salt movement inferred from the pattern of sedimentation shows the burial of a local salt sill and its remobilization into the South Eugene Island Block 330 minibasin with the Red Fault at its northern margin.
6. Detailed analysis of bottom hole temperature data shows a positive temperature anomaly of about 5^0C below the Pennzoil oil and gas fields roughly along the Red Fault and a negative (-5^0C) temperature anomaly above the oil reservoirs. Modeling shows that temperature anomalies of this magnitude or greater will be produced by the insulating hydrocarbon-filled sand reservoirs. Fluid flow could produce the positive anomaly below the reservoirs along the Red Fault, but not the negative anomaly above the reservoirs. This suggests that the present day temperature field in the South Eugene Island Block 330 minibasin is due to thermal conductivity anomalies associated with hydrocarbon reservoirs and not rapid fluid flow.

A variety of data support ongoing filling of the GA sand via rapid injection, and high fluid flux in the fault zone in the past Repeated sampling of wells over a period of 10 years has led to the finding that unbiodegraded oils are injected into the GA sand on the time scale of years

or less. Biodegradation occurs rapidly there, and the presence of unaltered oil is interpreted to reflect rapid influx from depths at which biodegradation does not take place. A variety of other organic geochemical data corroborate this conclusion. In the A6ST well, which penetrates the main growth fault at a point 1000 feet from the fault intercept in the Pathfinder Well, sediments from within the growth fault are characterized by anomalously high vitrinite reflectances relative to sediments outside the fault, indicating that the fault is locally a paleothermal anomaly. Combined with stable isotopic composition of minerals from the fault in that well, these data support the conclusion that the fault, at least 4 some locations, acted as a conduit of relatively high-temperature fluids.

The Pathfinder core contains three structurally distinct fault domains only the deepest of which contains oil. Based on structural and geologic data, this deepest domain is concluded to have been the most recently active. Structural and geochemical data indicate the other two fault domains were active prior to oil migration. The oil-barren domains contain fractures that are favorably oriented to transmit oil, and oil is furthermore present in sands in these domains. It is evident that fault zone oil migration took place only within that part of the fault that was active during the time migratable oil was available to the fault. Despite the variability of hydrogeologic characteristics of faults as evident in the core, the geochemical data indicate that none of these cored faults transmitted signLFicant amounts of fluid in the Pathfinder well. The same fault in the A6ST well has apparently acted as a fluid conduit, indicating relatively short-range lateral variability in fluid flow behavior in the fault.

Task Seven - Technology Transfer
Roger N. Anderson - Task Manager

OBJECTIVE:

The purpose of this task was to integrate the results into one comprehensive perspective of the project's objectives and to transfer the results to industry. We made special efforts to patent and license technology developed as part of this project so that it would become commercially available to the oil industry. We commissioned a study using the United States Geological Survey’s fractal oil and gas reserves techniques to identLFy whether we were dealing with an additional source of oil and gas in the Eugene Island 330 field’s recharge-along-faults.

SUMMARY:

The DOE field Demonstration Project “Dynamic Enhanced Recovery Technologies” has spawned important new technologies such as 4-D Seismic Monitoring, resulted in the placement of successful new wells to drain new and bypassed oil and gas in one of the most prolLFic oil fields in the U.S. offshore, grown into industry-only funding consortia for all its major tasks, and promoted Internet collaboration across institutional boundaries. In addition, there is every prospect that the U.S. Treasury will be repaid many times over for the direct investment of fluids into the future of the oil industry in America.

Task Two – Database Management

Software Development

LDEO 4-D Software was developed at Lamont-Doherty Earth Observatory of Columbia University. Software implementation started in 1994. It was initiated on the Global Basin Research Network (GBRN) which is headed by Dr. Roger N. Anderson. LDEO 4-D software was written by Liqing Xu with design input from Wei He and Albert Boulanger.

LDEO 4-D Software has applications to the interpretation of time dependent changes in multiple 3-D seismic surveys acquired over the same subsurface volume at different times to monitor the changes in impedance caused by drainage and migration of hydrocarbons and other subsurface fluids. A United States Letters Patent is pending. LDEO 4-D Software also has modules for seismic data processing, image processing, data interpretation and data visualization in 2-D and 3-D. It is built on top of Advanced Visual Systems, which provides the modular programming environment and basic modules for image display and 3-D rendering. The LDEO 4-D software currently contains more than 100,000 lines of code in the, which cover seismic data input, well log analysis, arid horizon data input into AVS. Modules are provided for 4-D seismic data interpretation, horizon extraction and interpretation, volume processing and imaging which form the backbone of the LDEO 4-D software. Because LDEO 4-D Software is built on top of AVS, users can dynamically connect our software modules to create 4-D seismic analysis networks. Each module is small and specifically designed to accomplish one task within the 4-D analysis framework. The LDEO 4-D Software divides major applications into groups of AVS modules which can be either independently executed in stages, or networked together to perform analyses of 4-D Seismic datasets.

The major purpose of the LDEO 4-D Software is to provide a "Quick Look" tool to track changes of seismic amplitude and impedance over the time as hydrocarbon pool drainage proceeds. The LDEO 4-Dsoftware modules are designed to extract dLFferences and similarities among multiple generations of 3-D seismic surveys (4-D seismic data). LDEO 4-D Software provides a methodology whereby hydrocarbon migration and drainage pathways and reservoir fluid locations and volumes can be mapped over time.

The LDEO 4-D Software provides all required data processing functions for 4-D analysis, such as amplitude and frequency spectral normalization, seismic attribute computation, and a rich set of data filters. The processing flow of the LDEO 4-D Software proceeds from the rebinning and pre-processing of multiple 3-D seismic data, to procedures for amplitude and frequency normalization, cross correlated to minimize spatial shLFt and navigation errors. Then each seismic dataset is converted to the seismic attribute domain, and reflection strength, or the amplitude envelope of the seismic signal, is computed for each waveform. The individual 3-D seismic datasets are then grown about seed points of the highest amplitudes within each seismic dataset to obtain volumetric representations of the hydrocarbon reservoirs. Another important part of the LDEO 4-D Software is visualization capabilities to display and recognize the dimouts, amplitude brightening and sustained amplitude regions that delineate drainage, water encroachment, gas cap formation, and most importantly, locations of bypassed pay. LDEO 4-D software provides a rich set of visualization modules such as slicing (orthogonal and arbitrary slicing), volumetric rendering of reservoirs, seismic and well log visualization along wellpaths

(regardless of deviation), multiple horizon slicing, amplitude extraction, horizon visualization, skeleton building, migration pathway manLFolding and 2-D particle flow simulation. All visualization is implemented in real 3-D space, but since we image only within grown regions, the datasets have been downsized for rapid manipulation with standard workstation graphics capabilities. LDEO 4-D Software provides an added set of utility modules to generate print-ready and Internet mountable html output easily.

LDEO 4-D Software contains five basic operations: data loading, data preprocessing, data interpretation, 4-D dLFferencing, arid visualization. It provides the ability to multiple 3-D seismic datasets for 4-D drainage and fluid migration changes.

Geologicl Analyses of Industry 3-D Seismic Surveys

Landmark compared the traditional interpretation of the horizons and faults, and the reinterpreted reflector horizons and faults in Phase I of this project. The reinterpreted geologic data was convened and exported to other databases. Integration of several data sets aided in the reassessment of the drilling location and the field demonstration experiment

Lincoln Fratson has completed the development of an algorithm for well log/time series correlation. Development of a robust, non-parametric correlation statistic for testing and ranking the similarity of any two, related time Series, specifically the well logs from Eugene Island 330, continues. A study of the morphology of the sea floor in the Gulf of Mexico has been completed and published in Geology. In this study, the intraslope basin morphology of the Louisiana slope, which is the evolutionary precursor of the Eugene Island 330 basin, is compared to the morphology of other US continental slopes. The study shows that the Louisiana Slope morphology, though rugged, is flatter and more random at both regional (>1,500 km2) and local (<0.1 km2) measurement scales than any of the other US continental slopes, which span a range of sedimentary and tectonic setting. The low grade of the Louisiana slope is undoubtedly tied to the allochthonous salt that underlies the region. It is suggested that the salt may not be competent enough to support steep seafloor slopes, and/or, in moving, it may frequently trigger slope re-adjustment through failure. Evidence for the latter are the numerous debris aprons that emanate from the base of the Sigsbee Escarpment where allochthonous salt has been thrusting seaward.

Real-Time Visualization of Database

Reservoir characterization of the LF reservoir in the Eugene bland Block 330 Field of offshore Louis- Gulf of Mexico

The dynamic changes we have observed in the LF reservoir during hydrocarbon production suggest that this reservoir is very complex and internally heterogeneous. We characterize this complexity with a fine-scale reservoir characterization model that describes petrophysical properties such as lithology, porosity, and effective oil saturation.

For many years, reservoir characterization has played an essential role in oil field management Reservoir simulations are used by geologists and reservoir engineers to optimize and maximize recovery efficiency. Traditionally, only wireline logging data and well production

histories have been used in these characterizations. Consequencly, the characterizations are often too smooth due to the lack of lateral resolution. As 3-D seismic imaging has improved, its usefulness in reservoir characterization has increased (Doyen et al., 1992; Martinez et al., 1992 and He et al., 1994). Reservoir characterization has become increasingly accurate and reliable. However, the static reservoir descriptions cannot predict dynamic behavior of hydrocarbon reservoirs under production.

The combination of static reservoir characterization and 4-D seismic monitoring techniques can be used to achieve much more accurate oil field management and higher economic returns (Anderson et al, 1995a and 1995b). We foresee that such a combination involving multiple 3-D seismic datasets will play a more and more important role in future reservoir management and surveillance, and become the industry norm in the near future.

Reservoir characterization can be performed in micro-, meso-, macro-, and megascales depending on data availability. Well logs and surface reflection seismic data are useful for mesoscopic and macroscopic scales (i.e., reservoirs are characterized in terms of bed boundaries, stratLFication types, lithology and porosity).

The lack *of* a unLFied theory that can account for all geophysical and geological observations at different scales severely affects the development of reservoir characterization techniques. Numerous empirical relationships between reservoir petrophysical and acoustic properties have been developed (Archie, 1942; Gardner et al., 1974; Brock, 1984 and Han et al., 1986). These relationships are of limited effectiveness because the correlation between petrophysical properties are imprecise. 'These hr *situ* relationships based on high frequency data (e.g., 10 KHz sonic log and 1 MHz ultrasonic core analysis frequency) are often very inaccurate when applied to lower frequency seismic surveys.

The imprecise relationship between rock lithology and acoustic properties is often a problem when multiple lithologies are present However, stochastic simulations can be used to assess this ambiguity and to determine the spatial distribution of reservoir properties. The physics behind the use of stochastic simulation is that the petrophysical and acoustic properties (e.g., impedance) made over the same reservoir are closely associated even though they have different frequency bandwidth. These associations can be imaged through cross-correlations between the properties and between the impedance data measured in space.

In this chapter, we present a systematic technique for determining reservoir lithology, porosity, and oil saturation distributions and applied it to the LF reservoir. Our method consists of a combination of well data analysis for lithology determination, spatial cross-correlation computations between lithology and acoustic impedance, and a robust stochastic simulation technique (Deutsch et al, 1992).

We first investigate the lithology distribution within the LF reservoir because lithology is the dominant factor affecting the acoustic impedances. Reservoir lithology interpreted from well log data analysis is assumed to be the most reliable (hard data), while lithology derived from estimated acoustic impedances is assumed to be imprecise (soft data). We used the Markov-Bayse conditional sequential indicator simulation technique to simulate the most probable Lithology distribution of the LF reservoir. This simulation technique integrates the shale volume fractions derived from the 1992 acoustic impedance volume with shale volume fractions derived from the wireline logging data. The porosity and effective oil saturation distributions are then inferred using a time-avenge equation along with the 3-D lithology model. The likelihood of the

Lithology model of the LF reservoir determines other properties, such as porosity and oil saturation.

Conditional soft inclicator simulations

The conditional soft indicator simulation is a stochastic optimization technique, which integrates data from different sources with various probability and confidence levels assigned to produce multiple images of the spatial distribution of an attribute related to these data. The simulated images provide a rich family of characterized attribute distribution with equal probability. When this technique is used to simulate spatial distributions of Lithology using well and seismic data, the estimated Lithology images preserve the spatial statistic of the original well data. In addition, the Lithology images also posses the higher lateral resolution of seismic data.

Uncertainties in an attribute, such as lithology, can be estimated by examining the statistics of an ensemble of estimated images to create probability maps. The simulated stochastic images are globally conditioned to all available information, and also locally conditioned by hard data. The sparse hard data is honored exactly while the soft data has influence in proportion to its degree of uncertainty.

The concept of indicator variables

Many geological properties, such lithology, permeability and pore fluid pressure, can be simulated as indicator variables because the classLFication of these parameters tends to be categorical For instance, the continuous variables, shale volume fraction, can be categorized into sandy and silty regions. The indicator is represented by a binary numbers that takes the value 0 or 1. The indicator is assigned to be either 0 or 1 depending on value of the underlying continuous variable. The indicator categorizes the value of the continuous variable. Thus indicator variables have the characteristics of both continuous and categorical variables. Indicator variables are useful when the number of hard data points is too few to produce reasonable statistical simulations of a continuous variable. The concept of indicator variables was introduced, developed and applied to spatial statistics by Switzer (1977), Joumel (1982, 1983, 1984 and 1986).

The sequential, condidonal, soft indicator simulation

The sequential, conditional indicator simulation is aggressive in practice. Once the lithology indicator at a location is simulated this location is recategorized into the hard indicator and joins the stochastic simulation for the next location, depending upon the physical and statistical analysis of the soft data. In our case, we simulate reservoir lithology using shale volume fraction from wells as hard data and those from impedance as soft data. Minimization only requires knowledge of the spatial autocovariance and cross variance of hard and soft indicators.

The simulations reproduce the indicator means, autocovariances, and cross covariances. The simulated spatial distribution of an indicator variable honors both hard data (directly, as constraint) and soft data (indirectly, through its indicator).

Geological and geophysical logging data analysis in the LF reservoir

Reservoir characterizations are performed in the same area where we have performed the 4-D analysis.

Well log analysis for lithology of the LF reservoir

The lithology of the LF reservoir is first studied using twenty logged wells in the study area. In sand and shale sequences gamma ray (GR) and spontaneous potential (SP) logs are used to calculate the fractional shale volume by using empirical relationships. The well log analysis is then used to derive the hard lithology data of the LF reservoir and its surroundings. Because the spatial cross-correlation plays a very important role in the conditional sequential indicator simulation algorithm, these 20 wells have been chosen very carefully to have a good spatial coverage.

Qualitative description of the LF reservoir

The LF reservoir belongs to a vertically stacked, deltaic sand package (JD~KE-LF sands) deposited during the proximal deltaic phase in the lowstand pro-ding wedge system tract in the EI-330 minibasin (Alexander et al., 1995). Holland et al (1990) used well logs and production data to analyze the overall reservoir properties.

The LF sand is a distributary-mouth bar deposit. The sand progressively thins up-dip and is shaled-out on the crest of the antic line. It is very fine-grained and clean, with a high irreducible water saturation. Unusually low resistivity is observed on resistivity logs. It consists of predominantly quartz with various, but minor amounts of detrital shale. Feldspars and other minerals may constitute as much as 30% of the total rock volume. Hard, unLFormly cemented "streaks" of calcite precipitates, along with authigenic clay, silica, dolomite, and pyrite, are found toward the top of the sand in two cores Flemings et al., 1996 and Hoover, 1996, personal communication).

As is typical with deltaic sand deposits, the sand bodies of the LF reservoir contain variable shale and other distributed fine-grained compositions that vary spatially. Using well data alone in traditional reservoir characterization, one must interpolate reservoir properties within each reservoir in order to estimate the spatial distributions of these properties. Simple contouring and kriging techniques are used to make the image of the characterized LF reservoir. The LF reservoir is the most prolLFic oil-producing reservoir in the field. It has excellent water drive support, and a gas cap exists near the structural crest of the EI-330 rollover anticline. The average porosity is about 30%, and the net pay thickness avenges about 17 m.

The characterizations of the LF reservoir from well data alone are qualitative. Only ranges of porosity and permeability have been estimated (Holland et al., 1990). These characterizations do not describe spatial variabilities, and cannot satisfy our needs for quantLFying the 4-D analysis, because the image is too smooth to capture the true heterogeneity of the reservoir. The addition of 3-D seismic data enables a much more realistic reservoir characterization.

The geometry of the LF reservoir

The estimated 1992 acoustic impedance volume contains the SD, KE and LF reservoirs. This impedance volume is used along with the reservoir lithology derived from well logs within it to characterize the lithology and porosity distributions of the LF reservoir.

The estimated acoustic impedance volume is converted from two-way traveltime to depth

using conversion table created by averaging fourteen sonic logs. The converted acoustic impedance volume is then resampled every 1.5 m. The top and bottom of the LF reservoir in this impedance volume are consistent with the well tops, indicating that the conversion from two way traveltime to depth has been successful.

The thickest part of the LF reservoir is in the center of the study area. There appears to be a thick sand trend running along the north-east to south-west direction, consistent with the interpretation that the LX sand is in a deltaic mouth bar deposit The map of depth to the top of the LF reservoir based on both seismic and log data has much greater spatial resolution than the map based on log data alone. Dramatic stratigraphic thinning of the SD, KE, and LF sands onto the crest of anticline in the study area is also seen in the east-west cross-section.

The relatiombip between acoustic impedances and lithology in the LF reservoir

Correlations between lithology, porosity and acoustic impedance are often ambiguous. The classLFied reservoir lithologies do not always correspond to a particular impedance interval, and impedance ranges of different lithologies often overlap one another. The more the overlap, the greater the ambiguity of direct classLFication.

The statistical distribution of the extracted acoustic impedance data and the shale volume fraction data dLFfer. Shale volume fraction data has strong bi-modal statistics, while acoustic impedance has is a single-modal statistics, but a long-tailed distribution. Empirical relationships between volume fraction and impedance are dLFficult to justLFy, given such large dLFference in their statistics. Even within the narrow specLFied depth interval (91 m), the relation between the shale volume fraction and acoustic impedance is very poor.

The variogram models estimated from hard and soft data

Variogram is the variance of a random variable with respect to discrete distance increments. The shale volume fractions in the hard data clearly exhibit sand and shale categories. However, the distribution of the soft data does have a long tail at the lower impedance end, which probably corresponds to clean sand saturated with either oil or gas.

The spatial correlation between the hard (shale volume fraction measured by logs) and the derived secondary data (shale volume fractions derived from the estimated acoustic impedance) is quantLFied using directional semivariograms. Experimental semivariograms of both hard and soft shale volume fractions in the east-west, north-south, and depth directions were computed and correspond to one another. The hard shale volume fractions have much greater spatial variability than the soft data in all three directions. Introduction of the soft data will signLFicantly improve estimates of the spatial distributions of reservoir properties.

We computed semivariograms of the three indicators using both hard and soft data. The observed semivariograms are then approximated by a simple, "spherical" semivariogram model (Deutsch et al., 1992). The hard and soft indicators have similar semivariograms. The maximum correlation length is larger in downdip and along-strike directions, than in the depth direction (152 m corresponds to 15 m). Sand has the least spatial variability with a maximum correlation length (183 m) in the across-strike (down-dip) direction. The variability of shaly sand and sandy shale is twice that of the sand in lateral directions.

Our stochastic simulation is carried out in a finite dLFference 3-D grid (it is also the 3-D seismic

grid) with dimensions of 134 node points in the downdip direction, 125 node points in the across-strike direction, and 61 node points in the depth direction. The spacing in the down-dip, across-strike, and depth directions are 23 m, 15 m, and 1.5 m, respectively.

The Markov-Bayes calibration of the hard and soft indicators

The Markov-Bayes calibration was performed using the calibration dataset, which contains 1235 collocated hard and soft data pairs. These collocated data pairs give the prior conditioned cumulative frequency table for each class. The table then gives the linear scaiing factors that ensure that the probability of random drawing of the realization at each data point is constrained to the collocated hard and soft data calibrations (Kulkarni, 1984). At this time, the shale volume fractions, which are not directly analyzed through the variogram studies, are incorporated implicitly into the simulation.

The simulated lithology distributions of the LF reservoir

Twenty simulations, using four different random seed points, were computed using the conditioned Markov-Bayes calibration table and the spatial semivariogram models. The simulated shale volume fraction realizations are compared with the estimated acoustic impedance distributions in the top, middle, and bottom of the LF reservoir. Remarkable lateral continuity of the simulated sand distributions is observed, even though such lateral continuity is not in either the estimated acoustic impedance or the well data. Similar sand and shale distribution patterns are observed in all twenty simulated images.

Because all the simulated lithologic images exactly honor the hard data, it is dLFficult to determine which image is the best description of the LF reservoir. We arithmetically average the twenty simulated shale volume fraction distributions to obtain a final estimate of the lithology. We then computed a probability volume that described the probability that the lithology is sand, shaly sand, silty shale, or shale at each point. The LF sand gradually shales out towards the east, as expected. The shale line runs nearly north-south even though the structural contours wrap around the anticline. The thickening of the LF sand reservoir in the center just north of the F fault defines the depocenter. The clean sand distribution shows the greatest discontinuity on the upper slice and the greatest continuity along the middle slice. On the lower slice, clean sands are primarily located in the depocenter.

Analysis of the estimated LF reservoir properties

The net sand thickness of the LF reservoir is computed by multiplying the reservoir thickness by the avenge sand volume fractions within LF sand interval. The LF sand thins toward the east. A sharp decrease in sand thickness is found in the eastern part of the reservoir along the structural highs. The boundary between signLFicant and insignLFicant net sand thickness runs north-south, and does not follow the structural contours. By the time the LF sand was deposited, the minibasin had signLFicant relief, and fresh sediments were transported to the depocenter. ModLFication to the LF sand thickness by the ocean waves was apparently not signLFicant. The cleaner sands are found in the depocenter.

We assess the accuracy of the simulated lithology and porosity distributions by

extracting four cross-sections of simulated shale volume fractions and estimated porosities along four well paths. Excellent correlation between the estimated and between resistivity and the estimated porosity are observed. The spatial consistency between the well logs and the simulated lithology and estimated porosity distributions is thus established In this sense, we have obtained accurate lithology and porosity volumes that both honor the well logs and estimated acoustic impedances.

Calcite precipitation near the top of the LF reservoir sand in the down-dip direction has been observed both in cores and sonic log measurements (Flemings et al., 1996). The thickness of the cemented sand is less than 5 m. Acoustic velocity and density of this interval tends to be greater than that of the sands without such precipitation, but less than that of surrounding shales. Thus seismic amplitudes observed near the top of the LF reservoir are primarily caused by two interfaces. The interfaces are located between the shale and cemented sand and between the cemented sand and uncemented sand. The calcite precipitation causes velocity of cemented sands to increase. The magnitude of such an increase is about one third to one half of the velocity dLFference between shale and uncemented sand. The increase of velocity in this zone is also observed in the estimated porosity distribution (low porosity zone), which is consistent with the well log data. The characterized main body of the LF reservoir is not signLFicantly affected by the occurrence of calcite precipitation.

In deriving the porosity, the fluid acoustic impedance was set to saline acoustic impedance. The estimated porosities may thus be considered "effective hydrocarbon saturation" indicators, because the porosities in the areas saturated with oil or gas are overestimated. Thus, the areas of higher porosities in the LF sand are, in fact, areas of high hydrocarbon saturations, enable us to derive a map of effective oil saturation from the estimated porosity volume. Remarkable similarities between the bypassed hydrocarbon map from our 4-D acoustic impedance analysis and the derived effective oil saturation map are observed. This observation substantiates the effectiveness of using acoustic impedance to estimate oil saturation. While the distinct oil and water boundaries have been smeared by the thickness of the LF sand, the map indicates that the thickest oil-saturated sand can be found in the depocenter of the LE reservoir.

In the future, we can use the effective oil saturations computed in this way as the soft data and the oil saturations derived from well log and production data as hard data to further simulate the hydrocarbon saturations. These saturations will substantially improve the accuracy of oil field management

Conclusion

We have presented an integrated method to quantitatively characterize the LF reservoir in the EI-330 Field in terms of lithology, porosity, and effective hydrocarbon saturation. The results show great consistency throughout the LF reservoir and the surrounding shale formations. The constructed lithology models exactly honor the well log data. The porosity model is less accurate than the lithology model because no porosity measurements are available in the study area. Inaccuracy of the estimated porosities is caused primarily by the hydrocarbon saturation in pore spaces. We developed a new concept that uses the discrepancy to locate hydrocarbons.

In practice, we have found the Markov-Bayes sequential indicator simulation technique to be powerful and robust. The technique systematically integrates the hard and soft data into a statistically optimized 3-D model.

Reservoir characterization based on the stochastic simulations is of great importance, especially in the integration of legacy 4-D seismic datasets. Multi-disciplinary data, including geological, geophysical, and production data, can all be
AVS analyzed system, and we dLFference that data set with the Pennzoil and Texaco/Chevron 3-D surveys. We have completed the inversion of the seismic volumes from Shell and Pennzoil and have performed the 4-D analysis of them.

Nonlinear inversion of 4-D seismic datasets in the Eugene Isand Block 330 Field of offshore Louisiana, Gulf of Mexico

Introduction

Parameters derived from seismic reflection data have been used to identLFy hydrocarbon reservoirs for decades. Variations of seismic amplitude, such as brightspots and flat spots, are associated with oil- or gas-bearing strata. As 3-D seismic technologies merge with the reservoir characterization, acoustic impedances estimated from seismic waveforms are becoming more and more important Unlike seismic amplitudes, which measure the acoustic impedance variations, the acoustic impedance itself is directly associated with petrophysical properties of sedimentary rocks and the fluids that fill pore spaces. The techniques by which the acoustic impedance are obtained are the bridge connecting reflection seismic data and rock petrophysical properties.

Acoustic impedance volumes estimated from 3-D seismic surveys have only recently begun to be used in reservoir characterization. The nonlinear seismic inversion technique described in Chapter 1 is a robust method of estimating acoustic impedance. It contains features particularly useful for analyzing 4-D (time-lapse 3-D) seismic datasets. The time-variant, dynamic wavelet extraction eliminates the dLFferences caused by most of the post-stack seismic processes applied to the various 3-D seismic datasets used in the 4-D analysis. The low-frequency constraints imposed on the estimated impedance functions can preserve the unchanging nature of the overall regional geological settings. As a result, dynamic changes of reservoir fluids can be imaged.

In this chapter, we have applied our nonlinear seismic inversion technique to two time-lapse 3-D seismic datasets to estimate acoustic impedance volumes in the EI-330 minibasin. The same geological and geophysical constraints derived from well log analysis are incorporated into the nonlinear seismic inversion of both seismic datasets. Both the technique and procedure used to construct the acoustic impedance constraints are presented in detail. Independent estimations of the accuracy and reliability of the estimated acoustic impedance are performed using acoustic well logging data. Our seismic inversion technique is found to be stable and consistent throughout the computation.

Geological background

The Eugene Island (EI) 330 minibasin is located approximately 270 Km southwest of New Orleans, which is one of the most prolLFic minibasins in the offshore Gulf of Mexico region. The EI-330 minibasin is oblong, approximately 19 Km by 15 Km (11.9 miles by 9.4 miles), and fault-bounded. It sits on a major shelf margin deltaic depocenter of Plio-Pleistocene

age. Hydrocarbons of the EI-330 Field are produced from over twenty-five different Plio-Pleistocene sand reservoirs that are segmented into at least a hundred structural and stratigraphic traps (Holland et al., 1990).

Alexander et al. (1995) suggest that the minibasin evolved in three phases: prodelta, proximal deltaic, and fluvial. In the prodelta phase, bathymal and outer neritic shales and turbidities loaded and mobilized an underlying salt sheet. During the proximal deltaic phase, salt continued to withdraw from beneath the minibasin and lowstand shelf margin deltas deposited large volumes of sediment. Regional growth faults bound the northern margin of the minibasin. Sediment accumulation and fault slip rates were high as thick sequences of deltaic sands were deposited adjacent to the fault system. During the final fluvial phase, salt withdrawal waned, and the creation of accommodation space within the minibasin ceased. The minibasin was filled and lowstands deltaic systems prograded southward (Alexander et al., 1995). Most of the hydrocarbon reservoirs discovered in the EI-330 Field were formed during the second and third phases. The seismic data input to the nonlinear inversion has a time window large enough to include all major sand reservoirs in the study area (O-3 seconds).

4-D seismic datasets: registration and wirelLFle logging database

Since the discovery of the EI-330 Field, more than five hundred wells were drilled to explore and produce this most prolLFic oil field in offshore US Gulf of Mexico. Well data collected in this area from several oil companies provide substantial control to the inversion and subsequent analyses. In addition to extensive 2-D seismic surveys, three partially overlapping 3-D seismic surveys have been acquired since 1985. Two of the 3-D seismic surveys, acquired in 1985 and 1992 were selected for 4-D analysis. The overlapping area is centered at the Block 330/331 boundary and covers approximately equal amounts of each block. Structurally, this area is situated on the western flank of the Block 330 rollover anticline, which forms the closure trapping hydrocarbons against the northern growth fault system.

Registration of 4-D seisimic datasets

To date, no 4-D seismic dataset has been acquired for the expressed purpose of fluid monitoring in the offshore Gulf of Mexico. The 3-D seismic surveys were acquired with different orientations and spacings, and processed with different parameters by different geophysical service companies. Despite these disadvantages, we found that these "legacy" 4-D seismic datasets are sufficiently similar to be used for fluid monitoring purposes.

Legacy 4-D seismic datasets must be properly registered in space and time. DLFferences between the results of two surveys can be caused by dLFferences in seismic data acquisition and processing as well as by dynamic changes that occur in the reservoirs. Changes caused by data acquisition and processing must be eliminated before hydrodynamic changes can be identLFied. DLFference caused by acquisition in different directions, at different spacing or different cable length, cannot be corrected after stacking and migration have been performed. Fortunately, modern seismic imaging technologies are much better than a decade ago. DLFferences due to different directions are often small in areas of low subsurface relief such as the Eugene Island Area. Especially helpful: the 1985 3-D survey was re-processed in 1992 using new processing techniques.

The general geology (1ocations of faults geometry, lithology and porosity) should be in

the same location between the surveys. Indeed, the two 3-D seismic datasets are remarkably similar, at least in regions where no steeply dipping geological structures (salt and large faults) occur. Salt withdrawal structures do occur in our study area, but do not distort the seismic images of the hydrocarbon reservoirs because they are usually deeper. We assume that the dLFferences observed in the stacked and migrated datasets are dominantly affected by hydrocarbon drainage caused by production and different post-stack processing parameters, and not by different acquisition geometry.

The 1985 seismic survey was acquired in the northwest-southeast oriented lines, while the 1992 survey was acquired in north-south lines. The "bin" spacing of the two surveys is also different A re-gridding process is applied to relocate the two surveys into a common grid before any farther seismic analysis is performed. We use an algorithm that interpolates one three-dimensional mesh into another three-dimensional mesh slice-by-slice in traveltime and orient the 1985 seismic survey onto the 1992 grid. The algorithm computes the areal weights in a moving window in depth, and interpolates new data values into the destination survey coordinates. After the re-gridding process, only data points common to both surveys are preserved, the rest being assigned null values. Seismic sections extracted from these two volumes at the same location from the two volumes are generally similar, although some dLFferences are evident. The loss of high frequency content in seismic data becomes signLFicant in the deeper portion of seismic volumes.

Spectral matching between the two seismic datasets is not necessary in the seismic inversion approach to the analysis of 4-D seismic datasets, unlike 4-D seismic amplitude dLFferencing technologies (Anderson et al., 1995). But phase matching is performed in order to compare the inversion results. Our nonlinear inversion technique is capable of eliminating other post-stack processing artLFacts using dynamically extracted seismic source functions. However, since the true amplitudes of seismic datasets are unknown, amplitude renormalization must be performed. We first normalize each seismic volume by mapping the histogram of amplitudes onto one another. The normalized seismic traces are rescaled to the proper amplitude by comparing them to synthetic seismograms computed from impedance measurements (i.e., sonic and density logs) from wells in the area- Scaling factors of 0.15 and 0.25 are used for the 1985 and 1992 seismic surveys, respectively. The extracted seismic source functions are normalized to unity so that the reflectivity functions derived from the estimated acoustic impedances are realistic (i.e., within the range of $\pm$ 0.15). Normally, Tertiary sedimentary basins filled with sand and shale sequences have mile seismic amplitudes less than $\pm$ 0.3.

Digital wireline logging database

The nonlinear inversion of seismic data requires a good a *priori* reference model. There are more than seventy wells in our study area overlapped by the two seismic datasets. However, sonic and bulk density logs, which are needed to compute impedance, are only available in fourteen of these wells. The limited sonic data availability may be overcome by using the correlation between sonic and other logs to empirically calculate a "pseudo" sonic log (a common technique in petrophysical analysis). In wells without density logs, we use the inverse Gardner relationship to calculate density logs from measured or estimated sonic logs (Gardner et al., 1976).

Well log analysis for the impedance inversion

The band-limited nature of observed seismic datasets requires that the estimated acoustic impedance functions, i.e., the short-wave length model parameter (Tarantola, 1982 and 1984), should also be within a confined frequency bandwidth in order to have physical meanings. Detailed trend analysis for predicting long-wavelength constraints on impedance is essential. Such constraints derived independently from acoustic measurements in wells not only increase accuracy of the estimated impedance, but also stabilize the iterative seismic inversion (He et al., 1995*)*. The low-frequency impedance constraints derived from well logs are sufficient to allow our nonlinear seismic inversion to converge on true acoustic impedance solutions.

The principles of wireline logging and data interpretation

Geophysical log data are recorded using probes, which are lowered, on the end of a wireline through the drillpipe and into the previously drilled borehole. The depth at which the measurements are made is determined by measuring the length of cable run into the hole. Modern logging technologies can measure many different physical properties. Three major types of log data are in general available for well data analysis: electrical, radioactive, and sonic logs. The well log database in our study area includes natural gamma my (GR), spontaneous potential (SP), resistivity (RES), induction %WD), bulk density (RHOB), sonic (DT) and caliper (CALl) measurements. Some wells also contain porosity measurements made on sidewall cores.

The natural gamma ray log utilizes a scintillation detector to measure the natural radiation emitted by the rocks surrounding the borehole. The response of the tool is a simple function of the concentration by weight of radioactive materials and the rock density. The average investigation depth into sedimentary formations is about 0.3 m, and actual resolution is 0.15 m. GR is used principally as a sand/shale discriminator since shales contain abundant radioactive minerals such as clays, whereas sandstones do not.

Density is measured by the lithodensity logging tool. A radioactive source is mounted in the tool body, and a bow-spring forces it and a pair of detectors against the borehole wall. The two detectors measure the returned flux of scattered gamma rays in a series of energy bands, which is used to determine formation density (RHOB) and photo-electric factor (PEF). A measure of tool performance based on the energy distribution at the near and far receivers (DRHO) is also provided. The interaction between the gamma ray and electrons in the formation causes Compton scattering. The density logging tool measures electron density direcily, and formation density is determined using the fact that in most rock-forming elements atomic weight is roughly twice atomic number. This measurement is almost independent of porosity and can be used as a matrix lithology indicator. The depth of investigation of the lithodensity tool depends on the density of the rock: the higher the density, the lower the penetration. In porous and permeable formations, the density tool does not read deeper than 0.15 m. The vertical resolution is about 0.3 m.

The array induction tool string indirectly measures electrical resistivity and gamma ray "shaliness", which are related to porosity and hydrocarbon content. The array induction tool is a resistivity logging device that provides measurements of spontaneous potential (SP) and resistivity. Resistivity is reported for three different depths (deep, medium, and shallow).

DLFferences between shallow and deep resistivity measurements can be related to the invasion of drilling fluids into permeable horizons. Resistivity is controlled mainly by the

amount and connectivity of the porosity and the conductivity of the pore fluids, since the solid constituents are orders of magnitude more resistive than pore fluids in most rocks.

Sonic tools are designed to measure the compressional wave velocity of the rock surrounding the borehole. The sonic tool can be thought of as a miniature seismic refraction experiment carried out within the cylindrical borehole. The tool is centered in the hole by means of bowsprings, and contains one or more acoustic sources and receivers. A source emits acoustic waves that are transmitted into the borehole fluid. A refracted compressional wave is generated when the wavefront impinges on the borehole wall. Waves arrive at the receivers at a time, which is linearly proportional to their offset from the source. Compressional wave velocities can be determined by dLFferencing the arrival times at multiple receivers a known distance apart

The Caliper log measures wellbore diameter, and is run at the top of both array induction and sonic combinations. It is primarily used to indicate "washouts", where other logs may read inaccurately, and to correct logs whose response is sensitive to hole diameter. However, caliper response can also be indicative of lithology. For instance, in zones with swelling clays, hole constrictions are observed where the caliper reads less than the bit size. Variations in hole diameter may correlate with lithologic changes, since hole conditions are in general a consequence of rock properties.

Lithology can be obtained from GR and SF logs. Resistivity and induction logs are used to identity pore fluid composition. Formation porosity is one of the primary physical property measurements made in a wellbore, and direct measurements are made by neutron logging tools. The dLFference between thermal and epithermal neutron porosity is a measure of the amount of bound water in clay minerals. Since neutron logging tools were not run in most of production wells drilled in the study area, porosities in our wellbores are indirectly derived from sonic, density, and resistivity logs. The relationship between resistivity and porosity has been quantLFied by "Archie's Law" (Archie, 1942), which relates the resistivity to an inverse power of the porosity. This empirical relationship works reasonably well in the sands found in hydrocarbon reservoirs.

Well log interpretation for nonlinear seismic inversion

The estimated acoustic impedance functions are sampled in traveltime whereas well logs are sampled in depth. We converted logs from depth to two-way traveltime using sonic logs and velocity measured by "checkshot" vertical seismic profiles (VSP). Synthetic seismograms, generated from the sonic logs, are compared with seismic data to verLFy the depth-time conversion.

Acoustic velocity and density logs estimated from other logs

Empirical relationships between well logs have been widely used in the oil industry for many years. In wells that have only density logs, the pseudo-sonic velocity can be estimated using the Gardner’s relationship (Gardner et al., 1974).

Velocity-depth profile varies laterally due to formation structure and stratigraphy. We compensate by adjusting the regressed sand and shale compaction curves according to stratigraphic horizons in our study area For example, the structure maps of two sand tops (the tops of JD and LF reservoirs) indicate that the sands dip about 20 degrees westwards along the west flank of the EI-330 roll-over anticline. The regressed sand and shale compaction curves are adjusted for the amount of structural uplLFt at each well location by an amount determined from wells with sonic measurements. The low-frequency trends are consistent with both geological structure, and direct measurements made in neighboring wells. Both the measured and estimated pseudo-sonic logs were then used to compute acoustic impedance logs and to convert logs in depth to logs in two-way traveltime. When no density log is available for a well, the pseudo-density log can be computed from the sonic log by using the inverse Gardner relationship.

Calibrations are performed on wells with full suites of log measurements to determine the constants in the above empirical relationships. Due to the crossover of the sand and shale compaction curves, the sand sections are high-velocity anomalies in the shallow portion of the well (above 1067 m) and are low-velocity anomalies at depth. We can see that the estimated velocity and density logs are very similar to the measured logs. The low-frequency trend in the estimated pseudo-velocity log agrees with the measured trend as well. The relative error between the estimated and measured velocity logs is 6% and that of density logs is 6.7%. The average relative error between the estimated and measured impedance logs is 5.5%. The velocity, density, and acoustic impedance logs are in agreement throughout the depth range, justLFying the use of the empirical relationships. These results also indicate that superimposing the regressed low-frequency trend of velocity to the high-frequency velocity variations derived from resistivity and lithology logs is viable. We will also use only the low-frequency impedance functions to constrain the estimation of high-frequency impedance functions.

The seismic section is an arbitrary seismic line extracted from the 1985 seismic survey. Several sand tops identLFied in well logs show good ties with the corresponding seismic reflectors in traveltime.

A priori acoustic impedance model construction

The nonlinear inversion employs a one-dimensional inversion algorithm. An a *priori* impedance model has to be constructed for each trace of both 3-D seismic surveys. We use impedance logs from twelve wells with sonic and density measurements in the study area to construct the reference impedance model. The acoustic impedance logs from these twelve wells are first analyzed to extract compaction trends at each location. Depth is then converted to two-way traveltime using the velocity logs at each well. We then construct a 3-D impedance model by linearly interpolating these impedance trend curves into the common seismic grid. The interpolated 3-D impedance model contains only the low-frequency trend of the acoustic impedance function. Each vertical trace of this model is then treated as the *a priori* impedance model and the initial model for the corresponding seismic trace. Data and model space covariance functions are also needed to constrain the inversion process, in addition to an *a priori* impedance model. These covariance functions represent uncertainties associated with data and model parameter optimization.

Nonlinear inversion of 4-D seismic datasets

The two seismic datasets are independently inverted with the same *a priori* low-frequency impedance and initial impedance models. The covariance functions that describe uncertainties m estimated impedance functions and the observed seismic traces are treated in the same mariner for each seismic trace of both seismic surveys, so the inversion of the two seismic datasets is under a unLForm constraints and uncertainties.

Dynamic extraction of seismic source functions

The first step of the full-scale nonlinear seismic inversion is to extract seismic source functions from the observed seismic trace. We dynamically extract a time-variant source function from each seismic trace in the dataset The time-variant source function actually contains three source functions that are applied to different time windows within the seismic trace. These source functions are determined from a moving-window autocorrelation function computed for each seismic trace, along with assumption that they are zero-phase. These dynamic source functions eliminate data processing artLFacts that were introduced by using different processing parameters after the stacking and migration processes. Using the method, the spatial variation of frequency bandwidth of the impedance function in the estimated acoustic impedance volumes are made internally consistent

Two seismic traces were extracted from the same location of the 1985 and 1992 3-D seismic surveys. The two traces have signLFicant dLFferences in frequency content and shape. The trace from the 1992 survey has the higher data quality, but its frequency content is lower than that of its 1985 counterpart. Frequency segmentation observed in both traces suggests that three seismic source functions are necessary to properly retain the frequency bandwidth of the estimated impedance functions, acting in three distinct time windows (0.1 seconds, 1-2 seconds and 2-3 seconds). Similar behavior is observed in other traces within the surveys, leading us to use three seismic source functions in three time windows for the inversion.

Estimation of impedance volumes from 4-D seismic datasets

We focus on seismic data from 0.9 to 2.8 seconds two-way traveltime. Each seismic trace in these surveys is sampled at 4 ms interval and contains 476 samples. The full-scale nonlinear seismic inversion is applied to each seismic trace of both surveys independently. The similarity in the estimated acoustic impedance volumes is an independent check of the success of the inversion.

The seismic data contain multiple reflections, side reflections, and noise, which affect the quality of the inversion. This contamination is modeled as random noise described by a Gaussian data covariance functions. Uncertainty in the model parameters is also modeled by a Gaussian distribution law. The a *priori* acoustic impedance at each sample location is expressed in terms of a mean and a covariance. The covariance expresses our degree of certainty that the true impedance is close to the *a priori* impedance. We use the low-frequency impedance model derived from well logs in section 2.4.4 as the a *priori* impedance. The variance of the impedance is taken to be about 20% of its mean.

Discussion and conclusion

Like the seismic volumes, the estimated 1985 and 1992 acoustic impedance volumes are in general similar to one another. However, signLFicant small-scale differences, occur. These changes are possibly caused by hydrocarbon production drainage in reservoirs.

Vertical wells drilled in offshore oil fields are rare, most of the wells were drilled with deviations. Thus the best way to compare the estimated impedance functions with the measurements from logs is to use arbitrary impedance cross-sections that follow the deviation pattern of the wells. Excellent match can be seen between the sonic logs and estimated impedance section along the well paths on both sections. The low impedance anomalies are often correlated to the hydrocarbon reservoirs.

There is significant evidence for hydrocarbon drainage from areas of low impedance observed in 1985. In 1992, these regions have matched of both increased impedances and decreased impedances. The increase in acoustic impedance often indicates that reservoir voids, which were occupied by hydrocarbons in 1985, have been replaced by formation brine by 1992 (Anderson et al., 1995).

Accuracy and reliability of estimated impedence volumes

Evaluation of the estimated acoustic impedance volumes is usually dLFficult to implement because we do not have exact knowledge of the acoustic properties in the entire sediment volume. We analyze the accuracy and reliability of our inversion results by examining the estimated impedances by using sonic, density, GR, and resistivity logs. These well logs are well-correlated to the acoustic impedance, in general. Because the initial and a *priori* impedance models are based on only the low-frequency part of impedance logs, the high-frequency data from those wells constitute independent data.

We plotted the measured impedance log in a vertical well, 33l-SH-l, against the estimated acoustic impedance function. The estimated impedance function has the same low-frequency trend as the impedance log. The high-frequency content in the estimated impedance is not as high as that of the impedance log. However, the relative error between the impedance log and the estimated impedance function in well 331_SH_1 is small, only 8.0%. A good linear correlation is observed between the impedance log and the estimated acoustic impedance. Similar results were also obtained from several other logs.

These tests demonstrate that the estimated acoustic impedance volumes are acceptable for use in 4-D and other geological analyses. Although the estimated impedance function has less resolution than the sparsely distributed well logs, the lateral continuity makes the impedance results much more useful.

2Conclusion

We have developed a full-scale, nonlinear 4-D seismic inversion technique to invert two-time lapse, 4-D seismic volumes under low-frequency acoustic impedance constraints. Prior to the inversion process, *a priori* information about the acoustic impedance model is constructed from a limited number of wells that have sonic and density logs. We do not use all available wells to construct the reference impedance model, so that control wells can be used after the inversion to analyze the reliability and accuracy of the computed impedance volumes. Independent examinations of the estimated acoustic impedance volumes using these control well logs indicate that the inversion is able to recover accurate acoustic impedance functions to less

than ± 10%. The consistency observed between impedance volumes suggests that our nonlinear inversion avoids serious artifacts.

The geological features observed in the two impedance volumes are remarkably similar. Good agreements between the estimated impedance functions and well logs are observed, suggesting that the nonuniqueness of the estimated impedance volumes is not significant The impedance volumes are now ready for 4-D seismic monitoring analysis and reservoir characterization.

Time-varying seismic source functions are also obtained for all seismic traces in the two inverted seismic data volumes. These wavelets may be of some usefulness in estimating spatial frequency variations caused by both acquisition and processing variability. We have not implemented phase adjustment into source extraction process. In the future, such refinements may further improve the inversion process.

Our estimated impedance volumes are well behaved and laterally continuous. We believe that the integration of high lateral resolution from the estimated acoustic impedance volumes and high vertical resolution from sparsely distributed well logs can be used to achieve a much better characterization of changes in oil and gas reservoirs overtime than today's standard analysis techniques.

References

Alexander, L., and P.B. Flemings, 1995, Geologic evolution of a Plio-Pleistocene salt-withdrawal minibasin: Eugene Island Block 330, offshore Louisiana: American Association of Petroleum Geologists Bulletin, v.79, p.1737-1756.

Anderson, R.N., A. Boulanger, W. He, Y.F. Sun, L Xu, and B. Han, 1995, 4-D seismic monitoring of drainage in the Eugene Island 330 Field in the offshore Gulf of Mexico: American Association of Petroleum Geologist special publication, in press.

Archie, G.E., 1942, The electrical resistivity log as an aid in determining some reservoir characteristics: Transactions AIME 146, p. 5~62.

Brock, J., 1984, Analyzing Your Logs, Vol. 11-Advanced Open Hole Log Interpretation: Petromedia, Tyler, 173 p.

Gardner, G.H.F., L.W. Gardner and A.L Gregory, 1974, Formation Velocity and Density-The Diagnostic Basics for Stratigraphic Traps: Geophysics, V.39, No.6, p.770-780.

He, W., R.N. Anderson, and Y. C. Teng, 1995, Application of seismic inversion to quantitative mapping geopressure transition zones in the Pleistocene, offshore Louisiana, Gulf of Mexico: The 2nd International Conference on Theoretical and Computational Acoustics, Honolulu, Hawaii.

Tarantola, A, and B. Valette, 1982, Inversion = Quest for information: Geophysics, v. 50, p.159-170.

Tarantula, A., 1984, Inversion of seismic reflection data in the acoustic approximation: Geophysics, v.49, p.1259-1266.

4-D seismic monitoring of subsurface fluids in the El-330 Field of offshore Louisiana, Gulf of Mexico

3-D seismic images have improved to the point that they are being applied to reservoir production and engineering problems. 4-D (time-lapse 3-D) seismic imaging may soon be applied to oil field monitoring. However, this technology will require a better understanding of the link between stratigraphy, fluid content and changes in seismic response.

Time-dependence of individual reservoirs has long been observed in production wells. The use of 4-D seismic datasets to monitor fluid movements dates back to more than a decade when thermal and CO2 injection enhanced oil recovery Projects were carried out (Nur, 1982; Dunlop et al., 1988 and Breitenbach et al., 1989). Petrophysical studies indicate that seismic datasets may be used to monitor subsurface fluid movement in sandstone reservoirs saturated with medium-to-light weight hydrocarbons (Wang et al., 1992). The acoustic contrasts caused by lightweight, gas saturated hydrocarbons (oils with high gas:oil ratio, GOR) can produce even greater seismic amplitude changes.

Changes in seismic amplitude within a given reservoir can be caused by changes in gas:oil:water ratios, fluid pressures and/or fluid contact levels. Time-lapse 3-D seismic surveys acquired can quantLFy these changes. These seismic datasets can be used to decipher both temporal and spatial distributions of oil, gas and water in reservoirs under production. We believe that such 4-D seismic technologies, integrated with petrophysics and other related multi-disciplinary principles, will become the industry standard in hydrocarbon exploitation.

4-D seismic technology is still in its infancy. New techniques are being developed yearly, as the great potential of using such datasets in reservoir surveillance and management is recognized Nur, 1989; Lumbly, 1995; Anderson, et al., 1995a, 1995b and 199Sc).

In order to extract 4-D seismic changes, we examine successive 3-D seismic surveys and examine their similarities and differences. The temporal changes allow us to predict the locations and compositions of bypassed hydrocarbons. We also use wireline logs (sonic, density, porosity, oil saturation variations over time) and production data (pressure, water cut, GOR variations over tune) to calibrate our models of acoustic impedance changes. The model results will allow us to predict the quantitative changes in seismic response.

Because the time-lapse 3-D seismic datasets used in this study were acquired for other purposes, we must pay special attention to their registration in space and time. The acquisition and processing parameters of different surveys were not the same, and thus we must correctly register the seismic datasets to preserve the maximum amount of common information of these surveys.

Despite these disadvantages, the results obtained from analyzing these "legacy" datasets are rather encouraging. Elimination of artLFacts caused by dLFferences in data processing enables us to distinguish the actual acoustic changes in hydrocarbon reservoirs. Many such legacy 4-D seismic datasets are available, especially for the producing oil fields in the offshore Gulf of Mexico. We expect that the application of 4-D seismic techniques to these seismic

datasets will result in the recovery of a large volume of bypassed oil. Nevertheless, much research will be needed to advance 4-D seismic techniques so that they can be used to view of the true dynamic of the drainage of oil and gas from reservoirs.

In this chapter, we present a seismic amplitude analysis technique, applied to the LF reservoir in the Eugene Island 330 Field. A 4-D seismic dataset consisting of two SD seismic surveys (acquired in 1985 and 1992, respectively) is used to locate regions where seismic amplitudes have changed over time. These changes are qualitatively analyzed in term of brightening, dim-outs, and unchanged areas that might contain bypassed hydrocarbons (pay). We then examine the spatial and temporal changes in acoustic impedance, as determined by the nonlinear 4-D seismic inversion techniques. The changes in the estimated 4-D acoustic impedances are better imaged than those changes observed in seismic amplitudes alone.

Seismic predicdon of dynarnic changes in hydrocarbon reservoirs

Laboratory experiments indicate that the acoustic reflection coefficients varies with oil, gas and water mix, effective pressure and temperature (Wyllie et al. 1958; King, 1965; Domenico, 1976; Gregory, 1976 and Wang et al, 1988). This behavior is also observed in the field in water and steam floods, which have produced noticeable acoustic differences over time (Nur, 1982 and 1989; Dunlop et a, 1988; Breitenbach et al., 1989 and Wang et al., 1992).

Changes in seismic data expected from the production of hydrocarbons in the LF hydrocarbon reservoir are summarized using a Simple seismic modeling approach. Seismic amplitudes were modeled by varying the acoustic properties across a hypothetical, constant thickness sandstone reservoir undergoing pressure depletion and GOR changes. The 1985-1992 petrophysical changes math the production data for the LF reservoir. The acoustic property changes are computed using the experimental data from Ottawa sand (Domenico, 1976). The changing gas/water contact (G/W), gas/oil contact (G/O), and oil/water contact (O/W) also causes changes in seismic amplitudes across the reservoir boundaries. Effective pressure (overburden pressure minus pore fluid pressure) increases as hydrocarbons are drained from a reservoir, reducing seismic amplitudes in both oil and gas sands. LF, however, a GOR increase occurs during production, as with the formation of a secondary gas cap, seismic amplitudes are predicted to increase (brighten) over time, because the acoustic affects of the fluid change dominate over the pressure depletion affects. Similarly, seismic amplitudes can dramatically decrease (dim-out), LF, in addition to pressure depletion of a high GOR oil, the O/W contact migrates across a reservoir, The amplitude decrease caused by pressure depletion is further enhanced by the drop in the impedance contrast caused by the replacement of low velocity oil and/or gas by relatively high velocity water.

Our seismic modeling investigation suggests that bypassed hydrocarbons are associated with near-zero changes in regions of high seismic amplitude over time, LF there has been little change in effective pressure (as within a water-drive reservoir). Areas of sustained high seismic amplitudes are either the highest permeability drainage pathways through which the hydrocarbons move, or isolated pressure compartments that are not connected to the wellbore drainage system. Bypassed hydrocarbon can be located on the basis of changes in seismic amplitudes only after the cause for impedance changes is understood.

4-D seismic monitoring technology

Our 4-D seismic analysis technology consists of imaging, feature extraction, and pattern recognition functions, coupled iteratively with high resolution, seismic forward and inverse modeling. Due to the practical limitations, systematic seismic forward modeling methods are only discussed briefly because they are still being developed. Pattern recognition, rather than interpolation and recomputation, is used to examine similarities and differences among the seismic amplitudes, and acoustic impedances of the datasets in the hope that we can use a large amount of legacy 3-D seismic datasets to monitor hydrocarbon drainage and to locate bypassed pay in the mean time.

The Eugene Island Block 330 Field

The Eugene Island Block 330 EI-330) Field has produced more than $5x10^8$ barrels of oil since 1972. The oil and gas are produced from more than twenty-five stacked sand reservoirs in rollover anticlines abutting against the large growth fault system (the Red fault) and associated smaller antithetic faults.

The ongoing development of this field and the remarkable amount of seismic, production, geological and wireline data available from the field make it an ideal location to research the effects of production and fluid migration on changing acoustic (seismic) signals over time. Multiple vintages of 3-D seismic data, large amounts of digital wireline logging data, and production histories from multiple wells enable us to study the reservoir fluid dynamics of the LF in great detail within the EI-330 Field.

The study area is centered along the Block 330/331 boundary where two vintages of 3-D seismic surveys overlap. The two 3-D seismic surveys are the 1985 survey centered on Block 330 and the 1992 survey centered on Block 331. Well logs and production data from nineteen wells are available in the overlap area .Combined stratigraphic, structural and seismic attribute analyses of the legacy 3-D seismic datasets have shown how depositional features and faults compartmentalize reservoirs in this field. Geopressures in the study area are also predicted and characterized (He et al., 1995a and 1995b) as part of the larger study. It is believed that hydrodynamic disequillibrium that has produced dramatic variations along the top-of-geopressure surface over short distances in the minibasin, coupled with periodic fluid release up the large regional growth fault system, is the primary cause for the active hydrodynamic fluid flow in this region. The well-connected aquLFer supporting the water drive mechanism within the LF is one result from this dynamic system.

4-D seismic data registration

Amplitude measurements from two 3-D seismic surveys cannot be directly used because the data acquisition and processing parameters applied to them originally were very different Seismic attributes, such as amplitude, phase, and frequency bandwidth, differ considerably. We use special matching, amplitude normalization, and phase corrections to correct the data

The 1985 and the 1992 3-D seismic surveys were first re-binned into the same common grid. When comparing the two 3-D seismic volumes acquired seven years apart, navigation efforts may have been introduced because the resolution of navigational systems at sea has been constantly improved. In our case, we found that there is a 62 m displacement in the east-west direction between the two seismic volumes. The offset was determined from a global cross-correlation between the two seismic volumes in both the north-south and the east-west directions.

The global cross correlations are computed from sequential time slices through the entire two volumes.

The frequency bandwidth of the 1985 volume differs from that of the 1992 seismic volume because seismic sources have been steadily improved over the years. To match the frequency bandwidth, we first computed the global frequency spectrum of each volume, determined the bandwidth that common to both, and used it to bandpass filter both datasets. A zero phase filter is used.

Different static shifts were applied to seismic datasets in the original processing. We correct for this shift by cross correlating corresponding traces to determine the relative offset The offset is then averaged over all the seismic traces, and the average is applied to the 1985 seismic survey to correct it to that the 1992 survey.

Phase shifts between legacy seismic surveys are determined using a cross-correlation technique to determine the phase angle difference between the two volumes. We held the seismic traces from the 1985 survey fixed, while phase-shifting the traces of the 1992 survey with all possible angles (Ck360 degree). The phase angle that maximizes the correlation between the two traces is applied to the 1992 survey to correct it. Numerical experiments carried out in our volume matching techniques indicate that the matching of conventional post-stack seismic volumes can be best performed by applying time-variant filters to different time windows because the seismic waveform characteristics vary wit traveltime.

Amplitudes of the two seismic volumes are normalized by requiring that the cumulative amplitude histograms of the two seismic volumes be similar. The two surveys have rather different amplitude distributions. We choose the 1992 seismic volume as the amplitude reference, performed a global histogram renormalization of the 1985 survey, The amplitudes are rescaled by a factor appropriate for real acoustic variations in the earth by comparison with synthetic traces computed from sonic and density logs. Amplitude of the two surveys are generally similar, but signLFicant.dLFferences occur within the producing reservoirs. We will next focus on the time window from 1.7 to 2.2 seconds, which includes the LF reservoir, to perform our 4-D seismic analysis.

The LF reservoir in the study area

The LF reservoir is centered along the boundary of blocks EI-330/331. It dips gently to the west from the crest of the rollover anticline in the center of EI-330, and is bounded on the north by the south-dipping B fault and on the south by the north-dipping F antithetic fault. It is one in a stack of reservoirs (JD-KE-LF) that are main oil and gas producers in the field. Structural dips are of the order of 10-20 degrees, and the sand top deepens from about 2,012 in (6600 ft) to over 2,316 m (7,600 ft) in this fault. The locations of production wells, and the positions of estimated fluid contacts at the beghining of production in 1972 and those estimated at the beginning of our 4-D study in 1992, indicate their movement with time as interpreted from the production data. The regions in red are the original gas cap. Regions in pink are areas that have had oil replaced by gas due to expansion of a secondary gas cap down-dip. Regions in green are predicted to be oil-filled and are thought to have undergone no change in fluid composition. Regions in dark blue are water. Regions in light blue in the west are water sweep occurred since 1972. A large region to the west that has been water swept between 1972 and 1992, whereas between the wells 330_Pz_C-iS and 330_Pz_A-I6ST to the east of the 330(331

block boundary, a secondary gas cap has grown between the time production started in 1972 and 1992. Low permeability gas is also detected from logs near the crest of the structure (regions in dark pink). The original oil-water contact in the LF reservoir is interpreted to be at the 2,307 m *(7,568* ft) level from the production data. UnLForm, gravity driven, up-dip movement of the oil-water contact is predicted from production data- The oil-water contact as deduced from the sparse well data is not horizontal in 1992, but appears to cut across structural contours in the south of the F fault The dip could indicate that the thick LF sand located in these zones is more permeable, and fluids are being preferentially drawn from these high quality sands.

4-D Seismic amplitude analysis technique

The region-growing algorithms

In practice, the amplitude normalization, frequency and phase matching techniques cannot totally correct for dLFferences in original seismic surveys, so the match is never perfect The inter comparisons are accomplished in attribute-derivative space since we have found that only the lowest frequency in amplitude spectra preserve the best commonality among the differently-processed seismic datasets. Comparison based on wavefleld envelope are more robust than those based on the seismic trace itself. Therefore, we use the reflection strength, or instantaneous amplitude (Taner et al., 1979) of the seismic amplitude in our analysis. These reflection strength volumes computed and divided into volumes of similar high amplitude regions (11ARs) through the use of region-growing algorithms that we have developed. The conventional isosurfacing technique bounds regions by connecting data points with the same amplitude values on the surface. The usefulness of this technique applied to as noisy seismic data is very limited. Our region-growing technique is more robust. The technique employs nonlinear, 3-D operators to isolate HAR’s within the seismic datasets. Beginning from a set of initial "seed" points (with large amplitude values), we track the magnitude of the change-in-amplitude in 3-D. A threshold value of amplitude gradient is selected to bound the regions. The HAR’s are bounded by surfaces of high amplitudes that exceed the threshold in the gradient of amplitudes away from the seed points. Data points outside HAR's are excluded from analysis, downsizing the overall amount of data. Rough-cut connectivity between HAR's within each dataset are obtained by properly choosing threshold operator so that lowpass spatial filtering, dilation and erosion "grows" the connections between segmented HAR seed points.

We then difference the two 3-D datasets within each of the HAR's. Corresponding HAR’S defined from the two separate surveys are merged into a single set of HAR’s by a volume union operation (Anderson et al., 1995b). Each HAR’s is characterleed as having undergone near-zero change, brightening, or dim-out. Fine-scaled structure within a single HAR may be indicative of bypassed pay. Intervals of sustained high amplitudes that are within 10% of each other can be used to reveal inter-connectivity. The 3-D pattern of bypassed hydrocarbons has a surprising inter-connectivity. The amplitude pattern is aligned 30 degrees to the major bounding faults in this portion of the LF reservoir. The apparent lineation may be due to small faults caused by westward shear in the vicinity of the LF reservoir. This pattern is not evident in either of the primary 3-D seismic surveys.

Misregistration errors can cause edge effects on the differentiated seismic data, as can be created by velocity differences caused by the changing fluid composition. For example, the

formation of a gas cap significantly lowers the velocities within the top of the reservoir, resulting in a mismatch between the two times. These edge effects must be removed from the final image of the reservoir.

Volumetric analysis of drainage of the LF reservoir

Regions of near-zero seismic amplitude dLFferences may possibly contain bypassed hydrocarbons. Dim-outs could be caused by water encroachment or pressure depletion. Brightened regions could be from GOR increases and secondary gas dissolution.

This detailed hydrocarbon distribution image can be combined with production data to further analyze the drainage patterns caused by production. More than 470,000 barrels of oil with low GOR has been produced from this part of the LF reservoir from 1985 to 1992, mostly from wells A- 12A, A-6, A-S, and *BA*. The other thirteen wells in both Blocks 330 and 331 stopped producing due to water intrusion or mechanical failure early in the production history (before the 1985 3-D survey was acquired).

The estimated initial (1972) and current (1992) oil/water and oil/gas contacts from the production data. The oil/water contact has moved about 107 m (350 ft) in vertical distance up-dip and to the east, and the gas expansion should have deepened the gas/oil contact by about 15 m (50 ft) down-dip and to the west. From these production history interpretations, new wells would have to be placed in a very narrow (< 610 m or 2,000 ft wide) band along the structure contours in the fault block B.

However, the 4-D image of the LF reservoir predicts a significant different drainage pattern from the interpretation derived based on the gravitational assumptions of the production history. The drainage is much more heterogeneous than indicated by the production data. The drainage patterns of the LF reservoir do not follow structure contours. Instead, the bypassed hydrocarbons appear to be related to fingered sands trending in the north-west to south-east direction. Water intrusions appear to have fingered into the reservoir in the same direction. The isolated regions with water invasion appear to be caused by water conning.

Horizon amplitude extraction of the LF reservoir

We sample the 3-D amplitude along the 2-D top horizon of the LF reservoir, which corresponds to a strong seismic reflector. The 1985 2-D image clearly shows dim-outs that are approximately parallel to structural contours, especially in the west and near the bounding faults B and F in the north and south. These amplitude boundaries correspond to the 1985 oil/water contacts. The amplitude pattern is more continuous in the east. However, by 1992, the amplitudes have become discontinuous. The total area of high reflectivity has decreased with time, as expected for an actively produced reservoir with decreasing fluid pressures and oil saturations.

Amplitude changes in the top of the LF reservoir also indicate brightened areas marking gas formation and dim-out areas marking water invasion. However, the boundaries are more complex and less clearly tied to structure than in the gravitational model derived from production data. Depletion of the gas cap from 1985 to 1992 is imaged as an amplitude dim-out in the eastern portion of the reservoir, with brightening indicated within the newly depleted oil zone (down-dip to the west). Areas of near-zero amplitude change are primarily located in regions where no active production wells were operated (e.g., Block 331). We predict that there is

signLFicant bypassed oil located in the LF reservoir of this fault block.

SignLFicant edge effects are caused by traveltime misalignment of the LF reservoir in the southwest and south of the fault block (just north of the F fault). This misalignment is probably caused by velocity changes from the significant drainage in the shallower JD reservoir , which is a large gas producer.

Volumetric variations of seisnic amplitude dLFferences

The HAR analysis measures the acoustic thickness of the LF reservoir, and allows variations within the volume to be examined. We difference HARs to create volumetric representations of the seismic amplitude changes between the 1985 and 1992 seismic surveys. Because 3-D variations are difficult to convey on paper, we slice the difference volume through its top, middle and bottom along planes parallel to the LF structure surface. We present both a fluid contact interpretation of the differences, and the absolute difference images.

We then compared these HAR slices with a slice made along the top of the reservoir, as defined by the seismic reflector. Both show the gas formation, but the HAR slices demonstrate that the high amplitude anomalies have migrated much deeper into the reservoir and to the west by 1992. However, in the eastern portion of the reservoir (up-dip), water sweep has changed the original gas distribution dramatically due to the active production in Block 330. For example, the A-6 well (in Block 330) produced oil since 1981. The A-6 well was shut-in in 1987 because of a sudden water intrusion, and it was producing hydrocarbon at a GOR of 3,000 before the shut-in. The case of amplitude increase (brightening) in Block 331 is unknown. It contains no active production wells. Perhaps pressure decreases within the overall reservoir caused gas to come out of solution. However, the brightened amplitudes moved more than 305 m (1,000 feet) to the northwest from 1985 to 1992, so we believe the amplitude increases to be real.

4-D acoustic impedance analysis technique

Volumetric reservoir descriptions based upon seismic amplitude data are less physical than those based upon acoustic impedance. Because acoustic impedance is more closely associated with the petrophysical and fluid properties of reservoirs than amplitudes, we apply the same region-growing technique to the estimated acoustic impedance volumes. We therefore inverted the amplitude-normalized, phase-matched seismic datasets to produce the estimated impedance volumes. The constrained, foil-scale nonlinear seismic inversion technique is applied. The estimated 4-D acoustic impedance volumes from the 1985 and 1992 seismic volumes is within the time window from 1.7 to 2.2 seconds. The hydrocarbon reservoirs correspond to low impedance regions within these two impedance volumes.

DLFferences in acoustic impedance between 1985 and 1992 in the LF reservoir

Using our region-growing algorithms, the 1985 and 1992 acoustic impedance volumes are then segmented into similar Low Impedance Regions (LIRs) and data from outside these LIRs are excluded from future analysis.

The shape of the LIRs (derived from acoustic impedice volumes) differs from that of the HARs (derived from seismic amplitude volumes). Because seismic amplitudes are sensitive to reservoir boundaries, to fluid contacts, and to impedance contrasts, while acoustic impedances are more sensitive to internal continuity and heterogeneity within the reservoir itself. Reservoir

thicknesses derived from the estimated acoustic impedance volumes are much more accurate than those resolved from seismic amplitudes. As we will see later in this section, our region-growing techniques are more robust when applied to the estimated acoustic impedance data.

Reservoir drainage from the shallower JD reservoir causes vertical traveltime delays in the LF reflections. There is up to 20 ms of delay in the 1992 survey versus the 1985 survey. We compensate the traveltime delays by applying a horizon-balancing technique. We interpreted the top of the LF reservoir sand on both estimated acoustic impedance volumes. We then corrected the traveltime dLFferences between the 1985 and 1992 LF reservoir tops by shLFting the 1985 data. The edge effects shown in are thus eliminated.

The dLFferences within the LIRs of the LF reservoir between 1985 and 1992 were then computed. Changes in acoustic impedance over time are quantitatively related to the drainage of hydrocarbons. Near-zero impedance differences indicate locations where there was minimal change within the LIRs of the surveys, which we interpret to be possible bypassed hydrocarbons. Increases in impedance are likely caused by water encroachment or pressure depletion between the times of the two surveys, and decreases from GOR increases and secondary gas dissolution. A visualization of the volumetric changes within the LF reservoir is created by slicing through the upper-, mid-, and lower-intervals of the LF LIR. Comparing this result to the similar figure made from seismic amplitude differences, more coherences are observed within the LIR than in the seismic amplitude HAR. However, water appears to have encroached in what might be fingers through high permeability sand from several directions, not just from the deeper portion of the reservoir in the west

Horizon acoustic impedance extraction of the LF reservoir

The acoustic impedances were extracted from along the LF reservoir top structure from each impedance volume. The extracted impedances can be directly used to delineate distributions of hydrocarbons remaining within the reservoir.

The reservoirs are outlined by the boundaries between high and low impedances. The reservoir dim-outs and brightenings have higher coherence than in the corresponding analysis that used seismic amplitudes. The hydrocarbon contacts are clearly seen on both images. The similarities and differences between the 1985 and 1992 extractions show the quantitative hydrocarbon changes that have occurred within the LF reservoir. Such changes indicate reservoir dim-outs and brightening inside the reservoir from 1985 to 1992.

As with the qualitative results obtained from the amplitude analysis, the dim-outs (increased impedance) are approximately parallel to structural contours, particularly in the western part of reservoir. These impedance boundaries correspond to the oil/water contact. No obvious water intrusion is detected perpendicular to structural contours in the northwest. However, long distance water encroachment perpendicular to the structural contours has occurred along the north of the F fault. In 1985, the region of low impedances show continuity to the eastern part of the reservoir. But by 1992, the continuity has markedly decreased. In general, the area of low impedances decreases with time, as might be expected for an actively produced reservoir.

Volumetric variations of acoustic impedance differences in the LF reservoir

Impedance differences within the LIRs are related to hydrocarbon movement. Brightened

volumes mark gas cap formation and volumes with dim-outs mark water sweep. But the boundaries are more complex and less tied to the reservoir structure than described by production data analysis. Low impedance regions above the initial gas/oil contact in fault block B are considered to be gas. Depletion of the gas cap from 1985 to 1992 is not obvious in these regions. However, areas with decreasing impedances occur further down-dip to the west within the oil zone, suggesting down-dip migration of the gas cap and gas dissolution from oil. The areas with near-zero impedance change in Block 331 are greater than those in Block 330, indicating that there may be more bypassed hydrocarbon reserves in Block 331 of the fault block. However, as we have noted previously, the cause of these regions with decreased impedance is unknown because there was no well producing from 1985 to 1992.

We present a fluid contact interpretation of the differences based on the analysis of images. Both volumetric impedance extractions and planar extractions show the low impedance anomalies migrated much deeper down-lip. This information is not present in the 2D surface extraction analysis.

The total volume of decreased impedance and near-zero impedance change is larger than those observed in the HAR analysis, and these volumes are more continuous as well. This improvement occurs because traveltime delays caused by production of shallower reservoirs have been eliminated.

The regions with near-zero impedance changes within the original gas cap to the east should still be gas. However, signficant water encroachment is detected, and the original gas distribution (gas/oil contact) has been changed dramatically by the production in Block 330.

The well data in Block 330 are consistent with the predicted hydrocarbon drainage patterns from the 4-D amplitude and impedance analyses. For example, in 1985, A-S well produced oil, gas, and water as the water front moves up-dip toward east and south, the well was shut-in in mid 1987 because of water encroachment. This well is located in the area of water sweep predicted by our 4-D analysis. The nearby A-6 well (in the up-dip direction to the south of A-S) has a similar history, but it saw water about six months earlier (instead of later) than A-S, indicating that either the water intrusion in the LF reservoir is preferentially oriented in certain directions or it is caused by water conning. Another example is the B-4 well, which came into production in 1984; it has produced oil steadily with low GOR into 1991. It is on the edge of the area of bypassed oil predicted by our 4-D analysis.

The water conning is observed much more clearly in the Block 331. Although production from wells in Block 331 has stopped because of water encroachment or sand-flow induced mechanical failures before 1985, there are water encroachment "halos" detected from our 4-D analysis existing around the watered-out wells (e.g., wells A-4, A-7 and A-S). Nevertheless, the predicted water encroachment are not radially isotropic, instead, the drainage appears to have been significantly affected by sand quality variations and other permeability heterogeneities.

Quantitative 4-D seismic monitoring technique

In an effort to further quantify our 4-D seismic monitoring techniques (He et al., 1994 and 1995b), we have used a multi-dimensional seismic forward model based on the finite element method (FEM) and fluid substitution technique (Sun, 1994) to verify whether the hydrocarbon drainage changes can produce the observable seismic amplitude changes. We constructed a velocity model of the LF reservoir as it appeared in 1985. To change the reservoir petrophysical properties, we use Gassman's equation combined with the dynamical theory of

porous media (Sun, 1994) for estimating the acoustic velocity of rock containing a multi-phase pore fluid. We incorporate changes in gas cap development, water intrusion, GOR increase and unchanged oil saturation into the 1992 model. We then compare its FEM seismic response to the 1985 response. The FEM model results indicate that surface seismic data can be used to monitor the hydrocarbon drainage process.

Conclusion

When applied to data from the LF reservoir in the EI-330 Field of offshore Louisiana, our 4-D seismic monitoring techniques are effective in determining the locations and volumes of bypassed hydrocarbons. Corrections for spatial data registration and traveltime from delays caused by drainage above the reservoir are very important. Without them, the resulting edge effects may cause the 4-D analysis to fail.

The application of our 4-D seismic monitoring techniques to seismic amplitude and estimated acoustic impedance data suggested that: a) the amplitude analysis is the better prediction of reservoir drainage patterns; and b) the impedance analysis is better prediction of reservoir petrophysical property changes. The integration of the two techniques produces quantitative understandings of the drainage of hydrocarbon reservoirs over time.

Our analysis suggests that drainage patterns are very sensitive to heterogeneities in lithology, porosity, and permeability of the reservoir. Water intrusion and gas cap expansion is found to be almost independent of the LF reservoir structure. Instead, we found that they are determined by potential fluid pathways provided by faults and fine-scale sediment fairways with high permeability.

Production wells within the LF reservoir in fault block B were found to have produced very limited, heterogeneous and contorted drainage radii. The drainage pathways in the LF reservoir are elongated along directions of high permeability (northwest-southeast) and shortened along directions with lower permeability (northeast-southwest), which indicates that the production wells have greater drainage efficiencies in selected directions. The wells that were shut-in because of water intrusions were seen to have "suffered" from much more water-conning from below than from lateral, up-dip gravity driven water invasion. The use of 4-D seismic data has significantly improved the understanding of reservoir dynamics of the LF reservoir, compared to what is possible with the traditional interpretations based on well logs and production history.

References

Alexander, L., and P.B. Flemings, 1995, Geologic evolution of a Plio-Pleistocene salt-withdrawal minibasin: Eugene Island Block 330, offshore Louisiana: American Association of Petroleum Geologists Bulletin, v.79, p.1737-1756.

Anderson, R.N., E. Bagdonas, A Boulanger, L. Xu, and W. He, 1995a, 4-D seismic interpretation techniques for the detection of drainage and migration in oil and gas reservoirs: US. Letters Patent Pending.

Anderson, R.N., A Boulanger, W. He, Y.F. Sun, L Xu, 1995b, 4-D seismic imaging of drainage and pressure compartmentalization in the Gulf of Mexico, Oil and Gas Journal, part 1, March28, part 2, April 4.

Anderson, R.N., P.B. Flemings, and S. Losh, 199Sc, The GBRN/DOE Eugene Island Dynamic Enhanced Recovery Project, CD-ROM, Lamont Press.

Breitenbach, E.A., G.A. King, and K.N.B. Dunlop, 1989, The Range of Applications of Reservoir Monitoring, Society of Petroleum Engineers Paper 19853.

Domenico, S.N., 1976, Effect of brine-gas mixture on velocity in an unconsolidated sand reservoir, Geophysics, v.41, p.882-894.

Dunlop, K.N.B., G.A. King, and E.A. Breitenbach, 1988, Monitoring of oil/water fronts by direct measurement, Society of Petroleum Engineers Paper 18271.

Gregory, A.R., 1976, Fluid saturation effects on dynamic elastic properties of sedimentary rocks: Geophysics, v.41, p. 895-921.

He, W., R.N. Anderson, and X. Wang, 1994, Constructing 3-D porosity and fluid pressure models in the Eugene Island Block 330 Area offshore Louisiana: American Association of Petroleum Geologists, Annual Convention Official Program, v.3, p.167.

He, W., and R.N. Anderson, 1995a, Seismic Attribute mapping of the geopressure surface in the Gulf of Mexico, Journal of Geophysical Research, submitted.

He, W., R.N. Anderson, X. Wang, and Y.-C. Teng, 1995b, Application of finite element seismic modeling in the Eugene Island Block 330 Field offshore Louisiana, Gulf of Mexico: American Association of Petroleum Geologists, Annual Convention Official Program, v.4, p. 41A.

Holland, D.S., LB. Leedy, and D.R. Lammlein, 1990, Eugene Island Block 330 Field-U.S.A. Offshore Louisiana: in Structural traps III: Tectonic fold and fault traps: Treatise of Petroleum Geology, Atlas of Oil and Gas Fields, E.A Beaumont and N.H. Foster, compilers, American Association of Petroleum Geologists, Tulsa, p.103-143.

Lumbly, D., 1995, Seismic monitoring of oil production: a feasibility study: presented at the 1994 Society of Exploration Geophysicist Annual Conference, Los Angeles.

King, M.S., 1965, Wave velocities in rocks as a function of changes in overburden pressure and pore fluid saturants: Geophysics, v.31, p. 5O-73.

Nur, A.M., 1982, Seismic Imaging in Enhanced Recovery, Society of Petroleum Engineers Paper 10680.

Nur, A.M., 1989, Four dimensional seismology and (true) direct detection of hydrocarbons: the petrophysical basis: The Leading Edge of Geophysics, v.9, p.30-36.

Sun, Y.F., 1994, 0n the foundations of the dynamical theory of fractured porous media and the gravity variations caused by dilatancy, Ph.D. Dissertation, Columbia University.

Taner, M.T., F Koehler, and R.E. Sheriff, 1979, Complex seismic trace analysis: Geophysics, v.44, p.1041-1063.

Wang, Z., and A.M. Nur, 1988, Effect of temperature on wave velocities in sands and sandstones with heavy hydrocarbons: Reservoir Engineering, v.3, p.158-164.

Wang, Z., and A.M. Nur, 1992, Aspects of rock physics in seismic reservoir surveillance: in Reservoir Geophysics, R.E. Sheriff, Editor, Society of Exploration Geophysics, p.285-300.

Wyllie, M.R.J., A.R. Gregory, and G.H.F. Gardner, 1958, An experimental investigation of factors affecting elastic wave velocities in porous media: Geophysics, v.23, p.459-493.

Task Three - Field Demonstration Experiment
Roger N. Anderson - Task Manager

OBJECTIVE:

The objective of task three was to drill one Well extension to test the Dynamic Enhanced Recovery Technologies objectives of this project In November and December, 1993, we drilled into the fault zone in Eugene Island Block 330 (A20-ST) and performed the following experiments: whole coring, wireline logging, sidewall coring, formation pressure tests, stress tests, completion with frac-pack, flow test, and pressure transient test.

SUMMARY:

Interpretation of Results of Well Experiments:

The A-2OST "Pathfinder" well was drilled by Pennzoil Exploration and Production Co., on behalf of partners Exxon. Mobil and Cockrell, into the 01-4 reservoir just above the "Red" growth fault zone that forms the northern boundary of the Eugene Island 330 minibasin. The well was then extended across the fault zone and into the footwall with DOE funding. The GBRN Field Demonstration Project consisted of three phases: whole coring, extensive logging, and stress and production testing in the Pathfinder extension. Measurements were made to determine in-situ conditions within and surrounding the fault zone and to test the hypothesis that hydrocarbons could be produced from a fault zone.

We found and sampled oil and gas from silty shales within the fault zone and discovered that the oils have similar chemistry to those being produced from the reservoirs directly above the fault zone. Whole coring revealed that faulting and fracturing extended at least 350 feet into the shales of the upthrown block. Many of the faults and fractures contained oil. Hydrocarbons would not flow at economically viable rates during drill-stem tests. The larger the drawdown pressure applied across the perforations, the lower the permeability of the fault zone became.

Where the A-2OST crossed the fault zone, the horizontal closure stress was found to be 500 psi greater than the fluid pressure. An increase in the pore pressure of 500 psi was then found to induce significant permeability within the fault zone.

A related well, the A-lOST, was drilled into the fault zone in El 330 in October. 1993, in anticipation of the Pathfinder well, completely with industry funds. In contrast to the "tight" fault encountered in the Pathfinder well, fluids flowed strongly when the fault zone was penetrated by the shallower A-lOST well. Fluid flow within the high-pressured fault zone was sufficient to cause differential sticking and the loss of two bottom-hole assemblies in the well. A pulsed-neutron, Thermal Decay Time log run through the stuck drillpipe recorded increased gamma ray radiation from oxygen activation indicating that water was flowing at rates of up to 700 barrels/day within the fault zone.

Introduction

The Global Basins Research Network (GBRN) is an electronic "Internet" organization that was formed to solve two very specific fluid flow problems: 1) the identification of expulsion mechanisms by which hydrocarbons migrate up fault zones from deep, geopressured strata into shallower reservoirs, and 2) the imaging of these hydrocarbon migration pathways so that wells can be drilled into these “streams” located within fault zones. As part of a GBRN/Department of Energy/oil industry cost-sharing project, we are experimenting with methodologies by which hydrocarbons can be economically produced from these natural conduits into deeper, as yet unexploited reservoirs. These deep reservoirs are targets of the sub-salt play currently receiving so much attention in the exploration community.

The specific hypothesis we are testing is that fluid pressures periodically exceed rock failure strength within the geopressured zone, reopening fault zones, which become transient conduits for fluids to rapidly exit the pressure chambers. The shallower reservoirs are filled by hydrocarbons that have migrated up these fault zones, but the timing, migration pathways, and rates of migration remain poorly understood. To address this hypothesis, we integrated a wide variety of geophysical, geochemical, geological and reservoir engineering technologies in order to image these ongoing fluid-flow processes in the Eugene Island 330 Field, and to site the test wells in Block 330 itself. In cooperation with the operator Pennzoil and partners Exxon, Mobil and Cockrell, we drilled, logged, sampled, Frac-Packed, and drill-stem tested a 700 foot extension of a development well into the deep fault zone (the A-20ST) in November-December, 1993, and logged an earlier extension of the A-lOST into the fault zone at a shallower level.

The Eugene Island 330 Field

We chose the Eugene Island 330 field for our oil migration study because it is the largest Pleistocene oil field in the world, it is geologically well-characterized, and most importantly, it shows a variety of indications of geologically recent hydrocarbon migration (Holland et al, 1990 and Whelan et al, 1994). The Eugene Island 330 Field is a typical Gulf of Mexico mini-basin (Alexander and Flemings, 1994). Structurally, a regional growth-fault system (the "Red Fault Zone") forms the northern boundary of alternating sequences of Plio-Pleistocene sands and shales overlying deep-water turbidities and basin-floor fan deposits from the ancestral Mississippi River delta. As the Red Fault Zone accommodated extension toward the deep-water Gulf of Mexico, the sediments in the depobasin formed rollover anticlines that are now filled with oil and gas. Extension was caused by withdrawal to the south of an extensive salt sill initially present near the surface of the mini-basin from 6 to at least 2.2 Ma (Rowan, Weimer and Flemings l994). A counter-regional, down-to-the-north fault zone forms the southern boundary of the mini-basin. A thick shale sequence separates the shallow-water shelf sands from geopressured. deep-water deposits (Alexander and Flemings, 1994). Remnant salt feeder stocks and remobilized salt diapirs bound the mini-basin, exclusively upthrown to the bounding fault system. The deep turbidities are still geopressured (He and Anderson, 1994), even after the removal of the impermeable salt seal, because high sedimentation rates combined with the thick, deepwater shale accumulations in the Pliocene resulted in rapid burial and permeabilities too low for the excess pore fluids to escape (Mello, et al, 1994).

Migration of hydrocarbons is occurring today in the Eugene Island 330 Field (Anderson. et al, 1993). Seeps are active at the sea floor outcrop of the Red Fault Zone system. Oil and gas are being produced in reservoirs as young as 400,000-years-old beneath these seeps. Geochemical monitoring over the last twenty years has recorded temporal changes in the composition of the oils being produced from the shallow reservoirs; these changes may reflect recent injection of wet gas and gasolines (Whelan, et al, 1994). Also, biodegraded oils have been replaced by less biodegraded oils over time in the shallowest reservoirs.

Locadons of the A-2OST Pathfinder and A-lOST Wells

Migration pathways of hydrocarbons can be imaged within the 3-D seismic surveys in the Eugene Island 330 Field by mapping high amplitude connectivity throughout the volume (Anderson, et al, 1993). The northern growth fault system is particularly involved in the migration of hydrocarbons. although the conduits are convoluted and more like 3-D "streams" than uniform, permeable, 2-D fault zone flow planes.

The GBRN focused on a strategy of testing the fault zone play concept by deepening appropriate development wells being drilled during the normal ongoing operations of the Eugene Island 330 Field. This strategy, though far more economical than drilling dedicated research wells, places practical limits to the targets available to the GBRN. In the A-2OST Pathfinder well, we penetrated the tightest, most shale-prone portion of the fault zone just beneath the deepest known reservoirs trapped against the Red Fault Zone in El 330 (the 01-4 and 5 sands). In this location, the stress field was predicted to be the most constrictive to fluid migration (Flemings, et al, 1994). and by testing the fluid flow properties here, we could better understand the migration process itself

In addition, we were able to participate in the logging of the A-lOST well that Pennzoil and partners drilled into the fault zone to the southeast of the A-2OST. At this location, the fault zone was intersected at a shallower depth, and the seismic signature was of two splays 180 feet apart with a high seismic amplitude anomaly trapped in-between.

The Field Demonstration Experiments in the A-20 ST Pathfinder Well Pennzoil and partners primary economic target in the A-205T well was the 014 sand located between the "D" and "A" fault splays of the Red Fault Zone. The well was spudded on November 2, 1993, and Pennzoil, as operator, drilled to 7035' Total Vertical Depth (TVD) and set 9 5/8" casing. They then drilled-out and penetrated a section of the 01-4 pay that was 50 feet thicker than the downdip section of this sand that is currently on-production in the A-23 well. Pennzoil and partners agreed to log-while-drilling the well extension from the 9 5/8" casing point through their 01-4 and 01-5 pay zones to the point where the GBRN began to core the fault zone. The GBRN/DOE extension was begun on November 23, at 7300'TVD, and ended at 8075' TVD on December 25, 1993. Experiments were carried out in three stages.

Stage I: Whole Coring

We cored the next 350 feet of the well below the 01-5 pay, and though the upper 60 feet of the cored interval was dominated by down-to-the-southwest, slickensided faults. The major deformation zone imaged by the logging tools (see below) was just above this interval. We used

an experimental anti-whirl PDC bit developed by Baker Hughes Inteq. and Amoco Production Co. that had not yet been used in a well. We coupled this new coring bit with a full-closure core catcher, and a water-based polymer mud containing a 3% synthetic, non-fluorescing oil additive developed by M-I Drilling Fluids Co. to prevent adhesion of clays to the bit (balling). A 60' core barrel with a 4" aluminum inner tube was chosen over the usual 30' barrel normally used in the Gull. We obtained a total of 343' of 4 1/4" diameter core from an attempted interval thickness of 360', a 95% recovery rate. The cutting rates averaged better than 70'/hour and at times exceeded 150'/hour in these "gumbo" shales, and the entire coring operation took less than three days. The core was split into alternating 3' chilled and frozen sections, and is available for further study at the GBRN Core Repository at the Pennsylvania State University.

The cored interval was from 7330' to 7680'T\ID, and overall, the rock consisted primarily of silty shale with minor sand beds. The Formation MicroImager (FMI) log indicates the cored interval begins just below the deformation zone mapped as the Red Fault Zone, and extends across a second, minor fault not imaged by the seismic surveys. Beds in the cored interval dip between 20 and 30 degrees to the north-northwest. The core sampled three primary structural domains. An upper faulted zone extends from 7330' to 7490', and containing slickensided faults at moderate to high angles. Many are filled with drilling mud, indicating fracture permeability. A middle zone from 7490' to 7560' is relatively unfaulted, and consists of silty shale, shaly silt, and thin, yellow fluorescing sand beds, the thickest measuring 9". Much of this interval corresponds with a slight increase in resistivity, and may be low resistivity pay. Finally, a lower fault zone was encountered from 7560' to 7680'TVD, consisting of silty shales with gouge zones that intersect the well at high angles. Slickensided faults are also present, and dip at a variety of angles. Much more fluorescence is apparent in both low- and high-angle structures in the lower fault than in the upper fault zone. The lowermost faulted zone in the core may reflect deformation associated with a fault beneath the Red Fault Zone.

The planning and execution of the coring stage of the project was a collaborative effort involving not only the GBRN scientists, but also many supporting oil and service companies, and the success was directly attributable to this collaboration. For example, an Exxon coring specialist, Mike Wooten, oversaw the on-site coring effort while Texaco, Chevron. Conoco, and M-I Drilling Fluids provided mud composition advice, CoreLabs processed and archived the core, a Chevron scientist collected gases, Shell and Exxon provided CAT-scanning of the core and other analyses, GERGI Texas A&M and Woods Hole, the organic geochemistry, Cornell, the structural and fracture mapping, Penn State. the acoustic correlation with seismic, Schlumberger, major element chemistry, the University of Michigan and Michigan Tech, the pore water chemistry of wells near the A-2OST, the University of Rochester, age dating of the pore fluids, Pennzoil, the paleontology and biostratigraphy, Woods Hole and Chevron, Mobil. Exxon and the University of Virginia, gas source and maturity analyses.

Stage II: Wireline Logging

The GBRN then logged from TD at 8010' to casing at 7046' TVD with a full suite of acoustic. nuclear and electrical "imaging" logs from Schlumberger to obtain as complete a picture of the fault zone as possible. The acoustic measurements made in the wellbore were from the dipole sonic log, which recorded compressional, shear, and stoneley waveforms throughout

the open-hole portion of the well. The fault zone was distinguished by a marked decrease in sonic velocities from the downthrown (shallower) to the upthrown (deeper) blocks. While compressional velocities decreased by 10% across the fault zone, the shear velocity decreased by more than 20%. The dipole shear source excited a shear wave only slightly faster than the stoneley wave. Fracturing. observed in the core, is thought to be the cause of the low shear velocities, and extensive acoustic measurements are planned at in situ conditions for the core samples.

An experimental nuclear geochemical logging tool developed by Schlumberger was then lowered across the fault zone. Using a controlled source of neutrons, this logging tool measures the elemental composition of the rock by neutron activation, in real time. The distribution of elemental abundances into a normative mineralogy model verifies that the rocks both above and below the fault zone are shales (quartz contents are less than 20% and clay mineral contents are greater than 40% in a rock with *25%* porosity). The fault zone itself appears to be somewhat more silty with quartz contents of slightly more than 25%. This logging tool also recorded neutron porosity and gamma ray density.

The electrical logs obtained were array induction and Formation MicroImager (FMI); the latter measures resistivity variations with resolution down to mm-scale along four orthogonal swaths along the wellbore wall. A fluxgate magnetometer orients the four pads relative to true north. Possible pay was indicated within the Red Fault Zone by the induction log, and the FMI showed that a considerable part of the 01-5 pay, thought to be above the fault zone, was in fact, significantly disrupted by movement downthrown to the fault zone. As indicated by dip "tadpoles", the 01-4 sand has normal, 10-20 degree regional dips to the north. Below this, the 01-5 dips first steeply to the west, then steeply to the east before the fault zone top is encountered at 7270' TVD. The fault zone is deformed by 40' of southwest-dipping faults imaged by the FMI. Below 7310', footwall deformation is seen to 7350', below which 20-30 degree dips to the north are the norm. No further southwest-dipping fractures are imaged by the FMI until the small fault zone, seen in the lower two cores, is encountered at 7560-7680' TVD. However, the core revealed that many such small faults exist throughout the footwall section.

In fact, the first core was repeatedly cut by down-to-the-southwest, slickensided faults that were too small to be imaged by the FMI. The FMI revealed that the lower half of the 01-5 target was within the fault zone itself, and consequently, we had begun our coring program about 10' BELOW the deepest down-to-the-southwest fracture within the fault zone imaged by the FMI.

From the bottom of the Red Fault Zone upward, the FMI revealed a zone of interbedded shales and silts with gentle dip, but cut by southwest dipping faults with increasingly more throw until a distinct surface dipping 55 degrees to the southwest was mapped at 7280' TVD. Above this discontinuity, highly deformed silty shale is found, cut by and rotated along an antithetic fault. Three large vertical fractures were mapped above this deformation zone, and each was found to have high electrical resistivity, possibly indicative of hydrocarbon charge. These natural fractures strike in the orientation of the fault zone, and may connect the fault zone hydraulically with the overlying 01-4 and 5 pay zones in the downthrown block. The composition of the oils recovered from the fault zone is identical to the 01-4 oils currently being produced in the A-23 well (see below).

The modular dynamics formation tester (MDT) was next run in the well. We intended to

use this tool to obtain at least 12 pressures throughout the well extension, but because of the hole conditions, the MDT was stuck obtaining the first pressure measurement. Pennzoil then acquired 75 sidewall cores from 7157'-7661' TVD in three coring runs in the hole, including valuable samples from within the major deformation zone of the fault zone.

Stage III: Stress and Production Testing

On December 2, 1993. we ran a 7 5/8" liner into the well extension. As a result of an incomplete cement job, we were required to squeeze cement through casing into the intervals directly above and below our test zone to insure isolation. Stress tests were performed below the fault at 7380-7384', within the fault at 7270-7310', and above the fault at 7240-7244' to obtain pore pressures and tectonic stress magnitude variations across the fault zone.

The difference between the minimum compressional stress (S3) and the fluid pressure (P) controls the hydraulic conductivity of the fault zone. As the fluid pressure converges upon the minimum horizontal stress, significant fracture permeability may be created. Our stress and pore pressure experiments allowed us to measure these in situ conditions above, below, and within the fault zone. We measured pore pressures that were 0.8 of the vertical stress (S1) above and 0.95 of S1 below the fault zone. Direct measurements of the stress field using hydraulic fracturing experiments show that fluid pressures of an additional 500 psi would be required to reopen fracture permeability and allow significant fluid flow within this segment of the fault zone.

It is also interesting to note that the maximum hydrocarbon columns in the OI reservoirs result in buoyant pressures of approximately 500 psi. Thus, it is possible that these large OI columns are in dynamic equilibrium with the closure stresses along the fault. This, in turn, implies that any new hydrocarbons migrating up the fault from depth would be able to naturally hydrofracture into lower pressured reservoirs. We believe the natural vertical fractures imaged just above the fault zone by the FMI log reflect this migration pathway. A fundamental question we continue to address is whether this process of ongoing vertical migration is presently occurring.

Drill-Stem Tests in the Fault Zone

We then perforated, frac-packed and flow tested a 40' interval within the fault zone. On December 14, 1993, the tubing conveyed perforating gun was fired at 7270-7310'. Since only a trickle of flow-back was seen at the surface, low permeability of the formation was assumed. We then hydraulically fractured the perforated interval using Dowell's new telemetry capability in which the test was monitored in real-time in the Dowell offices in Lafayette, Louisiana. The procedures followed were: a) an acid job was performed to clean the perforations and formation near the wellbore, b) a minifracture was created using stepped-rate injection into the formation, and several constant rate stress tests followed (essential for the final design of the frac-pack), then c) the well was shut-in to retrieve the downhole data recorded on the Schlumberger DataLink system. The fracture design was then finalized, and the hydraulic fracture completed. However, the fracture pumps stalled-out at the beginning of the final injection stage, preventing the downhole completion of the fracture job. Although a tip screen-out was thought to be observed at the surface, later retrieval of the downhole DataLink recorders showed that the

increased surface pressure was from frictional loss and not from fracture completion in the formation. Although the highest permeability recorded after the fracture was only 120 md, fluids began immediately to flow to the surface at a rate of 2 bbl/hr at 400 psi against a 16.3 lb/gal zinc bromide completion fluid.

Then the drill-stem testing assembly was tripped into the hole to flow test the fault zone interval. The flow test began with flow to the surface at a rate of 8 bbl/hr but within two hours, the rate had dropped to less than 2 bbl/hr. Pennzoil then used a coiled tubing unit to "jet-in" the well with nitrogen. Once this procedure began, the flow rate increased to 8 bbl/hr again but would not sustain itself, dropping within 24 hours to zero net flow. We did, however, recover several barrels of oil at the surface: hydrocarbons that came from within the fault zone. Fifteen gallons of this fault zone oil were collected for geochemical analysis, and samples are available through GERG/TAMU or WHOI.

As the nitrogen jetting drew higher and higher differential pressures against the formation, the well flowed at smaller and smaller rates, until it completely stopped at more than 5000 psi of drawdown differential. In other words, the more underbalanced we were, the less the formation flowed. At the end of each drawdown experiment, we shut-in the well to measure the permeability of the formation from the pressure rebound.

The fracture permeability in the fault zone is strongly pressure dependent, and as we drew-down the pressure in the wellbore, the fracture network supplying the permeability within the fault zone closed tighter and tighter. This observation was verified on the rig when we shut down the jetting, re-equilibrated the wellbore, then pumped fluid into the formation through the perforations to verify that they were not plugged-off. The fault zone took fluid easily at about 500 psi over ambient fluid pressures.

Pennzoil then plugged the fault zone interval on December 25, 1993, and will complete in their economic target, the 01-4 formation in 1994.

The Logging of the A-lOST Well

In preparation for the A-2OST well, and to examine targets on the upthrown side of the Red Fault, Pennzoil and partners extended the AIO-ST well through the fault zone in October 1993. The A-lOST well is located approximately 1300 feet shallower and 1000 feet to the southeast from the A-2OST.

In the A-lOST well, the first splay of fault zone was encountered at 7500' MD (6000 ft TVD), and a clear fault break was observed by the mudlogger. Significant shows of oil and gas (2000 units, with Cl through C4 components present) soon followed. The volumes of oil that flowed into the mud pits were estimated by the mud engineer to be 1% of 730 bbl of 14.2 LB/gal mud being cut by gas to 12.5 LB/gal in one 12 hour interval, and 2% of 530 bbl of 15.8 LB/gal mud cut to 13.5 LB/gal in 14 hours of circulation. An oil chromatogram of fault zone oil recovered from the mud pits was measured at GERG/TAMU, and it shows that the oil is unbiodegraded and does not have the light n-alkanes or gasolines stripped-off (as do the Pathfinder oils). The A- lOST oils are as complete, chromatographically, as any found in the producing reservoirs of EI-330.

The drillpipe became stuck as the second splay was being encountered 180 feet into the fault zone. Pennzoil backed off and whip stocked, re-entering the fault zone with significantly

heavier mud (16.2 LB/gal). Again, oil and gas (3000 units) shows were reported at the surface, this time against mud weights up to l6.5 LB/gal mud.

An open hole Array Induction resistivity log was then attempted, but was stopped by a borehole bridge 50 feet beneath the first splay of the fault zone. However, a clear fault zone break was observed at 7500' MD, (6010' TVD), in the Gamma Ray and Spontaneous Potential logs, with an oil show in shaley sand indicated by the resistivity log at the top of the fault zone.

While trying to clear this bridge, the drillpipe became stuck again at 7650' MD (6200' TVD), within 8 feet of the previous event. We believe the sharp lithologic break encountered at 7500' MD (6010' TVD) is the first splay of the fault zone, with porous and permeable, hydrostatically pressured IC sands of the downthrown block juxtaposed against low permeability shale or shale gouge. The resistivity log indicates high resistivity in the shale just below the fault break. Beneath this first splay, a slightly sandier zone was encountered at 7550-7570' MD (6060-6080' TVD). The second splay of the fault zone could be indicated by the low Sigma and low porosity logged from 7630-7660' MD (6140 to 6170' TVD).

A dual-burst, Thermal Decay Time (TDT) log was then run through the stuck drillpipe to TDT. Lithologies determined from gamma ray and neutron capture cross-section (Sigma) measurements indicate that the fault zone consists of shaly sand interbedded with shale streaks near the top and bottom of the fault zone. Gas (Neutron Porosity, NPHI <10% porosity) and possible oil shows were indicated by the minima in the Sigma capture cross-section log at 755O-7570' MD (6060'-6080' T\"D) and 7630-7660' MD (6140-6170' TYD). A water-wet, shaly sand was found at the base of this upper show at the center of the fault zone, with possible gas and oil shows measured both above and below. Gas continued to cut the mud from 16 to 13 lb/gal while the pipe was stuck. The oil-finding capability of the thru-pipe TDT was then verified by successfully logging the IC pay shallower in the well -- thru pipe, mud, casing, and cement.

Transient Fluid Flow from within the Fault Zone

In the most significant finding from the A-lOST, active, transient, fluid flow was recorded during four repeated TDT logging runs and subsequent station measurements within the fault zone. Water flow was detected by means of neutron activation of oxygen nuclii to produce the radioactive isotope ^{16}Nitrogen (Schnorr, 1993). The use of the oxygen activation technique to measure water flow in boreholes has been known since 1967 (Wichmann, et al, 1967), and an impulse-activation technique for the TDT log has been applied successfully in Alaska (Scott, et al, 1993, McKeon, et al, 1993). Water contains abundant oxygen atoms, but no oxygen atoms reside within the structure of hydrocarbons, so any possible oil/gas mix traveling with the flowing water was not determined by the following observations.

Gamma ray counts recorded by the natural gamma ray logging tool (NGT) in the TDT were routine during the lowering of the logging tool to the bottom of the well. Shales were emitting about 80 api units of natural radiation, as expected, and sands were recorded at about 60 api units. Then, at the bottom of the well, the neutron generator was activated and began to pulse neutrons into the formation as the logging tool was pulled up the hole at 12 feet per minute. A 10-millisecond burst of 10^8 neutrons was followed by a 100-millisecond quiescence as the photoelectric accumulator was counting gamma rays returning to the logging tool. The total capture cross-section (Sigma) of the formation is the intended measurement of the TDT tool.

As the TDT was logging Pass 1 across the fault zone, gamma ray counts quickly jumped to >200 api units above background, and steadily increased until at 7580' MD (6095' 'ND), a maximum radiation level of 290 api units was recorded--far in excess of the natural radiation level of any sedimentary rock. The gamma ray count then slowly decreased to 200 api units at 6030' TYD (7520' MD), then dropped to 60 api units at 7470' MD (5980' TVD), and remained near these background values that had been recorded on the trip into the hole for the rest of Pass 1. The minitron was then turned off, and the TDT logging tool lowered back to the bottom of the well. Normal gamma ray counts of 60-80 api units were recorded again on the trip back to the bottom of the hole with the neutron source turned off Passes 2 and 3 repeated the cycle of logging up the hole with the pulsed neutron source activated. Pass 2 recorded the highest gamma ray counts from the bottom of the hole to the most radioactive depth at 7580' MD (6095' TVD), but then the count rate dropped more precipitously from there to the top of the fault zone at 7500' MD (6010' TVD), where this time normal gamma ray counts were recorded by the TDT even with the minitron still pulsing neutrons. Pass 3 resulted in gamma ray counts that fall between those of Passes 1 and 2. Pass 4 was then recorded without turning the neutron source on, and only normal gamma ray counts were recorded by the tool. Clearly, some transient fluid flow phenomenon was being observed.

We believe this to be the first recorded case in which the TDT log measured water flow by oxygen activation while the tool was moving upward during a logging operation. The previous water flow studies reported in the literature (c.f., McKeon, et al. 1991. Scott, et al. 1993. Schnoor, 1993) all utilized the tool in stationary locations within the Wilber.

In our case, the TDT was activating oxygen nuclii within flowing water, sending radioactive ^{16}Nitrogen isotopes streaming uphole. The water must have been flowing at much faster rates than the logging tool was moving (12-17 ft/min) in order for the gamma rays emitted by the decay of the ^{16}N isotopes, which have a half-life of 7.13 seconds, to overtake and be recorded by the gamma ray detector which was 14.5 feet above the neutron source (McKeon, et al, 1991. Scott, et al, 1993, Schnoor, 1993).

The flux of gamma rays counted by the detector within the TDT logging tool quantitatively recorded the variations in water flow within the fault zone between the three activation passes logged in the well. That is, the number of oxygen nuclii streaming past the detector during the passes varied, and was measured direcily by the TDT log.

As shown by McKeon, et al. 1991, fast neutrons generated by the neutron generator have energies of approximately 14 MeV, high enough to activate oxygen nuclii to produce radioactive ^{16}N isotopes. ^{16}N decays by beta emission, emitting a 6.13 MeV gamma ray In most cases (69% of the time). Because of its high energy, the 6.13 MeV gamma rays penetrate several inches of borehole fluid, casing, drillpipe, and cement. However, these gamma rays are not ordinarily recorded by the natural gamma ray detector, because it is 14.5 feet above the minitron source, and logging is done while moving the tool uphole at 12-17 feet/minute. Water must be flowing at faster than the logging speed for the gamma ray detector to record the gamma rays emitted by this decay of ^{16}N.

McKeon, et al, (1991) report the development of a Monte Carlo neutron transport code that can be used to estimate the velocity and volume of the water flowing outside the drillpipe. Assumptions are that the 111/16" TDT logging tool is centered in the 5 1/2", 15.5 lbm/ft drillpipe, and stationary. The formation is assumed to be 30 porosity units of sandstone with water in the

pore spaces. The flow channel is a 2" thick annulus immediately outside the drillpipe.

The total number of activated oxygen nuclii passing the detector is proportional to a scaling factor and Avogadro's Number (there are 6.03 x 10^{23} oxygen nuclii in each gram molecular weight of water). Thus, the measurement appears. at first glance. to be independent of the flow velocity. However, the time that each activated nuclii remains in the vicinity of the detector is inversely proportional to the flow velocity, and since the activated ^{16}N signal decays exponentially after activation and before gamma rays reach the detector, the flow velocity can be estimated from the gamma ray detector count rate. The specific geometry of the flow pathway itself is irrelevant to the velocity calculation. The gamma ray count rate above background (Ct) is proportional to water flow velocity (v) by e (~L/v) /v, where A is the 16 N decay constant, and L is the distance from source to counter.

Thirteen station measurements were made after pass 4, and after a 17.5 lb/gal "kill-slug" was circulated to the bottom of the hole. In this mode, the TDT tool is held stationary in the Wilber while the minitron bursts neutrons for 10 msec, then passively counts for 100 msec, then the cycle is repeated many times (see Schnorr, 1993). Much slower flow rates were encountered overall after the kill-slug. but "bursts" of radioactive fluid were periodically encountered in 4 stations adjacent to the fault top. In these bursts, radioactivity first increases dramatically, then decays exponentially as the ^{16}N flu is dissipated across the stationary detector.

These velocity-versus-gamma-ray-count ratios were used to approximate the flow velocities logged by the moving TDT tool. although the gamma ray counts recorded by the moving tool were considerably higher than those recorded during the stations (because of the different mud weights in the wellbore). The assumption made is that the fluid flow was all in the same direction as the tool was moving. In fact, the tool velocity was added to the calculated flow velocity. Variations in water flow velocities are predicted for the gamma ray variations logged by the TDT to have been up to 160 ft/minute.

The variations in volume flux up the hole versus depth are interesting. The flux increases from about 150 bbl/day at in to a peak at 7580' MD (6095' 'ND). The maximum flow was encountered in all three activation passes at this depth, which is also the minimum Sigma "peak" within the fault zone. flow up the wellbore then steadily decreases between there and the top boundary of the fault zone. Very little flow is observed from the fault zone into the hydrostatically pressured IC sands above the fault zone (less than 50 bbl/day). The differential sticking of the drillpipe seems likely to have occurred where fluid was exiting the wellbore as the flow rate decreased within the wellbore from 7500' to 7680' MD (6010' to 6200' 'ND). Variations in the water flow were monitored by three separate repeat logging runs, and each time the maximum upward flow rate was encountered where the minimum neutron capture cross-section (Sigma) was found in the fault zone. However, the flow rate was variable, with the maximum flux encountered during the first pass, but the minimum measured by the second pass. By the time of the third pass, the flow rate had increased again.

An 18 lb/gal kill slug was then pumped downhole, and verification that flow had stopped was made by active TDT logging that reproduced the normal gamma ray values recorded from the fault zone and by several stations. The drillpipe was then severed, and the bottom of the well cemented-off.

In summary, what we believe happened in the bottom of the A-lOST well is that, after crossing the first fault splay a very large pressure increase was encountered (8.8 to 16 lb/gal

equivalent). Then as the well penetrated deeper into the second bounding splay of the fault zone, strong fluid flow began with water entering the wellbore from below the fault zone sand and moving uphole to exit the wellbore between the sand and the top-bounding fault splay. Interestingly, little of the flow appears to have gone into the overlying hydropressured sands, but instead was confirmed to the interval between the fault splays. This fault zone is clearly capable of producing fluids at high rates, especially if it were part of an interconnected fluid migration network.

Geochemistry of Hydrocarbons Recovered from El 330 Reservoirs and the Red Fault Zone

All of the biomarker and aromatic hydrocarbon maturation parameters measured to date in the Eugene Island 330 reservoir oils are consistent with these oils having been generated and expelled approximately from the beginning to the middle of the oil generation window, equivalent to a vitrinite reflectance, Ro_1 of about *0.75w* 0.8%, depending on the exact type of kerogen present However, gases from the same GOR mixes in wells have much higher maturity (1.1% to 1.2% Ro equivalent vitrinite reflectances, Whelan et al, 1994), suggesting a much deeper source for the gases. The biomarker maturation values from the A-2OST Pathfinder well's fault zone oils are also very constant and the same as those for the deeper "standard" EI reservoir oils from the KE, LF. MG, and OI reservoirs.

The ratio of (nC3 + nC4) *I* nCl7 was used by Whelan et al. (1994) to represent ratios of wet gas to oil. High wet gas to oil ratios may be diagnostic of recent hydrocarbon reinjection into reservoirs in El 330, since the lighter hydrocarbons are also more prone to escape from a reservoir undergoing leakage. In addition, in any reservoir undergoing active biodegradation which produces "humpane" type baselines, such as those observed for the GA and HB reservoirs, it would be expected that nC3 and nC4 should also be absent These low molecular weight compounds are easily and preferentially lost by biodegradation, as well as by a number of other processes, including water washing and evaporative fractionation (Thompson, 1983; 1987; 1988). Therefore, high (nC3+nC4)InCl7 ratios observed in the GA and HB oils of Eugene Island 330 are consistent with recent active oil migration anWor remigration.

Changes are noticeable over time as well, particularly in the ratios of light (C3-CS) to heavier (C7C8) components among samples taken in 1984, 1988, and 1992, with an ever higher proportion of lighter components being present in 1994. Ratios of B (toluene to n-heptane), F (n-heptane to methylcyclohexane), H (a maturity ratio based on the ratio n-heptane to the sum of branched and cyclo to n-alkanes), and I (ratio of branched C7 compounds to the sum of cyclic C7 dimethylcyclopentanes) also show systematic changes over the 6 year period indicative of changes in reservoir hydrocarbon composition and possibly of dynamic injection of hydrocarbons from deeper sources into the reservoirs over this interval time, Q.Yhelan et al, 1994).

The whole oil chromatograms of the A-2OST Pathfinder fault zone oils are identical to those of the deeper KE through Ol oils recovered from other "A" platform wells, and particularly the A-23 oils from the nearest reservoir "updip" to the fault zone, the 01-4. However, the Pathfinder oils from the fault zone show very low wet gas to oil ratios, suggesting no recent hydrocarbon injection of light hydrocarbons in this particular fault zone interval. In contrast, the A-lOST oils are from an interval of the fault zone with higher seismic amplitudes than are

present in the Pathfinder fault zone penetration, implying higher gas contents. Indeed, analyses of the A- lOST oils show them to have higher wet gas to oil ratios than do the Pathfinder oils. Perhaps the A-lOST oils are closer to a light hydrocarbon migration pathway within the fault zone than the A-20ST Pathfinder oils, or the Pathfinder oils have been stationary for long enough to lose their light components.

During drilling of the A-2OST Pathfinder well, gas samples were obtained by Martin Schoell, Chevron, using a new gas sampler technology. Initial molecular and isotopic compositions for these gases show that the gases from the cored interval beneath the fault zone contain a progressively higher biogenic versus thermogenic component with increasing depth. The biogenic gas represents that generated in organic rich sediments of the footwall at much shallower depth which was then carried down and buried. DLFflisive mixing is indicated, with more thermogenic gas entering the sediments through the fault zone at the top of the cored interval and mixing with biogenic gases in the shales from the upthrown block. Thus, the dl3C methane values for the Pathfinder well show that no significant fluid flow is occurring from the high-pressure footwall to the lower pressure reservoirs of the hanging wall sediments. Also, the source of the thermogenic gases found within the fault zone appears to be from deeper along the fault zone trajectory.

How to Produce Oil and Gas from a Fault Zone Conduit

Our current working hypothesis for hydrocarbon migration in the El 330 area is that deep in the geopressured turbidities, formation pressures periodically increase until fracture-reopening stresses are overcome in the fault zones that connect into these "chambers". At such times, large volumes of hydrocarbons are released rapidly in transient bursts up the fault zones towards the surface. and then the faults close back up. Put another way, with added pressure. oil is expelled up the fault zones, but then the very act of releasing the fluids drops the pressure and the faults become tight again. Over and over, the cycle repeats. Evidence from the Pathfinder well to support this hypothesis is that the fracture permeability within the fault zone is strongly pressure dependent. We have shown that oil and gas are present even in the tightest portion of the Red Fault Zone in Eugene Island 330, and that these would flow under fluid pressures 500 psi higher than those measured within the fault zone today. We have demonstrated that such pressurization increases the permeability of the fault zone to Darcy values. However, we have also found that the fluid-release from such a pressurized fault zone immediately lowers the permeability by several orders-of-magnitude. In addition, the A- lOST well provides strong evidence that once fluid flow is established within the fault zone, transient behavior can be expected.

The GBRN/DOE Field Demonstration Experiments have provided tests of likely strategies for future production:

1) Locate wells into high permeability pathways within the fault zones that have high-seismic amplitudes,
2) Change the angle of penetration from perpendicular to parallel to the fault zone in order to expose more surface area, such as drilling along a fault isolated sand lobe. Such strategies are likely to be profitable, since they increase permeability by drilling higher seismic amplitudes and

increase thickness by drilling along the plane of the fault zone.

We believe that technology transfer of the GB RN/DOE methodology of integrating geophysical and geochemical dynamics with the more traditional stratigraphic and structural techniques will lead to a more complete hydrocarbon-system view of the deep subsurface. In addition, these technologies led to a new play concept that could help locate and exploit large volumes of deep, geopressured reserves not only in the Gulf of Mexico, but also in other sedimentary basins where hydrocarbons are currently migrating out of deep geopressured chambers, such as in Nigeria, the North Sea, Indonesia and the Caspian Sea.

Task Four - Reservoir Chancterizadon
Peter Flennings - Task Manager

OBJECTIVE:

The purpose of this task was to integrate the geological and geophysical data to construct the minibasin and reservoir models in the SEI 330 Area in order to understand the hydrodynamics of the minibasins. The minibasins are analyzed through stratigraphic interpretation, salt analysis, pressure and temperature mapping. Temporal seismic amplitude analysis is to monitor the dynamic changes occurred in the reservoir

SUMMARY:

Through the final year of the project we continued to acquire important data for the 330 field. These included: 1) complete wire- line data for Blocks 338 and 339 (donated by Texaco), 2)fracture completion data, and leak off data for Blocks 330, 338, and 339. and 3) the entire 316 A-12 core (now housed in the Penn State Core Repository) which was recently drilled by Pennzoil. Throughout the year, Beth Bishop and Amanda Sbaw have continually updated the Landmark Openworks project and distributed data to all of our colleagues in this DOE-funded project.

The following work was performed by Parvel Peska of Standford University as consulting services to Columbia's Lamont-Doherty Earth Observatory from April 1, 1994 through July31, 1995:

CONSTRAINING IN SITU STRESS IN WE SOUTH EUGENE ISLAND FIELD, GULF OF MEXICO

Pathfinder well

We analyzed data from the GB RN/DOE Pathfinder well, block 330 of the South Eugene Island field (extension of the Pennzoil A-2OST production well, offshore Louisiana). The data include: 4-arm caliper leak-off/minifrac, pore pressure, FMI and hole orientation data.

Four-arm caliper measurements associated with an FM' log run in the Pathfinder well indicated systematic borehole enlargements from a depth interval 2158-2180m, about 150 m above the main growth fault The breakouts occur at an azimuth of N550E LF projected onto a horizontal plane. At these depths, the wellbore deviates 320 from the vertical at an azimuth

N350K

A leak-off test from a depth of 2148 m provides an estimate of the minimum principal stress. The corresponding vertical stress was computed from average density given by the density log, and the estimated formation pore pressure. These observations represent information that is typically available in many offshore reservoirs. The occurrence of naturally-occurring vertical extension fractures on the FMI log near the depth of interest indicates that *SV* is a principal stress Thus, to fully determine the stress state, two stress components are still unknown: the magnitude and azimuth of *SHmax* (or azimuth of *Shmin).*

The subsequent analysis revealed that the azimuth of *Shmin* must be between N37^{0}E and N49E and the corresponding values of SHmax must be between 39.5 MPa and 43 Mpa. No other values satisfy the observed wellbore breakouts. Although it is commonly assumed that in the Gulf Coast, the *SHmax* value determined in this case departs significantly from *Shmin.* The computed azimuth of *Shmin* deviates from the azimuth of observed breakouts (whereas in a vertical well the breakouts are at the same azimuth of *Shmin, and* it appears to be quite reasonable as it is orthogonal to strike of the major growth fault passing through the hole just below the measurement depth. No knowledge of either rock strength or elastic moduli was necessary in these computations.

Once the range of allowable magnitudes *of SHmxr and* azimuths of *Shmin* is computed, the uniaxial rock strength necessary to prevent borehole failure can be estimated. The occurrence of breakouts implies a strength less than about 22 MPa LF *SHmax* = 39.5 MPa and less than ≈32 MPa if *SHmax* =43 Mpa. These are reasonable values considering the sediments in question are poorly-indurated and clay-rich (Anderson et al. 1994).

The results of the study were presented in the paper "In situ stress and rock stren~h in the GBRN/DOE Pathfinder well. South Eugene Island. Gulf of Mexico" (Zoback and Peska 1995).

Surrounding well

Analysis of borehole breakouts detected in deviated wells by caliper logs was extended from the Pathfinder well to other wells in the South Eugene Island field where the logs were available. Borehole enlargements at azimuths, which do not correlate with the hole inclination, were detected in the wells at depths of 6000'-8000'. The caliper difference was relatively small and subsequent stress analysis revealed that either the breakouts are not stress-induced or the stress state is highly heterogeneous in the region of interest.

Miscellaneous

As a part of the stress studies in the South Eugene Island field, we also performed compilations on stress magnitudes in the Gulf Coast particularly on fracture gradients and pore pressures as a function of depth. This revealed that the Mohr-Coulomb frictional model controlling stress magnitudes in crystalline rocks in many parts of the world (e.g. Zoback and Healy 1984) is not working for overpressured formations in the Gulf Coast unless the coefficient of friction is extremely low. A theoretical model of stress distribution in overpressured sedimentary basins was developed to demonstrate changes in stress magnitude and orientation with depth in areas where gravitational sliding controls the extensional faulting. Also, a FORTRAN code was written for inverting breakout orientation data from deviated boreholes based on the method proposed by Qian and Pedersen (1991).

ANALYSIS OF THE RELATIONSHIP BETWEEN IN SITU STRESS AND BOREHOLE FAILURE FOR STRESS DETERMINATION AND

BOREHOLE STABILIZATION

An integrated methodology was developed to analyze the relationship between the in situ stress and failure of inclined boreholes. We have conducted a comprehensive series of calculations of the occurrence of borehole breakouts and drilling-induced tensile wall-fractures in arbitrarily inclined boreholes and showed how such observations can be used to determine stress orientation and magnitude, effective rock strength and the optimal mud weight for borehole stability. The results are summarized in the paper Compressive and tensile failure of inclined wellbores and direct determination of in situ stress and rock strength, Peska and Zoback 1995).

Optimally, there is a two-step procedure how to apply this methodology in practice:

1. Utilize observations of wall failures in inclined holes to constrain the in situ stress and effective rock strength assuming that independent information such as on the least principal stress, pore pressure and overburden is available.
2. Utilize the knowledge on the stress field from the previous step to predict optimal wellbore trajectories and mud weights to stabilize the wellbore.

Computer codes were written in Matlab programming environment to implement the methodology. The computations are based on the assumption that the rock is isotropic and it behaves elastically to the point of failure, which is controlled by the Mohr-Coulomb criterion.

The *GetStress* program computes the orientation and magnitude of the stress tensor (principal stresses are assumed to act vertically or horizontally) from the azimuth of borehole breakouts observed in an inclined borehole and from other a priori information. The program *may* be also used to constrain the rock strength as the conditions for failure are expressed by means of the critical strength and also the breakout width may be taken into account. The in situ stress may be also computed by the *BreakoutRotation* program, which is an improved version of the Barton and Zoback [1994] technique for stress magnitude measurement using observations of rotations in borehole breakout orientation in the vicinity of an active fault, penetrated by the borehole.

Once the stress state is known, the *GetFailure* program computes orientations of compressive and tensile failures in an arbitrarily oriented borehole and constrains mud weight or effective rock strength required stabilizing the wellbore. Directions of potential breakouts and tensile wall-fractures around holes of various inclinations and azimuths are shown using the "looking down the hole" convention, i.e. as if the reader is viewing the hole by looking down its axis and the breakout azimuth is displayed with respect to the bottom Side of the deviated borehole (the *FailureOrientation* program gives even a more detailed look at the stress concentration around an arbitrarily oriented borehole and makes it easier to understand the "looking down the hole" convention). The *Wellbore Trajectory* program also computes orientation and tendency to fail by compressive or tensile failure for the given stress field and borehole orientation but now the stress and hole orientation are functions of depth which makes possible to analyze stability along the whole borehole. Both programs are optimal to design a stable wellbore trajectory from the platform to the target under the assumption that the stress state was determined from observations in the surrounding wells.

REFERENCES

Anderson, R. N., P. Flemings, S. Losh, J. Austin, and R. Woodhams, In situ properties of a major Gulf of Mexico growth fault: Implications for behavior as a hydrocarbon migration pathway, *Oil*

Gas J., 92(23), 97-104, 1994.

Barton, C.. and M.D. Zoback, Stress perturbations associated with active faults penetrated by boreholes: Possible evidence for nearcomplete stress drop and a new technique for stress magnitude measurements, J. *Geophys. Res.,* 99, 9373-9390, 1994.

Hart, B. S., P. B. Flemings, and A. Deshpande, Porosity and pressure: Role of compaction disequilibrium in the development of geopressures in a Gulf Coast Pleistocene Basin, *Geology. 23(1), 4548,* 1995.

Peska. P., and M.D.Zoback, Compressive and tensile failure of inclined wellbores and direct determination of in situ stress and rock strength, J *Geophys. Res.,* in press. 1995. Qian, W., and L. B. Pedersen, Inversion of borehole breakout orientation data, *J. Geophys. Res.,* 96, 20093-20107, 1991.

Zoback, M.D., and J. H. Healy, Friction, faulting and in situ stress, *Ann. Geophys., 2,* 689-698, 1984.

Zoback M.D., and P. Peska, In situ stress and rock strength in the GBRN/DOE Pathfinder well, South Eugene Island, Gulf of Mexico, *J. Pet. TechnoL,* July 1995.

Temperature Mapping (G. Guerin, LDEO)

The mapping of the present day temperature distribution around Block 330 is now complete, and after 3-D numerical modeling of the conductive regime in this area, a 5-10 C° anomaly following the strike of the Red Fault can be observed in the depth range of the most productive sands. This observation is interpreted as the influence of warm hydrocarbon-bearing fluids migrating up along the fault, and will be used as a constraint for the 3-D numerical modelling of these circulations, under development.

Amplitude Mapping Analysis (R. Anderson, Wel He, LDEO)

This sub-task is now completed, with a patent filed and granted for geopressure mapping using seismic amplitude changes. In addition, considerable bypassed pay has been identified along the property line between Eugene Island blocks 330 and 338. New Wells to test the validity of the ~D analysis are in the planning stages by Pennzoil and Texaco for 1996 to be paid for entirely with industry funds. The A-8St continues to produce at about 1400 bbl/day, with total production now exceeding 800,000 bbl. At a royalty percentage of 18% and assuming oil prices of $20.bbl this entire Class I Oils study will be paid for in an additional 3 years through the royalties paid to the US Treasury on oil from just this one successful well, located in no small part through the use of 4-D technologies.

Predicting the geopressure transition zone in the Plio-PIeistocene of offshore Louisiana,

Gulf of Mexico

Geopressure or overpressure is abnormally high pore fluid pressure. This condition occurs when the formation pressure exceeds the hydrostatic pressure. The surface that marks the first occurrence of geopressure in a sedimentary basin is termed the top-of-geopressure surface. Geopressure is common in sedimentary basins of all ages (Ferti 1976 and Anderson et al., 1991). These abnormally high fluid pressures are an extreme hazard to drilling, since the undercompensation for borehole pressures results in blowouts. The top-of-geopressure is a hydrodynamic subsurface. The topography and dynamics of the geopressure surface are closely related to thermal-chemical and dynamic evolution of the basin. An accurately determined top-of-geopressure surface and a quantitatively evaluated geopressured transition zone is of great significance in studying the fluid dynamics and thermal maturation of the basin, because hydrocarbon generation and migration are usually controlled by the pressure distribution.

Geopressure can be caused by many different physical, chemical, or tectonic factors. Aquifer head (Levorsen, 1954), tectonic compression (Finch, l969 and Hubbert et al, 1959), sediment loading, compaction, and the absence of drainage systems (Dickinson, 1953; Hubbert et al, 1959; Jones, 1969 and Harkins et al., 1969), phase changes, or diagenesis, such as the water release from the phase change of montmorillonite to illite (Powers, 1967 and Burst, 1969), smectite dehydration (Bruce, 1984), gypsum to anhydrite (Heard et al., 1966), organic material maturation (Hedberg, 1974), aquathermal expansion of water due to the temperature variations (Levorsen, 1954), osmotic membrane phenomena (Hanshaw et at, 1965), and thick shale-sand sequences with the sand to shale ratio less than 15% (Harkins et at, 1969) have all been cited as causes of geopressure.

In the offshore basins of Gulf of Mexico, geopressure is caused by continuous sediment loading at fast sedimentation rates and to a lesser extent by clay phase changes (Jones, 1969). The excessive pore fluid pressure built up in such a short geological time frame (<2.5 ma) dissipates at an extremely slow rate due to the permeability bottle necks developed in interbedded sand and shale stratigraphic sequences (Mello et al, 1993).

The geopressure transition zone is the depth interval within which the hydrostatic pore fluid pressure gradually increases with depth to approach lithostatic pressure. The geopressure transition zone occurs at the permeability bottleneck. The bottom of the geopressured formation has not yet been reached by any wells drilled in the Gulf Coast region.

Acoustic velocity and bulk density are greatly effected by geopressure. Because the excessive pore fluid pressure partially supports the weight of rock column, the effective pressure exerted on the rocks is dramatically decreased. As a result the acoustic velocity and bulk density of geopressure formations are usually much lower than those of normally compacted formations at the same depth. For the same reason, a velocity inversion (from high to low) usually occur at the geopressure transition zone because velocity is proportional to the effective pressure. The decrease in velocity and density can be further enhanced by under-compaction of the rocks.

The original depositional porosity of sediments (often 65%) is partially preserved by under-compaction of sediments due to the geopressure. Under continuous loading at fast sedimentation rate, pore fluids of previously deposited sediments can not escape fast enough because of low vertical permeability, which effectively prevents further mechanical compaction of these sediments. With further burial, more fluids are generated from clay diagenesis and the

pore fluid pressure increases (Powers, 1967 and Spencer, 1987). We believe that the remarkable decrease in compressional-wave velocity and bulk density across the geopressure transition zone in the Gulf of Mexico is due to coupling of pore fluid pressure and porosity preservation.

The geopressure transition zone is also characterized by abnormally low vertical permeability, high salinity, and high temperature gradients (Dickinson, 1953: Bredeheoft et al., 1968; Burst 1969; Jones, 1975; Hunter, 1990 and Tigert et al., 1990). In a geopressure transition zone with fixed thickness, the higher the pore fluid pressure, the lower the acoustic velocity and density. A large negative seismic amplitude is expected. On the other hand, the thicker the geopressure transition zone, the lower the frequency of the seismic reflection.

In this chapter, we present a method that uses reflection strength of real seismic data to predict the top-of-geopressure surface. We use forward seismic modeling and cross-correlation to quantitatively estimate the thickness of the geo pressure transition zone. Once validated, these methods are applied to a 2D seismic survey acqulred in the South Eugene Island Area offshore Louisiana Gulf of Mtxico.

The acoustic velocity transition observed in sonic logs suggests that the geopressure transition zone can be quantified in terms of two variables: pore fluid pressure gradient and the transition zone thickness. The well data also suggest that the formations below the bottom of the geopressure transition zone are highly overpressured. The well data also indicate that the velocity changes are significant only when the pressure gradient ranges from 13.6 to 18.1 Mpa/Km (0.6 to 0.8 psi/ft). As the pore fluid pressure approaches the overburden pressure, no further decrease in velocity occurs. Our prediction technique is reliable only in defining the top portion of the geopressured zone.

Background of geopressure prediction techniques

Geophysical methods for detecting and predicting the top-of-geopressure surface can be classified into drilling methods, wireline logging methods, reflection seismic methods, and gravity or electric-magnetic potential field methods. The first two methods can only be performed when wells penetrate the top-of-geopressure surface. Seismic and potential field methods require only surface measurement. Potential field methods suffer from the limitation of being unable to distinguish overpressured formations from massive shale formations. The efficiency of reflection seismic methods are addressed in this chapter.

Many attempts to identify reflectors from the top-of-geopressure fail because the thickness of the transition zone can vary greatly over short distances (Anderson et al., 1992). Seismic interval velocity analysis (Pennebakker, 1968 and Reynolds et al., 197'1) and inverted pseudo velocity or acoustic impedance analysis Musgrave et al., 1965 and Martinez et al., 1991) attempt to detect interval velocity or impedance changes across the top-of-geopressure surface. Using velocity techniques, the top-of-geopressure surface is interpreted as the depth where the internal velocity trend departs from the velocity trend expected under normal compaction conditions. The velocity technique works well on sonic logging data, which have high resolution, but fails for lower resolution velocities determined by staking and migration. The pseudo velocity and impedance derived from seismic inversion, although have higher resolution, fails due to its lack of low frequency information (He et al., 1995). Missing the onset of geopressure can cause inconsistency in the predicted top-of-geopressure surfaces even within a single vintage of seismic data, this scenario deteriorates in areas where geopressure pressure transition zones

are thick or highly variable.

Changes in seismic reflection strength (instantaneous amplitude) of reflection seismic data can be used to detect geopressures as long as a sound relationship between the velocity transition and geopressure transition can be established. Our approach is to develop techniques that can distinguish seismic amplitude anomalies caused by geopressure transition zones from other reflections. We detect reflections from acoustic transition zones. Because reflection strength measurements contain low-frequency energy contained in original seismic traces. the reflections from acoustic transition zones can be enhanced and separated from other reflections by low-pass filtering. Reflection strength estimates derived from velocity transition models are used in the design of these filters. Top-of-geopressure can be directly detected as the uppermost boundary reflector between the high and low amplitude regimes in the reflection strength cross-sections (Anderson et al., 1992 and He et al., 1992 and 1994). The geopressure transition zone can also be imaged.

Characteristics of seismic reflections from geopressure transition zones

The appearance of geopressure on seismic data

In the Plio-Pleistocene basin of the Gulf of Mexico such as the South Eugene Island area geopressured formations produce observable features on reflection seismogram and wireline logging records. Substantial weakening of seismic amplitude is observable in time windows between about 1,500 ms and 3,000 ms on the eastern and western footwalls of the central Eugene Island basin and between 2,800 ms and 4,000 ms on the hanging wall. This weakening is caused by strata with less internal acoustic impedance contrast than normally pressured strata. Deepwater turbidities have reflectors of normal amplitudes; they are located beneath the weakening zones in the center of the basin. Salt diapir structures are seen beneath both footwalls. The boundaries of the weak reflection regions do not necessarily follow stratigraphic sequence boundaries.

Distinct features of the geopressure transition zone in seismic data

The generalized reflection coefficient of a transition zone in a laterally homogeneous acoustic medium has the form of a superposition integral (Wolf, 1937). The maximum amplitude is proportional to the ratio between the velocities at the top and bottom of the transition layer. The cut-off frequency (the highest frequency preserved) is inversely proportional to the thickness of the transition layer (Seo, 1978). An acoustic medium with a transition zone not only attenuates reflected seismic energy, but also greatly changes the phase of the reflected seismic waveforms (Bortfeld, 1960 and Gupta, 1965). We have generated two groups of seismic models to illustrate the seismic reflection effects of changing the velocity and thickness of the transition zones. Group I models have a transition zone with constant thickness and varying velocities of the underlying layer Group II models have a transition zone that varies in thickness with a constant velocities of the top and bottom layers. The cut-off frequencies are dramatically reduced as the transition thickness increases. The reflection energy increases with the velocity contrast. Small

increases of cut-off frequency are also observed for Group I models. These basic seismic characteristics of the geopressure transition zone are the main features on which our geopressure predicting technique is based.

In practice, the post-stack seismic data are usually treated as zero-offset seismic reflections. A seismic trace observed in an area with geopressured formations consists of reflections from both discrete geological events and the transitional zone. These seismic traces can be modeled as the convolution of a reflection coefficient function and a seismic source function. Using seismic data processing techniques, it is possible to separate the transitional events from the discrete events in an observed seismic trace.

Predicting top-of-geopressure surfaces using our seismic amplitude technique

We constructed a geological model consisting of an acoustic transition layer with varying thickness and several discrete layers with constant velocities. Using the first derivative of a 35 Hz, zero-phase, Ricker wavelet as seismic source, a synthetic seismic section was generated using a finite element seismic modeling algorithm (Teng, 1989).

Because our prediction technique is to detect the top-of-geopressure surface in two-way traveltime domain in which the convolution forward model is used in data processing, a synthetic model generated from a forward model other than convolution is necessary to test our prediction technique independently.

Our first step is to detect the low-frequency seismic reflections in the synthetic section. Using complex seismic trace analysis (Taner et al., 1979). The algorithm treats a real seismic trace as the real part of a complex signal. with an imaginary part is equal to Hilbert transform of the real part. The reflection strength is quantified by the envelope (magnitude) of this complex function. The complex seismic trace analysis was applied to compute the reflection strength of our test model. The reflection strength section is composed only of low frequency reflections.

Thick geopressure transition zones only contribute to low frequency contents in reflection seismic data, whereas large velocity contrasts between the top and the bottom of transition zone only contributes to large amplitudes. Therefore, our second step is to distinguish the reflections contributed by the transition layer from those contributed by discrete layers. Since the generalized reflection coefficient of typical transition zones contains mostly low frequencies, we designed a lowpass filter than enhance those frequencies. We took this filter to be simply the low-frequency part of the amplitude spectrum of the generalized reflection, up to the first zero. We then apply this filtered to the reflection strength. The bandwidth of the lowpass filter depends on the thickness of the velocity transition zone, which is unknown. We use a filter with an intermediate bandwidth (estimated from assumption), which is effective enough to enhance the majority of transition zone reflections. On the filtered reflection strength section, the top-of-geopressure surface can be interpreted as the uppermost boundary between the high (shallow) and low (deep) amplitude regimes. The top of the transition zone is interpreted as the enhanced (or unchanged) reflectors. The estimated top and bottom of the transition zone is almost identical to that of the true velocity model. Our processing technique can be visualized more clearly using a single seismic trace extracted from the synthetic section.

Verification of the prediction technique

We apply the technique to a synthetic trace generated from sonic and bulk density logs from Eugene Island well 33l-SH-1. Both sonic and density logs show a transition from high values to low values across the geopressure transition zone.

The top of sonic velocity transition is at 2,460 ms (2,621 m), and the measured pressure gradient is 13.6 Mpa/Km (equivalent to mud weight of 1,400 Kg/m^3). The bottom is at 2.600 ms (2,792 m), and it corresponds to a 18.1 Mpa/Km gradient (1,800 Kg/m^3). Acoustic velocity at the top and bottom of the geopressure transition zone are 2.772 m's and 2.242 m/s, respectively (a 19% decrease).

The reflection strength derived from the complex seismic trace analysis is lowpassed compared with data The highest frequency preserved in both traces is less than 30 Hz. A velocity transition model with thickness of 140 ms was constructed. The filter is obtained and applied to the reflection strength traces. The reflections from the geopressure transition zone are clearly seen at 2,460 ms on both filtered traces.

These results suggest that our geopressure prediction technique can be used to identify the top-of-geopressure surface using seismic amplitudes. However, the nonuniqueness introduced by the low frequency cyclicity of the sedimentary sequences may sometime affect the interpretation of the top-of-geopressure. Constraints from well logs are required for two reasons: 1) a well must be used to provide a *priori* knowledge of the geopressure transition zone at one location to construct the low-pass filter; and 2) the pressure detected in the well must be used to calibrate the occurrence and depth of the top-of-geopressure surface.

Prediction of the top-of-geopressure surface in the Plio-Pleistocene basin in offshore Louisiana Gulf of Mexico

We use a 2D seismic survey acquired in 1983 in the Eugene Island Area of offshore Louisiana to examine the feasibility and accuracy of our geopressure predicting technique. The survey area is about 90 Km (east-west) by 41 Km (north-south) with approximately 3.2 Km spacing between north-south "inlines" and 6.4 Km spacing between east-west "crosslines". There are 110 seismic lines contained in this survey. The survey covers the entire Eugene Island South Addition Area Block 330 minibasin, and its vicinity. The stacked and migrated seismic data of relative seismic amplitude ("true" amplitude) have a frequency range from 6 to 60 Hz.

Regional geology

The sedimentation history of the offshore Louisiana sub-basin is well studied by numerous authors (e.g., Galloway et al., 1991). Significant sedimentation in the offshore Louisiana did not occur until the Jurassic rifting of the Gulf of Mexico and the subsequent Laramide Orogeny and its uplift of the Rocky Mountains. Abundant terrigenous materials from erosion of the Rocky Mountains were delivered into the Northern Gulf of Mexico Basin, but were delayed by a lower Cretaceous barrier reef system that developed along the hinge zone of the Gulf. The Laramide erosional products finally breached the reef in the Tertiary, and the ancestral Mississippi River delta system rapidly dumped an enormous thickness of sediments

into the Gulf Coast basin. The thickness of progadationally deposited sand and shale sequences in the Cenozoic reached at least 12,000 m, and the thickness of the Pleistocene alone reached more than 3,000 m. This deposition took place in only about 5.3 ma (Galloway et al., 1991). The Pre-Tertiary sediments were buried, loaded, and heated with unusual rapidity. This rapid loading triggered the massive migration of the Louann salt toward the surface and to the south into the deepwater continental slopes. Pore pressures within the deeper sediments increased above hydrostatic, and large volumes of hydrocarbons were generated and migrated to shallow traps. These processes continue to this day (Anderson et al., 1991).

Large-scale hydrodynamic processes are coupled with the ongoing deposition of the massive sedimentary load. Convection is occurring in all three of the major hydrological regimes active in the Louisiana Gulf Coast At shallow depths, meteoric flow, controlled by topography and directed towards the shelf, mixes with upward moving connate water and diagenetic fluids from deeper in the basin. At mid-depths, considerable dissolution of salt occurs producing an unstable layer of heavy, dense, and highly saline pore fluids.

Salinities in Pleistocene sediments are often found to be more than 4 times greater than sea water. In the deepest portion of the basin, metamorphism and hydrocarbon maturation reactions release large volumes of high-temperature, gas-charged and extremely buoyant fluids. Thermal build-up and restricted fluid flow are associated with this geopressured zone which dominates the deeper compressional system within the basin. Hydrothermal fluids migrate both laterally and vertically for considerable distances (Anderson et al., 1991).

Several minibasins were formed in the survey area by the withdrawal of a salt canopy approximately 2 ma ago. These minibasins are situated on the major shelf-margin deltaic depocenters of Plio-Pleistocene age and are bounded by regional and counter-regional growth faulting systems. Their evolution is characterized by three sedimentary phases: prodelta, proximal deltaic, and fluvial (Alexander et al., 1995). In the prodelta phase, bathymal and outer neritic shales and turbidities loaded and mobilized an underlying salt sheet During the proximal deltaic phase, salt continued to withdraw from beneath the minibasin and low stand shelf margin deltas deposited across a regional growth fault zone system. which grew along the northern margin of the minibasin. Sediment accumulation and fault slip rates were high as thick sequences of deltaic sands were deposited on the footwall of the fault system. During the final fluvial phase, salt withdrawal waned and the creation of accommodation space within the minibasins ceased. The Eugene Island minibasin was filled less than 500,000 years ago and the lowstand deltaic system prograded southward (Alexander et al., 1995). Many hydrocarbon reservoirs discovered in the study area were formed during the second and third phases. Continuous sediment loading at fast sedimentation rates and clay diagenesis caused geopressures to occur widely.

Velocity characteristics of geopressure transition zone

Well logs provide the starting point for understanding the behavior of acoustic velocity in the geopressure transition zone. More than 500 wells have been logged in this area. Among them, 107 wells penetrated the to-of-geopressure surface. A 19% velocity decrease is observed in the geopressure transition, which has a pressure gradient that varies from 13.6 to 18.1 Mpa/Km within a 140 ms time window. We use one well to design the lowpass filter for the entire seismic survey.

The pore fluid pressure gradient measured at the bottom of the well is 19.7 MPa/Km,

well above the 10.5 Mpa/Km hydrostatic pressure gradient. Nevertheless, the sonic log does not show any transition at that depth, because only pressure gradients in between 13.6 Mpa/Km and 18.1 Mpa/Km can produce an observable velocity transition. The filter design for the velocity transition use a 30 Hz, zero-phase Ricker wavelet. This filter is applied to all the reflection strength traces computed for the entire 2D seismic survey in the next section.

Seismic data analysis to predict the top-of-geopressure surface

The top-of-geopressure surface is interpreted as the uppermost reflector that separates high amplitude region above from the low amplitude regions below, using the top-of-geopressure surface in the test well as reference. The geopressure surface is depressed in the center of the EI-330 minibasin due to the thick sediment load. The surface rises near bounding faults on both sides of the minibasin. It intersects stratigraphic and lithologic interfaces. Our results agree well with the top-of-geopressure surface detected in the another well.

Our technique allows the top-of-geopressure surface to be systematically interpreted across faults and other structural boundaries. The spatial consistency between stratigraphic horizons, faults, and the to-of-geopressure surface can be achieved. Such consistency is essential to integrate geopressure interpretations with other geological and geophysical data successfully.

By applying the same procedure to the other 109 seismic lines, we are able to predict the top-of-geopressure surface consistently with respect to faulting and stratigraphic configuration in these minibasins. The interpreted top-of-geopressure surface is then converted from two-way travel time to depth using the interval velocity derived from the corresponding stacking velocity of each seismic line. The compartmentalization of the predicted geopressure surface shows individual pressure chambers being bounded by major growth faults.

Accuracy and reliability of the predicted top-of-geopressure surface

The accuracy and reliability of the predicted depth to top-of-geopressure surface is investigated by comparing it with that detected by well logs and mud weights. Major discrepancies as well as some other subtle differences are present in a few places. The map based on seismic data includes faults, and thus it has much higher lateral resolution than the map based on wells. The agreement is better at the well locations themselves. The root-mean-square error is about ±107 m. The largest errors are introduced from eighteen wells, which are located in areas with complex geological structures, such as shallow salt diapirs. If we exclude these 18 wells, the root-mean-square error is reduced to ±46 m.

Quantitative evaluation of geopressure transition zone

If the geopressured formations share the same hydrodynamics, pressure differential between the top and bottom of the transition zone should be the same everywhere, regardless of the thickness of the transition zone. Quantitatively estimates of the geopressure transition zones can be obtained through the correlation of pressure gradients and acoustic velocities. The thickness of the geopressure transition zones in the wells is not constant, but the measured pressure gradients tend to linearly correlate with velocity contrasts across the geopressure transition zones. This correlation is used to define an empirical, linear relationship between pressure gradient and velocity.

We develop a suite of velocity transition models with fixed velocity contrast (22.7%) and

varying thickness of the velocity transition. Thirty models were generated with thickness increments of S ms, up to a maximum thickness of 240 ms. Using a 30 Hz, zero-phase Ricker wavelet as the source function. synthetic seismograms were computed for each of the thirty velocity models. Reflection strength tracts were then computed.

Using the previously interpreted top-of-geopressure surface, we can compute cross-correlation functions between the modeled and observed reflection strength functions. The velocity model corresponding to the maximum correlation among the thirty cross-correlation functions is then chosen as the best velocity transition model for that trace. The time lag of the maximum cross-correlation function is used to precisely locate the final, predicted top-of-geopressure surface. This technique produced an improved top-of-geopressure surface, an estimate of the thickness, as well as estimate of the thickness of the velocity transition and associated geopressure transition zone.

Minor time shifts are observed between the newly obtained and previously predicted top-of-geopressure surfaces. The topographic variations of the predicted bottom of geopressure transition zone are different from those of the top-of-geopressure surface. The largest deviations are observed near the large growth fault systems.

Using the interval velocity derived from the stacking seismic velocity, the final, predicted top-of-geopressure surface and the bottom-of-geopressure surface are converted from time to depth. The actual pore fluid pressure is computed from the predicted pressure gradients in the geopressure transition zone. The pore fluid pressures above the top-of-geopressure surface are at hydrostatic pressures. Pore fluid pressures below the bottom of geopressure transition zone are not estimated, because the pressure gradients are greater than 18.1 Mpa/Km in the study area and can not produce enough velocity contrast to be observable by our analysis. Two wells penetrating the top-of-geopressure surface are also projected onto the quantitatively predicted geopressure transition zone. The agreement between wells and prediction is good.

Geological significance of the predicted geopressure transition zone

The geopressures were developed in the early Cenozoic, when large amounts of clastic sediments were rapidly deposited. Subsequently, they have evolved along with the structural, stratigraphic, and thermal conditions. Large amounts of heat are trapped within the geopressured formations because no advective heat transport occurs across the top-of-geopressure. The effects of heat insulation on thermal evolution are two fold. On one hand, the heat transport to the hydrostatic zone is reduced, causing much lower formation temperatures in the hydrostatic zone than average temperatures observed in Tertiary basins without geopressuring. On the other hand, the trapped heat may have significant impact on the maturation of the deep Cenozoic organic source rocks. Strong thermal anomalies in the hydrostatic zone are observed along the red fault in the study area. They are caused by heat carried by transient fluids expelled from the overpressured formations along these faults (Anderson et al., 1991). These thermal anomalies indicate that many of the regional growth faults in the study area are still active at the present time. When pore fluid pressures within the geopressured formation continuously built up to exceed the minimum horizontal stress, periodic reopening of these faults occurs usually parallel to the regional faults. Consequently, the reopening releases tremendous amounts of fluid from the overpressured formations into the reservoirs in the hydrostatic zone.

The periodic reopening of growth faults every two thousand years is the mechanism for

present-day fluid migration. The pressurized fluid mixtures with high temperatures migrate from the geopressured formations to fill reservoirs in the hydrostatic zone and balance the pressure and temperature differences. Overproduction of some shallow reservoirs (Anderson, 1993) may be associated with this active fluid flow. To prove and quantify such a fluid recharging process, much work is still left to be done.

There is a good correlation between the locations of some large oil fields and areas with large horizontal pressure gradient. The horizontal pressures are highest near the top-of-geopressure surface, in regions where the topography of the surface is steep. The oil fields tend to occur in these areas. Since steep topographic gradients are probably associated with faults, we propose that the correlation is due to oil being forced up from greater depths along these faults by geopressure.

Conclusion

Geopressure transition zones are characterized by monotonically decreasing acoustic velocities in our study area. In our method, reflection strength is successfully used to extract the low-frequency content of seismic reflections needed to define acoustic transition zones. The top-of-geopressure surface, associated thickness and gradients of geopressure transition zones are obtained deterministically. Good agreement between the predicted results and measured results in wells is observed Our prediction method is robust and effective. The accuracy of the seismically predicted regional geopressure surface is within ±46 m, using only one well as control, which is more accurate than the results obtained from other seismic methods.

The cross-correlation technique has several advantages over the seismic inversion technique. Accurate phase information is not required, because the technique uses phase-free reflection strength information. The implementation of our technique does not suffer from numerical instability. The cross-correlation technique is a deterministic method, of which all possible models are already generated from the well logs. the results obtained can be directly used to other geological analysis.

Missing the onset of the geopressure is avoided in our geopressure prediction method even in areas with highly variable geopressure topography. The predicted and characterized geopressure transition zones are reliable and accurate. We have successfully tested our method in other basins besides the Gulf of Mexico.

References

Alexander, L., and P.B. Flemings, 1995, Geologic evolution of a Plio-Pleistocene salt-withdrawal minibasin: Eugene Island Block 330, Offshore Louisiana: American Association of Petroleum Geologists Bulletin, v.79, p.1737-1756.

Anderson, R.N., 1993, Recovering dynamic Gulf of Mexico reserves and the US. Energy future: Oil & Gas Journal, week of April 26, PennWell Publication.

Anderson, R.N., W. He. M.A. Hobart, C.R. Wilkinson, H.R. Nelson, 1991, Active fluid flow in the Eugene Island area, offshore Louisiana: The Leading Edge of Geophysics, v.10., p.12-17.

Anderson, R.N., and W. He, 1992. Method and apparatus for petroleum and gas exploration: US.

Patent No.5,311,484.

Bracewell. R.. 1965. The Fourier transform and its applications: M~raw-Hil1 Book Co.

Bredehoeft, LD., and B.B. Hanshaw, 1968, On the maintenance of anomalous fluid pressures. I. Thick sedimentary sequences: Geological Society of America Bulletin, v.79, p.1087-1106.

Bordeld, R., 1960, Seismic waves in transition layers: Geophysical Prospecting, v.8, p. 178-217.

Bruce, C.H., 1984, Smectite dehydration-Its relation to structural development and hydrocarbon accumulation in Northern Gulf of Mexico Basin: American Association of Petroleum Geologists Bulletin, v. 68, p.673-683.

Burst, J.F., 1969, Diagenesis of Gulf Coast claycy sediments and its possible relation to petroleum migration: American Association of Petroleum Geologists Bulletin, v.53. p.73-93.

Claerbout, J.F., 1985, Fundamentals of geophysical data processing with applications to petroleum prospecting: Mcciraw-llill Book Co.

Dickinson, G., 1953, Reservoir pressures in Gulf Coast Louisiana: American Association of Petroleum Geologists Bulletin, v.37, p. 410A32.

Fertl, W.H., 1976. Abnormal formation pressures-Implications to exploration, drilling, and production of oil and gas resources: Elsevier ScientLFic Publishing Company, Amsterdam-Oxford-New York.

Finch, W.C., 1969, Abnormal pressure in the Antelope field, North Dakota: Journal of Petroleum Technology, v.21, p.821-826.

Galloway, W.E., D.G. Bebout, J.B. Fisher, J.B. Dunlap Jn, R. Cabrera-Castro, J.E. Lugo-Rivera, and T.M. Scott, 1991, Cenozoic in The Gulf of Mexico Basin: Geology of North America, A. Salvador, Editor, v. J, p.245-324.

Gupta, R.N., 1965, Reflection of plane waves from a linear transition layer in liquid media: Geophysics, v.30, p.122-132.

Hanshaw, B.B. and E-an Zen, 1965, Osmotic equilibrium and over-thrust faulting: Geological Society of America Bulletin; v.76, p.1379-1386.

Harkins, K.L. and W. Baugher III, 1969, Geological signLFicance of abnormal formation pressures: Journal of Petroleum Technology, August, p.961-966.

He, W. and R.N. Anderson, 1992, A seismic amplitude analysis approach for mapping the top-of-geopressure surface in the Pleistocene, Offshore Louisiana: EOS Transactions, American

Geophysical Union, v.73, p.304.

He. W., 1994, Mapping the top-of-ge opressure surface in the Pleistocene, offshore Louisiana, Gulf of Mexico: M. Phil. thesis, Columbia University.

He, W., R.N. Anderson, and Y.&. Teng, 1995, Application of seismic inversion to quantitative mapping geopressure transition zones in the Pleistocene, offshore Louisiana, Gulf of Mexico: The 2nd International Conference on Theoretical and Computational Acoustics, Honolulu, Hawaii.

Hedberg, H.D., 1974, Relation of methane generation to undercompacted shales, shale diap irs, and mud volcanoes: American Association of Petroleum Geologists Bulletin, V.58, p.661-673.

Heard, H.C., and W.W. Rubey, 1966, Tectonic implications of gypsum dehydration: American Association of Petroleum Geologists Bulletin, v.77, p.741-760.

Hubbertt, M.K.. 1940, The theory of ground-water motion: Geology, v.48, Part 1, p. 785-944.

Hubbert, M.K.. and W.W. Rubey, 1959, Role of fluid pressure in mechanics of overdirust faulting. I. Mechanics of fluid-filled porous solids and its application to overthrust faulting: Geological Society of America Bulletin, v.70, p.115-166.

Hunt, J.M., 1990, Generation and migration of petroleum from abnormally pressured fluid compattments, American Association of Petroleum Geologists Bulletin. v.74, p.1-12. Jones, P.H.. 1969, Hydrodynamics of geopressure in the northern Gulf of Mexico Basin: Journal of Petroleum Technology, July, p.803-810.

Levorsen A.I., 1954, Geology of Petroleum: W.H. Freeman, San Francisco, 703 p.

Martinez, R.D., J.D. Schroeder, and G.A. King, 1991, Formation pressure predktion with seismic data from the Gulf of Mexico: Society of Petroleum Engineers, Formation Evaluation, no.3, p.27-32.

Mello, U.T., G.D. Karner, and R.N. Anderson, 1994, A physical explanation for the positioning of the top of overpressure in shale-dominated sequences in the Gulf Coast Basin: Journal of Geophysical Research, v.99, p.2775-2789.

Musgrave, A.W., and W.G. Hicks, 1965, Outlining shale masses by geophysical methods: American Association of Petroleum Geologists Bulletin, Memoir no.8, p.112-136.

Pennebaker, E.S., 1968, Seismic data indicate depth, magnitude of abnormal pressures: World Oil, v.166, p.73-78.

Powers, M.C., l%7, Fluid-release mechanisms in compacting marine mudrocks and their importance in oil exploration: American Association of Petroleum Geologists Bulletin, v. 51, p.1240-1254.

Reynolds, E.B., J.E. May, and A. KIaveness, 1971, The geophysical aspects of abnormal fluid pressures: Abnormal subsurface pressure, Houston Geological Society Study Group Report p.31-47.

Seo, J.H., 1978, Detection ofabnormal geopressure using seismic reflectivity: M.A. thesis, University of Texas at Austin.

Spencer, C.W., 1987, Hydrocarbon generation as the mechanism for overpressuring in the Rocky Mountain region: American Association of Petroleum Geologists Bulletin, v.77, p. 2006-2010.

Taner, M.T., F. Koehler, and R.E. Sheriff, 1979, Complex sejsmic trace analysis: Geophysics, v.44, p.1041-1063.

Tigert. V., and Z. Al-Shaieb, 1990, Pressure seals: their diagenetic banding patterns: Earth Science Reviews, v.29, p.227-240.

Teng, Yu-Chiung, 1989, Three-limensional finite element analysis of waves in an acoustic medium with inclusion: Journal of Acoustic Society of America, v.86, p.414422.

Wolf, K. 1937, The reflection of elastic waves from transition layers of variable velocity: Geophysics, v.2, p.357-363.

Wyllie, M.R.J., A.R. Gregory, and G.H.F. Gardner, 1958, An experimental investigation of factors affecting elastic wave velocities in porous media: Geophysics, v.23, p.459-493.

Task Five - Modeling
Larry Cathies - Task Manager

OBJECTIVE:
The objectives of the modeling task as set forth in the DOE proposal were to address:

- The cause of pressure, temperature, fluid chemical, and porosity anomalies near the Red Fault,
- The possible sources of oil and gas moving up the fault, and
- The causes of organic and inorganic chemical alteration near the fault

This was to be done realistically and with the aim of facilitating the interpretation of data collected in the study area. Particular attention was to be focused on: (1) porosity and excess pressure development in the RVE, (2) hydrocarbon maturation in the RVE, (3) detailed fluid flow near the fault focusing on the detailed distribution of high permeability sands, (4) the effects of salt diapirism on subsurface temperatures, (5) the effects of fault movement on fault permeability and fluid venting out of the fault, (6) the effects of gas venting on oil migration, (7) the transport of oil as a separate phase up the fault, and (8) the effects of fluid flow (water, gas. and oil) en rock chemistry and mineralogy. The modeling was to be carried out in 3D as well as 2D.

No computer software existed that was adequate to these tasks. To even attempt to interpret specific geologic data, the models needed to couple disparate phenomena such as faulting, salt diapirism, sealing and overpressure development, temperature and fluid flow. The software needed to do so realistically, specifically for the configuration of faults and salt domes in the South Eugene Island Block 330 area and in three dimensions. To fill these needs we have (in collaboration with a finite element modeling company, the Computational Mechanics Corp. of Knoxville, Tennessee) developed a basin modeling system capable of investigating the highly coupled phenomena associated with hydrocarbon migration up the Red Fault of the South Eugene Island Minibasin. The modeling system has been applied to the geologic data collected under other tasks of the DOE project.

The AKCESS.BASIN Modeling System we developed and applied to the SEI Block 330 region is described in full in this final report. Because there is a great deal of material to report. the report is organized hierarchically: Section II gives an executive summary of the principle accomplishments of Modeling Task 5. Section III reviews the plans and performance in each sub-task. References are given there to the detailed reports given in the various subsections of Sections IV. In this way it is hoped that an interested reader can both rapidly obtain an overview of what has been done and also rapidly find parts of the work of specific interest.

It is probably natural that not all of the work proposed has been accomplished in exactly the fashion proposed three years ago. Preparation of the geologic data in a fashion that takes account of diapirism, overpressuring, and faulting in three dimensions proved far more difficult and time consuming than we had anticipated. Substantial effort was also devoted to developing algorithms that accurately describe critical parameters such as thermal conductivity and permeability in the data cube. However some areas proceeded far better than originally envisioned, and many new results have been obtained. All the important principal subtasks will

be fully accomplished by the time the students involved in this project complete their Ph.D. theses. Furthermore, a powerful modeling capability has been created that is supported by a private company and a growing group of academics spread over five separate institutions. This is certain to impact basin studies for years to come.

SUMMARY:

The principal accomplishments to date under this proposal and the matching projects it encompasses are:

1. Development of a 3-D finite element basin modeling system with sound and fully articulated fundamentals and accurate algorithms for thermal conductivity and sand permeability. This provides for easy input of highly detailed three dimensional geologic data with options to infer salt diapirism from the surface pattern of sedimentation and sea level takes into account all major physical and chemical phenomena: (e.g., isostasy, salt diapirism, faulting, overpressuring, seals, hydrocarbon maturation, fluid flow driven by haline or thermal convection, water table topography, or overpressuring, salt dissolution and transport, etc.). It solves the coupled equations with an easy to use but versatile and controllable finite element solver, which can execute rapidly on parallel machines, and has convenient and easy to use visualization tools at all stages.

2. Distribution of that modeling system across 5 institutions (Cornell. LSU, Michigan Tech., and Bowling Green) with appropriate training of professionals and students at each.

3. Extensive benchmarking demonstrate the validity of various aspects of the modeling system (Section IV).

4. Application of the Modeling System to eight - 100 km long 2D seismic lines centered on the South Eugene Island Block 330 area of the Gulf of Mexico and one 1200 km interpreted N-S section. The modeling shows that the flexural rigidity of the Gulf lithosphere is less than about 10^{23} M-m. The history of salt movement over the last 20 Ma inferred directly from sedimentation shows evolution from a salt sheet to multiple minibasins and domes. The domes have a major impact on subsurface temperature ($\pm 70^0$C temperature anomalies above and below the salt domes) (Section II and V.)

5. Construction of a highly detailed 3-D data cube in the SEI 330 area resolving all principal sands and their displacement across four NE-SW faults over the last 3.4 Ma. The salt movement inferred from the pattern of sedimentation shows the burial of a local salt sill, and its remobilization into the South Eugene Island Block 330 Minibasin with the Red Fault at its northern margin.

6. Detailed analysis of bottom hole temperature date shows a positive temperature anomaly of about 5°C below the Pennzoil oil and gas fields roughly along the Red Fault and a negative (-5^0C) temperature anomaly above the oil reservoirs. Modeling shows that temperature anomalies of this magnitude or greater will be produced by the insulating hydrocarbon-filled sand reservoirs. fluid flow could produce the positive anomaly below the reservoirs along the

Red Fault, but not the negative anomaly above the reservoirs. This suggests that the present day temperature field in the South Eugene Island Block 330 minibasin is due to thermal conductivity anomalies associated with hydrocarbon reservoirs and not rapid fluid flow (Section V).

7. Fluid flow modeling shows that pulses of overpressured fluid through the Red Fault can expel large quantities of water (and hydrocarbons), and produce significant temperature anomalies provided the permeability of the overpressured zone is on average more than -0.05 md. Sand units below, in, and above the transition form hard overpressure to hydrostatic fluid pressures were found to be very important in controlling fluid flow and temperature anomalies associated with rapid venting. Clear vitrinite reflectance and isotopic anomalies in the A6 sidetrack (but not in the Pathfinder well 1000 ft away) suggest pulses of fluid have been expelled up the Red Fault, but that the flow channels are highly localized. (Section V).

8.. Under a matching grant from the Gas Research Institute a new concept for sealing in which the flow of water (and other phases) is inhibited where there are multiple sand-shale (coarse-fine) interfaces and a non-aqueous (especially gas) phase present was conceived, tested in the laboratory, and shown to be applicable to the pressure transition drilled and cored by the Pathfinder well. (Section I).

9. The discovery that the part of the Red Fault penetrated by the Pathfinder well had a Poisson's ratio very close to that of a fluid led to the conception and quantification of a new hypothesis that significant fluid (water and hydrocarbons) migration may take place through propagating fractures. (Section V.)

By
Roger N. Anderson

Work Performed Under Contract No. DE-FC22-93BC14961

Prepared for
U.S. Department of Energy
Assistant Secretary for Fossil Energy

Chandra Nautiyal, Technology Manager
National Petroleum Technology Office
P.O. Box 3528
Tulsa, OK 74101

Prepared by:
Columbia University
New York, NY 10021

Application of Akcess.Basin to SEI Block 330 Area

INTRODUCTION

The AKCESS.Basin Modeling System was developed to investigate phenomena associated wit hydrocarbon migration up the Red Fault of the South Eugene Island Minibasin. It is thought that hydrocarbons moved up this fault to charge Pennzoil's Block 330 oil and gas fields, which are among the largest accumulations of oil and gas in the Gull' of Mexico. Because the strata that host the oil and gas reservoirs are less than 1.5 ma old, and some only -0.46 ma, because there are temperature anomalies along the Red Fault tat are of the form that pulses of fluid flow up the fault might produce, and because some of the Pennzoil Reservoirs have produced more oil than is conventionally thought possible (up to and perhaps more than 100% of the oil originally in place), it is thought that hydrocarbon migration up the Red Fault may have occurred very recently taking place at the present day. As part of this project the Red Fault was drilled to investigate these possibilities. The fault was drilled at the transition zone between soft and hard overpressure; massive amounts of data were collected and analyzed.

The part of the project reported here is concerned with modeling. Our charge was to development a modeling methodology capable of realistically addressing temperatures and fluid flow in a data cube centered on the drilled portions of the Red Fault The modeling was to be of large enough scale to encompass phenomena associated with and recent hydrocarbon migration up the Red Fault The models were to address: (1) the cause of pressure, temperature, fluid chemical, and porosity anomalies near the Red Fault, (2) the possible sources of oil and gas moving up the fault, and (3) the causes of organic and inorganic chemical alteration near the fault. Specific attention was to be taken of: (1) porosity and excess pressure development, (2) hydrocarbon maturation, (3) detailed fluid flow near the fault focusing especially where high permeability sands were juxtaposed, (4) the effects of salt diapirism on subsurface temperatures, (5) the effects of fault movement on fault permeability and fluid venting out of the fault, (6) the effects of gas venting on oil migration, and (7) the effects of fluid flow (water, gas, and oil) on sediment mineralogy. The modeling was to be carried out in 3D as well as 2D.

These objectives, as reported below, have been largely met. Several new concepts of potential significance have emerged from the modeling. In particular it has been found that:

(1) Temperature anomalies may be cause by the low thermal conductivity of the hydrocarbon reservoirs.
(2) Hydrocarbons may migrate up faults as propagating fluid filled cracks.
(3) Hydrocarbon gas may cause sealing and fundamentally control the pattern of fluid flow.
(4) The porosity distribution in the study area is most compatible with a seal (pressure transition zone) that migrates upward through the section as sedimentation takes place.

THE GEOGRAPHIC CONTEXT OF THE MODELING

A critical question from the onset of the project was the size of the model volume required to capture the processes that drove and are driving fluid and hydrocarbon venting in up the Red Fault Almost certainly the process scale is larger that the -20 km dimensions South Eugene Island Block 330 Minibasin. Modeling was carried out on a range of scales to assure capture of the relevant processes: The largest scale was a 1200-km section running from the Arkansas-Louisiana boundary to the Sigsbee knolls. This line was used to constrain the flexural rigidity of the lithosphere and to show that salt diapirism is required to provide accommodation space for sediments deposited at the scales of the higher resolution modeling. Modeling on this scale was based on six interpreted seismic lines contributed by Arco, and two 2D seismic lines that were interpreted as part of this project by Mark Rowan and Colorado University.

The highest resolution modeling was carried out on a -30 x 30km scale. It focused on temperature the South Eugene Island Block 330 Minibasin. The geology up (n which the modeling is based was derived from the interpretation of well logs, 2D (Alexander, 1994 Cornell PhD thesis) and 3D (Coehlo, Cornell PhD thesis) seismic surveys, and well logs The detailed 3D modeling is based on nine NE-SW sections mapped across Pennzoil's 3D seismic survey. The sections capture all the major sand units in the cube.

REGIONAL MODELING

1200km Scale

100 km Scale Modeling

Modeling on this scale simulates the southward migration of the shelf edge and
Modeling was carried out utilizing a method by which the modeler could specify the position of the shelf margin as a function of time. The oceanward increase of water depth on the continental shelf and slope, and the maximum water depth in the oceanic parts of the Gulf Basin were assumed to be the same in the past as today. With this assumption the paleo-ocean depth profile can be specified by tabulating the position of the shelf break at all modeling timesteps. Estimates of the shelf break position were made from the thickness arid character of the sediments, and the position and geometry of salt domes.

The results of the modeling are described here for a single case. This case is known as Arco Line 10, and it is located to the west of the Eugene Island study area. The total length of the line is 199.54km. It extends from near the shoreline due south along the boundary between East Cameron/Vermillion and East Cameron South/Vermillion South. It extends slightly basinward of the latter boundary.

This model was constructed using 27 vertical pseudowells placed appropriately to capture the basic characteristics of the subsurface. Refinement of the model is possible and desirable in areas where this first pass does not accurately reflect the subsurface geology. The base of the salt section was assumed to be absent beneath minibasins, and to have a thickness below domes or walls so that its base was no deeper than the depth of the surrounding minibasin arid the salt thickness was minimized. It seems likely, in light of subsalt imaging that is now appearing in vendor's displays at technical conventions, that the salt beneath domes arid walls may actually be even thinner in some areas. We did not, however have extensive subsalt information so the estimates were made consistently. They can be modified in the future if necessary.

Temperature at the present time, after the basin is fully developed through forward modeling, shows that temperature increases with depth from a minimum of 3.9 degrees to a maximum of 412.6 degrees. The isotherms are elevated by up to 60^0C beneath minibasins and depressed up to 80^0C beneath salt domes. This is a result of the contrast in thermal conductivity between salt and sediment. Again, the anomalies may be somewhat exaggerated if the salt thickness in the model is larger than it should be. However similar magnitude temperature anomalies were computed by an extensive independent modeling study that was also part of this DOE project (Mello, 1994).

An important feature noticed by the simulations of compactive fluid flow is that fluid flow is significantly concentrated at the margins of the northernmost salt structure. This pattern of fluid flow out of minibasins and up along the margins of salt structures is observed for all of the modeled minibasins at various stages in their evolution. Most hydrocarbon migration occurs in conjunction (and possibly assisted by) connate water flow. The natural concentration of compactive flow at salt dome margins may in part account for the occurrence of hydrocarbon reservoirs above and along the margins of salt domes. It should be emphasized that the concentration of flow at the salt margins was not due to the margins having a greater than typical permeability. The permeability of the sediments adjacent of the domes in the models was the same as the permeability of the sediments elsewhere.

The modeling is described in more detail in Huntoon, et. al. (in preparation). The calculations reported there will include estimates of the regional hydrocarbon maturation arid the fluid flow driven by maturation reactions as well as compaction.

SEI BLOCK 330 AREA MODELING

The most intensive modeling addressed processes on a 30 x 30 km scale in the main SEI study area. A three dimensional data cube was assembled and analyzed through modeling. Modeling requires a computational grid. material properties, and heat, fluid flow, and chemical computation. Below we first describe the construction and geometric analysis of the computational grid, then we describe the determination of the proper material properties and the thermal state of the data cube. and finally we describe the modeling and conclusions reached from it.

1. **The 3D Modeling Grid** (L. M. Cathles. Cornell)

The 9 NE-SW sections.3 were processed to obtain the evolution of the SEI Block 330 area over the last 3.4 Ma. The grid consists of time horizons and appropriately-selected "pseudo-wells". Salt was redistributed in 3D by processing each section twice and solving a set of equations to make the salt redistribution as uniform as possible in 3D. The thickness of the present (0 ma) section is 8.5 km, and each section is about 12 km long. At 3.4 Ma the area that now holds the South Eugene Island minibasin and the Pennzoil oil and gas reservoirs was covered by a salt sheet about 2 km thick. Over the next 0.8 Ma this salt sheet was rapidly buried by thick shales. The sheet remobilized into a large dome at the right hand side (southern margin) of the data cube, in the area that is now the SEI minibasin. The salt dome was not uniform. It was large in the west, thinner in the middle, and very large on the far eastern side of the data cube. A salt ridge remains to this day on the eastern side of the data cube. Over the next 2.15 Ma this salt dome was itself loaded with sediments and remobilized. Its collapse provided the accommodation space for the SEI Block 330 minibasin. Starting about 1.5 Ma and continuing to the present, thin sands were periodically deposited over the whole area. Many of these sands are now filled with hydrocarbons.

The juxtaposition of sands across these faults is of interest, as many oil companies believe that fluids migrate up section by crossing the fault where a lower stratigraphic sand is juxtaposed against one higher in the stratigraphy. In this fashion fluids step up through the section. Fault plane (Allan-type) maps showing the juxtaposition of sands are often prepared from 3D seismic surveys, and the maps are then used to infer what connections there might have been at past times. The AGEOHIST pre-processor provides a way to automatically generate Allan-type sections over the full span of the basin's history, explicitly taking into account decompaction and eliminating the need for inference. Decompaction can be significant and can make a significant difference when specific sand-sand connections occur across the faults.

Sands on the upthrown (northern) side of the faults cut across the sands in the downthrown minibasin which black. There is a break in sand continuity in most of the faults about a third of the way across all the sections. This offset represents throw on the NE-SW trending fault captured between Lines 4 and 5. The fault plane sand connections captured by the grid allows Allan-type fluid flow to be calculated in our 3D basin simulations.

Present day temperature in South Eugene Island Block 330 is a particularly critical parameter for modeling. A principal hypothesis of this project, founded in geological/ geochemical reasoning most recently discussed by Whelan (1995), as well as in the geometry of the anomalies with respect to the main fault system (known as the "Red Fault System"), was that the migration of hot fluids along the fault planes could be responsible for a positive temperature anomaly observed there (Holland et al, 1990). Evidence for localized fluid migration through seepages along the fault system exists at the sea bottom in the South Eugene Island area (Holland et al, 1990). However, rapid fluid migration would be necessary to produce the observed anomalies.

Guerin (1995), using bottom-hole temperature data and a steady-state finite difference heat conduction model, concluded that if the temperature field is corrected for the effect of the salt domes a positive residue is left which is probably due to fluid advection. His model assumes the thermal conductivities are constant for each layer. By comparing the pure conductive heat transfer and pure advective one, Guerin conclude that the difference is due to fluid flow along the fault system.

McKenna (1994), did a similar study in the same area and, after recognizing the impossibility of resolving the spatially restricted thermal anomaly along fault planes, concluded that the thermal anomaly in the area could be explained by sedimentation differences between the downthrown and upthrown sides of the Red Fault System. Contrary to Guerin, McKenna concluded the same temperature anomalies attributed by Guerin to fluid flow were due to differential sedimentation across the Red Fault system.

Losh et al. (1994) observed that the well 330-PZ-6ST shows geochemical evidence of significant fluid flow but the Pathfinder Well located only 1000 fl away, does not. This suggests that the pathways for fluids along the Red Fault could be highly localized.

We followed the same steps as the previous authors, and compiled a database of bottom-hole temperatures. Our data set consists of approximately 400 measurements taken in vertical and inclined wells, as well as in exploratory and production wells. The information compiled was the depth of the temperature measurements, the temperatures and the time after stopping the mud circulation. Unfortunately, there is no data on the duration of mud circulation.

In the wells with more than one measurement at a single depth we applied the Homer plot technique as described in Dowdle and Cobb (1975) to correct for the cooling effect due to the mud circulation. The Homer method requires the mud circulation time as well as the time since the end of circulation at which multiple temperature measurements were made. Because the circulation time was not available, a sensitivity analysis was done to determine the impact of the mud circulation time on the magnitude of the Homer plot temperature correction. The Homer method gives similar corrected temperatures provided the circulation time is relatively short. The corrected temperatures shift significantly in the cases only when the circulation time exceeds about 14 hours. Dowdle and Cobb (op. cit.) pointed out that the Homer plot method is most reliable for short circulation times, basically for this reason. Common industry practice in the Gulf of Mexico makes it unlikely that circulation times exceeded 10 hours. Provided this is the case. It suggests it is possible to correct bottom hole temperatures to t 2 ^{0}F by assuming a circulation time of 6 hours. The time of circulation could be a few hours or as much as 10 hours and the correction would still be accurate to $\pm$ 2 ^{0}F(1.1 ^{0}C).

There is, however, another potentially larger source of error that must be assessed. Because of the difference in mud temperature compared to local ambient, differences in diffusivity etc., it is possible that the slope for 6 hours circulation line used in the Homer plot correction may not be the same for all depths in all wells. Data from different Blocks in South Eugene Island show the gradients for a 6 hours circulation time obtained from the Homer plots versus depth. The average gradient is 9.0 ^{0}F-^{1} with a standard deviation of $\pm$4.8 ^{0}F-^{1}.

Because most of the wells in the SEI 330 area are inclined, all the temperature measurements were located at their proper spatial position. Then, using a 3D Krigging algorithm from Spyglass with 500 meters cells, we built a 3D data cube with the interpolated observed temperatures. Slices through this data cube show the same basic features observed by the authors cited above: temperature anomalies follow the strike of the Red Fault System and change with depth.

Bottom Water Temperature (by L. M. Cathles)

The temperature of the top surface in *AKCESS. BASIN* calculations is controlled by water depth, the water temperature above the thermocline, and the depth to the top and bottom of the thermocline.

For the South Eugene Island data cube, excellent data is available on the position of the thermocline (see Cathles, et. al, 1991). We assume the thermocline was in this same position over the last 3.4 ma of basin history.

Material Properties of SEI Block 330 Sediments (by D. Coehlo, Cornell)

Material properties such as thermal conductivity and permeability, and chemical parameters characterizing the rates of organic and inorganic reactions are needed for modeling. This section briefly summarizes the parameters used in the SEI Block 330 modeling.

Long Term Sediment Compressibility

Under a matching grant from the Gas Research Institute and this DOE grant all available porosity logs in the SEI study area were obtained and interpreted. Density logs were found to give the most reliable estimates. Six wells on the hanging wall of the Red Fault, and six on the footwall were selected for analysis.

The wells nearest the Red Fault typically show an increase in porosity below the top of overpressure, whereas the wells more distant from the Red Fault show a flat porosity profile below the seal. From 200-m depth to 1500 to 2000 m depth porosity decreases linearly with depth. Porosities above 200 m decrease more rapidly with depth and were not addressed in the modeling.

Depth was convened to effective stress in the hydrostatic interval above the top of overpressure and porosity regressed linearly against effective stress.

Thermal Conductivity (M. Luo and J. Wood. MTU: L. Cathles. Cornell) Thermal conductivity is a particularly critical parameter for this study. Thermal conductivity is a strong function of temperature. sediment porosity. and pore fluid composition. The temperature dependent media conductivity was obtained by: (1) obtaining the temperature-dependence of the grain, water, oil, and gas thermal conductivities. and (2) then combining them in an appropriate fabric mixture:

A paper showing that a scheme very similar to the above replicates thermal conductivities of water-saturated sediments to within *10% has been published by Luo et. al. (1995) as part of this DOE project. The difference between the Luo et al. scheme and the one given above is that the parallel and series grain thermal conductivities are constructed from sums of the mineral grain thermal conductivities, rather than from sums of the grain thermal conductivities lumped into sand, shale, carbonate sand, etc., end members, where the end members are calculated from their average mineral grain compositions. We have shown that the difference between these two schemes is at most about 1.5%. The lumped approach is geological. simple, flexible (the lumped end members are easily modified), and easy to use. The errors associated with the lumping in to lithologic types are much less than the 10% uncertainty in the mineral composition estimates and thus insignificant.

The parameters used in our thermal conductivity model, plus some other parameters discussed above and below, are:

Permeability in Block 330 Data *Cube* (By D. Coeblo, Cornell)

An extensive database on sand permeabilities in the SEI Block 330 study area was obtained from Pennzoil. It consisted of porosity and permeability measurements from core wall samples in many reservoirs in Block 330. This database was used to develop an empirical model that describes permeability in terms of porosity and sand-shale ratio. The model fits the observed data very well and will

allow, since our model calculations predict porosity changes appropriate sand permeabilities to be ascribed at past geologic times.

Our log model was found to fit the observed relations between porosity and permeability much better than the Karmen-Kozeny relation. The quality of the log model fit can be appreciated if log k is plotted versus porosity. The base permeability of sediments is a function mainly of the size of the mineral grains that comprise the sediment and the lithology of those sediments. The effects of porosity are added to this reference value with the amplitude of the porosity dependence modified by the fraction -of coarse sediment component The sand permeabilities fit those observed in South Eugene Island Block 330 very well. The shale permeabilities are reasonable. The precise value of the shale permeability is not too critical as long as it is substantially smaller than the sand permeability, as is the case in our lithology-porosity model for permeability. The permeability model is a smooth function of porosity.

TTI and R Indices (M. Luo and J Wood, MTU; P. Meulbroek, Cornell)

TTI. a Lopatin-type time temperature index and vitrinite reflectance, R_0. are two measures of sediment maturity that are used in our modeling. 'TI is calculated as described in Waples (1985,1990) by summing the products of the time in millions of years a sediment has spent in each 10^0C temperature interval and a temperature factor. For example a temperature just above 1 10^0C would have a temperature factor of 2, and a temperature just below 100^0C would have a temperature factor of *0.5.*

A Sweeny and Burnham (1990) model for the R_0 measure of vitrinite reflectance is incorporated in Akcess.Basin. In this model:

These models have both been implemented in Akcess.Basin.

The chemistry of the light hydrocarbon gas and heavy oil can be specified in the program. The reactions have first order kinetics with the kinetic parameters as in Burnham and Braun.

The volume change associated with the hydrocarbon maturation reactions is calculated:
(1)The specific volumes of type I kerogen is 0.83 cc/g.
(2)The specific volumes of type II kerogen is 0.74 calg
(3)The specific volume of bitumen and all chars is 0.83 cclg
(4)The volume of hydrocarbon fluids is detenmined from an equation of state.

Hydrocarbon maturation is of interest in its own right because we need to know how much oil and gas could have been generated in the SEI minibasin. Hydrocarbon maturation is also important because the positive volume maturation reactions produce overpressures

With the bottom water temperature defined as a function of water depth, the material propensities of thermal conductivity, porosity, and sediment permeability defined in terms of calculable parameters, and a realistic evolution of the SEI minibasin defined from seismic data and well logs, we are in a position top model the SEI minibasin and interpret observations made there. In what follows we first discuss porosity modeling, then temperature modeling including the effects of episodic venting, and finally chemical modeling including hydrocarbon generation and maturity indicators.

Porosity Modeling (L. Cathles, Cornell; Matching funded by GRI)

Porosity depends on effective stress, but the porosity profile in a basin also

depends on whether there is relative movement of the pressure transition zone (seal) and the basin sediments. The Pathfinder well was logged from 6950 to 8300 ft depth in an interval where the pressure transitioned from soft (13.6 pound mud weight) to hard (16.3 pound mud) overpressure in two roughly equal steps. Below each of the major jumps in pore fluid pressure is a gas-filled sand. The gamma log indicates there are 40 to 50 transitions from sand to shale in the shale intervals above these gas sands. Shosa and Cathles (in preparation) have shown in laboratory experiments that under basin conditions of pressure and temperature and in the presence of a gas phase, an exit pressure of a few bars can be expected at each sand-shale interface within a basin. Since free gas is clearly present, and since the gamma logs show that there are enough sand-shale interfaces in both pressure transition zones to account for the increase in pressure by gas capillary exit pressure effects discussed by Shosa et. al., the pressure transition zones in the pathfinder well could be gas capillary exit pressure seals. If so, because gas exsolution is controlled by pressure and there is no lack of sand-shale interfaces in the upper part of the SEI minibasin, the position of the pressure transition zone there could have maintained a relatively constant depth, with sediments moving through the seal with time.

The porosity profile in a basin depends strongly on whether the seal is fixed to a particular strata or migrates through the sedimentary layers as sedimentation progresses. If there is no seal, compaction is linear until the minimum porosity of 0.1 is attained. If there is a seal overpressuring below the seal decreases the effective stress and inhibits compaction. If the seal is fixed to a particular strata, porosity increases under the seal. Compaction is arrested from shallow depths, and. since the pressure under the seal is limited to 0.8 times the reduced lithostatic load at the seal (e.g., the lithostatic load just under the seal minus the cold-water hydrostatic head there), compaction resumes once a certain amount of burial takes place. For a fixed seal the porosity under the seal is greater than the porosity just above the seal.

If the seal migrates through the stratigraphy so as to maintain a constant depth (e.g.,. the "migrating" seal), the porosity is arrested at the value just above the seal when the sediments move into the seal. The result is a constant porosity to depths at which the effective stress again attains the values it had just above the seal.

Porosity profiles of both the fixed and migrating style are observed in the Gulf Coast. However, it is clear that the porosity profiles in the SEI 330 study area are most similar to the migrating seal profiles. Porosity profiles near the Red Fault show a minor increase in porosity below the top of overpressure in most cases. Thus there is a tendency for seal migration to be more fixed near the Red Fault than further from it. The reasons for this are not clear, but it may be that shearing has disturbed the contiguity of sand-shale interfaces and made it more difficult for the gas-capillary seal to smoothly migrate upward through the section.

The porosities are calculated for the material properties calibrated to the SEI 330 area are slightly different for sands and shales. Thus the sands show up as relatively uncompacted (white) layers on the cross sections. Note that the porosities are calculated for the mid-point of each sedimentary layer.

Comparing the porosity-depth profiles and the observed profiles we conclude that at least since 1.5 ma it is likely that the pressure transition in the SEI 330 area maintained a relatively constant depth and thus the pressure transition zone migrated steadily upward through the sedimentary section as sedimentation took place.

Temperature Modeling (D. Coehlo, Cornell)

Introduction

A large number of 2D temperature simulations have been run for the. Most runs were made for Line 6, the line that passes through the center of the minibasin and passed directly under Pennzoil's Block 330 reservoirs. Several 3D simulations have also been made, and results from these runs are presently being analyzed. The thermal modeling proceeded in stages. First sensitivity analyses were carried out to

assess the relative importance of variable sedimentation, thermal conductivity, sea level variations, heat generation in the sediments by radioactive decay, etc., and to determine the best base case model. These studies revealed the importance of hydrocarbon-related temperature anomalies and radiogenic heat generation. Consequently hydrocarbons and radioactive heat generation were present in the base-case model.

Temperature in the base-case model was then calibrated to the present day temperatures by varying heat flow. Heat flow was not previously known in the SEI study site. Our calibration indicates that the heat flow at 8.5 km depth is be about 1.05 x 10^{-6} cal/cm^2-sec. This is about the value one might have estimated by interpolation from locations in the region where heat flow has been determined.

With the basal heat flow defined, we then calculated the thermal effects of hydrocarbon emplacement between 0.709 and 0.46 ma, and the consequences of this on vitrinite reflectance and other maturity indicators. The emplacement of hydrocarbons produces a thermal blanketing and heating, and this produces a small but potentially measurable vitrinite reflectance anomaly. The anomaly is small compared to that observed in the A6-sidetrack, however.

Table V 2 The impact of various parameter changes on subsurface basin temperature at the level of the Pennzoil reservoirs, ranked in order of magnitude.

	Variable Changed In Test Case	Nature of comparison	Maximum AT in Wells 6 and 17
Hydrocarbons	Hydroc. on reservoirs- dipole above reserve.		
	no hydrocarbons in reservoirs		+15° below
Paleobathymetry	max: always very shallow very deep		+12^{0}C
		probable: always present depth-variable	+2^{0}C
Salt	No salt under line 6 reservoirs - obsv sale		3^{0}C
Timing of HC emplacmt	Hydrocarbons from deposition-base case		3^{0}C
		Early plausible emplacement - base case	1.7^{0}C
Heat Generation		Reasonable maximum - reasonable minimum	+2^{0}C
Solid Advection	Building with hydroc. - steady state w. HC		2^{0}C
Fluid Advection	no flow - steady compactive *flow*		1.5^{0}C
Thermal Conductivity	all sand - all shale stratigraphy		- 1.4 ^{0}C
		realistic lithologic variations	$\pm$O.2^{0}C
		sand	from 9.5 to 11.5 TCU
		best HF changed	shale from 7.4 to 8 TCU
		from 1.05 to 1.25 RFU	
Seal Position		reasonable high - reasonable low seal	+0.08^{0}C

Hydrocarbon maturation calculations show that significant oil is matured only below the salt weld at the base of the SEI minibasin. Thus the oil in the SEI minibasin cannot have been sourced from within the minibasin, and must have been supplied from greater depths either locally or regionally.

Temperature perturbations produced by rupture of the seal were computed for the models and parameters described above, and much more intensively with a very refined grid and very high temporal resolution in an extensive series of calculations. This modeling shows that thermal anomalies of up to

30^0C can be produced by episodic rapid fluid venting. The critical parameter controlling the initial thermal anomalies (first - 100 years of venting) is the fault and sand permeability. The shale permeability is not important at these short time scales.

Temperature Sensitivity Analysis

Sensitivity analyses were carried out to assess the relative importance of the various factors that affect subsurface temperature. The impact of variable changes was generally assessed by calculating the difference in temperature between the test calculation and a reference calculation along pseudo wells 6 and 17 of Line 6 located in the upthrown and downthrown blocks respectively. Table V.2 lists the maximum temperature difference between the test and base models and the parameter varied.

Table V.2 shows that after hydrocarbons, which will be discussed below, the next most important factor is historical variations in water depth in the study, and the position of the sediment-water interface relative to the thermocline that this variation dictates. The water depths assumed for the study area are shown in TableV.3. The depths are constrained by paleontologic data reported in Alexander(1994) and Rowan (1994).

TableV3 Water depths used in the SEI Block 330 modeling as a function of time.

Time (ma)	Water Depth (m)	Time (ma)	Water Depth (m)
0	762.2	100	610
0.46	152.6	338	1.5
0.65	372.7	381	91
0.9	913.4	495	
1.1	914	495	
1.27	100	10	

Other variables affecting temperature have minor impact for various reasons. As can be seen from Table 3, only extreme variations in salt distribution significance affect subsurface temperatures at 1.5 to 4km depth. Heat generation is an important effect, but errors here will be transferred to errors in the inferred heat flow. Solid advection affects subsurface temperature but the differences across the faults are negligible at the depths of interest. This contrasts with McKenna's (1994) conclusion that the "Red Fault' temperature anomalies could have been caused by differences in sedimentation on the two sides of the fault. We find no such effect. Steady fluid advection produces no significant anomalies along the faults. Reasonable variations in the other variables in the Table have a negligible impact on subsurface temperatures.

The sensitivity analysis identified heat generation and hydrocarbons as important variables. Consequently a base case incorporating these variables was established. The base case model is described in Table V.4.

Table V.4. The Base Case Model for the SEI 330 Study Area.

Thermal Conductivity	K(T, f, So, Sg)
Compaction	Linear function of effective stress
Bottom Water T	Function of thermocline and paleodepth
Hydrocarbons	0.709 into GA and HB; 0.65 into OI-JD, 0.46 into DA
Permeability	Function of lithology and porosity
Heat Generation	Values determined by McKenna
Sedimentation History	Inferred from 3D seismic interpretation

Basal heat flux	1.05 x 10-6 call cm2-sec
Hydrocarbon Generation	Modified Burnham and Sweeney
Maturity Indicators	Burnham and Sweeney, Luo

Basal Heat Flow

The basal heat flow in the SEI 330 area was unknown at the start of this study. It was determined by varying heat flow in the base model (Table V.4) and determining the base heat flow that produces present-day temperatures in closest agreement with those observed. In Line 6 the present subsurface temperatures are best matched with a heat flow of 1.0 cal/ cm^2-sec. in the downthrown block and a heat flow of 1.1 cal/cm^2-sec in the upthrown block. In our base case we use a compromise heat flow of 1.05 x 10^{-6} call cm^2-sec. These heat flow values are compatible with the regional pattern of heat flow as inferred from measurements at other sites.

Subsurface T Anomalies produced by Hydrocarbons

The sensitivity analysis shows that the distribution of hydrocarbons is the most important factor affecting subsurface temperatures at 1.5 to 4km depths in the SEI 330 area. Even the timing Hydrocarbon emplacement can affect subsurface temperatures significantly.

The temperature pattern along line 6 with and without hydrocarbons in the Pennzoil reservoirs. When hydrocarbons are added to the appropriate sands and the impact of these hydrocarbons on thermal conductivity is considered, the subsurface temperature pattern changes significantly. Because the hydrocarbons make the sediments much more thermally insulating, their presence in reservoirs produces a steep temperature gradient in the reservoirs, a negative temperature anomaly (isotherm syncline) above the oil fields and a positive anomaly (isotherm anticline) below them. From the perturbation of the isotherms above and below the hydrocarbon reservoirs it can be seen that the positive anomaly below the reservoirs is about 15^0C in magnitude, and the negative anomaly above the reservoirs about 5^0C in magnitude.

The calculated and observed temperature anomalies are compared. The form of the temperature distribution is very similar. In both calculated and observed cases the temperature in the upper salt sill is 75^0C. The observed positive temperature anomaly along the Red Fault is 15^0C, the same magnitude as the calculated, and the negative anomaly above the reservoirs is 5^0C in both cases. The observed temperature distribution does not show the strong steepening in temperature gradient in the reservoirs that the calculated pattern shows so clearly. However, This we attribute to the 500 m cell size of the Krigging that was used to interpret the temperature data in three dimensions. When the 3D temperature simulations are run we will be able to compare the observed and calculated data without interpolation of the observed temperature data and make a much better comparison of the two. At this stage of the analysis we conclude that the present subsurface temperature field appears to be well explained by the thermal conductivity effects of the subsurface hydrocarbon distribution. Rapid fluid venting up the Red Fault is not required to explain present day subsurface temperatures.

Maturity Indicators

Vitrinite reflectance, illite-smectite, and TTI indices of maturity were calculated. Vitrinite reflectance was measured in the Pathfinder and A6 sidetrack wells. The Pathfinder vitrinite reflectance agree extremely well with the values calculated for our base case model. The effect of the differential movement on the Red Fault is clearly reflected in the reflectance Ro, mainly because of the shorter time sediments take to reach equal depths on the high sedimentation side of the fault.

Additional Maturity Caused by Introduction of Hydrocarbons

The thermal blanketing initiated with the introduction of hydrocarbons increased temperatures below the Pennzoil reservoirs. Over time this increased temperature can be expected to produce higher vitrinite reflectance in organic material under the reservoirs. The increased vitrinite reflectance due to the introduction of hydrocarbons was calculated. The increase is about 0.07%. This is not large enough to account for the 0.3% Ro anomaly observed in the A6 sidetrack. Thermal blanketing by hydrocarbons

cannot explain the A6 sidetrack anomaly. However, the maturity anomalies produced by hydrocarbon blanketing are large enough that there is some hope that their accurate definition might constrain the time of emplacement of hydrocarbons in some instances.

Hydrocarbon Maturation

Calculation of hydrocarbon maturation in the SEI data cube shows clearly that there is no hydrocarbon maturation in the minibasin itself. Oil is being generated below the salt weld at the base of the minibasin, but not in the minibasin itself. This is an important result. It shows that the hydrocarbons in Pennzoil's Block 330 fields cannot have been produced in the SEI Block 330 minibasin that hosts them, but must have been produced below the minibasin and introduced when the salt weld opened.

Steady Fluid Flow in the SEI Minibasin

The permeability of the seal is adjusted in nature and in our calculations such that the excess fluid pressures under the seal do not exceed 0.8 reduced lithostatic (lithostatic minus hydrostatic). Fluids leak through the seal where it is topographically highest because it is there that fluid pressures first exceed this fraction of lithostatic. Calculated subsurface fluid pressures agree well with the pressures inferred from mudweights.

Because of the interaction of the migrating seal with low permeability faults and salt, there are several fluid compartments in our simulations of the South Eugene island subsurface. The most interesting case is shown in Line 4 where the Red Fault is a nexus of 4 parallel faults. Flow is occurring into the horse between the two of the faults, and that this focussed leakage is producing a very localized finger of overpressure at shallow depths. Such a finger of overpressure is not observed in the study area, probably because flow leaks across the faults where sands are juxtaposed. However, narrow fingers of overpressure are know in the Gulf Coast. Another feature observed in the simulations is important. Fluids were observed to move horizontally through the sands both to the east and to the west. We are currently addressing this pattern and seeking to simulate Allen-type flow across the faults where sands are juxtaposed. The important point to be made at this stage is that these horizontal fluid flow through sands is intense and the pattern of flow is complex. It is therefore perhaps no surprise that the kinds of rock alteration that depend on fluid flow is complex and difficult to interpret. We hope that despite the complexities modeling can identify the robust aspects of the flow pattern and that these can be verified by alteration data.

T Anomalies Produced by Pukes of Fluid Flow

The temperature pattern 400 years after the seal on both sides of the Red Fault was ruptured, rapidly venting fluids through the permeable sand network in the section. The sides of the fault were given 5.2 Darcy permeabilities, and the sand network had the realistic permeabilities assigned by the porosity-dependent permeability model.

Sudden venting is one possible explanation for the temperature anomalies observed along the Red Fault. However the pattern is not as good a match as the hydrocarbon-generated anomaly pattern. The rapid venting anomaly is not as broad as the observed anomaly, and fluid flow could account for the positive temperature anomaly under the reservoirs and along the Red Fault, but not the negative temperature anomaly above the reservoirs. The temperature pattern produced by hydrocarbons produces the dipolar anomaly pattern observed; rapid fluid venting cannot produce this dipolar pattern.

Analysis of Highly Episodic Fluid Flow(Roberts, Boling Green, Nunn, LSU)

A great deal of modeling attention has been devoted to assessing the magnitude of thermal anomalies that could be produced by episodic rapid venting through ruptured portions of the seal in the Block 330 study area.

The studies that are reported there found that venting from the Red Fault can produce temperature anomalies up to 30^0C in magnitude 350 years after a 10 millidarcy fault is opened. The anomalies are localized within 0.5 km of the Red Fault and do not extend more than 0.75 km above the seal because flow is effectively diverted by the overlying sands. The depth extent of those parts of the fault that

become permeable during a rupture event is important. If the permeable part of the fault extends 0.5 km rather than 1.5 km below the seal, the maximum temperature anomaly after 100 years of venting is reduced from 24 to 15^0C. The permeability of the shale units in the basin does not significantly impact the temperature anomalies produced in the first few hundred years of venting. The permeability of the sands and fault are the important controls. For example, the maximum temperature anomalies calculated for cases where the permeability of the fault is a time-dependent function of fluid pressure (not a constant 10 millidarcies) is 7^0C at 100 years after the start of fluid expulsion. All sands were taken to have 1 millidarcy permeability in the simulations. This value is conservatively low.

These simulations show that temperature anomalies up to 30^0C can be produced along the ruptured parts of a fault in and below the seal. With higher sand and fault permeabilities the episodic flow events could be of very short duration and the temperature anomalies produced along the fault could be extremely local. Very short and intense rupture appear the best candidate to account for the elevated vitrinite reflectance Ro anomalies observed in the A6 sidetrack and the lack of any such anomalies in the Pathfinder 1000 ft away.

Vitrinite Reflectance Anomalies in the A6 Sidetrack

Highly episodic fluid venting can account for the vitrinite reflectance Ro anomalies observed in the A6 sidetrack and the curious feature that the same anomalies are not observed in the Pathfinder well only 300 m from the A6. We have calculated the effects of subjecting fault sediments near where the A6 intersects the Red Fault to temperatures to temperatures 10°C and 30^0C above present ambient for 150 years. These temperature perturbations cause an increase in vitrinite Ro of 0.14 and 0.21%, respectively. This level of additional maturation can easily account for the vitrinite anomaly observed in the A6 sidetrack. In addition, a thermal perturbation lasting 150 years will only propagate about 140 m on either side of the fault. Thus the lack of a vitrinite reflectance in the Pathfinder well 300 m distant from the A6 sidetrack can be explained providing the duration of the fluid venting episode was short.

Fluid Transport in Migrating Fluid-Filled Fractures (Nunn. LSU)

The conclusions of the previous section are very close to a new idea that came out of the DOE project: that upward propagation of water- and hydrocarbon-filled fractures could be a significant mechanism of fluid transport in the overpressured sediments below seals in the Gulf of Mexico and elsewhere. Analysis shows that such fractures could propagate at 1000 m/yr and could cumulatively accommodate mass flux rates of @100 kg / m^2-yr. This idea is described in Nunn (in press).

Thermohaline Convection, Salinity Distribution, and Salt Dissolution

Pore water salinity varies in the SEI 330 study area in ways that suggest fluid movement. Pore water salinities of reservoir sands were estimated from about 50 SP logs. Reservoirs in the SEI study area at <1600 m depth have higher salinities than reservoirs at >2000 m depth. The salinity of the shallower reservoirs has decreased significantly since the 1970's whereas the salinity of the deeper reservoirs has not changed. This may suggest that recent expulsion of low salinity waters from the overpressured zone that have diluted the deeper reservoirs in the recent past are only now diluting the higher reservoirs.

Calculations (Sakar et. al., *1995)* show that thermohaline convection can be a significant mechanism of salt dissolution even in sediments with permeabilities as low as 0.01 md. This shows that the high salinities in the upper Block 330 reservoirs could have been produced by convective dissolution of salt domes in the area.

CONCLUSIONS

Major conclusions from the modeling are:

(1) The present-day temperature distribution, contrary to the perceptions at the start of the project, is a steady state distribution. Thermal anomalies along the Red Fault are due to the blanketing effects of overlying hydrocarbons, not bursts of rapid fluid venting from the overpressured zone.

(2) Vitrinite reflectance and other maturity indicators in the Pathfinder drill hole are well matched by calculated maturity parameters assuming no rapid fluid venting.

(3) No hydrocarbons have matured in the SEI Block 330 minibasin. However kerogen has matured to oil below the salt weld at the base of the Miocene section. Oils and gases in the Block 330 reservoirs must have come from sources below the minibasin, perhaps when the salt weld opened.

(4) The blanketing effect of oil and gas in the Block 330 reservoirs causes the vitrinite reflectance of organic matter along the red fault to increase about 0.07%. This is a potentially observable increase and suggests that the time of hydrocarbon emplacement might be constrained by maturity anomalies. However the maturity increase by hydrocarbon blanketing is much smaller than the 0.3% anomaly observed in the part of the fault penetrated by the A6 sidetrack, a mere 1000 ft from the Pathfinder well. The Ro anomaly in the A6 is corroborated by connodont color changes and fluorescence data and thus the maturity anomaly thus appears to be real.

(5) The maturity anomaly in the AE sidetrack could potentially be caused by rapid episodic fluid venting. Very localized venting up the Red Fault is indicated by the lack of vitrinite anomalies in the Pathfinder well only 1000 ft from the A6 sidetrack. Calculations show that a short-lived (few hundred year) pulse of fluid up Red Fault could produce a localized temperature anomaly in the fault up to and perhaps somewhat greater than 30^0C in magnitude. This magnitude and duration of thermal pulse would be sufficient to produce an Ro anomaly of 0.2%, nearly the 0.3% recorded by the A6 sidetrack measurements.

E. REFERENCES

Alexander, L. (1995). Geologic Evolution and Stratigraphic Controls on Fluid Flow of the Eugene Island Block 330 Mini-basin, Offshore Louisiana. Gulf of Mexico. Cornell PhD Thesis, 25Op.

Dowdie, W. L. and W. M.. Cobb (1975). "Static Formation Temperature from Well Logs -An Empirical Method. Journal of Petroleum Technology' 27:1326-1330.

Guerin, G., Anderson, R. N.. He, W. (1994). "3D Temperature Distribution and Heat Flow Analysis for the Eugene Island 330 Area, Offshore Louisiana AAPG Abstract

Holland, D. S., W. E. Nunan, et al. (1980). "Eugene Island Block 330 Field - USA. Offshore Louisiana." in Halbouty. . ed.. Giant oil and gas fields of the decade:1968-l978 AAPG Memoir #30: 253-280.

Losh, S., L. Eglinton, et al. (1994). "Report on Geologic and Geochemical studies on rocks collected from the Pathfinder well and elsewhere in SEI Block 330 DOE annual report.

Luo, M., J. R. Wood, et al. (1994). "Prediction of Thermal Conductivity in Reservoir Rocks Using Fabric Theory." Journal of Applied Geophysics 32: 321-334.

McKenna, T. E (1994) Evaluation of Subsurface Temperature in Eugene Island Block 330 and Vicinity. AAPG Abstracts

McKenna, T. B. and J. M. Sharp (1995). "Thermal Conductivity and Radiogenic Heat Production from South Texas (Gulf of Mexico Basin)."GSA Abstracts 27(6):

McKenna, T E 3 M Sharp, et al. (1996). '17hermal Conductivity of Wilcox and Frio Sandstones in South Texas (Gulf of Mexico Basin)."Submitted to AAPG Bulletin:

Mello, U. (1994). Thermal and Mechanical History of Sediments in Extensional Basins, Columbia University PhD thesis, 350p.

Meulbroek, P. and L. M. Cathles (in Preparation). "Modeling the Effects of Evaporative Fractionation on Bulk Composition.".

Nunn, 3. A. (1996). "Buoyancy-Driven Propagation of Isolated Fluid-Filled Fractures: Implications for Fluid Transport in Gulf of Mexico Sediments. "Journal of Geophysical Research In Press:

Nunn, J. A., 5.3. Roberts, et al. (1995). Fluid Migration in Eugene Island Block 330 Area of Offshore Louisiana Archie Visualization Technology Conference, Woodlands, Texas,

Roberts, S.J. and J. A. Nunn (1995). “Episodic Fluid Expulsion From Geopressured Sediments." Marine and Petroleum Geology 12: 195-204.

Roberts, S. J., J. A. Nunn, et al. (1996). "Expulsion of Abnormally Pressured Fluids Along Faults." Journal of Geophysical Research In Revision:

Sarkar, A., J. A. Nunn, et al. (1995). "Free Thermohaline Convection Beneath Allocthonous Salt Sheets: An Agent For Salt Dissolution and Fluid Flow in Gulf Coast Sediments." Journal of Geophysical Research 100:18085-18092.

Shosa, S.D. and L. M. Cathles (in Preparation). "A Direct Investigation of Capillary Exit Pressure as a Basin Sealing Mechanism"

Whelan, 3. K., L. B. Eglinton, et al. (1994). "Organic Geochemistry of fluids and Kerogens from DOE Drilling in Eugene Island 330 Reservoirs Indicators of Fluid Flow Pathways." AAPG Abstracts:

Task Six - Geochemistry
Steven Losh - Task Manager

OBJECTIVE:

The purpose of the geochemical phase of this project was to analyze rock, brine, oil, and gas samples in order to test the hypothesis that oil and gas have recently migrated and are still migrating from depth, along growth faults, into the currently-producing reservoirs in the SEI Block 330 field. To accomplish this, analyses were performed on samples from the Pathfinder well, within and adjacent to the main growth fault abutting the Block 330 field, and compared with data obtained from samples from the reservoirs. For organizational purposes, the data so obtained are divided into two categories and are presented in this order in the report: 1) inorganic geochemistry, which includes: a) geology of the core, b) petrographic, mineralogic, whole rock geochemical, and stable isotopic investigations of rock samples, and a) brine chemistry; and 2) organic geochemistry, which includes a) hydrous pyrolysis experiments in order to evaluate controls on and kinetics of gas generation from sediments, and b) a wealth of analyses (many published separately) pertaining to whole oil, gas. and condensate compositions, compound-specific isotopic composition, and biomarkers. An on-line database (c) has been constructed to allow public access to the data collected as a part of the inorganic and organic geochemical investigations. The inorganic geochemical report summarizes the work carried out over the duration of the project, whereas the organic geochemical report summarizes the work accomplished over the past year.

SUMMARY:
Some of the main findings of the geochemical investigation regarding fluid ascent via the growth fault system in SEI Block 330 are:

- Although there is a considerable degree of compositional heterogeneity between reservoirs, the oils, gases, and condensates in SEI 330 appear to have a single source in Mesozoic rocks. The presently-observed variations in composition have resulted from processes that affected the oil and gas during and after migration, such as evaporative fractionation and biodegradation. Gas is characterized via higher thermal maturity than oil, suggesting that the oil is" swept up" by vertically migrating gas. Brine composition, specifically ^{129}I and $^{87}Sr/^{86}Sr$, supports the interpretation of large-scale vertical migration of fluid into the reservoirs. Systematic variations in major element, specifically chlorine, composition of brine between reservoirs indicate that brine entered the reservoirs at different times and/or from different directions.
- A variety of data support ongoing filling of the GA sand via rapid injection, and high fluid flux in the fault zone in the past. Repeated sampling of wells over a period of 10 years has led to the finding that unbiodegraded oils are injected into the GA sand on the time scale of years or less. Biodegradation occurs rapidly there, and the presence of unaltered oil is interpreted to reflect rapid influx from depths at which biodegradation does not take place. A variety of other organic geochemical data corroborate this conclusion. In the A6ST well, which penetrates the main growth fault a point 1000 feet from the fault intercept in the Pathfinder well, sediments from within the growth fault are characterized by anomalously high vitrinite reflectances relative to sediments outside the fault, indicating that the fault is locally a paleothermal anomaly. Combined with stable isotopic composition of minerals from the fault in that well, these data support the conclusion that the fault, at least at some locations, acted as a conduit of relatively high-temperature fluids.
- The Pathfinder core contains three structurally - distinct fault domains, only the deepest of which contains oil. Based on structural and geologic data, this deepest domain is concluded to have been most recently active. Structural and geochemical data indicate the other two fault domains were active prior to oil migration. The oil-barren domains contain fractures that are favorably oriented to transmit oil. Oil is furthermore present in sands in these domains. It is evident that fault zone oil migration took place only within that part of the fault that was active during the time migratable oil was available to the fault. Despite the variability of hydrogeologic characteristics of faults as evident in the core, the geochemical data indicate that none of these cored faults transmitted significant amounts of fluid in the Pathfinder well, indicating the operation of a higher-order control on fluid flow in the growth fault. The same fault in the A6ST well has apparently acted as a fluid conduit, indicating relatively short-range lateral variability in fluid flow behavior in the fault.

Tasks include:

- Development of protocol for acquisition, preservation, and complete analysis of core, involving research and meetings in Houston with oil company and service company personnel. The coring procedure was highly successful and has been adopted by Pennzoil and other operators in the Gulf.
- Overseeing coring while on rig. Funds were also redirected to cover cost overruns for core acquisition.
- Logging core in detail while Pathfinder was being drilled.
- Structural interpretation of core.
- Core preservation and curation.

SUBTASK 6.2
ORGANIC GEOCHEMISTRY
Sean Whelan, WHOI
October 9.1995

SUMMARY OF TECHNICAL PROGRESS:

Organic Geochemistry, Hydrous pyrolysis:

Introduction

Thermal maturation of sedimentary organic matter involves numerous chemical transformations that result in the production of hydrocarbon and non-hydrocarbon gaseous alteration products. These products play a critical role in the development of overpressure, the transport of petroleum, and sediment diagenesis in sedimentary basins (Hunt *et at*, 1995; Price *et at.*, 1983; Whelan *et at*, 1994a,b). Understanding fundamental processes that regulate the generation of gaseous products is essential to constrain factors influencing the accumulation of hydrocarbons in the Gulf Coast, USA. Owing to the extreme complexity of natural systems, key processes that regulate the timing, amounts, and composition of organic alteration products are often obscured. Laboratory beating experiments have proven to be an effective tool for constraining physical and chemical processes associated with the generation of hydrocarbons. In particular, the role of water during organic reactions in geologic environments has received much attention in recent years (Helgeson *et at*, 1993; Hoering 1984, Lewan 1991, 1993; Seewald 1994: Shock 1988; Siskin and Katritzky, 1991; Stalker *et at.*, 1994). Laboratory experiments have demonstrated that the presence of water during the maturation of sedimentary organic matter significantly influences the amounts and composition of liquid hydrocarbons. It is likely that water may also play an integral role in the generation of volatile hydrocarbons and non hydrocarbon such as carbon dioxide. Except for a few notable exceptions (Lewan 1992; Tannenabaum and Kaplan *1985;* Seewald 1994) laboratory studies focusing on the generation and stability of hydrocarbon and non-hydrocarbon gases have been conducted in the absence of added water.

The experiments presented here were conducted to constrain factors influencing the generation of natural gas and carbon dioxide during the thermal maturation of sedimentary organic matter from the Monterey, Smackover, and Eutaw formations. The experimental design reflects our attempts to duplicate natural conditions in the laboratory. Water is ubiquitously present in most sedimentary basins. Accordingly, our experiments involved heating bulk sediments in the presence of liquid water. Experiments were conducted at temperatures ranging from 125 to 360^{0}C at 350 bars pressure, conditions that are similar to those in most sedimentary basins during gas generation.

Methods

Sample Description and Preparation.

Samples of the Monterey, Smackover, and Eutaw Shale were used for the experiments presented here. These samples allow comparison of the gas generation characteristics of a sediment containing sulfur-rich organic matter primarily of marine origin (Monterey

Shale), with two sediment samples containing relatively sulfur-poor organic matter primarily of terrestrial origin (Eutaw and Smackover Shale).

The Monterey Shale is a thermally immature (bituminite reflectance = 0.25% expressed as R_0) consolidated sediment sample from the Miocene Monterey Fm. (ML9I-17). It was obtained from an outcrop at Naples Beach, CA. The sample was removed from a 10cm interval at the base of Unit 315, approximately 9 m below the lowest phosphorite horizon (M.D. Lewan, personal communication). The sample comprised a lenticularly laminated claystone and visually appeared fresh (i.e. unweathered) and blocky. The surfaces of the sample were scraped to expose pristine material and remove possible contaminants. This sample is organic rich (20.6 wt. % TOC) and based on petrographic observations and elemental analyses can be classified as a type Il-S kerogen.

The Eutaw Shale is a Cretaceous consolidated sediment obtained from core cuttings recovered at a depth interval of 3011 to 320 m from the Hampton/Nelson Ball well in Pike County, Mississippi. It is a relatively organic lean shale (0.97 wt. % TOC) and contains abundant quartz. A measured vitrinite reflectance value of 0.45% R_0 indicates that the kerogen has not yet reached the oil window. Petrographic observations indicate that this sediment contains mostly terrestrial derived organic matter that can be classified as type-Ill kerogen.

The third shale is a sample from the Upper Smackover formation (Jurassic). It is a consolidated sediment obtained from core cuttings recovered at a depth of 3260 m from the Amareda Scotch Well #1 in Clark County, Alabama. This shale is relatively organic-lean (0.917 wt. % TOC), contains abundant quartz, and has a measured vitrinite reflectance value of *0.52%* R_0. Petrographic observations indicate that the kerogen in this sample is type-III and characterized by a similar maceral type distribution as the Eutaw Shale.

During this study our primary goal was to constrain chemical processes that regulate the rate and extent of chemical reactions responsible for the generation of gaseous products. Accordingly, to minimize physical processes associated with expulsion of produced gases. The starting sediments were pulverized in a disc mill until the entire sample passed through a <125-mm sieve. In addition, existing hydrocarbons were removed prior to heating. This was achieved for the Eutaw and Smackover Shale by Soxhlet extraction in a 93:7 CH_2CI_2/CH_3OH mixture for 48 h. The Monterey was sequentially extracted by sonic disruption for 9 minutes in CH_2CI_2, a 1:1 mixture of CH_2CI_2/CH_3OH, and CH_3OH. Because we were concerned only with carbon dioxide generated from sedimentary organic matter, the starting sediments were treated with 10% HCl at 4)^{0}C for 2 h to remove sedimentary inorganic carbonate minerals that could dissolve during an experiment. For the Monterey Shale experiments at 225 and 275^{0}C, the sediment was not treated with HCl. Thus, generated carbon dioxide for these two experiments almost certainly includes a contribution from inorganic carbonate.

Experimental Apparatus and Conditions

The experiments were conducted in 316 stainless steel tubing reactors with a 20 cm^3 internal volume. The experiments described here are in many ways similar to the hydrous pyrolysis experiments described by Lewan (1991) in that bulk sediments are heated in the presence of excess liquid water, but there are important differences. For example, in our experiments the reactor vessel is filled completely with liquid water precluding the existence of a vapor head space during an experiment. This may be particularly significant for studying volatile products since they effectively partition into a vapor head space at the conditions of an experiment removing them from intimate contact with the water and sedimentary components. In addition the apparatus utilized for this study allows fluid samples to be withdrawn from the pipe-bomb at the temperature and pressure of an individual experiment avoiding potentially ambiguous reactions during a prolonged quench process. Moreover, because the experiments do not need to be cooled to determine the amounts of generated gases, fluid chemistry can be monitored as a function of time during an individual experiment.

During this investigation, it was assumed that all generated gases dissolved into the aqueous phase at the conditions of these experiments. To avoid the formation of a separate gas or oil phase, which might represent a sink for gaseous alteration products, relatively high water/sediment mass ratios were used. For each experiment 1.0 g of bulk sediment was loaded into the tubing reactor before sealing. Prior to heating, the air in the tubing reactor was evacuated and partially filled with argon-purged distilled water to ensure that the sediment was in contact with liquid water during heating. The entire reactor was heated to the experimental temperature in a horizontal tube furnace in approximately 30 minutes. Once at the desired temperature, the tubing reactor was completely filled with distilled water and pressurized to 350 bars so that only a single liquid phase was present (i.e., no head-space). Temperature was monitored (+- 2^0C) with a thermocouple at each end of the tubing reactor to ensure there were no thermal gradients. Experiments utilizing the Monterey and Smackover Shale were conducted isothermally for approximately 170 h. In contrast, the Eutaw Shale investigation was conducted by maintaining the tubing reactor at a constant temperature for a selected period of time before rapidly increasing the temperature to a new value. At each temperature condition gas generation was monitored as a function of time.

During the course of an experiment fluid samples were withdrawn into glass gas-tight syringes and monitored for the concentration of dissolved species. An internal 10 um steel mesh filter ensured particle free fluids. Pressure was maintained during the sampling process by pumping argon-purged distilled water into one end of the tubing reactor with an HPLC pump while the fluid sample was removed from the other. The sampling process was performed rapidly 1 to 2 minutes) to avoid dilution of the fluid samples with the freshly injected water. All subsequent concentrations of dissolved gases were corrected for the amount of water injected on each sampling occasion.

Analytical Procedures

Fluid samples were analyzed for the dissolved concentrations of CO_2, C_1-C_4 hydrocarbons, and for selected samples dissolved organic acid anions, H_2, and H_2S. The first aliquot of fluid (0.5 ml) withdrawn from the tubing reactor on any sampling occasion was discarded and. served only to flush the sampling valve and stainless steel lines. Dissolved CO_2 and C_1-C_4 hydrocarbons were analyzed in duplicate in subsequent aliquots (0.5 ml) by injecting the sample into a purge and trap apparatus interfaced directly to a gas chromatograph equipped with a flame ionization and thermal conductivity detector connected in series. The fluid samples were acidified with 1 ml of 25 % phosphoric acid in the purge cell to ensure complete evolution of dissolved CO_2. Separation of gases in the gas chromatograph was achieved with either a porapak-Q packed column or a poraplot Q megabore capillary column. Authentic standards were used to establish a three level calibration curve for CO_2 and each hydrocarbon. Analytical uncertainties are estimated to be <5 % for these species.

The concentrations of aqueous organic acid anions generated during the experiments were analyzed by ion chromatography on a Dionex DX-300 ion chromatograph equipped with an AS II column and a conductivity detector. Samples were preserved with 200 ppm mercuric chloride and stored in a refrigerator prior to analysis. Authentic standards were used to establish a three level calibration curve for all acids reported

Dissolved H_2 concentrations were determined by gas chromatography (thermal conductivity detector and a SA molecular sieve packed column) following a headspace extraction. Dissolved H_2O was determined gravimetrically by acidifying the fluid sample with 25 % phosphoric acid and precipitating the evolved H_2S as Ag_2S in a 3 wI.. % AgNO3 solution. Estimated uncertainties for the H_2 and H_2S analyses are <5 %.

Careful accounting of all fluid removed and added to the tubing reactor allowed the absolute amounts of generated products to be calculated from the dissolved concentrations, tubing reactor volume, and the mass of sediment in each experiment. The specific volumes of water at the temperature and pressure conditions of each experiment were calculated from the equation of state for water of Haar *et* at, (1980).

Elemental analyses (CRNSO) of the starting sediments and solid alteration products were conducted on either a Leco 932 or Fisons EAl 108 elemental analyzer. Inorganic carbonate (IC) was determined on a Coulometrics carbon analyzer. Total organic carbon (TOC) was determined by difference. The starting sediment and solid alteration products for the Monterey Shale experiments were demineralized by HCI and Hf acid digestions (Eglinton and Douglas, 1988) to isolate the kerogen. Iron sulfides were removed from the kerogen by treatment with $crci_2$ and HCI (Canfield *et at,* 1986; Acholla and Orr, 1993). The relatively pure kerogen isolate was analyzed for its elemental composition. Similar kerogen isolations for the Eutaw and Smackover Shale were not possible owing to the low organic matter content of these sediments.

Results

Volatile Products

Thermal maturation of organic-bearing sedimentary rocks is characterized by (lie generation or gaseous alteration products, the extent and rate, which are strongly dependent on time and temperature. For example, during the Monterey and Smackover experiments, methane generation increased by more than three orders of magnitude during heating at 360^0C relative to 125^0C, while methane generation was almost 3 orders of magnitude greater at 360^0C relative to 225^0C for similar reaction times during maturation of the Eutaw Shale. The concentrations of ethane and propane showed similar temperature trends although the absolute abundance of these hydrocarbons were substantially less than that of methane. Although, methane is the dominant hydrocarbon gas generated at all conditions during these experiments, its relative abundance shows a clear trend as a function of temperature. At 125^0C methane constitutes approximately 90% of the generated hydrocarbon gas while at 360^0C its relative abundance has decreased to approximately 40 %. Increasing maturation time results in decreasing relative abundance of methane on the time scale of these experiments.

In addition to alkanes significant quantities of alkenes were generated at all temperature for all sediments. In general the abundance of alkenes increased with increasing temperature. In contrast to the saturated hydrocarbons, however, the abundance of alkenes decreased with continued reaction at constant temperature, except during the 125°C experiments in which their abundance remained effectively constant. These results indicate that ethene, propene, and *n* butene are unstable at temperatures> I50~C. That the alkene abundance at 125^0C remained constant while the abundance of alkanes increased may suggest that alkenes were being generated but degradation reactions were occurring at a similar rate. These results confirm the hypothesis of Tannenbaum and Kaplan (l985) who suggested that alkenes are initially produced in small quantities under dry or hydrous conditions but represent an unstable intermediate during the formation of petroleum.

Although the thermal maturation of sedimentary organic matter results in the production of substantial hydrocarbon gases, carbon dioxide was unequivocally the dominant gaseous alteration product. During thermal maturation at 360^0C 312, 337, and 194 mg/g TOC carbon dioxide were produced from the Monterey, Smackover, and Eutaw Shale, respectively, and was still increasing in all experiments, even after heating the Eutaw Shale for 2716 h at 360^0C. These quantities are at least an order of magnitude greater than the total amount of hydrocarbon gases produced from each sediment. Carbon dioxide generation increased with increasing temperature, similar to the hydrocarbon generation trends.

Owing to the possibility that carbonate minerals such as calcite or siderite can precipitate during hydrous pyrolysis experiments, carbon dioxide values represent absolute minimums. Evidence for calcite precipitation is provided by the Monterey experiments MS5 and MS 13. In contrast to the other Monterey experiments in which the rate of release of carbon dioxide to solution showed continuously

decreasing rates with increasing reaction time, MS5 and MS 13 were characterized by initially rapid carbon dioxide increases in solution followed by relatively minor increases between the samples at 25 and 70 h. A subsequent rapid release of carbon dioxide was observed between 70 and 170 h. This trend suggests that carbon dioxide may have been precipitating as a carbonate mineral suppressing the amount observed in solution. The non-systematic increases in carbon dioxide released to solution as a function of temperature during the Smackover Shale experiments may also suggest carbonate mineral precipitation, since the solubility of carbonate minerals is particularly sensitive to pH and dissolved Ca or Fe concentration in addition to temperature, pressure, and dissolved carbon dioxide concentration. Requisite Ca and Fe for the formation of calcite and/or siderite was likely derived from feldspars, clays, and/or iron sulfides present in the sediment. Carbonate minerals were not observed petrographically at the termination of each experiment. Although mass balance calculations indicate that only trace amounts of carbonate minerals would form unless the majority of carbon dioxide precipitated. Immersion of some of the alteration products in dilute HCI resulted in minor effervescence suggesting the presence of a minor carbonate phase.

Determination of total dissolved $H_2$5 concentrations in the Monterey Shale experiments revealed increasing abundance in solution with increasing temperature in the range 250 to 360^{0}C At temperatures <225^{0}C dissolved H_2S concentrations were too low for gravimetric determination, but H_2S was detectable by odor in all experiments. No attempt was; made to determine H_2S abundance in the Eutaw and Smackover Shale experiments but a strong Pr2s odor in all fluid samples indicated its presence. The absolute abundance of total dissolved H_2S was likely regulated by the solubility of iron sulfides such as pyrite and/or pyrrhotite owing to the rapid dissolution precipitation kinetics for these minerals under hydrothermal conditions (Seewald and Seyfried, 1990). Pyrite was abundant in the unheated Monterey Shale and persisted along with newly formed pyrrhotite in the thermally altered sediments. Sources of sulfur during these experiments include diagenetic pyrite and organic matter. Although it is not possible to quantitatively determine the relative contributions from these two sources, the amounts of H_2S released to solution at 350 and 360^{0}C, 12.7 and 18.8 mg/g sediment, respectively, exceed the amount of sulfur present as diagenetic pyrite in the starting sediment (10.5 mg/g sediment as H_2S). Thus, these data indicate the release of organically bound sulfur to solution. Because sulfide is likely cycled through the solution into iron sulfide minerals, the amounts of organically bound sulfur indicated here represent minimum values.

Dissolved H_2 concentrations were determined in the final fluid samples from the Monterey Shale experiments at 200,300, 325,350, and 360^{0}C and in samples from the 325 and 360^{0}C phase of the Eutaw Shale experiment. During the Monterey Shale experiments the dissolved H_2 concentrations showed a systematic increase with increasing temperature, except for experiment M55 at 325^{0}C. Experiment MS5 was the first experiment conducted in a new tubing reactor and the relatively high dissolved H_2 concentrations may reflect R_2 released as a result of water disproportionation associated with oxidation of the stainless steel tubing reactor. Similarly, the Eutaw Shale experiment was also conducted in a new tubing reactor. Thus, the relatively high dissolved H_2 concentrations observed at 325^{0}C may reflect oxidation of the reactor walls. Continued reaction at constant temperature resulted in decreasing dissolved H_2 concentrations.

Organic Acids

The abundance of organic acid anions were determined in fluid samples from the Monterey and Smackover Shale experiments. Acetate was the most abundant organic acid anion in all samples. 'Thermal maturation of Monterey Shale also resulted in the production of formate and propionate and trace amounts of valerate, oxalate, and succinate. In contrast, thermal maturation of the Smackover produced significant formate but did not generate dectatable quantities of propionate, valerate, oxalate, and succinate, except for experiments SM6 and SM1 in which trace amounts of oxalate were detected. There is some indication that the abundance of acetate and propionate increased with increasing temperature

during Monterey Shale maturation. Continued reaction at constant temperature in the relatively high temperature experiments (>225^{0}C) resulted in decreasing acid concentrations, most likely the result of decarboxylation reactions (Kharaka *et at.*, 1983; Palmer and Drummond, 1986). The abundance of organic acids during the Smackover Shale experiments showed no clear trends with temperature.

Solid Alteration Products

In general, the bulk sediments were characterized by decreases in TOC contents consistent with the generation of hydrocarbons. The N and S content of the Monterey bulk sediment also decreased. Analyses of the Monterey Shale isolated kerogen, however, reveals chemical changes directly associated with kerogen maturation. For example, increasing C accompanied by decreasing O and H contents with increasing temperature indicates the residual kerogen was becoming more C-rich, a likely result of the generation of hydrocarbons and carbon dioxide.

Examination the data reveals a minor initial increase in the TOC content of the solid products during low temperature maturation. Because the sediment represents the only source of C present during the experiments, this increase likely reflects dissolution of the inorganic sediment components. Quantitative determination of the extent of inorganic mineral dissolution is not possible with the data available. However, to produce an increase from 20.6 wt. % TOC in the initial sediment to a value of 23.5 wt % in the alteration products from experiment MS 10 at 150^{0}C requires dissolution of 12.3 wt. % of the inorganic minerals present. This value is an absolute minimum because generation of liquid and gaseous C-bearing alteration products would result in decreasing TOC contents for the solid alteration products. If the amount of liquid and gaseous C-bearing products are accounted for, dissolution of approximately 15.0 wt. % of the inorganic minerals present is required.

Discussion

Generation of gas during the thermal maturation of kerogen involves a diverse and large set of reactions. Formation of low molecular weight hydrocarbons and carbon dioxide can occur as a result of the direct cleavage of functional groups from the kerogen macromolecule and/or secondary reactions involving generated long chain hydrocarbons that compose bitumen. The latter process is commonly referred to as "oil cracking". Current models that constrain the timing and amounts of carbon dioxide and hydrocarbon generation are to a large extent based on compositional trends observed for the maturation of kerogen in response to increased time and temperature. Examination of the data reveals that early stage maturation results in the loss of oxygen, a likely result of the cleavage of carboxyl, carbonyl, and methoxy functional groups, and little decrease in the hydrogen content of kerogen. Continued heating results in exhaustion of kerogen oxygen and decreases in the hydrogen content of kerogen. It is generally assumed that kerogen represents the only source of oxygen and hydrogen available for carbon dioxide and hydrocarbon generation involving organically derived carbon (Tissot and Welte, 1984; Ungerer 1990; Cooles *et al.*, 1985; Barker, 1990). Accordingly, peak carbon dioxide generation is generally viewed as an early-stage phenomenon that precedes peak hydrocarbon formation (Tissot and Welte, 1984). The results of this study, however, suggest that carbon dioxide generation may be substantially more pervasive. Although, significant quantities of carbon dioxide where generated during sediment maturation at low temperatures, carbon dioxide continued to be the dominant gaseous alteration product at 360^{0}C in all experiments. For the Monterey experiments, carbon dioxide production continued at temperatures significantly higher than those associated with peak bitumen formation which occurs during hydrous pyrolysis experiments at approximately 275^{0}C (Baskin and Peters, 1992; Nelson *et* at., 1995). Thus, based on experimental evidence carbon dioxide generation occurs before, during, and after peak hydrocarbon generation.

Variations in the compositional evolution of kerogen during the Monterey Shale experiments are consistent with maturation trends observed in nature. Large decreases in the oxygen kerogen content were observed in the relatively low temperature experiments with only a minor decrease

in the hydrogen content while maturation at relatively high temperatures resulted in only minor decreases in oxygen content and substantially greater decreases in the hydrogen content.

Possible sources of oxygen during these experiments include H_2O and oxygen bound in inorganic minerals. Considering the low ferric iron content of the Monterey Shale and thermodynamic barriers to reducing ferrous iron and aluminosilicate minerals, oxygen directly from these sources is not available for the formation of oxygen-bearing organic alteration products. Thus kerogen and H_2O represent the only additional source of oxygen during these experiments. H_2O has been implicated as a source of oxygen in other hydrous pyrolysis experiments at temperatures ~300^0C (Lewan 1992; Stalker et at.. 1993). Thus, H_2O may represent an important source of oxygen during kerogen maturation in these experiments and in natural systems.

Consumption of H_20-derived oxygen during the production of oxygen-rich alteration products would necessarily result in the release of hydrogen. Hydrocarbon formation represents a likely sink for excess-hydrogen during the thermal maturation of sedimentary organic matter. Results of redox-buffered hydrothermal experiments have demonstrated the incorporation of water-derived hydrogen during the saturation of ethene to form ethane at 325^0C (Seewald 1994). These experiments demonstrated that the relative abundance of ethene and ethane are controlled by a state of metastable redox dependent thermodynamic equilibrium that directly involves water. Similar reactions are likely during the present experiments. Alkenes which are a known product during the pyrolysis of sedimentary organic matter under dry and aqueous conditions (Tannenbaum and Kaplan, 1985; Esser and Schwochau 1991) were abundantly present in the early stages of these experiments and showed decreasing abundance with increasing time, even at temperatures as low as 150^0C. This trend is consistent with saturation of alkenes with H_20 derived hydrogen to form alkanes. Alkenes did not completely disappear during any of these experiments even after reaction 2716 h at 360^0C suggesting they were likely approaching a state of metastable thermodynamic equilibrium in response to the redox state of the chemical system.

The possibility that H_20 may represent a source of oxygen and hydrogen for the formation of carbon dioxide and hydrocarbons has important implications for the generation of oil and natural gas in sedimentary basins. Presently, most models that predict maximum oil and gas yields during from kerogen assume that requisite hydrogen and oxygen are only derived from kerogen only. Owing to the ubiquity of water in most sedimentary basins, these models may underestimate the oil and gas potential of sedimentary organic matter. Predicting maximum yields of organic-derived alteration products is a complicated and difficult task since the reactions involved are a function of numerous parameters including organic matter composition, temperature, pressure, and the chemical environment at the site of generation. It is unlikely that hydrogen availability represents the limiting factor during the initial generation of liquid hydrocarbons since it is generally believed that these products are produced to varying extents by the cleavage of intact fragments of kerogen which retain many of the compositional characteristics of the source kerogen. In addition, because early generated oil is composed of relatively long chain hydrocarbons only minor amounts of hydrogen are required to produce saturated products. With increasing thermal maturation, however, hydrogen demands increase as organic transformations result in a decrease in the average carbon chain length of hydrocarbons and associated increases in the H/C ratio. Thus, it is likely that H_2O-derived hydrogen may represent an important contributor to the overall hydrogen budget under high temperature conditions that result in the extensive cracking of oil to form natural gas.

Catalytic Processes

Reactions responsible for the production of natural gas via the cracking of long-chain hydrocarbons have been viewed as purely thermal processes during which sufficient thermal energy is available to result in cleavage of carbon-carbon bonds (Tissot and Welte, 1984; Barker 1990; Ungerer 1990) or as thermocatalytic processes in which the energy required to break carbon-carbon bonds is substantially lowered due to the presence of a catalyst (Mango et at., 1993). Mango et at. (1993) argues that a purely thermal model for the production of natural gas requires temperatures in excess of those

found to exist during natural gas production in natural systems and produces a gas that is compositionally distinct. In general, natural gas is composed predominantly of 50 to 100 wt. % methane with lesser amounts of ethane and propane. In contrast, laboratory experiments have demonstrated that thermal cracking of petroleum and pure hydrocarbons produces a hydrocarbon assemblage that contains significantly lower amounts of methane (Horsfield et at., 1992; McNab *et* at, 1952; Fabuss et at, 1962; Appleby et al, 1947). Mango (l993) demonstrated in the laboratory the catalytic activity of the Monterey Shale by producing a gas product via the thermocatalytic cracking of n-octadecene- 1 in a hydrogen at 1 atm total pressure at 190 to 220^{0}C under anhydrous conditions to produce a gas product with a strikingly similar composition to that of natural gas. He suggests that transition metals present in the sediment represent the catalytically active species.

Reactions occurring during laboratory heating of the Monterey, Smackover, and Eutaw shale results in the production of low molecular weight hydrocarbons whose relative abundance is consistent with those observed in nature. In all the experiments, methane constituted approximately 40 to 90 % of the generated hydrocarbon gas suggesting catalytic activity may be important. The relative abundance of methane varied systematically with temperature and time. Increasing temperature resulted in decreases in the relative abundance of methane. A possible explanation for this trend is that the selectivity of the operant catalyst varies with temperature. Alternatively, the temperature dependence may reflect a systematic shift in the individual reactions responsible for the production of methane. For example, methane generation at low temperature may reflect production directly from kerogen while high temperature generation may be the result of oil cracking reactions. Regardless of the reactions responsible, the rates of methane production observed during these experiments are sufficiently rapid to produce substantial accumulations of natural gas on a geologic time scale (see below).

Although the results of these experiments appear consistent with those of Mango et at. (1993), there are some important differences related to the experimental conditions. The experiments presented here were conducted at 350 bars in the presence of liquid water while those of Mango et at. (1993) were at 1 atm in a dry system. Mango et al. (1993) observed decreasing selectivity towards methane upon addition of high amounts of water. Perhaps more importantly, however, is the presence of abundant dissolved sulfur species in our experiments, which were essentially absent in the Mango et at. (1993) study. Sulfur is well known poison for the catalytic activity of transition metals due to the formation of transition metal sulfides. The presence of sulfur notwithstanding, the apparent catalytic activity in our experiments suggests that sediment components other than transition metals may represent the catalytically active species. Possibilities include dissolved sulfur species, inorganic minerals, and organic compounds such a~ NSO-rich asphaltenes.

Kinetic Modeling

Numerous models have been developed to predict the extent and timing of hydrocarbon generation in sedimentary basins (Sweeney et al, 1995; Hunt et al, 1991; Ungerer 1990; Braun and Bumham; 1990; Lewan 19S5; Lopatin 1971,1976; Karweil 1956; Waples 1980). In general, these models are based on reactions that are governed by first order reaction kinetics and the Arrhenius equation, but vary significantly with respect to the number of reactions that are used to describe the process of hydrocarbon generation. The thermal maturation of kerogen to produce oil and gas is an inherently complex process involving numerous sequential and parallel reactions. Accordingly, even the most complex kinetic models represent gross simplifications of naturally occurring processes. Nonetheless, they represent effective tools for petroleum exploration and predicting the geochemical evolution of sedimentary basins, provided of course that reliable data for activation energies and pre-exponential factors are available.

Laboratory experiments represent a unique opportunity to calibrate kinetic models under controlled conditions of time and temperature. Data from the present experiments are ideally suited to provide kinetic data for the generation of light hydrocarbons and carbon dioxide since gas generation was monitored as a function of time over a wide range of isothermal conditions. For this purpose we used computer code KINETICS (Braun and Burnham, 1990) to analyze the data from the experiments. This code fits an average pre-exponential frequency factor (A_0) and the relative fractions associated with a given activation energy (Ea) for by up to 25 first order parallel reactions. For the present analyses, the absolute amounts of gases generated were convened to fractions reacted relative to the maximum generated at 360^0C. A 2-kcal/mole spacing between consecutive values of Ea was used for all calculations.

Results of the kinetic analyses indicate that the generation of carbon dioxide and methane are characterized by different pre-exponential frequency factors and activation energy distributions that are also dependent on the composition of the source kerogen. Methane production from the Eutaw and Smackover Shale (type-III kerogen) is best accounted for by Ea values in the narrow range of 70 to 74 kcal/mole and A_0 values of 1.15 x $l0^{19}$ s^{-1} and 3.74 x $l0^{19}$ s^{-1} respectively while production from the Monterey shale (type II-s) requires Ea values in the range 66 to 68 kcal/mole and a an A_0 value of 6.37 x $l0^{18}$ s^{-1}.

In contrast to low molecular weight hydrocarbon generation, the Ea distributions for carbon dioxide production are characterized by a wide range of energies that vary from approximately 40 to 64 kcal/mole for both the Monterey and Eutaw shale. This distribution may suggest that a more diverse set of reactions is responsible for the generation of carbon dioxide. For example, it is likely that carbon dioxide production associated with low values of Ea is the result of the cleavage of oxygen-bearing functional groups directly from the kerogen macromolecule while that associated with high values of Ea may reflect reaction of organic compounds with water.

Application of the kinetic parameters retrieved from the experimental data to temperature and time conditions typical of petroleum producing sedimentary basins allows predictions to be made regarding the timing of gas generation. Gas generation curves for a hypothetical basin with a geothermal gradient of 25^0C/km that is subsiding at a rate of 2 km/My. The bulk of methane generation is restricted to a relatively narrow temperature range of 170 to 220^0C for the Monterey Shale while generation from the Eutaw and Smackover Shale is shifted to temperatures approximately 20^0C higher. Carbon dioxide generation from organic matter, however, is predicted to occur continuously from low temperatures that characterize early diagenesis to temperatures as high as 220^0C reflecting the wide range of activation energies associated with its production. Thus, extrapolation of the experimental results to natural conditions indicates that carbon dioxide production is not restricted to diagenetic processes that proceed peak hydrocarbon generation but can be expected to occur during all phases of kerogen maturation including natural gas formation deep within a sedimentary basin.

Comparison of the kinetic parameters derived here with previous studies shows both agreement and disagreement. Horsfield et al. (1992) used the results of confined anhydrous pyrolysis experiments to derive an Ea distribution that ranged from 66 to 70 kca1/mole and a A_0 value of 1.1 x 10^{16} s^{-1} for the cracking of a relatively immature crude oil from the North Sea to form C_1-C_4 hydrocarbons. These values correspond to the bulk of natural gas formation at temperatures of approximately 170 to 220^0C in the hypothetical basin described above, consistent with the results of our experiments. Generation of gas during our experiments is a two step process involving the initial generation of bitumen followed by thermocatalytic cracking to produce gaseous products. The striking similarity of Ea and A_0 values determined here with those Horsfield et at. (1992) for petroleum cracking suggest that generation of bitumen may be a relatively rapid process occurring at relatively low temperatures while the cracking of bitumen represents the rate limiting step that dominates the timing and extent of gas generation in our experiments.

Knaus et at. (1992) derived individual Gaussian distributions of activation energies for the generation of methane, ethane propane and butane from hydrous pyrolysis experiments examining the

New Albany Shale. Their results indicate Ea distributions centered on a value 55 kca1/mole for the generation of all gases. The significantly lower Ea values may be due to the fact that they assumed an A_0 value determined using a Pyromat II instrument applied to their hydrous pyrolysis experiments. There is no obvious reason to support such an assumption, however, since reactions occurring during open-system anhydrous, high temperature and low pressure pyrolysis are not likely to resemble those during closed system, hydrous, relatively low temperature and high pressurepyrolysis experiments. Alternatively, the discrepancy between Ea values determined by Knaus *et at* (1992) may be due to compositional differences between the New Albany Shale arid the sediments examined here.

Summary

Laboratory experiments represent an effective means to constrain processes responsible for organic transformations that occur in sedimentary basins. Results of hydrous pyrolysis experiments conducted as part of this project indicate that carbon dioxide is the dominant volatile alteration products generated during thermal maturation of the Monterey, Smackover, and Eutaw Shale. Carbon dioxide formation is not limited to early diagenesis but continues during and after peak hydrocarbon formation. Methane constitutes 40 to 90 % of the generated hydrocarbon gases. This distribution of hydrocarbon gases is consistent with those observed in nature and suggests that thermocatalytic cracking controls the generation of natural gas. Low molecular weight alkenes are generated but rapidly decrease in abundance with continued maturation to a level that may be controlled by metastable thermodynamic equilibrium.

Results of kinetic modeling indicate that Ea for the generation of methane range from approximately 66 to 74 kcal/mole while Ao values vary from 6.37×10^{18} to 3.74×10^{19} $s^{-1.}$ Calculated Ea and Ao values for carbon dioxide generation show a much wider range of values varying from 40 to 64 kcal/mole and 1.98×10^{14} to 2.95×10^{17} s^{-1}. Predictions based on these kinetic parameters suggest peak methane and carbon dioxide generation in the range of 200^0C, while carbon dioxide generation is predicted to occur continuously at both low and high temperatures in a typical sedimentary basin.

Organic Geochemistry, petrography, isotopes:

Summary of biomarker work

All analyses have been completed, and data is in process of being entered into an on-line data base which will be accessible though the Ethernet. Two papers have already been published on this work, Whelan et al, 1994 and 1995. A summary paper is also planned describing a plausible overall plumbing system for rapid injection of hydrocarbons into EI-330 reservoirs, as outlined below.

On the basis of biomarkers, all EI-330 oils have a common (Jurassic to Early Cretaceous marine) source. The Jurassic is currently estimated to be deeper than 30,000 ft. It is assumed to be directly beneath EI-330 or to the south because continental shelf oils to the north are compositionally different. The organic geochemistry is most consistent with the oils from the stacked faulted EI-330 reservoir system having been generated fairly early and then having been expelled into overlying reservoir rocks (Cretaceous or other rocks which currently lie at 20,000 to 25,000 ft or somewhat deeper). These, in turn, were buried further under impermeable cap rocks. possibly under salt. Later, as the salt receded, the oil remained trapped beneath overpressure until very recently when further gas formation and pressurization either in situ or from deeper formations caused ejection of the deep reservoired oil into modem Pleistocene reservoirs, in some cases through overpressure. This scenario fits the relative oil and gas maturities, with gases in all reservoirs being much more mature than the oil (R,= 1.5 to 1.7% for gas compared to 0.7 to 0.8% for oil, Whelan et al 1994a. 1995). The depths corresponding to these maturities at the present time is coupled with current best estimates on the limits on the oil and gas generation zones

beneath EI-330. We assume that the gases were generated in deeper, more mature formations and have subsequently moved upward to solubilize and pressurize the oil, although a combined marine source/reservoir facies below 25,000 ft is also a possibility. The gas/oil phase is envisioned as episodically having sufficient pressure to break through the overpressure in order to flow upward into the overlying Pleistocene reservoirs. From an exploration standpoint, this hypothesis is important because it implies deeper reservoirs, below overpressure and below reservoirs, which are producing and actively filling today.

This scenario is supported by ages of the inorganic fluids in EI-330 reservoirs. The ^{129}I ages are fairly uniform and are in the range of 35 to 58 Ma. The ^{129}I originates during kerogen maturation and, therefore, roughly reflects the age of sediments from which the oil was generated. These ages are minimum because of potential for contamination with younger fluids during upward migration. It is interesting that ^{129}I ages agree fairly well with those calculated by Qian et al, (1996) based on calculations or Younger et al, (1977) using ratios of gasoline range hydrocarbons. The ages calculated from the oil compositions are 2 to 59 million years at 100^{0}C, or 4 to 20 million years at 150^{0}C. The lower temperature gives ages closest to those measured by the ^{129}I data. Considering the numerous processes other than maturity are know to affect the hydrocarbon compositions, the agreement between the two ages is remarkable, particularly when one is made using the oils and the other on the aqueous fluids.

Whatever the exact age, all of the estimations above are consistent in suggesting that EI-330 fluids, both aqueous and organic, have spent considerable time in reservoirs much hotter than the EI-330 reservoirs are today, consistent with contemporary oil/gas migration from much deeper reservoirs.

Reproducibility of gas and oil compositions over time.

The manuscript by Qian et al, also presents additional evidence regarding the temporal changes in oil and gas described previously for EI-330 oils (Schumacher, 1992, Whelan et al, 1994). The new analyses are most consistent with these temporal changes being caused by recent migration for a deeper reservoir or source. Artifacts produced by sampling or storage or the analytical procedures have been pretty well ruled out. Evidence is presented against an alternative hypothesis of lateral migration as the cause of these temporal changes in composition.

TLC-FID (Iatroscan) results

Introduction

Petroleum migration conduits and reservoirs contain molecular records of petroleum as it migrates from source to trap. Compositional changes associated with increasing maturities of the sourcing kerogens and chemical interactions that occur along the migration pathways affect the bulk and molecular compositions of petroleum and rock extracts. Therefore, vertical and lateral differences in the molecular composition of petroleum streams can help identification of migration pathways and field filling directions (Karlsen and Larter, 1991). Bulk compositions of petroleum and the organic fingerprints left behind in the regional rocks through which petroleum has flowed can be used to interpret heterogeneities in reservoir sands and migration pathways (Karlsen and Larter, 1991). Comparison of the compositions of petroleum flowing through more permeable sand vein networks and/or fractured host-rock, in association with biomarker and phenol data (Taylor, 1994) from oils and fluids may provide further information relating migration pathways and field filling history (Karlsen and Larter, 19g9).

Our goal was to reveal compositional information to predict whether migrated hydrocarbons have penetrated host-rock. rock fractures and sandstone veinlets. Host-rock and rock fracture enrichment with saturated hydrocarbons may indicate the presence of lower molecular weight compounds which have faster diffusion coefficients, according to estimations by England et al., (1987) for oil migrating in tortuous media. This diffusion may be further enhanced by the degree of fracturing in the host-rock.

Methods

An Iatroscan TH-l0 MK-III, equipped with a flame ionization detector was used to quantify the bulk compositions of oils and core extracts separated by thin layer chromatography on Chromarod-S III silica rods. The solvent system used for separation into saturated hydrocarbons, mono-and di-aromatic hydrocarbons, poly-aromatic hydrocarbons, resins and asphaltenes was as follows:

Compound groups	Elution time		Solvent mixture	Solvent
1). Saturates	27 mins	100%	Hexane	
2). Mono-, di- and poly-aromatics	10 mins	100%	Toluene	
3). Resins and asphaltenes	3 mins	95:5%	Dichlorometliane: Methanol	

External standard quantification was performed using a calibration mixture containing known amounts of:

Surrogate standard	Compound group
n-Eicosane	Saturate response
n-Undecylbenzene	Mono-, di-aromatic response
Phenanthrene	Poly-aromatic response
2,6,-Dimethoxyphenol	Resins and asphaltene response

Samples

The Eugene Island Block-330 Pathfinder (A-20SJT) core provided high quality, contamination free core material ideal for detailed geochemical analysis. Core plugs were collected from the slabbed core, which had been stored in a frozen state, two weeks after core recovery.

To monitor detailed compositional heterogeneities throughout the Pathfinder cored interval, the dominant silty shale lithology was sampled in relation to a number of sand and silty laminae and thin-bedded sandstones. The Pathfinder core logging revealed three distinct major structural zones (Anderson et al, 1994). An upper faulted zone exists between 7670 - 7848' m.d. This zone contains slickensided faults at moderate to high angles. A middle structural zone between 7848-7923' m.d. is relatively unfaulted and unfractured but contains several thin, yellow fluorescing sand beds and laminae. The lower zone between 7923-8053'm.d. is faulted. Silty shales have gouge zones that intersect the well at both low and high angles. Fractures in this zone are fairly persistent and thin hairline faults are often slickensided and occasionally show fluorescence (Anderson et al., 1994).

Samples from all three structural zones were collected from the dominant medium-dark grey silty-shale, termed host-rock, and thin sand laminae and sandstone veins, termed vein-rock. The latter invariably showed fluorescence properties under blue-light excitation. Frozen core sub-samples were defrosted and. carefully sectioned to collect vein-rock without interference from host-rock and vice-versa. The vein- and host-rock samples were Soxhlet extracted for 48 hours using a 93:7 azeotroph of dichloromethane and methanol. The extracts were all reduced and diluted to a set volume ready for separation by TLC-FID (Iatroscan). Eight rods were spotted and eluted with 2 external standard rods loaded per rack of 10 rods. Data was acquired and quantified using Rainin Dynamax® software. Each

sample was analyzed in triplicate and relative abundances calculated. Relative abundance is used in preference to absolute concentrations to counter the effects of porosity changes (Karlsen and Larter. 1989).

Results and discussion

The sandy and silty vein-rock extracts bulk compositions show a fairly constant predominance (50%) of saturated hydrocarbons. Poly-aromatic hydrocarbons are the second most dominant compound group in these extracts with average abundances of 28%. The polar resins and asphaltenes are present in lower abundances, averaging 14% and 3.5% respectively. The resins show a small increase in abundance with depth below *7858.5'* m.d., which lies within the middle, relatively unfaulted structural zone.

Polar compounds are enriched in the deeper pans of the host extracts averaging about 75%. There is <5% relative abundance of poly-aromatics and less than 2% of mono- and di-aromatic hydrocarbons which remains fairly constant vertically. However, the saturates show a striking trend. There is a greater relative abundance of saturates (-40%) between 7678.8'm.d. and 7815.5'm.d. in the shallowest, more faulted structural zone followed by a sharp decrease (~8%) to 7893.70'm.d. within a polar enriched zone (89%), with the exception of one sample near 7846.4'm.d. which contains about 60% saturated hydrocarbons. Comparison of the compositions of the faulted host-rock extract and the adjacent vein-rock extract at 7846.4' m.d. show similar relative abundances of saturates (59% and 62% respectively). Most variance occurs in the amounts of poly-aromatics, which are more dominant in the vein-rock extract (18% vein-rock, 2% host-rock). This host-rock (7846.4'm.d.) was sampled from a small sub-vertical, sinistral fault zone that had no fluorescence properties, unlike adjacent thin, strongly fluorescing sand laminae. Since contamination can be ruled out, we conclude that detectable volumes of more volatile, saturated hydrocarbons have infiltrated the silty shale along this vertical fault plane. The host extract from 7894.5' m.d. contains -80% of saturated hydrocarbons and very few resins and aromatics but 16% asphaltenes. This sample was taken from a non-fluorescing zone within a section of core that had several thin fluorescing sand laminae and may indicate minor migration or diffusive action.
The high abundance of polar compounds in most of the host-rock extracts is consistent with other immature rock extracts (bitumens) which tend to be dominated by polar compounds (particularly asphaltenes) (Tissot and Welte, 1978). Figures II-B-iii-6-l0 show comparison relative abundances between host and vein samples for each compound group separated.

Summary and conclusions

TLC-FID has shown that vein extracts are compositionally quite distinct from the host-rock extracts in the Pathfinder core. The vein-rock extracts indicate petroleum is present in the sandy migration conduits and that petroleum composition is dominated by saturated hydrocarbons and relatively small abundances of polar compounds and is similar in composition to oils from producing reservoirs. Ternary plots were made of the summed aromatics, polars (NSO's) and saturated hydrocarbons for 47 reservoir and fault zone oils from Eugene Island Block 330 and vein-rock extracts, respectively. These data show a good correlation between the bulk compositions of vein-rock extracts and oils. It is reasonable to conclude that these thin sand and silty laminae form part of complex distributary migration networks, channeling petroleum to shallower, more extensive reservoir sandstones. The ternary plot shows the distribution of host-rock extracts from fractured and unfractured sections and shows that although, saturated hydrocarbons are enriched in some fractured samples, aromatic compounds remain in low relative abundance. One possibility to explain the low abundance of aromatics in host-extracts may reflect water-washing of the host rock. Since, aromatic hydrocarbons are more water soluble than saturated hydrocarbons they may be preferentially removed by water. Polar compounds are also water soluble but since they are so predominant in immature sediments they may not show such a

pronounced loss. However, host-rock samples that transect a fracture or small faulted zone do show evidence for the presence of migrated hydrocarbons. The relative intensity of the compound groups is also higher in fractured and faulted host-rock extracts relative to unfractured and faulted host-rock extracts. Phenol analysis may help to clarify some of these observations.

Phenol analysis

Twenty three representative EI-330 oil and their associated aqueous fluids from each of the stacked reservoirs described in Whelan et al., 1994 and from the Pathfinder well have been sent to Dr Steve Larter at the University of Newcastle for analysis of phenols. If successful, this analysis can potentially distinguish between rapid oil migration up faults versus slower migration through pore spaces. The analysis uses compositional changes in phenols, polar fractions of oil, which partitions between the moving oil and water migrating phases and the solid immobile mineral phase. The partition coefficients for phenol between the three phases are well known from the environmental literature. Measurement of the distributions of phenols between the three phases can then be combined with calculations for partitioning between the various possible phases and reservoirs, developed by Larter. The calculations place limits on the amount of time the oil has "seen" the walls of the migration conduit (Larter and Aplin, 1995; Taylor et al., submitted). Dr Steve Larter from Newcastle University in the U.K., who developed these procedures on fluids from North Sea reservoirs, spent the summer of 1995 at Woods Hole. He has agreed to collaborate with us in applying these procedures to Gulf Coast reservoirs, particularly EI-330. We hope this analysis will allow a distinction between fault-associated migration (fast migration; predicted for some GA and RB and SD and LF reservoirs) versus (predicted) slower migration through the capillary pore system (predicted for many of the shale associated OI oils from the Pathfinder well).

These procedures will also allow us to address several important questions regarding migration in EI-330 - is the migration occurring up fault or through pore space? A 3-D seismic profile of migration of a gas plume in S. South Marsh Island from underneath salt goes all the way to the surface and appears to be bypassing faults. Such plumes are evidently common in this area of the Gulf Coast

An alternative migration scenario also consistent with the EI-330 organic geochemical data is that oil is currently being generated and expelled from early Cretaceous (marine) rock already saturated with more mature gas derived from the underlying Jurassic rocks. The additional on-going gas generated from a marine Early-Cretaceous marine source rock is sufficient to move indigenous gas plus oil upward into Pleistocene reservoirs. In this case, the Lower Cretaceous marine oil source and reservoir rocks are the same. In marine carbonate and siliceous formations, source and reservoir rocks are commonly very closely associated, often being the same rock, *(e.g.* Hunt and McNichol, 1984). In this case, the whole source/reservoir rock system is carried downward, with efficient oil expulsion being impossible until a depth is reached where sufficient gas can be generated to aid in the expulsion and migration process.

The distinction between these two scenarios is important from an exploration point of view -the first implies deeper conventional reservoirs which could be produced; the other implies a lower porosity marine source/reservoir rock where the producing permeable zones might be much patchier and harder to find.

Limited data suggests that year time scales of oil/gas injection into reservoirs, which appears to be occurring at EI-330, is extremely fast on the scale of normal reservoir mixing processes. Therefore, it seems unlikely that rapid time scale injection could be occurring from a source rock. However, because marine rocks can act simultaneously as both a
source and reservoir, it is possible that some sort of combined deeper source/reservoir rock could be providing the "deep holding tank" required for rapid oil injection into shallower reservoirs.

Organic geochemistry, Modeling and technology transfer:

Description of data base

A data base has been created for all of the geochemical data gathered during the course of this project using commercially available "4D Database" on the MacIntosh. Entry into a CERN database folder allows access to other parts of the program. The data base has input sheets for data as well as for sample inventories. Data sheets and plots can be inserted into the "CERN share" files for transfer by ftp to any other organization. Currently, CERN members can access these files via the World Wide Web. This version of 4D replaces an earlier attempt using the same program designed by Chancy Rego and Mary Zawoysky.

For plotting, macros are utilized to export the data from the 4D data sheets to Excel, which has much more sophisticated plotting routines than are available within the 4D program. This has proved to be very advantageous in plotting the very complex data sets generated by the high resolution gas chromatograph mass spectrometer data (HRGCMS) of the biomarkers in the EI-330 oils. At the present time, loading of the most complex HRCCMS data set is complete.

Oil Migration in a Major Growth Fault: Structural Analysis of the Pathfinder Core, South Eugene Island Block 330, Offshore Louisiana

Steven Losh
Dept. of Geological Sciences, Cornell University

ABSTRACT

The Pathfinder core taken in the South Eugene Island field, offshore Louisiana, provides an outstanding sample of structures associated with a major growth fault that abuts a giant oilfield and which is thought to have acted as a conduit for hydrocarbon migration into the producing reservoirs. Where cored, the growth fault zone cuts semi-consolidated Plio-Pleistocene mudstone and is over 100 meters wide. The fault zone in the core consists of three structural domains, each characterized by distinct rock type, distribution of fault dips and dip azimuths, and distribution of spacing between adjacent faults and fractures. Although, all of the domains contain oil-bearing sands only faults and fractures in the deepest domain contain oil even though the oil-barren fault domains contain numerous faults and fractures that are parallel to those, which contain oil in the deepest domain, and are thus favorably oriented for transmitting oil. This deepest domain is also distinguished from the other two by a greater degree of structural complexity and by a well-defined power-law distribution of fracture spacings. The departure of the fault spacings in the upper two domains from a power-law distribution, combined with stable isotope data that points to low-temperature water-rock interaction within a gouge zone that separates these two fault domains, indicates that the faults in those domains may have been active only in the early stages of the growth fault zone. These faults may thus predate oil migration. In contrast the faults in the oil-bearing domain may have been active later in the fault zone's history, when geologic and organic geochemical investigations indicate oil migrated into the Block 330 reservoirs. Even though oil was present in sands throughout the core, its restriction to faults in the probably-youngest portion of the fault zone implies that oil migrated only through that part of the fault that was active during the time when oil was available. The absence of oil in favorably-

oriented fractures in the other, probably-older fault domains indicates that the oil was never sufficiently - pressured to hydraulically fracture its way up the fault zone, and instead migrated along faults and fractures that were opened primarily by tectonic stresses.

Introduction

High-angle faults in sedimentary basins should logically play a significant role in hydrocarbon migration from deep. overpressured reservoirs and "kitchens" to shallower reservoirs from which they can be economically produced. A number of studies have documented indirect and direct evidence of large-scale cross-formation fluid flow along growth faults (Jones and Wallace 1974: Weber et al. 1978; Hippler, 1993: Galloway et al, 1982, review of Hooper. 1991). While these examples provide valuable information about processes that affect such flow and also give permissive evidence that large volumes of hydrocarbons may migrate in such a fashion. There has remained a large uncertainty as to the actual connections between fault-conduit fluid flow and the filling of economically-producible oil and gas reservoirs. A clear understanding of fault charging could be extremely valuable as a prospect evaluation criterion. Although many reservoirs are spatially associated with faults, what role do the faults really play in charging of the reservoirs? Do some faults, or portions of faults, act as hydrocarbon migration conduits, while others do not? If fault charging does occur, what controls fluid migration up such faults and into the reservoirs?

In order to develop and test answers to these questions, the Global Basins Research Network, a consortium of universities and industry affiliates, undertook a multifaceted U. S. Department of Energy - funded project in South Eugene Island Block 330, offshore Louisiana. The goal was for simultaneously drilling and sampling a large, active growth fault and carrying out a variety of analyses of rocks, brines, and oil and gas from reservoirs adjacent to the fault. This particular location was selected because of a variety of evidence supportive of recent (even ongoing) reservoir filling linked to the bounding fault system (Anderson. 1993; Anderson et al, 1994). The fault was drilled and cored as an extension of a Pennzoil development well (the MO sidetrack) in the fall of 1993, a variety of logs were run and measurements made, and the fault was drill-stem tested as a potential reservoir (Anderson et al, 1994).

The purpose of this paper is to present a structural description of the core that was taken from the well. Particular attention is paid in this study to understanding why, although a wide fault zone was cored, only a discrete portion of it contained oil.

Core acquisition and processing

Because of the need to continuously sample the fault zone in order to fully characterize it, we utilized a whole-coring system designed to maximize recovery in the semi-consolidated sediments typical of the SEI Block 330 field. The bottom-hole assembly (BHA) consisted of the following:

Bit: Baker-Hughes INTEQ prototype RC 425 anti - whirl PDC bit The cutters were asymmetrically placed around the bit in order to minimize "walking" of the bit in the hole.

Core barrel: 18.3 meter x 0.1 meter (6(3-foot x 4 - inch) barrel with *6* - millimeter (1/4 inch) aluminum liner, with pressure release valves. Barrel was equipped with full-closure "clamshell" type doors just above the bit. Closure of these was activated from the surface before pulling out of the hole.

Coring was done at a mudweight of 1.97 kg/liter (16.3 pounds per gallon). There was no appreciable fluid pressure gradient associated with the fault in this well.

We anticipated that the core would be taken primarily in semi-consolidated smectite-mudstone. Industry experience with whole coring in this type of sediment led us to use an experimental mud formulation in order to stave off "balling", or adhesion of clay to the bit, which typically slows penetration rates to 60 centimeters an hour or, usually less. The requirement that we use a water-based mud constrained us to utilize an environmentally safe synthetic additive: we used a poly alpha olefin (Friedheim et al, 1991), such that it constituted 3% of the mud. This substance does not fluoresce. It is chemically distinct from nearly all of the organic compounds we anticipated finding in the core, and, at the low concentrations used, it did not interfere with sensitive electrical resistivity measurements required for the Formation MicroImager (FMI) log. We also used an additive to inhibit clay swelling which could have led to jamming in the core barrel.

The combination of the above enabled us to obtain unprecedented penetration rates with the core bit in the semi-consolidated mudstones, averaging 21 meters/hour, ranging as high as 52 meters/hour. We retrieved 104.6 meters of core out of 109.8 meters attempted for a recovery rate of 95%.

Because we initially anticipated slow (30 to 60 cm/hour) penetration rates during curing, we expected to retrieve perhaps 25 meters of core in the time available to us. Thus, we opted not to put on the coring BHA until we had drilled to within 12 meters of the fault, as determined from seismic data. Unfortunately, the uncertainty in picking the fault and converting time to depth for the seismic data resulted in our drilling through the upper bounding fault of the growth fault zone, which was marked by a gas show of 360 units (compared to a background of about 75 units), before changing to the coring RHA. This fault zone later produced several barrels of oil in a drill stem test (Anderson et al, 1994). The top of the core is thus about 8 meters below the first main fault in the growth fault zone.

On the rig, the core was marked with orientation stripes as it was pulled out of the core shuttle, then cut into 91-cm (three-foot) sections, or tubes. Every other tube, beginning with the second one, was placed in dry ice on the rig, and has been continuously frozen since in order to preserve organic compounds for geochemical analysis. The unfrozen tubes were placed on a tilted table in order to drain the drilling mud, and then capped and filled with non-fluorescing epoxy in order to stabilize the core in the liner and thus prevent damage during transport and storage.

In Houston, the cores were logged for spectral gamma radiation, oriented for slabbing by means of X-ray radiography, and logged on site at a scale of 1:5 as soon as they were slabbed. Wherever possible, tubes were slabbed perpendicular to the predominant set of fractures in order to facilitate sampling of them; where no fractures were present, tubes were cut perpendicular to bedding. The cores are presently stored at Pennsylvania State University. Frozen cores are kept at -15 C, the unfrozen ones are waxed and stored in a humidified room at 3 C.

Methods

All observed faults and fractures were recorded on the core logs, and their geometries in three dimensions were verified using X-ray fluoroscopy. A feature was considered a fault if it displayed gouge, breccia. pervasive slickensides, or offset beyond that which accompanied breakage of core in the inner tube. A disproportionately large share of faults are perpendicular to the long axis of the core, and at least some could represent breakage and rotation of core in the barrel as it was drilled (Kulander et al, 1990). However, many of these faults experienced only transnational offset, with no evidence of rotation either in the form of differences in apparent bedding dip across the fault s)r of circular grooves or slickensides on the fault surface. Where such evidence of coring-induced faulting was lacking, the fault was recorded as a natural feature. In contrast to faults, a fracture was indicated by a planar break across which no offset was observable, or which did not display any other fault characteristics.

Except for the fault at 2325 meters DD, faults and fractures were generally not detectable in the FMI log, perhaps owing to their tightness, so their orientations in real space had to be obtained indirectly. Structures in the core were oriented by the following procedure: 1) the core was co-registered with the FMI log by comparing the core gamma log with the downhole gamma ray log that was run with the FMI. as well as utilizing log header information. The depths recorded on the core (driller's depths) are 4.6 meters less than those recorded on the FMI log (logger's depths); this magnitude of discrepancy is not unexpected. 2) Places were identified where the bedding dip in the core matched the apparent bedding dip in the Formation MicroImager log. In those instances, the apparent azimuth of the bedding dip in the FMI and that of the slabbed face of the core were identical. 3) The apparent orientation of the stripes on the core inner tube was computed. It is assumed that this orientation does not vary over the length of a given 9.1 - meter (3- foot) core, as care was taken to maintain the core orientation when pulling it out of the shuttle on the rig. 4) The apparent azimuth of the slab face for each section was then computed, according to the angle between the orientation lines on the inner tube and the slab face. The azimuth was uniquely constrained by the direction of bedding dip in the core. 5) Apparent dip and dip azimuth were measured for all faults whose dip azimuth lay in the plane of the slab face. Because the slab faces were oriented to be cut parallel to the apparent dip azimuth of the majority of faults in a given section, the overwhelming majority of faults in the core were measured. However, the dataset of oriented faults and fractures does not contain planes that were oblique, rather than perpendicular. to the slab face: these account for about 20% of all observed planar features. 6) The apparent dip and dip azimuth data so obtained were then

rotated to account for the hole deviation, which in the cored interval was 22 degrees to the vertical in the 038 direction. Over four hundred data points were obtained in this fashion.

GEOLOGIC SETTING AND DESCRIPTION OF FAULTS

Geologic setting of the Pathfinder Well

The DOE-Pennzoil. well in SEI Block 330, the Pathfinder, was drilled in a fault-bounded salt withdrawal minibasin of Plio-Pleistocene age (Holland et al, 1990; Alexander and Flemings, 1995). This minibasin hosts the giant South Eugene Island field, presently the largest producing field in offshore Gulf of Mexico and the largest Pleistocene oil field in the world. Production is primarily from rollover anticlines in a section of deltaic and fluvial sands, and the reservoirs are segmented into a number of fault blocks (op cit). This sequence of sands, interbedded with mudstones overlies a thick (600-meter) mudstone and below that, turbidite/slope fan deposits (Alexander and Flemings, 1995).

The main growth fault zone penetrated by the Pathfinder well (the 'A' fault zone) is seismically imaged from> 5 seconds to approximately 0.4 seconds; at shallower depths, it is not resolvable in the data. The 'A' fault zone has a throw of approximately 600 meters at the level of the OI sand, just above where the Pathfinder intersected it, and displacement decreases approaching the surface. Based on stratigraphic evidence, the fault experienced its highest slip rate during deposition of the deltaic sand - shale sequence between 1.8 and 1.2 Ma (Alexander and Flemings, 1995). Current activity of the fault is implied by its presence at the shallowest resolvable depths in seismic data and by oil seeps along its trace on the seafloor. The geometry of the fault and hangingwall deformation in SEI Block 330 are consistent with dip-slip normal movement. Preliminary data on well-bore breakouts from the Pathfinder well indicate a minimum horizontal compressive stress direction nearly perpendicular to the fault trace (Peter Flemings, Penn State Univ., 1995, oral comm.), again consistent with normal faulting with no discernible strike-slip component.

Fault zone geometry and displacement in the Pathfinder well

In the Pathfinder well, the upper bounding fault for the A fault zone was intersected at 2325 meters driller's depth (DD), just below the 01-5 sand and 23 meters below the first appearance of the foraminifera Robulus 64 (1.8 Ma). This bounding fault has a dip of 53 degrees in the 213 (southwest) direction, according to the Formation MicroImager, and is about one meter thick in the well. Below this fault is a thick (>244 meters. to the bottom of the well at 2563 meters) section of variably faulted calcareous and non-calcareous silty mudstone, shaly silt, and rare sand, mostly as laminae but also, in one instance, in beds up to 25 cm thick. Using the paleontological picks and assuming a sedimentation rate of 1.3 mm/year for the D. brouweri - Robulus 64 interval (cf. Alexander and Flemings 1995), an omission of about 67 meters of section across the upper bounding fault at 2325 meters DD can be calculated taking true bed thickness into account. The first appearance of G. miocenica (2.0 my.) at 2476 meters DD. below the bottom of the core, is consistent with an apparent sedimentation rate of 1.04 mm/yr in the D. brouweri - G. miocenica interval. This is within the range of expected sedimentation rates, thus implying a small net throw on all of the cored faults. In contrast. D. pentaradiatus (2.2 my.) appears at 2503 meters DD. consistent with an omission of about 240 meters of section between that marker and the G. miocenica marker just 27 meters higher in the well, again assuming that a sedimentation rate of 1.3 mm/year applies to this interval. Additional faults may lie below this depth, but are not discernible from the paleontological. FMI, or seismic data.

In contrast to the gentle northeast bedding dips determined from seismic data and well intercepts for strata above the main fault zone, the FMI log shows consistent moderate (2040 degrees) north to northwest bedding dips below the main fault. Seismic and well top data from the upthrown block to the northeast of the fault zone indicate horizontal to gentle southwest dips. The cored portion of the Pathfinder well is best interpreted as a rotated horst between two or more faults, only the top one of which is evident on the seismic section. The northwest component of dip azimuth observed on the FMI in the cored interval can be accounted for by a modest counterclockwise rotation (looking northeast) about an

axis perpendicular to the plane of the upper bounding fault at 2325 meters. The northerly dips may be the result of rotation related to cross-faults that may lie within the faulted rock below the fault **.**

Nature of faults in core

Although we had drilled past the upper bounding fault before beginning to core, the core contains over 500 faults and provides much information about the nature and geometry of faults in the growth fault zone. In terms of physical appearance. there are two main types of faults logged in the core. The predominant type is a very thin to hairline slickensided fault across which displacement or truncation of beds can be observed in many cases. The slickensided fault surface is polished. and the slickenlines are very fine parallel grooves. Much less abundant than the "hairline" faults are gouge/breccia zones, which are up to 15 centimeters across in the core. In these, mudstone has been reconstituted into slickensided gouge that is slightly lighter colored than the adjacent mudstone and supports clasts of relatively undeformed mudstone up to 1.5 cm across, typically elongated parallel to the gouge foliation. A number of faults comprise zones up to 1 cm wide, mainly containing brecciated mudstone clasts with minor clay gouge infilling the interstices; these faults may represent a gradation between the two types above. No consistent cross-cutting relationships between sets of "hairline" faults was observed.
Shallowly-dipping faults cut steeply-dipping ones and vice versa, although the former situation is more common. However, the gouge zones, which typically dip shallowly to moderately to the southwest are almost never cut by any later structures in the core and in fact truncate more steeply-dipping faults and fractures.

Several faults and fractures in the core are mud-filled, but no natural fracture fillings or mineralized fault breccia were observed, and few open fractures or faults were detected in situ on the FMI log. However, about 25 faults and fractures in the core fluoresced strong gold, indicating the presence of oil, and will be described later. In addition, a weak gas show (increase of 70 units above background) was recorded in faulted mudstone at the bottom of the core.

Orientation of faults in core

Three structural "domains" can be identified in the core on the basis of plots of depth vs. fault dip and dip azimuth. The upper and lower thirds (more or less) of the core contain faults having a wide range of dips, and their dip azimuths nearly span the compass. The middle third. in contrast lacks shallow-dipping faults and faults whose dips lie in the northeast quadrant; southeast-dipping faults are present but rare. The boundary between domains I and 2 in the core corresponds to a 15-cm wide gouge zone that dips shallowly to the southwest and separates calcareous mudstones above from non-calcareous mudstones below. This fault zone is also marked by a high density of fractures and faults. Within domain 2 faults are scarcer and the rocks are siltier progressing downhole: the few notable sand beds in the core lie in the interval of minimal fault/fracture density. Although no distinct fault boundary was observed between domains 2 and 3, the rocks of domain 3 are much shalier than those immediately above, the faults typically contain more gouges than those in domains 1 and 2, and the fault+fracture density is also much higher. All but one of the 25 oil-bearing faults and fractures lie in domain 3.

Utilizing the above breaks, the fault data were analyzed separately for each domain. Dip/dip azimuth lines were plotted on an equal-area lower hemisphere stereographic projection. The number of lines per 1% area was then corrected for the angle between the line and the borehole orientation (Terzaghi, 1965; Barton and Zoback, 1992), and the resultant dip-corrected dataset was contoured using spherical Gaussian statistics (Kamb, 1959). Each domain is characterized by a distinctive concentration of fault orientations. The faults in domain 1 are predominantly shallow to moderately southwest dipping, although a weakly-developed set of east-dipping faults is also present. Domain 2 consists predominantly of moderately- west to west-northwest-dipping faults. Domain 3 contains two well-developed populations of faults, one moderately to steeply west-dipping, the other shallowly dipping to the southwest. A lesser population of northeast-dipping faults is also present. The dip/dip azimuths of oil-bearing faults are also plotted individually. They do not appear to have an affinity for any particular population.

In contrast to the fault domains, fracture orientations do not appear to show systematic variations with depth. A stereographic projection of the total population of fracture dip/dip azimuth data, corrected for the angle between the dipline and the drillhole, as done for the fault data above. shows a single broad maximum dipping steeply to the west-northwest (figure 6b).

Geometric distribution of fault/fracture spacing

As a way of evaluating each domain with respect to its propensity to act as a fluid conduit, some simple analyses of fracture/ fault spacing in each domain were carried out. The depth of every planar discontinuity that intersected the centerline of the core was recorded, including those for which orientations were not derived; spacings between immediately adjacent structures were figured directly from these depths. Log-log plots of fracture/fault spacing vs. the cumulative frequency of fractures/faults at or greater than a given spacing are, like the stereonet plots, distinctive for each domain. A plot of data using this transformation would be expected to yield a straight line for a power-law distribution of fracture/fault spacings (Gillespie et al, 1993). The data from domain 1 cannot be well fitted with a straight line over any significant range of spacings. Domain 2 spacings can be fitted with a straight line if the spacings below 10 centimeters are considered to be under-sampled and thus dropped from the dataset; the correlation coefficient (r^2) for the remaining data is then 0.96, with a slope of 1.00. The validity of considering fracture/fault spacings under 10 centimeters to be under-represented is questionable. however, as the practice during logging of this core was to record all distinguishable fractures and faults. Even in massive mudstones, fractures or faults 10 centimeters apart are readily distinguishable from one another. The lower threshold of spacing resolution for the core as a whole is on the order of 5 cm in well-laminated intervals. Fractures and faults as closely spaced as 5 mm were mapped as separate features. Including fractures and faults as closely-spaced as 5 cm in the domain 2 dataset results in a poorer straight-line fit to the data with a correlation coefficient of .926. Thus, the data for domain 2 do not appear to be well characterized by a power-law distribution or the closely-spaced fractures and faults are characterized by much different statistics than are the more widely-spaced ones.

Fracture/fault spacing data from domain 3 are well-fit by a straight line on a log-log cumulative frequency plot, using a lower spacing cutoff of 3 cm. The correlation coefficient for a straight line of slope 1.59 is 0.98, over a range of 1-1/2 orders of magnitude. The fracture/fault spacings in domain 3 clearly follow a power-law distribution.

The same data were also analyzed using an interval counting method. Intervals of varying sizes (d) were imposed on the core log. and the number of intervals (N) containing at least one fracture or fault was counted. Plots of log N vs. log (l/d) yield linear slopes for power-law distributions (Barton, 1995). The data for domains 1 and 2 are moderately characterized by such a distribution, having correlation coefficients of 0.98 and 0.97. respectively for interval sizes greater than 30 cm; however, the data also show a weak but continuous curvature. The data for domains 1 and 2 depart significantly from a power-law distribution at sampling intervals less than 30 cm. This departure is not believed to be an indication of a lower limit of perceptibility, as fractures much closer than 30 cm apart were logged routinely, as noted above. Thus, the fracture spacing data from these two domains are not characterized by a power-law distribution. In contrast to domains 1 and 2, and consistent with conclusions drawn from the cumulative frequency vs. spacing plots above, data for domain 3 are well-fit by a straight line on a plot of log N vs. log (1/d), yielding a slope of 0.88, with r^2 equal to 0.995 over 1-1/2 orders of magnitude of interval sizes. Analysis of residuals (Brooks, 1995) and incremental slopes between adjacent data points (Gilespie et al, 1993; Walsh and Watterson, 1993; Manning, 1995) corroborate the validity of a straight line fit to the domain 3 data.

Discussion

The above data demonstrate the structural complexity of a typical young growth fault zone in a mudstone-dominated section offshore Louisiana. Any conclusive interpretation for the cause of the uneven distribution of oil within the cored faults, as envisaged in the introduction to this paper is greatly hindered by the fact that the drill hole is a one-dimensional sample of what is clearly a three-dimensional system. For instance the presence of oil within domain 3 faults could be simply due to the proximity of an oil-charged sand in or adjacent to that particular fault zone near the Pathfinder well or to a locally complex fault pattern related to a nearby subsidiary fault. In fact, the structural data for domain 3 demonstrate the presence of two distinct fault sets, one of which is oblique to the main growth fault trend.

The interaction of these fault sets would be expected to result in an interconnected set of fractures that could constitute a permeable pathway for fluid flow.

Overlaid on the structural complexity, however, the analysis of fault spacing data indicates there may also be intrinsic differences in fault mechanics between the three structural domains in the core. The oil-barren domains are also characterized by a "deficiency" of closely-spaced faults and fractures relative to a power-law distribution, in contrast to domain 3. Because it is unlikely that this behavior is an artifact of a lower limit of perceptibility, this geometric difference may in fact reflect a difference in the mechanics of faulting. As shown above, fault/fracture spacings of domain 3 are well characterized by a power-law distribution, typical of "tectonic" faults/fractures documented elsewhere in consolidated rocks (Velde et al. 1991; Barton and Zoback. 1992; Gillespie et al, 1993; Barton. 1995). Departure from this behavior in domains 1 and 2 may reflect deformation of sediments whose material properties during faulting differed from those of consolidated rock, as suggested by Gillespie et al (1993). In this case, the faults in domains 1 and 2 may have been active earlier in the consolidation history of the sediment than were the faults of domain 3; the domain 3 faults could even be presently active.

Oxygen isotope data from which one may derive temperature and thus depths at which water-rock interaction took place were collected for calcite from two faults, including the low-angle gouge zone that separates domains 1 and 2. This gouge zone contains an unusually high amount of calcite (up to 9 weight %, determined by X ray diffraction (Losh et al, 1994), which is primarily diagenetic in origin. The ^{18}O values of this calcite are consistent with isotopic exchange with pore fluid having oxygen isotopic composition of 0 permil SMOW at temperatures of 14 to 22 C (fractionation equation of O'Neil et al, 1969). The fluid that circulated through the gouge zone precipitated calcite at temperatures not much higher than those that probably prevailed at the seafloor at the time. Thus indicating isotopic exchange took place at shallow burial depth, early in the fault's history. Oxygen isotopic equilibration between calcite and fluid at present day temperatures in the cored portion of the fault zone (about 65 C) would have produced
Distinctly different calcite 3180 values on the order of 2I permil, which are nowhere in evidence in the sampled faults in the core. Thus, the sampled faults in domains 1 and 2 have served as fluid conduits only early in the history of the growth fault zone, a finding consistent with the above interpretation of fault spacing data.

The coupling of relative timing of fault movement with the distribution of oil in faults, fractures, and sands in the core provides some insight into the timing and controls of oil migration relative to faulting. As was noted earlier, oil is present in all sands in the core, regardless of structural domain, but is (with one exception) present only in faults and fractures in domain 3. Furthermore, the stereograms illustrate the presence. in all three domains, of faults having "favorable" orientations for being oil-filled. The attitudes of faults that contain oil, a *de facto* indicator of favorable orientation, in domain 3 generally lie well within the population of fault orientations deduced for domains 1 and 2, but these features are barren of oil in those domains. Taken together, the above observations and interpretations indicate that: 1) faulting in domains 1 and 2 took place before the sands in those domains were charged with oil, 2) faults in domain 3 have been active more recently than those in domains I or 2 and may be active now, and 3) oil migration in the fault zone took place relatively late in the evolution of the growth fault, and may be occurring now. The relatively recent timing of oil migration into Block 330 reservoirs is indicated by organic geochemical and geologic studies (Whelan et al, 1994; Alexander, 1995). Thus, oil migration appears to have taken place within the same time interval as activity of faults in domain 3. The mere presence of favorably-oriented breaks, as defined above, did not appear to have enhanced oil migration in the upper two domains (Barton and Zoback, 1995). Rather, oil and gas migration in the fault zone probably took place only in those faults that were active when migratable hydrocarbons were available.

If fault-hosted oil migration was in fact restricted to the active part of the fault, some inferences may be made with respect to mechanisms of fluid migration within the fault zone. In particular, Anderson et al (1994) hypothesized that fluid ascent within the fault zone was described in terms of cycles of fluid pressure build-up followed by hydraulic fracturing, rapid fluid migration, fluid pressure dissipation, and ultimate closure of the fracture. In this interpretation, fluid migration up the fault is not directly linked to fault active. However, the temporal linkage between oil migration and tectonic activity as described above, and the lack of migration via faults that were evidently inactive when oil flushed through the sediments, implies that deviatoric tectonic stress sufficient to produce failure was a major control on

fracture and fault permeability in the Pathfinder core, and that fluid pressures alone were never sufficient to hydraulically open fractures.

Conclusions

The Pathfinder core provides a detailed traverse through much of a major growth fault, which is believed to have played a significant role in migration of hydrocarbons from deep to shallower levels. Detailed logging of the core shows that this growth "fault" is a zone at least 100 meters thick and that it consists in the core of three distinct domains, each characterized by its own distribution of fault orientations and fault/fracture spacings. Except for the upper bounding fault, only the faults in the lowest of the domains are known to contain oil. This domain is also characterized by a more complex fault pattern and is well described by a power-law distribution of fault/fracture spacings, in contrast to the other domains whose faults contain no oil. Both faulting and oil migration appear to have taken place in the same relatively recent time interval in domain 3, whereas faulting probably preceded oil charging of sands in the other two domains. The restriction of oil-bearing faults to the youngest portion of the fault zone, and their absence from portions of the fault that were active before migration, points toward fault activity as a major controlling factor on oil migration in the faults sampled by the Pathfinder core.

Acknowledgements

Funding for this work was provided by the Global Basins Research Network and Dept. of Energy grant DC-FC22-93BC14961 to Roger Anderson, Lamont-Doherty Earth Observatory. I especially thank Pennzoil Exploration and Production Co, without whose involvement the Pathfinder Well would not have been drilled. Paleontological analysis was carried out by Ardy Callender and Bernie Shaffer. Applied Biostratigraphix, Houston, and elucidated by Denise Butlen Pennzoil. Formation MicroImager interpretation was performed by Laura Foulk, Schlumberger, and Bruce Hart assisted with core logging. I thank Bruce Malamud, Ben Brooks and Prof. Don Turcotte for assistance with statistical analysis. Any shortcomings in interpretation are my own.

REFERENCES

Alexander, L. 1995, Ph.D. thesis, Cornell University

Alexander, *L.*, Flemings, P.. 1995. Geologic evolution of a Plio-Pleistocene silt withdrawal mini-basin, Eugene Island South Addition, Block 330, offshore Louisiana; Amer. Assoc. Petrol. Geol. Bull.

Anderson, R., 1993, Recovering dynamic Gulf of Mexico reserves and the U.S. energy future; Oil and Gas Jour., April 26, *p.85-91*

Anderson, R., Flemings, P., Losh, S., Austin, J., Woodharns. R., 1994, Gulf of Mexico growth fault drilled, seen as oil, gas migration pathway; oil and Gas Jour., June 6, pp.97-103

Barton, C.C., 1995. Fractal analysis of scaling and spatial clustering of fractures, in Barton, C.C., and LaPointe, P.. eds., Fractals in the Earth Sciences, Plenum Press, New York, pp.141-178

Barton, C.A.. Zoback, M.D., 1992, Self-similar distribution and properties of macroscopic fractures at depth in crystalline rock in the Cajon Pass scientific drill hole.; Jour. Geop. Res., vol. 97, pp.5181-5200

Barton, C.A., Zoback, M.D., Moos. D., 1995, Fluid flow along potentially active faults in crystalline rock; Geology vol.23, pp. 683-386

Brooks, B., 1994, Fractal clustering of metamorphic veins: Comment; Geology, v. pp. 1147-1148

Friedheim, 3., Hans, 0., Park, A.. Ray, C.. 1991. An environmentally superior replacement for mineral-oil drilling fluids; Soc. Petrol. Eng. preprint SPE 23062. pp.299-312

Galloway, W., Henry, C., Smith, 0.. 1982, Depositional. framework, hydrostratigraphy. and uranium mineralization of the Oakville Sandstone (Miocene), Texas Coastal Plain. Univ. of Texas at Austin Bur. of Econ. Geol. Rept. of Investigations 113, 51 pp.

Gillespie, P, Howard. C.. Walsh, 3., Watterson, 3.1993, Measurement and characterization of spatial distributions of fractures; Tectonophysics. vol. 226, pp. 113-141

Hippler, S., 1993, Deformation microstructures and diagenesis in sandstone adjacent to an extensional fault: Implications for the flow and entrapment of hydrocarbons; Amer. Assoc. Petrol. Geol. Bull., vol.77, pp.625-637.

Holland, D., Leedy, 3., Lammlein, D., 1990, Eugene Island Block 330 field - U.S. A., offshore Louisiana; in Beaumont, F., and Foster, N., eds., Structural Traps III: Tectonic Fold and Fault Traps; Amer. Assoc. Petrol. Geol. Treatise of Petroleum Geology, pp.103-143

Hooper, E. C. D., 1991. fluid migration along growth faults in compacting sediments; Jour. Petrol. Geol. vol. 14. pp.161-180

Jones, P., Wallace, R., Jr., 1974. Hydrogeologic aspects of structural deformation in the northern Gulf of Mexico basin; Jour. Res. U.S. Geol. Surv., vol. 2, pp.511-517

Kamb, W., 1959, Ice petrofabric observations from Blue Glacier, Washington, in relation to theory and experiment, Jour. Geop. Res.. vol.64, pp.1891 - 1910

Kulander, B., Dean, S., Ward, B., Jr., 1990, Fractured Core Analysis: Interpretation, Logging, and Use of Natural and Induced Fractures in Core; Amer. Assoc. Petrol. Geol. Methods in Explor. Series. vol.8,88 pp.

Losh, S., Eglinton, L., Wood, 3., 1994, Coring and inorganic geochemistry in the Pathfinder Well, in Anderson, R., Billeaud, L., Flemings. P., Losh, S., and Whelan, 3.. Results of the Pathfinder Drilling Program into a Major Growth Fault: Part of the GBRN/DOE Dynamic Enhanced Recovery Project in Eugene Island 330 Field, Gulf of Mexico; Annual Report (CD-ROM) to DOE. contract no. DE-FC22-93BC14961, pp.183-249.

Manning, C., 1994, Fractal clustering of metamorphic veins: Reply; Geology. vol. - pp. 1148-1149

O'Neil, 3., Clayton, R., Mayeda, T., 1969. Oxygen isotope fractionation in divalent metal carbonates; Jour. Chem. Phys., v.51, *pp.5547-5558*

Terzaghi, R., *1965.* Sources of error in joint surveys: Geotechnique, vol.15, pp. 287-304 Velde, B..

Dubois$_4$ J., Moore, D., Touchard. G., 1991, Fractal patterns of fractures in granites: Earth Planet. Sci. Lett., vol.104, pp 25-35

Walsh, 3.. Watterson, J., 1993, Fractal analysis of fracture patterns using the standard box-counting technique: Valid and invalid methodologies: Jour. Struc. Geol.v.. 15. pp. 1509-1512

Weber, K., Mandl, G., Pilaar, W., Lehner, F., Precious, R.. 1978, The role of faults in hydrocarbon migration and trapping in Nigerian growth fault structures; Tenth Annual Offshore Technology Conference Proc., vol. 4, pp.2643-2653 (OTC 3356)

Whelan, 3., Eglinton, L., Requejo, R., Kennicut, M., 1994, Pathfinder Well organic geochemistry: Indicators of oil source and maturity and fluid flow mechanisms, in Anderson, R., Billeaud, L., Flemings. P., Losh, S., and Whelan, 3., Results of the Pathfinder Drilling Program into a Major Growth Fault: Part of the GBFINIDOE Dynamic Enhanced Recovery Project in Eugene Island 330 Field, Gulf of Mexico, Annual Report (CD-ROM) to DOE. contract no. DE-FC22-93BC14961, pp.616-662.

Water - Rock Interaction in a Large Growth Fault, South Eugene Island Block 330 Field, Offshore Louisiana

Steven Losh

Dept. of Geological Sciences, Cornell University, Ithaca, NY

Lorraine Eglinton
Dept of Chemistry, Woods Hole Oceanographic Institution, Woods Hole, MA

James Wood
Dept. of Geological Sciences, Michigan Technological University, Houghton, MI

ABSTRACT

We examined whole core, sidewall core, and cuttings from seven wells that penetrated a large growth fault abutting the Plio-Pleistocene South Eugene Island Block 330 field, offshore Louisiana, for evidence that the fault acted as a conduit for fluid flow into the prolific reservoirs. The analytical program was designed to deduce mass and heat flux within the fault zone, and focused on comparing a variety of measurements on faulted and unfaulted rocks. Data include vitrinite reflectance and spore fluorescence measurements, standard petrographic and cathodoluminescence techniques, Rock-Eval pyrolysis, oxygen and carbon isotopic analysis, determination of bulk mineralogy and illite/smectite ratio by X-ray diffraction, and whole-rock major element and trace element geochemical determinations.

Rocks within and adjacent to the fault zone in the D.O.E.-Pennzoil Pathfinder well, taken at about 2226 - 2317 meters (7300 - 7600 feet) TVD, were characterized by low vitrinite reflectances, averaging 0.3%Ro, yellow to yellow-green spore fluorescence colors, moderate to high $\delta^{18}O$ and $\delta^{13}C$ values ($\delta^{18}O$ of calcite in faulted rocks ranged from 28 to 31 permil SMOW with $\delta^{13}C$ from 0.8 to –3.1 permil PDB), and, except for slight increases in K_20, $CaCO_3$. and Zn in some faulted samples, no differences in major or trace element composition between deformed and undeformed sediments. The lowest $\delta^{18}o$ value, 21.8 permil. was from a calcite-cemented siltstone 11 meters above the fault. The rocks were characterized by illite/illite+smectite ratios between 40% and 60%. unexpectedly high considering the low maturity of organic matter. and in most cases, there is no distinction between faulted and unfaulted rocks in terms of mineral assemblage or relative abundance. One gouge zone contained calcite in excess of that in the average mudstone, but oxygen and carbon isotopic data, noted above, indicate the calcite precipitated at shallow burial depth.

Rocks from the A6ST Well, which intersects the 'A' fault about 300 meters northwest of the Pathfinder at 1980 meters (6500 feet) TVD, exhibit higher vitrinite reflectances, averaging 0.55% Ro in the 'A' fault decreasing to 0.4%Ro at a distance of 50 meters (160 feet) feet above the top of the fault, yellow-orange to orange spore fluorescence colors, a distinct $\delta^{18}O$ and $\delta^{13}C$ shift to lower values (22.4 and -9 permil, respectively) at the top of the fault, and, like the Pathfinder, little evidence of mass influx into the sampled fault rocks. There are no observed mineralogical differences between faulted and unfaulted rocks, and the illite/illite+smectite ratios are a subject of dispute: one laboratory obtained a range of 40-55%, averaging 44%, whereas another obtained a range of *23-35%,* averaging 27%, from samples from the same interval within the fault zone.

Based on the existing data, the 'A' fault in the Pathfinder is concluded to have transmitted little fluid from depth, whereas the same fault in the A6ST well appears to have been a conduit for accent of a substantial amount of fluid.

Introduction

High-angle faults in sedimentary basins may be expected to play a significant role in hydrocarbon migration from deep, overpressured reservoirs and "kitchens" to shallower reservoirs from

which they can be economically produced. A number of studies have documented indirect and direct evidence of large scale, cross-formation fluid flow along growth faults (Jones and Wallace, 1974; Weber et al. 1978; Hippler, 1993; Galloway et al. 1982, review of Hooper. 199 1). While these examples provide valuable information about processes that affect such flow and also give permissive evidence that large volumes of hydrocarbons may migrate in such a fashion. there has remained a large uncertainty as to the actual connections between fault-conduit fluid flow and the filling of economicall5l-producible oil and gas reservoirs. A clear understanding of fault charging could be extremely valuable as a prospect evaluation criterion. Although many reservoirs are spatially associated with faults, what role do the faults really play in charging of die reservoirs? Do some faults, or portions of faults, act as hydrocarbon migration conduits, while others do not? If fault charging does occur, what controls fluid migration up such faults and into the reservoirs?

In order to develop and test answers to these questions, the Global Basins Research Network, a consortium of universities and industry affiliates, undertook a multifaceted U. S. Department of Energy - funded project in South Eugene Island Block 330, offshore Louisiana, having the twin goals of simultaneously drilling and sampling a large, active growth fault and carrying out a variety of analyses of rocks, brines, and oil and gas from reservoirs adjacent to the fault. The centerpiece of this project was the Pathfinder well, drilled into the main fault bounding a salt withdrawal minibasin of Plio-Pleistocene age (Holland et al, 1990; Alexander and Flemings, in press). This minibasin hosts the giant South Eugene Island field, presently the largest producing field in offshore Gulf of Mexico and the largest Pleistocene oil field in the world. Production is primarily from rollover anticlines in a section of deltaic and fluvial sands, and the reservoirs are segmented into a number of fault blocks (op cit). This sequence of sands. interbedded with shales, overlies a thick (600 meter) shale, and below that turbidite/slope fan deposits (Alexander and Flemings, in press). This particular location was selected because of a variety of evidence supportive of recent (even ongoing) reservoir filling linked to the bounding fault system (Anderson, 1993). The fault was drilled and cored as an extension of a Pennzoil infill development well (the A20 sidetrack) in the fall of 1993, a variety of logs were
run and measurements made, and the fault was drill-stern tested as a potential reservoir (Anderson et al, 1994, 1995).

Geochemical research on rocks from Block 330 has focused on ascertaining chemical and thermal signatures of fluid thought to have ascended the main growth fault (the 'A' fault) and flowed into reservoir sands. This paper presents petrographic, mineralogic, stable isotopic, and bulk geochemical data from fault zone Samples from the Pathfinder well, the A6ST well, which also penetrated the 'A' fault, and several other wells along the 'A' fault. Whole coring was carried out in the Pathfinder well in order to continuously sample a major growth fault abutting the Block 330 reservoirs. Continuous sampling, as opposed to sidewall coring, across the fault zone was considered important in that many features related to fluid flow in fault zones typically vary greatly over distances of centimeters. Thus, we attempted to obtain as much whole core as was practical, and recovered 109 meters (343 feet) of 10.2-cm (4-inch) diameter con in unfaulted to highly faulted rock, primarily mudstone. Sidewall cores were taken above the cored interval in order to evaluate evidence for fluid flux within the main 'A' fault, which was not cored, as well as in the downthrown block to the fault zone.

Analytical procedures

Vitrinite reflectance measurements were carried out on three different types of samples: 1) kerogen concentrate samples, cold set in epoxy resin and polished in accordance with ICCP protocol (1963.1971); 2) thin sections, prepared in accordance with the methods of Stach (1982), and 3) polished blocks of sediment. In whole-rock samples an "operator selective approach" (European method of Mukhopadhyay. 1992) is used, whereby morphology, color, relief quality. internal structure and other characteristics are used to identify vitrinite particles indigenous to the sediment. The whole rock approach is preferred for Gulf Coast sediments since one can distinguish autochthonous vs. allochthonous vitrinite, bitumen populations, cavings, and drilling contaminants. Rather than measuring a wide range of reflectances on a variety of macerals and then selecting the dominant or lowest-reflectance population as indicative of vitrinite maturity, as is frequently done for kerogen concentrates, we believe that more-reliable results can be obtained from these organic-lean, immature sediments by measuring fewer, but better characterized vitrinite particles in whole-rock mounts (Barker and Pawlewicz, 1993).

Vitrinite reflectance was measured using a Zeiss standard universal research microscope-photometer system (MPMO1K) equipped with a tungsten-halogen lamp (12V. 100W), a x40 Epiplan oil immersion objective, filtered *546* nm incident light, and Zeiss immersion oil (n_e 1.517 @ 23C). Three standards are measured in triplicate before analysis and every 30 minutes once analysis commences. Blue light fluorescence observations on spores (Mukhopadhyay, 1992) was performed on the same microscope fitted with a high-pressure mercury lamp (HBO100) for autofluorescence and an LP520, BP450-490 filter system.

Illite/smectite ratios were determined at Michigan Technological University on the <2 μm fraction with selected samples further separated to <1 μm. Samples from each size fraction were mounted on ceramic plates using a vacuum pump apparatus with XRD analysis carried out on an automated Dapplr/Noreko machine using CuKα and 1 degree slit size at a counting time of 2 seconds per step. Samples were then solvated with ethylene glycol in a desiccator for 24 hours at room temperature. Identification of I/S and estimation of percent expendables were made from techniques described by Moore and Reynolds (1989). A similar procedure was followed at Exxon Production Research for samples analyzed there.

Sample preparation and analysis for carbon and oxygen isotopic analysis of whole-rock carbonate was carried out by Krueger Enterprises, Cambridge, Mass. Carbon dioxide was liberated from the calcite by reaction with phosphoric acid at 90 C. Several calcite+dolomite samples were analyzed by timed extraction: a CO_2 sample was taken from the reaction vessel at 20 minutes, and is taken as representative of the isotopic composition of calcite, and a second sample was collected at 3 hours after initiation of reaction. and is taken to represent dolomite.

Whole - rock multielement geochemical analyses of whole core and sidewall core samples were obtained by X Ray Assay Labs. in Don Mills, Ontario. Major elements, Cl, Cr, Sn, Rb, Sr, Y, Zr, Nb, Ba. and LOI were analyzed by X-ray fluorescence, rare earths by neutron activation. S by LECO, and Li, Be, B, V, Co, Ni, Cu. Zn, Ge, Mo, Ag, Cd, Pb, and Bi by ICP spectroscopy. Gold. platinum. and palladium were analyzed by fire assay with DCP spectroscopy finish, but were found to be below the detection limits of 1, 1, and 10 ppb respectively. Major element oxides are computed without consideration of LOi or H_20+/H_20-. For all plots $BaSC_4$, taken as a tracer of drilling mud, is corrected for in samples having greater than 10,000 ppm Ba.

THE PATHFINDER WELL

General geology

In the Pathfinder well, the first detectable fault in the 'A' fault zone was intersected at a measured driller's depth (DD) of 2325 meters (7625 feet), after drilling through a 15-meter thick section of tilted sands and shales of the OI-5 sand. According to the Formation MicroImager, the main fault has a dip of 53 degrees in the 213 (southwest) direction, and is about 120 centimeters thick in the well. Below this fault is a thick *(>245* meters, to the bottom of the well at *2563* meters *(8405* feet) DD) section of faulted and unfaulted calcareous and non-calcareous silty mudstone, shaly silt, and rare sand. In contrast to the gentle northeast bedding dips determined from seismic data and well intercepts for strata above the main fault zone, the FMI log shows consistent moderate (2040 degrees) north to northwest bedding dips below the main fault. Seismic and well top data from the upthrown block northeast of the fault zone indicate horizontal to gentle southwest bedding dips. Thus, the cored portion of the Pathfinder well is best interpreted as a rotated horst between two or more major faults, only the top one of which is evident on the seismic section.

The core was taken from 2332 - 2442 meters (7650-8012 feet) DD, within the interval defined by Robulus 64(1.8 Ma), first encountered at 2303 meters DD, and Globorotalia miocenica (about 2 Ma), first encountered at 2476 meters. The average sedimentation rate of 0.7 mm/yr calculated for the above faulted interval is about half the 1.3 mm/yr rate calculated by Alexander and Flemings (in press) for unfaulted shales of this age elsewhere nearby in the minibasin, and is consistent with a stratigraphic omission on the order of 120 meters due to faulting in this interval.

Lithology and structure

The core consists of three lithologic "domains" that correspond to structural domains in the core. The uppermost 26.2 meters of core consists primarily of slightly to moderately calcareous, predominantly medium gray laminated to massive silty shale (mudstone) to shaly silt, also sampled by sidewall cores above the fault. The next 47 meters of core are significantly siltier but non-calcareous, and the thickest sand beds, up to 22 centimeters, are found in this interval. The bottom 36.6 meters comprise laminated, non-calcareous silty shale with only a paucity of sand. Siderite concretions to 4 cm in diameter are common. The boundary between domains 1 and 2 is a low-angle gouge zone at 2358.5 meters (7736 feet) DD that was sampled as part of this study. Oil was found almost exclusively in faults and fractures in the deepest structural/lithologic domain in the core.

The fault zone partly sampled by the core is believed to have a total throw on the order of 600 meters at the depth of the core (Alexander and Flemings, in press). The FMI log shows faults both above and below the cored interval, and paleontological data suggest that the cumulative throw on faults in the core is relatively minor. Nonetheless, the core contains over 500 faults and fractures, which are of two types: very thin slickensided, polished “hairline" faults that display mm to tens of cm of offset in the core and that have a range of orientations, and slickensided gouge/breccia zones to 15 cm thick that are of indeterminate offset and that have low to moderate dips to the southwest.

Petrography, Mineralogy, and Vitrinite Reflectance

Petrographic examination of faulted shale from the whole core and sidewall cores shows a variety of structures: microshears defined by bands of rotated clay from tens to a couple of hundred microns wide, rotated blocks bounded by microshears. and microduplex structures. In terms of cathodoluminescence, calcite/dolomite in these rocks comprises two populations: angular, bright red-orange luminescing calcite and redder dolomite grains that appear to be detrital, and subangular to subhedral dull red-orange luminescent ferroan calcite grains that are disseminated throughout the rock and in some instances lie in fractures. This latter type of calcite is believed to be authigenic. Foraminiferal calcite tends to be non-luminescent.

X-ray diffraction of shales from the core and sidewall cores was carried out at Exxon Production Research and Shell's Bellaire Laboratory, with one sample analyzed by Fourier Transform Infrared spectroscopy (FIIR) at Core Labs. The eleven shales consist primarily of clay (42 to 71%) and quartz (21 to 37%), and contain between 6 and 17% combined feldspars and a few percent calcite (0-9%). Clay and K-feldspar are negatively correlated. Only one sample had detectable dolomite, and one had detectable pyrite. Samples from within or near fault zones (7631, 7635-7636.1, 7734.9) tended to have more calcite than samples farther than a few feet from a known fault (7612, 7657), although the sidewall core at 2317.4 meters (7601 feet) consists largely of authigenic calcite. The fault at *2358.5* meters (77.36 feet) separates calcareous rocks above from noncalcareous ones below, and no sample below 2358.5 meters has more than trace amounts of calcite, regardless of position with respect to faults.

Clay mineralogy has been determined for a number of samples, both in terms of bulk mineralogy and smectite-illite ratios in the mixed-layer clays. The former was primarily performed at Exxon Production Research, Houston, with one sample analyzed at Shell Bellaire Labs, Houston. Smectite-illite ratios (Table. 1) were determined primarily at Michigan Technological University. with four samples analyzed at Exxon Production Research. Clays are predominantly mixed-layer smectite-illite (60-69%: four samples), with lesser detrital illite (16-22%), kaolinite ((14-17%), and chlorite (1-2%). Overall, smectite/(smectite+illite) ratios in the <2micron glycolated fraction from cuttings, sidewall cores, and the whole core show an gradual increase in I/S from about 30-40% at depths of 1200-1500 meters (4000 to 5000 feet) to 45-60% deeper in the hole. The shift to intermediate I/S ratios at depth is permissible given the bottom-hole temperature on the order of 70 to 75 degrees C (Abercrombie et al. 1994; J. Boles, oral comm., 1994)), although these ratios are not normally observed in rocks below temperatures on the order of 100 C (Hower et al. 1976: Milliken, 1985). However, the relatively high I/S ratios higher in the well (most published profiles for Plio-Pleistocene rocks show I/S ratios on the order of 20-30% at the depths of the Pathfinder well) suggest the initial composition of the smectite may favor transformation at lower temperature than usually observed. The elevated I/S ratio is probably not an effect of pore fluid chemistry, if the brine samples (Losh and Wood. 1995) are representative of fluids that interacted with the fault rocks, if anything, the potassium concentration is low (on the order of 300 mg/L), and the Na and Mg

concentrations are high (ca 40,000 and 1500 mg/L. respectively), which should suppress the smectite to illite transformation rather than enhance it (Huang et al. 1.993).

Vitrinite reflectance measurements were made at Woods Hole Oceanographic Institute (WHOI). Reflectance measurements were made on a variety of macerals, allowing distinction to be made between reworked and "indigenous vitrinite, with indigenous vitrinite reflectance measured on telocollinite.

In the Pathfinder well, indigenous vitrinite reflectance ranged from 0.25%Ro to 0.47%Ro (figure 5). The highest-reflectance sample comprised 2 readings: excluding this sample, the maximum reflectance was 0.37% Ro. Reflectance increases slightly with depth, and shows no increase relative to known faults at 2325 meters *(7625* feet DD) (A fault) and 2055 meters (6741 feet) (B fault). In addition, no petrographic evidence of oxidation or bitumen impregnation was observed. The vitrinite reflectance values are in accord with burial along a normal (20-25 C/km) geothermal gradient and do not allow for anomalous heating related to the fault zones. Yellow and yellow-green spore fluorescence colors corroborate the low thermal maturity of the sediments indicated by the vitrinite reflectance data.

Pyrolysis

Pyrolysis Tmax data were also obtained at Woods Hole on some of the same samples analyzed for vitrinite reflectance, using a Chemical Data Systems pyroprobe system interfaced for computer data acquisition and processing. Tmax data in general covaries with vitrinite reflectance, although they indicate a somewhat higher thermal maturity in terms of equivalent vitrinite reflectance than do the actual reflectance measurements. Elevated Tmax values for the Pathfinder well are commonly associated with organic assemblages containing greater than 60% reworked vitrinite and inertinite particles, and so may not be indicative of actual thermal maturity of the rocks themselves. In addition to providing evidence concerning thermal maturity, the pyrolysis measurements give evidence of migrated hydrocarbons in the form of P1 peaks or. pyrograms from the sidewall and whole core samples. Nearly all sidewall cores from the reservoirs penetrated by the Pathfinder well show enhanced P1 peaks indicative of migrated hydrocarbon; however, the fault zone samples show no such peaks.

Stable isotopes

Oxygen and carbon isotope data have been obtained from whole-rock shale samples taken from fault zones and undeformed shales near the faults. As expected, the δ^{18}o values of dolomite and calcite from the same samples differ by several permil, but the

minimum δ^{18}o value of the calcite obtained in this manner is virtually the same as that of the lowest - δ^{18}o calcite + dolomite sample. indicating that the δ^{18}o values of the; calcite + dolomite mixtures are reasonably representative of the calcite δ^{18}o. Because of the extremely fine-grained, disseminated nature of the calcite, separate samples of distinct cathodoluminescent character cannot be made. However, the isotopic composition of a shale containing both types of calcite and dolomite must be a mixture of the two end-point compositions of detrital and diagenetic carbonate, and thus useful information about the isotopic composition of diagenetic calcite + dolomite, which is of the greatest interest can be obtained from the presence or absence of an isotope shift from values in equilibrium with seawater at seafloor temperatures. Re-equilibration with higher-temperature fluid during burial would produce a shift to lower δ^{18}o values, which, even in a mixed sample, will be observable in the data.

In the case of samples from the Pathfinder whole core and sidewall cores, oxygen isotopic composition of calcite and calcite + dolomite mixtures ranges from 21.8 to 31.1 permil relative to SMOW, with no observable distinction in calcite δ^{18}o between undeformed and highly sheared samples at a given location. Calcite from sidewall cores near or in the 'A' fault at 2325 meters (7625 feet) DD yield δ^{18}o values between 26.3 and 28.2 permil, slightly shifted to lower δ^{18}o values relative to the deeper fault zone and to undeformed shales above and below the fault. Calcite from undeformed calcite-cemented shale around 2317 meters (7600 feet) (logger's depth) yields the lowest δ^{18}O values of all, at 21.8 permil. Calcite-cemented intervals are commonly known above fault zones in the Gulf of Mexico, and these samples probably represent such an occurrence. Carbon isotopic composition of calcite ranged from -0.7 to -9.5 permil relative to PDB; the low δ^{13}C value for the sample having 3180 of 31.1 permil may reflect contamination from epoxy, owing to the non-reproducibility of

the value (a second analysis of this sample gave δ^{13} C value of -8.2 permil), or less likely, it may indicate some of the calcite in that sample was precipitated from water containing oxidized methane or "kerogenic" CO2 at or near the seafloor. Generally, the carbon isotopic composition of the calcite is typical of normal marine shell and foraminiferal material, and is largely independent of δ^{18}o . On average, calcite δ^{13}C in faulted rocks is slightly higher than in undeformed ones (-1.7 permil vs. -2.5 permil).

In a well-developed gouge zone at 2358.5 meters (7736 feet). Both δ^{18}O and δ^{13}C of calcite are typical of values in equilibrium with seawater at seafloor (10-20 C) temperatures, and, particularly in the case of the oxygen isotope data, do not reflect re-equilibration with, or precipitation from higher-temperature fluids during burial. Even if the sediment were buried as a closed system, with only pore fluid available to exchange with calcite as temperature increased, an δ^{18}O shift would be observed as a result of moderate to high water-rock ratio: volumetrically, pore fluid occupies about 25% of the rock, whereas calcite + dolomite, considered to be the only phases to exchange significantly (by recrystallization) with fluid at these low temperatures, comprise only 2 to 3% of the rock, leading to a volumetric water/rock ratio W/R) on the order of 10, or an oxygen water/rock ratio of about 7. Even if clays were considered to exchange freely with water. the W/R would on the order of 0.5, still sufficient to produce a significant shift in calcite δ^{18}O during closed-system exchange during burial. At 70 C and W/R of 0.5, equal to an oxygen W/R of 0.35, calcite initially at 30 permil in the closed system described above would exchange with pore fluid and equilibrate to δ^{18}O value of 27.4 permil (fractionation of 0'Neil et al. 1969). As the calcite δ^{18}O values from the fault at *2358.5* meters show no shift away from pristine, seawater-equilibrated values, even resulting from closed-system exchange with pore fluid, they are interpreted to have been precipitated at low temperature, thus, at shallow burial depth. Since calcite is easily exchanged under ambient conditions by recrystallization, its high δ^{18}O indicates a lack of influx of even locally-derived fluid, which implies inactivity, in this fault during most of its burial history.

Along similar lines, calcite in the sidewall cores taken near the 'A' fault is' only weakly shifted in δ^{18}O from unexchanged values of about 30 permil, and reflects minor interaction with fluid during burial and/or faulting. The lowest δ^{18}O samples from 2317.4 meters (7601 feet), reflect interaction with aqueous fluid at or near present-day temperatures, as indicated by their near-agreement with the modeled δ^{18}O equilibrium trend for burial diagenesis at a geothermal gradient of 22 C/km, comparable with that observed presently in the Pathfinder well.

The calcite δ^{18}O values appear to correlate with sandiness of the sediment rather than with proximity to shear zones. In no case do the oxygen isotopic data reflect equilibration with ambient pore fluid at temperatures higher than those attributable to a normal geothermal gradient; if that were the case, the δ^{18}O values would lie to the left of the "equilibrium line". However, it is possible that, because the isotopic values were measured on whole-rock samples that include a mixture of detrital and diagenetic carbonate, a low δ^{18}O authigenic population exists and that it is masked by the presumably higher δ^{18}O detrital component. It is also possible that a fluid ascending rapidly from depth would have a δ^{18}O value higher than the ambient static values assumed in calculating the equilibrium curve, resulting in anomalously high-temperature calcite lying on the high δ^{18}O side of the curve. The data are insufficient to address these possibilities, and the simpler interpretation - that of an absence of thermally anomalous fluids affecting the oxygen isotopic composition of calcite in the Pathfinder well samples - remains.

Bulk Chemistry

Bulk chemical analysis was performed on 69 samples from the core, including all samples for which stable isotope data were obtained. Samples were collected every 60 centimeters (two feet) over a 3-meter (100- foot) interval in the relatively unfaulted middle of the core. Samples were also collected from gouge, fault breccia, sidewall con-as within and above the 'A' fault at 2325 meters (7625 feet) DD, and nearby undeformed rocks elsewhere in the core for the purpose of evaluating element flux in the fault zones.

Crossplots of typically immobile phases and elements, such as Al_20_3, Zr, and Sc show high correlation coefficients, indicating their usefulness as monitors of element flux in fault zones sampled in the Pathfinder well. Zirconium and Al_20_3 are inversely correlated: Zr (from zircon) tracks the sand

fraction, as indicated by the strong. positive correlation between Zr and SiO_2, whereas Al_20_3 tracks the clay fraction determined by XRD. These elements are less well correlated with other elements considered to be immobile in the sedimentary environment, but the correlations are sufficient to warrant the conclusion that these elements are immobile as a group. For the purposes of gauging mobility of other elements such as potassium, silica, and sodium, Al_20_3 and Zr are used as references.

The bulk geochemical data indicate little or no difference in chemical composition between faulted and unfaulted rocks in the Pathfinder well. Furthermore, the data indicate that many normally-mobile components, such as K_20, SiO_2, Zn, and Cu, are largely immobile in these rocks, even in samples characterized by a pronounced ^{18}O shift. Sample 7593, Zn shows a slight increase in gouge samples from the lowest of tie three fault domains in the core. A plot of K_2O vs. Al_20_3 shows a strong correlation (r^2=O.85) and a trend having a slope of 0.15, dominated by the stoichiometry of mixed layer smectite-illite clays. Potassium content in the samples is consistent with XRD data indicating the shales consist of approximately 30 to 45 weight percent I/S clay, compared with at most 11 percent K-feldspar in addition to kaolinite and detrital illite. However, a small group of samples from the fault zone at 2358.5 meters (7736 feet) DD plots at slightly elevated K_2O/Al_2O_3 ratio. XRD analysis of one of these samples (7736.4) shows a relatively high I/S ratio of 57% implying that the increase in K_2O content could be due to illitization of I/S clays. Addition of pure illite ($K_{0.5}Al_3Si_{3.5}O_{1O}(OH)_2$) would produce a trend having a slope of 0.3 on this plot. and addition of 11 weight percent illite to the I/S phase of these shales, which average 40% I/S clay by weight, could account for the observed departure from a linear trend; as noted, one gouge sample shows an elevated I/S ratio. Growth of potassic feldspar would be represented as a line having a slope of 1.7 on this plot, and addition of 0.7 weight percent K-spar could also account for the observed slight K20 increase this increase would not be resolvabled by XRD and would barely be perceptible by petrographic analysis.

Other frequently mobile components show strong correlation to immobile components in the Pathfinder rocks. SiO_2 shows no departure from immobility in faulted samples, and FeO and MgO correlate well with Zr. Similarly, zinc and copper, both soluble as chloride complexes at pressure and temperature conditions prevailing in the cored interval, show surprisingly good correlation with alumina. implying that even these elements were not introduced into the Pathfinder rocks by throughgoing fluids. In contrast $\delta^{18}O$ of whole-rock calcite is positively correlated with percent clay (3 data points) and negatively correlated with Zr, which tracks sand content. This relationship is interpreted to reflect the control of bulk permeability of rocks in and near the fault zone on calcite $\delta^{18}O$.

Na_2O in both faulted and unfaulted rocks is essentially independent of K_2O and Al_2O_3, implying that variations in sodium concentration in these samples is not due to mineralogy, but rather may be due to contamination. Assuming a pore fluid having 50,000 mg/l Na, similar to brines taken from the OI sands nearby, and a shale porosity of 25%, the deposition of salt in pore spaces due to evaporation is calculated to increase Na_2O by as much as 0.9% of the total rock mass, or equivalently, by as much as 40% over the Na_2O content of the rock itself. A number of samples were washed prior to analysis in order to circumvent this source of contamination, and generally show lower Na_2O content than do unwashed samples. No quality control was carried out at the lab in order to ascertain that all of the salt had indeed been washed away. Thus, none of the Na_2O values should be considered accurate.

Some of the above samples show elevated CaO content relative to Al_2O_3, indicating mobility, particularly in the fault zone at 2358.5 meters (7736 feet). Samples from that interval contain as much as 9% calcite, as determined by X-ray diffraction. As discussed above, the oxygen isotope data indicate that this calcite exchanged with fluid only at low temperature; thus, the calcite was precipitated at shallow burial depths.

Gas geochemistry

Martin Schoell, of Chevron Petroleum Technology Company. La Habra, California, collected 15 gas samples during drilling of the Pathfinder well by means of "...splicing a "T" into the gas stream of the mudlogging unit and transferring the gases with a hand pump into aluminum-coated gas bags at ambient pressure. The samples were analyzed for $^{13}C_1$ and $^{13}C_2$ using the newly developed Rapid Gas Isotope Analyzer (RGIA). A temperature programmable GC (equipped with a 30 m GS-Q megabore column), is on-line connected with a mass spectrometer via a combustion furnace. The mud gases were sampled with a gas tight syringe from the gas bags that were filled at the mud logging unit. Every unknown and

standard (NGS-2) was injected at a 6:1 split ratio. The reproducibility of the NGS-2 values is +1-0.25 permil. Our values were on average 0.9 permil more positive than the accepted value of the standard. Daily correction factors determined from the gas standards were applied to the methane and ethane isotope values...

"The methane isotope values become increasingly more negative with depth. The value of 47.8 permil above the fault zone in reservoir sand that will be likely a producer is fairly typical for gases in the Gulf of Mexico. The systematic trend to more negative values in the fault zone indicates two interesting aspects: 1) gases in the fault zone are not homogeneous and 2) the gases are mixtures of bacterial gas and thermogenic gas. Taken at face value the data are in many aspects surprising. Firstly bacterial gas in the fault zone suggests that gases of thermogenic and bacterial origin migrate as mixtures in the migration conduits. Secondly, the systematic trend within the fault zone would suggest unmixed discrete zones of compositionally different gases within the fault. This is difficult to rationalize as one would assume that the fluids are homogeneous in an active feeder fault..." (taken from Schoell and Haught. 1994)

DISCUSSION: Implication of geochemistry for fluid flow in the Pathfinder fault zones

The evidence concerning fluid flow can be divided into two categories: that bearing on thermal imprint of fluids on rocks (smectite-illite ratio, oxygen isotopes. vitrinite reflectance), and that bearing on chemical imprint of fluid (also smectite illite ratio, oxygen isotopes. mineralogy. bulk chemistry). The former type of data are useful only in determining whether fluid may have ascended the shear zone rapidly enough to produce thermal anomalies. Whereas, the latter type of data are sensitive to the passage of fluid from any source, at any flux, provided that major or trace elements are transported and precipitated. Thus, the first type of data may yield negative conclusions for the same rocks that are shown by the latter type to have hosted fluid flow. Such appears to be the case for the fault zone rocks studied in the Pathfinder core.

Vitrinite reflectance measurements indicate the fault zones in the Pathfinder well do not represent measurable thermal anomalies relative to unfaulted rocks or rocks at similar depths and geothermal gradients elsewhere in the region. These data yield a more definite insight into thermal maturity of fault rocks than do smectite-illite ratios in that the latter are highly susceptible to a variety of influences, such as fluid chemistry and initial clay composition. The smectite-illite data may equivocally be interpreted as reflecting unusually high temperatures (as discussed above). The vitrinite reflectance measurements, corroborated by spore fluorescence colors, preclude such a thermal anomaly in faults encountered in the Pathfinder well, including the main 'A' fault zone at 2325 meters *(7625* feet) DD. Oxygen and carbon isotopic composition of calcite in and near fault zones in the Pathfinder well does not support throughgoing fluid flow in the sampled shale dominated portions of the faults. If anything calcite composition points to fluid focusing into sandier sediments adjacent to the main 'A' fault. These data are in accord with carbon isotopic composition of gas samples collected and analyzed by Martin Schoell of Chevron, which indicate that the biogenic component of the fault zone gases has not been swept out by migrating thermogenic gases during burial.

As noted, scant data indicate flux of some elements in some fault zones in the core. In particular, calcite has been precipitated and illite appears to have formed from smectite in a gouge zone at 2358.5 meters (7736 feet). Although this particular mass flux is interpreted on the basis of stable isotope compositions to have taken place early in the burial history. The main 'A' fault at 2325 meters (7625 feet) DD is inferred to have hosted fluids on the basis of a modest calcite ^{18}O shift from unexchanged shale values; however, there is no evidence of mass gain or loss in the sidewall cores taken within or near this fault. The strongest evidence for fluid influx in the form of an ^{18}O shift is from a calcareous shaly silt some 11 meters above the main fault zone. Indicating that, on the basis of the available samples, fault-related fluid flow at the location of the Pathfinder well may have been focused in permeable rocks adjacent to the fault rather than within shale gouge zones of the fault itself. The fluid responsible for the ^{18}O shift in calcite did not introduce or remove mass from the affected rocks, implying either that the actual volume of fluid was small or that it in any event was in chemical equilibrium with the bulk shale mineralogy. Much or all of the observed ^{18}O shift in mudstone calcite could have been produced by water- rock interaction in a closed system undergoing burial. This stands in marked contrast to fault rocks

from the A6ST well, which penetrates the same fault as does the Pathfinder about 300 meters to the northwest.

The A6ST Well

The AE sidetrack well was drilled in 1991 to test a target in the KE sand at a TVD of approximately 1890 meters (6200 feet). A rathole was drilled through the 'A' fault, and a pressure surge was encountered, with oil-cut mud coming to the shaker. Pennzoil shot about 45 sidewall cores in the fault, but cased it off as reservoir dimensions could not be assigned to it. The sidewall cores form the basis of this investigation, which consists of petrographic and cathodoluminescence observations, stable isotope analysis of calcite, X-ray diffraction analysis, smectite-illite ratio determinations, and vitrinite reflectance measurements.

Petrography, Mineralogy, and Vitrinite Reflectance

Petrographic observations indicate the rocks are pervasively faulted, displaying numerous microshears characterized by rotated clays. In some instances showing coarser grain size than in the matrix, as well as rotation of clasts, duplex structures, and drag folding. As with the sidewall cores from the Pathfinder well, these fault structures are believed to represent *in* situ deformation not associated with the process of collecting the cores. At the outer edge of most cores a band of clay on the order of 1/4 mm wide has been rotated into parallelism with the core margin. This deformation and associated fracturing near the core margin is related to the coring procedure. However, the penetrative structures listed above show consistent displacement sense throughout the entire sidewall core; this, coupled with the observation that measured displacement on some of the faults is greater than that which would be expected on faults produced during the coring operation, implies a tectonic origin for the structures.

The A6ST samples contained essentially the same mineral assemblage as reported for the Pathfinder well. As is the case for the Pathfinder samples, there are two general types of carbonate with respect to cathodoluminescence: a bright red-orange, angular population, and a dull orange-red to red, subrounded to subhedral group that in some instances occurs as isolated grains in fractures. Both types of grains are disseminated throughout the rocks, are between 10 to 20 microns across, and are not mechanically separable. Calcite comprises an estimated 3 to 5 percent of the shale. As was the case with the Pathfinder samples, dolomite is not detectable in XRD scans made at Cornell University, but was detected in trace amounts in samples analyzed at Exxon Production Research Co, Houston. Electron microprobe analysis indicates dully-luminescent calcite in these rocks contains 2 to 3 percent iron as $FeCO_3$.

Smectite/illite ratios in rocks from the A6ST well varied considerably according to the laboratory carrying out the analyses. The first samples were analyzed at Michigan Technological University, and were concluded to have I/I+S ratios in rocks from within and just above the fault zone between 40% and 55%, averaging 44%. Significantly higher than "background" I/I+S ratios of 20-30% reported for Plio-Pleistocene rocks in the area by Milliken (1985). A second group of ten samples from the same interval was analyzed at Exxon Production Research (EPR) in Houston, and found to have I/I+5 ratios between 23% and 35%, averaging 27%, lying within the "normal" range as defined above. All samples are characterized by Reichweite = 0. The difference in reported values from the two laboratories could simply be due to different methods of interpreting the X-ray spectra. It must be noted that the two laboratories did obtain similar I/S ratios for samples from the Pathfinder well, but also that the A6ST and Pathfinder I/S determinations at MTU were carried out by different researchers. They were carried out by the same personnel using the same techniques at EPR. In view of the above considerations, the lower EPR numbers are taken as accurate. Their I/S determinations show a modest correlation with semi-quantitative degree of deformation in the fault rocks. Application of illite-smectite data to paleothermometry of the fault rocks awaits resolution of two issues. 1) The I/S ratios in the Pathfinder well are significantly higher than expected given the low vitrinite reflectance values and spore fluorescence colors; they also show no relation to the fault. 2) If the EPR I/S determinations for the A6ST well are indeed accurate, and there is no known reason to believe otherwise, the I/S ratios there are significantly lower than expected when compared with the vitrinite reflectance values and spore fluorescence colors.

Vitrinite reflectance measurements were made on polished thin sections and whole-rock blocks from fault rocks in the AEST. Five epoxy mounts of kerogen from fault rocks yielded an average reflectance of indigenous telocollisnite, using the same apparatus as described above, of 0.55%Ro. with a standard deviation of 0.08 (79 measurements). Other macerals were also measured; typically these were higher than those of the indigenous material and defined discrete populations on histograms. The relatively high reflectance of rocks from the fault zone in the A6ST well identifies that zone as a thermal anomaly with respect to rocks outside the fault zone, and to rocks elsewhere in the fault zone (i.e.. the Pathfinder well). The relatively higher reflectance is corroborated by yellow-orange to mid-orange spore fluorescence colors in the same samples; these indicate higher thermal maturity than do the green-yellow, yellow, and yellow-orange colors observed in the Pathfinder samples.

Stable isotopes

As is the case with the Pathfinder samples, dolomite in the samples is volumetrically minor in comparison to calcite and its presence does not appear to affect the $\delta^{18}O$ of the calcite + dolomite mixture to any significant extent. Oxygen isotopic composition of calcite (+ dolomite) shows a pronounced shift to lower $\delta^{18}O$ values, as low as 23.4 permil. The $\delta^{18}O$ shift actually involves unfaulted rocks just above the fault zone: calcite in rocks at the "top" of the fault shows a reverse $\delta^{18}O$ shift, back to higher $\delta^{18}O$ values with depth. Faulted rocks well below the top of the fault (for example, Samples at 2269 meters (7443 feet) DD) lie at high, unexchanged $\delta^{18}O$ values. These data suggest that, if the observed ^{18}O shift is related to fluid flow in the fault, that fluid preferentially flowed along the "top" of the fault.

As noted for the Pathfinder samples, the ^{18}O shift observed in the data may represent a mixing trend between low-$\delta^{18}O$ diagenetic calcite and high - $\delta^{18}O$ detrital and foraminiferal calcite, present in samples above and within the fault zone, and the low-$\delta^{18}O$ endpoint may lie to the high-temperature (low-$\delta^{18}O$, or left) side of the "equilibrium line". However, there does not appear to be a relationship between abundance of dully-luminescent calcite and whole-rock calcite $\delta^{18}O$. Alternatively, the calcite $\delta^{18}O$ values may simply be partially "frozen in" by partial equilibration with pore water during burial. The data are inconclusive in this regard: they permit, but do not unequivocally support, the interpretation of thermally anomalous fluids in the fault zone.

Calcite $\delta^{13}C$ values are correlated with the $\delta^{18}O$ values, such that the lowest-$\delta^{18}O$ samples also have the lowest $\delta^{13}C$, between -4 and -9 permil, whereas the highest-$\delta^{18}O$ samples have normal marine foraminiferal $\delta^{13}C$ values of around 0 permil. The ^{13}C depletion in the lower-$\delta^{18}O$ calcites may be due to incorporation of some carbon related to hydrocarbon maturation and/or organic acid decarboxylation, supporting a relatively deep source for the diagenetic fluid.

Whole rock geochemistry

The combined vitrinite reflectance, stable isotopic, and initial smectite-illite data lead us to conclude that at least part of the 'A' fault encountered in the A6ST well acted as a fluid conduit, and that at least some of the fluids were hotter than ambient temperatures. We then sought to corroborate the above evidence for fluid flow with whole rock geochemistry, anticipating that we might be able to determine the flux of major and trace elements into fault rocks.

As in the case of the Pathfinder well, Zr, Al203, and Sc are correlated with one another. Although the correlation coefficients are lower than for Pathfinder samples. Al_2O_3 was selected as a "reference" immobile component against which the behavior of other components can be measured. In terms of their geochemistry, the A6ST samples are nearly identical to the Pathfinder samples reported above, and can be plotted together with them. However, to facilitate analysis of the A6ST samples as a group, they are considered independently from the Pathfinder analyses.

Plots of normally mobile elements, such as SiO_2, K_20, Zn, and CaO versus Al_2O_3 indicate little to no mass influx into the fault zone samples. SiO_2 shows a negative correlation with Al_2O_3 and K_2)O is positively correlated with it. The former relationship indicating that SiO_2 content is controlled by abundance of detrital quartz (r^2 of SiO_2 vs. Zn which tracks zircon and thus tracks the coarser detrital fraction. is 0.75), and K_2O is controlled by abundance of clay. The slopes of the K_2O vs. Al_2O_3 plots for the A6ST and Pathfinder well samples are nearly the same, 0.13 and 0.15, indicating, as noted for the Pathfinder well samples, that K_2O occurrence is described by mixed-layer 115 stoichiometry. Unlike the Pathfinder samples, rocks from the A6ST well do not show even a weak relationship between K_2O content and extent of faulting. Zinc shows no enrichment in faulted versus unfaulted rocks. CaO does show possible weak enrichment in some weakly to moderately deformed rocks relative to undeformed ones, and the lack of correlation of CaO with Al_2O_3 indicates it is largely in the form of carbonate minerals rather than plagioclase or Ca-montmorillonite. $\delta^{18}O$ of calcite and mixed calcite+dolomite from these rocks is weakly inversely correlated with CaO content, suggesting that CaO, hence carbonate, in these rocks may be at least partly of diagenetic origin.

DISCUSSION: Thermal anomaly in the fault penetrated by the A6ST well

Modeling based on vitrinite maturation in the fault rocks, as described above. requires a significant thermal pulse in order to produce the average 0.55% Ro vitrinite reflectance at the depths from which these samples came. For this study, the first-order, distributed activation energy model of Burnham and Sweeney (1990) was used. In the simple situation rocks now in the fault zone are modeled as being buried along a constant, present-day. geothermal gradient of 30 C/km (present day temperature is about 80 C in the fault zone), with a pulse of instantaneous peak temperature of 120 C, or about 45 C above the ambient temperature, being required to produce the measured reflectance values. Longer-duration pulses (i.e., 20-30Kyr) need not have such high temperatures, but still are on the order of 35 degrees hotter than ambient temperature. The same burial history, without a temperature pulse, produces a calculated vitrinite reflectance of 0.27% Ro.

The combined vitrinite reflectance and stable isotope data support the interpretation of thermally anomalous fluid flow in the fault zone at the AEST well. Large volumes of fluid would be required in order to produce the interpreted thermal anomaly. Furthermore, if fluids are responsible for the thermal anomaly, they must have sourced below the massive shales that lie below the OI sands: only there are the temperatures sufficient to produce the thermal maturation recorded by the vitrinite. However, other interpretations for a temperature anomaly. such *as* influence of salt in the past are possible. Further study is required regarding the detailed history of salt movement in this area. as well a; the distribution and nature of other thermal anomalies, if any, within and outside of the fault zone in Block 330.

Vitrinite reflectance measurements elsewhere in Block 330

Vitrinite reflectance was measured from cuttings from five other wells in Block 330. In most cases the samples were of only fair to poor quality, and yielded only a few measurements: thus any conclusions drawn from these data must be considered tentative. That said, the data taken at face value highlights the Pathfinder well as a "cold spot" in the 'A' fault zone. The data imply that the imprint of an anomalous heating event or events, perhaps related to ascent of fluid in the 'A' fault, decreases to the southeast. Additionally, Rock-Eval pyrolysis data were obtained from a suite of cuttings through the fault in the C-7 well, Block 330, in order to evaluate thermal maturity and evidence for migrated hydrocarbons. The data shows a migrated hydrocarbon peak (P1) in the 5650-5680 sample, which corresponds to the 'B' fault intercept at 1732 meters (5680 feet*)* DD. No P1 peak in the sample taken below that fault, and weak P1 peaks in the 5980-6010 and 6010-6040 intervals, corresponding to the 'A' fault intercept at 1828 meters (5997 feet). Fault picks were based on marked logs provided by Pennzoil Exploration and Production Co.

In order to address the question of whether the fault represents a paleothermal anomaly and thus may have acted as a conduit for hot fluids, vitrinite reflectance measurements were made on four samples from the KE sand *(*1.5 My), of approximately the same age and depth as the fault samples at varying

distances from the fault system. Thin sections from these samples yielded significantly lower average vitrinite (telocollinite) reflectance, between 0.25 and 0.3% Ro, than did most samples from the fault zone.

CONCLUSIONS: Comparison of fluid flow between the Pathfinder and A6ST wells

Data in hand indicate the main ("A") fault zone is heterogeneous with respect to fluid flow, as is typically the case with fault zones. The evidence is against significant throughgoing fluid in the fault zone encountered in the Pathfinder well, while it supports the interpretation of such flow in the fault drilled in A6St well, only 300 meters away. Specifically, the elevated vitrinite reflectances and spore fluorescence colors in the A6ST fault rocks and the well-constrained extrapolation of vitrinite reflectances to "normal" values 100 meters above the fault identifies the fault as a paleothermal anomaly relative to rocks just above it. A thermal model for the vitrinite reflectance anomaly, while not a unique solution implicates fluids at temperatures compatible with oil generation.

Furthermore, the low $\delta^{13}C$ values, combined with low $\delta^{18}O$, of fault zone calcite combined with early- to mid-Tertiary brine iodine-129 ages (Losh and Wood, 1995) point to fluid that interacted with rocks at temperatures at which kerogen maturation was taking place (Udo Fehn, Univ. of Rochester, 1994, oral comm*)*. As the maximum ambient temperature at the A6ST well fault intercept was probably no greater than its present-day value of 80 C (and even this value is unusually high for this depth in this area), fluids of these temperatures and/or from these sources must have ascended from depth. Extrapolation of the 3OC/km geothermal gradient in the A6ST well indicates such fluids must have migrated a kilometer or more vertically: the brines have migrated considerably more than that since they first interacted with rocks undergoing kerogen maturati3n in the early to mid-Tertiary.

The lateral variability in fault-hosted fluid flow may result from lithologic and concomitant permeability variations along the fault zone: sandy intervals in the “massive shale" may have smeared out along the fault. providing channelways for fluid to ascend
from depth. Along the same lines, structural anisotropies in the fault, such as dilatant bends acting in concert with oblique slip, may produce fractured channelways. In the Pathfinder well, the deepest of the three fault domains in the core is interpreted to be the best suited to have acted as a fluid conduit and, as stated above, is the only portion of the cored fault that contained oil. However, even samples of oil-bearing fault rocks from this domain did not yield geochemical or mineralogical evidence for significant mass influx, nor did samples taken in or near the main 'A' fault. Unlike the A6ST well samples, there is no mitigating evidence for fluid flow: vitrinite reflectance values are uniformly low, and calcite $\delta^{13}C$, which is unfortunately obtainable only in the upper, calcareous portion of the core, is almost uniformly unaffected by products of kerogen maturation. Thus, even though oil is present within some of these deeper faults, indicating that they were capable of transmitting fluid to some extent. It is evident that some factor beyond local fault complexity or geometry of fault/fracture spacings controls large-scale fluid ascent in the 'A' fault. Both the Pathfinder and A6ST wells are distant from intersections of the 'A' fault with subsidiary structures as shown on structure contour maps interpreted from seismic and well data, and the 'A' fault has approximately the same trend and, probably, relationship to the stress field at both locations. Thus, a complete answer to the question of which factors exert control on fluid flow in the fault zone does not present itself on the basis of the above data alone. The seismic data and maps derived from them may not be of sufficient resolution to allow distinction of features that could indicate the propensity of the fault to transmit fluid. Answers to this question will probably be best derived from integrated geologic and geochemical studies at a number of points along the fault.

Acknowledgements

Funding for this research was provided by the Global Basins Research Network and Department of Energy grant DC-FC22-93BC14961 to Roger Anderson, Lamont-Doherty Earth Observatory. We are deeply grateful to Pennzoil Exploration and Production Co. for their matchless cooperation and generous access to samples and data; without their support, this entire project would not have been possible. SL also acknowledges the valuable help of Peter Vrolijk and Michael Wooten, Exxon Production Research, and the participants in the coring strategy meetings. Mm smectite-illite analyses were performed by Ahn Tu (Pathfinder samples) and Kirsten Price (A6ST), with the knowledgeable help of Prof. Doug

McDowell. Biostratigraphic analysis was performed by Applied Biostratigraphix, Houston, and elucidated by Denise Butler, Pennzoil.

REFERENCES CITED

Abercrombie, H., Hutcheon, I., Bloch, J. DeCaritat, P.., 1994. Silica activity and the smectite-illite reaction; Geology vol. 22. p 539-542

Alexander, L.. Flemings, P., in press. Geologic evolution of a Plio-Pleistocene salt withdrawal mini-basin. Eugene Island South Addition. Block 330. offshore Louisiana; Amer. Assoc. Petrol. Geol. Bull.

Anderson, R., 1993, Recovering dynamic Gulf of Mexico reserves and the U.S. energy future: Oil and Gas Jour, April 26. p.85-91

Anderson, R.. Flemings, P., Losh, S., Austin. J. Woodhams, R., 1994, Gulf of Mexico growth fault drilled. seen as oil, gas migration pathway: Oil and Gas Jour., June 6. pp.97-103

Galloway, W., Henry, C., Smith, G., 1982, Depositional framework, hydrostraigraphy. and uranium mineralization of the Oakville Sandstone (Miocene), Texas Coastal Plain. Univ. of Texas at Austin Bur. of Econ. Geol. Rept. of Investigations 113. 51 pp.

Hippler, 5., 1993. Deformation microstructures and diagenesis in sandstone adjacent to an extensional fault: Implications for the flow and entrapment of hydrocarbons; Amer. Assoc. Petrol. Geol. Bull., vol.77. pp.625-637.

Holland, D., Leedy, J., Lammlein, D., 1990, Eugene Island Block 330 field - U. S. A., offshore Louisiana; in Beaumont, B., and Fosten, N., eds.. Structural Traps III: Tectonic Fold and Fault Traps; Amer. Assoc. Petrol. Geol. Treatise of Petroleum Geology, pp.103-143

Hooper, E. C. D., 1991, Fluid migration along growth faults in compacting sediments; Jour. Petrol. Geol. vol 14, pp.161-iSO

Hower, 3., Eslinger, F., Hower. M.. Perry. F. 1976, Mechanism of burial metamorphism of argillaceous sediment I: Mineralogical and chemical evidence; Geol. Soc. Amen Bull., vol. 87, p.725-737

Huang. W.-L., Longo, 3., Pevear, D., 1993, An experimentally-derived kinetic model for smectite-to-illite conversion and its use as a geothermometer; Clays and Clay Minerals, vol. 41, p.162-177

International Committee for Coal Petrology (ICCP): International handbook of coal petrology. Centre Nat. Resch. Sci. (Paris), 2nd ed 1963,164 pp. 1st suppl. 1971,400 pp.; 2nd suppl. 1975.68 pp.

Jones, P., Wallace, R., Jr., 1974, Hydrogeologic aspects of structural deformation in the northern Gulf of Mexico basin: Jour Res. U.S. Geol. Surv., vol 2, pp.511-517

Land, L., MacPherson, 0., 1989, Geochemistry of formation waters, Plio-Pleistocene reservoirs, offshore Louisiana; Gulf Coast Assoc. Geol. Socs. Trans. vol.39, p. 421-430

Land, L., Lynch, F., Mack. L., Milliken, K.L., 1995, Regionally inhomogeneous potash metasomatism, Paleogene mudrocks, Texas Gulf Coast: Amer. Assoc. Petrol. Geol. Abstr. W/Prog., vol 4, p. 53A

Losh, S., Wood, 3., 1995. Brine chemistry. SF1 Blocks 316 and 330; in Anderson, R.. ed. Results of the Pathfinder Drilling Program into a Major Growth Fault; Part of the GBRNIDOE Dynamic Enhanced Recovery Project in South Eugene island 330 Field, Gulf of Mexico. CD-ROM available from Geosciences Dept.. Lamont-Doherty Earth Observatory. Palisades. NY 10964

Milliken, K., L., 1985. Petrology and burial diagenesis of Plio-Pleistocene sediments, northern Gulf of Mexico: unpub. PhD thesis, Univ. Texas at Austin. 112 pp

Moore and Reynolds, 1989

Mukhopadhyay, R.. 1992: In *Diagenesis III Developments in Sedimentology. 47:* pp. 435-510. Eds. K. H. Wolf and G.V. Chillingarian. Elsevier Science Publishers

O'Neil. J., Clayton, R., Mayeda. T.. 1969, Oxygen isotope fractionation in divalent metal carbonates: Jour. Chem. Phys., v.51.5547-5558

Schoell, M., Haught, M., 1994. Preliminary report on mudgas isotope analyses. GBRN well E1330 A2OST; Chevron Petroleum Technology Company. La Habra. CA. internal report TM94ooo()51. 7 pp.

Stach, E., Mackowsky, M-Th., Teichmuller. M., Taylor, G., Chandra, D., and Teichmuller, R.. 1982, Textbook of Coal Petrology, 3d ed. 536 pp. Gebruder Borritraeger

Sweeney. 3.. Burnham, A., 1990, Evaluation of a simple model of vitrinite reflectance based on chemical kinetics; Amer. Assoc. Petroleum Geol. Bull., vol 74, *p.155*[9] 1570.

Weber. K., MandI, G.. Pilaar, W., Lehner, F. Precious, R., 1978, The role of faults in hydrocarbon migration and trapping in Nigerian growth fault structures; Tenth Annual Offshore Technology Conference Proc., vol 4, pp.2643-2653 (OTC 3356)

Brine Chemistry, Blocks 330 and 316

Steven Losh
Cornell University: Jim Wood, Michigan Technological University

Twenty-two samples of brine were collected from producing wells in South Eugene Island Blocks 330 and 316 by Dr. Lynn Walter and Anna Martini (University of Michigan) over a three-day period during January, 1994. Seventeen phases were analyzed at the University of Michigan in addition to temperature at the wellhead, pH, density, and Sr isotopic composition. Chemically, the brines are similar to those documented in nearby Plio-Pleistocene reservoirs by Land and MacPherson (1989). They are NaCl waters that exhibit a sizeable range of chloride content, from 19,900 to 103.100 mg/L (however, the 10W-salinity sample from the A10ST well is probably contaminated by completion fluid, as that well has only recently gone into production), but lie on a seawater-halite dissolution line. Calcium concentration is somewhat higher than would be expected from dissolution of halite, but may reflect dissolution of gypsum associated with salt. Sulfate concentration is unusually low, in most cases below the detection limit, and may reflect ongoing sulfate reduction. The brines appear to be seawater mixed with varying proportions of halite-saturated fluid, or seawater that has simply dissolved varying amounts of salt as it migrated. These fluids have been further modified by limited fluid-silicate interaction.

Iodine-129 dating has been carried out at the University of Rochester, under the direction of Dr. Udo Fehn, on nearly all brines collected during this study. This method yields apparent brine ages between 31 and 61 Ma considering only a cosmogenic source of ^{129}I. However, even when accounting for likely fissiogenic contributions, an early Cenozoic age of the brine is indicated, and significant vertical fluid flow is implied. It is not anticipated that dissolution of Gulf Coast evaporites would significantly affect the measured brine age, as these materials contain very low concentrations of iodine (U. Fehn, 1994. oral comm.); indeed, no correlation between iodine age and chloride concentration is present. The brine age is likely strongly affected by the age of maturing kerogen from which much of the brine's iodine was derived, but even so, the ages imply that at least a component of the brines was present in rocks of at least mid-Cenozoic age.

Chloride concentration of the brines shows no systematic variation with depth. Nor does it appear to vary with respect to distance from faults, with one notable exception; however, it does show sizeable differences between reservoirs. It is highest in the shallowest reservoir, the GA, about half as high in the underlying HB sand, and high but variable in the deeper sands. Chloride concentration also shows no noticeable change from upthrown to downthrown blocks. As noted, chloride concentration in brines near faults is similar to that in brines far from faults, with the exception of the sample from the A2 well (OI-5 sand), which is unusually dilute for waters at this depth. This fluid may represent incorporation of water from shales undergoing dewatering below the OI sands. However, other brines collected near faults (the A6ST sample, for example, was taken from the KE sand, immediately above the 'A' fault) show no such decrease in chloride concentration. In a manner analogous to the distribution of chloride concentrations, ^{129}I ages show no systematic variation with respect to faults (although the range of 1291 concentrations **is** small), nor do there appear to be significant age variations between reservoirs.

The pronounced variations in brine chemistry between reservoirs and the evident compositional homogeneity within a reservoir using chloride as a monitor, indicate that the brine entered the reservoirs at different times and/or from different directions. As opposed to a model in which a single stream of fluid migrated up the fault and leaked into each reservoir it passed by. For example, the GA2 sand contains the highest - salinity brines in the dataset, yet is the shallowest reservoir sampled. Brines that entered that reservoir necessarily bypassed the HB I sand, in which brines have only half the salinity of the GA2 sand a few hundred feet above it. If S7Sr/865r ratios are interpreted as indicative of brine source (that is, neglecting water-rock interaction), comparison with the DSDP seawater Sr isotope curve implies that the least radiogenic brine with respect to Sr isotopes originated in 30 Ma sediments. This brine is also characterized by the lowest 1/Sr value in the dataset; other brines have higher 875r/S6Sr and lower 1/Sr, and thus appear to have been contaminated by a radiogenic component of sediment-derived strontium. The mid-Tertiary age deduced from Sr isotope ratios is consistent with the above iodine-129 data, and points to large-scale vertical migration of brine to its present location in the Pleistocene reservoir sands.

REFERENCE CITED

Land, L., MacPherson. 0, 1989, Geochemistry of formation water, Plio-Pleistocene reservoirs. offshore Louisiana: Gulf Coast Assoc. Geol. Socs. Trans. vol 39, p 421-430.

Reservoir Diagenesis, SEI Block 330

Steven Losh
Cornell University, with contribution from Jim Boles, Univ. California, Santa Barbara

The diagenesis of Pennzoil's Block 330 reservoir sediments has been studied in order to assess the possible relationship of cementation and alteration of these rocks to the fault that has presumably provided a conduit for diagenetic fluids. Approximately 200 thin sections from sidewall cores of reservoir rocks throughout Block 330 have been examined for diagenetic effects; the GA, 1413, JD, and OI reservoirs in particular have been studied in terms of cementation and grain alteration. In general, cement is sparse, less than 2 percent of the rock (in many cases, much less), and consists of calcite, ferroan dolomite, and siderite. Diagenetic pyrite, usually framboidal, is also present, whereas silica overgrowths are rare. Organic matter is scattered but ubiquitous, typically being found within formainifera, as layer-parallel stringers in shale (especially in the KR sands), and as discrete bitumen "patches" in sands.

These observations were made as a complement to the petrographic analysis of sediments from the same reservoirs carried out by David K. Davies Associates for Pennzoil. It was originally anticipated that cementation or grain alteration may be more intense as the fault is approached, and this study focused on obtaining samples in traverses across faults and examing for grain alteration, specifically albitization and plagioclase dissolution. Diagenetic minerals as determined both by Davies Associates and in this study show no apparent relationship with distance from the fault in terms of their abundance or type.

GA sands

Most of the sections are of sandy or silty shale to shaly silt; clean sand are not well represented in this suite, probably in part because sidewall cores of sand disaggregate very easily. Calcite cement in silty rocks is sparse (up to 3%) and extremely fine-grained. Plagioclase commonly shows weak to moderate pitting, but in any given sample, most plagioclase grains show no albitization. It is likely that any albitized plagioclase in these sands has been reworked from an older sand. Detrital carbonate grains are common, in many cases comprising 5-20% of the grain population.

Dr. Jim Boles, University of California, Santa Barbara, concluded his examination of selected sidewall cores from the GA sand, Block 330, wells B16, Al9ST, and B3ST. His report is as follows. Photographs are not included here.

"A petrographic study of 17 sidewall core samples of the "GA sand", Block 330 was undertaken to look for evidence of diagenesis resulting from fluid movement along faults. Results indicate that very little diagenesis has occurred.

The samples were received as loose particles and thus were prepared as grain mounts. Overall, samples are very fine to fine grain size sand with varying proportions of silt and clay matrix. Porosity could not be estimated from these samples due to their disaggregated condition.

The detrital components are quartz, K-feldspar, plagioclase, siliceous rock fragments, detrital carbonate shell material, micas, and trace minerals including glauconite, green hornblende, and garnet. A notable feature of some samples in the presence of zoned plagioclase feldspar indicating a hypabyssal or volcanic source component and rare volcanic rock fragments. No systematic changes in detrital or diagenetic mineralogy were noted with depth in the wells nor in comparison between wells.

Diagenetic smectite and illite are the most abundant authigenic phase but even these minerals do not exceed 10% by volume in the samples. The clays occur as thin rims on detrital grains and as pore-filling cement. In many cases diagenetic clay appears admixed with detrital clay matrix and it is difficult to distinguish the detrital from the authigenic phase. The samples with the most abundant, what is clearly authigenic clay, are B16@5074' which has up to 10% of small scattered lath-shaped birefringent illite clay particles. Curiously, these crystals are length fast, whereas typical illite is length slow. Other examples of diagenetic clay are in the A19ST well where a birefringent (illitic?) clay forms thin rims about detrital grains or in some cases, pores are partially filled with a yellowish-green to yellowish-grown clay.

Diagenetic carbonate occurs in trace amounts in some samples. Typically it occurs as scattered subeuhedral to euhedral grains or in some cases as grain coatings. In some cases, such as B3ST @5917' and 5930', the yellowish-brown color or the carbonate indicates it is probably siderite. Similar appearing siderite is found in Cretaceous sands from the Alaska North Slope and in this case they can be shown to have formed near the sediment-water interface.

Syntaxial quartz overgrowths are very rare in these samples, indicating that they have not undergone silica cementation due to upwelling hot fluids. The few samples with quartz overgrowths occur as incipient syntaxial overgrowths on a few grains in a few samples. The rarity of the overgrowths indicates that they could be reworked.

Feldspar diagenesis is a sensitive indicator of changing burial conditions. Neither dissolution of feldspar nor in situ albitization of detrital plagioclase can be demonstrated in these samples. Albitized feldspar occurs in the samples, but it in a mixed population with fresh plagioclase. This suggests that albitization is not an in situ process. In addition, zoned plagioclase, typically some of the most unstable feldspar, appears unaltered.

In summary, these samples are not extensively cemented. Clay minerals, which appear to be the dominant diagenetic phase, appear similar to those found in incipient diagenesis. The most compelling evidence for upwelling hot fluids from deep in the basin would be the presence of abundant authigenic silica. Such evidence is not found in these "GA" sand samples."

HR sands

Most sections are of moderately sorted shaly silts and shaly sands. Detrital calcite is common, in many cases comprising 10-20% of the rock. Authigenic calcite and ferroan dolomite occurs as ragged overgrowths on the detrital grains, and is thus more abundant in rocks containing more detrital carbonate. Aggregates and disseminations of extremely finegrained siderite are common, comprising perhaps 2% of many sands. At most, diagenetic carbonate comprises 10% of the rock, and is always extremely fine-grained. Plagioclase dissolution is minor to non-existent in many of the silts, but is moderately advanced in others. Michel-Levy analysis of albite twin angles for unaltered plagioclase indicates the feldspars may be as calcic as An60.

Diagenesis of the 70 examined HR sand samples (wells B16, B3ST, A7ST, C15ST, C13, C11, C9, C21, C2. #3, #4 (Al), A23, A19ST, C20, A6ST, A13, B12, C3, #1. #6;

is largely similar to that observed in the GA sand, except that carbonate (both detrital and authigenic) is slightly more abundant, and that dissolution of plagioclase, K feldspar, and in some cases quartz, is more common. In some cases involving all of the plagioclase and a significant percentage of other grains in a

sample (particularly samples from C2, C9, and C13). The dissolution is manifest both in the forms of uncommon skeletal grains and as microporosity, which may affect up to 15-20% of the quartz and feldspar grains in a sample. Skeletal grains are interpreted as reflecting in situ dissolution, whereas the intensely-pitted grains are similar in
appearance to pitted grains described from the vadose zone (i.e., soil profiles) in humid regions. In at least one case (B 16,6144') dissolution is inversely correlated with carbonate cement.
Where cement is abundant, feldspars are fresh, whereas uncemented zones contain pitted and rare skeletal plagioclase and K feldspar. This type of relationship indicates the dissolution is at least partly in situ, and that the carbonate cement in this sample predates at least some of the dissolution. Pronounced variations in proportion of pitted grains to unpitted ones exist over short vertical distances in the wells. Intergrown fine-grained calcite and dolomite were noted in two samples from the B16 well; these were analyzed for carbon and oxygen isotopic composition

(dolomite: $\delta^{18}O$ = 26.0-26.6 permil SMOW, $\delta^{13}C$ = I to 1.9 permil PDB; calcite $\delta^{18}O$ = 23.1-23.4 permil, $\delta^{13}C$ = 0.3 to 0.5 permil). These diagenetic indicators show little to no apparent spatial relationship between the extent of diagenesis and proximity to faults. Samples above the oil/water contact on the north side of a nearly east-west fault traversing the southern part of Block 330 have more carbonate cement and a higher proportions of pitted to unpitted grains than do samples south of this fault or samples below the OPY contact. There does not appear to be any correlation between abundance of pitted grains or authigernc carbonate and stratigraphic position within the HB 'sand. More work is being done to assess the possibility of in situ dissolution: if such a process were occurring, it would be unusual given the relatively low temperature of the 1413 sand. In situ dissolution generally begins at about 80-100 C, whereas the HB sand is at temperatures closer to 60 C.

JD sands

These are mostly clean sands, with high porosity. Calcite cement is sparse, at most 3-4 modal percent in rocks containing detrital carbonate, and is absent in many cases. Plagioclase is pitted to a varying extent in the sections: nearly all rocks show some pitting, and in some cases, up to half of the plagioclase shows weak to moderate dissolution. Clay coatings on sand grains are very rare; no pore-filling, authigenic clay has been noted.

OI sands

Clean to shaly silt and sand. Calcite cement is absent in most rocks, and is scarce (1%) at best. Several of the sands have clay coatings on sand grains or rare pore filling "felted" clays. Plagioclase dissolution and pitting is weak, typically affecting 10 - 25% of the plagioclase grains in a given section.

Temporal Variability in the Composition of Some Petroleum Fluids from Eugene Island Field-330 Over Short Time Scales

Mahlon C. Kennicutt H, Yaorong Qian and Adolfo G. Requejo
Geochemical and Environmental Research Group
Texas A&M University
College of Geosciences and Maritime Studies
833 Graham Road
College Station, IX 77845

Jean Whelan and Lorraine Eglinton
Department of Chemistry
Woods Hole Oceanographic Institute
Woods Hole, MA 02543

Introduction

While petroleum is often perceived as a rather uniform fluid, its composition, even within a field, can be quite heterogeneous (Baily et al. 1973; Milner et al. 1977; Hunt 1979; Tissot and Welte 1984; Connan 1984; Leythaeuser and Ruckheim 1939). Variations in the composition of petroleum can occur due to many factors including, source rock composition, thermal maturity, migration alteration, in-reservoir alteration, and mixing of fluids from multiple sources. The chemical characteristics of petroleum often provide clues for deciphering the evolution of a fluid in regard to temperature history, age of source rock, migration pathways, and the effects of post-generation alteration processes such as biodegradation, evaporative fractionation, water washing, in-reservoir maturation and gravity segregation. It has also been demonstrated that low rates of in-reservoir mixing of multiple charges of petroleum can lead to inhomogeneities (England et a'. 1987; England and Mackenzie 1989; Karlsen and Larter 1989; Larter et a'. 1989). These variations can be assessed on a variety of vertical and horizontal spatial scales. Regional (kilometers) trends in petroleum compositions provide insight into variations in organic facies, thermal maturity, reservoir filling history, and viable source horizons (England and Mackenzie 1989). Observations within a field can provide insight into post-generation alteration as well as communication amongst reservoirs, sands, and/or across fault blocks.

In contrast to spatial variations, temporal changes in fluid compositions have received little attention. Recent observations have led to the hypothesis that in certain geologic settings oil and gas may be migrating into producing reservoirs relatively recently compared to geologic time scales (Anderson et al.1991a,b; Anderson 1993; Schumacher 1993; Whelan Et al. 1994). A variety of circumstantial geological, geophysical and geochemical evidence has been presented in support of the "dynamic fluid injection" hypothesis. The evidence includes slower than predicted rates of reservoir fluid depletion, coherence of pressure and temperature profiles, the existence of deep seated conduits for fluid migration, displacement of heat flow anomalies away from salt features, intense present-day surface hydrocarbon seepage, temporal changes in oil and gas compositions, and secondary injection of non-biodegraded fluids into biodegraded fluids (Whelan et al. 1994; Anderson 1993; Schumacher 1992, 1993; Holland et al. 1990; Barnard and Bastow 1991; Anderson et al. 1991a,b.). To further define the origins of temporal variations in fluid compositions, the present study compares and contrasts the composition of fluids collected over an eight-year period at the site where "dynamic fluid injection'[1] was first suggested, the Eugene Island-330 Field in the northwestern Gulf of Mexico.

The geologic setting and chemistry of fluids recovered from the EI-330 field have been discussed in detail elsewhere (Holland et al. 1990; Kennicutt et al. 1992; Whelan et al. 1994). More than 25 Pleistocene sandstones are produced at depths from 701 to 3658 meters)Holland et al. 1990). The EI-330 field consists of more than 100 oil and gas reservoirs that are separated by faults and permeability barriers. The field is considered to be one of the giant oil and gas fields of the world (Carmalt and St. Johns 1986). Fluid compositions are highly variable and different sands produce a variety of admixtures of gas, condensate, and oil. Differences in oil compositions are apparent vertically within the section as well as between fault blocks and within single reservoirs (Schumacher 1993; Whelan et al. 1994, 1995). Despite these variations in composition it has been argued on the basis of biomarker data, that the majority of fluids at EI-330 are derived from the same or similar source facies (Whelan et al. 1994). However, it has been recognized that different molecular weight ranges (boiling points) exhibit characteristics typical of a range of thermal maturities suggesting more than one infusion of fluids (Thompson and Kennicutt 1990). Reservoired petroleum across the Gulf of Mexico exhibits a high incidence of alteration due to non-thermal processes such as biodegradation, evaporative fractionation, migration contamination, and extraction by water (Thompson anti Kennicutt 1990).

The objective of this study was to evaluate intra-field fluid compositions to document changes in fluid compositions over short-time scales (months to years.). The first goal of the study was to minimize variations due to non-geochemical processes. Variations in fluid composition due to collection, storage and analytical methodologies must be carefully considered. Most surface collection techniques do not recover fluids in their natural state in the reservoir. Physical alterations due to depressurization and cooling are expected. Partitioning of compounds among phases upon depressurization has been

demonstrated in the laboratory Thompson 1987, 1988, 1990). Long-term storage of collected fluids can result in the loss of the more volatile fractions. Gas chromatographic data are strongly influenced by the conditions of the analysis. Operating conditions such as the gas stream split between the vent and the column can lead to significant fractionation of volatile compounds. Differences in the liquid phases of chromatographic columns determine the elution order and the degree of resolution of components in complex mixtures. Chromatographic temperature programs and column gas flows effect the detector response of analytes. Effects related to variations in apparent fluid composition due to analytical conditions, storage, and the method of sample collection must be clearly delineated if variations in reservoired fluid compositions are to be attributed to natural processes occurring over short-time scales (months to years).

Variability Due to Analysis, Storage, and Sampling Conditions

Oil (including condensate) samples were collected from the producing s_4'inds of El330 in 1985.1988, and 1993. Oil and condensate samples were analyzed by high resolution capillary gas chromatography (CC) to quantify the percent composition of each fluid from propane to n-C34 (Kennicutt et al. 1992). Samples were also analyzed using a second gas chromatographic column to provide confirmation of peak identities.

Comparison of the results for samples collected and analyzed in 1988 and re-analyzed in 1994 provide an assessment of storage effects on fluid compositions and a comparison of analytical methodologies. An oil sample was also analyzed six times and then re-analyzed six months later to assess the reproducibility of successive injections and the effects of storage.

Replicate analyses were highly reproducible from one injection to the next. For the majority of the compounds the integrated peak areas exhibited less than t5% coefficient variation for six replicates. As expected, the coefficient of variation is directly related to the concentration of the compound being analyzed. Compounds accounting for less than 0.5% of the mixture exhibited larger coefficients of variation due to the precision of integrating small chromatographic peaks. However, a coefficient of variation of less than $\pm$10% was obtainable even for minor oil components. When the average results of six replicate analyses were compared to the results of an analysis conducted six months earlier, most compounds, with the exception of C3-C4 compounds, were within $\pm$5% of the mean area of the later analyses. The C3 and C4 compounds were reduced by 20 to 30% in the later analyses. This suggests that under these storage conditions, gases dissolved in the oil were partially lost. However, for compounds with five or more carbons the reproducibility over time approached that of replicate injections.

Comparison of the analyses of forty-two EI-330 oil samples analyzed in 1988 and then re-analyzed in 1994 showed significant variations in composition. On average, the C3-C5 compounds had greater relative abundances in the 1994 analysis than in 1988. Intuitively, the C3 and C4 compounds might have been lost during storage as already demonstrated for a six-month storage period. On the contrary, the most volatile components accounted for more of the gas chromatographically resolvable compounds after storage for six years. Variations in compositions between the two analyses were also apparent as over- and under-estimated. The most likely explanation is that gasoline range compounds were significantly effected by the chromatographic conditions, especially the split ratio, which is known to fractionate compounds based on boiling point or volatility. The over- and under-estimates can be partially attributed to the improved resolution of components using later analytical methodologies. Peaks occurring as shoulders in the 1988 analysis were either merged or more completely separated depending on the particular analyte. These differences in compositions suggest that variations due to analytical technique must be minimized to ensure comparability of results. Therefore all samples were reanalyzed within as short a period of time as possible under nearly identical chromatographic conditions. The following comparisons only utilize the later analytical results thus minimizing variations due to analytical conditions.

The effect of sampling technique on fluid chemistries is uncertain. Sampling which involves depressurization and cooling is known to cause changes in fluid chemistry (Price et al. 1983). Single step depressurization experiments produced relatively small variations in composition, whereas multiple episodes of depressurization are believed to cause fairly dramatic shifts in chemical composition (Thompson 1987, 1988, 1990; Larter and Mills 1991; Whelan et al. 1994). However, changes due to sample collection in this study equally affect all samples and only one episode of depressurization

occurred during sampling. Larter and Mills (1991) reported little change in gasoline range hydrocarbon compositions during a since stage depressurization and phase separation at STF'.

Origins of Fluids in EI-330 Field

Identical biomarker distributions and stable carbon isotope values (Holland et al. 1990; Kennicutt et al. 1992; Whelan et al. 1994) indicate that the fluids in the various reservoirs of EI-330 field have a common source.

Even though hydrocarbons in the GA and HB sands are relatively depauperate of C9+ n-alkanes, these fluids contain large amounts of hydrocarbons with three to eight carbons. The API gravities (2325° API) of the fluids from the GA and HB sands are in the range of a normal oil (Holland et al. 1990) despite the abundant light hydrocarbons. The co-occurrence of these light hydrocarbons with low API gravity fluids and the reduced C9+ aliphatic hydrocarbons suggests that the light hydrocarbons were added to these reservoirs after biodegradation had proceeded to an advanced stage (Whelan et al. 1994). This process has also been described for Trinidad Basin and Ecuadorian.

Spatial Variations in Fluid Compositions

Vertical spatial variations in hydrocarbon compositions are significant amongst producing sands in the EI-330 field. The heterogeneity in fluid compositions among sands is believed to be primarily caused by post-generation alteration processes such as remigration, biodegradation, and phase separation (Whelan et al. 1994). Among these processes, biodegradation causes some of the most dramatic changes in fluid compositions.

Variability within a sand (GA-2) and a block (A) was compared. Variability within the sand and the block are similar and significantly greater than analytical variability. However increased variability in normal alkanes with 9 to 12 carbons, isoprenoids with 11 and 13 carbons, and the low molecular weight aromatics benzene and toluene in the GA-2 sand is apparent. It is known that in this shallow sand reservoir biodegradation is quite common. The observed lateral variability in the GA sand fluids is most likely the result of variations in the degree of degradation. Degradation has been observed to be most rapid in alkanes with 9-10 carbons (Thompson 19__). The variability in benzene and toluene content is most likely related to the intensity of water washing. These two aromatic compounds are more water soluble than aliphatic hydrocarbons of similar molecular weight. Individual locations within a sand have been subjected to differing intensities of biodegradation and water washing.

A more detailed look at variability between sands and between fault blocks confirms these interpretations. Deeper in the section degradation decreases and the fluids within a given sand are more uniform. Therefore spatial variability can be most closely linked to in-reservoir alteration processes. The greatest variability in a fluid is in the shallowest sand (GA-2) which also contains the most altered fluids. Samples from other sands are less degraded or undegraded. Variability within a fault block reflects vertical spatial variability in fluid compositions. The characteristics of fluids within a fault block are controlled by the distribution of samples among the producing sand, for example, the fault block B sample collection contains a large number of samples from the GA-2 sand and thus the observed variability is primarily related to shallow reservoir alteration processes. However, it should be noted that fluids from the same sand but from different wells show variations on the order of -25-50%.

Another cause of spatial heterogeneity of hydrocarbon compositions in reservoirs is differences in the permeability of the reservoir sands (England et al. 1987; Leythaeuser and Ruckheim, 1989; Horstad et al. 1990; Hillebrand and Leythaeuser, 1192). Low permeability can restrict thc lateral diffusion and mixing of hydrocarbon fluids. The porosity and permeability of sands in the EI-330 field are high, with an average. porosity of 30% (Holland Et al. 1990). Permeability is in the range of 6 md to 6 darcys, with 80% of the sands having permeability of greater than 100 md (Holland et al. 1990). The heterogeneity in compositions within sands may be partially the result of restricted diffusion and mixing however the difference between sands is most likely related to the history of hydrocarbon charge.

Temporal Variability in Fluid Compositions

The amount of low molecular weight to high molecular weight hydrocarbons in fluids from the same well and sand within the EI-330 field increased with time over an eight year period. Gasoline hydrocarbon concentrations were highest during the latest samplings in many samples. Specifically, examining the GA-2 sands between 1988 and 1993 an envelope of compounds is recognizable as an addition. The additions include cyclohexane and a range of hydrocarbons with 7 and 8 carbons. The normal alkanes are particularly enhanced. These differences are most clearly apparent in the GA sand since most of the compounds in this carbon range were greatly reduced in the original charge due to biodegradation and water washing. The additional fluid is of a composition typical of a condensate.

The hydrocarbon ratios proposed by Thompson (1983; 1987) varied consistently from 1985 to 1993). The H, I, and F parameters are believed to reflect fluid maturity (Thompson 1983; 1987). These ratios increased from mature in 1985 samples to super-mature for most of the samples in 1993. The presence of abundant light hydrocarbons in the biodegraded GA and HB sands, the increase in the amounts of light hydrocarbons relative to the higher molecular weight compounds in the later samplings, and the increase in the maturity of light hydrocarbons in the latest samplings all point to a systematic variation in the light hydrocarbon compositions over a period of years.

The Origins of "injected" Hydrocarbons

The variation in the chemical composition of fluids from the sands of the EI-330 field over short-time scales indicates an influx of fluid into these reservoirs in the past several years. The observed temporal changes could be explained by inducing localized and lateral migration, migration from deeper intervals, and/or production induced depletion of the reservoir.

An influx of fluids from adjacent less permeable sands to the primary reservoir bodies as the field was depleted has been suggested. The concept of "feeder pays" was suggested by Holland et al. (1990) to explain the overproduction for the GA sands. It was suggested that even though adjacent sandstones had little capacity for significant lateral flow they may recharge the more permeable productive zones. However, the temporal change in fluid chemistry on the EI-330 field was characterized as an increase in fluids of higher maturity. In contrast, Leythaeuser and Ruckheim (1989) observed that fluids in high porosity/high permeability sand intervals bear a higher proportion of saturated hydrocarbons and have a higher apparent maturity compared to fluids from lower porosity/lower permeability zones. Therefore it would appear that adjacent "feeder pays" cannot be attributed with recharging the adjacent high porosity zones since it would be hypothesized that less mature fluid would arise from the lower permeability zones with time. Another words, the initial maturity of the fluids charging the sands could not be exceeded and yet maturity increases far beyond that documented throughout the field.

If the change in fluid composition was due to injection from much deeper strata, the latest influx of hydrocarbons would be expected to have had a more advanced thermal history different than the fluids originally emplaced. As well, the apparent age of the latest arriving hydrocarbons would be different from those of the originally reservoired hydrocarbon. Young et al. (1977) used the relative molar concentrations of paraffins, naphthenes, and aromatics in the light hydrocarbon range (C5-C7) arid the relative concentrations of the naphthenes with different numbers of rings in higher molecular weight ($_{C15+}$) hydrocarbons to calculate the ages of these hydrocarbons. The rationale was that the chemical composition of an oil from a single source is determined by the combined effects of time and temperature. With increased time and temperature, the chemical composition of the oil gradually shifts according to chemical kinetics. Based on this rationale the ages of several hundred oil samples were calculated.

Based on the equations and constants given by Young et al. (1977), the relative concentrations of naphthenes (C_n. relative to paraffins and aromatics) and the mean thermal history of light hydrocarbons in EI-330 field were calculated. Assuming that the thermal history during and after the generation of hydrocarbons is mostly responsible for the variation of the Cn values observed in the oils and assuming the temperatures of the reservoirs have not changed after the emplacement of oil in these sands, the apparent ages of the light hydrocarbons were calculated using the current reservoir temperatures and the C_n values.

The relative concentrations of naphthenes decreased uniformly from 0.35 in 1985 samples to about 0.25 in 1993 samples for all the reservoirs with the exception of GA-2 sand where the C_n value decreased from 0.4 to 0.34 over the same time period. This rapid diminishing of naphthenes might be the result of a temperature-time effect With increased exposure to high temperature, the oil would become

more mature (more paraffinic). However, if the C_n values had decreased from 0.35 to 0.25 within only 8 years at the current reservoir temperatures (55 to 86^0C) solely by the effect of temperature, then the C_n values of all of the fluids now in reservoirs should be much lower and the hydrocarbons should have been extensively cracked to gases. A more plausible explanation of the high C_n values of the hydrocarbon fluids at 1985 (0.35) and the rapid decrease to lower values (0.25) over the eight year period is that highly mature hydrocarbons have been added lowering the C_n values of the original hydrocarbon charge. Based on the analyses of several hundred different-aged oil samples a decrease in C_n value from 0.40 to 0.25 should be expected to take millions of years, depending on the temperatures experienced (Young et al. 1977).

The calculated ages of these oils lie between 8 and 133 million years. Given the age of the reservoir sands of 1 to 2 million years (Pleistocene), the calculated ages of the hydrocarbons are substantially older than the age of the reservoir sands. However, the age of the hydrocarbons was calculated based on current. reservoir temperatures. Petroleum must have been generated at higher temperatures in deeper sources than the present day reservoirs of EI-330. Young et al. (1977) and Quigley and Mackenzie (1988) concluded that temperature is the most critical factor that influences the generation, maturity, and compositions of oils and time is believed to be less influential than temperature (Quigley and Mackenzie, 1988, Mango, 1990, 1991). If the hydrocarbons were indeed derived from deeper sources (either from source rocks or deeper reservoirs), then higher temperatures should be used in the age calculations. Using the minimum hydrocarbon formation temperatures of l00 C to 150^0C (e.g. Quigley and Mackenzie, 1988) and assuming a constant thermal history, the calculated ages are substantially lower than the ages calculated. The ages range from 12 to 59 million at 100 C and 4 to 20 million years at 150 C, respectively. This wide variation in the calculated ages of the light hydrocarbons might indicate the presence of hydrocarbons of different ages in these reservoirs. The variation is most prominent among different sampling periods. The ages of the hydrocarbons at the same sampling times are similar between reservoirs. One exception is the GA sands where biodegradation may have obscured the age calculations. In addition, the ages of the hydrocarbons during the earlier sampling period, particularly 1985, are low ranging from 22 to 42 million years based on the current reservoir temperature. The ages are 15 to 21 millions years if 100 C is used in the calculation. These two groups of values are similar to the values reported by Young et al. (1977) for Eugene Island. The calculated ages of the light hydrocarbons are much older for samples from 1993 than those from 1988 and 1985 suggesting a further influx of highly mature (older age and/or higher temperature) hydrocarbons. The source of these hydrocarbons must be substantially deeper in the section and at much higher temperatures. If this is the case, the C_n values and their changes over the past several years in all the reservoirs (including GA-2 sand) could be explained by the ongoing process of "dynamic fluid injection".

Assuming the hydrocarbons were generated and emplaced in these reservoirs at similar time (i.e. the age of these fluids are similar), their thermal history should also be similar, or more precisely, the hydrocarbons in the shallow reservoirs should have experienced slightly less thermal stress than the deeper ones because the temperature of the shallow reservoirs are lower. The difference in the calculated mean thermal history (mean temperatures) between the shallow reservoirs at each using the OI from that time as a reference. For fluids in the OI sand, the deepest sand, secondary processes such as biodegradation are minimal. With the exception of the GA-2 sand and the HB sand, the difference in the temperatures between each reservoir and that in the OI sand at each sampling is small. suggesting that the thermal history of the fluids was similar. This conclusion agrees with oil maturities calculated from biomarkers and aromatic hydrocarbons (Whelan et al. 1994, 1995).

The calculated temperatures in GA and HB sands are substantially lower than the others. Several possible mechanisms can result in these lower calculated temperatures. The amounts of light hydrocarbons that were injected into the GA and HB sands might be small, whereas the amount of injection into the OI sand might be large. As a. result, the calculated thermal histories of GA and H13 sands relative to the OI sand are low. Alternatively, light hydrocarbons in GA arid HB sands have experienced biodegradation (Whelan et al. 1994) because of the lower reservoir temperatures and shallower depth. Biodegradation selectively removes n-alkanes leading to higher naphthene concentrations relative to paraffins and aromatics (higher Cn values). if this second interpretation is correct, the light hydrocarbons in GA and HB sands would appear to be less mature and have lower

apparent temperature histories. The calculated temperatures and ages would also be biased on the low side.

The ages of the hydrocarbons in all of the reservoirs are assumed to be similar and the average thermal history of the hydrocarbons in the OI sand over their life time is 86^0C (the current reservoir temperature, the actual thermal history of the hydrocarbons in OI sand might be slightly higher than this value), then the mean temperatures of the hydrocarbons in other reservoirs at different sampling periods can be calculated based on the measured C_n values for each reservoir at each sampling. These calculated temperatures are substantially higher in the 1988 and 1993 samplings than temperatures during the 1985 sampling. In addition, the calculated temperatures are substantially higher than the current reservoir temperatures for all the samples collected in 1988 and 1993. This higher temperature (higher thermal history) indicates that the light hydrocarbons were injected into these reservoirs recently from a deep, high maturity sources. As a result, the calculated thermal history (time-temperature effect) is higher in 1988 and in 1993 due to a continuing input of highly mature fluids. The increased calculated temperatures of GA sand in 1988 and 1993 is consistent with the injection of high maturity (high temperature 017 old aged) fluid into the GA reservoir in recent years, in spite of biodegradation, which lowered the calculated apparent temperature. The calculated temperatures for the hydrocarbons in most of the reservoirs in 1988, and particularly in. 1993, and close to the temperatures of the proposed source rock currently generating hydrocarbons (150 to 170^0C; Holland et al. 1990).

The H (heptane ratio), I (isoheptane ratio), and F (paraffinity parameter) values in all the samples show a consistent increase from 1985 to 1993 sampling period for each reservoir. Thompson (1983; 1987) proposed that these parameters reflect the maturity levels of oils, although Mango (1990) disputed this interpretation by arguing that the ratios might be controlled by kinetic mechanisms during the formation of hydrocarbons.

With an increase in maturity, these parameters should increase (Thompson, 1983, 1987). The consistent large increase in these parameters from 1985 to 1993 in all samples is consistent with fluid injection during that period. Such an input of high maturity, low carbon-number hydrocarbons derived from deep sources into these reservoirs would cause a rapid and concordant increase in these parameters. The relatively low values of H, I, and F parameters in GA and HB sands as compared with those of deeper reservoirs are probably the result of incipient biodegradation (Thompson, 1983; 1987; Whelan et al. 1994).

In contrast to EI-330, the C_n values from nearby South Marsh Island Block 128 (SMI-128) are nearly constant for all the sands, ranging from 0.32 to 0.34. The calculated ages of the hydrocarbons are in the range of 40 to 50 million years using the current reservoir temperatures. The H, I. and F parameters are also constant for all producing sands, with values of 22 to 25, 0.4 to 0.6, and 0.6 to 0.8, respectively. However, the SMI-128 field was not sampled at different production periods, as was EI-330.

Conclusions

Systematic changes in fluid chemistry have occurred over the time-scales of years at the EI-330 field. The changes are consistent with an on-going infusion of a relatively high maturity condensate fluid. Most evidence suggests that this change is a direct result of the influx of mature fluid from deep in the subsurface. One unknown is whether continued production of a field over long periods of time is sufficient to deplete the reservoired fluid to a degree that a compositional shift is observed. The EI-330 field is a mature field and believed to be in its decline, however less than 50% of the estimated reserves will be produced over the life-time of the field. The large amounts of unrecoverable fluids might argue against a shift in composition due to production. Intuitively it might be argued if anything was depleted over the lifetime of a field it would be the most volatile gaseous compounds that would be preferentially removed. This trend is contrary to the observed compositional variations where apparent maturity increases with time.

A range of observations suggest that fluids are being injected into the petroleum system of the EI-330 field at the present day causing measurable changes in fluid composition. If production induced changes in fluid composition are negligible., additions of highly mature fluids must be moving into the shallower reservoir sands from deeply seated horizons that are generating hydrocarbon fluids today or in

the recent past. This dynamic injection has resulted in compositional variations in fluids reservoired. in the El-330 field that occur on time-scales as short as months.

REFERENCES

Anderson, R.N. 1993. Recovering dynamic Gulf of Mexico reserves and the U.S. energy future. Oil and Gas Journal, 26 April: 85-91.

Anderson, R.N., M. A. Hobart, C.R. Wilkinson, and H.R. Nelson. 1991a. Active fluid flow in the Eugene Island area, offshore Louisiana. Geophysics: the Leading Edge of Exploration, April: 12-17.

Baily, N.3.L., A.M. Jobson, and M. A. Rogers. 1973. Bacterial degradation of crude oil: comparison of field and experimental data. Chem. Geol. 11: 203-2:21.

Barnard, P.C. and M. A. Bastow. 1991. Hydrocarbon generation, migration, alteration, entrapment and mixing in the Central and Northern North Sea. In: W. A. England and A.J. Fleet, eds., Petroleum Migration. Geological Society Special Publication No.59: 167-190.

Carmalt, S.W. and B. St. John. 1986. Giant oil and gas fields. In: M.T. Halbouty, ed., Future petroleum provinces of the world. American Association of Petroleum Geologists Memoir 40:11-54.

Connan, J. 1984. Biodegradation of Crude Oils in Reservoirs. In: J. Brooks and D.H. Welte, eds., Advances in Petroleum Geochemistry. Academic Press, London, pp. 299-335.

England, W.A. and A.S. Mackenzie. 1989. Some aspects of the organic geochemistry of petroleum fluids. In: R. S. Poelchau and U. Mann, Evolution of Sedimentary Basins. Geol. Research.

England, W.A., A.S. Mackenzie, D.U. Mann, and T.M. Quigley. 1987. The movement and entrapment of petroleum fluids in the subsurface. J. Geol. Soc. London 144: 327-347.

Hillebrand, T. and D. Leythaeuser. 1992. Reservoir geochemistry of Stockstadt oilfield: Compositional heterogeneities reflecting accumulation history and multiple source Input. Advances in Organic Geochemistry 19:119-131.

Holland, D.S., J.E. Leedy, and D.R. Lammlein. 1990. Eugene Island Block 330 field-U.S.A., Offshore Louisiana. APPG Treatise of Petroleum geology, Atlas of 011 and Gas Fields, Structural Traps III, pp.103-143.

Horstad, I., S.R. Larter, H. Dypvik, P. Aagaard. A.M. Bjornvik. P.E. Johansen, and S. Eriksen. Degradation and maturity controls on oil field petroleum column heterogeneity in the Gullfaks field, Norwegian North Sea. Advances in Organic Geochemistry 16: 497-510.

Hunt, J.M. 1979. Petroleum Geochemistry and Geology. Freeman, San Francisco.

Karlsen, D.A. and S. Larter. 1989. A rapid correlation method for petroleum population mapping within individual petroleum reservoirs-application to petroleum reservoir description. In: R. Steel. ed., Correlation in Hydrocarbon Exploration. Graham and Trotman, London.

Kennicutt II, M.C., T.J. McDonald, P.A. Comet, 6.3. Denoux, and J.M. Brooks. 1992. The origins of petroleum in the northern Gulf of Mexico. Geochim. Cosmochim. Acta 56:1259-1280.

Larter, S.R., K.O. Borlykke, D.A. Karlsen, T. Nedkvittne, T. Eglinton, E. Johansen, D. Leythaeuser, P.C. Mason, A.W. Mitchell, and G.A. Newcombe. 1989. Determination of petroleum accumulation histories. Examples front the Ula field, Central Graben, Norwegian North Sea. In: A.T. Huller, ed., North Sea Oil and Gas Reservoirs. Graham and Trotman, London.

Leythaeuser, D. and 3. Ruckheim. 1989. Heterogeneity of oil composition within a reservoir as a reflection of accumulation history. Geochim. Cosmochim. Acta 53: 2119-2123.

Mango, F.D. 1990. The origin of light hydrocarbons in petroleum: a kinetic test of die steady-state catalytic hypothesis. Geochim. Cosmochirn. Acta 54: 1315-1323.

Milner, C.W.D., M.A. Rogers, and C.R. Evans. 1977. Petroleum transformation in reservoirs. J. Geochem. Explor. 7:101-153.

Quigley, T.M. and A.S. Mackenzie. 1988. The temperatures of oil and gas formation in the sub-surface. Nature 339: 549-552.
Schumachen D. 1993. Eugene Island Block 330 Field, Offshore Louisiana: Geochemical Evidence for Active Hydrocarbon Recharging. AAPG Ann. Convention Abstracts. New Orleans. April.
Thompson, K.F.M. 1983. Classification and thermal history of petroleum based on light hydrocarbons. Geochim. Cosmochini. Acta 47: 303-316.
Thompson, K.F.M. 1987. Fractionated aromatic petroleums and the generation of gas-condensates. Org. Geochem. 11: 573-590.
Thompson, K.F.M. 1988. Gas-condensate migration and oil fractionation in deltaic systems. Marine Petrol. Geol. 5: 237-246.
Thompson, K.F.M. 1990. Contrasting characteristics attributed to migration in petroleums reservoired in clastic and carbonate sequences in the Gulf of Mexico region. Petroleum Migration Symposium, 1989. Special Publication. Geological Society of London.
Thompson, K.M. and M.C. Kennicutt II. 1990. Nature and frequency of occurrence of non-thermal alteration processes in offshore Gulf of Mexico petroleums. In: D. Schumacher and B.F. Perkins, eds., Gulf Coast Oils and Gases, Proc. Ninth Ann. Research Conf., pp.199-218. SEPM:.
Tissot, B.P. and D.H. Welte. 1984. Petroleum Formation and Occurrence. SpringerVerlag, Berlin.
Whelan. J.K., M.C. Kennicutt II, J.M. Brooks, D. Schumacher, and L.B. Eglinton. 1994. Organic geochemical indicators of dynamic fluid flow processes in petroleum basins. Org. Geochem. 22:: 587-615.
Young, A., P.H. Monaghan, and R.T. Schweisberger. 1977. Calculation of Ages of Hydrocarbons in Oils-Physical Chemistry Applied to Petroleum Geochemistry. AAPG Bulk 61:513-600.

Technology Transfer

Roger N. Anderson - Task Manager

OBJECTIVE:

The purpose of this task was to integrate all results into one comprehensive perspective of the project's objectives and to transfer the results to industry. This will involve the interactions between the various project task outputs and the transfer and dissemination of the major conclusions of the study. There were two main efforts related to technology transfer in the field demonstration project. First, we made special efforts to patent and license technology developed as part of this project so that it would become commercially available to the oil industry. Second, we commissioned a study using the United States Geological Survey's fractal oil and gas reserves techniques to identify whether we were dealing with an additional source of oil and gas in the Eugene island 330 field's recharge-along-faults.

SUMMARY:

The DOE field Demonstration Project "Dynamic Enhanced Recovery technologies" has been a resounding success by any gauge. It has spawned important new technologies such as 4D Seismic Monitoring, resulted in the placement of successful new wells to drain new and bypassed oil and gas in one of the most prolific oil fields in the U.S. Offshore, grown into industry-only funding consortia for all its major tasks, and promoted Internet collaboration across institutional boundaries at a time before Internet was such a household word. In addition, there is every prospect that the U.S. Treasury will be repaid many times over for the direct investment of funds into the future of the oil industry in America.

Patents and Licenses

Two patents and one license were developed during this project. Lamont; developed and filed U.S. letters patents for geopressure snapping and 4D Software technologies. These form the core of one of the outstanding accomplishments of the project--the development of 4D seismic monitoring techniques

to track the migration and drainage of oil and gas in reservoirs. Though not solely due to this Class project, 4D seismic technologies have become some of the newest and "hottest" in the industry. There are workshops, industry consortia, AAPG Distinguished lectures, the keynote address at the 1996 Offshore Technologies Conference, 4 separate symposia at the 1996 AAPG convention, all about 4D Seismic technologies. DOE is perceived to be one founder of the technology because of their support of this Class I project.

The 3D Finite Element Model the project developed for fluid flow was licensed to Computational mechanics, and a commercial version, ACCESS.BASIN is currently in the marketplace. ELF, Texaco and Phillips Petroleum are interested in buying it as of this writing.

A key determinant to whether a Class Program was successful might be whether its results were of sufficient interest to the oil industry for them to continue the funding of the Research and Development completely from industry funds. We are pleased to report that all 4 of the major tasks of the project have been continued by industry. Lamont and Penn State have formed a 4D seismic monitoring consortium with 7 oil company supporters. Penn State and Stanford have funded further stress analyses in fault zones through the Gas Research Institute, as have Cornell, Woods hole and LSU for the modeling. Oil companies are funding a continuation of the organic and inorganic geochemistry analyses in the Eugene Island 330 field through Cornell and Woods Hole.

In addition, the DOE funding of experiments in the Pathfinder well resulted in the subsequent placement of the A-SST by Texaco and partners along the boundary of El 330 and 338 blocks. That well is still producing at more than 1200 bb1/day, and has had cumulative production of over 800,000 bbl of oil. At the government's royalty rate of 18%, and assuming oil prices of $20/bbL $2.8 million of the DOE project's costs have already been returned to the U.S. Treasury, and the well is targeted to produce at least as much again over the net year or so. In addition. another horizontal well is being planned into 4D seismic targets to the west of the A-85T in 1996, again paid entirely by industry. The government should be "paid-back" for its direct investment in 2-4 years, and the long-term benefits from the use of 4D seismic technologies in old fields within the United States can hardly be underestimated.

Estimate of New Hydrocarbon Supplied

As part of the DOE project, we commissioned the University of South Florida, in cooperation with the United States geological Survey to conduct a "fractal" analysis of oil and gas reserves in the offshore Louisiana segment of the northern Gulf of Mexico. That report follows below, but the conclusions are that while substantial gas reserves might lie undiscovered in the currently-drilled portion of both the north and south additions of offshore Louisiana, no significant new oil reserves remain to be discovered. However, the report goes on to say that they do not detect possible new supplied remaining to be discovered at deeper depths--specifically, the sub-salt play.

At Lamont, we have analyzed the fractal distribution of the Eugene Island fields under study, and find that they depart from the fractal slopes detected for the overall offshore by the South Florida report. The oil and gas migrating up the Red Fault in El 330 appear to come from deeper, "sub-salt" sources. We believe there are substantial new reserves to be found in the sub-salt play of the South Additions. Our project began before the sub-salt play was initiated by the Mahogany discovery of Phillips, et al., in 1994. The industry as a whole now agrees that there are substantial new discoveries to be made deeper in the South Additions of the Gulf, as can be seen, from the increase in bidding prices and activity at recent MMS lease sales for the area.

Assessment of the Undiscovered Oil and Gas Potential, Offshore Louisiana in the South Marsh, Eugene Island, and Ship Shoal Areas

Sarah F. Tebbens

University of South Florida, Department of Marine Science,
St. Petersburg, FL 33701

Christopher C. Barton
U-S. Geological Survey, 600 4th Street, South, St. Petersburg, FL 33701

Gary L_1. Lore
Minerals Management Service, MS 5100, 1201 Elmwood Park Boulevard,
New Orleans, LA 70123-2394

ABSTRACT

For the South Marsh**,** Eugene Island and Ship Shoal areas of the U.S. Gulf of Mexico Outer Continental Shelf we calculate the size (volume) and number of undiscovered oil and gas fields. We use a new method (Barton and Scholz, 1995) to assess the size, number, and total volume of undiscovered, conventionally recoverable hydrocarbon fields based on fining a truncated fractal (power-law) distribution to a log-log plot of the cumulative size-frequency distribution of discovered fields in these three geographically defined areas. The results indicate that there are very few undiscovered oil fields above 1.0 million barrels volume in any of these areas. However, the analysis indicates significant volumes of undiscovered gas. In particular, estimates of remaining undiscovered gas in South Marsh North Addition, Eugene Island Area, and Eugene Island South Addition are 553, 674 and 487 MMBOE, respectively.

Introduction

The Gulf of Mexico basin holds approximately 9% of the worlds known recoverable petroleum liquids, and approximately 11% of the world's known recoverable natural gas *[Nehring,* 1991]. Only the Arabian -Iranian province (with nearly half the world's total) holds more petroleum liquids *[Nehring,* 1991] - Only the Arabian-Iranian and West Siberian provinces hold more natural gas *[Nehring,* 1991). No other province contains even 5% of the world's known conventionally recoverable resources of petroleum liquids or natural gas *[Nehring,* 1991]. The Gulf of Mexico Outer Continental Shelf is a significant source of domestic hydrocarbon resources. Cumulative production in United States Federal waters (3-200 miles offshore) through 1993 was 9.0 billion barrels of oil BBO) and 108 trillion cubic feet TCF) of gas. Ultimate known recoverable reserves in Federal waters in the Gulf of Mexico are 11.2 BBO and 137 TCF of gas *[Melcanon et al,* 1994]. For the entire Gulf of Mexico Basin, including reserves from Mexico. as of 1987, the ultimate known recoverable reserves (oil and gas combined) are 222.5 billion barrels of oil equivalent (BBOE). This includes 136.6 BB of petroleum liquids and 523.8 TFC of gas *[Nehring,* 1991]. During 1989, 22% of domestic gas and 10% of domestic oil were produced from the Gulf of Mexico Outer Continental Shelf United States Federal Waters) *[Lore,* 1991].

The reserve values cited above are minimum estimates based on known (discovered) reserves. These values demonstrate the significance of the Gulf of Mexico as a petroleum resource. This report assesses the remaining undiscovered oil and gas in South Marsh, Eugene Island. and Ship Shoal areas of the Central Gulf of Mexico, offshore Louisiana. These areas lie within the "Gulf Coast Offshore" sub province of the Gulf of Mexico basin, as defined by *Salvador* [1991] and *Nehring* [1991]. The assessment method of *Barton and Scholz* (1995) fits the population of known field sizes (past production plus reserve estimates, not "grown' to their ultimate sizes) with a power law distribution which is, in this report, then extrapolated down to an field size of 1 MMBOE. The total area under the power law distribution is a measure of the ultimate resource and the difference between is a quantitative estimate of the undiscovered conventionally recoverable resource.

Gulf of Mexico Basin Historical Production

A remarkable feature of the exploration. history of the Gulf of Mexico basin is the number of economically viable fields discovered annually. Unlike most other petroleum provinces, in which discoveries have been highly concentrated within a period of one to three decades, substantial numbers of new discoveries have been made in the Gulf of Mexico for the past seven decades *[Nehring,* 1991]. An explanation for this unusual development is that new exploration and development technologies have been developed to take exploration from onshore, to near shore, to progressively deeper waters *[Lore,* 1991] -This record of success is likely to continue through the 1990's *[Nehring,* 1991].

The first significant discovery of oil and gas in the Gulf of Mexico basin was made in 1895 at Corsicana, Mexico *[Nehrlng,* 1991). The rate of discovery in the basin accelerated in the 1920's with new geophysical exploration methods.

Prior to 1959, exploration in the offshore Gulf of Mexico was focused on shallow, near shore waters, reflecting extension offshore of active on-shore drilling. South Marsh, Eugene Island and Ship Shoals Block development was active at this time, located near the center of the area, in waters offshore Louisiana, from West Cameron to Main Pass . The average size of fields discovered was 139 MMBOE *[Lore,* 1991].

Between 1960 and 1969, exploration began to step further offshore, but still on the shelf (<200 m water depth) *[Lore,* 1991]. A 5-fold increase in the total number of both exploratory and discovery wells resulted in a near doubling of recoverable proved reserves and a 170% increase in the number of fields. In that decade, the average size of fields discovered decreased to 77 MMBOE *[Lore,* 1991].

In the next decade (1970 to 1979), drilling off Louisiana continued to extend further offshore. Activity on the upper continental slope was at water depths, greater than 200 m. Additionally, exploration and development in the western Gulf of Mexico, resulted primarily in the discovery of gas. During the 1970's, the average size of fields discovered on the outer continental shelf decreased to 42 MMBOE, with most of the larger fields discovered further offshore on the upper slope (average field size on the upper slope was 63 MMBOE).

In 1971, the Eugene Island Block 330 Field was discovered. The field now includes Eugene Island blocks 313, southern half of blocks 314,330,331,332,337 and *338 [Holland et at,* 1991]). From 1975 to 1980, the field was the largest producing field in United States Federal Outer Continental Shelf waters *[Holland et at, 1991]. As* of 1991, the field ranked second in annual hydrocarbon production (Minerals Management Service Data as reported in *[Holland et at,* 1991]) and fourth in cumulative hydrocarbon production (Dwight's Energy Data as reported in *[Holland et at,* 1991]). Estimated at 671 MMBOE of recoverable oil and gas *[Melcanon: et at* 1994] the Eugene Island field ranks 437th among the giant oil and gas fields of the world *[Carmalt and John,* 1986].

In the 1980ts, there was scattered development across the Central and Western Gulf of Mexico Shelf (figure 3D). Exploratory drilling had reached water depths in excess of 7,000 feet. The Auger field, discovered in 1987 in 2,862 feet of water, is estimated to hold 220 MMBOE of recoverable oil and gas *[Taylor, 1994;5hirley,* 1995]. Even with a few large discoveries, by 1989 the average field size had decreased to only 14 MMBOE.

The 1990s have witnessed discovery of the Mars field in 2,933 feet of water, which is estimated to hold 770 MMBOE *[Taylor* 1994; *Shirley,* 1995], making it the largest discovery in the Gulf to date. For a list of deepwater reserves (holdings in water 1,000 deep or greater) see *Taylor* [1994]. Near to shore and in shallow water, Ship Shoal, Eugene Island and South Marsh have been extensively explored through conventional methods and are in the mature stages of exploration and development.

Assessment Methodology

The methodology used to estimate the undiscovered oil and gas fields in the Eugene Island, South Marsh and Ship Shoal Areas was developed by Barton and. his colleagues *[Barton et at,* 1991; *Barton and Scholz,* 1995; *Barton and Troussov,* in press] *Barton and Scholz [1995].* We have determined that hydrocarbon fields ranging in size from a single play (i.e. Frio Strand Plain Play, Gulf Coast of Texas, and Cardium Scour Play of western Canada) to individual basins (Permian Basin, 0-5000' depths) to giant fields of the world follow a fractal (power law) distribution. In the following section we provide a brief

introduction to fractals in nature and then we describe the methodology as applied to oil and gas resource assessment. In. a later section, we discuss the results of this application to regions offshore Louisiana.

Background: Fractals in Nature

Objects in nature are commonly very irregular, such that, within the constraints of Euclidean geometry, one is forced to grossly approximate their shape. A rock fragment, for example, generally is treated as being spherical, and a coastline as straight or smoothly curved. Upon examination, however, these objects are found to be jagged over a wide range of length scales, and these irregularities do not diminish when viewed at ever finer scales. *Mandelbrot* (1982) developed fractal geometry, which is applicable to many irregular natural objects. Fractal objects have a number of definitive characteristics that are identifiable and described by the methods of fractal geometry. The analytical techniques for treating fractal geometry, and their interrelationships, have undergone rapid evolution and broad application (for example, *Feder,* 1988). Fractal geometry has been applied to a wide variety of geologic and geophysical objects and phenomena (for example, *Scholz and Mandelbrot;* 1989. *Turconne,* 1992; *Korvin,* 1993; *Turcone and Huang,* 1995; and *Barton and LaPointe,* 1995a,b).

Distribution Function of Hydrocarbon Fields

For the past forty years, the size-frequency distribution of mineral deposits, including oil fields, has been thought to be log-normal (for example, *Krige,* 1951; *Arps and Roberts,* 1958; *Kaufman.* 1962, 1983; *McCrossan,* 1968; *Barouch and Kaufiman,* 1976; *Lee and Wang,* 1983a, b; *Forman and Hinde,* 1985; *Davis and Chang,* 1989; *Power,* 1992). The log normal distribution resembles a power-law, or fractal, distribution in the middle of its range but is truncated at the lower end. Unlike the scale-independent power-law distribution, it has a characteristic size (mode) at which the distribution peaks and rolls off and has values below the mode. At the upper end, the log normal distribution tends quickly to zero and therefore has a thin tail. In contrast, the upper end of the power-law or fractal distribution tends to zero slowly and therefore has a fat tail. Note that only the fractal (power-law) distribution plots as a straight line. For size versus cumulative frequency distributions, the term fractal is used only for power-law distributions with slope (a) less than 2. Over small ranges in size portions of the other distributions can be approximated by straight lines with either steep slopes for large sizes or zero slopes for small sizes. It therefore is important to have data over a sufficient range so that the true distribution is observed. The general rule of thumb for a power law fit is that the data should range over as many orders of magnitude as the absolute value of the scaling exponent (slope of the line in log-log space) (Mandelbrot, pers. Com., 1995).

A power-law data set containing a perceptibility limit (the smallest size for which we have a complete census of the population) commonly is well fit by a log normal distribution. Because all observed distributors will have perceptibility limits; this misidentification is not uncommon. For example, a perceptibility limit occurs in earthquake detection. Because seismometers have lower-magnitude thresholds for event detection this results in a low-side truncation in observed earthquake sizes. Observed earthquake distribution is a power law distribution above the perceptibility limit. Installation of instruments with higher magnification results in detection of a multitude of smaller earthquakes that continue to belong to a power-law size distribution (which is called the Gutenberg-Richter law in seismology).

As progressively smaller hydrocarbon fields are discovered through time, the associated perceptibility limit moves to smaller field sizes, thus extending the power-law size distribution to progressively smaller field sizes. Such temporal change should not occur if the underlying distribution had a characteristic size, such as log normal distribution. A power law distribution, which has no characteristic size, appears to be the correct distribution to describe the size distribution of hydrocarbon fields.

Recognition that the size-frequency distribution of hydrocarbon fields may be a power-law was made by L.J. Drew and his colleagues *(Drew and others,* 1982; *Schuenemeyer and Drew,* 1983; *Attanasi and Drew,* 1985; *Drew and others,* 1988; and *Drew,* 1990; *Baker and others,* 1984; *Houghton,* 1988; *Scholz and Barton,* 1991; *Brett and Feldcamp,* 1993; *Barton and Scholz,* 1995; and *Crovelli and Barton,*

1995). An example from *Drew* (1990) shows the size distribution of discovered fields in the Frio Strand Plain play (onshore Texas) as a function of time, and as replotted by *Barton and Troussov* [in press] as a cumulative frequency versus field-size distribution in log-log space (figure SB). At any given time, the distribution in this play looks like a log normal distribution, but, as exploration proceeds, more small fields are discovered, with associated progressive decreases in the mode. We observe a similar pattern through time for the 200 top discovered oil and gas fields in U.S. Gulf of Mexico waters (based on original reserve estimates).

Drew and his colleagues maintained that the parent distribution in the Frio Strand Plain play is a power-law (or Pareto) distribution that is gradually being revealed by exploration. The rollover at any given time is determined by economics since uneconomic smaller fields are either undiscovered or not developed. This rollover is shifted to smaller sizes as price increases and more small fields are discovered and developed. The largest fields are commonly found early in the exploration cycle, and through time the population fills in with progressively smaller sizes. From this understanding of the discovery process we can infer that in any region at a mature stage of exploration, the right tail in die distribution provides a good estimate of the parent distribution down to the perceptibility limit, which is commonly at or near the economic truncation. Thus, the population in the largest size classes remains stable in time. Therefore, in order to obtain an estimate of the true or parent population of hydrocarbon deposits, we fit the right side of the size distribution in regions in the mature stages of exploration.

The Pareto distribution has been used by the U.S. Geological Survey (USGS) in past assessments of the undiscovered conventionally recoverable hydrocarbon resources of the United States. *Houghton and others* (1993) described application of the truncated shifted Pareto distribution in the 1989 USGS national petroleum assessment to fit geologists' estimates of the size and number of undiscovered hydrocarbon fields. In contrast, in the method proposed by Barton arid his colleagues, and used in this work, the size and number of undiscovered fields are forecast by fitting a power-law to the distribution of discovered fields larger than the perceptibility limit and then extrapolating to field sizes smaller than the perceptibility limit

Fractal Size-Frequency Distributions and their Application to Hydrocarbon Fields

A variety of geologic objects having this type of distribution are described by *Turcone* (1992); *Turcone and Huang (1995);* and *Barton and LaPointe (1995a.* 1995b). These collections of objects must be defined within some region, which we will call the distribution space. For hydrocarbon accumulations, this space may be a geographical region, such as the world, a basin, a country, or a State, or it may have a geologic definition, such as an oil province or a play. Members of the distribution must also be defined; these may be the field, for example, or the pool. These various members and spaces may constitute different hierarchies nested within one another. For example, there may be a distribution of pools within a reservoir and, at higher hierarchical levels, a distribution of reservoirs within a field within a play, and plays within a basin or province. In this report, we consider the hydrocarbon field sizes, as defined by Minerals Management Service *[Melcanon et at,* 1994, for example].

As mathematical expressions are defined over infinite ranges, but in any finite application the range must be limited by lower and upper fractal limits. The upper fractal limit (UFL) is always defined by the distribution space and is usually observable. For example,
the largest possible field in a basin is constrained by the size of the basin and its geology. One can always find or estimate this largest field; in regions of mature or semi-mature stages of exploration the largest deposit has probably been discovered, based on the discovery process (see *Drew,* 1990). On the other hand, the lower fractal limit (LFL) is arbitrarily defined. It may be the smallest structural trap within the basin or the smallest oil-filled pore space within the reservoir rock. In either case, we do not know its size. The lower fractal limit is not generally of practical importance because it is always well below a perceptibility limit (FL). the smallest size for which

For the Eugene Island South Addition oil fields, we predict that when all the oil is discovered, most of the total volume will be in the large fields. Because this convergence constraint is a general property of fractal distributions, it follows that, as exploration proceeds from development of large to small fields, the volume discovery rate decreases even though many more small than large fields are present.

If the fit to the data is a good representation of the parent population, the ultimate volume of hydrocarbons in the distribution space can be obtained by summing the discovered volumes greater than the perceptibility limit and adding to them the calculated undiscovered volume by evaluation. Using this method, the total residual volume of hydrocarbons can be calculated down to any lower threshold. The cumulative size-frequency distribution is used to
calculate because this distribution smoothes out the noise that results from inaccuracies in determining the volume of each field in the data sets.

Barton and Scholz (1995) fit a power law cumulative size frequency distribution to hydrocarbon populations at different hierarchical levels, each of which exhibits approximate fractal distributions. which means tat these populations consist of many nested fractal distributions. Such nesting may persist continuously over a wide range of sizes, all the way down to the porosity of the reservoir rock, which has also been shown to have a fractal size distribution (Krohn, 1988).

For several regions within the study area, the cumulative size-frequency versus field-size distribution will be shown to be strongly curved, concave downward, over the higher size ranges, such that the slope increases with size. if the data are truncated to a size about one order of magnitude smaller than the maximum field size, a power law is fit down to the perceptibility limit. The power law should not be extrapolated to the far right end of the distribution because it predicts an unrealistic maximum field size many times larger than that observed.

Curvature near the upper fractal limit is a local feature, affecting only the last one or two data points, and is expected because of the natural truncation associated with the upper fractal limit. Cases where the curvature, or enhanced slope, extends well below the last one or two largest field sizes cannot be explained in this way. We propose, instead, that the observed curvature in the large field sizes results from constructing data sets defined by the artificial boundaries of geographic areas tat contain portions of geologically defined plays, thereby including a diverse a set of sub populations. Consider the hypothetical case of five sub populations as solid lines. Each of these has cumulative-frequency size distributions with the same a value but different upper fractal limits. When combined$_1$. these produce the population shown by the ten data points. The line has curvature in the upper size ranges, whereas below the upper fractal limit, the a value for the total population is the same as for each of its parts.

This observation underscores the conventional wisdom in discovery process modeling (for example, *Kaufman,* 1983; *Drew* 1990) that one must carefully select data sets for homogeneity of geology and source. Data sets for larger regions *(Barton and Scholz,* 1995) are, however, still approximately fractal, and useful analysis can be made of them. The total resource in such a region can be estimated by summing the volume in the larger fields and integrating the remainder in the smaller fields in the way described above, stating from the point at which a becomes representative of the population as a whole.

Results

The assessment methodology presented above was applied to determine the size and number, and total volume of undiscovered conventionally recoverable oil and gas fields for Ship Shoal, Eugene Island and South Marsh areas. Based on the above discussion, we assume that the underlying distribution of oil and gas fields in these areas is fractal (power law). Field sizes (the sum of cumulative production through 1993, and remaining ungrown recoverable reserves) were provided by Minerals Management Service. They are defined and discussed in *Melcanon et al* [1994]. The lower fractal limit for this assessment is 1 mm BOE.

Cumulative frequency versus field size plots for oil, and gas in each of the three areas are presented. The following points made in the methodology section are particularly important for interpretation. 1) To infer a fractal distribution (i.e. to fit a line to a log-log plot (a power law, the data should span as many orders of magnitude as the absolute value of the slope of the line fit. For this work, the slope is usually less than one so that we need data with a range of values spanning a minimum of roughly one order of magnitude). 2) Rollover at smaller field sizes. suggests undiscovered fields at the smaller field sizes. 3) Rollover at larger field sizes suggests that data from several populations, each with fractal distributions, have been combined. The rollover at larger field sizes is expected for this work since the available data combine all fields at each area; the data are not separated by, for instance. stratigraphic source levels. We observe rollover at smaller field sizes (a perceptibility limit) for all three areas.

Rollover at larger field sizes is observed for South Marsh South Addition Gas, Eugene Island Oil and Gas, and all Ship Shoal Oil and Gas distributions. We note that for four of the fourteen assessments (South Marsh Gas, South Marsh South Addition Gas, Ship Shoal Oil, and Ship Shoal South Addition Gas), the data are sparse and the results should be considered tentative.

A summary of the oil assessment, including the volume of remaining undiscovered oil in each region down to a field size of 1.0 million barrels oil equivalent (mm BOE) was made. The calculated fractal scaling exponent represents the volume of discovered hydrocarbons, and the predicted ultimate volume of hydrocarbons. The remaining undiscovered volumes are further subdivided into the number of fields remaining to be discovered in each field class in each region.

In the seven regions studied, the region with the largest total volume of discovered oil is Ship Shoal block (1029 mm BOE) with the next largest discovered volumes in Eugene Island and Eugene Island South Addition areas (697 and *695* mmBOE, respectively).

The predicted volume of oil remaining undiscovered in each region is small (less than 90 mmBOE) or none. The largest predicted volume of oil remaining undiscovered is also in Ship Shoal block. We note that the Ship Shoal block oil assessment is one of the four assessments for which the data are scarce, so the results are tentative. if correct, the results predict 87 mmBOE oil remaining undiscovered in Ship Shoal block. These reserves are predicted to be comprised of two class S fields (mean field size 5.7 mmBOE), 10 class 7 fields (mean size 2.8 mmBOE) and 23 class 6 fields (mean size 1.4 mmBOE). The next largest predicted volumes of undiscovered oil are in South Marsh Island South Addition Area and Eugene Island South Addition Area, with 20 mmBOE and 11 mmBOE, respectively, remaining undiscovered. There are no remaining undiscovered fields larger than one mmBOE predicted in the South Marsh Island North Addition and South Marsh Island regions.

In the seven regions studied, the region with the largest total volume of discovered gas is Eugene Island South Addition (1449 mmBOE) with the next largest discovered volumes in Ship Shoal block and Eugene Island Block (1315 and 1283 mmBOE, respectively). The regions with the largest volumes of gas predicted to be remaining undiscovered are Eugene Island Area, South Marsh North Addition, and Eugene Island South Addition, with 674, 553 and 487 mmBOE, respectively. In the region with the largest volume of undiscovered fields, Eugene Island Area, the reserves are predicted to be comprised of 172 class six fields. 73 class seven fields, 30 class eight fields, and 10 class nine fields. The largest fields predicted are two class 10 fields (mean field size 23 mmBOE) in the Eugene Island South Addition Area.

We note that this analysis cannot evaluate the undiscovered resources located in plays at depths greater than those currently included in our data sets (subsalt); additional oil and gas plays at deeper horizons cannot be ruled cut

The scaling exponent can be used to inter the relative abundance of small fields to large fields. The smaller the (absolute value of the) scaling exponent, the greater the ratio of the large fields to the small fields. For gas fields, as one moves offshore, the scaling exponent decreases indicating the ratio of larger fields to smaller fields increases one moves offshore. For oil fields, the opposite trend is weakly suggest-md with the scaling exponent increasing slightly offshore in the South Marsh and Eugene Island Areas and observed to be roughly constant across the Ship Shoal Area.

Summary

Populations of hydrocarbon fields can be described by the power-law size distribution characteristic of fractal sets. This is true for all hierarchies of populations examined by *Barton and Scholz* (1995). ranging from pools in a play to giant fields in the world. *Barton and Scholz (1995)* suggest that any population of hydrocarbon fields consists of the combination of many fractal sub populations at different hierarchical levels nested within one another. We find that for the U.S. Gulf of Mexico Outer Continental Shelf, the underlying distribution of oil and gas fields appears to be fractal. For the South Marsh, Eugene Island and Ship Shoal areas we assume the underlying distribution is fractal (as is observed by *Barton and Scholz* (1995) to be the case for regions worldwide) and calculate the size, volume and number of undiscovered fields.

Our results indicate tat there are minimal (or no) remaining undiscovered oil reserves down to the 1.0 million barrel field size in the regions. However, the analysis indicates significant volumes of undiscovered gas. In particular, the gas remaining undiscovered is 674, 553 and 487 mmBOE, in Eugene

Island Blocks, South Marsh North Addition, and Eugene Island South Addition, respectively. These reserves are predicted to be contained within smaller size fields. The largest fields predicted are three class 10 gas fields (mean field size 23 mmBOE) in the Eugene Island South Addition area.

Acknowledgments: We are grateful to D. Gautier and D. Higley for critical reviews. We thank Roger Anderson and the Global Basins Research Network for encouragement and advice. This work was funded by the Department of Energy Cooperative Agreement DEFC22-93BC 14961 subcontract *1245-1*87-L3.

References

Arps, J.J., and Roberts, T.G., 1958, Economics of drilling for Cretaceous oil on the east flank of the Denver-Julesburg Basin: American Association of Petroleum Geologists Bulletin, v.42, p. 2549-2:566.

Attanasi, E.D., Drew, L.J., 1985, Lognormal field size distributions a consequence of economic truncation: Mathematical Geology, v.17, p.335-351.

Baker, R.A., Gehman, H.M., James. W.R., and White. D.A., 1984, Geologic field number and size assessments of oil anti gas plays: American Association of Petroleum Geologists Bulletin, v.68, p. 426-437.

Barouch, E. and Kaufman, G.M., 1976, Oil arid gas discovery modeled as sampling without replacement and proportional to random size: Sloan School Working Paper No.888-76.

Barton, C.C., and La Pointe, P.R., eds., 1995a, Fractals in the earth sciences: New York, Plenum Press, 265 p.

_____ 1995b, Fractals in petroleum geology and earth processes: New York, Plenum Press, 317 p.

Barton, C.C., and Scholz, C.H., 1995. The fractal size and spatial distribution of hydrocarbon accumulations--implications for resource assessment and exploration strategy, *in* Barton, C.C., and La Pointe, P.R. Eds. Fractals in petroleum geology and earth processes: New York, Plenum Press, p.13-34.

Barton, C.C., Scholz, C.H., Schutter, T.A., Herring, P.R.. and Thomas, W.J., 1991, Fractal nature of hydrocarbon deposits--2, Spatial distribution: American Association of Petroleum Geologists Bulletin, v.75, no.3, p.539.

Barton, C. C. and Troussov, G.L., Fractal methodology for petroleum resource assessment and FRA - A computer program that calculates the volume and number of undiscovered hydrocarbon accumulations: U.S. Geological Survey Circular 1128.23 p..

Brett, J.F., and Feldcamp, L.D.. 1993. The evidence for and implications of a fractal distribution of petroleum reserves: Society of Petroleum Engineers, SPE *25826*, p. 73-84.

Carmalt, S.W., and John, B. 5., 1986. Giant Oil and Gas Fields of the World, *in* Halbouty. M.T.. ed..' Future petroleum Provinces of the World: American Association of Petroleum Geologists Memoir 40, p.11-S[4].

Crovelli, R.A., and Barton, C.C., 1995, Fractals and the Pareto distribution applied to petroleum field-size distributions, *in* Barton, C.C., and LaPointe, P.R., eds., Fractals in petroleum geology and earth processes: New York, Plenum Press. P. 59-72.

Davis, J.C., and Chang, T., 1989. Estimating potential for small fields in mature petroleum province: American Association of Petroleum Geologists Bulletin, V. 73, p.967-976.

Drew, L.J., 1990. Oil and gas forecasting: Oxford, England, Oxford University Press, 252 p.

Drew, L.J., Attanasi, E.D., and Schuenemeyer, J.H., 1988, Observed oil and gas field size distributions--A consequence of the discovery process and prices of oil and gas: Mathematical Geology, v.20, p.939-953.

Drew, L.J., Schuenemeyer, J.H., and Bawiek, W.J., 1982, Estimation of the future rates of oil and gas discoveries in the western Gulf of Mexico: U.S. Geological Survey Professional Paper 1252, 26 p.

Feder, Jens, 1988, Fractals New York, Plenum Press, 283 p.

Forman, D.3., and Hinde, A.L., 1985. Improved statistical method for assessment of undiscovered petroleum resources: American Association of Petroleum Geologists Bulletin, v.69, p.106-118.

Holland, D. S., Leedy, 3. B., and Lammlein, D. R., 1991, Eugene Island Block 330 Field - USA Offshore Louisiana: American Association of Petroleum Geologists, Treatise of Petroleum Geology, p.10:3-143.

Houghton, J.C., 1988. Use of the truncated shifted Pareto distribution in assessing size distribution of oil and gas fields: Mathematical Geology, v.20, no.8, p.907-937.

Houghton. J.C., Dolton, G.L., Mast, R.F., Masters, C.D.. and Root, D.H., 1993, U.S. Geological Survey estimation procedure for accumulation size distributions by play: American Association of Petroleum Geologists Bulletin, v.77, no.3, p. 454-466. Kaufiman, G.M., 1962, Statistical decision and related techniques in oil and gas exploration: Englewood Cliffs, N.J., Prentice-Hall, 307 p.

1983, Discovery process models; *in* Adelman, M.A., Houghton, J.C., Kaufman, G.M., and Zimerman, M.B., eds.: Energy resources in an uncertain future: Cambridge, Mass., Bailinger Press, p.213-268.

Korvin, Gabor, 1993, Fractal models in the earth sciences: Amsterdam, Elsevier, 396 p. Krige, D.G., 1951, A statistical approach to some basic mine valuation problems on the Witwatersrand: South Africa *52,* no.6, p.119-139.

Krohn, C.E.. 1988, Sandstone fractal and Euclidean pore volume distributions: Journal of Geophysical Research 93, p.3286-3296.

Lee. P.3., and Wang, P.C.C., 1983a, Probabilistic formulation of a method for the evaluation of petroleum resources: Mathematical Geology, v.15. no.1, p.163-181.

_____ 1983b. Conditional analysis for petroleum resource evaluation: Mathematical Geology, v.15, no.2, p.349-361.

Lore, G. L., 1991, Exploration and discoveries, 1947-1989, Gulf of Mexico 0(5: An historical perspective: Minerals Management Report 91-0078.87 pp.

Mandelbrot, B.B., 1982, The fractal geometry)' of nature: San Francisco, W.H. Freeman, 460 p.

McCrossan, R.G., 1968, An analysis of size frequency distribution of oil and gas reserves of Western Canada: Canadian Journal of Earth Sciences, v.6, p.201-211.

Melcanon, J. M., Bacigalupi, S. M., Kinler, **C.** J., Marin, D. A, and Prendergast, M. T., 1994, Outer continental shelf estimated proved oil and gas reserves, Gun?. of Mexico, December31, 1993: Minerals Management Service Report 94-()045. 49 pp.

Middlebrooks, E. 3., 1976. Statistical calculations--How to solve statistical problems: Ann Arbor, Mich., Ann Arbor Science, 120 p.

Nehring, R., 1991, Oil and Gas resources; *in* Salvador, A., ed., The Gulf of Mexico Basin: Boulder, Colorado, Geological Society of America, The Geology of North America, *v.3,* p.445-494.

Power, M., 1992, Lognormality in the observed size distribution of oil and gas pools as a consequence of sampling bias; Mathematical Geology, v.24, no.8, p.929-945.

Salvador, A., 1991, Introduction; *in* Salvador, A., ed., The Gulf of Mexico Basin: Boulder, Colorado, Geological Society of America, The Geology of North America, v.3, p.1-12.

Scholz, C.H., and Barton, C.C., 1991, The fractal nature of hydrocarbon deposits--I. Size distributions: American Association of Petroleum Geologists Bulletin, v.75, no.3, p.668.

Scholz, C.H., and Mandelbrot, B.B., eds., 1989, Fractals in geophysics: Basel, Birkhauser, 313 p.

Schuenemeyer, J.H., and Drew, L.J., 1983, A procedure to estimate the parent population of the size of oil and gas fields as revealed by a study of economic truncation: Mathematical Geology, v.15, no.1, p.145-161.

Schuenemeyer, 3.H.. and Drew, L.J., 1991, A forecast of undiscovered oil and gas in the Frio Strand Plain trend--The unfolding of a very large exploration play: American Association of Petroleum Geologists Bulletin, v.75, no.6, p. 1107-1115.

Schuenemeyer, J.H., Drew, L.3., Root, D.H., and Attanasi, E.D., 1990, Estimating potential for small fields in mature petroleum provinces--Discussion: American Association of Petroleum Geologists Bulletin, v.74, no.11, p.176[1]-[17]63.

Schuster, H.G.. 1988, Deterministic Chaos: VCH. Weinheim, 270 p
Shirley, Kathy, 1995, Modeling proved a profitable cost: ALAPO Explorer, American Association of Petroleum Geologists, May 1995, p.11-12.
Taylor, 0., 1994, Deep Risks Paying off: Successes Buoy Gulf Hopes: AAPG Explorer, American Association of Petroleum Geologists. September 1994, p.l and 4.
Turcotte, D. L., 1992, Fractals and chaos in geology and geophysics: Cambridge, Cambridge University Press, 221 p.
Turcotte, D.L., and Huang. J., 1995, Fractal distributions in geology. scale invariance. and deterministic chaos; *in* Barton, C., and LaPointe, P.R., eds., Fractals in the earth sciences: New York, Plenum Press, p.1-40.

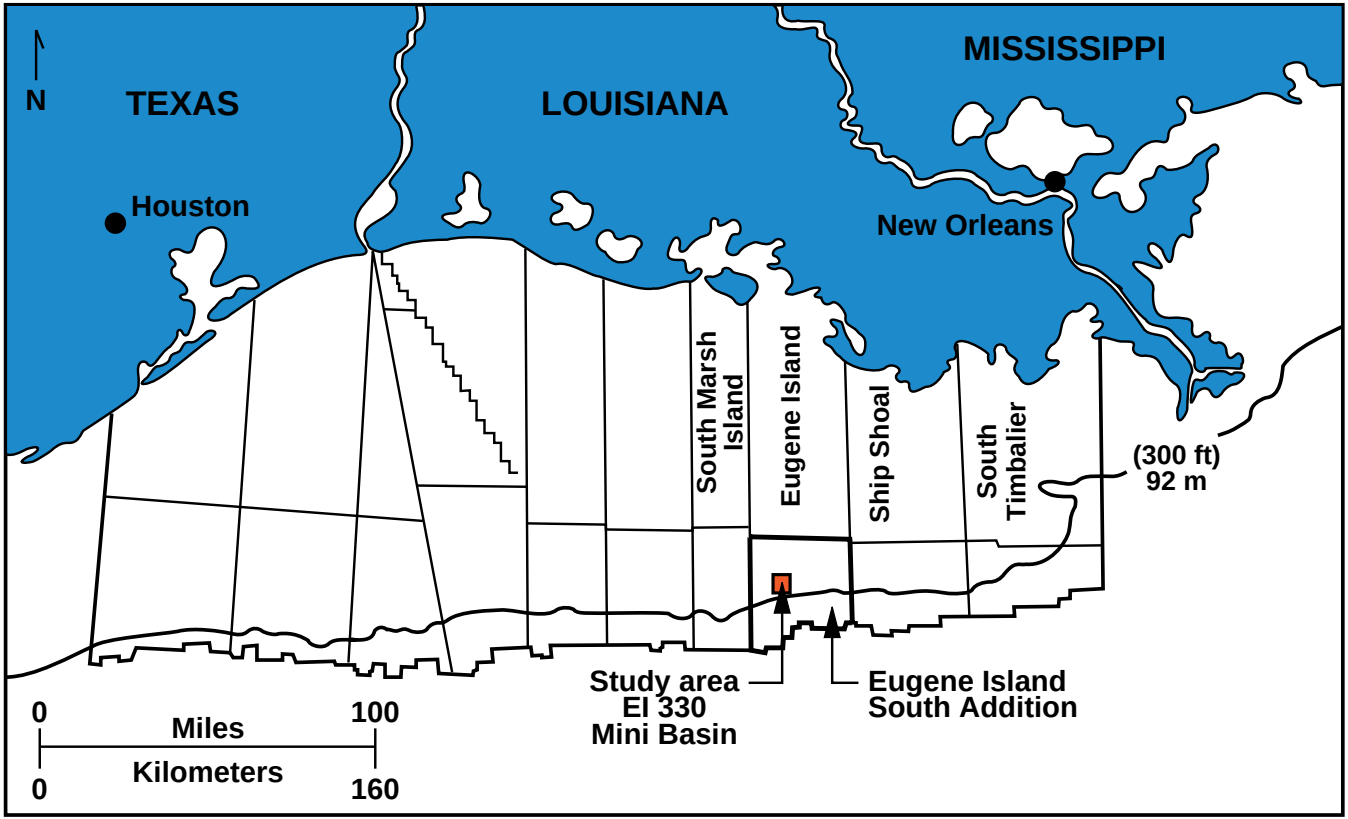

Figure I.i.1: Eugene Island 330, location of study area.

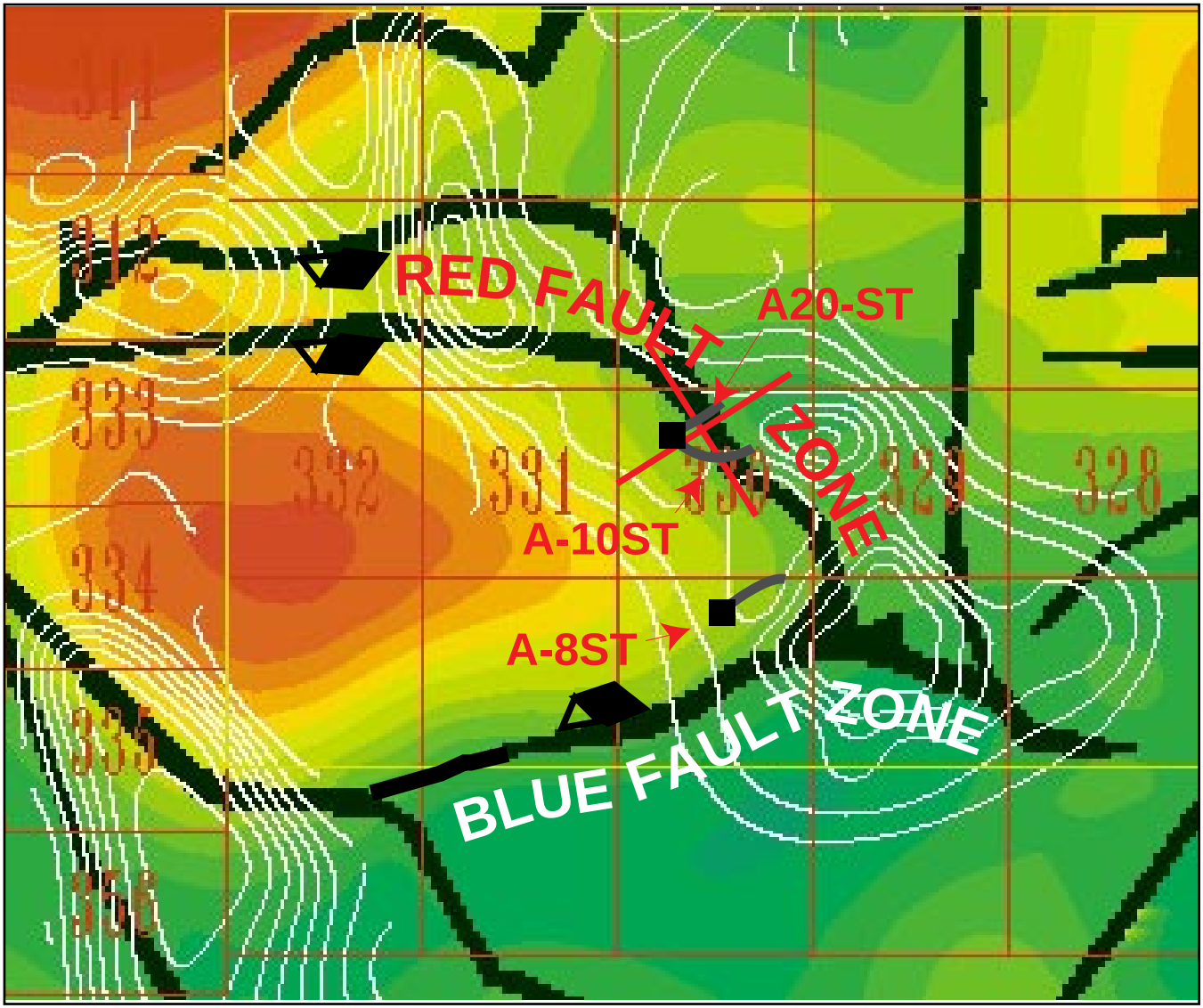

Figure I.i.2: The Eugene Island 330 minibasin is shown by depth to the top-of-geopressure surface (hot colors are deep, cold colors are shallow). White contours are top-of-salt, and black lines are faults. Pennzoil "A" platform and seismic profiles of Figures I.i.3 and I.i.5 are located within block 330 (from He and Anderson, 1994).

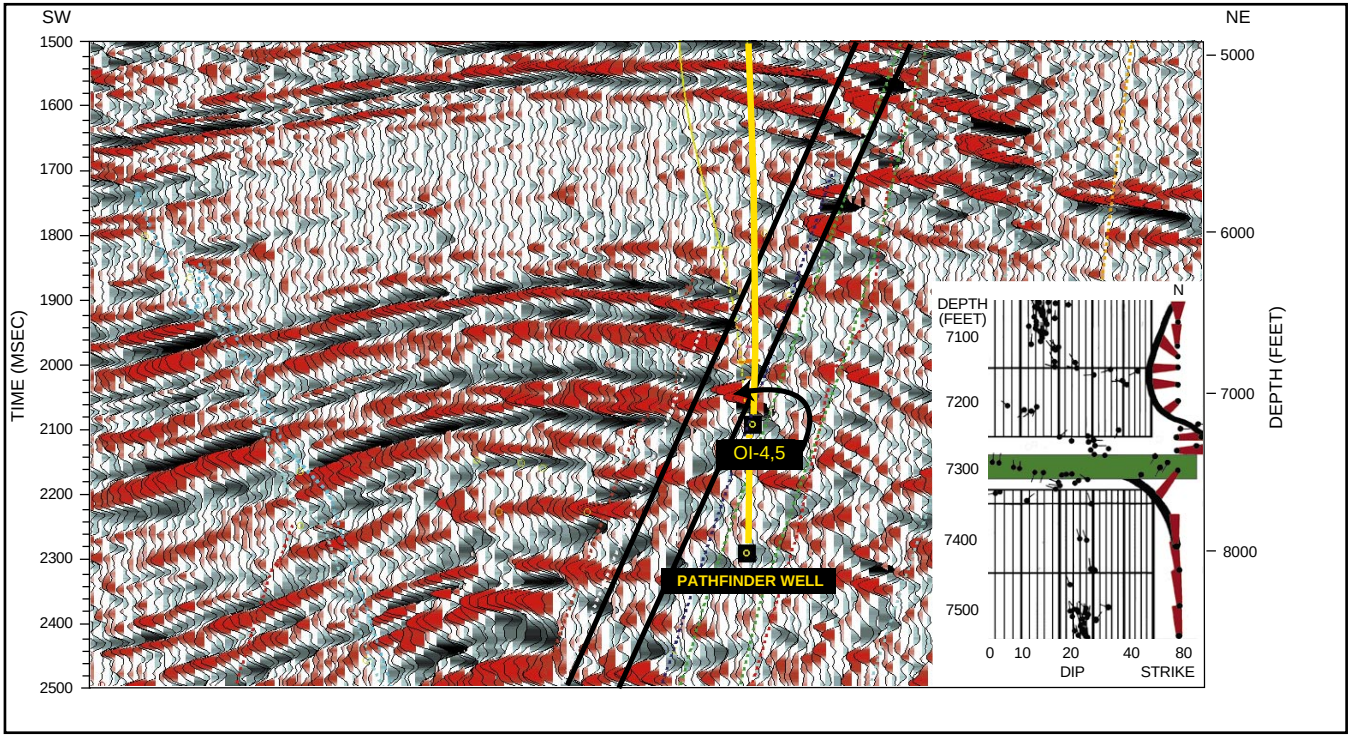

Figure I.i.3: Seismic reflection profile (courtesy Pennzoil, Exxon and Mobil) in-line to A-20ST "Pathfinder" well in Eugene Island block 330. Dipmeter "tadpoles" across fault zone shown in lower right. Note swing in strike of beds above, within, and below the fault zone.

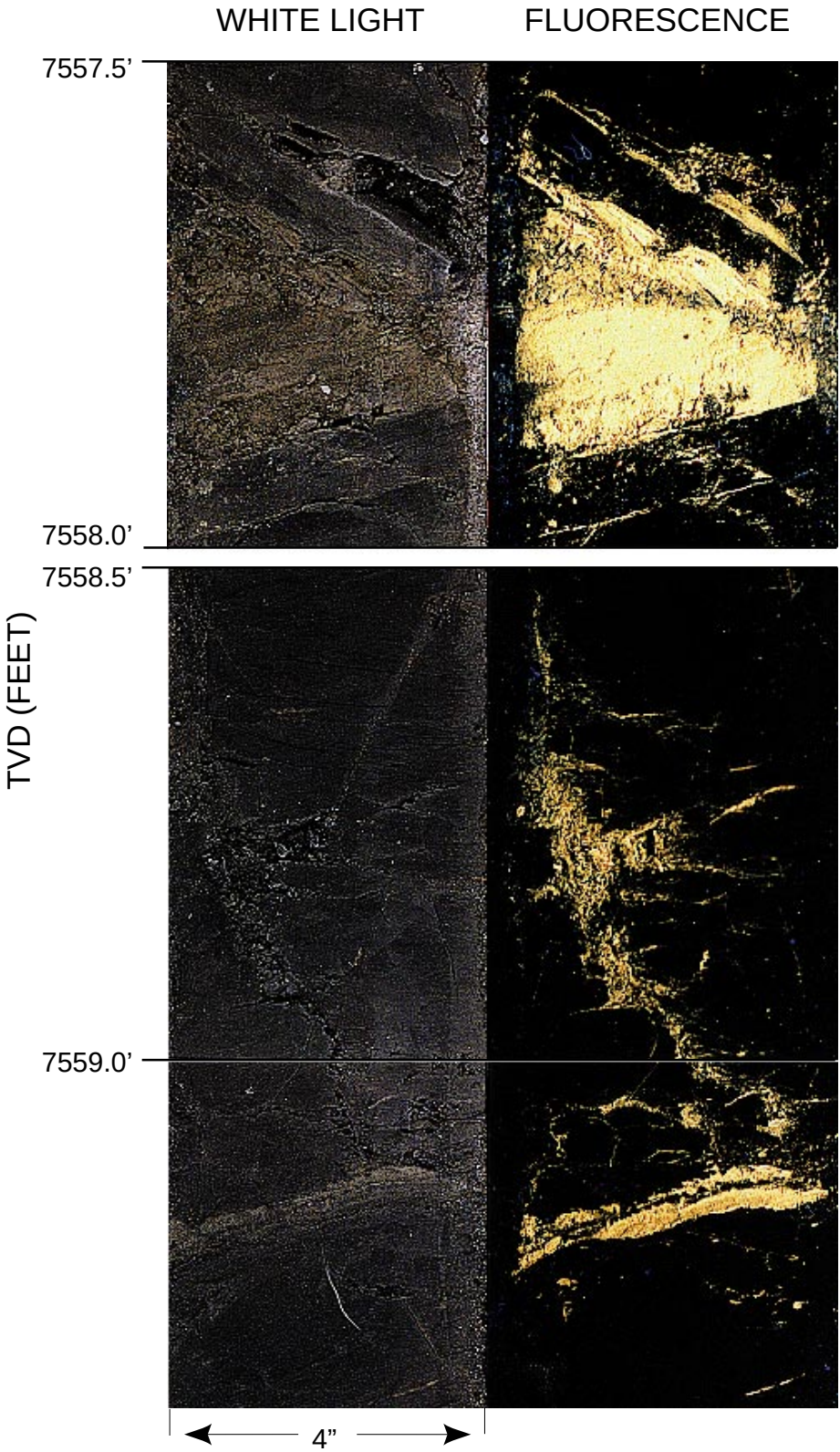

Figure I.i.4: Core photos from 7557.5'-7559' showing hydrocarbon-charged fault connected to small sand lens.

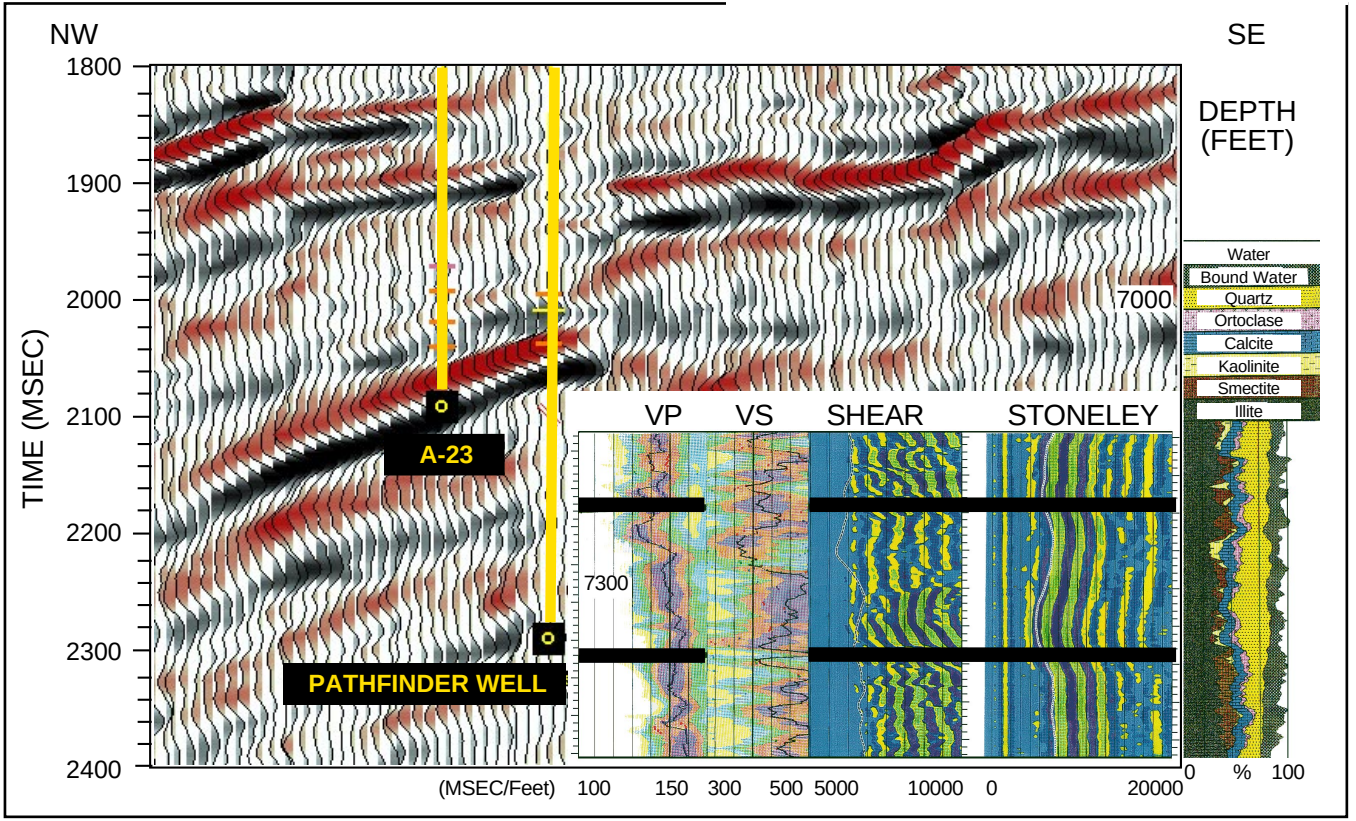

Figure I.i.5: Cross-line seismic reflection profile with dipole sonic and geochemical log inserts.

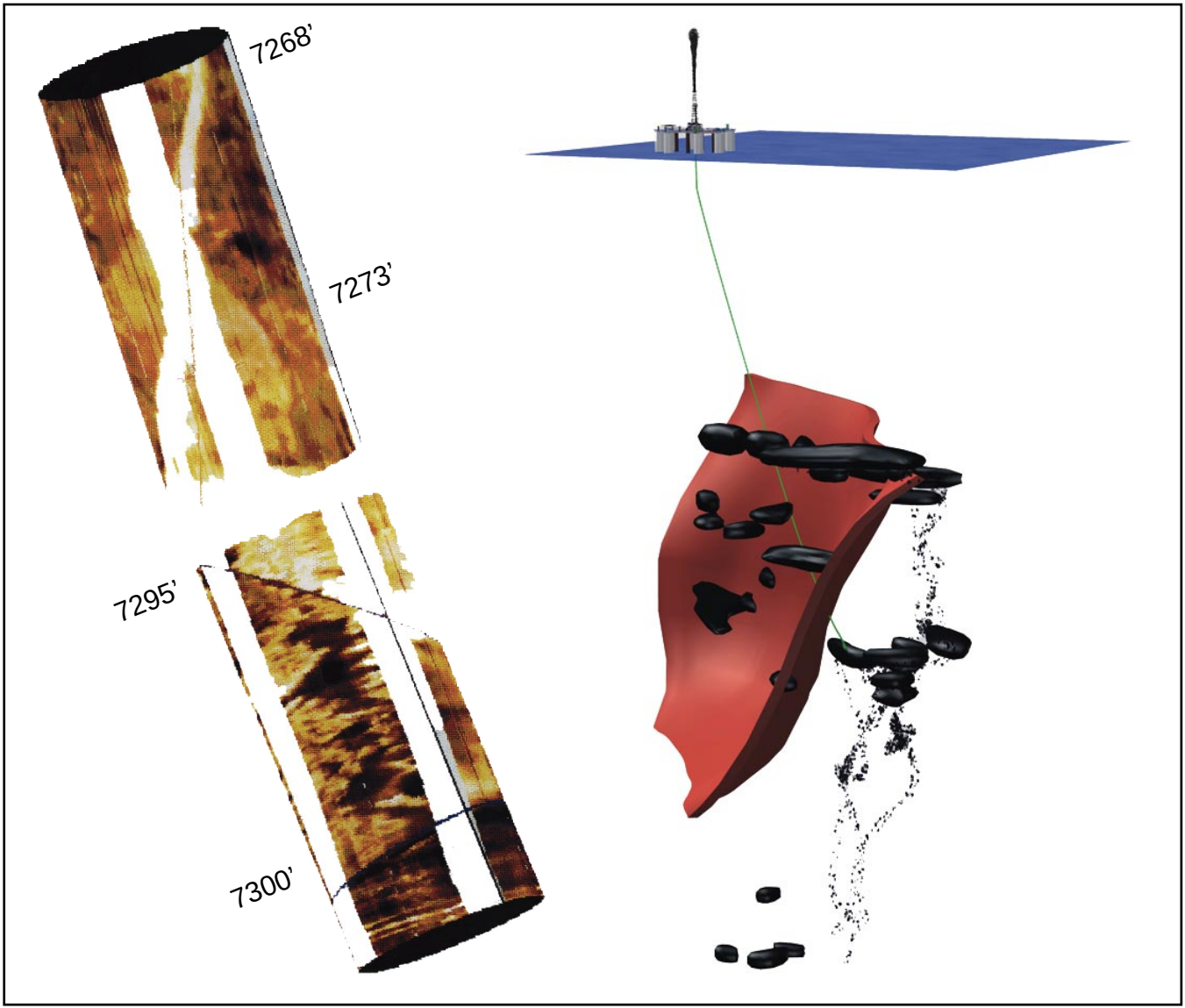

Figure I.i.6: Formation MicroImager of fault zone with well path image.

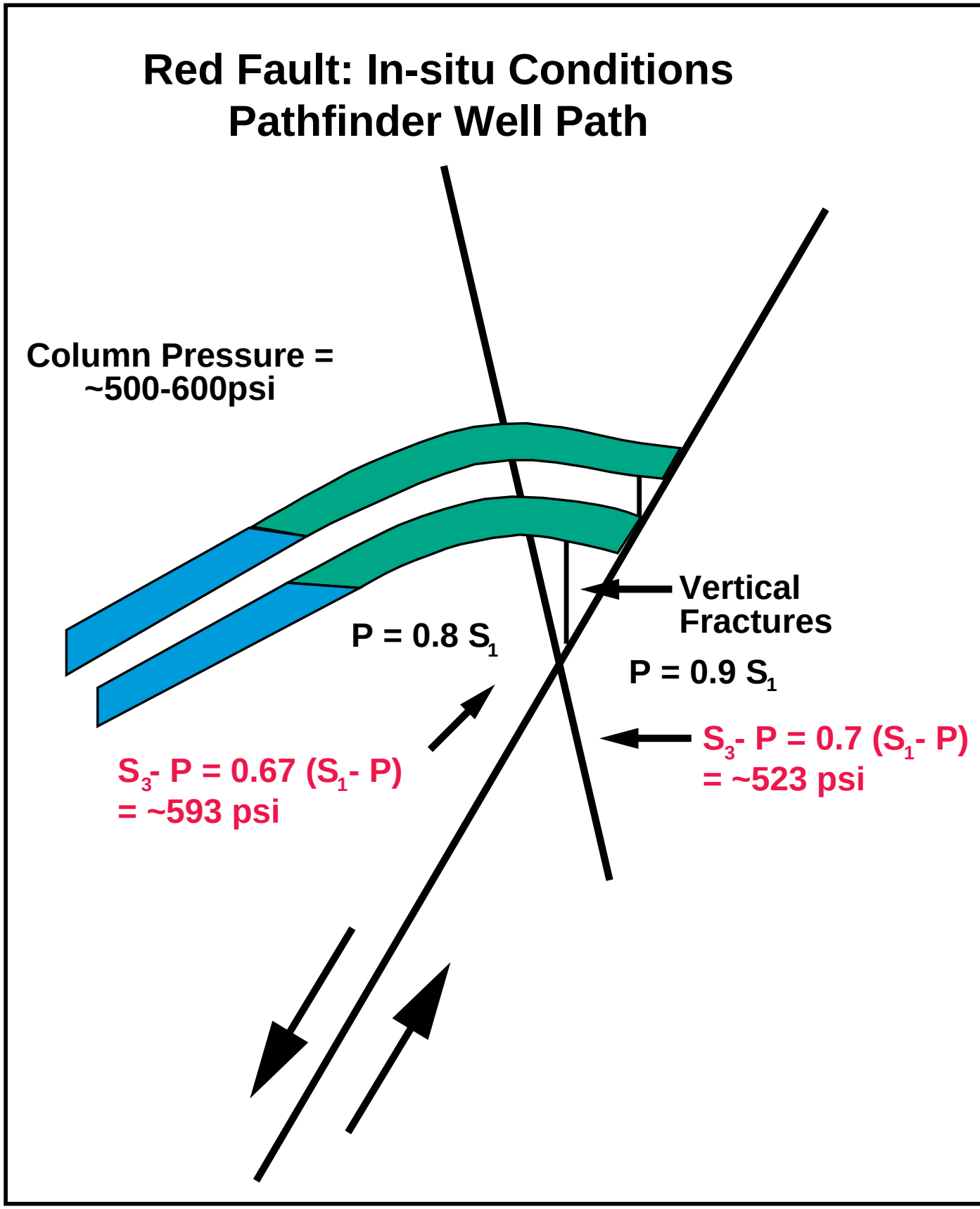

Figure I.i.7: In-situ stress and pressure measurements across fault zone.

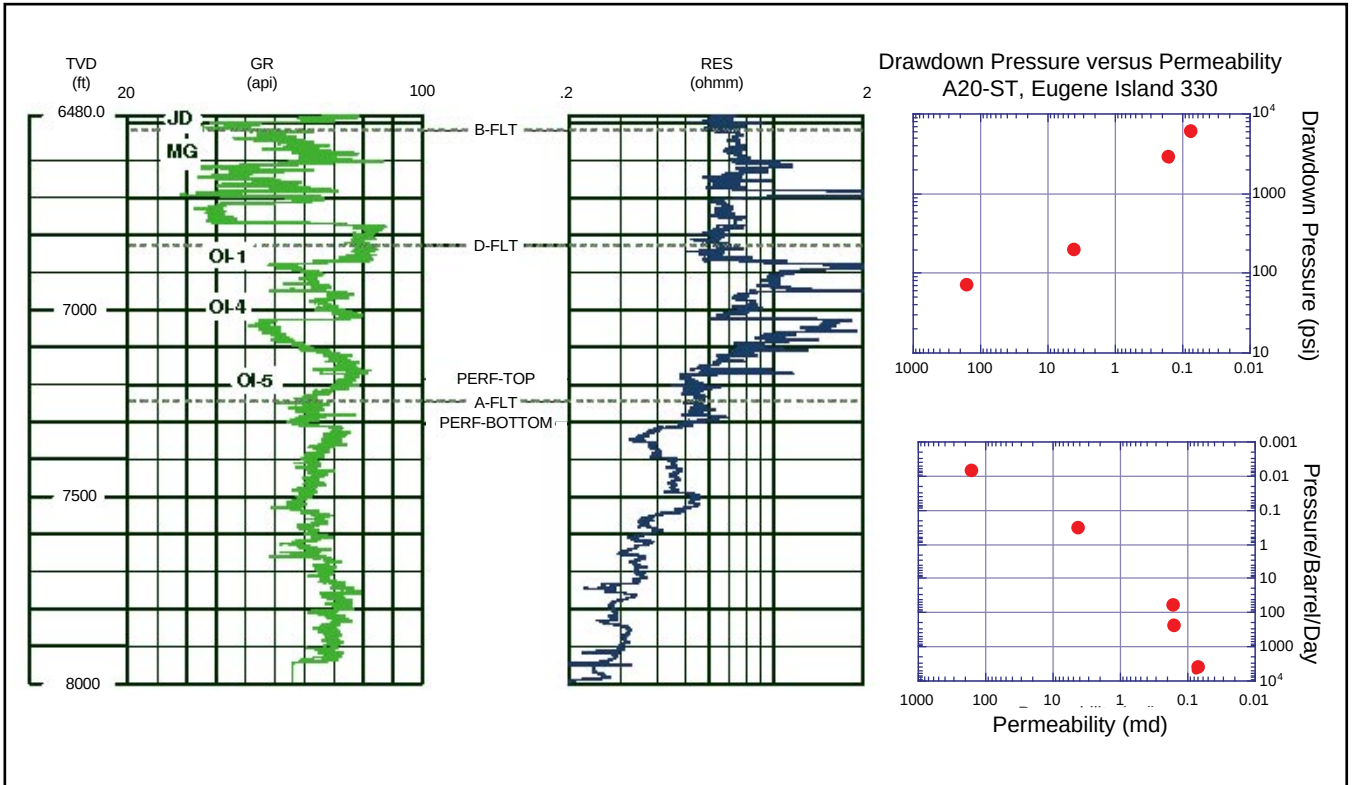

Figure I.i.8: Drill-stem test results.

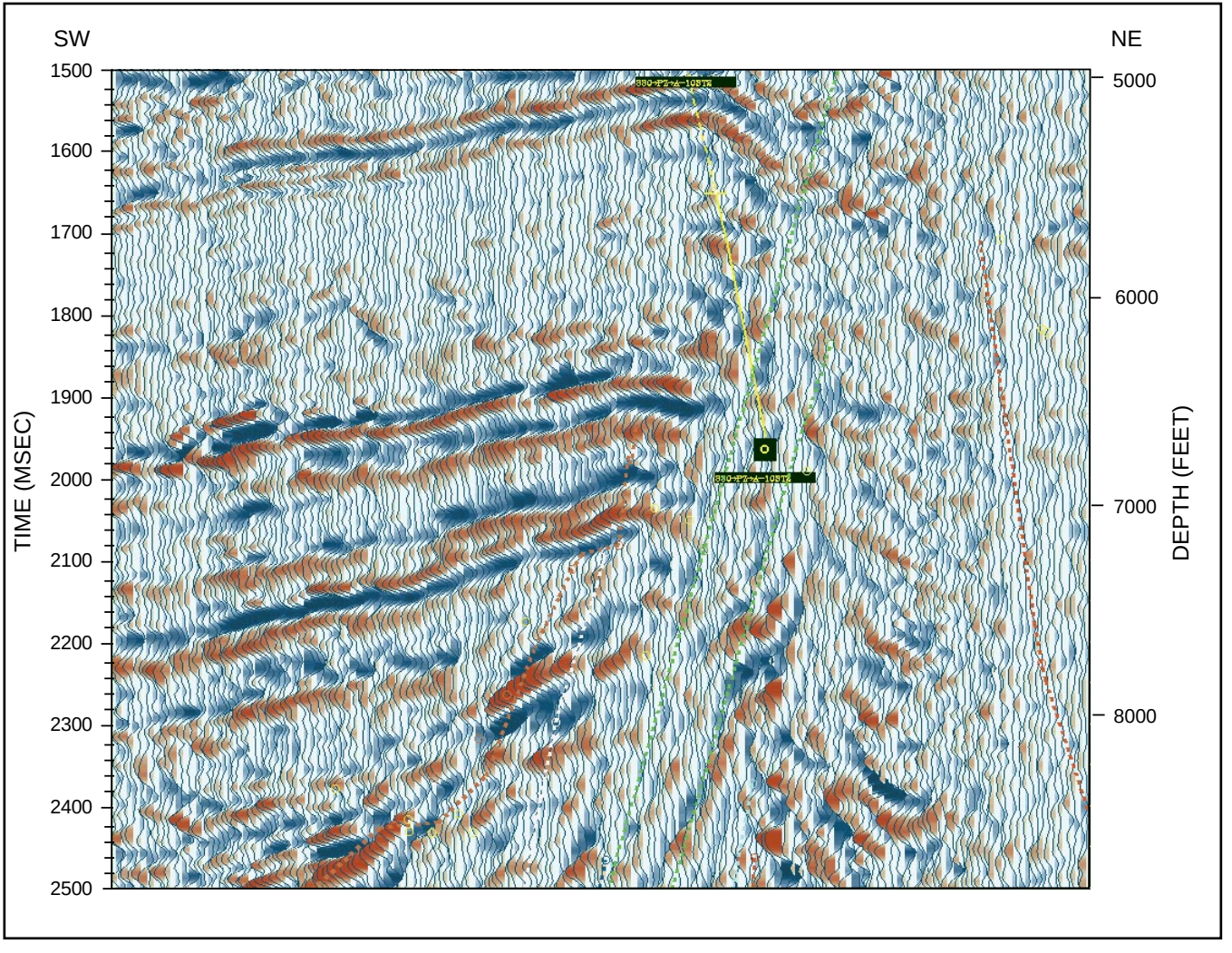

Figure I.i.9: Seismic profile along A-10ST wellpath.

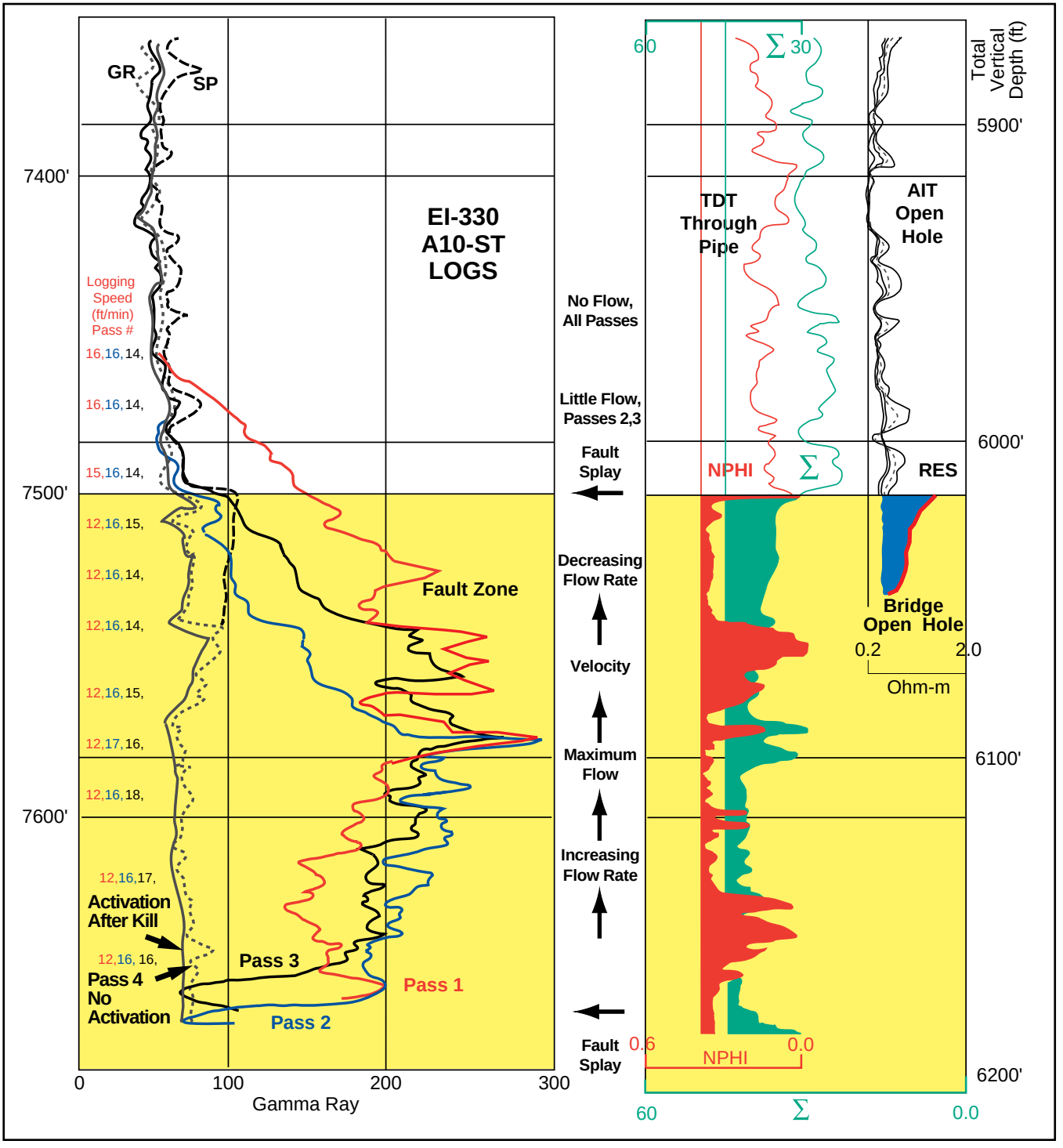

Figure I.i.11: Eugene Island 330 A-10ST open and cased-hole logs

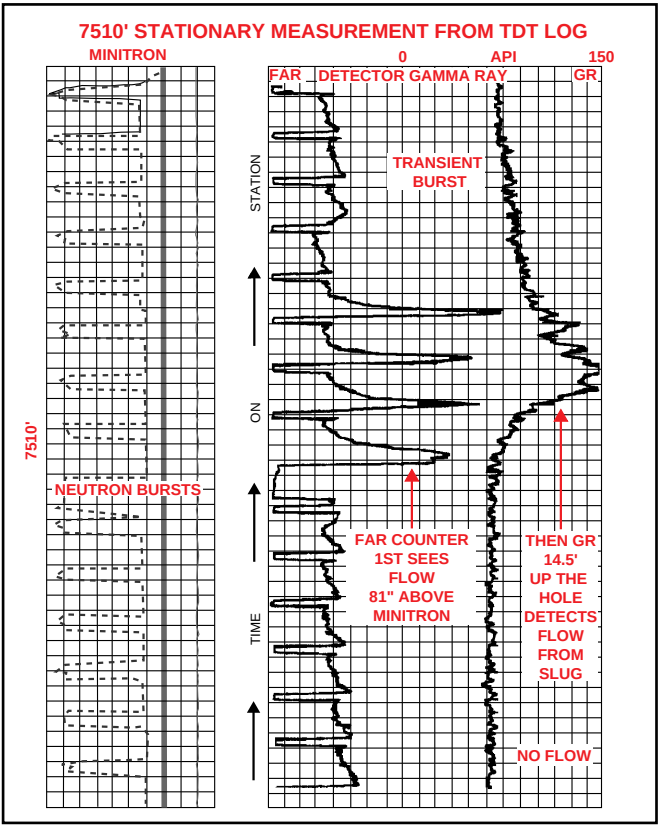

Figure I.i.12: Flow detected across a stationary TDT tool from a slug of water moving across the upper fault zone boundary against a 17.5 lb/gal (kill-slug).

	Depth (ft)	Gamma Ray	Vel (ft/min)	Vel (bbl/day)
Logging	7450.0	8.0000	37.700	48.900
	7475.0	10.000	48.000	64.000
	7495.0	80.000	110.00	160.00
	7500.0	110.00	120.00	170.00
	7505.0	90.000	115.00	150.00
	7510.0	145.00	103.00	180.00
	7520.0	125.00	100.00	175.00
	7520.0	120.00	130.00	185.00
	7525.0	175.00	145.00	195.00
	7530.0	155.00	130.00	180.00
	7535.0	175.00	145.00	195.00
	7545.0	245.00	160.00	220.00
	7550.0	215.00	150.00	200.00
	7555.0	150.00	135.00	180.00
	7570.0	75.000	103.00	150.00
	7575.0	175.00	135.00	200.00
	7580.0	130.00	125.00	175.00
	7595.0	25.000	68.000	90.000
	7600.0	60.000	100.00	140.00
	7605.0	80.000	110.00	150.00
	7625.0	15.000	52.000	70.000
	7630.0	30.000	85.000	115.00
	7635.0	30.000	85.000	115.00
Stations	7045.0	2.0000	3.5000	12.000
	7055.0	4.0000	6.0000	14.700
	7100.0	4.1000	7.4000	23.700
	7110.0	3.5000	5.8000	34.300
	7135.0	6.3000	33.500	50.000
	7145.0	5.4000	19.100	28.500
	7150.0	66.900	53.700	81.000
	7190.0	38.100	50.000	75.000
	7200.0	6.0000	14.700	20.000
	7395.0	7.4000	23.700	35.500
	7400.0	3.5000	12.000	18.000
	7450.0	37.700	48.900	73.000
	7490.0	10.400	12.500	19.000
	7500.0	43.200	64.300	96.000
	7510.0	3.3000	18.200	27.000
	7560.0	4.5000	10.500	15.000
	7570.0	44.500	56.200	84.000

Table I.i.1: Gamma Ray counts and flow velocities calculated for TDT log of fault zone, Pass 1 (Figure I.i.11), and station measurements made subsequently in A-10ST well.

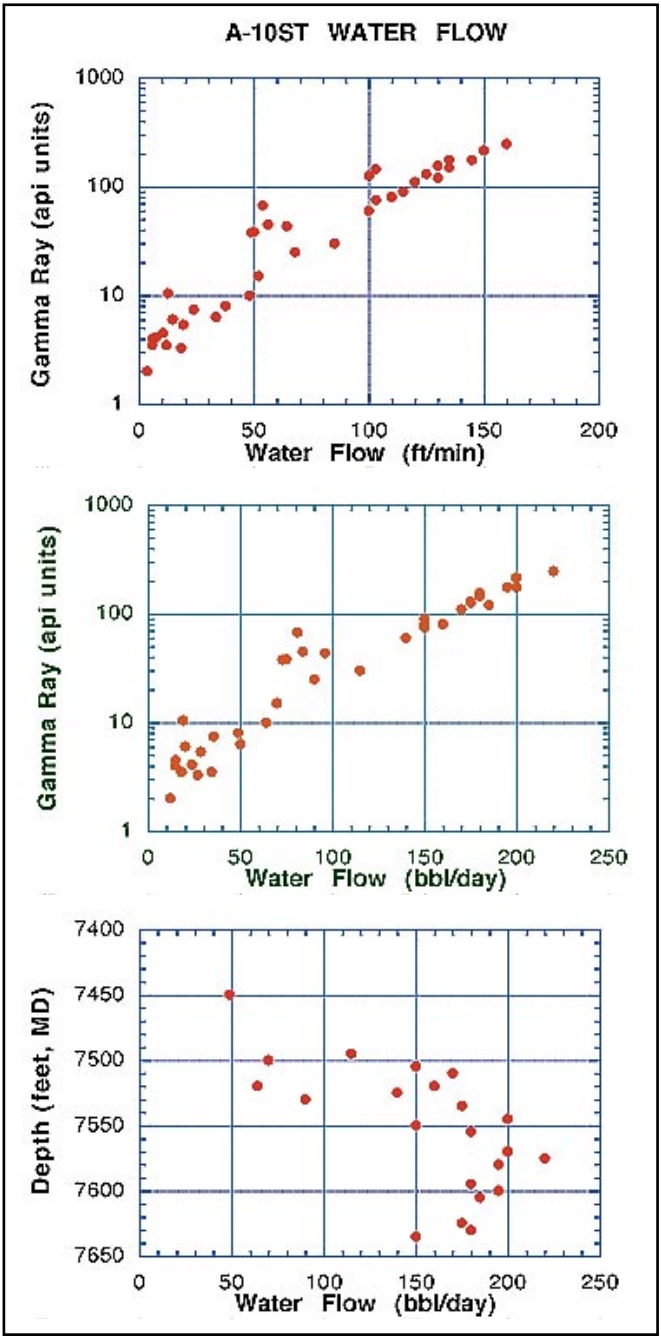

Figure I.i.13: Flow rates versus depth and gamma ray counts from TDT logs of fault zone in A-10ST.

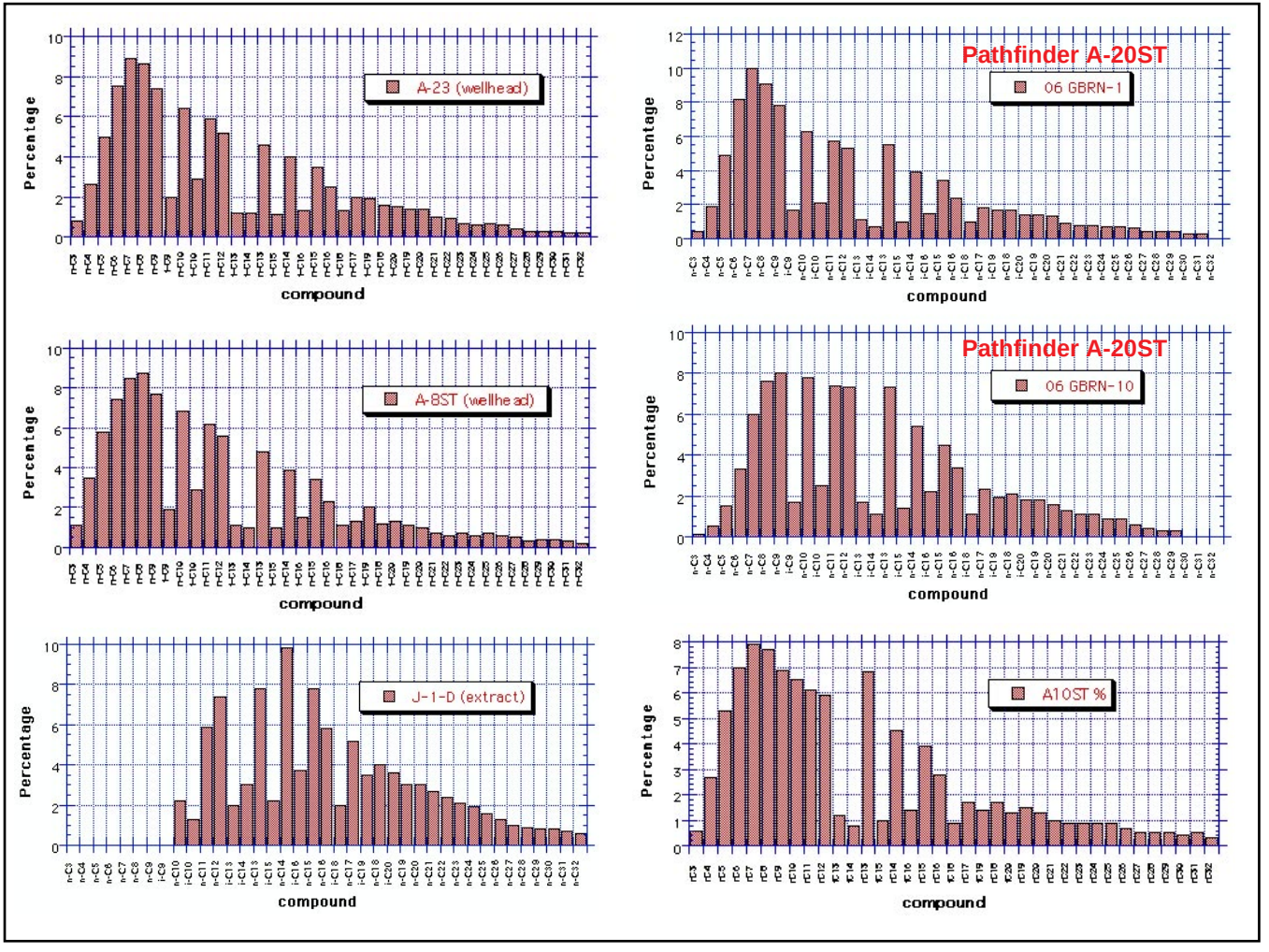

Figure I.i.14 :Whole oil chromatograms of oils sampled in 1993 from Eugene Island block 330 wells.

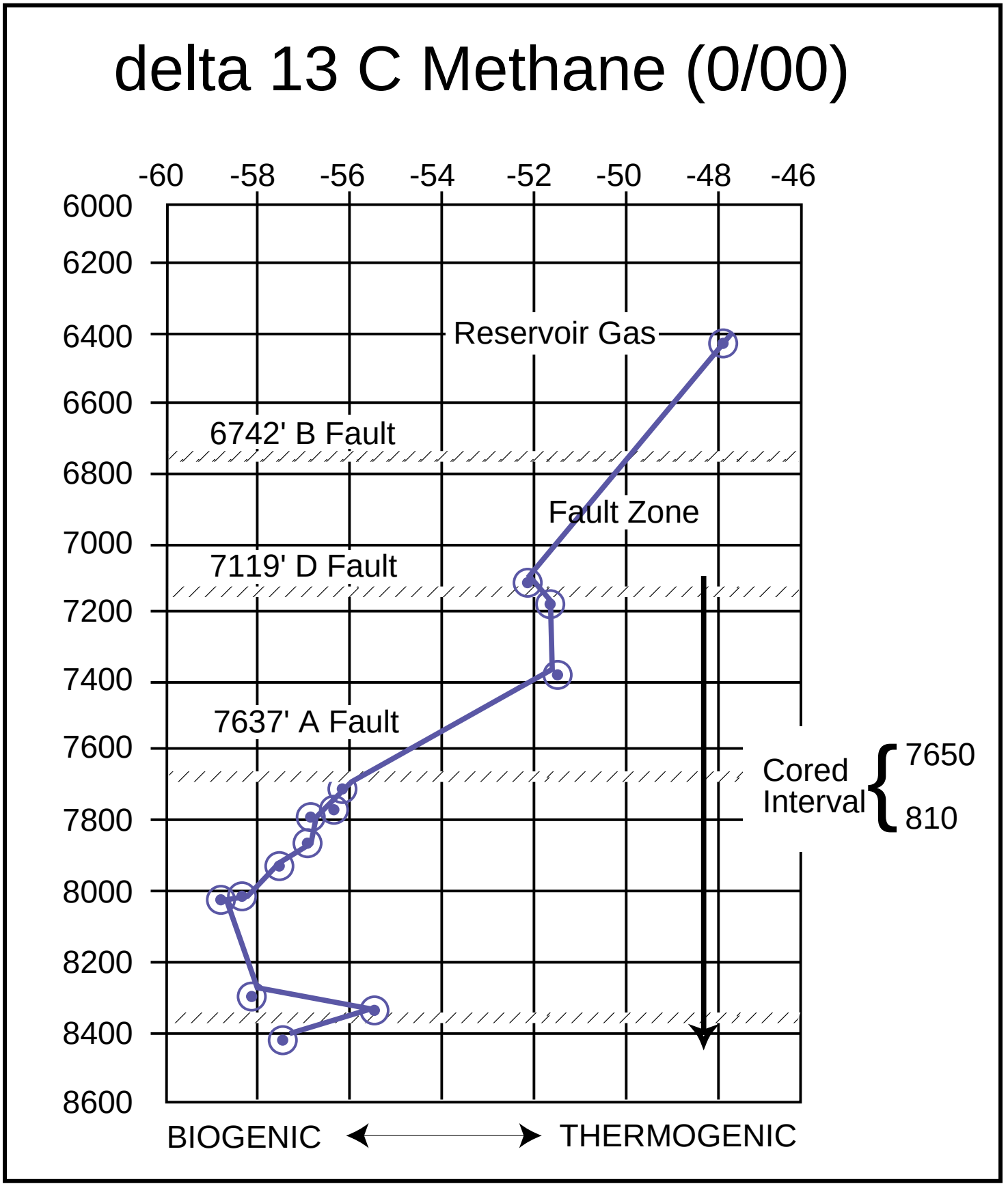

Figure I.i.15: del C17 analyses of gases collected from drilling muds from A-20ST well.

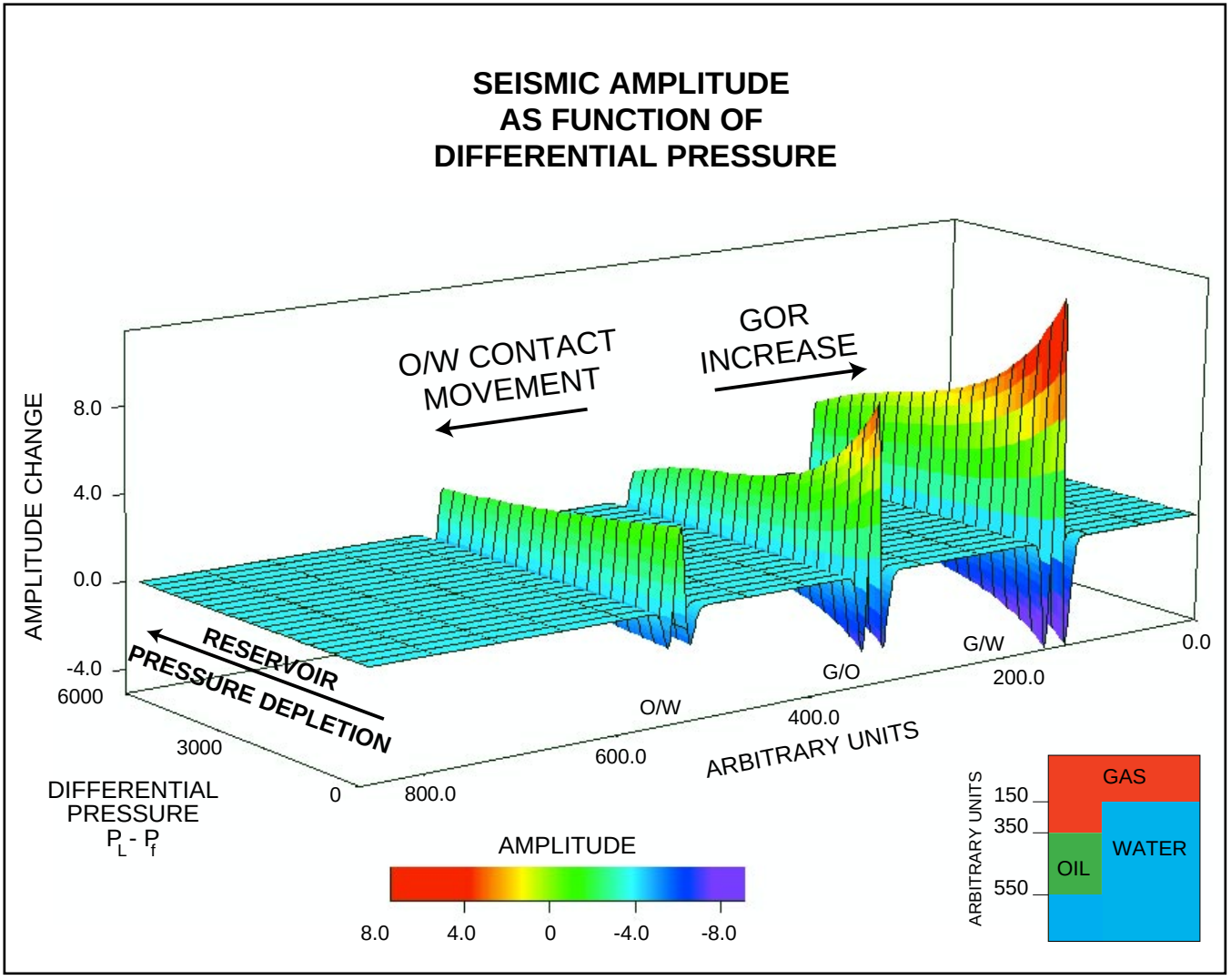

Figure I.ii.4: Modeling study of the effects on seismic amplitude of changes in pore pressure (P_f) relative to lithostatic pressure (P_L), oil/water, gas/oil and gas/water boundary movements. Gas/oil ratio increases cause amplitudes to increase, whereas oil/water movement causes amplitudes to dim out. Production-related drops in pore pressure cause both to decrease.

4D ADIP Seismic Analysis Steps

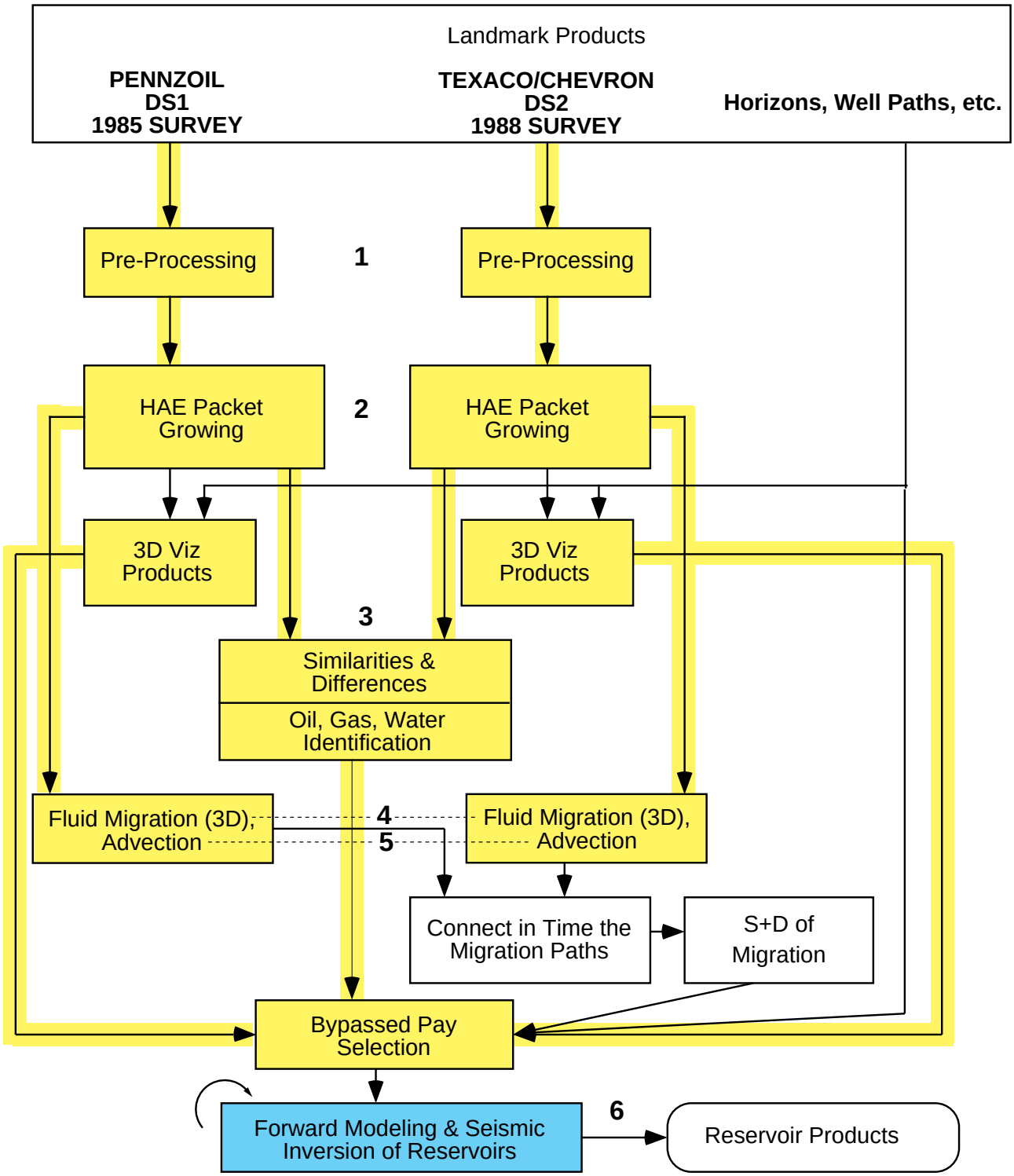

Table I.ii.1: Modules for 4-D seismic interpretation technique. Yellow boxes are operational; blue boxes are under development. (Click on any number above to go to detailed text on that subject).

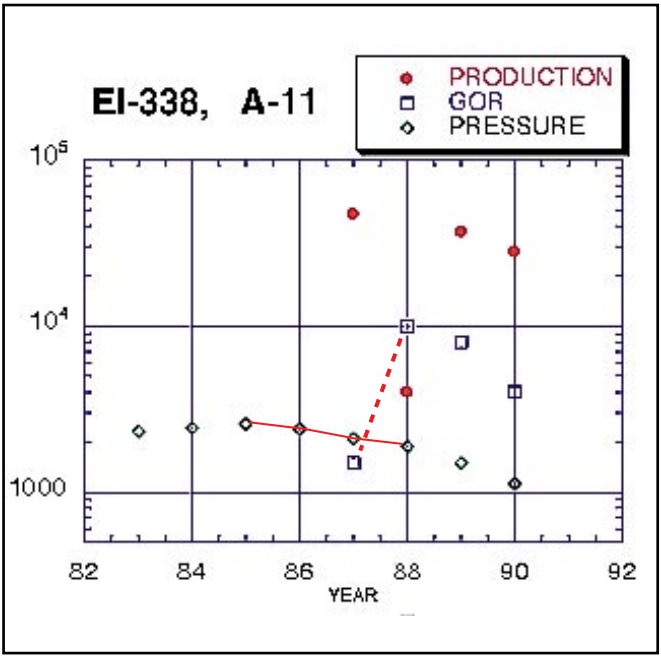

Figure I.ii.5: Production history of the A-11 well into the western fault block of the LF sand from 1982 until 1990.

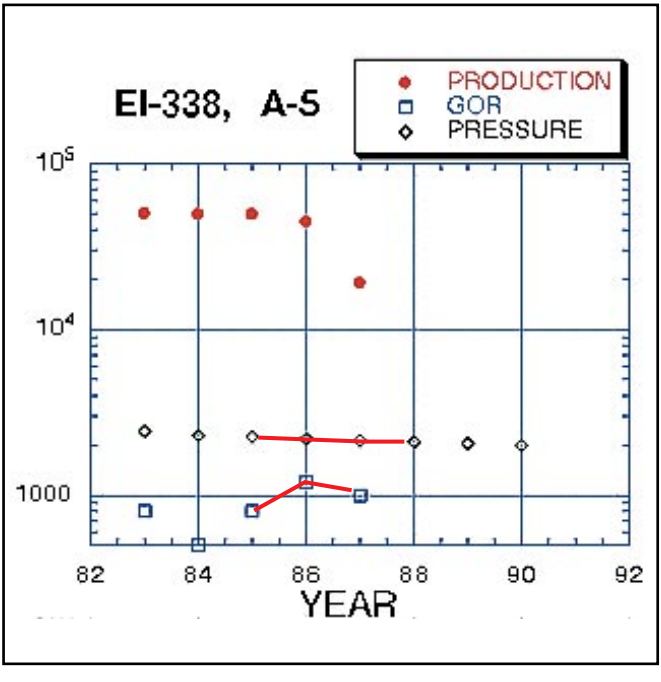

Figure I.ii.6: Production history of the A-5 well into the eastern block of the LF sand from 1982 until the well sanded out in 1988.

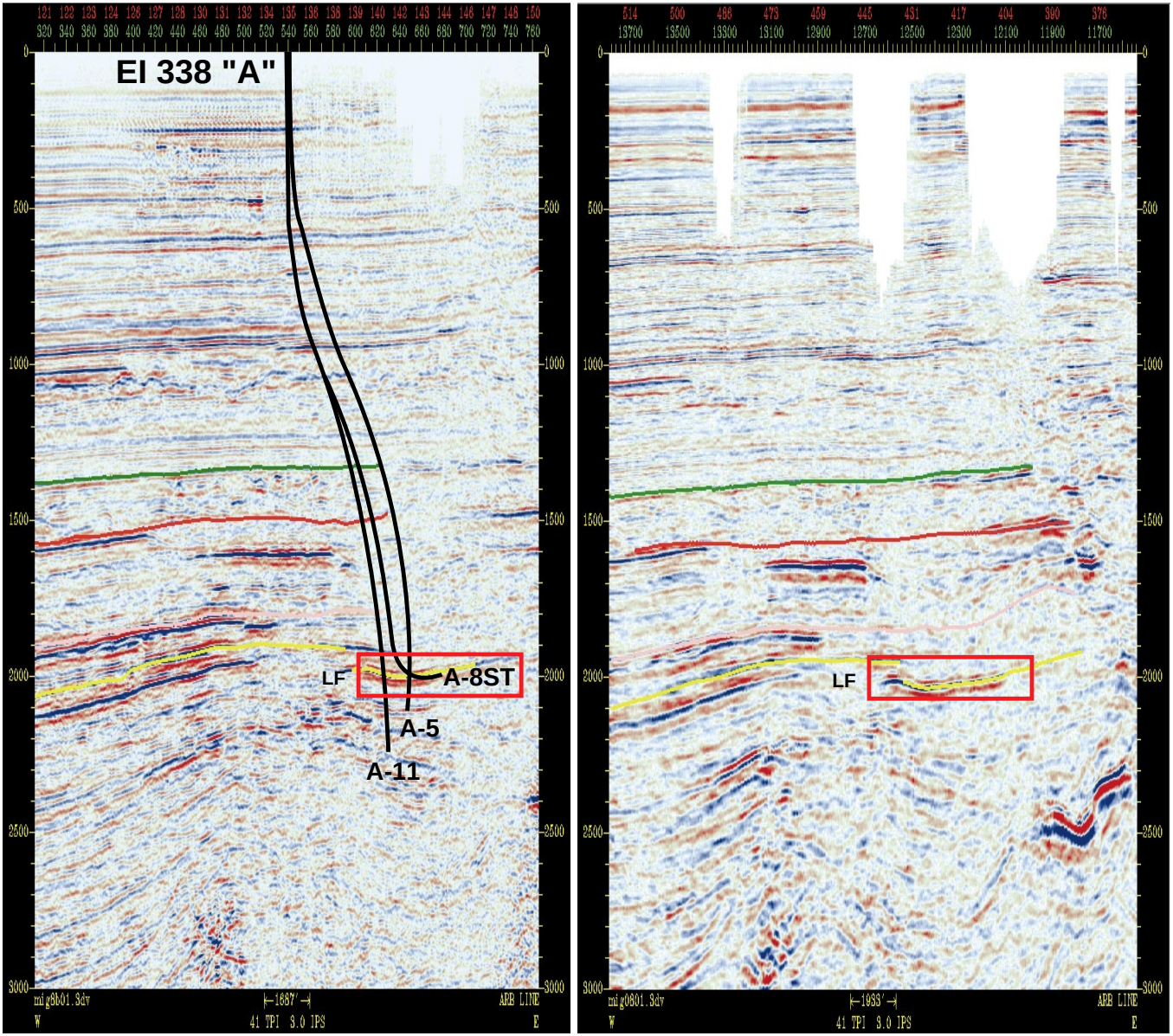

Figure I.ii.7: Seismic reflection profiles along the EI 330/338 boundary from 1988 survey (left) and 1985 survey (right), with A-8ST, A-5 and A-11 wells into the LF indicated. Note that horizontal scales are not quite the same.

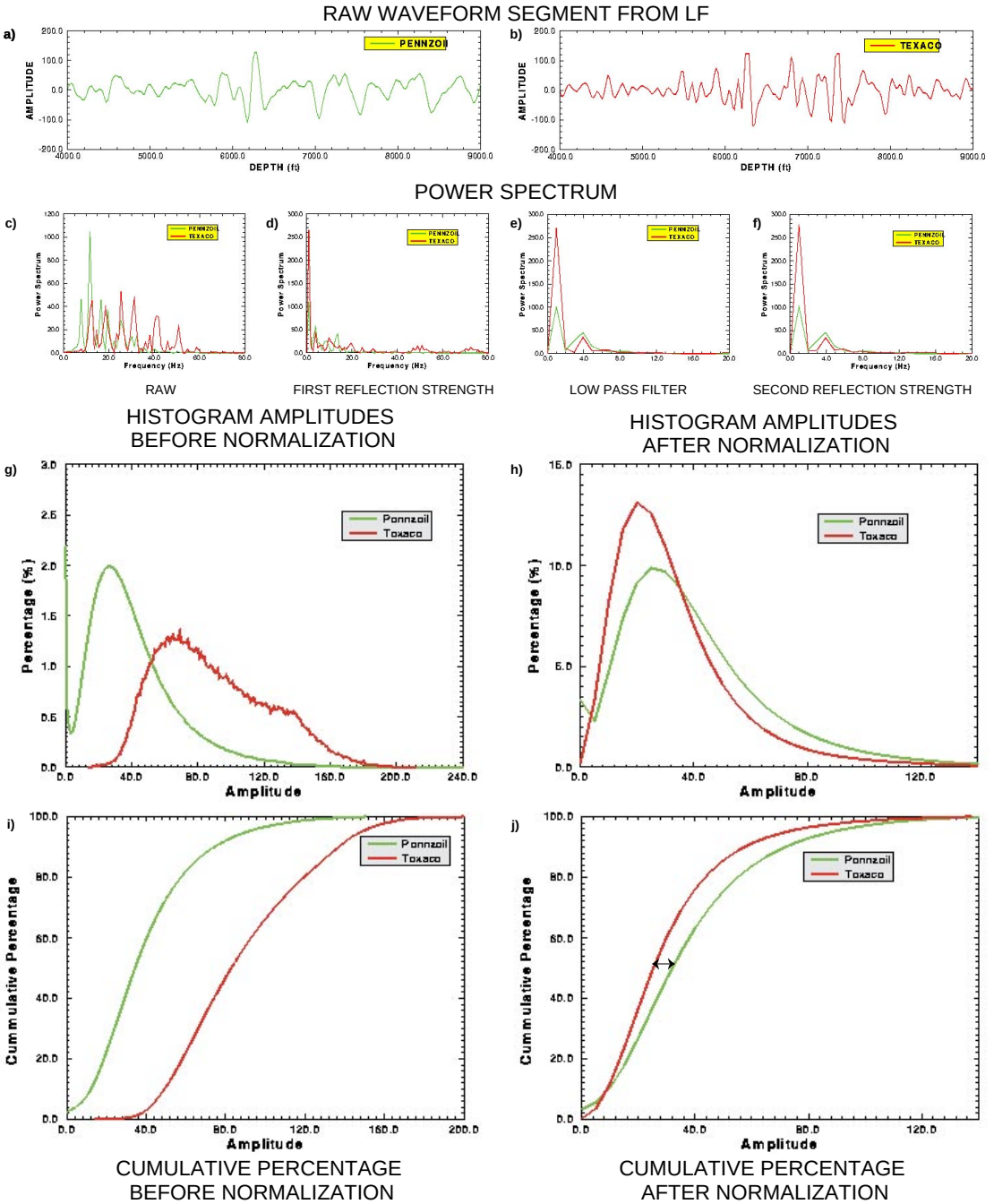

Figure I.ii.8: The first two graphs, a,b, are segments of two traces associated with LF from the Pennzoil and Texaco surveys, respectively. Note the differences in frequency content. The next graph, c, superposes the power spectra from Pennzoil and Texaco. Again, note the higher-frequency content in Texaco. The next graph, d, is the power spectra of the first-reflection strength (instantaneous amplitude) for the two datasets. Again, there is considerable difference in frequency content. The next graph, e, illustrates the use of a low-pass filter implemented via a 100ms moving window average. The frequencies are very much the same. The last graph, f, of power spectra illustrates the use of second-reflection strength after low-pass filtering. Note the similarity in frequency content. Histograms of the amplitude values of each voxel within the Pennzoil (1985) and Texaco (1988) surveys before and after normalization, g and h. Cumulative percentages of each before and after normalization, i and j, are also shown.

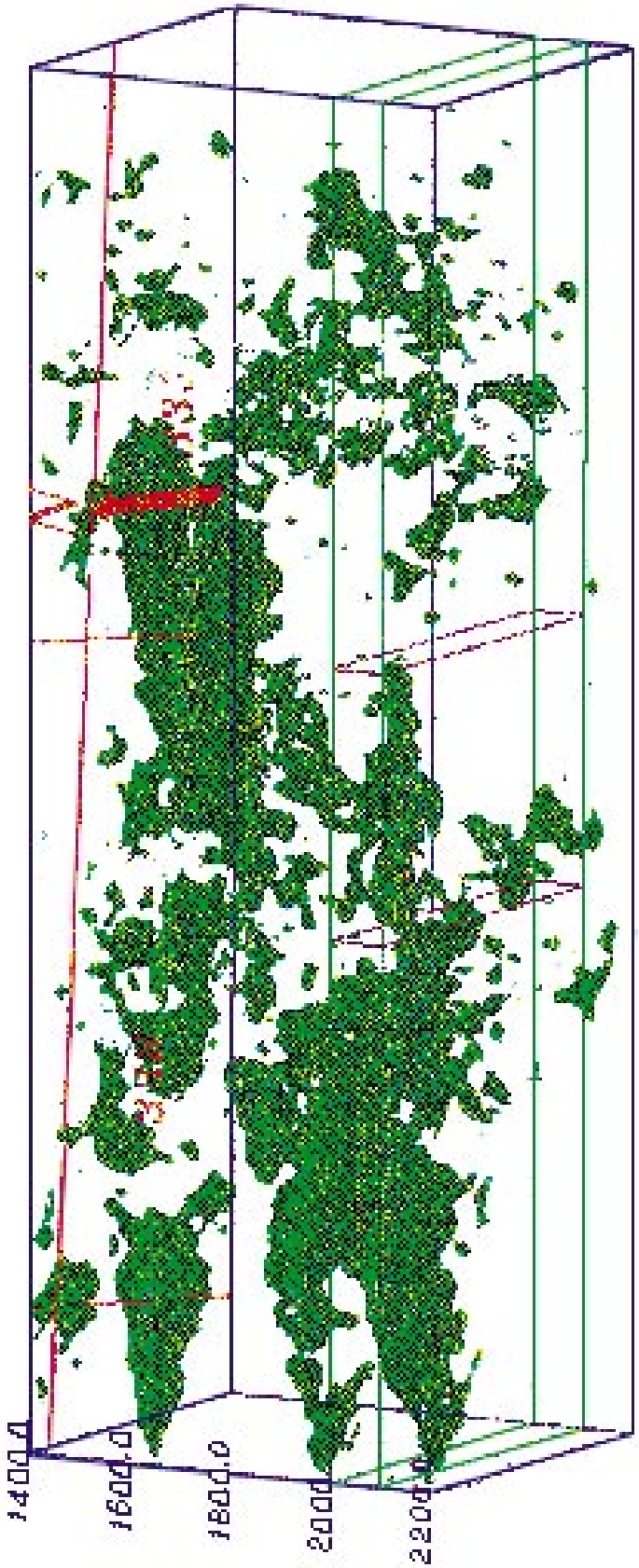

Figure I.ii.9.a: Amplitude envelopes around high seismic amplitudes from 1.4 to 2.2 seconds of travel time for the Pennzoil (1985) survey shown in green. The small box indicates the LF sand, blown up in Figure I.ii.12.

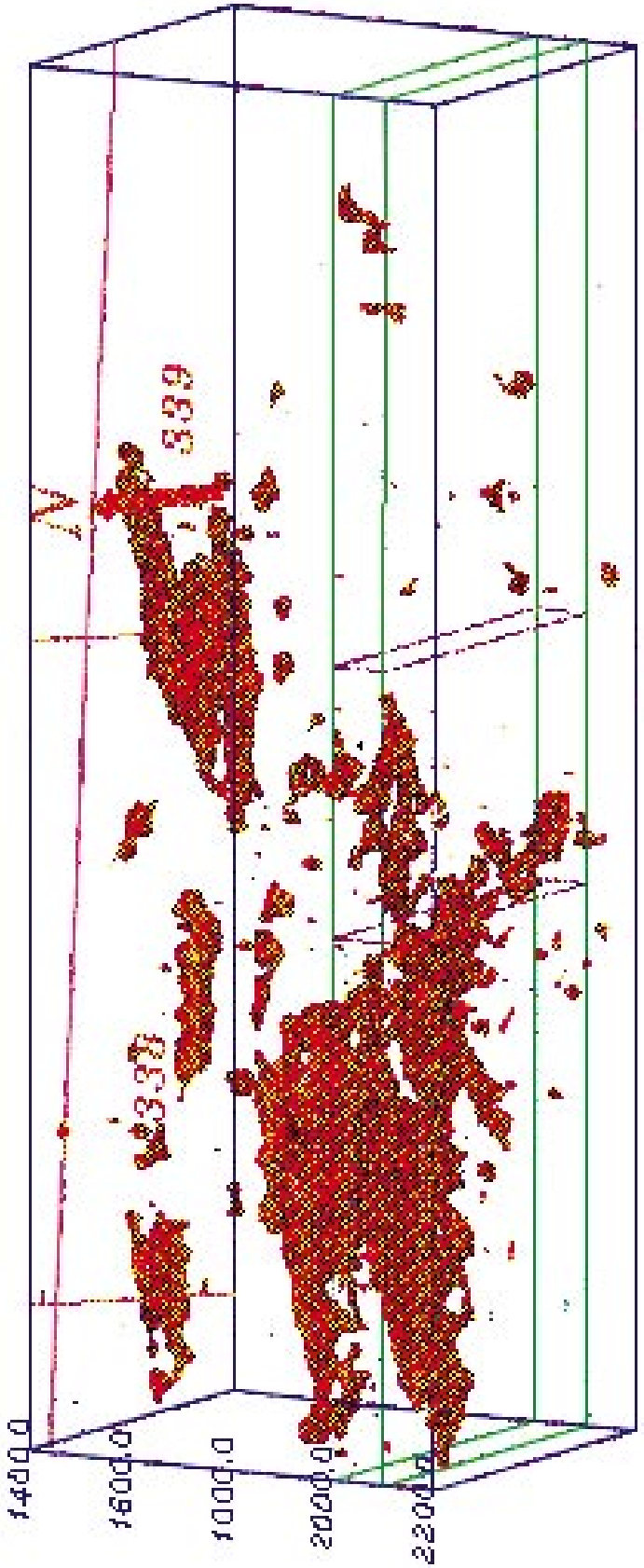

Figure I.ii.9.b: Amplitude envelopes around high seismic amplitudes from 1.4 to 2.2 seconds of travel time for the Texaco (1988) survey shown in red. The small box indicates the LF sand, blown up in Figure I.ii.12.

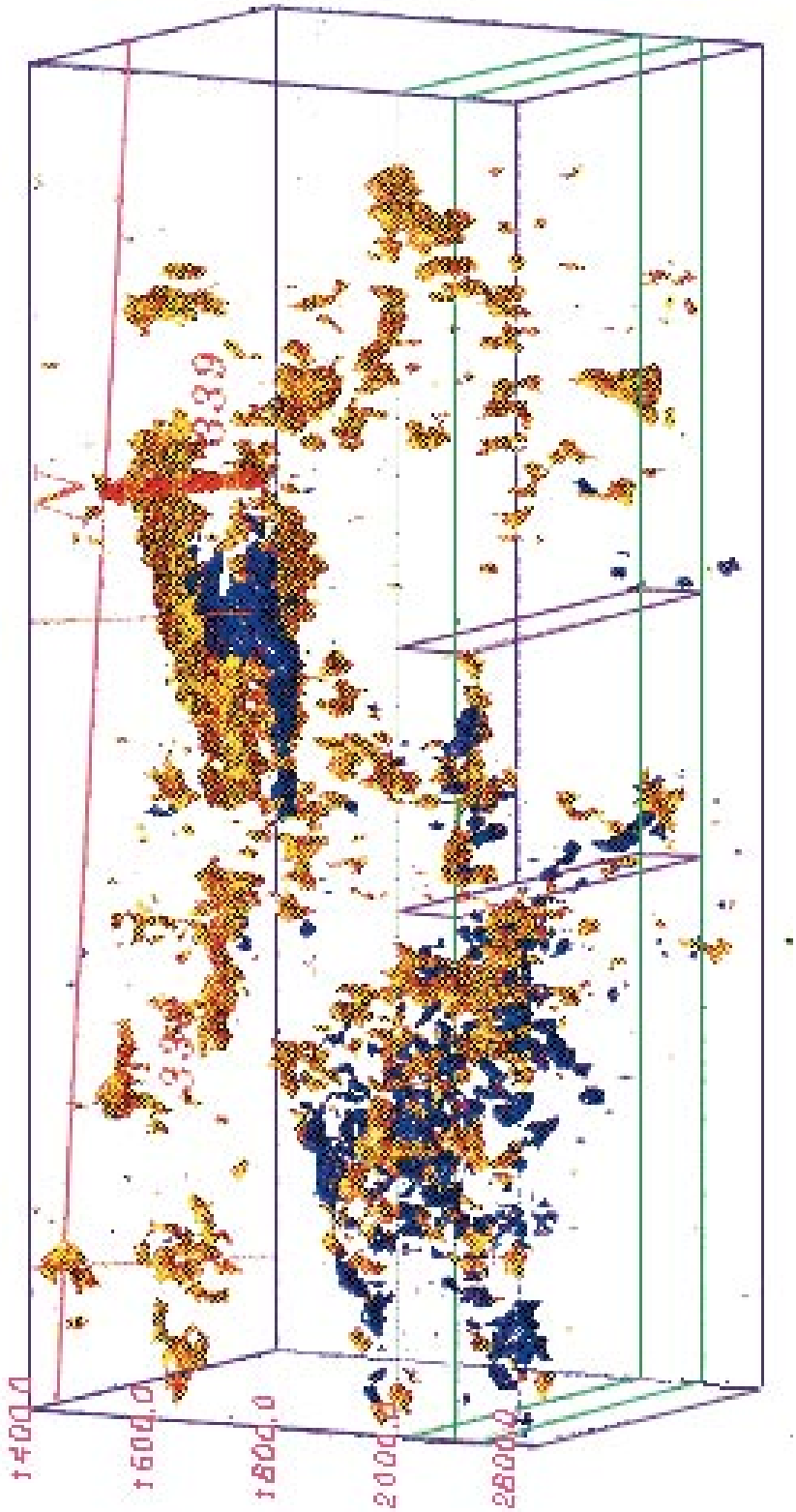

Figure I.ii.10: The differences in seismic amplitudes within the high-amplitude surfaces between Figures 1.ii.9 and I.ii.10, with dimouts from 1985 to 1988 indicated in blue and amplitude increases shown in gold. The small box indicates the LF sand, blown up in Figure I.ii.12.

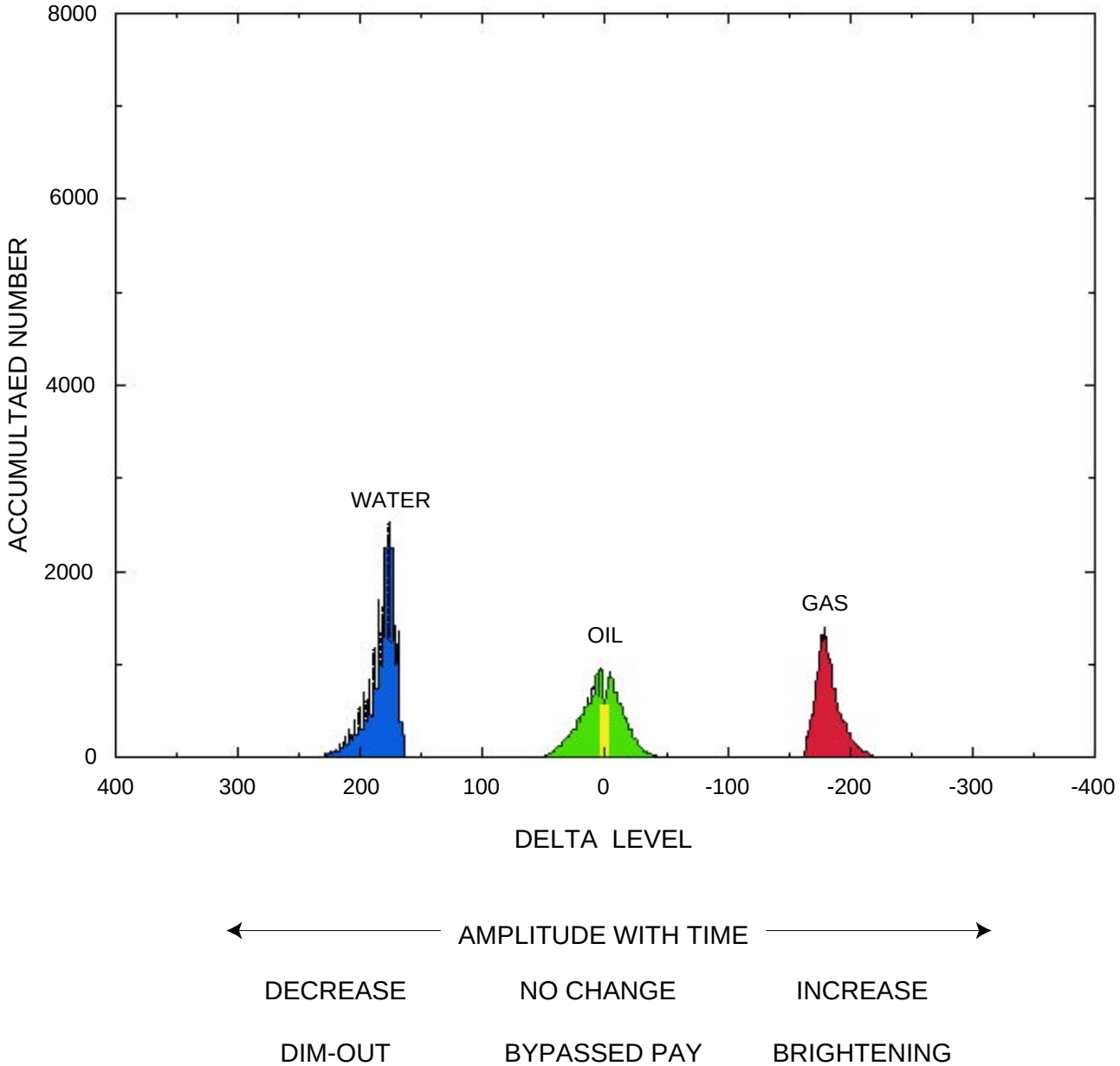

Figure I.ii.11: Histogram of reflection strength difference (1985 Pennzoil – 1988 Texaco). Color coded for use in Figure I.ii.12. These observations are consistent with model prediction in Figure I.ii.4.

Figure I.ii.12: Print onto transparency plastic each of the 11 time slices through the LF reservoir contained in this figure. Then tape onto transparency mounts, space with three blank mounts between each and assemble into 3-D physical model of the seismic changes within the LF sand caused by drainage from production from 1985 to 1988. Green is bypassed pay indicated by no change in high amplitudes, with yellow the most prospective, whereas the blue is waterfront advance that produced a dimout from production and the migration updip from the northeast of the oil/water contact. Red is amplitude increase caused by gas/oil ratio increase with production.

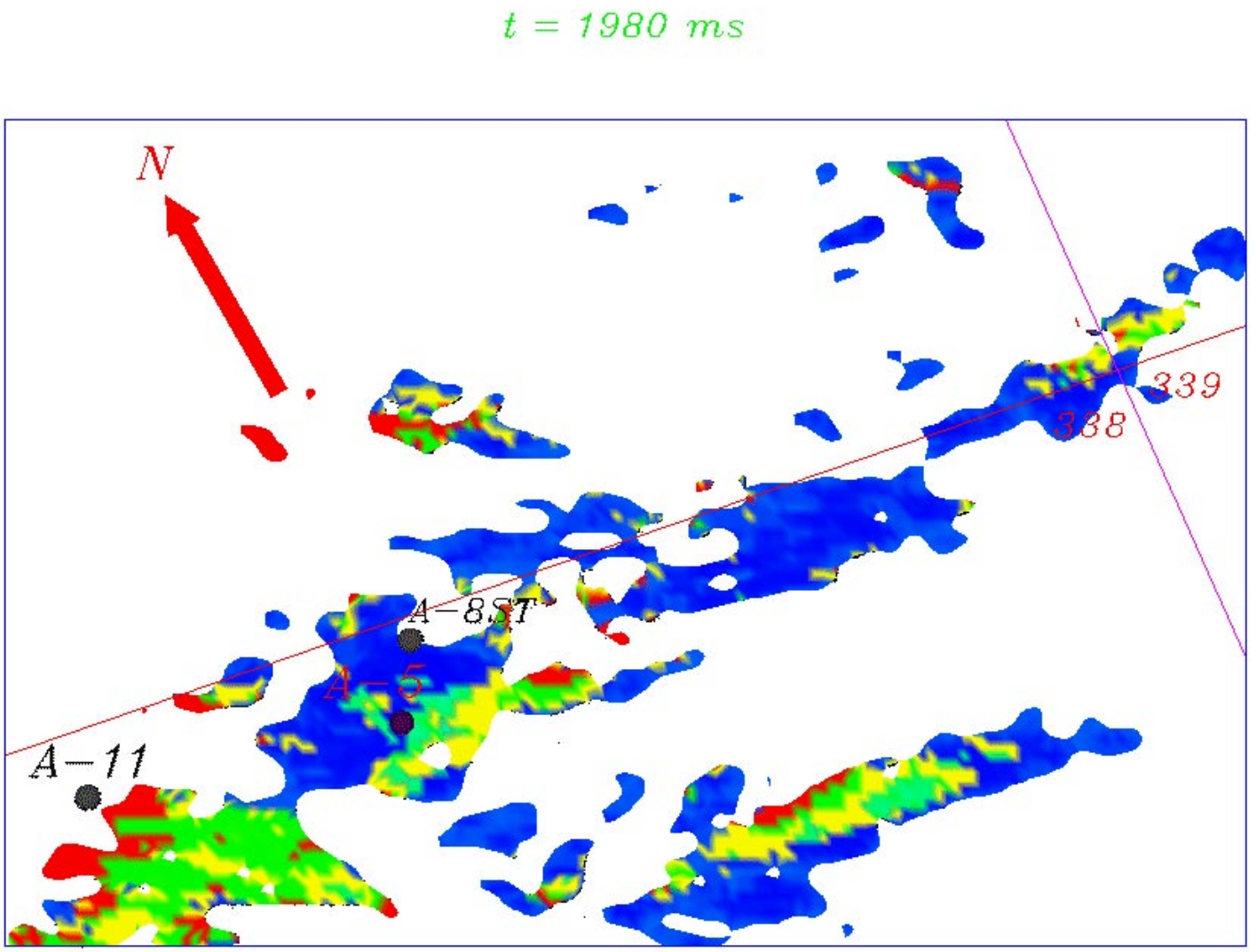

Figure I.ii.12 (continued): Print onto transparency plastic each of the 11 time slices through the LF reservoir contained in this figure. Then tape onto transparency mounts, space with three blank mounts between each and assemble into 3-D physical model of the seismic changes within the LF sand caused by drainage from production from 1985 to 1988. Green is bypassed pay indicated by no change in high amplitudes, with yellow the most prospective, whereas the blue is waterfront advance that produced a dimout from production and the migration updip from the northeast of the oil/water contact. Red is amplitude increase caused by gas/oil ratio increase with production.

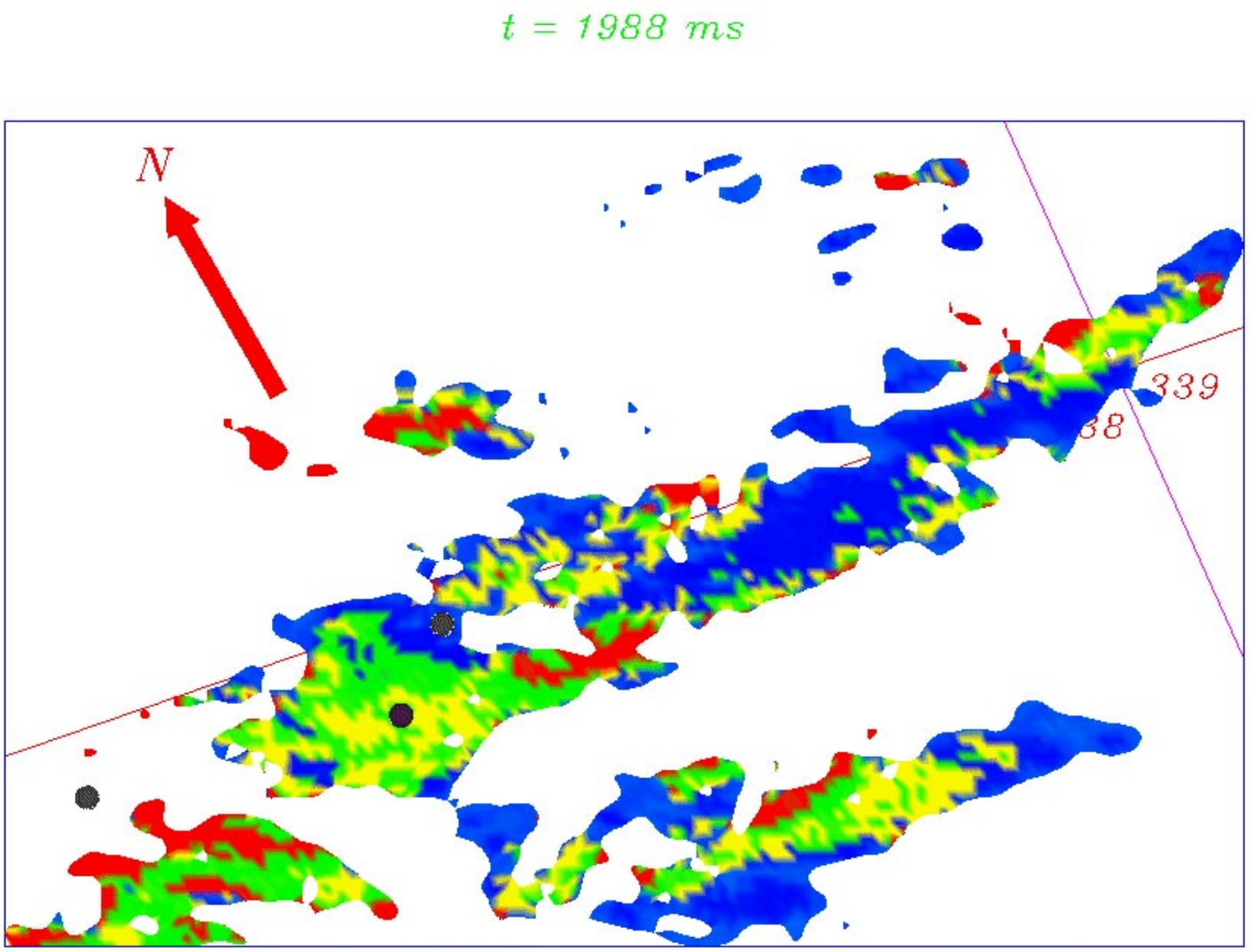

Figure I.ii.12 (continued): Print onto transparency plastic each of the 11 time slices through the LF reservoir contained in this figure. Then tape onto transparency mounts, space with three blank mounts between each and assemble into 3-D physical model of the seismic changes within the LF sand caused by drainage from production from 1985 to 1988. Green is bypassed pay indicated by no change in high amplitudes, with yellow the most prospective, whereas the blue is waterfront advance that produced a dimout from production and the migration updip from the northeast of the oil/water contact. Red is amplitude increase caused by gas/oil ratio increase with production.

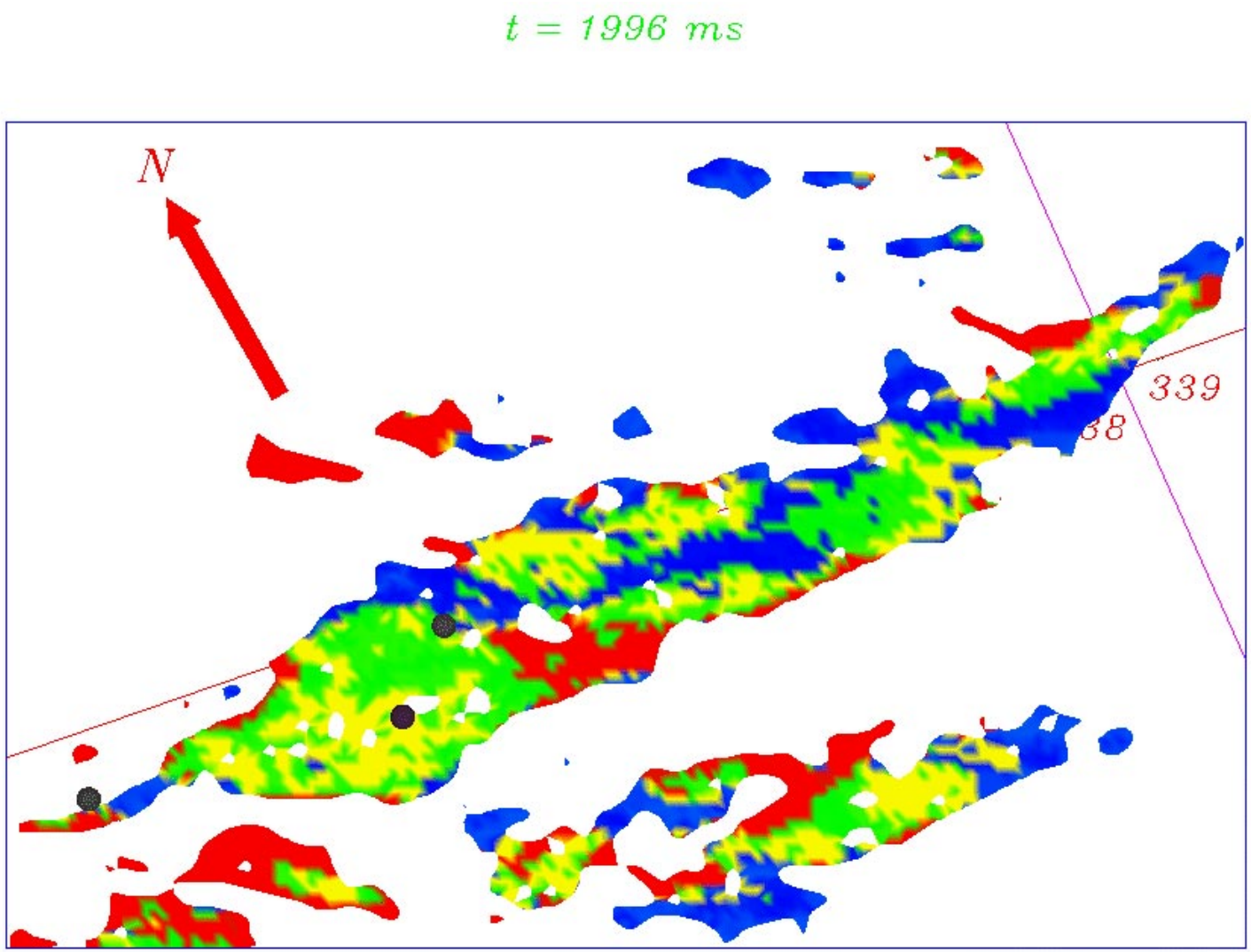

Figure I.ii.12 (continued): Print onto transparency plastic each of the 11 time slices through the LF reservoir contained in this figure. Then tape onto transparency mounts, space with three blank mounts between each and assemble into 3-D physical model of the seismic changes within the LF sand caused by drainage from production from 1985 to 1988. Green is bypassed pay indicated by no change in high amplitudes, with yellow the most prospective, whereas the blue is waterfront advance that produced a dimout from production and the migration updip from the northeast of the oil/water contact. Red is amplitude increase caused by gas/oil ratio increase with production.

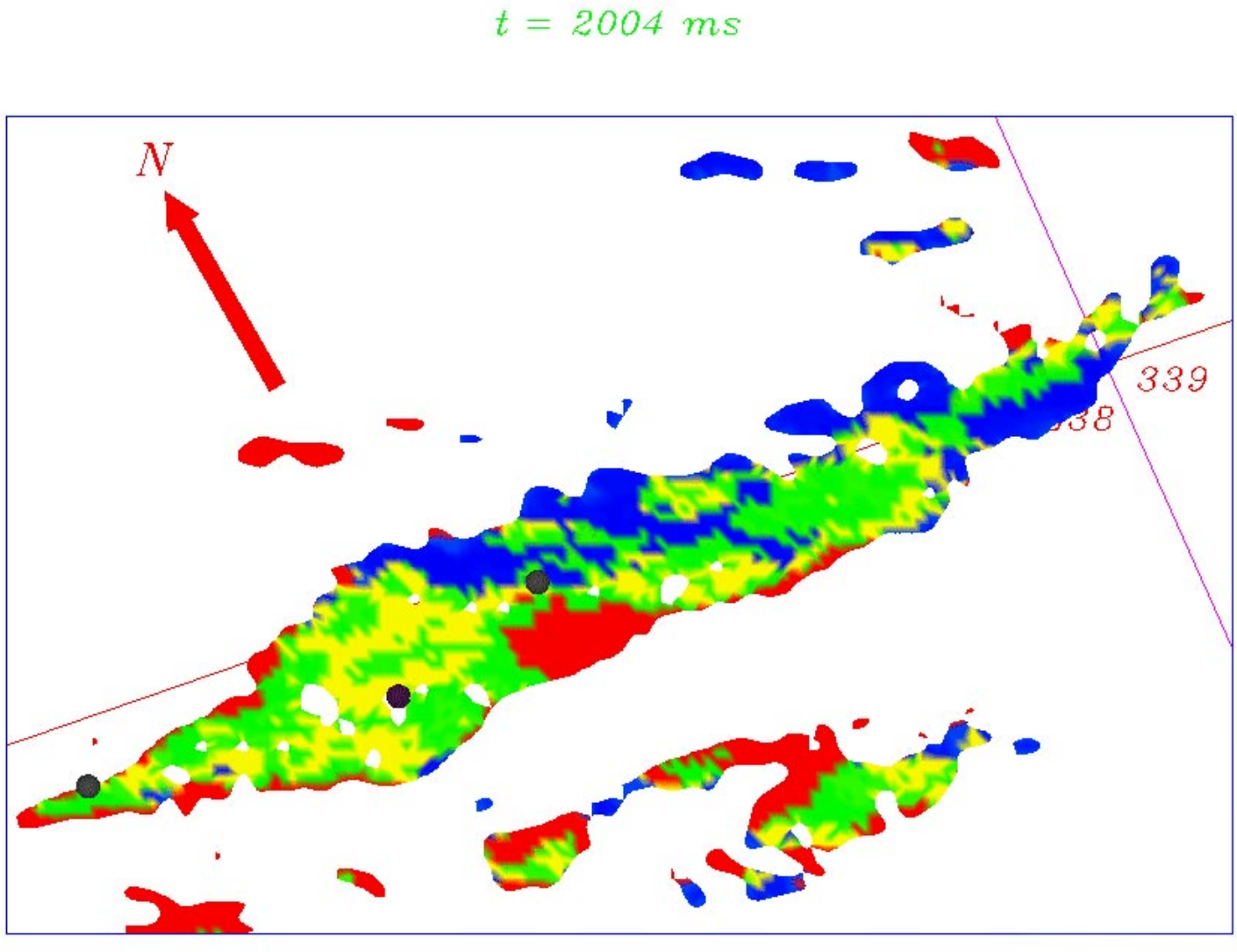

Figure I.ii.12 (continued): Print onto transparency plastic each of the 11 time slices through the LF reservoir contained in this figure. Then tape onto transparency mounts, space with three blank mounts between each and assemble into 3-D physical model of the seismic changes within the LF sand caused by drainage from production from 1985 to 1988. Green is bypassed pay indicated by no change in high amplitudes, with yellow the most prospective, whereas the blue is waterfront advance that produced a dimout from production and the migration updip from the northeast of the oil/water contact. Red is amplitude increase caused by gas/oil ratio increase with production.

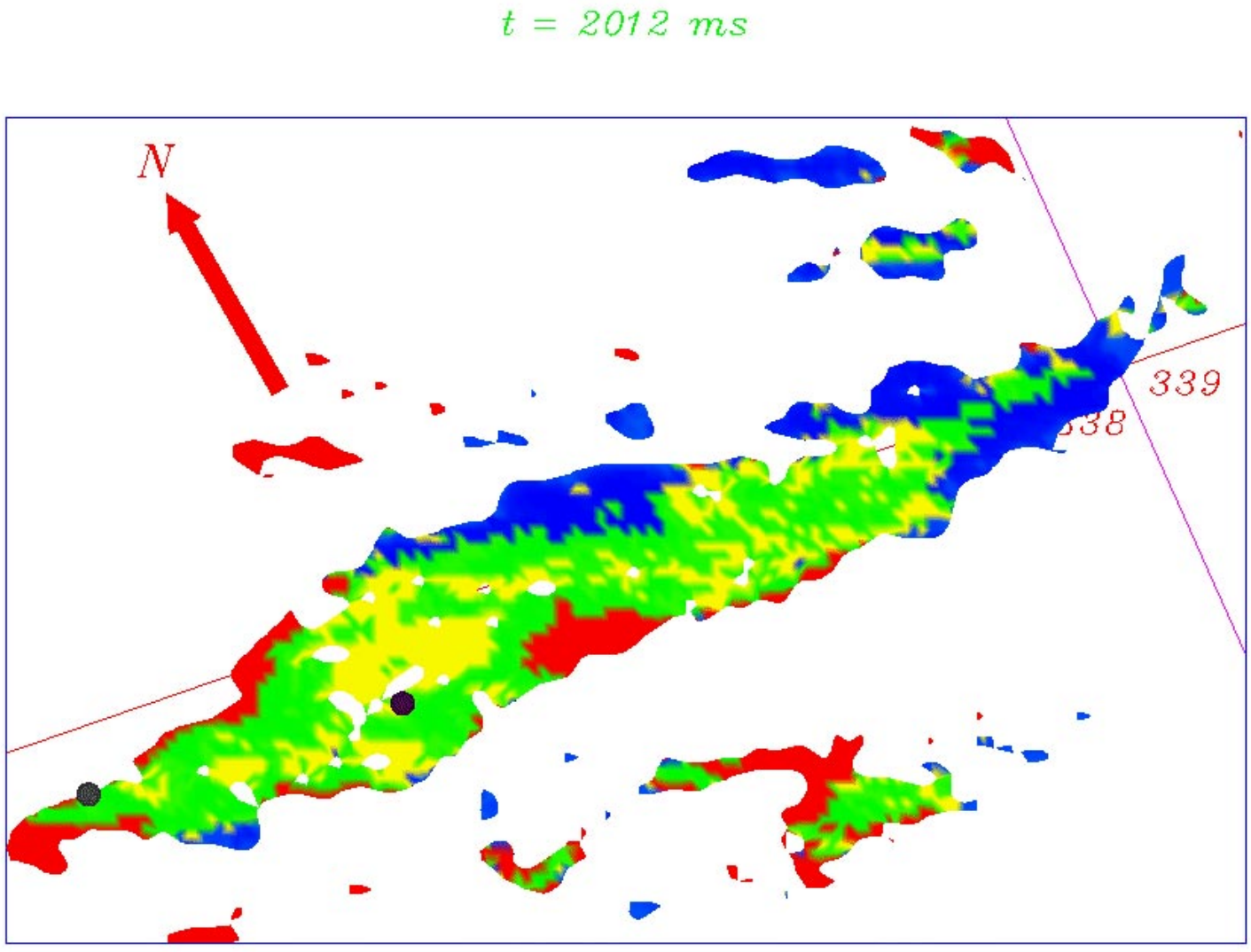

Figure I.ii.12 (continued): Print onto transparency plastic each of the 11 time slices through the LF reservoir contained in this figure. Then tape onto transparency mounts, space with three blank mounts between each and assemble into 3-D physical model of the seismic changes within the LF sand caused by drainage from production from 1985 to 1988. Green is bypassed pay indicated by no change in high amplitudes, with yellow the most prospective, whereas the blue is waterfront advance that produced a dimout from production and the migration updip from the northeast of the oil/water contact. Red is amplitude increase caused by gas/oil ratio increase with production.

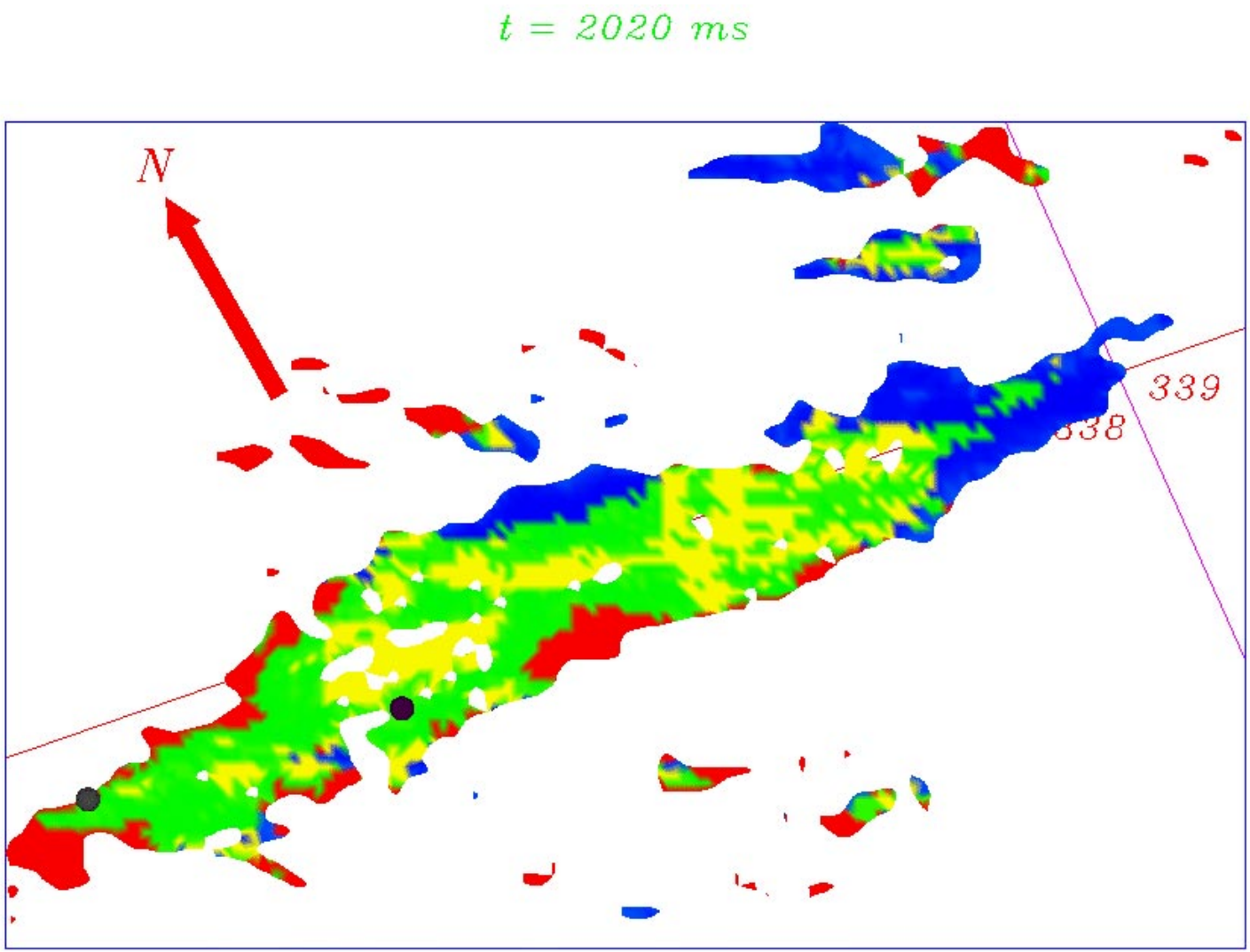

Figure I.ii.12 (continued): Print onto transparency plastic each of the 11 time slices through the LF reservoir contained in this figure. Then tape onto transparency mounts, space with three blank mounts between each and assemble into 3-D physical model of the seismic changes within the LF sand caused by drainage from production from 1985 to 1988. Green is bypassed pay indicated by no change in high amplitudes, with yellow the most prospective, whereas the blue is waterfront advance that produced a dimout from production and the migration updip from the northeast of the oil/water contact. Red is amplitude increase caused by gas/oil ratio increase with production.

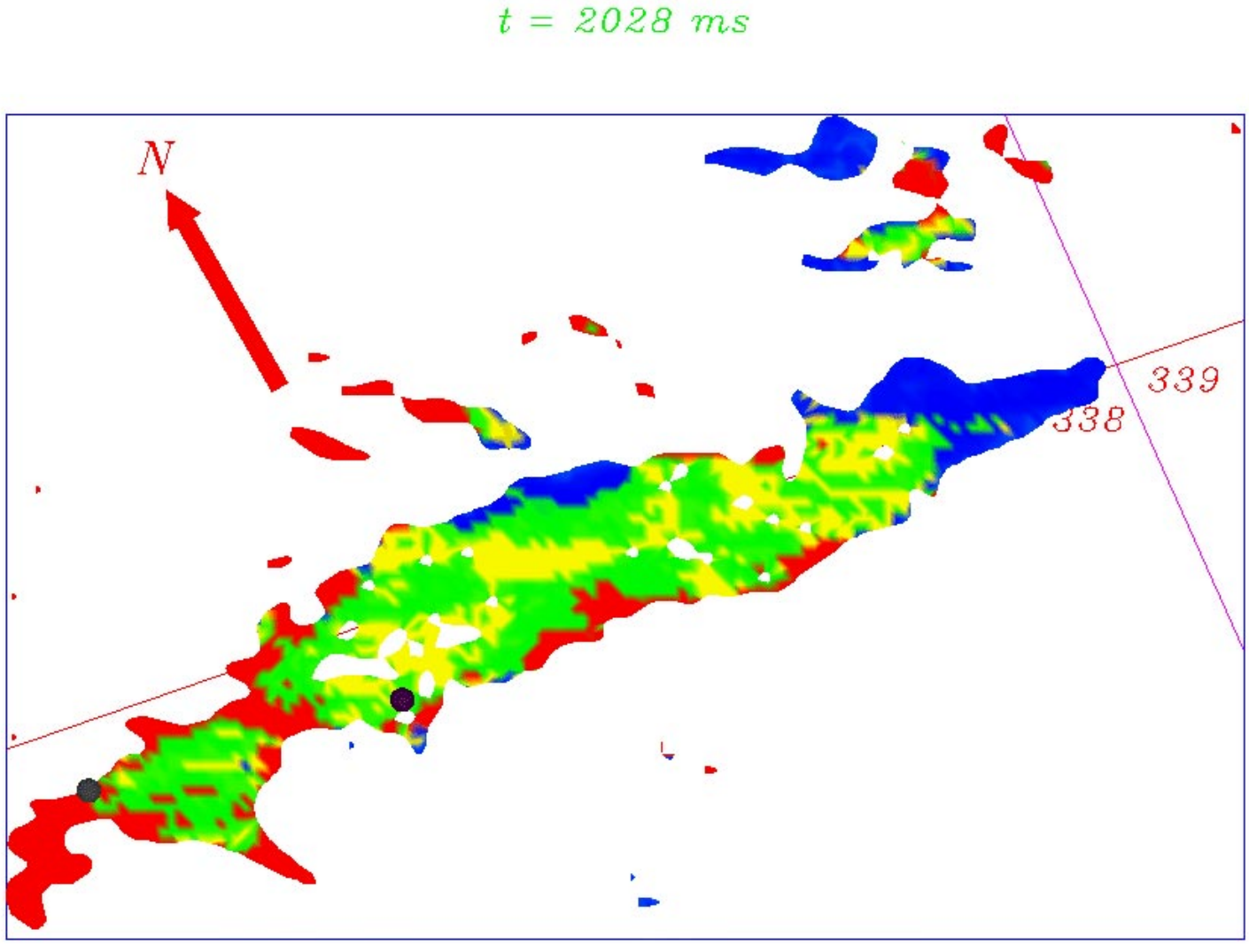

Figure I.ii.12 (continued): Print onto transparency plastic each of the 11 time slices through the LF reservoir contained in this figure. Then tape onto transparency mounts, space with three blank mounts between each and assemble into 3-D physical model of the seismic changes within the LF sand caused by drainage from production from 1985 to 1988. Green is bypassed pay indicated by no change in high amplitudes, with yellow the most prospective, whereas the blue is waterfront advance that produced a dimout from production and the migration updip from the northeast of the oil/water contact. Red is amplitude increase caused by gas/oil ratio increase with production.

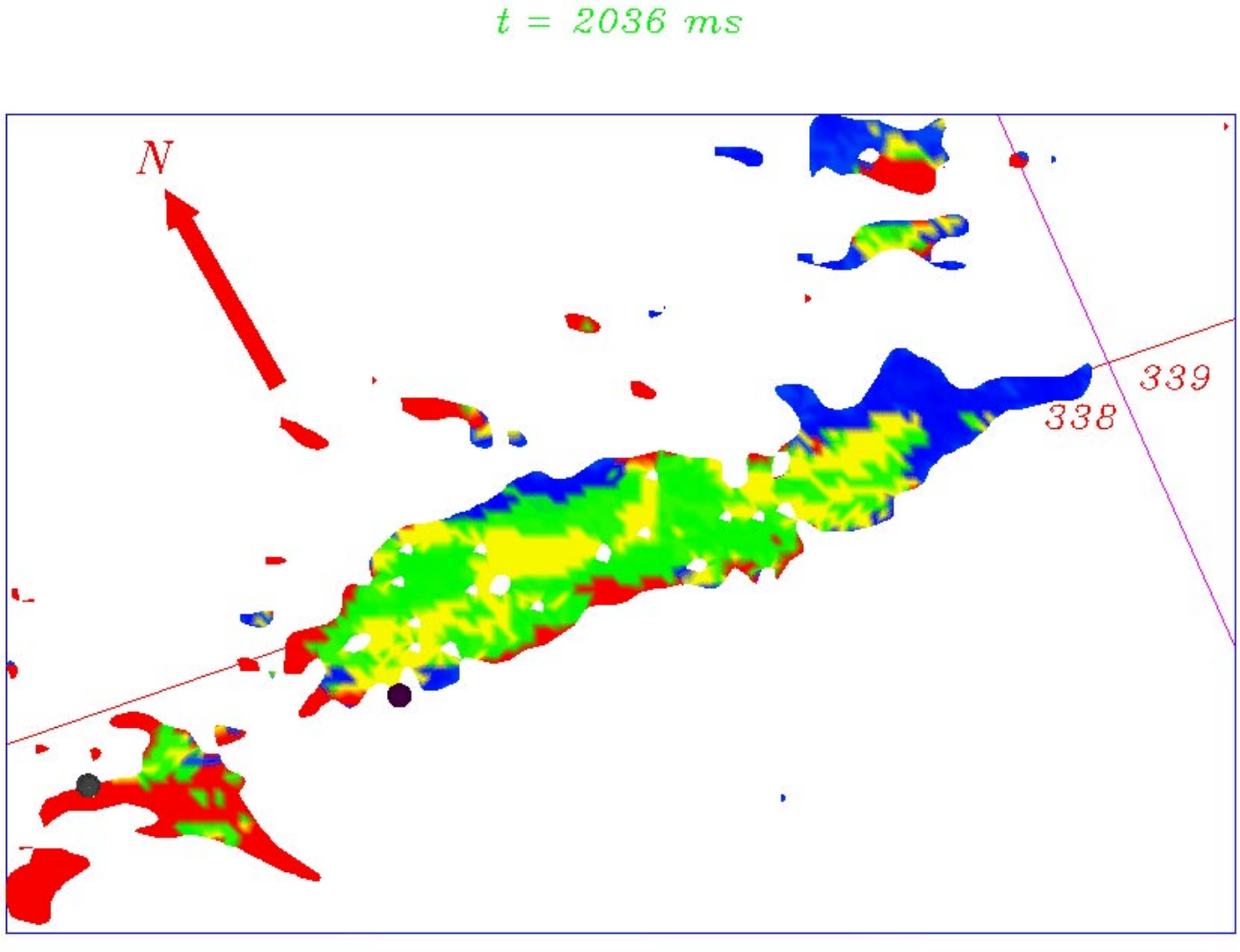

Figure I.ii.12 (continued): Print onto transparency plastic each of the 11 time slices through the LF reservoir contained in this figure. Then tape onto transparency mounts, space with three blank mounts between each and assemble into 3-D physical model of the seismic changes within the LF sand caused by drainage from production from 1985 to 1988. Green is bypassed pay indicated by no change in high amplitudes, with yellow the most prospective, whereas the blue is waterfront advance that produced a dimout from production and the migration updip from the northeast of the oil/water contact. Red is amplitude increase caused by gas/oil ratio increase with production.

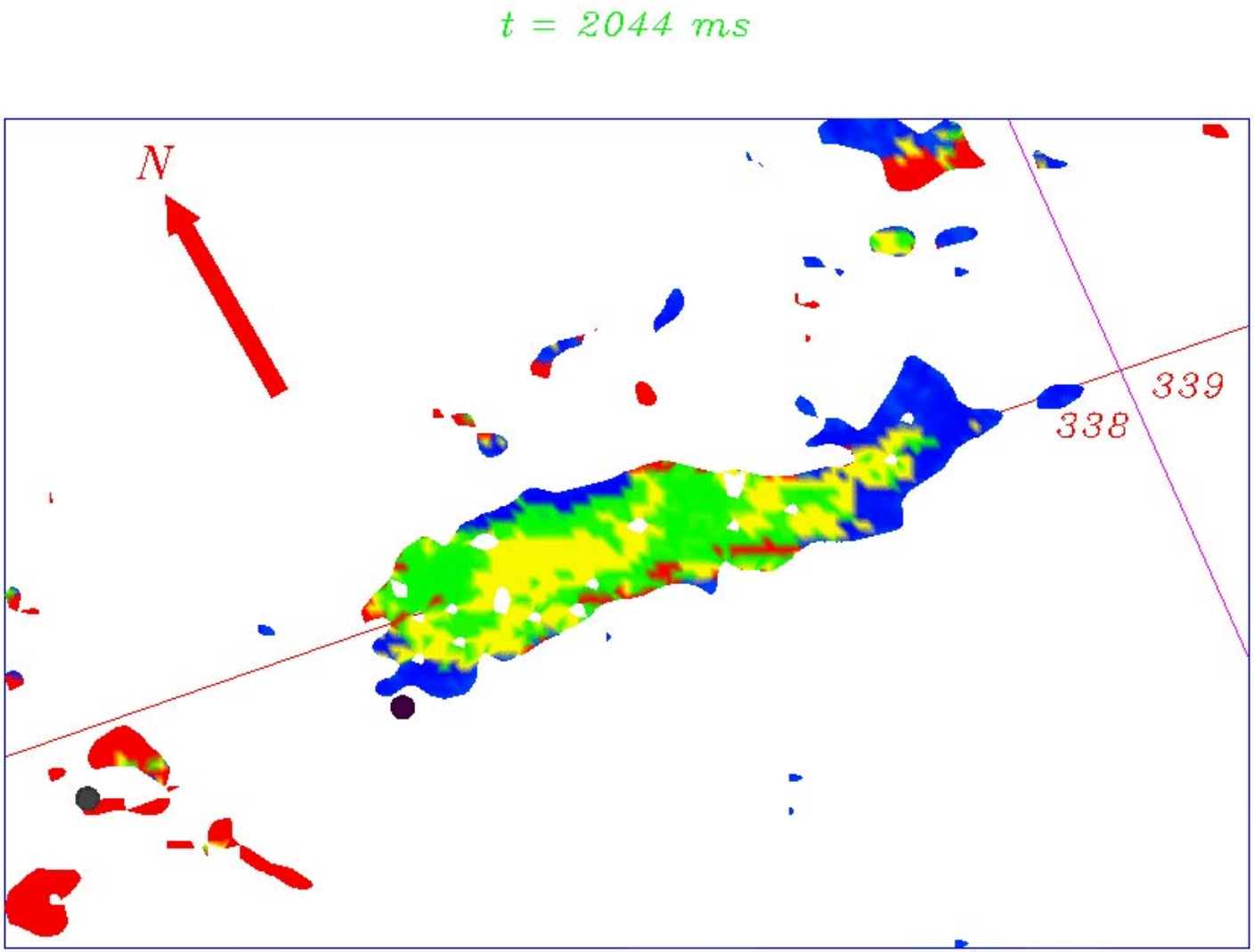

Figure I.ii.12 (continued): Print onto transparency plastic each of the 11 time slices through the LF reservoir contained in this figure. Then tape onto transparency mounts, space with three blank mounts between each and assemble into 3-D physical model of the seismic changes within the LF sand caused by drainage from production from 1985 to 1988. Green is bypassed pay indicated by no change in high amplitudes, with yellow the most prospective, whereas the blue is waterfront advance that produced a dimout from production and the migration updip from the northeast of the oil/water contact. Red is amplitude increase caused by gas/oil ratio increase with production.

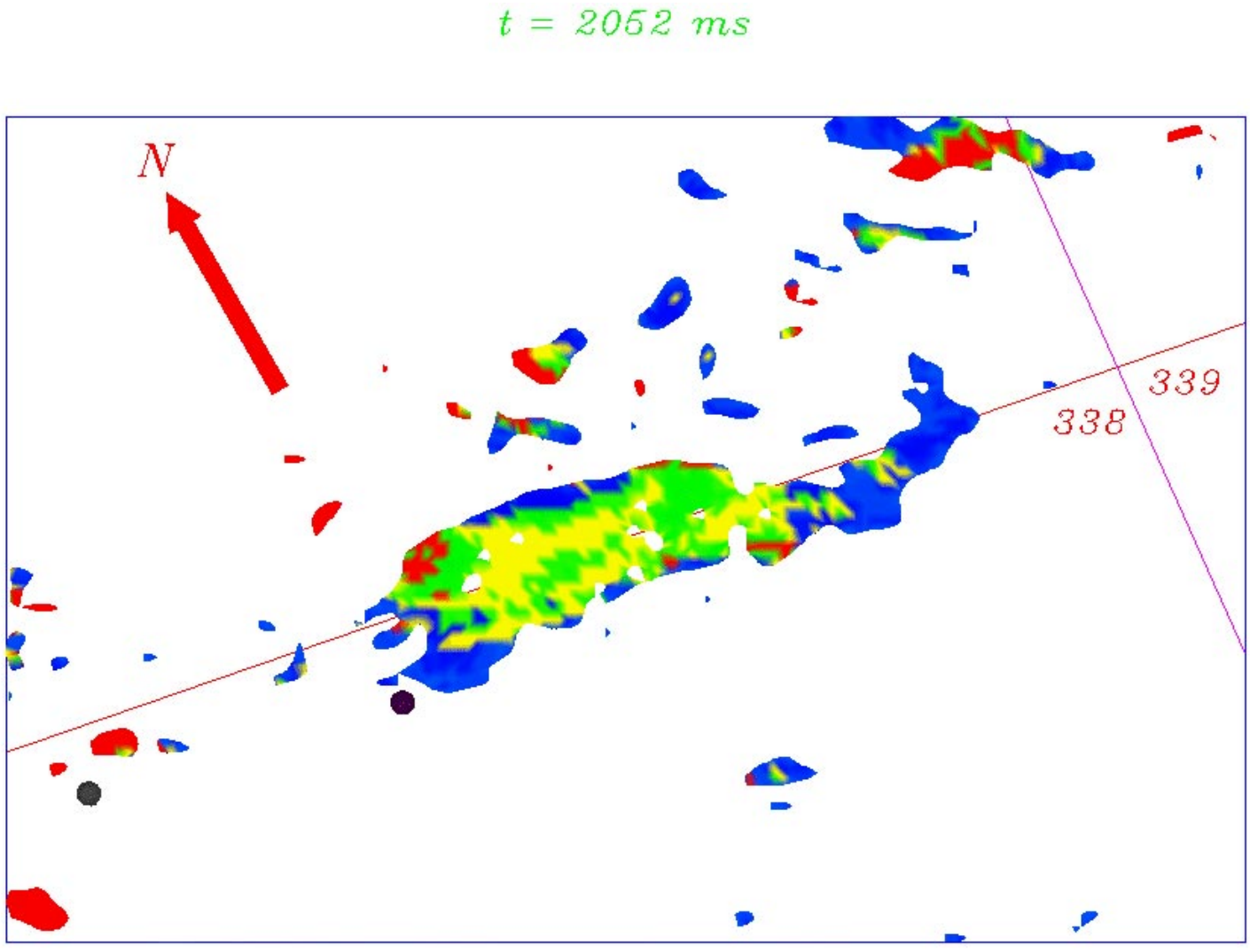

Figure I.ii.12 (continued): Print onto transparency plastic each of the 11 time slices through the LF reservoir contained in this figure. Then tape onto transparency mounts, space with three blank mounts between each and assemble into 3-D physical model of the seismic changes within the LF sand caused by drainage from production from 1985 to 1988. Green is bypassed pay indicated by no change in high amplitudes, with yellow the most prospective, whereas the blue is waterfront advance that produced a dimout from production and the migration updip from the northeast of the oil/water contact. Red is amplitude increase caused by gas/oil ratio increase with production.

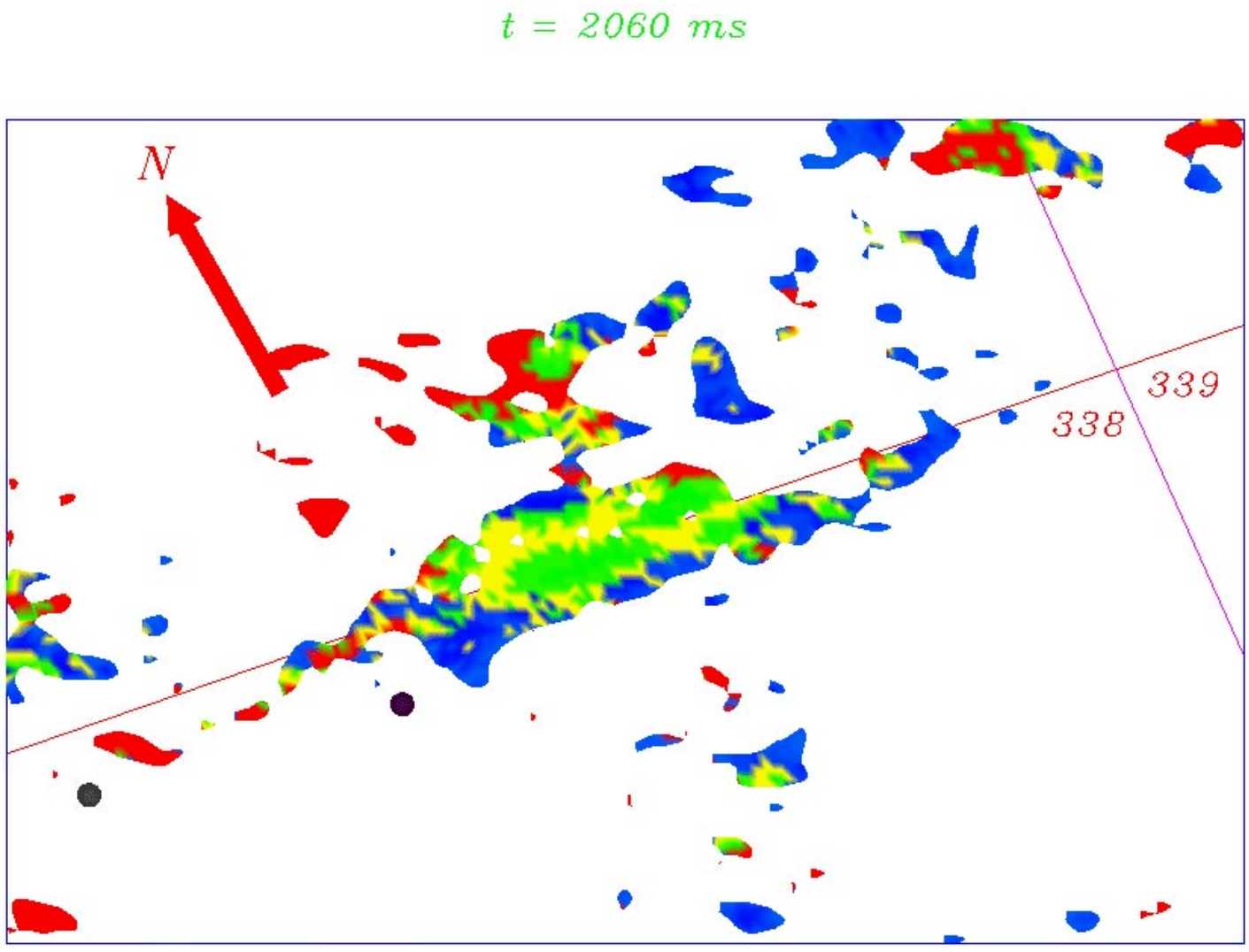

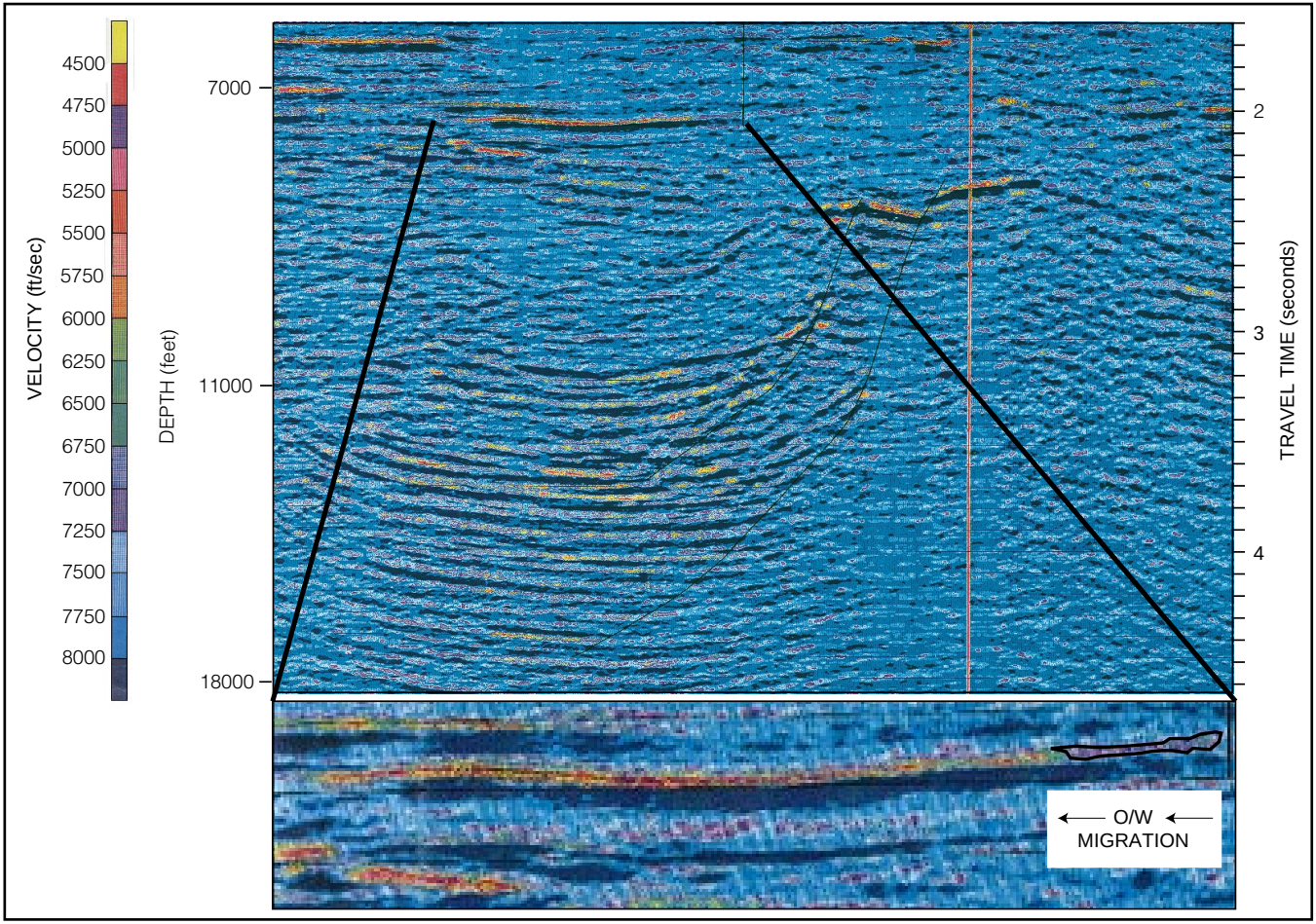

Figure I.ii.13: Seismic velocity inversion performed by Texaco along the seismic profile running along the EI 330/338 boundary, with the LF sand blown up (below). Increases in velocity are recorded in the easternmost part of the reservoir, perhaps from the movement of the oil/water contact as suggested by the 4-D seismic analysis.s.

Figure I.ii.14.a: The amplitudes extracted from a traditional "ZAP" of the trough that makes up the LF reflector from the Pennzoil (1985) survey (the yellow horizon in Figure I.ii.7, right). Hot colors are high amplitudes.

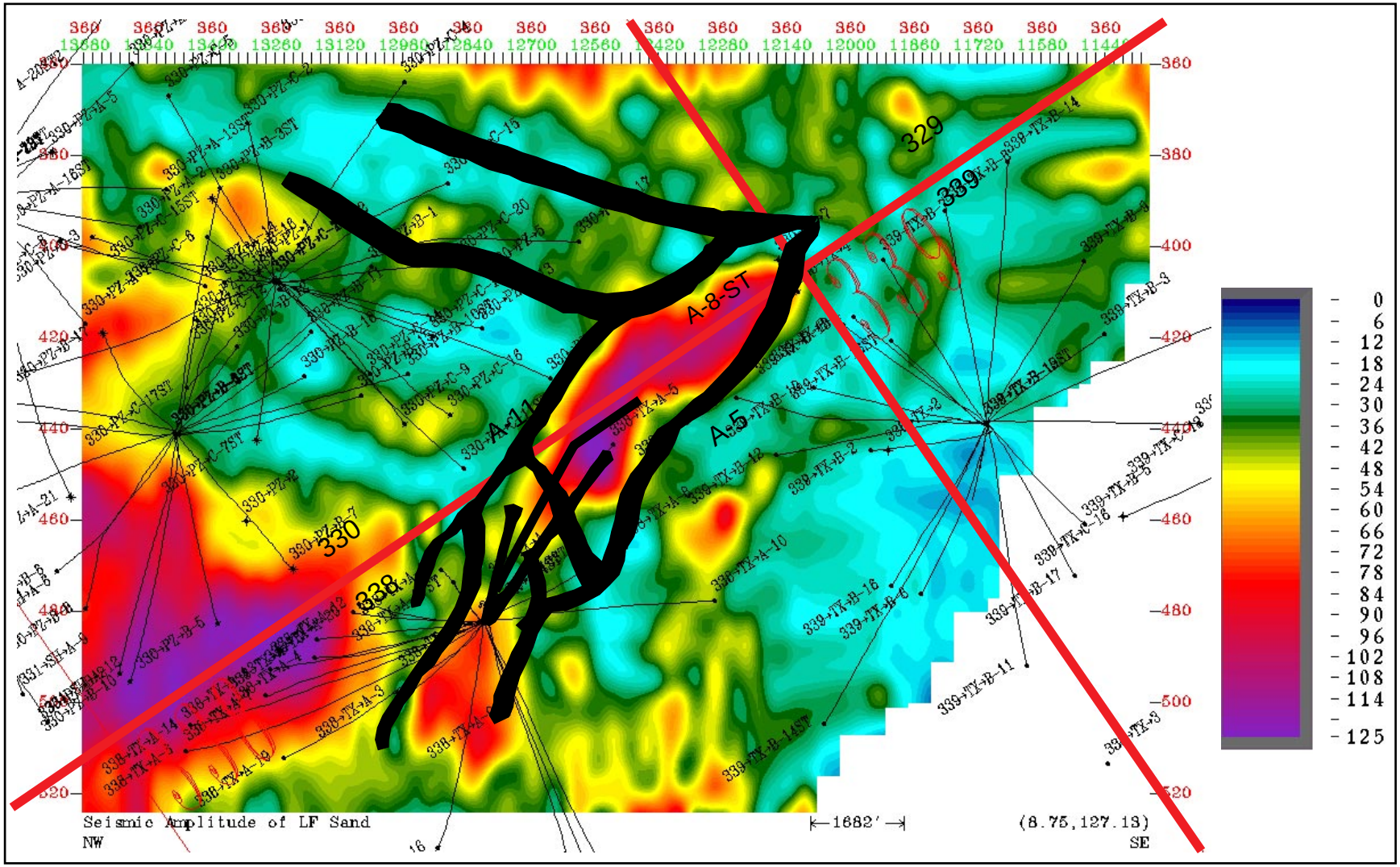

Figure I.ii.14.b: The amplitude extracted from a traditional "ZAP" of the trough that makes up the LF reflector from the Texaco (1988) survey (the yellow horizon in Figure I.ii.7, left). Note the dimout in the northeastern corner, thought to be caused by the oil/water contact movement.

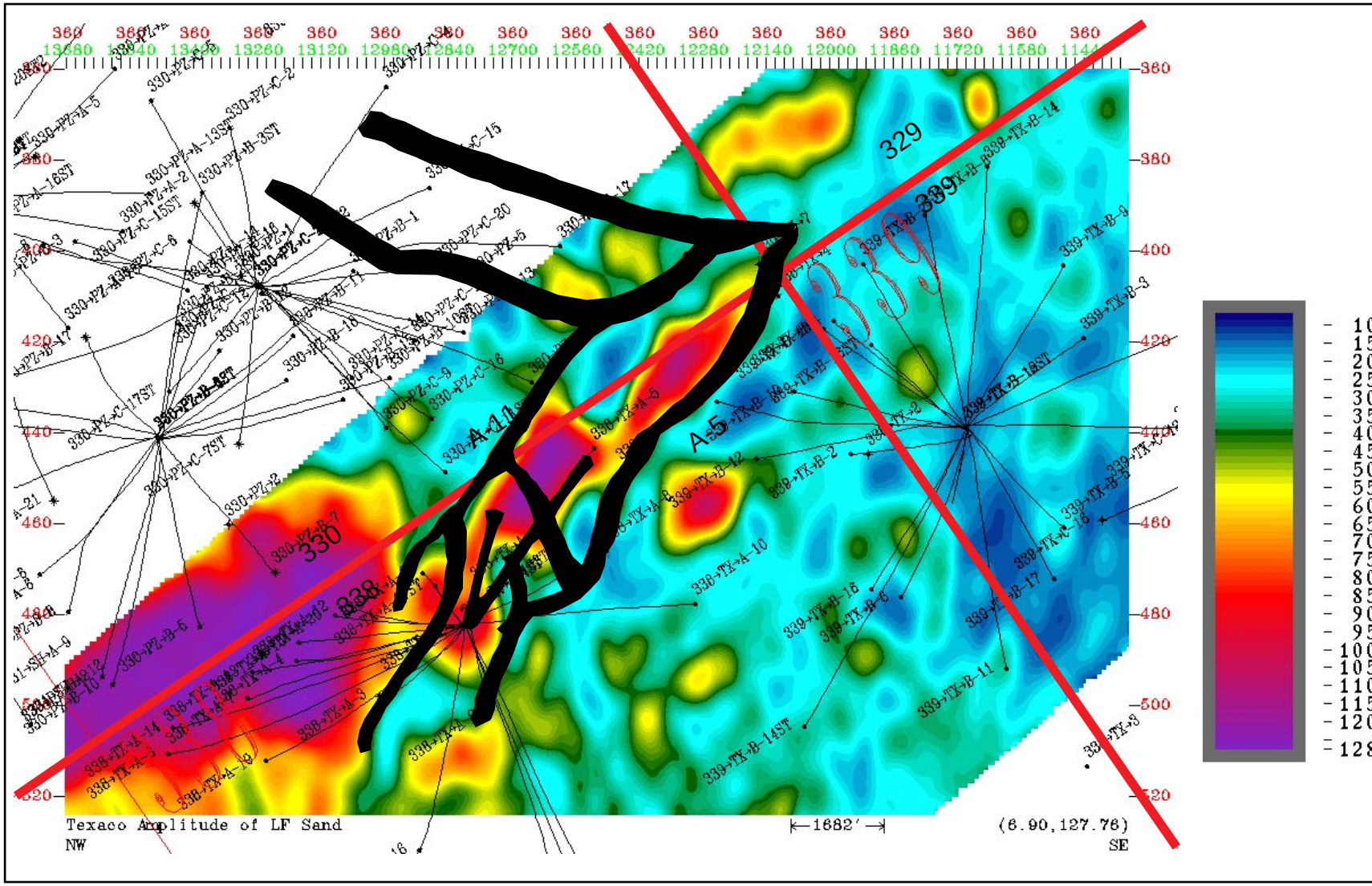

Figure I.ii.14.c: The differences between the LF seismic troughs from 1985 to 1988 (hot colors are decreased, dimmed-out amplitudes). Note the boundary between the western and eastern fault blocks is discernible as the A Fault of Figure I.ii.3.

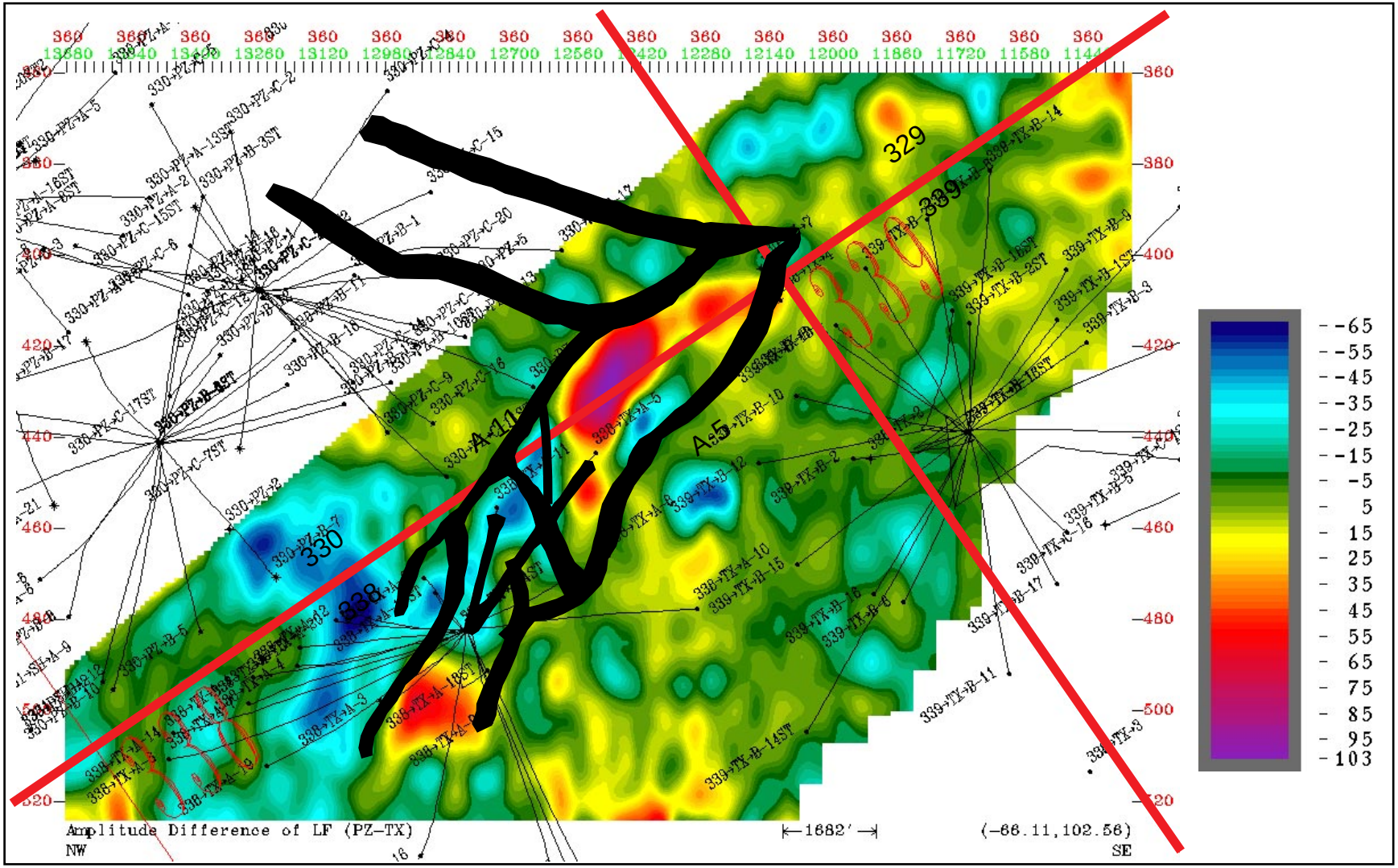

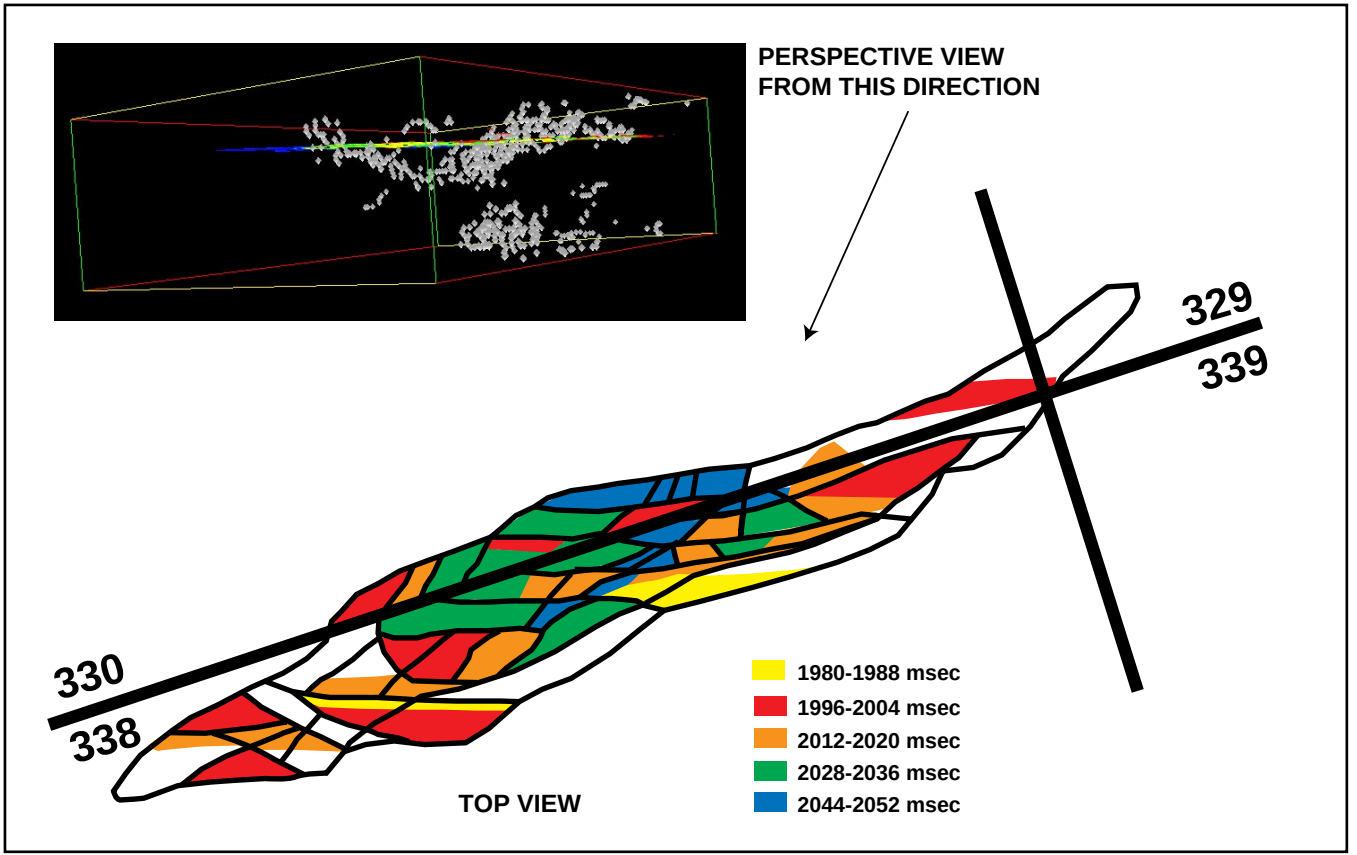

Figure I.ii.15: Permeability pattern in LF sand from connecting high-amplitude voxels, with no change between the 1985 and 1988 surveys (bypassed pay – the yellow region of Figure I.ii.12).

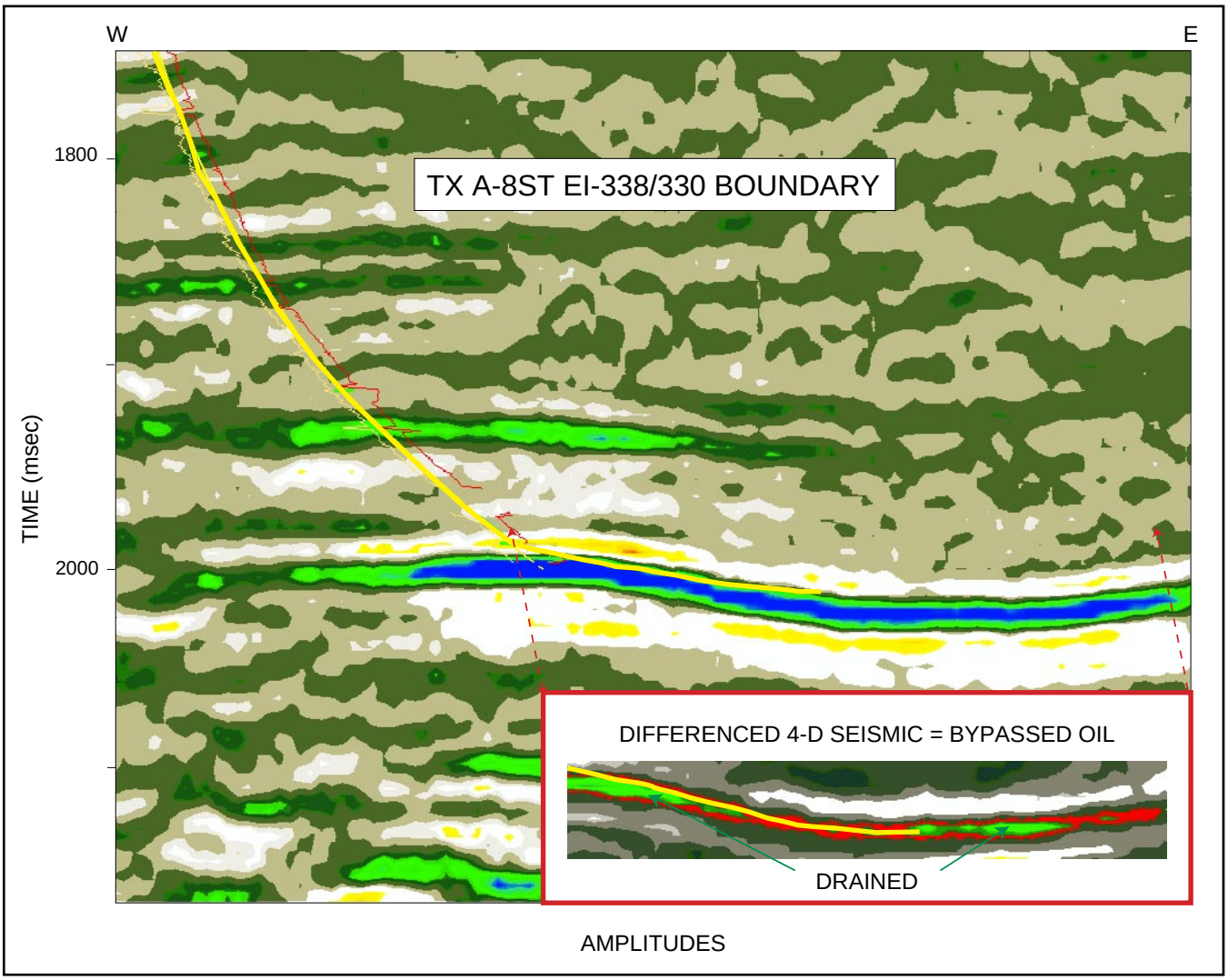

Figure I.ii.16: W-E seismic profile through the property boundary of EI 330/338 showing LF sand reservoir, and a blowup of the similarities and differences between seismic amplitudes from 1985 to 1988 (similar = red, dimmed out = green). The A-8ST horizontal well targeted bypassed pay, indicated by the red.

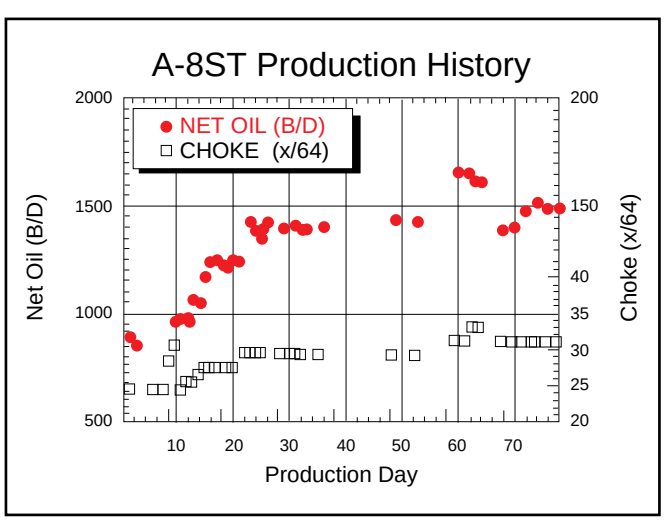

Figure I.ii.17: The production history of the A-8ST horizontal well.

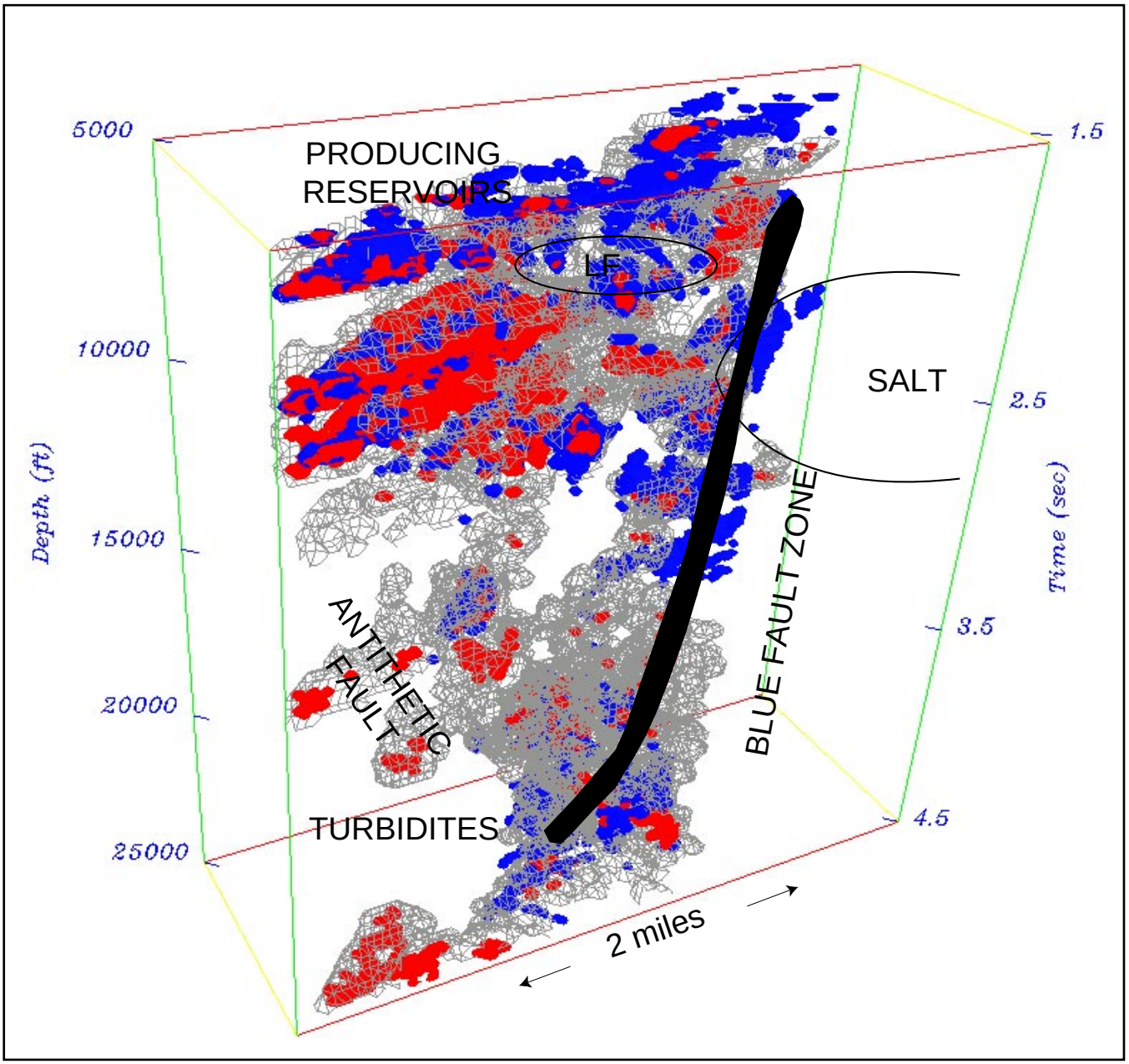

Figure I.ii.18: The gray mesh is the connectivity between the deep turbidites and the LF and shallower reservoirs, indicated by high-amplitude region tracking. Red = Texaco (1988) survey, Blue = Pennzoil (1985) survey.

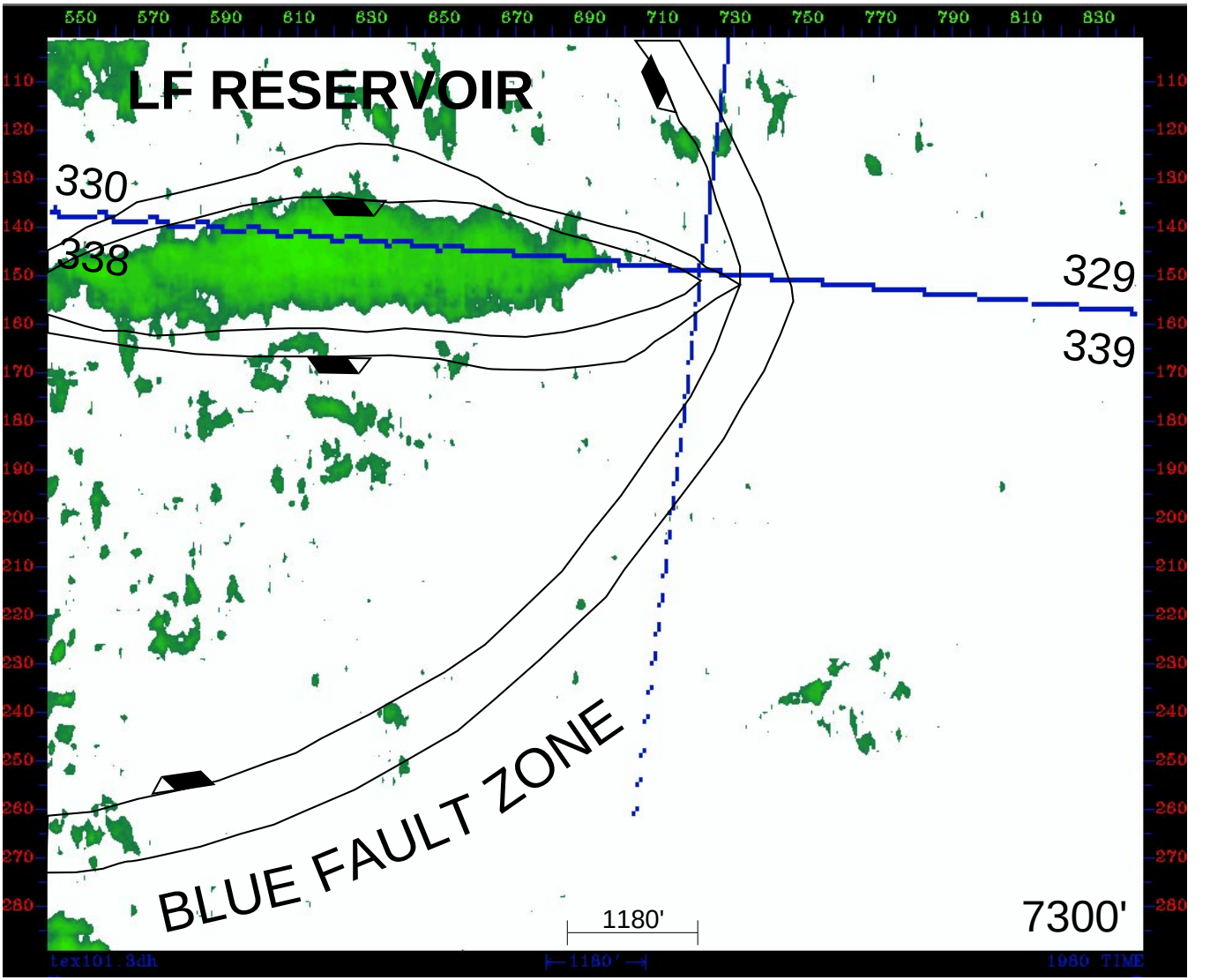

Figure I.ii.19.a: The connectivity in seismic amplitudes indicated by the white mesh in the previous figure can be illustrated by time slices through the seismic volume at 15,000', 8000' and 7300', with high amplitudes indicated in green. Note that the amplitude trail switches from the Blue Fault Zone at depth to the antithetic fault at 8000', which delivers the hydrocarbons to the LF and shallower reservoirs.

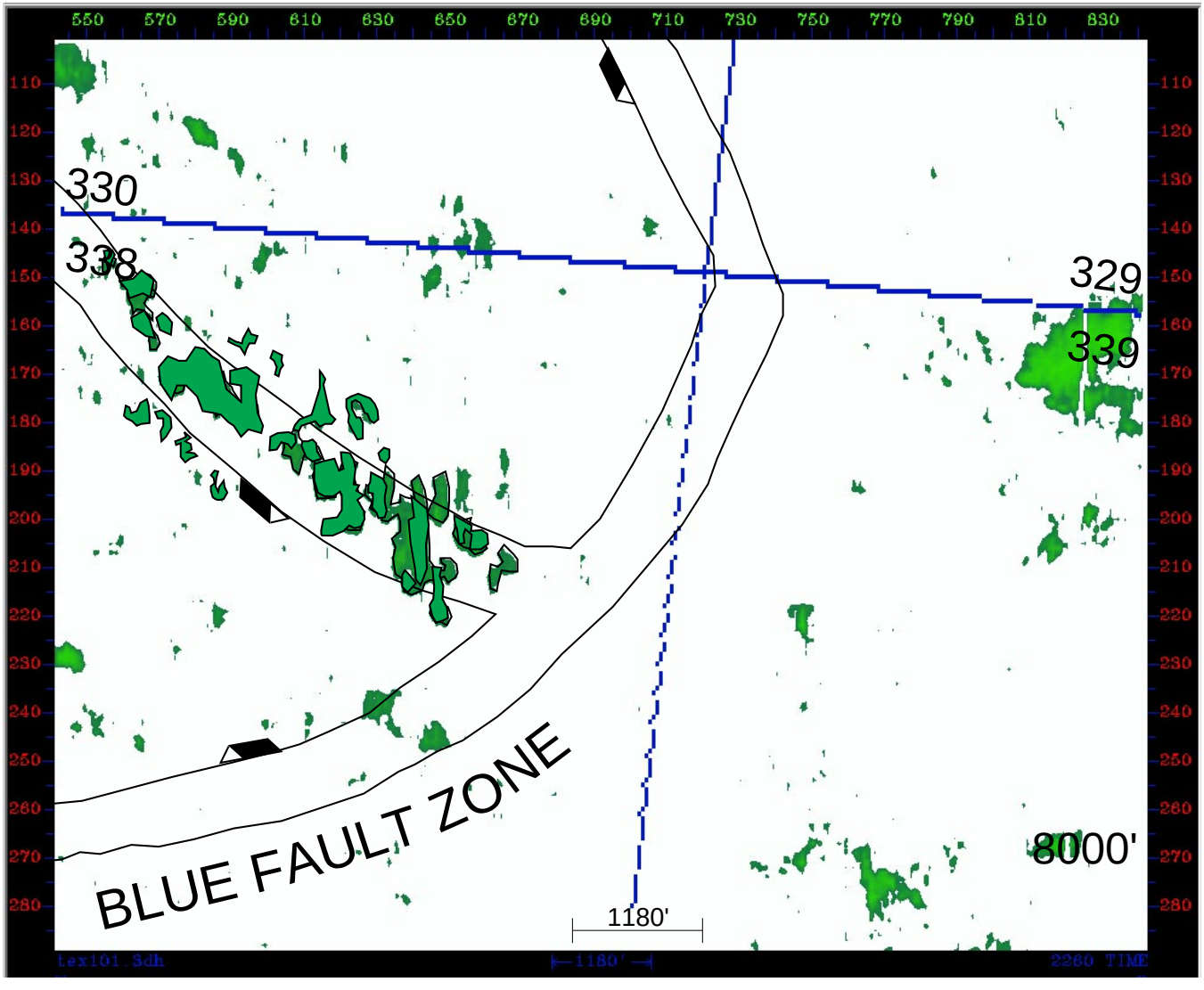

Figure I.ii.19.b (continued): The connectivity in seismic amplitudes indicated by the white mesh in the previous figure can be illustrated by time slices through the seismic volume at 15,000', 8000' and 7300', with high amplitudes indicated in green. Note that the amplitude trail switches from the Blue antithetic fault at depth to the antithetic fault at 8000', which delivers the hydrocarbons to the LF and shallower reservoirs.

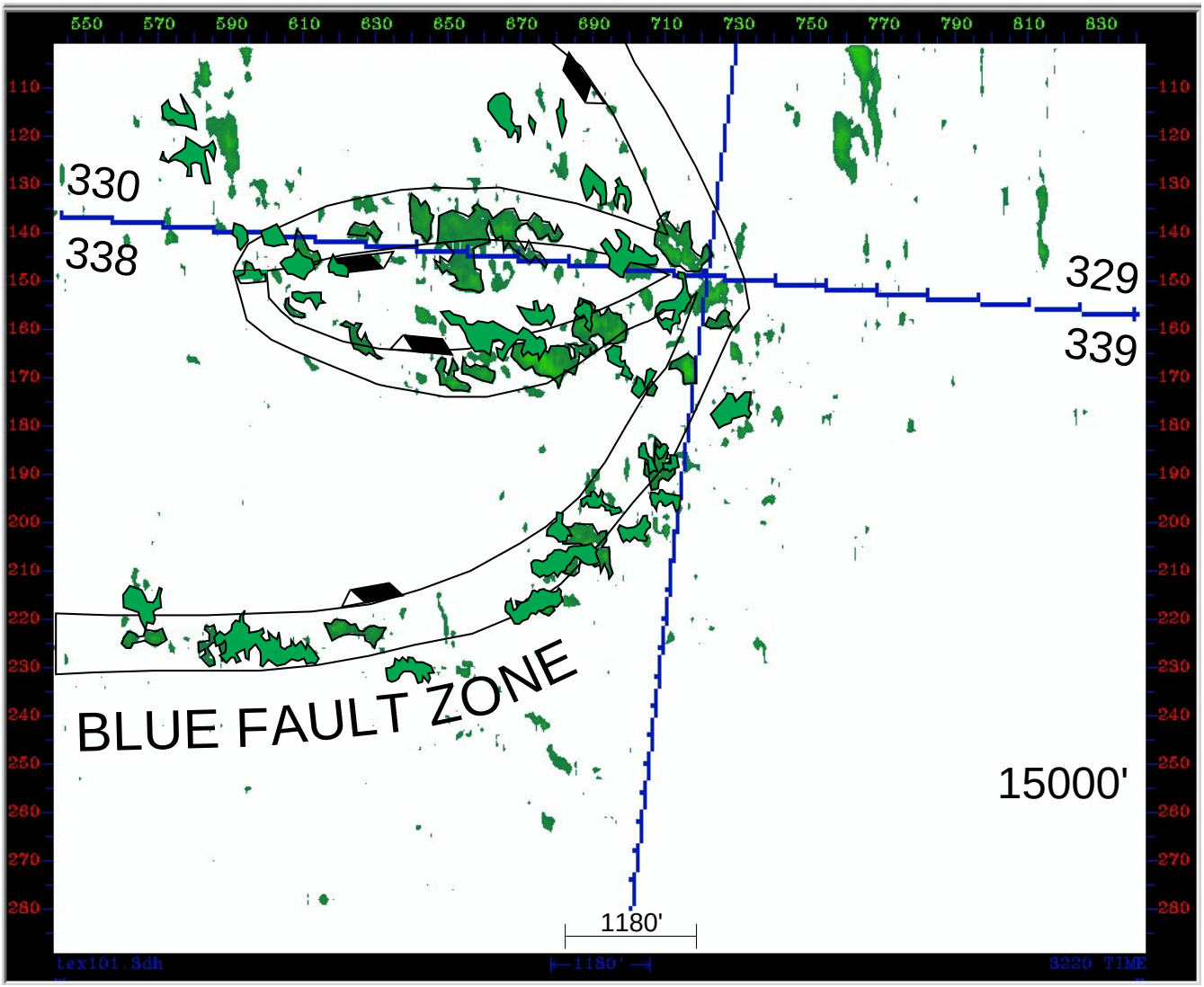

Figure I.ii.19.c (continued): The connectivity in seismic amplitudes indicated by the white mesh in the previous figure can be illustrated by time slices through the seismic volume at 15,000', 8000' and 7300', with high amplitudes indicated in green. Note that the amplitude trail switches from the Blue antithetic fault at depth to the antithetic fault at 8000', which delivers the hydrocarbons to the LF and shallower reservoirs.

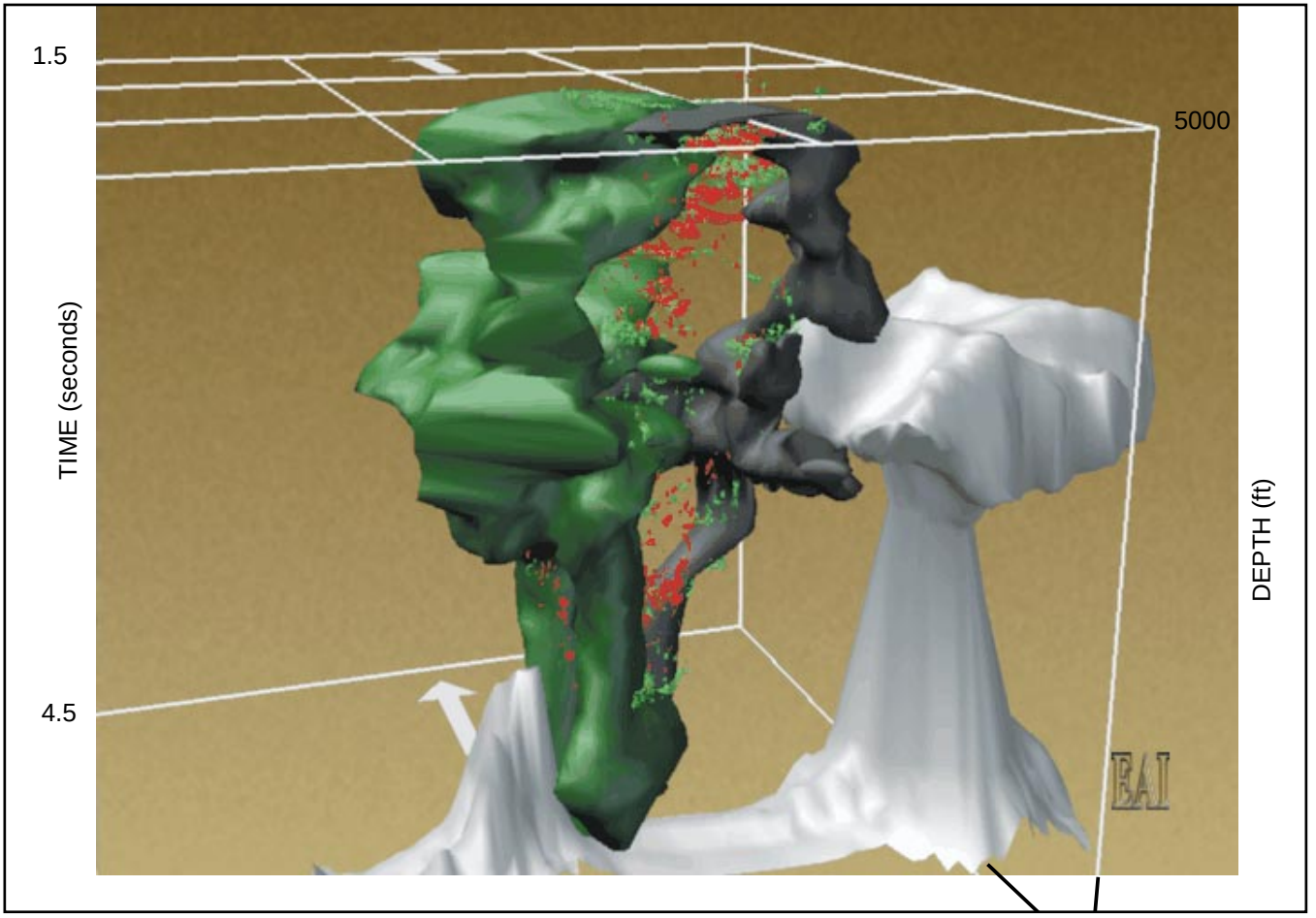

Figure I.ii.20: The migration pathway in 3-D as indicated by connectivity of seismic amplitudes. The large green and charcoal or dark gray columns are the two separate migration pathways that are discernible in the seismic data indicated by red (1988 Texaco) and green (1985 Pennzoil) surveys. White is salt.

Variations Caused by Dilatancy," *Ph.D. Dissertation*, Columbia University (1994).

Teng, Y.C. "Scattering of Transient Waves by Finite Cracks in an Anti-plane Strain Elastic Solid," *Journal of Computational Acoustics*, Vol. 1, No. 1, pp. 101-116 (1993).

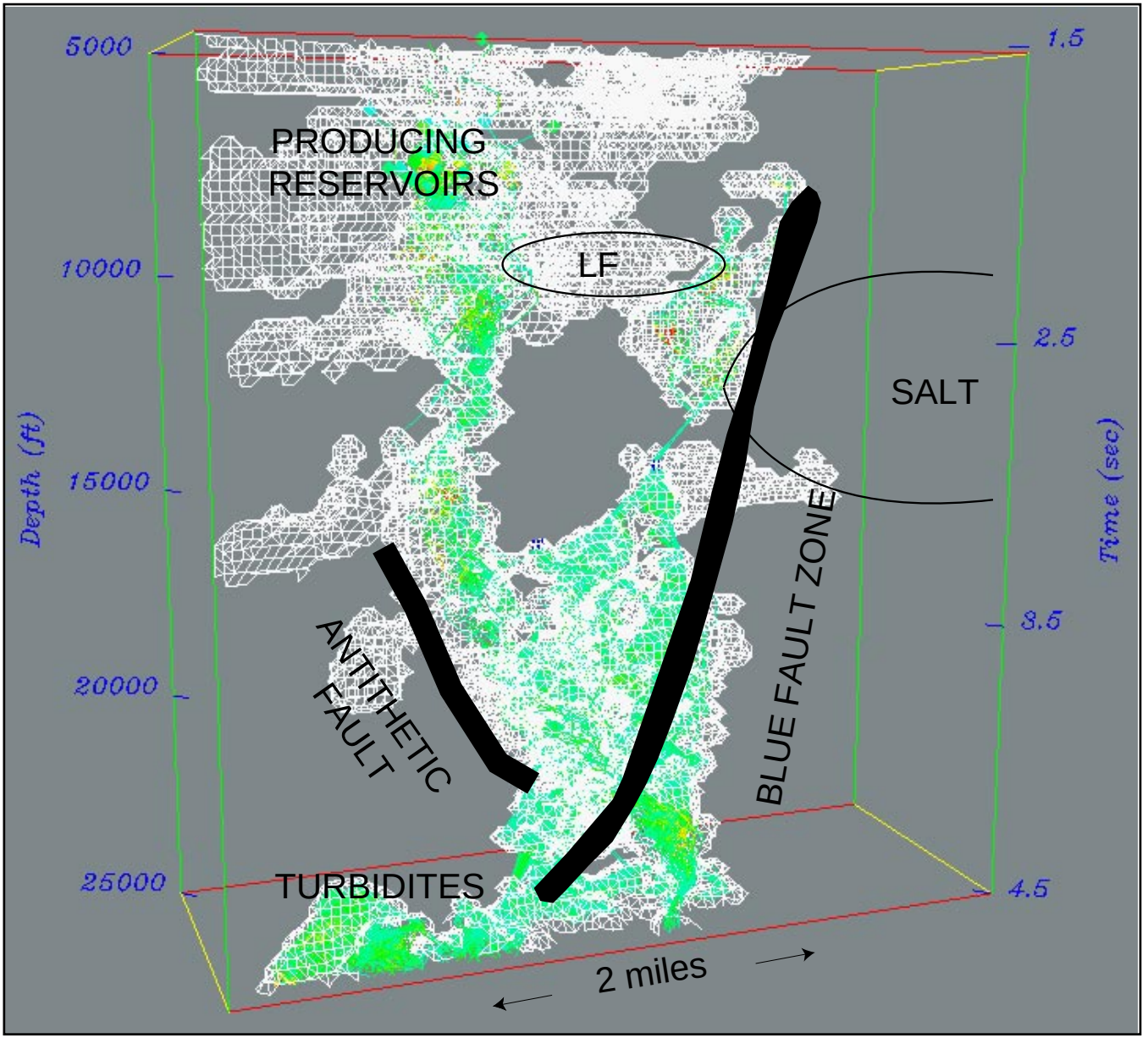

Figure I.ii.21: Buoyant balls convey the migration pathway through the high-amplitude, interconnected pathways identified within the seismic surveys.

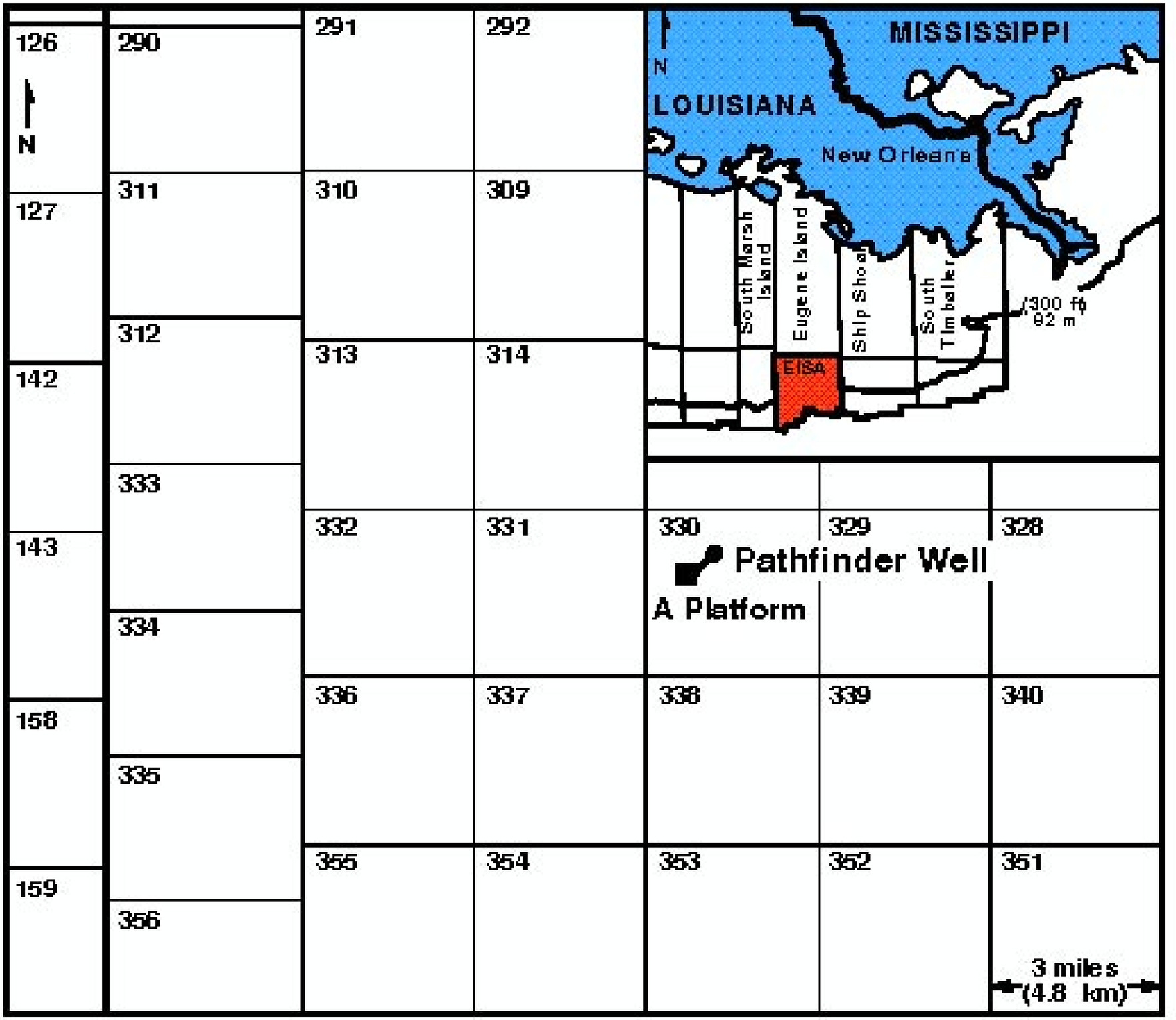

Figure I.iii.1: Basemap showing Eugene Island South Addition and location of the 330-A platform.

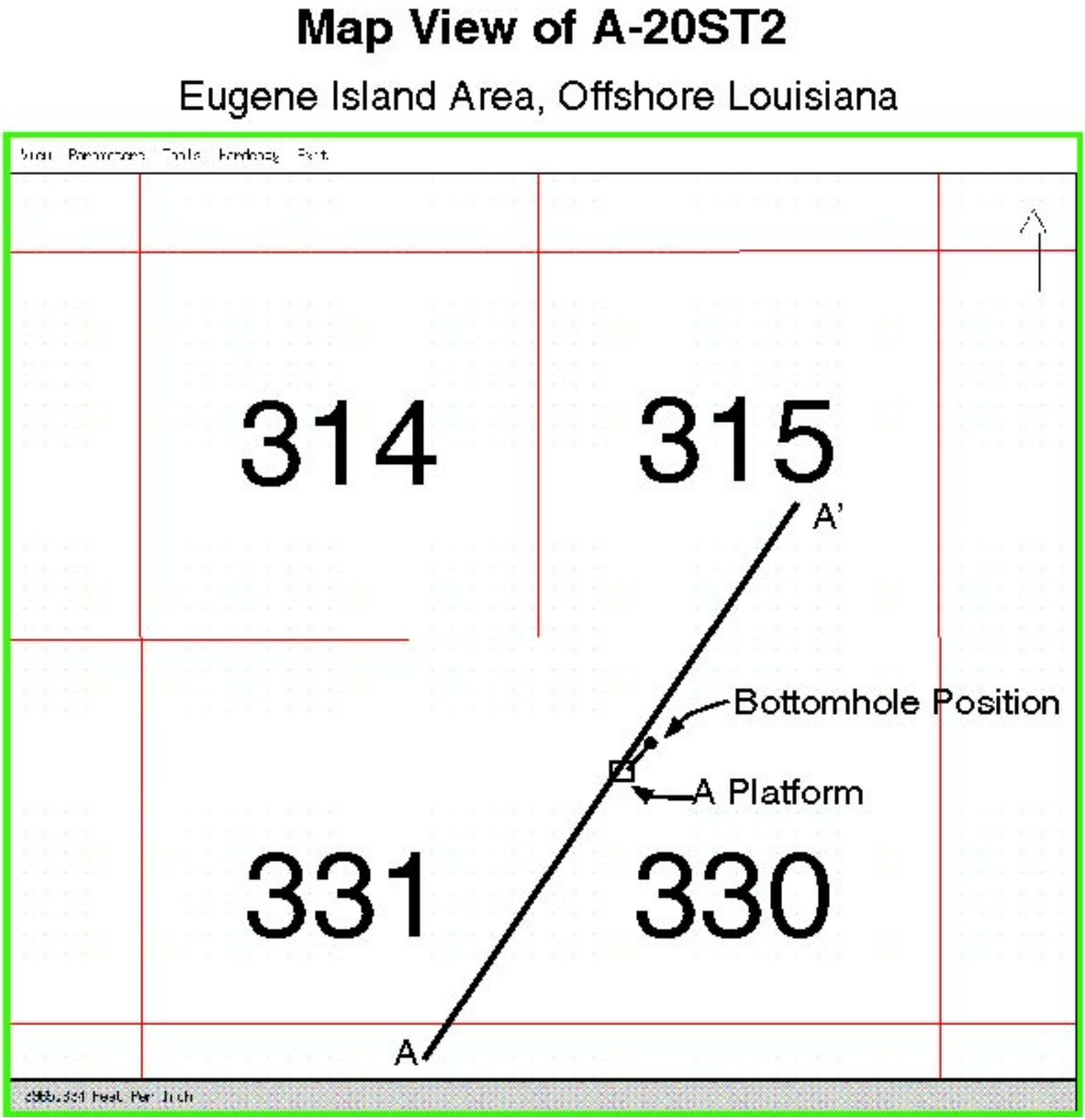

Figure I.iii.2: Expanded view of basemap, showing Pathfinder borehole path and the location of seismic line A-A'.

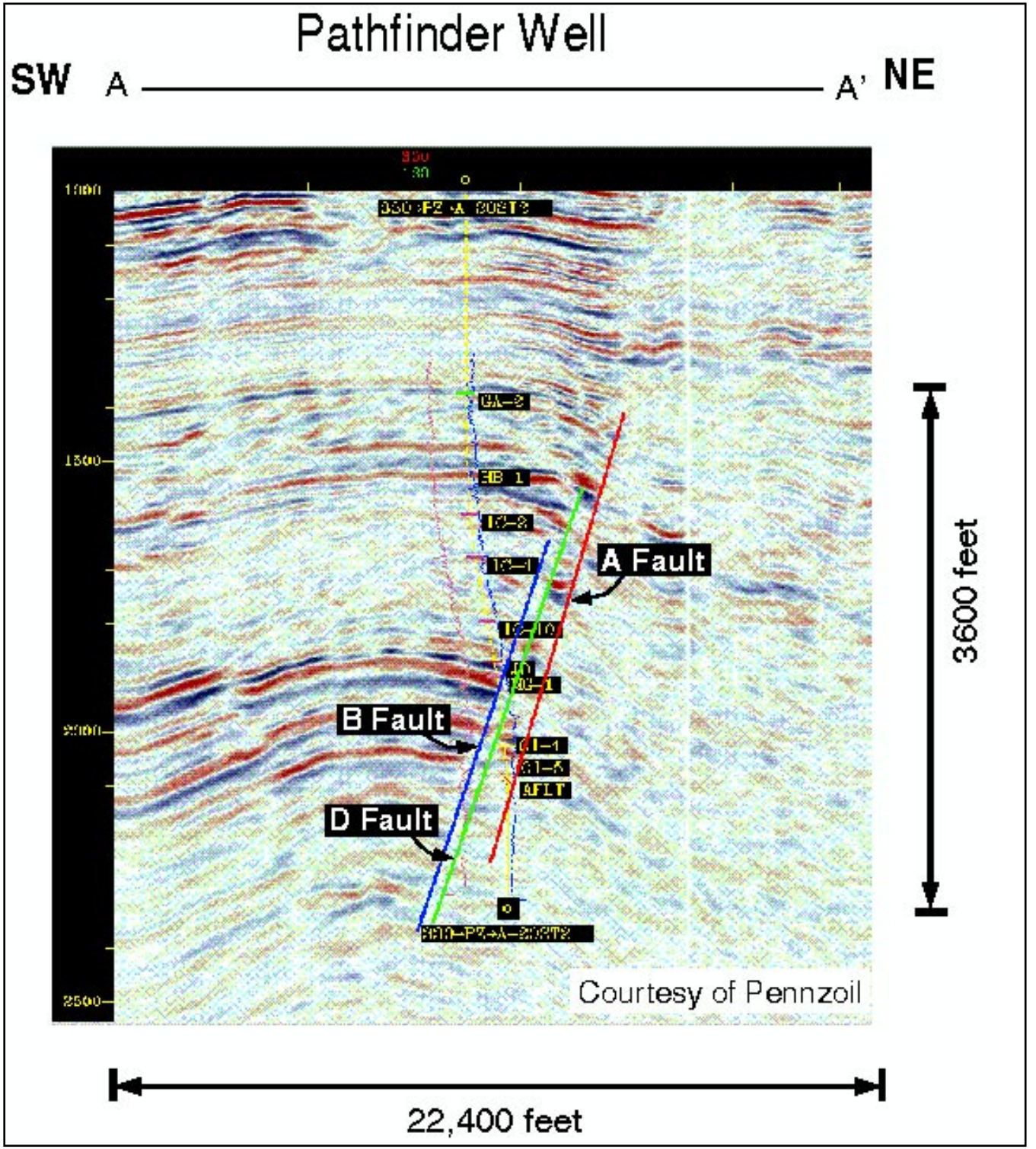

Figure I.iii.3: Seismic dipline (A-A') with Pathfinder well path, showing locations of interpreted sand tops and faults.

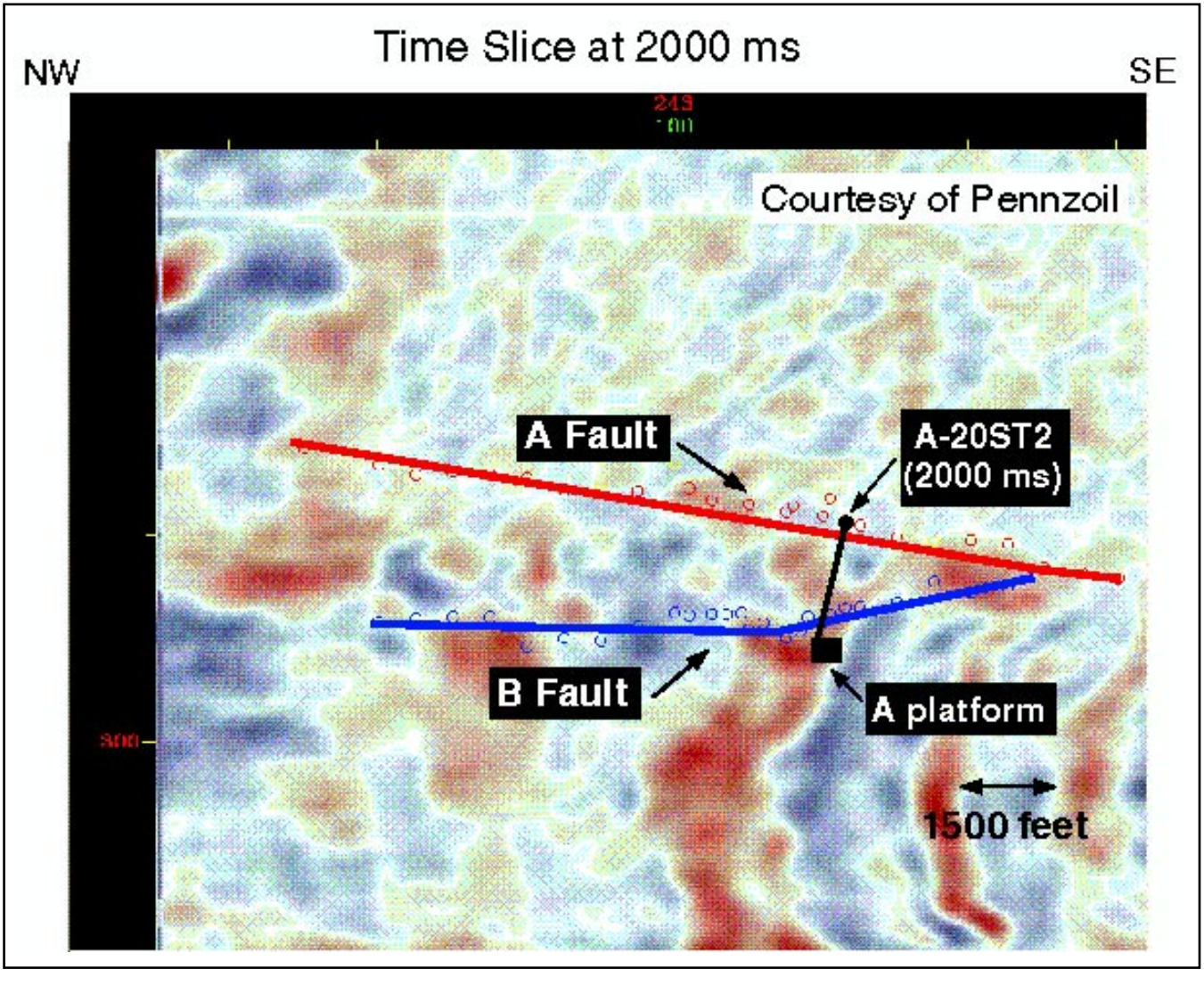

Figure I.iii.4: Seismic time slice taken at 2000 ms showing 330-A platform, Pathfinder well path and interpreted faults.

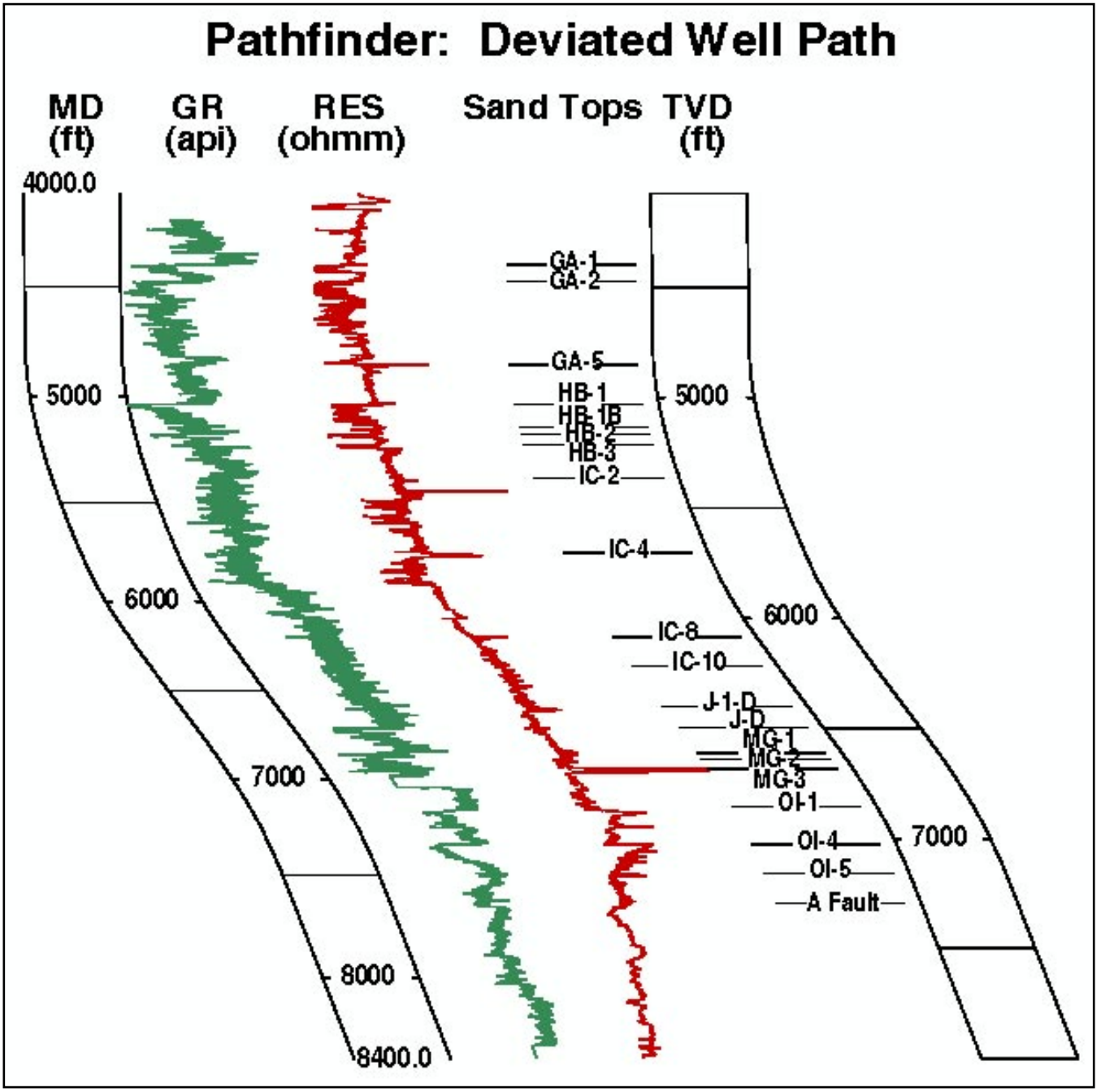

Figure I.iii.5: Deviated well display showing gamma ray, resistivity and sand tops. Reference is True Vertical Depth.

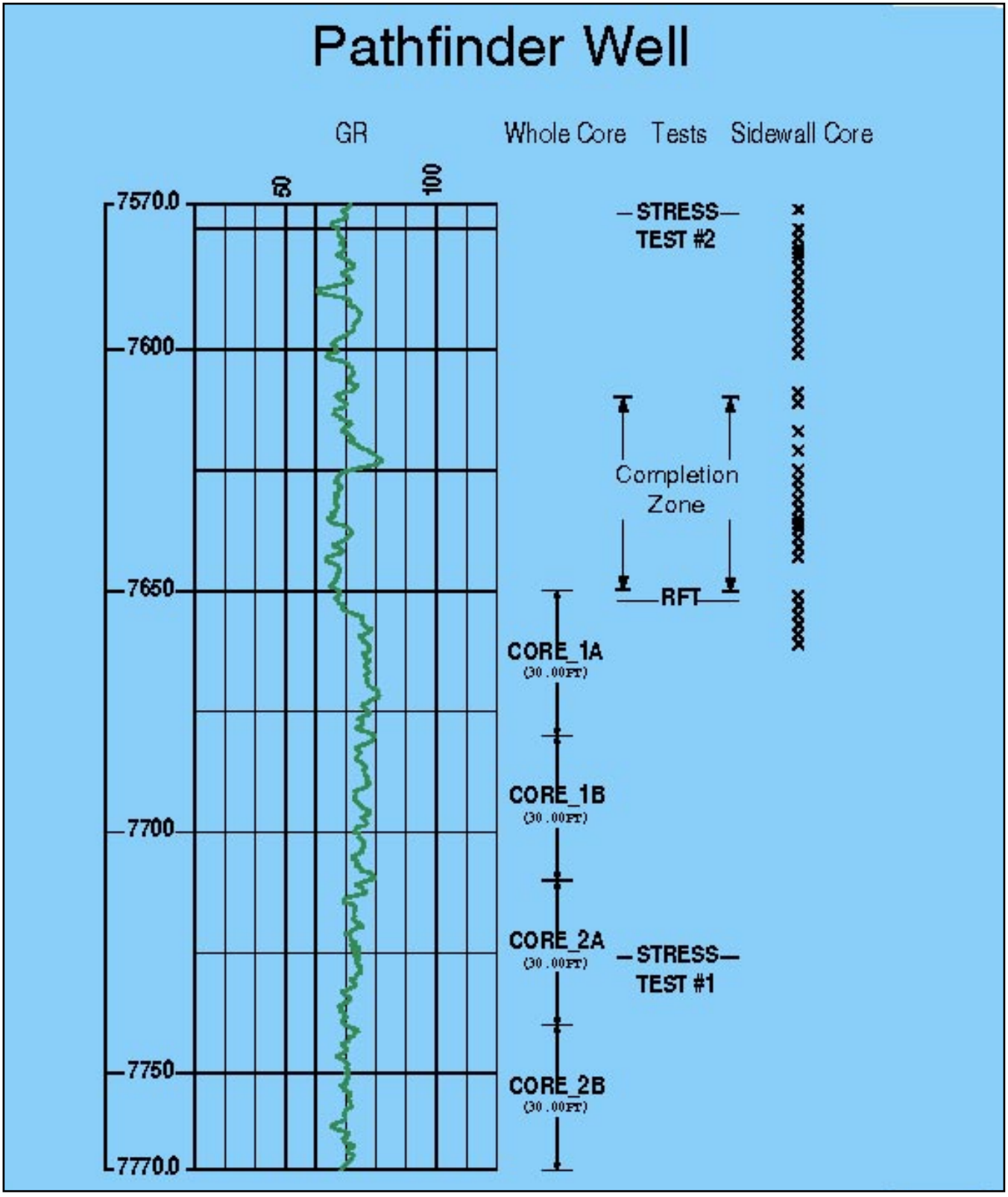

Figure I.iii.6: Type well expanded view of the fault zone showing experiment locations.

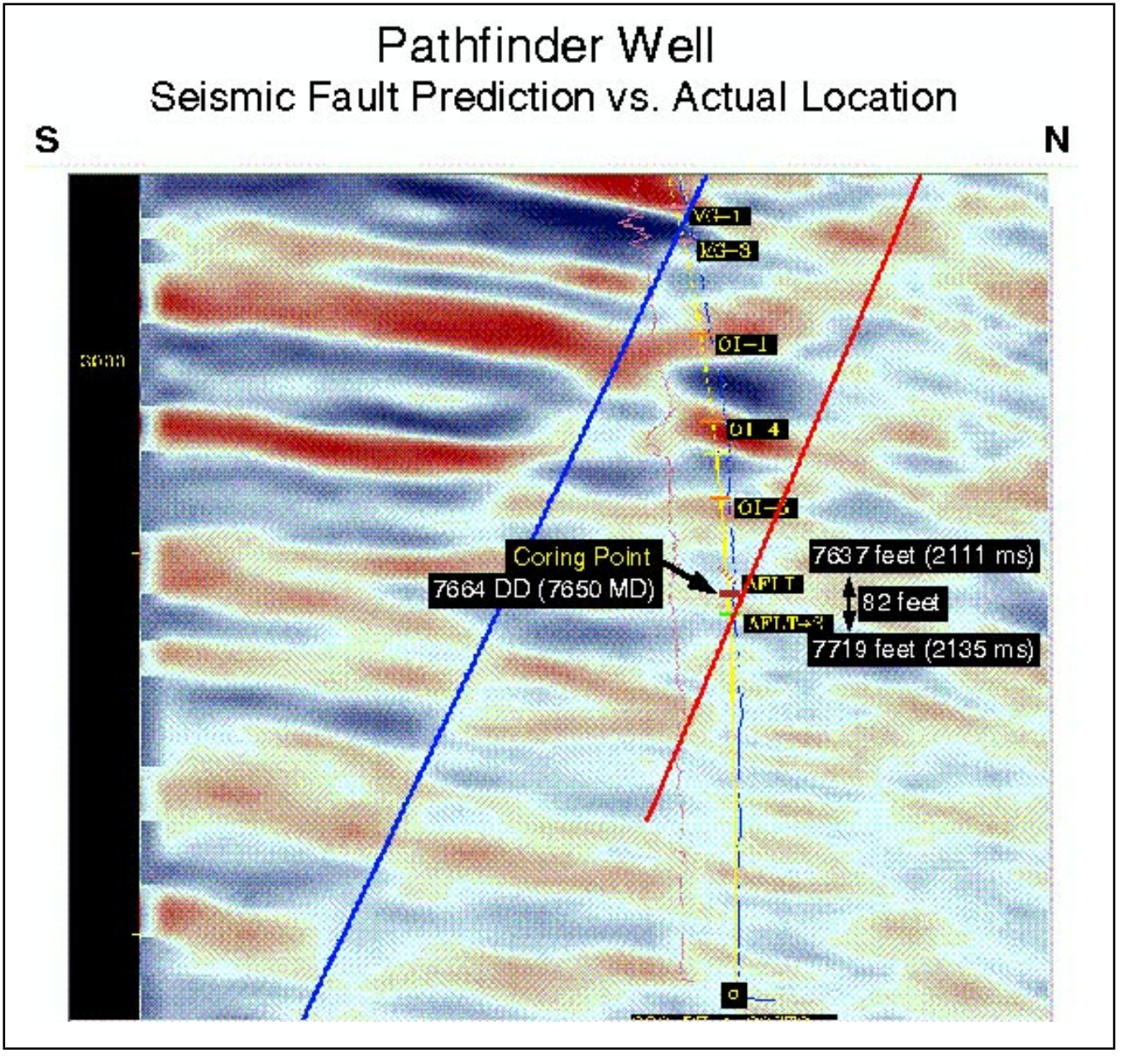

Figure I.iii.7: Expanded view of the seismic dipline showing the A Fault as it was interpreted on the seismic profile and where it was actually encountered.

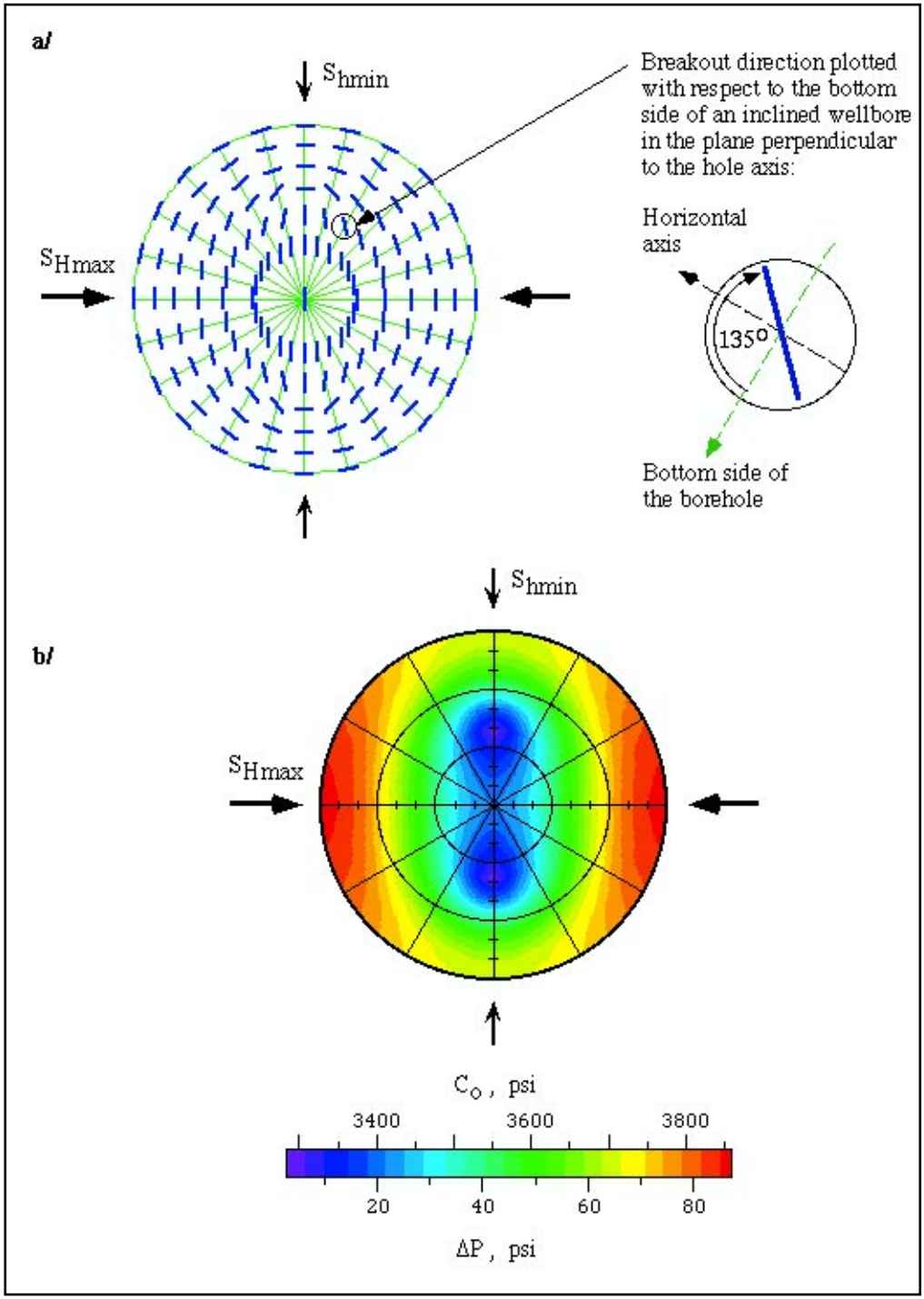

Figure IV.ii.1: Illustration of breakout directions (a) and tendency for failure (b) in boreholes of arbitrary orientations with respect to the horizontal principal stresses. The tendency for failure is expressed as a function of effective rock strength, C_0, or differential borehole fluid pressure, ΔP, necessary to prevent borehole failure. In this illustration, the coefficient of internal friction, μ_i, was assumed to be 1.0 and the magnitudes of in-situ stress and pore pressure are S_v=6528 psi, S_{hmin}=6226 psi, S_{Hmax}=6377 psi and P_p=4749 psi. The detailed illustration in the upper right indicates that breakout orientations are shown with respect to the bottom of the hole. In other words, the orientations of breakouts are shown as if the reader is looking "down the hole."

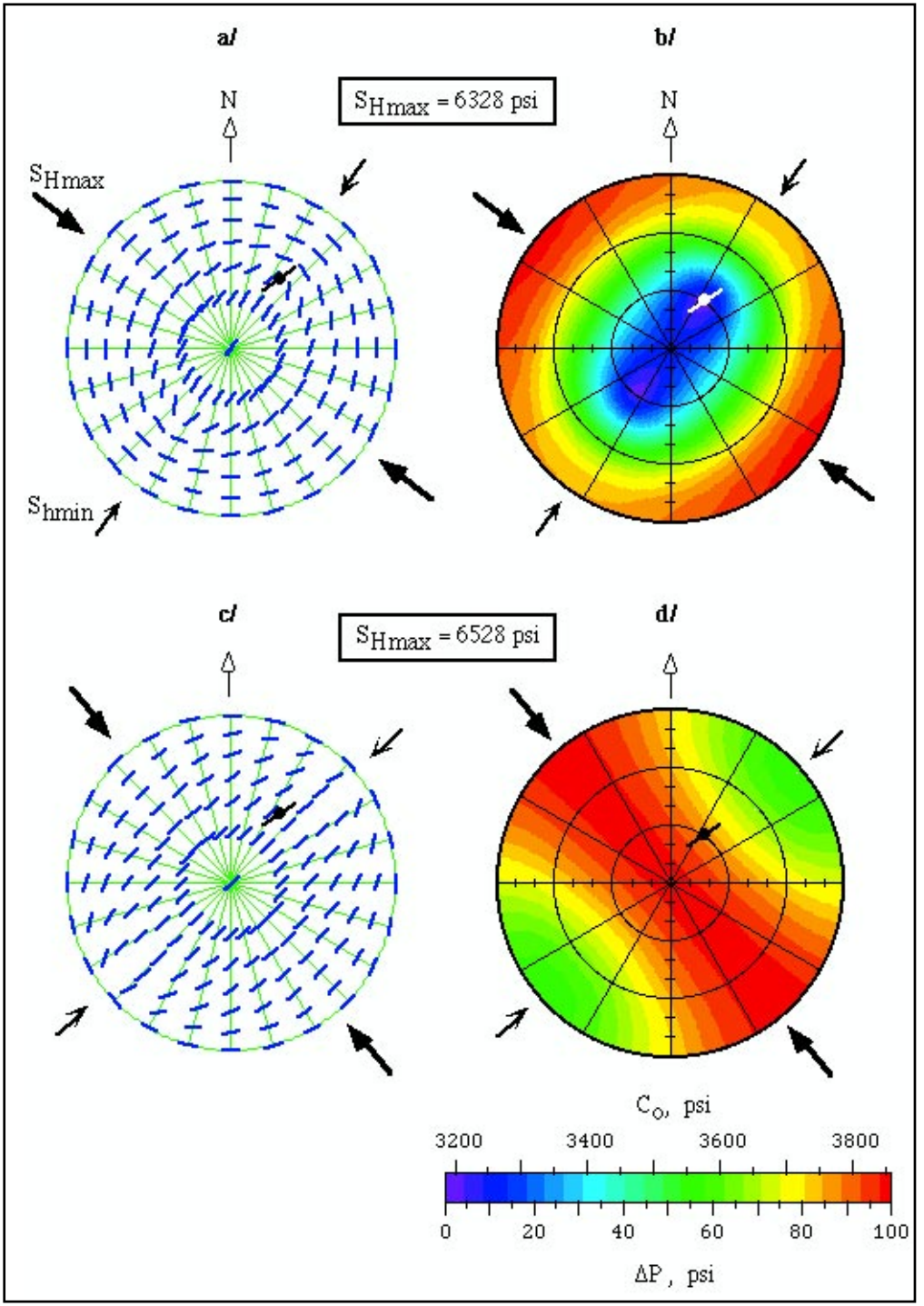

Figure IV.ii.2: Breakout orientations and the likelihood to occur in arbitrarily oriented wellbores for the orientation and upper-bound magnitude of S_{Hmax} of 6328 psi (a,b) and the orientation and lower-bound magnitude of 6528 psi (c,d). The other principal stresses and pore pressure are S_{hmin}=6226 psi, S_v=6528 psi and P_p=4749 psi. The tendency for failure is expressed in color either as a function of necessary uniaxial rock strength C_0 (for ΔP=0) or as a function of ΔP (for C_0=3180 psi) which is necessary to avoid borehole failure.

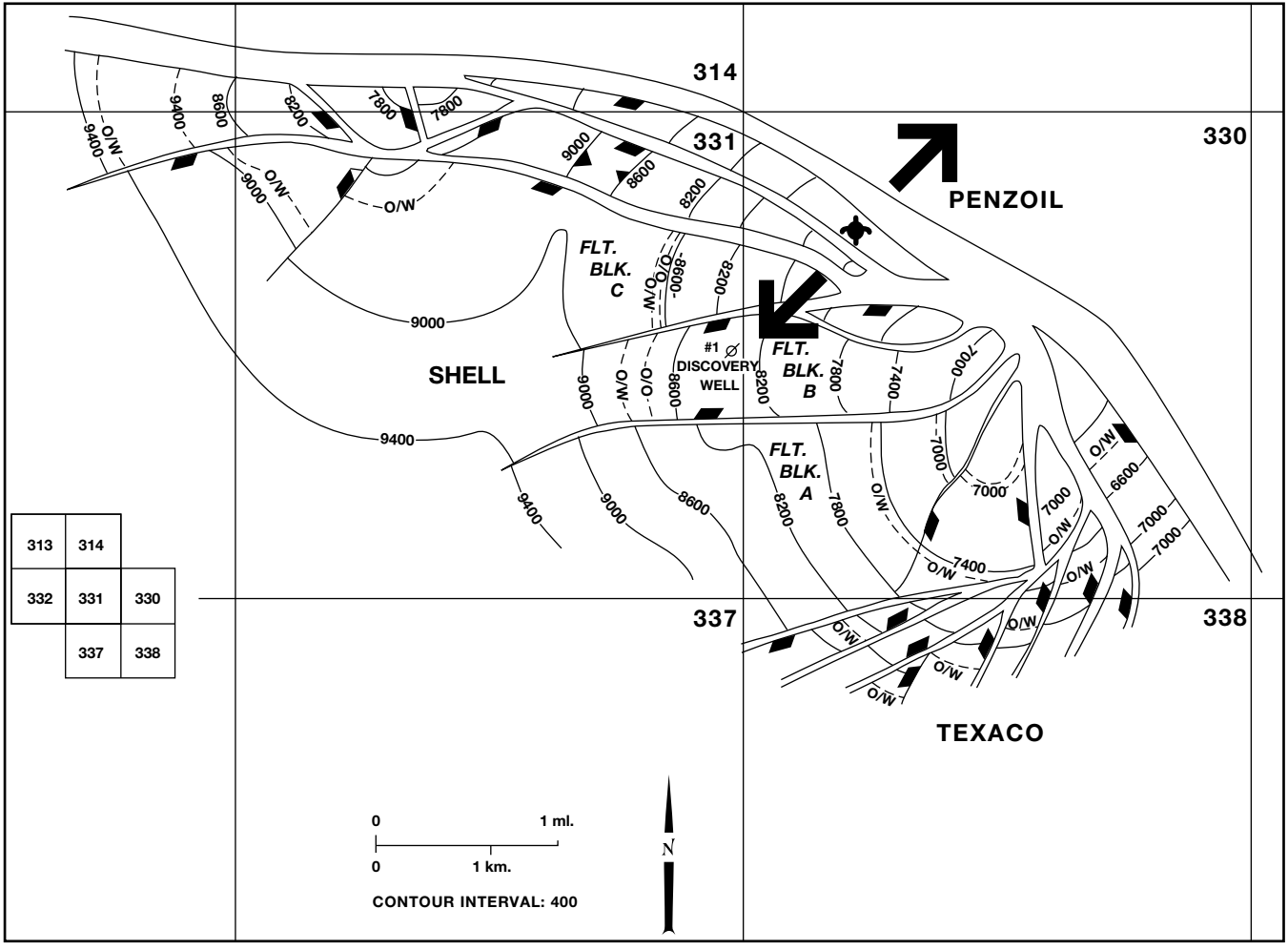

Figure IV.ii.3: Top OI sandstone structure map (after Holland et al.[32]) and direction of the least horizontal principal stress S_{hmin} obtained from the analysis of leak-off data and wellbore breakouts in the Pathfinder well.

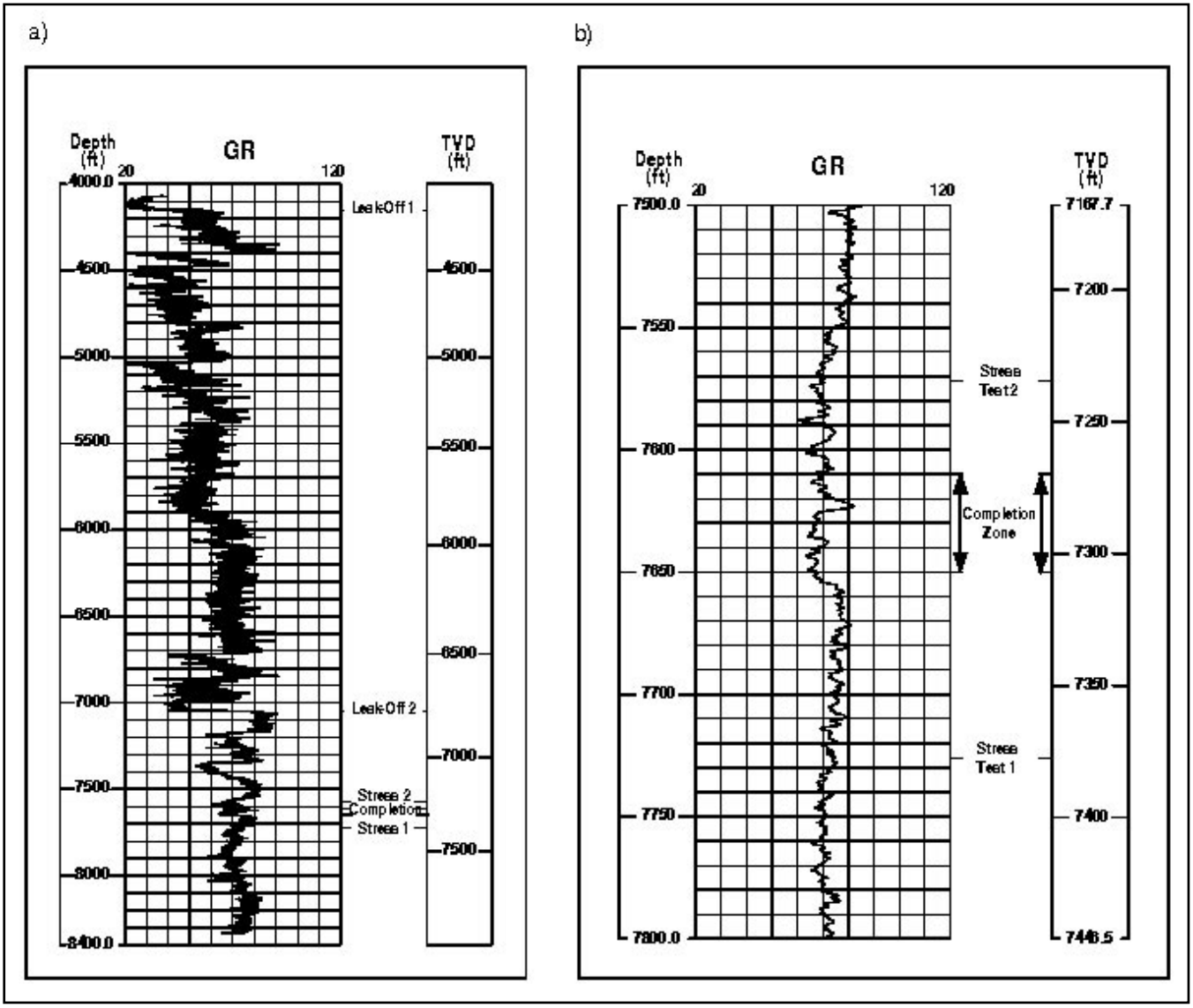

Figure IV.iii.1: Location of Pathfinder stress measurements. Measured depth in feet is on the left; true vertical depth (TVD) is on the right. Figure IV.iii.1.a: Entire interval. Figure IV.iii.1.b: Completion Zone interval.

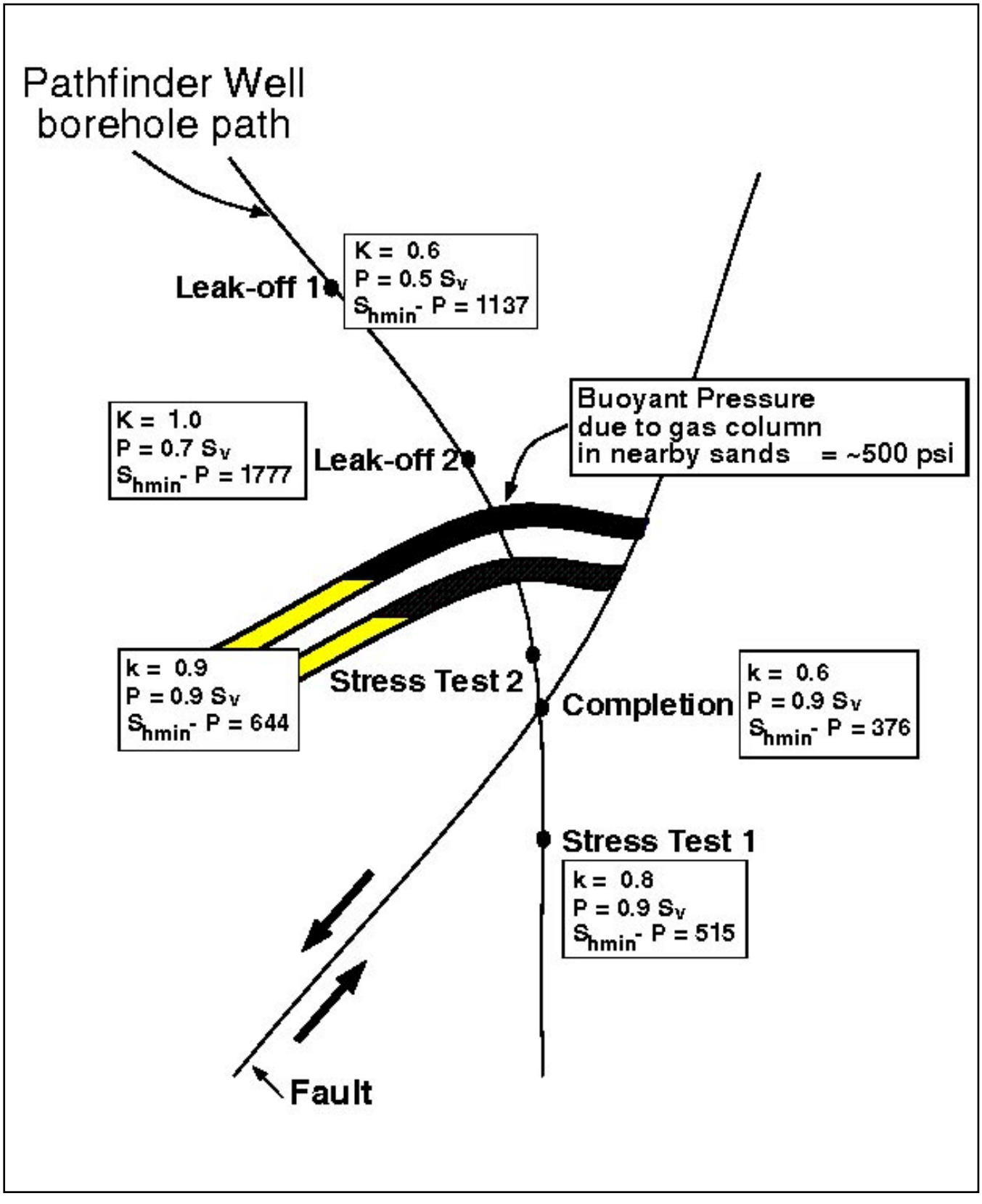

Figure IV.iii.19: Sketch of in-situ conditions in the Pathfinder well. K is the ratio of effective stresses (S_{hmin}-P/S_v-P); P is the formation pressure.

FOSSIL ENERGY

DOE/BC/14954-14
(DE96001265)

ADVANCED SECONDARY RECOVERY PROJECT FOR THE SOONER D SAND UNIT, WELD COUNTY, COLORADO

Final Report

By:
Diversified Operating Corporation

Date Published: November 1996

Work Performed Under Contract No. DE-FC22-93BC14954

Diversified Operating Corporation
Denver, Colorado

National Energy Technology Laboratory
National Petroleum Technology Office
U.S. DEPARTMENT OF ENERGY
Tulsa, Oklahoma

DISCLAIMER

This report was prepared as an account of work sponsored by an agency of the United States Government. Neither the United States Government nor any agency thereof, nor any of their employees, makes any warranty, expressed or implied, or assumes any legal liability or responsibility for the accuracy, completeness, or usefulness of any information, apparatus, product, or process disclosed, or represents that its use would not infringe privately owned rights. Reference herein to any specific commercial product, process, or service by trade name, trademark, manufacturer, or otherwise does not necessarily constitute or imply its endorsement, recommendation, or favoring by the United States Government or any agency thereof. The views and opinions of authors expressed herein do not necessarily state or reflect those of the United States Government.

This report has been reproduced directly from the best available copy.

DOE/BC/14954-14
Distribution Category UC-122

Advanced Secondary Recovery Project for the Sooner D Sand Unit
Weld County, Colorado

By
Diversified Operating Corporation
Principal Investigator: Mark A. Sippel
Project Manager: Terry J. Cammon

June 1996

Work Performed Under DE-FC22-93BC14954

Prepared for
U.S. Department of Energy
Assistant Secretary for Fossil Energy

Edith Allison, Project Manager
Bartlesville Project Office
P.O. Box 1398
Bartlesville, OK 74005

Prepared by
Diversified Operating Corporation
1675 Larimer St., Suite 400
Denver, CO 80202

ADVANCED SECONDARY RECOVERY PROJECT FOR THE SOONER `T" SAND UNIT, WELD COUNTY, COLORADO
COOPERATIVE AGREEMENT DE-FC22-93BC14954

Abstract

The objective of this project was to increase production at the Sooner D Sand Unit through geologically targeted infill drilling and improved reservoir management of waterfood operations. The Sooner D Sand Unit demonstration project should be an example for other operators to follow for reservoir characterization and exploitation methodologies to increase production by waterflood from the Cretaceous D Sandstone in the Denver-Julesburg (D=J) Basin. This project involved multi-disciplinary reservoir characterization using high-density 3D seismic, detailed stratigraphy and reservoir simulation studies. Tnfill drilling, water-injection conversion and re-completing some wells to add short-radius laterals were based on the results of the reservoir characterization studies. Production response were evaluated using reservoir simulation and production tests. Technology transfer utilized workshops, presentations and technical papers which emphasized the economic advantages of implementing the demonstrated technologies.

Table of Contents

Section Page

Disclaimer i
Abstract ii
Table of Contents
List of Figures iv
List of Tables v
Executive Summary vi
Introduction and Background I-1
History of the **Sooner "D"Sand Unit** .....)1 -1
Geology of the **Sooner "D" Sand Unit and** Adjacent Area III-1
Petrographical Analysis of the D **Sandstone** N-1
Core **and** Electrical Log Descriptions of the D **Sandstone** V-1
Pressure Transient Analysis of the **D Sandstone** VI-1
Seismic **Characterizations** of the **D Sandstone** VII-1
Reservoir Compartments VIII-1
Reservoir **Simulation** for **Waterflooding** ..... IX- 1
Targeted **infill Drilling and Economics** **X-1**
Summary and Conclusions XI4

List of Figures

Figure		Page
Figure 1-1	Limits of Denver Basin and D Sandstone Play	I-6
Figure 1-2	Denver Basin **and** D Sandstone Fields in Eastern **Colorado**	I-7
Figure II-1	Net Pay Interpretation of the D **Sandstone at the Sooner Unit in 1988**	**II-2**
Figure II-2	**Production History from the Sooner Unit `T" Sand Unit**	**II-3**
Figure III-1	Structure Map of D **Sandstone**	11I-4
Figure III-2	Type Log of D Sandstone and Adjacent Lithology	III-5
Figure III-3	**Isopach** Map of Huntsman Shale	III-6
Figure III-4	Structure Map of Huntsman Shale	III-7
Figure III-5	Depositional **Block** Diagram for **D Sandstone**	**III-8**
Figure III-6	**Isopach Map of'X' Bentonite to Mowry**	**III-9**
Figure DI -7	Log Cross-Section with Faulting	III-10
Figure III-8	Cross-Section of Thick Valley-Fill	III-11
Figure IV-1	Core Log of D Sandstone from SU 7-21	**IV-7**
Figure IV-2	**Density Log from** SU 7-21	**IV-8**
Figure IV -3	Density **Log from** SU 21-14-1	IV-9
Figure IV-4	Stratigraphic Comparison of SU 21-14-1 **and** 7-21	IV-10
Figure V-1	Porosity-Permeability Cross-Plot from D Sandstone Cores	V-3
Figure V-2	Permeability Distr**ibution** from D Sandstone Cores	V-4
Figure VI-1	Near-Well **Boundary** Example from Pressure Fall-Off Test	VI-3
Figure VI-2	Half-Slope Example from Pressure Fall Off Test	VI-4
Figure VI -3	**Quarter-Slope** Example from Pressure Fall-Off Test	VI-5
Figure VI-4	**Channel-Flow** Type-Curve Example from Pressure Fall-Off Test	VI-6
Figure VII- 1	Seismic Section from **Sooner** 3D Data **Volume**	VII-9
Figure VII-2	Synthetic Seismogram Cross-Section	VII-10
Figure VII -3	Stratigraphic West-East Cross-Section at the **Sooner Unit**	VII-11
Figure VII-4	Seismic Amplitude of the D Sandstone at the **Sooner Unit**	VII-12
Figure VII-5	Seismic **Isochron** of the D Sandstone at the **Sooner Unit**	VII-13
Figure VII-6	Prediction of Gross Thickness from Seismic Attributes	VII-14
Figure VII -7	Prediction of Net-Pay Thickness from Seismic Attributes	VII-15
Figure VII-8	Prediction of **Hydrocarbon-Feet** from Seismic Attributes	VII-16
Figure VIII-1	Schematic of Compartments in D **Sandstone** Reservoirs	VIII-3
Figure VIII-2	Map of Functional Reservoir Compartments	VIII-4
Figure VIII-3	3D seismic Attribute Map of Huntsman Shale	VIII-5
Figure IX- 1	Example of Single-Well History Matching	IX-7
Figure IX-2	History Match of Composite **Sooner** Unit	IX-8
Figure X-1	Map of Drilling Activity During the Project	X-4
Figure X-2	Map of Hydrocarbon-Feet from Seismic-Attribute Correlations	X-5

List of Tables

Table Page

Table I-1 Recovery by Waterflood from D Sandstone Fields Near the Sooner Unit..... I-4
Table N- i **Composition of D Sandstone from Thin-Section Analysis IV-4**
Table N-2 Grain Size for D Sandstone from Thin-Section Samples IV-4
Table N-3 **D Sandstone Petrographic Descriptions from SU 21-14-1 .....**N-5
Table V-1 Permeability Data from **D Sandstone** Cores in the **Sooner** Unit Area.....V-1
Table V-2 Summary of Log Calculations in the D Sandstone at the **Sooner** Unit V-2
Table VI- 1 Summary of Pressure Fall-off Analysis from Water Injection Wells ..... VI- 1
Table VII-1 Processing Flow Used for Sooner 3D Seismic Data VII-7
Table VI[-2 Correlation Coefficients of Seismic and Electrical Log Data VII-8
Table IX-1 Reservoir Properties **Used** for Simulation IX-2
Table IX-2 Results from History Matching by Well IX-4
Table IX-3 Results from History Matching Composite **Production **1X-5
Table IX-4 Economic Value of 2-Spot Waterflood Patterns IX-6
Table X-1 **Economic Model** for Comparison of Targeted and Blanket Jnflll Drilling X-3

Executive Summary

Production and Reserves

The oil producing rate at the Sooner Unit was increased nearly 200 bopd above pre-project projected trends. The projected ultimate developed reserves were increased from 1,556,000 bbl to 1,861,000 bbl. These production increases were the result of realignment of injection-production patterns and the drilling of one injection well and one production well. The original-oil-in-place (OOIP) calculated for the Sooner Unit were increased from 5,900,000 bbl to 6,900,000 bbl The increase in OOIP are the result of seismic mapping which was integrated with geological and engineering studies. The methodologies and development plan which evolved during the project lead to projections of 2,252,000 bbl (33 percent of OOIP) ultimate recovery after drilling of an additional five wells.

Seismic Modeling

Detailed synthetic seismic modeling was performed to determine resulting seismic signature and seismic frequency content necessary to resolve the internal stratigraphic architecture within the D Sandstone interval and to confirm the mapping and interpretation methodologies from earlier work during the project.

Seismic Attribute Correlation

Correlations of seismic attributes were made with petrophysical properties from electrical log data. It was found that direct attributes of the D Sandstone interval were inconsistent with reservoir development. Combination of attributes from the D Sandstone and adjacent temporal horizons through multiple-linear regression resulted in maps which were more consistent with geological and engineering interpretations. It is concluded that adjacent non-reservoir rock can provide important indicators of positive or negative development in adjacent reservoir rock.

Horizontal Completions

Attempts to drill a horizontal extension in a centrally located injection well were unsuccessful. Mechanical difficulties were encountered in the first attempt which utilized technology to drill an ultra-short radius curve with articulated drill collars and angled bottomhole assembly. The second attempt utilized a short-radius curve with a downhole mud-motor and steering assembly. A collapsing shale section above the target formation prevented completion of the lateral extension. A lithological or fault bather was penetrated during the second drilling attempt which confirms the objective and purpose of the horizontal extension. At a horizontal reach of 250 ft from the vertical wellbore, the mudmotor stalled and drilling angle abruptly changed. Drill cuttings contained clean sandstone and oil was flowing over the shale shaker.

Vertical Wells

Two conventional, vertical wells were drilled based on integrated studies. One well was an injection well and the other was a production well. The injection well encountered a thick

gross (55 ft) section of D Sandstone but had only 6 ft of net reservoir thickness. The producing well location was based on seismic attribute correlations. It encountered 26 ft of net reservoir thickness and was completed with a producing rate of over 200 **bopd.**

Petrography

Descriptions were made from whole and sidewall cores. Permeability ranges from 1 and to 100 and with a geometric-mean permeability of 21 md. Average porosity is 11.5 percent. Sidewall cores were taken from the SU 21-14-1 well. Petrographical studies and thin sections were made of these core samples. The study indicates that poor porosity and permeability development are primarily related to deposition. Clays and cements were found to be indicative of different facies. Low stand facies are characterized by kaolinite and feldspar. Abundance of calcite cement and chlorite clay suggest a transgressive setting with rising marine water. Low porosity and permeability rock results from fine laminations of clay and silty material.

Pressure Tests

Pressure tests taken during the project consisted of static shut-in measurements and transient surveys for injection and production wells. Pressure falloff tests were performed on three water-injection wells. Pressure buildup tests were taken from four producing wells. Permeability to water at injection wells ranged from 5 to 50 and and most wells indicate negative skin from -2 to-4. Nearly all pressure transient data indicate non-radial flow. The character from plots of the pressure transient data indicate late-time linear or bi-linear flow which is most likely resulting from reservoir heterogeneity. Evaluations of the pressure transient data using analytical simulation and type-curve matching indicate channel-widths which average 610 ft.

Realign Injection-Production

Four wells were converted from either production to injection or vice-versa in order to realign injection patterns which are better suited to the understanding of functional reservoir compartments. Reservoir management utilizing balancing injection with withdrawals of fluids and gas by compartments produced positive results. Gas-oil ratios decreased at some wells and high fluid levels were decreased at other wells. Balancing injection by compartment with the available wells appeared to improve oil production by 20 percent. Gas recycling was found to limit water-injection and was terminated. Gas injection pressure increased as water injection raised reservoir pressure. The pressure limit of the compressor (about 800 psi) prevented injecting the desired water volumes in certain compartments.

Inter-well Tracers

, Inter-well tracers were tested at three injection wells. Sodium bromide was used as the trace$_r$y material. Results were inconclusive. Water samples were taken on a daily basis for more than four weeks at selected producing wells which are in pressure communication with the tested injection wells. Laboratory analyses of water samples were performed by Marathon in Littleton. All samples indicated only background levels of tracer material.

Reservoir Simulation

Reservoir simulation was performed for two-spot situations to calculate recoverable oil in small, two-well compartments. The expected recovery from a hypothetical 2-spot, 40-acre pattern was found to be 24 percent of OOIP to economical limits. Oil and total fluid rates were matched by varying the oil-in-place at the start of the waterflood and injection rates. The average waterflood recovery of responding wells is about 78,000 bbl per well with a secondary recovery of 21 percent of the OOIP. This is equivalent to a secondary recovery of 115 bbl ac-ft. Total recovery after primary and secondary is indicated to be 37 percent in efficiently swept areas.

Technology Transfer

An oral presentation was made at the regional section meeting of AAPG in Reno, NV in July, 1995. The talk presented the case history of drilling a horizontal well at the Sooner Unit.

A workshop presentation was made on November 17, 1995 in Denver with the Rocky Mountain regional Petroleum Technology Transfer Council (PTTC). The Sooner project was one of three characterization studies presented from Eastern Colorado oil fields.

The project was presented on tour in six cities with the PTTC-BDM U.S. Department of Energy Class I traveling workshop during January and February, 1996.

All reservoir characterization data were donated to the Colorado School of Mines for use under the direction of Robert Thompson, John Curtis and Tom Davis. This data set includes electrical logs, production, pressure transient tests and 3D seismic. The data have been used in under-graduate classes and in graduate studies.

The Sooner 3D seismic survey was donated to the Rocky Mountain PTTC under the direction of Roger Slatt for use in the computer-technology demonstration lab.

Introduction and Background

Introduction and Project Objectives

The Sooner D Sand Unit (Sooner Unit) is considered a representative example of a waterflood project in the D Sandstone. The D Sandstone is a major oil and gas reservoir in the Denver Basin. Primary recovery from the D Sandstone is considered good with recoveries in the range of 14 to 18 percent. Waterflooding has not been very efficient, especially in the area around the Sooner Unit The Sooner Unit waterflood was also experiencing poor waterflood response at the start of the project after 4 years of injection.

The perceived reasons for poor waterflood recovery are primarily reservoir architecture, heterogeneity and compartmentalization. Reservoir rock and fluid properties indicate favorable waterflooding conditions. The D Sandstone has moderate permeability of about 21 and with a Dykstra-Parsons coefficient of about 0.75. The connate water saturation was initially at irreducible conditions. Oil gravity is 41° API and the oil water mobility ratio is less than one.

Integrated reservoir characterization with 3D seismic was used to better define the reservoir architecture. The Sooner Unit project was the first 3D seismic survey in the Denver Basin for exploitation of the D Sandstone. Since there was no previous experience for 3D interpretation techniques specifically for the D Sandstone, considerable effort was applied through model studies and trial-and-error to arrive at an interpretation methodology which was consistent with geological and engineering characterizations. The Sooner reservoir is interpreted as being deposited in a fluvial and estuarine environment. Narrow and sinuous reservoir patterns were imaged from the 3D seismic. The functionality of these images was confirmed by pressure transient tests which indicate bi-linear flow and channel widths which average about 600 ft. Functional reservoir compartments were found to average nearly 80 acres in size with a major axis of one-half mile and a minor axis of one-quarter mile. The orientation of reservoir compartments is generally parallel to the erosional valley system. It appears that an ideal well-spacing strategy would have been approximately 1980 ft along and 990 ft across the system axes (approximately 45 acres per well). The field was initially developed on standard 40-acre patterns.

It is concluded from the studies performed at the Sooner Unit that some infill drilling is required for a successful waterflood in D Sandstone compartments. There were three, targeted infill wells drilled during the project and there are plans for five additional wells to be drilled in late 1996. The drilling results confirmed the ability of 3D seismic to predict the D Sandstone reservoir and the presence of unswept reservoir compartments. Production rates were increased in 1995 from 200 bopd to over 400 bopd. The target ultimate recovery after drilling five additional wells is 32 percent of original-oil-in-place.

After reviewing the failed waterfloods in the area around the Sooner Unit, it is concluded that primary reasons for these failures were small reservoir compartments and inadequate number of wells, especially injection wells. Reservoir interpretation using integrated 3D seismic data indicates that heterogeneity in valley-fill reservoirs dictates targeted drilling of wells with unconventional spacing patterns for successful waterflood recovery.

Historical Background for D Sandstone Exploration

The D Sandstone play in the Denver Basin encompasses northeast Colorado and southwest Nebraska (Fig. I-1). The D Sandstone is a subsurface member of the Dakota Group

and is early Late Cretaceous age (Haun 1963). About 160 (42 percent) of the D Sandstone reservoirs in Colorado were abandoned or shut-in as of 1992 (Hemborg 1993). Although the D Sandstone may be considered a mature play, significant discoveries are still possible as shown by the discovery of Sooner Field in 1985 and Lilli Field in 1987, both in T. 8 N, R. 58 W., Weld County, Colorado.

The west side of the Denver Basin was the second area in the United States to produce oil from drilled wells. The early exploration was based on random wildcatting for fractured shale zones near oil seeps from 1862 through 1922. After 1920, exploration was based on surface geological surveys for anticlinal structures on the west side of the basin near the front range of the Rocky Mountains. Development of the east flank of the basin was slower than the west flank because of low, unreliable surface dips and blanket Tertiary gravel beds.

A 1930 wildcat discovery (sec. 24, T. 6 N., R. 61 W.) on a gentle surface anticline on the east flank of the basin in east Weld County, Colorado established the initial production from the D Sandstone and the first production from any reservoir on the east flank of the basin (Lavington 1941). This well, the Platte Valley Petroleum Corporation Patterson No. 1, initially flowed 184 barrels of oil a day from a depth of 6661 ft . This D field was named Greasewood (. 1-2). The operators who developed the field believed trapping in the Greasewood was a stratigraphic-structural combination. The discovery of Greasewood Field resulted in some additional nearby wildcat drilling. Interest in the Greasewood area and the east flank of the Denver Basin subsided quickly because of 1) lack of further discoveries, 2) the achievement of commercial production in only two of eight Greasewood Field development wells, 3) realization that surface structure did not mirror D Sandstone reservoir structure, and 4) erratic distribution of the D Sandstone in Greasewood Field (Rountree 1984).

After 1949, seismic exploration resulted in finding D Sandstone production on subsurface areas with structural nosing and anticlinal closures. In August 1949, the Ohio Oil Company completed a 225 barrel per day oil discovery from the D Sandstone near Gurley, Cheyenne County, Nebraska. This discovery, Egging No. 1, precipitated a decade and a half of active exploration on the east flank of the basin which caused the discovery of most Nebraska and Colorado D Sandstone reservoirs (Volk 1972). Many early D Sandstone fields were discovered from seismic leads, but as subsurface control accumulated, it became apparent that stratigraphic traps were dominant. In the 1970's, the primary interpretations of depositional environments for D Sandstone sediments were deltaic and fluvial with transitional and marine environments also represented.

By the late 1980's, a geological model was proposed which favored a valley-fill depositional system (Sonnenberg 1987). The D Sandstone interval, in this model, is divided into two sand-body types. The first or older unit was deposited during a regression at the end of Huntsman deposition. This unit is of regional extent and occurs across the entire western portion of the basin. The second or younger unit is a channel deposit (fluvial and estuarine) that accumulated as part of a valley fill. These valley-fill sediments were deposited in structurally low areas which are frequently associated with pre- D Sandstone faulting.

As the interpretation of D Sandstone reservoirs evolved from structurally to primarily stratigraphically controlled, interpreters of seismic data also began to realize that seismic amplitude of horizon-time events relating to the D Sandstone and adjacent formations should be indicators of reservoir development. As early as 1984, it was reported in the literature that channel complexes and valley-fill deposits could be located at Zenith Field (Fig. I-2) using seismic techniques (Sonnenberg 1987). Seismic modeling of a 52-ft reservoir produced an amplitude

peak and trough associated with the top and base of the D Sandstone, respectively, which diminished significantly as the sandstone thickness decreased. Amplitude responses were found in 2D seismic data across a D Sandstone valley-fill reservoir which were similar to the results from seismic modeling. Although stratigraphic interpretation of seismic data promised to be a boon for D Sandstone exploration, the method did not receive wide-spread acceptance. Possible reasons for this are 1) reluctance to look for D Sandstone reservoirs in areas which were structurally low during deposition and 2) inability to tie synthetic-seismogram events with actual survey data because of phase rotation or lack of adequate sonic logs.

Historical Background for Waterflooding the D Sandstone

Waterflooding of D Sandstone reservoirs began in the 1960's. Production by primary depletion from the D Sandstone has been good to excellent; however, secondary recovery by waterflooding has been disappointing. In 1974, there were 37 waterflood projects in the D Sandstone in Colorado according to a U.S. Bureau of Mines Report of Investigations (Biggs and Koch 1974). Data from the 37 D Sandstone waterfloods indicates incremental recovery of only 50 stb/ac-ft by waterflooding from 65 percent of the projects. Waterflood projects in the general vicinity of the Sooner Unit had marginal to negative incremental reserves compared to primary production extrapolations. Table 1-1 shows data from the waterflood projects in the area of the Sooner Unit.

Bureau of Mines Report of Investigations No. 7959, which tabulated statistics in 1974 on waterflooding oil fields in Colorado, is an excellent resource for production data from D Sandstone reservoirs in the Denver Basin. However, the authors of the report did not attempt to qualify the statistics on recovery by giving reasons for good or poor recovery. Coincidentally after the report was published, interest waned for waterflooding the D Sandstone in the Colorado portion of the Denver Basin. These statistics were subsequently used by engineers on technical committees for proposed waterflood projects to demonstrate that the D Sandstone was a poor waterflood candidate. Between 1974 and 1992, only two waterflood projects were approved by the Colorado Oil and Gas Commission. Some of the popular reasons which were proposed by engineers for poor waterflooding recovery were 1) high Dykstra-Parsons coefficient of permeability variation and 2) high gas-saturation at the end of primary depletion.

One of the D Sandstone fields found during the boom period for D Sandstone exploration is the Jackpot Field. The Jackpot Field is located in T. 6 N., R. 59 W. which is approximately 10 miles southwest from the Sooner Unit. Jackpot Field was discovered in 1955 from seismic mapping and subsurface controL Waterflood operations at Jackpot began in 1960. The D Sandstone sediments were described as discontinuous, lenticular transgressive sandstones (Webster 1982). The field was developed on 40-acre spacing with a maximum of 32 productive wells. The Jackpot Field project has the highest recovery by waterflood in the area around the Sooner Unit with a recovery factor of 31.9 percent of 001P as shown in table I-i. However, the ratio of incremental oil recovered by waterflooding to recovery by primary is only 25 percent. The calculated OOIP for this field may be too low. The Jackpot Field waterflood project is a technical success, but probably an economic failure.

The average primary recovery of D Sandstone waterflood projects in the area surrounding the Sooner Unit, shown in table I-1, is 16.1 percent of OOIP. The total recovery after primary and waterflooding is 17.7 percent. An average incremental recovery of only 1.6 percent after waterflooding is demonstrated by these fields. All of these waterflood projects, except the

Jackpot Field, are technical failures. The decision to risk waterflooding at the Sooner Unit was influenced to a large degree by the fact that the Sooner reservoir thickness is nearly double the average of the fields listed in table I-1.

Table I-1
Recovery by Waterflood from D Sandstone Fields Near the Sooner Unit

Field Name	Township - Range	Area - Acre	Acre-Feet	**OOIP-Mbbl**	Primary EUR-Mbbl	Waterflood EUR-Mbbl	Recovery Factor
Bijou	4-5N, 59-60W	1180	11800	7410	1400	1570	21.2%
Bijou-West	4N, 60W	1320	14520	7540	1198	1211	16.1%
Buckingham	8N, 58W	480	5760	2740	389	389	14.2%
Greasewood	6N, 61W	240	1920	1235	248	267	21.6%
Jackpot	6-7N, 59W	1440	11520	5515	1381	1762	31.9%
Orchard-East	4N, 60W	360	2160	1237	301	308	24.9%
Orchard-West	4N, 60W	200	1200	766	132	132	17.2%
Roggen-NW	2N, 63W	200	2000	1462	204	241	16.5%
Roggen-SE	2N, 63W	1050	10500	6267	496	552	8.8%
Masters	5N, 60W	360	2160	4070	335	354	8.7%
Total		6830	63540	38242	6084	6786	17.7%

Note: Waterflood EUR is total primary plus secondary recovery.

References

Biggs, Paul and Charles Koch. 1974. *Waterflooding of Oil Fields in Colorado.* U.S. Bureau of Mines Report of Investigations No. 7959.

Halm, John D. 1963. "Stratigraphy of Dakota Group and Relationship to Petroleum Occurrence, Northern Denver Basin." in *Guidebook to the Northern Denver Basin and Adjacent Uplifts,* eds. P.J. Katch and D.W. Bolyard (Denver: Rocky Mountain Association of Geologists): 119-134.

Hemborg, FL Thomas. 1993. `Denver Basin Plays - D Sand." in *Atlas of Major Rocky Mountain Gas Reservoirs,* ed. Carol L. Hjellming (Socorro: New Mexico Bureau of Mines and Mineral Resources): 111-112.

Lavington, C.S. 1941. "Greasewood Oil Field." in *Stratigraphic Type Oil Fields- A Symposium,* ed. A. L Levorsen (American Association of Petroleum Geologists): 19-42.

Rountree, Russ. 1984. *Rocky Mountain Oil History*. (Denver: Hart Publications, Inc.): 46-48.

Sonnenberg, Stephen A. 1987. "Tectonic, Sedimentary, and Seismic Models **for the D Sandstone,** Zenith Field Area, Denver Basin, **Colorado."** *The American Association of Petroleum Geologists Bulletin 45(11):* 1366-1377 (November 1987).

Volk, Richard W. 1972. "The Denver Basin and the Las Animas Arch", in *Geologic Atlas of the Rocky Mountain Region,* ed. W.W. Mallory, (Denver: Rocky Mountain Association of Geologists).

Webster, Mark. 1982. "Jackpot Field." in *Oil and Gas Fields of Colorado, Nebraska and Adjacent Areas,* (Denver: Rocky Mountain Association of Geologists).

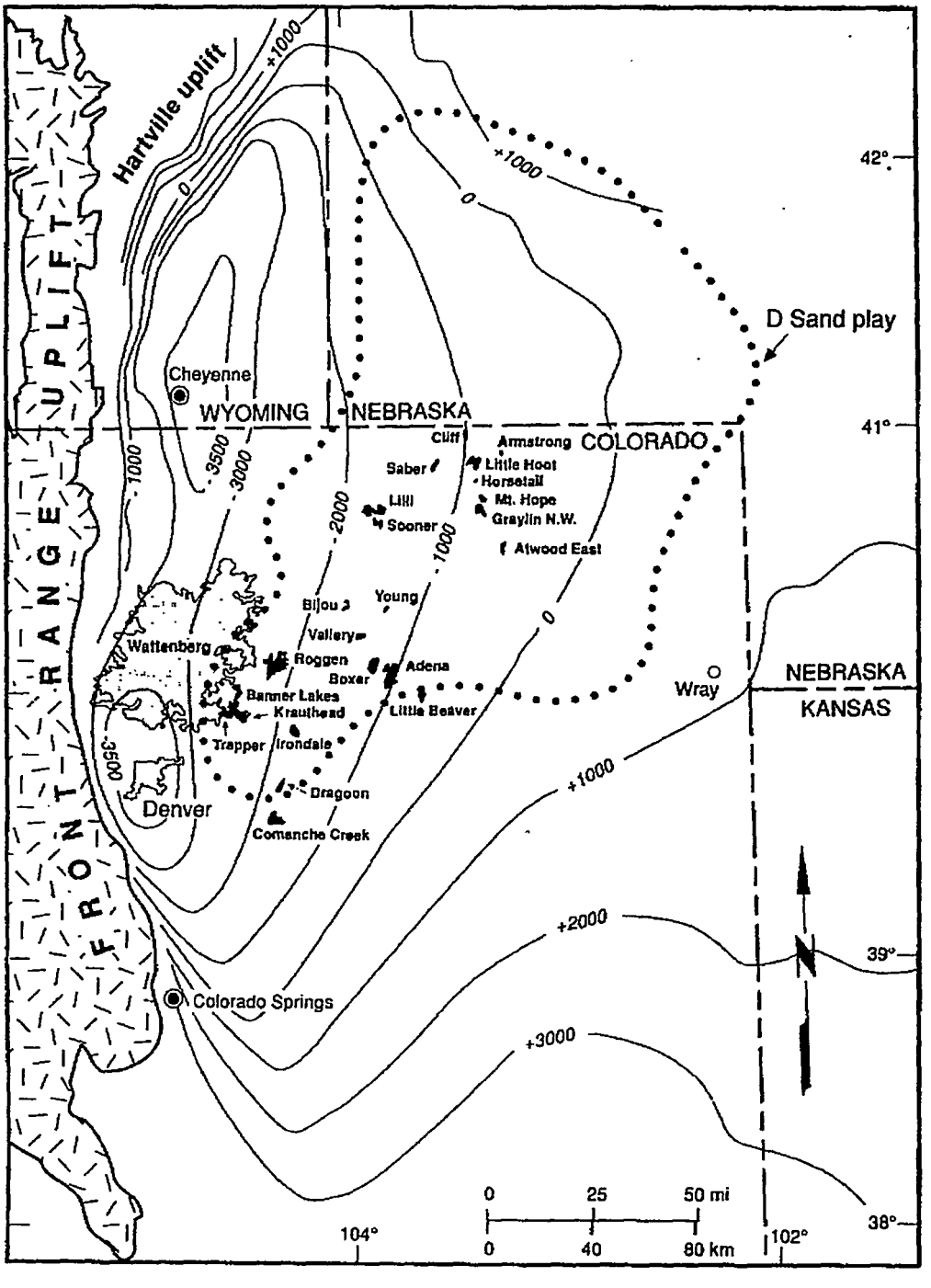

Figure I-1: Limits of Denver Basin and D Sandstone play. Contours are on top of the Cretaceous J Sandstone.

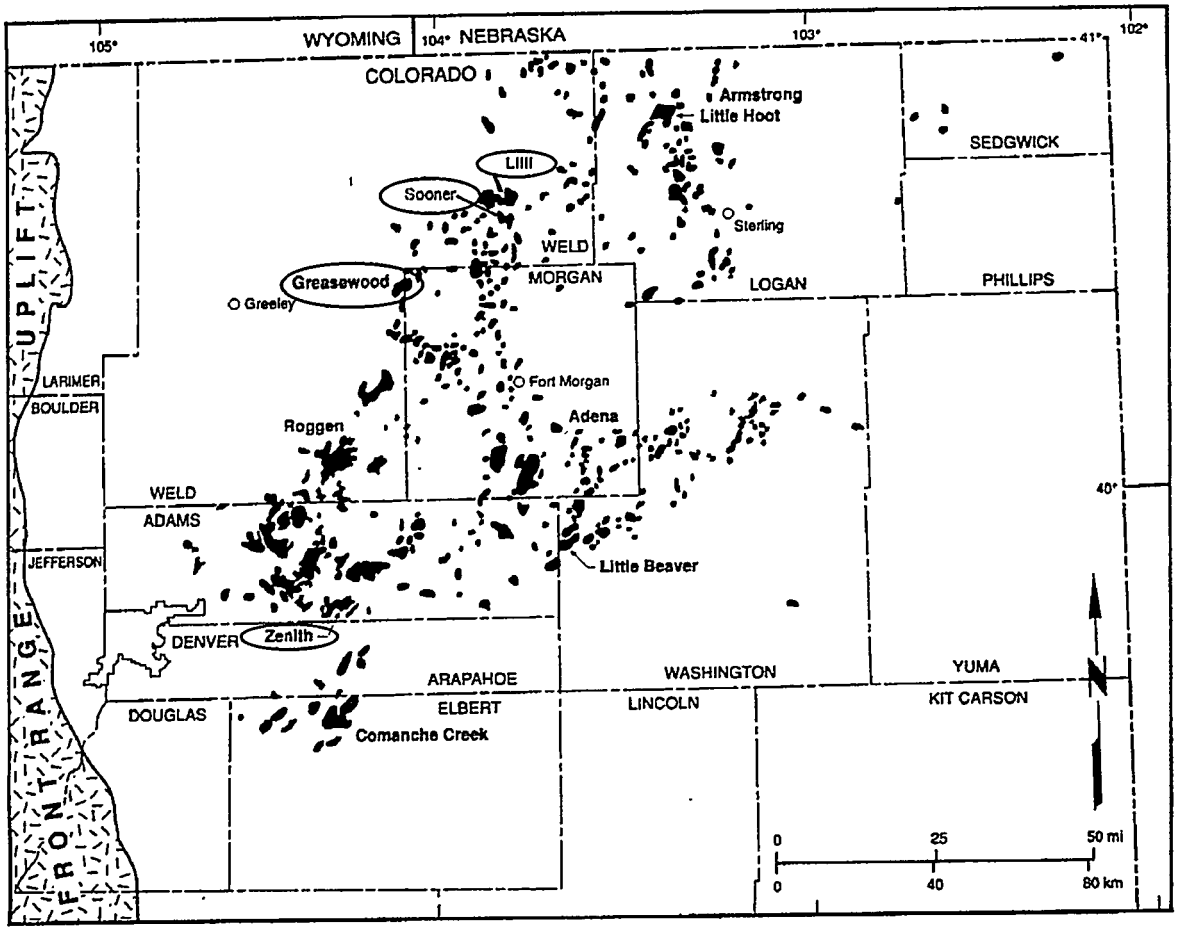

Figure I-2: Denver Basin and D Sandstone fields in eastern Colorado. The first D Sandstone discovery was Greasewood Field which was drilled by cable tools in 1930.

History of the Sooner "D" Sand Unit

Production from the D Sandstone was established in 1969 in the Sooner Field one mile east from the Sooner "D" Sand Unit (Sooner Unit) in section 27, T. 8 N., R. 58 W. Methods used for exploration and development in the area were geology from well logs and wildcatting. The field consisted of a single well until 1980, when four additional wells were completed. The first productive D Sandstone oil well within the confines of the current Sooner Unit boundary (NWSE section 28, T. 8 N., R 58 W.) was completed in December 1985. By 1988, the productive surface area of the Sooner Unit reservoir was defined at about 720 acres with wells spaced on regular 40-acre production units. The 1440-acre Sooner Unit was created in September 1989. At that time, the unitized area had produced 772,000 stock-tank bbl (stb) of oil and 3,000,000 mcf of gas. The reservoir did not have a gas cap or free-water contact. Negligible formation water produced during primary depletion. Estimates of original-oil-in-place (0 0 P) at the time the Sooner Unit was formed ranged from 5,300,000 to 5,900,000 stb. Estimates of ultimate primary recovery of oil by the unitization technical committee averaged 900,000 bbl and ranged from 850,000 to 1,100, 000 bbL

The geological interpretation of the reservoir at the time of unitization was predominately a fluvial channel with associated splay deposits. The strategy for water injection was to inject in the center of the channel and at the northern and southern ends. Production was curtailed during fill up for approximately one year.

At the time of unitization there were 17 active wells. Four wells were converted to water injection service. Figure 11-1 is a map of the reservoir area based on net-pay thickness and configuration of the original injection-production alignment. Water supply is from two wells completed in the J Sandstone which is approximately 100 ft below the top of the D Sandstone. These two sandstones are separated by 40 to 80 ft of Huntsman shale and Mowry siltstone.

When the Sooner Unit Class I project began in October 1992, there were 17 active D Sandstone wells, which consisted of 11 production wells, four water-injection wells and two gas-recycling wells. One well was shut-in and two wells were producing make-up water from the J Sandstone. Cumulative oil production was 1,086,133 bbL The average oil rate from the total Unit was 332 bbl oil per day.

By December 1995, and at the end of the project, there were 15 active D Sandstone wells, which consisted of 11 production wells and four water-injection wells. Four D Sandstone wells were shut-in. One water-supply well was active and the other water-supply well was shut-in. Three new wells were drilled and completed in the D Sandstone. The two gas-recycling wells were converted to production service. Two producing wells were converted to water-injection service. One well was plugged during the project after an unsuccessful horizontal completion attempt. At the end of December 1995, cumulative oil production was 1,436,707 bbl and the average oil rate from the total Unit was 442 bbl per day. Figure 11-2 shows the monthly production from Sooner Unit wells since discovery.

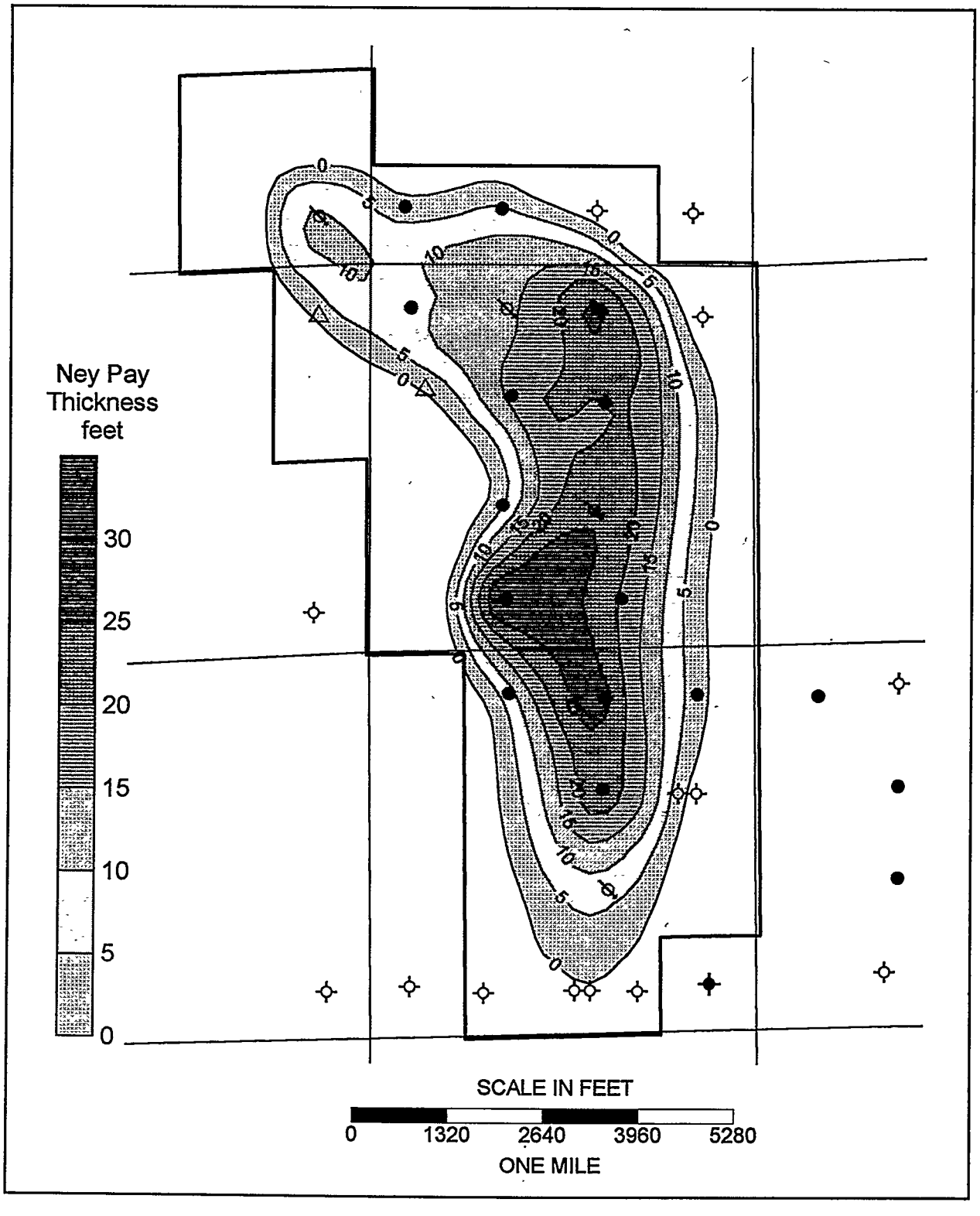

Figure II-1: Net pay interpretation of D Sandstone at the Sooner Unit in 1988.

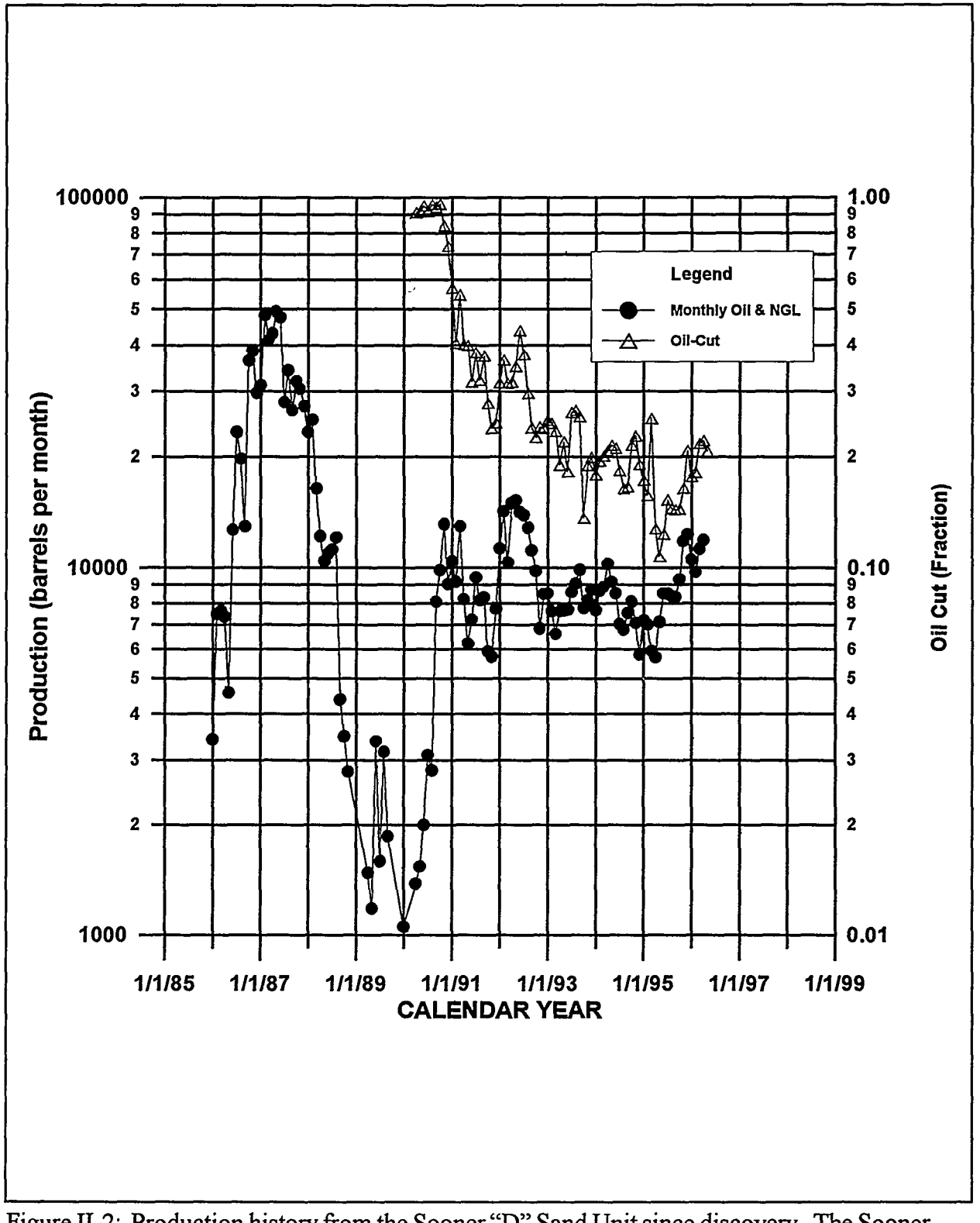

Figure II-2: Production history from the Sooner "D" Sand Unit since discovery. The Sooner Unit Class I project began in October 1992.

Geology of the Sooner Unit and Adjacent Area

The Sooner "D" Sand Unit (Sooner Unit) is located approximately 100 miles from Denver in the central portion of the Denver Basin in T. 8 N., R 58 W., Weld County, Colorado (Fig. I-2). The Denver Basin is asymmetric and trends north-south, with the deepest part of the basin near Denver where sedimentary rocks exceed 13,000 ft. The basin was formed during the Laramide orogeny and the western portion of the basin has the greatest dip near the flank of the Rocky Mountain Front Range. The producing reservoir at Sooner Unit is the D Sandstone with an average net pay of 17 ft at an average depth of 6,300 ft. The Sooner Unit reservoir is interpreted to be a valley-fill estuary. The predominant sedimentary features in the Sooner Unit are fluvial point bars and shallow water tidal bars. The reservoir is stratigraphically trapped on monocline with a dip angle of 0.4° oriented at 288° (Fig. III-1).

The D Sandstone, a member of the Dakota Group, is of Upper Cretaceous age and occurs between marine shales (Fig. III-2). The base of the overlying Graneros Shale is the top of the D Sandstone. It is black, organic-rich marine shale. The top of the Graneros is marked by the `X' bentonite bed, a wide-spread and correlative marker in the Denver Basin. The Huntsman Shale underlies the D Sandstone and is also a black, organic-rich, non-burrowed marine shale. The Graneros interval thickness is nearly constant from 94 to 106 ft over a large area surrounding the Sooner Unit. Any significant thinning of this interval is interpreted to be the result of post-depositional normal faulting. The Huntsman ranges in thickness from 18 to 48 ft (Fig. III-3). The variation of Huntsman thickness is related to erosion from the D Sandstone drainage system. A structure map of the top of the Huntsman shale shows the D Sandstone drainage system of the Sooner Unit reservoir (Fig. III-4).

At the end of Huntsman deposition, a regressive event (stage 1) began that deposited shoreline and shallow-marine sandstones across the basin (Fig. III-5). These sandstones are in transitional contact with the Huntsman. Slight fault-block movement influenced sedimentation. Streams and deltas were positioned in topographically low areas and inter-deltaic deposition occurred in topographically high areas. The regressive D Sandstone was deposited over the basin as the shoreline prograded seaward, approximately toward the northwest across the Sooner Unit area. Regional erosion and incisement occurred after the deposition of thin, regressive sandstones (stage 2). River and stream drainage incised through the older D Sandstone and into the underlying Huntsman Shale. The third stage of D Sandstone deposition occurred during a rise in sea level. During stage 3, the incised drainage were filled with fluvial and estuarine sandstones and siltstones.

There are several maps which can be made for reconstruction ofpaleo-structure. A map which corresponds well with production is the isopach from the `X' bentonite to the Mowry (Fig. III-6). The `X' bentonite-Mowry interval ranges from 158 to 184 ft and the thickest interval coincides with thickest D Sandstone and thinnest Huntsman Shale. The depositional model which most appropriately explains these thickness variations is that thicker D Sandstone-Huntsman Shale areas correspond to paleo-structurally low areas. These low areas are frequently bounded by normal faulting which occurred prior and concurrent with D Sandstone deposition (Sonnenberg 1982, Sonnenberg 1987 and Plybon 1983). This is demonstrated on log cross-sections (Fig. III-7) at the Sooner Unit and other fields. The faults in the Sooner Unit have a maximum displacement of 20 ft and are nearly verticaL Seismic indications of thick D Sandstone sediments (amplitude and wavelet isochron) frequently correspond to basement faults. Huntsman shale thickness of less than 38 ft at the Sooner Unit and adjacent area represents erosional down-

cutting by the D Sandstone drainage system. Productive valley-fill sediments are found in and immediately adjacent to these thin areas. Productive D Sandstone reservoirs associated with thick Huntsman exhibit a coarsening-upward character on electrical logs. These reservoirs are more marine in character and probably resulted from winnowing on subtle high areas.

The shape of the Sooner Unit reservoir is that of a funnel-mouth estuary. The mouth of estuary or valley-fill is located at to the north while the up-stream neck is located at the south end of the reservoir. To the north of the Sooner Unit is the Lilli Field (Fig. III-1). The Lilli Field is an east-west trending double-lobed marine bar. The Li ii Field produces from a stage-3 D Sandstone which was winnowed on a slight paleo-structural high. Immediately to the east of the Sooner Unit is another D Sandstone reservoir which is a bifurcation of the erosional valley system found in the Sooner Unit (Fig. III-3).

The predominant sedimentary features in the Sooner Unit are fluvial point bars and shallow-water tidal bars (stage-2 and stage-3 deposition). There are fine to medium-grained fluvial deposits with gross thickness of up to 55 ft. These are identified from a bell-shaped log character with the most permeable and porous rock at the base and a fining-upward character. Identification of valleys does not guarantee thick reservoir-quality rock. Some areas of thick sediments are filled with muddy siltstone with low porosity and permeability (Fig. III-8). Regional and non-productive stage-1 D Sandstone is found in all the dry holes surrounding the Sooner Unit (Fig. III-7).

A similar D Sandstone reservoir to the Sooner Unit can be found at Zenith Field in Adams County, Colorado (Fig. I-2). This field also produces from channel deposits in a valley-fill system (Sonnenberg 1987). The field is located on a regional monocline without structural closure as is the Sooner Unit reservoir. The Zenith reservoir is stratigraphically trapped as a result of fades changes of porous, permeable stage-2 and stage-3 deposits to more silty stage-1 deposits. The regional regressive stage-1 sandstones that are adjacent to the valley fill are non-productive. The field had a solution-gas drive and produced no water. The same criteria used at Zenith Field to identify productive intervals apply quite well at the Sooner unit. These include: 1) resistivity of greater than 30 ohm m, 2) gamma ray of less than 30 API units, micro-resistivity and caliper log readings indicating mud-cake buildup and 3) density-log porosities of greater than 8 percent. The similarities between the Sooner Unit and Zenith Field indicate that the valley-fill model is applicable across much of the Denver Basin.

Most of the petroleum produced from D Sandstone reservoirs has been from stratigraphic traps. In the Sooner Unit and adjacent area, the fields do not have structural-closure and do not produce formation water. The more prolific recoveries per well and per acre have been found in the thicker valley-fill reservoirs. Identification of areas with the most potential for prolific production depends on recognition ofvalley systems and paleo-structurally low areas by mapping the thickness of the Huntsman Shale and `X' bentonite-Mowry interval. While many D Sandstone exploration targets have been based on structural closure or nosing, these elements are often found to actually have negligible impact on reservoir quality or trapping after development drilling is finished.

References

Plybon, Steven C. 1983. "Seismic-Stratigraphic Investigation of the D Sandstone at Masters . Field, Weld County, Colorado." Masters Thesis No. 2781, Colorado School of Mines, Golden, Colorado.

Sonnenberg, Stephen A. 1982. "The Lanyard Field, a Structural-Stratigraphic Trap, Denver Basin, Colorado." *The Mountain Geologist* 19(3): 63-72 (July 1982).

Sonnenberg, Stephen A. 1987. "Tectonic, Sedimentary, and Seismic Models for the D Sandstone, Zenith Field Area, Denver Basin, Colorado." *The American Association of Petroleum Geologists Bulletin* 45(11): 1366-1377 (November 1987).

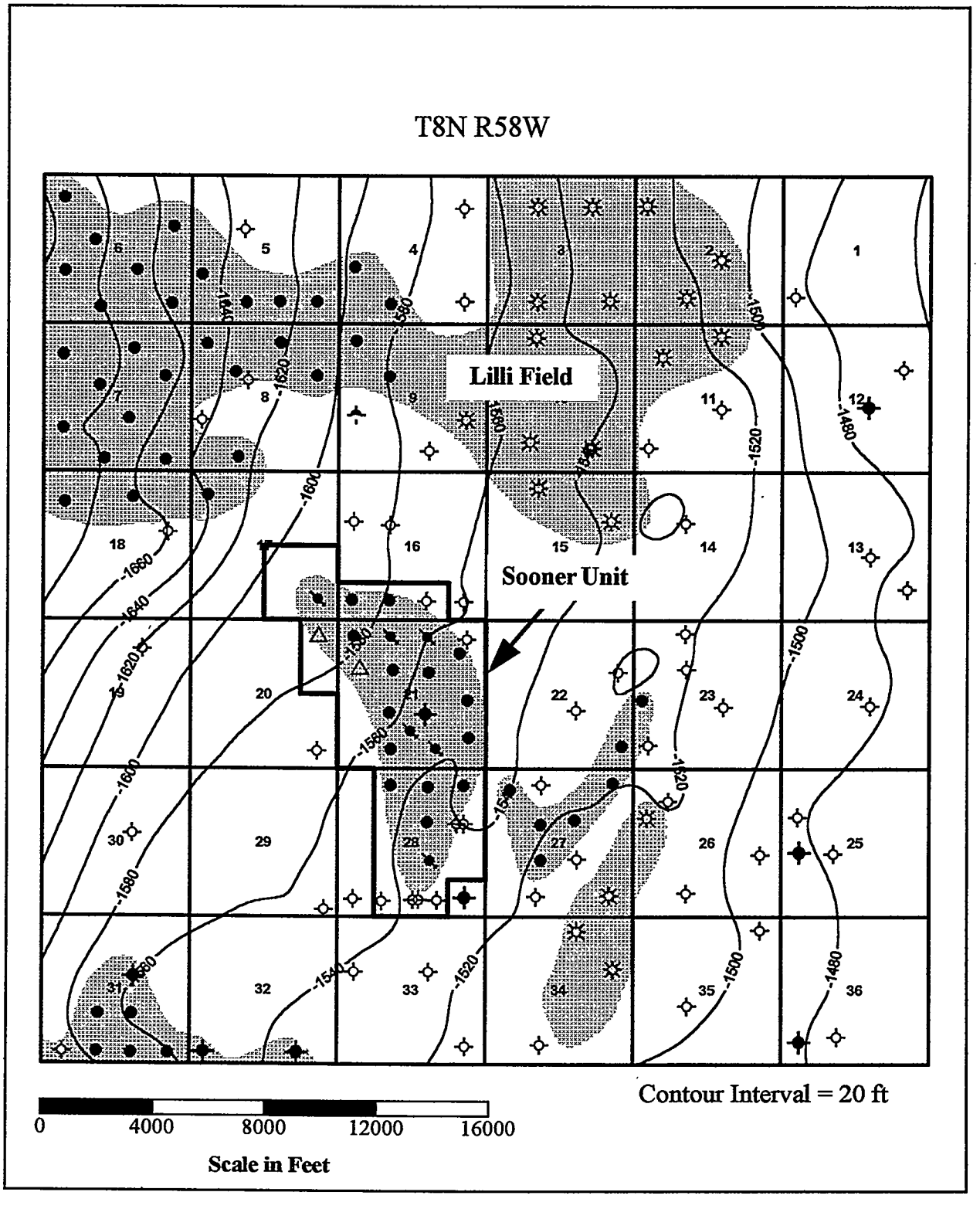

Figure III-1: Structure map on top of D Sandstone in area of Sooner Unit.

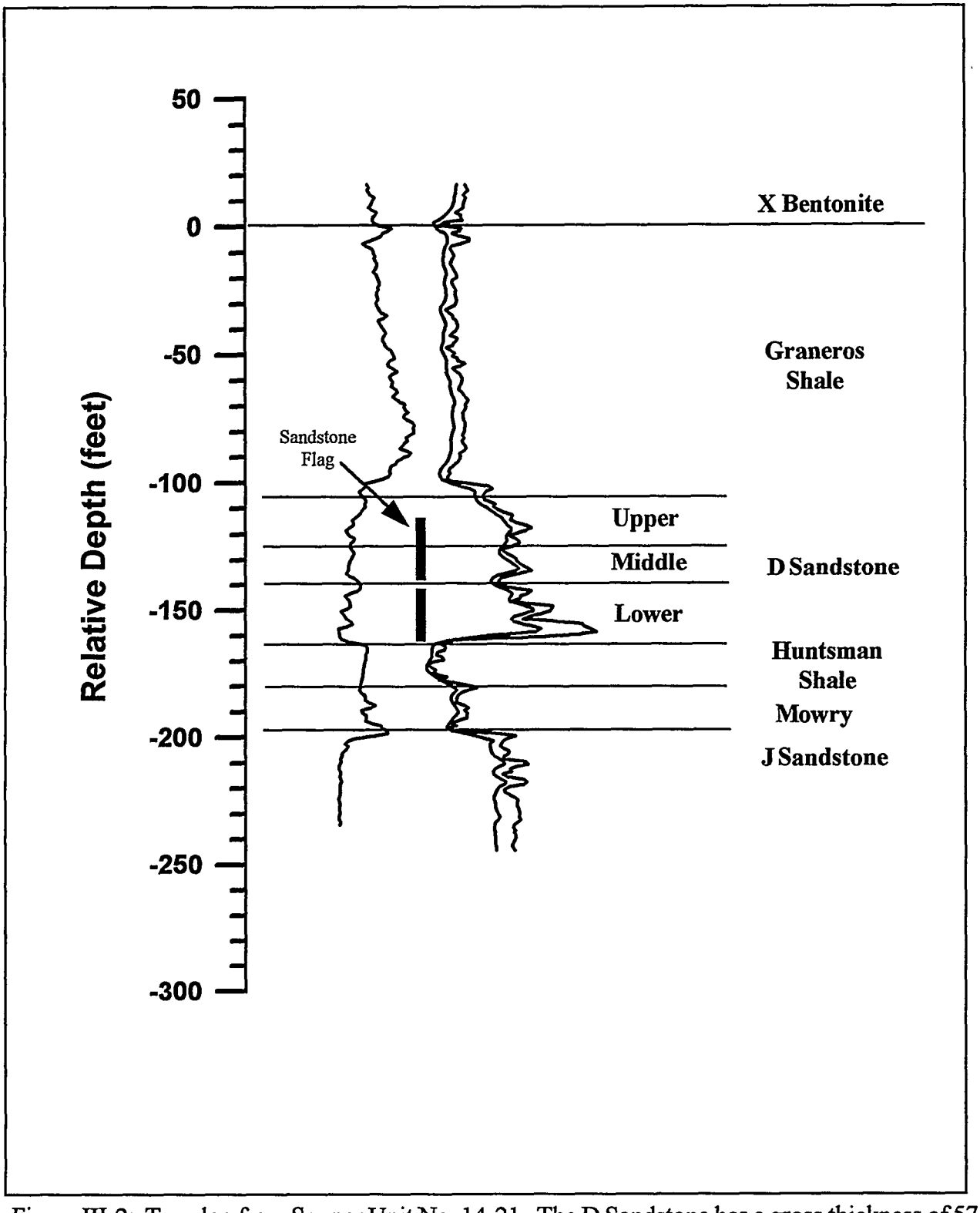

Figure III-2: Type log from Sooner Unit No. 14-21. The D Sandstone has a gross thickness of 57 ft. Net pay thickness is 34 ft. The D Sandstone was divided into three members for correlation work.

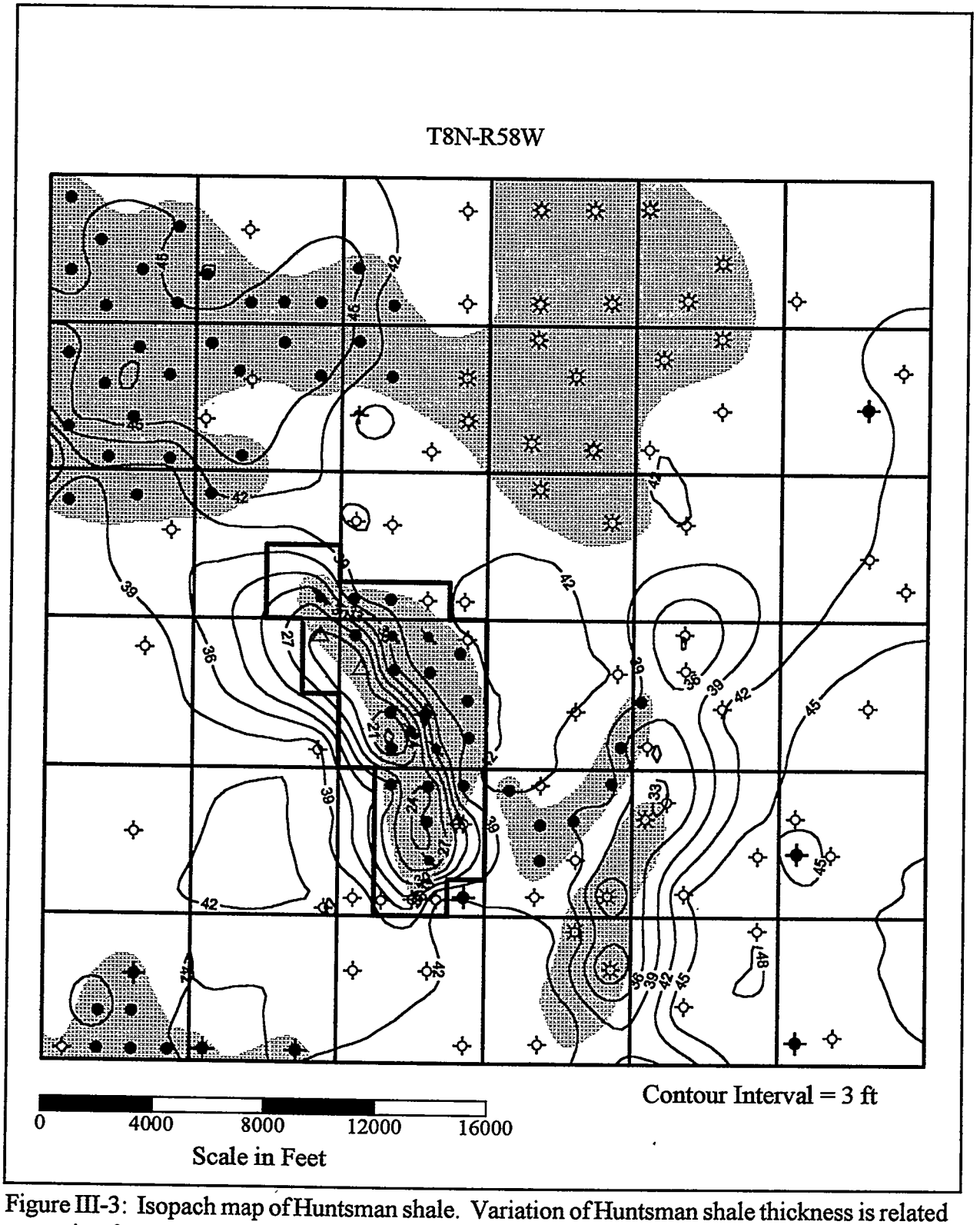

Figure III-3: Isopach map of Huntsman shale. Variation of Huntsman shale thickness is related to erosion from the D Sandstone drainage system. Contour interval is 3 ft.

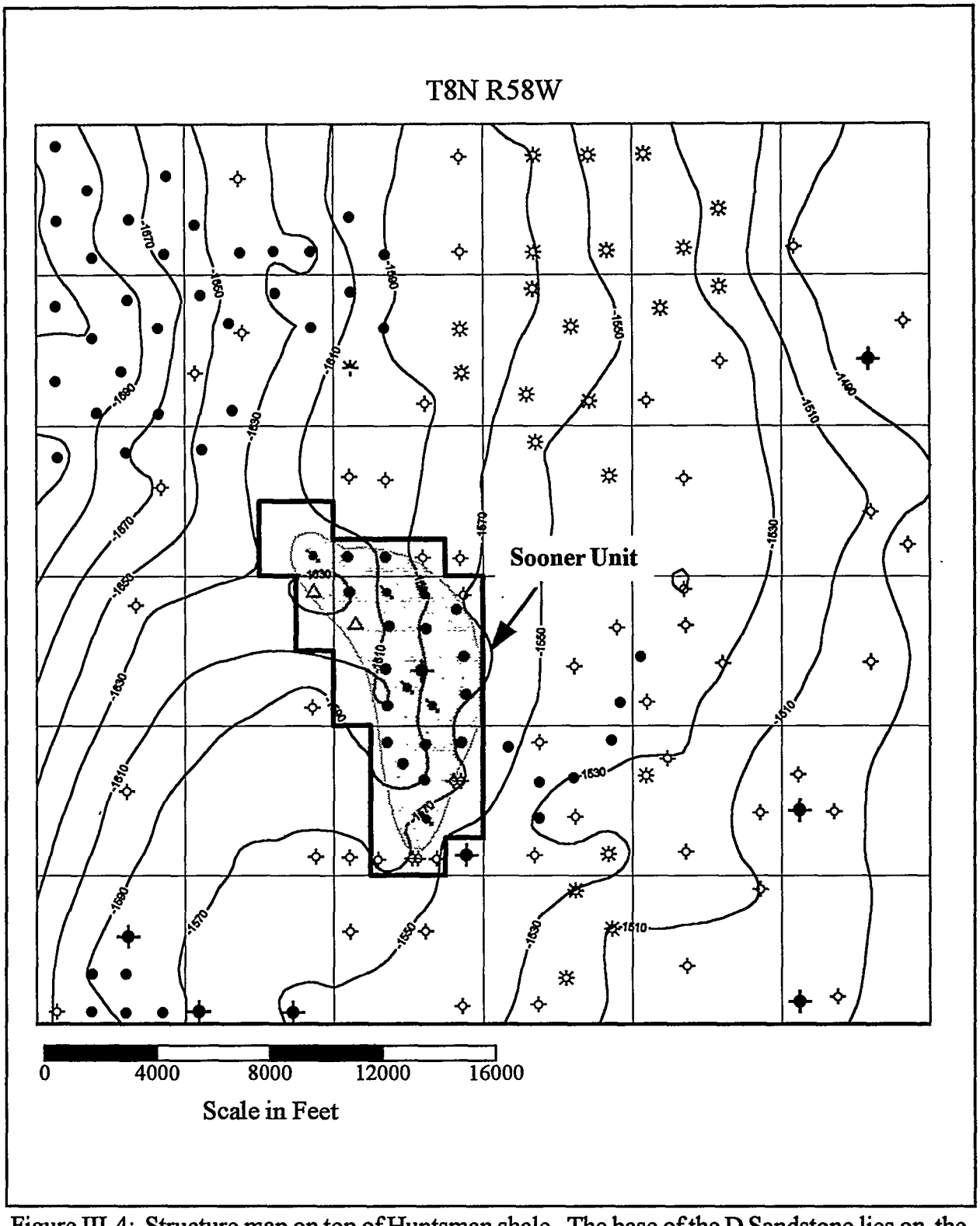

Figure III-4: Structure map on top of Huntsman shale. The base of the D Sandstone lies on the Huntsman. The erosional valley of the Sooner Unit reservoir is easily identified. Contour interval is 20 ft.

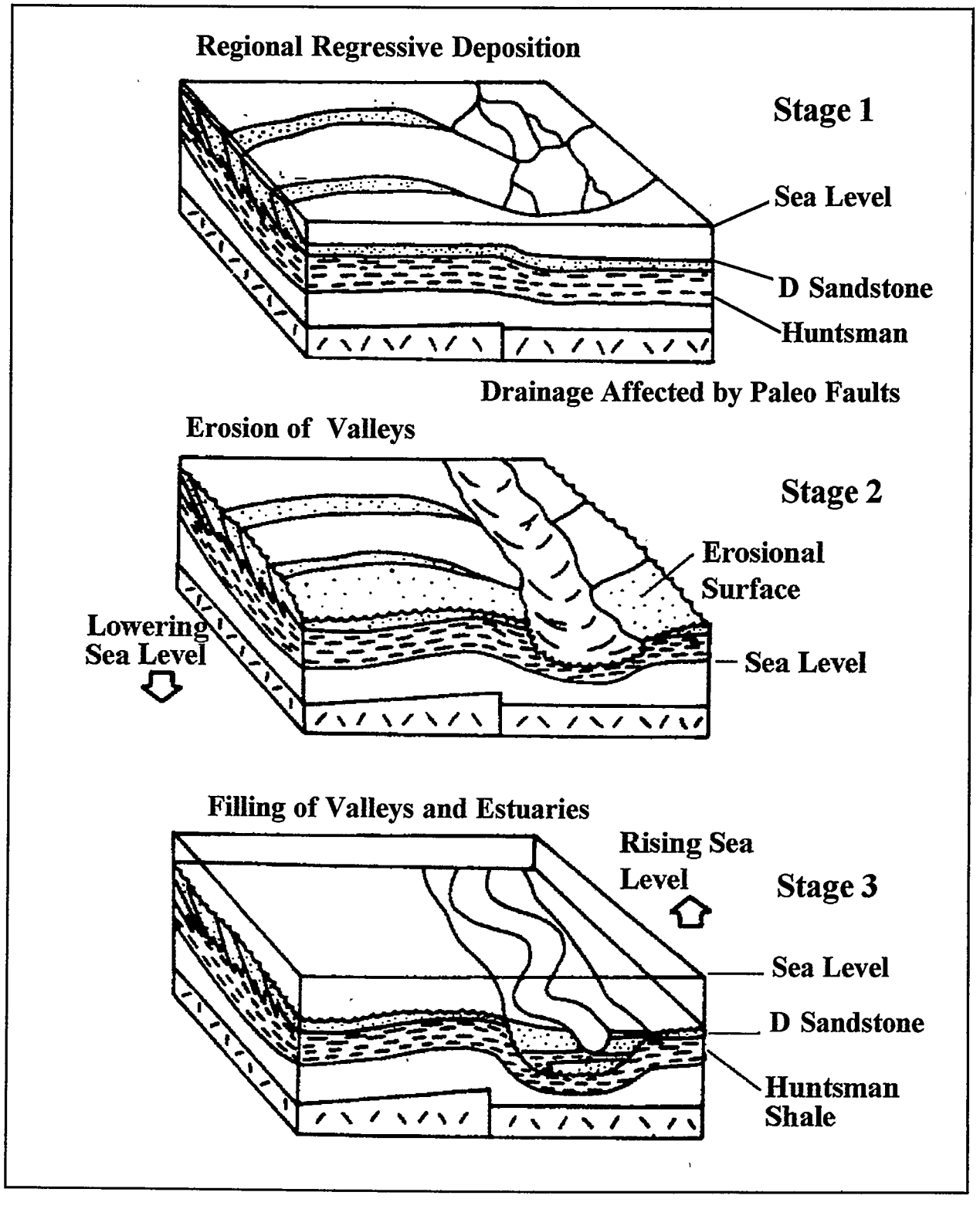

Figure III-5: Depositional block-diagram model for D Sandstone after Sonnenberg, 1987.

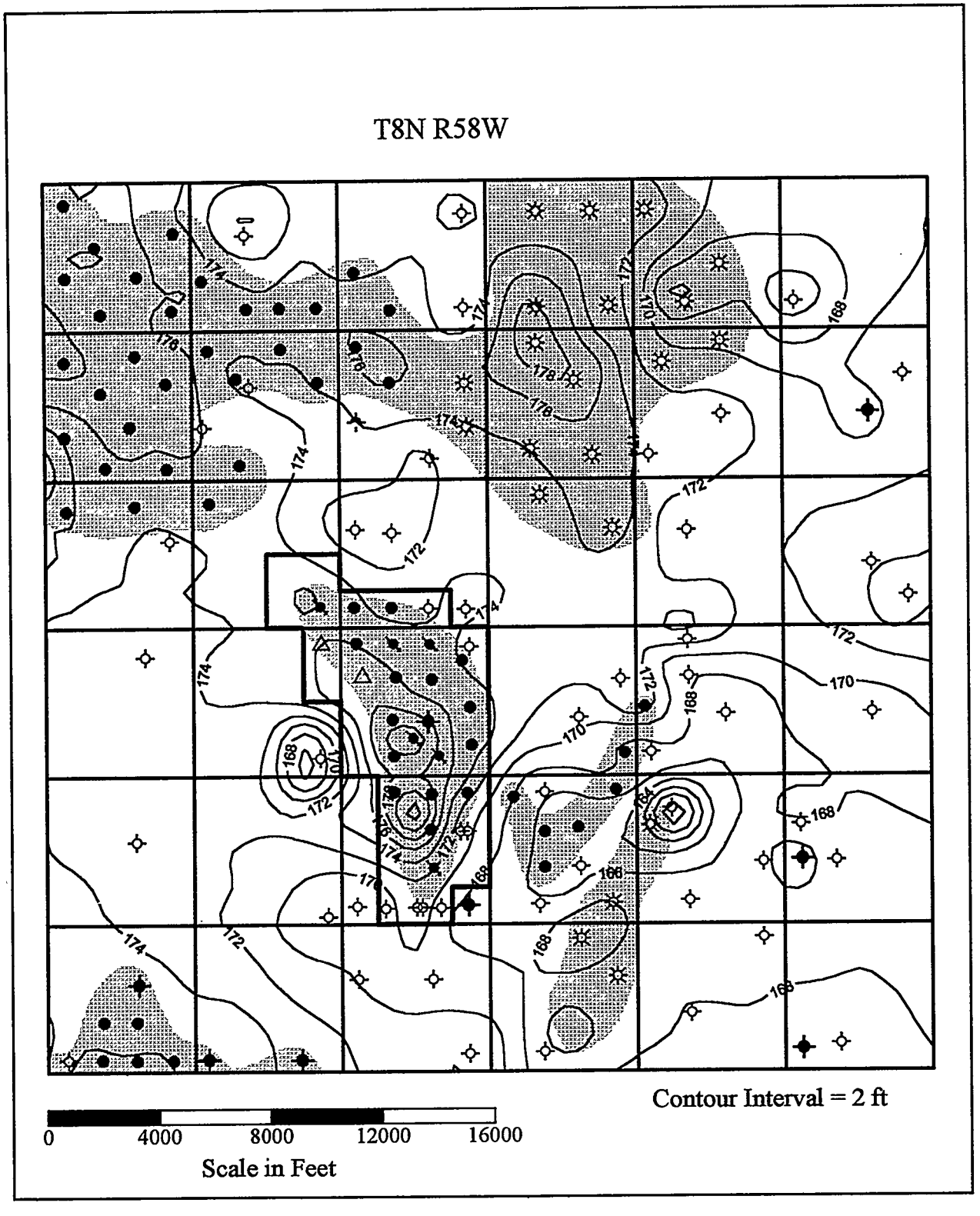

Figure III-6: Isopach map from X Bentonite to Mowry. Thick areas of this isopach represent structurally low areas during deposition of D Sandstone sediments. Contour interval is 2 ft.

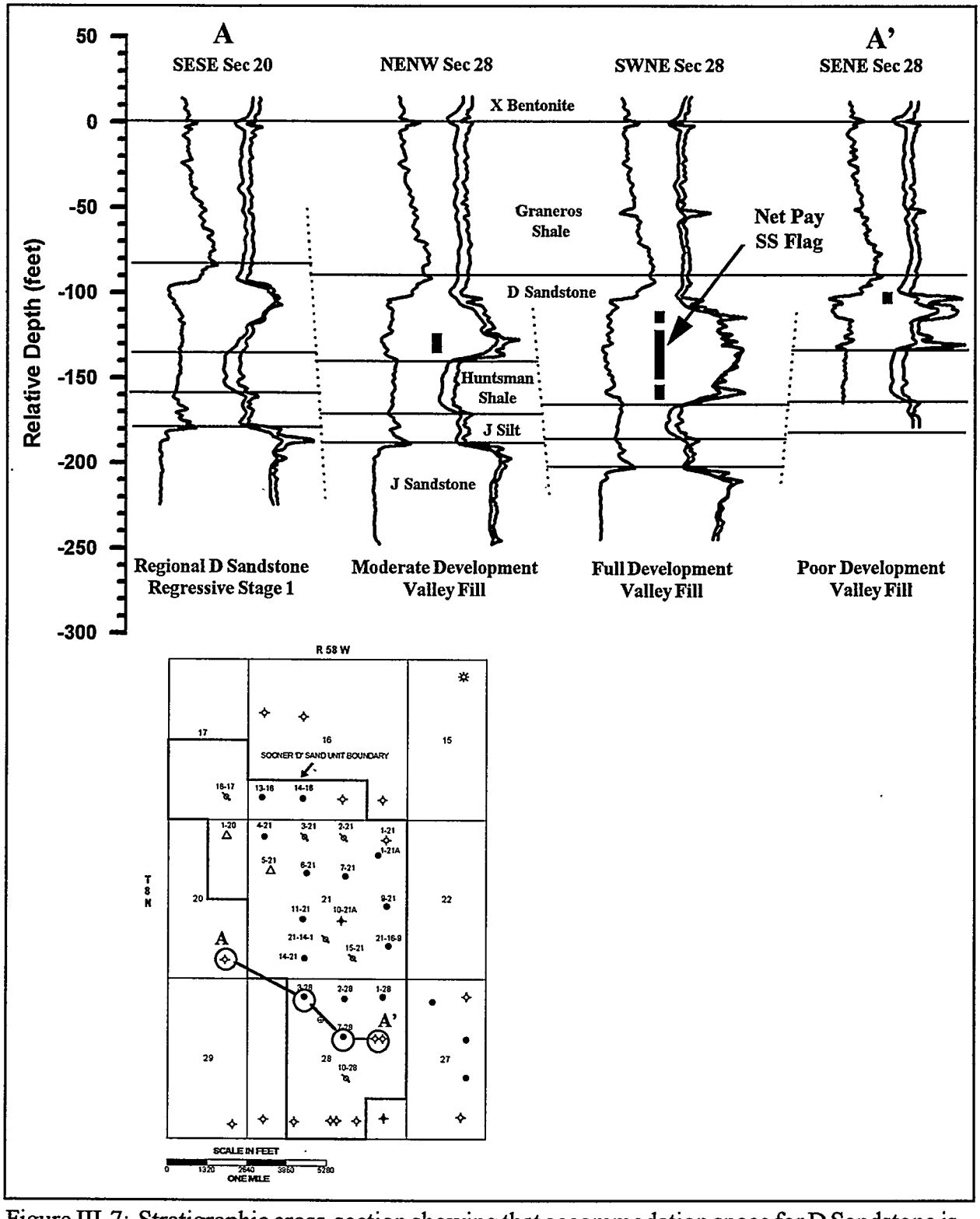

Figure III-7: Stratigraphic cross-section showing that accommodation space for D Sandstone is created by subtle paleo faulting and erosional thinning of Huntsman shale.

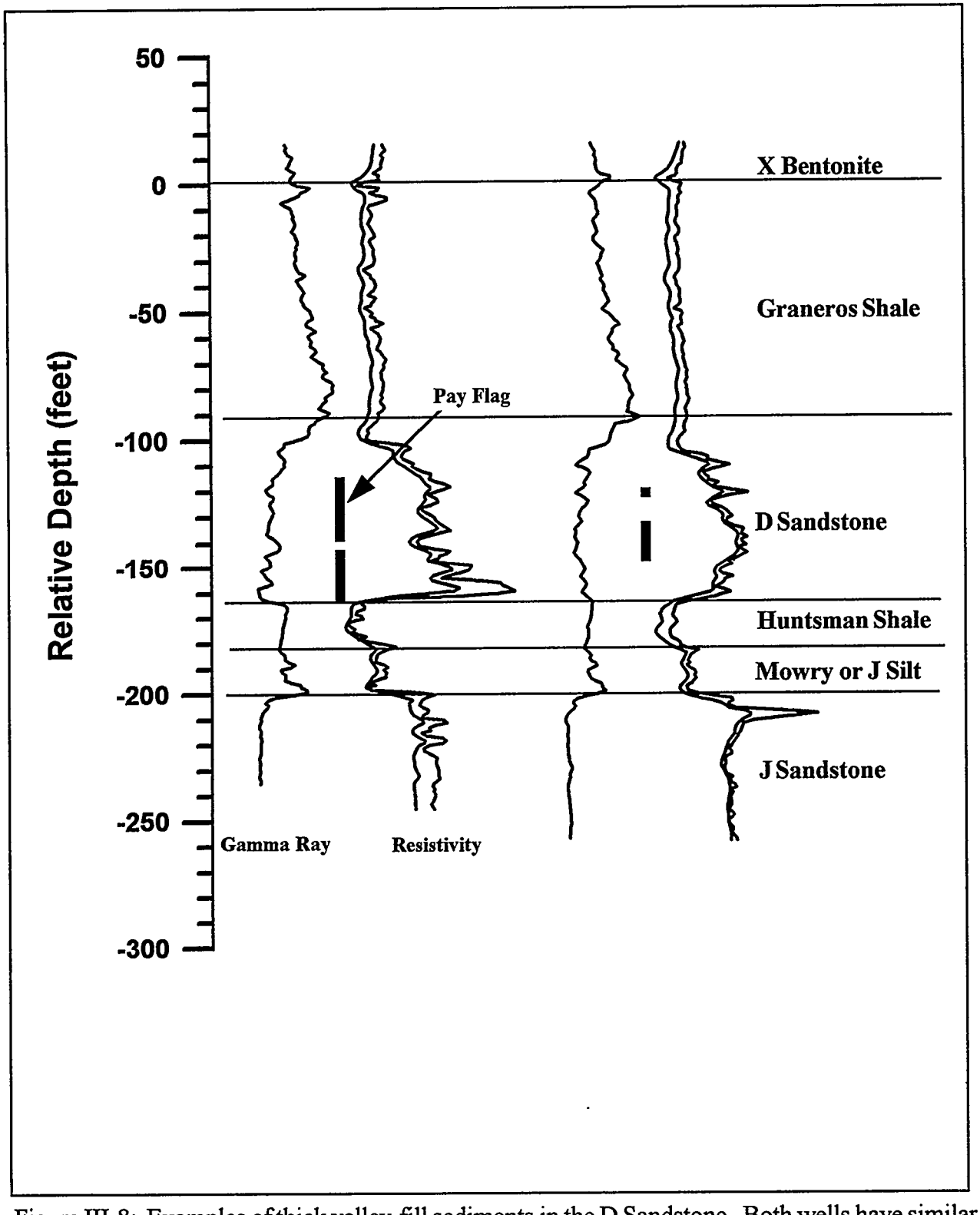

Figure III-8: Examples of thick valley-fill sediments in the D Sandstone. Both wells have similar gross thickness; however, the left log has 34 ft of net-pay thickness while the right log has only 11 ft. These wells are one 40-acre location (1320 ft) apart.

Petrographical Analysis of the D Sandstone

Introduction

Whole and sidewall cores were described from five wells. Two of these wells are in the Sooner Unit and four are in nearby fields. Thin-sections were taken and analyzed from the two wells in the Sooner Unit. The petrographical analysis helped define the estuarine depositional setting for the D Sandstone reservoir and support a basin-wide depositional model for the D Sandstone as a valley-fill system. Petrographical analysis shows two types of deposition in the Sooner Unit reservoir. Lower and older fluvial sandstones are characterized by kaolinite clays. Upper and younger sandstones are more estuarine in nature and are characterized by calcite and opal cements with burrowing by marine organisms. Root structures and carbonaceous shales also confirm the estuarine setting at the Sooner Unit D Sandstone reservoir. The primary component of D Sandstone at the Sooner Unit is mono-crystalline quartz which is fine-grained with a size of 0.163 mm +/- 0.045 mm. Tables IV -1 and W-2 summarize composition and grain size from D Sandstone thin section study. Major cements include iron oxide, clay and quartz. There are insufficient core data to determine if these cements constitute any significant component of reservoir compartmentalization. The main benefit derived from the petrographical analysis was from formulation of the depositional setting with well-log data.

Description of D Sandstone from SU 7-21

The reservoir rock from the SU 7-21 core contains very fine-grained sandstone, quartz to sub-arkosic arenite, styolites in thin clay laminae, ripple-drift cross-strata, trough class-beds, clay clasts, lenticular and flaser bedding (Fig. IV-1). The overlying cap rock is described as alternating shale and siltstone, with alternating laminate of high bioturbation and low to no bioturbation, horizontal and vertical burrows, some escape burrows, some laminae of shale with coal or organic with pyrite concretions. The underlying Huntsman Shale is described as uniform, dark grey shale with no obvious bioturbation. The density log from the SU 7-21 well is shown in figure IV-2.

Description of D Sandstone from SU 14-21-1

Nine sidewall-core samples were obtained and examined from the D Sandstone interval in SU 21-14-1. The samples were obtained with Schlumberger's sidewall drilling tool. A cut of each sample was impregnated with blue epoxy to allow estimation of porosity and thin sections were made. Detailed petrographic descriptions are found in table IV-3 and the density-porosity log from the SU 21-14-1 is shown in figure IV-3. These petrographical examinations were integrated with previous petrographical work from the SU 7-21 core (SWNE Sec 21).

Core samples show the D Sandstone interval to be fine-grained to very-fine-grained quartz arenite (to sub-arkose) sandstone which is inter-bedded with calcareous, organic-rich silt and clay. The sandstone is generally well sorted with sub-angular to rounded grains. Mono-crystalline quartz is the dominant grain type. Other grains include feldspar (often altered to sericite), chert, calcareous siltstone clasts, and muscovite mica. Quartz over-growths are the most volumetrically significant type of cement. They were preceded only by clay-rim cement. Other cements include calcite, brown clay (pelloidal texture, possibly iron oxide stained), opal, chlorite and illite clay, and kaolinite clay with vermiculite texture. The D Sandstone has been divided into three benches

from youngest to oldest; upper (Dl), middle (D2) and lower (D3),. Summary descriptions of each bench follow.

D1 and D2, Upper and Middle Benches (6269 - 6296 ft)

The upper and middle benches of the D Sandstone in the SU 21-14-1 well are generally finer grained, more finely inter-laminated with clay and silt-rich material, and have much less porosity than those found in the SU 7-21 well. Primary inter-granular porosity is almost always occluded by a variety of cements. The most volumetrically important of these include calcite, clay rims, and quartz over-growths. Non-kaolinitic clay pore-fill and minor amounts of opal pore-fill are also present. Secondary (leached) porosity is present in two samples at 6251 ft and 6258 ft (Fig. IV-3).

The abundance of calcite cement and chloritic, illitic (?) clay-types suggests a more marine-water composition of pore fluids. Finer grain size and abundant clays suggest deposition in a quiet water environment, possibly in a protected estuarine setting.

D3 Lower Bench (6238 - 6268 ft)

Porosity is best developed in the sample at 6279 ft (Fig. IV-3). This sample shows a combination of preserved primary inter-granular porosity (not occluded by quartz over-growths) and secondary porosity. The secondary porosity appears as oversized pores developed when feldspar grains or calcite cement were dissolved (leached). Permeability should be good in this interval since inter-granular pore systems generally have a high degree of connectivity. This zone and the one immediately below at 6290 ft are the best sorted, coarsest grained and with least clay-rim cement. Porosity is less at 6290 ft due to extensive development of quartz over-growths. Porosity occlusion in the zone at 6258 and 6272 ft is controlled by kaolinite clay pore-fill with a distinctive vermiculite texture. This interval is fine grained with clay rim cements, finely inter-laminated silty clay layers, and calcareous siltstone clasts.

Reservoir quality is best developed in sandstones which were deposited in higher energy environments, incompletely cemented by quartz over-growths, and exposed to waters that leach feldspar grains. Kaolinite is a clay typically associated with soil development in sub-aerially exposed environments. These characteristics are typical of fluvial deposits in an exposed alluvial-plain setting

Stratigraphic Analysis

Correlation between the Sooner Unit 21-14-1 and the Sooner Unit 7-21 (Fig. IV-4) indicates that the D Sandstone is thicker and more clay-rich in the Sooner Unit 21-14-1. The D Sandstone is bracketed between the high gamma-ray shales in the J Silt (below) and the Graneros Shale (above) which represent periods of quiet-water deposition during maximum marine transgression. These are maximum flooding surfaces (MFS) in sequence stratigraphy. Correlation from these flooding surfaces reveals that the D3 bench is an additional sand package in the SU 21-14-1 which includes the reservoir inter-valley and the kaolin clay-rich sands. This interval is bounded at the base by an erosional sequence boundary (SB) which was the floor of an incised valley system. It is bounded at the top by a transgressive surface (TS) and represents the low stand systems tract in this area. The upper-sandstone package (D1 and D2 benches) is of

similar thickness in the SU 21- 14-1 and 7-21 wells. These sands are characterized by calcite cements and burrowing by marine organisms. They were deposited during marine transgression into the valley system. Root structures and carbonaceous shales **found** in the SU 7-21 core suggest that these sands were deposited in an estuarine environment. They are bounded at the top eroding surface and generally fine upward. This interval is the transgressive-systems tract in sequence stratigraphy. The D1 and D2 benches are coarser grained and less clay-rich in the SU 7-21 than in the SU 21-14-1. They are oil reservoirs at the SU 7-21 and non-productive at the SU 21-14-1. The trend of quality sands is elongate parallel to the estuary margin. These sands were probably deposited as estuarine bar sands similar to those described by Allen and Posamentier at the Gironde Estuary, France.

Reservoir Compartmentalization

The low-stand and transgressive-systems tracts are characterized by different reservoir compartmentalization styles. Low-stand sands were deposited in fluvial point bars which were separated by clay-rich channel-fill along depositional strike (north-south to northwest-southeast). They are restricted to the deepest part of the incised valley and probably separated into reservoir pods along that trend. The most effective vertical-flow barrier is probably the kaolinitic clay pore-fill between the low-stand (D3) and transgressive (D1 and D2) sandstones.

Transgressive sands were deposited in a setting with increasing accommodation space during marine transgression. Consequently, they cover a wider area and are more aggradational in nature. Within the estuarine environment, elongate bar sands develop parallel to depositional strike. These bar sands form the reservoir compartments in the D1 and D2 benches.

Summary and Conclusions

Petrographic study of core data can tell much about reservoir heterogeneity by establishing elements indicative of depositional setting. The petrographic studies ofthe Sooner Unit D Sandstone established an estuarine setting. This allowed review of literature which described estuaries. Descriptions of modem estuaries helped visualize the Sooner Unit reservoir in the subsurface and orientation of sedimentary features.

Table IV -1
Composition of D Sandstone from Thin-Section Analysis

Component	Percentage
Mono-crystalline Quartz	66.5%
Poly-crystalline Quartz	7.2%
Potassium Feldspar	0.8%
Plagioclase	0.5%
Mica	0.8%
Rock Fragments	2.5%
Clay Cement	6.4%
Iron Oxide Cement	7.2%
Calcite Cement	1.0%
Opal Cement	2.9%
Quartz Cement	4.0%
Total	100.0%

Table IV-2
Grain Size for D Sandstone from Thin-Section Samples

Sample	Mean Size (mm)	Standard Deviation	Verbal
1	0.179	0.043	Fine
2	0.157	0.047	Fine
3	0.160	0.047	Fine
4	0.158	0.044	Fine
5	0.325	0.108	Medium
6	0.116	0.044	Very Fine

Mean size was determined by measurement of apparent long axes of 40 randomly selected mono-crystalline quartz grains per thin section.

Table IV-3
D Sandstone Petrographic Descriptions from SU 21-14-1

Depth	Description of thin-section from sidewall core
6243 ft	Calcareous siltstone inter-laminated with very-fine-gram quartz sandstone, no visible porosity, micaceous, abundant pyrite.
6247 ft	Very-fine-grain quartz sandstone inter-laminated with calcareous, clay-rich siltstone and organic-rich micro-styolites. Sandstone shows no visible porosity, primary inter-granular porosity has been occluded by cements; including clay rims, calcite pore-fill, opal and quartz overgrowths; rare, brown pelloidal clay clasts.
6251 ft	Very-fine-grain quartz sandstone inter-laminated with calcareous, clay-rich siltstone and organic-rich micro-styolites. Sandstone shows up to 10% porosity as over-sized pores (secondary porosity due to dissolution of feldspar grains and/or calcite cement). Primary inter-granular porosity has been occluded by clay rims, quartz overgrowths and minor opal and dark brown clay (possibly iron oxide) pore-fill.
6258 ft	Very-fine-grain quartz sandstone inter-laminated with calcareous, clay-rich siltstone and organic-rich micro-styolites. Ripple cross-lamination in sandstone layer. Sandstone shows up to 5% porosity as over-sized pores (secondary porosity due to dissolution of feldspar grains and/or calcite cement). Primary inter-granular porosity has been occluded by clay rims, quartz overgrowths and minor opal and dark-brown clay (possibly iron oxide) pore-fill.
6272 ft	Very fine grain quartz sandstone (40%), well-sorted, with no visible porosity. Primary inter-granular porosity has been occluded by kaolinite clay with vermiculite texture. Sandstone includes less than 10% feldspar (altered to sericite), chert, calcareous siltstone and muscovite grains. Sandstone is inter-laminated with calcareous, micaceous, clay-rich siltstone (60%) and organic-rich micro-styolites.
6276 ft	Fine-grain quartz sandstone with up to 10% feldspar, moderately well-sorted, 5% porosity (both primary inter-granular and secondary grain dissolution). Cements include quartz overgrowths, clay rims, and kaolinite clay pore-fill with vermiculite texture. Sample contains thinly laminated calcareous, micaceou^{g}, clay-rich siltstone and organic-rich micro-styolites in upper 20%.

Table N-3
D Sandstone Petrographic Descriptions from SU 21-14-1

6279 ft	Fine-grain quartz sandstone, well-sorted, with up to 10% feldspar (Plagioclase altering to sericite), muscovite mica, and distorted silty-clay clasts. Cement includes quartz overgrowths and possibly feldspar overgrowths. Observed 15% porosity, about half preserved primary inter-granular and half secondary dissolution of feldspar grains. Minor authigenic calcite rhombs, kaolinite clay, and chlorite clay associated with mafic grains.
6290 ft	Fine grain quartz sandstone, well sorted, with mineral assemblage as at *6279* ft. Primary inter-granular porosity is almost completely occluded by quartz (+/- feldspar) overgrowth cement. Observed *3%* porosity is entirely secondary dissolution of feldspar, mica, and/or calcite.
6295 ft	Very fine quartz sandstone inter-laminated with calcareous, micaceous, clay-rich siltstone and organic-rich micro-styolites. Cements include quartz overgrowths and kaolinite clay pore-fill with vermiculite texture. Observed less than 1% micro-porosity associated with incomplete clay pore-fill and possible calcite dissolution.

References

Allen, G .P. and IL W. Posamentier. 1993. "Sequence Stratigraphy and Facies Model of an Incised Valley Fill: The Gironde Estuary, France." *Journal of Sedimentary Petrology 63(3): 378-391* (May 1993).

Well No. Fed. Sooner #7-21
Location Sec 21, T8N, R58W
Weld County, CO

Date Dec. 31, 1992
Strat. Unit "p" Sandstone
Measured by F. G. Ethridge

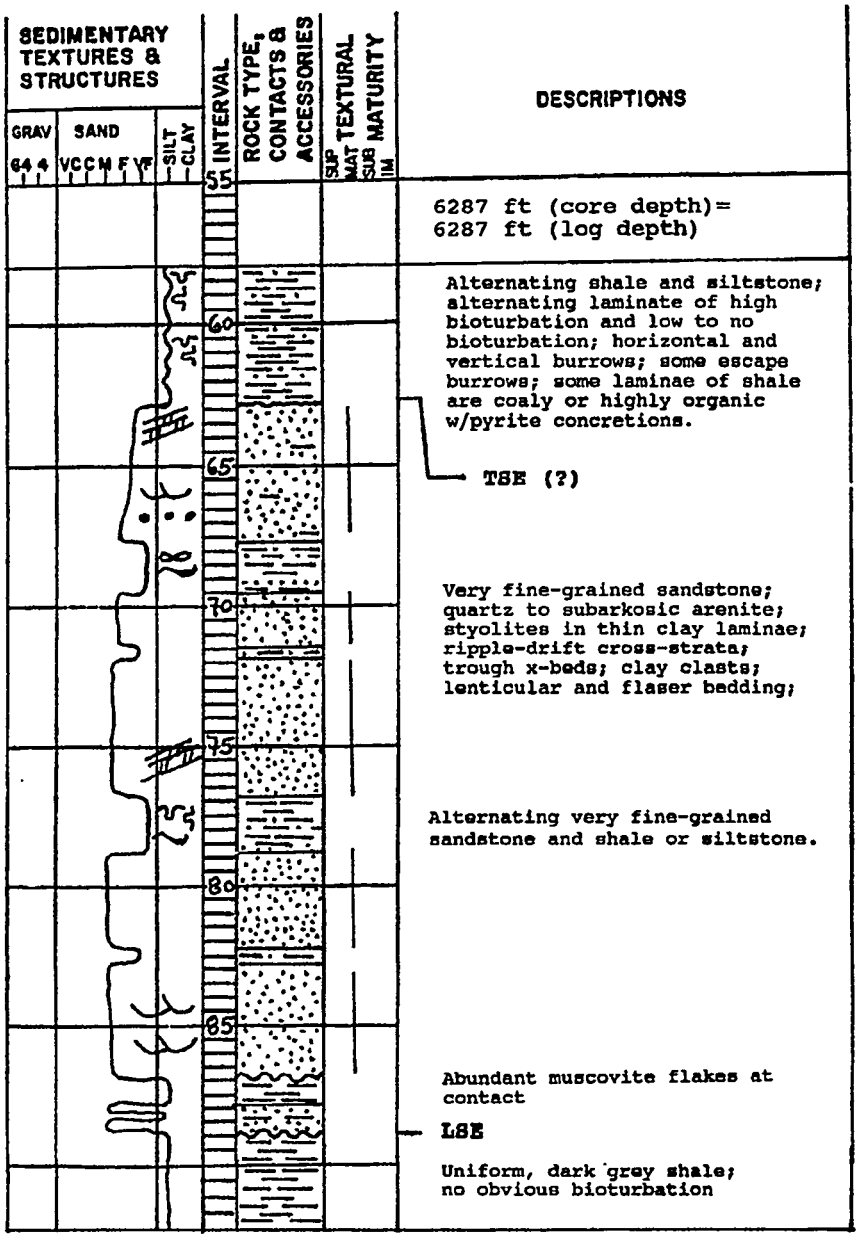

Figure IV-1: Description from whole core taken from SU 7-21 well.

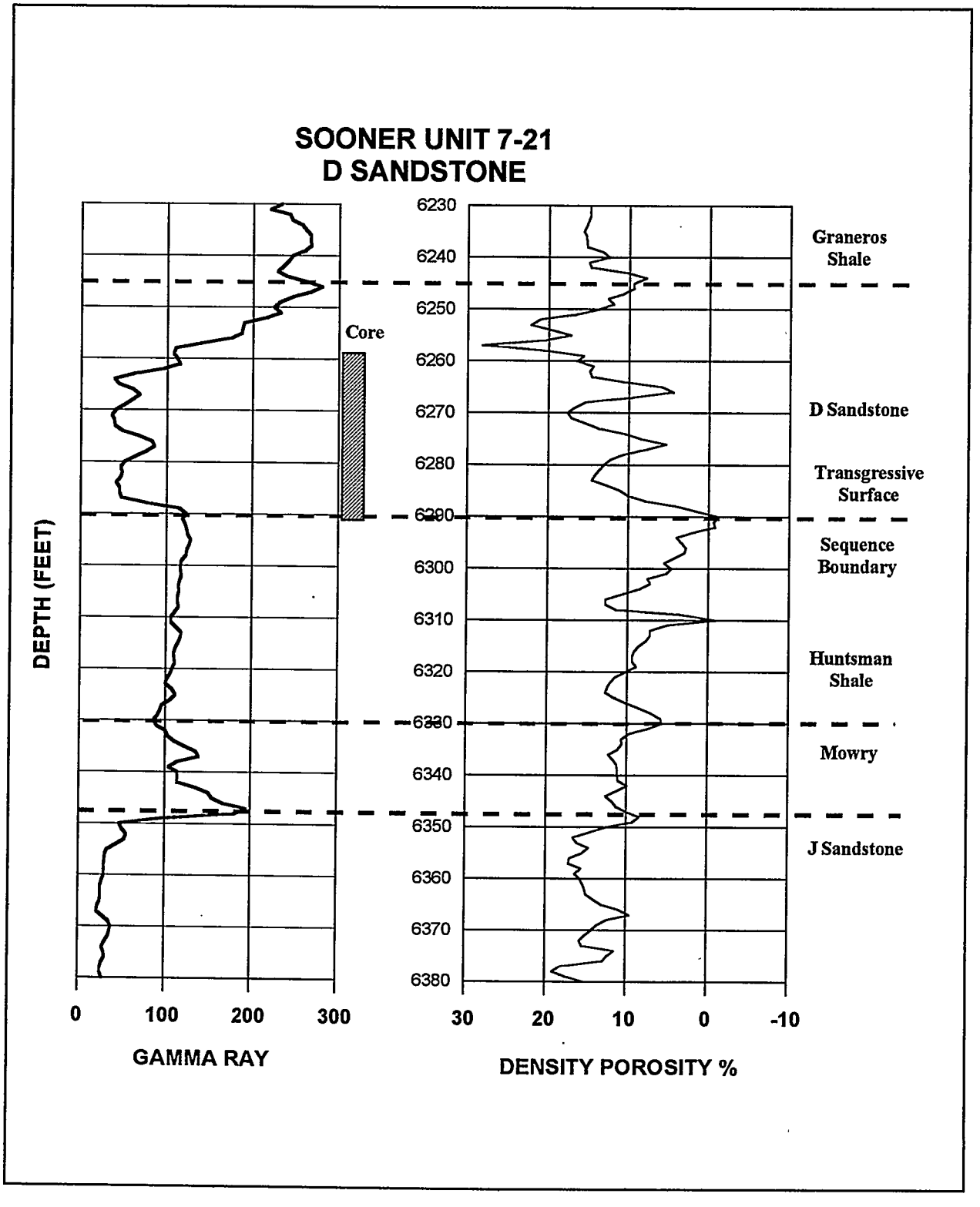

Figure IV-2: Density log from SU 7-21 well.

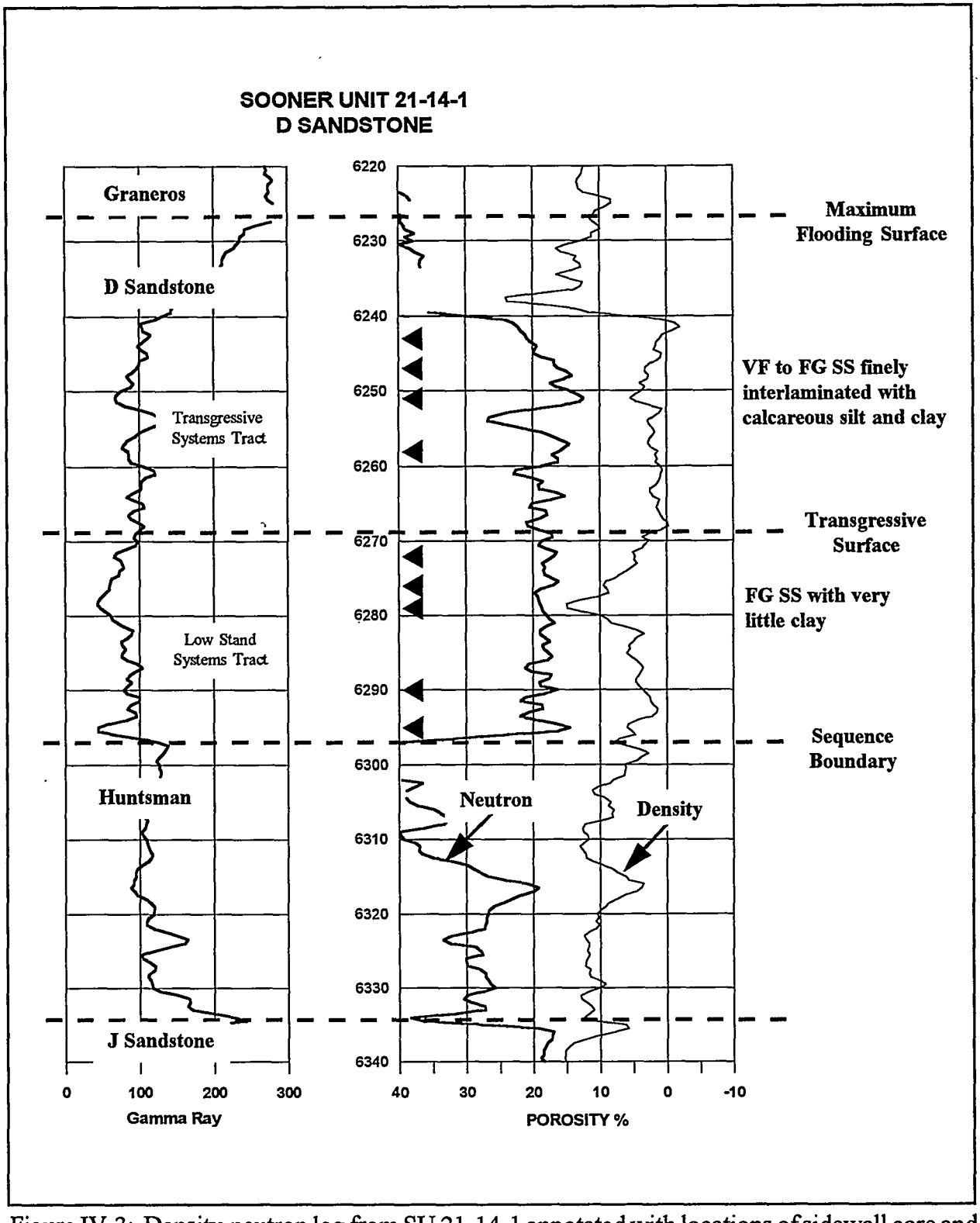

Figure IV-3: Density-neutron log from SU 21-14-1 annotated with locations of sidewall core and summary descriptions.

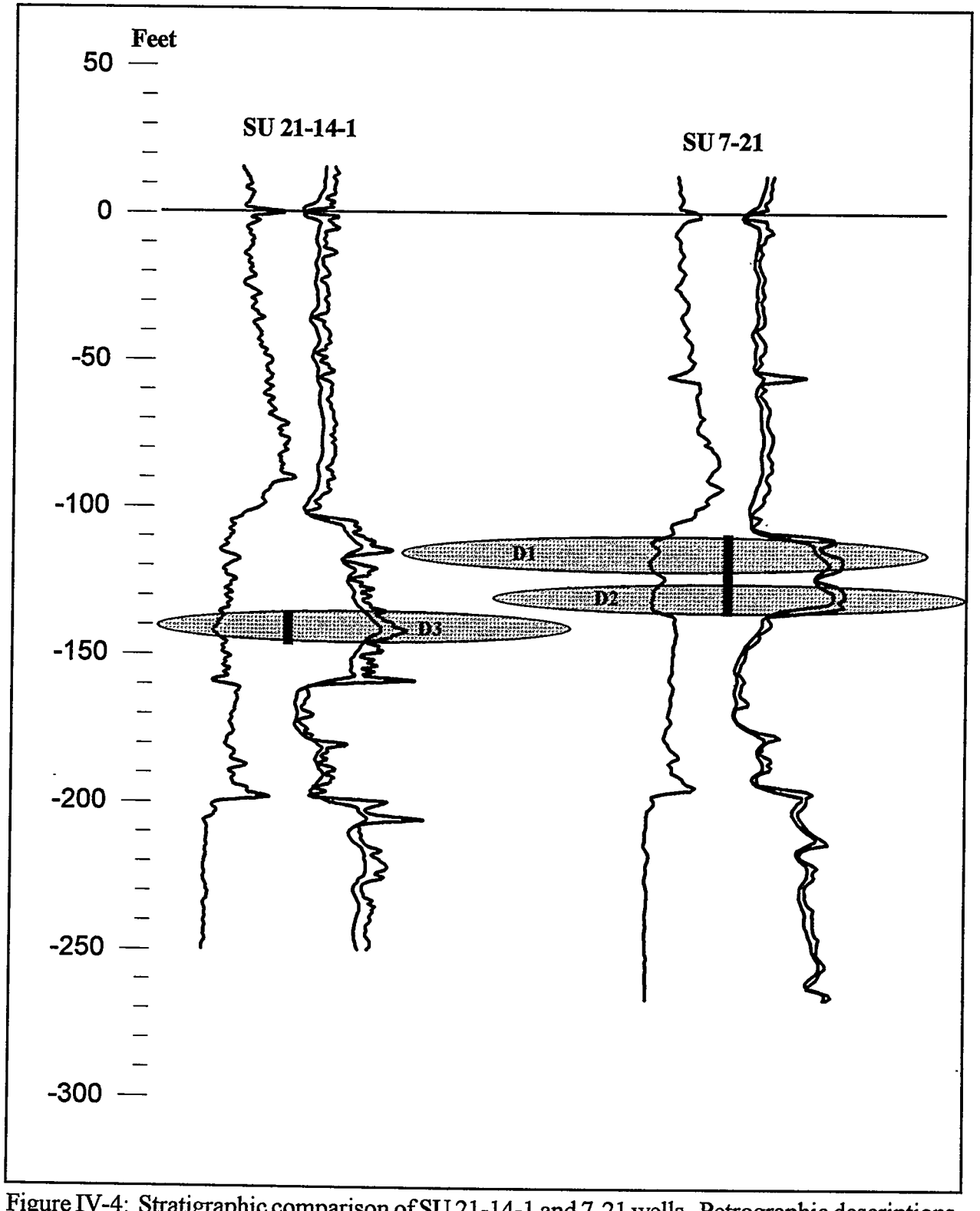

Figure IV-4: Stratigraphic comparison of SU 21-14-1 and 7-21 wells. Petrographic descriptions were made from core in these wells.

Core and Electrical Log Descriptions of the D Sandstone

Basic to the characterizations of the D Sandstone reservoir at the Sooner Unit are data from conventional core analysis and electrical log calculation. The permeability-porosity cross-plot from D Sandstone cores is shown in figure V-1. The plot suggests a porosity cut-off of between 6 and 8 percent for determination of net pay. The average net-pay porosity of the Sooner Unit reservoir is 11.5 percent. Statistics for permeability are summarized in table V-1. The tabulation is intended to show that a permeability cut-off of 0.5 and is probably appropriate and a value of 0.74 for Dykstra-Parsons coefficient of permeability variation results when a log-normal frequency plot is made as shown in figure V-2.

Calculations of net-pay properties from electrical logs are summarized in table V-2. Net-pay thickness averages 17 ft (+/- 8 ft) with a maximum of 34 ft. At the Sooner Unit, criteria used to identify productive intervals include 1) resistivity of greater than 30 ohm m, 2) gamma ray of less than 30 API units, micro-resistivity and caliper log readings indicating mud-cake buildup and 3) density-log porosities of greater than 8 percent. Calculations of water saturations are qualitative but are performed with reasonable success using a standard Archie equation for sandstones. The formation water is very fresh and a value of 0.06 ohm -m is used for water resistivity (R_W) at formation temperature of 220° F. Using the medium-induction curve value for formation resistivity (R_t) produces reasonable values for water saturation. A shale content of 35 percent from gamma-ray readings and water saturation of 60 percent are used to discriminate the net-pay from non-reservoir rock as summarized in table V-2. The D Sandstone did not produce formation water during primary depletion and it is assumed that the reservoir water saturation was initially at irreducible conditions. Special core analysis indicates a value for irreducible water saturation of 19 percent.

Table V-1
Permeability Data from Four D Sandstone Cores in the Sooner Unit Area

	0.1 and cutoff	0.5 and cutoff	1.0 and cutoff
Geometric Mean k	8.8	21.3	23.6
Median Value k	20.8	28.0	28.2
Dykstra-Parsons Co e£ of Variation	0.890	0.744	0.715
Cumulative Capacity	99.9%	99.8%	99.7%

Table V-2
Summary of Log Calculations from 23 wells in the D Sandstone at the Sooner Unit

	Net Pay Thickness (feet)	Porosity Thickness (feet)	Hydro-carbon Thickness (feet)	Average Porosity	Oil Saturation
Maximum	34.0	2.887	3.725	11.0%	77.5%
Mean	16.6	1.408	1.899	11.5%	74.1%
Median	19.0	1.363	2.052	10.8%	66.4%
Standard Deviation	8.2	0.892	1.110	1.4%	5.5%

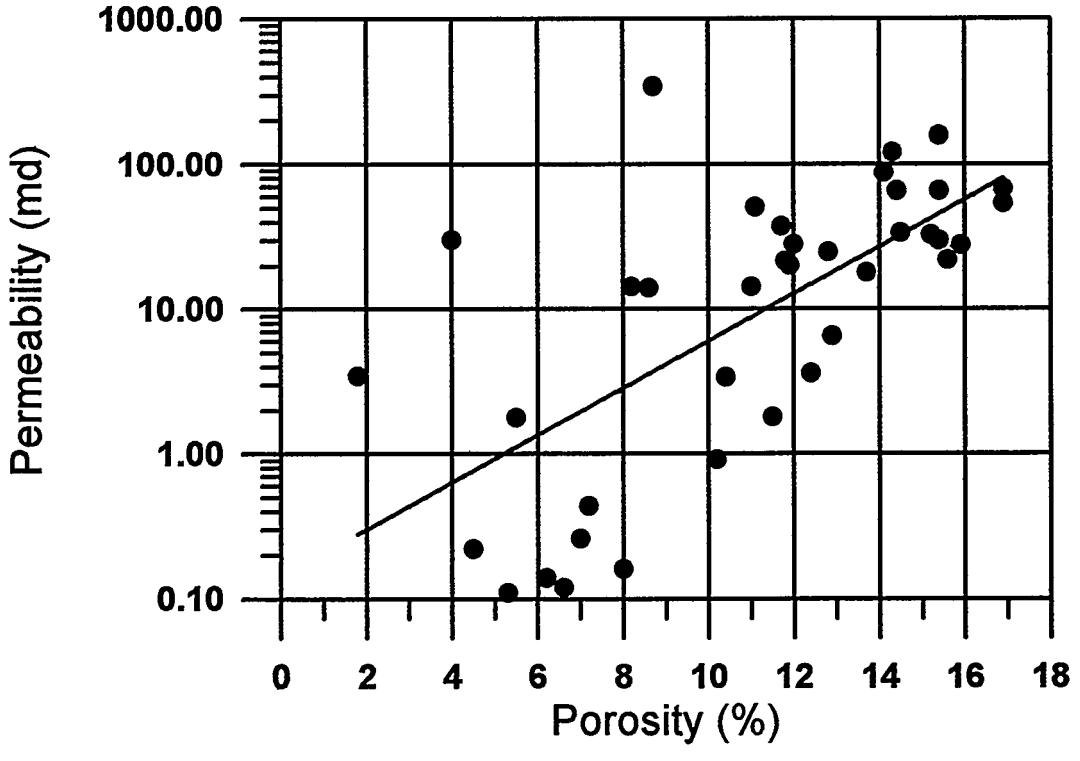

Figure V-1: Permeability-porosity cross-plot from D Sandstone core data.

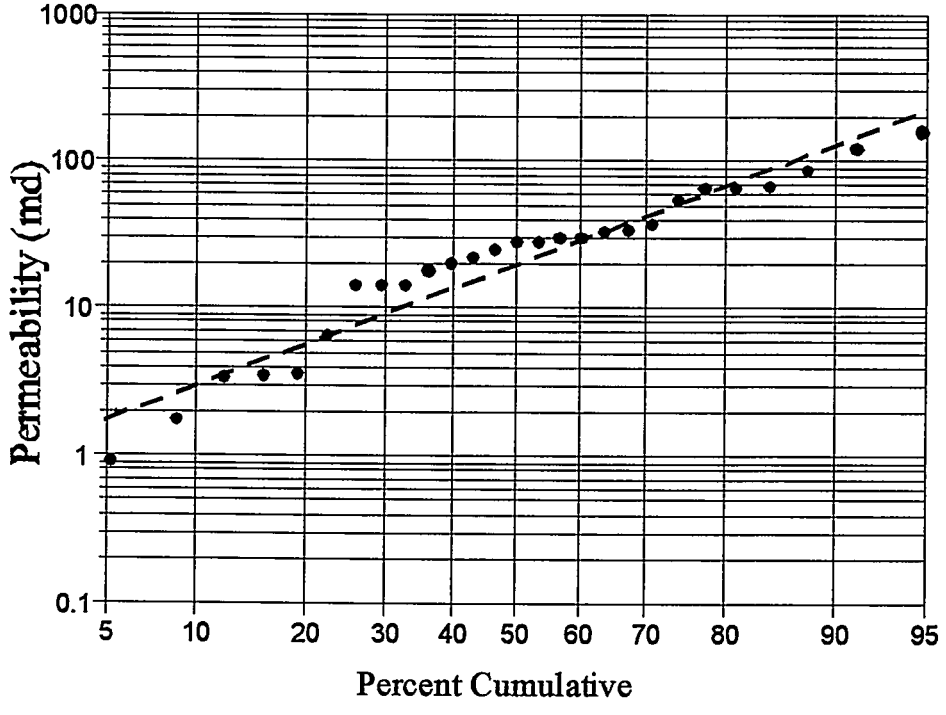

Figure V-2: Frequency distribution of D Sandstone permeability.

Pressure Transient Analysis of the D Sandstone

Pressure transient testing was performed at injection and production wells. The duration of these pressure tests were from 72 to 120 hours. Static reservoir pressures were found to vary from 200 psi to over 2000 psi. Permeability to water at injection wells ranged from 5 to 50 and and most wells indicate negative skins from -2 to -4. All wells in the Sooner Unit have been hydraulically fractured; however, the character from plots of the pressure transient data indicate late-time linear or bi-linear flow which is most likely resulting from reservoir heterogeneity. Evaluations of the pressure transient data using analytical simulation and type curves indicate channel-widths which average 610 ft. The analyses from injection-well data are summarized in table VI-1.

Table VI-1
Summary of Pressure Fall-off Analysis from Water Injection Wells

Well	Transmissibility kh/tB (md-ft/cp)	Skin	Bi-linear Flow Width (feet)
SU 2-21	3641	-4.3	905
SU 3-21	650	-3.3	684
SU 10-21A	1106	-4.6	490
SU 10-28	400	-2.0	363
Average	1449	-3.6	610

Most of the pressure tests could not be matched by type-curves or simulation without inclusion of nearby barriers in the analysis. These dimensions appear to be valid when compared to the dimensions and shapes on map displays of various 3D seismic attributes of the D Sandstone and related horizons.

Log-log plots and type-curve analysis of pressure transient tests of the D Sandstone at the Sooner Unit demonstrate classic examples of near-well bathers, linear flow and bi-linear flow. Although all the wells have been hydraulically fractured, linear-flow regimes exist in late time (20 to 100 hrs). Figure VI-1 shows a radial type-curve analysis from an injection well fall-off test. The pressure-derivative curve indicates non-radial flow and a near-well bather. This is interpreted from the pressure-derivative curve stabilizing at the 1.0 line (Pirard and Bocock 1986; Ehlig-Economides 1988). A very strong linear flow is demonstrated in figure VI -2 where the pressure-derivative curve follows a 1/2 slope. A slope of 1/2 is diagnostic of linear flow (Proano and Lilley 1986). Seismic interpretations of the D Sandstone reservoir surrounding this well clearly indicate narrow channel development. Bi-linear flow is diagnosed from a 1/4 slope of the pressure-derivative curve (Ehlig-Economides and Hegeman 1994). A 1/4-slope example is shown in figure VI-3. It is frequently difficult to interpret pressure-transient tests when there are indications of linear and bi-linear flow from the character of the pressure-derivative curve (1/2 or 1/4 slope). Channel flow type curves can provide meaningful insights to functional reservoir

architecture where this is the dominant case (Ehlig-Economides and Economides 1985). This is especially true if there are core and drill-stem test data for a supplemental source of permeability values. A channel flow type-curve analysis plot is shown in figure VI-4. The pressure data are the same as shown for a linear-flow example on figure VI-2. Reasonable reservoir and wellbore properties are calculated from this test using channel-flow analysis. The calculated channel width is 531 ft . The permeability to water is about 20 and and the apparent stimulation factor is -2.4. The permeability is in good agreement with core data and the channel width is supported by seismic interpretation.

The pressure-transient data from the D Sandstone at the Sooner Unit have characteristics which are consistent with linear and bi-linear flow. The log-log pressure and pressure derivative plots were found to be very diagnostic. Channel-flow type-curve analysis produced reasonable results for permebility and resevoir dimensions when compared to other data from core and seismic maps.

References

Ehlig-Economides, C. and M.J. Economides. 1985. "Pressure Transient Analysis in an Elongated Linear Flow System." *Society of Petroleum Engineers Journal* (December 1985): 839-847.

C. Ehlig-Economides. 1988. "Use of the Pressure Derivative for Diagnosing Pressure Transient Behavior." *Journal of Petroleum Technology* 40(10): 1280-1282 (October 1988).

Pirard, Y.M. and A. Bocock. 1986. "Pressure Derivative Enhances Use of Type Curves for the Analysis of Well Tests." paper Society of Petroleum Engineers 14101 presented at the 1986 SPE International Meeting on Petroleum Engineering, Beijing, March 17-20.

Proano, E.A. and I.J. Lilley. 1986. `Derivative of Pressure: Application to Bounded Reservoir Interpretation." paper Society of Petroleum Engineers 15861 presented at the 1986 SPE European Petroleum Conference, London, Oct. 20-22.

Ehlig-Economides, C. And Peter Hegeman. 1994. "Guidelines Simplify Well Test Interpretation." *Oil and Gas Journal* 92(29): 33-40 (July 18, 1994).

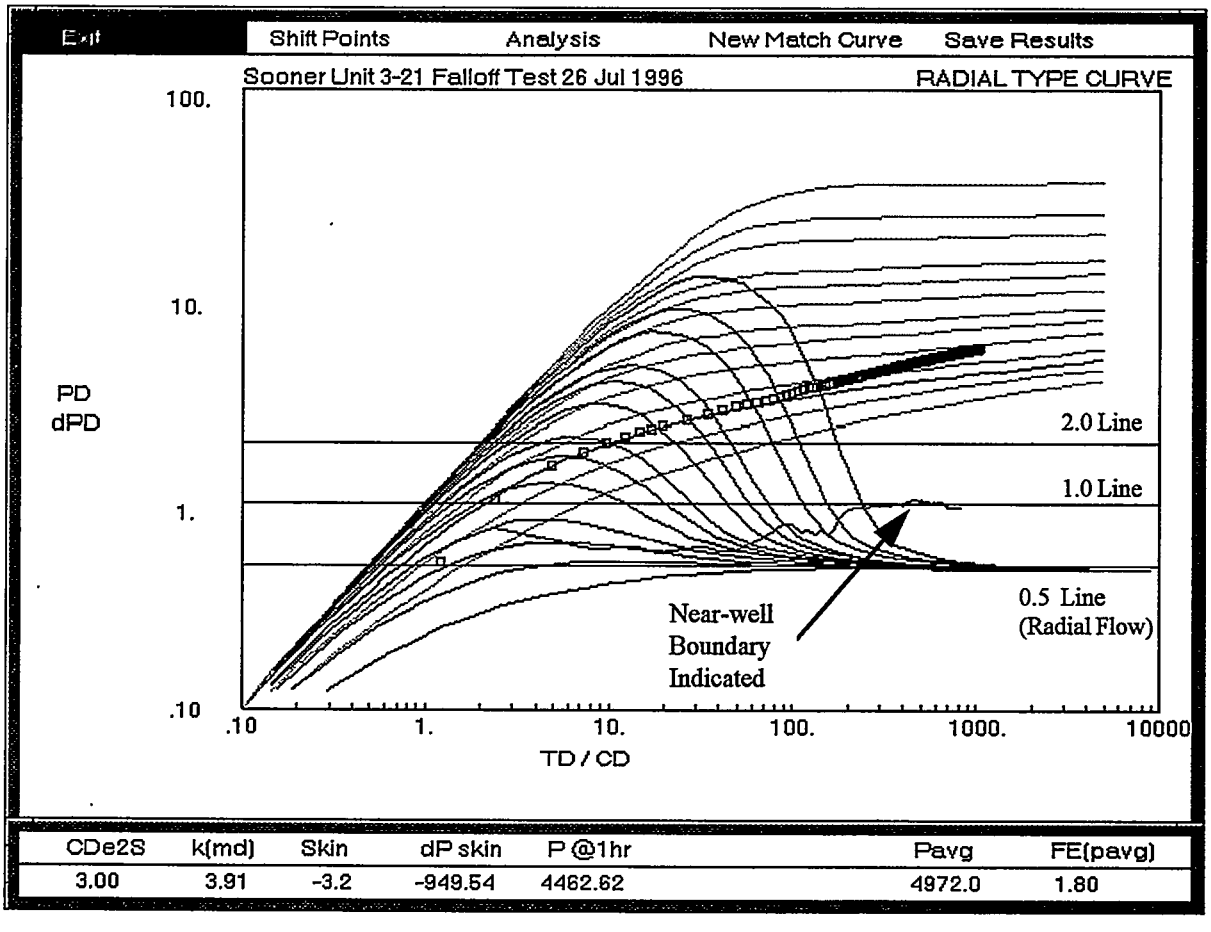

Figure VI-1: Near-well boundary example from radial type-curve analysis of a pressure fall-off test.

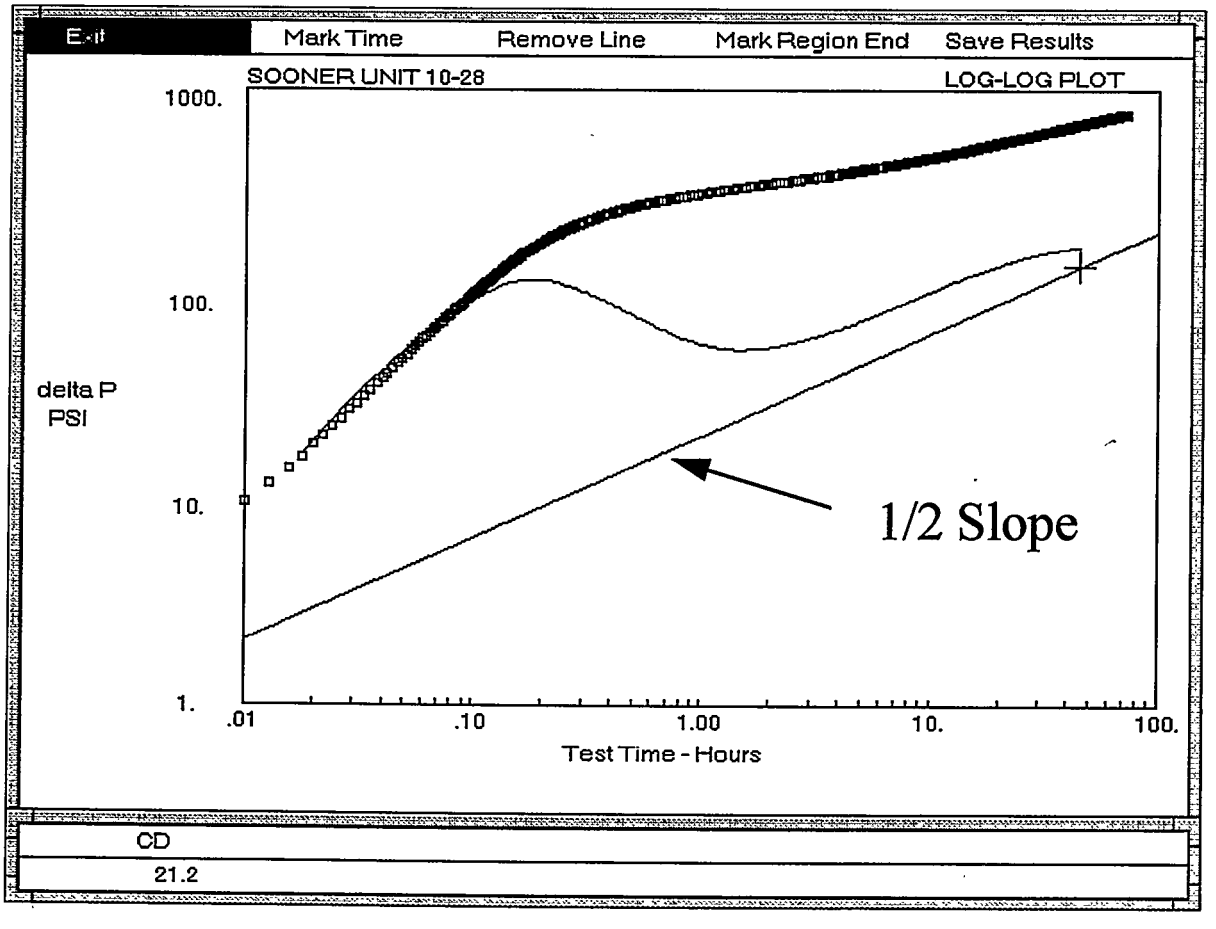

Figure VI-2: Half-slope example from a pressure fall-off test. A 1/2 slope of the derivative curve is indicative of linear flow.

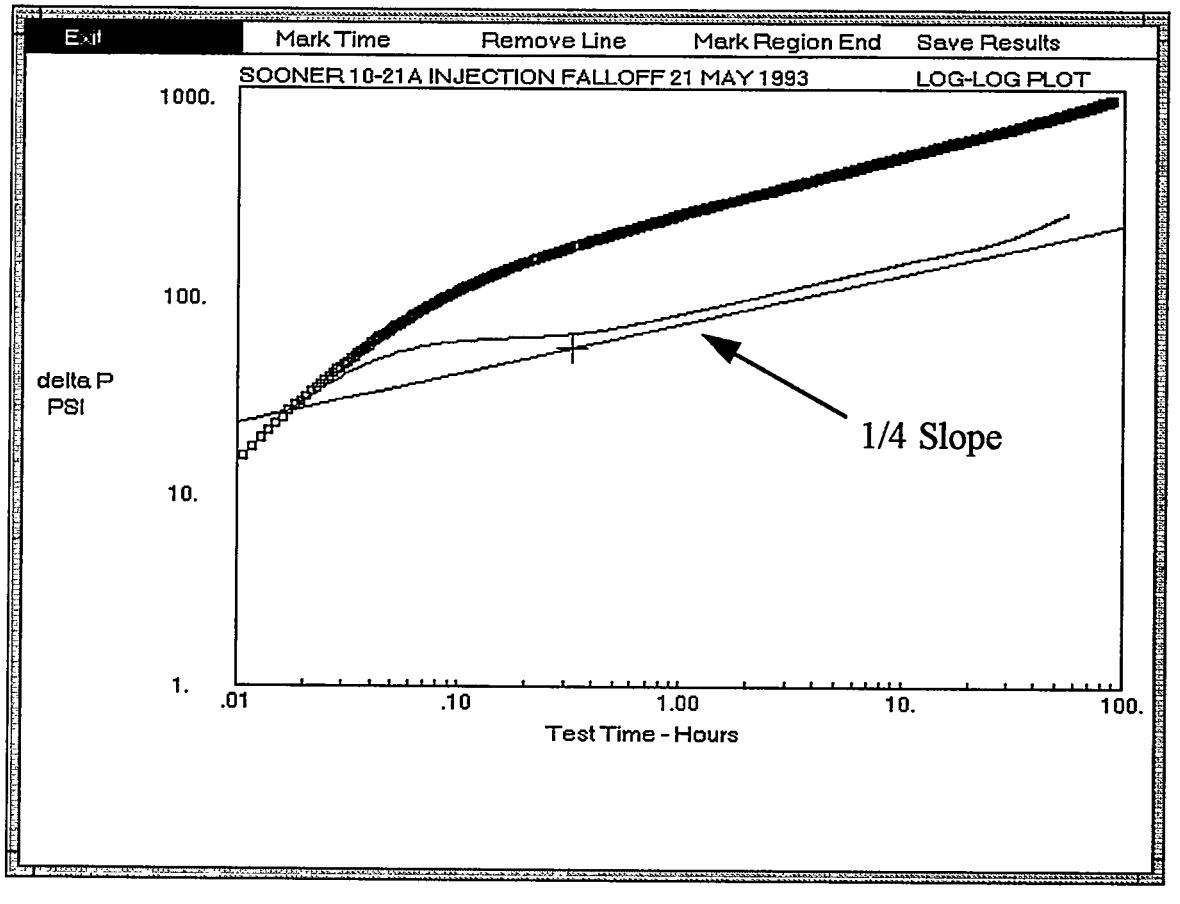

Figure VI-3: Quarter-slope example from a pressure fall-off test. A 1/4 slope of the derivative curve is indicative of bi-linear flow.

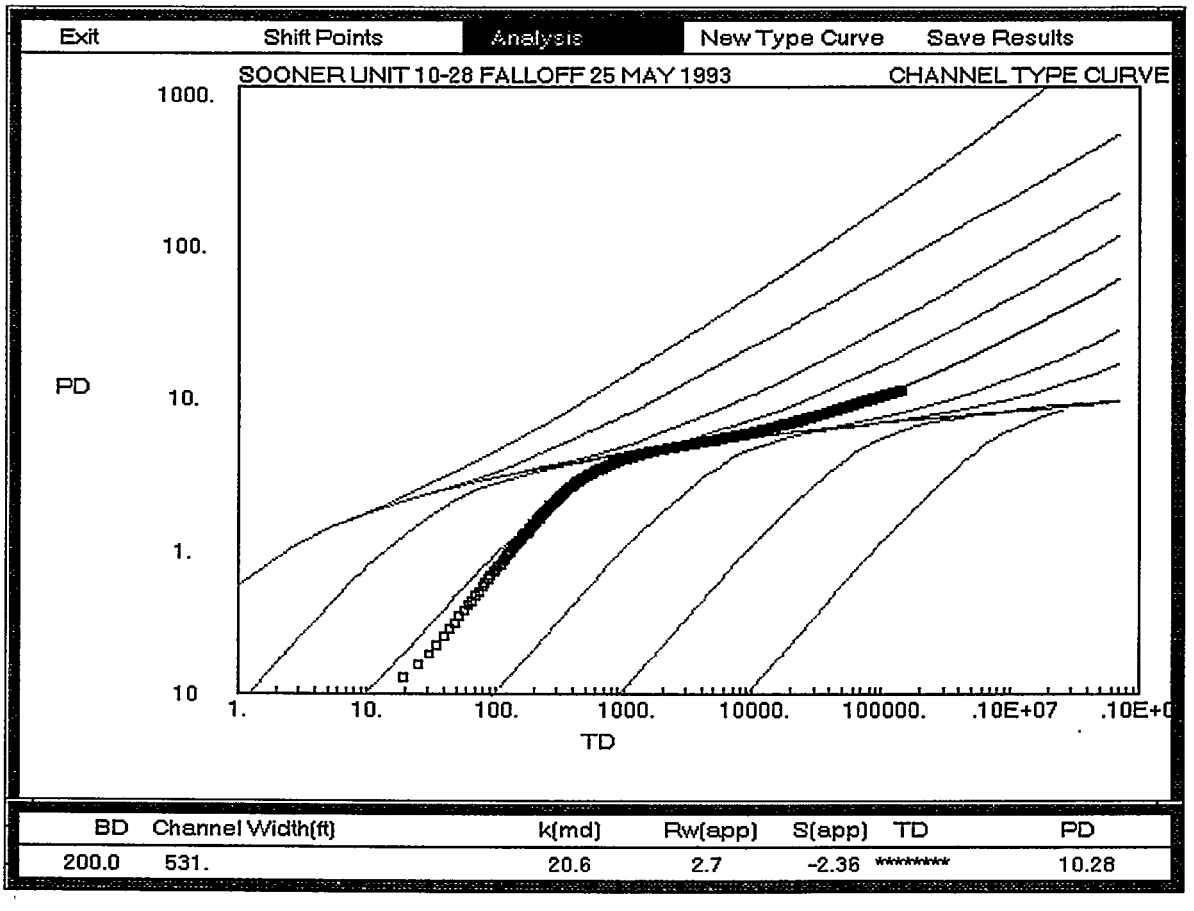

Figure VI-4: Example of channel-flow type-curve analysis. Supplemental permeability data from core or drillstem test aid interpretation from these curves.

Seismic Characterizations of the D Sandstone

Introduction

Fluvial and valley-fill hydrocarbon reservoir systems are frustrating to the explorationist and development engineer-geologist. This is because they exhibit a high degree of lateral and vertical heterogeneity. Countless examples can be given where near-offset and replacement wells encountered unpredicted and dramatic changes in reservoir development. During waterflood operations, effects from heterogeneity and anisotropy of the reservoir are magnified over what is observed during primary depletion. It is concluded that regular well spacing of 40-acre patterns is not efficient for waterflooding fluvial and valley-fill D Sandstone reservoirs in the Denver Basin. While infill drilling at 20-acre spacing and developing D Sandstone fields on regular five-spot injection patterns would recover most of the moveable oil, it is not economically efficient. Integrated reservoir characterization with 3D seismic can optimize infill locations with the minimum number of wells to maximize economic benefit. A method is presented which has successfully integrated 3D seismic attributes with electric-log and well-performance data for the purpose of drilling low risk and high-recovery wells. While interpreters of 2D and 3D seismic in the Denver Basin have been able to resolve the general limits and outline of valley-fill systems in the D Sandstone with single attributes such as amplitude, it is possible to improve resolution of compartmentalization by using multiple attributes of the D Sandstone and adjacent temporal horizons.

The acquisition of 3D seismic does not result in an easy and immediate interpretation of D Sandstone reservoirs. This is because reservoir development is primarily stratigraphic in nature and it is relatively thin at a maximum gross thickness of 70 ft with an average of 30 ft. It is possible with patience and systematic analysis to not only produce maps representing stratigraphic variability but to also quantify (with an error range) reservoir development in terms of net feet and porosity-feet.

Seismic Acquisition and Processing

The Sooner Unit 3D seismic data were recorded October 8-17, 1992. The source was created with four LRS-315FC vibrators. Twenty receiver lines were surveyed east-west and spaced•800 ft apart. Twenty-five source lines were oriented north-south and were spaced 600 ft apart. The 200-ft source-spacing used on each source line allowed four vibration points (VP) to be recorded between each pair of receiver lines. A total of 732 VPs were recorded to create the 3D data volume. The source and receiver coverage extended beyond the boundaries of the Sooner Unit so a stacking fold of 20 or more would begin immediately inside the Sooner Unit boundary. The initial processing steps of the Sooner 3D data are shown in table VII-1.

Interpretation

Three synthetic seismograms (from sonic and density log data in the 3D survey area) and a vertical seismic profile (VSP) taken in SU 10-21A at time of 3D data acquisition were used to calibrate initial interpretation efforts. The calibration identified the **D Sandstone** at **approximately** 1.456 sec two-way time (TWT): The analysis also indicated the zero-phase synthetic

seismograms best tie reverse-polarity seismic data. Picking of events was done on reverse-polarity (zero-phase) data. The correlation of the VSP to surface seismic data is good at the D Sandstone but deteriorates uphole. It is fortunate that one of the electrical-log suites used for construction of synthetic seismograms was from a well which was drilled to the Permian Ingelside (8133 ft total depth) as the Plainview (6646 ft) is a strong reflector below the D and J Sandstones (6308 ft and 6388 ft, respectively). A seismic section, shown in figure VII-1, from the Sooner 3D data volume shows the relationship of these reflectors. It is concluded that synthetic seismograms from good-quality sonic and density logs are *sufficient* to calibrate seismic data with formation horizons in the Sooner Unit area. A suite of logs **through** the Plainview formation is recommended for a high-confidence calibration.

The amplitude and isochron of the D Sandstone temporal event are good indicators of the general valley-fill system geometry and limits, but there are inconsistencies between these seismic attributes and good reservoir development. After additional study of synthetic seismograms and creating many maps of direct and complex seismic attributes of the D Sandstone and adjacent temporal horizons, it became clear that there was not a single attribute that best describes the Sooner Unit reservoir.

Synthetic Seismic Stratigraphic Modeling

As early as 1984, it was reported in the literature that channel complexes and valley-fill deposits could be located at Zenith Field in Adams Co., Colorado using seismic techniques (Sonnenberg 1987). Seismic modeling of the 52-ft reservoir at Zenith field produced an amplitude peak and trough associated with the top and base of the D Sandstone, respectively, which diminished significantly as the sandstone thickness decreased. Amplitude responses were found in 2D seismic data across the Zenith D Sandstone valley-fill reservoir which were similar to the results from seismic modeling. The initial seismic modeling for the Sooner 3D survey indicated that amplitude of the D Sandstone event would be a primary attribute for interpretation. Figure VII -2 is a synthetic seismogram section which shows amplitude variation with sandstone thickness from log data from the Sooner Unit. Amplitude decreases in the D Sandstone interval are primarily the result of thinning of valley-fill sediments or diminished acoustic contrast caused by lithological changes in the valley-fill sediments. Map view of the D Sandstone amplitude attribute displayed obvious inconsistencies with reservoir development of pay thickness and porosity-feet. This resulted in a lack of confidence for this attribute and other seismic attributes to produce maps suitable for targeted infill drilling. Further synthetic seismic modeling was performed with log data from the Sooner Unit reservoir to determine resulting seismic signature and seismic frequency content necessary to resolve the internal stratigraphic architecture within the D Sandstone interval and to confirm mapping and interpretation methodologies from earlier work during the project. Stratigraphic cross-sections of the D Sandstone interval were constructed across the central portion of the unit, running west to east. Stratigraphic correlation of well log data suggests that the D Sandstone interval can be subdivided into a series of vertically stacked reservoir flow units that may be related to sequence stratigraphic events or surfaces (Fig. VII-3). This reservoir unit correlation scheme was subsequently employed as geometric control for seismic modeling to determine the impact of the internal stratigraphic architecture on seismic response and potential vertical and lateral resolution limitations.

A seismic cross-section model was built across the Sooner Unit erosional valley. Synthetic seismograms were generated for each well using sonic-log data or transformed

resistivity-log data. All correlations between well locations and stratigraphic **boundary** conditions for the seismic cross-section modeling were based on the stratigraphic correlations. As a result, the synthetic seismic model geometry represents the D Sandstone internal stratigraphic architecture as interpreted from log correlation and **production** behavior.

A series of Ricker wavelet filters, at different frequencies, were applied to the synthetic cross-section model to determine the frequency content necessary to resolve internal stratigraphy. Ricker wavelets were used on all models and at all frequencies for simplicity and to remove any possibility of wavelet side-lobe interference of the modeled seismic response. Wavelet extraction from-the Sooner 3D seismic data, over the Niobrara to **Dakota** interval, reveals broad frequency spectra with central frequencies in the 45 to 50 Hz range and with usable, high-end frequencies in the range of 70 to 85 Hz.

Generation of a 50-Hz model shows that internal D Sandstone stratigraphy is not resolvable into separate seismic events at this frequency. A general broadening of the seismic peak associated with the D Sandstone is observed where the gross sand thickness is greatest (65 ft) in the stratigraphic cross-section. A model generated at 75 Hz does not differ greatly from the 50-Hz modeL No appreciable increase in resolution is gained at these slightly higher frequencies. Modeling at 50 and 75 Hz shows similar results as exhibited by the initial seismic modeling effort. As gross sand thickness increases, a corresponding increase is observed of the D Sandstone peak amplitude and Huntsman shale trough-amplitude. Isochron thickening is also observed between the D Sandstone and Huntsman events. As 50 to 75 Hz seismic data were recorded during the 3D acquisition at the Sooner Unit, observations from the synthetic seismic modeling offer the most reasonable and cost-effective methodologies for D Sandstone development and exploitation.

Seismic modeling at higher frequencies was also done to establish seismic parameters necessary to resolve internal stratigraphy. A 100-Hz model begins to show resolution of D Sand stratigraphy with initial development of a lower, secondary seismic peak within the D Sand interval in thicker D Sandstone fill. At 125 Hz, the seismic modeling shows full development of a secondary peak and trough pair which are coincident with increased erosion of the Huntsman and thicker D Sandstone fill in the valley system. This model also exhibits sharp lateral boundaries truncating the lower D Sandstone seismic peak. This sharp valley (channel) boundary is also observed in the dramatic isochron thinning of the Huntsman to J Sandstone (trough peak) interval.

A final model was created at 300 Hz which fully resolves internal D Sandstone stratigraphy. Tops and bottoms of individual sandstones of 8-12 ft are observable as separate seismic events. Abrupt channel boundaries are observable as sharp character and phase changes in the synthetic modeL At 300 Hz, a significant amount of background noise is evident in the modeling, both within and outside of the valley trend.

Synthetic seismic modeling, constrained by stratigraphic correlation, shows that D Sandstone internal stratigraphic architecture is resolvable into individual seismic events with data frequencies of 125 Hz or greater. While surface seismic data with frequencies in the range of 125 Hz to 150 Hz have been acquired in several producing fields, the increased cost related to this acquisition would be substantial due to the increased source effort and down-spacing of receiver and source points. Models with frequency content between 250 Hz and 300 Hz exhibit the greatest resolution of D Sandstone internal stratigraphy, with added background noise resulting from slight lithological and impedance variations. At present, it is not technically feasible to acquire 300 Hz surface seismic data at these depths. These very high frequencies can only be acquired with cross-wellbore seismic tomography techniques. At less than 125 Hz frequencies,

vertical stratigraphy is not resolvable and gross thickness variations can be estimated from analysis of seismic amplitude and isochron data. Higher frequencies would result in higher confidence for detection of stratigraphic variation, but at significantly higher seismic costs. Interpretation methodologies would vary slightly according to the frequency content of the data.

Seismic Attribute Correlation

The D Sandstone is a seismic thin bed at the frequencies recorded at the Sooner D Sandstone Unit (Sooner Unit) and produces a single wavelet at the D Sandstone temporal horizon at the frequencies recorded. Initial seismic modeling during this project indicated that the amplitude of the D Sandstone event would be the primary indicator of reservoir-quality sandstone development. Figure VII-2 shows modeled amplitude increasing with D Sandstone thickness. After mapping the D Sandstone amplitude at the Sooner Unit, it became clear that there were many places ofpoor correlation between good reservoir development and amplitude response, although the amplitude defines the approximate limits of the valley-fill or estuarine system. Figure VII-4 shows the amplitude from the D Sandstone horizon in map view. Notice the amplitude in the northeast portion of the Sooner Unit indicates a strong amplitude response over several dry holes which are thin and have no reservoir-quality rock. The amplitude map indicates several interesting features and patterns, but the use of this attribute alone for reservoir interpretation is not recommended. The isochron of the D Sandstone seismic event is shown in figure VII-5. The D Sandstone isochron is not exactly coincident with amplitude.

Ten seismic attributes were picked from the D Sandstone and adjacent horizons in an effort to find attributes with better correlation by empirical methods. These included simple attributes (such as amplitude and isochron) and more complex attributes (such as phase and frequency). The seismic data, measured at bin locations each 100 ft in the reservoir, provide higher spatial resolution than 1320-ft (40-acre) well spacing. Reservoir properties measured at the well locations were integrated with the 3D seismic data to provide correlation between data gathered at different spatial intervals. Petrophysical properties from 36 wells were calculated from digitized electrical logs. The petrophysical properties included gross thickness, net-pay thickness, porosity-feet and hydrocarbon-feet. Multiple linear regressions were then performed to correlate the seismic attributes with petrophysical values and it was found that correlation coefficients of multiple attributes are higher than for any single attribute. Maps were then constructed from these correlations of seismic attributes for gross thickness, net-pay thickness, porosity-feet and hydrocarbon-feet. Figures VII-6, VII-7, and VII-8 demonstrate the prediction of these reservoir attributes. Maps such as these can be used to directly estimate oil-in-place and its distribution across the field. These maps resulted in good agreement with the understanding of the reservoir from both geological and engineering perspectives. Calculation of original-oil-inplace (OOIP) from the hydrocarbon-feet map results in 6,900,000 stock-tank barrels (stb) inside the Sooner Unit boundary. This value for OOIP is slightly larger than was initially estimated by the unitization technical committee in 1988 at 5,800,000 stb. While it is comforting to be able to calculate a reservoir volume and OOIP that is in good agreement with the well data, it is more important to compare the distribution of OOIP. Comparison between the pre-unitization interpretation of net pay from log data shown in figure 11-1 with the seismic-attribute net-pay map in figure VII-7 indicates that the location of many of the regularly spaced wells are not optimal. The series of seismic attributes used for correlation with petrophysical attributes include the following:

1) COMBINATION AMPLITUDE (absolute difference of maximum D Sand peak-amplitude and Huntsman trough- amplitude),
2) **D SANDSTONE ISOCHRON** (measured for the D Sandstone peak to the Huntsman Shale trough),
3) D SANDSTONE ZERO-CROSSING ISOCHRON (measured from the -/+ zero-crossing above the D Sandstone peak to the +/- zero-crossing below the D Sandstone peak),
4) D SANDSTONE TO J SANDSTONE ISOCHRON (measured from the'ID **Sandstone** peak to the J Sandstone peak),
5) D SANDSTONE INSTANTANEOUS FREQUENCY,
6) HUNTSMAN INSTANTANEOUS FREQUENCY,
7) D SANDSTONE INSTANTANEOUS PHASE,
8) HUNTSMAN INSTANTANEOUS PHASE,
9) D SANDSTONE HILBERT REFLECTIVITY, and
10) HUNTSMAN HILBERT REFLECTIVITY.

These 10 seismic attributes were measured at 36 well locations within the 3D survey and then compared to reservoir properties from well logs by multiple linear regression analysis. The statistical and multiple regression analyses which allowed creation of correlation equations were performed with the PC software program WinStat^{7m}. Coefficients from multiple linear regression are shown in table VII-2.

The gross D Sandstone isolith is measured from the top of the D Sandstone where the shallow resistivity is greater than 10 ohm meters to the erosional contact at the Huntsman Shale where the shallow resistivity is less than 5 ohm meters. The net pay thickness is based on density porosity greater than 6 percent, shale volume of less than 30 percent and water saturation of less than 70 percent. Hydrocarbon porosity-feet is calculated using conventional Archie equations for sandstones and previously described cut-offparameters. Results of multiple linear-regression analyses are as follows:

$$Y = X1C1 + x_2c_2 + X_3C_3 + x_ac_4 + X5C5 + x_6c_6 + X7C7 + X_3C_3 + X9C9 + x_{10}c_{10} + Z$$

Where:

Y = reservoir attribute: gross, net or hydrocarbon-porosity thickness (ft)

X = Seismic attribute: amplitude, isochron, instantaneous frequency, etc.

C = Attribute coefficient from regression analysis

Z = constant

Results from the multiple linear regression analysis vary by reservoir property. The best correlation exists between 3D seismic attributes and the D Sandstone gross thickness with a correlation coefficient of 85 percent. As a result, there exists a 85 percent **probability** of predicting gross D Sandstone thickness with a standard error of 8.3 ft from the 3D seismic data. Linear regression of the well-log calculated versus 3D seismic predicted values for gross thickness

shows a 77 percent correlation. Cross-plotting of well-log calculated versus 3D seismic predicted net pay thickness shows a 68 percent correlation. The reservoir property with the greatest usefulness in reservoir management (hydrocarbon pore-foot thickness) exhibits the weakest correlation coefficient between log values and 3D seismic attributes. Seismic attributes allow for only a 49 percent probability of predicting with a standard error of 0.86 ft. Cross-plot comparison of well-log calculated versus 3D seismic predicted values of hydrocarbon pore-foot thickness yields a correlation coefficient of only 52 percent. While the use of 3D seismic attributes in the prediction of gross D Sandstone isolith thickness is strong, similar prediction of hydrocarbon pore-foot thickness is weak. Unfortunately, the prediction of gross sand thickness does not guarantee economic development of hydrocarbon pore-foot thickness in a given wellbore. Comparison of calculated gross thickness and correlative hydrocarbon pore-foot thickness for all wells in the Sooner Unit shows a linear regression correlation of 68 percent. It is unknown if the poor predictability of hydrocarbon pore-foot thickness is unique to this 3D survey or a function of the depositional system. One possibility for the poor correlation is that the reservoir sandstone has an average porosity of 12 percent. The regression correlations provided in table VII-2 are not offered as universal for the Denver Basin; it is the approach that is important. Each seismic survey should have different coefficients and correlations.

Summary and Conclusions

Mapping of seismic attributes from 3D surveys over D Sandstone reservoirs can produce images of complex reservoir heterogeneity. It appears from empirical observation that 25 ft is the minimum gross thickness required to image variability in the D Sandstone at the recorded frequencies of the Sooner survey. The acquisition of 3D seismic does not result in an easy and immediate interpretation of D Sandstone reservoirs. There are many steps to a successful interpretation of the D Sandstone from a 3D seismic survey.

The first step is correlation of seismic events with lithology. It was found that a vertical seismic profile (VSP) is not necessary and synthetic seismograms from density and sonic logs can provide sufficient lithological control. The Plainview formation (approximately 350 ft below the D Sandstone) produces a strong reflector below the D and J Sandstones and the inclusion of log data through the Plainview in synthetic seismograms should insure a correct tie of lithology to seismic events. Drilling an exploratory or development well through the Plainview for these data is concluded to be more useful and probably less expensive than a VSP survey. After successful correlation of seismic events and lithology, all seismic attributes of the D Sandstone and bounding lithologies should be measured.

Well logs in the 3D-seismic area should be digitized and carefully calculated for gross and net thickness, porosity-thickness and hydrocarbon-feet. A matrix of seismic-attribute and well log properties can be analyzed quickly by multiple linear regression with inexpensive statistical software such as WinStat^{TM}. If the 3D survey covers few existing wells, it is advisable to generate hypothetical synthetic seismograms from representative well-log data to cover the expected range of D Sandstone and adjacent lithological development. Seismic attributes from the synthetic seismograms can be also analyzed by regression analysis to identify which attributes should be most important. The correlation process should be performed step-wise fashion to identify the best three to five high-correlation attributes for each reservoir property. The correlation coefficients can be then used to quantify reservoir development.

The correlation coefficients are applied to each gridded attribute from the seismic survey.

These altered grids are then summed together with the correlation constant to produce a grid file containing the desired reservoir property. The resulting grid file can be displayed as a map of thickness or porosity-thickness, etc. Oil-in-place can be then calculated from these maps as would be done from contoured well-log data.

It is important to pay attention to correlation error. Drilling a location with a predicted thickness of 10 ft when the error is also 10 ft is not advisable; however, drilling a location with a predicted thickness of 20 ft with the same error may be acceptable. With these attribute-correlation maps it is possible to rank and prioritize drilling locations for infiii development or exploration. It is possible with patience and systematic analysis to not only produce maps representing stratigraphic variability but to also quantify (with an error range) reservoir development in terms of net feet and porosity-feet. The current cost of 3D seismic and interpretation covering approximately 7.7 sq miles at the Sooner Unit would be approximately $250,000. This is approximately equal to the cost of one completed well.

Table VII- 1
Processing Flow Used for Sooner 3D Seismic Data

1.	SEG-D Demultiplex	
	Process Sample Rate:	2 msec
	Process Record Length	4 sec
2.	Geometry Assignment	
3.	Deconvolution	
	Surface Consistent	
	Operator Length:	200 msec
	Gap:	2 msec
	Whitening:	0.01%
4.	Spectral Whitening:	10-129 Hz
5.	Reflection Statics	First Pass Miser
	Window:	100-2000 msec
	Maximum Shift:	24 sec
6.	Reflection Statics	Second Pass Miser
	Window:	300-1600 msec
	Maximum Shift:	36 sec
7.	NMO and First Break Suppression	First Miser Velocities 90% of Velocities
8.	Stack	
9.	Migration	

Table VII- 1
Processing Flow Used for Sooner 3D Seismic Data

10.	Filter:	10-100 Hz 0.0 sec 10-100 Hz 1.6 sec 10-60 Hz 4.0 sec
11.	FX Deconvolution	
12.	Spectral Whitening:	10-100 Hz

Table VII -2
Correlation Coefficients of Seismic and Electrical Log Data from Regression Analysis

Seismic Attribute	Gross Isolith Thickness	Net Productive Thickness	Hydrocarbon-Porosity Thickness
1	8.176e-04	1.018e-03	9.710e-05
2	-5.41 l e+00	-1.558e+01	-1.611e+00
3	-1.316e+01	-1.633e+00	-8.883e-03
4	-5.356e-01	3.3 17e+00	3.080e-01
5	-3.444e+00	-2.099e+00	1.717e-01
6	-1.535e+00	-6.446e-01	-5.333e-02
7	5.148e+01	1.570e+01	5.107e-02
8	-1.660e+00	-1.638e+00	-9.367e-03
9	1.647e+00	-1.443e+00	-1.922e-01
10	-2.122e+00	6.096e-01	3.661e+00
Constant	502.93	254.13	21.78
R^2	84.87%	65.40%	48.71%
Standard error	8.3 ft	8.2 ft	0.87 ft

References

Sonnenberg, Stephen A. 1987. "Tectonic, Sedimentary, and Seismic Models for the D Sandstone, Zenith Field Area, **Denver Basin, Colorado,"** *The American Association of Petroleum Geologists Bulletin,* 45(11): 1366-1377 (November 1987).

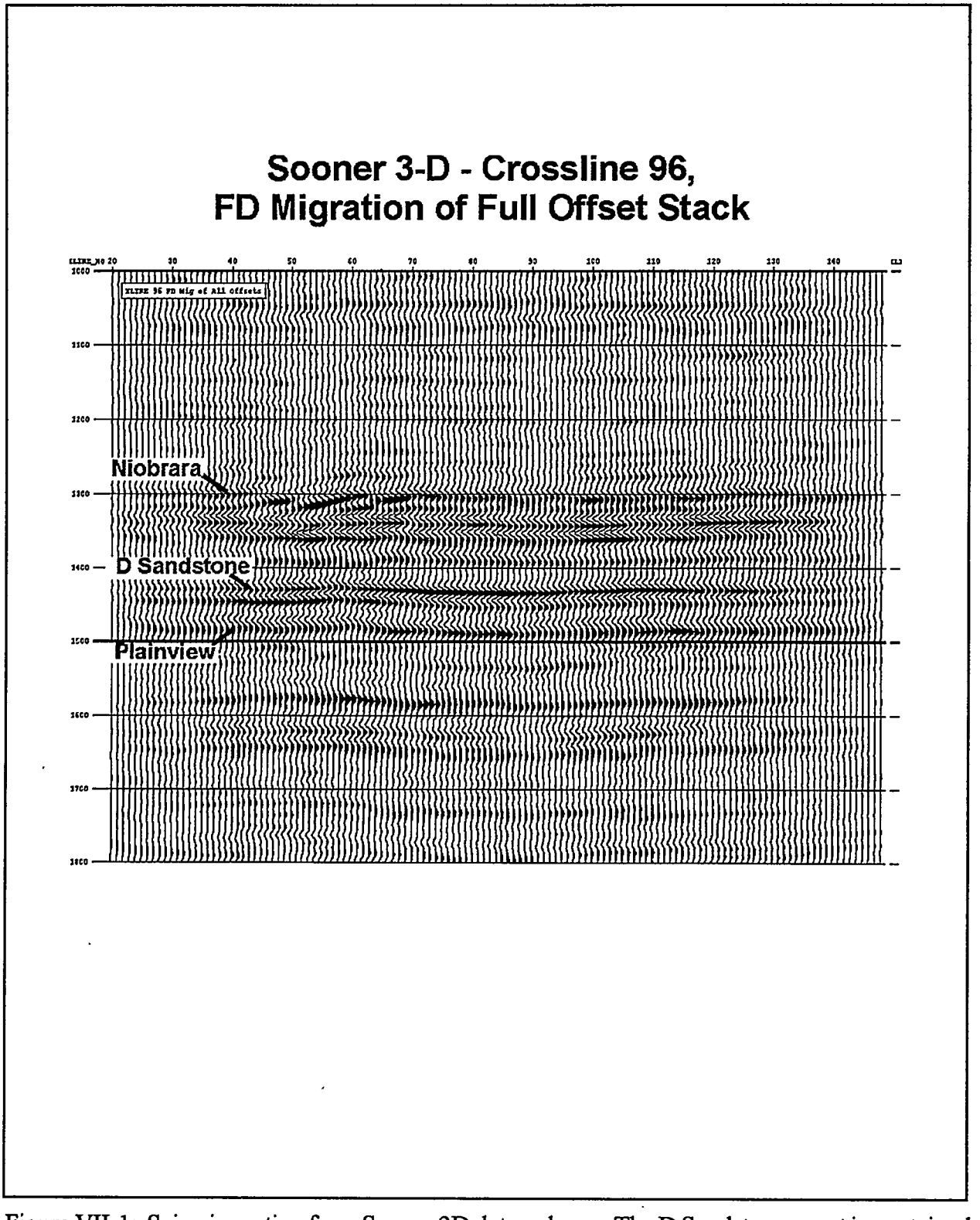

Figure VII-1: Seismic section from Sooner 3D data volume. The D Sandstone event is contained in a single peak at the frequencies recorded. The Plainview is a strong reflector below the D Sandstone which is helpful for correlation of seismic data with lithology.

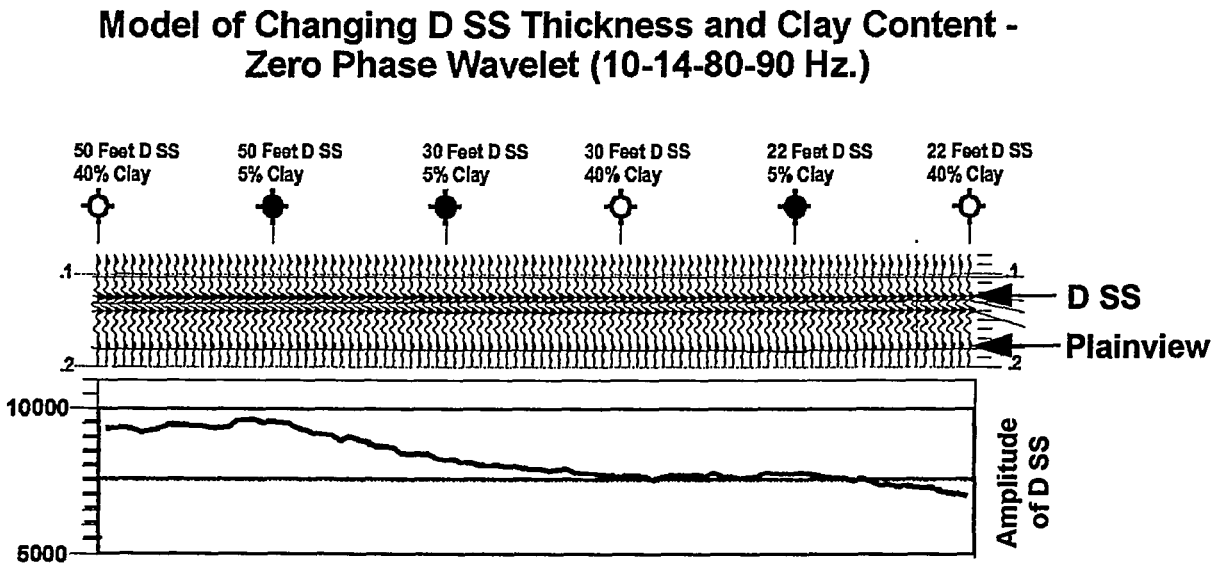

Figure VII-2: Synthetic seismogram section showing amplitude increase with thickness of D Sandstone.

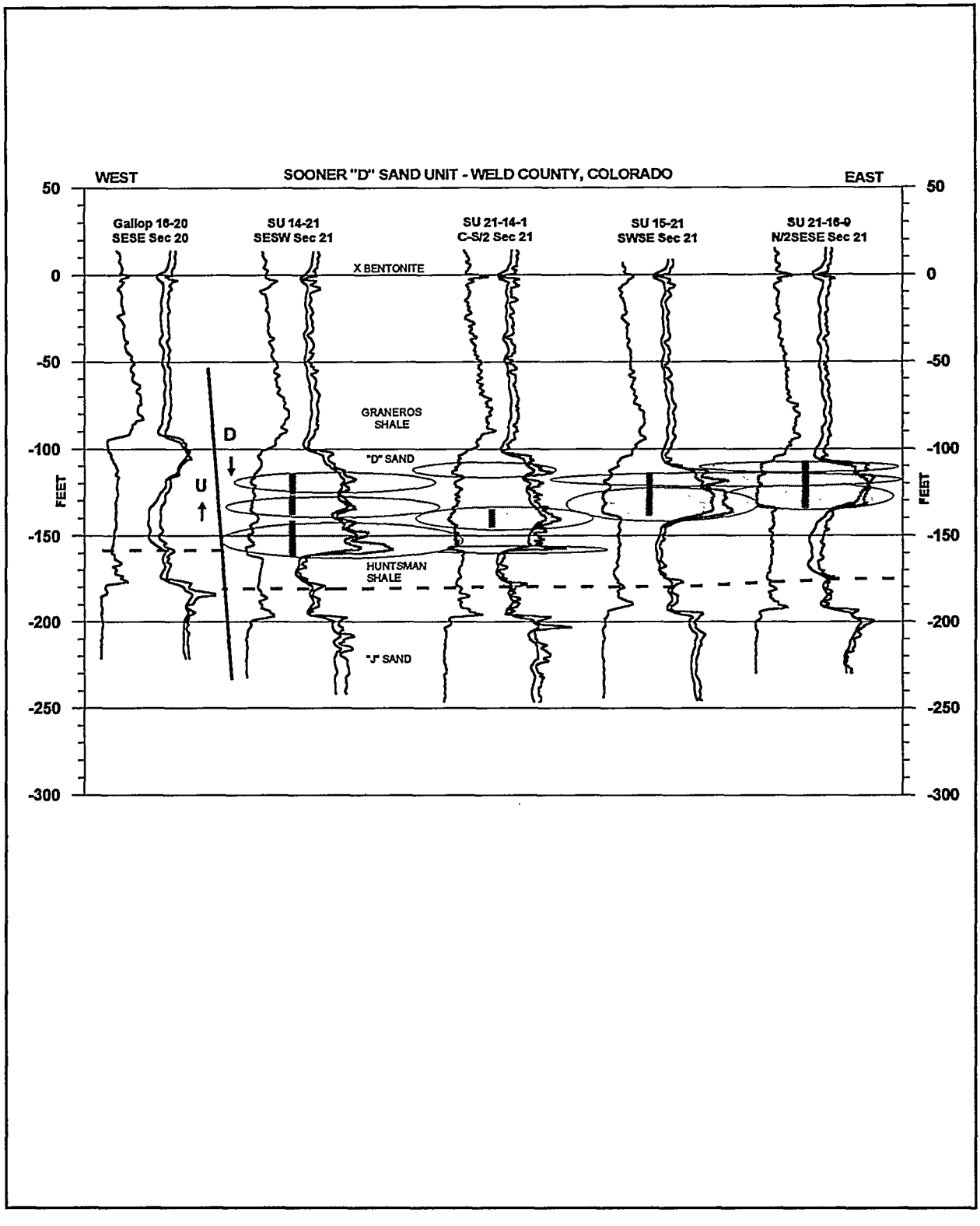

Figure VII-3: Stratigraphic east-west cross section of the D Sandstone at the Sooner Unit.

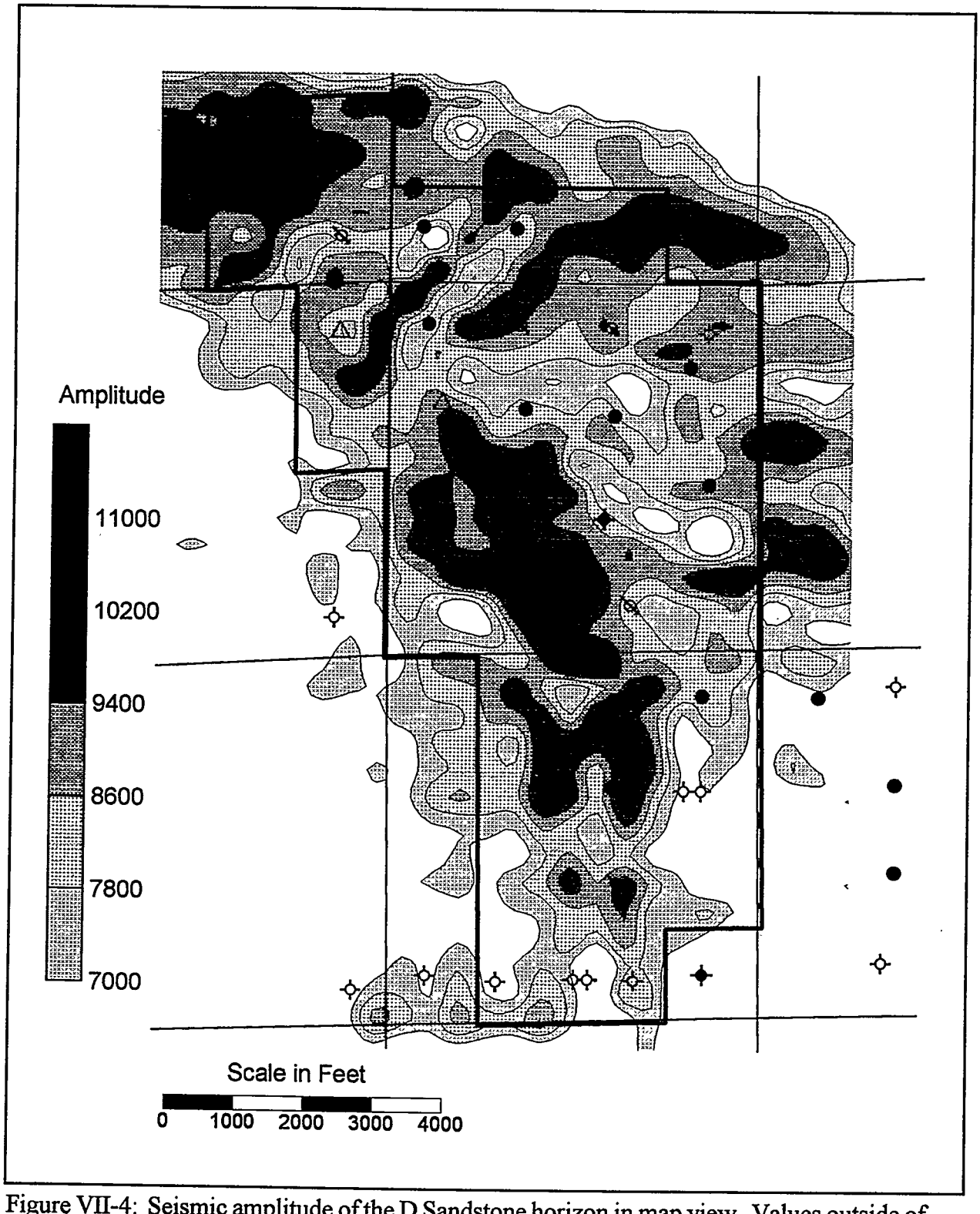

Figure VII-4: Seismic amplitude of the D Sandstone horizon in map view. Values outside of Unit boundary are affected by low fold.

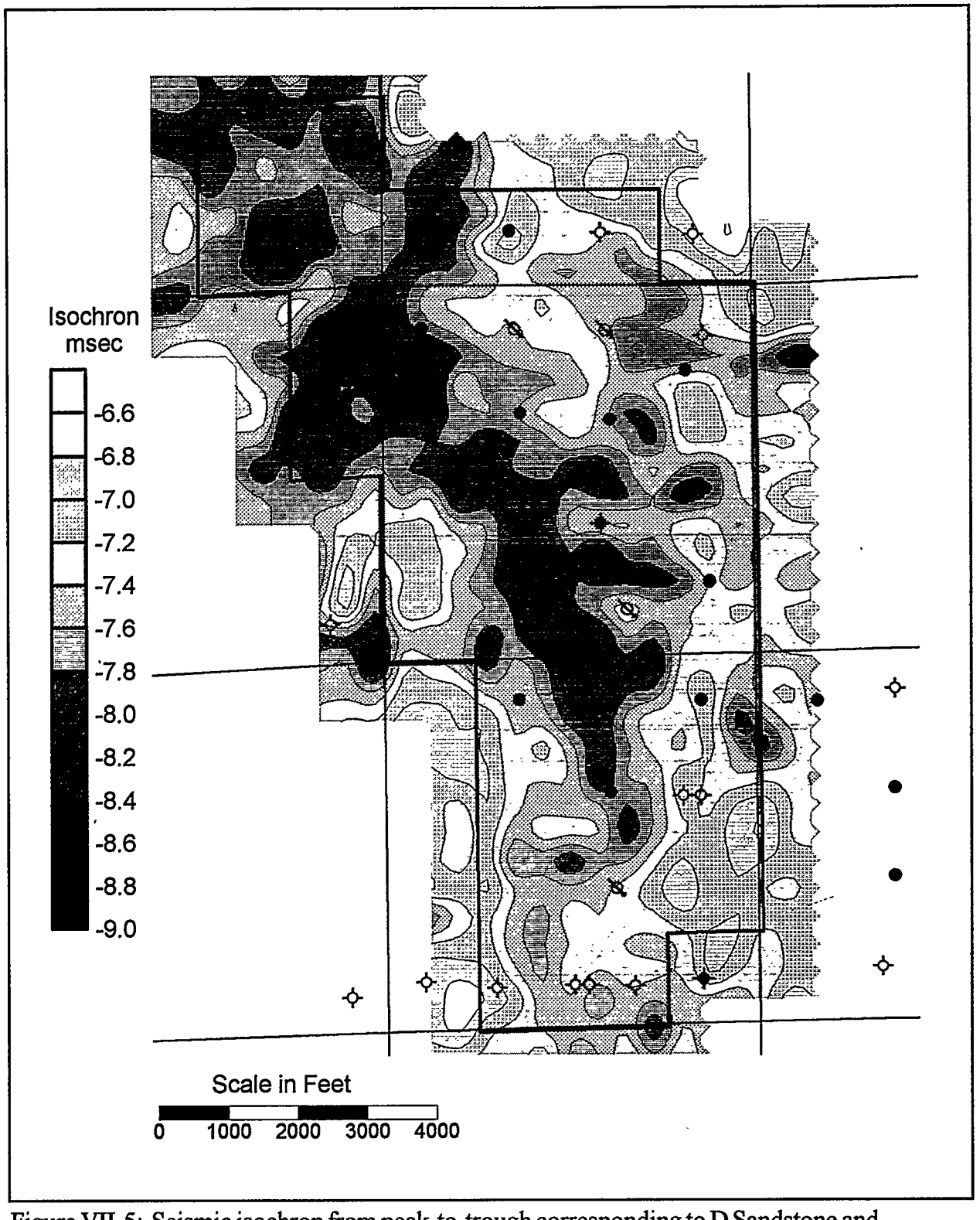

Figure VII-5: Seismic isochron from peak-to-trough corresponding to D Sandstone and Huntsman Shale events. Values outside of Unit boundary are affected by low fold.

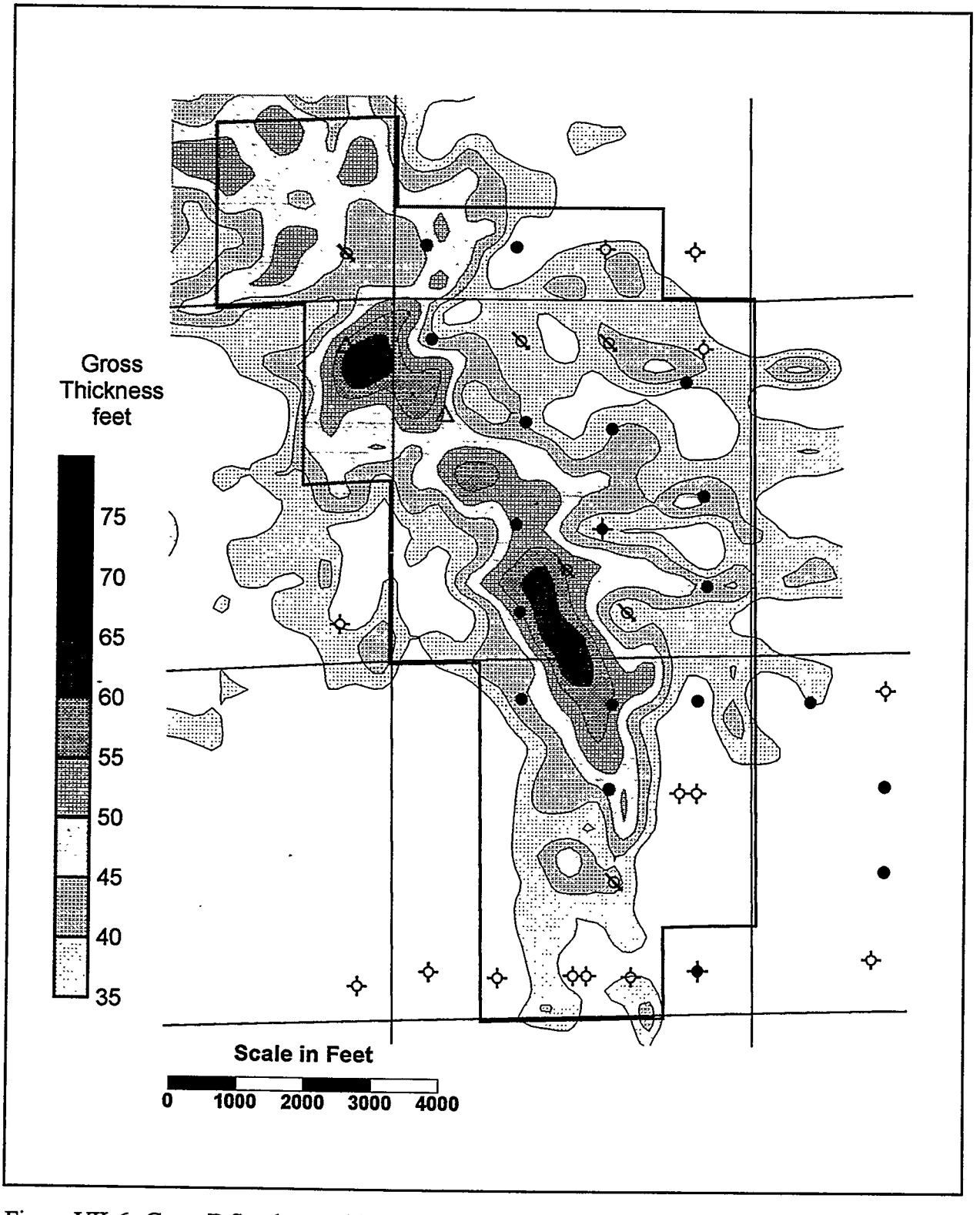

Figure VII-6: Gross D Sandstone thickness as predicted from seismic-attribute correlations.

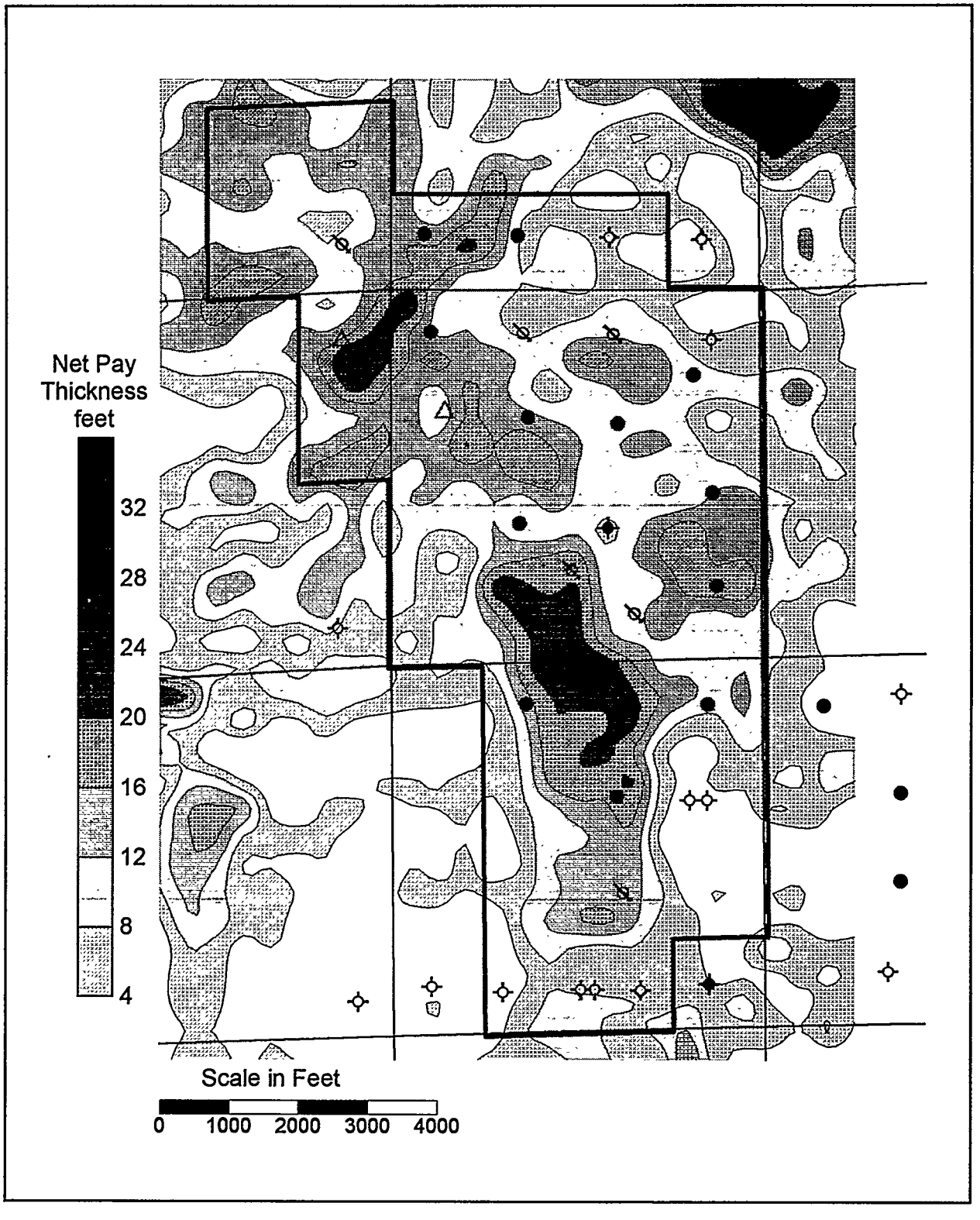

Figure VII-7: Prediction of net-pay thickness of D Sandstone from seismic-attribute correlations.

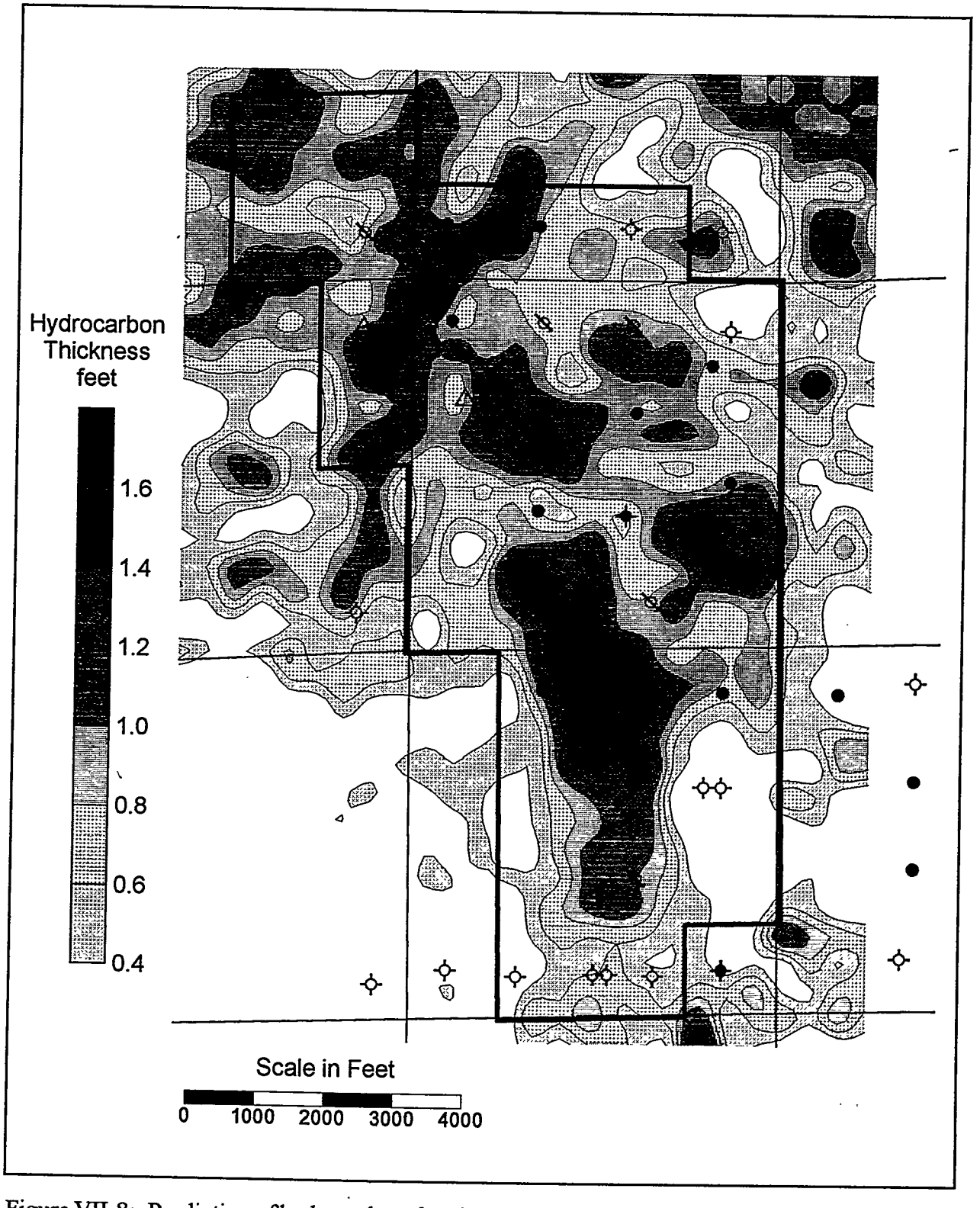

Figure VII-8: Prediction of hydrocarbon-feet from seismic-attribute regression correlations.

Reservoir Compartments in the D Sandstone

Geological-geophysical characterizations of the D Sandstone at the Sooner Unit indicate that both regressive and transgressive depositions which were influenced by recurrent movement of pre-Cambrian faults. Regional mapping of D Sandstone reservoirs at a field scale in the Denver Basin indicates length-to-width ratios of 2.5 to 1. Geostatistical evaluation of reservoir heterogeneity using variograms constructed with sandstone thickness from electrical logs in the Sooner Unit indicates a correlation trend of 2 to 1 at a scale ofnearly one mile by one-half mile. The major axis is oriented normal to paleo dip. Interpretation of functional data such as pressure and injection response leads to the conclusion that functional reservoir compartments have a major axis of one-half mile and a minor axis of one-quarter mile. The orientation of these functional reservoir compartments is generally parallel to the axis of the eroded valley. It is noted that the ratio of major-minor axes and orientations are the same at all scales, while functional dimensions of reservoir compartment size are approximately half that which is estimated from variogram analysis from electrical log data (Fig. VIII 1). These observations indicate that appropriate well spacing would have higher density across the axis of valley-fill systems. In the specific case at the Sooner Unit, it appears that wells should have been placed at approximately 1980 ft along and at 990 ft across the system axes (approximately 45 acre per well). This drilling strategy can only work if a relatively clear interpretation of the reservoir and depositional system exists at the time of discovery and prior to development drilling.

An interpretation of the **Sooner Unit** D **Sandstone reservoir before unitization** in 1988 is shown in figure II-1. The initial well spacing at the Sooner Unit was 40 acres per well, which is typical for D Sandstone fields. The map is a net-pay thickness contoured in a conventional manner used frequently for equity participation for waterflood units. While this map (and similar maps) is useful for unitization parameters and division of equity, it does little to describe the depositional and functional heterogeneity of the reservoir. Consequently, the use of this type of reservoir interpretation for implementing a waterflood or enhanced recovery project can result in **disappointing** recovery.

During the initial stages ofwaterflooding at the Sooner Unit, production was curtailed during re-pressurization of the reservoir by producing wells only a few days each month. This provided opportunity for pressure surveys at the producing wells which measured a stabilized static pressure. It became readily apparent from these pressure surveys that the reservoir was not pressurizing evenly across the field. An interpretation of functional reservoir compartments from the pressure data, injection breakthrough and non-reservoir development is shown in figure VIII-2. The functional reservoir compartments are depicted as a series of ellipses which show reservoir and drainage areas shared by wells. These reservoir compartments are not in all cases absolute permeability barriers. By 1995, it was determined that there were four single-well (40 acre) reservoir compartments.

Shape characteristics from electrical logs indicate several depositional styles in the Sooner Unit. These depositional styles and petrographical analysis of core data indicate a most likely depositional model would be valley-fill and estuarine. The establishment of a depositional model helped the interpretation of 3D seismic data. The initial seismic modeling studies indicated that the amplitude of the D Sandstone event would be the primary indicator of sandstone development. The D Sandstone is a seismic thin bed at the frequencies recorded at Sooner and produces a single wavelet at the event time which corresponds to the D Sandstone reservoir. After mapping the D Sandstone amplitude at the Sooner Unit, it became clear from even casual

observation that there were many places of poor correlation between good reservoir development and amplitude response, **although** the amplitude defines the approximate limits of the valley-fill or estuarine system.

Ten seismic attributes were picked from the D Sandstone and adjacent horizons. These include simple attributes (such as amplitude and isochrons) and more complex attributes (such as phase and frequency). The display of these attributes in map-view were visually inspected for features which appeared to depict erosional and sedimentary features which would be expected in a valley-fill and estuarine environment. Maps of attributes which produced patterns and textures which fit the depositional model gave comfort to cold statistical correlations of attributes with petrophysical properties from electrical logs. A map of instantaneous frequency at the Huntsman shale temporal horizon (below the D Sandstone) is shown in figure VIII-3. Maps such as this demonstrate the complexity and scale of depositional features in valley-fill reservoirs which cannot be mapped from well data at spacings of 40 acres (1320 ft).

It is concluded from the studies performed at the Sooner Unit that some in-fill drilling is required for a successful waterflood in D Sandstone compartments where normal well spacing is 40 acres or greater. After reviewing the failed waterfloods in the area around the Sooner Unit, it is also concluded that the primary reasons for these failures were small reservoir compartments and inadequate number of wells; especially injection wells. Reservoir interpretation using integrated 3D seismic data indicates that heterogeneity in valley-fill reservoirs dictates drilling of wells with unconventional spacing and patterns for successful waterflood recovery.

References

Mossel, L.G. 1978. "Hydrocarbon Accumulations in the `D' Sand, Adams and Arapahoe Counties, Colorado," (1978 Symposium, Rocky Mountain Association of Geologists, Denver): 75-80.

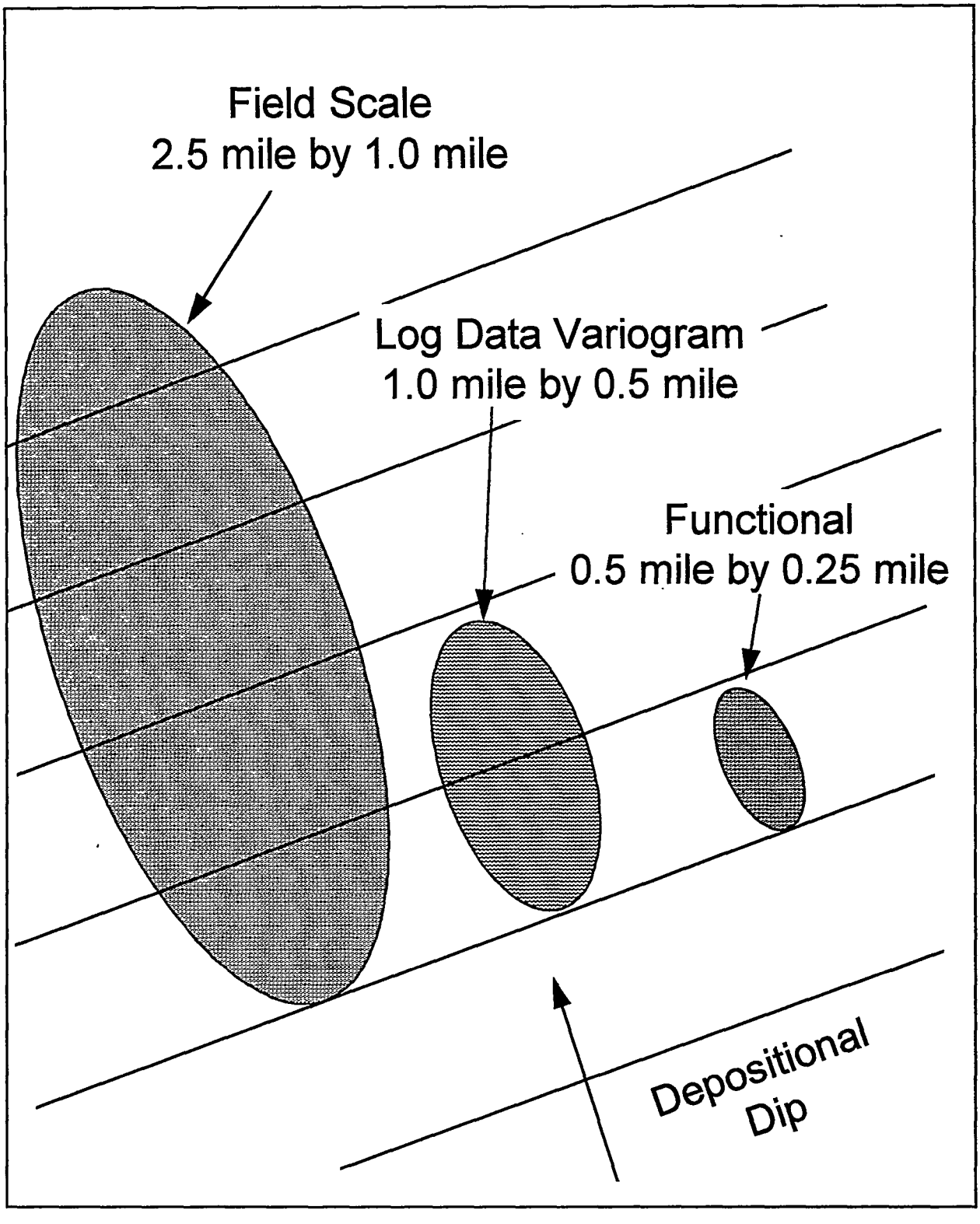

Figure VIII-1: Generalized schematic of compartments in valley-fill D Sandstone reservoirs.

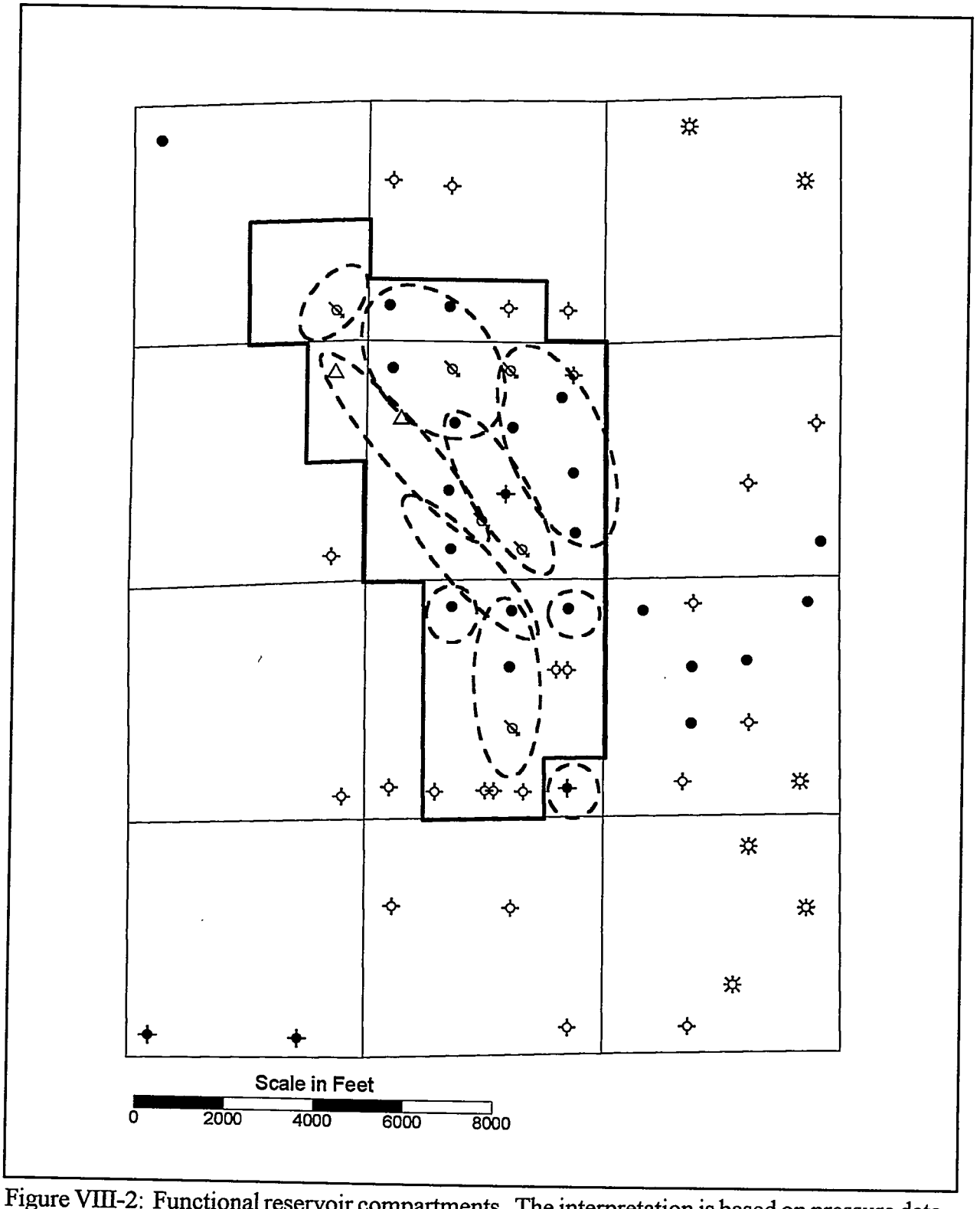

Figure VIII-2: Functional reservoir compartments. The interpretation is based on pressure data and response to water injection.

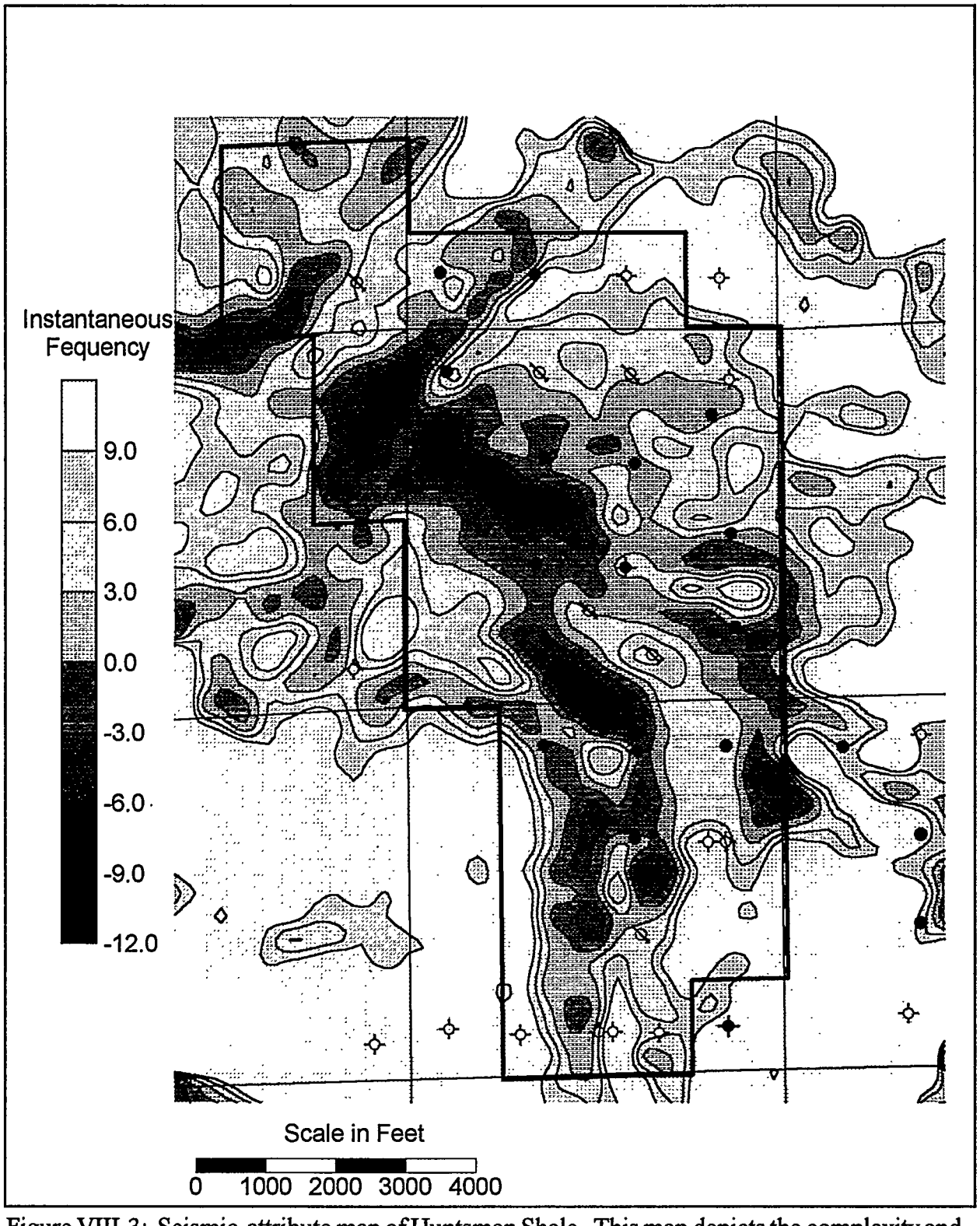

Figure VIII-3: Seismic-attribute map of Huntsman Shale. This map depicts the complexity and scale of erosional features in D Sandstone valley-fill reservoirs.

Reservoir Simulation for Waterflooding

Introduction

Using computer simulation to evaluate waterflood performance in a **heterogeneous** and compartmented reservoir can be a difficult task. Most small companies do not have the resources for sophisticated reservoir simulation nor is it economically justified in small reservoirs. Streamtube models for waterflood performance can provide a quick and effective evaluation of many elements expected from reservoir simulation. Simulations of individual well and composite-well production data with streamtube models were successfully employed in the Sooner Unit project. Reservoir simulations using core, fluid and relative permeability data from the Sooner Unit reservoir indicate that waterflooding the D Sandstone could incrementally recover 24 percent of the original-oil-in-place (OOIP) in fully swept reservoir regions. Simulation studies indicate that as of October 1992, between 8 to 12 additional wells would be required to fully develop the waterflood at the Sooner Unit.

Reservoir simulation is a tool which can be an effective means of reservoir description and prediction of future performance. Reservoir simulation at the Sooner "D" Sand Unit (Sooner Unit) was performed with the following objectives:

1) Determine appropriate reservoir parameters for evaluation by computer simulation,
2) determine contacted (swept) oil by well,
3) predict ultimate recovery by well,
4) calculate un-swept reservoir volume, and
5) estimate number of wells required to fully develop secondary reserves.

Type of Simulation Model

The pressure-production performance of the 1440-acre Sooner Unit indicates more than eight functional reservoir compartments (Fig. VIII-2). Imaging of the reservoir through 3D seismic, indicates many more potential reservoir compartments (Fig. VIII-3). There are three major vertical units in the D Sandstone reservoir and each of these vertical reservoir units are sometimes difficult to correlate laterally. This poses a challenge for deterministic reservoir simulation. The reservoir must be divided into several layers with lateral changes and permeability barriers. There is the additional problem of imperfect production allocations during the primary-depletion phase. The iterations required to produce a realistic full-field model is staggering and then the model would be still non-unique and ambiguous. After some experimentation with finite-difference, three-phase, black oil simulation; it was found that single-well and composite-well modeling with streamtube simulation software produced meaningful results in a time-efficient manner.

Two streamtube models were found to produce satisfactory results for evaluation by reservoir simulation of the Sooner Unit reservoir. These models should be also effective for other D Sandstone reservoirs. The first model is named *C02 Prophet.* It was developed as part of the U. S. Department of Energy Class I Oil program under contract number DE-FC22-93BC14960. The second model is named *Polymer Predictive Model.* Both models are free and available from the U.S. Department of Energy. These models generate streamlines for fluid flow between injection and production wells and then do displacement and recovery calculations along the

streamtubes. The streamlines form flow boundaries for the streamtubes. A finite-difference routine is used for displacement calculations. Layers are created from a Dykstra-Parsons coefficient for description ofpermeability variation. *CO2 Prophet* is a model for prediction by waterflood and enhanced recovery by CO_2. The *Polymer Predictive Model* is a waterflood and polymer-enhanced waterflood model. Both models work well with the **waterflooding-only** option. *CO2 Prophet* has several **options** for injection **patterns** and **the capability** to **construct** custom, multiple-well patterns. The *Polymer Predictive Model* allows only a five-spot pattern but has better graphical capabilities. While these streamtube models have limitations, they also have advantages over more complex finite-difference models. These advantages are simplicity and speed. It is also recommended that they be used before attempting to construct a model with complex lateral permeability variations and multiple relative-permeability rock regions.

Useful core and relative permeability data were obtained from the Sooner Unit reservoir. Additionally, all well logs were digitized and the data were used for net-pay and water-saturation calculations. The average reservoir properties found at the Sooner Unit are as listed in table IX-1.

Table DC-1
Average reservoir fluid and rock properties from the Sooner Unit D Sandstone reservoir which were used for reservoir simulation

Depth	6300 ft	Gas Gravity	1.0 Air = 1.0
Reservoir Temp.	220° F	Solution Gas	500 scflstb
Net thickness	17 ft	Oil Viscosity	0.48 cp
Porosity	12%	Oil Volume Factor	1.365 rb/stb
Air Permeability	21 and	Water Salinity	5000 TDS
Dykstra-Parsons Coef	0.74	Water Viscosity	0.27 cp
Oil Gravity	42° API	Water Volume factor	1.04 rb/stb

History Matching

The parameters which are important for history matching with streamtube models are oil-in-place, oil saturation, Dykstra-Parsons coefficient ofpermeability variation, and oil-water relative permeability. An oil saturation of 65 percent at the start of the waterflood was used for simulations of Sooner Unit production performance. This represented a gas saturation of 17 percent at the end of primary. Conventional core analysis from the Sooner Unit and adjacent reservoirs indicated Dykstra-Parsons permeability variations from 0.7 to 0.8. Water-oil relative permeability studies on the Sooner Unit core indicated an irreducible water saturation of 19 percent and a residual oil saturation of 65 percent. The initial relative permeability to oil is 0.80 and the final relative permeability to water is 0.35.

Relative permeability equations are used for constructing two-phase flow equations. An equation for the two-phase water relative permeability ($K_{rv}O$ is as follows with parameters from

the Sooner Unit data shown in parentheses:

$$K_m \quad K_{wro} \left[\frac{1 - S_{wir}}{1 \quad Sorw - S_{wir}} \right]^M$$

Where

$'S_W$	relative permeability of water
S_w	water saturation
M s	water equation exponent (2.5)
wir	irreducible water saturation (0.19)
SSOTW	residual-oil to waterflood (0.65)
K_W	endpoint relative permeability of water at residual oil saturation (0.35)

An equation for the two-phase oil relative permeability in the presence of water (Kn_{ow}) is as follows:

$$K_{row} = K_{rocw} \left| 1 \frac{1 \quad S_W \quad 'S}{S\ ores - S_{wir}} \right.$$

Where

K_{ro} S_w	relative permeability of oil
N	water saturation
S_{wir} s	oil equation exponent (2.5)
ores K	irreducible water saturation (0.19)
rocw	residual oil to waterflood (0.65)
	endpoint relative permeability of oil at irreducible water saturation (0.80)

Since injection patterns at the Sooner Unit are limited by the number of wells, narrow configuration of the reservoir and compartmented behavior, a two-spot injection pattern was concluded to be the best representation for history-matching and prediction by simulation. The expected recovery from a hypothetical 2-spot, 40-acre pattern was found to be 24 percent of OOIP to economical limits. Oil and total fluid rates were matched by varying the oil-in-place at the start of the waterflood and injection rates. An example of history-matching results for a single well is shown in figure IX-1.

Table IX-2 summarizes results from single-well history-matching using a 2-spot streamtube modeL The average waterflood recovery of responding wells is about 78,000 bbl per well with a secondary recovery of 21 percent of the 001P. This is equivalent to a secondary recovery of 115 bbl ac-ft. Total recovery after primary and secondary is indicated to be 37 percent in efficiently swept areas. However, the summation of contacted oil-in-place by wells at the start of the waterflood is only 3,514 MbbL

Table IX-2
Listing of results from history matching of production performance

Well	Oil-In-Place at Start of Waterflood (Mbbl)	Model Predicted Secondary Oil (Mbbl)	Secondary Recovery Factor of OOIP	Ratio of Pore-Feet in Model to Average in 40 acre
SU 13-16	212.8	48.5	12.9%	0.71
SU 14-16	89.0	9.9	2.6%	0.29
SU 1-21A	195.1	35.5	9.4%	0.65
SU 2-21	354.7	89.0	23.7%	1.18
SU 4-21	230.5	63.3	16.8%	0.88
SU 6-21	266.0	73.8	19.6%	1.18
SU 7-21	354.7	101.4	27.0%	1.32
SU 9-21	399.0	92.9	24.7%	0.65
SU 15-21	195.1	58.3	15.5%	1.53
SU 21-16-9	461.0	137.8	36.7%	0.59
SU 2-28	177.3	46.7	12.4%	1.92
SU 7-28	579.1	172.8	46.0%	0.97
Total of Wells	3514.3	929.9		
Average of Wells	292.9	77.5	20.6%	0.99
Standard Deviation	133.6	43.2	11.5%	0.44

This represents only 57 percent of the 6,200 Mbbl oil-in-place at the start of waterflooding which was estimated from volumetric and primary production calculations. This is not surprising because four of the 19 wells at the start of waterflooding were not in communication with the rest of the reservoir.

In similar fashion to history-matching individual well performance by adjusting hydrocarbon pore-volume and injection rate, the composite performance of the Sooner Unit can be simulated. Table IX-3 shows the results from history matching the total Unit production history prior to the commencement of the project in October 1992. Examples of production and history-matching curves for the 2-spot model listed in table IX-3 is shown in figure IX-2. Cumulative production prior to injection of water was 789 Mbbl. The total cumulative production (primary and secondary) from the Sooner Unit was 1,086 Mbbl on October 1992.

Table IX-3
Results from history matching the composite production from the Sooner Unit prior to October 1992

Streamtube Model	Oil-In-Place at Start of Waterflood (Mbbl)	Model Predicted Secondary Oil (Mbbl)	Secondary Recovery Factor of Volumetric OOIP
5 Spot	3287	825	12.0%
2 Spot	4696	1086	16.0%

Table IX-2 shows that on October 1992, the pore-volume being swept as efficiently as a fully developed 5-spot waterflood contained only 3,287 Mbbl or 53 percent of the volumetric OOP. Similarly, the less efficient 2-spot waterflood model indicates a swept reservoir volume containing 4,696 Mbbl or 75 percent of the volumetric O M . Both models predict incremental waterflood recovery of nearly 2,000 Mbbl (2,789 Mbbl total primary and secondary) should be possible if all portions of the Sooner Unit reservoir were fully developed with at least one injector and one producer in each functional reservoir compartment.

The difference between total volumetric oil-in-place and oil-in-place being contacted and swept by waterflooding represents the undeveloped potential of the reservoir. Both the single-well and composite-well simulations indicate non-contacted or poorly contacted reservoir oil of over 3,000 Mbbl at the start of the project in 1992. Using reservoir conditions on October 1992, and results from 2-spot composite-well simulation there were probable, undeveloped reserves of 914 Mbbl (2,000 Mbbl possible minus 1,086 Mbbl developed).

Having characterized the reserves and swept pore-volumes of effective waterflood producers, it is possible to quantify the number of wells which would be required to fully develop the waterflood and effectively sweep the entire reservoir. The average 40-acre recovery is indicated to be 78 Mbbl (+/- 44 Mbbl). Therefore, it would appear that 12 additional wells would be required to develop 914 Mbbl. This may be optimistic without clear imaging of reservoir compartment regions and boundaries. If 3D seismic can provide clear imaging of reservoir areas with thick net pay and compartment boundaries, it is possible that the expected reserves from targeted wells would be greater than the average of 78 Mbbl. Targeted wells could be expected to develop 122 Mbbl per well where 3D seismic indicates net-pay thickness of greater than 15 ft. Using this reserve model for targeted wells , full development of the 914 Mbbl might be achieved with as few as eight wells.

Simulation can also be used to quantify the economics of drilling locations and prioritize these locations by economic rank. A series of 40-acre, 2-spot locations were simulated using the average Sooner Unit reservoir parameters and varying the net pay thickness. The economic value of these hypothetical locations was calculated using an oil price of $17.00/bbl, net revenue interest of 82 percent, state taxes of 6 percent and lifting cost of $1,500 per month. The total fluid rate in each 2-spot pattern was fixed at 300 bbl per day. Table IX-4 shows there is a linear relationship between cumulative income and net pay thickness. This table also should be useful as a template to screen other D Sandstone reservoirs for economical potential by waterflooding.

Conclusion

Reservoir simulations using core, fluid and relative permeability data from the Sooner Unit reservoir indicate that waterflooding the D Sandstone could incrementally recover 24 percent of the OOP in fully swept reservoir regions. Using simple streamtube models, single-well and composite-well production data can be quickly history-matched to make estimates of swept reservoir volumes and probable undeveloped reserves. A development plan and economics can be prepared from expected reserves and the number of wells which would be required to exploit these undeveloped reserves.

Table IX-4
Economic Value of Various Net Thicknesses in a 40-acre, 2-Spot Waterflood Pattern Before Capital Expenditures

Thickness (feet)	Economic Life (years)	Secondary Recovery (Mbbl)	Cumulative , Income (M$)	Present Value (10% pv M$)
5	5	27.3	$269	$258
10	9	54.6	$538	$490
15	13	80.5	$807	$700
20	15	107.0	$1,075	$891
25	18	129.5	$1,337	$1,066
35	29	186.8	$1,883	$1,383

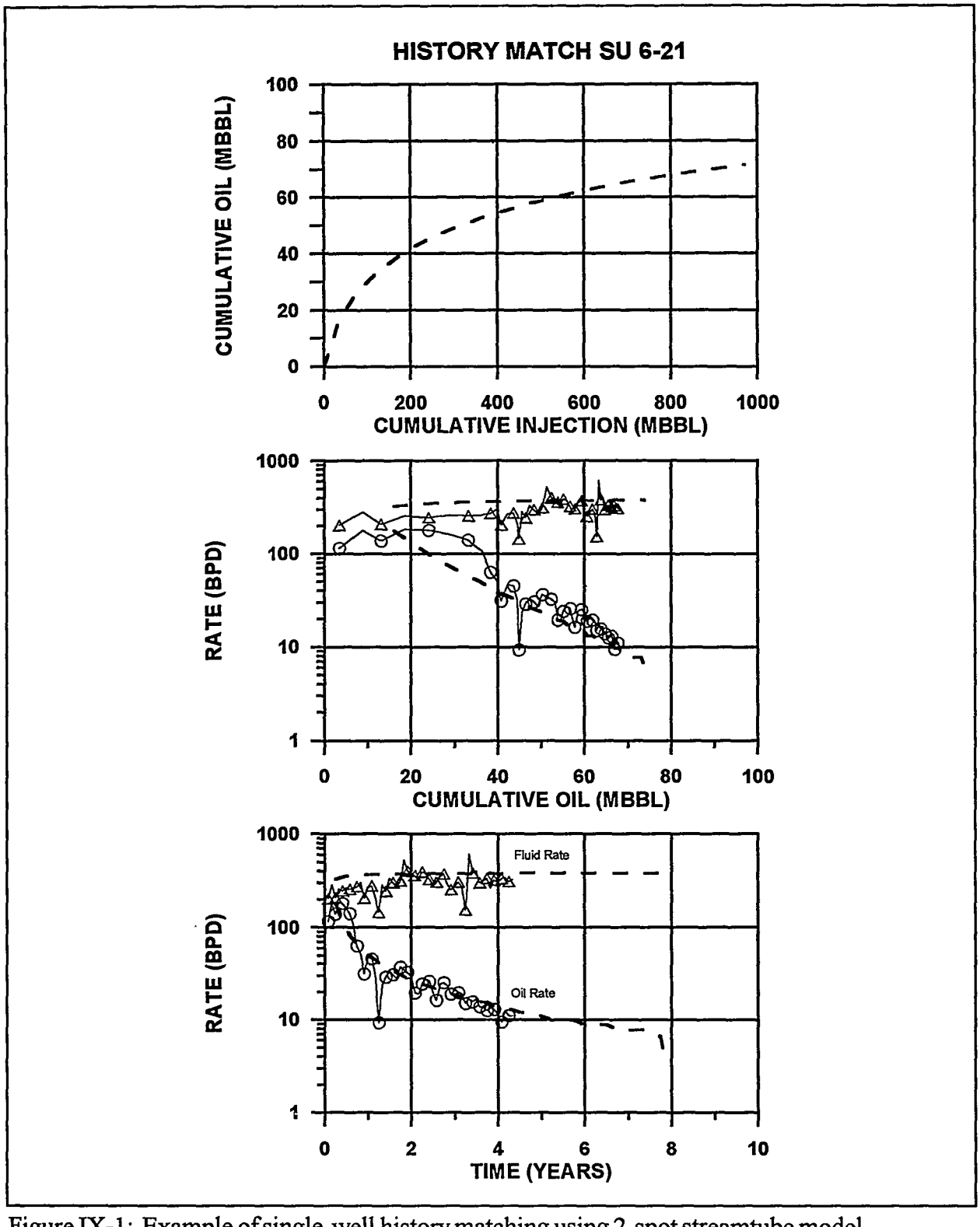

Figure IX-1: Example of single-well history matching using 2-spot streamtube model. Simulation output is shown as dashed line.

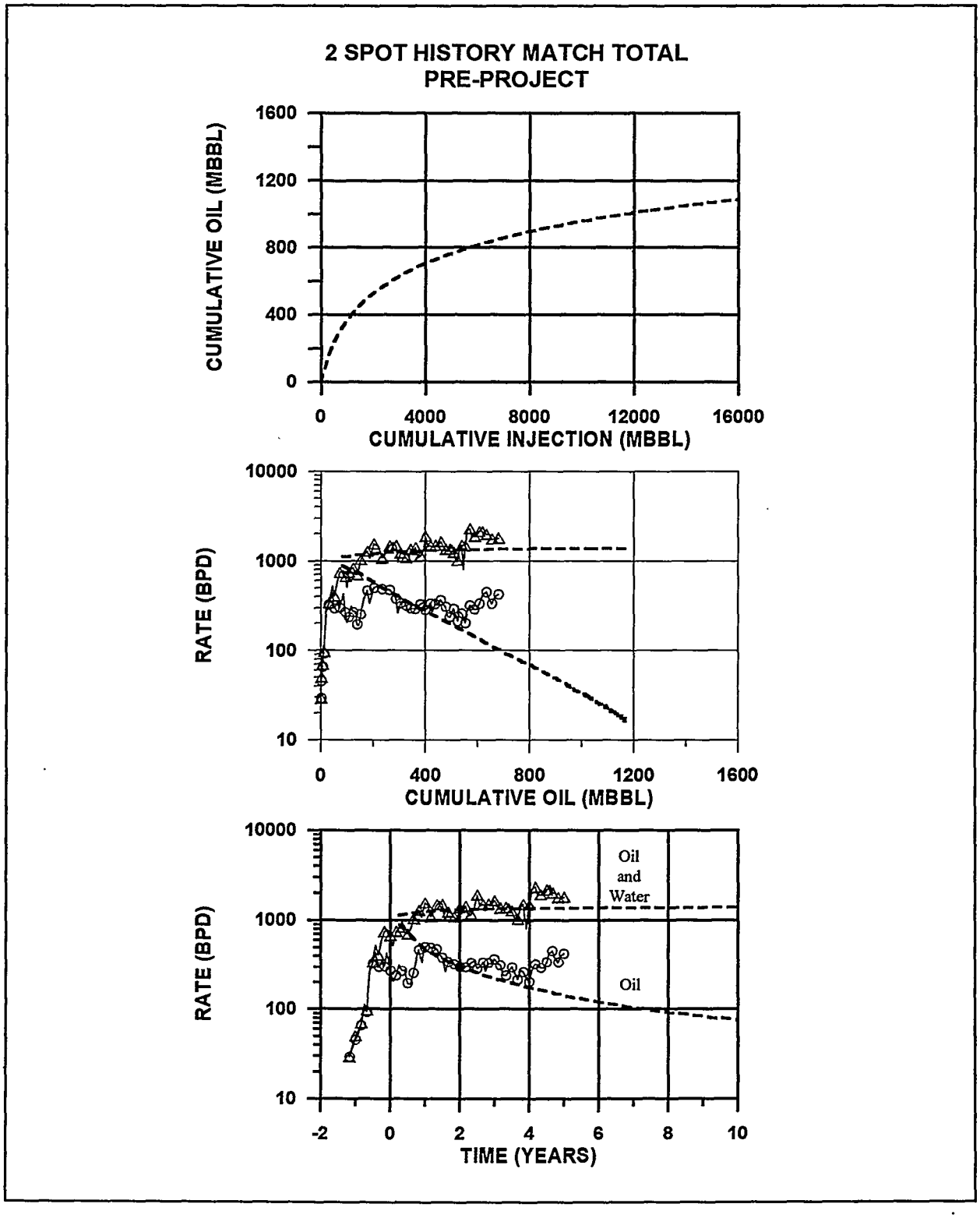

Figure IX-2: Results from history match of composite Sooner Unit production with a 2-spot pattern using a streamtube model. The history match was performed using production data prior to commencement of the Sooner Unit project. This is at year 2.5 on the rate-time graph.

Targeted Jnfill Drilling and Economics

Introduction

Three wells were drilled by the project based on 3D seismic and integrated reservoir characterization study. One well was completed for water injection and two wells were completed as producers. The two production wells were contributing more than half (over 200 bopd) of the total production from the Unit at the end of the project in December 1995. Combination of seismic attributes proved successful for predicting reservoir development and locating infill targets. Horizontal drilling and completion from a cased hole was unsuccessful. A conventional vertical well was finally drilled at the proposed objective of the lateral completion. The locations of drilling activities are shown in figure X-l.

Seismically Targeted SU 21-16-9

Combinations of attribute-correlations were developed from empirical relationships between seismic attributes of the D Sandstone and adjacent lithology and petrophysical data from well logs. Correlations were developed for gross thickness, net-pay thickness and hydrocarbon-porosity feet. An example of attribute correlation for hydrocarbon-feet is shown in figure X-2. These correlations predicted a net-pay thickness of 29 +/- 4 ft for the SU 21-9-16 location. The actual net-pay thickness of the SU 21-16-9 well is 26 ft with above-average porosity development. Net-pay maps, based solely on electrical logs, predicted much thinner reservoir development at the location of the new well. The multiple-regression correlation technique appears to be valid and offers the ability to selectively target higher-density drilling locations with confidence for improved waterflood sweep. The SU 21-16-9 was completed with a stabilized oil rate of 220 bopd.

Horizontal Completion at the SU 10-21A

After assessing the reservoir compartments from engineering and geological data, there was a sense of dismay. There were as many as nine functional compartments that had been identified in the 1440-acre unit. One proposed solution was to connect the compartments with horizontal completions from existing wells or new wells. The apparent advantages seemed compelling:

1) Effective use of existing infrastructure, such as roads, flowlines and power,
2) One well with laterals as effective as two vertical wells; and
3) Four ineffective, cased wellbores.

Functional reservoir compartments were identified from pressure and injection response data (Fig. VIII-2). It was decided to attempt a horizontal completion from the SU 10-21A water-injection well as it was not affecting waterflood response to the west or east 40-acre offset wells (Fig. X-1). The well had excellent injectivity and had ben injecting water at over 1000 bpd with no wellhead pressure. A radio-active and temperature survey indicated that water was being injected into the D Sandstone reservoir.

The drilling technology selected for the horizontal completion from the SU 10-21A well

was developed by Amoco (Warren, et al 1993). The technology appeared to be inexpensive. This technology consists of a rotary-guided short-radius curve drilling system and the system can be used to drill drainholes with curvatures of approximately 30 ft from existing wellbores. The curve-drilling assembly is composed of an anti whirl poly-crystalline diamond bit, flexible joint, eccentric deflection sleeve, orientation indicator, and flexible drillstring. The drill string is turned at the surface with a power swivel. The articulated drill collars are lined with high-pressure hose to allow circulation through the bit. The casing is section-milled and a cement plug is set at the kick-off point. The system can drill to 90° with a 30-ft radius when conditions are ideal and achieve lateral reaches of 300 ft or more. The use of lateral re-completions from injection wells was hoped to help contact un-swept oil and re-direct sweep in directions dictated by well spacing and geological heterogeneity. Two attempts were made with this technology to drill a lateral to the southwest from the SU 10-21A well. The technology was unable to achieve a full 90° curve or penetrate further than 30 ft beyond the casing.

This drilling system failed at the SU 10-21A for several reasons. The depth of operations for the D Sandstone is about 6300 ft. The weight on the razor-back knuckle joint and articulated drill collars is critical for proper drilling of the curve. A normal weight indicator is the only guide for the rig operator and provides inadequate control at a depth of 6300 ft and corresponding string weight. At much shallower depths of 3500 ft or less, there is much less string weight and the accuracy of the weight indicator is sufficient to properly load the bottom hole drilling assembly. Trip time with a slick line to check angle and orientation is slow. Frequent trips to check the bit and bottom-hole assembly limits effective time for drilling if operations are only working daylight tours.

After the failure of the USR lateral drilling, it was still believed important to determine if utilization of existing wells and infra-structure could be accomplished in the infill drilling and completion program. A more conventional mud motor with steering system and conventional drill rig were mobilized to the SU 10-21A well. A cement plug was placed in the wellbore across the casing window used for USR and a second 100 ft section of casing was milled for the medium-radius lateral drilling. Again, two unsuccessful attempts were made to drill horizontally. Final displacement of the second lateral was 680 ft (185 ft south and 655 ft west) at 6,239 ft total-vertical-depth (TVD). The horizontal drilling was unsuccessful because the Graneros Shale overlying the D Sandstone was unstable and the horizontal hole collapsed during trips despite careful attention to mud properties and hydraulics. The Graneros Shale section is not a problem during conventional vertical drilling operations.

Despite the failure to complete a lateral extension from the SU 10-21A well, it was determined that a significant Ethological or fault barrier exists at about 250 ft west from the well. At a horizontal reach of 254 feet from the wellbore (94 ft south and 236 ft west with a TVD of 6239 ft), the mud motor stalled and drilling angle changed abruptly. This barrier is in agreement with distance-to-bather calculations made from a pressure fall-off test performed on the well. The pressure transient behavior of this test indicates channel-like flow with a width of 400 to 500 ft. The 3D seismic also indicates a change west from the SU 10-21A well. The amplitude and isochron attributes of the D Sandstone waveform indicate rapid thickening of the section in the westerly direction.

Conclusions

The Sooner Unit D Sandstone reservoir has significant heterogeneity. Tnfill drilling to less

than 40 acres per well is required to allow efficient waterflooding of certain portions of the reservoir. Vertical wells to the D Sandstone in the Denver Basin are relatively inexpensive and are quickly drilled with little mechanical risk. Targeting vertical wells using 3D seismic appears to offer the most efficient method to for infitl drilling at low cost and with low risk.

Interpretation of functional data such as pressure and injection response leads to the conclusion that functional reservoir compartments have a major axis of one-half mile and a minor axis of one-quarter mile. The orientation of these fractional reservoir compartments is generally parallel to the axis of the eroded valley in the Huntsman Shale. These observations indicate that appropriate well spacing should have higher density across the axis of valley-fill systems. In the specific case at the Sooner Unit, it appears that wells for primary development should have been placed at approximately 1980 ft along and at 990 ft across the system axes (approximately 45 acre per well). This drilling strategy can only work if a relatively clear interpretation of the reservoir and depositional system exists at the time of discovery and prior to development drilling. Experience from the Sooner Unit waterflood and other nearby D Sandstone waterfloods indicates that regular spacing of wells on 40-acre patterns is inadequate for an *efficient* waterflood.

The experience from the Sooner Unit projects suggests that targeted drilling based on 1) a geological model, 2) understanding of functional reservoir compartments and 3) 3D seismic should be more efficient than blanket infitl drilling. An economic comparison of targeted drilling and blanket infitl drilling on 20-acre patterns is shown in table X-1. This table is based on incremental cost and recovery and assumes that the waterflood infrastructure is already in place. The revenue calculations are based on an oil price of $17.00 per bbL This economic model suggests a $2,280,000 advantage from targeted in-fill drilling in the best portions of the reservoir and effectively matching injection-production well pairs.

Table X-1
Economic Model for Comparison of Targeted and Blanket In-fill Drilling

	Blanket Tnfill Drilling	Targeted Infill Drilling
Number of Wells	20	8
Incremental Oil	768,000 bbl 11% of OOFP	640,000 bbl 9% of 001P
Capital Expenditures	$4,500,000	$1,800,000
Lease Operating Expense	$3,262,000	$1,902,000
Net Profit	$2,788,000	$5,068,000

Note: These numbers are incremental and assume the waterflood infrastructure is in place.

References

Warren, T.M., W. J. Winters and H.B. Mount, "Short-Radius Lateral Drilling System," *Journal of Petroleum Technology*, 45(2): 108-115 (February 1993).

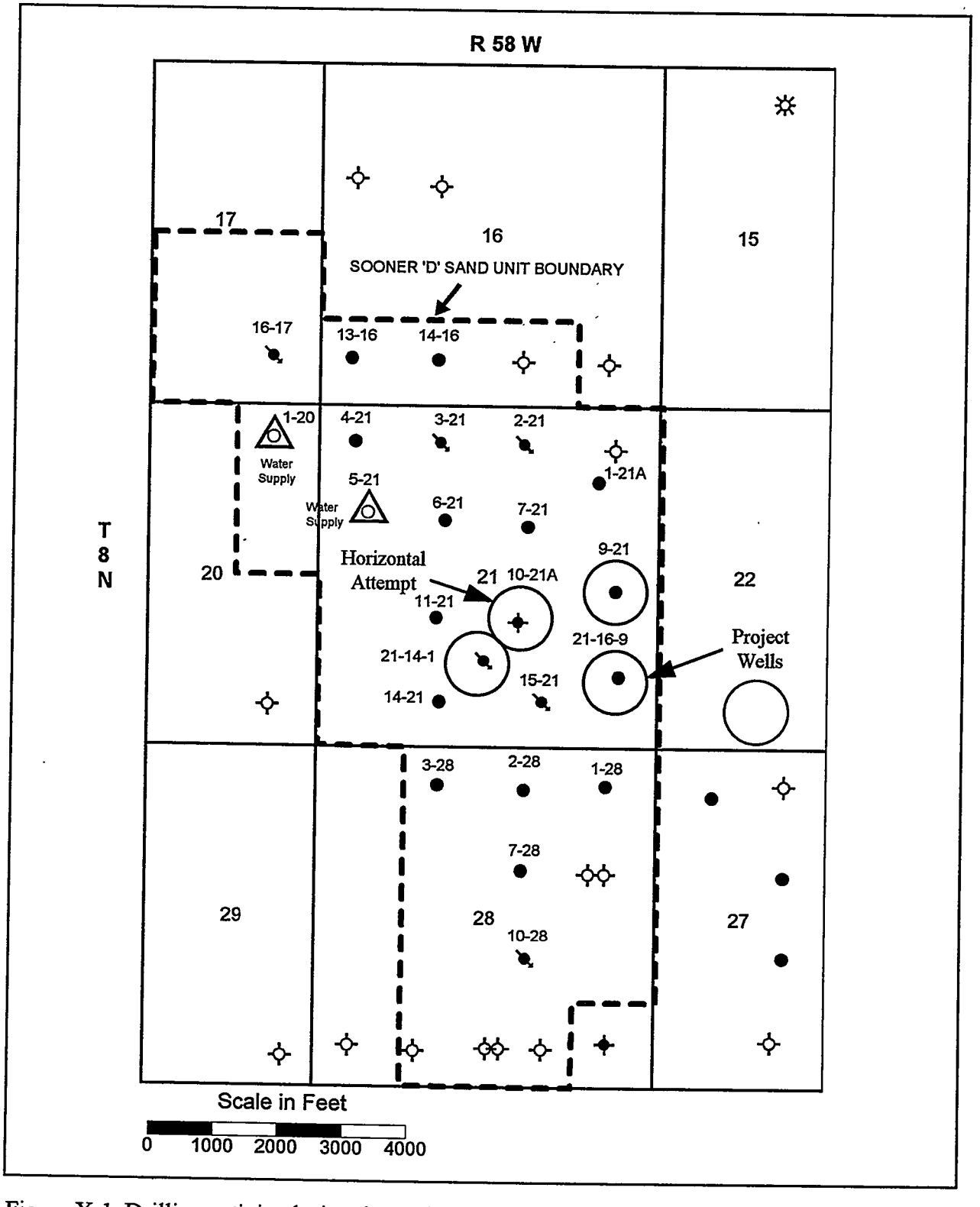

Figure X-1: Drilling activity during the project.

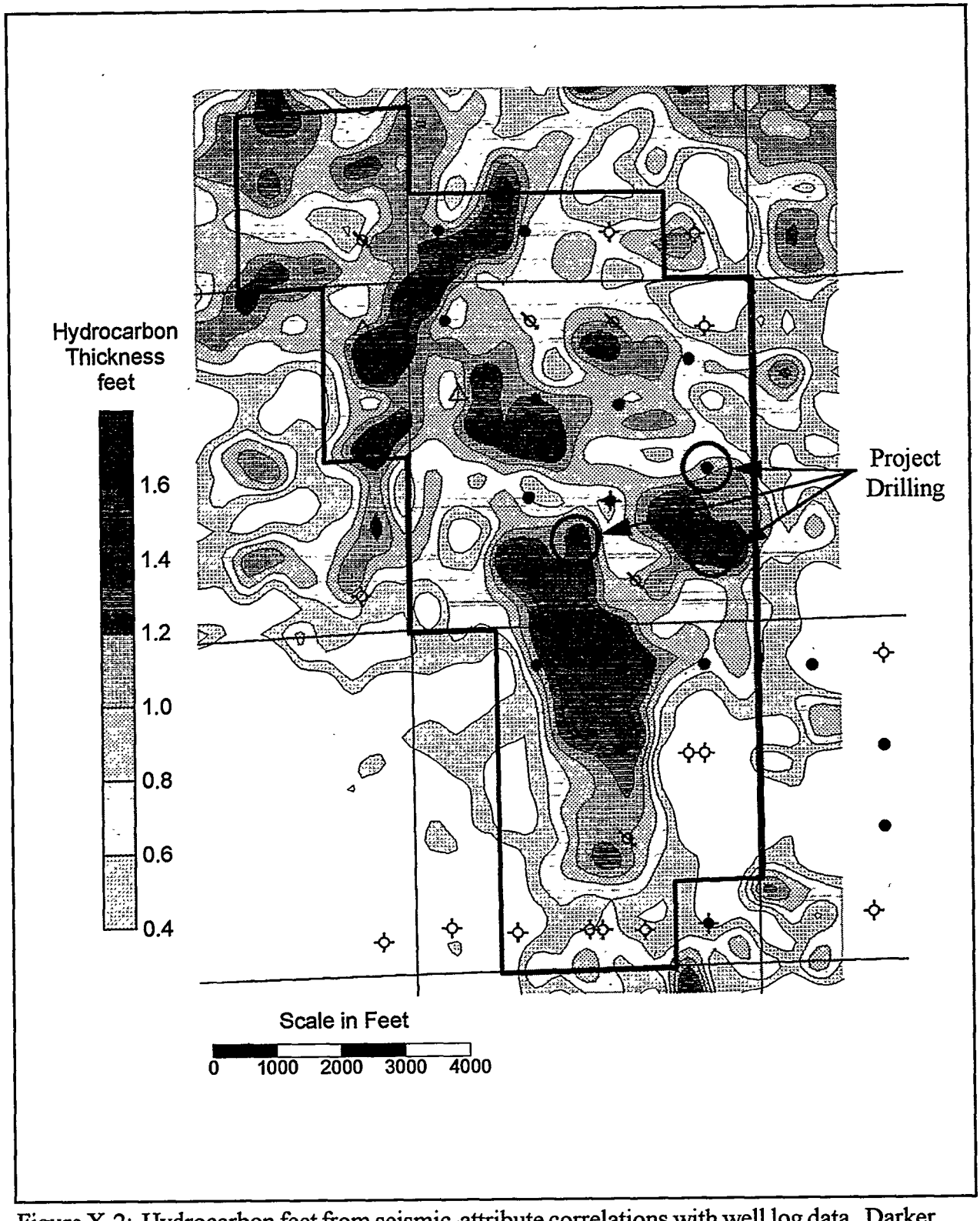

Figure X-2: Hydrocarbon feet from seismic-attribute correlations with well log data. Darker shading indicates thicker reservoir development.

Summary and Conclusions

The project objective to improve recovery at the Sooner Unit was achieved. Projected recovery was increased from 1,556,000 bbl to 1,861,000 bbL Daily production from the Sooner Unit increased more than 100% above the trend established before the project was initiated. A development plan was established to further increase total recovery to 2,252,000 bbl after the project term closed. Ultimate oil recovery from the D Sandstone reservoir is projected to be 32.6 percent of OOIP.

Several technologies were employed during the project. Successful elements of the project are 3D seismic imaging, selective infill drilling and reservoir management based on operational compartments, and reservoir description. The project acquired 3D seismic over a 7.7 sq-mile area. Transient and static pressure-test data were used with water-cut information for the delineation of operational compartments. Three vertical wells were drilled (one injector and two producers). Vertical drilling based on seismic-attribute maps proved effective while attempts at horizontal drilling and completion were unsuccessful. The greatest impact on describing the reservoir and developing an infill-drilling plan came from the 3D seismic. The greatest cost was incurred from horizontal drilling attempts.

Waterflood projects in the Cretaceous D Sandstone of the Denver-Julesburg Basin have been perceived as unattractive because of historically poor recovery. Reservoir heterogeneity and poor reservoir management practices are the major reasons for historically poor secondary recovery. The key to successfully developing a waterflood in the D sandstone is recognition of the depositional system and heterogeneity which is likely to have been created by that system. The waterflood must be designed to sweep oil from compartments and acknowledge anisotropy. Operators need to think in terms of non-standard well spacing and injection patterns to implement successful waterflood projects in the D Sandstone (and reservoirs with similar geological settings) .

Results from the project demonstrate that waterflooding the D Sandstone can yield secondary oil equal to that obtained by primary depletion. The important concept for successful waterflooding the D Sandstone is injection by reservoir compartment and unconventional patterns. While infill drilling at 20-acre spacing and developing the field on regular five-spot injection patterns would recover most of the moveable oil, it would not be economically efficient. Integrated reservoir characterization with 3D seismic can optimize infill locations with the minimum number of wells to maximize economic benefit.

Project studies concluded there were eight high-priority infill locations at the Sooner Unit. Three of these locations were drilled during the project. Work performed during the project increased production more than 100% and increased proved developed and undeveloped reserves by 696,000 bbL The Sooner Unit production rate was 400 bopd in October 1995, which is 220 bopd over the prior production trend. The current cost of the 3D seismic survey and three wells is $850,000. The incremental proved-developed oil reserves resulting from just 3D seismic and three wells are placed at 305,000 bbL The additional future income (using $17 per bbl) before income taxes is calculated to be $1,233,000 (undiscounted) and $876,000 (discounted at 10%). While the total project cost of $1,577,000 is not expected to payout from the current incremental reserves, future development is expected to result in a 2 to 1 return. The project cost and remaining development expenditures are estimated to be $2,700,000. Cash-flow and economic analysis of a $2,700,000 expenditure for 696,000 bbl projected reserves indicates incremental income before income taxes of $2,854,000 (undiscounted) and $1,901,000 (discounted at 10%).

*U.S. GOVERNMENT PRINTING OFFICE: 1996 - 559-031/40046

FOSSIL ENERGY

DOE/BC/14962-24
(OSTI ID: 750872)

THE UTILIZATION OF THE MICROFLORA INDIGENOUS TO AND PRESENT IN OIL-BEARING FORMATIONS TO SELECTIVELY PLUG THE MORE POROUS ZONES THEREBY INCREASING OIL RECOVERY DURING WATERFLOODING

Final Report
November 1999

By:
James O. Stephens
Lewis R. Brown
A. Alex Vadie

Date Published: February 2000

Work Performed Under Contract No. DE-FC22-93BC14962

Hughes Eastern Corporation
Ridgeland, Mississippi

National Energy Technology Laboratory
National Petroleum Technology Office
U.S. DEPARTMENT OF ENERGY
Tulsa, Oklahoma

DISCLAIMER

This report was prepared as an account of work sponsored by an agency of the United States Government. Neither the United States Government nor any agency thereof, nor any of their employees, makes any warranty, expressed or implied, or assumes any legal liability or responsibility for the accuracy, completeness, or usefulness of any information, apparatus, product, or process disclosed, or represents that its use would not infringe privately owned rights. Reference herein to any specific commercial product, process, or service by trade name, trademark, manufacturer, or otherwise does not necessarily constitute or imply its endorsement, recommendation, or favoring by the United States Government or any agency thereof. The views and opinions of authors expressed herein do not necessarily state or reflect those of the United States Government.

This report has been reproduced directly from the best available copy.

DOE/BC/14962-24
Distribution Category UC-122

The Utilization of the Microflora Indigenous to and Present in Oil-Bearing Formations to Selectively Plug the More Porous Zones Thereby Increasing Oil Recovery During Waterflooding

By
James O. Stephens
Lewis R. Brown
A. Alex Vadie

February 2000

Work Performed Under DE-FC22-93BC14962

Prepared for
U.S. Department of Energy
Assistant Secretary for Fossil Energy

Gary D. Walker, Project Manager
National Petroleum Technology Office
P.O. Box 3628
Tulsa, OK 74101

Prepared by
Hughes Eastern Corporation
403 Towne Center Blvd., Suite 103
Ridgeland, MS 39157-4803

TABLE OF CONTENTS

Page

LIST OF TABLES v
LIST OF FIGURES vi
EXECUTIVE SUMMARY ix

I. INTRODUCTION 1
- A. Review of MEOR 1
- B. Objective of the Project 2

II. DESCRIPTION OF THE OIL RESERVOIR 5

III. PRE-FIELD TRIAL STUDIES 7
- A. Experimental Design 7
- B. Acquisition of Live cores 7
- C. Analytical Methods 10
  - 1. Crushing Cores 10
  - 2. Enumeration of Microorganisms 10
- D. Results of Core analyses 12
  - 1. Geological Characterization 12
  - 2. Petrophysical Characterization 13
  - 3. Microbiological Characterization 15
- E. Formulation of Feeding Regime 16
  - 1. Preparation of Core Plugs 16
  - 2. Treatment of Core Plugs 16
  - 3. Analyses of Effluent from Core Plugs 18
  - 4. Core Flood Experiments 18
- F. Tracer Study 21
- G. Baseline Studies 22
  - 1. Methods 22
  - 2. Results 24

IV. FIELD TRIAL 25
- A. Design of Skid for Nutrient Injection 25
- B. Design of Field Trial 26
  - 1. Test Patterns for Field Demonstration 26
  - 2. Feeding Regime 29
- C. Modification of Experimental Design 31
- D. Drilling of Three New Wells 31
- E. Analysis of Cores 33
- F. Expansion of Injection Program 36
- G. Monitoring Program 36
  - 1. Petrophysical Analyses 37

2. Microbiological Analyses 38
3. Inorganic Ion Analyses 38
H. Results 39
1. Oil Production 39
2. Evidence of New Oil in Produced Fluids 41
3. Analysis of Produced Gas 42
4. Distribution of Nutrients Throughout the Reservoir 43
5. Evidence of Microbial Proliferation in Reservoir 43
6. Performance of Injector Wells 44
7. Overall Performance of Field Demonstration 45

V. DISCUSSION 49
VI. TECHNOLOGY TRANSFER 53
VII. SUMMARY AND CONCLUSIONS 57
VIII. ACKNOWLEDGEMENTS 59
IX. REFERENCES 61
APPENDIX 63

LIST OF TABLES

Table 1. Porosity and permeability of collected core samples 14

Table 2. Aerobic and anaerobic heterotrophs and oil-utilizing microorganisms in samples of core from newly drilled well 15

Table 3. Different physiological groups of microorganisms in the core from the newly drilled well 16

Table 4. Feed and feeding regime from November 1994-April 1996 30

Table 5. Feed and feeding regime from April 1996-June 1997 31

Table 6. Petrophysical properties of cores from three newly drilled wells 36

Table 7. Feed and feeding regime for all ten injector wells from July 1997-June 1998 37

Table 8. Oil production response from all wells included in project 40

Table 9. Numbers of microorganisms in sections of cores from three newly drilled Wells 44

LIST OF FIGURES

Figure 1. NBCU field location 5

Figure 2. Approximate location of two new wells in NBCU 8

Figure 3. Core from well 34-3 No. 2. (Note oil seeping from core) 9

Figure 4. Relative permeability as a function of gas saturation 14

Figure 5. Relative permeability as a function of water saturation 15

Figure 6. Live core assembly 17

Figure 7. Photograph of core in plastic wrap next to the rubber sleeve 17

Figure 8. Photograph of completely assembled core plug 18

Figure 9. Flow of simulated production water through control core in experiment 2 19

Figure 10. Flow rate of simulated production water containing potassium nitrate and disodium hydrogen phosphate through test core in experiment 2 19

Figure 11. Flow rate of simulated injection water through control core plug 20

Figure 12. Flow rate of simulated injection water containing nutrients through test core plug 21

Figure 13. Flow diagram for North Blowhorn Creek Unit nutrient injection skid 25

Figure 14. Picture of skid 26

Figure 15. Isopach of NBCU oil field showing locations of wells in the four test and control patterns 27

Figure 16. Locations of three new wells and injectors receiving nutrients during the final 12 months of the project 32

Figure 17. Electron micrograph of a sample of core from well 2-13 No.2, section 6. (Note the scattered microbial cells) 34

Figure 18. Electron micrograph of a sample of core from well 2-11 No.3, section 3. (Note the large number of microbial cells) 34

Figure 19. Electron micrograph of a sample of core from well 2-5 No.2, section 11. (Note the large number of microbial cells) 35

Figure 20. Electron micrograph of a sample of core from well 2-11 No.3, section 3. (Note the large number of microbial cells) 35

Figure 21. Total production from North Blowhorn Creek Unit excluding newly drilled wells 46

Figure 22. Mechanism of microbial enhanced oil recovery (MEOR) using *in situ* microbial permeability profile modification to enhance oil recovery 50

Figure 23. Comparison of MPPM EOR treatment (5-spot Pattern) vs. individual well MEOR Treatment 51

EXECUTIVE SUMMARY

This is the final report on a Department of Energy "Class I Oil Program-Mid Term Activities" project entitled "The Utilization of the Microflora Indigenous to and Present in Oil-Bearing Formations to Selectively Plug the More Porous Zones Thereby Increasing Oil Recovery During Waterflooding". The 5.5 year project was divided into three phases. Those phases and their duration were - Phase I Planning and Analysis (9 months), Phase II Implementation (45 months), and Phase III Technology Transfer (12 months). The laboratory portions of the project were carried out at Mississippi State University and the North Blowhom Creek Oil Field situated in Lamar Co., AL was the site of the field demonstration. Specifically, the objective of the project was to demonstrate the effectiveness of a microbial permeability profile modification technology (MPPM) to enhance oil recovery from a fluvial dominated deltaic reservoir and to document the scientific basis of the technology.

Simply stated MPPM involves adding nitrogen-containing and phosphorous-containing microbial nutrients to the injection water in a conventional waterflooding operation. . The resulting microbial growth redirects water flow from the more porous zones to new unswept oil-bearing channels, thereby increasing the efficiency of the waterflooding. Feed and feeding regimes employed in the field demonstration were formulated on the basis of core flood experiments conducted using live cores from a newly drilled well in an area of the field not influenced by the waterflooding operation. The field demonstration design involved injecting nutrients into four injectors (test) and monitoring the surrounding production wells. For control, the producing wells surrounding four other injectors not receiving nutrients were monitored. Thus, the results from producing wells in the test patterns could be compared to results from similar wells in the same field as well as the historical data.

The success of the technology was shown by the recovery of 10,970 m^3 (69,000 bbl) of incremental oil during the first 42 months with a projected recovery of 64,000-95,000 m^3 400-600 MBO) and an extension of the economic life of the field by 60-137 months. The field wide distribution of the injected nutrients was clearly demonstrated by their presence in producing wells and in cores obtained from three wells drilled in the field after 22 months of nutrient injection. The role of microorganisms was shown by the presence of large numbers of microorganisms in cores from the three wells cited above. Proof that oil from unswept areas of the reservoir was present in the produced oil was shown by changes in the gas chromatographic profile and by a change in the composition of produced gases.

Attractive features of the MPPM are that it (1) may be employed in many geological formations amenable to waterflooding, (2) does not interfere with normal waterflooding activities, (3) is environmentally friendly, and (4) is the least expensive of all FOR processes in terms of cost per barrel of incremental oil recovered.

I. INTRODUCTION

A. Review of MEOR

The concept of using microorganisms to enhance oil recovery, MEOR, was first proposed in 1926 by Beckman [1]; but, it was not until the 1950's that the concept was actively researched by ZoBell and his colleagues [2,5]. Since that time, a number of diverse microbiological technologies has been developed to enhance oil recovery. For example, some microbial methods aid in paraffin removal while others are designed to modify heavy oil. Still other methods use microorganisms to produce chemicals, such as surfactants, polymers, or solvents that are useful in oil recovery processes, either in above ground facilities or *in situ.* Most of the methods are designed to treat single wells, and not the entire fields. This diversity of MEOR applications has led to a great deal of confusion in the petroleum industry and skepticism as to the merits of MEOR. Since most of the early research on MEOR in this country was conducted by industry, the results were proprietary and the only references thereto are to be found in the patent literature.

The target for enhanced oil recovery processes is the tremendous quantity of unrecoverable oil in known deposits. Roughly two-thirds [approximately 55.6×10^9 m^3 (350 billion bbl)] of all of the oil discovered in the U. S. is unrecoverable economically using current technology. Since one of the major attributes of MEOR technologies is its low cost, the question arises as to why MEOR has not been generally accepted by the petroleum industry. One of the reasons for this state of affairs is that many of the processes simply don't work. They were either based on untried ideas or on laboratory work alone and when subjected to field tests, they failed. Also, many people in the petroleum industry do not understand that MEOR is a multiplicity of technologies, not a single process. While there has been an increasing number of publications in the open literature on laboratory studies, their value in the field is only speculative.

Furthermore, reports on the deleterious activities of microorganisms in the oil field contribute to the skepticism of employing technologies using microorganisms. Even most reports on field trials are poorly documented and fail to meet normal standards for scientific acceptance. For example, the lack of adequate controls is glaring. This lack of controls is understandable in light of the fact that they are an added expense and will not contribute a single barrel of oil to the operator involved. Thus, subsidy to acquire the data to scientifically document the success of MEOR technology is needed if MEOR is to become an accepted tool for the oil industry.

It is also clear that scientific knowledge of the fundamentals of microbiology must be coupled with an understanding of the geological and engineering aspects of oil production in order to develop a meritorious MEOR technology. Furthermore, funds must be available to pay for the collection of the scientific documentation necessary to validate that particular MEOR technology.

The MEOR technology being demonstrated in the current project was developed in the 1980's at Mississippi State University with funds provided in part by industry[6] and improved under a Dept. of Energy (DOE) Grant[7] in the early 1990's. The Reservoir Class Program initiated by DOE in 1992 presented the opportunity to not only demonstrate the effectiveness of a specific MEOR technology but also to be able to design and execute an experimental program that would allow for the scientific validation of the results. In order to accomplish this goal, Hughes Eastern Corporation and Mississippi State University joined forces with DOE in a cooperative agreement . The team of principal investigators assembled for the project consisted of a microbiologist, a petroleum engineer, and an oil company executive, thus insuring that expertise necessary for the successful execution of the project was actively involved in the design, implementation, and evaluation of the demonstration.

Since the MEOR technology in this project differs in several ways from other MEOR technologies, it is important that these differences be clearly delineated. The present project is designed to enhance oil recovery from an entire oil reservoir rather than treat single wells. Even more important is the fact that this technology relies on the action of the *in situ* microflora, not microorganisms injected into the reservoir. The MEOR technology being demonstrated in this project is a microbial permeability profile modification technology (MPPM) wherein the addition of nutrients to the reservoir enables the microflora present to grow, thereby altering the sweep pattern of the injection water in a conventional waterflood operation. Thus, injection water is diverted from the larger channels to previously unswept areas of the reservoir resulting in an increased efficiency of the waterflood operation. It is important to note that employing this MPPM technology does not interfere with the normal waterflood operation. Also, it should be emphasized that the technology is environmentally friendly in that neither microorganisms nor hazardous chemicals are introduced into the environment. The microorganisms upon which the technology depends are already present in the reservoir and the microbial nutrients are commonly used plant fertilizers. This process is the cheapest of all FOR processes.

B. Objectives of the Project

The objectives of this project were (1) to demonstrate that the *in situ* microbial population in a fluvial dominated deltaic reservoir could be induced to proliferate to such an extent that they will selectively restrict flow in the more porous zones in the reservoir thereby forcing injection water to flow through previously unswept areas thus improving the sweep efficiency of the waterflood and (2) to obtain scientific validation that microorganisms are indeed responsible for the increased oil recovery.

One expected outcome of this new technology was the prolongation of economical life of the reservoir, i.e. economical oil recovery should continue for much longer periods in areas of the reservoir subjected to the MPPM technology than it would if it followed its historic trend.

This five and a half year project was divided into three phases of nine months, forty-five months, and twelve months. Phase I was devoted to planning and analysis and involved the drilling of two new wells to obtain cores for laboratory experimentation. During Phase II the field demonstration was carried out and Phase III was devoted to technology transfer.

ll. DJ SCK1Y 1'IUN UI "111I UiL KESL+'KVOIK

The North Blowhom Creek Oil Unit (NBCU) is located in the Lamar County, AL about seventy-five miles west of Birmingham (See Figure 1). The field is in . what is known geologically as the Black Warrior Basin. The producing formation is the Carter Sandstone of Mississippian Age at a depth of about 700 m (2300 feet). The field was discovered in 1979 and initially developed on 80-acre spacing. Waterflooding of the reservoir began in 1983. The initial oil in place in the reservoir was about 2.54 x 10^6 m^3 (16 million barrels), of which 874,430 m^3 (5.5 million barrels) had been recovered by the end of 1995. To date, North Blowhom Creek is the largest oil field discovered in the Black Warrior Basin. Oil production peaked at almost 475 m^3/day (3000 BOPD) in 1985 and has since steadily declined. Currently there are 20 injection wells and 32 producing wells. Oil production at the outset of the field demonstration was about 46 m^3/day oil (290 BOPD), 1700 m^3/day gas (60 MCFD), and 493 m^3/day water (3100 BWPD) with a water injection rate at about 660 m^3/day (4150 BWPD). Projections at the beginning of the project were that about 1.59 x 10^6 m^3 of oil (10 MMBO) would be left unrecovered if some new method of enhanced recovery were not effective.

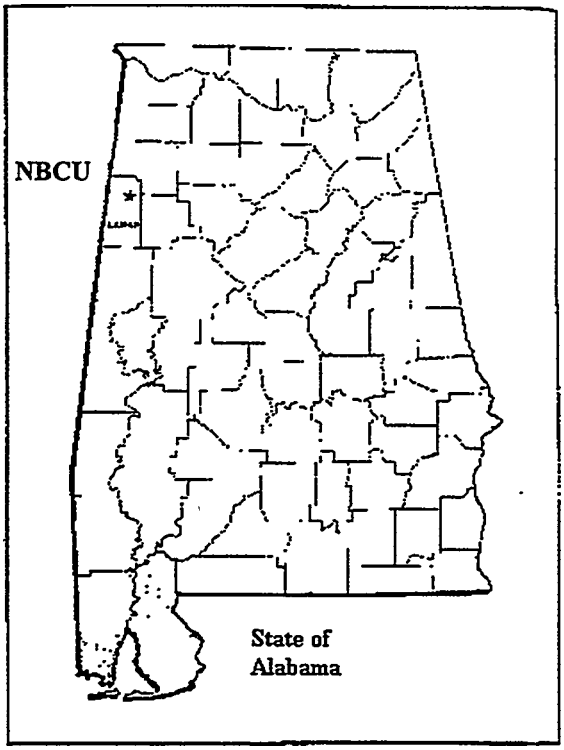

Figure 1. NBCU field location.

III. PRE-FIELD TRIAL STUDIES

A. Experimental Design

The concepts of the new technology evaluated in this project were scientifically sound and had been proven to be effective in laboratory experiments [illegible]. Nevertheless, it was deemed desirable to perform laboratory tests on live cores from the reservoir of interest. Two wells were drilled for this purpose and special core flood experiments were conducted in order to establish the exact concentration of, and schedule for additions of, nutrients to the injection water.

While the main purpose of drilling the two wells was to obtain cores suitable for use in the laboratory work, a secondary purpose was to obtain production data that would indicate the sweep efficiency of the existing waterflood.

At the conclusion of Phase I, two different feeding regimes were formulated for the field demonstration, each to be employed in two test injector wells.

B. Acquisition of Live Cores

Phase I of the project began with the drilling of two wells (see Figure 2) to obtain live cores and production data that would indicate how well the reservoir was being swept by the existing waterflooding. The two well locations were chosen in an area of the field where representative Carter sand thicknesses [approximately 6 m (20 ft)] could be expected and also in an area where bypassed oil could reasonably be expected to exist. The first well, NBCU 34-6 No. 3, was drilled in March 1994 and encountered 6.1 m (20 feet) of net Carter formation sand. However, probably due to the overbalanced drilling condition in the subnormally pressured reservoir, no increase in drilling rate occurred in the sand and the core point was missed.

The NBCU 34-6 No. 3 was completed and placed on rod pump. The well initially tested 4 m^3/day oil (25 BOPD), 0.16 m^3/day water (1 BWPD) and 142 m^3 (5 MCFD). By December 1994 the rate had decreased to 1.6 m^3/day oil (10 BOPD), 0 m^3/day water (0 BWPD) and 113 m^3/day gas (4 MCFD). Cumulative production was 533 m^3 oil (3354 BO), 38 m^3 water (241 BW), and 32.4 x 10^3 m^3 gas (1144 MSCF). The fact that the well exhibited low water cut compared to offset wells that typically produce 65-98% water was further evidence of the existence of bypassed oil. In December 1996, as a result of continued low fluid and low water cut production, the well was hydraulically refractured. The refracturing was very successful, resulting in an initial rate of 7.3 m^3/day oil (46 BOPD) with 0.08 m^3/day water (0.5 BWPD). The rate continued to improve and peaked at 13.7 m^3/day oil (103 BOPD) with 0.8 m^3/day water (5 BWPD) in May 1998. At this point the well accounted for almost one third of total unit production. After May the oil production began to decline as water production increased.

The second new well, NBCU 34-3 No. 2, was successfully drilled and cored during April, 1994. Because of the inability to pick a coring point by drilling rate increase in the first

well, the core point was picked in the second well strictly based upon where in the geologic section the sand should occur, without the necessity of actually having an increase in drilling rate

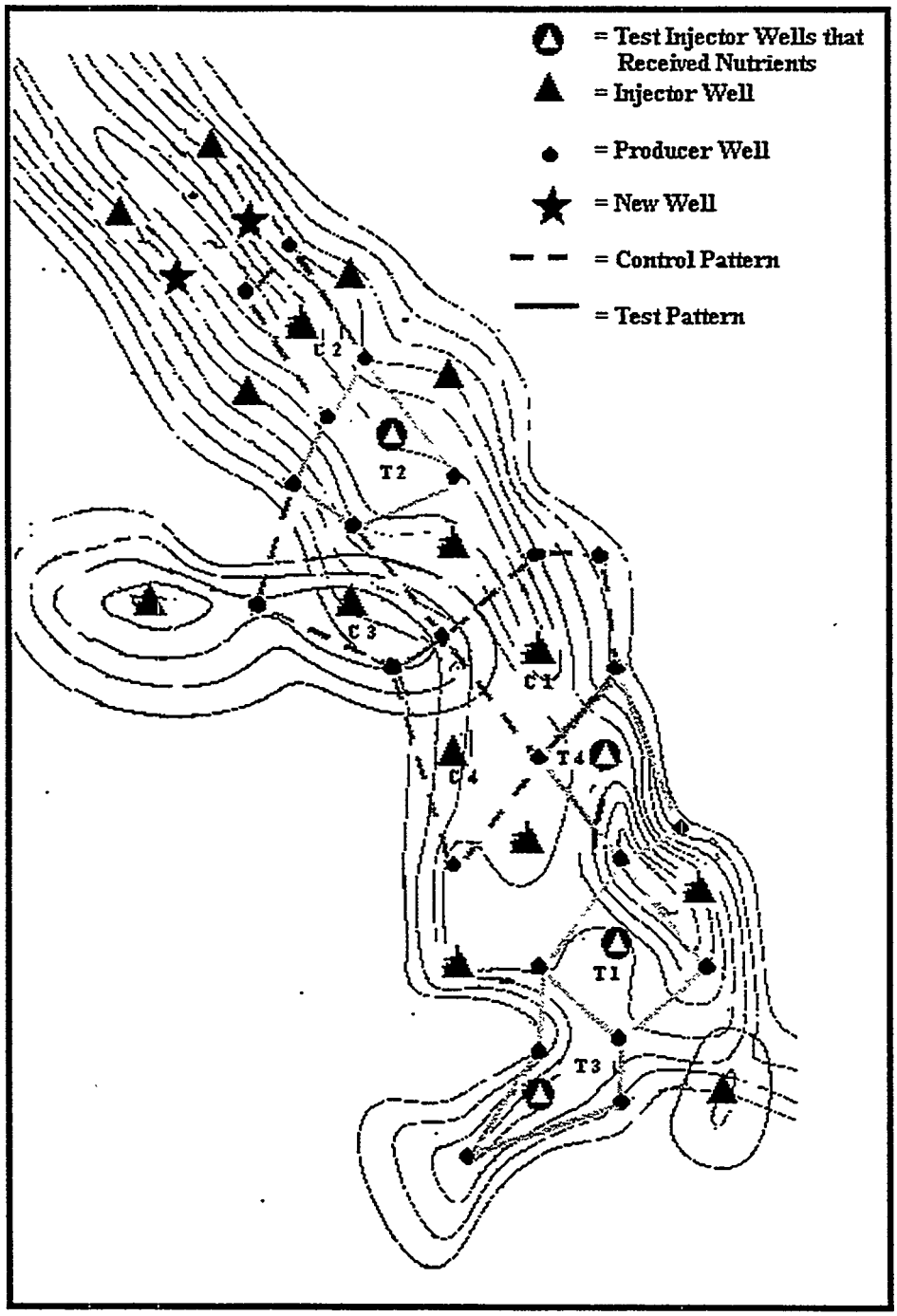

Figure 2. Approximate location of two new wells in NBCU.

to indicate penetration of the sand. The well encountered about 6.4 m (21 feet) of net Carter oil sand. About 6 m (20 feet) of the core was immediately collected using the special procedures outlined elsewhere in this report and transported to Mississippi State University for laboratory work. From visual observation of live oil running from the core (see Figure 3) as it was removed from the core barrel it was obvious that much oil remained in the reservoir. The well was completed and placed on rod pump for production.

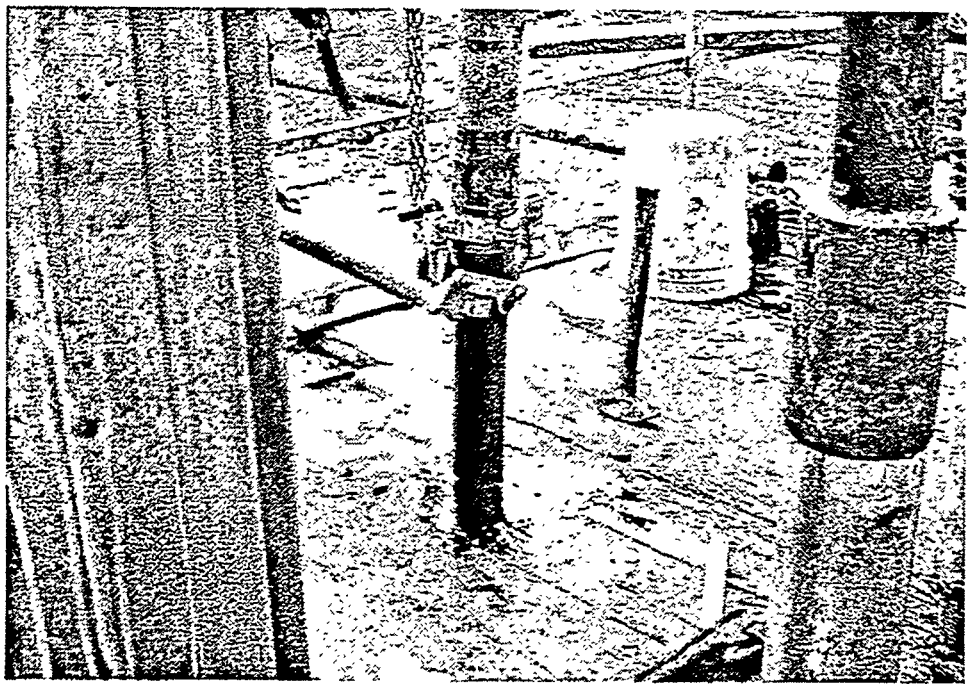

Figure 3. Core from well 34-3 No. 2. (Note oil seeping from core).

Representative production data could not be obtained initially due to the well pumping fluid containing large amounts of fracturing sand and relatively little fluid. The well tubing and pump had to be pulled several times to clean out sand. In June, the decision was made to re-fracture the well to remedy the sand production problem and obtain representative, commercial production from the well. The refracturing was successful in achieving both objectives, and soon afterward the well tested 6.8 m^3/day oil (43 BOPD), 6.8 m^3/day water (43 BWPD) and about -2265 m^3/day gas (80 MSCFD) on pump. By the end of December 1994, the producing rate had declined to 1.3 m^3/day oil (8 BOPD), 1.7 m^3/day water (11 BWPD), and 113 m^3/day gas (4 MSCFD). Cumulative production was 497 m^3 oil (3128 BO), 741 m^3 water (4659 BW), and 30,387 m^3 gas (1073 MSCF).

The cores were received as they were pulled from the core barrel (live cores). The cores were broken into 1-ft sections, wiped with 70% ethanol, and immediately placed in an anaerobic jar containing Gas Pak® disposable hydrogen and carbon dioxide generator envelopes to

produce anaerobic conditions in the jar (Becton Dickinson Gas Pak®). This procedure was completed within minutes, thus exposure to air was minimal which was of particular significance for microbiological studies. It should be pointed out that the pressure in the core tends to force fluid and/or gases outward, thereby reducing further the possibility of exposing the internal section of the core to air. The anaerobic containers were packed in ice, transported to the laboratory, and placed in a refrigerator at 4°C until needed.

C. Analytical Methods

1. Crushing of the Cores

When the cores were to be analyzed, they were removed from their containers under an atmosphere of nitrogen, again wiped with 70% ethanol, and cut into four-inch sections (top, middle, and bottom) using a sterile core saw (Rayteck Industries, Stanford, Spring, CT) and one inch cut from all sides of the core also using a sterile core saw blade. Each median part of a core was placed in a stainless steel core crusher under nitrogen gas and subjected to 1.4×10^4 kPa (20,000 psi) using a hydraulic press. Each portion of crushed core material was passed through a sterilized U.S.A. Standard Testing Sieve No. 40 [0.42 mm (0.0165 inch) openings] to make the inocula more uniform. All analyses were performed in a bacteriological hood containing an atmosphere of nitrogen gas.

2. Enumeration of Microorganisms

Fifty grams of sieved core material was mixed with 50 ml of sterile simulated production water described below that served as the diluent for this and subsequent dilutions. After mixing, 10 ml of the first dilution was transferred to a 90 ml dilution blank contained in a six-ounce prescription bottle. The second dilution was mixed thoroughly before transferring 10 ml to the next dilution blank. Precautions were taken to insure homogeneity in the suspensions prior to sampling, thus, particulate matter was present in all samples.

All work was conducted in a bacteriological hood containing a nitrogen atmosphere at a constant inlet pressure of 10 psi. The absence of oxygen in the atmosphere of the hood was confirmed by gas chromatographic (GC) analysis.

The conventional spread plate technique was employed in some enumeration procedures while the Most Probable Number (MPN) technique) was employed in others. All plate counts were performed in triplicate.

Simulated production water used for the core flood experiments was prepared with the following inorganic salts per 50 liters of distilled water.

$CaCl_2$	10.90 g
$MgCl_2$	2.71 g
$BaCl_2$	4.56 g

Na_2SO_4	1.84 g
$NaHCO_3$	34.86 g
NaCl	147.90 g

The pH was adjusted to 7.0 (±0.2) using 10% (v/v) HCI.

The following groups of microorganisms were enumerated.

Total Heterotrophs were enumerated using the conventional spread plate technique and Bacto Plate Count Agar (PCA) obtained from Difco Laboratories, Detroit, MI. Plate counts were conducted under both aerobic and anaerobic conditions with the anaerobic cultures incubated in the BBL Gas Pak® Systems containers. Plates were incubated at the temperature prevailing in the reservoir (32°C).

Oil-utilizing Bacteria were enumerated using the conventional spread plate technique and oil-overlay agar. Incubation was as described for the total heterotrophs. Oil-overlay agar was prepared with simulated production water supplemented with 0.1% KNO_3, 0.038% $K2HPO_4$, 1% filter-sterilized crude oil, and 2% Bacto-Agar. After the agar had been poured and had hardened in the petri plates, a thin overlay was added using oil agar prepared with oil-saturated water, but containing no added oil.

Two groups of Methane-producing Bacteria were enumerated, both using the Most Probable Number (MPN) technique (three tubes per concentration of sample). One set of tubes was supplemented with 10 g per liter of sodium formate, while the other set of tubes was incubated under an atmosphere of 80% H_2-20% CO_2 as described by Zeikus[9]. Tubes were incubated at the reservoir temperature (32°C). All tubes were closed with serum stoppers and methane production determined by GC analysis of the atmosphere in the tube.

Denitrifying and Nitrate-reducing Bacteria were enumerated using the Most Probable Number (MPN) technique (three tubes per concentration of sample) and Bacto-Nitrate Broth in test tubes containing Durham fermentation tubes. The tubes were incubated anaerobically for three weeks at the reservoir temperature (32°C). After incubation, tubes showing gas production were recorded as positive for denitrifying bacteria. Spot tests for nitrite were conducted using the sulfanilic acid and a-naphthylamine acetate reagents as described in Standard Methods for the Examination of Water and Wastewater [8]. Negative tubes were reexamined after 60 days.

Nitrate-reducing, Hydrocarbon-utilizing Bacteria were enumerated using the Most Probable Number (MPN) technique (three tubes per concentration of sample) and the hydrocarbon-utilizing, nitrate-reducing medium of Rosenfeld" [illegible] but modified by using simulated production water in place of synthetic seawater as follows:

$FeSO_4$	0.1 g
K_2HPO_4	0.5 g
KNO_3	1.0 g

Simulated production H_2O (400%)	25.0 ml
Distilled water	965.0 ml

The reaction mixture was adjusted to pH 7.8 prior to the addition of 1% crude oil (v/v).

After three weeks of anaerobic incubation at the reservoir temperature (32°C), the tubes were examined for the presence of nitrite as described above. Negative tubes were reexamined after 60 days.

Sulfate-reducing, Hydrocarbon-utilizing Bacteria were enumerated using the Most Probable Number (MPN) technique (three tubes per concentration of sample) and the hydrocarbon-utilizing, sulfate-reducing medium described by Rosenfeld [10], but modified by using simulated production water in place of synthetic seawater as follows:

$Fe(NH_4)_2(SO_4)_2 \cdot 6H_2O$	0.1 g
K_2HPO_4	0.5 g
$(NH_4)_2SO_4$	1.0 g
Simulated production H_2O (400%)	25.0 ml
Distilled water	965.0 ml
Crude Oil	10.0 ml

After three weeks of anaerobic incubation at the reservoir temperature (32°C), the tubes were examined for blackening of the agar. Negative tubes were reexamined after 60 days.

Test for Ultramicrobacteria was conducted by crushing fifty grams of core and vigorously mixing it with 200 ml of sterile saline solution (2.5% NaCl, w/v). The suspension then was filtered through a Whatman No. 1 filter paper to remove fines that would interfere with the filtration process. The suspension was immediately filtered through a pre-sterilized membrane filter (0.80 µm) and then through a pre-sterilized 0.45 µm membrane filter to trap normal size bacteria. The filtrate was next filtered through a pre-sterilized 0.22 gm membrane filter. One ml of the filtrate then was added aseptically to a test tube containing 10 ml of Tryptic Soy Broth (TSB) at a final concentration of one-eighth the strength of the original medium. The filters were placed into test tubes containing the same medium and incubated anaerobically at 32°C. Both the filters and filtrates were tested for the presence of viable microorganism weekly.

D. Results of Core Analyses

1. Geological Characterization

A general description of recovered cores is as follows.

Sandstone, grayish brown when dry and brownish gray when wet. The sandstone was a massive fine-grained quartz with less than 10% heavy minerals; well sorted; subrounded to subangular; and moderately well cemented with silica cement.

The sandstone had occasional silty clay clasts, more numerous near the top. The clay clasts were medium light gray when dry and toward the bottom; dark gray when wet and near the top. The clasts were up to 1 inch in diameter.

There were horizontal and vertical fractures present. The fractures and occasional near horizontal silty clay laminae were dark stained (particularly noticeable when wet).

The dark staining in the laminae and fractures, as well as some zones within the sandstone, appeared to be hydrocarbons. The core had a hydrocarbon odor and fluoresced purple from areas that correspond with dark s sins.

Most silts and clay laminae as well as clasts were visible in the faces of horizontal breaks in the cores and only occasional clasts noticed elsewhere. Occasional dark stained laminae were noticed throughout.

A typical identification and description of core samples is as follows: Sandstone, buff, fine, grain, well sorted, siliceous, laminated,•dolomite. X-ray diffraction analysis indicated the core was preliminary quartz (90%) with some 4% dolomite. The clay fraction consisted of 2% kaolinite and 3% mixed layer clay. Some traces of siderite ($FeCO_3$) were present in some samples.

X-ray diffraction Analysis	
Quartz	90%
Dolomite	4%
Kaolinite	2%
Mixed layer clay	3%
Siderite	<1%

For more detailed geological characterization of recovered cores, refer to Supplement0 i)

2. Petrophysical Characterization of Recovered Core Samples

Core sample porosity varied from 7 to 19 percent. Core sample permeability varied much more drastically from 1 to 198 md. Representative data are given in Table 1.

Connate water saturation was around 17 percent and irreducible oil saturation was between 34-45 percent (see Figures 4 and 5 for typical relative permeability curves for oil-water and gas-oil experiments). The relative permeability curves and contact angle photographs suggest that the core samples were oil-wet at the time of testing. For more detailed information on petrophysical characterization of recovered cores refer to Supplement(").

Table 1.
Porosity and permeability of collected core samples.

No.	Depth. Feet	Porosity pc	Permeability, md gas	liquid	Grain Density gr/cc
1	2333	18.90	24.80	11.00	2.35
2	2332	18.50	25.90	8.88	NA
3	2332	16.25	88.00	36.00	NA
4	2332	15.16	108.00	36.00	2.54
5	2331	15.16	4.70*	9.60*	NA
6	2330	NA	30.20	9.22	NA
7	2330	NA	21.38	8.82	2.25
8	2330	15.89	15.89	3.79	NA
9	2330	NA	24.77	3.51	2.41
10	2330	NA	14.79	10.96	NA
11	2329	15.16	30.20	9.00	2.73
12	2329	15.16	18.60	3.60	NA
13	2329	15.16	19.80	10.10	NA
14	2329	16.25	122.00	66.00	2.44
15	2329	15.60	108.00	36.00	NA
16	2329	16.25	88.00	36.00	NA
17	2323	19.79	26.80*	41.78*	NA
18	2323	14.98	42.00*	41.77*	2.81
19	2323	NA	39.00	41.00	2.27
20	2323	NA	26.80	8.10	2.30

*These data may not come from the same core cut.

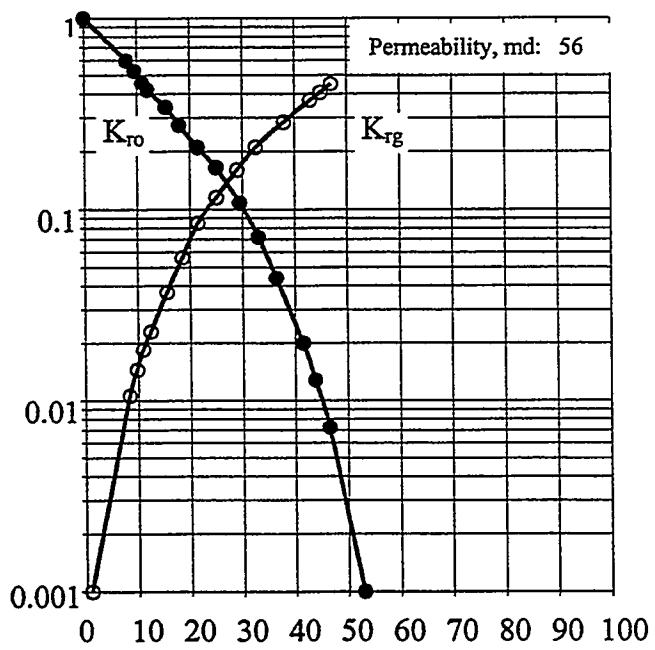

Figure 4. Relative permeability as a function of gas saturation.

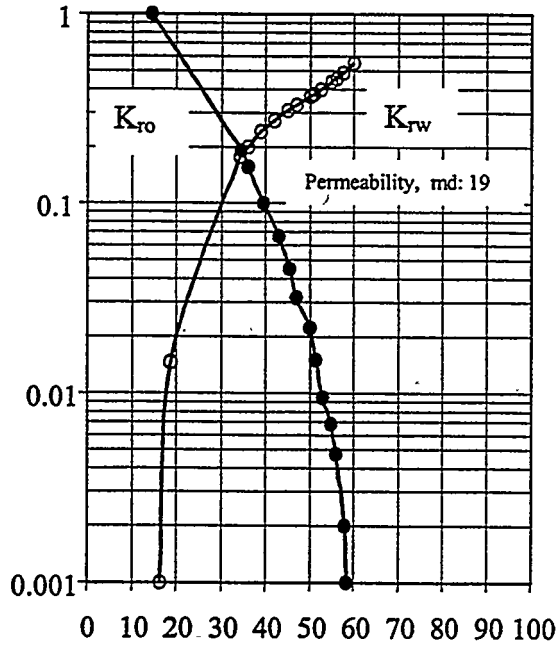

Figure 5. Relative permeability as a function of water saturation.

3. Microbiological Characterization

Each core was divided into three portions, (top, middle, and bottom) crushed, and analyzed for total heterotrophs and oil-utilizing bacteria by the conventional spread plate technique (as shown in Table 2) and for five physiological groups of microorganisms using the MPN technique (as shown in Table 3). It is interesting to note that there were no sulfate-reducing microorganisms (SRB) in any portion of the core. This was particularly surprising in that SRB's have been reported in the literature as the most prevalent organism in oil reservoirs, and SRB's had been recovered from fluids from other wells in this field. Thus, the results suggest that the area of the reservoir in which this well was drilled had not been swept by the, waterflooding. It is also interesting to note that in a previous study [12] no SRB's were found in live cores obtained from wells drilled in areas of 13 oil fields not impacted by FOR processes [13].

Table 2.
Aerobic and anaerobic heterotrophs and oil-utilizing microorganisms in samples of core from newly drilled well.

	PCA		Oil Agar	
Core	Aerobic	Anaerobic	Aerobic	Anaerobic
Top	1	0.3	<1.0	<1.0
Middle	43	2.0	193.0	<1.0
Bottom	36	2.0	0.3	<1.0

Numbers are No. of bacteria/g of core.
PCA = Plate Count Agar

Table 3.
Different physiological groups of microorganisms in the core from the newly drilled well.

Core	Methanogen CO_2:H_2 Broth	Methanogen Formate Broth	HC-utilizing NO_3-reducing Broth	HC-utilizing SO_4-reducing Broth	Difco Nitrate Broth
Top	4.6	<0.6	<0.6	<0.6	18.6
Middle	4.6	48.0	<0.6	<0.6	>220.0
Bottom	7.8	>220.0	<0.6	<0.6	18.6

Numbers are No. of bacteria/g of core.

No evidence of ultramicrobacteria (UMB) was found in any of the cores.

E. Formulation of Feeding Regime

1. Preparation of Core Plugs

Cores were removed from the GasPak® containers under a nitrogen atmosphere and two adjacent core plugs were cut radially from each core, one to serve as the test core and one as the control core. The plugs were 7.6-10.2 cm (3-4 inches) long and 3.8 cm (1.5 inches) in diameter. While still under a nitrogen atmosphere, each plug was inserted immediately into a special heat shrink plastic tube. The plastic wrap shrank as it was heated and wrapped tightly around the core. An entry and an exit port were placed on opposite ends of the core. These ports contained grooves for the reduction of end effects and for more homogeneous distribution of flowing fluids. The entire assembly then was inserted into a thick rubber sleeve [Viton Neoprene Sleeve, 3.8 cm (1.5 inches) diameter, with a 6 mm (0.24 inch) wall]. The ends of the entry and exit ports were fitted with rubber tubing and clamped shut. Both ends were completely sealed with high strength epoxy glue. The glue was allowed to harden for 24 hrs before the cores were used. Figure 6 is a diagrammatic sketch of the assembled core. Figures 7 and 8 are photographs of the cores.

2. Treatment of the Cores

Initially, simulated production water, contained in a five-liter carboy, was allowed to flow through the core. The carboy was situated approximately I m above the core and this hydrostatic head corresponds to 13.24 kPa (1.92 psi) and constituted the total pressure applied to the influent. The water was allowed to flow through a core plug for 48 hrs after which time experimentation commenced. Control cores received simulated production water only while the test cores received simulated production water containing added nutrients (nitrate as 0.06% potassium nitrate and orthophosphate as 0.04% disodium hydrogen phosphate).

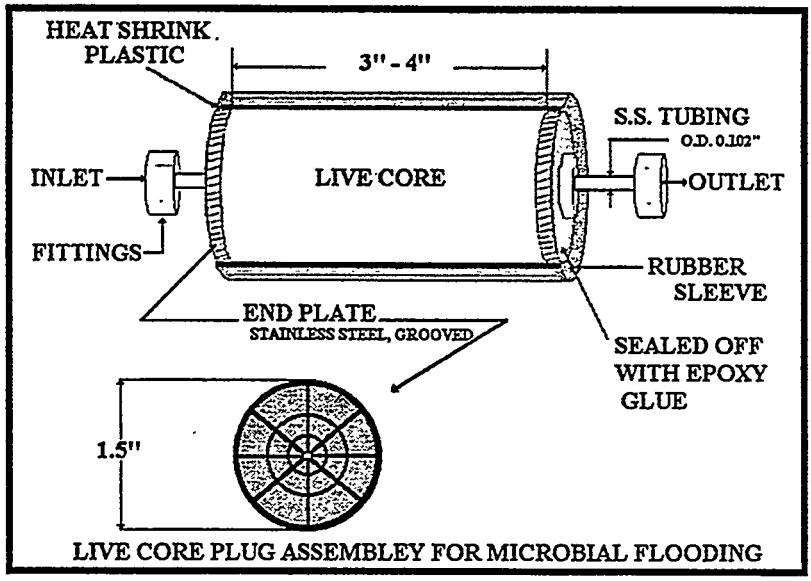

Figure 6. Live core assembly.

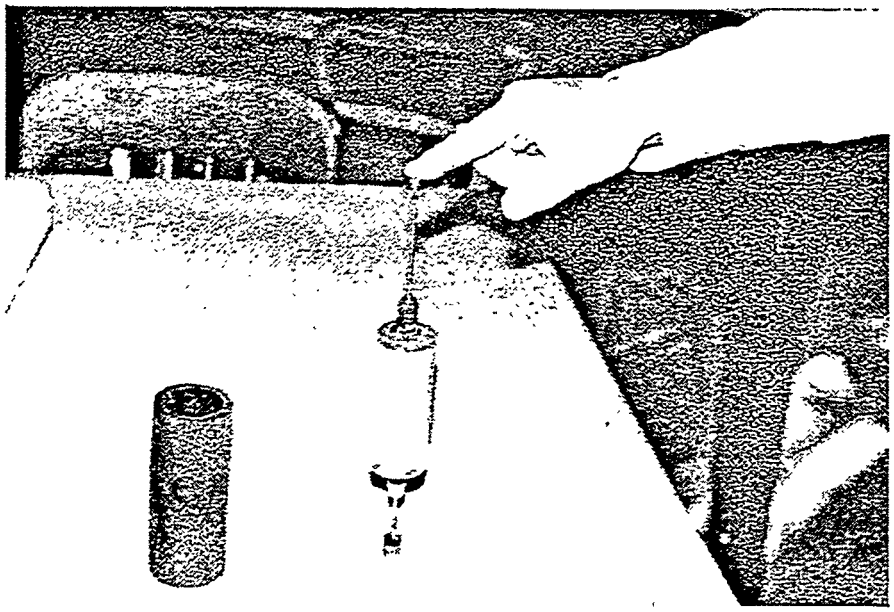

Figure 7. Photograph of core in plastic wrap next to the rubber sleeve.

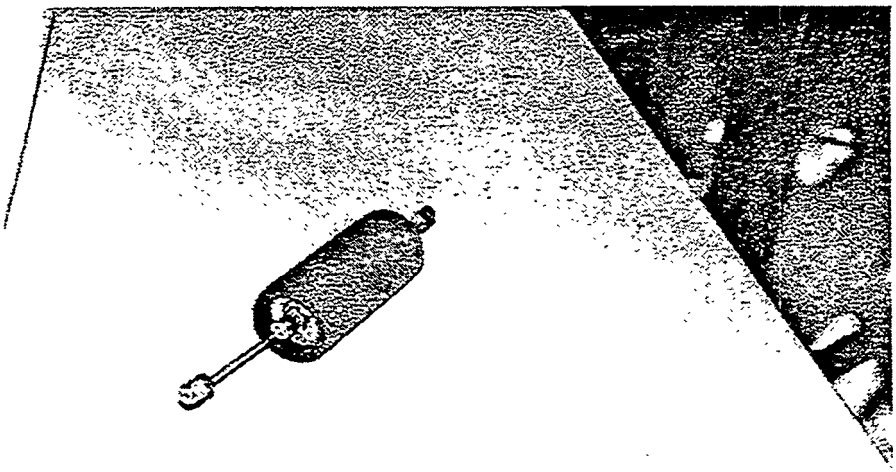

Figure 8. Photograph of completely assembled core plug.

3. Analyses of Effluent from Core Plugs

Fluid volume, pH, and microbial content were measured and recorded periodically for all cores and observations made as to the presence of oil in the effluent. Plate counts were conducted on selected samples using Bacto Plate Count Agar prepared with simulated production water. Plates were incubated for 72 hrs at 32°C under aerobic conditions or two weeks under anaerobic conditions.

4. Core Flood Experiments

The first series of core flood experiments were carried out as described above and as would be expected, flow through the cores varied from one core to another. The pH of the effluent from both cores ranged from 7.4 to 8.4 and the microbial content remained constant at about 10 organisms per ml for both the control and the test cores. It should be pointed out that most microorganisms grow attached to solid surfaces and therefore, the number of microbes in the effluent is not a reflection of the number in the cores.

The control cores showed a steady increase in flow rate while the flow rate in test cores decreased with time. In a typical experiment, oil was found in the effluent of the control core only once as shown in Figure 9, while in the test core, oil was found six times (day 11, 13, 14, 16, 19, and 25) as shown in Figure 10.

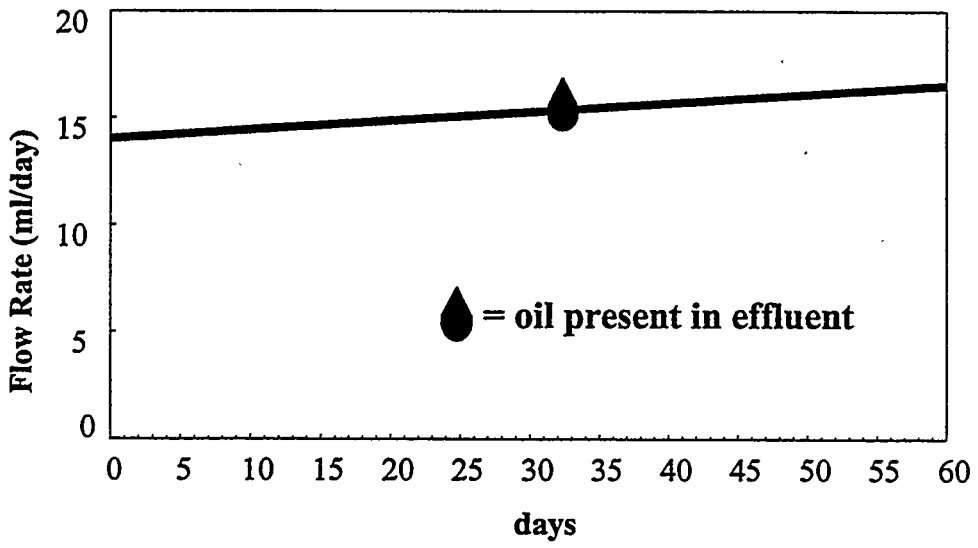

Figure 9. Flow of simulated production water through control core in experiment 2.

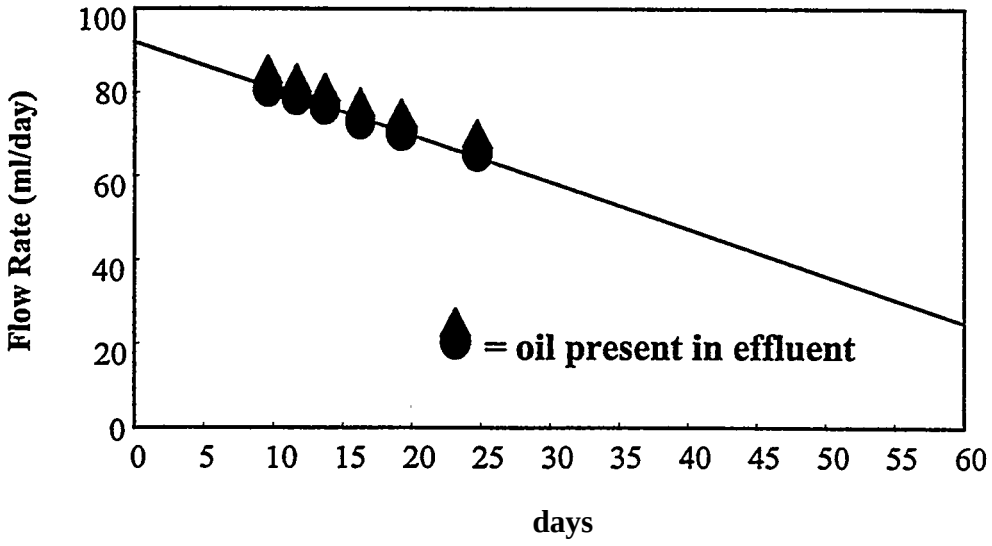

Figure 10. Flow rate of simulated production water containing potassium nitrate and disodium hydrogen phosphate through test core in experiment 2.

After the experiment was repeated three times, it was concluded that the addition of nitrate and orthophosphate should result in the stimulation of the *in situ* microflora with the subsequent generation of biomass that would decrease the flow in the pore throats of the reservoir formation. This decrease in flow through the main channels in the reservoir should

divert injection water to the less permeable areas of the formation, thereby increasing the sweep efficiency of the waterflooding operation.

Additional core flooding experiments were conducted using molasses as a microbial nutrient in addition to potassium nitrate and sodium orthophosphate. In a representative experiment, another set of core plugs was prepared as above. The control core received simulated injection water every day while the test core received simulated injection water plus nutrient supplements on the following schedule. Molasses in a concentration of 1% (v/v) on day 1, potassium nitrate in a concentration of 0.06% (w/v) on day 3, and disodium hydrogen phosphate in a concentration of 0.04% (w/v) on days 5, 7, and 9. This schedule was repeated every ten days for the duration of the experiment. As may be observed in Figure 11, the flow rate constantly increased in the control core plug.

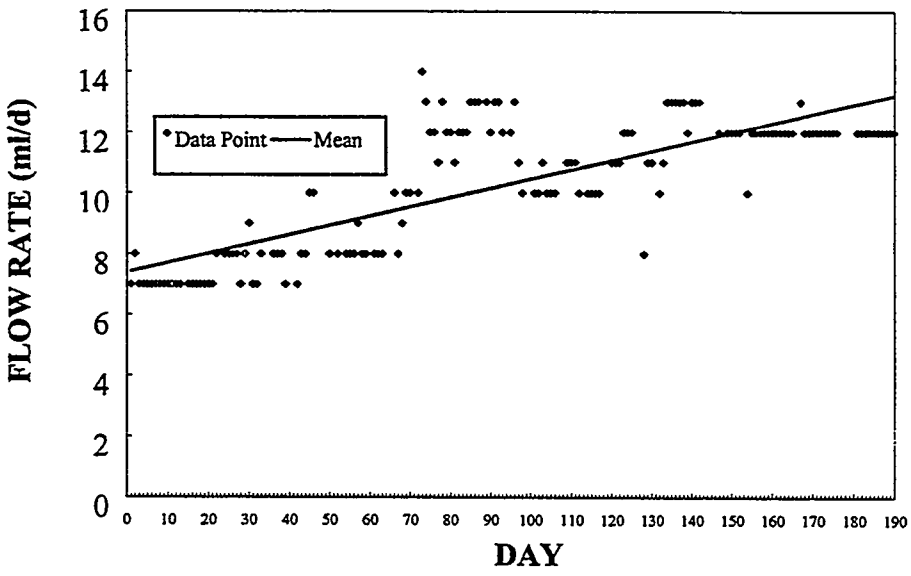

Figure 11. Flow rate of simulated injection water through control core plug.

Contrariwise, the- flow rate of injection water through the test core decreased with time (see Figure 12). After 61 days, the flow rate was increased by increasing the pressure on the influent (flushed) thereby increasing the flow of injection water through the core plug. Once again, flow rate decreased with time and the core plug was flushed a second time. This cycle was repeated one more time during the 187-day duration of the experiment. These data suggest that permeability profile modification could be accelerated by the addition of small amounts of molasses to the feeding regime.

The above experiment was repeated using the actual injection water from the North Blowhorn Creek Oil Field instead of simulated injection water. The results of this experiment paralleled those of previous experiments.

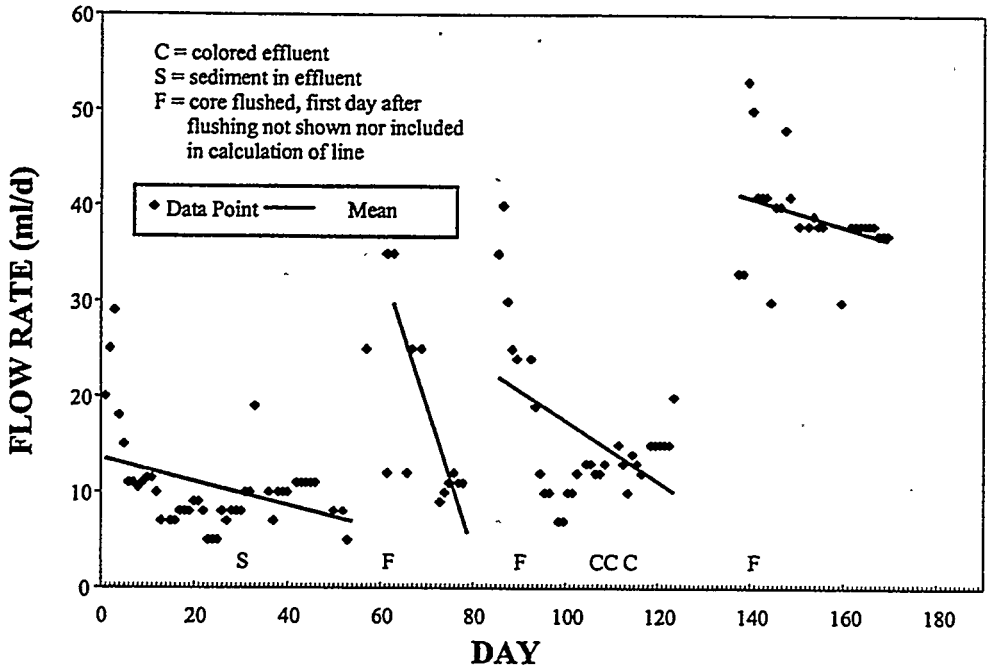

Figure 12. Flow rate of simulated injection water containing nutrients through test core plug.

F. Tracer Study

Early in the planning stages for the project, the first test well pattern was chosen for a tracer study because it had been observed in the field that the NBCU 2-14 No. 1 injection well seemed to be very well connected to the 2-13 No. 1 hydraulically. The 2-14 No. 1 allowed injection of relatively high rates, and the 2-13 No. 1 produced high fluid rates and was over pressured. It was theorized that the movement of water from the injector to producer would be quicker than in any other injection pattern. However, to quantify the time for fluid to travel from injector to the producers in the first pattern, the decision was made to conduct a radioactive tracer survey. If the travel time could be established, then some time frame for the effects of microbial activity to become detectable could be established.

On April 27, 1994, 2 Ci of tritiated water was injected into the 2-14 No. 1 well. Weekly and then monthly sampling of water from the four test pattern producing wells was carried out. No trace of the material was detected by the laboratory analysis of the water samples until October 12 when 14 pCi/ml was detected in 2-13 No. 1. On November 9, 1994 the concentration of tritium in the sample from well 2-13 No. 1 had increased to 41 pCi/ml and continued to be for the entire monitoring period which ended in March 1996. On October 18, 1996 1.6 +1.0 pCi/ml was detected in the sample obtained from well 11-3 No. 1 and continued to be present

throughout the monitoring program. On November 9, 1994, 1.9+0.3 pCi/ml was detected in the sample from well 2-15 No. 1 but was not found in any subsequent samples. Thus, on the basis of the tracer study evidence of microbial activity could not be expected to be detectable in less than seven months and probably closer to a year after initiation of nutrient injection.

G. Baseline Studies

1. Methods

Fluids from both injector wells and producer wells in all patterns were collected monthly in 5.7-liter (1.5 gallon) containers and brought to the laboratory for analysis. Oil and water were separated and a portion of the oil sample analyzed for its aliphatic profile by gas chromatography (GC). The remainder of the oil sample was used for measurement of gravity, viscosity, and interfacial tension (IFT). Additionally, the water samples were analyzed for surface tension (ST), pH, microbial content, and several inorganic ions. Production rates of fluids (oil, gas, and water) from the producer wells in all patterns were measured weekly by the field lease operator. These rates were plotted vs time to exhibit well production potential. For the most part, these graphs were consistent with actual plots of well production (based on sales) vs time. However, variations between the two plots were caused by well down time, freeze, or other production problems in which case these plots showed greater potential production than the actual production obtained (see Supplement [11],

Acquisition of Fluid Samples. Produced fluids were collected monthly from the wellhead of each producing well in all patterns. Injection make-up water samples were periodically collected from a deep well on site. Samples of injection water, which were a mixture of all produced waters from all the wells in the field, were collected monthly.

Enumeration of Microorganisms. Ten ml of a water sample was mixed with 90 ml of the distilled water, contained in a six-ounce prescription bottle. This dilution was examined using the conventional spread plate technique to enumerate total heterotrophs and oil-utilizing bacteria. All plate counts were performed in triplicate as described in the section III Cl above.

Chemical Methods

The following chemical tests were performed on produced water.

Orthophosphate was determined using the Ascorbic Acid Reduction method as given in the Standard Methods for the Examination of Water and Wastewater[8] .

Nitrate-nitrogen was determined using the Cadmium Reduction Method as given in the Standard Methods for the Examination of Water and Wastewater [8].

Sulfate was determined using the Barium Chloride Method as given in the Standard Methods for the Examination of Water and Wastewater [8].

Potassium was determined using the Tetraphenylboron Method as given in the Standard Methods for the Examination of Water and Wastewater [8].

Sulfide was determined using the Methylene Blue Method as given in the Standard Methods for the Examination of Water and Wastewater [8].

Chloride was determined using the Argentometric Method as given in the Standard Methods for the Examination of Water and Wastewater [8].

Calcium carbonate was determined using the EDTA Titrimetric Method as given in the Standard Methods for the Examination of Water and Wastewater [8].

Gas Chromatographic Analyses.

Analysis of oil samples collected from test and control producing wells was performed on a Varian® 3300 single column gas chromatograph (GC). The column was a J&W DB-1 30 x 0.53mm. Other GC operating settings are as follows.

Initial Col. Temp,°C.....40.00
Initial Col. Hold Time, min 2:00
Program Final Col. Temp.°C 290.00
Program Col. Rate in ml/min.....15.00
Program Col. Hold Time, min 5:00
Injector Temp.°C 290.00
Detector Temp.°C 300.00
FID B Initial Att.....1.00
FID B Initial Range.....10.00
Completion, min 35.00

The GC was connected to a desktop computer supported by Varian® GC Star Chromatograph version 4.0. All peaks were relayed into the computer and were saved in their entirety for future reference.

The carrier gas, helium, was employed at a flow rate of 35 ml/min, air pressure 414 kPa (60 psig), and the hydrogen running pressure 414 kPa (60 psig). Identification of paraffinic components was achieved by comparison of the retention time of peaks on the chromatogram to the retention time of standard samples. The area under the curves for different peaks was normalized. The standard sample used was ASTM Method D2287 Calibration Mixture.

The samples'were prepared for GC analysis as follows. Using an Eppendorf pipette, 100 µl of oil was placed in a five-ml beaker containing two ml of methylene chloride. The contents

of the beaker were poured over sodium sulfate (to remove water if present) and the filtrate placed in a two ml crimp-top vial with a tenon septum.

Petrophysical Analyses

The following characteristics of produced fluids from selected wells, test as well as control, were measured.

- Gravity (API) of produced oil (at room temperature)
- Viscosity of produced oil (at reservoir temperature)
- Interfacial tension (IFT) for produced and separated oil-water system
- Surface tension (ST) of air-water systems in IFT
- pH of produced water

2. Results

Since the baseline values were employed in the monitoring of the field demonstration, the results of these analyses are included in Section IV G1, 2, and 3 of the next section of this report.

IV FIELD TRIAL

A. Design of Skid for Nutrient Injection

After completion of the laboratory core flood experiments, the results were scaled up to field operating volumes which became the design basis for the nutrient skids (see Figure 13). It was determined that each injection skid needed the ability to mix and pump 380-1135 liters (100-300 gallons) of water containing 23-180 kg (50-4001b) of chemicals per day at a pressure of 8275 kPa (1200 psi). The ability to vary the pump rate over a wide range was required as well as the ability to maintain a precisely metered rate. With the exception of the molasses, the other nutrients were packaged dry in 23 kg (50 ibs) bags, so the ability to mix the chemicals and know that all went into solution was required. The skid was designed for simple maintenance and operation by the field lease pumpers. A small storage area to keep unused chemicals dry also was required.

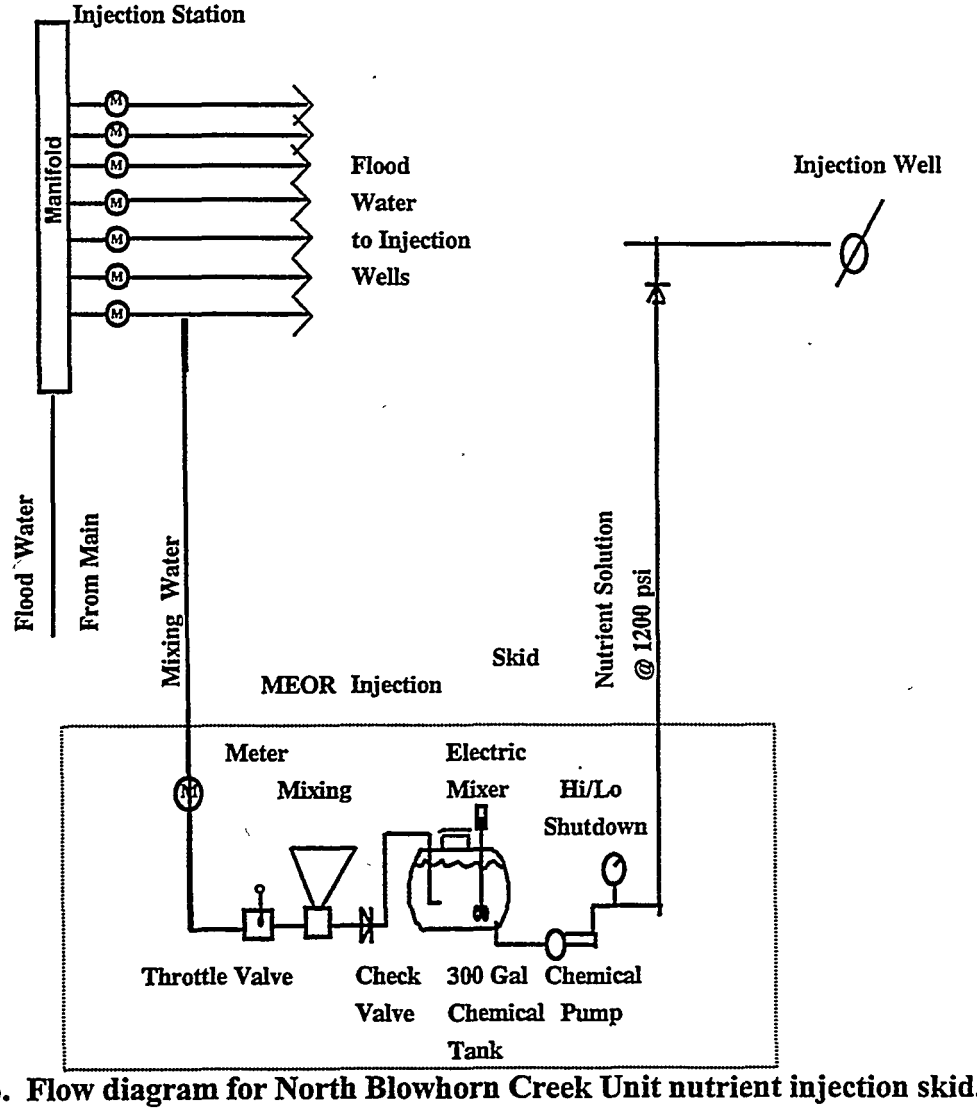

Figure 13. Flow diagram for North Blowhorn Creek Unit nutrient injection skid.

Based upon these requirements, the skid shown in (Figure 14) was constructed. It consisted of an oil field type skid with a metal roof and storage cabinet in one end. A mixing hopper was fabricated to make use of the 8275 kPa (1200 psi) waterflood water as a mixing jet for the dry sack chemicals. The mixture was stored in a 1135 liter (300 gallon) plastic tank which allowed direct observation and sampling of the solution. The tank contained an electric stirrer, which was generally run for a couple of hours after each batch of chemical was mixed to ensure that all of the chemical dissolved. The mixture was pumped downhole by a large air powered chemical pump which had a variable speed with precise displacement at any given speed. Subsequent designs switched to a small triplex pump driven by a DC electric motor with speed control. A high/low pressure switch shuts down the pump if the main waterflood pump quits or a line ruptures. The supply water line came directly from the waterflood line near the wellhead and the discharge line tied into the well just upstream of the wellhead.

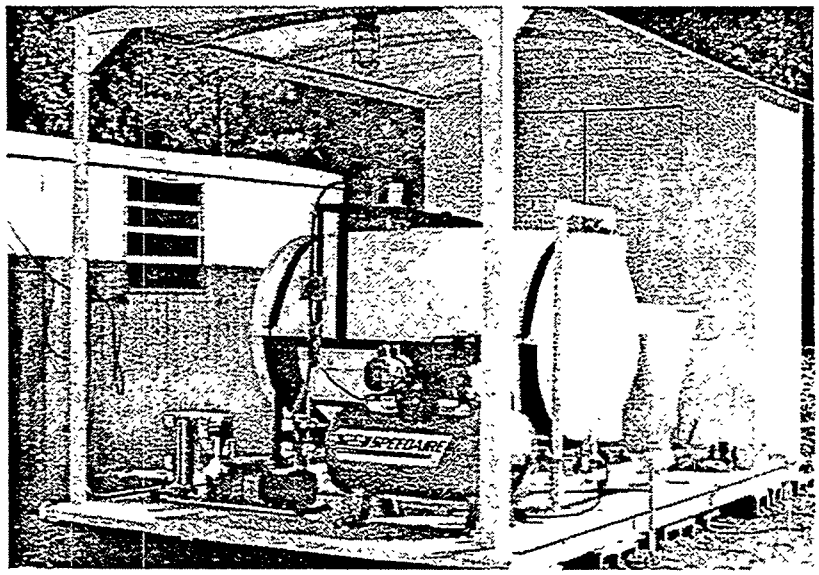

Figure 14. Picture of skid.

B. Design of Field Trial

1. Test Patterns for Field Demonstration

Figure 15 shows the locations of the wells in the four test and four control patterns.

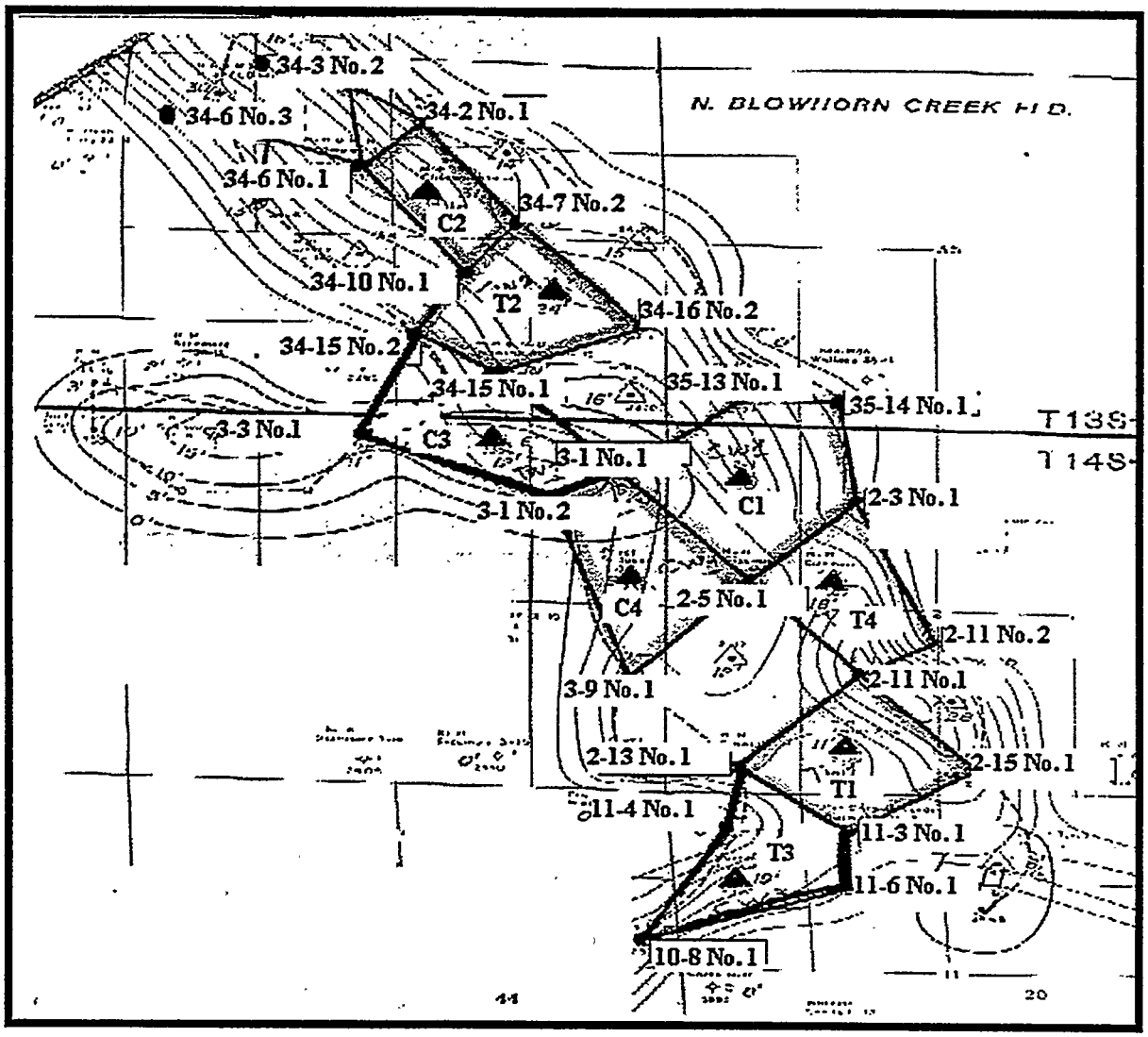

Figure 15. Isopach of NBCU oil field showing locations of wells in the four test and control patterns.

The wells included in the patterns are as follows:

<u>TP No. 1</u>
Injection-Production Pattern:

Injection Well:	NBCU 2-14 No. 1
Production Wells:	NBCU 2-11 No. 1*
	NBCU 2-15 No. 1
	NBCU 11-3 No. 1*
	NBCU 2-13 No. 1*

CP No. 1 (Control Set)

Injection Well:	NBCU 2-4 No. 1
Production Wells:	NBCU 35-13 No. 1
	NBCU 35-14 No. 1
	NBCU 2-3 No. 1*
	NBCU 2-5 No. 1*
	NBCU 3-1 No. 1*

TP No. 2

Injection-Production Pattern:

Injection Well:	NBCU 34-9 No. 2
Production Wells:	NBCU 34-7 No. 2*
	NBCU 34-16 No. 2
	NBCU 34-15 No. 1*
	NBCU 34-15 No. 2*
	NBCU 34-10 No. 1*

CP No. 2 (Control Set)

Injection Well:	NBCU 34-7 No. 1
Production Wells:	NBCU 34-2 No. 1
	NBCU 34-6 No. 1
	NBCU 34-7 No. 2*
	NBCU 34-10 No. 1*

TP No. 3

Injection-Production Pattern:

Injection Well:	NBCU 11-5 No. 1
Production Wells:	NBCU 10-8 No. 1
	NBCU 11-6 No. 1
	NBCU 11-4 No. 1
	NBCU 11-3 No. 1*
	NBCU 2-13 No. 1*

CP No. 3 (Control Set)

Injection Well:	NBCU 3-2 No. 1
Production Wells:	NBCU 3-3 No. 1
	NBCU 3-1 No. 1*

NBCU 3-1 No. 2*
NBCU 34-15 No. 1*
NBCU 34-15 No. 2*

TP No. 4

Injection-Production Pattern:

Injection Well:	NBCU 2-6 No. 1
Production Wells:	NBCU 2-11 No. 2
	NBCU 2-3 No. 1*
	NBCU 2-5 No. 1*
	NBCU 2-11 No. 1*

CP No. 4 (Control Set)

Injection Well:	NBCU 3-8 No. 1
Production Wells:	NBCU 3-1 No. 1*
	NBCU 3-1 No. 2*
	NBCU 3-9 No. 1
	NBCU 2-5 No. 1*

111U1liaL%,o WG11J i11G1ULIGU 111111ViG LLiG11 J. LGJL Vl GV11L1V1 p4LLGlll.

2. Feeding Regime

The test pattern No. 1 injector well (NBCU 2-14 No. 1) was injecting 76-80 m^3 (480-500 barrels) of water per day. Based on this rate of injection and the results obtained from the core flood experiments, it was decided to employ the addition of potassium nitrate at a concentration of 0.12% (w/v) and disodium hydrogen phosphate at a concentration of 0.034% (w/v). The nutrients were mixed in much higher concentrations on the skids (described below) and injected at such rates that the entire amount of injection water during a 24-hour period contained the above designated concentrations. In order to neutralize the effect of an increased pH of the injection water due to the phosphate addition, two gallons of 10% HCl(v/v) were added to each tank of phosphate solution. Subsequently, monosodium dihydrogen phosphate was substituted, thus obviating the need for adding the 10% HC1.

The following injection schedule was formulated on the basis of a waterflood injection rate of 76 -80 m^3/day (480-500 BWPD) in injector well NBCU 2-14 No. 1 (see Table 4).

Table 4.
Feed and feeding regime from November 1994-April 1996.

NUTRIENTS	PATTERNS 1	2	3	4
KNO_3	0.12% (w/v) Mondays	0.12% (w/v) Mondays	same as 1	same as 2
NaH_2PO_4	0.034% (w/v) Wednesday Fridays	0.034% (w/v) Fridays	same as 1	same as 2
MOLASSES	None	0.1% (v/v) Wednesdays	same as 1	same as 2

Nutrient Pumping Schedule

Monday - 91 kg (200 lbs, 4 bags) of potassium nitrate were mixed with 757 liters (200 gals) of water and pumped into the well in as close to 24 hrs as possible.

Tuesday - No chemical was pumped, but the tanks were washed out and the washings pumped down the well during the morning.

Wednesday - 45 kg (100 lbs, 2 bags) of disodium hydrogen phosphate and 7.57 liters (2 gals) of 10% HC1 were mixed with 757 liters (200 gals) of water and pumped down the well in as close to 24 hrs as possible.

Thursday - No chemical was pumped but the tanks were washed out and the washings pumped down the well during the morning.

Friday - 45 kg (100 lbs, 2 bags) of disodium hydrogen phosphate and 7.57 liters (2 gals) of 10% HC1 were mixed with 757 liters (200 gals) of water and pumped down the well in as close to 24 hrs as possible.

Saturday - No chemical was pumped but the tanks were washed out and the washings pumped down the well during the morning.

Sunday - No chemical added.

The above schedule was repeated each week for test patterns 1 and 3. The same concentrations were employed in test patterns 2 and 4 except that 0.1% molasses (v/v) was being added on Wednesdays instead of disodium hydrogen phosphate and HC1.

This project was initiated in January of 1994. The starting injection dates of nutrient additions to the test injectors in each test pattern were November 21, 1994 for test pattern 1; February 27, 1995 for test pattern 2; January 16, 1995 for test pattern 3; and February 27, 1995 for test pattern 4.

C. Modification of Microbial Feed and Feeding Regime

After a careful evaluation of the field results and additional' core flood experiments conducted in the laboratory, it was decided to modify the feed and feeding regimes as shown in Table 5.

Table 5.
Feed and feeding regime from April 1996-June 1997.

	PATTERNS			
NUTRIENTS	1	2	3	4
KNO_3	0.12% (w/v) Mondays	same as before	same as before	0.06% (w/v) Mondays
NaH_2PO_4	0.034% (w/v) Wednesdays	same as before	same as before	0.017% (w/v) Wednesdays
MOLASSES	0.2% (v/v) Fridays	same as before	same as before	0.3% (v/v) Fridays

D. Drilling of Three New Wells

Three new wells were drilled into the Carter formation sand during the Fall of 1996. The purpose of the three wells was to help evaluate the nutrient-induced *in situ* growth of microorganisms by analysis of recovered core samples and produced fluids. The locations of the wells are shown in Figure 16.

The first well drilled was the NBCU 2-5 No. 2 which started drilling on October 11 and reached a total depth of 701 m (2300 ft) on October 17. The well encountered 7.3 m (24 ft) of net Carter sand between 668 and 676 m (2192 and 2218 ft) and 13.1 m (43 ft) of core were recovered. The core analyses indicated that, as a general rule, the lower permeability rock retained a higher oil saturation while the high permeability rock was better swept resulting in a lower oil saturation. Visual observation of the core indicated much remaining oil in the low permeability rock. The well was cased for production, perforated from 668.4 to 676.0 m (2193 to 2218 ft) and fracture stimulated. Rod pumping equipment was installed and the well was placed on production. Initial production was 0.9 m^3/day oil (6 BOPD) with 27.7 m^3/day water

(174 BWPD). This production rapidly declined to 0.2 m^3/day oil (1 BOPD) with 27.7 m^3/day water (174 BWPD) by January 1998. The well is currently shut-in due to uneconomic rate of oil production.

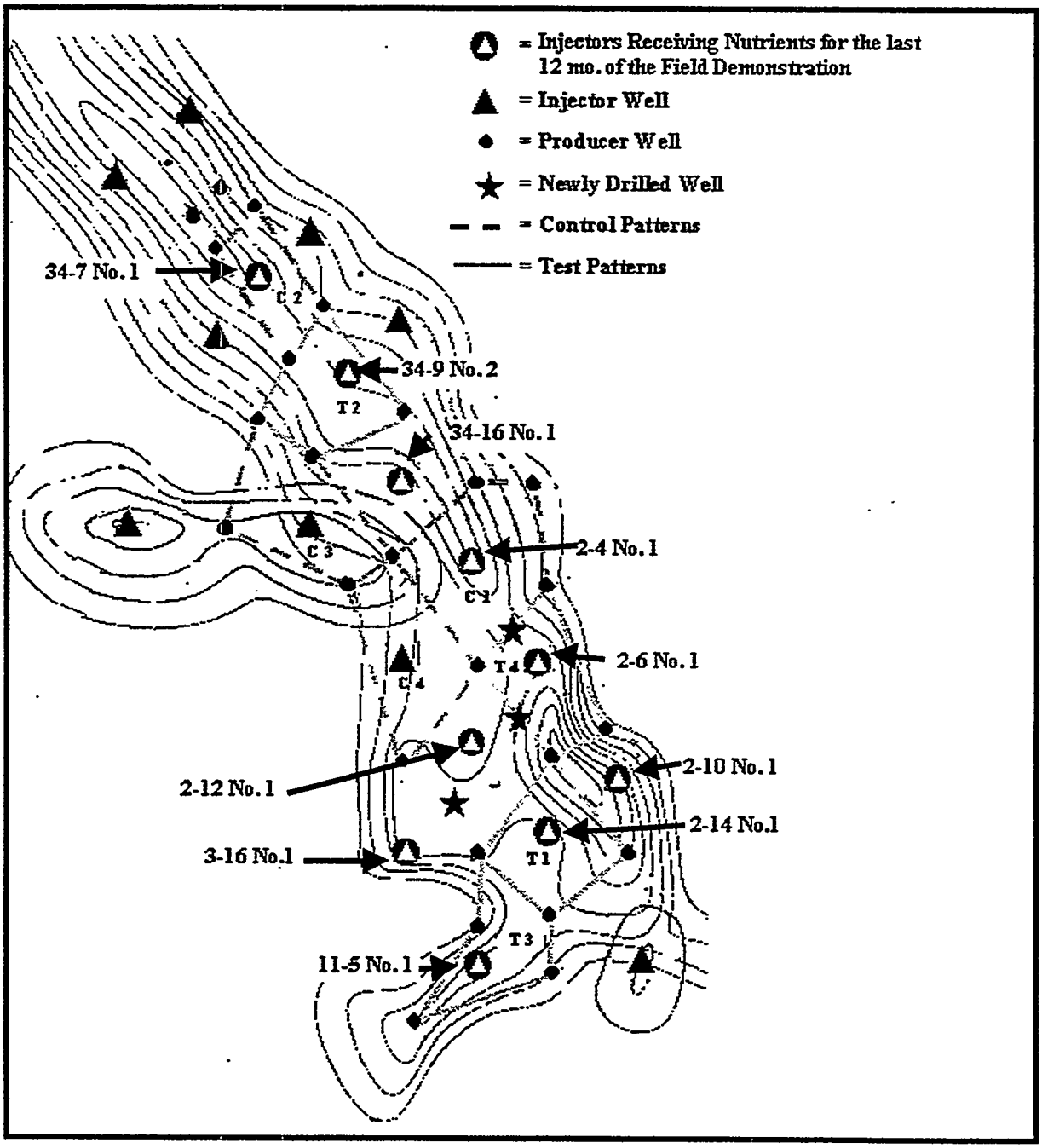

Figure 16. Locations of three new wells and injectors receiving nutrients during the final 12 months of the field demonstration.

The second well drilled was the NBCU 2-13 No. 2 which started drilling on October 22 and reached a total depth of 703 m (2305 ft) on October 30. The well encountered 6.4 m (21 ft) of net Carter sand between 664 and 672 m (2180 and 2205 ft) and 9.7 m (32 ft) of core were recovered. The core analyses indicated much higher permeability in the upper ten feet of the sand than in the lower portion. As in the previous well, the higher permeability rock generally had lower oil saturation than the lower permeability rock, which was harder to sweep by waterflood. Visual observation of the core indicated much remaining oil, as was observed in the previous well. The well was cased for production and perforated from 665-668 m and 669-670 m (2182-2192 ft and 2195-2199 ft). A packer and tubing were run and the well was swab tested at a rate of 76 m^3 (480 bbls) of fluid per day with 15-25% oil. Because the well initially swabbed at a high fluid rate, no fracture stimulation was performed. Rod pumping equipment was installed and the well was placed on production. Initial production was 2.9 m^3/day oil (18.5 BOPD) with 1.7-4.5 m^3/day water (11-28 BWPD). This production gradually declined to 1.6 m^3/day oil (10 BOPD) with 3.5 m^3/day water (22 BWPD) by July 1998.

The third well drilled was the NBCU 2-11 No. 3 which started drilling on November 6 and reached a total depth of 703 m (2306 *ft)* on November 13. The well encountered 11 m (36 ft) of Carter sand between 659.6 and 670.6 m (2164 and 2200 *ft).* The sand was much thicker than anticipated. Previous maps had indicated only 5.5 m (18 ft) of sand at this location. A 9.7 m *(32* ft) core was recovered which revealed significant remaining oil saturation, along with some portions which had obviously been swept by the waterflood. It was believed the water swept sections would provide the best opportunity to observe microbial growth as a result of nutrient injection into the NBCU 2-6 No. 1 well situated about 152 m (500 ft) north of this well. The well was cased for production, perforated from 659.6 to 670.6 m (2164 to 2200 ft), a packer' and tubing run, and the well was fracture stimulated. The well flowed without any stimulation for several months and then was put on rod pump in April 1997. Due to the well's close proximity to the 2-6 No. 1 injector, it produced a high rate of water and never produced oil at a commercial rate.

E. Analysis of Cores

Five sections of core from each of the three newly drilled wells were tested for nitrate ions and orthophosphate ions. Nitrate ions were present in 4, 3, and 5 sections of core samples from wells 2-5 No. 2, 2-13 No. 2, and 2-11 No. 3, respectively. Orthophosphate ions were found in 3, 0, and 1 sections of the core samples from wells 2-5 No. 2, 2-13 No. 2, and 2-11 No 3, respectively. It should be pointed out that phosphate can react with constituents (e.g. calcium ions) in the formation and, consequently, the data only reflect soluble orthophosphate. The results, however, clearly demonstrated that the nutrients were being widely distributed in the oil-bearing formation.

Using cultural methods, microorganisms were shown to be present in all sections of cores from all three newly drilled wells and, as may be expected, the numbers varied but, the larger numbers in some 'samples suggest that they had proliferated. Heterotrophs and oil-degrading microbes were present in all samples as were both aerobes and anaerobes.

Samples from each section were examined by electron microscopy and, as would be expected, many samples showed no microbial cells. Scattered microbial cells as illustrated in Figure 17 were observed in a number of samples from all three wells and in some cases (see Figures 18, 19, and 20) large clusters of cells were observed indicating that the added nutrients had had the desired effect of promoting microbial growth in the reservoir.

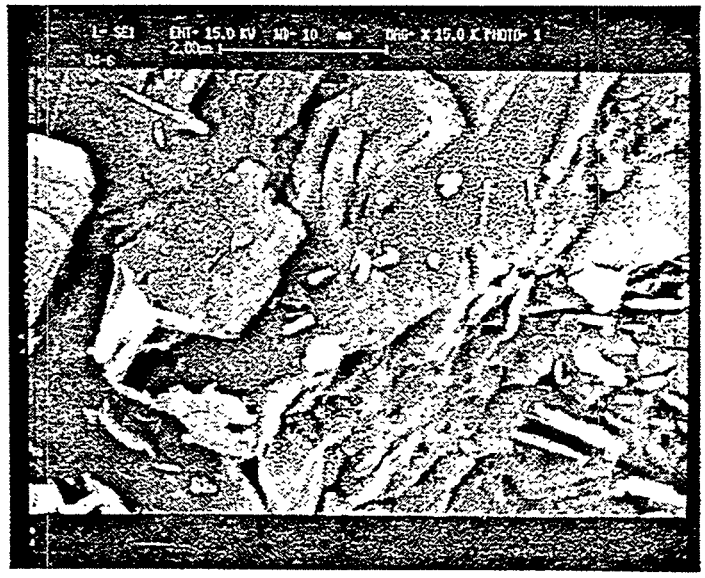

Figure 17. Electron micrograph of a sample of core from well 2-13 No.2, section 6. (Note the scattered microbial cells).

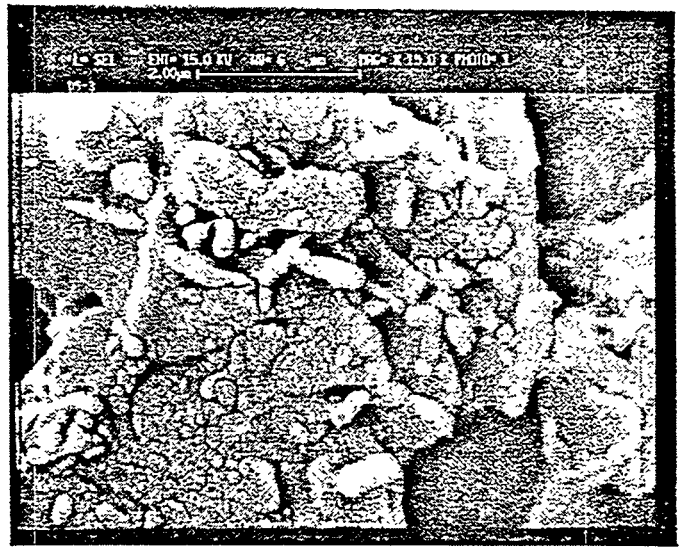

Figure 18. Electron micrograph of a sample of core from well 2-11 No.3, section 3. (Note the large number of microbial cells).

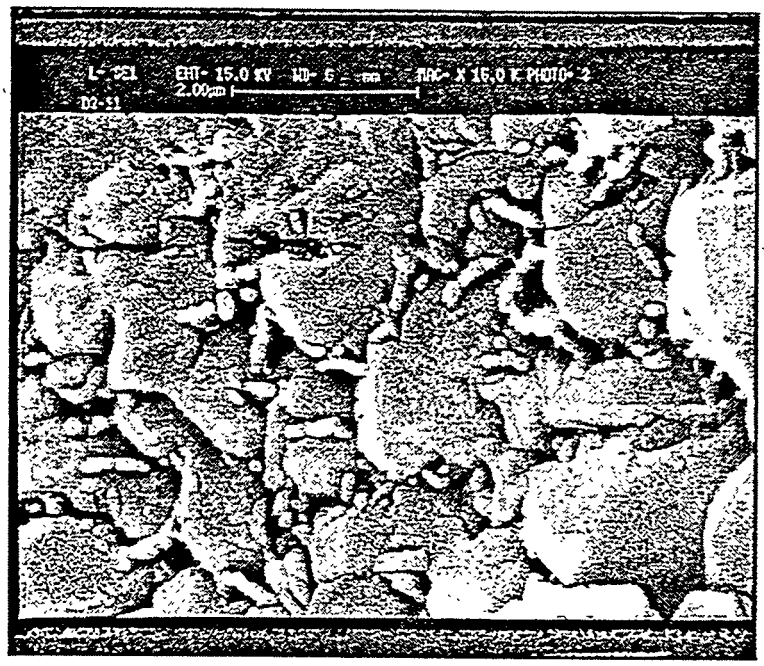

Figure 19. Electron micrograph of a sample of core from well 2-5 No.2, section 11. (Note the large number of microbial cells).

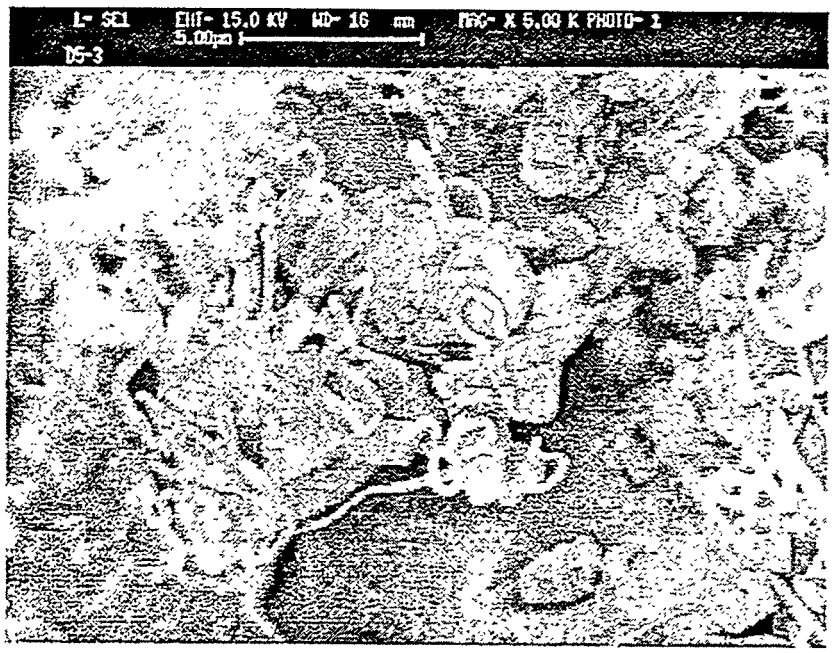

Figure 20. Electron micrograph of a sample of core from well 2-11 No.3, section 3. (Note the large number of microbial cells).

The core samples appeared to be massive, fine-grained, moderately mature, quartzarenite (a sandstone, Folk's classification) with abundant quartz, minor amount of feldspar, perhaps kaolinite, with minor calcitic cement component, probably ferroan dolomite.

The petrophysical properties of collected cores from the three newly-drilled wells are given in Table 6. In this Table, the lowest, the highest, and a median range of values are presented to show the heterogeneity of the reservoir formation.

Table 6.
Petrophysical properties of cores from three newly drilled wells.

Well Name	Depth		Porosity (%)	Permeability (md)	Fluid Saturation		Grain Density (g/cc)
	m	ft			%Oil	%H_2O	
2-5 No. 2	670.94	2200	4.3	0.70	31.7	28.1	2.74
2-5 No. 2	679.52	2207	12.9	11.60	11.6	23.3	2.62
2-5 No. 2	675.51	2215	12.9	38.00	8.0	18.7	2.68
2-13 No. 2	666.36	2185	13.9	141.00	9.8	24.3	2.59
2-13 No. 2	670.33	2198	9.9	34.00	7.7	22.3	2.62
2-13 No. 2	673.38	2208	3.9	1.60	9.4	23.1	2.66
2-11 No. 3	663.92	2177	12.1	13.29	2.4	14.5	2.64
2-11 No. 3	668.50	2192	13.9	61.02	13.8	26.0	2.59
2-11 No. 3	669.72	2196	11.0	1.35	15.9	21.3	2.60

F. Expansion of Injection Program

During July 1997, an additional nutrient injection skid was completed and installed at Test Station 4. Piping modifications were made to allow six more injection wells to accept nutrient. The NBCU 3-16 No. 1, 2-12 No. 1, 2-10 No. 2, 34-7 No. 1, and 2-4 No. 1 wells all began nutrient injection during July, 1997. The total number of nutrient injectors for the last year of the project was ten as is shown in Figure 16. The nutrient additions to the ten injectors are given in Table 7.

G. Monitoring Program

Fluids from both injector wells and producer wells in all patterns were collected monthly as described previously.

Table 7.
Feed and feeding regime for all ten injector wells from July 1997-June 1998.

WELL NO.	MON.	TUES.	WED.	THURS.	FRI.
34-16 No. 1		0.16 N 0.04 P	-	0.28 M	-
2-4 No.1	0.10 N 0.03 P	-	0.20 M	-	-
2-6 No. 1	0.05 N	-	0.30 M	-	0.02P
34-9 No. 2	0.11 N	-	0.18 M	-	0.05 P
3-16 No.1	-	0.19 N 0.05 P	-	0.32 M	-
34-7 No. 1	-	0.17 N 0.04 P	-	0.21 M	-
2-10 No.2	-	0.12 N 0.02 P	-	0.19 M	-
11-5 No. 1	0.15 N	-	0.29 M	-	0.04P
2-12 No. 1	-	0.26 N 0.07 P	-	0.43 M	-
2-14 No. 1	0.08 N	-	0.47M	-	0.02 P

N = percent potassium nitrate (w/v),
P = percent sodium dihydrogen phosphate (w/v),
M = percent molasses (v/v).

1. Petrophysical Analyses

One of the main concerns in the application of MEOR is the integrity of original oil in place since the selling price of produced oil is directly based on its petrophysical properties. To confirm the integrity of produced oil, the following tests were conducted on produced fluids from selected wells in test and control patterns:

- API gravity (at room temperature). It is expected that API gravity of produced oil from Test Patterns will either stay steady or show an upward trend due to infusion of new oil from previously unswept area of the reservoir. The upward trend may continue to the level of the gravity of the original oil in place.

- Absolute viscosity, (at reservoir temperature). It is expected that the viscosity of produced oil from test pattern wells will exhibit either a steady or downward trend

due to the infusion of new oil from previously unswept areas of the reservoir. The downward trend may continue down to the lower viscosity of the original oil in place.

- Water-oil interfacial tension, IFT. It is expected that the produced fluid may exhibit a steady or downward trend in water-oil interfacial tension due to microbial production of surfactants.

- Water-air surface tension, ST, and pH. To insure nothing out of the ordinary may happen that causes degradation of the produced fluid, these properties of produced water were measured regularly.

Based on the above considerations, no deleterious changes in the characteristics of the produced oil were observed. Table AI in the Appendix gives representative values for petrophysical characteristics of the produced fluids from selected wells in all patterns.

2. Microbiological Analyses

The microbiological analyses of production fluids did not show any significant changes attributable to the MEOR process. It should be pointed out however, that microorganisms prefer to grow attached to a substrate rather than be suspended in a medium. Consequently, numbers of microbes in production fluid do not necessarily reflect the size of the population in the reservoir.

3. Inorganic Ion Analyses

Production fluids were monitored for chloride ions, hardness, nitrate ions, phosphate ions, potassium ions, sulfate ions, and sulfide ions for the duration of the field demonstration.

No sulfide ions were detected in the fluids from any of the production wells (limit of detection 0.02 ppm) after six months of nutrient injection, but were present initially. This reduction in hydrogen sulfide was statistically significant. No significant changes attributable to the MEOR process were seen in the concentrations of chloride ions, hardness, potassium ions, or sulfate ions.

No nitrate ions were found in the produced fluids from any of the wells, although nitrate ions were found in some samples from all three of the newly drilled wells.

Phosphate ions were found in the produced fluids from producer wells in three of the four test patterns indicating that there was communication between the respective injector wells and those producer wells. The lack of the nitrate ions in samples indicates that they were either being consumed by the microflora or were reacting with materials in the reservoir since the presence of phosphate in samples demonstrates that there was communication between most injectors and some producer wells.

H. Results

1. Oil Production

The microbial permeability profile modification technology (MPPM) demonstrated in this project has resulted in, and continues to result in, the recovery of additional oil (hereinafter referred to as incremental oil recovery). The amount of incremental oil recovered from a well is the amount of oil that is recovered over and above that expected based on the decline curve of production from that well. It is interesting to note that with the passage of time, the incremental oil comprises an increasing percentage of the produced oil. Further, as will be pointed out later, incremental oil will continue to be produced long after the injection of nutrients has ceased.

In the present demonstration, the tracer study indicated that it would probably be at least seven months before evidence of microbial activity in the reservoir would become evident and indeed this proved to be the case. In fact, well 2-13 No. 1, that was shown to have good communication with test injector 2-14 No. 1, began to show enhanced production after seven months with a concurrent reduction in the rate of increase in the water-oil ratio (WOR). None of the other production wells in the program had veered from their natural decline curves at that time.

By the end of 1996 a total of eight of the fifteen production wells in test patterns showed a positive response to the nutrient injections (See Table 8). Conversely, two of the production wells in control patterns were abandoned due to an uneconomical production rate and five other wells continued their natural decline in oil production. The remaining producing well in the control patterns experienced increased oil production due to increased water injection into the nearby control injection well.

Thirty months after the first test injector well began receiving nutrients, there were no changes in the responses of the producing wells in the control patterns and one of the producing wells in a test pattern (well no. 2-3 No. 1) failed to continue its positive response and was therefore characterized as exhibiting a questionable response indicating that more time was needed to accurately evaluate the performance of this well. On the positive side of the ledger, three other producing wells in the test patterns showed evidence of responding positively to the nutrient injection and were classified as questionable at that time. These results clearly demonstrated that the nutrient injections were having a positive effect on oil production and it was requested (and approved by DOE) to expand nutrient injection by injecting nutrients into two control injectors [well 2-4 No. 1 (control pattern 1) and 34-7 No. 1 (control pattern 2)] and into four injector wells not previously included in the program (NBCU 34-16 No. 1, NBCU 2-12 No. 1, NBCU 2-10 No. 2, and NBCU 3-16 No. 1). Locations of the new injector wells are shown in Figure 16. Production data for all of the wells involved in the project with the exception of the two abandoned wells are given in Figures Al A21 of the Appendix. .

Twelve months after nutrient injection had been expanded to include 10 injectors, thirteen of nineteen producing wells had responded positively and two other wells yielded results

suggesting that they were beginning to respond positively. Only two of the producing wells in the original control patterns remained outside of the influence of the ten injectors receiving nutrients. Well 3-3 No. I continued on its natural decline while Well 3-1 No. 2 continued to exhibit increased oil production due to increased water injection in injector well 3-2 No. 1.

Table 8.
Oil production response from all wells included in the project.

Well No.	Pattern(s)	Response Evaluation Dec. 1996	June 1997	June 1998
2-11 No. 1	TP1, TP4	Positive	Positive	Positive
2-15 No. 1	TP1	None	Questionable	Questionable
11-3 No. 1	TP1, TP3	None	Questionable	Positive
2-13 No. 1	TP1, TP3	Positive	Positive	Positive
34-7 No. 2	TP2, CP2	None	Positive	Positive
34-16 No. 2	TP2	Positive	None	Questionable
34-15 No. 1	TP2, CP3	Positive	Positive	Positive
34-15 No. 2	TP2, CP3	Positive	Positive	Positive
34-10 No. 1	TP2, CP2	None	Questionable	Positive
10-8 No. 1	TP3	None	None	Positive
11-6 No. 1	TP3	Positive	Positive	Positive
11-4 No. 1	TP3	None	None	None
2-11 No. 2	TP4	Positive	Positive	Positive
2-3 No. 1	TP4, CP1	Positive	Questionable	Positive
2-5 No. 1	TP4, CP1, CP4	None	None	None
35-13 No. 1	CP1	Nat. Decline	Nat. Decline	Nat. Decline
35-14 No. 1	CP1	Shut-in	--	--
3-1 No. 1	CP1, CP3, CP4	Nat. Decline	Nat. Decline	Nat. Decline
34-2 No.1	CP2	Nat. Decline	Nat. Decline	Positive
34-6 No.1	CP2	Shut-in	--	--
3-3 No. 1	CP3	Nat. Decline	Nat. Decline	Nat. Decline
3-1 No. 2	CP3, CP4	*	*	*
3-9 No. 1	CP4	Nat. Decline	Nat. Decline	Positive

*Oil production increased due to an increase in the volume of injection water in control injector well 3-2 No. 1.

It is known that certain activities in the reservoir, such as the drilling of a new well, shutting-in a well, increasing the water injection rate in an injector well, etc., can alter the performance of other wells in the field. Indeed this was the case with well 2-11 No. 1, for when well 2-11 No. 3 was drilled and began producing, there was a steady drop in production from well 2-11 No. 1. However, when well 2-11 No. 3 was shut-in, production in well 2-11 No. 1

recovered. Also, as noted in Table 8, when the water injection rate in injector 3-2 No. 1 was increased, production from well 3-1 No. 2 increased.

There were, however, two wells that exhibited anomalous behavior. The first new well (well 34-6 No. 3) drilled during this project initially did not produce very well, but after fracturing, production increased appreciably. The interesting thing about this well is that production continued to increase slowly to over 16 m^3 (103 barrels per day) which is not characteristic of well performance in this reservoir. This unusual behavior could be a result of shutting-in well 34-6 No. 1, accessing a new oil pool, or a result of nutrient injection into injector well 34-7 No. 1.

In the second case, the fluid production from well 3-1 No. 1 also is unusual in that oil production remained essentially steady from July 1997 thru July 1998, while water production dropped drastically. The most logical explanation for this situation is that microbial growth had restricted water channels from injector wells 2-4 No. 1 and 34-16 No. 1. However, without other information this well was not characterized in Table 8 as yielding a positive response to the nutrient injections.

2. Evidence of New Oil in Produced Fluids.

Gas chromatographic profiles of the oil from all of the producing wells involved in this study were evaluated to determine if "new oil" (i.e. oil previously bypassed by the waterflood) was present in the produced fluid from the reservoir. Since the lighter hydrocarbons are produced earlier in the life of a reservoir and more of the water-soluble compounds are produced before the heavier less water soluble ones, their concentration in the oil fraction decreases as the reservoir ages.

Conversely, "new oil" contains a greater concentration of these lighter fractions of the oil. GC data collections began in 1995 and continued throughout the field demonstration. It is realized that quantitative comparisons for given compounds would not be fruitful because the multiplicity of steps involved in obtaining and preparing samples for analysis precluded having the exact same amount of oil for each analysis. On the other hand, the ratio of components in the samples should be more or less constant irrespective of the amount of sample analyzed. Therefore, the ratio of the lighter components in the oil to the heavier components should increase if "new oil" is present in the sample. Rather than make comparisons between single compounds, the area under the curve on the chromatograms was divided into four groups and comparisons made between the area under the curve on the chromatogram for the four groups. Group 1 compounds consist of the area under the curve from n-hexane (C_6) up to n-dodecane (C_{12}). Group 2 compounds consist of the area under the curve from n-dodecane (C_{12}) up to n-octadecane (C_{18}). Group 3 compounds consist of the area under the curve from n-octadecane (C_{18}) up to n-tetracosane (C_{24}). Group 4 compounds consist of the area under the curve from n-tetracosane (C_{24}) up n-triacotane (C_{30}).

When comparing the changes in ratio of different groups with time, it became apparent that there were very few changes in the ratios of the Groupl compounds to Group 2 compounds, Group 2 compounds to Group 3 compounds, or the Group 3 compounds to the Group 4 compounds. On the other hand, an increase in the ratio of Group 1 compounds to Group 4 compounds demonstrated the presence of "new oil" in the produced fluid from a given well. It was interesting to note that the changes in the ratio of Group 2 compounds to the Group 4 compounds parallel those of the ratio of the Group 1 compounds to the Group 4 compounds. Bar graphs showingthe ratios between the different groups of hydrocarbons for each well are shown in Figures Al-A21 in the Appendix. The same data for the two wells drilled in 1994 are shown to illustrate the normal change in ratios with time (see Figures A22-A23 in the Appendix).

The data given in the Appendix show that of the 13 wells characterized as having given a positive response in terms of oil production, nine were confirmed as positive (new oil) by the ratio of Group 1 compounds to Group 4 compounds. One may have contained a small amount of new oil, and three did not show evidence of "new oil".

Of the two wells characterized as being questionably positive from an oil production standpoint, one (34-16 No. 2) showed evidence of "new oil" while the other well (2-15 No. 1) did not.

Of the five wells characterized as not showing positive or questionable response in terms of enhanced oil production, one well gave no indication of "new oil" but four showed the presence of some "new oil" even though they did not exhibit a positive response from an oil production standpoint. Thus, it appears that some new oil was finding its way into the produced fluids of these two wells even though it did not manifest itself sufficiently to be considered a positive response. Production from the three new wells drilled in 1996 distorted production figures from one well (2-5 No. 1) to such an extent that no meaningful assessment could be made.

3. Analysis of Produced Gas

Another piece of evidence pointing to the infusion of "new oil" into the produced fluids was obtained from gas analyses performed on samples from a number of wells. Increased gas production that had been noted in some wells could have been the result of microbial activity or it could have come from previously unswept areas of the reservoir. Samples of gas were collected from selected production wells and analyzed by GC using a Fisher Gas Partitioner Model 1200 (dual column, dual detector chromatograph). Only a limited number of samples were analyzed but there was no evidence of changes in the composition of the produced gases due to microbial gas production, (i.e. no carbon dioxide or hydrogen was observed). The data suggest that the increase in gas production was due to gases from previously unswept areas of the reservoir since they contained a percentage of propane more closely like that of gas obtained from the field in earlier years.

4. Distribution of Nutrients Throughout the Reservoir

Indications are that nutrients are being distributed throughout the reservoir. It should be pointed out that phosphate ions were found in the produced fluids from producer wells in three of the four test patterns (1, 2, and 3) demonstrating that there was communication between the respective injector wells and the surrounding producer wells. The lack of the nitrate ions in samples indicates that it was either being consumed by the microflora or was reacting with materials in the reservoir since the presence of phosphate in samples demonstrates that there was communication between most injectors and some producer wells.

Fluid from cores from the three wells drilled nearly two years after nutrient injection began (Fall, 1996) were examined for the presence of nitrate ions and orthophosphate ions in five sections of core from each well. Nitrate ions were present in 4, 3, and 5 sections of core samples from wells 2-5 No. 2, 2-13 No. 2, and 2-11 No. 3, respectively. Orthophosphate ions were found in 3, 0, and 1 sections of the core samples from wells 2-5 No. 2, 2-13 No. 2, and 2-11 No. 3, respectively. These results clearly demonstrate that the nutrients were being widely distributed in the oil-bearing formation.

5. Evidence of Microbial Proliferation in Reservoir

Investigations into changes in the microbial population of the reservoir on the basis of their presence in produced fluids was of limited value in view of the fact that the wells did not contain packers. As a result, the microbial content of the produced fluids could be influenced by the microbial content of the fluid in the casing. Furthermore, since most microorganisms prefer to grow attached to the strata rather than free-floating in fluid, analysis of produced fluid may not reflect the true population in the reservoir. On the other hand, analyses performed on cores taken from the reservoir did yield valuable information. Cores from the second well drilled in 1994, in an area of the reservoir not being swept by the waterflood, were found to contain isolated microbial cells but no evidence of proliferation. The fact that sulfate-reducing bacteria (SRB) were present in the drilling fluid, but not in the core samples analyzed, was strong evidence that the microflora found in the core was indigenous to the reservoir, not contaminates from the drilling fluid.

Core samples from the three wells drilled in the Fall of 1996 were examined for the presence of microorganisms by cultural methods. All five sections of core from each of the three wells contained viable microorganisms. While some samples contained only a few microorganisms, most contained considerably more than the core samples taken from the earlier well (34-3 No. 2) drilled in 1994 as shown in Tables 2 and 9. Samples from each section also were examined by electron microscopy and, as would be expected, many samples showed no microbial cells. Scattered microbial cells as illustrated in Figures 17 were observed in a number of samples from all three wells and in some cases large clusters of cells were observed indicating

Table 9
Numbers of microorganisms in sections of cores from three newly drilled wells.

Well No.	Core Section (No.)	Depth m	Depth ft	Heterotrophs Aerobic (No./g)	Heterotrophs Anaerobic (No./g)	Oil-Degrading Aerobic (No./g)	Oil-Degrading Anaerobic (No./g)
2-5 No. 2	3	676.12	2217	3	*	0	*
2-5 No. 2	5	675.21	2214	29	*	3	*
2-5 No. 2	11	673.38	2208	7	*	11	*
2-5 No. 2	12	672.46	2205	138	*	250	*
2-5 No. 2	15	669.41	2195	>300	*	>300	*
2-13 No. 2	4	671.85	2203	250	4	175	<1
2-13 No. 2	6	670.94	2200	>300	14	103	<1
2-13 No. 2	11	670.02	2197	>300	11	>300	1
2-13 No. 2	13	667.89	2190	>300	41	125	<1
2-13 No. 2	15	666.06	2184	>300	20	105	1
2-11 No. 3	3	670.33	2198	231	30	182	48
2-11 No. 3	7	667.28	2188	250	71	163	50
2-11 No. 3	8	666.67	2186	179	59	102	38
2-11 No. 3	10	665.45	2182	>300	85	145	62
2-11 No. 3	14	663.92	2177	>300	52	153	33

*insufficient sample

that the added nutrients had the desired effect of promoting microbial growth in the reservoir (see Figure 18, 19, and 20).

Still one other piece of data supporting the widespread distribution of nutrients (nitrate) and/or the growth of microorganisms (nitrate-reducing bacteria) in the reservoir was the statistically significant reduction in sulfide content of fluids from the field six months after nutrient injection began. Both nitrate per se and the growth of nitrate-reducing microorganisms have been shown to inhibit SRB's and their production of sulfide from sulfate"[18].

6. Performance of Nutrient Injector Wells

Performance of injection well 2-14 No. 1 (Test Pattern 1)

The injection volume declined despite an increase in injection pressure. This performance may be an indication of permeability reduction due to microbial growth near the wellbore (see Figure A24).

Performance of injection well 34-9 No. 2 (Test Pattern 2)

Injection pressure increased and injection volume decreased. This performance may be an indication of permeability reduction due to microbial growth near the wellbore (see Figure A25).

Performance of injection well 11-5 No. 1 (Test Pattern 3)

The injection volume declined and there was a slight increase in injection pressure which may be an indication of permeability reduction due to microbial growth near the wellbore (see Figure A26).

Performance of injection well 2-6 No. 1 (Test Pattern 4)

This well's injection rate and pressure were very sensitive to production (or lack of) from well 2-11 No. 3. Injection pressure increased and the injection volume decreased over the last year (see Figure A27).

Performance of injection well 2-4 No. 1 (was injector for Control Pattern 1)

Injection volume declined as injection pressure increased (see Figure A28).

Performance of injection well 34-7 No. 1 (was injector for Control Pattern 2)

Injection volume declined as injection pressure increased (see Figure A29).

Performance of injection wells 34-16 No. 1 (not in original program)

Injection pressure increased and there was more water intake. There was no indication of plugging (see figure A30).

Performance of injection well 2-12 No. 1 (not in original program)

Injection pressure increased and there was more water intake. There was no indication of plugging (see Figure A31).

Performance of injection well 3-16 No. 1 (not in original program)

Injection pressure increased and there was more water intake. There was no indication of plugging (see Figure A32).

Performance of injection well 2-10 No. 2 (not in original program)

Injection pressure increased and there was more water intake. There was no indication of plugging (see Figure A33).

7. Overall Performance of Field Demonstration

In evaluating the overall performance of the MPPM treatment in the field, it must be remembered that only four of the twenty injector wells in the field received microbial nutrients before July 1997. Oil production for the field from Jan. 1992 through Aug. 1998 is given in Figure 21. The performance of each producing well in both control and test patterns and including the two wells drilled in 1994 is shown graphically in Appendix Al-A23. During the period May 1994 through Dec. 1998, total oil production was 74,700 m^3 (470 MBO). Based

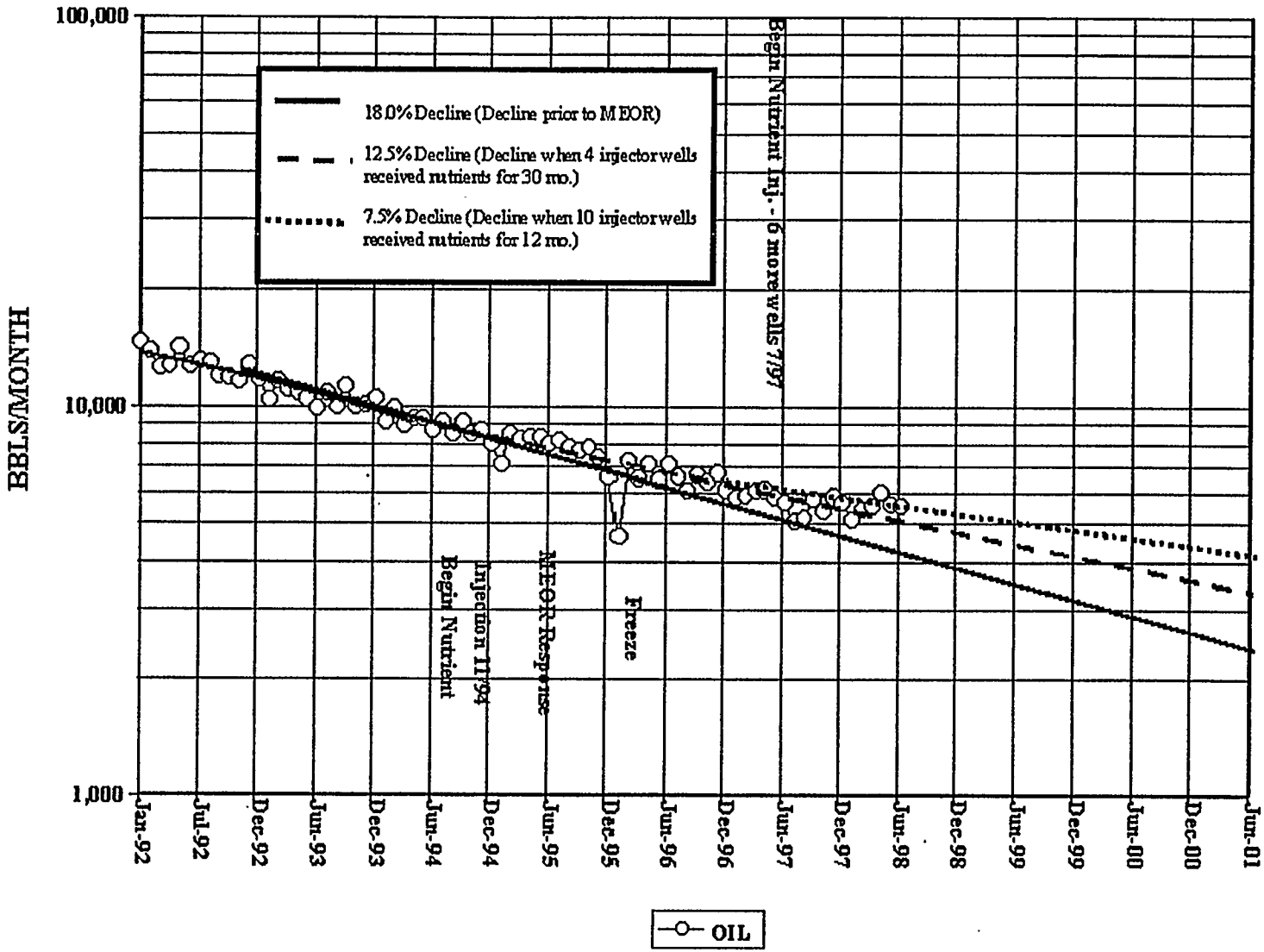

Figure 21. Total production from North Blowhorn Creek Unit excluding *newly drilled wells.*

on projections derived from the period of Jan. 1992-Apr. 1994, oil production from May 1994-Dec. 1998 should have been only 49,175 m^3 (309 MBO). Of this 25,000 m^3 (161 MBO) of incremental oil produced, 14,563 m^3 (92 MBO) were production from the five new wells, leaving a total of 11,000 m^3 (69 MBO) of oil attributable to the MEOR treatment.

Further, calculations based on production from Jan. 1992 through Apr. 1994 indicate that the field would reach its economic limit of 238 m^3 (1500 bbls) of oil per month on Jan. 1, 2003. Based on the current oil production rate, the expected economic life of the field has been extended by 60-137 mo. exclusive of any additional positive response from continued nutrient injection into the ten test injector wells. The expected total project incremental oil recovery is projected to be 63,600-95,400 m^3 (400-600 MBO).

V. DISCUSSION

When the primary production phase of an oil field approaches its economic limits, waterflooding is often the most promising and economical method of increasing oil recovery. Today over 50% of all the oil fields **in** the world are under waterflooding operations. As the waterflooding continues, fluid flow in the reservoir normally seeks larger channels, leaving smaller channels untouched. In time, water will sweep out all of the oil that was in its pathway, and a time will come when there will be no more oil for water to sweep out. Subsequently, water will be circulated in and out of the reservoir without sufficient oil recovery to sustain the operation (watered-out wells), resulting in a substantial volume of the original oil in place being left unrecovered:

The objective of this project was to use indigenous microbial biomass, generated by certain feed and feeding regimes in watered-out channels, to circumscribe the reservoir pore channels (microbial permeability profile modification, MPPM). Thus, injected water will be forced to alter its pathway and flow into unswept channels and sweep oil from them. The process of restricting watered-out channels and invading new and unswept oil-bearing channels will continue so long as the condition of a controlled growth and proliferation of *in situ* microbes prevails and other unforeseen reservoir characteristics or production activities do not create unpredicted obstacles.

The MPPM technology demonstrated in this project differs from most MEOR methods in a number of ways. For example, one of the distinctive features of the present technology is that it relies on the activities of the *in situ* microflora rather than on cultures that are injected into the reservoir. Early reports on the presence of microorganisms in petroleum reservoirs were viewed with extreme skepticism due to questionable sampling techniques [14]. More recently, however, it has been established beyond doubt that microorganisms are indigenous to oil reservoirs, not merely residents that have been introduced through drilling activities [14]. In fact, a previous DOE-sponsored project reported on the microbial population in cores from areas of 13 reservoirs uncontaminated by previous FOR activities [12]. In this earlier DOE-sponsored project or it was shown that these native microbial populations did respond to the introduction of simple inorganic nutrients (e.g. sodium nitrate and dipotassium hydrogen phosphate). Not only did the microorganisms reproduce but they also elaborated an array of byproducts that assisted the oil recovery endeavors. The advantage of relying on the *in situ* microbial population in the reservoir is that the microorganisms are already distributed throughout the reservoir and those in areas influenced by waterflooding will be supplied with nutrients that are required for growth. Furthermore, as new areas of the reservoir receive injection water, the microbial population already in place will be able to take advantage of the added nutrients. In the case of processes requiring the injection of microbial cultures, considering the slowness with which injection water travels in a reservoir (with the exception of fractures) coupled with the filtering effect of the oil-bearing strata itself, distribution of injected microorganisms to any appreciable extent has to be extremely limited.

To help understand how the present technology modifies the waterflood profile, the following explanation is offered. An average microbial cell is about one micron in length by 0.5 microns in diameter and most grow attached to a substrate rather than floating free in the water. Bacteria reproduce by a process known as binary fission which means one bacterial cell divides into two cells, they in turn divide into two more cells each and so on. Given the nutrients required for growth, the bacterial cells attached to the walls of water channels in the reservoir will begin to reproduce, thus reducing the orifice of the channel.

The question arises as to the length of time required for a microorganism to divide. Obviously, this varies from species to species and the environmental conditions under which they are growing. While some species will divide every 20 minutes during logarithmic growth under ideal conditions, the doubling time for the bacteria in the reservoir is probably hours, if not days. Even so, their impact on the waterflood profile will be dramatic in a relatively short period of time.

Thus, even with a doubling time measured in days, a significant shift in injection water flow would occur in a very short period of time. The MPPM accomplished by the microbial growth is illustrated in Figure 22. It must be remembered that when injection water is diverted to unswept areas of the reservoir, the nutrients included therein will be available for the microbes in these areas and the process described above will be repeated. A quantitative comparison of this whole field MEOR technology to single well MEOR treatment is given in Figure 23. Thus, where applicable, whole field (or a portion thereof) treatment significantly increases the potential incremental oil that can be recovered. This points up another major difference between the MEOR technology of this project and that of other MEOR methods.

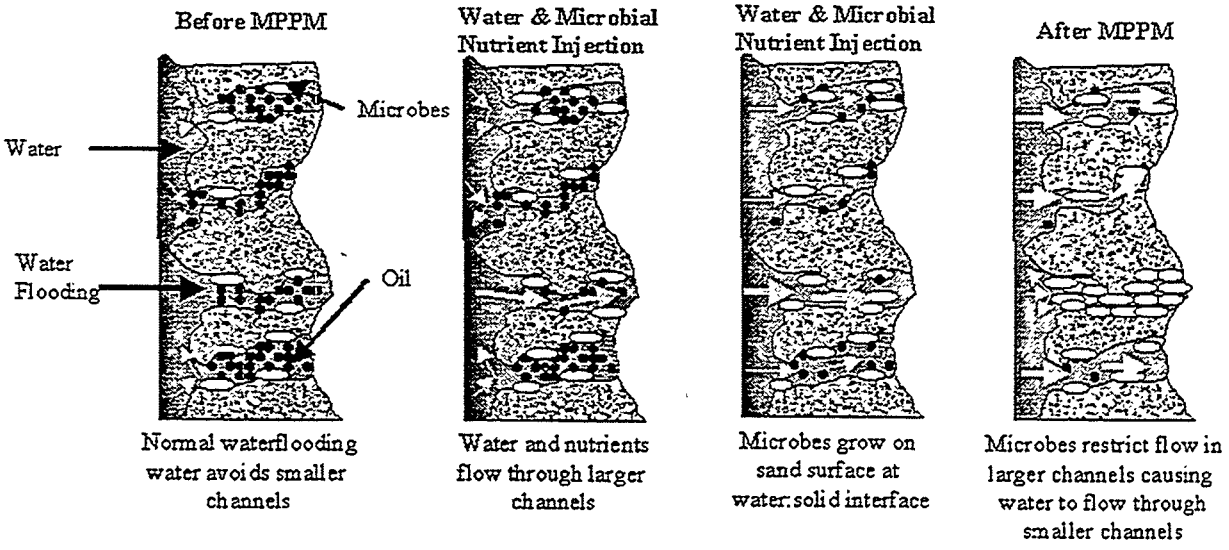

Figure 22. Mechanism of microbial enhanced oil recovery (MEOR) using *in situ* microbial permeability profile modification (MPPM) to enhance oil recovery.

Field Charcteristics of a Hypothetical Oil Reservoir:

Area:

MPPM[1] 161,880 m^2 (40 Acres)

Individual well MEOR[2] 2918.63 m^2

Pay zone thickness(h): 6.096 m (20 ft)

Porosity(φ): 18%

Oil saturation: 65%

Water: 35%

% Recovery:

MPPM 25%

Individual well MEOR 50%

1. Microbial Permeability Profile Modification EOR.

2. Injected microorganisms are assumed to have a 30.48 m (100 ft) (30.48 m) radius of travel in the pay zone.
Area = $(30.48\ m)^2 \times \pi = 2918.63\ m^2$ (0.72 acre)

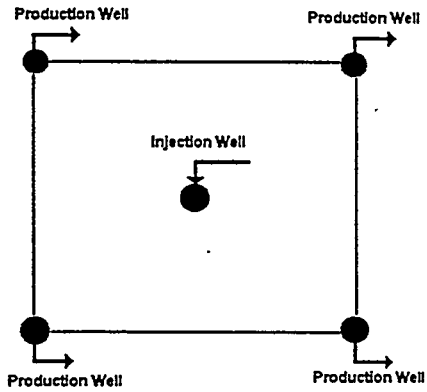

5-Spot Injection-Production Pattern

	MPPM		Individual well	
Bulk volume	986,785 m^3	34,848,000 ft^3	17,792 m^3	628,318 ft^3
Pore volume	177,621 m^3	6,272,640 ft^3	3,203 m^3	113,097 ft^3
Oil in place	115,343 m^3	725,483 barrels	2,080 m^3	13,080 barrels
Primary production	39,372 m^3	247,644 barrels	624 m^3	3,924 barrels
Remaining oil	80,740 m^3	507,838 barrels	1,456 m^3	9,156 barrels
Incremental Oil	20,185 m^3	126,959 barrels	727 m^3	4,572 barrels

The MPPM method produces 20,185 m^3 (126,959 barrels) of oil (using a 5-spot pattern with 4 producing wells) while the individual well MEOR also applied to 4 wells would yield 2,907 m^3 (18,287 barrels).

MPPM produces 694% more oil.

Figure 23. Comparison of MPPM FOR treatment (5-spot Pattern) vs. individual well MEOR treatment.

From an environmental perspective, the MPPM technology offers the advantage of not having to introduce microorganisms into the environment. This is especially important if genetically-engineered microbes are involved and where spills or eventual escape into the environment are possible. The nutrients employed in the MPPM are environmentally friendly, whereas in many MEOR processes the chemicals employed are proprietary and their environmental impact cannot be addressed herein.

Perhaps, one of the most important features of the MPPM is its relatively low cost per barrel of incremental oil. It is important to note that this technology does not interfere with normal waterflooding operations. In fact, all that is required is to add a facility to dissolve the chemical nutrients and feed them into the injection water stream. The number of such facilities required will, of course, depend upon the individual oil field. Similarly, the design can be simple to slightly more complex. The nutrients themselves are relatively inexpensive. For example, for the present project potassium nitrate cost $35/45.4 kg (100 lbs), sodium dihydrogen phosphate cost $100/45.4 kg (100 lbs), and molasses cost $67/387.5 liters (100 gal). On a weekly basis and assuming an injection rate of 521 m^3 (3275 bbl) of water/day, chemical costs would only be $1,400/ wk using the average schedule employed for the final 12 months of the project. Labor costs, of course, would vary but in the present project amounted to an average of 20 man-hours per week.

Finally, it should be emphasized that the MPPM technology can be employed in many fields where waterflooding is possible, irrespective of the geological formation involved.

VI. TECHNOLOGY TRANSFER

The last year of this project was devoted to analyzing data and to technology transfer. It is realized of course, that technology transfer is an on-going process and to date, the following papers have been published.

Brown L.R., A.A. Vadie, J.O. Stephens, and A. Azadpour, 1996. Enhancement of the Sweep Efficiency of Waterflooding Operations by the In-Situ Microbial Population of Petroleum Reservoirs. Proceedings of the Fifth International Conference on Microbial Enhanced Oil Recovery and Related Biotechnology for Solving Environmental Problems, pp. 95-114, Dallas, TX.

Vadie, A.A., J.O. Stephens, and L.R. Brown, 1996. Utilization of Indigenous Microflora in Permeability Profile Modification of Oil Bearing Formations. Proceedings 1996 SPE/DOE Tenth Symposium on Improved Oil Recovery, pp 459-471, Tulsa, OK.

Azadpour, A., L.R. Brown, and A.A. Vadie. 1996. Examination of Thirteen Petroliferous Formations for Hydrocarbon-Utilizing, Sulfate-Reducing Microorganisms. Journal of Ind. Micro. 16, 263-266.

Brown, L.R., A.A. Vadie, and J.O. Stephens, 1997. Field Demonstration of the Ability of *in situ* Microorganisms in Oil-Bearing Formations to Modify Waterflooding Profiles. Proceedings of the 1997 Eastern Section AAPG and TSOP Joint Meeting, pg 24-26.

Brown, L.R., A.A. Vadie, and J.O. Stephens, 1998. Going underground to spy on MEOR microbes and finding many MEOR barrels of incremental oil. The Class Act, DOE's Reservoir Class Program Newsletter. Vol. 411, Winter 1998.

A review of the project was published in "LORE" in Nov. 1998. [LORE is a publication of the Water Resources Research Institute of Mississippi.]

Prepared an update on the results of the project for Dr. Herb Tiederman of DOE for testimony for Congress.

In addition to presentations made at the Annual Contractors Review Sessions with DOE, the following presentations have been made.

Brown, L.R., A.A. Azadpour, and A: Vadie. 1996. Microbial Activity in Petroleum Reservoir Formations. Presented at the Society for Industrial Microbiology Meeting held in the Research Triangle, N.C. in Aug. 1996.

Brown, L.R., A.A. Vadie, J.O. Stephens, and A. Azadpour, 1996. Enhancement of the Sweep Efficiency of Waterflooding Operations by the In-Situ Microbial Population of Petroleum Reservoirs. Presented at the Fifth International Conference on Microbial

Enhanced Oil Recovery and Related Biotechnology for Solving Environmental Problems, Dallas, June 1996.

Vadie, A.A., J.O. Stephens, and L.R. Brown, 1996. Utilization of Indigenous Microflora in Permeability Profile Modifications of Oil Bearing Formation. Presented at the 1996 SPE/DOE Tenth Symposium on Improved Oil Recovery. Tulsa, OK.

Brown, L. R. 1997 made a presentation to the 1997 Eastern Section AAPG and TSOP Joint Meeting on Sept. 30, 1997, in Lexington KY, entitled "Field Demonstration of the Ability of Microorganisms in Oil-Bearing Formations to Modify Waterflooding Profiles.

Brown, L.R., 1998 presented a seminar to the Biology Dept. of the University of Nevada at Las Vegas entitled "Using Microorganisms to Improve Oil Recovery" on March 13, 1998.

Brown, L.R. 1998 made a presentation to the Southern Great Lakes Local Section of the Society for Industrial Microbiology on Oct. 10, 1998 at Michigan State University. "Microbial Enhanced Oil Recovery".

Brown, L.R. and A.A. Vadie made a presentation on Microbial Enhanced Oil Recovery at the Society of Petroleum Engineers Los Angeles Basin Section in Long Beach, CA in Nov. 1998.

Stephens, J.O., L.R. Brown and A.A. Vadie 1998 made presentations at the Petroleum Technology Transfer Council Workshop held in Jackson, MS on Nov. 4, 1998, "Microbial Enhanced Oil Recovery": North Blowhorn Creek Unit, Black Warrior Basin, Northwest Alabama. This presentation was sponsored by the Petroleum Technology Transfer Council.

A presentation to the Permian Basin Chapter-Society of Petroleum Engineers Recovery Study Group, was carried out on February 11, 1999 in Midland TX. The presentation was made by J. O. Stephens and L. R. Brown.

A presentation was made to the Society of Petroleum Engineers meeting in Bartlesville, OK on Feb. 18,1999. The presentation was made by J. O. Stephens, L. R. Brown, and A. A. Vadie. Discussions also were held with personnel from Phillips Petroleum Co. relative to use of MEOR in one of their projects.

A presentation was made to the Society of Petroleum engineers on May 13, 1999 in Jackson, MS by James O. Stephens.

A PTTC workshop entitled "Microbial Options for Increasing Oil Recovery" was held in Midland, TX on June 3, 1999. James O. Stephens, Lewis R. Brown, and A. Alex Vadie participated in the workshop.

A PTTC workshop entitled "Microbial Options for Increasing Oil Recovery" was held in Zanesville, OH on June 21, 1999. James O. Stephens, Lewis R. Brown, and A. Alex Vadie participated in the workshop.

A presentation entitled "A Low Cost Solution for Enhanced Waterflood Performance" was presented to the 1999 Oil and Gas Conference held in Dallas, TX, June 28-30, 1999.

Letters were sent to PTTC regional directors offering our services for a workshop on the project. Additionally, similar letters were sent to a large number of oil companies making the same offer.

There also were a number of cases where we have engaged in technology transfer on a more or less one-on-one basis. For example, L.R. Brown and A.A. Vadie had several hours of discussion with a group from Tidelands Oil Co. in Long Beach, CA. Also, material on our findings was sent to personnel at Chevron Pet. Tech. Co. as a result of the presentation.

A number of individuals throughout the country have inquired by phone and e-mail and appropriate responses have been made.

The three principal investigators on this project were indeed honored by the fact that this project was selected as the **Best Advanced Recovery** Project for the Gulf Coast area by *"Harts Oil* ***and*** *Gas World"*. This award was made even more meaningful by the fact that it was nominated by the National Petroleum Technology Office and that each principal investigator received a letter of congratulations from the Secretary of Energy, Bill Richardson.

VII. SUMMARY & CONCLUSIONS

The North Blowhorn Creek Unit (NBCU) oil field was discovered in 1979 with some 2.54×10^6 m^3 (16 MM bbls) of IOIP and was unitized in 1983. Following its primary oil production phase, waterflooding started in 1983. The economic life of the oil field was expected to terminate in 2003 with over 1.59×10^6 m^3 (10 MM bbls) of IOIP left unrecovered. This fluvial dominated deltaic reservoir was employed in a "Class I Oil Program - Mid Term Activities", project that demonstrated the effectiveness of a microbial permeability profile modification (MP IN) technology for enhancing oil recovery and extending the projected economic life of the field by 60-137 months. Initially the field program involved injecting microbial nutrients into four test injector wells and monitoring the performance of the surrounding producer wells. The performance of these test producer wells were compared to the performance of control producer wells surrounding four other injectors that did not receive nutrients. Thus, the performance of each test producer well was compared to the performance of similar wells in the same formation as well as to its own historical record. Chemical, microbiological, and petrophysical analyses were performed on fluids from all wells on a monthly basis for the duration of the demonstration. The feeding regime was modified twice during the course of the project and, for the last 12 months, 10 injector wells received nutrients. The nutrients employed were potassium nitrate, sodium dihydrogen phosphate, and molasses. Initially the feeding regimes were formulated on the basis of core flood experiments performed using cores from a well drilled in an area of the reservoir that had not been influenced by the waterflood.

The wide distribution of the injected nutrients was confirmed by:

- The presence of orthophosphate ions in producing wells in three of the four original test patterns and

- the presence of nitrate ions and orthophosphate ions in core samples from three wells drilled <u>within</u> the oil field after nutrient injection for 22 months.

Involvement of microorganisms in enhancing oil recovery and proof of ['new oil[' in the produced fluids as a result of microbial permeability profile modification was demonstrated by:

- The recovery of large numbers of viable microorganisms from cores of wells drilled within the field,

- electron micrographs showing large numbers of microbial cells in some of the cores cited above,

- analysis of the gas chromatographic profiles of produced oil illustrate the presence of ['new oil[' (oil from unswept areas of the reservoir), and

- changing the composition of produced gases to be more like that produced originally.

The microbial permeability profile modification technology demonstrated in this project resulted in:

- The production of 10,970 m^3 (69,000 bbl) of incremental oil by the end of December 1998,

- projections for the recovery of a total of 64,000-95,000 m^3 (400,000-600,000 bbl) of incremental oil by the end of the economic life of the field, exclusive of production . from the new wells drilled during the project, and

- extended the economic life of the field by 60-137 months.

The attractive features of the microbial permeability profile modification technology are:

- It does not interfere with normal waterflooding activities,

- may be used in any geological formation amenable to waterflooding,

- it is environmentally friendly since no microorganisms are added to the wells and only common plant fertilizers are employed,

- it enhances oil recovery and increases the economic life of the oil field, and

- it is the least expensive of all FOR processes in terms of cost per barrel of incremental oil recovered. [Based upon costs incurred in this project and the projected ultimate incremental recovery, the incremental cost per barrel of incremental oil is in the range of $1.10. to $1.65.]

VIII. ACKNOWLEDGEMENTS

The authors wish to express their sincere appreciation to the following individuals at Mississippi State University (MSU) for their contributions to the conduct of this project: to Todd and Scott French for their assistance in the preparation of reports and the conduct of laboratory experiments; to Michelle Badon and Robin Felder for their assistance in laboratory analyses; to Joanne Cotton for her secretarial assistance; to Jose Vasquez and John E. Parker for their efforts in the petroleum engineering phase of the project. A special thanks also goes to the late Dr. Ralph Powe, Vice President for Research at MSU, without whose help this project may never have come to fruition.

Special acknowledgements also should go to Angie Rushing for her tireless help in preparing all quarterly, yearly, and final reports and to field operators Thomas Keene, James Tate, William R. Brown, Paul Reynolds and the late Ronald Swindle for making the field end of the project work.

IX. REFERENCES

1. Davis, J.B., and D. Updegraff, 1954. Microbiology in the petroleum industry. Bacteriol. Revs., Vol. 18, pp. 215-238.

2. ZoBell, C.E., 1943. Bacteria as a geological agent, with particular reference to petroleum. Petrol. World, Vol. 40, pp. 30-43.

3. ZoBell, C.E., 1946. Bacteriological process for treatment of fluid-bearing earth formations. U.S. Pat., 2,413,278.

4. ZoBell, C.E., 1947. Bacterial release of oil from sedimentary materials. Oil and Gas J., Vol. 46(13), pp. 62-65.

5. ZoBell, C.E., 1953. Recovery of Hydrocarbons. U.S. Pat., 2,641,566.

6. Brown, L.R. 1982. Method for Increasing Oil Recovery. U.S. Patent No. 4,475,590.

7. Brown, L.R., A. Azadpour, and A.A. Vadie, 1992. A Study of the Interactions Between Microorganisms, Microbial By-Products, and Oil-Bearing Formation Materials. Final Report. DOE Contract No. AC22-90BC14665.

8. American Public Health Assoc., American Water Works Assoc., and Water environment Federation. 1992. Standard Methods of the Examination of Water and Wastewater. APHA, AWWA, WAF, Eighteenth ed.

9. Zeikus, J.G., 1977. The biology of methanogenic bacteria. Bacteriol. Revs., June 1977, vol. 41, No 2, pp. 514-541.

10. Rosenfeld, W.D. 1960. Petroleum Prospecting Method. U.S. Pat. 2,921,003.

11. To obtain a copy of the supplement and the electronic data file of production and analytical results contact National Petroleum Technology Office, One West 3 rd St., Suite 1400, P.O. Box 3628, Tulsa, OK 74101-3628 or on the intemet at www.npto.doe.com.

12. Azadpour, A., L.R. Brown, and A.A. Vadie, 1996. Examination of Thirteen Petroliferous Formations for Hydrocarbon-Utilizing Sulfate-Reducing Microorganisms. J. Ind. Microbiol. 16:263-266.

13. Reinsel, M.A., J.T. Sears, P.S. Stewart, and M.J. Mclnerry, 1996. Control of microbial souring by nitrate, nitrite, and glutaraldehyde injection in a sandstone column. J. Ind. Microbial. 17:128-136.

14. Amy, P. S. and D. L. Haldeman 1997. "The microbiology of Terrestrial Deep Subsurface". CRC, Lewis Publication, NY.

APPENDIX

NOTE

Figures Al-A21 show fluid production and oil characteristics for each producing well involved in this study with the exception of wells 34-6 No. 1 and 35-14 No. 1 that were abandoned. The same information is given in Figures A22-A23 for the first two wells initially drilled during this project and illustrate changes in the ratio of compounds in the oil with time.

Group 1 compounds consist of the area under the curve from n-hexane (C_6) up to n-dodecane (C_{12}). Group 2 compounds consist of the area under the curve from n-dodecane (C12) up to n-octadecane (C_{i}s). Group 3 compounds consist of the area under the curve from n-octadecane up to n-tetracosane (C_{24}). Group 4 compounds consist of the area under the curve from n-tetracosane up to n-tricotane (C30).

When comparing the changes in ratio of different groups with time, it became apparent that there were very few changes in ratio of the group 1 compounds to group 2 compounds, group 2 compounds to group 3 compounds, or the group 3 compounds to the group 4 compounds. As expected, the ratio of group 1 compounds to group 4 compounds (hereinafter referred to as 1:4) were the most significant and increases in this ratio with time indicate " new oil" in the produced fluid. Conversely, decreases in the 1:4 ratio indicate a weathering of the oil as the lighter, more soluble compounds are extracted by the water. It was interesting to note that the changes in the ratio of group 2 compounds to the group 4 compounds parallel those of the ratio of the group 1 compounds to the group 4 compounds.

Graphs showing pressure and rate of water injection for the ten injector wells that received nutrients are given in Figure A24-A33.

Table A1.
Petrophysical analyses of fluid from selected test and control wells.

PATTERN 1

Test Well 2-15 No. 1

	Gravity API	Viscosity cP	Surface Tension w-air, dyne/cm	Interfacial Tension o-w, dyne/cm	pH
Range	28.93-35.2	2.14-1.82	53-65	29.6-23.6	7.75-7.5
Trend	upward	downward	steady	downward	steady

Test Well 2-13 No. 1

	Gravity API	Viscosity cP	Surface Tension w-air, dyne/cm	Interfacial Tension o-w, dyne/cm	pH
Range	30-32	1.85-1.40	55.7-64.25	22.8-23.6	7-7.72
Trend	upward	downward	steady	steady	downward

Test Well 3-1 No. 1

	Gravity API	Viscosity cP	Surface Tension w-air, dyne/cm	Interfacial Tension o-w, dyne/cm	pH
Range	30.40-33.25	2.43-1.7	59-65	28.4-26	7.5-8.15
Trend	steady	downward	upward	downward	steady

PATTERN 2

Test Well 34-7 No. 2

	Gravity API	Viscosity cP	Surface Tension w-air, dyne/cm	Interfacial Tension o-w, dyne/cm	pH
Range	29.52-32.2	2.69-2.44	63-54	25.35-22.1	7.7-7.5
Trend	upward	steady	upward	steady	steady

Test Well 34-2 No. 1

	Gravity API	Viscosity cP	Surface Tension w-air, dyne/cm	Interfacial Tension o-w, dyne/cm	pH
Range	31-33.7	1.74-1.95	58-68	23-25.25	7.7-7.5
Trend	upward	steady	upward	steady	steady

PATTERN 3

Test Well 10-8 No. 1

	Gravity API	Viscosity cP	Surface Tension w-air, dyne/cm	Interfacial Tension o-w, dyne/cm	pH
Range	29.8-28	2.96-2.98	62.1-69.7	27.75-23.56	7.3-7.5
Trend	upward	upward	steady	steady	steady

Table A1. Continued

Test Well 11-4 No. 1

	Gravity API	Viscosity cP	Surface Tension w-air, dyne/cm	Interfacial Tension o-w, dyne/cm	pH
Range	28.9-30.47	3.65-1.98	64.4-56.1	24.65-21.3	7.7-7.55
Trend	upward	downward	steady	downward	steady

Control Well 3-3 No. 1

	Gravity API	Viscosity cP	Surface Tension w-air, dyne/cm	Interfacial Tension o-w, dyne/cm	pH
Range	34.11-30.8	2.32-2.45	61.9-57.6	26.9-22.7	7.75-7.25
Trend	steady	steady	steady	downward	steady

PATTERN 4

Test Well 2-11 No. 2

	Gravity API	Viscosity cP	Surface Tension w-air, dyne/cm	Interfacial Tension o-w, dyne/cm	pH
Range	32-33	2.3-2.16	60-63	22.8-22	7.8-7.25
Trend	steady	downward	steady	downward	steady

Control Well 3-9 No. 1

	Gravity API	Viscosity cP	Surface Tension w-air, dyne/cm	Interfacial Tension o-w, dyne/cm	pH
Range	33-32	2.2-2	59-64	20-22	7.6-7.25
Trend	steady	downward	steady	steady	steady

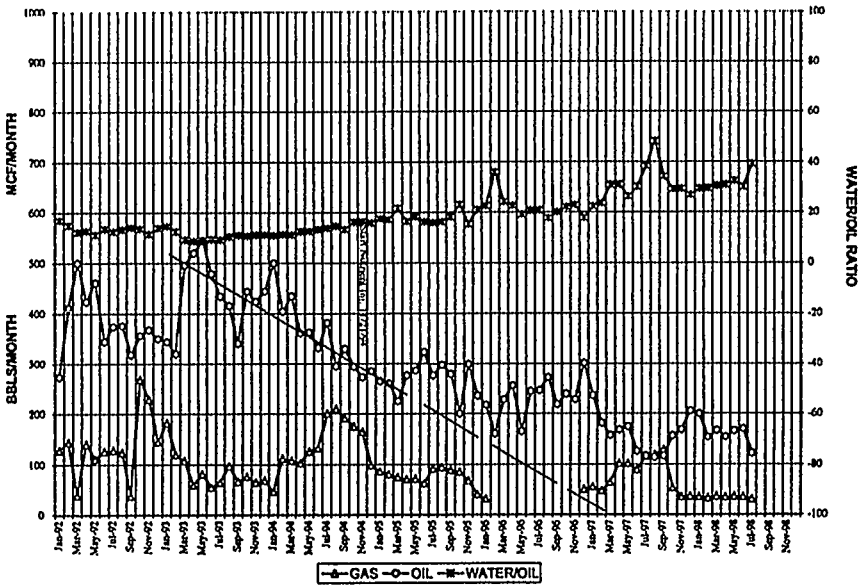

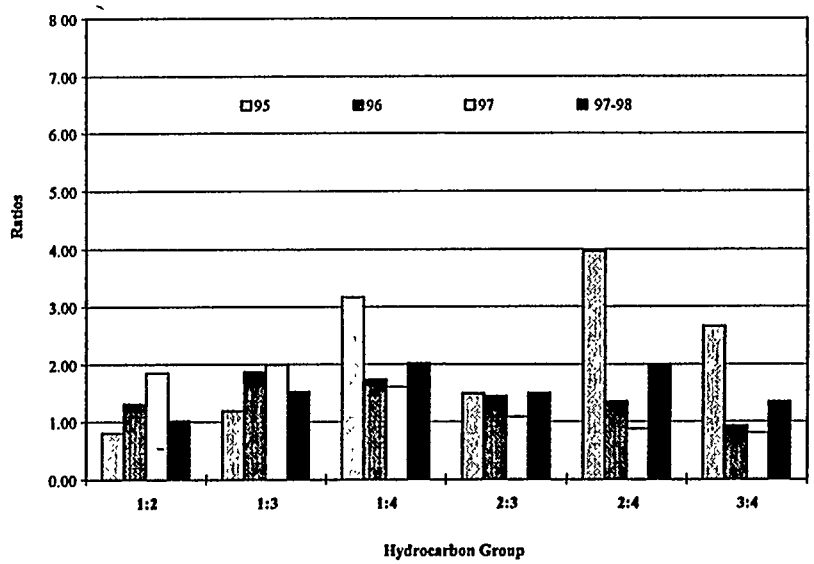

Figure A1. Well 2-11 No. 1 (2-14 No. 1, 2-6 No. 1, and 2-10 No. 2 Nutrient Injectors).

This well was classified as a positive response to MPPM as shown in Table 8.

This well is the northernmost well in Test Pattern 1 and the southernmost well in Test Pattern 4. It is situated north of test injector well 2-14 No. 1 and south of test injector well 2-6 No. 1. Approximately five months after beginning nutrient injection, there was an appreciable increase in oil production and the rate of decline in oil production became considerably less. WOR remained steady most of the time, then started to increase but at a lower rate. When production from well 2-11 No. 3 began, there was a steady drop in oil production (from Jan. to Sept. 1997). However, when well 2-11 No. 3 was shut-in, production began a steady increase. When the tracer study was performed in April of 1994, no evidence of communication with the injector well (well 2-14 No. 1) was obtained. It must be remembered, however, that this well could have easily been influenced by the injector well (well 2-6 No. 1) in Test Pattern 4.

Examination of the G.C. data on production fluid from this well fail to indicate an appreciable increase in the ratio of 1:4. The ratio of 1:4 dropped 45% from 3.17 to 1.73 from 1995 to 1996, respectively, and remained essentially constant at 1.60 in 1997. In 1998, however, the 1:4 ratio increased 26% to 2.01. While the increased oil production from this well prior to the drilling of well 2-11 No. 3 does not appear to be the result of the inclusion of previously bypassed oil as shown by GC analysis, it must be the result of some exogenous influence and the only known influence was microbial growth in the reservoir due to nutrient injection into either and/or both of the nearby test injectors.

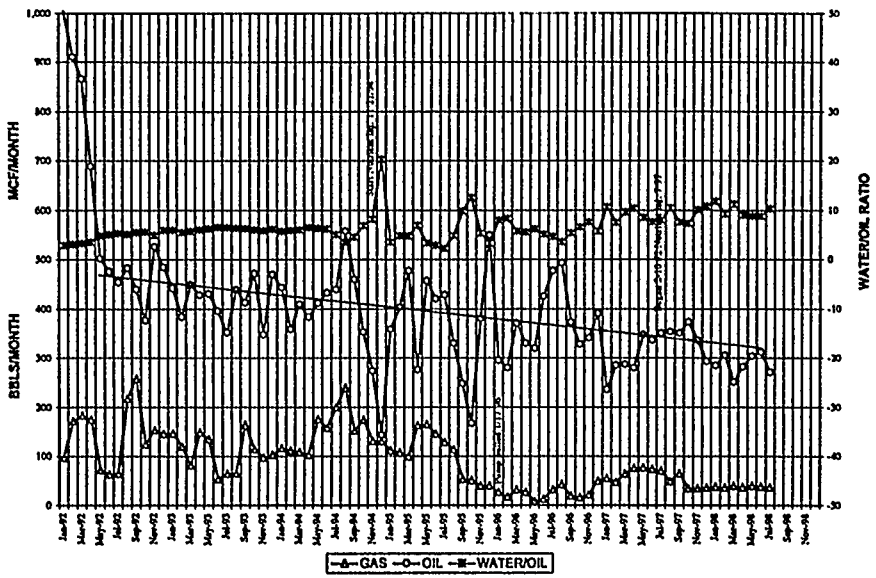

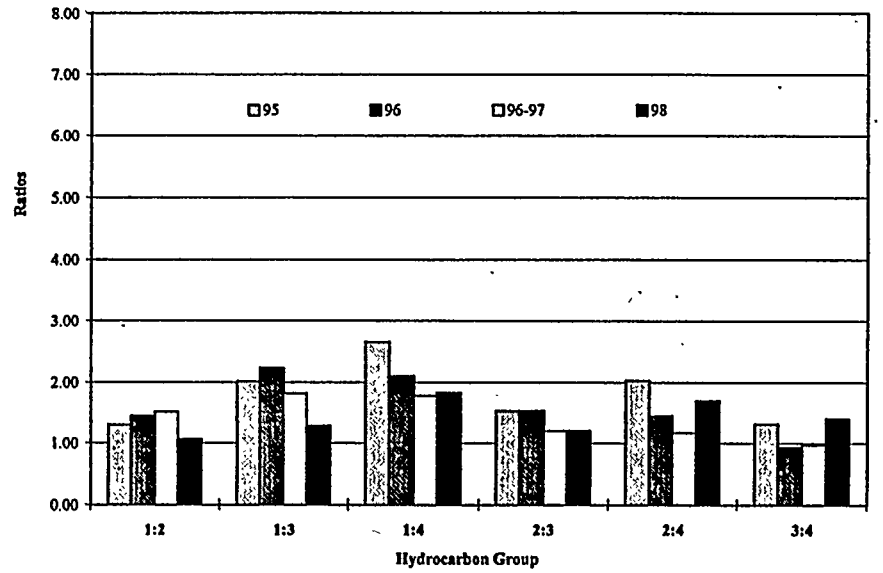

Figure A2. Well 2-15 No. 1 (2-14 No. 1 and 2-10 No. 2 Nutrient Injectors).

This well was classified as a questionable response to MPPM as shown in Table 8.

This well is in Test Pattern 1, due east of test injector well 2-14 No.1 and southeast of injector well 2-10 No. 1 that was not in the original experimental plan but did receive nutrient injections from July 1997 through June 1998. In the tracer test conducted in April 1994, communication between this well and injector well 2-14 No. 1 was demonstrated in one sample after seven months but never again so the connection between this well and the injector well 2-14 No. 1 did not appear to be consistent. Fluid production from this well has been erratic with no evidence of enhanced recovery due to microbial activity in the reservoir. The G.C. data from fluid out of his well tend to confirm this conclusion. Figure 4 shows that the ratio of 1:4 was rather low in 1995 as would be expected in a well that had been producing for years and declined from 2.65, to 2.10, to 1.78, to 1.82 in 1995, 1996, 1997, and 1998, respectively. The quantity of group1 compounds declined while the quantity of group 4 compounds increased.

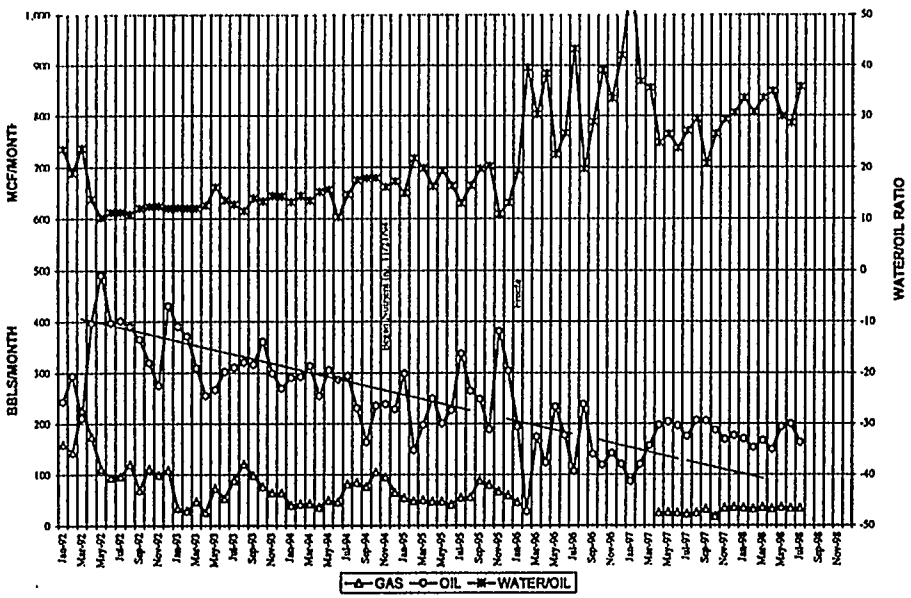

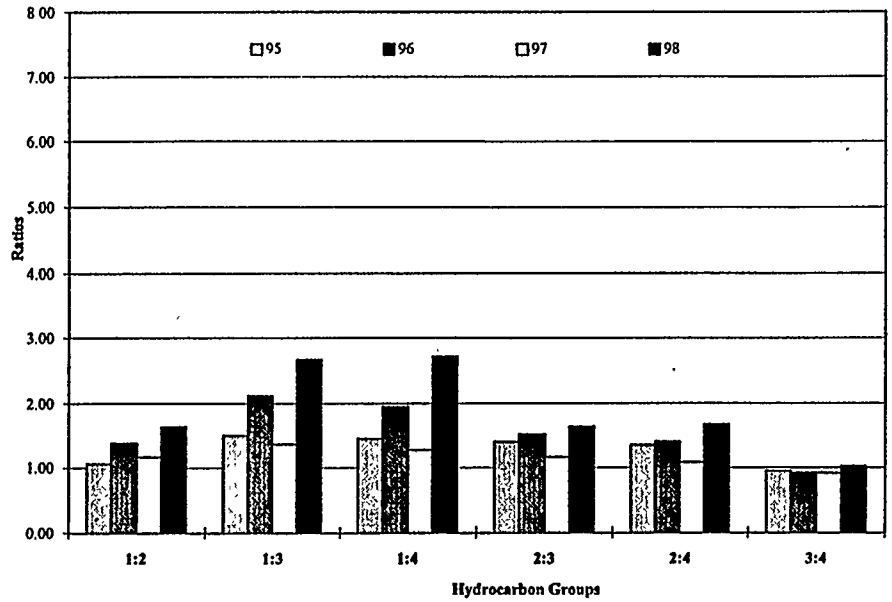

Table A3: Well 11-3 No. 1 (2-14 No. 1 and 11-5 No. 1 Nutrient Injectors).

This well was classified as a positive response to MPPM as shown in Table 8.

This well is in Test Pattern 1 and Test Pattern 3 and is situated almost due south of test injector well 2-14 No. 1 and northeast of test injector well 11-5 No.1. Oil production from this well was erratic until January 1997 when it increased and then remained essentially constant and WOR has generally remained steady. The ratio of 1:4 rose from 1.44 in 1995 to 1.95 in 1996 but fell back to 1.28 in 1997. In 1998 the ratio of 1:4 was 2.72 which is greater than a 100% increase. The quantity of group 1 compounds increased while the quantity of group 4 compounds decreased. These data definitely indicate the presence of bypassed oil in the produced fluid. Interestingly enough, the tritium injected into injector well 2-14 No. 1 in April 1994 required 18 months before it appeared in this well (well 11-3 No. 1). Therefore, it is not surprising that manifestation of the microbial growth in the reservoir was not apparent until 1998.

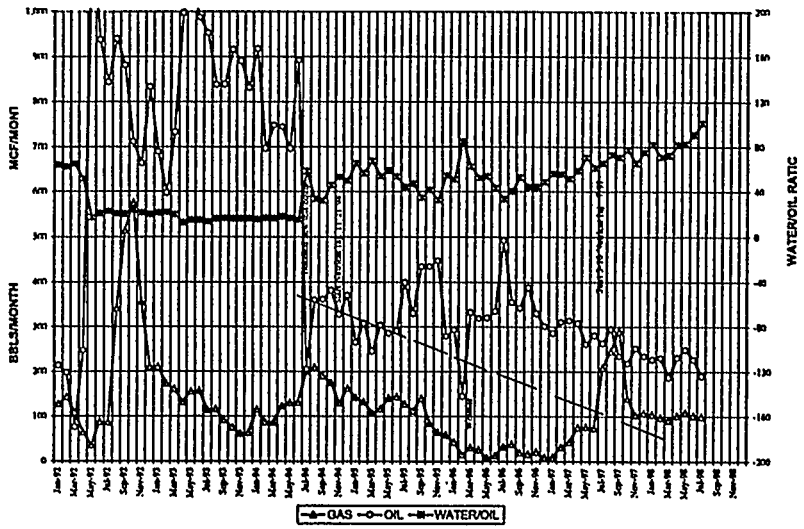

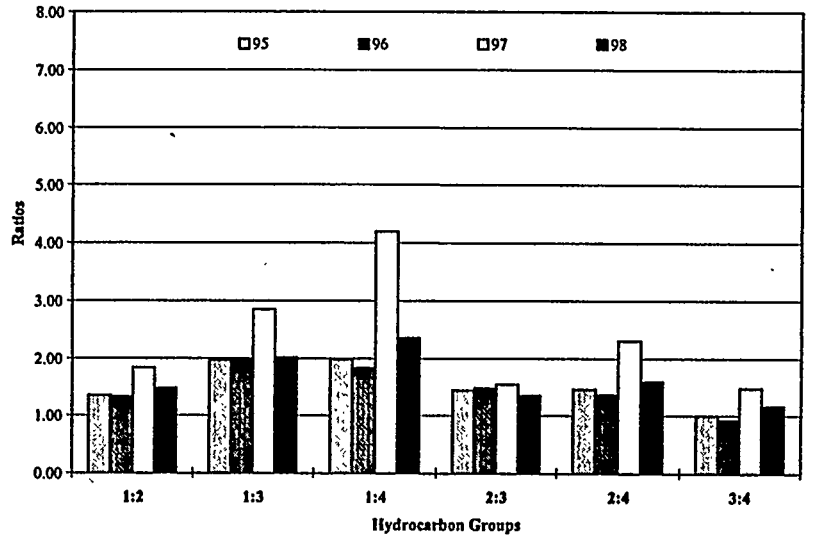

Table A4: Well 2-13 No. 1 (2-14 No. 1 11-5 No. 1, and 3-16 No. 1 Nutrient Injectors).

This well was classified as a positive response to MPPM as shown in Table 8.

This well is in Test Pattern 1 and Test Pattern 3. It is situated due west of test injector well 2-14 No. 1 and north of test injector well 11-5 No. 1 and east of test injector 3-16 No. 1 that was not in the original experimental plan but did receive nutrients from July 1997 through June 1998. In the tracer test conducted in April 1994, communication between this well and test injector 2-14 No. 1 was demonstrated in six months. Approximately six months after beginning the nutrient injection, there was an increase in oil production and the rate of decline in oil production decreased. The WOR remained steady, but recently has begun to increase slightly. The presence of bypassed oil was clearly demonstrated in 1997 when the ratio of 1:4 increased over 100% from 1.98 to 4.20 from 1995, to 1997, respectively. The amount of group 1 compounds increased while the amount of group 4 compounds decreased from 1995-96 to 1997-98.

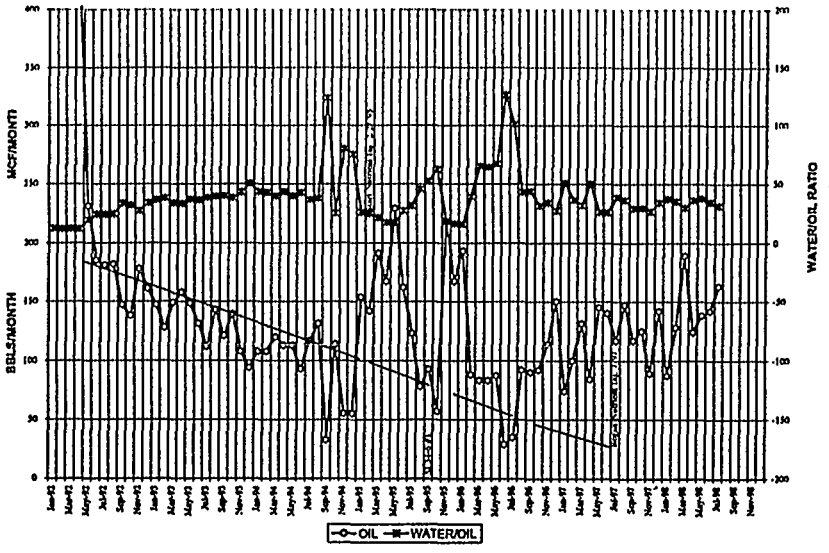

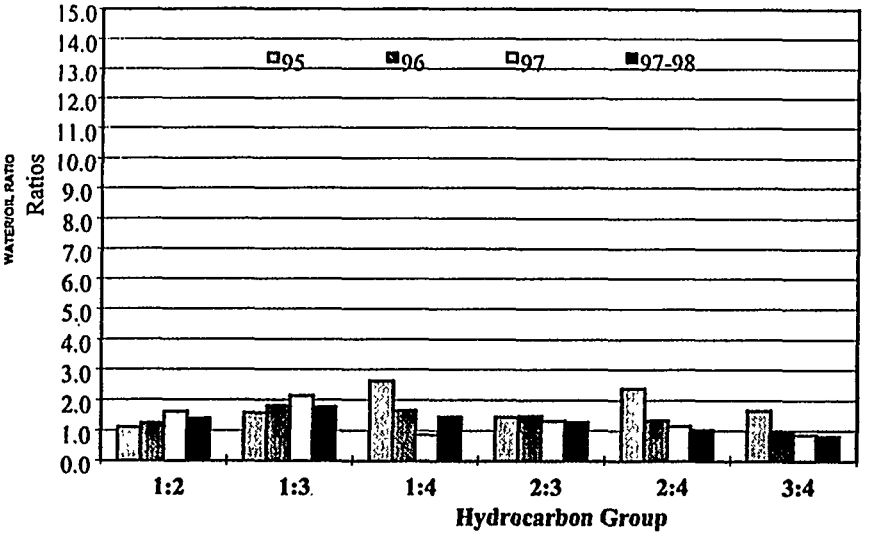

Table A5: Well 34-7 No. 2 (34-9 No. 2 and 34-7 No. 1 Nutrient Injectors).

This well was classified as a positive response to MPPM as shown in Table 8.

This well is located in Test Pattern 2 and in Control Pattern 2. It is situated north of test injector well 34-9 No. 2 and southeast of control injector well 34-7 No. 1 that was converted into a test injector well from July 1997 through June 1998. During the last 2 years, there was an increase in oil production and the WOR declined slightly. The increased oil production in this well does not appear to be due to the influx of previously unswept oil into the production fluid as determined by GC since there were no significant increases in the ratio of 1:4. Values for the 1:4 ratios were 3.02, 1.65, 1.86, and 1.44 for 1995, 1996, 1997, and 1998 respectively.

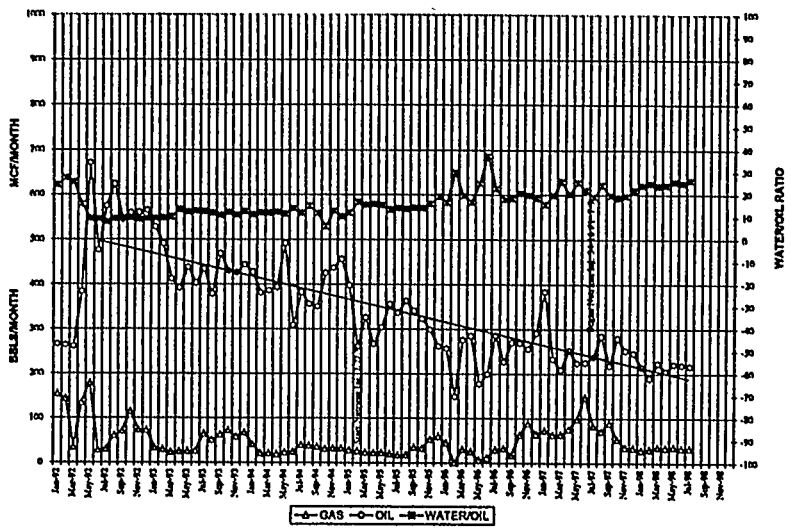

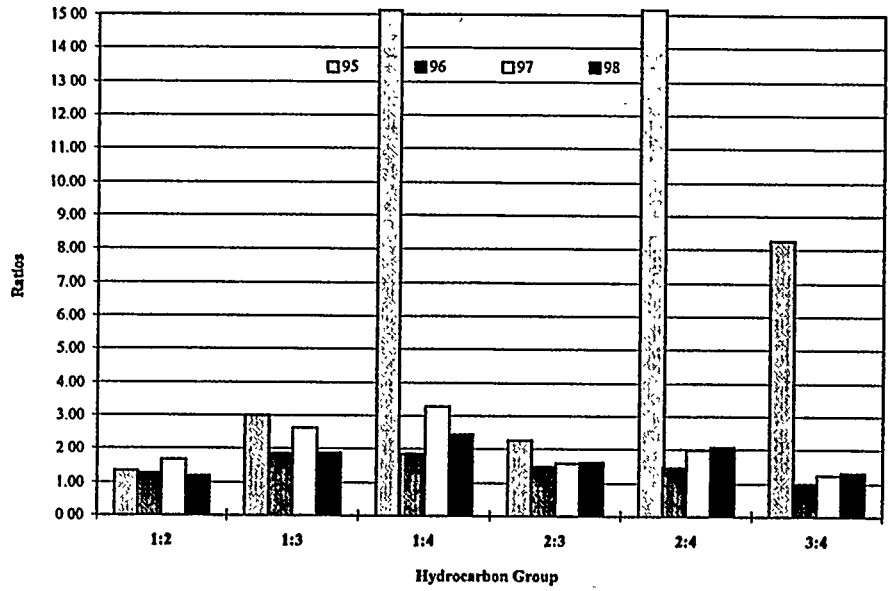

Table A6: Well 34-16 No. 2 (34-9 No. 2 and 34-16 No. 1 Nutrient Injectors)

This well was classified as a questionable response to MPPM as shown in Table 8.

This well is located in Test Pattern 2 and is situated southeast of test injector well 34-9 No. 2. It is almost due north of injector well 34-16 No. 1 that was not in the original experimental plan but did receive nutrients from July 1997 through June 1998. Oil production demonstrated a natural decline until July 1997 after which time the production decline decreased somewhat. The ratio of 1:4 increased from 1.85 to 3.27, a 77% increase, between 1996 and 1997 indicating the presence of previously bypassed oil in the production fluid from this well.

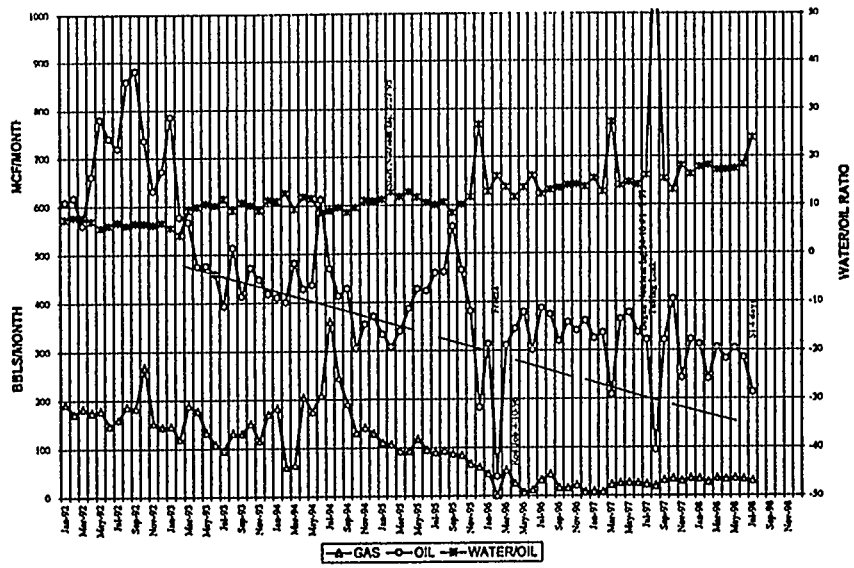

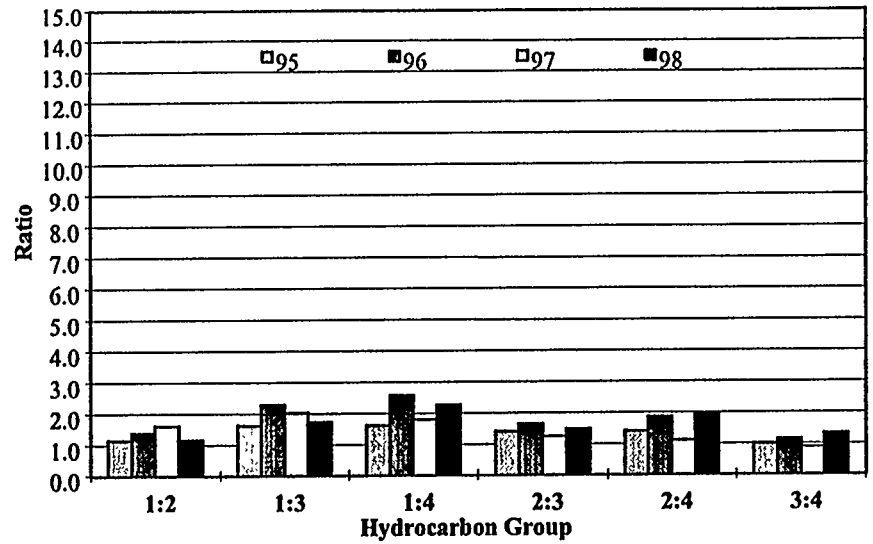

Table A7: Well 34-15 No. 1 (34-9 No. 2 and 34-16 No. 1 Nutrient Injectors).

This well was classified as a positive response to MPPM as shown in Table 8.

This well is located in Test Pattern 2 and Control Pattern 3. It is situated southwest of test injector well 34-9 No. 2 and west northwest of injector well 34-16 No. 1 that was not in the original experimental plan but did receive nutrients from July 1997 through 1998. Approximately 15 months after beginning the nutrient injection, there was an increase in oil production and subsequently the oil production rate declined at a lesser rate. WOR remained steady. The ratio of 1:4 increased 60% (1.61 to 2.58) from 1995 to 1996 as a result of an increase in group 1 compounds and a decrease in group 4 compounds. This ratio of 1:4 decreased from 2.58 to 1.80 in 1997 (28% decrease) but rose to 2.26 (a 26% increase) in 1998. These G.C. data indicate the appearance of bypassed oil in production fluid from this well.

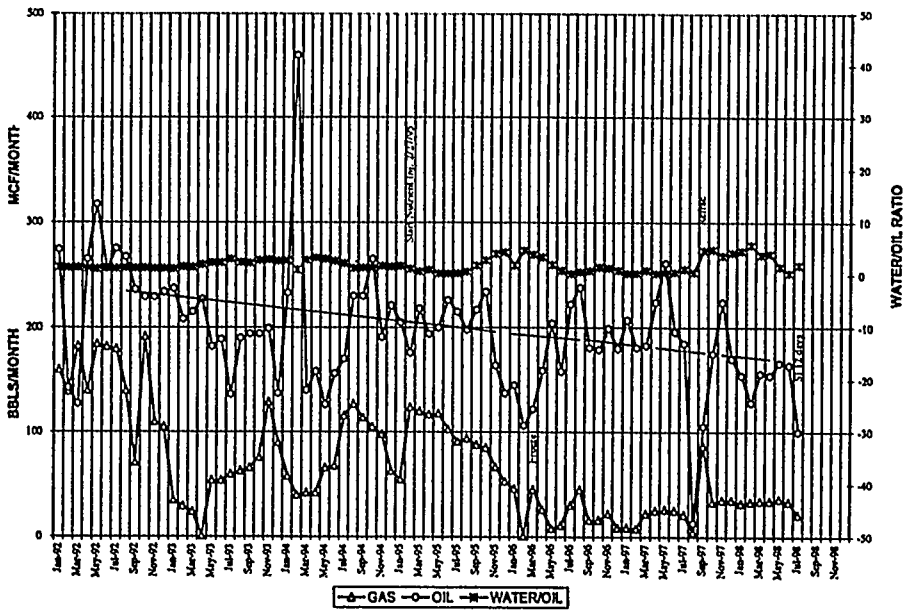

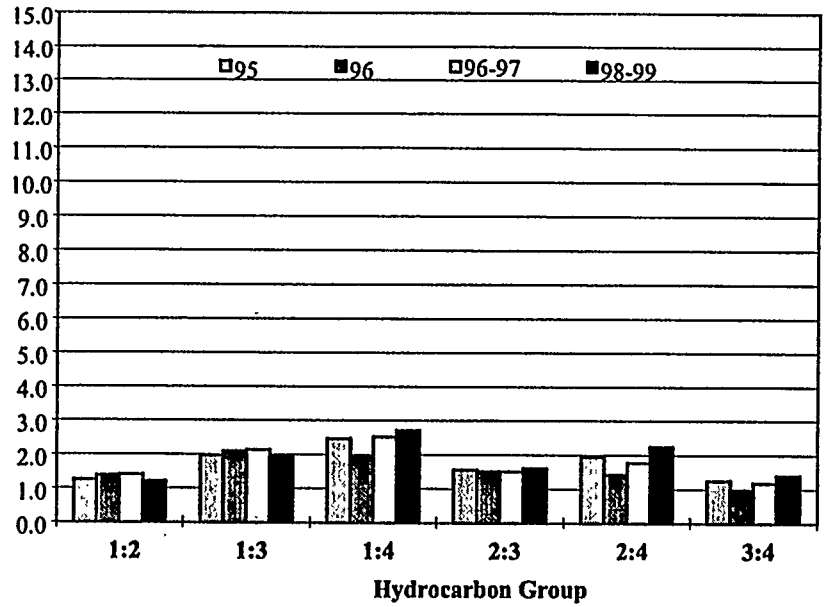

Table A8: Well 34-15 No. 2 (34-9 No. 2 Nutrient Injector).

This well was classified as a positive response to MPPM as shown in Table 8.

This well is in Test Pattern 2 and Control Pattern 3. It is situated west southwest of test injector well 34-9 No. 2. Approximately 16 months after beginning the nutrient injection, there was a slight increase in oil production and subsequently oil production remained steady except for the period in which the well was refractured (Aug. 1997). WOR remained steady except for the period in which the well was refractured. The ratio of 1:4 fluctuated from 2.46 to 1.96 to 2.52 to 2.70 for 1995, 1996, 1997, and 1998, respectively, and consequently did not clearly indicate the presence of bypassed oil.

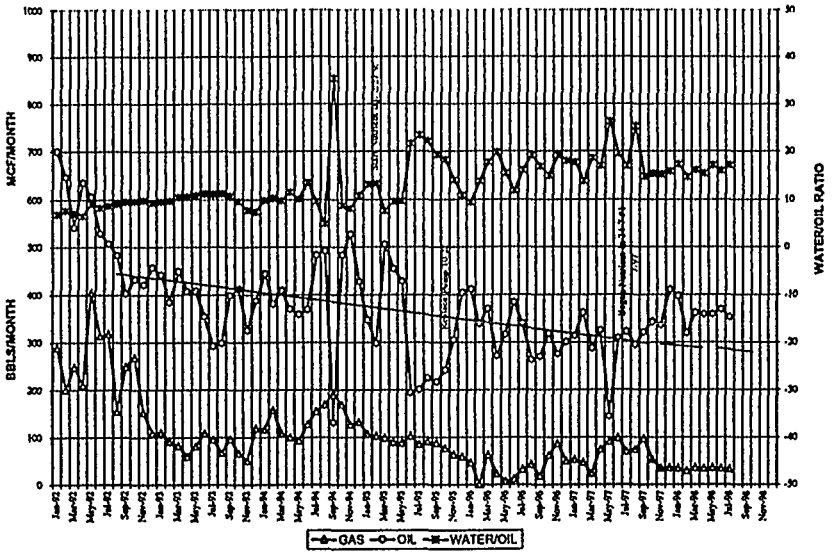

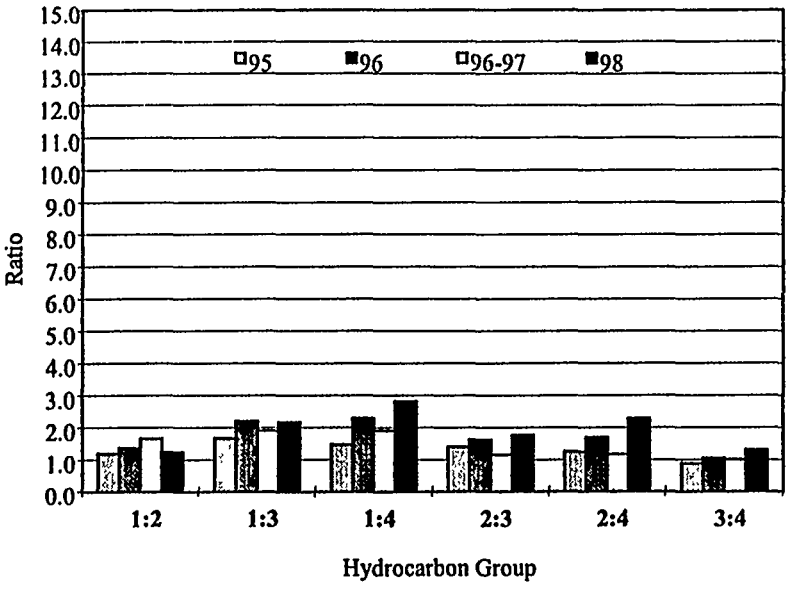

Figure A9: Well 34-10 No. 1 (34-9 No. 2 and 34-7 No. 1 Nutrient Injectors).

This well was classified as a positive response to MPPM as shown in Table 8.

This well is in Test Pattern 2 and Control Pattern 2. It is situated northwest of test injector well 34-9 No. 2 and south southwest of control injector well 34-7 No. 1 that received nutrients from July 1997 through June 1998. Oil production declined until Sep. 1997, at which time it increased and WOR declined. The low oil production in 1995 is reflected in the low ratio of 1:4 (1.48). When oil production increased in 1996 the ratio of 1:4 also increased to 2.28 or a 54% increase. There was a 19% decrease in this 1:4 ratio in 1997 but another increase of 47% (from 1.91 to 2.81) in 1998. These data suggest an influx of bypassed oil in the production fluid from this well.

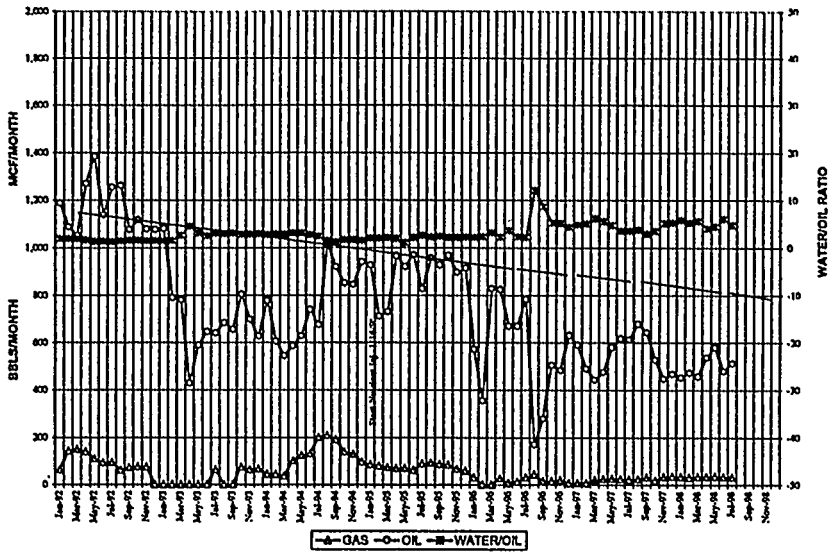

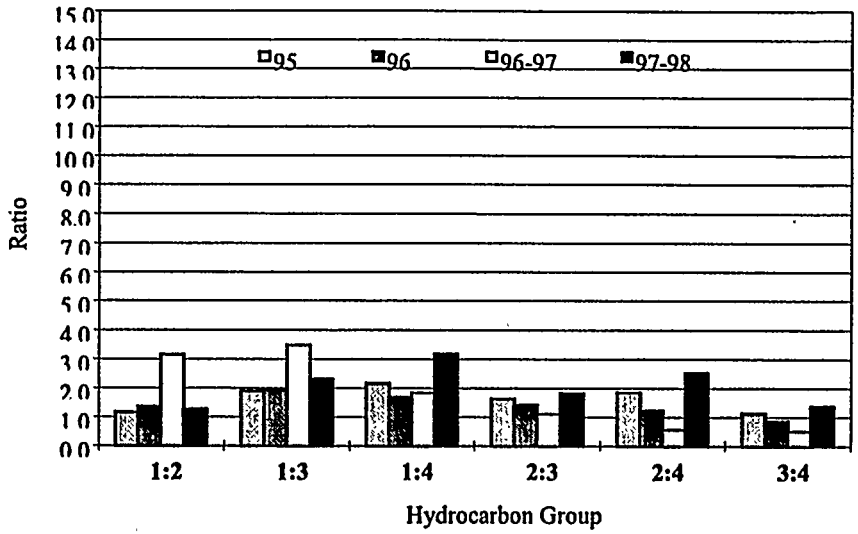

Figure A10: Well 10-8 No. 1 (11-5 No. 1 Nutrient Injector).

This well was classified as a positive response to MPPM as shown in Table 8.

This well is in Test Pattern 3 and is situated southwest of test injector well 11-5 No. 1. This well had mechanical problems. While oil production did not show a positive response initially, there were indications (aliphatic profile and petrophysical properties) that there had been a change in the characteristics of the produced oil suggesting new oil was being recovered. Both production and WOR have held steady since late 1997. The ratio of 1:4 went from 2.15 to 1.68 to 1.83 in 1995, 1996, and 1997, respectively. In 1998, however, the ratio of 1:4 increased 74% to 3.18 which clearly indicates the recovery of bypassed oil in the production fluids.

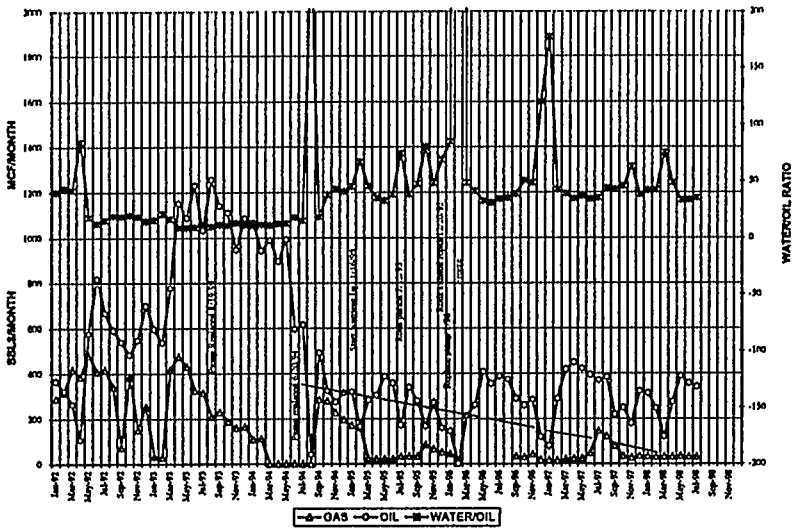

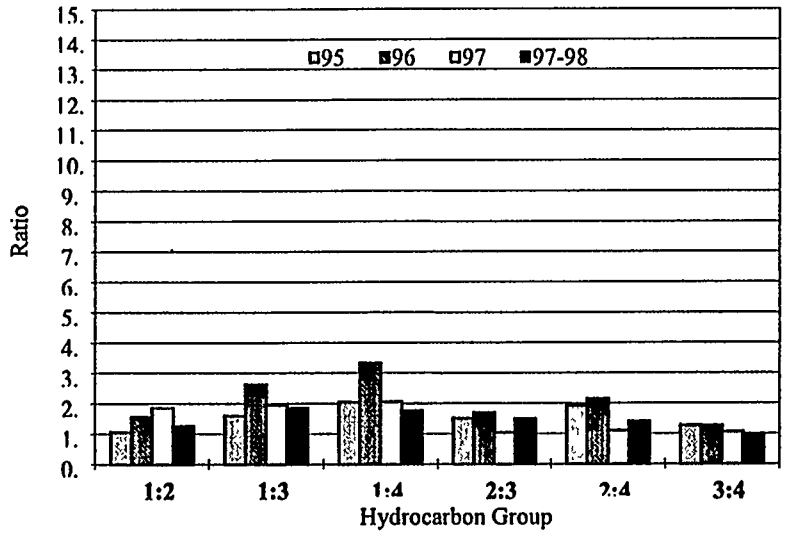

Figure A11: Well 11-6 No. 1 (11-5 No. 1 Nutrient Injector).

This well was classified as a positive response to MPPM as shown in Table 8.

This well is in Test Pattern 3 and is situated east of test injector well 11-5 No. 1. This well had mechanical problems. Approximately 15 months after beginning the nutrient injection, the oil production rate increased and subsequently held steady. WOR held steady. The ratio of 1:4 increased from 2.04 to 3.33 (63%) between 1995 and 1996 but then has steadily declined to 2.06 and 1.76 in 1997 and 1998, respectively. The big increase in oil production coincides with the big increase in the ratio of 1:4 and is characteristic of the presence of bypassed oil in the production fluid.

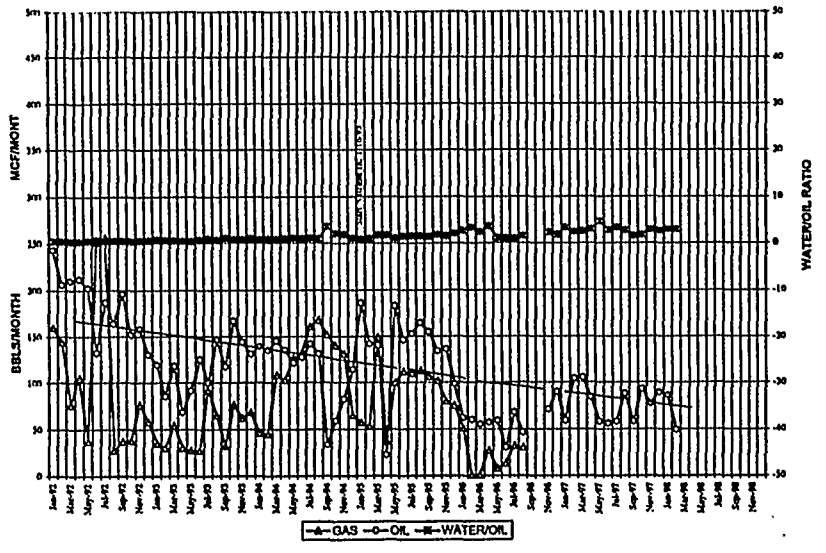

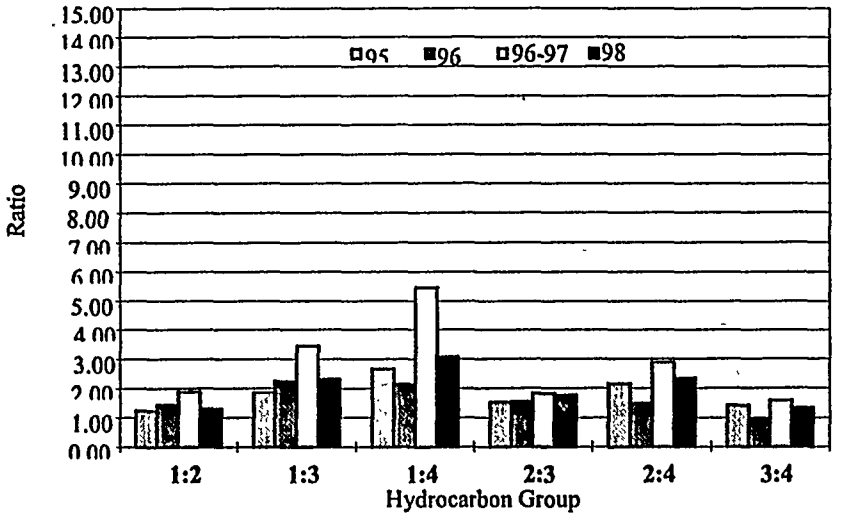

Figure A12: Well 11-4 No. 1 (11-5 No. 1 Nutrient Injector).

This well was classified as a no response to MPPM as shown in Table 8.

This well is in Test Pattern 3 and is situated north northeast of test injector well 11-5 No. 1 and southeast of injector well 3-16 No. 1 that was not in the original experimental design but did receive nutrients from July 1997 through June 1998. This well has exhibited natural decline in oil production with a concurrent increase in WOR. The ratio of 1:4 dropped from 2.66 to 2.15 (19%) between 1995 and 1996 but increased (153%) in 1997 due to an increase in group 1 compounds and a decrease in group 4 compounds. This increase in the 1:4 ratio definitely indicates the presence of a large percentage of bypassed oil in the produced fluid. In 1998 the ratio of 1:4 dropped to 3.08 which would be expected as time goes by, but is still relatively high.

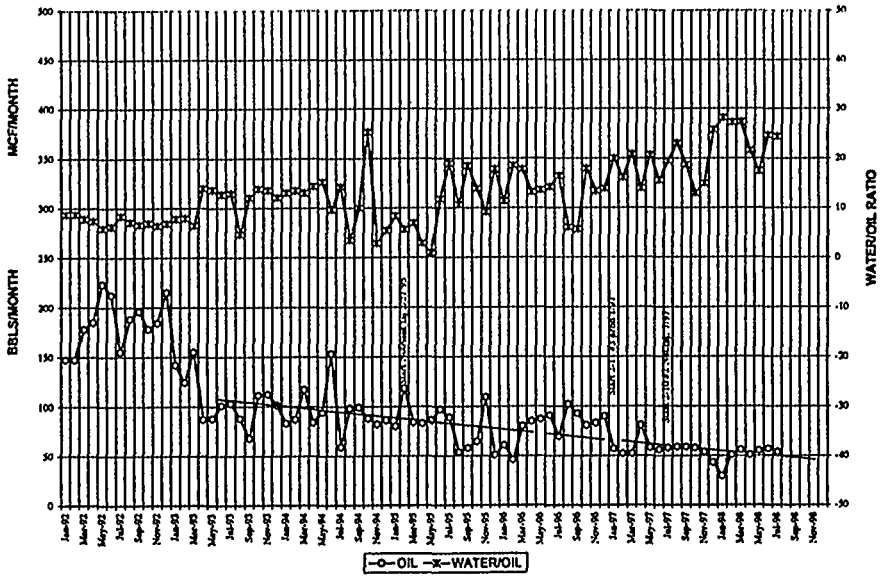

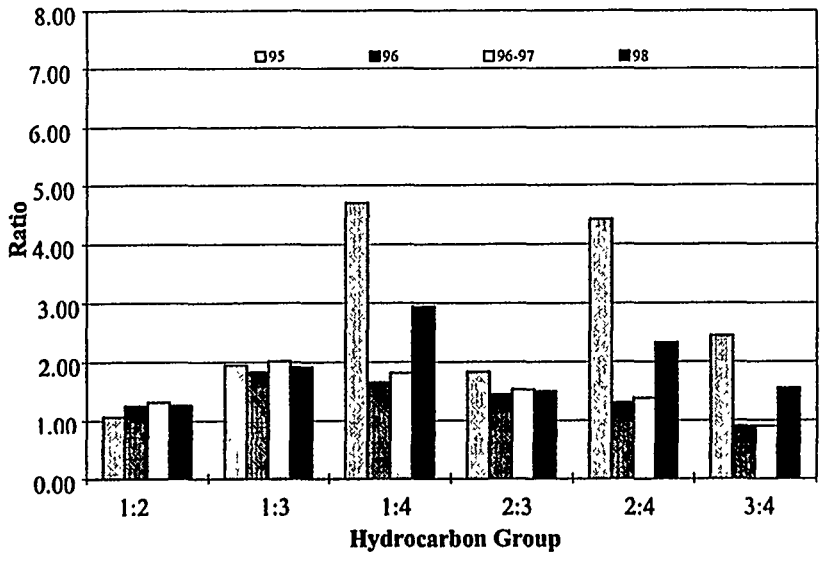

Figure A13: Well 2-11 No. 2 (2-6 No. 1 and 2-10 No. 2 Nutrient Injector).

This well was classified as a positive response to MPPM as shown in Table 8.

This well is in Test Pattern 4 and is situated southeast of test injector 2-6 No. 1 and north of test injector 2-10 No. 2 that was not in the original experimental plan but did receive nutrients from July 1997 through June 1998. Approximately 13 months after beginning the nutrient injection, oil production increased until Jan. 1997 when well 2-11 No. 3 began producing and production from well 2-11 No. 2 began to decline. After well 2-11 No. 3 was shut-in in Aug. 1997, oil production stopped its decline and WOR remained steady. (Well 2-11 No. 3 was drilled in Nov. 1996 and is located west northwest of well 2-11 No. 2.) The ratio of 1:4 in well 2-11 No. 2 dropped from 2.52 to 1.64 between 1995 and 1996 and rose only slightly (11%) in 1997 to 1.82. In 1998, however, the ratio climbed to 2.94, probably due to the impact of well 2-11 No. 3. Therefore, this increase in the 1:4 ratio may not be due entirely to microbial activity alone.

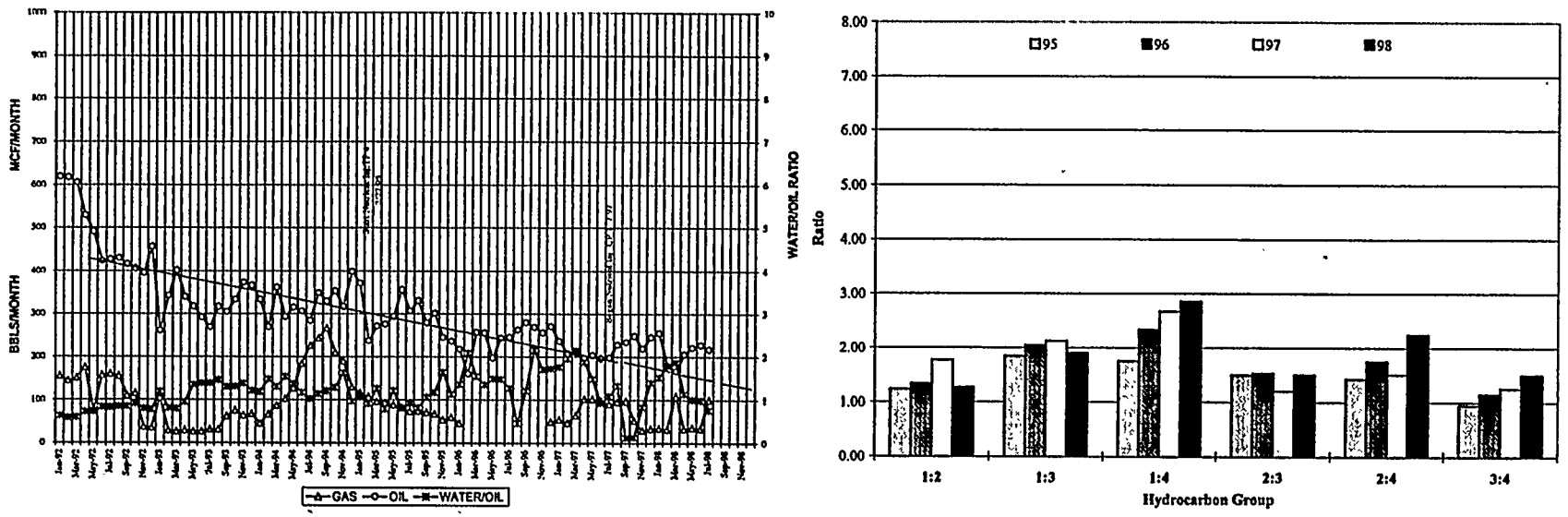

Figure A14: Well 2-3 No. 1 (2-6 No. 1 and 2-4 No. 1 Nutrient Injectors).

This well was classified as a positive response to MPPM as shown in Table 8.

This well is in Test Pattern 4 and Control Pattern 1. It is situated almost due north of test injector well 2-6 No. 1 and east of control injector well 2-4 No. 1 that was converted to a test injector well from July 1997 through June 1998. This well had shown a positive response and oil production had been consistently above the projected amount. Approximately 24 months after beginning the nutrient injection, WOR began to drop sharply. This well also benefited from the nutrient injection in control injector 2-4 No. 1. The ratio of 1:4 has steadily climbed from 1995 through 1998 showing an increase of 63% over that time period caused by an increase in group 1 compounds and a decrease in group 4 compounds. These data suggest a small but steady increase in previously bypassed oil in the production fluid.

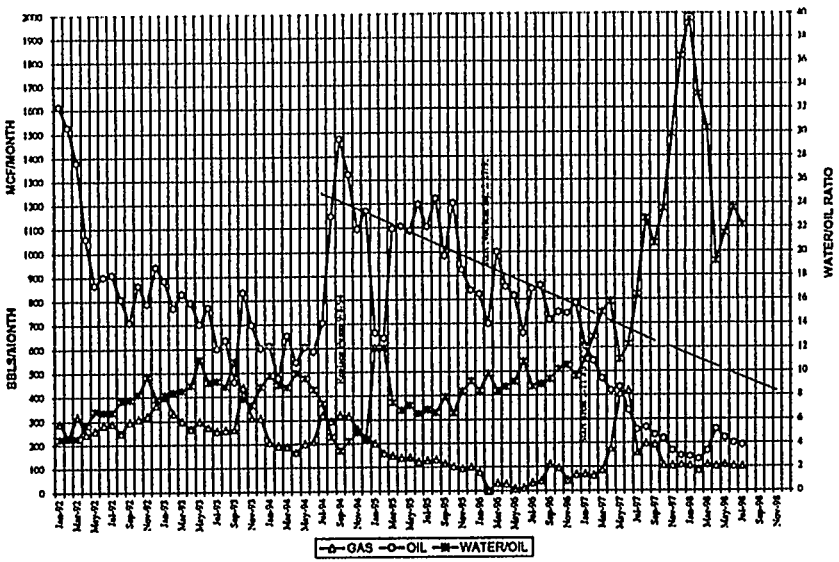

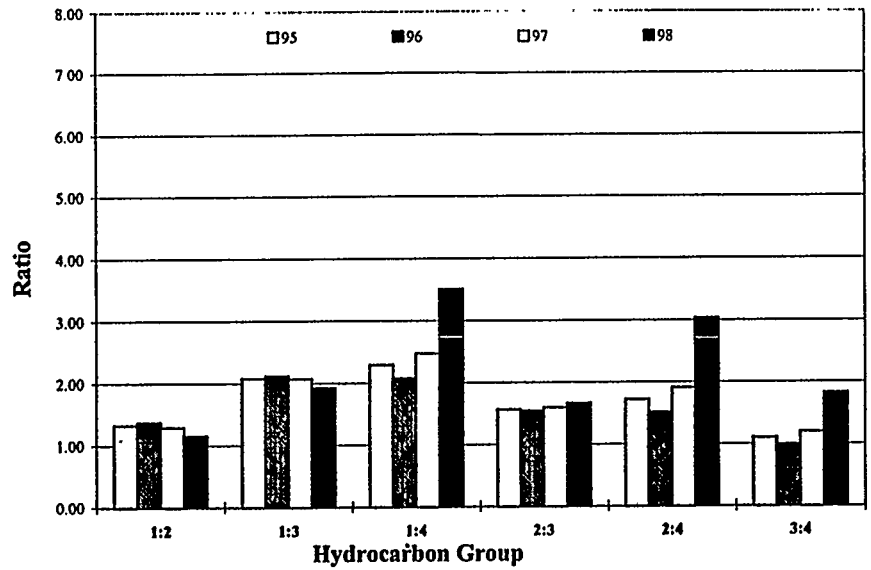

Figure A15: Well 2-5 No. 1 (2-6 No. 1, 2-4 No. 1, and 2-12 No. 1 Nutrient Injectors).

This well was classified as a no response to MPPM as shown in Table 8.

This well is in Test Pattern 4 and Control Patterns 1, and 4. It is situated west of test injector well 2-6 No. 1, south of control injector well 2-4 No. 1 that was converted to a test injector well from July 1997 through June 1998. It is due north of injector well 2-12 No. 1 that was not in the original experimental design but received nutrients from July 1997 through June 1998. This well had continued on a natural decline until approximately Nov. 1996 when production fell dramatically due to the production from newly drilled well 2-5 No. 2. WOR continued to increase. The ratio of 1:4 stayed essentially constant from 1995 through 1997 (2.29, 2.07, and 2.47, respectively) but increased 42% to 3.5 in 1998 caused by a drop in group 4 compounds. The new wells drilled nearby in late 1996 obviously impacted the performance of this well and consequently no meaningful conclusions about its performance can be drawn.

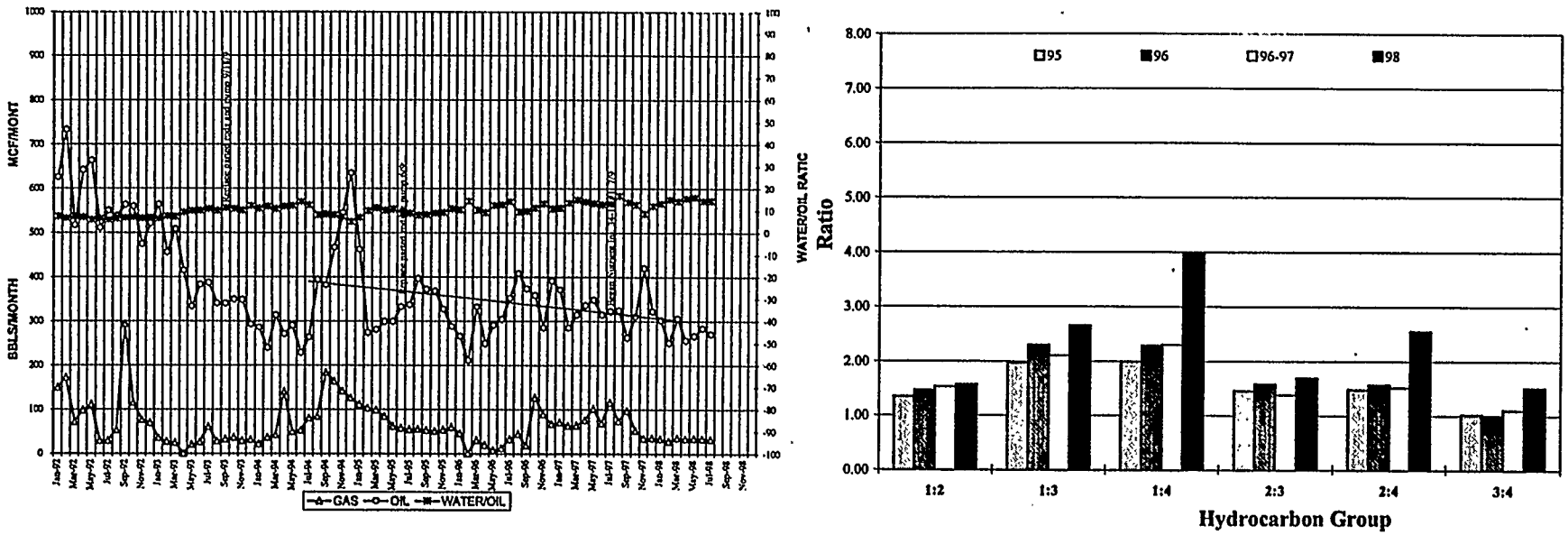

Figure A16: Well 35-13 No. 1 (34-16 No. 1 and 2-4 No. 1 Nutrient Injectors)

This well was classified as natural decline as shown in Table 8.

This well is in Control Pattern 1 and is situated due north of control injector well 2-4 No. 1 that was converted into a test injector from July 1997 to July 1998. Injector well 34-16 No 1, not included in the original experimental design, is due west of well 35-13 No. 1 and received nutrients from July 1997 through June 1998. The oil production rate has shown a steady decline since 1995 although the rate of decline is considerably less than it was prior to that time. This change in rate of decline is probably due to mechanical work on the well. The ratio of 1:4 remained virtually steady for 1995, 1996, and 1997 at 2.0, 2.28, and 2.31, respectively. In 1998, however, the ratio of 1:4 increased 75% to 4.0, strongly suggesting the presence of bypassed oil in the produced fluid even through total production of oil has not increased.

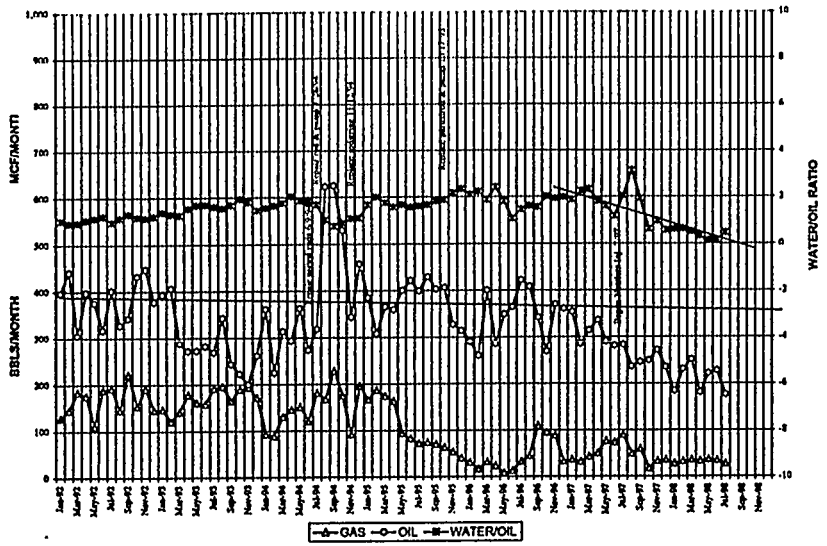

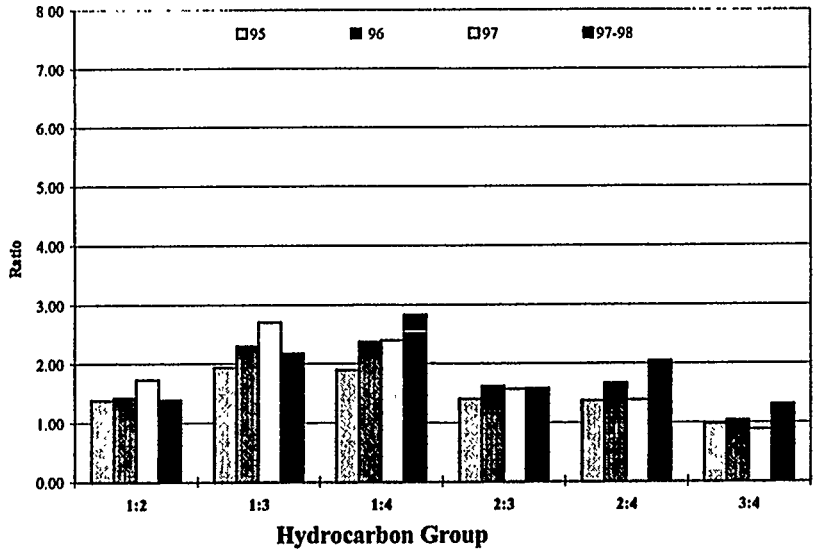

Figure A17: Well 3-1 No.1 (2-4 No. 1 and 34-16 No. 1 Nutrient Injectors).

This well was classified as natural decline as shown in Table 8.

This well is located in Control Patterns 1,3, and 4. It is situated west of control injector well 2-4 No. 1 that was converted into a test injector from July 1997 through June 1998. It is due south of injector well 34-16 No. 1 that was not in the original experimental plant but did receive nutrients from July 1997 through June 1998. This well had continued its natural decline up until Aug. of 1997 when WOR began an appreciable decline which may reflect a response to nutrient injection into two nearby injectors (34-16 No. 1 and 2-4 No. 1). The ratio of 1:4 did not show any dramatic changes indicating bypassed oil in the production fluid but rather showed a steady increase from 1.89, to 2.11, to 2.39, to 2.83, for 1995, 1996, 1997, and 1998, respectively.

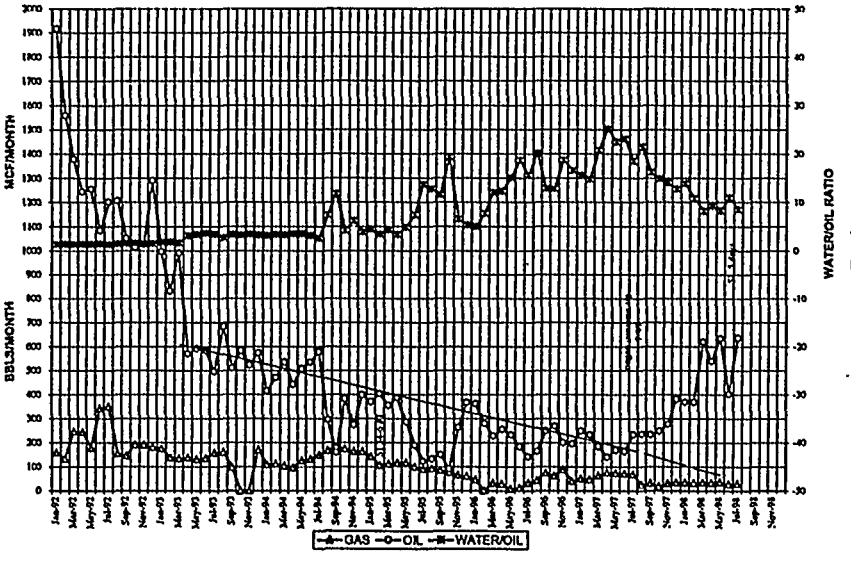

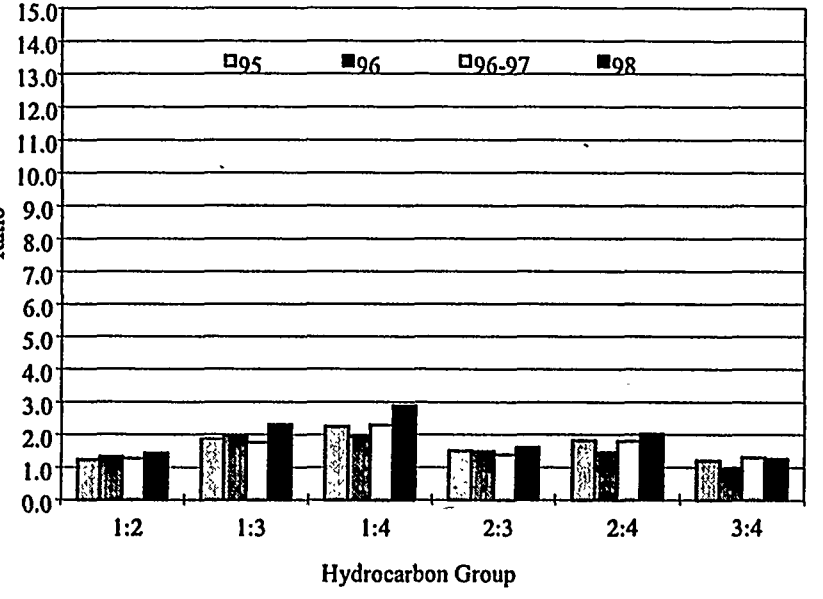

Figure A18: Well 34-2 No. 1 (34-7 No. 1 Nutrient Injectors)

This well was classified as a positive response to MPPM as shown in Table 8.

This well is in Control Pattern 2 and is situated due north of control injector well 34-7 No. 1 which received nutrients from July 1997 through June 1998. This well was exhibiting a natural decline until July 1997 at which time oil production began to increase appreciably due to nutrient injection into 34-7 No. 1. WOR decreased. The changes in the ratio of 1:4 were not nearly as dramatic as the large increase in oil production that began about four months after the control injector well started to receive nutrients. The ratio of 1:4 decreased 14% from 1995 to 1996 (2.25 to 1.94) but was back up to 2.30 in 1997. In 1998 the ratio increased to 2.90 (26% increase) due to an increase in group 1 compounds and a decrease in group 4 compounds.

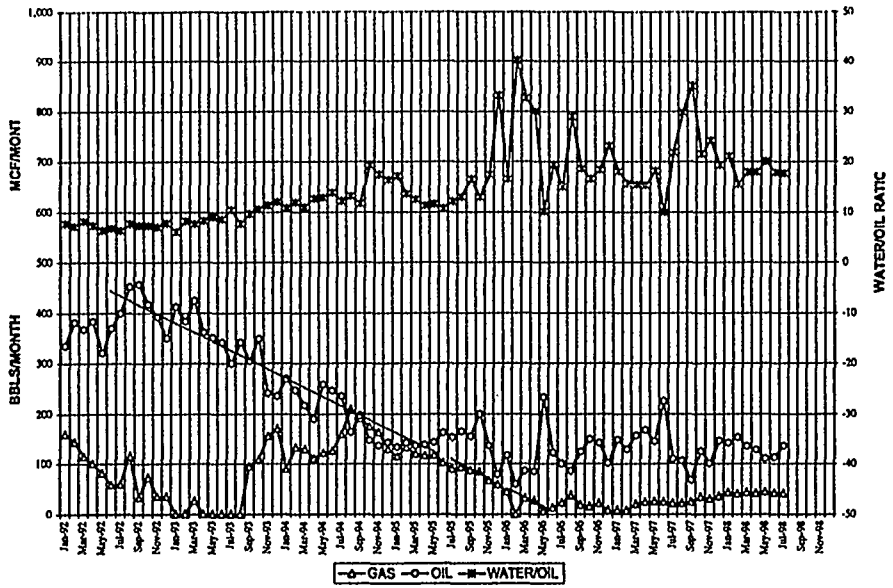

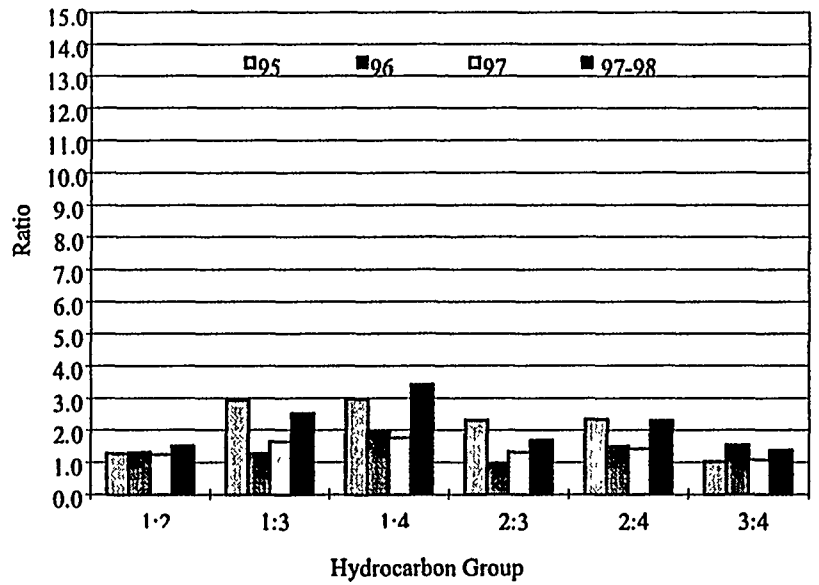

Figure A19: Table 3-3 No. 1 (3-2 No. 1 Injector).

This well was classified as natural decline as shown in Table 8.

This well is in Control Pattern 3 and is the westernmost well in this study. Oil production has remained essentially steady since May 1995 due to increased water injection in Control Injection well 3-2 No. 1. WOR increased. The ratio of 1:4 dropped from 2.98, to 2.12, to 1.76, in 1995, 1996, and 1997, respectively. Surprisingly, this ratio jumped to 3.42, a 94.3% increase, in 1998. These data suggest that some of the produced fluids are coming from previously bypassed oil and is result of the increased water injection initiated in 1995 or a reflection of other changes in the reservoir due to microbial growth.

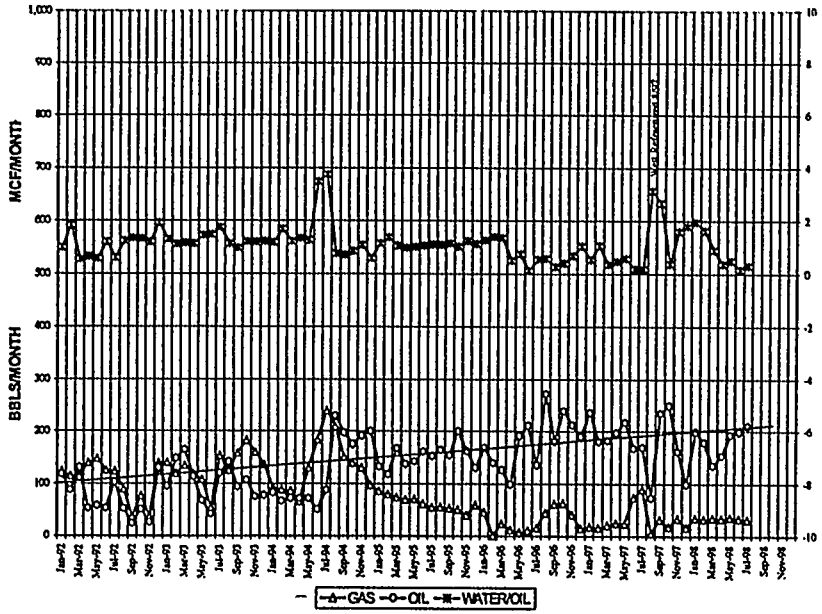

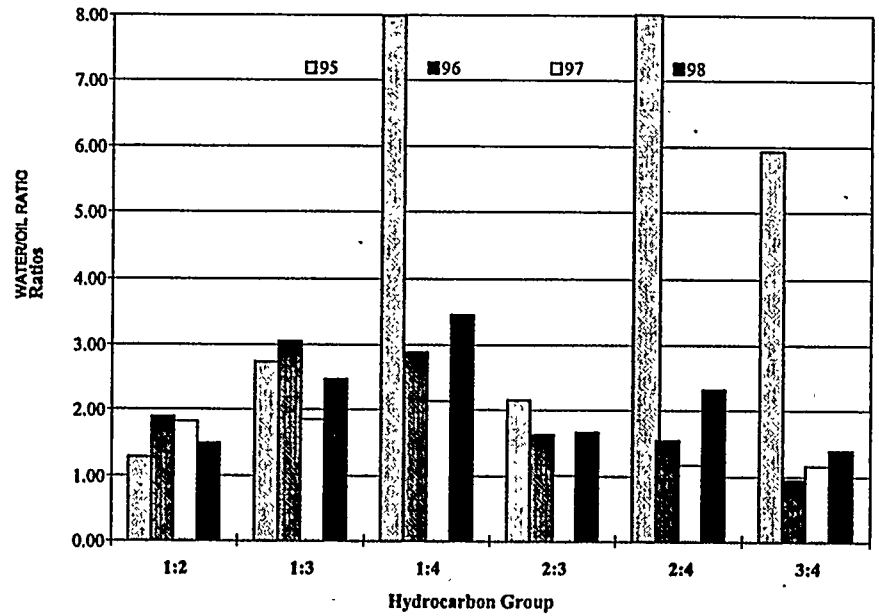

Figure A20: Well 3-1 No. 2 (3-2 No. 1 and 3-8 No. 1 Injectors).

This well was classified as a positive response as shown in Table 8 but was due to increased water injection in a nearby injector and not to MPPM.

This well is in Control Patterns 3 and 4. The positive response in oil production was due to an increase in water injection, not MEOR. WOR fluctuated due to refracturing of the well. Between 1996 and 1997 the ratio of 1:4 dropped 26%. As was the case with well 3-3 No. 1, the ratio of 1:4 exhibited a large increase (62%) in 1998, probably for the same reason(s) given for well 3-3 No. 1.

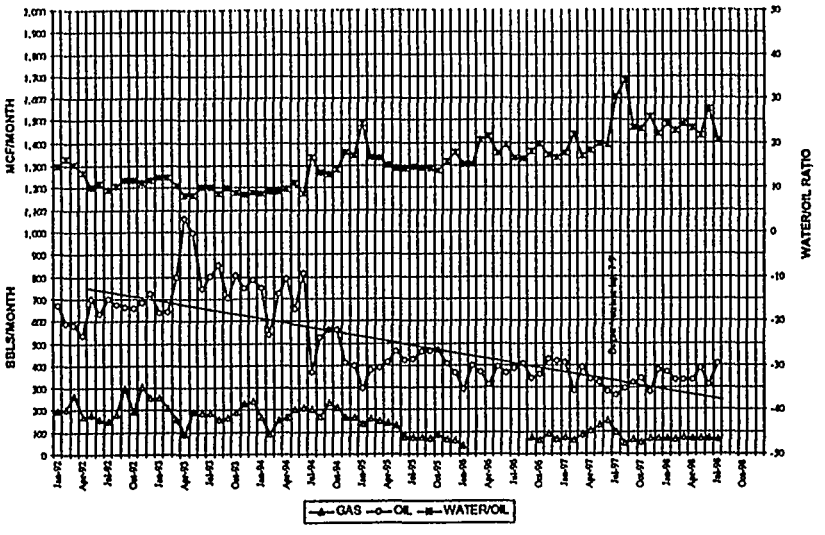

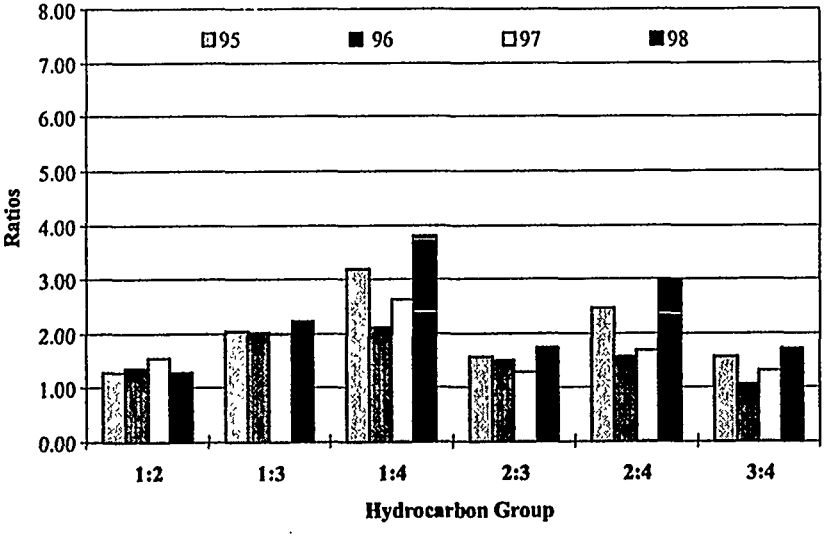

Figure A21: Well 3-9-1 (2-12 No. 1 and 3-16 No. 1 Nutrient Injectors).

This well was classified as a positive response to MPPM as shown in Table 8.

This well is in Control Pattern 4 and is situated west-southwest of injector well 2-12 No. 1 and north of injector well 3-16 No.1. Neither of these injectors was included in the original experimental plan but both received nutrients from July 1997 through June 1998. Oil production rate increased after the start of nutrient injection in 2-12 No. 1 and 3-16 No. 1. WOR leveled off and declined. The ratio of 1:4 decreased from 3.19 to 2.12 then rose slightly to 2.31 in 1995, 1996, and 1997, respectively. In 1998, however, the ratio rose 64% to 3.81. These data clearly indicate the impact of microbial activity in causing an increase in the amount of previously bypassed oil in the production fluid.

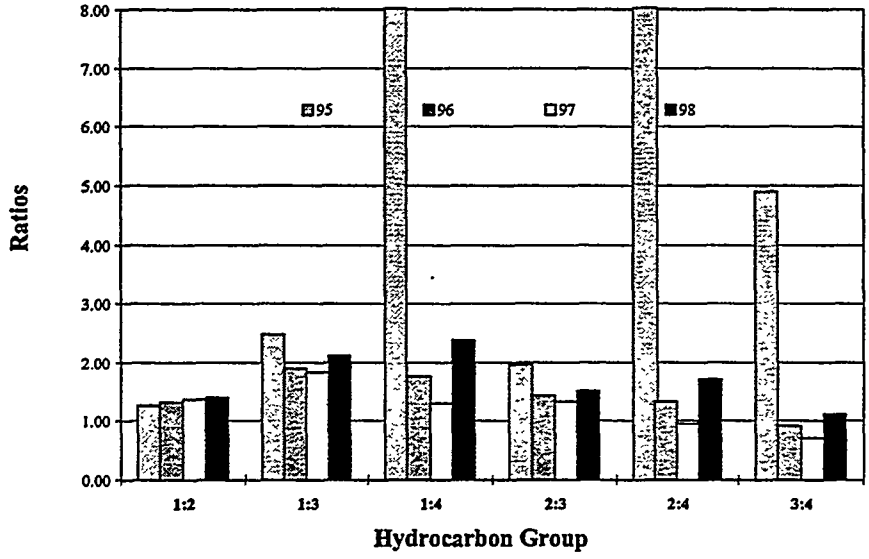

Figure A22. Well 34-6 No. 3.

This well was drilled in April 1994 in an area of the field that had not been swept by the waterflood. As may be seen, the ratio of group 1 **compounds** to group 4 compounds is extremely high (12.08) but dropped dramatically to 1.77 due to a 22% drop in group 1 **compounds** and a large increase (5.3x) in group 4 compounds. The ratio dropped even further to 1.30 in 1997 but increased to 2.38 in 1998. This 83% increase was due to an increase of 18% in group 1 **compounds** with a drop of 35% in group 4 compounds. The drop in the ratio of 1:4 in 1996 and 1997 was to be expected for a newly drilled well and generally this trend should continue or at least stabilize in subsequent years. Therefore, the increase of 35% in the 1:4 ratio in 1998, coupled with the steady increase in oil production suggests that production is being influenced by some exogenous force. The most likely influences would have been either (1) the shut-in of nearby well 34-6 No. l or (2) the nutrient additions into injector well 34-7 No. 1.

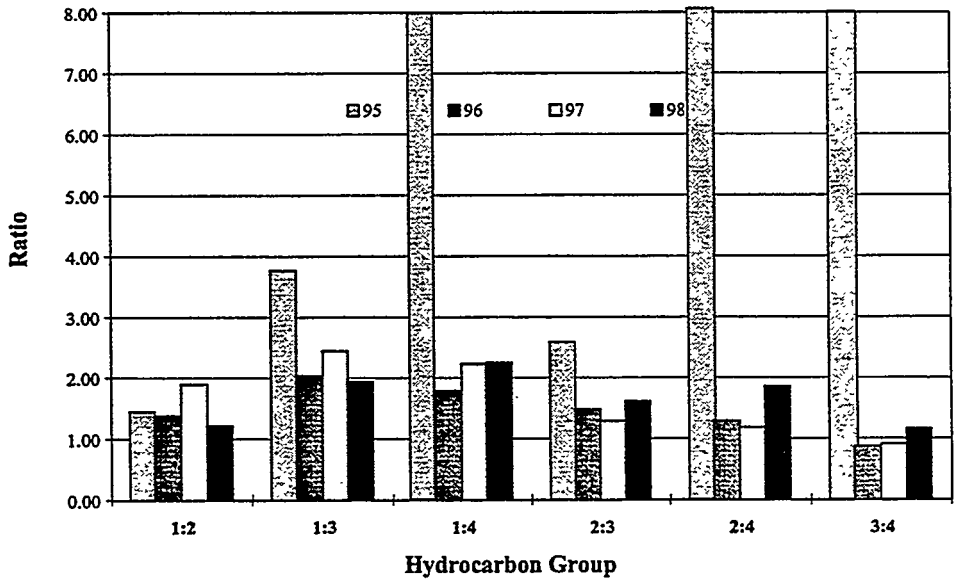

Figure A23. Well **34-3 No.** 2

This well was drilled in 1994 also in an area of the field that had been only partially swept by the waterflood. The ratio of 1:4 was 1.78 in 1996 and leveled off at 2.23 and 2.25 for 1997 and 1998. This is the type of pattern expected for a well not influenced by some exogenous force.

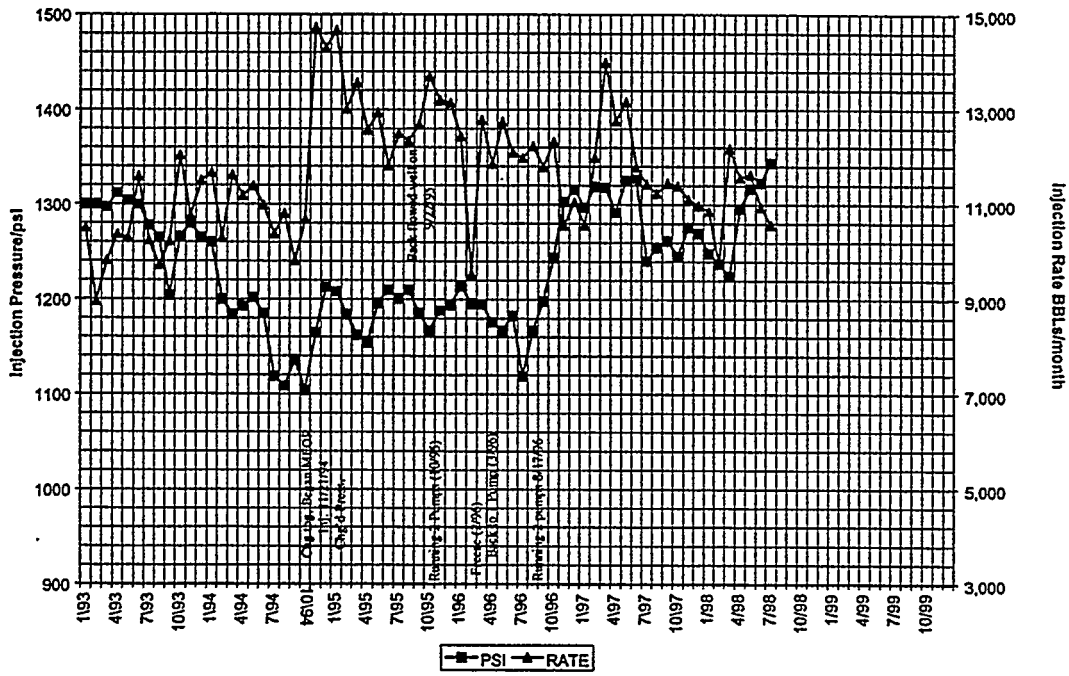

Figure A24. Injector Well 2-14 No. 1 (Test Pattern 1).

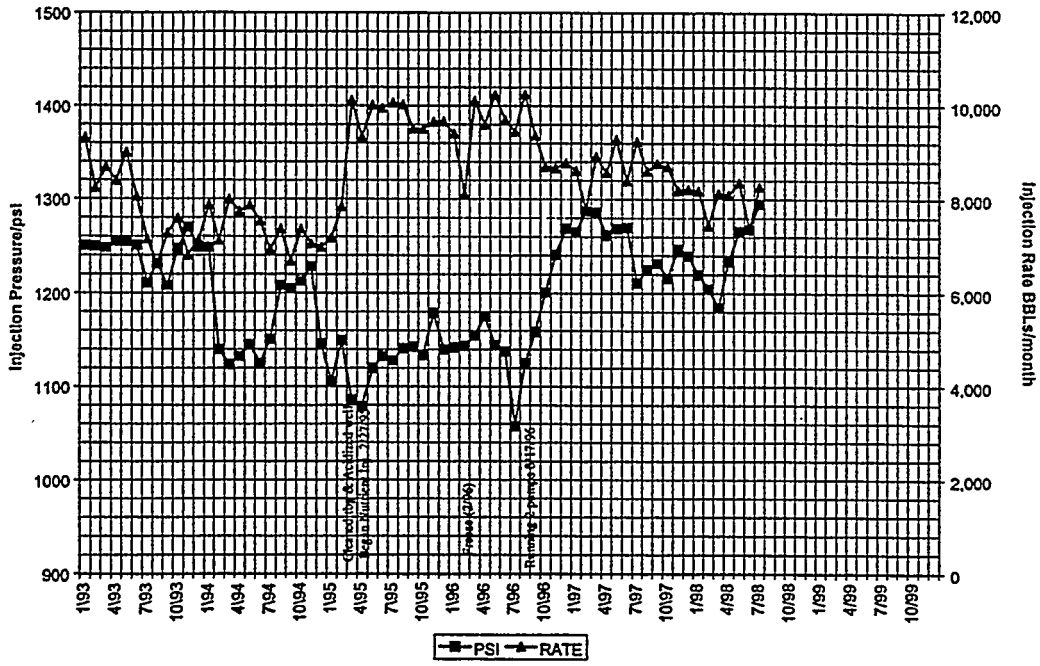

Figure A25. Injector Well 34-9 No. 2 (Test Pattern 2).

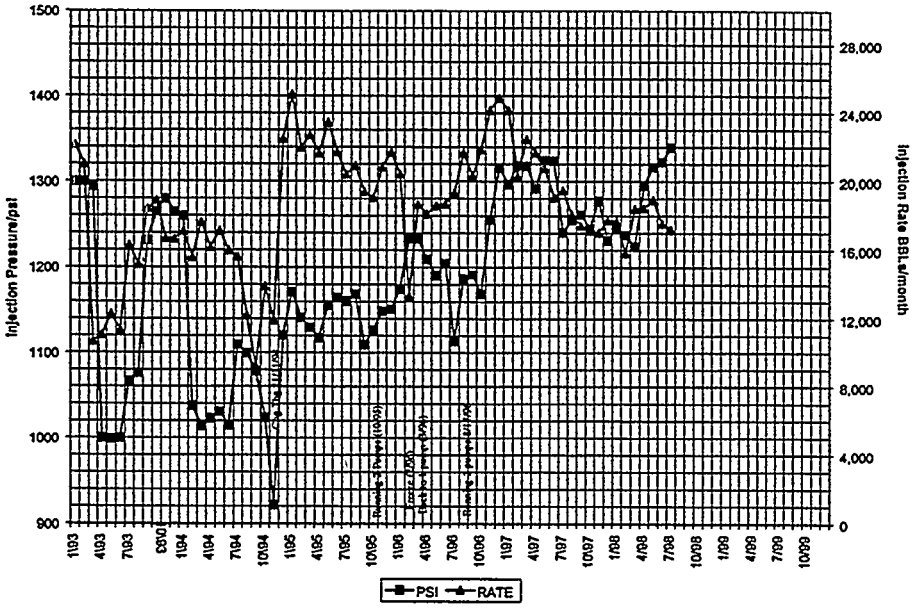

Figure A26. Injector Well 11-5 No. 1 (Test Pattern 3).

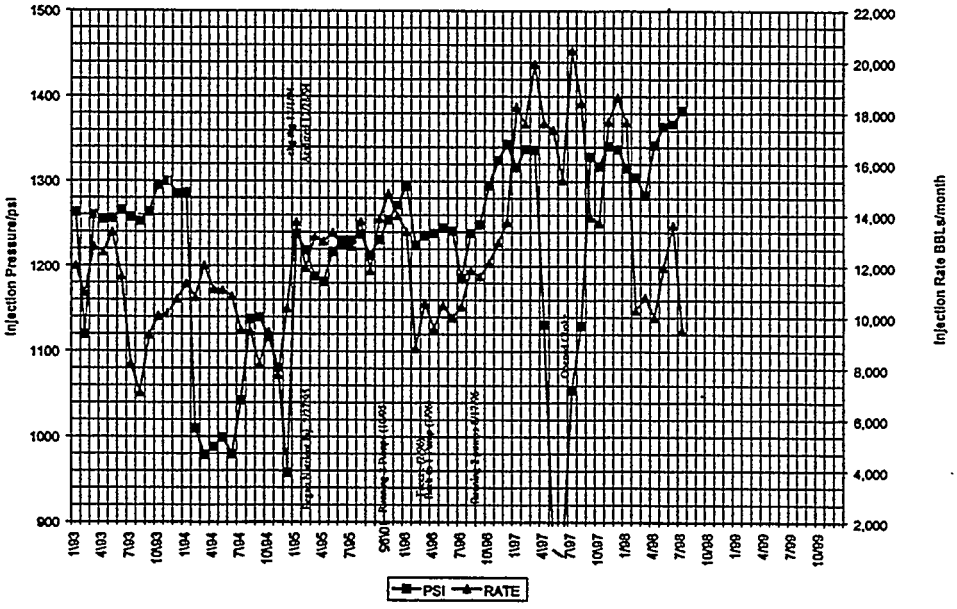

Figure A27. Injector Well 2-6 No. 1 (Test Pattern 4).

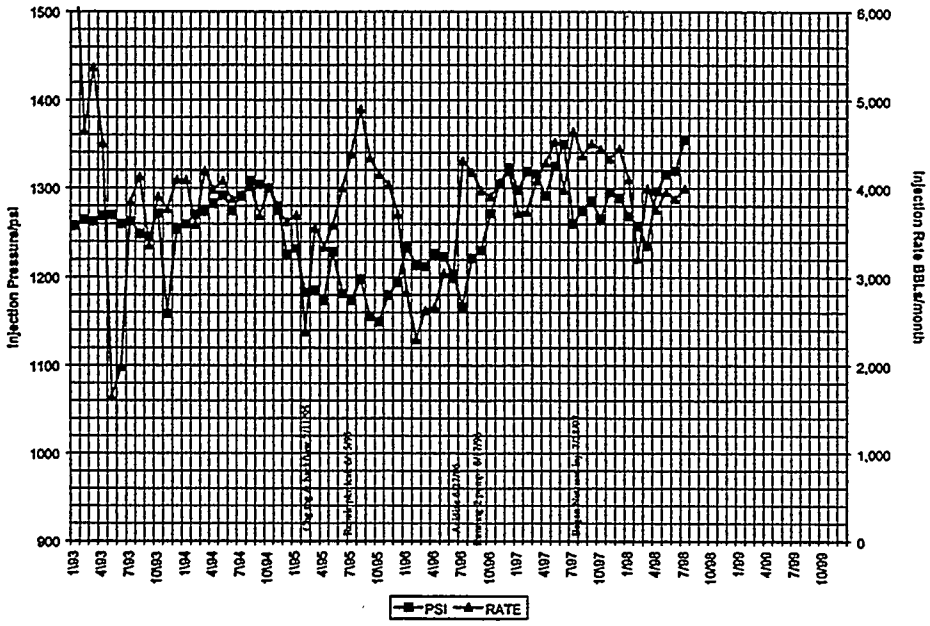

Figure A28. Injector Well 2-4 No. 1 (was injector for Control Pattern 1).

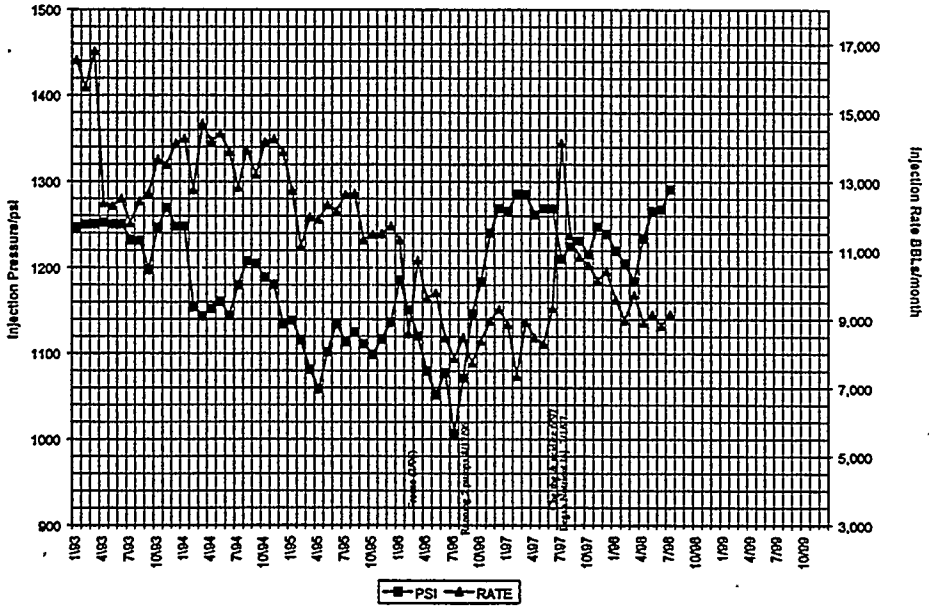

Figure A29. Injector Well 34-7 No. 1 (was injector for Control Pattern 2).

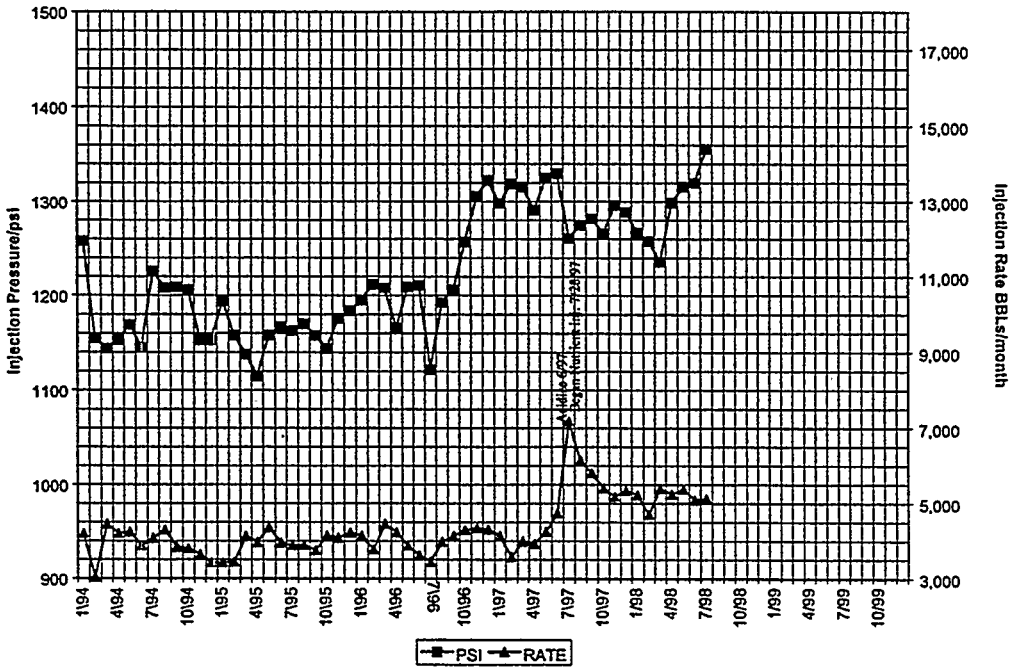

Figure A30. Injector Well 34-16 No. 1 (Not in Original Program).

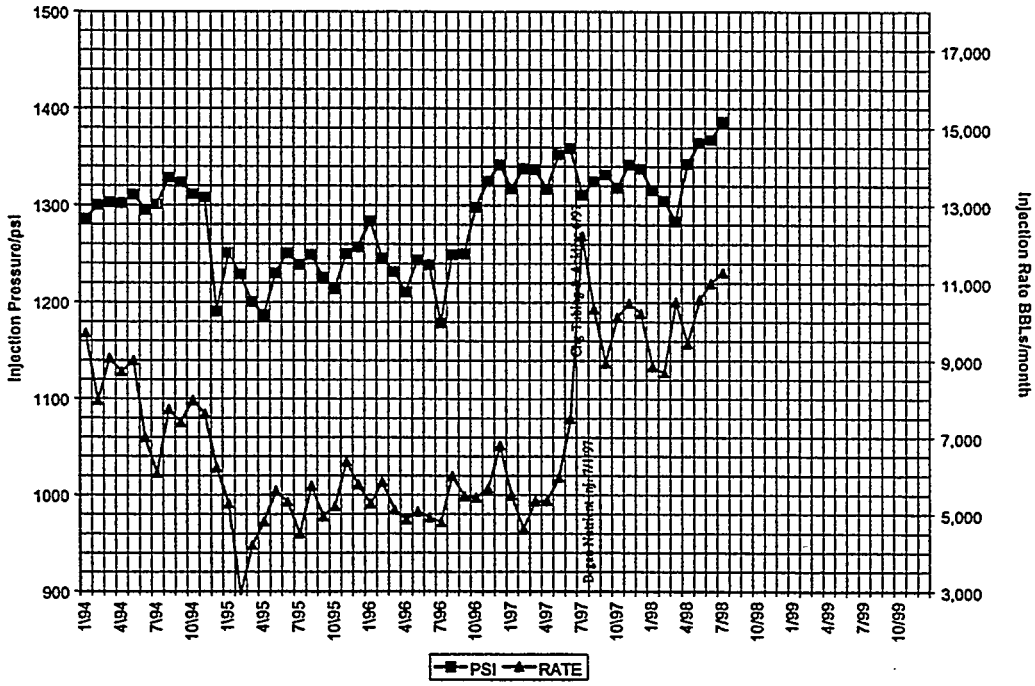

Figure A31. Injector Well 2-12 No. 1 (Not in Original Program).

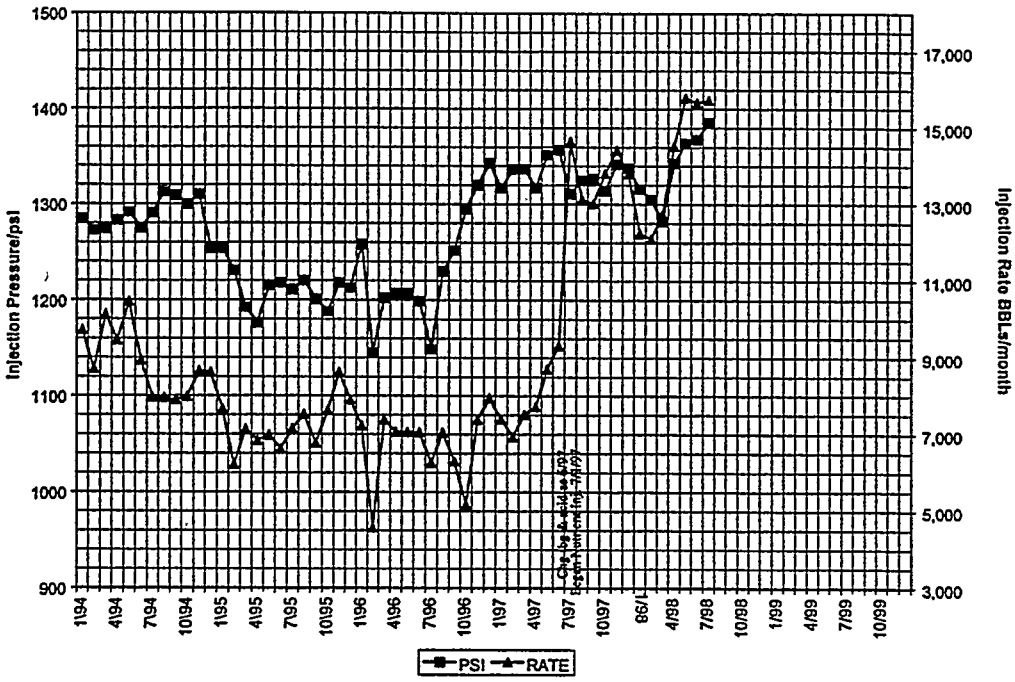

Figure A32. Injector Well 3-16 No. 1 (Not in Original Program).

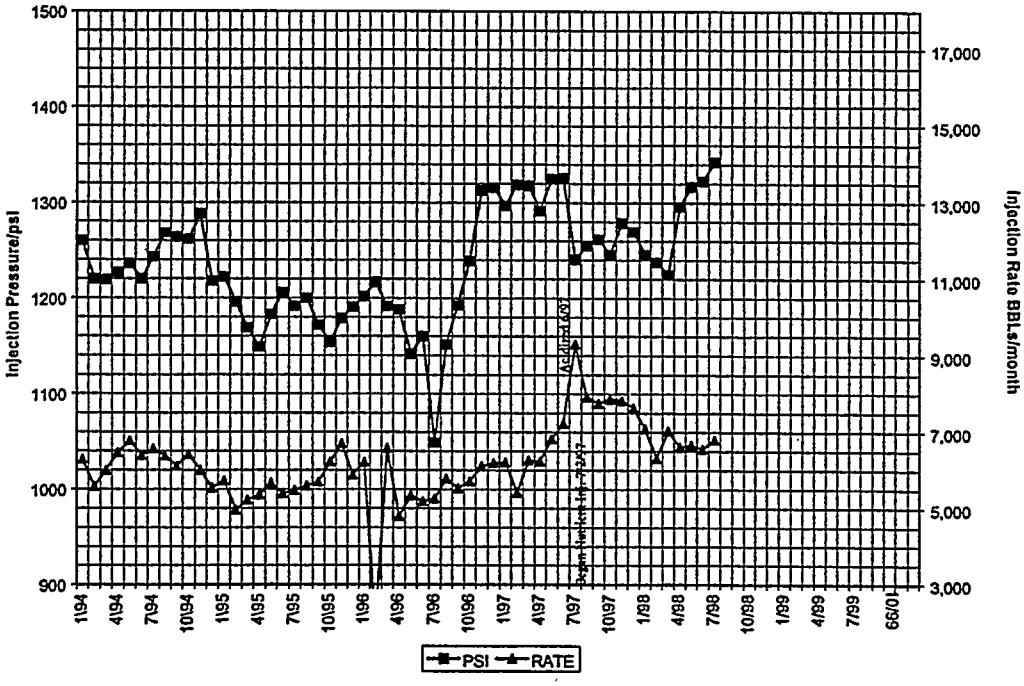

Figure A33. Injector Well 2-10 No. 2 (Not in Original Program).

DOE/BC/14958-15
(DE96001264)

FOSSIL ENERGY

GREEN RIVER FORMATION WATER FLOOC DEMONSTRATION PROJECT

RECEIVED
DEC 09 1997
OSTI

Final Report

By
Milind D. Doe
Dennis L. Nielson
John D. Lomax
John E. Dyer
Susan J. Lutz

November 1996

Performed Under Contract No. DE-FC22-94BC14958

Inland Resources, Inc./Lomax Exploration Co. and
University of Utah

Bartlesville Project Office
U. S. DEPARTMENT OF ENERGY
Bartlesville, Oklahoma

DISCLAIMER

This report was prepared as an account of work sponsored by an agency of the United States Government. Neither the United States Government nor any agency thereof, nor any of their employees, makes any warranty, expressed or implied, or assumes any legal liability or responsibility for the accuracy, completeness, or usefulness of any information, apparatus, product, or process disclosed, or represents that its use would not infringe privately owned rights. Reference herein to any specific commercial product, process, or service by trade name, trademark, manufacturer, or otherwise does not necessarily constitute or imply its endorsement, recommendation, or favoring by the United States Government or any agency thereof. The views and opinions of authors expressed herein do not necessarily state or reflect those of the United States Government.

This report has been reproduced directly from the best available copy.

Available to DOE and DOE contractors from the Office of Scientific and Technical Information, P.O. Box 62, Oak Ridge, TN 37831; prices available from (615) 576-8401.

Available to the public from the National Technical Information Service, U.S. Department of Commerce, 5285 Port Royal Rd., Springfield VA 22161

DISCLAIMER

Portions of this document may be illegible in electronic image products. Images are produced from the best available original document.

DOE/BC/14958-15
Distribution Category UC-122

Green River Formation Water Flood Demonstration Project

Final Report

By
Milind D. Deo, Dept. of Chemical & Fuels Engineering, University of Utah
Dennis L. Nielson, Energy & Geoscience Institute at the University of Utah
John D. Lomax, Inland Resources, Inc./Lomax Exploration Co.
John E. Dyer, Inland Resources, Inc./Lomax Exploration Co.
Susan J.Lutz, Energy & Geoscience Institute at the University of Utah

November 1996

Work Performed Under Contract No. DE-FC22-94BC14958

Prepared for
BDM-Oklahoma/
U.S. Department of Energy
Assistant Secretary for Fossil Energy

Edith Allison, Project Manager
Bartlesville Project Office
P.O. Box 1398
Bartlesville, OK 74005

Prepared by:
Inland Resources, Inc./Lomax Exploration Co.
and University of Utah

TABLE OF CONTENTS

LIST OF TABLES V

LIST OF FIGURES ..... **VI**

ABSTRACT ..... **IX**

EXECUTIVE SUMMARY ..... **X**

CHAPTER 1. INTRODUCTION **1**

REVIEW OF EARLY DRILLING AND **PRODUCTIONFROM** 1952 **THROUGH** *1996* *2*

SUMMARY OF YEARLY REPORTS *4*

SUMMARY OF YEARLY REPORT *1* *4*

***Summary** of **Yearly Report** 2* *7*

CURRENT REPORTING PERIOD *10*

CHAPTER 2. PRODUCTION REPORT **11**

CHAPTER 3. STRATIGRAPHY AND IMAGE LOG INTERPRETATION 17

REGIONAL GEOLOGY 17

THE GREATER MONUMENT BUTTE OIL FIELD 19

TYPE LOG (MONUMENT BUTTE FEDERAL #13-35) 20

REGIONAL STRATIGRAPHIC CORRELATION *22*

BOREHOLE IMAGING LOGS *22*

MAGNETIC RESONANACE IMAGING LOGS (MRIL) *24*

DESCRIPTION OF RESERVOIR UNITS *26*

Lower Douglas Creek Sandstone *26*

"A" ***Sandstone*** ***34***

"B" Sandstone *34*

"C" Sandstone *35*

" D' Sandstone *35*

FRACTURES 40

Fracturing in the LDC Sandstone Identified in Core *42*

Fracturing Identified Through FM! Logging *43*

FAULTING 44

CONCLUSIONS 45

REFERENCES 46

CHAPTER 4. RESERVOIR SIMULATION **89**

OBJECTIVES AND APPROACH **89**

INTRODUCTtON **90**

GEOSTATISTICAL MODELING 92

Data Employed *92*

Methodology *93*

RESERVOIR SIMULATION **95**

CONCLUSIONS **97**

REFERENCES **98**

CHAPTER 5. RESERVE CONSIDERATIONS AND ECONOMICS **109**

RESERVES **109**

ECONOMICS 112

Economics of the Monument Butte Unit *113*

Future Development Model *113*

Investment Units *114*

Type Decline Curve *114*

CONCLUSIONS *1 15*

CHAPTER **6.** TECHNOLOGY TRANSFER 119

LIST OF PAPERS AND PUBLICATIONS 119

CHAPTER 7. SUMMARY AND CONCLUSIONS 122

APPENDLY A. DETAILED L I T H O L O G I C LOG OF CORE AND X-RAY DIFFRACTION ANALYSES FROM TRAVIS FEDERAL #14A-28 .....

APPENDIX B. DETAILED L I T H O L O G I C LOG OF CORE AND X-RAY DIFFRACTION ANALYSES FROM TRAVIS FEDERAL #2-33 140

APPENDIX C. DETAILED LITHOLOGIC LOG OF CORE AND X-RAY DIFFRACTION ANALYSES FROM TRAVIS FEDERAL #6-33 146

LIST OF TABLES

TABLE 2-1. NEW WELLS DRILLED AS PART OF THIS PROJECT 12

TABLE 2-2. PRODUCTION FROM THE NEW PROJECT WELLS IN THE MONUMENT BUTTE UNIT AS OF 5/31/96 12

TABLE 2-3. PRODUCTION FROM SOME OF THE NEW WELLS IN THE MONUMENT BUTTE NORTHEAST EXPANSION AS OF 5/31/96 13

TABLE 2-4. WELLS IN THE MONUMENT BUTTE WEST EXPANSION: PRODUCTION AS OF 5/31/96 13

TABLE 2-5. WELLS IN THE MONUMENT BUTTE EAST EXPANSION: PRODUCTION AS OF 5/31/96 14

TABLE 2-6. PRODUCTION FROM SOME OF THE NEW WELLS IN THE MONUMENT BUTTE SOUTHEAST EXPANSION AS OF 5/31/96 14

TABLE 2-7. PRODUCTION FROM THE TRAVIS UNIT AS OF 5/31/96 14

TABLE 2-8. PRODUCTION FROM SOME OF THE NEW WELLS IN THE BOUNDARY UNIT AS OF 5/31/96 15

TABLE 3-1. LOGGED INTERVALS (FMI) OF WELLS IN THE GREATER MONUMENT BUTTE FIELD 53

TABLE 3-2. LITHOFACIES DESCRIPTION OF THE LOWER DOUGLAS CREEK SANDSTONES IN CORE FROM WELL TRAVIS FEDERAL #14A-28 54

TABLE 3-3. PHYSICAL PROPERTY MEASUREMENTS FROM THE LOWER DOUGLAS CREEK SANDSTONE 56

TABLE 3-4. PHYSICAL PROPERTY MEASUREMENTS OF THE B SANDSTONE RESERVOIR 57

TABLE 3-5. POROSITY AND PERMEABILITY MEASUREMENTS FROM THE D 1 RESERVOIR 58

TABLE 3-6. X-RAY DIFFRACTION ANALYSIS OF THE D1 RESERVOIR 59

TABLE 4-1. D 1 SANDS: DIFFERENT VARIOGRAM PROPERTIES 99

TABLE 4-2. DI SANDS: ADDITIONAL VARIOGRAM PROPERTIES 99

TABLE 4-3. B2 SANDS: DIFFERENT VARIOGRAM PROPERTIES 99

TABLE 4-4. B2 SANDS: ADDITIONAL VARIOGRAM PROPERTIES 100

TABLE 4-5. STATISTICAL VARIATIONS OF FLUIDS IN PLACE FOR SEVERAL GEOSTATISTICAL REALIZATIONS 100

TABLE 4-6. STATISTICAL VARIATIONS OF OOIP (MSTB) FOR B2 SANDS 100

TABLE 4-7. GEOSTATISTICAL PROPERTY SETS USED FOR RESERVOIR SIMULATIONS 101

TABLE 4-8. STATISTICAL VARIATIONS OF FLUIDS IN PLACE FOR THE EIGHT REALIZATIONS USED IN RESERVOIR SIMULATIONS ..... 10 I

TABLE 4-9. COMPARISON OF THE PERFORMANCE OFTHE MONUMENT BUTTE UNIT AT TWO DIFFERENT RESERVOIR SCALES 102

TABLE 4-10. STATISTICAL VARIATIONS IN PRIMARY PRODUCTIONS FOR EIGHT RESERVOIR SIMULATIONS USING PROPERTY SETS SHOWN IN TABLE 3 102

TABLE 4-11. STATISTICAL VARIATIONS IN TOTAL PRODUCTION FOR EIGHT RESERVOIR SIMULATIONS USING PROPERTY SETS SHOWN IN TABLE 3 103

List of Figures

FIGURE 2-1. THE THREE PROJECT UNITS, MONUMENT BUTTE, TRAVIS AND BOUNDARY WITH UPDATED WELL INFORMATION 16

FIGURE 3-1. MAP OFTHE UINTA BASIN SHOWING MAJOR FAULTS AND GILSONITE VEINS , AND THE LOCATIONS OF THE OIL FIELDS DISCUSSED IN THE TEXT 60

FIGURE 3-2. MAP OF THE MAJOR LARAMIDE TECTONIC ELEMENTS INFLUENCING THE UINTA BASIN 61

FIGURE 3-3. INTERPRETED LOG (TYPE LOG) OF THE MONUMENT BUTTE FEDERAL #13-35 SHOWING THE STRATIGRAPHIC NOMENCLATURE USED IN THIS REPORT 62

FIGURE 3-4. STRUCTURAL CONTOUR MAP CONSTRUCTED ON TOP OF THE DOUGLAS CREEK MARKER BED 63

FIGURE 3-5. PLANAR FEATURE INTERSECTING A WELL BORE AND BOREHOLE IMAGING LOG OF THE FEATURE 64

FIGURE 3-6. LOCATIONS OF WELLS DRILLED UNDER THE DOE PROGRAM FOR WHICH THERE IS DATA FROM THE FORMATION MICROIMAGER LOG 65

FIGURE 3-7. NET SANDSTONE ISOPACH MAP OF THE LOWER DOUGLAS CREEK SANDSTONE IN THE GREATER MONUMENT BUTTE AREA 66

FIGURE 3-8. SUMMARY OF LITHOFACIES AND INFERRED DEPOSITIONAL ORIGIN OF LOWER DOUGLAS CREEK SANDSTONE IN CORE FROM WELL TRAVIS FEDERAL #14A-28 67

FIGURE 3-9. DIP ANGLE AND AZIMUTH AS FUNCTION OF DEPTH INTERPRETED FROM THE FMI LOG IN THE LOWER DOUGLAS CREEK INTERVAL IN WELL TRAVIS FEDERAL # 14A-28 68

FIGURE 3-10. DIP VERSUS AZIMUTH (DVA) PLOT OF BEDDING FROM THE LOWER DOUGLAS CREEK FROM 5538 FT TO 5775 FT IN TRAVIS FEDEARL #14A-28 69

FIGURE 3-11. CORRELATED WELL LOGS OF LOWER DOUGLAS CREEK SANDSTONE IN THE TRAVIS UNIT..... 70

FIGURE 3-12. CROSS PLOT OF LOWER DOUGLAS CREEK NET SANDSTONE THICKNESS VERSUS DISTANCE BETWEEN THE B LIMESTONE AND THE CASTLE PEAK MARKER BEDS 71

FIGURE 3-13. NET SANDSTONE ISOPACH MAP OF THE B2 RESERVOIR 72

FIGURE 3-14. NET SANDSTONE ISOPACH MAP OF THE C RESERVOIR 73

FIGURE 3-15. NET SANDSTONE ISOPACH MAP OF THE D 1 RESERVOIR 74

FIGURE 3-16. LITHOLOGIC LOG OF THE D 1 RESERVOIR INTERPRETED FROM THE FMI IMAGES FROM MONUMENT BUTTE FEDERAL #9-34 75

FIGURE 3-17. LITHOLOGIC LOG OF THE D 1 RESERVOIR INTERPRETED FROM THE FMI IMAGE FROM WELL MONUMENT FEDERAL # 10-34 78

FIGURE 3-18. DIP VERSUS AZIMUTH (DVA) PLOT OF BED ORIENTATION FROM THE D 1 RESERVOIR IN WFT 1.S MONUMENT BUTTE FEDERAL #9-34 AND # 10-34 81

FIGURE 3-19. CORRELATED WELL LOGS OF THE D SANDSTONE INTERVAL IN THE MONUMENT BUTTE UNIT..... 82

FIGURE 3-20. FMI IMAGE OF A STRATIGRAPHICALLY BOUND FRACTURE FROM TRAVIS FEDERAL #5-33..... 83

FIGURE 3-21. TADPOLE PLOT OF ORIENTATION OF FRACTURES IMAGED BY THE FMI LOG IN BOUNDARY FEDERAL #12-21..... 84

FIGURE 3-22. ROSE DIAGRAMS SHOWING THE ORIENTATION OF FRACTURES IMAGED BY THE FMI LOG IN THE GREATER MONUMENT BUTTE OIL FIELD. DATA SHOWS THE ORIENTATION OF 140 FRACTURES..... 85

FIGURE 3-23. EQUAL ANGLE PROJECTIONS OF FRACTURES IMAGED BY THE FMI IN THE GREATER MONUMENT BUTTE FIELD..... 86

FIGURE 3-24. FMI IMAGE OF A MINOR FAULT IN WELL TRAVIS FEDERAL #5-33 87

FIGURE 3-25. EQUAL ANGLE PROJECTION OF POLES TO MINOR FAULTS MEASURED BY FMI LOGS IN THE GREATER MONUMENT BUTTE AREA 88

FIGURE 4-1. THE 12-SECTION AREA AROUND THE MONUMENT BUTTE UNIT USED IN RESERVOIR SIMULATIONS 104

FIGURE 4-2. POROSITY-PERMEABILITY CROSS PLOT 105

FIGURE 4-3. **THICKNESS DISTRIBUTION OF** DI **SANDS** IN THE **12-SECTION AREA** 105

FIGURE 4-4. **THICKNESS DISTRIBUTION FOR B2 SANDS** IN **THE 12-SECTION AREA** **106**

FIGURE 4-5. **POROSITY DISTRIBUTION OF** D I **SANDS** IN **THE 12-SECTION AREA** **106**

FIGURE 4-6. **PERMEABILITY DISTRIBUTION OF** D I SANDS IN THE **12-SECTION AREA** 107

FIGURE 4-7. **WATER SATURATION DISTRIBUTION FOR** D 1 SANDS IN THE **12-SECTION AREA** 107

FIGURE 4-8. **POROSITY DISTRIBUTION OF** B2 **SANDS** IN **THE 12-SECTION AREA** **108**

FIGURE 5-1. **INVESTMENT UNIT** IN **A FIVE-SPOT WATER FLOOD DEVELOPMENT** 117

FIGURE 5-2. **HISTORICAL (AVERAGE) MONUMENT BUTTE DECLINE CURVE** 1 17

FIGURE 5-3. **THE DECLINE CURVE USED FOR THE ECONOMIC ANALYSIS** **118**

Abstract

The objectives of the project were to understand the oil production mechanisms in the Monument Butte unit via reservoir characterization and reservoir simulations and to transfer the water flooding technology to similar units in the vicinity, particularly the Travis and the Boundary units. Comprehensive reservoir characterization and reservoir simulations of the Monument Butte, Travis and Boundary units were presented in the two published project yearly reports. The primary and the secondary production from the Monument Butte unit were typical of oil production from an undersaturated oil reservoir close to its bubble point. The water flood in the smaller Travis unit appeared affected by natural and possibly by large interconnecting hydraulic fractures. Water flooding the boundary unit was considered more complicated due to the presence of an oil water contact in one of the wells.

The reservoir characterization activity in the project basically consisted of extraction and analysis of a full diameter core, Formation Micro Imaging (FMI) logs from several wells and Magnetic Resonance Imaging (MRI) logs from two wells. In addition, several side-wall cores were drilled and analyzed, oil samples from a number of wells were physically and chemically characterized (using high-temperature gas chromatography), oil-water relative permeabilities were measured and pour points and cloud points of a few oil samples were determined. The reservoir modeling activity comprised of reservoir simulation of all the three units at different scales and near well-bore modeling of the wax precipitation effects.

Core analyses and examination of the results of the FMI logs were the principle tools utilized for the geologic characterization of the unit. Oil production from most units in the region is from multiple, largely distinct sand bodies. The geologic study identified the Lower Douglas Creek reservoir (which contributed to most of the production in the Travis unit) to form isolated lenses that can reach over 100 feet of net thickness. Localized nature of this reservoir combined with lithologic heterogeneity and complex architecture makes this a difficult water-flood candidate. The DI reservoir on the other hand, which contributed to over 2/3"' of the production in Monument Butte, is laterally continuous and lithologically homogeneous.

The reservoir characterization efforts identified new reservoirs in the Travis and the Boundary units. The reservoir simulation activities established the extent of pressurization of the sections of the reservoirs in the immediate vicinity of the Monument Butte unit. This resulted in a major expansion of the unit and the production from this expanded unit increased from about 300 barrels per day to about 2000 barrels per day.

The technology transfer component of the project was very successful. Ten technical papers and presentations resulted as a direct consequence of this project. Several new water floods were begun in the Greater Monument Butte region, modeled essentially after the Lomax/Inland Monument Butte flood.

Executive Summary

Despite successful water floods in nearby Wonsits Valley, Walker Hollow and Red Wash fields, secondary recovery via water flooding in the Monument Butte unit was assessed to be technically unfeasible. The fluvial deltaic geologic environment, low permeabilities of sands and waxy nature of the crude were some of the attributes that contributed to this preliminary assessment. The reservoirs in this region are undersaturated with the initial reservoir pressure close to the initial bubble point pressure resulting in a primary recovery of only about 5%. Thus, for the economic viability of any field in the region, some form of secondary recovery is a necessity. Based on these considerations, water flood operations were begun in Monument Butte. Contrary to initial expectations, the flood was quite successful and the production rate from the unit increased almost by an order of magnitude. The objective of this project was to learn about the Monument Butte flood and transfer the technology to other units/fields in the region in general and to the Travis and the Boundary units in particular.

The project essentially had three central activities.

- Drilling new wells to identify the expanse of each of the units.
- Performing detailed reservoir characterization using conventional and modern logging methods. Characterization also included fluid composition measurements, porosity-permeability measurements and determination of oil-water relative permeabilities.
- Understanding the reservoir performance using reservoir simulation.

Understanding of the performance of the Monument Butte water flood contributed toward a fast-paced unit expansion. More than 30 additional wells were drilled (by Lomax Exploration Company/Inland Resources Inc.) and production from the expanded unit has increased almost by an order of magnitude since the project began. The reservoir performance, both in the primary

and secondary phases was determined to be typical of an undersaturated oil reservoir. Simulations revealed that almost 30% of the injected water had migrated outside the boundaries of the unit. This had led to the pressurization of the outlying areas. Additional drilling and good responses from most wells corroborated this hypothesis. The Formation Microimaging Logs (FMI) and the Magnetic Resonance Imaging Logs helped identify thin pay zones saturated with hydrocarbons. The reservoir was modeled at various scales and images generated at different times were animated to create a video movie.

The FMI log in one of the wells in the Travis unit helped identify new reservoir horizons and oil was produced from these intervals in the primary mode. The water flood in the Travis unit was hampered by the presence of Iarge natural fracture systems which may have intersected the hydraulic fractures to create to high permeability conduit for water. Well spacing of only 20 acres may have exacerbated this problem. Whether water flood will ultimately be successful in this unit remains to be seen.

The primary production in the Boundary unit was also expanded. A 28-layer reservoir model was used to match the primary performance of the unit. Oil-water contact in one of the wells complicated the modeling process. The model revealed that hydraulic fracturing needs to be undertaken with care since there is a chance that the fracture may intersect the underlying aquifer. At the time of this writing, the C-sand interval in Boundary was being water flooded. Considering the expanse of the reservoir, the chances of a successful water flood in Boundary are fairly good.

A near well-bore analysis of the water injection process into a reservoir containing waxy crude was performed. A thermodynamic model was used to match the pour point of the Monument Butte crude oil. An analytical model used to study the effect of injection on wax precipitation

and oil recovery revealed that near well-bore wax precipitation was likely and that this would lower the ultimate recovery by about 5%. It was also determined that this effect would be felt late in the life of the flood.

Several new water floods were begun in the Greater Monument Region directly as a result of this project. Most of the technical papers and reports resulting from the project found wide circulation. Thus, the success of the Monument Butte unit water flood could be attributed to:

- Lateral continuity of the D I and the B2 sand bodies.
- Use of the best producers as injectors to get the reservoir pressurized quickly.
- Use of fresh water to maintain reservoir fluid compatibility
- Well designed hydraulic fracturing to provide enhanced injectivity and producibility. The

geologic characterization revealed that some of the sand bodies were not amenable to water flooding due to their lithologic complexity. The measured PVT properties showed that the initial reservoir pressure was close to the initial bubble point pressure. These measurements provided an accurate initial oil formation volume factor for oil in place computations. The fluid-rock properties measurements showed that the relative permeability to water at residual oil saturation was very low (between 0.07 and 0.1) and declined rapidly as the oil saturation increased. This explained, to a certain extent, the low water cuts in the Monument Butte water flood at a fairly mature stage.

The project was a demonstration of well-designed water flood technology. The methods and techniques employed in the project will be applicable to a large area (about 300 square miles) in the Greater Monument Butte Region.

Chapter 1. Introduction

In April, 1981, a discovery well, the Federal #1-35, was drilled in the Monument Butte field in Utah (Fig. 3-1) and completed in the Douglas Creek Member of the Green River Formation. Development proceeded on 40-acre spacing, concentrating principally on the "D" Sandstone (Lomax terminology). Primary production was anticipated to recover 309,000 STB of oil, or *5.5%* of the 5.67 million STB of the oil in place. Using primary methods, field production declined to 45 bbl/day. In order to improve the recovery of oil from this reservoir, Lomax Exploration Co. initiated a water flood. There was some historical precedence for this type of secondary recovery project in the Wonsits Valley field in the eastern part of the Uinta Basin. However, the technique had never been attempted in the vicinity of the Monument Butte field. Some reservoir engineering studies had predicted the procedure would not be successful based upon reservoir heterogeneity, the high paraffin content of the crude oil, and the low energy of the reservoir.

In 1987, Lomax Exploration Company formed a secondary recovery unit in order to initiate a water flood. Primary production had declined to 30 bbls/day as the flood was initiated. The flood proved successful and, as of November, 1991, production at Monument Butte had increased to 330 bbls/day. As a result of this water flood, estimated ultimate recoverable reserves of the "D" sandstone reservoir alone have increased from 300,000 bbls to over 1.2 million bbls, and recovery has increased from 5% to an estimated 20% of the oil in place. The water flood has since then expanded to include other sandstone reservoirs in the lower portion of the Green River Formation.

The three primary units which were the targets of this study (Monument Butte, Travis and Boundary) are all located in east-central Utah in Duchesne county. Details of the unit, unit maps, etc. were presented in the two earlier yearly reports (U.S. DOE, 1994; U.S. DOE, 1995). The early drilling activity in the region is summarized in the following paragraphs.

Review of Early Drilling and Productionfrom 1952 through 1996

In Townships 8 & 9 South, Ranges 15, 16, & 17 East, of Duchesne County, Utah; twenty five wells were completed for production during the period of 1952 through 1980. As of 01\01\84, the first annual and monthly production records reported by Dwight's, the cumulative production from the twenty five wells was 870,098 BBLS oil, and 566,635 MCF gas. Through 1983 these wells averaged cumulative production of 34,804 BBLS oil. During 1984 an average of fourteen wells were still producing, and total production for 1984 was 20,148 BBLS oil, and 52,432 MCF gas, the wells each were averaging approximately 4 BOPD. As of 12/31/1995 there were still ten wells producing, and the cumulative production for the twenty five wells was 1,076,688 BBLS oil, for an average of 41,187 BBLS per well over a forty three year period.

The high oil prices of the early eighties triggered new activity in the area, the following table indicates the completion activity since 01/01/1980:

Year	Completed wells	Comments
1980	3	
1981	18	activity created by high oil prices.
1982	46	continued development under high oil prices.
1983	34	
1984	20	Activity slowing down due to lower oil prices.

1985	13	Operators concerned about high decline rates.
1986	3	Operators concerned about reserve recovery.
1987	3	Primary recovery of the oil in place averaged less than 5%. Lomax pilot water flood started in November on the Monument Butte Unit.
1988		Decline arrested, production increased from 35 to 80 BOPD.
1989	4	Water flood production increased from 80 to 200 BOPD.
1990	12	Eleven well field development offsetting MBU by a minority partner in the Unit. MBU production increased to300 BPOD.
1991	3	In August Lomax formed the Travis Unit for its second water flood attempt.
1992	4	In July Lomax formed the Boundary Unit, and in October the Department of Energy-sponsored water flood test program, a three year field test on three secondary recovery units was approved.
1993	27	On the basis of the continuing success of the Monument Butte Unit, other operators started to develop water flood projects, and increased development drilling associated with water flood projects.

1994	34	Increased water flood activity, and development wells drilled to define new water flood projects.
1995	47	Extending water floods, and development wells defining new water flood areas.
1996	112*	Based on personal communication with active operators in the area under discussion. Forty five wells have been drilled so far this year and at least three rigs are currently running.

Summary of Yearly Reports

As part of this project, two yearly reports were published (U.S. DOE , 1994; U.S. DOE, *1995).*

Summary of Yearly Report 1

At the start of the project, Monument Butte unit was the most developed of the three units and currently had *22* wells, eight injectors and the rest producers. The unit contained about *9* MMstb of original oil in place (OOIP) primarily in two zones, the D and the B. About *4.5% of* the OO1P had been recovered by primary production, when the water flood was initiated in late 1987. Two wells were drilled in Monument Butte, *10-34* and *9-34.* Well *10-34* drilled in late 1992, did not appear to be affected by the water flood. The production from *10-34* resembled production from a well producing from a partially depleted undersaturated reservoir. Well *9-34* drilled in late *1993* penetrated producing sands and appeared to be producing from zones which were pressurized by the water flood. The production performances for these two wells were logical considering the distances of these wells from injection wells, *5-35* and *13-35.*

Formation Micro-Imaging (FMI) logs were obtained for these wells for better geologic understanding. Logs and stratigraphic sections from several wells were analyzed and a geologic model of the reservoir was constructed.

As part of the comprehensive engineering study of the unit, a general purpose core flooding, pressure-volume-temperature (PVT) system capable of measuring reservoir fluid properties was designed and built. Compositions of the Monument Butte oils were measured using a novel capillary chromatographic method. Most of the oils contained about 30% C„ + material. All the relevant reservoir fluid properties were measured. The geologic data and the reservoir fluid property data were integrated into a volumetric assessment and a detailed reservoir simulation study. The volumetric assessment was based on simple reservoir engineering calculations (zero-dimensional). Results from the simple volumetric study were found consistent with the comprehensive three-dimensional multiphase reservoir simulation study. The reservoir simulation study was successful in matching field history. The overall field production data was matched by the reservoir simulator within 10% and the individual well data were matched within 15%.

A thermal well bore model was developed to examine the temperature profiles in the well bore. The model showed that under the conditions of injection, injected water could be reaching the perforations at temperatures 50°-70° F lower than the reservoir temperature. Due to the high paraffin contents of the reservoir fluids, the study concluded that there was a strong possibility of paraffin deposition in the vicinity of the well bore.

The Travis unit had produced about 245 Mstb of oil and 1.08 MMMscf of gas in primary production. Most of the production was from the Lower Douglas Creek (LDC) sand. Injection in well 15-28 at 1000 stb/d appeared to pressurize the reservoir. However, when well 14-28a was

drilled in late 1992, injection in 1·5-28 had to be stopped due to water channeling in 14a-28. Producer 10-28, also had a water channeling problem. The new FMI logs in 14a-28 showed that LDC was extensively fractured. The fracture orientations were found to coincide with the channeling paths. The new logs in 14a-28 also revealed the existence of thin, but producible D sands. Based on this information, 14a-28 and also wells 14-28 and 10-28 were completed in the D-sand interval. The production from this zone was similar to production from an undersaturated reservoir close to the initial fluid bubble point (about 5% of OOIP recovery). Once the production from 14a-28 declined, it was-converted to an injector, injecting about 300 stb/d into the D-sands. Well 15-28 was started back on injection at a slower rate of about 300 stb/d, and well 3-33 was converted to an injector, injecting about 300 stb/d into LDC. The surface pressure data showed that the reservoir was being gradually pressurized. The water flooding operations in Travis appear to be dominated by natural or created (hydraulic) fractures. An engineering study of the Travis unit, similar to the Monument Butte was conducted. The geologic data and reservoir fluid properties were integrated into a dual-porosity, dual-permeability fractured reservoir model. The model provided a good match with the primary production history and predicted increased oil production on water flooding. Well 10-20 drilled in the Boundary unit did not intersect producing sand layers. This illustrated the risks involved in operating in fluvial deltaic environments.

The results of one of the Monument Butte unit simulation studies resulted in a paper SPE 27749, which was presented at the Improved Oil Recovery Symposium in Tulsa, Oklahoma in April 1994. The success of the water flood in the Monument Butte field and an understanding of the underlying mechanisms as a result of this project, resulted in the initiation of two major water floods in the Uinta Basin by Equitable Resources Inc. and by Pacific Gas and Energy.

Summary of Yearly Report 2

Lomax Exploration Company became a fully owned subsidiary of Inland Resources Incorporated. The project was continued by the new management team in partnership with the University of Utah (Earth Sciences Resources Institute and the Department of Chemical and Fuels Engineering).

All of the new wells drilled in the Monument Butte unit (10-34, 9-34 and 7-34) were reasonably successful. At the end of May 1996, well 10-34 had a cumulative oil production of 27,197 bbls. Cumulative production for wells 9-34 and 7-34 were 18,387 bbls and 19,592 bbls respectively. That in itself demonstrated the viability of water flood and pressure maintenance in fluvial deltaic reservoirs which were barely undersaturated (whose initial bubble point pressure was close to the initial reservoir pressure). The production from the unit appeared limited due to water injection limitations. The reservoir modeling showed that about a third of the injected water was migrating beyond unit limits. The response to the water flood was also affected by injection into sands which did not have direct communication with other wells. Finally, hydraulic fracturing also appeared to have played a role in determining the response of some of the wells. By December 31, 1994, the water flood had already produced 142% of the primary production and *34%* of the gas production. A cumulative gas oil ratio of about 940 scf/stb in comparison to the initial GOR of about 500 scf/stb shows that oil is still being produced from zones which are above the current bubble point and from zones which have free gas.

Continued water injection in the Lower Douglas Creek (LDC) sand pressurized this reservoir in the Travis unit. Surface pressures of nearly 2000 psia were reached in the two injectors, 15-28 and 3-33, indicating bottom hole pressures of about 4600 psia. Communication problems

between the injectors and producers (2-33 and 10-28) appeared to have caused the slow response to the water flood being observed in this unit. The well 5-33 drilled in the unit did not intersect the LDC sandstone. However, the well was completed in other sands.

New production and injection wells were planned for the Boundary unit. There was no field activity in the unit in 1994.

Detailed geologic and reservoir characterization of all the three units was continued. The FMI logs showed the fine structures in the sand bodies. Careful analysis and interpretation of these logs revealed detailed fracture information. The fractures were found oriented mostly in the east-west direction. A comprehensive core description of the core from well 14a-28 was also completed.

The reservoir simulation and modeling of all the three units was also continued. The Travis unit was modeled using three alternative models; a homogeneous model with locally adjusted permeabilities, a fractured model (dual-porosity, dual permeability) and a hydraulically fractured model. All of the three models were tuned to match the primary production data from the unit and were then used to predict the water flood response. All the three models predicted that a response to the water flood should have been observed in well 2-33 had the sands been in good communication. The model predictions were slightly different in terms of production rates and water oil ratios.

From the experience gained in modeling the Monument Butte and the Travis units, a comprehensive reservoir model of the Boundary unit was constructed. Data at 2 foot resolution was incorporated in the model. The model had 15 oil bearing layers separated by 13 non oil bearing layers for a total of 28 layers. The water-oil contact in one of the wells and the fact that the extent of the aquifer was not established, made this model the most complex of the three

reservoir models. The model oil and gas predictions matched the field results reasonably well. The logs for well 13-21, the Iargest producer in this unit did not show a water-oil contact. But the oil production from well 13-21 and the slow decline from that well could riot be explained on the basis of sands present in that well. Hence it was determined that the production from 13-21 was aided by water influx from the same aquifer which was seen in the logs of well 7-20. It was also determined that 13-21 communicated with this aquifer through its hydraulic fracture.

It was shown in the last yearly report that the crude oils from these reservoirs are extremely waxy with cloud points of about 120^0 F. Determining the conditions under which wax precipitation occurs and finding the effect of this precipitation on oil recovery were important tasks in this project. It was also shown that the injected water reaches the perforations at temperatures much lower than the formation temperatures. The thermodynamic aspects of these oils and wax formation at these temperatures as analyzed in this report and it was shown that wax precipitation models could be simplified to give equivalent results. It was also shown that wax appearance data as well as wax and oil composition data would be required to tune these models.

A first-generation model based on the generalized method of characteristics was developed. This model showed that wax precipitation causes lower oil recoveries and that the effect of precipitation is felt only in the later part of the water flood. For the parameters chosen in this study, the recovery reduction was nominal (4%), but for a certain combinations of parameters, the reduction in oil recovery could be as high as 10%.

The technology transfer aspect of the project was continued actively with presentation in the SPE-DOE Improved Oil Recovery Symposium in Tulsa, poster sessions at the AAPG meeting in Denver and the SPE Annual Fall Meeting in New Orleans, and a presentation at the International Oilfield Chemistry Symposium in San Antonio.

Current Reporting Period

The expansion of the Monument Butte unit on the west, north-east and on the east portions of the unit continued at a fast pace. A total of 30 wells were drilled either in the unit or in the expansion areas. Reservoir characterization continued with emphasis on gaining understanding regarding the expanse of each of the reservoir units. Reservoir modeling was also performed on areas much larger than the individual units. In this final report, expansion of the Monument Butte unit is summarized along with new production results. Detailed geologic and stratigraphic interpretation is presented next. Geostatistical modeling and large-scale reservoir simulations are the subject of the next chapter. An economic analysis, and project summary and conclusions complete this final report.

References

U. S. DOE 1994, Green River Formation Water Flood Demonstration Project, DE-FC22-93BC14958, Yearly Report, 1994.

U. S. DOE 1995, Green River Formation Water Flood Demonstration Project, DE-FC22-93BC14958, Yearly Report, 1995.

Chapter 2. Production Report

Wells drilled as part of this project are summarized in Table 2-1. Production from the new wells drilled, the expansion wells and unit productions are summarized in Table 2-2. The Monument . Butte unit has produced more than twice the oil produced during primary. The expansion units have also performed remarkably well. The sections involved in the unit expansion are shown in Figure 2-1. The wells in close proximity of the original flood, as expected, have responded most favorably with lower overall gas oil ratios. Most of the new wells drilled in Boundary have been successful. In Travis, the Lower Douglas Creek water flood is still a question mark. However, about 60,000 barrels of oil has been produced from newly identified reservoirs in Travis.

Table 2-1. New wells drilled as part of this project

Unit	Well	Date Drilled	Advanced Logs
Monument Butte	10-34	10/92	FMI, MRIL
Travis	14a-28	10/92	FMI
Boundary	10-20	4/93	None
Monument Butte	9-34	11/93	FMI, MRIL
Monument Butte	7-34	11/94	FMI, MRIL
Travis	5-33	10/94	FMI
Boundary	12-21		FMI

Table 2-2. Production from the new project wells in the Monument Butte unit as of 5/31/96

Well Number	Date on line	Oil Produced (Barrels)	Gas Produced (MCF)
10-34	11/26/92	17,330	27,197
9-34	01/09/94	22,566	18,387
7-34	12/24/94	13,668	19,592
2A-35	04/18/95	17,923	6,295
Unit	-	1,135,078	2,263,102

Table 2-3. Production from some of the new wells in the Monument Butte northeast expansion as of 5/31/96

Well Number	Date on line	Oil Produced (Barrels)	Gas Produced (MCF)
11-25	1995	18,388	21,579
12-25	1995	3,989	10,045
13-25	08/22/95	10,712	17,449
14-25	10/14/95	15,181	41,037
16-26	10/28/95	14,093	22,073

Table 2-4. Wells in the Monument Butte west expansion: Production as of 5/31/96

Well Number	Date on line	Oil Produced (Barrels)	Gas Produced (MCF)
3-34	1995	4,857	7,730
5-34	09/11/95	23,185	76,824
6-34	04/08/95	4,387	20,103

Table 2-5. Wells in the Monument Butte east expansion: Production as of 5/31/96

Well Number	Date on line	Oil Produced (Barrels)	Gas Produced (MCF)
3-36	10/28/95	4,038	7,528
10-36	10/16/95	26,470	29,883
14-36	06/20/95	20,558	39,725
15-36	10/14/95	6,437	3,996
16-36R	09/13/95	14,623	21,992

Table 2-6. Production from some of the new wells in the Monument Butte southeast expansion as of 5/31/96

Well Number	Date on line	Oil Produced (Barrels)	Gas Produced (MCF)
4-1	1995	2,582	4,337
5-1	1995	10,955	31,136
8-2	12/02/95	14,590	26,271

Table 2-7. Production from the Travis unit as of 5/31/96

Well Number	Date on line	Oil Produced (Barrels)	Gas Produced (MCF)
5-33	12/12/94	5,712	24,297
Unit	-	300,995	1,424,193

Table 2-8. Production from some of the new wells in the Boundary unit as of 5/31/96

Well Number	Date on line	Oil Produced (Barrels)	Gas Produced (MCF)
10-21	09/28/95	13,264	24,297
12-21	01/21/95	4,305	8,788
Unit	-	224,828	697,360

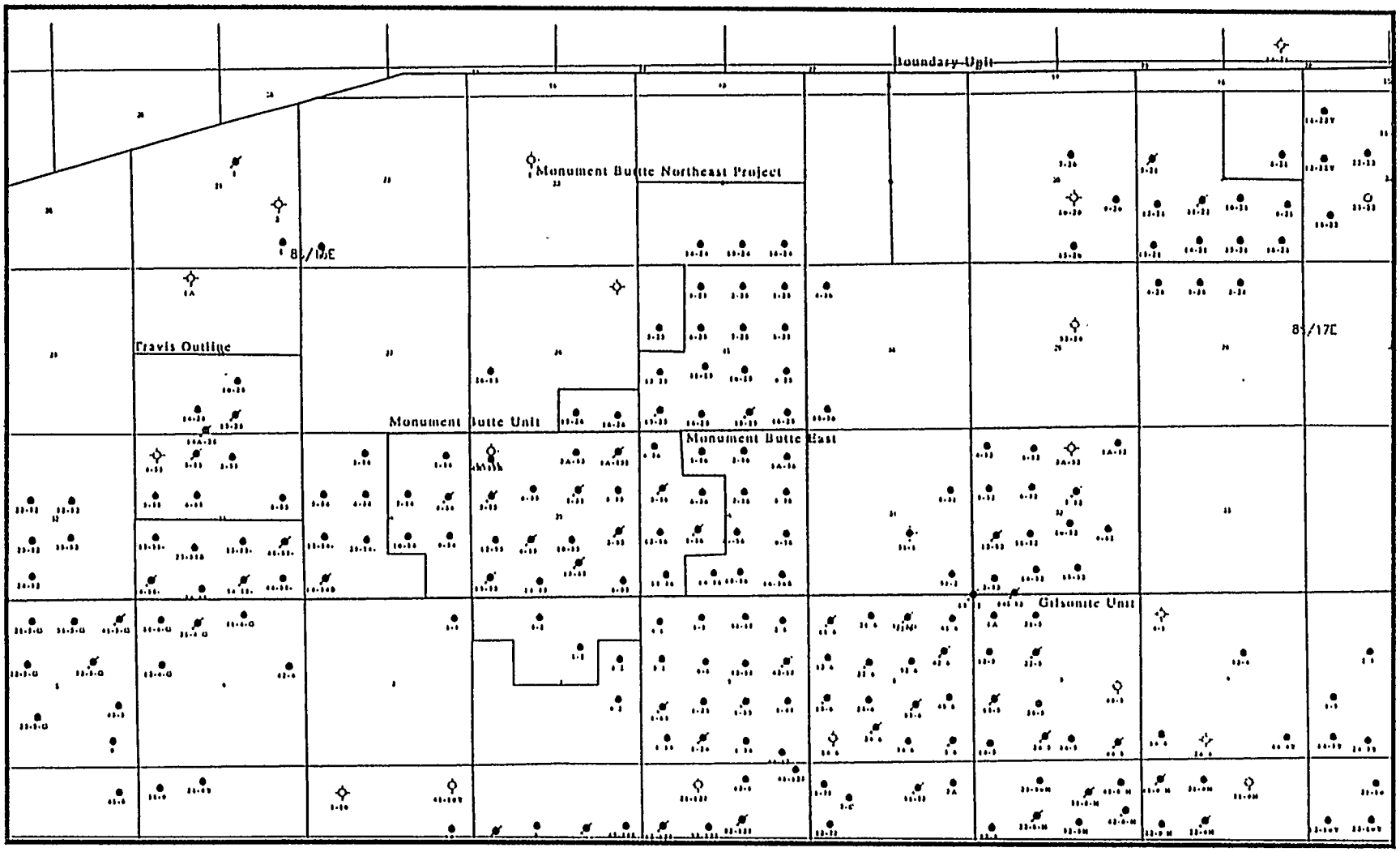

Figure 2-1. The three project units, Monument Butte, Travis and Boundary with updated well information.

Chapter 3. Stratigraphy and Image Log Interpretation

This project was initiated with the U. S. Department of Energy to improve the characterization of the sandstone reservoirs. Initially, the depositional origin of the reservoirs was poorly understood and all the sands were thought to be of fluvial origin. Correlation of sandstone bodies between adjacent wells was often difficult. And fracturing was not thought to play a significant role in reservoir heterogeneity in this part of the basin.

REGIONAL GEOLOGY

The Monument Butte oil field is located in the central portion of the Uinta Basin, Utah (Fig. 3-1). Reservoirs are principally developed in the Eocene Green River Formation. Recent summary articles present the level of understanding of the tectonic, climatic and sedimentological evolution of the basin (Fouch et al., 1992).

The structural development of the Uinta Basin started with the withdrawal of the Cretaceous inland sea and the beginning of the Laramide orogeny (Nary and Currie,1982). The late Cretaceous North Horn Formation is stratigraphically the lowest unit to reflect subsidence of the basin (Fouch, 1976). Within this basin, Lake Uinta formed and became the site for the deposition of both reservoir and source rocks in the Greater Monument Butte field. The uplift of the Uinta Mountains on the northern boundary of the lake provided a high relief source area. This uplift took place along high-angle reverse faults that trend in an east-west direction. At the southeastern boundary of the basin, the Uncompahgre uplift trends to the northwest (Fig. 3-2). Fractures parallel to this trend are present in the rocks of the Monument Butte area, and, on a regional basis, form the hosts for gilsonite veins. In general, fracture orientations will change within the basin and be related to the older structural trends in the vicinity. Narr and Currie show

that regional joints follow north-south, northwest-southeast and northeast-southwest trends. The sedimentary rocks of the basin have undergone a single cycle of deposition, subsidence and uplift. The Uinta Basin developed in an asymmetric fashion which has, in general, controlled the style of sedimentation. High-angle normal faults form the northern boundary adjacent to the Uinta Mountains. This resulted in a source area of relatively high relief and the deposition of a coarser-grained stratigraphic section. The southern portion of the basin was a zone of low relief and finer-grained sedimentary deposits.. The half graben sedimentation style is similar to that observed in many modern (Cohen, 1990; Johnson et al., 1995) and ancient (Lambiase, 1990) lacustrine basins. Oil and gas bearing strata of the Eocene Lower Green River Formation consist of fluvial-deltaic deposits. Sandstones were deposited along shorelines, in deltas, and in distributary and fluvial channels. Carbonates were deposited in marginal lacustrine environments. Along the southern and eastern margins of the Uinta Basin, fluvial-deltaic sediments of Eocene age represent over one-third of the total stratigraphic section. In the southern Uinta Basin, oil and gas reservoirs are concentrated along an east-west paleoshoreline trend that extends for a distance of about 60 miles. Within this zone, sandstones form fluvial-deltaic reservoirs. The southern, updip portion of the productive area is characterized by the transition from marginal lacustrine deposits into clayey lower delta plain facies. The northern boundary of the fairway is characterized by the transition from sandy shoreline deposits to fine-grained open lacustrine rocks. The open lacustrine facies consist of nonreservoir organic-rich mudstones and calcareous claystones. The fairway is present across portions of both Uintah and Duchesne counties, where it extends from the Greater Red Wash field westward to the Brundage Canyon field. The Greater Red Wash

field, discovered in 1950, occcupies the easternmost portion of the fairway in which numerous marginal lacustrine sandstone and carbonate reservoirs have combined production of over 135 million STBO. The western portion of the fairway has undergone limited development and is characterized by small, localized oil fields.

Within the project area, there are two major structural trends observed on the surface, gilsonite veins and the Duchesne fault zone. The Duchesne fault zone (Fig. 3-1) is an east-west trending zone of surface fracturing and faulting (Ray et al., 1956). The zone has been traced for a total distance of 42 miles and has a width of up to 2 miles. The mapped fault zone is located to the north of the Monument Butte unit, approximately through Lomax's Boundary Unit. There is little information published on the character of this zone. Nielson et aI. (1993) showed that fracturing associated with the Duchesne fault was prominent in the Duchesne oil field and had important controls on production of oil from that field.

Northwest trending gilsonite veins form another obvious structural element in the vicinity of Monument Butte (Fig. 3-1). The Pariette Mine produced gilsonite in the northeast corner of section 31, about 1.5 miles to the east of the Monument Butte Unit. Both Verbeek and Grout (1992) and Monson and Parnell (1992) ascribe the formation of these dikes to high formation pressures that cause natural hydraulic fracturing and injection of liquid bitumen into the fracture zones.

THE GREATER MONUMENT BUTTE OIL FIELD

This enhanced recovery project specifically targeted sandstone reservoirs in the Travis, Monument Butte and Boundary units (Fig. 3-1) that constitute the Greater Monument Butte field. Producing reservoirs within the Green River Formation are discontinuous sandstone bodies, hence, correlation of individual sandstones between adjacent wells is often difficult. The

common practice in this portion of the basin is to formulate a stratigraphic nomenclature that is consistent within a field. Regional marker beds have been identified (Fouch, 1981; Colburn et al., 1985) and can be used in correlating between producing fields.

Although the discontinuous nature of many of the sandstone reservoirs has made it difficult to predict their thickness before drilling, the large number of reservoir units has allowed most wells to be completed for production.

Type Log (Monument Butte Federal #13-35)

Figure 3-3 is a log of Monument Butte Federal #13-35 that shows the local stratigraphic nomenclature that will be used in this report. Note that this nomenclature is specific to Lomax Exploration. Other companies active in the area use different terms, but the stratigraphic markers used are Iargely the same. The sands between the marker horizons have been designated A, B, C, D, and Lower Douglas Creek. These designations will give a gross picture of the sandstone thickness within the interval, but a more detailed breakdown of A 1, A2, etc. is needed to understand the geometry of the sandstone bodies that will be the subject of the water flood.

The top of the Wasatch Formation is located at 6357 feet in the type log. There is no oil production from the Wasatch Formation in the Lomax property although it is productive for gas in many fields in the basin. Above this is a thick carbonate sequence that is termed the basal Green River Limestone. This unit is approximately 150 feet thick.

Above the basal Green River Limestone is a section of sandstones and carbonates that is termed the Black Shale Facies (Colburn et al., 1985). In Lomax's terminology, this is the Castle Peak section, and it terminates at a prominent carbonate marker bed known as the Castle Peak

Limestone. The Castle Peak section is about 330 ft thick and contains sandstones that produce hydrocarbons, however, these reservoirs are not part of the current water flood project. The next prominent marker is the "B" Limestone. In the 475 ft section between the Castle Peak and the "B", a number of productive sandstones are often encountered. These are termed the Lower Douglas Creek (LDC) Sandstones. The LDC sandstones are thin in the Monument Butte Unit, but thicken considerably to the west to form important reservoirs in the Travis Unit. In the upper part of the section, thin (generally less than 10 feet thick) channel sandstones constitute the "A" Sandstones. The prominent marker above the "B" Limestone is termed the Bicarb or B1 Carbonate. In the section between these two markers, sandstones termed the "B" Sandstones constitute important petroleum reservoirs in the Greater Monument Butte area.

The 240 ft thick section between the Bicarb and the Douglas Creek markers contains the most important sandstone reservoir units in the Monument Butte unit. The lower part of this section contains the "C" Sandstone. Above this are three "D" sandstone sections which are named in ascending order "D3", "D2" " and "D_I". The character of the Douglas Creek Marker can be inferred from imaging logs in the #10-34 and #14A-28 wells. The unit is thinly bedded and consists of carbonate and siltstone. In both wells, the Douglas Creek marker is fractured. These fractures probably contribute to the occasional high values observed on the porosity log. Figure 3-4 is a structural contour map constructed on the top of the Douglas Creek marker bed. This map shows the general northwest dip of the reservoir section, toward the axis of the Uinta Basin.

Regional Stratigraphic Correlation

Correlation with the regional terminology of Fouch (1981) is based upon interpretation of available logs from the Duchesne Field to the west of Monument Butte. The significant marker horizons occur at the contact between the Green River Formation and the underlying Wasatch Formation, and at the contact between the Black Shale Facies of the Lower Green River Formation and the Green Shale Facies of the Upper Green River Formation (Wiggins and Harris, 1994). Fouch's (1981) "Top of the Carbonate Marker Unit" is equivalent to the "Bi-Carbonate Marker" in Lomax's terminology that separates the Lower, from the Upper, Green River Formation.

The following sections discuss the more important reservoir units in the greater Monument Butte field. The Lower Douglas Creek and D sandstones were the principal focus of this investigation, and are therefore discussed in greater detail than the other units. As a general note, the net sandstone isopach maps included in the detailed discussion are characterized as having >10% neutron log porosity and a gamma ray response of <105 API.

BOREHOLE IMAGING LOGS

Borehole imaging logs commonly use either acoustic impedence or electrical resistivity to image the inside of a borehole. Importantly, the features imaged by the logs are oriented, providing a method for describing and characterizing both sedimentologic and structural information. In this project, the Formation MicroImager (FMI) log of Schlumberger was used. This is a high-precision electrical resistivity imaging tool with a total of 192 microresistivity sensors. The sensors are arranged on four arms and provide appoximately 80% coverage of an 8-inch diameter well.

Structural and stratigraphic features are generally planar, and cut a borehole that is, in general, cylindrical. The image log is displayed unwrapped, with a horizontal axis between 0 and 360 degrees. This display convention is shown schematically in Fig. 3-5. When the borehole image is displayed flat, the planar element takes the form of a sinusoid whose amplitude is a function of the dip angle of the planar feature and whose trough is located in the direction of dip. By convention, the orientation of the planar element will be designated as dip angle and dip azimuth. The utilization of a workstation to analyze the features on the log allows for the efficient collection of large data bases of dip information. .

Although borehole imaging logs were originally used for structural interpretation, there has recently been an emphasis on stratigraphic interpretation. In this project, imaging logs were used to determine sedimentary structures, depositional facies, and paleocurrent directions to evaluate depositional environments and sand body geometries. We also use these logs to determine the character and orientation of fractures. We have found it more useful to plot orientation data as dip angle or dip azimuth as a function of depth (Bengtson, 1981; Nielson et at., 1992) rather than the more traditional tadpole plot. We also use the. dip versus azimuth (DVA) cross plot of Bengtson (1981) to help characterize stratigraphic orientation data. In general, all data used for stratigraphic interpretation will have the structural dip removed, restoring orientation, as much as possible, to that of the depositional environment.

The FMI log was run through parts of the reservoir interval in the following wells: Travis Federal #14A-28 and #5-33, the Monument Federal #7-34, #9-34 and #10-34, and the Boundary Federal #12-21 (Fig. 3-5). Data from the #7-34 well were lost by the contractor and, therefore, are not available for quantitative interpretation. The FMI provided bed resolution of less than one inch, more definitive lithology, and most important, good definition of fracturing or faulting with the

ability to determine the azimuth of the fractures. Some of the more general aspects of interpretation will be discussed in this section while the more detailed stratigraphic interpretation will be presented below.

Table 3-1 lists the intervals where FMI logs were run, and it also shows the regional dip interpreted from the logs. This dip has been removed for discussions of depositional orientation: The regional structural dips are small throughout the Greater Monument Butte area where the study wells are located to the south of the Duchesne fault zone. Information from the Duchesne field to the west (Fig. 3-1 and Nielson et al., 1993) shows that the Duchesne fault acts as a hinge with dips similar to that at Monument Butte to the south of the fault and higher dips (7° - 8°) to the north of the fault.

MAGNETIC RESONANACE IMAGING LOGS (MRIL)

The Magnetic Resonance Imaging Log (MRIL) is a relatively new tool that may prove to be very valuable in the evaluation of petroleum reservoirs. This log is a product of NUMAR Corporation, and is described in several publications (Miller et al., 1990; Coates et al, 1991). The log uses magnetic resonance imaging to determine porosity, irreducible fluid saturation and fluid diffusion coefficients in a manner that is independent of lithology.

Magnetic Resonance Imaging Logging (MRIL) was used on five wells. Three of the wells were in the Monument Butte unit and one each in the Boundary and Travis units. Two additional wells were scheduled to be logged with the MRIL, but in one case the salinity of the mud was to high, and in the other case deteriorating hole conditions precluded running the log. The logs were run in 1992, 1993, and 1994. The primary purpose of running the logs was to determine if this log could give an indication of permabiiity and if it could indicate moveable oil and water.

The Federal 10-34 located in the NW SE of Section 34 T8S, R16E Duchesne County, Utah was the first in the program to run the full suite of logs designed to aid in reservoir characterization, and provide an evaluation of MRIL, and the Formation Micro Imager [FMI]. In addition Rotary Sidewall Cores were taken so that log data could be compared directly to actual reservoir rocks. The full suite of logs included the Dual Laterolog-Gamma Ray, Litho Density-Compensated Neutron-Gamma Ray, Formation Micro Imager-Gamma Ray, and the Magnetic Resonance Imaging Log. There was reasonable correlation between the comparable traits of the logs, but certain features of the new logs were not available on the conventional resistivity, and porosity logs. The MRIL provides good effective porosity data, but the main function of this log is to provide more data on effective permability, and the mobility of oil water in the reservoir. In the Federal 10-34, at a depth of 5796 to 5816, the density curve exhibited a porosity of 13 to 16 percent: however the gamma ray, and the compensated neutron indicated possible shaley sand. Rotary sidewall cores at 5800' and 5810' indicated porosity of 14.8 and 10.6 percent respectively. permeability was .43 and .15 md. The lithology of both cores was described as Ss, It gy, of--f gr, calc. The conventional Iog interpretations and core data was similar to other sands in this interval in other wells in which completion attempts were not successful. In this case the MRIL log indicated 8 to 13 percent porosity and 6 to 35 and permeability. The porosities using side-wall cores in the same interval were about 15% and 11% respectively, while the permeabilities were 0. 43 and and 0.15 md. It was observed in the reservoir simulation study that even though reservoir permeability, as determined by side-wall cores is very low (usually less than 1 md), the reservoir behaves as if it has higher overall permeability (of the order of 25 md). From that point of view, the MRIL permeabilities are more indicative of the actual reservoir

permeabilities. The moveable hydrocarbon- curve indicated commercial volumes of oil and no moveable water.

DESCRIPTION OF RESERVOIR UNITS

Lower Douglas Creek Sandstone

The Lower Douglas Creek (LDC) interval lies between the B Limestone and the Castle Peak markers. The thickest accumulations of Lower Douglas Creek sandstones occur in the western portion of the Greater Monument Butte field (Fig..3-7). As shown in this map, the LDC is characterized by discontinuous sandstone bodies that can reach over 100* feet in net thickness. The LDC sandstones are normally oil-saturated and are often productive reservoirs. The unit forms in an approximate east-west trending belt and is an important oil producer as far west as the Duchesne field (Fig. 3-1).

The LDC has been characterized through a variety of techniques including core description, net . sandstone isopach mapping, well log correlation and porosity and permeability measurements on core. In addition, our knowledge of the geology of the LDC has been greatly improved by the collection of Formation Microlmaging (FMI) logs in the Travis Federal #14A-28. Facies analysis based on the FMI log allows interpretation of the sandstone beds below the depth where core was collected. In addition, orientation data for both depositional trends and fracture analyses were determined from the imaging logs through the entire LDC section.

As part of this project, a continuous core was collected from the upper portion of the LDC sandstone from depths of 5550 to 5646 feet in the Travis Federal #14A-28. This is one of the few continuous, full-diameter cores from this important reservoir unit, and the core has been described and analyzed in some detail. The core description and inferred depositional origins for

the sedimentary facies are shown in Figure 3-8. A more detailed lithologic log is presented in Appendix A. Small amounts of continuous core are also available from the LDC in wells #6-33 and #2-33 from the Travis unit.

The core collected in the Travis Federal #14A-28 represents deposits of sediment gravity flows (Lutz et al., 1994). The core is comprised of two packages of planar-laminated fine-grained sandstone that exhibit various degrees of dewatering and soft-sediment deformation, which are separated by thin disrupted or massive very fine grained sandstone and siltstone beds (Fig. 3-8). The planar-laminated sandstones occur in 15 ft thick packages with an intraclast-rich base and a dewatered top, and are interpreted as moderate to low-density turbidite channel deposits. One of the packages, from 5632.7 to 5623.5 ft forms a complete Bouma sequence (Bouma, 1962). Both of the planar-laminated sandstone units are strongly oil-stained.

In the following discussion, classification of the type of mass transport (slump, debris flow, grain flow, fluidized flow, and turbidity current flow) is based on sedimentologic criteria established by Nardin et al. (1979). The LDC Sandstone in well #14A-28 consists of nine lithofacies that are described in Table 3-2.

Although planar-laminated fine grained sandstones may occur in many different depositional environments, it is the association of this facies with the other facies in complete and incomplete Bouma sequences that allows the interpretation of their origin as turbidite deposits. The lower thick turbidite unit has been divided into the various Bouma units based on the vertical sequencing of facies (Fig. 3-8). The sixfold subdivisions of the turbidite units (Ta through Te_t) are based on a modified Bouma sequence (Bouma, 1962; Scholle and Spearing, 1982). The base of the turbidite channel from 5632.6 ft to 5631 ft is characterized by disrupted medium to fine-grained sandstones with abundant flat shale rip-up clasts. This facies represents

the Ta unit. The bulk of the channel from 5631 ft to 5626 ft consists of dewatered laminated fine grained sandstone that represent the Tb unit. Ripple laminated fine grained sandstone occurs from 5626 ft to 5625 ft and can be interpreted as the Tcd units. The top of the channel sequence up to 5623.7 ft is composed of massive very fine grained sandstone and siltstone with abundant very fine clasts. The association of this facies with the underlying units suggests its formation as a Bouma Te_t unit rather than as a separate grain flow.

Above this classic turbidite channel sequence is a sequence of disrupted fine grained sandstone beds with abundant very fine clasts that are interpreted as debris flow and grain flow deposits, each about 2 to 3 ft thick (from 5614.2 ft to 5623.7 ft). Above this debris flow-grain flow sequence and below the next thick turbidite channel sequence (from 5607.3 ft to 5614.2 ft) is a stack of disrupted Iaminated fine grained sandstone beds that are interpreted as slumped thin turbidite units or fluxoturbidites, each about 3 to 4 ft thick. Because the lithologic contacts within the debris flow sequence and within the slumped sequence are gradational, it is difficult to subdivide these sequences into individual flow units.

The overlying thick turbidite unit does not appear to have been deposited as a result of fluidized flow. Overlying an intraclast-rich base, the planar-laminated fine grained sandstone is not disrupted by any dewatering or slumping features from its base at 5603 ft up to 5590.1 ft (15 ft thickness). From the slightly rippled top of this unit to the top of the cored interval are thin slumped and rippled calcareous sandstone beds and finer-grained silty mudstones.

The increase in bioturbation, ripple lamination and carbonate content in sandstones upward suggests a shallowing-upward facies succession. The fluidized turbidite channels, debris flows and slumps in the lower portion of the LDC Sandstone suggest deposition along the upper part of a sublacustrine slope. The upper less deformed (and possibly, less channelized) turbidite

sandstone unit and generally fining-upward sequence suggests shallower deposition in a marginal lacustrine environment.

Below the cored intervals, our knowledge of the LDC sands is based on analysis of FMI logs from well # 14A-28, core and facies descriptions from well #2-33 and well log correlations across the Travis unit. Figure 3-9 shows the dip angle and dip azimuths as a function of depth interpreted from the FMI log. The zones of slumping are clearly evident from the high dip angles measured. Note that these zones generally correspond with dip directions to the northwest (Fig. 3-10). This is approximately at right angles to the trend of the thickest accumulation of Lower Douglas Creek sandstones (Fig. 3-7). Both the paleocurrent data and the sandbody morphology suggest that the thick LDC sands represent sublacustrine fans.

Figure 3-11 illustrates the geometry of the sandy portion of the LDC along a southwest-northeast cross section that uses the B Limestone marker as an elevation datum. Overall, the sandstone appears to have a funnel-shaped geometry,. with a localized, channelized base and a flat, more widespread top. The turbiditic sandstones beds described in the #14A-28 core represent only the upper half to third of the sandy portion of the LDC section, or the flat top of the unit. There is a thick (up to 60 ft) sandstone bed present below the cored interval in wells #3-33 (5650-5700 ft), #14A-28 (5646-5690 ft), and #15-28 (5660-5740 ft). Generally, the shape of this sandstone interpreted from the gamma-ray logs indicates a fine base and a fining-upward top, which could be consistent with its origin as either a thick slump or a channel with shale rip ups at its base. The base of the sand appears to cut into relatively flat, underlying units.

In well #2-33, core from the LDC (Appendix B) appears to represent slumped debris flow and fluxoturbidite deposits that correlate with the thick slumped sandstone unit in wells #14A-28 and #3-33, located directly to the west. The lower portion of the core from #2-33 (5677 ft to 5669.5

ft) is mostly shale with a few thin (less than a ft thick) slumped sandstone beds. From 5669.5 to 5659 ft, there are four stacked debris flow units composed of muddy, medium-grained sandstone with variable sizes of shale intraclasts which are distributed randomly through the sandstone. Steeply dipping silty laminations are present in thin shales between the sandy debris flow units. The upper portion of the core from 5659 ft to 5650 ft consists of thick (2-5 ft) beds of clean, laminated, fine-grained sandstone with abundant dewatering features (pipes and synsedimentary microfaults). These sands- are interpreted as slumped fluxoturbidites, as the laminations are disrupted, and some, steeply inclined (up to 70%).

In well #14A-28, the section of the image log that correlates to the lower portion of LDC appears to represent slumped channel sands. Convoluted laminations and high-angle cross-laminations are present in the thick sands between 5645 ft and 5689 ft. The bases of the channels and the crossbedding suggest depositional trends to the north. In addition to the sedimentary structures evident on the image logs, large-aperture fractures are present from 5660 ft to 5675 ft and from 5700 ft to 5710 ft. In shales below 5710 ft, isoclinal folds can be recognized on the image log. These folds probably represent local deformation associated with loading caused by the deposition of the overlying LDC sands.

Most of the beds between the Castle Peak and the LDC Carb markers can be traced continuously across the Travis unit (Fig 1-12). Successive landward pinchouts of thin beds to the southwest below the LDC Carb may indicate onlapping with a baselevel rise and lake expansion. The LDC Carb marker shows a good coarsening upward pattern, wave-working and a shallowing-upward sequence. The LDC Carb may represent the capping phase of the lake level rise.

The LDC sand exhibits an erosive base that cuts into relatively flat, underlying units. This downcutting implies a lacustrine lowstand. In wells #15-28 and #10-28 (Fig. 3-11), another

channel sand body appears to overlie the basal sandstone unit. This vertical stacking of channels implies a lacustrine highstand and backfilling of the channel scour with the subsequent rise in lake level. The deposition of the sediment gravity flows (slumps, turbidites and sandy debris flows) probably occurred during a wet climatic cycle, when both water and sediment inflow was high and the lake was deep.

The correlated well logs in Figure 3-11 show that the turbiditic and debris flow sands in the upper portion of the LDC sand are relatively flat-lying and uniform in thickness compared with the channel-fill sands in the lower part of the sandbody. The basal turbidite can be traced up onto the proposed shelf or margin of the lake (Fig. 3-11, well #4-33), but the underlying channel-fill sands can not. This would imply that the channel scour was filled by the slumped sands by the time the turbidite unit was deposited.

The calcareous sands that cap the LDC interval seem to have a channelized, fining-upward base and a wave-worked, coarsening upward top. Overall, the entire LDC section appears to represent a shallowing-upward sequence.

When the B Limestone marker is used as an elevation datum as it is in Figure 3-11, the Castle Peak marker shows a systematic offset that appears to relate to the thickness of the overlying LDC sands. Figure 3-12 is a crossplot of the LDC net sandstone thickness versus the thickness between the B Limestone and the Castle Peak markers. This plot suggests that the deepest channel incisions, produced during the lake lowstand, provided the most accomodation space for the deposition of the gravity flow sands.

To summarize, our studies of the Lower Douglas Creek indicate the following depositional history for this relatively unusual lacustrine sandstone. The LDC sands appear to have been deposited as slumps, debris flows, and turbidites in sublacustrine fans during a lake highstand

and wet climatic cycle. The geometry of the fans suggest a funnel shape, with a slumped, channelized base and a laterally more extensive top. The occurrence of these fans appears to have been controlled by the location of deep channel incisions which were produced during a previous lake lowstand. These channel incisions into marginal lacustrine deposits occurred along an east-west trending zone that may be related to the Duchesne fault zone. The Duchesne fault zone may have acted as a knickpoint for both the creation of the lowstand incised channels and the subsequent loci of deposition for the highstand gravity flows.

The reservoir potential of the LDC Sandstone has been assessed using five core plugs in the upper portion of the sandstone interval from well #14A-28 and from seven samples taken from the #2-33 core, representing the lower portion of the sandy interval. These plugs have been analyzed by the following methods: the measured porosity, permeability and saturations by Dean-Stark analysis (Table 3-3) and visual examination by petrographic techniques.

The most strongly oil-stained sandstones are those that are planar-laminated, whether or not they are disrupted or undeformed. Presumably, these laminated facies are also the best reservoir units. Moderately stained sandstones of the lower turbidite channel sequence have oil saturations that range from 49.6 to 40.5%, horizontal permeabilities in the .46 to .77 and range and vertical permeabilities in the .50 to .99 and range. The plug from 5638 ft has the highest vertical permeability (Table 3-3) of any of the measured samples because the laminations are steeply inclined at this depth. Porosities in this facies range from 9 to 11.7%.

Strongly oil-stained planar-laminated sandstones in the upper turbidite unit are 67 to 70.7% oil saturated. Horizontal permeabilites in this sandstone unit are much higher than those of the lower turbidite unit and range from 2.5 to 13 md. Porosities range from 14.8 to 16.6%.

Calcite and dolomite cement the planar-laminated sandstones. By XRD analysis, the lower turbidite sandstone unit contains between 13 and 18% calcite and dolomite. In contrast, the upper sandstone unit contains 7 to 8% calcite and dolomite cement. Petrographically, these sandstones appear clean and well sorted. The grains are angular to subangular and most of the primary intergranular porosity is preserved in the sandstones. Some compaction effects are evident where mica grains and shale intraclasts drape or deform around the quartz and feldspar grains. Minor quartz overgrowths can be observed, but the dominant authigenic cements are calcite and dolomite. Dissolution of feldspars, especially in volcanic rock fragments, has created some secondary porosity in the sandstones.

X-ray diffraction analysis indicates that most of the clay in the planar-laminated sandstones consists of non-swelling illite (and fine mica) and chlorite. Petrographically, the chlorite can be attributed to chloritized detrital biotite. The illite and mica are detrital rather than authigenic clays. Two samples were found to contain illite-rich mixed-layer illite-smectite (from 5615 and 5639 ft). Thin-sections from these depths contain thin shale laminations or shale rip-up clasts.

The sequence of diagenetic events for the upper portion of the LDC Sandstones appears to be 1) early quartz overgrowths, 2) dolomite cementation with rhombs bridging pores, and 3) calcite cementation. Dissolution of the feldspars probably occurred after the carbonate cementation. In contrast to clean, laminated sandstones from the upper turbiditic units of the LDC, the sandy debris flow units in the lower LDC contain abundant mixed-layer illite-smectite. The muddy sandstones that make up the debris flows contain between 13% and 19% illite-smectite, as analyzed by X-ray diffraction. The shales in the bottom of the core contain about 53% to 58% illite-smectite. In both the shale and in the clayey sandstone, the clay was probably smectitic and detrital in origin, and has undergone burial diagenesis to an illite-smectite with about 15%

smectite interlayers. Similar to the planar-laminated sandstones in the upper portion of the LDC, the sands that are interpreted to be turbiditic in origin are strongly carbonate-cemented. By XRD analysis, the fluxoturbidites contain about 20% calcite, 3-5% dolomite and a trace to 2% siderite.

"A" Sandstone

The "A" Sandstone is a somewhat arbitrary designation for probable channel sandstones that lie above the Lower Douglas Creek reservoirs. As such, they represent a fall in base level and superposition of a fluvial section above the deeper water turbidites of the LDC. Due to their discontinuous nature, the "A" Sandstones are not currently considered a candidate for water flooding.

"B" Sandstone

The "B" Sandstone is another unit that is currently being produced as part of the Monument Butte water flood. The unit occurs within the stratigraphic interval between the B Limestone and the Bicarbonate markers (Fig. 3-3). There appear to be at least three, and perhaps five, stratigraphically distinct sands. The important sandstones in terms of thickness and porosity are located near the base of the section, above the B Limestone. In some places, thick sandstones occur directly on a truncated and thinned B Limestone, and it is clear that there is an erosional contact. Since the B Limestone is a clearly recognizable unit across the southern portion of the basin, we assume that it represents a stable marginal lacustrine environment.

Figure 3-13 is a net sandstone isopach map of the B2 sandstone, and physical property measurements are presented in Table 3-4. Correlations between adjacent wells suggests this unit represents a meandering channel system. The relationships shown in 3-13 suggest it is a

distributary channel system in a lower delta plain environment. Note also that the isopach shows accumulation along an east-west zone, similar to that of the LDC sandstone (Fig. 3-7). The northwest trend of the thickest portions of the B sandstone in the Monument Butte unit are noteable (Fig. 3-13). This trend is parallel to the trends of gilsonite dikes, which are younger than the channel system, but the two may have resulted from similar structural controls. From the standpoint of the water flood, the sandstones are probably well confined by shale horizons providing a good geometry for the water flood sweep.

"C" Sandstone

The next prominant reservoir unit above the B is the C sandstone. The C sandstone is present in about one half of the wells in the project area. It is normally thin, but is over 30 feet thick in some wells (Fig. 3-14). To the south of the Monument Butte unit, this sandstone forms a very prominant northeast trending thick accumulation. The C sandstone is not being produced under water flood at the present time in the project area.

"D" Sandstone

The "D" sandstone lies above the "C" and'is the principal target for water flood in the project area. A discontinuous channel sandstone, the "D2" is only of minor importance. However, the "D 1" sandstone is thick, widespread and continuous as shown on the net sandstone isopach map (Fig. 3-15).

The "D" Sandstone interval has been characterized from full-diameter core taken in the Monument Federal #6-35 and #12-35 wells (Davies, 1983; Lomax files). Davies characterizes these sandstones as "deposits of a playa environment formed along the margins of a larger

permanent lake. Terrigenous clastics were carried onto the playa by unchanneled sheetfloods and braided fluvial channels."

Although no continuous core of the D1 Sandstone has been taken, detailed description of the sandstone is possible from the FMI image logs from wells #9-34 (Fig. 3-16) and #10-34 (Fig. 3-17) in the Monument Butte Unit. Through identification of sedimentary structures and bedding contacts on the images, the FMI logs can be used to create a lithologic log and to interpret depositional facies, just as this information would be obtained from a core description. In addition, the borehole imaging logs can be used to orient features such as fractures and bed boundaries and allow the estimation of fracture apertures and sandstone bed thicknesses.

In well #I0-34, two 6-7 ft thick sandstone beds comprise the DI reservoir (Fig. 3-17). On the image logs, both sandstone beds appear to be finely planar laminated with some coarser and more calcareous laminations near the middle of the bed, and ripple laminations at the top of the beds. The basal contacts with shale are sharp but planar. The upper contacts exhibit some relief with a rippled or cross bedded top. In well #10-34, the sandstones are separated by thin shales interbedded with rippled to burrowed siltstones. In well #9-34 (Fig. 3-16), two upward-coarsening sequences (7-9 ft thick) are present, from shale at the base, to interbedded planar-laminated siltstone and shale, to sandstone upward. These sands are interpreted to represent open lacustrine bars near a deltaic environment.

Petrography of sidewall core plugs from- the sandstones reveals the presence of abundant rounded micrite clasts and micrite-coated quartz and feldspar grains that suggest formation of the grains in a marginal lacustrine environment and then transportation into the open lake. The overall fine grain size and lack of strong normal grading preclude deposition as channelized sands. The textures observed on the image logs are similar to those in cores of the upper black

shale facies of -the Green River Formation described by Wiggins and Harris (1994). They describe siliciclastics that alternate with carbonates arranged in a cyclical fashion. These siliciclastic cycles are thought to reflect increases' in the supply of silt to very fine sand to the nearshore lacustrine environment during periods of high fluvial discharge, while the sedimentary structures are typical of migrating sand bars. Because there is no erosion at the cycle bases, they envision sands/silts spewing out of channels , that emptied into the lake from a delta-front environment.

The bar crests are represented-by the coarsest part of the cycles. These are the slightly coarser laminations recognized. in the middle of the sandstone beds on the image logs (5008 ft and 4998 ft in #10,-34). Where the base of the bar crest facies is sharp into underlying rippled siltstone (such as at 5007 ft in well #9-34), the presence of an erosive pan out in front of the bar crest is indicated. The rippled silty upper parts of the cycles (such as 4995 ft in well #10-34) are interpreted as the lee side of bars riding up over the bar crest.

Bed orientations from the D1 reservoir in wells #9-34 and #10-34 interpreted from the FMI logs are summarized in Fig. 3-18. The data from the #10-34 shows a bedding orientation of about 80^0 while the orientation of beds in the #9-34 is much more scattered. This absence of strong orientation is probably a function of the high degree of reworking of the sediments.

Petrographically, laminations in the core plugs are commonly symmetrically graded, with the coarsest sand in the middle of the lamination. These fine laminations are also observed on the image logs of the D 1 sands. Wiggins and Harris (1994) describe pulses of sandstone and siltstone that are characterized by repetitions of uniformily 1 cm-thick, sand-silt rhythms without any jumps in grain size or evidence of truncation. They interpret these sedimentary structures as a

result of continuous sedimentation in the delta front, without wave reworking or erosion, possibly as a result of storm deposition and high stream discharge from the fluvial source area. An isopach of the D_I sandstone (Fig. 3-15) shows a maximum thickness of 34 ft (net) with a general lensoid shape oriented WNW-ESE. Although thicker portions of the body occur as a single unit, sections through the margins show that as the body gets thinner, it also breaks up into two or three separate sands separated by shale horizons that are 2-4 ft thick. The position of well #10-34 along the western margin of the body is consistent with the interpretation of the DI sands as sublacustrine bars. The #9-34 well is located slightly closer to the center of the sand body. The coarsening-upward sequences in the DI interval in this well are indicative of more deltaic deposition closer to the mouth of the river.

Correlation of well logs along a west-east cross-section through the D interval allows a detailed stratigraphic analysis of the sandstone facies. Figure 3-19 shows the gamma-ray logs in an east-west section across the thickest portion of the D 1 reservoir. Although the gamma ray logs are of little use in discriminating carbonate from sandstone beds, depositional patterns are indicated by pinchouts and downlap or onlap of individual packages of sediment below the DI interval. Packages a-c (Fig. 3-19) show successive westward (lakeward) downlapping in a forward-stepping pattern that is suggestive of falling lake levels. The b package that represents the D2 sand in well #12-35 is a thin progradational unit. The d beds and the D1 sands are vertically stacked and represent a lake highstand. Hence, in this 50 ft section, one cycle of lake level fall and then, rise is recorded.

The D 1 sands appear to cut down into the vertically-stacked beds, especially in wells #4-35, #10-35 and #2-35 where the sands are the thickest. Because the base of the D 1 sand appears to

be erosive and downcutting, the sands could represent a lake lowstand, with an abrupt landward shift in depositional facies from marginal lacustrine carbonates to deltaic sandstones upward. Alternatively, we propose that the D 1 sand represents a highstand delta that formed during a wet climate cycle, as described by Wiggins and Harris (1994). High stream discharge from the fluvial source area could have increased sediment supply to form a delta in the already-expanded lake. Although not definitive, it is likely that the increased amount of sediment was related to a short-term change in climate rather than renewed tectonics in the San Rafael Swell and/or Uncompahgre Uplift.

The reservoir potential of the D 1 sandstone has been assessed using four core plugs from well #10-34 and three core plugs from well #9-34. These plugs have been analyzed by the following methods: the measured porosity, permeability and saturations by Dean-Stark analysis (Table 3-5) , the bulk and clay mineralogic analyses by X-ray diffraction techniques (Table 3-6), and visual examination by petrographic techniques.

In well #10-34, core plugs at 5006 ft and 5007 ft from the middle of the lower D_1 reservoir are characterized by very fine to fine sand grains in well-sorted, parallel laminations. The grains are predominantly composed of quartz, plagioclase and potassium feldspar. From the X-ray diffraction (XRD) analysis, quartz makes up 48 wt.% , plagioclase makes up 24 wt.%, and potassium feldspar makes up 10 wt. % of the sample. Minor mica, polycrystalline quartz, volcanic rock fragments, and rounded micrite and micrite-coated grains are also present. The grains are cemented with minor quartz overgrowths and common calcite and dolomite. From the XRD, the calcite and dolomite contents of the sandstone are each 6 wt. %. The porosity types are mostly intergranular with some intergranular porosity in the volcanic rock fragments. Measured porosity is 14%, horizontal permeability is 5.5 md, and the oil saturation is 36%. The

clay X-ray diffraction analysis indicates only the presence of detrital clays, chlorite and illite with fine mica.

The sands at top of the D_I reservoir (4989 ft) in well #10-34 are more texturally and compositionally mature, and more strongly carbonate-cemented, than the underlying sands. The rounded to subrounded grains are cemented by quartz as overgrowths, and by carbonates (mostly dolomite) that poikilotopically enclose the grains in some places. Abundant micrite clasts occur along some Iaminations. There is very little visible porosity. Measured porosity is 5.8%, permeability is .04 md, and oil saturation is 39.9%.

The base of the DI sandstone in well #9-34 is similar in texture and mineralogy to the D1 in well #10-34, but it has undergone a different cementation history. Extensive, early quartz overgrowth formation can be recognized, calcite cementation is very minor (2-4% calcite by XRD), and the feldspars have undergone extensive dissolution. The result is a porous rock with good intergranular and intragranular porosity. The measured porosity is 13.5%, permeability is 2.7 md, and oil saturation is 51.5%. The upper portion of the D 1 sand interval in well 9-34 (4994 ft) is similar to that in well 10-34, with lower porosities and permeabilities as a result of strong quartz and calcite cementation (14% calcite by XRD). In addition, a brown authigenic clay is present in the intergranular pores. From the X-ray diffraction analysis, this clay is a chlorite or a mixed-layer chlorite-smectite.

FRACTURES

The importance of fracturing to petroleum production in the Unita Basin has been recognized for some time (Steams and Friedman, 1972; Lucas and Drexler, 1976; Chidsey and Laine, 1992). Narr and Currie (1982) studied fracturing in the Altamont field and concluded that, because of

low permeability, oil production was dependent upon the presence of extensional fractures. Their evidence suggests that fractures were initiated at about the maximum depth of burial and continued to form as the beds were uplifted. Nielson et al. (1993) documented the abundance and orientation of fracturing in the Duchesne field. These fractures were principally oriented east-west, parallel to the Duchesne fault zone. Northwest- and north-trending fractures are also present. The northwest trending fractures are parallel to the trend of the gilsonite veins, and the north-south fractures may reflect the influence of Basin and Range normal faulting that becomes more prominent on the western side of the Uinta Basin (Fig 1-1).

Studies in the eastern part of the Unita Basin (Verbeek and Grout, 1992) have documented five regional joint orientations. From oldest to youngest, these are: F1 = N 15^0-30^0 W, F_2 = N55°-85° W, F_3 = N 60^0-80° E, F4 = N 15°-40° E and F5 = N 65°-85° W. The F_2 and F_4 orientations are characterized as being very abundant and the F3 event is of moderate abundance.

The joints• are near-vertical and extend into the Piceance Basin in Colorado (Lorenz and Finley, 1991). Although the gilsonite dikes have an orientation similar to F2, Verbeek and Grout (1992) concluded that there were significant differences in morphology, age and orientation. They suggest that the gilsonite dikes were forcefully emplaced during the early stages of regional extension following the Laramide orogeny.

The orientation and character of fractures from the Greater Monument Butte area was determined using core from well #14A-28 and FMI logging. A typical example of a fracture imaged in reservoir units is shown in Fig. 3-20. In general, fractures are developed in sandstones and are terminated or decrease in intensity in overlying and underlying shales. Thus, they tend to develop in the more brittle lithologies and are either not formed or preserved in the more ductile

units. In most cases, there is no offset of bedding associated with the fractures, and they are more appropriately termed joints (Pollard and Aydin, 1988). These joint-like fractures contribute to horizontal permeability within the sandstone reservoirs, but have little influence on vertical permeability. Lorenz and Finley (1991) found that similar fracturing in Mesaverde reservoirs in the Piceance basin produced a horizontal anisotropy of 100:1. In addition, the horizontal permeability will be anisotropic and can be assumed to follow the predominant fracture trend in a particular well. The process of hydrofracturing during well completion will only increase the effect of fracture-related reservoir heterogeneity.

Fracturing in the LDC Sandstone Identified in Core

The core from well #14A-28 is moderately fractured (Fig. 3-8; Appendix A). In general, fractures are developed in cemented sandstone beds rather than in more ductile, finer-grained Iithologies. In the upper portion of the core, fractures are present in carbonate-cemented sandstone beds at 5570-5572', 5582' and at 5589-5590'. In these beds, the fractures are open, subvenical and planar. Fractures in the upper and lower turbidite sandstone units are more irregular. At 5608-5611' and 5625-5627', open fractures are subvertical but tend to mimic the orientation and geometry of dewatering pipes in the laminated sandstones and are nonplanar. The dewatering pipes appear to be oil-stained; the pipes may be filled with migrated fines (clay) that preferentially absorb oil. The correlation of dewatered facies to fractured zones is not strong because many of the dewatered sandstones do not contain fractures.

In general, the open, throughgoing (planar), natural fractures have dips greater than *60%*. The dewatering pipes exhibit similar dips and are commonly subvertical. Synsedimentary microfaults also developed as a result of dewatering. However, these microfaults generally dip less than 45% and probably don't extend for appreciable distances.

Fracturing Identified Through FMI Logging

Fractures imaged by the FMI logs are of higher electrical conductivity than the surrounding rock. We assume this results from the ingress of drilling fluid into these zones. The FMI images also suggest that, if the fractures are cemented by calcite or quartz, which are electrically resistive minerals, the cement is minor.

The Boundary Federal #12-21 well has FMI coverage through much of the lower Green River and upper Wasatch Formations (Table 3-1). Interpretation of the imaging log shows that fracturing is ubiquitous through the Green River Formation, but dies out in the upper part of the Wasatch Formation (Fig. 3-21). This stratigraphic distribution of fracturing is similar to that shown for gilsonite veins by Monson and Parnell (1992).

The orientation of fractures determined by interpretation of the FMI log from the five wells that were part of this project are shown in Fig. 3-22. These fracture orientations generally correspond with the F_2 trend of Verbeek and Grout (1992). The east-northeast strike of the fractures is similar to the regional east-northeast trend of faults that cut outcrops of the Green River Formation in the southern part of the Uinta Basin. The strong east-west trend in Monument Federal #9-34 is more closely parallel to the Duchesne fault zone.

The orientations of all the fractures measured in the imaging logs are shown in Fig. 3-23. This diagram illustrates the preponderance of steep fractures. From a statistical standpoint, there is a low probability of intersecting a steeply dipping fracture with a near vertical well. We therefore suspect that the sandstone reservoirs, where the measured fractures predominantly occur, are pervasively fractured. In the Duchesne field, Nielson et al. (1993) reported that a near-horizontal well drilled toward the north encountered fracturing of variable frequency. However, the

maximum concentration was nearly 2 fractures/ft in Duchesne, and it is not unreasonable to believe that similar concentrations are present in the Greater Monument Butte field. The character of fracturing intersected in wells in the Greater Monument Butte field is similar to those described by Lorenz et al. (1991) in the Piceance Basin. These similarities include the lack of shearing, vertical orientation, and their presence in the more brittle lithologies and termination by more ductile mudstones and shales, in addition to the similar orientations mentioned above. Also, we have seen no evidence for the formation of fractures by natural hydraulic fracturing, although that does not preclude the process in zones of overpressuring (Bredehoeft et al., 1992). We subscribe to the model. of Lorenz et al. (1991) for the formation of these fractures during burial in an environment of differential horizontal stress with pore pressures approaching the least horizontal principal stress. A possible exception to this may be the fractures that are parallel the Duchesne fault zone. Nielson et al. (1993), in a study of the Duchesne field, did document flexure across this fault that could be the mechanism for the generation of these fractures.

Faulting

Faulting with minor offset was observed in several wells in the project area. Figure 3-24 illustrates an example of one of these faults from the Travis Federal #5-33. There were no large zones of brecciation or offset observed in the imaging logs, and most of the fault activity appears to have taken place during sedimentation.

Figure 3-25 is a stereoplot of the orientation of all faults measured in FMI images from the Greater Monument Butte area. There does not appear to be a strong concentration of fault orientations. The observed faulting may have resulted from localized conditions produced

during during sedimentation, which would have Iittle influence on the petroleum production in this area.

CONCLUSIONS

The petroleum reservoirs of the lower Green River Formation owe their character to both sedimentary and structural processes. Stratigraphic information collected during this project has provided detailed information on the origin of the D 1 and LDC sandstone bodies that are the principal reservoirs being exploited by the water flood.

The Lower Douglas Creek reservoir forms isolated sandstone lenses that can reach over 100 feet of net thickness. The sandstones are concentrated in channel scours that formed during a lowstand in lake level. The channel incisions were subsequently filled with slumps, debris flows and turbidites during a lake highstand. The lithologic heterogeneity of this unit, complex reservoir architecture, and pervasive fracturing makes it a less than ideal candidate for water flood. In addition, its localized nature makes it a difficult exploration target.

The D sandstone reservoir formed as a sublacustrine bar complex that was associated with a nearby delta system. In contrast to the LDC sandstones, the D_1 reservoirs are laterally continuous and lithologically homogeneous. This unit provides an excellent geometry and lithology for the water flood project.

The other reservoir sandstones in the lower Green River Formation are fluvial and are not candidates for water flood at the present time. They do, however, contribute to oil production and are important for the overall economics of the field.

The lower Green River Formation in the Greater Monument Butte area reflects deposition from a long-lived fluvial-deltaic system. This river system was developed along the shallow gradient

margin of the lake and probably drained the San Rafael uplift to the south. In the marginal lacustrine enviroment, the presence of fluvial and distributary channels reflect lowstands of Lake Uinta. Open lacustrine mudstones and shales that separate the reservoir sandstones were deposited during highstands. In the nearshore environment, most of the deltaic units represent highstand deposits when a wet climate increased the amount of fluvial discharge of sand and water into the lake. It is these deltaic sands in which the water flood has been most effective.

From a structural standpoint, the Greater Monument Butte field is located on the gently dipping flank of the asymmetric Uinta Basin. A structural contour map constructed on the Douglas Creek marker shows the homoclinal dip to the northeast. In contrast to this simple structural setting, the reservoir sandstones within the project area are pervasively fractured. These fractures trend east-west to northwest-southeast and are comparable with the orientations of the regional F2 fracture set described by Verbeek and Grout (1992) and the orientation of gilsonite dikes. A

strong east-west trend in wells #14A-28 and 49-34 may also reflect the influence of the Duchesne fault zone. The fracturing is stratigraphically bound in that the more brittle sandstones are fractured while adjacent mudstones and shales are not. Therefore, the fracturing will produce an anisotropic horizontal permeability in the reservoirs, but will not contribute to vertical permeability. Hydrofracturing during well completion will enhance this permeability heterogeneity.

REFERENCES

Bengtson, C. A., 1981, Statistical curvature analysis technique for structural interpretation of dipmeter data: American Association of Petroleum Geologists Bulletin, v. 65, p. 312-332.

Bouma, A. H., 1962, Sedimentology of some flysch deposits, a graphic approach to facies interpretation: Elsevier, Amsterdam, 168p.

Bredehoeft, J. D., Wesley, J. B. and Fouch, T. D., 1994, Simulations of the origin of fluid pressure, fracture generation, and the movement of fluids in the Uinta Basin, Utah: American Association of Petroleum Geologists Bulletin, v. 78, p. 1729-1747.

Carter, R.M., 1975, A discussion and classification of subaqueous mass-transport with particular application to grain-flow, slurry-flow and fluxoturbidites: Earth Science Review No. 11, p. 145-177.

Castle, J. W., 1990, Sedimentation in Eocene Lake Uinta (Lower Green River Formation), northeastern Uinta Basin, Utah, in Katz, B. J. (Ed.) Lacustrine basin exploration - case studies and modern analogs: American Association of Petroleum Geologists Memoir 50, p. 243-263.

Chidsey, T. C. and Laine, M. D., 1992, The fractured Green River and Wasatch Formations of the Uinta Basin, Utah: Targets for horizontal drilling, in Fouch, T. D., Nuccio, V. F. and Chidsey, T. C. (eds.), Hydrocarbon and mineral resources of the Uinta basin, Utah: Utah Geological Association Guidebook 20, p. 123-134.

Coates, G. R., Peveraro, R. C. A., Hardwick, A. and Roberts, D., 1991, The magnetic resonance imaging log characterized by comparison with petrophysical properties and laboratory core data: Society of Petroleum Engineers paper SPE 22723, p. 627-635.

Cohen, A. S., 1990, Tectono-stratigraphic model for sedimentation in Lake Tanganyika, Africa, in Katz, B. J. (Ed.) Lacustrine basin exploration - case studies and modern analogs: American Association of Petroleum Geologists Memoir 50, p. 137-150.

Colburn, J. A., Bereskin, S. R., McGinley, D. C. and Schiller, D. M., 1985, Lower Green River Formation in the Pleasant Valley producing area, Duchesne and Uinta Counties, Utah, in Picard, M. D. (ed.) Geology and Energy Resources Uinta Basin of Utah: Utah Geological Association Guidebook 12, p. 177-186.

Fouch, T. D., 1981, Distribution of rock types, lithologic groups, and interpreted depositional environments for some lower Tertiary and upper Cretaceous rocks from outcrops at Willow Creek-Indian Canyon through the subsurface of Duchesne and Altamont oil fields, southwest to north central parts of the Uinta basin, Utah: U. S. Geological Survey, Chart OC-81.

Fouch, T. D., Nuccio, V. F., Osmond, J. C., MacMillan, L., Cashion, W. B., and Wandrey, C. J., 1992, Oil and gas in uppermost Cretaceous and Tertiary rock, Uinta basin, Utah, in Fouch, T. D., Nuccio, V. F. and Chidsey, T. C. (eds.), Hydrocarbon and mineral resources of the Uinta basin, Utah: Utah Geological Association Guidebook 20, p. 9-47.

Hintze, L. F., 1980, Geologic map of Utah, scale 1:500,000: Utah Geological and Mineral Survey.

Johnson, T. C., Wells, J. D. and Scholz, C. A., 1995, Deltaic sedimentation in a modern rift lake: Geological Society of America Bulletin, v. 107, p. 812-829.

Lambiase, J. J., 1990, A model for tectonic.control of lacustrine stratigraphic sequences in continental rift basins, in Katz, B. J. (ed.) Lacustrine basin exploration - case studies and modern analogs: American Association of Petroleum Geologists Memoir 50, p. 265-276.

Lorenz, J. C. and Finley, S. J.,-199I, Regional fractures II: fracturing of Mesaverde reservoirs in the Piceance Basin, Colorado: American Association of Petroleum Geologists Bulletin, v. 75, p. 1738-1757.

Lorenz, J. C., Teufel. L. W. and Warpinski, N. R., 1991, Regional fractures I: a mechanism for the formationof regional fractures at depth in flat-lying reservoirs: American Association of Petroleum Geologists Bulletin, v. 75, p. 1714-I737.

Lucas, P. T. and Drexler, J. M., 1975, Altamont-Bluebell: a major fractured and overpressured stratigraphic trap, Uinta Basin, Utah, in Bolyard, D. W. (ed.) Deep drilling frontiers in the central Rocky Mountains: Rocky Mountain Association of Geologists Symposium, p.265-273.

Lutz, S.J., Nielson, D.L., and Lomax, J.D., 1994, Lacustrine turbidite deposits in the lower portion of the Green River Formation, Monument Butte Field, Uinta Basin, Utah: American Association of Petroleum Geologists Annual Convention Program, v. 3, p. 203.

Middleton, G.V. and Hampton, M.A., 1976, Subaqueous sediment transport and deposition by sediment gravity flows, in D.J. Stanley, and D.J.P. Swift (eds.), Marine sediment transport and environmental management: John Wiley and Sons, Inc., p. 197-218.

Miller, M. N., Paltiel, Z., Gillen, M. E., Granot, J. And Bouton, J. C., 1990, Spin echo magnetic resonance logging: porosity and free fluid index determination: Society of Petroleum Engineers paper SPE 20561, p. 321-334.

Monson, B. and Parnell, J., 1992, The origin of Gilsonite vein deposits in the Uinta basin, Utah, in Fouch, T. D., Nuccio, V. F. and Chidsey, T. C. (eds.), Hydrocarbon and mineral resources of the Uinta basin, Utah: Utah Geological Association Guidebook 20, p. 257-270.

Narr, W. and Currie, J. B., 1982, Origin of fracture porosity- example from Altamont field, Utah: American Association of Petroleum Geologists Bulletin, Vol. 66, p.1231-1247.

Nardin, T.R., Hein, F.J., Gorsline, D.S., and Edwards, B.D., 1979, A review of mass movement processes, sediment and acoustic characteristics, and contrasts in slope and base-of-slope systems versus canyon-fan-basin systems: SEPM Special Publication No. 27, p. 61-73.

Nielson, D. L., Chidsey, T. C., Morgan, C. and Zhao, W., 1993, Fracturing in the Duchesne field, Utah: Importance for horizontal drilling: 1993 American Association of Petroleum Geologists Annual Convention Official Program, p. 156-157.

Nielson, D. L., Lutz, S. J. and Anderson, P. B., 1992, Evaluation of reservoir heterogeneity using the statistical curvature analysis technique: Gas Research Institute, report GRI-92/0321, 141p.

Pollard, D. D. and Aydin, A., 1988, Progress in understanding jointing over the past century: Geological Society of America Bulletin, v. 100, p. 11181-1204.

Ray, R. G., Kent, B. H., and Dane, C. H., 1956, Stratigraphy and photogeology of the southwestern part of Uinta Basin Duchesne and Uinta Counties, Utah: U. S. Geological Survey Map OM 171.

Scholle, P.A. and D. Spearing, eds., 1982, Sandstone Depositional Environments; Continental Slopes by H.E. Cook, M.E. Field, and J.V. Gardner; Submarine Fans by D.G. Howell and W.R. Normark: AAPG, p. 329-404.

Stearns, D. W. and Friedman, M., 1972, Reservoirs in fractured rock, in King, R. E. (ed.) Stratigraphic oil and gas fields - classification, exploration methods, and case histories: American Association of Petroleum Geologists Memoir 16, p.82-106.

Verbeek, E. R. and Grout, M. A., 1993, Structural evolution of gilsonite dikes, eastern Uinta basin, Utah, in Fouch, T. D., Nuccio, V. F. and Chidsey, T. C., eds., Hydrocarbon and mineral resources of the Uinta basin, Utah: Utah Geological Association Guidebook 20, p. 237-255.

Wiggins, W.D. and Harris, P.M., 1994, Lithofacies, depositional cycles and stratigraphy of the Lower Green River Formation, southwestern Uinta Basin, Utah, in Lomando, A.J., Schrieber, B.C. and Harris, P.M. (eds.), Lacustrine reservoirs and depositional systems, SEPM Core Workshop No. 19, Denver, June 12, 1994.

Zemanek, J., Glenn, E. E., Norton, L. J. and Caldwell, R. L., I970, Formation evaluation by inspection with the borehole televiewer: Geophysics, v. 35, p. 254-269.

Table 3-1. Logged intervals (FMI) of wells in the Greater Monument Butte field

Well	Regional Dip	Depth Interval Logged (ft)
Travis 14A-28	1^{0} @30^{0} in D zone	2911-3190
		4910-5124
		5480-5780
Travis 5-33	2.2^{0} @ 8^{0}	4430-4470
		4650-4690
		5032-5140
		5410-5480
		5898-5960
		6010-6080
Monument Butte 9-34		3060-3310
		4940-5100
		5290-5420
		5530-6065
Monument Butte 10-34	1^{0} @ 30^{0}	4900-5022
		5458-5530
		5730-5976
		6240-6320
Monument Butte 7-34		5020-5060
		5450-5490
		5530-5580
		5680-5760
		5900-6040
		6080-6130
		6210-6310
Boundary 12-21	0	5175-5809
		6062-6587
		6624-7332

Table 3-2. **Lithofacies** description of the Lower Douglas Creek Sandstones in core from well Travis Federal #14A-28

Shale	Fissile to conchoidal partings, commonly silty, common at the top of the cored interval.
Bioturbated mudstone.	Rare sand-filled burrows (slightly smeared or deformed) in shaly siltstone, mudstone is interbedded with shale at the top of the cored interval.
Disrupted siltstone.	Variably calcareous siltstone to very fine grained sandstone with vague sandy laminations or mottles that appear slightly deformed. These homogeneous light gray siltstones commonly occur in thin beds between the planar-laminated sandstone units. Their calcareous composition suggests deposition in a quiet marginal lacustrine area.
Ripple laminated sandstone.	Rippled sandstone occurs at the top of thin planar-laminated or dewatered sandstone beds in the upper portion of the cored interval and also at the top of the upper thick turbidite sandstone unit. In the lower sandstone unit, the presence of ripples is attributed to waning current energy after active channel deposition. In the upper portion of the core, the ripples may indicate shoaling upward channels within reach of wave-base.
Planar laminated sandstone.	Most of the cored interval is composed of well-sorted, slightly calcareous fine grained sandstone in planar laminations. This facies comprises nearly all of the upper turbidite unit where it is also strongly oil-stained.
Dewatered sandstone.	The sandy laminations in this facies are cut by many thin vertical fluid escape pipes, or more rarely, exhibit flame structures. The dewatered sands are common at the top of fine-grained turbidite units (= "fluxoturbidite" of Carter, 1975; Middleton and Hampton, 1976). The bulk of the lower turbidite sandstone unit is composed of this facies, which indicates its deposition as a result of fluidized flow. Compared to the other lithofacies, this one is preferentially fractured where the fractures have propagated along the planes of weakness presented by the fluid escape routes.

Disrupted sandstone. The sandy laminations in this facies are commonly folded to steeply inclined indicating slumping of originally horizontally-laminated sandstone. The laminations in some of these slumped packages are offset (rarely in an en-echelon pattern) by synsedimentary microfaults. This facies is common to the thin slumped beds between the two turbidite sandstone units and also, in sandstone beds underlying the Iower turbidite unit.

Shale rip-ups in sandstone. Thin beds containing flat to possibly algal-laminated shale clasts are common at the bases of the turbidite sandstone units. They are interpreted to represent the bases of the turbidite channels. The sandstone containing the shale rip-ups is slightly coarser (up to medium-grained) than the overlying sandstone and is commonly carbonate-cemented and less oil-stained than the overlying, more porous sandstone. Some deformation of the laminations and of the shale clasts in this facies may indicate minor loading at the channel bases.

Massive sandstone. This facies is either massive or contains scattered rounded fine to coarse clasts that are occur in random orientations within the siltstone to very fine grained sandstone. These massive but thin (2-3 ft thick) beds are common above the dewatered fine sandstone at the top of the lower turbidite unit and also below the turbidite at the bottom of the cored interval. This facies is interpreted to represent grain flow to debris flow units.

Table 3-3. Physical property measurements from the Lower Douglas Creek sandstone

Well	Depth (ft)	Permeability (md)		%Porosity	Saturation (%)		Grain Density (g/cc)	Neutron Log Porosity
		Horiz.	Vert.		Oil %	Water %		
14A-28	5595	2.5	.07	14.8	67.0	20.4	2.65	16.3
	5598	13	.43	16.6	70.7	16.4	2.65	15
	5615	0.14	.07	12.5	29.1	44.2	2.66	10
	5638	0.77	0.99	11.7	40.5	20.2	2.66	10
	5639	0.46	0.50	9.0	49.6	34.2	2.66	9
10-34	5800	0.43		14.8	41.8	25.9	2.67	16.2
	5810	0.15		10.6	48.2	16.4	2.69	14.4
9-34	5650	0.11		9.0	64.8	27.4	2.67	14
	5651	0.63		13.1	69.4	12.3	2.66	16.8

Table 3-4. Physical property measurements of the B sandstone reservoir

Well	Depth (ft)	Permeability (md)		%Porosity	Saturation (%)		Grain Density (g/cc)	Neutron Log Porosity
		Horiz.	Vert.		Oil %	Water %		
9-34	5338	0.80		14.4	55.7	20.7	2.66	16.2
	5344	0.03		2.8	75.1	18.7	2.67	7
	5356	0.16		10.4	57.5	20.2	2.69	11

Table 3-5. Porosity and permeability measurements from the D1 reservoir

Well	Depth (ft)	Permeability (md)		%Porosity	Saturation (%)		Grain Density (g/cc)	Neutron Log Porosity
		Horiz.	Vert.		Oil %	Water %		
9-34	4994	0.04		6.3	55.0	24.9	2.66	10
	5004	0.45		11.0	50.1	20.2	2.66	13
	5006	2.7		13.5	51.5	12.5	2.66	15
10-34	4989	0.04		5.8	39.9	18.8	2.67	10
	4998	1.2		13.3	37.6	48.5	2.66	14
	5006	0.60		12.2	47.3	17.4	2.66	15
	5007	5.5		14.0	36.0	39.4	2.66	14

Table 3-6. X-ray diffraction analysis of the D1 reservoir

Sample No.	Quartz	Plagioclase	K- Feldspar	Siderite	Calcite	Dolomite	Pyrite	Smectite	Chlorite	Illite+ Mica	Mixed-layer Illite-smectite	Mixed-layer Chlorite-smectite	Amorphous	Below Detect.	% smectite in illite-smectite	
Well #10-34																
5007.0-08.0 Bulk	48	24	10		6	6			3	3	Tr					
5800.0-01.0 Bulk	43	22	8	Tr	4	7			3	3	10					
Clay									18	10	72			20		
5810.0-11.0 Bulk	50	20	4	2	16	6	Tr		1	1						
Clay									15	54	31			20		
5880.0-81.0 Bulk	54	27	10		2	*3			Tr	1	3					*ferroan dolomite
Well #9-34																
4994 Bulk	36	30	8		14	4				4	Tr	2	2	Tr		
5004 Bulk	48	27	7		4	6		Tr		3	1	2	2			
5006 Bulk	45	35	4		2	3				3		2	6			

Tr = Trace

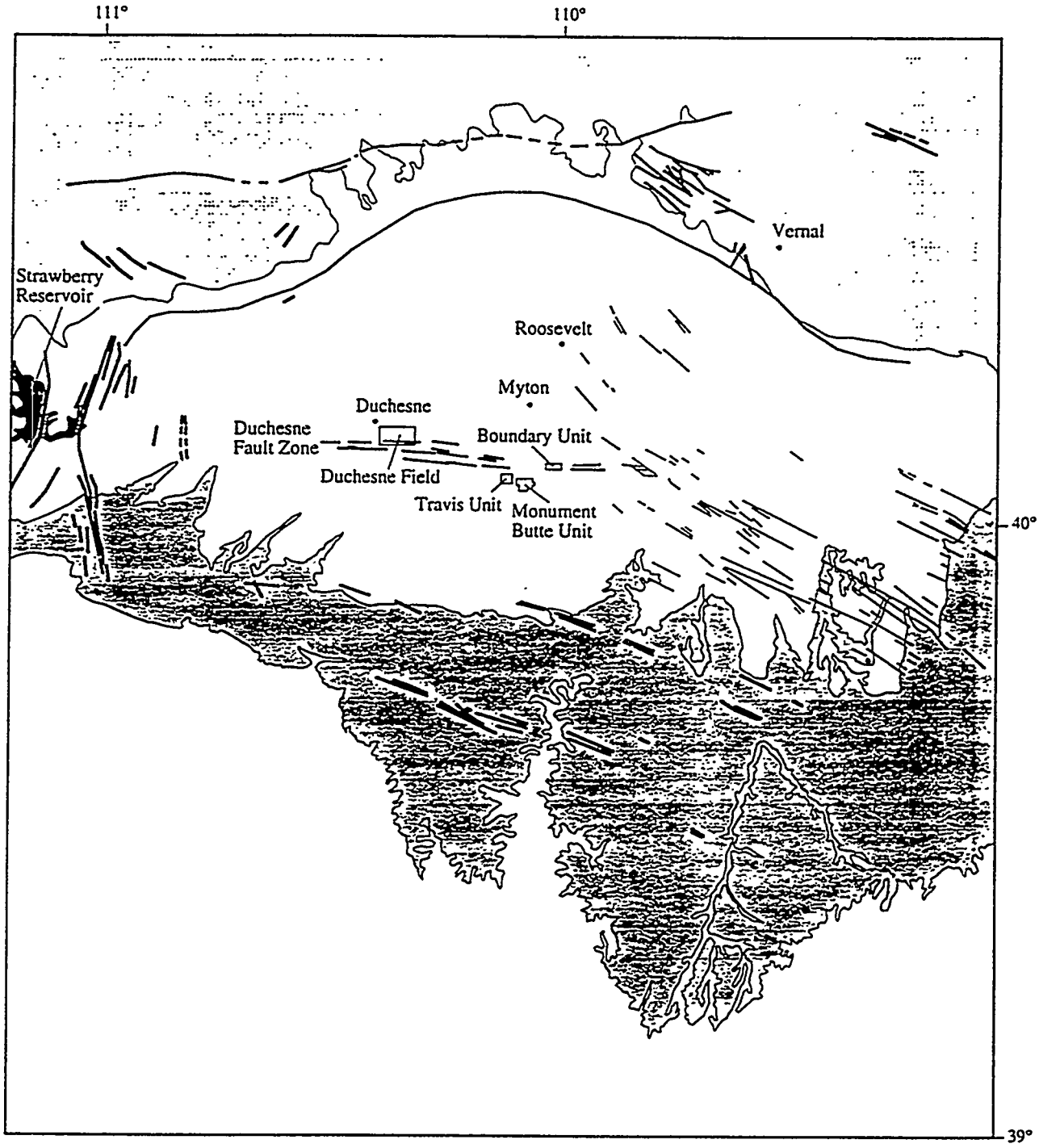

Figure 3-1. Map of the Uinta Basin showing major faults (light dashed lines) and gilsonite veins (heavy dashed lines) after Hintze (1980) and the locations of the oil fields discussed in the text

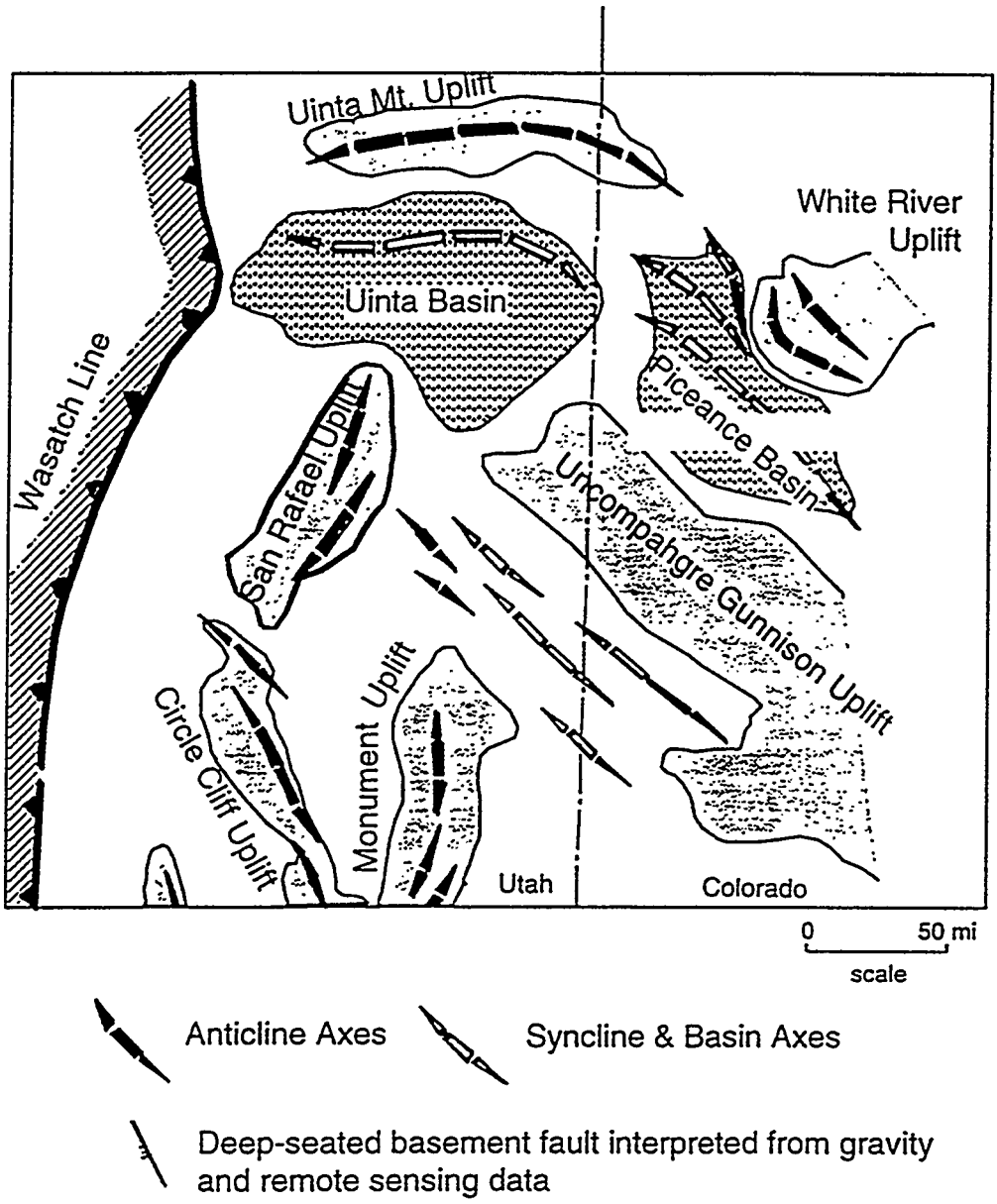

Figure 3-2. Map of the Major Laramide tectonic elements influencing the Uinta Basin

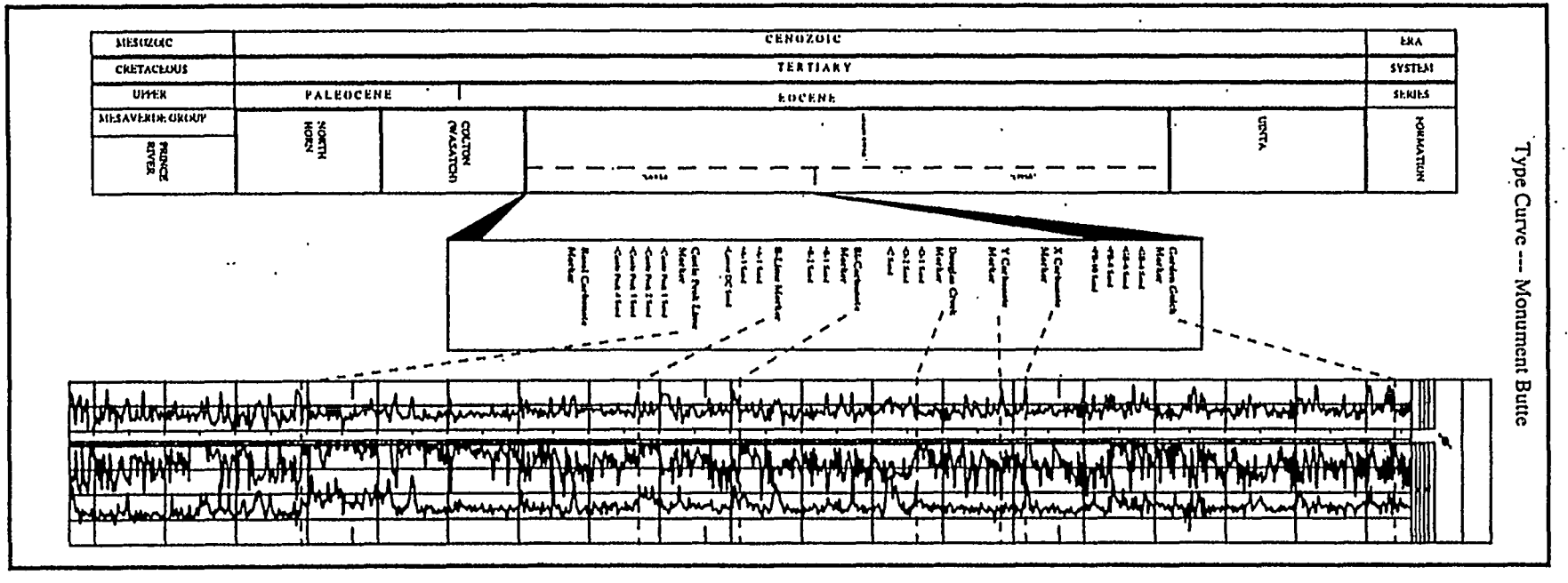

Figure 3-3. Interpreted log (type log) of the Monument Butte Federal #13-35 showing the stratigraphic nomenclature used in this report

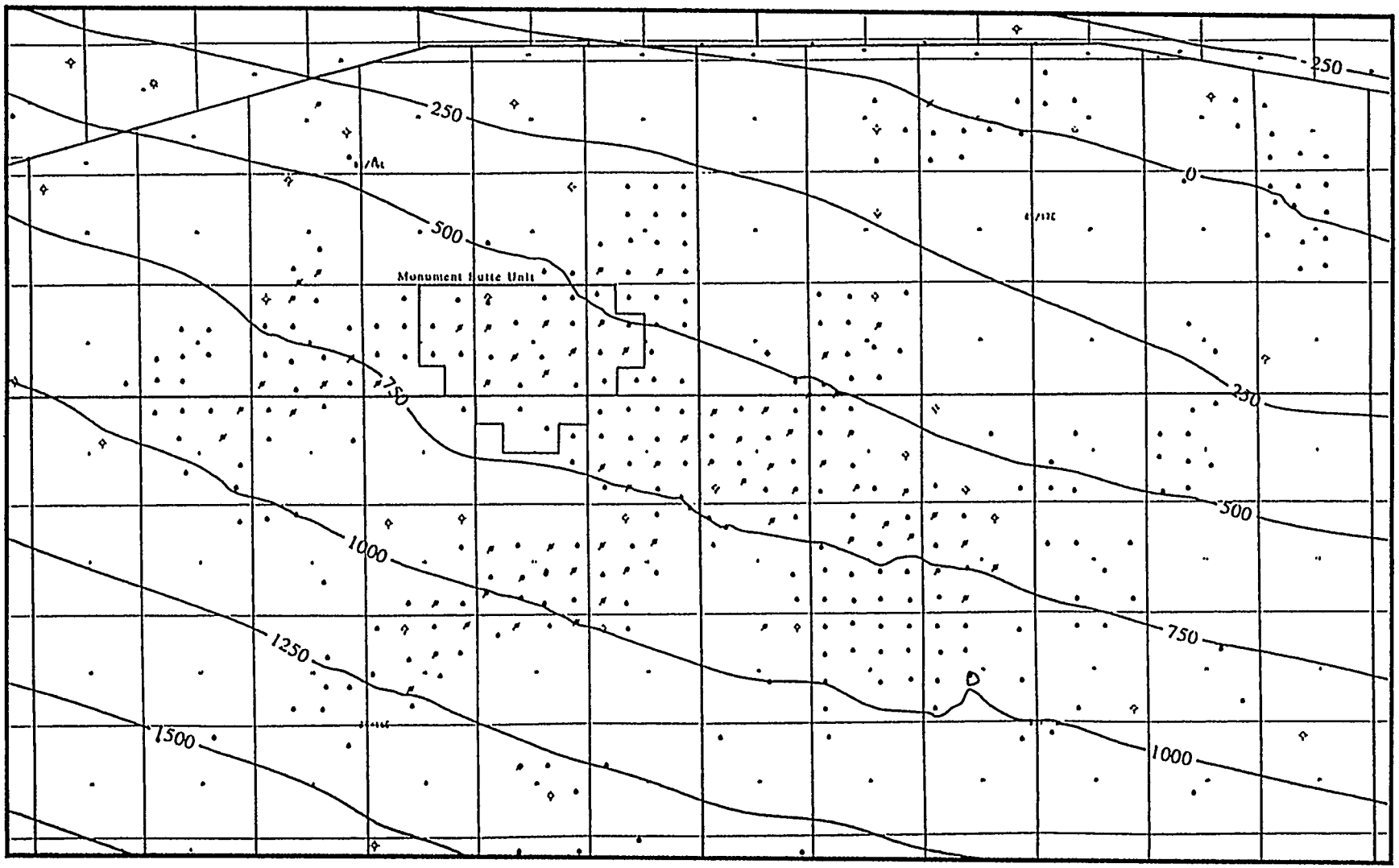

Figure 3-4. Structural contour map constructed on top of the Douglas Creek marker bed

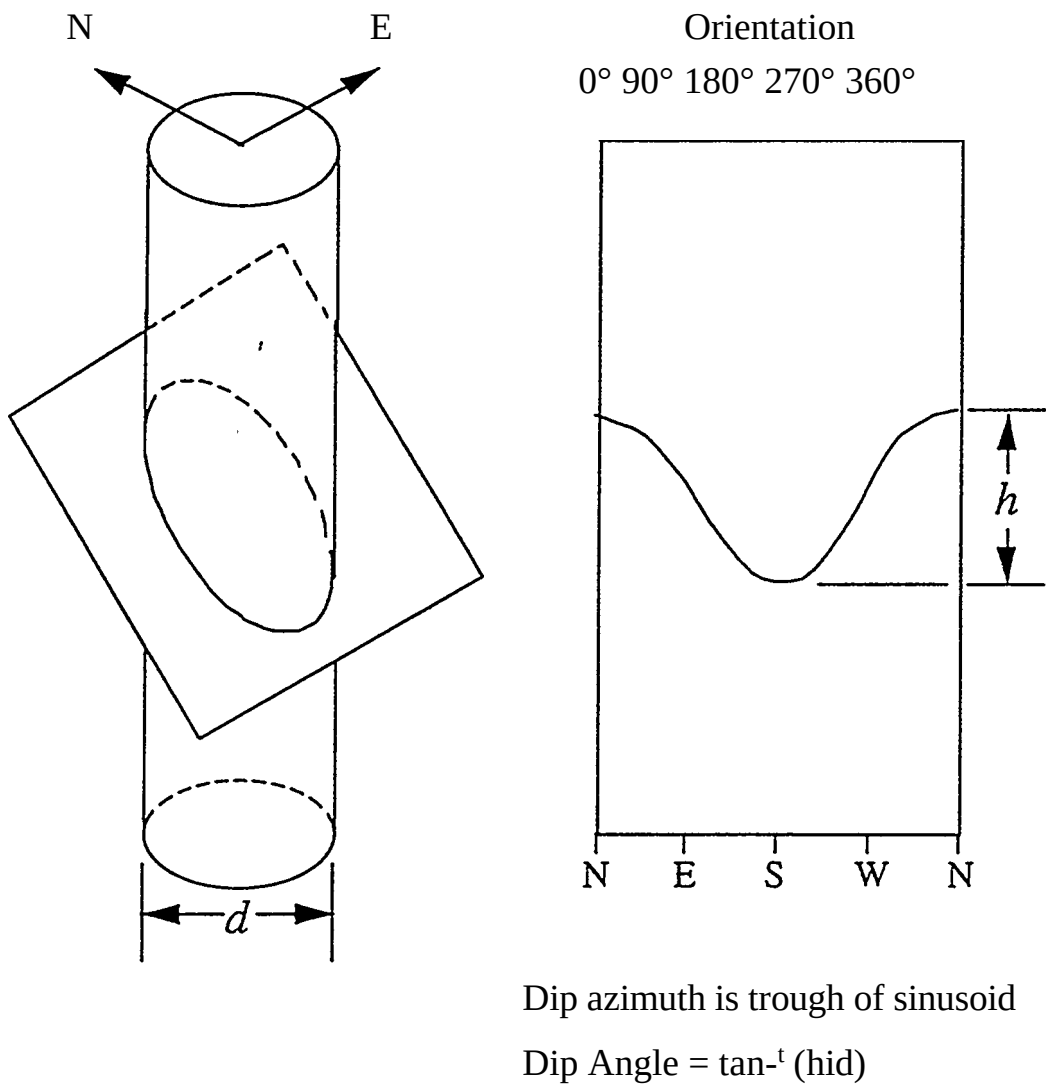

Figure 3-5. Planar feature intersecting a well bore and borehole imaging log of the feature (modified from Zemanek et a1.1970).

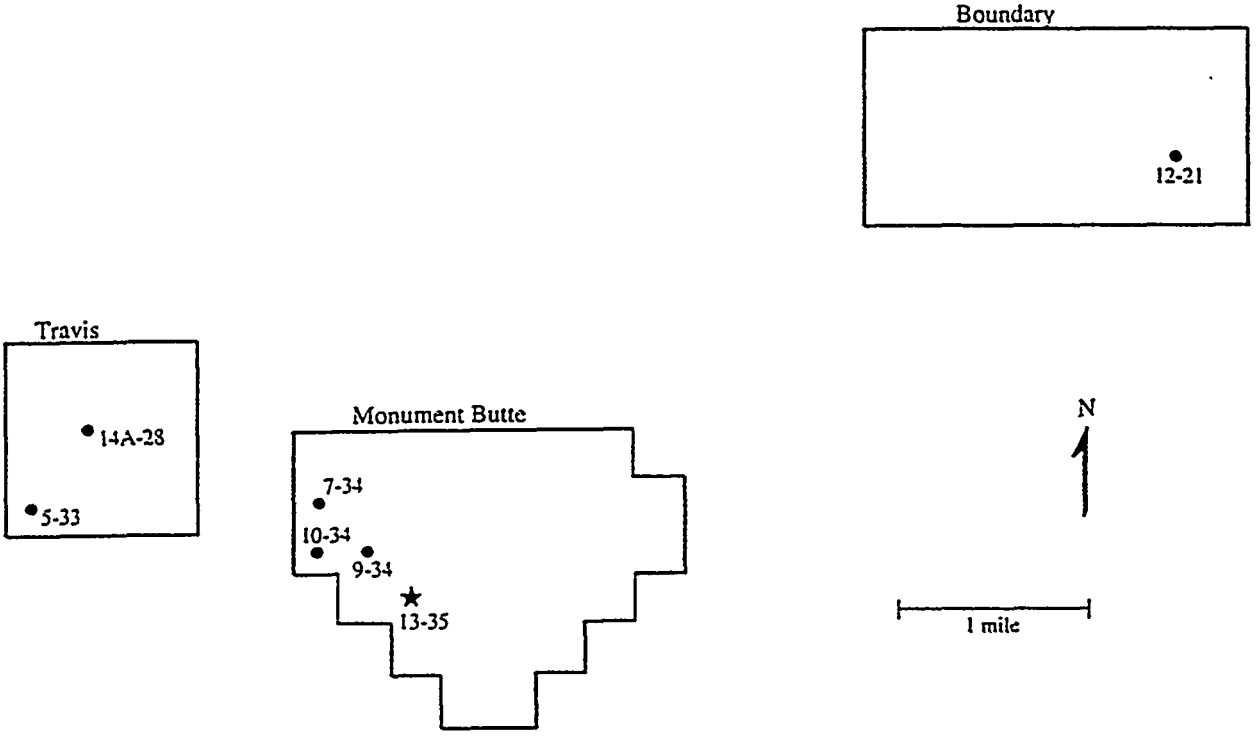

Figure 3-6. Locations of wells drilled under the DOE program for which there is data from the Formation MicroImager log.

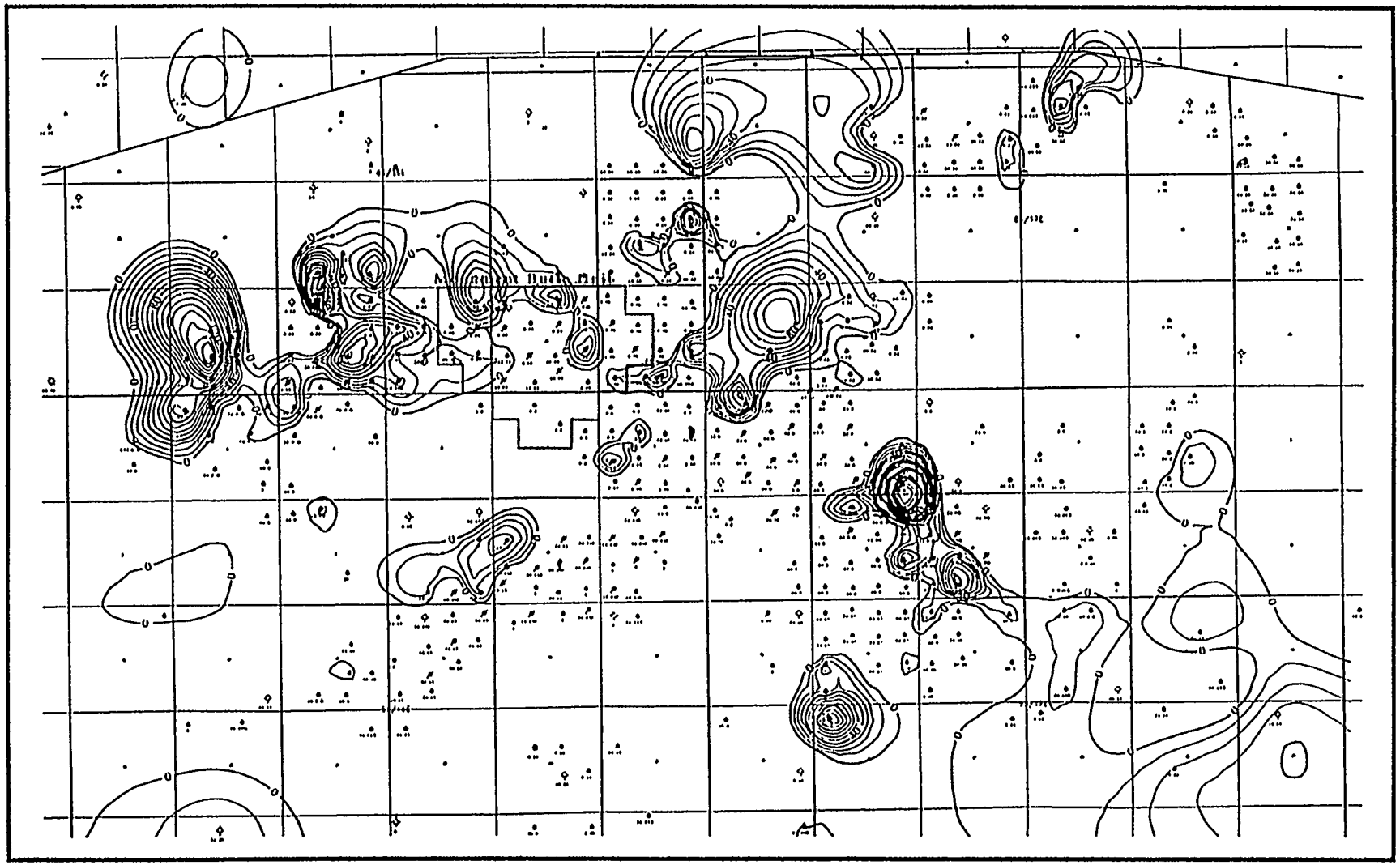

Figure 3-7. Net sandstone isopach map of the Lower Douglas Creek sandstone in the Greater Monument Butte area

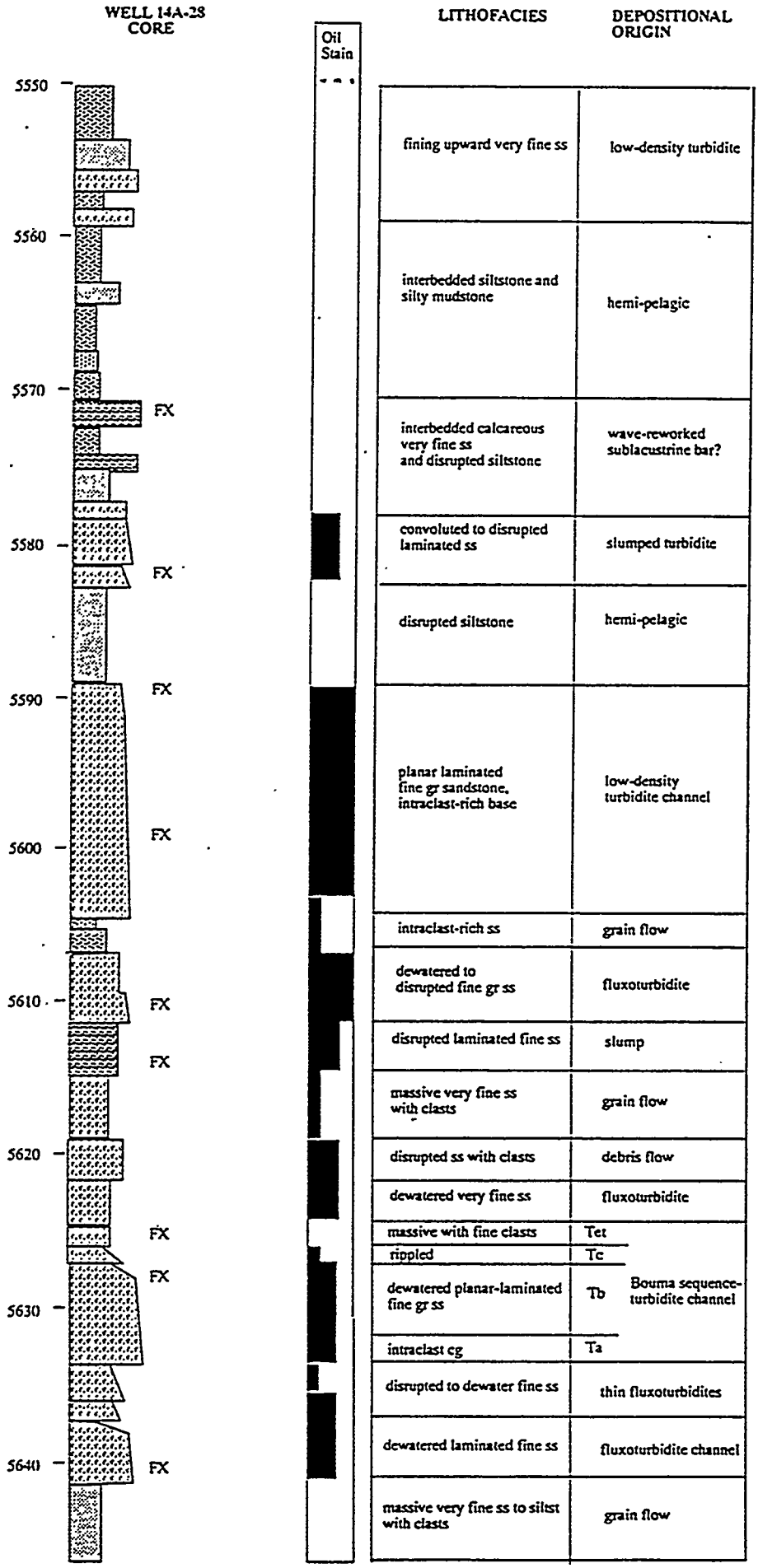

Figure 3-8. Summary of lithofacies and inferred depositional origin of Lower Douglas Creek sandstone in core from well Travis Federal #14A-28. (FX=Fracture)

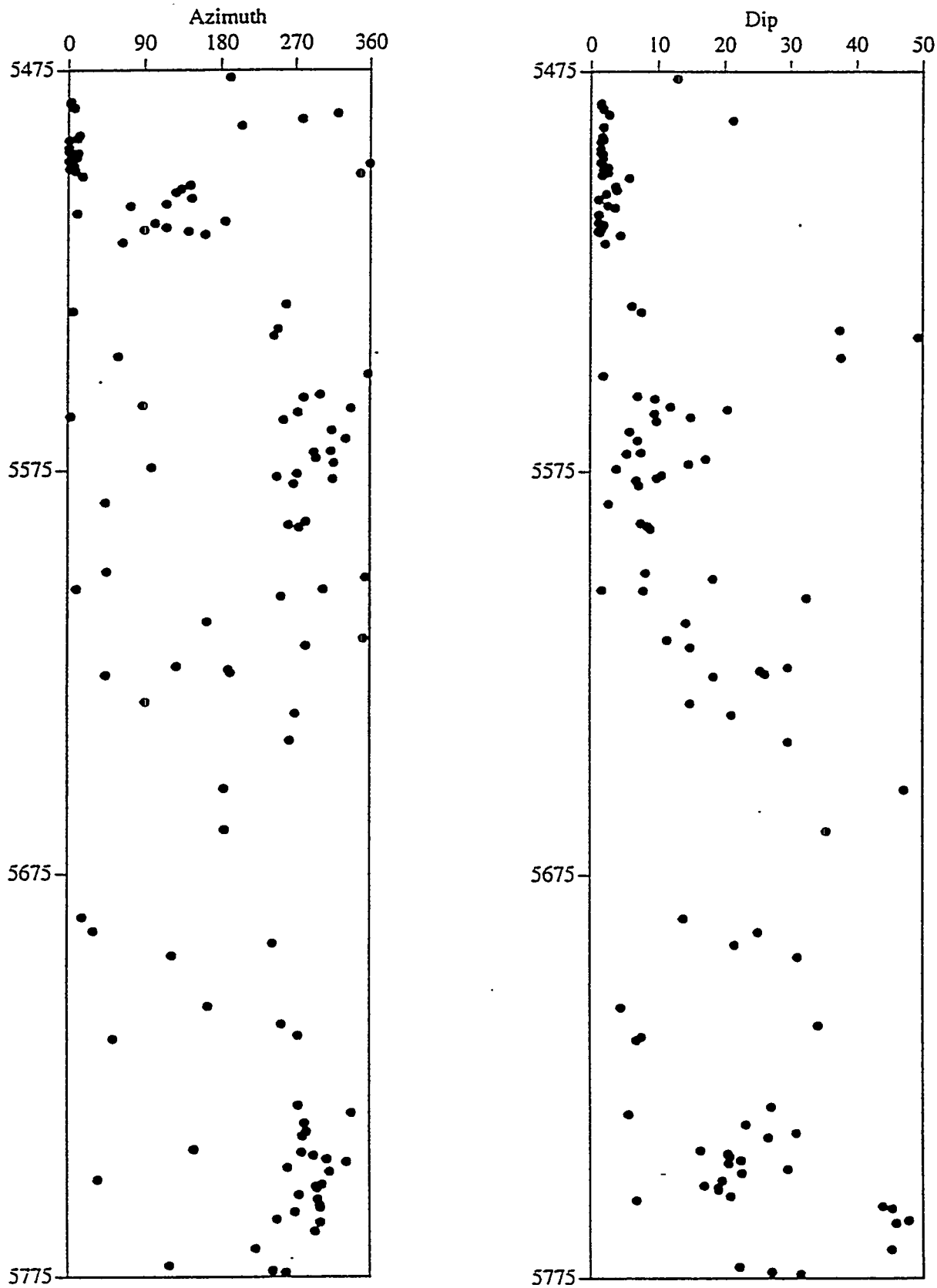

Figure 3-9. Dip angle and azimuth as function of depth interpreted from the FMI log in the Lower Douglas Creek interval in well Travis Federal #14A-28

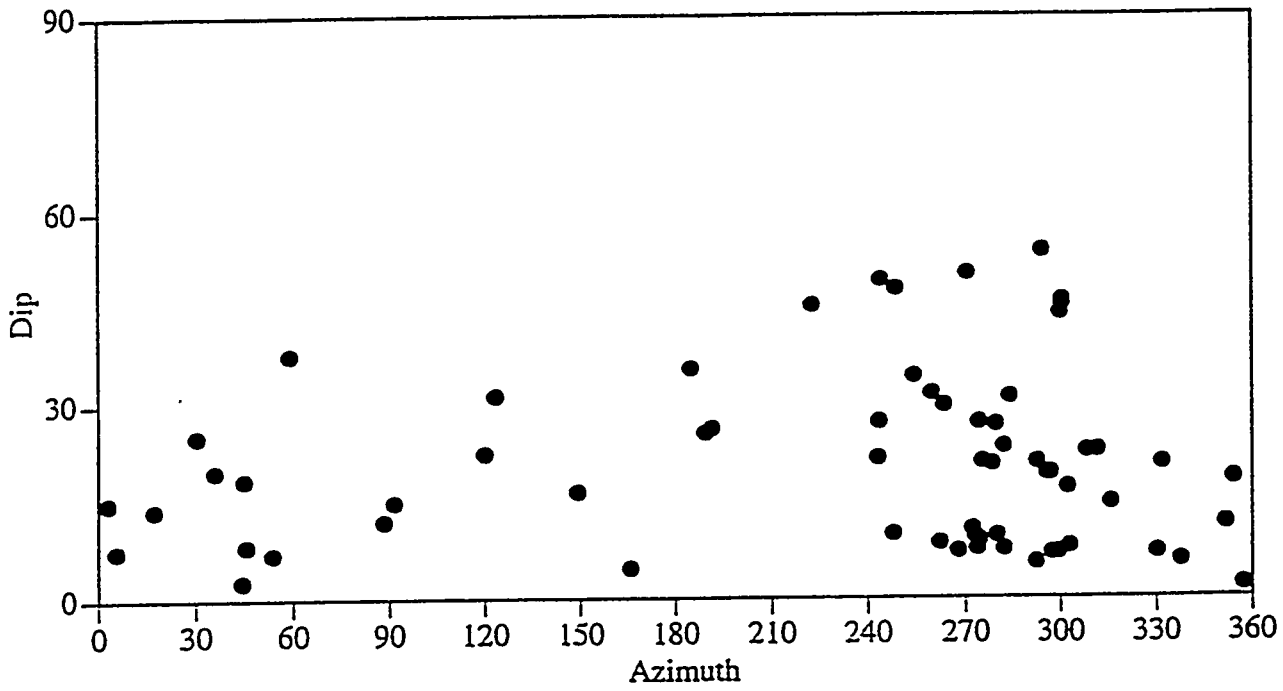

Figure 3-10. Dip versus azimuth (DVA) plot of bedding from the Lower Douglas Creek from 5538 ft to 5775 ft in Travis Fedearl #14A-28

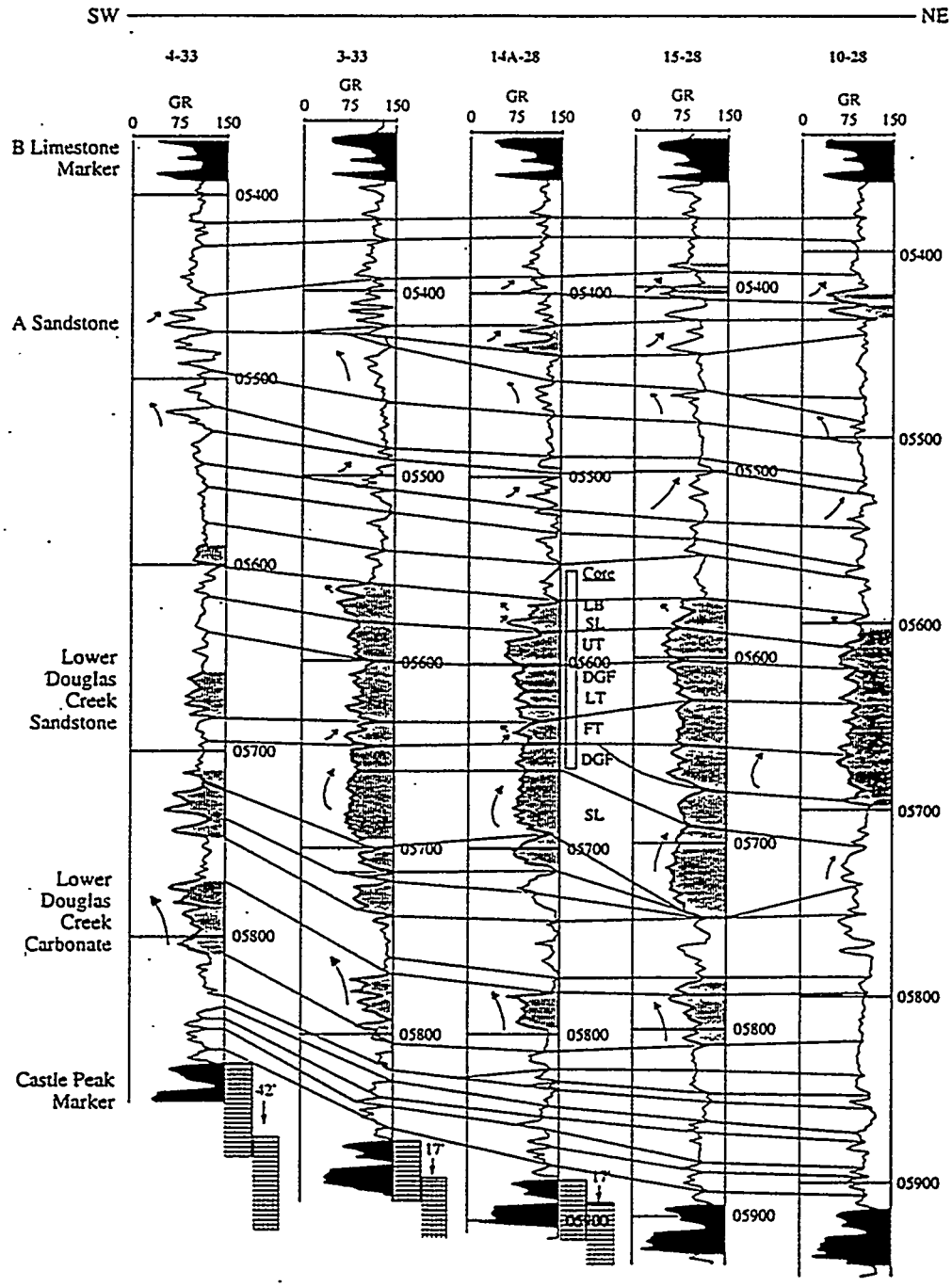

Figure 3-11. Correlated well logs of Lower Douglas Creek sandstone in the Travis unit. Channelized sands show a general fining-upward pattern (arrows to right). Wave worked sublacustrine bars coarsen upward (arrows to left). SL=slump, FT=fluxoturbidite, DGF=debris and grain flows, UT=upper turbidite, LB=lacustrine bar

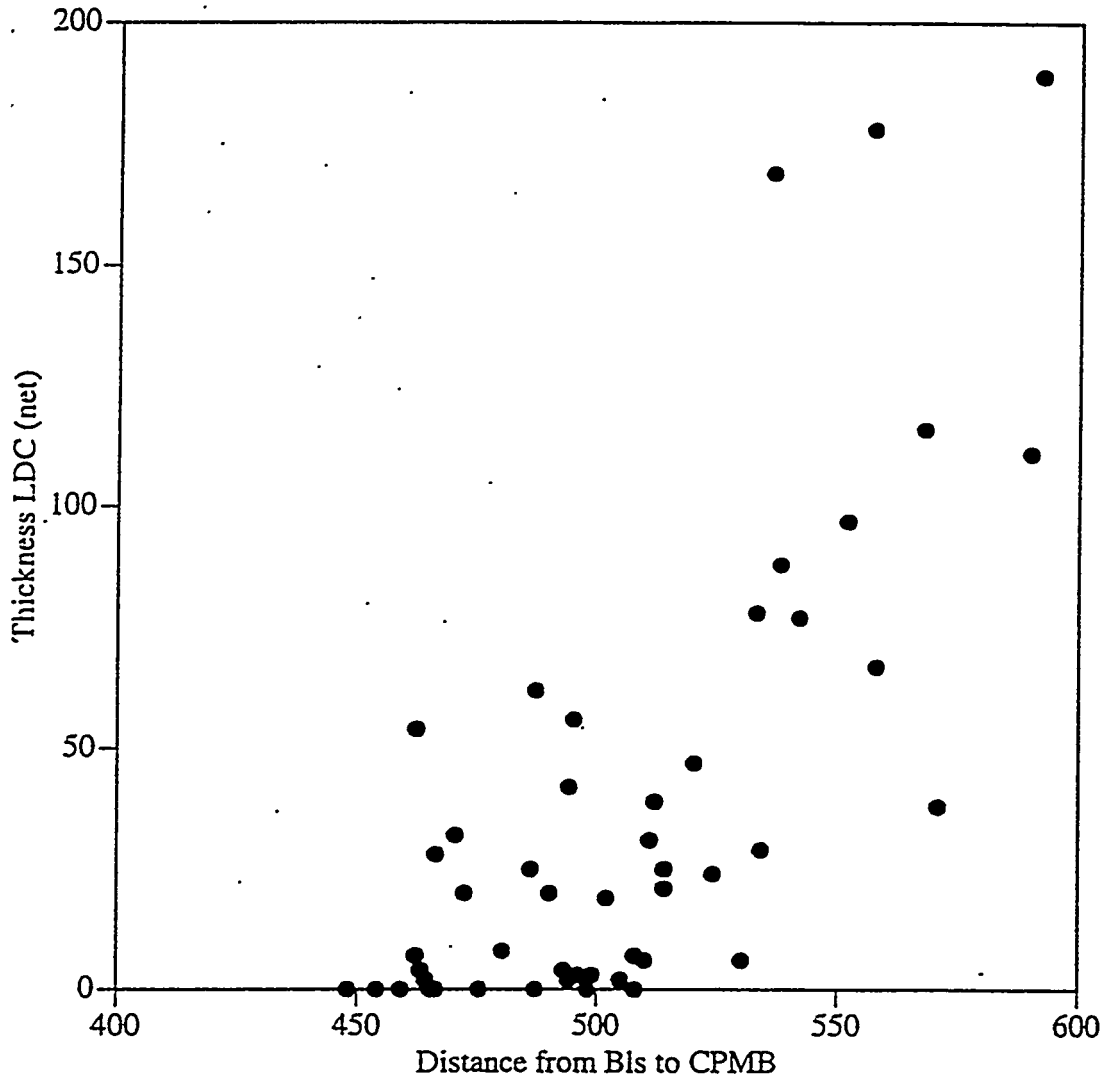

Figure 3-12. Cross plot of Lower Douglas Creek net sandstone thickness versus distance between the B Limestone and the Castle Peak marker beds

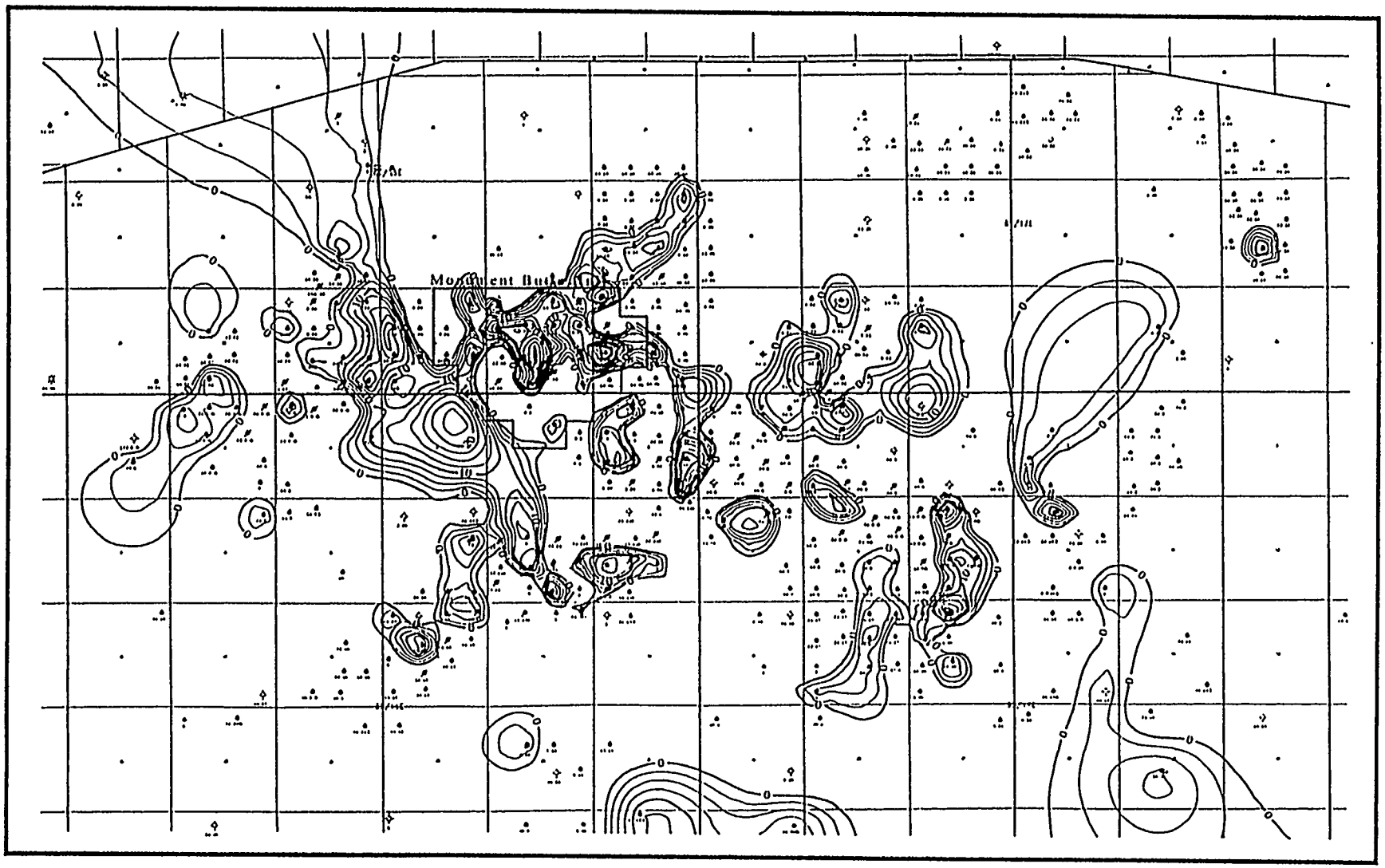

Figure 3-13. Net isopach sandstone map of the B2 reservoir

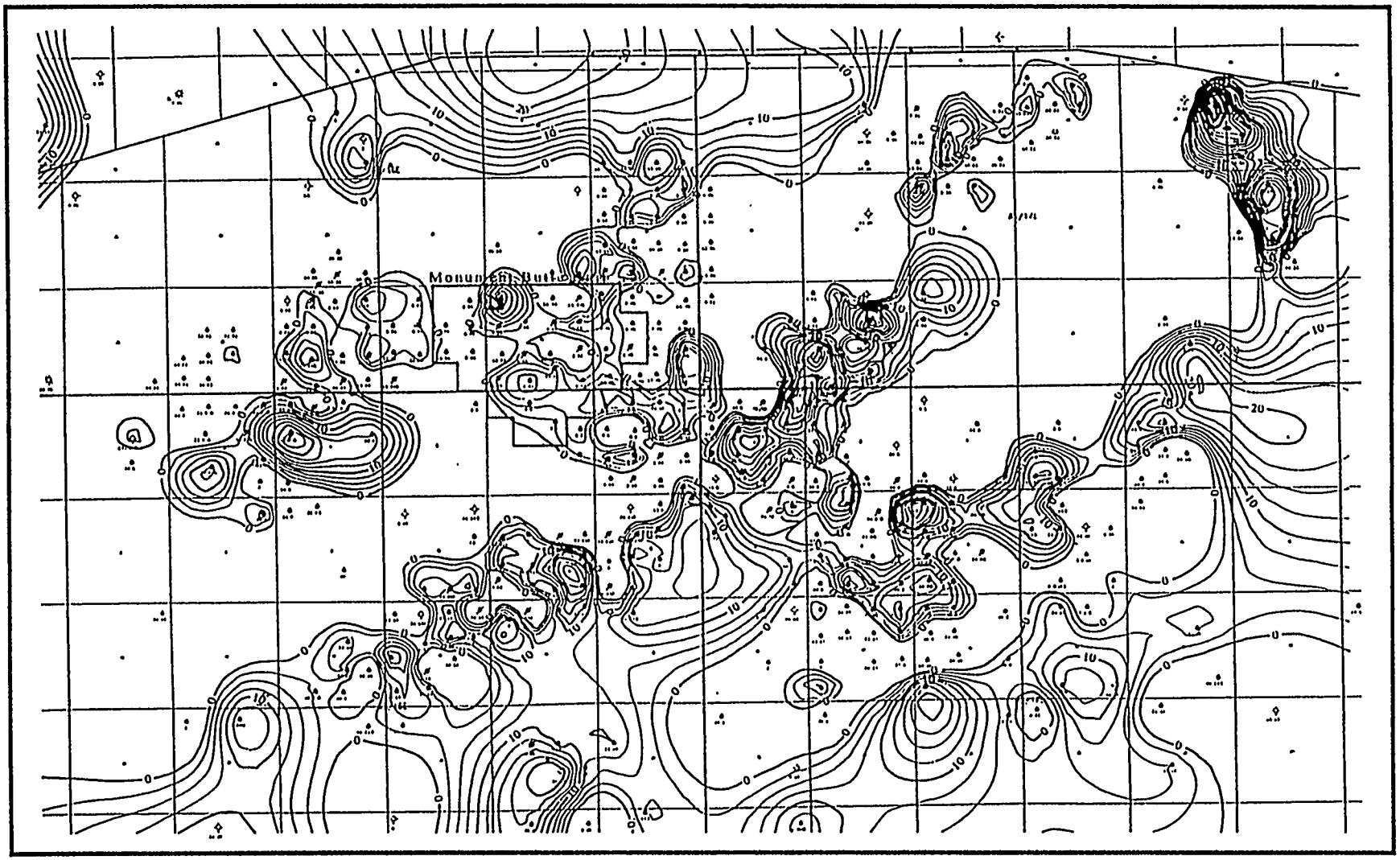

Figure 3-14. Net isopach sandstone map of the C reservoir

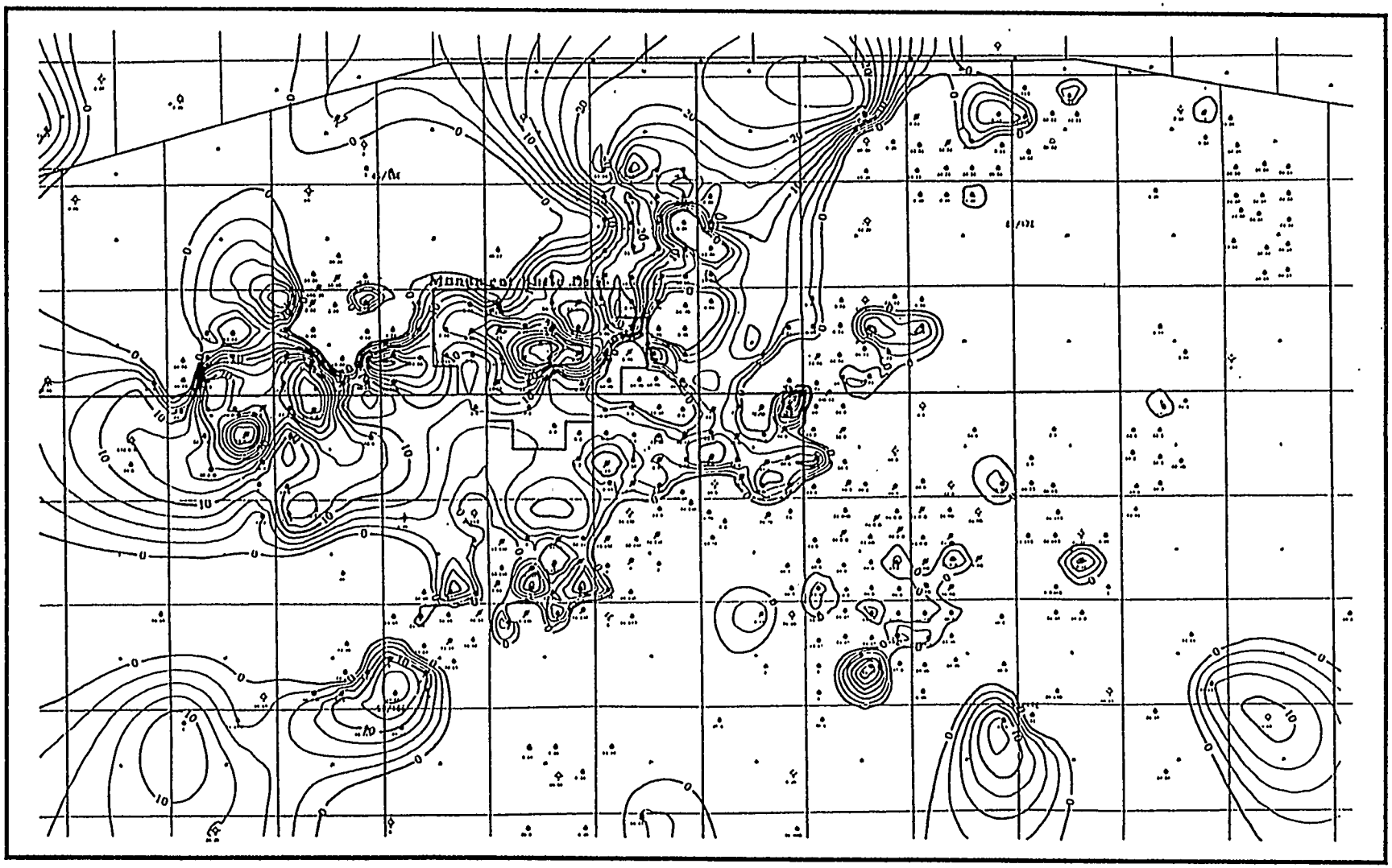

Figure 3-15. Net isopach sandstone map of the D1 reservoir

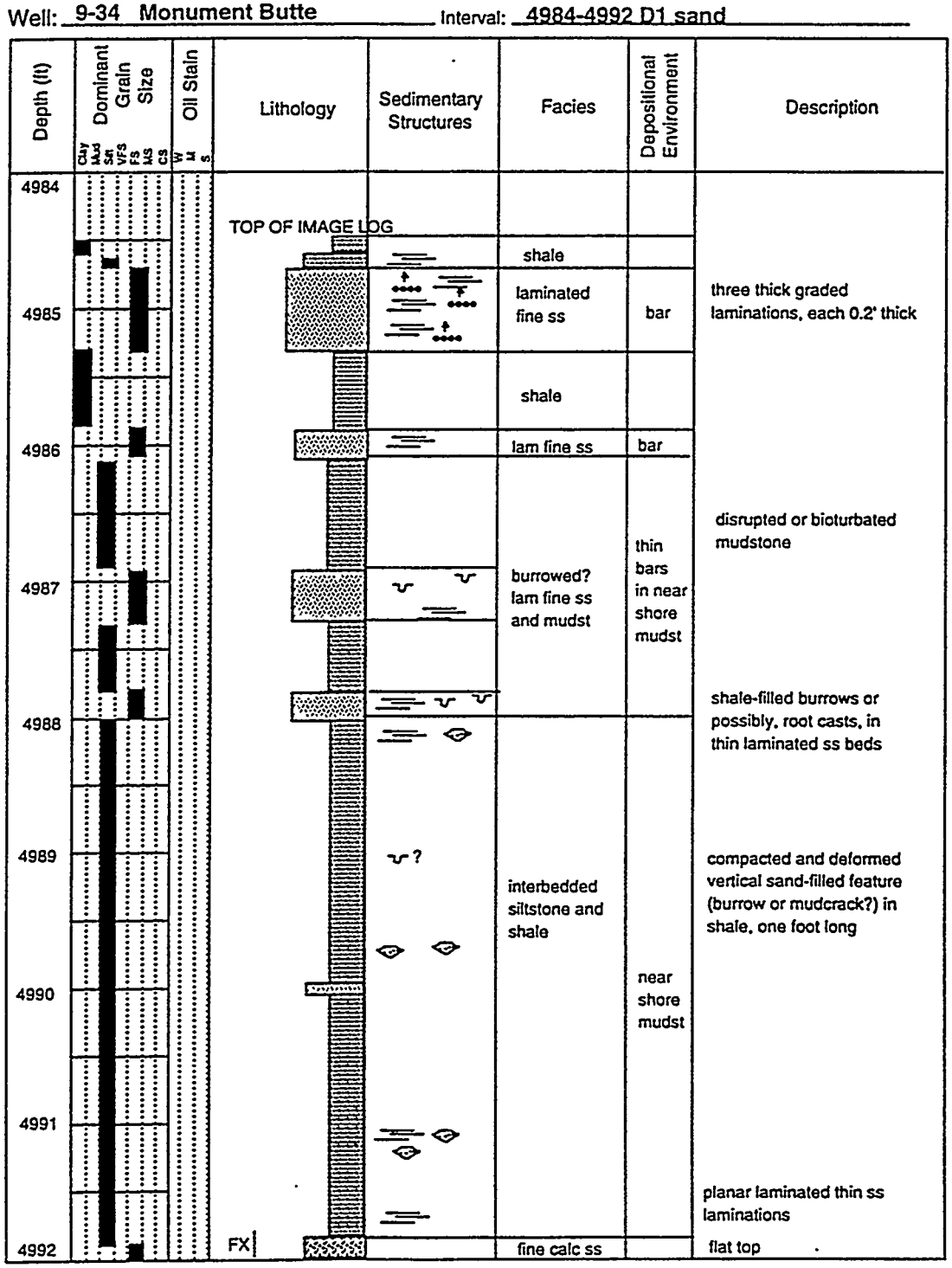

Figure 3-16. Lithologic log of the DI reservoir interpreted from the FMI images from Monument Butte Federal #9-34

Well: 9-34 Monument Butte Interval: 4992-5000 D1 sand

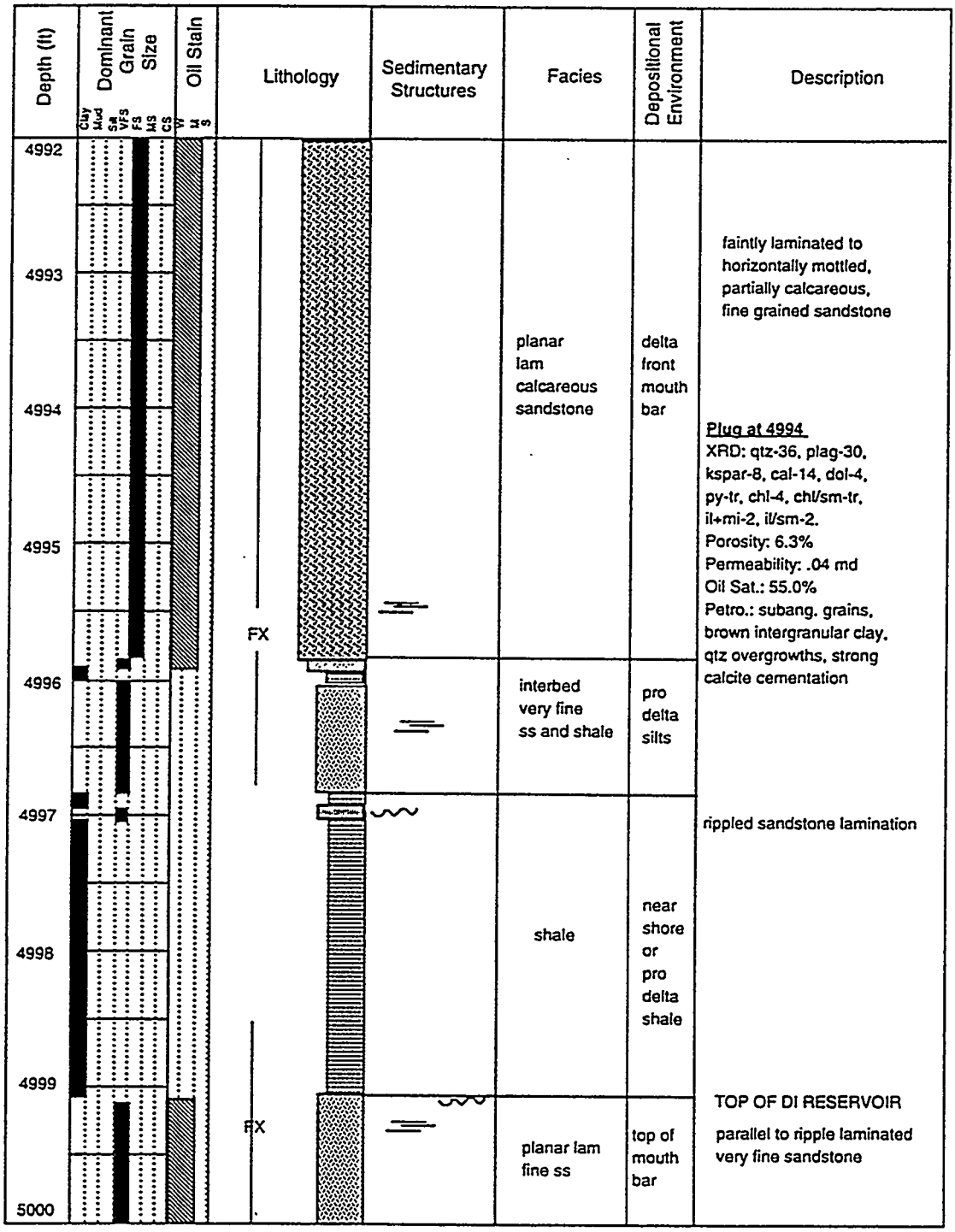

Figure 3-16 continued

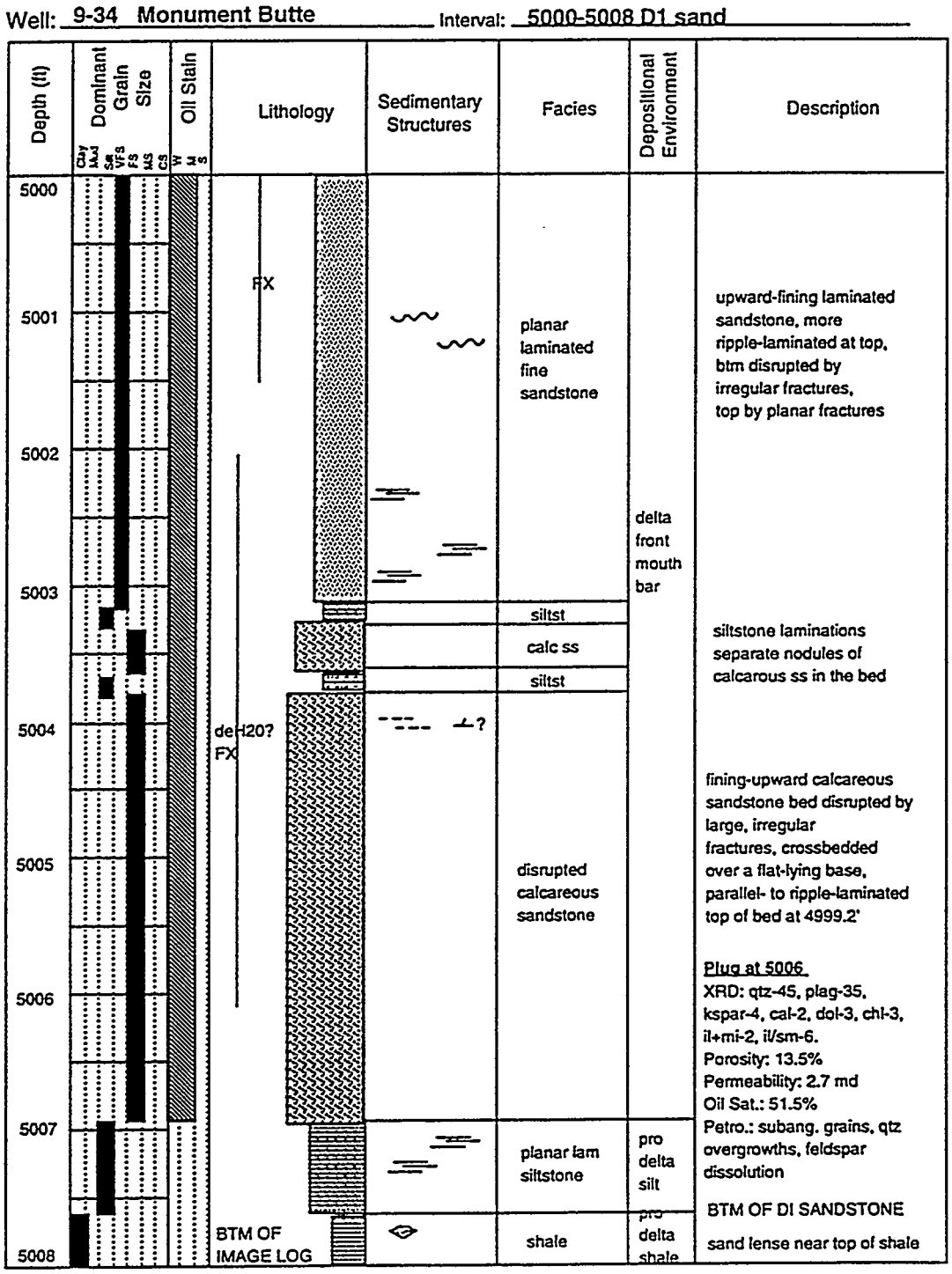

Figure 3-16. Continued

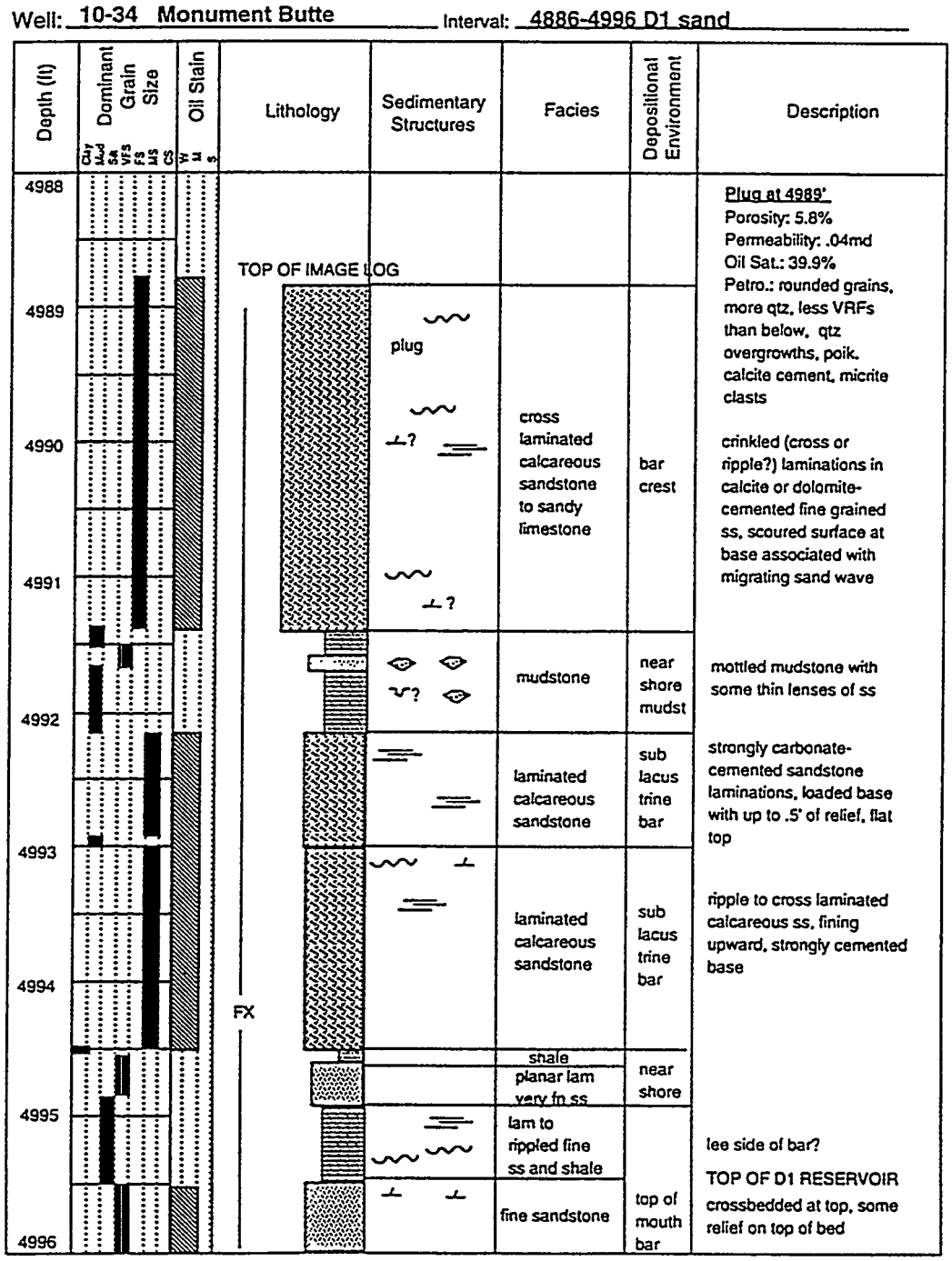

Figure 3-17. Lithologic log of the D1 reservoir interpreted from the FMI image from well Monument Federal #10-34

Well: 10-34 Monument Butte Interval: 4996-5004 D1 sand

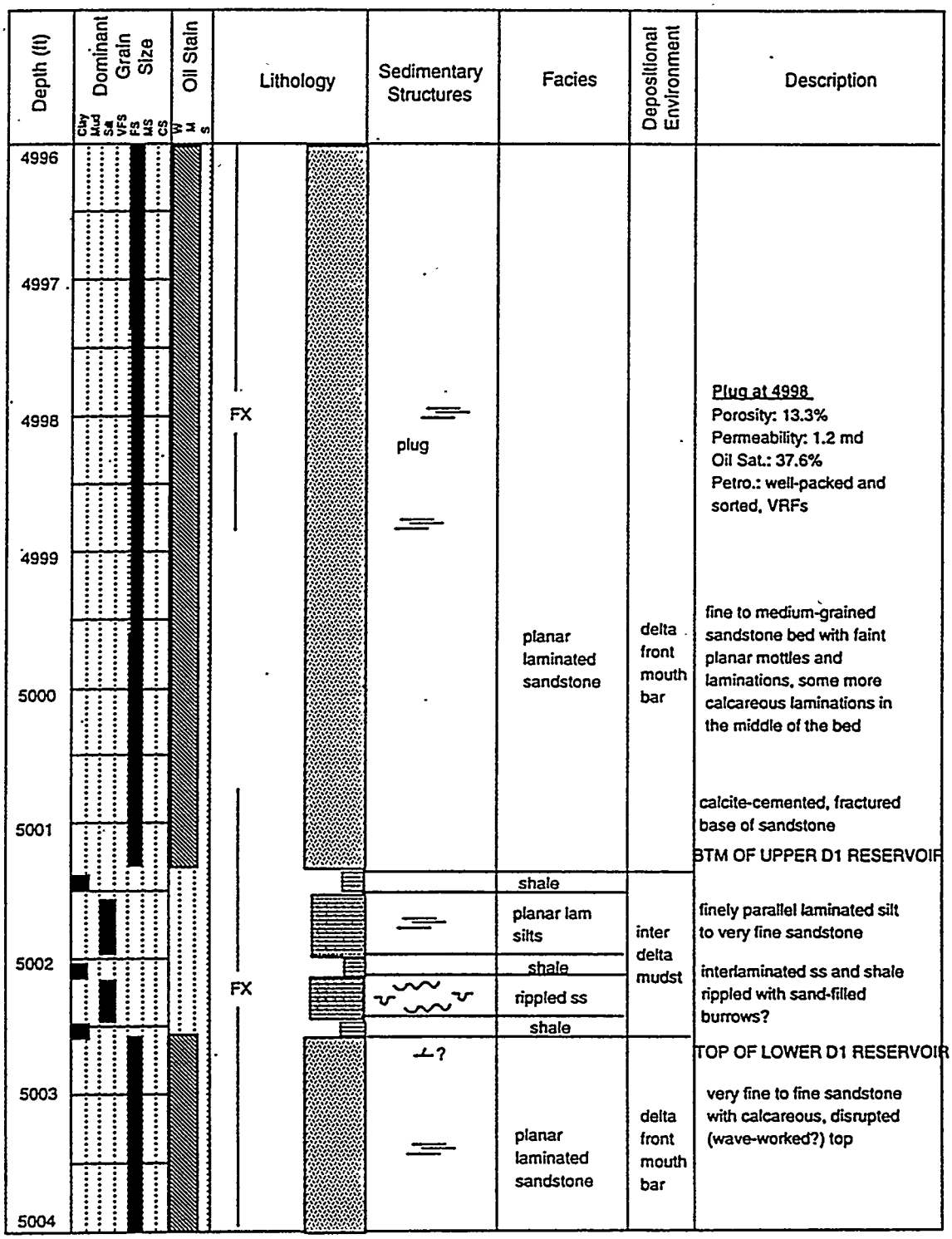

Figure 3-17. Continued

Well: 10-34 Monument Butte Interval: 5004-5012 btm of D1 sand

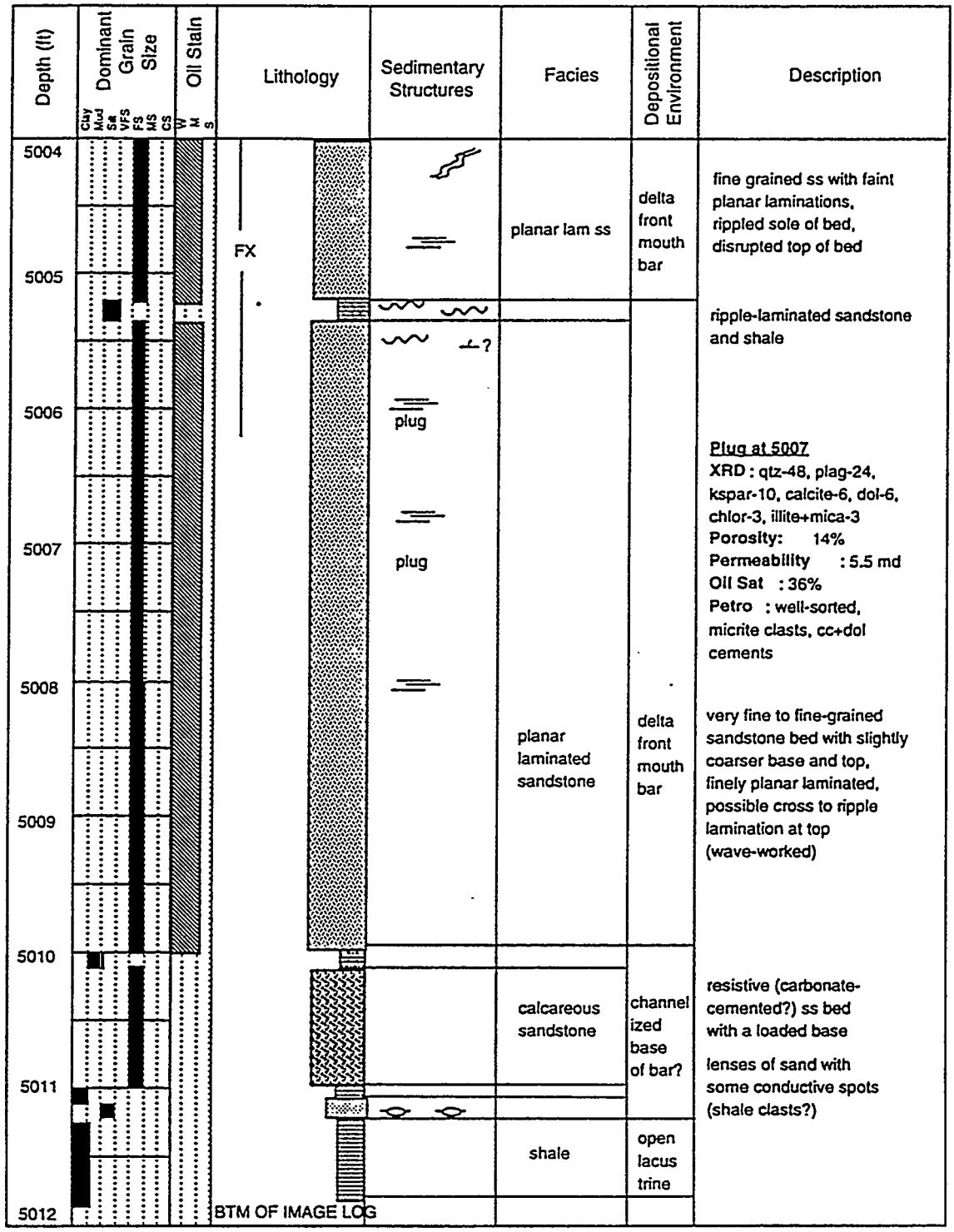

Figure 3-17. Continued

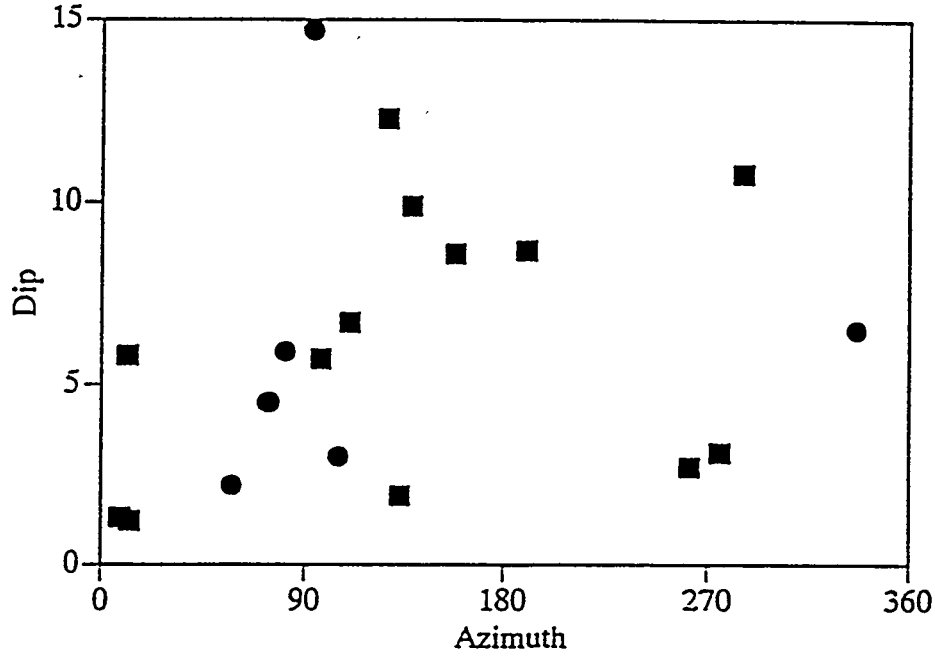

Figure 3-18. Dip versus azimuth (DVA) plot of bed orientation from the D1 reservoir in wells Monument Butte Federal #9-34 (squares) and #10-34 (circles)

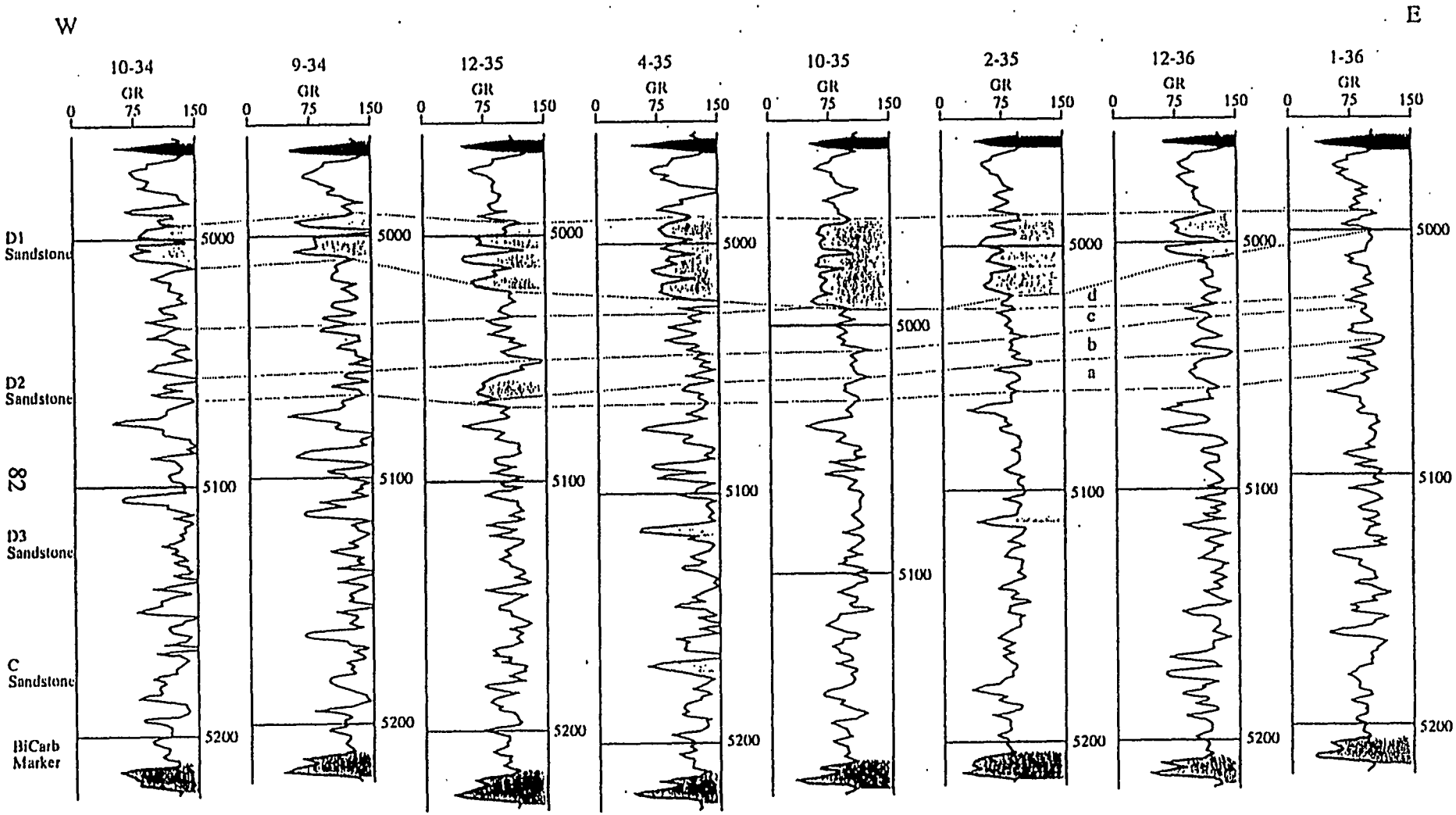

Figure 3-19. Correlated well logs of the D sandstone interval in the Monument Butte unit. The D1 sands consist of sublacustrine bars, separated by thin shales. The underlying packages of rock, labelled a, b and c, downlap in a lakeward-stepping pattern. The d beds and the D1 sands are vertically stacked in an aggradational pattern.

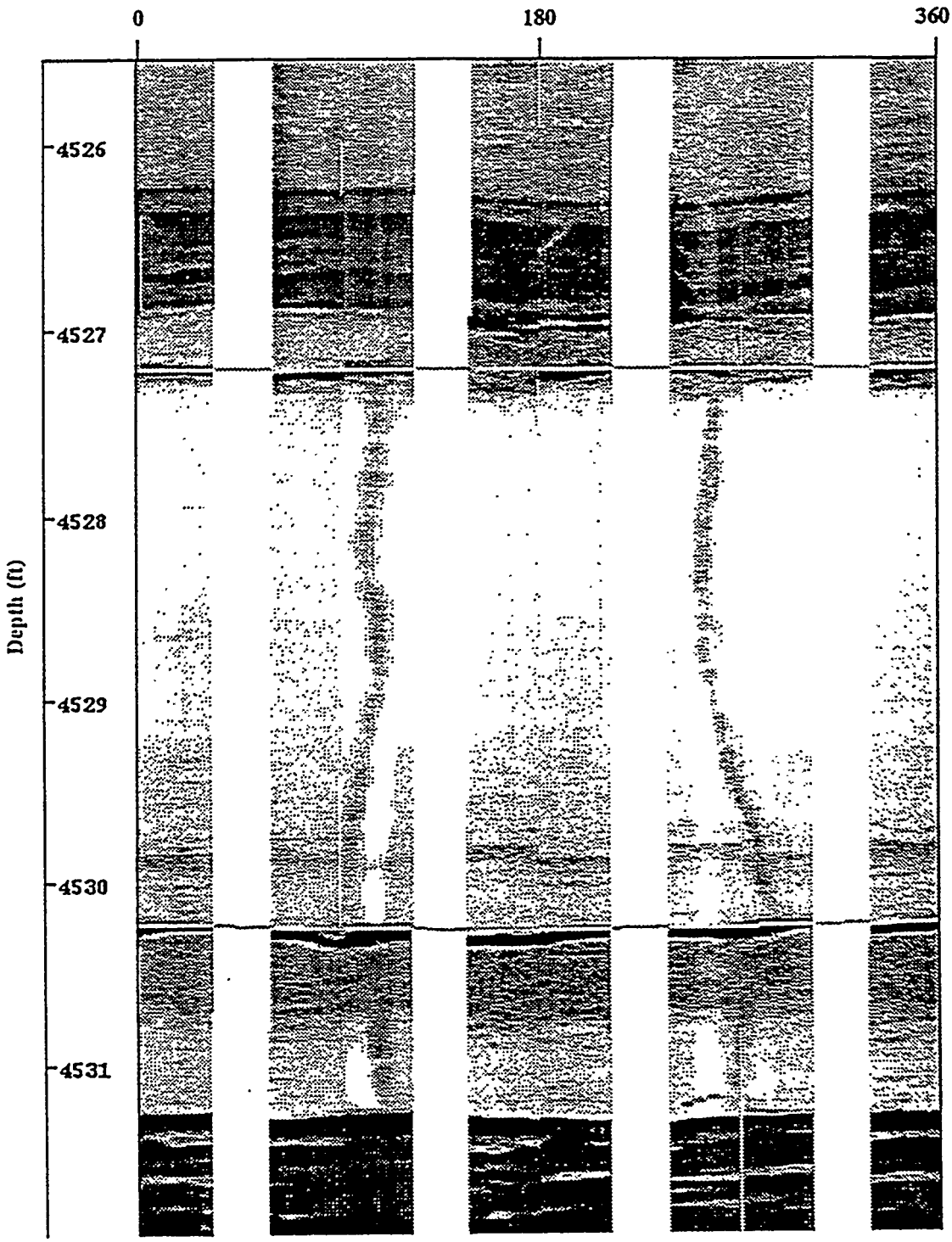

Figure 3-20. FMI image of a stratigraphically bound fracture from Travis Federal #5-33.

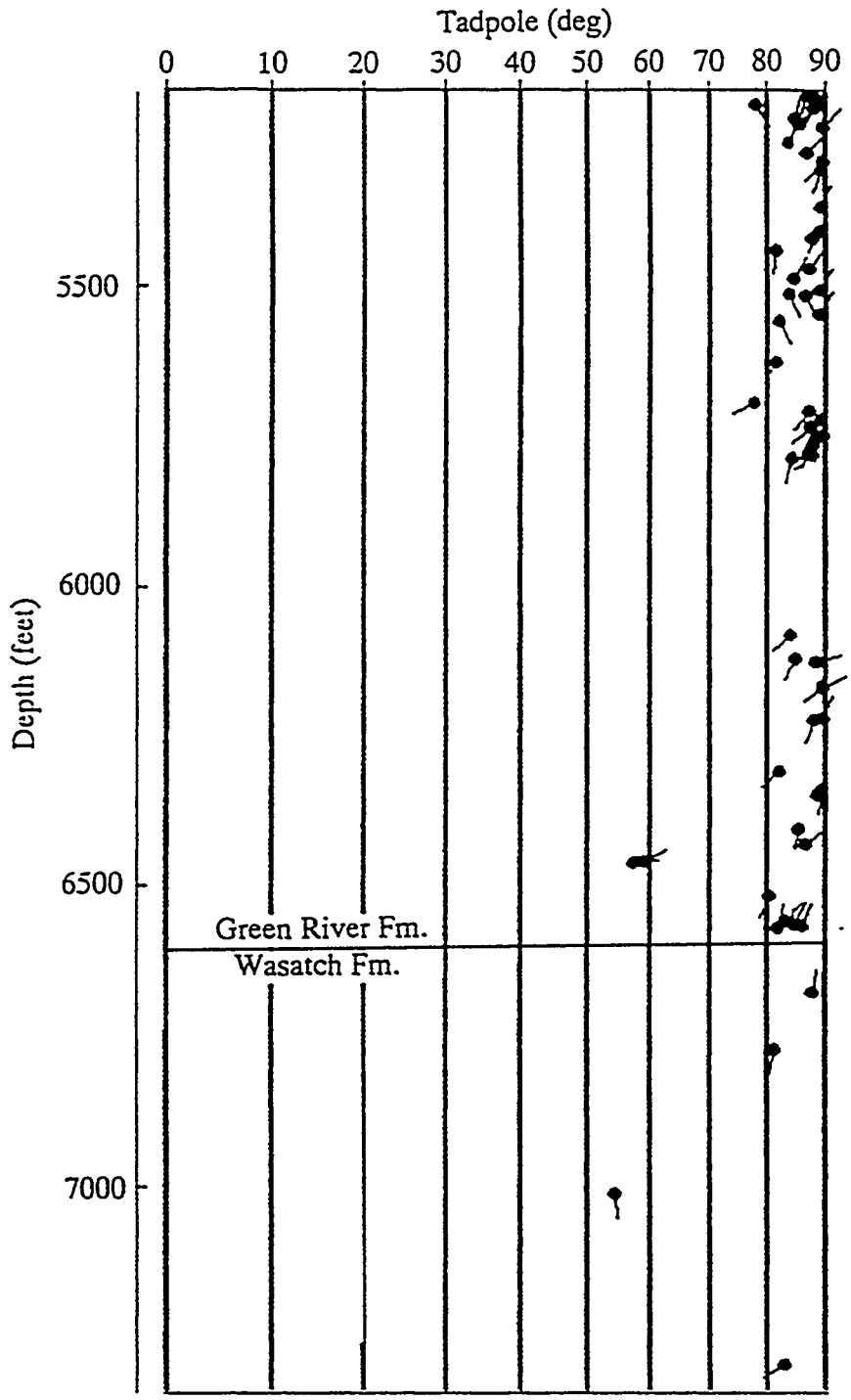

Figure 3-21. Tadpole plot of orientation of fractures imaged by the FMI log in Boundary Federal #12-21. The depth of contact between the Green River and the Wasatch Formations is shown.

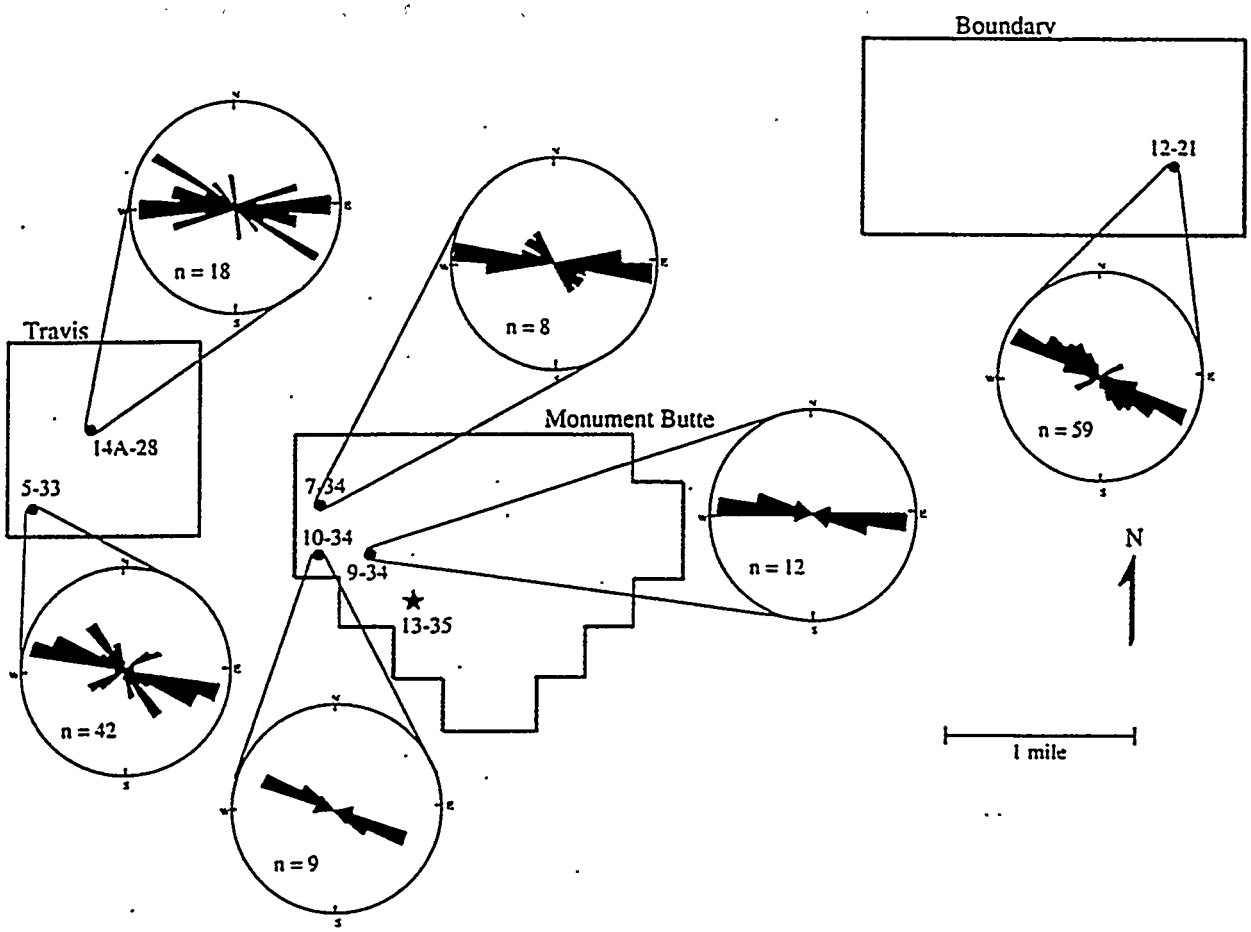

Figure 3-22. Rose diagrams showing the orientation of fractures imaged by the FMI log in the Greater Monument Butte oil field. Data shows the orientation of 140 fractures. Well #13-35 is the type log for the project.

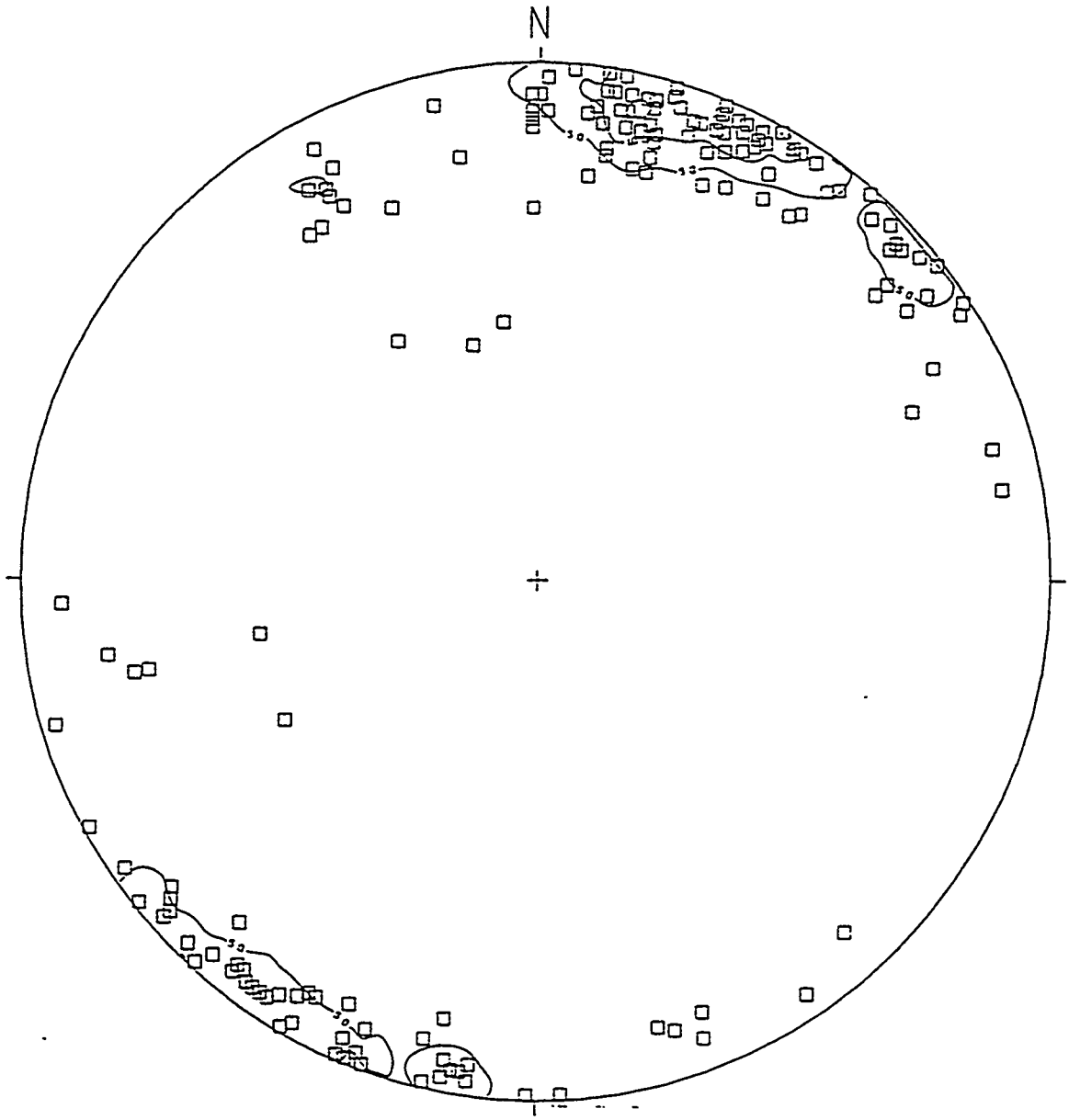

Figure 3-23. Equal angle projections of fractures imaged by the FMI in the Greater Monument Butte field. Contours at 5% and 10%. 165 samples.

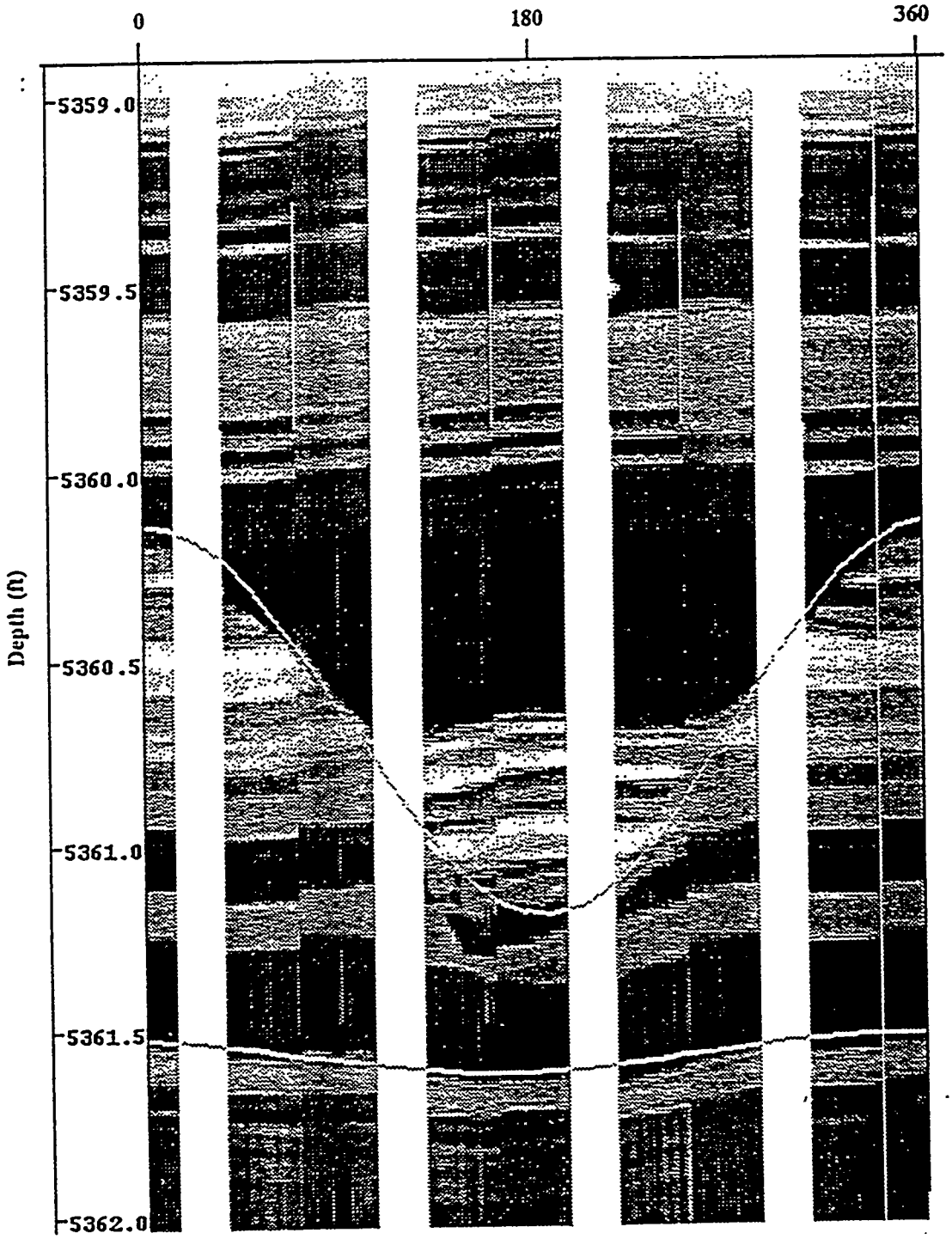

Figure 3-24. FMI image of a minor fault in well Travis Federal #5-33.

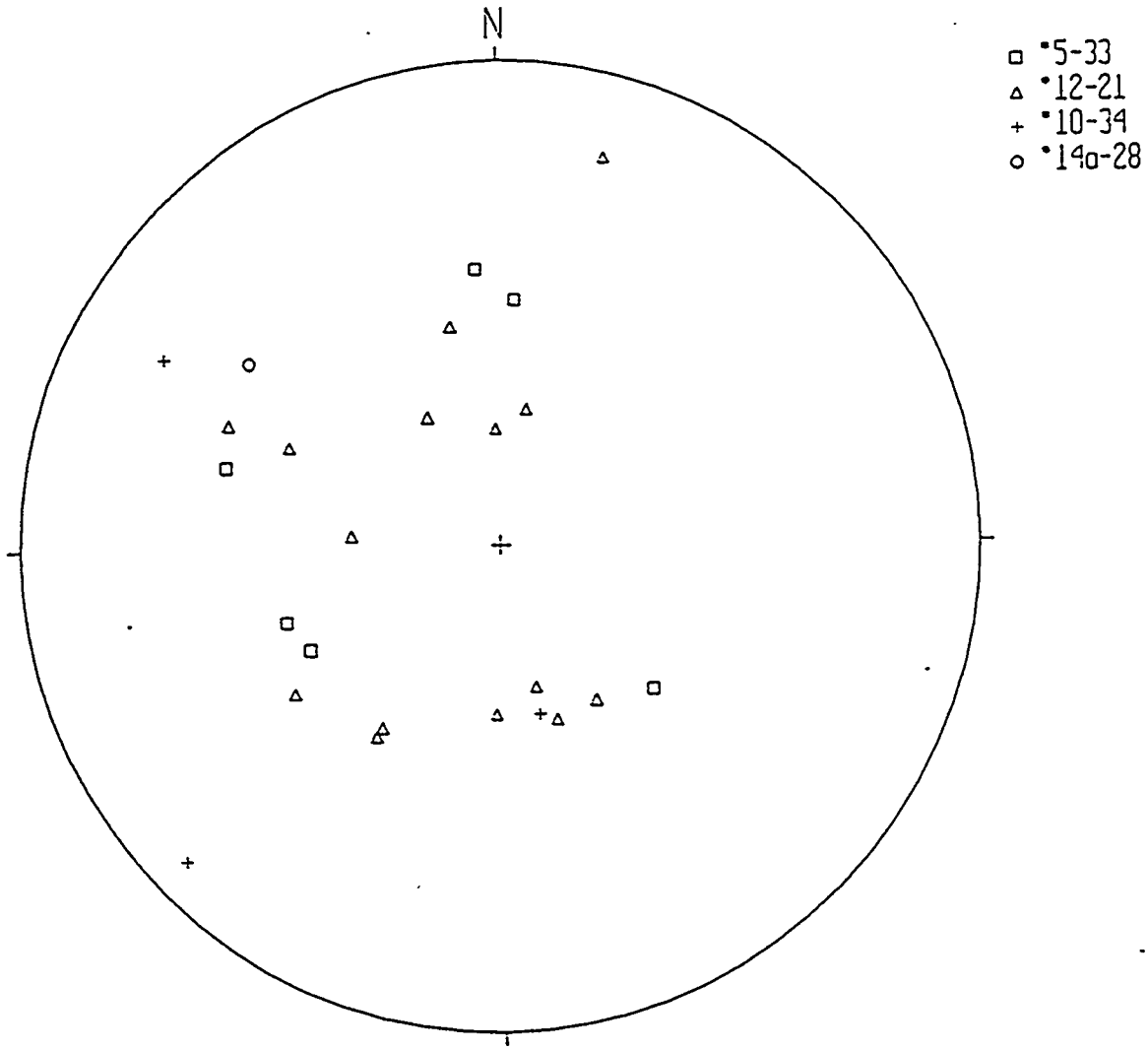

Figure 3-25. Equal angle projection of poles to minor faults measured by FMI logs in the Greater Monument Butte area

Chapter 4. Reservoir Simulation

Objectives and Approach

The preliminary objective of the reservoir simulation study was to develop a history match of the oil production from the Monument Butte unit. It was believed that this in turn, would provide credible evidence that the underlying production mechanisms were well captured by the model. The reservoir model could then be used for production forecasting. Initially, only the reservoir sands within the Monument Butte unit were modeled and the oil and gas production performance was matched unit-wide and on a well by well basis (U. S. DOE, 1994; Deo, et al., 1994).

As the unit expansion continued, it became evident that the multiple reservoir bodies within the Monument Butte unit extended well beyond the unit. At this time, the original model was expanded to include additional 80-acre strips on all four sides. In order to visually depict the basic mechanisms of solution gas drive and gas evolution during primary production, and reservoir pressurization and gas redissolution during secondary production, the time-dependent output data from the model was animated to create a video movie. The movie clearly showed which regions of the reservoir depleted first, which got pressurized and pockets of oil that was bypassed.

Geologic and production analyses of the nearby Wellsdraw and Jonah units, which were placed on water floods after the success of the Monument Butte unit water flood, showed that there was some degree of connectivity between sand bodies in these units. The question then was, what was the appropriate scale for representing and simulating these sand bodies ? In order to answer

this question, a 12-section area surrounding the Monument Butte unit was considered. First, the logs for about 200 wells in the region were digitized and geostatistical modeling was performed to generate reservoir images. Even though five to six sand bodies contribute to production in a typical well in the region, only DI and B2 reservoirs were simulated, since water flood in the Monument Butte unit targeted only these two sand bodies. Results of the geostatistical simulations and flow simulations using resulting reservoir images are presented in this report.

Introduction

In the Monument Butte region, it is common to produce oil from four to five (sometimes as many as twenty) productive sands typically arranged in a distinct layered format. The reservoirs in these sand units can be considered, for modeling purposes as distinct. Most of the reservoirs are undersaturated with the initial reservoir pressure close to the initial bubble point pressure. As a result, the gas oil ratios (GORs) increased precipitously a few weeks into the primary production process. The increased gas production slowed the oil production significantly causing low primary recovery. Had water flood not been implemented at this stage, the unit would not have been economically viable. A unique water flood strategy was implemented to revitalize the unit wherein the largest producers were converted to injectors. In keeping with the lacustrine depositional environment, fresh water was injected into the formation. The water flood strategy was successful and the secondary production from the unit has already exceeded the primary production.

A comprehensive reservoir simulation and history matching effort was undertaken to understand the production mechanisms underway in MBU. The results were published in an earlier paper (Deo, et al., 1994). In this study, thicknesses of the reservoir sands were assigned using geologic isopachs and knowledge about perforated intervals. Thicknesses of internal grid blocks (where

data was not available) were determined by conventional interpolation methods. The model area consisted of the unit with an additional 40-acre margin on each side. The geologic heterogeneity in the MBU was represented only through varying sand thicknesses. A thickness-weighted average porosity was assigned to each sand unit. For history matching purposes, permeabilities of well-containing grid blocks were adjusted until reasonable responses were obtained for the overall oil and gas production from the unit. All the wells in the unit and in the region in general, are hydraulically fractured and thus the near well bore permeabilities are markedly different from measured core permeabilities. The above approach yielded excellent history match with the field data, unit-wide as well as for most individual wells. The exercise also revealed that the reservoir performance in primary and secondary recovery closely resembled that of a undersaturated reservoir close to its initial bubble point pressure. The model also established that about 30% of the injected water migrated outside the unit boundaries.

The objectives of this study were the following:

1. To use all of the available data (mostly in the form of digitized logs) to generate geostatistical reservoir images of all relevant reservoir properties; thicknesses, porosities-permeabilities and water saturation.
2. To study the production performance of the Monument Butte unit in isolation and as a subset in a large 12-section area.
3. To combine the different reservoir property data sets and generate multiple realizations.
4. And to examine the resulting variability in primary and secondary production response for the unit and for the 12-section area.

A map of the 12-section area is shown in Figure 4-1. This area partially includes two other large water floods in the region. In this report, geostatistical analyses of two of the most productive

sands from the unit (DI and B2) and reservoir simulations of the D1-reservoir have been presented.

Geostatistical Modeling

The greatest advantage of geostatistical simulations is that the calculations provide equally probable reservoir images based on the data at known control points (wells). These realizations, in turn, give statistical variability in parameters such as initial oil and gas in place, etc. When different realizations from geostatistics are used in flow simulations, statistical variability in production can be obtained.

Data Employed

Usually the first step in generating a geologic model of a reservoir is distribution of different facies or rock types (Hand et al., 1994; Begg et al., 1994). Next, the distributions of lithotypes or sands are determined in individual facies, followed by porosities, permeabilities etc. Data on facies or lithotype distributions were not available for this study area. For each of the wells in the 12-section area, log data were available at 2 feet resolution. Porosity and water saturation values were calculated from the log data. Different sand intervals and thus thickness of the sands were identified in each well based on high porosity and low water saturation values. Approximately, 65 cores were obtained from some of the wells in the region. Air permeabilities were measured from these cores. Measured core permeabilities (horizontal direction) were in the 0.01-50 and range. Vertical permeability data were not available. A crossplot of permeability versus porosity was also available. The porosity-permeability crossplot is shown in Figure 4-2. The crossplot correlation was generated using data from a number of sands in the region. For the purpose of this study, it was assumed that the crossplot correlation was true for the D1 and the B2-sands.

The data were used to obtain distributions of thickness, porosity and saturations using geostatistical principles. In the absence of the facies data, individual sands were distributed through sand thickness as the first step. Once sand thickness and thus sands were distributed throughout the study area, porosities and water saturations were distributed independent of each other.

' Methodology.

Principles of sequential Gaussian simulations were used to obtain distributions of different properties. The SGSIM algorithm developed by Deutch and Journel (1992) was used to perform the simulations. The algorithm requires the data to be normally distributed. The data sets for each of the above mentioned attributes were transformed to obtain normal distributions. After the simulations they were transformed back to their original values. Following sections give information on individual properties.

Thickness

A horizontal variogram determined for the sand thicknesses was omni-directional. A model was obtained for this variogram. The variogram model had two components, one of which was spherical with a correlation length of 2000 feet and the other exponential with a correlation length of 4000 feet. The model for B2-sands was also omni-directional but had only a spherical component with a correlation length of 1450 feet. Both the D I and B2 sands models did not show any nugget effect. The details of the models are given in Tables 4-1 to 4-4. The distribution of D 1 and the B2 sand thicknesses in the I2-section model (one of the realizations) are shown in Figures 4-3 and 4-4. The sinuous nature of the reservoir is captured by these images.

Porosity and water saturation

Variograms were calculated to find spatial variability in the vertical and the horizontal directions. The vertical coordinates were normalized to obtain a uniform coordinate system, as the thickness of the sands varied from well to well. An average thickness was calculated. The thickness in each well was converted to the average thickness and the vertical coordinates were transformed' accordingly. A vertical variogram was calculated for these converted coordinates. A horizontal variogram was also calculated from all the available data values. These horizontal variograms were also omni-directional. Just like the thickness variogram, both the horizontal and vertical variograms were modeled by nested structures.

The correlation lengths for thickness and porosities were greater than the average well spacing of 1320 feet. For water saturations the first part of the model had a range of about 1200 feet, but the second structure showed correlation length greater than the average well spacing. Horizontal permeabilities were calculated from the simulated porosity values and the porosity-permeability cross-plot. The values of the permeabilities were constrained between 0.01-50 md, because the measured core permeabilities varied between those limits. The vertical permeabilities were assumed to be 50% of the horizontal permeability values.

The distributions of porosity, permeability and water saturations in the twelve section area are shown in Figures 4-5, 4-6 and 4-7 for the D 1 sands. The porosity distribution for B2 sands is presented in Figure 4-8. Only one of the several realizations generated has been chosen for presentation. Two different types of grids were used for generating distributions. A 33X25X 100 grid was used to generate data used for the analysis of fluids in place (grid block dimensions 660 ft. X 660 ft.), while a 17X13X100 grid was used to generate data sets for flow simulations (grid

block dimensions 1320 ft. X 1320 ft.). The correlation lengths for all the properties were greater than the block dimensions.

Reservoir Simulation

Reservoir simulation results for the D I sands are reported in this section. Geostatistical reservoir images for the unit and for the 12-section area were used as input in the black oil simulator IVIEX, developed by Computer Modelling Group (CMG). The grid size was 17X 13X5. This was a variable thickness, variable depth model. Each block was characterized by its own thickness, porosity, permeability and water saturation. For reservoir simulation purposes, geostatistical realizations were generated on a 17X 13X 100 grid. The vertical grid blocks were upscaled 1:20 using conventional single-phase upscaling algorithms. The reservoir properties (block thicknesses, porosities and water saturations) were generated independent of one another. Multiple realizations were generated and variation in initial fluids in place were calculated. Table 4-5 shows OOIP (original oil in place) and initial water in place statistics for the entire 12-section area and for the MBU for the D1-sands. Similar statistics for B2 are summarized in Table 4-6. As expected the variability is much greater for the 12-section area, where large portions are yet to be developed.

Two completely different realizations of individual properties were used in generating input data for reservoir flow simulations. In order to assess the effect of employing results of different realizations in reservoir simulation, only one or two of the property sets were changed. This resulted in a total of eight different input files for reservoir simulation. The data sets employed in each of the eight simulations are shown in Table 4-7. As explained previously, these data sets were generated on a larger grid and in general the models had more fluids in place than the

smaller grid models (Table 4-8). Once again the statistical deviation for the well-defined MBU were much lower than that for the entire 12-section area.

Results of reservoir simulation using one of the generated realizations are discussed below. In Dl-sands, the Monument Butte unit contained 10.3 MMstb of oil compared to a total of about 58 MMstb in the entire 12-section area. The average oil saturation in the unit was about 76% compared to 74% in the total area. The initial reservoir pressure was assumed to be 2500 psia based on a gradient of about 0.5 psi/ft. When the water flood was initiated in the unit in September of 1987, the average pressure in the unit had dropped to about 1400 psia compared to an average pressure of 2160 psia for the entire region. These numbers provide the extent of drawdown that the unit as a whole created with respect to the surrounding reservoir. The cumulative production from the unit was about 370 Mstb or about 3.5% of the original oil in place. The total primary production for the unit was about 420 Mstb and about two-third (281) to three-fourth (315) of this production is believed to be from the D sands. Thus, the model overpredicted primary production. The model results are still reasonably close to the field results considering that there are no adjustable parameters in the model. At the end of 1995, the model predicted a production of about 520 Mstb. The total production from the unit as of December 1995 was about 1.1 MMstb. The D-sand contribution is believed to be between 700 Mstb to 800 Mstb. Thus, the model underpredicted water flood performance significantly. The model does not take into account hydraulic fractures. The results obtained thus far indicate that it is very important to consider the effect of hydraulic fractures on production. A material balance on water does indicate that most of the water injected into the unit stays in the unit.

In order to assess the impact of the model scale on primary and secondary recovery performance, reservoir simulations of the 12-section area, where the unit was essentially a subset were

compared to simulations of the unit with only additional 40-acre strips on all sides. The simulation data sets for this comparison were developed using identical geostatistical data sets. The results of the MBU primary and secondary production at smaller and larger scales are compared in Table 4-9. The reservoir performance is almost identical at both the scales considered. Based on the extent of sands and on field experience, it was believed that the model scale would have a larger impact than what was observed in the simulation study. Hydraulic fractures were not accounted for in the simulations. Thus, the overall low reservoir permeabilities may have contributed to the observation concerning the effect of model scale on primary and secondary production performance.

The variability in primary and secondary production observed using the abovementioned eight statistical realizations is summarized in Table 4-10 for the Monument Butte Unit. The deviations in primary production for MBU were low, even in comparison to the deviations observed in the unit fluids in place values. This trend basically continued for the remainder of the unit history (total production-Table 4-11). The deviations in gas production were higher in primary production and lower in secondary production. The deviations for total oil and gas production from the 12-section area were as expected greater (on a normalized basis) than deviations for equivalent values for the unit.

Conclusions

Variations in original oil and gas in place were greater for the relatively unexplored 12-section area in comparison to the variations of the same parameters in the well defined Monument Butte Unit. The reservoir scale used in representing the MBU did not affect the production response from the unit significantly. The variability in primary and secondary production from MBU for different geostatistical realizations was low. Thus, reservoir heterogeneity at this scale did not

affect primary and secondary response from MBU. No adjustable parameters were used in matching reservoir performance. This approach did not yield good history match, particularly because effect of hydraulic fractures was not incorporated in reservoir description.

References

Deo, M. D., Sarkar, A., Nielson, D. L., Lomax, J. D. and Pennington, B. I.: "Monument Butte Unit Case Study: Demonstration of a Successful Water flood in a Fluvial Deltaic Reservoir," paper SPEIDOE 27749, *Proc.*, SPE/DOE Ninth Symposium on Improved Oil Recovery, Tulsa, Oklahoma (1994) 143.

Hand, J. L., Moritz Jr., A. L., Yang, C-T and Chopra, A. K.: "Geostatistical Integration of Geological, Petrophysical, and Outcrop Data for Evaluation of Gravity Drainage Infill Drilling at Prudhoe Bay," paper SPE 28396, *Proc.*, SPE Annual Technical Conference and Exhibition, New Orleans, LA (1994) 347.

Begg, S. H., Kay, A., Gustason, E. R. and Angert, P. F.: "Characterization of a Complex Fluvial-Deltaic Reservoir for Simulation," paper SPE 28398, *Proc.,* SPE Annual Technical, Conference and Exhibition, New Orleans, LA (1994) 375.

Deutsch, C. V. and Journel, A. G.: GSLIB *Geostatistical Software Library and User's Guide*, Oxford University Press, New York City (1992).

U.S. DOE (1994), *Green River Formation Water Flood Demonstration Project*, Yearly Report.

Table 4-1. D1 sands: Different variogram properties

Property	Variogram: Nested Structure 1			
	Model	Range	Sill	Vertical anisotropy
Thickness	Spherical	2000	0.75	1.0
Porosity	Spherical	2000	0.80	0.000956
Saturation	Spherical	1200	0.75	0.00119

Note - The lateral anisotropy is 1.0 for all the properties.

Table 4-2. D1 sands: Additional variogram properties

	Variogram: Nested Structure 2			
Property	Model	Range	Sill	Vertical anisotropy
Thickness	Exponential	4000	0.25	1.0
Porosity	Exponential	4000	0.20	0.000797
Saturation	Spherical	3000	0.25	0.00159

Table 4-3. B2 sands: Different variogram properties

Property	Model	Range	Sill
Thickness	Spherical	1450	1.0
Porosity	Spherical	2400	1.0
Saturation	Spherical	1700	1.0

Table 4-4. B2 sands: Additional variogram properties

Property	Major anisotropy angle	Lateral anisotropy	Vertical anisotropy
Thickness	Omni	1.0	1.0
Porosity	Omni	1.0	0.0003
Saturation	Omni	1.0	0.0018

Table 4-5. Statistical variations of fluids in place for several geostatistical realizations

Statistics	Entire 12-section area		Monument Butte Unit	
	OOIP (Mstb)	OWIP (Mstb)	OOIP (Mstb)	OWIP (Mstb)
Mean	54176	23477	10073	4019
Standard Deviation	8446	4333	653	336
High	70998	33175	10926	4440
Low	40490	17268	8518	3187

Table 4-6. Statistical variations of OOIP (MSTB) for B2 sands

Statistics	12-section area	MBU
Mean	64365	10145
Standard Deviation	11368	1154
High	84159	12307
Low	48502	7768

Table 4-7. Geostatistical property sets used for reservoir simulations

Simulation ID	Thickness	Porosity/permeability	Water saturation
1	Set 1	Set 1	Set 1
2	Set 2	Set 1	Set 1
3	Set 1	Set 2	Set 1
4	Set 1	Set 1	Set 2
5	Set 2	Set 2	Set 1
6	Set 2	Set 1	Set 2
7	Set 1	Set 2	Set 2
8	Set 2	Set 2	Set 2

Table 4-8. Statistical variations of fluids in place for the eight realizations used in reservoir simulations

Statistics	Entire 12-section area		Monument Butte Unit	
	OOIP (Mstb)	OWIP (Mstb)	OOIP (Mstb)	OWIP (Mstb)
Mean	65328	27603	11221	4218
Standard Deviation	5147	2595	755	283
High	72734	31336	12474	4673
Low	57973	23432	10275	3873

Table 4-9. Comparison of the performance of the Monument Butte unit at two different reservoir scales

	Simulation of MBU as an isolated reservoir		Simulation of MBU as a subset of the 12-section area	
	Oil (Mstb)	Gas (MMscf)	Oil (Mstb)	Gas (MMscf)
Primary Production	376	1162	375	1198
Secondary Production	522	2235	519	2253

Table 4-10. Statistical variations in primary productions for eight reservoir simulations using property sets shown in Table 3

Statistics	Entire 12-section area		Monument Butte Unit	
	Oil Produced (Mstb)	Gas Produced (MMscf)	Oil Produced (Mstb)	Gas Produced (MMscf)
Mean	563	1522	385	1212
Standard Deviation	49	207	7	26
High	616	1763	395	1254
Low	500	1295	375	1177

Table 4-11. Statistical variations in total production for eight reservoir simulations using property sets shown in Table 3

Statistics	Entire 12-section area		Monument Butte Unit	
	Oil Produced (Mstb)	Gas Produced (MMscf)	Oil Produced (Mstb)	Gas Produced (MMscf)
Mean	1181	6177	538	2298
Standard Deviation	85	335	14	24
High	1288	6648	565	2338
Low	1076	5717	519	2253

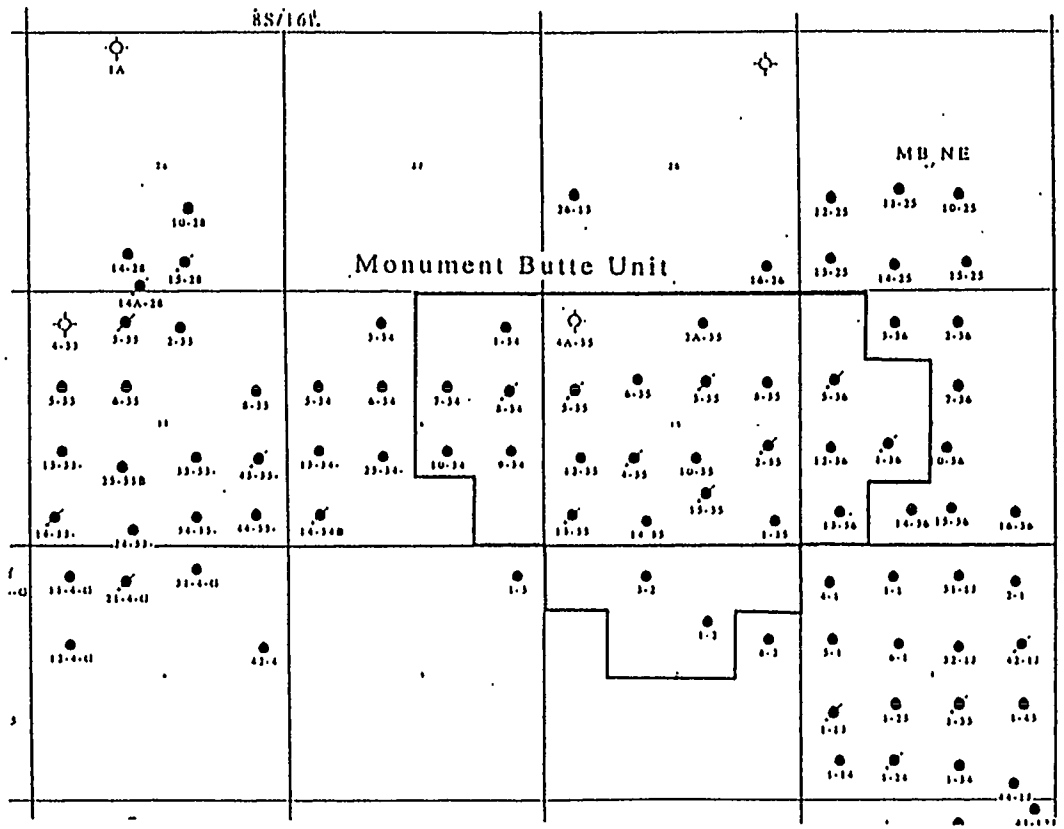

Figure 4-1. The 12-section area around the Monument Butte unit used in reservoir simulations

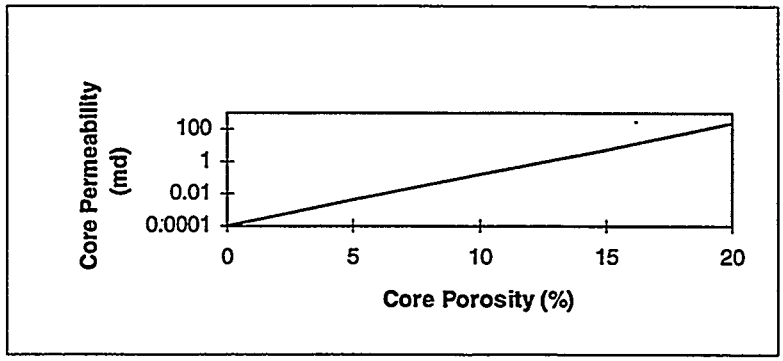

Figure 4-2. Porosity-permeability cross plot

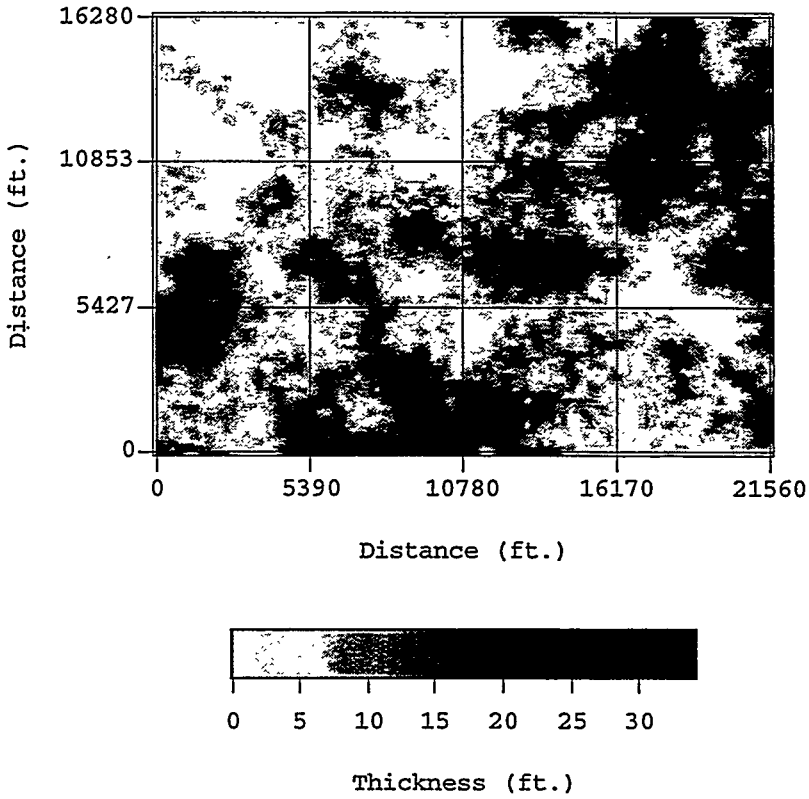

Figure 4-3. Thickness distribution of D1 sands in the 12-section area

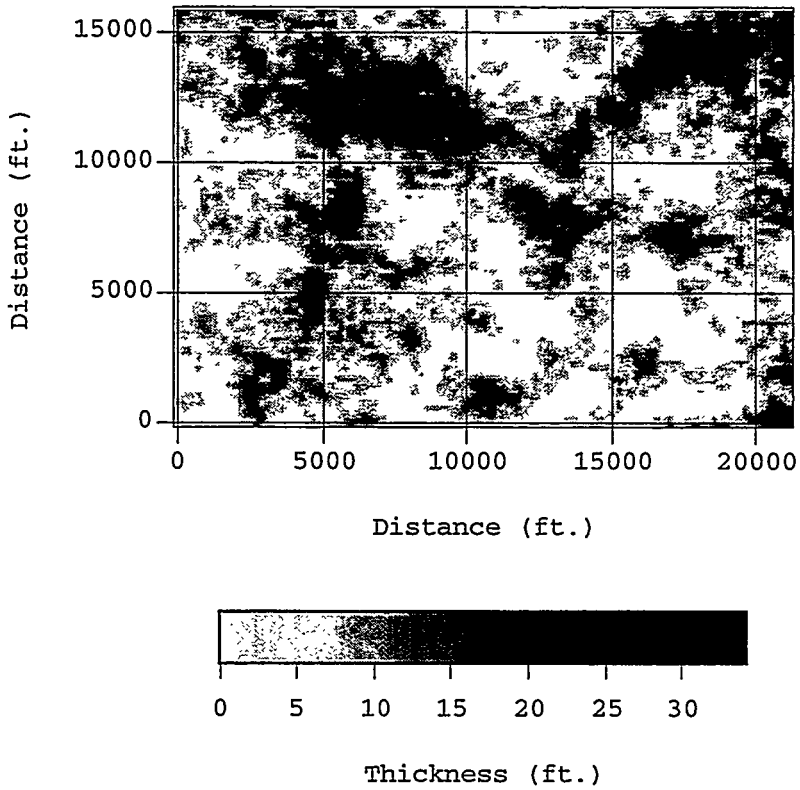

Figure 4-4. Thickness distribution for B2 sands in the 12-section area

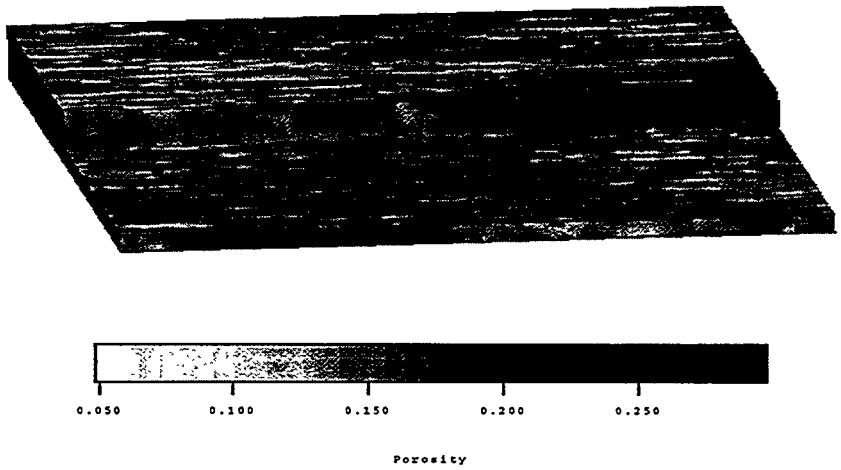

Figure 4-5. Porosity distribution of D1 sands in the 12-section area

5 10 15 20 2S 30 3S 40 45 SO

Permeability (ad)

Figure 4-6. Permeability distribution of Dl sands in the 12-section area

0.1 0.2 0.3 0.4 0.5 0.6 water

saturation

Figure 4-7. Water saturation distribution for Dl sands in the 12-section area

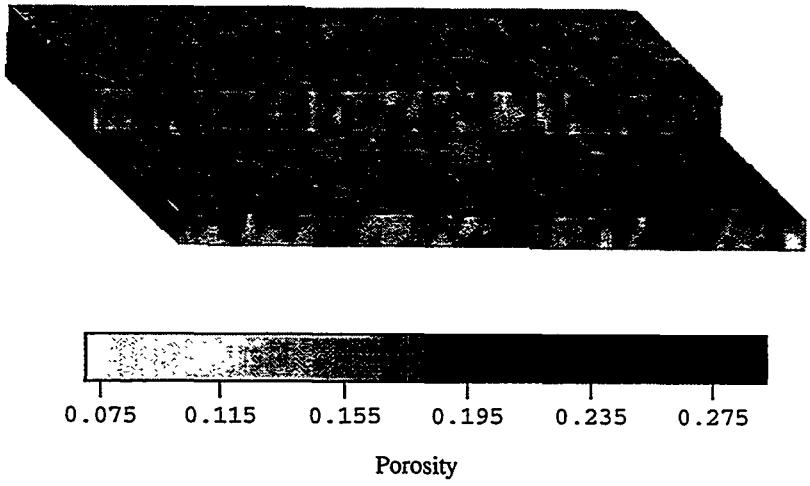

Figure 4-8. Porosity distribution of B2 sands in the 12-section area

Chapter 5. Reserve Considerations and Economics

Reserves

Eighteen wells were drilled and completed in the Monument Butte Unit as of November 1987, and the cumulative production from these wells from September 1981 through November 1987 was 413,830 bbls of oil, 1,646,968 MCF of gas and 11225 bbl of water. The unit reservoir engineering committee in their reserve report estimated remaining primary oil reserves at 27,000 bbls oil using production decline analysis techniques. The field was rapidly becoming uneconomic. Further primary development was not economic, and unless a secondary recovery project could be implemented, the Green River sand play was over.

In November 1987 water injection was commenced on a pilot water flood. At that time the field was producing approximately 40 bbls of oil per day (BOPD), 410 MCF of gas per day, and 2 bbls of water per day. Over the next six months, production continued to decline to about 35 BOPD. At that time, the decline in production rate appeared to cease, and by April, 1989 after an additional 12 months of injection and cumulative injection volume of 355, 927 bbls of water, oil production had increased to 125 BOPD, and the gas-oil ratio had declined from 7750 scf/bbl to 1800 scf/bbl. In August 1991, 46 months after initial injection and with a cumulative injection volume of 1,287,726 bbls of water, production peaked at an average of 360 BOPD. A consulting reservoir engineering firm on January 1, 1992, estimated remaining recoverable reserves to be 1, 382,319 bbls of oil, representing ultimate reserves of 2,021,445 bbls (about 20% OOIP). On January 1, 1996 the cumulative oil production was 1,342,146 bbls of oil with remaining oil reserves estimated at 1,001,806 bbls of oil representing an ultimate recovery after

water flood of 2,343,952 bbls of oil, versus estimated ultimate recovery under primary of 440,830 bbls of oil. This recovery represents about 21% of the original oil in place in the D and the B sands, the only sands being waterflooded in the Monument Butte unit.

The secondary to primary recovery ratio for the Monument Butte unit (as of April 30, 1996) was about 2.6 and is estimated to be about 5.6 ultimately. The primary recovery was low due to the fact that the initial reservoir pressure was very close to the initial bubble point pressure leading to high gas production and precipitous decline. High paraffin content of the crude also contributed to well bore plugging and production problems, lowering primary recovery. The ultimate recovery of 21% is low compared to other water floods and is due to poor areal sweep.

Normally individual Green River sand fields in this part of the basin will be approximately the same size as the Monument Butte Unit; however, there are other considerations that need to be taken into account prior to forming a unit or commencing a water flood. In most wells there are three to five sands that are potential commercial reservoirs, although usually only one or two will have enough lateral extent for three or more wells to intersect the sand. Therefore, when one or two sections are drilled up on forty acre spacing, there may be two or more water floods active in separate reservoirs. This situation currently exists in the Monument Butte Unit Green River formation D and B sands. The D sand was first water flooded as an individual sand to establish the viability of secondary recovery in this sand. When this was successful, water flooding of B sand began. Production rates, injection rates, and pressures were monitored, and the results indicated that the additional water flood was also successful. This is an important concept because, unlike many reservoirs that cover large areas, in this area there is considerable oil in place but the reservoirs are relatively small in areal extent, although they stack up and overlap so

that more than one sand can be water flooded simultaneously. Being able to combine water floods enhances the economics through increased reserves and increased production rates. Detailed geological mapping with extensive cross section evaluation, will define the reservoirs that need to have extensive reservoir evaluation. In some cases, rotary sidewall cores, and or one or more of the sophisticated logging programs will be needed to aid the reservoir evaluation. The FMI log is most helpful for evaluating fracturing, thin bed stratigraphy, and picking appropriate core points. The MIRL log is valuable for determining effective permeability, fluid content of the reservoir along with the relative mobility of the oil and water. Good reservoir characterization and definition will determine the potential for development of a commercial water flood. Even though the FMI and the MRIL logs provide useful reservoir data, it is not practical (in an economic sense) to use these tools on every well that is drilled. These logs should be used to calibrate the reservoir information from other suite of logs. It is difficult to generalize the frequency with which these logs ought to be employed. From a reservoir characterization viewpoint, it is advisable to use the FMI at least once in a one to two square mile area while MRIL could be used once in a two to three square mile area. Once again, these guidelines are valid only in the immediate vicinity of the field and are likely to change depending on the complexity of the geologic environment and the economics of the entire project. Success of the Monument Butte Unit, and the indication of response in the Jonah Unit, Gilsonite Unit, and Wells Draw Unit, all of which have had indications of response to injection, supports the theory of the floodability of the Green River sands. These last three units are not part of the DOE Study, although, they were all started as a result of the Monument Butte success. The water flood in the Travis unit was put on hold due to water channeling problems. This is believed to be due to the lithologic complexity of the Lower Douglas Creek reservoir (please see the

discussions in Chapter 3) and due to the 20-acre spacing and hydraulic fracturing practices. At the present time, the unit is being reevaluated. The Boundary Unit had not started water injection as of January 1996. The Boundary unit has eight to ten possible water flood targets, some of which have oil-water contacts. This makes. designing and operating the water flood more complicated. As of April 1996, in the study area, there are eight active water flood units, with two more being formed. In the immediate area of the trend play there are six more active water flood units, all of which have been started after Monument Butte Unit became successful. With fourteen active units, and others being formed, the. magnitude of this play begins to take on significant proportions. It is projected that with the water floods now active the potential recoverable reserves will exceed more than thirty million barrels of oil, and when the trend is fully developed the potential reserves will exceed one hundred million barrels of oil.

Economics

As water flood operations continue throughout the Monument Butte area of the Uinta Basin, operators continue to evaluate their investment decisions in order to obtain the best possible internal rate-of-return. Considerations such as taxes, drilling and completion cost, cost of capital and oil prices become increasingly important as additional water flood projects are implemented. Oil and gas companies typically value reserves on *a time value of money* basis commonly referred to as the Net Present Value (NPV). Each Net Present Value calculation must be discounted for the imputed cost of capital. The assumed cost of capital for this analysis is 10% (NPV- 10).

Economics of the Monument Butte Unit

As of September 1987 primary production had been 405,000 barrels of oil. Reservoir engineers estimated approximately 27,000 barrels remaining reserves and the field was producing 40 barrels of oil per day. At this time the field was S I,635,000 from payout and with the remaining reserves it would never payout. Water injection began in October, 1987 and by September, 1993 the field had a positive net revenue of $1,733,000 for this period (October 1987 - September 1993). From September, 1993 to August, 1996 the Unit had an additional positive net revenue of about $751, 624, for a total net revenue of about 52,484,624. In addition, the discounted value (NPV-10) of the remaining reserves within the Monument Butte Unit, as of July 1, 1996 was S11,851,260.

Future Development Model

Due to the success of the Monument Butte water flood project, and the successful transfer of technology, development drilling within the area is being pursued by Inland Resources as well as other operators. As development drilling advances, new economic scenarios evolve as oil production rates verses time change from those observed at the Monument Butte Unit. At the Monument Butte Unit, primary depletion of the reservoir was allowed to persist for the first 5-6 years of production before the first water was injected into the reservoir. In most cases, revenue from oil production was not adequate to provide a return in excess of the initial capital required to drill and complete the wells. This situation allowed a large portion of time to elapse during which net revenue from oil production was providing only a marginal, if any, rate-of return on the initial capital investment. In order to maximize the rate-of-return, current development drilling programs allow for the conversion of producers to injectors within the first 6-8 months of

the initial production of the well. This practice has allowed the reservoir pressure to be maintained, as opposed to allowing the well to cycle through a full depletion history and subsequent repressurization, as experienced at the Monument Butte Unit.

Investment Units

Economic modeling of the development program has been broken down into basic building blocks called "Investment Units". An Investment Unit considers the cost of drilling and completion operations for two wells versus the revenue generated by oil production over time. The economics of an investment unit assumes that both well are drilled and completed as producers with one well being converted to an injector 6 months after the production is established. Each well is drilled on a 40 acre tract, thus each investment unit consists of 80 acres (2 wells x 40 acres). Investment units are intended to be drilled in groups with a minimum of 8 investment units drilled contiguously. Multiple investment units must be drilled in order to achieve full five-spot injection pattern. Without full five-spot injection patterns, an investment unit may not perform to its full potential. (See Figure 5-1).

Type Decline Curve

Production histories from wells within the Monument Butte area (Figure 5-2) were analyzed in order to develop a most likely case scenario for production rates versus time. Since both wells within the investment unit are initially produced, the historical decline curve is multiplied by a factor of 2. Average historical initial production (I.P.) rates were observed to be approximately 125 BOPD. During the first 6 months of production both wells are produced. During this period, production declines at approximate 85% exponential decline,typical of wells with no pressure support. After 6 months of production from both wells, one of the wells is converted to

an injection well for the purpose of providing pressure support for the offset well. At this point, the production from the investment unit is reduced by' , in order to reflect the dedication of one well to a water injection well. Over the next six months, .production continues to decline from the one ' remaining producer until the effects of injection have been realized. At this time, production begins to gradually rise as reservoir pressure builds. The single producing well eventually peaks at a stabilized production rate of approximately 65 BOPD. This rate declines slightly at 8% per year over the next 4 years until water breakthrough occurs. At water breakthrough, the decline accelerates to a 25% exponential decline until the investment unit reaches its economic limit of approximately 7 BOPD (Figure 5-3). At the economic limit, the cost to operate both the injection well and the producing well are in excess of the revenue from the producer.

Conclusions

The model requires assumptions to be made regarding the cost of drilling and completion, taxes, royalties, operating cost and oil price. The following model assumptions have been made based on historical data:

Assumptions:

DRILLING AND COMPLETION COST (2 WELLS)	$700,000.00
WORKING INTEREST	100.0%
NET REVENUE INTEREST (Working Interest minus royalty)	85.0%
OIL PRICE	$17.75
TAXES	4.5%
LEASE OPERATING EXPENSE	$1400.00/MO

Conclusions:

NET PRESENT VALUE @10%	$865,857.00
LIFE OF PROJECT IN YEARS	16.0 YEARS
RATE-OF-RETURN	48.8%
PAYOUT	3.12 YEARS

Based on the assumptions above, the economic model was run in order to value a typical investment unit. The main purpose of the economic model is to calculate the value of the investment unit at the time the initial investment is made. The Net Present Value calculation is used to discount the value of the investment based on the time require to recover the cost of the initial capital requirements and realize a return on the investment. The profit of the investment unit is $865,857.00. It is important to note that the profit of the investment unit is net of the 8700,000. 00 initial investment cost, i.e. the discounted revenue pays back the capital investment in 3.12 years and has a cumulative discounted cash flow of an additional $865,857.00. In addition, payout, rate-of return, and project life were evaluated by evaluating cash flows on a monthly basis and are summarized below. The economic results of the Development Drilling Type Decline curve are superior in all categories to the actual Monument Butte Decline. The difference is attributable to the commencement of injection at a much earlier time. Early injection allows higher volumes of oil to be recovered within a shorter period of time and thus provides a higher rate-of-return.

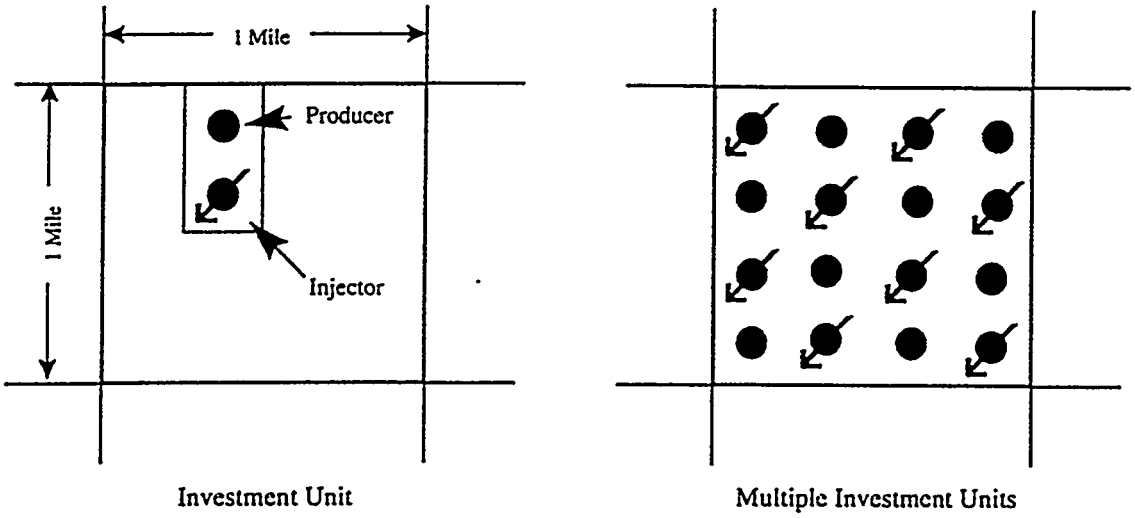

Figure 5-1. Investment unit in a five-spot water flood development

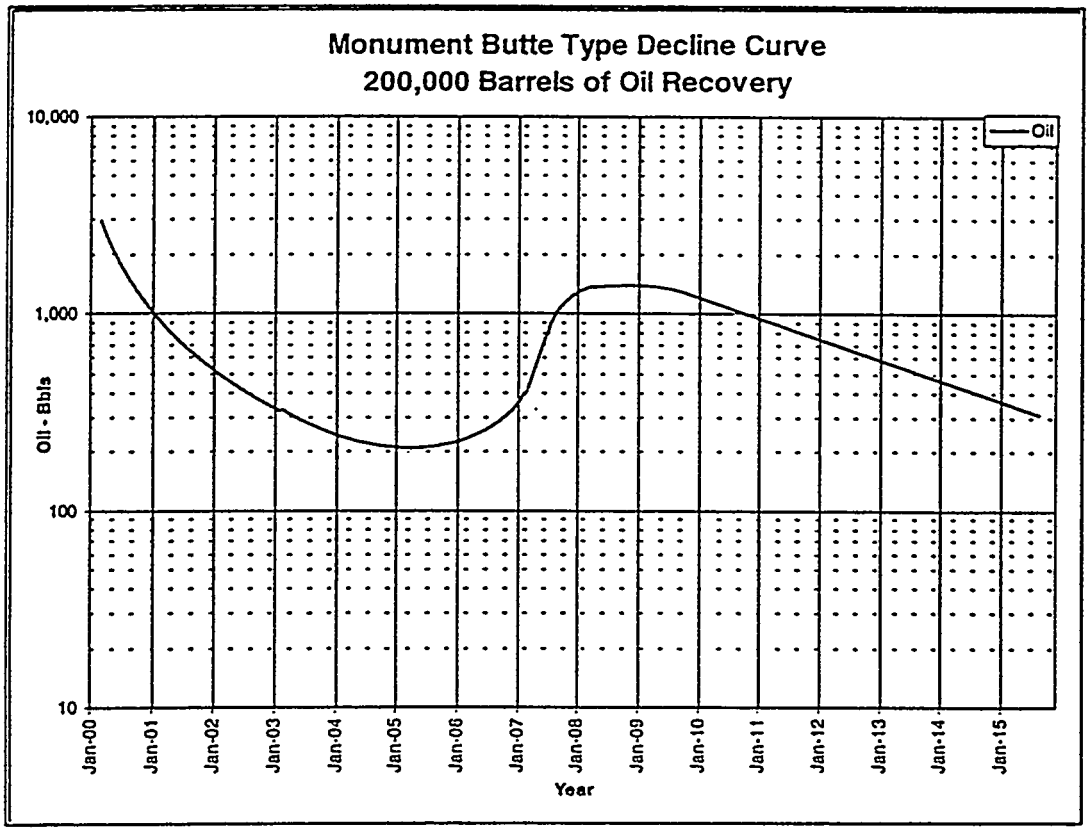

Figure 5-2. Historical (average) Monument Butte decline curve

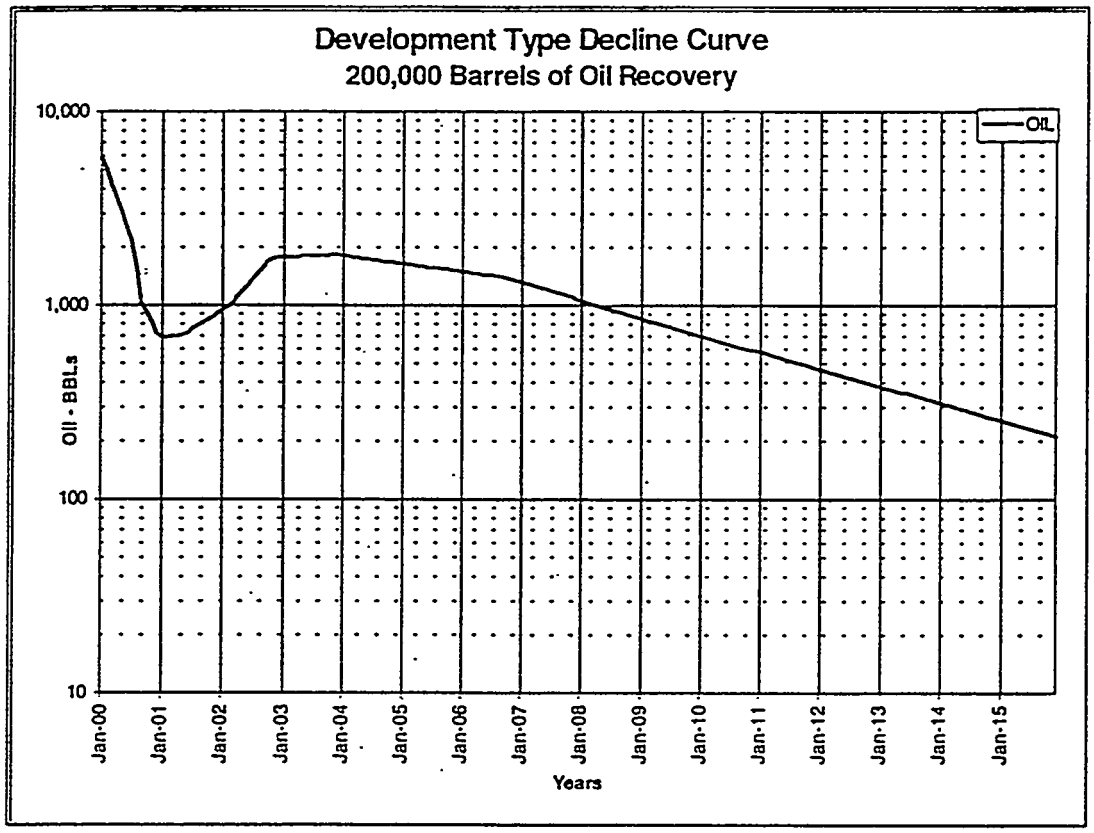

Figure 5-3. The decline curve used for the economic analysis

Chapter 6. Technology Transfer

As part of the Monument Butte expansion, more than 30 wells have already been drilled. Primary production from each of these expansion units has been better than the original Monument Butte unit at around the same stage in the life of the reservoir. Water floods have been started in the expansion units recently and production wells have not yet responded. The water floods in the Jonah and the Wellsdraw units were begun as a direct consequence of the success of the Monument Butte water flood. These floods have had good success. The oil production rate in the Jonah unit has approximately tripled while that in the Wellsdraw unit has nearly doubled since the inception of their respective water floods.

The following is a list of papers and other publications that resulted due to this project.

List of Papers and Publications

1. Water Flood Project in the Monument Butte Field, Uinta Basin, presented by John D. Lomax, Annual meeting of the Interstate Oil and Gas Compact Commission, December 6-8, 1992, Salt Lake City, Utah.
2. Water Flood Project in the Uinta Basin, presented by Milind D. Deo, Monthly meeting of the Salt Lake section of the Society of Petroleum Engineers, February 16, 1993, Salt Lake City, Utah.
3. Potential of Water Flooding in the Uinta Basin, presented by Milind D. Deo, Monthly meeting of the Uinta Basin section of the Society of Petroleum Engineers, March 25, 1993, Vernal, Utah.

4. Green River Formation Water Flood Demonstration Project Showing the Development of New Reserves in the Uinta Basin, presented by John D. Lomax, meeting of the Workshop for Independent Oil & Gas Producers in the Appalachian & Illinois Basins, June 4, 1993, Lexington, Kentucky.

5. Green River Formation Water Flood Demonstration Project Showing the Development of New Reserves in the Uinta Basin, presented by John D. Lomax, meeting of the Subcommittee on Renewable Energy, Energy Efficiency and Competitiveness of the U.S. Senate

6. Committee on Energy and Natural Resources held on November 30, 1993, Roswell, New Mexico.

7. Monument Butte Case Study, Demonstration of a Successful Waterflood in a Fluvial Deltaic Reservoir, Deo, M. D., Sarkar, A., Nielson, D.L. and Lomax, J.D. and Pennington, B.I.,

8. SPE 27749, Paper presented at the Improved Oil Recovery Symposium of the SPE and the U.S. DOE in Tulsa, Oklahoma, April 17-20, 1994.

9. Green River Formation Water Flood Demonstration Project, Yearly Report published by the U.S. DOE, 1994, 89pp.

10. Description and Performance of a Lacustrine Fractured Reservoir, Deo, M. D., Neer L. A., Whitney, E. M., Nielson, D. L., Lomax, J. D. and Pennington B. I., SPE 28938, Paper to be presented in the Poster Session of the Annual Fall Meeting of the Society of Petroleum Engineers.

11. Solids Precipitation in Reservoirs Due to Nonisothermal Injections, Deo, M. D., SPE 28967, Paper presented at the SPE International Symposium on Oil Field Chemistry, San Antonio, Texas, February, 1995.

12. Green River Formation Water Flood Demonstration Project, Yearly Report published by the U.S. DOE, 1995, 60pp.

13. Effect of Reservoir Connectivity on Primary and Secondary Recovery, Pawar, R. J., Deo, M. D. and Dyer, J., SPE 35414, Paper to be presented at the SPEIDOE Improved Oil Recovery Symposium in Tulsa, Oklahoma, April, 1996.

Chapter 7. Summary and Conclusions

The primary objective of the project to understand the Monument Butte water flood and to encourage the implementation of secondary recovery processes in similar units was successful. Continued application of water flood in the unit increased production more than twice the total primary production. The total reserves estimated after primary production increased more than five times once results from the flood were considered. Water flood was applied in the nearby Jonah and Wellsdraw units with significant success.

Water flood in Monument Butte was successful because it targeted sands that were laterally continuous and lithologically homogeneous. The performance of the reservoir was similar to that of a typical undersaturated reservoir whose initial reservoir pressure was close to the initial bubble point pressure. The repressurization of the reservoir in secondary recovery was accelerated by converting some of the best producers to injectors. Fresh water was injected to maintain compatibility with the reservoir fluids.

Lower Douglas Creek unit, a lensy, isolated, lithologically heterogeneous reservoir was the target of the water flood in the Travis unit. Over the duration of the project, the Travis water flood was unsuccessful. A list of reasons for the failure of the water flood in Travis is given below. The failure may have resulted due to any one or any combination of these reasons.

- Geologic complexity, lithologic heterogeneity.
- A hydraulic fracture in well 15-28 (the primary injector in Travis) that channeled water to units other than the target.

Opening of and short circuiting through natural fractures due to the high injection rate in well 15-28.

The FMI log in well 14a-28 did help identify the D 1 producing horizon in Travis, which was later opened in a few other wells. This. proved to be a decent primary production target. However, water flood in D1 also resulted in premature water breakthrough without significant . additional oil production. The interconnecting hydraulic fractures between the injector and the producer may have contributed to this. This established that caution should be exercised when creating hydraulic fractures particularly at 20-acre-spacing.

The planning and implementation of a water flood in the Boundary unit highlighted the difficulty in the application of this technology in these reservoirs. There were about eight target zones and the lateral continuity of several of these zones was questionable. There were only six control points (wells). Water-oil contact was observed in one well in the D 1 horizon. Of the possible targets, the C sandstone unit appeared most promising and water flood was begun in early 1996. At the current time (April 1996), all indications are that this water flood will be successful.

The reservoir characterization activities undertaken in this project such as advanced well Iogs (Formation Micro Imaging and Magnetic Resonance Imaging), full-diameter and side-wall cores, etc. provided better understanding of reservoirs involved. In some cases, these methods led to the discovery of commercially producible zones. PVT properties, permeabilities, relative permeabilities, etc. were measured, primarily since they were required as input for reservoir simulation. Reservoir simulation was performed at different resolutions and scales. History of all of the three units was matched reasonably well. In addition, geostatistical reservoir images were generated of large areas in the Greater Monument Butte region. Thermodynamics of wax precipitation in these waxy-oil reservoirs was modeled along with an analysis of reduction in

recovery that might result due to wax precipitation in injection operations. A modest microbial treatment program undertaken in Monument Butte to address the wax problem in production wells was reasonably successful, reducing hot-oil treatments required.

Technology transfer was the most successful component of the project. The project resulted in four (4) SPE papers, two(2) AAPG papers and presentations in several national and international meetings. This project revived the oil-drilling activity in Utah's Uinta basin. This is evidenced by the fact that the drilling planned for 1996 (112 wells) exceeds the wells drilled in the region in 1993 fourfold. Wells in the Gilsonite unit are showing a good response while the oil production rate in Balcron's Jonah unit has increased about three times the pre-water flood production. Production rate in the Wellsdraw unit has also almost doubled.

There is no reason why the successful Monument Butte flood technology can not be applied to about 300 square miles in the Greater Monument Butte region. The targets must be chosen carefully, and the hydraulic fractures must be carefully designed.

APPENDIX A - Detailed lithologic log of core and X-ray diffraction analyses from Travis Federal #14A-28.

Well: #14A-28 Monument Butte Interval: Top 5550 - 5552

Depth (ft)	Dominant Grain Size (Clay, Mud, Sh, VFS, FS, MS, CS)	Oil Stain (W, M, S)	Lithology	Sedimentary Structures	Facies	Depositional Environment	Description
			TOP OF CORE				
5550							
5551					Shale	off shore	increasing shale and fissility upwards
5552							

Well: #14A-28 Monument Butte Interval: 5552 - 5560

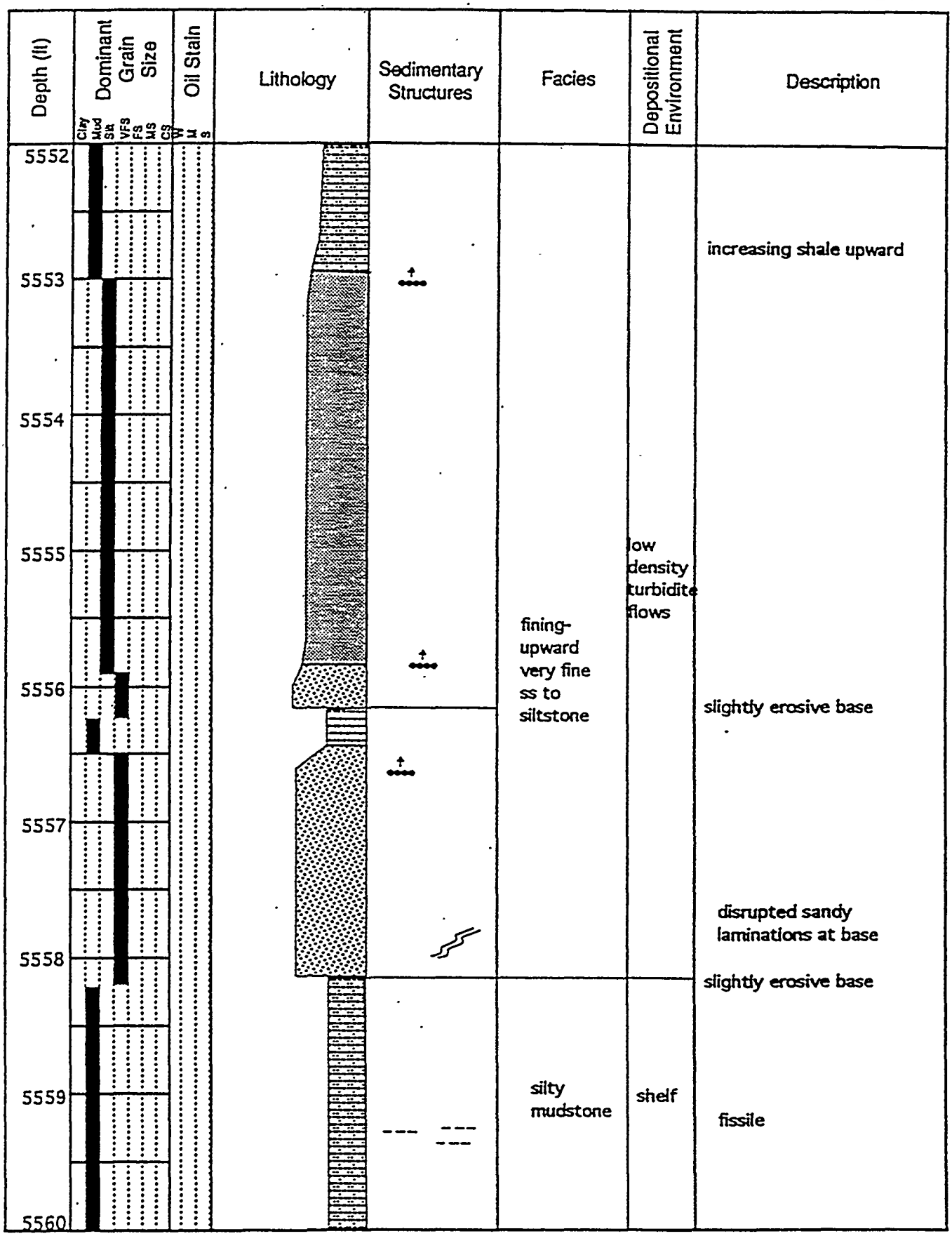

Well: #14A-28 Monument Butte Interval: 5560-5568

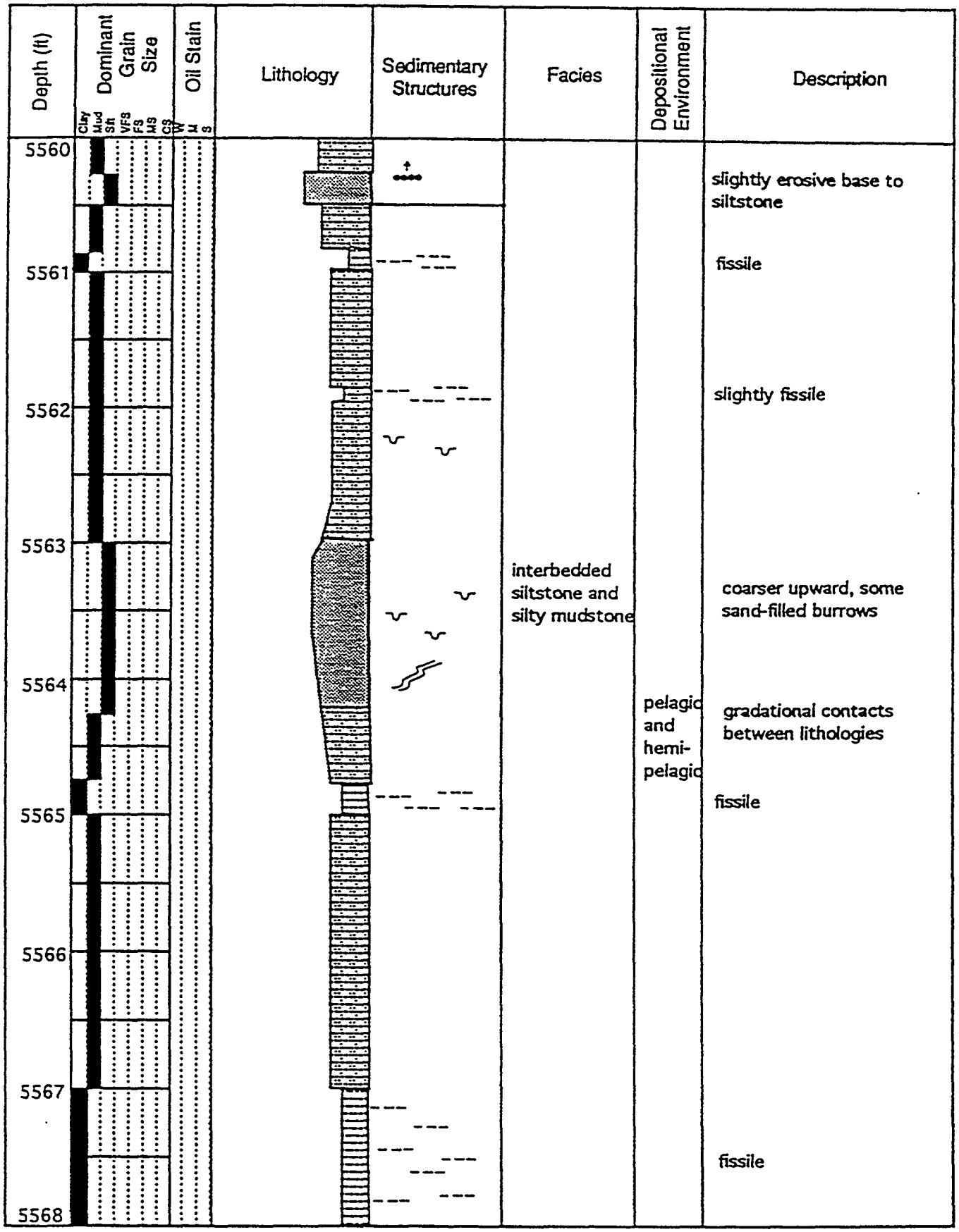

Well: #14A-28 Monument Butte Interval: 5568-5576

Depth (ft)	Dominant Grain Size (Clay, Mud, Slt, VFS, FS, MS, CS)	Oil Stain (W, M, S)	Lithology	Sedimentary Structures	Facies	Depositional Environment	Description
5568					silty mudstone	hemi pelagic	medium gray mudstone, breaks conchoidally, abundant very fine organic material
5569							
5570							
5571			FX		planar laminated very fine gr calcareous ss	shelf bar	light gray very fine grained sandstone, carbonate cement, sharp basal contact and gradational upper contact
5572					bioturbated shaly siltstone	hemi pelagic	fining-upward to mudstone, slightly smeared Chondrites burrows at base
5573							
5574					disrupted laminated ss	slump	disrupted and inclined laminations in a semicoherent block of sediment, sharp upper and lower contacts
5575					slightly disrupted siltstone	shelf	light gray siltstone, one sandy lamination is offset by a synsedimentary fault
5576							

Well: #14A-28 Monument Butte Interval: 5576-5584

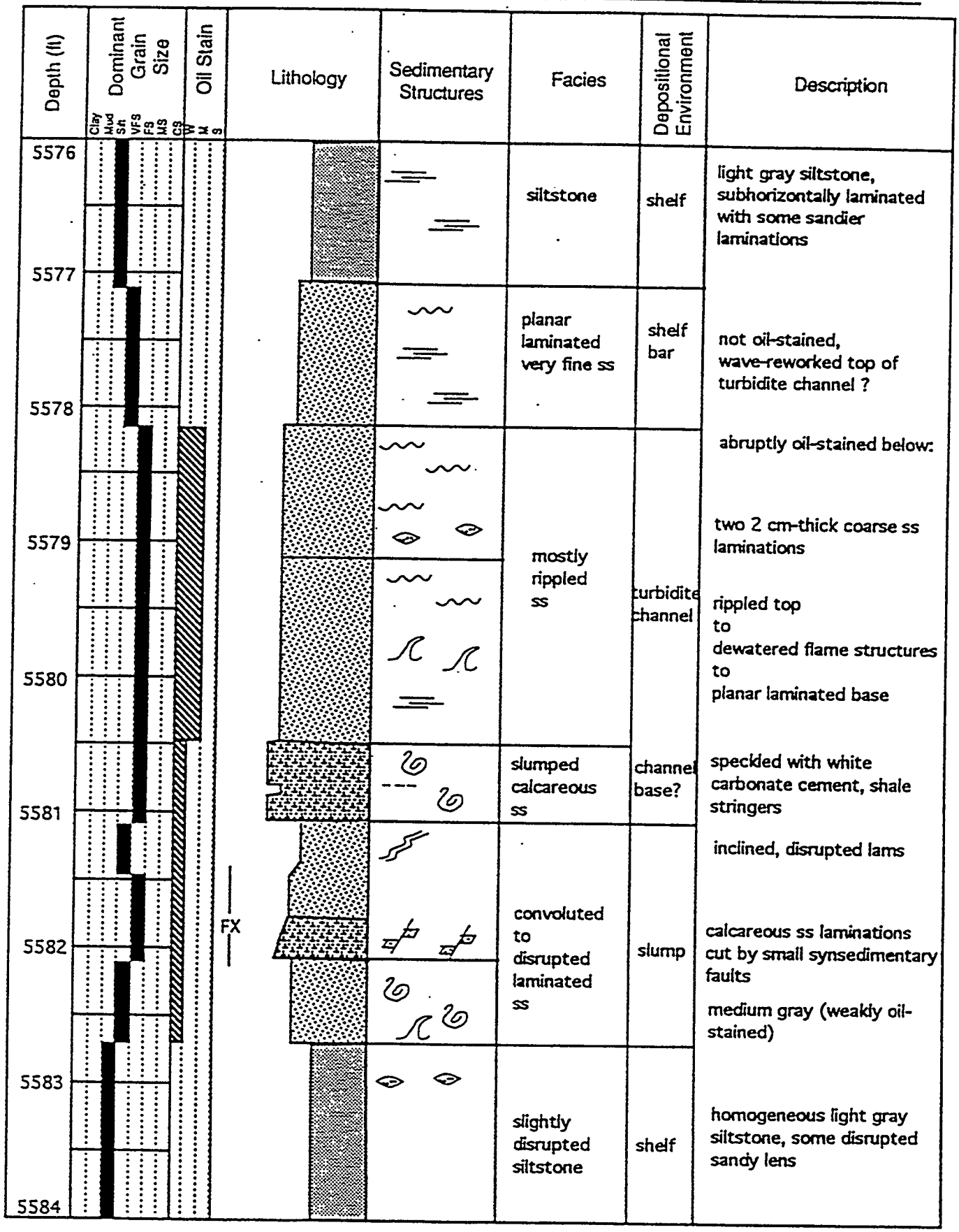

Well: #14A-28 Monument Butte Interval: 5584-5592

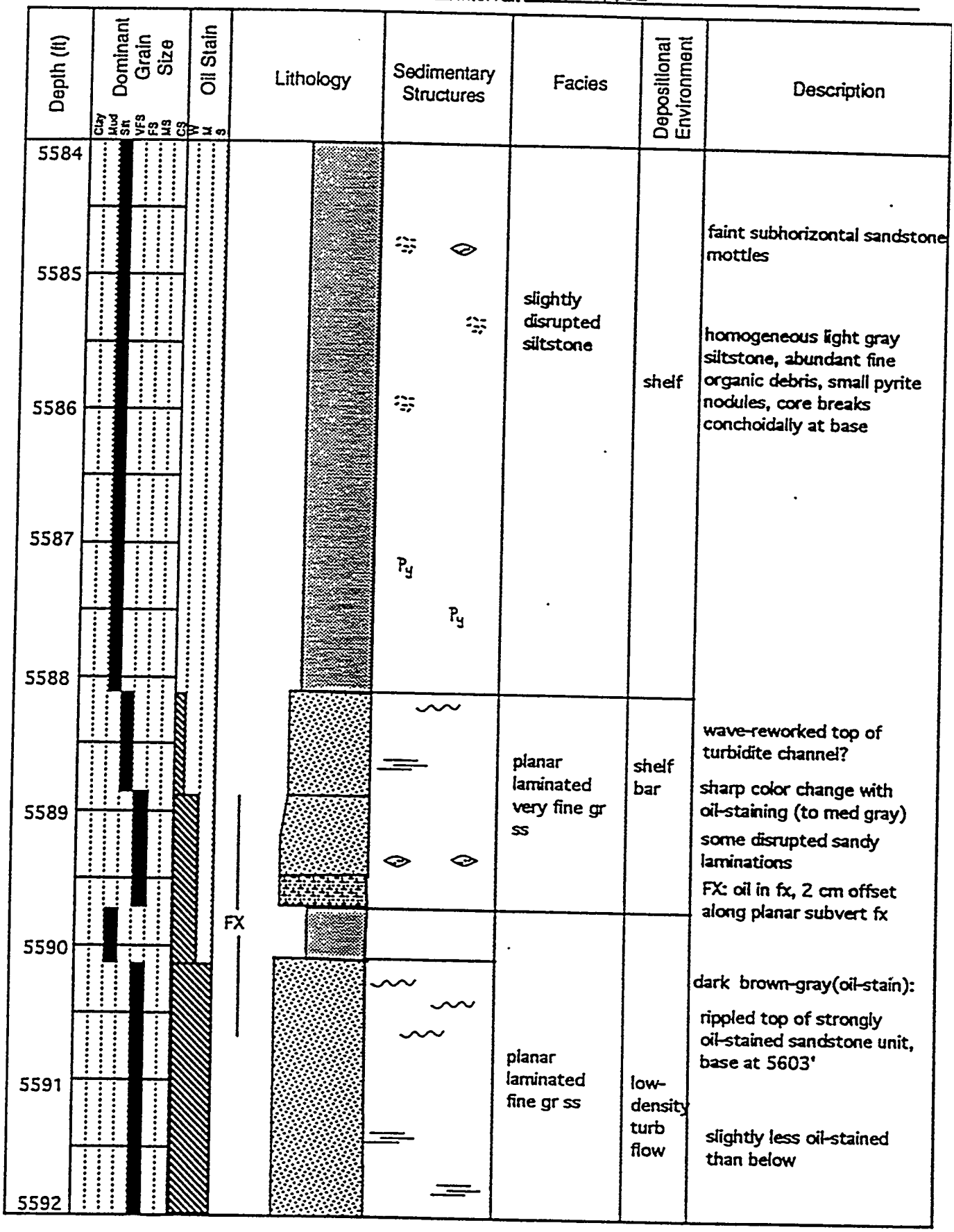

Well: #14A-28 Monument Butte Interval: 5592-5600

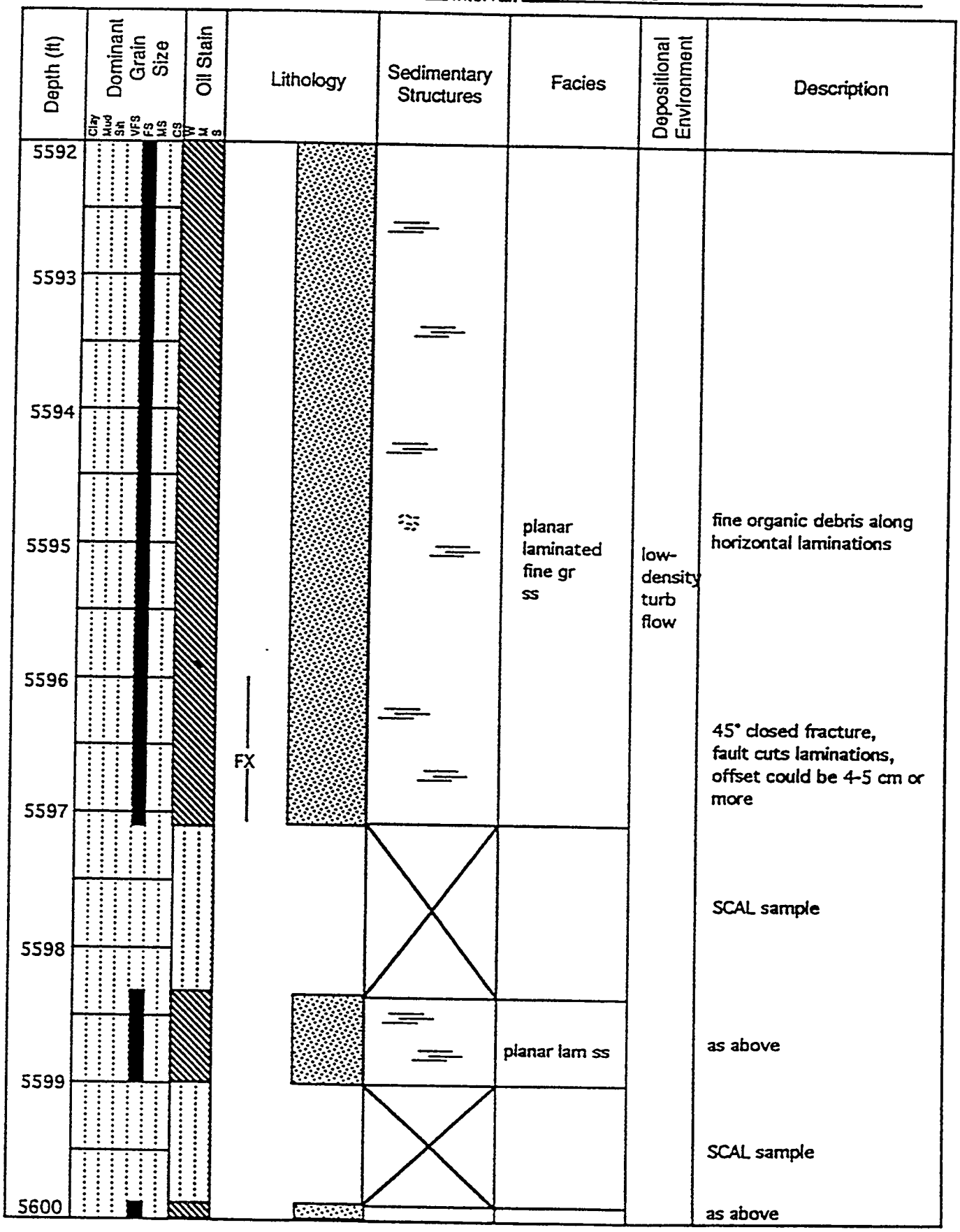

Well: #14A-28 Monument Butte Interval: 5600-5608

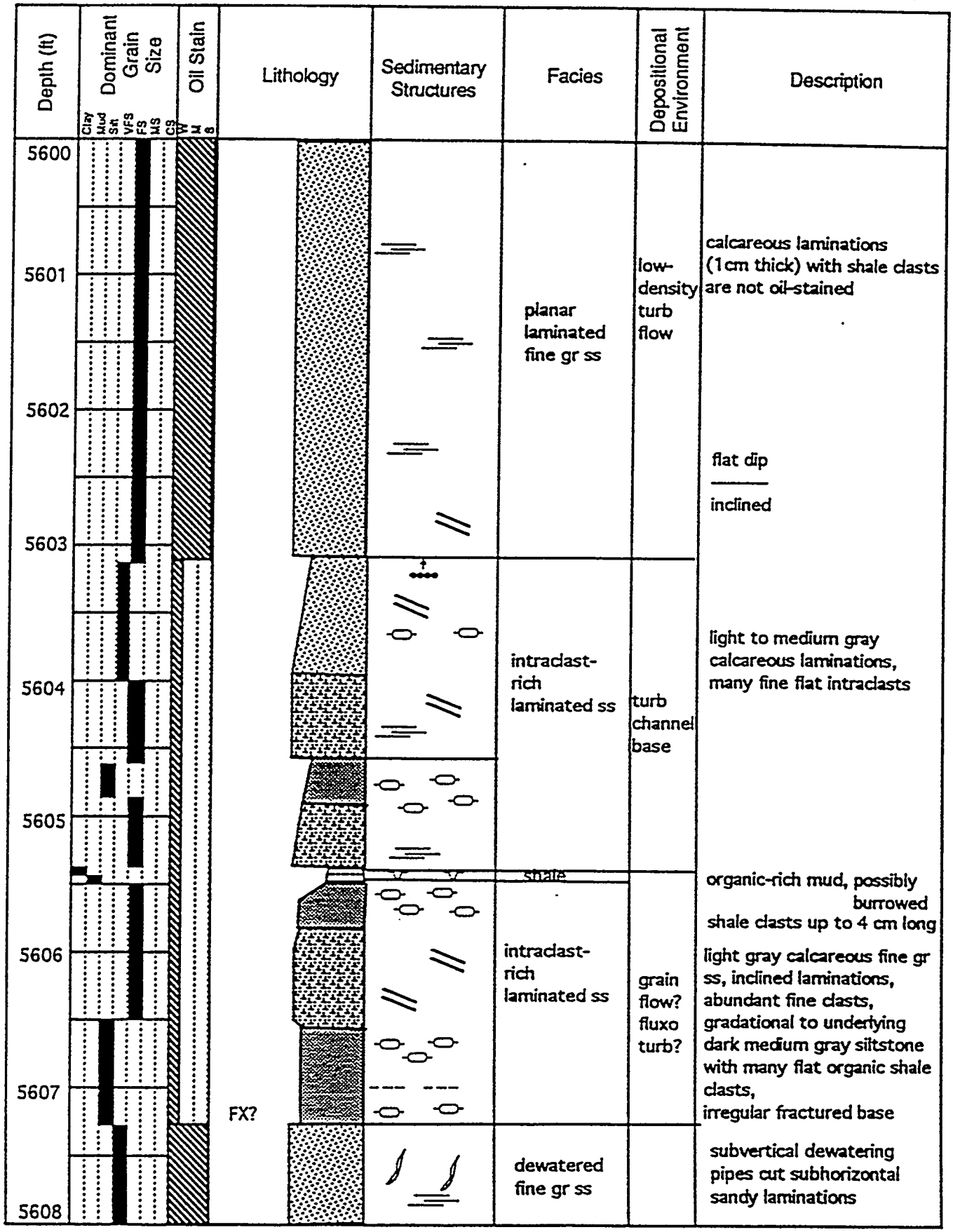

Well: #14A-28 Monument Butte Interval: 5608-5616

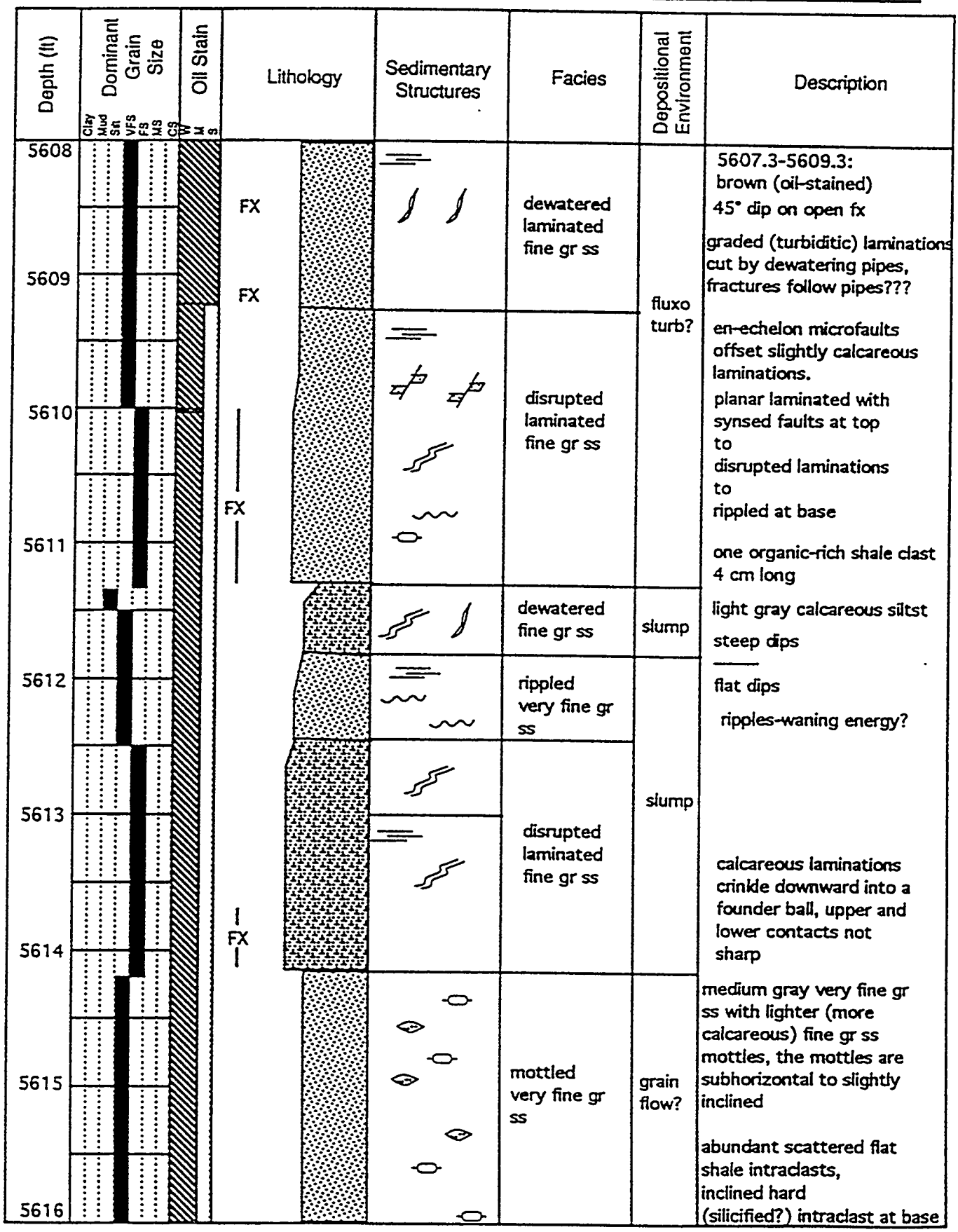

Well: #14A-28 Monument Butte Interval: 5616-5624

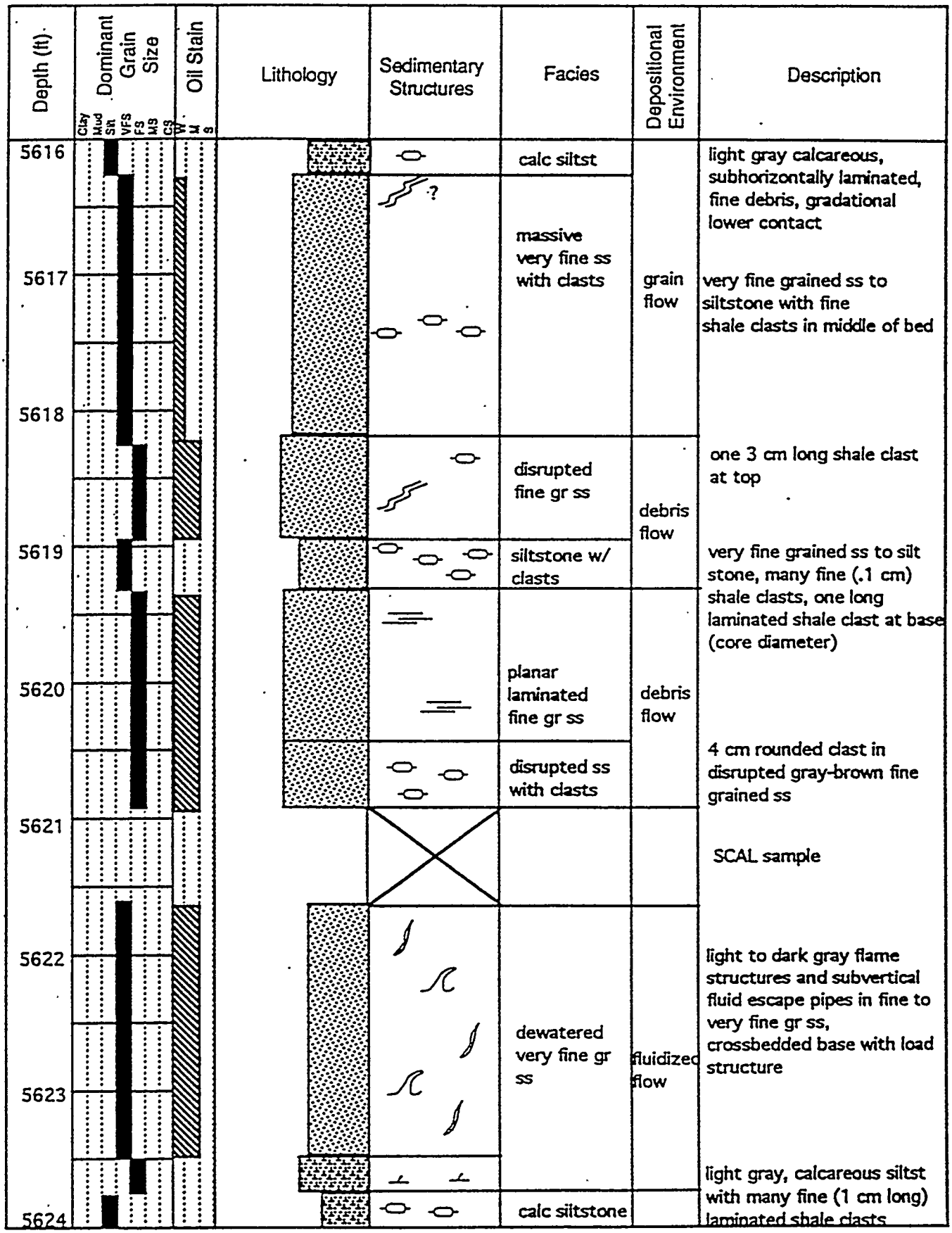

Well: #14A-28 Monument Butte Interval: 5624-5632

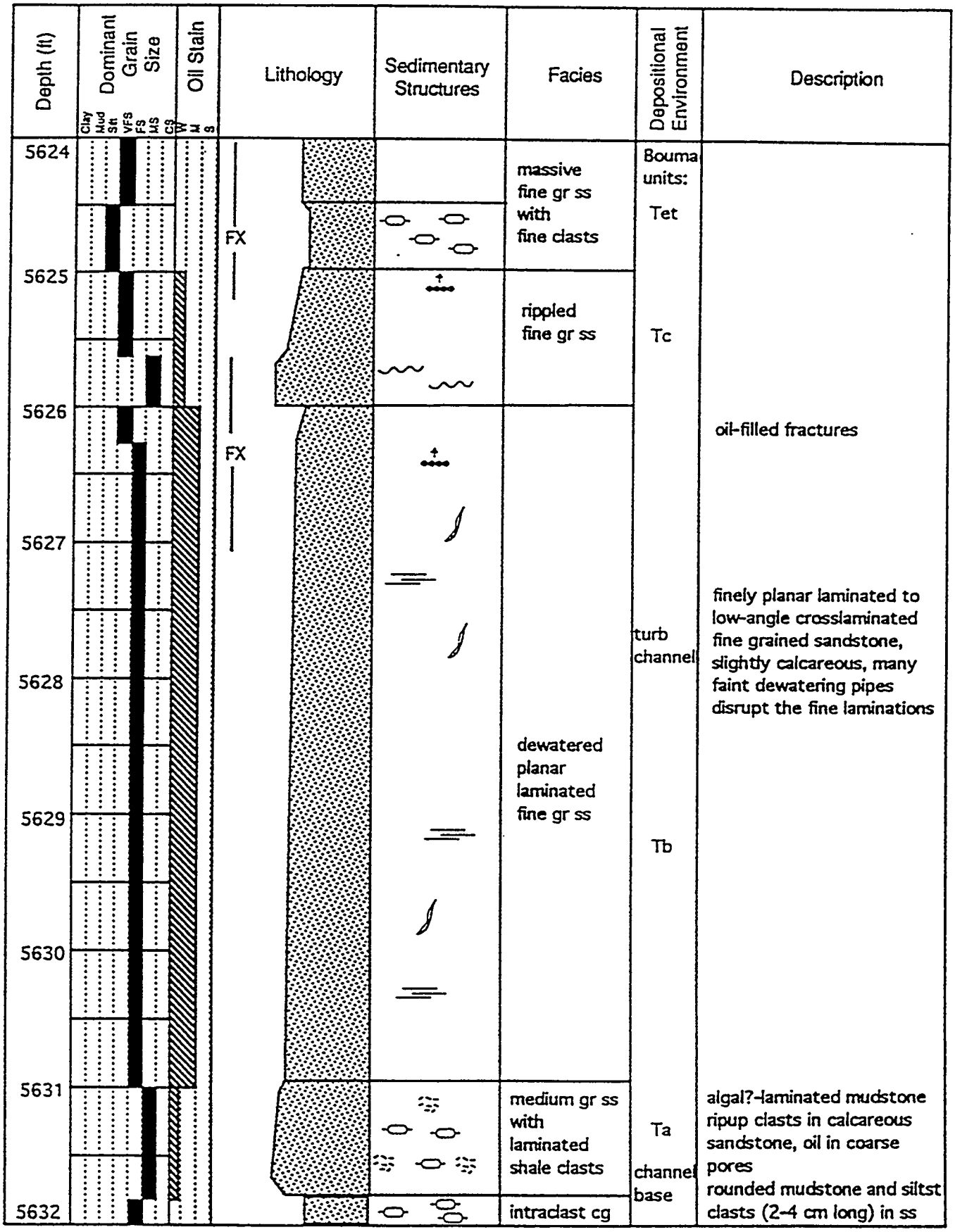

Well: #14A-28 Monument Butte Interval: 5632-5640

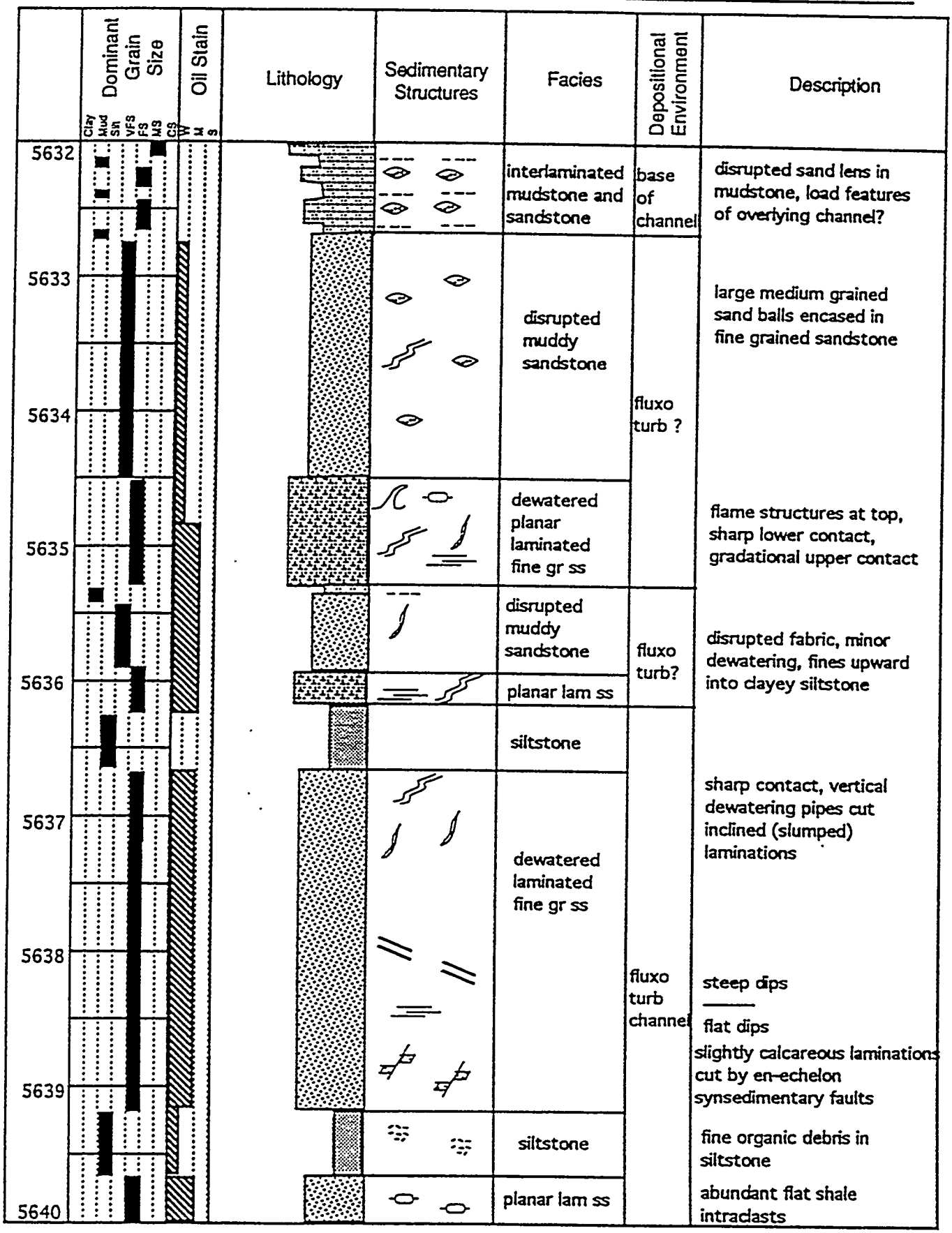

Well: #14A-28 Monument Butte Interval: 5640-5646 Btm

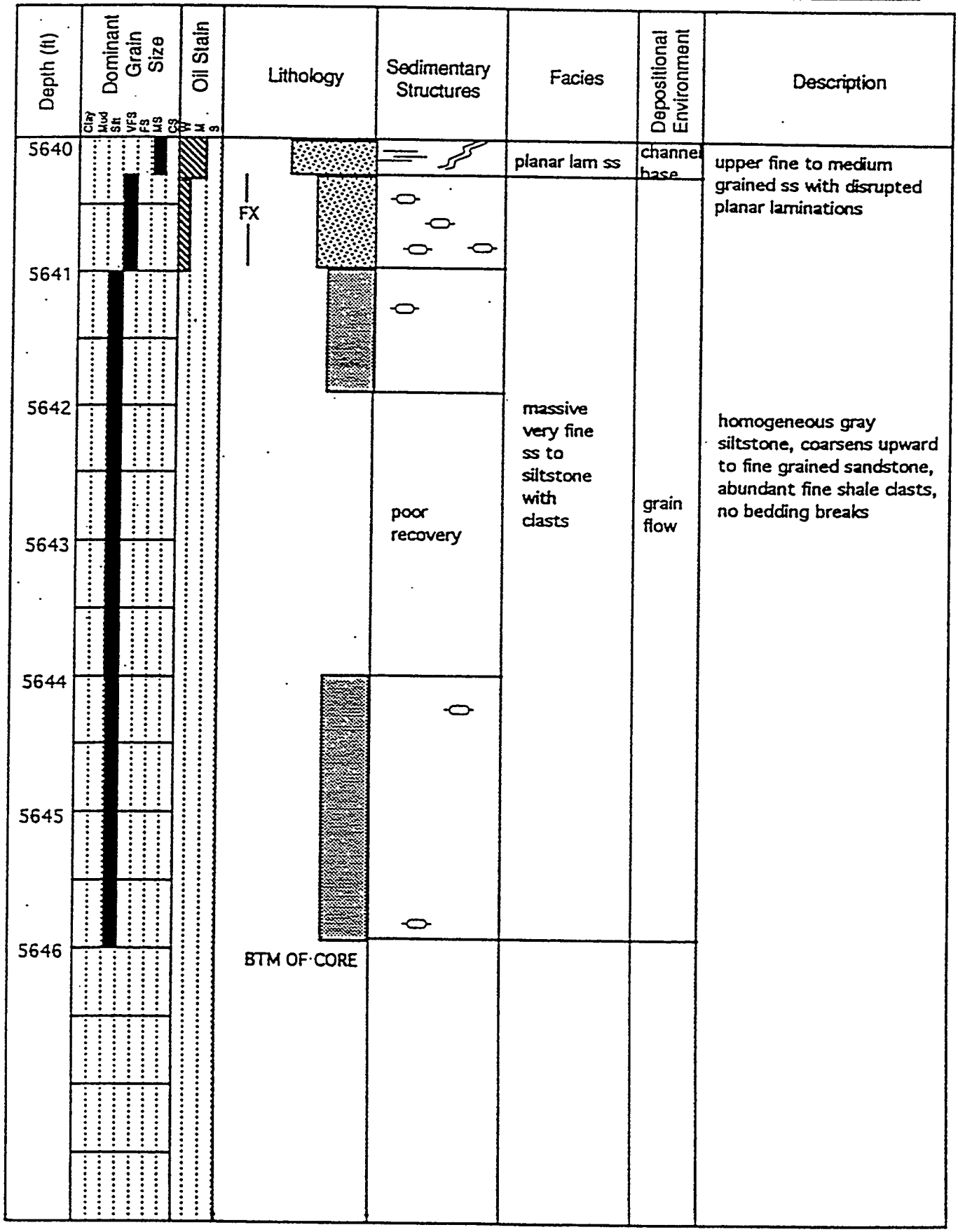

Lomax Exploration Co.

Fed #14A-28

Mineralogy, Approx. Wt.% [X] (or) Relative Abundance [ ]

Sample No.	Quartz	Plagioclase	K- Feldspar	Siderite	Calcite	Dolomite	Pyrite	Chlorite	Illite+ Mica	Mixed-layer illite-smectite	Amorphous/ Below Detect.	% smectite in illite-smectite	
5595.0-96.0 Bulk	49	32	7		3	4		2	3		-		
Clay								26	74				
5598.0-99.0 Bulk	48	32	6	1?	3	5	Tr	3	2		-		
Clay								25	75				
5615.0-16.0 Bulk	46	26	6	Tr?	5	6	1	4	2	4	-		
Clay								27	28	45		10	illite-rich illite-smectite
5638.0-39.0 Bulk	51	21	6	Tr	14	4	Tr	2	2		-		
Clay								25	75				
5639.0-40.0 Bulk	43	21	5		3	10	3	3	4	8	-		
Clay								9	35	56		10	

MM = Predominant M = Major m = Minor Tr = Trace ? = Tentative Identification

Figure 2. SUMMARY OF X-RAY DIFFRACTION ANALYSIS

UNIVERSITY OF UTAH RESEARCH INSTITUTE, EARTH SCIENCE LABORATORY

APPENDIX B - Detailed lithologic log of core and X-ray diffraction analyses from Travis Federal n2-33.

Well: #2-33 Monument Butte Interval: Top 5647-5654

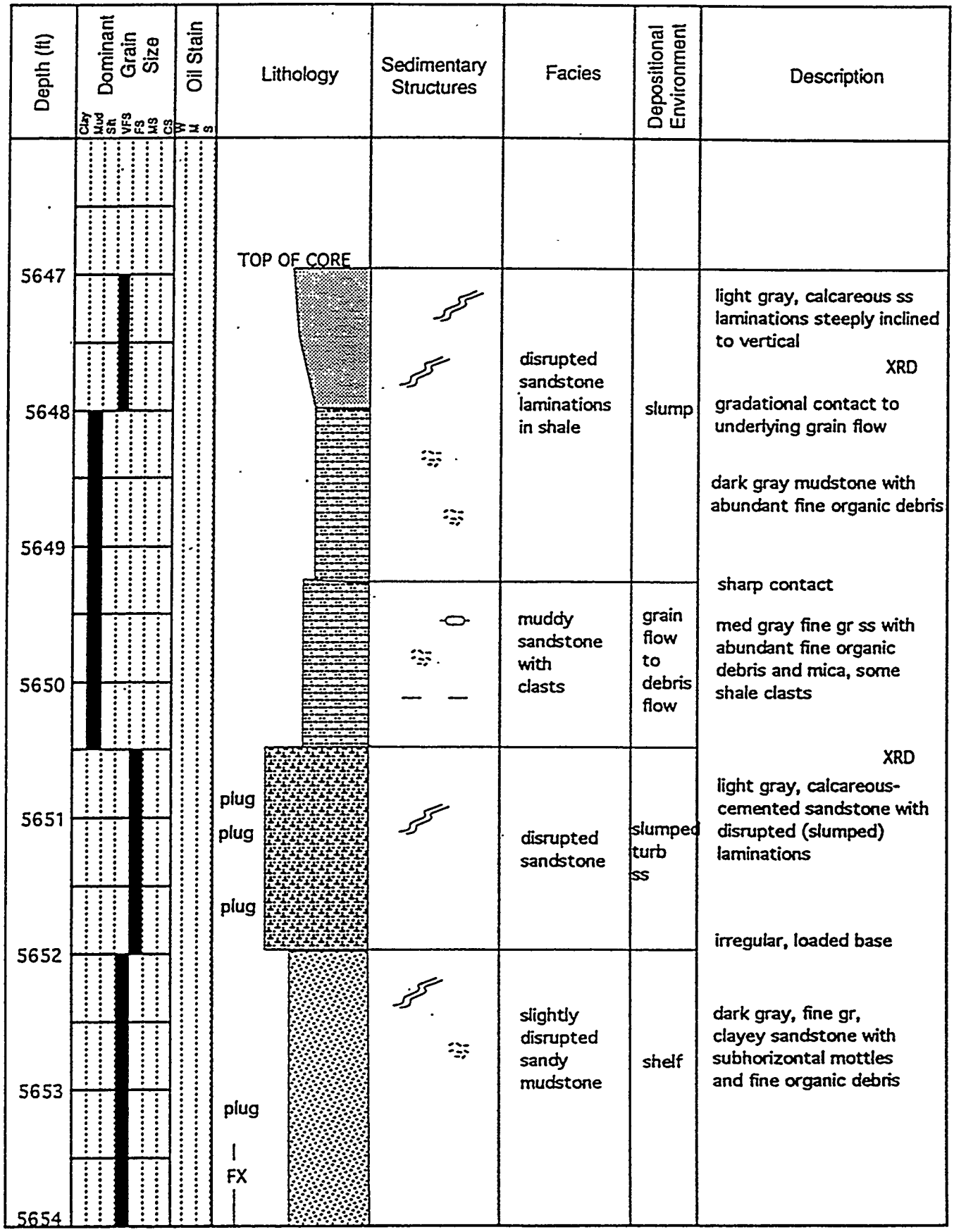

Well: #2-33 Monument Butte Interval: 5654-5662

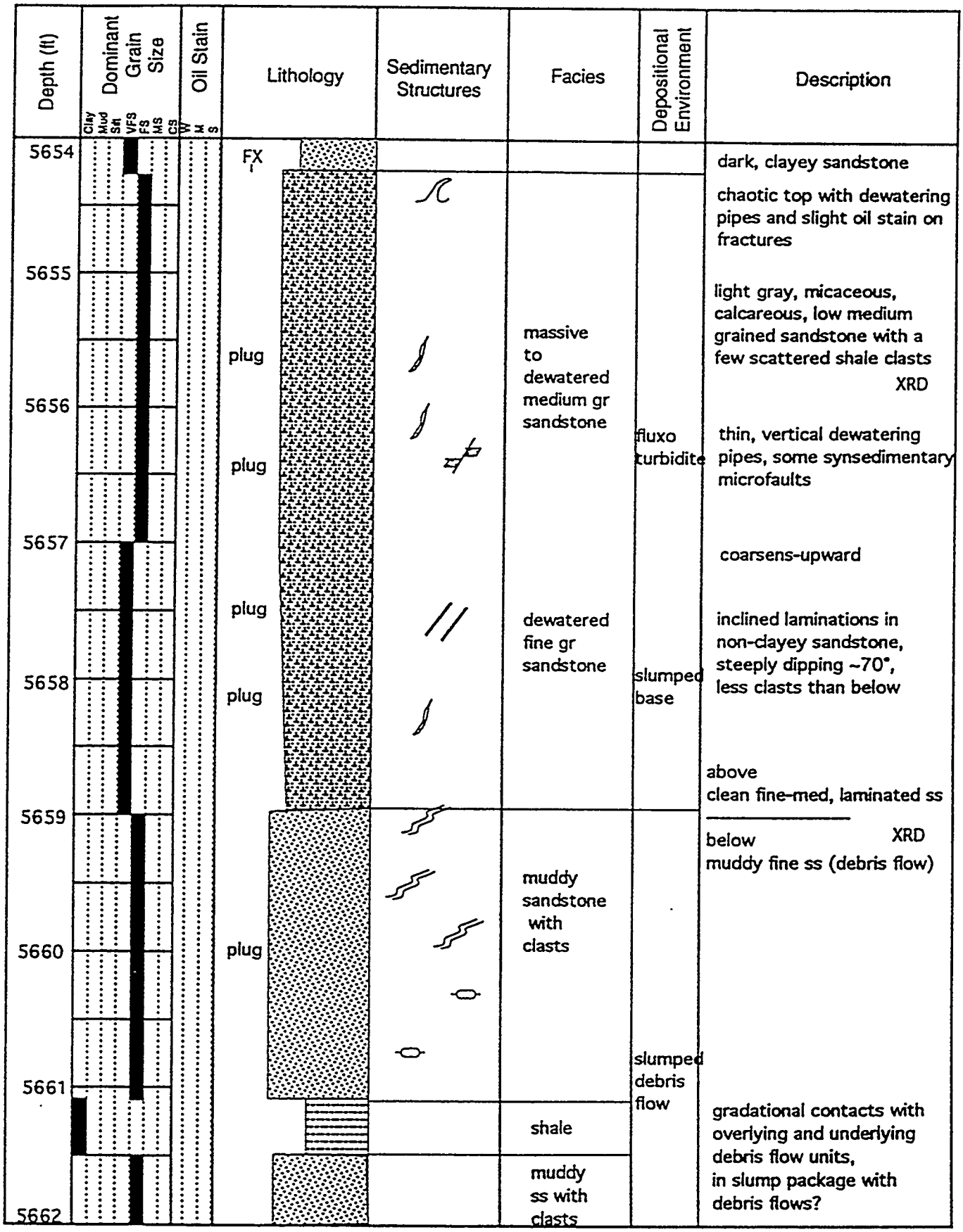

Well: #2-33 Interval: 5662-5670

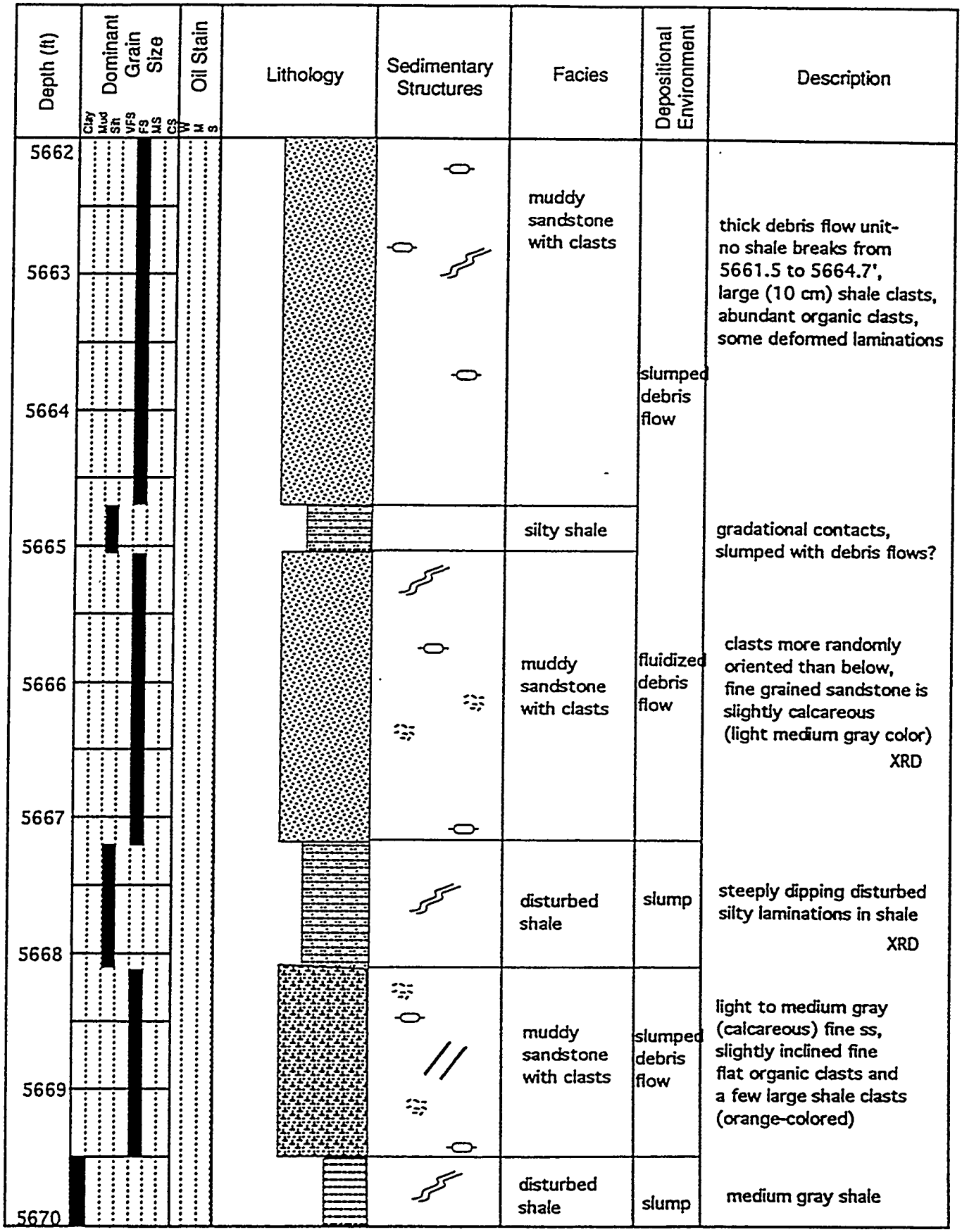

Well: #2-33 Interval: 5670-5676 Btm

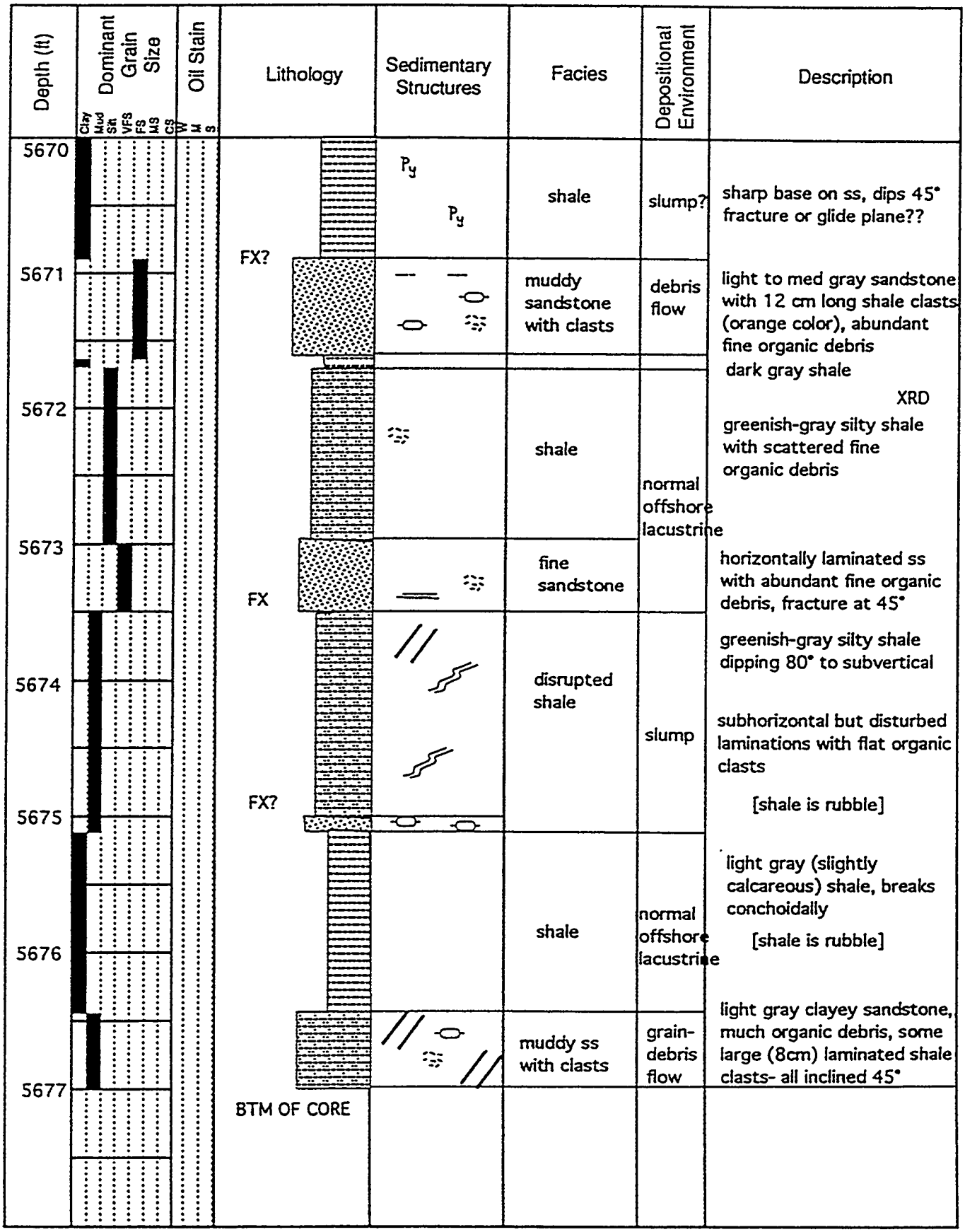

Lomax Exploration Co.

Lower Douglas Creek Sandstone
Well 2-33
Travis Unit,
Greater Monument Butte field

Mineralogy, Approx. Wt.% [X] (or) Relative Abundance [ ]

Sample No.	Quartz	Plagioclase	K- Feldspar	Siderite	Calcite	Dolomite	Pyrite	Chlorite	Mixed-layer Chlor-smectite	Illite+ Mica	Mixed-layer ~~Illite-smectite~~	Smectite	Amorphous/ Below Detect.	% smectite in illite-smectite
5648 core Bulk	36	15	12		2	8	1	2	tr	4	20		-	
Clay								13	4	10	73			15
5650.5 core Bulk	43	14	5	2	20	5		4	tr	2	5		-	
Clay								7	9	14	69	1		15
5656 core Bulk	43	19	6	tr	20	3		2		1	5		-	
5659 core Bulk	40	17	6	tr	3	5	tr	4		5	19		-	
5666 core Bulk	42	17	8	1	7	7	tr	3		2	13		-	
5668 core Bulk	20	9	4	2	3	3		2		4	53		-	15
5672 core Bulk	16	6	5		4	3	3	2		3	58		-	15

MM = Predominant M = Major m = Minor Tr = Trace ? = Tentative Identification

SUMMARY OF X-RAY DIFFRACTION ANALYSIS

UNIVERSITY OF UTAH RESEARCH INSTITUTE, EARTH SCIENCE LABORATORY

S. Lutz
revised
3-3-95

APPENDIX C - Detailed lithologic log of core and X-ray diffraction analyses from Travis Federal #633.

Well: #6-33 Monument Butte Interval: Top 5596-5602

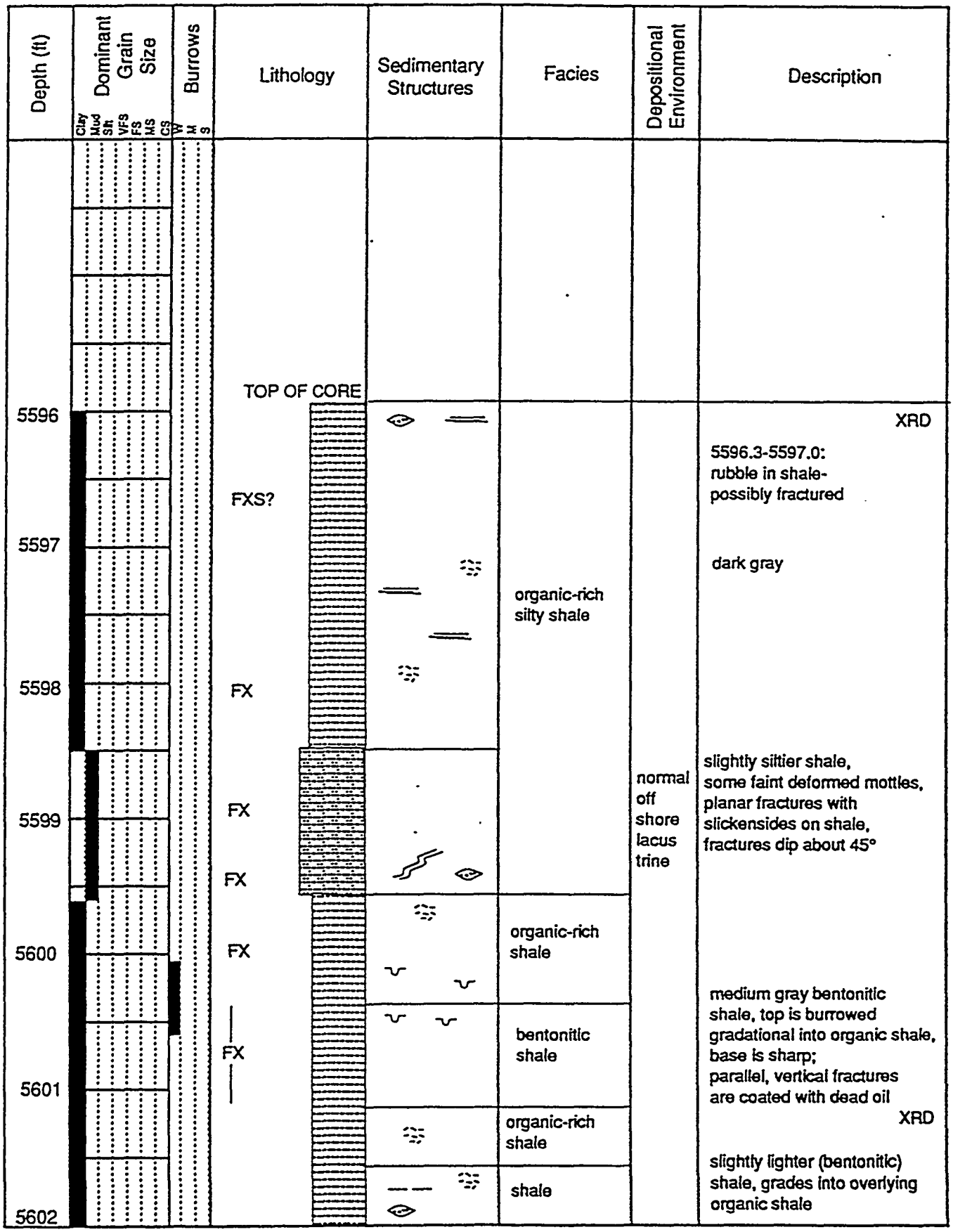

Well: #6-33 Monument Butte Interval: 5602-5610

Depth (ft)	Dominant Grain Size (Clay, Mud, Slt, VFS, FS, MS, CS)	Burrows (W, M, S)	Lithology	Sedimentary Structures	Facies	Depositional Environment	Description
5602					organic-rich shale	normal off shore lacus trine	a few lighter (silty) mottles
5603							dark gray shale with abundant flat organic debris
5604					burrowed organic-rich shale		slightly compacted Planolites in organic-rich shale XRD
5605			FX		bentonitic shale		T.S. + XRD: light to medium gray shale with expandible clay, disrupted fabric, sharp upper and lower contacts are fractures, dipping at 45°
5606			FX FXS?	py?	organic-rich shale		rubble in shale XRD
							lighter silty lamination dipping abut 30°
5607							
5608							dark gray organic-rich shale with subhorizontal flat organic debris
5609							
					disrupted silty shale	slump	one 4 cm thick medium gray silty lamination dipping 30° smeared fabric, gradational upper contact
5610							

Well: #6-33 Monument Butte Interval: 5610-5617 Btm

Depth (ft)	Dominant Grain Size (Clay, Mud, Slt, VFS, FS, MS, CS)	Oil Stain (W, M, S)	Lithology	Sedimentary Structures	Facies	Depositional Environment	Description
5610					disrupted silty shale	slump?	mostly shale with some faint deformed mottles of silty material, gradational lower contact
5611					organic-rich shale	normal off shore lacus trine	dark gray shale, a few silty mottles at the top
5612					disrupted mudstone		medium gray shale with silty mottles, possibly smeared burrows, subhorizontal
					bentonitic shale		medium gray shale with expandible clay, sharp upper and lower contacts
5613				Py Py	organic-rich shale		XRD dark gray shale, flat organic debris is horizontally oriented, gradational base
5614					disrupted silty mudstone	slump	
5615			FXS?		disrupted shale		dark gray waxy shale with a few silty mottles, dipping 30°, slumped nodular texture; 5615.1- 5615.5 rubble in shale, green material on rubble pieces
5616					burrowed organic-rich shale	normal off shore lacus trine	dark gray, organic-rich shale, possibly some burrows, a few silty mottles at the top
5617			BTM OF CORE				

Lomax Exploration Co.

Lower Douglas Creek
Well 6-33 Core
Travis Unit,
Greater Monument
Butte field

Mineralogy, Approx. Wt.% [X] (or) Relative Abundance [ ]

Sample No.	Quartz	Plagioclase	K- Feldspar	Siderite	Calcite	Dolomite	Ferroan Dolomite	Pyrite	Chlorite	Mixed-layer Chlor-smectite	Illite+ Mica	Mixed-layer Illite-smectite	Amorphous/ Below Detect						% smectite in illite-smectite
5596 Bulk	15	6	4			13		5	tr	2	3	52		-					~20
5601 Bulk	30	11	4				5	3	3	1	5	38		-					
5604.5 Bulk	26	9	5			5		4	1	tr	2	48		-					
5605 Bulk	29	12	7			4	2	1	2	tr	3	40		-					
5606 Bulk	16	9	4	2		8		2	1		1	48		9					
5613 Bulk	23	12	5			4		12	2	2	4	36		-					

MM = Predominant M = Major m = Minor Tr = Trace ? = Tentative Identification

SUMMARY OF X-RAY DIFFRACTION ANALYSIS

UNIVERSITY OF UTAH RESEARCH INSTITUTE, EARTH SCIENCE LABORATORY

S. Lutz
revised
3-3-95

PROJECT facts

U.S. DEPARTMENT OF ENERGY
OFFICE OF FOSSIL ENERGY
NATIONAL ENERGY TECHNOLOGY LABORATORY

Petroleum Exploration and Production

02/2004

GREEN RIVER FORMATION WATER FLOOD DEMONSTRATION

Waterflooding high paraffin content reservoirs

PARTNERS

Inland Resources, Inc.
Denver, CO

Lomax Exploration Co.
Denver, CO

University of Utah
Salt Lake City, UT

MAIN SITE

Monument Butte Field
Duchesne and Uintah, Cos.
Uinta Basin, UT

Well site showing the typical terrain of Monument Butte Field.

Background/Problem

The Monument Butte waterflood project, which started in 1992 and completed in 1996 by Lomax Petroleum, was one of the major success stories of the Class I Fluvial-Deltaic program. Waterflooding technology was not commonly used in the Uinta Basin due to the low permeability, heterogeneity and high paraffin content (12%) of the lacustrine reservoirs. Primary production from the Eocene age, Green River formation in Monument Butte field averaged only 5% of original oil in place (OOIP). Lomax Petroleum was bought by Inland Resources as the project successfully demonstrated how to waterflood a high paraffin oil reservoir. Inland Resources completed the DOE project in 1996.

In 2003 NETL began reviewing the field demonstrations of the Class projects to determine the long term benefits of DOE funding. Inland Resources expressed great satisfaction with the original DOE Class I project and credited the expansion of the pilot from a 2-section Monument Butte Unit to the entire 125,000 acre field to technology developed under DOE's funding. DOE's return on investment has an average annual rate of 33% from 1992 to 2003.

Project Description/Accomplishments

The objectives of the project were to identify the recovery mechanisms operating in the waterflood, to evaluate the success of the Monument Butte Unit waterflood and extend the waterflood to Travis and Boundary Units.

Reservoir characterization of Monument Butte reservoirs provided key information, which resulted in a successful waterflood. Core analysis identified the most laterally continuous and lithologically homogeneous zones. The ability to isolate and waterflood a single zone, making use of fracture orientation data, rather than targeting multiple zones significantly increased production and improved economic efficiency. Reservoir simulation models based on core and log analysis identified the need to quickly pressurize the reservoir by waterflooding to move the waxy crude into the wellbore.

The successful waterflooding technology was expanded to the Travis and Boundary Units with as estimated ultimate recovery of 20% OOIP from secondary recovery. The first use of FMI logs in northern Utah proved valuable in identifying zones for perforation and data for geologic modeling. One of the keys to waterflooding the reservoir was the importance of using fresh water for injection. Oil recovery from Monument Butte Unit increased from 300 BOPD to 2000 BOPD, and the number of wells increased from 20 to 60 during the project. Independent operators in neighboring leases picked up the technology and initiated eleven new waterflood projects in the Uinta Basin. Reservoir life was extended by over 10 years.

Green River Formation Water Flood Demonstration

Waterflooding high paraffin content reservoirs

Benefits/Impacts

Since the end of the DOE project in 1996 Inland Resources has continued to expand the waterflood technologies. Current production is at 6,000 barrels of oil and 11 million cubic ft of gas per day. Cumulative production of 25 million barrels of oil and 70 billion cubic feet of gas has reached 20% of OOIP and continues to rise. The strategy developed from the DOE project is to drill wells on a 5-spot pattern. All wells are put on production and after 18 months, the center producer is converted to a water injector. As of May 2003, 740 wells are on production and Inland plans to drill an additional 1,000 wells on 40-acre spacing over the next 4 to 5 years. Inland Resources controls over 125,000 acres, the vast majority of Monument Butte field. The original DOE project has expanded from 2 sections to cover over 60 sections. Currently, the drilling rate averages 5 days per well to a depth of 5,000 to 6,000 ft. To meet both environmental regulations and to maintain year round production each producer has its own surface facilities including 800 bbl oil storage tanks and 400 bbl water storage tanks and each injector has a heated wellhead. Hydrocyclones have been installed to remove particulate matter prior to water injection. Fresh water for injection remains a critical factor in expansion of the field in the arid Uinta Basin. At present, Inland is injecting 18,000 bbl of water per day (including 4,000 bbl of produced water) in 5-spot patterns. Decline curves of Monument Butte field prove the technical success of the waterflood technology, as a positive response is shown with each new waterflood cycle.

Main water injection facility showing a series of water separation tanks and the building housing the hydrocyclone.

The financial benefits in the Uinta Basin are demonstrated by increased royalties, state and federal taxes and increased employment. Inland Resources employs over 100 people. Three large independent operators, Petrocliffe, Questar and Berry Petroleum have acquired leases in the area and continue to expand the waterflood technologies across the Uinta Basin. Inland Resources has installed a gas stripping plant that enables the company to meet pipeline specifications and environmental regulations for selling oil and gas liquids. The gas liquids recovered from the plant provide an additional $150,000 per month profit. Paraffin is also sold as a by-product of oil and gas liquids production. The life of the Monument Butte reservoir has been extended from a short period on primary to 10 to 20 years on secondary production. The economic success of the project can be inferred from the aggressive expansion by Inland Resources and from other area operators using the waterflood technology developed.

CONTACT POINTS

William Pennington
President
Inland Resources
Phone: (303) 292-2000

William T. War
Vice-president
Inland Resources
Phone (303) 382-4417
E-mail: billw@inln.com

Roy Long
Technology Manager
U.S. DOE
Phone (918) 699-2017
E-mail: roy.long@netl.doe.gov

Rhonda L. Jacobs
Project Manager
U.S. DOE
Phone: (918) 699-2037
E-mail:
rhonda.jacobs@netl.doe.gov

TOTAL ESTIMATED COST

$4.4 million

COST SHARING

DOE	- $1.8 million
Non-DOE	- $2.6 million

WEBSITE

www.netl.doe.gov

FOSSIL ENERGY

DOE/BC/14957-27
(OSTI ID: 756344)

IMPROVED OIL RECOVERY IN FLUVIAL DOMINATED DELTAIC RESERVOIRS OF KANSAS - NEAR TERM

Final Report
June 18, 1993-September 30, 1999

By
Don W. Green
G. Paul Willhite
Rodney R. Reynolds
A. Dwayne McCune
Michael J. Michnick
Anthony W. Walton
W. Lynn Watney

Date Published: June 2000

Work Performed Under Contract No. DE-FC22-93BC14957

The University of Kansas Center for Research, Inc.
Lawrence, Kansas

National Petroleum Technology Office
U.S. DEPARTMENT OF ENERGY
Tulsa, Oklahoma

DISCLAIMER

This report was prepared as an account of work sponsored by an agency of the United States Government. Neither the United States Government nor any agency thereof, nor any of their employees, makes any warranty, expressed or implied, or assumes any legal liability or responsibility for the accuracy, completeness, or usefulness of any information, apparatus, product, or process disclosed, or represents that its use would not infringe privately owned rights. Reference herein to any specific commercial product, process, or service by trade name, trademark, manufacturer, or otherwise does not necessarily constitute or imply its endorsement, recommendation, or favoring by the United States Government or any agency thereof. The views and opinions of authors expressed herein do not necessarily state or reflect those of the United States Government.

This report has been reproduced directly from the best available copy.

DOE/BC/14957-27
Distribution Category UC-122

Improved Oil Recovery in Fluvial Dominated Deltaic Reservoirs of Kansas - Near Term

By
Don W. Green
G. Paul Wilthite
Rodney R. Reynolds
A. Dwayne McCune
Michael J. Michnick
Anthony W. Walton
W. Lynn Watney

June 2000

Work Performed Under Contract No DE-FC22-93BC14957

Prepared for
U.S. Department of Energy
Assistant Secretary for Fossil Energy

Dan Ferguson, Project Manager
National Petroleum Technology Office
P.O. Box 3628
Tulsa, OK 74101

Prepared by
The University of Kansas Center for Research , Inc.
4008 Learned Hall
Lawrence, KS 66044-7526

Table of Contents

LIST OF FIGURES v

LIST OF TABLES v

CHAPTER 1 - INTRODUCTION 1

Abstract 1

Executive Summary 2

CHAPTER 2 - STEWART FIELD PROJECT 5

Objectives 5

Background 5
History 5
Pressure 6
Production 7
Field Data Summary 7

Reservoir Modeling 11
Overview of Reservoir Simulation 11
Simulation Conducted at the University of Kansas 12
Simulation Conducted by Sharon Resources 22
Economic Analysis 29

Laboratory Testing 31
Commercial Laboratories 31
University of Kansas Laboratory 31
Utilization 37

BUDGET PERIOD 2 ACTIVITIES 38

Design and Construct Waterflood Plant 38

Design and Construct Injection System 39

Design and Construct Battery Consolidation and Gathering System 40

Waterflood Operations and Reservoir Management 40

TECHNOLOGY TRANSFER ACTIVITIES FOR STEWART FIELD PROJECT FOR BUDGET PERIODS 1 AND 2 46
CONCLUSIONS 47

STEWART FIELD FIGURES 49-58

CHAPTER 3 - SAVONBURG FIELD PROJECT 59

Objectives 59

Background 59

BUDGET PERIOD 1 ACTIVITIES 60
Geological and Engineering Analysis 60
Database Development 60
Zone Description and Mapping Methods 60
Reservoir Parameters 61
Volumetric Analysis 61
Simulation Study 66
Geological Analysis 68
Discussions of Field Recommendations 69
Conclusions and Summary 70
BUDGET PERIOD 2 ANALYSIS 70
Waterplant Development 70
Permeability Modification Treatments 71
Pattern Change and Wellbore Cleanups 72
Reservoir Development 72
Field Operations 81
Technology Transfer 81
POST-PROJECT DEVELOPMENTS 83
Observations from the Field 83
CONCLUSIONS 83
APPENDIX A 85
APPENDIX **B** 103
APPENDIX C 125
APPENDIX D 139

List of Figures

Figure 1 Location Plat for Stewart Field 51
Figure 2 Stewart Field Well Location Plat 51
Figure 3 Stewart Field Primary Production Curve 52
Figure 4 Polymer Flooding versus Waterflooding Plot in the Stewart Field 52
Figure 5 Actual Versus Simulated Production for the Original Model fo the Stewart Field 53
Figure 6 Cumulative Oil Production versus Cumulative Water Injection for Waterflood Patterns Investigated for the Stewart Field 53
Figure 7 Relative permeability versus pore volumes injected for synthetic formation brine 54
Figure 8 Relative permeability versus pore volumes injected for filtered produced water 54
Figure 9 Relative permeability versus pore volumes injected for 3.0% potassium chloride solution 55
Figure 10 Original Modified Six Line Drive Pattern Selected for Waterflooding the Stewart Field 55
Figure 11 Average Daily Totals for Injection and Production by Month for the Stewart Field 56
Figure 12 Plot of Pressure Versus Shut-in Time for the Fall-Off Test Conducted on Mackey #6 56
Figure 13 A Schematic Illustrating a Vertical Fracture of Infmite Conductivity that is Confined on Two Sides by Parallel Faults Each Equidistant from the Injection Well 57
Figure 14 Plot of Pressure Versus Shut-in Time for the Fall-Off Test Conducted on the Meyer 10-2 57
Figure 15 Revised History Match for the Stewart Field 58
Figure 16 Computer Model Illustration of Oil Saturation Distribution in the Stewart Field as of June 1998 58
Figure 17 Nelson Lease Production & Injection 63
Figure 18 Nelson Lease Water: Oil Ratio 63
Figure 19 B2 Net Pay 64
Figure 20 B3 Net Pay 64
Figure 21 Location of RW-20 75
Figure 22 RE-20 Core Chloride Content 75
Figure 23 RW-20 Core Water Sat'n 75
Figure 24 RW-20 Porosity 75
Figure 25 RW-20 Permeability (air) 76
Figure 26 RE-20 Permeability (water) 76
Figure 27 RW-20 Residual Oil Sat'n 76

List of Tables

Table 1 Composition of Synthetic Formation Brine Used for the Stewart Field Experiments 32
Table 2 History of Experiments Performed on Scott 4-4 Core Plug 34
Table 3 History of Experiments Performed on Sherman 3 Core Plug 35
Table 4 History of Experiments Performed on Meyer 10-1 Core Plug #1 36
Table 5 History of Experiments Performed on Meyer 10-1 Core Plug #2 36

Table 6 December 1998 Stewart Field Surface Injection Pressures 41
Table 7 Stewart Field Water Injection Summary 41
Table 8 Summary of Reservoir Parameters Computed from Match of Mackey #6 FalloffData 43
Table 9 Summary of Reservoir Parameters Computed from Match of Meyer 10-2 Falloff Data 43
Table 10 Fluid Production and Their Simulated Values for Different Regimes in the Stewart Field 46
Table 11 Savonburg Pattern Volumetric Analysis 65
Table 12 Input Parameters for Steamtube Simulator - Savonburg Field 66
Table 13 Nelson RW-20 Core Anlaysis; Data 77

Chapter 1

Introduction

ABSTRACT

Common oil field problems exist in fluvial dominated deltaic reservoirs in Kansas. The problems are poor waterflood sweep efficiency and lack of reservoir management. The poor waterflood sweep efficiency is due to 1) reservoir heterogeneity, 2) channeling of injected water through high permeability zones or fractures, and 3) clogging of injection wells due to solids in the injection water. In many instances the lack of reservoir management results from 1) poor data collection and organization, 2) little or no integrated analysis of existing data by geological and engineering personnel, 3) the presence of multiple operators within the field, and 4) not identifying optimum recovery techniques.

Two demonstration sites operated by different independent oil operators were involved in this project. The Stewart Field is located in Finney County, Kansas and is operated by PetroSantander, Inc. This field was in the latter stage of primary production at the beginning of this project and is currently being waterflooded as a result of this project. The Nelson Lease (an existing waterflood) is located in Allen County, Kansas, in the N.E. Savonburg Field and is operated by James E. Russell Petroleum, Inc. The objective was to increase recovery efficiency and economics in these types of reservoirs. The technologies applied to increase waterflood sweep efficiency were 1) in situ permeability modification treatments, 2) infill drilling, 3) pattern changes, and 4) air flotation to improve water quality. The technologies being applied to improve reservoir management were 1) database development, 2) reservoir simulation, 3) transient testing, 4) database management, and 5) integrated geological and engineering analysis.

The Stewart Field project results included 1) the development of a comprehensive reservoir database using personal computers, 2) the completion of a simulation study to history match the primary production, 3) the simulation of waterflooding and polymer flooding, 4) an economic analysis to assist in identifying the most economical waterflood pattern, 5) completion of laboratory analysis conducted on reservoir rock, 6) unitization of the field so that a field-wide improved oil recovery process could be implemented, 7) design and construction of waterflood facilities, and 8) initiation and operation of the waterflood utilizing improved reservoir management techniques.

Water injection began on October 9, 1995 in the Stewart Field. In March 1996 oil production in the field began to respond to the water injection. Oil production continued to increase and through December 1998 total incremental waterflood response was approximately 2900 BOPD. Total field production was over 3150 BOPD. Total incremental waterflood production through December 1998 was 1, 634,782 BO.

The Stewart Field project's activities and plans consisted of the operation of the waterflood utilizing state-of-the-art technologies in an attempt to optimize secondary recovery. Production and reservoir data were analyzed using reservoir characterization techniques and by updating the existing reservoir simulation. The analysis of results was utilized to optimize the waterflood plan and flooding techniques to maximize secondary oil recovery. This project was awarded the "Best Advanced Recovery Project in the Midcontinent" for 1995 by Hart's Oil and Gas World.

The Savonburg Field project results were; 1) the installation and proving of the air flotation device to be effective in water cleanup in mid-continent oil reservoirs, 2) the development of a database which includes injection and production data, and reservoir data, 3) the development of a reservoir description, 4) the completion of a pattern volumetric study to select high potential areas, 5) completion of a streamtube waterflood simulation, 6) an analysis of injectivity on individual wells as a result of clean water/wellbore cleanups, and 7) the results of infill drilling and pattern changes.

EXECUTIVE SUMMARY

This project involved two demonstration projects, one in a Morrow reservoir located in the southwesjern part of the state and the second in the Cherokee Group in eastern Kansas. Morrow reservoirs of western Kansas are still actively being explored and constitute an important resource in Kansas. Cumulative oil production from the Morrow in Kansas is over 400,000,000 bbls. Much of the production from the Morrow is still in the primary stage and has not reached the mature declining stage of that in the Cherokee. The Cherokee Group has produced about 1 billion bbls of oil since the first commercial production began over a century ago. It is a billion-barrel plus resource that is distributed over a large number of fields and small production units. Many of the reservoirs are operated close to the economic limit, although the small units and low production per well are offset by low costs associated with the shallow nature of the reservoirs (less than 1000 ft. deep).

Common recovery problems in both reservoir types include poor waterflood sweep efficiency and lack of reservoir management. The poor waterflood sweep efficiency is due to 1) reservoir heterogeneity, 2) channeling of injected water through high penneability zones or fractures, and 3) clogging of water injection wells with solids as a result of poor water quality. In many instances the lack of reservoir management results from 1) poor data collection and organization, 2) little or no integrated analysis of existing data by geological and engineering personnel, 3) the presence of multiple operators within the field, and 4) not identifying optimum recovery techniques.

The technologies being applied to increase waterflood sweep efficiency were 1) in situ penneability modification treatments, 2) infill drilling, 3) pattern changes, and 4) air flotation to improve water quality. The technologies being applied to improve reservoir management were 1) database development, 2) reservoir simulation, 3) transient testing, 4) database management, and 5) integrated geological and engineering analysis.

In the Stewart Project, the reservoir management portion of the project conducted during Budget Period 1 involved performance evaluation. This included 1) reservoir characterization and the development of a reservoir database, 2) volumetric analysis to evaluate production performance, 3) reservoir computer modeling and simulation, 4) laboratory work, 5) identification of operational problems, 6) identification of unrecovered mobile oil and estimation of recovery factors, and 7) identification of the most efficient and economical recovery process.

To accomplish these objectives the initial budget period was subdivided into three major tasks. The tasks were 1) geological and engineering analysis, 2) laboratory testing, and 3) unitization. Due to the presence of different operators within the field, it was necessary to unitize the field in order to demonstrate a field-wide improved recovery process. This work was completed and the project moved into Budget Period 2.

Budget Period 2 objectives consisted of the design, construction, and operation of a field-wide waterflood utilizing state-of-the-art, off-the-shelf technologies in an attempt to optimize secondary oil recovery. To accomplish these objectives the second budget period was subdivided into five major tasks. The tasks were 1) design and construction of a waterflood plant, 2) design and construction of a water injection system, 3) design and construction of tank battery consolidation and gathering system, 4) initiation of waterflood operations and reservoir management, and 5) technology transfer. All the tasks were completed and water injection began in October 1995.

The Stewart Field project results were 1) the development of a comprehensive reservoir database using personal computers, 2) the completion of a simulation study to history match the primary production, 3) the simulation of waterflooding and polymer flooding, 4) an economic analysis to assist in

identifying the most economical waterflood pattern, 5) completion of laboratory analysis conducted on reservoir rock, and 6) unitization of the field so that a field-wide improved oil recovery process could be implemented, 7) design and construction of waterflood facilities, and 8) initiation and operation of the waterflood utilizing improved reservoir management techniques.

Water injection began on October 9, 1995 in the Stewart Field. In March 1996 oil production in the field began to respond to the water injection. Oil production continued to increase and through December 1998 total incremental waterflood response was approximately 2900 BOPD. Total field production was over 3150 BOPD. Total incremental waterflood production through December 1998 was 1, 634,782 BO.

The Stewart Field project's activities and plans consisted of the operation of the waterflood utilizing state-of-the-art technologies in an attempt to optimize secondary recovery. Production and reservoir data were analyzed using reservoir characterization techniques and by updating the existing reservoir simulation. The analysis of results was utilized to optimize the waterflood plan and flooding techniques to maximize secondary oil recovery. This project was awarded the "Best Advanced Recovery Project in the Midcontinent" for 1995 by Hart's Oil and Gas World.

In the Savonburg Project, the reservoir management portion involved performance evaluation. This work included 1) reservoir characterization and the development of a reservoir database, 2) identification of operational problems, 3) identification of near wellbore problems such as plugging caused from poor water quality, 4) identification of unrecovered mobile oil and estimation of recovery factors, and 5) identification of the most efficient and economical recovery process.

To accomplish this work the initial budget period was subdivided into four major tasks. The tasks included 1) geological and engineering analysis, 2) waterplant optimization, 3) wellbore cleanup and pattern changes, and 4) field operations. This work was completed and the project has moved into Budget Period 2.

The Budget Period 2 objectives consisted of continual optimization of this mature waterflood in an attempt to optimize secondary and tertiary oil recovery. To accomplish these objectives the second budget period was subdivided into six major tasks. The tasks were 1) waterplant development, 2) profile modification treatments, 3) pattern changes, new wells and wellbore cleanups, 4) reservoir development (infill drilling), 5) field operations, and 6) technology transfer.

-- The Savonburg project results included a complete geological and engineering analysis and fieldwork. The geological and engineering analysis included, 1) development of a database which includes injection and production data, and reservoir data, 2) development of a reservoir description, 3) completion of a pattern volumetric study to select high potential areas, and 4) completion of a streamtube waterflood simulation. The field work completed included, 1) the installation of the air flotation device for improvement of water quality, 2) wellbore cleanups throughout the field, 3) completion of six in-situ permeability modification treatments, 4) three pattern changes, and 5) an in-fill well drilled and completed as an injection well.

Chapter 2

Stewart Field Project

OBJECTIVES

The objective of this project was to address waterflood problems in Morrow sandstone reservoirs in southwestern Kansas. The general topics addressed were 1) reservoir management and primary drive performance evaluation, and 2) the demonstration of a recovery process involving off-the-shelf technology which could be used to enhance waterflood recovery and increase reserves.

The reservoir management portion of this project conducted during Budget Period 1 involved performance evaluation. This included 1) reservoir characterization and the development of a reservoir database, 2) volumetric analysis to evaluate production performance, 3) reservoir computer modeling and simulation, 4) laboratory work, 5) identification of operational problems, 6) identification of unrecovered mobile oil and estimation of recovery factors, and 7) identification of the most efficient and economical recovery process.

To accomplish these objectives the initial budget period was subdivided into three major tasks. The tasks were 1) geological and engineering analysis, 2) laboratory testing, and 3) unitization. Due to the presence of different operators within the field, it was necessary to unitize the field in order to demonstrate a field-wide improved recovery process. This work was completed and the project moved into Budget Period 2.

Budget Period 2 objectives consisted of the design, construction and operation of a field-wide waterflood utilizing state-of-the-art, off-the-shelf technologies in an attempt to optimize secondary oil recovery. To accomplish these objectives the second budget period was subdivided into five major tasks. The tasks were 1) design and construct waterflood plant, 2) design and construct injection system, 3) design and construct battery consolidation and gathering system, 4) waterflood operations and reservoir management, and 5) technology transfer. All the tasks were completed and water injection began in October 1995.

BACKGROUND

History

The Stewart Field is located approximately 12 miles northeast of Garden City in Finney County, - Kansas. The Field is about 1/4 - 1/2 mile wide, 4;5 miles long and is approximately 2400 acres. A location plat is shown in Figure 1.

In August of 1967, Davidor and Davidor drilled the Haag Estate #1 well in the NE NE of Section 12-T23 W R31 W, attempting to extend Mississippian production found to the northeast in Section 6. This was the discovery well for the Stewart Field. The Haag Estate #1 well was completed from a basal Pennsylvanian Morrow sand from 4755-4767 ft. for 99 BOPD. Davidor and Davidor drilled two additional producers (Haag Estate #2 and Mackey #1) and one marginal well (Mackey #2) in Section 12 (refer to the well location plat in Figure 2).

In 1971, Beren Corporation acquired the lease and attempted to extend the field to the west with the Mackey #3 located in the NE NW of Section 12. The well was drilled in November 1971 and temporarily abandoned in June 1972 after minimal production.

In 1985, Sharon Resources, Inc. drilled the Shennan #1 located in C E/2 E/2 NE of Section 11 and penetrated 45 ft. of Morrow sand. This well was completed for 60 BOPD. This resulted in a more active development of the field. Sharon drilled four more producing wells in Section 11 through 1985 and early 1986, followed by two dry holes. Beren drilled two offset wells on the Mackey lease, both near the west line of Section 12. In 1986, Sharon extended the field north to Section 2 (four producers and two dry holes) on the Nelson and Carr leases. In 1987, Sharon continued a westward extension in Section 3 (four producers and two

dry holes) and drilled the Bulger #7-1 east of the Haag lease in the C W/2 SW NW Section 7-T23S-R30W. Four producing wells were drilled on the Meyer lease in Section 10, around 1988, followed by wells on the Scott lease, in Section 4, in 1988 and 1989. North American Resources Company (NARCO) leased Section 9 and drilled a total of three producers and one dry hole in the north half of Section 9 during 1988. The eastern end of the field, the Bulger lease, was extended with two more Morrow producers, one St. Louis producer, and three dry holes in 1987.

Some locations were drilled during 1990 and 1991. Competitive forces resulted in development drilling with two additional wells in Section 12, one in Section 4 and three stepout wells in Sections 3 and 10. The Scott 4-8 was drilled in January 1992. During 1994, the final two wells, the Bulger 7-8 and 7-10, were drilled on the eastern end of the field.

The western extent of the field is currently defined by three tight Becker wells on the east edge of Section 5 and a wet Morrow test in Section 8. The eastern extent of the field is not as well defined with a suspected permeability barrier east of Bulger 7-10. Total primary field development resulted in 43 producers and 14 dry or abandoned wells.

All wells were drilled through the Morrow, cased with 4.5 or 5.5-inch production casing, perforated through a majority of the net pay interval and stimulated. Most wells utilized approximately 450 ft. of 8-5/8 inch surface casing and a DV or stage collar around 2050 ft. with top stage cement to surface. Early completion practices included acid or diesel breakdown jobs. Some wells were hydraulically fractured with gelled diesel. In 1990 and 1991, Sharon Resources implemented a field wide fracture program consisting of a water based gel with 3,000 to 43,500 lbs. of sand. All Morrow wells have currently been fracture stimulated, with the exception of Mackey #1. All wells during primary production were produced with pumping units and insert rod pumps.

Three wells within the Stewart Field were completed as St. Louis producers, namely Bulger #7-2, Sherman #5 and Nelson #2-3. The two latter wells have been recompleted into the Morrow, whereas the Bulger #7-2 remains a St. Louis producer with no Morrow sand present.

Pressure

The Stewart Field primary pressure history consisted of drill stem tests (DSTs) on 31 producers drilled from August 1987 to October 1991, and two field-wide shut-in surface buildup pressure tests in September 1989 and November 1991. The average field pressure at the beginning of this project was estimated to be 100-150 psig.

The first well, the Haag Estate 1, was DSTd 8/14/67 with a final shut-in pressure of 1080 psig. The Haag Estate 2 was DSTd on 1/28/68 with a final recorded pressure of 1102 psig. No extrapolated pressures were available on these wells. Given the good permeability and no pressure depletion in the reservoir, the 1100 psig value was considered representative of an initial stabilized reservoir pressure. Subsequent extension wells proved the continuity of the reservoir over the 4.5-mile length of the field.

The initial two wells were drilled on the Mackey lease in 1968, on the west offset quarter section to the Haag wells. Only the Mackey 1 (SE NW Section 12) encountered productive Morrow sand. It tested with 1102-psig bottomhole pressure (BHP). No further Morrow wells were drilled until the Sherman 1 was DSTd on 7/10/85. This well is near the east line of Section 11 and showed depleted pressures of 847 psig measured shut-in and 862 psig extrapolated. In the 18 years between 1968 and 1985 the two Haag wells and the Mackey well produced 323,196 bbls of oil. The field was extended west with drilling from 1985 to 1992. In 1987 the initial wells were offset to the east with the Bulger 7-1 DST having a final shut-in pressure of 718 psig. The latest Morrow DST producer during primary was the Scott #4-8 which had a static BHP of 300 psig in January 1992. Two additional wells were drilled on the Bulger lease in the latter part of 1993 and early 1994. Pressure data on these wells were not available.

In September 1989, surface measured bottomhole pressure buildup tests were run on 12 wells after 2-6 days of shut-in (depending on the well) to obtain an average reservoir pressure. Bottomhole pressure calculations and an isobar map resulted in an average reservoir pressure of 575 psig.

In November 1991, the field was shut-in for 4 days and surface measured bottomhole pressure buildup tests (6 wells) and static fluid levels (31 wells) were used to calculate bottomhole pressures. Eliminating wells with high fluid levels due to St. Louis water communication, the field-wide average pressure was planimetered to be approximately 215 psig.

Production

Initially most of the wells in the Stewart Field were completed in the Morrow formation. Three wells were completed in St. Louis and Ste. Genevieve initially. Therefore, production was mainly from the Morrow. Production increased approximately 8 fold due to the fracture stimulation work in 1990-1991. There was also substantial increase in water production that is believed to be due to communication with the underlying St. Louis formation.

The Morrow wells produced approximately 3,365 Mbbl of oil and 1,143 Mbbl of water, through May 1994. Using decline curve analysis, extrapolation of this production data indicated estimated primary recovery to be 3.88 million barrels of oil. May 1994 average daily production was 600 BOPD.

Gas production from the field was used to power the pumping units and to fire the gun barrels and heater treaters. Gas volumes were insufficient to market and any excess gas not being used on the leases was vented. No gas volume measurements from the field were available.

Field Data Summary

General		
State:	Kansas	
County:	Finney	
Location:	Section 7, T23S - R30W and Sections 2,3,4,9,10,11,12, T23S - R31W	
Primary Well Count:	43 Producers	
Operators:	3	
Reservoir Data		
Formation	Morrow	
Elevation (Field Average KB)	2884 ft.	
Depth to Top of Morrow Sand	4764 ft.	
Temperature	125° F	
Original Pressure	1102 psig (estimated)	
Average Initial Water Saturation	32.2%	
Area within Zero Contour of Net Sand Map	1,356 Ac.	
Original Oil In Place (estimated)	22,653	MSTB
Cumulative Production (as of 6-1-94)	3,365.035	MSTB
Cumulative Recovery Factor	14.9%	
Estimated Ultimate Primary Reserves	3,881	MSTB
Primary Recovery Factor	17.1%	
Estimated Incremental Secondary Reserves	3,738	MSTB
Incremental Secondary Recovery Factor	16.5%	
Estimated Primary plus Secondary	7,619	MSTB
Primary plus Secondary Recovery Factor	33.6%	
Rock Properties		
Lithology	Sandstone	

Average Thickness	26 ft.
Average Porosity (11% cutoff)	16.5%
Arithmetic Average Permeability (from Cores)	138 md
Compressibility	10×10^{-6}
Archie Equation Parameters:	a = 1 m = n = 2

Fluid Properties

Crude Oil -	
API Gravity	28
Viscosity at P_i and T_{res}	12.1 cp
Initial Solution Gas-Oil Ratio	37 SCF/STB
Gas Specific Gravity	1.234
FVF at Pi	1.038 RB/STB
Bubble Point Pressure (P_{BP})	180 psig
FVF at P_{BP}	1.045 RB/STB
Compressibility at P_i	5.83×10^{-6} psi^{-1}
Avg. Compressibility above P_{BP}	7.88×10^{-6} psi^{-1}
Produced Water-	
Resistivity at 125° F	0.04 ohm-m
Chlorides	55,500 mg/l
Total Dissolved Solids	91,300 mg/l
Compressibility at P_i	3.07×10^{-6} psi^{-1}

BUDGET PERIOD 1 ACTIVITIES

Geological and Engineering Analysis

Geology Summary

The Stewart Field is situated on the northeastern edge of the Hugoton Embayment of the Anadarko Basin. Morrowan or Atokan aged sands filled an incised valley into the underlying Ste. Genevieve and St. Louis formation of the Mississippian age. This incision occurred from regressive sequences during the period of the Central Kansas Uplift. The incised valley is filled with at least three and as many as six stacked, partly eroded silielastic sedimentary intervals. Each sequence represents a transgressive and regressive succession reflecting flooding and then reemergence of the shelf and valley system. Local erosion and reworking of the sediments is common. The sands may be at least partially sourced from erosion of a local sandy Ste. Genevieve limestone. It is believed that marine reworking of the sands from the west contributed to cleaning up the sands.

Log, core and dipmeter data indicate that the deposits prograded from east to west, landward to basinward. The channel thickens from around 20 ft. in the eastern end in Sec. 7-T23S-R30W to around 45 ft. in Sec. 9-T23S-R31 W with a notable exception in the east half of Sec. 12-T23S-R31 W, where a suspected karstic feature results in 61.5 ft. of gross sand. The lower half of this sand is poorly developed, possibly due to lack of marine reworking. The channel dips 3 to 5 degrees per mile until the paleogradient steepens in the western end of Sec. 3-T23S-R31 W before emptying into a deltaic environment with shale and silty sandstones in Sec. 5-T23S-R31 W. Deep fault planes or zones of weakness may have contributed to rapid directional changes of the center of the channel.

Sourcing of the reservoir is believed to have occurred along fault lines and porous reservoir rocks from the Woodford shale deep in the Anadarko Basin. A thick black oil stain is found in some of the core samples, possibly indicative of an earlier hydrocarbon migration. The Morrow reservoir was initially underpressured, but a higher pressure region was tested in the west end.

The lithology is described as glauconitic quartzarenite to quartzarenite with varying grain size distribution from very fine to medium sized grains. In some wells, a coarse grained conglomerate is reported at the base of the sand. Samples are typically subangular to subrounded, moderate to well sorted with intergranular to intercrystalline porosity development. Quartz overgrowths are abundant. X-ray diffraction indicates 0 - 6 % clay volume with a majority of smectite along with detrital chlorite and illite.

The fluvial influence of the channel is exemplified by the tributary channels and by the thickening and dipping sand strata towards the west. In addition, the cores show layers of coarse grains fming upwards with numerous instances of cross-bedding within the individual strata.

A strong marine influence is shown by numerous lime streaks. Even though individual lime streaks cannot be correlated across the whole length of the channel, the Pe curve identifies common no flow boundaries across 4-5 well distances. In actual core recovery, these lime streaks were tested impermeable with no oil saturation. An abundance of glauconite, pyrite, coals, shales, fossils, burrows and caliche zones are also found within the sand sequences.

Database Development

All the electric log data for the field were digitized into a computer database. The log data were analyzed by digitizing the Morrow interval of the printed logs using a commercial "Logdigi" computer program by "Logic Group". Existing core analyses and log data were analyzed to find a relationship between core porosity versus log porosity and porosity versus permeability. A cumulative porosity plot was used to determine a porosity cut-off as related to net pay. The porosity cut-off was determined to be 11%, which corresponds to about 8% of the total porosity feet. Net pay thicknesses for individual wells were completed using this porosity cut-off value. A net pay map was constructed for the purpose of the waterflood feasibility study. This map was planimetered to determine the reservoir volume of the Morrow and oil recovery factors.

Water saturation calculations from electric logs were done in order to be included in the database. The water saturations could not be calculated with sufficient accuracy to tabulate values for individual wells. Key problems identified were thin bed effects, thin conductive beds from pyrite cementation material, and conductive chloride clays. Capillary tests on cores were employed to estimate initial water saturation.

Production data for all wells in the Stewart Field was also entered into the computer database. Production data was tabulated by month since the discovery of the field. The wells were grouped by tank battery so that allocations for each well could be monitored. The production was allocated to each well by monthly barrel tests. Water production was estimated by applying the percent of water as determined by a grind-out test and relating that to the oil volume produced. The sales numbers for each tank battery were also listed to compare with the production numbers supplied by the operators. Production was divided between Morrow and non-Morrow for the wells that had produced from other zones. Gas production from the field was minimal and was used to power the pumping units or vented.

The Stewart Field primary pressure history, including drill stem tests (DST) conducted on 31 wells, two field wide shut-in surface pressure tests, and individual well fluid level tests was also tabulated into the database. Pressure tests indicated the continuity of the reservoir over the 4.5-mile length of the field. Isobar maps were constructed for the field. Pressure history of all DST's, shut-in pressures, bottomhole pressure (BHP) from fluid levels, and BHP versus cumulative production plots were made for each well and the entire field.

A log stratification study was completed which indicated the Morrow formation could be divided into as many as eight different flow units. Three main flow units were identified as separate depositional sequences that appeared to possess similar porosity and permeability characteristics. These three flow units correlate along the deepest parts of the channel, with some minor discrepancies within the thinner boundary wells. The three flow units were identified as the Red zone on top, Purple zone in the middle, and Yellow zone on the bottom. The depth and subsea elevation for the top and bottom of each zone was entered into the database for each well.

Porosity and resistivity log data (foot by foot) were cross-plotted on log-log paper (Pickett plot) keeping track of depth trends. The three primary zones in the Morrow formed distinct clusters of points on these plots indicating that the zonation identified nicely grouped the levels of heterogeneity. While most of the field is above the oil-water contact, several wells in the west half of the field indicate a transition zone and water leg.

Wettability tests, petrographic data, and standard core analysis were compared as series of plots with log analysis results to define correlations. In particular, relationships between bulk volume water (water saturation and porosity) and relative permeability data, grain size and sorting, and mineral composition (clays) were sought.

Permeability was estimated using different relationships utilizing porosity and water saturation. One method investigated was the Timor relationship. This empirical relationship provided only fair results when comparing measured core permeability versus estimated permeability.

The possibility of open fractures in the Morrow reservoir was evaluated through three potential sources of information:

1. 4-arm dipmeters from the reservoir to examine for borehole breakouts to establish minimum horizontal compressive stress direction.
2. Paleomagnetic measurements of core samples to orient the cores to define directions of any open fractures that might be present.
3. Examination of the oriented core from the Sherman #3.

The presence and characterization of fractures helped to define any anisotropy in the reservoir in addition to the influence of sedimentary structures on fluid flow.

Volumetric Analysis

Decline curve analysis from existing production data was completed for all the wells within the field. Utilizing a straight exponential decline analysis, calculated remaining primary reserves as of June 1, 1994 were 516,000 barrels of oil for an ultimate primary oil recovery of approximately 3,881,000 barrels. A plot of the field's primary production is shown in Figure 3.

Over the last year of primary production a substantial flattening of the production decline occurred for many leases, as more of the field was affected by gas expansion.

Material Balance

Material balance calculations were performed from initial pressure to the 1989 and 1991 field wide tests. Assuming no water influx and pressure above the bubble point, the fluid produced should have been due .to fluid and rock- expansion over the given pressure drop.-These calculations gave original reserves in excess of 100 million barrels of oil in place. Volumetric mapping of the net sand indicated only 22 million barrels in place.

It was determined that uncertainties in fluid and rock properties would not resolve the difference in determining the original oil in place between volumetric mapping of the net sand and material balance calculations. Either a large volume of the reservoir was yet to be defined or a limited water influx (pressure support) existed within the field.

Development drilling and seismic data indicated that the reservoir boundaries were defined with reasonable certainty. Therefore, potential pressure support sources were investigated and identified. This was accomplished through the geological examination of well logs and drill stem test data from locations adjacent to the field. A complete collection of well logs from adjoining areas to the field was assembled.

Three potential sources of pressure support were identified. A water aquifer associated with the Morrow formation is present at the west end of the field. Underlying formations, the Ste. Genevieve and St. Louis, appear to be in communication with the Morrow reservoir in certain areas of the field.

Polymer Flood Analysis

Relative permeability tests were conducted on cores taken from the Stewart Field. Using the endpoints from the relative permeability curves, mobility ratios were calculated. All the mobility ratios calculated based on the average saturation behind the flood front were less than 1.0, which was highly favorable.

Analysis was conducted utilizing the Polymer Flood Predictive Model developed by Scientific Software-Intercomp for the National Petroleum Council's (NPC) 1984 survey of U.S. enhanced oil recovery potential (NPC, 1984). Using average reservoir properties the model did not predict significant incremental amounts of oil recovery for polymer flooding versus waterflooding. Figure 4 is a plot illustrating the results of this analysis.

Based on these fmdings there was no justification for considering a polymer flood in this project.

Reservoir Modeling

Independent reservoir simulation studies were undertaken by Sharon Resources and the University of Kansas. Sharon Resources, located in Englewood, Colorado, was connected via Internet to the workstation at the University of Kansas. The studies were performed using a Silicon Graphics workstation with Western Atlas VIP Executive simulation software. The VIP simulator is a conventional black oil simulator, equipped with graphics interface. A major portion of the technology transfer associated with this budget period pertains to University personnel assisting Sharon Resources in their simulation efforts.

The objectives of each study consisted of: (1) the characterization and distribution of the various reservoir parameters, (2) a material balance model to establish a history match with the primary production, and (3) a waterflood predictive model to select the optimum waterflooding pattern for maximum economic oil recovery. The independent studies resulted in different models, however, the two models provided similar results.

Overview of Reservoir Simulation

A. Introduction

Reservoir simulation is a tool to increase profitability of a reservoir through proper reservoir management. Simulation can be a tool to determine -optimum well pattern and spacing, design of a facility, optimum recovery method, optimum well completion, etc. Simulators can also be used to match the history of the reservoir with updated seismic and geological data. It can serve as a tool to judge the actual performance of the reservoir and also predict the future performance. Based on the predictions, proper reservoir management can be applied to reduce operating costs and thereby increasing profitability.

B. Data Requirements

The approach for reservoir description entirely depends on the available reservoir database. Data required for a reservoir description can be classified as follows:

1. Rock property data at initial static conditions.
    a. Formation structure: Tops and bottoms of the formation.
    b. Net pay thickness.
    c. Porosity at initial pressure.
    d. Drainage and capillary pressure data.
2. Fluid properties at static conditions.
    a. Oil, gas and water formation volume factors.
    b. Oil, gas and water densities at standard conditions.
3. Rock and fluid data for oil/gas displacement
    a. Absolute permeability of rock.

b. Gas and oil relative permeability curves.
c. Fonnation, oil and water compressibility.
d. Oil and gas formation volume factor as a function of pressure.
e. Gas in solution as a function of pressure.
f. Oil and gas viscosity as a function of pressure.

4. Rock and fluid data for water/oil displacement
a. Oil and water relative permeability curves.
b. Water formation volume factor as a function of pressure.
c. Water viscosity as a function of pressure.

Porosity and permeability distributions are normally derived from core analysis, well-log, and well test data. The most difficult reservoir property to define is the permeability distribution areally and vertically between wells. Adequate knowledge of permeability distribution is more important than the porosity to understand the flow of reservoir fluids. Porosity can be measured by logging, but permeability cannot be measured reliably by logging. Thus, it is necessary to estimate the permeability from permeability/porosity correlations developed from core analysis data. Correlations will be most reliable if they are developed for each major rock type present in the reservoir.

After developing the reservoir description, it is necessary to test the description. This is carried out by matching the available history of the reservoir. Simulation of the past history can identify the weaknesses in the reservoir description and modifications to the description can then be implemented. In some cases the reservoir description is changed to match the history, considering that the changes should be rational and consistent. History matching can also be used to study the current status of the reservoir, to identify the depletion mechanism, and to determine the fluid distribution in the reservoir.

Simulation Conducted at the University of Kansas

A. Data Availability

Necessary data required for simulation was provided by Sharon Resources. The most important data for reservoir description was the porosity /permeability correlations for the three major zones within the Morrow. These correlations were derived by Sharon Resources and the results of the correlations were used in the simulation for distribution of properties in the reservoir. Relative permeability data representative of the field was also required. Sharon Resources also supplied this data.

B. Reservoir Description

The Stewart Field model was developed in stages. Sharon Resources initially identified the three major pay zones in the reservoir. Based on core/log and permeability/porosity correlations they assigned porosity and permeability values to the zones present in all the producing wells. Digitized logs were also provided to get the tops and bottoms of each zone. Initially it was decided to divide the field in four different sections, which were assumed to be isolated from each other. The first section of the field consisted of the Sherman, Nelson, Carr and Mackey leases. These leases comprise 912,000 barrels of oil production from the Morrow, which is approximately 35% of the total field production from the year 1985. The assumptions used to match the production history of this section were also used in the subsequent sections.

Initially it was necessary to assign X and Y coordinates to each well from a zero reference point. The NE corner of section 10 was chosen as the zero reference point.

To identify the distributions in the regions between the wells, it was necessary to contour the tops, bottoms, porosity, permeability and water saturations of each zone. Data files were created and CPS Radian software was used for contouring. Due to the absence of control points, other than the wells, CPS Radian mathematically extrapolated the reservoir boundaries. In order to get a more accurate reservoir description, about 100 Dry holes were introduced around the reservoir to force a NO FLOW boundary in the desired

locations. The necessary files were converted to a format that was acceptable to the VIP black oil simulator's GRIDGENR, a preprocessor program to generate grids graphically for simulation purposes.

C. Reservoir Simulation using VIP Simulator

The VIP black oil simulator was developed by Western Atlas Inc. It is one of the most powerful commercial software packages available for reservoir simulation. Its graphic interface enables the user to import geological and other data from various engineering and geological software. GRIDGENR is a utility of VIP that allows the user to import reservoir parameters in the form of contours. Based on the grid system selected, it calculates and assigns values to each grid block.

Using the VIP PRCORE utility, all rock and fluid parameters were input and the necessary data files relating to the formation structure, porosity and permeability distribution were imported into GRIDGENR. The initial simulation grid of 150x20x3 blocks was created and the values were calculated using the program. This allowed creation of the VIP-CORE initialization module file.

Once the initialization file was created, the next step was to create the VIP-EXEC file. This file consists of the history of all the wells which includes location, date of completion, perforation intervals, wellbore radius, skin factor, stimulation history, production history, pressure constraints, and any other information related to the wells. Sharon Resources provided all relevant information. Using the VIP PREXEC utility, all data was imported and a recurrent run file was created. The field consisted of 44 producing wells.

D. History Matching of Primary Production

The model had the following initial assumptions:

1. Initial reservoir pressure was assumed to be 950-1000 psi (depending on the first date of production in the four sections). No external pressure support was provided.
2. The reservoir was under natural depletion drive.
3. There was no initial skin damage on the wells.
4. Based on the pressure buildup tests an average skin factor of -3 was assigned to each well after the fracture stimulation work.

Several cases were run to get an optimum history match of each section. The details of the simulation results for section "C" consisting of Sherman, Nelson, Carr and Mackey leases are described below. Similar assumptions were used for all the other three sections.

<u>Details of the Simulation Conducted at the University of Kansas of Section "C" of the Stewart Field</u>

The model had the following initial assumptions:

1. Initial reservoir pressure was assumed to be 950 psi and there was no external pressure support for the reservoir.
2. The reservoir was under natural depletion drive.
3. There was no skin damage on the wells.
4. Based on the pressure buildup tests an average skin factor of -3 was assigned to each well after the fracture stimulation work.

Several cases were run to get an optimum history match. Tables of all cases are included. During the initial run it was observed that the simulated production was much less than the actual production, especially during the period from 1989-1992 (Case 1). This was the period when Sharon Resources had conducted the field wide fracture stimulation program. The actual peak rate of production in this period was about 850 BOPD. The simulated results showed a peak rate of production of about 250 BOPD. During the analysis of the results it was observed that most of the wells became pressure limiting and were unable to produce the rates due to low pressures. These results lead to a hypothesis that there was a source of external pressure support. One possible scenario for providing pressure support was from the underlying St. Louis

formation acting as an active aquifer. Based on various data available, the St. Louis formation was implemented into the model as a layer which was 95% water saturated and had a slightly higher pressure compared to that of the Morrow formation. The simulated results after the introduction of the St. Louis formation (at 1250 psi) increased, but were still below actual production (Case 2).

The St. Louis formation pressure was then increased to 1550 psi with a very low vertical permeability (Case 3). There was some increase in the production, but simulated results were still off in the post fracture production by a factor of 3.

In the next two runs, a skin factor of +1 was introduced during the pre-frac period and -3 in the post-frac period. Low vertical permeability of 0.002md and 0.0015 were introduced in all the layers (Case 4 and 5). In both the runs, there was substantial increase in post-frac production, but the pre-frac production was reduced by a factor of 3 due to the skin factor.

Vertical permeability was then increased by a factor of 10, i.e to 0.015 and (Case 6). It was observed that the initial simulated peak production during the pre-frac period was approximately 150 BOPD less than actual and the post-frac production was about half the actual production.

At this point the perforations were changed in the wells. It was assumed initially, all the wells were perforated in all the zones present in the wells. To maintain the reservoir pressure during the post-frac period and achieve the peak production rate, it was decided to have perforations only in the top two layers during the pre-frac period and have perforations in all the zones including the St Louis formation during the post-frac period (Case 7). Also, a -2 skin factor was implemented during the pre-frac period and a skin factor of -4 during the post-frac period (Case 8). The St. Louis formation pressure was also increased to 1750 psi. Simulated results were still much below the actual until the permeability of the system was increased by a factor of 2. In this model the initial peak production rate during the pre-frac period was off by about 30-40 BOPD and the post-frac rate was off by about 250 BOPD.

Analysis of each well's simulated production compared with the actual production history revealed that some of the edge wells did not have enough reservoir volume to produce properly. It was decided to extend the NO FLOW boundary and give these wells additional reservoir volume. This increased the original-oil-in-place-(OOIP) in the model by about 35%. The results of this model were 96.013% of the actual production from the wells in the section (Case 9). The match from this model was considered adequate for the reservoir section in question.

Conclusions

The following changes to the original description enabled the model to have a history match of the reservoir section chosen for simulation:

1. Permeability of the reservoir was increased by a factor of 2.
2. Reservoir volume had to be added to the northern portion of the simulated area. This leads us to question whether the reservoir boundaries have been properly defined in this area.
3. Outside pressure support had to be included. It appears most logical that this support was coming from the underlying St. Louis formation. This would result in the primary drive mechanism being a combination of depletion drive and water influx.

Results and Cases

Case 1

Layer #	Perf	KZ md	Sw %	P psi
1	Yes	0.002	31	950
2	Yes	0.002	31	950
3	Yes	0.002	31	950
4	No	0.0015	99	950

Pre-frac Skin = 0
Post-frac Skin = -3

Analysis: The prefrac results are about 100 BOPD less than the peak production and Post frac results are about 1/4th of the actual production.

Case 2

Layer #	Perf	KZ md	Sw %	P psi
1	Yes	0.002	31	950
2	Yes	0.002	31	950
3	Yes	0.002	31	950
4	No	0.002	95	1250

Pre-frac Skin = 0
Post-frac Skin = -3

Analysis: There was not much difference from the case one.

Case 3

Layer #	Perf	KZ md	Sw %	P psi
1	Yes	0.001	31	950
2	Yes	0.001	31	950
3	Yes	0.001	31	950
4	No	0.001	95	1550

Pre-frac Skin = 0
Post-frac Skin = -3

Analysis: The prefrac results are about 80 BOPD less than the peak production and Post frac results are about 1/4th of the actual production. Not much increase in cumulative production.

Case 4

Layer #	Perf	KZ md	Sw %	P psi
1	Yes	0.002	31	950
2	Yes	0.002	31	950
3	Yes	0.002	31	950
4	No	0.002	95	1550

Pre-frac Skin = +1
Post-frac Skin = -3

Analysis: There was decrease in pre-fracture production by a factor of three but increase in post fracture production by a factor of 2.

After this the permeability in x and Y direction were increased by a factor of 2, resulting in some major changes which are discussed in the cases below.

Case 5

Layer #	Perf	KZ md	Sw %	P psi
1	Yes	0.0015	31	950
2	Yes	0.0015	31	950
3	Yes	0.0015	31	950
4	No	0.0015	95	1550

Pre-frac Skin = +1
Post-frac Skin = -3

Analysis: Due to the low vertical permeability there was some pressure support but was not substantial to increase the cumulative production by factor of 2 to match the actual production.

Case 6

Layer #	Perf	KZ md	Sw %	P psi
1	Yes	0.015	31	950
2	Yes	0.015	31	950
3	Yes	0.015	31	950
4	Yes	0.015	95	1550

Pre-frac Skin = +1
Post-frac Skin = -3

Analysis: The vertical permeability was increased by a factor of 10, resulting in increase of the total production substantially. post fracture production by a factor of 2.

It was then decided to produce from Zone 1 & 2 to match the pre-fracture production and then open all the zones after the fracture job.

Case 7

Layer #	Perf	KZ md	Sw %	P psi
1	Yes	0.0	31	1000
2	Yes	0.09	31	1000
3	Yes	0.002	31	1000
4	Yes	0.002	60	1700

Pre-frac Skin = +1
Post-frac Skin = -3

Analysis: No substantial changes in production observed.

Case 8

Layer #	Perf	KZ md	Sw %	P psi
1	Yes	0.025	31	950
2	Yes	0.025	31	950
3	Yes	0.025	31	950
4	Yes	0.0095	95	1750

Pre-frac Skin = -2
Post-frac Skin = -4

Analysis: Initial peak production was about 30-40 BOPD less than the actual production, but the post fracture peak production was about 250 BOPD less than the actual production.

Reservoir Model OOIP:	7523.140 MSTB
Total production:	817757 STB
Actual production:	912540 STB
% of Actual Production:	88.846 %

It was found that the edge wells namely Nelson #2-2, Nelson #2-3, Sherman #4 and Carr #2-1 were not producing at the rate they should have been producing. Looking into the maps and contours, it was found that there was not enough reservoir volume in that area for the wells to produce. In order to increase the reservoir volume the no flow boundary was moved further outside. this increased the total reservoir OOIP by about 35%.

Case 9

Layer #	Perf	KZ md	Sw %	P psi
1	Yes	0.002	31	950
2	Yes	0.09	31	950
3	Yes	0.095	31	950
4	Yes	0.09	99	1650

Pre-frac Skin = -2
Post-frac Skin = -4

Analysis: Substantial changes in production observed. The final results gave us history match of about 99.013%

Reservoir Model OOIP:	100288 MSTB
Total production:	876153.9 STB
Actual production:	912540 STB
% of Actual Production:	96.013 %

Conclusions:
1. Permeability increased by factor of 2.
2. Increased reservoir volume at the edges.
3. Pressure support from the aquifer.

Case to prove aquifer support:

Case 10: No vertical permeability in either layer.

Layer #	Perf	KZ md	Sw %	P psi
1	Yes	0.0	31	950
2	Yes	0.0	31	950
3	Yes	0.0	31	950
4	Yes	0.0	95	1750

Pre-frac Skin = -2
Post-frac Skin = -4

Analysis: Initial peak production was about 60-80 BOPD less than the actual production, but the post fracture peak production was about 250 BOPD less than the actual production.

Reservoir Model OOIP:	10288 MSTB
Total production:	730160.2 STB
Actual production:	912540 STB
% of Actual Production:	80.01%

Case 11: No aquifer present in the model.

Layer #	Perf	KZ md	Sw %	P psi
1	Yes	0.002	31	950
2	Yes	0.09	31	950
3	Yes	0.0095	31	950

Pre-frac Skin = -2
Post-frac Skin = -4

Analysis: Initial peak production was about 60-80 BOPD less than the actual production, but the post fracture peak production was about 250 BOPD less than the actual production.

Reservoir Model OOIP:	10007 MSTB
Total production:	762144.7 STB
Actual production:	912540 STB
% of Actual Production:	83.51%

The following is a summary of the assumptions used and changes implemented to the field description in order to obtain a history match of the primary production for all four sections:

1. **Permeability of the reservoir was increased by a factor of 2. Justifications for this could be that there was uncertainty in the porosity permeability correlations developed using the core/log data or damage to the cores during the drilling process.**
2. **Reservoir volume was added to the northern portion of the Nelson and Carr leases. This led us to question whether the reservoir boundaries had been properly defined in this area.**
3. **Outside pressure support was included. It appeared most logical that this support was coming from the underlying Ste. Genevieve/St. Louis formations. This would result in the primary drive mechanism being a combination of depletion drive and water influx.**
4. **The initial skin had to be changed to +1 and the average skin after fracture stimulation remained at -3 for all wells. This post fracture skin used in the simulator was in agreement with the pressure transient analysis where the post fracture stimulation skin was within the range of -2.8 to -3.6.**
5. **The initial reservoir pressure was 1200 psi and the pressure of the underlying formation was assumed to be 1500 psi. Initially it was assumed that the underlying formation was in pressure communication with the entire field, but based on the geological analysis and production history it was observed that the direct communication of the permeable underlying formation is in the area of the Mackey and Scott leases. This assumption was built into the model in order to describe the reservoir more realistically.**

Based on the above assumptions the model was developed. An external aquifer, as described above in assumption 5, was included as the fourth layer in the model. None of the wells were perforated in the fourth layer.

A model of the entire field was developed. The model was built using a grid of 150x20x4. Each gridblock had average dimensions of 190 x 250 ft. The resulting model had about 2-3 gridblocks between each well. The model contained a total of 12000 gridblocks. The OOIP for this model was 25256 MSTB. This figure did not match with the estimated OOIP based on the net sand map provided by Sharon Resources. One reason for this discrepancy could have been the uncertainties associated with the reservoir boundaries. The following parameters were added to the reservoir description to obtain a history match.

1. Water saturations in the four layers:

Layer 1: 31 %
Layer 2: 31 %
Layer 3: 31 %
Layer 4: 99 %

2. Vertical permeability distribution within and between the layers.

Layer 1: $K_z = 0.05$ md
Layer 2: $K_z = 0.01$ md
Layer 3: $K_z = 0.05$ md, Only at the west end and in section 12.
Layer 4: $K_z = 0.05$ md, Only at the west end and in section 12.

The vertical permeability in the rest of the field in layers 3 & 4 was zero.

3. Initial pressure for the layers:

Layer 1: 1200 psi
Layer 2: 1200 psi
Layer 3: 1200 psi
Layer 4: 1500 psi

These values provided a primary history match in which the simulated production was 95.74% of the actual production. The actual and simulated results are plotted in Figure 5.

This was assumed to be a representative model of the field. This model looked different from the actual field in certain aspects, but it behaved similar to the actual reservoir in terms of the production and pressure history. One of the reasons for possible discrepancies could have been the description of the reservoir properties within the interwell region. Many different models were capable of producing a history match for the same field.

E. Waterflood Simulation

Reservoir simulators have served as an effective tool to predict and design the optimum recovery processes. The VIP simulator has the capability to simulate many of the enhanced oil recovery processes, including waterflooding. During the initial stages of this study it was observed that the mobility ratio was favorable for waterflooding. Thus, there was minimal incremental increase in oil production due to polymer flooding. Polymer flooding was analyzed using the DOE streamtube waterflood/polymer flood predictive model. Based on the results of the predictive model, it was decided to design an optimal waterflood recovery pattern.

F. Waterflood Patterns Investigated

Working Interest Owners (WIO) and University personnel proposed six different patterns. The injection rate was restricted by the water availability of about 6000 BWPD (as informed by Sharon Resources). Thus, in each case the total water of 6000 BWPD was distributed equally between each injection well within the waterflood pattern. The different waterflood patterns simulated were 3 line drive, 5 line drive, 7 line drive and three other line drive type patterns.

All the patterns were run for a waterflood period of ten years. The production wells were set to a watercut limit of 90%. Figure 6 is a plot of cumulative oil production versus cumulative water injection for the different patterns investigated. During the waterflood predictive runs convergence failures were observed. To avoid excessive failures, timestep control was implemented in the simulation. Timestep control restricts the maximum change in the saturation profiles, pressure, etc, in order to avoid convergence failures by solving the fluid flow equations at small time intervals. This had no significant effect on the calculated results.

G. Conclusions of the Waterflood Simulation

The Stewart Field simulation indicated favorable results for waterflood. The following conclusions were derived for waterflood prediction based on the simulation results.

1. Based on the simulations, the cumulative oil production and the WOR for all the patterns varied by less than 10%.
2. Simulation results suggested that the total oil recovery was a function of the volume of water injected, but not a strong function of the injection pattern.

Simulation Conducted by Sharon Resources

The simulation conducted by Sharon Resources was designed in two phases. A two-dimensional (2D) study was done with radial and linear models using a range of reservoir characteristics and sensitivities. Also a three dimensional (3D) study was conducted to history match the Morrow production history and predict the optimum waterflooding pattern.

A. **Two-Dimensional Study**

The objectives of the 2D simulation were to study oil recovery changes as reservoir characteristics varied within a range of known field data. This would acquaint Sharon Resources personnel with the simulator, assist in the understanding of the reservoir, and would also help simplify history matching in the 3D simulation. The following objectives were stated:

1. In a radial model, history match a typical fracture stimulation response.

2. a. In a linear model, study the effect of layering and cross-flow between layers. Study oil recovery as a function of permeability variation and permeability ordering.

   b. Study the impact of wells with St. Louis communication. Study the effect of shutting in first line producing wells at various water cuts and converting them to injectors.

   c. Vary relative permeabilities and capillary- pressures within known field parameters to ascertain their effect on oil recoveries.

1. Radial Model

Sherman #3 was selected as the well to model via radial simulation. This well had good logs with clearly identified flow units, core analysis, pre- and post stimulation pressure transient analysis and was an excellent example of the increased production rates obtained from hydraulic fracture treatments. The purpose - of the radial model was to history match the fracture results.

Core porosities and penmeabilities were used to represent eight layers identified from the logs. Production declined from a peak rate of 47 BOPD in January 1986 to 3 BOPD in October 1990. The well was fractured in November, 1990 with 11,000 gallons of 40 lb. Boragel with 1,300 lbs. 100 mesh sand and 18,200 lbs. 20/40 sand. Production reached a stable rate of around 120 BOPD before declining to 13 BOPD in December 1993. This production response could not be explained by changing from a +1 pre-frac skin to a -2 post-frac skin factor, but was augmented by additional thickness opened at the wellbore. An eight layer radial model with 20 concentric cylinders with increasing radii away from the wellbore was used to match production from a 32-acre drainage area. The production could not be matched by depletion drive alone without substantial pressure support. This support was likely water influx, possibly from hydraulic fractures communicating with the St. Louis. It was also necessary to double the core penneabilities to match the actual flow rates.

The after-frac peak production rate was best modeled by adding a large outer cylinder of water reservoir, surrounding the drainage area, to represent an external pressure source. A no-flow boundary was needed to isolate half of the reservoir at original pressure. Half of the thickness was initially perforated, with the pressure support, and allowed to produce down to the pre-frac rate. The fracture was then responsible for opening up the other half of the thickness, releasing oil that was still at original pressure, matching the production increase. This was a plausible explanation, as several shale and limestone streaks were evident in the core and pressure support could be seen from different sources.

The external pressure source and isolation of part of the reservoir accomplished the goal of approximating the well's performance. The model did not sustain the peak rate for as long as the actual production, but this could be accomplished by increasing the drainage area. The model required a pressure

constraint at the producing well. The well was allowed to produce at the actual rate if the BHP stayed above 50 psi. If the actual rate was too great and required a lower pressure than 50 psi, the pressure limit was invoked thereby reducing the rate at which the well could produce. The model performance showed that the well was able to produce at the actual rates while keeping the well essentially pumped off as evidenced by the pressure staying above 50 psi but not exceeding 200 psi. The only portion of the model where the well was unable to keep up with the actual production was the extended peak rate after the frac.

2. Linear Model

a. Layering, Cross-Flow, Permeability Variation and Ordering

The linear model was built using 25 x 5 x 8 gridblocks in the X, Y and Z directions, respectively. Each gridblock was 55 feet in the X and Y direction and 5 feet in the Z direction. One well at each end of the model approximates the 40-acre spacing seen across most of the field. (This is referred to as a 2D model since the purpose of including the Y-direction was to judge the directionality of the solution algorithm and not to describe the width of the channel.) The flow units were described by eight layers, two in the Red (top) and Purple (middle) and four in the Yellow (bottom). Eight layers represented the maximum amount of flow units identified in any well and were felt necessary to adequately describe the reservoir with a proper permeability variation. Since the permeability-porosity transforms were based on log analysis that averages data over several feet, the permeabilities calculated from the logs were too uniform. As an example, Sherman #3 plotted a permeability variation (V) = 0.7 from point specific lab measurements, but V=0.3 based on the log transforms. The linear model was run at V=0.3, 0.5 and 0.7 to quantify how much the log derived permeability transforms over-estimate waterflood performance. The recovery of reserves in the 2D model was very high as each layer will flood out eventually and areal sweep was complete for each case. Therefore, comparing ultimate recovery is not an indication of waterflood performance. The method chosen to compare waterflood performance in the 2D study was the number of months to recover 72,000 barrels of oil. The more efficient floods will have later water breakthrough, thereby recovering more reserves sooner and without the added operational cost of produced water. The V=0.7, 0.5 and 0.3 cases recovered 72,000 BO in 47, 28 and 24 months respectively. The 03 permeability variation case recovered the oil in almost half the time of the case with V=0.7.

The different permeability variation cases were all run with 1 and of cross-flow between layers.-The effect of cross-flow on a reservoir with V=0.7 was studied at 0, 1 and 100 md. The model uses the vertical permeability as the permeability to flow between the gridblocks. The 0, 1 and 100 and cases recovered 72,000 BO in 48, 47 and 27 months, respectively. The no-flow barriers isolated the layers creating different pressure profiles in each layer. Cross-flow between layers allows the pressure to equalize so that a uniform pressure drop from the injector to the producer exists across all the layers. Based on these results, wells with low stratification would make better injection wells.

The impact of permeability ordering was seen to be negligible in the case of wells with no-flow boundaries. This was expected since cross-flow is not occurring and the pressure transients move through each zone individually with no effect of gravity. What was more surprising, however, was the small effect of permeability ordering in the presence of vertical permeability.

Sensitivity to number of layers was tested by comparing a three layer model with the eight layer model to see the validity of representing a $V = 0.7$ with only three layers. Three layers recover 72,000 BO in 37, 31 and 24 months for the 0, 1 and 100 and cases, respectively. This was an improvement of 23%, 34% and 11% over the eight layer model with the same vertical permeability. The difference was caused not from the difficulty of representing a V=0.7 with three or eight data points, but from the vertical permeability. Seven no-flow barriers exist in an eight layer system as opposed to only two in a three layer. At low vertical permeability this causes considerable differences. Increasing vertical permeability reduces the contribution of the barriers and puts more priority on the permeability variations. At high vertical permeability a three layer system only differs from an eight layer model by 11%.

The continuity of layers must be considered. The low vertical permeability in the Stewart Field would suggest that more layers are required, but if the eight layers are of limited extent it may not be necessary to model that many layers. The following cases are defined as follows:

Case 8>3:	Eight layer model with seven no-flow barriers in the injector and two no-flow barriers in the producer.
Case 3>8:	Same as above, inject from the other direction.
Case 8:	Eight layer model, vertical permeability = 100 and with two no-flow barriers.
Case 3-0:	Three layer model with two no-flow barriers.
Case 8F:	Eight layers, vertical permeability = 100 md, communication in all layers near well-bore, two no-flow barriers.
Case 3F:	Three layers, vertical communication near wellbore (100 md), and two no-flow barriers.

Again, comparisons were based on time to breakthrough and time to recover 72,000 BO. Case 8>3, with the more stratified well used as the injector, showed water breakthrough in 12.6 months, two months sooner than Case 3>8. A well with more uniform stratigraphy makes a slightly better injector, but the two cases were not much different. Case 8 had slightly later breakthrough (15.7 months) and recovered the reserves in the same amount of time as Case 3>8. Therefore, it is not necessary to model eight layers if the no-flow barriers are discontinuous.

Case 8 was compared to Case 3-0 to see if a vertical permeability variation of 0.7 was better described with eight layers as **o**pposed to three layers if only three continuous flow units exist in each well. The three layer case had water breakthrough in 15.2 months as compared to 15.7 months for the eight layer, but it recovered the reserves much faster than the eight layer model (35 months vs. 43.8 months). In comparing results with V=0.7, with three vs. eight layers, breakthrough occurred in the high penneability layer at about the same time. The three layer model was more efficient and resulted in more optimistic results regarding reserve acceleration.

Cases 8F and 3F were designed to study the same effects as above where fractures result in communication around the wellbores. Note, both cases have only two no-flow barriers. The results were - similar to the comparison of Case 8 and 3-0 in the preceding paragraph. The eight layer model showed no difference between the fractured and non-fractured cases. The three layer model had a three month delay in-- breakthrough and recovered reserves three months sooner than the non-fractured**.** The three layer results were slightly optimistic as compared to the eight layer. Therefore, the configuration used in the 3F case was used in the 3D simulation.

b. St. Louis Communication

The effect of communication with the St. Louis in a linear model was duplicated by a thick, water aquifer underlying the Morrow. A third well was inserted between the two previous wells in the center block (20-acre spacing). No vertical flow was present between the Morrow and St. Louis except in the one gridblock containing the center well. A vertical penneability of 1.0 and was allowed in the 55 foot by 55 foot block containing the well to simulate the conductivity of a hydraulic fracture into the St. Louis. The pressures in the Morrow and St. Louis were 200 psia and 800 psia, respectively. The cases were run on a V=0.7 and kz=1 and in the Morrow. The center well was shut-in at different watercuts to determine the optimum time to shut-in the well and to observe any cross-flow into the St. Louis.

The first model had a fixed injection rate of 110 BWPD (approx. 1 ft/day advance rate in the reservoir). The center well was shut-in at 0 (not producing), 50, 80 and 98 percent watercut. The model showed that the center well accelerates recovery of reserves. The cumulative production after one year was. 36,000 BO, 36,667 BO, 42,000 BO and 42,000 BO for the 0, 50, 80 and 98 case, respectively. Although producing the first well at high watercuts (80% and 98%) recovered more oil in the first year, producing the injection water is not cost effective as compared to keeping it in the ground. Shutting in the first line producer as soon as it begins to cut water allows the flood front to advance to the next well.

The model allowed for injection to be controlled by a constant rate or constant injection pressure. The bottomhole pressure in the 110 BWIPD case remained low enough that no cross-flow into the St. Louis occurred. Another case was run with the bottomhole pressure in the injection well held constant at 3000 psia. The rate was allowed to vary to accommodate the pressure. Again, the recoveries were accelerated by producing the center well with the added cost of handling more produced water. A producing well pressure limit of 400 psia on the 40 acre producer was able to keep the pressure low enough at the center well to prevent cross-flow. Therefore, it appeared that a communicated well might be shut in without the reservoir pressure building high enough to cross-flow into the St. Louis. This would need to be verified in the field with BHP tests in the communicated wells. Initial water influx from the St. Louis into the base of the Morrow was seen in both cases.

B. Three **Dimensional Study**

The 3D study was divided into a material balance (MB) study and a reservoir description study. The objective of the MB portion of the simulation study was to utilize the simulator as a volumetric tool to establish a history match with the primary production. More attention was paid to reservoir volumes and areas of influx than to detailed reservoir description.

The results showed that reservoir volume of the Morrow channel was insufficient to match produced volumes from depletion drive alone. The study identified three possible sources of influx that may contribute to the reservoir performance. These sources are 1) a Morrow or St. Louis reservoir communicated at the west end of the channel, 2) a juxtaposed productive Ste. Genevieve found in the E/2 of Section 11, Section 12 and the W/2 of Section 7 and 3) Mackey #3 (a temporarily abandoned well with fracture stimulation into the St. Louis, isolated behind a bridge plug).

The MB simulation was done with a two layer model to reduce computer run time associated with multiple layer models. The Morrow channel for the Stewart Field was represented by a single layer of varying thickness and average reservoir characteristics. The second layer served as the source for "other" zones that may provide pressure support.

A net sandmap.was digitized using GridGenerator software included in the VIP Program package. The Morrow interval was mapped on screen and included some dry holes within the area mapped. However, the volume of the map calculated a satisfactory 26,468 MSTB OOIP. The field was mapped to include the production from the Chief operated wells found in Section 8, T23S-R30W. These wells were drilled beginning in July of 1990 and had a discovery pressure around 700 psig. The less than original pressure found in this section may have been an indication of pressure communication with the Stewart Field, but this was later found to be questionable. The final match did not include the estimated 86,000 barrels of oil produced from the Chief wells as part of the MB. The volume mapped for the Chief wells was left in the model to compensate for additional Morrow reservoir beyond the Bulger 7-10 or in the N/2 of Section 7.

A thick (up to 100 feet) aquifer was modeled underlying the Morrow that represents multiple geologic intervals. This "influx" zone was divided into four sections, using zero permeability barriers around each section. This was done to prevent pressure communication between the influx zones and to reduce the number of gridblocks required studying three or four layers. The GridGenerator puts an overlying grid on the maps and assigns reservoir parameters to each gridblock including: structure top, gross and net thickness, porosity, water saturation and permeability in the X, Y and Z directions. The grid orientation chosen for this run had 100 blocks along the channel (east - west) and 15 blocks across the channel (north - south) approximately 320 by 320 feet. With 1,500 blocks for the Morrow and the influx zone, the entire model required 3,000 gridblocks.

The Stewart Field was divided by sections with reservoir parameters assigned to each as follows:

Section	kx-ky-kz	porosity
4 and 9	150 md	18%
3 and 10	120 md	17%
2 and 11	90 md	15%

12	80 md	16%
7	65 md	16%

These values were based on average log calculated data that showed an increasing trend in permeability toward the west. The initial pressure of the Morrow was set at 1200 psig and an initial water saturation of 31% was used across the field.

The initial run had no aquifer influx and represented a total depletion drive system in the Morrow. The field recovered 2.11 MMBO (including Chief) as compared to 3.23 MMBO actual production through 7/1/93 (including Chief), or a 65% match.

Due to an increase in water production in the Scott 4-4, 4-5 and on the Pauls lease along with the presence of a permeable, high pressured zone DSTd in the Scott 4-3, the west end was chosen as the first area to introduce water influx. The influx support was represented by a 100% water saturated zone with 5 and permeability in the X and Y directions with a pressure of 1400 psig. Communication between the Morrow and the aquifer was modeled with vertical permeability between the layers of 0.07 and over an area of approximately 40 acres on the west end of the field, south of the Scott 4-4 and 4-5 and west of the Pauls 9-3. After trying varying values of vertical permeability, 0.07 and was selected as the value providing the most pressure support without excessive water production.

The influx from the aquifer supported the early production from 1967 to 1985. In this time period only 3 wells in Section 12 were producing and the withdrawal from the Morrow was small compared to the size of the reservoir. From 1985 and forward, production increased sharply due to the drilling activity. As the production increased, the water influx becomes less.adequate in supporting the producing wells.

Modeling wells fractured into the St. Louis was initially attempted, but water production from these wells caused the pressure in the aquifer to be drawn down too quickly. The influx from the 'west end was assumed to be from a different source than the St. Louis "C" zone in the fracture communicated wells. The water production from the St. Louis is from an independent zone and contributes little pressure support to the Morrow if the communicated wells remain on production or are only shut-in for short periods of time. Since only the Mackey #5 was shut-in for some of the recent months, modeling the water production from the-St. Louis is unnecessary.

The west end influx increased the model recovery from 2.11 MMBO to 2.23 MMBO or 69% of - actual. The model was still having trouble keeping up with the post 1985 drilling program. The pre-frac skin was then reduced from +3.0 to +1.5 and the producing BHP was reduced from 50 to 15 psi. The skin was lowered to reduce the severity of the pressure drop from the grid block to the wellbore. Since the wells had historically been "pumped off', the BHP could be lowered to allow for lower fluid levels. These changes increased the model production to 2.49 MMBO, a 77% match.

Having obtained the maximum benefit from the west end influx, the Ste. Genevieve was identified as another source of influx. Many well logs calculate a productive Ste. Genevieve interval underlying the Morrow channel, especially in an area extending from the east half of Section 11 to the west half of Section 7. A study map of the Ste. Genevieve resulted in 1.5 MMBO in place. One section of the influx layer was allocated to represent the Ste. Genevieve. An area extending from the Sherman #1 to the Bulger 7-1 on the south side of the channel was used as the Ste. Genevieve source in the model. It was necessary to use a porosity of 1% and 40% water saturation to obtain an oil volume approximating that of the study map. The low porosity was only a means of adjusting the storage volume in the model and does not affect the flow capacity of the reservoir. The saturation value means both oil and water will flow from the Ste. Genevieve. These values increase the oil volume of the model by 1,703 MSTB for an OOIP of 28,171 MSTB. The Ste. Genevieve was given 0.07 and communication with the Morrow channel. The Ste. Genevieve influx increased the model history match to 2.53 MMBO or 78% of actual.

In December 1971, the Mackey #3 was drilled and encountered 1 foot of Morrow sand. A fracture attempt communicated with the St. Louis, and the well tested 160 BWPD and was temporarily abandoned. In

1986, holes in the casing were repaired. Fluid levels after swab tests showed pressures to be 900-1100 psig. The well was again temporarily abandoned. Wells had been producing from Section 12 since 1967. In 1985, an offset well in Section 11 (Sherman #1) DSTd an extrapolated pressure (p*) of 862 psig, less than the original pressure. From 1972 to 1986 (and forward) the fracture in the Mackey #3 potentially allowed water influx from the St. Louis to cross-flow into the Morrow as the Morrow was being depleted. This represents the third source of pressure support used in the simulation.

Multiple runs showed that a high conductivity fracture between the Morrow and St. Louis in the Mackey #3 could be simulated by allowing 1 and of vertical permeability in the gridblock containing the well without watering out offset wells. Fluids were allowed to move between the zones due to the pressure differential. No fluids were produced from the well. The simulation of the Morrow channel with these three sources of influx produced 2.57 MMBO through 7/1/93 as compared to an actual 3.23 MMBO (including Chief), an 80% match. Even though oil production only increased 40 MBO, the pressure history match was improved.

Core work performed by TORP on extracted cores from the Sherman #3 and Scott 4-4 indicated sensitivity to water resulting in a reduction in permeability. Meyer 10-4 and Mackey #1 had exhibited lower production rates subsequent to being exposed to water from casing leaks. The coring procedure itself is likely to reduce the permeability found in the routine core analysis due to water and mud filtrate. For these reasons and the need to increase transmissibility along the length of the channel, the permeability in the Morrow was doubled. This brought the model results up to 2.98 MMBO produced, a 92% match.

The fine tuning of the MB simulation case included removing the Chief production from the match and updating the production data to 1/1/94. Adjustments were made to the skin of individual wells to improve each well's match. The final case had a 98% match with 3.19 MMBO (without Chief) compared to the actual production of 3.27 MMBO as of 1/1/94.

The pressure was evaluated visually in the 3-D graphical display. Particular attention was paid to reservoir pressure as wells were drilled westward. Although the model pressure of the Sherman #1 was higher than actual (1000+ vs. 862 psig), the majority of the wells in the model were drilled with reservoir pressure around 800 psig. The simulation also showed a reservoir pressure of approximately 800 psig at the time of drilling the western-most wells on the Scott lease. This coincides with the p* of 775 psig exhibited by the DST of Scott 4-4 in January 1989.

The final MB history match utilized the following parameters:

1. Three sources of water influx
   a. West end, kz=0.07 md, kx and ky = 5 md, Porosity = 12%, Sw = 100%, area of influx approximately 43 acres, pressure = 1400 psig.
   b. Ste. Genevieve, 1.7 MMB OOIP, kz = 0.07 md, kx and ky = 5 md, Porosity = 1%, Sw = 40%, pressure = 1400 psig.
   c. Mackey #3 cross-flow, one grid block with kz = 1.0 md, kx and ky = 5 md, Porosity = 12%, Sw = 100%.

2. A producing BHP of 15 psig.

3. A pre-frac skin = 1.5 and post-frac skin = -3.0 with the following exceptions:
   Bulger 7-4, 7-5 and Sherman 3-5 have post-frac skin = -4.5
   Sherman #5, Pauls 9-1 and Haag #4 have pre/post-frac skin =0.0/-4.5

4. Permeability and porosity values of:

Section	kx-ky	kz	porosity
4 and 9	300 md	150 md	18%
3 and 10	240 md	120 md	17%
2 and 11	180 md	90 md	15%

12	160 md	80 md	16%
7	130 md	65 md	16%

5. Morrow pressure = 1200 psig.

6. OOIP Morrow = 26,468 MSTB, Morrow and Ste. Genevieve = 28,171 MSTB

C. Waterflood Study

The 3D reservoir description study was used in a predictive mode to quantify secondary reserves and to select the best pattern for waterflood operations. The objective of the predictive portion of the simulation study was to create a model with the reservoir characteristics that would affect waterflood performance, yet simple enough to maintain the history match found in the material balance portion of the simulation study.

A net sand map for each flow unit (Red, Purple and Yellow) was drawn using GridGenerator. Each zone was mapped honoring all data, including dry holes surrounding the field. The Red and Purple intervals were mapped with a maximum thickness of 10 feet. The Yellow zone was mapped with a maximum net thickness of 30 feet with a 15 foot contour being carried the entire length of the field. At an initial water saturation of 31%, the field was calculated to contain 27.8 MMSTB OOIP. The OOIP includes approximately 1.7 MMSTBO from the Ste. Genevieve leaving 26.1 MMSTB of Morrow oil.

No vertical permeability was allowed for the three Morrow layers except at the wellbore. A vertical permeability of 1 and was assigned to each gridblock (approximately 300-320 feet square) containing a fracture stimulated well. Permeability was assigned to each zone so as to establish a 0.70 permeability variation. Utilizing the permeability-porosity transform derived from the core-log relationship, the most frequently occurring permeability ordering was the Yellow (bottom) zone with the highest permeability, the Purple (middle) zone with the lowest permeability and the Red (top) zone with the median permeability. The permeability distribution across the field was described as follows:

	Sec 4&9	Sec 3&10	Sec 2&11	Sec 12	Sec 7
Red (Top)	300	240	180	160	130
Purple (Middle) 130	105	79	70	58	
Yellow (Bottom) 680	550	400	350	285	

Vertical permeability allows cross-flow from the three sources of influx into the Yellow zone. The bottomhole pressure in each producer was reduced to 10 psig and all fractured wells were given a post-frac skin of -4.5. Increasing the post-frac skins on all wells in reality affected only a few wells, since most were limited by their actual producing rate. The pre-frac skins were retained from the material balance simulation study.

This predictive model was first run to compare the history match by using the same three sources of influx described in the material balance study. Ninety six percent of the historical production was matched with the new and more detailed model.

Several injection patterns were modeled. Each pattern was modeled with 6,000 and 10,000 barrels of water injected per day (BWIPD) for the field. The two injection rates were chosen to see the effect of injection rate and to bracket the range of available source water, which was unknown until the waterflood, is implemented. The injection volume was equally distributed among the number of injection wells with a maximum allowable BHP of 3000 psig. A favorable mobility ratio allows oil to move more easily than the water. As the reservoir fills with water, the injectivity goes down. The field injection curves show that the maximum rate (6,000 or 10,000 BWIPD) is sustained for 2 to 4 years until injection wells become pressure limited. The three line drive pattern was not modeled with 10,000 BWIPD because of insufficient number of injection wells to allow such a large volume. The majority of the net present value of the waterflood occurred in the first five years. The predictive model was designed for a ten year life with all producing wells being shut in at an 80% watercut. Reserves are recoverable at a higher watercut, but would be recovered late in the

life of the project having a small effect on the NPV. The 3, 5 and 7 line drive patterns were chosen in order to select the optimum number of line drives. An additional run was made on the 5 line drive pattern where the producing wells are shut in at a 20% watercut and then returned to production on 7/1/97 and produced to a 97% watercut (labeled 5 L-D 20/97). Each pattern was associated with a different oil and water production curve, capital requirement and operating expense. Once the optimum number of line drives had been established, the results of the 2D and the reservoir characteristics could be used in selecting individual wells in the fmal pattern.

The cases run with the high injection rate exhibit higher peak oil rates and earlier water breakthrough. The low injection rate cases break through later and recover more reserves. The ten year reserves and the recovery factors for the different cases were as follows:

	Waterflood Recovery	Recovery Factor
3 L-D	2,986,000	11.4%
5 L-D Lo	2,776,000	10.6%
5 L-D Hi	2,764,000	10.6%
7 L-D Lo	2,796,000	10.7%
7 L-D Hi	2,713,000	10.4%
Beren Hi	2,710,000	10.4%
5 L-D 20/97	3,622,000	13.9%

Economic Analysis

Cost estimates were prepared for the purpose of determining a waterflooding pattern that optimizes the net present value. Higher water injection volumes will recover secondary oil reserves sooner, but at higher capital and operating costs. Price quotes were obtained from supply and service companies on major items in order to approximate total costs. Extensive cost analyses was performed on injection lines, injection wells; potential water supply sources, waterflood plant, and tank battery consolidation.

Footages for the injection lines were estimated for the different patterns. Bids were obtained for different materials for injection line pipe and downhole tubulars in the injection wells. The three possibilities investigated were: (1) fiberglass, (2) coated steel line pipe, and (3) PVC lined tubing.

Extensive cost analyses were performed on potential source water for the waterflood. Six potential water sources were identified and are summarized as follows:

Ogallala - A fresh water formation 300 feet deep with an estimated potential of 10,000 barrels of water per day (BWPD). Positive aspects are cheap lifting costs and the Conservation Reserve Program may help make water available. Negative aspects include field cores have displayed sensitivity to fresh water and political issue with farmers concerning depletion of irrigation water source.

Glorietta - A saltwater formation 600 -feet deep with an estimated potential of 1,500 BWPD. The formation is currently being used for saltwater disposal. Positive aspects are three existing saltwater disposal wells could be converted to supply wells, cheap lifting costs, this water was successfully used in the Ingalls Field and minimal capital costs. Negative aspects are sand production problems and the expense to treat this water.

Topeka - A saltwater formation 4,400 feet deep with an estimated potential of 1,000 to 1,500 BWPD.

Morrow/St. Louis - Approximately 670 BWPD is currently being produced from Morrow and Morrow/St. Louis commingled wells in the field.

St. Louis - Two production wells in the field are completed in the St. Louis. These wells produce approximately 200 BWPD. This formation is approximately 5,000 foot deep and the water is very corrosive.

Devonian/Ordovician - A saltwater formation 5,700 feet deep with an estimated potential of 10,000 BWPD. Water quality from this formation was unknown.

The maximum design rate of 10,000 BWPD injection could be met several ways. Total cost per barrel of water produced was calculated from the potential sources including capital and operating costs. These costs included drilling and completion, appropriate pump size, electrical usage, service life, chemical usage, etc. It was determined a deep water source that can deliver all the water required was more economic than drilling numerous shallow lower deliverability wells.

Cost estimates were conducted for the water injection plant. The cost estimates included supplying electricity to the plant site, plant costs and injection pumps. Plant costs included the plant building, filtration system, valves, gauges, emergency shut-off systems, alarms, etc.

The preliminary design called for the consolidation of the existing 19 tank batteries to three satellite batteries. Consolidation of the production facilities would result in the following benefits: (1) replacement of inefficient or inadequately sized equipment, (2) relocation of facilities to achieve operating and production data gathering efficiencies that will save on manpower and maintenance, (3) less potential for environmental damage, and (4) simpler produced water collection and handling.

Total capital costs used in the economic analysis for the installation of the waterflood ranged from approximately $1.4 to $1.7 million dollars. The range was due to variables associated with the different patterns investigated (length of line pipe, number of injection wells, etc).

Economic analyses were run on all the waterflood patterns investigated in the simulation study. The economics were run based on 100% working interest with an 80% net revenue interest. The price of oil was held constant at $18.00 per barrel. The lease operating expense was $1600 per well per month. The economics were run using six month time units instead of yearly production to more accurately reflect discounting of future production back to the initial time of investment.

The lease operating expense included a fixed cost for the water injection plant operation, a variable water handling expense and a fixed per well cost. Injection water was made up of both water supply and produced water. The early life of the project primarily uses injection water from the supply well. As the production wells began to produce water, this water was reinjected requiring less water from the supply well. The produced water was reinjected at one-third the cost of the water from the water supply well. Initially, all wells were shut in when they reached an 80% water cut. This prevents the producer from starving the flood front and allows the front to move to the next producer. Later, all the wells were reinstated to producing status and allowed to produce to a 97% water cut.

When the production profile of each pattern was subjected to the assumptions of the economic analysis, some of the production was below the economic limit. Thus, only economically recoverable reserves were used in the economic analysis. The net present value of the economic reserves was run at discount rates of 10 and 40 percent.

Due to the favorable mobility ratio, the reserves recovered were similar for most patterns. The different patterns recover oil reserves at different rates throughout the project, since oil recovery is primarily a function of the volume of water injected. The net present value of economic reserves at a discount rate of 10% for the different patterns ranged from approximately $23 to $27 million dollars and at a discount rate of 40% ranged from approximately $11 to $17 million dollars. The sensitivity of the net present value to oil price was also investigated.

LABORATORY TESTING

Commercial Laboratories

Cores were recovered on the following six producing wells: Meyer 10-1, Scott 4-4, Scott 4-8, Sherman #3, Sherman #5 and Pauls 9-2, with a directional whole core routine analysis performed on Sherman #3. The other five wells were analyzed with plug analysis.

A special core analysis was run by Core Laboratories on the Meyer 10-1 with steady state relative permeability tests on four extracted samples. The cores represent a slight water-wet condition. Connate water saturations ranged between 18 and 29%, whereas residual oil saturations varied between 33 and 42%. Formation compressibilities were measured over a range from 2400 to 800 psig to be 10X10 No apparent water sensitivity was experienced.

Laboratory tests were also conducted on preserved cores taken from the Stewart Field. These tests were conducted by Surtek, Inc. located in Golden, Colorado. The tests consisted of a fluid-rock linear core study to determine the relative permeability characteristics using reservoir fluids. Capillary pressure was determined by mercury injection method. The linear corefloods also defined the initial and residual oil saturation, effective and absolute permeability, fractional flow, wettability of the reservoir rocks and the mobility ratio between water and oil. The capillary pressure test results were used to calculate the pore size distribution and saturation data.

The average initial oil saturation from three linear corefloods using Scott 4-8 core was 71% and the average waterflood residual oil saturation was 44%. The average oil recovery was 38% OOIP.

The average initial saturation in the laboratory for two relative permeability determinations was at 0.67 PV, and the waterflood residual oil saturation was 0.48 PV for a recovery of 35% OOIP.

The mobility ratio averaged 1.0 using endpoint permeability and saturation values for water displacing crude oil. This indicated that water was a good fluid for displacing Stewart Field crude oil.

Fractional flow data from the two relative permeability tests indicated the producing water-oil ratio would be approximately 3.5 after water breakthrough. The average oil saturation at water breakthrough would be 0.62 for 7.5% OOIP recovery at breakthrough. Assuming an economic limit of 99% water, the average residual oil saturation would be 0.509 or a total of 24% OO1P recovered economically by waterflooding.

Total waterflood recovery in coreflood 2 was 40.6% 00W, and in coreflood 3 was 30.1% 001P for an average recovery of 35.4% 001P. This indicated that approximately 11.4% of this waterflood oil couldn't be recovered economically.

Mercury injection capillary pressure curves generated on the Meyer 10-1 and Sherman #3 cores suggested that the average initial non-wetting phase saturation would be 76% of the pore volume. Using the imbibition curve, the change in oil saturation by both primary production and waterflooding processes would be about 31%.

University of Kansas Laboratory

The objective of the laboratory testing conducted at the University of Kansas was to analyze the water sensitivity of Stewart Field cores. Initially the testing was to be done to determine the reservoir sensitivity to the proposed injection water. However, in the early stages of the testing, it was determined that the reservoir rock displayed sensitivity to formation brine. The following summarizes the results of these experiments.

Introduction

Water sensitivity analysis of Stewart Field cores was conducted through permeability measurements of the cores. Core plugs of known dimensions were cut, evacuated and saturated. Permeability measurements were made on these cores using different solutions at room temperature (z68°F) and reservoir temperature (125°F). Experiments were performed on the core plugs from the following wells:

(i) Scott 4-4 (depth 4796 ft.)
(ii) Sherman 3 (depth 4781 ft.)
(iii) Meyer 10-1 (depth 4800 ft.)

The following solutions were used for performing permeability measurements:

(a) 2.0% sodium chloride
(b) synthetic formation brine (composition given in **Table** 1)
(c) injection water (proposed)
(d) filtered produced water from Scott 4-5
(e) 3.0% potassium chloride
(f) 500 ppm aluminum (aluminum citrate)

Table 1: Composition of Synthetic Formation Brine

Salt	Concentration (mg/l)
NaCl	76,470
$NaHCO_3$	430
Na_2SO_4	1,700
$CaCl_2.2H_2O$	15,010
$MgCl_2.6H_2O$	9,930

pH adjusted to 6.5

Experimental Procedure

The core plugs were cut having approximate dimensions of 1" length and 1" diameter. The plugs were cut using fresh water unless specified otherwise. The core plugs were then evacuated and saturated with the desired solution. The experimental set-up consisted of placing the core plugs in a rubber sleeve within a metal casing. The rubber sleeve was subjected to a pressure of approximately 200 psi, which resulted in an airtight seal around the plug. This was done in order to ensure no bypassing of the plug by the injected fluid.

The injection fluid was pumped into the core and the flow rate was measured by collecting the fluid from the effluent line. The pressure drop across the core was measured using two pressure ports situated upstream and downstream of the core, which were connected to a transducer to measure the pressure differential. Experiments were performed at room temperature and reservoir temperature by placing the apparatus in a water bath maintained at 125°F. The procedure for calculating the permeability from these measurements is outlined in the following:

Calculations for Permeability Measurements Conducted at the University of Kansas

$$k = Q\mu L/(A\Delta p)$$

where: k = permeability, darcys
Q = flow rate, cc/sec

μ = liquid viscosity, cP
L = core length, cm
A = cross-sectional area of core, cm^2
Δp = pressure drop across the core, atmospheres

Core Dimensions:

Core	Average length (cm)	Average diameter (cm)
Berea	2.478	2.506
Scott	2.616	2.506
Sherman	2.908	2.504
Meyer #1	2.682	2.508
Meyer #2	2.533	2.505

Viscosity:

2.0% Sodium Chloride Solution: Viscosity assumed to be same as water

For distilled water,

$$= \exp(1.003 - 1.479*10^{-2}T + 1.987*10^{-5}T^2), \text{ viscosity in cp}$$

where: T is the temperature in degrees Fahrenheit

Synthetic Formation Brine:

Viscosity at 125°F = 0.67 cp
Viscosity at 77°F = 1.07 cp
Viscosity at 68°F ≈ 1.20 cp

Injection Water:

Viscosity assumed to be same as water

3.0% Potassium Chloride Solution:

Viscosity at 125°F = 0.66 cp
Viscosity at 77°F = 0.98 cp
Viscosity at 68°F ≈ 1.10 cp

Filtered Produced Water:

Viscosity assumed to be same as synthetic formation brine

500 ppm Aluminum (Aluminum Citrate) Solution:

Viscosity assumed to be same as water

Porosity:

Berea core: porosity = 20.0 %

Field cores: porosity assumed to be 16.0 %

Results of Permeability Measurements

This section gives a brief summary of the results obtained from the permeability measurements of the core plugs from the three wells. Preliminary experiments were performed on Berea core plugs to validate the measurements by the apparatus being used.

The experiments performed on core plugs from the wells are summarized in Tables 2 through 5. Data for all the measurements are also shown in the following.

Berea core: Experiments were performed on berea core using synthetic formation brine solution at room temperature (-,-,68°F) and reservoir temperature (125°F). Normally the injection was done at three different flow rates. The flow rate was measured from the effluent line and typical values were around 1.2 ml/min, 2. 4 ml/min and 3.6 ml/min.

Scott 4-4: The core plug was cut from the rock sample using fresh water. The plug was then evacuated and saturated with synthetic formation brine. Injection was typically done at measured flow rates of about 1.2 ml/min, 2.4 ml/min and 3.6 ml/min.

The core plug was removed from the apparatus and on visual inspection no damage could be observed. The plug was stored in a bottle containing 3.0% potassium chloride solution. The history of the series of experiments performed on the core plug is summarized in chronological order in Table 2.

Table 2: History of experiments performed on Scott 4-4 core plug

Time	Experimental Process	Permeability (md)
Day 1	Core plug cut using fresh water. Core evacuated and saturated with synthetic formation brine (SFB). Permeability measurements performed using SFB at room temperature (≈68°F). Overnight the core was left in contact with SFB at room temperature.	189-187
Day 2	Injection started with SFB at room temperature and good reproducibility was obtained. Injection started with SFB at reservoir temperature (125°F). A decrease in permeability was observed and the behavior continued during the entire injection period of about 3 hours. Overnight the core was left in contact with SFB at room temperature.	184-140
Day 3	Permeability measurements performed with SFB at room temperature giving a value of about 139 md. Measurements were then performed at 125°F and further decrease in permeability was observed for the entire injection period of about 2 hours. Overnight the core was left in contact with SFB at room temperature.	139-107
Day 4	After an initial permeability measurement with SFB at room temperature (90 md), the direction of flow was reversed. No change in permeability was observed. Injection at 125°F yielded further reduction in permeability. Overnight the core was left in contact with SFB at room temperature.	90-70
Day 5	The direction of flow was reversed again and SFB was injected at 125°F. The decrease in permeability was observed for the entire injection period of about 2 hours. The core was left in contact with SFB overnight at room temperature.	70-59

Time	Experimental Process	Permeability (md)
Day 6-10	The core was left in contact with SFB at room temperature.	-
Day 11	The core was injected with injection water from the field. Permeability measurements at room temperature remained constant but injection at high temperature resulted in a further reduction in permeability. Overnight the core was left in contact with the injection water at room temperature.	65-40
Day 12	The core was injected with 3.0% KCl solution at room temperature. An increase in permeability was observed with KCl injection at various flow rates. The core was left in contact with KCl solution overnight.	43-94
Day 13	Further injection with KCl solution resulted in a decrease in permeability. Overnight the solution was left in contact with KCl solution at room temperature.	82-55
Day 14	Permeability measurements performed with 3.0% KCl solution at 125°F. A continuous decrease in permeability was observed for the injection period of about 6 hours. The core was left in contact with the KCl solution overnight at room temperature.	48-30
Day 15	Injection was started with KCl solution at 125°F. A further drop in permeability was observed. Injection was continued at a fixed flow rate for about 6 hours until the permeability reached a constant value. The flow rate was changed and the injection was continued overnight at 125°F.	30-21
Day 16	No further change in permeability was observed. Changing the flow rates did not show any significant change in the permeability values. The core plug was removed from the apparatus and on visual inspection, no damage could be observed. The core plug was stored in a bottle containing 3.0% KCl solution.	20-25

***Sherman** 3:* The core plug was cut using fresh water. It was then evacuated and saturated with filtered produced water from the Scott 4-5. The produced water obtained from the field was filtered at atmospheric conditions and then used for saturation and injection.

The core plug was removed from the apparatus and no anomalies could be observed on visual inspection. The plug was stored in a bottle containing filtered produced water. The history of the series of experiments performed on the core plug is summarized in chronological order in Table 3.

Table 3: History of experiments performed on Sherman 3 core plug

Time	Experimental Process	Permeability (md)
Day 1-4	Core cut using fresh water. Evacuated and saturated with filtered produced water from Scott 4-5. Injection started with produced water at 125°F and was continued for a period of three days. A constant decrease in permeability was observed. At the end of three days, the flow rate was reduced by 50% and injection continued for another day. Decrease in permeability was still observed. The core	7-2

Time	Experimental Process	Permeability (md)
	plug was stored in a bottle containing filtered produced water.	

Meyer 10-1 Core #1: The core plug was cut using 3.0% potassium chloride solution. It was then evacuated and saturated with the same solution. Injection was typically done at the flow rates of 1.2 ml/min, 2.4 ml/min and 3.6 ml/min at reservoir temperature.

The core plug was left in contact with the salt solution at room temperature. The history of the series of experiments performed on the core plug is summarized in chronological order in **Table** 4.

Table 4: History of experiments performed on Meyer 10-1 core plug #1

Time	Experimental Process	Permeability (md)
Day 1	Core cut using 3.0% KCl solution, evacuated and saturated with the same solution. Injection started with 3.0% KCl solution at 125°F. Solution was injected at three different flow rates and a continuous decrease in permeability was observed. Overnight the injection was continued at the reservoir temperature.	30-16
Day 2	Injection was done at three different flow rates and the permeability values appear to have reached a constant value. Overnight the core was left in contact with the 3.0% KCl solution at 125°F.	9-12
Day 3	Injection was done at different flow rates and the permeability values did not show any change. Overnight the core was left in contact with the 3.0% KCl solution at 125°F.	9-12
Day 4	Injection was continued with the same solution and no change in permeability was observed. The core was left in contact with 3.0% KCl solution at room temperature.	10-12

***Meyer** 10-1 Core #2:* The core plug was cut using 3.0% potassium chloride solution. It was then and **evacuated** and saturated with 500 ppm aluminum (aluminum citrate) solution. Injection was done at different flow rates for permeability measurements.

The core plug was left in contact with synthetic formation brine at room temperature. The history of the experiments performed on the core plug is summarized in a chronological order in Table 5.

Table 5: History of experiments performed on Meyer 10-1 core plug #2

Time	Experimental Process	Permeability (md)
Day 1	Core cut using 3.0% KCl solution. It was evacuated and saturated with 500 ppm aluminum (aluminum citrate) solution. Injection started with 500 ppm aluminum solution at 125°F. Solution was injected at three different flow rates and a continuous decrease in permeability was observed. After approximately 6 hours of injection the injection fluid was changed to synthetic formation	29-16

Time	Experimental Process	Permeability (md)
	brine. Overnight the core plug was left in contact with the synthetic formation brine at the reservoir temperature.	
Day 2	Injection was done at different flow rates. For all the different injection rates the permeability values appear to have reached a constant value. The core was left in contact with synthetic formation brine at room temperature.	6-5

Figure 7 shows the results of the experiment performed on a core plug from Scott 4-4. The core was injected with synthetic formation brine at 125°F. The results show the relative permeability as a function of the pore volumes injected. A continuous decrease in the permeability was observed for the entire injection period. Figure 8 shows similar results for a core plug from Sherman 3 injected with filtered produced water from Scott 4-5 at 125°F. The plug was continuously injected with produced water for a period of four days and a continuous decrease in permeability was observed. Figure 9 shows the results of the experiment performed on a core plug from Meyer 10-1. The core was injected with 3.0% potassium chloride solution at 125°F and for the entire injection period a continuous decrease in permeability was observed.

From the results obtained it was observed that there is a reduction in permeability for all the field cores. This behavior was observed with all the injection fluids at reservoir temperature, indicating a high sensitivity of the cores to the injection fluids.

Conclusions

Permeability reduction of at least 50% will occur in the immediate vicinity of the wellbore where large volumes of water flow through the porous rock. Consequently, there will be in an increase in the skin factor. Injection rates would be expected to decrease with time at constant pressure or injection prressure would be expected to increase with time at constant rate.

UNITIZATION

A critical task associated with the initial budget period of this project was the unitization of the field. Unitization needed to occur in order to implement a field-wide improved oil recovery process. Initially, there were three operators and multiple working and royalty interest owners owning production interests within the field. A minimum of 75% of all interest owners needed to be in agreement on equity issues in order for the field to be unitized.

The Kansas Corporation Commission is the governing body concerning unitization in the State of Kansas. If 100% of the working and royalty interest owners agree to a unit operating agreement, then formal unitization by the Kansas Corporation Commission for waterflooding operations is not required. If 100% agreement cannot be reached, then a minimum of 75% of both working and royalty interest owners would have to be in agreement prior to initiating forced unitization proceedings with the Kansas Corporation Commission.

A technical committee was formed in order to help resolve some of the equity issues. Regular meetings and correspondence took place between the technical committee members and the working interest owners throughout the duration of this project. Difficulties arose concerning resolving equity issues necessary for unitization, with one major issue being the selection of the unit operator.

North American Resources Company (NARCO) resolved the unitization issue by offering to purchase the working interest of the other operators in the field. NARCO purchased Sharon Resources et al working interest in the Stewart Field and took over operations of their properties effective February 1, 1995. NARCO was successful in purchasing 100% working interest in the Stewart Field and proceeded in implementing the waterflood.

BUDGET PERIOD 2 ACTIVITIES

Design and Construct Waterflood Plant

A centrally located area in the middle of the field was selected for the waterplant, central tank battery, and field office facilities. The area is located on the Sherman Lease and is approximately 2.5 acres in size. This area is leased from the landowner on an annual basis.

A pre-fabricated injection plant was purchased from Power Service, Inc. The injection plans is skid mounted and enclosed in an all weather insulated metal building. The building is 12 ft wide, 43 ft long, and 8 ft tall. The plant has a maximum design of 10,000 BWPD at 2000 psi. The plant consists of two quintiplex positive displacement pumps powered by two 200 Hp electric motors, filtering equipment, suction and discharge piping, pressure recorders, flowmeter, and control equipment. All internal piping and electrical wiring was included with the plant.

The filtering equipment consists of a two-canister system using standard bag type filters. Each canister contains three bag filters and total injection volume passes through one canister at a time. Flow is switched from one canister to the other at a pre-set pressure differential. All water injected during the waterflood has passed through 3-5 micron filters. There are two pressure recorders, one for each injection pump. One master Halliburton flowmeter indicates total injection volume leaving the plant. The controls consist of high and low pressure shutdowns for both discharge and suction.

The water supply tankage consists of three 1000 bbl and one 300 bbl fiberglass tanks. The first 1000 bbl tank is used as a separation tank or retention tank for water off the heater treater and source water from the supply wells. The 300 bbl tank is a slop tank coming off the separation tank. _The two additional 1000 bbl tanks are source tanks from which the injection plant draws from. All the tanks are gas blanketed to keep oxygen out of the system to minimize corrosion. The water supply tankage is part of the central tank battery facility.

The waterplant is also equipped with a computerized emergency shutdown (ESD) and call out system. This is a part of the computerized monitoring system for the central tank battery facility. The majority of the central facility monitoring and control system is packaged by Remote Operating Systems (ROS). The system uses industry standard data acquisition and control techniques that provide the facility with state-of-the-art automation. The system consists of three basic components:

1. *Master Terminal* (computer workstation consisting of personal computer with Pentium 100+ MHz chip, 16 MB RAM, 800 MB hard drive, monitor, modem, tape backup, one color printer, and one dot matrix printer). The master terminal monitors the operation of the system and provides a man-machine interface for input of setpoints, printing of reports, and alarm notification. The master terminal is located in the field office at the central facility.
2. *Remote Terminal Unit (RTU).* The RTU is similar to an industrial use computer. All control functions are programmed into the RTU that directly monitors all the measurable parameters and makes decisions based on those measurements. The RTU is located on the east wall of the injection building.
3. *End Devices.* Are used for measuring user parameters. End devices include level sensors for tank fluid levels and temperature measurement, flowmeters, status lights, etc. End devices are presently located as follows:
   a. 1000 bbl separation tank - oil and water level sensor
   b. 1000 bbl water suction tank - level sensor on closest tank to injection plant
   c. Two 1000 bbl oil stock tanks - level sensors
   d. Heater treater - oil and water dump line flowmeters
   e. Injection discharge line flowmeter
   f. Water source inlet line flowmeter
   g. Status light and ampmeter for each of the two quintiplex injection pumps
   h. LACT unit totalizer and BS&W

i. Heater treater overflow tank - level sensor
J· Filter bypass switch
k. Source water inlet valve (ESD)
1. East and west emulsion (flowline) inlet valves (ESD's)
m. Injection discharge valve (ESD)

The master terminal unit is equipped with the following primary software programs:

1. *ROSSERVER* - performs communication with the RTU
2. *In Touch* by Wonderware - provides the man-machine interface
3. *ROS VOICE* - provides a voice callout alarm system
4. *Remotely Possible* - enables remote access to the computer

The monitoring and control system provides the following main functions:

1. Automated monitoring which reduces safety risks.
2. Automated monitoring and corresponding automated emergency shut down in the case of a problem, thereby minimizing spill and/or environmental damage potential.
3. Call out via pagers in the case of an alarm.
4. Ease of operation and trouble shooting problems.
5. Cost effectiveness.
6. Data gathering and analysis.

After PetroSantander bought the Stewart Field waterflood they installed a horizontal injection pump to increase the injection capacity from approximately 10,000 to **15,000** BWPD.

Design and Construct Injection System

Two existing wells in the field were recompleted as water supply wells. The Can 2-2, which was a temporarily abandoned well that tested uneconomical in the Morrow and the Sherman 3-9, which was an existing producing well. These wells were recompleted in the Topeka formation. The Topeka is a saltwater bearing dolomitic limestone formation at approximately 4400 ft. Each well was tested for water supply quantity and quality. Following the tests both wells were equipped with a 175 Hp electrical submersible pump with variable speed drive. The pumping equipment for each supply well was designed to produce approximately 3000 BWPD. The supply wells were plumbed into the central injection facility using fiberglass pipe and put into operation in October 1995. The running of the supply wells were alternated to test the productivity of each well for approximately the first four months of the waterflood.

The geometry of the Morrow reservoir at the Stewart Field lended itself to the design of a trunidine injection system along the length of the field with short laterals branching from the trunkline to the individual injectors. A 4 inch 2500 psi working pressure fiberglass injection trunkline was trenched and installed over 3.5 miles of the length of the field. Lateral lines off the trunkline were 3 inch fiberglass pipe to the injection wells.

Originally a modified six line drive pattern **(Figure** 10) was selected for waterflooding the field based on the geological and engineering analysis conducted in Budget Period 1. Six existing producing wells were selected to be recompleted as water injection wells. The original six injection wells were the Bulger 7-1, Mackey #6, Meyer 10-2, Scott *4-2,* Sherman #3 and Sherman 3-1. Numerous items were considered in selecting the injection wells. The major selection criteria were based on good net pay characteristics throughout the Morrow interval, no evidence of communication to the underlying formations resulting from hydraulic fracturing, peak primary production rates, and cumulative primary production. Recompletion consisted of running PVC lined tubing and packer with corrosion inhibiting fluid in the annulus. Each injector was equipped with an injection meter and pressure recorder. New valves, chokes, and wellhead equipment were installed on each injector to enable adjustment or shut off of injection rates. Subsequently, after PetroSantander bought the Stewart Field, an additional six existing wells were converted to injection to improve the sweep efficiency in several areas of the waterflood. December 1997 conversions were:

Well	**Previous Status**
Scott 4-5	Producing approx. 10-12 BOPD

Sherman 3-8	Producing < 1 BOPD
Nelson 2-2	Shut-in

Downhole injection profiles were attempted on several injection wells during the latter part of 1997. Difficulties with the plastic coated tubing prevented completion of this program. Profiles were obtained on the Sherman 3-1, Mackey #6 and Meyer 10-2 to evaluate injection distribution. The vertical injection distribution for these three injectors was good.

March 1998 conversions were:

Well	Previous Status
Haag Estate No. 2	Shut-in
Bulger 7-5	Producing 4 BOPD
Bulger 7-10	Producing < 1 BOPD

Design and Construct Battery Consolidation and Gathering System

The existing 19 tank batteries were consolidated into one central tank battery facility. Benefits of consolidation of the production facilities were 1) replacement of inefficient or inadequately sized equipment, 2) relocation of facilities to achieve operating and production data gathering efficiencies that saves on manpower and maintenance, 3) less potential for environmental damage, and 4) simpler produced water collection and handling. All the old tank batteries were reclaimed.

A concrete foundation and dike was poured for the central tank battery. The battery consists of four 1000 bbl welded steel oil stock tanks, 8 ft by 20 ft horizontal heater treater, and a truck liquid automated control terminal (LACT). As stated earlier, two of the 1000 bbl oil tanks have level sensors as part of the computerized monitoring system. Additional computerized monitoring equipment in the tank battery are oil and water dump line flowmeters off the heater treater, a level sensor in the heater treater overflow tank, and LACT unit totalizer and BS&W. The totalizer monitors oil sales and the BS&W sounds an alarm if the basic sediments and water content in the oil are to high.

A 4 inch fiberglass gathering line was trenched and installed across the length of the field which tied all the producing wells into the central tank battery. Two computer controlled emergency shut down valves were installed on the inlet to the tank battery from produced fluids coming in from the east and west sides of the field.

Waterflood Operations and Reservoir Management

North American Resources Company (MARCO) was the operator who implemented the waterflood. NARCO entered into a sales agreement on the Stewart Field waterflood with PetroSantander, Inc. of Houston, TX in September 1997. PetroSantander took over operations on October 11, 1997. PetroSantander, as did NARCO, conducts the secondary field operations with a full-time company lease operator and a full-time contract lease operator. The company and contract lease operators are supervised by a company production foreman who coordinates and supervises all field operations. A company project engineer is responsible for the reservoir and production engineering, as well as operations supervision. A company geologist provides geologic support for the project. The project engineer, production foremen, and geologist comprises PetroSantander's reservoir management team who are responsible for monitoring, recommending, coordinating, and implementing the development and enhancement plans/work for the field. University of Kansas personnel, including engineers from the Tertiary Oil Recovery Project and geologists from the Kansas Geological Survey complemented NARCO's and PetroSantander's reservoir management team.

PetroSantander, as did NARCO, utilizes an in-house field data capture program which allows field employees to input tank gauges, produced water meter readings, water cuts, well tests, injection rates, pressures, and other vital field information into a computer. The data is transmitted via modem on a daily basis to the project engineer and production accounting system. This near instantaneous access to detailed production and operations information aids in efficiency of the overall waterflood operations and assists in preventing problems before they are compounded which could result in loss of production or expense.

Total oil and water production for the field is recorded daily. Daily injection volumes and pressure are monitored at each injection well. Portable well test trailers are used for production tests on individual producing wells. Individual well tests and fluid level measurements are normally run twice a month. Water supply volumes and fluid levels are monitored on both water supply wells.

Water injection began on October 9, 1995 into four injection wells. Water was being injected into the original six injection wells by the end of October. Initial injection rate was approximately one half the design rate of 6000 BWPD due to alternating production of the supply wells to test their productivity. The injection rate was increased to 5600 BWPD the first week in February 1996. December 1998 injection rate into twelve injection wells was approx. 9,800 BWPD. Both supply and produced water are being injected. Initially, all the injection wells were taking water with the surface pressure being a vacuum. Surface injection pressures in December 1998 ranged from a vacuum to 1080 psi. December 1998 injection pressures are shown in Table 6.

Table 6
December 1998 Stewart Field Surface Injection Pressures

Well	Surface Injection Pressure (psi)
Nelson 2-2	1080
Sherman #3	675
Haag Estate #2	820
Mackey #6	570
Sherman 3-1	520
Scott 4-5	460
Sherman 3-8	380
Meyer 10-2	280
Scott 4-2	430
Bulger 7-1	240
Bulger 7-5	vacuum
Bulger 7-10	170

Cumulative water injection in the field from flood startup through December 1998 was 7,781,980 BW. Monthly and cumulative injection volumes for the twelve injection wells are shown in Table 7.

Table 7
Stewart Field Water Injection Summary (all values in bbls of water)

Date	Bulger 7-1	Mackey #6	Meyer 10-2	Scott 4-2	Sherman #3	Sherman 3-1	Nelson 2-2	Sherman 3-8	Scott 4-5	Haag Est. #2	Bulger 7-5	Bulger 7-10	Total Injection
Oct '95	7026	9857	8561	9945	10008	9810							55207
Nov '95	15276	14301	13738	14091	14329	13912							85647
Dec '95	15657	14833	15237	14879	14849	14549							90004
Jan '96	14590	13822	14199	13865	13837	13558							83871
Feb '96	24850	24227	26030	24994	25198	24384							149683
Mar '96	28460	23410	34977	29205	28429	28516							172997
Apr '96	23618	19184	35069	34973	27575	28091							168510
May '96	27534	17056	34664	36381	31034	25792							172461
Jun '96	29382	17132	31117	34987	28904	22126							163648
Jul '96	33353	17439	31412	37216	30520	23356							173296
Aug '96	33277	17145	29430	36915	31909	23395							172071
Sep '96	28561	15055	22549	31826	28535	20513							147039
Oct '96	30884	16034	25275	35285	29858	20853							158189
Nov '96	33427	16341	28970	39391	30765	20681							169575
Dec '96	36044	17370	28205	43279	31429	21447							177774
Jan '97	35980	16826	30695	41950	30782	21043							177276
Feb '97	32862	15255	27909	38889	27553	16293							158761
Mar '97	37848	17212	32131	40647	30457	20169							178464
Apr '97	35374	17310	30874	37885	27194	21442							170079
May '97	36391	17944	31844	40300	30039	21985							178503
Jun '97	34775	17722	28592	38826	28367	21067							169349
Jul '97	39172	19320	30475	42271	30968	22979							185185

Aug '97	39721	19776	31016	42472	32151	23449							188585
Sep '97	39086	18710	30311	41122	30835	21811							181875
Oct '97	40363	19199	30314	42014	30856	22867							185613
Nov '97	41084	19965	27450	41716	30067	27627							187909
Dec '97	39953	21581	26121	40440	29456	22030	2304	2435	2409				186729
Jan '98	43203	25224	31069	42826	32778	33922	26802	29004	37310				302138
Feb '98	40513	25017	27958	40516	45716	38656	15752	21017	39183				294328
Mar '98	38811	25386	26958	39949	29894	39959	8703	9465	23494				242619
Apr '98	36051	24056	28954	39546	31009	32749	13860	20062	24204	13798	13645	12818	290752
May '98	44935	24051	29189	38724	31030	31235	13874	19952	24879	14089	17961	11287	301206
Jun '98	41404	24119	31305	38301	31459	31180	12540	19068	22900	11191	18057	10886	292411
Jul '98	40077	24692	34694	39686	32500	31602	12524	19645	26071	13358	23847	20592	319288
Aug '98	39450	24497	33629	39634	30750	30577	12823	20085	24703	14847	19961	18572	309528
Sep '98	38024	23660	32204	38851	29346	29986	14228	18996	24675	13928	24044	22677	310619
Oct '98	40152	25293	34142	40598	30779	31277	14478	19574	25408	14066	24779	22720	323266
Nov '98	39045	24453	33187	38932	29557	30197	14538	19488	24032	7841	20353	12131	293754
Dec '98	28445	17522	24050	28045	21398	21780	11304	14112	17407	9034	13360	7288	213745
Total	**1304664**	**762002**	**1104512**	**1391374**	**1112123**	**956867**	**173730**	**232903**	**316675**	**112152**	**176007**	**138971**	**7781980**

Individual well injection volume adjustments have been made based on response (both injection well pressure response and offset producing well response) and reservoir volume near each injector.

In March 1996 following the injection volume increase in February, oil production in the field began to respond to the water injection. Approximately 550,000 BW was injected prior to observing any increase in oil production. Oil production has continued to increase and as of December 1998 total incremental waterflood response is approximately 2900 BOPD. Total field production is over 3150 BOPD. Total incremental waterflood production through December 1998 was 1,634,782 BO. Figure 11 is a plot showing average daily totals for injection and production data by month for the field since the initiation of the waterflood.

In April 1996 injection profile and channel indicator tests were run on 1) Mackey #6, 2) Sherman #3, and 3) Sherman 3-1. The tests indicated that all the injected water is going into the Morrow reservoir with no near wellbore channeling. Attempts to log the other three injection wells failed due to restricted internal diameter in the injection tubing resulting from the PVC lining which would not allow the logging tool to go down.

In May 1996 the Mackey #6 was shut-in for a pressure falloff test to evaluate reservoir properties. The well was selected for testing because it appeared pressure had begun to build up in the region around this well. The test was conducted for 72 hrs using Echometez's computerized Well Analyzer. This test was also conducted to evaluate the effectiveness of the fluid level instrument to obtain liquid levels inside the tubing string while the well was on a surface vacuum. Bottomhole pressures were computed from the fluid level data. The data were analyzed using PanSystem Version 2.3, a commercially available well test analysis program. Figure 12 is a plot of pressure versus shut-in time. Also shown in Figure 12 is the match obtained by assuming the well had a vertical fracture of infinite conductivity which was confined on two sides by parallel faults each equidistant from the injection well, as shown in Figure 13. The analysis confirmed the existence of a vertical fracture, but the fracture half-length was estimated to be 855 ft. This is not consistent with an estimate of 100-150 ft calculated from a review of the hydraulic fracture treatment conducted in June of 1990. The distance to parallel faults (reservoir boundaries) of 1055 ft is approximately the distance from the well to the edges of the productive channel. Other parameters are summarized in Table 8.

Table 8 Summary of Reservoir Parameters Computed from Match of Mackey #6 Falloff Data		
C_s	0.2365	bbl/psi
k_w	49.9	md
S_f	2.37	
x_f	855	ft
L	1055	ft

Where C_S is the wellbore storage constant, k_W is the permeability to water, S_f is the skin factor on the fracture, x_f is the fracture half-length, and L is the distance to the reservoir boundary. These parameters are not unique, but with the exception of the fracture half-length, appear to be consistent with estimates of reservoir parameters.

Electrification of the producing wells in the field began in May 1996. Electrification of the field has provided a more reliable and lower maintenance power source that can be automated much easier. Electrification of the field was completed in November 1996. The only wells in the field that were not electrified are three current producers which are planned as future injection wells (Meyer 10-5, Carr 2-1, and Scott 4-7) and two temporarily abandoned wells the Haag Estate #1 and #2.

In January 1997 the Meyer 10-2 was shut-in for a pressure falloff test to evaluate reservoir properties. The test was conducted for 72 hours using Echometer's computerized Well Analyzer. Bottomhole pressures were computed from the fluid level data. This data was also analyzed using PanSystem Version 2.3. Figure 14 is a plot of pressure versus shut-in time. Also shown in Figure 14 is the match obtained by assuming the well had a vertical fracture of infinite conductivity that was confined on two sides by parallel faults. The analysis confirmed the existence of a vertical fracture with the fracture half-length being 231 ft. Other parameters are summarized in **Table** 9.

Table 9 Summary of Reservoir Parameters Computed from Match of Meyer 10-2 Falloff Data		
C_s	0.1619	bbl/psi
K	4.97	md
S_f	0.1694	
X_f	231	ft
L_1	11637	ft
L_3	256	ft
P_i	376	ft

Workovers were attempted on the Haag Estate #1 and #2 wells to return both wells to production status (both wells have been temporarily abandoned since NARCO took over operations on 4-1-95). Due to downhole mechanical problems neither workover attempts were successful and the wells were shut-in.

The Sherman #5 (which had been shut in since late 1-96) was placed back on production with a progressive cavity pump. The Sherman #5 was producing 3 BOPD and 170 BWPD when it was shut-in. The high water production was due to fracture communication between the Morrow and primarily water producing Mississippian formation. The progressive cavity pump was designed to produce over 500 BFPD and was installed in an attempt to lower the fluid level to allow the Morrow to produce into the wellbore. The Sherman #5 was placed on production 11-26-96 at a rate of approximately 9 BOPD and 220 BWPD during the last 5 days of November. Production from the Sherman #5 tested at 330 BWPD and 14 BOPD at the beginning of December 1996 and was increased to a semi-stable near pumped-off rate of 385 BWPD and 25 BOPD at the end of December 1996. This well became inactive in 1997 due to its high water oil ratio.

Larger bottomhole pump, rods and larger pumping unit were installed on the Bulger 7-4 on 12-27-96 to lower the fluid level that had increased over the past few weeks. Production prior to installing the larger lift equipment was 135 BOPD and 8 BWPD and post installation tests have been as high as 240 BOPD and 15 BWPD.

Upgraded artificial lift equipment were installed on the following wells:

Mackey #4 - installed 456 pumping unit with 144" stroke length
Meyer 10-2 - installed low profile 320 pumping unit and 2" bottomhole pump
Sherman #2 - installed low profile 320 pumping unit and 2" bottomhole pump
Haag Estate #3 - installed 228 pumping unit with 74" stroke length Scott 4-7
- installed low profile 160 pumping unit with 74" stroke length

Two additional pumping unit changes were made on the Scott 4-1 and Sherman 3-2, where it was necessary to install low profile units to accommodate new overhead farm sprinkler systems. A 640 pumping unit and 2-inch insert pump was installed on the Bulger 7-4 to replace a 320 unit and 1.75-inch pump. A 320 pumping unit was installed on the Meyer 10-1, also lowered the tubing and installed a 1.75-inch pump. The 320 unit replaced a 114 unit on the Meyer 10-1. These two artificial lift upgrades were performed as a result of rising fluid levels. Several additional pumping units were upsized to lower producing fluid levels. New units were purchased for the Scott 4-7, Carr 2-1, and the Haag Estate #5. Two of the pumping units released from these. wells were transferred to the Sherman #4 and Haag Estate #4. Also four new progressive gravity pumps were installed on producing wells to increase fluid production.

Resizing pumping units, bottomhole pump upgrades and increasing strokes per minute on pumping units were performed as a result of the well testing program which assists in identifying wells with production problems such as: rising fluid levels, abnormal production trends, and low pump efficiencies. The artificial lift upgrades were performed to handle increasing fluid production, lower the producing fluid level to a near pumped off condition and to maximize oil production.

The Pauls 9-5 (infill well) located 355 ft FNL - 1400 ft FEL in Sec.9-23S-31W and the Haag Estate #6 (replacement well) located 920 ft FNL - 420 ft FEL in Sec.12-23S-31 W were drilled during the Spring of 1997. The Haag Estate #6 did not encounter any Morrow sand and was subsequently plugged and abandoned. The Pauls 9-5 was completed with 27 ft of Morrow perforations. The perforations were broken down with diesel and the well was placed on production 6-5-97. The Pauls 9-5 was producing over 100 BOPD and 6 BWPD during the later part of June 1997.

Long term static fluid levels were taken (to estimate bottomhole pressure) on the Meyer 10-5 and Nelson 2-2. Also the bottomhole pressure of the Pauls 9-5 was measured on a drill stem test. The pressures were as follows:

Well	Date	Shut-in Time	Pressure
Meyer 10-2	6-9-97	6 days	1072 psi
Nelson 2-2	6-9-97	5 days	35 psi
Pauls 9-5	5-23-97	DST	307 psi

A pressure build-up test was performed on the Mackey No.l that indicated positive skin damage. An acid treatment was performed that resulted in a minor increase in production. Subsequently, this well was hydraulically fracture treated in an attempt to remove skin damage and increase production. The treatment was unsuccessful, as post treatment production was the same as before.

The computer model developed at the Tertiary Oil Recovery Project at the University of Kansas was revised to history match waterflood production and injection. The availability of waterflood data necessitated these modifications to the model. The basic structure of the model, the four layers, was retained but changes in the petrophysical (skin, x and y permeability) properties were made to get a reasonable match in the oil and water production peaks and the arrival of the waterflood front. The fluid levels were maintained equal to the reservoir reported data and well production was predicted accordingly, i.e. the simulation was performed under bottomhole pressure as the limiting constraint.

To arrive at a reasonable value for the gas-oil ratio, a series of runs were performed by changing gas-oil ratios and the flood front arrivals were compared with the actual water front arrival in the field. The original ratio of 37 SCF/STB turned out to be the most reasonable value. A revised set of relative permeability data regressed from the old relative permeability data were used. Also, the relative permeability data were further adjusted to reduce water production and the early arrival of the water response to the flood. The vertical permeability of the fourth layer was adjusted to study the effect of the pressure support of the fourth layer on water and oil production and on the arrival of the flood response. It was found that a vertical permeability factor of 0.005 (0.5%) of the original core value gave adequate pressure support. Different simulation runs were performed by varying the permeability of the top three layers and observing its effect on the match. It was observed that permeability values of 67.5 % of the original core permeability values produced a reasonable match. This was acceptable and justified because the original core values were measured with respect to air, and a factor of 0.7 is generally used to get the permeability with respect to liquid phase.

To history match fluid production of individual wells, the skin values of each well were modified. The skin only modifies the permeability of the well grid block. In cases where the maximum negative skin was reached (the negative maximum skin is a function of the grid block size) local modifications to the permeability were made to get better history matches. The local modifications typically extended to a 3 X 3 grid, and in some instances to a 5 X 5 grid, with the well located at the center. These modifications were applied to all the layers and were done at the time of completion and when hydraulic fracturing occurred, if needed.

A few wells had their flood front arriving later or earlier than observed in the field. To correct this, the grid permeability between the injector and the producing wells was altered. The altered path was as narrow and direct as possible. These modifications were applied to individual layers as needed. A few wells showed both oil and water responses to the flood when there was none observed in the field. These wells were generally directly above or near the region in communication with the underlying Ste. Genevieve and St. Louis formations (the fourth layer in this model). The communication between the third and fourth layer near these wells was removed by closing the vertical permeability (i.e., K = 0). In other instances, some wells did not show a response or the water response to the flood was not large enough. These wells had some surrounding grid blocks opened to the fourth layer to allow additional water influx. The grid blocks altered were usually a 5 X 5 grid with the well located at the center. A few wells had two to three distinct oil spike responses to the flood indicating that different layers had broken through at different times. These wells were modeled by altering the path permeability, as needed, of the individual layers.

The revised history match for the field is shown in **Figure 15.** There are three distinct peaks in oil production. The first is due to the field-wide development, the second due to the hydraulic fracturing of the field and the third peak is the response to the waterflood. The data points indicate actual production figures while the solid lines indicate the simulated values. The recent decline in actual oil production is due to excessive downtime due to workovers to upsize pumping equipment, rod parts, pump changes, water supply well downtime and work on the injection system. This temporarily effected the normal trend in production, which has since stabilized and is following the trend predicted by the simulation. Oil production rates, cumulative oil, and water production rates are presented in red, green, and blue,

respectively. Field wide oil, water, and gas cumulative productions are reported in Table 10. There are three regimes of production. The first is the primary production match, the second is the matching of the waterflood period to date and the third is the prediction of the field performance through the year 2010.

Table 10
Fluid Production and Their Simulated Values for Different Regimes

	Primary Production through 9/1995		Production through 4/1998		Production through 12/2010	
	Actual	Simulated	Actual	Simulated	Actual	Simulated
Cumulative Oil (MSTB)	3.593	3.776	4.62	4.645	N/A	8.872
Cumulative Water (MMSTB)	1.348	1.186	2.51	2.026	N/A	38.06
Cumulative Gas (MMSCF)	N/A	814	N/A	841	N/A	848
Pressure Drop (psi)	~1000		N/A		N/A	

The prediction indicates additional production of approximately 4 million barrels of oil. Figure 16 illustrates the oil saturation distribution of the field as of June 1998. The three layers are separated from each other to provide better visualization. The color scale can be seen at the bottom. The first layer clearly indicates the presence of large areas of unswept oil that should be considered for further exploitation. These regions are represented in blue.

A meeting between PetroSantander and University personnel was conducted in May 1998 to discuss the model behavior and the prediction. PetroSantander presented two locations that they suspected had potential for oil production. These sites corresponded with the regions that had unswept oil on the simulated oil saturation distribution. This provided additional support to the accuracy of the model. Two simulated wells were drilled in these areas and their combined output was estimated to be 300,000 barrels from October 1, 1998 through the year 2010. A few additional runs were perfonned by drilling new wells at other sites that the model indicated had potential. The model predicted economic wells could be drilled at these locations.

Technology Transfer

Technology transfer activities for this project includes the demonstration of data collection and analysis, the importance of a multi-disciplinary reservoir management team, and monitoring waterflood performance such that real-time changes can be made to optimize oil recovery. The following are the technology -transfer activities conducted during this project:

1. A paper titled, "Stewart Morrow Field - DOE Class 1 Project" was presented in March 1995 at the TORP Oil Recovery Conference in Wichita, KS and was published in the conference proceedings.
2. The project was awarded the "Best Advanced Recovery Project" and was runner-up as the "Best Field Improvement Project" in the Midcontinent by Hart's Oil and Gas World for 1995.
3. Project information was presented as a poster session at the SPE Forum Series titled, "Multidisciplined Analysis and Solutions to Rejuvenating Old or Marginal Fields" in August 1995 at Snowmass Village, Colorado.
4. Methodologies used in this project were presented as a case study at seminars titled, "Increasing Profitability in Marginal Oil Fields" in August 1995 in Great Bend, Kansas and November 1995 in Wichita, Kansas.
5. Presentations were made on the Stewart Field as part of the Traveling Workshop Series for selected Class 1 near-term projects sponsored by BDM-OK *and* the Petroleum Technology Transfer Council. Presentations were made in Bartlesville, OK, Wichita, KS, Denver, CO, Billings, MT, Oklahoma City, OK, and Grayville, IL. A paper on the project was also published as part of the workshop proceedings.
6. A paper titled, "Evaluating Waterflood Potential in a Morrow Sandstone Reservoir" was presented at the SPE/DOE Tenth Symposium on Improved Oil Recovery in April 1996 at Tulsa, Oklahoma and was published in the conference proceedings.

7. A tour of the waterflood facilities was held in conjunction with the mid-year meeting of the Kansas Independent Oil and Gas Association in Garden City, Kansas in May 1996.
8. Articles pertaining to the increase in oil production due to waterflood response were published in Enhanced Energy Recovery News, Improved Recovery Week, and local newspapers throughout western Kansas.
9. An article on the Stewart Field waterflood was published in the University of Kansas Petroleum Technology Newsletter dated fourth quarter 1996.
10. Presentations on the Stewart Field project were made at the API Chapter meeting in Great Bend, Kansas on 1-8-97 and Society of Independent Professional Earth Scientists (SIPES) meeting in Wichita, Kansas on 2-19-97.
11. A paper titled "Implementation and Monitoring of the Stewart Field Waterflood" was presented and published as part of the proceedings for the Twelfth Oil Recovery Conference held March 19-20, 1997 in Wichita, Kansas.
12. A presentation on the Stewart Field waterflood was presented on August 25, 1997 at the annual meeting of the Kansas Independent Oil and Gas Association in Wichita, KS.
13. A presentation on the Stewart Field waterflood was presented on September 11, 1997 at the Noon Kiwanis Club meeting in Lawrence, KS.
14. A presentation titled, "Waterflooding Using Improved Reservoir Management: Stewart Field Case Study", was presented at a symposium sponsored by the University of Wyoming Enhanced Oil Recovery Institute on October 29-30, 1997 in Casper, WY.
15. Presentations on the Stewart Field waterflood were presented to the Tertiary Oil Recovery Project's advisory board meetings on November 7, 1997 in Lawrence, KS, April 7, 1998 in Wichita, KS and October 30, 1998 in Lawrence, KS.
16. Information pertaining to the Stewart Field waterflood was displayed on the exhibition booth for the Tertiary Oil Recovery Project at a workshop titled, "Horizontal Drilling Applications in Kansas", sponsored by the North Midcontinent Regional Lead Organization of the Petroleum Technology Transfer Council on June 16, 1998 in Wichita, KS. A brochure containing detailed information on the Stewart Field waterflood was developed, printed and distributed at the workshop.
17. Papers on the Stewart Field project were presented at the North American Prospect Expo (NAPE) in Houston, TX on January 27-28,1998; the Society of Independent Earth Scientists (SIPES) 1999 Annual Convention and Seminar in Wichita, KS on March 10-12, 1998; and the Tertiary Oil Recovery Project's 13th Oil Recovery Conference in Wichita, KS on March 17-18, 1998.
18. An article on the Stewart Field Waterflood was published in the 2°d Quarter 1999 University of Kansas Petroleum Technology Newsletter.
19. A presentation on the Stewart Field waterflood was conducted at the Department of Energy (NPTO and FETC) Oil and Gas Conference in Dallas, TX on June 29,1999.
20. A paper titled "Waterflood in Kansas field should boost recovery by five million bbl" was published in the PTTC/World Oil Petroleum Technology Digest in September 1999.
21. Operators throughout the area continue to visit the field to view the state-of-the-art waterflood installation and computerized monitoring system.

CONCLUSIONS

A waterflood was designed and implemented for the entire field based on the geological and engineering analysis conducted in Budget Period 1. The waterflood installation includes state-of-the-art computerized monitoring and emergency shut down systems. The installation design places special emphasis on production, injection, and pressure data access and recording.

Water injection began in October 1995 and the field has responded favorably to waterflood operations. Through December 1998 a total of 7,781,980 BW had been injected resulting in an increase in oil production of approximately 2900 BOPD or 1,634,782 bbls of incremental secondary oil recovery through December 1998.

Stewart Field Figures

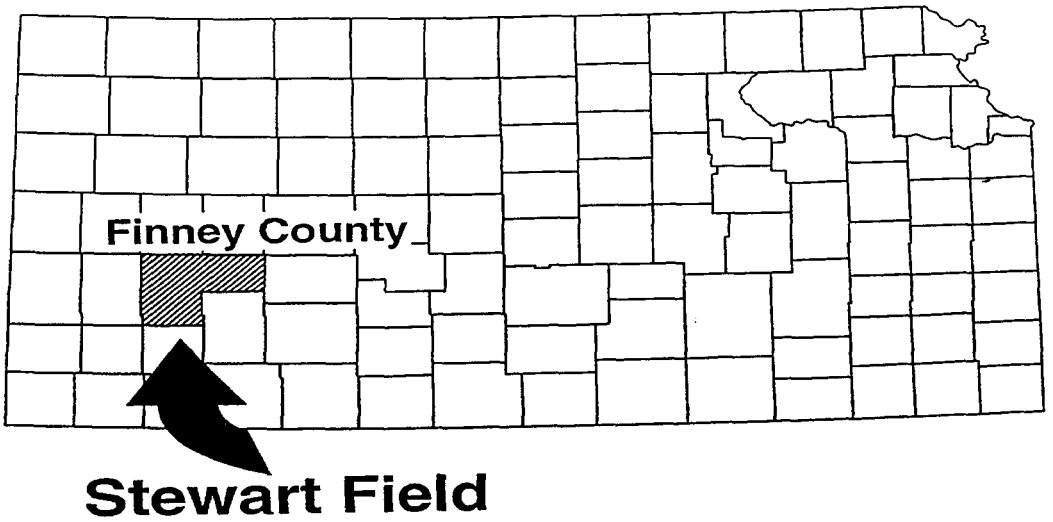

Figure 1 **Location Plat for Stewart Field.**

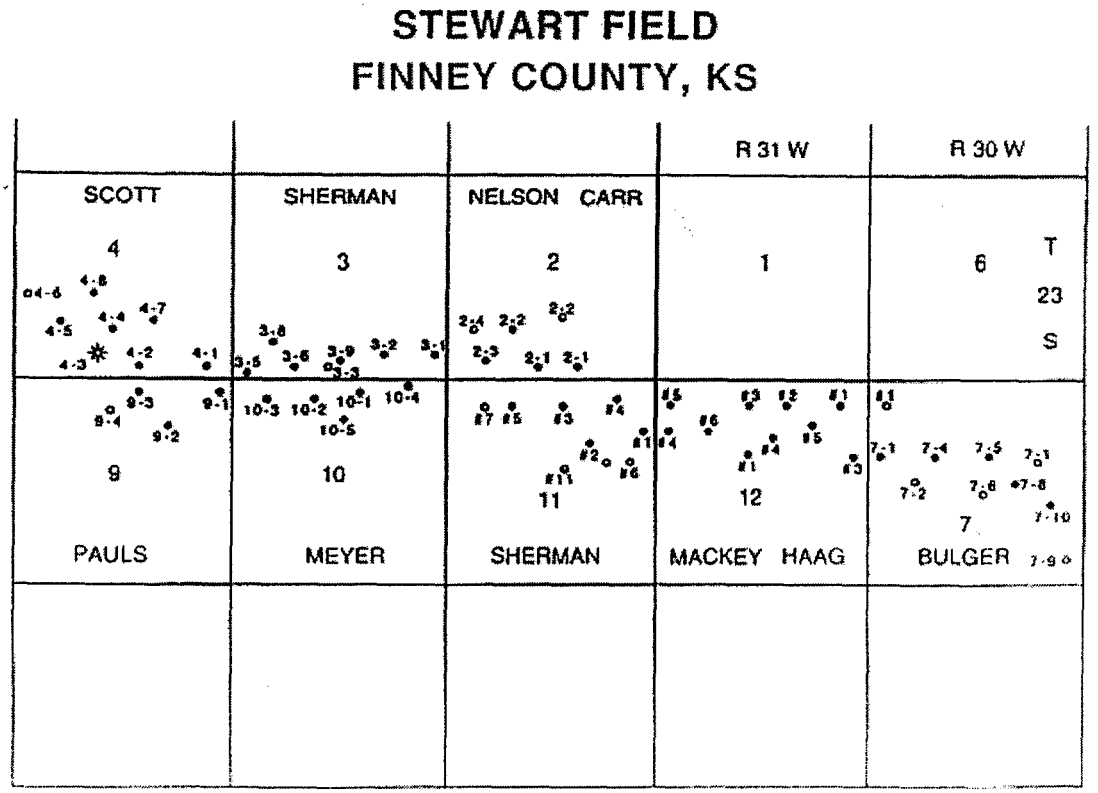

Figure 2 **Stewart Field Well Location Plat.**

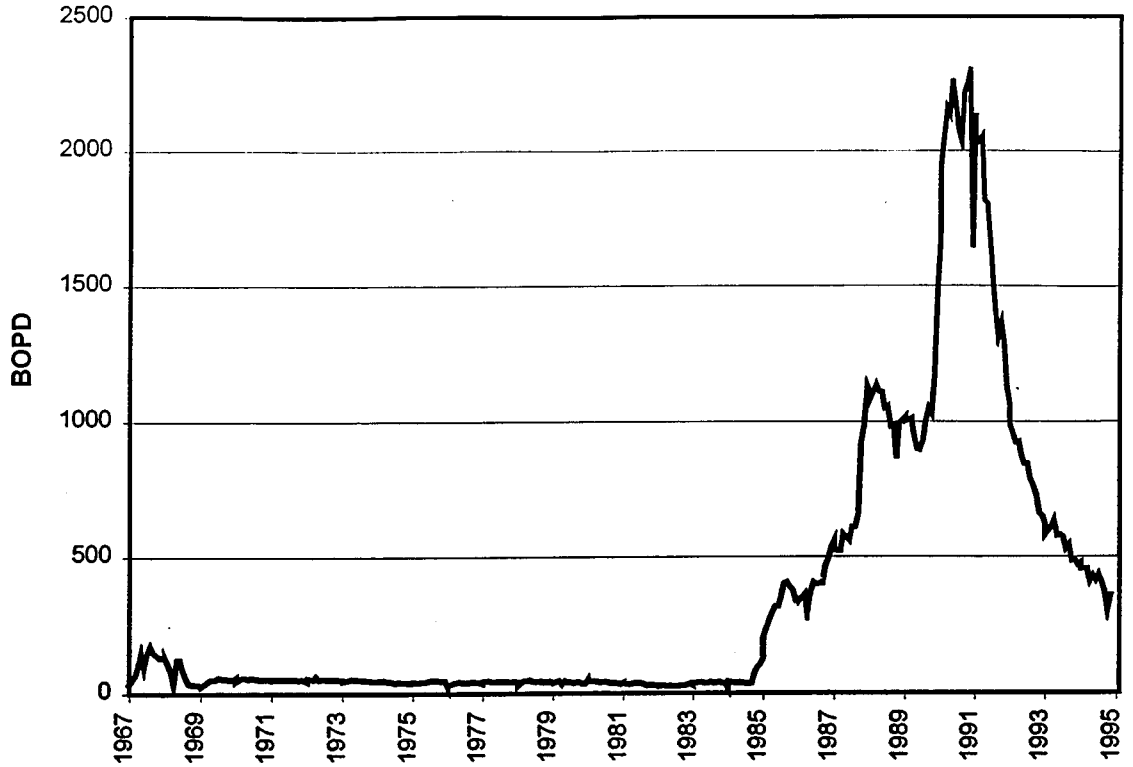

Figure 3 **Stewart Field Primary Production Curve.**

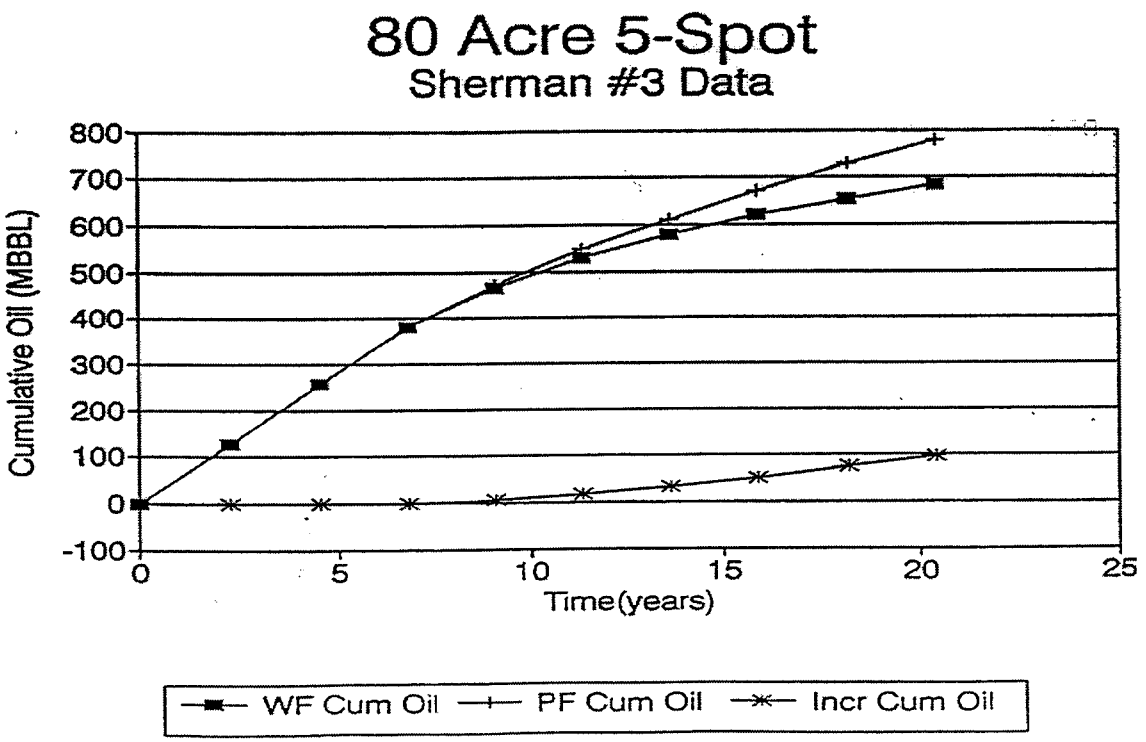

Figure 4 **Polymer Flooding versus Waterflooding Plot in the Stewart Field.**

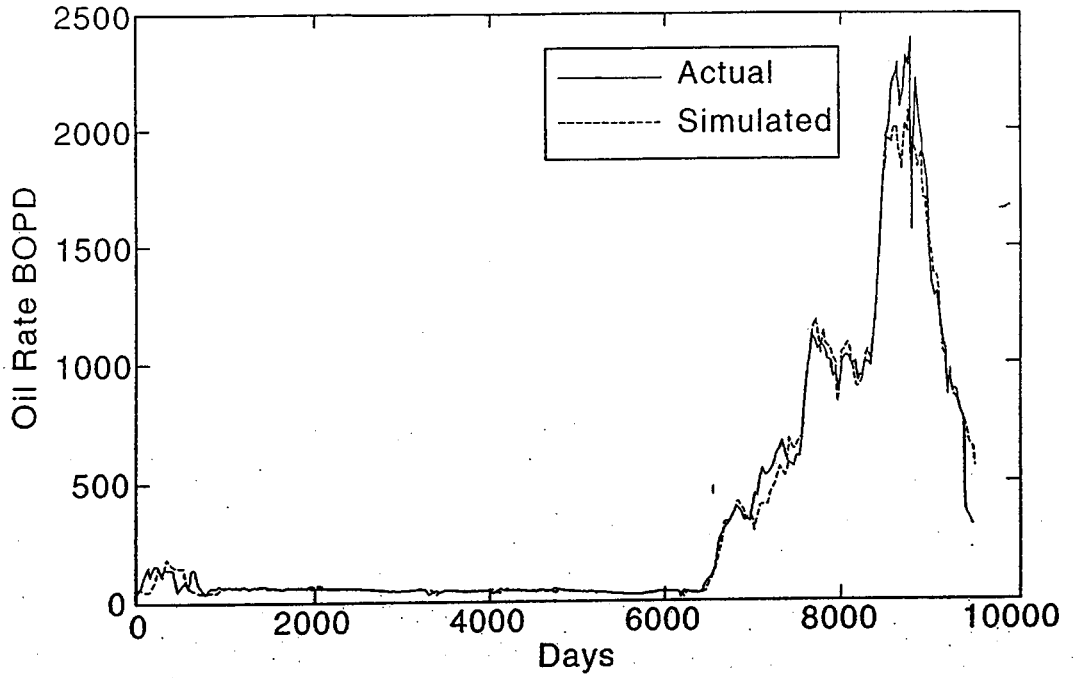

Figure 5 **Actual Versus Simulated Production for the Original Model of the Stewart Field.**

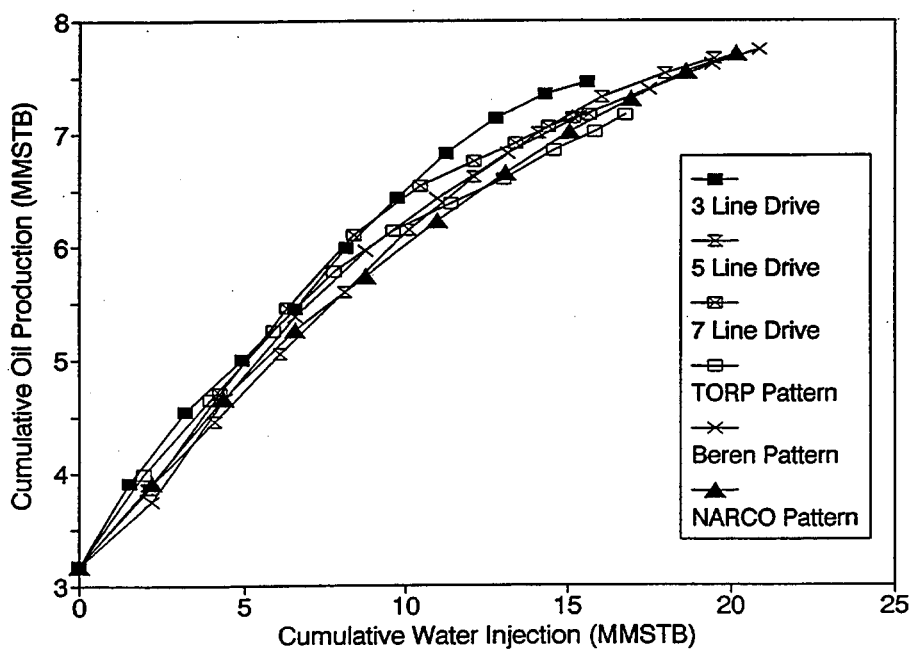

Figure 6 **Cumulative Oil Production versus Cumulative Water Injection for Waterflood Patterns Investigated for the Stewart Field.**

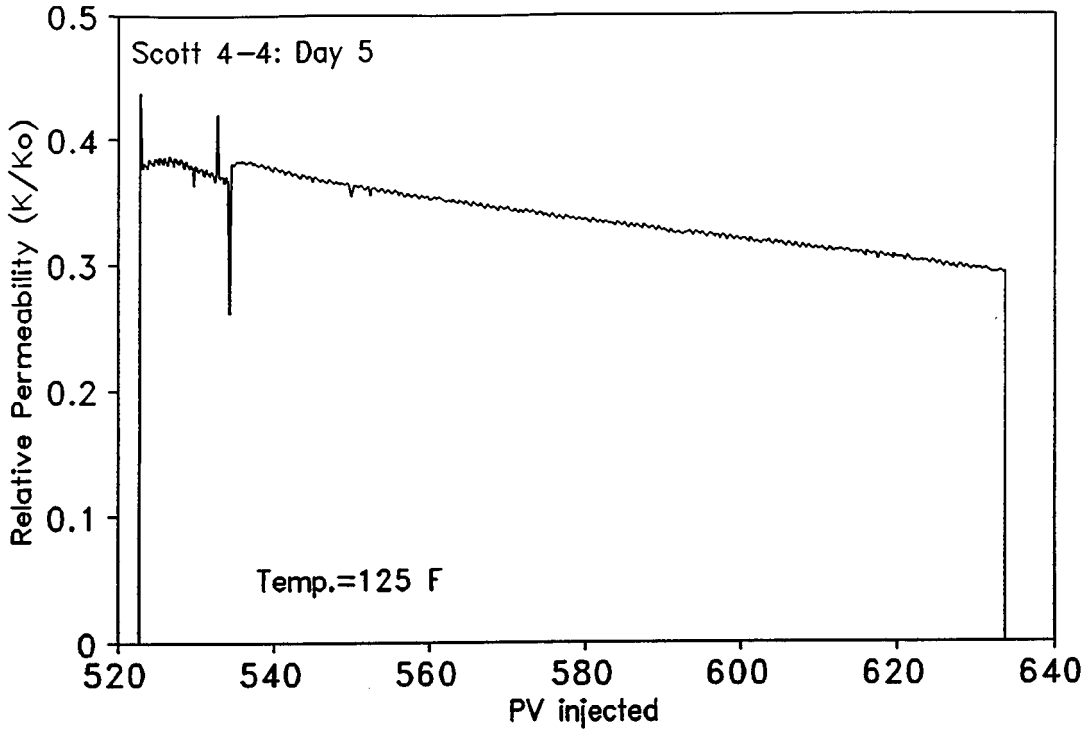

Figure 7 **Relative permeability versus pore volumes injected for synthetic formation brine.**

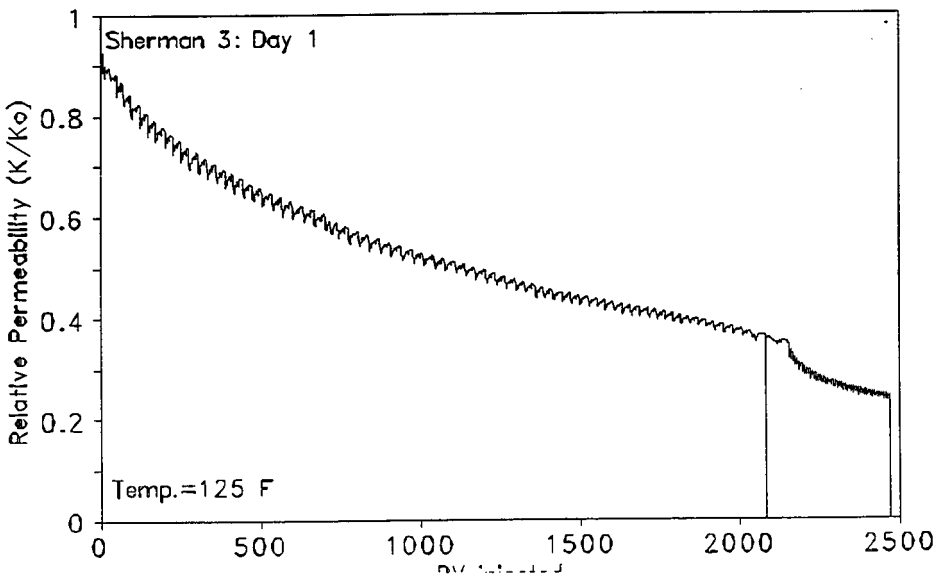

Figure 8 **Relative permeability versus pore volumes injected for filtered produced water.**

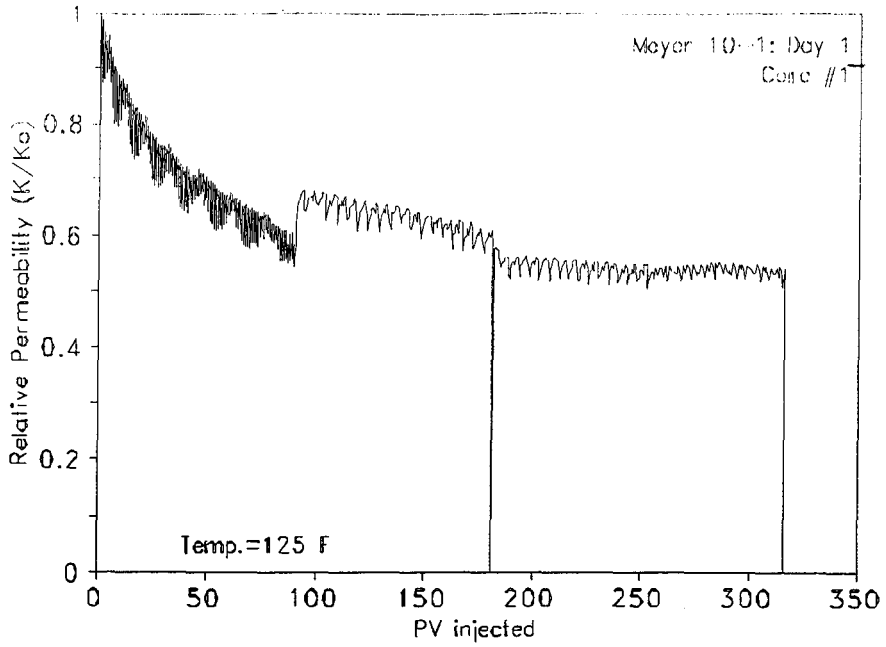

Figure 9 **Relative permeability versus pore volumes injected for 3.0% potassium chloride solution.**

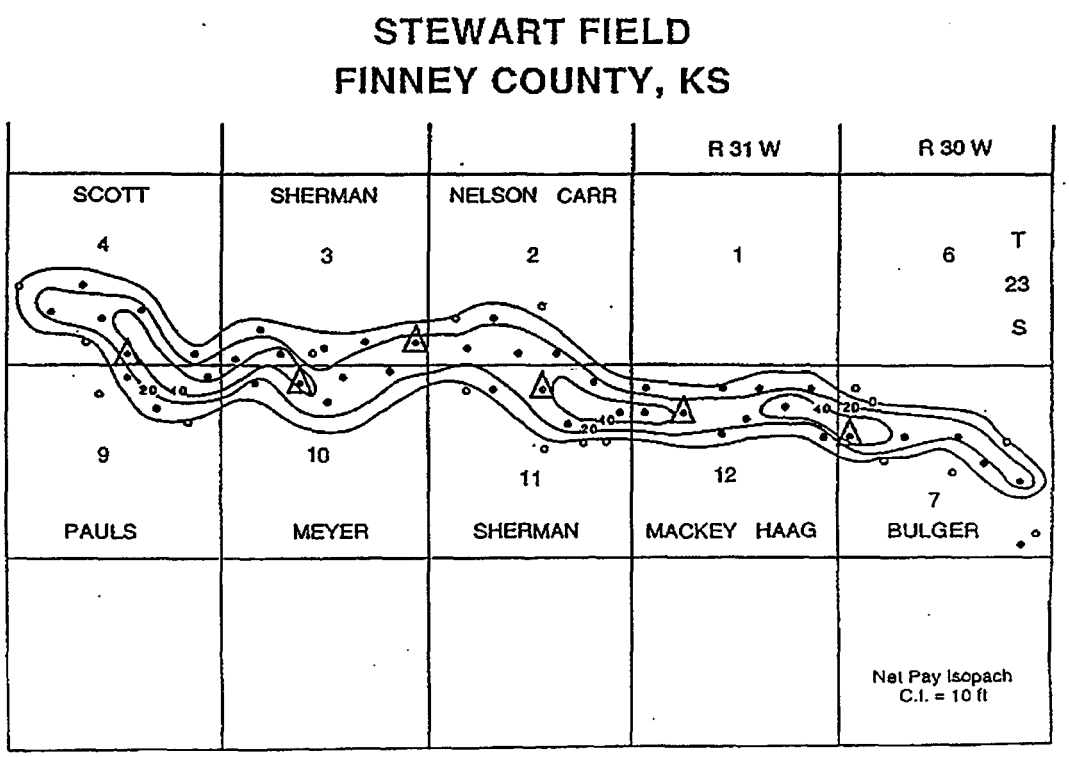

Figure 10 **Original Modified Six Line Drive Pattern Selected for Waterflooding the Stewart Field.**

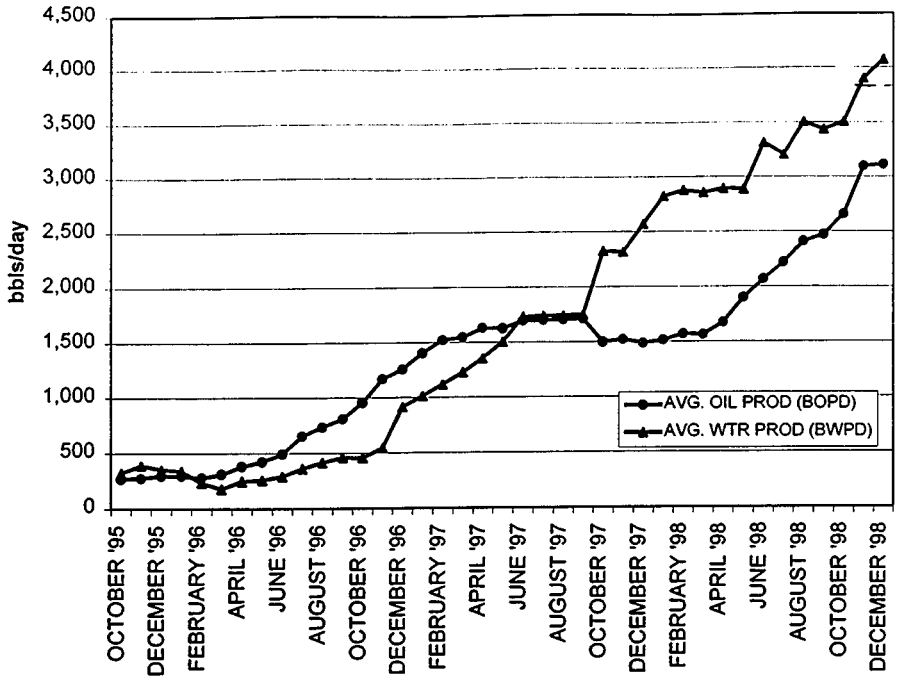

Figure 11 **Average Daily Totals for Injection and Production by Month for the Stewart Field.**

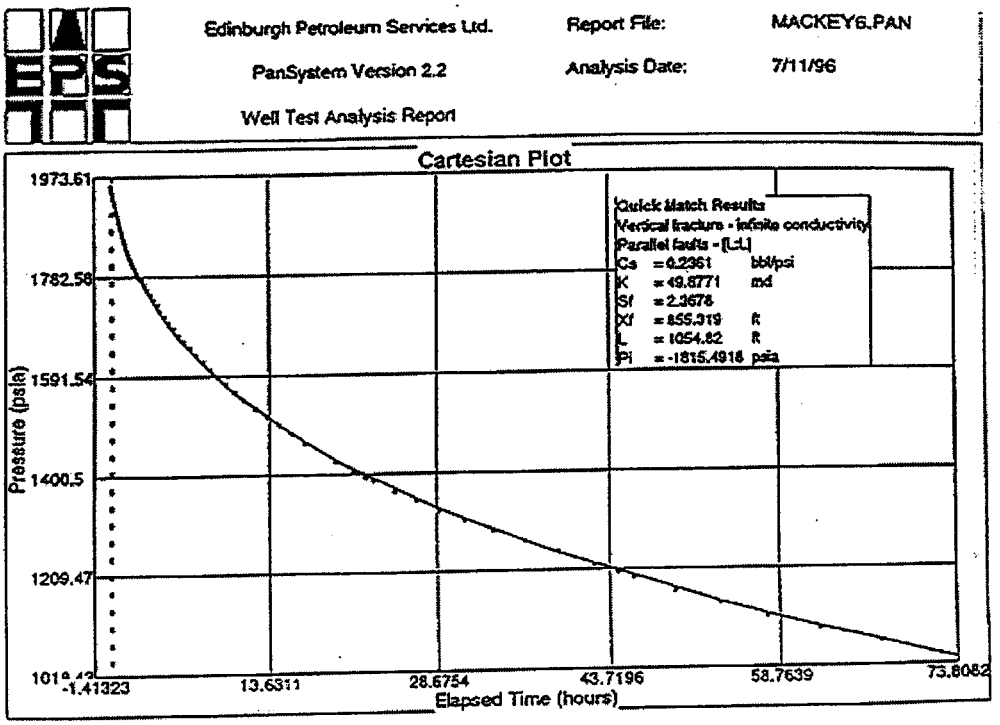

Figure 12 **Plot of Pressure Versus Shut-in Time for the Fall-Off Test Conducted on the Mackey #6.**

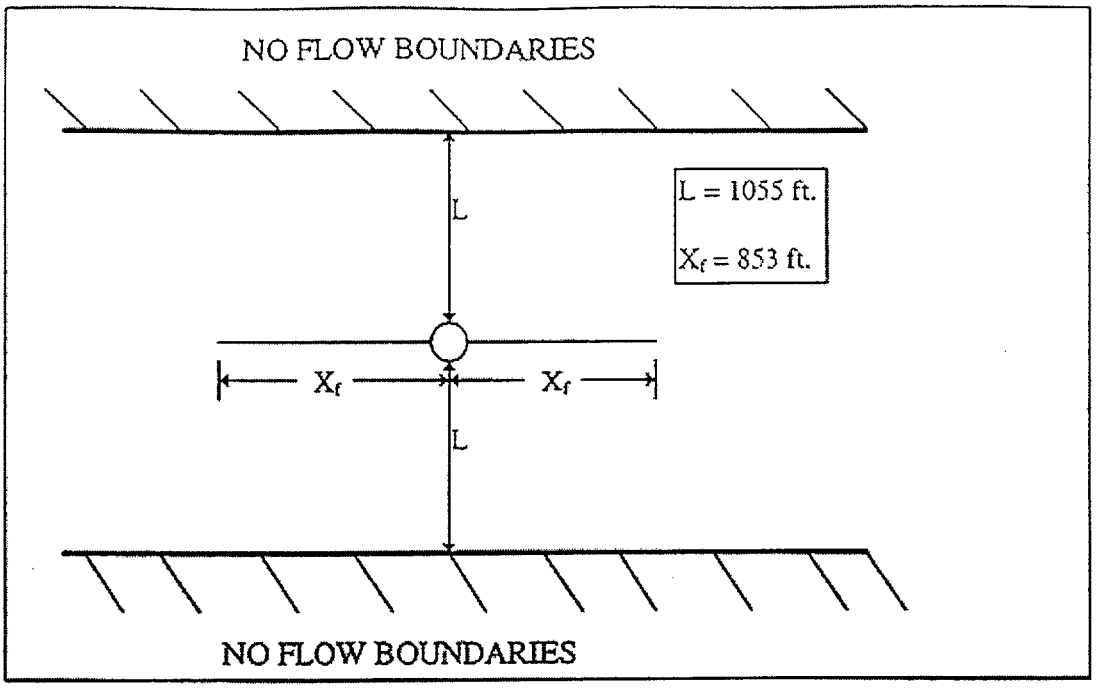

Figure 13 **A Schematic Illustrating a Vertical Fracture of Infinite Conductivity that is Confined on Two Sides by Parallel Faults Each Equidistant from the Injection Well**

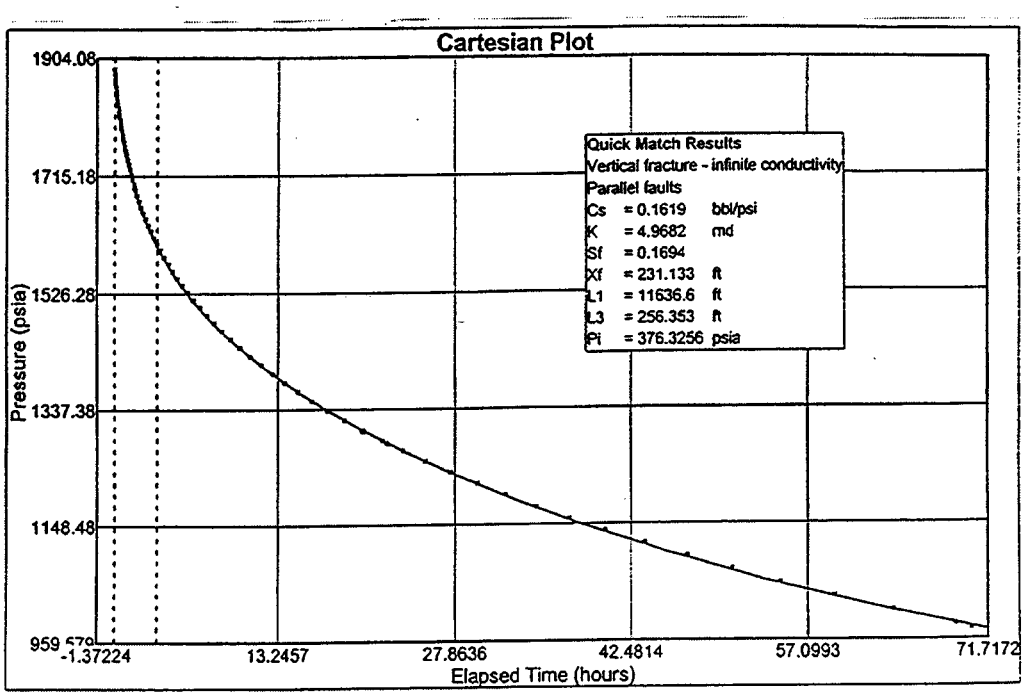

Figure 14 **Plot of Pressure Versus Shut-in Time for the Fall-Off Test Conducted on the Meyer 10-2.**

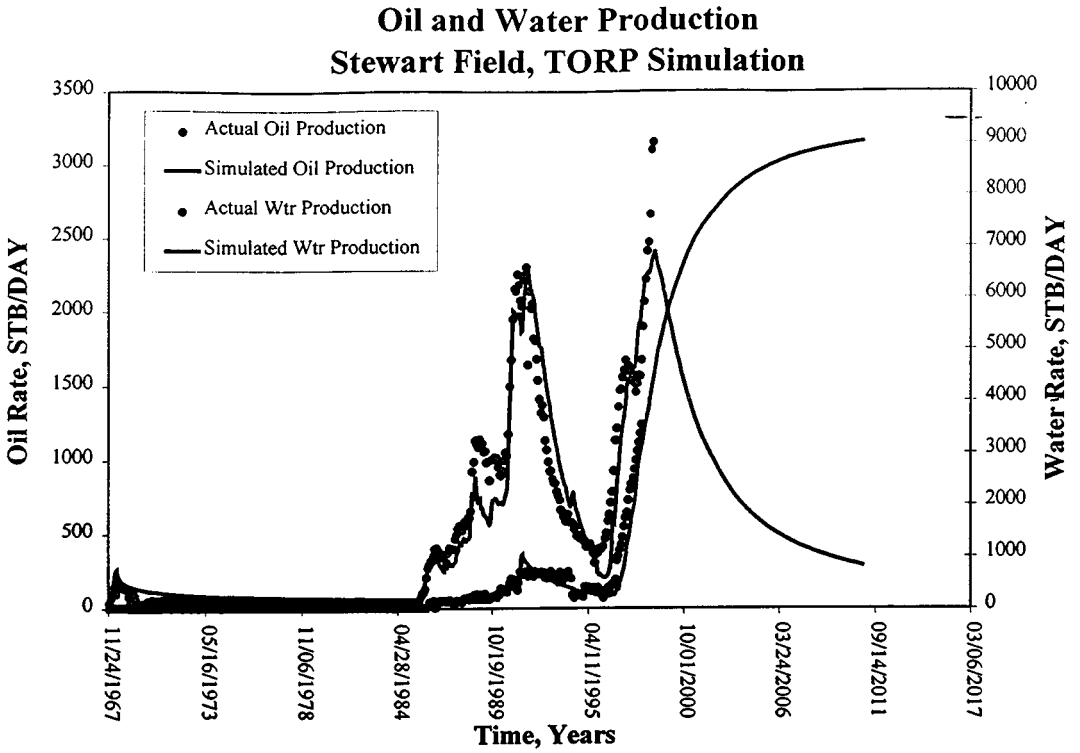

Figure 15 **Revised History Match for the Stewart Field**

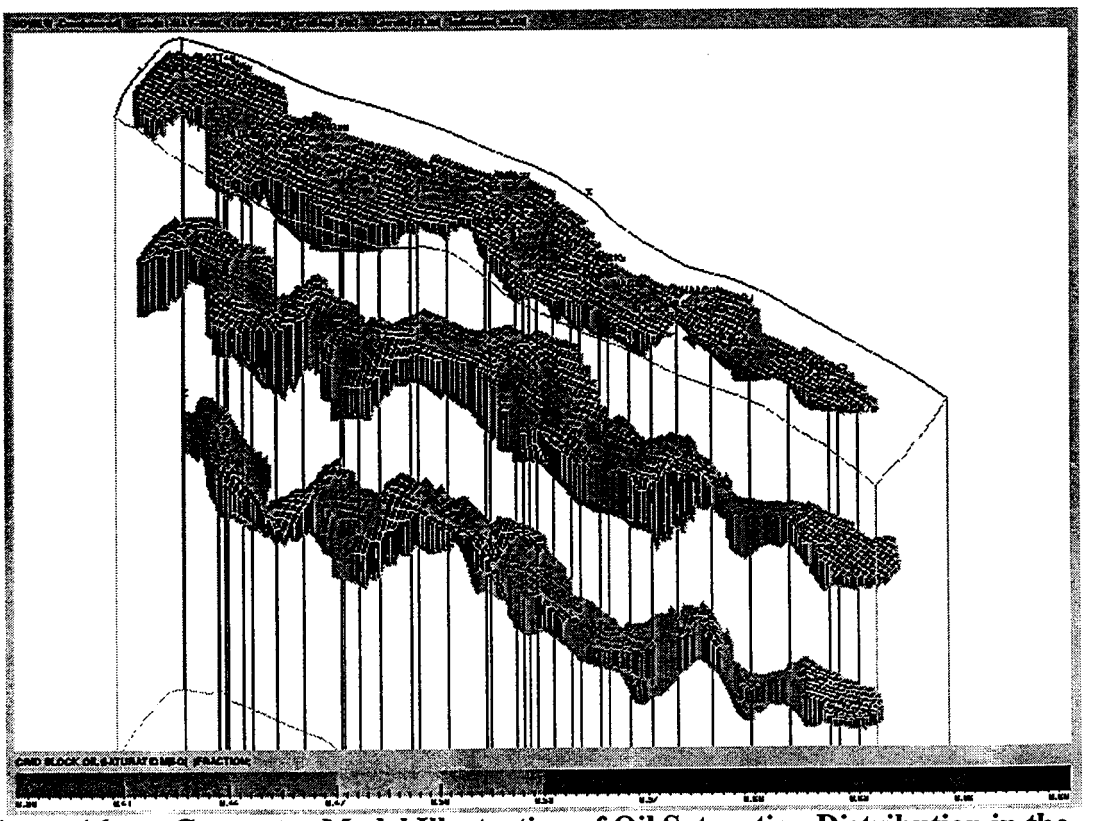

Figure 16 **Computer Model Illustration of Oil Saturation Distribution in the Stewart Field as of June 1998.**

Chapter 3

Savonburg Field Project

OBJECTIVES

The objective of this project was to address waterflood problems in Cherokee Group sandstone reservoirs in eastern Kansas. The general topics addressed were 1) reservoir management and performance evaluation, 2) waterplant optimization, and 3) demonstration of off-the-shelf technologies in optimizing current or existing waterfloods with poor waterflood sweep efficiency. It is hopeful that if these off-theshelf technologies are implemented the abandonment rate of these reservoir types will be reduced.

The reservoir management portion of this project involved performance evaluation and included such work as 1) reservoir characterization and the development of a reservoir database, 2) identification of operational problems, 3) identification of near wellbore problems such as plugging caused from poor water quality, 4) identification of unrecovered mobile oil and estimation of recovery factors, and 5) preliminary identification of the most efficient and economical recovery process i.e., polymer augmented waterflooding or infill drilling (vertical or horizontal wells).

To accomplish these objectives the initial budget period was broken down into four major tasks. The tasks included 1) geological and engineering analysis, 2) waterplant optimization, 3) wellbore cleanup and pattern changes, and 4) field operations.

Budget Period 2 objectives consisted of the continual optimization of this mature waterflood in an attempt to optimize secondary and tertiary oil recovery. To accomplish these objectives the second budget period was broken down into six major tasks; 1) waterplant development, 2) profile modification treatments, 3) pattern changes, new wells and wellbore cleanups, 4) reservoir development, 5) field operations, and 6) technology transfer.

In Budget Period 1, it was determined that the lower B3 zone had not been flooded effectively and contained unswept mobile oil. The in-fill injection well drilled in December 1995 confirmed this assumption. The core results are presented in the July 1996 annual report, and included in this report as **Appendix** B. In the past few years, main emphasis of all tasks was to target water injection into this B3 zone.

BACKGROUND

The Nelson Lease is located in Allen County, Kansas in the N.E. Savonburg Field about 15 miles northeast of the town of Chanute and one mile northeast of Savonburg. The project is comprised of three 160-acre leases totaling 480 acres in Sections 21, 28, and 29, Township 26 South, Range 21 East.

The first well drilled in the location of this project was in 1962. Fifty-nine production wells and forty-nine injection wells have been drilled and completed since 1970. A pilot waterflood was initiated in March 1981 and expanded in 1983. Full development occurred in 1985.

Production of oil in the Nelson Lease in the Savonburg NE Oil Field is from a valley-fill sand in the Chelsea Sandstone member of the Cabaniss Formation of the Cherokee Group. This lease is similar to a large number of small oil fields in eastern Kansas that produce from long, narrow sandstones, "shoestring

sandstones" (Bass, 1934), at shallow depth.

The most productive part of the reservoir sand in the lease lies in the eastern half of the SW/4 of Section 21 and is a narrow valley cut to a depth of up to 40 feet (12 m) through the Tebo and Weir-Pittsburg horizons into the Bluejacket A coal (Harris, 1984). The deepest part of the valley is less than 300 m wide. Wells that encountered the most sandstone in the valley are the most productive.

In 1986, eleven gel polymer treatments were implemented successfully on the Nelson Lease. Overall incremental oil recovery was 3.5 barrels per pound of polymer placed which totaled 12,500 barrels. The production increase was not sustained due to wellbore plugging as a result of poor water quality.

Cumulative production through December 1998 has been 393,511 barrels. Of this production, 131, 530 barrels were produced by primary depletion. Water injection began in March 1981 and over 261,000 barrels have been produced under waterflood operations. Cumulative water injection is 5,628,660 barrels. The graph of waterflood production and injection data is presented in **Figure** 17. Water-oil ratio since waterflood start-up is presented in **Figure** 18.

In 1993, this Class 1 project started Budget Period 1. The tasks included 1) geological and engineering analysis, 2) waterplant optimization, 3) wellbore cleanup and pattern changes, and 4) field operations, which have been completed and are presented in the 1994 annual report. In that report, the high potential areas for development were defined.

BUDGET PERIOD 1 ACTIVITIES GEOLOGICAL

AND ENGINEERING ANALYSIS Database

Development

Due to the abundance of data on the field, a computer database was set up to make data easily accessible. Spreadsheets were utilized in the development of the database. The computer database included, 1) reservoir properties from core analysis on a well basis, 2) production and injection data on a well basis since waterflood start up, and 3) lithology picks on a well basis.

This study used materials provided by J.E. Russell Petroleum Inc., including cores, unscaled gamma ray-neutron logs and core data. While cores collected before 1983 were discarded after description and analysis, cores were available for 23 wells drilled since Russell became operator of the field. Russell cores are simply designated by their well number, either RW-n (n=1 through 19) or 0-n (n=1 through 4). The Russell cores were described and were the basis for much of the depositional interpretation of the reservoir rocks and associated strata. Core data provided was collected by Oil Field Research in Chanute, Kansas, except for two descriptions carried out by CoreLab. Core data included a text and graphic description, measurements of porosity, permeability, and fluid saturation for nearly all wells, and, for the Russell cores, recoverable oil and effective permeability at residual oil saturation.

Zone Description and Mapping Methods

Sandstone was mapped and identified utilizing two methods, 1) core reports to determine net floodable sand for volumetric analysis, and 2) gamma-ray logs to determine sand thicknesses and differences in lithologies for geological analysis. Both methods proved valuable.

In the volumetric study, net pay was determined from core analysis utilizing a porosity cut-off of 13% and effective water permeability cut-off of 1 md.

In the geological study, a shale line and a sand line were drawn on the g-ray log. The shale line was drawn at a deflection which was consistently reached by beds which did not appear to be anomalously radioactive. The sand line was drawn at the gamma-ray reading in the Cherokee Group. Rocks with a

deflection greater than 1/2 of the difference between the sand and shale lines were considered to be shale and those with a smaller deflection were considered to be sandstone.

Reservoir Parameters

The reservoir characteristics were defined from log and core analyses. Average porosity and permeability are 18.4% and 27 and respectively. Average residual oil saturation, based on laboratory flood pot tests was 34.9 percent. Connate water saturation of 24 percent was estimated from core data and by applying an empirical relationship using permeability data. The gravity of the crude oil is 31.2 degrees API at 60° F. The viscosity of the reservoir crude oil at reservoir temperature is 15.4 cp.

Volumetric Analysis

A pattern volumetric analysis was conducted to determine recovery factors in BBL/Ac-ft for given segments of the field. Net pays were determined from flood pot data. From the database three grids and maps were developed; 1) net pay, 2) porosity, and 3) water saturation. The net pay grid was multiplied with the porosity grid to develop a porosity-foot grid for the field. Each segment or pattern was then integrated to determine acre-ft. The patterns or reservoir segments are presented in Figure 15. Areas of high potential are also presented in the figure.

Initial-oil-in-place at waterflood start up was determined by multiplying the porosity-ft with the initial oil saturation of 24%. A formation volume factor (FVF) of 1.06 was included in the calculations.

A simulation study was conducted to determine waterflood and polymer flood recoveries. The study (along with input parameters) is presented in the following section. It was found that the recovery factor for waterflood and polymer flood were 255 and 335 BBL/Ac-ft respectively. Table 3 presents the remaining waterflood and polymer flood reserves remaining per segment. It also presents volumetrics for the B2 and B3 zone, and (oil & water) production by segment.

Estimates of oil recovery by polymer injection were computed by assuming that the polymer flood started at the same time and same initial saturations as the waterflood. Producing water-oil ratios in the field (Figure 18) were in excess of 30 during the waterflood. The model used to simulate polymer **flooding** does not account for the fact that a substantial portion of the reservoir was waterflooded when the polymer flood was initiated. Polymer injected into these portions of the reservoir will displace large-amounts of water with additional oil and the response to polymer injection will be delayed when compared to the simulated response. Consequently, polymer flood estimates were considered optimistic.

FIGURE 17: NELSON LEASE PRODUCTION & INJECTION

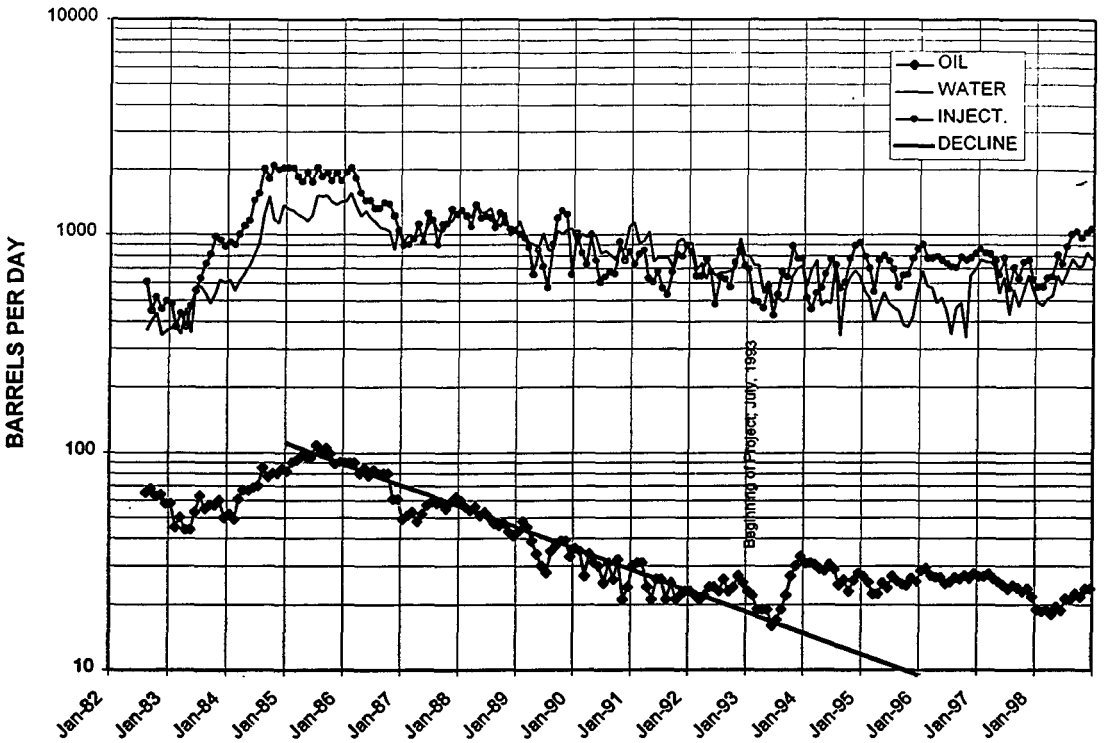

FIGURE 18: NELSON LEASE WATER:OIL RATIO

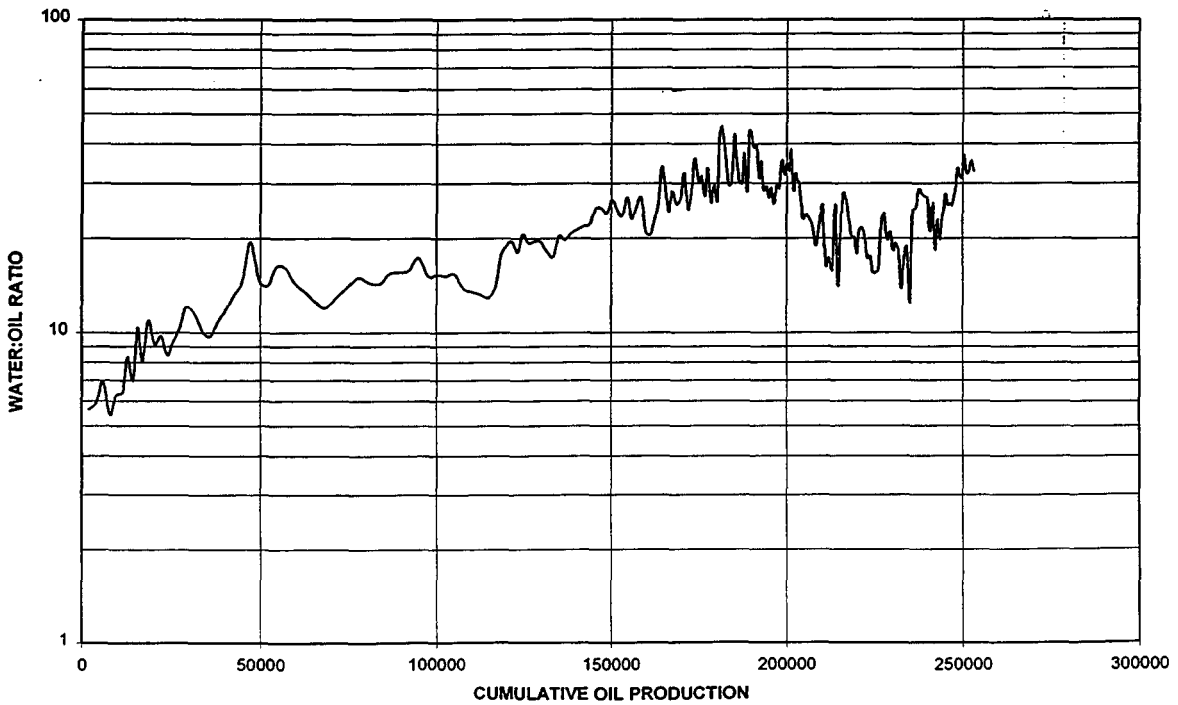

B2 Net Pay

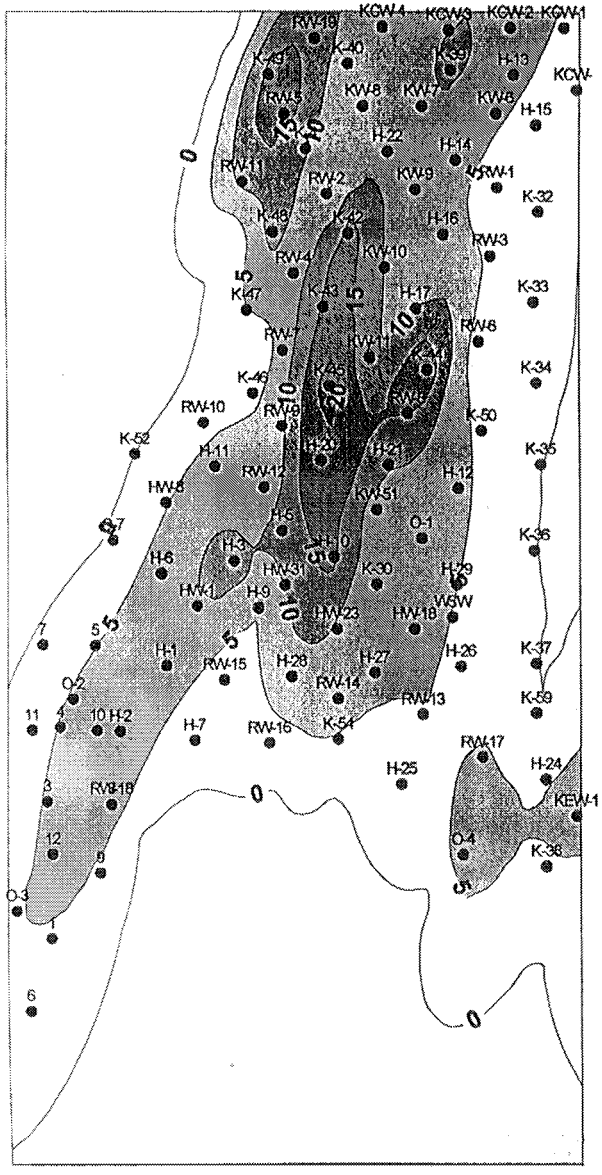

FIGURE 19

B3 Net Pay

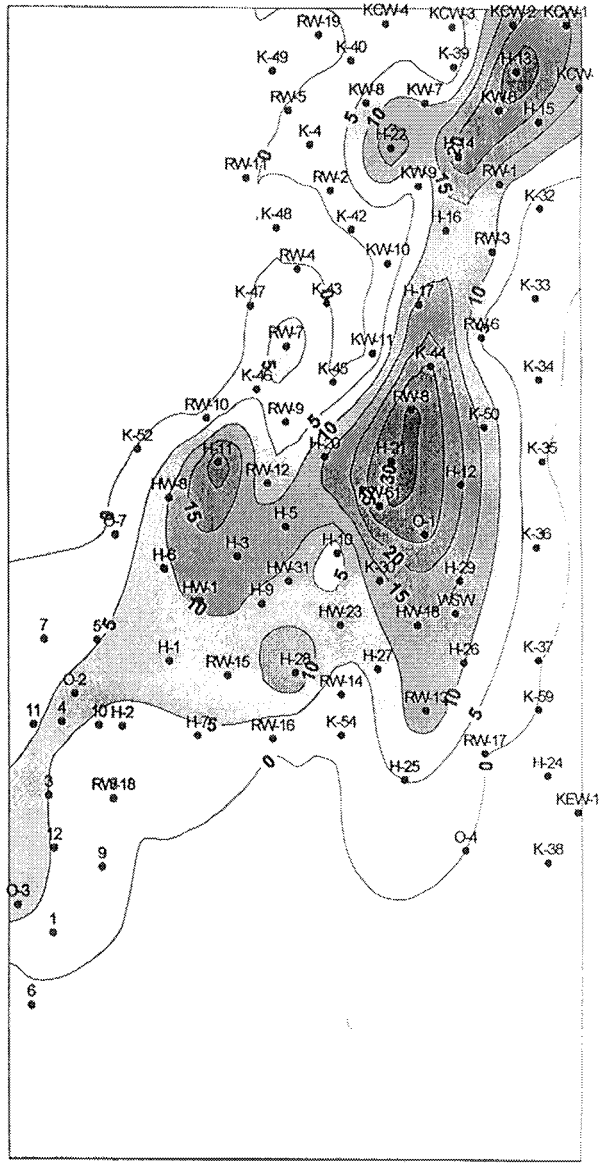

FIGURE 20

Table 11: Pattern Volumetric Analysis

Well	Oil Prod. BBL/ Ac-ft	Oil Left BBL/ Ac-ft	Remaining Sec. Oil	Remaining Poly Oil	Remaining Tot. Oil	Segment Acres	B2 Vol. Ac-ft	B3 Vol. Ac-ft	Total Vol. Ac-ft	Oil Prod. June 94	Water Prod. June 94
H-1	117	138	9,149	5,298	14,447	4.09	33.89	32.34	66.23	7,740	113,625
H-11	75	180	9,708	4,304	14,012	2.47	19.81	33.99	53.80	4,012	92,014
H-14	259	(4)	(274)	5,504	5,231	2.51	18.72	50.09	68.81	17,819	192,372
H-15	184	71	2,043	2,312	4,355	1.01	4.56	24.34	28.90	5,327	58,965
H-16	226	29	1,990	5,398	7,388	3.32	20.54	46.94	67.48	15,217	202,476
H-17	127	128	12,377	7,709	20,086	3.82	40.13	56.24	96.37	12,196	203,703
H-20	144	111	24,216	17,504	41,720	6.74	94.10	124.70	218.80	31,579	221,003
H-22	134	121	6,656	4,389	11,046	2.49	23.22	31.65	54.87	7,335	101,718
H-26	236	19	602	2,480	3,082	1.34	9.40	21.59	31.00	7,302	63,697
H-27	21	234	10,430	3,568	13,999	2.57	19.98	24.62	44.60	944	76,606
H-28	69	186	9,304	4,000	13,305	2.96	23.12	26.88	50.01	3,447	144,798
H-3	65	190	30,164	12,681	42,846	6.46	79.33	79.19	158.52	10,258	169,577
H-30	220	35	5,968	13,731	19,700	6.75	67.24	104.41	171.64	37,801	310,339
K-36	35	220	9,401	3,415	12,816	2.83	11.65	31.04	42.69	1,485	34,205
H-9	82	173	9,931	4,591	14,522	3.02	25.87	31.51	57.38	4,701	101,352
K-39	153	102	16,361	12,880	29,242	6.69	56.04	104.97	161.01	24,695	345,730
K-40	21	234	6,250	2,133	8,383	2.10	24.38	2.27	26.66	547	30,563
K-41	129	126	4,256	2,694	6,950	2.55	31.71	1.97	33.67	4,331	131,973
K-42	75	180	8,207	3,645	11,852	2.78	38.05	7.51	45.56	3,410	98,335
K-43	178	77	4,115	4,280	8,394	3.08	49.52	3.98	53.50	9,527	107,389
K-44	144	111	10,101	7,260	17,362	2.72	35.72	55.03	90.75	13,041	188,887
K-45	85	170	12,295	5,773	18,068	3.01	55.02	17.14	72.17	6,107	130,939
K-47	36	219	12,901	4,717	17,618	7.27	46.73	12.23	58.96	2,134	36,524
K-49	112	143	1,460	815	2,275	0.31	9.88	0.31	10.19	1,137	18,253
K-54	184	71	2,182	2,450	4,632	3.09	15.11	15.51	30.62	5,626	127,719
TOTALS			219,793	143,531	363,331	85	856	942	1,794	237,812	3,302,856

Simulation Study

To determine the potential recovery from waterflooding in the Savonburg Field, a streamtube simulator was utilized. The following input parameters were used in the simulation:

Table 12: Input Parameters for Streamtube Simulator

FORMATION PROPERITIES AND PATTERN VOLUMES

FORMATION DEPTH	620.0 FT
FORMATION TEMPERATURE	70.0 DEG.F
FORMATION AVE. PERMEABILITY	27.0 MD
FORMATION POROSITY	0.2
TOTAL NET THICKNESS	17.2 FT
TOTAL PORE VOLUME	61.4 MBBL
ORIGINAL OIL IN PLACE	45.8 MSTB
OIL IN PLACE AT START OF FLOOD	42.2 MSTB
DYKSTRA-PARSONS COEFFICIENT	0.63 VDP
PATTERN AREA	2.50 ACRE
WELLBORE RADIUS	0.50 FT
INJECTIVITY COEFFICIENT	1.00 PSI/FT
INJECTION RATE OVERRIDE	40.0 RB/D
WATER-OIL MOBILITY RATIO	7.38
POLYMER-OIL MOBILITY RATIO	1.00
POLYMER CONCENTRATION	500.0 PPM
POLYMER ADSORPTION	200.000 LB/AC FT
POLYMER ADSORPTION PARAMETER	0.147 VOL SLUG/PV
POLYMER VISCOSITY	12.700 CP
RESISTANCE FACTOR	7.40
RESIDUAL RESISTANCE FACTOR	2.000
POWER-LAW COEFFICIENT	4.774 CP*SEC**(N-1)
POWER-LAW EXPONENT	0.600
POLYMER SLUG SIZE	0.300 PV
MAXIMUM INJECTED PV, POLY+CHASE WAT	2.000 PV

FORMATION PROPERTY TABLE

DISCRETE LAYER CALCULATION OPTION	1 LYROPT
NUMBER OF LAYERS	5 NLAYER OR NLDP
AVERAGE POROSITY	0.1840
AVERAGE PERMEABILITY	27.0 MD
TOTAL NET THICKNESS	17.2 FT
AVERAGE INITIAL WATER SATURATION .	0.30

LAYER NO.	PHIL	PERML MD	PAYL FT	SWIL
1	0.18	75.69	3.44	0.30
2	0.18	28.35	3.44	0.30
3	0.18	16.64	3.44	0.30
4	0.18	9.84	3.44	0.30
5	0.18	4.48	3.44	0.30

RELATIVE PERM CURVES

IRREDUCIBLE WATER SATURATION .	0.240 SWC
RESIDUAL OIL SATN AFTER WATER	0.349 SORW
OIL RELATIVE PERM END-POINT	0.800 XKROE
WATER RELATIVE PERM END-POINT	0.300 XKRWE
OIL RELATIVE PERM CURVATURE	2.00 XNO
WATER RELATIVE PERM CURVATURE	2.00 XNW

RELATIVE PERMEABILITY TABLE

WATER SATURATN	OIL KRO	WATER KRW	FRACTION WATER	FRACTION POLYMER
0.2400	0.8000	0.0000	0.0000	0.0000
0.2811	0.6480	0.0030	0.0835	0.0038
0.3222	0.5120	0.0120	0.3157	0.0190
0.3633	0.3920	0.0270	0.5755	0.0539
0.4044	0.2880	0.0480	0.7664	0.1211
0.4455	0.2000	0.0750	0.8807	0.2367
0.4866	0.1280	0.1080	0.9432	0.4109
0.5277	0.0720	0.1470	0.9757	0.6280
0.5688	0.0320	0.1920	0.9916	0.8322
0.6099	0.0080	0.2430	0.9983	0.9617
0.6510	0.0000	0.3000	1.0000	1.0000

WATERFLOOD REPORT PATTERN PRODUCTION SUMMARY

PATTERN LIFE RATIO	10.80
PATTERN AREA .	2.50 ACRE
PATTERN PORE VOLUME	61.4 MBBL
ORIGINAL OIL IN PLACE	45.8 MSTB
OIL IN PLACE AT START OF FLOOD	42.2 MSTB
TOTAL OIL PRODUCTION	11.0 MSTB
OIL RECOVERY	255 BBL/AC-FT @ WOR - 25

POLYMERFLOOD REPORT PATTERN PRODUCTION SUMMARY

PATTERN LIFE RATIO	10.80
PATTERN AREA	2.50 ACRE
PATTERN PORE VOLUME	61.4 MBBL
ORIGINAL OIL IN PLACE	45.8 MSTB
OIL IN PLACE AT START OF FLOOD	42.2 MSTB
TOTAL OIL PRODUCTION	15.1 MSTB
OIL RECOVERY	335 BBL/AC-FT @ WOR - 60
TOTAL POLYMER INJECTED	3.2 MLB
OIL/POLYMER RATIO	4.67 STB/LB

The simulation run indicates that the recovery factors for waterflood and polymer flood are 255 and 335 BBL/Ac-ft respectively. This recovery factor is larger than most of the recovery factors in the volumetric pattern study. This would indicate that many of the patterns have a high potential for incremental oil if the continued development was optimized.

Geological Analysis

The primary zone of oil production is a sandstone that is part of the Chelsea Sandstone of the Cabaniss Formation, Cherokee Group. The sandstone, with associated mixed lithology (rippled sandstone, wavy-and linsen-bedded sandstone, siltstone and shale) and shale, fills a valley that was cut during a low stand of sea level. The low stand occurred after deposition of the Tebo Coal and some overlying strata but before deposition of the Scammon Coal. The most productive reservoir is a structureless, fine-grained sandstone associated with the first stage of filling this valley, called the B_3 zone in this report. Rippled sandstones of the overlying interval, the B_2 zone, are potentially productive in the NW part of the lease, but are generally either saturated with dead oil, have low initial oil saturations, or are thin and discontinuous, making poor reservoirs.

Geological understanding of this reservoir results from two factors. One is the availability of good data. The operators, J.E. Russell Petroleum, Inc. provided cores, core descriptions and analyses, and logs. The other factor was the application of sedimentologic and stratigraphic principles that have emerged in the past few years, especially sequence stratigraphy and the understanding of the features of sediments deposited by tidal currents.

The stratigraphic framework of the Cherokee Group in the field area is a series of regional marker intervals that consist (ideally) of an underclay, a coal, a caprock of marine sandstone or limestone, and a dark gray or black shale. In terms of sequence stratigraphy, the boundary of the underclay and coal represents a sequence boundary, a surface of subaerial exposure. The boundary between the coal and the caprock represents the initial surface of marine transgression, with the caprock representing a lag deposit on a ravinement surface cut during transgression. The surface of maximum transgression lies in the overlying dark gray or black shale or in the medium gray shale that gradationally overlies it. These strata thus reflect the effects of rise and fall of sea level relative to the area of deposition of these sediments. Regional marker intervals extend across the Cherokee basin of southeastern Kansas and into the Forest City and Sedgwick basins (northeastern and south-central Kansas, respectively). They may continue into Iowa and southwestern Kansas.

Locally, the regional marker intervals are missing, notably in the vicinity of the Nelson Lease. The . pattern of their absence in the field area suggests a valley eroded into underlying deposits; this is the valley referred to above. The sediments that fill this valley appear to carry indications of deposition by tidal currents. The sediments show gradational changes from shale to wavy- and linsen-bedded sandstone and mudrocks to rippled sandstone on a dm scale. The gradational nature of these changes suggests no little erosion between depositional events. The changes of grain size suggest frequent changes of current intensity, from essentially no current, when mudstone and macerated plant material accumulated in wavy-or linsen-bedded successions to times of current when ripples or sand or silt accumulated. This may correspond to currents during individual tidal cycles. The dm-scale gradation of shale to mudrocks to sand may reflect changes in intensity of ripple-forming episodes of the kind that would result from the neap-spring cycles of tidal activity. Because the mixed lithologies of the B_2 and B_3 zones suggest tidal activity, the sandstones and shales of these zones may also have formed in tidal environments. Tidal sandstones occur in mounded masses, convex upward, rather than in the convex-downward patterns of fluvial channels.

Planning for further development of this field should take into account the linear nature of the primary reservoir, the lower (or B_3) sandstone, and the sheet-like nature of the upper sand (B_2) in the northwestern part of the field, if that area is developed further. Additional drilling for improved waterflood recovery may be warranted in the central part of the deep valley and in the northwestern part of the lease. Several wells are completed in sandstones where petrophysics, saturations, and continuity of beds are unfavorable for either injection or production. Each well should be evaluated in view of current subsurface information, and those that are not likely to be productive should be abandoned. The field contains substantial amounts of dead oil, which not only cannot be produced but which act as a barrier to flow of fluids thought the reservoir. Wells drilled during further development the wells logged at least with g-ray--neutron logs. The wells should be cored and the cores analyzed for normal petrophysics, fluid saturations, recoverable oil and

effective permeability. Cores should be described geologically and their character used to improve knowledge of the distribution of rocks in the field.

The geological study identified two sandstones, B_2 and B_3, which have potential for additional oil recovery. The study utilized regional marker horizons to form the basis for correlation of Cherokee Group rocks over the Cherokee Basin and to adjacent basins. East-West cross sections were developed on nearly all the wells identifying the continuity of the B_2 and B_3 pay zones. The cross sections are presented in Appendix E. Isopach maps were developed for the B_2 and B_3 sandstones.

It was concluded that the sandstones of the B_3 zone of the Chelsea valley fill in the eastern- 1/2 of section 21 may not be completely drained by the current arrangement of wells. Specifically, injection wells may be needed between wells H-14 and H-16, between H-16 and K-44, between H-20 and H-21, and between H-30 and H-27. These locations lie along the trend of thickest sandstone in the axis of the Chelsea valley fill and adjacent injection wells are on the margins of the sandstone. While these steps would reduce spacing substantially, very high original oil saturations along the valley (as high as 5000 bbls/acre recoverable oil) and the potential for improved recovery may justify the step.

Cores of the B_2 zone in the northwest part of the Nelson Lease indicate recoverable oil averaging 2000 Bbls/acre, but production from that area has been low. Recompletion, additional development drilling, or some expansion of the field in this direction may be desirable, under the right economic conditions.

The complete geological analysis of the field is included as **Appendix** A.

Discussion of Field Recommendations

As part of the Phase 1 work, selected field testing of the waterflood was completed. Based on the volumetric pattern study and geological evaluation, several recommendations were made. Field recommendations included well cleanups. Recommendations were based on zone potential. From examining the geological report, Zone B-3 is of better quality and of higher potential than Zone B-2. As a result, it was suggested that initial work be conducted on Zone B-3 in Phase 1. -Once these recommendations were implemented, areas of high potential would be identified in. Zone -B-2 and work continued.

The following injection wells had gel polymer treatments conducted, and wellbore cleanups occurred.

Well RW-8 - The original differential survey indicated that the fluid was entering above the oil producing horizon. A gel polymer treatment was conducted to plug the thief zone. A wellbore cleanup was conducted on the oil producing horizon with success. The final differential survey indicated that the water was entering the B3 zone, which was the targeted formation. After treatment, approximately 60 B/D was being injected at a pressure of 460 psi.

Well RW-3 - A gel polymer treatment was implemented to plug the channel to H-17. The wellbore was cleaned and a differential temperature survey indicated the water was being injected into the B2 and B3 oil zones.

Well RW-6 - A gel polymer treatment was implemented to plug the channel to K-44.

The following injection wells were cleaned to improve injectivity.

Well KW-51 - Placed on injection in September 1994, utilizing 1-inch pipe and a packer. The wellbore was cleaned within the following two weeks. Injection later averaged 50 B/D.

Wells (KW-6, KCW-1, RW-7, RW-9, RW-12, RW-13, RW-1, HW-23) were cleaned and reactivated as injectors.

The following producing wells were cleaned and remediated: H-17, H-21, K-44, H-13, H-26, H-22, H-30, H-5, H-14, and O-1.

Producing Wells H-5 and H-14 were converted to injection wells in the April 1995, and July 1995, respectively.

Conclusions and Summary

An engineering and geological study was conducted on the Savonburg Field with many conclusions and findings to date. Also a water cleanup process was selected to cleanup the low quality injection water in the field.

Air flotation was selected as the process to improve water quality. The air flotation unit was installed along with additional tanks and lines needed for proper installation. Steady-state operation was achieved. A flocculation chemical was selected to aid in the performance of the air flotation unit. Economics looked favorable.

Results from the engineering study included, 1) a volumetric study of selected patterns throughout the field, and 2) a waterflood and polymer flood simulation study of a five-spot with average properties of the Nelson Lease. The volumetric study provided waterflood efficiencies on a pattern basis to determine patterns of highest potential for additional recovery. The simulations indicated that a total recovery factor of 225 BBLS/Ac-ft could be achieved through continued operation of the waterflood and if a polymer flood was installed 335 BBLS/Ac-ft could be achieved. These recovery factors are larger than most of the recovery factors in the volumetric pattern study. This would indicate that many of the patterns have a high potential for incremental oil if the waterflood were optimized. If a polymer flood is installed incremental oil is estimated at 363,000 barrels.

BUDGET PERIOD 2 ACTIVITIES

Waterplant Development

The water supply for the Nelson Lease is a mixture of produced water-from the Bartlesville formation and makeup water from the Arbuckle formation. The produced water contains barium and soluble iron, whereas, the make-up water contains sulfate and sulfide. The combination of the two waters causes barium sulfate and iron sulfide to precipitate from solution. Depending on the ratio of the two waters the resulting water is either black due to the iron sulfide or red due to the formation of insoluble iron oxide. Prior to the Department of Energy Project, these waters were mixed in a single tank. The produced water was filtered through a 75-micron bag filter. This water was pumped into the supply tank where the make-up water was added. The mixed water was black and contained iron sulfide, iron oxide, barium sulfate, and oil. This black water was then pumped to the injection wells. Barium sulfate scale and particulate matter collected in the flow lines and in the injection wells, creating continual injectivity problems and workover expense. Various scale inhibitors, detergents, and other chemicals were added at the produced water tank to reduce the scaling and plugging problems experienced.

The water supply system was redesigned. An air flotation unit was added to improve the quality of the injection water by removal of oil and suspended solids. Flotation was selected over sand filtration in order to demonstrate available technology not used by Kansas operators. The premise for selecting the flotation unit was that it would be easier to operate than a sand filtration system, and the chemical treatment costs per barrel of water would be less than the prior system used. A 1000 barrel per day unit was purchased from Separation Specialists, Inc. of Bakersfield, California in June of 1994. The flotation unit was designed for off-shore operations for the removal of oil to less than 30 ppm for water discharged to the ocean. The flotation unit was installed and began operation on July 13, 1994. A complete write-up on the water quality improvement by air flotation on the Savonburg project is included in **Appendix** D.

Permeability Modification Treatments

Phase I analysis indicated that numerous channels exist in the reservoir between injection and producing wells. Profile modification treatments were designed and implemented to plug the channels so water will be injected in oil bearing porous media. A variety of gel systems was considered

During 1997 two wells on the Nelson lease were subjected to permeability modification treatments. In September 1997 a channelblock treatment was performed on well No. H-14. A sixty-barrel batch of freshwater polymer solution was prepared with salts and thiosulfate added while agitating and hydrating the polymer. Sodium dichromate was added during the treatment at a concentration from 650-750 ppm. The injection treatment lasted slightly less than six hours.

Initial Pressure	450 PSI
Maximum Pressure	662 PSI
Final Pressure	620 PSI
Average Pressure	625 PSI
Polymer Injection Rate	3.64 BPH
Treatment Volume	60 Bbls.
pH of Solution	5.8-6.3
Viscosity	36.0-43.5 cp
Temperature	26.5-29.5° C
Polymer Alcoflood 935	137.5 lbs.
Sodium Dichromate	14.2 lbs.
Sodium Thiosulfate	10.5 lbs.
Sodium Chloride	100.0 lbs.
Calcium Chloride	65.0 lbs.

Offset producers were sampled throughout the treatment for evidence of polymer breakthrough. All tests were negative. The wellhead pressure increased well above prior levels when the well was placed on injection, indicating that the primary water channel was plugged. However, a tracer test conducted five weeks after the treatment indicated communication with H-15 in 23 hours and H-16 in 24.5 hours...

In October a 62 barrel channelblock treatment was performed on well RW-8 due to the injection entering only the B2 perforations. After setting a sand pack over the B3 zone the polymer solution was injected at 41 barrels per day and 540 psi. Sodium dichromate was added continuously at concentrations of 650-750 ppm.

Initial Pressure	420 psi
Final Pressure	500 psi
Average Pressure	500 psi
Polymer Injection Rate	3.68 bbl/hour
Treatment Volume	62 bbls
pH Solution	5.4-6.2
Viscosity	49.5-52 cp
Temperature	27.5° C
Polymer Alcoflood 935	137.5 lbs
Sodium Dichromate	14.2 lbs
Sodium Thiosulfate	10.5 lbs
Sodium Chloride	100.0 lbs
Calcium Chloride	65.0 lbs

A second channelblock treatment was performed six weeks later on November 19. The well was treated with two batches of polymer solution.

	FIRST BATCH	SECOND BATCH
Initial Pressure	335 psi	755 psi
Final Pressure	490 psi	590 psi
Average Pressure	480 psi	585 psi
Polymer Injection Rate	3.6 BPH	3.7 BPH

Treatment Volume	32.6 bbls	31.8 bbl
pH Solution	5.7	5.8-4.4
Viscosity	No measurements taken	
Temperature	51-43° F	11.8-9.3° C
Polymer Alcoflood 935	70 lbs	84 lbs
Sodium Dichromate	6.8 lbs	7.4 lbs
Sodium Thiosulfate	5.25 lbs	5.25 lbs
Sodium Chloride	50.0 lbs	50.0 lbs
Calcium Chloride	32.5 lbs	32.5 lbs
28% HCL Acid	None	2 quarts

Actual injected volume in batch two was reduced to 28.1 bbl.

A month later, on December 18, the well was washed to the plugged back total depth of 675'. An injection test of 3.68 BPH @ 550 psi indicated the treatment did not hold. Subsequently, about four weeks later, injection was again attempted and, although pressures were in excess of 700 psi, no water could be injected into the B2 zone. The well was then washed out and injection resumed in the B3 zone through tubing under a packer.

Pattern Changes and Wellbore Cleanups

Pattern Changes. Since the geological and engineering analysis conducted in Budget Period 1 indicated that the B3 zone had not been waterflooded completely and that unrecovered oil existed, pattern changes were implemented to increase the volume of water injected into the B3 zone. Since production wells H-14 and H-5 showed good continuity in the B3 zone, these two wells were converted into injectors in 1995. Well 0-1, also recommended to be converted to injection in the Budget Period 1 analysis was converted to injection in late 1998.

Injection well KW 51 and producer H-9 were plugged in February 1998 as both wells were in serious communication with other wells on the lease. During late 1998 many of the comparatively poor quality wells were also plugged - Wells 2, 6, 7, K-32, K-33, K-34, K-35, K-36 and Cox 1, 5 and 502.

Wellbore Cleanups. 1997 was a period of relatively clean injection wells, but in 1998 a large number of wellbore cleanouts were required due to the inconsistency of injection water quality. Prior to the cleanouts," the injection volumes were much lower than normal, resulting in lower total fluid and oil producing rates. A series of mid-year 1998 wellbore cleanouts coupled with the development of excellent injection water resulted in an increase in injectivity to over 1000 BWPD.

Injectivity improvement was obtained by wellbore cleaning. Clean-up treatments have involved acid and a wide variety of additives. Techniques include hydraulic jetting, jetting with air and foam, placement with a coiled tubing unit, and simply lubricating in the treatments. The principal functions of the acid additive are to remove wellbore emulsion, sludge and deposits, prevent iron precipitation, prevent clay swelling, and the attendant migrations of clays and fines.

A typical treatment involves the following chemicals: 1) 50 gallons of 28% hydrochloric acid, 2) two gallons of an iron control additive (ESA-91), 3) one-half gallon of clay stabilizer (ESA-50), and 4) two gallons of micellar acidizing additive (ESA-96).

Reservoir Development

In 1996 an infill injection well was drilled to further develop the reservoir. Figure 19 presents the location of the in-fill well. The core analysis showed a watered out B2 zone at an approximate depth of 646-661 ft. and appreciable mobile oil in the B3 zone at an approximate depth of 678-715 ft. This can be qualified with measuring the core water saturations and chloride content in the brine. Table 13 presents the core analysis measurements and the B2 and B3 zones. Since the injected water is of much lower concentration chloride, any watered out zones will show lower concentrations of chloride in the brine from

core analysis. **Figure 20** presents this phenomenon with footages (647-660) showing low concentrations of chlorides. **Figure** 21 presents water saturation in the core verifying the watered out zone in the upper B2.

Figure 22 presents porosity measurements that are somewhat uniform averaging approximately at 18%. **Figure** 23 presents the permeability to air measurements that identifies the permeable sandstones. This plot presents the separation of the B2 and B3 sandstone reservoirs. There is an eight-foot impermeable barrier between the zones. This is also presented in Figure 24 presenting the effective permeability to water in millidarcys.

On March 13, 1996, the well was perforated from 678 to 688 ft. A 3 1/8" diameter hollow steel carrier casing jet gun was utilized. Waterflood injection was initiated on April 11, 1996.

The original proposal included evaluation of the possibility of installing a polymer flood in the Savonburg Field. Until the latest months of operations a consistently clean water supply was not available (a necessity in polymer flooding), plus, the producing water/oil ratio is becoming critically high.

FIGURE 21: LOCATION OF RW-20

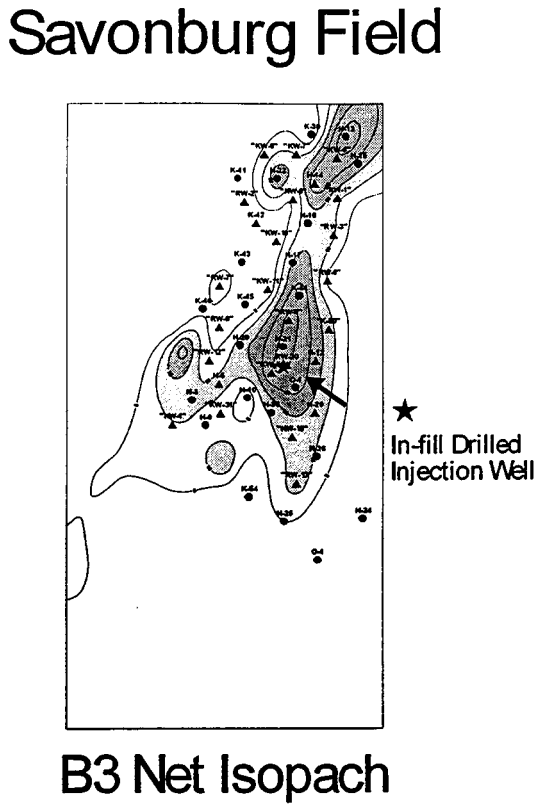

FIGURE 22: RW-20 CORE CHLORIDE CONTENT

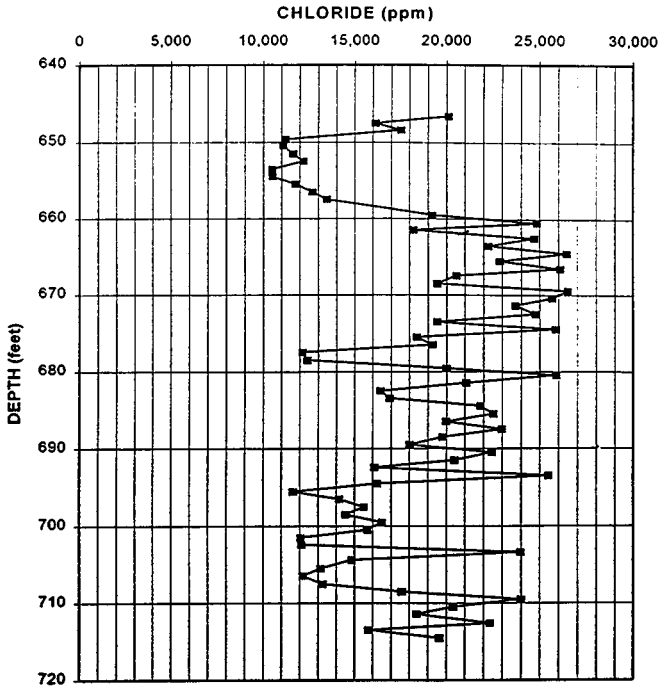

FIGURE 23: RW-20 CORE WATER SAT'N

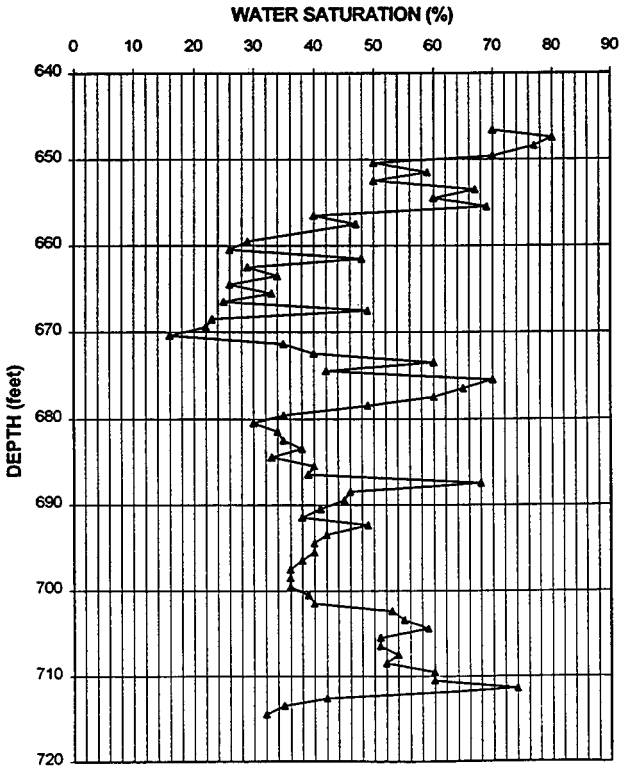

FIGURE 24: RW-20 POROSITY

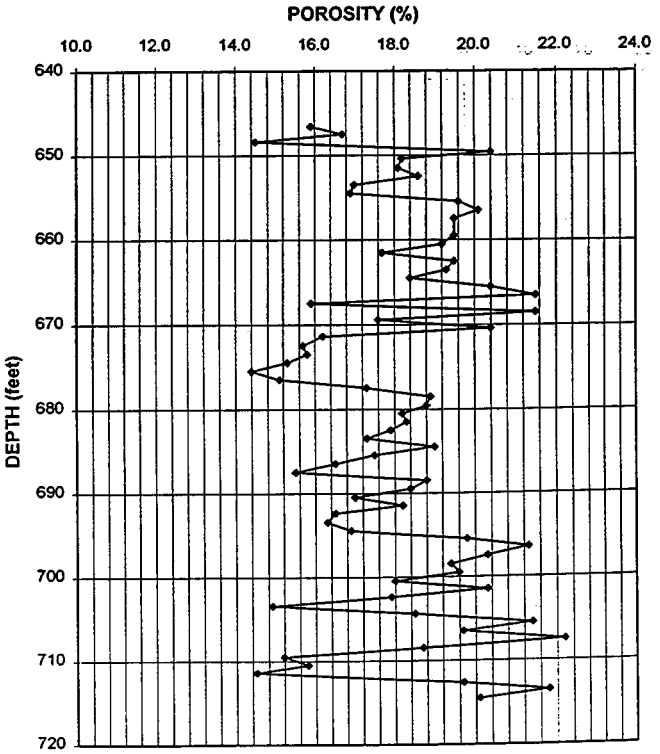

FIGURE 25: RW-20 PERMEABILITY (air)

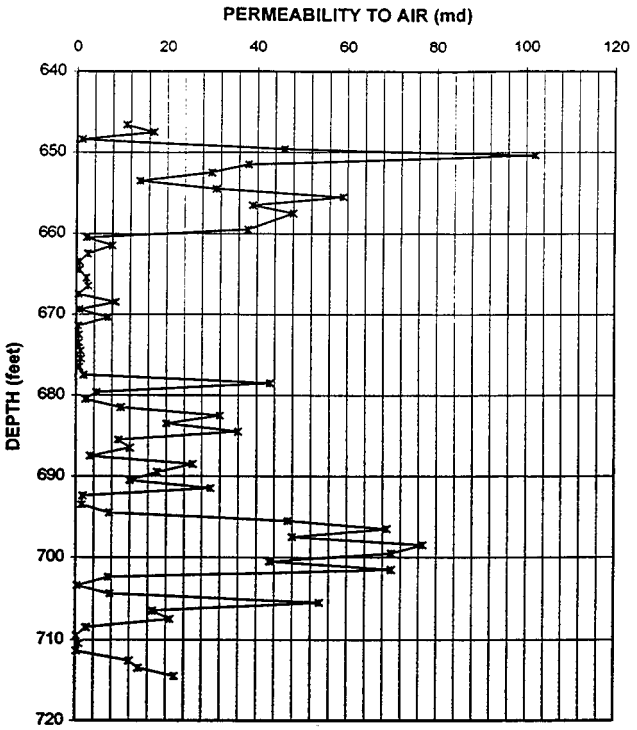

FIGURE 26: RW-20 PERMEABILITY (water)

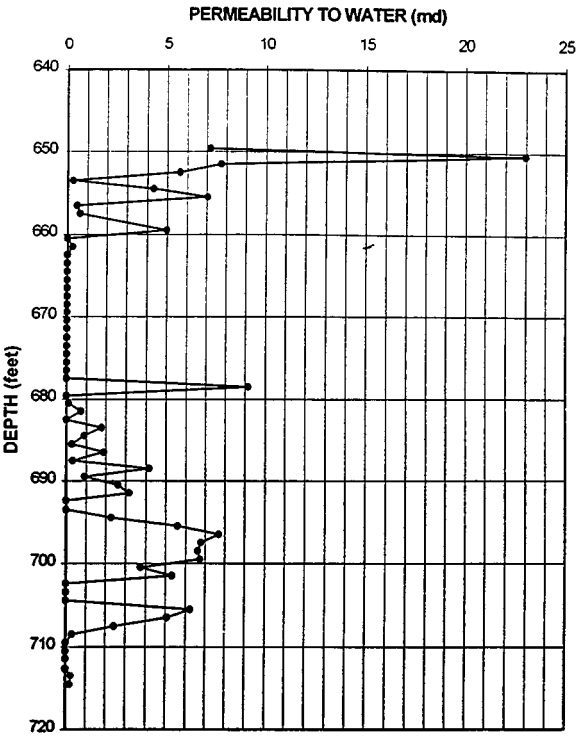

FIGURE 27: RW-20 RESIDUAL OIL SAT'N.

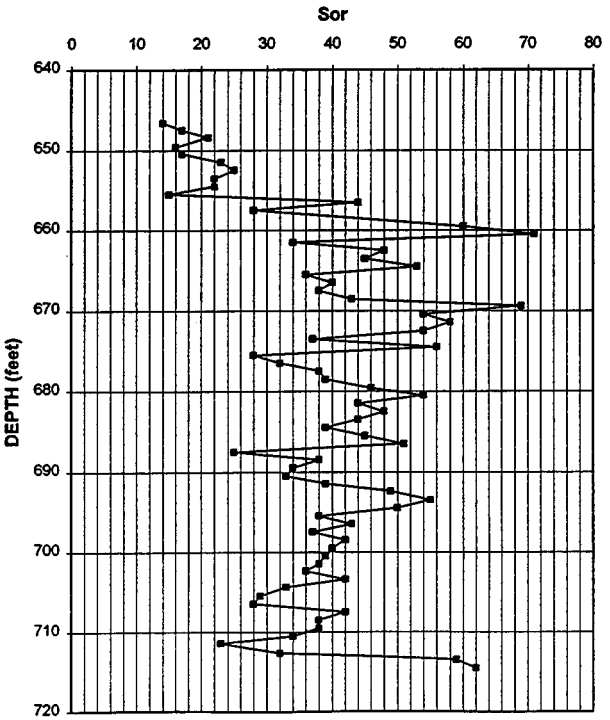

Table 13

RW-20 **BASIC CORE ANALYSIS DATA**

Sample #	Depth Feet	Eff. Porosity Percent	Percent Oil Saturation Oil	Water	Total	Perm. Mill
1	646.6	15.9	14	70	84	11
2	647.5	16.7	17	80	97	17
3	648.4	14.5	21	77	98	1.1
4	649.6	20.4	16	70	86	46
5	650.4	18.2	17	50	67	102
6	651.5	18.1	23	59	82	38
7	652.5	18.6	25	50	75	30
8	653.5	17.0	22	67	89	14
9	654.5	16.9	22	60	82	31
10	655.5	19.6	15	69	84	59
11	656.5	20.1	44	40	84	39
12	657.5	19.5	28	47	75	48
13	659.5	19.5	60	29	89	38
14	660.5	19.2	71	26	97	2.2
15	661.5	17.7	34	48	82	8
16	662.5	19.5	48	29	77	2.5
17	663.5	19.3	45	34	79	0.72
18	664.5	18.4	53	26	79	0.66
19	665.5	20.4	36	33	69	2.2
20	666.5	21.5	40	25	65	2.6
21	667.5	15.9	38	49	87	0.47
22	668.5	21.5	43	23	66	8.8
23	669.4	17.6	69	22	91	0.71
24	670.4	20.4	54	16	70	7.2
25	671.4	16.2	58	35	93	0.43
26	672.5	15.7	54	40	94	0.63
27	673.5	15.8	37	60	97	0.6
28	674.5	15.3	56	42	98	1
29	675.5	14.4	28	70	98	1.1
30	676.5	15.1	32	65	97	0.79
31	677.5	17.3	38	60	98	1.7
32	678.5	18.9	39	49	88	43
33	679.6	18.8	46	35	81	4.6
34	680.5	18.2	54	30	84	2.1
35	681.5	18.3	44	34	78	10
36	682.5	17.9	48	35	83	32
37	683.5	17.3	44	38	82	20
38	684.5	19.0	39	33	72	36
39	685.5	17.5	45	40	85	9.5
40	686.5	16.5	51	39	90	12
41	687.5	15.5	25	68	93	3.2
42	688.5	18.8	38	46	84	26
43	689.5	18.4	34	45	79	18
44	690.5	17.0	33	41	74	12
45	691.5	18.2	39	38	77	30
46	692.4	16.5	49	49	98	1.5
47	693.5	16.3	55	42	97	1.3
48	694.5	16.9	50	40	90	7.5
49	695.5	19.8	38	40	78	47
50	696.5	21.3	43	38	81	69
51	697.5	20.3	37	36	73	48
52	698.5	19.4	42	36	78	77
53	699.5	19.6	40	36	76	70
54	700.5	18.0	39	39	78	43
55	701.5	20.3	38	40	78	70
56	702.4	17.9	36	53	89	7.3
57	703.4	14.9	42	55	97	0.35
58	704.4	18.5	33	59	92	7.7
59	705.5	21.4	29	51	80	54
60	706.5	19.7	28	51	79	17
61	707.5	22.2	42	54	96	21
62	708.5	18.7	38	52	90	2.4
63	709.5	15.2	38	60	98	0.28
64	710.5	15.8	34	60	94	0.81
65	711.4	14.5	23	74	97	0.23
66	712.6	19.7	32	42	74	12
67	713.5	21.8	59	35	94	14
68	714.5	20.1	62	32	94	22

Table 13

RW-20 **BASIC CORE ANALYSIS DATA**

Sample #	Depth Feet	Eff. Porosity Percent	Percent Oil Saturation Oil	Water	Total	Perm. Mill
1	646.6	15.9	14	70	84	11
2	647.5	16.7	17	80	97	17
3	648.4	14.5	21	77	98	1.1
4	649.6	20.4	16	70	86	46
5	650.4	18.2	17	50	67	102
6	651.5	18.1	23	59	82	38
7	652.5	18.6	25	50	75	30
8	653.5	17.0	22	67	89	14
9	654.5	16.9	22	60	82	31
10	655.5	19.6	15	69	84	59
11	656.5	20.1	44	40	84	39
12	657.5	19.5	28	47	75	48
13	659.5	19.5	60	29	89	38
14	660.5	19.2	71	26	97	2.2
15	661.5	17.7	34	48	82	8
16	662.5	19.5	48	29	77	2.5
17	663.5	19.3	45	34	79	0.72
18	664.5	18.4	53	26	79	0.66
19	665.5	20.4	36	33	69	2.2
20	666.5	21.5	40	25	65	2.6
21	667.5	15.9	38	49	87	0.47
22	668.5	21.5	43	23	66	8.8
23	669.4	17.6	69	22	91	0.71
24	670.4	20.4	54	16	70	7.2
25	671.4	16.2	58	35	93	0.43
26	672.5	15.7	54	40	94	0.63
27	673.5	15.8	37	60	97	0.6
28	674.5	15.3	56	42	98	1
29	675.5	14.4	28	70	98	1.1
30	676.5	15.1	32	65	97	0.79
31	677.5	17.3	38	60	98	1.7
32	678.5	18.9	39	49	88	43
33	679.6	18.8	46	35	81	4.6
34	680.5	18.2	54	30	84	2.1
35	681.5	18.3	44	34	78	10
36	682.5	17.9	48	35	83	32
37	683.5	17.3	44	38	82	20
38	684.5	19.0	39	33	72	36
39	685.5	17.5	45	40	85	9.5
40	686.5	16.5	51	39	90	12
41	687.5	15.5	25	68	93	3.2
42	688.5	18.8	38	46	84	26
43	689.5	18.4	34	45	79	18
44	690.5	17.0	33	41	74	12
45	691.5	18.2	39	38	77	30
46	692.4	16.5	49	49	98	1.5
47	693.5	16.3	55	42	97	1.3
48	694.5	16.9	50	40	90	7.5
49	695.5	19.8	38	40	78	47
50	696.5	21.3	43	38	81	69
51	697.5	20.3	37	36	73	48
52	698.5	19.4	42	36	78	77
53	699.5	19.6	40	36	76	70
54	700.5	18.0	39	39	78	43
55	701.5	20.3	38	40	78	70
56	702.4	17.9	36	53	89	7.3
57	703.4	14.9	42	55	97	0.35
58	704.4	18.5	33	59	92	7.7
59	705.5	21.4	29	51	80	54
60	706.5	19.7	28	51	79	17
61	707.5	22.2	42	54	96	21
62	708.5	18.7	38	52	90	2.4
63	709.5	15.2	38	60	98	0.28
64	710.5	15.8	34	60	94	0.81
65	711.4	14.5	23	74	97	0.23
66	712.6	19.7	32	42	74	12
67	713.5	21.8	59	35	94	14
68	714.5	20.1	62	32	94	22

Table 13

RW-20 CORE FLOODPOT DATA

Sample #	Residual Sat.			Vol of Water	Effective Perm.	I.F.P.	Chloride Content
	% Oil	% Water	Bbls./A.Ft.	Rec. cc.	Millidarcys	#/Sq.	of Brine, ppm
1	14	82	178	124	0.94	25	20,094
2	18	80	236	216	1.5	15	16,131
3	21	77	235	0	imp	-	17,526
4	16	80	248	440	7.2	5	11,196
5	17	78	245	288	22.99	5	11,093
6	23	73	318	528	7.73	5	11,616
7	25	73	367	516	5.66	15	12,181
8	22	76	295	26	0.27	35	10,487
9	23	74	302	550	4.33	15	10,492
10	15	81	225	464	7.06	10	11,742
11	44	52	686	30	0.48	40	12,674
12	28	69	417	40	0.63	40	13,466
13	60	38	908	608	5	25	19,204
14	71	26	1041	0	0	-	24,838
15	34	63	456	30	0.28	40	18,180
16	48	29	722	0	0	-	24,695
17	44	35	649	0	0	-	22,248
18	53	26	757	0	0	-	26,433
19	36	34	564	0	0	-	22,862
20	39	27	647	0	0	-	26,079
21	38	49	469	0	0	-	20,525
22	43	24	717	0	0	-	19,484
23	68	24	918	0	0	-	26,477
24	54	17	846	0	0	-	25,643
25	58	35	729	0	0	-	23,696
26	54	40	649	0	0	-	24,774
27	38	60	469	0	0	-	19,477
28	56	42	665	0	0	-	25,835
29	29	68	315	0	0	-	18,371
30	32	65	375	0	0	-	19,235
31	38	60	498	0	0	-	12,137
32	29	69	432	282	9.16	10	12,418
33	46	35	657	0	0	-	19,997
34	54	44	750	8	0.11	50	25,883
35	40	56	562	52	0.72	40	21,045
36	48	35	655	0	0	-	16,414
37	40	58	549	134	1.78	40	16,906
38	39	57	584	64	0.89	40	21,799
39	45	53	604	20	0.28	45	22,501
40	42	56	548	170	1.89	35	19,984
41	25	71	301	18	0.33	50	22,961
42	36	60	536	342	4.16	20	19,792
43	32	65	456	82	0.94	35	17,997
44	29	69	391	288	2.61	20	22,429
45	33	65	469	282	3.16	30	20,432
46	49	49	627	0	0	-	16,083
47	55	42	687	0	0	-	25,464
48	37	61	494	212	2.28	35	16,214
49	36	62	553	442	5.61	25	11,632
50	32	66	523	212	7.7	20	14,169
51	34	65	543	298	6.79	25	15,497
52	37	60	566	382	6.65	25	14,510
53	37	61	572	480	6.77	20	16,493
54	37	60	517	344	3.78	30	15,692
55	36	62	575	452	5.33	30	12,057
56	36	53	500	0	0	-	12,084
57	42	55	479	0	0	-	23,967
58	33	59	474	0	0	-	14,838
59	29	69	490	262	6.26	15	13,136
60	28	68	434	518	5.11	15	12,176
61	42	54	720	298	2.44	20	13,247
62	38	58	563	36	0.33	35	17,570
63	38	60	442	0	0	-	23,996
64	34	60	417	0	0	-	20,342
65	22	75	246	0	0	-	18,381
66	32	43	484	0	0	-	22,336
67	59	38	989	22	0.28	40	15,760
68	62	34	981	28	0.22	35	19,581

Field Operations

Field operations consisted of 1) monitoring and modifying the waterplant, 2) monitoring all wells and lines in field, and 3) testing each well at least on a monthly basis. Russell Petroleum supplied monthly reports, which consist of monthly activities and barrel test/meter reading on active wells.

Producing wells were tested and the data were posted to a computer and updated monthly. The data consisted of oil and water volumes produced, pumping unit stroke length, net effective stroke length, pumping speed (strokes per minute), and general comments. These data were utilized to estimate oil and water production for each well.

Russell Petroleum has been responsible for all field activities, 1) plant development, 2) wellbore cleanups, and 3) permeability modification treatments.

Technology Transfer

A mid-year 1997 test on Well No. RW-20 proved that successful pressure transient tests could be performed in shallow, slim-hole wellbores utilizing a computerized Echometer (fluid-level detector).

POST-PROJECT **DEVELOPMENTS**

Observations from the Field

During the eight months immediately following the end of the project, the operator's field personnel have experienced a noticeable decrease in the frequency of certain maintenance obligations which at one time were very time consuming.

In order to prepare for the polymer injection the operator implemented in the summer of 1999, all the injection wells were acidized, jetted and cleaned. In only two wells was any "fill-up" detected, and then only minor amounts. Most of the wells exhibited a very clean wellbore with little or no filtrate or particulate matter accumulated. It is the opinion of the field personnel that the ability of the air-flotation unit (AFU) to maintain the clean water for an appreciable period of time has resulted in the clean wellbores in the injection wells.

In previous years, each flow meter on the wells needed to be removed approximately once per month for maintenance and/or cleaning. For the first eight months of 1999 this maintenance requirement has become almost non-existent. In each occasion to work on a meter, the problem was not related to scale accumulation or corrosion, but the fact that the meters had worn out.

Prior to the clean water era, the 75-micron filters used in the field required changing an average of once each week. Now, using 10-micron filters, changes occur about once every sixty days. This level of filter maintenance has been prevalent for all of 1999.

Basically, the advent of consistently clean injection water has 1) increased injectivity, 2) reduced downtime, 3) lowered well servicing costs, 4) reduced meter maintenance, 5) reduced filter changes, 6) reduced chemical requirements, and 7) allowed personnel labor to be applied to other functions.

Experience is a good teacher and the Russell field personnel are good students. Much was learned utilizing the AFU, but improvements on future applications can be made. Future AFUs need not be built above ground, but can be set lower, if not level with the ground surface, and still perform its functions. The tank does not need to be but a few feet deep to accomplish its purpose, rather than ten foot tall as in the Savonburg setup. The building housing the AFU at Savonburg has suffered from serious corrosion to the exposed steel, wood and electrical components. Future designs should be built with more corrosion proof - materials, better ventilation and placement of electrical boxes, etc. away from the corrosive elements.

For small operations where iron compounds are a problem, an AFU may not be justifiable, the air-injection system used to pretreat the water may be all that is needed. Field personnel noted significant water improvement by virtue of this application alone, possibly even a greater impact than that of the AFU.

CONCLUSIONS

Obviously, the initial estimates of waterflood recovery were too optimistic, evidently because mobile oil saturation estimates were too high. Despite the concentrated effort to sweep the B_3 reservoir, the operator was unable to mobilize significant quantities of oil - much less than originally anticipated. Occasional limited production surges or slight prolonged increases were witnessed at individual producing wells, however, field wide, the responses were only capable of stabilizing the producing rate and decreasing the rate of production decline. Only one well (11-17) experienced an appreciable, sustained increase in production. This well went from 2.5 BOPD to 8 BOPD then produced with a shallow decline for several years. In most cases, when an increase was detected, it was only an increase of 1-3 BOPD and lasted but a few months. Although simulations performed in Budget Period I indicated appreciable oil reserves would be produced by polymer augmented waterflooding, polymer applications were never utilized during the project period due to 1) inability, until late in the project, to process clean water, 2) performance of waterflood suggested lower residual oil saturation than originally thought - consequently, less reserve potential -, and 3) very high producing water/oil ratio (> 30:1).

Throughout the life of the project numerous wellbore cleanouts were necessary due to the inconsistency of injection water quality. Only in the most recent months has the water quality been consistently acceptable. The included Hall Plots of certain injection wells graphically indicate the response of well treatment. After performing a cleanout the plot usually returns to its historical slope, indicating the removal of damage and a return to the well's normal injectivity.

Operation of the air flotation unit was improved. Solids content of 10 mg/L appears to be attainable in the injected water during continuous operation with proper maintenance and supervision

Chemical costs for water treating were reduced to $4.50/day or about 0.5 cents/barrel of water.

Permeability profile treatments on two wells were successful in deterring interwell communication and improving wellbore injection profiles within the scope of this project.

The operator concludes the property currently requires less maintenance and is operating more efficiently than in prior years, particularly pertaining to the water injection system. However, sufficient cost data histories are not available to quantify this conclusion.

Individual producing well and injection well performance curves are included in **Appendices** B **and C.**

Appendix A

APPENDIX A

Geological Description of the Savonburg Field

Correlation of the well logs provided the stratigraphic framework of the field and the basis for interpreting lithology in wells or parts of wells where no core description was available. Stratigraphic markers, either regional or local, were traced through the field area to provide detailed correlation on a scale of 10 to 40 feet. Some of the markers, which are designated "marker intervals" can be tied into the regional stratigraphic correlation previously developed by Harris (1984) and applied by Staton (1987) and Huffman (1991). Where such correlations could be made, the marker intervals were referred to by the name of the associated coals, either those that have been formally recognized (Weir-Pittsburg, Tebo, Scammon, etc.) or those that Harris (1984) informally named (Fig. D-2). A few markers, especially those that are only of local significance, are still designated by the color of the press-on dots that were used to identify them on logs during the phase of the study when the internal stratigraphy of the field was being worked out (red, brown, dark blue, silver, etc.). Others, below the silver marker, were referred to by the letters A, B, C, and D because no additional colors were available to differentiate them. Traces of this usage remain in this report. Names of sandstones are based upon Jewett et al. (1968), as modified by Hulse (1978), Ebanks (1979), Staton, and Huffman.

Nomenclature of Mud rocks

The geological study uses *shale* in an informal sense that is common both in the oil industry and among professional geologists. Usage here does not differentiate between fissile or laminated rocks, which are strictly called clay- or mud shales, and non-fissile, non-laminated rocks which are given the suffix - stone. Clay and mud differ in particle size. Claystones and clay shales consist dominantly of clay (particles less than 4mm), whereas mudstones and mud shales consist of sub equal mixtures of clay particles and silt particles (4 to 62mm).

Contouring

Isopach maps of good quality reservoir sandstone, especially that in the B_3 and B_2 zone, were contoured to represent the geological interpretation of them as the result of deposition in a tidal estuary"-. These maps are presented in Figure D-6 and D-7, respectively.

Regional Geology

The valley-fill deposit that is productive on the Nelson Lease is in the Chelsea Sandstone member of the Cabaniss Formation (Jewett, et al., 1968), the lower part of the Skinner interval (younger than the Tebo Coal and older than the Scammon Coal; Staton, 1987), or the informal Cattlemans interval (Hulse, 1978). Rocks of the Cabaniss Formation are assigned to the Desmoinesian stage of the Middle Pennsylvanian Series. The Nelson Lease includes the SW/4 of Section 21, and the NW/4 of Section 28, Township 26 South, Range 21 East (Fig. D-1, D-2) and lies on the SW flank of the Bourbon Arch, a subtle structure that separates the Cherokee basin to the south from the Forest City basin to the north.

Both of these shallow basins lie in the marginal part of the craton of North America, on the shelf north of the Arkoma Basin, a foreland basin that, in turn, lies north of the Ouachita Tectonic Belt. The Ouachita belt was most active in the early and middle Pennsylvanian, with orogeny climaxing in Desmoinesian time, simultaneous with deposition of the Cherokee Group. Deposition in the Arkoma basin began in early Middle Pennsylvanian time (Atokan). Despite intense contemporary tectonic activity a few hundred kilometers to the south, sediments for the Cherokee Group appear to have come from sources that lay to the north and east.

The Cabaniss Formation consists mostly of shale, but includes beds of sandstone, coal, and limestone. In the area of the Nelson Lease, only the sandstones reach large thickness, with single sandstone lenses making up to 10 to 25 percent of the entire thickness of the Cabaniss Formation in many wells. Shale intervals are broken up by marker intervals, which are described below, into sequences 10 to 40 feet thick.

Previous descriptions

Operators of this field have divided the reservoir into informal A, B and C sandstone intervals (named from top to bottom). These intervals were defined primarily upon their depth, and the boundaries were drawn between them on the basis of shale interbeds that were approximately at the same elevation in adjacent wells. The A sand was not present in all parts of the field and was not productive of where it was found. The B sandstone was traced throughout the field and is perforated in most, if not all, productive wells. The C sandstone, as defined by the operators, is best developed in the eastern part of the _northern 1/4 section lease, but was correlated over the entire field area. The operator's C sand is the major productive sands in the most productive wells, and intervals that appeared to have C sand in them were perforated in many wells throughout the field.

Results of restudy of the field

The analysis presented below has used the same designations for the intervals containing sandstone in the reservoir (A, B, and C), but has defined them according to their age with respect to regional stratigraphic marker intervals, described below, which are more continuous than the shale breaks used by the earlier analysis. The C sandstone, as used in this study, is older than the Tebo marker interval and younger than the Weir-Pittsburg marker interval, although it locally is deposited in a valley that was eroded through the Weir-Pittsburg marker interval. The B interval post-dates the Tebo marker interval and predates the Scammon marker interval, but includes a valley-filling succession that is lower in elevation than the projected position of older markers down as far as the Abj coal (Harris, 1984). The most productive sandstones in the field, which were designated C by the operators, have been reassigned to the B interval, based upon their situation as part of the fill of that valley. The B interval has been subdivided into B_3, B_2, and B_1 zones (listed from bottom to top) to differentiate sandstones that formed during different parts of the history of valley filling. All of the oil production- in the field comes from beds designated as part of the B_2 and B_3 zones, according to revised correlations. Sandstones of the A interval are younger than the Scammon marker interval and older than the Mineral marker interval. Locally A sandstone beds are deposited in a shallow valley that cuts through the Scammon marker interval.

Regional marker intervals of the Cherokee Group

Regional marker intervals are characteristic of the Cherokee Group and other dominantly siliciclastic Pennsylvanian strata of eastern Kansas. Where these marker intervals are completely developed, they include, in ascending order, an underclay or paleosol, a coal bed, an argillaceous limestone or shelly sandstone, and a dark gray to -black shale (Fig. D-3). Commonly small concretions of siderite, called " birdshot siderite" are found in the strata just below the underclay. The strata containing siderite may be very light gray claystone or siltstone that has a bleached appearance and is tightly cemented.

Marker intervals can be correlated for distances of hundreds of kilometers, and from basin to basin on the shelf of the US interior. Some of those in the Cherokee can be correlated into Iowa and, across the Mississippi River Arch, into the Illinois Basin (Brenner, 1989; Coveney et at., 1987). Regional marker intervals may also correlate with markers that divide the Atokan and Desmoinesian succession in southwestern Kansas (Youle, 1993). Marker intervals have been successfully used to subdivide the Cherokee Group of Kansas, especially the Cabaniss Formation, and traced over southeastern and south-central Kansas (Killen, 1986; Staton 1987; Huffman, 1991) and into the Kansas City area. They are generally the stratigraphically equivalent to the coal beds used by Hulse (1978), Ebanks (1979), and Harris (1984), but are easier to correlate because they consist of a suite of lithologies, not all of which need to be present to establish the position of the marker interval. In characterizing reservoirs, as well as in other geological activities in the Cherokee section, these markers make possible a detailed stratigraphy and fine subdivision of the section into temporally distinct units (Fig. D-2, D-4). Marker intervals are 10 to 40 feet apart, for the most part, they are thus the most precise basis for correlation of Cherokee successions.

Marker intervals are remarkably recognizable in gamma ray-neutron logs. The underclay commonly washes out, which can be reflected in the caliper log. Underclays may also be depleted of potassium,

compared to other shales, and resemble shaley sandstone on the gamma ray log, while the neutron log shows a "high porosity" response (leftward deviation) to bound water in the clay. Underclays are almost invariably present beneath Pennsylvanian coals in Kansas, and commonly beneath dark shales where no coal is present. A gamma ray low and a neutron deflection toward the right (low apparent porosity) is common just below the underclay. This corresponds to the tightly cemented, apparently bleached shales or siltstones that contain birdshot siderite.

Coal beds by themselves have leftward neutron responses to the left because they contain abundant water and hydrogen. Coal has low gamma ray intensities, but the gamma ray response is commonly masked by overlying highly radioactive dark gray or black shales, which are actually more common and continuous than the coals.

Argillaceous limestone and sandstone beds are not common in the Savonburg NE Field area, and are generally very thin, so that their log response is masked. They are common in other parts of the Cherokee elsewhere in SE Kansas. Harris (1984) reports that about 50% of coal occurrences have overlying limestones in the Krebs Formation (lower Cherokee Group) in cores and in natural and artificial outcrops in Cherokee, Crawford, and Bourbon counties.

Dark shales, either dark gray or black and either massive or fissile, are the fourth member of the complete marker interval. They contain a concentration of uranium and organic matter, which makes their response strong on both the gamma ray and neutron sides, although the gamma ray response is the most marked. Dark shales of one type or the other are almost invariably present above thin limestones or sandstones, above coal where the limestones are not present, or above underclay, where both coal and thin limestones and sandstones are missing. In the Nelson lease, such shales were the most recognizable unit of marker intervals.

Sequence Stratigraphy

The paleosols and underclays of the marker successions represent subaerial exposure of the succession during periods of low relative sea level. Thus they meet the definition of boundaries of stratigraphic sequences (Van Wagoner et al., 1990). The overlying part of the marker successions (coal, limestone or sandstone, if present, and dark gray or black shale; Fig. D=3) are probably the-result- of deposition during a rise in relative sea level with accompanying landward _shift of :adjacent depositional environments. The successive environments would be subaerial coal swamp, erosional region (associated with passage of the shoreline and shoreface across the area, which may leave residual deposits), and deposition in a shelf environment in a stratified water column, respectively. Between the coal (or underclay if no coal is present) and the next overlying bed is a surface of initial transgression, marking the passage from non-marine to marine deposition. The dark gray shale or a gradationally overlying medium gray shale would represent the surface of maximum transgression for each sequence.

Strata in the interval between marker successions reflect filling of available accommodation space (space beneath local base level that is not already filled with sediment) during conditions of rising, steady, or falling sea level. All of the sediment above a particular marker interval is younger than all of the sediment beneath that marker interval, e.g. all of the sediments between the Tebo and Scammon marker intervals are older than all beds between the Scammon and Mineral markers, so that temporal ordering of inter marker intervals is unequivocal.

In the valley region in the eastern part of the NW/4 of Section 21, T26S R21E (filled by Chelsea Sandstone; Fig. D-2, D-4), and elsewhere wherever erosion has removed the sequence boundary, the boundary lies at the base of the erosive cut, commonly just below a sandstone or a conglomerate. The depth of incision of the Chelsea valley is sufficient to indicate that sea level fell below a shelf edge during its incision (van Wagoner et al., 1990).

Marker intervals in the Nelson Lease

In the lower and middle Cabaniss of the Nelson Lease, six regional marker intervals are present, correlated (from top to bottom) to "V" Shale -Croweburg Coal, the Mineral Coal, the Scammon Coal, the Tebo Coal, Weir-Pittsburg Coal, and the Bluejacket "A" coal (Fig. D-2, D-4). In addition, several characteristic kicks of the gamma-neutron logs carry across the field, or parts of it, and are useful as additional stratigraphic markers (Fig. D-4). The following section of the report describes the individual marker intervals present close to the reservoir sandstones in the Savonburg Field and correlates them into a regional framework developed by Harris (1984). The correlation is based upon a study of the Cherokee Group in the Bourbon Arch region by Huffman (1991). While this report uses a nomenclature for the marker intervals based upon existing correlations, it does point out a few places where correlations are questionable and possibly subject to revision. This section also describes other stratigraphic markers in the field, the stratigraphic position of sand bodies, including the reservoir sand body in the Chelsea Sandstone, and non-reservoir rocks between markers in the Nelson Lease.

Stratigraphic Succession in the Nelson Lease - Bluejacket A marker interval

The Bluejacket A marker interval consists of the Bluejacket A coal bed ("A" coal bed on logs used in this study) and overlying dark shale. The coal bed itself was penetrated in the core from well RW-8, where it was 0.8' thick. The presence of this coal bed is inferred from a spike of low gamma ray intensity and high neutron porosity occurs in all other wells that penetrate deeply enough . The designation of the Bluejacket A coal bed was introduced informally by Harris (1984) to distinguish one of several previously unrecognized coal beds between the Weir-Pittsburg and Dry Wood coals. Staton (1987) and Huffman (1991) did not fmd the Bluejacket A coal easy to correlate across the Cherokee basin and Bourbon arch areas.

The coal of the Bluejacket A marker is underlain by a poorly developed underclay that is the lowest 3. 1' of core RW-8. The underclay grades from laminated mudrock at the base, with vertical fractures filled with siderite and some slickensides, to mottled claystone with slickensides at the top. Above the Bluejacket A coal is less than 0.1' of very fine sandstone with pebbles of shale, siderite, and carbonaceous material, and medium gray streaked, burrowed shale that forms a small gamma peak. This shale bed was penetrated by the core of well 0-1 (Fig D-5C), where it consisted of 3' of dark gray laminated shale.- This dark gray shale is overlain directly by the silver marker.

Silver marker

The silver marker is a distinct kick to the right on the neutron log and moderate kick toward lower gamma ray values, compared to shales above and below. The top of this marker is 6 feet above the top of the Bluejacket A coal. The silver marker is present in the core RW-15, and its lower part is present in core 0-1 (Fig. D-5C),. In RW-15, it consists of 3.7' of near white, light gray and dark gray mudstone that is firmly cemented. Siderite concretions of mm-scale ('birdshot siderite") are common in it. It was originally wavy bedded or laminated, but has since been disturbed by the action of organisms. Its boundaries with dark gray clay beneath (part of the Bluejacket A marker interval) and medium gray claystone above are sharp.

In core RW-12, light gray shales of the silver marker are overlain by just over 1' of siltstone and very fine sandstone with disturbed bedding. This bed grades into 1.1' of poorly stratified, dark gray silty shale. In RW-15, the silver marker is again overlain by light to medium gray shale, here 0.5' of laminated clayey mudstone below and 0.8' of blocky, slickensided clay above. The upper contact of the slickensided clay is gradational with laminated olive medium gray claystone that becomes light gray at the top.

The succession from the silver marker to the dark gray or olive clay above it appears to be a marker interval that lacks a coal at this locality. It differs from the normal marker interval in that its dark gray clay overlies the underclay or paleosol component gradationally, rather than sharply. Correlation of this horizon, referred to below as the Silver marker interval, is problematical and is discussed further below.

Silver marker to light blue marker

Dark clays at the top of the silver marker interval grade into a succession characterized by decreasing gamma ray intensity and rightward-shifting neutron values upwards, followed by sharper shifts of the gamma ray and neutron curves toward values characteristic of shales. The succession is about 14' thick. In part this sequence reflects a coarsening- then fining-upward succession of dark gray to light gray, weakly laminated shale, light gray streaked and linsen-bedded shale, and light gray linsen- to wavy-bedded silty shale. The shaley part of the succession may contain a few fossils of fragmented plants, especially 1/4 of the way up.

Some of the log deflections may be related to tight cementation and presence of siderite, like those of the silver marker. Several parts of the upper 6.5' of this interval have beds with moderate to high concentrations of birdshot siderite. In such beds, disruption of bedding by root marks or brecciation is common, especially in the upper part of the bed, where it grades into the underclay beneath the overlying Weir-Pittsburg marker. Maximum deflection of gamma ray and neutron curves corresponds to a light gray or light olive gray, cemented layer with red, birdshot siderite concretions in cores 0-2, RW-7, RW-9 (Fig. D-5B), RW-10, RW-12, RW-15, and RW-16. The peak of this apparently upward coarsening upward succession lies about 16 feet above the top of the silver marker and was correlated as the dark blue marker. The topmost part of this sequence decreases in grain size to shale and changes from linsen-bedded to streaked with thin laminae of silt. It has higher gamma ray values and deflection to the left of the neutron curves.

Weir-Pittsburg marker interval

The Weir Pittsburg marker appears in logs as a prominent gamma-ray peak and the immediately underlying peak of a-neutron deflectionto the left; both have a sharp deflection below and a gradational one above, unless the overlying succession has been removed by erosion and the marker is overlain by a valley-filling succession. This marker is partially or completely present in cores from wells 0-3, RW-3, RW-6, RW-7, RW-9 (Fig. D-5B), RW-10, RW-12, and RW-16. This marker is very persistent, Harris (1984), - Staton (1987) and Huffman (1991) were able to trace it across southeastern Kansas. It is absent in part of the Nelson Lease where it is apparently truncated by erosion before deposition of the B or C sandstones. The Weir-Pittsburg marker generally lies a few feet above the dark blue marker and is 21 feet above the silver marker.

Generally, the Weir-Pittsburg marker consists of an underclay overlain by a dark gray shale. Coal, limestone, and sandstone are not present in any of the cores from this field, but bleached, sideritic, cemented light gray shale and siltstone is present in the dark blue marker beneath. The correlation with the Weir-Pittsburg Coal is based upon the work of Huffman (1991). Reasons why this correlation is only tentative are discussed below.

The underclay of the Weir-Pittsburg marker interval grades from the light gray, cemented, sideritic mudrocks of the underlying dark blue marker. No bedding is preserved in the underclay, but it is friable and breaks into chunks that are slickensided and show root marks. The clay has a waxy appearance. Fractures are filled with brecciated fragments of the bed itself. This bed is 3.3' thick where completely preserved in core RW-7. The dark gray to black shale (actually claystone) bed in the Weir-Pittsburg marker is 0.75' to 2' thick and is laminated. It includes some phosphatic concretions and, at least in one well, a bed of fossil shells and shell fragments. Dark gray to black shale grades into overlying beds of medium gray or olive medium gray shale of the Weir-Pittsburg--Tebo interval.

Weir-Pittsburg-Tebo interval and C Sandstone

Dark gray, fissile, phosphatic shales of the Weir-Pittsburg marker interval grade into medium gray shales then into an upwards-coarsening mudrock sequence that has birdshot siderite and disturbed bedding as widespread features. This sequence is remarkably like the silver and dark blue markers and like the development between the Tebo marker interval and the brown marker outside the channel area, as

described below. It is present in cores 0-3, RW-6, RW-7, RW-10, RW-11, RW-16, and RW-17. Core descriptions from Oil Field Research commonly describe the top of this succession as "light gray sandstone" . The total CU succession is about 6 feet thick. The shale bed is about two feet thick and is generally of an olive medium gray color. It is laminated and fissile. The coarser beds are shale and siltstone, apparently structureless, well indurated, and of light gray or perhaps olive light gray to very light gray color. They have disturbed bedding, root marks, and birdshot siderite in their upper part. Calcite cements may also be present. The top of this siltstone interval grades into the underclay at the base of the Tebo interval.

In the southeast corner of the southwest corner of section 21, T26S R21 E, the interval between the base of the Tebo marker and the top of the Weir-Pittsburg marker includes a sandstone bed up to 11 feet thick. It has an erosional base and cuts through the Weir-Pittsburg marker interval into the dark blue marker below. According to the usage in this report, this sandstone is the C sandstone. The C sandstone has a upward-fming log pattern on the gamma ray-neutron log. This sandstone was encountered in only a few wells and no cores are available. Some sandstone assigned to the Chelsea valley fill that postdates the Tebo marker interval might actually be older than the Tebo marker interval and actually part of the C sandstone. Only where the Tebo marker is present is it possible to differentiate the B and C sandstones unequivocally. Sandstone in deep part of the valley fill (wells H-27, H-30, KW-51, H-21, RW-8, K-44, H-16, KW-6, H-13) was mapped as part of the B_3 zone, rather than being incorporated into the laterally adjacent C sandstone because the trend of the valley, as defined by the truncations of markers was at right angles to that apparent trend of the C-sandstone.

Tebo Marker Interval

In cores RW-16 and RW-17, the Tebo marker interval is a coal bed about six inches thick that overlies a poorly developed underclay. This marker was also encountered in cores RW-4, RW-5, and RW 11. In all of these cores, the coal was overlain by sandstone or conglomerate**,** rather than black shale. Despite the lack of **a** dark shale in those wells, the Tebo marker interval is marked on their logs by a distinct kicks, with the neutron peak just above the gamma ray peak. In wells on the east bank of the Chelsea erosional valley, the Tebo appears to be overlain by a black shale that grades up into a upward-coarsening succession, because logs of those wells display a sharper gamma ray peak than the Tebo marker interval does in other wells on the Nelson lease.

The underclay is at least 1.3' thick in the cores of the Tebo marker interval, and is a mottled, medium to very light gray, very friable claystone that gradationally overlies the sideritic upward-coarsening succession described above. The coal is less than one foot thick. In one well, the coal is split by layer of sandstone 0.3' thick, in another, by a shale bed. In the core from RW-16, the Tebo coal is overlain by a thin (0.4") limy sandstone interval with rip ups and other intraclasts that passes up into medium gray laminated mudstone. The mudstone passes, over a thickness of a foot, to medium gray siltstone and then into wavy-bedded mudrock or very fine sandstone. The log from this well shows a stronger gamma ray peak than other occurrences of the Tebo marker interval.

Bluejacket A Coal through Tebo Marker Interval

Correlation. The Weir-Pittsburg and Tebo marker intervals, as defined above, correlate exactly to markers Huffrnan (1991) identified in the Yemon #54 Dotson well in the NW SW of Section 26, T26S R21E, about 2 miles east of the Nelson Lease in the Savonburg NE Oil Field. Huffman (1991) and Staton (1987) had correlated their nets of wells back to the Pittsburg and Midway #20 core (SE NE NE Section 8, T32S R22E in Cherokee County, Kansas), which includes all of the Cherokee except the few feet above the Breezy Hill Limestone (Fig. D-2). Harris (1984) described this core and identified several key beds in it. Because Huffinan's and Staton's correlations appear consistent and are already available, they are used in this report.

However, it is suspected that the correlation is incorrect with regard to the Tebo and Weir-Pittsburg coals. The marker called Weir-Pittsburg in this study normally has a phosphatic dark gray to black shale, similar to the shale assigned to the Tebo marker interval elsewhere, but no coal, whereas the Weir-Pittsburg

is dependably a mineable coal with no black shale just 30 miles to the east, near the outcrop in Crawford County. It is suspected that the marker called "Weir-Pittsburg" in this study is actually includes the horizon of the Tebo Coal Bed.

If this is true, the identity of the marker called Tebo (i.e. the green marker) in this study then becomes a problem. However, Harris (oral comm., 1983) found that the Tebo coal is commonly split into two beds. For an example of this, see Harris's (1984, p. A-45) description of the P&M #21 core. It is possible that both markers (Weir-Pittsburg and Tebo, as referred to in this study) should be correlated with the Tebo. Unfortunately, where the Tebo is split into two beds elsewhere, the beds are generally not separated by as much section, 13 feet, as they are here.

Making the light blue marker part of the Tebo requires that another bed be the Weir-Pittsburg. It is possible that the silver marker is actually the Weir-Pittsburg horizon, with a well-developed paleosol and underclay, but no coal and little black shale. Final judgment on exact identity of beds awaits re-evaluation of Huffman's (1991) and Staton's (1987) correlations with the P&M 20 core. For the meantime, I have used their nomenclature.

Spacing between the Marker Intervals

Generally the spacing between the markers, especially the upper markers in the succession, vary from well to well. That is not true of the spacing between the Tebo marker interval, the Weir-Pittsburg marker interval, and silver marker and the Bluejacket A coal bed. Wherever the Bluejacket A coal bed and the silver markers are both present in a well, it is six feet from the top of the A bed to the top of the silver marker. The Weir-Pittsburg marker (defined as the cross-over from high neutron values (leftward deflection) to high gamma values) lies 21 feet **above** the top of the silver marker. Thirteen feet separates the Weir-Pittsburg marker from the Tebo marker, again defined as the crossover from high neutron to high gamma values. These distances serve as very reliable guides in reconstructing the depth of erosion of th**e** valley now filled by the B_2 and B_3 sands and to projecting the depth of an underlying marker not penetrated by the drill.

The Reservoir Interval, the B_2 B_3 Interval

The reservoir interval is younger than the Tebo marker interval and older than the brown marker. It appears to be part of the fill of a valley cut through the Tebo and Weir-Pittsburg marker intervals, the dark blue marker, and, in places, the silver marker into the top of the Bluejacket A coal bed (Fig. D-2, D-4). Lithology of the valley-filling succession is complex. It consists of three basic lithologies: sandstones; interbedded sandstones, siltstones, and shales; and shales. It can be divided into two separate units, referred to here as the B_2 and B_3 zones. Stratigraphy and lithology of the reservoir interval are described below.

At places along the eastern side of the Nelson lease, the wall of the valley is preserved. Beds that predate cutting of the valley, but post -date the Tebo marker interval, are encountered in wells K-34, K-35, K-36, and K-37 (Fig. D-2, D-4). The succession in these wells has a log character like that of the coarsening upward successions between the Silver and Weir-Pittsburg markers and the Weir-Pittsburg and Tebo markers. No cores penetrate these rocks, but they are believed to be similar to the other successions with the same log character. If so, they would consist of medium gray shale and streaked shale grading into medium to light gray shale and siltstone, with linsen-, wavy- and ripple bedding. Their log character suggests that they have the same kind of siderite cement as the upper parts of the similar successions. While these beds lie between the Tebo marker interval and the brown marker, it may be interpreted as being slightly older than the valley-filling succession that lies between the same markers and is the main reservoir interval in the field. The western edge of their distribution marks the eastern margin of the valley succession.

East - West cross sections were developed presenting the B_2 and B_3 zones and their continuity. These cross sections are presented in Appendix D.

Brown Marker

The brown marker overlies the reservoir interval. Of the markers recognized in this field, this is the most difficult to identify and trace. It was recognized as a distinct, but neither sharp nor very high, gamma ray maximum that occurs below the Scammon marker interval and above reservoir sandstones and interbedded sandstones, siltstones and shales of the B_2 and B_3 intervals. However, this marker is not identifiable on logs from all wells and is well developed in only a few. In many wells, the brown marker was placed at the top of a sequence of interbedded sandstones, siltstones, and shales, and below a sequence of shale several feet thick. The brown marker was identified in cores 0-1 (Fig. D-5C), RW-6 and RW-7. In those cores, it consists an interval of gray shale, which may contain pyrite concretions or plant fragments and is distinctly darker than overlying or underlying shales, although not very dark gray or black. It lacked any hint of development of coal, underclay, limestone, dark gray to black shale, or siderite-cemented, upward-coarsening sequence, which are all parts of the regional marker intervals as described in this report, and it is not known to extend beyond the boundaries of this field. It does, however, extend into wells along the east side of the Nelson lease where the valley-fill succession is not present and the interval above the Tebo marker interval has upward-coarsening character. This provides precise age control on the valley fill.

Brown Marker to Scammon Marker Interval, the B_1 Zone

The interval between the brown and Scammon markers contains light gray to medium gray shale at most places with moderate to extensive development of birdshot siderite and an underclay beneath the Scammon Coal Bed. The interval is 5 to 20' thick and is especially well developed above the deepest part of the Chelsea valley in the eastern part of the SW/4 of section 21. In RW-6, shales in this interval are at least 9.9 feet thick and consist of an upward-coarsening succession of clayshale and mudshale, with intense mottling and slickensides at the top. Shales contain pyritized plant remains and birdshot siderite. Siderite commonly is associated with near-vertical features that may be rhizocretions or expansion-contraction cracks related to drying during exposure at the earth's surface and soil formation. In RW-8, =20 feet of shale are present above the top of interbedded sandstone, siltstone, and shale of the B_2 zone; including a well developed underclay that probably is part of the Scammon marker interval. All of this shale has been assigned to the B_1 zone. The remarkable feature of this zone in RW-8 is the vertical fracture lined with birdshot siderite that reaches 20 feet down from the pre-Scammon underclay.

There is little development of sandstone between the brown marker and the Scammon marker interval, except in the southwestern part of the field. In the northwest corner of section 28, T26S R21E, sandstone reaches a thickness of over 10' between these markers. No preserved cores contain this sandstone. It does not appear to be productive.

Scammon Marker Interval

The Scammon marker interval includes the Scammon coal; an underlying underclay and an overlying dark shale. Birdshot siderite is common in the shales beneath the underclay, but the underlying succession does not display the nicely defined decrease in natural gamma-radiation and rightward deflection of the neutron log. However, a sharp, but low, rightward neutron kick in logs of some wells between the coal and overlying dark gray shale probably indicates a limestone. Many of Harris's (1984) descriptions of cores from the upper Cherokee in Crawford and Cherokee counties, Kansas, show a limestone above the Scammon Coal.

The Scammon marker interval is present in cores 0-1 (Fig. D-5C), RW-4, and RW-8. The Scammon Coal Bed is the among the thickest cored in the Nelson leases, reaching 1.5' in core RW-4. The Scammon marker interval is present in most wells, but has been partly to completely removed by erosion preceding deposition of the overlying "A" sandstone in one well, H-17, in the center of the E 1/2 of the SW 1/4 of section 21, and the coal has been removed in both RW-4 and RW-8, where underclay is overlain by sandstone. Dark shale of the Scammon marker interval is rather thin and not highly radioactive. It is commonly a foot or less thick.

The Overlying Section - Scammon-Mineral Interval

Between the Scammon marker interval and the overlying Mineral marker interval is a sequence of shale, with some sandstone. This interval was designated as the "A" sandstone by the operators of the field. It contains sand along the eastern margin and in the center of the field, both in the SW 1/4 of section 21. This sand shows a distinct upward-fining pattern where it is thick enough that the gamma ray curve can be interpreted to show a pattern. In this interval, core RW-8 encountered 3.7' of light olive tan, fine, structureless sandstone, with a few inches of very fine to fine sandstone at the base. No other cores sampled this interval. This sandstone fills a shallow valley eroded through the Scammon marker in well H-17, and sandstone overlies the sub-Scammon underclay in several wells in the valley region in the east or southeast center of the SW/4 of section 21, T26S, R21E.

Mineral Marker Interval

The Mineral marker interval includes the Mineral Coal and an overlying dark shale. In many wells the dark shale is not present, so the Mineral coal is marked by a kick to the left on both the neutron and gamma logs. In other wells, it has a thin dark shale immediately above it. The dark shale may have additional spikes of high gamma count, making a gamma kick up to about five feet thick. This marker lies 15 to 30 feet below the "V" shale marker and is present in nearly all wells in the Nelson Lease. In core RW-6, the Mineral marker interval included 2.3' of coal overlain by 2' of fissile, very dark gray claystone with streaks of silt in places and 0.5' of light gray, laminated shale.

Red marker

The red marker is a sharp neutron kick to the right and lower gamma kick about 10 to 20 feet below the "V"-shale marker. In some wells, the red marker appears to be similar to, but not as well developed as, the dark blue marker, which is an upward-coarsening succession with siderite cement in the upper part. In some wells, one or more sharp kicks on gamma-ray or neutron are present above and below the red marker. The red marker is a persistent, but is not attributable to any horizon previously identified regional marker, although Jewett et al. (1968) and Harris (1984) have identified the Flemming and Robinson Branch coals between the Mineral Coal and the "V" shale.

"V" Shale marker interval

The most persistent and easily identified marker in the upper Cherokee is the "V" shale marker, which includes the associated beds of the Croweburg Coal, with its underclay and a very persistent black shale. This succession is overlain-by the Verdigris (or Ardmore) Limestone, which occupies the position of a regressive limestone in limestone-shale cyclothems of the later Desmoinesian, Missourian, or lower Virgillian. Brenner (1989) referred the interval between the Croweburg Coal and the top of the Verdigris (Ardmore) Limestone to the Verdigris Formation. This marker succession is easily correlated into Iowa, where the black shale is called the Oakley Shale and the coal is called the Whitebreast Coal (Brenner, 1989). Schlinsog and Angino (1983) called this dark shale the "V" shale in southeastern Kansas.

Extent of Marker Intervals in the Nelson Lease

The Tebo and Weir-Pittsburg marker intervals and the dark blue and silver markers do not extend all the way across the Nelson Lease (Fig. D-2, D-4). Because some of these markers are regional in their extent, their local absence must be explained. The absences of marker beds form a pattern in which the lowest one, the silver marker, has a small area from which it is absent and subsequent overlying markers have progressively greater areas of absence. The most consistent interpretation of this pattern is that an erosional valley that developed after deposition of the Tebo marker interval, and cut through to the level of the silver marker or below (in places).

As pointed out above, the brown marker extends on to the bank of the valley, as defined by the presence of the Tebo marker and an upward-coarsening succession above it, which implies that the cutting took place before deposition of the brown marker. Sand and mud filled the valley before accumulation of

the brown and younger markers, although a depression may have been left or developed by differential compaction after deposition of the brown marker.

Valley-fill **Succession and Reservoir Sandstones**

Reservoir sandstones of the Nelson Lease are part of a lithologically complex interval that lies stratigraphically between the Tebo marker interval and the brown marker (Fig. D-4). It includes a valley fill that is set into the underlying beds as far down as the Bluejacket A coal, but not the upward-coarsening succession of slightly older (but still post-Tebo) age found in wells K-34-37, in the bank of the valley. In addition to sandstones ranging from a few cm to over 10 m thick, this succession includes interbeds (called mixed lithologies or interbedded lithologies) of shale, siltstone, and sandstone on a scale of mm to dm, and beds of shale that are up to a few meters thick.

This interval can be divided fairly unequivocally into B_2 and B_3 zones, because a discontinuous horizon of conglomerate or a sharp increase of grainsize can be correlated from well to well across the lease, marking the base of the upper, or B_2 zone (Fig. D-4, D-5). In most wells, an interval of shale or mixed lithology lies at the top of the B_3 zone. This change is noted in preserved cores, and can be inferred in several of the core descriptions prepared by Oil Field Research. The B_3 zone fills the deepest part of the erosional valley in the eastern 1/2 of the SW/4 of section 21 and extends westward and southwestward across much of the lease. The B_3 zone includes the thickest and most productive sandstones in the study area. Thickness of the entire B_3 interval ranges up to 54 feet. The B_2 zone is more sheet-like and sandstone bodies in it are also thinner and more laterally extensive. However, they have distinctly less productive capability than the B_3 sandstones, although a small area in the NW part of the field in section 21 has recoverable oil results suggesting possible future development may be warranted.

Component Lithologies - Sandstone

Two types of sandstone that may have good reservoir properties are present in the Chelsea Sandstone, reservoir interval in the Nelson leases. Generally, structureless sandstones, with some rippled or laminated intervals, are present in the B_3 zone and B_2 sandstones are structured with ripples and some laminated intervals. Some B_2 sandstones do contain structureless intervals. Not all such sandstones are good reservoir, however, because some contain dead oil with initial saturations of greater than 50%;- bid no recoverable oil and zero effective permeability at residual oil saturation.

It is possible to recognize sandstone with good reservoir properties in the B_3 and B_2 intervals from the gamma ray pattern developed on logs, even on the unscaled logs available for this study (Fig. D-4). Good reservoir quality sandstones had sharp deflections and did not appear to be broken into thinner intervals by shale, because the gamma ray curve was consistently below the 50% deflection line that differentiated sandstone and shale. Mixed lithologies, such as those described below, have higher and more irregular gamma ray readings than the good reservoir sandstone. This difference permitted differentiation of good reservoir sandstones in logs of wells for which cores are no longer available.

Both structureless and structured sandstone commonly have conglomerates or conglomeratic sandstone at their base and may have one or more conglomeratic horizons above the base. Thickness of conglomeratic beds ranges from a few inches to several feet. Pebbles, cobbles and boulders are intraclasts of siltstone and concretions, with coalified fossil wood also present.

Structureless Sandstone

Structureless sandstones are especially common in the B_3 interval, in the paleovalley in the eastern part of the SW/4 of section 21. These sandstones are displayed in cores 0-1 (Fig. D-5C), RW-1, and RW-8. Good quality B_3 sandstone is up to 35 feet thick in the core from well RW-8, which is in the valley center. Thickness decreases rapidly to the east and west of the axis of the valley and varies somewhat along the valley trend. The rock is heavily oil stained. For the most part, bedding is absent or so subtle that it is not detectable during description of core that has not been slabbed. Broken surfaces of the core are irregular or hackly with no tendency to have smooth, angled, or undulating surfaces, as beds with

sedimentary structures would. Mica flakes show neither strongly preferred orientation nor concentration into zones. A few intervals of this sandstone, a few feet thick at most, do display ripples and lamination. The sandstone contains a few plant fossils.

The base of the good, structureless sandstone, although sharp and apparently erosive, is not necessarily the base of the erosional valley. In cores from both RW-8 and 0-1 (Fig. D-5C), which are the best ones from the deep valley fill, the base of such sandstone lies several feet above the base of the valley fill, above a conglomerate bed and an interval of mixed lithology. The top of the good structureless sandstone of the B_3 interval in the valley fill grades into overlying successions of mixed litho logy.

In the NE/4 of the NW/4 of section 28, the deep channel of the eastern part of the SW/4 of section 21 broadens, becomes less deeply incised, and contains thinner, less productive sandstones. Cores RW-13, RW-14, and RW-17 are from this area. B_3 sandstone reaches 16 feet thick in this area, and is mostly not structured, although beds do contain intervals of rippled, laminated, or cross-bedded sandstone. The base of sand beds and intervals within them contain mud intraclasts, in some places these are common enough to make the rock a conglomerate. Beds of structureless B_3 sandstone in this area have sharp, possibly erosive bases and gradational tops. They are overlain by interbeds of sandstone, siltstone, and shale.

West of the deepest part of the valley, in the center and south center of the SW/4 of section 21 and extending into the NW/4 NW/4 of section 28, B_3 sandstones are thinner, more laterally extensive, and not as productive. Cores are available from wells 0-2, RW-7, and RW-15. Sandstone beds in this region is up to 15 feet thick and generally very fine grained and structureless. Sand beds may have coarser intervals with sharp bases at the base and within them, dividing the overall succession into units 5 to 10 feet thick. Coarser intervals at the base of units of the succession may be coarser sand (fine or on the border of fine and medium) or they may be conglomerates containing intraclasts of granule to boulder size. Conglomerates are up to 2.5 feet thick and may contain siderite cement. Coalified wood fragments are common in conglomerates and in parts of the section immediately overlying conglomerates but are scattered throughout sandstone beds. Some relatively thin intervals of the sandstone are laminated or rippled. Calcite cement is present in a few places.

Rippled Sandstone

Sandstones of the B_2 zone, in contrast, generally display clear ripple cross-lamination, plane lamination, small-scale to medium-scale cross-bedding, or other sedimentary structures. They have sharp bases and their lower few feet are commonly conglomeratic or slightly coarser grained-fine to very fine sandstone as opposed to the very fine sandstone above. Conglomerate clasts are intraclasts of mudrock. Internally, structured sandstones of the B_2 zone are very fine micaceous sandstones. B_2 sandstones grade upward into interbeds of sandstone, siltstone, and clay. Beds of sand range up to nearly 17 feet thick, but generally are thinner, commonly less than 10 feet thick. Layers of wavy-bedded sandstone and mudrock may break them into packages a few feet thick. Coalified wood fragments are present and may be common in B2 sandstones; macerated plant debris commonly defines bedding in ripple marked or plane laminated intervals. Birdshot siderite is present in bands and layers in many occurrences of B_2 sandstone.

Structured sandstones of the B_2 zone are thickest, up to nearly 17 feet, in the valley region in the eastern part of the SW/4 of section 21. Cores 0-1 (Fig. D-5C), RW-1, RW-3, RW-6, and RW-8 are all that part of the field. Several of the sandstones in the B_2 interval in the valley region are partially to completely saturated with "dead" oil. These beds have no recoverable oil, despite measured saturations of over 50%, and no permeability to water at residual oil saturation. Not only are they not reservoir, but they are barriers to movement of fluids through the sand.

In the NW/4 SW/4 of section 21, west of the main valley trend and in the northwest corner of the Nelson Lease, several wells encountered thick, potentially productive sandstone in the B_2 interval. Average recoverable oil saturations reach 2000 bbls per acre in wells RW-4, RW-5, RW-7, and RW-11, for which cores are available. Sandstones in this region may exceed 15 feet in thickness, but are commonly less than 10 feet thick. They are rippled very fine sandstones with a few silty partings. Macerated organic debris and mica fragments mark bedding surfaces. Some intervals, up to a few feet thick, are actually

wavy-bedded intercalations of sandstone and mudrocks. Intervals of parallel-laminated intercalations of macerated plant debris and sandstone and intervals of wavy bedded sandstone and shale divide thicker sand-rich successions into intervals a few feet to several feet thick. Such intercalations have gradational bases and tops.

Sandstones are also found in the B_2 zone in the center of the SW/4 of section 21 and in the northern part of the NW/4 of section 28. Cores RW-9 (Fig. D-5B) and RW-12 represent the center of the SW/4 of section 21 while cores from wells 0-2, 0-3, RW-13, RW-14, RW-15, and RW-17 are from the northern part of the NW/4 of section 28. Cores RW-16 and RW-18 represent accumulation of the B_2 zpne in a erosional remnant left between arms of the Chelsea valley.

In the RW-8 core, B_3 sandstone had recoverable oil of a few hundred barrels per acre-foot and total recoverable oil of 5500 bbls per acre, according to core analyses conducted by Oil Field Research in Chanute, Kansas. Wells developed in this sand where it lies in the paleovalley of the E 1/2 of the SW 1/4 of Section 21 have produced 10,000 to over 20,000 bbls of oil during water flood operations and may have produced for long periods before the water flood was installed in the area.

Interbedded sandstone, siltstone, and shale (mixed lithologies)

A characteristic suite of lithologies in the B_2 and B_3 zones of the Chelsea valley fill of the Nelson Lease comprises rippled very fine sandstones and siltstones, linsen- and wavy-bedded sandstones and mudrocks, and shale, including structureless mudrock, laminated shale, and streaked shale. In such sequences, the predominant lithology is wavy-bedded sandstone, siltstone, and shale, with linsen-bedded shale and siltstone second in importance. Burrowing is common but by no means sufficient to destroy the primary lamination of the sediment. Sandstone beds in most such successions are subordinate in abundance, but they are a plurality or a majority of the beds in some wells. They can be described as very fine grained, rippled, and tan, although some sandstone beds are apparently structureless or contain parallel lamination. Some sandstones contain a few shaley intraclasts or mud flasers. Sandstones commonly contain carbonaceous debris on lamina surfaces and may be sparsely burrowed.

In this suite, lithologies are interstratified at two scales. At the larger scale, the sequence is thin to medium bedded, with beds a several cm to a few dm thick. Rippled very fine sandstone and siltstone in beds several cm to a few tens of cm thick alternate with similarly thick beds of either interbedded shale and wavy- or linsen-bedded siltstone or beds of shale alone. At the smaller scale of interstratification, in wavy or linsen-bedded sequences, laminae of silt, sand, or shale are less than one mm to one cm thick and form coarse-fine alternations.

Characteristic of these rocks are gradational boundaries between beds in which rocks of different grain size prevail. This describes the beds at the several cm to a few dm scale, not the mm to cm laminations within wavy-bedded successions or streaked shales. Examples of such changes are from a bed where sandstone or siltstone predominates to one where linsen or wavy bedding is common or from a linsen- and wavy-bedded interval to shale. It is important to note that sharp-based sequences, progressively grading from coarse lithology (fine sand or conglomerate) to finer grained lithology (very fine sandstone to siltstone to mudrocks) are not common in interbedded intervals, although they are present.

Interbeds of sandstone, siltstone, and shale are found in both the B_2 and B_3 zones. Wells 0-1 (Fig. D-5C), RW-3 and RW-8 represent the B_3 zone in the valley fill of the eastern part of the SW/4 of section 21. Commonly, a zone of interbeds overlies a thin sandstone or conglomeratic bed at the base of the valley fill. Such intervals are a few feet thick. In well RW-8 for example, the interbedded succession, 9 feet thick, at the base of the valley fill is overlain by structureless reservoir sandstone of excellent quality. Elsewhere, notably in wells KW-10, KW-11, RW-9 (Fig. D-5B), and RW-12, the entire B_3 zone is composed of such interbeds. The B_3 zone is 28 and 21 feet thick, respectively, in KW-10 and KW-11 which lie in the Chelsea valley. Logs of wells containing mixed lithologies show an irregular pattern, indicating interbedding at about the scale of resolution or finer. Cores from RW-9 (Fig. D-5B) and RW-12 confirm the lack of good quality sand in the B_3 interval, but they lie on an erosional remnant between the eastern valley and the western patch of B_3 sand. A similar set of thin to medium interbeds of sandstone, siltstone, and shale

occurs in core RW-14 from along the western side of the eastern branch of the Chelsea valley in the NE/4 of the NW/4 of section 28 and in the core from well 0-2 in the NW/4 of the NW/4 of section 28. Log patterns indicate that the upper 5 to 15 feet of the B_3 zone throughout its extent is composed of interbeds of sandstone, siltstone, and shale.

Interbedded successions of sandstone, siltstone, and clay are common in the B_2 zone as well, but they are generally absent from the bottom of that succession, because the base of the B_2 zone was generally placed at a sharp increase in grain size from the underlying B_3 zone. Some B_2 successions, however, consist of a thin conglomerate and a few feet (1 or 2 feet) of fine to very fine sandstone above it with and then interbedded successions above that range to over 20 feet thick. Elsewhere, the bulk of the B_2 succession is rippled sandstone, as described above, and only the upper few to several feet is interbedded lithologies. Contacts between thick beds of rippled sandstone and overlying interbedded successions are gradational in all occurrences.

Cores from wells RW-3, RW-6, and RW-8 contain interbedded lithologies in the B_2 zone from the region where the Chelsea valley is best developed, in the eastern half of the SW/4 of section 21. Interbedded sequences in the B_2 zone range from 4 to 18.9 feet thick in these wells, and are divided into beds 0.1 to 2.6 feet thick. Some of the thicker sandstone beds have scoured bases.

RW-2, RW-4, RW-10, and RW-19 display interbedded lithologies from the west part of the productive area in the SW/4 of section 21. Interbedded successions range from 9.5 to 16 feet. Sandstone occurs in beds from a few tenths of a foot to 6 feet thick, with thickest beds at the base of the B_2 zone. The thicker of these sandstone beds, over about 2-3 feet thick, might be separated from the mixed lithology successions and considered as individual sandstones. Sandstone is very fine grained, except at the base of the B_2 zone, where. conglomeratic sandstone or conglomerate up to 0.9 feet thick may be present. Sandstone layers are rippled, inter laminated with mica and macerated organic matter, or structureless. Shale strata range from laminae to over 1 foot thick. They are streaked with sand or silt and may be burrowed. Large plant fragments are present in some beds.

The main Chelsea valley occupies two branches in the northern part of the NW/4 of section 28. Cores from wells 0-2, 0-3, and RW-15 contain interbedded lithologies in the B_2 zone above western branch, while 0-4, RW-13, and RW-14 sample that zone overlying the eastern branch. In this area, interbedded lithologies may reach a total thickness of 8 to 21 feet, including beds of shale up to 1.8 feet thick and wavy-or linsen-bedded sandstone and siltstone up to 5.7 feet thick. Wavy- or linsen-bedded successions display variation in the proportion of sandstone or siltstone ripples to intervening mudstone drapes on a scale of several inches to a foot. Shale beds are commonly laminated, or contain streaks or lenses of sand or silt. Interbedded sequences in this part of the field contain sparse burrows, large plant fossils, and macerated plant debris, which is common on bedding surfaces. A series of upward fining beds of siltstone and shale, including linsen-bedded and streaked shale is present in RW-15. In 0-2, an associated bed four feet thick consists of inter laminations of fine sandstone and macerated organic matter with mica.

RW-16 represents deposition of interbedded lithologies on the divide between the two branches of the Chelsea valley in the NW/4 of section 28. The B_2 zone is 17 feet thick and contains at least 5 feet of good sand at the top. The basal foot is pebbly sandstone, and the overlying 9 feet is interbedded sandstone, sandstone, siltstone and shale. Wavy-bedded sandstone is in beds some 2 feet thick, streaked shales are in beds 0.6 to 1.5 feet thick, laminated shales in beds 0.5 to 0.8 feet thick, and rippled sandstones in beds some 0.5 feet thick. Siderite is present in some beds.

Parallel-Bedded Sandstone and Organic Matter

Several cores from the B_2 zone (0-2, RW-6, and RW-8) contain distinctive successions of parallel stratified inter laminations of fine to very fine sand and organic matter, with mica. Laminae are on the mm scale. Sand laminae either display little in the way of sedimentary structures or the inter laminations may be wavy-bedded. Parallel-bedded sandstone and organic matter may be interbedded with rippled successions. Interlaminated successions range up to 6.7 feet thick.

Shale

Shale is a common component of the fill of the Chelsea valley in both the B_2 and B_3 zones. Much of it occurs intimately interstratified with silt and sandstone or as flasers or other inclusions in coarser rocks, as described above. In addition there are beds of shale about 2 feet to 11 feet thick in the succession. Such beds are most common in the upper part of either of the two zones, where they represent the culmination of gradational sequences from conglomerate or sandstone through interstratified lithologies. Shale beds are thickest in the area of the deep part of the Chelsea valley fill in the eastern part of the SW/4 of section 21.

Shale ranges over the gamut from mudstone and mudshale, which have subequal amounts of silt and clay, through claystone and clayshale. Shales in the B_2 and B_3 zones range from very light gray to dark gray, in places with an olive cast to the color. The range of shale lithologies includes laminated or bedded shales, structureless shales, streaked shales, with laminae of silt or sand as thin as a grain or two thick, and linsen-bedded shales, with scattered lenses of silt or sand. Generally, shale intervals at the top of both the B_2 or B_3 zones of the valley fill grade finer upwards, from linsen-bedded to streaked to laminated or structureless. Some cores of apparently structureless shale break easily along planar surfaces that parallel bedding in nearby rocks and indicate that the shale is stratified, although layering may not be visible because of fine grain size and little or no contrast between adjacent beds.

Shales contain fossilized plant material, either macerated or as pieces that may be larger than the diameter of NX core. Shale beds are commonly bioturbated normally in particular zones. Rarely are primary bedding structures in them completely destroyed by burrowing. Shale commonly contains pyrite, especially in the form of pyritized plant remains, and birdshot siderite, which may be in beds or may follow vertical structures that appear to be related to soil formation in overlying strata.

Tidal Features

Intervals of interbedded sandstone, siltstone, and shale display several features indicative of deposition by tidal currents. The most prominent is gradational alternations of thickness of sand laminae in wavy- and linsen-bedded intervals. These variations occur over intervals of several centimeter. Detailed counting of beds has not been attempted, and none of the intervals of wavy- and linsen-bedded siltstone and shale that have been examined had obvious periodicity of bed thickness of 14 or 28, which may form from-diurnal or semi-diurnal tidal frequencies. Despite the lack of the compelling periodicity in thickness variation, the interval shows repeated rapid variations of current intensity, both fine-coarse alternations at the scale of mm to one cm and bed thickness variations at the scale of several cm it a few dm. Such variations are characteristic of tidal environments.

The sequences of varying thickness of bedding are also unlike wave-rippled sequences because they do not have scoured basal surfaces and thin dm-scale fining-upward sequences that are produced by storms. Individual thin laminae in linsen-bedded intervals can be traced across the entire width of the core, which is also a common feature of tidal deposition during the neap part of the tidal cycle, when deposition takes place from suspension and each successive current from the rising and falling tide does leads to accumulation without erosion of previous deposits. Boundaries between laminae are commonly thin, continuous layers of mica and carbonaceous trash, which imply cessation of current activity between depositional events. Current ripples from river deposits or other sites of activity of unidirectional currents, on the other hand, have macerated plant debris in troughs and part way up the foresets, where they are trapped in eddies rather than deposited during pauses of current activity.

Interbeds of wavy- and linsen-bedded sandstone, siltstone, and shale with shale, of possible tidal origin, are common in the B_2 zone. As a result, the B_2 zone is interpreted as a series of tidal sand bars with intervening tidal flat or mud bank deposits. Tidal indicators are also present in the mixed lithologies of the B_3 zone.

Another characteristic lithology in the Nelson Lease is best understood if it is assigned to formation by tidal activity. Sandstone interlaminated with organic matter and mica, which may make up units a few

m thick, are unlikely to be the result of accumulation in flow-regime bed forms, because the rapid fluctuation from conditions where plant debris and mica would accumulate to those where plane beds of very fine sand are deposited seems unlikely, especially with no evidence of erosion between depositional events. Tidal ebb and flood cycles, with periods of slack water, seem to be a more likely explanation. Again, no obvious 14- or 28-bed cyclicity was noted during core description. Tidal deposits of interlaminated sandstone and organic matter, like tidal deposits of very fine sandstone, siltstone, and shale, are not rocks of reservoir quality.

Shapes of Sand Bodies

In drawing cross sections of the B_3 and B_2 intervals, it was necessary to depict the shape of the sandstone bodies. They could be either channels, which are convex downward with a broad, relatively flat top, or bars, with a convex upward top and a bottom conforming to the pre-existing surface. Which configuration one chooses has considerable significance in terms of the continuity of the reservoir. In this report, sandbodies in the B_2 interval are depicted as bars for several reasons. First, the B_2 interval commonly overlies a rather flat, apparently erosional surface, and the sand accumulations are of smaller scale than the width of the valley (Fig. D-4, D-7). Above this apparent erosion surface, even where thick sandstones were absent, thin layers of conglomerate and sandstone are present at the base of the interval. Tidal features, listed above, in the mixed lithology intervals suggest tides were important processes in depositing these sediments. The shape of the sediment accumulation in the B_2 zone is similar to an estuary, which is a common environment where tidal processes are important today. Tidal estuaries often contain **convex** upward sand bars, which form elongate, irregular mounds. Choosing to make the accumulations of sand in the B_2 interval convex-upward bars avoided the necessity of inferring large quantities of sand in areas between wells, where no available evidence bore on the shape of sand bodies.

Diagenesis

Ten thin sections were cut from several different layers of the B sandstone interval. These have been only cursorily examined. They show development of three minerals that are of significance for recovery efforts in the Nelson Lease. Two of these are iron carbonates, siderite ($FeCO_3$) and ankerite $Ca(Mg,FeXCO_3)_2$. Iron may be released from these minerals during acidification of wells or other recovery operations, and be oxidized to form iron hydroxide, an insoluble precipitate. Particles of iron hydroxide may migrate to pore throats, where the plates of iron hydroxide can be trapped, blocking the pore.

The other mineral is kaolin, $A1_2Si_2O_1o(OH')_8$. Kaolin is a clay mineral that forms accumulations of flaky particles in pores. During recovery operations, the clay particles may be moved to pore throats, blocking them. The sandstone also contains pyrite, which may oxidize during recovery operations and provide an important source of iron.

Appendix B

H-1

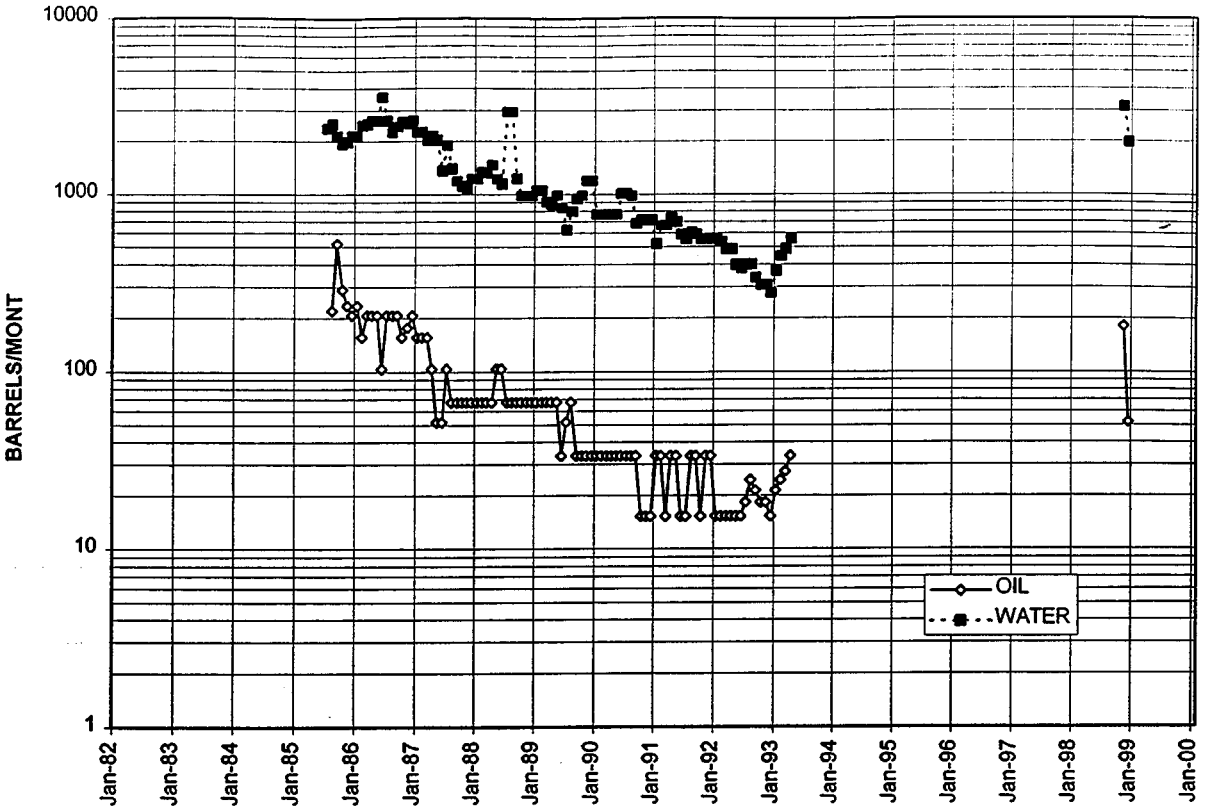
10000
1000
100
10
1
BARRELS/MONT
OIL
WATER
Jan-82
Jan-83
Jan-84
Jan-85
Jan-86
Jan-87
Jan-88
Jan-89
Jan-90
Jan-91
Jan-92
Jan-93
Jan-94
Jan-95
Jan-96
Jan-97
Jan-98
Jan-99
Jan-00

H-1

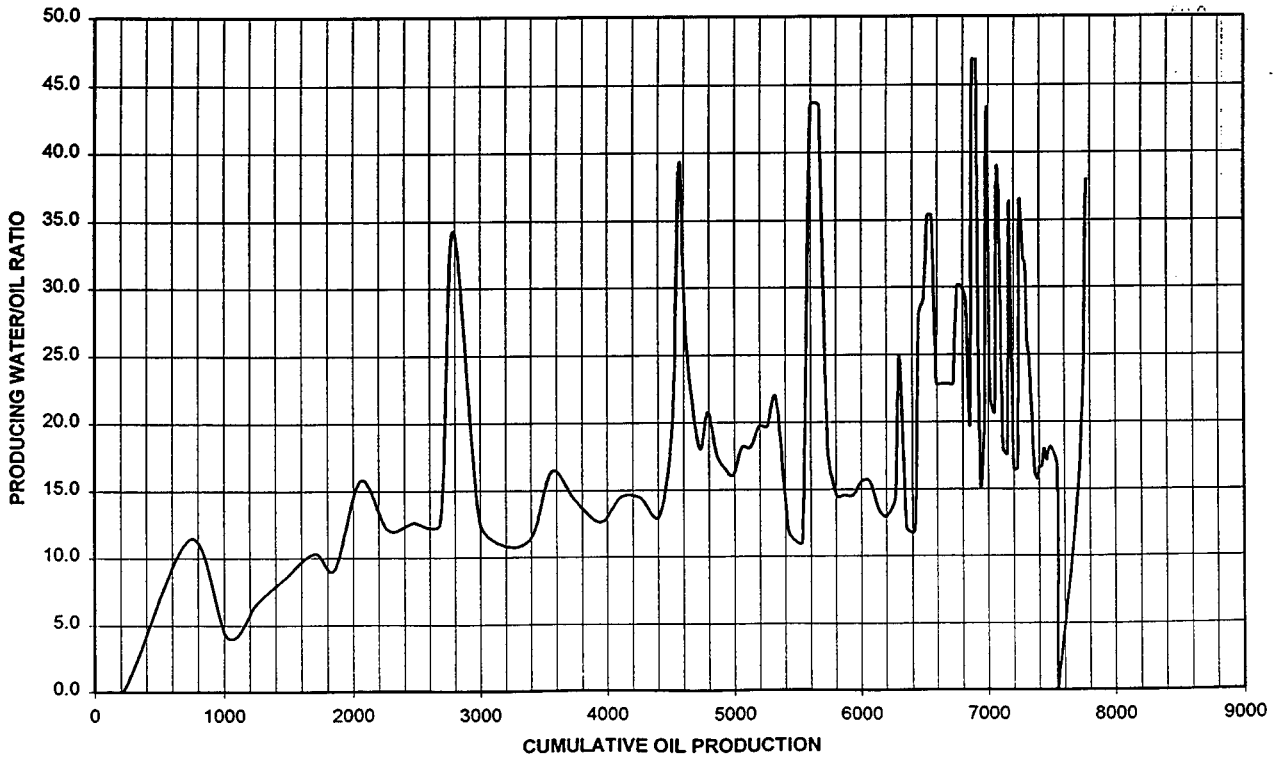
50.0
45.0
40.0
35.0
30.0
25.0
20.0
15.0
10.0
5.0
0.0
PRODUCING WATER/OIL RATIO
0
1000
2000
3000
4000
5000
6000
7000
8000
9000
CUMULATIVE OIL PRODUCTION

H-3

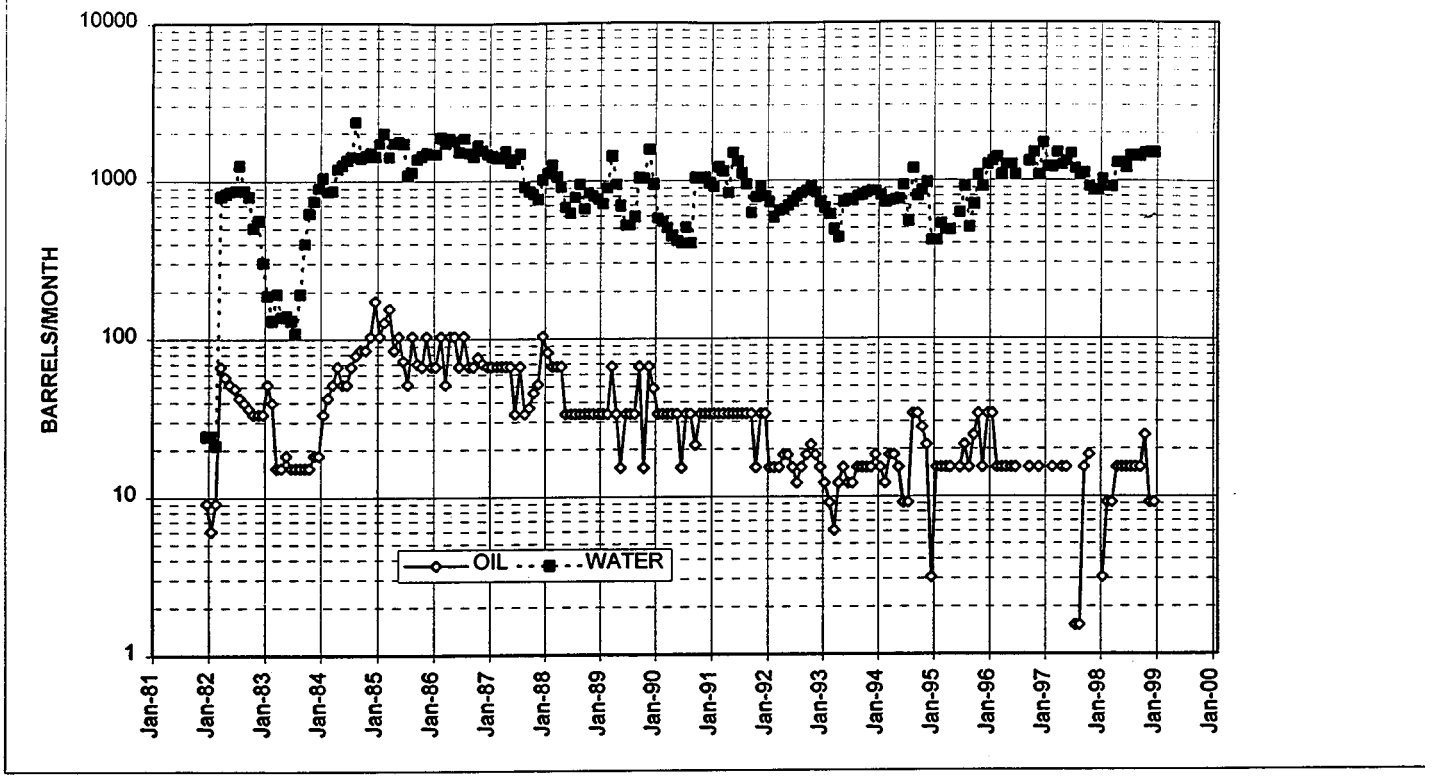
10000
1000
100
10
1
BARRELS/MONTH
OIL
WATER
Jan-81
Jan-82
Jan-83
Jan-84
Jan-85
Jan-86
Jan-87
Jan-88
Jan-89
Jan-90
Jan-91
Jan-92
Jan-93
Jan-94
Jan-95
Jan-96
Jan-97
Jan-98
Jan-99
Jan-00

H-3

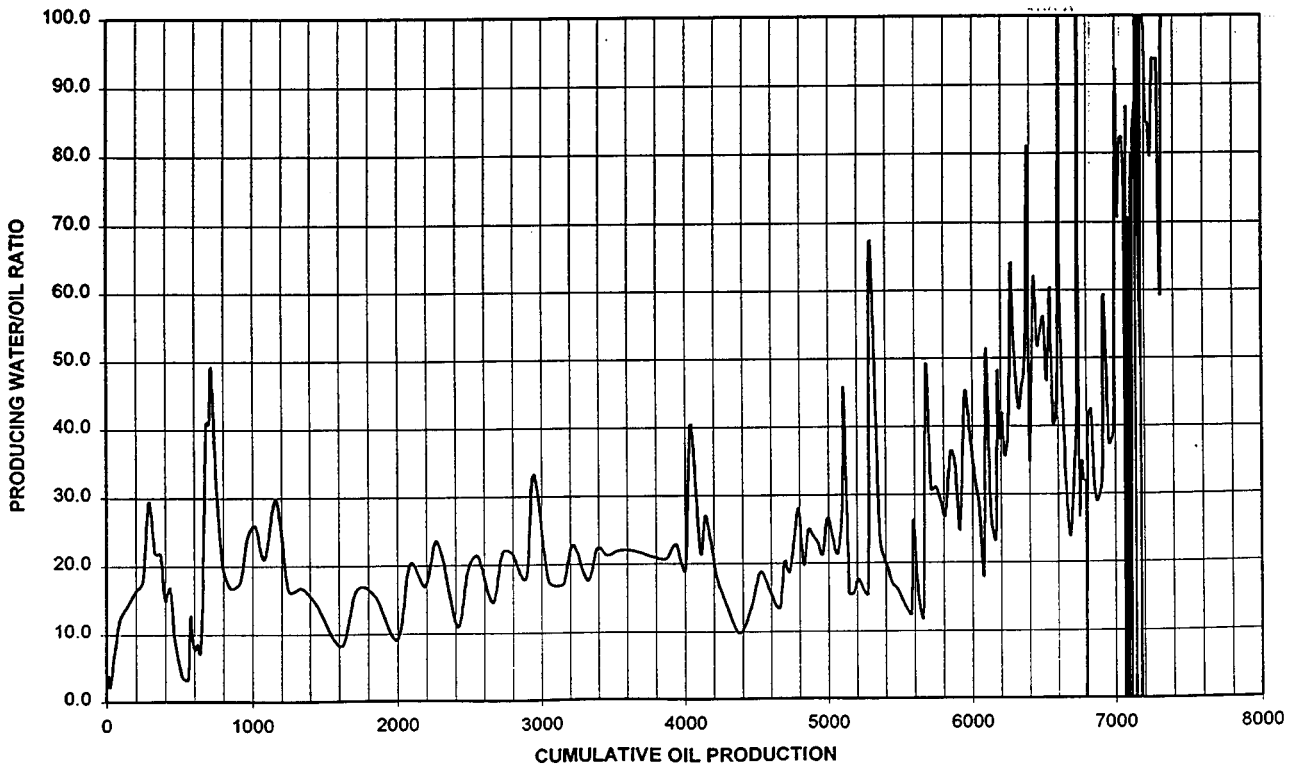
100.0
90.0
80.0
70.0
60.0
50.0
40.0
30.0
20.0
10.0
0.0
PRODUCING WATER/OIL RATIO
0
1000
2000
3000
4000
5000
6000
7000
8000
CUMULATIVE OIL PRODUCTION

H-5

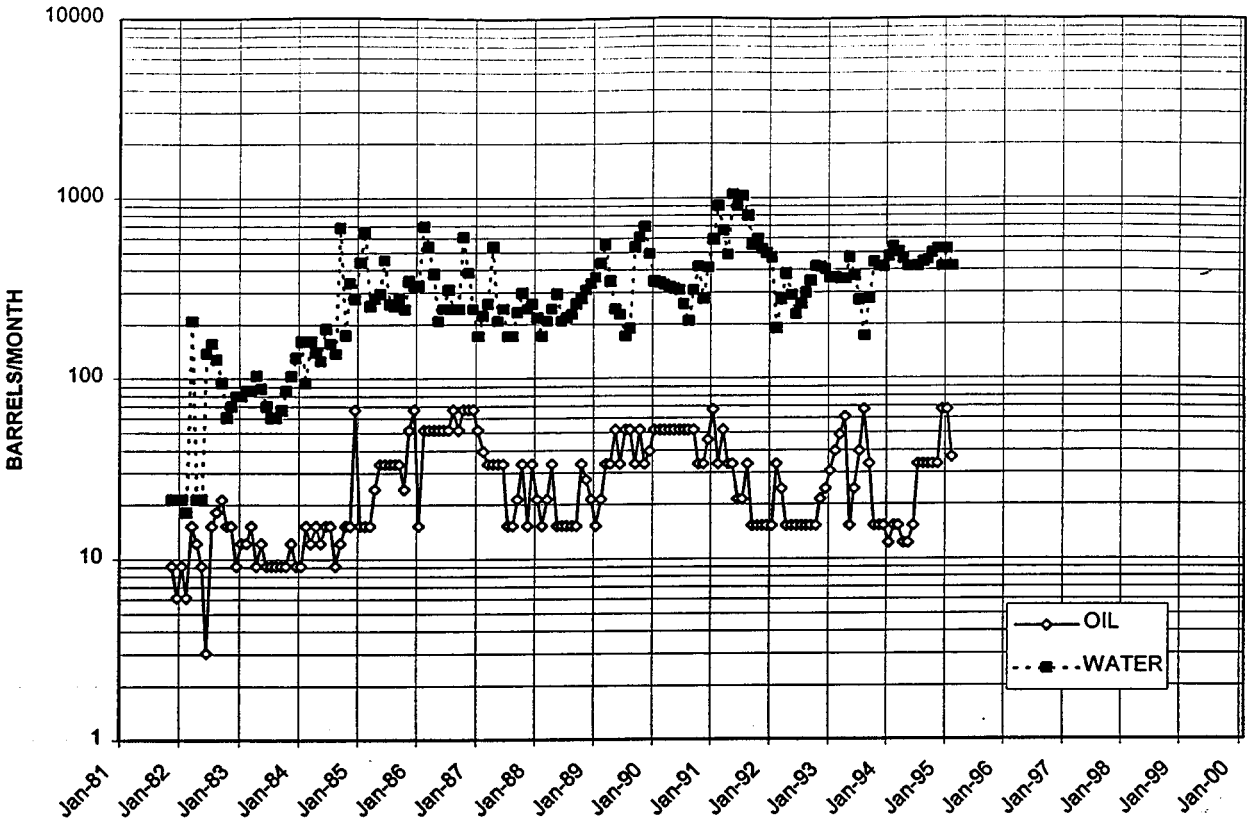
10000
1000
100
10
1
BARRELS/MONTH
OIL
WATER
Jan-81
Jan-82
Jan-83
Jan-84
Jan-85
Jan-86
Jan-87
Jan-88
Jan-89
Jan-90
Jan-91
Jan-92
Jan-93
Jan-94
Jan-95
Jan-96
Jan-97
Jan-98
Jan-99
Jan-00

H-5

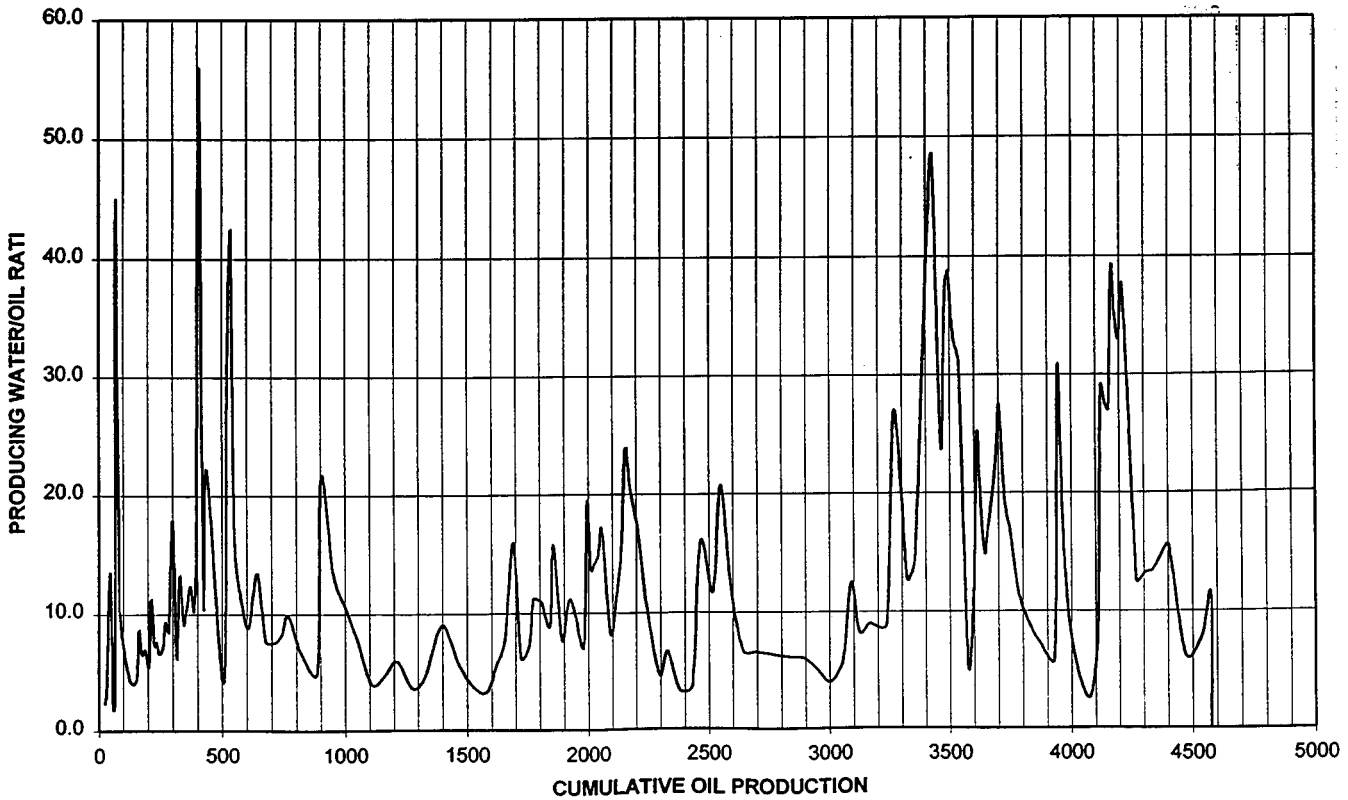
60.0
50.0
40.0
30.0
20.0
10.0
0.0
PRODUCING WATER/OIL RATI
0
500
1000
1500
2000
2500
3000
3500
4000
4500
5000
CUMULATIVE OIL PRODUCTION

H-10

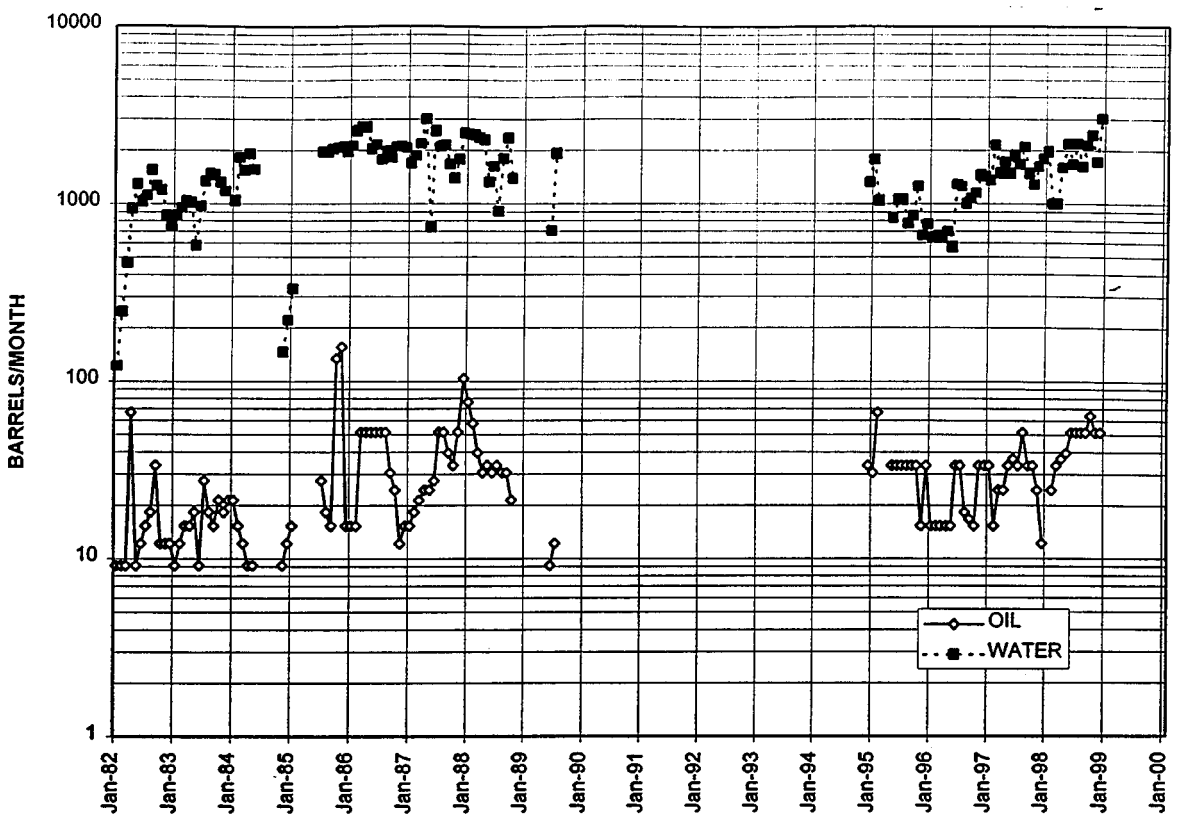
10000
1000
100
10
1
BARRELS/MONTH
OIL
WATER
Jan-82
Jan-83
Jan-84
Jan-85
Jan-86
Jan-87
Jan-88
Jan-89
Jan-90
Jan-91
Jan-92
Jan-93
Jan-94
Jan-95
Jan-96
Jan-97
Jan-98
Jan-99
Jan-00

H-10

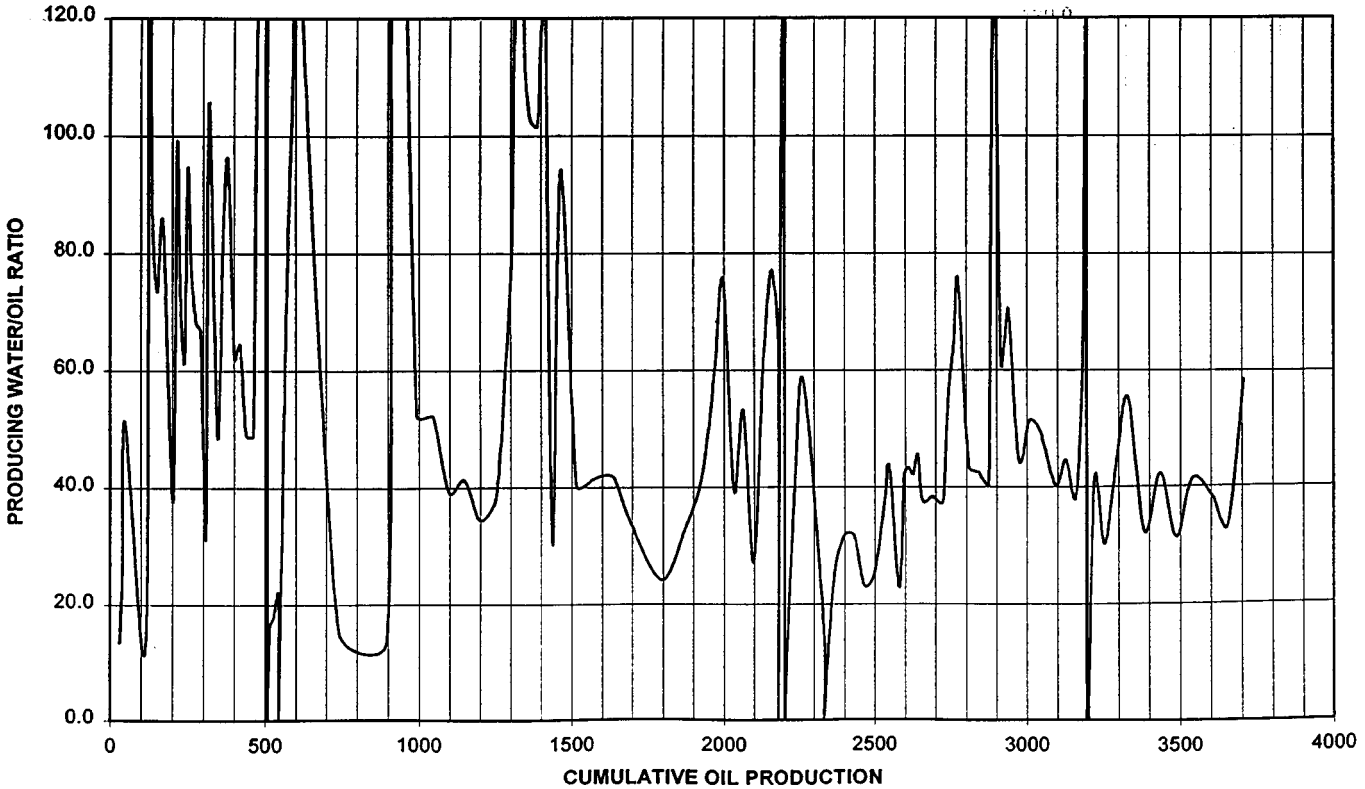
120.0
100.0
80.0
60.0
40.0
20.0
0.0
PRODUCING WATER/OIL RATIO
0
500
1000
1500
2000
2500
3000
3500
4000
CUMULATIVE OIL PRODUCTION

H-13

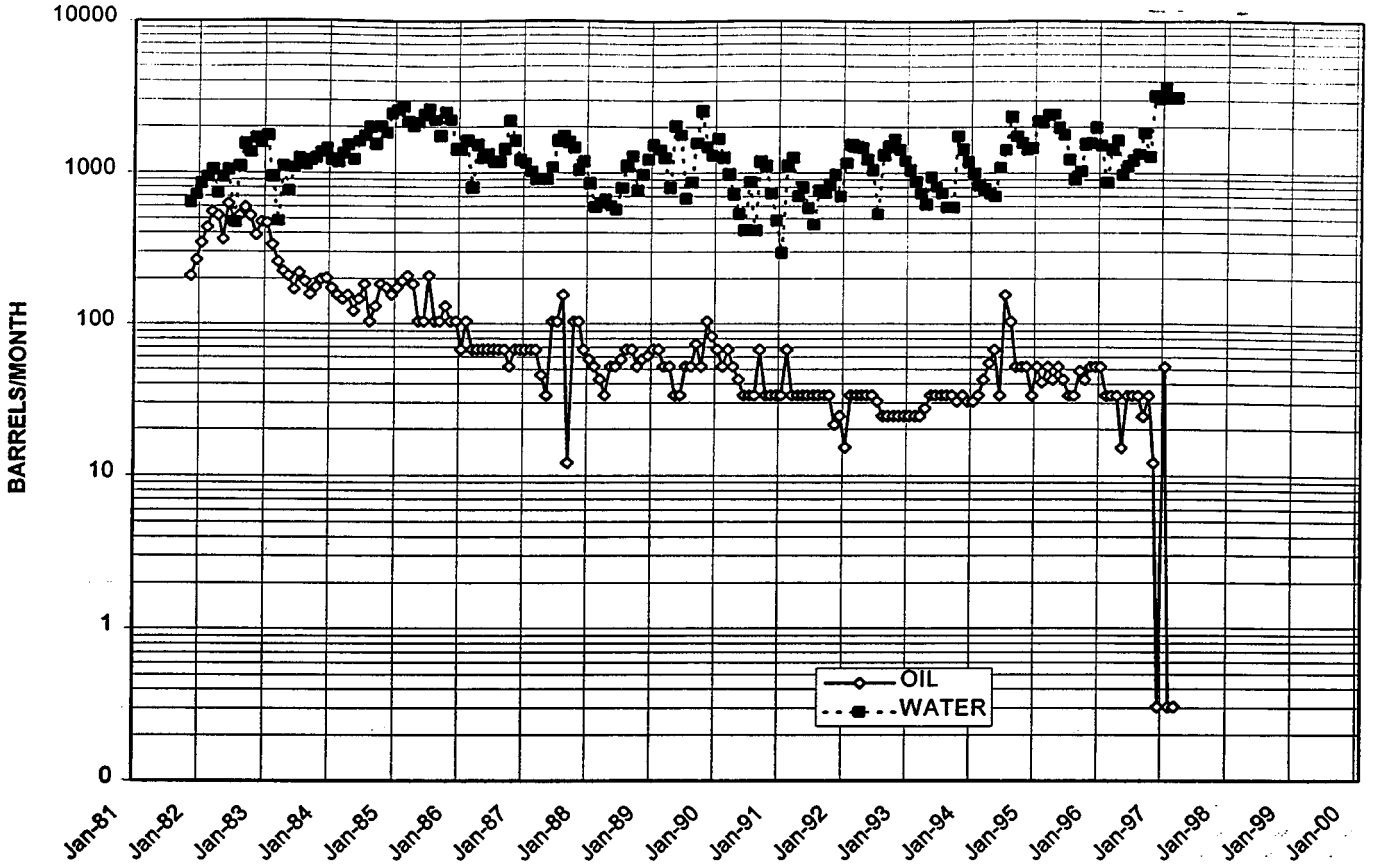
10000
1000
100
10
1
0
BARRELS/MONTH
OIL
WATER
Jan-81
Jan-82
Jan-83
Jan-84
Jan-85
Jan-86
Jan-87
Jan-88
Jan-89
Jan-90
Jan-91
Jan-92
Jan-93
Jan-94
Jan-95
Jan-96
Jan-97
Jan-98
Jan-99
Jan-00

H-13

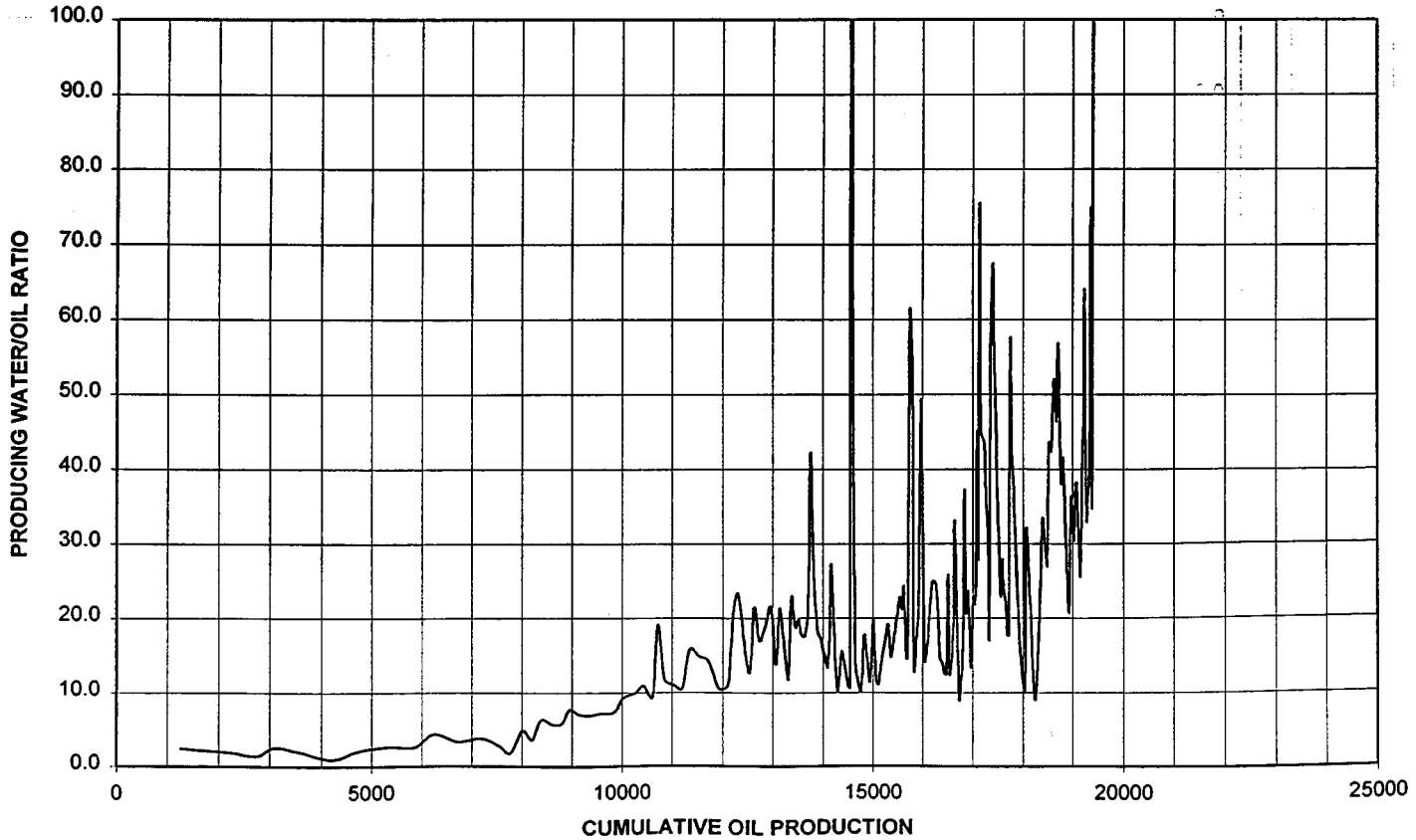
100.0
90.0
80.0
70.0
60.0
50.0
40.0
30.0
20.0
10.0
0.0
PRODUCING WATER/OIL RATIO
0
5000
10000
15000
20000
25000
CUMULATIVE OIL PRODUCTION

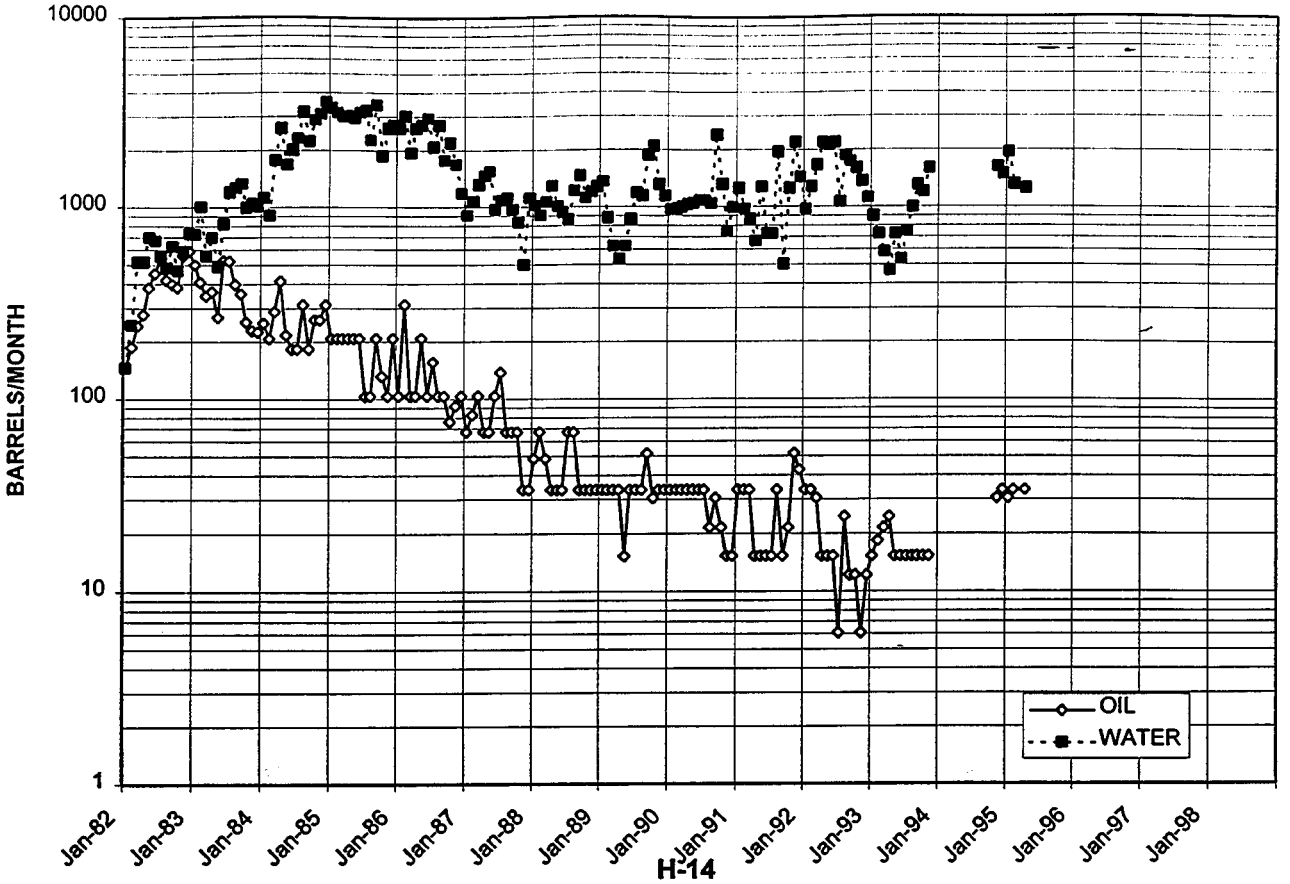
10000
1000
100
10
1
BARRELS/MONTH
OIL
WATER
Jan-82
Jan-83
Jan-84
Jan-85
Jan-86
Jan-87
Jan-88
Jan-89
Jan-90
Jan-91
Jan-92
Jan-93
Jan-94
Jan-95
Jan-96
Jan-97
Jan-98
H-14

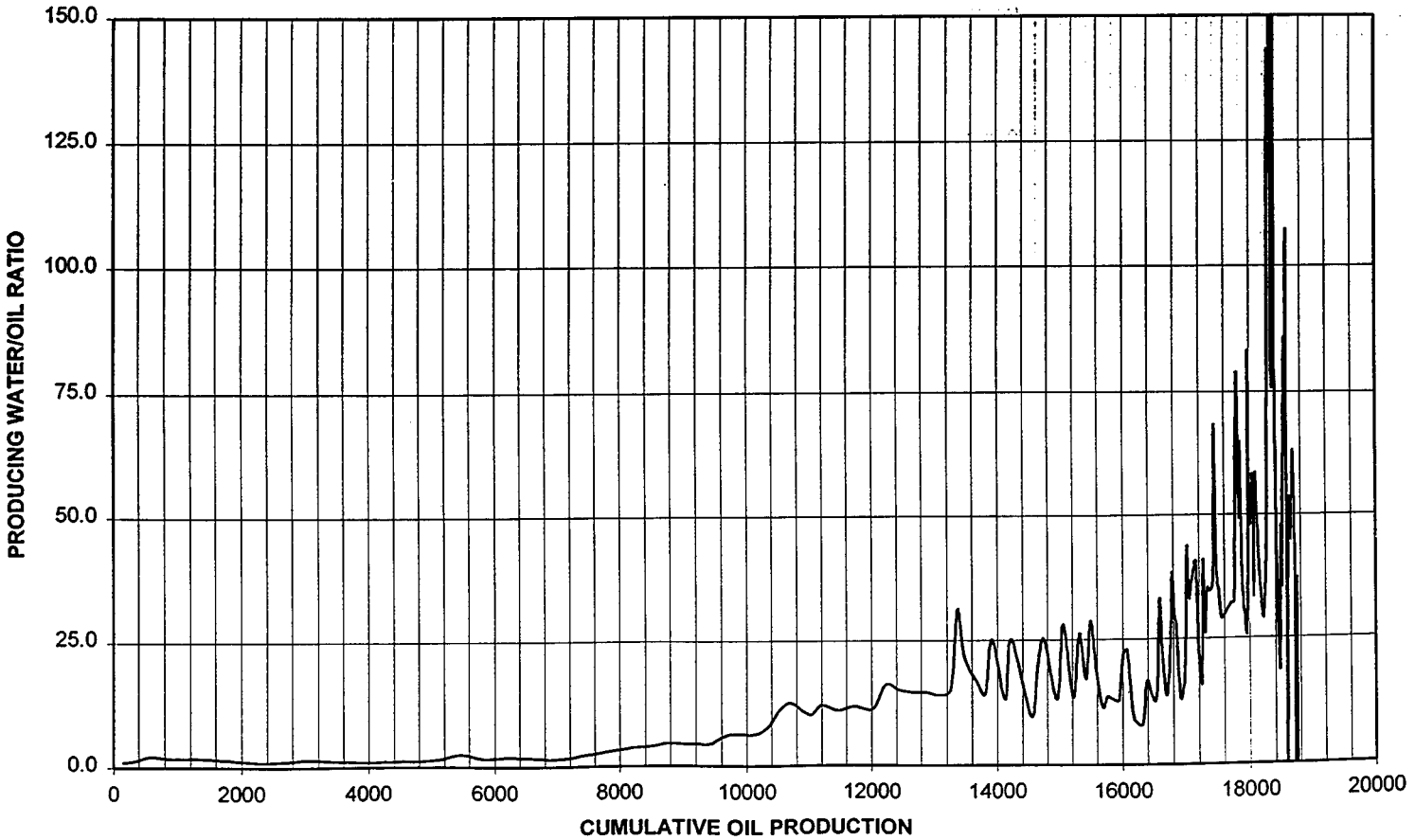
150.0
125.0
100.0
75.0
50.0
25.0
0.0
PRODUCING WATER/OIL RATIO
0
2000
4000
6000
8000
10000
12000
14000
16000
18000
20000
CUMULATIVE OIL PRODUCTION

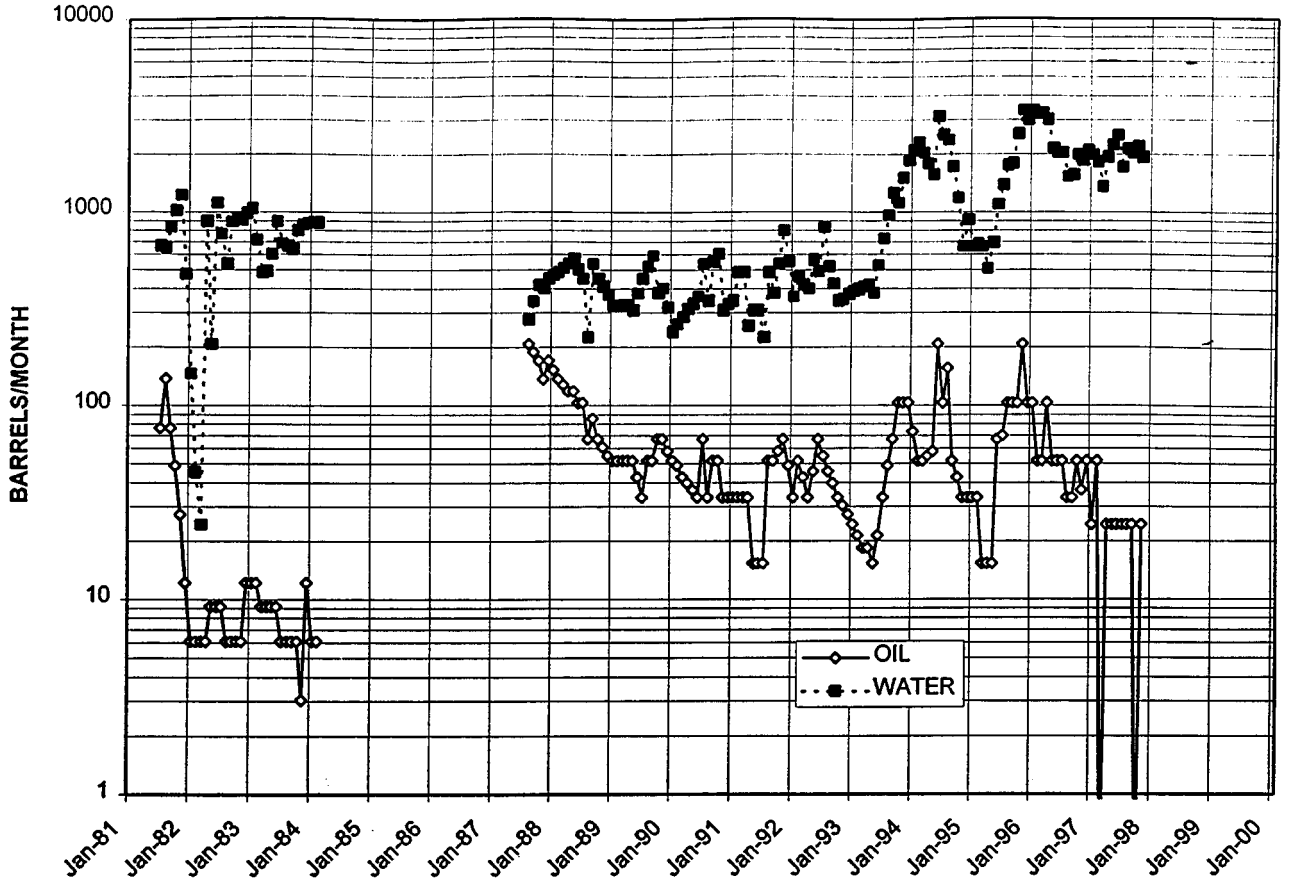
10000
1000
100
10
1
BARRELS/MONTH
OIL
WATER
Jan-81
Jan-82
Jan-83
Jan-84
Jan-85
Jan-86
Jan-87
Jan-88
Jan-89
Jan-90
Jan-91
Jan-92
Jan-93
Jan-94
Jan-95
Jan-96
Jan-97
Jan-98
Jan-99
Jan-00

H-15

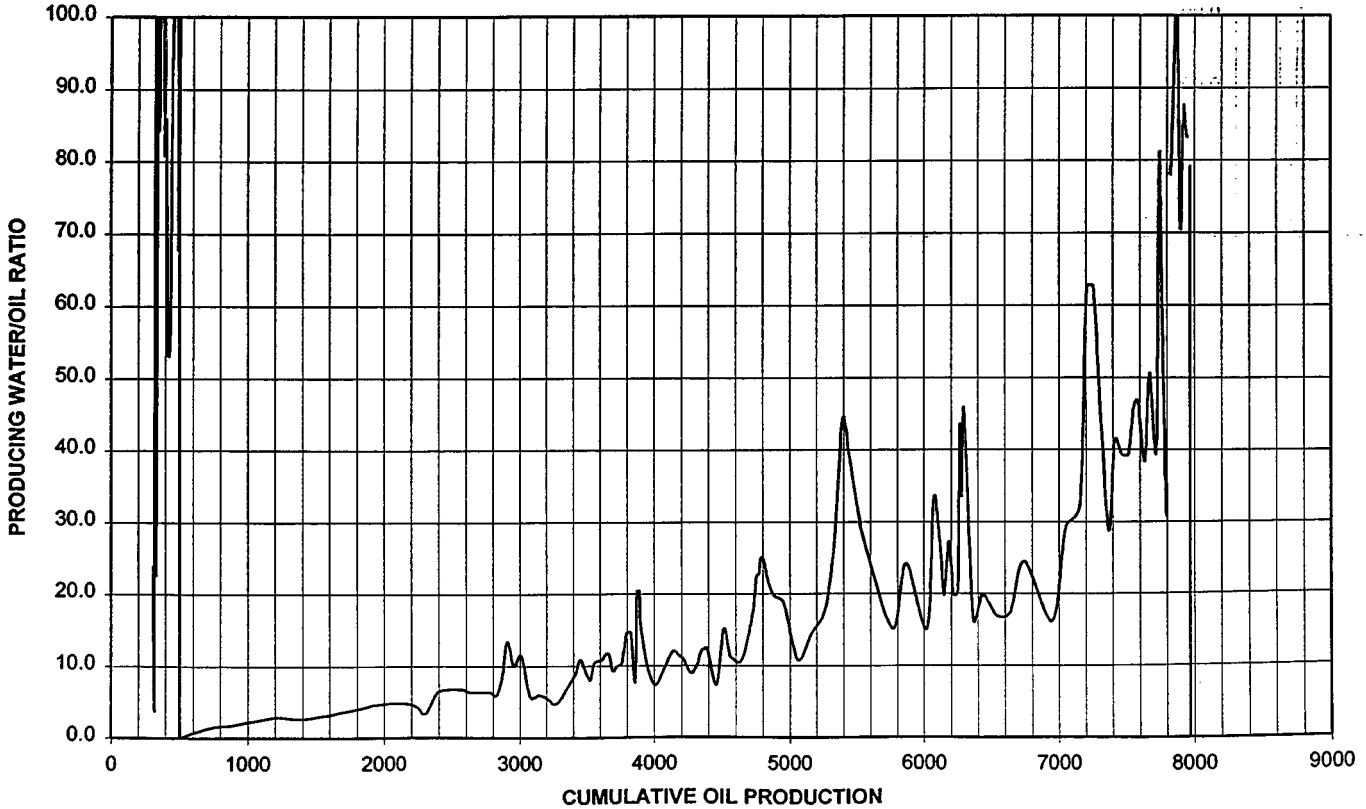
100.0
90.0
80.0
70.0
60.0
50.0
40.0
30.0
20.0
10.0
0.0
PRODUCING WATER/OIL RATIO
0
1000
2000
3000
4000
5000
6000
7000
8000
9000
CUMULATIVE OIL PRODUCTION

H-16

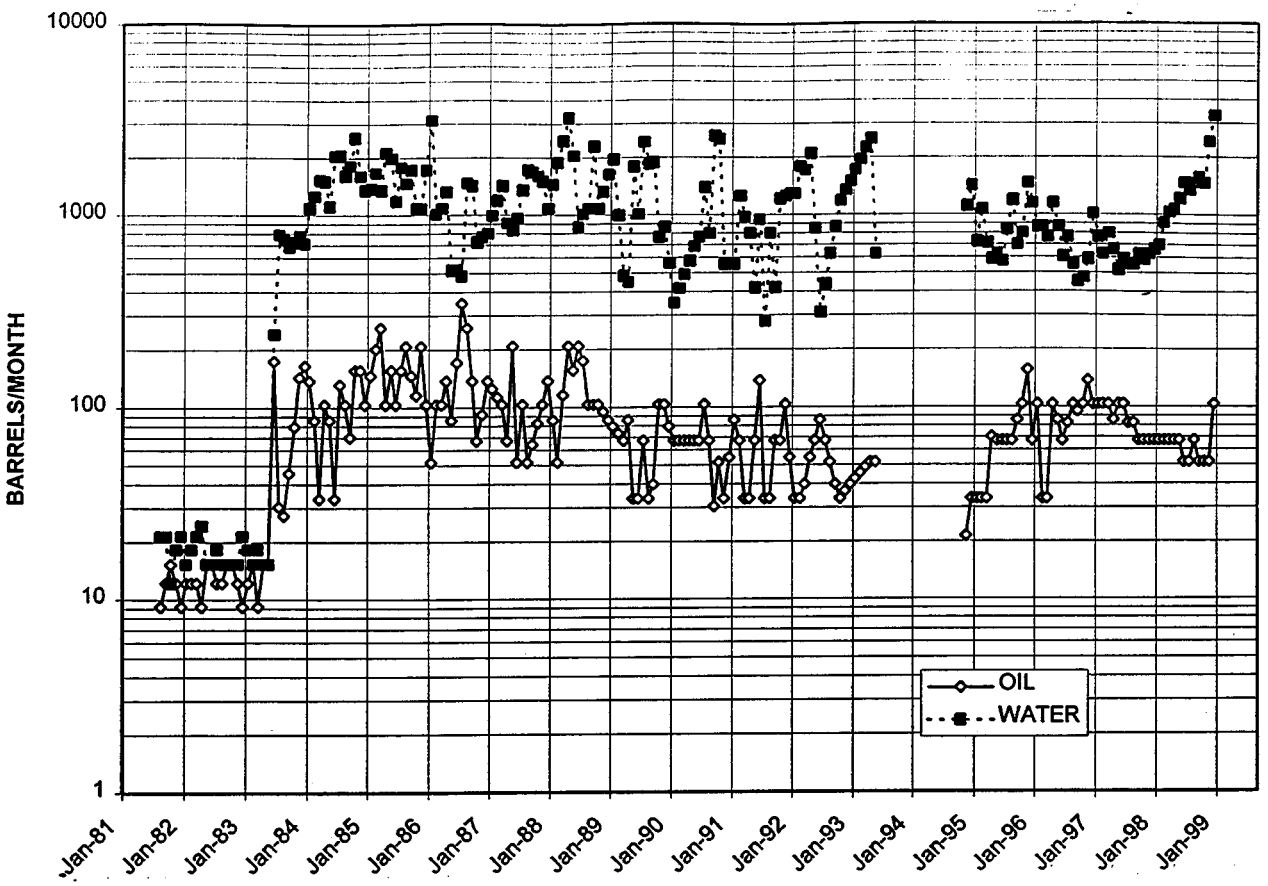
10000
1000
100
10
1
BARRELS/MONTH
OIL
WATER
Jan-81
Jan-82
Jan-83
Jan-84
Jan-85
Jan-86
Jan-87
Jan-88
Jan-89
Jan-90
Jan-91
Jan-92
Jan-93
Jan-94
Jan-95
Jan-96
Jan-97
Jan-98
Jan-99

H-16

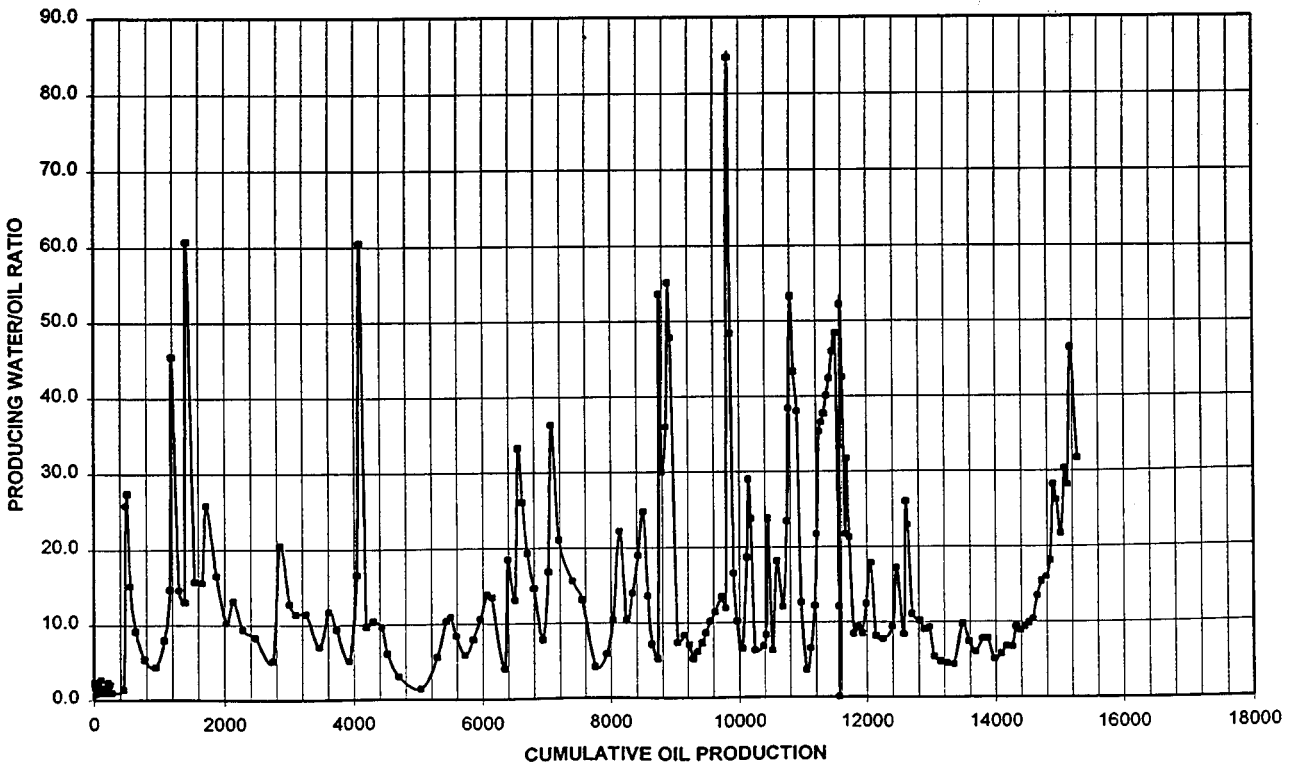
90.0
80.0
70.0
60.0
50.0
40.0
30.0
20.0
10.0
0.0
PRODUCING WATER/OIL RATIO
0
2000
4000
6000
8000
10000
12000
14000
16000
18000
CUMULATIVE OIL PRODUCTION

H-17

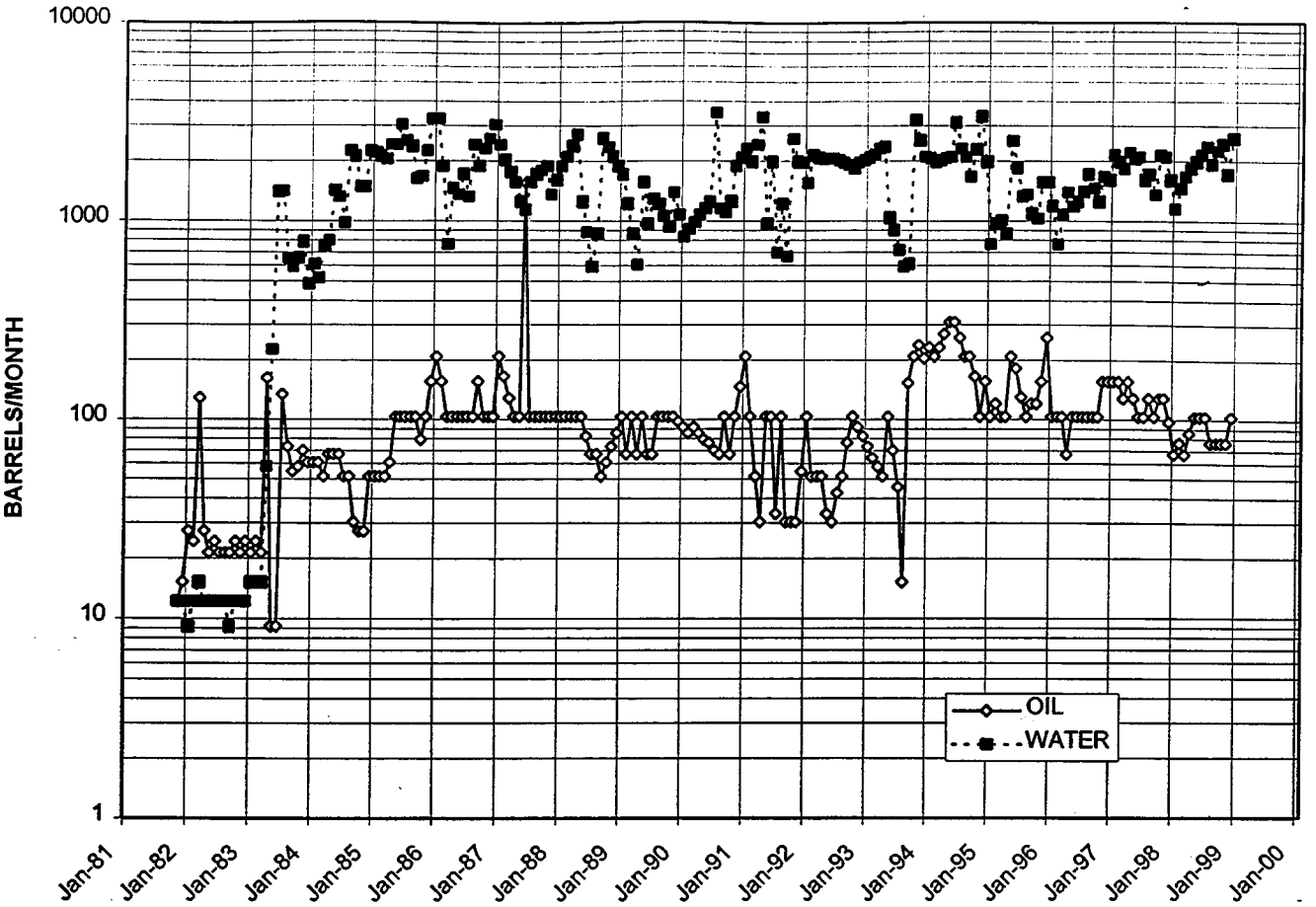
10000
1000
100
10
1
BARRELS/MONTH
OIL
WATER
Jan-81
Jan-82
Jan-83
Jan-84
Jan-85
Jan-86
Jan-87
Jan-88
Jan-89
Jan-90
Jan-91
Jan-92
Jan-93
Jan-94
Jan-95
Jan-96
Jan-97
Jan-98
Jan-99
Jan-00

H-17

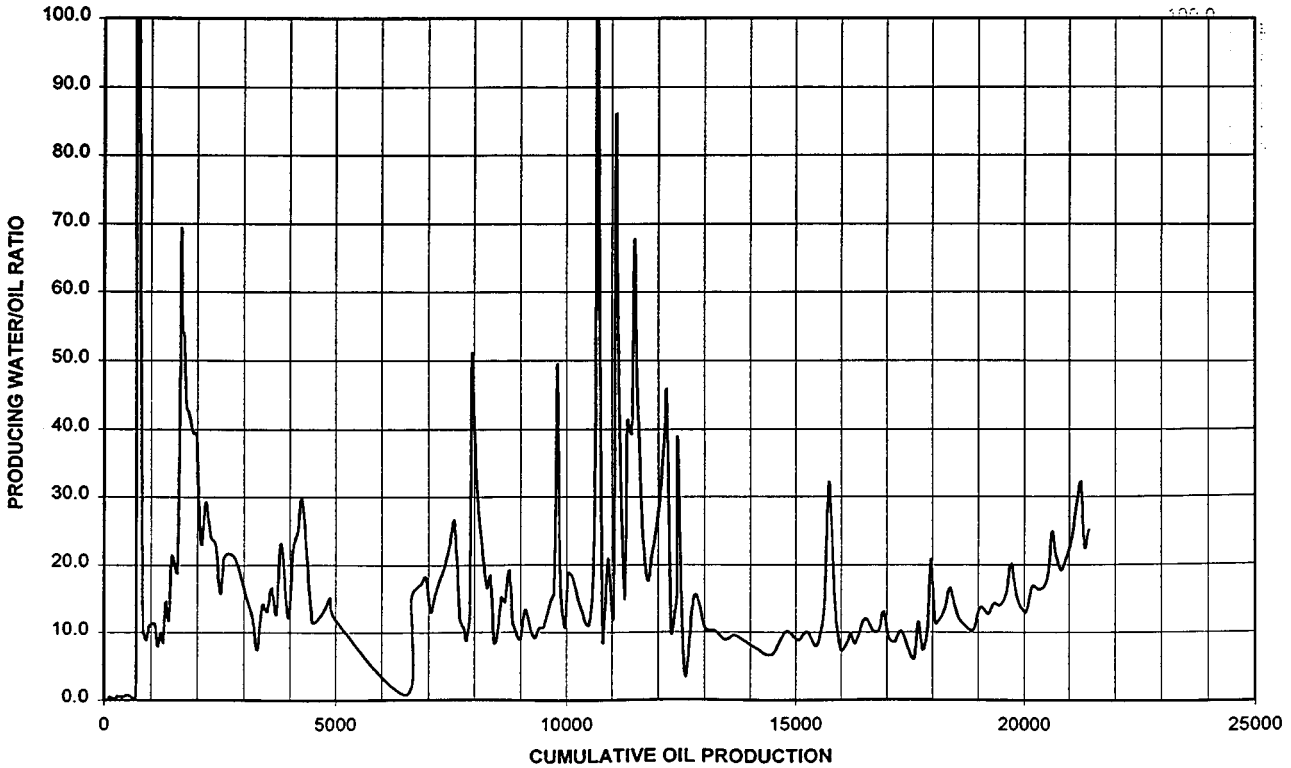
100.0
90.0
80.0
70.0
60.0
50.0
40.0
30.0
20.0
10.0
0.0
PRODUCING WATER/OIL RATIO
0
5000
10000
15000
20000
25000
CUMULATIVE OIL PRODUCTION

H-20

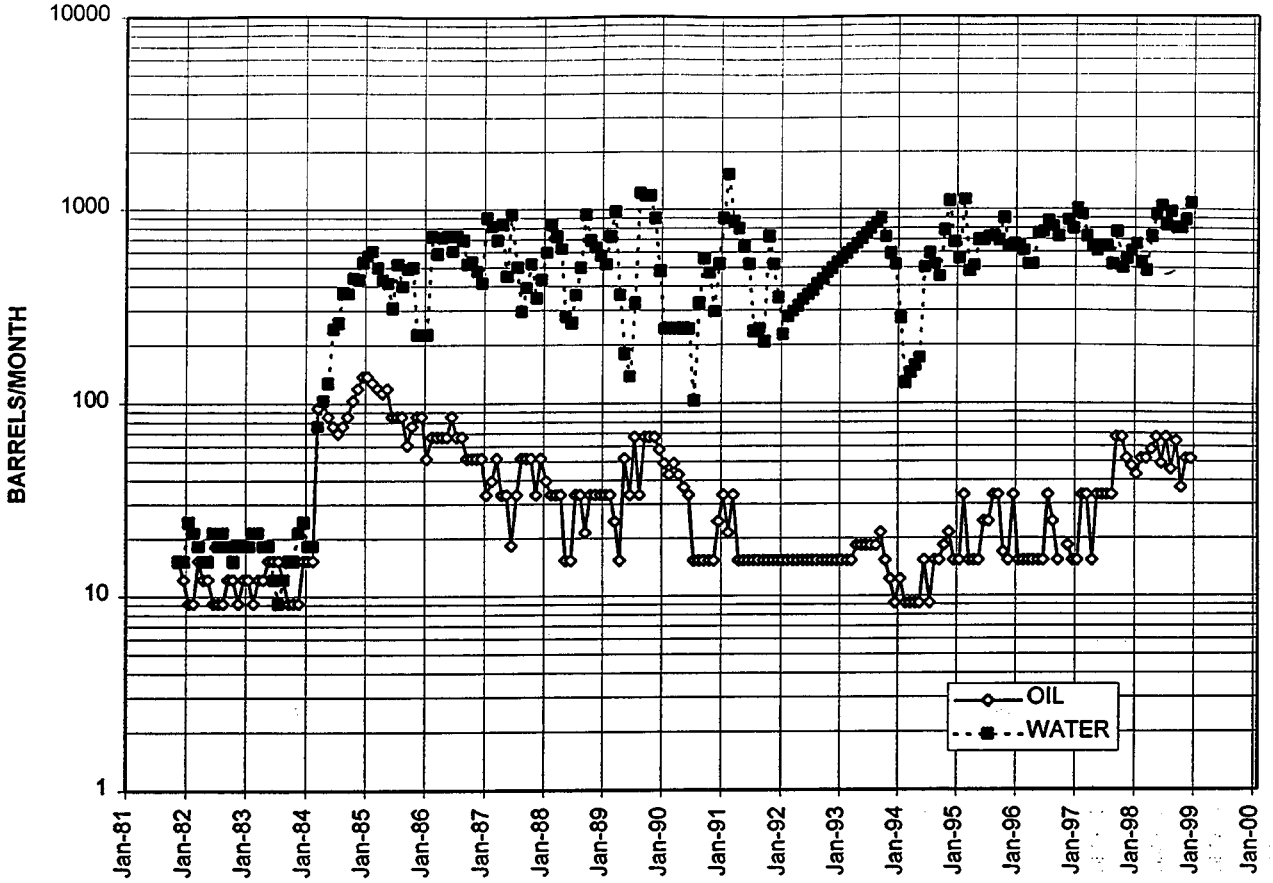
10000
1000
100
10
1
BARRELS/MONTH
OIL
WATER
Jan-81
Jan-82
Jan-83
Jan-84
Jan-85
Jan-86
Jan-87
Jan-88
Jan-89
Jan-90
Jan-91
Jan-92
Jan-93
Jan-94
Jan-95
Jan-96
Jan-97
Jan-98
Jan-99
Jan-00

H-20

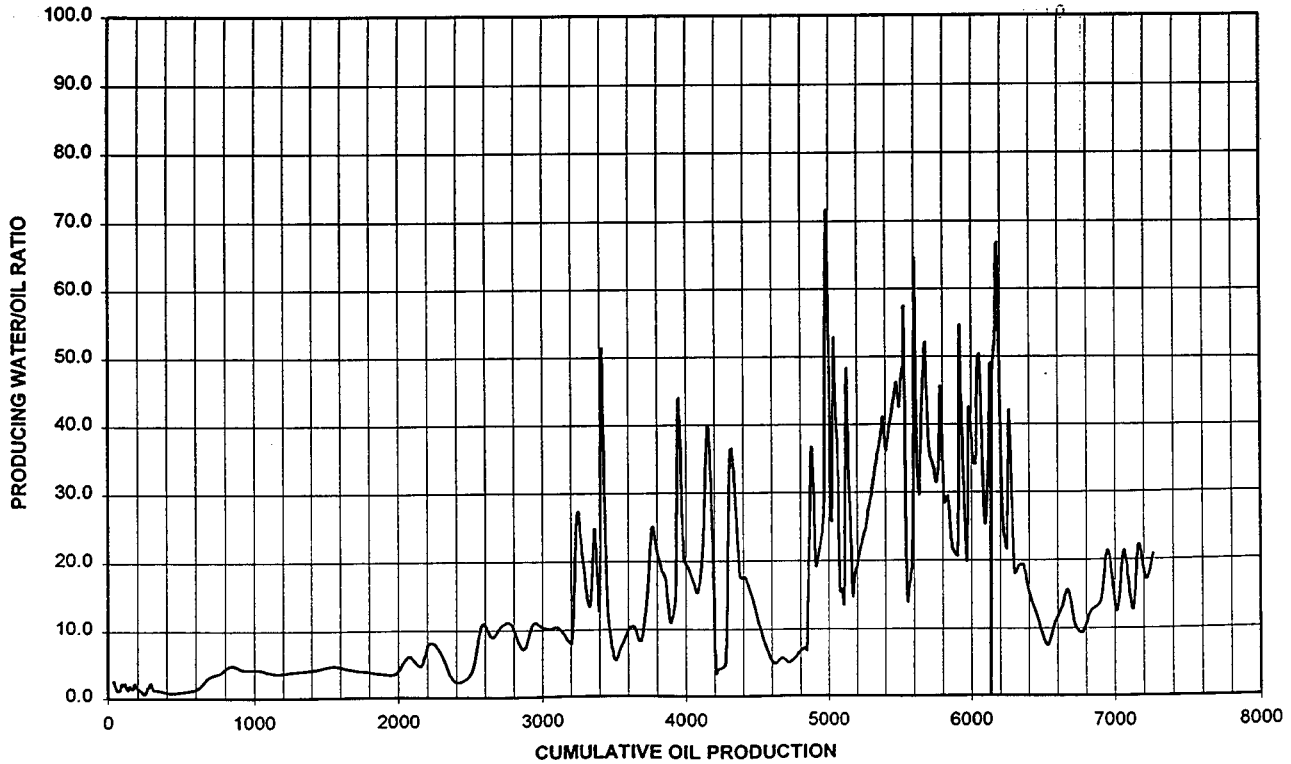
100.0
90.0
80.0
70.0
60.0
50.0
40.0
30.0
20.0
10.0
0.0
PRODUCING WATER/OIL RATIO
0
1000
2000
3000
4000
5000
6000
7000
8000
CUMULATIVE OIL PRODUCTION

H-21

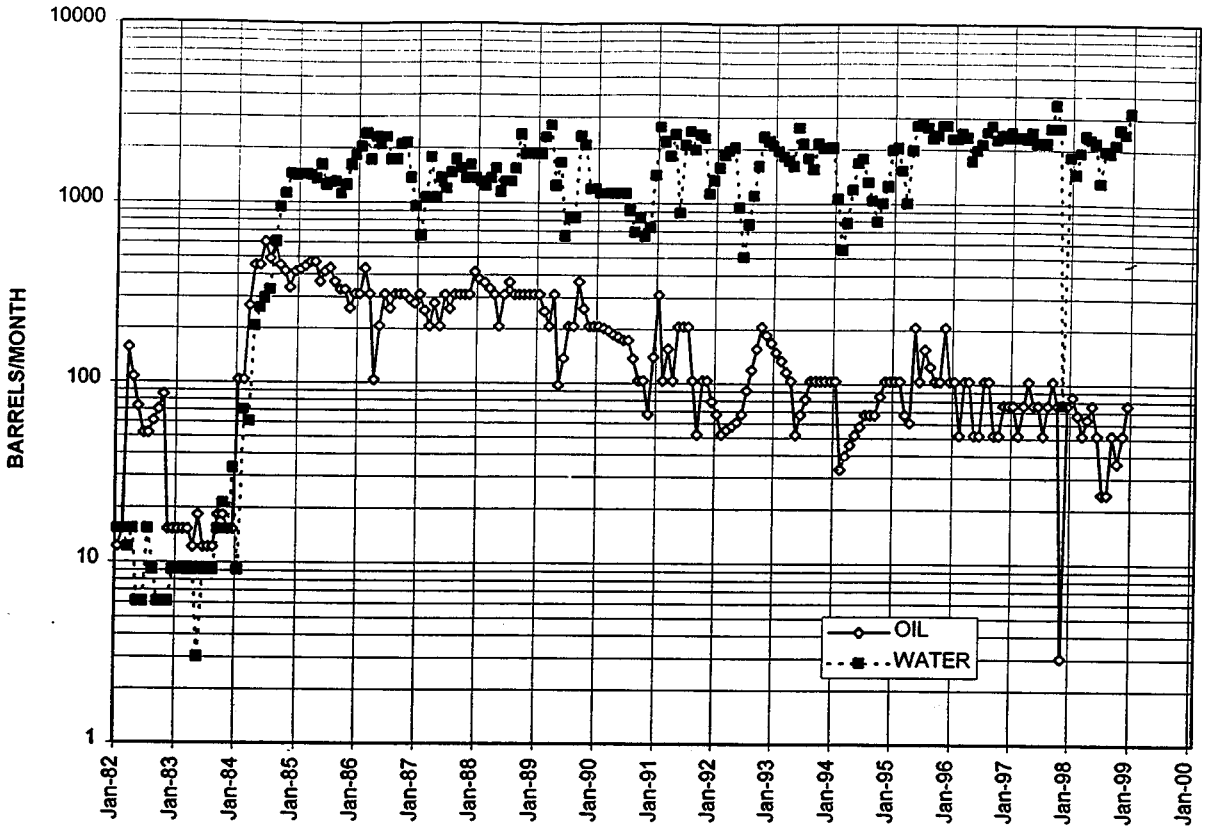
10000
1000
100
10
1
BARRELS/MONTH
OIL
WATER
Jan-82
Jan-83
Jan-84
Jan-85
Jan-86
Jan-87
Jan-88
Jan-89
Jan-90
Jan-91
Jan-92
Jan-93
Jan-94
Jan-95
Jan-96
Jan-97
Jan-98
Jan-99
Jan-00

H-21

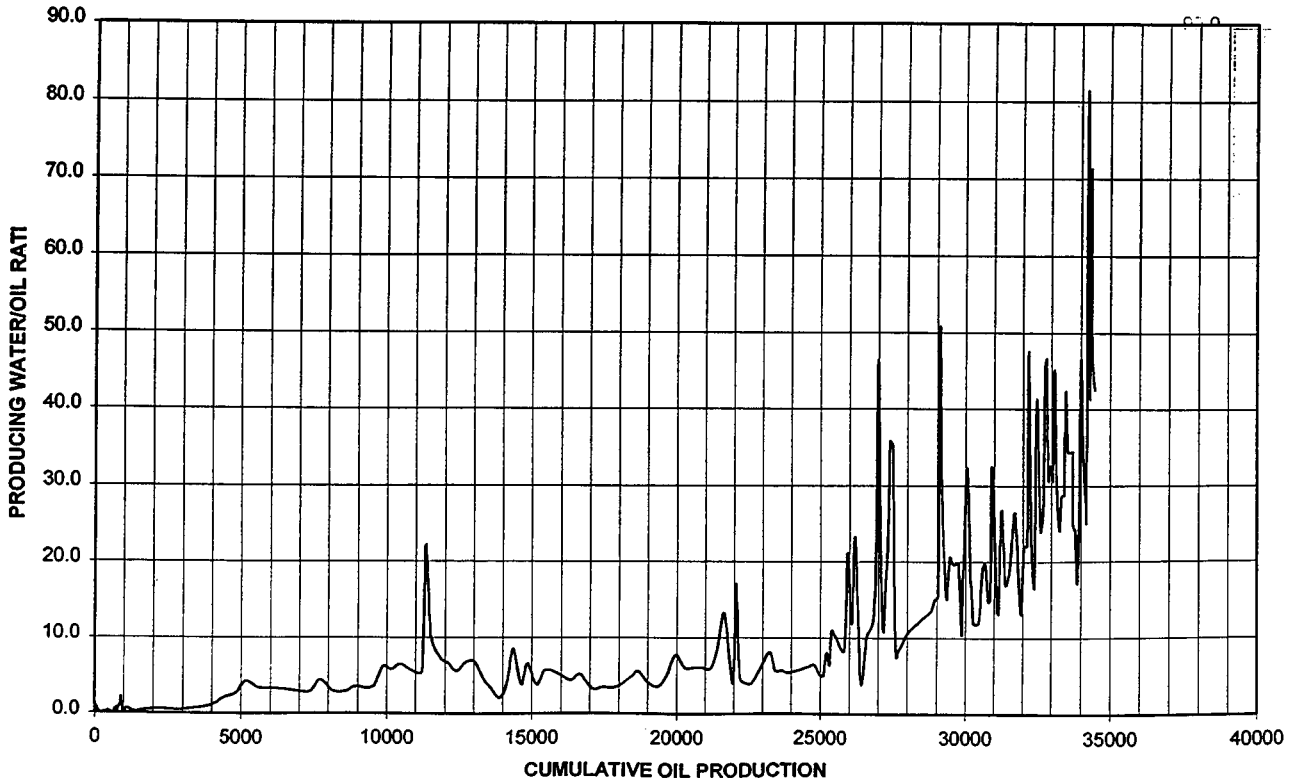
90.0
80.0
70.0
60.0
50.0
40.0
30.0
20.0
10.0
0.0
PRODUCING WATER/OIL RATI
0
5000
10000
15000
20000
25000
30000
35000
40000
CUMULATIVE OIL PRODUCTION

H-22

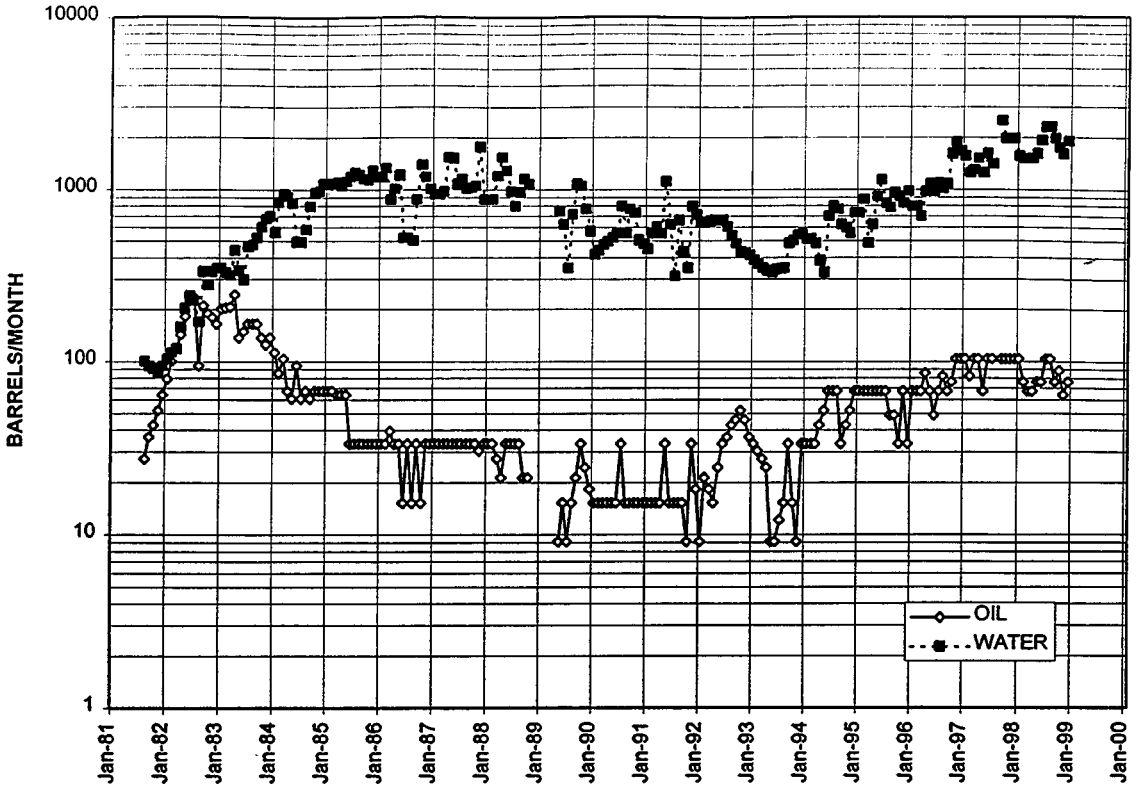
10000
1000
100
10
1
BARRELS/MONTH
OIL
WATER
Jan-81
Jan-82
Jan-83
Jan-84
Jan-85
Jan-86
Jan-87
Jan-88
Jan-89
Jan-90
Jan-91
Jan-92
Jan-93
Jan-94
Jan-95
Jan-96
Jan-97
Jan-98
Jan-99
Jan-00

H-22

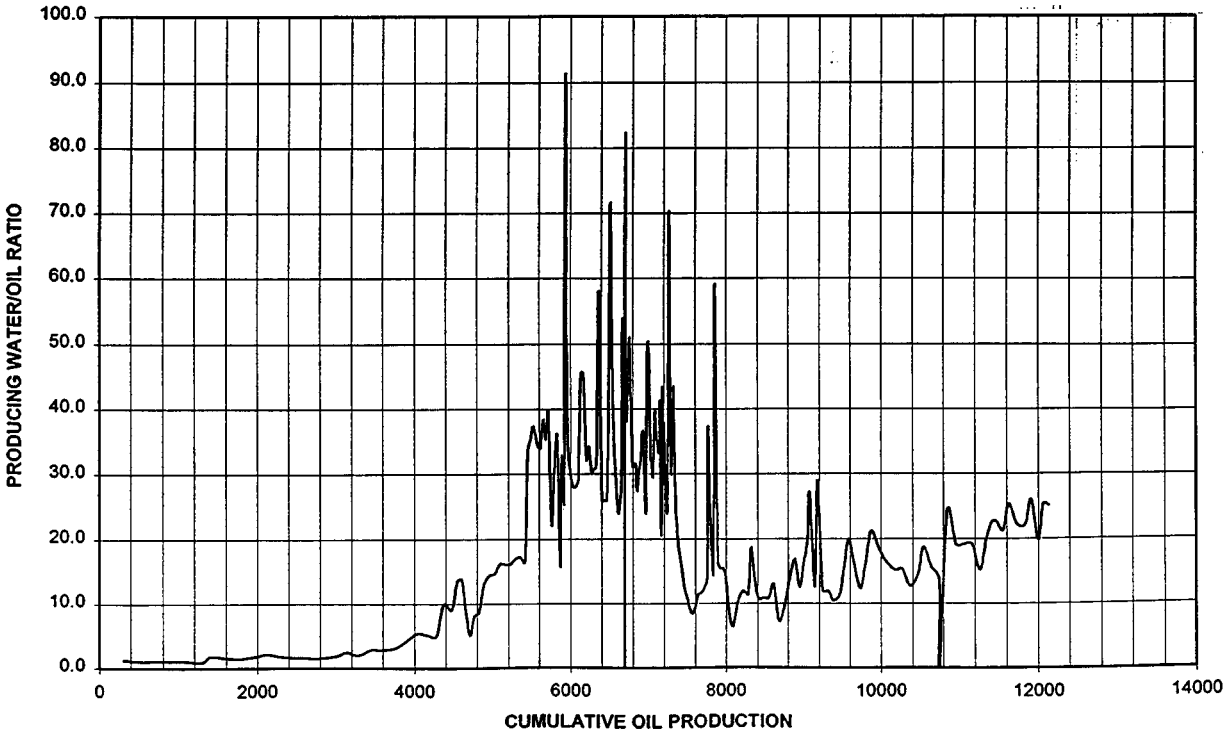
100.0
90.0
80.0
70.0
60.0
50.0
40.0
30.0
20.0
10.0
0.0
PRODUCING WATER/OIL RATIO
0
2000
4000
6000
8000
10000
12000
14000
CUMULATIVE OIL PRODUCTION

H-30

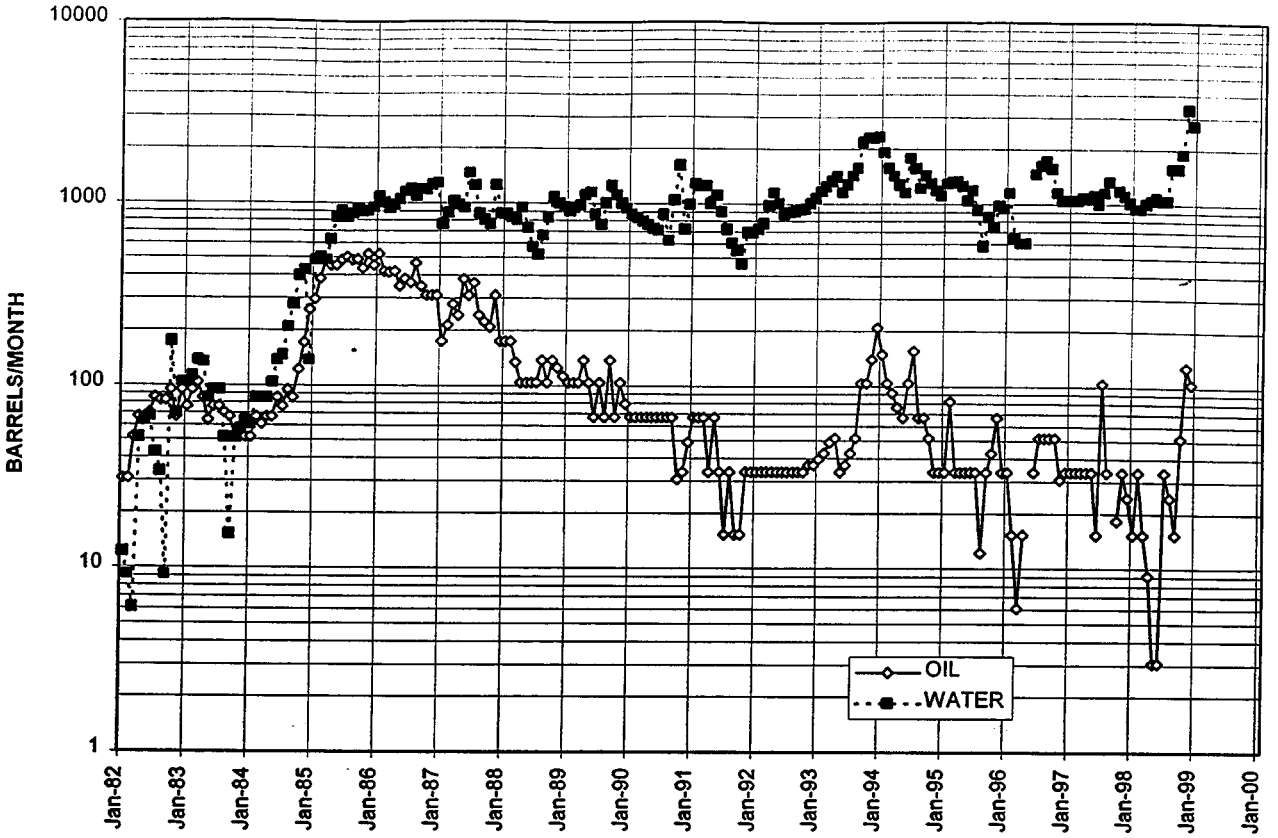
10000
1000
100
10
1
BARRELS/MONTH
OIL
WATER
Jan-82
Jan-83
Jan-84
Jan-85
Jan-86
Jan-87
Jan-88
Jan-89
Jan-90
Jan-91
Jan-92
Jan-93
Jan-94
Jan-95
Jan-96
Jan-97
Jan-98
Jan-99
Jan-00

H30

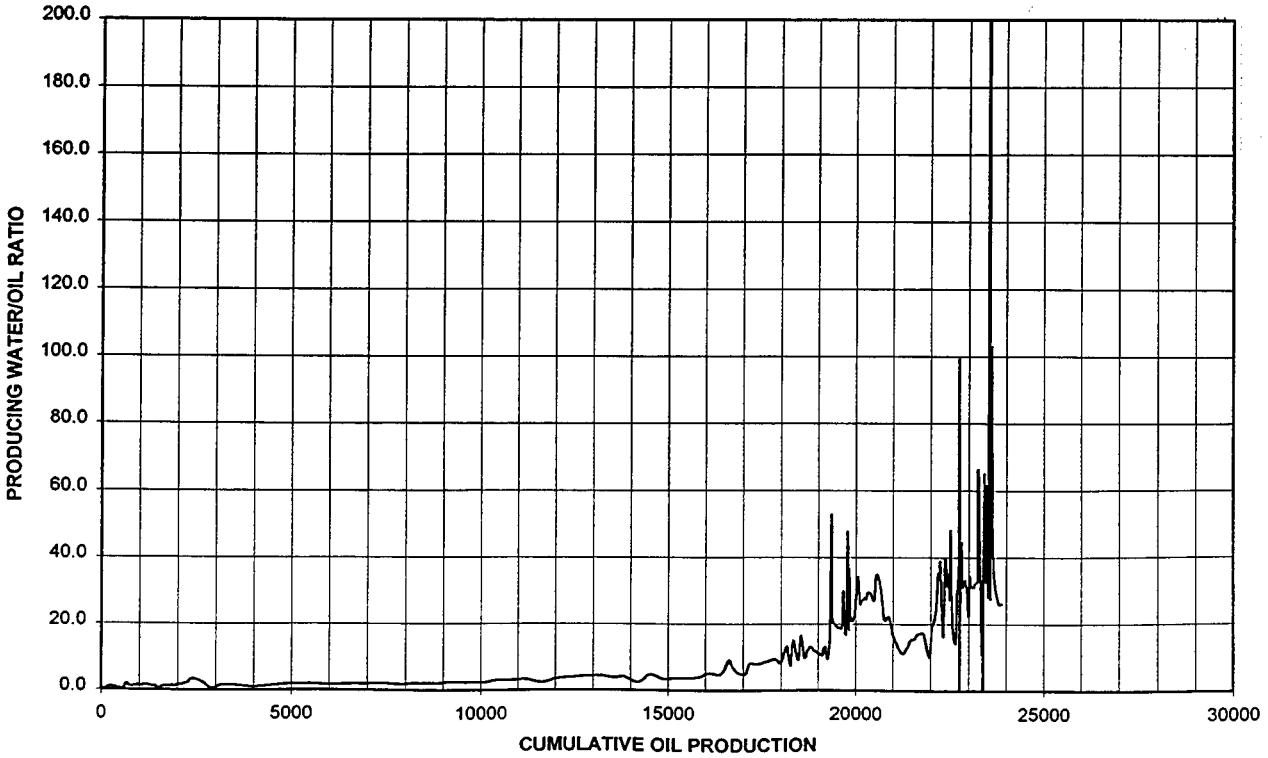
200.0
180.0
160.0
140.0
120.0
100.0
80.0
60.0
40.0
20.0
0.0
PRODUCING WATER/OIL RATIO
0
5000
10000
15000
20000
25000
30000
CUMULATIVE OIL PRODUCTION

K-41

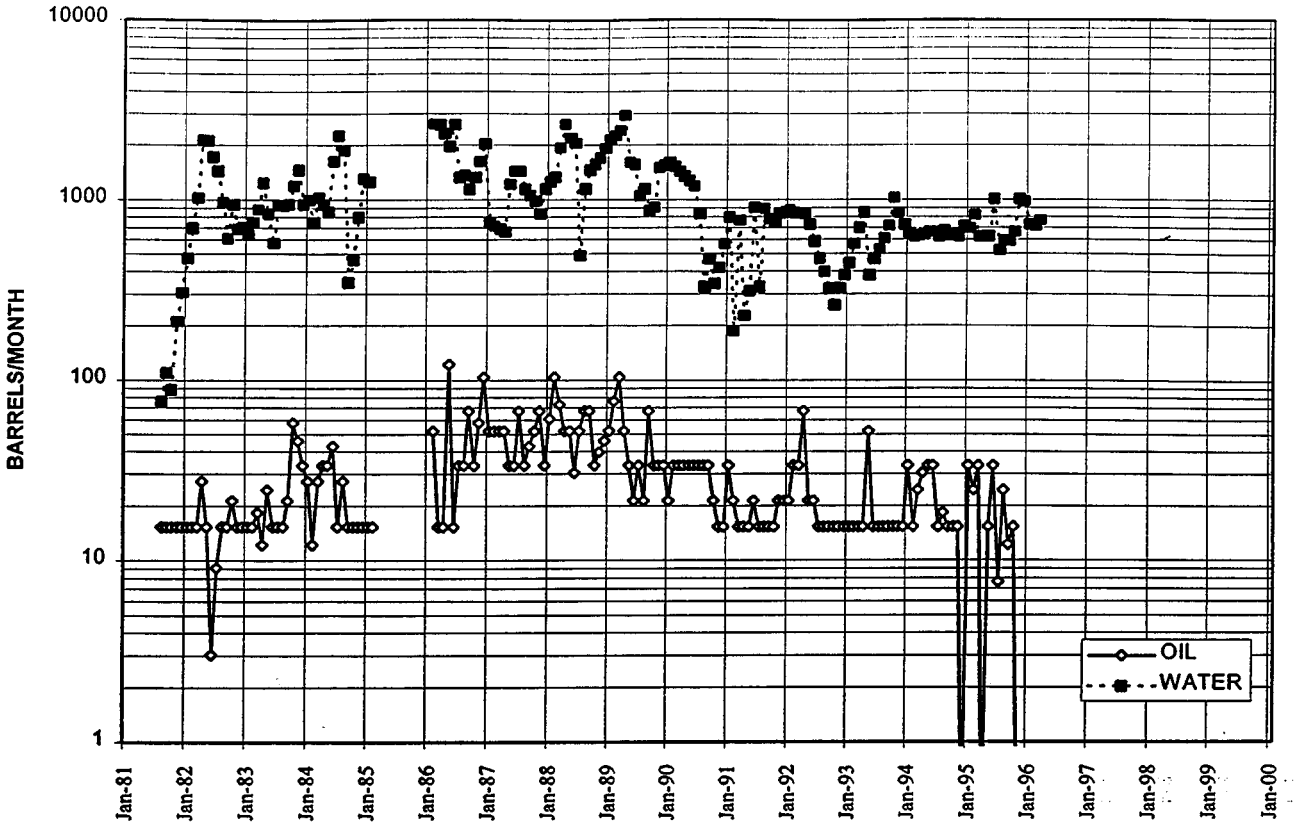
10000
1000
100
10
1
BARRELS/MONTH
OIL
WATER
Jan-81
Jan-82
Jan-83
Jan-84
Jan-85
Jan-86
Jan-87
Jan-88
Jan-89
Jan-90
Jan-91
Jan-92
Jan-93
Jan-94
Jan-95
Jan-96
Jan-97
Jan-98
Jan-99
Jan-00

K-41

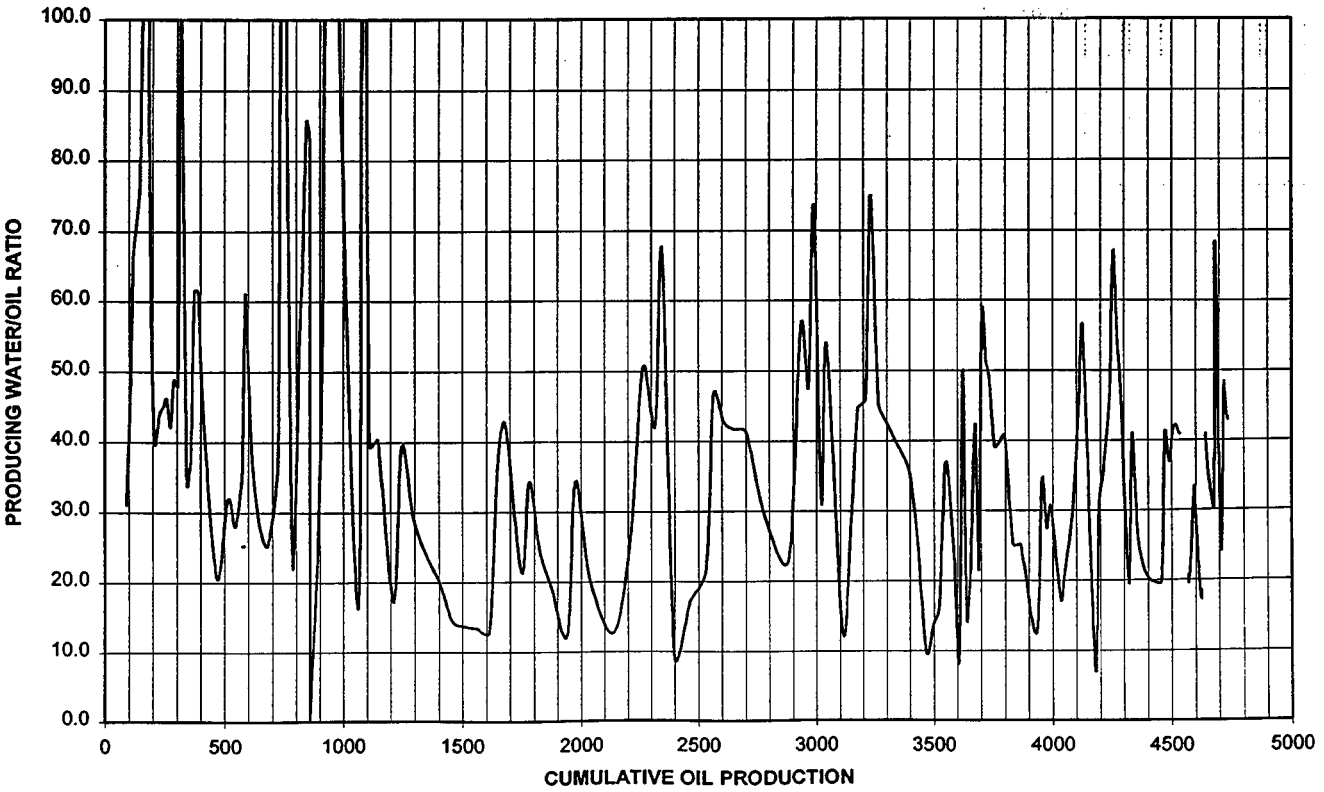
100.0
90.0
80.0
70.0
60.0
50.0
40.0
30.0
20.0
10.0
0.0
PRODUCING WATER/OIL RATIO
0
500
1000
1500
2000
2500
3000
3500
4000
4500
5000
CUMULATIVE OIL PRODUCTION

K-43

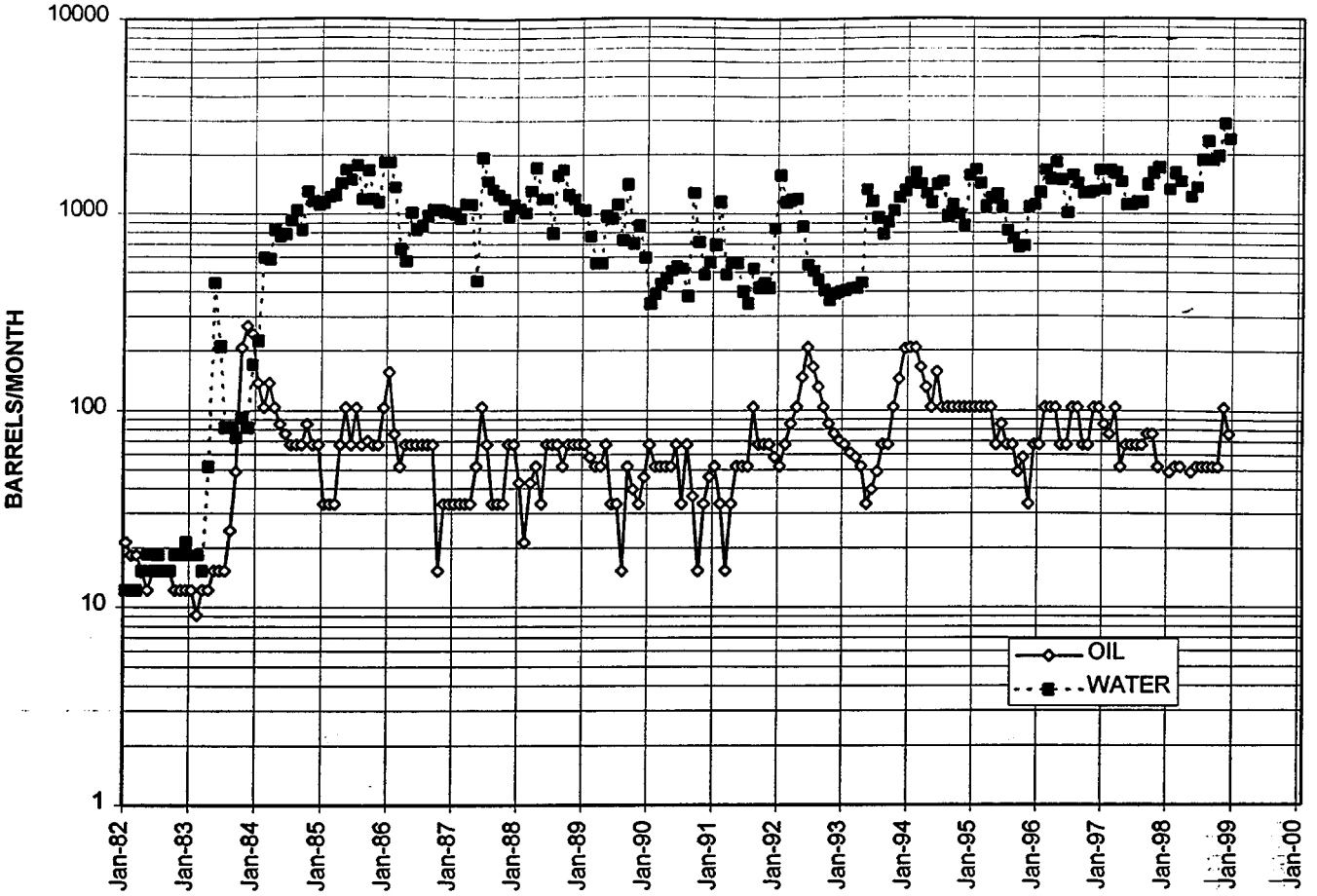
10000
1000
100
10
1
BARRELS/MONTH
OIL
WATER
Jan-82
Jan-83
Jan-84
Jan-85
Jan-86
Jan-87
Jan-88
Jan-89
Jan-90
Jan-91
Jan-92
Jan-93
Jan-94
Jan-95
Jan-96
Jan-97
Jan-98
Jan-99
Jan-00

K-43

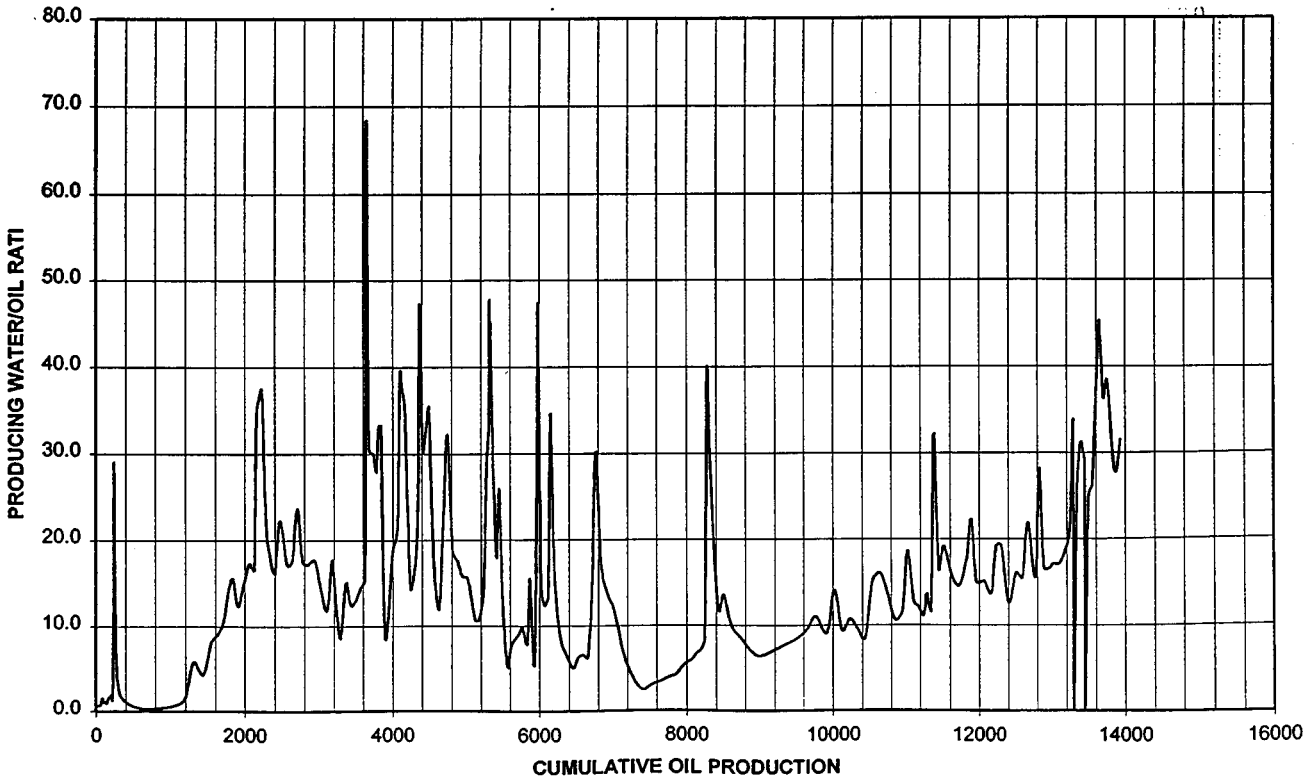
80.0
70.0
60.0
50.0
40.0
30.0
20.0
10.0
0.0
PRODUCING WATER/OIL RATI
0
2000
4000
6000
8000
10000
12000
14000
16000
CUMULATIVE OIL PRODUCTION

K-44

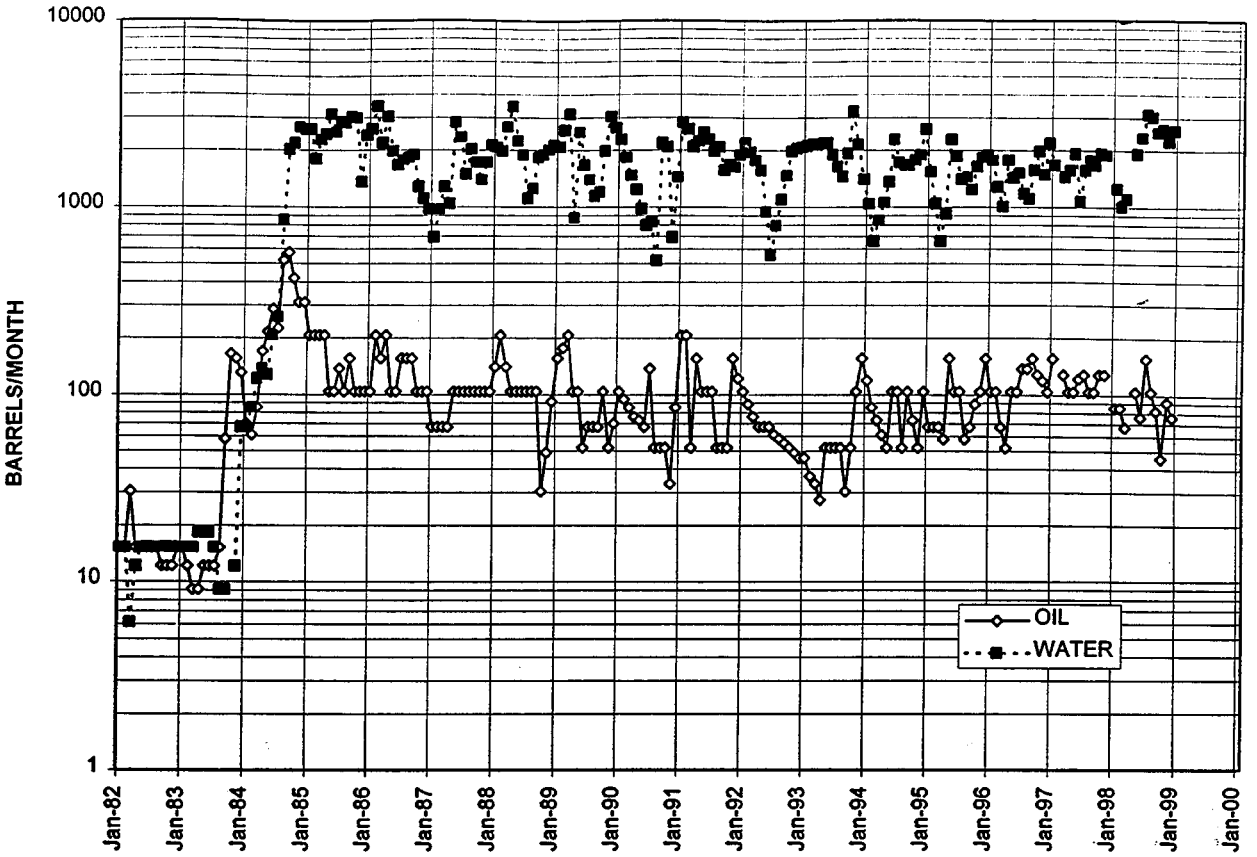
10000
1000
100
10
1
BARRELS/MONTH
OIL
WATER
Jan-82
Jan-83
Jan-84
Jan-85
Jan-86
Jan-87
Jan-88
Jan-89
Jan-90
Jan-91
Jan-92
Jan-93
Jan-94
Jan-95
Jan-96
Jan-97
Jan-98
Jan-99
Jan-00

K-44

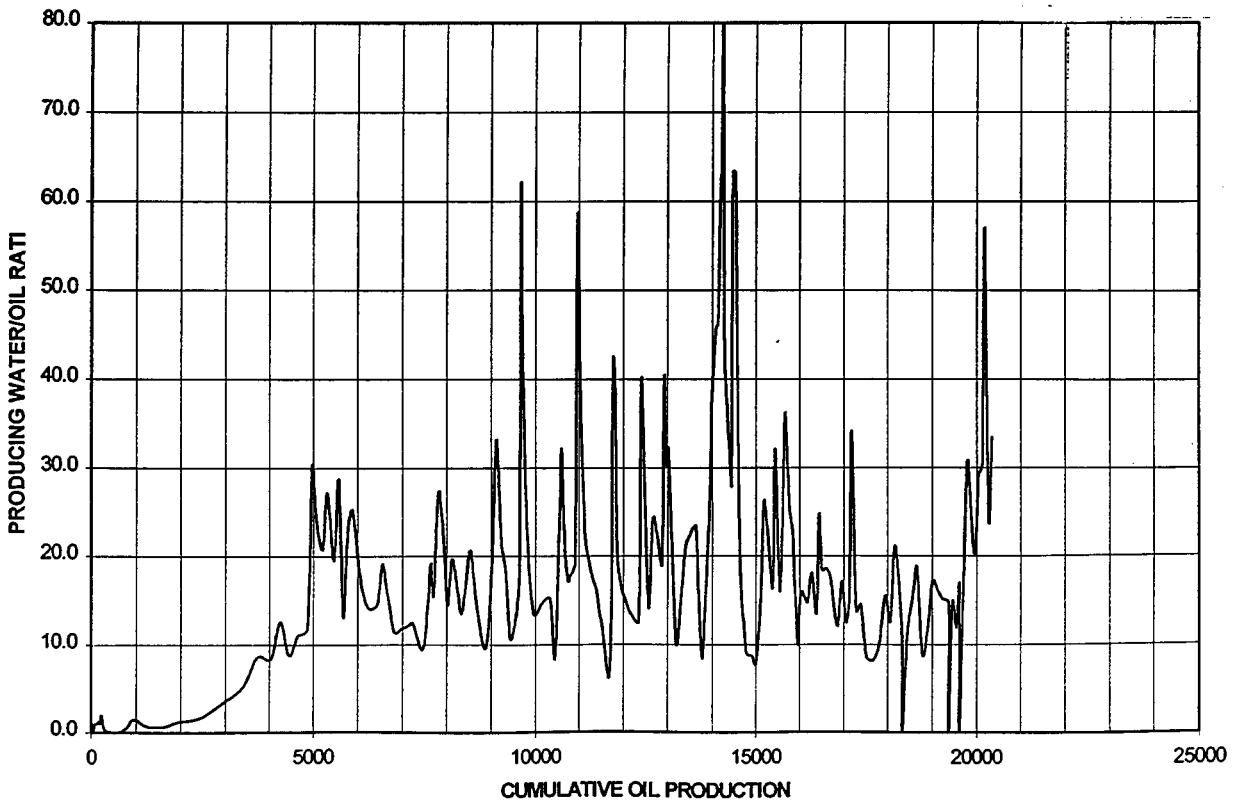
80.0
70.0
60.0
50.0
40.0
30.0
20.0
10.0
0.0
PRODUCING WATER/OIL RATI
0
5000
10000
15000
20000
25000
CUMULATIVE OIL PRODUCTION

K-45

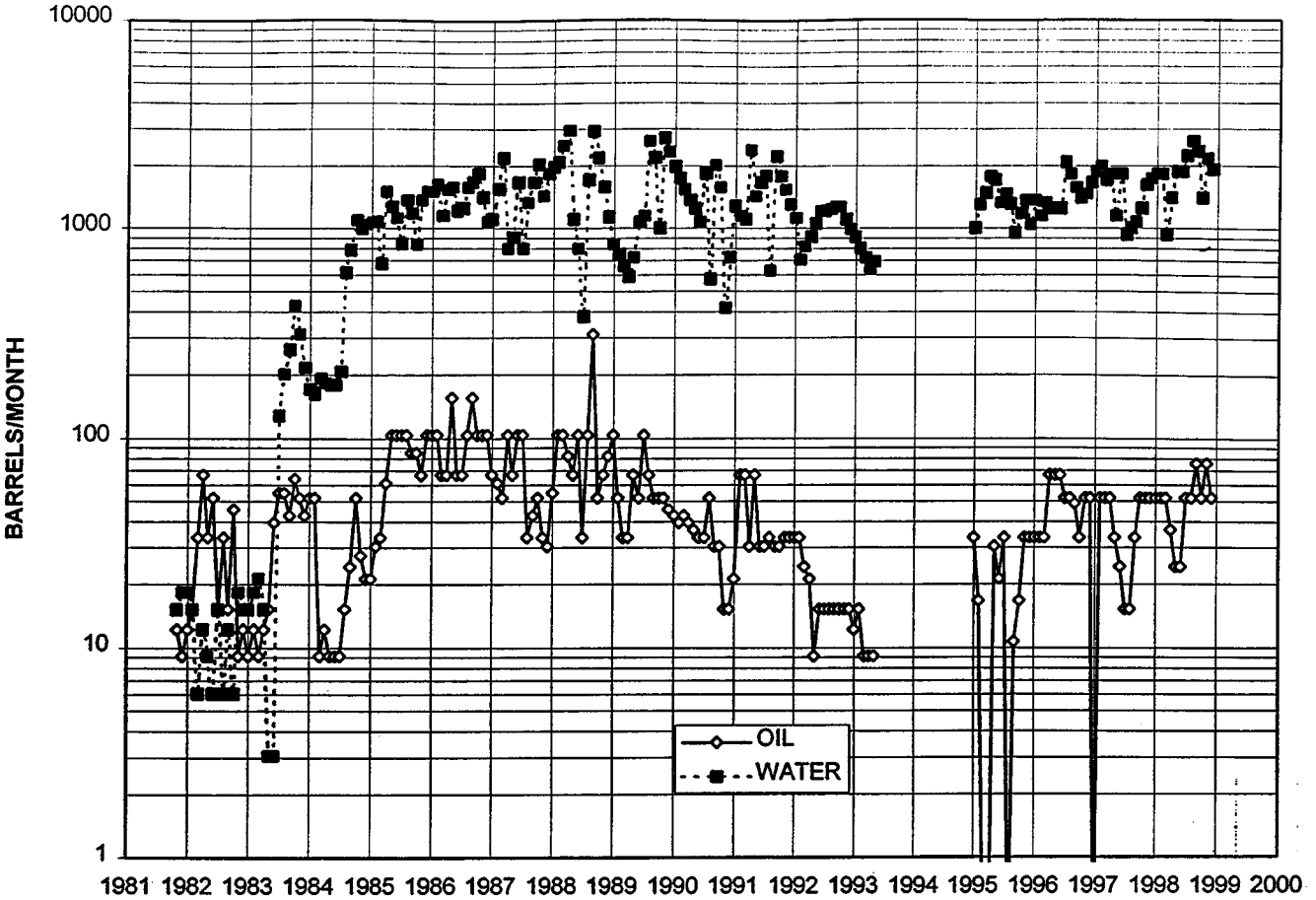
10000
1000
100
10
1
BARRELS/MONTH
OIL
WATER
1981 1982 1983 1984 1985 1986 1987 1988 1989 1990 1991 1992 1993 1994 1995 1996 1997 1998 1999 2000

K-45

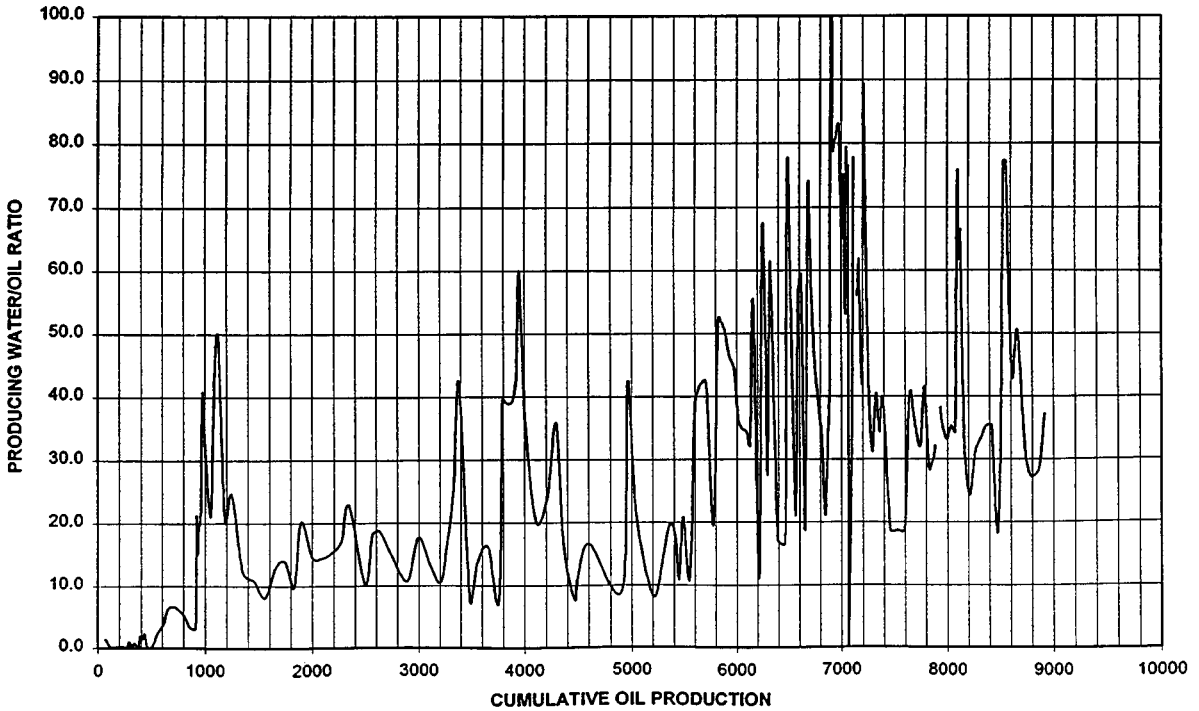
100.0
90.0
80.0
70.0
60.0
50.0
40.0
30.0
20.0
10.0
0.0
PRODUCING WATER/OIL RATIO
0 1000 2000 3000 4000 5000 6000 7000 8000 9000 10000
CUMULATIVE OIL PRODUCTION

K-54

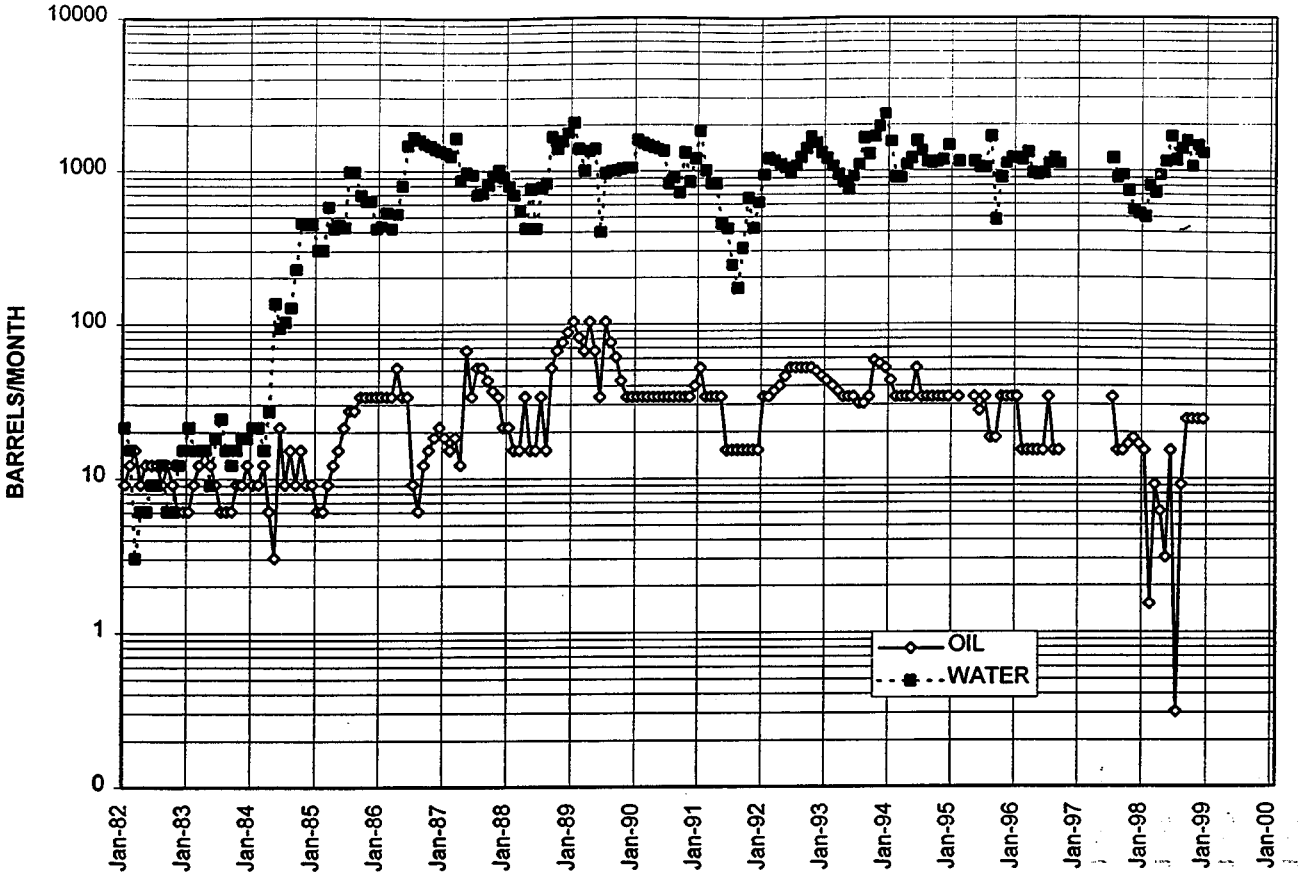
10000
1000
100
10
1
0
BARRELS/MONTH
OIL
WATER
Jan-82
Jan-83
Jan-84
Jan-85
Jan-86
Jan-87
Jan-88
Jan-89
Jan-90
Jan-91
Jan-92
Jan-93
Jan-94
Jan-95
Jan-96
Jan-97
Jan-98
Jan-99
Jan-00

K-54

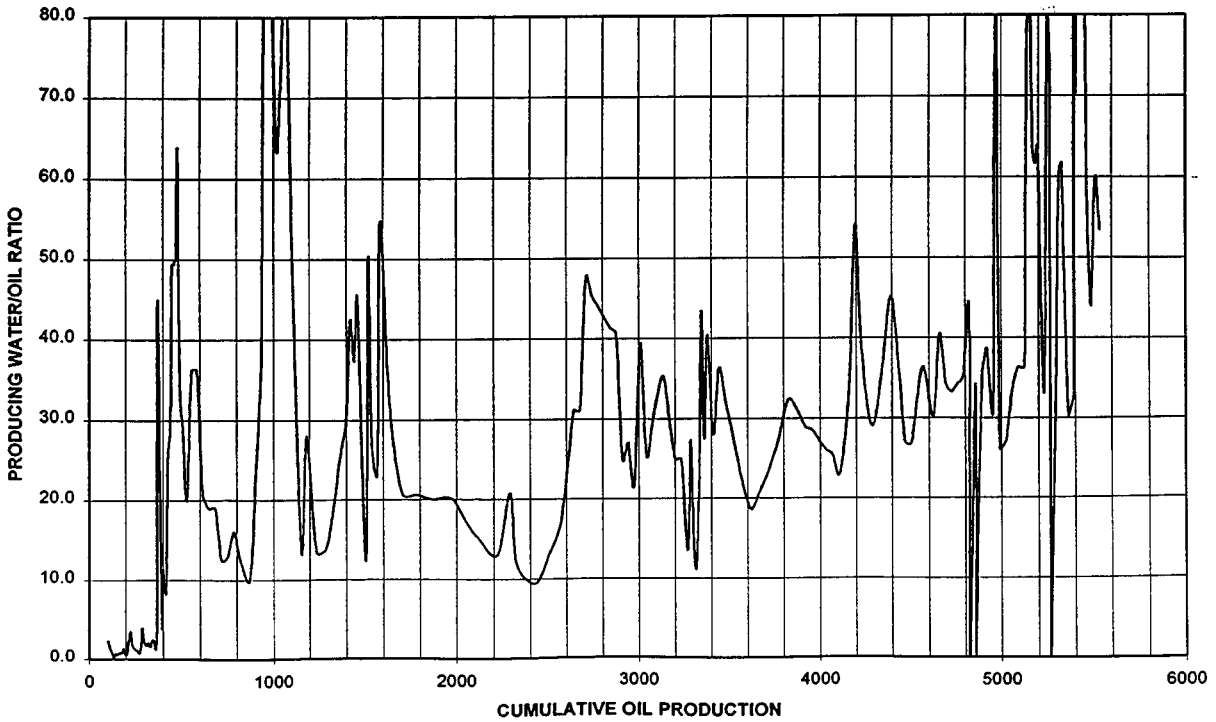
80.0
70.0
60.0
50.0
40.0
30.0
20.0
10.0
0.0
PRODUCING WATER/OIL RATIO
0
1000
2000
3000
4000
5000
6000
CUMULATIVE OIL PRODUCTION

O-1

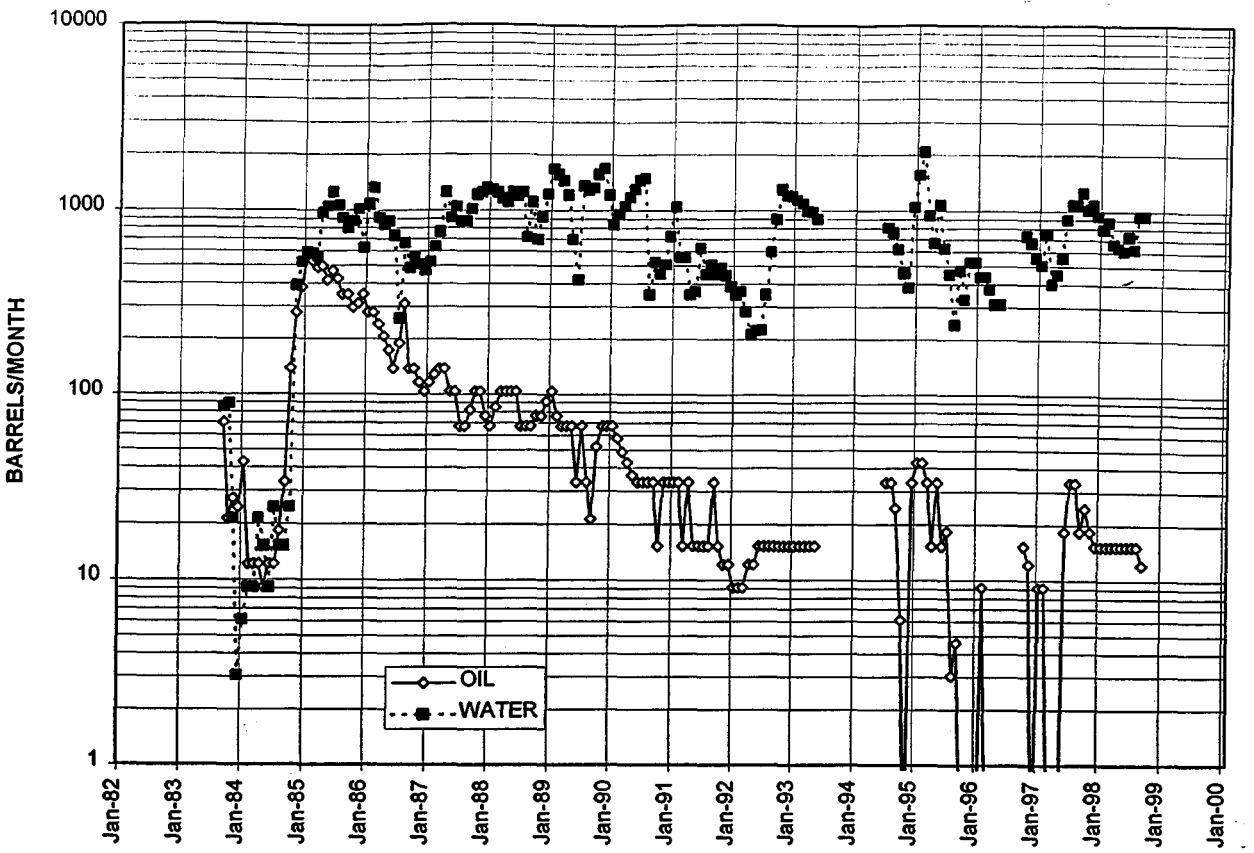
10000
1000
100
10
1
BARRELS/MONTH
OIL
WATER
Jan-82
Jan-83
Jan-84
Jan-85
Jan-86
Jan-87
Jan-88
Jan-89
Jan-90
Jan-91
Jan-92
Jan-93
Jan-94
Jan-95
Jan-96
Jan-97
Jan-98
Jan-99
Jan-00

O-1

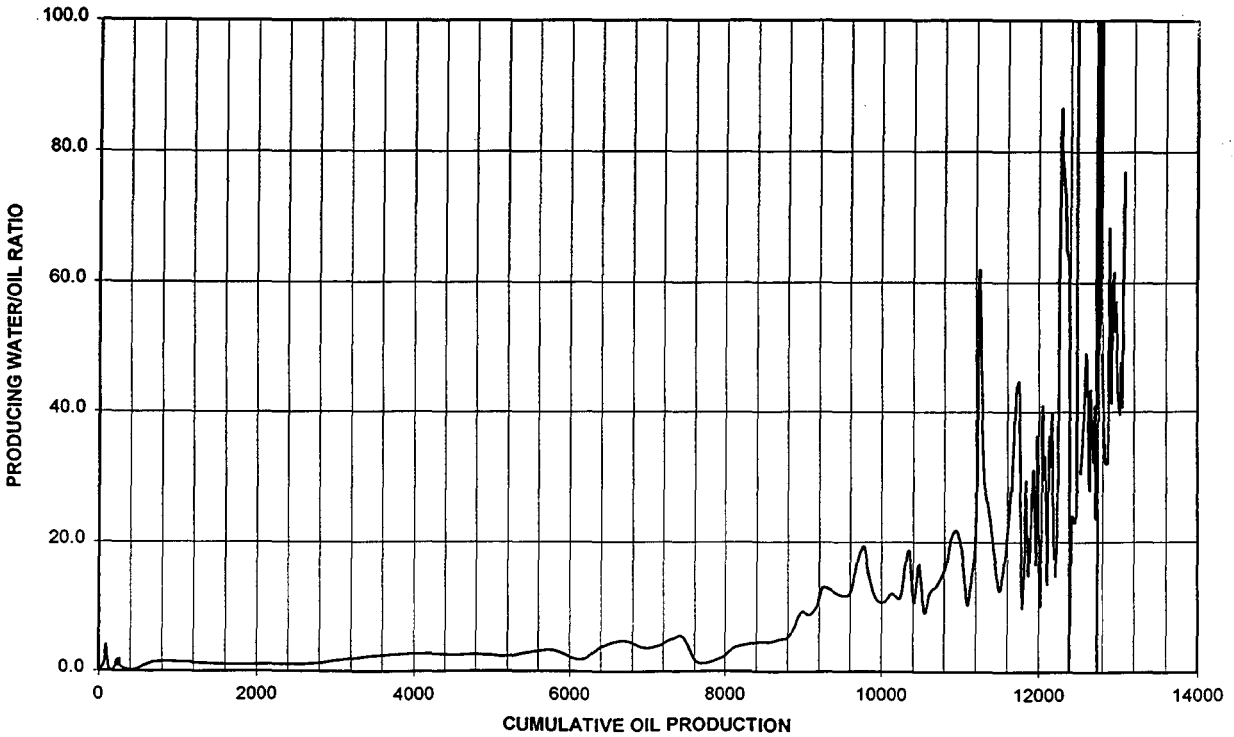
100.0
80.0
60.0
40.0
20.0
0.0
PRODUCING WATER/OIL RATIO
0
2000
4000
6000
8000
10000
12000
14000
CUMULATIVE OIL PRODUCTION

Appendix C

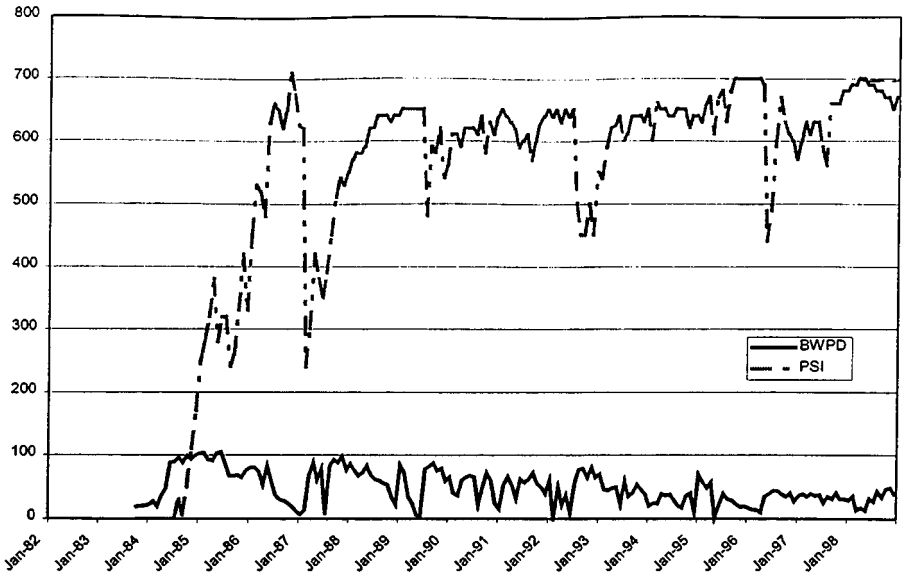

H-12 INJECTIVITY INDEX

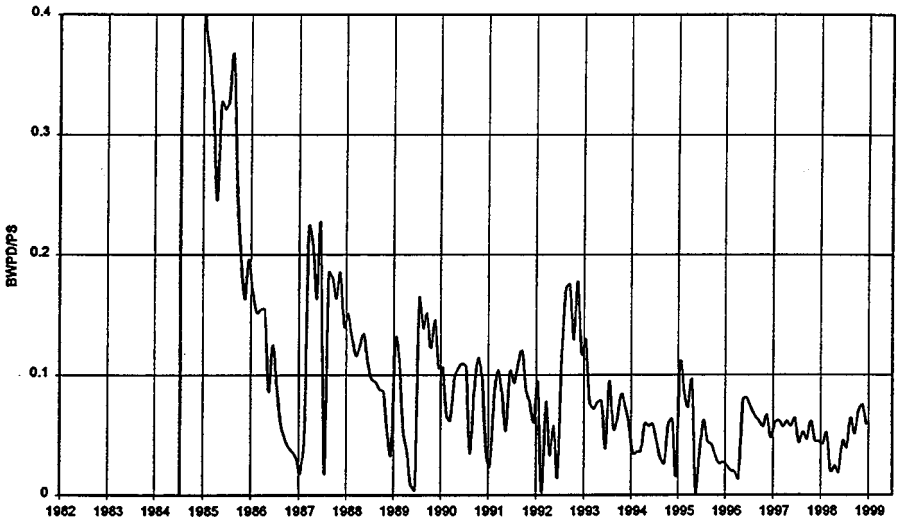

H-12 HALL PLOT

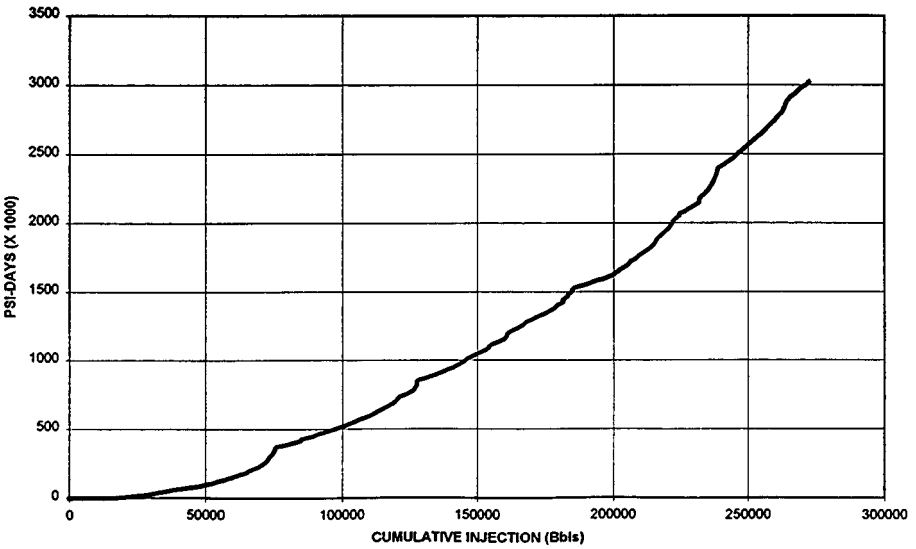

H-14 INJECTION HISTORY

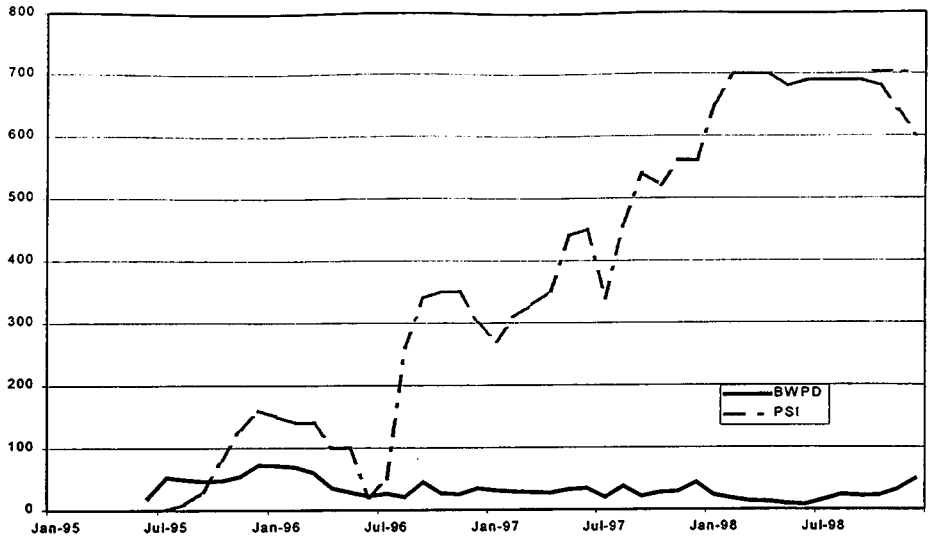

H-14 INJECTIVITY INDEX

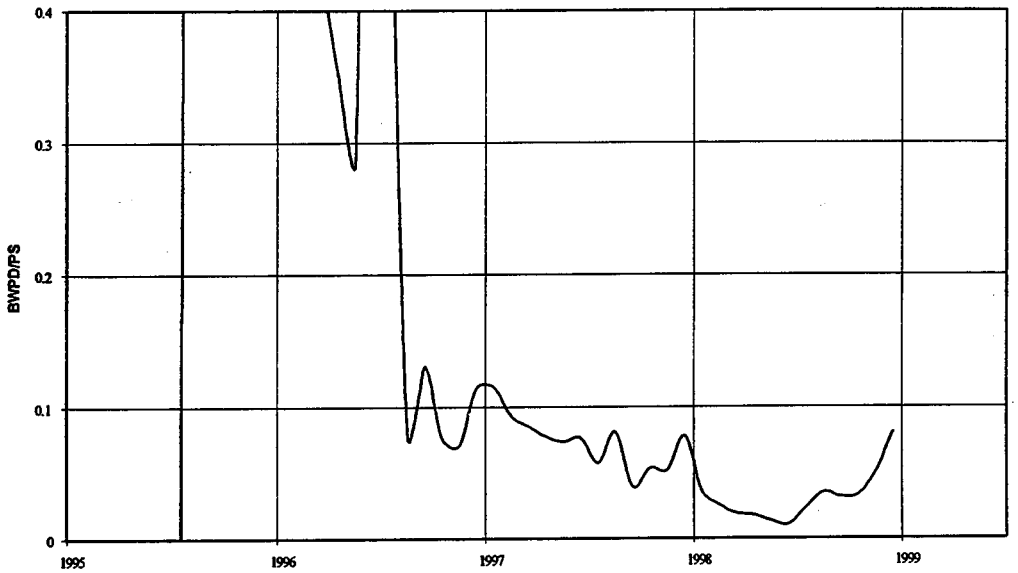

H-14 HALL PLOT

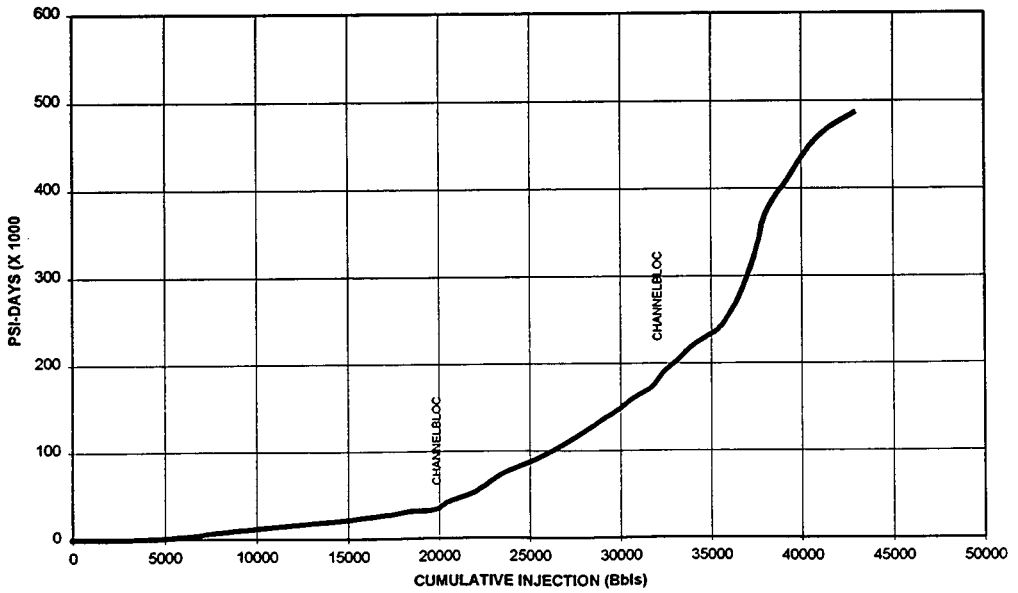

KW-7 INJECTION HISTORY

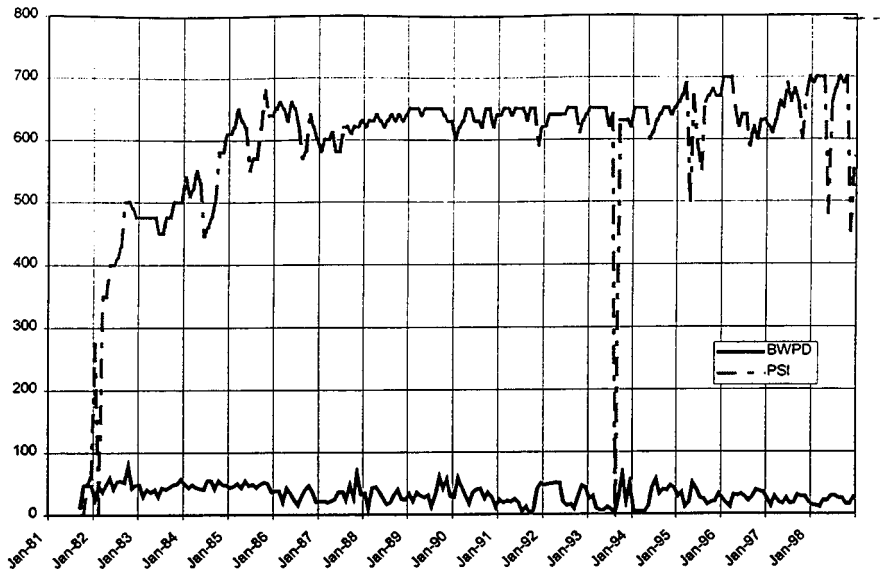

KW-7 INJECTIVITY INDEX

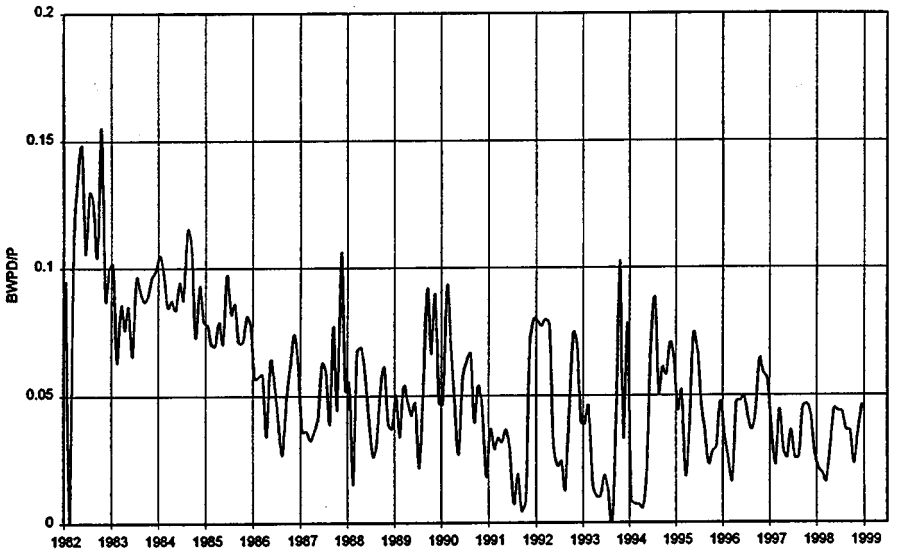

KW-7 HALL PLOT

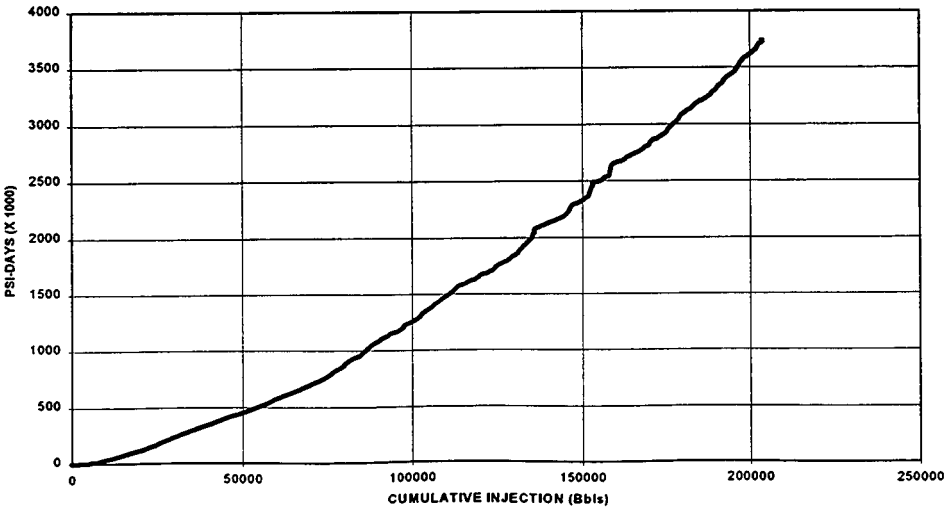

KW-9 INJECTION HISTORY

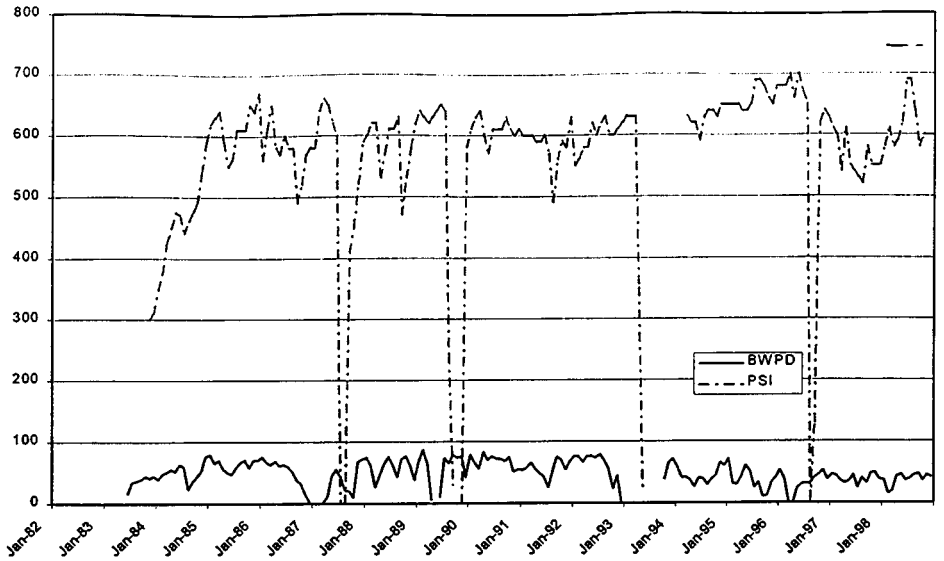

KW-9 INJECTIVITY INDEX

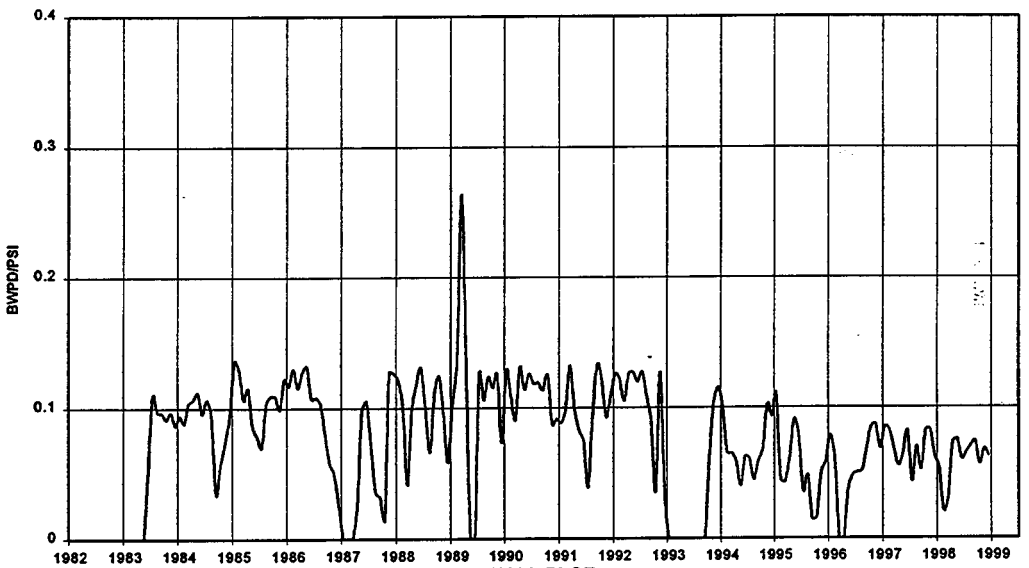

KW-9 HALL PLOT

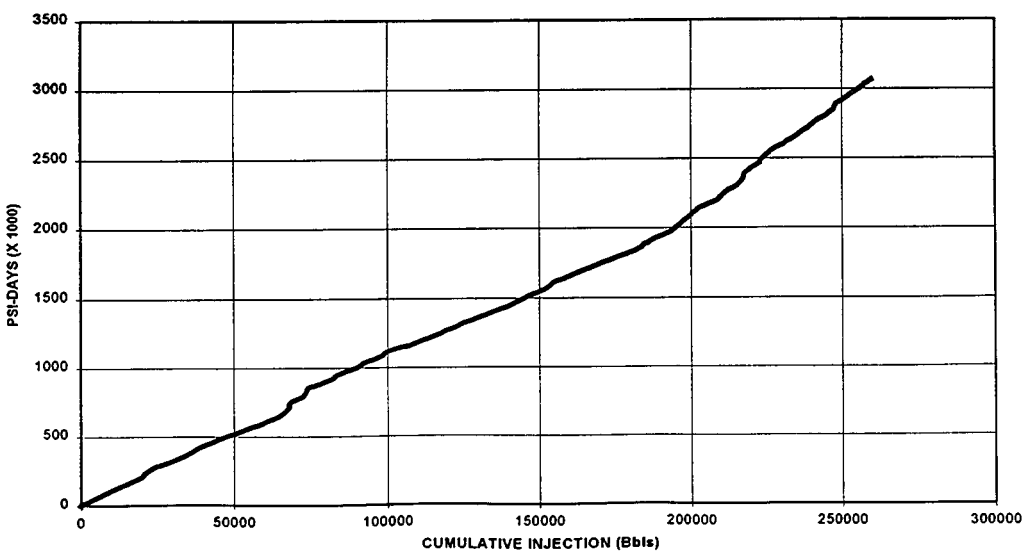

KW-11 INJECTION HISTORY

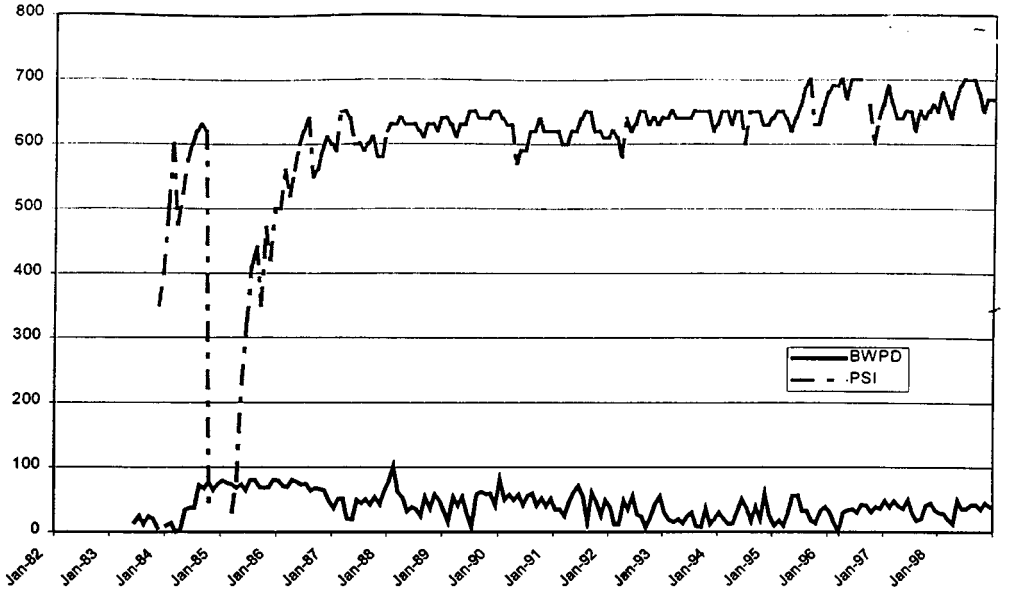

KW-11 INJECTIVITY INDEX

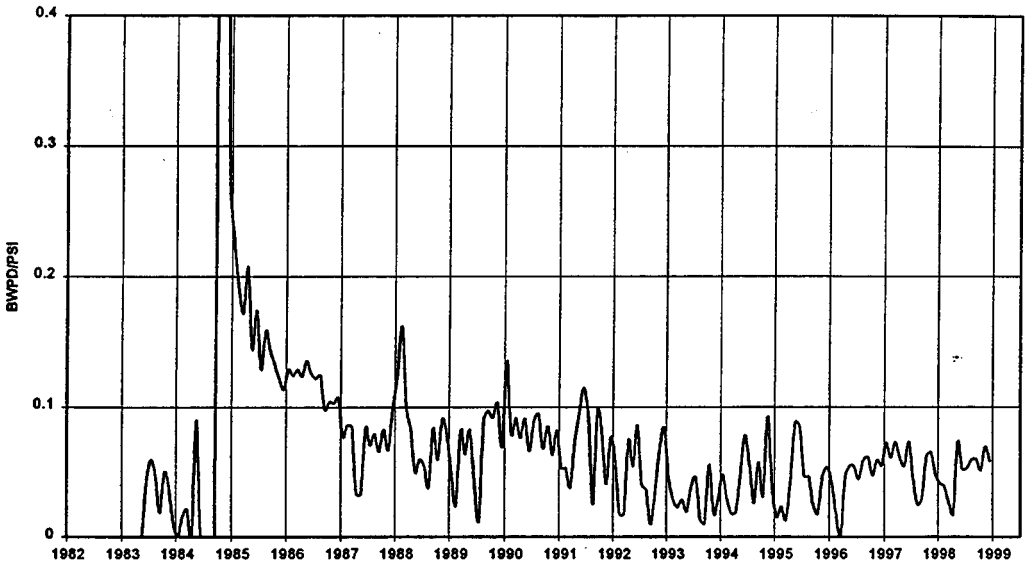

KW-11 HALL PLOT

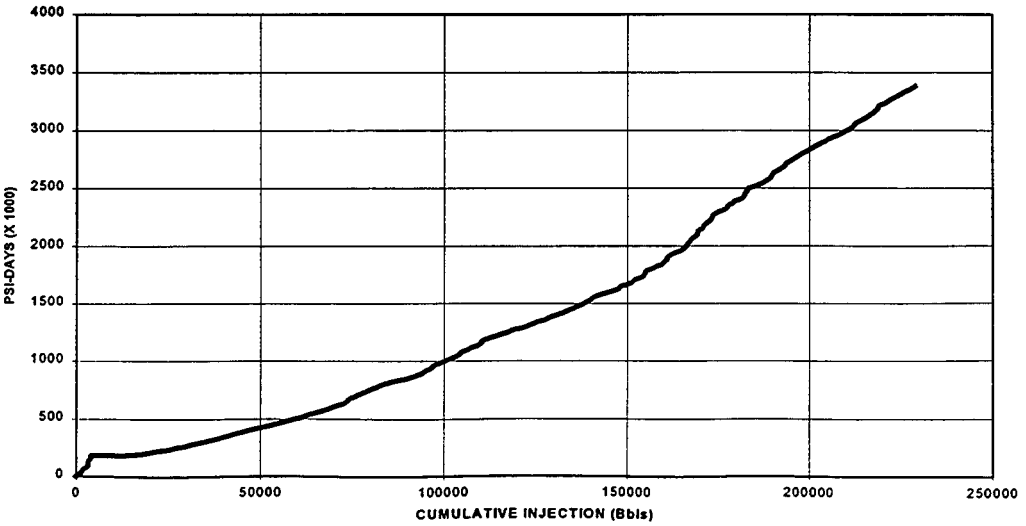

RW-3 INJECTION HISTORY

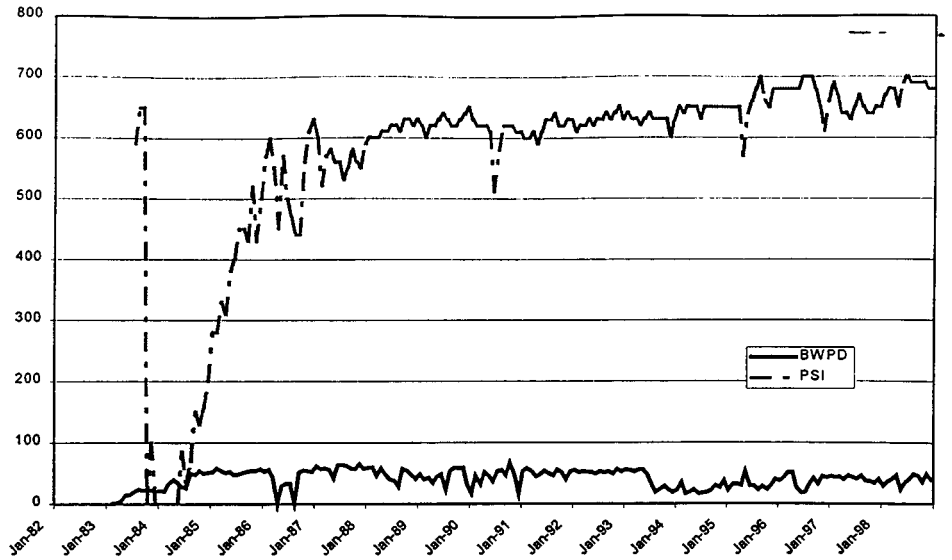

RW-3 INJECTIVITY INDEX

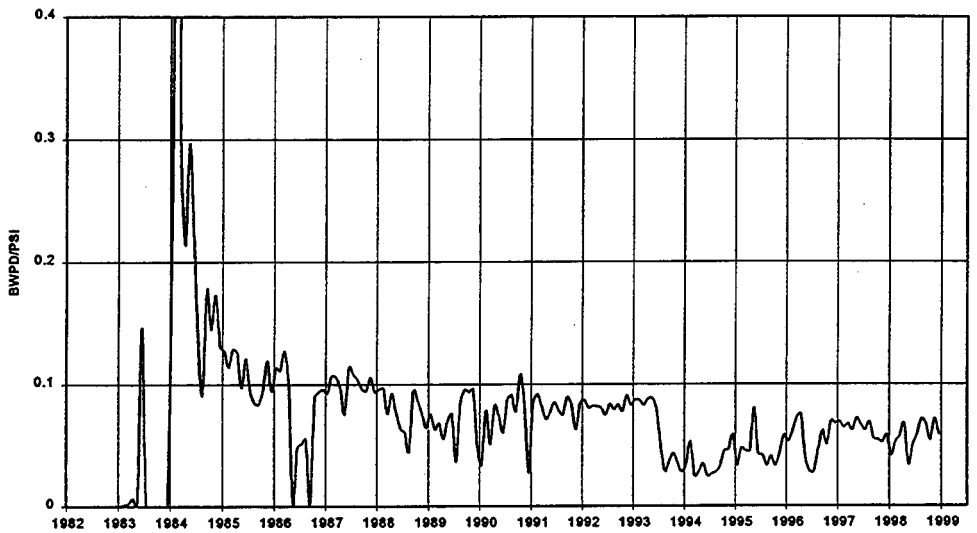

RW-3 HALL PLOT

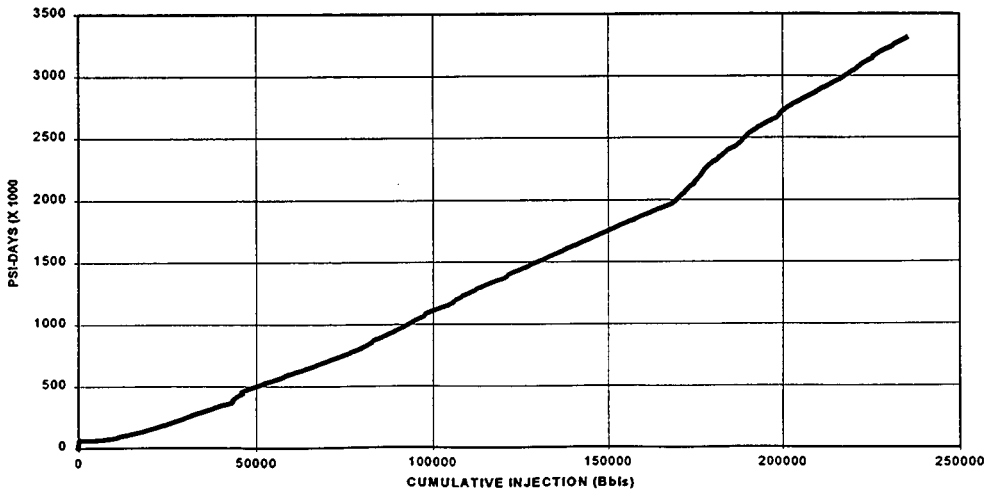

RW-8 INJECTION HISTORY

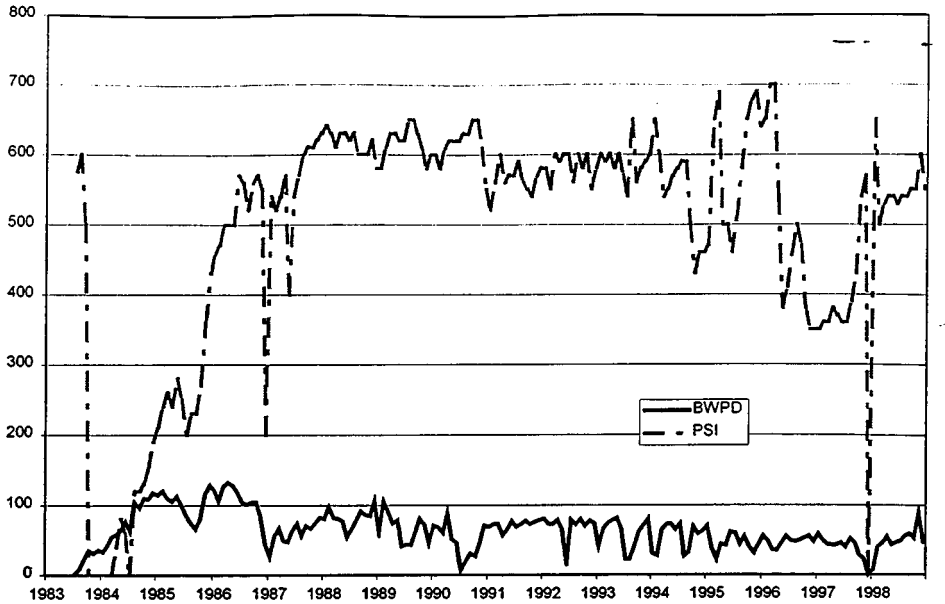

RW-8 INJECTIVITY INDEX

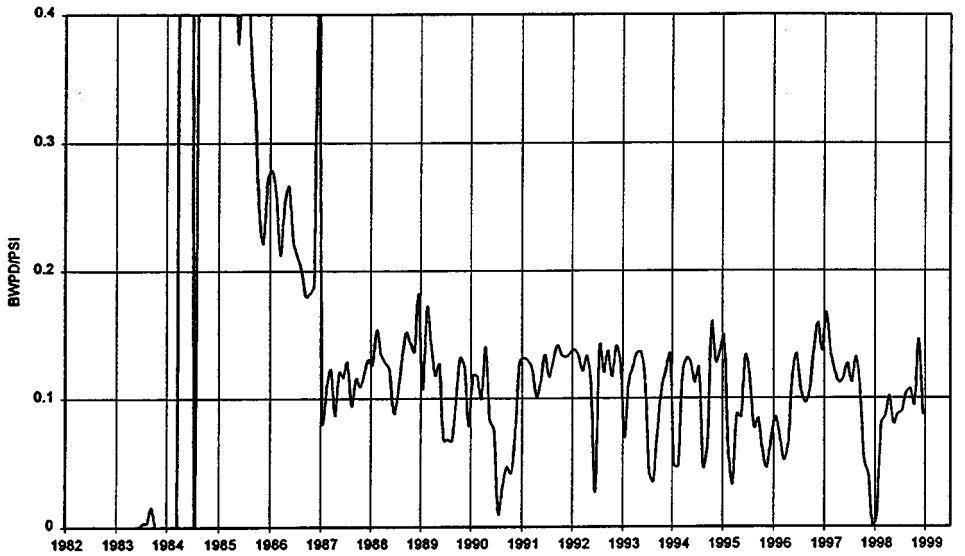

RW-8 HALL PLOT

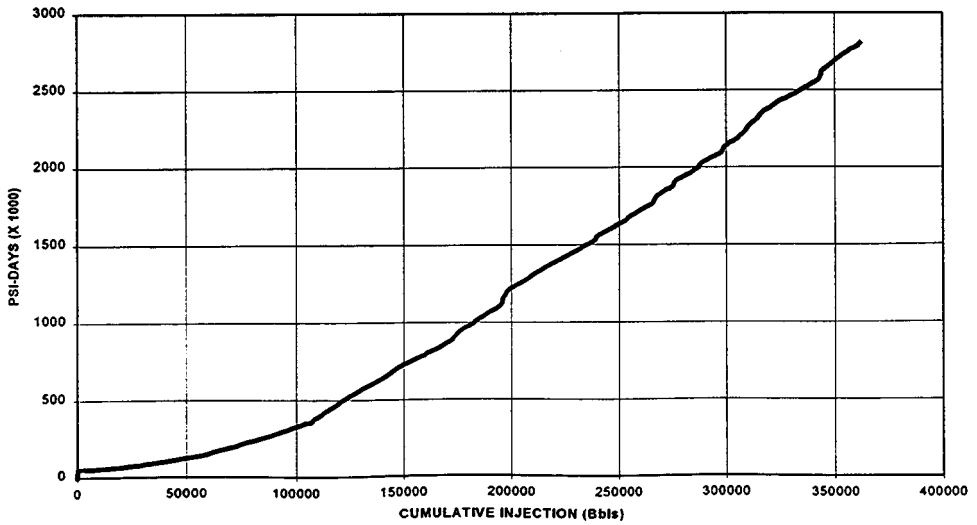

RW-20 INJECTION HISTORY

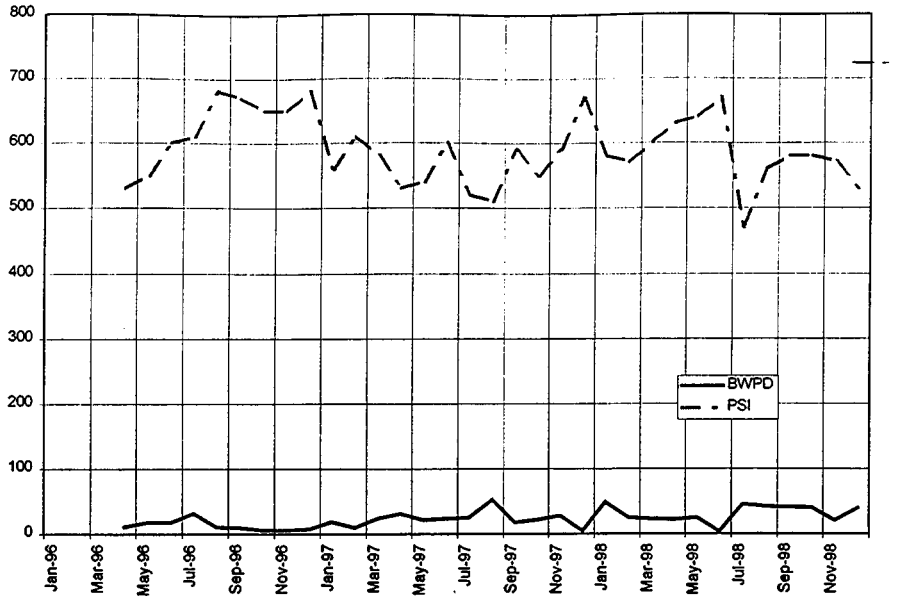

RW-20 INJECTIVITY INDEX

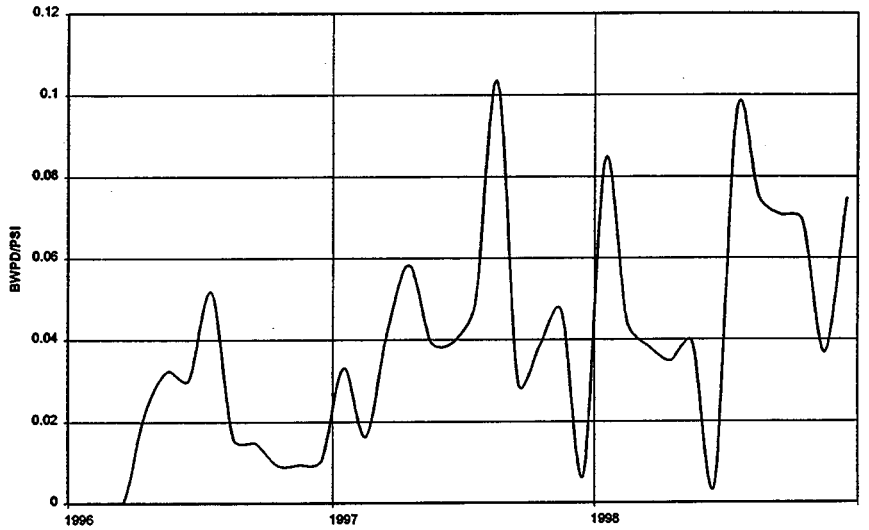

RW-20 HALL PLOT

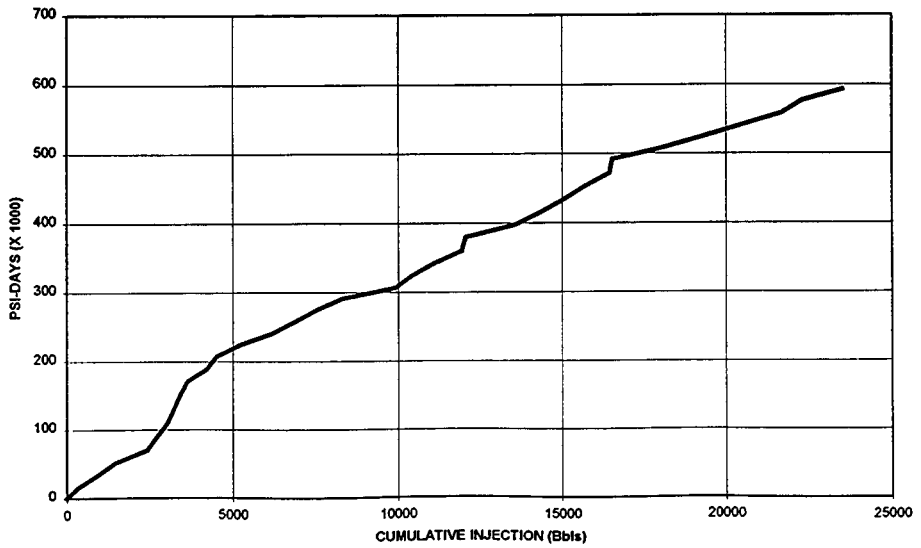

H-12; LATE-TIME HALL PLOT

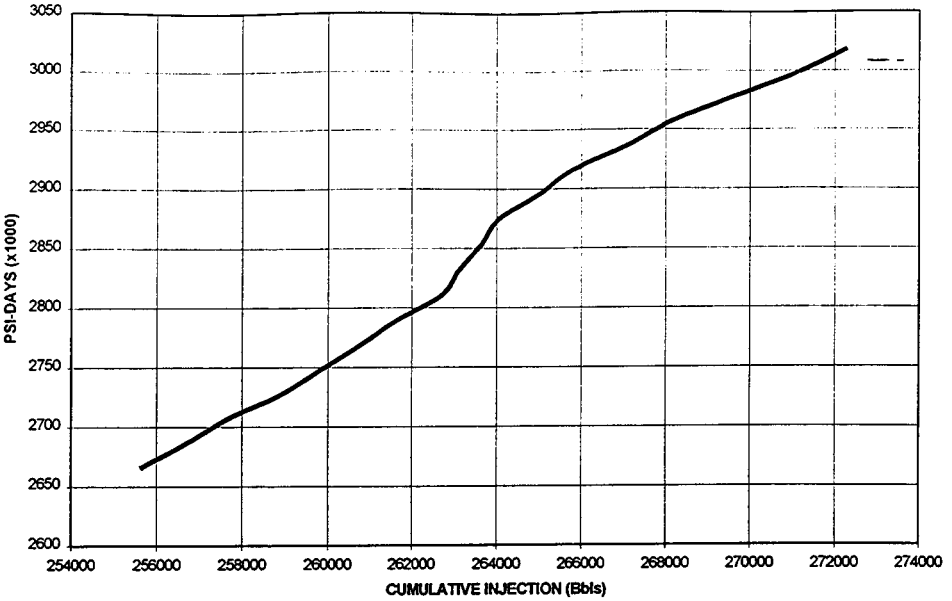

H-14; LATE-TIME HALL PLOT

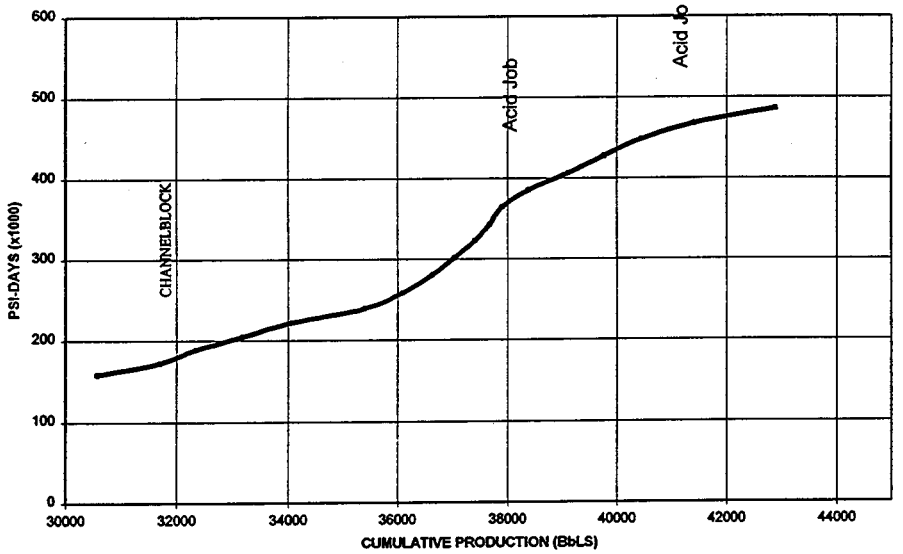

KW-7; LATE-TIME HALL PLOT

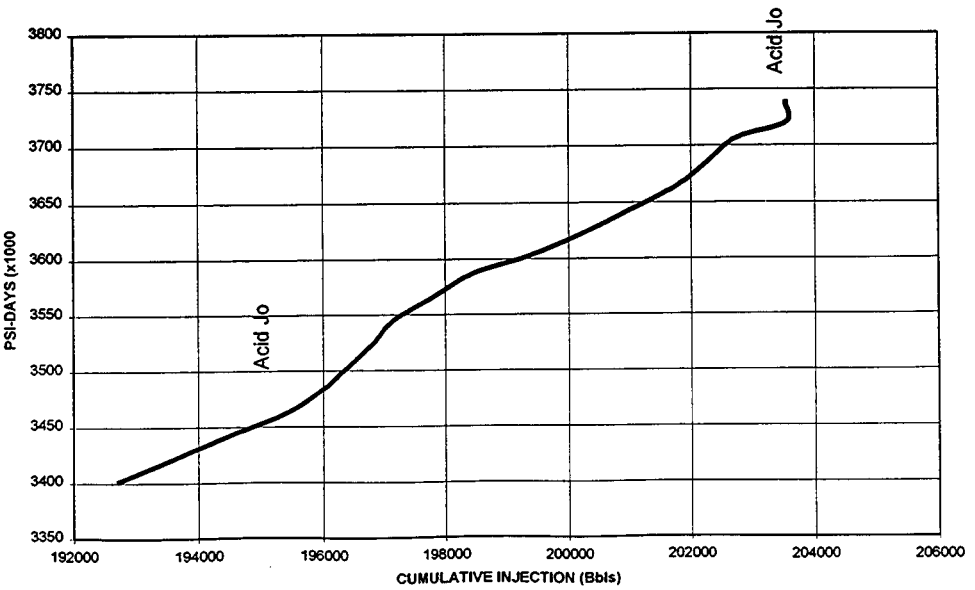

KW-9 HALL PLOT

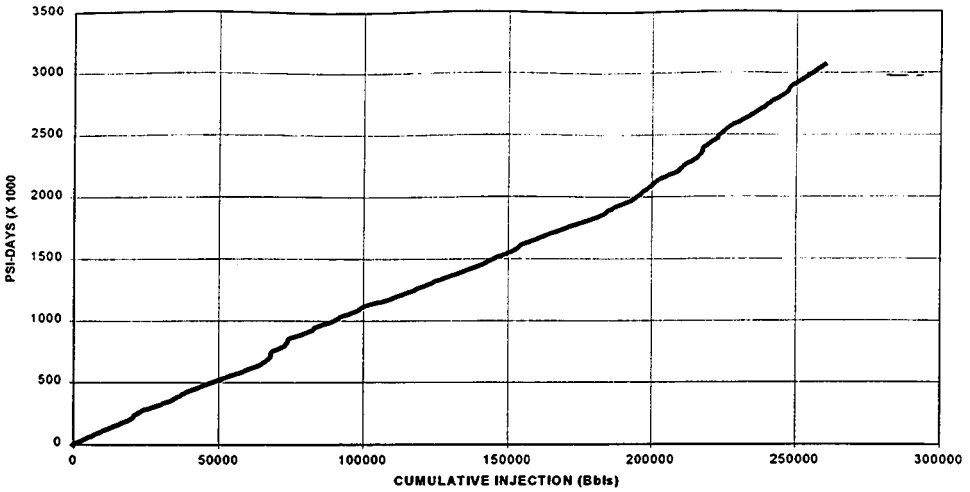

KW-11; LATE-TIME HALL PLOT

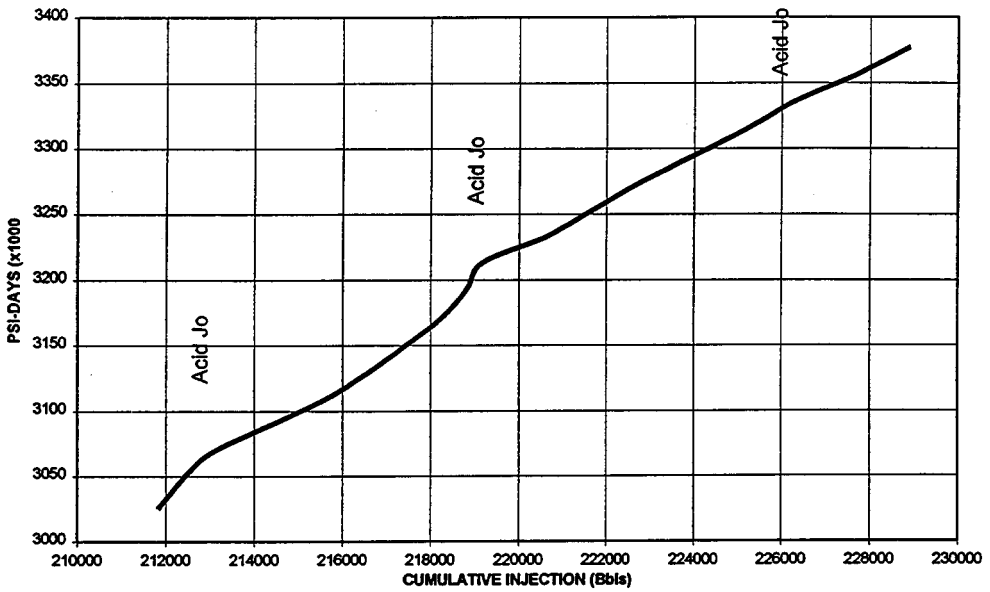

RW-3; LATE-TIME HALL PLOT

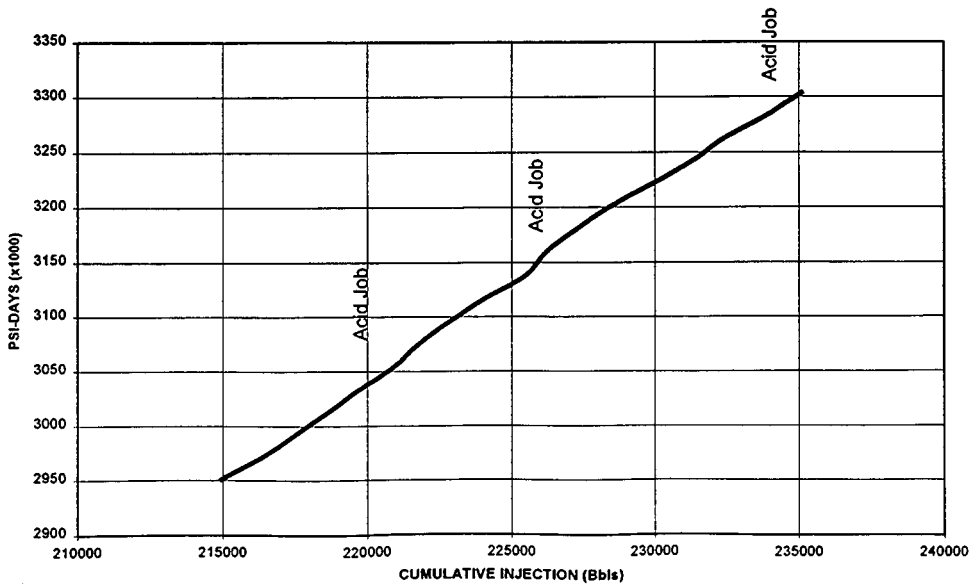

RW-8; LATE-TIME HALL PLOT

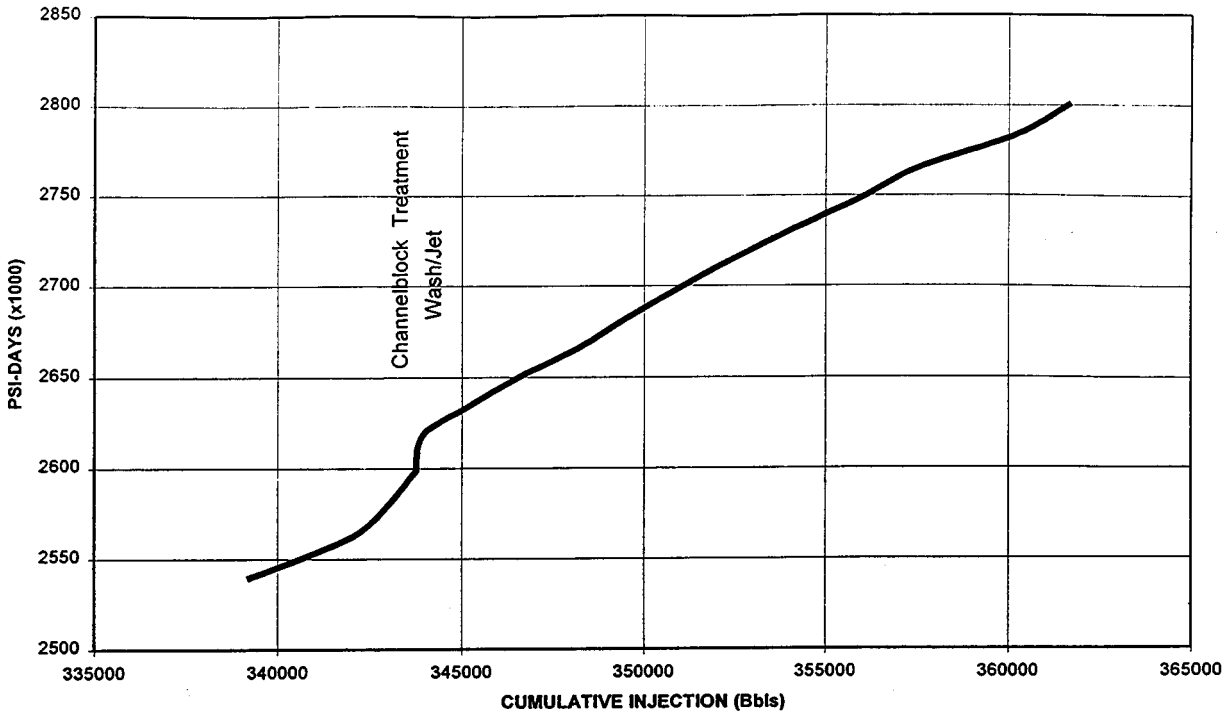

RW-20; LATE-TIME HALL PLOT

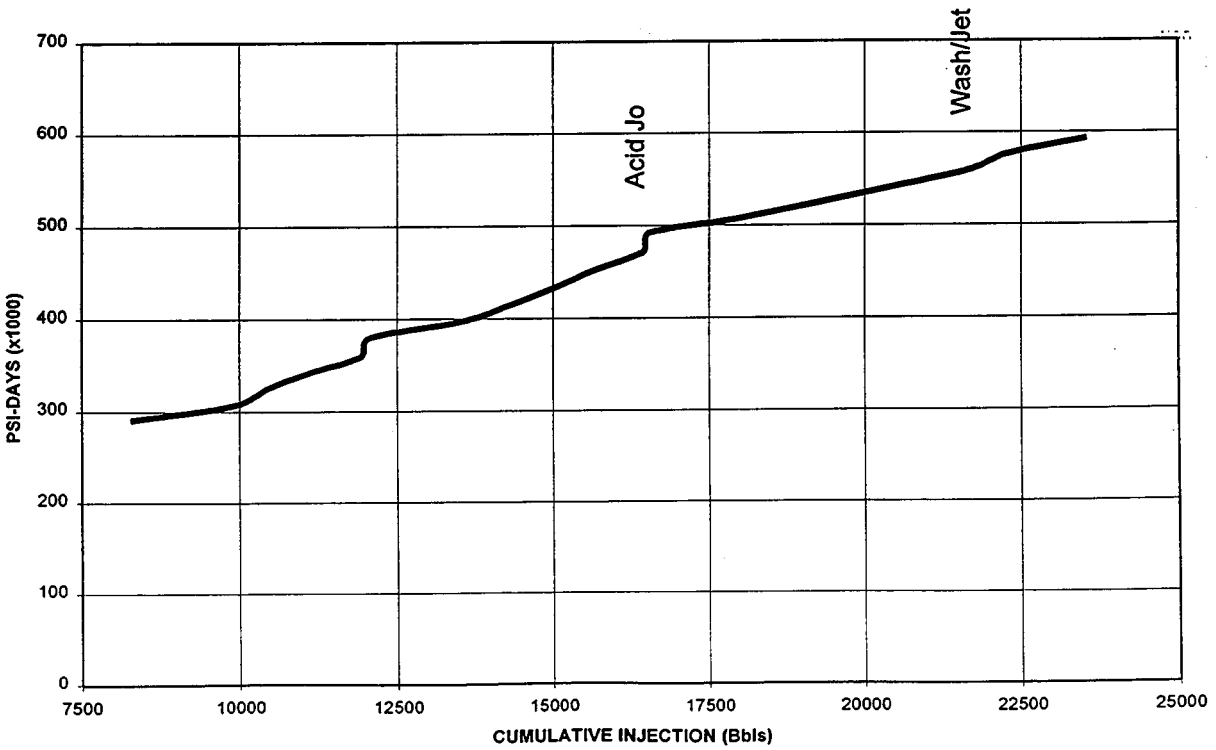

Appendix D

Water Quality Improvement by Air Flotation
Savonburg Project, Nelson Lease

Michael J. Michnick, Senior Scientist
Tertiary Oil Recovery Project
University of Kansas

The success of a waterflood for the recovery of petroleum from a reservoir depends on the quality of the water injected into the reservoir and the path the water takes between injection and production wells. The injection water will take the path of least resistance through the formation. Imbibition of water by the rock and the pressure gradient from injection to production well allows the flood water to contact a greater area of the reservoir than just close to natural and man caused fractures. Water quality can affect and alter the water path. The five harmful constituents in flood water, in order of importance are; (1) dispersed oil; (2) bacteria and algae; (3) suspended solids; (4) dissolved solids; and (5) dissolved gases. Both oil and solids plug the entrance to the pores at the well bore or fracture face near the well bore, and thus, diminish the water volume that can enter the pores of the reservoir rock. An attempt is made periodically to remove this accumulation of debris by treating the well with hydrochloric acid and other cleaning chemicals. Removal of dissolved and suspended solids is generally incomplete, even when the injection well is back flowed after an acid-chemical treatment. Insolubility of oil, silica, clay, bacterial and algae debris, and scale deposit such as barium sulfate in hydrochloric acid prevents the restoration of the injection well to its full potential.

Typical waterflood operations and problems

When an operator decides to start a waterflood to prolong the economic life of the lease, three questions need to be answered. First, where can the flood water be obtained on or near the lease? The source of the flood water is generally from a saline zone other than the oil zone. This water zone must supply a sufficient quantity of water to meet the needs of the waterflood. This water is generally of excellent quality and causes no problems at the injection wells, unless the source zone contains traces of oil or has been contaminated by the disposal of water into the zone. Bacteria are always a problem in all wells. Chemical incompatibility between the injected and connate waters can lead to serious formation plugging and is discussed below.

Second, what will be done with the produced water when it appears at. the production wells? The operator of the lease has three choices. The first choice is that all the produced water is sent to a disposal well(s) on or near the lease. The second choice is that the produced water is re-injected into selected injection wells. This requires two water handling systems on the lease. The third choice is that the produced water is combined with the injection water before the water is sent to the injection wells. This latter practice commonly occurs in waterflood operations, especially by the small independent operators, and leads to major problems in the injection wells. Precipitation of minerals when incompatible waters are combined and the carryover of oil from the produced water eventually plugs the injection wells.

Third, how will the injection water affect the properties of the reservoir? Each zone in a reservoir is from a different geological era, and therefore, the water frequently has a different dissolved mineral content. When incompatible waters are mixed, precipitation of barium and calcium sulfate, calcium carbonate, and iron sulfide or oxide commonly occurs. A check for compatibility of the proposed injection water with the connate water in the oil reservoir, if considered, is frequently ignored because of a limited source of supply water or immediate economic needs. Many oil operators will inject an incompatible flood water into the oil reservoir based on the assumption that the damage in the mixing zone will be small, or treatment of the injection well with acid and/or chemicals will restore the capability of the well to take water, or that any future problems will not be their concern.

The Proposal to the Department of Energy

The Tertiary Oil Recovery Project at the University of Kansas, in cooperation with several independent oil operators, submitted a proposal to investigate typical problems faced by operators in Kansas in response to a Department of Energy notice. The following excerpts, taken from the proposal submitted to the Department of Energy on January 10, 1992, describe the problem and the solution to the water quality problem.

"Project Overview - The major emphasis of this project will be to address waterflood problems of the type found in Cherokee Group reservoirs in southeastern Kansas. General topics addressed will be (1) reservoir management and performance evaluation, (2) waterflood optimization, and (3) the demonstration of a recovery process involving off-the-shelf technology . . . (page 47)."
"Phase II - Processes to be Implemented - The implementation phase will be conducted in two stages, (1) the waterflood optimization stage, and (2) the reservoir development stage . . . (page 58)." "The waterflood optimization will consist of, (1) the development of a water plant, and (2) profile modification treatments to reduce channeling of injected water, (3) well bore cleanup treatments and, (4) pattern changes . . . (pages 58-59)." "A water plant will be designed and constructed which is capable of producing high quality brine continuously. The water plant will be monitored daily for water quality. Five-micron filters will be placed at each well to act as monitoring devices. If the 5-micron filters plug, the water plant will be redesigned until acceptable water quality is achieved ... (page 59)."

From this broad statement in the proposal, one goal of the Savonburg Project was to improve the quality of the injection water with the premise that cleaner water would reduce the cost of injection well operations. The equipment and chemicals were to be "off the shelf technology" and require no long term support from Tertiary Oil Recovery Project personnel after installation and startup of the equipment.

This report describes the water problem at the Nelson Lease, the choice of using air flotation to clean the water, the principles of air flotation, and the installation of the equipment into the then current water plant. Next the "off the shelf technology" approach is covered with its achievement and failure. A description follows of the necessary changes needed in the flotation equipment, the water handling practices, the need for flow meters, and the analytical measuring equipment with the training of field personnel in the use of the equipment.

Nelson Lease Water Plant

The Nelson Lease that is in Allen County, Kansas in the N. E. Savonburg Field is operated by Russell Petroleum, Incorporated. The projects consist of three 160-acre leases in Sections 21, 28, and 29, Township 26 South, Range 21 East. The lease is 1.5 miles east of the county road that connects the towns of Elsmore and Savonburg both which are 1 mile east of US 59. The first well was drilled in 1962. A pilot waterflood was initiated in March 1981, expanded in 1983, and a full waterflood was started in 1985. The water plant currently consists of a single triplex pump to pump water at sufficient pressure and volume to the individual injection wells via a pipe-manifold system. Water for two to six individual injection wells are supplied from a single manifold. Control valves, flow meter, and filter are installed at the manifold in the flow line to each well.

At some point in the waterflood operations, Russell Petroleum decided that the produced and supply (makeup water) waters would be mixed before re-injection into the reservoir. Figure 1 is a schematic of the water flow through the plant in early 1993. All the produced water was reused. This water was passed through a 7x32 inch, 75-micron bag filter and sent to the clean water tank. The additional water needed for the flood was obtained from the supply well that was also sent to the clean water tank. The water in the clean water tank was grayish-black to reddish-brown in color depending on the ratio of produced and supply water, and the oxygen in the water.

The produced water contained oil and solids smaller than 75 microns that passed through the bag filter. Additional solids formed when the two incompatible waters were mixed. Bacteria and algae in the clean water storage tank added to the problem. Each injection well was protected with 75-micron cartridge filters. A significant quantity of solids would pass through the cartridge filters and eventually reduce the water flow at the injection well to the point that the well had to be cleaned. The removal of solids from the well bore by periodic cleaning with hydrochloric acid with or without addition chemicals would partially restore the injection well capability to take water. The net results of the solids in the injection water were an increase in pressure on the formation at the injection wells, decrease in injection water volume, and an increase in frequency of well cleaning.

Water flow through the plant was controlled by three water level switches in the clean water tank. The out-of-water switch shuts off the injection system to protect the triplex pump. The high water switch at the top and the low switch found two feet lower in the clean water tank controlled the transfer of water from the produced water tank or supply well. The low water switch began the pump to transfer produced water to

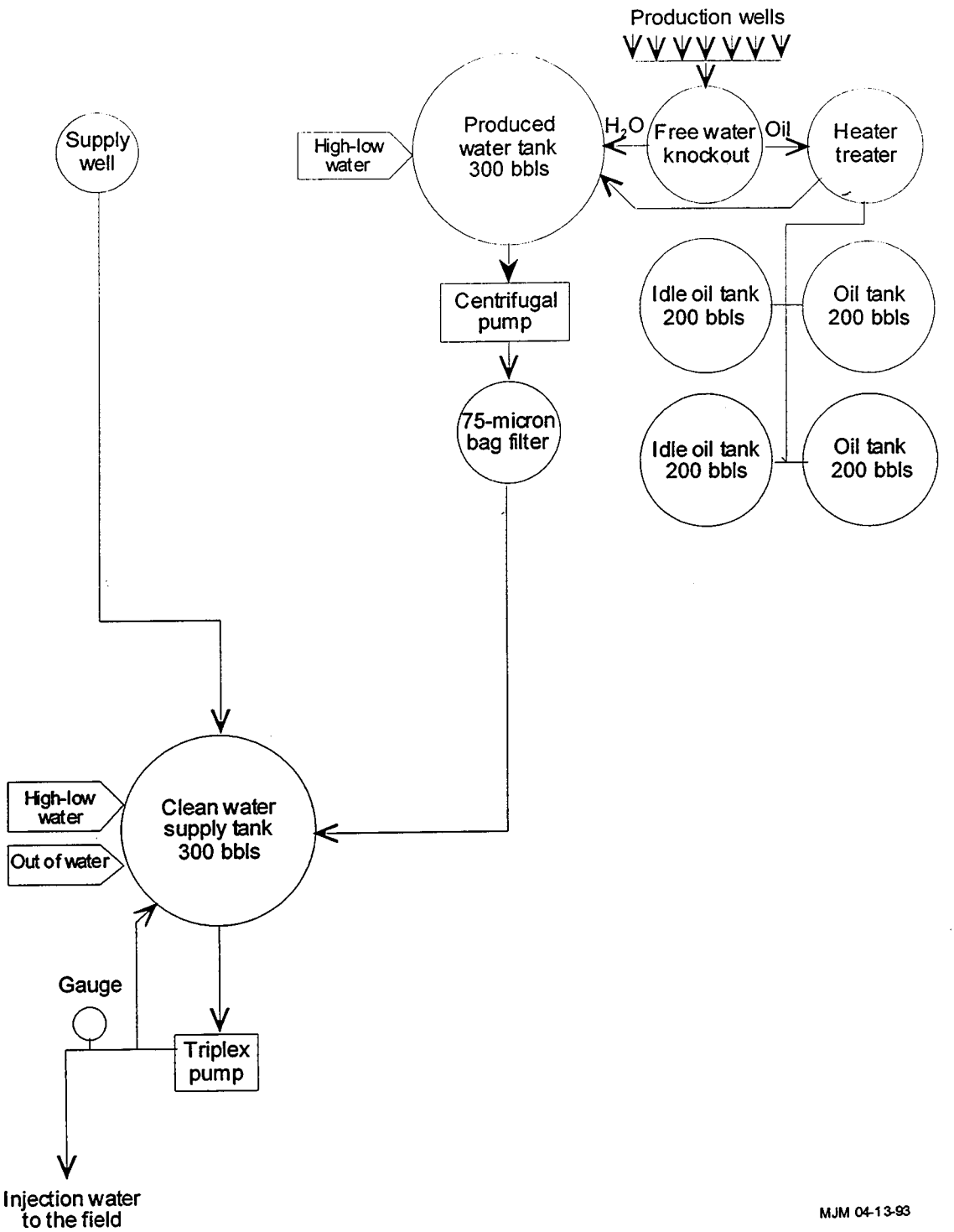

Figure 1. Flow of water through the Nelson Lease water plant before the installation of the air flotation unit in 1994.

the clean water tank. If water level in the produced water tank was low then a low water switch would shutoff the transfer pump and start the supply well pump that sent water to the clean water tank. The high water switch in the clean water tank would shut off the supply well or the produced water transfer pumps. Various treatment chemicals were added at the produced water tank in an attempt to alleviate the filter plugging in the plant and at the injection well by scale formation and aggregation of suspended solids.

Russell Petroleum and Tertiary Oil Recovery Project personnel meet several times in early 1992 to discuss the potential and value of submitting a proposal to the Department of Energy as a Class I PON demonstration project. One facet of the proposal would be to improve the quality of the injection water used for the waterflood. The premise being, that removal of oil and solids from the injection water would reduce the costs of operating the injection well system. The proposal would most likely require modification of the water plant and a change in the operational procedures for the water plant.

The Nelson Lease Water Problem

The injection water for the Nelson Lease consists of a mixture of produced water and make-up water. Production water comes from three sandstone beds from the 630 to 700-foot depth of the Chelsea Sandstone, a member of the Cabaniss Formation of the Cherokee Group. Makeup water is obtained at 1475 foot depths of the Arbuckle Formation that is 700 feet below the Cherokee formation. The two waters have a different chemical composition that leads to precipitation of solids on mixing. Injection well problems arose when the mixed supply-produced water was used in the waterflood operation. The use of 75-micron cartridge filters at the wellhead permitted sufficient quantity of suspended solids to reach the well bore. This required an increase in pressure to maintain water volume in the injection wells. As pressure increased and water volume decreased, the need to treat the injection wells with acid increased in frequency.

The water injection problem arose from the incompatibility between the produced and supply waters. Factors identified was (1) carryover of 300 mg/L or greater of disbursed oil in the produced water, (2) the precipitation of barium sulfate and iron sulfide on mixing of the two waters, and (3) the clay, sand, organic solids, and bacterial debris in the mixed water. The presence of iron sulfide and oil are known to cause problems in the injection wells. The removal of the oily solids from the well bore required frequent treatment with hydrochloric acid along with other treatment chemicals. In an attempt to alleviate the injection well plugging problem various treatment chemicals were added to the mixed water at the plant. A typical daily cost for these chemicals was approximately $35.00 per day to treat 1000 barrels of water in 1992. The 21 and 20 injection wells required 24 and 21 extensive clean outs in 1992 and 1993., respectively.

Difficulty was experienced in filtering 700 to 1000 barrels of supply-produced water per day through a 75-micron bag filter. Eventually, the supply water was added to the filtered produced water in which case the barium sulfate and iron sulfide formed in the water in the tank feeding the water injection pump. The mixed water generally varied from reddish-brown to gray or black in color. Table 1 lists the ion analysis as reported by Oil Field Research of Chanute, Kansas.

Table 1. Water analyses for produced, supply, and combined waters at the Nelson Lease, October 28, 1993

Ion	Produced mg/L	Makeup mg/L	Combined mg/L	Produced meq/L	Makeup meq/L	Combined meq/L
Sodium	3924	1247	3157	170.68	54.24	137.32
Iron	0	0	3	0.01	0.00	0.16
Barium	145	6	82	2.11	0.09	1.19
Calcium	200	116	152	9.98	5.79	7.58
Magnesium	101	46	79	8.31	3.79	6.50
Chloride	6241	1986	4964	176.04	56.02	140.02
Bicarbonate	920	429	776	15.08	7.03	12.72
Sulfate	0	42	0	0.00	0.87	0.00
Total	11531	3872	9213			
Cation meq/L				191.10	63.91	152.76
Anion meq/L				191.11	63.92	152.73
Difference meq/L				-0.01	-0.02	-0.03

From the analyses in Table 1 the ratio of produced to supply waters was estimated at 7 to 3. From this ratio, 30 mg/L of barium sulfate precipitated on combining the two waters. The black color of the water is typical of oil field waters in which iron sulfide has precipitated. Insufficient information was available to estimate iron sulfide in the water. Sulfide analysis was not reported and the iron values are low due to oxidation of ferrous ion and the precipitation of iron oxide before soluble iron analysis was done.

Potential solutions to the water quality problem at the Nelson Lease consisted of three approaches:

1. Keep the produced water separate from the supply water and divide the field into two injection systems. This would require two injection pumps and water distribution lines.
2. Install a better filtration system than the current 75-micron cloth bag filter.
   a. A sintered metal filter was considered. The sintered metal filter unit is automatically back washed when the pressure reaches a set limit. The problems with a sintered metal filter system were the disposal of the backwash water, what size a system would be required, the cost for equipment, and could the manufacture assure successful operation in the oil field.
   b. Install a graded sand filtration system. Sand filtration systems have been used in the oil field and Russell Petroleum had experience. The problems with a graded sand filter system were the disposal of the backwash water, and the failure of sand to resettle properly when oil causes the sand grains to agglomerate. These clumps of sand disrupt the sand bed and reduce the filtration capability of the sand.
3. Install an air flotation unit to remove oil and solids from the water. Air flotation has been used in cleaning water in the oil field. An air flotation system would not be new technology, but would be new to Russell Petroleum and to the oil operators in Kansas. The air flotation system would test the concept of rapid assimilation of a "new method" for Kansas independent oil operators by using "Off the Shelf Technology".

Choice of Air Flotation

An air flotation unit was selected as the process to remove oil and solids from the mixed produced-supply water used as source water for the waterflood at the Nelson Lease. The principal reasons for selecting air flotation were; (1) air flotation has been used in the oil field for the removal of oil and solids from produced water before disposal of the water, particularly in California and offshore in the gulf of Mexico; (2) air flotation is not used by the oil operators in Kansas and would serve as a demonstration site; and (3) air flotation would be a test of assembling "Off the Shelf Technology" to serve a need in the production of oil and reduce the problems and cost of operating a waterflood. The equipment would be installed and operated by professional personnel from Russell Petroleum and the Tertiary Oil Recovery Project. Then the operation would be turned over to field personnel for daily operation and maintenance under the supervision of an engineer from Russell Petroleum.

The Principles of Air Flotation

Oil is insoluble in water. That is, oil is hydrophobic and will float to the surface of the water. When the oil is dispersed as small droplets or emulsified, and especially in the presence of solids such as iron sulfide to which the oil will adhere, then the individual droplets will not coalesce and will not float to the surface of the water. Air bubbles, which are also insoluble in water, rapidly rise to the surface of the water. Air, being hydrophobic, will stick to an oil drop. This combination of air bubble and oil drop increases the effective size and decreases the effective density that aids in the flotation of the oil. The steady stream of rising, minute air bubbles bouncing off the oil droplet helps to move the oil to the water surface. The same is true for suspended solids in the water. If the solid can be made hydrophobic by adsorption of an appropriate chemical then an air bubble will attach itself to the solid particle. Specific minerals have been separated from ores by this process. The problem is to find a chemical formulation that will make all solids hydrophobic in the produced-supply water mixture. A hydrophobic wetting agent that imparts a charge to the particle can also aid in the removal of d^{i}rt from the water. In this case, a hydrophobic flocculation material that has a charge opposite of the wetting agent is used. The solid particles are attracted to the flotation agent by coulombic force. The principles are simple, but fmding the correct formulation that works well with the specific water in the field is the problem.

Air flotation works well for the removal of solids between 10 and 100-microns in size. The surface of the particle is important in that it must be hydrophobic or made hydrophobic by adsorption of a chemical. The adsorption of a hydrophobic chemical on the particle surface depends on the zeta potential of the solid, i.e., whether the particle carries a positive, negative, or no charge. Zeta potential depends on the pH of the

water that affects the isoelectric point of the solid. The isoelectric point is the pH of the system in which the particle such as iron oxide has a zero charge. The pH of the system also affects interaction between solid(s) and chemical(s) and between two or more chemicals used in the flotation process.

The air or gas bubble size is also important. Smaller bubbles are more effective than larger bubbles. Air is commonly used as the gas, but natural gas, nitrogen, and other gases have been used. The bibliography contains a selected list of references that describe in greater detail the process of air flotation overall and the use of air flotation in the cleaning of produced water in the oil field before reuse or disposal.

Methods of Generating Small Air Bubbles

The generation of air bubbles in an air flotation unit is accomplished by one of two principal methods, dissolved air and induced air. The dissolved air method requires air to be dissolved in the water by increasing the air pressure above the water to 50 or greater pounds per square inch. When the pressure of the system is reduced to atmospheric pressure, then the air comes out of solution forming small bubbles. A variation of the induced air system is a vacuum desorption process. The water is saturated with air at atmospheric pressure and then the water is placed under a vacuum that causes the dissolved air to come out of solution forming small bubbles. In the induced air system, the bubbles are generated by a high speed rotating impeller. The rapid rotation of the impeller creates a low pressure area at the center of the hollow shaft that sucks in air. The air is then forced against a perforated shroud by the impeller where small bubbles are formed. A venturi tube has also been used to generate small air bubbles. As the water flows through the constriction of the tube, air is sucked into the tube at the low pressure location and the flow of water provides the shearing force to generate the small air bubbles. The electrolysis of water to form oxygen and hydrogen has also been used to form the gas bubbles.

Purchase and description of the air flotation unit.

Four potential suppliers were invited to submit bids for an air flotation unit to clean the produced water at the Nelson Lease. Two companies responded with information and prices; two of the companies no longer produced air flotation equipment. A flotation unit from Separation Specialists Incorporated of Bakersfield, California was selected based on the best price and was the only company to send a system engineer to the site. The systems engineer tested the proposed feed water in February 1994 in a bench model flotation unit. The results showed promise even with the limited chemicals in his test kit. The unit was ordered in March and delivered in June 1994.

The unit was designed to remove oil from produced water in offshore operations in the Gulf of Mexico. The unit was guaranteed to reduce the oil in water to less than 30 mg/L. No other warranty of specifications were implied as to removal of solids from the water.

The flotation vessel is a 4-foot diameter by 4-foot tall with a top and bottom dome, epoxy coated, enclosed tank. Figure 2 is a photograph of the flotation unit as received. The working volume of the tank is 375 gallons. Air bubbles are generated by impeller air turbines mounted tangentially at one, two, and three feet below the surface of the water. Figure 3 is an exploded drawing of an impeller-air turbine assembly. The impeller forces water past the edge of the air turbine where the velocity of the water shears off small air bubbles as air exits the turbine. The air turbine is a closed impeller for a centrifugal pump. The lip of the inlet for the impeller fits into a plastic block which serves as a bearing and seal between the water and air inlet. The plastic bearing block is held in place by a retainer bar that also aligns the impeller-air turbine shaft through a water seal at the tank wall and then connects to the shaft of the motor.

The impeller-air turbine units cause a counterclockwise rotation of the water in the tank. This rotation of the water is the only mechanism to sweep the oil and dirt at the surface of the water into the waste water weir mounted at the water surface. The waste weir is pie shaped and mounted at the side and extending to the center of the tank at the water surface. Feed water enters just below the water surface in the tank and clean water exits from the center bottom of the tank. Treatment chemicals are added to the feed water before it enters the tank or at the air turbine-impeller ports.

Clean water exits the flotation unit at the bottom center and rises in a pipe to a 12x12x12-inch weir box on the side of the tank. The clean water weir is set to maintain a fixed height of water in the flotation tank. Water exits the clean water weir box and flows by gravity into a water storage tank. As the flow of feed water increases, the clean and waste water flow also increases. For steady-state operation of the flotation unit the feed water rate needs to be held constant.

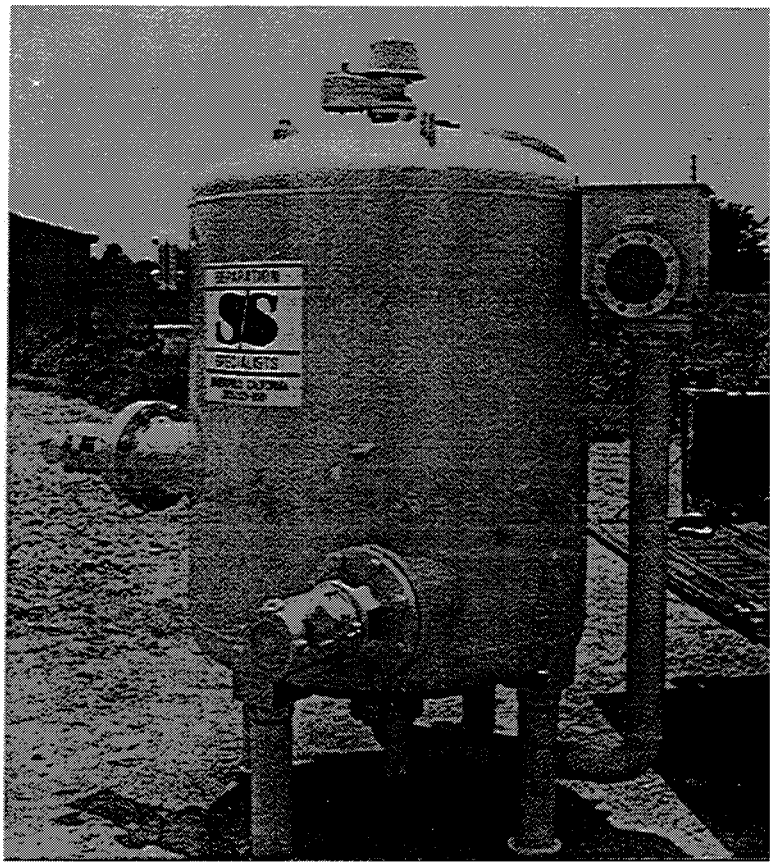

Figure 2. Photograph of the air flotation unit as received from Separation Specialist of Bakers-field, California, June 1994. Two of the air turbine mounts are visible on left and lower front. The clean water exit weir is on the top right. Note the tank is enclosed for off-shore application.

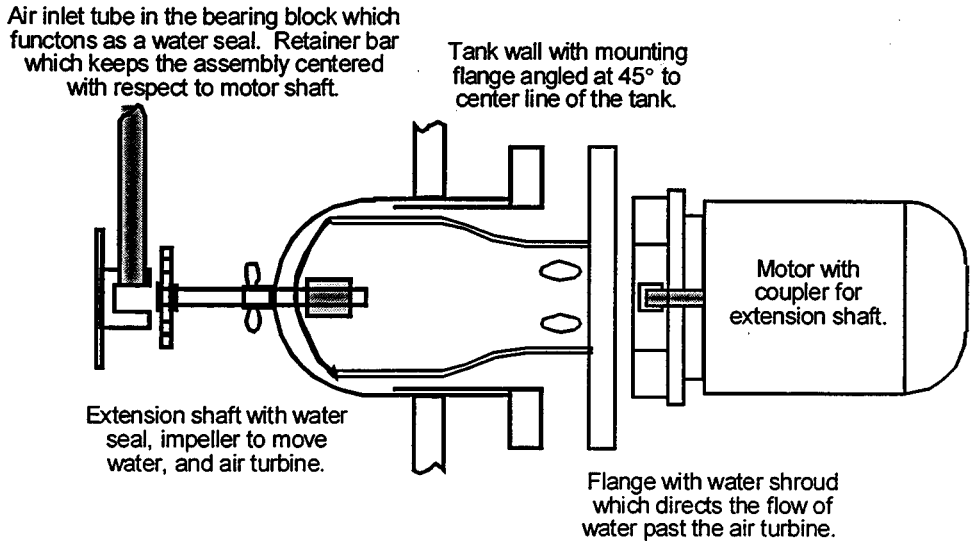

Figure 3. View of components which constitutes the impeller–air turbine assemble for the generation of air bubbles in the flotation unit. Each component is shifted to the left with respect to the motor to more clearly show the various parts.

Air Flotation Chemical Formulations

Before the installation of the air flotation unit, various chemical vendors were invited to test the combined supply-produced water for potential chemical formulations to be used with the flotation unit. Only Petrolite Corporation responded. The field engineer tested 30 formulations that Petrolite supplied as floatation aids and recommended two formulations in June 1994. The best formulation, FLW-162, is a high molecular weight cationic polymer prepared in an oil emulsion. This formulation, on contact with water releases the water soluble cationic polymer along with a surfactant and/or wetting agent. However, shear is needed to disperse the polymer into the water.

In early 1996 a water soluble anionic flocculation polymer was recommended by field engineer from Separation Specialists. This material is used in water clarification and is not a formulation for air flotation. Additional chemicals are required with the anionic polymer. Details of the use of the anionic polymer with other chemicals are described later. The anionic polymer was tried when the water plant ran out of the FLW-162 and a new supply could not be obtained in time.

Installation of the Air Flotation Unit

The flotation unit was placed in operation at the Nelson Lease water plant on July 13, 1994. The FLW-162 flotation chemical was started at one pint per day, the slowest feed rate on the chemical pump, and added to the water inlet line just before the flotation tank. All previously used water treatment chemicals was stopped. Instructions from the manufacture as to the operation of the flotation unit were a minimum. Engineers from the Tertiary Oil Recovery Project and Russell Petroleum directed the installation and startup of the equipment. Two 200-barrel fiberglass tanks and one 50-barrel steel tank were added to the water plant tankage. One 200-barrel fiberglass tank served as a feed tank to the flotation unit and the second served as the receiver of the clean water from the flotation unit. The 50-barrel steel tank received the froth from the top of the flotation tank. The flotation unit was mounted on a 7-foot high platform with no protection from the elements. A corrugated metal and fiberglass shed was constructed around the flotation unit to protect the unit in the winter. Figure 4 is a schematic of the flow of water from the field and supply well, through the air flotation unit, and then back to the field.

Water flow through the plant is controlled by water level switches in the clean water and the produced water tanks. An out-of-water switch near the bottom of the clean water tank shuts off the triplex pump to protect the pump. A pair of switches about two feet apart near the top of the clean water tank begins the transfer of water from the produced water tank to the air flotation supply tank. A low water switch on the produced water tank shuts off the produced water pump and starts the supply well pump.. The high water switch on the produced water tank will reverse the source of water sent to the air flotation supply tank. The high water switch in the clean water tank shuts off all water transfer. Activation of the air turbines in the flotation unit is also controlled by the high-low water switches on the clean water supply tank. Water from either the produced water tank or supply well enters at the bottom the flotation supply tank and exits by gravity to the air flotation unit via a 2-inch PVC pipe. This arrangement of water transfer caused the flow rate through the flotation unit to fluctuate with the level in the flotation supply tank.

Initially, water flowed through the air flotation by gravity from the 200-barrel fiberglass air flotation supply tank via a 2-inch PVC line. The feed water entered the flotation unit 3-inch below the surface of the water. Water from the produced water tank was transferred to the feed tank by a centrifugal pump using a buried flow line that had been in place between the produced water tank and the clean water tank. When the produced water tank was empty, then water was obtained from the supply well. This configuration was changed in September 1994 when the feed water transfer pump was used to sent produced water directly to the air flotation unit. The air flotation supply tank was no longer used. This eliminated the surge of water through the unit experienced in the gravity flow feed. The supply water was rerouted from the air flotation feed tank to the produced water tank. The waste water that was initially sent to the air flotation tank was rerouted to the produced water tank when use of the air flotation supply tank was abandoned in September 1994. The reason for the change was that a chemical feed rate could not be established for the flotation chemical when the flow rate varied through the flotation unit. Starting in September, the specified feed rate for FLW-162 was one pint per day, the lowest feed rate of the chemical pump. However, the flotation polymer feed rate varied widely as the field personnel adjusted the rate as they thought best. The FLW-162 was initially feed directly from the 55-gallon drum and then later from a five-gallon plastic tank. Difficulty was experienced with the chemical feed pump. A small amount of moisture from the air would interact with the oil emulsion allowing lumps of the cationic polymer to form which would plug the check valves on the chemical pump. This would require frequently cleaning of the chemical pump.

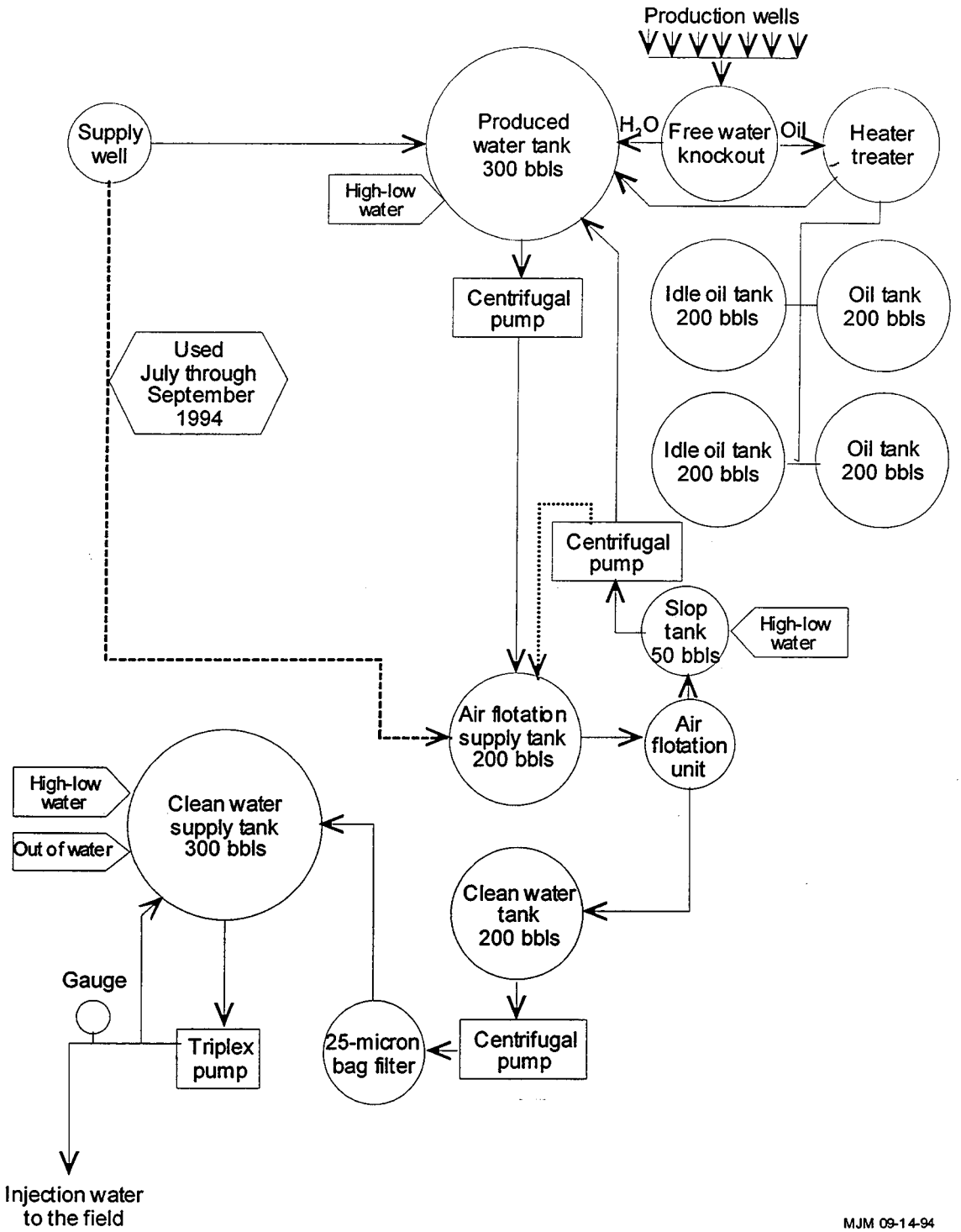

Figure 4. Flow of water through the Nelson Lease water plant after the installation of the air flotation unit in July 1994.

The quality of the water exiting the flotation unit was better than the feed water, however, no test equipment was available to evaluate water quality other than the ASTM D-4189 "Silt Density Index for Water. A modified version was adapted to measure water quality. One liter of water was passed through a 0.5-micron, 47-mm diameter fiberglass filter using a 10 psi pressure from an air pump. The square root of time versus cumulative volume generally results in a straight line. The slope of the line times 100 was used as a water quality index. The filter can be dried and weighed to measure the suspended solids in the water. This filtration test will give a water quality index of 0.5 for pure water. Before the startup of the flotation unit the water quality index for the flood water was 26.4. The first water from the flotation unit had a water quality index of 2.62. However, this tenfold improvement could not be maintained consistently. The fluctuation in water flow through the flotation unit, the frequent stop and start of the unit as controlled by the need for water, and the varying composition of the feed water all affected the water quality from the air flotation unit. Nevertheless, the daily operation of the flotation unit was turned over to Russell Petroleum field personnel in September of 1994.

Initial problems with the air flotation unit

After seven and one-half months the air flotation unit stopped working, the air turbines produced no bubbles. On March 2, 1995, the field engineer from Separation Specialties arrived and the three air turbines were removed from the flotation unit and found completely plugged with solids. The tank was cleaned and three new air turbines were installed. Difficulty was experienced with the alignment of the air turbines since the plastic bearing block had to have the mounting holes drilled and tapped in the field. This caused some misalignment of the air turbine to the water seal. The air turbines started failing within weeks and required constant cleaning of the solids that would accumulate in-the turbine.

The black to brown water fluctuation requires a different concentration of flotation chemical. This observation leads plant personnel to adjust the chemical feed rates to the unit frequently. The result was either over or under treatment with flotation chemical. Under treatment would result in minimum removal of suspended solids in the feed water. Over treatment would result in a sticky froth that would not flow into the waste weir at the surface of the water. The solids would build on the surface of the water and then be drawn into the air inlet tubes for the air turbines. This was thought to be part of the problem in plugging of the air turbines with solids. Extension of the tubes through the manhole of the closed tank where solids could not be sucked back into the air turbines did not relieve the plugging of the air turbines.

An in depth evaluation was undertaken by the engineers from Russell Petroleum and the Tertiary Oil Recovery Project in early 1995 as to operational parameters that affected the quality of water from the air flotation unit. Thus, begun a study of the equipment, waters, and chemicals used in the air flotation unit. The results are summarized in the following sections. Ten problems were identified. The problems are discussed as individual items but in reality are interrelated and cover the time from late 1995 through the end of 1998 when a viable air flotation unit requiring minimum attention was in operation.

The first problem was the frequent start and stopping of the air flotation unit. The second problem was the appearance of a hard barium sulfate scale on the injection well meters. The third problem was the fluctuation in the supply to produced water ratios that caused the feed water color to vary from black, containing iron sulfide, to reddish-brown, containing iron oxide. This variation in solids composition required a different concentration of flotation chemical. The fourth problem was the flotation chemical and the plugging of the chemical metering pump. The fifth problem was fmding the optimum location for the addition of the flotation chemical with respect to the flow of feed water to the flotation unit. The sixth problem was the constant failure of the air turbines and replacement with venturi tubes. The seventh problem was insufficient pump power to generate sufficient air volume from the venturi tubes. The eighth problem was the type and placement of the waste water weir. The ninth problem was the lack of measurement equipment to measure flow rates and water quality quantitatively, and a data base to identify causes and effects. The tenth problem was the need to keep water flowing to the field always, especially in winter months when freezing would become a problem in the pipes under no flow condition.

Problem One. Reduce the frequency of starting and stopping the air flotation unit.

Initially the quality of the water from the flotation unit would be poor and then improve as the unit ran. With each stoppage of the flotation unit it was observed that some solids in the water would sink to the bottom of the tank and exit with the clean water. The length of stop time did not appear to relate to the

solids that appeared in the clean water. To reduce the frequency of stopping and starting the air floatation unit, two 300-barrel fiberglass tanks were installed in September 1995 for the clean water that feeds the triplex pump. This increased the clean water storage capacity by 200 barrels. In addition, the high-low water switches were placed further apart, and thus, decreased the frequency of calling for water about one-half. This additional working volume in the clean water tanks allowed the air flotation unit to run for a longer time on each call for water. The decrease in the number of stops for the air flotation unit per day resulted in a small increase in the overall water quality of the clean water leaving the unit.

An additional benefit with the two clean water tanks was that it provided for a 50 percent increase in injection time before the out-of-water switch would shut down the injection system. This increase in storage capacity generally provided ample time to solve water plant problems. The two tanks were connected such that water from the filter could be sent to either tank and likewise water could be drawn by the triplex pump from either tank. The new arrangement of tanks permitted one water tank to be taken out of service at a time for cleaning. During the normal operation, the water levels in the two tanks are equalized by a direct connection between the tanks. With the two tanks connected the frequency in the call for water was reduced by one-half. Figure 5 illustrates the new arrangement of the flow of water through the Nelson Lease water plant.

Problem Two. Barium sulfate scale in the injection well meters and air turbines.

Before the start of the air flotation unit, the individual injection well meters had to be removed frequently and cleaned of scale deposits. This scale on the meters was soft and mushy and could be easily removed from the rotor and body of the meter. The scale consisted of a mixture of barium sulfate, iron sulfide, and iron oxide, all coated with oil. The deposit in the meters changed from a soft to a hard and very difficult to removal scale over a year after the startup of the flotation unit. Oil and iron sulfide was absent from the hard scale. Apparently it took almost a year to flush the accumulated solids and scale inhibitor from the flow lines.

The precipitation of barium sulfate past the air flotation unit was not expected. The precipitation of barium sulfate on combination of sulfate with barium, in salt water, is rapid in the laboratory, but with formation waters the precipitation of barium sulfate is much slower. The cause for the retarded precipitation of barium sulfate in the mixed waters is not known nor was any attempt made to study this phenomenon.

All the barium can be precipitated from the produced water by the addition of sulfate from sulfuric acid or sodium sulfate to the water in the supply water tank. However, this resulted in a serve scaling problem in the lines between the produced and supply tank and to the air flotation unit. The barium in the water leaving the plant was reduced to 0 ppm during this test period.

It was the consensus that a longer residence time for the feed water would allow the barium sulfate to form and thus not precipitate after the air flotation unit. Plans were made to increase the residence time of the mixed waters before transfer to the flotation unit. This is discussed in details in Problem Three.

The deposition of the hard barium sulfate at the meters on each injection well was remedied by restoration of a scale inhibitor to the clean water in November 1995. This was done as a precautionary measure until the residence time of the mixed waters could be increased. The addition of the scale inhibitor in the flood water immediately affected the injection well meters. No injection well meters have had to be replaced due to barium sulfate scale after December 1995. This rapid response is in contrast to the time for the hard scale to appear. This was an early indication that clean water was helping to clean the injection lines of solids.

The failure of the air turbines due to solids was also attributed to the barium sulfate scale problem. Thus, the location for injection of the scale inhibitor was moved from the clean water tank to the air flotation unit. Addition of the scale inhibitor to the water in the flotation unit did not affect the action of the flotation chemical nor on the quality of the water leaving the flotation unit. The scale inhibitor did not stop the solids accumulating in the air turbines. The cause is discussed in Problem Five. The addition of the scale inhibitor to the flotation unit did solve the problem of barium sulfate scale on the screens of the bag filter units. The filters are between the flotation water tank and the clean water tanks.

Problem Three. The varying composition of the feed water.

The feed water to the air flotation unit is a mixture of produced and supply water. Produced water on the Nelson Lease comes from three sandstone beds from the 630 to the 700-foot depth of the Chelsea Sandstone member of the Cabaniss Formation of the Cherokee Group. Makeup supply water is obtained at

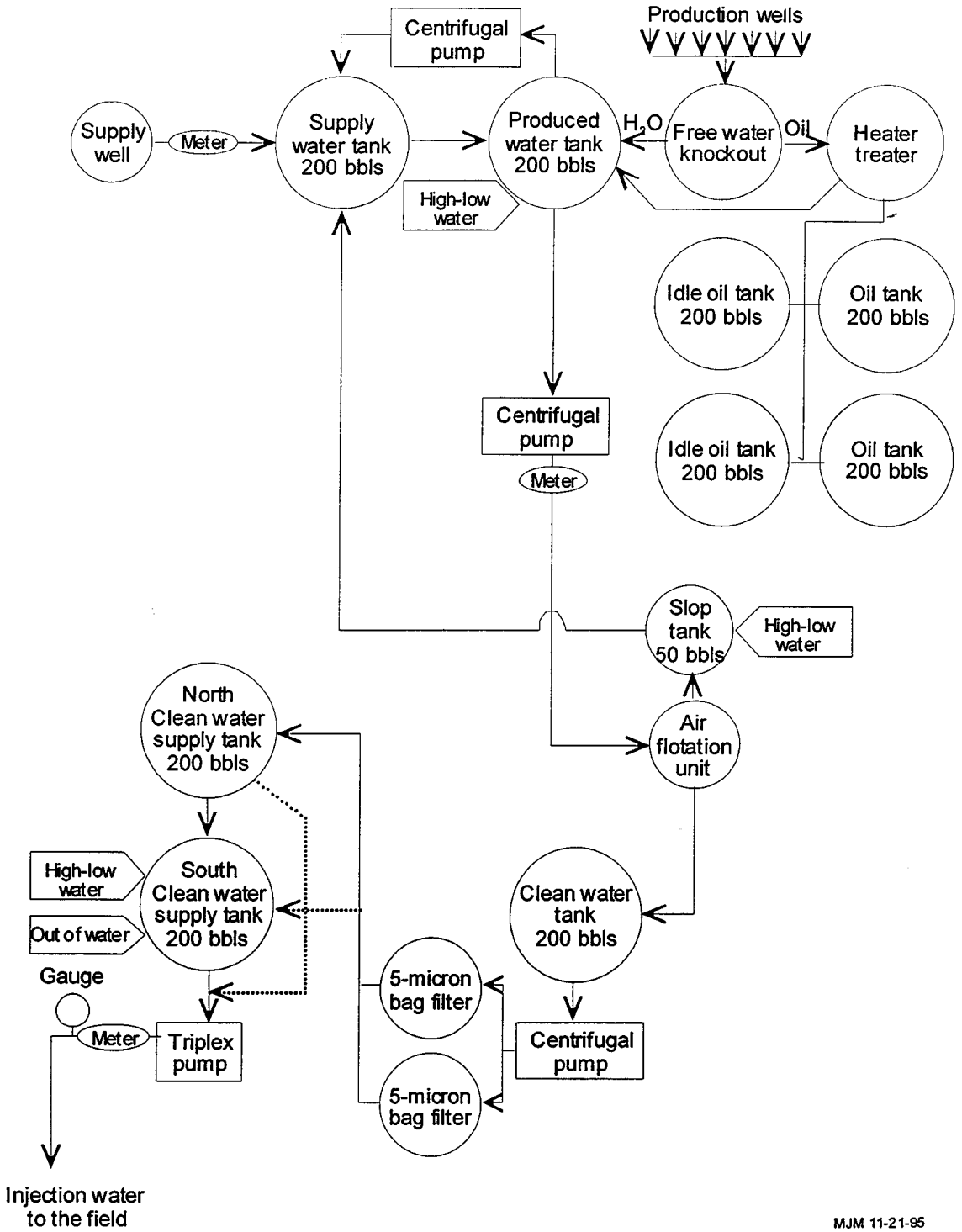

1475-foot depth of the Arbuckle Formation that is 700 feet below the Cherokee formation. The two waters have a different chemical composition that leads to precipitation of solids on mixing. The produced water

Figure 5. Flow of water through the Nelson Lease water plant after addition of additional tanks for water storage in September 1995.

contains approximately 120 mg/L barium and 10 to 20 mg/L of ferrous iron. The supply water has approximately 40 mg/L sulfate and from 10 to 70 mg/L of sulfide. Barium sulfate forms a soft to hard scale depending on oil and other solids in the water. On exposure of the water to oxygen from the air the ferrous iron is converted to ferric iron and precipitates as brown ferric oxide or black iron sulfide, if sulfide is present. Oxidation of the ferric sulfide by oxygen slowly forms brown ferric oxide.

On startup of the flotation unit it was quickly observed that treatment of brown water, due to ferric oxide, required less flotation chemical than treatment of black water, due to ferric sulfide. Throughout the day the water would cycle between brown and black in color depending on whether the supply well was on or off. The produced water from the field for a given period is nearly constant. Variation of supply water depends on the pumping rate and the number of injection wells in operation.

The daily variation in the amount of produced water can be related to the temporary shutdown of one or more production wells. A long term change in the amount of produced water can be attributed to a change in pump size at one or more production wells, or the shutdown of a well for a prolonged period. In contrast, the supply water in the mixed feed water varies throughout the day. This variation in amounts of supply water is caused by the need for additional water and is controlled by the high and low water switches in the produced water tank. The amount of clean water needed depended on the number of injection wells in operation and the water scheduled for the flood. The produced water averaged 695 and the supply water averaged 245 barrels per day for 1998.

The produced water is separated from the oil in a gun barrel separator with the water going to the produced water tank. The water stream falls through the air, an average, about ten feet, before splashing into the water in the tank. This allows for the oxygenation of the water. During the period that no supply water is added to the produced water tank, the water becomes brown from the oxidation of ferrous hydroxide-oxide to insoluble ferric hydroxide-oxide. When the water level reaches the low water switch in the produced water tank, then the supply well pump is started and pumps water to the produced water tank. The supply water enters at the bottom of the tank. The sulfide in the supply water reacts with the iron in the produced water to form ferrous and ferric-sulfides. Ferrous sulfide is oxidized to by the oxygen in the water to form insoluble ferric sulfide as the two waters mix. Likewise, the sulfate in the supply water reacts with the barium in the produced water to form insoluble barium sulfate as the two waters mix.

The approximate 100-barrel fluctuation in the produced water tank with the changing ratio of supply to produced water caused the over and under treatment with the flotation chemical in the flotation unit. The ratio of produced to supply water ranges from 100 to 50% during a water transfer cycle to the air flotation unit, and several transfer cycles occur in a 24-hour period. No provision was made to coordinate the feed rate of the chemical pump used for injection of the flotation chemical to the time when the supply well pump was in operation.

An attempt was made to oxidize the ferric sulfide in the produced water tank using 10% sodium hypochlorite. The supply water, at the start of pumping, contains 10 to 15 mg/L of sulfide. It was assumed that the initial water from the supply well would contain the highest concentration of sulfide. Test of the mixed water on startup of the supply well with sodium hypochlorite suggest that 3 to 4 gallons of 10% hypochlorite should be sufficient to oxidize all the ferric sulfide to ferric oxide. However, continuous injection of hypochlorite into the supply tank never solved the black water problem.

In September 1995 the tankage at the Nelson lease was increased in capacity and arrangement changed. Two 300-barrel fiberglass tanks were installed for clean water storage. This reduced the frequency of stop and start for the air flotation unit. A 300-barrel fiberglass tank was set to receive the supply well water. The deteriorating 300-barrel steel, produced, a water tank was replaced by a 200-barrel fiberglass tank. This increased the total water storage to 1000 barrels. In the replacement 200-barrel fiberglass tank the float switches were again placed to allow for about 100-barrel difference in water level. The water from the gun barrel separator was allowed to fall approximately ten feet through the air before splashing into the water surface in the tank. This again caused the produced water to be fully oxygenated. The supply and recycle water were diverted to the bottom of the new 300-barrel fiberglass supply water tank. Water from this tank flows by gravity to the 200-barrel produced water tank. This water is allowed to fall through the air again for approximately ten feet that oxygenates the water from the supply water tank.

The original plan was to add supply water to the produced water at a rate that provided a more consistent water composition. As the supply tank was filled the first time, it was found that the sulfide content increased from 15 to more than 80 mg/L in the first hour of pumping from the supply well. The

sulfide slowly decreased to 40 mg/L after three hours of pumping. The high sulfide content of the water in the supply tank clearly showed that hypochlorite oxidation of sulfide to sulfur of sulfate was not economically feasible. Air sparging was tried and found to release hydrogen sulfide to the atmosphere. The hydrogen sulfide content in the free space in the tank posed an unacceptable environmental hazzard. The presence of hydrogen sulfide in the air space in the produced water tank was never a problem when the produced and supply waters were combined in the original produced water tank. Thus, a pump was installed between the supply and produced water tanks and the two tanks continuously circulated. This procedure reduced the hydrogen sulfide in the air space above the supply tank to less than 5 ppm and generally below detection limits (0.5 ppm) of the Drager sampling equipment used. The hydrogen sulfide in the water was essentially removed by reaction with ferrous and ferric ions in the produced water.

With no free hydrogen sulfide in the produced-supply water mixture, then air sparging of the supply tank water with air from a venturi tube in the line between the supply and produced tanks, or from an air compressor greatly reduced the presence of black water in the air flotation unit. Advantage was taken of the oxygen in the air to oxidize the ferric sulfide in the water to ferric oxide. The circulation of the supply and produced water tanks doubled the residence time of the feed water before transfer to the flotation unit. However, this increase in reaction time still does not prevent the formation of barium sulfate scale at and after the flotation unit. Thus, the water is currently treated at the air flotation unit with a scale inhibitor.

The elimination or reduction of the ferric sulfide in the water by air oxidation reduced the flotation chemical needed. This permitted the feed rate for the flotation chemical to be optimized, and eliminated the need for field personnel to change the feed rate constantly. The result was an improvement in the water quality from the flotation unit. A new chemical pump was obtained in July 1997 that allowed lower and more precise metering of flotation chemical.

Problem Four. The chemical pump for the flotation chemical.

Part of the problem with consistently obtaining clean water from the air flotation unit was related to the injection of flotation chemical into the feed water. Chemical metering pumps from Liquid Metronics Division of Milton Roy were available in the water plant for metering the various treatment chemicals. The first problem was the Model Z14 pump failed to deliver a constant amount of the cationic polymer to the flotation unit. The field engineer from Petrolite Corporation reported that 1 to 2 ppm FLW-162 would be needed to treat the feed water. For 1000 barrels of water per day at 2 ppm would require 0.08 gallons of chemical per day. The lowest setting on the Model Z14 pump is 0.08 gallons per day. However, at the lowest speed setting the flow rate becomes unreliable. The speed of the pump is controlled by adjusting a variable resistor. A small change in resistance caused by a change in temperature or humidity at the minimum setting caused the pump to stop pumping or to speed up. The speed rate was frequently increased by field personnel to insure chemical would be pumped, especially over night or weekends. This resulted in excess flotation chemical which caused problems in the flotation unit with the stiffness of the froth that would plug the waste weir.

The second and major problem was failure of the pump check valves. Sticky globs of the flotation chemical or flakes of a white solid would coat the balls of the check valves and stop the flow of chemical. This failure was attributed to the typical handling procedure of treatment chemicals by plant personnel. The chemical was pumped directly either from a drum or from a smaller container that is open to the atmosphere. For the cationic flotation formulation prepared as an oil emulsion a small amount of moisture would cause premature inversion of the emulsion. This resulted in a very viscous fluid that would not flow though the feed line or pump. Any emulsion on the surface of the container would dry and form a white flake that would also cause the check valves to malfunction. Thus, many pump failures occurred between July 1994 and April 1996.

In April 1996 a switch was made to a water solution of an anionic flocculation polymer. The reason for the change was (1) the plant was out of cationic polymer and immediate delivery was not possible, and (2) the desire of the plant personnel to have a chemical that would be easier to handle in the water plant. The field engineer from Separation Specialists suggested an anionic polymer from Rohm and Haas Company would be easier to handle in the water plant. The anionic polymer, ROMAX™ 7000, was supplied by Rohm and Haas Company as a 50% solution in water. This material was not formulated as a flotation agent and therefore required additional chemicals. A foaming agent was necessary to create a froth at the water surface that holds the solids until the froth reaches the waste weir. Various anionic and nonionic materials were tried. The nonionic materials, such as Triton X-100, worked best but created two problems. First, an excess of the Triton X-100 would generate too much foam that would plug the waste weir. Second, the

waste water is recycled to the feed water and the buildup of nonionic surfactant caused excess foam at the flotation unit. In addition, the anionic polymer always removed fewer solids from the water than the cationic polymer. This was probably caused by part of the suspended solids that carried a negative charge and were not flocculated by the anionic polymer. The main advantage of the anionic polymer was that the material could be diluted with water and thus allow the metering pump to run at a faster speed and/or stroke length. This allowed the pump to be operated in a favorable speed and stroke range. However, the handling procedures in the plant still caused failure of the chemical pump due to solids in the check values. When the anionic polymer solution dried out on the upper portion of the reservoir, then flakes of an insoluble polymer would cause the check valves to fail. In addition, the use of the anionic polymer required second metering pump for the injection of an additional chemical such as the nonionic or anionic surfactant tried. Combination of additional chemicals and pumps only compounded the problem with the operation of the flotation unit by plant personnel.

In December of 1997 the decision was to return to use of the cationic polymer and find a practical solution to the chemical pump plugging problem. The problem in handling the oil emulsion of the cationic polymer was twofold. The first problem was the plugging of the check valves on the Model Z14 metering pump when the FLW-162 emulsion was exposed to moisture. Elimination of moisture and dirt from the air eliminated the pump check valve problem

The second problem was the FLW-162 feed rate of 0.08 gallons per day required the Model Z14 pump be operated at the slowest speed and shortest pump stroke. At this setting the feed rate varied and the pump would fail to deliver chemical. For a period the FLW-162 emulsion was diluted 50 percent with kerosene. This allowed the chemical pump to be operated above the minimum speed and stoke which caused problems in the uniform delivery rate for the flotation chemical. The problem of moisture and failure of check values remained when an open container was used for the kerosene-diluted polymer. The collapsible plastic container solved the problem of moisture reacting with the oil emulsion polymer. However, a new problem appeared in the settling of the polymer rich phase to the bottom of the container. A heavy mineral oil as diluent was also tried. The FLW-162 diluted with mineral oil would still slowly settle into a polymer rich layer at the bottom of the container. This-settling of the internal phase in kerosene or mineral oil would cause a slow decrease in the amount of polymer added to the water over a period of one week as fluid was withdrawn from the bottom of the container.

The problem of varying chemical feed was eliminated when a new metering pump, A model A971-151P pump that had digital controls for pump rates was purchased in July 1997. This pump provides a constant rate at the lowest pump setting. With the new chemical pump and the use of a collapsible container as polymer reservoir, no-metering pump problems were encountered over a 12-month period. A preventive maintenance check- on the pump showed no problems with the balls and seats of the check valves nor the accumulation of solids on the diaphragm of the pump after six months of operation. The Model A971451P pump allows the plant personnel to increase the flotation chemical rate, if needed, and then return to the one stroke per minute, theminimum rate, which delivers the required 1 ppm FLW-162. The 1-ppm of flotation chemical was verified by preparing a 3 to 1 dilution of the FLW-162 in heavy mineral oil. The minimum amount of cationic polymer needed on 19 May 1998 was 037 pounds per day (0.34 pints, 0.8 ppm by volume). From July through November 1998 the flotation unit has performed well with the 0.5 pounds per day (1 ppm) of FLW-162. Occasionally, the flotation chemical needs to be increased to 2 or 3 ppm when the feed water composition is altered, due to return of treating fluids from a production well.

Problem Five. Location for the addition of flotation chemical to the feed water.

For the cationic flotation chemical to work it must be released from the internal phase of the oil emulsion and then the high molecular weight cationic polymer must be dispersed in the water. After inversion and dispersion is achieved the polymer can then start coagulation of the suspended solids and finally the flocculation of the polymer laden solids. Originally, the cationic polymer was injected into the 2-inch flow line as the feed water entered the flotation unit. A tap for a 1/4-inch valve was threaded into the 2-inch PVC pipe that connected the 1/4-inch feed line from the metering pump. This tap was 12-inches in front of the inlet to the flotation tank. The viscous polymer emulsion would flow along the surface of the pipe and slowly start to invert and release the cationic polymer on contact with water. This resulted in lumps of the polymer in the flotation tank. Moving the injection point to the flange that held the air turbine assembly provided better dispersion of the polymer as the lumps of the viscous polymer flowed past the impeller and across the lip of the air turbine. The best solution was to inject the polymer in front of the centrifugal pump

that transferred the water to the flotation unit. The impeller in the centrifugal pump provides the shear needed to invert the emulsion and disperse the polymer in the feed water. The 2-inch feed line to the centrifugal pump was tapped and a 1/4-inch ball valve was installed. The valve was drilled to allow the 1/4-inch polypropylene feed line to be inserted through the ball valve and to the center of the 2-inch pipe. This injection of chemical into the water prevented the polymer from adhering to the pipe wall and provided a uniform feed rate of flotation chemical. The addition of the cationic polymer to the transfer line some 75 feet before the flotation unit provided additional time for the coagulation and flocculation of the solids before the water reached the flotation unit. Installation of a 1.5-inch venturi tube in the transfer line provided air for entrainment of the solids as they passed through the transfer line. This air also reduced the tendency of solids to accumulate in the transfer line. The addition of polymer and air in the transfer line improved the efficiency of the flotation unit since the air entrained solids remained in the top 6-inch of water in the flotation unit. Repeated water samples from 2-inches below the surface of the water in the flotation unit and from the bottom of the unit gave the same suspended solids values.

Problem Six. Failure of the air turbines and replacement with venturi tubes.

The sixth problem was the failure of the unit to generate air bubbles. After nine months of operation (27 February 1995) the generation of air bubbles ceased. The air turbines were completely plugged with solids. Initially, the cause was attributed to the formation of barium sulfate scale in the air turbines and throughout the flotation unit. Replacement of the impeller-air turbine units required two men for eight hours,-and excessive time for repair. Each air turbine and plastic bearing block was replaced. The bearing blocks needed to have mounting holes drilled and taped in the field. The new impeller-air turbine units started to fail within weeks and lasted four months before bubble generation ceased. The air turbines were again plugged with solids.

In July 1995, the first air turbine-impeller assembly with the mounting flange and shroud was brought to the repair shop at the Tertiary Oil Recovery Project for evaluation and redesign of parts if necessary. The plastic bearing block from the February repair was found to be off-center which caused the water seal in the flange and the water seal between the air-.turbine and bearing block to fail. A new bearing block retainer - was cut from stainless steel stock and aligned with the center of the motor shaft. A 1/4-inch hole was drilled in the retainer bar to aid the alignment of the plastic bearing block. A new bearing block was machined from 3-inch diameter, high density polyethylene. The new block had a 1/4-inch diameter by 1/4-inch heigh protrusion on the end that fit into the alignment hole on the retainer bar. The new bearing block also had a recess cut into the face for a spring-loaded lip seal to-receive the lip of the air turbine. A 1-inch threaded hole on the side of the block for the 1-inch PVC air pipe completed the new design for the bearing block. The air turbine assembly with a new air turbine was installed in the air flotation unit on 27 July 1995. The second and third air turbine assemblies were removed and brought to the Tertiary Oil Shop for a similar repair with the new design for the bearing blocks. It was found that each assembly was customly built and the parts were not interchangeable with respect to retainer bars and bearing blocks. Thus, future repairs, if necessary, had to account for the difference in each part of the air turbine assembly.

The new water seals on the bearing blocks did not stop the water leakage problem of the seal. Field personnel reported that they thought the air volume was decreasing daily. Installation of air flow meters on each of the air turbines verified their observation. A representative of the seal manufacture stated that a watertight seal required no more than a 0.005-inch lateral movement and a 0.002-inch radius of gyration of the air turbine lip in the seal. The lip of a new air turbine, which is an enclosed impeller for a centrifugal pump, was found out-of-round and/or off-center by more than 0.009 inches. Thus, a watertight seal between the air turbine and bearing block could not be achieved by any commercially available seal. The evaporation of water in the air turbine would always lead to plugging by solids accumulation. Removal of the solids from an air turbine was impractical. This led to consideration of alternate methods for the generation of air bubbles in the flotation unit.

A porous plastic, muffler assembly was built in December 1996 in which air was pumped through the porous plastic and a centrifugal pump was used to pump water past the plastic muffler to shear off small air bubbles. This device showed promise, but was a custom build item in the shop at the Tertiary Oil Recovery Project. Two of the air bubble generators were installed and used for six weeks. The air bubble generators required an air compressor for air and a centrifugal pump. Clean water from the bottom the flotation unit was pumped to the bubble generators. Difficulty was experienced in regulating the flow of air and water to the two bubble generators using valves.

An advertisement for a high air volume venturi tube used to aerate sewage lagoons appeared as a potential solution to the air bubble problem in the air flotation unit. A 0.5 and a 1-inch venturi tube manufactured by Ma77i Injector Corporation were purchased and tested in the laboratory for bubble generation. A quick field test in the flotation unit revealed that the 1-inch venturi tube driven by a 5-gpm centrifugal pump generated as much air as one bubble generator. For the air bubble generators a mounting flange had been fabricated from 1-inch thick PVC sheet. This flange had a 1.5-inch mounting hole for the pipe that contained the outside pipe of the bubble generator. On 10 December 1997 the bubble generator was removed from the south air turbine port and the 1-inch venturi tube was installed in the flange using a 1.5 to 1-inch reducing nipple. The hose that supplied water to the bubble generator was used to power the 1-inch venturi tube. The pressure across the venturi was 9.5 psi against a hydrostatic head of 30 inches of water, the deepest air turbine port in the flotation unit. This venturi tube produced 15 SCFH air. The second 1-inch venturi tube was installed on 10 January 1997 in the west air turbine port located 20 inches below the water surface and 900 from the south air turbine port. The south and west venturi tubes showed no scale buildup after 75 and 29 days of operation, respectively. Later the west venturi tube was moved to the north air turbine port, 10 inches below the surface of the water, to get a better rotation of solids at the water surface.

The venturi tubes were inexpensive, easy to install, and performed better than the original impeller-air turbine equipment or the porous plastic air compressor system. In May 1997 flow meters for measuring air volume were installed and daily measurements of air were recorded. The south and north venturi tube each generated 20 SCFH air flow in the flotation tank. A portable third 1-inch venturi tube was installed in June 1997. This venturi was attached to 1-inch PVC pipe and a 90° elbow to allow the venturi to be placed horizontally at any depth and position in the flotation tank. This was done in an attempt to move the dirt to the waste water weir and away from the sides of the flotation tank. The three venturi tubes produced as clean a water as the three air turbines, however, judging water quality was difficult due to the lack of a simple method to measure suspended solid content. The cause of excess solids in the clean water was not apparent until later and is discussed below. The fmal locations of the venturi tubes in the air flotation unit are discussed in the next section.

Problem Seven. Pump power for the venturi tubes and location of the venturi tubes.

Originally one TEEL 2P377 centrifugal pump was used to power the two or three-venturi tube configuration. A set of valves was used to control the water to each venturi tube. This form was inadequate for two reasons. First, the flow rate to any venturi tube was difficult to control. Different water flow rates to - the venturi tubes affected the water circulation at the water surface. When one venturi tube received more water, then the accumulation of solids at the water surface would move from the center toward the side of the tank, which affected removal of solids. Second, one centrifugal pump did not produce sufficient pressure across the venturi tubes to generate the needed air volume. This was discovered when a bench model air flotation. unit was built. A sample of water exiting from the flotation unit would produce water of less than 10 mg/L solids without the addition of any flotation cationic polymer. All needed was the additional air volume in the bench unit. This was confirmed by testing the water at the top of the flotation unit when water transfer to the unit was stopped. The venturi tubes were kept operational during this stopped water transfer period.

The installation of a second TEEL 2P377 centrifugal pump, which is an open-face impeller pump, allowed each of the two venturi tubes to be powered by an individual pump. This allowed maximum water flow, i.e., a maximum pressure differential across each 1.5-inch Mazzi 1585-X venturi tube. The original 1-inch venturi tubes were replaced by 1.5-inch venturi tubes as the larger size provided more air. The cost per venturi tube increased from $59 to $83. At an inlet pressure of 20 psig, the air flow is 2.4 SCFM for each tube or 4.8 SCFM air to the flotation unit. It was found, from a test in the bench unit, that a minimum of 4 SCFM air was needed per 40 gpm-of feed water to produce water with less than 10 mg/L solids in the clean water. This was also true in the plant air flotation unit. As indicated in Figure 6, the goal of less than 10 mg/L solids was approached when the second pump was installed in May of 1998.

The combination of the two venturi tubes, 180° apart, mounted at 45 ° to the center axis of the tank, and 1-foot from the bottom of the tank was the optimum location for the venturi tubes. The air from the venturi tubes sweeps the wall of the tank with the small rising bubbles and prevents solids from adhering to the wall of the tank. The placement of the venturi tubes at a 45° angle cause the water to rotate at 3 to 5 rpm. This top-to-bottom and tank wall-to-center circulation of the water moves the solids from bottom to top and from wall to the center of the tank at the water surface. Quality water of less than 10 mg/L was achieved

starting in July with the new waste weir in the center of the tank and with a centrifugal pump for each 1.5-inch venturi tube.

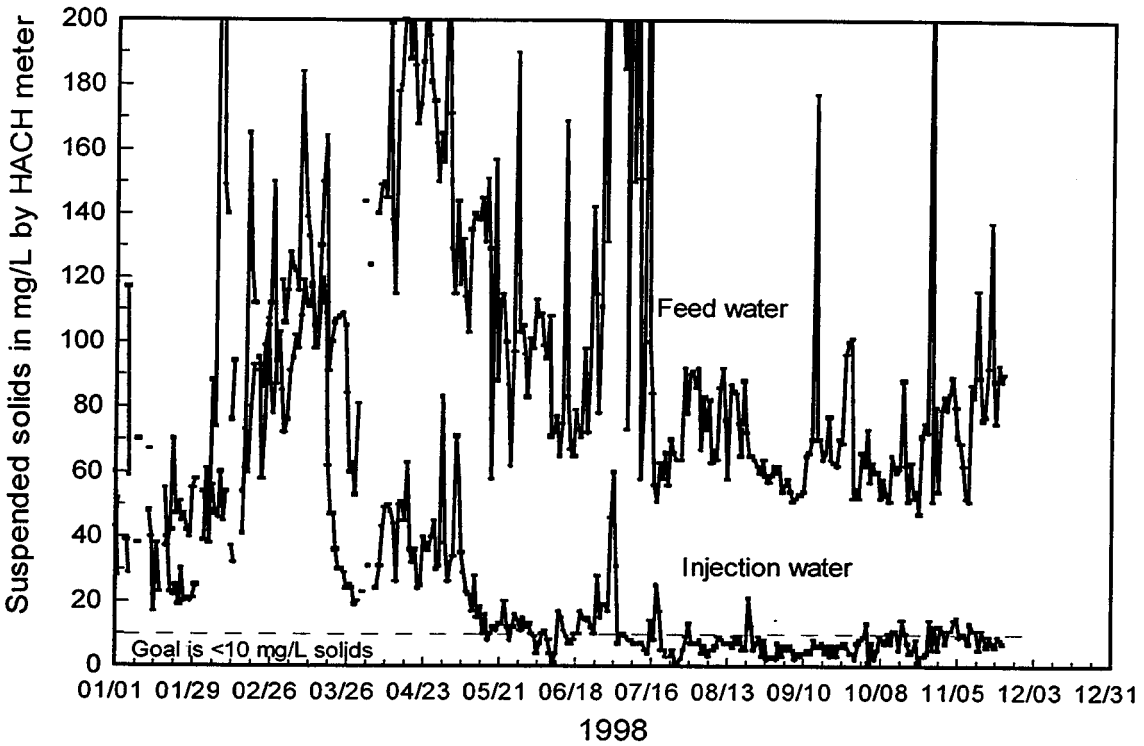

Figure 6. The successful removal of suspended solids from the mixed supply-produced water by air flotation. The goal of less than 10 mg/L of solids in the clean water as measured by HACH colorimeter was achieved in July and sustained when an air to water ratio of 4 SCFM air to 40 gpm water was attained. The air flotation unit was rebuilt with two 1.5-inch venturi tubes locatated 12-inches above the bottom of the tank and a 6-inch diameter waste weir located in the center of the tank at the water surface.

Problem Eight. Shape and placement of the waste water weir. The original waste water weir was a pie-shaped collector that extended from the wall of the center of the tank at the water surface. A b-inch wide opening for froth was 4-inches from the wall of the tank. The waste weir had an adjustable weir plate to allow the froth to pass into the weir with a selected amount of water. Observation of the froth at the water surface was difficult due to the enclosed tank construction. From the port hole one could observe the froth collecting at the wall and at the apex of the waste weir. A piece of paper dropped on the surface of the water would take an erratic path as it moved through various eddy areas at the water surface. The problem -of the solids accumulating on the surface of the water became evident when the top of the enclosed flotation tank was cut open in September 1995. Figure 7 illustrated the eddy areas observed at the water surface A new waste weir was constructed from a "U" shaped a PVC floor drain and extended across the tank at the water surface. This improved the removal of solids, but did not eliminate the accumulation of solids on the air pipes for the air turbines. A 4-rpm wiper arm was constructed to skim the surface of the water and force the froth into the "U"shaped, waste water weir. This wiper could not gather all the froth due to the air tubes near the wall for the air turbines. The first wiper arm used rubber to skim the surface of the water. After a few weeks the rubber became stiff and the wiper would catch on the waste weir. Next the rubber was replaced with fiber bristles, but suffered the same problem when it became coated with dried froth.

The final solution to the waste weir problem coincided with the optimum location of the venturi tubes. When the two venturi tubes were 12-inches from the bottom of the flotation tank, 180 ° apart, and at a 45 ° angle with respect to the diameter line of the tank, then the water would circulate at 3 to 5 rpm with the bubbles rising around the perimeter of the tank. This top-to-bottom and wall-to-center circulation of the water with the bottom-to-top and wall-to-center movement of the air moved the froth to the center of the

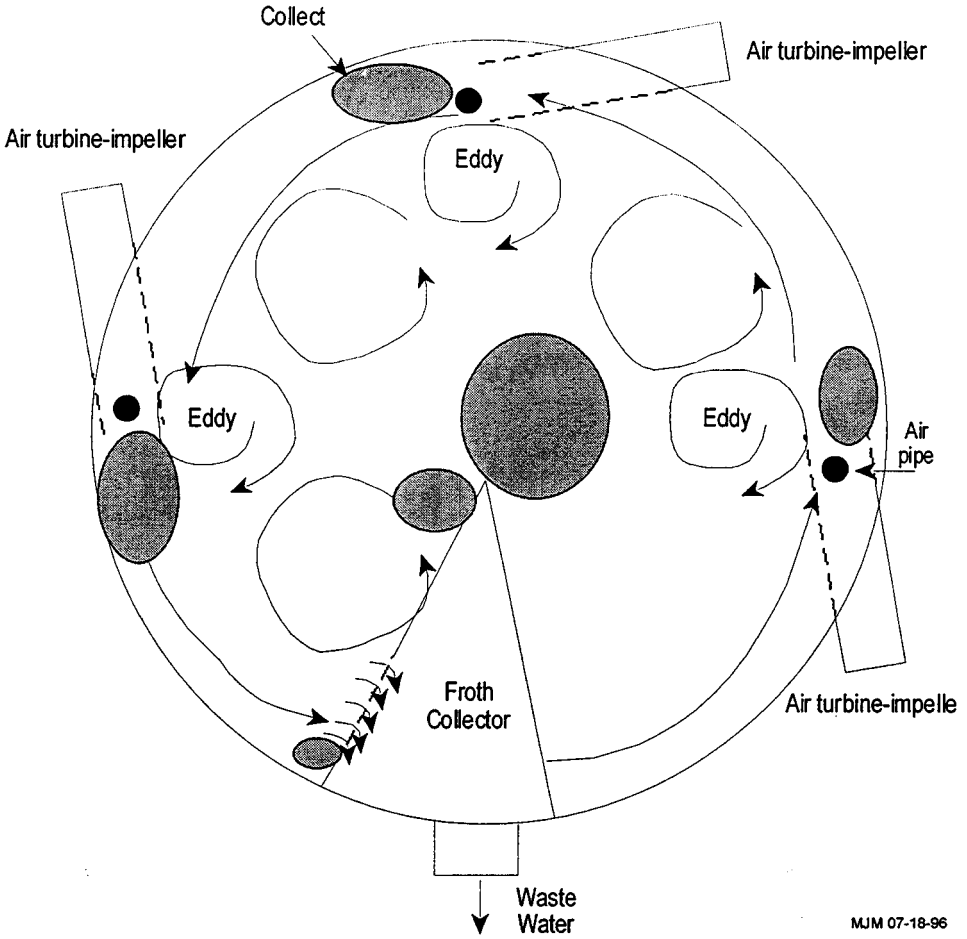

Figure 7. Location of eddy areas on the water surface of the air flotation tank which allowed solids to accumulate on the surface of the water at the tank wall.

tank at the water surface. The impingement of the water jets from the venturi _tubes on the wall of the tank forced the air bubbles to sweep the wall of the tank. The air bubbles rising along the wall of the tank prevent solids from accumulating on the wall of the tank, especially at the water surface. A 6-inch pipe at the center of the tank was adequate to catch and remove the froth. Figure 8 is a schematic of the air flotation tank with the modified waste water weir and the two venturi tubes used to_generate the air bubbles. The location of the venturi tubes at the bottom of the tank, and the waste weir in the center of the tank, along with sufficient volume of air, resulted in quality water from the air flotation unit of less than 10 mg/L by turbidity (2.2 mg/L solids by weight).

Problem Nine. Analytical Measurements.

Relationships and conclusions in engineering and science can only be made from quantitative data. All else is speculation. From startup of the flotation unit in July 1994 until February 1996 no quantitative measuring equipment was available at the Nelson Lease for routine measurement of flow rates or suspended solids in the feed and clean water.

A. Water flow measurements.

The schematic of the water plant in Figure 3 shows five flow lines for which flow rates were needed to understand and quantify the functionality of the air flotation unit. From July 1994 to July 1996 the flow rate through the flotation unit was estimated from the sum of the individual injection well flow meters. In July 1996 a turbine flow meter was installed in the clean water line leaving the plant and provided a daily

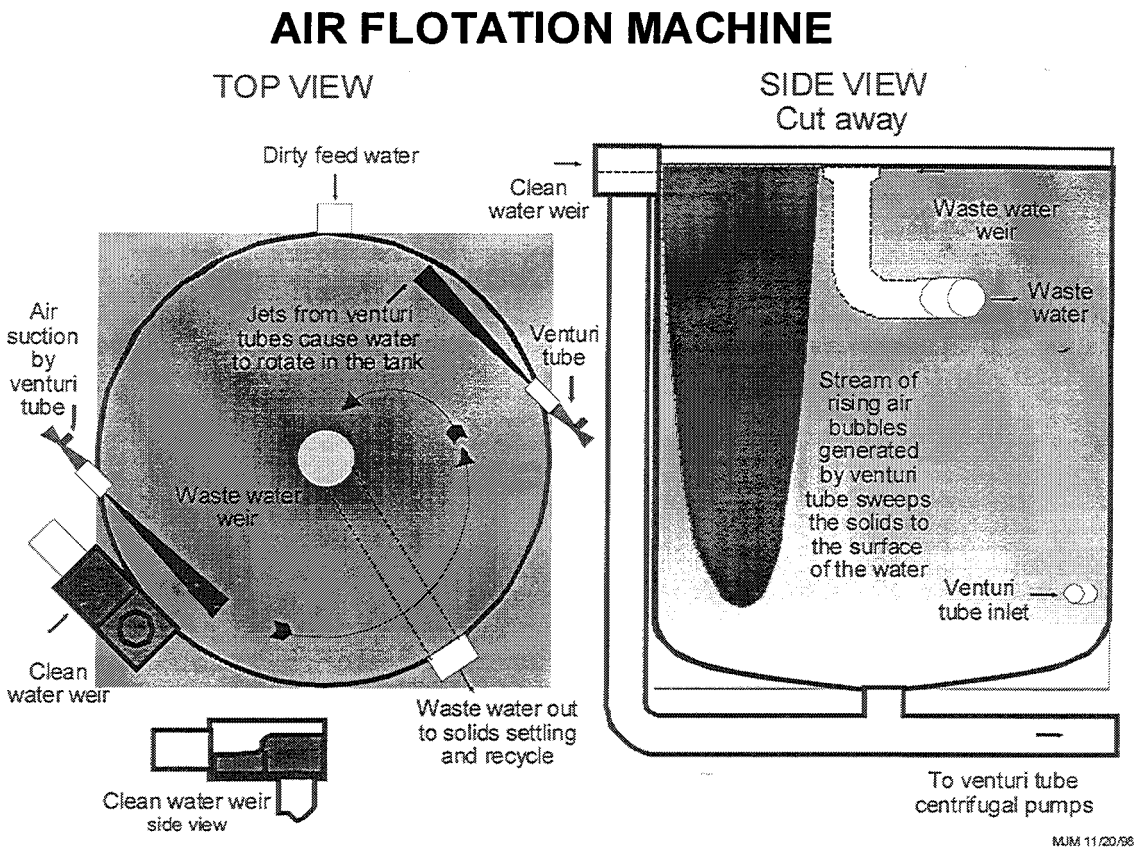

Figure 8. Modified air flotation unit with two 1.5-inch venturi tubes mounted 12-inches from the bottom of the tank and at a 45° angle with respect to the diameter of the tank. The water jets from the venturi tubes cause the water in the tank to rotate at 3 to 5 rpm. The water jets also carry the entrained air to the tank wall where the rising bubbles sweep the dirt to the water surface and also keep the wall free of solids. The waste weir is 6-inches in diameter and located in the center of the tank. The water enters near the surface of the tank and descends in a spiral counter to the spiral of rising bubbles.

volume for water leaving the plant. A paddle type meter was installed also on the transfer line to the air flotation unit, but due to location gave high daily water volumes. This meter is in the harsh, scaling water and requires frequent removal for cleaning. A turbine flow meter was installed on the supply well in January 1997, damaged in April 1997, and replaced in February 1998. Flow of waste water was determined by periodic sampling of flow with a 5-gallon bucket starting in July 1998. The waste water bucket test was done on most days, except weekends.

An attempt was made to meter- the produced water in February 1997. A paddle meter was installed in the flow line from the gun barrel to the produced water tank. However, no useful data was collected for the short time the meter was in use. A good estimate of the daily water volume to the flotation unit was made by using the daily water volume sent to the field, the waste water volume, and the supply well volume. Table 2 summarizes the results from July 4 through November 22, 1998. This information was vital in that it supplied the basis for evaluation of the functionality of the air flotation unit. From the flow rate data accumulated, the deficiency in the quality of the water exiting the flotation unit was not due to the suspected variation in the feed water rate, but was due to lack of sufficient air volume in the unit to sweep all the dirt to the surface of the water. This was verified in the bench air flotation unit.

B. Quantitative measurement of suspended solids in water.

The second important measurement needed was an instrument to measure water quality. Water quality requires a knowledge of the constituents in the water and, for a waterflood operation, how well the water flows through the porous media, a filter. The flood water problem at the Nelson lease was due to

Table 2. Summary of water flow from July 4 through November 23, 1998 in barrels per day.

Water	Low	High	Average
Supply well	5	1035	260
Produced	115	1120	780
Transfer to AFU[1]	522	1930	1420
Transfer to AFU by difference[2]	1030	1420	1230
Triplex to the field	835	1240	1050
Recycle from waste	90	380	220
Ratio of produced to supply water	0.1	11	3

1. Results are unreliable due to location and fouling of the paddle meter.
2. Transfer is based on sum of the water sent to the field and returned from air flotation as waste water.

suspended and dissolved solids in the water. Table 1 (Nelson Lease Water Problem) lists the ion analysis or the produced, supply waters, and combined waters for October 23, 1993. Analysis of the produced, supply, and mixed waters on other dates before and after October 1993 gave similar values as determined by Oil Field Research Laboratory of Chanute, Kansas. Analysis by other laboratories also gave comparable values. However, the analysis of the water is incomplete and does not represent the water at the time the - water sample(s) was obtained. Carbonate, bicarbonate, sulfide, pH, and iron values can change between sample and analysis time, and frequently some essential analyses are not routinely done.

As mentioned in the "Nelson Lease Water Problem" section, the quality of the water is compromised when the supply and produced water are mixed. The sulfate and sulfide in the supply water and the barium and iron in the produced water causes barium-sulfate and iron sulfides to form. Both waters also contain bacteria, clay, sand, and organic matter. The solids in the water along with oil caused plugging problems at the injection wells. In this study no attempt was made to improve or expand the scope of the water analysis. Instead the filtration characteristics became the important measurement for the mixed supply-produced water.

The quantification of the mixed water as to filtration was accomplished by using a modified ASTM procedure D-4189-82, "Silt Density Index of Water". A 10 psi air pressure differential was used since this permitted a polyethylene water reservoir to be used. Initially, 0.45-micron polycarbonate filters were used, but later 0.5-micron fiberglass, 47 mm diameter filters were found more practical for the filtration of one liter of water. Fiberglass filters are classified as a depth filter whereas the polycarbonate filters are classified as a sieve filter. The depth filter removed the same quantity of solids from the water in a shorter filtration time. In appendix A, a description of the filtration procedure is given. The parts list and sources are also given for the construction of the filtration apparatus.

A plot of the square root of time versus cumulative water volume results in a straight line for non compressible solids collecting on the filter. The slope of the line-can be used as index of water quality. Excessive amounts of oil in the water, and especially cationic polymer, will cause an excessively long filtration time, which results in a large "Water Quality Index" value. Addition of 0.1 mL of 5% sodium hypochlorite to the liter of water would deactivate the cationic polymer and results in a realistic filtration time and "Water Quality Index". The actual solid content in the liter of water was measured by weighing the filter before and after the filtration. Solid content required the filter to be washed with distilled water in the field, which was not convenient, or in the laboratory to remove dissolved salts in the water on the filter.

Fiberglass filters were superior in that the solids could be treated with acid to separate the soluble from the insoluble solids collected. The polycarbonate or nylon filters disintegrated in acid.

The filtration of a liter (quart) of water was time consuming and too complicated for field personnel to do daily, and thus, was done by a professional from either the Tertiary Oil Recovery Project or Russell Petroleum. Filtration procedure took from 15 minutes to several hours depending on the amount of solids and the presence of the cationic polymer in the water. A second filtration with hypochlorite in the water would distinguish between polymer interference and other cause. The results required returning the filter to the laboratory for drying and weighing on the analytical balance. Thus, the results were not available to the field personnel or the engineers in time to make reasonable changes in the air flotation operational parameters. From the startup of the flotation unit in July 1994 until February 1996, the performance of the unit in response to changes made was subjective and depended on whether field personnel, the engineer from Russell Petroleum, or the engineer from the Tertiary Oil Recovery Project was operating the unit.

The filtration measurement was done one to five times per week by professional personnel from Tertiary Oil Recovery Project or Russell Petroleum. The data obtained from the filtration test was useful in verifying the practicality of a portable, inexpensive colorimeter used to measure turbidity (suspended solids) at the various water sample points.

The purchase of a simple, easy-to-use, HACH DR/700 colorimeter for $500 by Russell Petroleum in February 1996 provided the means to make an essential measurement of suspended solids on a daily basis. A HACH colorimeter was then purchased by the Tertiary Oil Recovery project in April 1996. Field personnel were trained in the use of the colorimeter in fifteen minutes. It takes only 30 seconds to turn on the instrument and set the zero, and then each water sample takes 15 seconds for a suspended solid measurement. The effect of a change in a flow rate through the flotation unit or amount of flotation chemical could be detected by the turbidity measurement. The quantitative numbers eliminated the subjective judgement as to water quality and eliminated the long periods of operating the flotation unit with excess flotation chemical. The daily measurements of suspended solids in the feed, the air flotation, the filtered, and the triplex water provided a basis in the evaluation of the air flotation unit. The HACH meter along with a bench air flotation cell was the key in determining cause and effect as the operational parameters of the air flotation unit were varied.

In addition, the HACH DR/700 colorimeter has interchangeable modules that permit many analyses to be done in the field, such as oxygen, oil, barium, ferrous, ferric and other constituents in water. This instrument provided the quantification necessary in relating cause and *affect*. The calibration incorporated in the 81.01 Module (810 nm) for suspended solids is for sewage containing solids with a density close to one (Method 8006). Actual solid content by weight is possible is possible by a calibration with test solids. Figure 9 is an example of the relationship between the HACH value with the weight for a fine silica sand. Figure 10 is for the solids in the mixed water that was serial diluted with the same water in which the solids had been removed by filtration. During the two years the HACH colorimeter was used in testing the air flotation water, the HACH meter values were used without correction as to actual solids content since a reading of 10 mg/L or less was within the goal of less than 10 mg of solids per liter of water by weight. Figure 11 shows the relationship between the HACH meter readings for suspended solids and the actual weight of solids as determined by the filtration procedure.

C. The bench air flotation cell.

A change of an operational parameter for the air flotation unit, such as change in flotation chemical feed rate or type, or water flow rate, or residence time, would take 3 to 72 hours before a noticeable change observed in the effluent at the flotation unit or at the clean water exiting the plant. A quicker method was needed to evaluate change in water quality, due to change in an operational parameter for the air flotation unit. Thus, a bench model air flotation unit was designed by Michnick and constructed in the machine shop of the Tertiary Oil Recovery Project in March 1997. This bench air flotation cell consisted of a one gallon (4 liters) clear plastic tank. Water is withdrawn at the bottom center to feed a small centrifugal pump that powers a 0. 5-inch venturi tube mounted at the side, near the bottom of the tank. The venturi tube is mounted at an angle of 45°with respect to the diameter of the tank. This configuration causes the water in the bench air flotation unit to rotate as in the water plant flotation unit. The solids move to the water surface and accumulate at the center within seconds after the addition of the flotation chemical into the inlet of the centrifugal pump. The clear plastic tank allows visual observation in the improvement in water quality as the flotation chemical coagulates and flocculates the solids. A water sample port near the bottom of the

tank allows the withdrawal of water for turbidity measurement in the HACH colorimeter every minute during the test.

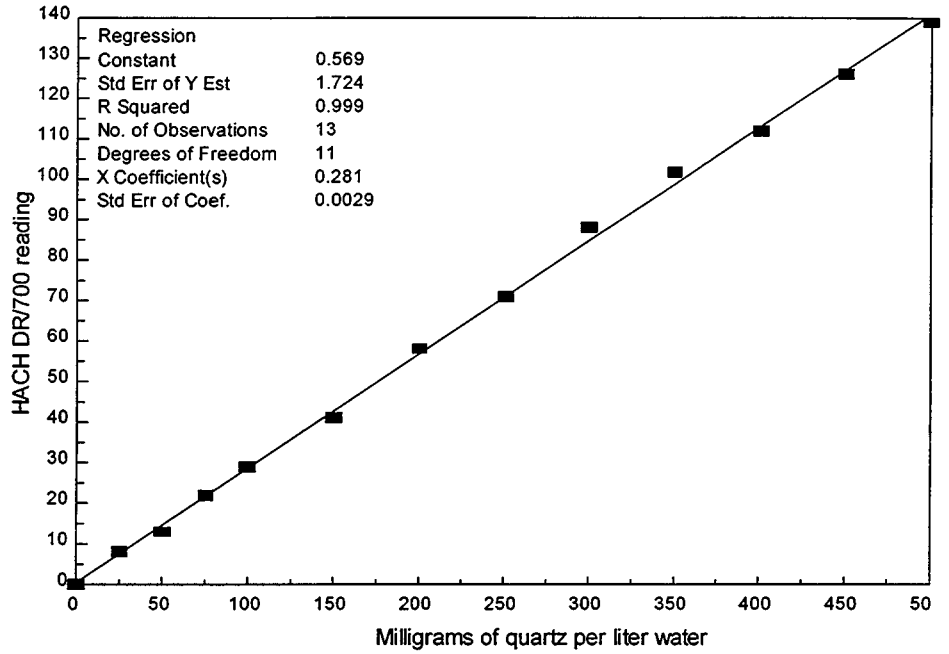

Figure 9. Comparison of suspended solids reading by HACH DR/700 colorimeter with known weight of quartz powder in water. Solid boxes are experimental data and the line is best fit by least squares regression of the data.

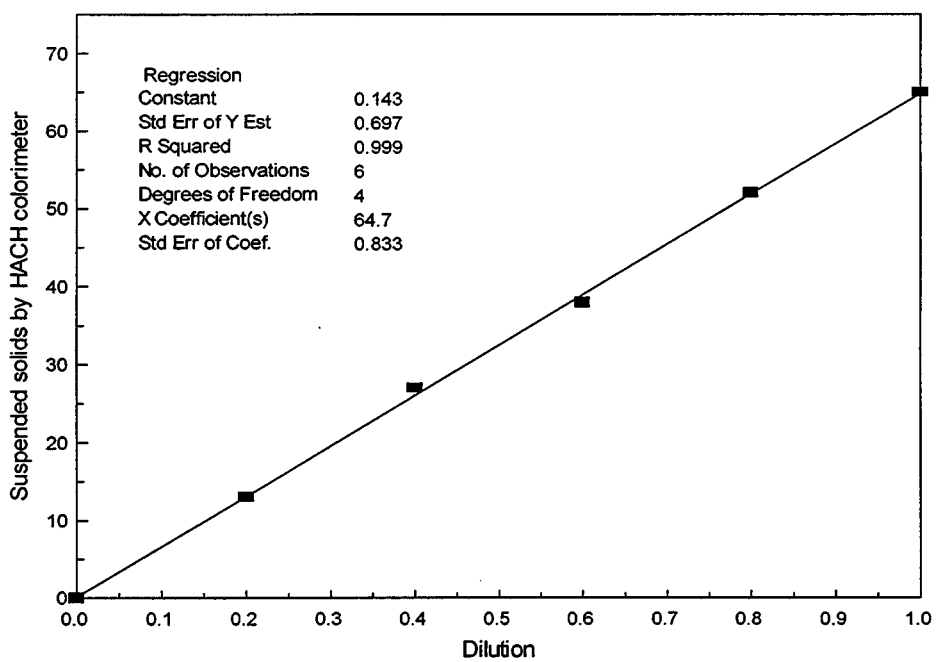

Figure 10. Comparison of suspended solids in the feed water as measured by the HACH DR/700 colorimeter as the water sample was diluted with the filtrate from the same water sample. The solid boxes are the experimental data and the line is the best fit of the data by least square regression of the data.

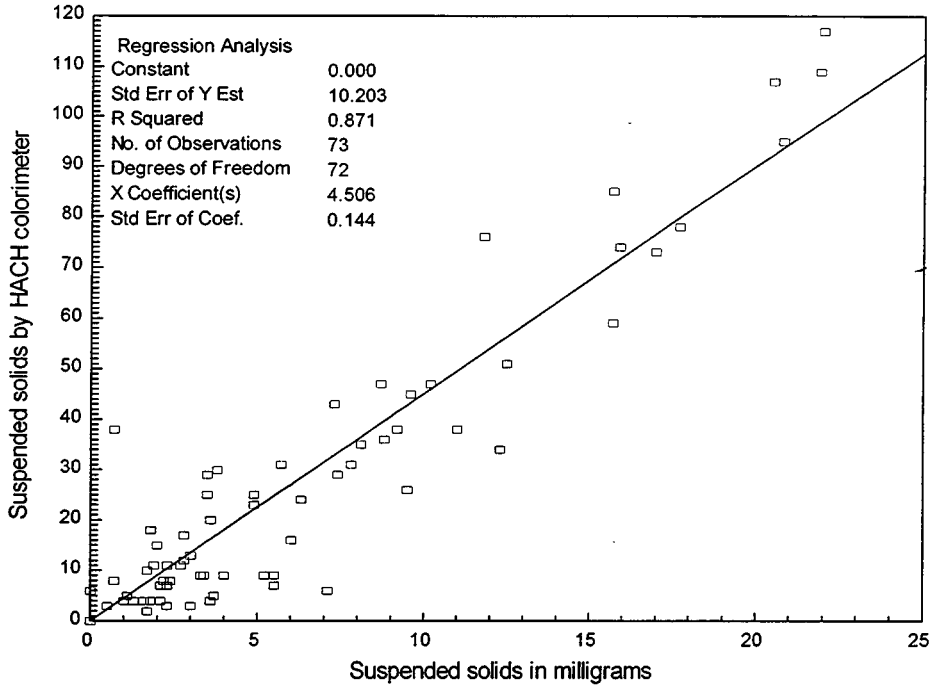

Figure 11. Correlation between weight of suspended solids collected on a filter and HACH colorimeter reading. Filtration consists of passing one liter of water through a 0.5-micron fiberglass filter using a 10 psi pressure differential. Each filter weight was corrected for the 6.6 mg of dissolved solids in the water which adheres to the filter. Data set is for the clean water at the exit of the triplex pump for the year 1998.

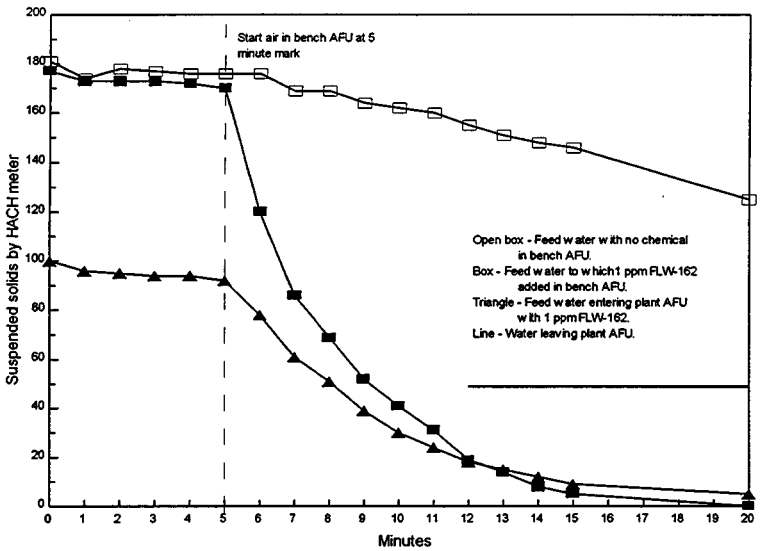

Figure 12. Comparison of water quality between bench and plant air flotation units. The feed water contained 177 mg/L suspended solids as measured by HACH meter. Treating 1-gallon of feed water in bench flotation cell with 1 ppm FLW-162 resulted in water with 0 mg/L solids. The water entering flotation unit measures 100 mg/L solids due to coagulation and flocculation that takes place in the transfer line and exits the unit with 49 mg/L solids. The same water when placed in bench flotation cell and exposed to air for 15 minutes had only 9 mg/L solids showing that more air is needed in the plant flotation unit.

Figure 12 is an example of the results obtained from the bench air flotation unit. The feed water to the flotation unit contained 177 mg/L of suspended solids. A sample of the feed water was placed in the bench flotation cell and treated with 1 ppm FLW-162 and air for 15 minutes. The resulting clean water had no solids by HACH meter. A sample of the water entering the plant flotation unit, which had 1 ppm FLW-162, was then paced in the bench unit and exposed just to air for 15 minutes. The resulting water tested at 9 mg/L solids compared with 49 mg/L solids in the water from the plant flotation unit. This clearly showed that the plant flotation unit did not have sufficient air to remove the solids in the water. Appendix B describes the bench air flotation unit along with the materials for construction of the unit. The bench air flotation unit was used extensively by the engineer-chemist from the Tertiary Oil Recovery Project to test and compare the results from the 1-gallon bench unit and the 1000-barrel a day air flotation unit from April 1997 through July 1998. A typical test would require 30 to 60 minutes to perform. This included the filtration test of the feed water being tested plus the clean water from the bench unit. The filtration tests provided the information to verify the mass of solids in the feed and clean waters, respectively. Various proposed flotation chemicals were tested such as the anionic polymer with and without various additives. The bench unit clearly showed that an air flotation formulation was superior to any combination of chemicals tried, although the anionic polymer with a cationic wetting agent showed promise. Since the proposal was for "Off the Shelf Technology" , little time was spent in developing a simpler to use formulation than the FLW-162 formulation, which is a high molecular weigh, cationic polymer prepared as the internal phase in an oil emulsion.

The bench air flotation unit demonstrated that the remaining deficiency in the air flotation unit was in air volume necessary to float all the solids to the surface. It was not as suspected in the variation in the flow rate of water through the flotation unit, or in the change in the ratio of produced to supply water, or the amount of cationic flotation chemical.

Problem Ten. The need to keep water flowing to the field at all times.

The major constraint in the study was that injection water had to be kept flowing to the field always, especially in the winter. Once the air flotation unit had been purchased and installed the only option left was to bypass the unit and send the untreated mixture of supply-produced water to the field. This was done only in the early days when the air turbines were being repaired. This was necessary since insufficient tankage was available to store the incoming produced water for the eight or more hours during the repairs to the unit. Although the flotation unit did not produce the best quality water for the first four years, Russell Petroleum saw the advantage that the improvement in water quality had on the cost in maintaining the injection wells. Therefore, all changes in the operational parameters were constrained by water needed for. the waterflood of the lease. For 1998 the demand for injection water ranged from 725 to 1050 BPD. The produced water tank could only take about three hours of production before an overflow condition would be reached, thus, water had to be withdrawn from the produced water tank continuously. Operation the flotation unit at desired test rates of 500 or 1500 barrels per day was not possible because of lack of tanks to store produced or clean water.

Oxygen in water

In many typical produced water handling systems the water is exposed to oxygen from the air. A water stream falling through- the air from a separator or heater-treater into the produced water tank will be oxygenated between 6 and 10 ppm oxygen, depending of salt content. The use of an oil pad on the tank does not prevent oxygen from entering the water even if the incoming water is introduced below the oil pad. Surprisingly, the solubility of oxygen in oil is greater than in water. Bacteria in the water are the main reason many produced water tanks have almost no oxygen in the water, especially tanks with stagnant water at the bottom of the tank.

The air flotation unit will produce water that is fully oxygenated. In the past, corrosion was no problem at the injection wells at the Nelson Lease. A check for oxygen at individual wells was negative until recently. Table 3 shows some values at selected points in the water plant and at individual wells. The presence of oxygen was detected at 3 mg/L at test well RW-20 and at the extreme end of the lease at H-7 when bacteria and algae were controlled in the clean water storage tanks. Whether corrosion will become a problem at the Nelson Lease, will depend on control of the growth of algae in the unpainted fiberglass clean water storage tanks, especially in warm weather. The technology and chemicals are readily available to remove the oxygen from the water as it leaves the plant, when it becomes necessary, due to corrosion at the injection wells.

Table 3. Typical oxygen values in mg/L for the feed water, air flotation unit water, clean water, and injection water at test well RW-20 and H-7.

Date	Feed water	Flotation	Clean water	RW-20	H-7
11/06/96	—	7.2	4.0	0.0	—
11/13/96	—	7.2	6.9	—	—
11/21/96	4.1	6.4	6.1	—	—
10/06/98	5.4	7.9	5.7	1.3	—
10/20/98	3.9	7.6	6.3	1.8	6.0[1]
11/04/98	7.4	8.4	7.4	5.1	—
11/17/98	6.4	8.6	7.3	3.2	3.2

1. Fiberglass flow line from plant to north end of field was flushed for 15 minutes before sampling.

Results

The air flotation unit was modified to provide an economical alternative to cleaning produced water for re-injection into the reservoir. The original cost of the flotation unit from Separation Specialists of Bakersfield, California was $30,000. Figure 3 is a photograph of the unit as received in June 1994 and Figure 8 is a schematic of the unit with the venturi tubes and center waste weir. This is the arrangement of the flotation now in operation. A similar size-flotation can be built for an estimated $10,000. Figure 13 is a schematic for the same size flotation unit constructed from a 4-foot diameter by 4-foot tall steel tank. 4-foot diameter by 4-foot tall tank. A bare steel, flat bottom tank is the-least expensive and easiest in which to install the necessary fittings. A dish-bottom, fiberglass tank is desirable, but more expensive. However, note that this is a schematic for a planned flotation unit that has not been tested and actual costs can vary.

The clean water sent to the injected wells allowed the replacement of the 75-micron cartridge filters with 5-micron filters. Filter change at each injection well was no more frequent with the 5-micron cartridges than was the case with the 75-micron cartridges; field personnel stated that the 5-micron filters appeared to have fewer solids with the air flotation water than the 75-micron filters before t$e start of the air flotation unit. A test injection well used a 2-micron cartridge filter. Filter changes for the 2-micron filter were no more frequent than the other injection wells with the 5-micron filters.

Important fmdings of the investigation are; (1) An air to water ratio of at least 4 SCFM of air to- each-40 gpm water is needed to sweep the solids to the surface of the water; (2) A stream of small air bubbles rising at the sides of the tank is needed to keep solids from accumulating at the tank wall, especially at the water surface; (3) By angling the venturi tubes at 45° to the center line of the tank, the water jets from the venturi tubes with the air bubbles can be directed to the wall of the tank and cause the water to rotate in the tank at 3 to 5 rpm; (4) Removal of waste solids and water at the center of the tank at the water surface instead at the tank wall improved-the efficiency of the flotation unit; (5) Introduction of air near the bottom of the tank further reduced the solid content of the clean water exiting the flotation unit; (6) A preventive maintenance schedule for pumps and meters is necessary to insure the continuous operation of the flotation unit, particularly on the raw water side of the flotation system; (7) Good records on the daily operation of the water plant are essential; and (8) The injection well filters were changed from 75 to 5-micron with no more frequent change of filters.

From July 4 through November 22, 1998 the air flotation unit reduced the suspended solids from an average daily value of 80 to 7 mg/L as measured by the HACH meter, 19 to 2 mg/L by weight. Solids in feed water ranged from 40 to 367 mg/L by HACH, 9 to 90 mg/L by weight. This corresponds to an average of 90% in the removal of solids from the water by the flotation unit, which reduced the solids entering the injection wells in the flood water from 2400 to 240 pounds per year. The cost of chemicals for the water plant has been reduced from $35 to $15 per day. Table 4 contains a list and cost of chemicals used from July 4 through November 22, 1998 in the operation of the flotation unit at the Nelson Lease. Future chemical costs are expected to be less because the averages calculated contains days when one or more chemicals were used at a greater rate than necessary due to a malfunction of a metering pump or a planned test.

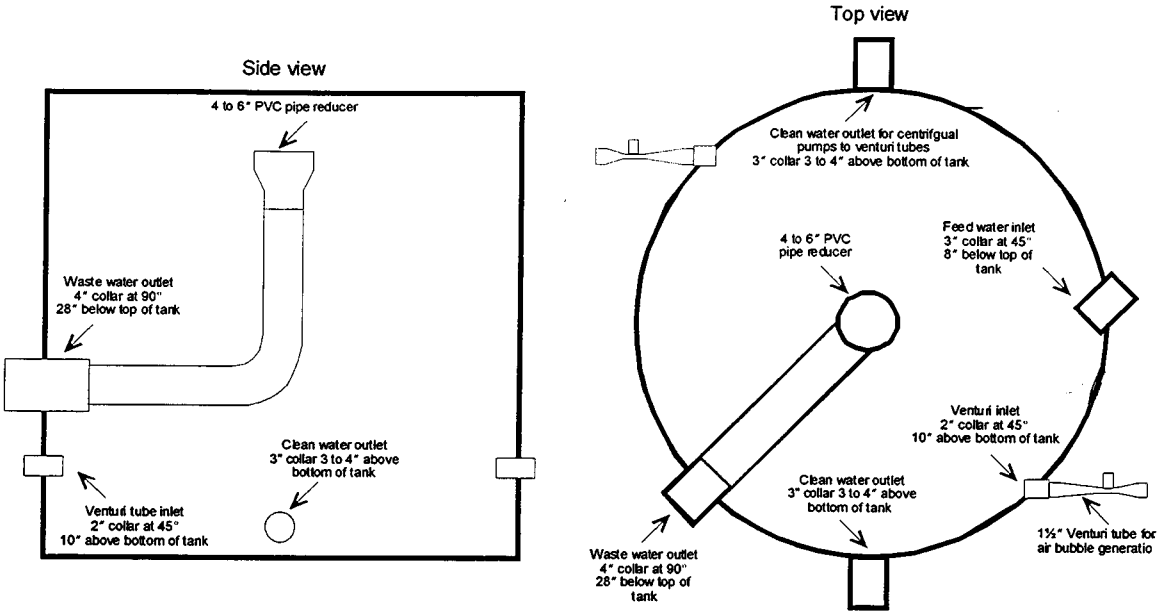

Figure 13. Schematic of proposed air flotation unit constructed from a 4-foot tall by 4-foot diameter steel tank. Note this flotation unit has not been built and tested.

Table 4. Chemical used in operation of flotation unit from July 4 through November 23, 1998 with costs.

Chemicals	Low	High	Average	$/gal	$/day
Hypochlorite, gal	1.5	5.0	2.7	2.10	5.70
Scale inhibitor, qts	0.0	5.5	3.0	10.00	7.50
Flotation chemical, lbs	0.30	1.17	0.51	20.00	1.20
Total					14.40

Conclusions

1. The "Off the Shelf Technology" approach has limitations. One must have some knowledge of the technology and should have some experience. Otherwise, time and money will be spent in learning the technology and operation of the equipment.
2. Air flotation is an economic alternative to cartridge, bag, or sand filtration of produced water that is re-injection into the reservoir.
3. A 1,000 barrel per day air flotation unit can be constructed from a 4-foot diameter by 4-foot tall tank for about $10,000. This estimate includes centrifugal pumps to power the venturi tubes and to recycle the waste water, venturi tubes, a HACH DR/700 colorimeter, and chemical metering pumps. Installation costs depend on the current or anticipated plant configuration. The estimate does not include tanks for storage of produced, supply, and clean waters.
4. Time required to monitor and maintain the flotation unit should be about one hour per day, mainly in keeping operation records, and in preventive maintenance of pumps.
5. Chemical costs were reduced from $35 per day in 1993 to less than $15 per day for 1998.
6. Clean injection water will reduce the frequency, and thus the cost, of maintaining the injection system.
7. The mixed feed water will always contain oxygen whenever the tanks are open to the atmosphere. Air flotation added only 2 to 3 mg/L more oxygen to the water. The oxygen in the clean water decreased rapidly due to algae growth in the clean water tank. Aerobic bacteria in the water also consume oxygen.
8. Oxygen was detected at the injection wells only when the algae and bacteria in the clean water storage tanks were vigorously treated with appropriate chemicals.
9. A preventive maintenance schedule for pumps and meters, and a set of daily water plant operation data will permit management to spot problems before they become serious.

Bibliography

1. K.J. Ives, "The Scientific Basis of Flotation" Martinus Hijhoff Publishers, 1984.
2. M.W. Ranney (Editor), "Flotation Agents and Processes; Technology and Applications", Noyes Data Corporation, 1980.
3. B. Yarar, "Flotation", *"Kirk-Othmer Encyclopedia of Chemical Technology"*, Fourth Edition, Vol. 11, 1992, 81-107.
4. H.I. Heitner, "Flocculating Agents", *"Kirk-Othmer Encyclopedia of Chemical Technology"*, Fourth Edition, Vol. 11, 1992, 61-81.
5. D.S. Kocurek and G. Woodside, "Water (Waste Treatment, Hazardous Waste)';. *"Kirk-Othmer Encyclopedia of Chemical Technology"*, Fourth Edition, Vol. 25, 1992, 284-324.
6. W.W. Eckenfelder, Jr., "Water (Wastes, Industrial)", "*Kirk-Othmer Encyclopedia of Chemical Technology"*, Fourth Edition, Vol. 25, 1992, 325-361.
7. J.D. Hem, "Water (Sources and Quality Issues)", "*Kirk-Othmer Encyclopedia of Chemical Technology"*, Fourth Edition, Vol. 25, 1992, 361-382.
8. W.W. Eckenfelder, Jr., "Water (Pollution)", "*Kirk-Othmer Encyclopedia of Chemical Technology"*, Fourth Edition, Vol. 25, 1992, 406-424.
9. None listed, "Water (Analysis)", "*Kirk-Othmer Encyclopedia of Chemical Technology"*, Fourth Edition, Vol. 25, 1992, 424-437.
10. J. Robinson and B. Dearborn, "Water (Industrial Water Treatment)", *"Kirk-Othmer Encyclopedia of Chemical Technology"*, Fourth Edition, Vol. 25, 1992, 487-526.
11. J.E. Singley, "Water (Municipal Water Treatment)", "*Kirk-Othmer Encyclopedia of Chemical Technology"*, Fourth Edition, Vol. 25, 1992, 526-540.
12. None listed, "Water (Sewage)", "*Kirk-Othmer Encyclopedia of Chemical Technology*", Fourth Edition, Vol. 25, 1992, 540-560.
13. None listed, "Water (Reuse)", *"Kirk-Othmer Encyclopedia of Chemical Technology"*, Fourth Edition, Vol. 25, 1992, 561-569.
14. *Annual Book of ASTM Standards"*, Section 11, Water and Environmental Technology, (D 4189-95) 400-402.
15. None listed, "DR/700 Colorimeter Procedures Manual" HACH Company, 1994, Method 8006, 81-69-81-72.
16. G.F. Bennett, "The Removal of Oil from Wastewater by Air Flotation: A Review", *Critical Reviews in Environmental Control*, Vol. 18, Issue 3, 1998, 189-252.
17. M.C. Sport, "Design and Operation of Dissolved-Gas Flotation Equipment for the Treatment of Oilfield Produced Brine", *Journal of Petroleum Technology*, August 1970, 918-920.
18. M.M Ellis and P.W. Fisher, "Clarifying Oilfield and Refinery Waste Water by Gas Flotation", *Journal of Petroleum Technology*, April 1973, 426-430.
19. M.G. Bassett, "WEMCO Depurator System", Rocky Mountain Regional Meeting of Society of Petroleum Engineers of AIME, Billings, MT., June 2-4, 1971, SPE 3349.
20. M.A. Carrell, "Reclaiming Produced Water for Steam Generation in the Kern River Field", 5[1] Annual Technical Conference and Exhibition of Society of Petroleum Engineers of AIME, Las Vegas NV, September 23-26, 1979, SPE 8411.
21. A.H. Bayer and L.L. Palmer, "Biological Oxidation of Dissolved Compounds in Oilfield-Produced Water by a Pilot Aerated Lagoon", *Journal of Petroleum Technology*, February 1979, 241-245.
22. N.D. Sylvester, "Oil/Water Separation by Induced-Air Flotation", *Society of Petroleum Engineers Journal*, December 1980, 579-590.
23. C.A. Leech et al., "Performance Evaluation of Induced Gas Flotation Machine Through Mathematical Modeling", *Journal of Petroleum Technology*, January 1980, 48-58.

Appendix A. Water quality index by filtration (as modified by Michnick).

A modified procedure, along with the equipment used, is described here for the measuring the quality of a water by filtration. The procedure is a modification of the ASTM D-4189-95 "Silt Density Index for Water". The ASTM procedure calls for recording the times for passage of the water volumes through a 0.45-micron, 47 mm diameter membrane filter using a 30 psi gas pressure. A lower pressure permits simpler and lighter weight equipment to be used in the field. Figure Al is a schematic of the simplified

apparatus and contains a list of parts with prices as of 1999. The only additional item is a tape recorder to record times at selected volumes of water collected for those samples which filter rapidly.

Assembly of the apparatus and operation is simple. A filter is placed in the filter holder connected to the polyethylene water reservoir through a ball valve and flexible plastic tubing. The bottle is filled with more than one liter of water. The air pump is started and pressure adjusted to 10 psi. The air hose is connected to the polyethylene bottle cap using the quick connectors to pressurize the system. The valve is opened and the time recorded for uniform volume increments in the collecting cylinder. A plot of the square root of time versus cumulative volume generally results in a straight line. The slope of the line times 100 can be used as a water quality index. The smaller the slope the better the quality of the water. Filtration time, using a 0.5-micron fiberglass filter, ranges from one minute for clean water to hours depending on solids and other organic contaminants in the water. The pressure is released from the apparatus, the filter removed, blotted on paper toweling and stored until it can be dried and weighed in the laboratory.

Ideally, the air in the filter line and filter should be displaced with water and the filter wetted with clean water. However, from experience I found this only increased the time to perform the test and provided little or no improvement in the precision or quantitative values in the index number as calculated from the slope of the line. This plot can be made in the field on graph paper and the slope estimated without the aid of a calculator. The actual weight of solids in one liter of water can be determined by pre-weighing the filter before the test. The filter should be washed in the field with 50 to 100 mL of water, but I have found this again to be inconvenient. A filter can be mounted in a simple filter holder in the laboratory and washed, either before or after they have become dry during storage. For the Nelson Lease water the solid contribution from the soluble salts in the water sticking to the filter was essentially constant over a twelve-month period at 6.6 mg per filter. Duplicate filtrations made in the field in which one was washed in the field and the other washed in the laboratory gave the same results to within 0.1 mg. The same 6.6 mg weight average for soluble salts-vas obtained for nine filters soaked in filtered Nelson Lease water, blotted, and dried A balance weighing to the 0.1 mg is necessary to obtain the weight of the dried solids.

The limitation of the method is the time to filter samples. The presence of a few milligrams per liter of the cationic flotation polymer caused very long filtration times. Addition of 0.1 mL of 5% sodium hypochlorite to the liter of test water reduced the filtration time to within the expected time for the solid load in the water. Excessive amounts of dispersed oil or bacteria can also lead to long filtration times, but this is a true indication of the quality of the water. Hypochlorite does not change the water quality index by oxidation of the oil or bacteria. The method is to time consuming for field personnel to do and results are not as useful as a turbidity measurement in the operation of the flotation unit.

Appendix B. The design and fabrication of a bench air flotation test unit.A chemical change made as an operational parameter of the air flotation unit would take 3 to 72 hours before a noticeable change observed in the effluent at the flotation unit or at the clean water exiting the plant. A quicker method was needed to evaluate change in water quality due to changes in how much flotation chemical needed. Thus, a bench model air flotation unit was constructed in the machine shop of the Tertiary Oil Recovery Project. Figure B1 is a schematic of the bench flotation unit and with a list of parts and prices as of 1999. The unit consists of a one gallon (4 liters) clear plastic tank. Water is drawn from the bottom center to feed a small centrifugal pump that powers a 0.5-inch venturi tube mounted at the side, near the bottom of the tank. The water action in the bench unit is very similar to the field flotation unit. A tee with a septum port allows for injection of micro liter amounts of test chemical to the circulating water. A ball value is used to control the water to the venturi tube. This valve is adjusted so that a vortex is not created in the tank. A valve on the air inlet to the venturi tube controls the air to the flotation cell. A sample port near the bottom of the tank allows for periodic withdrawal of water for suspended solid measurements in the HACH colorimeter. At the end of the test a liter of water is withdrawn for water quality index measurement and solid content by weight using the filtration apparatus. Testing time for a water sample is usually 15 minutes in the flotation unit, and then another 2 to 30 minutes for the filtration test. The solids in the water from the bench and the plant air flotation unit agreed within 1 to 5 mg/L, by turbidity, for the same amounts of flotation chemical(s) in the two flotation units.

WATER FILTRATION APPARATUS

Part	Number	Price
Air pump	P-07059-40	$440.00
Tubing, per 50 ft	P-06408-66	19.50
Quick dicsonnect	P-06360-50	13.25
	P-06360-75	8.75
Carboy with tubulation	P-06080-10	14.00
¼″ ball valve	P-06225-54	13.50
Filter holder	P-06623-22PP	20.50
0.5-micron glass fiber filters	09-730-61	37.00
500 mL graduate cylinder	P-06137-80	8.25
Stopwatch	P-99410-20	36.00

All part numbers refer to Cole-Parmer catalog, except filters from Fisher Scientific. Other vendors supply similar or identical items at comparable prices.

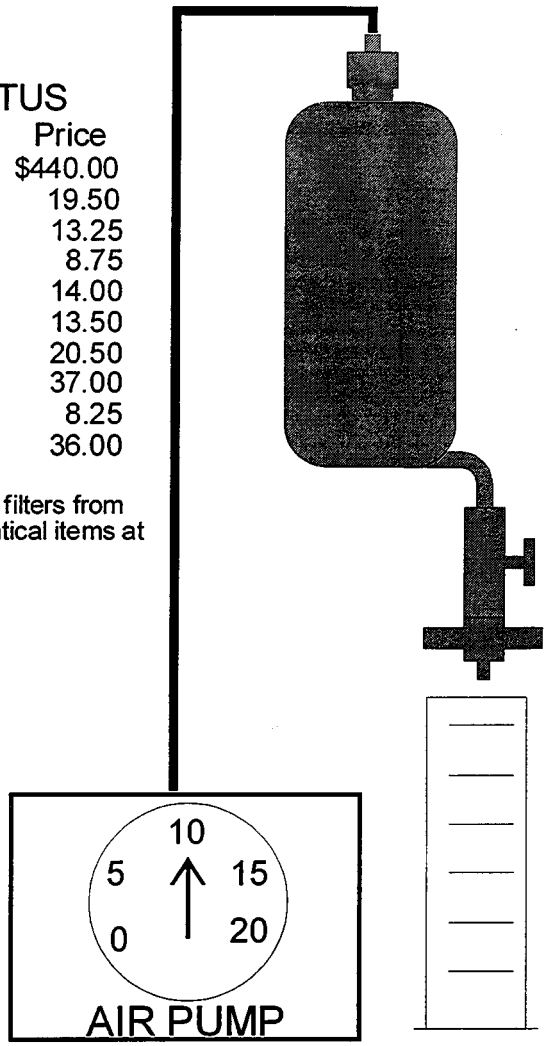

Figure A1. Apparatus to measure water quality by filtration time and to obtain solids by weight.

BENCH AIR FLOTATION UNIT

LIST OF MATERIALS

Magnetic drive centrifugal pump, 5 gpm	E-07021-01	$140.00
Ball valve, PVC ¼"	E-06225-50	12.00
Metering ball valve, PVC ½"	E-01360-40	73.40
Polycarbonate jar, 1¼ gal	E-06761-12	52.17
Polycarbonate rod, 2×12"	8751K22	27.38
Polycarbonate sheet 12×12× ½"	8574K32	15.94
Venturi tube ½"	283	24.50
Plastic cement	HW store	—
4 to 6" PVC to clay pipe	HW store	—
Electric box and switch	HW store	—
NPT pipe to barb fittings	HW store	—
Tygon tubing, d " OD	HW store	—

Parts with E- are from Cole Parmer, -K- from McMaster-Carr, and Venturi tube from Mazzi Injector Corporation.

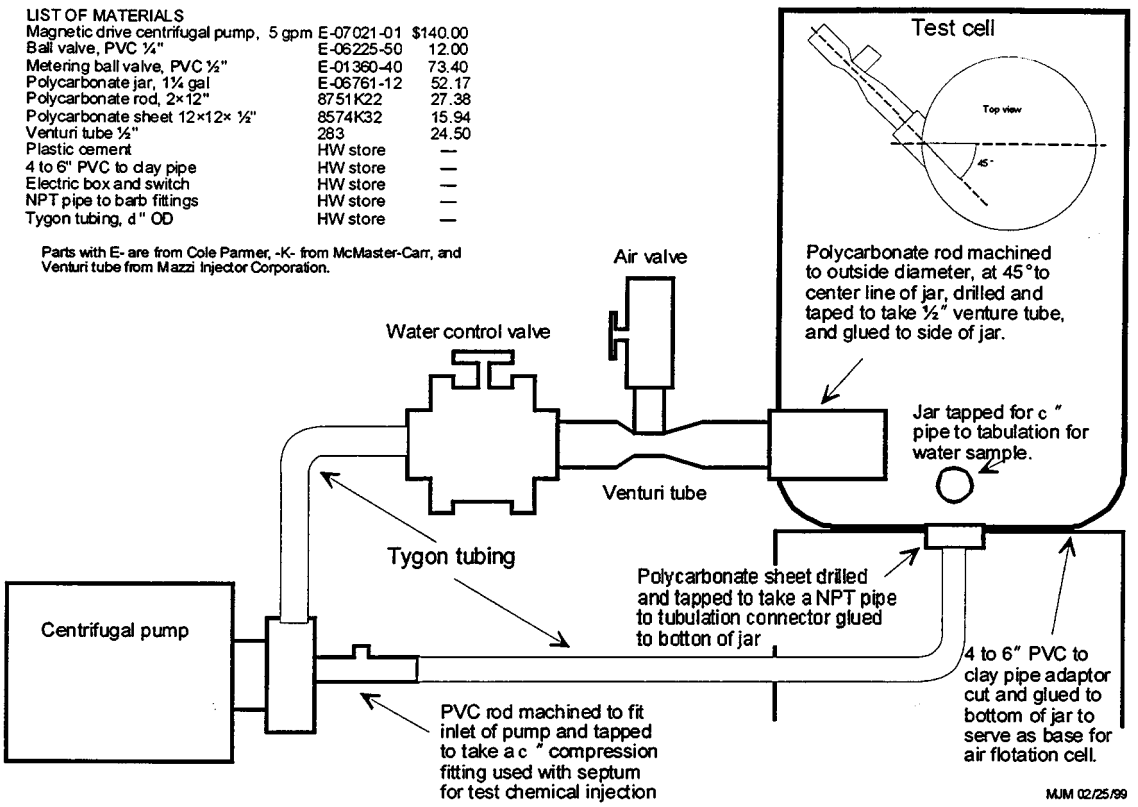

Figure B1. Bench unit for testing water for solids removal by air flotation.

FOSSIL ENERGY

DOE/BC/14956-16
(DE98000547)

IDENTIFICATION AND EVALUATION OF FLUVIAL-DOMINATED DELTAIC (CLASS I OIL) RESERVOIRS IN OKLAHOMA

Final Report
August 1998

By:
Mary K. Banken

Date Published: November 1998

Work Performed Under Contract No. DE-FC22-93BC14956

Oklahoma Geological Survey
University of Oklahoma
Norman, Oklahoma

National Energy Technology Laboratory
National Petroleum Technology Office
U.S. DEPARTMENT OF ENERGY
Tulsa, Oklahoma

DISCLAIMER

This report was prepared as an account of work sponsored by an agency of the United States Government. Neither the United States Government nor any agency thereof, nor any of their employees, makes any warranty, expressed or implied, or assumes any legal liability or responsibility for the accuracy, completeness, or usefulness of any information, apparatus, product, or process disclosed, or represents that its use would not infringe privately owned rights. Reference herein to any specific commercial product, process, or service by trade name, trademark, manufacturer, or otherwise does not necessarily constitute or imply its endorsement, recommendation, or favoring by the United States Government or any agency thereof. The views and opinions of authors expressed herein do not necessarily state or reflect those of the United States Government.

This report has been reproduced directly from the best available copy.

DOE/BC/14956-16
Distribution Category UC-122

Identification and Evaluation of Fluvial-Dominated Deltaic (Class I Oil) Reservoirs in Oklahoma

By
Mary K. Banken

November 1998

Work Performed Under DE-FC22-93BC14956

Prepared for
U.S. Department of Energy
Assistant Secretary for Fossil Energy

Rhonda Lindsey, Project Manager
National Petroleum Technology Office
P.O. Box 3628
Tulsa, OK 74101

Prepared by
Oklahoma Geological Survey
University of Oklahoma
1000 Asp, Room 314
Norman, OK 73019

II. TABLE OF CONTENTS

I. ABSTRACT v

III.EXECUTIVE SUMMARY

IV. INTRODUCTION 1

V. DISCUSSION 2

- **Task 1: Database and Applications Development** 2
- **Task 2: Play Analyses, Publications, and Workshops** 5
  - **The Morrow Play** 6
  - **The Booch Play** 10
  - **The Layton and Osage-Layton Plays** 13
  - **The Skinner and Prue Plays** 17
  - **The Cleveland and Peru Plays** 26
  - **The Red Fork Play** 31
  - **The Tonkawa Play** 34
  - **The Bartlesville Play** 36
- **Industry Responses** 39
- **Task 3: Professional Outreach** 40

VI. CONCLUSIONS 41

VII. REFERENCES 43

List of Tables and Figures

Table 1 - Fluvial-Dominated Deltaic Oil Reservoirs: Oklahoma PIays 5
Table 2 - GeologicalEngineering Data for the Lower Morrow Sandstones 6
Table 3 - Oil Production Statistics for Upper Morrow Purdy Sands 10
Table 4 - Oil Production Statistics for the Wewoka N.W. Booch Sand Unit 12
Table 5 - Oil Production Statistics, Booch Oil Reservoirs 13
Table 6 - Reservoir Properties, Osage-Layton Reservoir 16
Table 7 - Oil Recovery Comparisons for Different Development Cases 16
Table 8 - Annual Oil Production from Oklahoma Skinner and Prue Reservoirs, 1979-95 17
Table 9 - Reservoir Properties for the Perry SE nd Guthrie SW Skinner Sand Units 19
Table 10 - Oil Production Statistics for the Guthrie S.W. 20
Table 11 - Reservoir Properties for the Salt Fork North Field Skinner Sandstones 22
Table 12 - Reservoir Properties for the Prue Sandstone in Long Branch Field 25
Table 13 - Ten-Year Production Forecast Based on Reservoir Simulations 25
Table 14 - Reservoir Properties for the Peru Oil Reservoir in Hogshooter Field 28
Table 15 - Crude Oil Production from Cleveland Sand Reservoirs, 1979-1995 29
Table 16 - Reservoir Properties of the Cleveland Sand Reservoir, Pleasant Mound Field 30
Table 17 - Oil Recovery Comparisons from Different Development Cases, Cleveland Sand Reservoirs 30
Table 18 - Oil- and Gas-Production Statistics for the Bartlesville Sandstone in Paradise Field 37
Table 19 - Annual Production and GOR for the Three Wells Completed Exclusively In the Bartlesville Sandstone 38
Table 20 - Summary of FDD Play Workshops Operator Responses 39

Figure 1 - Generalized location map showing Morrow FDD areas 6
Figure 2 - Oil-production decline curve for lower Morrow sandstones in the Canton study area 8
Figure 3 - Oil-production decline curve for upper Morrow sandstones in S. Balko field 9
Figure 4 - Generalized location map showing Booch FDD area 11
Figure 5 - Maximum net thickness of Layton and Osage-Layton sandstones in the deltas area 14
Figure 6 - Information map of the East Lake Blackwell oil field area 15
Figure 7 - Paleogeography of the central Mid continent region during deposition of Skinner and Senora 18
Figure **8** - Generalized location map of Perry S.E. field study area 19
Figure 9 - Generalized location map of Guthrie S.W. field study area 20
Figure 10 - Generalized location map of the Salt Fork North study area in SE Grant County, OK 21
Figure 11 - Predicted outcome of exploitation schemes from 1996 to 2010 22
Figure 12 - Generalized location map of the Long Branch field Prue oil pool, Payne County, OK 24
Figure 13 - Generalized location map showing Peru FDD areas 26
Figure 14 - Maps showing the Hogshooter field, areas with Peru production 27
Figure 15 - Generalized location map showing Cleveland FDD areas 28
Figure 16 - Generalized distribution & depositional environments of the Red Fork sandstone in OK31
Figure 17 - Regional insopach map of the interval from the top of the Pink lime to the top of the Inola Limestone 32
Figure 18 - Map showing location of the N. Carmen Field in southwestern Alfalfa County, OK 32
Figure19 - Long Branch study area 33
Figure 20 - Generalized location map of the Tonkawa play 34
Figure 21 - Generalized location map of Blackwell field study area, Kay County, OK 35
Figure 22 - Generalized location map of the Bartlesville play 36
Figure 23 - Map showing location of the Bartlesville oil pool in the NW Russell field area 37

Appendix A. Attendee Evaluation Summaries 45

I. ABSTRACT

The Oklahoma Geological Survey (OGS), the Geo Information Systems department, and the School of Petroleum and Geological Engineering at the University of Oklahoma have engaged in a five-year program to identify and address Oklahoma's oil recovery opportunities in fluvial-dominated deltaic (FDD) reservoirs. This program included a systematic and comprehensive collection and evaluation of information on all FDD oil reservoirs in Oklahoma and the recovery technologies that have been (or could be) applied to those reservoirs with commercial success.

The execution of this project was approached in phases. The first phase began in January, 1993 and consisted of planning, play identification and analysis, data acquisition, database development, and computer systems design. By the middle of 1994, many of these tasks were completed or nearly finished including the identification of all FDD reservoirs in Oklahoma, data collection, and defining play boundaries. By early 1995, a preliminary workshop schedule had been developed for project implementation and technology transfer activities. Later in 1995, the play workshop and publication series was initiated with the Morrow and the Booch plays. Concurrent with the initiation of the workshop series was the opening of a computer user lab that was developed for use by the petroleum industry. Industry response to the facility initially was slow, but after the first year lab usage began to increase and is sustaining. The remaining six play workshops were completed through 1996 and 1997, with the project ending on December 31, 1997. The play workshop and publication listing (in order of production) was as follows: Morrow, Booch, Layton and Osage-Layton, Prue and Skinner, Cleveland and Peru, Red Fork, Tonkawa, and Bartlesville.

This program has been described by numerous industry representatives as the most valuable program that the Oklahoma Geological Survey has ever implemented. Since there is no direct way to measure the impact that this program has had on the volumes of FDD oil production in Oklahoma, the success of the program must be measured in terms of the accomplishments and the industry evaluations of those accomplishments. Eight highly successful workshops and accompanying publications were completed on eleven FDD horizons. A computer user laboratory was established and continues to be a resource to the industry. Industry relationships with the project participants have shown vast improvements. Industry feedback to the program has been overwhelmingly positive. The development of this FDD program and the support of the U.S. Department of Energy have set the stage for a strong technology transfer foundation for Oklahoma's petroleum industry.

III. EXECUTIVE SUMMARY

The Oklahoma Geological Survey (OGS), the Geo Information Systems department, and the School of Petroleum and Geological Engineering at the University of Oklahoma engaged in a five-year program to identify and address Oklahoma's oil recovery opportunities in fluvial-dominated deltaic (FDD) reservoirs. This program included a systematic and comprehensive collection and evaluation of information on all FDD oil reservoirs in Oklahoma and the recovery technologies that have been (or could be) applied to those reservoirs successfully. This data collection and evaluation effort was the foundation for an aggressive, multifaceted technology transfer program that was designed to support all of Oklahoma's oil industry. However, particular emphasis of this program was directed toward smaller companies and independent operators in order to help them maximize oil production from FDD reservoirs.

Specifically, this project identified all FDD oil reservoirs in the State; grouped those reservoirs into plays that have similar depositional and geologic histories; collected, organized and analyzed all available data; performed characterization and simulation studies on selected reservoirs in each play; and implemented a technology transfer program that targeted operators of FDD reservoirs. These elements of the FDD program provided the kind of assistance that could allow operators to extend the life of existing wells with the ultimate objective of recovering more oil.

The execution of this project was approached in phases. The first phase began in January, 1993 and consisted of planning, play identification and analysis, data acquisition, database development, and computer systems design. By the middle of 1994, many of these tasks were completed or nearly finished including the identification of all FDD reservoirs in Oklahoma, data collection, and defining play boundaries. Later in 1994, a preliminary workshop schedule was developed for project implementation and technology transfer activities. In early 1995, a specific workshop agenda was formatted and play publication requirements were identified. Later in 1995, the play workshop and publication series was initiated with the Morrow play in June and the Booch play in September. The remaining six play workshops were completed through 1996 and 1997, with the project ending on December 31, 1997.

The following is a summary of tasks completed as part of the implementation and technology transfer activities of this FDD project:

Task 1: Database and Applications Development: Computer support activities included ongoing database development and maintenance, applications development, and user lab development and operation. An operator database was designed to track operators (and other interested parties) who were working with FDD reservoirs in Oklahoma. These operators were targeted to participate in the data collection process as well as the technology transfer program. A variety of computer applications programs were developed for data analysis, for publication and workshop preparation, and to support users. Computerized mapping and report programs were necessary for reservoir analysis and regional play interpretations. Database development also involved reformatting NRIS well, lease and field mainframe databases for p.c.-level access through a computer user lab, which was one of the primary technology transfer tools implemented during this project. The lab was opened on June 1, 1995, in conjunction with the Morrow play presentation. Industry response to the facility initially was slow, but after the first year lab usage began to increase and is sustaining.

Task 2: Play Analyses, Publications, and Workshops: During the project, eight FDD workshops involving 11 plays with accompanying folio publications were completed.

The Morrow Play was the first in the series, presented on June 1 and 2, 1995 at the Sarkeys Energy Center in Norman, Oklahoma. A total of 215 people attended either day. Morrow fluvial systems are found principally in three regions within Oklahoma: the Dewey-Blaine Counties embayment, the Woodward "trench'; and the Panhandle region comprising of Texas, western Beaver, and eastern Cimarron Counties. Detailed information was provided for three Morrow field studies: the Canton field area in Dewey County, the South Balko field in Beaver County, and the Northeast Rice field in Texas County. A reservoir characterization and waterflood simulation study was completed and presented for the Northeast Rice field.

The Booch Plav was presented next, on September 11, 1995 at the Indian Capital Vo-Tech School in Muskogee, Oklahoma. A total of 128 people attended that workshop. The Pennsylvanian sandstones in the Booch were significant oil reservoirs during the early history of the oil industry in Oklahoma; Booch reservoirs are still important today for potential recovery of additional oil by water-flooding or other enhanced recovery methods. The Booch play is located on the Cherokee Platform in northeastern Oklahoma and extends southward beyond the hinge line of the McAlester Formation into the Arkoma basin. Detailed information was provided for two Booch field studies: the Northwest Wewoka field area in Seminole County, and the Greasy Creek field in Hughes County. Additionally, a reservoir characterization and waterflood simulation study was completed and presented for the Greasy Creek field.

The Layton and Osage Layton Play was presented on April 17, 1996 at the Francis Tuttle Vo-Tech Center in Oklahoma City. It was well attended by 103 people. The Layton and Osage Layton sands constitute two different zones or formations (the Layton lies 100 ft or more below the Osage-Layton). The names have been so misused by industry, that it is nearly impossible to differentiate between the two reservoirs from production records or from formation tops recorded on completion reports. This problem was addressed in the workshop but because it is so widespread, both formations were treated as one play in the regional discussion. Detailed geologic field studies within this workshop and play publication include the East Lake Blackwell and South Coyle fields. East Lake Blackwell field is an Osage-Layton sand reservoir that also was used in the waterflood simulation study. South Coyle field is a Layton sand reservoir that lies stratigraphically below the Osage-Layton interval.

The Prue and Skinner plays were presented on June 19 and 20, 1996 in Oklahoma City, and on June 26, 1996 in Bartlesville. Because of the large number of operators and high interest in these plays, three workshops were necessary to accommodate the 201 attendees. Similarities in depositional origin, stratigraphy, age, and environments of deposition made it convenient to group the Prue and Skinner plays into one workshop. Major topics included in the publication and workshop consisted of the regional analysis of each play along with three Skinner field studies and one Prue field study. The four fields have diverse geologic characteristics that typify many of the clastic reservoirs in the Cherokee Platform of eastern Oklahoma. Two of the fields have alreacly been water flooded which provided a good analogy for this technology. Enhanced recovery simulation studies were completed on one Prue and one Skinner reservoir. Computer modeling utilized software demonstrated in previous workshops (Eclipse) in addition to Boast III which is more widely available to the public.

The Cleveland and Peru workshop was completed October 17, 1996 in Bartlesville, Oklahoma with 85 attendees. Each play was presented individually using the adopted protocol of stratigraphic interpretations, a regional overview, and detailed field studies. Two field studies were completed including the Pleasant Mound Cleveland oil pool and the Hogshooter Peru oil pool. A waterflood simulation was completed for the Pleasant Mount Cleveland oil pool. The Peru field study was not considered suitable for waterflood simulation because of the lack of production data. Instead, a guest lecturer presented a talk on formation evaluation of the Peru sand in the Hogshooter oil field.

The Red Fork Play was the subject of a workshop that was presented twice: on March 5, 1997 in Norman, and again on March 12 in Bartlesville, to a total of 195 attendees. The Red Fork sandstone has been, and continues to be, one of the main producers of oil and gas in Oklahoma, as well as one of the most widespread Cherokee plays in Oklahoma. The Red Fork interval extends from the Cherokee platform, across the Nemaha fault zone and the central Oklahoma uplift to the Anadarko basin. Field studies were completed on the North Carmen Field in Alfalfa County and the Long Branch Field, located in east-central Payne County. This is the same field area in which a Prue reservoir had been the subject of a previous study and workshop.

The Tonkawa Plav has been of continued interest for many operators and geologists for a long time, but recently has become very active in western Oklahoma. The renewed interest in the Tonkawa centers in the Anadarko Shelf and Basin areas where production is prone to gas from marine sands. Because of this high interest, the Tonkawa FDD workshop was partnered with a presentation on the Tonkawa gas play. The workshop was presented on July 9, 1997 in Norman with 101 attendees. Portions of north central Oklahoma have significant areas containing FDD deposits, but only scattered areas within the FDD portion of the play produce oil. The Virgilian age sandstones of the Tonkawa play are the youngest of the fluvial-deltaic reservoirs to be investigated in the FDD workshops, with drilling depths of about 2,200-4,400 ft. A field study was completed on the Blackwell Field in Kay.

The finale of the FDD program was the Bartlesville Plav. Oil reservoirs in the Bartlesville sandstone were the foundation for the dominance of Oklahoma as an oil producing state, beginning with the No. 1 Nellie Johnstone in 1897. This workshop was presented three times and locations: on October 29, 1997 in Tulsa, on October 30 in Bartlesville, and on November 12, 1997 in Norman. Attendance for the three sessions totaled 183. The Bartlesville play is situated on the Cherokee platform of northeastern Oklahoma. Bartlesville field studies included the Paradise field in Payne County and the Northwest Russell field in Logan County.

Since the inception of the workshop program in 1995, industry responses to the program have been very positive. In short, this program has been described by numerous industry representatives as the most valuable program that the Oklahoma Geological Survey has ever implemented. The operator registration statistics for the various workshops support this assertion. There were 1,211 total workshop registrations in the program, reflect **584** individuals, many with multiple registrations. Of the 584 individuals, 355 (61%) are from active operating companies, based on a comparison of company names to gross production tax records, and 145 (25%) are from other industry interests such as service companies, or are "consultants"(31) or "independents"(30), that could not be linked to the gross production tax records.

Task 3: Professional Outreach: Three levels of professional outreach have been identified as part of this overall project effort. The first, technical advising, refers to those industry contacts that take place as follow-ups to the workshop presentations. Second, the ongoing reservoir characterization and simulation studies provide opportunities for individualized efforts with operators. Third, professional activities such as conferences provide a forum for promoting the FDD program activities.

CONCLUSIONS

There is no direct way to measure the impact that this program has had on the volumes of FDD oil production in Oklahoma. Throughout Oklahoma, as in the rest of the domestic petroleum industry, oil well abandonments have continued to increase and production has continued to decline throughout the five years of the program. There is no way of knowing what that decline would have been if this program had not been implemented. Furthermore, most of the volumetric impacts of this program will in fact be realized in future years. If this program has served its function, it will be demonstrated through the ongoing viability of FDD reservoirs five to ten years in the future.

Since volumetric measures cannot be provided, the success of the program must be measured in terms of the accomplishments and the industry evaluations of those accomplishments. Eight highly successful workshops and accompanying publications were completed on eleven FDD horizons. A computer user laboratory was established and continues to be a resource to the industry. industry relationships with the project participants have shown vast improvements. Industry feedback to the program has been overwhelmingly positive.

Numerous operators and industry people provided positive feedback for the overall program. Due to the nature of the Oklahoma FDD project, it is recognized as one of the most successful and respected programs to assist operators throughout the entire Mid-Continent region. Nearly everyone wants this program continued or expanded. Because of this, arrangements have been made with the Oklahoma City Geological Society to present "repeat"workshops of some of the workshops, and requests for copies of the play publications continue to be received. Furthermore, the Oklahoma Geological Survey has plans to continue with the "play analysis" format as a permanent component of their overall program. The development of this FDD program and the support of the U.S. Department of Energy have set the stage for a strong technology transfer foundation for Oklahoma's petroleum industry.

IV. INTRODUCTION

The Oklahoma Geological Survey (OGS), the Geo Information Systems department, and the School of Petroleum and Geological Engineering at the University of Oklahoma engaged in a five-year program to identify and address Oklahoma's oil recovery opportunities in fluvial-dominated deltaic (FDD) reservoirs. This program included the systematic and comprehensive collection and evaluation of information on all of Oklahoma's FDD oil reservoirs and the recovery technologies that have been (or could be) applied to those reservoirs with commercial success. This data collection and evaluation effort was the foundation for an aggressive, multifaceted technology transfer program that was designed to support all of Oklahoma's oil industry. However, particular emphasis of this program was directed at smaller companies and independent operators in order to help them maximize oil production from FDD reservoirs.

Project efforts included identifying all FDD oil reservoirs in the state; grouping those reservoirs into plays with similar depositional and geologic histories; collecting, organizing and analyzing all available data; conducting characterization and simulation studies on selected reservoirs; and implementing a technology transfer program that targeted operators of FDD reservoirs.

The elements of the technology transfer program included developing and publishing play summaries in the form of folios, holding workshops to release play analyses and discuss opportunities in each of the plays, and establishing a public-access computer user laboratory within the OGS. The user lab contained all the play data, as well as other oil and gas data files, together with the necessary hardware and software to analyze the information. Technical support staff were available to assist interested operators in the evaluation of their producing properties, and professional geological and engineering outreach staff were available to help determine appropriate recovery technologies for those properties.

The FDD project assisted numerous operators in Oklahoma by providing them with practical ways to improve production from existing leases and/or to reduce operating costs. Currently-available technologies can improve recovery factors in these FDD reservoirs when sufficient information is available to determine the most appropriate course of action for an operator. This project developed the needed reservoir-level information and worked with interested operators in the implementation of the appropriate improved recovery technologies.

Light oil production from Class I Oil fluvial-dominated deltaic reservoirs is a major component of Oklahoma's total crude oil output. These types of reservoirs provide approximately 15 percent of the State's total oil production. Most of this production is by small companies and independent operators. This segment of Oklahoma's oil industry typically does not have ready access to the information and technology required to maximize the exploitation of these reservoirs.

Oil production from FDD reservoirs is at high risk. Individual well production is often very low (one to three barrels per day) and operating costs continue to rise. These factors, in addition to cyclic crude oil prices, resulted in oil well abandonment rates that have more than doubled in recent years. Successful implementation of appropriate recovery technologies and field development practices could help to sustain production from these reservoirs throughout much of the 21st century. Without such action, most oil production from Oklahoma FDD reservoirs will be abandoned by the beginning of the next century.

V. DISCUSSION

The execution of this project was approached in three phases. Phase I began in January, 1993 and consisted of planning, play identification and analysis, data acquisition, database development, and systems design. By the middle of 1994, many of these tasks were completed or nearly finished including the identification of all FDD reservoirs in Oklahoma, data collection, and the definition of play boundaries. Later in 1994, a preliminary workshop schedule was developed for the implementation and technology transfer activities of Phases 2 and 3, respectively. In early 1995, a specific workshop agenda was developed and folio publication requirements were identified. Later that year, the Morrow and Booch workshops were completed along with the accompanying folio publications. During 1996, three more workshops were completed involving six separate plays. These were the Layton and Osage-Layton, the Prue and Skinner, and the Cleveland and Peru plays. By this time, the workshop format had evolved to include better organization of data, more information, and better allocation of time for presentations and demonstrations. During the final year of the program, workshops and publications were completed for the Red Fork, the Tonkawa, and the Bartlesville plays.
The following sections briefly describe technical activities relating to the tasks of this project.

Task 1: Database and Applications Development

Technical computer database development activities were divided into three primary tasks:

1) Database Development and Maintenance. This activity included efforts to develop and upgrade FDD databases and to capture the information gathered during this project. Database development also involved reformatting NRIS well, lease and field mainframe databases for p.c.-level access through a computer user lab.

Initially, three databases were developed for this project. A reservoir database was designed to record reservoir characteristics, engineering, and production data for each identified FDD oil reservoir in Oklahoma. A bibliographiic database was designed to track the reference information related to the Oklahoma FDD reservoir research. For the early plays, considerable effort was devoted to gathering and coding information to enter into these databases. However, after the first year of workshops and publications it became clear that the demand for these databases, and the value achieved from them, did not warrant the level of effort required to maintain them. Project staff efforts were utilized much more effectively to prepare the publication and workshop materials. Thus, the maintenance of these two databases became a lower priority for the overall project.

In contrast, the operator database was a fundamental tool throughout the entire project. The operator database was designed to track operators (and other interested parties) who were working with FDD reservoirs in Oklahoma. These operators were targeted to participate in the data collection process as well as the technology transfer program. The operator database originally was developed at the mainframe level, but work was completed during the program to convert the operator file to the personal computer to allow tracking participation in various activities of this project, and help measure the overall effectiveness of the technology transfer program. That conversion was completed prior to the Morrow workshop held in June, 1995.

Operator mailouts, registrations, and summary data in this report were made possible though this database.

One fundamental precursor to the analysis of FDD reservoirs was the appropriate delineation of the oil field boundaries in which these reservoirs occur. Project staff worked with the Oklahoma Nomenclature Committee (ONC) of the Mid-Continent Oil & Gas Association to identify updates to the official field boundaries based on field and lease data from the Natural Resources Information System (NRIS)

2) Applications Development. A variety of computer applications programs were required for data analysis, for publication and workshop preparation, and to support users. Many of these programs were standardized for repeated applications in the various plays. These programs were mostly developed prior to 1995 as part of the *Phase* I planning and analysis, but were modified and enhanced during subsequent years to prepare for new plays. Computerized mapping and report programs were necessary for reservoir analysis and regional play interpretations. These included programs to generate standard reports and tables, perform statistical analyses, generate graphical displays of the data, and produce surface and subsurface maps. The outputs from some of these programs were incorporated into the play folio publications and/or used as exhibits during the play workshops. At the mainframe level, commercial software systems such as SAS (Statistical Analysis System) were used for most of the applications, editing, and data manipulation. At the personal computer level, applications are based on a variety of commercial packages. Mapping was completed through application programs such as Arc/Info and ARCVIEW, GeoGraphix and Easycad.

3) User Lab Development and Operation. One of the primary technology transfer tools implemented during this project was a computer user laboratory. The user laboratory was developed as one mechanism for allowing industry, especially small independents, to access the resources developed as part of this project. Capabilities of the laboratory were supplemented through software and support provided by the Petroleum Technology Transfer Council program. Housed within the offices of the Oklahoma Geological Survey, and staffed with technical advisors who can assist users in developing their own applications, the computer user laboratory is advantageous for those who have little or no experience using computerized resources for their decision-making.

User lab development activities included both the acquisition of hardware and software, and the development of user interfaces for the data and software applications that are available through the user lab. Currently, the computer facility is equipped with 4 Pentium microprocessors, a laser printer and E-size plotter, and a scanner on a Novell network. User lab software includes both commercial and public domain packages, since a technology transfer goal of the user lab is to provide examples of applications that operators might want to adopt for their own use. The in-house software development that was completed for the project was primarily for site-specific activities such as developing user interfaces and user lab accounting processes. Standard word processing, spreadsheet, project management and graphics packages are all available. Geologic mapping is possible through application programs such as GeoGraphix contouring package, and spatial analyses will be possible through Arc/Info and ARCVIEW.

In late 1994 a decision was made to use an Oracle database engine with Visual Basic programming language to develop the user interfaces. The actual installation of Oracle took

place in early 1995 after the network software was upgraded to Novell Netware 3.12. Efforts then were initiated to develop the Visual Basic interfaces to allow easy access to the NRIS and FDD data.

The lab was opened on June 1, 1995, in conjunction with the Morrow play presentation. Industry response to the facility initially was slow, primarily due to the lack of visibility for the facility and difficulty accessing the facility on campus. During the first year of operation, the lab averaged four users and 50 hours of usage per month. After the first year, the lab was moved to a more accessible location on the north side of Norman, and lab usage began to increase to an average of 11.5 visitors and 196 usage hours per month during the second year. This usage level is sustaining, and despite the close of this FDD project, the lab operation is continuing through the support of the Petroleum Technology Transfer Council.

Task 2: Play Analyses, Publications, and Workshops

The concept of a "play" is used to describe reservoirs that are subject to petroleum exploration or development. For the purposes of this project, the plays were characterized by a geologic formation or horizon that contains FDD reservoirs. In Oklahoma, all of the FDD oil reservoirs are Pennsylvanian in age. A list of Oklahoma's FDD oil reservoirs, in order of geologic age from youngest to oldest, is summarized in Table 1. These reservoirs were grouped into plays and delineated on regional sand trend maps that showed play boundaries and regional depositional environments.

TABLE 1 - FLUVIAL-DOMINATED DELTAIC OIL RESERVOIRS: OKLAHOMA PLAYS

PLAY	Reservoirs	Location	Class*	Leader	Comments
1. Tonkawa Play (Virgilian)	**Tonkawa sd**	**NE Oklahoma Platform** **Nemaha** Uplift **NW Anadarko Shelf**	**B**	**Campbell**	**Workshop completed** 7/97
2. Layton & **Osage-Layton Plays (Upper Missourian)**	**Osage-Layton sd** 'True" Layton	**NE Oklahoma Platform** **Nemaha** Uplift **NE Flank Anadarko Basin**	**B**	**Campbell**	**Workshop completed 4/96**
3. Cleveland Play (Lower Missourian)	**Cleveland sd**	**NE Oklahoma Platform** **Nemaha** Uplift **NE Flank Anadarko Basin**	B/C	**Campbell**	**Workshop completed 10/96**
4. Peru Play (DesMoinesian)	**Peru sd**	**NE** Oklahoma **Platform**	C	**Northcutt**	**Workshop completed 10/96**
5. Prue & **Skinner Plays (DesMoinesian)**	**Prue sd** **Skinner sd**	**NE** Oklahoma **Platform** **Nemaha** Uplift **NE Flank Anadarko Basin**	**A**	**Andrews**	**Workshops completed 6/96**
6. Red Fork Play (DesMoinesian)	**Red Fork sd**	**NE Oklahoma Platform** **Nemaha** Uplift **NW Anadarko Shelf** **NE Flank Anadarko Basin**	**A**	**Andrews**	**Workshops completed 3/97**
7. Bartlesville Play (DesMoinesian)	**Bartlesville sd**	**NE Oklahoma Platform** **Nemaha** Uplift	**A**	**Northcutt and Andrews**	**Workshops completed 10/97**
8. Booch Play (DesMoinesian)	**Booch sd**	**NE Oklahoma Platform**	**B**	**Northcutt**	**Workshop completed 9/95**
9. Morrow Play (Morrowan)	Upper & **Lower Morrow sd**	**NW Anadarko Shelf** **Hugoton Embayment**	**B**	**Andrews**	**Workshops completed 6/95**

*** "Class"is an estimate of the overall size of the play, based on geographic extent and on the number of reservoirs and operators in the play. Class** "A"plays **are the largest plays.**

For each of the plays, a consistent format was developed for the presentation of materials. Presentations included both general materials regarding FDD depositional environments that were consistent for all of the plays, and specific materials that uniquely described the characteristics of each individual play.

For each workshop and folio publication, a series of tasks was completed. These tasks included data analysis and preparation of the publication by the authors; drafting of illustrations, figures, maps, and plates by the cartographic staff; editing; and publication. The workshop agenda was fairly standardized for all of the play presentations. Publicity for the workshops was through press releases and by mailouts to play operators as well as to all other operators and others who had attended past OGS workshops. For each workshop,

announcement mailouts were to about 6,000 individuals and companies. Materials prepared for the workshops include 35mm slides, overhead transparencies, cores, field rock samples, and computer-generated production information maps. Each attendee at each workshop received a copy of the publication, and play operators who did not attend the workshops were given an opportunity to receive a complementary copy of the play publication.

Workshop sites for the various plays were identified based on areas of the greatest expected interest level. Lists of operators with recent production from the FDD plays were generated from the *NRIS* database. On the basis of operator addresses along with the number of operators in each FDD reservoir, potential sites were identified for each workshop presentation. Thus, for example, the Layton, Cleveland and Peru workshops were held in the Oklahoma City while the Prue and Skinner workshops were held in both Oklahoma City and Bartlesville.

The following paragraphs contain brief summaries of the play analyses and workshops completed for this program, in the order in which the workshops were completed.

THE MORROW PLAY

Primary author:	Richard Andrews
Workshop dates:	June 1 and 2, 1995
Workshop site:	Sarkeys Energy Center, Norman, OK.
Publication:	Oklahoma Geological Survey SP 95-1, Fluvial-Dominated Deltaic (FDD) Oil Reservoirs in Oklahoma: The Morrow Play.

Pennsylvanian Morrow sandstones are some of the most important oil and gas reservoirs in Oklahoma. Morrow sediments are Lower Pennsylvanian in age and consist of sandstone, shale, and limy clastics. The name is primarily a subsurface term that is used by the oil and gas industry in northwestern Oklahoma. The term Morrow is applied to the section of rock that extends from the base of the Atokan Thirteen Finger lime to the top of the Mississippian Chester limestone. This interval is highly variable, usually about 200-400ft thick throughout much of the Anadarko shelf, and thickens to over 4000ft in the basin depositional center in western Oklahoma. Wireline log responses change suddenly and correlations can be very difficult even over short distances. Additionally, fluvial sandstones often are interbedded with marine sediments and limestone indicating an unstable geological setting involving the interaction of several depositional environments in close proximity to one another.

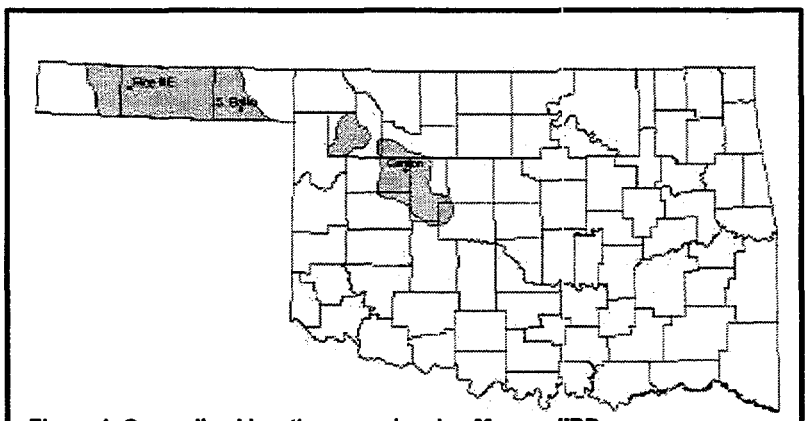

Figure 1 Generalized location map showing Morrow FDD areas.

Morrow fluvial systems are found principally in three regions within Oklahoma. The first area is the Dewey-Blaine Counties embayment. A second area in central Woodward County is located within a north-south trending paleo-valley and is commonly referred to as the Woodward "trench". The most extensive area of fluvial domination stretches across the Panhandle region comprising of

Texas, western Beaver, and eastern Cimarron Counties (Fig. 1). Distribution of fluvial or FDD sediments is directly related to the type of hydrocarbon produced from the Morrow. Morrow oil production occurs almost entirely in areas identified as FDD. One reason for this occurence is that sediments of fluvial origin are typically coarser grained and have better porosity than the relatively tight marine sands that mainly produce gas.

Detailed information was provided for three Morrow field studies: the Canton field area in Dewey County, the South Balko field in Beaver County, and the Northeast Rice field in Texas County. A reservoir characterization and waterflood simulation study was completed and presented for the Northeast Rice field.

Canton Field: The Canton study area consists of four sections that were originally part of Canton Southwest field before their assignment to the Watonga-Chickasha trend. Selection of the site was based upon oil production characteristics of the Morrow that are unique to the geologic province in which it occurs. It also has favorable well spacing (40 acres) and available current data such as cores, modern well logs, and production information. Table 2 gives a summary of geological/engineering data for the Canton study area.

TABLE 2 - Geological/Engineering Data for the Lower Morrow Sandstones in the Canton Study Area, Dewey County, Oklahoma

	lower Morrow "B" sand	lower Morrow "C" sand
Reservoir size	1,503 acres	1,960 acres
Well spacing (oil)	40 acres	40 acres
Oil/water contact	none	none
Gas /oil contact	none	none
Porosity	5-20% (10% avg)	5-20% (10% avg)
Permeability	1-200 and (1-10 avg)*	1-200 and (2-10 avg)*
Water saturation	20-45%	20-45%
Thickness (net sand in field)	10-20 ft (10.2 ft avg)	10-30 ft (12 ft avg)
Reservoir temperature	160-1700 F	160-1700 F
Oil gravity	40-470 API	40-470 API
Initial reservoir pressure	4,200 PSI**	4,200 PSI*"
Initial formation-volume factor	1.2 reservoir barrels/stock tank barrels**	
Original Oil in Place (volumetric)	**6,442 MSTBO**	**9,884 MSTBO**
Cumulative primary oil	2,360 MSTBO (combined)	
Recovery efficiency (oil)	**14.5%** (combined)	
Cumulative gas	12.4 BCF (combined since 1979)	

*Source: South (1983). 'Source: Colton (1974a).

The Canton study area constitutes one of the most complicated assemblages of sediments in the entire Morrow FDD play. Numerous sand zones occur in a stratigraphic interval of only a few hundred feet and their thickness and lateral continuity is highly variable. Depositional origin apparently is very complicated since facies representative of marine, semimarine, and subaerial environments are in close proximity both vertically and laterally. The principal Morrow sandstones beds identified in the Canton area informally are called, in descending order, the "B; "C; and "D" sands. The structure of the Canton area is characteristic of a stable shelf or shelf-transition environment. Structure contours indicate basinward dip to the southwest at -100 ft per mile which is equivalent to a 1° dip. There are no known faults or structural closures in the four-section study area.

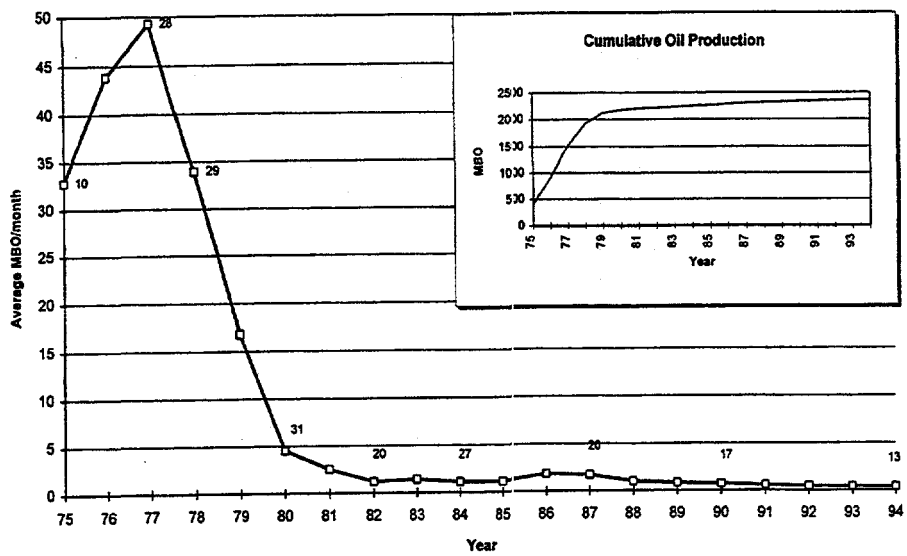

Figure 2. Oil-production decline curve for lower Morrow sandstones in the Canton study area. Numbers on the curve designate the number of wells that had Morrow production at various years. Inset plot shows cumulative production from the "B" and "C" sands combined.

Field development in the Canton area took place in the late 1970's and early 1980' s. There was a success rate of 92% for the 39 wells drilled: 35 produced from the Morrow, three were dry, and one produced from a deeper horizon. Almost all completions in the Morrow are classified as oil wells since they generally have a gas/oil ratio of <5,000:1. Cumulative primary oil production from all lower Morrow sandstones in the four section study area is estimated at 2,360 MSTBO, which is 14.5% of the estimated 16,326 MSTBO in place originally. The initially rapid recovery rate of oil followed by a quick decline in production is attributable to a strong solution-gas-drive mechanism within the reservoir. Once this energy was lost, oil production was reduced to very small quantities (Fig. 2).

South Balko Field: Production from the main part of the S. Balko field was established in December 1959, with the discovery of gas in the Oklahoma Natural Gas Co. No. 1 Custer well in sec. 9, T.1 N., R.23ECM. The accredited discovery well was completed as a gas well in the western updip part of the field, now known as a gas cap. Production from this well is from the upper Morrow "A"sand at a depth of -7,400ft. Initial calculated open-flow was estimated at 15MMCFGPD with a shut-in tubing pressure of 1,667 PSI. Total cumulative production from the No. 1 Custer well is estimated at 1.7 BCFG.

There are three main sandstones intervals in the upper Morrow section of the S. Balko field. In descending stratigraphic order they are called informally the "A, upper "B; and lower "B" sands. The upper Morrow "A"sand is the most continuous and uniformly deposited sandstone in the S. Balko area. It is present in two general areas in the study area and usually occurs as a single bed with a gross thickness of 20-40ft. The "A" sand is best developed within a meandering thalweg that is oriented in a northwest-southwest direction. The upper "B" is composed of several individual sandstone beds that occupy a stratigraphic interval of about 80-120ft. Predominant sandstones appear to be fluvial channel fill in nature, lenticular in aerial extent, and have scoured basal contacts. Only the lower sandstone in the upper"B"interval is productive. This zone seems to be the direct result of fluvial channel deposition. The lower "B" sand contains the most extensive distribution of sandstone in the S. Balko field and is commonly >40ft thick. However, this thickness includes many intervals that are shaley and that do not show significant GR or SP log responses. The lower"B"is only productive in a few

wells in extreme northern parts of S. Balko field, and is not considered to be a significant reservoir.

Cumulative oil production through 1994 from the upper Morrow sands in S. Balko field is estimated at 4.8 million barrels. S. Balko field was unitized in 1972, but its not known whether it was successfully water flooded. A sharp decrease in the slope of oil production (Fig. 3) occurred during this time, and the number of producing wells dropped from 30 to 22. Since mid-1985, average production for individual wells has been <3 BOPD.

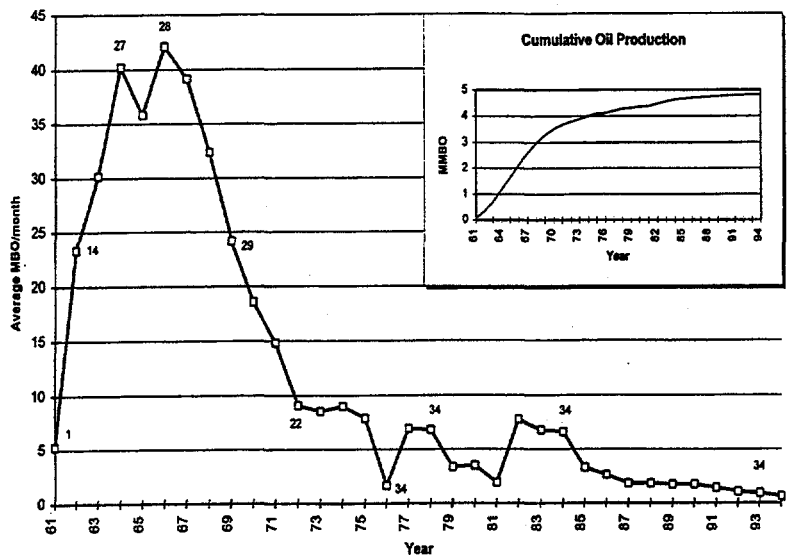

Figure 3. Oil-production decline curve for upper Morrow sandstones in S. Balko field. Numbers on the curve designate the number of wells that had Morrow oil production at various years. Inset plot shows cumulative oil from the "A" and "B" sands combined.

Rice Northeast Field is located along the east flank of Keyes dome which is part of the north-south trending Cimarron uplift that crosses the Oklahoma Panhandle. It was discovered by Apache Corp. in 1963 with the completion of the Gaither No. 1 well in sec. 23, T.3N., R.10ECM. That well was perforated from 5,192-5,220 ft and had an initial potential flowing of 140 Bbls of 36 gravity oil per day. Cumulative production from this well is estimated at 82MBO, which is generally better than average for this field.

The Morrow is subdivided into two intervals that are called informally the upper and lower Morrow. The lower Morrow is entirely marine in origin and consists mostly of shale. The upper Morrow contains multiple sands of both marine and nonmarine origin, but there are only two main sandstones which produce hydrocarbons, identified informally as the upper Purdy "a' and the lower Purdy "C" sands. Cumulative primary oil production through 1994 from the Purdy sands (combined) in Rice NE is estimated at -1 million barrels (Table 3). An estimated 66% of the total primary oil recovery in Rice NE is attributed to the lower Purdy "C"sand. This zone had relatively stable oil production from only a few wells until the early 1980's, when Rice NE field expanded due largely to lower Purdy "C"completions in the southern part of the field.

Both of the Purdy reservoir sandstones are interpreted to have fluvial origins in a transgressive valley-fill depositional setting. They are separated from one another stratigraphically by about 10 to 40 ft of shale. Rice NE is bounded by major fault blocks on the east and west sides of the field. The updip fault in the west part of the field is interpreted to be the principal trapping mechanism for the upper Purdy "B"sand. The trapping mechanism for the lower Purdy "C"is predominantly stratigraphic.

TABLE 3. - Oil Production SI:atistics for Upper Morrow Purdy Sands (Combined) in Rice NE Field, Western Texas County, Oklahoma

Year	Number of Oil Wells* (estimated)	Annual Oil Production (Barrels)	Average Monthly Oil Production (Barrels)	Average Daily Oil Production Per Well (BOPD)	Cumulative Oil Production (Barrels)
63	4	28,750	2,396	19.7	28,750
64	5	40,896	3,408	22.4	**69,646**
65	4	35,721	2,977	24.5	105,367
66	4	**40,458**	3,372	27.7	**145,825**
67	4	33,617	2,801	23.0	179,442
68	4	27,873	2,323	19.1	207,315
69	4	25,411	2,118	17.4	**232,726**
70	6	26,029	2,169	11.9	**258,755**
71	5	25,622	2,135	14.0	**284,377**
72	5	24,294	2,025	13.3	308,671
73	4	21,052	1,754	14.4	329,723
74	4	20,825	1,735	14.3	**350,548**
75	5	18,076	1,506	9.9	**368,624**
76	5	16,288	1,357	8.9	384,912
77	5	13,100	1,092	7.2	**398,012**
78	6	**15,465**	1,289	7.1	413,477
79	6	12,506	1,042	5.7	**425,983**
80	6	10,081	840	4.6	436,064
81	5	8,655	721	4.7	**444,719**
82	8	26,403	2,200	9.0	471,122
83	12	94,978	7,915	21.7	566,100
84	14	**138,648**	11,554	27.1	**704,748**
85	12	83,199	6,933	19.0	787,947
86	12	68,463	5,705	15.6	856,410
87	13	46,971	3,914	9.9	**903,381**
88	13	32,085	2,674	6.8	**935,466**
89	11	25,002	2,084	6.2	960,468
90	12	20,452	1,704	4.7	980,920
91	12	17,598	1,467	4.0	998,518
92	11	16,206	1,351	4.0	1,014,724
93	10	9,938	828	2.7	1,024,662
94	10	7,525	627	2.1	1,032,187

*Based on number of producing leases. Individual leases may contain more than one producing unit

THE BOOCH PLAY

Primary author: Robert Northcutt
Contributing authors: Kurt Rottmann, Roy Knapp, X. H. Yang
Workshop date: September 11, 1995
Workshop site: Indian Capital Vo-Tech School, Muskogee, OK
Publication: Oklahoma Geological Survey SP 95-3, Fluvial-Dominated Deltaic (FDD) Oil Reservoirs in Oklahoma: The Booch Play.

The Pennsylvanian sandstones in the Booch were significant oil reservoirs during the early history of the oil industry in Oklahoma. The Booch sands are the informal subsurface equivalents of the sandstone members cif the McAlester Formation in the Krebs Group of the Desmoinesian Series. Booch reservoirs are still important today for potential recovery of additional oil by water-flooding or other enhanced recovery methods. Booch reservoirs

dominantly occur in stratigraphic traps in fluvial-dominated deltaic environments, such as fluvial, upper and lower delta plain and delta-front deposits. Local uplifting and faulting, as well as sediment compaction, have influenced the localization of oil and gas in these traps.

The Booch play is located on the Cherokee Platform in northeastern Oklahoma and extends southward beyond the hinge line of the McAlester Formation into the Arkoma basin. The play area in Oklahoma is limited on the east and south by the outcrop of the McAlester Formation and on the west by depositional limit of sandstone in the Booch. The depth of the Booch sand increases from the surface outcrop in the east to 3,200 feet at the western limit of the play. A regional distribution map of the Booch sand in the play area is shown in Fig 4.

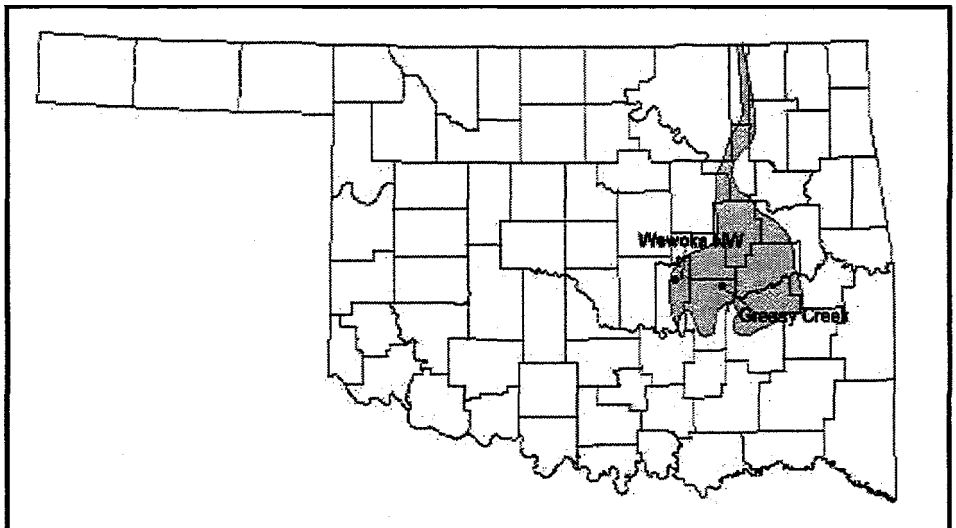

Figure 4. Generalized location map showing Booch FDD area.

Booth sediments are Middle Pennsylvanian in age and consist of shale, sandstone, and coal. Shales were deposited in marine, delta-front, lagoonal, and coastal-plain environments. Sandstones were deposited in distributary channels on the delta plain. Coals were deposited in the lagoonal areas associated with the delta plain. The top of the Booch is now recognized at the base of the overlying Savanna Formation or Brown Lime. The base of the Booch is at the top of the Hartshorne Formation, represented by the upper Hartshorne sand of the subsurface. This study of FDD reservoirs that produce the majority of the Booch oil includes only the play area on the Cherokee Platform, which produces both oil and gas.

Detailed information was provided for two Booch field studies: the Northwest Wewoka field area in Seminole County, and the Greasy Creek field in Hughes County. Additionally, a reservoir characterization and waterflood simulation study was completed and presented for the Greasy Creek field.

Wewoka Northwest Booch Sand Unit was originally part of the Cheyarha field and eventually was incorporated into the Seminole field in 1948. In 1989, Beard Oil Company unitized portions of secs. 4,5,7, and 8 of T.9N., R.7E. and portions of secs. 32 and 33 of T.10N., R.7E., and named it the Wewoka N.W. Booch Sand Unit. Production from the area of this unit had been established in 1944, with the discovery of oil from the Troup-Moore-Hall No. 1 Austin in sec 33, T.10N., R.7E. The discovery well was completed with an initial potential flow of 170 BOPD. Within two years, 55 additional oil wells had been completed and the field was fully developed (see Table 4). Cumulative oil production through 1994 was 2,539,922 BO for the Wewoka N.W. Booch unit. Secondary recovery in this field has yielded 4,710 BO through December 1991.

TABLE 4. - Oil Production Statistics for the Wewoka N.W. Booch Sand Unit, Seminole County, Oklahoma

Year	Number of Oil Wells	Annual Oil Production (barrels)	Average Monthly Oil Production (barrels)	Average Daily Oil Production (BOPD)	Cumulative Oil Production (barrels)	Year	Number of Oil Wells	Annual Oil Production (barrels)	Average Monthly Oil Production (barrels)	Average Daily Oil Production (BOPD)	Cumulative Oil Production (barrels)
1944	2	11,366	3,789	63	1'1,366	1970	23	10,478	873	1	2,445,365
1945	31	305,739	25,478	27	317,105	1971	23	12,540	1045	2	2,457,905
1946	54	728,361	60,697	37	1,045,466	1972	23	10,612	884	1	2,468,517
1947	56	559,021	46,585	28	1,604,487	1973	23	9,935	828	1	2,478,452
1948	56	126,315	10,526	6	1,730,802	1974	23	7,408	617	1	2,485,860
1949	56	145,843	12,154	7	1,8'76,645	1975	22	7,484	624	1	2,493,344
1950	53	113,600	9,467	6	1,990,245	1976	21	5,257	438	1	2,498,601
1951	52	68,335	5,695	4	2,058,580	1977	15	4,237	353	1	2,502,838
1952	52	51,787	4,316	3	2,110,367	1978	15	4,647	387	1	2,507,485
1953	52	45,032	3,753	2	2,155,399	1979	18	3,128	261	0	2,510,613
1954	52	41,553	3,463	2	2,196,952	1980	18	2,564	214	0	2,513,177
1955	48	30,460	2,538	2	2,2:27,412	1981	18	1,545	129	0	2,514,722
1956	48	23,537	1,961	1	2,250,949	1982	18	545	45	0	2,515,267
1957	48	19,390	1,616	1	2,270,339	1983	18	528	44	0	2,515,795
1958	46	18,669	1,556	1	2,2139,008	1984	3	152	13	0	2,515,947
1959	33	14,553	1,213	1	2,31)3,561	1985	0	0	0	0	2,515,947
1960	31	13,952	1,163	1	2,3'17,513	1986	0	0	0	0	2,515,947
1961	29	14,398	1,200	1	2,331,911	1987	0	0	0	0	2,515,947
1962	29	13,468	1,122	1	2,345,379	1988	0	0	0	0	2,515,947
1963	27	12,319	1,027	1	2,357,698	1989*	8-4**	0	0	0	2,515,947
1964	27	12,567	1,047	1	2,370,265	1990	17-7**	2,712	226	0.4	2,518,659
1965	26	13,201	1,100	1	2,3133,466	1991	3-7**	1,998	167	2	2,520,657
1966	26	14,187	1,182	2	2,397,653	1992	4-4**	14,969	1247	10	2,535,626
1967	23	12,854	1,071	2	2,410,507	1993	1-2**	3,240	270	9	2,538,866
1968	23	12,815	1,068	2	2,423,322	1994		1,056	88	0	2,539,922
1969	23	11,565	964	1	2,434,887	1995			0	0	2,539,922

*Wewoka N.W. **area** unitized into N.W. **Wewoka Booch Sand** Unit **
Denotes number of injectors.
NOTE: The **average daily oil production per well was calculated by dividing the average monthly production by 30 days and the number of active wells.**

Greasy Creek Field, located in north-central Hughes County, Oklahoma, was discovered in 1945. Production is primarily gas from Pennsylvanian sandstones, although there are isolated instances of oil production in this large field. One of these reservoirs is the Booch oil reservoir discovered in the No. 1 Hall (sec. 4, T. 8 N., R. 11 E.), drilled by Bell Oil and Gas Company and completed in 1961. The well had an initial pumping potential of 36 BO and 96 BSWPD from perforations at 2,314-2,316 ft in the thick Booch channel sandstone. The reservoir was not fully developed until 1971, and it is still producing marginal amounts of oil.

The Booch oil reservoir is in a stratigraphic trap formed in sandstones deposited in a distributary channel that is incised into the prodelta marine shales of the lower Booch. The surrounding marine shales provide a logical source for the hydrocarbons in this reservoir although oil also may have migrated updip into the reservoir from the Arkoma basin before faulting sealed the reservoir. Oil production statistics for the Greasy Creek Booch oil reservoir through December 31, 1994, are shown in Table 5. Cumulative oil production from the reservoir was 692,315 BO. The reservoir only produced 4,120 Bo in 1994, an average of

6BOPD for the remaining two wells. The production peak in 1971 was the result of completion of 10 new oil wells.

TABLE 5. - Oil Production Statistics, Booch Oil Reservoir, Greasy Creek Field, Hughes County, Oklahoma

Year	Number of producing wells	Annual oil production (barrels)	Average monthly production (barrels)	Average daily **production** (barrels)	Average daily production **per** well (barrels)	Cumulative production (barrels)
1961	3	4,873	1,218	41	14	4,873
1962	4	21,212	1,768	59	15	26,085
1963	4	34,864	2,905	97	24	60,949
1964	4	41,195	3,433	114	29	102,144
1965	4	28,342	2,362	79	20	130,486
1966	4	26,520	2,210	74	18	157,006
1967	5	39,286	3,274	109	22	196,292
1968	5	45,657	3,805	127	25	241,949
1969	5	30,018	2,502	83	17	271,967
1970	10	77,064	6,422	214	21	349,031
1971	13	102,065	8,505	284	22	451,096
1972	11	49,576	4,131	138	13	500,672
1973	11	27,824	2,319	77	7	528,496
1974	10	20,647	1,721	57	6	549,143
1975	10	13,959	1,163	39	4	563,102
1976	8	11,416	951	32	4	574,518
1977	7	13,866	1,156	39	6	588,384
1978	7	10,006	834	28	4	598,390
1979	7	11,090	924	31	4	609,480
1980	5	11,376	948	32	6	620,856
1981	5	9,720	810	27	5	630,576
1982	5	10,308	859	29	6	640,884
1983	5	7,668	639	21.	4	648,552
1984	5	6,709	559	19	4	655,261
1985	5	5,621	468	16	3	660,882
1986	5	3,378	282	9	2	664,260
1987	5	3,058	255	8	2	667,318
1988	5	2,661	222	7	1	669,979
1989	5	3,704	309	10	2	673,683
1990	5	3,466	289	10	2	677,149
1991	5	3,261	272	9	2	680,410
1992	5	3,896	325	11	2	684,306
1993	4	3,889	324	11	3	688,195
1994	2	4,120	343	11	6	692,315

Sources: Petroleum Information **Corporation, Oklahoma Crude Report, and Natural Resources Information System (NRIS).**

THE LAYTON AND OSAGE-LAYTON PLAYS

Primary author Jock Campbell
Contributing authors: Dennis Shannon, Victoria French, Roy Knapp, X. H. Yang
Workshop date: April 17, 1996
Workshop site: Francis Tuttle Vo-Tech Center, Oklahoma City, OK
Publication: Oklahoma Geological Survey SP 96-1, Fluvial-Dominated Deltaic (FDD) Oil Reservoirs in Oklahoma: The Layton and Osage-Layton Play.

The Layton and Osage-Layton sands are informal names that have become part of the subsurface geologic nomenclature in northeastern Oklahoma. Layton is a driller's name that dates to the early part of this century. The name Osage-Layton originated from an attempt to

correct a recognized misidentification of a younger sandstone interval as Layton. The Layton and Osage-Layton sand occur in the Missourian Series of Pennsylvanian System but have never been defined by the geological community, and the applications of those names continue to vary locally according to individual discretion.

The Layton sand is now well understood to occur high in the shale, sandstone, and carbonate sequence above the Checkerboard Limestone and below the Hogshooter Limestone. These strata belong to the Coffeyville Formation or the Coffeyville Subgroup. The Layton sand is most commonly described as a fine- to very-fine-grained sandstone with common associations of mica and clay minerals. The Osage-Layton sand is now correctly identified as the Cottage Grove Sandstone, a member of the Chanute Formation. In common industry usage, Osage-Layton designates the "eastern facies of the Cottage Grove Sandstone, which is largely of flood-plain and deltaic in origin. The name Cottage Grove most commonly is used in association with the " western" facies, which is of marine origin. The Osage-Layton is commonly described as a fine- to very fine-grained sandstone. It is commonly silty and micaceous, indicating low-energy environments of deposition. The Cottage GrovelOsage-Layton sand is commonly thicker and exhibits a much greater area of distribution than the Layton sand.

The FDD Osage-Layton and Layton plays occur in a relatively small area in northeastern Oklahoma (Fig. 5). Within this area, hydrocarbon production from the Layton sands is attributed to several horizons within a stratigraphic interval of several hundred feet. Although historical production records are not available, the Layton sands in the FDD study area are generally prone to oil rather than gas production. During the last 17 years, the Layton sands have produced about 11,467,000 barrels of oil. Two detailed geologic field studies were prepared for this workshop. South Coyle field is a Layton sand reservoir and the geologic study for this field was completed by Jock Campbell and Victoria French. The geologic interpretation of East Lake Blackwell also was used in the waterflood simulation study of Roy Knapp and X.H. Yang.

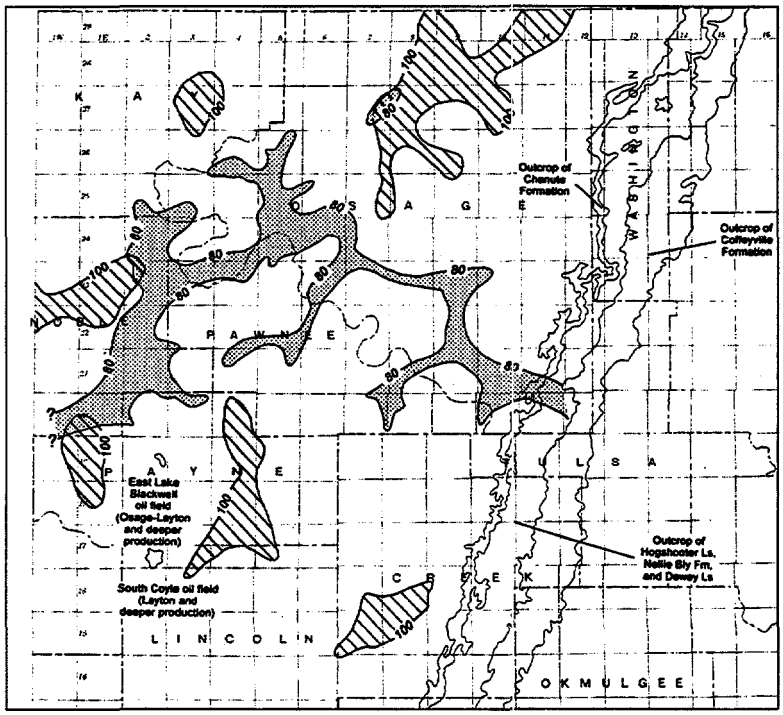

Figure 5. Maximum net thickness of Layton and Osage-Layton sandstones in the deltas area. Layton sand (stippled); minimum thickness shown is 80 ft (after Ekebafe, 1973). Osage-Layton sand (hachured); minimum thickness shown is 100 ft (after Lalla, 1975a). Outcrop areas from Miser (1954).

South Coyle Field is located in T. 17N R. 1E in Logan and Payne Counties, Oklahoma. The Layton sand is defined stratigraphically as sandstones in the interval between the Hogshooter Limestone and the Checkerboard Limestone. Layton production in the field area originally was established in 1947, with the discovery of oil in Layton sand in the Gulf Oil Corporation No. 1 Bliss well, sec. 26, T. 17N, R. 1E from perforations at 3,634-3,658 ft. This well was completed for an initial potential pumping of 11 BOPD + 125bbl of water per day with an oil gravity of 47.6° API. This first producing well was abandoned at an unknown date after producing only 2,042 BO. The next Layton completion didn't occur until 34 years later, when the Funk Exploration, Inc., No. 1 Woods well in section 28 produced from perforations at 3,704-3,730 ft. The Layton was completed in that well in June 1981 and had an IPF of 26 BO, 2 BW, and 150 MCFGPD.

Oil production occurs in an indistinctly defined shaley interval approximately 40-80 ft below the top of the Hogshooter Limestone. The producing sandstones in the Layton interval typically are very shaley. Resistivities are low, ranging from -1 to 5 ohm-meters, due in large part to the shaliness of the sandstones. The South Coyle field occurs on a structural terrace, seen as a slight flattening of a homoclinal dip to the west at 75-150 ft/mi. Structural position seems to have played no part in the Layton accumulations.

Field development continued from November 1983 through August 1988. By June 1995 the Layton reservoir in the South Coyle field had a total of 14 wells, with a cumulative production of almost 190,000 BO. The cumulative production for the best single well was 35,756 BO over a ten year period. The average for the 14 field wells is slightly more than 13,500 bbl/well. Casinghead gas has been reported from only one well and is minor, with a cumulative production of 17,324 MCF over a 3.5 year period. This reservoir is difficult and economically risky as a primary exploration objective, however, it provides for understanding of the keys to production. The Layton sand will continue to be a secondary, and locally a primary zone of interest over a large geographic area.

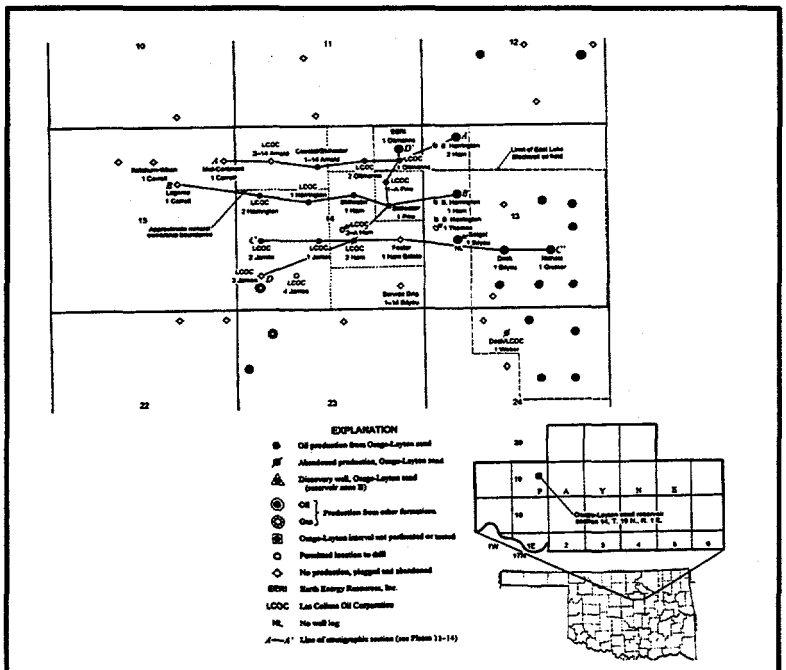

Figure 6. Information map of the East Lake Blackwell oil field area, sec. 14, T. 19N., R. 1E., northwestern Payne County, Oklahoma.

East Lake Blackwell Field **is in** north central Oklahoma in western Payne County (Fig. 6). It was discovered in 1987 as a recompletion of the Coastal #1 Arnold well in sec. 14, T. 19N., R. 1E., and had initial production of 22 BOPD. It was found that the Osage-Layton interval consisted of several producing sand zones. Mapped together, the sandstone comprising the stacked channel sequence has a gross thickness of about 20-100 feet, but in the field area the cumulative sandstone thickness is only about 35-40 feet thick. Thickening occurs down-dip to the west and thinning occurs up-dip to the east. The reservoir lies at a depth of about 3300 feet and hydrocarbon

trapping results from a combination of structural nosing and an up-dip reduction in net sandstone and porosity.

Total cumulative primary oil production from East Lake Blackwell Field is estimated to be 320,000 BO which is about 12% of the original oil in place (2.6 MMBO). The field produces from four different zones and by the end of 1994, there were 10 producing oil wells completed in the Osage-Layton interval. Reservoir properties are very favorable for secondary water flooding since the sandstone generally has relatively high porosity (-15-18%) and permeability (-10-50 md). These data are summarized in Table 6.

TABLE 6 - Reservoir Properties, Osage-Layton Reservoir, East Lake Blackwell Field, Payne County, Oklahoma

Estimated properties	Zone A	Zone B	Zone C	Zone D
Porosity	12-22%	**15.5%**	17%	18%
Permeability	10-5G and	35md	40md	**35md**
Average Gross Pay	70 ft	50 ft	60 ft	20 ft
Average Net Pay	11ft	Eft	14ft	8ft
Initial Water Saturation	46%	**46%**	46%	46%
Initial Bottom-Hole Pressure	**1,450** PSIA	1,440 PSIA	1,430 PSIA	1,430 PSIA
Initial Gas-Oil Ratio	400 SCF/STB	400 SCF/STB	400 SCF/STB	400 SCF/STB
Initial Formation-Volume Factor	1.22 RB/STB	1.22 RB/STB	1.22 RB/STB	1.22 RB/STB
Reservoir Temperature	110^0 F	110^0 F	110° F	110° F
Oil Gravity	43.0° API	43.0° API	43.0° API	43.0° API
Specific Gas Gravity	0.95	0.95	**0.95**	**0.95**
Initial Oil in Place	1.6 MMSTB	0.51 MMSTB	0.39 MMSTB	0.10 MMSTB

The summary of oil production is included in Table 7 which also indicates the secondary oil recovery expected for different development cases. Waterflood modeling by Knapp and Yang indicates that unproduced mobile oil amounts to about 1.4 MMSTBO or 52% or the OOIP. Various secondary recovery scenarios were examined and they indicate that the amount of additional recoverable oil varies from 32% to 233% of primary production (Table 7). The various scenarios include production from existing well completions in addition to cases involving recompletions and infill development drilling.

TABLE 7 - Oil Recovery Comparisons for Different Development Cases, usage-Layton Keservoir, Last rsiacicwe ı mesa, rayne county, uicianoma

	Primary (9/30/1995)			**Base** (12/31!2005)			Recompletion (12/31/2005)			**Infill Wells** (12/31/2005)		
Formation	**Cum Oil (STB)**	**Rec. Factor** (%)	Cum Wtr (Barrels)	Cum Oil **(STB)**	Rec. Factor (%	Cum Wtr (Barrels)	Cum Oil **(STB)**	Rec. Factor (%)	Cum Wtr (Barrels)	Cum Oil **(SIB)**	**Rec. Factor** (%)	Cum Wtr (Barrels)
ZoneA	227,000	14	850,000	310,000	19	1,800,000	500,000	31	1,500,000	**570,000**	**36**	1,800,000
Zone B	75,000	15	28,000	82,000	15	44,000	260,000	50	160,000	**280,000**	**55**	160,000
Zone C	6,000	1.5	240,000	7,000	1.8	470,000	165,000	**42**	690,000	**186,000**	**48**	**580,000**
Zone D	12,000	12	42,000	22,000	22	90,000	15,000	15	56,000	30,000	30	70,000
Total	320,000	12	1,200,000	421,000	1'5	2,400,000	**940,000**	**36**	2,400,000	1,066,000	41	2,600,000

THE SKINNER AND PRUE PLAYS

Primary author: Richard Andrews
Contributing authors: Kurt Rottmann, Roy Knapp, Z. N. Bhatti, X. H. Yang
Workshop dates: June 19 and 26, 1996
Workshop sites: Francis Tuttle Vo-Tech Center, Oklahoma City, and Phillips Petroleum Co. Research & Development Center, Bartlesville, OK.
Publication: Oklahoma Geological Survey SP 96-2, Fl uvial-Dominated Deltaic (FDD) Oil Reservoirs in Oklahoma: The Skinner and Prue Plays.

Similarities in depositional origin, stratigraphy, age, and environments of deposition made it convenient to group the Prue and Skinner plays into one workshop. Major topics included in the publication and workshop consisted of the regional analysis of each play along with three Skinner field studies and one Prue field study. Fields were selected because of their appropriate size (aerial extent and cumulative oil production), availability of core data and modern electric well logs, and availability of recent production information. The four fields have diverse geologic characteristics that typify many of the clastic reservoirs in the Cherokee Platform of eastern Oklahoma. Two of the fields have already been water flooded which provided a good analogy for this technology. Enhanced recovery simulation studies were completed on one Prue and one Skinner reservoir. Computer modeling utilized software demonstrated in previous workshops (Eclipse) in addition to Boast III which is more user-friendly and widely available to the public.

The Skinner Play

In terms of stratigraphic thickness and aerial distribution, the Skinner is probably the largest single play in the Oklahoma FDD series. During the past 17 years, estimated annual Skinner oil production has been between 1.2 and 3 MMBO. The actual production rate is probably considerably higher due to the fact that much of the Skinner oil production is commingled and not always distinguished separately. These data are summarized in Table 8.

TABLE 8. - Annual Oil Production from Oklahoma Skinner and Prue Reservoirs, 1979-95

	Skinner only		Skinner commingled with other reservoirs		Prue zones only		Prue commingled with other reservoirs	
Year	**Production (MBO)**	**# of leases**	**Production (MBO)**	**# of leases**	**Production (MBO)**	# of leases	**Production (MBO)**	**# of leases**
79	1,174	**581**	3,958	1,078	1,347	332	3,077	562
80	1,279	680	4,091	1,283	1,283	361	3,062	656
81	2,110	791	5,214	1,523	1,267	**385**	3,152	729
82	2,298	891	5,619	1,756	1,634	472	3,956	889
83	**2,265**	937	5,648	1,861	1,800	**534**	4,256	990
84	2,669	1,032	6,125	2,019	1,959	597	4,197	1,089
85	2,706	1,087	5,947	2,106	2,179	647	4,360	1,168
86	2,791	1,094	6,016	2,098	1,995	650	4,079	1,179
87	2,973	1,069	5,581	2,061	**1,549**	610	3,150	1,135
88	2,776	1,018	**5,232**	1,989	1,260	606	2,671	1,107
89	2,329	1,043	4,511	2,045	1,127	640	**2,534**	1,157
90	2,080	1,057	4,117	2,040	1,246	627	2,611	1,132
91	2,128	968	**4,045**	1,902	1,177	614	**2,457**	1,084
92	1,877	906	3,718	1,823	1,078	602	**2,335**	1,063
93	1,497	883	3,238	1,781	884	513	2,037	974
94	1,439	792	3,093	1,602	820	490	1,963	897
95	1,592	808	3,112	1,579	742	477	1,831	910
Total **(MBO)**	**35,982**		79,264		**23,346**		51,726	

NOTE: Production **data** from NRIS. MBO = thousand barrels of oil.

The Skinner interval is typically defined as the interval between the Verdigris limestone and the Pink lime. Skinner sands are middle Pennsylvanian in age and belong to the upper "Cherokee" Group. The Skinner interval is commonly 100-250 ft thick and is informally divided into an upper and lower zone, although in many areas a middle zone is also distinguishable. Skinner sands are generally very fine to fine grained, although medium- to coarse grained sand is sometimes observed. The sand consists mostly of quartz, averaging 66-80% depending on location. Porosity is primarily secondary and fracturing was not documented in most references used in this study.

Sandstones in the Skinner interval originated from major fluvial systems that advanced across much of the Cherokee platform in a southwest direction (Fig. 7). The Skinner sand was probably deposited in a transitional environment ranging from subaerial coastal plain and deltaic to shallow marine. The depositional slope throughout most areas in the Cherokee platform was very small, which inhibited thick accumulations of sediment particularly basinward. Therefore, some of the thickest Skinner sandstones occur in fluvial channels. Certain episodes of Skinner deposition were suppressed in central Oklahoma by positive elements along the Nemaha fault zone. A few major fluvial systems did advance into the western part of the Anadarko basin. These depositional phases occurred primarily during upper Skinner time and are mapped in western Oklahoma as far as Roger Mills County. Much of the Skinner sandstone occurs east of the Nemaha fault zone and lies stratigraphically in the lower or middle part of the Skinner section. In the southeastern part of Oklahoma, the Skinner merges with a much thicker depositional system in the Arkoma basin. In this area, the stratigraphic equivalent of the lower Skinner sand interval is referred to as the lower Senora Formation, Chelsea Sandstone, or Allen sand. In general, the Skinner FDD system was sourced by the Ouachita uplift and advanced to the northwest.

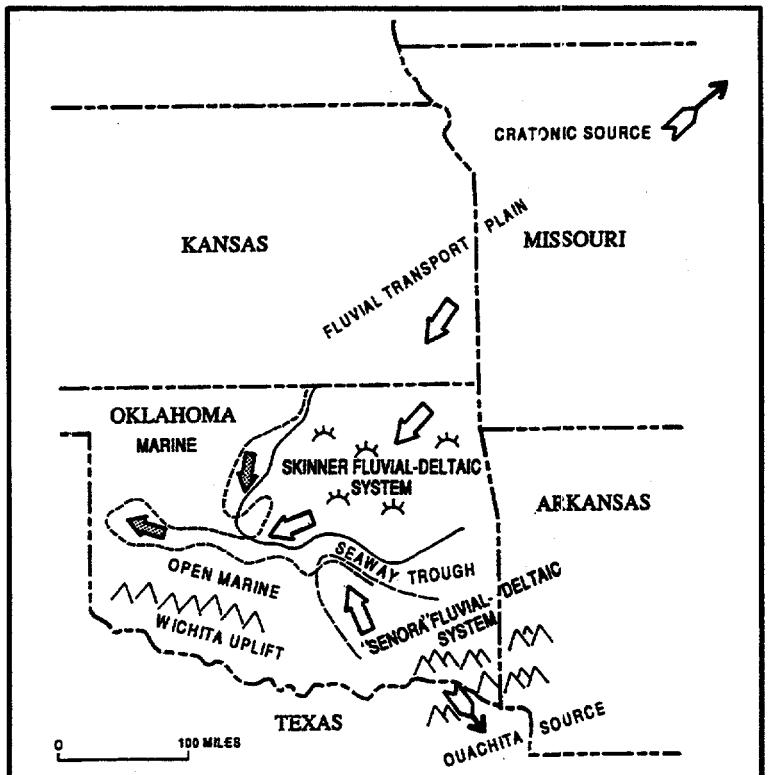

Figure 7. Paleogeography of the central Midcontinent region during deposition of Skinner and Senora (often called Allen or Chelsea) sandstones. Solid outline indicates areas of lower and middle Skinner sandstone and equivalents, whereas the dashed outline indicates the regional extent of the upper Skinner sandstone.

Production from the Skinner and Senora sands is highly gas prone, and becomes entirely gas in the deeper portions of the Anadarko and Arkoma basins. Most marine and fluvial reservoirs have good-to-excellent reservoir properties, with some problems from compartmentalization and highly variable permeability. In order to characterize these important reservoirs, three detailed geologic field studies were completed involving reservoirs of fluvial origin. Two of the Skinner fields have already undergone successful water flooding and are useful analogies to

this commonly employed secondary recovery technique. These are the Perry SE field and Guthrie SW field, with basic reservoir and engineering data as shown in Table 9.

TABLE 9 - Reservoir Properties for the Perry S.E. and Guthrie S.W. Skinner Sand Units

	Perry S.E.	*Guthrie S.W.*
Reservoir size	610 acres	583 acres
Spacing (oil)	40 acres	40 acres
Oil/water contact	none	**-4625** feet
Gas/oil contact	none	none
Porosity (average)	15%	15%
Permeability (average)	15 and average	not determined
Water saturation (calculated)	36%	20%
Average Gas-Oil Ratio (GOR)		
Initial	492 SCF/BO	800 SCF/BO
Final	n.a.	**4808 SCF/BO**
Average Thickness	12.5 feet	6.8 feet
Reservoir Temperature	122° F	128° F
Oil Gravity	41° API	42° API
Initial reservoir pressure	-2000 PSI	-2367 PSI
Initial formation-volume factor	1.24 RB/STB	1.4 RB/STB
Original Oil in Place (volumetric)	4,591,000 STBO	2,467,000 STBO
Cumulative primary oil production	639,000 STBO	312,761 STBO
Cumulative primary oil recovery	84 BO/acre-ft	79 BO/acre-ft
Recovery efficiency (oil)	-13.9%	-12.6%
Cumulative primary gas production	Not determined	-1.5 BCF

Southeast Perry Skinner Sand Unit *is* located in Noble County in north-central Oklahoma in the southern part of the Perry Townsite field (Fig. 8). The Perry S.E. study area lies about 18 miles east of the Nemaha fault zone and in an area often referred to as the Cherokee platform province. The first well in the study area that produced oil from the Skinner was the MacKeller, Inc. No. 1 Warren well (sec. 25, T. 21 N R. 1W). The well was completed in 1983, with an initial pumping potential of 45 BO, 175 MCFG, and 20 BLW per day. Within two years, 22 additional oil wells were completed in the lower Skinner. The log signatures of the thick Skinner sandstone generally display a sharp basal contact, blocky SP and gamma-ray profile through the body of the sandstone, and at the top, a fining-or shalier-upward gamma ray profile, which indicates that this is a channel sandstone in a fluvial depositional environment.

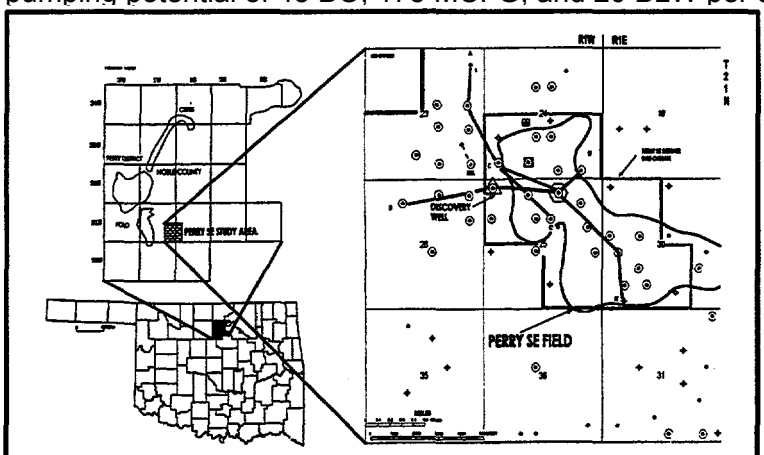

Figure 8. Generalized location map of Perry S.E. field study area, Noble County, Oklahoma. Solid black line is the outline of the Perry S.E. Skinner Sand Unit pool..

Primary oil production was 639,000 BO for the Perry S.E. Skinner Sand Unit, with an oil recovery factor prior to unitization of -13.9%. The field was utilized for secondary recovery on December 1, 1989. Water injection started on January.

1, 1990, resulting in a production increase that has led to cumulative production of 1,318,268 BO through the first six months of 1995.

Southwest Guthrie Field *is* located in southern Logan County in central Oklahoma (Fig. 9). Regionally, the field is located just east of the Nemaha fault zone in the region between the Cherokee platform to the east and the Anadarko basin and shelf provinces to the west. Most of the Guthrie S.W. production is from the lower Skinner sandstone. Commercial production was first established with the 1983 completion of the Harper Oil Co. No. 1 Davis well in sec. 36, T. 16N., R. 3 W. The initial potential flow reported was 38 BOPD and 442 MCFGD from the lower Skinner sand. The field was fully developed within three years by the completion of seven lower Skinner oil wells.

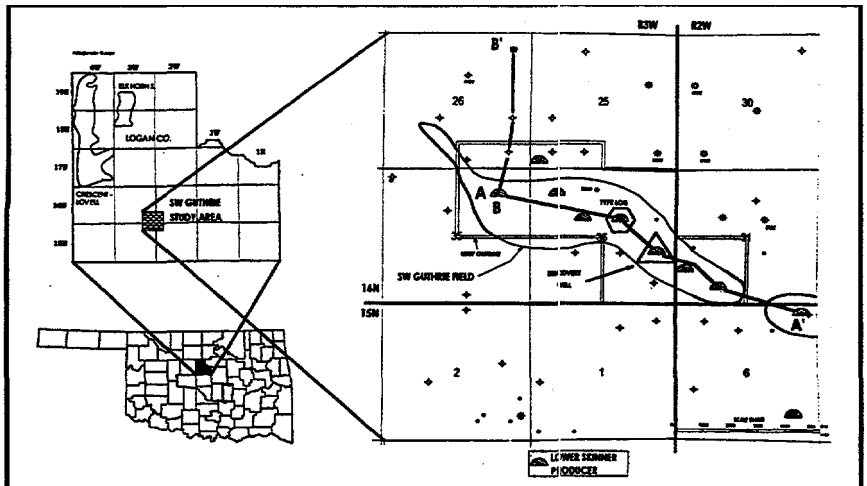

Figure 9. Generalized location map of the Guthrie S.W. field study area in southern Logan County, central Oklahoma.

The Pink limestone, which generally defines the base of the Skinner zone, is absent in the study area. So, the Skinner zone is the interval from the base of the Verdigris Limestone to the unconformity, which is at the top of the Woodford Shale. The log signature of the sandstone is very similar in all the wells in the cross section and suggests that this could be a channel facies of a fluvial depositional environment. The Skinner sand within the reservoir approaches 20 ft in thickness in the center of the channel. Table 10 shows oil production statistics for the unit.

TABLE 10. - Oil Production Statistics for the Guthrie S.W. Skinner Sand Unit, Logan County, Oklahoma

Year	Number of Oil Wells	Average Annual Oil Production (Barrels)	Average Monthly Oil Production (Barrels)	Average Daily Oil Production (BOPD)	Cumulative Oil Production (Barrels)
1983	1	19,781*	1,978	66	19,781
1984	3	89,283	7,440	83	109,064
1985	6	97,842	**8,154**	45	206,906
1986	7	39,542	3,295	16	**246,448**
1987	7	21,832	1,819	9	268,280
1988	7	15,782	1,315	6	284,062
1989	7	8,677	723	3	292,739
1990	7	**8,594**	716	3	301,333
1991	7	6,961	580	3	**308,294**
1992**	5	4,467	372	2	312,761
1993	5	3,741	312	2	316,502
1994	5	72,391	6,033	40	**388,893**
1995	5	65,949***	**8,244**	**55**	454,842

* 10 months of production
** unitized **Feb.** 1, 1992, 2 producers were converted tc water injection wells *** 8 months of production

Salt Fork North Field was discovered in 1981 and developed by DEM Operating - a small Oklahoma operator. The field is located in Grant county in north central Oklahoma (Fig. 10) and consists of 15 producing wells. The field was unitized for purposes of water flooding in

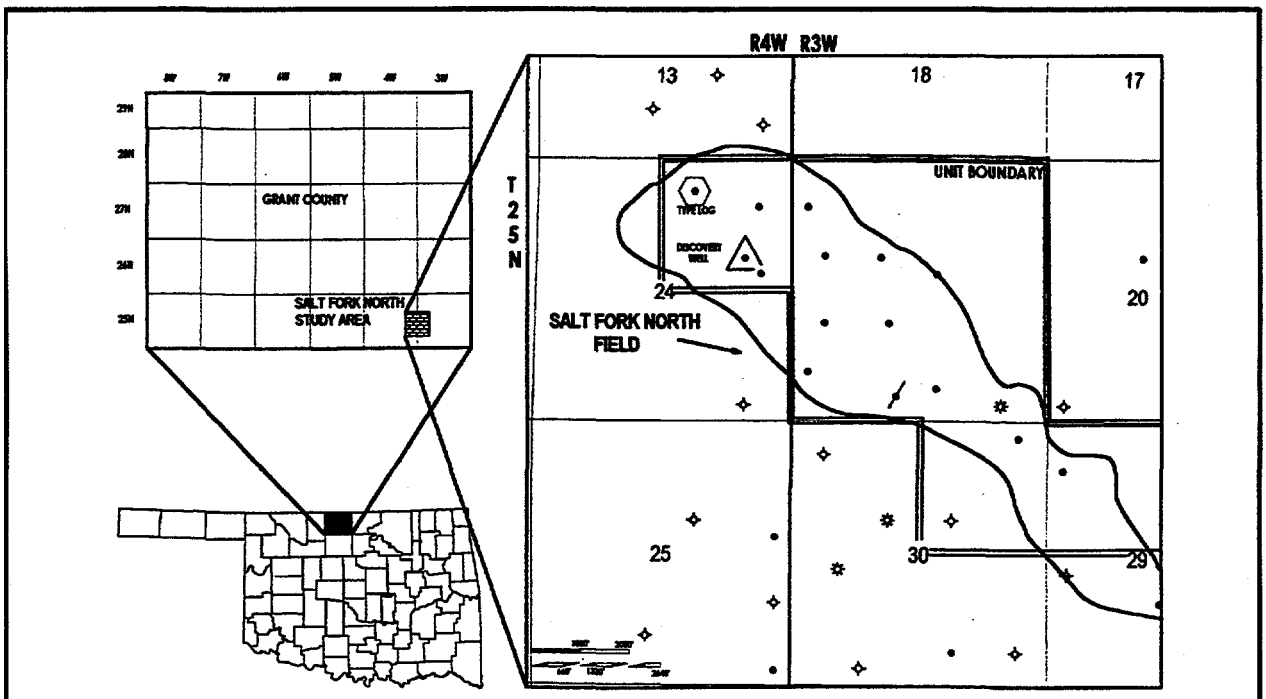

Figure 10. Generalized location map of the Salt Fork North study area in southeast Grant County, Oklahoma.

December 1994 and "experimental" water injection was attempted the following year. However, because of rapid breakthrough of the water in a nearby well, the waterflood was discontinued. Total primary production is estimated at 232 MBO and '1.6 BCF.

The Skinner reservoir consists of an upper and lower sand zone. The upper sand has a net thickness of about 10-20 feet and is productive throughout the field. Within the field boundary however, the upper sand occurs in two pods that might be compartmentalized (secs. 19 and 24, T. 25N., R. 3W). The upper Skinner sand also is productive in a field just to the south (sections 25 and 30) and is inferred within the western portion of section 29. The lower Skinner sand is generally thicker and has a net sand accumulation of about 10 to over 30 feet. It occurs in a narrow meandering band that is about 1/3 mile wide and at least two miles long. Hydrocarbon production from the lower Skinner is highly affected by the structural position of the sand and is best in the southeastern part of the field that is sufficiently above an inferred oil/water contact.

During the initial evaluation of this field, it became apparent that oil production was not very good considering the thickness of reservoir sand and the apparent good porosity. Then, reservoir data was acquired from cores for two wells just south of Salt Fork North that is believed to be representative of reservoir conditions within the field study. These data indicate that the Skinner reservoir is relatively tight since the average permeability is only about 4 md. With such low permeability, it is understandable why a large sand fracture was necessary to bring the wells on-line. The summary of geologic and engineering data for the Skinner sands in Salt Fork North field is shown in Table 11.

TABLE 11 - Reservoir Properties for the Salt Fork North Field Skinner Sandstones in Grant County, Oklahoma

	Lower Skinner Sand	*Upper Skinner Sand*
Reservoir size	-375 acres	-645 acres
Spacing (oil)	40 acres	40 acres
Oil/water contact	- -3950	above - -3950
Gas/oil contact	undetermined	undetermined
Porosity	10-18% (avg 12%)	10 - 19% (avg 13%)
Permeability[1]	0.25-8 and (avg 4 md)	0.25-8 and (avg 4 md)
Water saturation (calculated)	26-60% (avg 41%)	33-50% (avg 43%)
Thickness[2]	10-20 ft (avg 16 ft)	10-35 ft (avg 12 ft)
Reservoir Temperature	125° F	125° F
Oil Gravity	40-42° API	40-42° API
Initial reservoir pressure	1,826 PSI	1,826 PSI
Initial formation-volume factor	1.3 RBISTB	1.3 RB/STB
Original Oil in Place (volumetric)	2,376,000 STBO	3,137,000 STBO
Cumulative primary oil production	73,337 STBO (est)	159,313 STBO (est)
Recovery efficiency (oil)	3.1%	5.1%
Cumulative gas[3] production	336,044 MCF	1,286,000 MCF

[1] Based on permeabilities measured in cores from two Skinner wells located a few miles south of the study area.
[2] Entire sand bed thickness. In places, adjacent to the oil-water contact, the thickness of net sand above the oil-water contact is somewhat lower than the entire sand bed thickness.
[3] Not including produced gas used for on-site power generation.

Primary oil production in Salt Fork North was essentially complete by early 1996 when modeling for this project was initiated. Because the low permeability of the Skinner reservoir meant that simple water flooding had a very long response time, alternative recovery techniques were modeled by Knapp and Bhatti. Immiscible gas injection and alternating gas/water injection (WAG) scenarios were tried which significantly reduced the oil production response time. The predicted outcome of exploitation schemes are compiled in Figure 11. Based upon this modeling effort, it was learned that in a relatively tight sand reservoir, an alternating gas/water injection program (WAG) was optimal without regard to economics). In this study, using the WAG model, recovery of more than 500 (MSTBO (15% 001P) was predicted over a 15 year period, which is over 2.1 times the primary recovery. This assumed injection of 4.2 MMMCFG and 2.2 MMSTBW. The simulation projected that most of the injected fluids and gas were ultimately recovered by the end of the 15 year enhanced recovery period.

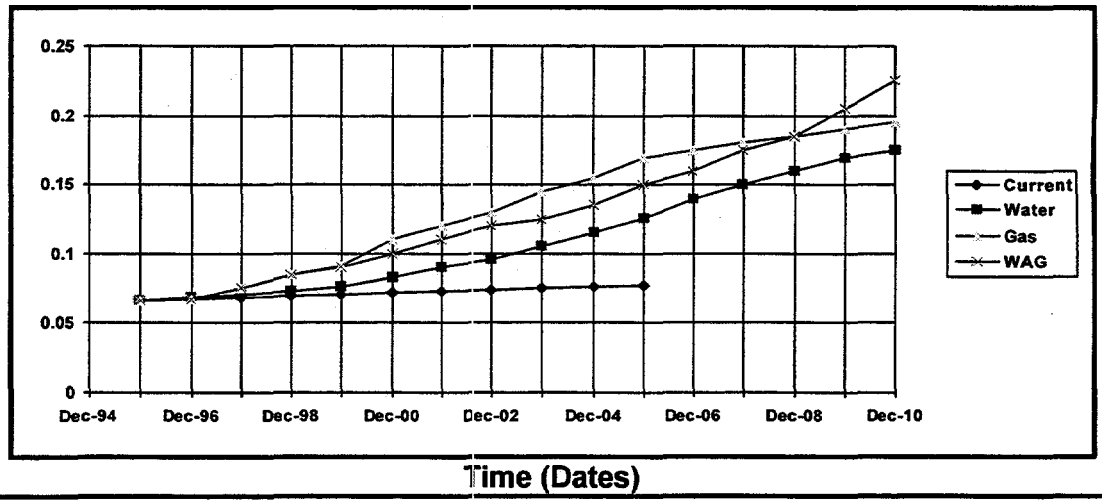

Figure 11: Predicted outcome of exploitation schemes from 1996 to 2010: % Recovery of Original Oil in Place based on Simulation Results

The Prue Play

The upper "Cherokee"Prue sand was first referenced in 1921, by White and Green from its occurrence in the Prue Field in Osage County, Oklahoma. During the early 1900's, Prue oil production was quickly exploited in northeastern Oklahoma, particularly in structural closures where it was often the shallowest productive "Cherokee" reservoir. The Prue sandstone is confined to the Cherokee platform and shallow shelf area of the Anadarko basin. In the northern part of this area, Prue sandstones are primarily fluvial; however they become increasingly more marine southward. Sandstones in this section are usually about 10-50 ft thick and fine to very fine grained.

Prue oil production is commonly commingled with production from other reservoirs, making statistical compilations of production misleading. Overall, Prue oil production is characterized by moderate annual fluctuations and has ranged from about 0.75-2 MMBO over the past 10 years, with a moderate decline since 1987. Since the mid-1980's annual Prue oil production was consistently about 0.75-1.0 MMBO less than that from the Skinner. These data were summarized in Table 8.

The Prue is a very commonly-used subsurface term that refers to a sand interval consisting of usually one or two individual sand zones. When more than one distinct sand zone is present, they are not always separated by a distinctive marker bed such as coal, limestone, and/or hot shale beds as are the Skinner zones. At outcrop, the formal equivalent name of the Prue sand is the Lagonda Sandstone, although this terminology is seldom used by the oil industry. Because of correlation problems in southeastern Oklahoma, the Prue sands are commonly referred to as the Calvin Sandstone - a formal surface name.

The Prue play is located primarily in the eastern half of the state in the Cherokee Platform Province. Progradation of the Prue FDD system to the southwest took place in a manner similar to the Skinner but deposition was not as extensive or intensive. As a result, Prue deposition was redirected southward away from structurally positive areas arising along the Nemaha Uplift, thereby inhibiting the transport of coarser grained sediments into the Anadarko basin. The stagnation of the Prue FDD system resulted in very dirty reservoirs containing abnormally high amounts of clay and mica. Subsurface evidence marking the maximum westward extent of Prue FDD occurs along the southern extent of the Nemaha fault zone just west of Oklahoma City. The southern limit of the Prue FDD system adjoins a marine seaway. In approximately the same stratigraphic position, a similar depositional sequence originated in far southeastern Oklahoma (Arkoma Basin) and prograded to the northwest. The Prue "equivalents"in this part of the state are referred to as the Calvin sands, and are much thicker than the Prue interval of the Cherokee Platform Province farther to the north.

Hydrocarbon production from the Prue and Calvin sands is highly oil prone although a significant proportion of well completions are classified as gas wells. Since this play does not extend into the deeper part of the Anadarko basin, there are no large areas of production that are entirely gas. Most of the reservoirs, whether marine or fluvial, are second-rate and do not produce as well as the cleaner reservoirs found in the Bartlesville, Red Fork, and some Skinner zones. Another problem with Prue reservoirs is formation evaluation because the sands often calculate wet. This is due to errors in the interpretation of true (deep) resistivity which is suppressed" by the high interstitial clay content. Clean sands in the Prue interval are sometimes difficult to interpret from gamma-ray logs because of the unusually high mica

content in the reservoir. Other drawbacks that are inherent to this class of reservoirs include compartmentalization and highly variable permeability. These problems were addressed in the evaluation of the Prue oil pool in Long Branch field.

Long Branch Field, Prue oil pool *is* located in Payne county in north central Oklahoma (Fig. 12). The field is in the western part of the Cherokee platform province and is -45 mi east of the Nemaha fault zone. Prue production was discovered and commercially produced early in 1993 despite several earlier Prue penetrations in the center of the field. These earlier wells

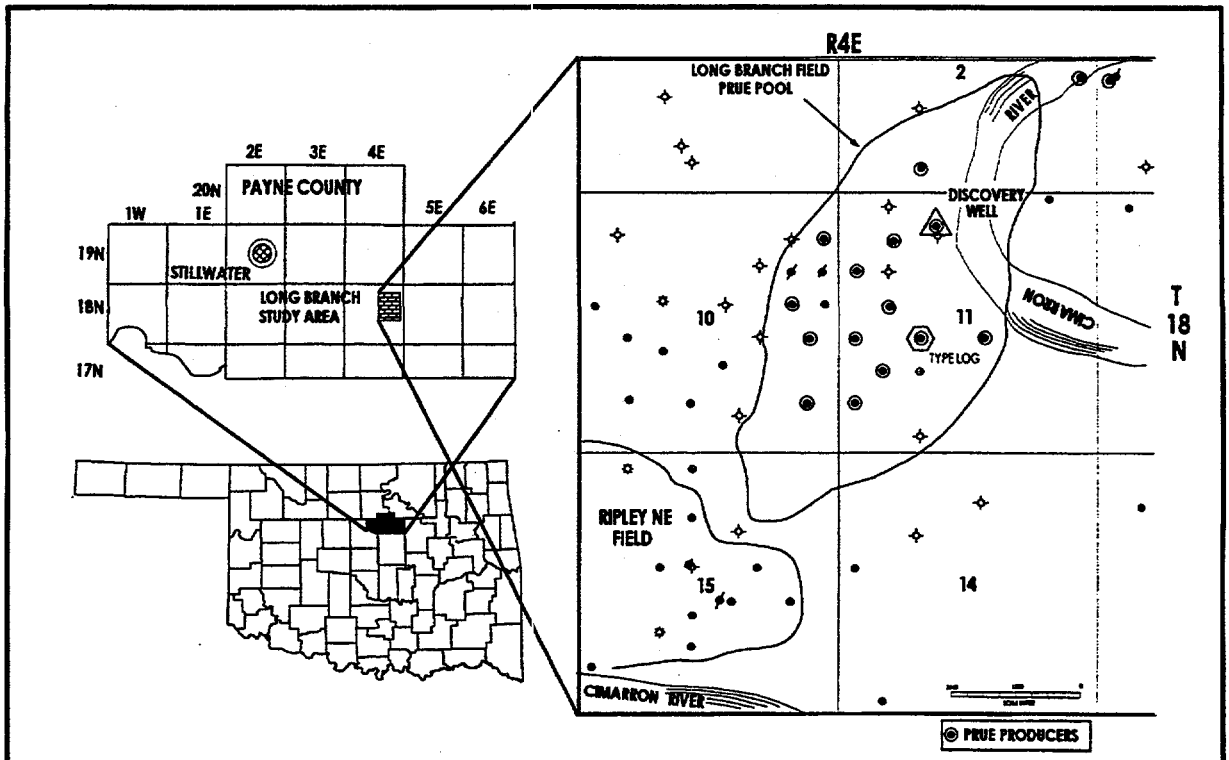

Figure 12. Generalized location map of the Long Branch field Prue oil pool, Payne County, Oklahoma.

were drilled to deeper targets and often had live oil shows in the Prue although the electric logs calculated wet. Completion of the discovery well was pursued by an alert consulting geologist who recognized the oil potential of the zone in spite of high water saturation calculations. The field opener tested at least 15 BOPD and subsequent drilling or recompletions led to 15 Prue oil wells with primary reserves of at least 200-300 MSTBO. The exact amount of oil production will never be known because it is commingled with production from several other pay zones.

The Prue reservoir sand in Long Branch field has a net thickness of 20-40 feet. The sandstone pinches out rapidly along the edges of the channel and is discontinuous up-dip to the northeast. The down-dip limit of the field is defined by an oil/water contact. The field is about 1 1/2 miles long and about 2/3 mile wide.

The basic reservoir and engineering data for this field are shown in Table 12. Despite the large volume of oil in-place (-10 MMSTBO), only about 15-30MSTBO are expected to be recovered on a per-well basis. This very low recovery is due to the relatively high water saturation calculated to be 50-60%. The porosity (-16%) and permeability (-23 md) are

relatively high, but without massive stimulation the Prue reservoir probably would not be productive.

TABLE 12 - Reservoir Properties for the Prue Sandstone in Long Branch Field
Payne County, Oklahoma

Reservoir size	-800 acres
Spacing (oil)	20-40 acres
Oil/water contact	- - 2475 feet
Gas/oil contact	none
Porosity	10-22% (avg. -- 16%)
Permeability)	10-63 and (avg. - 23md)
Water saturation (calculated)	44-60%
Average Gas-Oil Ratio (GOR)	probably < 1000 SCF/BO
Thickness	15-42 ft (avg -27 ft)
Reservoir Temperature	108° F
Oil Gravity	40-41° API
Initial reservoir pressure	NA
Initial formation-volume factor	1.25 (est from GOR, BHT, oil gravity)
Original Oil in Place (volumetric)	10,725,000 STBO
Cumulative primary oil production	undetermined, commingled with Peru
Estimated cumulative primary oil per well	15,000 - 30,000 BO
Recovery efficiency (oil)	undetermined, probably < 10%
Cumulative gas production	undetermined, commingled with Peru 1 All

wells have been fracture treated, possibly resulting in preferentially oriented enhanced permeability.

Waterflood simulations by Knapp and Yang indicate that the estimated volume of unproduced mobile oil is about 5.6 MMSTBO which is about 52% of the OOIP. Results of a 10-year model simulation show that this oil pool would be a very attractive secondary recovery operation using any alternative considered in this study. These include water flooding using existing wells versus water flooding with infill wells. The performance of these two scenarios is compared to a base case whereby current operations are maintained (Table 13). The incremental oil recovery due to water flooding is estimated to be as much as about 1,700 MSTBO or 20% OOIP. This is 4.7 times the amount that would be recovered by continuing the current operation conditions for 10 years.

TABLE 13 - Ten-Year Production Forecast Based on Reservoir Simulations

	Current operations	Waterflood with existing wells	Waterflood with infill wells
Cumulative oil production (mstb), 1/01/96	210	210	210
Expected cumulative oil production (mstb), 1/01/06	**460**	1,800	2,150
Incremental recovery from waterflood (mstb), 1101/06		1,340	1,700
Cumulative water production (mstb), 1101/06	1,700	12,000	15,250
Cumulative water injected (mstb), 1/01/06		**14,350**	18,100
Cumulative gas production (mmscf), 1/01/06	1,660	6,900	8,400
Maximum field oil production rate (stbid)	70	700	900
Time at maximum oil rate (date)	1/01/06	2/01/00	5/01/00
Oil production rate (stb/d), 1/01/06	70	250	**275**

THE CLEVELAND AND PERU PLAYS

Primary authors:	Jock Campbell - Cleveland
	Robert Northcutt - Peru
Contributing authors:	Bruce Carpenter, Roy Knapp, X. H. Yang
Workshop date:	October 17, 1996
Workshop site:	Phillips Petroleum Research & Development Center, Bartlesville.
Publication:	Oklahoma Geological Survey SP 97-5, Fluvial-Dominated Deltaic (FDD) Oil Reservoirs in Oklahoma: The Cleveland and Peru Plays.

The Peru and Cleveland sands are important oil-producing FDD plays in Oklahoma. They were combined for a dual workshop because of the relatively small number of operators attributed to each play in addition to the relatively small amount of oil production recorded during the past 17 years. The Peru sand is the informal subsurface name of the Englevale Sandstone and lies at least 100 feet beneath the Cleveland sand interval. The Cleveland sand also is an informal subsurface name and the sand interval is often comprised of an upper and lower sand horizon. The formal surface equivalents are the Tulsa and Jenks Sandstones, respectively.

The **Peru Play**

The Peru fluvial-dominated deltaic (FDD) play has centered on the Cherokee platform in northeastern Oklahoma (Fig. 13) and extends into southern Kansas. The play is limited by the outcrop on the east and by the depositional limit of the sand on the south and west. Peru is an informal subsurface term for the Englevale Sandstone in Kansas that lies within the Labette Shale of the Marmaton Group. In the subsurface terminology, the Labette is the shale interval between the Big Lime and the Oswego lime. The Peru sand is not as prolific as some of the other Cherokee sands, and has been overlooked as an objective reservoir. The Peru is quite shaley and commonly appears "wet" on resistivity logs; however, the Peru does produce oil and can be economic in spite of its poor appearance on wireline logs.

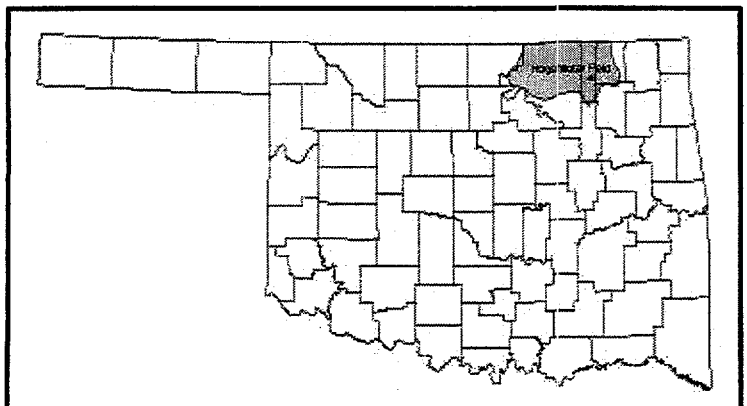

Figure 13. Generalized location map showing Peru FDD areas.

The shallow Peru sand lies in that part of Oklahoma where extensive oil reservoirs have been developed since 1904. Most wells in the area were drilled through the Peru zone and into the Bartlesville, therefore a lot of subsurface data and a large number of existing wells are available for calculating the oil potential of the Peru sand. The Peru sandstone reservoirs have been developed primarily in distributary-channel deposits of a fluvial-dominated deltaic environment. The reservoirs are generally stratigraphic traps where the sand is present on local structural noses or where the sand pinches out updip. Local uplift and sediment compaction also influence the localization of these oil reservoirs. The Peru sandstone in

Oklahoma covers an area only 42 miles north to south and 84 miles from east to west. However, most of the leases that produce from the Peru are in an area that extends only about 30 miles south from the Kansas state line and roughly 40 miles west from the outcrop. This area corresponds roughly to the eastern half of the sandstone area, where the Peru is generally thicker, up to 75 ft.

In terms of aerial extent and oil production, the Peru play is the smallest in the FDD series. During the past 17 years, estimated cumulative oil production is between 1 to 2 million barrels. The higher estimate includes commingled oil production whereas the lower estimate includes only Peru oil production. Typically, annual Peru oil production accounts for about 40-50 MBO. The play was developed primarily during the early 1900' s and producing reservoirs are generally very shallow - less than 3000 feet.

Most fields having Peru production were developed in the early 1900's which inhibits any kind of detailed geologic field study. Log records are generally poor, and production records of individual wells are often incomplete or lost to history. Because of these problems, a suitable field study for waterflood modeling was not identified. Instead, an area of recent Peru production was identified and studied in as much as the data permitted. This area occurs within the Hogshooter field in central Washington county. The area of interest is confined to about 160 acres.

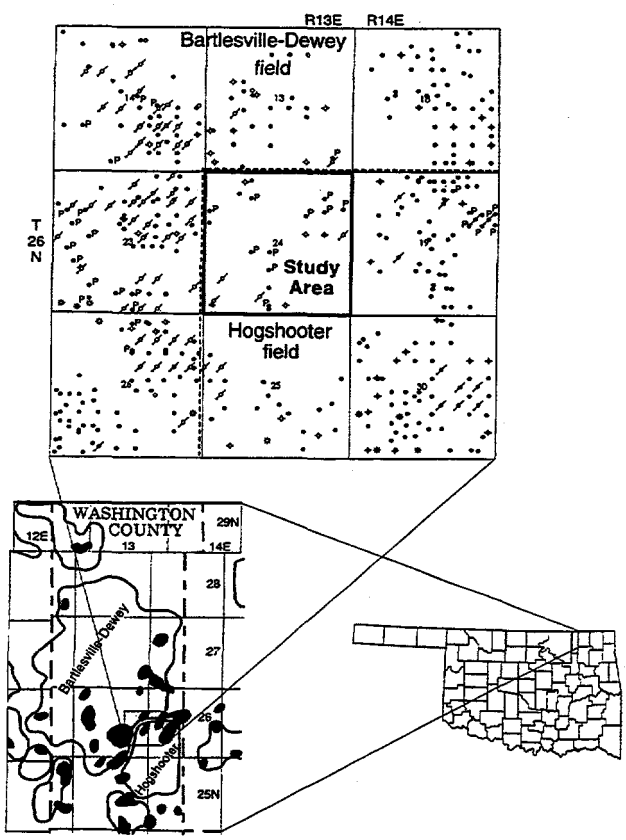

Figure 14. Maps showing the Hogshooter field, areas with Peru production (shown in black), and the Peru oil-reservoir study area in sec. 24, T. 26N., R. 13E., Washington County, Oklahoma. On the detailed map, large well spots with *P* denote wells that produce(d) oil from the Peru or from the Peru commingled with oil from another reservoir.

Hooshooter Field, in east-central Washington County, Oklahoma (Fig. 14) was discovered in 1906. The first oil production was from the Bartlesville sand, with an initial potential ranging from 225 to 500 barrels of oil per day (BOPD). Production from the Peru oil reservoir in sec. 24, T. 26N., R. 13E. was established in 1981 with the 'completion of the Chatauqua Oil, Inc., No. 2 Mayberry. The well had an initial pumping potential of 10 BOPD and 190 barrels of salt water per day (BSWPD) from perforations at 739-743 ft in a 50 ft thick Peru channel sandstone.

The reservoir is a local stratigraphic trap in a distributary-channel sandstone at the top of a progradational deltaic sequence. The seal for this stratigraphic trap is formed in part by the Labette Shale, which surrounds the Peru channel sandstone. Production was established during the early 1980's from a very thick channel sand (-80'). Most wells produced

only a few barrels of oil per day and upwards to 275 barrels of water. The initial oil/water ratio varied from about 2-5% and because of this high water cut, the reservoir was essentially being produced under waterflood conditions during primary production. The reservoir lies at a depth of about 700 feet and hydrocarbon trapping results from structural nosing. Only the very upper part of the channel is perforated since the sand is mostly wet.

Total cumulative primary oil production from the Peru sand in the Hogshooter field is estimated to be about 42,000 barrels of oil. The original oil in place was not determined. Peru oil production was established in up to 8 wells. Reservoir properties (Table 14) are very good as the sandstone generally has relatively high porosity (~20%) and permeability (~28 md).

TABLE 14 - Reservoir Properties for the Peru Oil Reservoir in Hogshooter Field, Washington County, Oklahoma

Reservoir size	~230 acres
Spacing (oil)	10 acres
Oil/water contact	~ 40 ft above mean sea level
Gas/oil contact	none
Porosity	20%
Permeability	28 md
Initial water saturation	<56%
Thickness (net sand in reservoir)	48 feet average
Reservoir temperature	85° F
Oil gravity	35° API
Initial reservoir pressure	unknown
Initial formation-volume factor	unknown
Original Oil in Place (volumetric)	unknown
Cumulative primary production (Peru-only)	42,040 BO (13 wells)
Recovery efficiency	unknown
Cumulative primary gas production	no data

However, because of the strong water drive and high water cut during production, this reservoir is not suitable for secondary water flooding since the reservoir is being water-flushed concurrent with primary production (an induced water flood).

The Cleveland Play

The Cleveland sand is an informal subsurface term first used by drillers at the Cleveland oil field in eastern Pawnee County. The Cleveland sand interval consists of as many as three persistent, but not continuous bodies of sandstone. The lowermost (lower"Cleveland) occurs most widely and commonly is the thickest. The upper two sandstone bodies are less widespread, but are significant hydrocarbon reservoirs locally. It is generally recognized that the Dawson coal splits the upper and lower Cleveland sands.

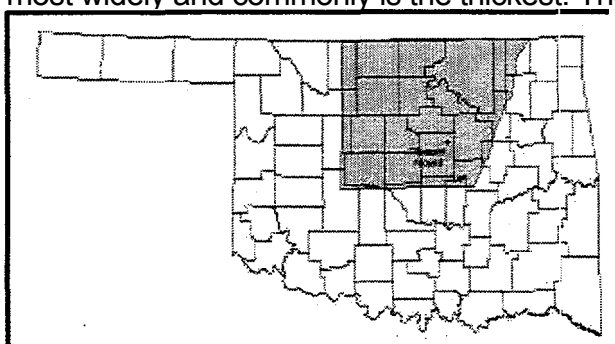

Figure 15. Generalized location map showing Cleveland FDD areas.

This play occurs throughout much of north central Oklahoma (Fig. 15). It consists largely of fluvial and delta front (marine) sediments that prograded in a westerly direction. This is very unlike many of the Cherokee plays that advanced in a southerly direction. Although FDD components constitute a large part of

the Cleveland interval, there are scattered areas of sandstone deposition that are probably entirely of marine origin rather than deltaic. These areas are primarily located in western Oklahoma.

Over the past 17 years, Cleveland production was reported from 158 fields and the total estimated oil production is about 12,500,000 barrels (Table 15). During the past six years, annual production was typically about 500 MBO. The play was developed primarily during the early 1900's but is now more often regarded as a secondary objective. Field mapping and regional _production data indicate that there are still local areas containing significant oil potential in this play. Cleveland reservoirs are generally shallow - less than 6000 feet.

Table 15. Crude Oil Production from Cleveland Sand Reservoirs, 1979-1995

Reservoir	Leases reporting'	Cumulative oil	Average bbl/lease	Other leases[1,2]
Cleveland sand	326	11,445,443	35,109	264
"Jones"[3] sand	56	999,696[4]	17,852	34

1 Average number of leases during the time frame, 1979-95.
2 Commingled production with that from other formations.
3 "Jones"sand is a local equivalent of the Cleveland.
4 "Jones"sand reservoirs include production from Cleveland sand and other formations.
SOURCE: Natural Resources Information System (KRIS) oil and gas production data base

Pleasant Mound Field, **Cleveland sand** reservoir is in northeastern Lincoln County, secs. 10,11,14, 15 and secs. 22-26, of T. 16N., R. 6E. The study area consists of -2,000 productive acres that are bounded by oil-water contacts on the west and by the sand-body limits on the east. The southern boundary is assumed to be a no-low boundary. The oil-bearing Cleveland sand appears to have been deposited in three layers: B, C, and D.

The Cleveland sand was discovered by the Nadel & Gussman No. 1 Alice Teters well in September 1956. Twenty-six additional wells were drilled and completed in zones B and C during the next three years. Most of the production has been from zone B, which was perforated in all 36 producing wells. Total cumulative oil production from the Cleveland sand prior to water flooding in Pleasant Mound field is estimated to be 400,000 BO which is about 3% of the original oil in place (13.6 MMSTBO). In 1960, because of a steep decline in oil production, the Pleasant Mound Cleveland sand unit was formed. Initially, there were six injectors and up to 18 producing wells although not all of the producing wells were completed in the zone being water flooded. Water was injected at a rate of about 100-400 BWPD per well. However, response to water injection did not occur for nine years until 1970 at which time four more injectors were added. The biggest response in oil production occurred the following year when it more than tripled to about 2000 BO/month in 1971. By the end of 1995, primary plus secondary oil production totaled about 860,000 BO, the field oil-production rate was <2 BOPD and the water cut had reached 99%.

The original oil in place in the Pleasant Mound Cleveland sand reservoir was estimated to be 13.6 MMSTB. Only -6% of that amount has been recovered after 40 years of primary and waterflooding production. The estimated volume of unproduced mobile oil in this field (-6.8 MMSTB, or 50% of OOIP) provided a strong motivation for considering future oil recovery

opportunities. The reservoir lies at a depth of about 2,200 feet, and hydrocarbon trapping results from an up-dip stratigraphic pinch-out of net sandstone. Reservoir properties are very favorable for secondary water flooding since the sandstone generally has relatively high porosity (-20-23%) and permeability (-50-130 md). These data are summarized in Table 16.

TABLE 16 - Reservoir Properties, Cleveland Sand Reservoir, Pleasant Mound Oil Field, Lincoln County, Oklahoma

Estimated properties	Zone B	Zone C	Zone D
Porosity	23%	20%	20%
Permeability	130 rnd	50 and	50 and
Average Gross Pay	20 ft	20 ft	25 ft
Average Net Pay	10ft	15ft	13ft
Initial Water Saturation	32%	32%	32%
Initial Bottom-Hole Pressure	**950** PSIA	**950** PSIA	950 PSIA
Initial Gas-Oil Ratio	385 SCF/STB	385 SCF/STB	**385** SCF/STB
Initial Formation-Volume Factor	1.20 RB/STB	1.20 RB/STB	1.20 RB/STB
Reservoir Temperature	106° F	106° F	106° F
Oil Gravity	**48°** API	**48°** API	48° API
Specific Gas Gravity	0.8	0.8	0.8
Initial Oil in Place	7.5 MMSTB	5.6 MMSTB	0.6 MMSTB
Initial Gas in Place	3,800 MMSCF	3,000 MMSCF	220 MMSCF

Table 17 summarizes the reservoir's oil production history as well as projected outcomes for several different secondary oil recovery development cases based on the models developed by Knapp and Yang. Waterflood modeling indicates that unproduced mobile oil amounts to about 6.8 MMSTBO or 50% or the OOIP. Various secondary recovery scenarios were examined which indicate that up to 2,800,000 STBO could be recovered in 10 years which is about 3.3 times the recovery during the past 40 years. The various enhanced recovery scenarios include the recompletion of several wells for injection (for a total of 14 injectors), and varying water injection rates and bottom-hole pressures (300 vs. 1800 psi - Options I and 2, respectively). The base case assumed that there were no changes in field development and well operating conditions.

TABLE 17 - Oil Recovery Comparisons for Different Development Cases, ~ievelana sane Keservoir, rieasani mouna oil rieia, Lincoln okianoma

Formation	Primary & Water-flooding (12/1995)			**Base** (12/2005)			Recompletion -Option 1 (12/2005)			**Recompletion -Option 2** (12/2005)		
	Cum Oil **(STB)**	**Rec. Factor** (%)	Cum Wtr **(MSTB)**	**Cum Oil (STB)**	**Rec. Factor** (%)	Cum Wtr **((MSTB)**	Cum Oil **(STB)**	**Rec. Factor** (%)	Cum Wtr **(MSTB)**	Cum Oil **(STB)**	Rec. Factor (%)	Cum Wtr **(MSTB)**
Zone B	**835,000**	11.1	2,700	940,000	12.5	2,900	1,550,000	21	11,000	2,000,000	**26.7**	40,000
Zone C	25,000	0.4	400	30,000	0.5	500	470,000	**8.4**	**380**	650,000	11.6	2,000
Zone D	0	0	0	0	0	0	80,000	13	20	150,000	25	1,000
Total	860,000	**6.3**	3,100	970,000	7.2	3,400	2,100,000	**15.5**	11,400	2,800,000	**0.6**	43,000

THE RED FORK PLAY

Primary author:	Richard Andrews
Contributing authors:	Kurt Rottmann, Roy Knapp, X. H. Yang
Workshop dates:	March 5 and 12, 1997
Workshop sites:	Postal Service Technical Training Center, Norman, and the Phillips Petroleum Research & Development Center, Bartlesville.
Publication:	Oklahoma Geological Survey SP 97-1, Fluvial-Dominated Deltaic (FDD) Oil Reservoirs in Oklahoma: The Red Fork Play.

The Red Fork sandstone has been, and continues to be, one of the main producers of oil and gas in Oklahoma. Unlike some of the other shallower Cherokee sands, such as the Prue and Skinner, the Red Fork is relatively clean. Therefore, Red Fork oil potential was generally not overlooked because of a shaley or wet appearance on wireline logs. Thus, during the past fifty years numerous fields have been discovered and developed as a result of deliberate exploration for the Red Fork.

Figure 16 shows the generalized distribution and depositional facies of the Red Fork sandstone. The Red Fork interval is mostly shale and sandstone that lies between the Pink lime and the Inola Limestone. In most places, the entire interval is -100ft thick and contains one or two 10- to 50- ft thick sandstones with an occasional thin limestone or coal bed. Sandstones in the Red Fork interval are mostly fine to very fine grained, with some medium-grained sandstone. In general, the Red Fork FDD system has a northerly source and advanced to the south and west. Sandstone in the Red Fork interval originated from a major fluvial system that advanced across much of the Cherokee Platform in a southerly direction.

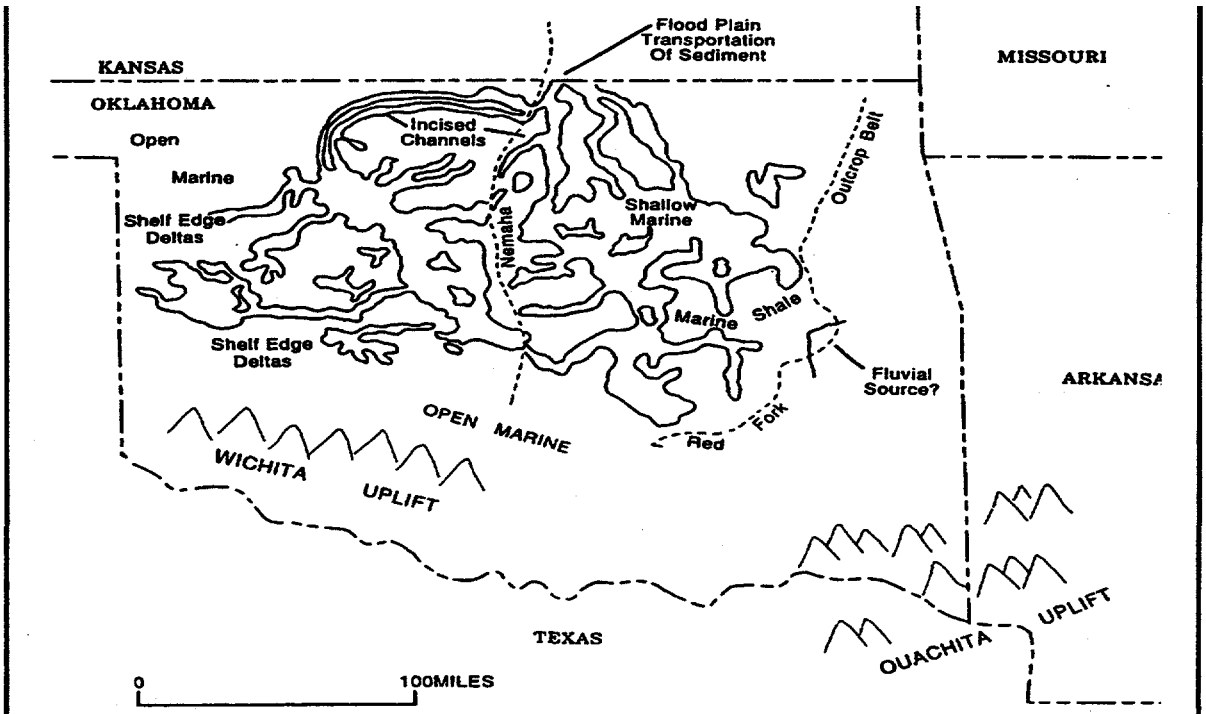

Figure 16. Generalized distribution and depositional environments of the Red Fork sandstone in Oklahoma.

The Red Fork sandstone is one of the most widespread Cherokee plays in Oklahoma. A regional isopach map of the interval from the top of the Pink lime to the top of the Inola Limestone reflects the location and the geometry of the basins and platform areas that existed during the deposition of the Red Fork (Fig. 17). The thickness of the Red Fork interval was apparently controlled mostly by the configuration of the Cherokee platform, the Nemaha fault zone, the central Oklahoma uplift, and Anadarko basin. The Red Fork interval is relatively thin (s100ft thick) and relatively uniform in thickness throughout much of central and northeastern Oklahoma. This indicates that Red Fork deposition was significantly attenuated along the Nemaha uplift and possibly eroded. The relatively uniform thickness of the Red Fork interval also suggest that the depositional gradient was relatively low on the Anadarko shelf and Cherokee platform. This is in sharp contrast to the Anadarko Basin, where the Red Fork interval thickens considerably over a short distance.

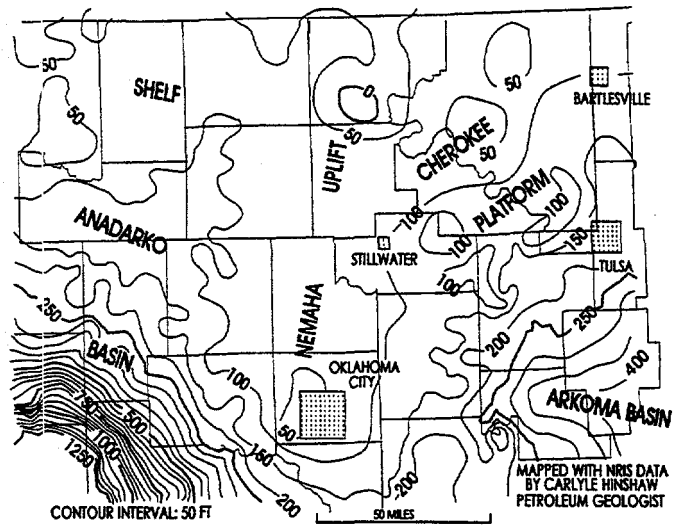

Figure 17. Regional isopach map of the interval from the top of the Pink lime to the top of the Inola Limestone (Red Fork interval plus the Pink lime), Oklahoma. Contour interval is 50 ft.

North Carmen Field is located in Alfalfa County in northwestern Oklahoma (Fig. 18). The field is about 60 miles west of the Nemaha uplift, in the area commonly referred to as the Anadarko Shelf Province. Early wells drilled in N. Carmen were completed in the Mississippi lime in 1965. The Red Fork in these early wells were shaley.

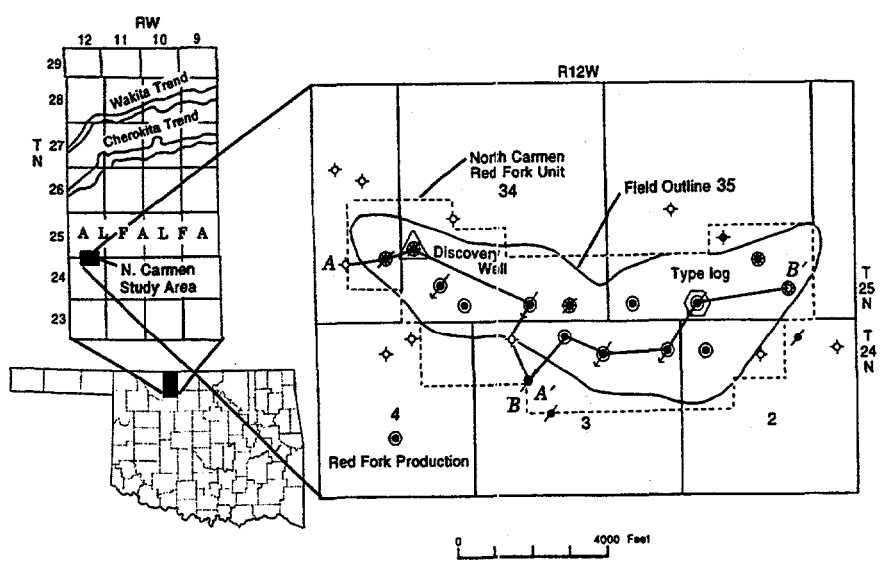

Figure 18. Map showing location of the N. Carmen Field in southwestern Alfalfa County, Oklahoma. The field boundary is shown by the solid line; the N. Carmen Red Fork Unit boundary is shown by the dashed line. The Cherokita and Wakita trends also produce from the Red Fork sand.

In December 1984, Duncan Oil drilled the field opener for the Red Fork oil pool. The No. 1 Zoa (SW¼ NW¼ SW¼ sec. 34 T. 25N., R. 12W.) had an initial potential flowing 108 BOPD, 344 MCFGD, and no water from 14 ft. of Red Fork

sandstone. During the next year, nine additional Red Fork wells were drilled in the area east of the discovery well. By mid-1986, 14 wells had been completed in the Red Fork.

The N. Carmen Red Fork has an oil gravity ranging from 40° to 50° API. The lighter oil is found structurally lower in the reservoir. N. Carmen is fully developed on 40 acre spacing. Most of the wells were shut-in during the early 1990's when individual well production fell only to a few barrels of oil per day. In late 1995, the field was unitized by Ensign Oil and Gas and a waterflood was initiated.

Regional dip of the Pink lime in the study area is to the south at -50ft/mi. In the study area, the regional southward dip is interrupted by a pronounced northeast trending trough that plunges to the south in the eastern part of the study area, and a smaller northwest trending trough in the western part of the field. These deviations from the regional structure are probably the effects of small-scale basement faulting. Because there is no dominant structure feature as incentive for exploratory drilling, this field was discovered by extending the known geologic trend of the Red Fork channel that was delineated further to the west in the early 1980's.

The estimated cumulative oil and gas production from the Red Fork in N. Carmen field from December 1984 through June 1996 is 415,082 BO and 2,315685 MCFG. The peak in annual oil production was in 1985 when 10 wells produced 166,375 BO; average daily production was 46 BOPD per well. In 1988, 12 wells were producing and production had fallen to 17,931 BO; 4 BOPD per well.

Long Branch Field, located in east-central Payne County in north-central Oklahoma (Fig. 19). This is the same field area in which a Prue reservoir had been the subject of a previous study and workshop (see Figure 11). The first commercial Red Fork well was completed in November 1983. Statex Petroleum's No. 1 Snyder, (sec. 10 T. 18N., R. 4E.) was completed in about 6ft of net Red Fork sand and had an initial flowing potential of 238 BOPD, 100 MCFGPD, and no water. During the next year development in the area progressed to the northwest where a much thicker Red Fork sand was encountered. As of April 1996, nine wells had been completed in the Red Fork pool; however, the only two Red Fork wells still active were making only a few barrels of oil per day. Because of the shallow depth and well spacing patterns, this field appears to be an excellent candidate for a waterflood.

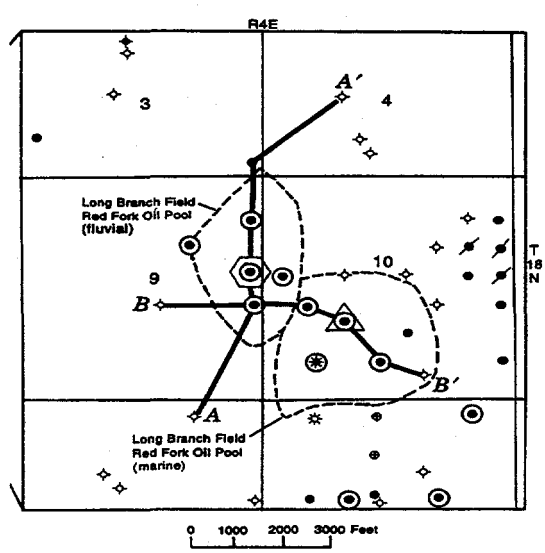

Figure 19. Long Branch study area. The field outline is differentiated between fluvial and marine reservoir facies as determined from well logs.

Regional dip in the area surrounding Long Branch Field is to the west-southwest toward the Anadarko basin at ~50ft/mi. The Red Fork channel sandstone that is productive is interpreted to be a point bar deposited within a meandering river of a flood plain. The point bar sandstone was interpreted mainly from the character of the gamma ray and resistivity logs. The sandstone has a fining-upward textural profile

that includes shale breaks in the upper half of the sandstone. The point bar sands contain a major portion of the oil within the Red Fork oil pool in Long Branch field. Productive marine sandstone is interpreted to have been deposited on a shallow marine shelf, as bars, or poorly developed shoreface. Estimated cumulative oil and gas production from the Red Fork in Long Branch field from November 1983 through April 1996 was 247,206 BO and 158,849 MCFG. The principal drive mechanism is interpreted to be a solution gas expansion rather than a water drive. Wells in this field were diminished to strippers by the late 1980's when the average daily oil production was only 2-3 BOPD.

THE TONKAWA PLAY

Primary authors: Jock Campbell, Carlyle Hinshaw
Contributing authors: Kurt Rottmann, Roy Knapp, X. H. Yang
Workshop date: July 9, 1997'
Workshop site: Postal Service Technical Training Center, Norman, OK.
Publication: Oklahoma Geological Survey SP 97-3, Fluvial-Dominated Deltaic (FDD) Oil Reservoirs in Oklahoma: The Tonkawa Play.

The Tonkawa Play has been of continued interest for many operators and geologists for a long time, but recently has become very active in western Oklahoma. The renewed interest in the Tonkawa centers in the Anadarko Shelf and Basin areas where production is prone to **gas** from marine sands. Although portions of north central Oklahoma have significant areas containing FDD deposits, only scattered areas within the FDD portion of the play produce oil. (Figure 20.) Because of the nature of hydrocarbon distribution patterns within the Tonkawa play and the high interest in the predominantly gas prone areas of the state, it was decided to complete the Tonkawa play in two parts: FDD oil and non-FDD gas. The funding support for the effort was divided between the FDD (fluvial oil reservoirs) and the Petroleum Technology Transfer Council projects (marine gas reservoirs). The Oklahoma Geological Survey SP publication however, included only information and maps relevant to Tonkawa FDD (oil) play. Information concerning the Tonkawa gas play in the predominantly marine facies of the Anadarko Basin is available as an OGS open file report.

Relatively little has been published about the Tonkawa play, and the interpretation supporting FDD deposition is documented in only a few thesis and by well log evaluations by the primary author. The basic patterns of deposition appear to be primarily FDD along the outcrop belt and into the shallow subsurface. In western Oklahoma, the Tonkawa is interpreted to be primarily of marine origin although some investigations indicate that lower delta-plain and/or deep marine deposition took place. These contradictory interpretations have provided an incentive to more accurately evaluate the regional depositional environment of the Tonkawa play and better identify the principal sandstone trends.

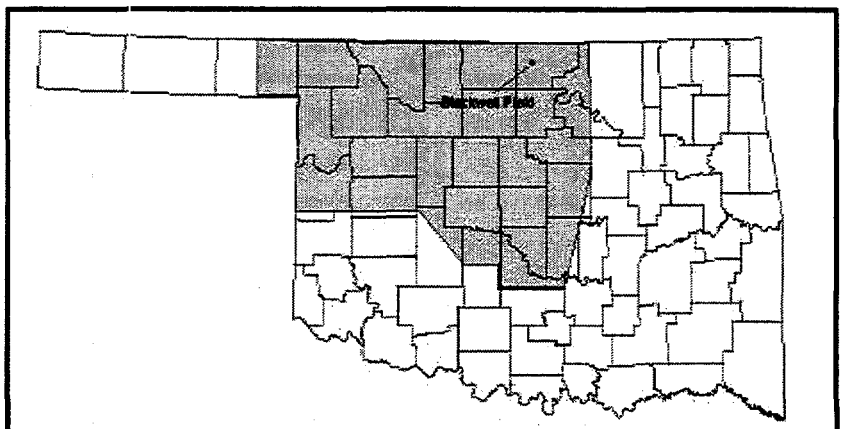

Figure 20. Generalized location map of the Tonkawa play.

The Virgilian age sandstones of the Tonkawa play are the

youngest of the fluvial-deltaic reservoirs to be investigated in the FDD workshops, with drilling depths of about 2,200-4,400 ft. Tonkawa reservoirs have produced oil and gas for 76 years in Oklahoma. The historical record of that production is incomplete; however, from 1979 through 1996, 29 fields produced oil from the Tonkawa sand in the area of fluvial-dominated deltaic sand deposition.

The Tonkawa play consists of the widely occurring, uppermost sandstone unit below the Haskell Limestone. Several sub-commercial plays have been found above and below the Haskell, but are minor in comparison to the Tonkawa production. The Tonkawa and related sand units are bounded below by the Wildhorse Limestone and equivalents. The regional structural dip is westward to southwestward at about 300 ft/mi. The accumulation of commercial amounts of oil and gas in Tonkawa sand reservoirs is associated mainly with the Nemaha uplift and Nemaha fault zone. Fault controlled structures are common in the area, and anticlines associated with basement-rooted faults have trapped hydrocarbons in many of the producing fields.

Blackwell Field's Tonkawa oil reservoir lies in secs. 9 and 10, T. 27N., R. 1W., and secs. 3 and 4 in T. 27N., R. 1W., Kay County, Oklahoma (Fig. 21). The Tonkawa sand in this field is at depths of ~2,300 ft or ~1,300 ft subsea. Its average thickness is ~35 ft, and its aerial extent, ~850 acres. Production from the Tonkawa was first established in 1923 in the Blackwell Oil and Gas Co. No. 1 Humphrey (SE¼ NW¼ SW¼ sec. 10 T. 27N., R. 1W.). The well was completed with an initial flow of 220 BOPD. The field was expanded with the drilling of 15 additional Tonkawa producers developed on 10-acre spacing from 1923 through 1941. For this time period, it is not known how much oil was recovered from these wells, thus the production history is incompletely known for the reservoir.

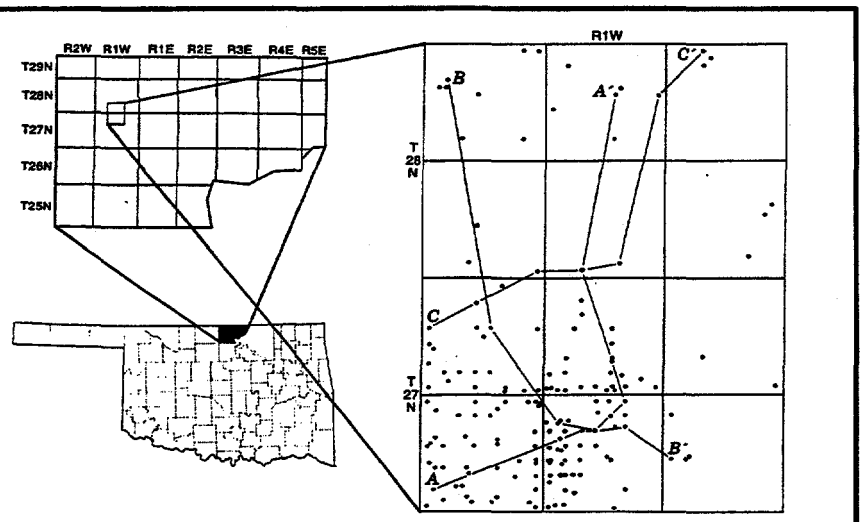

Figure 21. Generalized location map of Blackwell field study area, Kay County, Oklahoma. Lines of cross-sections included in the study are indicated.

The "B"sandstone, the main oil and gas reservoir, has an average porosity of 24% with an oil gravity of 44° API. Bottom-hole temperature was measured at 100°F, and a bottom-hole pressure of 950 PSI. Drill-stem test results from early in the life of the reservoir and from more recent tests indicate the same BHP. The persistence of reservoir pressure without pressure maintenance indicates the reservoir has a very strong water drive. Many early wells were completed flowing oil naturally. The original oil in place (OOIP) is calculated to -9.1 million stock barrels of oil (MMSTBO). The reported primary production from 1956 through 1995 is 1.282 MMSTBO, which is a recovery factor of 14%.

THE BARTLESVILLE PLAY

Primary authors: Robert Northcutt
Contributing authors: Richard Andrews, Roy Knapp, X. H. Yang
Workshop dates: October 29 and 30, and November 12, 1997
Workshop sites: U.S. Army Corps of Engineers Facility, Tulsa; Phillips Petroleum Research & Development Center, Bartlesville; Postal Service Technical Training Center, Norman.
Publication: Oklahoma Geological Survey SP 97-6, Fluvial-Dominated Deltaic (FDD) Oil Reservoirs in Oklahoma: The Bartlesville Play.

Oil reservoirs in the Bartlesville sandstone were the foundation for the dominance of Oklahoma as an oil producing state. On April 15, 1897, Cudahy Oil Co. No. 1 Nellie Johnstone, a Bartlesville sand oil well, opened the first commercial oil field in Oklahoma. Subsequent discoveries of Bartlesville oil fields made Oklahoma the leading oil producing state from statehood in 1907 until 1923. The Bartlesville play is situated on the Cherokee platform of northeastern Oklahoma (Fig. 22). The play is limited on the east at the outcrop, where the Bartlesville surface equivalent is the Bluejacket Sandstone, and on the south by its outcrop along the front of the Ouachita Mountains uplift. To the west the play is bounded by the limit of deposition of sand or onlap of the Bartlesville interval around the Nemaha uplift. Southwest of the Cherokee platform, the Bartlesville interval either was not deposited or was removed by erosion on the Oklahoma City uplift. Only marine deposits occupy the Bartlesville interval of the Anadarko basin, outside of the play area.

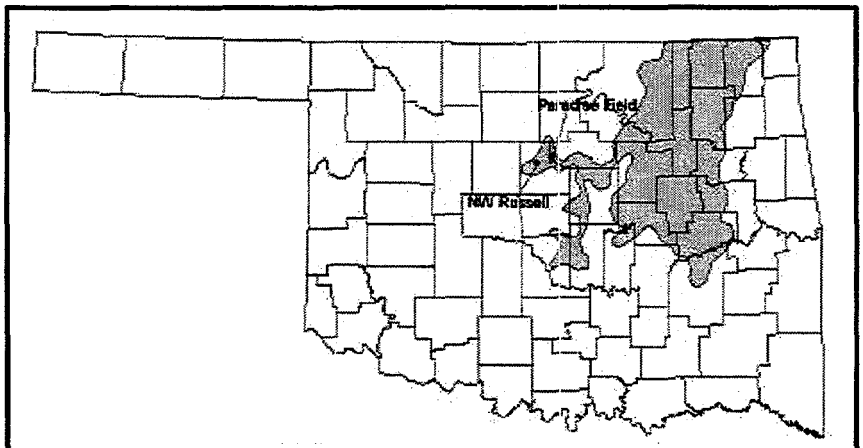

Figure 22. Generalized location map of the Bartlesville play.

The Bartlesville sand increases in depth from the outcrop on the east to -2, 400 ft at the western sand limit in southeastern Osage County. The depth of the Bartlesville sand increases to -4,800 ft in the lower Anadarko shelf area. The regional dip of the Bartlesville sand zone is to the west from the Ozark uplift in the northeastern Oklahoma. The thickness of the Bartlesville interval is generally controlled by intensity and duration of the depositional processes and the spatial relationship to structural provinces. The interval thickens bainward of the Cherokee platform and away from the Nemaha uplift. The sand is up to 200 ft thick in places along the main transport direction. The Bartlesville interval generally thins from the southeast to the northwest, where it onlaps older strata. It is absent over some the structural features in northeastern Oklahoma, either by nondeposition or erosion.

Paradise Field is located in southwestern Payne County in north-central Oklahoma. The field area is about 25 miles east of the Nemaha uplift on the Cherokee platform. Paradise field produces oil and gas from several types of Bartlesville sand deposits, including various kinds of channel deposits such as point bars in addition to tidal-mouth bars. Oil production was first established in the Paradise study area in the 1950's with the completion of two wells in the

northern part of sec. 34, T.18N., R.1 E. These wells were completed in the marine facies of the Bartlesville sand for up to 174 BOPD. In an effort to extend the original Misener oil production to the south, Canadian Exploration drilled the No. 3 Downey well (SE% SW%4 SE% sec. 33, T.18 N., R.1 E.), and accidentally discovered the Bartlesville oil pool in Paradise field. This well was completed in March 1986 and had an initial flowing potential of 290 BOPD, 133 MCFGPD and 2 BWPD from 30 ft of net Bartlesville sandstone. A total of 13 wells were completed in the Bartlesville reservoir, with oil gravities ranging from 34° to 40° API.

Paradise field is fully developed on 10-20 acres spacing. The peak in annual oil production was in 1990, when 12 wells produced 83,866 BO averaging 20 BO per well. In March 1994, the eastern part of the field was unitized by Pennacle Oil, and waterflood was initiated. In mid-1995 the first significant response in oil production was measured. The estimated oil and gas production from the Bartlesville in Paradise field from March 1986 through July 1996 is 427,752 BO and 450,718 MCFG (Table 18).

TABLE 18. - Oil- and Gas-Production Statistics for the Bartlesville Sandstone in Paradise Field, Payne County, Oklahoma

Year	Number of wells		Annual production		Average GOR	Average monthly production per well		Average daily production per well		Cumulative production	
	Oil	Gas	Oil BBL	Gas MCF		Oil BBL	Gas MCF	Oil BBL	Gas MCF	Oil BBL	Gas MCF
1986[8]	2	1	**30,349**	**11,348**	**374**	1,686	1,135	**56**	**38**	**30,349**	**11,348**
198r	4	2	**53,564**	**25,688**	480	1,275	1,284	**43**	**43**	**83,913**	37,036
1988[8]	10	**5**	**80,429**	52,661	**655**	1,072	1,699	36	57	**164,342**	89,697
1989	10	6	**80,308**	87,824	1,094	669	1,220	22	41	**244,650**	177,521
1990	12	8	**83,866**	78,619	**937**	612	1,062	20	**35**	**328,516**	**256,140**
1991	12	**9**	**38,399**	91,236	2,376	267	**861**	9	**29**	**366,915**	**347,376**
1992	12	**9**	22,321	**48,640**	2,179	155	450	**5**	15	**389,236**	396,016
1993	12	**9**	16,697	32,111	1,923	116	297	**4**	10	**405,933**	428,127
1994[b]	11	**8**	**8,445**	19,011	2,251	**64**	198	2	7	**414,378**	**447,138**
1995	11	7	6,577	**3,580**	**544**	50	37	2	1	**420,955**	**450,718**
1996[a]	9	0	6,797	0	0	**63**	0	2	0	427,752	**450,718**

[a] Includes wells having only a partial year's production. [b] Unitization occurred January 1994. Production through July 1996.

Northwest Russell Field is located in Logan County in north-central Oklahoma (Fig. 23). The field area is about 11 miles east of the Nemaha uplift on the Cherokee platform. NW Russell field produces oil and gas from several reservoirs, although the Bartlesville sand, Mississippi lime and the Oswego lime are the principal supply sources. Oil and gas production from these reservoirs is generally commingled, and only a few wells produce from a

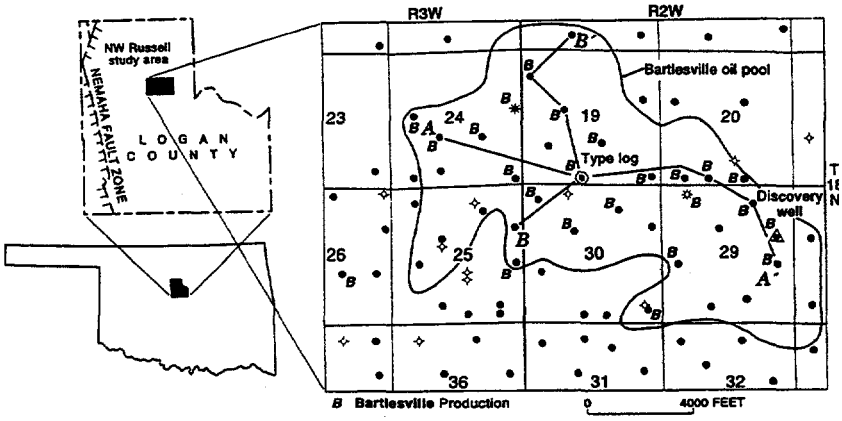

Figure 23. Map showing location of the Bartlesville oil pool in the NW Russell field area, Logan County, Oklahoma.

single-zone completion. Oil production from the Bartlesville sand was first established in the field when Bobby Darnell drilled the No. 3 Brown in sec. 29, T. 18N., R. 2W. The NW Russell Bartlesville oil pool probably was discovered in a deliberate effort to extend known productive fluvial trends farther to the west. This same trend is productive in Paradise field, 12 miles to the east. The discovery well was completed in 1977 with an initial flowing potential of 18 BOPD from 8ft of net Bartlesville sandstone. A total of 27 wells were completed in the Bartlesville with oil gravities ranging from 39° to 42° API.

NW Russell field is fully developed on 80-acre spacing. Most if not all wells continue to produce small amounts of oil and gas, and the field has never been developed for secondary oil recovery. The cumulative oil and gas production volumes from the Bartlesville are unknown due to the commingling of production from several reservoirs. Three wells have single zone Bartlesville completions and are presented in Table 19. These wells typically have sand development in the non-channel facies with about 17,500 BO and 176,000 MCFG per well.

TABLE 19. - Annual Production and GOR for Three Wells Completed Exclusively in the Bartlesville Sandstone

Year	SE SW 20,18N-2W 1 Dunsmore Oil (BBL)	Gas (MCF)	GOR	NE SE 29,18N-2W #2 Acton Oil (BBL)	Gas (MCF)	GOR	SE NW 29,18N-2W #1 Miller Oil (BBL)	Gas (MCF)	GOR
1978	0	0		0	0		0	0	
1979	5,214	**15,134**	2,903	**4,859**	10,376	2,135	**6,593**	22,465	**3,407**
1980	2,523	2,016	799	**6,868**	**28,952**	4,215	2,911	**45,004**	**15,460**
1981	1,322	5,912	4,472	2,757	**29,963**	**10,868**	1,330	**32,959**	24,781
1982	750	6,070	8,093	1,462	21,921	**14,994**	724	15,370	21,229
1983	**532**	8,014	15,064	1,263	**14,615**	11,572	757	14,122	**18,655**
1984	691	**4,578**	**6,625**	**866**	17,560	20,277	**738**	13,806	18,707
1985	205	**3,992**	**19,473**	864	16,086	18,618	**540**	11,424	21,156
1986	300	**2,096**	**6,987**	574	**14,992**	26,118	**543**	11,113	**20,466**
1987	260	2,203	**8,473**	**345**	9,720	28,174	**360**	10,321	**28,669**
1988	262	1,631	6,225	517	10,268	**19,861**	**352**	8,205	23,310
1989	**332**	**2,434**	7,331	**351**	10,520	29,972	181	8,712	**48,133**
1990	**396**	1,774	**4,480**	**350**	**9,597**	27,420	**364**	8,107	22,272
1991	**364**	1,830	5,027	**350**	**8,668**	**24,766**	178	7,417	**41,669**
1992	227	1,425	6,278	126	**5,675**	**45,040**	180	6,519	36,217
1993	264	1,350	5,114	**333**	**7,538**	22,637	179	**5,589**	31,223
1994	**397**	1,730	**4,358**	87	**5,525**	**63,506**	175	**5,633**	**32,189**
1995	0	**1,399**		0	6,656		171	3,712	21,708
1996	327	1,064	**3,254**	0	**5,518**		0	0	
Cumulative	**14,366**	**64,652**	4,500	21,972	234,150	10,657	16,276	230,478	14,161

Industry Responses

Since the inception of the workshop program in 1995, industry responses to the program have been very positive. In short, this program has been described by numerous industry representatives as the most valuable program that the Oklahoma Geological Survey has ever implemented. The operator registration statistics for the various workshops support this assertion, as shown in Table 20.

TABLE 20. - Summary of FDD Play Workshops Operator Responses

Play	Workshop Dates & Locations	Total Regis-trations	of play o • - rators	Registered Play o . - rators	Registered Operators not in • la	Total Workshop O • - rators
1. Morrow	June 1 & 2, 1995 Norman	215	604	**95**	5	100
2. **Booch**	September 11,1995 Muskogee	128	**432**	31	20	51
3. Layton & Osage-Layton	April 17, 1996 OKC	103	342	21	25	46
4. Prue & Skinner	June 19 & 26, 1996 OKC & Bartlesville	201	**1599**	72	23	**95**
5. Cleveland & Peru	October 17, 1996 Bartlesville	85	516	24	14	38
6. Red Fork	March 5 & 12, 1997 Norman & Bartlesville	**195**	**1478**	69	29	**98**
7. **Tonkawa**	July 9, 1997 Norman	101	347	23	25	48
8. Bartlesville	**October,** 1997 Tulsa, Bartlesville, & Norman	183	1420	**49**	31	80
	TOTALS:	1,211	**6,738**	**384**	**172**	**556**

The 1,211 total workshop registrations reflect 584 individuals, many with multiple registrations. Of the 584 individuals:

- 355 (61%) are from active operating companies, based on a comparison of company names to gross production tax records
- 145 (25%) are from other industry interests such as service companies, or are "consultants" (31) or "independents"(30), that could not be linked to the gross production tax records.
- 44 (8%) are OGS, University, and program staff members
- 40 (7%) are from other State and Federal agencies, and from "data suppliers" such as the OCGS and PI/Dwights.

Excluding the OGS, University, and program staff members from consideration, of the remaining 541 individuals,

- 181 (33%) have attended at least two of the workshops
- 92 (17%) have attended three or more workshops
- 41 (8%) have attended four or more workshops
- 21 (4%) have attended five or more workshops.

All of these statistics are based on registration records and a post hoc linking to the gross production records. Because of this, it is possible that some company identifications and operator designations have been missed. Therefore, these should be considered "conservative"estimates of the operator contacts through the FDD program.

By the third workshop of the FDD series, an attendee workshop evaluation process was implemented. At each of the workshops given during 1996 and 1997, attendees were asked to complete evaluation forms reflecting their assessments of the materials and presentations.

For all of the plays, attendee evaluations were overwhelmingly positive, with average scores ranging from "very good"to "great"on nearly every item in the evaluation form. A summary of the compiled evaluations for each of the plays is provided in Appendix A.

Task 3: Professional Outreach

Several levels of professional outreach were identified as part of this overall project effort.

Technical Advising: Following each of the workshops that were held in the program, the workshop participants (particularly the play leaders and the engineering staff) were called on to serve in an advisory role to respond to various industry inquiries. Operators called with specific questions about how to best manage a property they may have in the play. In this role, the project staff typically could not fully research the property to recommend a course of action, but generally were able to direct people towards the kinds of information and issues they should address. These contacts were fruitful not only for industry, but also for the project staff as they obtained feedback on the value of the publications and workshop materials.

Reservoir Characterization and Simulation Studies: These studies were conducted in cooperation with the operators of the selected reservoirs, with the goal of identifying opportunities for increasing recovery from those reservoirs. Operators were selected for these studies based on the quality of data they had for the reservoir, their willingness to participate and contribute resources to the study, and their willingness to allow the project results to be published and otherwise made available 1:o industry.

A primary goal for these reservoir characterization studies was to develop methodologies that are affordable, understandable, and usable for the small independent oil operator. While the data collection for these selected reservoirs was in far greater detail than for other reservoirs in the plays, it was still at a "minimized" level of detail relative to comprehensive reservoir studies that are performed in research facilities or by major companies in industry. The typical reservoir for these studies had about 15 to 40 wells, and fields with current production data and modem well logs were preferred. Lithology, estimates of the original hydrocarbons-inplace, and production profiles (oil, gas and water) for the reservoir were important components for the reservoir characterization. When necessary, algorithms were developed to estimate water and gas production from the reservoir, and to describe the geologic framework. The level of precision resulting from these studies was necessarily limited, but accomplished the basic goals of helping operators target the remaining resource.

Professional Activities: Information on the FDD project activities was distributed through a number of professional outlets. During the project, OGS displays provided information about the FDD program at events such as the annual meetings of the American Association of Petroleum Geologists and the Geological Society of America, and at various regional and local meetings and events. Additionally, the play leaders from each of the work shops were periodically called upon to present short summaries of their work in area professional gatherings, such as the monthly meetings of the Oklahoma City Geological Society.

VI. CONCLUSIONS

There is no direct way to measure the impact that this program has had on the volumes of FDD oil production in Oklahoma. Throughout Oklahoma, as in the rest of the domestic petroleum industry, oil well abandonments have continued to increase and production has continued to decline throughout the five years of the program. There is no way of knowing what that decline would have been if this program had not been implemented. Furthermore, most of the volumetric impacts of this program will in fact be realized in future years. If this program has served its function, it will be demonstrated through the ongoing viability of FDD reservoirs five to ten years in the future.

Since volumetric measures cannot be provided, the success of the program must be measured in terms of the accomplishments and the industry evaluations of those accomplishments. Eight highly successful workshops and accompanying publications were completed on eleven FDD horizons. A computer user laboratory was established and continues to be a resource to the industry. Industry relationships with the project participants have shown vast improvements. industry feedback to the program has been overwhelmingly positive.

Numerous operators and industry people provided positive feedback for the overall program. They indicated that the workshops were extremely valuable and provided important reservoir, geologic, and engineering information. Participants also said they gained a better insight regarding depositional environments and reservoir characteristics which would help them in exploration and development strategies. The regional trend analysis and detailed field study protocol combined with waterflood simulation exercises were directly applicable for most people. Due to the nature of the Oklahoma FDD project, it is recognized as one of the most successful and respected programs to assist operators throughout the entire Mid-Continent region. Nearly everyone wants this program continued or expanded. Because of this, arrangements have been made with the Oklahoma City Geological Society to present "repeat" workshops of some of the workshops, and requests for copies of the play publications continue to be received. Furthermore, the Oklahoma Geological Survey has plans to continue with the "play analysis" format as a permanent component of their overall program. The development of this FDD program and the support of the U.S. Department of Energy have set the stage for a strong technology transfer foundation for Oklahoma's petroleum industry.

VII. REFERENCES

Colton, E.G., Jr., 1974a, S.W. Canton field, *in* Berg, O.R. (ed.), Oil and gas fields of Oklahoma: Oklahoma City Geological Society Reference Report, Supplement 1, p. 6.

Ekebafe, Samson B., 1973, Stratigraphic analysis of the interval from the Hogshooter Limestone to the Checkerboard Limestone: a subsurface study in north-central Oklahoma: University of Tulsa unpublished M.S. thesis, 89 p.

Krumme, G.W., 1975, Mid-Pennsylvanian source reversal on the Oklahoma platform: University of Tulsa unpublished Ph.D. dissertation, 151 p.

Lalla, Wilson, 1975a, A stratigraphic study of the Osage-Layton format in northeast Oklahoma: University of Tulsa unpublished M.S. thesis, 35 p.

Miser, Hugh D., 1954, Geologic map of Oklahoma: Oklahoma Geological Survey, scale 1: 500,000.

South, M.V., 1983, Stratigraphy, depositional environment, petrology and diagenetic character of the Morrow reservoir sands, southwest Canton field, Blaine and Dewey Counties, Oklahoma: Oklahoma State University unpublished M.S. thesis, 140 p.

ATTENDEE EVALUATION SUMMARY REPORT
FDD WORKSHOP: LAYTON & OSAGE-LAYTON PLAY

April 17, 1996 **Oklahoma City, OK**

DEMOGRAPHIC INFORMATION

Type of Company	Small Independent	Major Producer	Service Co.	Govern-ment	Mid/Large Independent	Acad-emia	Con-sultant	Other	# of responses
TOTALS	16	1	1	1	1	0	8	0	28
Technical Background	Geol/Geoph	Engr	Both	Other					
TOTALS	21	3	0	2					26

How did you learn about this workshop?

- mailing 13
- conversation with OGS staff 2
- attending other workshops 2
- word of mouth 2
- OGS 3
- Tulsa Geol Soc Newsletter 1
- SPE newsletter 1

OVERALL WORKSHOP EVALUATION

	1 (Poor)	2	3 (Avg.)	4	5 (Great)	# of responses	Average
Was this workshop useful?	0	0	2	14	13	29	4.38
Was this workshop worth your time and money?	0	1	1	7	19	28	4.57

WORKSHOP AUXILIARY COMPONENTS

	1 (Poor)	2	3 (Avg.)	4	5 (Great)	# of responses	Average
Preconference materials	0	0	4	13	11	28	4.25
Registration process	0	0	1	8	20	29	4.66
Presentation facilities	0	0	1	7	21	29	4.69
Supplemental Materials	0	0	3	7	19	29	4.55
Breaks and lunch arrangements	0	0	0	4	25	29	4.86
Overall location	0	0	1	7	21	29	4.69

Please provide any suggestions or comments that you believe would help to improve these workshops.

- more, more, more
- Basically an excellent job...everyone did an excellent job
- Have presenters refer to page #'s and/or figure #'s in their discussions to minimize page flipping
- I would like to attend a seminar on the Bartlesville sand.
- Would like to see a repeat of the Morrow workshop sometime in the future.
- Closer relationship between sample descriptions, core analysis and thin sections with available electric logs.
- Computer demo useful but hard to follow
- Motel/Hotel number on registration form to correlate to map.
- More info on lithology - thin sections, clay minerals, etc.
- Keep up this high quality!
- Great job, keep it up.

• • Very well done.

Do you see an opportunity to apply the information and/or technologies discussed in today's workshop? YES: 21 NO:1

If so, what information and/or technologies?

- We have recompletions in both the True Layton and the Corrage Grove that have been proposed and approved. This information will prove very useful in recompletion choices.
- This type of study emphasizes the work that is yet to be done in order to maximize OK production, both in terms of production enhancement and exploration. You have uncovered a lot of potential areas for further study.
- Geologic info & review of things I have not used lately. Reservoir simulation was interesting and possibly useful.
- The fact that it is not at all unusual for low resistivity changes to be the difference between production and water makes our observations more important and encourages me to map sands for recompletion that at first glance appear wet.
- Being employed by an independent operator, I no longer have the opportunity to increase skills & knowledge by attending in-house schools. This workshop is a fantastic substitute. I predict this idea will be a great help to the independent petroleum operator.
- Reservoir simulation & care that must be given low resistivity reservoirs.
- Regional data as well as specific prospect areas.
- Logs & x-sections for correlation purposes;nomenclature;production analogs;reservoir simulation study;sequence stratigraphy
- In mapping & prospecting
- Investigation of passed-over potential
- Knowledge gained from regional perspectives,

PRESENTATION DETAILS	1 (Poor)	2	3 (Avg.)	4	5 (Great)	#of responses	Average
Mankin: Opening Remarks: Technical content	0	0	9	13	9	31	4.00
Mankin: Opening Remarks: Value of the info	0 _	0	6	16 .:	9	31	4:10
Mankin: Opening Remarks: Applicability to you	0	_ 1	**8**	11	10	30	4.00
Campbell: Intro to FDD: Technical content	0 °	0	6	13	12	31	4.19
Campbell Intro to FDD: Value of the info	1	0	4	12	14	31	4.23
Campbell Intro to FDD: Applicability to you	0"	1'	**5**	12	13	31	4.19
Campbell: Lower MissourianStrat: Technical	0	0	4 ,	15	12 ;	31	**4:26**
Campbell: Lower Missourian Strat:Value of the	**0"**	0	**3**	15	13	31	**4.32**
Campbell: Lower Missourian Strat: Applicability to	0	0	6	13	12	31	4.19
Campbell: Regional Overview: Technical content	0	0	2	17	11	30	**4.30**
Campbell: Regional Overview: Value of the info	0	0	**4**	12	14	30	**4.33**
Campbell: Regional Overview: Applicability to	0 '	0	**4 "**	12	14	30	**4.33**
Shannon: South Coyle Field: Technical content	0	1	8	14	7	30	**3.90**
Shannon: South Coyle Field: Value of the info	0	1	10	10	9	30	3.90
Shannon: South Coyle Field: Applicability to you	0	**4**	8	11	7	30	**3.70**
Campbell: East Lake Blackwell Technical content	0	0	6	15	9	30	4.10
Campbell: East Lake Blackwell: Value of the info	0	1	7	10	12	30	4.10
Campbell: East Lake Blackwell: Applicability to you	0	3	6	11	10	30	**3.93**
Knapp & Yang: Res. Simulation: Technical content	0	1	**5**	11	13	30	4.20
Knapp & Yang: Res. Simulation: Value of the info	0	4	6	11	9	30	**3.83**
Knapp & Yang: Res. Simulation: Applicability to you	1	**4**	9	7	9	**30**	**3.63**
Core Exhibits Technical content	-0	1	7	11	9	28	4.00
Core Exhibits Value of the info	0	1	7	9	11	28	4.07
Core Exhibits Applicability to you	0	2	7	9	10	**28**	**3.96**
Computer Demonstrations Technical content	0	0	6	13	8	27	4.07
Computer Demonstrations Value of the info	0	3	6	11	7	27	**3.81**
Computer Demonstrations Applicability to you	0	_ 2	7	11	7	27	**3.85**

FDD WORKSHOP: SKINNER AND PRUE PLAYS

June 19 & 20, 1996 — **Oklahoma City, OK**
June 26, 1996 — **Bartlesville, OK**

DEMOGRAPHIC INFORMATION

Type of Company	Small **Independent**	Major Producer	Service Co.	Govern-ment	Mid/Large Independent	Acad-**emia**	**Con-**sultant	Other	# of responses
TOTALS	47	2	2	0	6	0	19	2	78
June 19	20	0	1	0	3	0	9	0	33
June 20	10	1	0	0	2	0	3	0	16
June 26	17	1	1	0	1	0	7	2	29
Technical Background	**Geol/Geoph**	Engr	**Both**	Other					
TOTALS	**54**	9	5	6					74
June 19	26	1	3	2					32
June 20	11	4	1	0					16
June 26	17	4	1	**4**					26

How did you learn about this workshop?

	June 19	**June 20**	**June 26**	**TOTAL**
mailing	17	9	**15**	**41**
company announcement			1	1
other workshops	4	1	3	8
OGS	3	1	1	5
TGS Newsletter			2	2
Newsletter		1	2	3
OGS Advertisement			1	1
OKC Geol Library	2	1		3
Friends/word of mouth	4	**3**		7
FDD literature	1		1	2
OGSIOIPA		1		1
Shale Shaker		1		1
Tulsa World News		1		1

OVERALL WORKSHOP EVALUATION

	1 (Poor)	2	3 (Avg.)	4	5 **(Great)**	# of **responses**	Aver **age**
Was this workshop useful?	0	0	7	40	29	76	4.29
June 19	0	0	2	17	13	32	**4.34**
June 20	0	0	3	7	5	**15**	**4.13**
June 26	0	0	2	16	11	29	**4.31**
Was this workshop worth your time and	. 0	0	5	27	42	74	4.50
June 19	0	0	1	10	21	32	**4.63**
June 20	0	0	3	7	5	15	**4.13**
June 26	0	0	1	10	16	27	4.56

WORKSHOP AUXILIARY COMPONENTS

	1 {Poor)	2	3 (Avg.)	4	5 (Great)	# of responses	Average
Preconference materials	0	1	20	27	26	74	4.05
June 19	0	1	6	11	12	30	4.13
June 20	0	0	6	**5**	4	15	3.87
June 26	0	0	8	11	10	29	4.07
Registration process	0	0	6	29	41	76	4.46
June 19	0	0	3	11	18	**32**	4.47
June 20	0	0	1	6	8	15	4.47
June 26	0	0	2	12	15	29	**4.45**
Presentation facilities	0	0	1	28	47	76	4.61
June 19	0	0	0	13	19	32	**4.59**
June 20	0	0	0	**4**	11	15	4.73
June 26	0	0	1	11	17	29	**4.55**
Supplemental Materials	0	**0**	**5**	34	37	76	4:42
June 19	0	0	3	12	17	32	**4.44**
June 20	0	0	1	7	7	15	**4.40**
June 26	0	0	1	15	13	29	4.41
Breaks and lunch arrangements	0	0	**5**	17	**53**	75	4.64
June 19	0	0	2	**5**	**25**	**32**	4.72
June 20	0	0	0	2	12	14	4.86
June 26	0	0	3	10	16	29	**4.45**
Overall location	1	0	**3**	20	50	74	4.59
June 19	1	0	1	7	23	**32**	**4.59**
June 20	0	0	0	1	12	13	4.92
June 26	0	0	2	12	15	29	4.45

Please provide any suggestions or comments that you believe would help to improve these workshops.

June 19:

- This is a first class workshop in all respects. Very professional. I'm impressed.
- You must come to Tulsa, half of industry excluded when you don't. All previous presentations (Morrow, etc.) should be done in Tulsa.
- Great workshop & lecture data
- Continue the good work. Geologists need the education & networking.
- A+!
- Show slides of cores or have us look @ photos in book @ 9:10 a.m.: (1) explain main features (2) encourage us to see the features on our own during break (3) rotate core expert between core tables during break to answer questions we may have.
- Waterflood segments too short, hard to understand. Please let us know when Boast 3 is available.
- Best location yet.

June 20:

- Allow more time for engineering discussion.
- Keep lights up a little more (too dark during some of the presentations for note taking.)
- Great place to have these workshops.
- I got a flyer about the workshop but not any registration material. I had to ask around to get the registration form. I missed the earlier workshops for the same reason.
- Limited access of telephone at breaks for the use of attendees. Noticed some staff held the phone for many minutes.
- I feel these workshops are great, I wish our survey (Kansas) would contribute half of what the OGS has been doing!
- Try to present the materials in a manner that can be easily understood by company personnel that may not have a strong geology background, such as workover and completion engineers.
- Leave lights on (dim at least) during slide presentations. It was too dark for me to see to take notes during the first couple of talks.

- Would appreciate including data regarding stimulation procedures, injection rates & volumes

June 26:

- Good workshop.
- Phillips has uncomfortable chairs!
- Excellent overheads - these really help the presentation
- Scales on logs!
- Have producers do these vs. school teachers.
- Since the bulk of the data that is available to an independent geologist is electric logs, it would really be helpful to see what log signatures correspond to the cores. A small display of the electric log showing the cored intervals and a short description of all or just noteworthy lithologies would just be great.
- Maybe supply economic discussion - Feasibility of each study field; or even separate study of mature floods and their economic impact - failure or success although no one would comment on their failures.
- Workshop presentations and cost is excellent. Cant think of any suggestions. Very helpful!
- More information regarding initial treatment of wells.
- Great format. Excellent materials provided for follow-up research.
- Have E-logs laid out along cores.
- Come to Tulsa. I am surprised no one studied the fracture pattern in the field study areas.
- How about Tulsa U or TJC?

Do you see an opportunity to apply the information and/or technologies discussed in today's workshop?

June 19: YES: 22 NO: 0
June 20: YES: 10 NO: 1
June 26: YES: 17 NO: 2

If so, what information and/or technologies?

June 19:

- Fine regional studies.
- I made a list of prospect and further investigation ideas.
- Reservoir simulations
- Secondary Recoveries
- Computer Mapping
- Injection patterns & waterflood evaluation criteria. Regional Skinner correlations will help understanding of local terminology.
- The general approach to sand reservoirs and how to plan secondary recoveries from those reservoirs.
- All of it!
- Software USA

June 20:

- Clearer understanding of regional framework of both reservoir systems.
- Study and development of Skinner wells. Will use study for mapping & sales.
- It always helps seeing field interpretations to help give ideas of how to make environment interpretations.
- There was no new information or technology introduced. Admitted that not all available data was used to make the interpretations.
- Continuation of log curve analysis as exploration tool.
- Field studies, regional overview.
- I will use this information for modeling
- NRIS; exposure to reservoir simulators and mapping software.
- Found out what is really happening (geologically) in my L. Skinner field.

June 26:

- Boast 3 - Excel links
- Regional geology very helpful; interpretation of log characteristics as relating to specific environments.
- Interesting demonstration of Boast
- information of the regional Skinner & Prue in Oklahoma plus examples of existing fields
- computer simulation
- Greater understanding of Fluvial environments will aid our exploration process.
- Uphole potential

• • Geological interpretations/evaluations for Analogy. Geographic localvalued if applicable (??)
- All except computer
- Geological mapping & interpretation

PRESENTATION DETAILS	z (Poor)	2	3 (Avg.)	4	5 (Great)	#of responses	' Average
Mankin: Opening Remarks: Technical content	0	**3**	25	29	19	76	**3.84**
June 19	0	2	8	16	9	**35**	3.91
June 20	0	0	6	**5**	**3**	14	3.79
June 26	0	1	11	8	7	27	3.78
Mankin: Opening Remarks: Value of the info	0	0	23	**34**	20	77	**3.96**
June 19	0	0	9	18	**8**	**35**	3.97
June 20	0	0	**5**	**5**	**5**	15	4.00
June 26	0	0	9	11	7	27	**3.93**
Mankin: Opening Remarks: Applicability to you	1	1	24	30	19	75	**3.87**
June 19	1	1	7	17	9	**35**	3.91
June 20	0	0	7	3	**4**	14	3.79
June 26	0	0	10	10	6	26	**3.85**
Andrews: Intro to FDD: Technical content	1	1	12	40	**30**	**84**	4.15
June 19	0	0	**5**	21	13	39	4.21
June 20	1	0	**3**	6	**5**	15	**3.93**
June 26	0	1	**4**	13	12	**30**	4.20
Andrews: Intro to FDD: Value of the **info**	1	1	18	36	27	**83**	4.11
June 19	0	0	7	18	13	**38**	**4.16**
June 20	1	0	**4**	6	**4**	15	**3.80**
June 26 -	0	1	4	13	12	30	**4.20**
Andrews: Intro to FDD: Applicability to **you**	1	2	17	37	26	**83**	**4.02**
June 19	0	0	7	19	12	**38**	**4.13**
June 20	1	1	3	6	4	15	3.73
June 26	0	1	7	12	10	30	**4.03**
Andrews: Skinner/Senora Regional: Technical	0`	0	6	47	**35**	**88**	**4.33**
June19	0	0	2	21	16	39	**4.36**
June 20	0	0	2	10	**4**	16	**4.13**
June 26	0	0	2	16	15	**33**	**4.39**
Andrews: Skinner/Senora Regional: Value of the info	0	0	9	44	**35**	**88**	**4.30**
June 19	0	0	**3**	19	17	39	4.36
June 20	0	0	3	9	**4**	16	**4.06**
June 26	0	0	3	16	14	**33**	**4.33**
Andrews: Skinner/Senora Regional: Applicability to	0	2	13	46	27	**88**	411
June 19	0	1	**5**	20	13	39	**4.15**
June 20	0	1	**4**	8	3	16	3.81
June 26	0	0	**4**	18	11	**33**	**4.21**
Rottmann: Guthrie SW Technical content	0	**4**	22	40	19	**85**	**3.87**
June 19	0	2	6	20	10	**38**	4.00
June 20	0	1	3	6	4	14	**3.93**
June 26	0	1	13	14	5	33	3.70
Rottmann: Guthrie SW Value of the info	0	**3**	17	47	18 _	**85**	**3.94**
June 19	0	0	**5**	22	11	**38**	4.16
June 20	0	1	**4**	6	3	14	3.79
June 26	0	2	8	19	4	**33**	3.76
Rottmann: Guthrie SW Applicability to you	0	3	28	37	17	**85**	**3.80**
June 19	0	0	11	17	10	**38**	3.97
June 20	0	2	**5**	**4**	3	14	3.57
June 26	0	1	12	16	**4**	**33**	3.70
Andrews: Salt Fork North Technical content	0	1	12	**53**	19	**85**	4.06
June 19	0	0	**5**	25	8	**38**	4.08

June 20	0	1	2	8	3	14	3.93
June 26	0	0	**5**	20	8	33	4.09
Andrews: Salt Fork North Value of the info	0	**3**	12	45	**25**	**85**	4,08
June 19	0	0	**5**	22	11	38	4.16
June 20	0	1	2	8	3	14	3.93
June 26	0	2	**5**	15	11	33	4.06
Andrews: Salt Fork North Applicability to you	0	**5**	16	39	**25**	**85**	3:99
June 19	0	0	6	21	11	38	4.13
June 20	0	2	4	**5**	3	**14**	**3.64**
June 26	0	3	6	13	11	33	3.97
Knapp & **Bhatti: Salt Fork North:** Technical content	3	4	23	36	20	86	.3.77
June 19	2	3	13	14	7	39	**3.54**
June 20	1	0	1	9	**4**	15	4.00
June 26	0	1	9	13	9	32	**3.94**
Knapp & **Bhatti: Salt Fork North:** Value of the info	2	**5**	**35**	31	13	**86**	**3:56**
June 19	1	4	15	13	6	39	**3.49**
June 20	1	0	**5**	6	**3**	15	3.67
June 26	0	1	15	12	**4**	32	**3.59**
Knapp & **Bhatti: Salt Fork North:** Applicability to you	1	8 "	37	26	14	86	**3.51**
June 19	0	**4**	19	10	6	39	**3.46**
June 20	1	2	**5**	**4**	**3**	15	**3.40**
June 26	0	2	13	12	**5**	32	**3.63**
Rottmann: Perry SE Technical content	0	1	16	42	26	**85**	4:09
June 19	0	0	6	18	14	38	4.21
June 20	0	0	**4**	7	**4**	15	4.00
June 26	0	1	6	17	8	32	**4.00**
Rottmann: Perry SE Value of the info	0	**3**	16	39	27	**85**	**4:06**
June 19	0	1	**4**	18	15	38	4.24
June 20	0	0	5	6	**4**	15	3.93
June 26	0	2	7	15	**8**	32	3.91
Rottmann: Perry SE Applicability to you	0	2	18	40	**24**	**84**	4102
June 19	0	1	6	18	13	**38**	4.13
June 20	0	0	**5**	7	3	15	**3.87**
June 26	0	1	7	15	8	31	**3.97**
Andrews: Prue/Calvin Regional Technical content	0	1	11	42	29	**83**	4.19
June 19	0	1	**5**	17	13	36	4.17
June 20	0	0	3	**8**	**4**	15	4.07
June 26	0	0	3	17	12	32	4.28
Andrews: Prue/Calvin Regional Value of the info	0	3 `	12	**34**	34	**83**	4.19
June 19	0	2	**5**	14	15	36	4.17
June 20	0	0	3	7	**5**	15	**4.13**
June 26	0	1	**4**	13	14	32	**4.25**
Andrews: Prue/Calvin Regional Applicability to you	1	3	15	35	28	82	4.05
June 19	0	3	7	15	11	36	**3.94**
June 20	0	0	**4**	6	**4**	14	4.00
June 26	1	0	**4**	14	13	**32**	4.19
Andrews: Long Branch Technical content	1	1	10	38	32	**82**	4.21
June 19	0	1	3	17	14	**35**	4.26
June 20	1	0	2	7	**5**	15	4.00
June 26	0	0	**5**	14	13	32	**4.25**
Andrews: Long Branch Value of the info	1	1	11	37	32	82	4.20
June 19	0	1	3	17	14	**35**	4.26
June 20	1	0	1	8	**5**	15	4.07
June 26	0	0	7	12	13	32	4.19
Andrews: Long Branch Applicability to you	**3**	0	16	**34**	28	81	4.04
June 19	1	0	7	15	12	35	4.06

June 20	1	0	2	7	4	14	3.93
June 26	1	0	7	12	12	32	4.06
Knapp & **Yang: Long Branch** Technical content -	0	4	17	30	17	68	**3.88**
June 19	0	2	7	14	6	29	**3.83**
June 20	0	0	5	2	5	12	4.00
June 26	0	2	5	14	6	27	**3.89**
Knapp & **Yang: Long Branch** Value of the info	A	4	25	25	14	68	3.72
June 19	0	1	10	12	6	29	3.79
June 20	0	0	5	4	3	12	**3.83**
June 26	0	3	10	9	5	27	**3.59**
Knapp & **Yang: Long Branch** Applicability to you	4	7	21	23	13	68	**3.50**
June 19	2	1	11	10	5	29	**3.52**
June 20	0	1	4	4	3	12	**3.75**
June 26	2	5	6	9	5	27	**3.37**
Core Exhibits Technical content	0	1	7	32	30	70	**4.30**
June 19	0	0	3	16	11	30	4.27
June 20	0	0	1	3	7	11	**4.55**
June 26	0	1	3	13	12	29	4.24
Core Exhibits Value of the info	0 -	2'	6	37	25	70	**4.21**
June 19	0	0	4	17	9	30	4.17
June 20	0	0	1	3	7	11	**4.55**
June 26	0	2	1	17	9	29	**4.14**
Core Exhibits Applicability to you	1	0	9	**33**	26	69	**4.20**
June 19	0	0	6	15	9	30	**4.10**
June 20	0	0	1	3	6	10	**4.50**
June 26	1	0	2	15	11	29	4.21
Computer Demonstrations Technical content	0.	1	11	23	16	51	4.06
June 19	0	1	5	8	7	21	4.00
June 20	0	0	1	2	4	7	**4.43**
June 26	0	0	5	13	5	23	4.00
Computer Demonstrations Value of the info	1	1	10	26	13	51	**3.96**
June 19	0	0	6	10	5	21	3.95
June 20	0	0	1	3	3	7	**4.43**
June 26	1	1	3	13	5	23	**3.87**
Computer Demonstrations Applicability to you _	2	2	9 `	24	14	51	**3.90**
June 19	0	1	5	9	6	21	**3.95**
June 20	0	0	2	2	3	7	4.14
June 26	2	1	2	13	5	23	3.78

FDD WORKSHOP: CLEVELAND AND PERU PLAYS

October 17, 1996 **Bartlesville, OK**

DEMOGRAPHIC INFORMATION

Type of Company	Small independent	Major Producer	Service Co.	Govern-ment	Mid/Large Independent	Academ is	Con-sultant	Other	# of responses
TOTALS	13	0	0	1	1	0	2	2	19
Technical Background	**GeoVGeoph**	Engr	**Both**	Other					
TOTALS	15	1	0	3					19

I you learn about this workshop?

	TOTAL
mailing	**8**
other workshops	**3**
OGS	**2**
Friends/word of mouth	**3**

	1 (Poor)	2	3 (Avg.)	4	5 (Great)	# of **responses**	Aver age
Was this workshop useful?	0,	2	4	$	**5`**	19	3.84
	0	2	2	6	9	19	4.16

	1 (Poor)	2	3 (Avg.)	4	5 (Great)	# of responses	Aver age
Preconference **materials**	0	2	6	**6**	4	18	3.67
Registration process	0	0 ,	4	1	**14**	19	**4.53**
Presentation **facilities**	0	0 '	0:	**5**	14	19	4.74
Supplemental Materials	0	0	4	10	**5**	19	4.05
Breaks and lunch **arrangements**	0	0	3	**3**	13	19	**4.53**
Overall location	0	0	2	7	10	19	4.42

Please provide any suggestions or comments that you believe would help to improve these workshops.

- A great job as usual.
- 1 have rated all presentations as average. All presenters did an excellent job but presented very little that could be considered new. I found the Pleasant Mound Reservoir simulation to be most interesting from a content point of view.
- Field studies of more general interest, even though e. fogs, cores, etc. may not be available. Computer simulations are not helpful to average attendee.
- All of the presenters did a really good job, however I was left with the feeling that there is not a lot of future to these two reservoirs. Neither of the field studies were very economic, or was that the point?
- The seminar proved valuable by showing a zone which we always wondered about but never had time to map.
- Why Bartlesville location? It would seem that more might avail themselves to the workshop if in OKC & Tulsa primarily....1 have been to several workshops, but never in Tulsa...Are there facilities here? Also, I felt the Peru portion was practically a waste of time due to the lack of economic significance of this reservoir. Based on the presentation, I don't know many operators that would re-complete this zone, much less drill for it.
- Could have found some better Peru wells in Osage - Even made workovers behind pipe not feasible for Peru. Should have spent one day per zone study - Some old geologists never change.
- The "plays"presented were not commercially feasible.

- This was the poorest of the series. Previous workshops were better prepared & discussed in more detail. Overall the series has been great. Please keep the program expanding even into other geologic areas.
- Provide core analysis of cores on display and full log suite.
- I would like to see upcoming workshops held in Bartlesville again.
- Great facility - good for folks operating in central & NE Oklahoma.
- Wish all day on Cleveland!
- Core was very good - Could have used core analysis data & correlative core/log relationship quantification. Discussion of secondary projects needs more than 1 project, and info on what works, what are problems to be aware of, etc.

Do you see an opportunity to apply the information and/or technologies discussed in today's workshop? YES: 17 NO: 0

If so, what information and/or technologies?

- Log analysis by Bruce Carpenter contained a great deal of universal information that I have found useful.
- This workshop provided me with review of Cleveland and Peru sand information that I need for my present job.
- Watertood technology
- Overview of formations studied
- Bruce Carpenter's talk was very helpful in evaluating logs.
- The history matching at Pleasant Mound is deemed worthy of further investigation. Excellent program!!
- Extent of Cleveland production.
- Infield drilling on Cleveland sand leases - most studies say wont flood? I believe it will & has in some compartmental instances. As usual you guys & gals do an excellent job!
- Fluvial vs. marine
- Geological info will help in future prospecting
- Engineering reservoir simulations give insight into secondary recovery operations.
- Location of Clev. fields wrn whole depositional setting...as explanation for some probs. w/ low Rt, grain size (pore size) vs. perm. distribution - & need for core!

PRESENTATION DETAILS

	1 (Poor)	2	3 (Avg.)	4	5 (Great)	#of responses	Average
1. Mankin: Opening Remarks	0	0	**5**	7	6	18	4.06
2. Jock Campbell: Introduction to FDD Concepts	0	0	6	9	3	18	**3:83**
3. Jock Campbell: Cleveland Regional Overview	0	0	**5**	11	2	18	**3:83**
4. Kurt Rottmann: Pleasant Mound Field Study	0	1	6	9	2	18	3:67
5. Knapp & Yang: Pleasant Mound Reservoir Simulation	0	**5**	**4**	6	3	18	3.39
6. Robert Northcutt: Peru Regional Overview	1	4	7	4	1	17	3.11
7. Robert Northcutt: Hogshooter Field Study	1	4	**5**	6	0	16	3.11
8. Bruce Carpenter: Hogshooter Log Analysis	0	1	3	10	2	16	**3.81**
9. Core Exhibits	A	0	3	11	3	17	**4.00**
10. Computer Demonstrations	0	0	3	10	3	16	4.00

FDD WORKSHOP: RED FORK PLAY

March 5, 1997 — **Norman, OK**
March 12, 1997 — **Bartlesville, OK**

DEMOGRAPHIC INFORMATION

Type of Company	Small Independent	Major Producer	Service Co.	Govern-ment	Mid/Large Independent	Acad-ems	Con-sultant	Other	*#'of* **responses**
TOTALS	52	5	**5**	2	9	0	10	0	83
March **5**	24	3	3	1	6	0	4	0	41
March 12	28	2	2	1	3	0	6	0	42
Technical Background	**Geol/Geoph**	Engr	**Both**	Other					
TOTALS	56	12	**5**	9 _					**82**
March **5**	34	4	0	3					41
March 12	22	8	**5**	6					_ 41

How did you learn about this worksho[p]?

	March 5	**March 12**	**TOTAL**
mailing	**30**	**20**	**50**
company announcement	**1**	**1**	**2**
other workshops	**3**	**2**	**5**
OGS	**2**	**6**	**8**
OKC/Tulsa Gaol Soc.	**1**	**3**	**4**
Friends/word of mouth	**2**	**4**	**6**
Newspaper		**5**	**5**
Web page		**1**	1

OVERALL WORKSHOP EVALUATION

	1 (Poor)	2	3 (Avg.)	**4**	5 (Great)	# of responses	Aver **age**
Was this workshop useful?	0	0	2	44	36	82	4.41
March **5**	0	0	1	23	17	41	**4.39**
March 12	0	0	1	21	19	41	**4.44**
Was this workshop worth your time and money?	0	0	1	36	**45**	**82**	4.54
March **5**	0	0	1	21	19	41	**4.44**
March 12	0	0	0	_ 15	26	41	4.63

WORKSHOP AUXILIARY COMPONENTS

	1 (Poor)	2	3 (Avg.)	4	5 **(Great)**	# of **responses**	Aver **age**
Preconference materials	0	1 `	11	40	27	79	4.18
March **5**	0	1	**5**	20	**14**	40	**4.18**
March 12	0	0	6	20	13	**39**	**4.18**
Registration *process*	0	0	7	22	**54**	**83**	4.57
March **5**	0	0	5	11	25	41	**4.49**
March 12	0	0	2	11	**29**	**42**	**4.64**
Presentation facilities	0	0	0	17	**66**	83	**4.80**
March **5**	0	0	0	**5**	**36**	41	**4.88**
March 12	0	0	0	12	30	42	4.71
Supplemental Materials	**Q'**	0	**5**	**26**	52	83	4.57
March **5**	0	0	**4**	11	26	41	**4.54**
March 12	0	0	1	15	26	**42**	4.60
Breaks and lunch arrangements	0	1	**3**	25	**53**	82	**4.59**
March 5	0	0	2	9	30	41	4.68
March 12	0	1	1	16	23	41	**4.49**
Overall location	0	2	6	**34**	40	**82**	4.37
March **5**	0	1	2	11	26	40	**4.55**
March 12	0	1	**4**	23	14	42	**4.19**

Please provide any suggestions or comments that you believe would help to improve these workshops
March 5:

- Might be good to have more presentations from Redfork operators - I recall at Morrow workshop you had a couple of private companies give talks on their fields/3D etc. - which was excellent.
- Better directions/location within postal service center (i.e., building at far end, etc.)
- Would like to have seen one field study where the Red Fork was split into upper & lower members.
- Meeting facilities were good.
- OK is primarily a gas producer. Have similar programs on Red Fork gas reservoirs.
- As a small independent operator, I need technical support which is not available except to major companies.
- Continue program.
- Keep up the good work!
- Can you do additional field studies, such as Red Fork Play II?
- Need to do more for the low resistivity Redfork sand with high porosity, in say Lincoln Co.
- Too much time spent on production models. Reviewing one case and summary of variables is all that is needed because it is just a model! Shows quickly how well model matches data.
- Would like to see more workshops.
- Place logs along side of core samples.
- The Red Fork play is the best yet: Excellent slides, excellent food, excellent speakers.
- Keep up the good work.
- Add wireline log/core.
- The organization - management - & conduct of the workshop was outstanding.
- This entire series of FDD sessions has been superlative - keep them coming!
- Expand into gas producing areas. I would be very interested in an Ordovician Clastics study.
- Better directions to room location.
- Someday repeat the early workshops - Booch, etc. Many people missed the opportunity!
- Need a sign outside!
- More of them - other sand dep. environments & carbonates too! Also, a workshop on the application of Geology in Secondary (recovery) may help lots of operators who are interested in that type of development. Probably should include work in increased density drilling of "deeper"reservoirs and the compartmentalization of them - lots of potential here in Oklahoma.
- All of you have done incredible jobs in gathering and presenting data. I am amazed at how much work you have done.
- Field Studies? Any work on grain-size/perm. relationships & transition zones?

March 12:

- Keep using this facility.
- Excellent! Speaker should repeat aloud questions from the floor.
- From Tulsa - can't really complain, a very nice facility & setup. The price is obviously right too!
- Lobby **displays needed** more room.
- More field studies...the reservoir simulation wasn't of interest to me: too far from my geologic interest.
- The types of computer models are nebulous ᵍit best. I much preferred the waterflood presentation on the Morrow. (Actual **case** history.)
- Enjoyed photos at beginning, especially the surface outcroppings. I did purchase some OGS publications onsite.
- Given costs etc., Bartlesville is fine.
- More plays significant in Oklahoma, or potential plays.
- Workshop on intemet & NRIS resources.
- Would like workshop on Coal seam gas in Oklahoma. Other exploration methods, seismic, areomag, gravity, 3D seismic. Limestone reservoirs, deep Arbuckle, and other zones.
- More workshops on geological techniques and concepts. More workshops on other reservoirs and depositional environments.
- Excellent information, well compiled and presented at a most reasonable fee. Marvelous facility!
- I hate Phillips chairs tho the visibility in the room is excellent.
- Have them more often.
- Ask Amoco Research to cooperate!
- Rick Andrews' presentations were excellent.

Do you see an opportunity to apply the information and/or technologies discussed in today's

March **12: YES: 36 NO: 0**

If so, what information and/or technologies?

March 5:

- % recovery of OOIP with waterflood is striking.
- mapping facies distributions.
- Fluvial vs. Marine deposits.
- Use of API oil gravity to help identify different prod. facies
- Improve knowledge for exploration and future operations.
- Case/field studies for lease evaluation & "protection"
- Great info about application of waterflooding
- Locations of Red Fork sands and how they were developed
- Detailed field studies
- Water flood applications
- Better evaluation of reservoir geometry from aerial photo overview and field studies. Great job by Rick Andrews!
- Adds to my overall regional understanding of the Red Fork plays. How about a follow up workshop on deeper Anadarko Red Fork "tite"gas sands & fields.
- Gravity and facies analysis using it.
- The graphic materials give ideas and aid in recognizing the different depositional features, especially in conjunction with one another.
- Geologic framework for future prospects. Background info regarding reserves & anticipated secondary recovery.
- The study of fluvial dominated systems has changed my outlook on mapping the Cherokee - Made me money.
- We are presently putting in 2 Red Fork waterfloods in Grant & Alfalfa Co. Wish it had been 18 months earlier.
- Reconstructing depositional environments. Redevelopment of older fields. Playing off key wells to find new fields.
- This presentation provides me the incentive to revisit many of my Red Fork plays. By using the more subtle log variations, I should be able to extract more prospects.
- Have some basis to contour point bars with little (no) control.
- Field studies show potential for discoveries of additional hydrocarbon reservoirs.
- Reservoir compartmentalization effects on waterflooding
- Evaluation of reservoirs for secondary. Application of depositional environment to determination of infill/development foes.

March 12:

- E log signatures. Overall maps.
- Transverse vs. lateral permeability for additional drilling locations.
- Reservoir identification through logs
- Facies analyses
- All of it.
- The general interpretation & specific correlations.
- Geographic areas of Red Fork plays.
- Mainly exploration and water flood techniques.
- Red Fork - facies variations in the context of exploration and exploitation.
- Boast 3. Geological concepts.
- Cherokee sd. devel. in N. Okla.
- Environmental interpretation from E-log signatures.
- Identifying what type reservoir that we produce in.
- Secondary potential. General depositional info.
- Review logs in areas working.
- Strong background for consulting/prospect generation.

PRESENTATION DETAILS

	1 (Poor)	2	3 (Avg.)	4	5 (Great)	# of responses	Average
1. Mankin: Opening Remarks:	0	0	11	36	25	72	4.19
March 5	0	0	6	14	13	33	4.21
March 12	0	0	5	22	12	39	**4.18**
2.Andrews Intro to FDD:	0	0	4	31	**38**	73	4.47
March 5	0	0	3	13	17	33	**4.42**
March 12	0	0	1	18	21	40	**4.50**
3.Andrews: Red Fork stratigraphy/regional	0	0	1	30	43	74	**4.57**
March 5	0	0	1	13	20	**34**	**4.56**
March 12	0	0	0	17	23	40	**4.58**
4. Andrews: N. Carmen Field Study	0	0 '	5	28	39	72	**4.47**
March 5	0	0	1	14	19	**34**	**4.53**
March 12	0	0	4	14	20	**38**	**4.42**
5. Knapp &Yang: N. Carmen waterflood model:	1	5	15	26	**23**	70	**3.93**
March 5	0	1	8	11	14	**34**	4.12
March 12	1	4	7	15	9	36	**3.75**
6. Rottmann: Otoe City S. Field Study	0	0	15	36	22	73	4.10
March 5	0	0	7	16	11	**34**	4.12
March 12	0	0	8	20	11	39	**4.08**
7 **Andrews: Long Branch**	0	0	4	32	37	73	**4.45**
March 5	0	0	0	14	20	**34**	4.59
March 12	0	0	4	18	17	39	**4.33**
8. Core Exhibits	0 .	0	6	30	31	67	**4:37**
March 5	0	0	3	9	20	32	**4.53**
March 12	0	0	3	21	11	**35**	**4.23**
9. Computer Demonstrations	0	2	13	25	19	59	4.03
March 5	0	0	6	9	13	28	**4.25**
March 12	0	2	7	16	6	31	**3.84**

Footnotes based on comments written on the back page (by section number):

March 5:

1. OK
2. Aerial photos - excellent
   We all appreciate this segment & do not tire of it as perhaps you think.
   Good
3. Very good - Puts all else into perspective
4. Mapping of facies is good - Should describe characteristics of each zone separately, two types of"flow units". What are wells in "trend"to east/west?
5. Would be of interest to see economics.
   Need to work more closely with geologists; & operators - Also keep in mind dual perm of reservoir!
6. Fades mapping would be good - Any fracturing present? What was ultimate primary vs. secondary?
7. Nice study - Be careful w/ flood pettem! Enjoyed work on separate fades.
8. Great - Adjoining notes are helpful. This info is rare. Thanks.
9. Good - first exposure of many participants to availability and scope of information.

March 12:

1. Nice sum. of program's past & possible future.
2. Excellent photos
3. Exhibit "plates"will be very useful (no matter what depo environ interpretation one subscribes to!)
   Good discussion on controversies
4. Appreciate information on production response to waterflood
5. Thanks for metrics of secondary production estimated from 1997-2001.
   Torpedoed by bad electronics - normally very good presentations.
6. Core from the main field study area woulcl have been nice for interpretation.
8. Good! The vote was an interesting idea to get people to really look at
   core.

FDD WORKSHOP: TONKAWA PLAY

July 9, 1997 **Norman, OK**

DEMOGRAPHIC	INFORM								
Type of Company	Small Independent	Major Producer	Service Co.	Govern-ment	Mid/Large **Independent**	Mad-emia	Con-sultant	Other	# of responses
TOTALS	26	0	0	1	5	0	5	1	38
Technical Background	**Geol/Geoph**	Engr	Both	Other					
TOTALS	28	7	0	3					**38**

How did you learn about this workshop?

	TOTAL
mailing	**21**
other workshops	**6**
OGS	**5**
OKC Geol Library	**2**
Friends/word of mouth	**4**
Newspaper	1

OVERALL WORKSHOP EVALUATION	1 (Poor)	2	3 (Avg.)	**4**	5 (Great)	# of responses	Aver **age**
Was this workshop useful?	0	1 .	5	24	9	39	.4.05
Was this workshop worth your time and	0 `	1	3	19	16	39	4.28

WORKSHOP AUXILIARY COMPONENTS	1 (Poor)	2	3 (Avg.)	4	5 (Great)	# of responses	Aver age
Preconference materials	0	[illegible]	9	18	11	38	4.05
Registration process ,	1	0	1	11	26	39	**4:56**
Presentation facilities	1	0 -	0	**S**	30	39	4.69
Supplemental Materials	0	0	3`	19	17	39	4:36
Breaks and lunch arrangements	1	0	1	7	29	38	4.66
Overall location	1 '	1	3	9	**25**	39	4.44

Please provide any suggestions or comments that you believe would help to improve these workshops

- Try to extend this play into NE Texas Panhandle of Lipscomb & Ochiltree Counties
- Slides were great this time & tied with book. Cant really make any improvement suggestions. Keep up the good work.
- Good Job!
- More speakers on the correlation of depositional environment with log correlation.
- More field studies.
- Well economics. Tonkawa Play economics overall.
- 1) Analysis of water samples, i.e. RW's; 2) sem- x-ray analysis, i.e. clay contents; 3) any unusual log evaluations and/or what is best logging suite; 4) responses of reservoirs to stimulations (any damage problems?).
- More attention to slide quality. Overheads are hard to read. On technical material, try to pick strat. markers below the Tonkawa to use as datum, use shale markers not the top of the sand or limestone. Show porosity curves as well as induction curves.
- Obtain more data from operators, i.e. water production data, corrosion? gas quality? Also, field check these studies - view production equipment, disposal wells, casing problems, etc.
- This was one of the best workshops I have been to.
- Provide more (longer) breaks to allow people to go through displays and information.

- Discussion of problems common to Tonkawa production in Northwest Oklahoma gas play, e.g. low resistivity production and causes.
- 1) Please include slide show of the core so that we can at the breaks view the salient points. 2) Use this workshop to add facts in future Geology Notes or other publications: Example thin sections of key lithologies or core.
- I would have liked more information on the cores. What in the cores supports your interpretation of the depositional environment? How do the marine bar cores differ from the deltaic?.
- I appreciate the "down-to-earth"approach which makes workshops helpful to my engineering discipline and operations, not just academic geology.

Do you see an opportunity to apply the information and/or technologies discussed in today's workshop? YES: 35 NO: 0

If so, what information and/or technologies?

- In everyday drilling & completion activities in the Tonkawa formation.
- Currently working areas to the west of study.
- Suggestions by speaker as to how to map reservoir sands (i.e. using pessimistic cut-off for net picks) could be helpful in determining compartmentalization within reservoir!
- Better understanding of Tonkawa trend. Useful in further exploration.
- Log analysis correlated w/ production.
- Techniques for estimating depositional environment from mechanical log analysis.
- Interpretation of reservoir character as related to water flood potential.
- Depositional environment determinations
- The correct stratigraphy in sorting out true Tonkawa production. Fades analysis and core descriptions in lobby. Sand body orientations.
- Material presented by Kurt Rottmann.
- Will use regional info to help focus my efforts for detail work.
- Tonkawa production.
- FMI logs.
- Continuing plays into the basin and further TX Panhandle areas.
- General idea of environment of deposition
- Infill & offset potential in existing field based on facies trends.
- My company has 2 gas storage projects in the Tonkawa in N. OK for which the basic geology was very fundamental for understanding of additional development w/ multiple lenses, etc..

PRESENTATION DETAILS	1 (Poor)	2	3 (Avg.)	4	5 (Great)	# of responses	Average
1. Mankin: Opening Remarks:	0	0	8	17	9	34	**4.03**
2. Campbell: Intro to FDD:	0	/	9	18	6	34	**3:85**
3. Campbell: Tonkawa FDD regional overview:	0``	1	12	14		**34**	**3.79**
4. Rottmann: Blackwell Field Study	0-	0	1	19	14	**34**	**4.38**
5. Knapp, Samad & Xie: Blackwell Simulation	0		14	14	3	34	**3.50**
6. Hinshaw: Tonkawa Anadarko Regional Overview	0	1	7	16	10	**34**	**4.03**
7. Rottmann: WaynokaNE Field Study	0`	0	1	18	13	32	**4.38**
8. Core Exhibits	0 `	0	6	19	9	**34**	**4.09**
9. Computer Demonstrations	0	1	10	15	4	30	**3.73**

Footnotes based on comments written on the back page (by section number): 1.
Some colors don't show up well on overheads.

FDD WORKSHOP: BARTLESVILLE PLAY

October 29, 1997 — **Tulsa, OK**
October 30, 1997 — **Bartlesville, OK**
November 12, 1997 — **Norman, OK**

DEMOGRAPHIC INFORMATION

Type of Company	**Small Independent**	Major Producer	Service Co	Govern-ment	Mid/Large **Independent**	Acad-**emia**	Con-sultant	Other	# of responses
TOTALS	46	0	1; `	5	5	1	10	3	71
October 29	22	0	0	5	2	0	5	0	34
October 30	7	0	0	0	0	0	3	0	10
November 12	17	0	1	0	3	1	2	3	27
Technical Background	**GeoVGeoph**	Engr	Both	Other					
TOTALS	47	12	6	7					72
October 29	20	4	4	6					**34**
October 30	7	2	0	1					10
November 12	20	6	2	0					28

How did you learn about this workshop?

	October 29	**October 30**	**November 12**	**TOTAL**
mailing	**26**	**6**	**13**	**45**
other workshops	**6**	**3**	**6**	**15**
OGS	**3**	**0**	**5**	**8**
TGS	**3**	**0**	**0**	**3**
OKC Geol Library	**0**	**0**	**1**	**1**
Friends/word of mouth	**1**	**1**	**2**	**4**
Newspaper	**0**	**1**	**0**	**1**

OVERALL WORKSHOP EVALUATION

	1 (Poor)	2	**3** (Avg.)	**4**	**5** (Great)	*# of* responses	Aver **age**
Was this **workshop useful?**	0	0 ',	7	**38**	**25**	70	4.26
October 29	0	0	4	18	10	32	4.19
October 30	0	0	1	3	6	10	4.50
November 12	0	0	2	17	9	28	4.25
Was this **workshop** worth **your** time **and money?**	0	0	5	31	35	71	**4.42**
October 29	0	0	4	16	13	**33**	4.27
October 30	0	0	0	2	8	10	4.80
November 12	0	0	1	13	14	28	4.46

WORKSHOP AUXILIARY COMPONENTS

	1 (Poor)	2	**3** (Avg.)	**4**	**5 (Great)**	*# of* responses	Aver **age**
Preconference materials	**0**	0	12	30	27	69	**4.22**
October 29	0	0	9	12	11	32	**4.06**
October 30	0	0	1	5	3	9	4.22
November 12	0	0	2	13	13	28	4.39
Registration process	**0**	0	2	23	46	71	4.62
October 29	0	0	2	11	20	**33**	**4.55**
October 30	0	0	0	2	8	10	4.80
November 12	0	0	0	10	18	28	4.64
Presentation facilities	**0**	0	3	19	49	71	4.65
October 29	0	0	3	14	16	33	4.39
October 30	0	0	0	0	10	10	5.00
November 12	0	0	0	5	23	28	4.82

Supplemental Materials	0	0	4	33	32	69	4.41
October 29	0	0	3	20	8	31	4.16
October 30	0	0	0	**4**	6	10	4.60
November 12	0	0	1	9	18	28	4.61
Breaks and lunch arrangements	2	9	9	14	36	70	**4.04**
October 29	2	9	8	6	7	32	3.22
October 30	0	0	1	1	8	10	4.70
November 12	0	0	0	7	21	28	**4.75**
Overall location	0	2	12	20	37	71	**4.30**
October 29	0	2	10	13	**8**	33	3.82
October 30	0	0	0	0	10	10	5.00
November 12	0	0	2	7	19	28	4.61

Please provide any suggestions or comments that you believe would help to improve these workshops

October 29:

- Lunch outdoors on a cool windy day...otherwise"4':
- Please do Hunton, Viola, Simpson, & Arbuckle workshops.
- Need Gamma Ray of outcrop to compare to CSR of core. Purchase a hand-held Gamma Ray Tool to measure the weathered response of the rocks that crop out. In this manner your photos of the outcrops are meaningful to us who look at your cores and logs. Keep up the excellent core photos in the guidebook. I would send out these core photos with promotion on the school or at least to those who are registered. Expand core photos to **all** major Rh/environments. In this manner an operator will buy your guidebook for the core that is in his garage.
- When you have a seminar this late in the year, don't arrange to have lunch outdoors.
- Get preconference materials out earlier to help with planning. Move along more quickly - leaving more time for questions/discussion. Work the operators for the data ...too much is never reported via state records. Roy Knapp (& others) - include some economics in these studies.... Don't worry if your **#'s** are inexact, but do make some financial evaluation!
- Use more non technical language.
- Rather than reduce the number of projects in the future (due to loss of funding) I would reduce the amenities (break food & beverages).
- Do a workshop on strat-trap reservoirs.
- Good food, poor conditions for lunch. How about other seminars on 1. NRIS, 2. Seismic for really small operators, 3. Mississipian, Devonian, (older formations), 4. computer software applications for small operators, i.e. reservoir simulator usage, contour & isopach mapping.
- Great job! Can we something on the Arbuckle, or deeper potential below old eastern Oklahoma oil fields?

, More data on understanding seismic data. Seminar on Misener/Simpson Series etc.

- Don't have lunch outside. I was disappointed that there was not much concentration on a wide variety of B-ville producers in the heart of the Bartlesville through big producing areas such as Creek Co.
- Excellent - good planning. Possibly different type lunch, but not complaining. Appreciate these workshops.
- Almost perfect! Don't change the format.
- Very good meeting - thanks so much!
- I would like to see similar workshop like this for the Mississippi Lm in c. Oklahoma.

October 30:

- Don't Stop.
- Your continuation, even at more conservative pace, would be helpful - Suggested topics of Mw/Spr, Deep Red Fork, & Arkoma basins would be helpful.
- Continue the "excellent"work.
- Closer interfingering of publication figures with slides presented with lectures.
- Would really like to see a regional workshop on Mississippian Rocks for central and eastern Oklahoma.

November 12:

- Case studies of completed, successful, secondary recovery projects.
- This is really hard to improve and I'm serious. Keep up the good work. As a taxpayer - this is money well spent.
- Maybe more emphasis on larger fields and/or infill drilling opportunities.
- Onward to Carbonates!
- Chester limestone in northwest Oklahoma - porosity types/systems - stratigraphic complexities.
- Field Trips. Proper completion techniques for a given reservoir.
- Do a field trip in conjunction with the workshop.
- Very impressive, "user friendly"environment for conferences; presenters were well prepared - good job!

Do you see an opportunity to apply the information and/or technologies discussed in today's workshop?

October 29:	YES: 29	NO: 1
October 30:	YES: 9	NO: 0
November 12:	YES: 20	NO: 0

If so, what information and/or technologies?

October 29:

- Analogous comparisons...reinforcement of general information from previous FDD's too.
- Log correlations & environments in the type log & x-section displays. Each time I attend one of these I hear something a little differently and thus re-think the previous schools.
- This was helpful in using facies to predict where to drill the next well. The facies mapping can be applied to other similar formations.
- Waterflooding in small fields - but need some economic evaluation of various case studies...Possibility of using 2-D seismic for stratigraphic boundary interpretation.
- Log signature interpretation in determination of facies within an environment of deposition, mapping style, etc.
- Environmental facies recognition.
- Regional facies interpretation into a depositional model.
- Utilize data that is available to review old areas. .
- Mapping and prospecting for Bartlesville Sand.
- Ideas about how to prospect for Bartlesville sand.
- Point bar deliveation in more detail.
- Be alert to low rt values in prod. Bartlesville sands. Use of log characteristics to define depositional environments.
- More familiar w/fluvial log signatures
- Assist in regulating lease provisions on drainage, diligent development.
- General interpretation of localized depositions.

October 30:

- Analysis of individual sands on log to better define what is happening in the B'ville and to refine beyond isopach/structural trends.
- Will request one operator to assign shut-in leases.
- All.
- Exploration methods.
- Should be helpful in tracking channel sands of all formations, not limited to Bartlesville.
- 1.) The use of well log character in determining depositional environment. 2.) the regional Bartlesville depositional map and direction of deposition.
- Starting new water floods.

November 12:

- Differentiation of sand developments within the usual depositional environment.
- Information from production that confirms barriers mapped and interpreted on environments from log data that encourages the use of such interpretations to design flood programs.
- Seismic stratigraphy application to sand prediction.
- Potential waterflood project.
- Facies signatures on electric logs.
- Geo information systems - water quality, shallow aquifers - enjoyed visit w/Mary Banken (GIS).

PRESENTATION DETAILS	1 (Poor)	2	3 (Avg.)	4	5 (Great)	# of responses	Average
1.Mankin: Opening Remarks:	0	0	10	**33**	23	66	4.20
October 29	0	0	6	12	14	32	4.25
October 30	0	0	1	6	2	9	4.11
November 12	0	0	3	15	7	25	4.16
2. Northcutt: Intro to FDD:	0	2	17	29	18	66	3.95
October 29	0	1	9	15	7	32	3.88
October 30	0	0	2	3	**4**	9	4.22
November 12	0	1	6	11	7	25	3.96
3. Northcutt: Bartlesville regional overview:	f	1	15	**33**	16	66	3.94
October 29	1	0	10	15	6	32	3.78
October 30	0	0	1	**4**	**4**	9	**4.33**
November 12	0	1	**4**	14	6	25	4.00
4. Andrews: Paradise Field Study	0;	0	**5**	30	31	66	4.39
October 29	0	0	**4**	14	14	32	4.31
October 30	0	0	0	2	7	9	4.78
November 12	0	0	1	14	10	25	4.36
5. Knapp et al.: Paradise Waterflood Model:	0	**3**	20	30	11	64	3:77
October 29	0	2	12	14	3	31	**3.58**
October 30	0	0	2	**3**	**3**	**8**	4.13
November 12	0	1	6	**13**	**5**	25	**3.88**
6. Andrews: Russell NW Field Study	0	1	**8**	32	24	**65**	4.22
October 29	0	1	6	**14**	10	31	4.06
October 30	0	0	1	3	**5**	9	**4.44**
November 12	0	0	1	15	9	25	4.32
7. **Riepl: Seismic Stratiaraphv**	0	4	20	28	14	66	3.79
October 29	0	4	12	12	**4**	32	3.50
October 30	0	0	2	**5**	2	9	4.00
November 12	0	0	6	11	8	25	4.08
8. Campbell: Ohio-Osage Field Study	0	1	19	23	11	54	3.81
October 29	0	1	9	12	6	28	3.82
October 30	0	0	1	4	1	6	4.00
November 12	0	0	9	7	**4**	20	3.75
9. Core Exhibits	0'	0	6 '	31	18	**55**	4:22
October 29	0	0	**5**	16	7	28	4.07
October 30	0	0	0	**5**	2	7	4.29
November 12	0	0	1	10	9	20	4.40
10. Computer Demonstrations	1	0	9	21	15	**45**	4:04
October 29	0	0	**5**	12	**4**	21	**3.95**
October 30	1	0	1	1	2	**5**	3.60
November 12	0	0	3	8	9	19	4.26

Footnotes based on comments written on the back page:

- Smoking in DoD facilities has been limited since the late 80's. The recent exec. order was to move the cloud of cigarette smoke away from the entrances where the non-smokers would have to"hack"their way through the smoky maze, scrum, huddle, etc.
- *re Northcutt Intro to FDD:* Seems rambling. *re Andrews Paradise field study:* Did better w/ Red Fork study. re *Knapp:* No economics, No explanation of problems. *re Andrews* Russell *NW field study:* Stick to interpretations - too much talk here on "maybe this, but maybe not..." *overall:* Maybe I'm being a bit harsh on presenters, but I feel they have done, and really can do a better job of this - Move along, be enthusiastic and don't try to be funny - State the interpretation and invite discussion.
- *re Riepl Seismic* Stratigraphy: He didn't convince me of the correlation between his amplitude anomaly and Bartlesville sand quality.
- *re Robert summary:* rates a 5 (Great)
- *re Northcutt Bartlesville Regional Overview:* presented fine - regional data is poorest of any workshop.
- *re Northcutt Intro* to *FDD:* slides good. *re Supplemental Materials:* Need more time allotted - room was full!
- 300 MBO historically & these were the 2 fields chosen to be studied?

FOSSIL ENERGY

DOE/BC/14951-26
(OSTI ID: 13821)

INTEGRATED APPROACH TOWARDS THE APPLICATION OF HORIZONTAL WELLS TO IMPROVE WATERFLOODING PERFORMANCE

Final Report
January 1, 1993-August 31, 1999

By:
Mohan Kelkar
Chris Liner
Dennis Kerr

Date Published: October 1999

Work Performed Under Contract No. DE-FC22-93BC14951

The University of Tulsa
Tulsa, Oklahoma

National Energy Technology Laboratory
National Petroleum Technology Office
U.S. DEPARTMENT OF ENERGY
Tulsa, Oklahoma

DISCLAIMER

This report was prepared as an account of work sponsored by an agency of the United States Government. Neither the United States Government nor any agency thereof, nor any of their employees, makes any warranty, expressed or implied, or assumes any legal liability or responsibility for the accuracy, completeness, or usefulness of any information, apparatus, product, or process disclosed, or represents that its use would not infringe privately owned rights. Reference herein to any specific commercial product, process, or service by trade name, trademark, manufacturer, or otherwise does not necessarily constitute or imply its endorsement, recommendation, or favoring by the United States Government or any agency thereof. The views and opinions of authors expressed herein do not necessarily state or reflect those of the United States Government.

This report has been reproduced directly from the best available copy.

DOE/BC/14951-26
Distribution Category UC-122

Integrated Approach Towards the Application of Horizontal Wells to Improve Waterflooding Performance

By
Mohan Kelkar
Chris Liner
Dennis Kerr

October 1999

Work Performed Under DE-FC22-93BC14951

Prepared for
U.S. Department of Energy
Assistant Secretary for Fossil Energy

Dan Ferguson, Project Manager
National Petroleum Technology Office
P.O. Box 3628
Tulsa, OK 74101

Prepared by
The University of Tulsa
Tulsa, OK 74104

TABLE OF CONTENTS

TABLE OF CONTENTS ii

LIST OF ILLUSTRATIONS iv

LIST OF TABLES xi

DISCLAIMER xii

ACKNOWLEDGMENT xiii

ABSTRACT xiv

EXECUTIVE SUMMARY xvi

INTRODUCTION 1

BACKGROUND 2

BUDGET PERIOD I 10

INTRODUCTION 10
SELF UNIT 10
GEOLOGICAL FACIES ARCHITECTURE 19
Facies and Subfacies Elements *20*
Discrete Genetic Interval (Parasequence) Elements *29*
Systems Tracts and Sequence Stratigraphic Elements *31*
Petrophysical Properties and Architectural Elements *32*
Structure Southeast Side of Glenn Pool Field *34*
GEOPHYSICAL ANALYSIS 35
Introduction *35*
Data Processing *38*
Interpretation and Integration *39*
Crosswell Seismic Test *39*
Tomograms and Interpretation *47*
Anisotropic Ray Tracing *53*
3-D Seismic *53*
GEOSTATISTICAL MODELING 54
Multiple-Attributes Simulation *54*

FLOW SIMULATION 69
Deterministic Model *69*
Stochastic Model without Tomography Information *86*
Stochastic Model with Tomography Information *99*
Reservoir Management *111*
IMPLEMENTATION OF RESERVOIR MANAGEMENT PLAN 130
Recommendations *130*
Field Implementation - Problems and Solutions *130*
Results *131*
Economic Evaluation *132*
EVALUATION OF VARIOUS TECHNOLOGIES 133
Integrated Approach *133*
Cross Borehole Tomography *133*
Formation Micro-Resistivity Borehole Imaging *134*
Discrete Genetic Interval (DGI) Evaluation *134*
Geostatistics *135*
Flow Simulation *135*

BUDGET PERIOD II 137

INTRODUCTION 137
DATA COLLECTION 137
GEOLOGICAL ANALYSIS 143
ENGINEERING EVALUATION 153
Introduction *153*
Screening Test for High Potential Areas *154*
Evaluation of Production Information *158*
Chevron's Micellar-Polymer Unit *163*
Tract 9 Evaluation *169*
Tract 7 Evaluation *185*
FIELD IMPLEMENTATION 198

TECHNOLOGY TRANSFER ACTIVITIES 204

PUBLICATIONS AND PRESENTATIONS 204
TECHNOLOGY TRANSFER WORKSHOPS 207
NEWSLETTERS 208

REFERENCES 209

LIST OF ILLUSTRATIONS

Figure 1 – Location of Glenn Pool field 3

Figure 2 – Stratigraphic location of Bartlesville sandstone 7

Figure 3 – Marker beds for Glenn Pool field 8

Figure 4 – Self-unit location 11

Figure 5 – Well locations 13

Figure 6 – Production history of Self-unit 17

Figure 7 - Self-82 log with stratigraphic units and core oil-staining observations 20

Figure 8 – Self-82 core description of DGI F braided channel-fill facies 22

Figure 9 – Self-82 core description of DGI C meandering channel-fill facies 24

Figure 10 - Microresistivity borehole image for meandering channel-fill facies of DGI C 27

Figure 11 – Self-82 core description of DGI D splay facies 28

Figure 12 – Cross-section through Self-82 well showing discrete genetic intervals and facies 30

Figure 13 – Permeability vs. porosity from core plug measurements in Self-82 32

Figure 14 - Vertical permeability vs. horizontal permeability from core plug measurements in Self-82 33

Figure 15 – Map and shooting schedule for crosswell seismic data acquisition 40

Figure 16 – Photo of source and some characteristics 41

Figure 17 – Photo of receiver and some characteristics 42

Figure 18 – Details of shooting geometry for the test survey 43

Figure 19 – Comparison of 63-82 tomograms processed by Memorial Univerity and software from the U.S. Bureau of Mines 49

Figure 20 – Comparison of MUN and Amoco tomograms 50

Figure 21 – Comparison of MUN and The University of Tulsa tomograms 50

Figure 22 – MUN tomogram and zoom of Glenn interval with interpreted sand body 51

Figure 23 – Detailed stratigraphic interpretation 52

Figure 24 – The tomogram interpretation (left) compared to the geological model (right) 52

Figure 25 - Schematic diagram of the co-simulation technique 55

Figure 26 - Conditional distribution procedure for porosity 57

Figure 27 - Example of the use of conditional distribution technique in porosity simulation 58

Figure 28 - Conditional distribution technique for permeability 59

Figure 29 - Geologist's interpretation of facies distribution in the vicinity of track-7 62

Figure 30 - Multiple realization of facies distribution of DGI A - track 7 unit 63

Figure 31 - Global PDF comparison between simulation and data for all realizations 64

Figure 32 - Porosity and permeability distribution of DGI A for track 7 unit from one of the realization. Permeability is sampled using random sampling 65

Figure 33 - Computation time comparison for different grid block configurations and different number of realizations 66

Figure 34 – 3-D view of DGI distribution of the Self-unit data. 67

Figure 35 – 3-D view of porosity distribution of the Self-unit data. 68

Figure 36 – 3-D view of permeability distribution of the Self-unit data. 68

Figure 37 – Deterministic north-south and east-west sand cross section 71

Figure 38 - Deterministic - sand thickness well 43 and 37 72

Figure 39 – East west porosity cross section – deterministic model 74

Figure 40 - Porosity comparison at Self-82 75

Figure 41 – North-south permeability cross section – deterministic model 77

Figure 42 – Permeability comparison at Self-82 – deterministic model....78

Figure 43 – Permeability thickness product (kh) comparison – deterministic model....79

Figure 44 – Initial potential comparison – deterministic model....81

Figure 45 – Field oil production rate (FOPR) – deterministic model....82

Figure 46 – Original oil in place estimation – deterministic model....83

Figure 47 – Simulated field water cut – deterministic model....84

Figure 48 – Oil saturation comparison at Self-82 – deterministic model....85

Figure 49a - DGI comparison at well no. 43 - DGI model....87

Figure 49b - DGI comparison at well no. 37 - DGI model....87

Figure 50 - Porosity comparison at Self-82 - DGI model....88

Figure 51 - Permeability distribution – north-south cross section - DGI model....90

Figure 52 – Permeability comparison at Self-82 – stochastic model....91

Figure 53 – Permeability – thickness (kh) comparison – stochastic model....92

Figure 54 – Initial potential comparison – stochastic model....94

Figure 55 – Field oil production rate comparison – stochastic model....95

Figure 56 – Original oil in place (FOIP) and cumulative oil production (FOPT) at 1946 comparison – stochastic and deterministic models....96

Figure 57 – Field water cut prediction for stochastic and deterministic models....97

Figure 58 – Oil saturation comparison at Self-82 – stochastic and deterministic models....98

Figure 58 - Porosity distribution at tomogram panels after applying the correlations....101

Figure 59a – Horizontal porosity variogram of the tomogram data (DGI's B and D)....103

Figure 59b – Horizontal porosity variogram of the tomogram data (DGI's B and D)....103

Figure 60 – Porosity comparison at Self-82 104

Figure 61 – Permeability comparison at Self-82 106

Figure 62 – Permeability – thickness (kh) product comparison – all models 107

Figure 63 - Comparison of field oil production rate (FORP) – all models 108

Figure 64 – Comparison of original oil production rate (FOIP) and cumulative production at 1946 for different models 108

Figure 65 – Comparison of field water cut – all models 109

Figure 66 – Comparison of oil saturation at Self-82 – all models 110

Figure 67 - Increase of oil production using scenario 1A 115

Figure 68 - Increase of oil production using scenario 1B 115

Figure 69 - Increase of oil production using scenario 1C 116

Figure 70 - Increase of oil production using scenario 1D 116

Figure 71 - Increase of oil production using scenario 1E 117

Figure 72 – Comparison of additional oil production – all models 118

Figure 73 - Increase of oil production using scenario 2A 119

Figure 74 - Increase of oil production using scenario 2B 120

Figure 75 - Increase of oil production using scenario 2C 121

Figure 76 - Increase of oil production using scenario 2D 121

Figure 77 - Increase of oil production using scenario 2E 122

Figure 78 – Increase of oil production using scenario 3A 123

Figure 79 – Increase of oil production using scenario 3B 124

Figure 80 – Rate of return estimation for different case study stochastic model without tomography information 125

Figure 81 – Pay out time estimation for different cases stochastic model without tomography information 126

Figure 82 - Rate of return estimation for higher operating cost - DGI model 127

Figure 83 - The effect of oil price - scenario 1D - DGI model....128

Figure 84 - ROR and pay out time comparison for different models 129

Figure 85 – Results of field implementation 132

Figure 86 – Index map showing the locations of six cross sections constructed 139

Figure 87 - Area of concentration....140

Figure 88 - Expanded coverage of core and log data....141

Figure 89 – Data availability within section 16 and surrounding areas 142

Figure 90 – A sketch map showing the general stratal relationship from Self-unit to tract 7 (figure not drawn to scale; thickness variation of each DGI is not shown)....144

Figure 91 – Shale thickness between DGI D and E....147

Figure 92 – Core oil saturation (%) profile (Chevron's micellar-polymer unit)....151

Figure 93 – DGI A map for the area of interest....152

Figure 94 – Average net/gross ratio determined from 120 logs 153

Figure 95 – Potential index map for DGI C and cumulative index map for DGI A-E....157

Figure 96 – Raw production data overlain with extrapolated data....160

Figure 97 – W/P and G/P ratios for tracts 1-18 and micellar-polymer unit 161

Figure 98 – Total oil (primary + secondary) recovered as % of OOIP (all tracts + Chevron's micellar-polymer unit)....163

Figure 99 - (a) Completion practices in the Chevron unit. (b) Completion practices in section 16 and tract 9....165

Figure 100 – WOR and oil production response of the Chevron unit 166

Figure 101 – Sample porosity and permeability areal profiles 167

Figure 102 – WOR and field oil production plots for the Chevron unit.....168

Figure 103 – Production analysis plot for tract 9 showing the primary gas injection and water flooding stages of depletion.....169

Figure 104 – Gamma ray versus core porosity correlation developed from the data compiled from Self-82.....171

Figure 105 – Composite diagram showing areal maps of porosity, permeability and thickness honoring the facies distribution.....173

Figure 106 – Areal reservoir pressure map that is tied to DGI E in psi.....175

Figure 107 – Well base map of existing/proposed wells for tract 9 176

Figure 108 – Oil production and water cut plot for scenario plug/recomplete all wells 178

Figure 109- Proposed well base map with multilateral well locations.....179

Figure 110 – Well locations of the existing/proposed wells along with a sample potential index map.....181

Figure 111 – Oil production and the water cut plot for ancillary scenarios.....182

Figure 112 – ROR histogram with sensitivity on oil price.....183

Figure 113 – Rate of return and net present value charts for ancillary scenarios 184

Figure 114 – Well map for tract 7 185

Figure 115 – Shift in pdf to align gamma ray probability distribution functions.....187

Figure 116 – Gamma ray versus porosity relationship.....188

Figure 117 – Histogram of perforations in tract 7.....192

Figure 118 – Oil production and water cut plot for scenario with $S_w \times 1.2$ 193

Figure 119 – Oil production and water cut for scenario with $S_w \times 1.4$ 195

Figure 120 – Rate of return and net present value charts for tract 7 197

Figure 121 - Proposed management plan for tract 9 199

Figure 122 - Profile of a deviated hole 200

Figure 123 - Direction of a deviated hole 201

LIST OF TABLES

Table 1 – Historical Information on Self-unit 14

Table 2 – Properties of tomography software used in this project.....41

Table 3 - Case definition used in flow simulation.....82

Table 4 - Definition of sub-scenario used in future production forecast.....113

Table 5 - Vertical separation condition, tract 7 and adjacent area 148

Table 6 - Comparison of core porosity and permeability between Self-unit and tract 7 area 149

Table 7 - Oil in place estimates 162

Table 8 – Comparison of miceller-polymer versus conventional waterflood.....168

DISCLAIMER

This report was prepared as an account of work sponsored by an agency of the United States Government. Neither the United States Government nor any agency thereof, nor any of their employees, makes any warrant, expressed or implied, or assumes any legal liability or responsibility for the accuracy, completeness, or usefulness of any information, apparatus product, or process disclosed, or represents that its use would not infringe privately owned rights. Reference herein to any specific commercial product, process, or service by trade name, trademark, manufacturer, or otherwise does not necessarily constitute or imply its endorsement, recommendation, or favoring by the United States Government or any agency thereof. The views and opinions of authors expressed herein do not necessarily state or reflect those of the United States Government or any agency thereof.

ACKNOWLEDGMENT

The research effort described in this report was supported by the U.S. Department of Energy under Contract DE-FC22-93BC14951. Additional support is provided by Amoco Production Company and Uplands Resources, Inc. The computer facilities were provided by the University of Tulsa.

We would like to thank Dan Richmond from Uplands Resources, Inc. for his valuable contribution and insight to our work. We also would like to acknowledge the guidance provided by Rich Chambers, Henry Tan, John Eager and Chandra Rai from Amoco Production Co. Lastly, our special thanks go to Rhonda Lindsey and Dan Ferguson from the Department of Energy for their enthusiasm and valuable suggestions.

September, 1999

Mohan Kelkar

ABSTRACT

This final report describes the progress during the six years of the project on "Integrated Approach Towards the Application of Horizontal Wells to Improve Waterflooding Performance." This project was funded under the Department of Energy's Class I program which is targeted towards improving the reservoir performance of mature oil fields located in fluvial-dominated deltaic deposits. The project involved an integrated approach to characterize the reservoir followed by drilling of horizontal injection wells to improve production performance.

The project is divided into two budget periods. In the first budget period, many modern technologies were used to develop a detailed reservoir management plan; whereas, in the second budget period, conventional data was used to develop a reservoir management plan. The idea was to determine the cost effectiveness of various technologies in improving the performance of mature oil fields.

In the first budget period, we applied several new technologies. These included integrated approach, use of cross borehole tomography, detailed geological analysis using micro-resistivity logs, facies biased mapping of sands using a concept of discrete genetic intervals (DGI), geostatistics and flow simulation. Out of these technologies, integrated approach, geological description using DGI's, geostatistics and flow simulation proved to be very effective. The other two technologies – cross borehole tomography and micro-resistivity logs – were not effective because of either the cost and/or uncertainties in application of these technologies.

The field implementation at the end of the first budget period resulted in significant increase in oil production. More important, our predictions matched very well with the observed performance.

In the second budget period, we concentrated on using conventional data to develop a detailed reservoir description. We used the existing well core and log data as well as production data to develop reservoir description. We continued to use technologies which were proven to be effective in the first budget period – namely, use of DGI's to describe geology, geostatistics and flow simulation.

Based on the evaluation of conventional data, we proposed drilling a deviated well using surface steered drilling assembly. Unfortunately, due to problem during drilling, the well had to be abandoned. We, therefore, never had the opportunity to test our reservoir management plan in the second budget period. Based on the experience during the first budget period, we are confident that we would have been able to improve the performance had the well been successful.

To compliment our technical effort, we also conducted vigorous technology transfer activities. These included publications and presentations at various technical meetings and journals, conducting technology transfer workshops for small operators and independents, and publishing two newsletters for interested audience. These activities resulted in reaching a wide cross section of audience, and making the operators aware about technologies that can help them in the future.

EXECUTIVE SUMMARY

This final report discusses the various approaches used in attempting to improve the performance of mature oil field. The results of the implementation and the lessons learned from the implementation are also included in the report. The field selected for the implementation is Glenn Pool oil field, which has been producing for more than 90 years. Overall, the technologies that proved to be effective include integrated approach to describe reservoirs, geological description using Discrete Genetic Intervals (DGI's), ranking of reservoir using productivity index mapping, geostatistics and flow simulation. The technologies which proved to be only marginally effective or ineffective include: use of micro-resistivity logs for detailed geological description, cross borehole tomography and drilling of deviated hole using surface steered drilling assembly.

The first budget period of the project focused on the Self-unit, a 160-acre tract of Glenn Pool field operated by Uplands Resources, Inc. The data available from the unit were wireline logs and core reports, and historical production records. Using log and core data, the reservoir was first divided into seven DGI's, each composed of contiguous facies deposited during a limited, discrete increment of time. Based on the preliminary geological evaluation, a test well (Self-82) was drilled and cored. Additional log data including micro-resistivity log (Formation Microscanner Imaging) data were collected from the same well. Using this well as a source well, three cross borehole tomography surveys were conducted between Self-82 and the surrounding three wells. With the help of a modified geological description as well as geophysical and engineering data, a detailed reservoir description was constructed. After validating the description by comparing the simulated flow performance with the historical data, several operating scenarios were simulated to optimize the flow performance under modified conditions. A combination of recompletion and stimulation of most wells followed by increasing the water injection rate in the field was observed to be the most optimal change to improve the flow performance of the Self-unit.

The proposed reservoir management plan was implemented, and the unit performance was monitored for over three years. At the base level, the Self-unit was producing between 15 to 17 bbls/day. The initial increase in the incremental oil production was predicted to be in the range of 18 to 21 bbls/day.

The actual increase was 21 bbls/day. After 3 years, the incremental increase was predicted to be about 10 to 12 bbls/day. Currently, the field is producing 10 incremental bbls of oil per day over its base rate. In short, we were able to correctly predict the performance of the reservoir. Although in terms of actual production, this increase is not much, note that it still represents about 150% increase in the production rate. Further, the field is more than 90 years old, and has been subjected to many technologies in the past. If we can cost effectively increase production from such a mature field, we would be able to do better in other, relatively younger, fields. The economic evaluation indicated finding cost of oil is in the range of $4.50 to $6.00 per barrel. This cost can be reduced substantially if we only use the cost-effective technologies and eliminate the use of other technologies.

The effectiveness of technologies applied during the first budget period was critically examined. The use of integrated approach in developing reservoir description was found to be very useful. By combining various disciplines, we were better able to identify the uncertainties in reservoir description as well as were better able to understand the importance of most relevant scales in describing the reservoirs. The use of DGI's was helpful in identifying the intervals where the remaining oil is most likely located. Geostatistics helped us in developing tools that were capable of integrating various types of data, and quantifying uncertainties in the description. Flow simulation allowed us to evaluate various scenarios in determining an appropriate reservoir management plan. On the other hand, use of micro-resistivity logs did not add significantly more information compared to the actual core. For shallow, marginal reservoirs like Glenn Pool, the use of micro-resistivity logs was not very effective. The cross borehole imaging was expensive, and resulted in images that were dependent on the algorithm used to process the data. The cross borehole technology is relatively new, and technical uncertainties in the evaluation simply do not allow us to use the technology on a routine basis in a cost-effective manner.

For the second budget period of the project, we expanded the scope to other parts of the Glenn Pool field. Unlike the first budget period, we did not collect any new data during this period. Instead, we concentrated on using the existing data to develop a detailed reservoir description. We evaluated the entire area operated by Uplands Resources for the second budget period. In addition, we also evaluated an adjacent unit, which used to be operated by Chevron. The Chevron miceller-polymer unit

was successfully flooded in early 80's using miceller-polymer flood. We wanted to understand the reasons for the success.

Since it was difficult to study all parts of the reservoir in great details, we graded the reservoir based on a method of potential index mapping. This mapping involves evaluating various areas in the reservoir based on the permeability, thickness, porosity, saturation as well as prior access to that area by already existing wells. In addition to potential index mapping, we also examined the primary and secondary recovery production from various units. Based on the grading of various parts of the reservoir, we decided to concentrate on tracts 7 and 9.

We began our evaluation by studying the Chevron unit. Our evaluation indicated that the success of the Chevron unit could be partly attributed to re-completion of the upper intervals in the Glenn sand. Unlike other operators, Chevron concentrated on the upper and middle Glenn sand, and implemented the miceller-polymer flood in those sands. The increase in oil production as well as reduction in water cut was substantial. We re-simulated the Chevron unit assuming that it is water flooded with same completion as Chevron had used. The response indicated that Chevron would have achieved a substantial increase in the oil production with reduction with water cut just by using water flood. Although not as impressive as the miceller-polymer flood, the simulation indicated to us that we could use a similar approach in other parts of the field. We studied both tracts 7 and 9, and investigated various scenarios for improving the performance of those units.

Based on our evaluation, we decided to drill a deviated well in tract 9, which would be completed in the upper and middle part of the Glenn sand. To achieve the drilling in a cost-effective manner, we employed a relatively new technology of surface steered drilling which is much cheaper than conventional deviated hole drilling. Unfortunately, drilling of deviated hole proved to be much more challenging than anticipated. We lost the drilling assembly twice. During the second time, we could not fish it, and the hole had to be abandoned. As a result, our reservoir management plan during the second budget period could not be validated. Because of budget constraints, another attempt at drilling the deviated hole could not be made. Hopefully, private owners will take an initiative, and with favorable oil price, drill deviated wells in the same field to validate the concept.

To compliment our technical effort, we vigorously pursued various technology transfer activities. These activities resulted in 26 publications and 10 presentations. In addition, four technology transfer workshops were conducted for the benefit of small operators and independents. These workshop locations included Tulsa, Houston, Denver and Ft. Worth. We also published two newsletters and sent them to over 300 interested parties.

To summarize, although the project ended with a failure of deviated well, we accomplished a great deal. We demonstrated that even a ninety-year old field could be rejuvenated using cost effective technologies. We evaluated various technologies and determined their cost-effectiveness. We were able to transfer many aspects of the technology to small operators and independents.

INTRODUCTION

The overall report is divided into four sections. In the first section, we provide the background of the field that was the subject of investigation. The project was divided into two budget periods. In the second section, we describe the activities during the first budget period. The first budget period involved using modern technology to describe the reservoir in part of the field followed by implementing an appropriate reservoir management plan to improve the performance. In the third section, we describe the activities during the second budget period. The second budget period involved using conventional technology to develop a reservoir description followed by implementing an appropriate reservoir management plan to improve the performance. Comparing the two periods, we were successful in improving the performance of the field during the first budget period. In contrast, due to problems in drilling the horizontal well, we were unable to validate our approach during the second budget period. In the last section of the report, we summarize some of the technology transfer activities carried out as part of the project.

BACKGROUND

The DOE Class I Program is targeted towards improvement of production performance of existing mature oil fields located in fluvial-dominated deltaic sandstone reservoirs. This project was selected under the near-term program which required that existing new technologies be applied in these fields to prevent any premature abandonment of these mature fields. The Glenn Pool field selected for this project fits the desired characteristics under this program.

The Glenn Pool field is located in portions of Tulsa and Creek Counties of Oklahoma. The field was discovered in 1905, and it is estimated as having produced 330 MM barrels of oil from the Middle Pennsylvanian (Desmoinesian) age Bartlesville sandstone. Glenn Pool field, like other fields developed in the Bartlesville sandstone, is located on the northeastern Oklahoma platform, a paleotopographic and structural depression of mid-Mississippian-Pennsylvanian age lying between the Ozark uplift to the east, the Nemaha ridge on the west and the Arkoma basin to the south (see **Figure 1**). The figure also shows the area of study for this project. The Self-unit indicated in the figure was the subject of first budget period investigation, whereas the gray area surrounding the Self-unit was the subject of the second budget period.

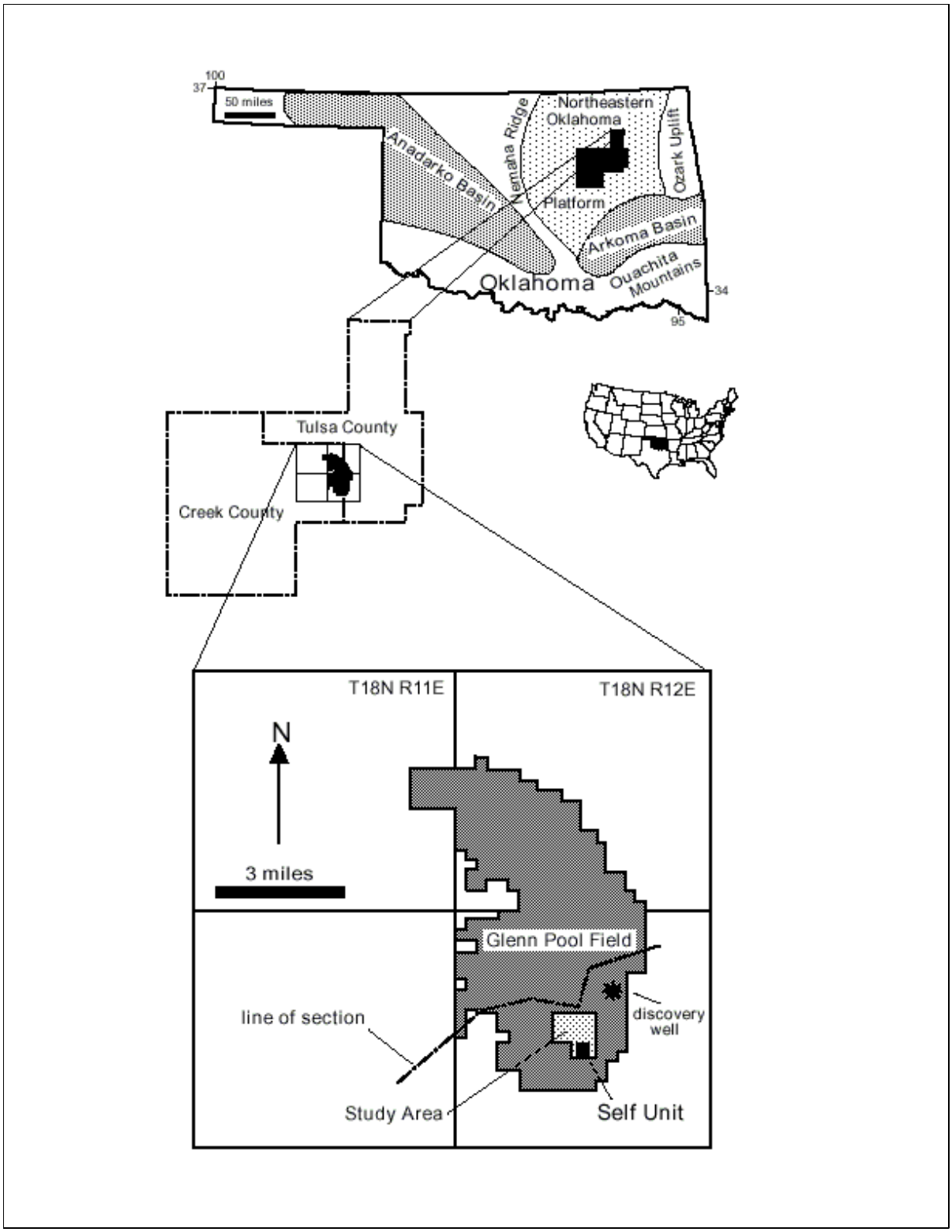

Figure 1 – Location of Glenn Pool field

The field encompasses 27,440-acres. Initial production from the wells ranged from 75-500 BOPD to 4,000 BOPD. After discovery in 1905, the field reached peak production in 1907. The first well in the field was drilled in fall of 1905. The well was located on the Ida Glenn farm near the center of the SE/4 of section 10, T17N, R12E, in Tulsa County (see Figure 1). The well was 1,458-ft deep and produced at a flowing rate of 75 BOPD. The producing interval was called "Glenn sandstone" and in the subsequent years became the target pay zone. The average producing span was estimated to be close to 240-ft and was the most productive compared to the other nearby fields.

Initial wells were drilled by cable tools. Surface casing of 8-5/8 inch size was set at 275-ft and open hole drilling was carried out to the top of Bartlesville reservoir. The hole size was reduced to 6 inches through the pay zone interval. The producing interval was shot with 250-300 quarts of nitroglycerine, casing set to the top of the sandstone, and the shot hole cleaned out. By 1906, well drilling averaged at the rate of 3 wells per day. In this process, orderly spacing of the wells was neglected. Subsequently, the completion was on a ten-acre pattern. Earthen lakes were used for storage on many leases, and oil was shipped to the Texas Gulf Coast by railroad. In 1908, 100 companies were operating in the field. By 1912, several BCF of natural gas is estimated to have been flared, vented or used as fuel for lighting field operations. The field limits had been defined by 1920. A pipeline through Coffeyville, Kansas connected the field to the Chicago and Great Lakes markets. By 1926, 22 refineries served the area.

With depletion of production, gas injection was introduced in 1940, and gas collected at producing wells was recycled to injection wells. Water flooding operations began in 1944. Cumulative oil production records prior to field-wide water flooding are incomplete. By 1943, it was estimated that the production throughout the field was between 222 and 236 MMBO. Over 100 MMBO had been produced up to 1990 by secondary gas repressuring, water flooding, and tertiary recovery methods bringing total production to 330 MMBO. The field is being depleted at present. Several large production units are under water flood, and a few units have undergone testing and implementation of micellar-polymer enhanced recovery methods. Results have shown the possibility for significant additional volumes of recoverable oil.

The Glenn sand has been conventionally divided into 3 units: upper, middle and lower Glenn.[1] Each is separated by apparent permeability barriers consisting of interbedded siltstones and shales. In the central portion of the Glenn Pool field the Glenn sand is present at a depth of approximately 1,500 feet, and the thickness varies from 100 to 185-feet. The upper and middle Glenn are the producing intervals in the central portion of the field and the lower Glenn is below the oil-water contact.

Oil from the Glenn sand has a gravity of 35.8° to 41.3°. It contains 3.12 to 11.46% paraffin and a sulfur content of 0.3%. Initial reservoir pressure has been estimated in the range of 600 to 700 psi. Current water flooding injection pressure ranges from 100 to 1,100 psi.[1]

From regional studies, the Bartlesville sandstone is regarded as having been deposited by a fluvial-dominated delta system.[2] In the Glenn Pool field area, the Glenn sand is predominantly the deposits of delta plain depositional environments. The lower Glenn sandstones are subangular to subrounded, moderately sorted, silty fine- to medium-grained sandstone, with abundant sand-size rock fragments, and thin beds of shale and siltstone.[1] The lower non-porous break consists of interbedded, laminated silty sandstone and shale with localized thin beds of shale, sideritic clay pebbles and with intervals of carbonate-cemented sandstone.[1] The middle Glenn is subangular to subrounded and well-sorted fine- to very-fine-grained sandstone.[1] It is primarily massively bedded, with portions containing medium-scale crossbedding.[1] The middle Glenn forms the major part of the reservoir.

The upper non-porous break consists of thin silty shale or interbedded laminated, silty sandstone and silty shale.[1] It is an effective permeability barrier but limited lateral extent may result in localized contacts between the upper and middle Glenn. The upper Glenn is in part massively bedded and in part medium-scale crossbedded. It is angular to subangular, moderately sorted very fine- to medium-grained sandstones,[1] and contains abundant carbonaceous fragments and a few sand-sized rock fragments. The upper portion of the upper Glenn contains poorly sorted very fine- to medium-grained sandstones with silty interlaminations, sparse carbonate or silica cement, and visible porosity.

Tectonism associated with the Ouachita collisional event caused the platform to tilt southward into the subsiding Arkoma foreland basin of southeastern Oklahoma.[2-4] Regional uplift during the Jurassic and

Cretaceous resulted in a gentle, westward dipping monocline with locally developed low-relief closures.[1, 5] Glenn Pool field structure contour data at the top of the Bartlesville (Glenn) sandstone show a broad feature, open to the northwest, with about 200-ft (61 m) of relief.[1] The productive limits of Glenn Pool field only generally coincide with this feature. Within the field, structural relief is variable (50-75-ft, 15-23 m) as a result of Bartlesville (Glenn) sandstone thickness variations and stratigraphic termination along the eastern margin of the field.

Stratigraphically, the Bartlesville sandstone and its outcrop equivalent, the Bluejacket sandstone, are members of the Boggy formation, which is included within the Krebs group of the Desmoinesian series (**Figure 2**). The Bartlesville is underlain by the Savanna formation (Krebs group) and is overlain by the Inola limestone and, locally, by the Red Fork member (zone). Black shales within the Inola limestone, a member of the Boggy, and Brown limestone, a member of the Savanna, are used as marker beds for detailed stratigraphic correlation (**Figure 3**). Within Glenn Pool field, the Bartlesville (Glenn) has been traditionally divided into upper, middle, and lower Glenn sand intervals, all of which pinchout at the eastern edge of the field.[1] Entrapment within the field is a result of this updip termination of reservoir-quality sandstones (Figure 2).

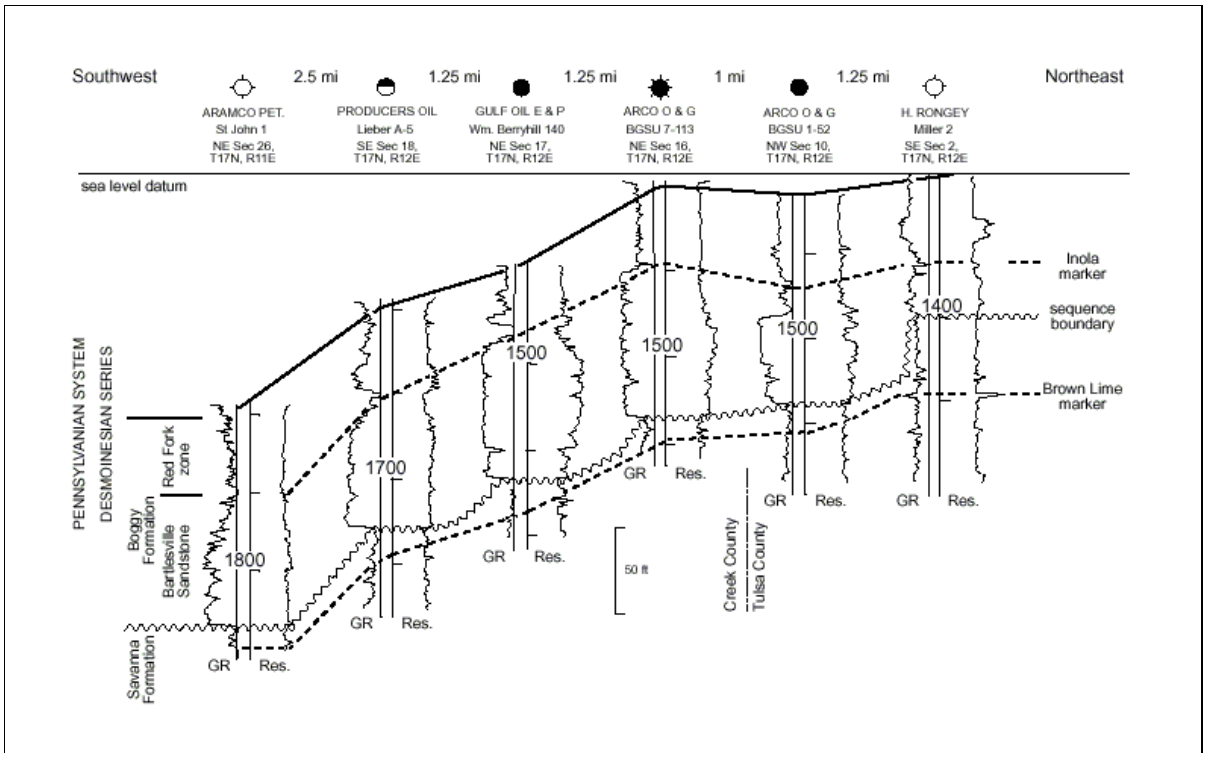

Figure 2 – Stratigraphic location of Bartlesville sandstone

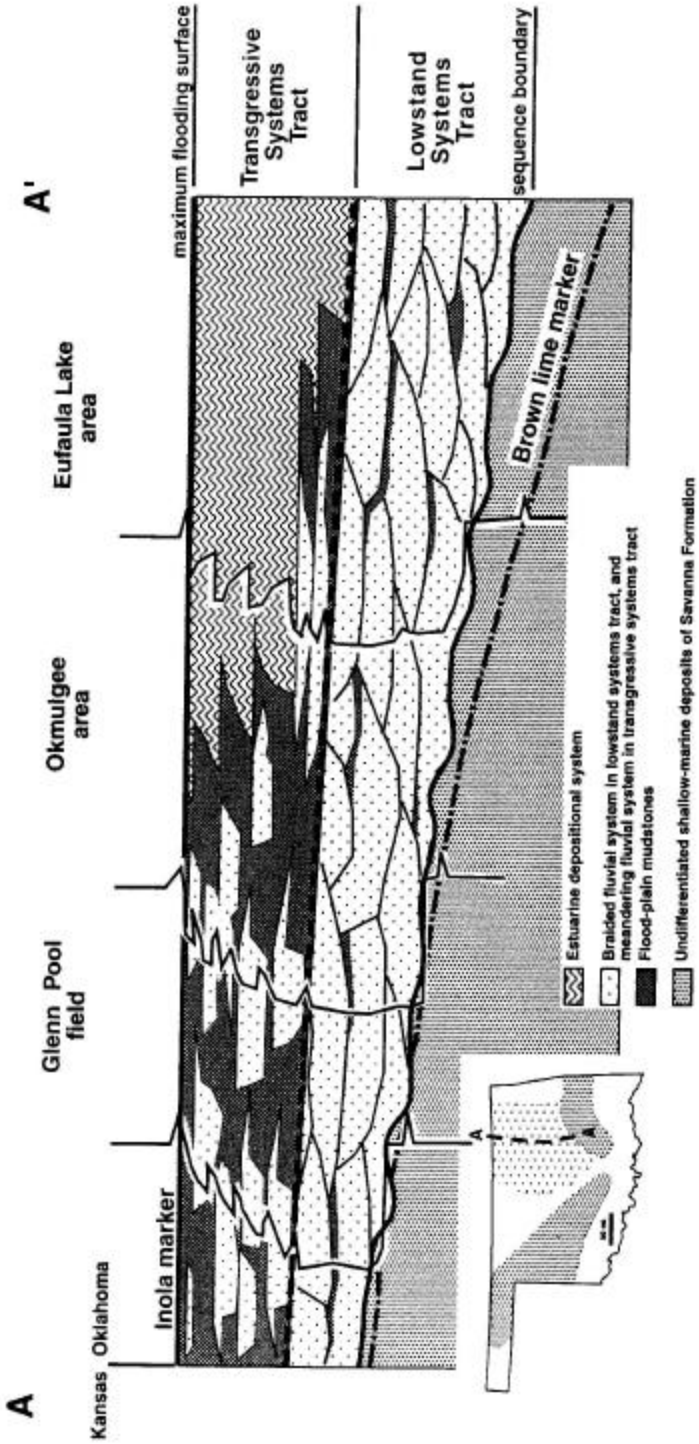

Figure 3 – Marker beds for Glenn Pool field

The conventional interpretation of the Bluejacket (outcrop) and Bartlesville (subsurface) sandstone was established in studies conducted by Visher[2] and his students at The University of Tulsa during the 1960s and 70s. This interpretation proposes that the Bartlesville was deposited within a fluvial-dominated deltaic system that prograded southward into the subsiding Arkoma Basin (see Figure 1), essentially during a single regressive event. An alluvial valley system extending from the Kansas-Oklahoma state line is inferred to show southward transition to a fluvial-dominated deltaic system across northeastern Oklahoma. Within this scheme, Glenn Pool field lies well within the deltaic portion of the overall system, close to the depositional boundary between upper and lower delta plain facies.

During this investigation, the conventional geological model of Bartlesville sandstone has been substantially revised in light of new information. The details of this revision are discussed in the following sections.

BUDGET PERIOD I

Introduction

In the first budget period, our effort concentrated on Self-unit located in the southeast portion of the Glenn Pool field (see Figure 1). During this period, we applied several new technologies to improve the reservoir description. These technologies include integrated reservoir description, geological description using DGI's (discrete genetic intervals), modern logs, cross borehole tomography, geostatistics and reservoir flow simulation. The description and success of each of these technologies is discussed in this section.

Self-Unit

The Self-unit, area of investigation of project during budget period one is a 160-acre tract located in southeast portion of Glenn Pool oil field in section 21-17N-12E (**Figure 4**). Currently Uplands Resources, Inc. operates the unit. The first well on the lease was put on production November 6, 1906. In all, 5 wells were put on production in 1906. Out of the three Glenn sand intervals, the upper and middle are present while lower Glenn is absent in the Self-unit. ARCO's report by Heath[6] on the Glenn sand unit gives a brief history about the performance of the Self-unit.

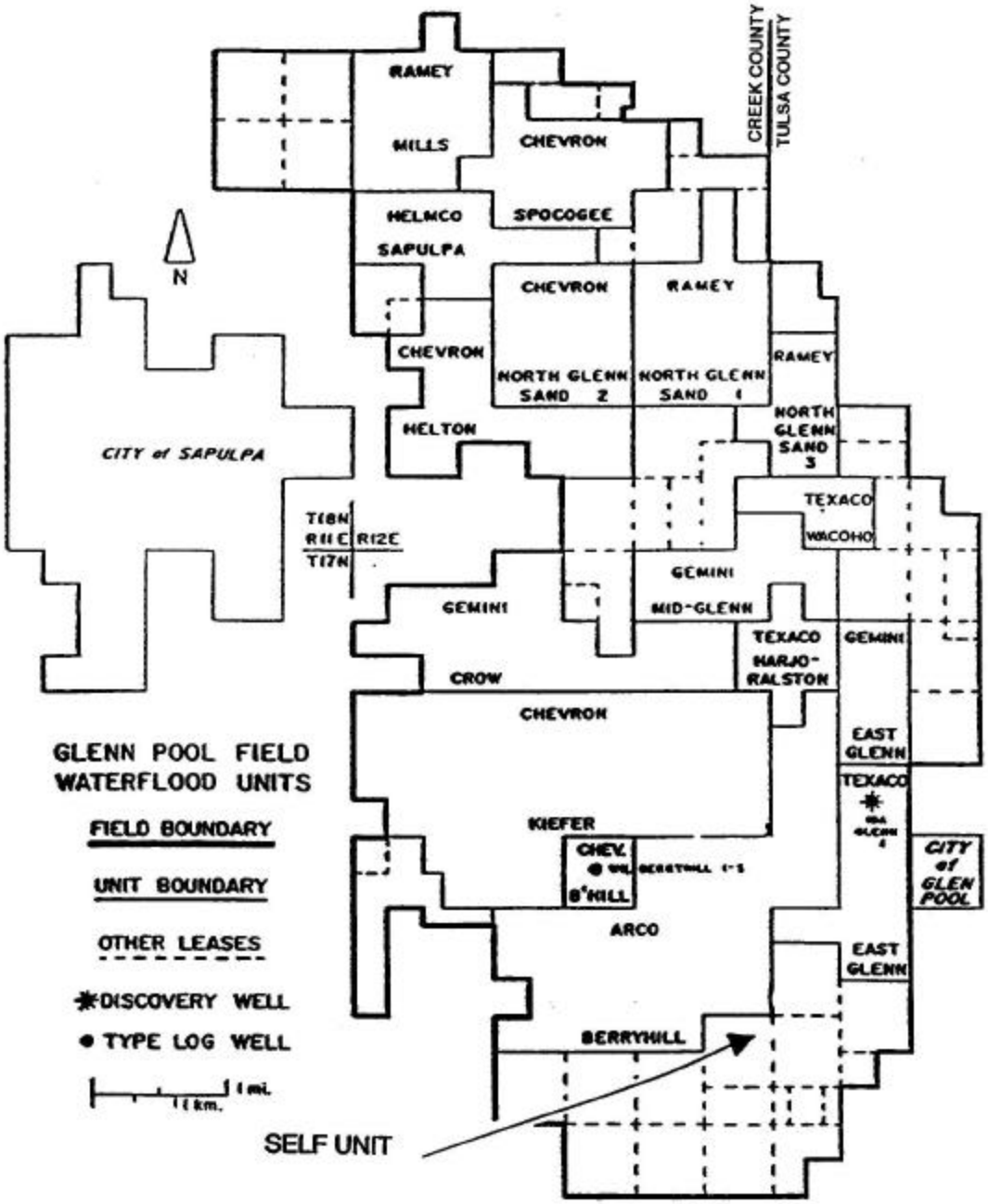

Figure 4 – Self-unit location[1]

The original oil in place (OOIP) for the unit has been estimated to be 13.009 MMBO. Primary production during 1906-1945 resulted in the production of 1.809 MMBO representing 13.91% of

OOIP. In 1945, gas repressuring began in the unit. This resulted in a recovery of 0.231 MMBO representing 1.8% of OOIP. During 1954-1966 the unit was put on a pilot water flood resulting in production of 0.169 MMBO (1.3% of OOIP). The recoveries were higher in the areas surrounding the pilot and the gas injectors. In 1966, water flooding was extended to the majority of the field. In the initial period of water flooding, the production increased across the entire Self-unit. The total production during 1966-1978 was 0.235 MMBO, representing 1.8% of OOIP. The unit was re-drilled in 1978 on a ten-acre 5-spot pattern. During 1978-1983, 0.146 MMBO production representing 1.12% of OOIP was obtained. From 1984-1992, production was 0.157 MMBO representing 1.2% of OOIP. Total production obtained to date from the unit is around 20% of the OOIP.

The Self-unit experienced good primary recovery, but response to the subsequent secondary recovery efforts has not been encouraging. Study of the available well logs and core reports indicate that lithologic heterogeneities and permeability vary throughout the lease. Well logs taken in the 1980's indicate higher water saturations in middle Glenn portions rather than in the upper Glenn. Upper Glenn portions could not be swept by water flooding, perhaps, because of lower permeabilities in these portions and inadequate perforation coverage.

Despite subsequent water flooding, water injection could not be contained on the lease and water possibly migrated to other parts of the field. Large permeability variations in upper and middle Glenn also contributed to this inefficient use of water injection. Injection pressures and rates vary throughout the lease; pressures range from 50 to 700 psi, and the rates range from 40 to 2,000 barrels of water per day. At the start of budget period one, oil production from the unit was less than 18 bbls/d with water cut of 99%.

In total, 81 wells have been drilled on the Self-lease. The study required the availability of all well records. Though starting production and abandonment data for most of the wells are available, information with regards to the production history for individual wells could not be traced. The lease-wide production records are not available before the year 1935. Well chronology has been established by analyzing two well maps, well map as of 12-August-1955, well map as of 15-May-1981 and the

other sparsely available well records. Information pertaining to the number of producing wells each year is available from production documents but information regarding the location or respective number had to be estimated based on the documents mentioned above. The chronological development of the Self-unit on a well by well basis till the start of the project is included in **Table 1**. The well map depicting all the wells drilled in the Self-unit is shown in **Figure 5**. Initial development occurred along the periphery of the unit; subsequently, development occurred in the interior.

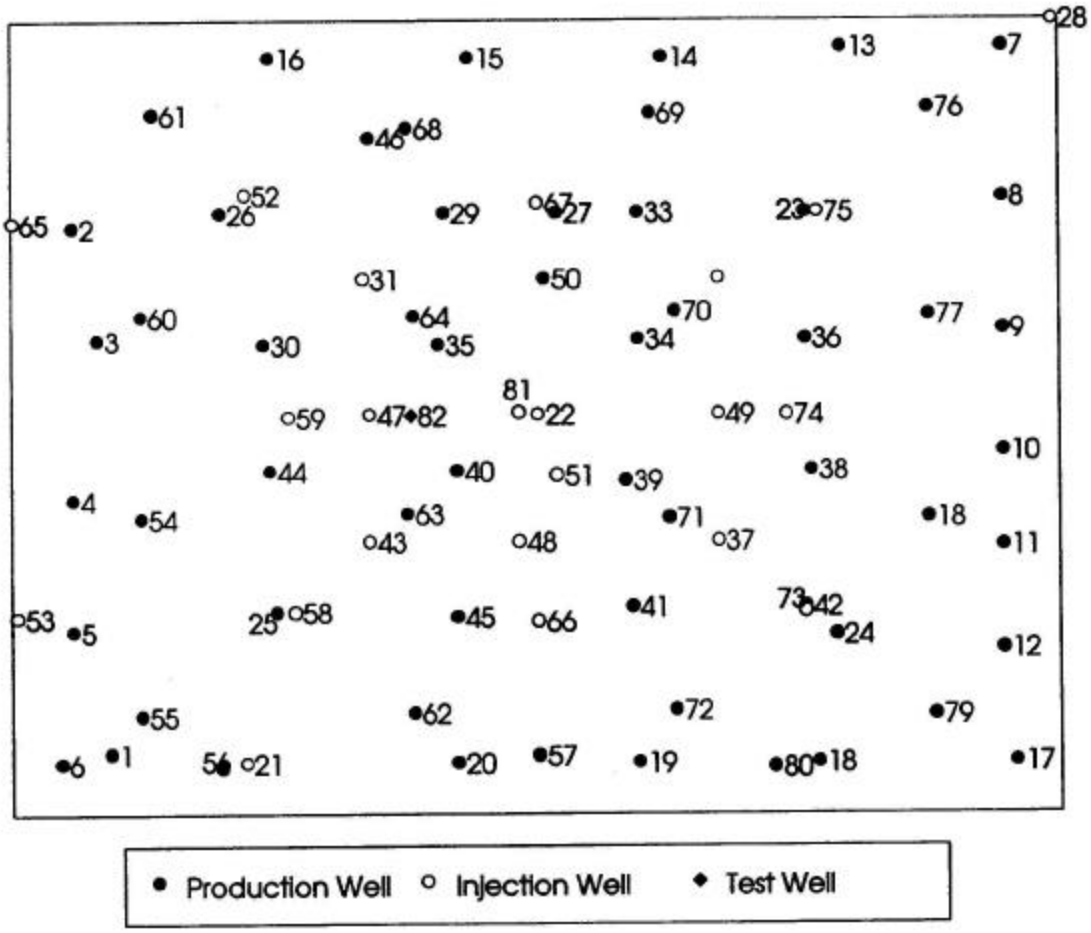

Figure 5 – Well locations

Table 1 – Historical Information on Self-unit							
Year	Number of Producers	Gas Injectors	Water Injector	Water Disposal	Wells Drilled	Wells Plugged	Well Number
1906	5	-	-	-	5(1, 2, 3, 4, 7)	-	1, 2 ,3, 4, 7
1907	27	-	-	-	22(5, 6, 8-27)	-	1-27
1911	26	0	0	0	0	1(4)	1-3,5-27
1923	24	-	-	-	-	2(3, 5)	1,2,6-27
1927	20	-	-	-	-	4(11, 12, 17, 18)	1, 2, 6-10, 13-16, 19-27
1930	18	-	-	-	-	2(19, 24)	1, 2, 6-10, 13-16, 20-23, 25-27
1936	18	-	-	-	-	-	1, 2, 6-10, 13-16, 20-23, 25-27
1946	16	4(21, 28, 31, 32)	-	-	5(28-32)	1(27)	1, 2, 6-10, 13-16, 20, 22, 23, 25, 26 Inactive 29, 30
1947	19	5(21, 28, 31, 32, 37)	-	-	7(33-39)	-	1, 2, 6-10, 13-16, 20, 22, 23, 25-26, 29, 30, 33 Inactive 34-36, 38-39
1948	25	6(21, 28, 31, 32, 37, 43)	-	-	6(40-45)	-	1, 2, 6-10, 13-16, 20, 22, 23, 25-26, 29, 30, 33, 34, 35, 36, 38, 39, 40 Inactive 41, 42, 44, 45
1950	27	8(21, 28, 31, 32, 37, 43, 47)	-	-	2(46, 47)	-	1, 2, 6-10, 13-16, 22, 23, 25, 26, 29, 30, 33-36, 38-42, 44 Inactive 20, 45-46

Year	Number of Producers	Gas Injectors	Water Injector	Water Disposal	Wells Drilled	Wells Plugged	Well Number
1954	27	8(21, 28, 31, 32, 37, 43, 47)	3(22, 48, 49)	1(20)	2,(48,49)	-	1, 2, 6-10, 13-16, 23, 25, 26, 29, 30, 33-36, 38-42, 44-45 Inactive 46
1957	28	-	11(21, 22, 28, 31, 32, 37, 43, 47, 48, 49, 50)	1(20)	1(50)	-	1, 2, 6-10, 13-16, 23, 25, 26, 29, 30, 33-36, 38-42, 44-45, 46
1965	28	-	12(21, 22, 28, 31, 32, 37, 43, 47, 48, 49, 50, 51)	1(20)	1(51)	-	1, 2, 6-10, 13-16, 23, 25, 26, 29, 30, 33-36, 38-42, 44-45, 46
1967	28	-	12(21, 22, 28, 31, 32, 37, 43, 47, 48, 49, 50, 51)	1(20)	1(52)	-	1, 2, 6-10, 13-15, 23, 25, 26, 29, 30, 33-36, 38-42, 44-45, 46, 52 Inactive 16
1970	28	-	12(21, 22, 28, 31, 32, 37, 43, 47, 48, 49, 50, 51)	1(20)	-	1(16)	1, 2, 6-10, 13-15, 23, 25, 26, 29, 30, 33-36, 38-42, 44-45, 46, 52
1971	27(1st ½) 23(2nd ½)	-	12(21, 22, 28, 31, 32, 37, 43, 47, 48, 49, 50, 51)	1(20)	-	5(7, 9, 13, 14, 15)	1, 2, 6, 8, 10, 23, 25, 26, 29, 30, 33-36, 38-42, 44-46, 52

Year	Number of Producers	Gas Injectors	Water Injector	Water Disposal	Wells Drilled	Wells Plugged	Well Number
1972	20	0	12(21, 22, 28, 31, 32, 37, 43, 47, 48, 49, 50, 51)	1(20)	-	3(29, 33, 34)	1, 2, 6, 8, 10, 23, 25, 26, 30, 35, 36, 38-42, 44-46, 52
1973	20(1st ½) 17(2nd ½)	-	12(21, 22, 28, 31, 32, 37, 43, 47, 48, 49, 50, 51)	1(20)	-	3(10, 35, 36)	1, 2, 6, 8, 23, 25, 26, 30, 38-42, 44-46, 52
1978	16	-	11(21, 22, 28, 31, 37, 43, 47, 48, 49, 50, 51)	1(20)	-	2(2, 32)	1, 6, 8, 23, 25, 26, 30, 38-42, 44-46, 52
1979	6(1st ½) 9(2nd ½)	-	10(21, 22, 28, 31, 37, 43, 478, 49, 50, 51)	1(20)	3(53-55)	8(8, 23-26, 44-47)	1, 6, 30, 38, 42, 52, 53-55 Inactive 39-41
1980 (Jun)	6	-	2(48, 50)	-	-	17(1, 20, 21, 22, 28, 31, 37-43, 49, 51)	6, 30, 52, 53, 54, 55
1981 (Dec)	21	-	11(48, 52, 53, 58, 59, 65, 66, 67, 73-75)	-	24(56-80)	1(6)	30, 50, 54-57, 6-64, 68-72, 76-80
1982	20	-	11(48, 52, 53, 58, 59, 65, 66, 67, 73-75)	-	-	1(30)	50, 54-57, 60-64, 68-72, 76-80
1984	20	-	11(52, 53, 58, 59, 65, 66, 67, 73-75, 81)	-	1(81)	1(48)	50, 54-57, 60-64, 68-72, 76-80
1992							Same status
1993							Same status

As already mentioned, the unit was put to production in 1906, though no exact date could be found. Heath's report[6] lists the cumulative production through 1946 as 1.809 MMBO. Yearly production information from 1935-1906 has been extrapolated based upon the number of wells operating in the respective years and the production information for the years 1935-1946. From 1936-1972, the yearly estimation has been carried out on the basis of production information available for one month, three months, or in some cases six months. 1972 onwards production data availability are complete and detailed. Annual water injection and production rates are available for Self-unit and the adjoining Burrows lease combined. Data for individual leases has been obtained based upon their respective oil production fraction. The overall production history based on the above information is summarized in **Figure 6**. As evident from this figure, every time new technology was implemented in Self-unit the field responded with substantial increase in production. This is evident in 1946, 1965 and 1978. This also gives an indication that if new technology is properly used and a good reservoir management plan is implemented, the Self-unit can respond with an increase in oil production.

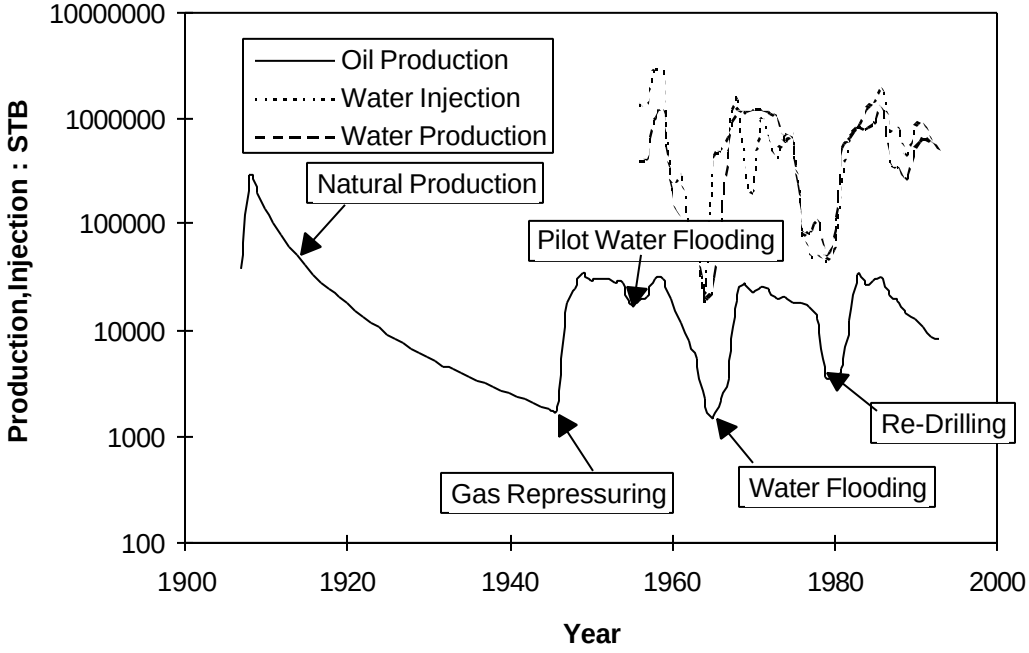

Figure 6 – Production history of Self-unit

For information related to the petrophysical properties, 3 well logs for wells drilled after 1978 are available. Permeability data availability for the Self-unit is not that abundant. Though eight core reports are available from the wells operating during 1940's and 1950's, the logs for those wells could not be traced and as a result no relation between the core and well log of the same well could be established. Furthermore, the existing wells have only been logged and there is no core report relevant to these wells.

Well schedule, water injection and production data have been summarized based on 1002-A forms, production reports, PI forms and other miscellaneous documents available from Uplands Resources, Inc. and the Oklahoma Well Log Library.

Although significant production data were available, the project team believed that an additional well was needed to be drilled for the following reasons.

- We did not have a single core from the Self-unit. The only core available to us was from northern part of the Glenn Pool field. We did not believe that it would be representative of Self-unit.
- We intended to run micro-imaging log to obtain detailed geological architecture. To run the micro-imaging log, we needed an open hole. With the existing wells, no open hole was available.
- We wanted to use cross borehole tomography to generate cross section information between two wells. To properly obtain the image of the reservoir, the well needs to be drilled deeper than the formation. All the existing wells were drilled to the total depth of Glenn sand. To properly obtain the cross borehole imaging information, we needed to have at least one well 400-ft deeper than the bottom of the Glenn sand.

In view of the above considerations, a vertical well was drilled in the Self-unit at the end of 1993. The location of the well, Self-82 is shown in Figure 5. The location was decided based on preliminary geological mapping, as well as distance considerations from the surrounding wells. The well was drilled 400-ft deeper than the Glenn sand. It was cored, a suite of modern logs, including micro-imaging log, was run successfully. The well was completed in January 1994.

In the following sections we will describe various technologies used in improving the reservoir description.

Geological Facies Architecture

Conventional geological analysis has divided the Glenn sand into upper, middle and lower sands. Recent well log, core, and outcrop analyses, however, have resulted in significant revisions to the conventional model.[7-9] These studies strongly suggest the Bartlesville sandstone in Glenn Pool field and much of northeastern Oklahoma consist of incised valley-fill deposits. Advanced reservoir characterization efforts in the southern portion of the field, including the Self-unit, propose a new facies architectural scheme based on a three-level spatial hierarchy of elements.[9] These elements, in increasing volumetric order, include: 1) facies/subfacies; 2) discrete genetic intervals (parasequences); and 3) systems tracts and stratigraphic sequence (Figure 3).

Much valuable data for re-interpretation of the Bartlesville sandstone came from a project cooperative well, the Self-82. A full suite of logs, including a microresistivity borehole image log, as well as a core (87-ft, 26 m) through nearly the entire Bartlesville interval, supplied considerable information for detailed characterization of reservoir sandstones and remaining reserves (**Figure 7**).

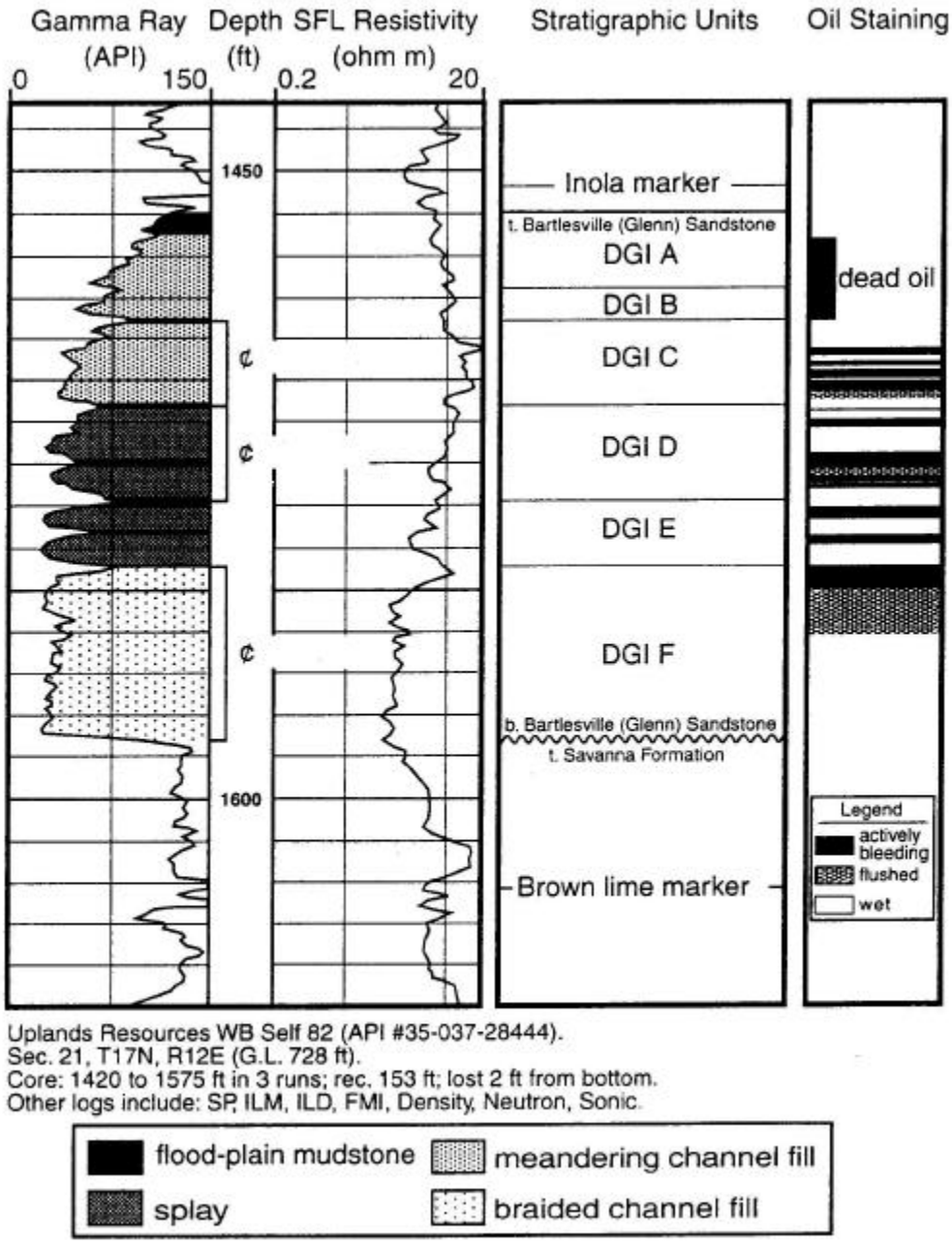

Figure 7 - Self-82 log with stratigraphic units and core oil-staining observations[10]

Facies and Subfacies Elements

The use of the term facies and subfacies is consistent with the traditional concept of sedimentary facies. Each facies and subfacies is characterized by its texture, sedimentary structures and wireline log profile.

Although they are given interpretative names, each is based on its distinctive descriptive characteristics. As architectural elements, facies, and to a more limited degree subfacies, are the volumetrically smallest elements in the hierarchy resolvable by conventional subsurface technologies.

Braided Channel-Fill Facies

Braided channel-fill facies compose the lower 40 to 80 ft (12-24 m) of the Bartlesville sandstone in Glenn Pool field. These deposits consist of structureless to less commonly parallel-bedded, moderately to well-sorted, upper medium- to lower coarse-grained sandstones (**Figure 8**). The basal contact is erosional with the underlying Savanna formation (sequence boundary, Figures 3 and 7). In outcrop, thick, structureless sandstones grade laterally to cross-stratified and/or parallel-bedded sandstone with parting lineations.[9]

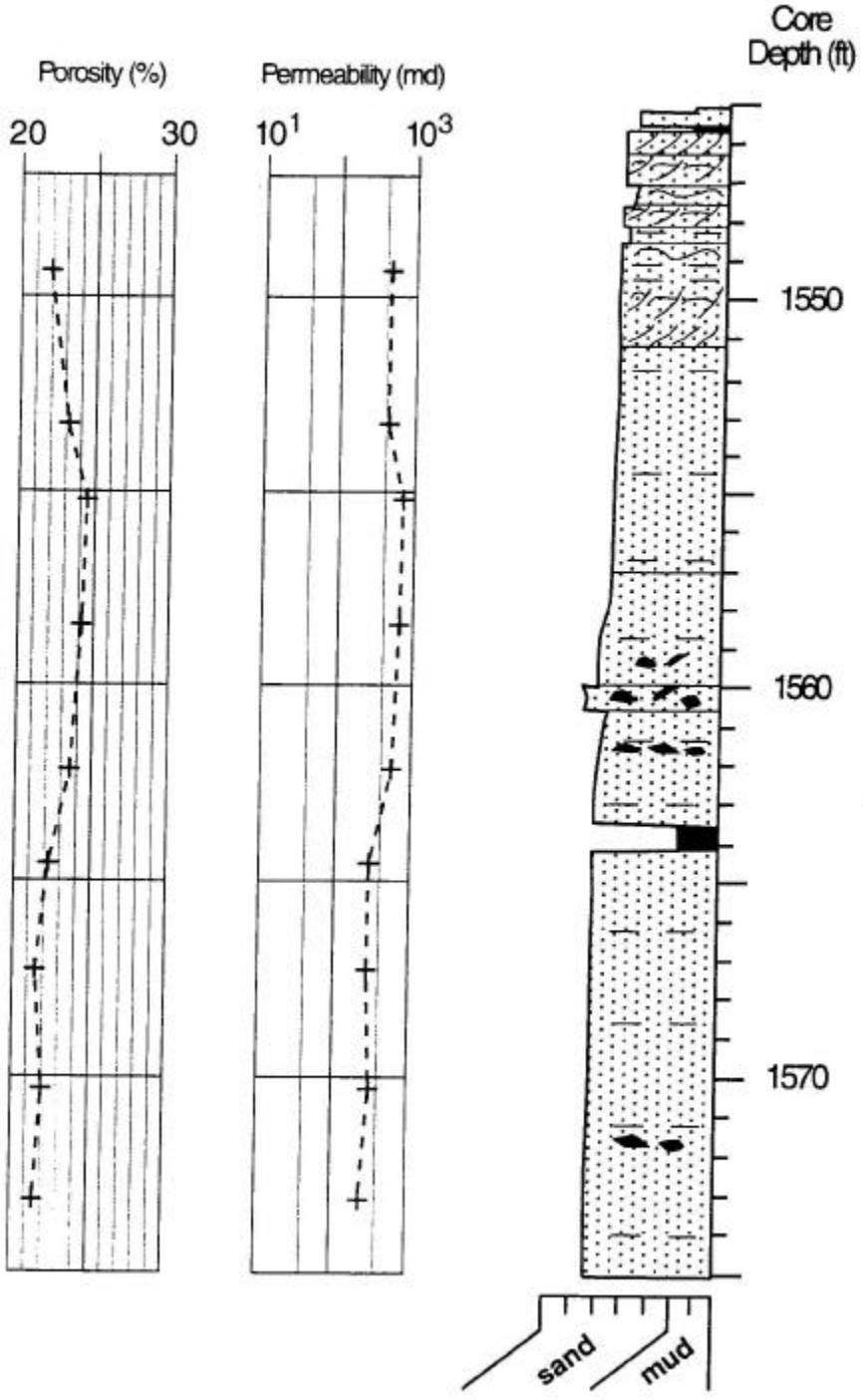

Figure 8 – Self-82 core description of DGI F braided channel-fill facies[10]

Subsurface correlations suggest that braided fluvial sandstones cover much of the southern part of Glenn Pool field. Mapping reveals localized areas where net sand thickness is 40 to 60-ft (12-18 m) over an area of 120 ac (48 ha), elongated in an east-northeast to west-southwest direction. In outcrop, the lateral limits of sand-body complexes are rarely seen, but numerous internal erosional surfaces define individual sand-bodies with width to maximum-net-sand-thickness ratio averaging about 30% and ranging between about 15-50%.[9]

Deposits of this facies exhibit blocky gamma ray well log profiles and excellent reservoir characteristics, as determined by core analysis (Figure 7). Porosities and permeabilities are commonly in the range of 20-25% and 100-1000 md.

Meandering Channel-Fill Facies and Subfacies

Meandering channel-fill deposits dominate the upper 100 to 150-ft (30-45 m) of the Bartlesville sandstone in Glenn Pool field. This facies is further subdivided into lower, middle, and upper channel-fill subfacies that together display a fining upward progression in grain size and an upward increase in proportion of interstratified mudstone. This texture profile and upward increase in mudstone content is also reflected in serrated bell-shaped well log (gamma ray and resistivity) profiles (**Figure 9**).

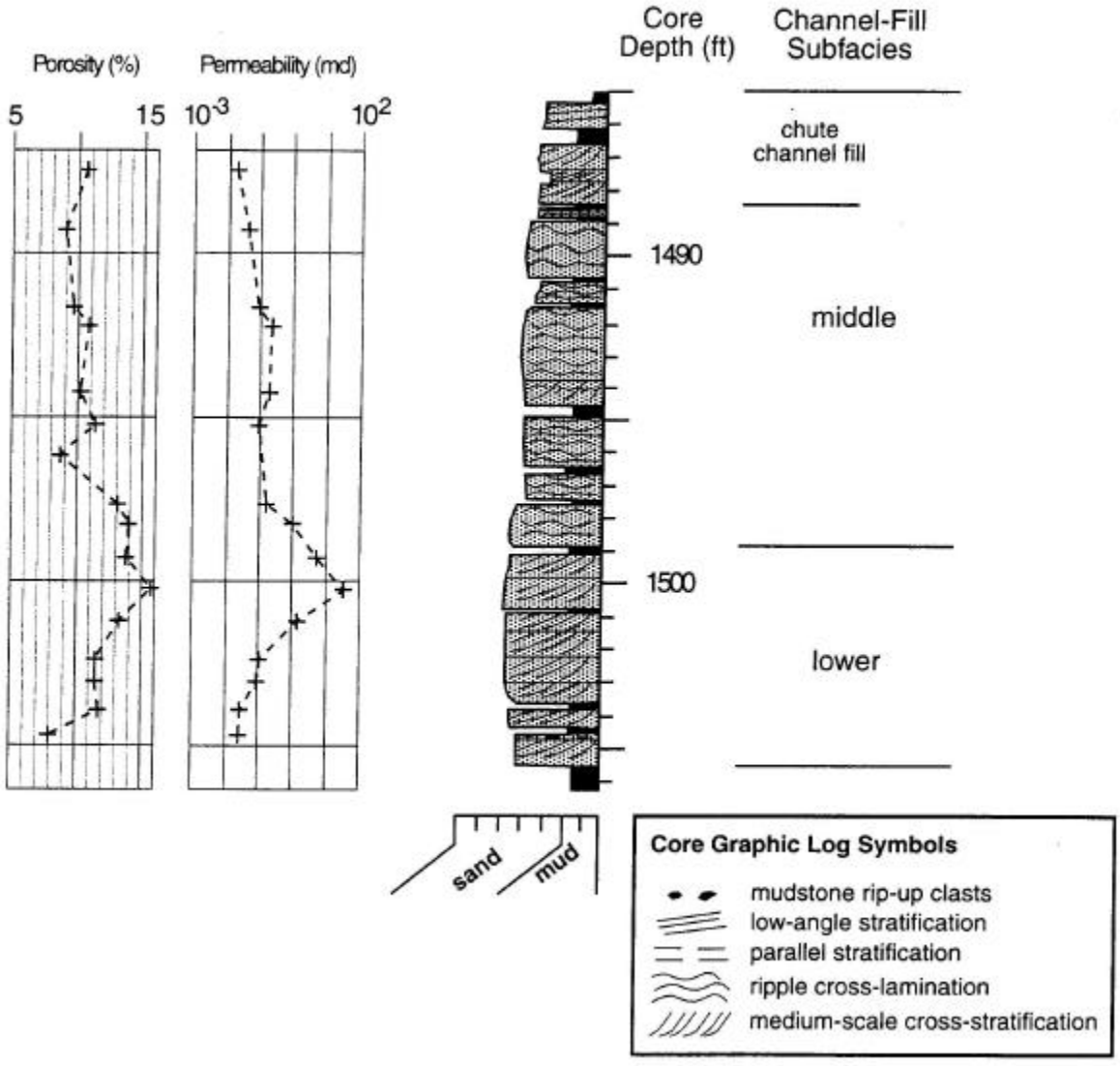

Figure 9 – Self-82 core description of DGI C meandering channel-fill facies[10]

Lower Channel-Fill Subfacies

Consists of moderately to well-sorted, medium-grained sandstone with medium-scale cross stratification. Intraclast lag deposits are common at the base, with similar clasts and mudstone drapes typically occurring along cross strata.

Middle Channel-Fill Subfacies

Deposits include moderately sorted, lower medium-grained sandstones; poorly sorted, silty fine-grained sandstones; and mudstone to silty mudstone with carbonaceous debris. Other physical structures include horizontal stratification and ripple lamination. Medium grained sandstones tend to be cleaner and better sorted. Low-angle bedding planes identified as lateral accretion surfaces show drapes of medium- to very thin-bedded mudstone and silty mudstone containing carbonaceous debris (Figure 9). Inversion in the overall fining-upward texture profile and medium-scale trough cross stratification are regarded as chute channel-fill deposits within the middle channel-fill subfacies. Chute channel-fills are not common in Glenn Pool field, but are common in outcrop exposures northeast of Glenn Pool.[7]

Upper Channel-Fill Subfacies

This subfacies consists of non-reservoir mudstone and silty claystone.

Interpretation of the above described facies and subfacies as meandering channel-fill deposits is consistent with published literature.[11-12] The basal erosional contact is regarded as the record of the channel thalweg (thread of deepest flow) eroding laterally as the channel evolves. The lower channel-fill subfacies are the deposits of crescentic dunes deposited near the thalweg but in shallower, lower current-strength parts of the channel. The middle channel-fill subfacies is the record of lateral accretion bar deposition. The presence of sand-mud couplets and abundance of mudstone interbeds strongly suggests influence by tidal fluctuations.[13] The upper channel-fill subfacies represents the abandonment phase of channel filling; it is expected to be thickest at the last location of the thalweg.

Log correlation and facies mapping in southern Glenn Pool field define north-south oriented meandering channel-fill sand bodies, in contrast to the more east-west orientation of braided channel-fill facies.[9] Meandering channel-fill sand-body geometry is characterized by a width to maximum net sand thickness ratio ranging from 30-80%. Channel-fill widths vary from a typical 1,500-ft (500 m) at lower stratigraphic levels to 200-ft (67 m) at upper stratigraphic levels. Within each channel-fill deposit localized net-sand isopach thicks are interpreted as complex lateral accretion bar deposits.

Analysis of a microresistivity borehole image log run in the Self-82 well demonstrated the utility of using these data for refining the facies architecture at a particular location (**Figure 10**). The meandering channel-fill facies is interpreted as the deposit of a complex lateral accretion bar with the major sand thickness located to the north-northeast of the Self-82. The acute azimuthal angle between the dip of lower channel-fill subfacies cross strata (azimuth average = 153°) and the dip of middle channel-fill subfacies lateral accretion surfaces (azimuth average = 183°) indicates the Self-82 is located on the downstream side of a lateral accretion bar.[14] In addition, the upward rotation observed in lateral accretion surface dip directions suggests that this bar developed by amplitude increase (i.e. increasing thalweg sinuosity) and included secondary nodes.[15]

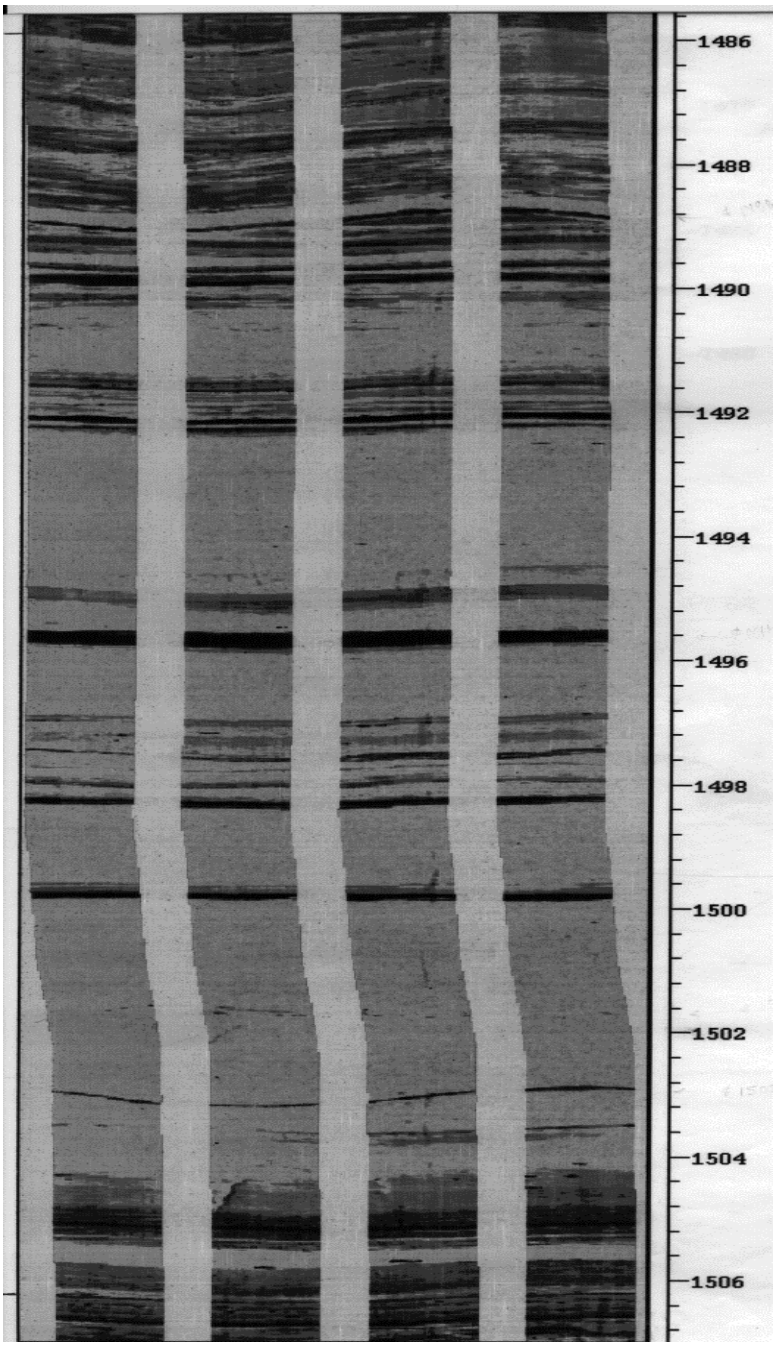

Figure 10 - Microresistivity borehole image for meandering channel-fill facies of DGI C[10]

Splay Facies

Splay facies has a characteristic coarsening-upward textural profile that results from interbedded silty mudstone and fine-grained sandstone grading upward to medium-grained sandstone (**Figure 11**).

Low-angle parallel bedding and ripple cross-lamination are the most common sedimentary structures, with medium-scale cross stratification and contorted bedding less frequently observed. Thin mudstone beds (up to several inches, centimeters) are interstratified throughout and become more numerous in the uppermost portions of the Bartlesville sandstone.

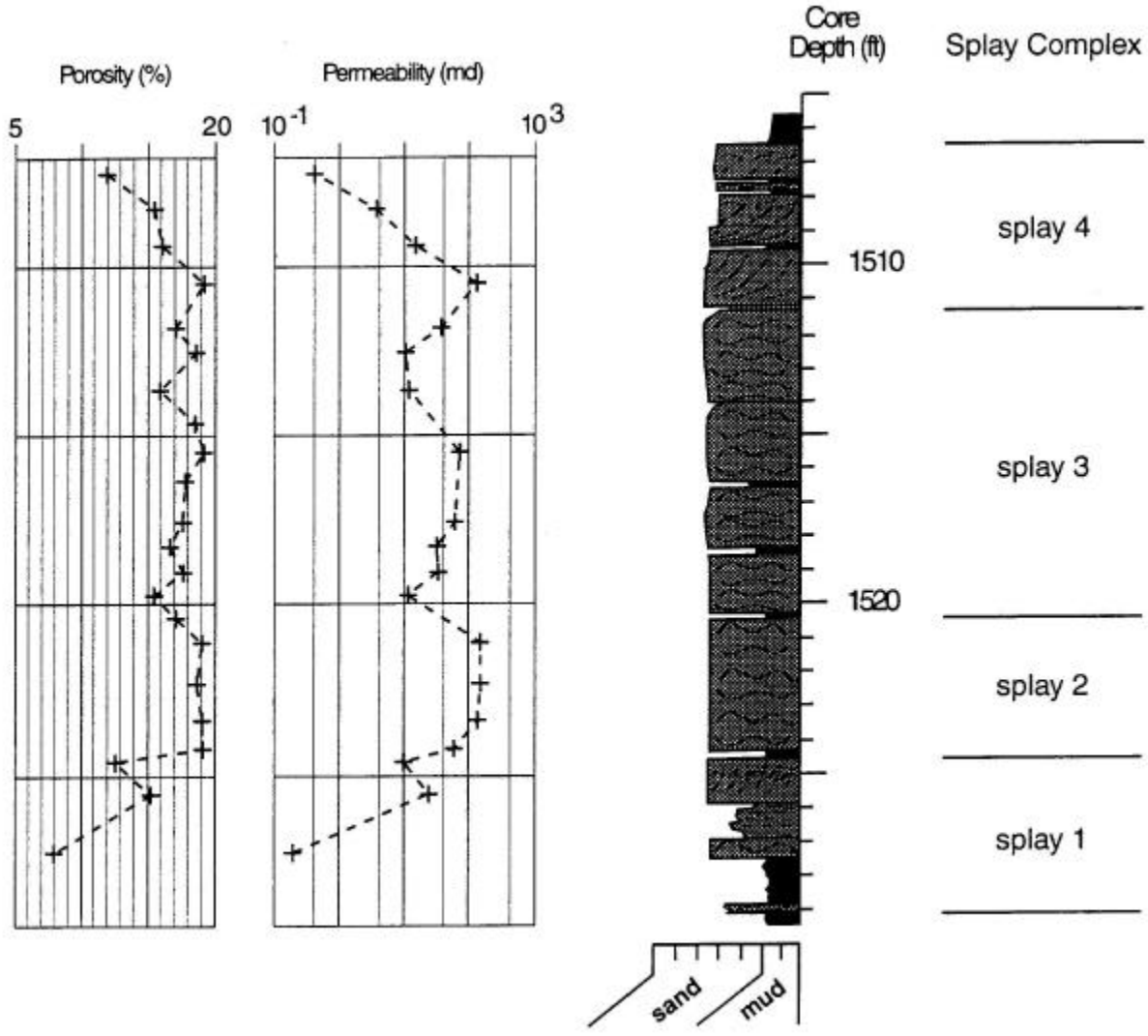

Figure 11 – Self-82 core description of DGI D splay facies[10]

Solitary occurrences of splay facies typically generate a funnel-shaped log profile (Figures 7 and 11). However, where splay complexes formed from two or more crevasse breaks, vertical stacking of

sandstone and mudstone beds, as well as grain size profiles, are more complicated and exhibit undiagnostic log responses (Figure 7).

Floodplain Mudstone Facies

Floodplain mudstone facies consist of strata ranging from siltstones with ripple cross lamination to dark gray mudstones and carbonaceous shale. High gamma ray and low resistivity well log values are characteristic. However, the log response may not reach the "mudline" where these mudstones form thin beds between thick sandstones.

To the south and northwest of Glenn Pool field, the floodplain facies contain coal deposits that are mined locally.[16-17]

Discrete Genetic Interval (Parasequence) Elements

A discrete genetic interval (DGI) is defined as a collection of genetically related contiguous facies deposited during a discrete increment of time. Kerr and Jirik[18] developed the concept of a DGI for the purposes of subsurface mapping of Tertiary fluvial deposits in the south Texas onshore gulf coast region. Thus, a DGI is an operational unit for subsurface mapping. A single DGI is correlated as having a common elevation from the top of gross channel-fill thickness to a stratigraphic datum (marker bed). After correlation through a cross section network has been completed, the facies and their thickness are plotted at each well site for each DGI. If the facies genetic relationships are logical, then the task is complete. If, however, the facies genetic relationships do not make sense, then the correlation must be reconsidered and another iteration is required. Once satisfied with the DGI correlation, facies-biased isopach mapping is performed.

A DGI can also be thought of as a lithostratigraphic unit whose boundaries have chronostratigraphic significance and whose definition in the case of the Bartlesville sandstone is equivalent to that of a parasequence[9] in sequence stratigraphic parlance.[19] Identification of DGI's for the Self-unit portion of Glenn Pool field are indicated in Figure 7. As shown, each DGI is commonly associated with a single facies type in individual wells but will exhibit lateral distribution of coexisting facies in cross sections

(**Figure 12**). The DGI is considered the major subsurface unit for mapping purposes. Within the productive, sand-rich portion of the Bartlesville sandstone, individual DGI's are separated by laterally extensive (except for localized erosional windows) floodplain mudstone horizons. Facies occurrences within a DGI share a common depth relative to the Inola limestone marker (Figures 7 and 12). In correlating Bartlesville DGI's in southern Glenn Pool field, a 5-ft (1.5-m) tolerance is required due to local variations in early compaction and syndepositional slumping off the valley margin.

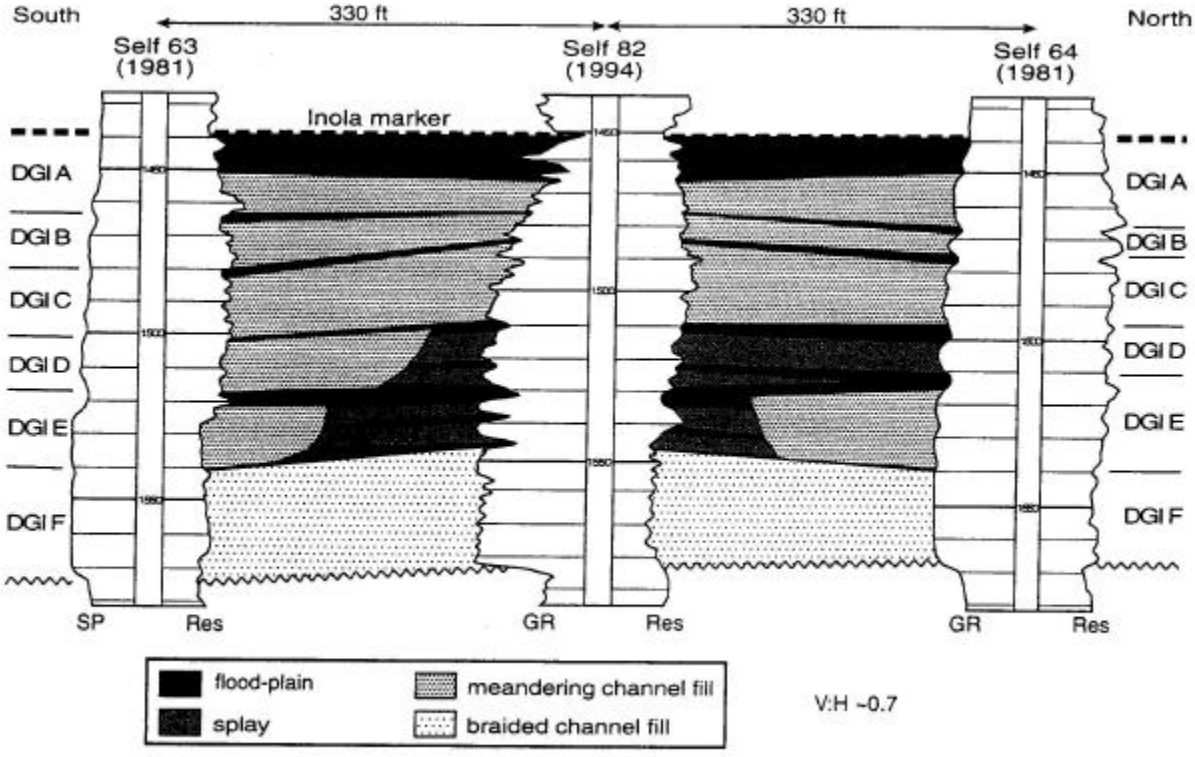

Figure 12 – Cross-section through Self-82 well showing of discrete genetic intervals and facies[10]

In the southern part of Glenn Pool field, a total of 7 DGI's are recognized, labeled A through G in descending order; however, DGI G is not present in the Self-unit (Figure 12).[9] DGI's G and F consist of braided channel-fill facies and limited occurrences of floodplain mudstone facies. DGI's A-E are made up of meandering fluvial facies (channel-fill and splay facies) (Figure 12), with an overall upward increase in the proportion of non-reservoir floodplain mudstone facies. Within the limits of the Self-unit,

DGI G is absent due to onlap pinchout to the south. South of Glenn Pool field, DGI A through E show transition to estuarine bayhead delta facies deposits.[9]

Systems Tracts and Sequence Stratigraphic Elements

The largest stratal volumes considered in study of the Bluejacket (Bartlesville) sandstone are equivalent to systems tracts and stratigraphic sequences. A stratigraphic sequence is a succession of genetically related strata bounded by unconformities and their correlative conformities.[20] A systems tract is a contemporaneous three-dimensional assemblage of facies whose designation is based on position within a stratigraphic sequence and a distinctive parasequence stacking pattern.[19-20] The original conceptualization of sequence stratigraphy has the incised valley being filled during the later stages of relative sea level lowstand.[21-22] However, if the erosional accommodation provided by incision of the former shelf is not filled during relative sea level lowstand, then the incised valley may be filled during subsequent rise in relative sea level.[23]

Based on analysis of facies distribution and DGI (parasequence) stacking patterns, the Bluejacket (outcrop) and Bartlesville (subsurface) sandstone comprises two systems tracts (see Figure 3). In Glenn Pool field, the low-stand systems tract is represented by DGI G and F, which include braided channel-fill facies sandstones in an aggradational stacking pattern. An overlying transgressive systems tract is interpreted for DGI A through E, with meandering fluvial facies dominant in the area of Glenn Pool field. The Inola marker is considered to represent a compressed section associated with the maximum flooding surface (Figure 3).

The basal contact of the Bartlesville sandstone with the underlying Savanna formation is an unconformity identified as a type-1 sequence boundary. This conclusion is based on outcrop observations and detailed subsurface correlations and conforms to the overall interpretation of the Bartlesville as representing the lower portion of a type-1 stratigraphic sequence.[9] The sub-Bartlesville unconformity shows truncation of parasequences in the Savanna formation and, as noted, is onlapped by Bartlesville parasequences (DGI's).[9]

Petrophysical Properties and Architectural Elements

The above analysis of facies architectural elements is considered of direct importance to defining, mapping, and explaining the distribution of reservoir quality and remaining oil reserves in the Bartlesville sandstone. Core analysis performed on samples from the Self-82 well demonstrated that porosity and permeability are strongly DGI-related, with both parameters showing progressive increase from DGI B downward to DGI F (**Figure 13**). Highest reservoir quality and the greatest degree of homogeneity are indicated for DGI F, with *Kv/Kh* ratios as high as 0.8-0.9 (**Figure 14**). Moderate to good reservoir quality exists in meandering channel-fill and splay facies sandstones, which display considerably greater permeability anisotropy (*Kv/Kh* of 0.3-0.5) than do braided channel-fill deposits. Figure 14 suggests that both lateral and vertical fluid flow are significantly more complex in meandering channel-fill and splay sandstones, and that large portions of these potential reserves remain unflushed by waterflooding to date.

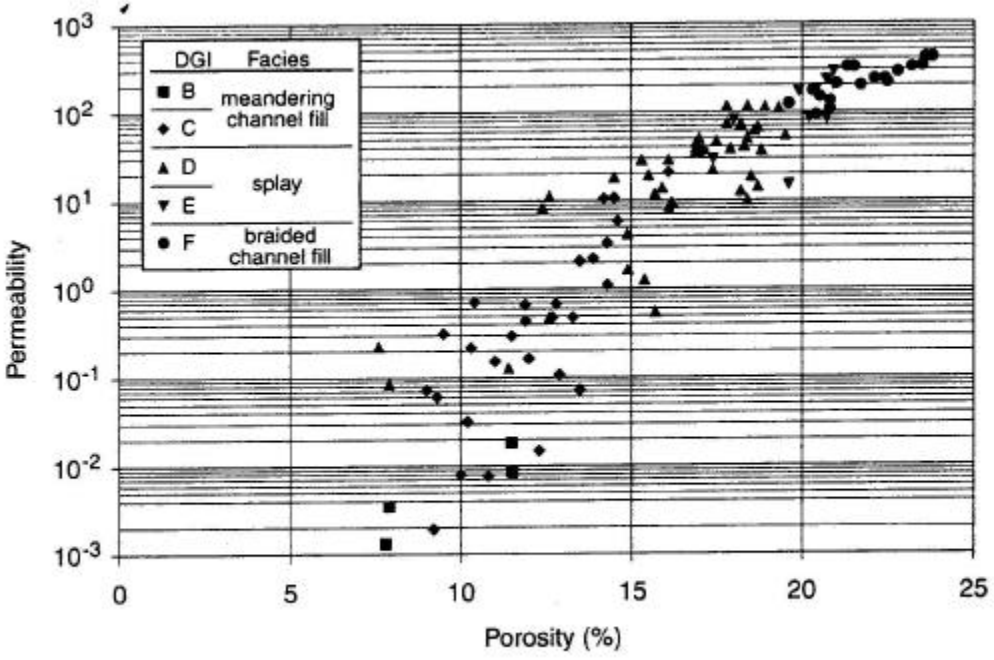

Figure 13 – Permeability vs. porosity from core plug measurements in Self-82[10]

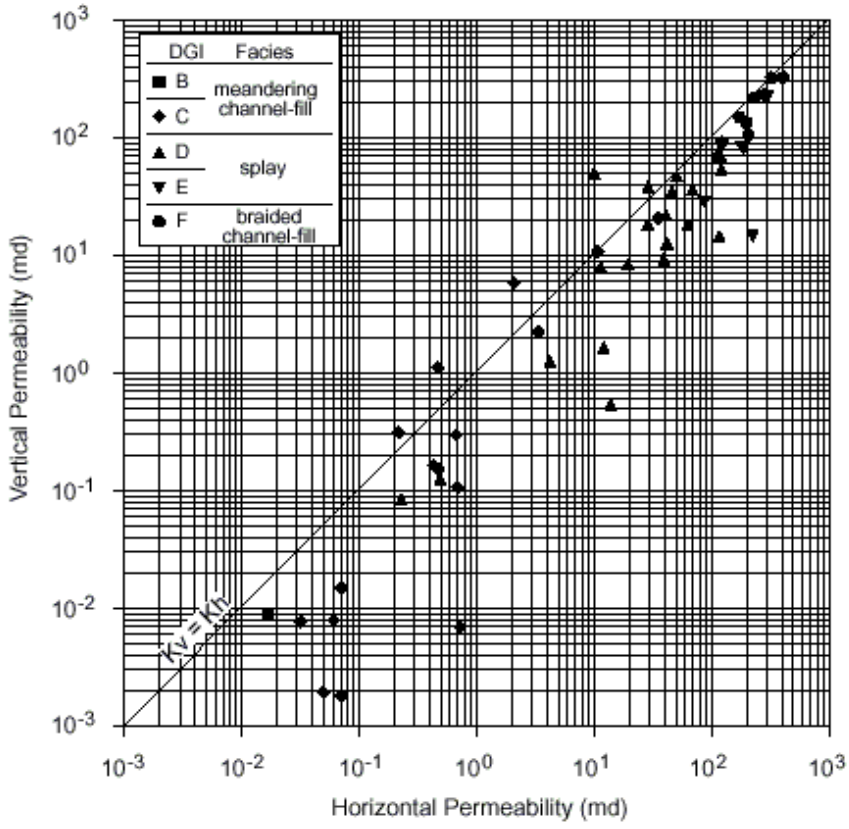

Figure 14 - Vertical permeability vs. horizontal permeability from core plug measurements in Self-82[10]

This conclusion is strongly supported by observations of oil staining in the Self-82 core (see Figure 7). Such observations showed that DGI C, the lower channel-fill subfacies, was water bearing (i.e., appeared to be flushed), whereas actively bleeding oil was seen in middle channel-fill sandstones between mudstone drapes on lateral accretion surfaces. For DGI D, in which individual splay sandstone layers are separated by mudstones, oil was observed bleeding from all except one of the sandstones, assumed to be flushed (see Figure 7).

The combined quantitative and qualitative data on the Self-unit indicate that the largest amount of remaining oil reserves, after nine decades of development, are concentrated in middle channel-fill subfacies and splay facies of DGI A through E (transgressive systems tract).

Structure Southeast Side of Glenn Pool Field

Preparation for drilling the Self-82 well included picking the expected depths to the top of the Inola limestone and Glenn sandstone for establishing a coring point. Offset wells were about 600-ft apart from the Self-82 staked location. The coring point was picked at 1420-ft drill depth; the point was estimated independently by two geologists whose estimations were very similar. After coring and logging of the Self-82, it was realized that the estimated and actual depths were 30-ft off. This discrepancy was most puzzling given the close distance to offset wells. Consideration to the possibility of additional structural relief within the broad Glenn Pool field closure was discussed, but not given a high priority within the project work schedule.

A study area was selected along the southeastern margin of Glenn Pool field (sections 27, 28, 33 and 34 of T17N R12E) for the investigation of this question of localized structural relief. The working hypothesis was that such structures are large-scale slumps located along the incised valley margin. The study area is located closer to the margin than the Self-unit. Logs from 21 wells were available for this effort. Well spacing ranges from 2,600-ft to less than 300-ft apart. Structure cross sections were compiled through the well array.

The stratigraphic interval of interest spanned the Pink limestone to the Brown limestone. Top of the Pink is about 260-ft above the Glenn sandstone. Top of the Brown is about 120-ft below the top of the Glenn sandstone. The interval thickness between the top Brown and base of Glenn is highly irregular as a result of erosional relief along the base of the Glenn. Structure maps were produced for top Pink, top Inola, and top Brown.

The top Inola structure map provides evidence of localized structures similar to what would be expected for slumping. The relief within the study area measured from well log tops is 50-ft over about 1 mile. Locally, however, the relief is as high as 30-ft vertically in 400-ft laterally; relief comparable to that developed around the Self-82 well. From careful correlation, it is clear that stratigraphic section if faulted out of wells where the structural relief is high. The faults appear to be listric normal in geometry, with associated antithetic faults and rollover anticlines. The normal faults trend northeast southwest

(parallel to the local orientation of the incised valley margin) with open curvature to the northwest and down to the northwest separation. Laterally discontinuous antithetic faults mirror the normal faults. Structural separation is 30-ft across the listric faults with localized antithectic faults; is 15-ft across listric faults without antithetic faults; and is 10-ft across antithetic faults. Separation up through the Pink limestone is only locally developed.

The implication for reservoir compartments depends on the stratigraphic level within the Glenn sandstone. Faulting of the braided fluvial section probably has little effect in that fault gouge of this sand-rich interval is not likely to be a barrier to fluid flow. On the other hand, faulting of the meandering fluvial section could produce reservoir compartments in that fault gouge of this mud-rich interval that will likely produce reservoir barriers/baffles. Thus, DGI A through E reservoir compartments could be developed locally in these listric faulted areas.

Geophysical Analysis

As part of applying new technology, we evaluated the effectiveness of cross borehole tomography in improving the reservoir description. In this section we detail our efforts and provide some results.

Introduction

Seismic crosswell tomography is a method of determining seismic velocity (wave speed) between boreholes. The tomographic image has a resolution of 10 to 25-ft and can supply otherwise unavailable information on geological and reservoir characterization parameters.

Seismic tomography is similar in principle to medical tomographic methods, but several factors conspire to make seismic tomography more difficult than the medical case. This is illustrated in the comparison below.[24]

Medical X-Ray Tomography

- Imaged object can be completely surrounded by sources and receivers (full aperture).
- Image rays travel at constant velocity (speed of light) and are straight.

- Uniform ray coverage.
- Resolution dictated by x-ray wavelength on the order of Angstroms.

Seismic Tomography

- Imaged object cannot be completely surrounded by sources and receivers (limited aperture).
- Image rays travel at variable velocity (sound speed in rocks) and are bent.
- Irregular ray coverage due to ray bending and limited recording aperture.
- Resolution dictated by seismic wavelength on the order of 25-ft.

These differences mean that medical tomography technology has not been of direct use in the seismic case. Rather, it has been necessary to develop methods of acquisition, processing and interpretation that directly account for the nature of seismic tomography measurements. This new technology has, until recently, only been available in research labs of major oil companies. We feel that seismic tomography an important tool for reservoir analysis. The information to be gained from seismic tomography includes details of geological variations within the reservoir and estimates of parameters of interest to petroleum engineering.

In this project we acquired seismic tomography across a five-spot well pattern in order to visualize and understand important parameters controlling reservoir quality. The acquisition and initial processing of this data was performed by Amoco Production Company under the direction of Larry Lines and Henry Tan of the Tulsa Research Center. The survey planning and interpretation was integrated with petroleum engineering and geological data.

Four separate tomography data sets were acquired inside the Self-unit of the Glenn Pool field. The geometry included a centrally located source well, S, and four receiver wells, R. Each tomography survey results in an image plane between the source well and the receiver well active for that survey. By shooting in four substantially perpendicular directions, we planned to maximize the probability of observing geologic trends in the data (e.g., channels, depositional fabric, etc.).

The source well is referred to as Self-82. This was drilled as part of this research project. The advantages of using a new well for the source, as opposed to an existing well, are:

1) Hole will be clean, uncased and untreated.
2) Hole will be logged, including sonic.
3) TD approximately 500-ft below reservoir level.
4) Hole will be cored through the reservoir.
5) Hole will have micro-imaging log through the reservoir.

Items 1 through 3 are of direct importance to the tomography, while 4 and 5 are critical to integrating tomography results with reservoir parameters. In addition to the logs mentioned here, a deviation survey was performed in the source and receiver wells.

The tomography acquisition was done with equipment and personnel provided by Amoco Production Company, under the direction of Dr. Larry Lines and Dr. Henry Tan. This team had extensive experience in the acquisition of tomography data[25-29] including several surveys in Oklahoma.[30-31]

The four tomography surveys were not be acquired in one continuous effort. Aside from questions of field crew efficiency in a lengthy shooting program (see below), there was a need to review data from the first survey for data quality and processed image fidelity. This review pointed out the need for modifications to the acquisition parameters.

The field equipment needed for tomography acquisition is two wireline trucks, a down-hole source and a string of down-hole receivers.

There were many tomography sources in use or being developed[32-33] at the time of this project. This study used a Piezoelectric transducer source.[28, 34] Physically, the source is a steel-encased ceramic piezobender with 4 3/4 inch outside diameter (OD), and requires a fluid-filled borehole of inside diameter (ID) not less than 5 inches. It can generate a useful signal up to 2000 Hertz (cycles per second) and actual tests in Oklahoma rocks similar to those at Glenn Pool have shown 1500 Hz signal received across distances of 400 to 500-ft.

The basic receiver for this study is a string of hydrophones connected through wireline cable to a truck-mounted recording system. The use of hydrophones requires the receiver hole, like the source well, to be fluid filled. An important efficiency factor is the number of receivers that can be operated down-hole at one time, termed a receiver group. Current technology (as of the project date) limited this number to about 6 receivers per group. The receivers, wireline cable and recording instruments deliver a time sampling rate of 50 microseconds, with 8000 samples per trace and 24 bits/sample. This general kind of source/receiver tomography acquisition set-up has seen extensive field use.[26, 28, 35]

Data Processing

Once the data is collected it must be processed to create an image of the subsurface between the source well and receiver well. This involves picking first arrival times for each source and receiver then inverting a large, sparse system of algebraic equations. The result is a velocity tomogram which estimates the seismic velocity on a regular grid in the vertical plane between the source and receiver wells. The method is capable of determining interwell velocity variations of 5%, or better.

The plan was to process the data in two fundamentally different ways. First, the data would be processed by Amoco using the system they had developed over the course of several years.[36-37] We considered this to be state-of-the-art processing technology. Second, we planed to process the data at The University of Tulsa using public domain software. We used a seismic tomography processing program written by the U. S. Bureau of Mines called BOMTOM (Bureau Of Mines TOMography).

Since BOMTOM is free and could be run on a standard PC, it is typical of the processing capability that any small operator could possess. By processing the data in two ways we could compare the processing capability available to small operators (e.g., BOMTOM) with the state-of-the-art solution (Amoco processing). This gave some indication whether tools available to the small operator are adequate for reservoir characterization studies using seismic tomography.

Interpretation and Integration

Once the seismic tomography data has been acquired and processed it must be interpreted. It is at this stage, more than any other, that the integration of geophysics, geology and petroleum engineering is required. The raw product of tomography processing is a velocity tomogram showing variations in seismic wave speeds between the source and receiver boreholes. This must be correlated with all available information, including well logs, cores, geological parameters (lithology, porosity, stratigraphy, etc.) and petroleum engineering parameters (oil saturation, fluid contacts, etc.). Our project generated one image between the source well and each of four receiver wells. We planed to interpret this data and gain information on several characteristics of the reservoir. First, structure and lithostratigraphy,[28, 38-40] second, reservoir inhomogeneities,[38] third, acoustic continuity[30, 41] which is a tool for determining whether beds that appear to be the same unit in two wells are physically continuous; and fourth, correlation of stratigraphic units between tomography surveys to determine their orientation in three-dimensional space.

Any interpretation goal depends on data quality, but these require only average data quality. In addition, if the data quality were excellent it might also be possible to infer porosity[31] and/or oil saturation.[38, 42]

Crosswell Seismic Test

The primary goal before acquisition was to test operational procedures and data acquisition parameters in advance of the full crosswell test scheduled in late 1993 or early 1994.

The test was conducted on 24-25 August between wells 62 and 72 of the Self-unit. The well locations are shown in **Figure 15**. The acquisition team consisted of equipment and personnel from Amoco Production Company's Tulsa Research Center (H. Tan, L. Colethorp and J. Beck). Also represented were The University of Tulsa (C. Liner, M. Kelkar, D. Kerr, and graduate students), Uplands Resources, Inc. (D. Richmond, J. Helm), and the Department of Energy (R. Lindsey).

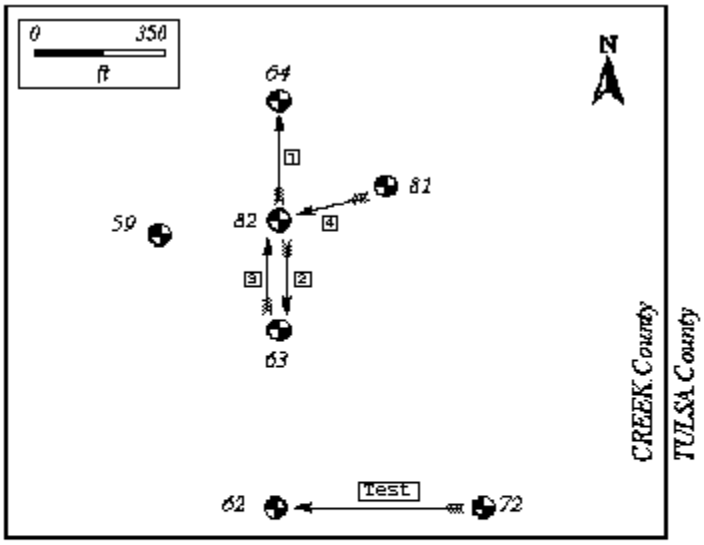

Well Pair	Distance (ft)	Data	Survey	Date
72-62	660		Test	24 August 93
82-64	341	14736	1	27 January 94
82-63	324	17759	2	28 January 94
81-82	361	16696	3	29 January 94
82-59	347	travel times	4	30 January 94

Figure 15 – Map and shooting schedule for crosswell seismic data acquisition

These particular wells were chosen because they were widely spaced (about 660-ft) and intermittently shut down. Well 62 served as the receiver well and 72 as the source well. The seismic source, **Figure 16**, is an annular piezoelectric transducer, which produces a swept signal. For day 1 shooting the signal sweep contained frequencies from 200-2000 Hz. Other acquisition parameters are listed in **Table 2**. The recorded data traces were cross-correlated with the pilot sweep to create impulse-like correlated data traces. The correlation process allows more energy to be input over a time window (0.25 seconds) than could be injected by an impulsive source. An impulsive source of similar strength would be damaging to downhole equipment and the borehole. The test operation involved two wireline trucks, one each for source and receiver well, and a control truck. Each shot generated 6 channels of time-dependent data: one channel for each of the 3 receivers, one channel for the pilot signal, and two dead channels.

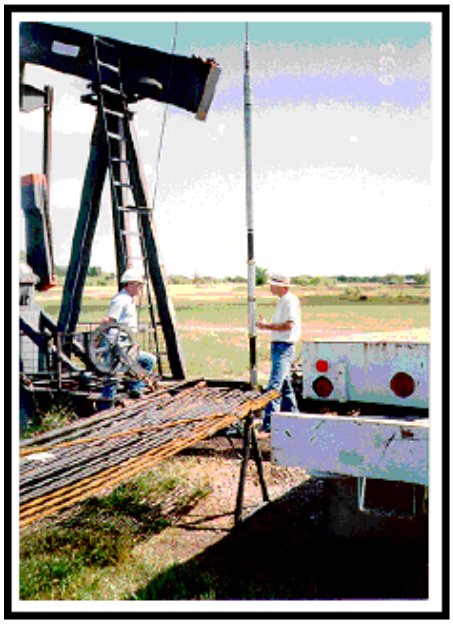

- Piezoelectric Transducer
- Sweep Signal
- 200-2000 Hz
- 0.25 s Sweep Time
- 4 ft Source Interval

Figure 16 – Photo of source and some characteristics

Table 2 – Properties of tomography software used in this project

Group	Rays	Anisotropy	Access
Utulsa	Curved	Yes	In development
Amoco	Curved	Yes	Proprietary
MUN	Curved	Approximate	Consortium
BOMTOM	Straight	No	Public

The receiver apparatus, **Figure 17**, consisted of three hydrophones on wireline spaced 8-ft apart. The hydrophones return electrical signals in response to the passage of acoustic, or sound, waves. The receivers are suspended freely in the borehole while the source is continuously moved in the receiver well. Both source and receiver wells must be fluid-filled for the crosswell system to operate.

- Hydrophones
- Fluid-filled Borehole
- Array of 15
- 8 ft Spacing

Figure 17 – Photo of receiver and some characteristics

Four common receiver fans were shot on day 1, as shown in **Figure 18**. Also shown are the fan numbering system, extent of fans, lithology in source and receiver wells, well separation, and starting/ending depth associated with each fan. Some formation depths are also indicated. The lithology and formation depth information was supplied by the geological team based on well-log interpretation. The deepest sand unit in each well is the Glenn sand, which is the productive interval in the field. From the acquisition geometry we did not expect to determine velocity in the Glenn sand itself during this limited test. The fans were acquired in the order 1, 2, 3, 4.

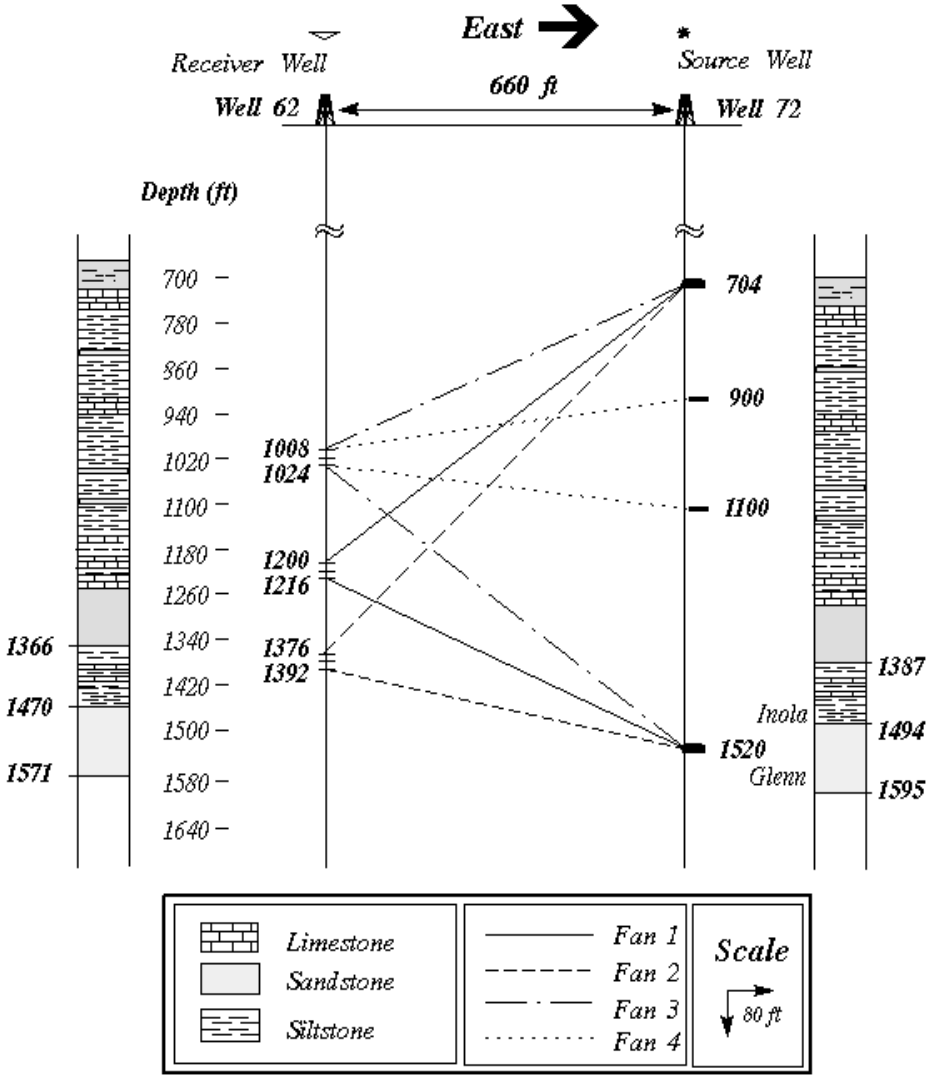

Figure 18 – Details of shooting geometry for the test survey

Fans 1-3 had source spacing of 16-ft, which allowed rapid traverse of the entire section of interest. This source spacing is very large, even for a typical tomographic survey. It was used for testing purposes only, and the total interval covered by sources in Fans 1-3 was approximately 700 to 1,500-ft. High-resolution reflection surveys require smaller source intervals. To test the feasibility of reflection work at Glenn Pool, Fan 4 was shot with source spacing of 4-ft. This was accomplished by moving the source up one-half of the fixed receiver interval of 8-ft.

Vertical stacking is a method of improving data quality and suppressing random noise. The idea is to make repeat measurements without moving source or receiver and summing the repeat results to create a final trace. The signal-to-noise improvement achieved by this process in SQRT[N] where N is the number of vertical stacks. Only random noise is suppressed by this technique. Source generated noise (such as tube wave energy) is not suppressed.

All fans from day 1 used an 8-fold vertical stack. As the source is continuously moved uphole, the source is activated 8 times in a 2-ft zone centered on the stacked source location. The resulting traces are summed to form the stack trace at this level. The vertical stacking process is valid if the stacking interval is much less than a seismic wavelength. We estimate the P-wave wavelength in the data to be approximately 12 to 13-ft, and the S-wave wavelength approximately 6-ft. Therefore, the 2-ft vertical stacking interval is valid.

Data acquired on day 1 showed good data quality and signal transmission. First arrivals (which are the basis of tomographic processing) were well defined, and significant events beyond first arrival energy are also present. These are some combination of direct shear waves, reflected P & S waves, and tube waves. The 16-ft source spacing on Fans 1-3 give the direct arrivals large time delays as source/receiver separation increases. Four 4-ft source spacing on Fan 4 resulted in observation of reflection energy beyond the first arrival. These reflections are important as a source of high-resolution information about the rock configuration.

Detailed examination of Fan 1 showed first arrivals with good continuity and amplitudes significantly above background noise levels. When first break amplitudes fall below background level first breaks cannot be picked for use in tomography. This gives a constraint on the maximum operating range of the crosswell acquisition system. This operating range varies with geographic location and reservoir depth.

Direct arrivals weaken with angular source/receiver separation. Calculations based on data from Fans 1-3 indicate the maximum transmission distance for direct arrivals at the Glenn Pool site is about 735-ft. In the full crosswell test we expected well separation of 450-ft, so the 735-ft maximum range corresponds to a maximum source/receiver angle of 52š. This is well in excess of the design criteria of

45š. Therefore, we expected good direct arrival energy at maximum acquisition angles in the full crosswell test.

A major attraction of crosswell seismic data, relative to surface data, is its higher frequency content. Spectrum analysis of the test data indicated significant frequency content from 300-1300 Hz. No surface seismic data exists at Glenn Pool, but typical surface seismic frequencies are 20-80 Hz. Thus, crosswell seismic data gives a 10 to 20-fold increase in resolution relative to surface seismic data.

The second day of the crosswell test followed up ideas and concerns identified on day 1. Four additional fans were acquired. Fans 5 and 6 have source level spacing of 16-ft. These were designed to test maximum signal range by shooting with large vertical source/receiver separation. The longest source/receiver separation occurs in Fan 6, where the signal clearly faded into background noise levels. At this range no useful source-generated energy is present. This test fan reinforced the maximum range calculations derived from day 1 data.

All of the day 2 data was shot with a source bandwidth of 400-2000 Hz. This change from 200-2000 Hz on day 1 was in response to low frequency tube wave noise (about 200 Hz) interpreted on the day 1 data. The 400 Hz low-cut had a nominal effect on the data quality.

Fans 7 and 8 are reflection-quality common receiver fans with 4-ft source spacing. These are near in depth to the reservoir level and may contain reflections from the reservoir itself. These two fans were shot with the first source in each fan vertically offset by 2-ft. That is, the source levels in Fan 7 are at depth levels 1488, 1484, Š, 1276, while Fan 8 has source levels 1490, 1486, Š, 1278. This acquisition geometry allows the data traces to be interleaved to an effective spacing of 2-ft. Strong tube wave energy was seen to interfere with reflection events. Some advantage was gained by the 2-ft spacing, but no further interpretation was attempted.

Also on day 2, a vertical stack test was performed as part of Fan 5. The source interval 800-928 (fixed receiver location) was shot once with 8-fold vertical stack and again with 32-fold vertical stack. The 32-fold data (lower plot) stands out slightly better from background noise level. The 32-fold data

shows some improvement in signal strength in the 1500-2000 Hz range. Overall the effect is a minor improvement in data quality.

Crosswell tomography involves picking first arrival times on crosswell seismic data and inverting for a velocity distribution between the wells. The quality and reliability of the tomogram depends on highly redundant data. If a great number of travel times are available then the velocity field is well-constrained. With fewer travel times the solution is highly non-unique. The crosswell data acquired on days 1 and 2 was insufficient for full tomographic reconstruction. However, using all day 1 data we were able to estimate velocities, which should be viewed with caution due to insufficient data for full inversion. The average velocity in well-illuminated zones was about 12,000-ft/sec. This is in very good agreement with sonic log velocities from the Self-82, which was drilled in December 1994. The average sonic velocity at a depth of 1,000-ft in the Self-82 is 11,800-ft/sec.

The location of Self-82 was decided in a series of team meetings during third and fourth quarters of 1993. From a geophysical point of view, this location was acceptable because the four surrounding wells were close (about 330-ft) and formed perpendicular seismic image planes. This configuration seemed optimum for delineating reservoir features of interests.

After the Self-82 well was drilled, well preparation began on the 59, 63, 81 and 64 wells. These wells served as receiver wells in the full crosswell survey. It was discovered at this time that the receiver wells were either plugged back or sand-filled to near the top of the Glenn sand.

An important parameter in tomographic acquisition is aperture. This is a measure of how well the acquisition geometry "surrounds" the object of interest. If the object is surrounded then the aperture is good and a well-constrained image can be produced. If the aperture is incomplete, the object is not surrounded and an incomplete image results. The nature of crosswell acquisition is such that it is never possible to acquire full aperture data, but it is important to get the best aperture possible. By having the receiver wells only open through the uppermost Glenn sand, the survey aperture was seriously compromised. It was decided to re-enter these wells for cleaning and/or reaming to the base of the

Glenn. As cleaning these wells was an unanticipated cost, the geophysical team was requested to prioritize the receiver wells in order of importance.

A meeting with geological team members was held on 17 January 1994, and priorities were established. These priorities are given here, together with related comments.

1. 82 → 81
   - Edge of DGI "B" sand (subtle)
   - Thickening of DGI "C" (15 feet)
   - Thinning of DGI "A" (10 feet)
   - Best image plane perpendicular to channel

2. 82 → 63
   - Point-bar to point-bar cross section
   - Erosional edge of DGI "B"
   - Thinning of DGI "A" (10 feet)

3. 82 → 64
   - Thickening of DGI "C" (10-15 feet)
   - Edge of DGI "B"
   - Thinning of DGI "A" (10 feet)

4. 82 → 59
   - Small well casing (4.5" OD; 3.875" ID)
   - Unlikely it can be cleaned well enough to admit seismic receivers
   - Suggest no cleaning of well 59, but run receivers from PBTD.

Tomograms and Interpretation

By late 1994 there were tomography results available from The University of Tulsa (G. Bozkurt), Amoco (A. Vassiliou), Memorial University of Newfoundland (L. Lines), and BOMTOM (G. Bozkurt). Table 2 lists the tomography software characteristics used in this study.

It was quickly apparent that the data presented a difficult geophysical problem because of strong P-wave anisotropy present in shaly rocks above the Glenn sand. This was first recognized by A. Vassiliou of Amoco, and independently discovered by L. Lines of Memorial University. The following discussion is based on ideas originated by A. Vassiliou.

P-wave anisotropy means that the velocity of P-waves depend on direction of propagation. It is customary to refer to speed of horizontally traveling P-waves as *Vh* (horizontal velocity) and vertically traveling ones as *Vv*. If $Vh > Vv$ then the rocks are said to be weakly anisotropic, while $Vh >> Vv$ indicates strong anisotropy. In the Glenn sand itself, we observe negligible anisotropy. However, the presence of strong anisotropy above the Glenn must be accounted for if accurate tomography results are to be obtained. Furthermore, the level of anisotropy observed at Glenn Pool is such that surface reflection data (such as 3-D seismic) may require special processing. For independent operators in the area, this fact could be very important.

Velocity anisotropy is usually indirectly indicated. This can be through core plug measurements at frequencies 100 times (or more) greater than surface seismic frequencies, or tomographic results that are highly processed products or even non-hyperbolic normal move out curves on surface seismic data. At Glenn Pool we have rare direct evidence of strong P-wave anisotropy.

The first piece of evidence is the sonic log on the interval 1200 - 1600. Sonic logs measure velocity by refracting a high-frequency P-wave pulse vertically along wall of the borehole. Thus, sonic measurements indicate *Vv*. For example at the 1,250-ft level in Self-82 the sonic reading is 90 microsecs/ft, corresponding to a *Vv* of 11,110-ft/sec.

From the crosswell data, we can extract traces that have source and receiver at the same level (depth). The pertinent wells at Glenn Pool were surface surveyed to determine relative wellhead location, and a deviation survey was run on each to track subsurface (x, y, z) coordinates of each well bore. From this information, it is possible to construct a constant-level gather for each survey. Since the source and receiver for each trace are at the same depth, the direction of energy travel is horizontal and therefore indicates *Vh*. The crosswell horizontal distance and travel time can be combined to provide a *Vh*

Pseudo-Sonic reading in microsecs/ft. For example, at the 1,250-ft level in the 82->64 survey, the first arrival energy indicates a *Vh Ps*-Sonic value of about 71.5 microsecs/ft, corresponding to a *Vv* of 13,990-ft/sec. This value is consistent in all three crosswell surveys.

To summarize, the sonic log in Self-82 gives *Vv*=11,110-ft/s at 1,250-ft while the crosswell data shows that *Vh*=13,990-ft/s at the same depth. This represents direct evidence for a *Vh* about 26% greater than *Vv* in the rocks at this level. Generally, P-wave anisotropy greater than 10% is considered strong, which makes the level of anisotropy seen at Glenn Pool quite remarkable.

As it relates to the tomography results, the first clear evidence of anisotropy was a characteristic X feature seen in the BOMTOM result. This processing was done at The University of Tulsa using picks from A. Vissiliou of Amoco. This X feature is typical of constant velocity tomography results in an area where anisotropy is present. As seen in **Figure 19**, this feature is present in the constant velocity tomogram (BOMTOM), but not the MUN tomogram, which honors anisotropy and curved rays.

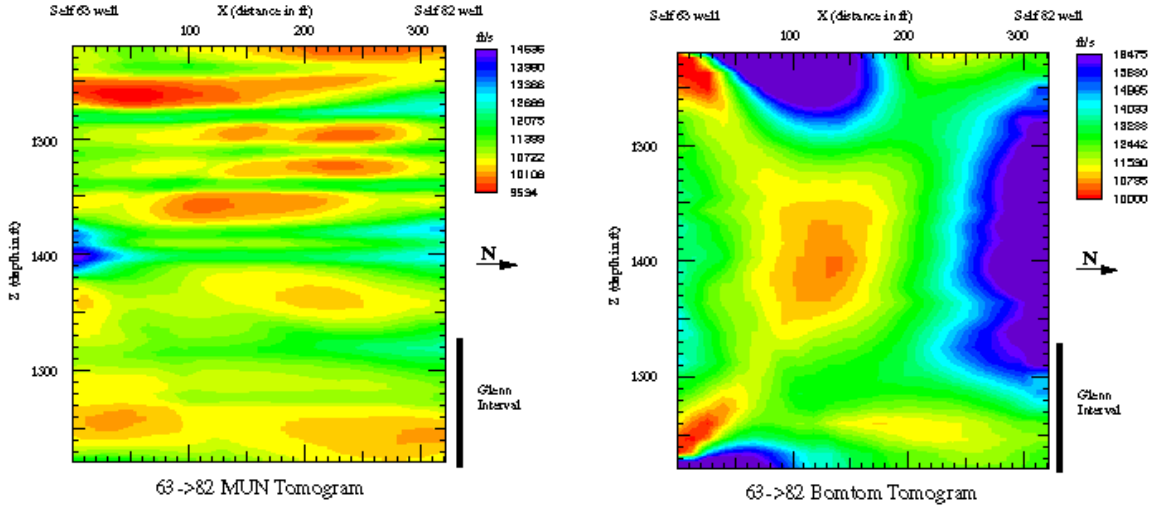

Figure 19 – Comparison of 63-82 tomograms processed by Memorial Univerity and software from the U.S. Bureau of Mines

The Memorial University tomograms were discussed at length at a meeting in Tulsa between Dr. Lines and TU team members on June 29, 1994. This tomogram was significantly different from the Amoco result, particularly the level of detail in lateral variations of velocity. The original of this tomogram was

forwarded to TU for final display and interpretation. **Figure 20** is a side-by-side comparison of the MUN and Amoco results. Finally, The University of Tulsa result is compared with MUN in **Figure 21**.

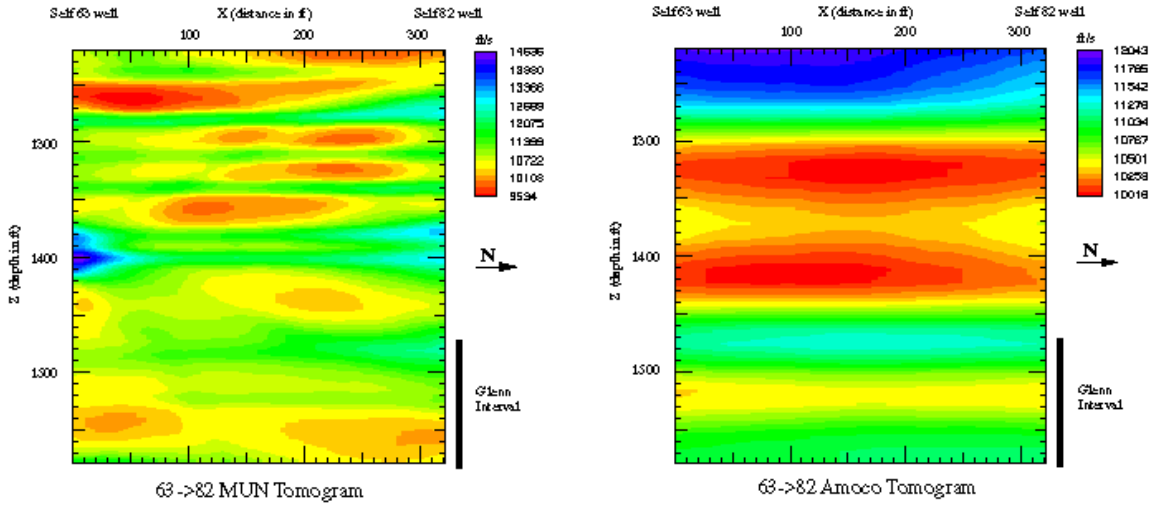

Figure 20 – Comparison of MUN and Amoco tomograms

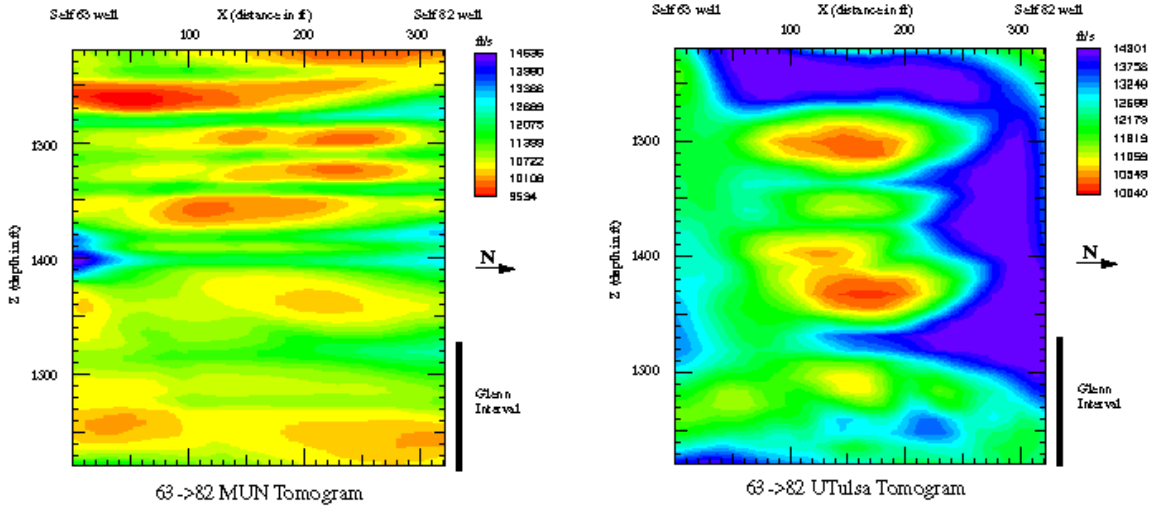

Figure 21 – Comparison of MUN and The University of Tulsa tomograms

Based on discussions with the geological and engineering teams, it was decided that the MUN result best represented the subsurface as tested by well control. Detailed interpretation of the MUN tomogram was undertaken. **Figure 22** shows the full tomogram and a zoom of the Glenn interval showing an interpreted sand body. Properties of the imaged sand body are listed, including width,

height, etc. This is a level of detail that is unavailable from surface seismic measurements, and illustrates the added value of crosswell studies.

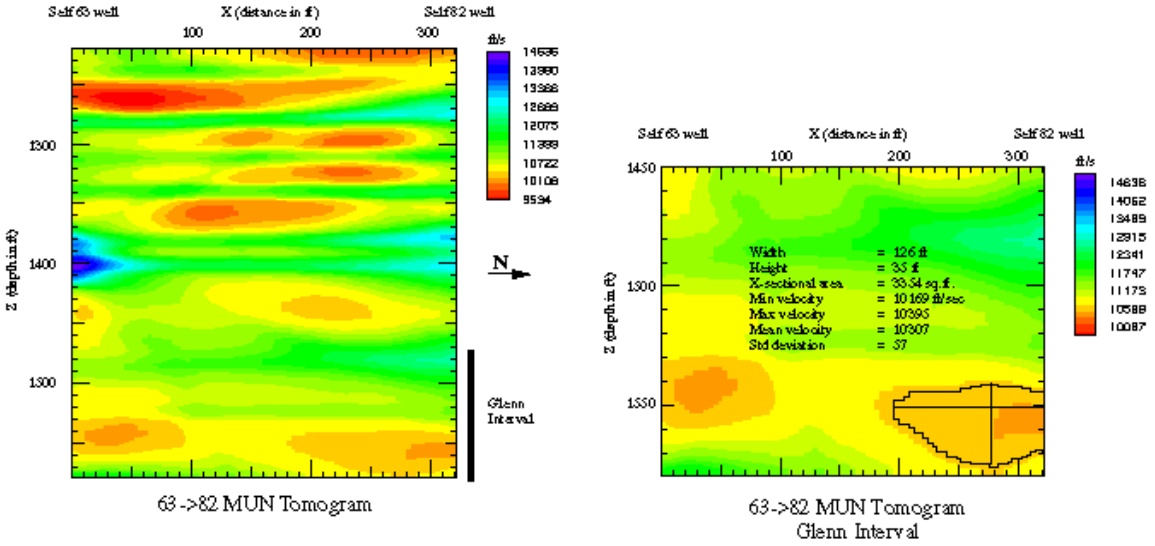

Figure 22 – MUN tomogram and zoom of Glenn interval with interpreted sand body

Using well log data, the geological team had developed a sequence stratigraphic interpretation of the rocks encountered in the 63 and 82 wells. In **Figure 23**, these interpretations are brought into the tomogram. Finally, the interpreted tomogram is shown along side a line drawing of the sequence stratigraphic interpretation in **Figure 24**.

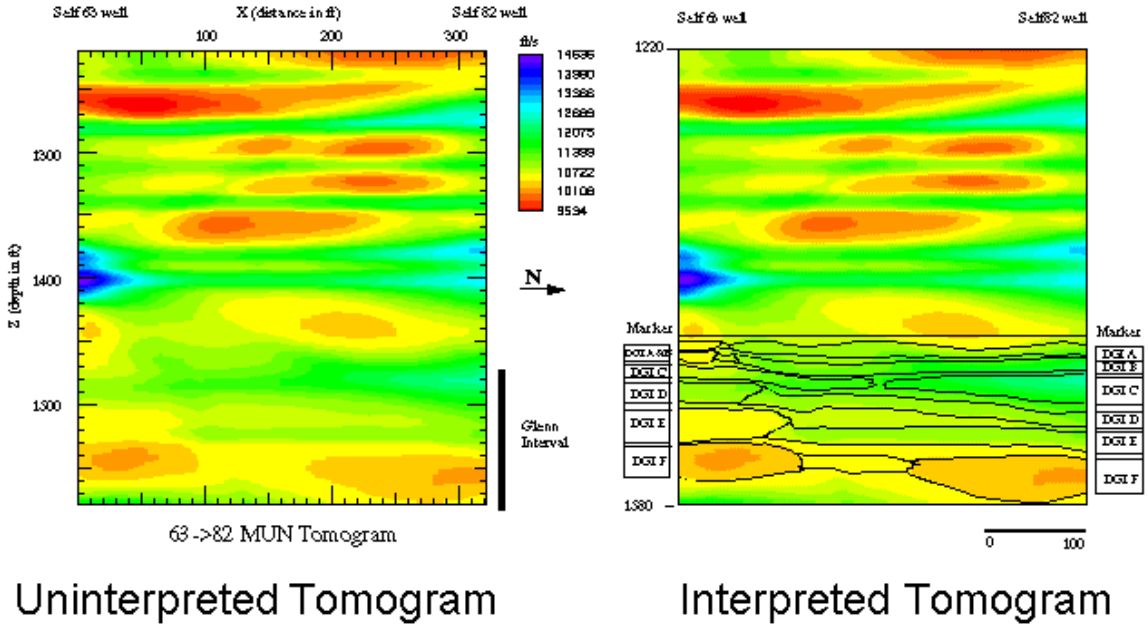

Figure 23 – Detailed stratigraphic interpretation

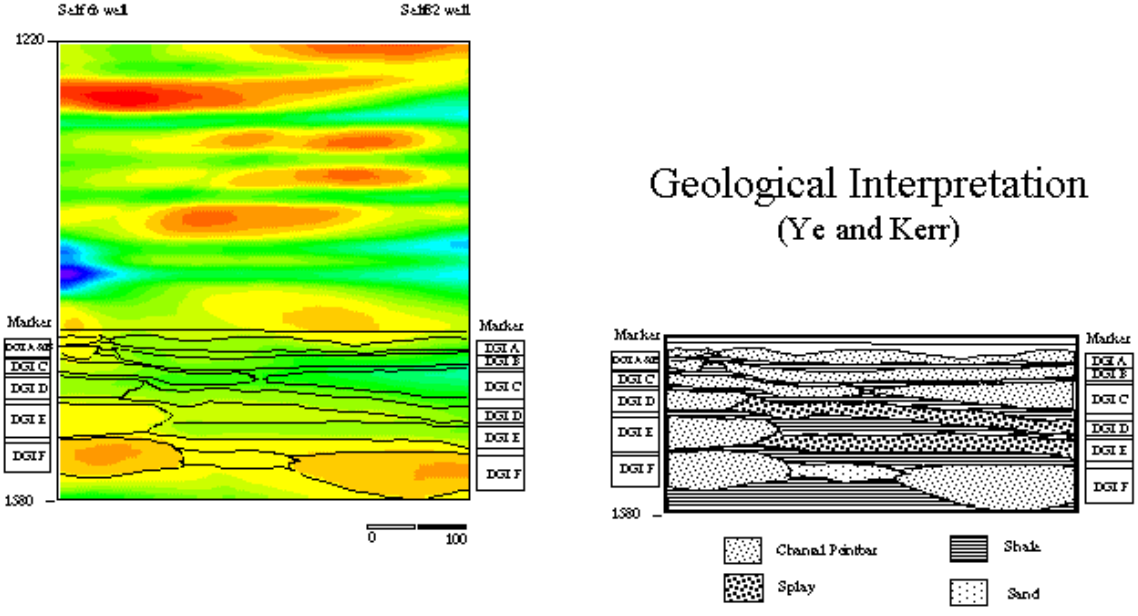

Figure 24 – The tomogram interpretation (left) compared to the geological model (right)

Anisotropic Ray Tracing

As noted above, the Glenn Pool site is characterized by strong seismic anisotropy. This means that seismic wave speed in a vertical plane depend on the direction of travel, which leads to complications with processing crosswell seismic data. If it is not properly taken into account, the resulting tomograms exhibit artifacts, which have no geological meaning. Software has been developed at The University of Tulsa to deal with this problem. The software is an extension of earlier work by Epili and McMechan[43] and is the subject of G. Bozkurt's Ph.D. dissertation.[44]

3-D Seismic

In addition to cross borehole tomography survey, a 3-dimensional surface seismic survey was acquired on the western edge of the Glenn Pool field. This did not include the Self-unit. This survey was organized by C. Liner of The University of Tulsa on the basis of in-kind contributions by Uplands Resources, The University of Tulsa, Mercury International Technology, and Nemeha Resources. Unrelated to the DOE research project involving Uplands Resources and The University of Tulsa, this seismic survey was acquired, processed, and interpreted through in-kind contributions and without use of DOE funds. The market value of the survey is approximately $50,000. The total area of the survey is approximately 2 square miles.

The objective was to acquire (Nemeha), process (MIT), and interpret (TU) a 3-D seismic survey over an area of known Wilcox (Devonian) production.

Specific interpretation objectives included:

- Analysis of the Glenn sand interval for evidence of channels and/or reservoir quality indicators.
- Structural interpretation of the Wilcox formation.
- Structural interpretation of the Arbuckle formation.

With the growing trend toward 3-D seismic use in all phases of exploration and production, we feel this project served as an example and a stimulus to 3-D work in the shallow oil province of northeastern Oklahoma. The data may be released in whole or in part at the discretion of each partner individually.

This is an important project that benefited all parties involved, and enhanced the existing DOE Glenn Pool project.

Geostatistical Modeling

Once the geological and geophysical data are gathered, the next step was to integrate this information. We generated petrophysical properties description such that the description is consistent with underlying geology. The geophysical cross sections generated by cross borehole tomography were used to improve the spatial modeling of different attributes. In this section we describe the approach used to integrate geological and petrophysical properties information. For additional details, please refer to Bahar.[45] The technique is based on the combination of simultaneous sequential Gaussian simulations and conditional distribution technique.

Multiple-Attributes Simulation

The approach used for this work in performing the co-simulation procedure is the combination of simultaneous sequential Gaussian simulation (sGs)[46] and conditional distribution technique. Additionally, the truncated Gaussian technique and indicator kriging are also employed since it involves the simulation of indicator variable in the Gaussian domain. **Figure 25** presents the schematic diagram of the co-simulation technique used in this study.

The key techniques in this procedure are the implementation of the simultaneous sGs and the use of conditional distribution to back transform the secondary and tertiary variables, i.e., porosity and permeability. The back transform of the first variable, i.e., facies, is performed using the truncated Gaussian method.[47] Using this technique, there will be no cross covariances/cross variograms required and no large co-kriging system to solve. This improves the practical application of the technique.

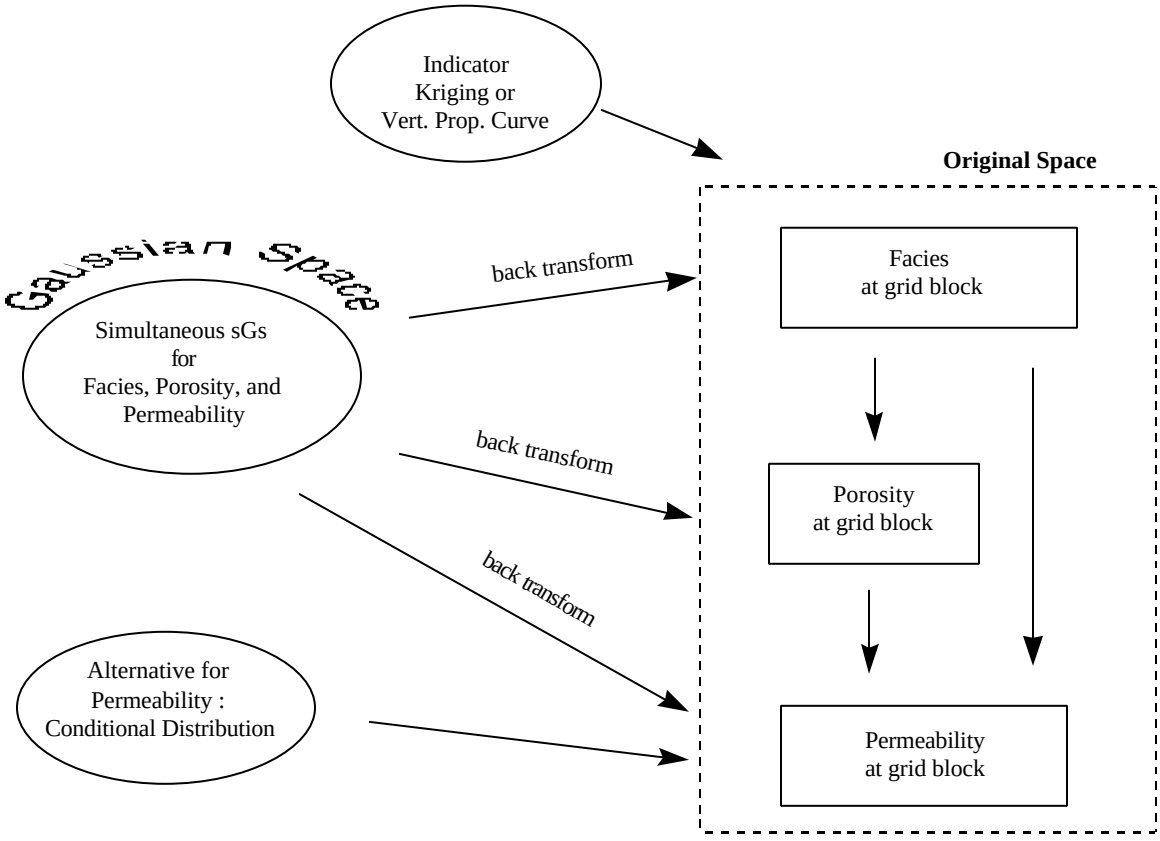

Figure 25 - Schematic diagram of the co-simulation technique

Theoretically, the technique is not limited to only three variables. We can extend it to as many variables as we wish, but the implementation of this technique in this study is limited to these three variables only since these are the most important variables, based on the log and core data, that directly relate the geological information and petrophysical properties.

The first most important aspect about the co-simulation technique developed here is the simultaneous use of sGs procedure for facies, porosity, and permeability. It provides two advantages. First, the ability to incorporate the spatial relationship of each variable. Second, by selecting the same simulation procedure for all three variables, a single search neighborhood can be applied where the same data points are used in the kriging process of each variable. This technique makes the program computationally efficient. As in any sGs procedure, the sample points could either be the original data or the previously simulated nodes and each simulation node is visited only once using the selected random path.

The application of single search neighborhood during the simulation may not always be possible if some data for one or two variables are missing at one particular location. For example, consider the case where at one location facies have been identified but porosity and permeability are not available. For facies, this location is considered as the sampled point but for the other two variables this location needs to be treated as the unsampled location. So, when sampled points are searched during the sought neighborhood process, this point can not be fully used to perform the kriging process of all three variables. It is only good for kriging of facies. Additional search is required for porosity and permeability until the requirement of the minimum number of nodes to complete the kriging is satisfied.

In the most common situation, however, there will be porosity data for each location where facies are identified and limited number of permeability data are available. In this case, it is better to perform the single search neighborhood for facies and porosity simulations only and do separate search for permeability simulation.

In the case where the locations for permeability data are unknown, then only conditional distribution technique can be applied for permeability simulation, i.e., without the sGs. This is the case where the "alternative" procedure of Figure 25 is applicable.

Since the technique uses independent sGs for each variable, the spatial analysis required are the Gaussian variograms for facies, porosity, and permeability. No cross variogram is necessary. Additionally, for the purpose of indicator kriging where its result is used in the truncated Gaussian procedure[47] to back transform the Gaussian facies value, a set of indicator variograms is required. One variogram is needed for each facies.

The second most important aspect of this co-simulation procedure is the use of conditional distribution technique to perform the back transformation from the Gaussian space into the original space. The idea of using conditional distribution is similar to the use of vertical proportion curves in the truncated Gaussian technique. The vertical proportion curves represent the probability or the percentage of geological facies at a particular depth. By using this proportion curve, it restricts the appearance of certain facies and allows other facies at certain depth with some probability. In this case, the use of

conditional distribution technique will restrict the distribution of the simulated value which is consistent with the local relationships between the new and prior simulated variables.

In the standard sGs, the back transform procedure is conducted using the distribution of all data. In this technique, the back transform of porosity, as the secondary variable, is constrained to the porosity distribution for certain facies only. **Figure 26** shows the schematic diagram of the conditional distribution procedure for porosity simulation. From this figure, we can see that, first, distribution functions or correlations between porosity and each facies are built (Figure 26a). Then, the cumulative distribution function (cdf) of porosity data in the original space (Figure 26b) is calculated. The cdf in Gaussian space can be calculated for later use as shown in Figure 26c.

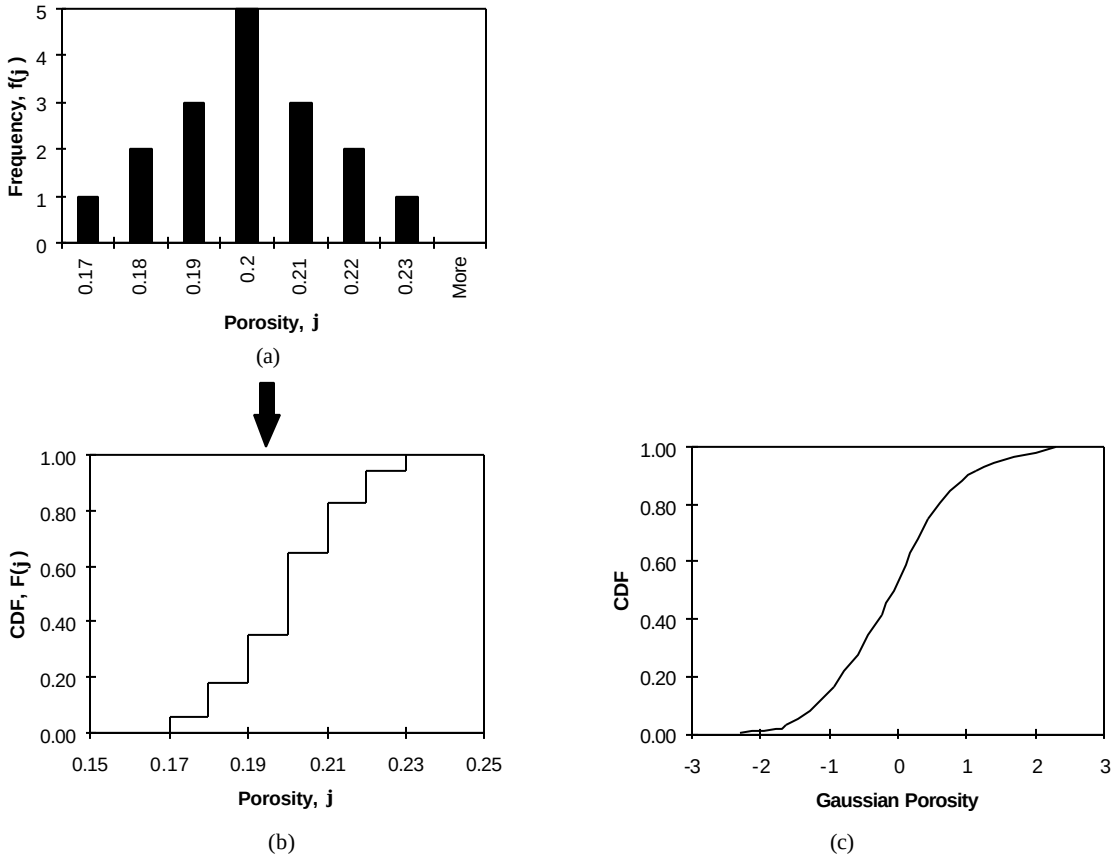

Figure 26 - Conditional distribution procedure for porosity: (a) the frequency plot of porosity data for certain facies type, (b) cumulative distribution function (cdf) of the corresponding porosity correlation, and (c) cdf in Gaussian space

Once a facies is assigned for a certain location, then the cdf for this facies is used to back transform porosity as shown in **Figure 27**. In the example shown in this figure, the facies for a certain location is identified as Facies A. Using the cdf of porosity for Facies A only, the Gaussian porosity obtained from the sGs procedure is back transformed to get the final porosity value. The dotted line on the cdf curve is calculated using linear interpolation of the data in the cdf curve. This line is used in assigning the final porosity. The dotted line with the arrowhead shows the direction of the process during back transform procedure.

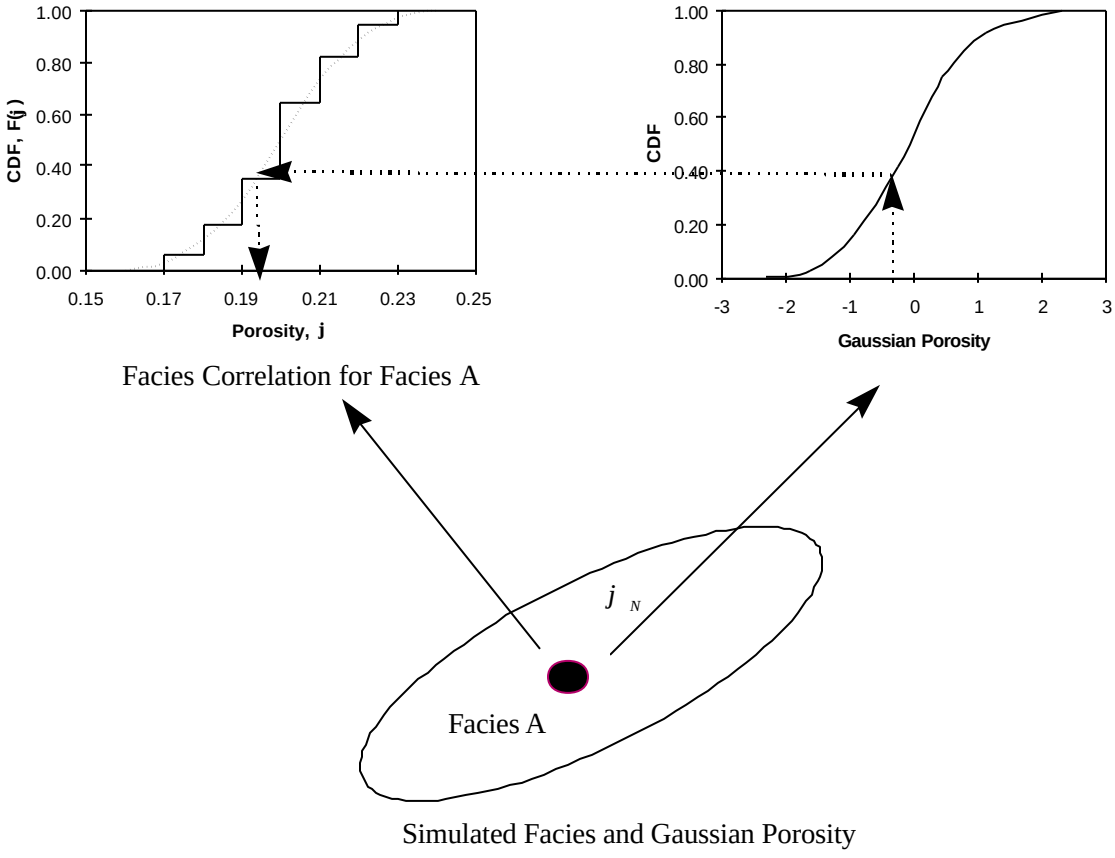

Figure 27 - Example of the use of conditional distribution technique in porosity simulation

The use of this technique can be extended to next variable, the tertiary variable, i.e., permeability. Since permeability is a function of porosity, and porosity is a function of facies then permeability needs to be constrained to both of these variables. **Figure 28** shows the schematic diagram of the back

transformation using conditional distribution technique for permeability. Figure 28a shows the porosity-permeability correlation for one of the facies. As we can see from this figure, several porosity classes are defined in this correlation. This is to minimize the variation of the permeability values. In general, the number of the class can be set as the square root of the number of data points. However, in the implementation of this program the number of class is always set as 4 which corresponds to the quartiles of data. The histogram of permeability for one of the porosity class is shown in Figure 28b. Using this histogram, we can build the cdf of this histogram as shown in Figure 28c. The cdf for Gaussian space can be calculated for later use as shown in Figure 28d.

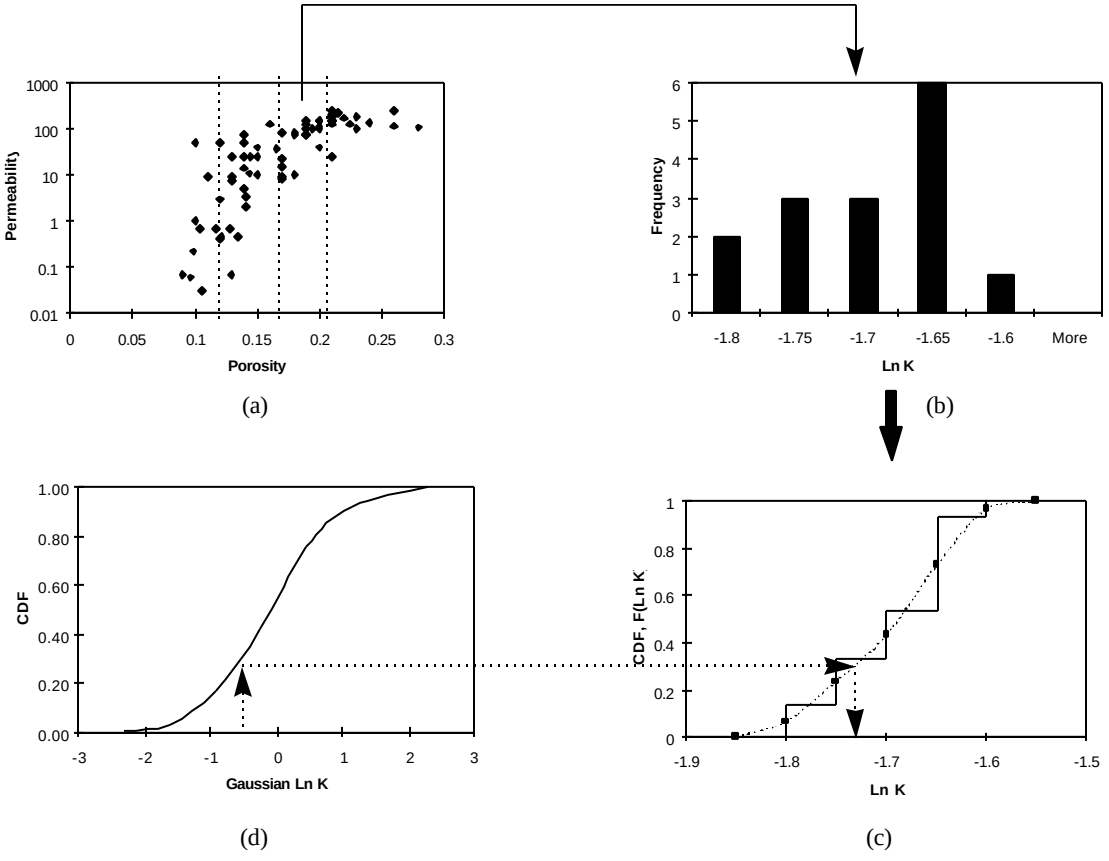

Figure 28 - Conditional distribution technique for permeability

In the simulation procedure, once facies and porosity are assigned for a certain location, then we can assign permeability using the appropriate cdf, i.e., the cdf from the corresponding porosity class, and the Gaussian permeability value from the sGs procedure.

For the case where the sGs is not performed for permeability simulation due to the missing location information, a random number between 0 and 1 can be used instead of the Gaussian transformed value to simulate a permeability value from conditional cdf.

The co-simulation technique described in the previous section uses the data that originate mainly from well logs and well cores. Using these data and other information, the geologist will produce geological interpretation of the reservoir that includes the description of facies at well location. Facies distribution at, for example, 1-ft interval in each well could be generated based on this interpretation. This distribution becomes the hard data for the co-simulation technique. It is considered as hard data since it is based on measured values.

The goal of the geological simulation is to closely replicate the geologist's interpretation. To achieve this goal, it may be important that some other information, other than the hard data, to be incorporated in the geological simulation procedure. This information is commonly known as the soft data.

One type of information that can be considered as the soft data is the geologist's interpretation of facies distribution for the whole reservoir, e.g., the isopach map of the facies. This interpretation is considered soft information since it is not based on measured values. Hard data in the indicator simulation technique are represented by an indicator value that has the value of 1 if present and 0 if absent, e.g. $I(\vec{x}) = [0 \quad 1 \quad 0 \quad 0]$, means facies 2 is present and others are absent at location $\vec{x}$. To incorporate the soft information, certain probability values can be assigned for each facies at one location. This information can be incorporated in the simulation procedure by modifying the definition of indicator function. For example, if there is 50% chance of facies 1 and 50% chance for facies 2 to exist at a certain location, then for a system with 4 facies, the indicator function becomes $I(\vec{x}) = [0.5 \quad 0.5 \quad 0 \quad 0]$. A question mark can be assigned if the probability of one facies is not known with certainty. That is, if the probability of facies 1 is 25% but there is no certainty about the other three facies, then we can assign a question mark for other facies, i.e., $I(\vec{x}) = [0.25 \quad ? \quad ? \quad ?]$.

The value specified in the soft data can be assigned as the result of indicator kriging for that location. In the case where the question mark is provided for several facies then indicator kriging for those facies

needs to be performed. The cumulative value of the kriging results must be rescaled to 1 minus sum probability of the known facies. So, the cumulative value of all facies becomes exactly 1.0. For example, if the soft data for a location $\vec{x}$ are $I\ (\vec{x}) = [0.25\ \ ?\ \ ?\ \ ?]$, the kriging for facies 2, 3, and 4 must result with the probabilities that satisfy the following condition,

$$\sum_i p_i = (1 - 0.25) = 0.75, \qquad \text{where } 0 \le p_i \le 0.75, \text{ and } i = 2,3,4 \tag{1}$$

The method was used to generate reservoir description in the Glenn Pool field. The geological unit used by the geologist in describing the Glenn sandstone in the Glenn Pool field is the discrete genetic interval (DGI). Ye[10] has defined 6 DGI's in the vicinity of Self-unit, namely DGI A through F, and 7 DGI's in the vicinity of track 7 unit, namely DGI A through G. Each DGI may consist of several facies such as channel fill, crevasse splay, and flood plain mudstone. Due to the unavailability of porosity log for track 7 unit, at half of the wells, porosity data are simulated using the remaining well data. Permeability data are available from few of the cored wells in track 7.

The first result shown here is the 2-D simulation of DGI A of track 7 unit. In the vicinity of this unit, three facies exist for the DGI A, namely channel-fill, crevasse splay, and shale/mudstone. For simulation purposes, these three facies are named facies 1, 2, and 3, respectively. The dimension of the track 7 unit is 2,640 $\times$ 2,640 sq. ft. The simulation is conducted using 80 $\times$ 80 grid blocks in x and y directions or a total of 6,400 grid blocks.

The detailed spatial modeling analysis is not included here. Only the results of the simulation are presented. **Figure 29** presents the geologist's interpretation of facies distribution for DGI A in the vicinity of track 7. The simulation results for 4 different realizations are shown in **Figure 30**. Total number of realizations simulated is 100. Comparing these figures, we can see that the simulation matches the geologist's interpretation very well.

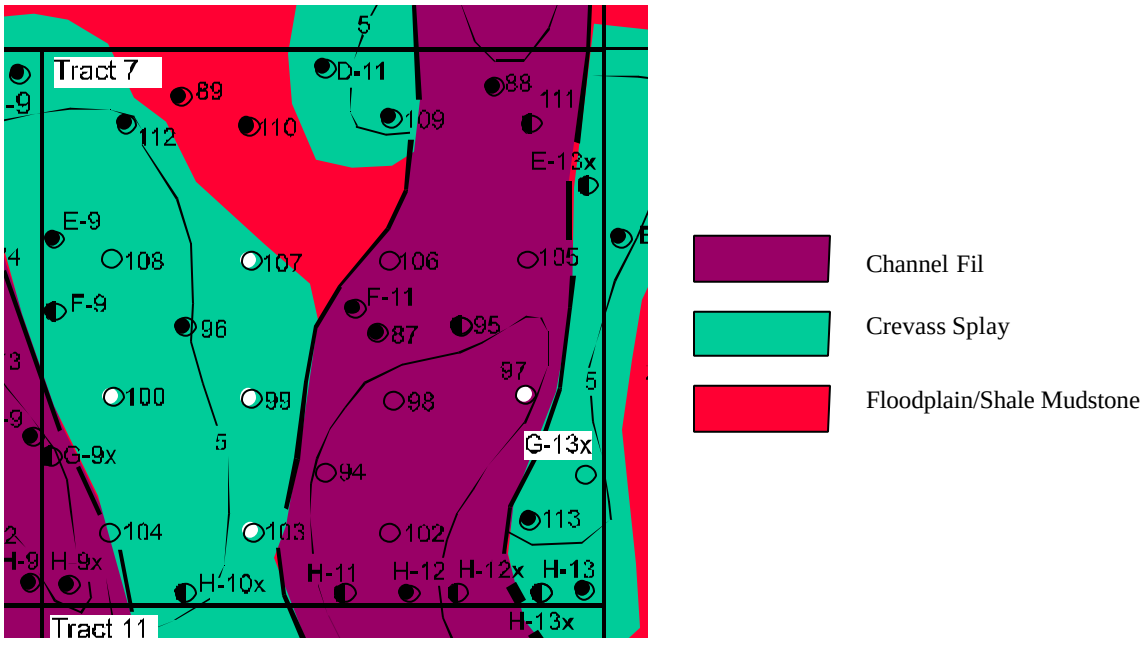

Figure 29 - Geologist's interpretation of facies distribution in the vicinity of track-7 (after Ye)[10]

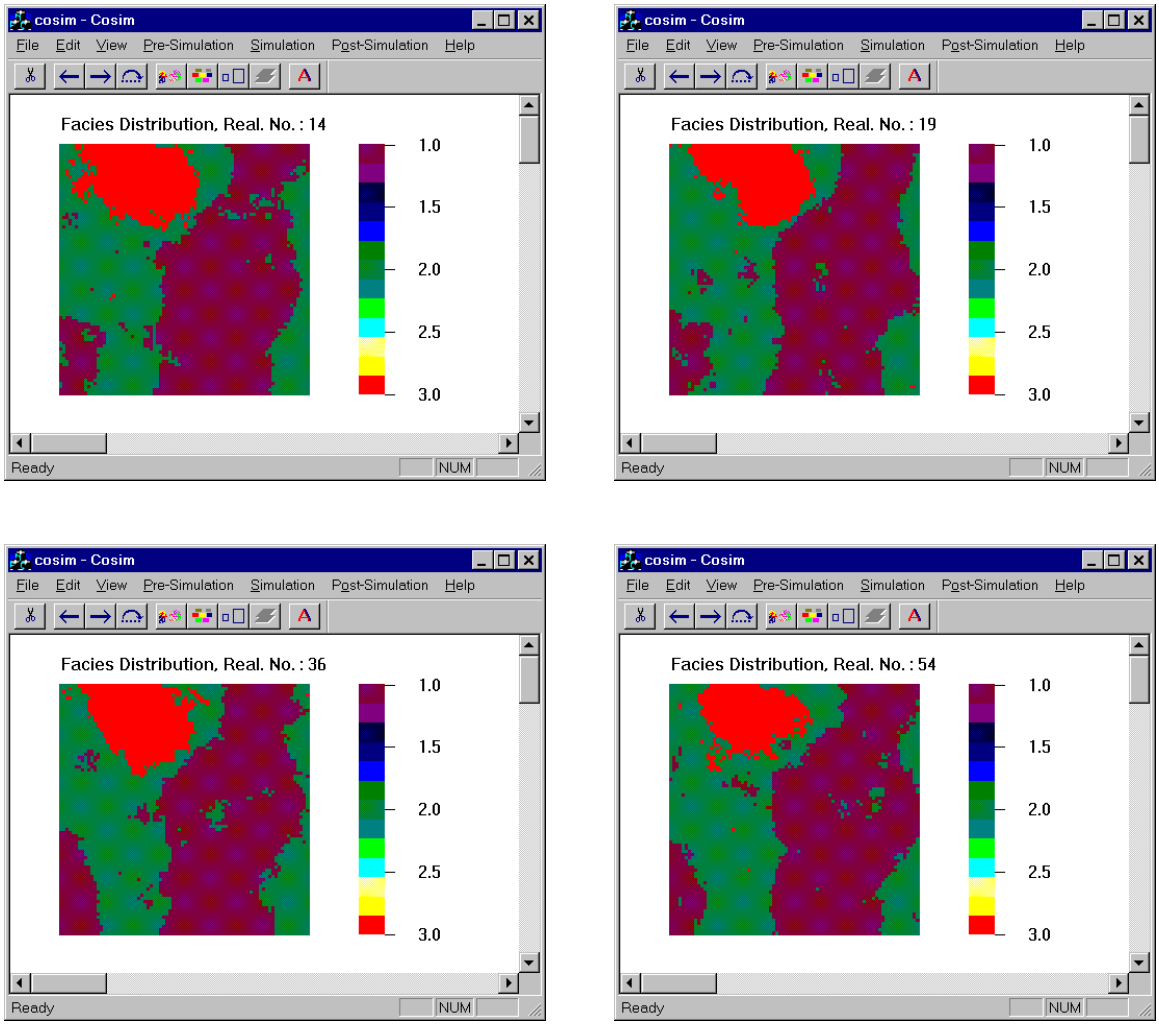

Figure 30 - Multiple realization of facies distribution of DGI A - track 7 unit

The global pdf comparison between the simulation and the conditioning data for all realizations is shown in **Figure 31**. From this figure we can see that, with respect to the conditioning data, the simulation under-estimates the proportion of facies 2 and over-estimates the proportion of facies 3. But, as we refer to Figure 29, we can observe that we only have two samples of facies 3. Therefore, the discrepancy between the two results prevail.

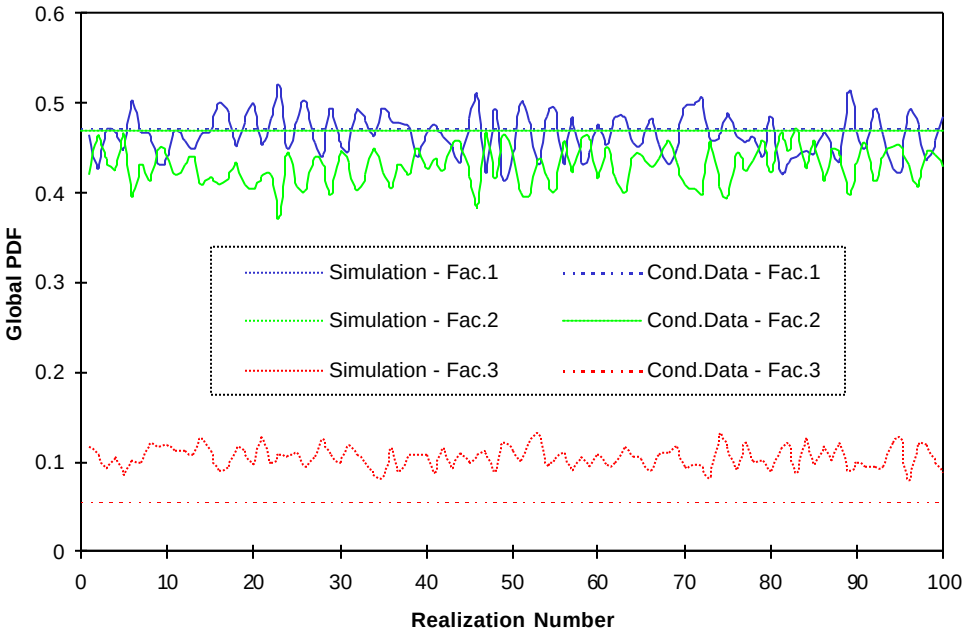

Figure 31 - Global PDF comparison between simulation and data for all realizations

The corresponding petrophysical properties distribution for one of the realizations is shown in **Figure 32**. From this figure we can clearly see that both porosity and permeability distributions follow facies description very well. This result confirms that the petrophysical properties are controlled by underlying geological description. The local variation of the permeability distribution is due to the use of random sampling method since collected permeability data are from wells other than the ones used as conditioning data. The other aspect that is important in this work is the efficiency of the program in replacing the traditional technique, i.e., the two stage approach.[48-49] This aspect will be discussed in the next paragraph.

The amount of time required to complete one simulation run can be considered very small. With the Pentium 200-Pro machine, it takes about 7 seconds. The variation in simulation time using different grid block configuration and different number of realizations is shown in **Figure 33**. As expected, the amount of time varies significantly depending on the number of grid blocks as well as the number of realizations.

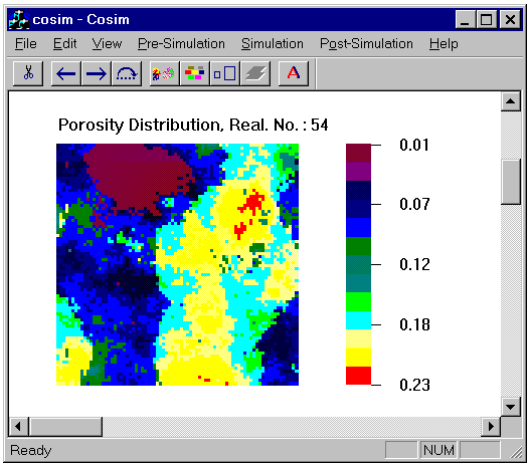

(a)

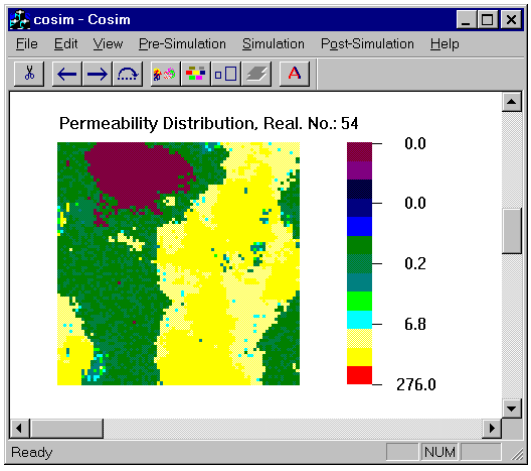

(b)

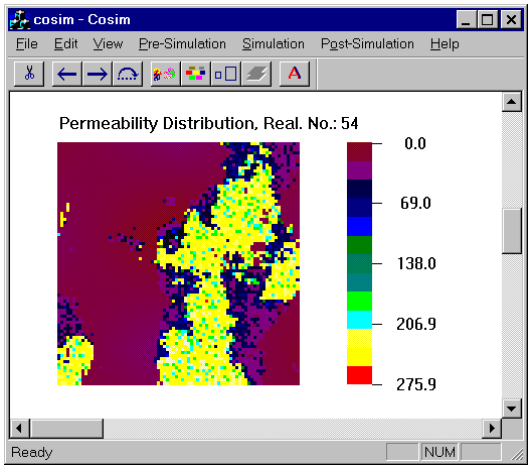

(c)

Figure 32 - Porosity and permeability distribution of DGI A for track 7 unit from one of the realization. Permeability is sampled using random sampling. (a) Porosity distribution. (b) Permeability distribution shown in log scale. (c) Permeability distribution shown in decimal scale.

The efficiency of the program can be much more appreciated if we directly compare the actual time required to complete one case study starting from raw data until the distributions of facies, porosity, and permeability are obtained. This include data preparation and variogram analysis. Using the traditional approach it is estimated that an order of magnitude time will be required compared to the approach proposed here.[45] We have to include the data preparation time in this comparison since the traditional

approach requires a lot of human intervention to complete the work while the co-simulation technique has eliminated a big part of it.

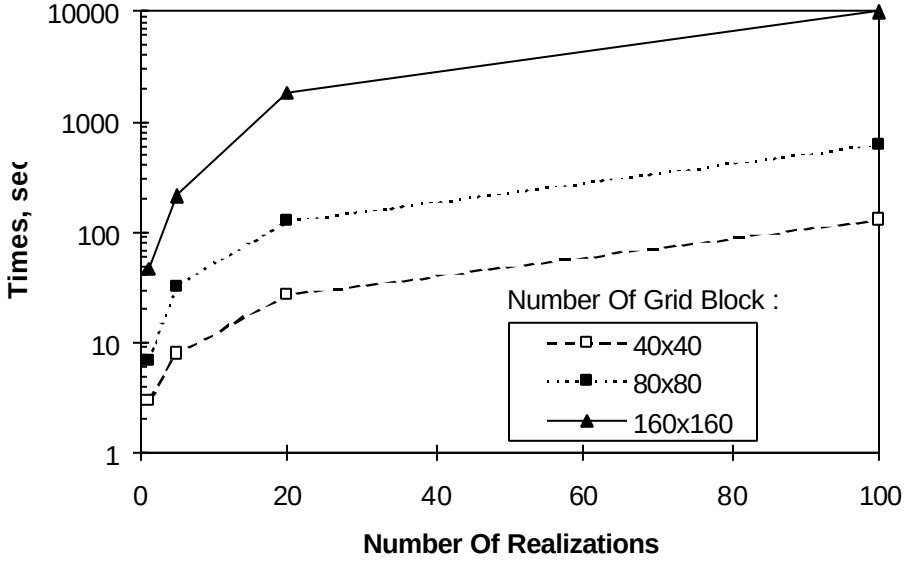

Figure 33 - Computation time comparison for different grid block configurations and different number of realizations

The second result shown in this section is taken from the Self-unit data where the 3-D simulation of DGI, not facies, is conducted. The purpose of this simulation is to show that the simulation is capable of simulating the sequence stratigraphic characteristic of the DGI. The number of grid blocks used in this example is 256,000 ($40 \times 40 \times 160$) grid blocks where the size of each block is $66 \times 66 \times 1$ ft^3. The 3-D view of DGI distribution is shown in **Figure 34**. The corresponding petrophysical distribution is shown in **Figure 35** and **Figure 36**.

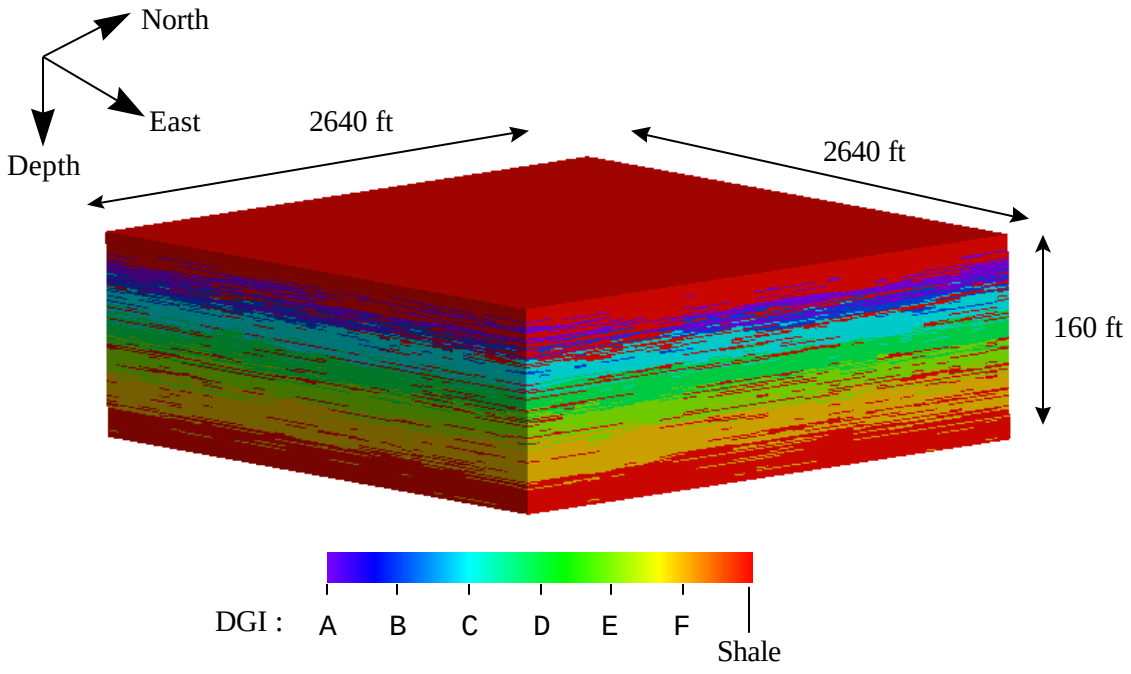

Figure 34 – 3-D view of DGI distribution of the Self-unit data.

From these figures we can see clearly how the DGI's vary from top to bottom with shale on the top and the bottom borders. This distribution is followed very well by the petrophysical properties distribution as shown in Figure 35 and Figure 36. The increase in porosity and permeability from top to bottom are matched very well with the field observation, i.e., from well log and core data.

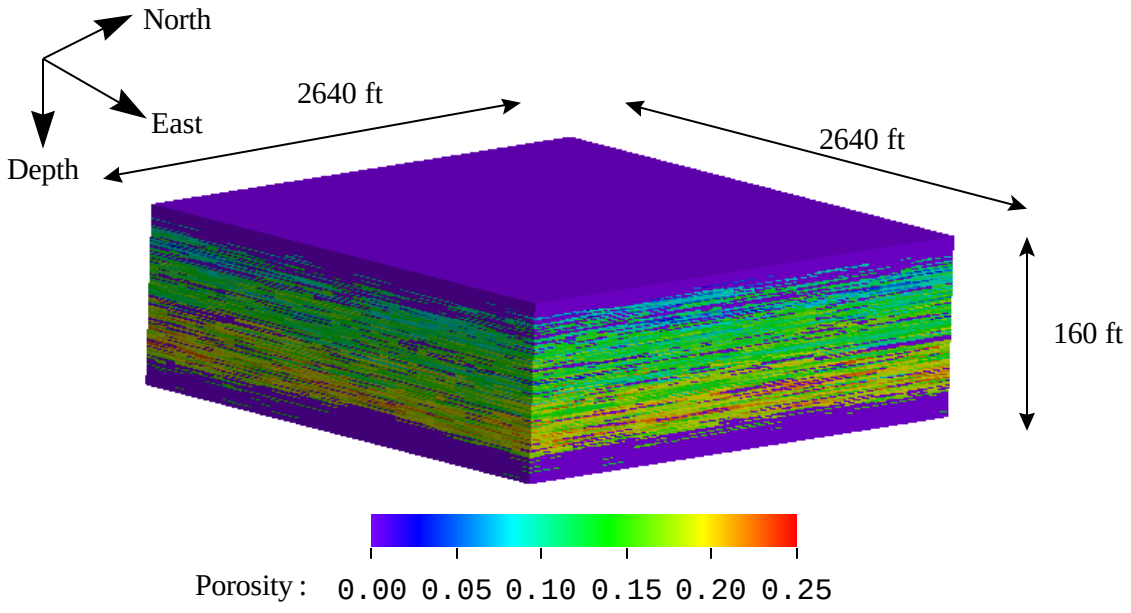

Figure 35 – 3-D view of porosity distribution of the Self-unit data.

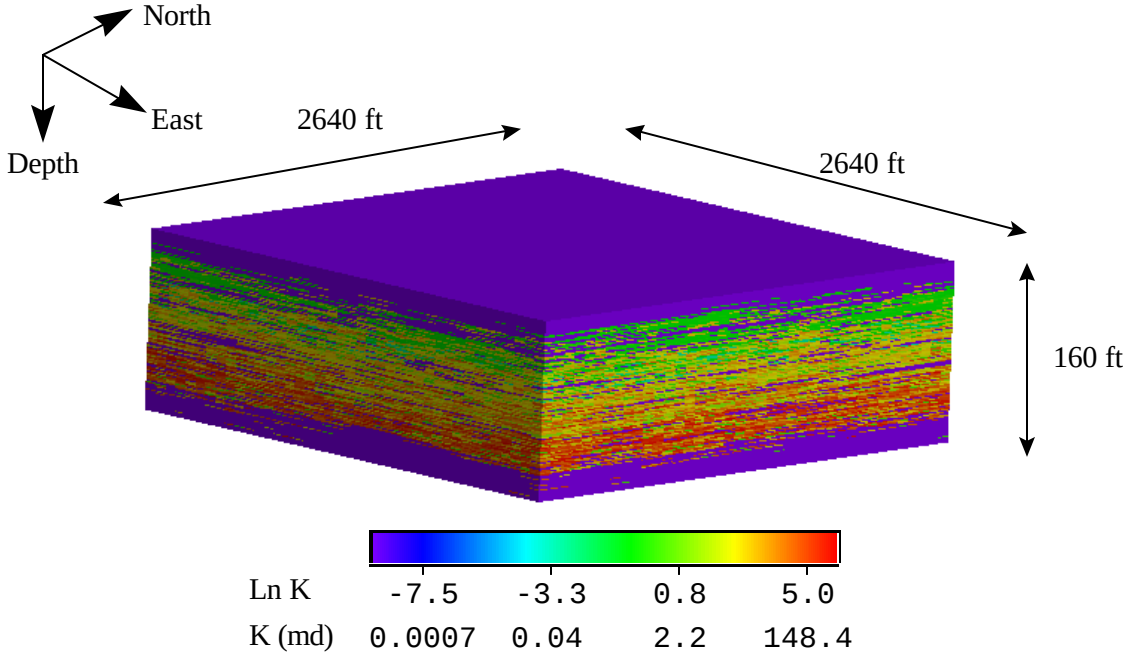

Figure 36 – 3-D view of permeability distribution of the Self-unit data.

The approach used in incorporating tomographic data is very similar to the above discussion. The only difference was the construction of variogram model, which is required for spatial analysis. Instead of

using data from vertical wells only, we also used the data from various cross sections generated by tomography. As a result of incorporating tomographic data, the variogram model improved substantially. However, as discussed in the next section, the overall flow simulation results did not improve substantially.

Flow Simulation

In conducting flow simulation to simulate the reservoir performance, we used three alternative models. These are:

- Deterministic model: It represents traditional approach where cross correlations at interval locations were established based on geological correlations. The petrophysical properties were estimated using traditional interpolation techniques given the well data.
- Stochastic model: This model represents a geostatistical approach where an integrated description was used to generate a detailed reservoir description. Some of the results are shown in the previous section.
- Stochastic model with tomogram: This model represents incorporation of cross borehole seismic data in stochastic model.

Following the reservoir description task, the flow simulation was conducted to match the past performance and also to predict the future production using three different scenarios. Based on the flow simulation results, the economic analysis was conducted as to the most feasible scenario that is applicable to the Self-unit.

Deterministic Model

Geological Simulation

The common problem encountered in generating the reservoir description is how to fill in the information at the unsampled locations, i.e. at the interwell regions. The conventional way of solving this problem is to assume that a certain relationship (correlation between wells and/or based on similarity) exists in these

regions, and that there is a unique set of model output data for a given set of inputs. This is known as a deterministic approach. A model that is commonly used in the conventional approach is known as the layer-cake model.

The geologists involved in this project, Kerr and Ye, have established a stratigraphic framework of the Self-unit that divided the unit into 6 Discrete Genetic Intervals (DGI's). Using each DGI as a layer, a model with 6 sandstone-layers can be developed. From their interpretation, it is observed that for some intervals an impermeable layer exists between two consecutive DGI's. To accommodate this fact, the model is modified to contain this layer in between two DGI's.

For the purpose of flow simulation, each layer is divided into several grid blocks. To cover the 160-acres of the Self-unit, 400 grid blocks (20×20 in X and Y directions respectively) are assigned to each layer. Using this configuration, the dimension of each grid block in X and Y directions becomes 132-ft whereas its thickness is determined using bilinear interpolation based on the well data. **Figure 37** shows the interpolation result for north-south cross section. This figure clearly indicates how each layer is stacked against one another.

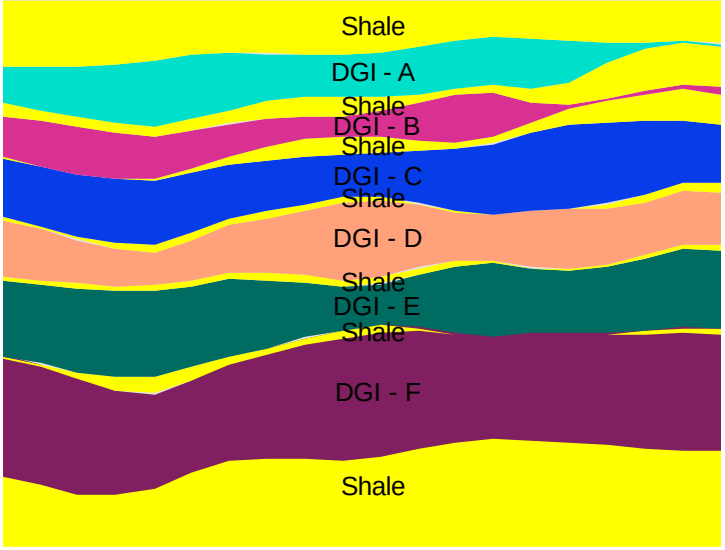

(a)

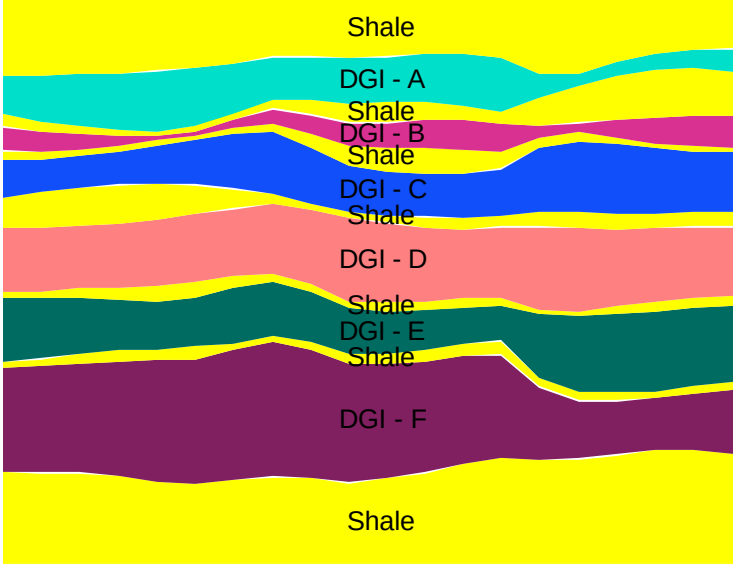

(b)

Figure 37 – Deterministic north-south and east-west sand cross section

Figure 38 shows the thickness comparison of each layer between well data and the model at wells No. 43 and No. 37 respectively. The data from these wells were not used as input in the interpolation process. Thus, these comparisons should validate the interpolation used in generating the model. As these figures indicate, the model conforms to the geological architecture as is commonly observed in the conventional method.

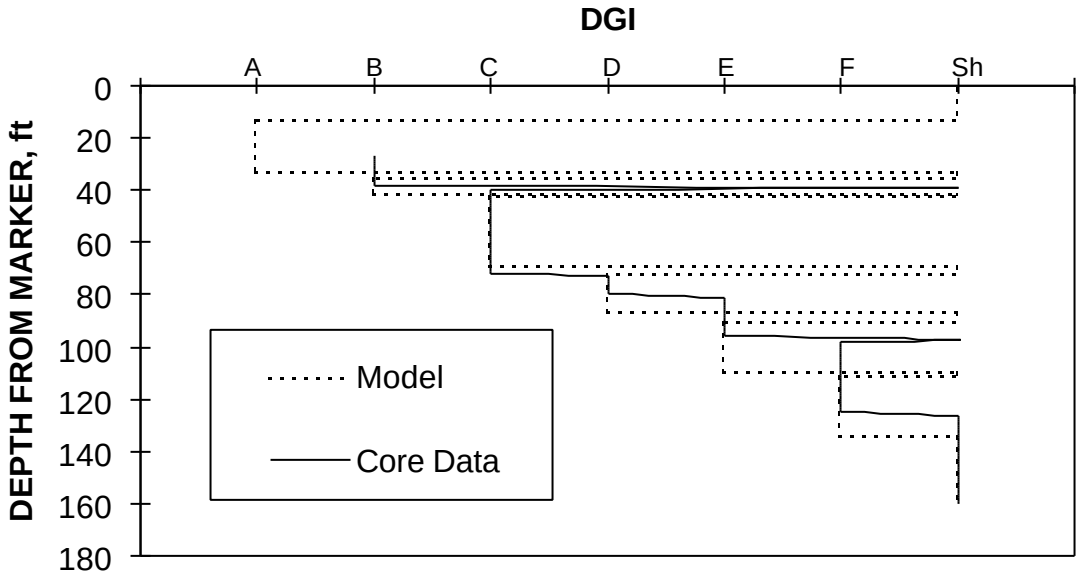

(a) Well 43

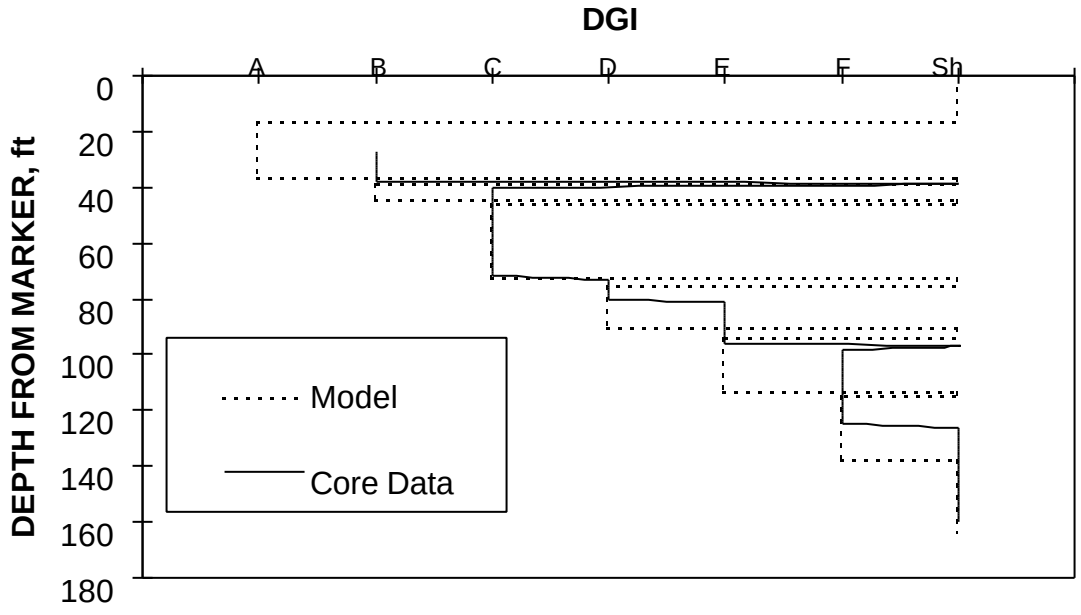

(b) Well 37

Figure 38 - Deterministic - sand thickness well 43 and 37

Porosity Description

In assigning the porosity value to each grid block, the well data is first superimposed on the geology data, i.e.; the porosity of each DGI/layer is separated from the others. An average value is calculated for each layer at each well. Then, the porosity of a grid block at an unsampled location is calculated using bilinear interpolation of the well data that has been averaged previously. The porosity of the impermeable (shale) grid blocks is set as zero. All of the porosity data used in this study were gathered from the log of currently existing wells. No corrections or correlations to core data are made since none of these wells were cored.

Figure 39 shows the porosity distribution of the east-west cross section. It can be observed that the porosity distribution is almost uniform in each layer. Thus, it is clear that this model can not capture the heterogeneity of the reservoir. **Figure 40** presents the porosity at Self-82 to show the comparison of the estimated value with the field data at a specific well. It can be observed that the porosity value from the model seems to be inconsistent. It underestimates at the top part of the reservoir (DGI's A, B, and C), but overestimates at the bottom part of the reservoir (DGI's E and F).

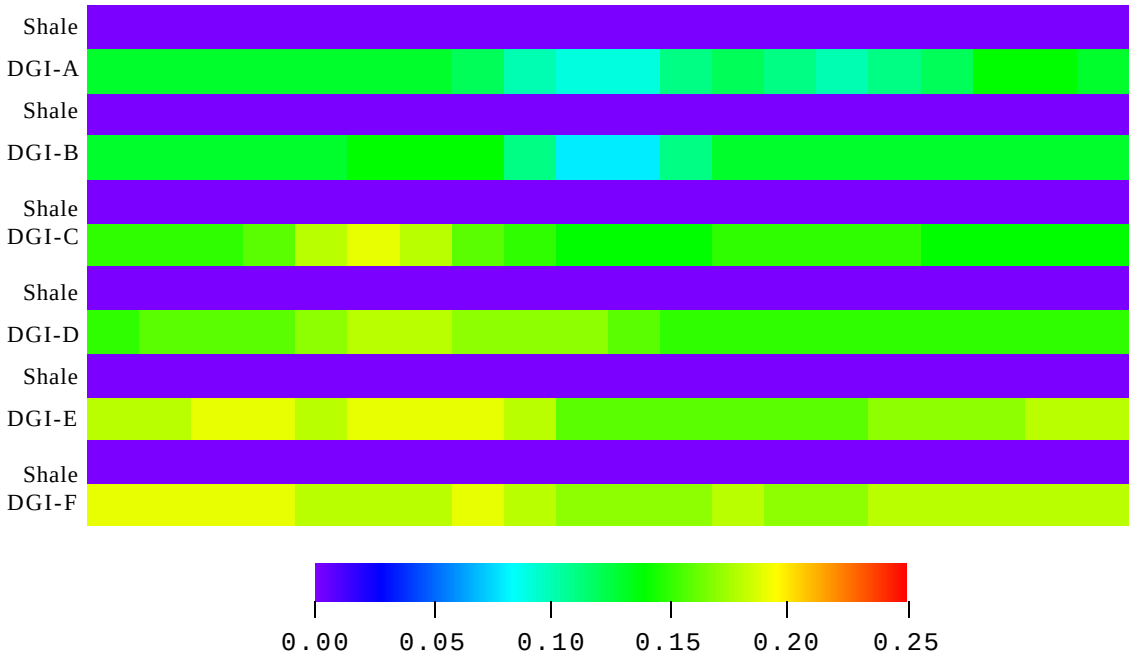

Figure 39 – East west porosity cross section – deterministic model

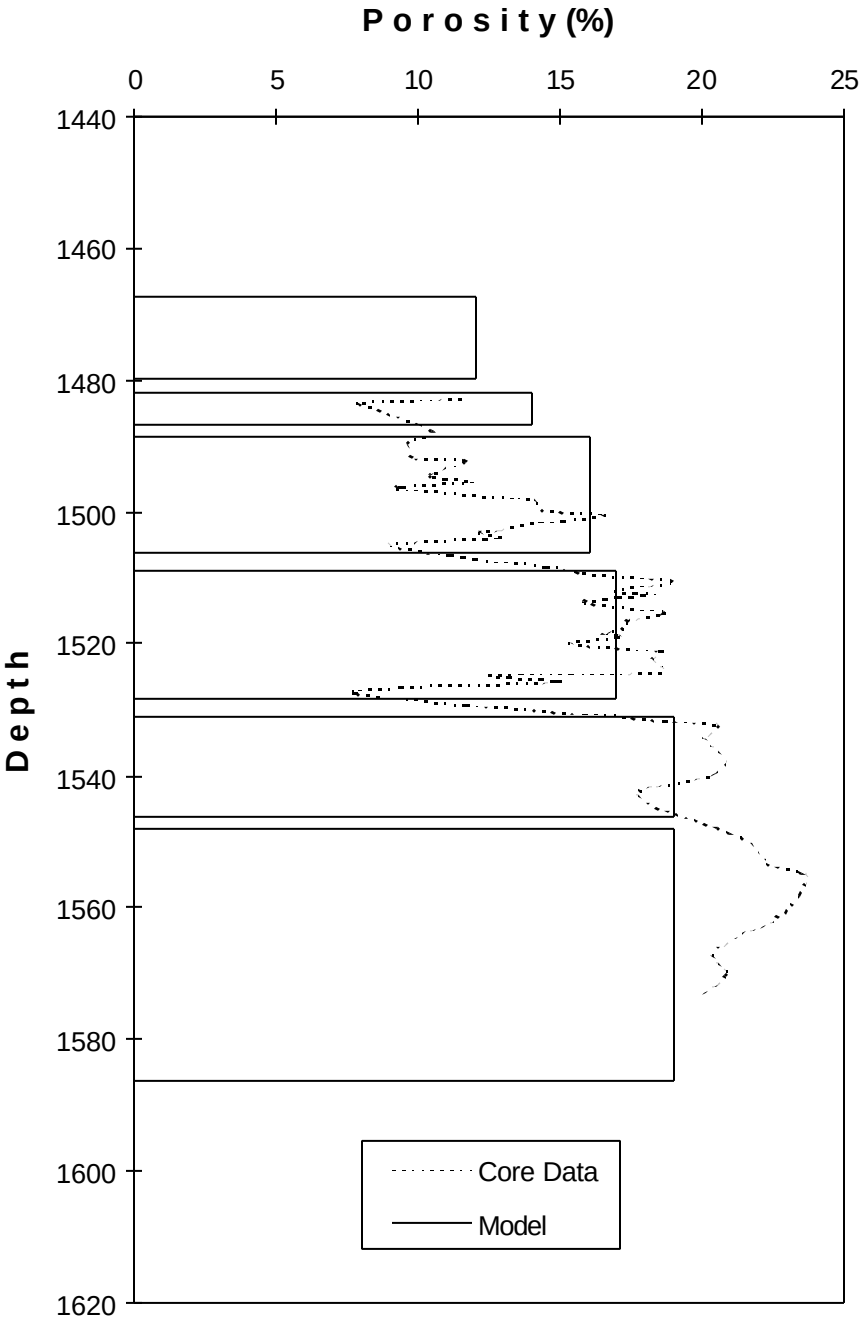

Figure 40 - Porosity comparison at Self-82

Permeability Description

The permeability value for each grid block for this model is estimated using a linear relationship assumption between porosity and the logarithm of the permeability. The only source of data for permeability available for this study is from the core measurements of several old wells, i.e. Well No.'s 28, 31, 32, 37, 43, and 47. Unfortunately, the core data from these wells are not available for the whole intervals. Mostly, they are only from the bottom intervals since those were the most productive intervals. This situation creates difficulty in generating the correlation. In fact, there is no data available for DGI-B and only a few points for DGI-A.

Figure 41 shows the permeability distribution of the north-south cross section. As in the porosity distribution, it can be observed that the areal heterogeneity cannot be captured by this model. Observing the average value for each layer, it is found that the permeability of DGI A (*k*-average = 15.6 md) and DGI B (*k*-average = 15.5 md) is higher than the permeability of DGI C (*k*-average = 8.5 md). This is inconsistent with the field data. The reason for this is the poor quality of the data that were used in generating the porosity-permeability relationship for these DGI's. The core study of Self-82 indicates that the porosity for DGI's A and B is about 12 - 15% with the permeability in the range of 0.1 to 1 md, while the average value from the old core which was used as input data was 17% for porosity and 60 md for permeability. Overestimated distributions resulted for DGI's A and B. **Figure 42** presents the permeability distribution at Self-82. In general, the model predicts a very narrow range of permeability. It overestimates at the top intervals but underestimates at the bottom intervals. Again, the heterogeneity of the reservoir is not captured very well.

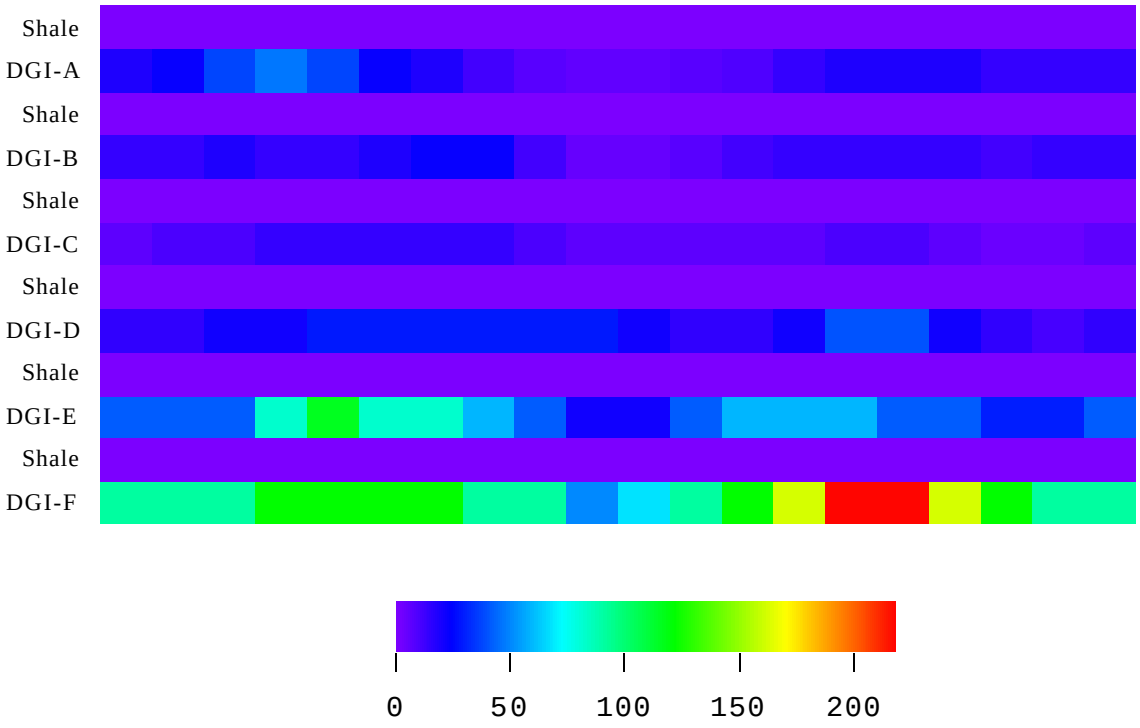

Figure 41 – North-south permeability cross section – deterministic model

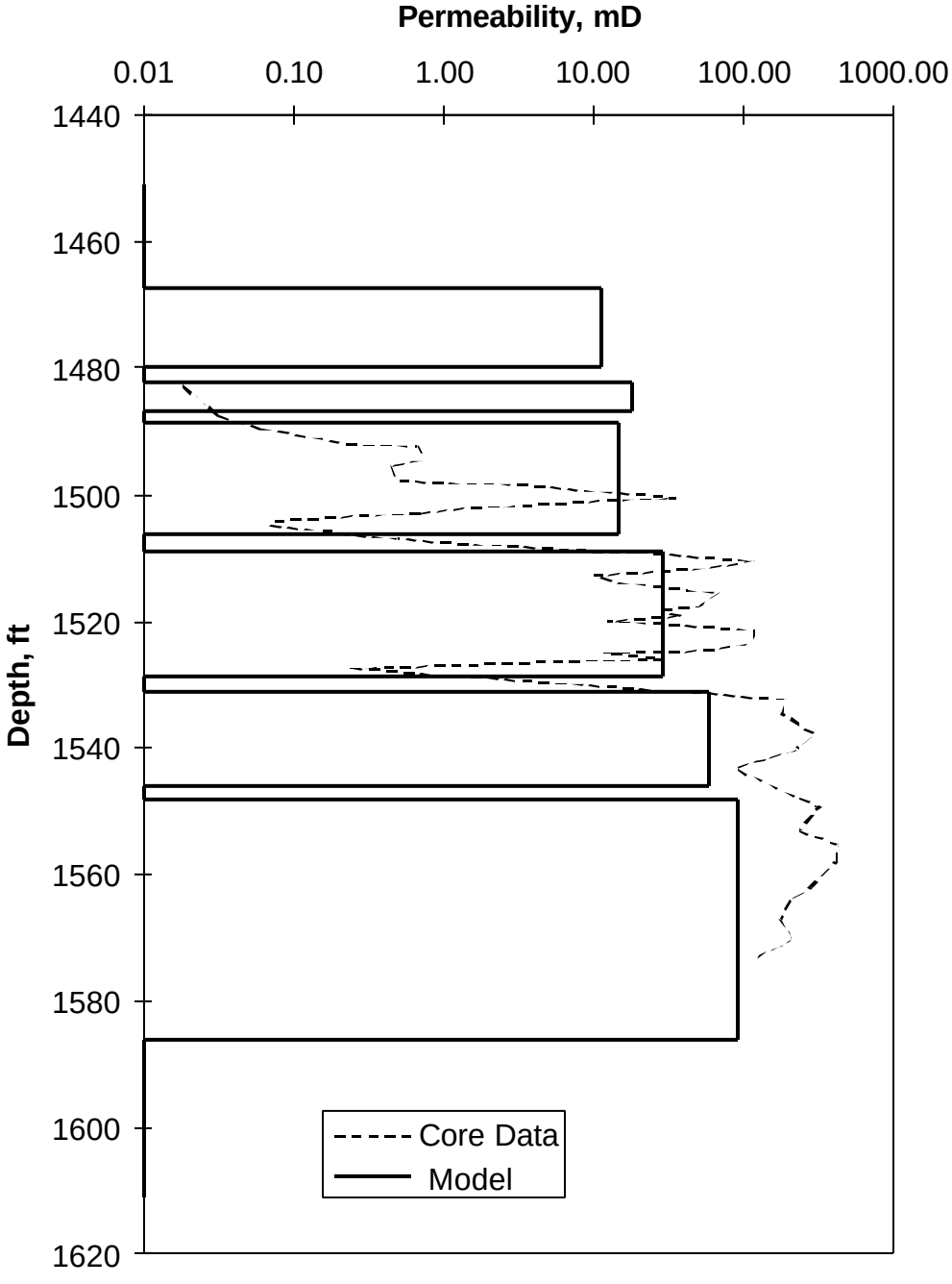

Figure 42 – Permeability comparison at Self-82 – deterministic model

Figure 43 presents the comparison of the permeability thickness product (kh) between the well test interpretation and the model. In this figure, any point that lies on the 45° line is a perfect match. Since

most of the results lie above this line, it indicates that the model overestimates the kh value when compared to the well test results. The procedure that was applied in calculating the kh for the model is as follows.

1. A radius of investigation is defined as half the distance between adjoining wells.
2. The permeability inside this radius was averaged geometrically. The geometric average was calculated only for layers, which are perforated.
3. The kh of the model then was calculated as the summation of kh for each of the layers.

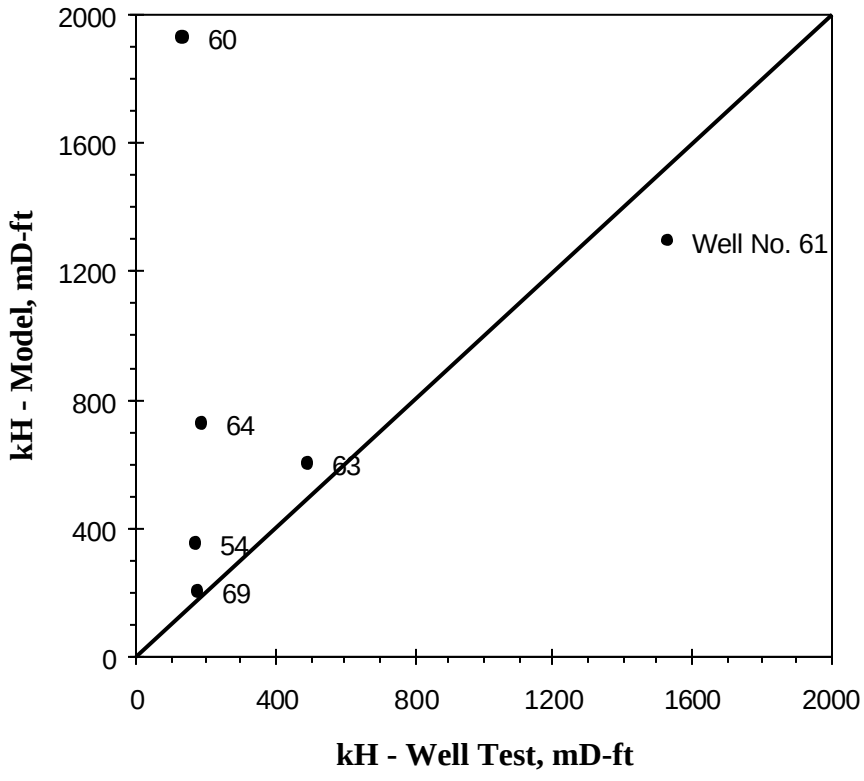

Figure 43 – Permeability thickness product (kh) comparison – deterministic model

The permeability of the model used for comparison with the well test, such as in Figure 43, is the absolute permeability whereas in practice the permeability calculated from the well test is the effective permeability. Considering that most of the field has been flushed with water, especially at the bottom

part of the reservoir, and has been produced with 99% water cut, it is reasonable to assume that the flow in the reservoir is approximately single-phase. Thus, the use of absolute permeability for this comparison is justifiable.

Flow Simulation

In order to have confidence in predicting the future performance of the reservoir, a reasonable match in the flow simulation of the past performance has to be achieved. The next task after generating the reservoir description is to conduct a flow simulation. All of the flow simulations presented in this report were conducted using ECLIPSE-100 Black Oil Simulator.

The flow simulation was performed to match the past production from November 6, 1906 until January 1, 1994. In this model, the same number of grid blocks used in the reservoir description is used in the flow simulation, i.e., $20 \times 20 \times 12 = 4800$ grid blocks. Therefore, no upscaling process required for this model.

In running the flow simulation, at least one parameter should be available as a control parameter. This parameter could be oil production rate, water production rate, or bottom hole pressure, etc. Using one control parameter, the other parameters can be used as the match parameters, to which the flow simulation result is compared. The problem that was encountered in running the simulation is the limited information on any of these parameters. Accurate information about the original oil-water contact was not known. Thus, it was quite difficult to determine the initial conditions of the reservoir. The production data were not available for the early times until 1946. The only data that was available was the first 24 hours production, or the initial potential, of a few early wells. It was decided to make trial and error runs in searching for the bottom hole pressure that could produce the initial potentials at those wells. **Figure 44** presents the initial potential comparison between the simulation and field data using uniform bottom hole pressure (BHP) at all wells of 400 psi. Except for Wells No. 1 and 16, the match is considered reasonable. In order to have a better match for these two wells, a lower BHP value should be used, but lowering the BHP would affect the other well matches. Thus, it is decided to use the BHP of 400 psi for the early production time. Using this value as the control parameter, the

simulation is continued until the reservoir pressure is depleted to this pressure. When this happens a lower value of bottom hole pressure is used as the control parameter and the simulation resumes. This process is repeated until the year 1946.

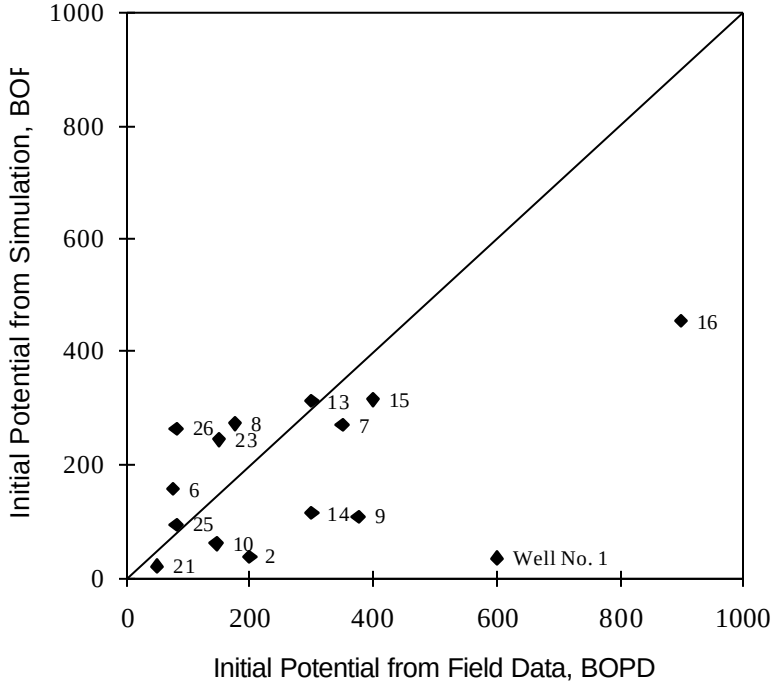

Figure 44 – Initial potential comparison – deterministic model

The production profile derived from this method is presented in **Figure 45**. In this figure, the results from 4 case studies were presented. These case studies were conducted due to the uncertainty of the relative permeability data and the initial water saturation. The definition of each case study is presented in **Table 3**. From Figure 45, it can be seen that at the beginning, the production is optimistic, but close to 1946 the production is low compared to the field data. The flow simulation in the period after 1946 was run using water production rate as a first control parameter with a restriction of a maximum value of oil production rate. These water and oil production rates are the yearly field wide data available for the Self-unit. It can be observed that the simulated results match the field data.

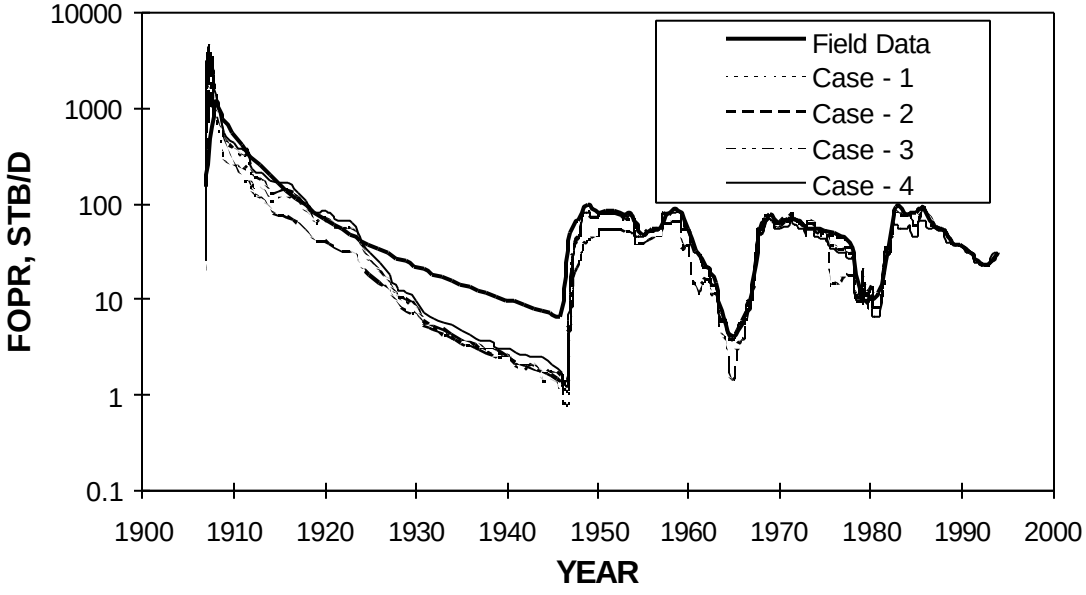

Figure 45 – Field oil production rate (FOPR) – deterministic model

Table 3 - Case definition used in flow simulation	
Legend	Description
Case 1	Uniform Kr (Glenn Pool Data), Uniform $Swi = Swr$
Case 2	Uniform Kr (Modified - Glenn Pool Data), Variable Swi
Case 3	Variable Kr (3 zones - Glenn Pool Data), $Swi = Swr$ (3 zones)
Case 4	Kr as measured by BDM-Oklahoma (2 zones), $Swi = Swr$ (2 zones)

Figure 46 presents the Original Oil In Place (OOIP) calculated using this model. As a comparison, the calculated OOIP as reported by Heath[6] is also presented. The difference that is observed among the case studies is due to the difference in the initial water saturation that was assumed in each case.

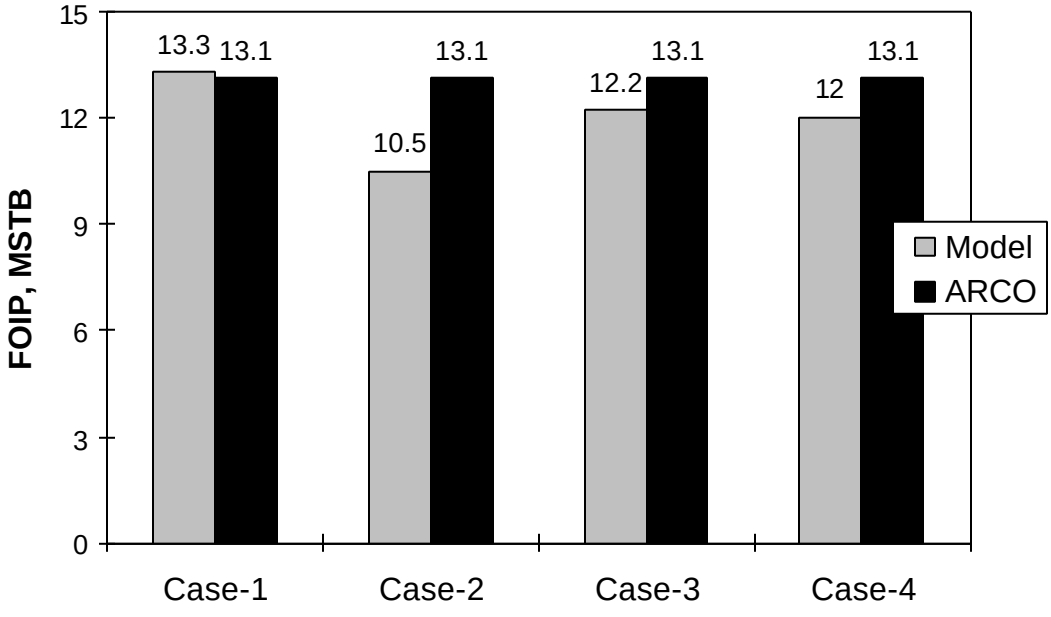

Figure 46 – Original oil in place estimation – deterministic model

Figure 47 presents the water cut predicted from the simulation. The field presently produces with a water cut of 99%. It can be seen that the simulated water cut does not match the field data very well. This is probably due to the limited information about the oil-water contact as well as the relative permeability as suggested by case 2 that gives higher water cut compared to the other cases. In this case the bottom interval (DGI F) was assumed to be saturated with water at the initial conditions and a higher water relative permeability (k_{rw}) was used. Overall information about oil-water contact indicates that water may present in part of the F zone. However, due to limited information, no aquifer model has been used.

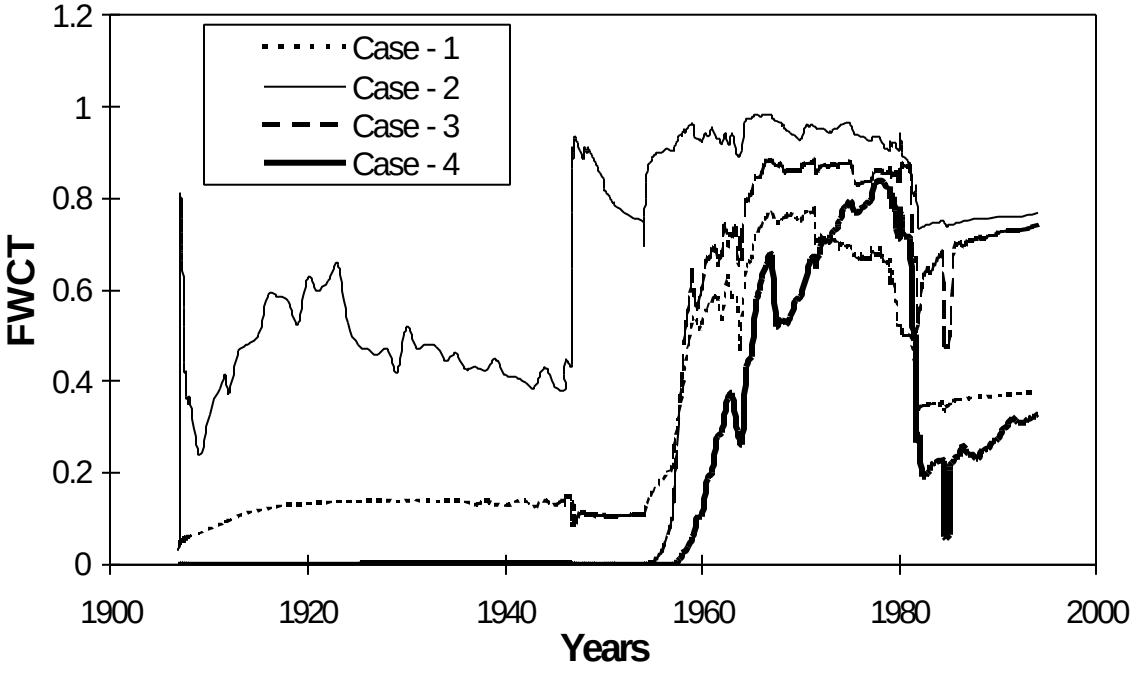

Figure 47 – Simulated field water cut – deterministic model

In order to see the potential for future use, the oil saturation map had to be analyzed. **Figure 48** shows the oil saturation comparison between the simulation and log-derived values at Self-82 for each case. The comparison is reasonable. In general, the simulation shows an optimistic result. All cases predicted high oil saturation at almost all units except unit F. In this unit, cases 2 and 3 predict a relatively lower oil saturation value as observed from the log data. The assumption that the formation is flushed by water at this interval can be justified. Thus, based on this model all the units, except unit F, can be considered good candidates with future potential.

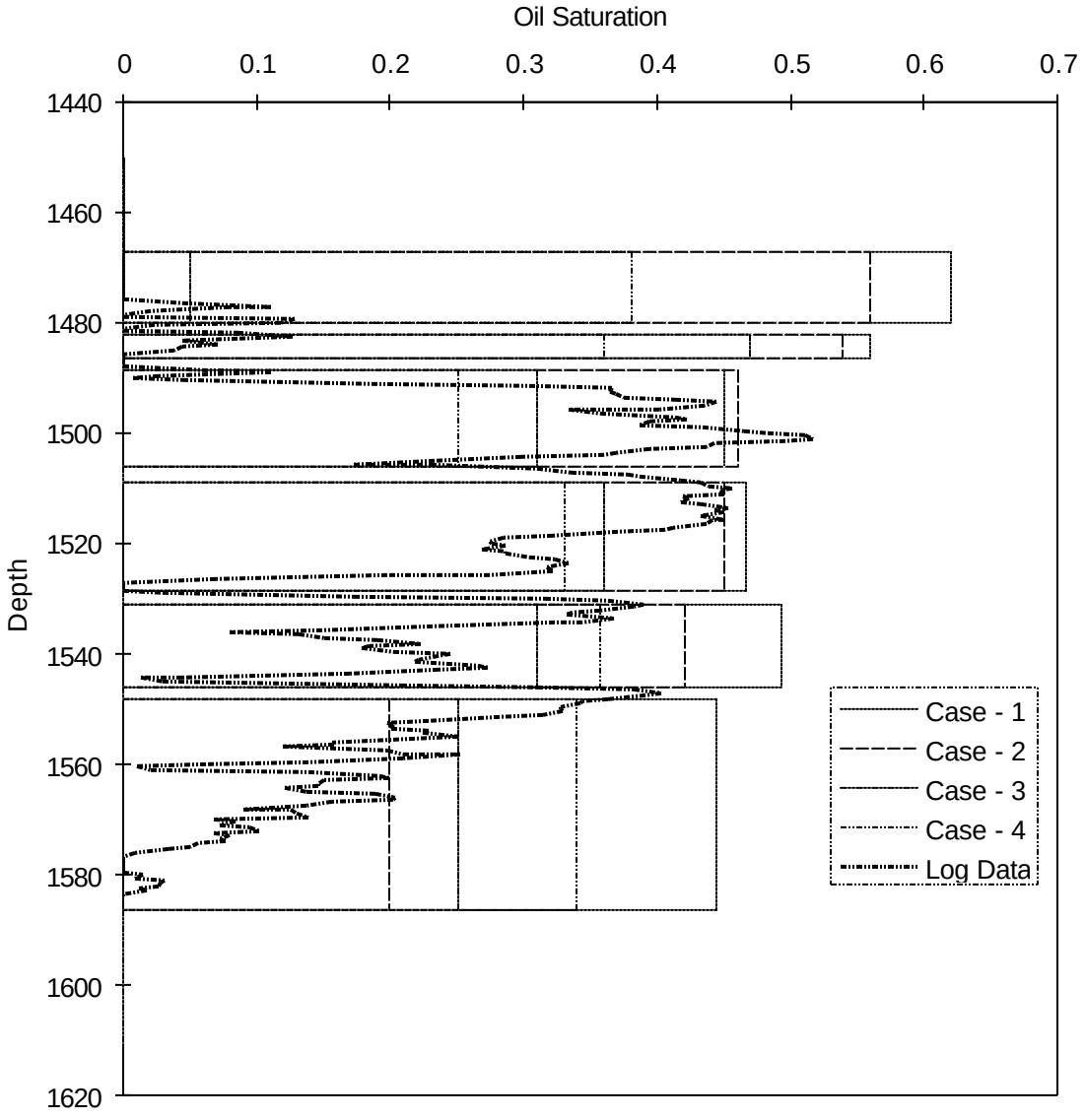

Figure 48 – Oil saturation comparison at Self-82 – deterministic model

Summary

To summarize the findings from this model, a deterministic model was developed for the Self-unit using available log and core data as well as the geological interpretation. The overall results based on the deterministic model are optimistic when compared to the field data. The kh values from the well tests are lower than predicted by the model. In general, variability of the properties observed in the field data

is not preserved when using a deterministic model. In the next two sections, the comparison of this model with the stochastic approach is be presented.

Stochastic Model without Tomography Information

Geological Simulation

The geological facies simulation was carried out using a geostatistical approach. The details and some of the results are already presented in the previous section and will not be repeated here. To summarize, the DGI's were simulated as categorical variables. The description was observed to be consistent with geological mapping developed by geologists. The total number of grid blocks simulated was equal to 256,000.

Porosity Description

Once the geological facies were simulated, the porosity values were simulated consistent with underlying geology. The details are provided in the previous section and will not be repeated here. **Figures 49a** and **b** show the comparison between simulated DGI's and observed DGI's at two wells which were not used in simulation. As can be seen from these two figures, the comparison is reasonable. The porosity from Self-82 was not used as conditioning data. **Figure 50** compares the simulation results with the observed data. Compared to deterministic model, the stochastic model captures the reservoir heterogeneity much better. It also tracks the variation in porosity better than the deterministic model.

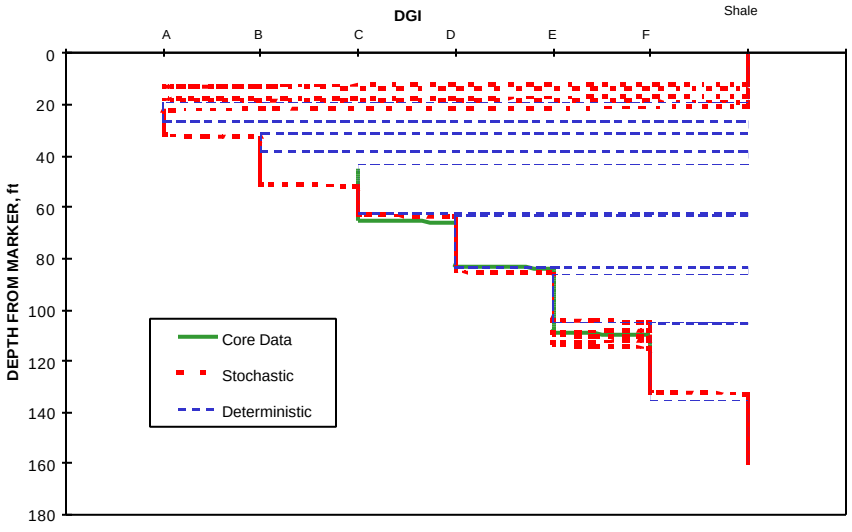

Figure 49a - DGI comparison at well no. 43 - DGI model

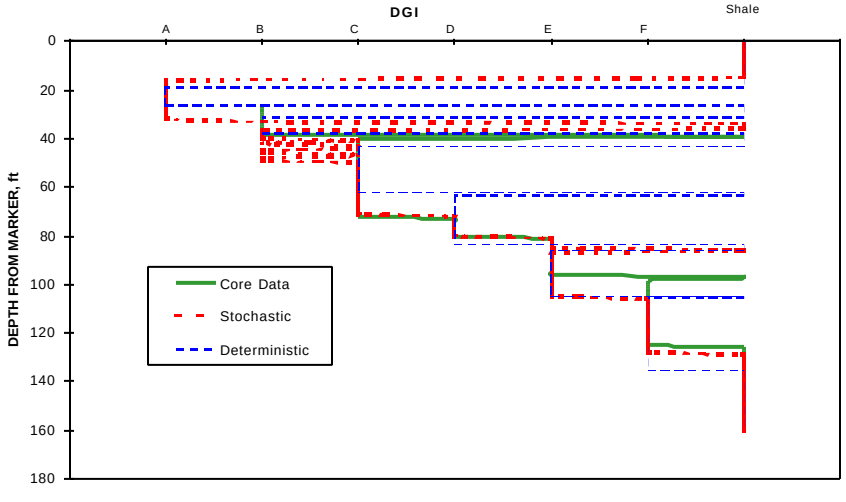

Figure 49b - DGI comparison at well no. 37 - DGI model

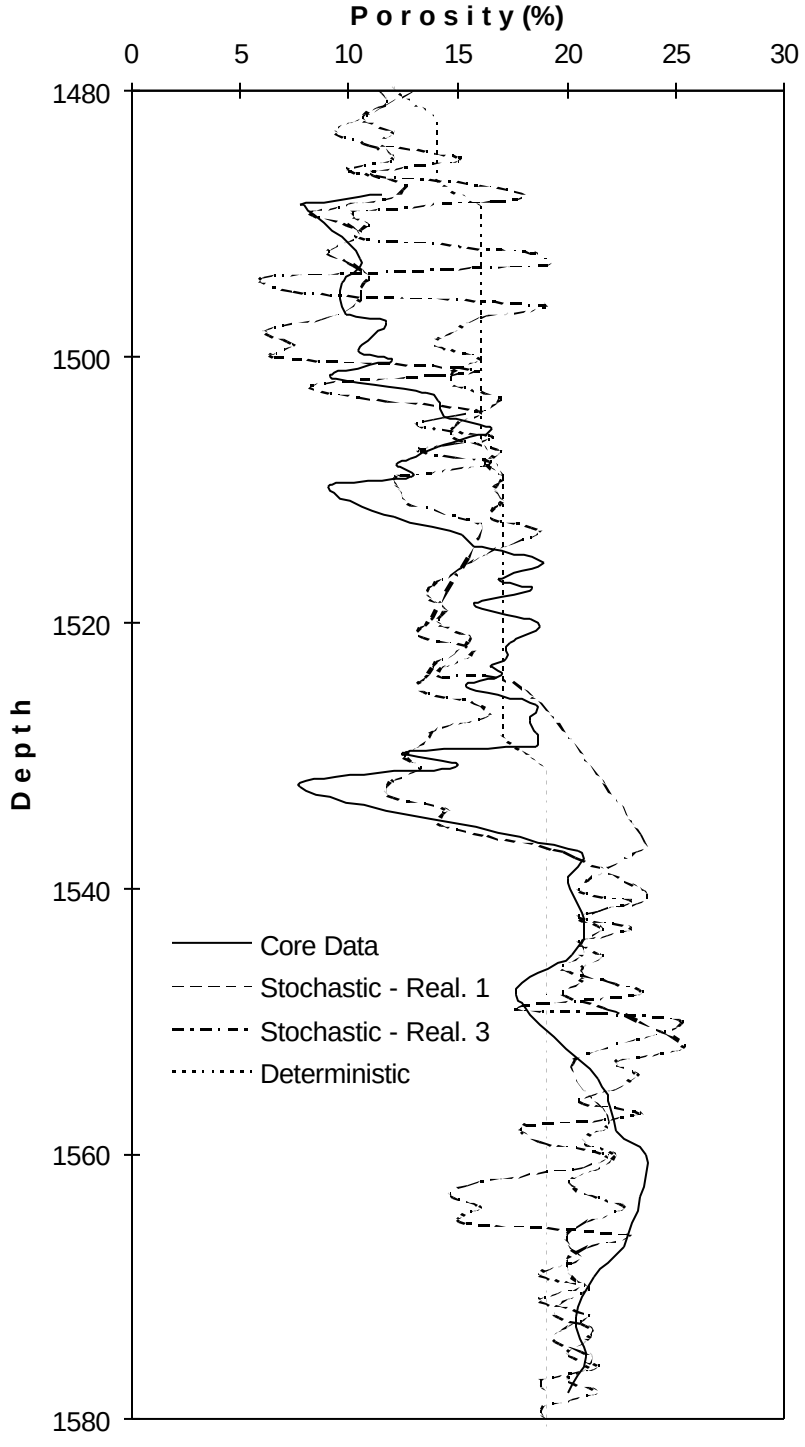

Figure 50 - Porosity comparison at Self-82 - DGI model

Permeability Description

After simulating the porosity values, permeability values were simulated using the relationship between log of permeability and porosity. A conditional distribution technique was used whereby for given porosity, permeability value was sampled from a given class. **Figure 51** shows a typical cross section of simulated permeability values.

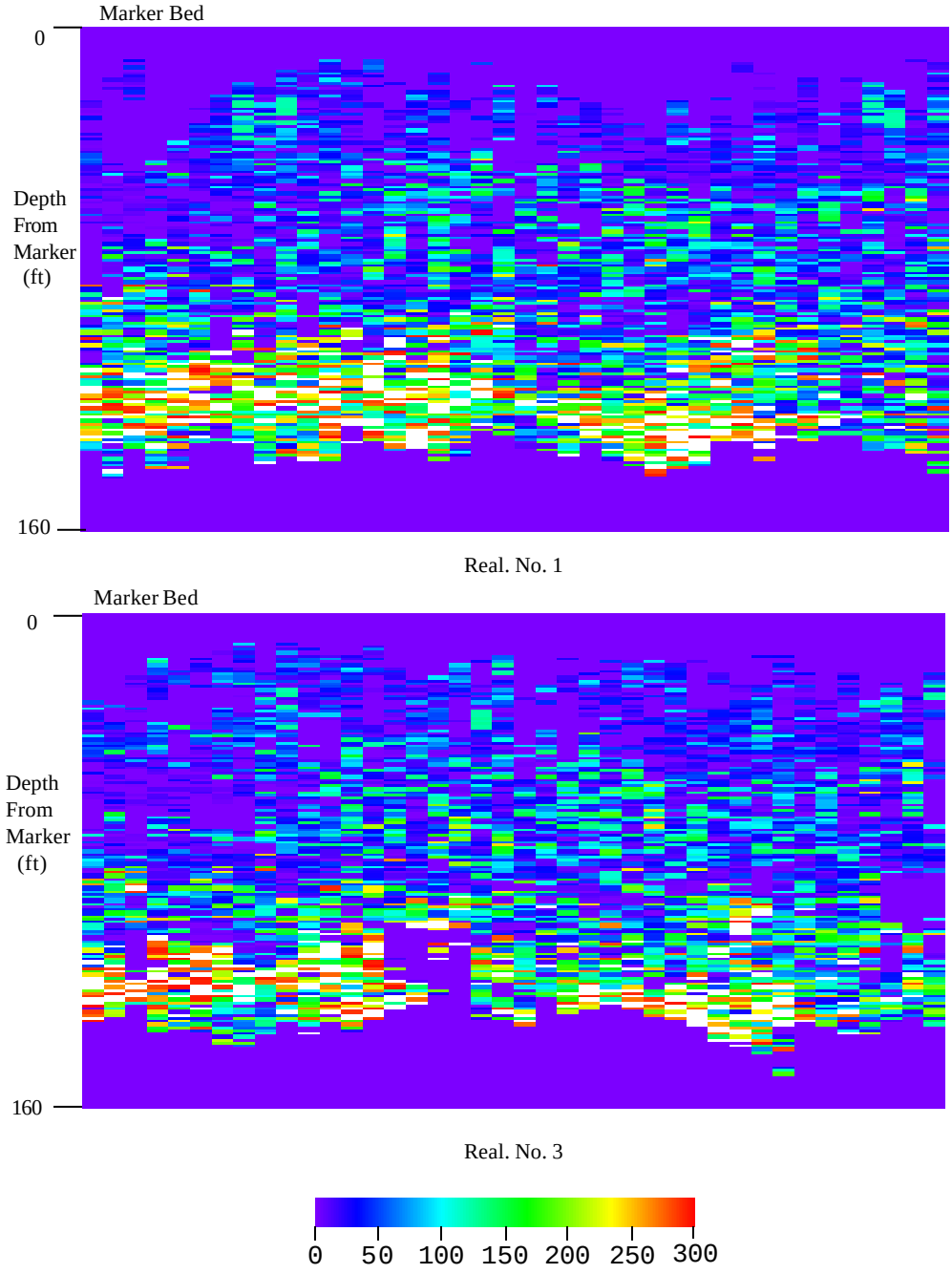

Figure 51 - Permeability distribution – north-south cross section - DGI model

Figure 52 shows the comparison between simulated permeability values and observed permeability values at Self-82. As can be seen, the permeability heterogeneity is better captured by stochastic model compared to deterministic model.

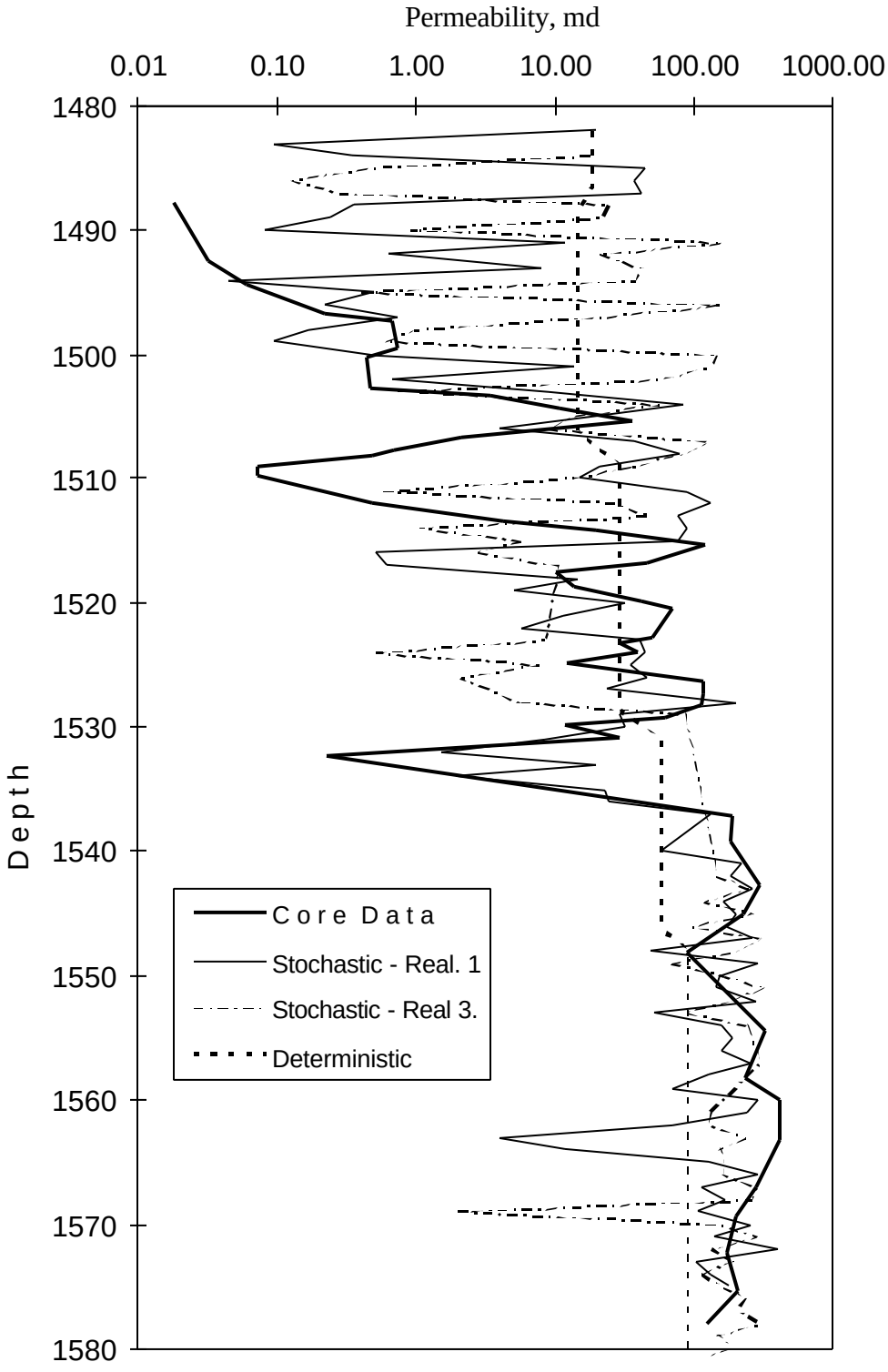

Figure 52 – Permeability comparison at Self-82 – stochastic model

To cross validate the result, the permeability-thickness product (kh) value from the model with the well test is compared. The comparison is shown in **Figure53**. Except for Well No. 61, where an anomaly was observed during the test, this figure clearly indicates that the stochastic model does a good job. The overestimated prediction of the deterministic model can be observed from the comparison presented in this figure.

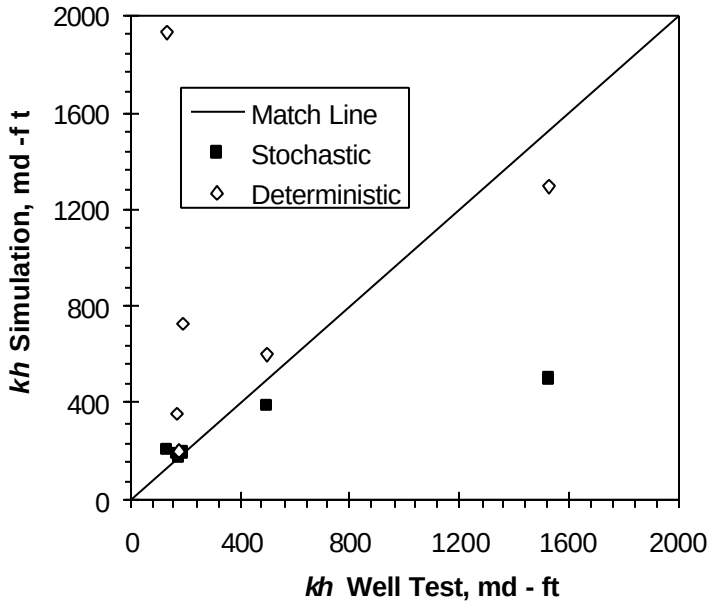

Figure 53 – Permeability – thickness (kh) comparison – stochastic model

Upscaling of Petrophysical Properties

The reservoir description generated in this model used 256,000 ($40 \times 40 \times 160$) grid blocks. This huge number of grid blocks can not be used in the flow simulation due to hardware (memory) limitations. The common number of simulator grid blocks used in the industry is in the range of 15,000 - 30,000 grid blocks. Unfortunately, the facility that was available for this study can handle only up to about 6,400 grid blocks. Thus, an upscaling process of the petrophysical properties is required before the simulation can be run. To get the total 6,400 grid blocks the configuration is reduced to $20 \times 20 \times 16$. This means that every 4 blocks in the horizontal plane have to become 1 super block, while for the

vertical direction average, every 10 blocks have to become 1 super block. All together, 40 blocks have to become 1 super block.

The upscaling of porosity was performed using a simple arithmetic average while the permeability is upscaled using the combination of arithmetic and harmonic average as follows.

1. Permeability average in either X or Y direction (Kx or Ky).

   •The permeability generated by the simulation was assumed to be the permeability in the horizontal direction ($Kx = Ky = Ksimulation$).

   •For blocks in the horizontal plane:

   -Two harmonic averages (kh_1 and kh_2) were calculated for 2 pair blocks in the direction of flow, as follows:

$$kh_i = \frac{2\,kx_1\,kx_2}{kx_1 + kx_2}$$

   -The super block average is calculated as the arithmetic average of kh_1 and kh_2, as follows:

$$k_x = k_y = \frac{kh_1 + kh_2}{2}$$

   -The arithmetic average is used to calculate the average for vertical blocks.

2. Permeability Average in Z direction (Kz)

   •Kz is assumed to be some percentage of Kx.

   •Harmonic average kh_i was calculated for blocks in the direction of flow (vertical direction).

   •The super block average for Kz is calculated as the arithmetic average of the 4-neighbor horizontal blocks.

Flow Simulation

The number of grid blocks to be used for the flow simulation as mentioned in the previous section was 6,400 ($20 \times 20 \times 16$) blocks. The dimension of each grid block in the horizontal directions (Δx and Δy) was chosen to be fixed at 132-ft. Several cases were run in the beginning of this study using a uniform size in z direction with Δz = 10-ft. It was observed that the results were not satisfactory. Thus, it was decided to run the simulation using a variable size in the vertical direction. This size is determined by observing the significant changes in the formation as given by the well log. The resulted size is as follows: 15, 15, 10, 5, 5, 5, 5, 5, 5, 5, 5, 10, 10, 20, 20, 20-ft. All of the simulation results presented below use this configuration.

The first result presented is the comparison of the initial potential of the reservoir between the simulation and the field data as shown in **Figure 54**. The bottom hole pressure used in this model is not a uniform value as was used in the deterministic model, but rather a variable value that is unique for each well. The result was derived using realization no. 1 of the reservoir description generated. It can be seen that the match is good.

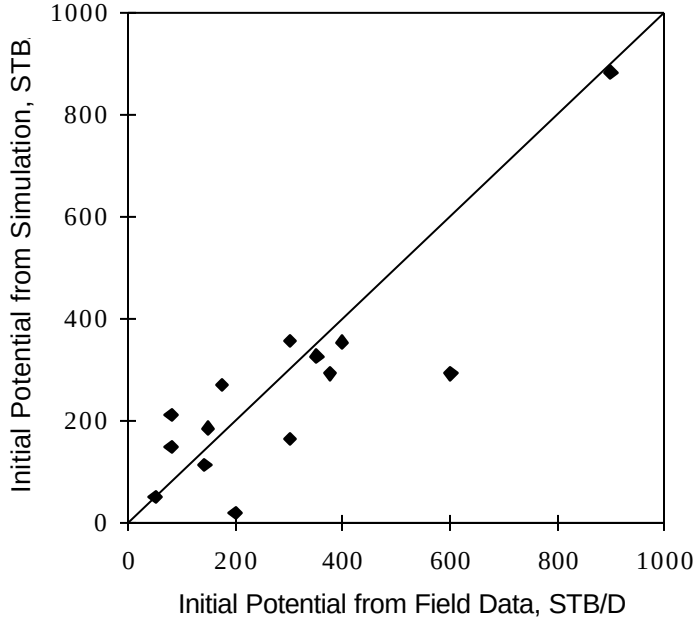

Figure 54 – Initial potential comparison – stochastic model

Figure 55 presents the field oil production rate for cases 1, 2 and 3. These cases represent use of different relative permeability curves. Similar results are observed for other realizations as well.

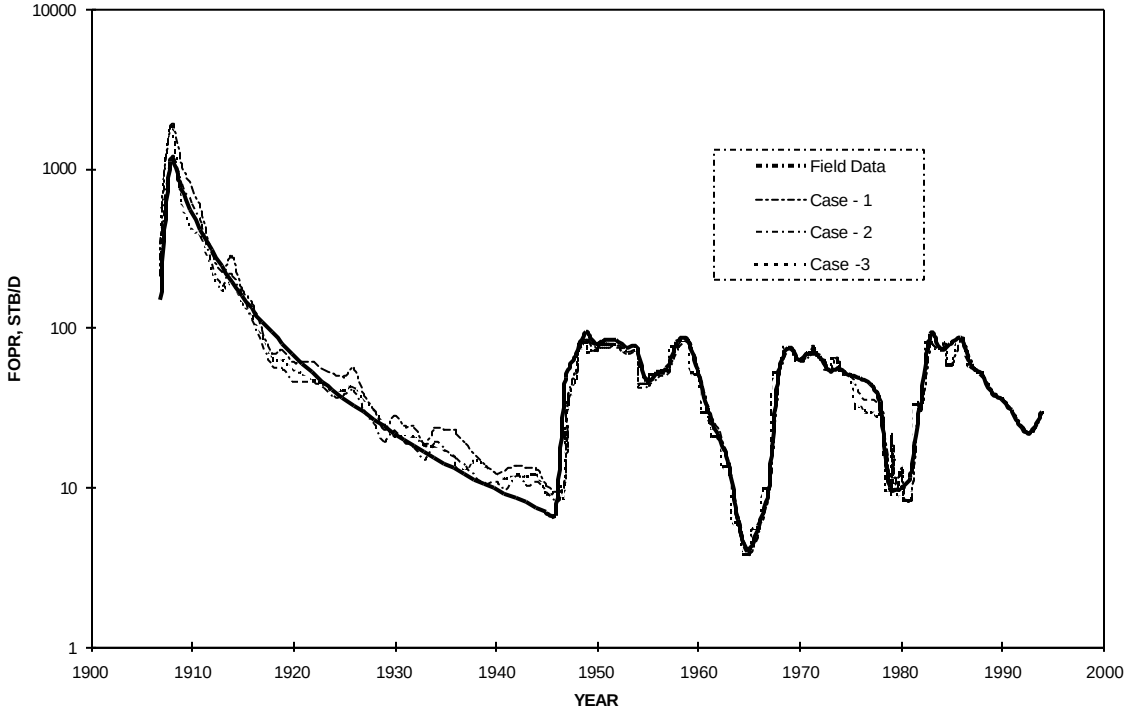

Figure 55 – Field oil production rate comparison – stochastic model

Figure 56 shows the results of OOIP and cumulative production at 1946 for different realizations and the deterministic model using case 4. The three realizations show a consistent result, even though some uncertainties can be observed. The mean value from these realizations is 11.77 MSTB, which is less than what is estimated by the deterministic model. Thus, this result shows that the deterministic model is more optimistic compared to stochastic models.

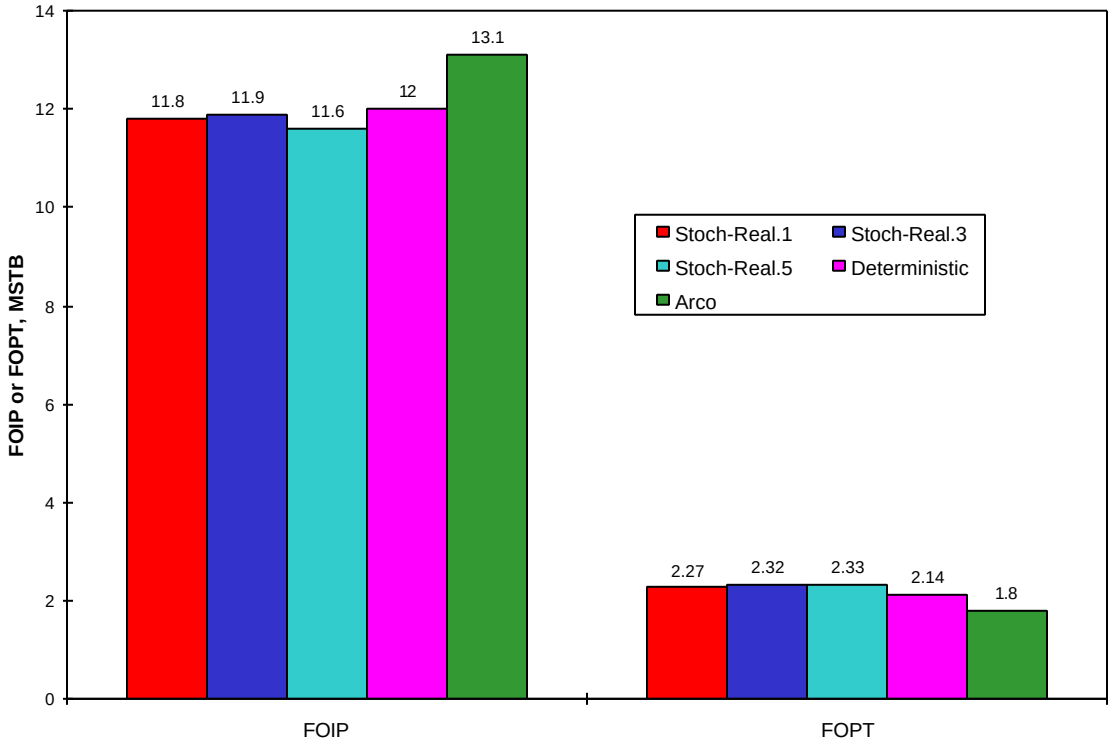

Figure 56 – Original oil in place (FOIP) and cumulative oil production (FOPT) at 1946 comparison – stochastic and deterministic models

Figure 57 shows the field water cut predicted by the simulation for different realizations. As in the deterministic model, the simulation does not match the field conditions very well. The comparison presented in Figure 57 once again supports the argument about the optimistic result of the deterministic model. Its water cut prediction is much lower (thus, the oil cut is much higher) than the ones that are predicted by the stochastic model.

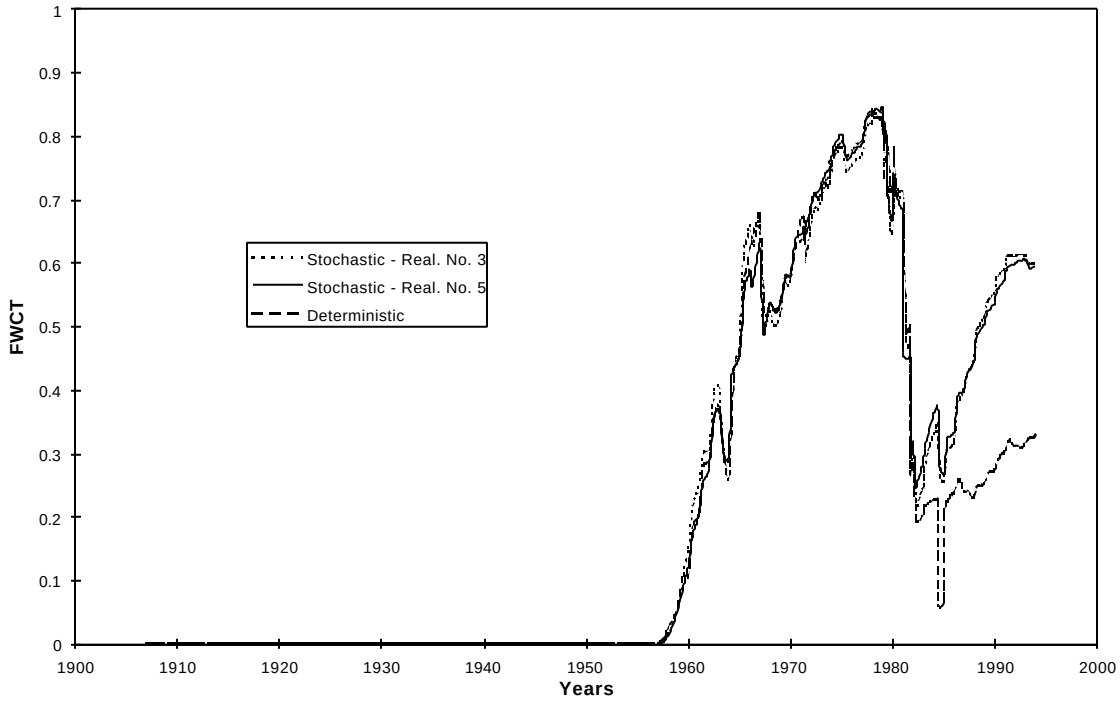

Figure 57 – Field water cut prediction for stochastic and deterministic models

The comparison of the simulation result with respect to the log data of Self-82 is presented in **Figure 58**. From this figure it can observed that the saturation heterogeneity of the reservoir was not really captured very well. This may be related to the grid resolution (number of grid blocks and its size at a particular location) that is very difficult to solve at the present condition.

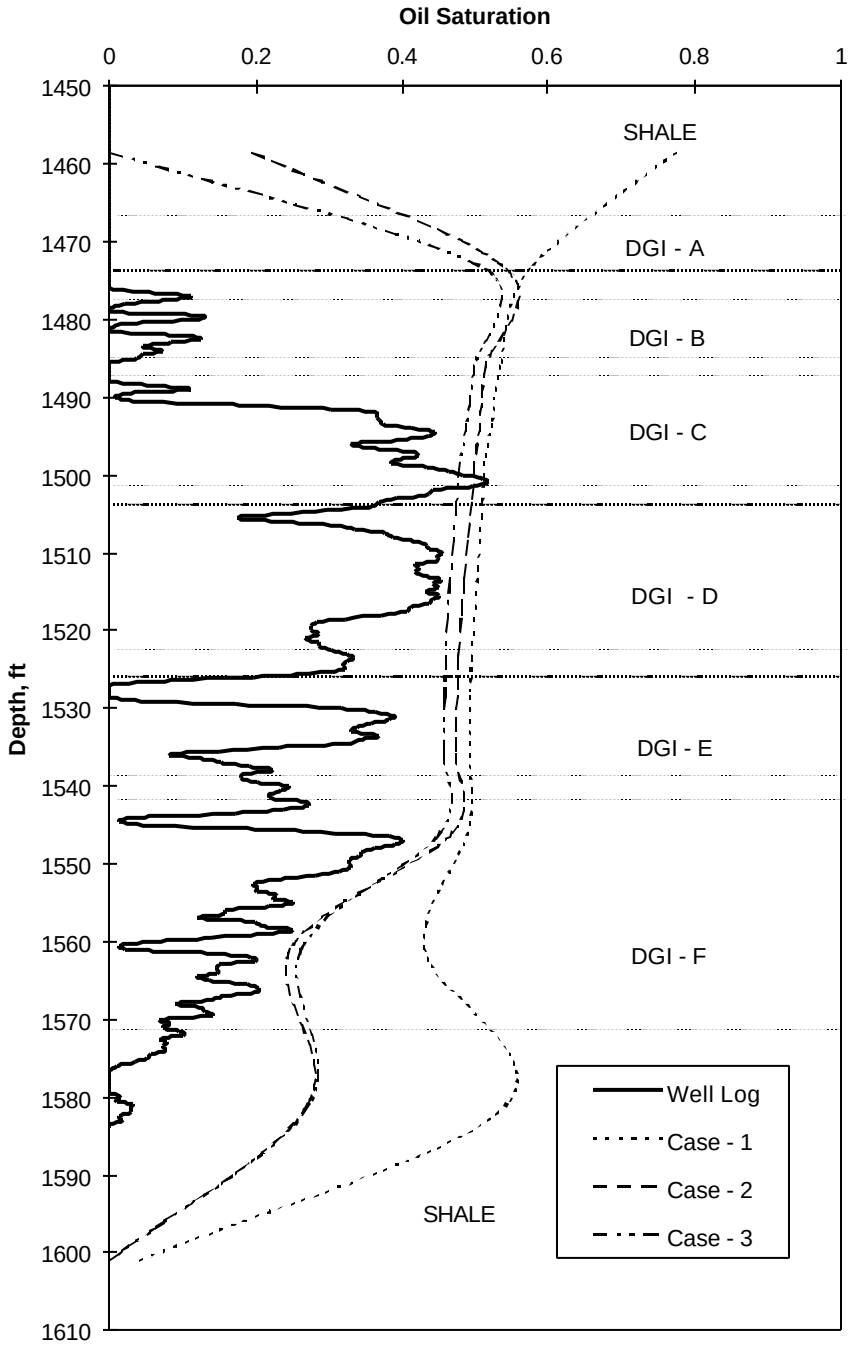

Figure 58 – Oil saturation comparison at Self-82 – stochastic and deterministic models

Summary

The stochastic model performed a very good job of capturing the reservoir description. It replicated the geological architecture very well. It matched the porosity as well as the permeability data at wells not used as conditional data and performed a reasonable job of matching the historical production performance.

Stochastic Model with Tomography Information

Porosity Description

This section presents the integration of the seismic data into reservoir description based on the stochastic model presented previously. The same geological model was used in this model but the porosity simulation contains extra information. Since the permeability description is related to the porosity distribution then the permeability distribution will also contain extra information. The term seismic in the above statement refers to the tomogram as interpreted from a series of cross well seismic field test surveys that were performed in the Self-unit between wells no. 82 - 63, 82 - 64, and 82 - 81 in January, 1994. Three tomogram panels were available for this study. The inversion of seismic data into velocity distributions at each panel was discussed in the previous section. The discussion presented here started from the assumption of known velocity distributions in each tomogram panel.

The use of velocity data in the reservoir description is related to the porosity distribution as given by the Wyllie Equation where the porosity is linearly related to the reciprocal of velocity, which is known as transit time. The main advantage of having these data is to get a better spatial relationship (variogram) in the interwell region, which is missing from the usage of log or core data alone. It was expected that the tomogram data would improve the variogram model with respect to the range of the model.

To superimpose the geology, the data were separated according to the type of the DGI at each location. In this case, the separation is not a straightforward process due to the differences in the grid block configuration. The velocity distribution had poor vertical resolution but better horizontal resolution compared to the simulated geological model. Horizontally, the changes of geology are known for every

66-ft whereas the changes of velocity are known for every 13-ft. Since the simulation of porosity follows the grid block configuration of the geological model, it was decided to take the average of 5 velocity data values before the conversion is done. On the other hand, in the vertical direction the geology is known on a one-foot interval whereas the velocity is only known for every 12-ft. For this case, no averaging process is required.

Figures 58 presents the porosity distribution at each tomogram panels after applying the correlation between porosity and transit time. It is assumed that the transit time and porosity are correlated using linear relationship. It can be observed that the layer of highest porosity occurs at the middle of the formation (DGI D). This result does not match with the observed field data where porosity increases with depth. There are two reasons that can be suggested for this result. The first one is related to the velocity distribution itself. The velocity distribution indicates that a layer of low velocity (high porosity) exists in the middle of the Glenn sand. The other reason may be that the correlation used in transforming the velocity into the porosity is not accurate. In spite of this concern, we decided to use this distribution since we wanted to preserve the information in the original form as much as possible.

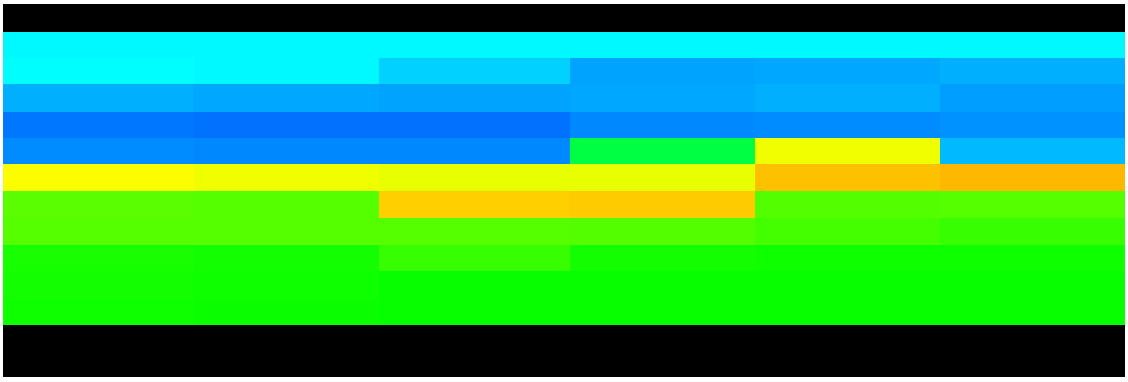

Wells 63 - 82

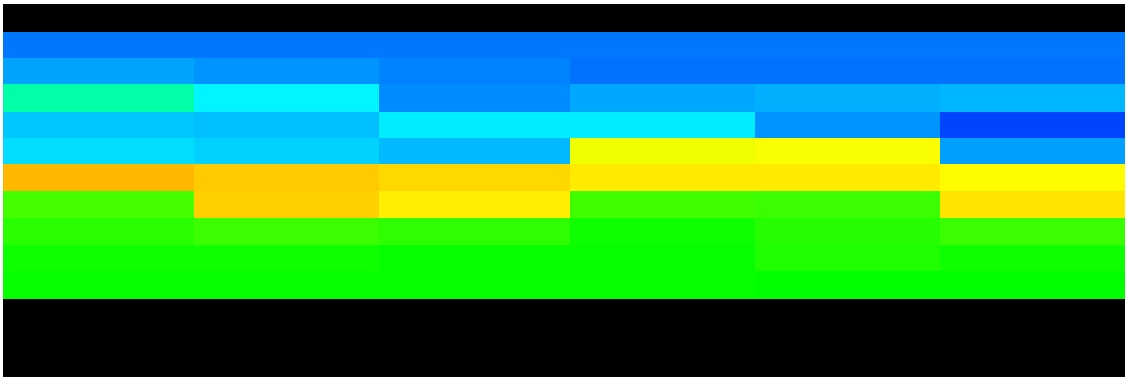

Wells 82 - 64

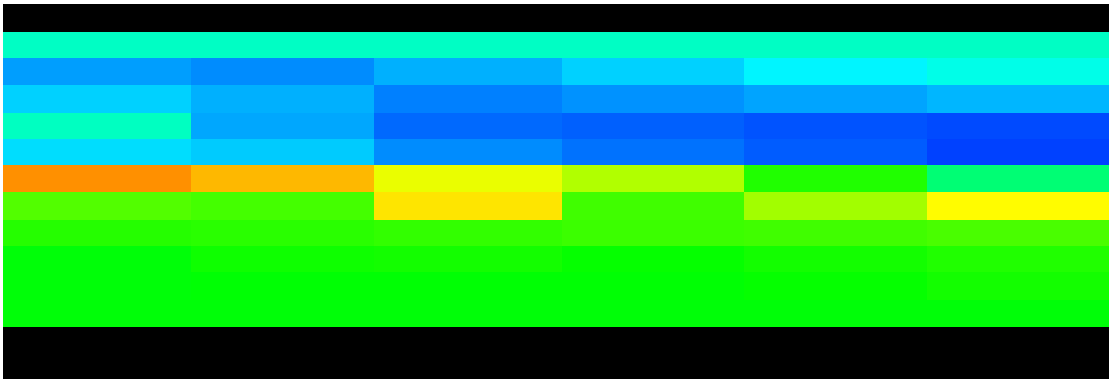

Wells 82 - 81

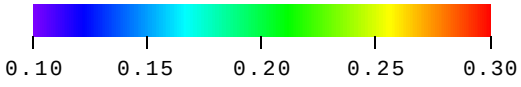

Figure 58 - Porosity distribution at tomogram panels after applying the correlations

The variograms for each DGI generated using the porosity distribution in each panel are shown in **Figure 59**. The separation of porosity of DGI's B and D from the other DGI's is due to the difference in the sill value in each DGI. It can be observed that in all DGI's the variogram of the conditional data can be represented by the spherical model. This observation is consistent with the assumed spherical model in the previous section where only limited data were used.

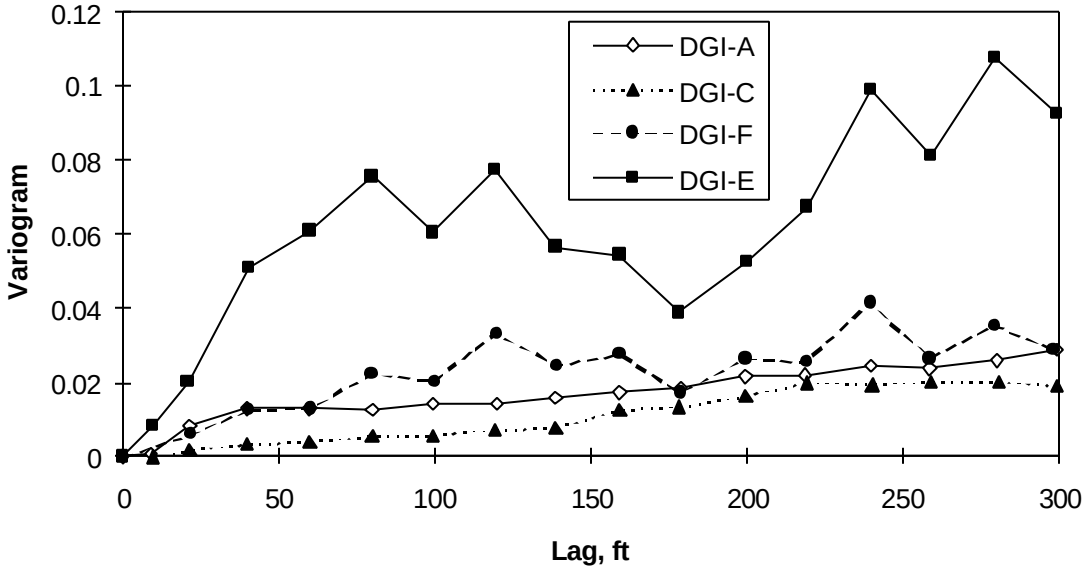

Figure 59a – Horizontal porosity variogram of the tomogram data (DGI's B and D)

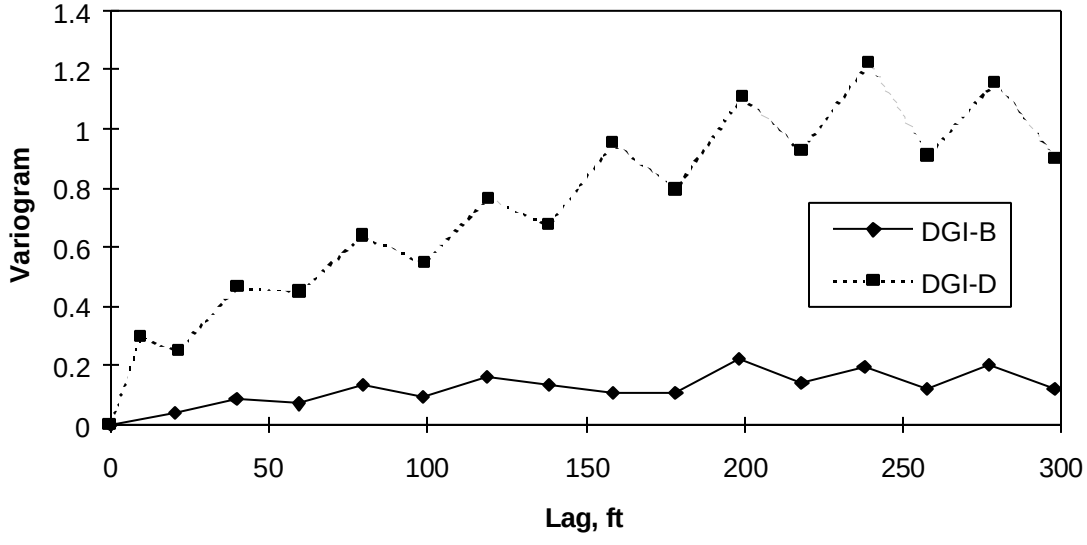

Figure 59b – Horizontal porosity variogram of the tomogram data (DGI's B and D)

The second observation that can be drawn from the variograms generated is related to the range parameter. It can be observed that the range of the porosity spatial relationship is at least the distance between two wells, i.e., about 300-ft. Thus, the assumption of using a range equal to the distance of the

closest well pair can also be justified. This assumption was used for DGI's B, E and F. The porosity variogram for DGI's A, C, D was modeled previously using soft geological information where the range is assumed to be a number that is greater than the distance between the wells and is related to length of the channel-fill in each DGI. Thus, this assumption can also be justified.

The simulation of the porosity distribution was conducted using the same method as discussed before. The only difference between this distribution and the previous one is in the conditioning data. The variogram models are the same since the assumptions used previously are justified.

The comparison of the porosity at Self-82 is presented in **Figure 60**. In general the match of porosity at Self-82 from this model can be considered good except in the zone of DGI D where two peaks occur. This discrepancy may be due to the high velocity region in the D zone found from the velocity distribution.

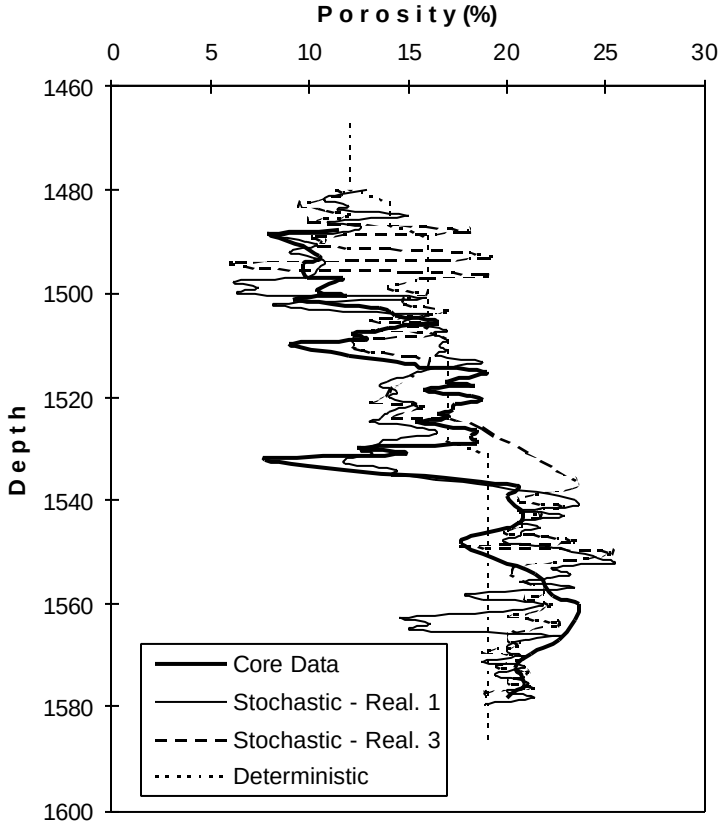

Figure 60 – Porosity comparison at Self-82

Permeability Description

Following the same method used previously, the permeability distribution was generated using the conditional distribution method where it is calculated using the distribution function of the permeability in a given porosity class.

The comparison of the permeability at Self-82 is presented in **Figure 61**. This figure shows that the model with tomogram data performed a better job than the model without the tomogram data. This statement can be verified by observing the top and bottom zones. In the top zone, the previous model (no tomogram) tends to give a higher value whereas the present model (with tomogram data) remains in the range 0.1 to 1 md. The core data show a very low value. At the bottom interval, the present model follows the core data consistently whereas the previous model predicted a layer with a lower permeability value. At the middle of the formation, both models give the same result.

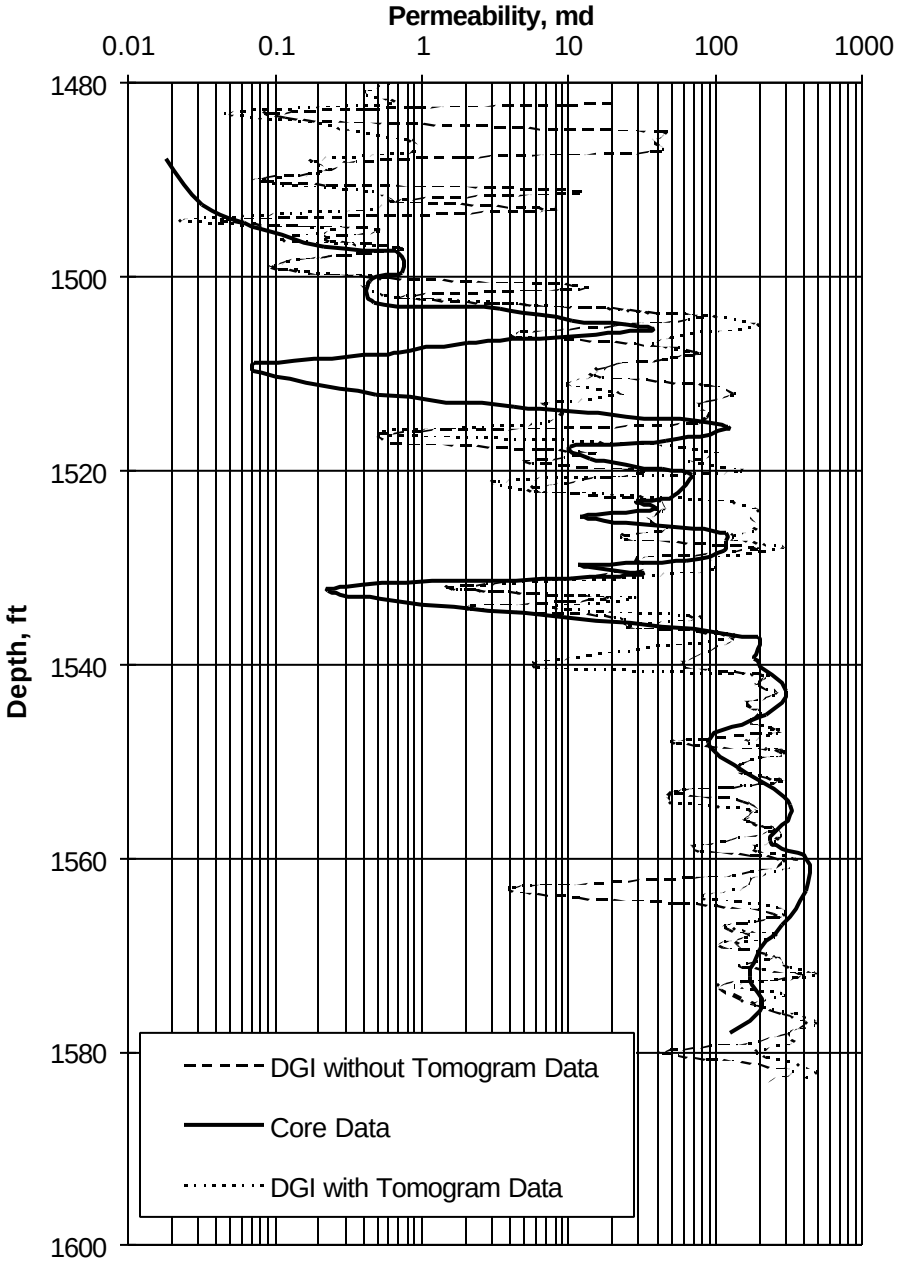

Figure 61 – Permeability comparison at Self-82

The validation of the permeability distribution generated using this model is done by comparing the product of permeability and thickness (kh) as was done for each model. This comparison is presented in **Figure 62**. This figure clearly indicates that the tomogram model performs an excellent job. The matches are good for all wells including the result of well No. 61 where a kh value of 1,530 md-ft was

calculated from the well test and the model predicted 1,405 md-ft. This figure is an important illustration of the principle that addition of different information reduces uncertainty in the reservoir description.

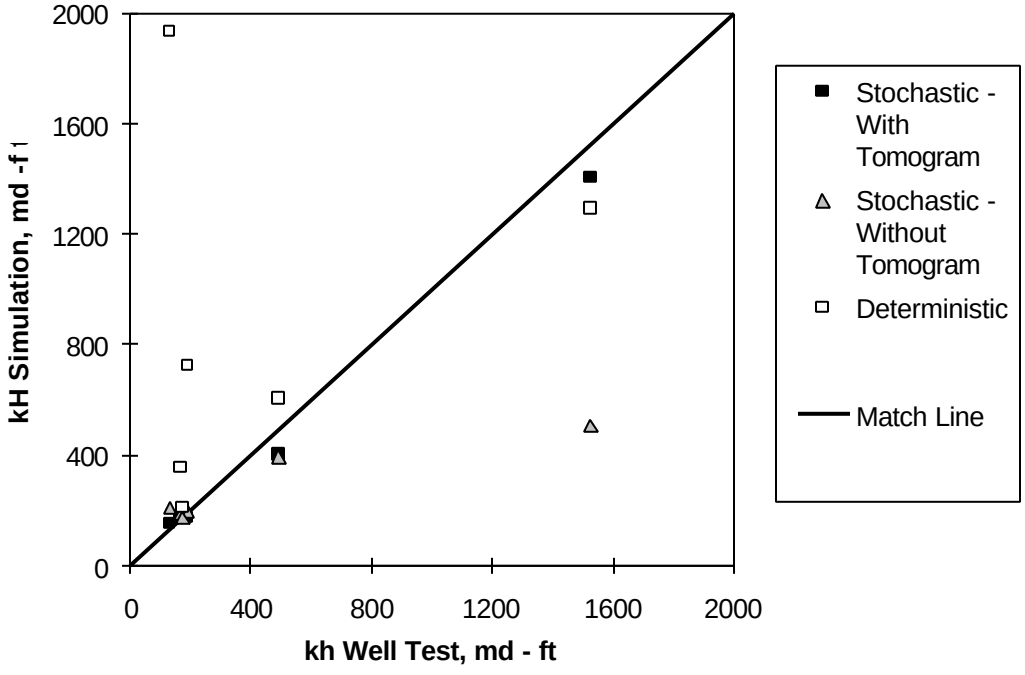

Figure 62 – Permeability – thickness (*kh*) product comparison – all models

Flow Simulation

Figure 63 presents the field oil production rate predicted by the simulation. For the early period, the tomogram model shows a slightly higher production rate compared to the non-tomogram model. The higher production rate for the same relative permeability curve may be due to the higher initial oil in place, which means a higher pore volume generated from the reservoir description. To see if this is the case, **Figure 64** compares the original oil in place calculated using several models. It can be seen that the tomogram model estimated the most optimistic original oil in place.

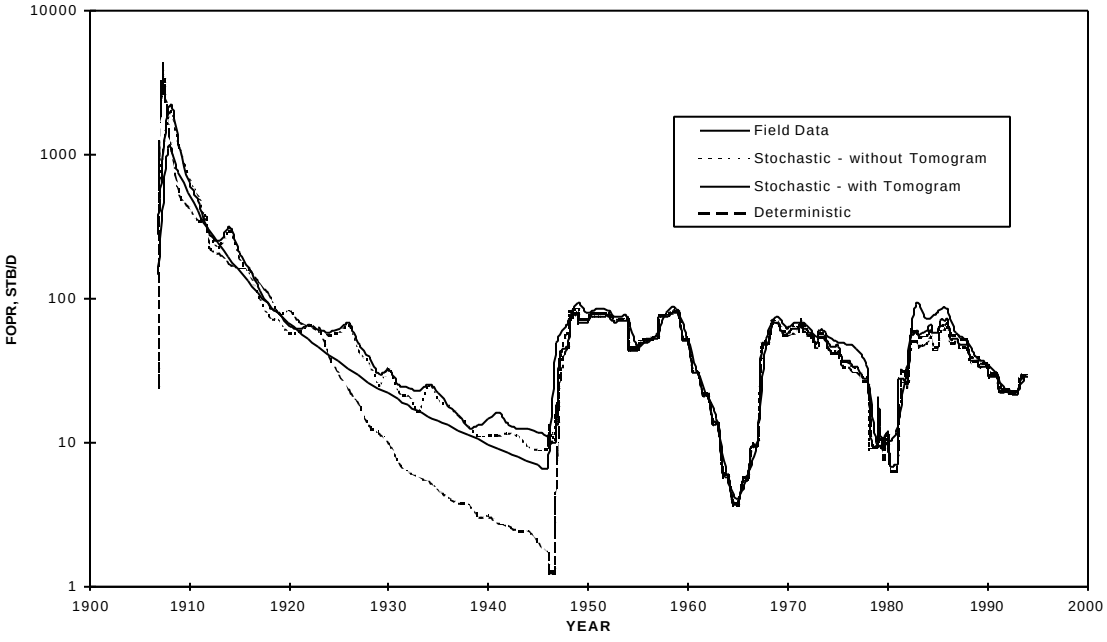

Figure 63 - Comparison of field oil production rate (FORP) – all models

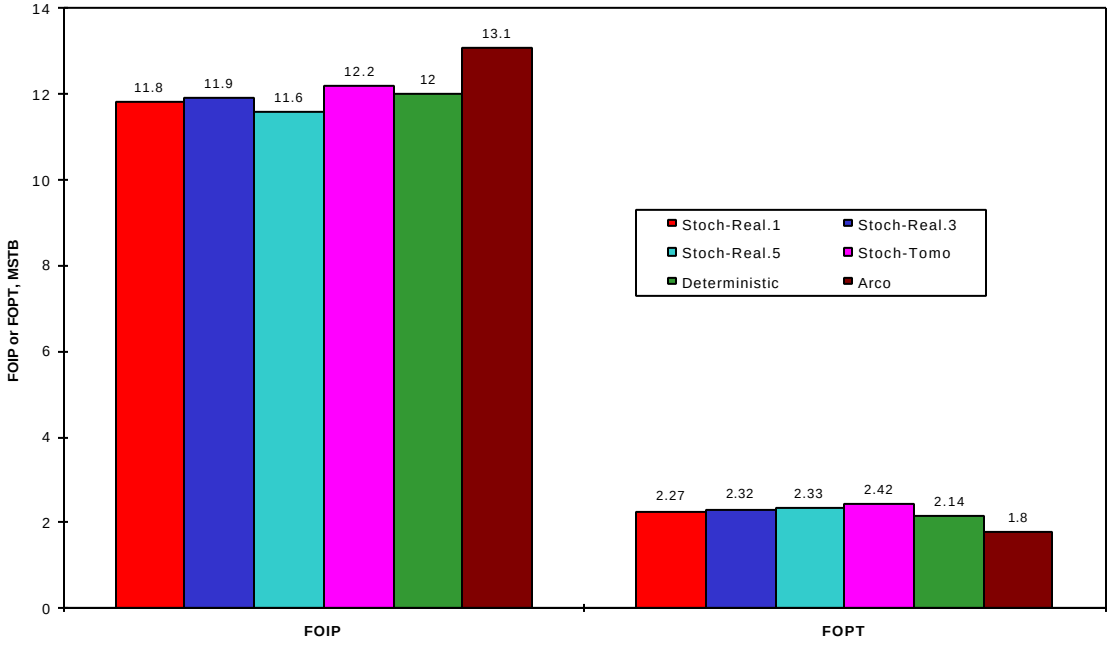

Figure 64 – Comparison of original oil production rate (FOIP) and cumulative production at 1946 for different models

Figure 65 compares the field water cut predicted using this model with respect to the other models. It can be seen that the two stochastic models give about the same prediction of water cut during the life of the reservoir even though it does not match very well with the field data. The deterministic model remains the optimistic model since it predicts the lowest water cut while the field was operated with a very high water cut.

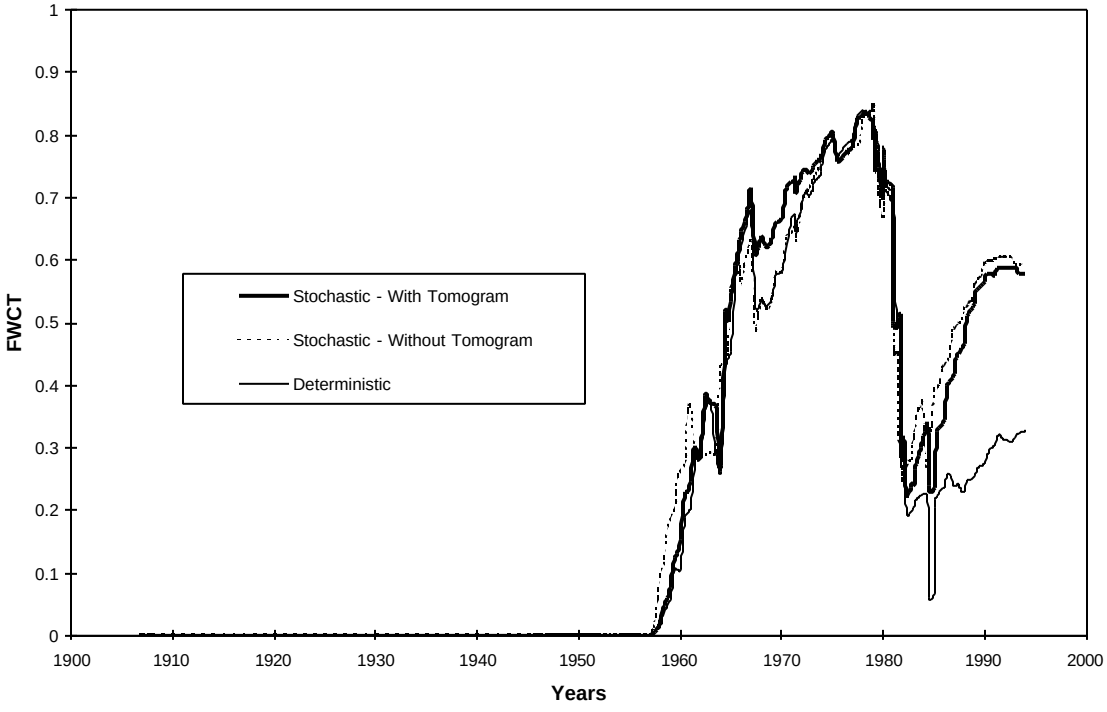

Figure 65 – Comparison of field water cut – all models

Finally, the comparison between the simulated and the measured oil saturation at Self-82 is presented in **Figure 66**. As it is shown in this figure, there is no significant difference among the models with respect to the oil saturation at Self-82. The three models do not follow very well the heterogeneity of the oil saturation profile. This is mainly due to the resolution of the grid blocks configuration.

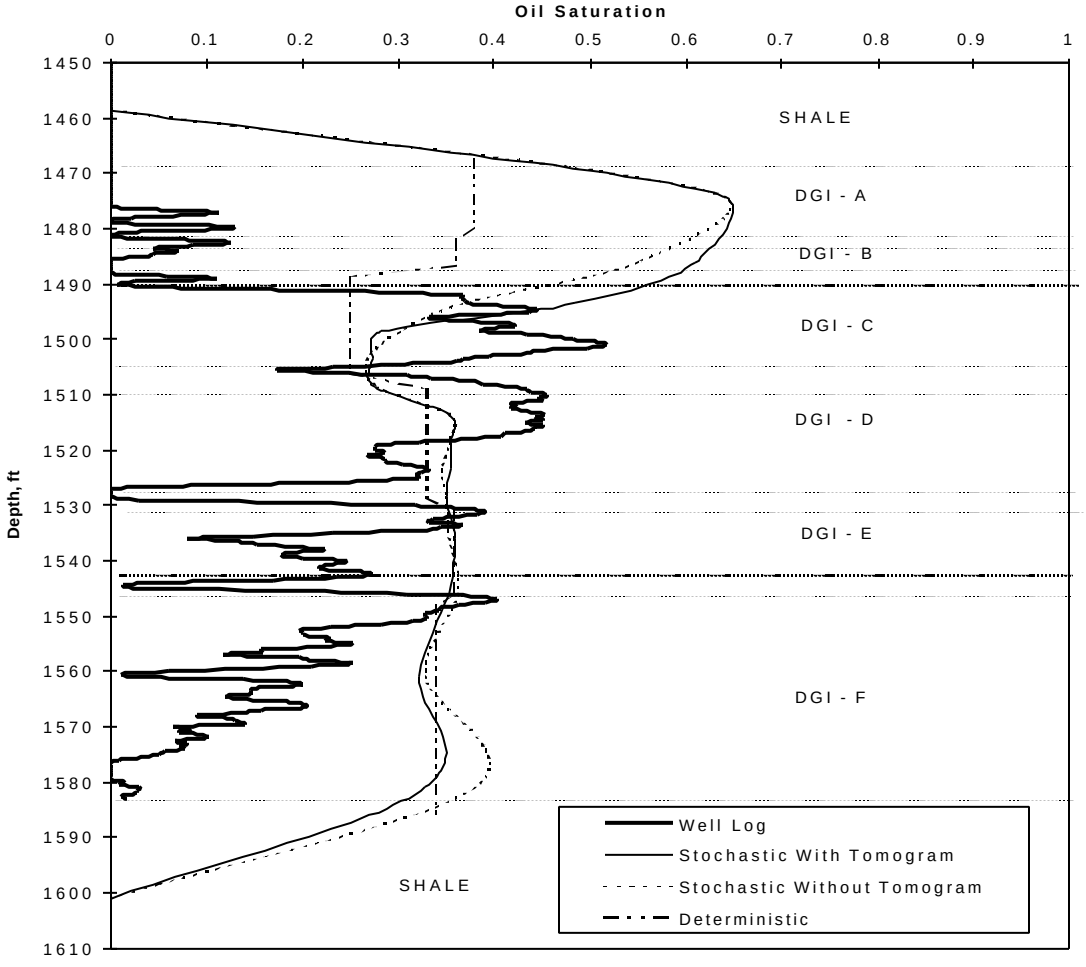

Figure 66 – Comparison of oil saturation at Self-82 – all models

Summary

To summarize the findings in this model, the tomogram data could be incorporated into the reservoir description through velocity porosity transformations. The main use of the tomogram data in this model was to estimate the variogram models used in the previous model. It was found that the spherical model was adequate for the modeling purposes and the range of the porosity variogram was not less than the distance between two wells. In general, the results were in good agreement with the other stochastic model except for the permeability distribution where the model with tomogram data performed a much better job. Especially, the dynamic reproduction of the well test permeability data was much improved

after incorporating the tomogram data. This indicates that additional information can improve the reservoir description.

Reservoir Management

The overall goal of the study is to improve the secondary recovery performance through the use of a better reservoir description and better reservoir management. This section presents the analysis that led to the reservoir management plan of the Self-unit for future production. The analysis started with the discussion of the future production forecast using three different scenarios for three reservoir description models discussed in the previous sections, i.e., the deterministic model, the stochastic-model without tomography information, and the stochastic model with tomography information. The three scenarios are:

1. Drilling no additional wells.
2. Drilling a horizontal well.
3. Drilling new vertical production wells.

Each scenario was related to the well completion and the water injection rate. To cover several possibilities of this configuration, several sub-scenarios were defined within each scenario. The flow simulation was run for each sub-scenario until the year 2000 and the increase of production (if any) was compared with the base case which is the simulation with current field conditions (based on 1993 data).

Following the flow simulation, an economic analysis was performed for several selected sub-scenarios that would give the best increase of production. The analysis was based on the data provided by Uplands Resources, Inc. Conservative estimates are used for the cost of production to avoid over optimistic forecasts of the profits. The best scenario was determined by the rate of return and the payout time as criteria based on a constant oil price at the current level of $17.00 per barrel.

Future Production Forecast

The definition of each sub-scenario (presented in **Table 4**) was determined based on the following two reasons: the Self-unit was completed very well at the middle to the bottom interval (DGI's D and E),

and it was feasible to increase the injection rate. Since the deterministic model predicted relatively high permeability and high oil saturation in DGI's A and B then these two DGI's cannot be ignored for this model. Thus, for the deterministic model the future forecast also include DGI's A and B in addition to DGI's D and E whereas for the stochastic model only DGI's D and E are to be considered for recompletion. The exclusion of DGI C is due to the relatively low permeability (in both models) and the fact that it has been opened within most of the Unit. The DGI F was excluded from any sub-scenario since it has been flushed by water as observed on the flow simulation runs.

Table 4 – Definition of sub-scenario used in future production forecast	
Name	Description
Scenario - 1A	Open well 82 as producer Convert well 81 as producer
Scenario - 1B	Reopen DGI's* at all wells Base Injection rate
Scenario - 1C	Current perforation Double injection rate
Scenario - 1D	Reopen DGI's* at all wells Double injection rate
Scenario - 1E	Reopen DGI's* at all wells Triple injection rate
Scenario - 2A	Horizontal injection well with injection rate of 1000 BWPD, Reopen DGI's*, double rate at old wells
Scenario - 2B	Horizontal injection well with injection rate of 2000 BWPD, Reopen DGI's*, double rate at old wells
Scenario - 2C	Horizontal injection well with injection rate of 3000 BWPD, Reopen DGI's*, double rate at old wells
Scenario - 2D	Horizontal injection well with injection rate of 3000 BWPD, Reopen DGI's*, base rate at old wells
Scenario - 2E	Horizontal producer well Reopen DGI's*, base rate at old wells
Scenario - 3A	4 new vertical wells (producer) Base rate at old wells
Scenario - 3B	4 new vertical wells (producer) Double rate at old wells

*Reopen DGI's means: Reopen DGI's A, B, D, and E for deterministic model and DGI's D and E for stochastic model

The possibility of increasing the injection rate was based on the data from 1992 and 1993 where the production increased 38% (from 21 BOPD to 29 BOPD) when the field was flooded with a 125% higher injection rate. This fact suggested that the field responded to an increase in the amount of water

injected. We expect that, in the future, by increasing the water injection rate, we can increase the oil production.

Scenario 1: Drilling No Additional Wells / Current Field Configuration

From Table 4, there are 5 sub-scenarios defined for scenario 1, i.e., scenario 1A through 1E. For each of these sub-scenarios, the results of the 4 case studies (defined in Table 3) of the stochastic model without the tomogram data are presented. For the purpose of comparison and also to evaluate the uncertainty of the result, case 4 is run using scenario 1D for other models, i.e., deterministic, stochastic description without tomogram for 3 realizations, and stochastic description with tomogram data. The result is presented at the end of this section.

Figures 67-71 present the result of scenario 1A through 1E respectively. The result of scenario 1A shows that there will be no increase of production if this scenario is applied in the Unit. Thus this scenario can be ignored. Figure 63.B shows that the range of additional oil production that can be expected by implementing scenario 1B is between 10 to 16 barrels of oil per day. In this scenario, case 4 shows almost a steady performance whereas the other cases seem to decline faster. In scenario 1C the first three cases predicted almost the same result, but case 4 is very pessimistic. A contrasting performance can be observed by comparing the result of case 4 between scenarios 1B and 1C. This result indicates that case 4 is more sensitive to the opening of new intervals (scenario 1B) than to increasing the injection rate (scenario 1C).

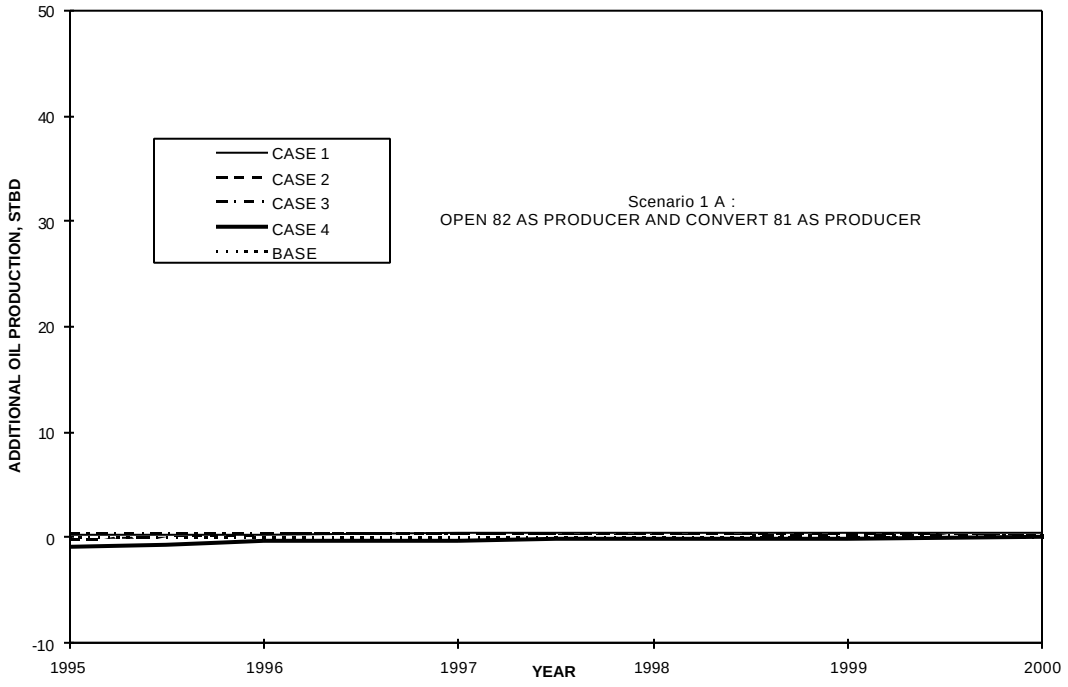

Figure 67 - Increase of oil production using scenario 1A

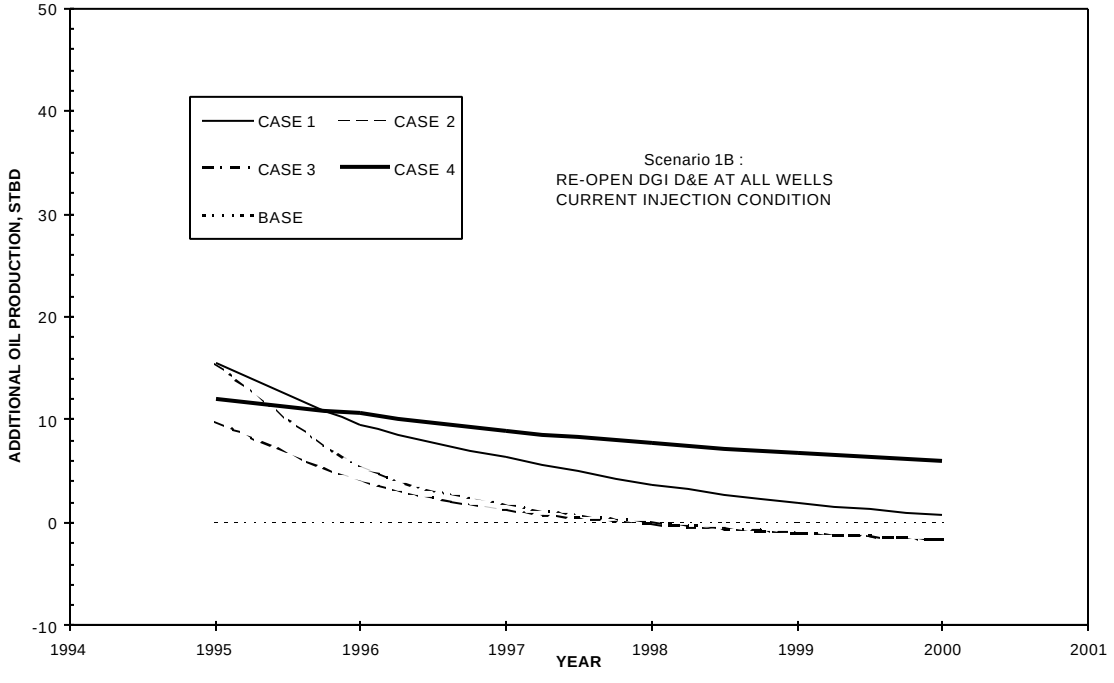

Figure 68 - Increase of oil production using scenario 1B

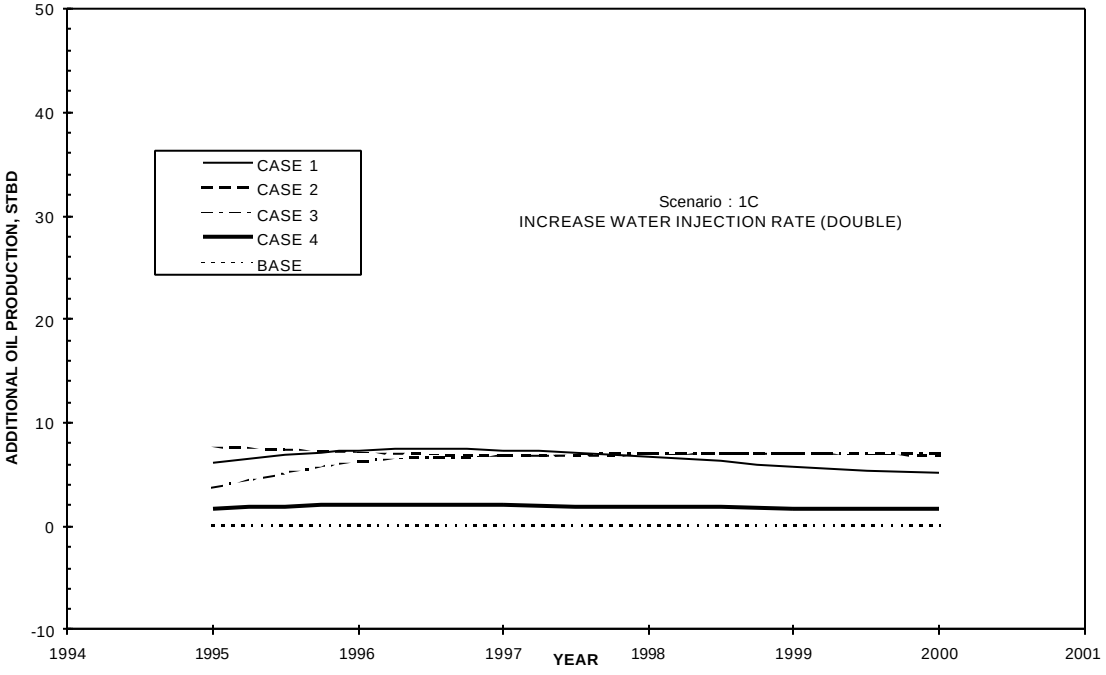

Figure 69 - Increase of oil production using scenario 1C

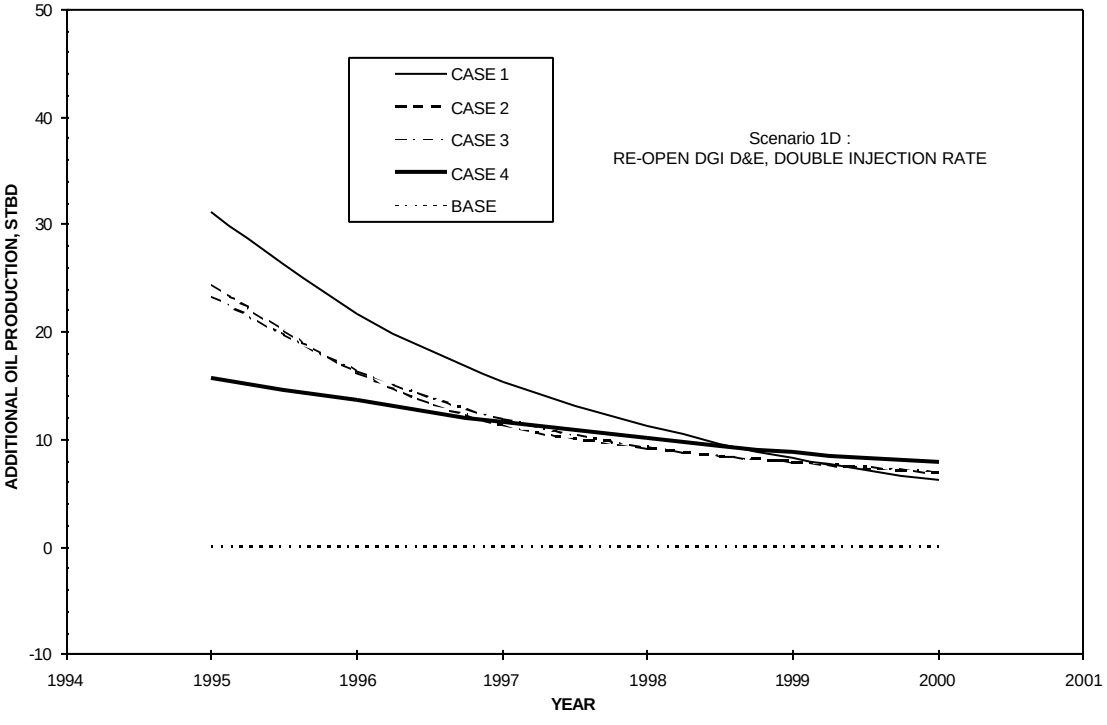

Figure 70 - Increase of oil production using scenario 1D

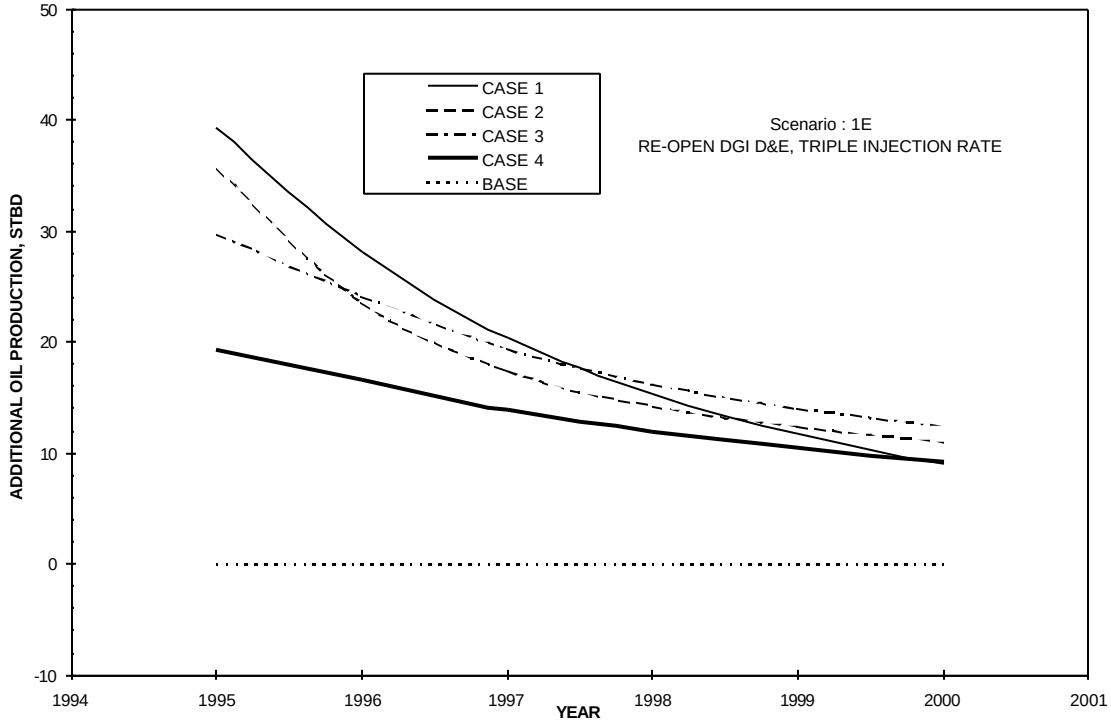

Figure 71 - Increase of oil production using scenario 1E

The result of scenario 1D, which is the combination of scenarios 1B and 1C, shows the combined effect of the previous two scenarios. It can be seen that more additional production can be expected from this scenario. Thus, by simultaneously opening DGI's D and E and increasing the injection rate, a better result will be achieved. Scenario 1E shows the effect of higher injection rate. Intuitively, the result should be better and this is proved from Figure 71. Overall, it was concluded that significant increase of oil production can be obtained if the formation is reopened at DGI's D and E and simultaneously the water injection rate is increased.

The comparison of the simulated future production for different models using scenario 1D - case 4 is presented in **Figure 72**. There are two important points that can be concluded from this figure. First, the stochastic model demonstrates its capability of giving an estimation of the uncertainty (for a given set of information) of the future production whereas the deterministic model predicts only one value. The increase of oil production from the stochastic model ranges from 18 - 21 barrels of oil per day in 1995

whereas from the deterministic model this value is 21 barrels of oil per day. Secondly, the deterministic model is more optimistic. It can be seen that at any time in future the deterministic model always provides a higher prediction.

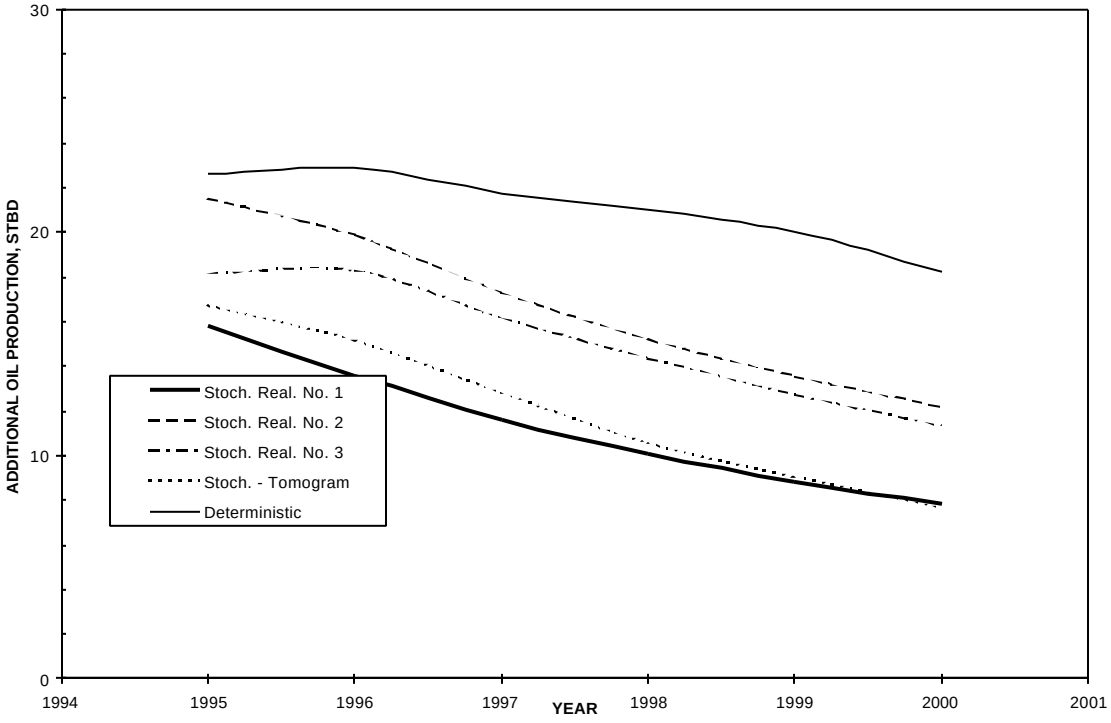

Figure 72 – Comparison of additional oil production – all models

Scenario 2: Drilling Horizontal Well

The purpose of this scenario was to explore the feasibility of drilling a horizontal well in the Self-unit. This prediction is very critical since the cost of drilling a horizontal well is very high (cost ~ $400,000). We investigated the effect of three sub-scenarios as defined in Table 5. The first one is related to the amount of injection rate either in the horizontal well or at other wells if this horizontal well is to be used as the injector. The second one is to see the effect of re-completing other old wells. The last one is to see whether the horizontal well should be an injector or producer.

The horizontal well investigated in this study is located in the vicinity of the Self-82. The simulation has been run for 3 different areal locations and 6 different vertical positions, but no significant difference in

the results is observed. **Figures 73-77** present the results of scenario 2A through 2E respectively. Figures 73-75 show the effect of injection rate in the horizontal well on the production performance. It can be observed that only a slight increase of additional production can be obtained. Figure 76 shows the effect of injection rate at the old wells. It can be observed that the result of case 4 almost remains the same. This result is also observed in scenario 1, where case 4 is more sensitive to reopening DGI's than increasing the injection rate. In addition, this result also shows the importance of opening DGI's simultaneously with increasing the injection rate. Finally, Figure 77 shows that an injector horizontal well is preferable to a producer horizontal well.

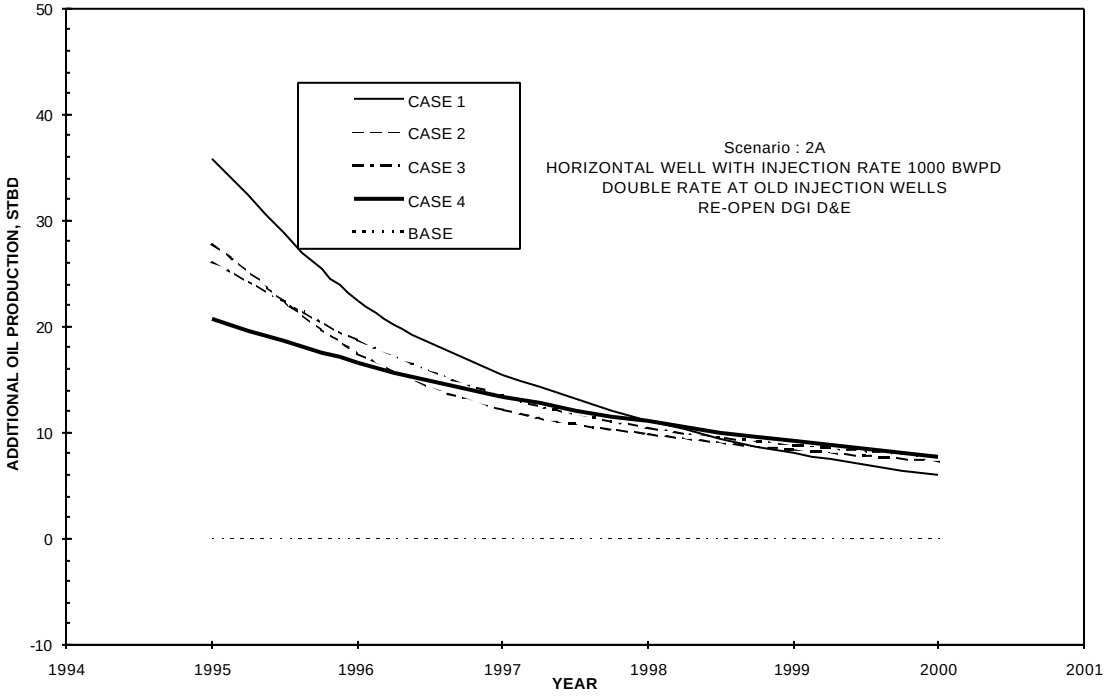

Figure 73 - Increase of oil production using scenario 2A

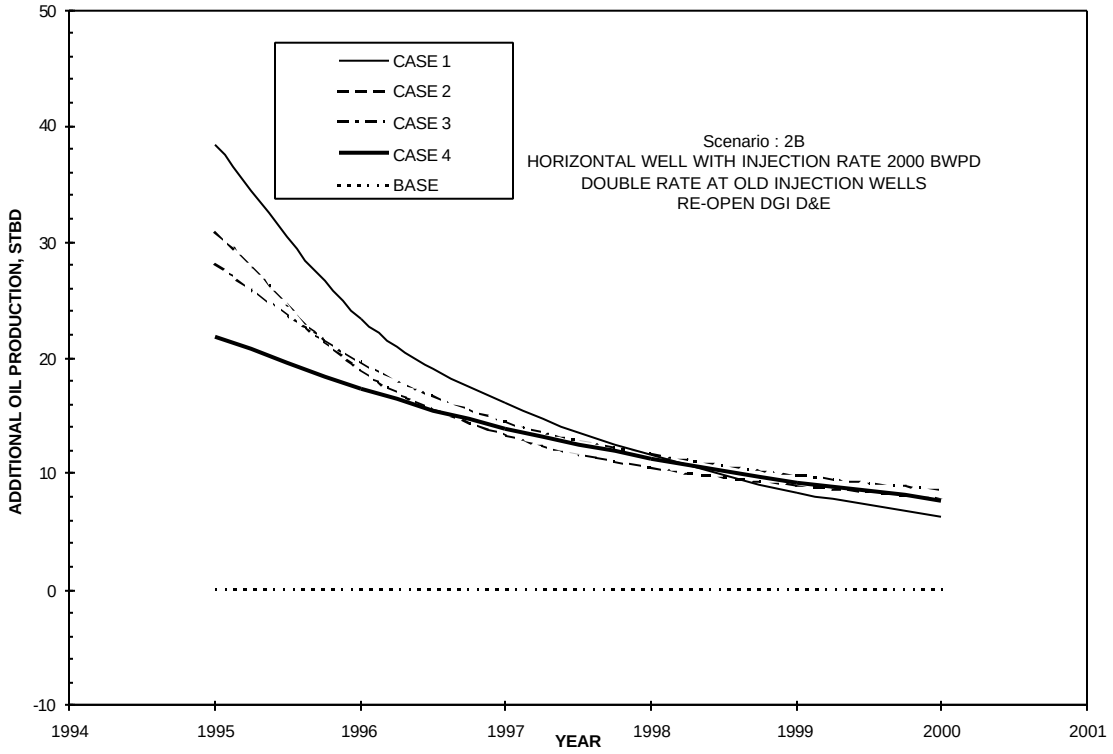

Figure 74 - Increase of oil production using scenario 2B

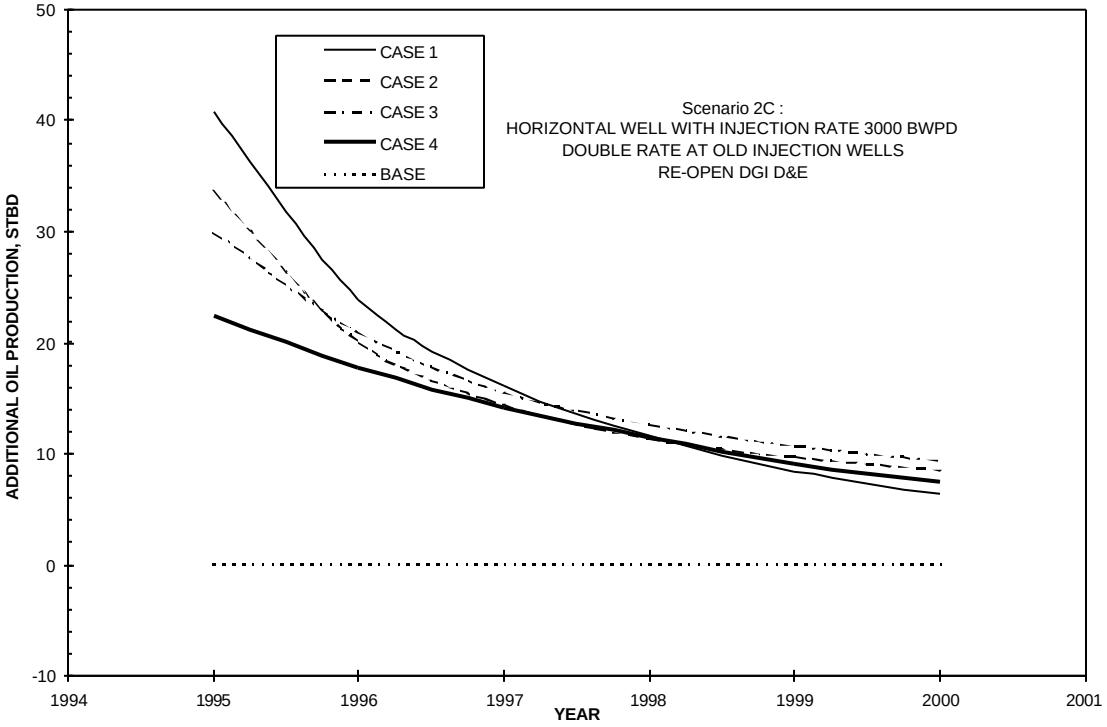

Figure 75 - Increase of oil production using scenario 2C

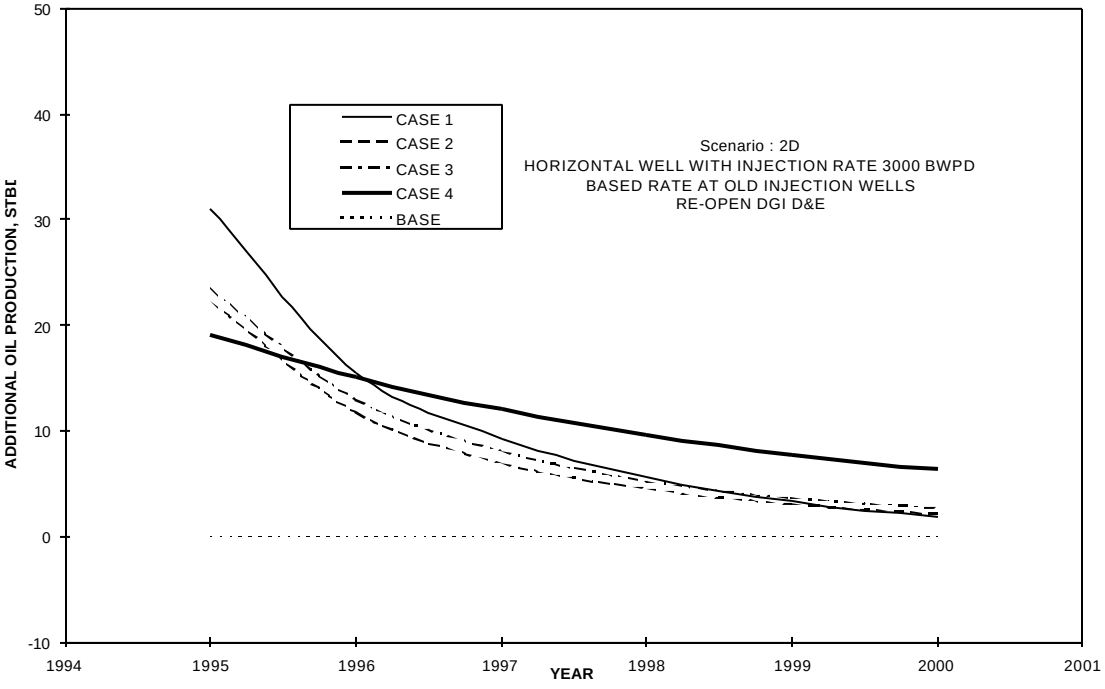

Figure 76 - Increase of oil production using scenario 2D

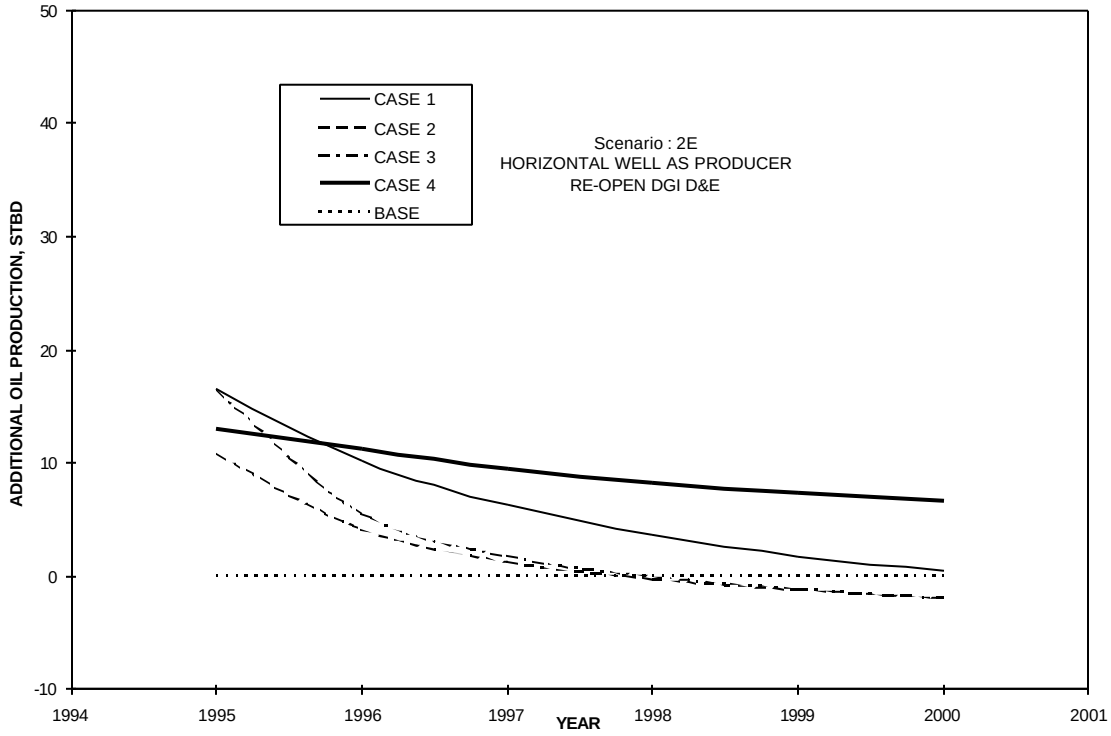

Figure 77 - Increase of oil production using scenario 2E

Overall, excluding scenarios 2D and 2E, the additional oil production from this scenario ranges between 21 - 41 BOPD whereas the range for the first scenario is 16 - 39 BOPD. It was evident that drilling horizontal well does not provide significantly better performance compared to the first scenario. Intuitively, this additional oil production would not have been able to cover the cost of drilling a horizontal well at the existing level of oil price.

Scenario 3: Drilling New Vertical Production Wells

An additional 4 vertical wells were used in this simulation. The locations were determined based on the oil saturation map and also by considering the vacant space that exists in the Self-unit. **Figures 78-79** show the simulation for this scenario. The conclusion about the importance of increasing injection rate as found from the previous scenarios could also be observed from this scenario by comparing the results of scenarios 3A and 3B. From Figure 78 it can be observed that the overall additional oil production using this scenario is about the same as for the previous scenarios, which ranges from 18 to 37 BOPD.

Thus, there is no significant increase in oil production after implementing this scenario. Comparing the results of the three scenarios, it was concluded that the best alternative from an economic standpoint is scenario 1 since there are no drilling costs associated with this scenario.

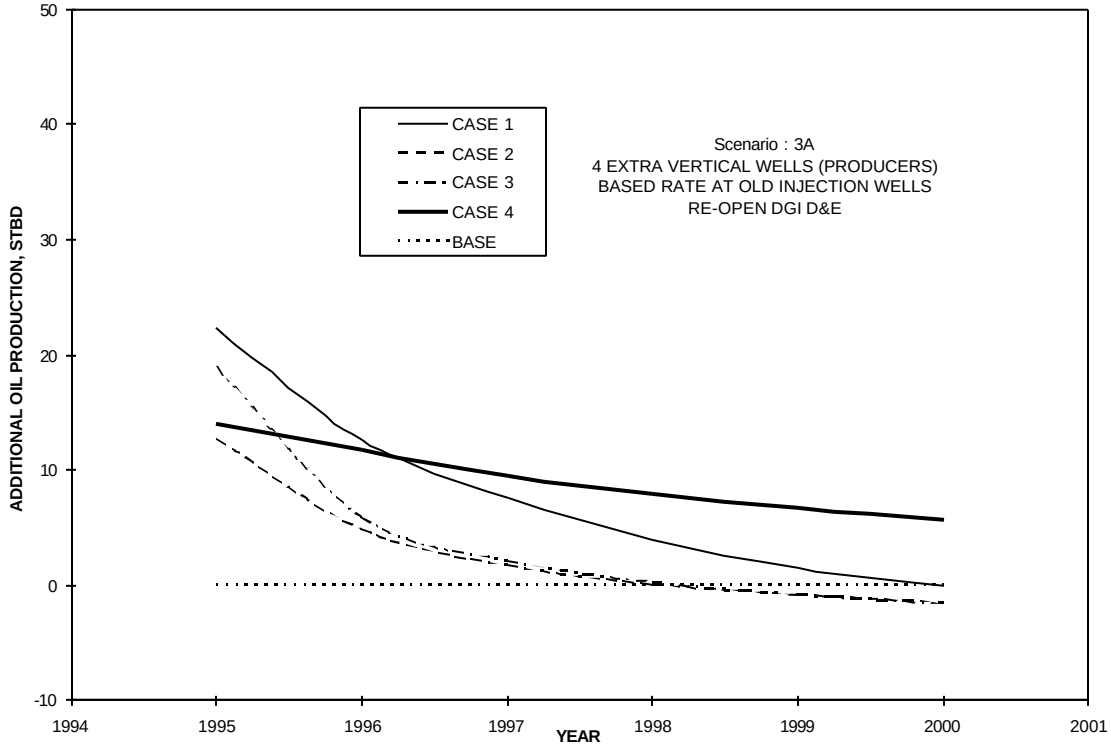

Figure 78 – Increase of oil production using scenario 3A

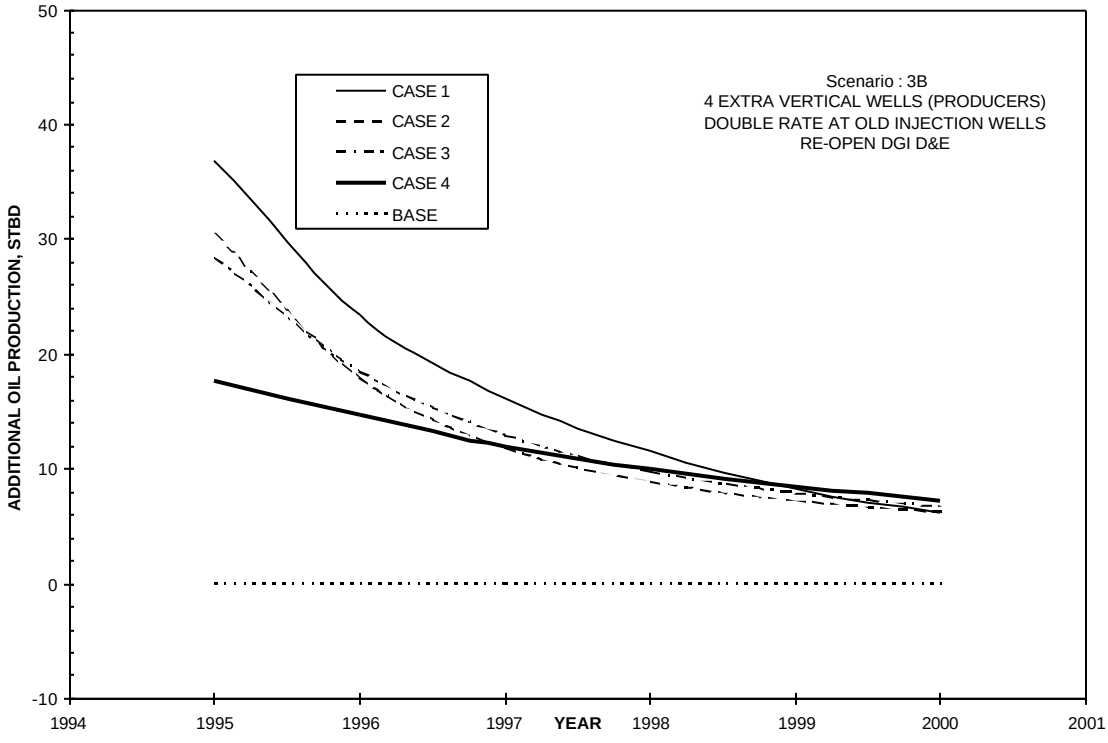

Figure 79 – Increase of oil production using scenario 3B

Economic Analysis

As mentioned previously, the criteria used in the economic analysis are the rate of return and the pay out time. These parameters were calculated using the first scenario (except scenario 1A) which was found to be the only scenario that is feasible for the Self-unit. Before this calculation is performed, the simulations were rerun for another 4 years so that a 10-year projection can be made. The revenue was calculated using the constant oil price of $17.00 per barrel. The capital and operating costs were provided by Uplands Resources, Inc. The capital cost includes the cost to improve the water injection system that is capable of doubling or tripling the injection rate and the cost that is related to opening new intervals (perforation, stimulation, etc.). The fixed cost to improve the water injection system is $87,495, whereas the cost to reperforate DGI's D and E is predicted as $61,600. The fixed cost provided is applicable to tripling the injection rate.

The operating cost is mainly due to chemical treatment of water, electrical, and maintenance costs. This cost varies significantly for the Self-unit. It ranged between $6 per bbl of oil to $9 per barrel of oil during 1993-1994. The value of $9.50 per barrel of the produced oil is considered to be a conservative estimate under current conditions. In this study, this value is used for the condition where no increase of injection rate is applied (scenario 1B). For the scenario where the injection rate is to be doubled (scenario 1C and 1D), the operating cost of $10.50 per barrel of produced oil is used. For scenario 1E (tripled injection rate) the operating cost is assumed as $11.50 per barrel of produced oil.

Figure 80 presents the different rates of return (ROR) estimated for the 4 case studies using 4 different scenarios (1B through 1E). The ROR shown in Figure 80 is the rate of return for the period where the production is still profitable (non-negative cash flow). **Figure 81** presents the result of pay out time predictions for the cases investigated.

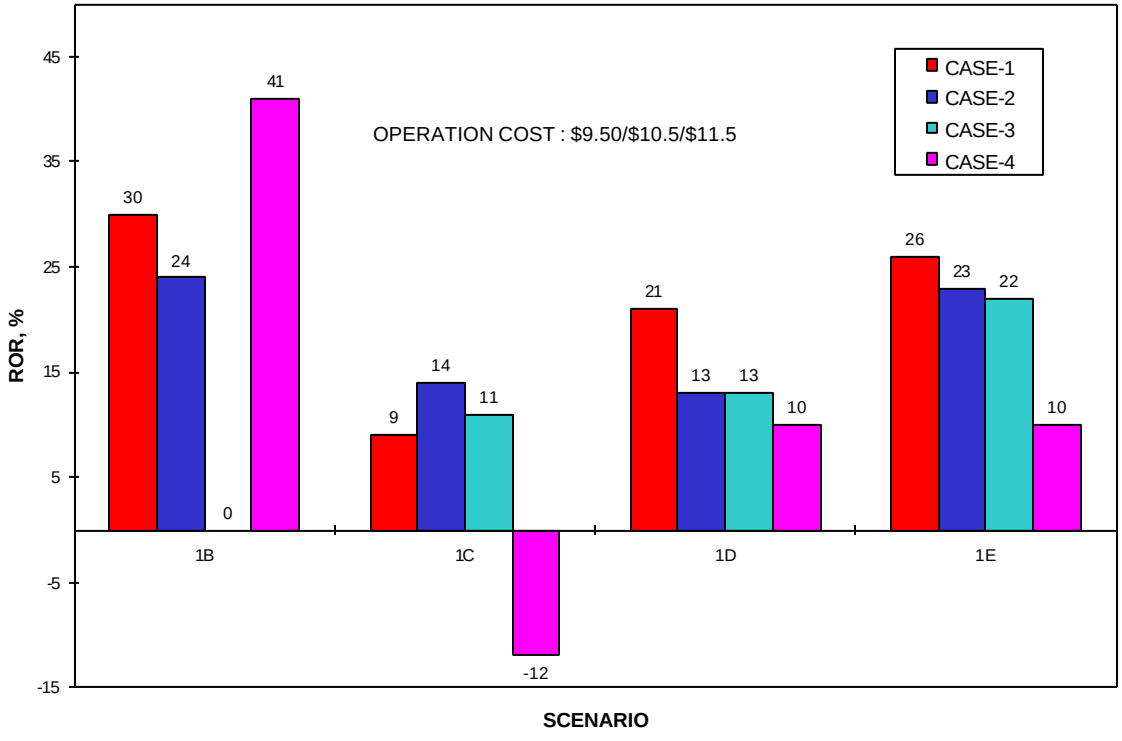

Figure 80 – Rate of return estimation for different case study stochastic model without tomography information

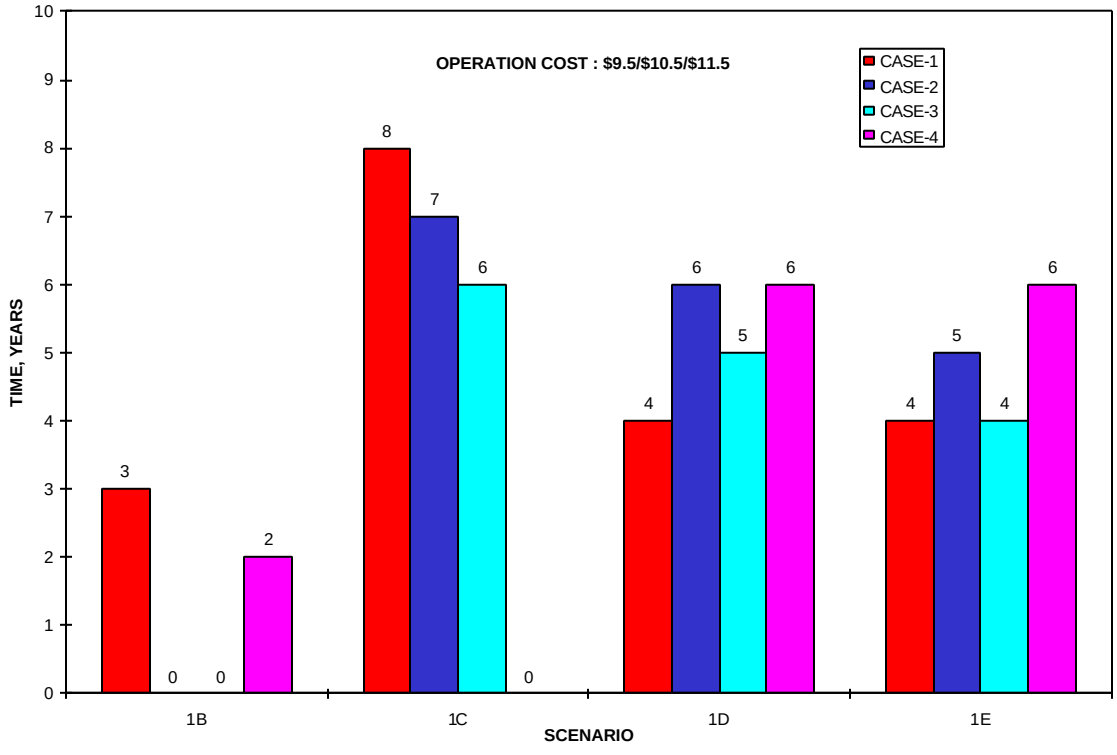

Figure 81 – Pay out time estimation for different cases stochastic model without tomography information

As Figure 80 indicates, the highest ROR is indicated from scenario 1B. This is mainly due to the lowest capital costs (equal to the cost of reopening DGI's D and E only). But the uncertainty among the four cases in this scenario was significant. To further examine the effect of the operating cost, a sensitivity study was conducted by increasing the operating cost by $1.00, so that it becomes $10.50 / $11.50 / $12.50 for no increase in injection rate, double injection rate, and triple injection rate respectively. The result is shown in **Figure 82**. It can be seen that scenario 1B is not very stable (negative ROR for case 2 and 3) and very sensitive to the operating cost. **Figure 83** presents the effect of oil price on the ROR prediction. It can be seen that in order for this scenario to work the oil price can not be lower than $15.00 per barrel.

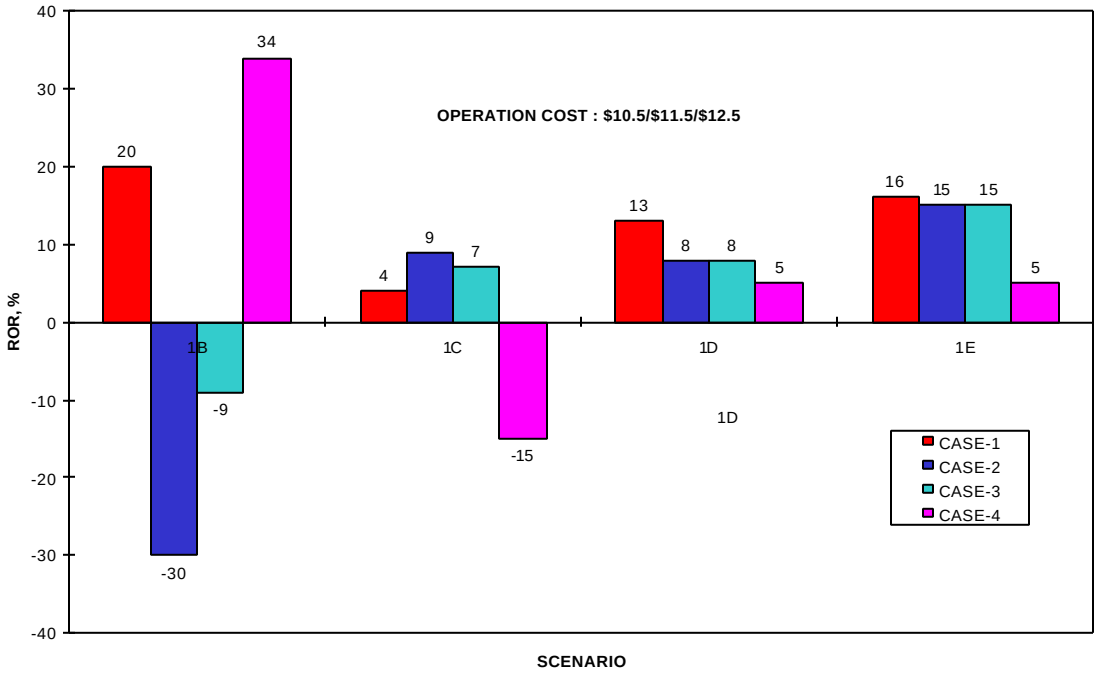

Figure 82 - Rate of return estimation for higher operating cost - DGI model

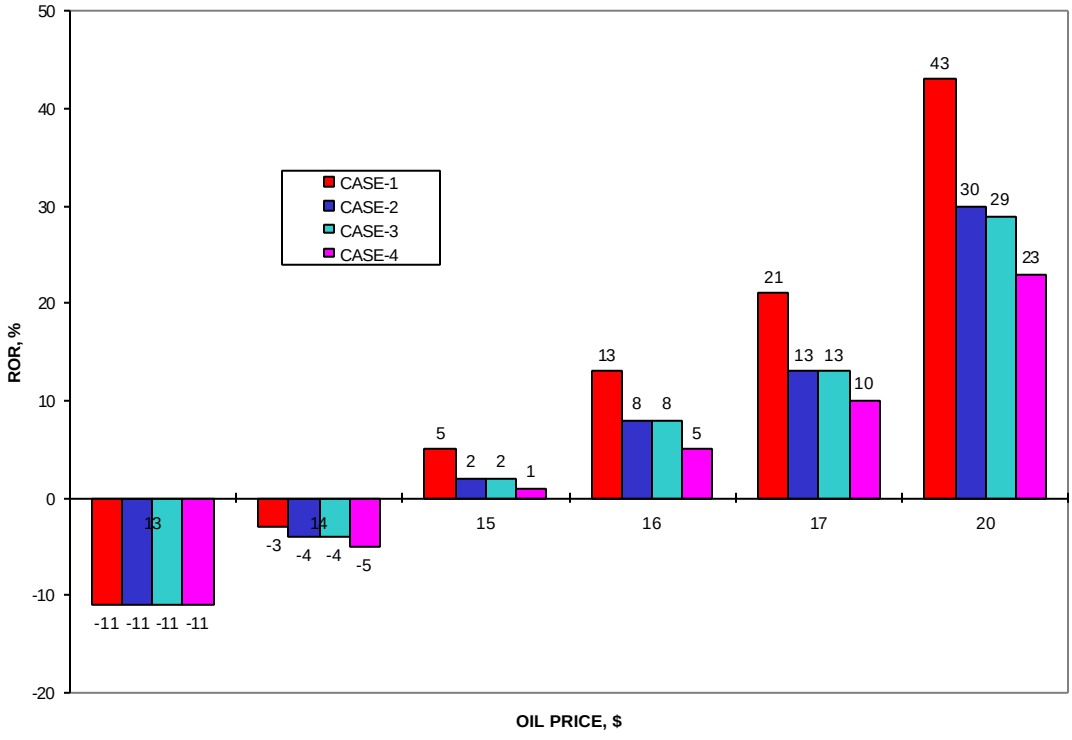

Figure 83 - The effect of oil price - scenario 1D - DGI model

Figure 84 presents the comparison of the ROR and pay out time estimated from the different models using scenario 1D of case 4. This figure shows one of the advantages of the stochastic model whereby it provides the estimation of uncertainty. In this case, the predicted ROR ranges from 10 to 22 percent and the pay out time varies between varies 4 to 6 years, whereas the deterministic model predicted one single value of 31% for ROR and 3 years for pay out time. This figure also confirms the optimistic nature of the deterministic model.

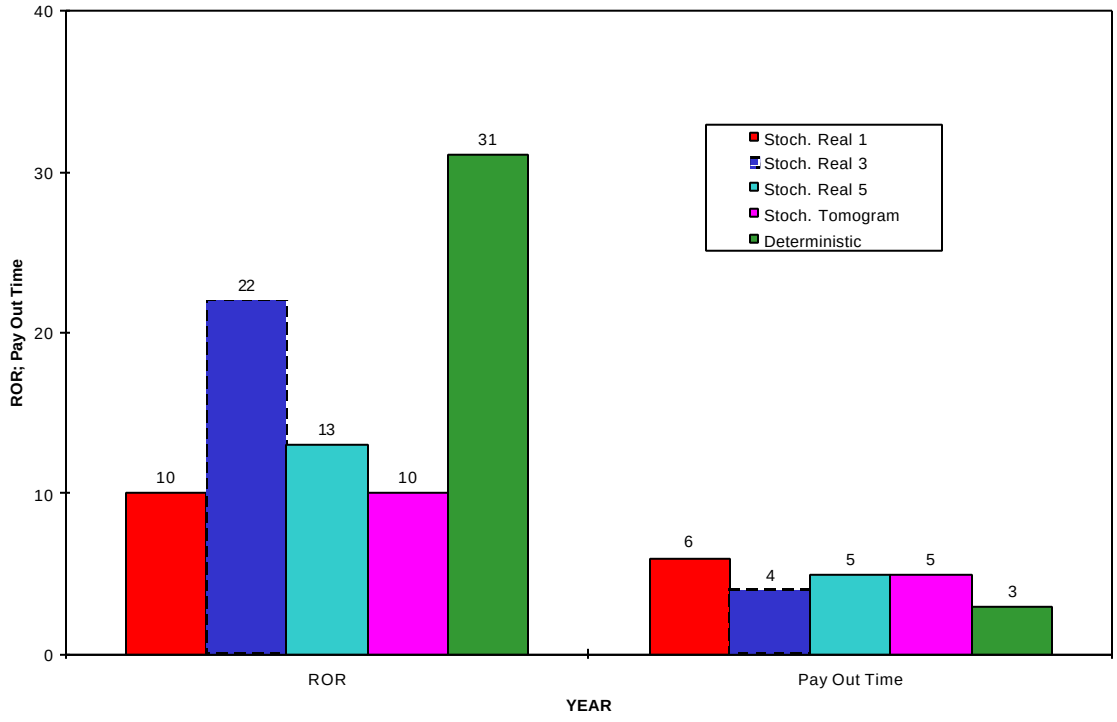

Figure 84 - ROR and pay out time comparison for different models

Summary

The flow simulation to forecast the future production was conducted. It was found that the additional oil production that can be expected from the Self-unit is in the range of 16 - 41 barrels per day depending on the specific scenario applied to the unit. The drilling of any extra wells, either one horizontal well or several vertical wells, was not feasible for the Self-unit at the current level of oil price since the increase of oil production can not justify the cost that was required to drill those wells. The scenario of reopening DGI's D and E and simultaneously increasing the injection rate was found to be the most feasible. The economic analysis was done for this scenario. A rate of return in the range of 10 - 25% was expected by applying this scenario. The deterministic model consistently predicted optimistic results compared to the stochastic model.

Implementation of Reservoir Management Plan

Based on the sensitivity analysis, we decided to implement our reservoir management plan. The details are discussed below.

Recommendations

Our evaluation of the reservoir and production data indicated that the DGI's A and B probably contain immovable oil, DGI F (lower unit) has already been flooded, and DGI's C, D and E had the most potential in terms of additional recovery. DGI C is already open in most of the existing wells. This left us with two possible DGI's for further exploitation, DGI's D and E. We also noticed that an increase in the injection rate had resulted in an increase in the oil rate in the past. Based on the well configuration, the injection wells are capable of taking a lot more water without any modifications.

Based on our understanding of the reservoir, we considered several strategies to improve the performance of the unit. These included: i) re-perforating selected intervals and stimulating them; ii) increasing the injection rate; iii) drilling a horizontal injection well; and iv) drilling additional vertical wells. We also considered combinations of these alternatives. Assuming an oil price of $17/bbl over the life of the project, we determined that the best alternative is to re-perforate some of the intervals and double the injection rate. Drilling of a horizontal injection well may have resulted in higher production rates; however, the cost of the horizontal well did not justify the additional production. Drilling of additional vertical wells did not result in any significant increase in production. The results of recompletion are already presented in the previous section. To repeat, our prediction was incremental oil recovery between 18 to 21 barrels per day without any increase in water injection. If we would increase the water injection rate, the predicted range was between 18 to 32 barrels per day.

Field Implementation - Problems and Solutions

Upon identification of the additional intervals to be perforated in each of the 28 wells on the Self-unit, a prognosis was developed for up-sizing the water injection station, and re-completing each of the wells. Several concerns were considered with regard to recompletions. These included the current integrity of

casing, condition of the injection well packers and tubing, and the actual increase of fluid volumes that would come from the producing wells after completion. Five producers and two injectors were selected for initial recompletion so that the operator can test the recompletion methodology and obtain actual production data to evaluate the economic viability of the project in stages. This also ensured that the lease continued to produce without undue loss of production.

The steps involved in recompletion are: i) pull all the equipment out of casing; ii) run the bit and scraper to clean casing; iii) re-perforate the desired intervals as indicated by the simulation results; iv) acidize both new and old perforations; and v) test wells. No substantial problems were encountered through the perforation process. However, acidization took longer than expected. The breakdown took longer because the formation needed to be pre-soaked with acid before acidizing. The pre-soaking helped reduce the time required for acidizing. Through a learning experience, the costs of recompletion for the last two wells were less than the AFE. The up sizing of the water plant was done without significant deviation from the construction plan.

All wells were initially swabbed back to recover the spent acid and flush, and the producers were swab tested. It became apparent that the fluid volumes being produced were substantially greater than expected. To measure the maximum possible rates, variable speed submersible pump was used. Both the volume and the oil cuts were monitored for three weeks for each well. The initial production from the wells was essentially all water. However, as the time progressed, the oil cut from the well increased gradually. At present, the oil cut varies between 1 to 1.5%. This was an improvement over previous observations.

Results

Based on the implementation of the reservoir management plan, we observed an increase in the oil production. As can be seen in **Figure 85**, the oil production increased from initial value of 17 to 18 barrels per day to about 42 barrels per day. This increase of about 24 barrels per day was consistent with our original model observation. In addition to recompleting the wells, we also increased the injection rate. Currently (1999), the unit is producing about 28 barrels per day. This is an increment of

10 barrels per day. This is also consistent with our prediction (see Figure 70). Currently, only make-up water is injected. This change is due to a significant reduction in oil price.

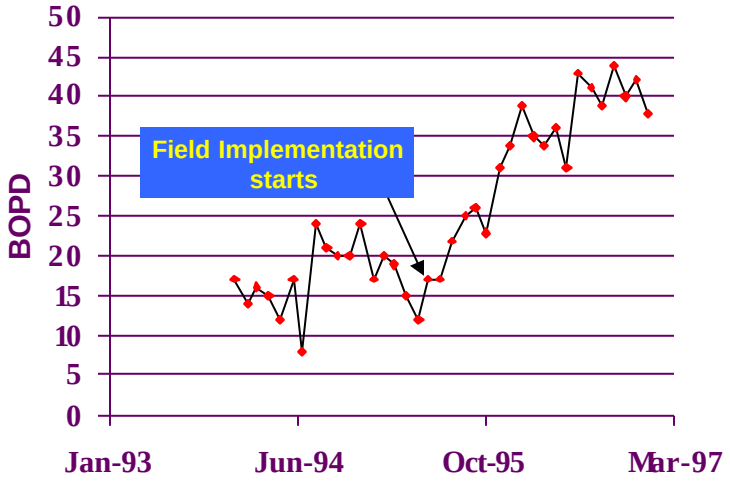

Figure 85 – Results of field implementation

Economic Evaluation

One of the important goals of this project was to investigate the economic feasibility of the implemented strategies. For an effective transfer of technology, it is critical that the technology be cost effective.

By assuming that the production will decline at 6% per year, we estimated the range of additional oil that can be recovered from the unit in the next 15 years. This amount ranged between 200,000 barrels to 250,000 barrels. The anticipated cost of this project is approximately $1.2 million. This translates into finding cost per barrel of $4.80 to $6. This number may be unattractive. However, we can also calculate the finding cost based on the knowledge gained in this project. Some technologies in this project were either proven to be ineffective or marginal. If we assume the same field costs and further assume that a typical consultant in the oil patch can apply the methodology proposed in this project, the overall cost of the project will be in the range of $500,000 to $600,000. This translates into finding cost of $2 to $3 per barrel. This is significantly less than the present acquisition cost used in the market. This reduction in the cost, although dramatic, is not unrealistic. For example, the cost associated with cross borehole seismic data acquisition and analysis was $250,000. The cost of drilling a new well and

acquiring the modern suite of logs was $120,000. Additional costs associated with the administration of the project as well as technology transfer costs can be paired down substantially as well.

It is also worth remembering that the Glenn Pool field is one of the oldest fields in the United States. Most of the fields are much younger than this field. If we can apply better reservoir management techniques to improve the performance of this field in an economically viable manner, we sure will be able to do the same for other fields, which are much younger.

Evaluation of Various Technologies

In this budget period, we used several modern technologies. In this section, we briefly describe the technologies and their value to the project.

Integrated Approach

We made a concerted effort to integrate information from various sources to better understand the reservoir. Geophysical, geological, and engineering data were used to better describe the reservoir properties. In addition to interdisciplinary nature of the project, this project also involved active participation from government, the university, a small oil company and a major oil company. The biggest benefit of working together among such a diverse group of people is understanding and appreciating each other's language and perspective on the issues at hand. Communication between different disciplines helped us better understand what each discipline considers to be an important part of the reservoir description. We tried to create a good balance between the form of the reservoir (architecture) and the function of the reservoir (production performance). Interaction among various entities during the project made us aware of each other's priorities and each other's objectives. Although the objectives of each organization did not always coincide, we learned to appreciate and respect each other's objectives. This helped us in proceeding in the project in an optimal way.

Cross Borehole Tomography

Cross borehole tomography is a method by which an interwell image of reservoir characteristics is constructed by using an acoustic source in one well and receivers in another well. We conducted three

such surveys with the help of Amoco Production Company and Conoco. The surveys were conducted between well pairs 82-63, 82-64 and 82-81. The collected data were processed by Amoco, using public domain software and by Memorial University in Newfoundland, Canada. In addition, data were also provided to a group of scientists from Imperial College. Depending on the assumptions involved in the software, the results obtained from the three methods were significantly different. The results are in the form of sonic velocity distribution across the well pair. We used this information by relating the velocity to the porosity and the facies at the well location. The use of these data slightly improved our reservoir description. Because of the high cost of acquisition and significant uncertainty in the interpretation, the use of cross borehole data was limited.

Formation Micro-Resistivity Borehole Imaging

We used this tool in the newly drilled Self-82. Along with the resistivity imaging, we also cored the desired interval. Formation micro-resistivity imaging tool produces a high-resolution resistivity of the wellbore. Analysis of the image provides spatial orientation of architectural elements in the vicinity of the wellbore. By combining the information from the core data and the imaging tool, we were able to describe the geological heterogeneties at higher resolution level than otherwise possible with conventional well logs. Unfortunately, we were not able to use this detailed information in an effective way in flow simulations due to computer memory limitations. For a mature, shallow, oil field with marginal oil production, the detailed knowledge of geological structure may not be important in predicting unswept reservoir and preferential flow paths. The cost benefit analysis of using micro resistivity log versus taking an oriented core needs to be evaluated further before reaching the final conclusion on the utility of these type of logs. The preliminary analysis indicates that micro-imaging log may not be very valuable in terms of adding incremental value compared to taking a core sample.

Discrete Genetic Interval (DGI) Evaluation

Using the data collected from all the wells, we were able to construct a detailed description of geologically distinct units deposited during a limited time interval. This information was extremely valuable in understanding the vertical as well as areal heterogeneties. Previously, Glenn sand was

divided into three basic units - upper, middle, and lower. With the help of DGI approach, we were able to divide the sand in six geological units. This detailed geological description helped us in flow simulation as well as in our overall reservoir management planning.

Geostatistics

Geostatistics is a procedure by which interwell properties are described using all the available information. Geostatistics assumes that the reservoir properties are spatially correlated, and this correlation can be quantified by a method called variogram analysis. Geostatistics further allows us to quantify uncertainties in describing these properties. Using geostatistics as a tool, we were able to describe the spatial relationships for geological facies as well as the petrophysical properties. By using the relationship between the seismic velocity and the porosity, we were able to use the cross borehole data to improve the spatial relationship for porosity at interwell distances. Using a geostatistical technique called conditional simulation; we generated geological facies image. The comparison between the simulated image and the geologist's view of the reservoir indicated good results. This provided us the confidence that the architecture of the reservoir is preserved. Using the geological description as a starting point, alternate images of the petrophysical properties (permeability and porosity) are constructed by further integrating engineering and geophysical information. Overall, geostatistics was a valuable tool in constructing realistic reservoir descriptions.

Flow Simulation

Once the reservoir description was constructed, we used the ECLIPSE commercial simulator to simulate the reservoir performance. We used both the deterministic (conventional, "layer-cake") as well as geostatistical reservoir descriptions for simulation purposes. Typically, the number of grid blocks in the simulator is less than the number of grid blocks in geostatistical simulation. As a result, appropriate up scaling procedure is used to scale the petrophysical properties suitable for simulation purposes. Since the performance data from individual wells were not available, we could only match overall unit performance. After matching the historical oil production performance, we projected the future oil

production performance under various scenarios to understand the benefits and the drawbacks of various alternatives.

With increasing speed of computers, flow simulation technology is becoming increasingly viable for small operators. Field simulations can be conducted on personal computers without much difficulty. We believe that flow simulation will be an integral part of future reservoir evaluation procedures.

BUDGET PERIOD II

Introduction

In the second budget period, we extended our efforts to other parts of the Glenn Pool field (see Figure 1). This part of the Glenn Pool field was also operated by Uplands Resources. The main idea behind the second budget period was to apply conventional technology to develop reservoir management plan. Unlike the first budget period, where modern technologies such as micro-resistivity logs and cross borehole tomography data were collected, in the second budget period, the analysis relied on more conventional data. Any use of modern technology was restricted to the analysis and interpretation of the data.

Data Collection

During the second budget period of the project, we intended to concentrate on tract 7 and surrounding areas. Tract 7, another 160-acre unit in southern Glenn Pool field, is located about 1 mile north of the Self-unit. The emphasis of second budget period is to use conventional technology and knowledge gained from advanced technology in budget period one (FMI, cross-well tomography etc.) in developing an effective reservoir management plan.

Study of tract 7 and adjacent area involved data compilation, well log correlation of DGI's, and facies architecture reconstruction. For a better and more complete description of tract 7, its adjacent areas including tract 6, tract 10, tract 12, tract 13, tract 11, part of tract 3, tract 4, tract 33, and Corbray unit are included into the mapping area (**Figure 86**), with total area about 1.6 square miles. Subsequently, the area of coverage was expanded to include additional areas in the southern part of the Glenn Pool field including tract 9 and Chevron miceller-polymer unit which is directly north of tract 9, and is directly west of tract 6. See **Figure 87.** Figure 87 shows the area of concentration, whereas, **Figure 88** shows the areas from where additional log and core data were collected. In addition to the existing logs, six new Gamma Ray logs were acquired to compliment the existing data. Five of them are in the tract 7 unit (well numbers: 7-97, 7-99, 7-100, 7-103, and 7-107), and the other one (11-82) is in the

tract 11 unit. There is a suspicion that upper part of the Bartlesville sandstone in tract 7 area may contain a gas cap. Thus cased-hole neutron logging (TDT) was also performed for three wells (well numbers: 7-97, 7-103, 7-107). These TDT logs do not show any evidence of gas.

In addition to the data available from Uplands Resources, Inc. data were also collected from Hyperion Oil Company's office. Data from 23 cores (which includes oil saturation information), well logs and many other materials regarding the micellar-polymer project were collected.

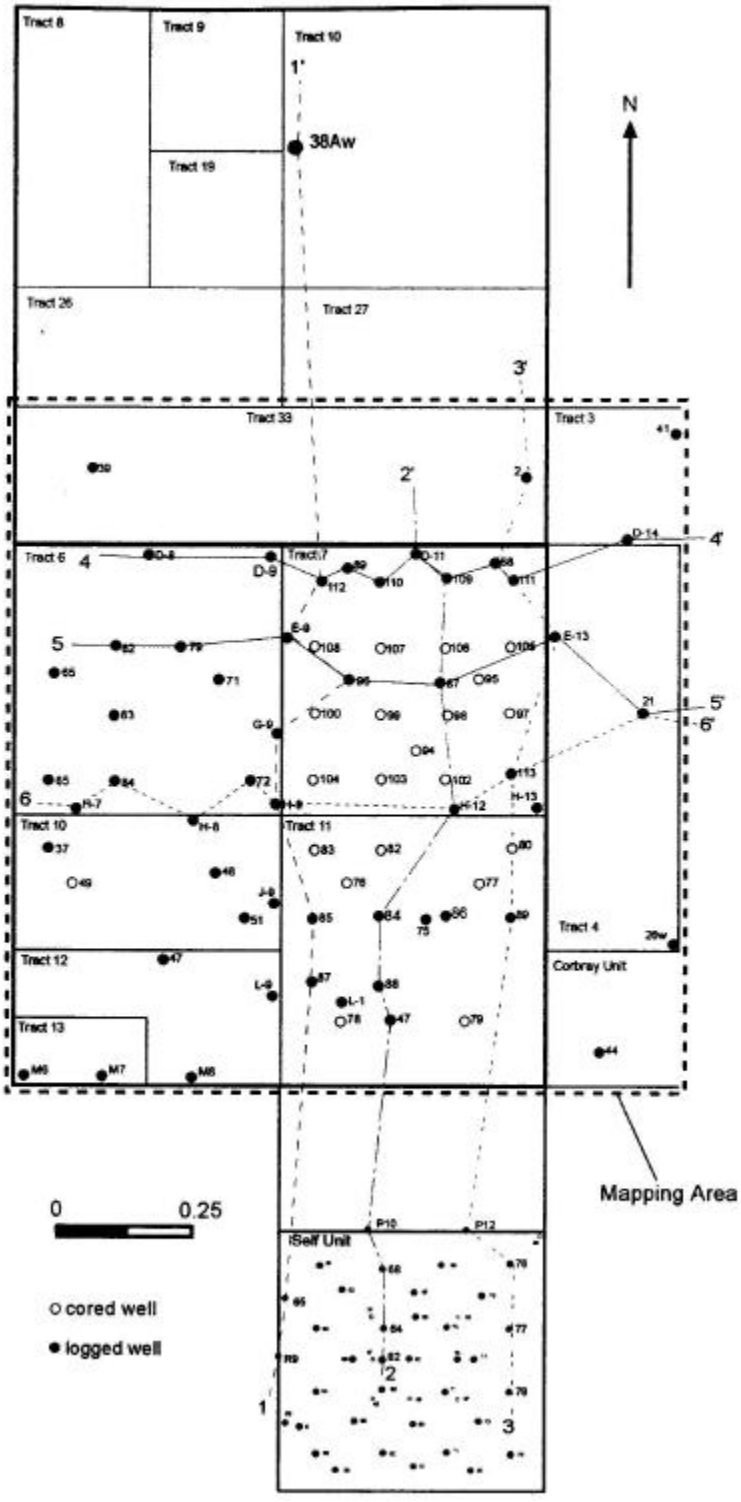

Figure 86 – Index map showing the locations of six cross sections constructed

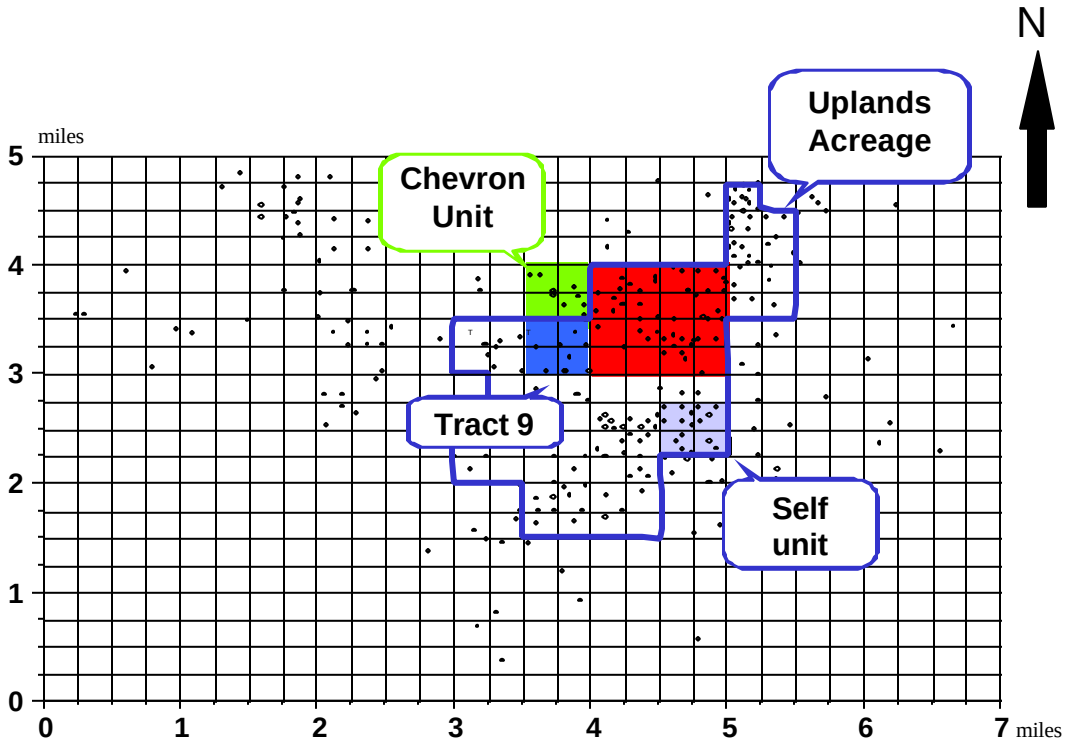

Figure 87 - Area of concentration

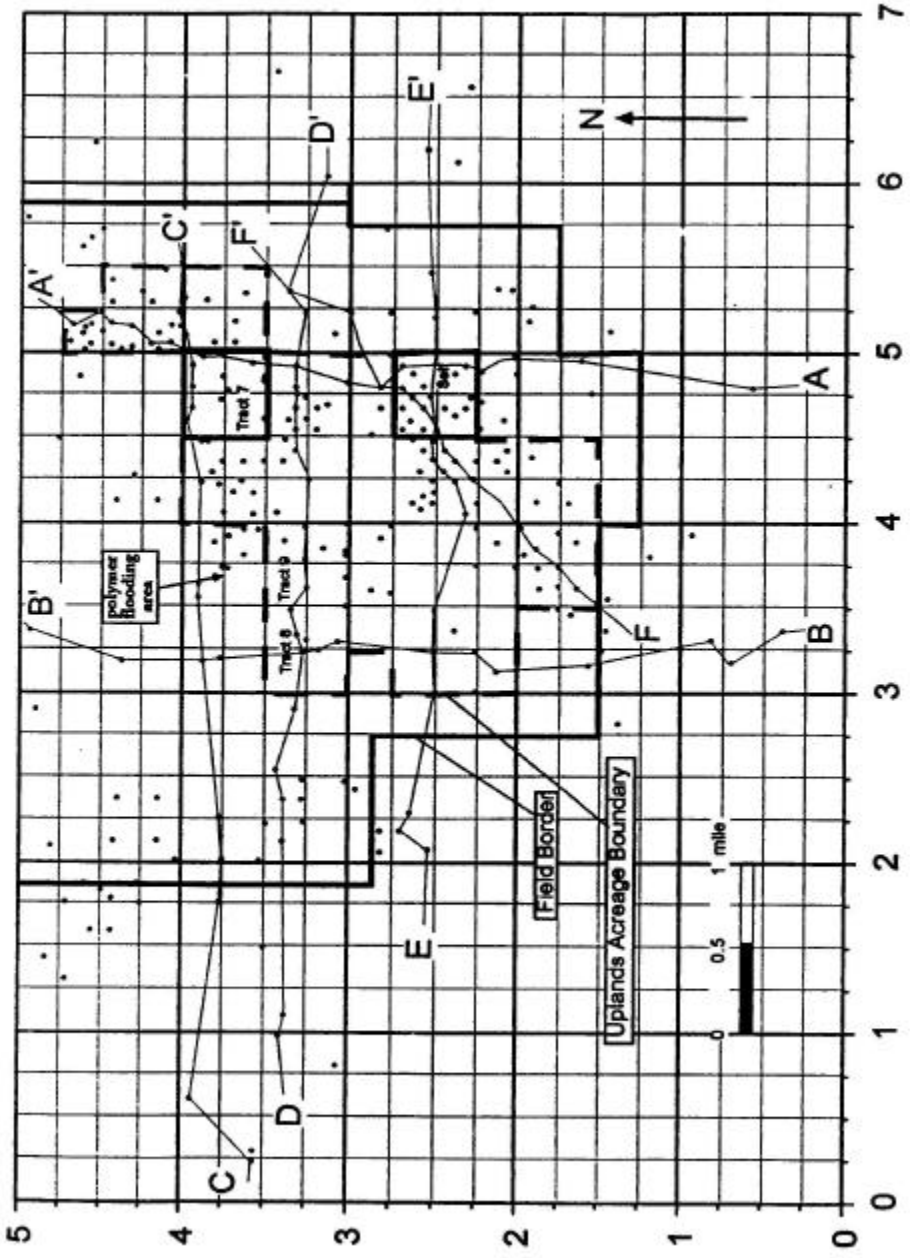

Figure 88 - Expanded coverage of core and log data

Data compilation included collecting all logs and core data available in the office of Uplands Resources and Oklahoma Well Log Library and constructing the well location map (**Figure 88 and 89**).

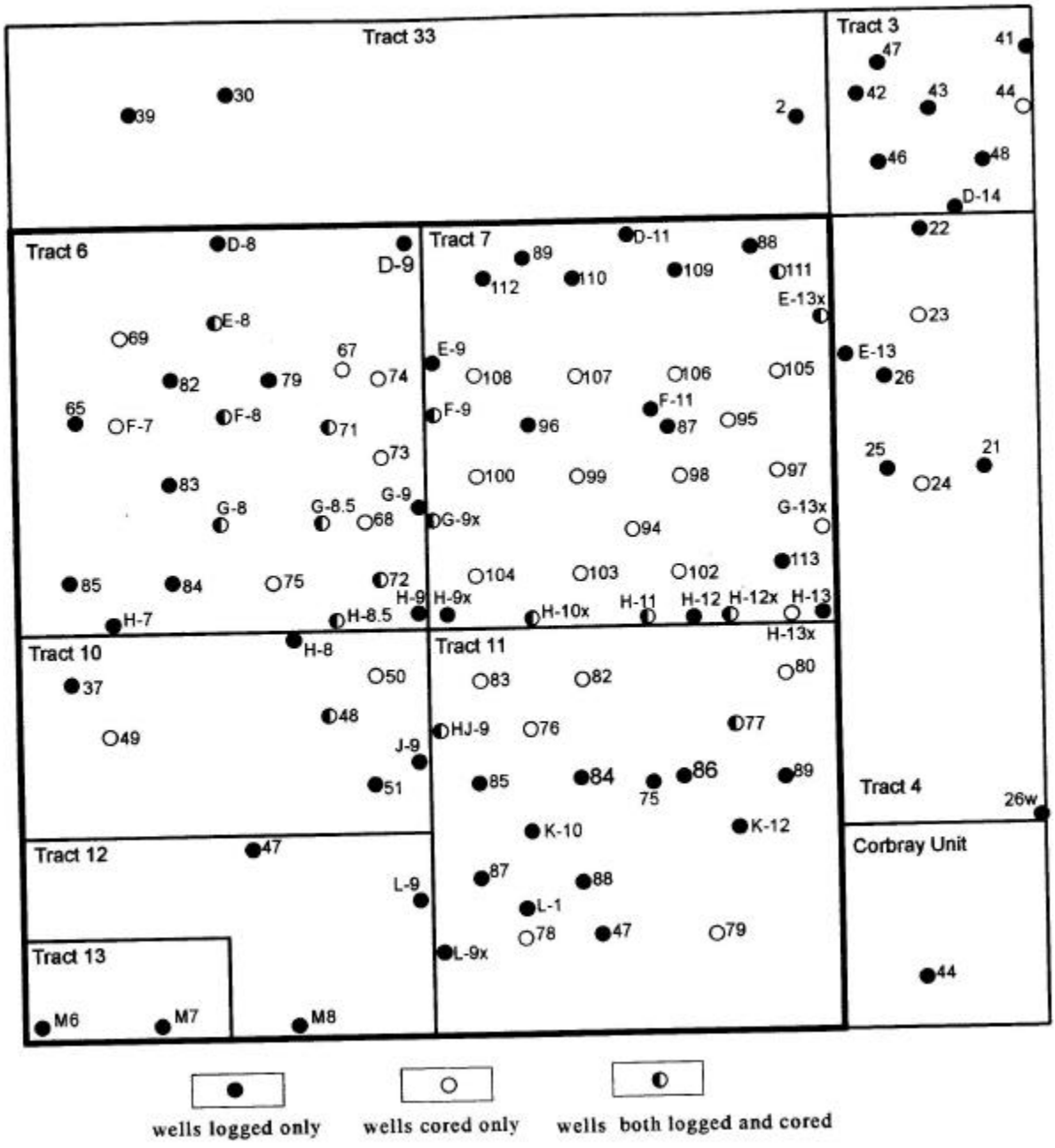

Figure 89 – Data availability within section 16 and surrounding areas

Tract 7 includes 36 wells which have some sort of data available to use: 14 wells were logged (8 open-hole logs and 6 cased-hole logs) but not cored; 9 wells were both cored and logged (8 cased-hole logs and 1 open-hole log); and 13 wells were cored but not logged.

In areas adjacent to tract 7, information from 80 wells were collected and used for the study. Of these 80 wells, 9 wells were both logged and cored (in some intervals), 18 wells were cored but not logged, and the remaining 53 wells have log data only. In total, core and/or log data from 116 wells were collected and used for the mapping area. Unfortunately, the 23 wells with logs in tract 7 are not uniformly distributed across the unit but mainly concentrated along the edge of the unit (Figure 89), cores of this unit are from the lowest part (DGI F & G) of the Glenn sand only. In addition, all cores within tract 7 have been physically missing and are likely not to be found.

In addition to the area of concentration, additional core and log data were collected within a 25-sqaure mile area (see Figure 88). This covers Glenn Pool acreage of several independent oil companies, including Uplands Resources, Producers, ELS, Hyperion, Reddy and part of Bazneet.

320 logs were available in the public domain within the area; 280 of them cover the whole Bartlesville interval. Correlation was completed to the DGI level for all these logs, with reference to the Pink lime, Inola lime, and Brown lime markers. Six cross sections, showing the interval from the Pink lime to the Brown lime, were constructed (see Figure 88 for cross section locations, designated as A-A' to F-F'').

Geological Analysis

The geological analysis concentrated on developing DGI relationships for the expanded area. We started with well log correlation. Well log correlation aims at investigating the stratal relationship between Self-unit and tract 7. Detailed correlation at a level of individual DGI's was performed and six cross sections were constructed, three of them are in north-south direction connecting the Self-unit and tract 7 (Figure 86). Correlation results show that the Glenn sand interval thickens from Self-unit to tract 7 (160-ft to about 200-ft). In Self-unit, six DGI's (DGI A to F) are recognized, but seven DGI's (DGI A to G) in tract 11 and eight DGI's (DGI A to H) in north-central part of tract 7 are recognized. DGI G and H are equivalent to the lower Glenn sand of Kuykendall and Matson.[1] Thus, the lower Glenn sand (DGI G and H) is absent in Self-unit, and DGI H is absent in tract 11. **Figure 90** shows schematically the stratal relationship from Self-unit to tract 7.

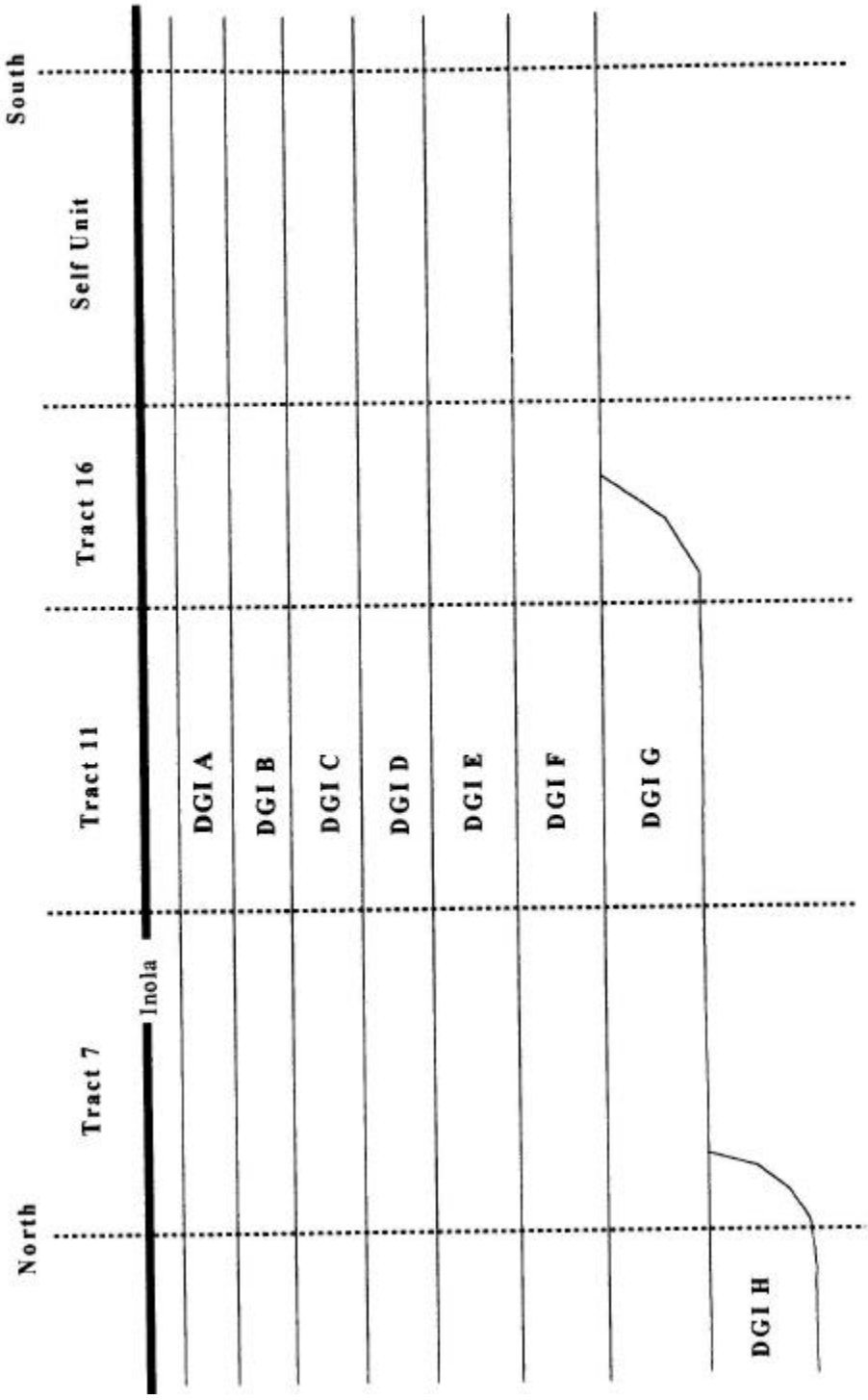

Figure 90 – A sketch map showing the general stratal relationship from Self-unit to tract 7 (figure not drawn to scale; thickness variation of each DGI is not shown)

Based on the correlation results, tables of sandstone depth intervals for each DGI at each well used were developed, which served as an important database for further mapping and reservoir simulation.

One important aspect of the tract 7 study had focused on the revision of sand isopach and facies maps constructed for each DGI in the area (1.6 square miles). This revision was deemed necessary after the acquisition of additional well data. Also insights into the reservoir architecture of the Bartlesville sandstone gained from outcrop studies benefited this revision greatly. In this version of the facies architecture reconstruction, the Bartlesville sandstone (especially intervals DGI A-C) is less layer-caked than earlier believed. It was observed that a thick and blocky sandstone, if it exists, is within the top part of the Bartlesville sandstone. It is more likely to be placed into one DGI rather than divided into more multiple DGI's. This resulted in the interpretation that sandstones of DGI A to C are more channelized than described in the earlier interpretation.

Also the outcrop study resulted in a new facies interpretation for the DGI F sandstone (about 40-50 ft thick). DGI F was interpreted as channel mouth bar deposits based on the Self-82 core characteristics and persistent blocky log shapes. Similar rocks have been observed in the lower part of Bartlesville sandstone outcrops in the Eufaula Dam area. These "massive" thick sandstones may laterally transition to cross-stratified and/or parallel-bedded thick sandstone. They are highly channelized, showing unidirectional paleoflow; vary greatly in thickness according to their position relative to the channel thalwegs; and are made of many small individual channels which are stacked together and cut each other horizontally and vertically, resulting in a widespread distribution.

Thus, while the facies interpretation of DGI A to E was kept unchanged, DGI F was re-interpreted as braided-stream deposits. Facies interpretation for DGI G was undertaken on the only available core from Crow 9-43, which is on the property of Gemini Oil Company. Observation of this core indicated that the DGI G sandstone is analogous to the DGI F sandstone, except that the DGI G is often more shaly than the DGI F because of a higher rip-up class content.

As has been done for the Self-unit study, several maps showing the shale thickness between DGI's were constructed for investigating the vertical separation of the reservoirs. As an example, **Figure 91**

shows the shale thickness between DGI D and E. Generally speaking, Bartlesville sandstone has a good vertical separation between DGI's. **Table 5** presents the separation between different DGI's in terms of shale thickness and the number of wells which show no shale break. This indicates that the reservoirs of the upper part of the Bartlesville sandstone (DGI A to C) have a worse vertical separation than those of lower part (DGI D to G).

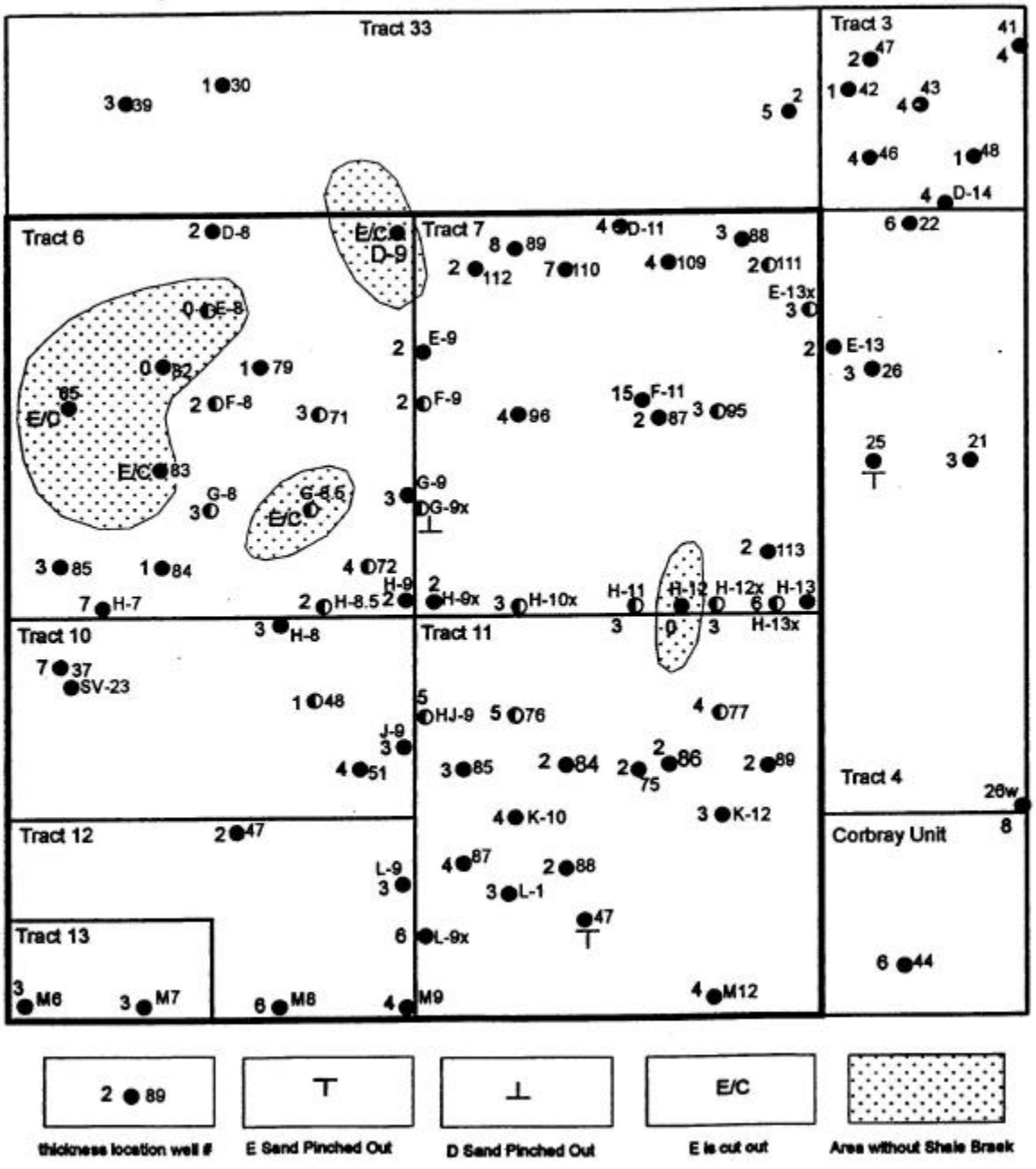

Figure 91 – Shale thickness between DGI D and E

Table 5 - Vertical separation condition, tract 7 and adjacent area

Shale Break	Typical Thickness Range (Ft)	NWI*	NWWNS*	PWWNS*
A vs. B	1 to 3	89	27	30
B vs. C	2 to 4	89	19	21
C vs. D	2 to 6	89	7	8
D vs. E	2 to 6	89	7	8
E vs. F	2 to 6	89	9	10
F vs. G	3 to 8	116	4	3

Note: NWI* = number of wells investigated

NWWNS* = number of wells which shows no shale break

PWWNS* = percentage of wells which shows no shale break

It is difficult to evaluate the petrophysical properties for reservoirs in tract 7, because all cores (20 in total) were cut for DGI F and G only. Fortunately, there are three longer cores cut in nearby area of tract 7 (i.e., well 6-F8, 10-49, 4-24), data of which can be used as a reference for tract 7. **Table 6** shows core porosity and permeability data for these three wells, as well as some core data for DGI F and G in tract 7, in comparison to the data of Self-82 core.

The data presented in Table 6 indicates that for DGI E to F (or G if present), the tract 7 area and Self-unit have comparable porosity and permeability. However, for DGI B to D, the tract 7 area has a much higher porosity and permeability than that of the Self-unit. There is no core sample for DGI A in tract 7 area, however well logs show good reservoir quality for DGI A sandstone in the tract. This implies that the upper part of Bartlesville sandstone in tract 7 area could have very good potential for further development.

Table 6 - Comparison of core porosity and permeability between Self-unit and tract 7 area

	Well Self 82			Well 6-F8			Well 10-49			Well 4-24		
DGI	Phi (%)	K (md)	Facies	Phi (%)	K (md)	Facies	Phi (%)	K (md)	Facies	Phi (%)	K (md)	Facies
A	NS	NS	CH	NC	NC	FP	NC	NC	FP	NC	NC	FP
B	9.1 (3)	0.018 (1)	CH	11.5 (2)	1.6 (2)	CH	0.1 (1)	13.3 (1)	FP	NS	NS	FP
C	11.8 (16)	0.57 (15)	CH	22.3 (19)	397 (19)	SP	20.6 (17)	148 (17)	CH	5.1 (22)	2.3 (22)	CH
D	16.5 (20)	26.4 (19)	SP	20.7 (17)	237 (17)	SP	17.8 (12)	105 (12)	SP	11.9 (4)	18.2 (4)	SP
E	19.9 (5)	181.8 (5)	SP	19.3 (20)	151 (20)	CH	18.1 (26)	77.6 (26)	CH	15.7 (8)	66.9 (8)	SP
F	21.8 (9)	246 (9)	BS	20.5 (56)	137 (56)	BS	22.2 (24)	217 (24)	BS	18.5 (43)	146 (43)	BS
G		Not developed		17.9 (34)	30 (34)	BS	16.2 (49)	18.2 (49)	BS	19.4 (36)	91.4 (36)	BS

	Well 7-100			Well 7-102			Well 7-103		
DGI	Phi (%)	K (md)	Facies	Phi (%)	K (md)	Facies	Phi (%)	K (md)	Facies
A-E	NC	NC		NC	NC		NC	NC	
F	21.2 (22)	162.3 (22)	BS	15.4 (4)	32 (4)	BS	20.2 (20)	141.3 (20)	BS
G	15 (40)	35.5 (40)	BS	17.8 (50)	14.9 (50)	BS	17.2 (36)	29.5 (36)	BS

Note: The number within parenthesis is the number of samples.

NC = not cored

NS = not sampled

CH = channel-fill sandstone

FP = flood plain mudstone

SP = splay sandstone

BS = braided stream sandstone

The geological analysis of tract 16, based on the limited data available, showed that the DGI G sandstone is absent in the southern two-thirds part of the unit. DGI A to C has the most likely potential for further oil recovery.

56 wells have been drilled on tract 9, however, only 11 logs were available for geological interpretation. As was done in other tracts, the Bartlesville sandstone was subdivided based on the correlation of these 11 logs and logs in other tracts. DGI A to DGI G was recognized. Log facies interpretation was performed for each well, and each DGI facies map was completed for each DGI in conjunction with other tracts. Characteristics of the vertical profiles are very similar and correlatable to what was observed in tract 7 area.

Chevron's miceller-polymer flooding acreage, also a 160-acre unit, is located in the northeast quarter of section 17-17N-12E, i.e., immediately north of tract 9 and west of tract 6 (Figure 87). The miceller-polymer flooding project was conducted during the early 1980's and is considered to be very successful in terms of oil production increase. Currently this unit is operated by Hyperion Oil Company.

An investigation of the factors leading to this success was intended, in the hope of gaining insight into our proposed reservoir management planning. Fourteen logs were collected from public domain in Tulsa. Correlation to DGI level and sandstone classification for each DGI was made for each of these wells. Facies maps for each DGI were constructed for this unit in conjunction with other reservoir units.

In addition to conventional logs, we also had detailed log descriptions from micellar-polymer unit. This included information about saturation (see **Figure 92**). As can be seen from this figure, oil saturation tends to be much higher in the upper part of the Glenn sand than the lower part. This is an indication that more potential for recovering additional oil existed in the upper part of the Glenn sand.

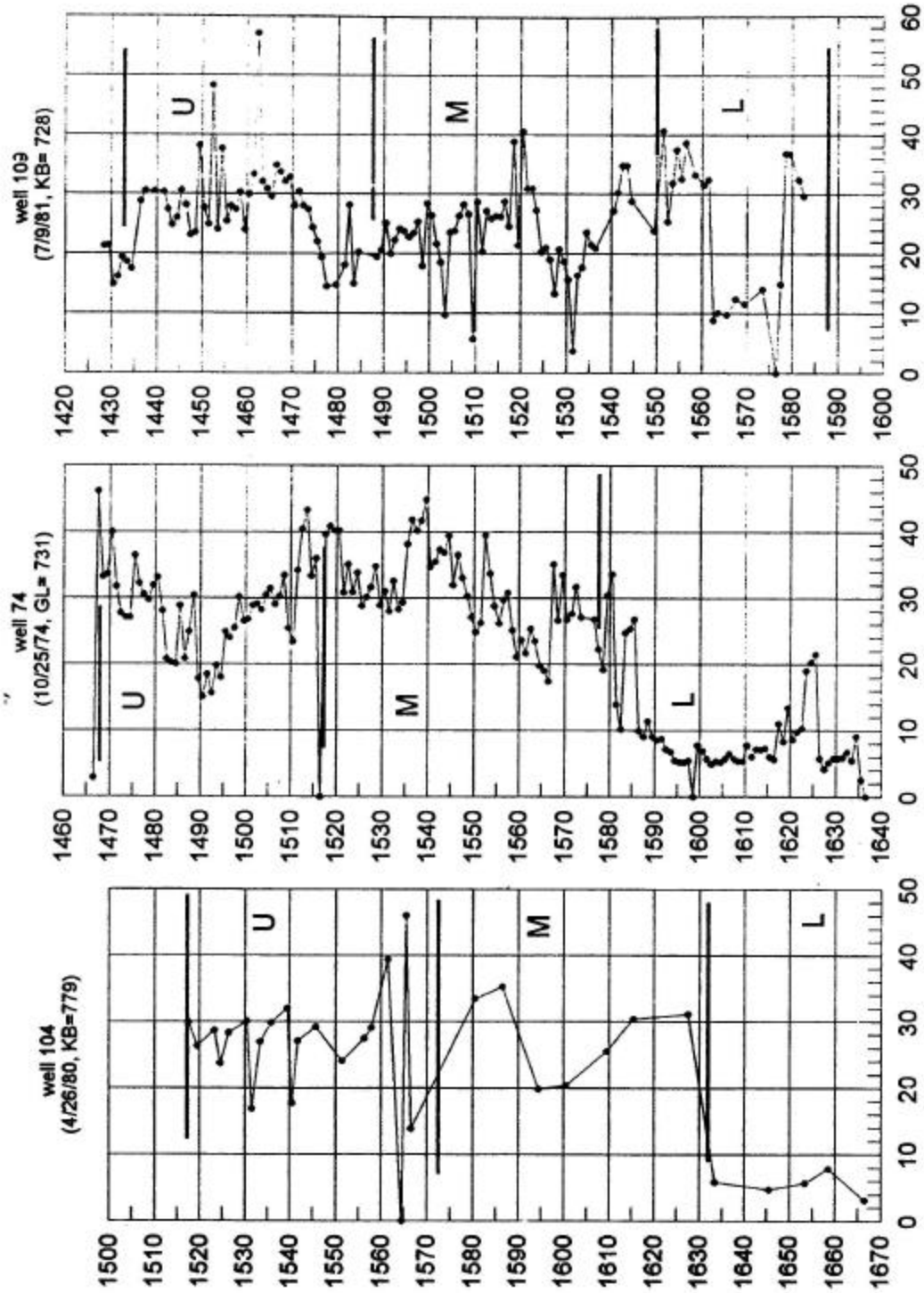

Figure 92 – Core oil saturation (%) profile (Chevron's micellar-polymer unit)

With inclusion of tract 16, tract 9, and the Chevron miceller-polymer flooding acreage, the area mapped for detailed facies architecture over the course of the project was about 1,500 acres. It was helpful to construct a unified facies map for entire area including the Self-unit, and tracts 3, 4, 6,

7, 9, 10, 11, 12, 13, 16, and the Chevron miceller-polymer flooding acreage. The unified facies map was completed for each DGI and shows the depositional relationship among different tracts very clearly. **Figure 93,** as an example, shows the unified facies map of DGI A for the entire area.

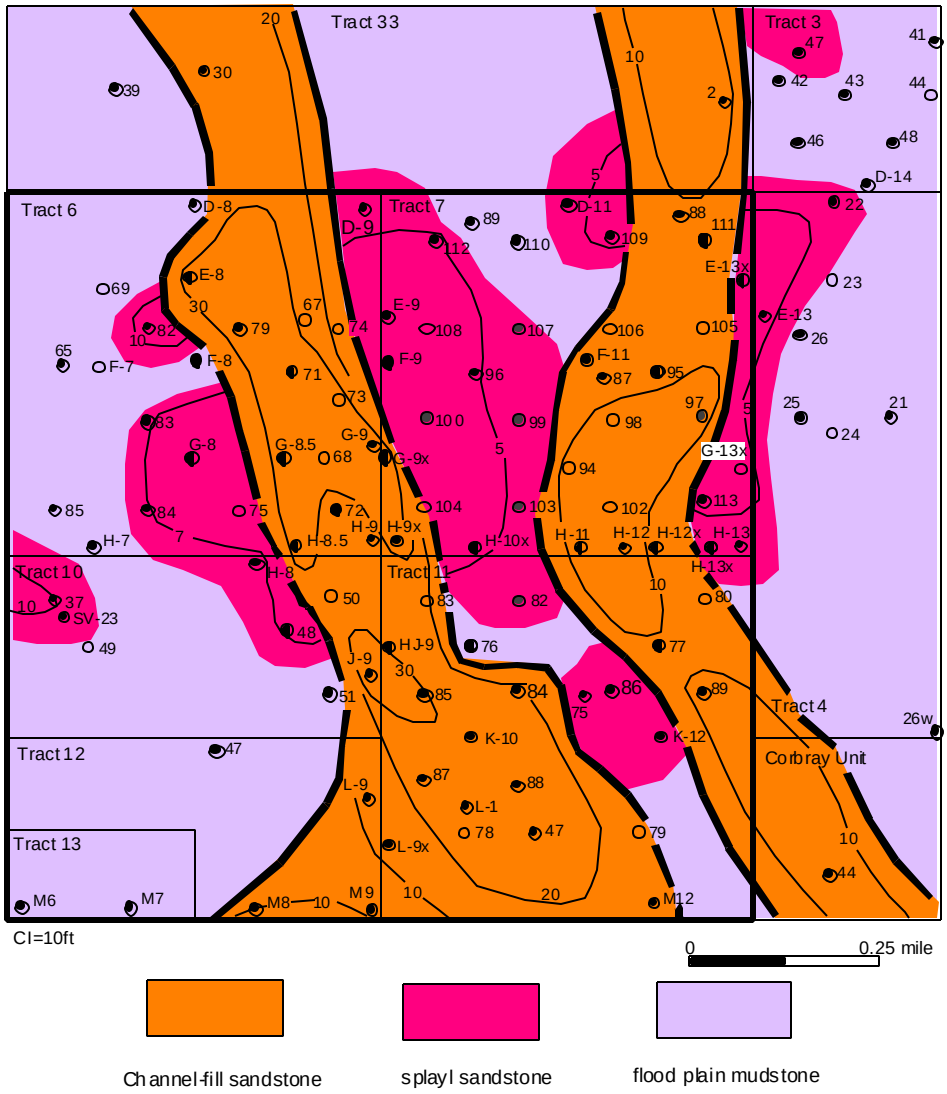

Figure 93 – DGI A map for the area of interest

To form a more accurate estimate of oil reserves in tracts 6, 7, 9, 10, 11, 12, 13, 16 and the Chevron miceller-polymer flooding acreage, net sand thickness was evaluated by using well logs. The "50% method" was adopted for determining the net sand thickness, which is the portion of sandstone with reservoir quality. About 120 logs were analyzed for this purpose.

Figure 94 displays the ratio of net sand thickness to gross sand thickness (i.e., the interval thickness from sandstone top to sandstone bottom within a DGI) for each DGI. The ratio displayed is the average value calculated from all 120 logs. From this figure we can see that the ratios for DGI A and DGI G are slightly smaller than those for other DGI's. This implies that at least in these tracts, DGI A and G are more muddy or shaly than other DGI's. As was mentioned earlier, the Bartlesville sandstone was deposited in a regressive manner, thus it is easy to understand why DGI A is shalier than the lower DGI's. But why is DGI G different? One possible explanation is that the lower part of Bartlesville sandstone contains more rip-up class shale originated from the erosion of underlying Savanna shale.

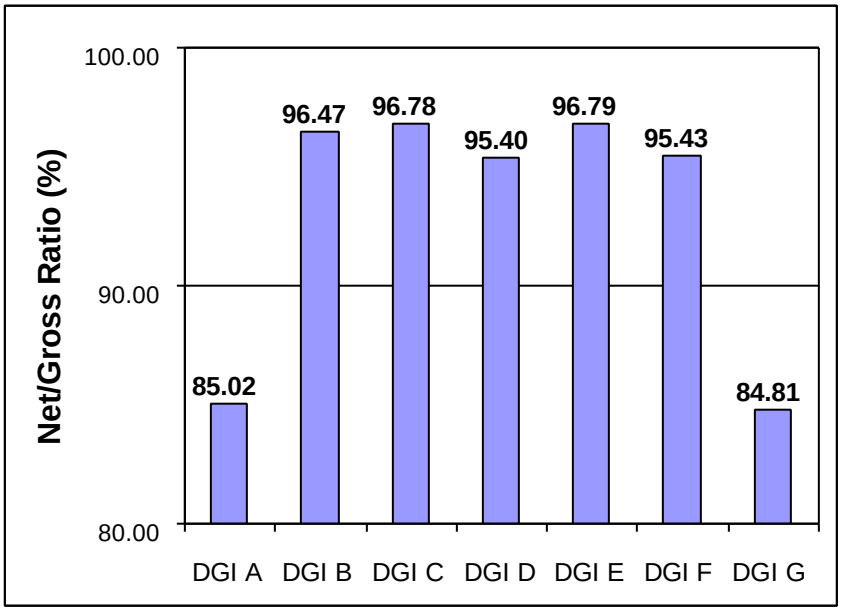

Figure 94 – Average net/gross ratio determined from 120 logs

Using this geological analysis as input, a detailed engineering evaluation was conducted as discussed in the next section. No geophysical component was involved in this budget period.

Engineering Evaluation

Introduction

This section discusses the engineering evaluation of the Glenn Pool field, which was the subject of interest in the second budget period. In addition to the part of the field operated by Uplands

Resources, we also investigated the Chevron's miceller-polymer flood. This flood was very successful in recovering significant additional oil.

A database of all the wells that have been drilled was compiled detailing information pertaining to the location of the well and the perforation depths. A total of 280 wells were included in this database, including both producers and injectors. Perforation maps were generated for each DGI displaying only those wells that have been completed in that DGI with an estimate of the interval that has been completed out of the thickness of the DGI under consideration. The conclusion derived from these maps was that the upper zones were not perforated as densely as the lower zones. Since most of the available completion data are skewed towards the years 1942-1995 this conclusion is appropriate during the course of secondary flooding implementation in the field.

Perforation interval maps were plotted for the Chevron lease to understand the completion practices before and after the miceller-polymer flood implementation in l980. These maps showed that Chevron had concentrated its completions in the upper intervals. There was very little activity in the lower DGI's especially DGI G. We believe that the rationale used was upper zones have a lot of potential owing to ineffective flooding practices. This is supported by the TDT logs in tract 7, which shows clean sands with high oil saturations in the upper regions.

Screening Test for High Potential Areas

It was difficult to determine which part of the study area we need to concentrate further. A screening procedure needed to be developed so that we can high-grade and low-grade some of the areas. A procedure was developed as a screening test to identify the areas with high potential for oil recovery in terms of the petrophysical properties.

The investigation area was divided into 60-ft $\times$ 60-ft grid blocks. The area of interest spans 7,920-ft in the x direction and 5,820-ft in the y direction and 5 DGI's (A-E) in the z direction. DGI's F and G were not included in this analysis since it was believed that they have already been effectively flooded by previous water floods. This results in a 3-dimensional grid block setup of $132 \times 88 \times 5$ (x, y, z) respectively. Each DGI was represented as a slice independent of a physical magnitude associated with it.

Mapping of Petrophysical Properties

(a) Porosity

Logs were collected and digitized wherein the combination of logs for a particular well is sufficient to make a reasonable estimation of porosity and saturation. The number of such wells is extremely small. Typically a combination of Spontaneous potential, Gamma ray, Density and Neutron logs is used to compute porosity. The computation validity is then established by comparing it with the core porosity data for the lower intervals since the upper intervals are predominantly uncored. The porosity values at the well locations are averaged for each DGI. These average values are kriged to estimate porosity values at all other grid blocks for a particular DGI. The result is seven areal slices (DGI A-G); each slice represents a particular DGI.

(b) Permeability

Log permeability versus porosity relationships is established for each DGI individually by combining all available core data. Permeabilities are evaluated based on the above relationships for all wells where porosity is computed. The permeability values at the well locations are averaged for each DGI. Precautions are taken to strip any unreasonable permeability value. These average values are kriged to estimate permeability values at all other grid blocks for a particular DGI.

(c) Saturation

Typically a combination of porosity, induction or resistivity logs is used to compute saturation. The saturation values at the well locations are averaged for each DGI. The computation validity is then established by,

- Comparing the log derived profile with the core profile.
- Comparing S_w averaged for each DGI with TDT saturations using compatible R_w and s_w values.

The average values are kriged to estimate saturation values at all other grid blocks for a particular DGI.

Potential Index Estimation

The potential for a particular location is a cumulative effect of the production capacity, storage capacity and access to the existing wells. The potential should be directly related to the production, storage capacities and inversely proportional to the access by existing wells.

(a) Conductivity Index (CI)

This index quantifies the production capacity and is related to the product of permeability and thickness $(k \times h)$. Since k and h are defined at all grid blocks in all the seven DGI slices (A-G) the productivity can be estimated at each grid block. Since F and G have been drained considerably, further indexing is done only from DGI's A-E. The productivity data for the DGI's A-E are then combined to establish quartiles X_{25}, X_{50} and X_{75}. Ranks are then assigned from 1-4 by comparing data points at each grid block with the quartiles. For instance if the productivity for a particular grid block is less than X_{25} then it is assigned a rank 1. If it is between X_{25} and X_{50} then the grid block is assigned a rank 2. If it is between X_{50} and X_{75} then the grid block is assigned a rank 3 and if the value is greater than X_{75}, it is assigned a rank 4.

(b) Storativity Index (SI)

This index quantifies the storage capacity, and is related to the product of porosity, oil saturation and thickness $(f \times S_o \times h)$. Since porosity, saturation and thickness are known at all grid blocks in all the five DGI slices (A-E), the storativity can be estimated at each grid block. The storativity data for the DGI's A-E are then combined to establish quartiles X_{25}, X_{50} and X_{75}. Ranks are then assigned from 1-4 by comparing data points at each grid block with the quartiles as was done for the conductivity index.

(c) Accessibility Index (AI)

This index defines the access to a particular area by drilled wells. It is assumed that a fully penetrated well in a particular DGI contacts 10 acres. Although arbitrary, this assumption is consistent with the overall observations in the field that indicate low areal continuity. If partially

penetrated, the area is proportionately reduced. The area contacted by a well is assumed to be proportional to the square of the ratio of perforated interval to the total thickness for each DGI. If a grid block is contacted by a drilled well (i.e., it falls within the assigned drainage area), the accessibility index is assigned 0 and if grid block is not contacted, the accessibility index is assigned 1.

(d) Potential Index (PI)

The productivity and storativity indexes are combined by summing up their individual ranks at all grid blocks. The maximum value of the sum is 8 denoting that the area has the highest potential both in terms of its productivity and storativity. Conversely, the least value of the sum is 2 denoting low potential. Since the essence of the procedure is to identify areas of high potential it was decided to use a combined sum of 4 as the index of demarcation between high and low potential areas. Hence if the sum is greater than 4, the grid block is categorized as 1 (high potential) and if sum is less than 4, the grid block is categorized as 0 (low potential). The category value is then multiplied by accessibility index to calculate the final potential index as,

$$PI = (CI + SI) \times AI \tag{2}$$

Irrespective of a grid block having a high or low potential, if the area is being contacted by a well, its accessibility is 0, which also reduces the PI value to a 0. By including the accessibility, we essentially mask all the regions that are being drained and treat them as being equivalent to areas having zero potential (see **Figure 95**).

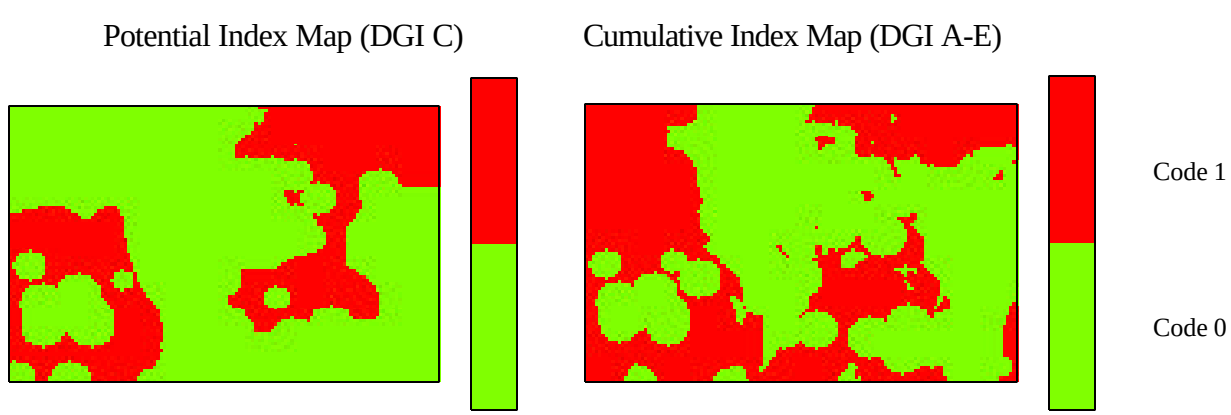

Figure 95 – Potential index map for DGI C and cumulative index map for DGI A-E

Cumulative index is estimated by adding the PI values at corresponding grid blocks for all DGI's A-E. For each areal location, 5 indices are added corresponding to each DGI. By collapsing all the DGI's into one unit we can examine which areas have the highest potential both areally and vertically. (see Figure 95). In Figure 95, code 1 represents high potential, whereas, code 0 represents low potential.

Evaluation of Production Information

In addition to generating the Production Index maps, the cumulative production data from the individual tracts was evaluated to assess the relative success of secondary recovery to primary recovery. The specific objectives were,

- To make a comparative analysis of the primary production and incremental secondary recovery production for tracts numbering 1 - 18.
- Estimate original oil in place (OOIP) and total recovery as a percentage of the OOIP in tracts 1-18.

Tracts 1-18 cover the areal expanse where the Berryhill Glenn Sand Unit (BGSU) has been identified. We also included Chevron miceller-polymer unit for comparison purposes.

Analysis of Primary Production and Secondary Recovery

Primary and secondary recovery production data were obtained from Reference 50. The report lists year wise production data from the field inception time in 1908 through 1988. It also lists the contribution from each tract provided the tract was in commercial operation in the year of question. The field wide production history can be summarized as follows,

1908- 1955-60:	Primary Depletion
1940- 1961-66:	Gas Injection
1965 - 1985-95:	Waterflooding

The production data for each tract is plotted as a function of time. Then the area under the curve is estimated to obtain the cumulative primary production and incremental recoveries due to 1) gas injection and 2) waterflooding.

A typical example is shown in **Figure 96.** It can be noted from the production response that the data compares well with the field wide history mentioned above. The production data was extrapolated as in decline curve analysis for the cumulative production estimates and the area under the curve was adjusted accordingly during the time spans when two processes are in effect simultaneously. For instance, in Figure 96 during 1940-52 primary depletion and production due to gas injection are occurring simultaneously. The following ratios were then estimated and the values were compared for all tracts under consideration

G/P	=	Incremental cumulative production due to gas injection (G) / cumulative production due to primary depletion (P)
W/P	=	Incremental cumulative production due to injection of water or other fluids (except gas) (W) / cumulative production due to primary depletion (P)

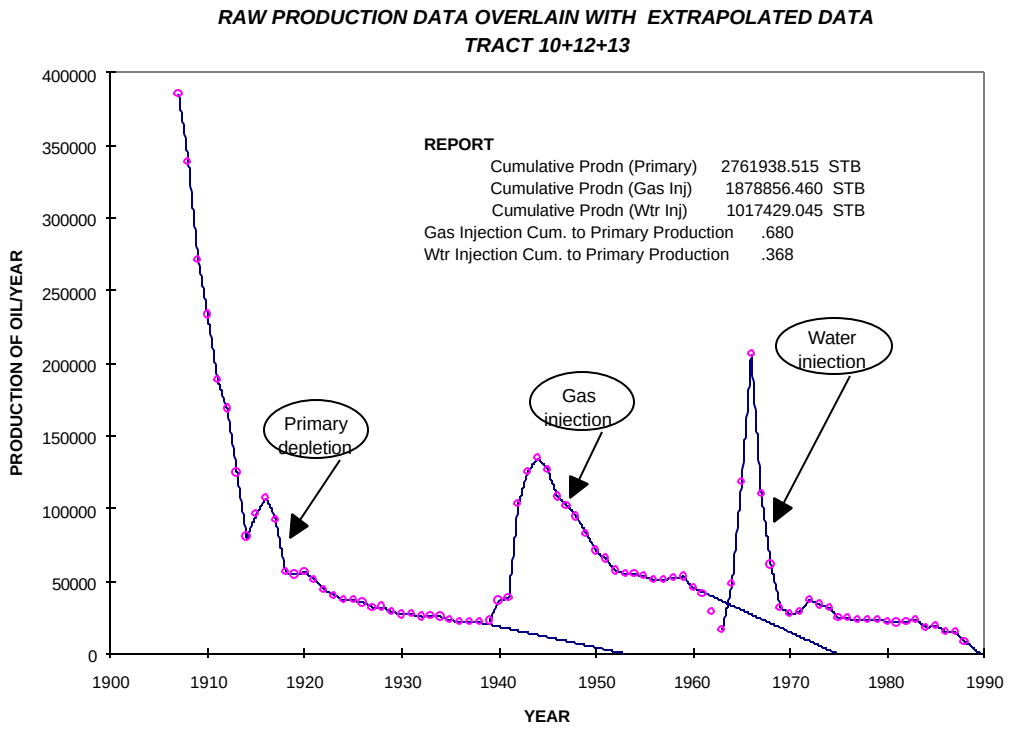

Figure 96 – Raw production data overlain with extrapolated data

Figure 97 is a representation of this information. In Figure 97, tract 10 represents the combined area of tracts 10, 12 and 13. It was obvious that gas injection response is poor over the entire field with the exception of tracts 7, 6 and 3. The most interesting feature of the plot was the W/P value for the micellar-polymer unit. It stands out in comparison to other tracts demonstrating the success of the Chevron miceller-polymer unit.

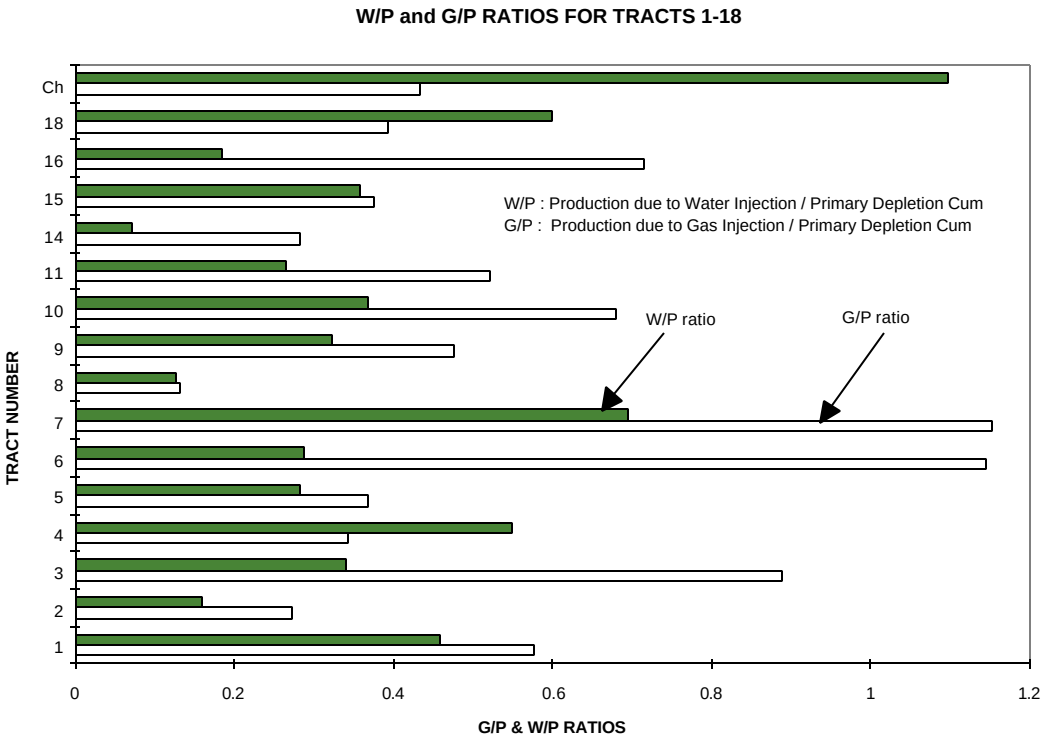

Figure 97 – W/P and G/P ratios for tracts 1-18 and micellar-polymer unit

Original Oil in Place (OOIP) Estimations

The net sand volume figures as quoted in Reference 50 for the upper, middle and lower Glenn sands were summed to get the total sand volume. This was then multiplied by an assumed constant field wide initial oil saturation of 0.78 and formation volume factor of 1.15 RB/STB to get the original oil in place. The calculated values are shown in **Table 7**.

Table 7 - Oil in place estimates

Tract	OOIP MMstb	Tract	OOIP MMstb
Chevron	9.745	10	6.003
1	8.148	11	12.388
2	1.739	12	4.717
3	9.216	13	1.792
4	6.026	14	2.494
5	4.403	15	9.940
6	14.660	16	7.320
7	14.717	17	2.071
8	6.794	18	3.809
9	13.428		

The OOIP estimates were also used to calculate the total recovery of each tract from primary and incremental production from secondary methods. **Figure 98** shows the result. It can be seen that tract 7 has a lot of potential that can still be tapped. Tract 7 is a good candidate for secondary process implementation since the OOIP is large. Tract 9 is also attractive for the same reason coupled with the fact that it has an extremely low well density in terms of number of wells drilled.

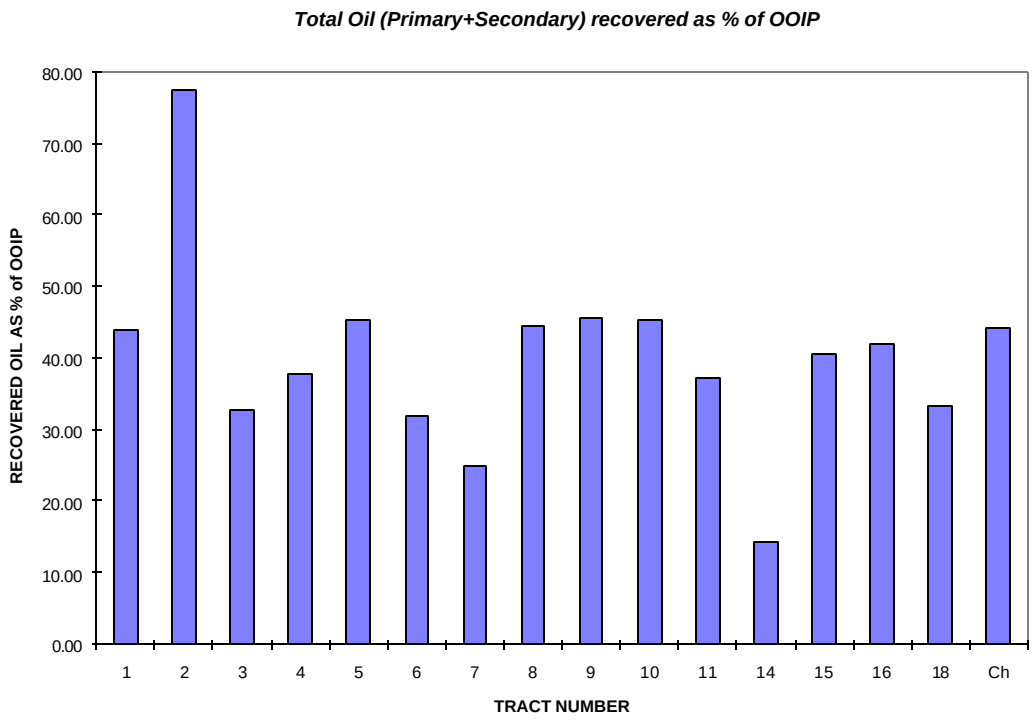

Figure 98 – Total oil (primary + secondary) recovered as % of OOIP (all tracts + Chevron's micellar-polymer unit)

Summary

Using our screening criteria, the areas with the highest potential for additional recovery were identified. The areas with the highest potential for recompletions were identified as tracts 9 and 7. These tracts were investigated in more detail as discussed below. In addition, Chevron's micellar-polymer unit was studied further to understand why the micellar-polymer flood was successful in that unit.

Chevron's Micellar-Polymer Unit

The area of analysis was the Chevron micellar-polymer unit, which is north of tract 9. Chevron implemented a micellar-polymer flood pilot from 1979-1983, which was based on selective isolation of the upper zones. Chevron initiated field-wide implementation in 1983-1984 that resulted in a remarkable increase in oil production, which will be discussed later in more detail. The obvious success of the Chevron micellar-polymer flood prompted us to analyze the unit in more

detail. Further, the performance and the completion strategies in this unit could be used as a focal point to compare and contrast it against tract 9 which is a geologically similar unit with comparable oil saturation profiles.

Perforation Strategies

Chevron used the prevalent upper Glenn, middle Glenn and lower Glenn divisions of the Bartlesville sandstone to describe the reservoir. Chevron believed that the upper and middle Glenn layers were separated by a continuous shale barrier and implemented the pilot flood by isolating the perforations in the upper zones. This was later proved to be untrue. The strategy during the field-wide implementation was to complete the wells both in the upper and middle Glenn layers. **Figure 99a** shows the contrast in completion strategies during the pilot and field implementation. The lower Glenn was avoided since it is known to be water bearing. This is in sharp contrast to the completion practices in section 16 and tract 9 wherein the completion density increases as we progress down to the lower intervals. **Figure 99b** shows this in graphical form.

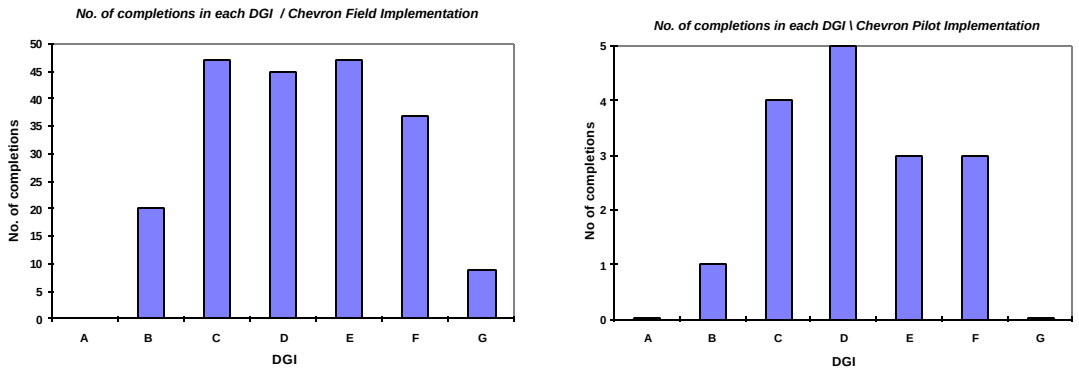

a

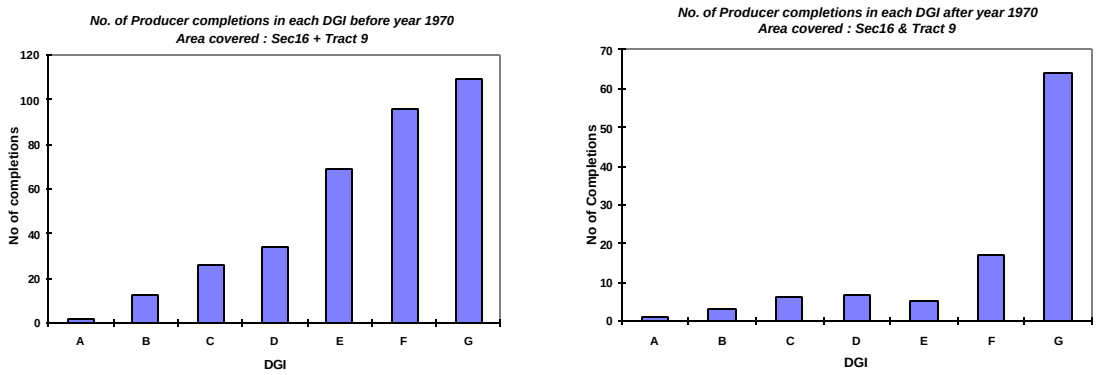

b

Figure 99 - (a) Completion practices in the Chevron unit. (b) Completion practices in section 16 and tract 9

Effects of the Micellar-Polymer Flood

The micellar-polymer flood implementation resulted in 52-times increase in oil production and a WOR decrease of almost 10 times as shown in **Figure 100**. Chevron increased the number of completions dramatically in 1982-83 prior to micellar-polymer flood field implementation. We believed that at least part of the additional oil response could be attributed to better completion practices. Hence it was decided to conduct a flow simulation to study the effect of additional completions by waterflooding the reservoir as opposed to a micellar-polymer flooding effort. This enabled us to quantify the additional recovery that could be expected out of a similar program in tract 9.

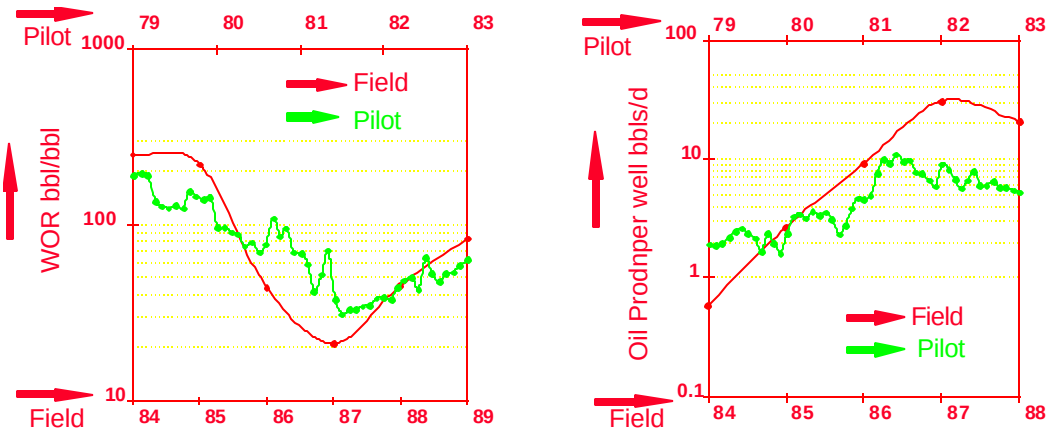

Figure 100 – WOR and oil production response of the Chevron unit

Chevron Unit Flow Simulation

The following data were collected for the area courtesy of Hyperion Energy Resources, the current operator for the lease. In general the porosity in the Chevron area is higher as compared to section 16 although this is not true for permeability.

- Core and log data
- Production data as a function of time
- Perforation/completion data

The core data at each well location was averaged for each DGI. The average values were then interpolated at interwell locations to create areal maps of porosity and permeability (**Figure 101**) for each DGI. The shale barriers between the DGI's were assumed to be continuous since the vertical permeability is observed to be negligible as compared to the horizontal permeability.

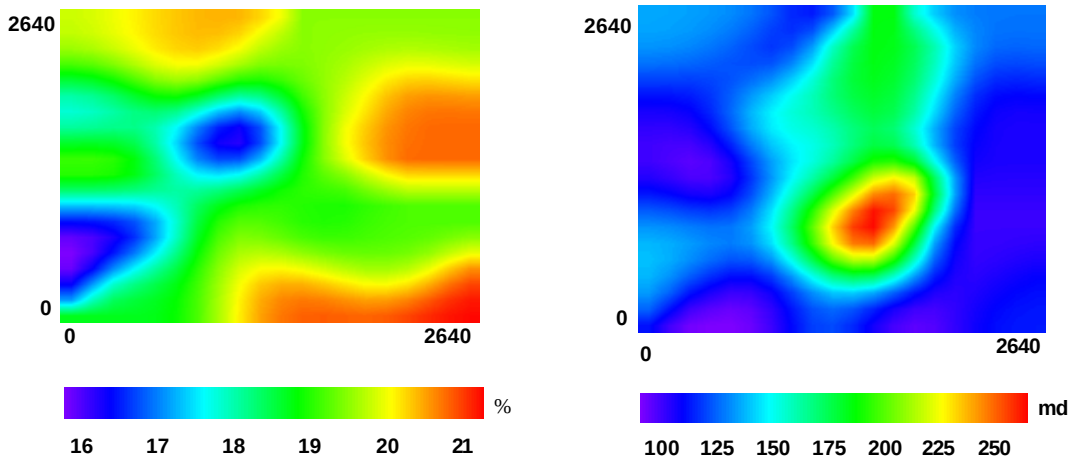

Figure 101 – Sample porosity and permeability areal profiles

The PVT properties input requires oil and gas properties as a function of pressure. The minimum bottom hole pressure is known to be around 20 psi and the initial pressure of the reservoir was around 900 psi. Therefore the working range of pressure is 20-900 psi. All the properties were generated using standard black oil model correlations for the above working range in discrete increments of pressure.

The parameterization of the relative permeabilities was done using the power law model with reasonable end point permeabilities suggested by the Kuykendall.[2] The exponents of the oil and water curves were varied as a function of time.

A commercial simulator, ECLIPSE, was used for simulation purposes. The primary depletion stage simulation was carried out so as to approximate the field oil production response by standard hyperbolic decline with a reasonable guess value of initial oil production. The secondary recovery stages of the simulation were constrained to match the oil rates. The relative permeabilities were fine-tuned as a function of time to get the observed water cuts. Every effort was made to closely monitor the number of active wells and the average reservoir pressure at any time to get a reasonable forecast.

The areal expanse of the Chevron unit is 160 acres. It was decided to divide the area into 132-ft x 132-ft grid blocks so that any layer is split in 400 grid blocks. The thickness of each grid block is assigned to be the thickness of the layer itself, which is obtained by interpolating at interwell

locations. The system has 11 layers, which is the sum of all DGI's B through G and the intermediate shale layers between any two DGI's.

The results are as shown in **Figure 102**. The simulated water flooding response shows a much lower kick in the field oil production (FOPR) as compared to the actual micellar-polymer flood response. Similarly the WOR plot shows decrease by a larger factor for the actual micellar-polymer flood response as compared to the simulated water flooding response. **Table 8** quantifies the responses observed.

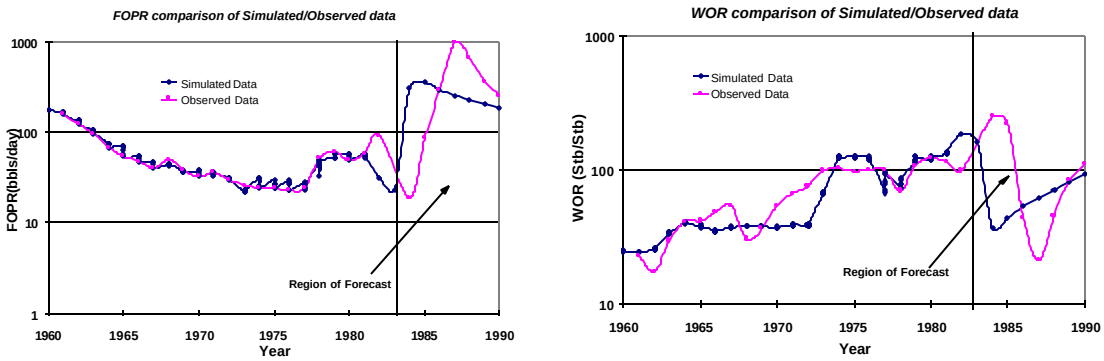

Figure 102 – WOR and field oil production plots for the Chevron unit

Table 8 – Comparison of miceller-polymer versus conventional waterflood

Response	Miceller-Polymer	Waterflood
Field oil production (bbl/d)	51 times increase	15 times increase
WOR (bbl/bbl)	10 times decrease	4 times decrease

Summary of Simulation of Chevron's Unit

Based on the simulation results from Chevron's unit, it was clear that the favorable response observed during the miceller-polymer flood was partly due to better completion strategies and partly due to the addition of chemicals. Conservatively, if only water flooding would have been used in the Chevron unit, the oil production would have increased by 15 times as compared to 51 times. The WOR would have decreased from 200 to 50 instead from 200 to 20. Although not as impressive, re-completion of upper zones would have added significant oil production. This type of completion

strategy is relatively cheap as compared to injecting expensive chemicals. We evaluated the usefulness of these strategies for tracts 9 and 7 in the following two sub-sections.

Tract 9 Evaluation

Tract 9 is located south of the Chevron unit and has an areal expanse of 160-acres (see Figure 87). The unit is operated by Uplands Resources Incorporated and has very similar reservoir conditions to the Chevron unit. The well schedule information was very difficult to reconstruct. It is known with a fair degree of certainty that number of wells that have been drilled so far from the time of discovery is close to 65. The unit currently has six active producers and ten active injectors providing pressure support. Tract 9 is one of the units that rank high with respect to the original oil in place (15 MMStb). From the report compiled by Welch[50] it was observed that tract 9 had produced cumulatively 6.058 MMStb of oil through primary depletion and secondary recovery operations as shown in **Figure 103**. This amounts to a recovery of 40% of the original oil in place.

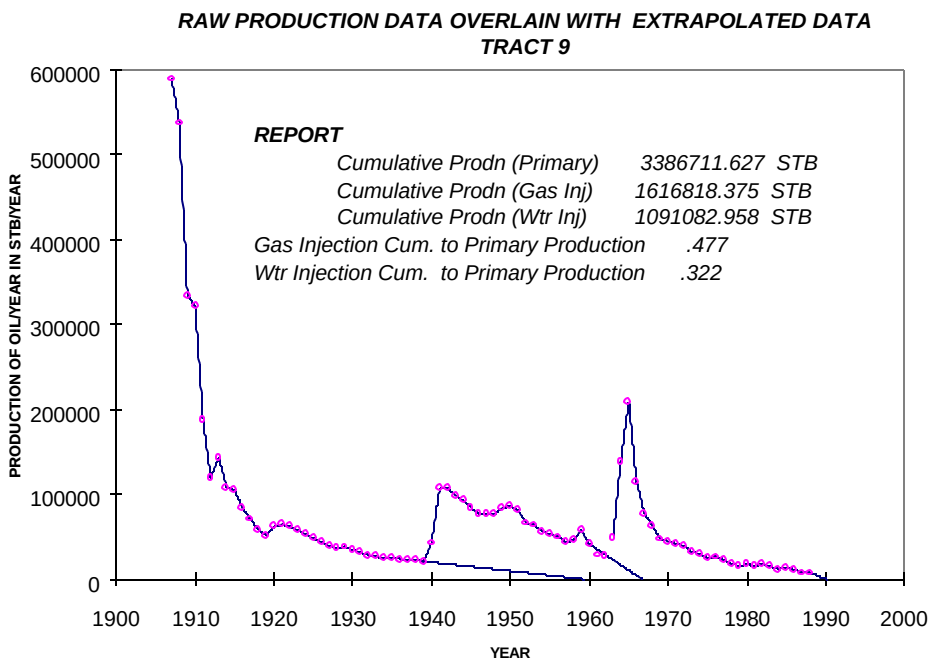

Figure 103 – Production analysis plot for tract 9 showing the primary gas injection and water flooding stages of depletion

Geostatistical Estimation of Petrophysical Properties[51]

The A-G DGI model provided by the geologist was directly used as input for a thirteen layer system into the simulator with each DGI constituting one layer with shale interbedding between successive DGI's. The facies divisions used within each DGI are channel sand, splay sand and flood plain mudstone as provided by the geologist.

A well base map for each DGI was constructed with the facies code assigned at the well locations. The facies type was determined by the type of SP or Gamma ray log response observed at the well. The facies code was assigned based on the following convention:

- Channel sand
- Splay sand
- Flood plain mudstone, shale

Indicator variograms were then generated for each facies, which were then input into the indicator simulation program-Sisimpdf[52] for constructing the areal facies map. The Sisimpdf program honors the input proportion of each facies. In this study a multi-layered model was used which compromised the variability of the petrophysical properties to a certain degree but the depositional hierarchy was strictly honored. Unlike the Chevron unit study an attempt was made to simulate the shale layers between successive DGI layers to identify areas where the shale barrier is discontinuous permitting sand upon sand stacking.

The thickness of sand in each DGI at well locations was estimated from the data provided by the geologist. These estimates were then kriged at interwell locations using the ordinary kriging procedure to generate thickness maps for each DGI. It should be noted that the thickness of sand is explicitly forced to zero for interwell locations where the simulated facies is known to be shale.

The porosity at each well location was estimated based on the gamma ray logs due to insufficient density-neutron or sonic logs. A gamma ray to core porosity regression relationship was established based on data from the Self-82 well located in the Self-unit (**Figure 104**). This was the only physical core situated proximal to the study area. The gamma ray values were then averaged

within each DGI and then kriged at interwell locations to produce gamma ray maps for all DGI's. The kriging was performed with the previously simulated facies maps as external drift.[52] The regression relationship was then used to translate this to a porosity map.

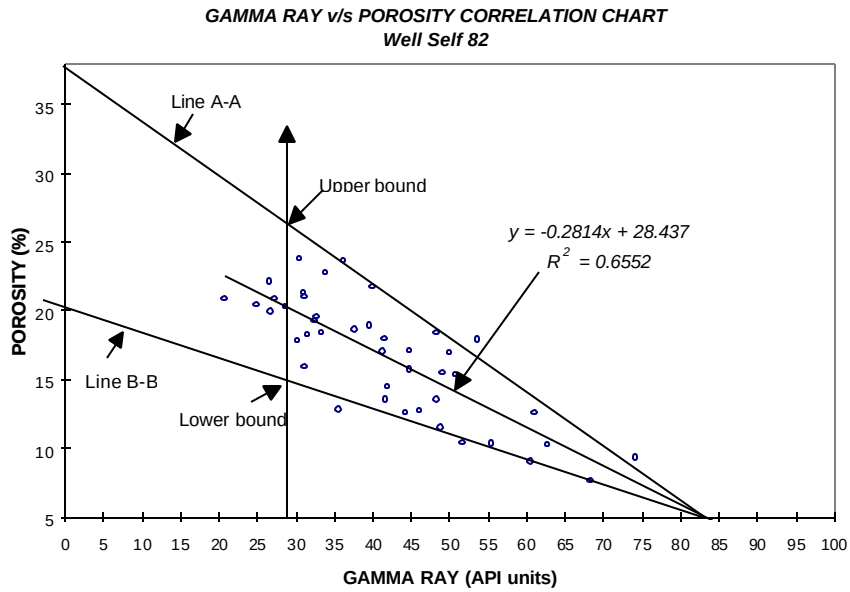

Figure 104 – Gamma ray versus core porosity correlation developed from the data compiled from Self-82

Gamma-ray values have a direct dependence on the shale content of the reservoir, which is inversely proportional to the porosity of section. Since gamma-ray logs show a pulsating response as opposed to the blocky response shown by SP logs, foot by foot measurements of gamma ray logs may be misleading. When they are averaged over the thickness of the DGI itself the value should be representative of the shale content and in turn porosity at a particular location.

Figure 104 shows a large scatter identified by the lines A-A and B-B around the trendline for which the equation is provided. Hence it was proposed to feed the straight-line equations of A-A and B-B and use a random number generator for determining the porosity value for a given gamma ray measurement. For example a gamma ray measurement of 30 API units could be representative of a porosity value between 15% and 26% marked on the plot as Lower and Upper bounds respectively. It should be noted that the lower the gamma ray value, the higher the uncertainty in the correlation.

Even though the correlations between $\ln(k)$ and porosity are quite good it was not used since the regression relationship may yield unreasonable values when extrapolated beyond the input porosity range used to construct the correlation. Once the porosity maps were generated for all DGI's the values in each DGI were transformed into a standard normal Gaussian distribution. It is known that the porosity values are related to permeability without a large scatter. So the values in the Gaussian domain obtained from porosity are back transformed into permeability (real space) using the cumulative distribution function (cdf) from Chevron unit data as input. This is done DGI by DGI with the input cdf for the corresponding DGI generated from the Chevron unit.

Figure 105 presents a composite diagram of the facies, thickness, porosity and permeability map. It can be observed that the thickness and the petrophysical property maps carry the geological facies imprint.

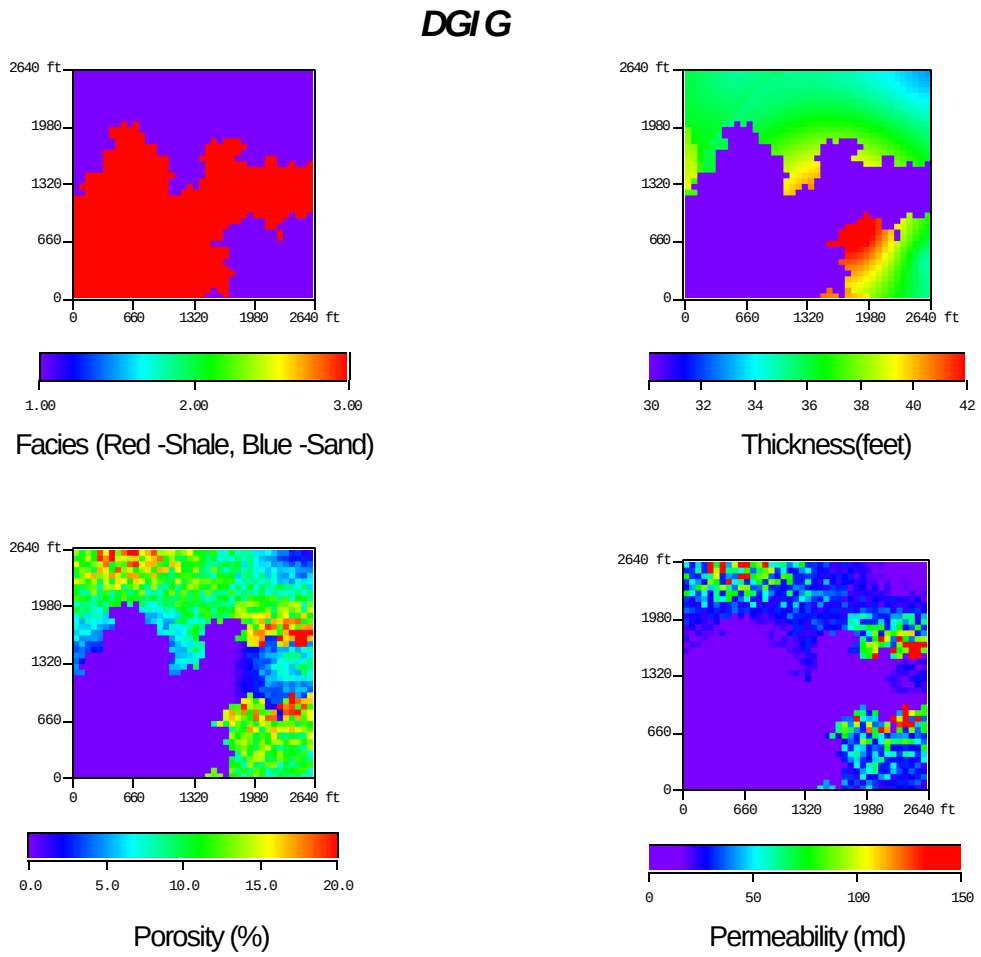

Figure 105 – Composite diagram showing areal maps of porosity, permeability and thickness honoring the facies distribution

Flow Simulation Procedure

Tract 9 simulation study used total liquid production as the flow constraint instead of oil production. The rationale used was that if the total liquid production were matched, discrepancies in simulated water cuts compared to the actual field values would result in unacceptable errors in simulated oil production. This should be understood in light of the fact that typical water cuts in producing wells are 99%. If a small difference in simulated versus observed water cut is observed it results in significant difference in water production. It would have happened if we had used oil rate as a constraint.

Another difference from conventional history matching procedure was the entire history of tract 9 was not matched. Significant uncertainty exists as to the well locations during the early life of tract 9. Further data on individual wells – production, completion, and abandonment – was not available. Even the total production on tractwide basis was missing for many years. This made it very difficult to simulate the historical performance. Instead of trying to match an "estimated" historical performance, it was decided to concentrate on the last five years of production history for which better quality data were available. We initialized the model in 1992, and estimated the prevalent conditions at that time using available data as described below.

The areal expanse of the tract 9 is 160-acres. It was decided to divide the area into 66 × 66-ft grid blocks so that any DGI is divided in 1,600 gridblocks. The thickness of each gridblock was assigned to be the thickness of the DGI itself, which was obtained by interpolating the values at interwell locations. The system had 13 layers, which is the sum of all DGI's A through G and the intermediate shale layers between successive DGI's.

The PVT properties input requires oil and gas properties as a function of pressure. The minimum bottom hole pressure is known to be around 20 psi and the initial pressure of the reservoir was around 900 psi. Therefore the working range of pressure is 20-900 psi. All the properties were generated using standard black oil model correlations for the above working range in discrete increments of pressure.

The well test data provided an estimate of the average reservoir pressure around the well. Four well tests were conducted within tract 9. These average pressures were gridded using the kernel smoothing technique to generate an areal base map of pressure for the year 1992. Since all the DGI's are in vertical communication with the exception of DGI's A and B vertical equilibrium was assumed to calculate the areal pressure profile for each DGI. It should be noted that the base pressure map is tied to DGI E since this layer represents a median depth in the vertical structure of Glenn sand. All other DGI pressure profiles were determined based on the hydrostatic pressure difference. **Figure 106** shows the base pressure map that is tied to DGI E. It can be seen that the southwestern corner pressures are lower as compared to other areas. This might be an indication of lack of support to the existing producers from the current injectors.

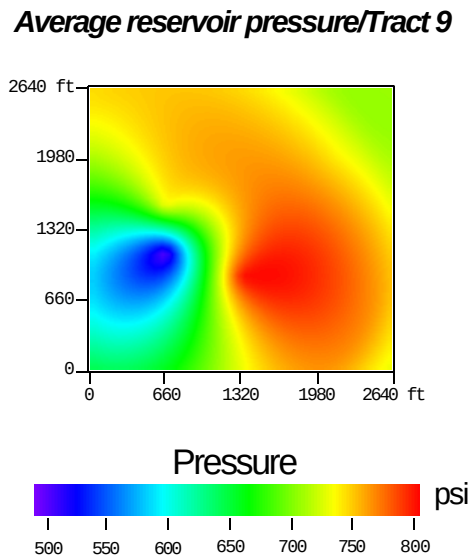

Figure 106 – Areal reservoir pressure map that is tied to DGI E in psi

The saturation profile was derived from resistivity logs. It was then scaled using a multiplier to make it representative of the year 1992. The methodology used to determine the multiplier is as follows. The effective permeability (product of relative permeability and absolute permeability) was estimated from the model at all wells where well testing was carried out. The effective permeability, which is a function of saturation, was then compared with the observed effective permeability derived from the well test. Since the effective permeability has a direct dependence on saturation, the saturation was scaled so as to bring the model derived effective permeability closer to the well test derived effective permeability at all the wells. Using this method, the multiplier selected was 1.4.

Flow Simulation Results

The well map is presented in **Figure 107**. It shows only the active wells for clarity and does not include all the wells that have been drilled in this unit. Initially it was proposed to restrict the recompletion/redrilling program to the area marked by dotted lines in the well base map. In accordance, the following scenarios were proposed.

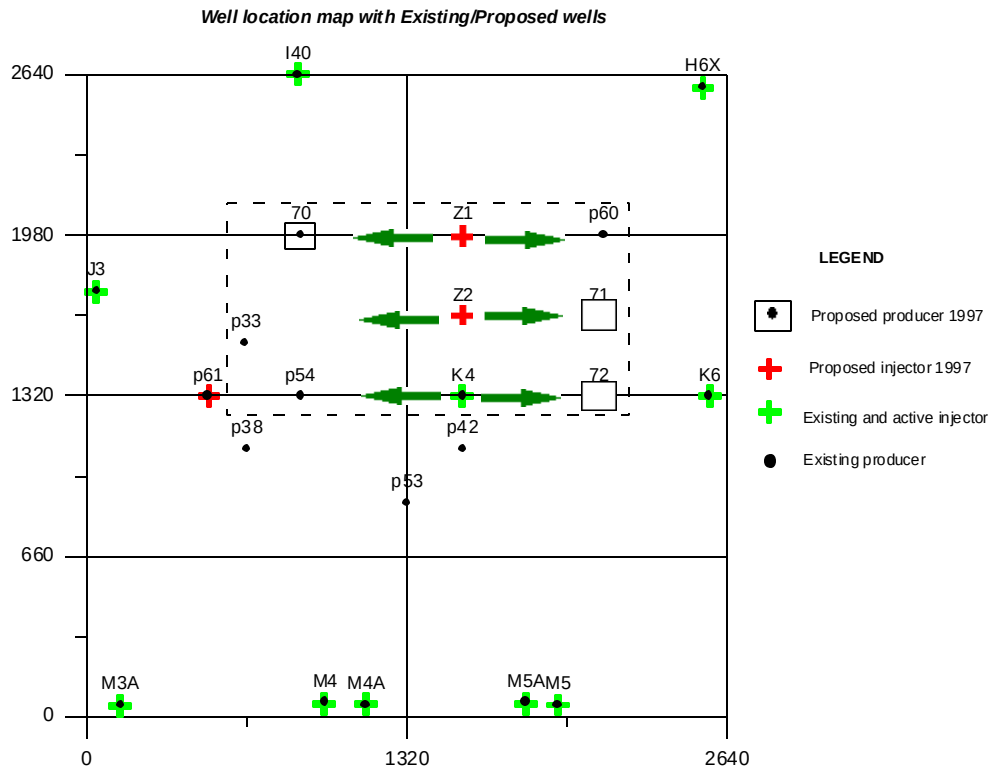

Figure 107 – Well base map of existing/proposed wells for tract 9

Scenario Base

It was proposed to plug the lower DGI's (E, F, G) and then complete upper DGI's (A, B, C, D) for all existing wells within dotted area namely p33, p54, p60 and K4. Two new injectors and three new producers 70, 71 and 72 were proposed. It was intended that the injectors Z1, Z2 and K4 would form a water bank and sweep the oil east and west of the line of injectors toward the producers as shown by the green arrows in Figure 107.

Anisotropy Favorable/Unfavorable

It was proposed to investigate the effect of anisotropy $K_{N-S} = 3 \times K_{E-W}$ for the base case. This would be favorable for the proposed intent since the water bank formation is promoted owing to the North-South permeability being higher. It was also decided to consider the adverse case where $K_{N-S} = (1/3) \times K_{E-W}$ to get an idea of the possible downside if the truth is an exact converse to the favorable case.

The history matching for all the cases was done from the year 1992-1997. The forecasting was done from May 1997. It should be noted that the history matching was done with total liquid production as the flow constraint. Hence the oil production curve during the history matching stage would be case dependent because of variations in the oil cuts.

Scenario Plug/Recomplete All Wells

Scenario base did not yield a good response. Hence it was decided not to restrict the scope of operations to the dotted area mentioned in the base scenario. It was proposed to plug all injectors and producers in the lower DGI's (E, F, G) and complete them in the upper DGI's (A, B, C, and D) without redrilling new wells.

The proposal did not look attractive at first glance (**Figure 108**) since the incremental oil production on implementation of recompletion/redrilling program was not significantly higher as compared to the case in which existing conditions were allowed to prevail. This was indicated by the closeness of the two curves in the oil production plot. The water cut plot showed a decrease of 98.7% to 97.3% that translates into a considerable reduction in water production. Hence despite the fact that incremental oil production was not encouraging the proposal was economically viable since the water production was cut drastically resulting in a remarkable reduction in operating costs.

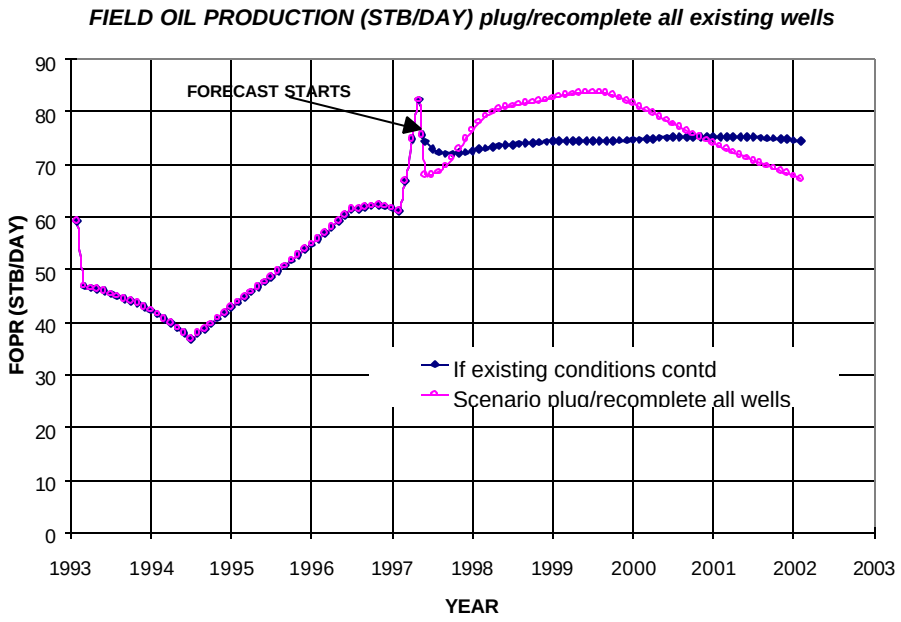

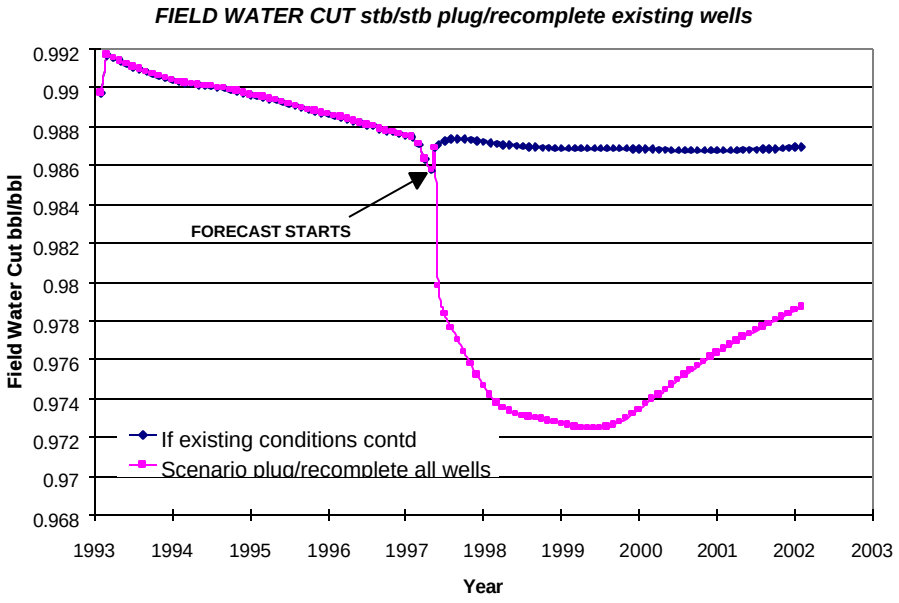

Figure 108 – Oil production and water cut plot for scenario plug/recomplete all wells

Scenario Plug/Recomplete Old Well and Drill New Vertical Wells

This scenario was a combination of the base case and the scenario detailed in the previous section. The proposal for new wells was not changed. Hence in this scenario the new wells are p70, p71 and p72 as producers and Z1, Z2 as injectors. The intention was to capture the advantages of

plugging the lower intervals in terms of reduction in water cut and still gain incremental oil production by virtue of the new wells drilled.

The incremental oil production, after implementation of the proposal over the existing condition case, was at best about 35 bbls/d. The water cut goes down from a value of 98.7% before implementation to a low of 97.8% which was a reduction of 0.9% as compared to a cut of 1.4% brought about by the plug/recomplete program.

Scenario Plug/Recomplete Old Wells and Drill New Multilaterals

It was proposed to drill multilateral wells (**Figure 109**) with lateral sections penetrating each of the upper DGIs A, B, C, D. The well would penetrate the formation in the North-South direction. Well Z1 would be a multilateral injector and well 71 would be a multilateral producer. The intention was to gain advantage of the horizontal sections of the multilateral wells. It was hoped that multilateral injector would provide good sweep and that the multilateral producer would yield more incremental oil production as compared to vertical wells.

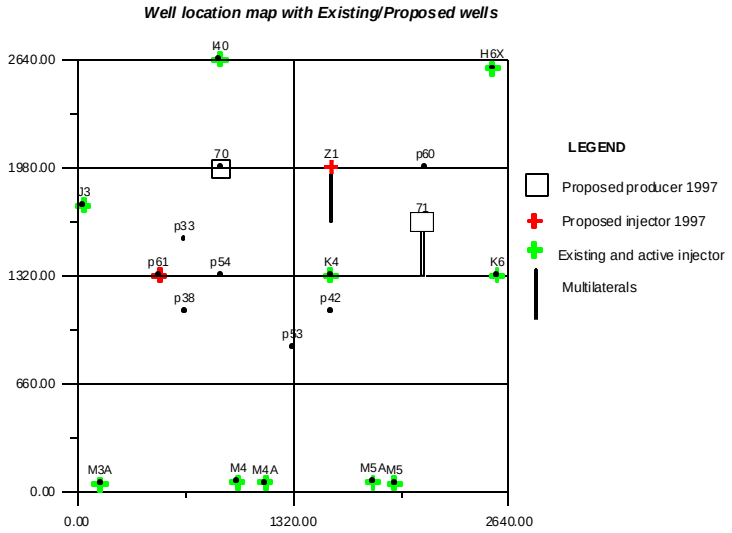

Figure 109- Proposed well base map with multilateral well locations

The incremental oil production after implementation of the proposal over the existing condition case was at best about 70 bbls/d which was considerably larger than the vertical well scenario (35 bbls/d). The maximum reduction in water cut was about 1%.

Scenario Plug/Recomplete Old Wells and Drill Deviated Wells

Since the multilaterals proved not to be cost ineffective it was proposed to investigate a scenario wherein the multilateral wells were substituted by deviated wells. The idea was drill at an angle of 80 degrees to the vertical (almost horizontal) and penetrate all upper DGI's namely A, B, C, D with an approximate span of 80 feet in each layer. The principal direction of penetration would be North-South.

The incremental oil production after implementation of the proposal over the existing condition case was at best about 70 bbls/d, which was lower as compared to the scenario in which multilaterals were proposed. The maximum reduction in water cut was once again about 1%. Since the cost of drilling a deviated well is a cheaper proposition as compared to the cost for a multilateral well, it was economically more attractive.

Ancillary Scenarios

In addition to the above scenarios, we also considered scenarios that were based on our understanding of potential index mapping of tract 9. Based on the mapping of potential index, we had noted that all the areas of tract 9 were not equally explored. Based on the potential maps, we investigated three additional scenarios that involved either drilling vertical producing wells, or either drilling deviated injection or production wells. These scenarios are shown in **Figure 110**.

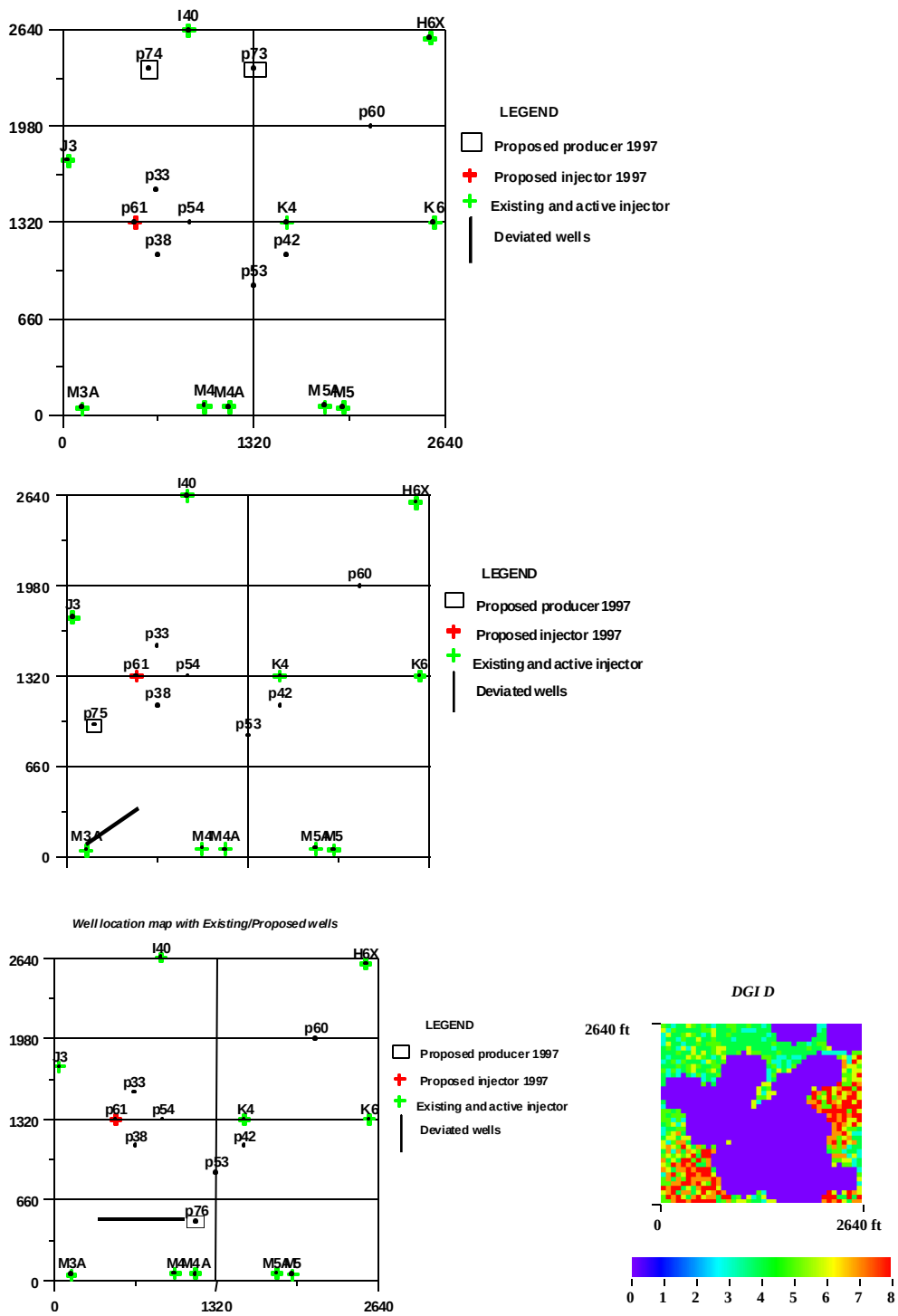

Figure 110 – Well locations of the existing/proposed wells along with a sample potential index map

The response from these scenarios is shown in **Figure 111**. The results are compared with the base line where existing conditions are allowed to prevail. The best response is given by drilling a

deviated producing well – P76, and is second only to the scenario when all the individual scenarios are implemented simultaneously.

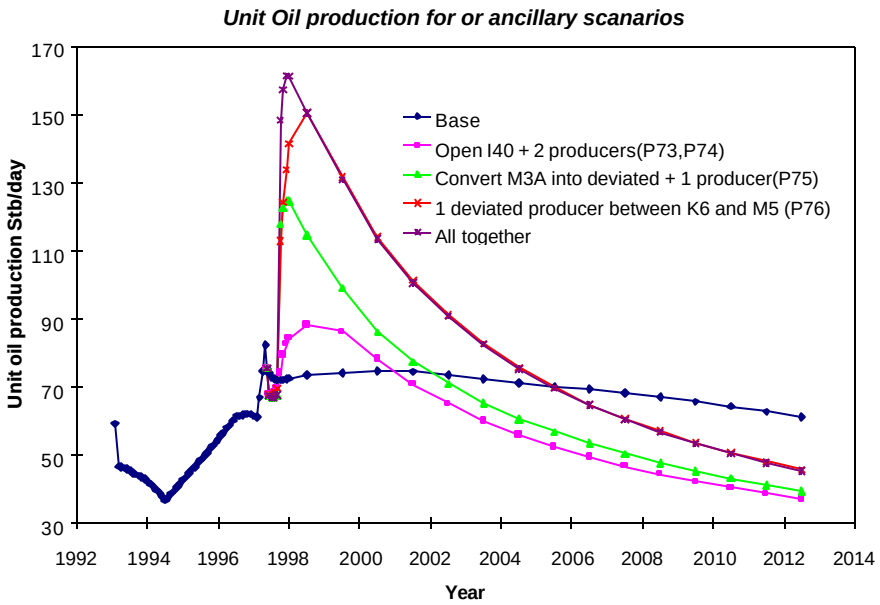

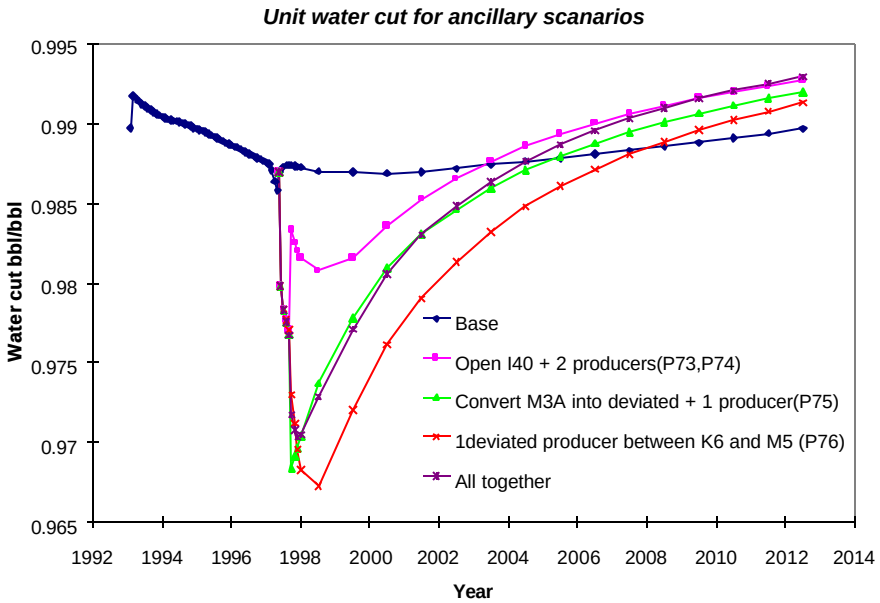

Figure 111 – Oil production and the water cut plot for ancillary scenarios

Economic Evaluation

A simple economic evaluation was conducted to identify the most favorable scenarios.[51] The rate of return histogram is presented which is a compilation of all scenarios (with the exception of ancillary

scenarios) together arranged in ascending order. It was decided to incorporate sensitivity analysis on the oil price with variations as shown in **Figure 112**. The ROR figures do not show a large variation for any given scenario. It can be noted that the plug lower DGI's/ recomplete upper DGI's flow scenario stands out among all the proposals. However, it should be noted that the production increase in plug/recompletion scenario was not significant. Most of the cost savings were achieved by reducing the water cut, and hence cost of lifting.

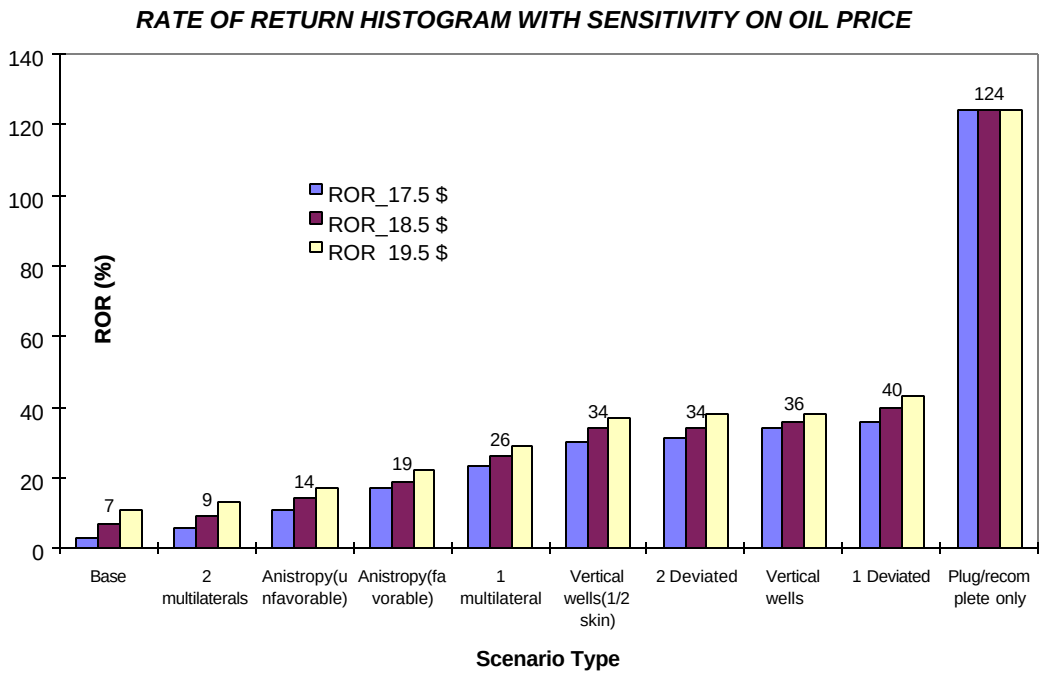

Figure 112 – ROR histogram with sensitivity on oil price

The ancillary scenarios were investigated separately because of the method with which locations of the wells were selected. The results of the economic analysis are presented in **Figure 113**. The deviated producer resulted in an impressive ROR with a positive NPV at both 15 % and 25 % interest rate. In these scenarios, we have assumed that the existing wells were selectively plugged/recompleted for three months, and the new wells were drilled following the three-month observation period.

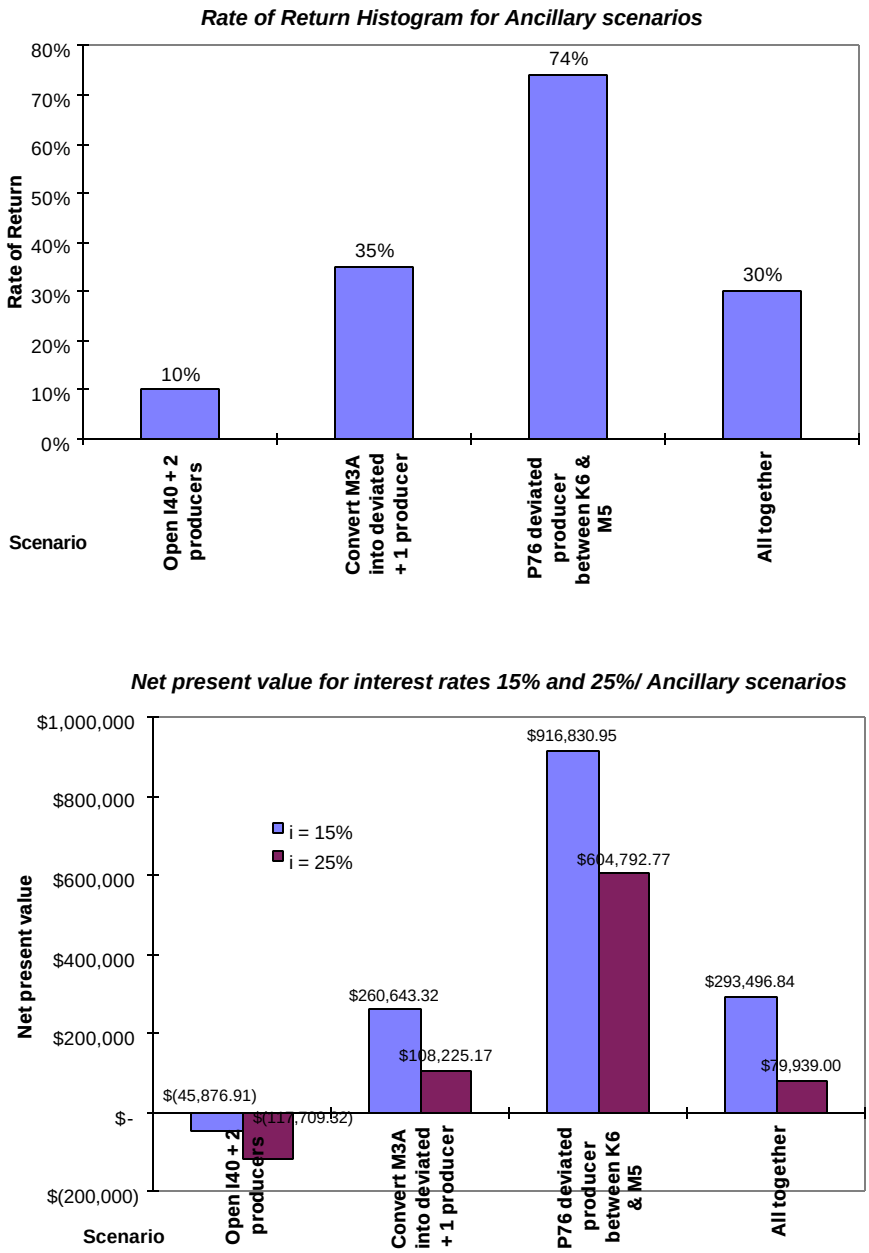

Figure 113 – Rate of return and net present value charts for ancillary scenarios

Summary from Tract 9 Simulation

Based on the evaluation of several scenarios, we observed that the most feasible scenario was drilling of a deviated well, p76. This well would result in most incremental oil production with a significant reduction in water cut.

Tract 7 Evaluation

Tract 7 is located north and east of tract 9 and is also operated by Uplands Resources, Inc. The well density is higher as compared to tract 9, and the unit has a history of good response to water flooding. The present well locations are shown in **Figure 114**. It is estimated that tract 7 has close to 15 MMStb of Original Oil in place (OOIP). From Welch[50] it was noted that tract 7 has produced about 3.9 MMStb through primary depletion and secondary recovery operations. This means that the total recovery is about 26% of the OOIP, implying there is still a lot of untapped potential in the reservoir as compared to tract 9 which has a cumulative recovery closer to 40%. The well density being high, it was not advisable to drill new wells, but a plugging/recompletion program to exploit the upper zones may yield significant additional oil recovery.

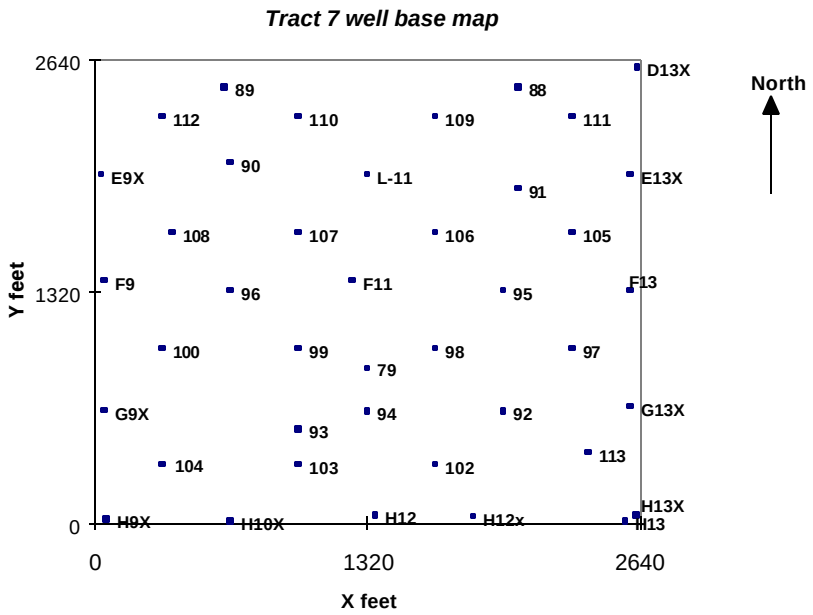

Figure 114 – Well map for tract 7

Data Input and Flow Simulation Technique

The facies maps for all DGI's were generated using similar methodology as discussed in the previous sub-section. Several realizations were performed, and the realization which closely matches the map generated by the geologist, was chosen for petrophysical property estimation. In this work, this selection was done by visual observation.

As discussed in the previous sub-section, we used gamma ray values to estimate the porosity data. Although gamma ray logs are common in the field, one of the major drawbacks of estimating porosity from gamma ray logs in mature fields is as follows. The engineer has to contend with the fact that calibration of the gamma ray tool is not uniform since the logs are performed by different service companies.

Open hole logs always give a higher gamma ray reading as compared to cased hole logs. Since gamma ray logs measure the natural radioactivity of the formation, cased hole logs are affected by the presence of the casing between the recording tool and the formation. Conceptually, if two different wells are logged with the same tool, a pure shale interval in the two wells would have the same reading of gamma ray API units. This is not observed in practice since the shale found at two different vertical sections may have different sand content, varying organic material content, contrasting compaction levels, all of which affect the value of the gamma ray readings.

If the raw values of gamma ray readings from different wells are translated to porosity without accounting for the facts mentioned above, it would lead to under or over estimation of porosity. It should be noted that the gamma ray to porosity regression correlation is one single relationship and the same relationship is used for all the wells uniformly. By itself, the correlation does not take into account the variations in the gamma ray readings between the wells. To overcome this problem, we used a procedure of multiwell normalization.

The objective of the procedure is to bring the shale base line for different logs in alignment so that all deviations from this base line, which are indicative of sand, are referenced from a common base datum, thus making the use of gamma ray-porosity relationship more reliable. It is observed that most of the wells in this study area are cored in the lower interval. Gamma-ray logs are transformed into porosity values for wells, which are cored in the lower intervals. Then the gamma ray derived porosity is compared with the core porosity. Only those gamma-ray logs are selected which demonstrate a good comparison. Foot by foot gamma-ray readings for such logs are pooled together to construct a probability density function (pdf) and this pdf is termed as the standard distribution. Individual well gamma-ray logs are then used to construct pdf(s) for the respective

wells. The well pdf is then plotted against the standard distribution to determine the amount of linear shift in gamma-ray absolute value required to bring the shale base lines in alignment.

Figure 115 graphically exhibits the procedure. It can be observed that pdf curves exhibit two peaks, one for a range of gamma ray values between 15-60 units and the other centered around 90 API units. The first peak represents the range of possible gamma ray values representative of sand and splay. The range of values exhibited by the second peak is representative of shale. The underlying principle in shifting individual well pdf's is that even though the probability of occurrence of a gamma ray value representative of shale may not be the same in two different wells, the range of gamma-ray values which represent shale should be centered approximately around the same gamma ray reading. For well E-9 it was determined that a linear correction of -25 API units is appropriate. It can be seen that originally the centerline of the shale peak, which was 125 API units, after adjustment is about 100 units. This was done for all the wells other than those that were used to generate the standard distribution.

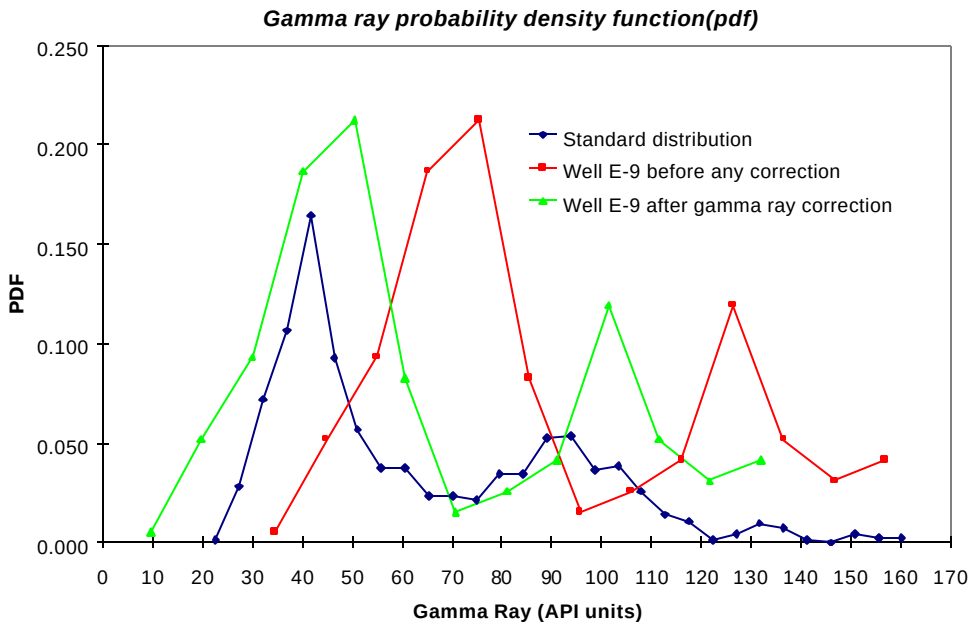

Figure 115 – Shift in pdf to align gamma ray probability distribution functions

Once the normalization procedure was completed the gamma ray values were averaged within each DGI at all wells. These average values were then kriged at all interwell locations DGI by DGI to produce areal maps of gamma ray readings with the simulated facies maps as external drift.

The areal gamma ray maps were transformed into porosity maps by using the gamma ray-porosity relationships with the use of a random number to aid the reproduction of the scatter seen in the gamma-ray vs. porosity plots (**Figure 116**). The correlations were generated with the use of digitized gamma ray values and density-neutron log porosity values. It can be observed that the wells show a fairly consistent relationship. In this study a cutoff was used with respect to the gamma ray values beyond which transformation of gamma ray values to porosity is meaningless. The cutoff in this case was fixed as 140 API units. Beyond this range, the porosity was fixed as 1%.

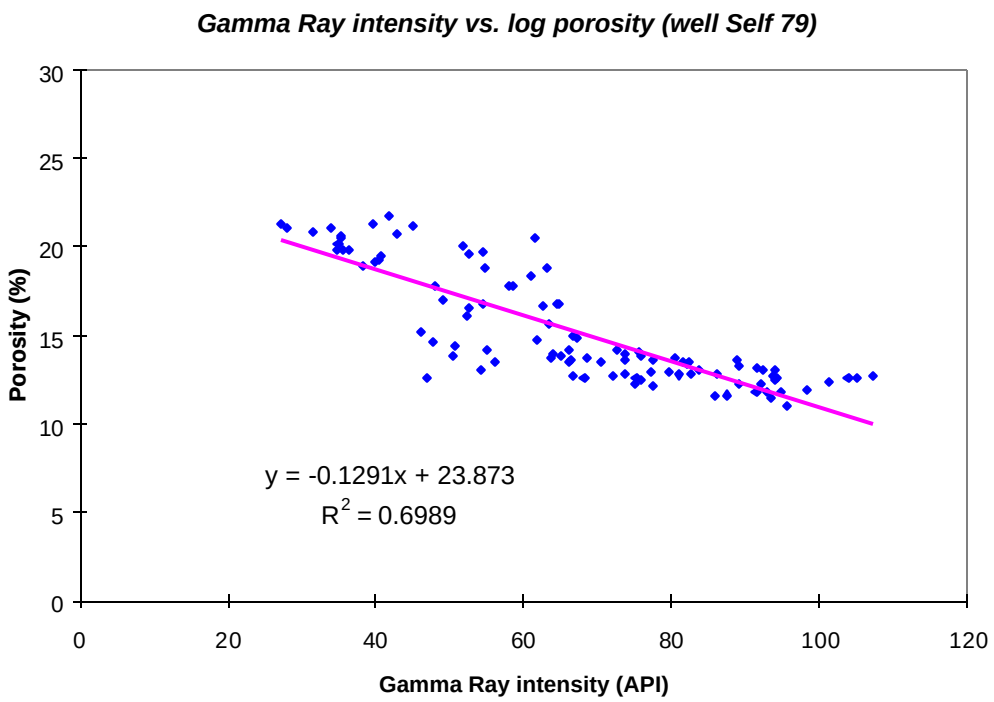

Figure 116 – Gamma ray versus porosity relationship

Regression relationships between *log(k)* and porosity were used to generate the permeability distribution from the porosity maps.

The thickness maps for all DGI's were generated by using the ordinary kriging procedure at interwell locations. The thickness of all gridblocks for which the facies type is known as shale/flood plain mudstone was forced to zero. Since thickness is a continuous variable as opposed to facies which is a discrete variable kriging on thickness even with zero thickness points need not necessarily capture the facies boundary between sand and shale. It was therefore necessary to use explicit procedures to make the simulated facies and kriged thickness maps consistent with each other.

Flow Simulation Process

The conventional history matching procedure involves reconstructing the well history from inception time to present time. A deterministic initial pressure and saturation profile is mapped, and then field flow performance is matched by tuning the input parameters. In this case study the saturation and pressure profiles were derived for the year 1993 and history matching is initiated at this time. This eliminates the need for reconstructing the well schedule history from inception time of the field. The history matching was performed for a short segment of time 1993-1997, during the course of which the input model was calibrated. It should be noted that the production and injection data were provided by the operator for this unit and is far more reliable than public sources of data.

The areal expanse of the tract 7 is 160 acres. It was decided to divide the area into 66 $\times$ 66-ft grid blocks so that any DGI is split in 1600 grid blocks. The thickness of each grid block was assigned to be the thickness of the DGI itself, which was obtained by kriging at interwell locations. The system has 13 layers, which is the sum of all DGI's A through G and the intermediate shale layers between successive DGI's.

The PVT properties used for this case study are essentially the same as those used for the Chevron unit study. The saturation profile derived from the resistivity logs was scaled up so as to match the water cuts. It can be recalled that the tract 9 case study uses well test data to match the effective permeability calculated from the model with the effective permeability derived from the well test. In this simulation study, this approach could not be realized since only a single well was tested within this study area. Hence the reserves in place and the saturation multiplier used for tract 9 were used as a guidelines for estimating the possible range of scaling coefficients of saturation. Recall that

saturation multiplier was necessary because we did not begin the simulation right from the beginning of production. Since our well log data were collected earlier compared to when we began the simulation, we needed to adjust the well log derived saturation so as to match the initial oil production as well as water cut. This was done by adjusting initial water saturations. The saturation multiplier represents the increase in water saturation required to match the observed production as well as water cut at the beginning of simulation period.

First, a multiplier of 1.4, which was used for tract 9, was used for this study also. The ratio of oil phase effective permeability to water phase effective permeability was similar in both the study areas justifying use of the same multiplier.

Second, a multiplier of 1.2 was chosen based on the fact that it is the lowest possible multiplier that would still yield a good history match with regard to the accuracy necessary in simulated water cuts.

It was known that reserves in place at the time when history matching is started (1993) is around 11.1 MMstb. Based on the use two multiplier coefficients 1.2 and 1.4 on the water phase saturation S_w, the reserves in place were calculated as 10.653 and 9.43 MMstb respectively. These numbers are consistent with the estimated reserves (11.1 MMStb) which were based on initial oil in place and cumulative oil production so far. The objective is to get an idea of the incremental oil production obtainable with a worst case $(S_w \times 1.4)$ and best case $(S_w \times 1.2)$ scenarios.

The pressure profile was guessed for DGI E, based on which all the other DGI pressure maps were generated assuming that the pressure difference between DGI's is equal to the hydrostatic head. The guess profile was then input into the simulator and the performance of this profile was gauged by determining if it satisfies the field injection and production rates. If not, the pressure data were altered so as to be able to match the production and injection data. It should be noted that the BHP for producers (pumping wells) is about 20 psi and the BHP for the injectors is known to be 1,250 psi. Hence there is only a certain range of input average reservoir pressure (year 1993) for which the production data/injection data can be matched. This obviously assumes that there is no leverage with regard to alteration of the petrophysical property fields. If a typical fracture gradient of

0.75psi/ft is assumed, the formation fracture pressure is calculated as 1,163 psi. It was found that the BHP of injectors is very close and sometimes above the fracture pressure. This is taken into account in the simulator by multiplying well transmissibility based on the instantaneous pressure difference between BHP and the calculated fracture pressure.

It should be noted that the single well test (well 7-111) that was performed in this study area demonstrated an average reservoir pressure of 1,050 psi. It was also known that the row of injectors located in the southern part of the study area take in water at very high pressures only. Considering these facts there was enough reason to believe that the average reservoir pressure is high and close to about 1,000 psi. Well 7-111 produces the highest volume of fluid and contributes one half of the total liquid production at any given time.

Flow Simulation Results

The completion density in this study area is largely skewed towards DGI G (**Figure 117**). Considering the well density in tract 7, it was decided that a plugging/recompletion program is the most appropriate future implementation. All perforations in DGI G are plugged, and then DGI's B-F are recompleted. Recompletion of DGI A is avoided since the permeability for this layer is observed to be smaller as compared to all other DGI's. Independent simulations were conducted with two different S_w scaling factors mentioned before.

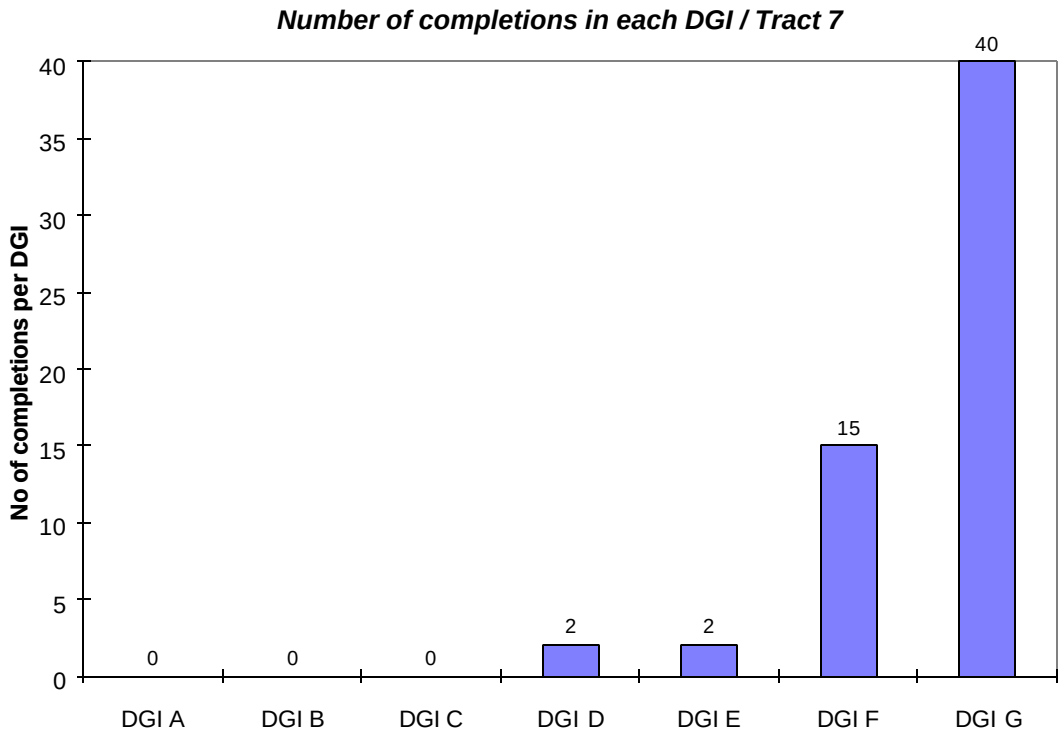

Figure 117 – Histogram of perforations in tract 7

Scenario $(S_w \times 1.2)$

This is the optimistic scenario wherein it is deemed sufficient that the resistivity log derived saturation profile, when scaled up by a factor 1.2, is adequate to bring it in tune with the initial time of history matching (1993). It should be noted that the saturation profile captures the global profile of the reservoir but the relative highs and lows predicted in this profile need not necessarily be valid. Extending this logic, it could be said that when the unit is considered as one unified system, the flow simulation gives an approximate idea of how the system would behave in response to a stimulus, but there is no guarantee that wells at selected locations will honor the simulated performance in truth. The reduction in water cut for this scenario was about 2%, and the incremental production obtainable after implementation of the plug/recompletion program was about 375 bbl/d. The simulated response is shown in **Figure 118**.

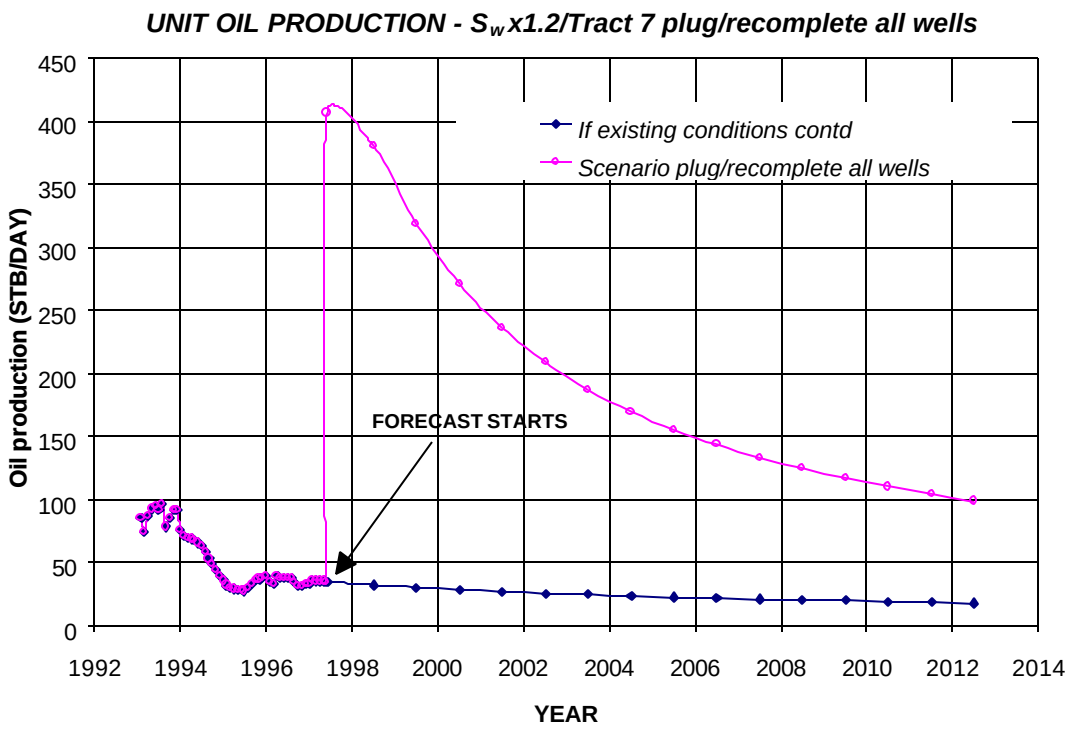

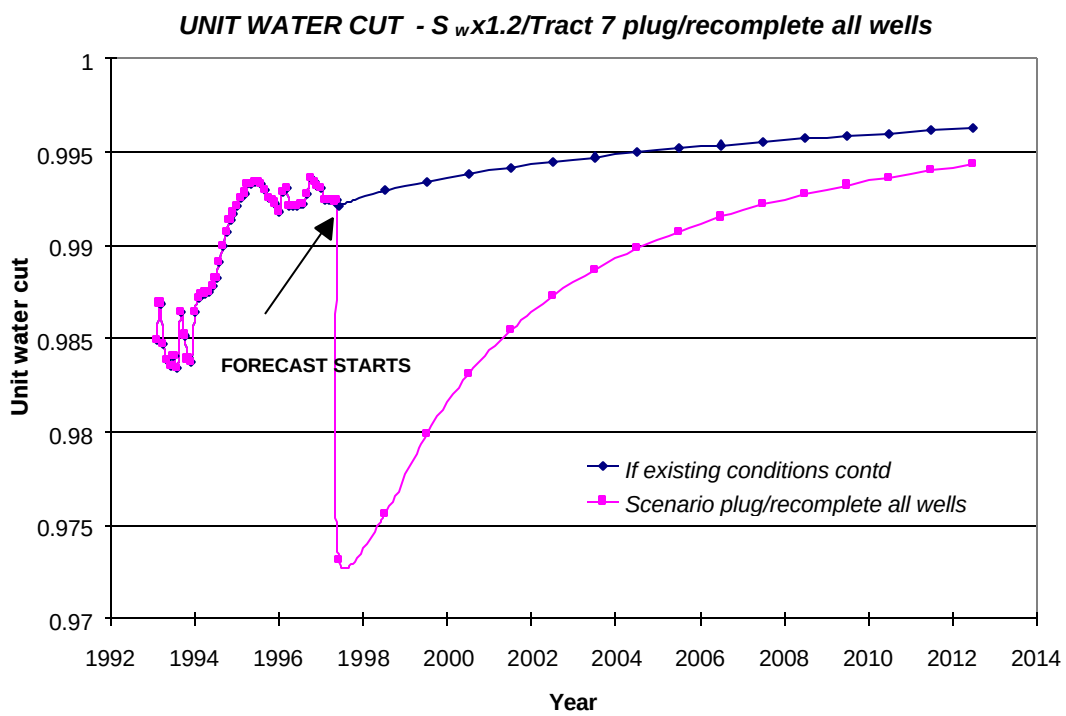

Figure 118 – Oil production and water cut plot for scenario with $S_w \times 1.2$

Scenario $(S_w \times 1.4)$

This is the pessimistic scenario, wherein the effect of a very large multiplying coefficient for the S_w profile at 1993 is simulated, and is contrasted against the previous case. It can be observed that the incremental oil production is still quite high but the reduction in water cut is small after implementation of the plug/recompletion program. The governing factor for a proposal to be viable or not, is the possible reduction in water cut coupled with the incremental oil production that could be obtained. In this case, oil production increases since more total fluid (oil+water) is being withdrawn. The high rates of total liquid withdrawal also result in increase of lifting or operating costs. It should be noted that, before implementation of the recompletion program, the wells were primarily producing from one DGI. But after implementation of the program fluid is withdrawn from DGI's B-F yielding more total liquid production.

It can be observed from **Figure 119** that the water cut shows a decrease of about 0.2% at best. It will be shown below in the economic analysis section that the incremental oil production does not generate enough revenue to offset the increase in lifting costs. If the saturation profile in reality is close to the saturation profile estimated in this scenario, then it can be concluded that a plug/recompletion program is not economically viable.

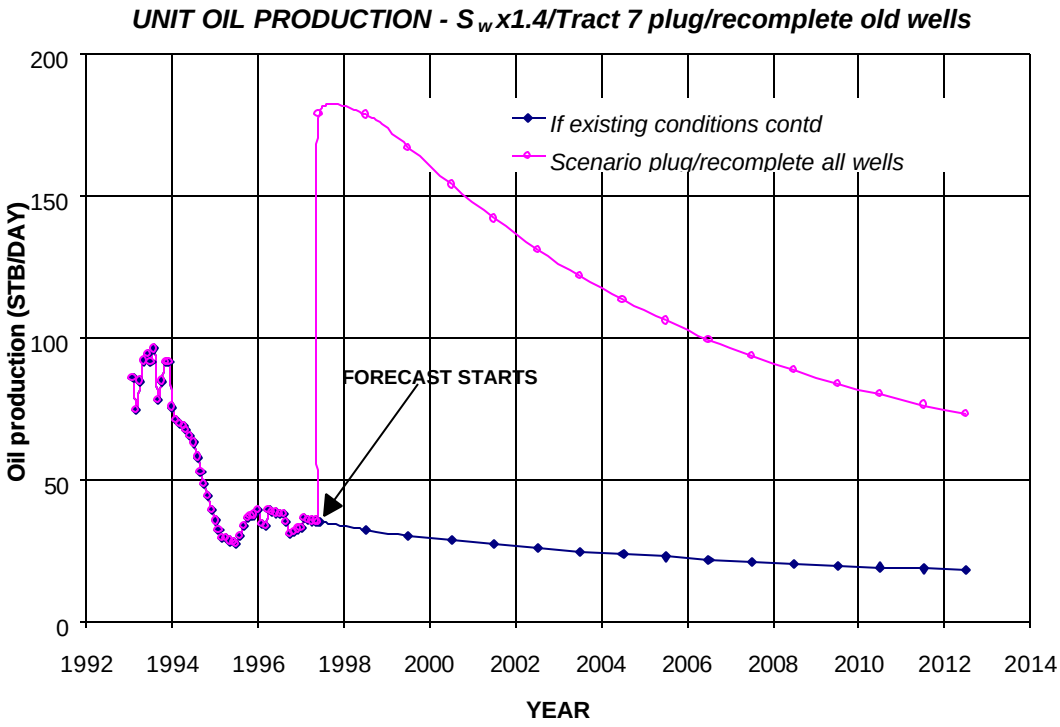

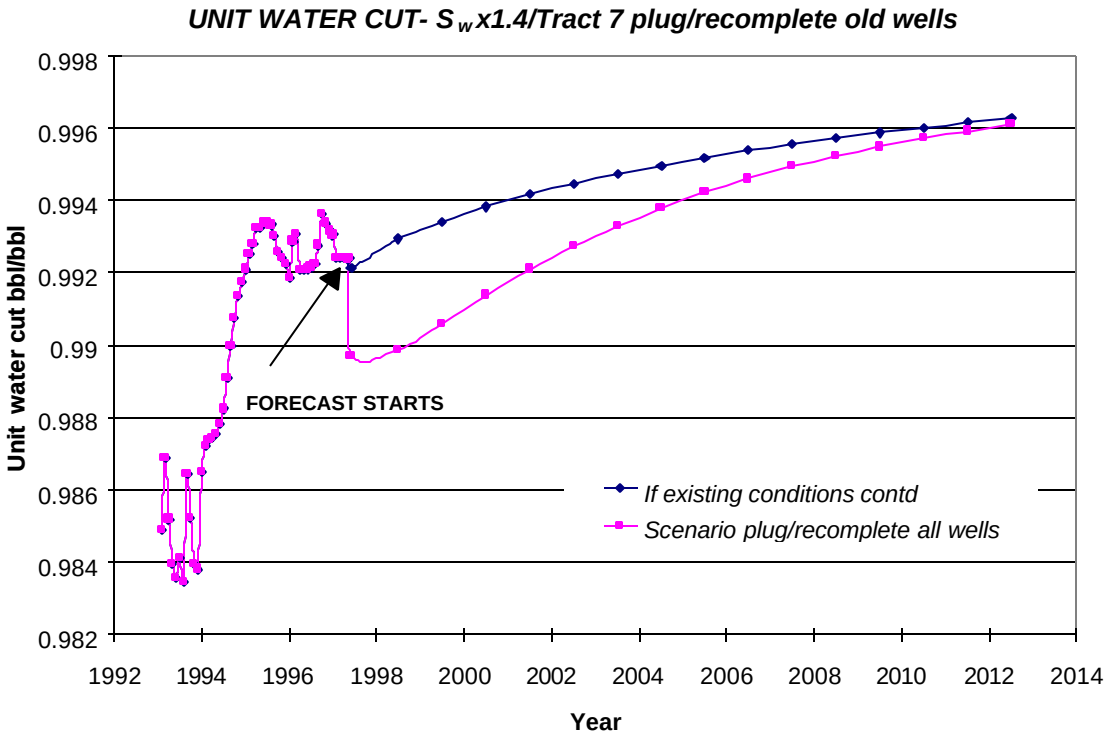

Figure 119 – Oil production and water cut for scenario with $S_w \times 1.4$

Economic Analysis of Tract 7

Only two scenarios were incorporated in the analysis of tract 7. The forecasting was performed for observing the response of plug/recompletion program but the simulation itself was initiated with two different base maps of resistivity log derived water saturation maps. This was accomplished by using two scaling coefficients for saturation namely $S_w \times 1.2$ and $S_w \times 1.4$. **Figure 120** presents the rate of return and the net present value charts for the two scenarios. The unit has 37 active wells for which the approximate plug/recompletion cost is $500,000. It can be observed that if the water saturation profile is scaled up by a factor of 1.4, the plug/recompletion program was unfeasible as indicated by the zero rate of return and negative net present value. Conversely, if in reality the saturation profile corresponds to the resistivity log derived profile scaled up by a factor of 1.2, the implementation of the plug/recompletion program would have been largely successful. These two extremes could be considered as the bounding cases for actual field implementation.

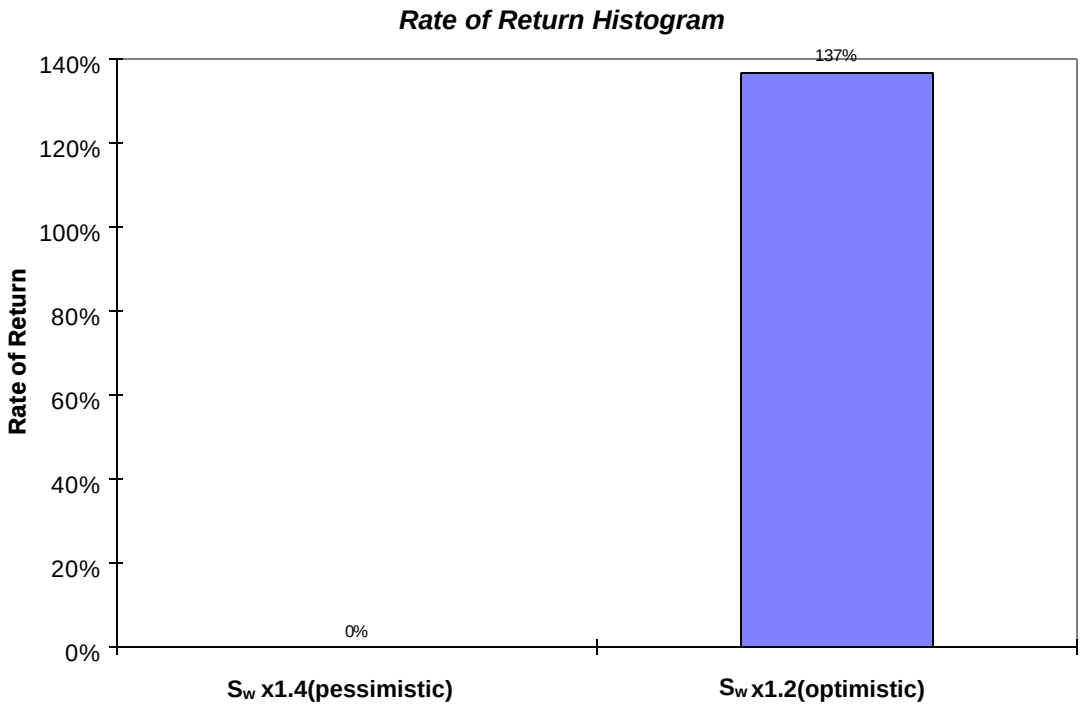

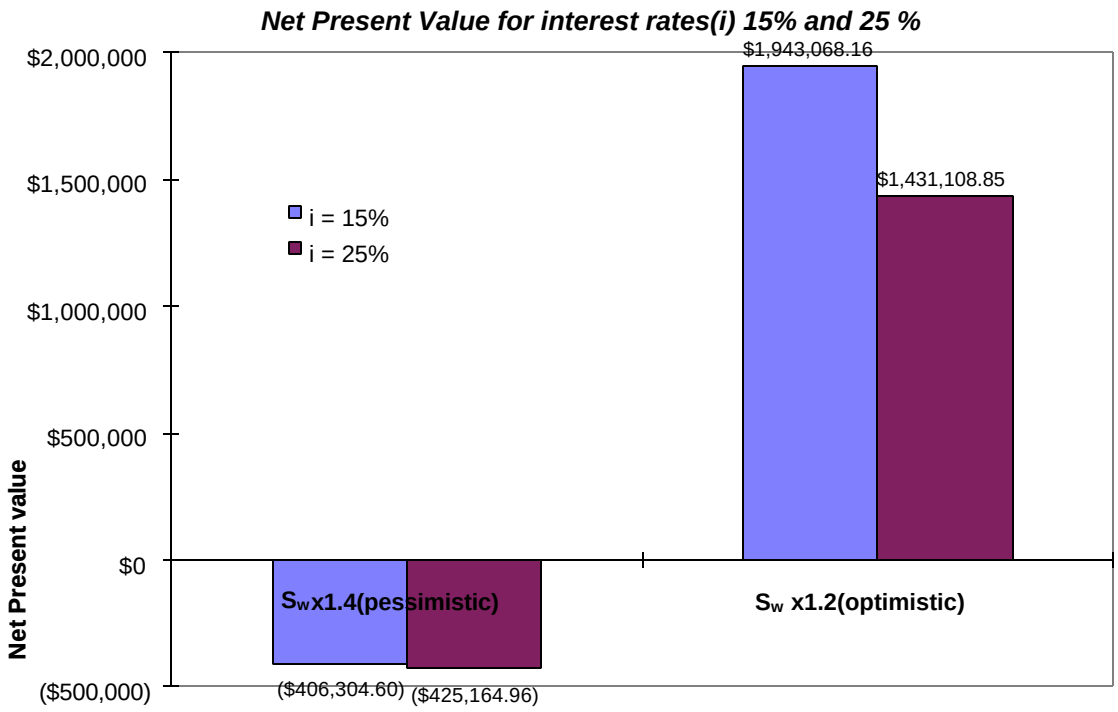

Figure 120 – Rate of return and net present value charts for tract 7

Summary of Tract 7 Simulation

Owing to the high well density and completion skewed towards the lower zones in tract 7, the most appropriate program is plug/recompletion. Most likely, the procedure would result in successful recovery of additional oil. The bounding extremes, discussed above, have been defined by performing simulations with different saturation profiles for the time instant when history matching is started.

Field Implementation

In the previous section, we discussed various detailed field implementation plans for tracts 7 and 9. We decided to concentrate on tract 9 because of the limited number of wells producing in that tract. Also, more economic uncertainty existed with respect to field implementation plan for tract 7. Initially, our plan was to re-complete the existing wells in the upper portion (DGI's A, B, C and D) of the reservoir and shut in the lower portions of the reservoir in the same wells. Unfortunately, these old wells were treated with nitroglycerine. As a result, we were not confident about the formation of caverns, which may have been left behind in these wells. After receiving several bids from various contractors, it became apparent that completing the lower portions of the existing wells is not an easy task. The amount of cement required cannot be known unless we start completing these wells, and it was possible that the cost would exceed the cost of drilling a new well. With this scenario in mind, we decided not to re-complete the old producing wells.

In addition to concern about the existing wells, we were also concerned with the possibility of a gas cap in tract 9. Earlier reports had indicated that there is a possibility of a gas cap in other parts of the reservoir. Although TDT logs in tract 7 had indicated an absence of a gas cap; we did not have any direct proof of presence of oil in the upper zones in tract 9. To test the presence or absence of gas, we completed well 9-60. The well was selectively completed in the upper intervals, and a bridge plug was placed to separate the bottom zones from the top zone. After the well was re-completed, there was no indication of the presence of gas – this is consistent with our model, and the well showed a slight improvement in the oil cut – also consistent with our model. We were

encouraged by this result which indicated that the oil saturation is higher in the upper zone, and there is no free gas present in the top zones.

Armed with all the information in the previous studies, as well as the information from well 9-60, we designed a deviated production well to be selectively completed in the upper four zones (A, B, C and D). The location is shown in **Figure 121**. This overall implementation includes converting well no 61 into an injector, reperforating wells M-3A and M-4A, and drilling a deviated production well between 61 and M-3A/M-4A in an east-west direction. The total length is expected to be about 500-ft, and the well would be completed in zones A through D. **Figure 122** shows the well plan proposed for the deviated hole and **Figure 123** shows the direction in which the well is to be drilled. With this configuration, we can take advantage of the portion of the tract 9 that has not been drained, and also support the production through three injectors that are completed in the same zone. In addition to testing the concept of a deviated hole, we also decided to test the concept of drilling a vertical well using air drilling.

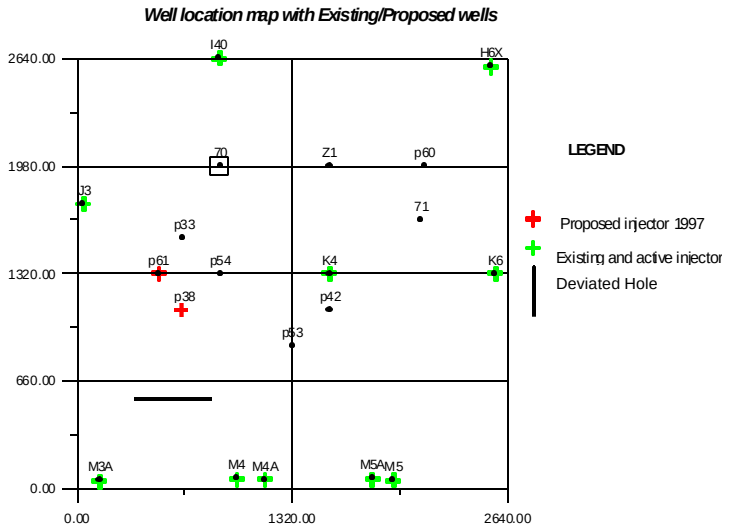

Figure 121 - Proposed management plan for tract 9

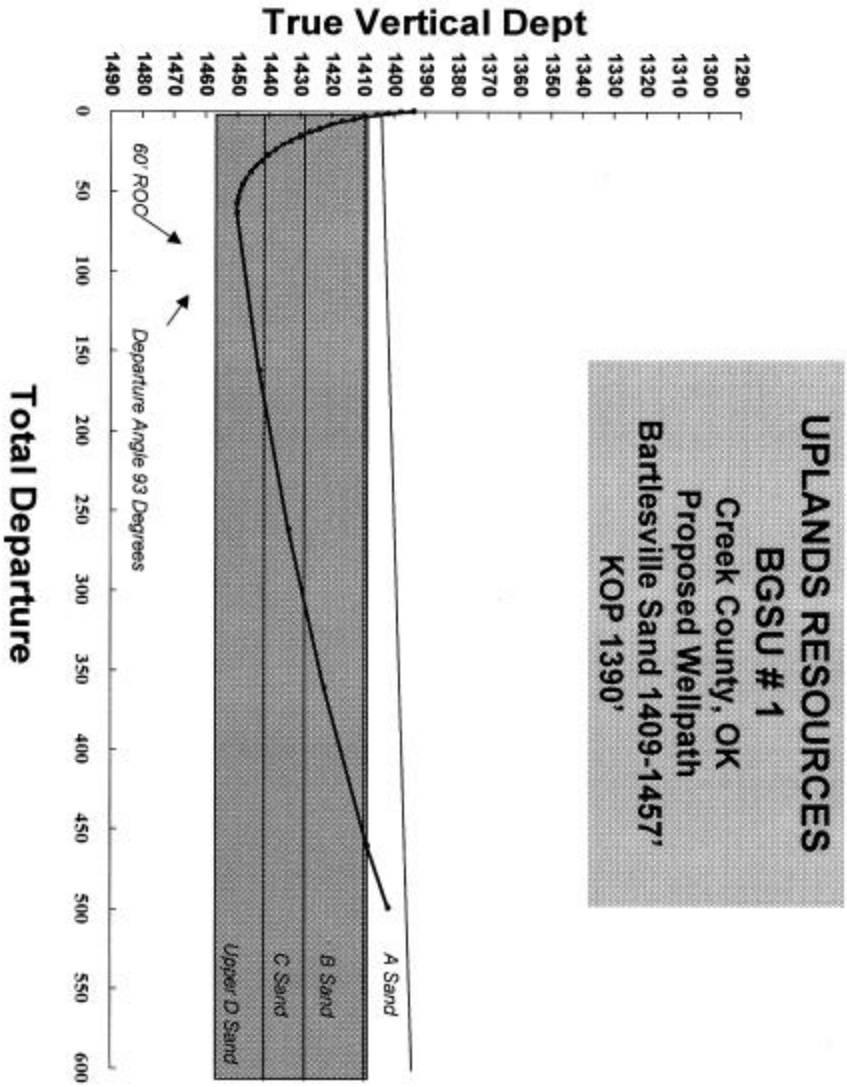

Figure 122 - Profile of a deviated hole

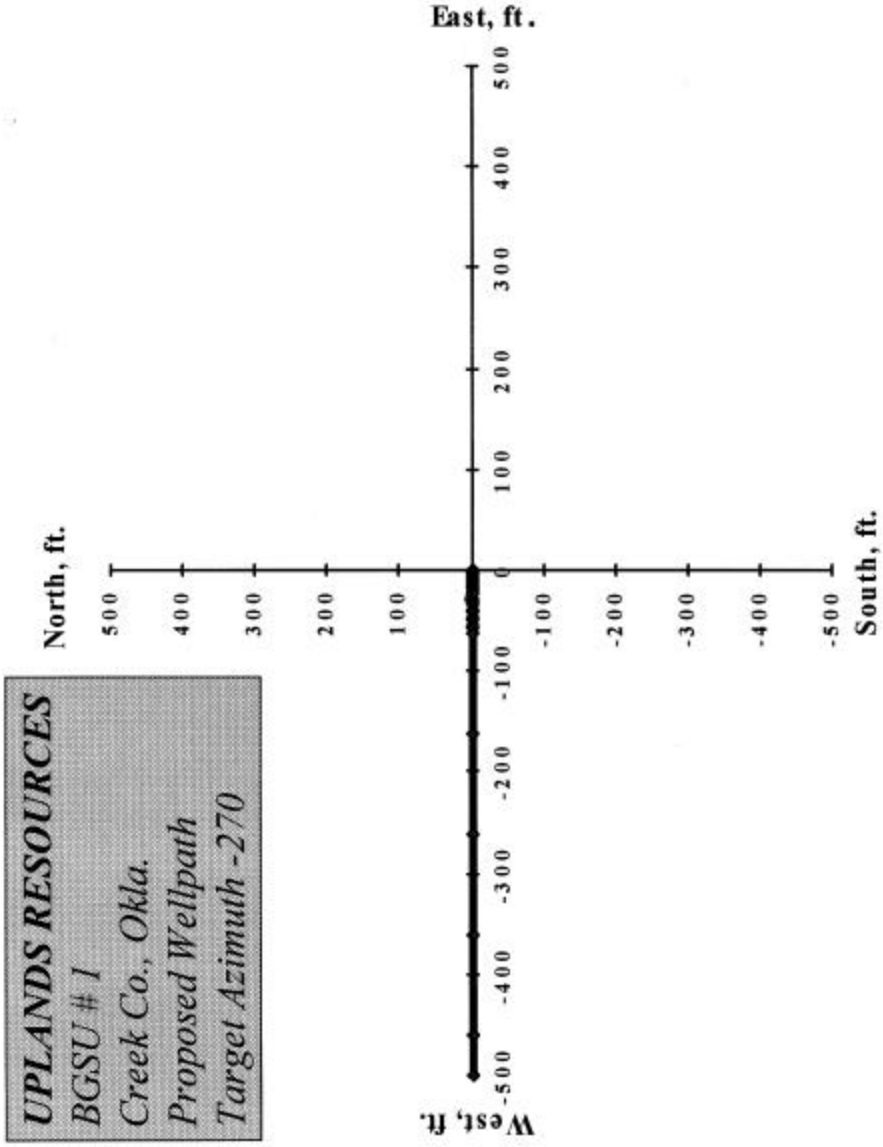

Figure 123 - Direction of a deviated hole

The drilling of the vertical portion of the well was initiated at the end of November 1998. The drilling encountered no problem, and we completed the vertical portion in the allocated time within our budget. For drilling the deviated hole portion, we gave a contract to Integrated Directional Resources (IDR), a company specializing in drilling directional wells through use of surface rotary equipment. The drill bit is steered from the surface rather than using mud motors. This is a relatively

new technology, and, if successful, can result in substantial savings in drilling horizontal holes in the future.

The drilling of the deviated hole was initiated on December 1, 1998. The bottom hole tool assembly included 6" PDC bit, CDA double joint, 2 Monel collars followed by 6 joints of drill pipe (PH6). The initial attempt to drill the well failed, because after drilling the well up to a depth of 1,363-ft, it was realized that the tool was not building any curve. Instead it was drilling a straight hole. The possible cause for this was assumed to be the double joint, and the decision was made to use a single knuckle tool. The well was plugged back using cement on December 2nd. On December 3rd, the drilling resumed with a slightly different assembly. Instead of double joint, a single knuckle tool was used. To control the direction, a gyro tool was used. From the surface, after drilling of 1-ft, the gyro was run and seated, a tool face was marked at the surface, and then gyro tool was pooled back and the rig resumed drilling. The drilling went smoothly with the angle being built according to the expectations. On December 5th, the gyro tool broke. The possible cause was determined to be high torque and high dogleg severity. After changing the tool, the drilling resumed at a very slow rate. After drilling a few more feet, the up hole Monel collar failed. The steel drill pipe failed at the pin due to high stress exerted by the Monel collar. A fishing operation was initiated and the fish was successfully brought to the surface with 3.5" basket grapple. To avoid a repeat, the decision was made to run with only one Monel collar.

After drilling another 24-ft on December 6th, the Monel collar failed at the connection on top of the non-magnetic cross over. The pipe was pulled and numerous fishing attempts were made over the next two days. The fish could not be caught. Because of significant cost over-runs, a decision was made to abandon the well by plugging back inside the casing.

An attempt was made to reinitiate the drilling in the first quarter of 1999. However, we were not able to come up with a successful cost effective strategy to re-drill the hole. Hence, the plan to complete the well was abandoned and the site was restored. It was an unfortunate end to the budget period two considering the fact that a significant effort was vested in developing a detailed reservoir management plan. In addition, with our ability to predict the performance of the reservoir, as evidenced in budget period one, gave us a lot of confidence in proposing a plan for budget

period two. We still believe that, with cost-effective technology to drill a deviated hole, we would be able to recover additional oil from the Glenn Pool field. However, this effort will have to be carried out by private oil companies.

TECHNOLOGY TRANSFER ACTIVITIES

During this project, several technology transfer activities were conducted. These activities can be broadly divided into two three categories – publications and presentations, technology transfer workshops and newsletters. These three activities are discussed below.

Publications and Presentations

Kerr, D.R., Martinez, G., Azof, I. and Kelkar, M.: "Integrated Reservoir Description Using Outcrop Studies: Example from Bartlesville Sandstone Northeast Oklahoma," presented at the Deltaic Reservoirs Workshop, Norman, Oklahoma (March 23-24, 1993).

Liner, C.L. and Lines, L.R.: "Simple Prestack Migration of Crosswell Seismic Data," Expanded Abstract, 63rd Annual International Meeting of the Society of Exploration Geophysicists (1993) pp 308-312.

Ahuja, B.: "Integration of Geological and Petrophysical Information Using Geostatistical Methods – "Self-Unit" Study," Thesis, The University of Tulsa, Tulsa, Oklahoma (1993).

Liner, C.L. *et al.*: "Glenn Pool Project: Initial Tomographic Results," Expanded Abstract, 64th Annual International Meeting of the Society of Exploration Geophysicists (1994) pp 302.

Ahuja, B.K., Bahar, A., Kerr, D.R. and Kelkar, M.: "Integrated Reservoir Description and Flow Performance Evaluation of Self-Unit, Glenn Pool Field," paper SPE 27748, presented at the Improved Oil Recovery Symposium, Tulsa, Oklahoma (April 17-20, 1994).

Kelkar, M.: "Integration of Interdisciplinary Information for Reservoir Characterization," presented at the Symposium on Multidisciplinary Approaches to Reservoir Characterization, The University of Tulsa, Tulsa, Oklahoma (May 9-12, 1994).

Bahar, A.: "Integrated Reservoir Description and Flow Performance Evaluation: Glenn Pool Field – Self-Unit Study," M.S. Thesis, The University of Tulsa, Tulsa, Oklahoma (1994).

Liner, C.L. and Lines, L.R.: "Simple Prestack Migration of Crosswell Seismic Data," Journal of Seismic Exploration, 3, (1994) pp 101-112.

Bozkurt, G. and Liner, C.L.: "Straight Ray Tomography: Synthetic and Real Data Examples," Expanded Abstract, 64th Annual International Meeting of the Society of Exploration Geophysicists (1994) pp 174-177.

Liner, C.L. *et al.*: "Glenn Pool Project: Crosswell Seismic Data Acquisition Overview," Expanded Abstract, 64th Annual International Meeting of the Society of Exploration Geophysicists (1994) 298-302.

Liner, C.L.: "Crosswell Seismic Research at the Glenn Pool Field," presentation to Geophysical Society of Tulsa, Tulsa, Oklahoma (April 1994).

Liner, C.L.: "Crosswell Seismic: Overview and Glenn Pool Project," presentation at the TGS/GST/AAPG/SPWLA Spring Symposium on Multidisciplinary Approaches to Reservoir Characterization, Tulsa, Oklahoma (May 1994).

Bahar, A., Kelkar, M. and Thompson, L.G.: “Integrated Reservoir Description and Flow Performance Evaluation - Glenn Pool Study,” paper SPE 30622, presented at the Annual SPE Meeting, Dallas, Texas (October 22-25, 1995); also presented at the AAPG Mid-Continent Section Meeting, Tulsa, Oklahoma (October 8-10, 1995).

Ye, L. and Kerr, D.R.: "Characterization of Fluvial-Dominated Deltaic Reservoirs in a Mature Oil Field: Glenn Pool Field, Northeastern Oklahoma," Abstract, American Association of Petroleum Geologists Annual Convention, Houston, Texas (1995)

Kelkar, M. and Richmond, D.: “Implementation of Reservoir Management Plan - Self Unit, Glenn Pool Field,” paper SPE 35407 presented at the 1996 SPE/DOE Tenth Symposium on Improved Oil Recovery, Tulsa, Oklahoma (April 21-24, 1996).

Liner, C.L., Bozkurt, G. and Cox, V.D.: "Shooting Direction and Crosswell Seismic Data Acquisition," Geophysics, 61, No. 5 (1996) 1489-1498.

Ye, L. and Kerr, D.R.: "Use of Microresistivity Image Logs in Detailed Reservoir Architecture Reconstruction of Glenn Sandstone, Glenn Pool Field, Northeastern, Oklahoma," Transactions of the 1995 AAPG Mid-Continent Section Meeting, Tulsa, Oklahoma (1996) pp 203-213.

Kelkar, M. and Richmond, D.: "Reservoir Management Plan Implemented in Glenn Pool Field," *Petroleum Engineer International* (July 1996) pp 45.

Kerr, D.R., Ye, L., Kelkar, M. and Bahar, A.: "Reservoir Characterization and Improved Waterflood Performance in Glenn Pool Field: A DOE Class I Project," presented at the American Association of Petroleum Geologists Annual Convention, Dallas, Texas (1997).

Ye, L., Kerr, D.R. and Yang, K.: "Facies Architecture of the Bluejacket Sandstone in the Eufaula Lake Area, Oklahoma: Implications for the Reservoir Characterization of the Bartlesville Sandstone, presented at the Fourth International Reservoir Characterization Technical Conference, Houston, Texas (1997).

Paranji, S.: "Integrated Reservoir Description and Flow Simulation Case Study: Glenn Pool Field," Thesis, The University of Tulsa, Tulsa, Oklahoma (1997).

Bahar, A. and Kelkar, M.: "Integrated Lithofacies and Petrophysical Properties Simulation," paper SPE 38261, presented at the Western Regional Meeting, Long Beach, California (June 25-27, 1997).

Bahar, A. and Kelkar, M.: "Journey from Well Logs/Cores to Integrated Geological and Petrophysical Properties Simulation: A Methodology and Application," paper SPE 39565, presented at the 1998 SPE India Oil and Gas Conference and Exhibition, New Delhi, India (February 10-12, 1998).

Ye, L., Kerr, D. R., and Yang, K.: "Facies Architecture of the Bluejacket Sandstone in the Eufaula Lake Area, Oklahoma: Implications for Reservoir Characterization of the Subsurface Bartlesville Sandstone," in Jordan, J. F. and Schatzinger, R., eds., Recent Advances in Reservoir Characterization (selected contributions from the Fourth

International Reservoir Characterization Conference), American Association of Petroleum Geologists Memoir Series, in press, scheduled for release for Spring, 1999.

Kerr, D. R., Ye, L., Bahar, A. and Kelkar, M.: "Glenn Pool Field, Oklahoma: A Case of Improved Production from a Mature Reservoir," American Association of Petroleum Geologists Bulletin, v. 83 (January 1999) pp 1-18.

Ye, L. and Kerr, D.R.: "Sequence Stratigraphy of the Middle Pennsylvanian Bartlesville Sandstone, Northeastern Oklahoma: A Case of an Underfilled Incised Valley," American Association of Petroleum Geologists Bulletin. Accepted, anticipated publication January, 2000.

Kerr, D.R., Ye, L., Aviantara, A. and Martinez. G.: "Application of Borehole Imaging for Meandering Fluvial Facies Architecture: Examples from the Bartlesville Sandstone, Oklahoma," American Association of Petroleum Geologists Bulletin, in preparation.

Technology Transfer Workshops

As part of the technology transfer program, Mohan Kelkar and Dan Richmond participated in a traveling workshop series organized by BDM-Oklahoma, Inc. The purpose of the workshop series is to make small operators aware of the technologies used in the Class I projects. The workshop included four Class I projects including this project. A total of six workshops were held at the following locations: Bartlesville, Oklahoma; Wichita, Kansas; Denver, Colorado; Billings, Montana; Oklahoma City, Oklahoma; and Grayville, Illinois. The average attendance for these workshops was 30 or more people. The response was extremely favorable and a lot of positive feedback was received from the attendees.

As the most important part of the technology transfer program, one-day-workshops regarding this DOE Glenn Pool project were offered in Tulsa, Denver, and Houston in October 1996. In addition, a workshop was also conducted in April 1997 in Fort Worth, Texas at the invitation of local SPE chapter. Workshop preparation included preparing materials for the workbook, poster exhibit, and slide presentation. This effort resulted in a notebook summary and more than 250 slides and photos for the workshop. Participants were provided with workshop materials and computer software to

generate the reservoir description. The response to the workshop was good. The average attendance to the workshop was 27. The audience represented a wide cross section of small and large operators, service companies and consultants.

Newsletters

As part of the technology transfer activities, two newsletters were prepared and were mailed to approximately 300 operators and independent producers. The newsletters contained progress about the project, and provided operators practical information regarding the implementation of reservoir management plan.

REFERENCES

1. Kuykendall, M. D., and Matson, T. E.: "Glenn Pool Oil Field, Northeast Oklahoma Platform," American Association of Petroleum Geology - Treatise of Petroleum Geology Atlas of Oil and Gas Fields: Stratigraphic Traps III (1992) pp 155-188.

2. Visher, G. S., Saitta, B. S., and Phares, R. S.: "Pennsylvanian Delta Patterns and Petroleum occurrences in Eastern Oklahoma*," American Association of Petroleum Geology Bulletin*, V.55, pp 916-926.

3. Johnson, K.S., Amsden, T.W., Denison, R.E., Dutton, S.P., Goldstein, R.B., Sutherland, P.K., and Thompson, D.M.: "Geology of the Southern Mid-Continent," Oklahoma Geological Survey Special Publication 89-2 (1989) pp 53.

4. Roberts, M.T.: "Geologic Relations along a Regional Cross Section from Spavinaw to Broken Bow, Eastern Oklahoma," (Suneson, N.H., and Hemish, L.A., eds.) Geology and Resources of the Eastern Ouachita Mountains Frontal Belt and Southeastern Arkoma Basin, Oklahoma: Oklahoma Geological Survey Guidebook 29, (1994), pp 137-160.

5. Miser, H.D.: Geologic Map of Oklahoma, 1:500,000: U.S. Geological Survey, (1954).

6. Heath, E. S.: "Evaluation of the William B. Self and T. R. Burrows Leases, Glenn Pool Field," ARCO Reservoir Engineering Report (April 4, 1984).

7. Martinez, G., 1993, *Reservoir Heterogeneity in a Portion of the Bartlesville Sandstone (Desmoinesian), Mayes County Northeastern Oklahoma*, M.S. Thesis, The University of Tulsa, Tulsa, Oklahoma, pp 147.

8. Mishra, J., 1996, *Sequence Stratigraphy of the Bartlesville Sandstone in parts of Okmulgee, Creek, and Okfuskee Counties*, M.S. Thesis, The University of Tulsa, Tulsa, Oklahoma, pp 68.

9. Ye, L., 1997, *Reservoir Characterization and Sequence Stratigraphy of the Pennsylvanian Bartlesville Sandstone, Oklahoma,* Ph.D. Dissertation, The University of Tulsa, Tulsa, Oklahoma, pp 256.

10. Kerr, D. R., Ye, L., Bahar, A., Kelkar, B.M., and Montgomery, S.L.: "Glenn Pool Field, Oklahoma: A Case of Improved Production from a Mature Reservoir," *American Association of Petroleum Geologists Bulletin,* V. 83 (1999) pp 1-18.

11. Allen, J.R.L.: "Studies in Fluviatile Sedimentation: Six Cyclothems from the Lower Old Red Sandstone, Anglo-Welsh Basin," *Sedimentology*, V. 3 (1964) pp 163-198.

12. Miall, A.D.: *The Geology of Fluvial Deposits*, New York, Springer-Verlag (1996) PP582.

13. Thomas, R.G., Smith, D.G., Wood, J.M., Visser, J., Calverley-Tange, E.A., and Koster, E.H.: "Inclined Heterolithic Stratification -- Terminology, Description, Interpretation and Significance," *Sedimentary Geology,* V. 53 (1987) pp 123-179.

14. Grace, M., and Newberry, B.M.: "Geologic Applications of Borehole Electrical Images and Dipmeter," Schlumberger Education Services, Houston, Texas (1990) pp 724.

15. Ye, L., and Kerr, D.: "Use of Microresistivity Image Logs in the Detailed Reservoir Architecture Reconstruction of Glenn Sandstone, Glenn Pool Field, Northeastern Oklahoma," Transactions of the AAPG Mid-Continent Section Meeting (1995) pp 203-213.

16. Hemish, L.A.: "Coal Geology of Rogers County and Western Mayes County, Oklahoma," *Oklahoma Geological Survey Bulletin,* No. 144 (1989) pp 118.

17. Suneson, N.H. and Hemish, L.A., eds.: "Geology and Resources of the Eastern Ouachita Mountains Frontal Belt and Southeastern Arkoma Basin, Oklahoma," Oklahoma Geological Survey Guidebook 29 (1994) pp 294.

18. Kerr, D. R., and Jirik, L. A.: "Fluvial Architecture and Reservoir Compartmentalization of the Oligocene Middle Frio Formation, South Texas," Gulf Coast Association of Geological Societies Transactions, v. 40 (1990) pp 373-380.

19. Van Wagoner, J.C., Mitchum, R.M., Campion, K.M., and Rahmanian, V.D.: "Siliciclastic Sequence Stratigraphy in Well Logs, Cores, and Outcrops," AAPG Methods in Exploration Series No. 7 (1990) pp 55.

20. Van Wagoner, J.C., Posamentier, R.M., Mitchum, Jr., R.M., Vail, P.R., Sarg, J.R., Loutit, T.S., and Hardenbol, J.: "An Overview of the Fundamentals of Sequence Stratigraphy and Key Definitions," in Wilgus, C.K., Hastings. B.S., St. C. Kendall, C.G., Posamentier, H.W., Ross, C.A., and Van Wagoner, J.C., eds., Sea-Level Changes -- An Integrated Approach: SEPM Special Publication No. 42 (1988) pp 39-46.

21. Posamentier, H.W., Jervey, M.T., and Vail, P.R.: "Eustatic Controls on Clastic Deposition I -- Conceptual Framework," in Wilgus, C.K., Hastings. B.S., St. C. Kendall, C.G., Posamentier, H.W., Ross, C.A., and Van Wagoner, J.C., eds., Sea-Level Changes -- An Integrated Approach: SEPM Special Publication No. 42 (1988) pp 109-124.

22. Posamentier, H.W., and Vail, P.R.: "Eustatic Controls on Clastic Deposition II -- Conceptual Framework," in Wilgus, C.K., Hastings. B.S., St. C. Kendall, C.G., Posamentier, H.W., Ross, C.A., and Van Wagoner, J.C., eds., Sea-Level Changes -- An Integrated Approach: SEPM Special Publication No. 42 (1988) pp 110-154.

23. Shanley, K.W., and McCabe, P.J.: "Perspectives on the Sequence Stratigraphy of Continental Strata," *AAPG Bulletin*, V. 78 (1994) pp 544-568.

24. Stork, C. and Clayton, R. W.: "Analysis of Issues in Transmission Tomography using Ray Trace Tomography," 58th Annual International Meeting of Society of Exploration Geophysicists, Expanded Abstracts (1988) pp 1224-1227.

25. Lines, L. R.: "Applications of Tomography to Borehole and Reflection Seismology," *The Leading Edge*, 10, no.7 (1991) pp 11-17.

26. Lines, L. R., Tan, H., and Treitel, S.: "Velocity and Density Imaging Between Boreholes," CSEG Recorder, 16, no.6 (1991) pp 9-14.

27. Lines, L. R., Jackson, R., and Covey, J. D.: "Seismic Velocity Models for Heat Zones in Athabasca Tar Sands," *Geophysics,* 55 (1990) pp 1108-1111.

28. Harris, J. M., Tan, H., Lines, L., Pearson, C., Treitel, S., Mavko, G. Moos, D., and Hoeksma, R. N.: "Cross-Well Tomographic Imaging of Geological Structures in Gulf Coast Sediments," 60th Annual International Meeting of Society of Exploration Geophysicist, Expanded Abstracts (1990) pp 37-40.

29. Lines, L. R., and LeFehr, E. D.: "Tomographic Modeling of a Cross-Borehole Data Set," *Geophysics,* 54 (1989) pp 1249-1247.

30. Lines, L. R., Kelly, K. R., and Queen, J.: "Channel Waves in Cross-Borehole Data," 61st Annual International Meeting of Society of Exploration Geophysicist, Expanded Abstracts (1991) pp 850-854.

31. Lines, L. R., and Tan, H.: "Cross-Borehole Analysis of Velocity and Density," 60th Annual International Meeting of Society of Exploration Geophysicist, Expanded Abstracts (1990) pp 34-36.

32. Owen, T. E., Balogh, W. T., and Peters, W. R.: "Arc Discharge Pulse Source for Borehole Seismic Applications," 58th Annual International Meeting of Society of Exploration Geophysicist, Expanded Abstracts (1988) pp 151-154.

33. Kennedy, W., Wiggins, W., and Aronstam, P.: "Swept-Frequency Borehole source for Inverse VSP and Cross-Borehole Surveying," 58th Annual International Meeting of Society of Exploration Geophysicist, Expanded Abstracts (1988) pp 158-160.

34. Balogh, T. W., Owen, T. E., and Harris J. M.: "New Piezoelectric Transducer for Hole-to-Hole Seismic Applications," 58th Annual International Meeting of Society of Exploration Geophysicist, Expanded Abstracts (1988) pp 155-157.

35. Harris, J. M.: "Cross-Well Seismic Measurements in Sedimentary Rocks," 58th Annual International Meeting of Society of Exploration Geophysicist, Expanded Abstracts, (1988) PP 147-150.

36. Scales, J. A: "Tomographic Inversion via the Conjugate Gradient Method," Geophysics, 52 (1987) pp 179-185.

37. McGaughey, W. J., and Young, R. P.: "Comparison of ART, SIRT, Least-Squares, and SVD Two-Dimensional Tomographic Inversions of Field Data," 60th Annual International Meeting of Society of Exploration Geophysicist, Expanded Abstracts (1990) pp 74-77.

38. Justice, J. H., Vassiliou, A. A., Mathisen, M. E., Bulau, J. R., Singh, S., and Cunningham, P. S.: "Cross-Hole Seismic Tomography-Reservoir Interpretation Case Histories," 60th Annual International Meeting of Society of Exploration Geophysicist, Expanded Abstracts (1990) pp 41-42.

39. Inderwiesen, P. L., and Lo, T.: "Cross-Hole Seismic Tomographic Imaging of Reservoir in Homogeneities in Midway Sunset field, California," 60th Annual International Meeting of Society of Exploration Geophysicist, Expanded Abstracts (1990) pp 22-25.

40. Paulsson, B. N. P., Fairborn, J. W., Cogley, A. L., Howlett, D. L., Melton, D. R., and Livingston, N.: "McKittrick Cross-Well Seismology Project: Part I. Data Acquisition and Tomographic Imaging," 60th Annual International Meeting of Society of Exploration Geophysicist, Expanded Abstracts (1990) pp 26-29.

41. Krohn, C. E.: "Cross-Well Continuity Logging using Seismic Guided Waves," 60th Annual International Meeting of Society of Exploration Geophysicist, Expanded Abstracts (1990) pp 43-46.

42. Lo, T., Inderwiesen, P. L., Howlett, D. L., Melton, D. R., Livingston, N. D., Paulsson, B. N. P., and Fairborn, J. W.: "McKittrick Cross-Well Seismology Project: Part II. Tomographic Processing and Interpretation," 60th Annual International Meeting of Society of Exploration Geophysicist, Expanded Abstracts (1990) pp 158-160.

43. Epili, Duryodhan and McMechan, George A.: "Parallel Implementation of 3-D Prestack Kirchhoff Migration with Application to Field Data," 65th Annual International Meeting of Society of Exploration Geophysicist, Expanded Abstracts (1995) pp 168-171.

44. Bozkurt, G.: *Crosswell Tomography in Anisotropic Media: Glenn Pool Field, Oklahoma,* Ph.D. Dissertation, The University of Tulsa, Tulsa, Oklahoma (1998).

45. Bahar, A.: *Co-Simulation Of Lithofacies And Petrophysical Properties,* Ph.D. Dissertation, The University of Tulsa, Tulsa, Oklahoma (1994).

46. Verly, G.: "Sequential Gaussian Co-Simulation: a Simulation Method Integrating Several Types of Information", Proceedings of 4th International Geostatistical Congress, pp 11.

47. Xu, Wenlong, and Journel A. G.: "GTSIM: Gaussian Truncated Simulations of Lithofacies," Report-6, Stanford Center for Reservoir Forecasting (May 1993).

48. Damsleth, Elvind, et al.: "A Two Stage Stochastic Model Applied to a North Sea Reservoir," paper SPE 20605, presented at the 65th SPE Annual Meeting (1990).

49. Ahuja, B. K.: *Integration of Geological and Petrophysical Information Using Geostatistical Methods – Self-Unit Study,* M.S. Thesis, The University of Tulsa (1993).

50. Welch R.A.: "Berryhill Glenn Sand Unit Reservoir Study," Internal Report of ARCO Oil & Gas Company (1989).

51. Paranji, S.: *Integrated Reservoir Description and Flow Simulation Case Study: Glenn Pool Field*, MS Thesis, The University of Tulsa (1997).

52. Deutsch, C.V and Journel, A.G: *Geostatistical Software and Library and User's Guide*, Oxford University Press (1992).

FOSSIL ENERGY

DOE/BC/14953-26
(OSTI ID: 750285)

INCREASED OIL PRODUCTION AND RESERVES FROM IMPROVED COMPLETION TECHNIQUES IN THE BLUEBELL FIELD, UINTA BASIN, UTAH

Final Report
September 30, 1999

By:
Craig D. Morgan and J. Wallace Gwynn, Ph.D., Utah Geological Survey
Milind D. Deo, Ph.D. and Richard Jarrard, Ph.D., University of Utah
Richard Curtice, Halliburton Energy Services
Thomas H. Morris, Ph.D., Brigham Young University
DeForrest Smouse, Ph.D., Quinex Energy Corporation
Carol N. Tripp, Consulting Geologist

Date Published: January 2000

Work Performed Under Contract No. DE-FC22-92BC14953

Utah Geological Survey
Salt Lake City, Utah

National Energy Technology Laboratory
National Petroleum Technology Office
U.S. DEPARTMENT OF ENERGY
Tulsa, Oklahoma

DISCLAIMER

This report was prepared as an account of work sponsored by an agency of the United States Government. Neither the United States Government nor any agency thereof, nor any of their employees, makes any warranty, expressed or implied, or assumes any legal liability or responsibility for the accuracy, completeness, or usefulness of any information, apparatus, product, or process disclosed, or represents that its use would not infringe privately owned rights. Reference herein to any specific commercial product, process, or service by trade name, trademark, manufacturer, or otherwise does not necessarily constitute or imply its endorsement, recommendation, or favoring by the United States Government or any agency thereof. The views and opinions of authors expressed herein do not necessarily state or reflect those of the United States Government.

This report has been reproduced directly from the best available copy.

DOE/BC/14953-26
Distribution Category UC-122

Increased Oil Production and Reserves from Improved Completion Techniques in the Bluebell Field, Uinta Basin, Utah

By
Craig D. Morgan and J. Wallace Gwynn, Ph.D., Utah Geological Survey
Milind D. Deo, Ph.D. and Richard Jarrard, Ph.D., University of Utah
Richard Curtice, Halliburton Energy Services
Thomas H. Morris, Ph.D., Brigham Young University
DeForrest Smouse, Ph.D., Quinex Energy Corporation
Carol N. Tripp, Consulting Geologist

January 2000

Work Performed Under DE-FC22-92BC14953

Prepared for
U.S. Department of Energy
Assistant Secretary for Fossil Energy

Dan Ferguson, Project Manager
National Petroleum Technology Office
P.O. Box 3628
Tulsa, OK 74101

Prepared by
Utah Geological Survey
Box 146100
Salt Lake City, UT 84114-6100

CONTENTS

ABSTRACT vii

EXECUTIVE SUMMARY ix

INTRODUCTION 1
- Project Status 1
- Geology and Field Background 1

TASK 1: LOG ANALYSIS AND PETROPHYSICAL INVESTIGATIONS 5
- Objectives 5
- Accomplishments 5
- Results 5

TASK 2: OUTCROP STUDIES 7
- Objective 7
- Accomplishments 7
- Results 7

TASK 3: CORE ANALYSIS 9
- Objective 9
- Accomplishments 9
- Results 9

TASK 4: SUBSURFACE MAPPING 11
- Objective 11
- Accomplishments 11
- Results 11

TASK 5: ACQUISITION AND ANALYSES OF NEW LOGS AND CORE 13
- Objective 13
- Accomplishments 13
- Results 13

TASK 6: FRACTURE ANALYSIS 15
- Objective 15
- Accomplishments 15
- Results 15

TASK 7: GEOLOGIC CHARACTERIZATION SYNTHESIS 17
- Objective 17
- Accomplishments 17

Results 17

TASK 8: ANALYSIS OF COMPLETION TECHNIQUES 19
Objectives 19
Accomplishments 19
Results 19

TASK 9: RESERVOIR ANALYSIS 21
Objectives 21
Accomplishments 21
Results 22

TASK 10: BEST COMPLETION TECHNIQUE IDENTIFICATION 25
Objective 25
Accomplishments 25
Results 25

TASK 11: BEST ZONES OR AREAS IDENTIFICATION 27
Objectives 27
Accomplishments 27
Results 27

OIL WELL DEMONSTRATION PROGRAM 29
Recompletion of the Michelle Ute 7-1 Well 29
Objective 29
Accomplishments 30
Results 30
Recompletion of the Malnar Pike 17-1 Well 30
Objectives 30
Accomplishments 31
Results 31
Completion of the Chasel 3-6A2 Well 32
Objectives 32
Accomplishments 32
Results 32
Completion of the Wade Cook Well 33
Objectives 33
Accomplishments 33
Results 33

TASK 12: TECHNOLOGY TRANSFER 35
Objective 35
Accomplishments 35
Results 35

REFERENCES 41

ILLUSTRATIONS

Fig. 1. Index map of the Uinta Basin 3

ABSTRACT

The Bluebell field is productive from the Tertiary lower Green River and Colton (Wasatch) Formations of the Uinta Basin, Utah. The productive interval consists of thousands of feet of interbedded, fractured, clastic and carbonate beds deposited in the ancestral Lake Uinta. Wells in the Bluebell field are typically completed by perforating 40 or more beds over 1000 to 3000 vertical ft (300-900 m), then stimulating the entire interval with hydrochloric acid. This technique is often referred to as the "shotgun" completion technique. Completion techniques used in the Bluebell field were discussed in detail in the Second Annual Report (Curtice, 1996). The shotgun technique is believed to leave many potentially productive beds damaged and/or untreated, while allowing water-bearing and low-pressure (thief) zones to communicate with the wellbore.

A two-year characterization study involved detailed examination of outcrop, core, well logs, surface and subsurface fractures, produced oil-field waters, engineering parameters of the two demonstration wells, and analysis of past completion techniques and effectiveness. The study was intended to improve the geologic characterization of the producing formations and thereby develop completion techniques specific to the producing beds or facies instead of a shotgun approach to stimulating all the beds. The characterization did not identify predictable-facies or predictable-fracture trends within the vertical stratigraphic column as originally hoped. Advanced logging techniques can identify productive beds in individual wells. A field-demonstration program was developed to use advanced, cased-hole logging techniques in two wells and recomplete the wells at two different scales based on the logging. The first well (Michelle Ute) was going to be recompleted at the interval scale using a multiple-stage completion technique (about 500 ft [150 m] per stage). The second well (Malnar Pike) was recompleted at the bed-scale using a bridge plug and packer to isolate four beds for stimulation. The third demonstration involved the logging and completion of a new well (Chasel 3-6A2) using the logs to reduce the number of perforated beds from more than 40 to just 19. The 19 perforated beds were stimulated in two separate treatments, greatly reducing the gross vertical interval and net perforated feet normally treated.

The first demonstration was to be a high-pressure, high-diversion, three-stage acid stimulation. Because of a leak in the tubing the operator could not treat the reservoir at as high a pressure as planned. Also, the treatment was pumped from a single packer location instead of from three intervals as planned. Dipole shear anisotropy and dual burst thermal decay time logs were run before treatment, and an isotope tracer log was run after treatment. These logs were effective tools for identifying fractures and fluid-flow communication within the reservoir. Only the first 500 ft (150 m) of the gross perforated interval received acid, the lower 1000 ft (300 m) remained untreated. The demonstration did show how difficult it is to treat large vertical intervals from a single packer seat. The second demonstration resulted in increased production. This demonstration successfully treated four beds but two were bridged off after limited testing. The operator felt the lower two treated beds might produce water. The increase in production is encouraging considering it is coming from only two beds. Cased-hole logs indicate several beds exist in the well with potential equal to or greater than the beds that were treated. During the third demonstration, completion testing of the Chasel 3-6A2 well appeared very promising. The well began flowing oil with no water but the casing collapsed. Because of the collapsed casing the well will probably not produce anywhere near its potential.

EXECUTIVE SUMMARY

The objective of the project was to increase oil production and reserves by the use of improved reservoir characterization and completion techniques in the Uinta Basin, Utah. To accomplish this objective, a two-year geologic and engineering characterization of the Bluebell field was conducted. The study evaluated surface and subsurface data, currently used completion techniques, and common production problems. It was determined that advanced cased- and open-hole logs could be effective in determining productive beds and that staged-interval (about 500 ft [150 m] per stage) and bed-scale isolation completion techniques could result in improved well performance. In the first demonstration well (Michelle Ute), dipole shear anisotropy (anisotropy) and dual-burst, thermal decay time (TDT) logs were run before treatment, and an isotope tracer log was run after treatment. The logs were very helpful in characterizing the remaining hydrocarbon potential in the well. Significant improvement in the oil production from the well was not obtained due to mechanical problems during the recompletion.

The second demonstration well (Malnar Pike) was a recompletion of four separate beds which resulted in increased hydrocarbon production. Anisotropy, TDT, and isotope tracer logs were used to identify beds for recompletion and to evaluate the effectiveness of each treatment. The third demonstration (Chasel 3-6A2) was a newly drilled well which was logged with anisotropy, TDT and isotope tracer logs. The logs were used to select 19 beds for perforating and acidizing, compared to more than 40 beds that are typically perforated in a new well. It was expected that fewer perforated beds would result in lower treatment costs, more effective treatment of each of the selected beds, and more oil production with less production of associated formation water. Initial testing was encouraging but the casing collapsed and the operator was unable to complete the well.

A portable, parallel, fractured-reservoir simulator was developed to carry out reservoir analysis of the Bluebell field. The development and performance of the simulator on a shared-memory machine (Silicon Graphics Power Challenge) was reported in earlier quarterly and annual reports. The performance of the parallel program was also studied on a distributed memory machine. The results of parallel computing on the distributed memory machine were rather disappointing. If the code was ported to a cluster of workstations, the cluster would be expected to perform as a distributed memory virtual machine. The way in which the equations are solved and the communication protocol will have to be optimized to improve the performance of the code on distributed memory platforms.

Technology transfer activities for the final year of the project included one paper in the American Association of Petroleum Geologists (AAPG) Bulletin, a poster presentation at the National AAPG meeting in Salt Lake City, and an oral presentation at the Department of Energy/ Petroleum Technology Transfer Council Symposium in Denver. Information exhibits were displayed at the Utah Geological Survey (UGS) booth during the National AAPG meeting and Vernal Petroleum Days exhibition in Vernal, Utah. Inquiries and general discussion at the poster session and exhibitor booth indicate a strong interest by oil industry personnel. Daily activity reports for the second and third demonstration were posted on the Bluebell project Internet home page. Previous technology transfer activities have been reported in earlier annual technical reports.

INTRODUCTION

Project Status

The contract with the U.S. Department of Energy ended September 30, 1999. The two-year characterization study of the Bluebell field, Duchesne and Uintah Counties, Utah, consisted of separate, yet related tasks. The characterization tasks were: (1) log analysis and petrophysical investigations, (2) outcrop studies, (3) cuttings and core analysis, (4) subsurface mapping, (5) acquisition and analyses of new logs and cores, (6) fracture analysis, (7) geologic characterization synthesis, (8) analysis of completion techniques, (9) reservoir analysis, (10) best completion technique identification, (11) best zones or areas identification, and (12) technology transfer. The study helped identify advanced logging techniques that can be effective in selecting beds for stimulation in old and new wells. A three-part field demonstration was developed using advanced logging techniques to selectively identify productive beds and test the effectiveness of treating at different scales (interval about 500 ft [150 m] and bed scale).

The first demonstration was a recompletion at the interval scale and was discussed in the previous technical report. The second demonstration was a recompletion of the Malnar Pike well at the bed scale. The recompletion resulted in an increase in the daily oil production from the well. The production is still being monitored and the long-term production increase is being evaluated. The third demonstration was the logging and completion of the Chasel 3-6A2, a newly drilled well. Reservoir characterization using the anisotropy and TDT logs resulted in perforating and acidizing of 19 beds in the new well, far fewer than the more than 40 beds that are typically perforated in new wells. Fewer perforated beds should result in lower completion cost, improved oil production, and less production of formation water. Preliminary test results were encouraging until the casing collapsed in the well. As a result, the operator was unable to complete the well as an oil producer.

Geology and Field Background

The Uinta Basin is a topographic and structural basin encompassing an area of more than 9300 square miles (24,000 km^2) (Osmond, 1964). The basin is sharply asymmetrical, with a steep north flank bounded by the east-west-trending Uinta Mountains, and a gently dipping south flank bounded by the northwest-plunging Uncompahgre and north-plunging San Rafael uplifts. In Paleocene to Eocene time, the Uinta Basin had internal drainage forming ancestral Lake Uinta. Deposition in and around Lake Uinta consisted of open- to marginal-lacustrine facies that make up the Green River Formation. Alluvial, red-bed deposits that are laterally equivalent and intertongue with the Green River lacustrine deposits make up the Colton (Wasatch) Formation. The depositional environments are described in detail by Fouch (1975, 1976, 1981), Ryder and others (1976), Pitman and others (1982), Stokes (1986), Castle (1991), Fouch and others (1990), Fouch and Pitman (1991, 1992), and Franczyk and others (1992).

The Bluebell field is the largest oil producing field in the Uinta Basin. Bluebell is one of three contiguous oil fields: Bluebell, Altamont, and Cedar Rim (Fig. 1). The Bluebell field is 251 square miles (650 km^2) in area and covers all or parts of Townships 1 North, 1 and 2 South and Ranges 1 and 2 East and 1 through 3 West, Uinta Base Line and Meridian (Fig. 1). More than 139 million barrels of oil (MMBO [19.5 million MT]) and nearly 182 billion cubic feet (BCF [5.2 billion m^3]) of associated gas have been produced as of September 30, 1997 (Utah Division of Oil, Gas and Mining records). The spacing is two wells per section except within the Roosevelt unit, but much of the field is still produced at one well per section. Although some wells have produced over 3.0 MMBO (420,000 MT), most produce less than 0.5 MMBO (70,000 MT).

The majority of the production and the focus of the demonstration is the Flagstaff Member of the Green River Formation reservoir (lower Wasatch transition in operator terminology). The Flagstaff reservoir consists dominantly of carbonate and sandstone beds that were deposited in marginal- to open-lacustrine environments and is productive throughout most of the field. The Flagstaff is overlain by the alluvial sandstone, siltstone, and shale (red beds) deposits of the Colton Formation. The Colton is overlain by the lower Green River lacustrine facies.

The complex, heterogeneous lithology of the Colton and Green River Formations makes it very difficult to identify which beds are potential oil producers. As a result, the operators have taken a shotgun approach to completing and recompleting the wells; they typically perforate 40 to 60 beds over a vertical interval of 1500 ft (460 m) or more, and acidize the entire interval. Operators believe this completion technique may leave many potentially productive beds damaged and/or untreated, while allowing water-bearing and low-pressure (thief) zones to communicate with the wellbore (Allison, 1995). Our study found that oil productive beds can be identified using advanced open- and cased-hole logs, which would allow operators to perforate and treat smaller intervals and result in more effective completions. The demonstrations were designed to show the effectiveness of treating more selective beds at different scales.

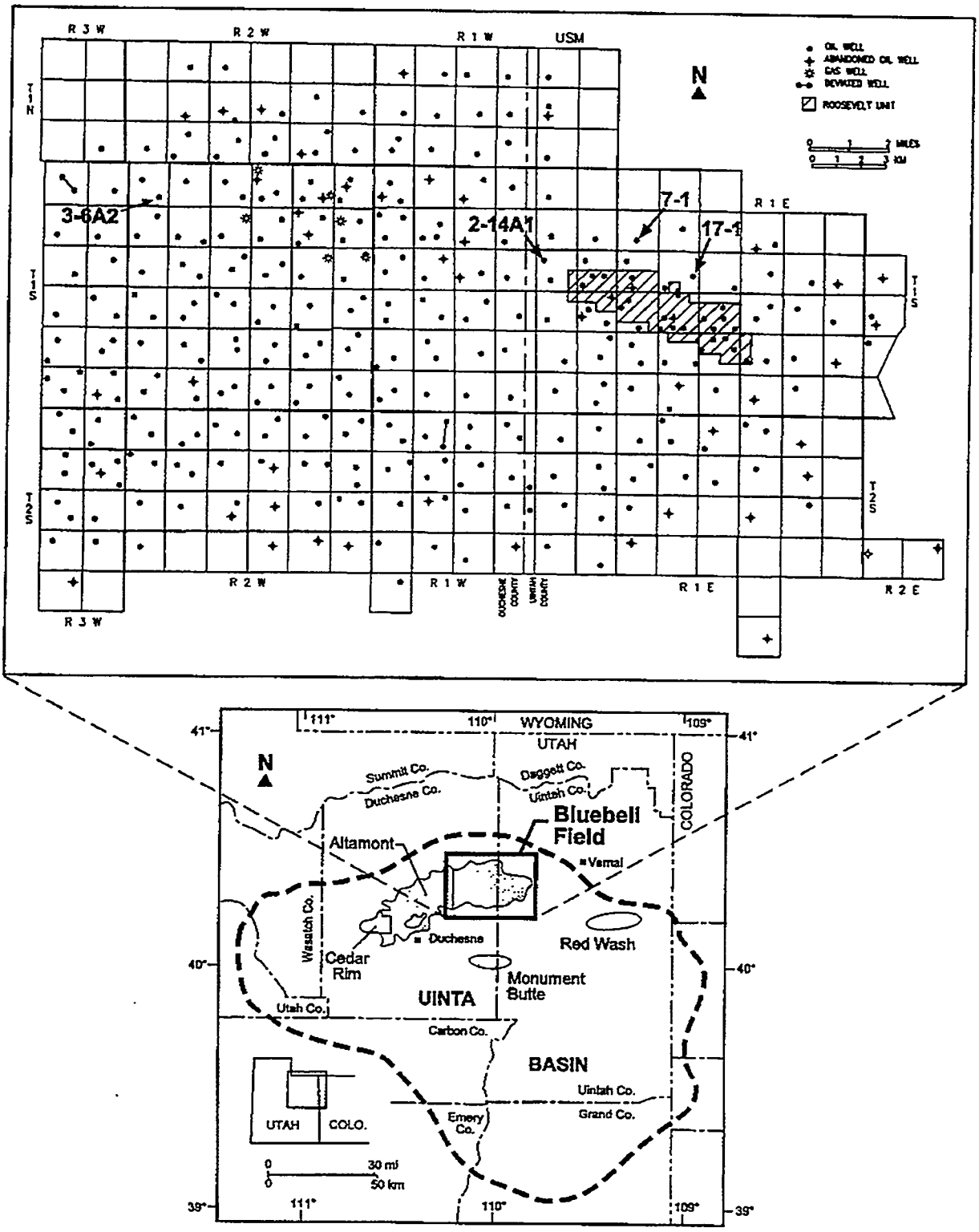

Fig. 1. Index map of the Uinta Basin showing major oil fields producing from Tertiary-aged reservoirs. Dashed line approximating the basin extent is the base of the Tertiary-aged rocks. Enlarged map is the Bluebell field with the location of the demonstration wells labeled, 7-1, 17-1, 3-6A2, and 2-14A1.

TASK 1: LOG ANALYSIS AND PETROPHYSICAL INVESTIGATIONS

Objectives

The objectives of task 1 were to: (1) develop a digital well-log database useful for correlating horizons between wells and drawing field-wide, structure maps and cross sections; (2) calculate lithology, porosity, and pore fluids from those wells with a full suite of digitized logs; and (3) evaluate the reliability of log-based estimation of these parameters.

Accomplishments

Geophysical well logs from 80 wells distributed across the Bluebell field were digitized. Logs were quality checked and only the better quality logs were digitized. Poor log quality often resulted from irregular borehole diameter. Correlation was done primarily by using the gamma-ray curve. A wide suite of logs (gamma-ray, sonic, neutron, density, resistivity, and sprectral gamma ray) was digitized and analyzed from a subset of wells. Lithology and porosity derived from core plugs and cuttings were used to calibrate the geophysical well log calculations.

Formation-water resistivities were difficult to determine. As a result, calculated water saturations were unreliable. We originally planned to calculate lithology and porosity by inversion, then do a shaley-sand hydrocarbon analysis. However, the relative proportions of quartz, dolomite, and limestone were poorly resolved, causing the inversion to give unreliable porosity values. Core-plug measurements showed that the relative proportions of quartz, dolomite, and limestone are of minor importance to calculating porosity from well logs. The best method for calculating porosity from logs was determined to be neutron-density averaging.

Results

The results of this task are discussed in detail by Jarrard (1996). Geophysical log analyses and petrophysics were used to better evaluate potentially productive beds. Natural fracture permeability is believed to play an important role in hydrocarbon production, but for long-term production, intergranular permeability (>0.1 milliDarcy [mD]) and intergranular porosity are also important. Core studies determined that fractures exist in carbonate and sandstone, but are rare in shale. Based on core-plug analyses, intergranular permeability of >0.1 mD exists only when clay content is 4% or less and intergranular porosity is >4%.

Log analysis of wells in the Bluebell field has shown that clay content can be accurately estimated from a computed gamma-ray (CGR) log using the potassium (K) and thorium (Th) contributions to total gamma radiation. Uranium is not present uniformly in the clays and is therefore

not correlated with K or Th. As a result, total gamma ray is a less reliable indicator of clay content than is CGR from spectral gamma-ray logs.

Analyses of core plugs shows that grain densities are generally lower than had been expected, averaging 2.66 g/cc, in contrast to the normally-assumed matrix value of 2.68 g/cc in the eastern part of the field and 2.71 g/cc in the western part of the field. As a result, the density porosity is often overestimated. The presence of feldspar may account for the lower than expected grain density.

The biases found in both the neutron-porosity and density-porosity measurements are opposite in sign and roughly the same magnitude (within about one porosity unit). Therefore, the best log-based estimate of porosity for shale-free rocks is the average of density-porosity and neutron-porosity, both calculated using a limestone matrix. Wash out zones in well logs must be avoided because they give unreliably high porosity readings, but fortunately washouts are less common in shale-free rocks than in shaley rocks. For wells in which a sonic log was run without a density/neutron log, porosity cannot be accurately determined even when the analysis is confined to shale-free rocks, because of lithology-dependent variations in matrix travel-time.

Without quantifying the role of fractures, the best reservoirs were predicted to be beds with, CGR of < 20 API units (or less reliably GR < 45 API units), neutron/density porosities of >6% (4% intergranular plus 2% fracture), and high resistivities. This was based on the assumption that fractures are important in the permeability of the rock but that intergranular porosity is necessary for sufficient storage capacity. Detailed mapping of beds that meet the above criteria (Morgan, 1997) failed to established a correlation between net reservoir thickness and cumulative production. Also, wells in which a fluid entry log was run showed that the majority of the production was often coming from beds that did not meet the minimum criteria. There are several reasons why the predictive criteria failed: (1) the storage capacity of the fracture network is much larger than expected, (2) the storage capacity of some beds with high GR values is much larger than expected, and (3) ineffective completion techniques has resulted in poor reservoir rocks producing and the better quality reservoir rocks being damaged or untreated and not contributing to the production. The third possibly is considered the least likely since some of the wells where fluid entry logs show the production coming from very poor quality beds are high-volume producers. If the reservoir beds were as poor as the geophysical well logs indicate, then the well should have been a very poor producer. The most likely explanation of the well's performance is that fractures play a much larger role in both permeability and storage capacity than originally anticipated.

TASK 2: OUTCROP STUDIES

Objective

The objective of task 2 was to delineate the general stratigraphic framework and broad facies of the Green River and Colton (Wasatch) Formations in order to understand facies heterogeneity and reservoir capacity within each facies.

Accomplishments

About 2790 ft (850 m) of vertical section in the lower Green River Formation was measured and described from outcrop in Willow Creek Canyon. Samples representing the volumetric majority of rock types present in the outcrop were petrographically analyzed. Core plugs from the lithologic samples were analyzed for porosity, vertical and horizontal permeability, and grain density. Thin sections were made from 33 of these samples, and each thin section was petrographically classified. The sand-dominated clastic rocks (16 in all) were each subjected to a 300-grain point-count. All samples were analyzed for clay type by x-ray diffraction (XRD).

Lithologic units in the outcrop were so discontinuous and varied that we were unable to draw distinct boundaries that delineate the open lacustrine facies from the marginal lacustrine facies, or from the lower delta plain or fluvial facies. Throughout most of the stratigraphic section, the facies commonly intertongue with each other within a few feet, both vertically and laterally.

Results

The results of this task are discussed in detail in Garner (1996), and Garner and Morris (1996a and 1996b). The upper 600 ft (183 m) of the Willow Creek Canyon outcrop is mostly marginal to open lacustrine facies with abundant silty limy mudstone and crystalline limestone. The lower portion of the outcrop is a mix of marginal and open lacustrine as well as fluvial facies. There are abundant channel and overbank sandstone deposits intermixed with red to green siltstone and silty limy mudstone. About 360 ft (110 m) above the base of the measured section is an 82-ft (25-m) thick unit of limestone/dolomite which clearly represents an open lacustrine environment.

The Flagstaff Member of the Green River Formation, which underlies the Colton Formation, was also measured and described. The predominant rock types were shale/mudstone, limy mudstone, and limestone which represents a marginal to open lacustrine environment.

The arenites in the Green River Formation outcrop tend to have the best porosity and permeability and therefore the best storage capacity. The most porous arenites were found in the bottom half of the section just above the Colton Formation. These arenites are extensively interbedded with shale and mudstone which are potential source rocks. There are clays and relatively abundant

swelling mixed-layer clays present in the outcrop. The amount of swelling clays decreases towards the base of the section.

Comparison of the outcrop study with the limited data from subsurface core analyses of the Green River Formation shows that there is more smectite present in the outcrop than in core and that the arenites at the outcrop contain more feldspars and lithics than those in the core. This may be due to different provenances and transportation distances. The outcrop represents the south shore of Lake Uinta with streams transporting sediment hundreds of miles from the south. The core samples from Bluebell field represent the north shore of Lake Uinta with sediment transported miles to a few tens of miles from the Uinta Mountains to the north.

The arenites have the best reservoir characteristics of the rocks studied in outcrop. The majority of the oil production at Bluebell field is from the Flagstaff Member of the Green River Formation. Where the Flagstaff outcrops it is relatively thin and consists mostly of marginal lacustrine carbonates. In the subsurface at Bluebell the Flagstaff is much thicker and much more varied in lithology and environment of deposition. Therefore, the lower Green River strata in Willow Creek may be more representative of the types of facies found in the subsurface at Bluebell, even though they come from a different part of the stratigraphic section and had a different source. There are no truly representative outcrops for the Flagstaff Member as found in the deep Bluebell area.

Studies of the reservoir at Bluebell field failed to correlate oil production to specific facies or lithology. Therefore, understanding the facies relationships and distributions of the Green River Formation on outcrop did not directly improve our understanding of the reservoir in the Bluebell field.

TASK 3: CORE ANALYSIS

Objective

The objective of task 3 was to identify the facies and rock types in the subsurface with the best potential for oil production in the Bluebell field. If specific facies could be identified as the primary pay in the Bluebell field then identification and mapping of those facies could result in better selection of well sites and improved completion techniques by limiting the number of beds being perforated and treated.

Accomplishments

A total of 1613 ft (492 m) of core from the Bluebell field was described. The cores are from the lower Green River and Colton Formations, and Flagstaff Member of the Green River Formation. Seventy-two thin sections were made from a broad sampling of rock types throughout the cores and were petrographically examined. The sandstone samples were subjected to a 300-grain point-count. Thirty-five samples were analyzed for clay type using XRD. Fracture data were analyzed to determine how lithology, bed thickness, and/or depth control fracture density. Porosity and permeability data were determined from plug analysis.

Results

The results of this task are discussed in detail in Wegner (1996) and Wegner and Morris (1996). Natural fractures identified in the core were carefully described because of the importance of fractures in the reservoir quality. Fractures in sandstone beds are commonly perpendicular, to near-perpendicular, to bedding, with a measured length greater than 3.3 ft (1 m) (many fractures extend out of the sample). The width of the fractures ranges from 0.03 to 0.13 inches (0.5-3.0 mm) wide, and the fractures are only partially calcite-filled. Fractures in mudstone beds have multiple orientations and have a higher fracture density than is found in the sandstone beds. However, fractures in mudstone beds are very short (commonly less than 4 inches [10.2 cm]), generally less than 0.03 inches (0.5 mm) wide, and almost completely calcite-filled.

Dominant rock types in the core are sandstone of varying composition (39 %), and limy mudstone (15 %). In general, feldspar and lithic fragments seem to be present in nearly equal amounts in most thin sections counted.

Of the total core described, 78 % was siliciclastic, while only 22 % was carbonate. This is probably not an accurate reflection of the true ratio of siliciclastic to carbonate rocks in the subsurface, because it probably reflects operator bias to core siliciclastic intervals since sandstone beds are considered the best reservoirs in the Bluebell field.

Based on the semi-quantitative analyses, core samples show very low concentrations of smectitic mixed-layer clays throughout. Where they do exist, they are primarily illite-smectite or chlorite-smectite mixed layers, with only minor kaolinite-smectite mixed layers present. Nearly pure illite dominates the core samples, but chlorite is also found, in smaller amounts, in many of the samples. Kaolinite is less prevalent.

Of the 219 samples tested, 85 % have less than 4 % porosity and less than 0.05 mD permeability. In general, porosity and permeability tend to be slightly higher in the arenite beds that contain significantly more quartz than lithic fragments and feldspar. Overall, most rock types sampled have very low intergranular porosity and permeability

Limited core studies, such as this, do not result in a very large database, and therefore, the results may be biased. The study may also be biased because companies typically target the clastic beds for coring. These facts must be kept in mind when interpreting the core results and making recommendations.

Analyses of core from the Bluebell field indicate that the most promising hydrocarbon reservoirs are arenitic with high quartz content, low concentrations of swelling clays, relatively high porosity and permeability, large, open fractures, and that overlie fractured mudstone.

Limited core data makes an accurate description of the depositional processes in the Green River Formation in the Bluebell field inconclusive. The fluvial-dominated deltaic depositional environment often applied to the Green River Formation cannot be proven or disproven from the few available cores. Another possible interpretation is deposition of sand by wave-dominated transport derived from fan deltas developed along the slopes of the ancestral Uinta Mountains.

TASK 4: SUBSURFACE MAPPING

Objective

The objective of task 4 was to use geophysical well logs to correlate and map important oil producing beds or facies from well to well. Thickness mapping of individual units helps establish reservoir distribution and depositional patterns. Thickness mapping of thicker intervals helps to delineate depositional trends and regional thinning. Contour mapping shows the structural setting and potential migration direction of hydrocarbons and, in combination with thickness mapping, can show stratigraphic traps and identify potentially productive beds in old wells and new well locations.

Accomplishments

Field-wide structure contour, production, and gas-to-oil ratio maps were published (Morgan, 1994). Fourthy-nine sandstone isochore maps covering a 20-square-mile (51.8 km^2) area in the eastern portion of the Bluebell field were published by Morgan (1997). Isochore mapping of large stratigraphic intervals within the lower Green River and Colton Formations showed a general east-west strike with north to south thinning (Morgan and Tripp, 1996). The sandstone beds selected for mapping were based on critical parameters determined by the characterization study. The minimum standard in selecting a sandstone unit was that the bed must have a gamma-ray count of 60 API units or less, be at least 6 ft (1.8 m) thick, and have 6 percent or more porosity (density/neutron averaging) in at least one well. Average porosity and water saturation were determined for every sandstone bed in every well that was mapped.

Results

The thickness, porosity, and water saturation data were used to develop a reservoir simulation model. The sandstone isochore maps were compared to cumulative oil production from each of the wells. Neither the thickness, porosity development of individual beds nor the summation of beds could be correlated with well productivity. In wells where fluid-entry log data were available there was very little correlation between actual versus predicted production. Many of the producing beds did not meet the minimum criteria while many of the beds with the best parameters did not produce at all. The role of natural fractures, which we were unable to quantify due to a lack of core and bore-hole imaging, appears to have a dominant effect on the reservoir productivity.

Correlation of many of the beds and depositional cycles defined by log character, showed good lateral continuity with generally minor thickness variations over several miles. Fining-upward log character, typical of fluvial channels, and anomalous thick sandstone buildups, typical of distributary mouth bars, were not found. The Flagstaff Member and lower Green River Formation may best be

described as wave-dominated shoreface deposits, not fluvial-dominated deltaic deposits. The dominant factor controlling hydrocarbon entrapment is fracturing, not stratigraphy or structure. The hydrocarbons in the Flagstaff reservoir are believed to have been generated in-situ. The expansion caused by the conversion of kerogen to hydrocarbon is responsible for most of the fracturing in the reservoir. The greatest volume of hydrocarbons is found where the largest volume of source rocks in the Flagstaff has reached maturity, generally at the greatest depth. Near the northern limits of the field the Flagstaff thins. As a result, that area is thermally mature, but has less source rock to generate hydrocarbons. Near the southern limits of the field the Flagstaff has abundant source rock, but was not buried as deep. As a result, in the southern part of the field there is an abundance of source rock, but it is less thermally mature.

TASK 5: ACQUISITION AND ANALYSES OF NEW LOGS AND CORE

Objective

The objective of task 5 was to gather borehole imaging logs and cores from new wells drilled in the Bluebell field. There was no core taken during the project period. The new logs were used to better understand the sedimentary structure, bedding, and natural fractures. At the beginning of budget period two, the definition of new logs was expanded to included cased hole logs that can determine fracturing and oil saturation.

Accomplishments

The level of drilling activity in the Bluebell field dropped dramatically from the time the proposal was written till the project began. It was initially estimated that we would gather borehole imaging logs and core from at least five wells per year. However, during budget period one only three wells were drilled. All three wells were logged with borehole imaging tools, but none were cored. The fracture analysis of these logs, and a very limited number of older directional cores, is discussed by Allison and Morgan (1996). New cased hole logs were run in each of the demonstration wells, but other operators did not take advantage of the funding for logging before recompleting any of their wells.

Results

Borehole imaging logs are an effective tool to identify fractures in the well even though rugose hole conditions resulted in portions of the section without data. Unfortunately, the operators ran the logs but didn't use them. The wells were completed in the usual fashion of perforating every bed that had a drilling show. If fracturing is the most important reservoir property it would have been logical to perforate only the beds that have fractures. If the well was drilled in a partially drained portion of the field, then an operator should perforate and acid-stimulate the beds with shows but no fractures, and then perforate the fractured beds, thus avoiding sending all the acid down a few drained fractured beds.

Dipole shear anisotropy (anisotropy) logs for fracture data, and thermal decay neutron (TDT) logs for oil saturation, were run in the three demonstration wells. Both logs can be run in a cased hole or open hole environment. The logs were used selectively by the operator. Fracturing identified on the anisotropy log was considered when selecting beds to be perforated and acid stimulated, but it was never a deciding criterion: both fractured and nonfractured beds were selected. Good oil saturation indicated on the TDT log was used as a criterion for selecting beds for perforating and acid-stimulating, but low oil saturation indicated on the TDT log was not used as a criterion to eliminate a bed from consideration. The role of fracturing cannot be quantified in the demonstration wells because both fractured and nonfractured beds were perforated and fluid entry logs were not run after the stimulations.

The TDT log was the primary tool used to select beds to be perforated in the third demonstration which was a new well. Only 19 beds were selected, far fewer than the 40 or more that are normally perforated in Bluebell wells. During swab testing the casing collapsed and the lower portion of the hole (covering all 19 perforated beds) had to be abandoned before the effectiveness of the selection could be evaluated.

TASK 6: FRACTURE ANALYSIS

Objective

The objective of task 6 was to determine the nature and characteristics of fracturing in the Bluebell reservoir. It was intended to use the fracture information to determine if there is a preferred orientation of productive fractures, what fracture characteristics affect production, and recognize stratigraphic intervals and areas or conditions where an operator might take advantage of natural fractures. New fracture data were gathered from both the surface and subsurface.

Accomplishments

Surface fracture data were gathered and analyzed by B.J. Kowallis and are discussed in Allison (1995). Analysis of the subsurface fracture data is discussed in Allison and Morgan (1996). Fewer imaging logs were obtained from the Bluebell field during the new logs task than anticipated due to a sharp decrease in the number of wells drilled during the project. As a result, we were only able to collect five sets of subsurface data during the characterization phase: three modern imaging logs and two oriented cores.

Results

Variations in the fracture orientation were determined from the limited data set both areally across the field, and vertically through the stratigraphic section. The data set was spread out over several tens of miles so continuity of fracturing between wells could not be determined. Fracture data gathered in cased holes using dipole shear anisotropy logs were used to determine statistical fracture information used in the reservoir simulation model. Cased hole anisotropy logs can detect fractures but cannot determine an orientation. Since the operators did not limit the perforations to fractured beds, and fluid entry logs were not run after perforating and acid stimulation, the importance of naturally occurring fractures in the reservoir performance cannot be quantified.

TASK 7: GEOLOGIC CHARACTERIZATION SYNTHESIS

Objective

The objective of task 7 was to coordinate and compile the other characterization tasks (1 through 5) into a single geologic evaluation.

Accomplishments

Regularly scheduled meetings resulted in good communication and cooperation among all of the task leaders of the project.

Results

The primary result was the production and submission of the Project Evaluation Report (unpublished report), and the recommended field demonstrations. The final product will be two reports, currently in review, that will hopefully be published by the UGS. The first report is the geological characterization of the Bluebell field, and the second report contains the details and evaluation of the field demonstration program.

TASK 8: ANALYSIS OF COMPLETION TECHNIQUES

Objectives

The objectives of task 8 were to compile and analyze existing completion data from wells which had been previously treated, and determine what specific type of previous treatment was the most effective. Based on past successes and failures, recommendations were whether to change the current completion technique or to develop an entirely new technique.

Accomplishments

Completion data were gathered from the Utah Division of Oil, Gas and Mining, and from companies currently operating wells in the Bluebell field. Treatment data were compiled on a spreadsheet containing 108 different categories, on 67 wells with a total of 246 stimulation treatments (original and recompletions). The database was sent to Halliburton Energy Services Tech Team in Denver, Colorado, and Reservoir Department in Houston, Texas, for analyses.

Results

The results of the analyses of completion techniques are reported by Curtice (1996). The treatment methods used by operators in the Bluebell field have not changed significantly over the years except for treating larger intervals and more perforations. As a result, no treatment method appears better than another because there is such little difference between them. As treatment intervals get larger, it is apparent that many of the beds are not getting treated because of the difficulty of diverting the acid into so many different beds. Some operators have begun staging the acid treatments and greatly increasing the amount of diversion material used. Typically, an operator treating a 1500-ft (457-m) interval will treat the lower 500 ft (152 m), move the packer up and treat the middle 500 ft (152 m), and then do the upper 500-ft (152-m) interval. Ideally, the diversion material plugs the perforations of a stage before moving uphole so only 500-ft (152-m) sections are being treated at a time.

Older wells that have been recompleted many times eventually become uneconomical to retreat. In the older wells only a minor incremental increase in the oil production rate occurs after treatment because so much of the acid is going into beds that are depleted of oil. In these older wells it is recommended that treatment of a few individual beds be attempted using a dual packer tool. This way, only the few beds with remaining oil potential are acidized, reducing the size of the treatment needed, and providing more effective stimulation of the beds with remaining potential.

TASK 9: RESERVOIR ANALYSIS

Objectives

The objectives of task 9 were to develop a reservoir model, and use that model to understand the performance of the reservoir based on model properties. If reservoir production history could be matched, based on a predefined reservoir description, then ultimate oil-producing potential could be projected with some level of confidence. Both reservoir characterization and simulation were studied. The objectives of reservoir characterization were to generate accurate petrophysical models of various portions of the reservoir using the available data, and to evaluate the possibility of projecting available fracture information field wide. The goals of reservoir simulation were to model the reservoir at various scales to see if reservoir simulation could be used as a production history matching tool and ultimately as a planning and forecasting tool. Since one of the objectives was to develop a detailed reservoir model which consists of hundreds of thousands of grid cells, it was necessary to create a computational infrastructure to accommodate such a model. Hence, a parallel, (multiprocessor) fractured reservoir simulator was developed.

Accomplishments

Reservoir data such as fluid property, production, fracture data, log-derived pay-zone thicknesses, porosities, water saturations, as well as core-derived permeabilities and porosities were compiled for the modeling effort. Single-well homogeneous and dual-porosity, dual-permeability, fractured-reservoir simulation models were constructed for the Michelle Ute and Malnar Pike demonstration wells. Homogeneous and fractured simulation models were constructed covering a 4-square-mile (10.4 km^2) area encompassing two of the demonstration wells in the eastern portion of the Bluebell field, and a 4-square-mile (10.4 km^2) area in the western portion of the field. Each of the reservoir simulation models were subjected to internal analysis and the following reservoir properties were examined: (1) original-oil-in-place in each of the perforated zones, (2) original reservoir pressure, (3) oil produced and oil remaining in each of the modeled layers, and (4) current reservoir pressure.

A significant problem in this task was the uncertainty in the reservoir data. Data at well locations, such as porosities, thicknesses, fracture permeability, and other reservoir parameters had to be interpolated between well locations. Since oil originates from tens of producing layers, establishing realistic correlations of these layers between wells is difficult. Fracture information is also limited; it was derived from a few cores and a few imaging logs. To extrapolate a fracture pattern for the field from this limited data set is problematic. The confidence level for the reservoir fluid and rock properties data is higher than the confidence level in the fracture data since the rock and fluid properties data were defined in laboratories.

Reservoir models were constructed for: (1) the Michelle Ute and Malnar Pike wells representing all of the perforated beds, (2) a 4-square-mile area in the eastern portion of the field area

consisting of five correlated beds, and (3) a 4-square-mile area in the western portion of the field. Internal analyses of the reservoir models were performed and beds with the most potential for additional oil production were identified.

Various methods used for generation of fracture networks and fracture property distributions have had limited success in past petroleum reservoir characterization efforts. Most of the methods generate fracture property distributions that are not suitable for conventional methods of reservoir model development and flow simulations, like the dual-porosity, dual-permeability approach. A new method for fracture property distribution is suggested in this study. This new method uses principles of stochastic simulations. Analysis of sample data from Bluebell field shows that the fracture frequency distributions are functions of rock types. This information was used as an additional constraint while generating fracture frequency distributions, using Markov-Bayes principles. Two types of conditioning were used during the stochastic simulation procedure. The observed values of fracture frequency were fully honored (hard conditioning), while the rock type information was used for soft conditioning. The fracture frequency distributions generated through this approach were compared with the distributions generated using principles of sequential Gaussian simulations and sequential indicator simulations.

A parallel (multiprocessor) fractured reservoir program, based on the dual-porosity principles, was developed using a portable parallel library (Message Passing Interface). The parallel program was compiled and run on two types of parallel environments: shared memory, and distributed memory. In each case, the performance of the parallel program was compared against the serial version of the program. The comparison was made in terms of the time required to perform different computations in the program. These computations included calculation of coefficients and formulation of coefficient matrices, solution of fracture flow equations, solution of matrix flow equations, and all the calculations involved in an entire time step.

Results

The results of the reservoir analyses are reported in Allison (1995), Deo and Pawar (1996, 1997a, 1997b), Deo and Morgan (1998), Morgan and Deo (1998), and Pawar (1998). The modeling indicates that there is a great deal of oil remaining to be recovered from the Bluebell field and that some form of stimulation is necessary in order to recover this oil. In some wells, certain thick beds contain significant quantities of oil that might be possible to target for individual bed treatment.

Incorporating water saturations calculated from geophysical well logs into the reservoir simulators results in much larger volumes of water in the model than is actually produced from the wells. This problem could be caused by: (1) calculating water saturations lower than actually exist in the reservoir, (2) water saturations averaged over the entire bed while only a small portion actually produces, (3) the percentage of bound water is much higher than anticipated, or (4) many of the beds perforated have high water saturations but don't actually produce.

The production performance of parts of the naturally fractured reservoirs in the Bluebell field was studied through flow simulations performed on numerical models. Models were developed for two four-section areas on the east and the west portions of the field. The east-side model was a preliminary

model that only took into account some of the beds responsible for the oil production. The west-side model incorporated each bed into the model, as it was perforated during the life of the well. Two comprehensive models were developed for two wells on the east portion of the field. These models took into account all the perforated beds. Lack of data on some of the required parameters made model development a challenging task. The numerical values of these parameters were calculated through production history match. Extremely low values of matrix rock permeability and fracture properties were needed to match the production history. Such low rock permeability values are in agreement with the core values. On the other hand, low values of fracture properties suggest that either the fractures are not contributing to the flow, or the field operations have resulted in extensive formation damage near the well bore rendering the fractures noncontributing. The amount of formation damage was quantified through time dependent permeabilities of well bore blocks. A 20-section area on the east side of the Bluebell field was used to study the effect of fractures on production variability from stochastically generated data. Geophysical logs were used to identify and characterize all the oil-bearing beds in the entire 20-section area. Reservoir rock properties were calculated for all the beds based on properties calculated from log analyses. Stochastic simulations were performed to generate distributions of rock properties. These simulations were then used to study the variability in fluids in place. A number of beds in the 20-section area were estimated to contain significant amounts of fluids in place. Most of the beds in the 20-section area were not continuous over the entire area. Inclusion of fractures reduced the variability in the production from the 20-section area. In the dual-porosity, dual-permeability approach, the fractures are the main pathways for the flow while the rock matrix is the main storage area for the fluids. Only the rock matrix properties were generated through stochastic simulations while the fracture properties were assumed to be continuous over the study area. Since the fractures dominated the flow, the variability in production due to matrix properties was reduced. The effect of various fracture properties on the production behavior of the fractured reservoir was also studied. As fracture porosity increased, oil and gas production also increased due to increased oil contained in the fractures. Increasing the fracture permeability increased the oil production up to a certain value of permeability, but beyond that the production was limited by the rate of fluid transfer between matrix and fractures. Increase in fracture frequency also increased the oil and gas production only up to a certain fracture frequency. Beyond that particular frequency, the increase in fracture frequency had only a marginal effect on production. The effect of variations in fluid thermodynamic properties on production was also studied. Increasing the oil API gravity resulted in increased oil production and reduced gas production. Increasing the reservoir temperature did not have any effect on the production performance.

The effect of scale was studied on the production for two wells in the reservoir. The study was performed only for one layer. The results showed that the production performance of Michelle Ute well was affected by scale of study. The production for single well model, where only a 40-acre area around the well was studied, was lower than the production for 20-section area. The continuity of the sand around the well did increase the production significantly even with low values of fracture and matrix flow properties.

Wells in the fractured reservoir models exhibit radii of influence (up to about 1000 ft [304.8 m]) that are larger than those in the homogeneous models. Most wells in the field are more than 1000 ft

(304.8 m) apart, but generally the second well drilled in a section is partially depleted. The difference between the modeled and actual production data could result fromeither of the following conditions: (1) the fractures are closed and not a significant part of the reservoir property, or (2) the production is from fractures, but from only a few of the perforated beds, and most of the other beds are not contributing to the production.

When the model included soft conditioning, the relationship of fracture frequency distribution on the rock type could be duplicated. The frequency distributions generated through the other two approaches did not reproduce this important trend. Reservoir models were developed with the fracture frequency distributions generated through these three approaches. The production performances of these three reservoir models, as expected, were different.

The parallel program was compiled and run on Silicon Graphics Power Challenge. The Power Challenge was a shared memory computer with 12 processors. The machine had 2 gigabytes of random access memory (RAM) and 12 gigabytes of hard disk space. The processors were MIPS R8000 chips with clock speed of 75 megahertz each. The parallel program was run with two and four processors. Four different input models were used. The grid configurations for the four models were 16X16X16, 32X32X16, 64X64X16 and 128X128X16.

Considerable speed up was observed with the parallel codes on the SGI Inca. The addition of processors was beneficial only for larger size problems, where even with the additional time required for communications, the total time required to complete one computational time step decreased. Performance degradation of the parallel program on IBM SP may be due to the waiting during the communications. A simple parallel solution technique was successfully implemented to achieve faster computational performance.

TASK 10: BEST COMPLETION TECHNIQUE IDENTIFICATION

Objective

The objective of task 10 was to recommend completion techniques for recompletion of older wells and completion of new wells based on the results of task 8 (Analysis of Completion Techniques) and Task 9 (Reservoir Analysis).

Accomplishments

A detailed analysis of prior completion techniques (task 8) identified many ways current completion practices could be improved. It is evident that many of the beds are not getting treated, and that smaller treatment intervals, and more effective diversion of treatment fluids is needed.

A detailed study was conducted by Gwynn (1996) of the produced water compositions from wells in the Bluebell field, including computer simulations to restore in-situ conditions. Production of water with varying composition was computer simulated. Production at varying reservoir conditions, with changes in pressure, temperature, and gas content, was simulated to identify the amount and composition of potential scaling materials precipitated. Changes in simulation parameters were used to determine ways to reduce scaling problems during production. The study did not find any unique or unusual water chemistries in any particular facies or area of the field that might affect completion techniques.

Reservoir analysis indicates that there is a significant amount of oil left to be produced in the Bluebell field wells. Accurately identifying which beds actually contribute to the production and the role that naturally occurring fractures play in the reservoir remains a major problem.

Results

Almost all the completions in the Bluebell field follow the same procedures, generally varying only slightly in the volume of acid and the types of additives used. As a result, analyses of past completion techniques did not identify one technique that was more effective than another. In newer wells, perforating fewer beds and treating shorter gross intervals can result in more effective completions. In recompleting wells, staging the treatments over shorter intervals and more effective diversion of the treatment fluid to the desired interval, will result in better completions. In older wells, where expensive staged completions are no longer economical, identifying remaining oil with cased holes and then acid treating individual beds with a dual packer tool may help extend the life of the well.

TASK 11: BEST ZONES OR AREAS IDENTIFICATION

Objectives

The objectives of task 11 were to identify the most productive facies, and the areas within the Bluebell field with the most remaining oil potential. A better definition of what beds are the oil pay and prediction of where these beds can be found in undrilled portions of the field would identify new drill locations and help reduce the number of perforations needed in a well.

Accomplishments

Detailed correlation and log analyses of thousands of feet of section from all the wells in a 20-square-mile area allowed stratigraphic cross sections, isochore maps of individual beds, evaluation of production histories, and reservoir simulation modeling to be completed as part of the Bluebell geologic characterization and reservoir analysis. A lack of detailed information on which beds actually contribute to the oil production in a well, and very limited amount of core, made it impossible to identify (if it exists) any specific facies or fracture trend that is responsible for the production at Bluebell field.

Results

It is recommended that operators in the Bluebell field use geophysical and imaging logs as the primary tool for selecting perforations in new wells, not drilling shows as is commonly done. This should result in a reduction of the number of beds perforated, and more effective treatment. In recompletion of existing wells, cased hole logs can help identify additional beds to be perforated, and if necessary, identify beds that can be treated individually.

OIL WELL DEMONSTRATION PROGRAM

The oil well demonstration program carried out by Quinex Energy Corporation, Bountiful, Utah, involved three parts. The first demonstration well was a recompletion of the Michelle Ute 7-1 well using a three-stage, high-diversion, high-pressure, acid treatment. Each stage was about 500-ft (150-m) vertical interval with over 10 beds perforated in each interval. The second well demonstration was a recompletion of the Malnar Pike 1-17 well using an acid treatment of four separate beds using a bridge plug and packer to isolate individual beds in a well with over 60 beds previously perforated. The third well demonstration was the logging and completion of a new well, the Chasel 3-6A2. The Michelle Ute and Chasel 3-6A2 wells were both severely hampered by mechanical problems. The Malnar Pike recompletion was mechanically successful but the incremental increase in oil production was less than most recompletions in the Bluebell field.

The Wade Cook 2-14A1 well was not originally part of the demonstration program. The well was drilled by Quinex Energy Corporation about 2 miles from the Michelle Ute well. Financial support from the project was provided for running dipole shear anisotropy and TDT logs in the well which were run in each of the three demonstration wells.

Recompletion of the Michelle Ute 7-1 Well

Objective

The recompletion of the Michelle Ute well is discussed by Deo and Morgan (1998). Most wells in the Bluebell field have 40 or more beds perforated over a 1500-ft (460-m) or more, vertical interval. Some operators have improved their recompletions by acidizing the large intervals in stages, but it remained unclear if they were opening up more of the perforated beds to production or if they were more effectively treating a few beds that account for most of the production. The objective in the recompletion of the Michelle Ute well was to use cased-hole logs to better understand what was being accomplished with a staged treatment. Prior to the treatment, cased-hole logs would be used to determine which beds have fractures (dipole shear anisotropy), and which beds show evidence of depletion (TDT). After the treatment, dipole shear anisotropy and isotope tracer logs would be run to determine the effectiveness in diverting the acid to each of the beds, and if most of the acid went into the beds with fractures or if the treatment opened up new fractures. Fluid-entry logs would be used to determine if production was coming from significantly more beds than in the typical Bluebell well, and if production was coming from only beds with fractures.

Accomplishments

Cased-hole logs were run before the treatment and showed fracturing in many of the beds that was confined by the bed boundary. This had been seen in other wells, in both core and open-hole imaging logs. The TDT log identified several beds with oil potential that had not been previously perforated. A leak was detected when the tubing was pressure tested prior to pumping the acid. Rather than come out of the hole and delay the treatment, the operator decided to pump the acid from a single packer location over the entire 1500-ft (460-m) interval. The tubing parted after the acid was pumped as the operator was attempting to come out of the hole. As a result, the spent acid was left in the hole for several days until the tubing could be fished out of the hole.

Results

The isotope tracer log was run after the treatment and showed a pattern of dispersal of the acid similar to the fractures, providing some confidence in the interpretation of the fracture log. A qualitative analysis of the TDT log indicates an equal oil saturation in both perforated and non-perforated beds which suggests vertical communication in the reservoir. Some of the beds shown to have good oil potential on the TDT log are correlatable to neighboring wells where fluid-entry logs indicate that the beds are oil productive. The isotope tracer log showed that only beds in the upper 500 ft (150 m) of the 1500 ft (460 m) tested interval received any significant amount of acid; the lower 1000 ft (300 m) were not treated. The dipole shear anisotropy log was not run after the treatment as planned, but since the acid was pumped at lower than normal pressures, and only a third of the interval received any acid, it is unlikely that any fractures were induced.

The demonstration was not a valid test of the staged completion because of the mechanical problems encountered. A minor incremental increase in the daily oil production did occur for a few months, which was encouraging considering how few beds were actually treated. Although the interpretation of the cased-hole logs was not proven by the demonstration, the limited results did increase our confidence in the data.

Recompletion of the Malnar Pike 17-1 Well

Objectives

The recompletion of the Malnar Pike well is discussed in Morgan and Deo (1998). Wells in the Bluebell field are initially completed, and periodically recompleted, by treating tens of beds at a time. The objective of the Malnar Pike recompletion was to use cased-hole logs that were shown to be of value in the Michelle Ute demonstration, to select individual beds for treatment and determine the effectiveness of treating Bluebell wells at the bed scale.

Accomplishments

Dual-burst thermal-decay-time (TDT), dipole shear anisotropy, and isotope tracer logs were used to identify beds for treatment and testing, and for post-treatment evaluation. Four separate treatments and tests were applied. The intervals were isolated using a bridge plug at the base and a packer at the top of the test interval. The first two treatments resulted in communication above and below the test interval. Swab tests recovered water from both intervals after the treatment. The third and fourth treatments were mechanically sound, and resulted in an increase in the daily oil production.

Results

A bridge plug was placed above the first and second intervals because the operator felt these intervals would produce water. The daily oil-production rate did increase as a result of the treatment of the third and fourth intervals. The incremental increase in the oil production was less than most recompletions in the Bluebell field.

Initially we planned to do the treatments with a dual-packer tool so that all four treatments could be done in a day. The operator decided to use the bridge plug and packer method which is mechanically safer but took about two weeks, greatly increasing the cost. As a result, the incremental increase will probably not pay for the cost of the treatment.

Communication above and below the test intervals was a major problem. The Malnar Pike well has numerous perforations that have been acidized several times, and this increases the potential for communication behind the casing. It is very likely that conventional acid treatments (typically a 500 to 1500 ft [150-460 m] interval) of older wells in the Bluebell field cause a similar problem. Much of the acid may be moving vertically through the cement and not into the formation.

The bed-scale completion technique can be an effective treatment, especially in older wells where the incremental increase in oil no longer justifies the expense of a larger single or multi-staged recompletion. The bed-scale completion should be conducted using a dual packer tool to reduce cost, and the anisotropy and TDT logs should be used to select beds that are fractured and have relatively low water saturation. Both the upper and lower packer should be placed between perforated beds that are at least 50 ft (15 m) apart to reduce the risk of communication behind the pipe.

Completion of the Chasel 3-6A2 Well

Objectives

The objective of completing the 3-6A2 well was to use geophysical well logs that were shown to be effective in the first two demonstrations. This would hopefully reduce completion costs, increase the production rate, and greatly reduce the volume of water produced. The completion of the John Chasel 3-6A2 well is discussed in Morgan and Deo (1998). Most wells in the Bluebell field are completed by perforating 40 or more beds. Perforations are usually selected based on drilling shows with minor reliance on geophysical well logs.

Accomplishments

Quinex Energy Corporation drilled the John Chasel 3-6A2 well to a total depth (TD) of 15,872 ft (4837.8 m) in the Flagstaff Member of the Green River Formation. Neighboring wells have produced as little as 2000 bbl to over a million bbl of oil (280-140,000 MT). The 3-6A2 well is the second deep well in the section and, like most second wells, it appears to have been partially depleted. In this part of the Bluebell field, the first wells typically required 14 lbs/gal (1.7 kg/L) drilling mud. The 3-6A2 well encountered numerous oil and gas shows in the Green River and Colton Formations, but was drilled to TD with a maximum mud weight of 11 lbs/gal (1.3 kg/L).

Open-hole geophysical well logging consisted of a suite of logs including the dual induction, compensated neutron lithodensity, dipole shear anisotropy, gamma ray, and spontaneous potential. The TDT log was run after the hole was cased. Nineteen beds were selected for perforating, far fewer than in most other wells in the Bluebell field. The TDT log was the primary tool used for selecting perforations, along with consideration given to fracturing identified on the dipole shear anisotropy log and exceptional drilling shows. The density-neutron porosity log was evaluated but log porosity was not a deciding factor.

The 3-6A2 well was stimulated by acidizing the perforations in two separate treatments. The first treatment was of the lower 12 perforated beds, and the second treatment was of all 19 perforated beds.

Results

The isotope tracer log indicated that most of the acid went into perforated and nonperforated beds in the interval from 15,130 to 15,340 ft (4611.6-4675.6 m). The log showed extensive communication behind the casing in this interval. The interval was cement squeezed, and many of the beds were reperforated, and the entire perforated interval was acidized. Swab testing began recovering drilling mud, and then the tubing had to be pulled because it was plugged with cement chips.

While the tubing was out of the hole the well began to flow. The shut-in pressure at the well head was 2500 psi (17,160 kPa). The operator flowed the well in an attempt to reduce the pressure so they could run the tubing back in the hole. One day the well flowed 124 BO (17.4 MT), 255 MCFG (7220 m^3), and no water. The next day it flowed 133 BO (18.6 MT), 125 MCFG (3550 m^3), and no water. The operator eventually stopped the flow and ran the tubing back into the hole. It was discovered that the casing had partially collapsed at 15,354 ft (4682.9 m) and 15,573 ft (4749.8 m) with a tight spot at 14,700 ft (4480.6 m). The swedge became stuck while trying to open the tight spot resulting in the swedge and some of the tubing being left in the hole. The well is shut in and was completed based on the earlier flow rate up the casing. The effectiveness of the selection of perforations and the completion technique cannot be evaluated in this well because of the mechanical problems that developed.

Completion of the Wade Cook Well

Objectives

The Wade Cook 2-14A1 (NW1/4NW1/4, section 14, T. 1 S., R. 1 W.) well was not originally scheduled as part of the demonstration program. However, the Wade Cook well is about 2 miles from the first demonstration well, the Michelle Ute, and we felt the data from the Wade Cook could help the study. Therefore, we supported the logging of the well to ensure that dipole shear anisotropy and TDT data were gathered.

Accomplishments

Quinex Energy Corporation drilled the Wade Cook well to a total depth of 14,212 ft (4331.8 m) in the Flagstaff Member of the Green River Formation. The well was logged with a suite of logs including the spontaneous potential, gamma ray, compensated neutron and formation density, dual induction, dipole shear anisotropy, and dual burst thermal decay time (TDT). Twenty-eight beds between 12,001 and 14,104 ft (3657.9-4298.9 m) were perforated and acidized. After swab testing another eight beds between 10,536 and 10,938 ft (3211.4-3333.9 m) were perforated and acidized. The well was completed flowing 285 BOPD (39.9 MTPD), 148 MCFGPD (4000 m^3/d) and no water.

Results

The Wade Cook well provided only limited data. The operator selected 28 beds for perforating based primarily on the TDT and drilling shows. Both fractured and nonfractured beds, as well as some beds that appeared tight or wet on the TDT log, were selected for perforating. As a result, the role of naturally occurring fractures in production of the well cannot be determined. The 2000-ft (610 m) gross interval was acidized from a single packer location instead of staging it in smaller intervals, as recommended by our study. Isotopes were not used in the acid so the effectiveness of

diverting acid into the desired beds is unknown. The operator believes most of the acid went into the lowermost perforations. The well would flow oil for a few days and then stop; swabbing would start the well flowing again. The operator believes the stoppage of production occurred when the wellbore filled with oil and load water to the top of the perforated interval and blocked the set of perforations that were producing gas. When the gas-producing perforations became blocked, there wasn't enough gas in the wellbore to lift the fluids. To increase the gas to the wellbore, another eight beds (10,536-10,938 ft gross) were perforated and acidized.

The well is currently producing from 36 beds in a gross vertical interval of 3568 ft (1087.5 m). It is believed that only a few of the beds are actually contributing to the production. It is unknown if the nonproductive beds are incapable of producing, or if the inefficient completion technique failed to adequately divert acid into those beds.

TASK 12: TECHNOLOGY TRANSFER

Objective

The objective of technology transfer was to get the data and results of the study to explorationists and operators of wells in the Uinta Basin and other fluvial-dominated deltaic reservoirs, as well as to people involved in regulatory and land use planning, and anyone with a general interest in the geology and hydrocarbons of the Uinta Basin.

Accomplishments

Information was provided through:

1. Cooperation between team members from academia, state agencies, oil field service companies, and oil well operators;
2. the Utah Geological Survey Industry Outreach Program;
3. visits to the demonstration sites;
4. posting of technical reports on the UGS web site;
5. publications of technical papers and graduate theses; and
6. presentation of papers at professional meetings and industry trade shows.

Results

Team cooperation: The mutidisciplinary team met quarterly during the characterization phase to coordinate our efforts and share findings and new ideas. Service companies and operators carried the ideas back to offices and shared the information with other industry personnel and companies.

Industry outreach: The UGS Industry Outreach Program compiled and maintained a contacts list of all people and companies that expressed interest in the project. These people received copies of the quarterly and annual technical reports as well as the UGS Petroleum News and Survey Notes. The Outreach Program set up an exhibitor booth displaying information about the project at the following industry conventions and programs:

1. AAPG National Conventions from 1993 through 1999,
2. AAPG Regional Meetings from 1993 through 1999,
3. Society of Petroleum Engineers National Convention 1994,
4. Vernal (Utah) Petroleum Days 1994, 1996, and 1998;
5. Utah Geological Association and Four Corners Geological Society Symposium 1996,
6. Petroleum Technology Transfer Council 1998,
7. Interstate Oil and Gas Council National Meeting 1998.

Site visits: Site visits to each of the demonstration well locations were coordinated with the Quinex Energy Corporation. There was little interest in visiting the sites except by people directly involved in the project.

Internet web page: The UGS maintains a Bluebell home page on its web site containing the following information: (1) a description of the project, (2) a list of project participants, (3) each of the Quarterly Technical Progress Reports, (4) a description of planned field demonstration work, (5) portions of the First and Second Annual Technical Reports with information on where to obtain complete reports, (6) a reference list of all publications that were a direct result of the project, (7) an extensive, selected reference list for the Uinta Basin and lacustrine deposits worldwide, and (8) daily activity reports of the Michelle Ute 7-1, Malnar Pike 17-1, and Chasel 3-6A2 demonstration wells. Numerous inquiries resulted from the web page.

Publications: The following publications resulted from the Bluebell study:

Garner, Ann, 1996, *Outcrop study of the lower Green River Formation for the purpose of reservoir characterization and hydrocarbon production enhancement in the Altamont-Bluebell field, Uinta Basin, Utah:* Provo, Brigham Young University M.S. thesis, 192 p.

Garner, Ann, and Morris, T.H., 1996, *Outcrop study of the lower Green River Formation for the purpose of reservoir characterization and hydrocarbon production enhancement in the Altamont-Bluebell field, Uinta Basin, Utah:* Utah Geological Survey Miscellaneous Publication 96-2, 61 p.

Montgomery, S.L., and Morgan, C.D., 1998, *Bluebell field, Uinta Basin: reservoir characterization for improving well completion and oil recovery:* American Association of Petroleum Geologists Bulletin, v. 82, no. 6, p. 1113-1132.

Morgan, C.D., 1994, *Oil and gas production maps of the Bluebell field, Duchesne and Uintah Counties, Utah:* Utah Geological Survey Oil and Gas Field Study 15, 4 p., 7 plates, scale 1 inch = 0.8 miles.

Morgan, C.D., compiler, 1995, *Increased oil production and reserves from improved completion techniques in the Bluebell field, Uinta Basin, Utah - second annual report:* Utah Geological Survey Open-File Report 330, 115 p.

Morgan, C.D., Sprinkel, D.S., and Waite, K.A., 1995, *Bluebell field drill-hole database, Duchesne and Uintah Counties, Utah:* Utah Geological Survey Circular 90 DF, 23 p. 1 diskette.

Pawar, R,J, 1998, *Reservoir characterization and reservoir simulations: fractured and nonfractured systems:* Salt Lake City, University of Utah Ph.D. dissertation, 401 p.

Wegner, MaryBeth, 1996, *Core analysis and description as an aid to hydrocarbon production enhancement - lower Green River and Wasatch Formations, Bluebell field, Uinta Basin, Utah:* Provo, Brigham Young University M.S. thesis 233 p.

Petroleum News is a newsletter published by the UGS that keeps petroleum companies, researchers, and other parties who are interested in Utah's energy resources, informed on the progress of various energy-related projects of the UGS. The following articles were published in *Petroleum News.*

January 1994, *DOE Class I Oil Program.*
June 1994, *DOE Class I Program.*
July 1995, *Bluebell project begins second successful year.*
May 1996, *Bluebell project readies for demonstration program.*
April 1997, *Bluebell field demonstration: new logs show fractures, oil.*
January 1998, *Bluebell field: second demonstration completed.*
April 1999, *Demonstration nearly completed in Bluebell field.*

The UGS *Survey Notes* is a newsletter that reaches a wide audience including industry, teachers, government, and the general public. The following articles were published in *Survey Notes.*

1995, *Bluebell project to test well-completion techniques:* v. 28, no. 1, p. 12-13.
1997, *Energy News:* v. 29, no. 2, p. 9.
1997, *Oil recovery demonstration program begins with acid treatment in the Bluebell field:* v. 29, no. 3, p. 10.
1997, *Energy News: Oil demonstration programs move into advanced phases:* v. 30, no. 1, p. 10-11.

Presentations: The following talks or poster presentations often with an associated published abstract, have discussed the Bluebell study:

Deo, M.D., 1998, *Fractured reservoir modeling in the Bluebell filed, Uinta Basin, Utah:* Petroleum Technology Transfer Council Symposium, Salt Lake City, UT.

Garner, Ann, 1995, *Reservoir characterization through facies analysis of the lower Green River Formation for hydrocarbon production enhancement in the Altamont-Bluebell field, Uinta Basin, Utah:* American Association of Petroleum Geologist Annual Convention Program with Abstracts p. 32A.

Garner, Ann, 1995, *Reservoir characterization through facies analysis of the lower Green River Formation for hydrocarbon production enhancement in the Altamont-Bluebell field, Uinta Basin, Utah:* Physical and Mathematical Sciences and the Central Utah Section of the American Chemical Society Ninth Annual Spring Research Conference Program with Abstracts.

Garner, Ann, and Morris, T.H., 1994, *Reservoir characterization through facies analysis of the lower Green River Formation for hydrocarbon production enhancement in the Altamont-Bluebell field, Uinta Basin, Utah:* Geological Society of America Program with Abstracts, v. 26, no. 7.

Morgan, C.D., 1995, *A multi-disciplinary team approach to reservoir characterization of the Bluebell field, Uinta Basin, Utah:* American Association of Petroleum Geologists Bulletin, v. 79, no.6, p. 923.

Morgan, C.D., 1995, *Bluebell field: increasing production in a fluvial-deltaic reservoir:* Utah Geological Association August Newsletter and luncheon.

Morgan, C.D., 1997, *Improving primary oil recovery from a (DOE Class I) fluvial-dominated deltaic lacustrine reservoir Uinta Basin, Utah:* American Association of Petroleum Geologists Annual Convention Program with Abstracts, p. A85.

Morgan, C.D., 1998, *Use of dipole shear anisotropy, dual burst thermal decay time, and isotope tracer logs for recompletion design and post-recompletion evaluation in complex reservoirs:* Petroleum Technology Transfer Council Symposium, Denver, CO.

Morgan, C.D., 1998, *Increased oil production and reserves from improved completion techniques in the Bluebell field, Uinta Basin, Utah:* Petroleum Technology Transfer Council Symposium, Salt Lake City, UT.

Morgan, C.D., 1998, *Second field demonstration of completion techniques in a (DOE Class I) fluvial-dominated deltaic lacustrine reservoir, Uinta Basin, Utah:* American Association of Petroleum Geologists Annual Convention Abstracts CD ROM.

Tripp, C.N., 1995, *Reservoir characterization of potential targets for horizontal drilling in the Tertiary Green River and Wasatch Formations, Bluebell field, Uintah County, Utah:* American Association of Petroleum Geologists Bulletin, v. 79, no. 6, p. 925-926.

Wegner, MaryBeth, 1995, *Facies analysis of well cores from the lower Green River Formation, Bluebell field, Uinta Basin, Utah: implications for identifying highly productive zones:* Physical and Mathematical Sciences and the Central Utah Section of the American Chemical Society Ninth Annual Spring Research Conference Program with Abstracts.

Wegner, MaryBeth, Garner, Ann, and Morris, T.H., 1995, *Reservoir characterization through facies analysis of core and outcrop of the lower Green River Formation: hydrocarbon production enhancement in the Altamont-Bluebell field, Uinta Basin, Utah:* American Association of Petroleum Geologists Bulletin, v. 79, no. 6, p. 926-927.

Wegner, MaryBeth, Garner, Ann, and Morris, T.H., 1995, *Reservoir characterization through facies analysis of core and outcrop of the lower Green River Formation: hydrocarbon production enhancement in the Altamont-Bluebell field, Uinta Basin, Utah:* American Association of Petroleum Geologists National Convention (abstract not published).

REFERENCES

Allison, M.L., 1995, Increased oil production and reserves from improved completion techniques in the Bluebell field, Uinta Basin, Annual Report for the period October 1, 1993 to September 30, 1994: U.S. National Technical Information Service DE95000171, 123 p.

Allison, M.L., and Morgan, C.D., 1996, Fracture analyses, *in* Allison and Morgan, compilers, Increased oil production and reserves from improved completion techniques in the Bluebell field, Uinta Basin, Annual Report for the period October 1, 1994 to September 30, 1995: U.S. National Technical Information Service DE96001227, p. 48-51.

Castle, J.W., 1991, Sedimentation in Eocene Lake Uinta (lower Green River Formation), northeastern Uinta Basin, Utah, *in* Katz, B.J., editor, Lacustrine basin exploration - case studies and modern analogs: American Association of Petroleum Geologists Memoir 50, p. 243-263.

Curtice, Richard, 1996, Completion techniques, *in* Allison, M.L., and Morgan, C.D., editors, Increased oil production and reserves from improved completion techniques in the Bluebell field, Uinta Basin, Annual Report for the period October 1, 1994 to September 30, 1995: U.S. National Technical Information Service DE96001227, p. 77-92.

Deo, M.L., and Morgan, C.D., 1998, Increased oil production and reserves from improved completion techniques in the Bluebell field, Uinta Basin, Annual Report for the period October 1, 1996 to September 30, 1997: U.S. National Technical Information Service DE98000481, 62 p.

Deo, M.D., and Pawar, R.J., 1996, Numerical simulation modeling of hydrocarbon production from the Green River and Wasatch Formations, *in* Allison and Morgan, compilers, Increased oil production and reserves from improved completion techniques in the Bluebell field, Uinta Basin, Annual Report for the period October 1, 1994 to September 30, 1995: U.S. National Technical Information Service DE96001227, p. 60-76.

---1997a, Non-fractured geostatistical modeling and reservoir simulations, *in* Morgan, C.D., compiler, Increased oil production and reserves from improved completion techniques in the Bluebell field, Uinta Basin, Annual Report for the period October 1, 1995 to September 30, 1996: U.S. National Technical Information Service DE96001297, p. 8-15.

---1997b, Fractured geostatistical modeling and reservoir simulations, *in* Morgan, C.D., compiler, Increased oil production and reserves from improved completion techniques in the Bluebell field, Uinta Basin, Annual Report for the period October 1, 1995 to September 30, 1996: U.S. National Technical Information Service DE96001297, p. 16-30.

Fouch, T.D., 1975, Lithofacies and related hydrocarbon accumulations in Tertiary strata of the western and central Uinta Basin, Utah, *in* Bolyard, D.W., editor, Symposium on deep drilling frontiers in the central Rocky Mountains: Rocky Mountain Association of Geologists Special Publication, p. 163-173.

---1976, Revision of the lower part of the Tertiary system in the central and western Uinta Basin, Utah: U.S. Geological Survey Bulletin 1405-C, 7 p.

---1981, Distribution of rock types, lithologic groups, and interpreted depositional environments for some lower Tertiary and Upper Cretaceous rocks from outcrops at Willow Creek - Indian Canyon through the subsurface of Duchesne and Altamont oil fields, southwest to north-central parts of the Uinta Basin, Utah: U.S. Geological Survey Oil and Gas Investigations Map, Chart OC-81, 2 sheets.

Fouch, T.D., and Pitman, J.K., 1991, Tectonic and climate changes expressed as sedimentary cycles and stratigraphic sequences in the Paleogene Lake Uinta system, central Rocky Mountains, Utah and Colorado: American Association of Petroleum Geologists Bulletin, v. 75, no. 3, p. 575.

---1992, Tectonic and climate changes expressed as sedimentary and geochemical cycles - Paleogene Lake systems, Utah and Colorado - implications for petroleum source and reservoir rocks, *in* Carter, L.J., editor, U.S. Geological Survey Research on Energy Resources, 1992 McKelvey Forum Program and Abstracts: U.S. Geological Survey Circular 1074, p. 29-30.

Fouch, T.D., Pitman, J.K., Wesley, J.B., Szantay, Adam, and Ethridge, F.G., 1990, Sedimentology, diagenesis, and reservoir character of Paleogene fluvial and lacustrine rocks, Uinta Basin, Utah - evidence from the Altamont and Red Wash fields, *in* Carter, L.J., editor, Sixth V. E. McKelvey Forum on Mineral and Energy Resources, U.S. Geological Survey Research on Energy Resources - 1990 - Program and Abstracts: U.S. Geological Survey Circular 1060, p. 31-32.

Franczyk, K.J., Fouch, T.D., Johnson, R.C., Molenaar, C.M., and Cobban, W.A., 1992, Cretaceous and Tertiary paleogeographic reconstructions for the Uinta-Piceance Basin study area, Colorado and Utah: U.S. Geological Survey Bulletin 1787-Q, 37 p.

Garner, Ann, 1996, Outcrop study of the lower Green River Formation for the purpose of reservoir characterization and hydrocarbon production enhancement in the Altamont-Bluebell field, Uinta Basin, Utah: Provo, Brigham Young University M.S. thesis, 192 p.

Garner, Ann and Morris, T.H., 1996a, Outcrop study of the Green River Formation, Willow Creek Canyon, *in* Allison and Morgan, compilers, Increased oil production and reserves from improved completion techniques in the Bluebell field, Uinta Basin, Annual Report for the period October 1, 1994 to September 30, 1995: U.S. National Technical Information Service DE96001227, p. 24-34.

---1996b, Outcrop study of the lower Green River Formation for reservoir characterization and hydrocarbon production enhancement in the Altamont-Bluebell field, Uinta Basin, Utah: Utah Geological Survey Miscellaneous Publication 96-2, 61 p.

Gwynn, J.W., 1996, Factors affecting the formation and rate of calcium carbonate scaling, *in* Allison and Morgan, compilers, Increased oil production and reserves from improved completion techniques in the Bluebell field, Uinta Basin, Annual Report for the period October 1, 1994 to September 30, 1995: U.S. National Technical Information Service DE96001227, p. 93-110.

Jarrard, Richard, 1996, Log analysis and petrophysics, *in* Allison and Morgan, compilers, Increased oil production and reserves from improved completion techniques in the Bluebell field, Uinta Basin, Annual Report for the period October 1, 1994 to September 30, 1995: U.S. National Technical Information Service DE96001227, p. 12-23.

Morgan, C.D., 1994, Oil and gas production maps of the Bluebell field, Duchesne and Uintah Counties, Utah: Utah Geological Survey Oil and Gas Fields Studies 15, 5 p., 8 pl., 1" = 0.8 mile.

---1997, Increased oil production and reserves from improved completion techniques in the Bluebell field, Uinta Basin, Annual Report for the period October 1, 1995 to September 30, 1996: U.S. National Technical Information Service DE96001297, 35 p.

Morgan, C.D., and Deo, M.D., 1998, Increased oil production and reserves from improved completion techniques in the Bluebell field, Uinta Basin, Annual Report for the period October 1, 1997 to September 30, 1998: 46 p.

Morgan, C.D., and Tripp, C.N., 1996, Formation evaluation and mapping, *in* Allison and Morgan, Increased oil production and reserves from improved completion techniques in the Bluebell field, Uinta Basin, Annual Report for the period October 1, 1994 to September 30, 1995: U.S. National Technical Information Service DE96001227, p. 52-59.

Osmond, J.C., 1964, Tectonic history of the Uinta Basin, Utah, *in* Sabatka, E.F., editor, Guidebook to the geology and mineral resources of the Uinta Basin: Intermountain Association of Petroleum Geologists Thirteenth Annual Field Conference, p. 46-58.

Pawar, R.J., 1998, Reservoir characterization and reservoir simulations: fractured and nonfractured systems: Salt Lake City, University of Utah Ph.D. dissertation, 401 p.

Pitman, J.K., Fouch, T.D., and Goldhaber, M.B., 1982, Depositional setting and diagenetic evolution of some Tertiary unconventional reservoir rocks, Uinta Basin, Utah: American Association of Petroleum Geologists Bulletin, v. 66, no. 10, p. 1581-1596.

Ryder, R.T., Fouch, T.D., and Elison, J.H., 1976, Early Tertiary sedimentation in the western Uinta Basin, Utah: Geological Society of America Bulletin, v. 87, p. 496-512.

Stokes, W.L., 1986, Geology of Utah: Utah Geological Survey Special Publication no. 6, 280 p.

Wegner, MaryBeth, 1996, Core analysis and description as an aid to hydrocarbon production enhancement - lower Green River and Wasatch Formations, Bluebell field, Uinta Basin, Utah: Provo, Brigham Young University, M.S. thesis, 233 p.

Wegner, MaryBeth, and Morris, T.H., 1996, Core analyses of the lower Green River and Wasatch Formations, *in* Allison and Morgan, compilers, Increased oil production and reserves from improved completion techniques in the Bluebell field, Uinta Basin, Annual Report for the period October 1, 1994 to September 30, 1995: U.S. National Technical Information Service DE96001227, p. 35-47.

FOSSIL ENERGY

DOE/BC/14953-27
(OSTI ID: 758140)

DELIVERABLE 3.1.4 – INCREASED OIL PRODUCTION AND RESERVE FROM IMPROVED COMPLETION TECHNIQUES IN THE BLUEBELL FIELD, UINTA BASIN, UTAH

Topical Report
June 7, 1999

By
Milind Deo
Craig D. Morgan

Date Published: July 2000

Work Performed Under Contract No. DE-FC22-93BC14953

Utah Geological Survey
Salt Lake City, Utah

National Petroleum Technology Office
U.S. DEPARTMENT OF ENERGY
Tulsa, Oklahoma

DISCLAIMER

This report was prepared as an account of work sponsored by an agency of the United States Government. Neither the United States Government nor any agency thereof, nor any of their employees, makes any warranty, expressed or implied, or assumes any legal liability or responsibility for the accuracy, completeness, or usefulness of any information, apparatus, product, or process disclosed, or represents that its use would not infringe privately owned rights. Reference herein to any specific commercial product, process, or service by trade name, trademark, manufacturer, or otherwise does not necessarily constitute or imply its endorsement, recommendation, or favoring by the United States Government or any agency thereof. The views and opinions of authors expressed herein do not necessarily state or reflect those of the United States Government.

This report has been reproduced directly from the best available copy.

DOE/BC/14953-27
Distribution Category UC-122

Deliverable 3.1.4

Increased Oil Production and Reserves from Improved Completion Techniques in the Bluebell Field, Uinta Basin, Utah

By
Milind Deo
Craig D. Morgan

July 2000

Work Performed Under Contract No DE-FC22-92BC14952

Prepared for
U.S. Department of Energy
Assistant Secretary for Fossil Energy

Gary Walker, Project Manager
National Petroleum Technology Office
P.O. Box 3628
Tulsa, OK 74101

Prepared by
Utah Geological Survey
1594 West North Temple, Suite 3110
Salt Lake City, Utah 84114-6100

TABLE OF CONTENTS

Deliverable: Field-scale Reservoir Models

DELIVERABLE: FIELD-SCALE RESERVOIR MODELS iii

SYNOPSIS 1
BACKGROUND: FLUID FLOW THROUGH FRACTURED ROCKS 1
Explicit discrete fractures 2
Discrete fracture network (DFN) 2
Single equivalent continuum 3
Dual continuum approach 3
Naturally fractured reservoirs and their simulations 4
THE STUDY AREA 6
Geology of the area 6
Available data and study sites 9
East study area 10
West study area 12
Reservoir fluid properties 13
RESERVOIR MODELS 14
East-side four-section mode 14
West-side four-section model 15
Twenty-section models 16
Available data 17
Generation of spatial property distributions 18
Thickness distribution 18
Porosity distribution 19
Saturation distribution 20
Variation in fluids in place 20
Flow simulations 20
Reservoir models 21
Production results 21
Effect of scale on production 23
CONCLUSIONS 25
REFERENCES 26

Synopsis

Bluebell field in east-central Utah is a large, extensively fractured reservoir. Conventional dual-porosity, dual-permeability simulators were used to study production performance in parts of this reservoir. Lack of data on a number of different reservoir parameters made modeling a difficult task. The main objectives were to:

- Simulate parts of the reservoir using the conventional dual-porosity, dual-permeability approach. Generate progressively complex reservoir models and use the production history match results to quantify formation damage.
- Examine the effect of the numerical aspects such as grid sizes and fracture properties on the simulations results
- Evaluate the effect of fluid thermodynamic properties on production.
- Study effect of inclusion of fractures on variability in production from stochastically generated reservoir models.

Background: Fluid flow through fractured rocks

Various approaches have been suggested to simulate fluid flow through fractured rocks. These approaches have been applied to petroleum reservoir simulations, simulations of multiphase contaminant transport, and groundwater flow simulations. The approaches can be divided loosely into four categories (Bear, 1993).

1. Explicit discrete fracture
2. Discrete fracture network
3. Single equivalent continuum
4. Dual continuum

Above classification which is based on how the fractures are represented depends to a certain extent on scale of study. The scale starts at a few feet for explicit discrete fracture representation to thousands of feet for single equivalent continuum simulations.

Explicit discrete fractures

These models incorporate explicit, discrete representation of fractures. This approach is also been described as "very near field approach" by Bear (1993). The approach which considers flow in single fractures, consists of writing mass balance equations explicitly in individual fractures. The models allow explicit representation of fluid potential gradients and fluxes between individual fractures and between fractures and porous media. Travis (1984) and Ward et al. (1993) have developed models for explicit discrete fracture flow approach. Murphy and Thomson (1993) have solved two phase flow in a single fracture of variable aperture with the boundary element method. Other single fracture flow studies have been reported by Schrauf and Evans (1986), Tsang (1984), Tsang and Tsang (1987), Wang and Narasimhan (1985). As the number of fractures increases, the data acquisition and computational burden increase significantly. It is difficult to extend this approach to a network of fractures.

Discrete fracture network (DFN)

In this approach, the fractures are represented as a network of fractures. The flow occurs only through the fracture network and the matrix system is not considered at all. Bear (1993) calls this a "near field" approach. The individual fractures are approximated with parallel plates or planes and simplified transport equations are written for each fracture. The flow through the network is written by using mass and energy balance equations at fracture intersections. A large number of models have been developed using the discrete fracture network approach, most of which have been for applications in contaminant transport and ground water flow modeling. Rasmussen (1991) and Rasmussen and Evans (1989) have used the discrete fracture network approach and principles of the boundary element method to investigate steady state flow of water through a fractured medium. Smith and Schwartz (1984) have used two-dimensional DFN model where the flow and mass transport occur through two orthogonal fracture sets. Long et al. (1982) developed a two-dimensional DFN model where fractures were assumed to be circular disks with uniform aperture. Long et al. (1985) later extended this approach to three-dimensional computational domain. Huang and Evans (1985) have also proposed a three-dimensional

DFN approach for steady, saturated flow. A one-dimensional flow tube formulation was used to describe flow through the fracture plane.

Single equivalent continuum

This approach is also known as the "very far field approach" (Bear, 1993). When the volume of interest is large enough, the fractures and the matrix are considered to be a single equivalent continuum. This approach essentially combines the separate representation of fractures and matrix into a single medium. Various techniques are used to calculate the single set of equivalent properties for the fractured rocks. Pruess et al. (1986) developed a model for single equivalent continuum in fractured rock, where the equivalent permeability was sum of the rock and fracture permeability. Travis (1984) and Reeves et al. (1986) have proposed finite difference numerical models. Wang and Narasimhan (1985) used finite element approximations to study the fractured systems using the single equivalent approach. Brebbia and Maier (1985), Elsworth (1986, 1987), Andersson and Dverstorp (1987) applied boundary element methods with single equivalent continuum approach to solve for flow in fractured rock.

Dual continuum approach

This approach is also known as the "far field approach" (Bear, 1993). This approach was first introduced by Barenblatt et al. (1960) and later extended by Warren and Root (1963). The dual continuum approach considers the fracture and matrix as two equivalent and interacting continua. Equations of flow are written for each continuum and solved together to describe flow through fractured rock. This approach has been extremely popular in oil reservoir simulations.

Various other approaches have also been proposed for flow through fractured rocks. Bai et al. (1993) introduced a generalized multiporosity, multipermeability approach. It was shown that the dual continuum or single fracture approaches can be derived from this general approach. Pruess and Narasimhan (1982, 1985) proposed a multiple interacting continua (MINC) method. The matrix was represented as nested blocks. The fractures were on the outside of the nested matrix blocks. Since only part of the matrix interacts with the fractures during actual flow, the nested blocks are used to represent the varying

interaction between the fractures and the matrix. The innermost block has a very limited interaction with the fractures, representing parts of matrix which are not in immediate contact with the fractures. Saidi (1987) used a numerical simulator where the entire fractured reservoir was divided into a small column of matrix blocks, each representing smaller reservoirs. The fractures were used to specify the boundary conditions for each small reservoir.

The single fracture and discrete fracture network approaches are widely used in hydrology and aquifer modeling. These approaches need detailed characterization of fracture networks and are useful when the study area is small (few hundred square feet). In petroleum reservoir applications, usually the field of study is very large (several hundred acres). It is impractical if not impossible to perform detailed characterization of fracture networks for these systems. Also, implementation of these techniques will result in computationally intensive problems. The single continuum equivalent and the dual continuum approaches can be used in the field scale problems where the need for small scale variability is not that important.

Naturally fractured reservoirs and their simulations

A number of oil reservoirs in the world are naturally fractured. Some of the giant oil fields in the Middle East are fractured. These reservoirs have a wide variety of rock mineralogy. The fractured reservoirs in the middle east are mainly fractured limestones. These fields include, Ain Zalah, Kirkuk fields in Iraq, Dukhan field in Qatar, Asamari field in Iran. The Gela and Ragusa fields in Sicily are fractured dolomite reservoirs. Examples of fractured sandstone reservoirs include the Altamont-Bluebell field in Utah and the Spraberry Trend in west Texas. The Santa Maria basin in western California and La Paz-Mara field in Venezuela are examples of fractured shale reservoirs. In all of these reservoirs, the porosity and permeability of the reservoir rocks are moderate to low. Fractures provide a means of production in otherwise unproductive reservoirs. Some of the reservoirs in middle east are so extensively fractured that two to three well placed wells can drain the entire field (Van Golf-Racht, 1982).

Even though a number of fractured reservoirs exist very few numerical flow simulation studies have been reported on these reservoirs. Two studies are described below.

1. Saidi (1983) developed a numerical simulator where fractures were used to assign boundary conditions for matrix blocks. He used this simulator to simulate two fractured reservoirs in Iran, namely the Asamari formation and the Kirkuk field. Unlike the dual-porosity, dual-permeability approach, this approach did not need explicit specification of fracture properties. The fracture frequencies were characterized from core studies and flow-meter surveys. These fracture frequencies were used to determine the matrix block size. The matrix block size used was about 8 feet. The observations from limited samples were generalized over the entire reservoir. Values of a number of parameters were unavailable. These values were determined by trial and error through a production history match. This approach was used to successfully match part of the production data.
2. Thomas et al. (1987) reported results of simulations study performed on the Ekofisk reservoir. The simulations were performed with dual-porosity, dual-permeability simulators. The fractured areas were determined through comparing the well test derived permeability with rock permeability values. Blocks with effective permeability larger than the rock permeability were considered fractured and the fractures were assigned the effective permeability values. The effective permeability values were used to determine the matrix block lengths and thus fracture frequencies using following relation: $k_e = k_m + 1.69 \times 10^{10}\, b^3/L$. The fracture width, b was assumed to be 50 μm. The fracture porosity was assumed to be 0.01. The matrix block lengths were then used in the calculation of shape factors. These parameters were used to obtain a production history match. Values of various matrix and fracture properties were adjusted to obtain a satisfactory history match. The model that obtained a satisfactory history match was used to study the waterflood performance.

Above studies used various sources of information to characterize fracture properties. The fracture networks were not characterized over the entire study areas, since it will be difficult to do so. Trends in fracture properties were determined from available test results like well-test derived permeability. Approximations were made about some of the

fracture property values and their distributions. Trial and error methods were also used to obtain satisfactory history match.

There have been no field-wide flow simulations of Altamont-Bluebell field. Models were developed to study different parts of this field using the conventional modeling methods as reported by Thomas et al. (1987) and Saidi (1983).

The study area

The study area is part of the Bluebell field in eastern Utah. The Bluebell field is the largest oil producing field in the Uinta Basin. Bluebell is one of the three contiguous oil fields, Bluebell, Altamont, and Cedar Rim, shown in Figure 1. The Bluebell field is 251 square miles in size and has produced over 127 million barrels of oil and 155 billion cubic feet of associated gas so far. Most of the field is produced at a spacing of one oil well per section, though some sections have two wells.

Geology of the area

The Bluebell field produces oil from the Eocene-Paleocene Green River and Wasatch Formations near the basin center. Figure 2 shows a north-south cross-section of the Uinta Basin. The distribution of the depositional environments of the ancient lake Uinta is shown in Figure 3. Fouch (1975) has discussed different formations in the Altamont-Bluebell fields.

- North Horn Formation: The North Horn Formation includes variegated claystone, sandstone, conglomerate, and local deposits of coal and carbonate which are identified as alluvial, paludal and isolated lacustrine depositional facies.
- Flagstaff Formation: The lacustrine Flagstaff Formation lies between the fluvial beds of the North Horn and Colton Formations. The Colton Formation pinches out northward into the basin where laterally equivalent lacustrine rocks of the Green River Formation were deposited. It is difficult to distinguish between the two formations where Green River lies directly on Flagstaff. It is common practice to refer to the section as Green River Formation when Green River and Flagstaff can not be broken out, or the Flagstaff Member of the Green River Formation.
- Colton Formation: The Colton Formation lies between the Green River and Flagstaff Formations on the southwestern side of the basin. Sandstone and red claystone form

this formation. The Colton intertongues with and pinches out northward into the Green River Formation. In the southeast portion of the basin the underlying Flagstaff is absent. Where the Flagstaff is absent, the red-bed sequence below the Green River is called the Wasatch Formation. On the eastern side of the basin, the contacts between the Green River, Wasatch and North Formations are gradual and hard to define.

- Green River Formation: The Green River Formation lies on top of and interfingers with the Wasatch and Colton Formations. As can be seen from Figure 2, large portions of the Uinta Basin tertiary aged rocks are part of the Green River Formation.

The Green River and Wasatch or Colton Formations were deposited in inter-tonguing relationship. The contacts between these formations are transitional and inter-tonguing, as a result they are difficult to identify accurately. The depositional cycles indicate rapid lake level fluctuations and changes in water chemistry (Fouch, 1975). The Green River and Wasatch Formations were deposited in alluvial-fluvial, marginal lacustrine, and open lacustrine environments. The oil production in the Bluebell field comes from three primary intervals belonging to these two formations:

1. Lower Green River/ upper Wasatch transition
2. Wasatch Formation
3. Lower Wasatch transition

The Lower Green River/ upper Wasatch transition defines the transition between the top of the Wasatch Formation and the lower part of the Green River Formation, while the lower Wasatch transition defines the transition between the lower part of Wasatch and the Flagstaff Member of the Green River Formation. These three intervals are shown on a cross sectional map between two wells in the Bluebell field in Figure 4. There are a number of subsurface markers that can be identified through out the Uinta Basin. The middle marker is one of the most prominent markers identifying the top of Lower Green River.

Production from the Bluebell field was first established in the Roosevelt Unit from the Lower Green River/upper Wasatch transition at depths less than 11,000 feet. The

Productive beds in this interval are interbedded calcareous sandstone, limestone, marlstone and ostracodal limestone, deposited in fluvial-deltaic and carbonate mud-flat environments. Many of the lower Green River beds laterally extend into the Wasatch Formation. The Wasatch Formation is primarily made up of sandstone and siltstone deposited in alluvial to fluvial-deltaic environments. The source for Wasatch redbeds (sandstone, siltstone and red shale) in Bluebell field was the Uinta Mountains to the north. The Wasatch redbeds thin rapidly from north to south through the field, with the best sandstone development located in the west portion of the field. The lower Wasatch transition consists dominantly of carbonates with minor sandstone that were deposited in marginal to open lacustrine environments. The lower Wasatch is productive throughout most of the field. On the east portion of the Bluebell field, lower Wasatch is the primary productive interval, while on the west portion both the Wasatch sandstone and lower Wasatch carbonate are productive.

The oil fields in the Uinta Basin have extremely high reservoir fluid pressures (Bredehoeft et al., 1994). The average pressure gradient is around 0.5 - 0.6 psi/ft. Pressure gradients as high as 0.8 psi/ft have been reported in the central part of the field (Lucas and Drexler, 1976). The abnormally high pressures have been attributed to tight low-permeability reservoirs and local generation of hydrocarbons from kerogen within the formations due to high formation temperatures. Due to the tight nature of the reservoir rocks the fluid pressures are localized. As a result even closely spaced reservoirs have considerable pressure differential.

The Altamont-Bluebell fields are naturally fractured reservoirs (Lucas and Drexler, 1976; Narr and Currie, 1982). Because of the low permeability of the reservoir rock, oil production is dependent on the presence of natural, joint type fractures. The generation of subsurface fractures has been attributed to the regional geology, high pore-fluid pressures, temperatures, tectonic stresses and the depositional sequences (Narr and Currie, 1982). The evolution of the fracture network was gradual and formed before the generation or secondary migration of the hydrocarbons (Lucas and Drexler, 1976; Narr and Currie,

1982). Most of the fractures in the Altamont-Bluebell fields are vertical and have north-northwest orientations. The surface fracture pattern has been studied in the Bluebell field (Allison, 1987). The fracture trends follow the regional geologic structural trends. There are two dominant sets of fractures, one set has orientations north northwest while the other set is orthogonal to the first set. The fracture frequency is strongly dependent on the lithology (Lucas and Drexler, 1976). Narr and Currie also observed that the compositional and physical properties of the rocks controlled the amount of fracturing observed in a bed.

Individual beds in the lower Green River and Wasatch producing intervals are difficult to evaluate for production characteristics. Fracturing and complex formation water chemistries make conventional geophysical log analysis highly questionable. Due to the economics involved, production tests of individual beds have been discouraged. Therefore, it is not clearly understood which beds in any particular well are potentially significant producers, limited producers, water producers or thieves. As a result, the common practice is to perforate numerous beds over thousands of vertical feet and apply acid-frac treatment. A typical well in the Bluebell field has between 1,500 to 2,000 feet of gross perforations. Figure 5 shows a histogram of gross perforations in thousands of feet from a data set of 132 wells in the eastern portion of the Bluebell field. As can be seen from the figure most of the wells are perforated over thousands of feet of intervals.

Available data and study sites

The present study was concentrated in two different study areas from the Bluebell field. The reservoir rock properties were calculated from geologic logs. The following logs were available for the wells in the region:

1. Gamma Ray
2. Neutron Porosity
3. Density Porosity
4. Resistivity

The logs were available for thousands of feet of formation interval as shown in Figure 4. The geologic characterization became progressively complex in terms of number of beds identified. The logs were used to identify the middle marker and subsequently the three

productive intervals in each well. Once the productive intervals were identified, the oil-bearing beds were identified based on 60 API or less gamma ray readings (only those beds with thickness greater than 6 feet were taken into consideration). The thickness of the beds were calculated from the gamma ray readings. After the oil-bearing beds were identified, the porosity values were calculated as the average of the neutron and density porosity logs. The porosity readings were used along with the resistivity log readings in Archie's equation to calculate the fluid saturation in each bed. The porosity and saturation values represented the average values over the entire bed. Thus, the following information was available for each zone in each well.

- Thickness
- Average porosity
- Average saturation

All the identified beds were correlated through each well over the entire study area. The two study areas are described in the following sections in detail.

East study area

As the name suggests, the east study area is in the eastern portion of the Bluebell field. A 20-section area was chosen on the eastern side of the field. Figure 6 shows a map of the 20-section area and the wells in the region. This study area included the Roosevelt Unit. This area has lower Green River/upper Wasatch transition, Wasatch, and lower Wasatch transition intervals. These intervals are commingled in some of the wells. This part of the field has the poorest producers. Typically the wells from this area have produced less than 200,000 barrels of oil, some have produced even less than 100,000 barrels. Most of the sections in the Roosevelt Unit have two wells per section, while some sections have only one. As mentioned before, some of the wells in the east study area are perforated in all the three intervals over intervals spanning thousands of feet. The characterization of different beds in these intervals was performed in steps and became progressively complex. The three stages of characterizations and the different study areas are as follows.

1. A four-section area, which is part of the 20-section area was chosen for primary characterization and modeling. The four sections chosen were sections 7, 8, 17 and 18 in Township 1 South, Range 2 West. Figure 7 shows a map of the four

sections and the wells present in those sections. The area included the following wells.

a) Michelle Ute

b) A1E Ute

c) 1-18A1E

d) Chasel Sprouse

e) RU C-11

f) Malnar Pike

g) 1-17A1E Ute

The logs were used to identify five different beds in this four-section area. These beds were correlated through all the wells. The thickness, porosity and saturation values were calculated for each bed. Figure 8 shows a cross section through two of the wells, showing the five correlated beds identified as QEL1 - QEL5. All the wells with the exception of 1-17A1E are perforated in one or more of these beds.

2. Comprehensive single well models were developed for two wells in the four-section area. The two wells were Michelle Ute in section 8 and Malnar Pike in section 17. Michelle Ute is perforated in 69 different beds, while Malnar Pike is perforated in 50 different beds. The geophysical logs were used to calculate the reservoir properties for each of the perforated beds. The information included thickness of each bed, the average porosity and saturation present in each bed. A report on comprehensive single-well models has been submitted previously.

3. A detailed characterization of the entire 20-section area was performed. The logs were used to identify all the possible oil bearing beds in each well. The identified beds were correlated through all the wells in the entire 20-section area. The information on each bed included thickness, average porosity and saturation.

Side-wall core samples were available for some of the wells in the Bluebell field. Permeability values of these cores were measured by core flooding experiments (Wagner, 1996). Figure 9 shows a porosity versus permeability cross plot. The permeability data indicates extremely tight formations with very low permeability values. The fracture characterization in this area is very limited. Narr and Currie (52) reported results of

fracture analysis in the Altamont field. Utah Geological Survey has reported results of a surface fracture pattern study for parts of the Bluebell Field (Wagner, 1996). The surface fracture study was limited to orientations of fractures. No quantitative information was available in terms of subsurface or surface fracturing frequency, widths of fractures, etc. Wagner analyzed cores available from some of the wells in the Bluebell field. The results of the core analysis were reported qualitatively for fracturing densities.

West study area

The west study area is located in the western portion of the Bluebell field. Figure 10 shows the west study area and the wells in the area. The study area included sections 9, 10, 15 and 16 in Township 1 South, Range 2 West. There are seven wells drilled to the lower Green River Formation or deeper in the four sections.

1. 2-9A2 Lamicq
2. 3-10C State
3. 2-10C Springfield
4. 2-16A2 Lamb
5. 6-16A2 Boren
6. 3-15A2 Boren
7. 4-15A2 Sundance

This study area includes some of the best producing wells with cumulative production of over three million barrels of oil per well. Many of the wells were originally drilled and completed in the lower Green River/upper Wasatch transition. Oil production from this formation ranged from 93 - 436 MSTB of oil. The wells were later deepened and completed in the Wasatch Formation and lower Wasatch transition. The wells produced greater than one million barrels of oil per well. Of the above mentioned wells only Lamicq 2-9C, Springfield 2-10C and State 3-10C were perforated in the Lower Green River/ upper Wasatch transition.

The reservoir characterization for the wells in this area was performed only for the lower Green River/upper Wasatch formation. Eleven different beds were perforated in one or

more of the wells. For each of the beds, information in terms of thickness, average porosity and saturation was available. These beds were correlated through all the wells in the four-section area. Figure 11 shows a cross section of the reservoir through two of the wells in the area. Nine of the 11 correlated beds are present in these two wells. As can be seen from the figure, most of the beds have significant thickness in both the wells. The beds had cumulative thickness of 20 to 90 feet. No data on permeability of the reservoir rock were available. Similar to the east study area, quantitative information on fracture properties and their distribution was not available.

Reservoir fluid properties

Oil and gas samples from two of the wells in the region were collected. Experiments were performed to measure the oil API gravity, oil viscosity and thermodynamic properties. The details of the experiments and the results were provided in earlier annual reports. The gas specific gravity was 0.75. The geologic and fluid property information was used to develop a number of different models for parts of Bluebell field. The API gravity of two oils from the wells in the Roosevelt unit were 31.5 and 32 respectively. Glasso (1980) has derived empirical relationship between the bubble point pressure and dissolved gas as a function of oil API gravity, gas specific gravity and temperature. The relationship was derived from experimental measurements of properties of a number of gas and oil samples from the North Sea reservoirs. These empirical relations were used to calculate the pressure versus dissolved gas relationship. The gas gravity of 0.75 was used. The oil API gravity was varied from 22 API to 32 API. The reservoir temperature was varied between 200 to 250 °F. Figures 12 a and b show the variation of pressure and oil formation volume factor with dissolved gas for three oil API gravity values. As the API gravity increases the gas solubility increases. On the other hand, changes in API gravity do not have a significant impact on the oil formation volume factor. As shown in Figures 13 a and b, varying the temperature from 200 to 250 °F does not have a significant impact on either the pressure or oil formation volume factor at a particular solution gas volume. These thermodynamic properties and bulk properties were used to develop reservoir models and to study their effect on production behavior of a fractured reservoir model.

Reservoir models

The numerical models developed were fractured models based on the conventional dual-porosity, dual-permeability approach. In this approach, the fractures are treated like a continuum similar to the nonfractured rock (also known as the matrix). For every grid block the fractures are characterized in terms of the properties such as porosity, permeability, frequency, etc.

- Fracture frequency: The fracture frequency denotes the number of fractures per unit length. The fractures are assumed to be orthogonal and present in the principle coordinate directions. The fracture frequency determines, to a large extent, the amounts of fluids transferred between the matrix and fractures.
- Fracture porosity: Fracture porosity is defined as the fraction of the reservoir volume occupied by fractures. The fracture porosity is equivalent to the matrix porosity. The changes in rock fracturing can be taken into account by specifying spatially varying fracture porosity.
- Permeability of fractures.

In addition to these properties, fluid saturations, initial pressure, initial bubble point pressure, and relative permeability-saturation curves are also required for fractures. Assumptions were made about the numerical values of fracture properties due to the lack of quantitative information. Various numerical models are described below.

The four-section models

The east-side four-section model was a preliminary model, since it took into account only some of the beds responsible for production. On the other hand, the west-side model was developed for all the beds that were responsible for the production.

East-side four-section model

The numerical parameters used for various properties are listed in Table 1. The reservoir extended from 13000 to 14000 feet. The model had 20 grid blocks in the x and y directions. The x and y dimensions of the grid blocks were 528 feet each. Low porosity and low permeability layers separated the five correlated zones, which resulted in nine blocks in the vertical direction. The reservoir rock porosity varied between 0.0 and 0.18.

The initial reservoir pressure varied with the depth at a gradient of 0.5 psi/foot. The initial GOR was 900 scf/stb at a initial bubble point pressure of 4146 psi. The initial oil saturation was constant at 0.7.

The thickness, porosity and saturation data were calculated from the well logs and thus represented properties at the well bore. The values observed at well bore were assumed continuous over the area surrounding the wells. The values of matrix permeability and fracture properties were obtained through field production history match. The values used for these properties are listed in Table 1. Limited fracturing was assumed. Only about a million square feet area surrounding each of the wells was assumed fractured. The fractures were vertical and present only in the x and y directions. The fracture frequency was 1 fracture per 10,000 feet. The fracture porosity was constant at 0.05 % of the reservoir volume.

Figures 14a and b compare the model predictions for cumulative oil and gas production for the entire four-section area with the field data. The production performance for Michelle Ute well is compared in Figures 15a and b. As seen from the figures, the model does a good job of matching the cumulative oil production. For the four-section area, the gas production predictions are higher than the field data, while for the Michelle Ute well, the gas production prediction lags the field data. The final pressure distributions for the model are plotted in Figure 16 along with the individual well locations. As can be seen from the figure, except for the Chasel Sprouse and RU C11 wells, the drainage radius of wells does not extend over to the next well. The history match was obtained with very low values for matrix permeability as well as fracture properties. The values used for matrix permeability were in the range of 0.018 - 0.33 mD. The values of fracture porosity, permeability and frequency were also very low.

West-side four-section model

Information in terms of bed thickness, average porosity and saturation were calculated from the logs. Similar to the east-side model, the reservoir properties were available at the

well locations. The property values were assumed to be continuous over the area surrounding the wells. The parameters used to develop the model are listed in Table 2.

The vertical extent of the reservoir was from 10,250 to 10628 feet. The entire four square mile area was divided on a grid with 20 blocks in x and y directions each. The x and y dimensions of the grid blocks were 528 feet each. The 11 oil bearing zones were separated by low-porosity and low-permeability zones, which resulted in 21 layers. The vertical dimensions of the grid blocks varied according to the individual bed thickness. The matrix porosity varied between 0 % and 26 %. The initial oil saturation varied between 0.7 and 0.9. Similar to the east-side model, the pressure varied at a gradient of 0.5 psi/foot. The initial GOR was 400 scf/stb and the initial bubble point pressure was 2100 psi. Field production history match was obtained by adjusting the values of rock permeability and fracture properties. The values that obtained the final production match are tabulated in Table 2.

Figures 17a and b show the comparison between the model predictions and the field data for cumulative oil and gas production for the four-section area. The production predictions for well 3-10C State are compared with the field production data in Figures 18a and b. As seen from the figures, the model does a good job of matching the final field production data.

Twenty-section models

Stochastic simulations are widely used to generate reservoir property distributions. These property distributions can be used to assess the reservoir production variability. This section discusses the effect of inclusions of fractures on the production variability. A 20-section area was chosen on the eastern side of the Bluebell Field. The details of the study area were described earlier.

The geophysical logs were used for detailed characterization of most of the beds present in the 20-section area on the eastern side of the Bluebell field. Most of the oil-bearing beds were identified and correlated through out the 20-section area. The characterization led to information in terms of thickness, porosity and saturation for all the beds. No

information on rock types or lithotypes distributions was available. Principles of geostatistics were used to generate property distributions from the available data. Reservoir models were developed to study the effect of stochastic distribution of properties on fluid production.

Available data

The general geology of this region was presented earlier in the report. The oil bearing zones are part of three different intervals; lower Green River/upper Wasatch transition, Wasatch and lower Wasatch transition. Most of the wells in this region are perforated in at least one of these intervals. The middle marker is a major geologic marker that can be correlated throughout the 20-section area. The middle marker identifies the top of the lower Green River/ upper Wasatch formation.

The oil-bearing beds were identified based on Gamma Ray readings of 60 API or less and 6% porosity. Once the beds that met the above criterion were identified in each well, they were correlated through all the other wells in the 20-sections area. Some of the beds did not have property values above the cutoff threshold in all the wells. These beds were still considered in model development. In all, 85 different beds were identified over the entire 20-section area. However, none of the wells had all the 85 beds present.

The two comprehensive single well models discussed earlier were developed using only the perforated beds. Michelle Ute well was perforated in 69 different beds, but for this study 77 different beds were identified in Michelle Ute. Some of the perforated beds did not qualify for present analysis due to their failure to meet the cutoff criterion. Limited information on matrix permeability values was available and no information on fracture properties was available. The reservoir characterization resulted in the following information for 20-section area:

- Correlated beds in different wells
- Thickness of beds in each well
- Average porosity in each bed
- Average saturation in each bed

The information about various property values was available at the well locations. In order to develop reservoir models, property distributions in the 20-section area were necessary. For the four section area models and the single well models, the property values observed at the well bore locations were assumed continuous through out the model area. For this study, the available data were used to generate stochastic spatial distributions of reservoir properties over the 20-section area.

Generation of spatial property distributions

The conventional methods used to develop reservoir models using stochastic techniques are described in geostatistical text books. The specific methods used in this study are presented in detail elsewhere (Pawar, 1998). In order to use those methods, information on rock type distributions, sands distributions within individual rock types and porosity-permeability distributions is required. For the present study such information was not available. Due to lack of the data, the reservoir models were not generated for all the beds. Instead the stochastic distributions of properties for different beds were obtained individually and independent of other beds. Stochastic simulations were performed using the principles of sequential Gaussian simulations. In order to perform the stochastic simulations, the parameters for spatial variability were calculated for each property in each zone. The calculation of spatial variability and subsequent simulations were performed with normally transformed data sets.

Thickness distribution

The spatial variability was calculated in terms of two-dimensional thickness variograms. Principle directions of continuity and anisotropy factors were determined by comparing a number of semivariograms in multiple directions. Figure 19 shows a semivariogram of thickness for bed 30. The thickness data in this zone did not show any principle direction of continuity hence an omni-directional semivariogram was chosen. The semivariogram did not show any structural anisotropy. The semivariogram was calculated at a minimum lag spacing of 220 feet. Figure 19 also shows a model fit to the semivariogram. The model was an exponential model. The model had no nugget effect. The semivariogram had a range of 3000 feet. A sill of 1.0 was used, since the semivariogram was calculated

for a normal data set. The semivariograms for thickness of all the zones were calculated in similar fashion. The model parameters for thickness semivariograms for all the beds are compiled in Pawar (1998).

The structure of the semivariograms for different beds was similar. All of the semivariograms were omni-directional. Different beds in parts of the 20-section area different beds might have exhibited local anisotropy, but when the entire 20-section area was considered, none of the semivariograms showed a principle direction of continuity. Some of the beds had higher correlation lengths than others. Since all of the semivariograms were calculated for the normally transformed data sets a sill of 1.0 was used.

The spatial variability information was used to generate multiple thickness realizations. These realizations were conditioned to the observed thickness values at the well locations. The output of stochastic simulations was transformed back to the original data format (from normal distributions). Figure 20 shows one realization for thickness distribution in bed 30. Multiple thickness distributions were generated for all the beds.

Porosity distribution

The distributions of porosity were also generated in two dimensions for each bed. two-dimensional semivariograms were calculated to determine measures of continuity. Figure 21 shows an omni-directional variogram for porosity in bed 30. The omni-directional semivariogram was chosen due to lack of structural anisotropy calculated through number of different directional semivariograms. The semivariogram was calculated at a lag spacing of 220 feet. Figure 21 also shows the model fit to the semivariogram. The model had one exponential structure. The correlation range was 1320 feet. There was no nugget effect and the sill was 1.0. The semivariogram structures were similar to the thickness semivariograms. Multiple, conditional realizations of porosity distributions were generated using the semivariogram model. Figure 22 shows a realization of porosity in bed 30.

Saturation distribution

The spatial distributions of saturation data were generated using similar steps. A semivariogram for saturation in bed 30 is shown in Figure 23. Figure 23 also shows the model fit to the semivariogram. The model had an exponential component with a range of 1320 feet. The nugget effect was 0.0 and the sill was 1.0. Multiple conditional realizations of saturations were generated with the spatial variability parameters. The realizations were conditioned to the observed saturation data. Figure 24 shows one such realization for saturation distribution in bed 30 through the 20-section area. Similar distributions were generated for all the beds. The stochastic realizations of various properties were generated for all the beds independent of one another.

Variation in fluids in place

The information on thickness, porosity and saturation was used to generate models for different beds. These models were used to study variations in fluids in place. Four different realizations of porosity, thickness and saturations were generated for each of the beds. The resulting property distributions were combined to generate 64 different models for each bed.

Some of the beds have high average OOIP compared to others. Most of the beds have average OOIP of the order of 1-8 million STB. These beds are not continuous over a large part of the 20-section area. Thickness realizations for four beds are compared in Figure 25. The four beds are 18, 25, 30, and 38a. Beds 25 and 38a have low average OOIP, 5.75 MSTB and 5.0 MSTB respectively. As can be seen from the figure, these beds have zero thickness over most of the 20-sections area. On the other hand, beds 18 (42.5 MSTB) and 30 (37.2 MSTB) have high average OOIP due to thicker oil bearing zones over the domain, as can be seen from Figure 25.

Flow simulations

The stochastically generated data sets were used to develop reservoir models. Due to the large number of beds and limitations of flow simulator, it was impossible to take all the beds into account. In order to study the flow performance, independent and separate

reservoir models were developed for different beds. Six different, reasonably continuous beds were chosen. All the chosen beds had high average OOIP. The six beds were 13, 18, 19, 23, 30 and 31.

A number of different reservoir models were developed from multiple property data sets. Flow simulations were performed with these models to study the effect of fractures on production variability. Flow simulations were performed on ten different reservoir models for each bed. The 10 models considered were chosen randomly from the 64 models used for OOIP studies.

Reservoir models

The flow simulations were performed with both fractured as well as nonfractured models. The fractured models were conventional dual-porosity, dual-permeability models. The numerical values for different parameters are tabulated in Table 3. The models had 41 and 33 blocks in the x and y directions. The x and y dimensions of each block were 660 feet. There was only one block in the vertical direction. The thickness of the grid blocks varied according to the stochastically generated thickness values. The porosity and saturation of the matrix also varied according to geostatistically generated data. The permeability of the matrix was assumed to be constant at 0.5 mD. The fracture porosity was assumed to be 0.005. The fracture frequency was 1 per 220 feet. The permeability of the fractures was assumed to be 1.5 mD. The fracture properties were assumed to be continuous over the entire 20-section model. The reservoir fluid and thermodynamic properties were similar to the earlier models. The variations in the production performance of these models are discussed below.

Production results

The flow simulations were performed over a period of 8 years. All of the wells were open during this period of time. The statistics of the production results for both fractured and nonfractured reservoir models for each zone are summarized in Table 4. Production from

the entire 20-section area, and Michelle Ute and Malnar Pike wells are compared in the table.

As can be seen from the table the presence of fractures makes a big difference in the amount of oil produced. The production in bed 18 tripled due to the presence of fractures; however, the gas production increased six times. The GOR for the fractured model thus increased from 945 scf/stb to 1660 scf/stb. GOR values of about 1000 scf/stb are more common in the field than values around 1500 scf/stb. The Michelle Ute and the Malnar Pike wells appeared to be affected differently due to the presence of fractures. The production in Michelle Ute increased by an order of magnitude while the production from Malnar Pike only doubled. Since the fracture representation is uniform around both the wells, the production is related to other reservoir characteristics around the wells, such as bed thickness, porosity and saturation. Production responses from beds 19 and 23 are similar to the trends observed for bed 18. Oil production from these beds for the fractured model increases two to four times while the gas production increase is six to eight times. Thus the effective GOR values for the fractured model are 1.5-3 times higher than the nonfractured models. Once again, the production from Michelle Ute increases significantly more than the production from Malnar Pike. The water saturation for Michelle Ute in zone 23 is 100%. In a nonfractured environment, there is no avenue for the drainage of oil that lies beyond the well grid block. The fractures provide this drainage capability and as a result the oil production in Michelle Ute for bed 23 goes up almost two orders of magnitude. Fractures provide a much larger drainage radius and the fact that Michelle Ute is the only well in its section (section 7) obviously contributes to the observed enhancement in production. The quality of the reservoir around each of the wells also plays an important role.

Beds 30 and 31 also show the same trends with respect to overall oil and gas productions (for the 20-section area). However, the increase in oil and gas productions for the Michelle Ute and Malnar Pike wells is comparable for these two beds. The standard deviation in both the oil and gas production is significantly lower in the fractured model

compared to the nonfractured model. Thus, introduction of a uniform fracture network reduces production uncertainties resulting due to the use of equally probable reservoir images of the nonfractured rock mass. In the dual-porosity dual-permeability approach the fractures act as the main pathways for production. The matrix rock acts only as a source of oil to the fractures. Once the fractures are introduced, they dominate production and reduce the importance of a more accurate representation of the matrix. Even with low values of fracture property parameters, the production from the fractured models for these six zones is much greater than the actual field production. This points to the following possibilities.

- Most of the fractures are closed and for all practical purposes, the reservoir behaves as if it is nonfractured.
- There are even fewer fractures than are represented in the fractured models.
- There is an extensive formation damage at the well bore preventing the realization of the full production potential of each well.

These results are similar to the results for the four-section area models and the single well models. The sensitivity of these models to following fracture properties were studied (Pawar, 1998).

- Fracture frequency
- Fracture porosity
- Fracture permeability

The results were similar to the single well model results, details of which were provided in an earlier report.

Effect of scale on production

It was observed that the low values for different fracture parameters result in low drainage radius for the wells. The reservoir models described earlier were used to study the effect of scale of representation. The single well models for Michelle Ute and Malnar Pike wells were described in a previous report. The effect of scale was studied by using reservoir models for one bed.

In the twenty section models, the production was studied for six different beds. Of the six beds both Michelle Ute and Malnar Pike wells are perforated only in bed 18. The reservoir models for this bed were used to compare the production performance of the single well models and the 20-section area models. The values of fracture properties and matrix permeability used for the 20-section area models were different from the values used for single well models. In the present study, the values of these properties were the same as the ones used for single well models. Limited fracturing was assumed for the area surrounding the well block. Values of fracture porosity, permeability and frequency were listed in Table 3. All the other properties like initial pressure, bubble point pressure, thermodynamic and rock-fluid properties were also the same as the single well models. Flow simulations were performed for 10 different models.

The production results for this bed are compared in Table 5. The table compares the average of cumulative oil and gas production from the layer for Michelle Ute and Malnar Pike wells for the single well model and 20-section model. The total oil production for the Michelle Ute well is about 100,000 stb, while the gas production is about 90 MM scf. For the Malnar Pike well the total oil production is about 84,000 stb, while the gas production is about 80 MM scf. As can be seen from the table for Malnar Pike model there is not a significant difference between the two predictions. For this well the matrix permeability values used were extremely low (0.0001 mD), hence the production is not very significant for both the models. For the Michelle Ute well the oil and gas production are significantly different. The matrix permeability values used for Michelle Ute well were 0.14 mD. For the single well model only a 40-acre area surrounding the well was considered for production. The pressures around this well for the two cases are compared in Figure 26. As can be seen from the pressures for the single well model, the average pressure is much lower than the 20-section model. Due to the surrounding high pressure blocks the production for Michelle Ute well for the 20-section model is more. The average pressure for the 20-section model is still above the bubble point pressure. Thus, for this layer the scale has an effect on production for Michelle Ute well but not for Malnar Pike well.

Conclusions

The production performance of parts of the naturally fractured reservoirs in the Bluebell field was studied through flow simulations performed on numerical models. Two models were developed for Four Sections areas on the east and the west portions of the field. The east-side model was a preliminary model as it took into account only some of the zones responsible for production. The west-side model was developed for the zones responsible for production at the time. Two comprehensive models were developed for two wells on the east portion of the field. These models took into account all the perforated zones. All the models were developed based on the information available through geophysical log analysis. Lack of data on some of the required parameters made model development a challenging task. The numerical values of these parameters were obtained through production history match. Extremely low values of matrix rock permeability and fracture properties were needed for matching production history. The low values of the rock permeabilities are in agreement with the observed values. On the other hand, low values of fracture properties suggest that either the fractures are not contributing to the flow or the field operations have resulted in extensive formation damage near the well bore rendering in noncontributing fractures. The amount of formation damage was quantified through time dependent permeabilities of well bore blocks. A 20-section area on the east side of the Bluebell Field was used to study the effect of fracture on production variability from stochastically generated data. The available geophysical logs were used to identify and characterize all the oil-bearing zones in the entire 20-section area. Reservoir rock properties were calculated for all the zones based on properties calculated from log analyses. Stochastic simulations were performed to generate distributions of rock properties. These simulations were then used to study the variability in fluids in place. A number of zones in the 20-section area had significant amounts of fluids in place. Most of the zones in the 20-section area were not continuous over the entire area. Inclusion of fractures reduced the variability in the production from the 20-section area. In the dual-porosity, dual-permeability approach, the fractures are the main pathways for the flow while the matrix acts as source of fluids. Only the matrix properties were generated through stochastic simulations and the fracture properties were continuous over the study area. Since the fractures dominated the flow, the variability in production due to matrix

properties was reduced. Effect of various fracture properties on the production behavior of the fractured reservoir was also studied. As fracture porosity increased, oil and gas production also increased due to increased oil in place in fractures. Increasing the fracture permeability increased the oil production up to a certain value of permeability, but beyond that the production was limited by the rate of fluid transfer between matrix and fractures. Increase in fracture frequency also increased the oil and gas production only up to a certain fracture frequency. Beyond that particular frequency, the increase in fracture frequency had only a marginal effect on production. Effect of variation in fluid thermodynamic properties on the production was also studied. Increasing the oil API gravity resulted in increased oil production and reduced gas production. Increasing the reservoir temperature did not have any effect on the production performance.

The effect of scale was studied on the production for two wells in the reservoir. The study was performed only for one layer. The results showed that the production performance of Michelle Ute well was affected by scale of study. The production for single well model where only a 40-acre area around the well was studied was lower than the production for 20-section area. The continuity of the sand around the well did increase the production significantly even with low values of fracture and matrix flow properties.

References

Allison, M., 1995: "Increased Oil Production and Reserves from Improved Completion Techniques in the Bluebell Field, Uinta Basin, Utah," Annual Report, USDOE Contract No. DE-FC22-92BC14953 (1995) 1-38.

Andersson, J. and Dverstorp, B., 1987: "Conditional Simulations of Fluid Flow in Three-Dimensional Networks of Discrete Fractures," *Water Resources Research* (Oct. 1987) 1876-1886.

Bai, M., Elsworth, D. and Roegiers, J. C., 1993: "Multiporosity/Multipermeability approach to the Simulation of Naturally Fractured Reservoirs," *Water Resources Research* (June 1993) 1621-1633.

Barenblatt, G. I., Zheltov, I. P., and Kochina, I. N., 1960: "Basic Concepts in the Theory of Seepage of Homogeneous Liquids in Fissured Rocks," J. *Applied Mathematics* (USSR), (1960) **24**, No. 5, 1286-1303.

Bear, J., 1993: "Flow and Contaminant Transport in Fractured Rock," ed. Bear, J., Tsang, C., and de Marsily, G., Academic Press Inc., CA (1993) 1-40.

Brebbia, C. A. and Maier, G. (Eds.), 1985: "Boundary Elements VII - Volume 2, Proceedings of the 7th International Conference," Villa Olmo, Loake Como, Italy, Springer-Verlag (1985) .

Bredehoeft, J. D., Wesley, J. B. and Fouch, T. D., 1994: "Simulations of the Origin of Fluid Pressure, Fracture Generation, and the Movement of Fluids in the Uinta Basin, Utah," *AAPG Bulletin* (Nov. 1994) 1729-1747.

Elsworth, D., 1986: "A Model to Evaluate the Transient Hydraulic Response of Three-Dimensional Sparsely Fractured Rock Masses," *Water Resources Research* (Dec. 1986) 1809-1819.

Elsworth, D., 1987: "A Boundary Element-Finite Element Procedure for Porous and Fractured Media Flow," *Water Resources Research* (Apr. 1987) 551-560.

Fouch, T. D., 1975: "Lithofacies and Related Hydrocarbon Accumulations in Tertiary Strata of the Western and Central Uinta Basin, Utah," in Bolyard, D. W. ed., Symposium on deep drilling frontiers in the central Rocky Mountains: Rocky Mountain Association of Geologists Special Publications (1975) 163-173.

Glasso, O., 1980: "Generalized Pressure-Volume-Temperature Correlations," *JPT* (May 1980) 785-795.

Huang, C. and Evans, D. D., 1985: "A 3-Dimensional Computer Model to Simulate Fluid Flow and Contaminant Transport Through a Rock Fracture System," Report NUREG/CR-4042, U. S. Nuclear Regulatory Commission, (1985) 100-108.

Long, J. C. S., Remer, J. S., Wilson, C. R. and Witherspoon, P. A., 1982: "Porous Media Equivalents for Networks of Discontinuous Fractures," *Water Resources Research* (June 1982) 645-658.

Long, J. C. S., Gilmour, P., Witherspoon, P. A., 1985: "A Model for Steady Fluid Flow in Random Three-Dimensional Networks of Disc-Shaped Fractures," *Water Resources Research* (Aug. 1985) 1105-1115.

Lucas, P. T. and Drexler, J. M., 1976: "Altamont-Bluebell- A Major Naturally Fractured Stratigraphic Trap," *AAPG Memoir* (1976) **24**, 121-135.

Murphy, J. R. and Thomson, N. R., 1993: "Two-Phase Flow in a Variable Aperture Fracture," *Water Resources Research* (Oct. 1993) 3453-3476.

Narr, W. and Currie, J. B., 1982: "Origin of Fracture Porosity-Example from Altamont Field, Utah," *AAPG Bulletin* (Sep. 1982) 1231-1247.

Pawar, R. J., 1998: "Reservoir Characterization and Reservoir Simulation of Fractured and Nonfractured Systems", Ph.D. Dissertation, (1998), University of Utah, Salt Lake City, UT.

Pruess, K. and Narasimhan, T. N., 1982: "On Fluid Reserves and the Production of Superheated Steam from Fracture, Vapor-Dominated Geothermal Reservoirs," *Journal of Geophysical Research* (Nov. 1982) **87**, No. B11, 9329-9339.

Pruess, K. and Narasimhan, T. N., 1985: "A Practical Method for Modeling Fluid and Heat Flow in Fractured Porous media," *SPEJ* (Feb. 1985) 14-26.

Pruess, K., Wang, J. S. Y. and Tsang, Y. W., 1986: "Effective Continuum Approximation for Modeling Fluid Flow in Fractured Porous Tuff," Report SAN F86-7000, Sandia National Laboratories (1986) 1-60.

Rasmussen, T. C., 1991: "Steady Fluid-Flow and Travel-Times in Partially Saturated Fractures Using a Discrete Air-Water Interface," *Water Resources Research* (Jan. 1991) 67-76.

Rasmussen, T. C. and Evans, D. D., 1989: "Fluid Flow and Solute Transport Modeling Through Three-Dimensional Networks of Variably Saturated Discrete Fractures," Report NUREG/CR-5239, (1989) 1-15.

Reeves, M., Ward, D. S., Johns, N. D. and Cranwell, R. M., 1986: "Theory and Implementation for SWIFT II," Report NUREG/CR-3328, U.S. Nuclear Regulatory Commission, (1986) 185-189.

Saidi, A. M., 1983: "Simulation of Naturally Fractured Reservoirs," paper SPE 12270 presented at the SPE Symposium on Reservoir Simulation, San Francisco (1983).

Saidi, A. M., 1987: "Reservoir Engineering of Fractured Reservoirs," Total Edition Presse, Paris (1987) 35-105.

Schrauf, T. W. and Evans, D. D., 1986: "Laboratory Studies of Gas Flow Through a Single Natural Fracture," *Water Resources Research* (May 1986) 1253-1265.

Smith, L. and Schawrtz, F. W., 1984: "An Analysis of the Influence of Fracture Geometry on Mass Transport in Fractured Media," *Water Resources Research* (Sep. 1984) 1241-1252.

Thomas, L. K., Dixon, T. N., Evans, C. E., and Vienot, M. E., 1987: "Ekofisk waterflood Pilot," *JPT* (Feb. 1987) 221-232.

Travis, B. J., 1984: "TRACR3D: A Model of Flow and Transport in Porous/Fractured Media," LA-9667-MS, Los Alamos National Laboratory, Los Alamos, NM (May 1984) 1-35.

Tsang, Y. W., 1984: "The Effect of Tortuosity on Fluid Flow Through a Single Fracture," *Water Resources Research* (Sep. 1984) 1209-1215.

Tsang, Y. W. and Tsang, C. F.,1987: "Channel Model of Flow Through Fractured Media," *Water Resources Research* (Mar. 1987) 467-479.

Van Golf-Racht, T. D., 1982: "Fundamentals of Fractured Reservoir Engineering," Elsevier, Amsterdam (1982) 1-215.

Wagner, M.: "Core Analysis and Description as an Aid to Hydrocarbon Production Enhancement: Lower Green River and Wasatch Formation, Bluebell Field, Uinta Basin, Utah," M. S. Thesis, Brigham Young University (1996).

Wang, J. S. Y. and Narasimhan, T. N., 1985: "Hydrologic Mechanism Governing Fluid Flow in a Partially Saturated, Fractured, Porous Medium," *Water Resources Research* (Dec. 1985) 1861-1874.

Ward, D. S., Harrover, A. L. and Vincent, A. H., 1993: "Data Input Guide for SWIFT/486, Release 2.53", GeoTrans, Inc., Sterling, VA (1993) 1-60.

Warren, J. E., and Root, P. J., 1963: "The Behavior of Naturally Fractured Reservoirs," *SPEJ* (Sep. 1963) 245-255.

Table 1: Parameters for east-side four-section model.

Parameter	Value
Reservoir extent	13000 - 14000 feet
Grid	20 * 20 * 9
Grid block size (x and y)	528 feet
Porosity	0.0 - 0.18
Permeability	0.018 - 0.33 mD
Fracture frequency	1 per 10000 feet
Fracture porosity	0.0005
Fracture permeability	0.023 - 0.04 mD
Pressure	0.5 psi / foot
Oil gravity	35 API
Gas gravity	0.75
Initial GOR	900 scf/stb
Initial bubble point pressure	4146 psi
Initial oil saturation	0.7
Bottom hole pressure	3000 psi

Table 2: Parameters used for the west-side four-section model.

Parameter	Value
Reservoir extent	10250-10628 feet
Grid	20 * 20 * 21
Grid block size (x and y)	528 feet
Porosity	0.0 - 0.26
Permeability	0.08 - 0.18
Fracture porosity	0.0005
Fracture frequency	1/5000 feet
Fracture permeability	0.07 - 0.1
Pressure	0.5 psi / foot
Oil gravity	35 API
Gas gravity	0.75
Initial GOR	400 scf/stb
Initial bubble point pressure	2100 psi
Initial oil saturation	0.7 - 0.9
Bottom hole pressure	2500 psi

Table 3: Numerical parameters for the 20-section models.

Parameter	Value
Grid	41* 33 * 1
Grid block size (x and y)	660 feet
Matrix Permeability	0.5 mD
Pressure	0.5 psi / foot
Oil gravity	35 API
Gas gravity	0.75
Initial GOR	900 scf/stb
Initial bubble point pressure	3950 psi
Initial oil saturation	0.7 - 0.9
Bottom hole pressure	2500 psi

Table 4: Statistics of production from 20-section area for five beds.

Bed 18 (nonfractured)

Statistics	20-section area			Michelle Ute			Malnar Pike		
	Oil (MSTB)	Gas (MMSCF)	Water (MSTB)	Oil (MSTB)	Gas (MMSCF)	Water (MSTB)	Oil (MSTB)	Gas (MMSCF)	Water (MSTB)
Average	785.38	742.24	42.45	20.48	16.73	11.92	35.33	36.84	0.06
Minimum	681.07	680.40	41.06	18.48	11.72	10.84	13.58	19.56	0.0
Maximum	897.95	809.67	43.66	22.44	19.07	18.10	49.33	44.65	0.21
Standard deviation	60.83	37.58	0.86	1.35	2.11	2.20	12.47	8.99	0.08

Bed 18 (fractured)

Statistics	20-section area			Michelle Ute			Malnar Pike		
	Oil (MSTB)	Gas (MMSCF)	Water (MSTB)	Oil (MSTB)	Gas (MMSCF)	Water (MSTB)	Oil (MSTB)	Gas (MMSCF)	Water (MSTB)
Average	247.40	4228.20	19.41	231.06	260.57	7.43	89.95	136.82	0.001
Minimum	2321.70	3925.60	16.30	194.21	242.04	6.53	64.06	89.60	0.00
Maximum	2994.50	4497.60	23.23	263.25	289.00	8.98	132.56	173.24	0.009
Standard deviation	136.40	150.07	1.42	21.53	11.98	0.51	20.09	22.37	0.002

Table 4 continued.

Bed 19 (nonfractured)

Statistics	20-section area			Michelle Ute			Malnar Pike		
	Oil (MSTB)	Gas (MMSCF)	Water (MSTB)	Oil (MSTB)	Gas (MMSCF)	Water (MSTB)	Oil (MSTB)	Gas (MMSCF)	Water (MSTB)
Average	967.11	898.94	39.44	96.25	80.27	7.41	29.11	26.66	0.88
Minimum	894.44	874.15	38.58	82.98	70.49	7.11	17.34	16.51	0.62
Maximum	1003.00	912.60	40.65	110.01	90.88	7.67	38.23	33.29	1.02
Standard deviation	31.65	13.38	0.66	8.66	6.43	0.18	7.17	5.43	0.13

Bed 19 (fractured)

Statistics	20-section area			Michelle Ute			Malnar Pike		
	Oil (MSTB)	Gas (MMSCF)	Water (MSTB)	Oil (MSTB)	Gas (MMSCF)	Water (MSTB)	Oil (MSTB)	Gas (MMSCF)	Water (MSTB)
Average	2850.31	5401.70	12.92	345.31	508.86	3.00	78.19	152.18	0.15
Minimum	2699.40	5123.20	11.18	315.56	469.93	2.60	59.72	99.90	0.00
Maximum	3043.70	5756.10	14.81	373.11	553.13	3.43	105.93	191.22	0.35
Standard deviation	101.13	173.15	0.89	16.42	14.70	0.29	14.04	24.77	0.11

Table 4 continued.

Bed 23 (nonfractured)

Statistics	20-section area			Michelle Ute			Malnar Pike		
	Oil (MSTB)	Gas (MMSCF)	Water (MSTB)	Oil (MSTB)	Gas (MMSCF)	Water (MSTB)	Oil (MSTB)	Gas (MMSCF)	Water (MSTB)
Average	993.23	846.47	274.84	1.71	1.51	73.01	18.24	15.31	8.27
Minimum	681.36	754.64	221.01	0.00	0.00	0.00	11.81	9.91	4.87
Maximum	1106.70	944.67	349.62	8.55	7.49	129.63	31.99	26.50	11.86
Standard deviation	77.28	65.16	35.28	3.44	3.05	46.87	6.85	5.61	2.32

Bed 23 (fractured)

Statistics	20-section area			Michelle Ute			Malnar Pike		
	Oil (MSTB)	Gas (MMSCF)	Water (MSTB)	Oil (MSTB)	Gas (MMSCF)	Water (MSTB)	Oil (MSTB)	Gas (MMSCF)	Water (MSTB)
Average	4441.68	8156.44	179.04	161.28	215.33	44.85	132.76	228.94	7.94
Minimum	4228.90	7689.00	121.23	146.39	197.75	18.97	108.92	200.45	2.15
Maximum	4799.4	8508.5	279	185.17	237.91	63.7	171.71	280.4	14.73
Standard deviation	140.99	172.50	42.91	9.62	9.47	15.71	19.09	18.96	3.98

Table 4 continued.

Bed 30 (nonfractured)

Statistics	20-section area			Michelle Ute			Malnar Pike		
	Oil (MSTB)	Gas (MMSCF)	Water (MSTB)	Oil (MSTB)	Gas (MMSCF)	Water (MSTB)	Oil (MSTB)	Gas (MMSCF)	Water (MSTB)
Average	431.80	370.78	268.57	21.73	18.45	29.96	15.71	13.25	22.97
Minimum	351.28	301.11	217.24	12.41	10.55	23.58	7.58	6.37	19.99
Maximum	496.39	422.1	374.22	28.29	24.05	42.06	27.79	23.59	26.45
Standard deviation	46.85	39.99	47.77	6.13	5.20	6.12	6.66	5.68	2.14

Bed 30 (fractured)

Statistics	20-section area			Michelle Ute			Malnar Pike		
	Oil (MSTB)	Gas (MMSCF)	Water (MSTB)	Oil (MSTB)	Gas (MMSCF)	Water (MSTB)	Oil (MSTB)	Gas (MMSCF)	Water (MSTB)
Average	3492.84	6255.07	214.93	340.49	505.51	31.34	235.06	432.78	22.93
Minimum	3142	5771	146.97	305.1	446.66	15.9	186.72	361.05	15.48
Maximum	3819.2	6710	312.66	377.43	576.28	52.19	313.14	519.57	32.91
Standard deviation	202.35	243.60	41.60	16.52	26.82	9.22	35.28	38.74	4.45

Table 4 continued

Bed 31 (nonfractured)

Statistics	20-section area			Michelle Ute			Malnar Pike		
	Oil (MSTB)	Gas (MMSCF)	Water (MSTB)	Oil (MSTB)	Gas (MMSCF)	Water (MSTB)	Oil (MSTB)	Gas (MMSCF)	Water (MSTB)
Average	298.07	256.42	263.89	28.43	24.16	22.08	36.67	29.40	20.77
Minimum	243.00	212.91	223.4	17.89	15.21	15.58	23.96	19.07	16.24
Maximum	370.97	314.43	330.56	43.91	37.32	31.70	62.51	51.64	27.66
Standard deviation	48.39	38.03	30.72	8.65	7.35	5.51	12.96	11.21	4.69

Bed 31 (fractured)

Statistics	20-section area			Michelle Ute			Malnar Pike		
	Oil (MSTB)	Gas (MMSCF)	Water (MSTB)	Oil (MSTB)	Gas (MMSCF)	Water (MSTB)	Oil (MSTB)	Gas (MMSCF)	Water (MSTB)
Average	2824.33	4720.75	208.43	342.69	425.56	24.51	324.28	576.83	19.06
Minimum	2546.1	4346.9	126.38	309.51	388.35	12.35	276.58	494.88	13.28
Maximum	3222.2	5090.3	324.02	372.2	473.41	33.94	425.48	691.76	27.98
Standard deviation	192.73	183.56	41.43	18.33	22.28	7.0	39.21	45.58	3.57

Table 5: Comparison of production for two model scales.

Michelle Ute				Malnar Pike			
20 Section model		Single well model		20 Section model		Single well model	
Oil (MSTB)	Gas(MSCF)	Oil (MSTB)	Gas(MSCF)	Oil (MSTB)	Gas(MSCF)	Oil (MSTB)	Gas(MSCF)
9.607	8.400	6.896	6.900	0.080	0.060	0.050	0.045

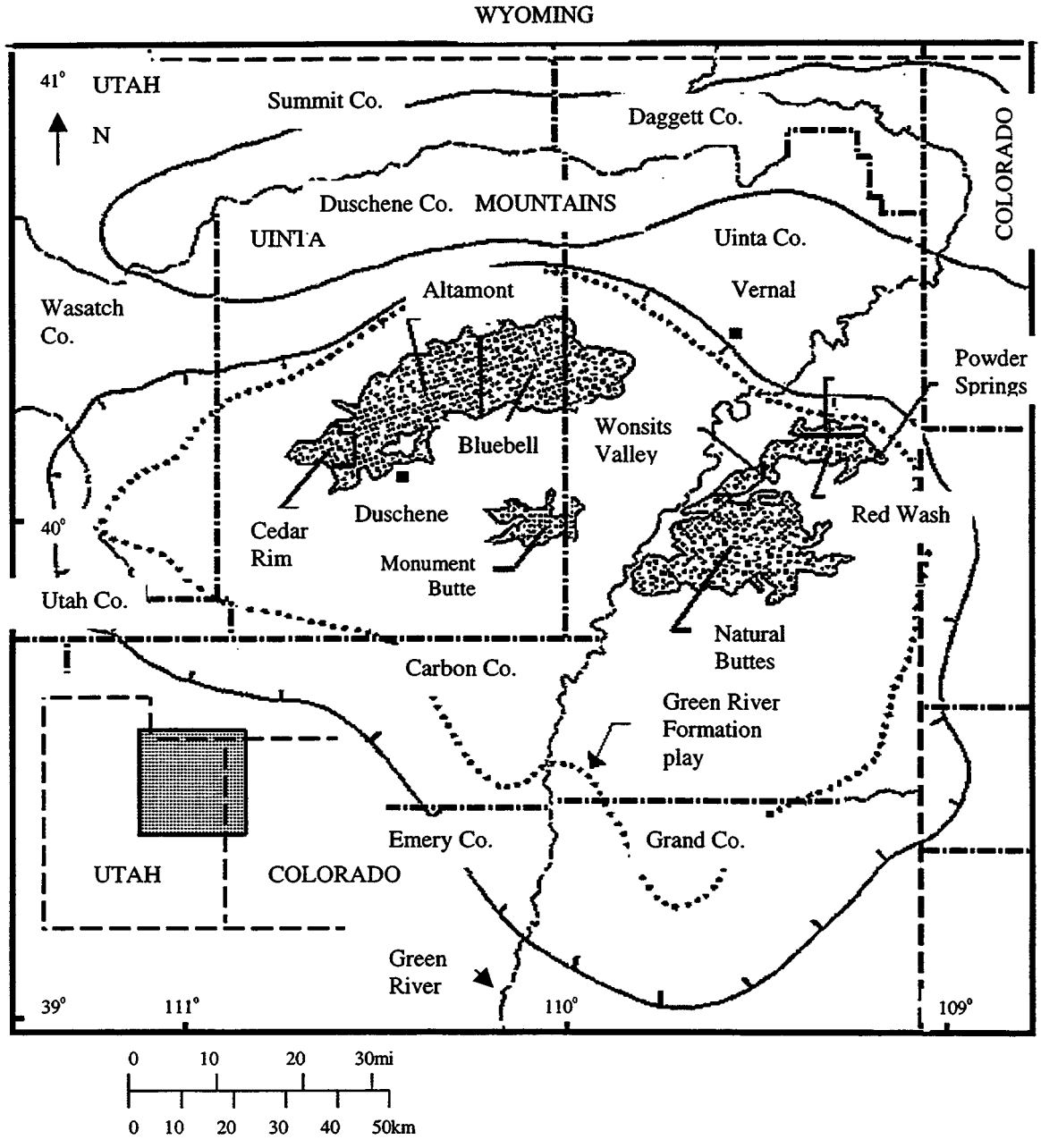

Figure 1: A map of the oil fields in Uinta Basin (Allison, 1995).

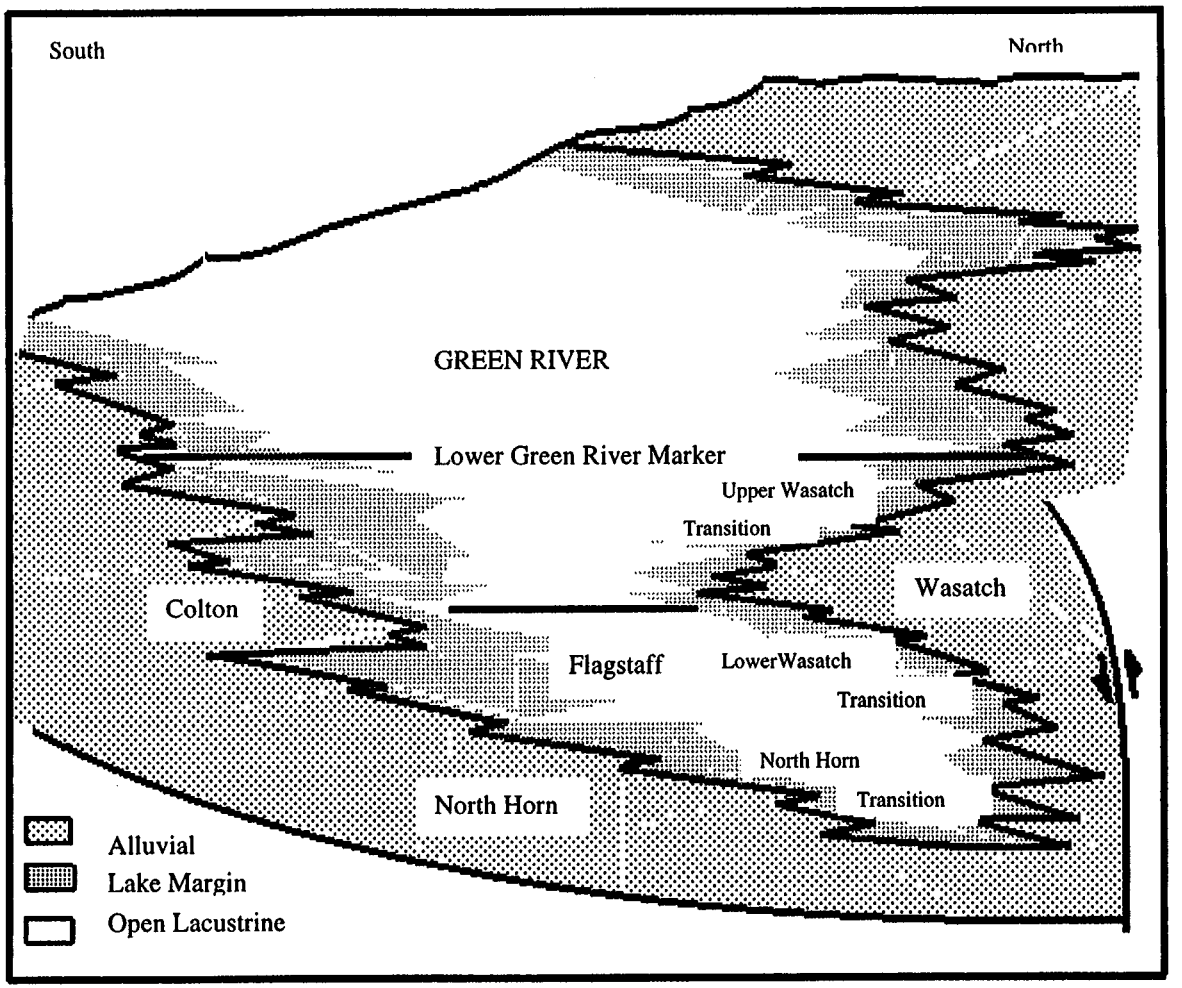

Figure 2: A north-south cross section through Uinta Basin.

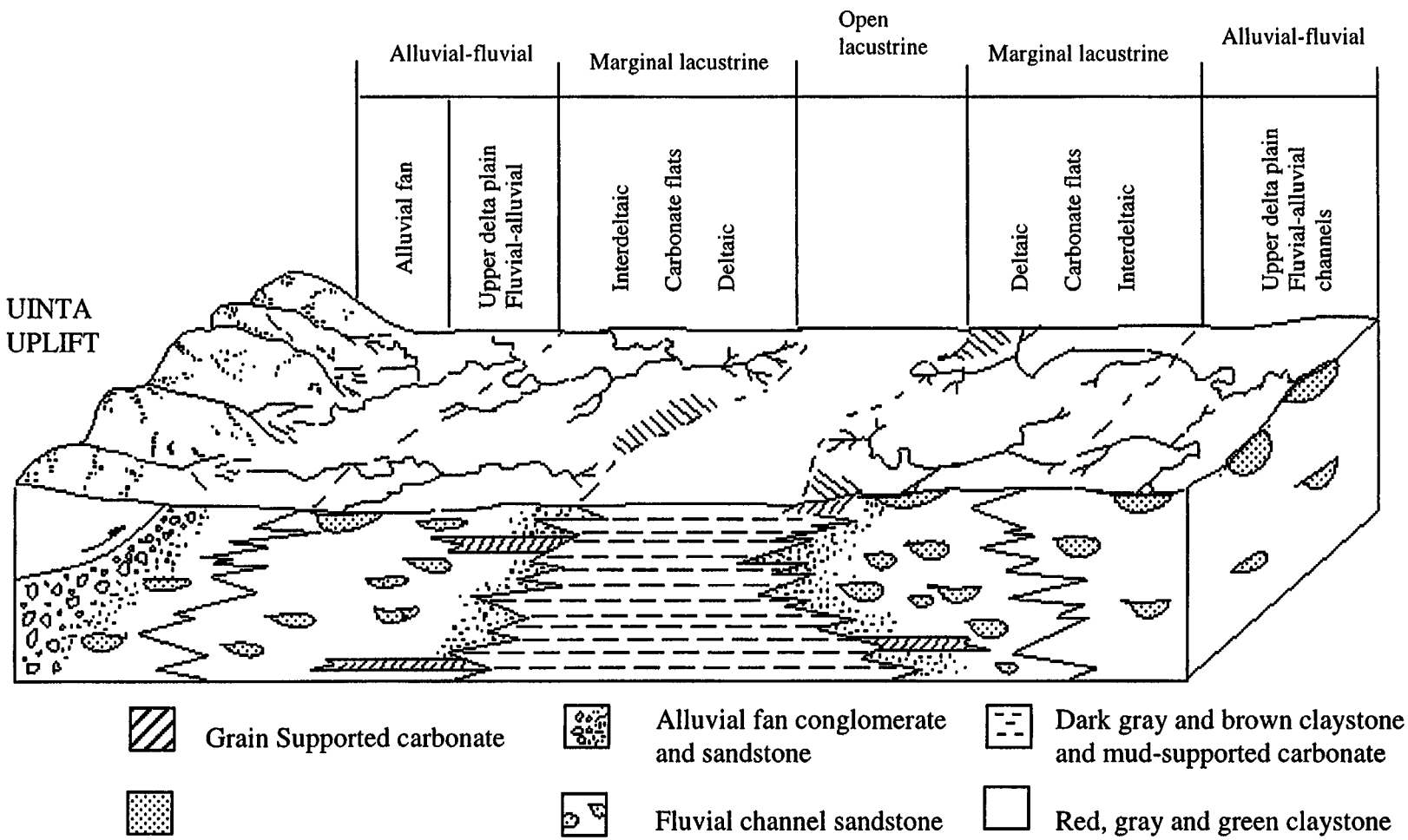

Figure 3: A Conceptual diagram of various depositional environments in the Uinta Basin (Allison, 1995).

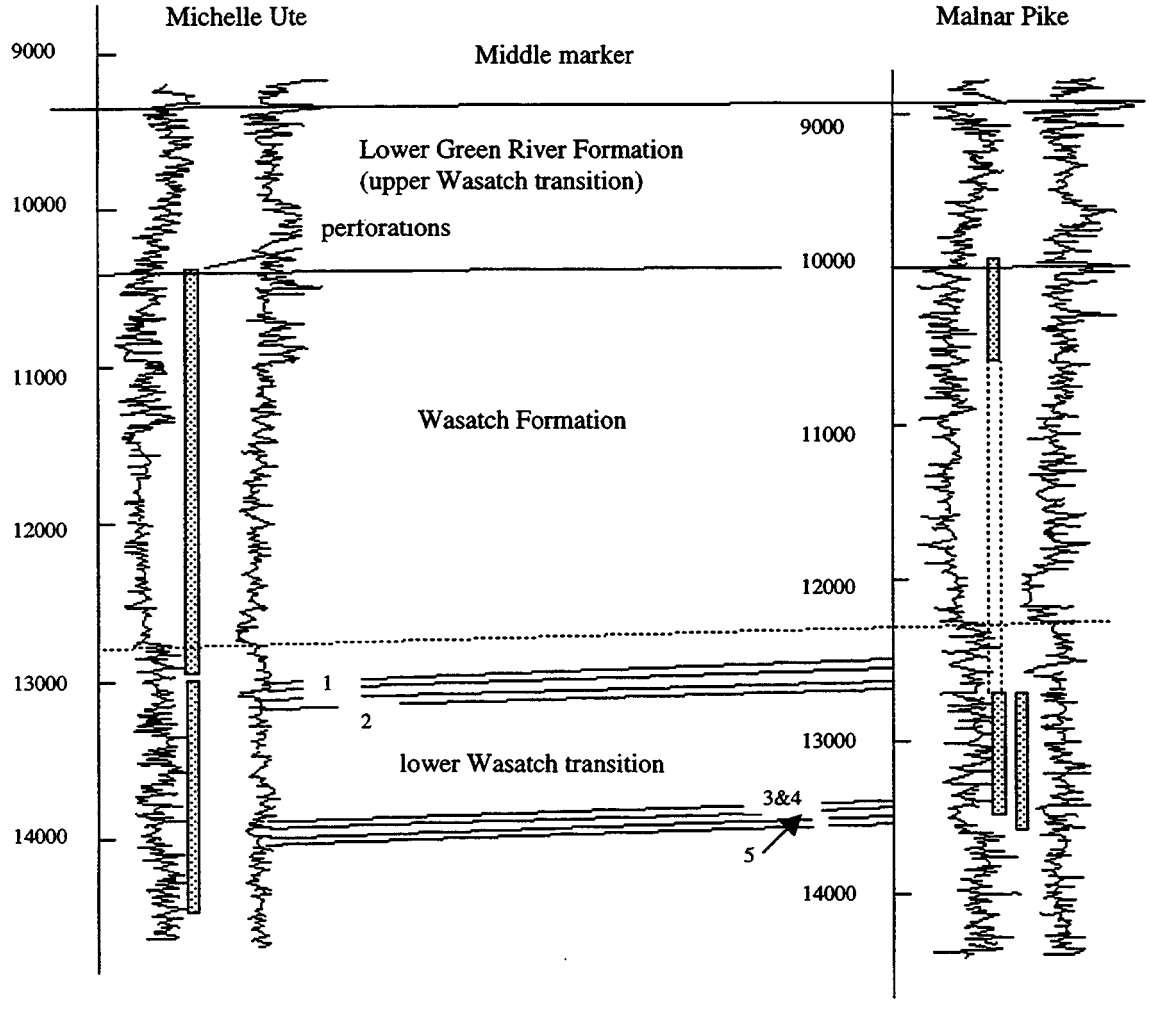

Figure 4: A cross-sectional map showing three intervals in the Bluebell field (reproduced from Allison, 1995).

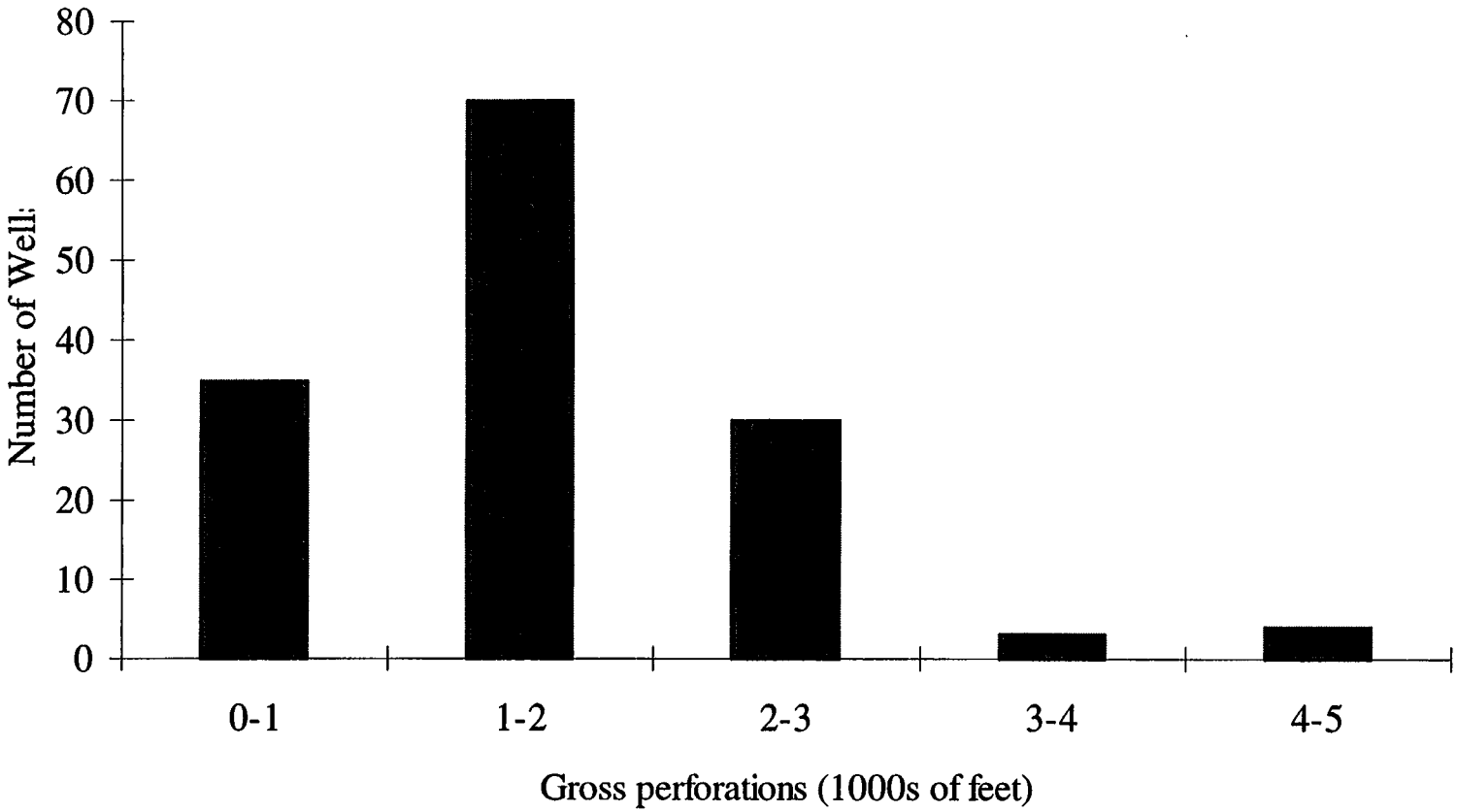

Figure 5: A histogram of gross perforations in the eastern portion of the Bluebell field.

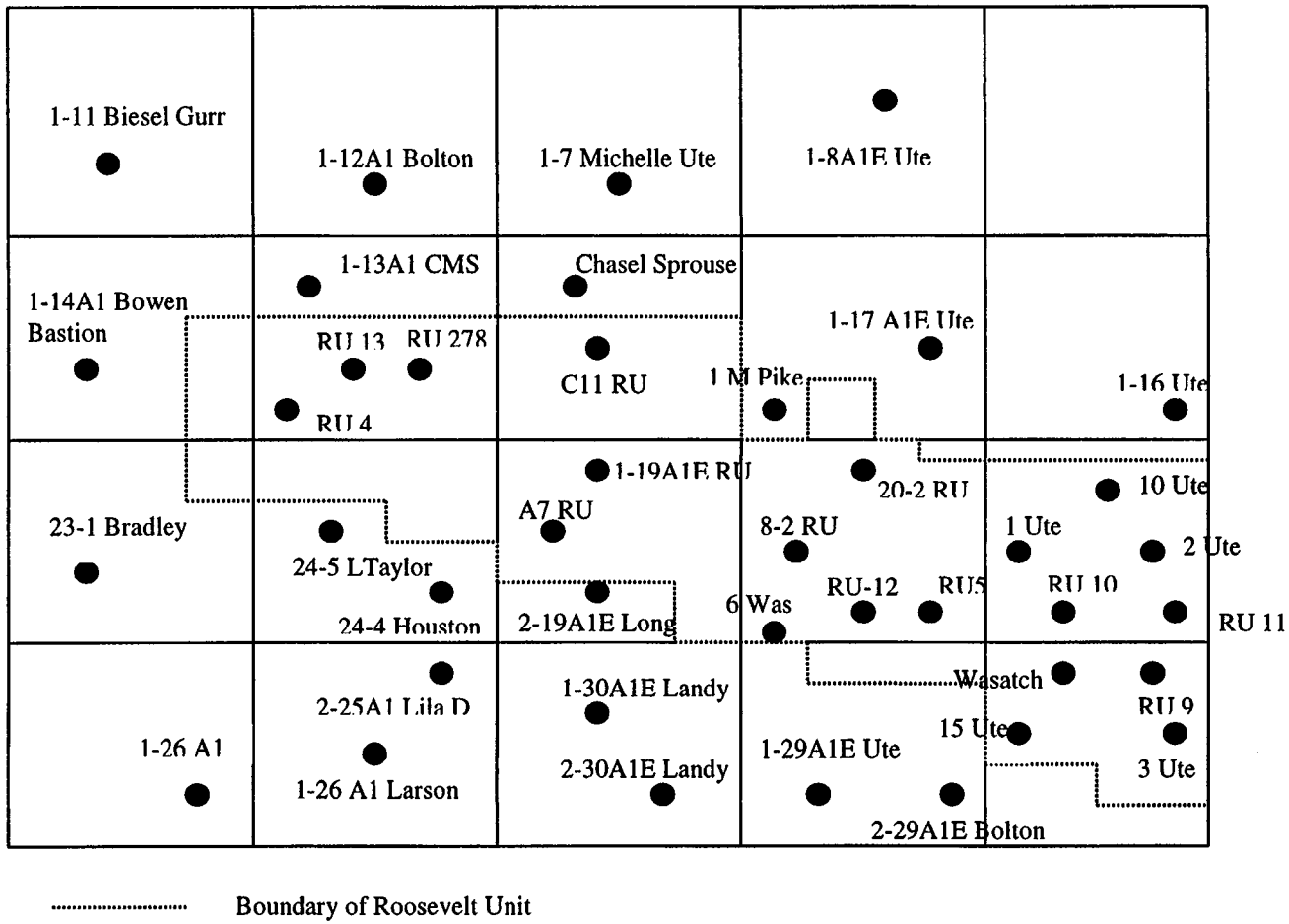

Figure 6: A map of the 20-section study area on the east-side of the Bluebell field.

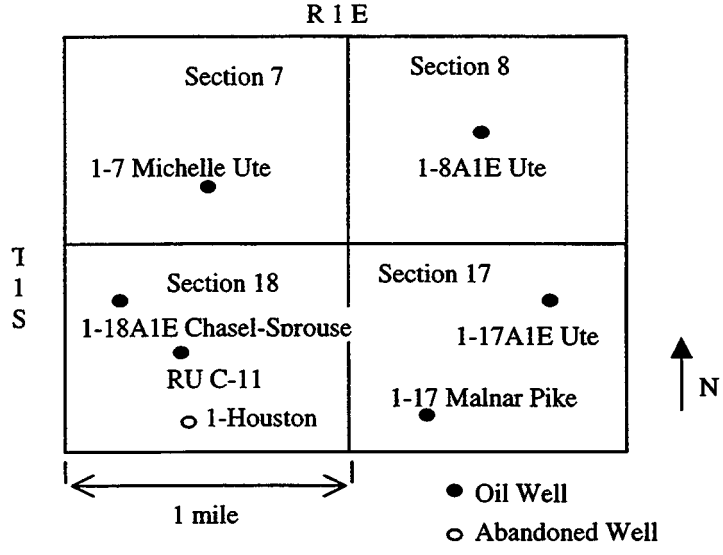

Figure 7: A map of the four-section area on the east-side of the Bluebell field.

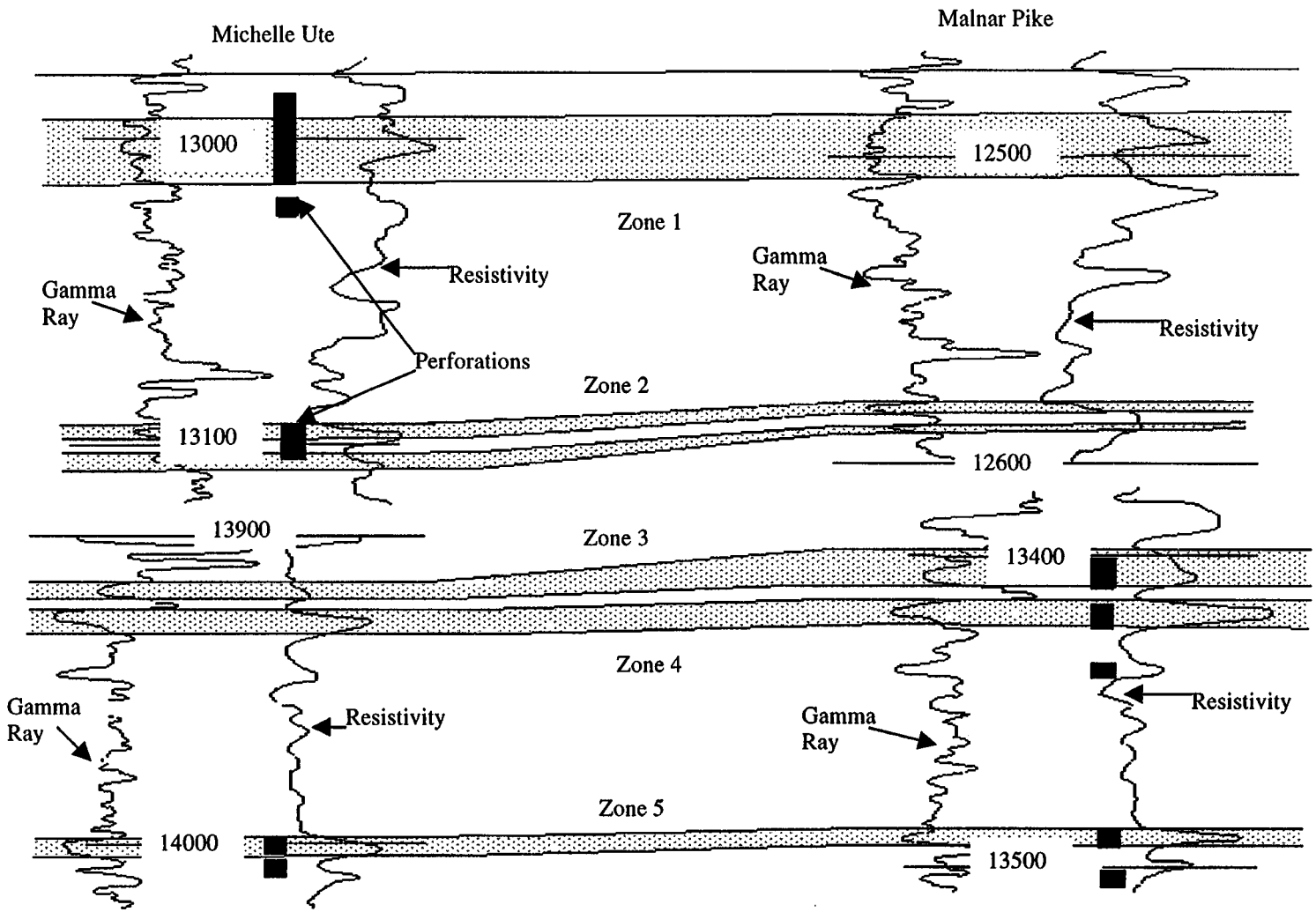

Figure 8: A cross section of the east-side four sections showing the five correlated zones (Allison, 1995).

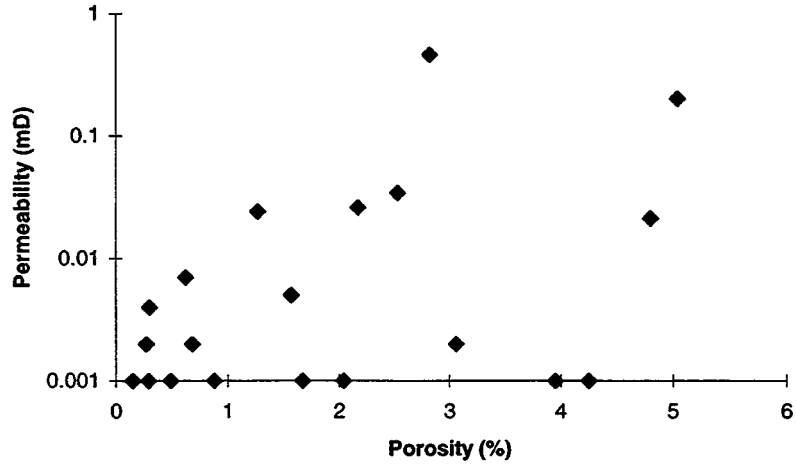

Figure 9: A porosity versus permeability cross plot for core plugs from the Bluebell field.

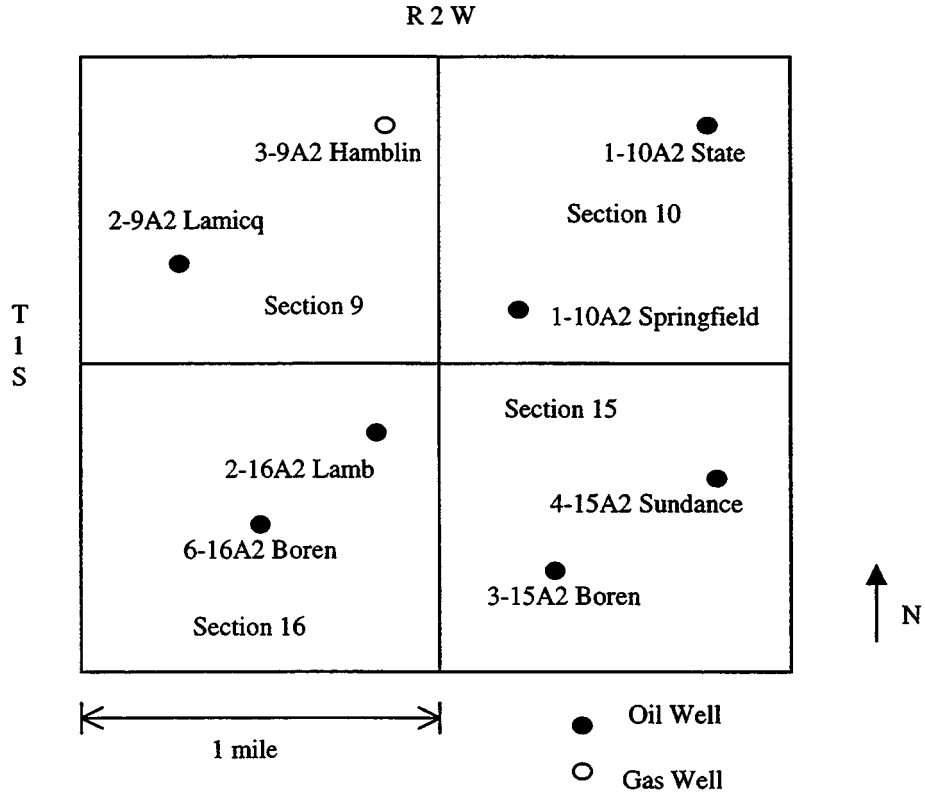

Figure 10: A map of the four-section area on the west-side of the Bluebell field.

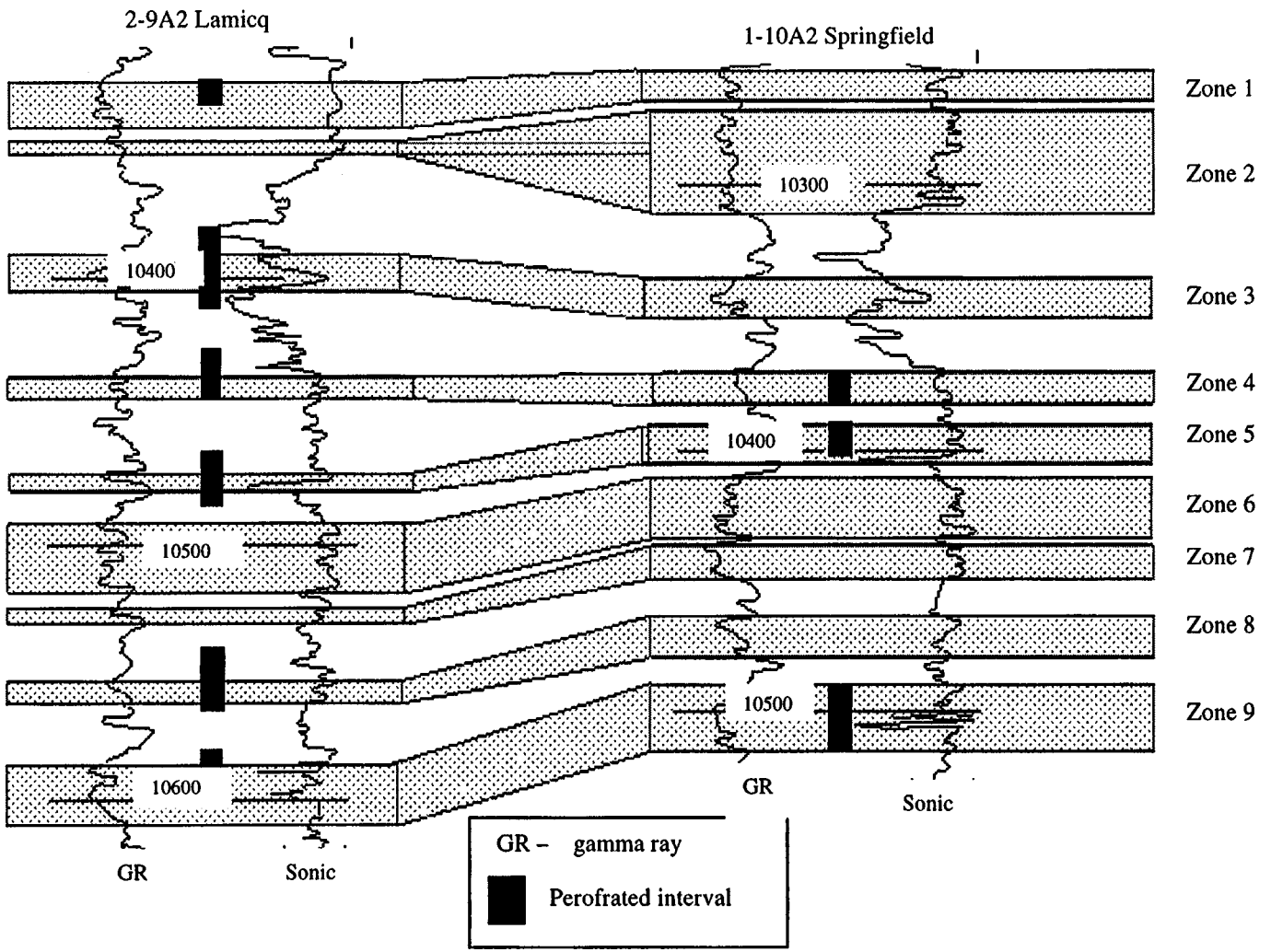

Figure 11: A cross section of the west-side four sections showing 9 of 11 correlated beds (Allison, 1995).

a)

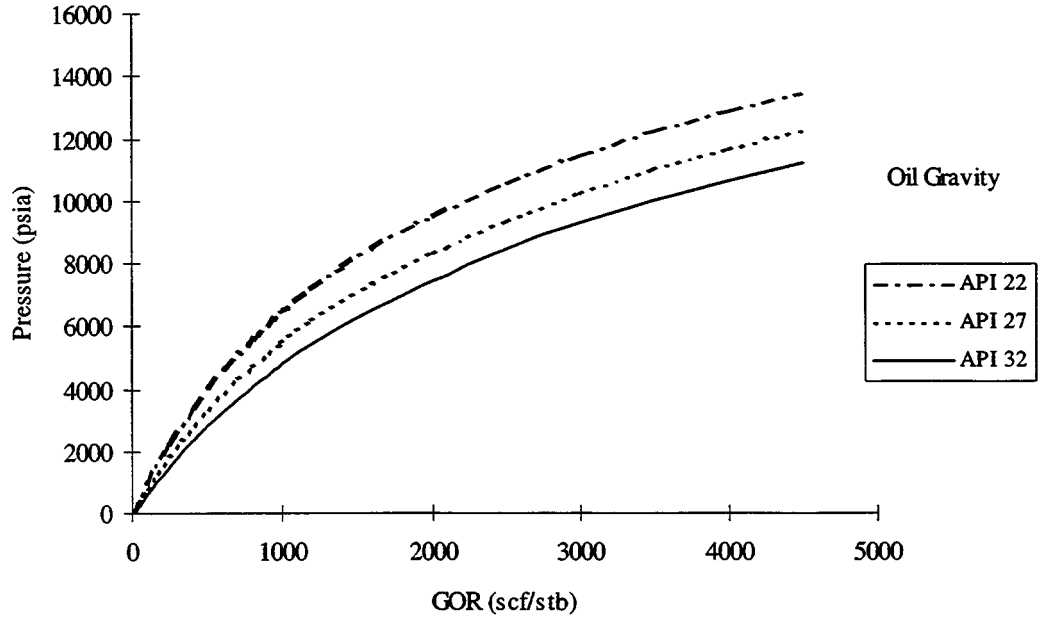

b)

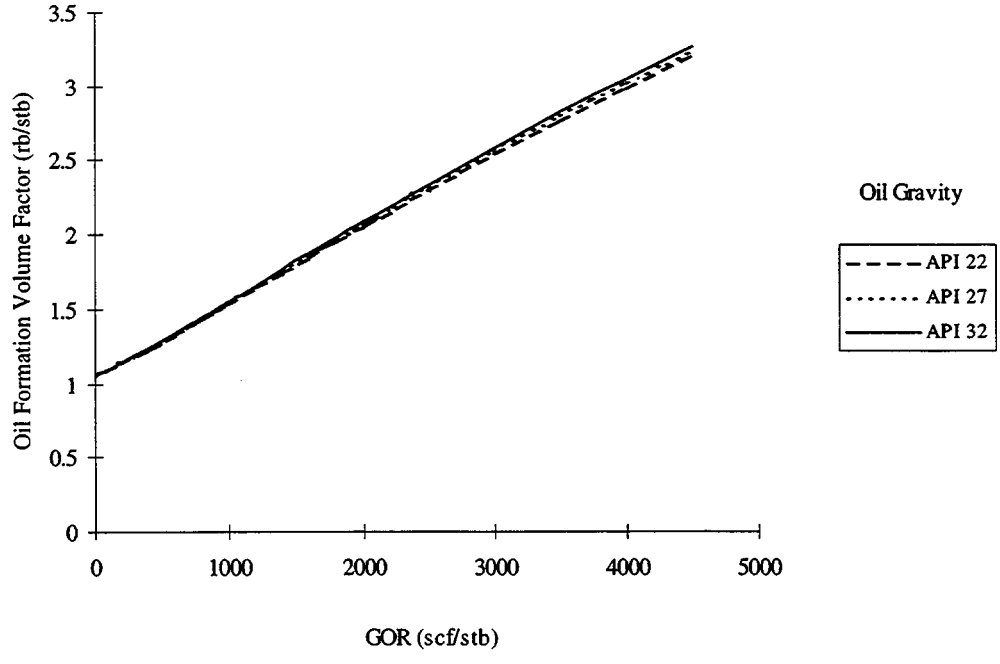

Figure 12: Effect of API gravity on thermodynamic properties at 240 °F: a) bubble point pressure versus GOR, b) oil formation volume factor versus GOR.

a)

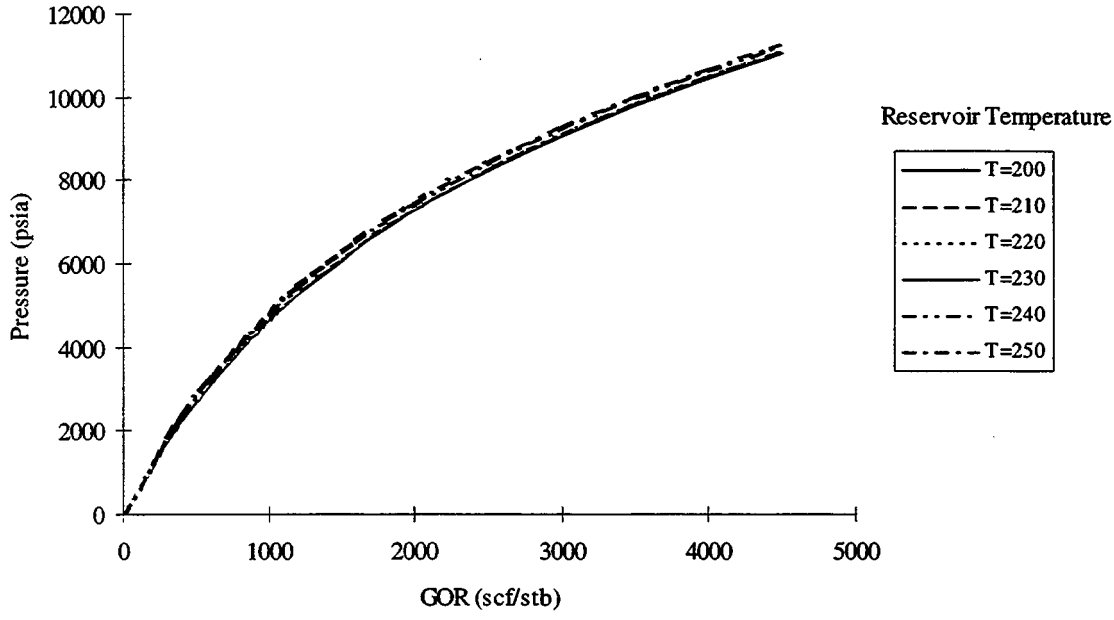

b)

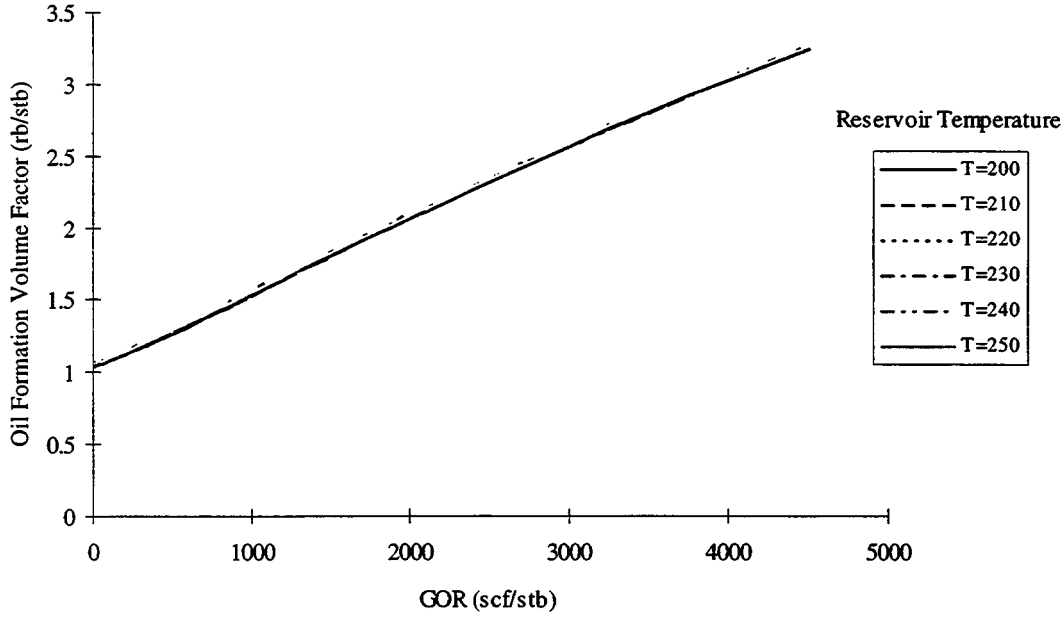

Figure 13: Effect of temperature on thermodynamic properties for 32 API oil and 0.75 gas gravity: a) bubble point pressure versus GOR, b) oil formation volume factor versus GOR.

a)

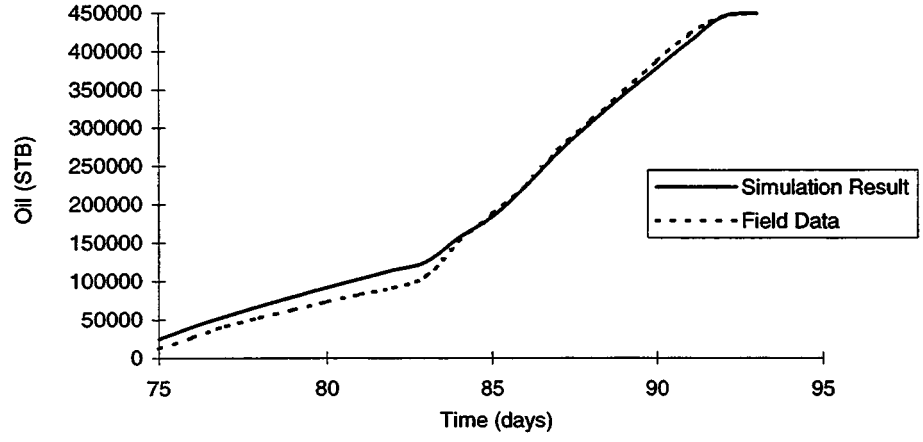

b)

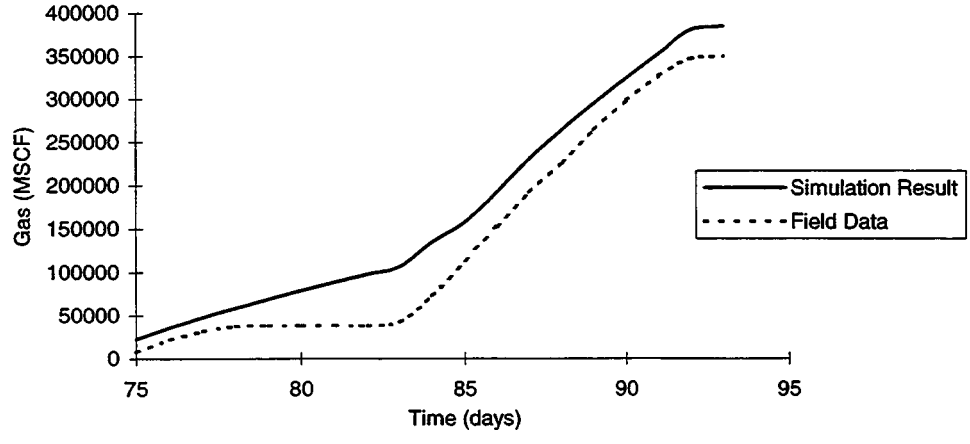

Figure 14: Comparison of the field production data to the simulation results for the east-side four-section area: a) cumulative oil production, b) cumulative gas production.

a)

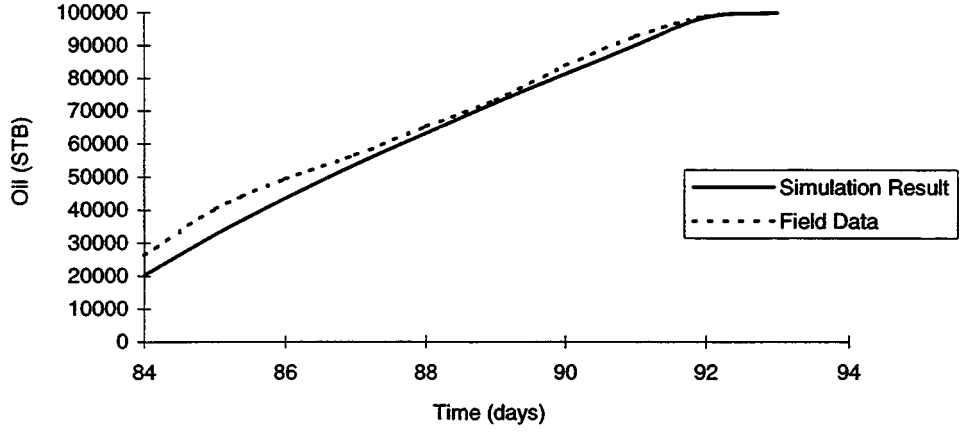

b)

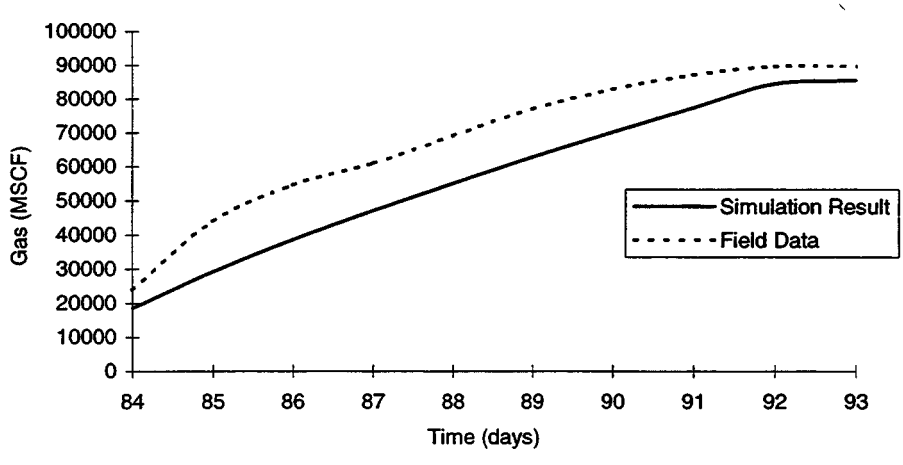

Figure 15: Comparison of the field production data to the simulation results for Michelle Ute well in east-side four-section model: a) cumulative oil production, b) cumulative gas production.

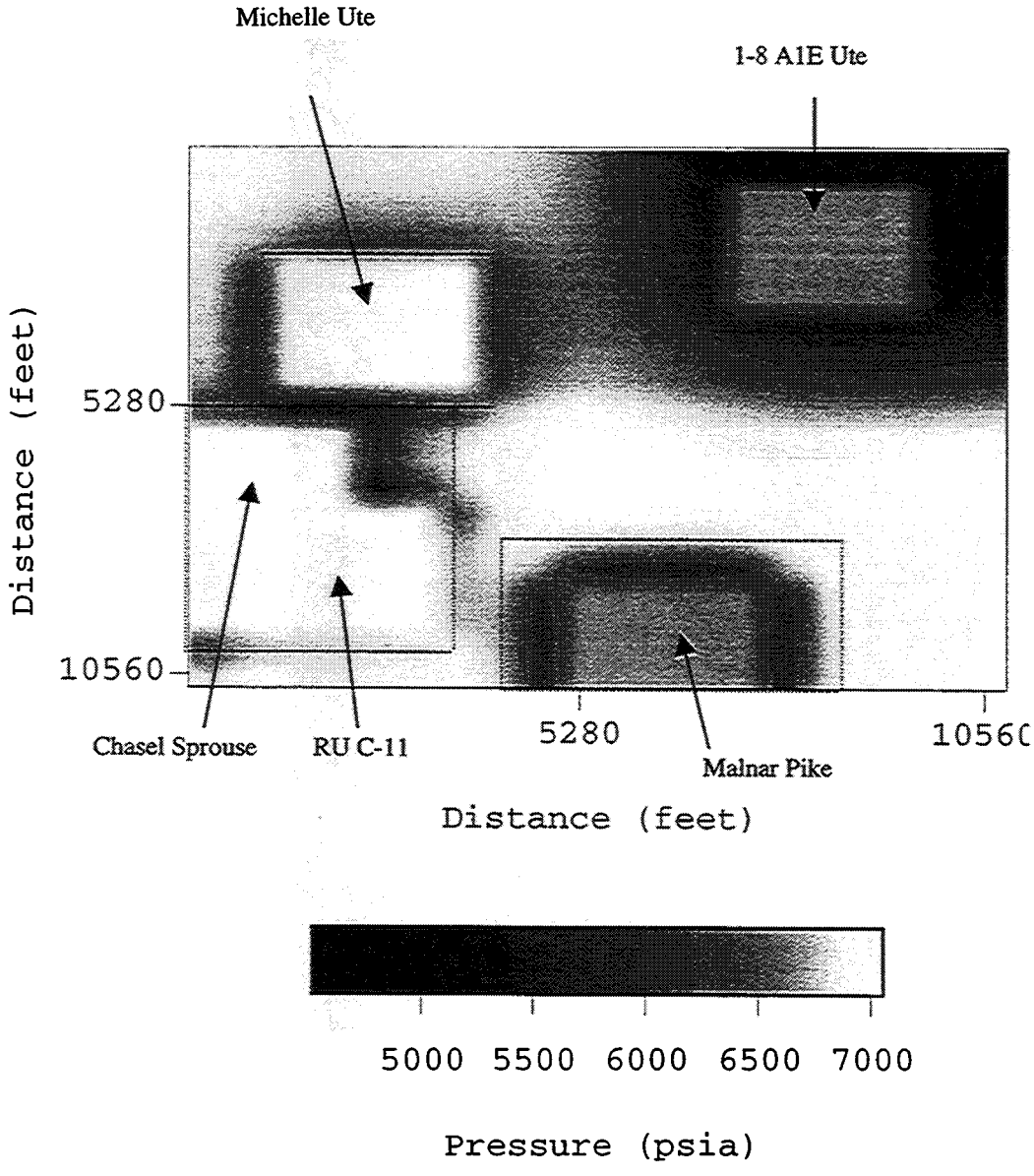

Figure 16: Pressure distribution throughout the east-side four-section area at the end of simulation.

a)

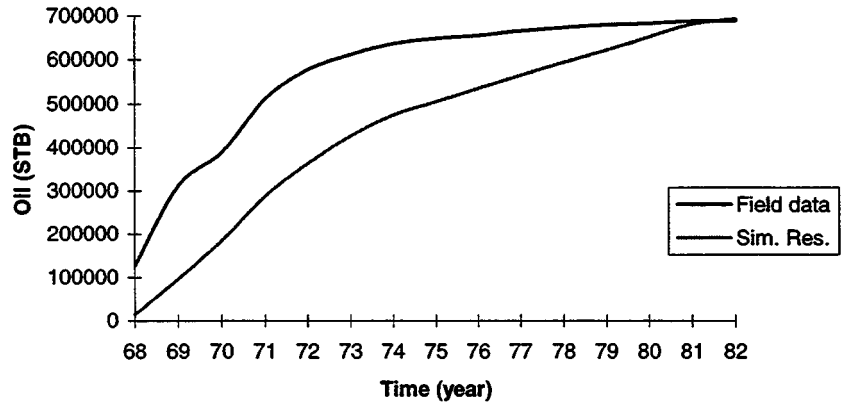

b)

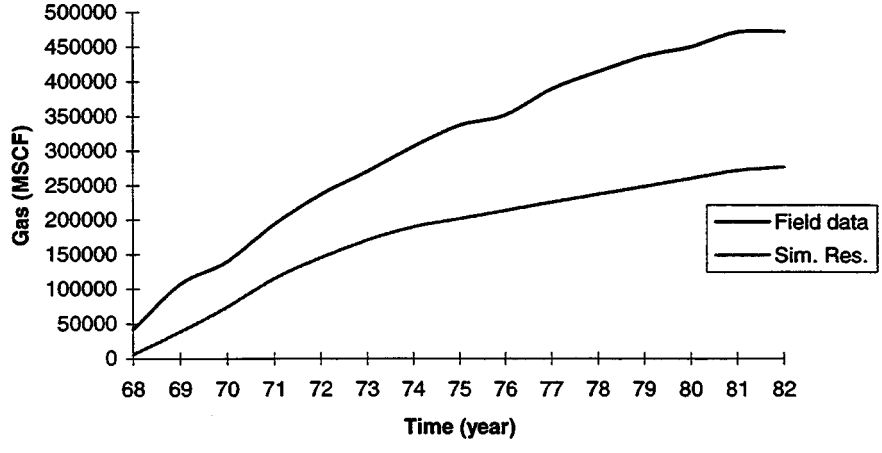

Figure 17: Production history match for the West side four section area model a) oil b) gas.

a)

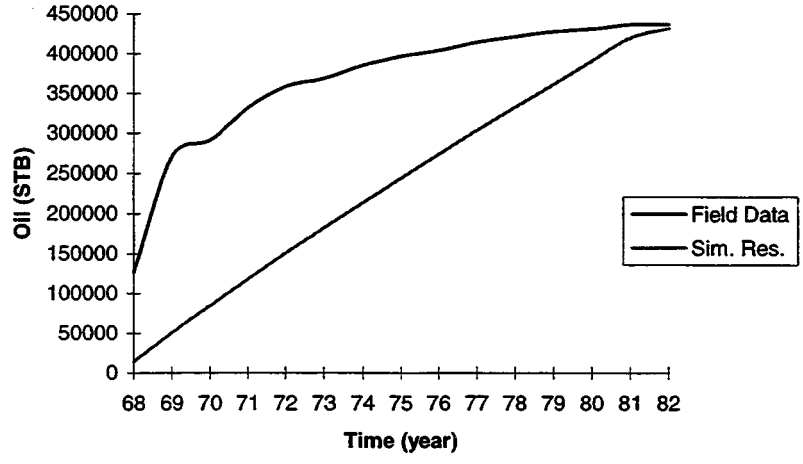

b)

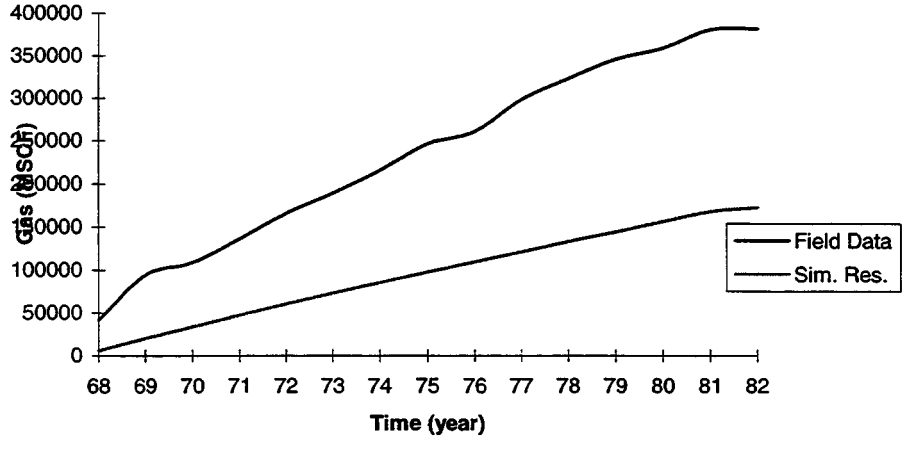

Figure 18: Production history match for well 3-10C a) oil b) gas.

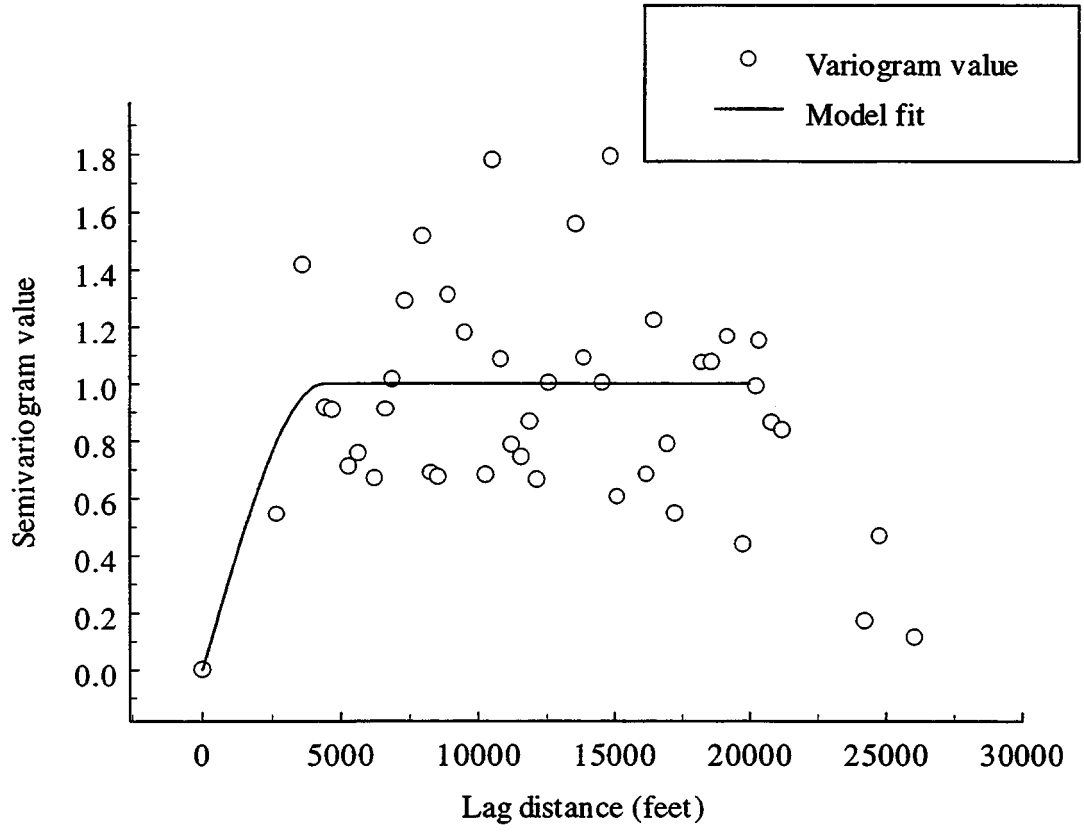

Figure 19: Semivariogram for thickness in bed 30.

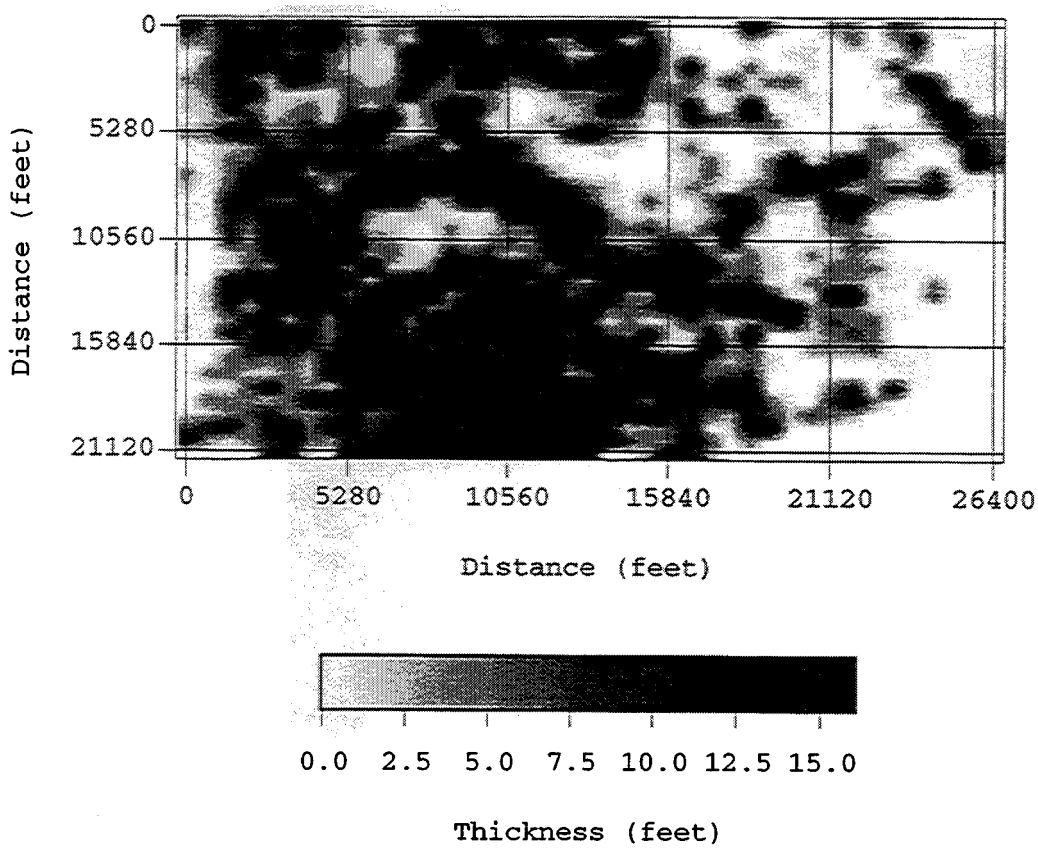

Figure 20: A realization of thickness in bed 30.

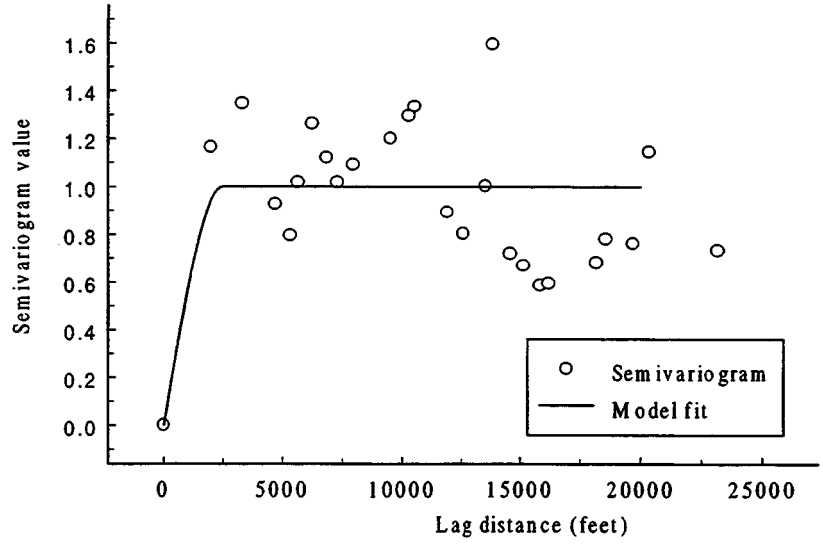

Figure 21: Semivariogram for porosity in bed 30.

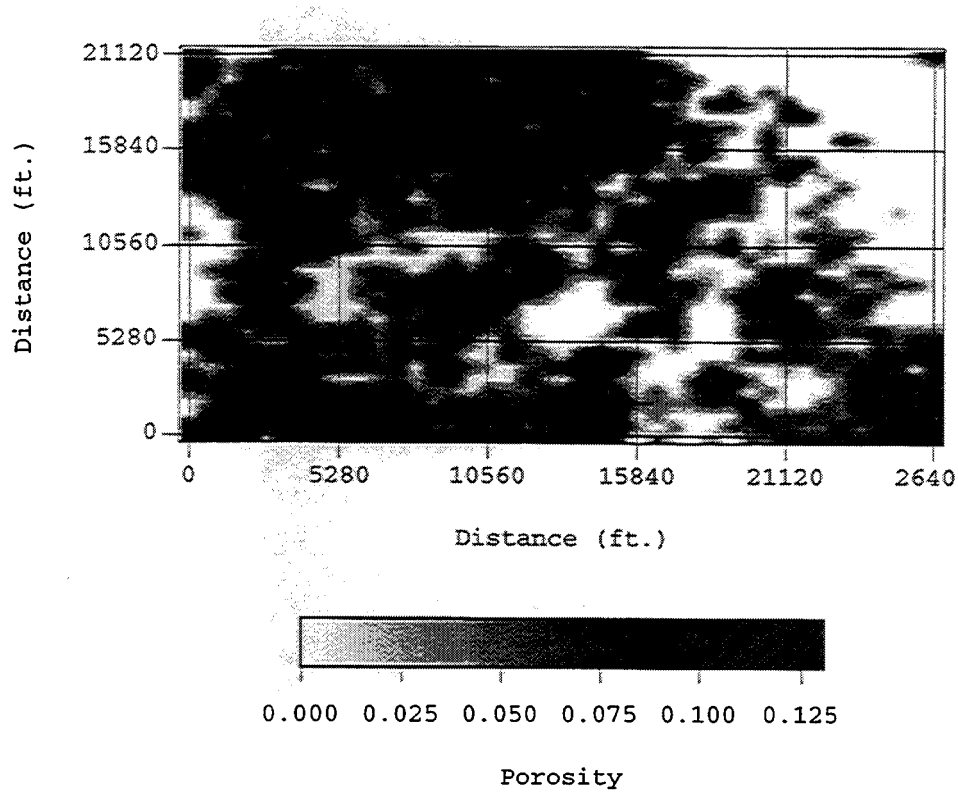

Figure 22: A realization of porosity in bed 30.

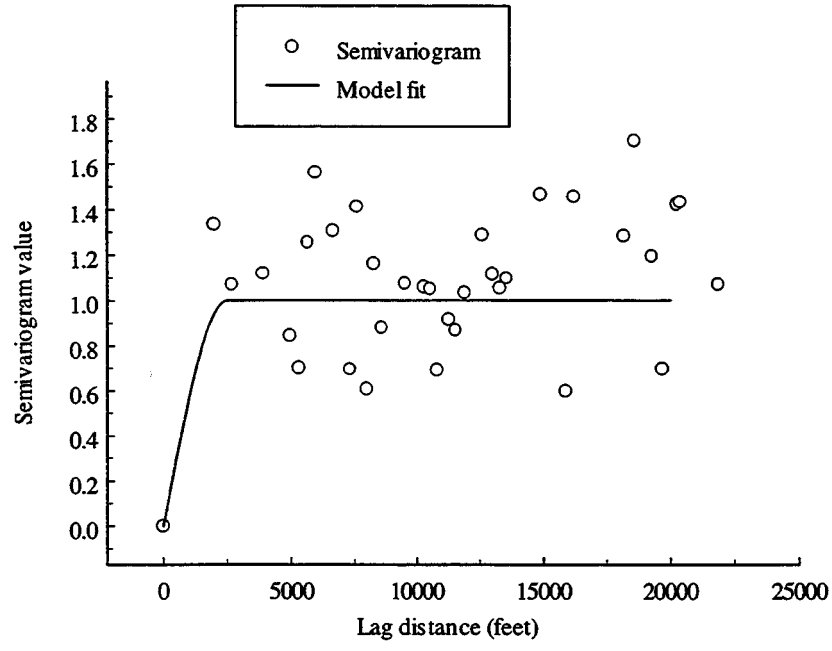

Figure 23: Semivariogram for saturation in bed 30.

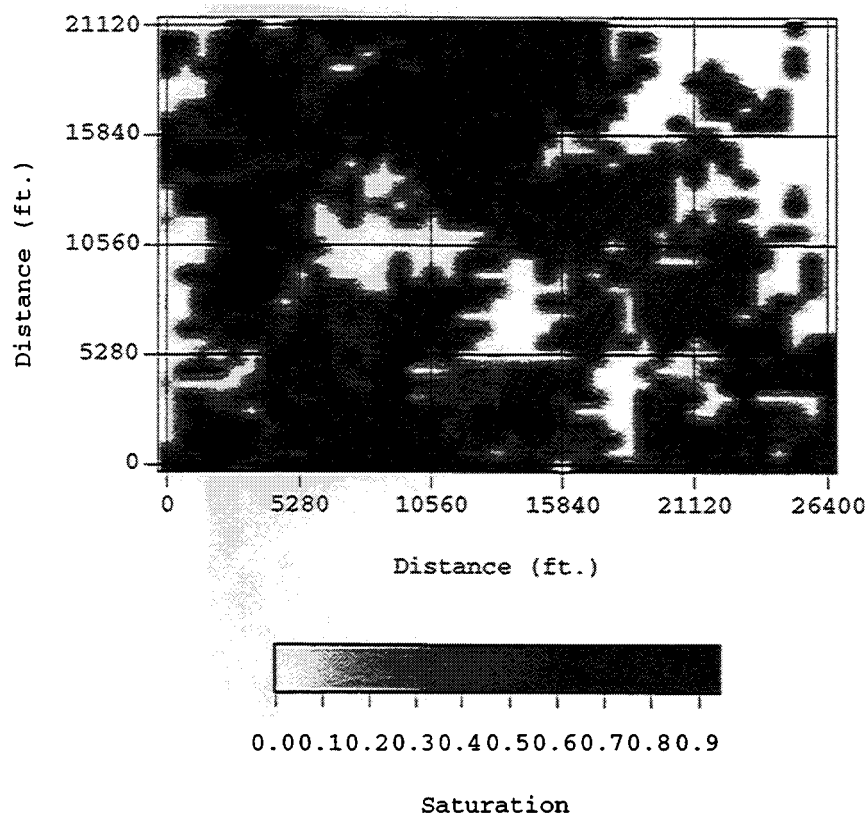

Figure 24: A saturation realization in bed 30.

a)

6180	6159	6104	6169	6184
5863	5579	5263	5814	6058
5427	4387	3134	5111	5831
5381	4988	4524	5210	5735
-	-	5071	5326	5607

Well block

b)

3421	2895	2713	2923	3499
3341	2413	2131	2435	3434
3322	2409	2088	2430	3420
3399	2420	2138	2442	3480
3516	3001	2829	3027	3583

Figure 26: Pressure distributions for well blocks surrounding Michelle Ute well: a) 20-section area model, b) single-well model.

FOSSIL ENERGY

DOE/BC/14953-28
(OSTI ID: 758141)

DELIVERABLE 2.4.4 – EVALUATION AND SINGLE WELL MODELS FOR THE DEMONSTRATION WELLS

Topical Report
March 22, 1999

By
Milind Deo
Craig D. Morgan

Date Published: July 2000

Work Performed Under Contract No. DE-FC22-93BC14953

Utah Geological Survey
Salt Lake City, Utah

National Petroleum Technology Office
U.S. DEPARTMENT OF ENERGY
Tulsa, Oklahoma

DISCLAIMER

This report was prepared as an account of work sponsored by an agency of the United States Government. Neither the United States Government nor any agency thereof, nor any of their employees, makes any warranty, expressed or implied, or assumes any legal liability or responsibility for the accuracy, completeness, or usefulness of any information, apparatus, product, or process disclosed, or represents that its use would not infringe privately owned rights. Reference herein to any specific commercial product, process, or service by trade name, trademark, manufacturer, or otherwise does not necessarily constitute or imply its endorsement, recommendation, or favoring by the United States Government or any agency thereof. The views and opinions of authors expressed herein do not necessarily state or reflect those of the United States Government.

This report has been reproduced directly from the best available copy.

DOE/BC/14953-28
Distribution Category UC-122

Deliverable 2.4.4

Evaluation and Single-Well Models for the Demonstration Wells

By
Milind Deo
Craig D. Morgan

July 2000

Work Performed Under Contract No DE-FC22-92BC14952

Prepared for
U.S. Department of Energy
Assistant Secretary for Fossil Energy

Gary Walker, Project Manager
National Petroleum Technology Office
P.O. Box 3628
Tulsa, OK 74101

Prepared by
Utah Geological Survey
1594 West North Temple, Suite 3110
Salt Lake City, Utah 84114-6100

TABLE OF CONTENTS

Single-well models and Evaluation of Treatments 1
Model parameters 1
Initial History match 1
Model Sensitivity 3
Model Updates and Prediction of the Performance of the Treatment 6
Summary and Conclusions 8

Tables 9-11
Figures 12-21

Deliverable 2.4.4

Single-well models and Evaluation of Treatments

Two single-well models were developed for Michelle Ute and Malnar Pike wells. The perforated intervals span thousands of feet in both the wells. Geological properties were calculated for all the perforated beds. The information was used to develop models for these two wells. These were comprehensive models since they took into account all the perforated beds.

Model parameters

Both Michelle Ute and Malnar Pike wells are perforated in multiple beds. Michelle Ute is perforated in 69 beds, while Malnar Pike is perforated in 55 beds. The models were developed for a 40 acre (1320 feet in the x and y directions) area surrounding the wells. The property values observed at the well bores were assumed continuous over the entire 40-acre area surrounding the well. The numerical values used for various parameters are listed in Table 1.

The models had 8 blocks with x and y dimensions 165 feet (in the x and y directions each). Low-porosity, low-permeability blocks separated the blocks representing perforated zones. This resulted in 109 layers in the vertical direction for the Malnar Pike model and 137 layers for the Michelle Ute model. The thickness of the grid blocks varied according to the log calculated thickness data. The initial saturation varied according to the values calculated from logs. The initial pressure varied with depth at a gradient of 0.5 psi/foot. The bottom-hole pressure was 3000 psi for the first year of production and 2000 psi in subsequent years of production. The initial GOR was set to the average GORs observed during the first month of production in each well.

Initial History match

The field production operations were duplicated for the history match. Therefore, it is not clearly understood which beds in any particular well are responsible for production. Even

though the wells were perforated in multiple beds, all the beds were not perforated at the same time. This was taken into account in the models by opening up the respective beds at appropriate times. The permeabilities of the grid blocks representing the perforated beds were adjusted to match the field oil and gas production. Initially, only the permeabilities of the beds perforated at that time were adjusted until the next sets of perforations were added. When the new set of perforations were added, only the properties of newly perforated beds were adjusted. The properties of the set of perforations already open were not changed. In order to match the production data, the overall permeabilities were reduced after the last sets of perforations were added for both the wells. For Michelle Ute well the overall permeabilities were reduced to 8% of the original values, while for Malnar Pike well the overall permeabilities were reduced to 1% of the original value.

The model predictions for the cumulative oil and gas productions for Malnar Pike well are compared with the field data in Figures 1a and 1b. Figures 2a and 2b show the comparisons for Michelle Ute well. As can be seen from the figures, the model predictions are in close agreement with the field data. The oil production match is better than the gas production, though the gas production predictions are not significantly different than the field data.

The permeabilities and the fracture properties used to obtain the history match are listed in Table 1. Extremely low permeability values of these properties were needed to obtain the production history match. There was a significant difference between the matrix permeability values used for the two models. The matrix permeability for Malnar Pike model varied between 0.1 - 2.5 mD, while for Michelle Ute model it varied between 0.005 - 0.09 mD. For both the models, the fracture porosity was only 0.02% of the reservoir volume. The fracture frequency was 1 per 165 feet for Michelle Ute model and 1 per 125 feet for Malnar Pike model. The fracture permeability was constant at 0.23 mD for Michelle Ute model and varied between 0.02 - 0.22 mD for Malnar Pike model. These were adjusted when evaluating the performances of treatments in these wells.

The numerical models (four-section, as well as single-well) do a reasonably good job of matching the field production data. The numerical parameters used for the matrix rock permeability and the fracture properties are extremely low. The low values of the matrix permeability are close to the experimentally observed values. Other researchers also have observed extremely tight reservoir bed rocks in the Bluebell Field (1, 2). Because of the tight nature of the reservoirs, the production from the Altamont and Bluebell fields is due to the presence of naturally occurring fracture networks (1, 2, 3). The high production from the wells in the west four-section area is due to the good quality of the reservoirs. These reservoirs have sands with high cumulative thickness and average porosity. Even these good quality sands do not produce up to their full potential due to the low values of fracture properties used. The extreme low values of the fracture properties in all the models suggest that the fractures are not fully contributing to the production. Wagner (4) analyzed some of the cores from the Bluebell Field for fractures. A large number of the fractures were filled with calcite, pyrite or clay. One of the other reasons for non-contributing fractures could be damage to the formation near the well bore. Frequent treatment to the reservoir rocks could damage the near well bore region. It could also fill the fractures near well bore, rendering them ineffective for fluid flow. For the Michelle Ute and Malnar Pike wells, the overall permeability values had to be reduced significantly to match the production. The permeability reductions were applied only to the well bore blocks and not to the entire model. The values were reduced after the final sets of perforations were added to the wells. These extreme reductions in the permeability values (92 % for Michelle Ute and 99% for Malnar Pike) suggest that the near well bore formations have been damaged with time. The reductions required can be used to quantify the level of damage.

Model Sensitivity

The numerical values of a number of parameters required for the development of the models were unknown and obtained by trial and error during the history match. This reduced the uniqueness of the numerical models. The sensitivity of the models to changes in various parameters was studied for Michelle Ute model. The variation in oil and gas production was studied with respect to the following parameters.

- Block dimensions
- Fracture porosity
- Fracture frequency
- Fracture permeability

Effect of variation in block dimensions

The initial models were developed with 8 grid blocks with x and y dimensions of 165 feet. The number of blocks were varied by varying the block size from 82.5 to 660 feet in both the x and y directions. Due to the limitations in the flow simulator, the lowest possible block size was 82.5 feet. The production results for various block sizes are plotted in Figure 3. The change in block size did not have significant effect on oil or gas production. The fracture frequency was kept the same for all the models to ensure the same amount of fracture to matrix fluid transfer.

Effect of variation in fracture porosity

The value of the fracture porosity used to obtain the history match was extremely low. The total fracture volume was $2x10^{-6}$ times the entire reservoir volume. The fracture porosity was varied from $2x10^{-6}$ to $2x10^{-2}$ and the effect on overall production was studied. The results are shown in Figure 4

Increasing the fracture porosity from $2x10^{-6}$ to $2x10^{-2}$ had little effect on the cumulative oil production. Comparing the gas production results it can be seen that except for the highest porosity, the cumulative gas production numbers are close to each other. For porosity of 0.02, the gas production was higher than the other models. The average pressure in the reservoir for the models with fracture porosity lower than 0.02 is about 4170 psia. For the model with fracture porosity 0.02 the average pressure is 4090 psia. Comparing the fracture pressures, it can be seen that during most of the production, the pressure for model with high fracture porosity is lower than the models with low fracture porosity. Increased fracture porosity means larger fractured reservoir volume resulting in faster depletion of the reservoir. As the pressure drops below the bubble point pressure, free gas is formed in the reservoir, which is produced preferentially.

Effect of varying the fracture frequency

Fracture frequency is one of the most important parameters characterizing the fracture networks. Fracture frequency is defined as the number of fractures per unit length. For the Michelle Ute well, the fracture frequency used was 1 fracture per 165 feet in the x and the y directions. The fracture frequency was varied from 1 per 165 feet to 1 per 10 feet. The resulting oil and gas production predictions are compared in Figures 5a and 5b.

As can be seen from Figure 5a, a as the number of fractures is increased, the cumulative oil increases steadily. In the dual-porosity, dual-permeability models, the fracture frequency is used to calculate the shape factor in the matrix to fracture transfer function. The shape factor is calculated from effective matrix block dimensions. The effective matrix block dimension decreases with increased fracture frequency, which results in higher value of shape factor. Thus, the amount of oil transferred from matrix to fracture increases with the fracture frequency. With the increased amount of oil transferred to the fracture, the rate of oil production and cumulative oil production increases. Even though reservoir models with higher fracture frequency produce more oil than the ones with lower frequency, the total amount of oil in place is the same for all the models. Increased oil production results in reduced average pressure. The average pressure at the end of the simulations for the model with a frequency of 1 fracture per 10 feet was 4090 psi. For the model with a frequency of 1 fracture per 1320 feet the average pressure was 4370 psi. For the models with high fracture frequency, the amount of gas produced increased due to two reasons. Increased oil production results in increased gas production because of the dissolved gas associated with the produced oil. The second reason is that the lower reservoir pressure results in increased amount of free gas in the reservoir. As the amount of free gas in the reservoir increases, gas is produced preferentially. Thus, for the models with high fracture frequency along with the increased oil production the gas production also increases.

Effect of variation in fracture permeability

To obtain the production history match, both the matrix and the fracture permeability values were varied. The effect of variation in permeability was studied by varying the values of fracture permeability while keeping the matrix permeability values constant. In

the Michelle Ute model, the value of fracture permeability used was 0.23. To see the effect of fracture permeability, it was varied between 0.1 to 50 mD. The oil and gas production results for different fracture permeability values are compared in Figures 6a and 6b.

Increasing the fracture permeability increases the oil as well as gas production for fracture permeabilities up to 5 mD. Above 5 mD, increasing the fracture permeability does not have a significant effect on the production. In the dual-porosity, dual-permeability approach, the oil present in fractures is produced faster since only fractures are connected to the production well. As the amount of oil present in the fracture systems decreases, the production is limited by the rate of oil transfer between matrix and fracture. Since matrix has large storage capacity (hence more oil in place than fractures) it acts as the source of oil to the fractures. The transfer between the matrix and fractures is limited by matrix permeability as well as fracture density. If the values of matrix permeability and fracture frequency are kept constant, increase in fracture permeability above 5 mD does not result in higher production. For the values of different properties used in this model, the fracture permeability cutoff appears to be 5 mD. For another set of values this value may be different.

Model Updates and Prediction of the Performance of the Treatment

In Malnar Pike, two test intervals were treated; test interval 3, between 12950 to 13050 feet and test interval 4 between 12,680 to 12,730 feet. A bridge plug was set at 13060 feet so that the perforations below this depth were not contributing to production. Because of the treatment, the oil production increased from about 20 barrels/day to about 35-40 barrels a day.

The dual-porosity, dual-permeability model employed previously to match oil and gas production from Malnar Pike was modified to assess the treatment. Relevant matrix and fracture properties used in the model are presented in Table 1. The model aerial extent was 40 acres. The well intersected 109 layers; 55 oil bearing layers separated by 54 non oil bearing zones. Each of the zones were assigned appropriate depths.

When measured water saturations were used in the model, water produced from the model was two times the actual water produced in the field. In order to match the field water production, water relative permeabilities were altered. The new set of relative permeabilities are shown in Table 2.

The cumulative oil, gas and water production by October 1997 as predicted by the model are compared with the field totals in Table 3. As can be seen from the table, the agreement between the model predictions and field data is excellent. Even though this end-point history match reasonably good, the oil, gas and water production results from the model differ considerably from the field results (Figures 7, 8 and 9). The oil production from the field is still reasonably well matched; however water and gas data could be improved. Considering the complexity of the data set and the interdependency of data types, the history match is reasonable. The difference between this history match exercise and that reported previously is that an attempt has been made to match the water production data as well.

The model predicted a total oil rate of 16 barrels/day in October 1997. Several different strategies were attempted to match the post treatment rate of about 40 barrels/day. Only the properties in the affected zones were changed at the treatment time. All of the strategies and corresponding rates after treatment are listed in Table 4. It was hypothesized that the treatment would have increased fracture permeabilities, extent of fracturing and or frequency of fracturing. Each of these options were examined either in isolation or in combination with other options. One final option of adding a new zone was also examined.

As seen in Table 4, it is possible to realize the gains in production by a variety of methods. Increasing the fracture permeability to 22 md appeared to provide the most realistic increase in production. However, in most of the strategies examined, the production rate decreased to about 25 barrels/day after about 6 months. Only in the scenario where an equivalent new zone was added to the reservoir, the production

remained steady at around 31 barrels/day well after the zone was opened. The zone was 30 foot thick with a porosity of 0.14 and an initial oil saturation of 0.7. The zone had a matrix permeability of 1.5 and fracture permeability of 2.2 md (properties of the older zones). Assuming only 3% recoverable oil from the zone (based on the performance of the well) it was hypothesized that net reserves of about 27,000 barrels were added the well.

The Michele-Ute model was also revised. Field water production from Michele-Ute is shown in Figure 10. There are apparently two distinct regimes in the water production behavior. The water production rate is very low for about 2700 days of production (December 1992). Only about 5300 barrels of water are produced to this point. The rate drastically increased at this time and the total production reached about 25,000 barrels at 4600 days of production (June 1998). In order to match this behavior, two sets of water relative permeabilities were employed; a set for the first 2700 days and a different set after 2700 days. These relative permeabilities are shown in Table 5.

Michele Ute treatment did not change the oil production rates over the long term. The treatment once again could have increased fracture permeabilities or extent of fracturing. However, since the production rate did not increase over the long run, the fractures must have gone back to their original characteristics.

Summary and Conclusions

The initial history match of the two project wells was reasonably successful. All of the perforated intervals were included. The key feature of both the models was time-varying permeabilities. In the modified models, apart from being able to match the post-treatment rates, attempt was made to match water production from the project wells. In the Michele-Ute well time-varying relative permeabilities were employed. The end-point match for the Malnar Pike well for the cumulative oil, gas and water was excellent. The comprehensive history match over the entire time period was reasonable.

Of the five different possibilities identified in having caused the post-treatment production rate enhancement in Malnar-Pike, increase in fracture permeability was determined to be the most likely factor leading to consistent increase in production rate. Analysis performed by adding a new producing zone showed that the treatment added additional reserves of about 27,000 barrels of oil.

Table 1- Parameters for the comprehensive models for Malnar Pike and Michelle Ute wells.

Parameter	*Malnar Pike*	**Michelle Ute**
Reservoir extent (ft.)	9582 - 14360	10,413 - 14,445
Grid	8 * 8 * 99	8 * 8 * 137
Grid block size (x and y)	165 feet	165 feet
Porosity	0.0 - 0.21	0.0 - 0.16
Matrix permeability	0.1 - 2.5	0.005 - 0.09
Fracture porosity	0.000002	0.000002
Fracture frequency	1 per 125 feet	1 per 165 feet
Fracture permeability	0.02 - 0.22	0.23
Pressure	0.5 psi / foot	0.5 psi/feet
Oil gravity	35 API	35 API
Gas gravity	0.75	0.75
Initial GOR	1100 scf/stb	900 scf/stb
Initial bubble point pressure	4795 psi	4146 psi
Initial oil saturation	0.1 - 1.0	0.0 - 0.86
Bottom hole pressure	3000 psi	3000 psi

Table 2: Relative permeabilities used to obtain the history match for the Malnar Pike well

Water Saturation	Relative permeability to water	Relative permeability to oil
0.22	0.0	1.0
0.3	0.05	0.1
0.35	0.1	0.05
0.4	0.15	0.0175
0.5	0.5	0.0073
0.6	0.7	0.005
0.8	0.9	0.003
0.9	0.96	0.001
1.0	1.0	0.0

Table 3: Production match between the model and field data - Malnar Pike well

* -extrapolated from available data

Production as of December 1993				Production as of October 1997			
Field Data		Model Predictions		Field data		Model Predictions	
Oil (Mstb)	93	Oil (Mstb)	100	Oil (Mstb)	113	Oil (Mstb)	125
Gas (MMscf)	79	Gas (MMscf)	87	Gas (MMscf)	96*	Gas (MMscf)	119
Water (Mstb)	100	Water (Mstb)	102	Water (Mstb)	122*	Water (Mstb)	110

Table 4: Different strategies used in emulating the treatment in Malnar Pike

Strategy	Production rate immediately after treatment (stb/day)	Production rate 4 months after treatment (stb/day)
1. Increase fracture permeability in affected zones from 2.2 to 22 md	39	25
2. Increase extent of fracturing in the affected zones from 495 feet to 660 feet	29	22
3. Combine strategies 1 and 2	35	23
4. Increase fracture frequency to one every 5 feet	41	24
5. Add a new zone 12 feet thick of porosity 0.1 and oil saturation 0.7	39	31

Table 5: Relative permeabilities used is matching water production from Michele-Ute over the entire time interval

Water Saturation	Water relative permeability for the first 2700 days	Water relative permeability for the after 2700 days	Oil relative permeability
0.22	0.0	0.0	1.0
0.3	0.0	0.0	0.7
0.4	0.0	0.0	0.4
0.5	0.003	0.02	0.3
0.6	0.009	0.06	0.05
0.8	0.015	0.1	0.03
0.9	0.021	0.14	0.0
1.0	0.03	0.2	0.0

a)

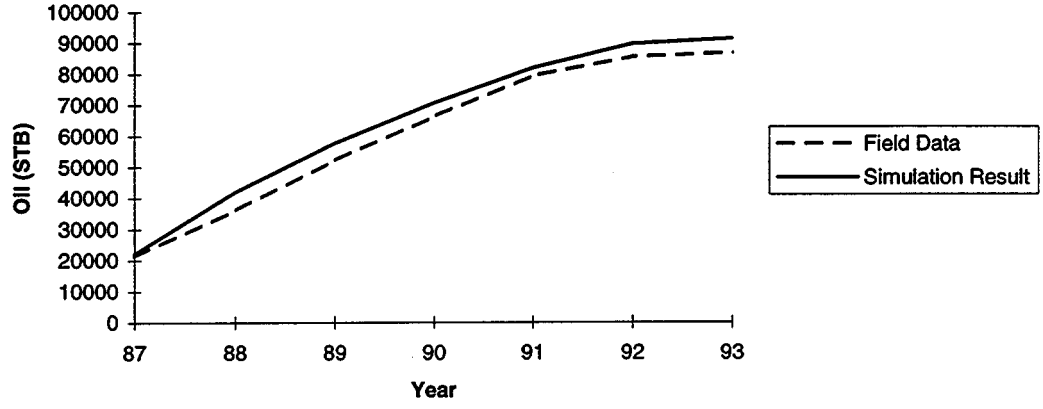

b)

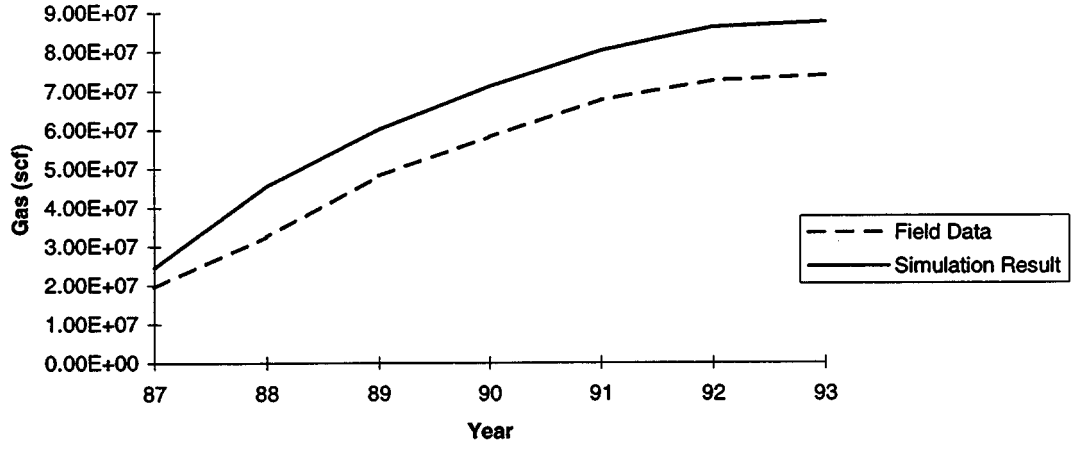

Figure 1: Field production comparison with the original model predictions for the Malnar Pike well: a) cumulative oil production, b) cumulative gas production.

a)

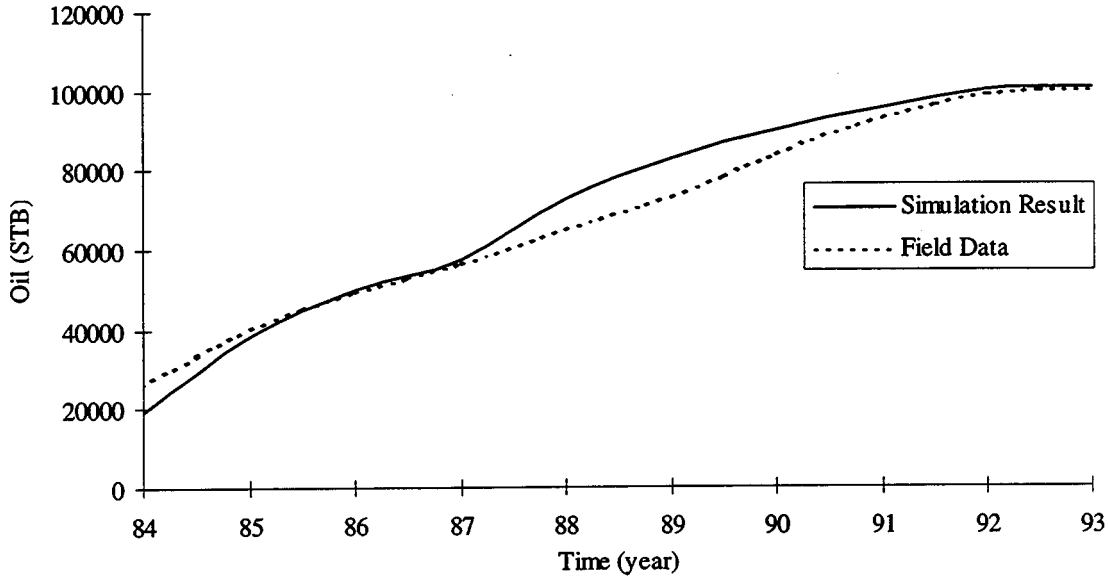

b)

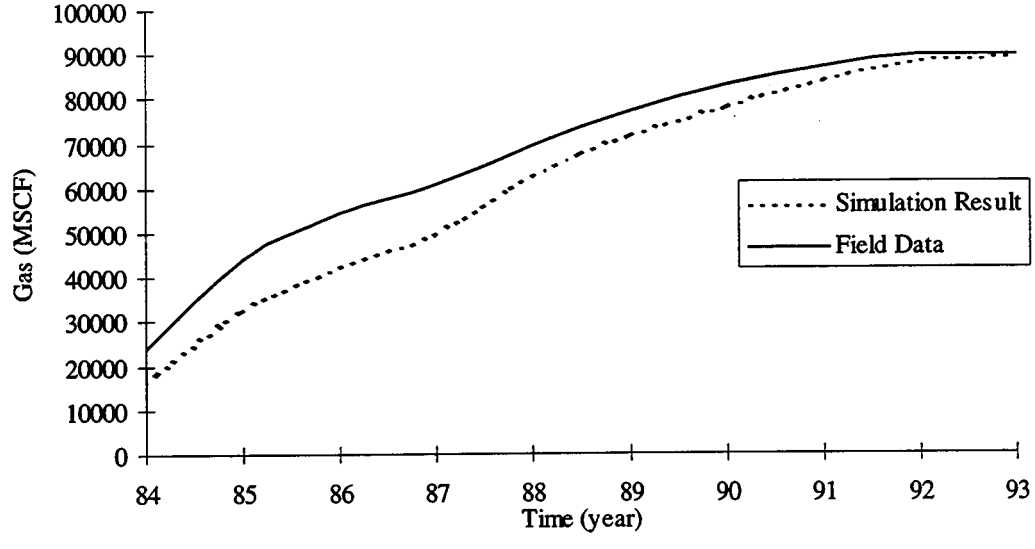

Figure 2: Field production comparison with the original model predictions for Michelle Ute well: a) cumulative oil production, b) cumulative gas production.

a)

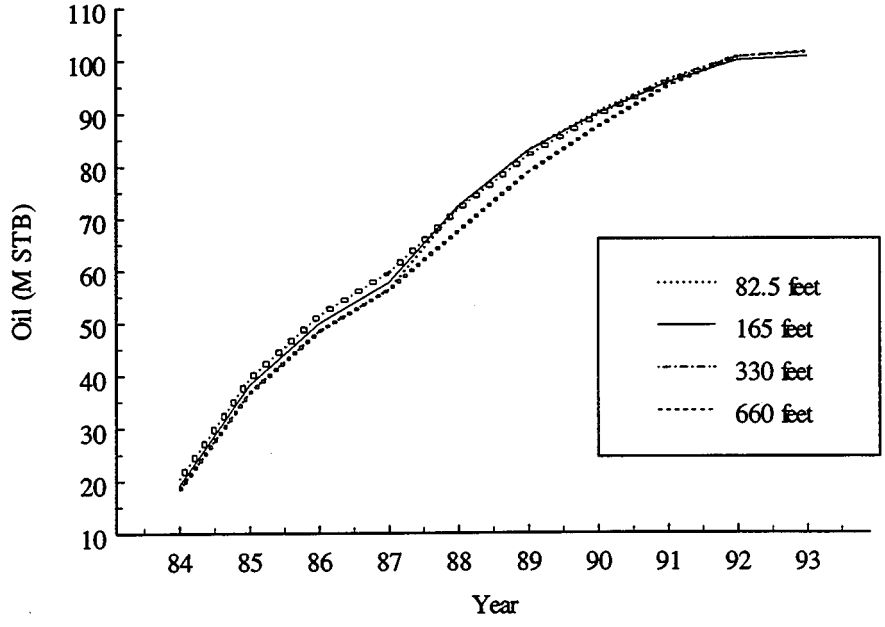

b)

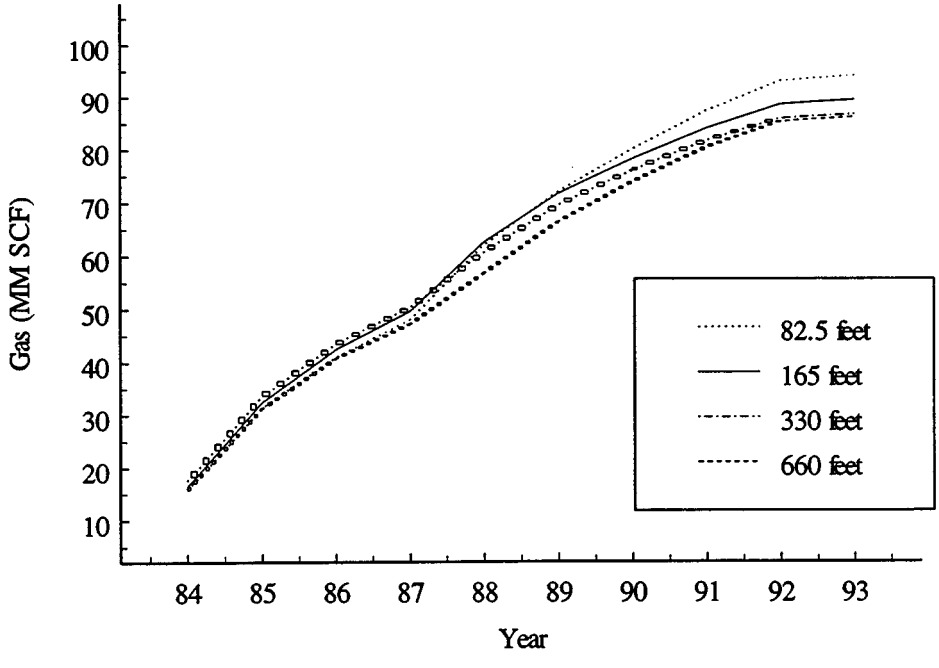

Figure3: Effect of block size on cumulative production for Michelle Ute well: a) oil, b) gas.

a)

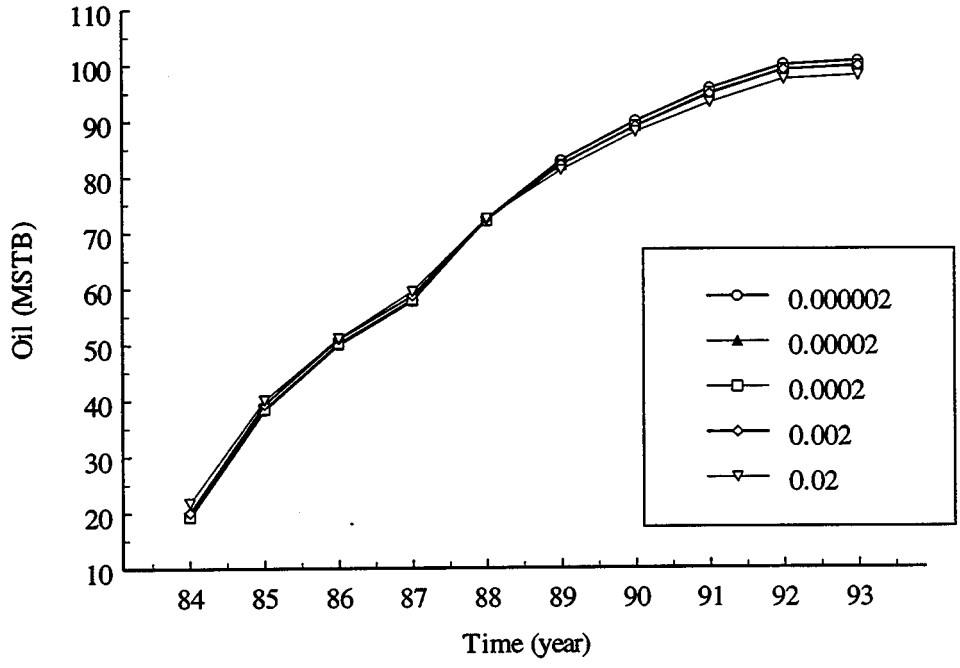

b)

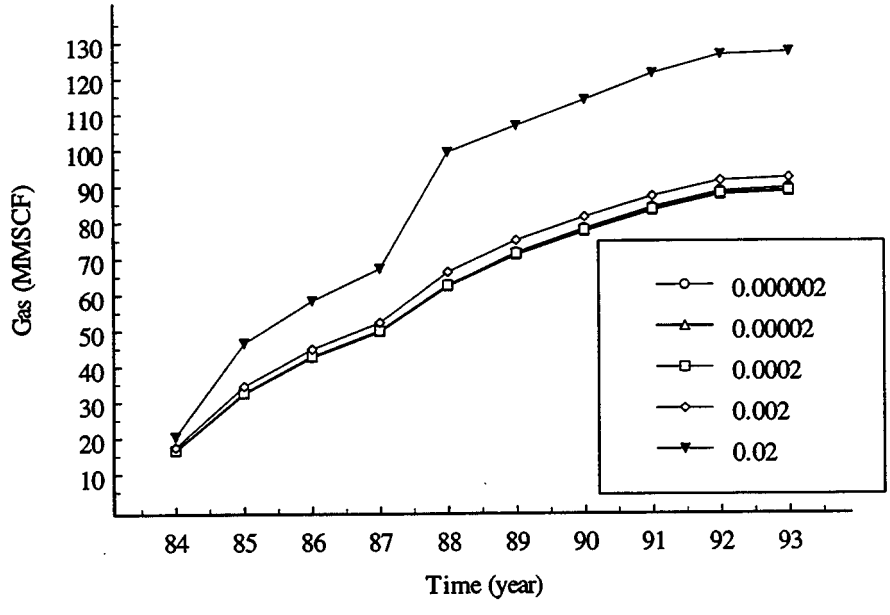

Figure 4: Effect of fracture porosity on cumulative production from Michelle Ute well: a) oil, b) gas.

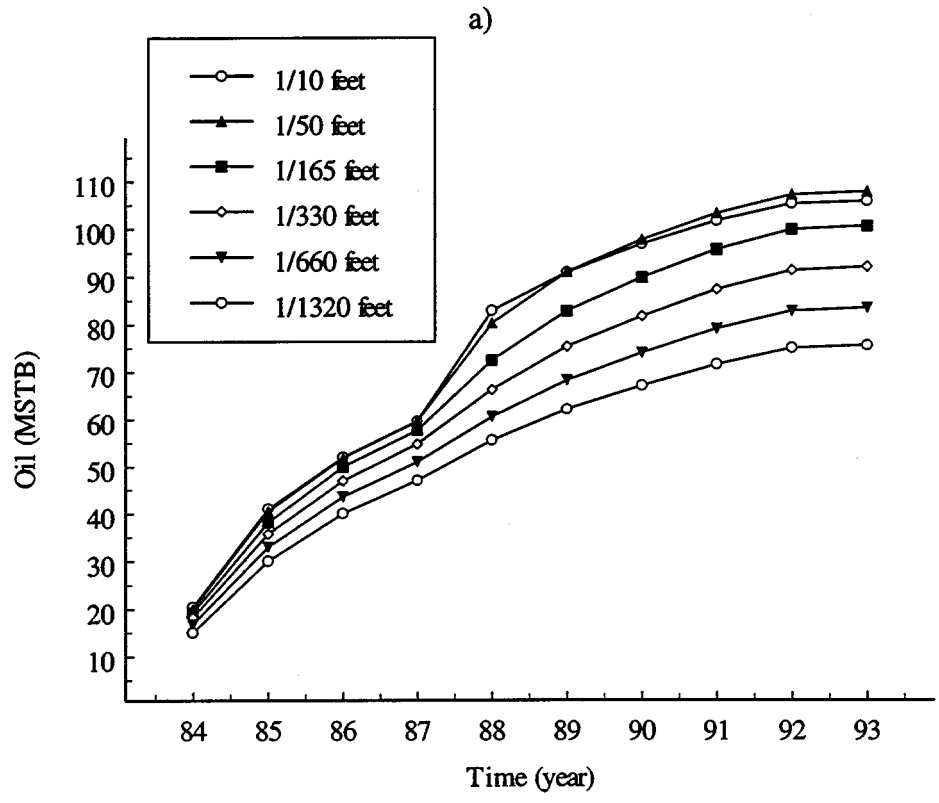

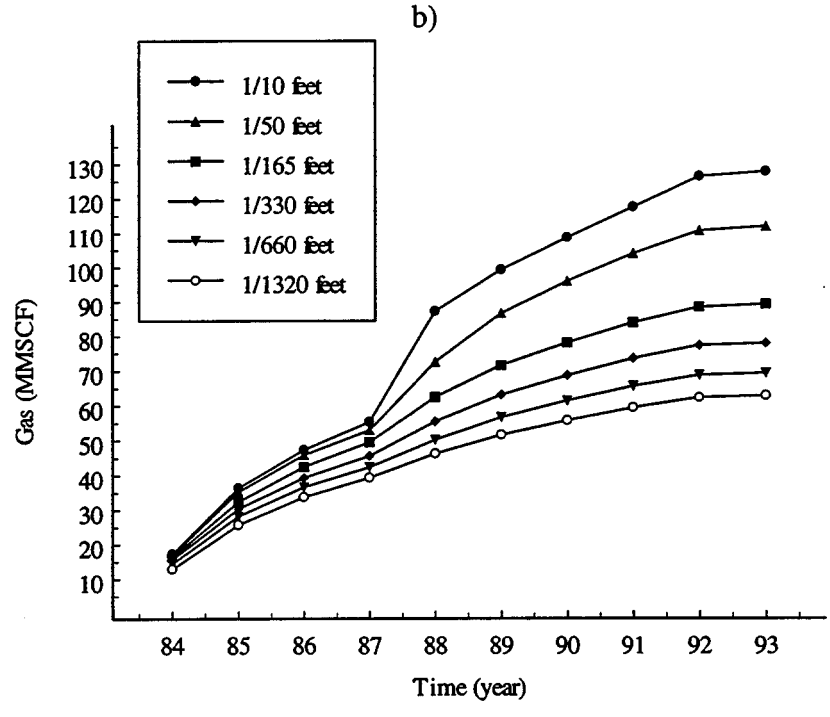

Figure 5: Effect of fracture frequency on cumulative production for Michelle Ute well: a) oil, b) gas.

a)

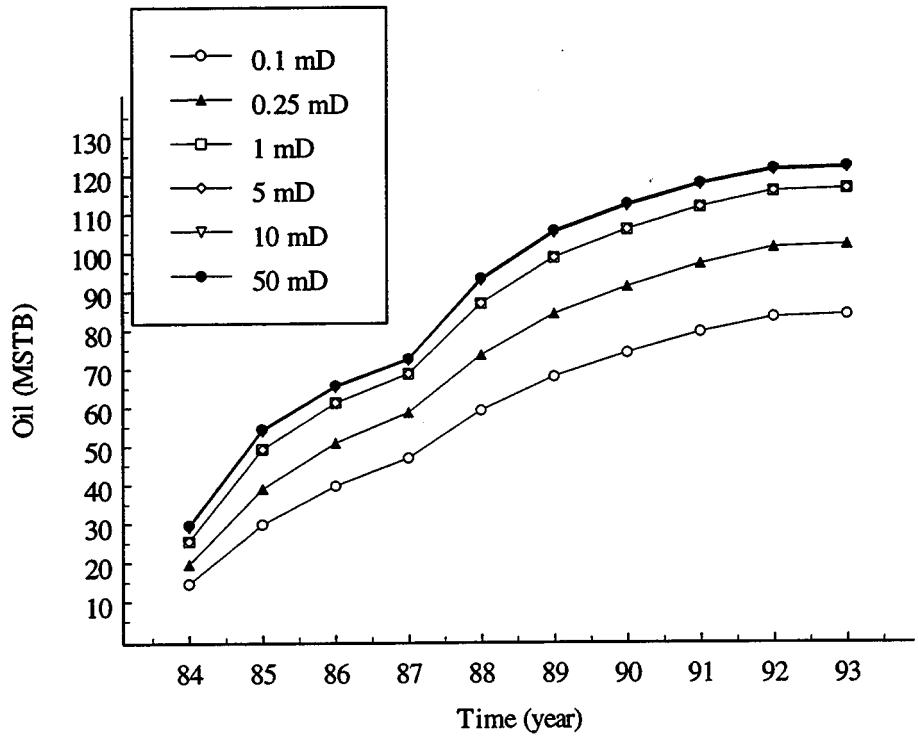

b)

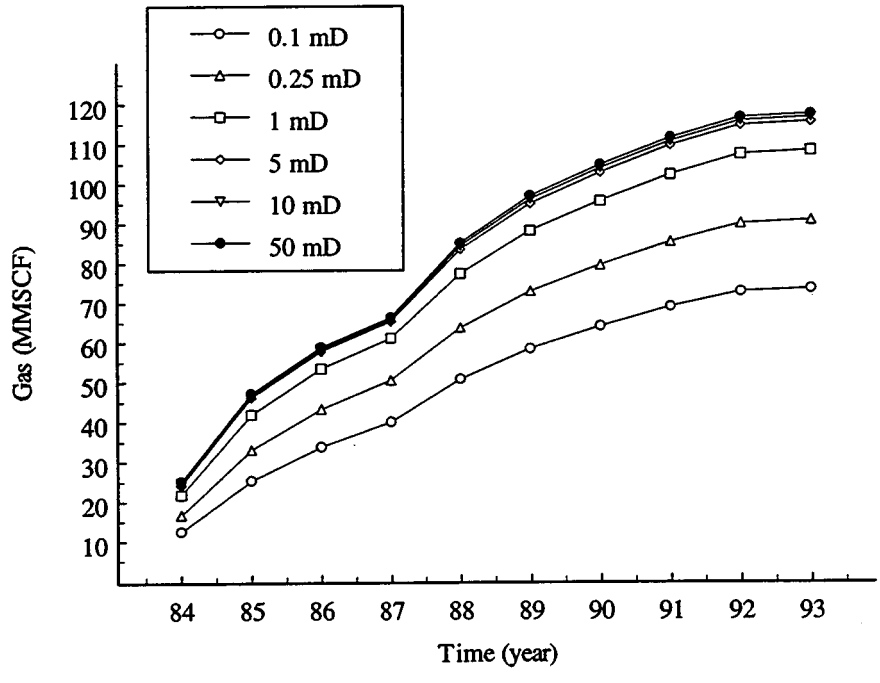

Figure 6: Effect of permeability on cumulative production from Michelle Ute well: a) oil, b) gas.

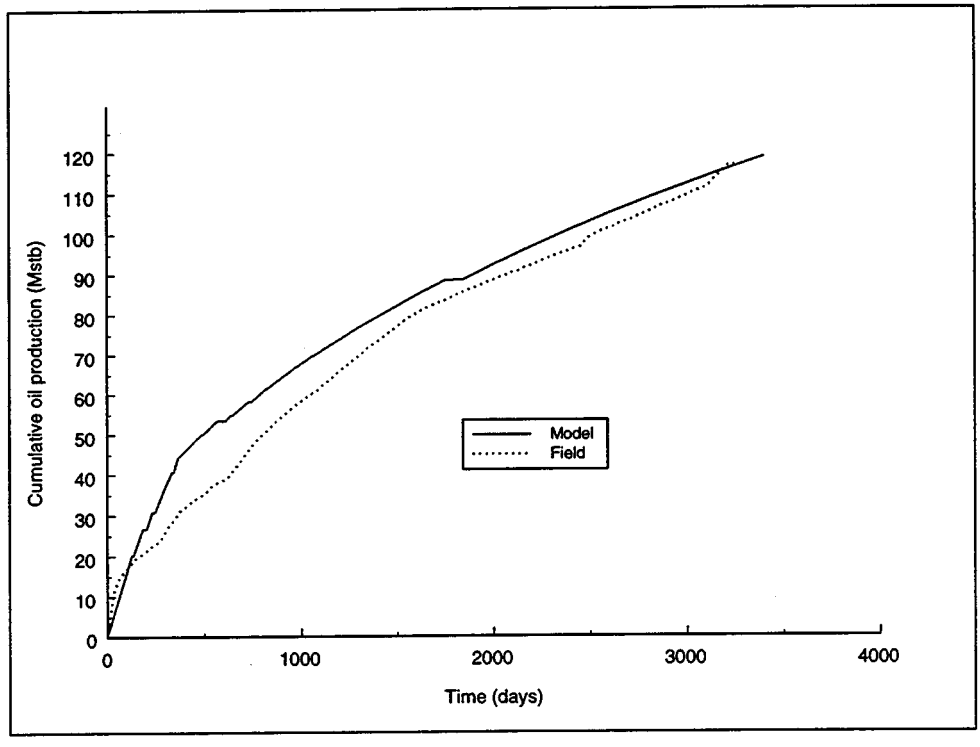

Figure 7: Comparison of oil cumulative production in Malnar Pike with the modified model predictions

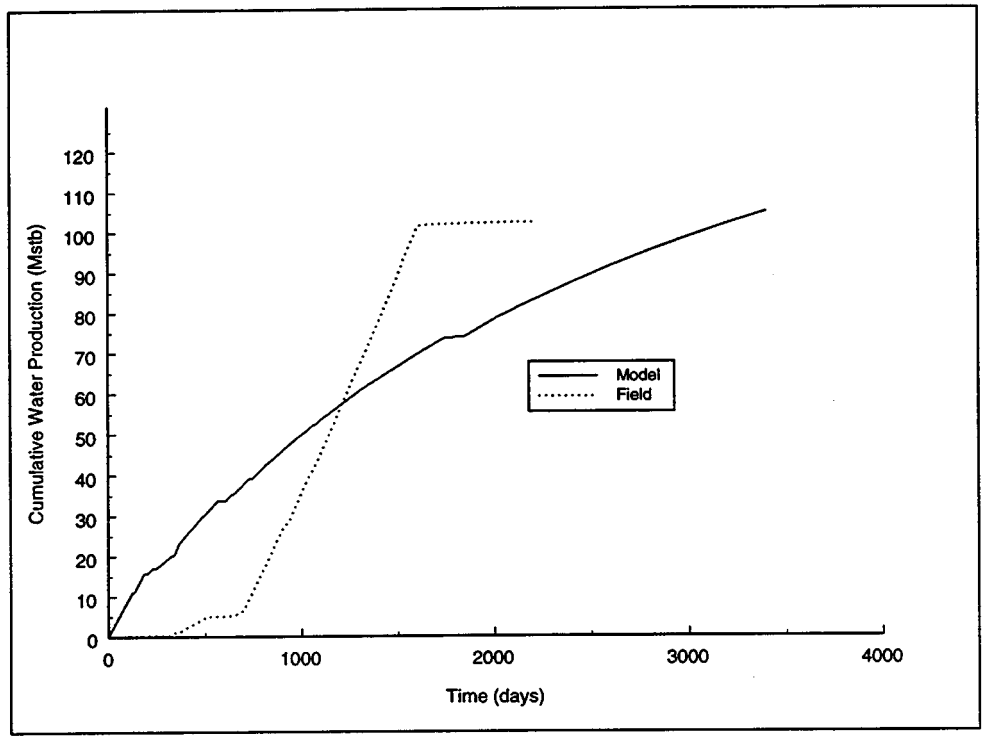

Figure 8: Comparison of water cumulative production in Malnar Pike with the modified model predictions

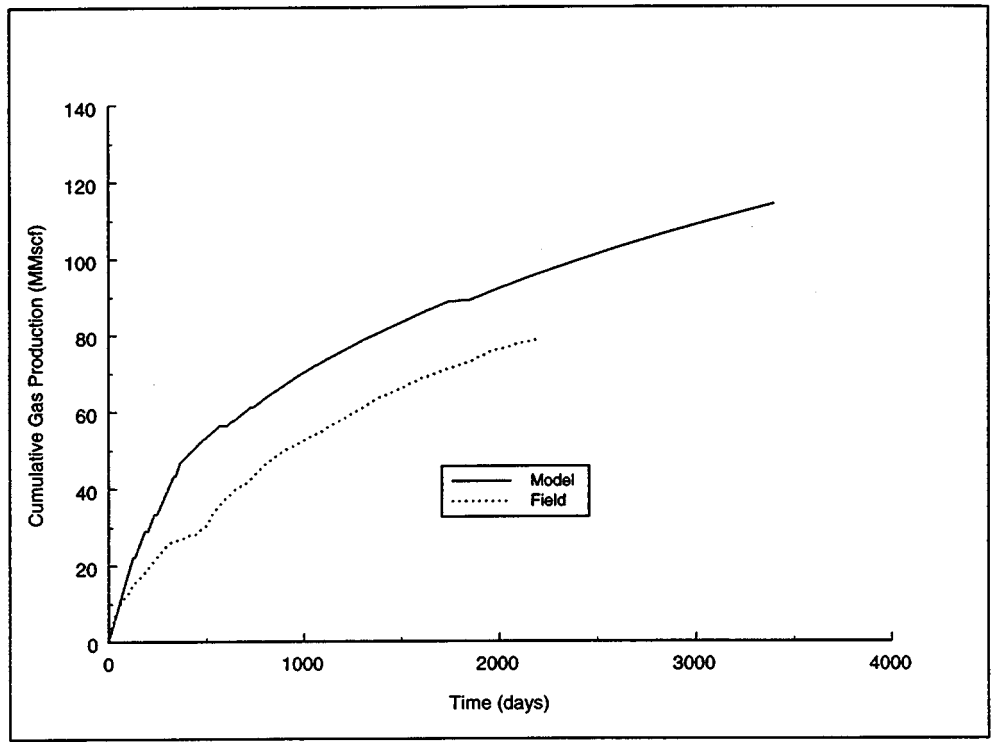

Figure 9: Comparison of gas cumulative production in Malnar Pike with the modified model predictions

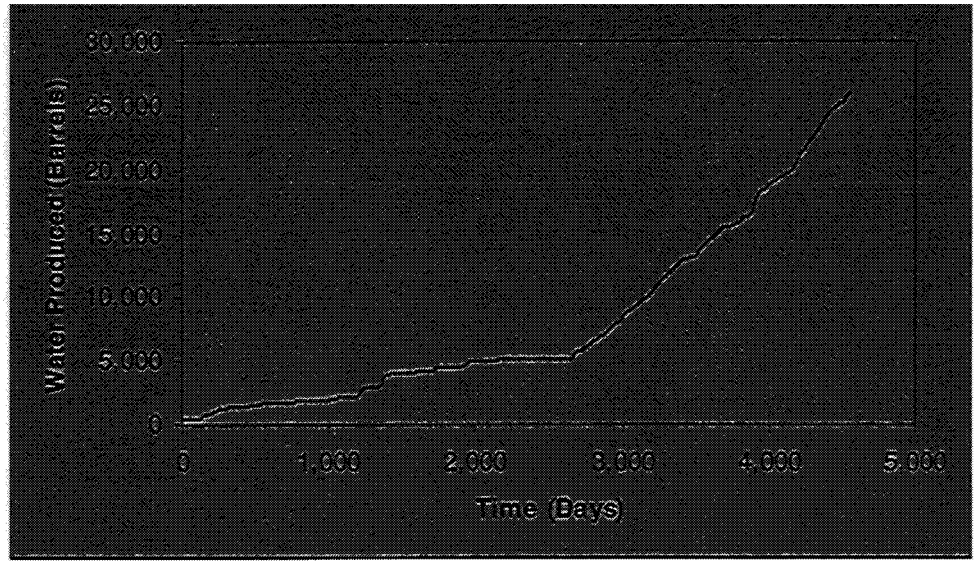

Figure 10: Water produced from the Michele-Ute; observe the sharp transition at around 2700 days.